second edition

SKELETAL IMAGING

ATLAS OF THE SPINE AND EXTREMITIES

TAYLOR HUGHES RESNICK

SAUNDERS

SKELETAL IMAGING

ATLAS OF THE SPINE AND EXTREMITIES

TAYLOR HUGHES RESNICK

SAUNDERS
ELSEVIER

second edition

VISIT…

LANZAROTE
Caliente.COM

SAUNDERS
ELSEVIER

3251 Riverport Lane
Maryland Heights, Missouri 63043

SKELETAL IMAGING: ATLAS OF THE SPINE AND EXTREMITIES, SECOND EDITION ISBN 978-1-4160-5623-2

Copyright © 2010, 2000 by Saunders, an imprint of Elsevier Inc.

All rights reserved. No part of this publication may be reproduced or transmitted in any form or by any means, electronic or mechanical, including photocopying, recording, or any information storage and retrieval system, without permission in writing from the publisher. Permissions may be sought directly from Elsevier's Rights Department: phone: (+1) 215 239 3804 (US) or (+44) 1865 843830 (UK); fax: (+44) 1865 853333; e-mail: healthpermissions@elsevier.com. You may also complete your request on-line via the Elsevier website at http://www.elsevier.com/permissions.

Notice

Neither the Publisher nor the Authors assume any responsibility for any loss or injury and/or damage to persons or property arising out of or related to any use of the material contained in this book. It is the responsibility of the treating practitioner, relying on independent expertise and knowledge of the patient, to determine the best treatment and method of application for the patient.

The Publisher

Library of Congress Control Number: 2009935763

Vice President and Publisher: Linda Duncan
Senior Acquisitions Editor: Kellie White
Associate Developmental Editor: Kelly Milford
Publishing Services Manager: Catherine Jackson
Senior Project Manager: Karen M. Rehwinkel
Design Direction: Jessica Williams

Printed in the United States of America

Last digit is the print number: 9 8 7 6 5 4 3 2 1

Working together to grow
libraries in developing countries

www.elsevier.com | www.bookaid.org | www.sabre.org

ELSEVIER BOOK AID International Sabre Foundation

To my parents and siblings,
who taught me the importance of hard work and persistence;
to my mentors who taught me the importance of lifelong learning;
to my students who provide continuous motivation;
and to my co-authors, Tudor Hughes and Donald Resnick.
JAMT

To my coauthor, John, who is clearly the first author.
And to my always-supportive family: my loving wife Kelly;
my three wonderful boys, Geraint, Griffith, and Rhett;
and my learned parents, Dorothy and Fred.
THH

It was a great pleasure and a distinct honor for me to work with two
skilled colleagues and friends, John Taylor and Tudor Hughes,
whose efforts far overshadow my contributions to this text.
They brought organization, dedication, and enthusiasm to
the project, sprinkled with good old-fashioned energy.
DR

PREFACE

BACKGROUND

We initially intended the Second Edition of *Skeletal Imaging* to be merely a modification of the First Edition. We planned only on updating the original and adding new case material that illustrates the more recent advances in the imaging diagnosis of musculoskeletal disorders. After all, only 9 years had elapsed between publication of the first edition, and the beginning of research for this edition. However, our survey of the literature published since 2000 persuaded us that a wealth of new information deserved synthesis and recognition. Our major dilemma was not so much to decide what to include, but what to exclude, and still meet our two principal objectives—to limit the atlas to a single volume and to address the most important musculoskeletal disorders. Accordingly, we have focused on disorders most frequently encountered in practice and on how those disorders appear on conventional radiography, CT scans, MR images, and to a lesser extent, radionuclide imaging and diagnostic ultrasonography.

WHO WILL BENEFIT FROM THIS BOOK?

Radiologists, chiropractors, and other clinicians who routinely interpret images of the musculoskeletal system will find the second edition an indispensable everyday reference. Radiology residents, chiropractic students, and other clinicians-in-training who are preparing for certification examinations can use it in the classroom, at the viewbox or monitor, and as a helpful study guide.

ORGANIZATION

The second edition retains the same organizational strategy: arranging musculoskeletal disorders according to anatomic region. This organization enhances the book's value as a reference tool for practitioners and is a practical way for students to learn a logical and methodical approach to patient assessment. Each chapter includes a description of the appearance of normal developmental anatomy and major anomalies and anatomic variants. It also demonstrates the full range of the most frequently encountered pathologic conditions, including dysplasias, physical injuries, internal derangements of joints, articular disorders, and bone tumors, as well as metabolic, hematologic, and infectious diseases.

Specifically, Chapter 1, "Introduction to Skeletal Disorders: General Concepts," consists of 19 tables summarizing the general characteristics of the most common disorders discussed and illustrated throughout the text. These tables offer an overview of information, such as age of onset, sites of involvement, clinical features, and general imaging features. This chapter was developed to avoid repetition of background material about disorders that affect several anatomic regions. Chapters 2 to 17 represent stand-alone monographs, each dealing with a specific anatomic site. The tables in these chapters emphasize only the site-specific manifestations of each entity, and they provide a sense of the range of disorders that characteristically affect that site. Furthermore, in each of these regional chapters, most of the important conditions are illustrated with routine radiographs, some of which are supplemented with conventional tomograms, CT or bone scans, MR images, or combinations of these. In addition, the chapters dealing with spinal regions and joints contain tables and illustrations of the normal developmental anatomy of that region through infancy, childhood, and adolescence. When reading these chapters, it may be useful, or even necessary, to refer to Chapter 1 for a more detailed discussion of the general features of a particular disorder.

The major emphasis of this work, however, is on the illustrations that the authors believe represent the most characteristic or typical presentations of disease entities. For the most part, the cases include commonly encountered disorders, although some disorders that are seen less commonly also are included because they are important to consider with regard to differential diagnosis. Purposely, the illustrations are as large as possible to best display the imaging findings. Each is accompanied by a detailed legend beginning with the primary diagnosis followed by a discussion of the imaging findings and any available and important clinical data. When MR imaging is displayed, detailed imaging parameters are included in the legend.

At least one useful reference for each condition has been included. The references are cited not only in the tables but also in the figure legends. These reference citations indicate the major sources of material and serve to direct the reader to further discussion. In Chapter 1, a bibliography of recommended readings includes many textbooks dealing with various aspects of skeletal radiology that served as sources for information.

It is our hope that by retaining the successful features and format of the First Edition, updating the text to reflect new information, and adding more case material that this edition will be as favorably received by readers and reviewers.

John A. M. Taylor
Tudor H. Hughes
Donald Resnick

ACKNOWLEDGMENTS

For the Second Edition

Many colleagues and friends who generously contributed so much to the first edition have done so again, in a variety of ways, for this revised second edition of *Skeletal Imaging*. We are enormously indebted to Dr. Brian Howard for contributing many more excellent case studies from his teaching files; to Stephanie Brown, DC, for compiling research material in the formative stages of revision; and to Gary Smith, DC, DACBR, Matthew Richardson, DC, and Laurie Rocco, DC, for carefully and thoroughly proofreading every chapter, word by word. We thank Pete Broomhall for editorial advice and assistance and Karen Rehwinkel and the other professionals of the Elsevier team and Saunders for providing encouragement, advice, and assistance at every turn. We are particularly indebted to our editors, Kellie White and Kelly Milford, for patiently and gently guiding us through every stage of production and for attempting to keep us on task and on schedule.

John A. M. Taylor
Tudor H. Hughes
Donald Resnick

The original two authors of *Skeletal Imaging* are enormously indebted to Dr. Tudor Hughes, a well-respected musculoskeletal radiologist and educator at the University of California, San Diego, and the second edition's recently recruited third author. His extensive knowledge and understanding of musculoskeletal disorders is matched by equally impressive skills in researching, fact-checking, writing, and editing. In addition to contributing hundreds of fascinating cases from his vast digital teaching files, he improved every chapter of *Skeletal Imaging* by making them more accessible to and productive for the reader.

John A. M. Taylor
Donald Resnick

ACKNOWLEDGMENTS

For the First Edition

The authors wish to acknowledge their appreciation of several persons who have generously contributed their time, effort, and case material during the production of this text. First, as is indicated in the legends associated with the illustrations, approximately 140 colleagues contributed one or more cases for inclusion in this atlas. Their willingness to share case material with us is very much appreciated. Of these persons, many deserve special mention for their donation of several cases: Drs. John Amberg, Appa Anderson, Richard Arkless, Felix Bauer, Gabrielle Bergman, Eve Bonic, Enrique Bosch, Sevil Kursunoglu Brahme, Thomas Broderick, Ann Brower, Clement Chen, Armando D'Abreu, Larry Danzig, Steven Eilenberg, Douglas Goodwin, Guerdon Greenway, Jorg Haller, Al Nemcek, Beverly Harger, Brian Howard, Roger Kerr, Phillipe Kindynis, Michael Mitchell, Arthur Newberg, Mini Pathria, Carlos Pineda, Jean Schils, Jack Slivka, Gary Smith, Richard Stiles, Phillip VanderStoep, Christopher Van Lom, and Vinton Vint. Numerous radiographs illustrating normal developmental anatomy were donated by Dr. David Sartoris from the University of California, San Diego; Dr. Jeffrey Cooley from Los Angeles College of Chiropractic; and Dr. Beverly Harger from Western States Chiropractic College. The authors also wish to acknowledge a number of persons who have willingly proofread portions of the manuscript at various stages of completion: Bill Adams, Eve Bonic, Todd Knudsen, Chad Warshel, Peter Broomhall, and especially Gary Smith, who was kind enough to carefully read and re-read every chapter.

The atlas would not have been possible without the input of a team of professionals at WB Saunders: Lisette Bralow, Frank Polizzano, Mary Reinwald, Walt Verbitski, Nicholas Rook, and Nancy Matthews. Their expertise and advice were crucial to the production of the atlas.

Finally, two members of our team who from the outset were absolutely essential to the completion of the text deserve recognition for their extraordinary efforts. Debra Trudell, our technical assistant, produced the photographic reproductions. Catherine Fix, our copy editor, meticulously edited every table, caption, and reference throughout the text. Their expertise, attention to detail, and demand for excellence are evident throughout the atlas. The authors are deeply indebted to Debra and Catherine and, indeed, to all of the persons cited here.

PART I

Introduction

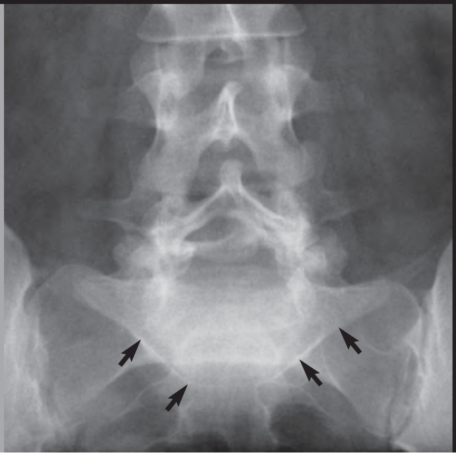

CHAPTER 1

Introduction to Skeletal Disorders: General Concepts

Many bone and joint disorders affect multiple regions of the skeleton. The tables in this chapter list anomalies and anatomic variants (Table 1-1), skeletal dysplasias (Table 1-2), spinal dysraphisms (Table 1-3), fractures (Tables 1-4 and 1-5), articular injuries (Table 1-6), articular disorders (Tables 1-7 to 1-11), bone tumors (Tables 1-12 and 1-13), tumorlike lesions of bone (Table 1-14), metabolic, nutritional, and endocrine disorders (Table 1-15), hematologic disorders (Table 1-16), osteonecrosis (Table 1-17), osteochondroses (Table 1-18), and infectious disorders of bones and joints (Table 1-19). These tables are intended to provide the reader with an overview of the common clinical, laboratory, and radiographic features of the more common disorders that typically appear in more than one skeletal location. Site-specific findings and features unique to each anatomic region are discussed further in subsequent chapters.

TABLE 1-1 Developmental Anomalies, Anatomic Variants, and Sources of Diagnostic Error: Concepts and Terminology*

			Examples	
Entity	**Characteristics**	**Terminology**	**Spine**	**Extremities**
Developmental anomaly	Marked deviation from normal standards as a result of a congenital or hereditary defect; such malformations usually represent a primary problem in the morphogenesis of a tissue	Nonsegmentation or synostosis	Block vertebrae	Tarsal coalition
		Aplasia or agenesis	Odontoid agenesis	Radial aplasia
		Hypoplasia	Hypoplastic C1 posterior arch	Glenoid hypoplasia
	May be asymptomatic or associated with significant clinical manifestations	Hyperplasia	Transverse process hyperplasia	Focal gigantism
	Spinal anomalies—general concepts: 1. Most spinal anomalies occur at transitional areas, such as the craniocervical, cervicothoracic, and thoracolumbar regions 2. When one anomaly is identified, always search for more because anomalies may be multiple 3. Anomalies may be isolated or associated with a syndrome 4. Osseous anomalies may be associated with underlying neurologic or visceral anomalies	Supernumerary bones	Transitional segments	Polydactyly
Anatomic variant	A modification of some anatomic characteristic that is considered normal Usually not associated with clinical manifestations; often encountered as an incidental finding	Areas of normal trabecular diminution or prominence	Prominent Hahn venous channels	Humeral pseudocyst Ward triangle of femur Pseudocystic region of calcaneus
		Normal sites of osseous irregularity	Cupid bow configuration of vertebral body simulating endplate fracture or Schmorl nodes	Avulsive cortical irregularity of the femur
Sources of diagnostic error	Misdiagnosis may occur under various conditions: Normal structures may be interpreted as abnormal owing to overlying shadows created by gas, soft tissue, or malpositioned structures	Overlying normal anatomy	Mach effect overlying odontoid, simulating fracture	Quadriceps muscle plane overlying femur, simulating fracture
	Rarefactions, irregularities, depressions, or proliferations of bone may be mistaken for evidence of disease	Anatomic irregularities	Normal notch in superior articulating process, simulating cervical pillar fracture	Normal sclerosis and fragmentation of calcaneal apophysis, simulating osteochondrosis
	Slight modifications in osseous anatomy may be judged to be significant	Anatomic variants	Osteosclerotic anterior arch of atlas, simulating an osteoblastic lesion	Rhomboid fossa in clavicle, simulating a destructive lesion

Data from Jones K: Smith's recognizable patterns of human malformation. 6th ed. Philadelphia, Saunders, 2005.

* The differentiation of anomalies, anatomic variants, and sources of error is often indistinct, owing to considerable overlap in the definitions.

TABLE 1-2 **Skeletal Dysplasias and Other Congenital Disorders**

Entity	General Characteristics	General Imaging Findings
Achondroplasia	Relatively common rhizomelic dwarfism Accentuated lumbar lordosis, waddling gait, prominent forehead, depressed nasal bridge, trident hand Short proximal extremities, normal length of spine ***Complications*** Spinal stenosis Brain stem compression from narrow foramen magnum	Spinal stenosis with posterior scalloping of vertebral bodies and decreased spinal canal diameter Vertebral bodies may be flattened or wedge-shaped Diaphyseal widening of long bones Narrow thorax, champagne glass pelvis Splayed and cupped metaphyses of long bones
Diastrophic dysplasia	Rare autosomal recessive dwarfing dysplasia	Short stature, progressive scoliosis, kyphosis
Spondyloepiphyseal dysplasia	***Congenita form*** Autosomal recessive, rhizomelic dwarfism Short trunk, respiratory and visual complications	***Congenita form*** Decreased height of vertebral bodies, pear-shaped vertebrae in childhood, kyphoscoliosis, accentuated kyphosis and lordosis, pectus carinatum, delayed ossification, hypoplasia of the odontoid with atlantoaxial instability
	Tarda form Milder, X-linked recessive form seen only in males	***Tarda form*** Heaped-up vertebrae, platyspondyly, disc space narrowing
	Rare lethal form Also termed *hypochondrogenesis*	
Dysplasia epiphysealis hemimelica	Trevor disease Uncommon developmental disorder Asymmetric cartilaginous overgrowth in one or more epiphyses May be localized or generalized Joint dysfunction, pain, limitation of motion, and a mass may accompany the disease	Resembles large eccentric osteochondroma arising from epiphyses particularly about the knee and ankle Bulky irregular ossification extending into soft tissues Computed tomographic (CT) or MR imaging may be useful to show the exact location and extent of the lesion and the presence of joint involvement
Mucopolysaccharidoses (MPS)	Enzyme deficiencies result in radiographic changes termed *dysostosis multiplex* Two types most commonly encountered: Hurler and Morquio syndromes	***MPS I-H (Hurler syndrome)*** Atlantoaxial instability may be present Rounded anterior vertebral margins with inferior beaking Posterior scalloping of vertebral bodies Paddle ribs, flared ilia, coxa valga, and coxa vara deformities ***MPS IV (Morquio syndrome)*** Hypoplastic or absent odontoid process with atlantoaxial instability Flattened vertebral bodies (platyspondyly) Posterior scalloping of vertebral bodies Short, thick tubular bones
Fibrodysplasia ossificans progressiva	Rare autosomal dominant disease Progressive ossification of skeletal muscle Results in limitation of motion, weakness, and eventual respiratory failure	Sheetlike ossification within soft tissues of neck, trunk, and extremities Hypoplastic vertebral bodies and intervertebral discs Apophyseal joint ankylosis Shortening of thumbs and great toes
Cleidocranial dysplasia	Rare autosomal dominant disorder characterized by incomplete ossification Widened cranial vault Drooping shoulders Abnormal gait, scoliosis, hypermobility, and dislocations of shoulders and hips Deafness, severe dental caries, and infrequently, basilar impression	Absent or hypoplastic clavicles Spine: multiple midline defects of the neural arch (spina bifida) *Pelvis:* widened symphysis pubis, coxa valga, coxa vara, underdeveloped bones with small pelvic bowl *Skull:* wormian bones, persistent metopic suture
Osteopetrosis	Sclerosing dysplasia Benign (autosomal dominant), intermediate, and lethal (malignant autosomal recessive) forms *Complications:* anemia, osteomyelitis, blindness, deafness, hemorrhage; brittle bones predispose to bone fragility and pathologic fracture	*Patterns of osteosclerosis:* diffuse osteosclerosis, bone-within-bone appearance, sandwich vertebrae

Continued

TABLE 1-2 Skeletal Dysplasias and Other Congenital Disorders—cont'd

Entity	General Characteristics	General Imaging Findings
Osteopoikilosis	Asymptomatic sclerosing dysplasia No associated complications	Multiple 2- to 3-mm circular foci of osteosclerosis Symmetric periarticular lesions resembling bone islands predominate about the hip, shoulder, and knee
Osteopathia striata	Extremely rare asymptomatic sclerosing dysplasia No associated complications	Regular, linear, vertically oriented bands of osteosclerosis extending from the metaphysis for variable distances into the diaphysis Metaphyseal flaring also may be seen May be related to cranial sclerosis and focal dermal hypoplasia (Goltz syndrome)
Melorheostosis	Rare sclerosing dysplasia ***Clinical findings*** May be associated with intermittent joint swelling, pain and limitation of motion, muscle contractures, tendon and ligament shortening, growth disturbances in affected limbs, and other musculoskeletal abnormalities	*Usual pattern:* hemimelic involvement of a single limb Peripherally located cortical hyperostosis resembling flowing candle wax on the surface of bones Para-articular soft tissue calcification and ossification may occur and may even lead to joint ankylosis May be positive on bone scans
Mixed sclerosing bone dystrophy	Rare condition in which patients have radiologic findings characteristic of more than one, and occasionally all, of the sclerosing dysplasias	Combinations of osteopetrosis, osteopoikilosis, osteopathia striata, and melorheostosis
Chondrodysplasia punctata	Conradi-Hünermann syndrome or stippled epiphyses Several different types of this rare multiple epiphyseal dysplasia have been identified, including mild and lethal forms Mild dwarfism, mental retardation, and joint contractures	Stippled calcification of vertebral bodies and epiphyses of the extremities In the rhizomelic form, coronal clefts are present within the vertebral bodies
Osteogenesis imperfecta	Inherited connective tissue syndrome Type II, congenital lethal form, has a high infant mortality rate Type I, the more common form, exhibits milder changes and is associated with a normal life expectancy Associated with osteoporosis and bone fragility, various degrees of dwarfism, blue sclera, ligament laxity, dentinogenesis imperfecta, and premature otosclerosis Complicated by multiple fractures, deafness, and pneumonia	Severe osteoporosis Pencil-thin cortices Multiple fractures of vertebrae and long bones Bowing deformities of long bones, especially lower extremity Rare cystic form—ballooning of bone, metaphyseal flaring, and honeycombed appearance of thick trabeculae
Progressive diaphyseal dysplasia	Rare autosomal dominant disorder also termed *Camurati-Engelmann disease* Typically bilateral and confined to the diaphyseal region of bone Progressive diaphyseal dysplasia affects predominantly the lower extremity Usually self-limited, resolving by 30-35 years of age	Bilateral fusiform thickening of the diaphysis of the long bones Cortical thickening and hyperostosis result in increased diaphyseal radiodensity
Hereditary osteo-onychodysostosis syndrome	Also termed *Fong syndrome*, *HOOD syndrome*, and *nail-patella syndrome* Associated with abnormalities of the fingernails and toenails	Absent or hypoplastic patellae Patellar dislocation, iliac horns, and radial head dislocation
Marfan syndrome	Autosomal dominant connective tissue disorder Muscular hypoplasia, joint laxity, dislocations, cataracts *Complications:* aortic aneurysm, lens dislocation	Long slender bones, arachnodactyly, thin cortices Kyphoscoliosis in 40%-60% of persons Posterior vertebral body scalloping from dural ectasia Significant osteopenia independent from body mass index (BMI)
Ehlers-Danlos syndrome	Rare connective tissue disorder characterized by joint hypermobility, blood vessel fragility, and skin elasticity; many forms identified *Complications:* valvular insufficiency, aortic aneurysm and dissection	Posterior scalloping of vertebral bodies Platyspondyly and kyphoscoliosis Genu recurvatum and other joint subluxations Heterotopic myositis ossificans Subcutaneous hemangiomas (calcified phleboliths)

For more detailed discussion, refer to:

Murray RO: The radiology of skeletal disorders. 3rd ed. New York, Churchill Livingstone, 1989.
Taybi H, Lachman RS: Radiology of syndromes, metabolic disorders, and skeletal dysplasias. 5th ed. St Louis, Mosby-Year Book, 2007.
Yochum TR, Rowe LJ: Essentials of skeletal radiology. 3rd ed. Baltimore, Williams & Wilkins, 2004.

TABLE 1-3 Classification of Spinal Dysraphisms*

Entity	Description
Open spinal dysraphisms • Myelomeningocele • Myelocele • Hemimyelomeningocele • Hemimyelocele	In open spinal dysraphisms, nervous tissue is exposed to the environment
Closed spinal dysraphisms	Closed spinal dysraphisms are covered by skin and therefore are not exposed to the environment 50% have cutaneous birth marks
With subcutaneous mass—lumbosacral • Lipomas with dural defect: lipomyelomeningocele and lipomyelocele • Terminal myelocystocele • Meningocele	
With subcutaneous mass—cervicothoracic • Nonterminal myelocystocele • Meningocele	
Without subcutaneous mass—simple dysraphic states • Intradural lipoma • Filar lipoma • Tight filum terminale • Persistent terminal ventricle • Dermal sinus	
Without subcutaneous mass—complex dysraphic states • Disorders of midline notochordal integration a. Dorsal enteric fistula b. Neurenteric cysts c. Diastematomyelia • Disorders of notochordal formation a. Caudal agenesis b. Segmental spinal dysgenesis	

* Modified from Rossi A, Gandolfo C, Morana G, et al: Current classification and imaging of congenital spinal abnormalities. Semin Roentgenol 41:250, 2006.

TABLE 1-4 Fractures in Adults: Concepts and Terminology

Entity	Classification	Typical Sites of Involvement	Characteristics
Acute fractures	Orientation	Any tubular bone	*Transverse:* bending or angular forces in long bones; tensile or traction forces in short bones; also pathologic fracture such as occurs with tumors *Oblique:* compression, bending, and torsion forces *Oblique-transverse:* combination of axial compression and bending forces *Spiral:* torsion forces
	Alignment	Any tubular bone, particularly lower extremity	*Varus angulation:* angulation of the distal fragment toward the midline of the body *Valgus angulation:* angulation of the distal fragment away from the midline of the body *Anterior or posterior angulation:* anterior or posterior angulation of the distal fragment
	Position	Any tubular bone	*Relationship of fracture fragments, exclusive of angulation:* displaced or undisplaced fractures *Displacement:* abnormalities of apposition and rotation *Apposition:* degree of bone contact at the fracture site: undisplaced fractures have 100% apposition; fracture surfaces may be separated and are termed *distracted fractures*; overlapping of fracture surfaces with consequent shortening is termed a *bayonet deformity* *Rotation:* rotation about the longitudinal axis; difficult to assess from routine radiographs
	Open fracture	Any site, particularly femur, tibia, and humerus	Communication between fracture and outside environment because of disruption of the skin ***Imaging findings*** Soft tissue defect, bone protruding beyond soft tissues, subcutaneous or intraarticular gas, foreign material beneath skin, absent pieces of bone Associated with high-impact trauma; high rate of infection
	Closed fracture	Any bone Most fractures are closed	Simple fracture in which the bone does not break through the skin
	Comminuted fracture	Any bone, especially long, tubular bones	Fracture with more than two fracture fragments Associated with high-impact injuries and crush injuries
	Butterfly fragment	Femoral and humeral diaphyses	Wedge-shaped fragment arising from the shaft of a tubular bone at the apex of the force input
	Segmental fracture	Femur, rib (flail chest)	Fracture lines isolate a segment of the shaft of a tubular bone
Impaction fractures	Depression fracture	Tibial plateau	One hard bone surface is driven into an apposing softer bone surface
	Compression fracture	Vertebral body	Forceful flexion of the spine resulting in a wedge fracture of the vertebral body with depression of the endplate within the spongiosa bone of the vertebral body
Pathologic fractures		Sites of skeletal metastasis, simple bone cyst, enchondroma, giant cell tumor, plasma cell myeloma, lymphoma, Ewing sarcoma, and other large osteolytic or osteosclerotic lesions	Fracture through a bone weakened by a disease process (such as osteoporosis, neoplasm, infection, or metabolic disease) with forces insufficient to fracture a normal bone *Insufficiency fracture* is a term commonly applied to pathologic fractures occurring at sites of nontumorous lesions (see stress-related bone injuries)
Stress-related bone injuries*	Fatigue fracture	Pars interarticularis of lumbar vertebrae (spondylolysis), metatarsal bones in military recruits (march fracture), and the lower extremity in athletes, joggers, and dancers	Fracture resulting from repeated cyclic loading applied to normal bones, with the load being less than that which causes acute fracture of bone Athletic, recreational, and occupational injuries are most common causes Tibial or femoral fatigue fractures may be longitudinal, involving a major portion of the diaphysis
	Insufficiency fracture	Sacrum, pubic rami, and lower extremity about the ankle, foot, knee, and hip	Pathologic fracture through a bone weakened by a disease process, initiated with forces insufficient to fracture a normal bone Disease processes include rheumatoid arthritis, osteoporosis, Paget disease, osteomalacia or rickets, hyperparathyroidism, renal osteodystrophy, osteogenesis imperfecta, osteopetrosis, fibrous dysplasia, and irradiation High signal intensity on T2-weighted and low signal intensity on T1-weighted spin echo MR sequences; scintigraphy also positive

Bone contusions (bone bruises)		Sites of trauma as a result of direct blow, shear forces, impaction of one bone upon another, or traction forces from avulsion injury	Not visible on radiographs Bone marrow edema seen on MR imaging; decreased signal intensity on T1-w images; increased signal on short tau inversion recovery (STIR) May be associated with microfractures
Acute chondral and osteochondral fractures		Distal portion of femur, patella, humeral head, glenoid rim, elbow, or hip	*Fracture of cartilage alone:* chondral fracture *Fracture of bone and cartilage:* osteochondral fracture Shearing, rotational, or tangentially aligned impaction forces generated by abnormal joint motion may result in fractures of two apposing joint surfaces Momentary, persistent, or recurrent dislocations and subluxations may result in these injuries Associated with painful joint effusion, joint locking, clicking, and limitation of motion; intraarticular bodies common; bodies may attach to synovium and eventually resorb
Osteochondritis dissecans		Femoral condyles and talus are most typical sites Less common sites: other tarsal bones, tibia, humeral head, glenoid cavity, acetabulum, and elbow (capitulum) Patellar involvement is rare	Fragmentation and possible separation of a portion of the articular surface Adolescent onset most frequent, but occurs from childhood to middle age Male > female Symptoms and signs usually begin in patients between ages 15 and 20 years; painful or painless joint effusion, joint locking, clicking, and limitation of motion Significant history of trauma in 50% of cases MR arthrography and computed tomographic arthrography are the most useful imaging techniques
Avulsion injuries	Avulsion fracture	Tibial tubercle, olecranon, pelvis, hip, tibial eminence, spinous process	Osseous fragment is pulled from the parent bone by a tendon, ligament, or portion of the joint capsule
Improper fracture healing	Delayed union	Scaphoid and improperly immobilized fracture sites	Conversion of fibrocartilage to bone is delayed or temporarily stopped
	Nonunion	Scaphoid, femoral neck, tibia, clavicle, odontoid process (os odontoideum), or any site improperly immobilized Also occurs in neurofibromatosis and fibrous dysplasia	Fracture site fails to heal completely during a period of 6-9 months after the injury Characterized by a pseudarthrosis consisting of a synovium-lined cavity and fluid typically related to persistent motion at the nonunion site *Local causes*[†]*:* infection, mechanical instability, inadequate vascularity, poor bone contact, and iatrogenic causes *Systemic causes*[†]*:* malnutrition, vitamin deficiency, smoking, medications, systemic medical conditions (diabetes), metabolic bone disorders
	Malunion	Any bone, especially long bones, such as the tibia and clavicle	Fracture that heals in an improper position Excessive angular or rotational deformity *Adults:* leads to deformity that may require surgical correction *Children:* often temporary phenomenon that may disappear spontaneously with further skeletal growth

---

[*] From Datir AP, Saini A, Connell A, et al: Stress-related bone injuries with emphasis on MRI. Clin Radiol 62:828, 2007.

[†] From Perumal V, Roberts CS: (ii) Factors contributing to non-union of fractures. Curr Orthop 21:258, 2007.

TABLE 1-5 Fractures in Children: Concepts and Terminology

Entity	Classification	Typical Sites of Involvement	Characteristics
Incomplete fractures	Greenstick fracture	Proximal metaphysis of the tibia and the middle third of the radius and ulna	Incomplete fracture that perforates one cortex, extends into the medullary bone, and compresses the opposite cortex
	Torus fracture	Distal end of radius and ulna and, less commonly, the tibia	Incomplete fracture resulting in buckling of the cortex Usually involves a longitudinal compression force insufficient to create a complete discontinuity of the bone Most frequent in children and osteoporotic persons
	Lead pipe fracture	Radius	Combined compressive and angular forces result in a combination of greenstick and torus fractures Most frequent in children
	Bowing fracture	Radius and ulna; less commonly, the clavicle, ribs, tibia, humerus, fibula, and femur	Plastic response of a long tubular bone to longitudinal stress Bowing occurs in the absence of cortical discontinuity; in the case of neighboring bones (radius and ulna or tibia and fibula), one bone typically fractures or dislocates, whereas bowing is identified in the adjacent bone Seen almost exclusively in children
Toddler fractures		Distal tibial diaphysis, fibula, femur, metatarsal bones, and, less commonly, the calcaneus, cuboid bone, pubic rami, or patella	Acute onset of fracture in children between the ages of 1 and 3 years Radiographs may initially be negative; scintigraphy useful in detecting such occult fractures *Classic toddler fracture:* nondisplaced, oblique fracture of the distal tibial diaphysis
Trauma to synchondroses (growth plate injuries)		Distal end of radius (50%) Distal end of humerus (17%) Distal end of tibia (11%) Distal end of fibula (9%) Distal end of ulna (6%) Proximal end of humerus (3%)	Up to 15% of all fractures to the tubular bones in children younger than 16 years of age involve the growth plate and neighboring bone 25%-30% of patients develop some degree of growth deformity
	Salter-Harris classification:		
	Type I (6%)		Pure epiphyseal separation; fracture of cartilaginous growth plate; no fracture of adjacent bones Slipped capital femoral epiphysis
	Type II (75%)		Growth plate fracture with associated metaphyseal fracture; metaphyseal fragment termed *Thurston-Holland fragment* or "corner sign"
	Type III (8%)		Growth plate fracture with associated vertically oriented epiphyseal fracture
	Type IV (10%)		Vertical fracture through the epiphysis, growth plate, and metaphysis
	Type V (1%)		Crushing or compressive injury of the growth plate with no associated osseous fracture Frequently overlooked
	Chronic stress injury	Growth centers of the distal end of the radius and ulna in competitive gymnasts; also proximal portion of the humerus, distal ends of the femur and tibia in other young athletes	Chronic application of stress to the developing growth center in vigorous or repetitious physical activity Part of the physis appears widened and irregular with accompanying sclerosis of the adjacent metaphysis; often unilateral or asymmetric distribution

TABLE 1-5 Fractures in Children: Concepts and Terminology—cont'd

Entity	Classification	Typical Sites of Involvement	Characteristics
Child abuse	Traumatic abuse of children	Fractures: • Ribs • Humerus • Femur • Tibia • Small bones of hands and feet • Skull • Spine (rare) • Sternum (rare) • Lateral portion of clavicle (rare) • Scapula (rare)	An estimated 2.8 million children are abused and 2000-5000 deaths are attributed to child abuse in the United States annually About 10% of children younger than the age of 5 years seen for trauma by emergency room physicians have inflicted injuries that are detectable radiographically in 50%-70% of cases Typical age range is between 1 and 4 years; after this age, children generally are able to escape the abuser or at least verbalize what has occurred Humeral fractures in infants and femoral fractures in crawling children should raise suspicion of abuse ***Imaging findings*** Fractures in different phases of healing, subperiosteal hemorrhage with periostitis, metaphyseal corner fractures, physeal injuries, and transverse diaphyseal or metaphyseal fractures ***Differential diagnosis*** Accidental fractures such as torus fractures of the distal end of radius, toddler's fractures of the tibia, clavicular and skull fractures; normal periostitis of infancy, metaphyseal changes of normal growth, congenital insensitivity to pain, rickets, osteogenesis imperfecta, metaphyseal and spondylometaphyseal dysplasia, Menkes kinky hair syndrome, congenital syphilis, and infantile cortical hyperostosis (Caffey disease)

TABLE 1-6 Articular Injuries: Concepts and Terminology

Entity	Typical Sites of Involvement	Characteristics
Joint effusion	Knee Elbow Tibiotalar joint Hip Glenohumeral joint	Accumulation of excessive synovial fluid within joint Bland effusion associated with acute injury or internal joint derangement Nonbloody effusions usually appear 12-24 hours after injury Absence of effusion with severe trauma may indicate capsular rupture of such a degree that fluid extravasates into the soft tissues surrounding the joint (especially the knee) Proliferative effusion associated with synovial proliferation as in inflammatory arthropathy and villonodular synovitis *Pyarthrosis:* purulent material in joint from pyogenic septic arthritis
Hemarthrosis	Any injured joint	Accumulation of blood within joint Hemarthroses usually result in joint effusion within the first few hours after injury May result from acute ligament injury, villonodular synovitis, hemophilia, synovial hemangioma, or other articular diseases
Lipohemarthrosis	Knee Glenohumeral joint Hip	Accumulation of blood and lipid material within synovial joint Fat-blood interface seen on cross-table horizontal beam lateral radiographs and on transaxial and sagittal MR images Double fluid-fluid levels on MR images are more specific for lipohemarthrosis than a single fluid-fluid level Usually related to acute intraarticular fracture
Pneumolipohemarthrosis	Hip	Accumulation of gas, blood, and lipid material within synovial joint Typically seen after fracture-dislocation Most evident on CT scans
Sprain	Acromioclavicular joint Tibiotalar joint Knee Elbow	*Grade I:* Mild sprain—stretching of the ligament but no tear *Grade II:* Moderate sprain—partial ligamentous disruption *Grade III:* Complete ligamentous rupture (with or without dislocation)
Subluxation	Glenohumeral joint, patellofemoral joint, and many other sites	Partial loss of contact between two osseous surfaces that normally articulate
Dislocation	Glenohumeral joint, acromioclavicular joint, patellofemoral joint, hip, apophyseal joints, and many other sites	Complete loss of contact between two osseous surfaces that normally articulate
Trauma to symphyses	Symphysis pubis, discovertebral joint, and manubriosternal joint	Abnormal separation of a joint containing fibrocartilage that normally is only slightly movable Cartilaginous nodes, posttraumatic annular vacuum cleft, limbus vertebrae, and apophyseal ring avulsion fractures resulting from discovertebral trauma
Heterotopic ossification	Large muscle groups in thigh, leg, upper arm	Self-limiting posttraumatic myositis ossificans Usually results from ossification of a chronic muscle hematoma ***Imaging findings*** Faint calcific intermuscular or intramuscular shadow may appear within 2-6 weeks of injury Well-defined region of ossification aligned parallel to the long axis of the tibia and fibula may be evident within 6-8 weeks Zonal phenomenon—ossific periphery with radiolucent center Cleavage plane may be evident between ossification and adjacent bone, helping to differentiate it from parosteal osteosarcoma Associated periostitis may relate to subperiosteal hemorrhage May be surrounded by edema seen on MR images ***Differential diagnosis*** Aggressive neoplasms such as parosteal, periosteal, and soft tissue osteosarcoma, and Ewing's sarcoma, liposarcoma, and synovial sarcoma

TABLE 1-7 Degenerative Joint Disease and Related Disorders

Entity	Typical Age of Onset (Years)	Sex	Target Sites of Involvement	Clinical Characteristics	General Imaging Findings
Primary osteoarthrosis	>40	Female : male, 10 : 1	Knee Hip Hand Foot Acromioclavicular joint Sacroiliac joint	Articular degeneration in the absence of any obvious underlying abnormality Accompanies aging ***Clinical findings*** Variable, depending on site of involvement Periarticular bony enlargement; e.g., Heberden nodes Pain and tenderness variable Joint stiffness and decreased mobility Joint crepitus Occasional instability Subluxation and deformity	Nonuniform or, less commonly, uniform joint space narrowing Osteophytes Subchondral sclerosis Subchondral cysts Subluxation, deformity, malalignment Buttressing Intraarticular osseous bodies; rarely, secondary synovial osteochondromatosis Absence of soft tissue swelling Absence of osteoporosis Fibrous ankylosis (rare) Unilateral or bilateral asymmetric distribution
Secondary osteoarthrosis	>25	Male = female	Glenohumeral joint Elbow Knee Hip Hand Foot Sacroiliac joint Acromioclavicular joint	Articular degeneration that is produced by alterations from a preexisting affliction; some of these are as follows: Previous septic arthritis or inflammatory arthritis, slipped capital epiphysis, developmental dysplasia of the hip, fracture or dislocation, obesity, Legg-Calvé-Perthes disease, osteonecrosis, acromegaly, ochronosis, and occupational or athletic injury Also occurs with crystal deposition diseases, synovial inflammatory processes, and other articular diseases ***Clinical findings*** Same as those of primary osteoarthrosis; findings may coexist with, or be obscured by, those of the primary disorder	(See Primary osteoarthrosis) Appearance of osteoarthrosis may obscure (or be obscured by) that of the primary articular process
Erosive inflammatory (Erosive) osteoarthritis	>40	Female	Hand	Unique form of inflammatory interphalangeal osteoarthritis ***Clinical findings*** Acute, inflammatory painful episodes of swelling and erythema overlying the interphalangeal joints of the fingers Prominent subluxation and osseous nodules (Heberden nodes) May clinically resemble synovial inflammatory diseases	Central erosions Nonuniform joint-space narrowing Subchondral sclerosis Osteophytes Subluxation

Continued

TABLE 1-7 Degenerative Joint Disease and Related Disorders—cont'd

Entity	Typical Age of Onset (Years)	Sex	Target Sites of Involvement	Clinical Characteristics	General Imaging Findings
Degenerative spine disease	>30	Male = female	C5-C7 T2-T5 T10-T12 L4-S1 Discovertebral junction Uncovertebral joint Apophyseal joint Costovertebral joint	Degenerative spine disease includes: Intervertebral osteochondrosis Spondylosis deformans Uncovertebral osteoarthrosis Apophyseal joint osteoarthrosis Costovertebral joint osteoarthrosis ***Clinical findings*** Variable, depending on anatomic site and severity Symptoms range from absent to severe and include acute or chronic pain, stiffness, radiculopathy (rare), and associated muscle spasm Poor correlation between symptoms and radiographic findings; patients with severe degenerative changes may have minimal or no symptoms, whereas those with minimal degenerative changes may have considerable symptoms	*Spondylosis deformans:* Osteophytes and osseous ridging *Intervertebral osteochondrosis:* Disc space narrowing Intradiscal vacuum phenomenon Disc calcification (rare) Subchondral bone sclerosis Schmorl (cartilaginous) nodes *Uncovertebral joint osteoarthrosis:* Sclerosis, hypertrophy, and joint space narrowing *Apophyseal (facet) joint osteoarthrosis:* Sclerosis, hypertrophy, joint space narrowing, subluxation, capsular laxity, and synovial cysts Frequently contributes to foraminal stenosis
Diffuse idiopathic skeletal hyperostosis (DISH)	>50	Male > female	Thoracic spine Cervical spine Lumbar spine T7-T11 most common segments	DISH affects 25% of men and 15% of women older than 50 years of age ***Clinical findings*** Symptoms are mild in comparison with the often dramatic radiographic signs Middle to lower back pain and stiffness Restricted motion Recurrent Achilles tendinosus Recurrent "tennis elbow" Cervical dysphagia Palpable calcaneal, patellar, and olecranon enthesophytes	*Axial skeleton:* *Flowing hyperostosis:* thick (1-20 mm) linear shield of ossification along the anterolateral aspect of the spine (see Diagnostic criteria below) *Appendicular skeleton:* Enthesopathy and ligament ossification about the pelvis, hip, knee, foot, heel, and other extraaxial sites ***Diagnostic criteria*** 1. Flowing calcification and ossification along the anterolateral aspect of at least four contiguous vertebral body segments with or without associated localized pointed excrescences at the intervening vertebral body—intervertebral disc junctions 2. Relative preservation of intervertebral disc height in the involved vertebral segment and absence of extensive degenerative disc disease 3. Absence of apophyseal joint bony ankylosis and sacroiliac joint erosion, sclerosis, or intraarticular osseous fusion

TABLE 1-8 Inflammatory Articular Disorders

Entity	Typical Age of Onset (Years)	Sex	Target Sites of Involvement	Clinical Characteristics	Laboratory and Imaging Findings
Rheumatoid arthritis	25-55	Female : male, 2 or 3 : 1	Hand Foot Wrist Knee Elbow Glenohumeral joint Acromioclavicular joint Cervical spine	Bilateral symmetric polyarticular synovial inflammatory process Five to 15 times as common as ankylosing spondylitis ***Clinical findings*** Acute or chronic episodes of painful joint swelling Prodromal symptoms: fatigue, anorexia, weight loss, malaise, muscular pain, and stiffness Capsular and ligamentous laxity Muscular contraction and spasm Bursitis, tendinitis, and tenosynovitis ***Diagnostic criteria**** 1. Morning stiffness in and around joints lasting at least 1 hour before maximal improvement 2. Soft tissue swelling (arthritis) of three or more joint areas observed by a physician 3. Swelling (arthritis) of the proximal interphalangeal, metacarpophalangeal, or wrist joints 4. Symmetric swelling (arthritis) 5. Rheumatoid nodules 6. The presence of rheumatoid factor 7. Radiographic erosions or periarticular osteopenia, or both, in hand or wrist joints, or in both Rheumatoid arthritis is defined by the presence of four or more criteria; criteria 1 through 4 must have been present for at least 6 weeks	***Laboratory findings:*** Normochromic or hypochromic normocytic anemia (common) *Leukocytes:* normal, elevated, or, infrequently, decreased *Erythrocyte sedimentation rate:* markedly elevated *Rheumatoid factor:* present in high titers Positive LE phenomenon (8%-27% of patients) ***Imaging findings*** Fusiform soft tissue swelling (early finding) Concentric joint space narrowing (early finding) Marginal and central subchondral erosions Subchondral cysts Cortical atrophy and osteolysis Absent or mild sclerosis Periarticular osteoporosis Synovial cysts Joint instability, particularly atlantoaxial joint Fibrous ankylosis, and infrequently, bony ankylosis Deformity, subluxation, dislocation Pathologic fractures
Juvenile idiopathic arthritis[†]	5-10	Variable, depending on disorder	Hand Wrist Knee Cervical spine Foot Ankle Elbow Heel Hip	Several arthropathies have been identified in children ***Disorders*** 1. Systemic arthritis 2. Oligoarthritis Persistent Extended 3. Polyarthritis Rheumatoid factor negative Rheumatoid factor positive 4. Enthesitis-related arthritis 5. Psoriatic arthritis 6. Other ***Clinical findings*** Variable, depending on disorder Subcutaneous nodules Acute joint swelling, pain, and erythema *Systemic manifestations:* Vasculitis Hepatosplenomegaly Iridocyclitis	Soft tissue swelling Periarticular osteoporosis with metaphyseal lucent bands Diffuse joint space loss (late finding) Erosions (late finding) Periostitis Growth disturbances Apophyseal joint ankylosis Extraaxial joint ankylosis Atlantoaxial instability Bony proliferation and periostitis Epiphyseal compression fractures

Continued

TABLE 1-8 Inflammatory Articular Disorders—cont'd

Entity	Typical Age of Onset (Years)	Sex	Target Sites of Involvement	Clinical Characteristics	Laboratory and Imaging Findings
Ankylosing spondylitis	15-35	Male : female, 4 : 1 to 10 : 1	Sacroiliac joint Thoracolumbar spine Cervical spine Symphysis pubis Hip Shoulder Heel	Most common seronegative spondyloarthropathy ***Clinical findings*** *Axial skeleton:* Middle and low back pain and stiffness Limited lumbar and thoracic spine motion Limited chest expansion (1 inch or less) Sacroiliac joint pain Radiating pain to lower extremity (50%) Muscle spasm Increased thoracic kyphosis *Extraaxial skeleton:* As many as 50% of patients affected Mild symmetric involvement is typical Pain, tenderness, and swelling *Extraskeletal findings:* Iritis (20% of cases) Aortic insufficiency and aneurysms Pulmonary fibrosis (upper lobes) Pleuritis Inflammatory bowel disease Amyloidosis (especially kidney)	***Laboratory findings:*** Elevated erythrocyte sedimentation rate Negative rheumatoid and LE factors HLA-B27 histocompatibility antigen present in 90% of patients (6 to 8% of general population) ***Radiographic findings*** *Spine:* marginal syndesmophytes, erosions, ligament ossification (see Tables 3-9 and 3-10) *Sacroiliac joints:* bilateral symmetric involvement; joint erosion initially with eventual ankylosis *Extraaxial skeleton:* joint erosions; partial or complete osseous ankylosis; enthesopathy
Psoriatic arthropathy	20-50	Male = female	Hand Foot Sacroiliac joint Thoracolumbar spine Cervical spine	Seronegative spondyloarthropathy Less common than ankylosing spondylitis Two to 6% of patients with psoriatic skin lesions have associated psoriatic arthropathy ***Clinical patterns*** 1. Polyarthritis with distal and proximal interphalangeal joint involvement 2. Deforming arthritis characterized by ankylosis and arthritis mutilans 3. Symmetric rheumatoid-like arthritis (rare) 4. Asymmetric oligoarthritis or monoarthritis 5. Combination of spondyloarthropathy and sacroiliitis ***Signs and symptoms*** *Long history of psoriatic skin lesions:* patchy, scaly macular lesions *Nail changes:* pitting, discoloration, splintering, erosion, thickening, and detachment	***Laboratory findings*** HLA-B27 antigen present in as many as 60% of patients with psoriatic arthropathy Mild anemia Elevated erythrocyte sedimentation rate Elevated serum uric acid levels (occasionally) Negative for rheumatoid factor ***Imaging findings*** *Axial skeleton:* Paravertebral ossification (nonmarginal parasyndesmophytes) Unilateral or bilateral asymmetric sacroiliitis Atlantoaxial instability *Extraaxial skeleton:* Soft tissue swelling: periarticular or involving entire digit (sausage digit) Absence of osteoporosis Severe joint space destruction with marginal erosions

				Low back pain, fever, fatigue, stiffness, conjunctivitis, iritis, and scleritis Sternocostoclavicular hyperostosis; pustular lesions of the skin in the hand and foot (pustulosis palmaris et plantaris) are observed in some patients with hyperostosis of the clavicles, ribs, and sternum and may be related to psoriasis, chronic recurrent multifocal osteomyelitis, and the synovitis-acne-pustulosis-hyperostosis-osteomyelitis (SAPHO) syndrome or pustulotic arthro-osteitis (PAO)	New bone formation: whiskering, enthesopathy *Ray pattern:* involvement of all joints in one digit, frequently associated with sausage digit Tuft resorption and proliferation (ivory phalanx)
Reactive arthritis associated with Reiter syndrome	15-35	Male : female, 5 : 1 to 50 : 1	Foot Heel Ankle Knee Hip Sacroiliac joint Spine Hand (rare) Shoulder (rare) Elbow (rare)	***Clinical findings*** Urethritis (often first symptom) Ocular abnormalities *Early:* transient conjunctivitis (common) *Later:* episcleritis, keratitis, uveitis Circinate balanitis Keratoderma blennorrhagicum Keratosis of the nails ***Other findings*** Fever, weight loss, thrombophlebitis, amyloidosis, arthritis	***Laboratory findings*** HLA-B27 antigen present in as many as 75% of patients Leukocytosis Anemia Elevated erythrocyte sedimentation rate ***Imaging findings*** *Axial skeleton:* Paravertebral ossification (nonmarginal parasyndesmophytes) Unilateral or bilateral asymmetric sacroiliitis Atlantoaxial instability *Extraaxial skeleton:* Soft tissue swelling: periarticular or involving entire digit (sausage digit) Absence of osteoporosis Diffuse joint space loss *New bone formation:* whiskering, enthesopathy
Enteropathic arthropathy	Variable, depending on underlying condition	Variable, depending on underlying condition	Sacroiliac joint Spine	Seronegative spondyloarthropathy resembling ankylosing spondylitis radiographically Associated with many inflammatory enteropathic diseases, as follows: ulcerative colitis, Crohn disease, Whipple disease, *Salmonella*, *Shigella*, and *Yersinia* infections, and intestinal bypass surgery Frequency of chronic inflammatory bowel disease in ankylosing spondylitis varies from 2%-18%	***Laboratory findings*** HLA-B27 antigen present in 90% of patients with ulcerative colitis and Crohn disease who develop spondylitis or sacroiliitis ***Imaging findings*** Spondylitis and sacroiliitis identical to those of ankylosing spondylitis Occasional peripheral joint abnormalities

Continued

TABLE 1-8 Inflammatory Articular Disorders—cont'd

Entity	Typical Age of Onset (Years)	Sex	Target Sites of Involvement	Clinical Characteristics	Laboratory and Imaging Findings
Dermatomyositis and polymyositis	5-10 and 30-50	Female : male, 2 : 1	Soft tissues of the thigh, leg, and arm	Diseases characterized by diffuse inflammation and degeneration of striated muscle with widespread sheetlike calcification in soft tissues Unknown cause; affects patients of all ages Dermatomyositis affects skin and muscle, and polymyositis affects only muscle ***Clinical findings*** Progressive, symmetric, proximal weakness, Raynaud phenomenon (33% of cases) and arthralgia (50% of cases)	***Laboratory findings*** Elevated serum muscle enzyme or urinary creatinine excretion levels Abnormal electromyogram results Abnormal muscle biopsy ***Imaging findings*** Initial soft tissue edema Soft tissue atrophy Sheetlike soft tissue calcification and infrequently, ossification Phalangeal tuft resorption
Scleroderma (progressive systemic sclerosis)	20-50	Female > male	Hand Wrist Foot Ribs Spine (rare)	Uncommon collagen vascular disease that affects skin, lungs, gastrointestinal tract, heart, kidneys, and musculoskeletal system *Two types:* 1. Localized scleroderma: scleroderma without systemic involvement 2. Progressive systemic sclerosis: scleroderma with systemic involvement ***Clinical findings*** Raynaud phenomenon or syndrome Muscle weakness Dysphagia (smooth muscle weakness) Edema, rigidity, thickening, and tightening of the skin of the hands, feet, and face Melanotic hyperpigmentation, vitiligo, and telangiectasis Secondary infection Pulmonary or renal involvement	***Laboratory findings*** Elevated erythrocyte sedimentation rate (60%-70% of patients) Positive rheumatoid factor (30%-40% of patients) Presence of antinuclear antibodies (35%-96% of cases) High levels of protein in aspirated synovial fluid ***Imaging findings*** Globular accumulations of periarticular and subcutaneous soft tissue calcinosis Phalangeal tuft erosion Conical appearance of fingertips resulting from soft tissue resorption Erosions of superior aspect of ribs Paraspinal calcification

Systemic lupus erythematosus (SLE)	20-45	Female > male	Hand Osteonecrosis in femoral head, femoral condyles, and humeral head	Relatively common connective tissue disorder characterized by significant immunologic abnormalities, involvement of numerous organ systems, and musculoskeletal involvement ***Clinical findings*** Variable depending on organ system involvement; most common manifestations include malaise, weakness, fever, anorexia, weight loss, polyarthritis, skin rashes (erythema nodosum and butterfly rash on face), neurologic findings, and several visceral inflammatory processes	***Laboratory findings*** Anemia (70%-80% of patients) Leukopenia Plasma protein abnormalities False-positive serologic test for syphilis Formation of LE cells and other antinuclear factors Autoagglutination of red blood cells ***Imaging findings*** Symmetric, deforming nonerosive arthropathy Acrosclerosis Erosions and subchondral cysts (rare) Phalangeal tuft resorption *Osteonecrosis:* occurs in patients regardless of whether they received corticosteroid therapy; possibly caused by vasculitis; hip most common site Tendon weakening and rupture Insufficiency fracture Osteomyelitis and septic arthritis
Mixed connective tissue disease	20-50	Female > male	Hand Wrist Foot	Overlap syndromes and mixed connective tissue diseases include combinations of rheumatoid arthritis, dermatomyositis, scleroderma, and systemic lupus erythematosus ***Clinical findings:*** Variable, depending on predominant connective tissue diseases involved	***Laboratory findings*** Presence of ribonuclease-sensitive extractable nuclear antigen ***Imaging findings*** Imaging features variable; may result in diffuse joint space narrowing, erosions, soft tissue calcinosis, deforming nonerosive arthropathy, osteonecrosis, phalangeal tuft resorption, marginal erosions

[*] From Arnett FC, Edworthy SM, Bloch DA, et al: The American Rheumatism Association 1987 revised criteria for the classification of rheumatoid arthritis. Arthritis Rheum 31:315, 1988.

[†] From Johnson K, Gardner-Medwin J: Childhood arthritis: classification and radiology. Clin Radiol 57:47, 2002. Classification according to the International League for Rheumatology.

TABLE 1-9 Articular Disorders: Crystal Deposition Diseases and Metabolic Disorders

Entity	Typical Age of Onset (Years)	Sex	Target Sites of Involvement	Clinical Characteristics	Laboratory and Imaging Findings
Calcium pyrophosphate dihydrate (CPPD) crystal deposition disease	>50	Male = female	Knee Symphysis pubis Hand Wrist Hip Shoulder Elbow Spine	Common disorder characterized by CPPD crystal deposition within soft tissues May be precipitated by local damage ***Clinical patterns*** Most persons are asymptomatic; several types of symptomatic disease include the following: 1. Pseudodegenerative joint disease 2. Pseudogout 3. Pseudorheumatoid arthritis 4. Pseudoneuropathic osteoarthropathy 5. Miscellaneous patterns ***Clinical findings*** Asymptomatic, or may be characterized by acute, subacute, or chronic self-limited attacks of joint pain, swelling, and erythema Flexion contractures, morning stiffness, fatigue, restricted joint motion Many associated diseases and disorders have been reported	***Laboratory findings*** Pyrophosphate crystals in synovial fluid aspirate Elevated erythrocyte sedimentation rate ***Imaging findings*** Bilateral asymmetric involvement Local soft tissue swelling Calcification of intraarticular hyaline cartilage and fibrocartilage, synovium, capsules, tendons, and ligaments *Pyrophosphate arthropathy:* articular space narrowing, prominent subchondral sclerosis, cyst formation, and osteophytes *Advanced disease:* articular destruction and fragmentation resembling neuropathic osteoarthropathy Features characteristic of CPPD crystal deposition disease allowing differentiation from degenerative joint disease include prominent calcification, involvement of unusual joints and compartments, and the presence of extensive sclerosis, cysts, fragmentation, osseous debris, and variable osteophyte formation
Calcific bursitis and tendinitis	40-70	Male = female	Shoulder *Rare sites:* Wrist Hand Elbow Hip Neck	Calcium hydroxyapatite crystal deposition in tendons and bursae about the joints Calcific tendinitis of the rotator cuff is the most common clinical condition ***Clinical findings*** Solitary or multiple periarticular calcific deposits can be asymptomatic or may be associated with painful episodes *Acute symptoms:* pain, tenderness on pressure, local edema or swelling, restricted active or passive motion and, infrequently, mild fever *Chronic symptoms:* mild, nonincapacitating pain and tenderness More common in manual workers than sedentary workers Often associated with acute or chronic trauma	***Laboratory findings*** Elevated erythrocyte sedimentation rate Identification of calcium hydroxyapatite crystals by electron microscopy, radioisotope techniques, or x-ray diffraction analysis (tests that are performed only infrequently) ***Imaging findings*** Single or multiple cloudlike, linear, triangular, or circular soft tissue calcifications at tendon insertion sites and within bursae Occasionally, large tumorlike accumulations of calcification are seen about joints in patients with chronic renal disease or collagen vascular disorders Associated osseous destruction, marrow changes and soft tissue calcification may be confused with tumor radiologically and pathologically

Gouty arthropathy	>40	Male : female, 20 : 1	Common: Foot Hand Wrist Elbow Knee Uncommon or rare: Hip Shoulder Spine	Hyperuricemia develops from overproduction of uric acid, decreased renal excretion of uric acid, or a combination of both Primary gout results from an inborn error of uric acid metabolism; secondary gout arises as a consequence of other disorders ***Clinical findings*** *Four phases:* 1. *Asymptomatic hyperuricemia:* prolonged hyperuricemia without signs or symptoms; 20% of patients develop acute arthritis or renal calculi, marking the end of this phase 2. *Acute gouty arthritis:* often dramatic acute inflammatory episode; monoarticular, oligoarticular, or occasionally polyarticular; severe pain, tenderness, swelling, erythema overlying affected joints 3. *Interval phase of gout (intercritical gout):* asymptomatic period between gouty attacks 4. *Chronic tophaceous gout:* visible tophaceous deposits with repeated episodes of pain	***Laboratory findings*** Hyperuricemia Monosodium urate crystals in synovial fluid aspirate ***Imaging findings*** Most commonly present with chronic gouty arthropathy Extraarticular erosions with overhanging edges of cortex Intraarticular erosions Tophi (soft tissue deposition of urate crystals) Absence of osteoporosis Relative absence of joint space narrowing Subperiosteal bone apposition Intraosseous calcification Predilection for first metatarsophalangeal joint
Hemochromatosis	40-60	Male : female, 10 : 1 to 20 : 1	Hand Wrist Knee Hip Shoulder	Rare progressive disorder involving articular damage from excessive iron deposition Classified into primary and secondary forms ***Clinical findings*** *Classic triad:* bronze skin pigmentation, liver cirrhosis, and diabetes mellitus Joint pain, stiffness, and swelling; usually bilateral	***Laboratory findings*** Elevated erythrocyte sedimentation rate Elevated serum iron concentration Increased saturation of the plasma iron-binding protein transferrin Characteristic findings on liver biopsy ***Imaging findings*** Bilateral symmetric involvement Osteoporosis Chondrocalcinosis related to CPPD crystal deposition Signs of secondary osteoarthrosis Predilection for metacarpophalangeal joints
Alkaptonuria	Present at birth, but asymptomatic until 30 or 40 years of age	Male = female	Spine Hip Knee	Rare hereditary metabolic disorder characterized by absence of homogentisic acid oxidase ***Clinical findings*** Usually asymptomatic until adulthood *Ochronosis:* brown-black pigmentation in connective tissues (rare in patients younger than age 20 years) Discoloration of urine *Ochronotic arthropathy:* acute exacerbations of arthritis, joint effusions, stiffness and restriction of motion, low back pain, thoracic kyphosis, lumbar hypolordosis, or disc prolapse Ochronotic deposition in other organs may lead to various systemic abnormalities	***Laboratory findings*** When urine is allowed to stand, homogentisic acid oxidizes to a melanin-like product, causing the urine to turn black Presence of homogentisic acid in urine and plasma ***Imaging findings*** Ochronotic arthropathy: accelerated degenerative disc and joint disease, disc calcification and peripheral joint chondrocalcinosis, diffuse joint space narrowing, sclerosis, fragmentation, osteophytosis, and eventual bamboo spine from syndesmophyte formation

TABLE 1-10 Miscellaneous Articular Disorders

Disorder	Typical Age of Onset (Years)	Sex	Target Sites of Involvement	Clinical Characteristics	General Imaging Findings
Hemophilic arthropathy	2-3	Male	*Common sites:* Knee Elbow *Rare sites:* Ankle Hip Shoulder Hand Foot	Group of disorders characterized by deficiency in specific plasma clotting factors and defective blood coagulation Results in easy bruising and prolonged and excessive bleeding Manifested in men and carried by women Two main X-linked recessive types result in musculoskeletal manifestations *Hemophilia A:* Classic form; deficiency of factor VIII (antihemophilic factor) *Hemophilia B:* Christmas disease; deficiency of factor IX (plasma thromboplastin component) ***Clinical findings*** Three phases: 1. Acute hemarthrosis. Rapid onset of bleeding; tense, stiff, red joint; pain, tenderness, muscle spasm; fever and leukocytosis; symptoms decrease with administration of clotting factor 2. Subacute hemarthrosis. After two or more acute hemarthroses; periarticular swelling, contractures, muscle spasm, and mild pain 3. Chronic hemarthrosis. Six months to 1 year after subacute phase; more severe and persistent fibrosis, joint destruction, and contractures	Radiodense joint effusions Osteoporosis Epiphyseal overgrowth Accelerated localized skeletal maturation Osseous erosions and cysts Joint space narrowing Sclerosis and osteophytes Osteonecrosis Imaging appearance of joints closely resembles that of juvenile chronic arthritis Hemophilic pseudotumors (<2% of patients); intraosseous hemorrhage with multiloculated osteolytic lesions
Neuropathic osteoarthropathy	Variable, depending on cause	Variable, depending on cause	Knee Hip Ankle Spine Shoulder Elbow Wrist Foot	Central (upper motor neuron) and peripheral (lower motor neuron) lesions can lead to neuropathic osteoarthropathy ***Underlying disorders*** Syringomyelia, diabetes mellitus, tabes dorsalis, meningomyelocele, trauma, multiple sclerosis, leprosy, alcoholism, amyloidosis, infection, and congenital insensitivity to pain	Hypertrophic and atrophic forms *Axial skeleton:* widespread discovertebral and zygapophyseal joint destruction May resemble infectious spondylodiscitis Joint collapse, bone fragmentation, pseudarthrosis, and kyphosis *Appendicular skeleton:* joint disorganization, osseous debris, distention, dislocation, fragmentation, increased density, deformity, and subluxation

Neurologic injury: heterotopic ossification	Any age	Male > female	Hip Knee Shoulder Elbow	Extensive periarticular soft tissue ossification occurs in as many as 53% of paraplegic and quadriplegic patients after brain and spinal cord injury—as a result of burns, mechanical trauma, and venous stasis ***Clinical findings*** Some patients have no symptoms other than those of their primary neurologic disorder itself Others have pain, swelling, restricted joint motion, or synovitis	Periarticular osseous deposits begin to appear 2-6 months after injury Begin as poorly defined opaque areas, typically progress to large accumulations possessing trabeculae Often result in complete osseous ankylosis
Pigmented villonodular synovitis	20-40	Slight male predominance	Knee Hip Elbow Ankle	Monoarticular synovial proliferative disorder of unknown cause 50% of patients have history of trauma Extraarticular form is termed *giant cell tumor* of the tendon sheath and is seen most commonly in the hand and foot ***Clinical findings*** Monoarticular distribution is typical May have symptoms of internal joint derangement Slowly progressive joint pain, swelling, warmth, tenderness, and stiffness *Aspiration:* acute or chronic hemorrhage	Soft tissue swelling Cystic erosions on both sides of the joint Hemorrhagic joint effusion Eventual osteoporosis Well-preserved joint space until late in the disease Radiographs may be normal Magnetic resonance (MR) imaging is useful in evaluation
Idiopathic synovial osteochondromatosis	20-50	Male : female, 2 : 1	Knee Hip Elbow	Monoarticular metaplastic or neoplastic proliferation of cartilaginous and osteocartilaginous bodies by the synovial membrane *Idiopathic form:* unknown cause *Secondary form:* secondary to degenerative disease or trauma ***Clinical findings*** Several years of joint pain with limitation of motion; pain may resemble that of an internal joint derangement Joint locking and instability may occur Focal recurrence after surgery Malignant degeneration (rare)	Multiple intraarticular or periarticular collections of calcification of variable size and density Erosion of adjacent bone Secondary osteoarthrosis Noncalcified bodies are best demonstrated with arthrography or MR imaging Secondary synovial osteochondromatosis may occur as a result of degenerative joint disease

TABLE 1-11 Articular Disorders With Skin and Joint Findings*

Entity	Skeletal Findings	Skin Findings
Disorders of the Epidermis		
Psoriasis	Peripheral arthritis, sacroiliitis	Scaling erythematosus papules on scalp and extensor surfaces
Ulcerative colitis	Like psoriasis and other seronegative spondyloarthropathies	Maculopapular eruptions, purpura, aphthae, erythema nodosum, erythema multiforme, pyoderma gangrenosum
Disorders of the Dermis		
Ehlers-Danlos syndrome	Joint effusion, dislocation, and contracture	Hyperelasticity and fragility of skin, soft tissue calcification
Disorders of the Sebaceous Glands		
Pustular acne (Pustulotic arthro-osteitis (PAO) or SAPHO)†	SAPHO: abbreviation for synovitis, acne, pustulosis, hyperostosis, and osteitis Osteoarticular inflammation involving anterior chest wall, spine, pelvis, sacroiliac joints Polyarthralgia Hyperostosis	Nodulocystic pustules with scarring primarily on the palms of the hands and plantar surface of the feet
Acne fulminans	Sacroiliitis, synovitis, and osteolytic lesions	Acute ulceration and hemorrhage
Acne conglobata	Small joint erosions, sacroiliitis, and syndesmophytes	Large inflamed cysts
Disorders of Sweat Glands		
Hidradenitis suppurativa	Sacroiliitis, phalangeal periostitis	Infected sweat glands with abscesses in groin and axilla
Tumors and Tumorlike Conditions		
Disseminated ovarian or other carcinoma	Shoulder and hand arthritis and contractures	Palmar fasciitis
Immunologic and Allergic Cutaneous Disorders With Arthralgia		
Drug reaction/serum sickness	Arthralgias	Urticaria
Infections, Behçet syndrome, drugs	Arthralgias	Erythema nodosum
Collagen Vascular Diseases		
Systemic lupus erythematosus	Subluxations without erosions	Malar butterfly rash
Systemic periarteritis nodosa	Migratory polyarthralgia	Ulceration, nodules, purpuric plaques
Scleroderma	Inflammatory arthritis	Tight skin, fibrosis, telangiectasia
Rheumatoid arthritis	Symmetric small joint erosive synovitis	Subcutaneous nodules, petechiae, and purpura
Juvenile rheumatoid arthritis	Asymmetric large joint erosive synovitis	Maculopapules on limbs, trunk and face
Multicentric reticulohistiocytosis	Destructive polyarthritis, erosive synovitis	Multiple cutaneous nodules, characteristically around fingernails
Relapsing polychondritis	Rheumatoid-like arthropathy	Swollen ears, saddle nose, erythema nodosum

* Reprinted with permission from Kilcoyne RF: Arthritis associated with dermatologic conditions. Semin Musculoskeletal Radiol 7:227, 2003.

† From Hyodoh K, Sugimoto H: Pustulotic arthro-osteitis: Defining the radiologic spectrum of the disease. Semin Musculoskeletal Radiol 5:89, 2001.

TABLE 1-11 Articular Disorders with Skin and Joint Findings—cont'd

Entity	Skeletal Findings	Skin Findings
Infections		
Viral	Arthralgias	Urticaria and other rashes
Measles, rubella, parvovirus, viral hepatitis, herpes simplex, vaccinia		
Bacterial		
Rheumatic fever	Transient arthralgia/arthritis	Erythema marginatum
Disseminated gonococcal infection	Septic arthritis or reactive allergic arthritis	Scattered acral papular and vesicopustular lesions
Leprosy	Osteomyelitis, infective arthritis, neuropathic joints	Thickening of skin over face and extremities; autoamputation
Spirochetal		
Syphilis, acquired	Neuropathic joints	Different skin lesions in primary, secondary, and tertiary stages
Lyme disease	Mono- or migratory arthritis, chronic erosive arthritis	Erythema chronicum migrans
Fungal		
Sporotrichosis	Direct contiguous spread or hematogenous infection	Suppurating nodular lesions of wrist, ankle, and elbow
Coccidioidomycosis (valley fever)	Acute desert rheumatism or chronic arthritis	Erythema nodosum
Possibly infectious		
Sarcoidosis	Phalangeal cysts and arthralgia/arthritis	Erythema nodosum, lupus pernio
Reiter syndrome	Asymmetric arthritis and sacroiliitis	Circinate balanitis, keratoderma blennorrhagicum of palms
Diseases of Nutrition and Metabolism		
Acromegaly	Widened joint spaces, early degeneration	Skin thickening of hands, feet, and face
Ochronosis	Chondrocalcinosis, early degeneration	Slate blue skin pigmentation
Hemochromatosis	Generalized arthropathy, chondrocalcinosis	Bronze diabetes
Gout	Discrete articular erosions, especially toe	Tophi, soft tissue swelling, erythema
Environmentally Caused or Drug-Related Diseases		
Vinyl chloride exposure	Acro-osteolysis	Scleroderma-like
Retinoids	Hyperostosis, DISH-like changes, enthesopathy, osteoporosis, premature closure of physes	Dry skin, epilation, reduced sebum

TABLE 1-12 Malignant Bone Tumors and Myeloproliferative Disorders

Entity	Typical Age of Onset (Years)	Sex (Male: Female)	Most Frequent Skeletal Locations* (%)	General Characteristics	General Imaging Findings
Secondary Malignant Tumors of Bone					
Skeletal metastasis	50-75	Variable: depends on source	Spine (40) Pelvis (15) Ribs, sternum (30) Skull (10) Femur (<10) Humerus (<10) Hand and foot (rare)	Most common malignant tumor of bone *Most frequent primary sources in adults:* carcinoma of the breast, prostate, lung, kidney, bladder, and thyroid gland *Most frequent primary sources in children:* neuroblastoma, Ewing sarcoma, and osteosarcoma ***Clinical findings*** Bone pain, bone tenderness, soft tissue mass, osseous deformity, unexplained weight loss ***Laboratory findings*** Elevated serum calcium, serum alkaline phosphatase, and urinary hydroxyproline levels; anemia; elevated prostate-specific antigen level in prostate carcinoma	Multiple skeletal sites typically involved Permeative or moth-eaten osteolysis (75% of patients) Diffuse or patchy osteosclerosis or mixed pattern of osteolysis and osteosclerosis (25% of patients) Pathologic fracture Soft tissue mass (rare) Periosteal reaction (rare) Bone expansion (rare) ***Cortical metastasis*** Prevalent in the long bones, especially in patients with metastasis resulting from bronchogenic carcinoma Small radiolucent, eccentric, saucer-shaped, scalloped erosions, which sometimes occur near the entrance of nutrient arteries into the bone (cookie-bite lesions)
Primary Malignant Tumors of Bone					
Osteosarcoma (conventional)	10-25	2:1	Femur (46) Tibia (21) Humerus (11) Pelvis (7)	Readily metastasizes to other bones and lung and may result from malignant transformation of benign neoplasms ***Clinical findings*** Pain, swelling, restriction of motion, warmth, and pyrexia	Osteolytic, osteosclerotic, or mixed patterns of medullary and cortical destruction Prominent aggressive periosteal reaction common Preferential involvement of the metaphysis
Osteosarcoma (parosteal)	20-45	1:1	Femur (64) Humerus (15) Tibia (11)	***Clinical findings*** Insidious onset of pain, swelling, and palpable mass (often about the knee)	Osteosclerotic surface lesion of bone Large radiodense, oval sessile mass with smooth or irregular margins Lesion may have cleavage plane separating it from the parent bone Ossification begins centrally and progresses outwardly, opposite that of benign heterotopic bone formation (myositis ossificans)
Osteoblastoma (aggressive)	10-30	2:1	Spine (23) Tibia (13) Pelvis (13) Femur (11) Foot (11)	Aggressive (malignant) osteoblastomas recur in 50% of cases, whereas only 10% of conventional (benign) osteoblastomas recur Aggressive osteoblastomas have histologic and radiographic characteristics of malignancy and can be difficult to differentiate from osteosarcoma May lead to patient's death in some cases	Variable appearance that may resemble osteosarcoma or conventional osteoblastoma Expansile osteolytic lesion that may be partially ossified or contain calcium Metaphyseal location; may extend into epiphysis Soft tissue involvement

Chondrosarcoma (conventional)	30-60	3:2	Femur (24) Pelvis (24) Humerus (10) Ribs (8) Tibia (7) Spine (6)	*Several forms:* conventional, juxtacortical, clear cell, mesenchymal, and dedifferentiated types Further classified as peripheral or central Patients with peripheral chondrosarcoma tend to be slightly younger than those with central chondrosarcoma ***Clinical findings*** Pain, tender soft tissue mass, pathologic fracture, warmth, and erythema	***Central chondrosarcoma*** Elongated poorly defined lesions May have soft tissue mass Multilobulated, osteolysis, cortical destruction, cortical thickening, periostitis, endosteal scalloping, and calcification ***Peripheral chondrosarcoma*** Arise from preexisting osteochondroma or, infrequently, from the periosteal membrane in the form of juxtacortical chondrosarcoma ***Calcification characteristics*** Present in more than 60% of cases Well-organized calcific rings in low-grade chondrosarcomas Amorphous, punctate, scattered, or irregular calcification in high-grade chondrosarcomas
Giant cell tumor (aggressive)	30-50	3:2	Femur Tibia Radius Spine Humerus	Locally aggressive or malignant form of giant cell tumor is more common in men than in women Five to 10% of giant cell tumors are malignant; radiographic appearance is an inaccurate guide to determining malignancy of lesion; biopsy is necessary Vast majority of malignant giant cell tumors develop after irradiation of benign giant cell tumors Forty to 60% recurrence rate for all giant cell tumors Tumor implantation may occur at distant sites, typically the lung, 2-5 years after surgical resection of tumor; more prevalent with lesions of the distal end of the radius ***Clinical findings*** Pain, local swelling, pathologic fracture, and limitation of motion in adjacent joint Pain usually mild and of several months' duration, relieved by bed rest, aggravated by activity	Eccentrically located, subarticular osteolytic lesion extending into the metaphysis of long bones Cortical destruction and soft tissue mass are variable findings Spinal lesions predominate in the vertebral body and may result in vertebral collapse
Fibrosarcoma	25-55	1:1	Femur (39) Tibia (16) Humerus (11) Pelvis (10)	Rare malignant neoplasm of bone Fibrosarcomas of bone have a poorer prognosis than fibrosarcomas of soft tissue *Two main types:* 1. De novo form 2. Secondary form: in areas of Paget disease, osteonecrosis, chronic osteomyelitis, or previously irradiated bone ***Clinical findings*** Local pain, swelling, limitation of motion Pathologic fracture present at initial evaluation in 33% of patients	Purely osteolytic destruction with wide zone of transition Large solitary metaphyseal lesion: 1.5-20 cm in size Usually moth-eaten or permeative destruction; may exhibit geographic destruction Sequestrum may be seen Minimal sclerotic reaction or periostitis Central or eccentric location in tubular bones Soft tissue masses are common

Continued

TABLE 1-12 Malignant Bone Tumors and Myeloproliferative Disorders—cont'd

Entity	Typical Age of Onset (Years)	Sex (Male: Female)	Most Frequent Skeletal Locations* (%)	General Characteristics	General Imaging Findings
Chordoma	30-60	2:1	Spine (75) Skull (25)	Rare locally aggressive lesion of notochordal origin Predominate in the sacrum and clivus and, less commonly, the axis or thoracolumbar vertebral bodies ***Clinical findings*** Vary according to location; symptoms may be mild initially and result from pressure on adjacent structures (rectum, bladder, nerve roots, and spinal cord)	Central vertebral body lesion; osteolytic destruction with expansion is the most common pattern; rarely osteosclerotic or mixed; soft tissue mass frequently encountered
Adamantinoma (malignant angioblastoma)	Women, 10-30; men, 30-50	5:4	Tibia (85) Humerus (6) Ulna (4) Femur (3)	Rare locally aggressive or malignant lesion of bone May be related to ossifying fibroma in the immature skeleton	Longitudinally oriented mid-diaphyseal lesion; central or eccentric, multilocular, slightly expansile, sharply or poorly delineated osteolytic lesion Reactive bone sclerosis Periostitis rare
Ewing sarcoma	10-25	3:2	Femur (22) Pelvis (18) Tibia (11) Humerus (10) Fibula (9) Ribs (8) Scapula (5)	Rare in African Americans (fewer than 2% of patients) Pain most common presenting symptom	Permeative or moth-eaten osteolysis, aggressive cortical erosion or violation, laminated (i.e., onionskin appearance) or spiculated periostitis, and soft tissue involvement Occasional bone sclerosis Pathologic fracture (15% of patients) Most lesions central and diametaphyseal in location
Myeloproliferative Disorders					
Plasma cell (multiple) myeloma	60-70	2:1	Spine (75) Pelvis (27) Ribs (26) Humerus (15)	Plasma cell (multiple) myeloma is a malignant disease of plasma cells and represents the most common primary malignancy of bone 75% of cases of plasma cell myeloma are multiple myeloma Particularly common in African Americans ***Clinical findings*** Bone pain, particularly in the back and chest, weakness, fatigue, fever, weight loss, bleeding, neurologic signs, and many other signs and symptoms Rare osteoblastic form may be associated with peripheral neuropathy ***Laboratory findings*** Serum immunoelectrophoresis is positive in 80%-90% of cases, and Bence Jones proteinuria is present in 40%-60% of patients Normocytic normochromic anemia, rouleaux formation, thrombocytopenia, leukopenia, hypercalcemia, hyperuricemia, elevated erythrocyte sedimentation rate	*Early:* Normal radiographs or diffuse osteopenia *Later:* Widespread well-circumscribed osteolytic lesions with discrete margins, which appear uniform in size Vertebral collapse common Pathologic fracture 97% osteolytic; 3% osteoblastic False-negative bone scans common

Solitary plasmacytoma	45-55	2:1	Spine (50) Pelvis (13) Femur (16) Sternum (15)	Localized form of plasma cell myeloma 25% of cases of plasma cell myeloma are solitary plasmacytoma, but 70% of these eventually develop into multiple myeloma ***Clinical findings*** Bone pain is a common finding ***Laboratory findings*** Serologic test results may be negative or similar to those of multiple myeloma	Solitary, geographic, expansile, multicystic osteolytic lesion with thickened trabeculae Frequently results in pathologic vertebral collapse If calcified, may relate to secondary amyloidosis
Hodgkin disease	15-35	1:1	Spine (43) Ribs (16) Pelvis (11) Femur (10)	Skeletal abnormalities occur in 10%-25% of patients; more common in adults than in children More than 60% of patients have multiple sites of skeletal involvement ***Clinical findings*** Lymphadenopathy, masses, hepatomegaly, splenomegaly, fever, night sweats, weight loss	75% of lesions are osteolytic; 25% are osteosclerotic (ivory vertebra) Permeative or moth-eaten osteolysis Anterior vertebral body scalloping may occur secondary to direct invasion of lymph nodes
Primary lymphoma (non-Hodgkin)	20-40	1:1	Femur (24) Pelvis (18) Spine (13) Tibia (9)	No race predilection ***Clinical findings*** Localized pain and swelling, lymphadenopathy and splenomegaly Systemic signs and symptoms characteristically are absent Skeletal involvement in up to 30% of patients with non-Hodgkin lymphoma	May result in multiple moth-eaten or permeative osteolytic metaphyseal lesions Common cause of pathologic fracture Diffuse or localized sclerotic lesions are rare
Leukemia	Acute *Childhood type:* 2-5; chronic *Adult type:* 35-55	1:1	Long bones Spine	Poor correlation between the extent of bone lesions and the progress of leukemia ***Clinical findings*** Vary according to type Lymphadenopathy, splenomegaly, bone pain, arthralgia, tenderness, swelling, bleeding episodes, recurrent infections ***Laboratory findings*** Anemia, leukocytosis, neutropenia, and thrombocytopenia	Imaging abnormalities more prevalent in childhood form (up to 70% of cases) than adult form (less than 20% of cases) Findings in acute childhood leukemia: Diffuse osteopenia (15%-100% of cases) Radiolucent or radiodense transverse metaphyseal bands (10%-55% of cases) Osteolytic lesions (30%-50% of cases) Periostitis (10%-35% of cases) Osteosclerosis (5%-10% of cases) Radiodense metaphyses more frequent in patients undergoing chemotherapy for leukemia; may resemble appearance of lead poisoning

* Numbers in parentheses indicate approximate percentages of the neoplasms that affect each skeletal site based on analysis of major reports containing the greatest number of cases. In cases in which no numbers are provided, the relative frequency at each site is unknown.

TABLE 1-13 Benign Bone Tumors

Entity	Typical Age of Onset (Years)	Sex (Male: Female)	Most Frequent Skeletal Locations* (%)	General Characteristics	General Imaging Findings
Enostosis (bone island)	Any age	1:1	Femur (25) Pelvis (25) Ribs (12) Humerus (9) Wrist, hand (9)	Not a true neoplasm; painless, circular zone of osteosclerosis ***Clinical findings*** Usually encountered as an incidental finding on radiographs obtained for unrelated reasons ***Differential diagnosis*** Other osteosclerotic processes, such as osteoblastic metastases, osteomas, osteoid osteomas, enchondromas, bone infarcts, fibrous dysplasia, and osteopoikilosis	Solitary or multiple, discrete foci of osteosclerosis within the spongiosa of bone Round, ovoid, or oblong with brush border composed of radiating osseous spicules that intermingle with the surrounding trabeculae of the spongiosa Lesions may grow in size and, when large, exhibit activity on a bone scan even though they are benign Giant bone islands have been reported to reach proportions of up to 4 × 4 cm in diameter
Osteoid osteoma	7-25	3:1	Femur (32) Tibia (24) Wrist, hand (9) Humerus (7) Spine (6)	***Clinical findings*** Often results in severe dull or aching pain, classically worse at night and relieved by salicylates *Spinal lesions:* torticollis, scoliosis, spinal stiffness *Intracapsular lesions:* joint tenderness, swelling, synovitis, limitation of motion Laboratory studies usually are unremarkable	Cortical or subperiosteal lesion with reactive sclerosis surrounding central radiolucent nidus: nidus usually less than 1 cm in diameter and may not be visible on routine radiographs Computed tomography is gold standard to show nidus Intracapsular lesions provoke less reactive sclerosis and are more likely to cause joint pain
Osteoblastoma (conventional)	10-30	2:1	Spine (30) Femur (14) Tibia (10) Foot (7)	Approximately 95% of osteoblastomas are benign ***Clinical findings*** Mild local pain; usually not relieved by rest or salicylates Spinal lesions may be accompanied by muscle spasm, scoliosis, and neurologic manifestations	Osteolytic, osteosclerotic, or both Partially calcified matrix in many cases Often resembles large osteoid osteoma *Spine:* expansile, multiloculated lesion of the neural arch *Tubular and flat bones:* Cortical thinning Diaphyseal (75% of cases) or metaphyseal location May be subperiosteal in location
Osteofibrous dysplasia (Ossifying fibroma)	<1-20	1:1	Facial bones Tibia	Rare fibro-osseous lesion of tubular bones occurring almost exclusively in the tibia (and, infrequently, the ipsilateral fibula) Closely related to fibrous dysplasia and may resemble adamantinoma or a large nonossifying fibroma	Long diaphyseal lesion with intracortical osteolysis clearly marginated by a band of osteosclerosis Hazy or ground-glass appearance reminiscent of fibrous dysplasia Occasionally purely osteosclerotic Osseous expansion Bowing, deformity, and pathologic fracture
Enchondroma (solitary)	15-35	1:1	Wrist, hand (57) Femur (11) Foot (7) Humerus (7) Ribs (5)	Lesions usually are asymptomatic or associated with painless swelling Onset of pain should arouse suspicion of malignant transformation to chondrosarcoma (fewer than 1% of cases) or pathologic fracture	Solitary, central or eccentric, medullary osteolytic lesion Metaphyseal location; may extend to include entire diaphyseal and subarticular regions of bone Lobulated endosteal scalloping Stippled calcification (50% of lesions)

Enchondromatosis (Ollier disease)	<10	1:1	Tibia Fibula Femur Hand, wrist	Rare nonhereditary disease ***Clinical findings*** Palpable masses, asymmetric limb shortening, osseous deformities related to pathologic fracture *Malignant transformation rate:* 5-30%	Multiple enchondromas Tubular radiolucent areas extending into the metaphysis from the physis Shortening and deformity of affected bones Frequent calcification of matrix
Maffucci syndrome	<10	1:1	Tibia (50) Fibula (50) Hand, wrist Foot	Rare, congenital, nonhereditary mesodermal dysplasia Multiple enchondromas and soft tissue hemangiomas Unilateral distribution in 50% of cases *Malignant transformation rate:* 20%-40% of cases (occurs in both bone and soft tissue)	*Soft tissue hemangiomas:* multiple phleboliths in the soft tissues Multiple central or eccentric radiolucent lesions containing variable amounts of calcification Shortening and deformity of affected bones
Chondroblastoma	10-25	2:1	Femur (33) Humerus (22) Tibia (18) Hands and feet (10)	Benign epiphyseal tumor of cartilage origin Frequently results in joint pain	Circular osteolytic lesion 1 to 6 cm in diameter Arise from epiphyses and apophyses of long bones; metaphyseal extension in 25%-50% of cases Thin sclerotic margin Calcification in matrix (30%-50% of cases) Soft tissue mass and pathologic fracture rare Occasionally periosteal reaction may be seen on routine radiographs and edema may be seen on magnetic resonance images
Chondromyxoid fibroma	10-25	Slight male predominance	Tibia (38) Femur (17) Fibula (8) Foot (6) Pelvis (6)	Least common benign tumor of cartilage Slowly progressive pain, tenderness, swelling, and restriction of motion; may infrequently be asymptomatic Pathologic fracture (rare)	Eccentric, elongated metaphyseal lesion 2-10 cm in length Cortical expansion, coarse trabeculation, endosteal sclerosis Calcification is rare (5% to 27% of cases) May appear aggressive with large "bite" lesion penetrating cortex
Osteochondroma (solitary)	10-30	2:1	Femur (31) Humerus (19) Tibia (18) Foot (6) Hand, wrist (5) Fibula (4)	Represents either a true primary benign bone tumor, a developmental physeal growth defect, or a cartilaginous metaplasia within the periosteal membrane May occur spontaneously or secondary to injury or irradiation ***Clinical findings*** Nontender, painless, slow-growing mass ***Complications*** Fracture, osseous deformity, bursa formation, vascular injury, neurologic compromise, and malignant transformation (fewer than 1% of solitary lesions)	Pedunculated or sessile cartilage-covered osseous excrescence arising from the surface of the metaphyses of long bones or, infrequently, flat bones Composed of cortex and medulla, which are continuous with the host bone Cartilage cap frequently contains calcification visible on radiographs Grows in a direction away from the adjacent joint Spinal lesions arise from the posterior arch ***Signs suggesting malignant transformation*** Pain, soft tissue swelling, and soft tissue mass; growth of a previously stable lesion, bone erosion, irregular or scattered calcification, thick cartilage cap (>1 cm) These signs are not always reliable; a normal bone scan virtually excludes presence of malignancy; microscopic biopsy findings are most definitive

Continued

TABLE 1-13 Benign Bone Tumors—cont'd

Entity	Typical Age of Onset (Years)	Sex (Male: Female)	Most Frequent Skeletal Locations* (%)	General Characteristics	General Imaging Findings
Hereditary multiple exostoses	10-30	1:1	Femur Tibia Fibula Humerus Pubis	Autosomal dominant disorder of metaphyseal overgrowth Also referred to as *diaphyseal aclasis* and *multiple osteochondromatosis* Characterized by multiple osteochondromas *Malignant transformation rate:* 3%-25% of cases	Multiple sessile and pedunculated osteochondromas numbering from a few to more than 100 Osseous deformities and abnormalities of modeling
Nonossifying fibroma and fibrous cortical defect	10-20	2:1	Tibia (43) Femur (38) Fibula (8) Humerus (5)	The terms *nonossifying fibroma* and *fibrous cortical defect* often are used interchangeably Common benign lesions consisting of whorled bundles of connective tissue cells Present in about 2% of persons younger than 20 years of age, according to some estimates ***Clinical findings*** Clinically silent; usually discovered incidentally or after fracture	Eccentric, multiloculated osteolytic lesion arising from metaphyseal cortex Resembles a well-circumscribed, blisterlike shell of bone arising from the cortex Cortical thinning often is present Most lesions are replaced by normal bone, gradually disappearing over time; others grow large and may result in pathologic fracture Often bilateral and symmetric On serial radiographs, the lesion may appear to migrate away from the physis owing to normal longitudinal metaphyseal growth between the physis and the lesion
Giant cell tumor (benign)	20-40	Benign, 2:3; aggressive, 3:2	Femur (31) Tibia (27) Radius (10) Spine, especially sacrum (7) Humerus (6)	90%-95% are benign; 5%-10% are locally aggressive or malignant 40%-60% recurrence rate ***Clinical findings*** Pain, local swelling, limitation of motion Pathologic fracture (10%) Neurologic symptoms may accompany spinal or sacral lesions	Elongated, eccentric osteolytic neoplasm with a predilection for the subarticular region and metaphyses of the long bones Multiloculated, expansile, with delicate trabecular pattern Spinal and sacral lesions affect the vertebral body in an eccentric fashion and may extend into the posterior elements or cross the sacroiliac joint Radiographs are inaccurate in distinguishing benign from aggressive giant cell tumors

Intraosseous lipoma	30-50	1 : 1	Fibula (20) Calcaneus (15) Femur (15) Tibia (14) Humerus (9) Ribs (8)	Uncommon tumor or tumor-like osseous lesion that may be related to osteonecrosis or fat necrosis ***Clinical findings*** Symptoms (in 66% of patients) include localized pain and variable amounts of soft tissue swelling and tenderness to palpation Infrequent compression of adjacent neurovascular structures	Solitary osteolytic lesion surrounded by a thin, well-defined sclerotic border Central calcified or ossified focus is common Occasional lobulation or internal osseous ridges Osseous expansion (rare) Cortical destruction and periostitis absent
Hemangioma (solitary)	25-50	1 : 2	Skull (40) Spine (25) Ribs (9) Foot (5)	*Vascular channels within bone:* cavernous, capillary, or venous types Single lesions predominate, but multiple lesions occasionally are encountered ***Clinical findings*** Usually discovered as an incidental finding Occasional soft tissue swelling or pain, particularly in presence of pathologic fracture Spinal lesions infrequently may be complicated by spinal cord compression from bone expansion, epidural tumor extension, epidural hemorrhage, or compression fracture	Radiolucent, slightly expansile intraosseous lesion Radiating, latticelike or weblike trabecular pattern Spinal lesions exhibit characteristic corduroy cloth appearance: prominent vertical trabecular ridges within radiolucent spongiosa bone of vertebral body; may extend into neural arch Occasional cortical thinning Rarely, periostitis, soft tissue mass, or osteosclerosis Intracortical and periosteal hemangiomas (extremely rare) predominate in the tibia and fibula
Simple bone cyst	5-25	2 : 1	Humerus (56) Femur (27) Tibia (6) Fibula (5)	Fluid-filled solitary cyst of unknown cause and pathogenesis; not a true neoplasm Also termed *solitary* or *unicameral bone cyst* Flat bones (pelvic bones and calcaneus) more frequently involved in persons older than 20 years of age ***Clinical findings*** Asymptomatic unless pathologic fracture occurs	Mildly expansile, solitary osteolytic lesion within metaphyseal medullary cavity of long bones May be multiloculated On serial radiographs, the lesion may appear to migrate away from the physis owing to normal longitudinal metaphyseal growth between the physis and the lesion May observe fallen-fragment sign in patients with pathologic fracture
Aneurysmal bone cyst	10-30	2 : 3	Tibia (15) Spine (14) Femur (13) Pelvis (9) Foot (8) Fibula (7) Hand, wrist (5)	Benign non-neoplastic lesion containing blood-filled cavities May develop after trauma or may accompany other benign processes, such as giant cell tumor, fibrous dysplasia, and chondroblastoma ***Clinical findings*** Pain and swelling Spinal lesions may lead to neurologic compromise	Eccentric, thin-walled, expansile osteolytic lesion of the metaphysis of long bones Spinal lesions arise from the neural arch but often extend into the vertebral body Thin trabeculation with multiloculated appearance Buttressing at edge of lesion Typically more expansile than osteoblastoma

* Numbers in parentheses indicate approximate percentages of the neoplasms that affect each skeletal site based on analysis of major reports containing the greatest number of cases. In cases in which no numbers are provided, the relative frequency at each site is unknown.

TABLE 1-14 Tumorlike Lesions of Bone

Entity	Typical Age of Onset (Years)	Sex (Male : Female)	Most Frequent Skeletal Locations* (%)	General Characteristics	General Imaging Findings
Paget disease	>55	2 : 1	Pelvis Femur Skull Tibia Spine Humerus	Unknown cause Results in deformity of bone ***Clinical findings*** Asymptomatic in 90% of patients Mild bone pain, worse with bowing deformities, pathologic fractures, and malignant transformation ***Laboratory findings*** Elevated alkaline phosphatase, urinary hydroxyproline, and serum calcium levels; vary according to stage of involvement ***Malignant transformation*** *Malignant transformation rate:* fewer than 2% of cases; osteosarcoma, chondrosarcoma, and fibrosarcoma; femur is the most frequent site of malignant transformation Ominous signs for malignant transformation include increased pain, enlarging soft tissue mass, enlarging osteolytic lesion, further elevation of serum alkaline phosphatase levels	Usually polyostotic and may have unilateral involvement Coarsened trabeculae, cortical thickening, and bone enlargement Pathologic fracture Bowing deformities of bones Pseudofractures (i.e., insufficiency fractures) on convex surface of bowed bones Blade of grass (flame-shaped advancing edge of osteolysis) appearance seen in tubular bones Stages of involvement: I: osteolytic (50%) II: osteosclerotic (25%) III: mixed (25%) IV: malignant transformation (fewer than 2%)
Neurofibromatosis Type I (von Recklinghausen disease)	Birth	1 : 1	Cranium Spine Ribs Tibia Femur	Inherited, autosomal dominant mesodermal dysplasia 50% of patients develop skeletal lesions Approximately 5% rate of malignant transformation to neurofibrosarcoma ***Clinical findings*** Café-au-lait macules, neurofibromas, inguinal or axillary freckling, optic glioma, Lisch nodules, osseous lesions	Dysplastic bones with overconstriction, bowing deformities, pathologic fractures, and remodeling *Circumscribed cystlike intraosseous lesions:* may result from subperiosteal hemorrhage with subsequent periosteal proliferation and repair or from the incorporation or overgrowth of periosteum around a previously external soft tissue lesion, such as a neurofibroma *Pseudarthroses:* may occur when deformed bones fracture; precise cause of pseudarthrosis and defective fracture healing is not clear *Spinal involvement:* 60% of patients; scoliosis or kyphoscoliosis, pedicle erosion, foraminal enlargement, penciling and spindling of transverse processes and ribs

Fibrous dysplasia				Nonhereditary, idiopathic, developmental anomaly of bone-forming mesenchyme in which osteoblasts fail to undergo normal morphologic differentiation and maturation	
Monostotic (70%-80%)	10-20	1:1	Rib (28) Femur (15) Tibia (10) Skull (common) Humerus (4)	***Clinical findings*** Monostotic lesions tend to be asymptomatic unless pathologic fracture or stress fracture occurs ***Laboratory findings*** Elevated serum alkaline phosphatase levels in one third of patients; poor correlation with extent of skeletal involvement	Thick rim of sclerosis surrounding a central or eccentric radiolucent lesion; hazy ground-glass appearance of matrix Lesions in long bones usually are intramedullary and diaphyseal in location Focal bone expansion and minimal bowing may occur
Polyostotic (20%-30%)	5-20	Slight female predominance	Femur (92)[†] Tibia (81) Pelvis (78) Foot (75) Fibula (62) Ribs (55) Hand, wrist (55) Humerus (50)	***Clinical findings*** Initial symptoms may include osseous deformity or pathologic fracture May be associated with McCune-Albright syndrome; precocious female sexual development and cutaneous pigmentation	Polyostotic lesions are bilateral and asymmetric, or occasionally unilateral; tend to be larger, more expansile, and more multiloculated than monostotic lesions Bowing deformities more prominent
Langerhans cell histiocytosis	5-10	Slight male predominance	Skull (>50) Pelvis (20) Femur (15) Ribs (7) Spine (6)	Histiocytic infiltration of tissue; unknown cause *Three major conditions:* 1. *Eosinophilic granuloma:* 80% of patients; mildest, benign form characterized by single or multiple lesions of bone; usually asymptomatic 2. *Hand-Schüller-Christian disease:* 10% of patients; most varied form with chronic dissemination of osseous lesions; associated with diabetes insipidus, exophthalmos, and severe visceral involvement 3. *Letterer-Siwe disease:* 10% of patients; acute form with rapid dissemination, severe visceral involvement, and poor clinical prognosis; usually affects children younger than 3 years of age	*Long bones and flat bones:* osteolytic lesions may be multiloculated and expansile *Spine:* *Vertebra plana:* with healing, the height of the pathologically collapsed vertebral body may be reconstituted, a finding more common in younger persons; bubbly, osteolytic, or expansile spinal lesions without collapse also may occur

[*] Numbers in parentheses indicate approximate percentages of lesions that affect each skeletal site based on analysis of major reports containing the greatest number of cases. The relative frequency of involvement in each location for Paget disease and neurofibromatosis type I is unknown.

[†] Numbers add up to more than 100% because several sites are involved simultaneously.

TABLE 1-15 Metabolic, Nutritional, and Endocrine Disorders of Bones and Joints

Entity	Typical Sites of Involvement	General Characteristics	General Imaging Findings
Generalized osteoporosis*	Predominates in the axial skeleton Osteoporotic fractures: Thoracolumbar spine Hip Distal end of radius Proximal end of humerus	***Causes*** Senile and postmenopausal states (most common) Medication Corticosteroids Heparin Endocrine states Hyperthyroidism Hyperparathyroidism Cushing disease Acromegaly Pregnancy Diabetes mellitus Hypogonadism Deficiency states Scurvy Malnutrition Calcium deficiency Alcoholism and chronic liver disease Anemic states Osteogenesis imperfecta Idiopathic conditions	Uniform decrease in radiodensity, thinning of vertebral endplates, accentuation of vertical trabeculae Insufficiency fractures of the spine and hip common Wedge-shaped vertebral deformities caused by compression fractures are most common in thoracic spine; biconcave deformities are more common in the lumbar spine; vertebra plana deformities are more likely to be related to pathologic fracture caused by plasma cell myeloma, skeletal metastasis, or other destructive process Quantitative bone mineral analysis (densitometry) is necessary for accurate assessment of the presence and extent of diminished bone mineral content Dual energy x-ray absorptiometry is the most widely used method to assess bone mineral density because of its ease of use, high precision, and low radiation exposure to patients
Regional osteoporosis*	Hip Knee Foot Hand Immobilized extremity	***Causes*** Transient regional osteoporosis Idiopathic transient osteoporosis of the hip Regional migratory osteoporosis Complex regional pain syndrome Immobilization and disuse Periarticular osteoporosis associated with inflammatory arthritis Usually self-limited	Patchy, spotty, linear, or diffuse patterns of osteopenia in a regional distribution Regional involvement Magnetic resonance imaging findings of marrow edema
Osteomalacia	Diffuse skeletal involvement	Inadequate or delayed mineralization of osteoid in mature cortical and spongiosa bone ***Causes*** Vitamin D deficiency Inadequate exposure to ultraviolet radiation Gastrointestinal malabsorption Abnormal vitamin D metabolism Liver disease Kidney disease Phosphate loss Associated tumors Anticonvulsant drugs	Diminished radiodensity and prominent coarsened trabeculae Bilateral and symmetric transverse insufficiency fractures: pseudofractures or Looser zones, which, when seen in tubular bones, occur on the concave aspect of the bone Thickening of tubular bones from excessive osteoid deposition

Rickets	Findings are more prominent in the appendicular skeleton	Interruption in orderly development and mineralization of the growth plate ***Causes*** Similar to those in osteomalacia ***Clinical findings*** Muscle tetany, weakness, delayed skeletal maturation, small stature, irritability, osseous bowing deformities, rachitic rosary	General retardation in body growth Osteopenia Rachitic rosary (masses on anterior chest wall) at costochondral junctions ***Deformities*** Bowing deformities of long tubular bones Scoliosis may develop with overall decrease in height Concave vertebral body deformities Basilar impression and acetabular protrusion **Growth plate changes** Widening, cupping, and fraying of the metaphyses Decreased density at the metaphyseal zone of provisional calcification Irregularity of the metaphyseal zone of provisional calcification
Hyperparathyroidism	Resorption: phalangeal tufts, sacroiliac joint, symphysis pubis, periarticular regions, discovertebral joints, patellofemoral joints, medial tibial metaphysis, skull Brown tumors: tubular and flat bones	*Three forms:* primary, secondary, and tertiary *Primary form:* elevated parathyroid hormone secretion as a result of parathyroid gland hyperplasia or adenomas *Secondary form:* excessive parathyroid hormone secretion secondary to sustained hypocalcemic states such as those encountered in chronic renal failure, malabsorption syndromes, sprue, and gluten enteropathy *Tertiary form:* occurs in patients with chronic renal failure or malabsorption and long-standing secondary hyperparathyroidism who develop relatively autonomous parathyroid function and hypercalcemia ***Clinical findings*** Widely variable owing to the many organ systems that can be involved; some findings include urinary tract calculi, peptic ulcer disease, pancreatitis, symptomatic bone disease (10%-25% of patients), and abnormalities of the skin, central nervous system, and cardiovascular system	*Bone resorption:* subperiosteal, subchondral, subligamentous, subtendinous, intracortical, endosteal Urate and calcium pyrophosphate dihydrate (CPPD) crystal deposition Osteosclerosis *Rugger-jersey spine:* horizontal bands of osteosclerosis adjacent to the superior and inferior surfaces of the vertebral body *Brown tumor (osteoclastoma):* solitary or multiple expansile osteolytic lesions containing fibrous tissue and giant cells; may disappear after treatment for hyperparathyroidism Tendon rupture Soft tissue and vascular calcification
Renal osteodystrophy		Uremic osteopathy in patients with chronic renal insufficiency Combination of osteomalacia or rickets and secondary hyperparathyroidism ***Clinical findings*** Most patients have chronic renal disease and may be undergoing dialysis treatment	Findings of osteomalacia, rickets (in children), and hyperparathyroidism Osteosclerosis may be prominent
Dialysis spondyloarthropathy	Cervical and lumbar spine	Seen in as many as 25% of patients who receive long-standing hemodialysis Middle-aged or elderly men or women May be related to amyloid deposition or, less commonly, calcium hydroxyapatite or calcium oxalate crystal deposition in disc Additional sites of amyloid deposition include shoulder with large masses (shoulder-pad sign), wrist with carpal tunnel syndrome, and hip (which may lead to fracture of the femoral neck)	Discovertebral joint erosions at one or more levels resembling those of infectious spondylodiscitis, neuropathic osteoarthropathy, and CPPD crystal deposition disease Rapidly progressive disc space narrowing, erosion, and sclerosis of vertebral endplates

Continued

TABLE 1-15 Metabolic, Nutritional, and Endocrine Disorders of Bones and Joints—cont'd

Entity	Typical Sites of Involvement	General Characteristics	General Imaging Findings
Hypervitaminosis D	Tubular bones	Acute or chronic vitamin D poisoning occurs particularly in patients with preexisting renal or gastrointestinal dysfunction ***Clinical findings*** *Acute:* vomiting, fever, dehydration, abdominal cramps, bone pain, convulsions, coma *Chronic:* lassitude, thirst, anorexia, polyuria, vomiting	***Infants and children*** Metaphyseal bands of increased density alternating with areas of increased radiolucency Cortical thickening or osteoporosis Widespread osteosclerosis and soft tissue calcification ***Adults*** Focal or generalized osteoporosis Massive intraarticular and paraarticular metastatic soft tissue calcification
Scurvy (hypovitaminosis C)	Long tubular bones	Ascorbic acid (vitamin C) deficiency Radiographic evidence of skeletal changes in scurvy is seen only in advanced disease of long duration *Infantile scurvy:* occurs in babies who are fed pasteurized or boiled milk; heating the milk disrupts vitamin C *Adult scurvy:* rarely encountered, only in severely malnourished persons, especially the elderly ***Clinical findings*** Pale skin, petechial hemorrhage, bleeding gums, anorexia, weight loss	***Infantile scurvy*** Periostitis secondary to subperiosteal hemorrhage Transverse radiodense zone of provisional calcification (white line of Frankel) Transverse radiolucent metaphyseal line (scurvy line, Trümmerfeld zone) Beaklike metaphyseal excrescences (Pelken spurs, corner or angle sign) Radiodense shell surrounding epiphyses (Wimberger sign of scurvy) Healing scurvy may result in increased radiodensity of the metaphyses and epiphyses
Hypervitaminosis A	*Hyperostosis:* ulnae, metatarsal bones, clavicles, tibiae, fibulae, metacarpal bones, other tubular bones, ribs *Metaphyseal and epiphyseal changes:* most prominent at distal end of femur	Acute or chronic vitamin A poisoning occurs in both children and adults ***Clinical findings*** *Acute form:* nausea, vomiting, headache, drowsiness, irritability, and, in children, bulging of the fontanelles, drowsiness, and vomiting *Chronic form:* anorexia, itching, dry scaly skin, hair loss, digital clubbing, soft tissue swelling of the extremities, and osseous abnormalities on radiographs Similar findings may be seen with medications (e.g., *cis*-retinoic acid) used to treat skin disorders	Imaging findings usually confined to children at the end of the first year of life Soft tissue nodules *Hyperostosis and periostitis:* cortical thickening of tubular bones involving the diaphysis Cupping, splaying, and shortening of the metaphysis; irregularity and narrowing of the growth plates; hypertrophy and premature fusion of the epiphyseal ossification centers
Fluorosis	Axial skeleton involvement is characteristic Infrequently may affect bones of the extremities	Endemic or industrial exposure to high concentrations of fluorine in water or air; also occurs in osteoporotic patients treated with sodium fluoride ***Clinical findings*** *Acute exposure:* nausea, vomiting, constipation, anorexia, toxic nephritis *Prolonged exposure:* joint pain, restriction of motion, back stiffness, restriction of respiratory movements, dyspnea, paraplegia, and palpable thickening of superficial tubular bones ***Differential diagnosis*** Osteopetrosis, Paget disease, skeletal metastasis, other causes of diffuse osteosclerosis, and diffuse idiopathic skeletal hyperostosis (DISH)	*Spine:* osteosclerosis and ossification of the posterior longitudinal ligament, prominent osteophytosis, and periostitis *Tubular bones (rare):* osteosclerosis, periostitis, or osteoporosis (early in the disease) *Flat bones:* osteosclerosis, ligament calcification, and enthesopathy

Hypothyroidism	Entire skeleton, particularly long bones and spine	Thyroxine and triiodothyronine deficiency Primary and secondary forms ***Clinical findings*** Dry, coarse skin and hair, fatigue, lethargy, edema, pallor, cold intolerance, decreased sweating, hoarseness, constipation, weight gain, hair loss, paresthesias	*General findings:* osteopenia, delayed skeletal development, epiphyseal dysgenesis and deformity, dystrophic calcification, slipped capital femoral epiphysis, CPPD crystal deposition, erosive osteoarthritis *Spine findings:* bullet vertebrae, thoracolumbar gibbus deformity, and widened disc spaces
Hyperthyroidism	Entire skeleton	Thyrotoxicosis from overproduction of thyroid hormone by the thyroid gland; common causes are Graves disease and thyroid adenomas ***Clinical findings*** Nervousness, hypersensitivity to heat, palpitation, fatigue, weight loss, tachycardia, dyspnea, weakness, hyperorexia, goiter, tremor, thyroid bruit, and eye signs and symptoms	Hyperthyroid osteopathy Osteoporosis Accelerated skeletal maturation
Thyroid acropachy	Metacarpals, metatarsals, middle and proximal phalanges, and, occasionally, long tubular bones	Occurs in patients after treatment for hyperthyroidism Unknown cause Present in less than 1% of patients with thyrotoxicosis ***Clinical findings*** Exophthalmos Soft tissue swelling Pretibial myxedema	Digital clubbing Asymmetric diaphyseal periostitis of tubular bones Periostitis is irregular or spiculated and is more prominent on the radial or tibial side of the bones
Acromegaly and gigantism	Acromegalic changes most prominent in acral parts, skull, mandible, and soft tissues Gigantism affects entire skeleton proportionately	Hypersecretion of growth hormone (somatotropin) results in acromegaly in adults and gigantism in children Often associated with acidophilic or chromophobic adenomas of the anterior lobe of the pituitary gland ***Clinical findings*** Enlarged acral parts, menstrual disturbances, headaches, amenorrhea, increased basal metabolic rate, hyperhydrosis, cutaneous pigmentation, weight gain, hypertrichosis, back ache, limb arthropathy, compression neuropathy, neuromuscular symptoms, Raynaud phenomenon	***Acromegaly*** Widening or enlargement of costochondral junctions, mandible, phalangeal tufts, heel pad, sella turcica, articular spaces, and disc spaces Enthesopathy, thickening of cranial vault, cortical thickening of tubular bones, osteophytosis, and premature degenerative disease *Spine:* elongation and widening of the vertebral bodies; ossification of the anterior portion of the disc; posterior scalloping of vertebral bodies occurs infrequently; increased disc height; premature degenerative disease, exuberant osteophytosis ***Gigantism*** Symmetric and proportionate overgrowth of all tissues within the body
Growth recovery lines (Harris lines)[†]	Tubular bones, including femur, tibia, humerus	Transverse radiodense lines representing a sign of new or increased growth, presumably after a period of inhibited bone growth In children, growth recovery lines may be related to a previous episode of trauma, infection, malnutrition, or other chronic disease state Also seen in normal children without episodes of trauma or disease	Transverse radiodense lines across the metaphyseal region of tubular bones In adults, transverse bone bars or reinforcement lines may be present in persons with chronic osteoporosis and do not appear to be related to growth recovery or arrest

---

[*] See also: Quek S-T, Peh WCG: Radiology of osteoporosis. Semin Musculoskeletal Radiol 6:197, 2002.

[†] See also: Ameen S, Staub L, Ulrich, et al: Harris lines of the tibia across the centuries: a comparison of two populations, medieval and contemporary in Central Europe. Skeletal Radiol 34:279, 2005.

TABLE 1-16 Hematologic Disorders of Bone

Entity	Typical Sites of Involvement	General Characteristics	General Imaging Findings
Mastocytosis	*Axial skeleton:* diffuse or focal lesions *Appendicular skeleton:* focal lesions predominate	Systemic mastocytosis is characterized by mast cell proliferation and histamine release ***Clinical findings*** Resembles lymphoma and leukemia and typically results in edema, flushing, shocklike episodes, diarrhea, vomiting, anaphylaxis, bronchoconstriction, hepatosplenomegaly, weakness, and malaise	*Skeletal changes include combinations of the following:* Diffuse or focal osteosclerosis Diffuse osteopenia Focal osteolysis Pathologic fracture
Myelofibrosis	Axial skeleton and proximal long bones Spine, pelvis, skull, ribs	Rare disease of unknown cause characterized by fibrotic or sclerotic bone marrow and extramedullary hematopoiesis Middle-aged and elderly men and women *Malignant or acute form:* patients may die within a few months of initial diagnosis ***Clinical findings*** Weakness, fatigue, weight loss, abdominal pain, anorexia, nausea, vomiting, and dyspnea; abdominal swelling, purpura, and hepatosplenomegaly Diagnosis established by bone marrow biopsy Elevated serum or urinary uric acid levels (50%-80% of patients) lead to secondary gout in as many as 20% of patients	Osteosclerosis is a predominant pattern (40% to 50% of patients) Occasional sandwich vertebra appearance Normal or osteopenic bones or osteolytic lesions may be present Cortical thickening and endosteal sclerosis lead to obliteration of the normal demarcation between cortical and medullary bone
Gaucher disease	Spine Long tubular bones Pelvis	Rare familial lipid storage disease characterized by marrow infiltration with Gaucher cells Caused by a deficiency of a specific enzyme (glucocerebroside hydrolase or beta glucosidase) that leads to abnormal accumulation of lipid material in reticuloendothelial cells *Type I:* chronic or adult form; most frequent form; Ashkenazic Jews; bone involvement common *Type II:* acute form: rare fatal neurodegenerative disorder; survival usually is 1 year or less *Type III:* subacute form: juvenile onset; convulsions and other neurologic signs ***Clinical findings*** Hepatosplenomegaly, mental retardation (variable), spasticity, seizures, anemia, leukopenia, bleeding diathesis	Vertebral changes include diffuse vertebral body collapse and, infrequently, H-shaped steplike defects in the vertebral bodies Marrow infiltration results in osteopenia, osteolytic lesions, cortical diminution, and medullary widening Osseous weakening results in pathologic fractures Modeling deformities: *Erlenmeyer flask deformity* is the term applied to widening of the distal diametaphysis of the femur and other tubular bones Osteonecrosis

TABLE 1-16 Hematologic Disorders of Bone—cont'd

Entity	Typical Sites of Involvement	General Characteristics	General Imaging Findings
Sickle cell anemia	Can involve any skeletal site	Common disease among North American and African blacks characterized by the presence of HbS, sickle-shaped erythrocytes ***Clinical findings*** Symptomatic painful crises begin during second or third year of life and include anemia, fever, icterus, nausea, vomiting, abdominal pain, and prostration	Diffuse osteopenia Vascular occlusion leading to osteonecrosis Growth disturbances Osteomyelitis and septic arthritis Uric acid and calcium pyrophosphate dihydrate (CPPD) crystal deposition Marrow hyperplasia Joint effusion and hemarthroses
		Other findings include hepatosplenomegaly, cardiac enlargement, chronic leg ulcers, infection, pulmonary infarction and pneumonia, abdominal pain, cholelithiasis, peptic ulcer disease, hematuria, priapism, neurologic findings, and lymphadenopathy Death may result from infection, cardiac decompensation related to severe anemia, or thrombosis and infarction of various organs	H-shaped vertebral body indentations occur as a result of vascular occlusion to the vertebral body growth centers; commonly encountered in severe cases of sickle cell anemia and other hemoglobinopathies; may simulate Schmorl nodes or biconcave (fish) vertebrae associated with osteoporotic vertebral body fractures; compensatory vertical growth of adjacent vertebral bodies results in "tower vertebrae"
β-thalassemia	Skull, spine, ribs, and appendicular skeleton	Severe form of anemia associated with hepatosplenomegaly and bone abnormalities Typically encountered in patients of Mediterranean ancestry ***Clinical features*** *Homozygous β-thalassemia (thalassemia major):* severe anemia, prominent hepatosplenomegaly, and early death, often in childhood Anemia leads to pallor, fatigability, jaundice, icterus, deficient growth, and significant osseous deformities, especially in the face *Heterozygous β-thalassemia (thalassemia minor):* milder signs and symptoms, including slight to moderate anemia, splenomegaly, and jaundice; most common in Mediterranean populations and affects 1% of American blacks, most of whom are asymptomatic	Findings similar to those of sickle cell anemia Severe osteopenia—lacelike trabecular pattern H-shaped vertebral bodies (rare) *Modeling deformities:* Erlenmeyer flask appearance Multiple and recurrent fractures secondary to osteoporosis Uric acid and CPPD crystal deposition along with hemochromatosis secondary to repeated transfusions

TABLE 1-17 Osteonecrosis

Entity	Typical Sites of Involvement	Causes and Associations	General Imaging Findings
Epiphyseal osteonecrosis and osteonecrosis of the small or irregular bones	Femoral head Talus Distal femoral condyle Carpal lunate Humeral head	Trauma Hip dislocation Intracapsular hip fracture Hemoglobinopathies Sickle cell anemia Corticosteroid compounds Exogenous corticosteroid therapy Cushing disease Inflammatory articular disorders Systemic lupus erythematosus Dysbaric disorders Divers Astronauts Pregnancy Irradiation Pancreatitis (alcoholism) Gout Renal transplantation Lymphoproliferative disorders Idiopathic	Routine radiographs may be negative Bone sclerosis Cysts Subchondral collapse (crescent sign) May be focal or segmental area of involvement Joint space narrowing in advanced cases Intravertebral vacuum phenomenon with pathologic vertebral body collapse Scintigraphy, computed tomography, and magnetic resonance imaging are important in assessing osteonecrosis
Medullary osteonecrosis	Long tubular bones, especially lower extremity	Same associations as epiphyseal osteonecrosis (above)	Metadiaphyseal involvement: also termed *bone infarct* Patchy intramedullary sclerosis with areas of radiolucency Irregular calcific deposits Closely resembles appearance of enchondroma Occurs within areas of fatty marrow Malignant transformation extremely rare
Vertebral body osteonecrosis	*Vertebral body:* lumbar and thoracolumbar segments	Frequently associated with corticosteroid use	Vertebral body collapse with linear zone of intraosseous gas (intravertebral vacuum)

TABLE 1-18 Osteochondroses and Other Epiphyseal Alterations

Entity	Site of Involvement	Age (yr)	Probable Mechanism
Legg-Calvé-Perthes disease	Femoral capital epiphysis	4-8	Osteonecrosis, perhaps caused by trauma
Freiberg infraction	Metatarsal head	13-18	Osteonecrosis caused by trauma
Kienböck disease	Carpal lunate	20-40	Osteonecrosis caused by trauma
Thiemann disease	Phalanges of hand	11-19	Osteonecrosis, perhaps caused by trauma
Osgood-Schlatter disease	Tibial tubercle	11-15	Trauma or abnormal stress
Blount disease	Proximal tibial epiphysis	1-3 (infantile) 8-15 (adolescent)	Trauma or abnormal stress
Scheuermann disease	Discovertebral junction	13-17	Trauma or abnormal stress
Sinding-Larsen-Johansson disease	Patella	10-14	Trauma or abnormal stress
Köhler disease	Tarsal navicular	3-7	Osteonecrosis or altered sequence of ossification
Panner disease	Capitulum of humerus	5-10	Osteonecrosis or abnormal ossification
Sever disease	Calcaneal apophysis	4-10	Variation of normal ossification (no clinical significance)
Van Neck disease	Ischiopubic synchondrosis	4-8	Normal bulbous appearance of ossification center (no clinical significance)

TABLE 1-19 Infectious Disorders of Bones and Joints

Entity	General Characteristics	General Imaging Findings
Acute pyogenic osteomyelitis	Intravenous drug abusers, diabetics, and immunocompromised patients have a predisposition to osteomyelitis and septic arthritis of adjacent joints Routes of contamination: hematogenous, contiguous source, direct implantation, and postoperative *Organisms: Staphylococcus, Actinomyces, Pseudomonas, Brucella,* and many others	Metaphyses in children Spine and pelvis in adults Poorly defined permeative bone destruction
Pyogenic septic arthritis	*Predisposing factors:* intravenous drug abuse, joint surgery, immunocompromised states *Routes of contamination:* hematogenous, contiguous source, direct implantation, and postoperative *Common organisms: Staphylococcus aureus, Streptococcus, Hemophilus, Pseudomonas,* gonococcus, and *Escherichia coli* Mycobacterial and fungal agents also may be implicated Neonatal septic arthritis is more common than childhood septic arthritis Infectious spondylodiscitis occurs most frequently after spine surgery	***Adult septic arthritis*** Rapid concentric joint space narrowing Periarticular osteoporosis Capsular distention from joint effusion Loss of definition and destruction of subchondral bone Marginal and central osseous erosions Bony ankylosis (rare) ***Neonatal and childhood septic arthritis*** Soft tissue swelling or capsular distention *Pathologic subluxation or dislocation:* lateral displacement of ossification center Slipped capital femoral epiphysis Metaphyseal osteomyelitis Concentric joint space narrowing
Chronic osteomyelitis	***Signs of reactivation*** Change from a previous radiograph Poorly defined areas of osteolysis Thin linear periostitis Sequestration ***Complication*** Marjolin ulcer—squamous cell carcinoma at site of cloaca	Osteosclerosis and cortical thickening Thick, single layer of periosteal bone proliferation Areas of osteolysis and poorly defined areas of sclerosis Sequestrum and involucrum
Brodie abscess	Subacute pyogenic osteomyelitis Most frequently found in children Predilection for the distal tibial metaphysis Rarely crosses into the epiphysis Tibia is the most common site of such infections Usually staphylococcal organisms Aspirate is frequently sterile	Circular, geographic zone of osteolysis Sharply circumscribed sclerotic margin Metaphyseal location Radiolucent channel may communicate with growth plate May resemble osteoid osteoma or stress fracture
Chronic recurrent multifocal osteomyelitis (CRMO)*	Unknown cause Occurs mainly in children and adolescents *Diagnosis of exclusion:* 1. Lack of causative organism 2. No abscess formation 3. Atypical location compared with infectious osteomyelitis 4. Often multifocal lesions 5. Imaging findings suggesting acute or subacute osteomyelitis 6. Laboratory and histologic findings suggesting acute or subacute osteomyelitis 7. Prolonged, fluctuating course with recurrent episodes of pain occurring over several years, usually without systemic manifestations 8. May accompany pustulosis palmoplantaris or other skin lesions and may be closely related to synovitis, acne, pustulosis, hyperostosis, and osteitis (SAPHO) syndrome	Initial osteolytic destruction of metaphysis adjacent to growth plate with no periosteal bone formation or sequestration Magnetic resonance imaging also useful in the diagnosis

* Data from Jurik AG: Chronic recurrent multifocal osteomyelitis. Semin Musculoskeletal Radiol 8:243, 2004; Jurik AG, Egund N: MRI in chronic recurrent multifocal osteomyelitis, Skeletal Radiol 26:230, 1997.

Continued

TABLE 1-19 Infectious Disorders of Bones and Joints—cont'd

Entity	General Characteristics	General Imaging Findings
Tuberculous osteomyelitis: extraspinal sites	Tuberculosis confined to extraspinal bone is infrequent; bone involvement usually is associated with tuberculous arthritis of adjacent joints Affects persons of any age, especially those with underlying disorders, corticosteroid users, intravenous drug abusers, immigrants, and immunosuppressed persons *Most common organism: Mycobacterium tuberculosis* *Can affect any bone:* pelvis, phalanges and metacarpals (tuberculous dactylitis), long bones, ribs, sternum, scapula, skull, patella, and the carpal and tarsal regions	Osteolytic lesions Surrounding sclerosis and periostitis may occur Intracortical lesions are rare Cystic tuberculosis: disseminated lesions throughout the skeleton rarely occur Often begins in epiphysis and spreads to adjacent joint Metaphyseal lesions in children may violate the growth plate (helping to differentiate tuberculous osteomyelitis from pyogenic osteomyelitis)
Tuberculous arthritis: extraspinal sites	Affects persons of any age, especially those with underlying disorders, corticosteroid users, intravenous drug abusers, immigrants, and immunosuppressed persons *Most common organism: Mycobacterium tuberculosis* Other sites include the hip, knee, wrist, and elbow	Various degrees of soft tissue swelling Gradual joint space narrowing Juxtaarticular osteoporosis Peripherally located erosions Subchondral erosions Periarticular abscess
Tuberculous spondylitis	*Tuberculous spondylitis:* spine is involved in 25%-50% of all cases of skeletal tuberculosis Thoracolumbar region most frequent site of involvement May affect solitary vertebra, but most cases affect two or more vertebrae In more than 80% of patients, tuberculous infection begins in the vertebral body; less commonly affects posterior elements *Most common organism: Mycobacterium tuberculosis* Men > women; occurs in adults and children	*Discovertebral lesions:* osteolytic destruction of vertebral body margins and usual extension into the intervening intervertebral disc; eventual obliteration of the disc space and adjacent subchondral endplates; vertebral collapse and consequent kyphosis (gibbus) deformity may occur *Paraspinal extension:* frequent spread of infection from vertebral bodies and discs to adjacent ligaments and soft tissues; usual extension is anterolateral; rare epidural extension; subligamentous extension underneath the anterior and posterior longitudinal ligaments; abscesses (i.e., psoas abscesses) may extend for great distances and may penetrate adjacent viscera Other infrequent radiographic findings include bony ankylosis, ivory vertebrae, atlantoaxial instability (fewer than 2% of tuberculous spondylitis patients), and spinal canal involvement
Congenital syphilis	Affects babies born to mothers who have been infected during pregnancy with the spirochete *Treponema pallidum*	Symmetric, transverse, radiolucent, metaphyseal bands or linear, longitudinal, alternating lucent and sclerotic bands (the "celery stalk" appearance) Other osseous abnormalities include osteochondritis, diaphyseal osteomyelitis, and gumma formation
Poliomyelitis	Paralysis results in muscle and bone atrophy May result in scoliosis and mechanical disorders of the spine and lower extremities	Asymmetric hypoplasia and osteopenia of the pelvic bones and femur Prominent scoliosis
Leprous osteomyelitis	Leprosy is an infectious disease caused by *Mycobacterium leprae,* rarely encountered in the United States; most common in Africa, South America, and Asia Patients also may contract neuropathic osteoarthropathy, secondary infection, and leprous arthritis	Periostitis Osteitis Osteomyelitis Neuropathic osteoarthropathy

TABLE 1-19 Infectious Disorders of Bones and Joints—cont'd

Entity	General Characteristics	General Imaging Findings
Unusual bacterial and fungal forms of osteomyelitis	*Disorders include the following:* Actinomycosis Nocardiosis Cryptococcosis (torulosis) North American blastomycosis Coccidioidomycosis Histoplasmosis Sporotrichosis Candidiasis Maduromycosis (mycetoma)	Findings variable depending on causative organisms

PART II

Spine

CHAPTER 2

Cervical Spine

NORMAL DEVELOPMENTAL ANATOMY

Accurate interpretation of pediatric cervical spine radiographs requires a thorough understanding of normal developmental anatomy. Table 2-1 outlines the age of appearance and fusion of the primary and secondary ossification centers. Figures 2-1 to 2-3 demonstrate the radiographic appearance of many important developmental landmarks at selected ages from birth to skeletal maturity.

DEVELOPMENTAL ANOMALIES, ANATOMIC VARIANTS, AND SOURCES OF DIAGNOSTIC ERROR

Radiographic interpretation of disease processes in the cervical spine may be difficult owing to many anomalies, variations, and other sources of diagnostic error that are frequently encountered in this region of the spine (Table 2-2 and 2-4). Although most of these processes are of no clinical significance, some anomalies may result in atlantoaxial instability and are of vital concern to the clinician and the patient (Table 2-3). Table 2-5 details the features of Klippel-Feil syndrome. Figures 2-4 to 2-40 show examples of many of these entities.

SKELETAL DYSPLASIAS AND OTHER CONGENITAL DISEASES

Table 2-6 outlines a number of dysplastic and congenital disorders that affect the cervical spine; Figures 2-41 and 2-43 illustrate some of these disorders.

PHYSICAL INJURY

Fractures, dislocations, and soft tissue injuries involving the spine are frequent, and often these lesions are associated with serious clinical manifestations. Tables 2-7 and 2-8 detail the Canadian Cervical Spine Decision Rule for determining the need for imaging. Table 2-9 stratifies cervical spine injuries according to their relative degree of instability. Tables 2-10 and 2-11 address injuries of the upper cervical spine, whereas Tables 2-12 to 2-14 address injuries to the lower segments of the cervical spine. The injuries are classified according to their anatomic locations, presumed mechanism of injury, and presence or absence of spinal instability. In addition, Figures 2-44 to 2-65 demonstrate the most characteristic imaging manifestations of some of the more common examples of physical injury.

ARTICULAR DISORDERS

The cervical spine is a frequent and characteristic site of involvement for many forms of spondyloarthropathy. Tables 2-15 and 2-16 discuss degenerative, inflammatory, crystal-induced, infectious, and other articular diseases that commonly afflict the cervical spine, and Figures 2-66 to 2-91 reveal some of their radiographic manifestations.

BONE TUMORS

A wide variety of malignant tumors, benign tumors, and tumorlike lesions affect the cervical spine. Table 2-17 reveals the spectrum of neoplasms that may affect the entire vertebral column (including the thoracic, lumbar, sacral, and coccygeal segments). The table also indicates some of the typical characteristics of each lesion as it is manifested in the cervical spine. Figures 2-92 to 2-106 illustrate some of the more common examples. Table 2-18 lists some causes of enlarged cervical intervertebral foramina.

METABOLIC DISEASES

The skeletal manifestations of many metabolic disorders are frequently exhibited in the cervical spine. Some of the more common conditions are outlined in Table 2-19 and illustrated in Figures 2-107 to 2-109.

INTERVERTEBRAL DISC ABNORMALITIES

Herniation of one or more intervertebral discs in the cervical spine is a common cause of signs and symptoms in the cervical spine and upper extremity. Table 2-20 describes acute disc herniations and chronic degenerative spondylosis. Figure 2-110 illustrates the imaging of this common problem. Degenerative spine disease also is discussed under the heading of articular disorders earlier in this chapter.

CERVICAL SPINE SURGERY

Numerous surgical procedures are performed for pathologic conditions of the intervertebral disc, spinal stenosis, or other disorders. Tables 2-21 and 2-22 list a few of these procedures and some of their complications; Figures 2-111 to 2-116 show some of their imaging manifestations.

VASCULAR DISORDERS

Vascular disease may be encountered in the evaluation of cervical spine radiographs. Table 2-23 contains a description of three of these conditions, two of which are illustrated in Figures 2-117 and 2-118.

TABLE 2-1 **Cervical Spine: Approximate Age of Appearance and Fusion of Ossification Centers[1-3] (Figures 2-1 to 2-3)**

Ossification Center	Primary or Secondary	No. of Centers	Age of Appearance* (Years)	Age of Fusion* (Years)	Comments
C1 posterior arch	P	2	Birth	3	
C1 anterior arch	P	1	Birth-1	6-7	
C1 tip of transverse process	S	2	18	21-25	
C2 odontoid	P	2	Birth	4	Fuses to body
C2 tip of odontoid	S	1	3-6	8-12	Fuses to odontoid
C2 body	P	1 or 2	Birth	4	Fuses to laminae
C2 neural arches (laminae)	P	2	Birth	2	Fuse together
C2 endplate ring apophysis	S	1	Puberty	22-25	Fuses to body
C3-C7 body	P	1	Birth	3	Fuses to laminae
C3-C7 neural arches (laminae)	P	2	Birth	1	Fuse together in order from C7-C3
C3-C7 endplate ring apophyses	S	2	11-12	17-18	Fuse to body

P, Primary; *S*, secondary.

* Ages of appearance and fusion of ossification centers in girls typically precede those of boys. Ethnic differences also exist.

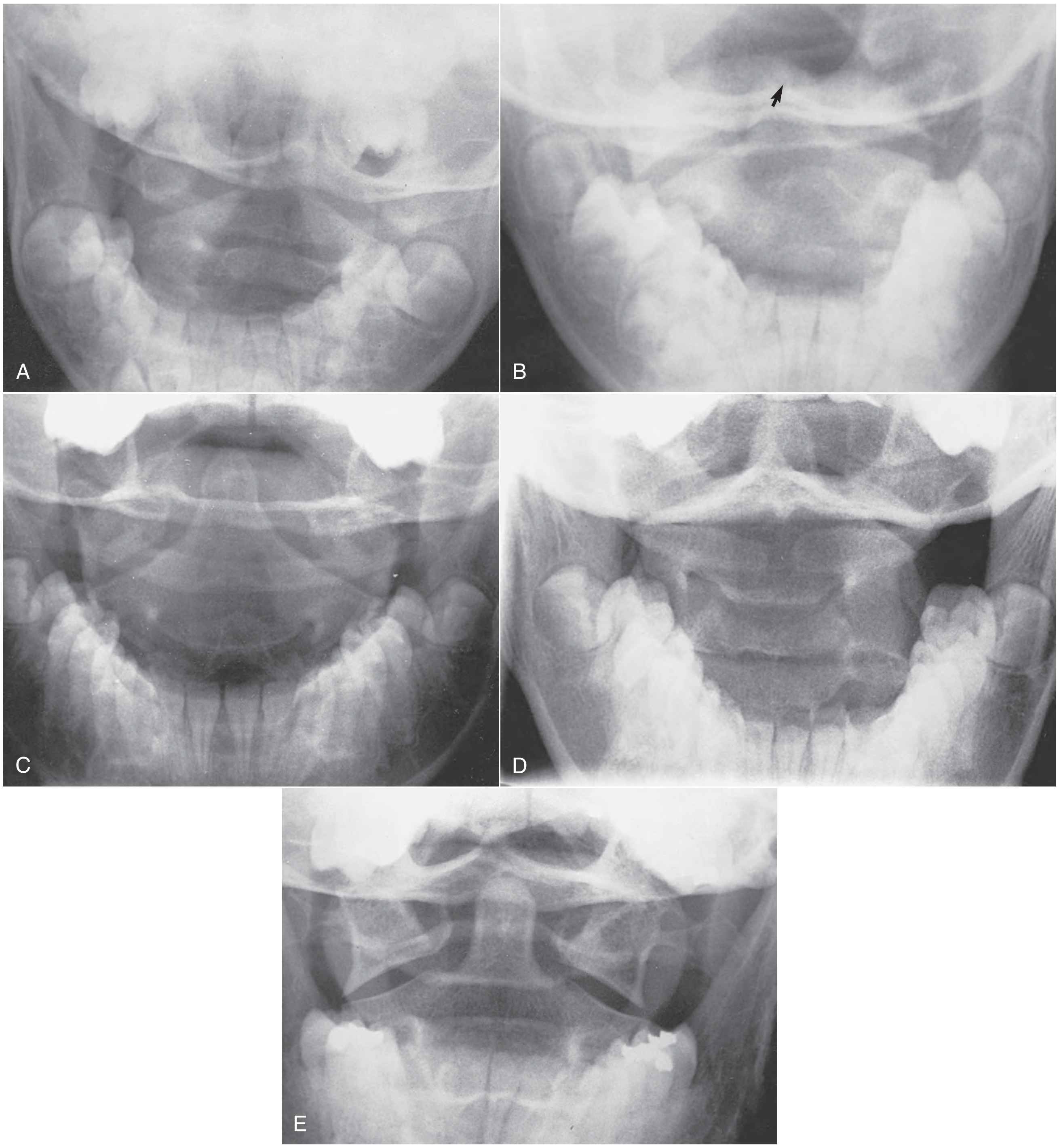

FIGURE 2–1 Skeletal maturation and normal development: anteroposterior open mouth upper cervical spine radiographs.[1-3] **A,** A 3-year-old girl. The odontoid and lateral masses of the atlas are obscured by the occipital and dental structures. The atlas often appears wider than the axis until about the age of 5 years. **B,** A 5-year-old boy. The ossification center at the tip of the odontoid *(arrow)* typically appears at the age of 2 years and fuses to the odontoid by the age of 12 years. If it persists into adulthood, it is termed an *os terminale of Bergmann* and is considered a normal variant. **C,** An 11-year-old girl. The odontoid process usually is completely developed by this age. **D,** A 14-year-old girl. The posterior arch of the atlas, which usually fuses at about the age of 3 years, remains ununited in this child. Such incomplete fusion (spondyloschisis) at this level is a frequent occurrence. **E,** Adult: 28-year-old man. The secondary ossification centers of the transverse processes typically are the last centers to fuse, usually by age 25 years, and such fusion signals complete development.

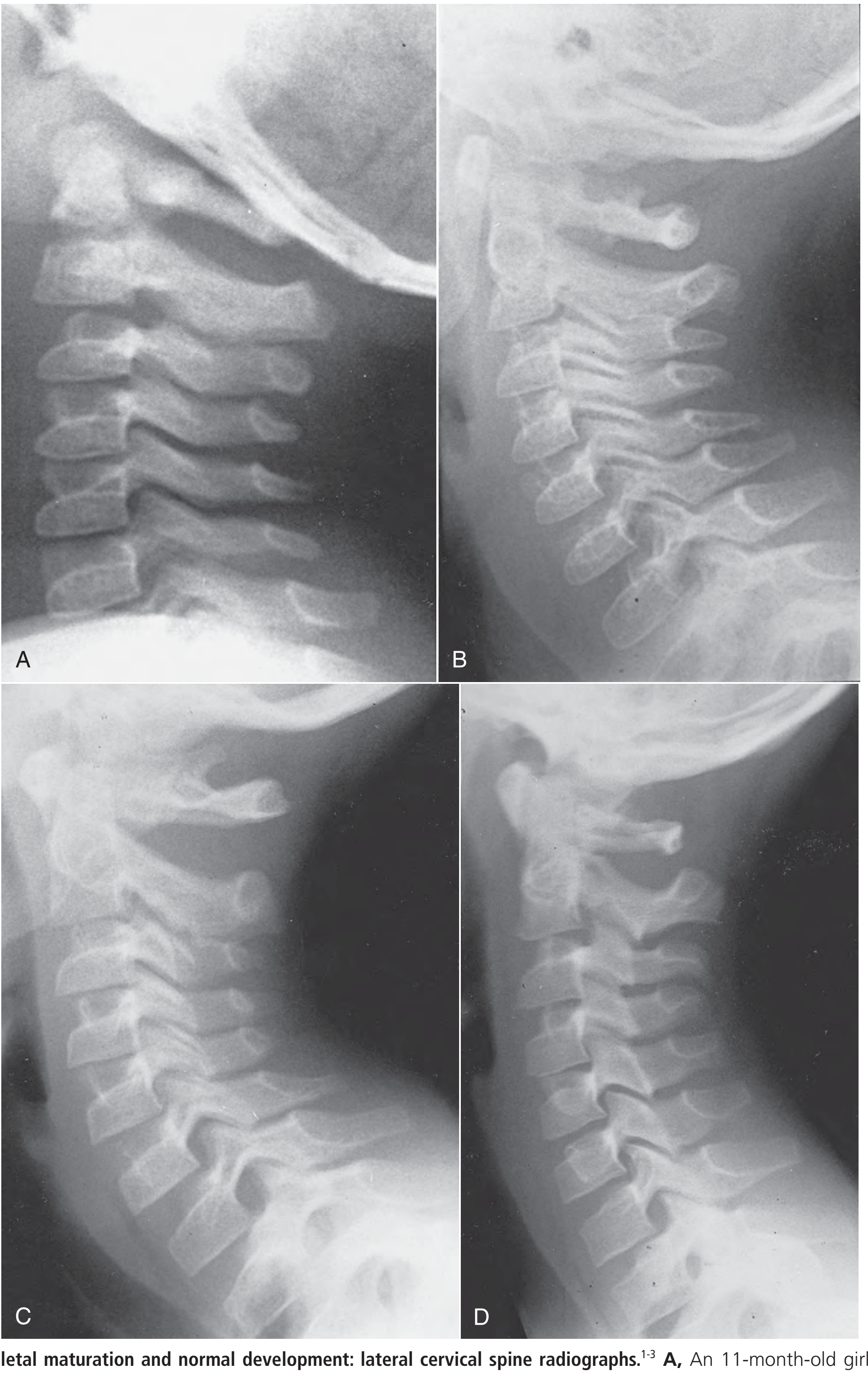

FIGURE 2–2 **Skeletal maturation and normal development: lateral cervical spine radiographs.**[1-3] **A,** An 11-month-old girl. The odontoid is not yet fused with the body of C2. The vertebral bodies appear flattened, and the sagittal spinal canal diameter is disproportionately wide. **B,** A 3-year-old girl. The odontoid typically fuses to the body of C2 about the age of 3 years, and it is almost completely fused in this child. The superior aspects of the vertebral bodies are rounded, the spinal canal remains proportionately wide, and the posterior margins of the vertebral bodies are scalloped. The anterior arch of the atlas appears to be displaced superiorly in relation to the tip of the odontoid. This normal finding is the result of incomplete ossification of the odontoid and should not be mistaken for subluxation of the atlas. **C,** A 5-year-old boy. The vertebral bodies are wedge-shaped and their anterosuperior margins remain rounded. **D,** An 8-year-old boy. The superior margins of the vertebral bodies are beginning to appear less wedge-shaped.

Continued

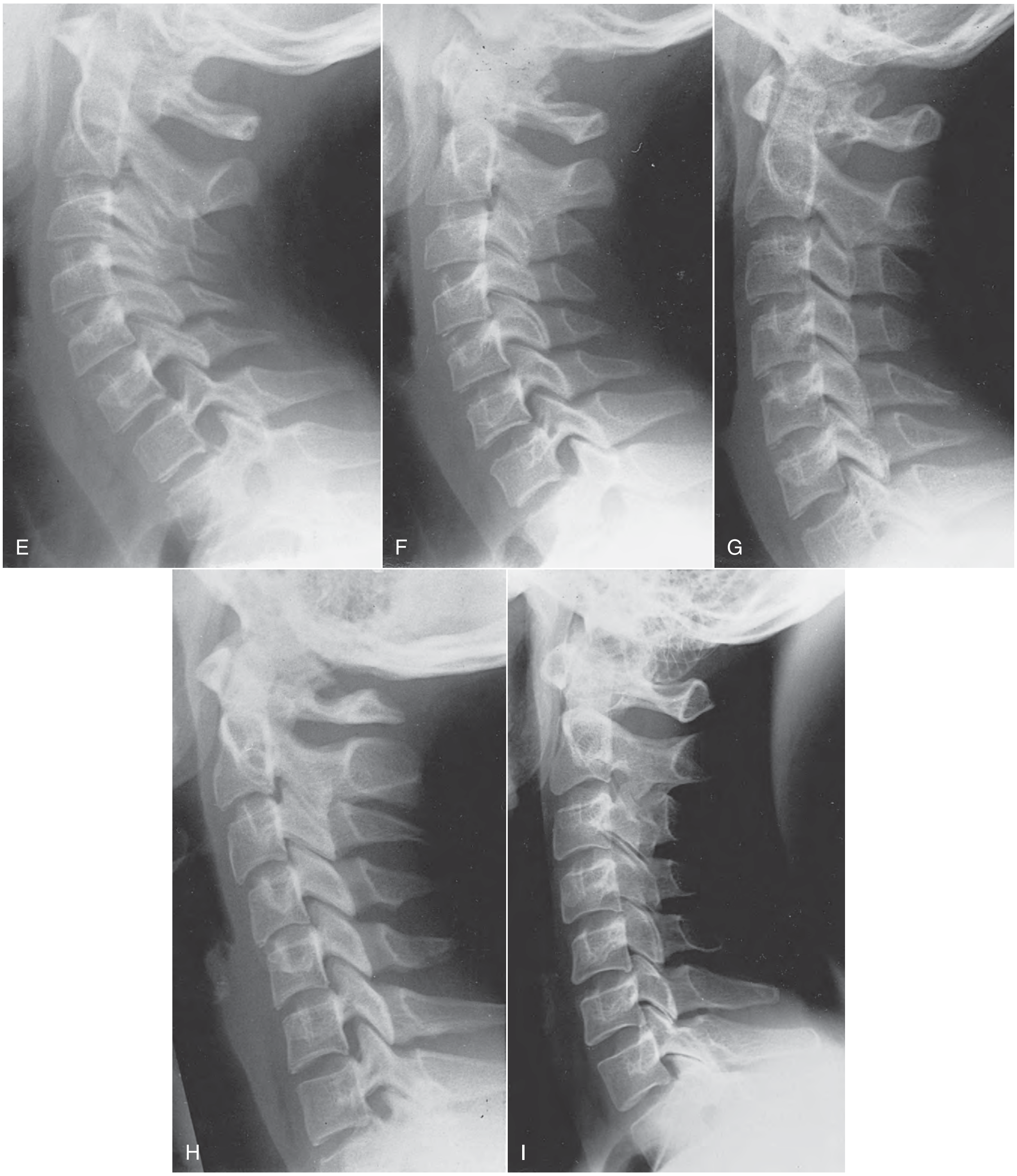

FIGURE 2–2, cont'd **E,** An 11-year-old girl. The secondary ring apophyses adjacent to the superior and inferior vertebral endplates begin to appear at puberty but may appear as early as age 7 years. The odontoid process usually is fully developed at this age. **F,** A 12-year-old boy. The midcervical vertebral bodies maintain a somewhat wedged appearance. Observe the ring apophyses and scalloped posterior body margins. **G,** A 15-year-old boy. The vertebral bodies have a more adult shape. Note the V-shaped predens space, a normal variant. **H,** A 16-year-old girl. The ring apophyses usually fuse with the vertebral bodies by the age of 17 years in girls and 18 years in boys. C3 often is the last cervical vertebra to retain its wedge-shaped configuration. The cervical lordosis is flattened in this girl. **I,** Adult: 43-year-old woman. The vertebral bodies are squared, but their anterosuperior margins remain slightly rounded. The C2-C3 facet joints are not well visualized owing to their normal orientation. The superior articulating surface of the C7 articular process is notched, a normal variant frequently encountered in this region. The normal mastoid air cells overlying the atlanto-occipital region should not be confused with an expansile mass.

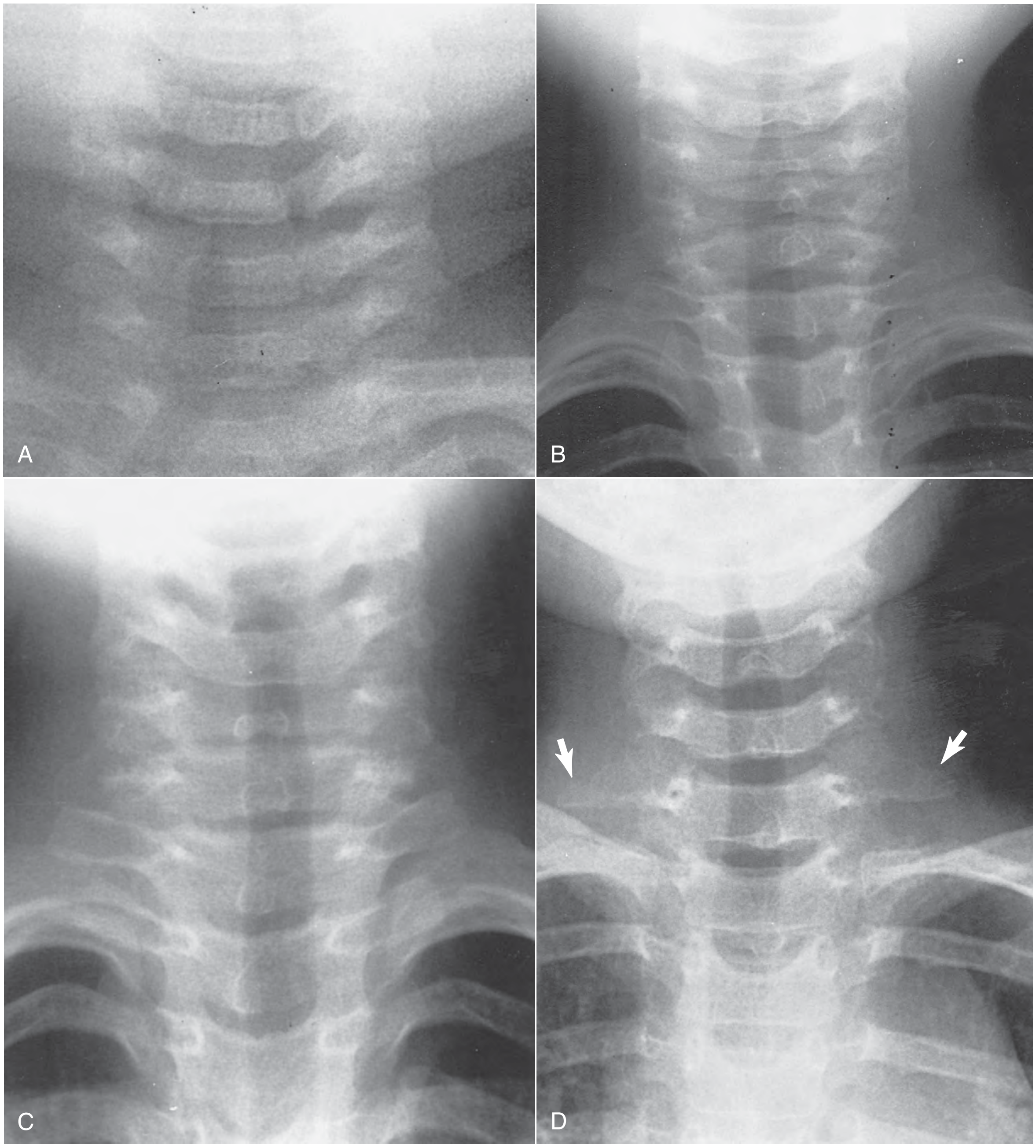

FIGURE 2–3 **Skeletal maturation and normal development: anteroposterior cervical spine radiographs.**[1-3] **A,** An 11-month-old girl. Bilateral neural arch ossification centers, which usually fuse between 1 and 7 years of age, are evident in this infant. Incomplete development of the osseous structures results in a proportionately wide appearance of the spinal canal. Patient rotation has resulted in tracheal deviation. **B,** A 3-year-old girl. **C,** A 5-year-old boy. **D,** An 8-year-old girl. The C7 transverse processes are somewhat elongated *(arrows),* a common developmental anomaly. The obliquely oriented clavicles result from elevation of the patient's arms during exposure.

Continued

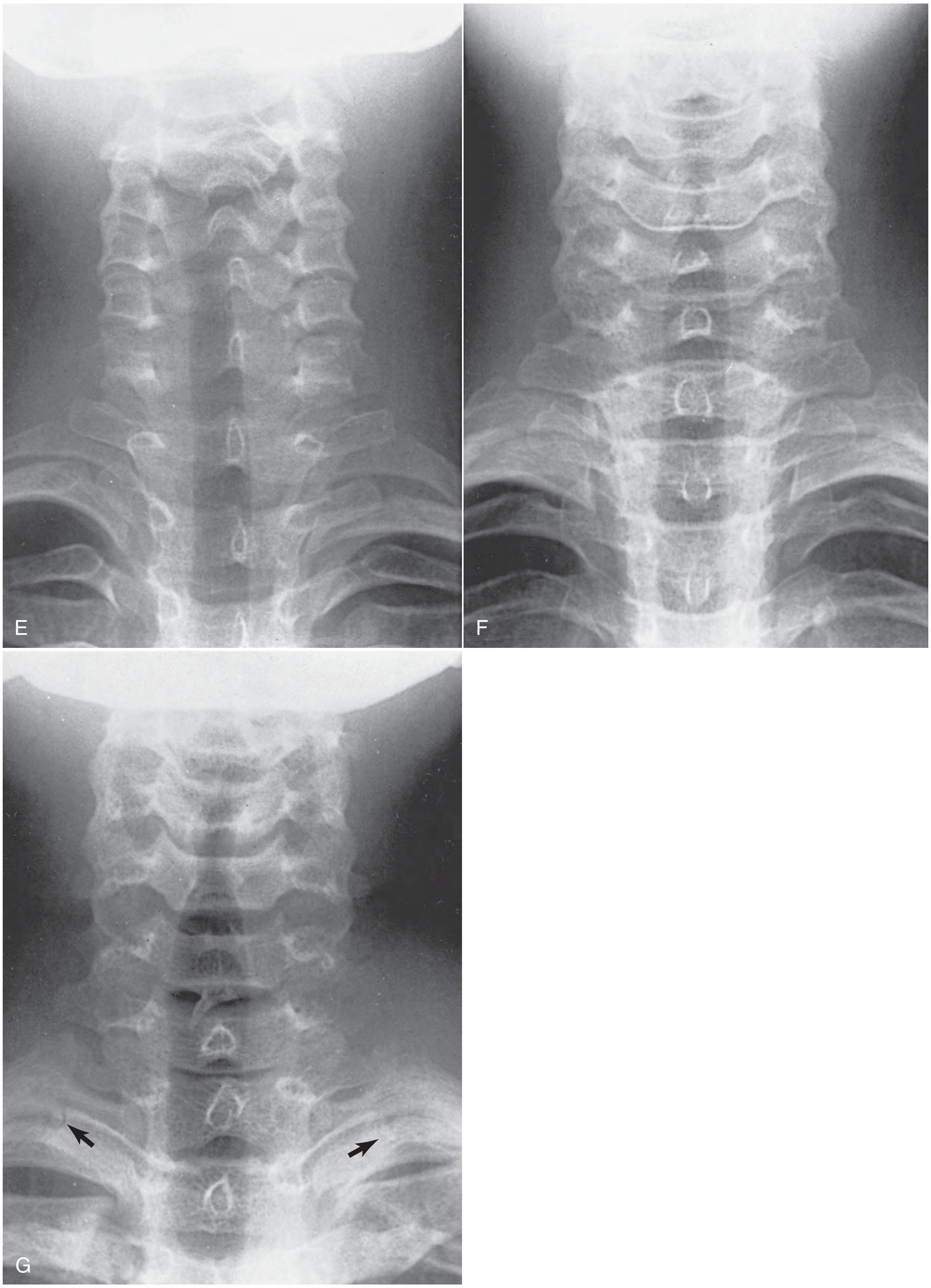

FIGURE 2–3, cont'd **E,** A 10-year-old boy. Inferior angulation of the x-ray beam allows visualization of the facet joint spaces. **F,** A 13-year-old boy. The cervical spine approaches adult proportions. **G,** A 15-year-old boy. The secondary ossification centers of the transverse processes usually appear about the age of 16 years. They are obvious at T2 *(arrows)* but indistinct at T1 in this person.

TABLE 2-2 Some Developmental Anomalies, Anatomic Variants, and Sources of Diagnostic Error Affecting the Upper Cervical Spine*

Entity	Figure(s)	Characteristics
Atlas (C1)		
Atlas assimilation[4] (occipitalization)	2-4	Failure of segmentation of the most caudal occipital sclerotome; atlas is fused to base of occiput Usually asymptomatic, but may be associated with pain, limitation of cervical motion, and neurologic signs May be associated with platybasia, basilar invagination, Chiari type I malformation, Sturge-Weber syndrome, and Klippel-Feil syndrome Atlantoaxial instability present in 50% of persons with associated C2-C3 synostosis: flexion and extension radiographs should be considered to evaluate for such instability Premature degenerative disease at subjacent levels, especially C1-C2, observed in some patients with this anomaly
Posterior arch agenesis[4-8]	2-5, 2-6	Complete agenesis of posterior arch of atlas (a rare, usually asymptomatic anomaly characterized by incomplete ossification of the secondary growth center of the posterior arch) Partial agenesis, usually manifest as a midline cleft (spondyloschisis); present in 4% of adults: a much more common anomaly than complete agenesis Often accompanied by compensatory hypertrophy and sclerosis of the anterior arch of C1 and hypertrophy of the spinous process of C2 (megaspinous process)—reliable signs that this is a long-standing condition rather than a rapid destructive process A cartilaginous or fibrous posterior arch is usually present, typically not resulting in instability; flexion and extension radiographs are useful in evaluating the integrity of the transverse ligament.
Anterior arch agenesis[4,7]	2-7	*Anterior spondyloschisis:* midline radiolucency on anterior arch from incomplete fusion of the ossification centers is extremely rare (0.1% of persons); best seen on axial radiographs and computed tomographic (CT) scans. Posterior arch of atlas spondyloschisis is nearly always present when there is anterior arch spondyloschisis, suggesting that the anterior arch spondyloschisis could be a secondary stress fracture.
Accessory ossicles[9]	2-8	A variety of small ossicles may be present in the region of the atlas Usually of no clinical significance
Posterior ponticulus[6]	2-9	Ossification of posterior atlanto-occipital membrane present in 15% of normal persons Arcuate foramen allows passage of the vertebral artery and C1 nerve Usually stable and benign; rarely related to vertebral artery compression, posttraumatic basal subarachnoid hemorrhage, and the Barré-Liéou syndrome
Sclerotic anterior tubercle[6]	2-10	Normal variant, not associated with osteosclerotic disorders Sclerosis and hypertrophy may be associated with chronic altered stresses related to posterior arch agenesis, os odontoideum, and other atlantoaxial anomalies
Asymmetry of atlas[7]	2-11	Lateral masses of atlas often develop asymmetrically and should not be mistaken for evidence of a compression injury of the lateral mass
Axis (C2) and C1-C2 Articulations		
Normal transverse foramen[5,7]	2-9	*Normal anatomy:* transverse foramen is seen on lateral radiograph as a circular radiolucency
Rotation simulating fracture[5,7]	2-12	Rotation of lateral radiograph results in overlap of lateral masses simulating fracture
Mach band effect[10]	2-13	Transverse zone of relative radiolucency overlying the base of the odontoid adjacent to the edge of the overlapping posterior arch of the atlas, simulating an odontoid fracture
Paraodontoid notch[5,7]	2-14, *A*	Normal bilateral notches adjacent to the base of the odontoid may simulate fractures
Incisors overlying odontoid[5]	2-14, *B*	Normal space between incisors overlapping the odontoid may simulate a vertical fracture on anteroposterior open mouth radiograph
Os terminale of Bergmann[5,7]	2-15	Unfused ossification center at the tip of the odontoid persisting past the age of 12 years, which may simulate a fracture

* See also Table 1-1.

Continued

TABLE 2-2 Some Developmental Anomalies, Anatomic Variants, and Sources of Diagnostic Error Affecting the Upper Cervical Spine—cont'd

Entity	Figure(s)	Characteristics
Os odontoideum[4,7,11]	2-16	Incomplete fusion of odontoid to C2 body Most likely represents a nonunion of a type II odontoid fracture rather than an anomaly Frequently results in multidirectional atlantoaxial instability that may lead to transient or progressive neurologic deficit and even death with trivial trauma
Odontoid agenesis and hypoplasia[7]		Incomplete development or absence of the odontoid Frequently results in atlantoaxial instability
Posterior inclination of odontoid[12]	2-17	Normal variation in the inclination of the odontoid that may simulate posterior displacement from an odontoid fracture or os odontoideum
V-shaped predens space[13,160]	2-2, *G*, 2-18	Normal variation in which the predens space (atlantodental interspace) is V-shaped rather than parallel Accentuated on flexion radiographs Present in about 9% of persons In some cases, may be due to increased flexion mobility with elongated or lax transverse ligament
Absence of transverse ligament[14]	2-19	Up to 20% of children with Down syndrome (trisomy 21) are born with this anomaly, and many have hypoplasia or agenesis of the odontoid resulting in atlantoaxial instability and possible cord compression; these children should be screened with flexion and extension radiographs before participating in Special Olympics and other sporting events
Anomalous articulations[5,7]	2-20	C1-C2 junction is a common site for several anomalies
C2 congenital spondylolysis[15]	2-21	Incomplete fusion of the C2 neural arches to the vertebral body results in a radiolucent defect and potential instability
Pseudosubluxation of C2[16,17,135]	2-22	Normal variant present in up to 24% of infants and children up to age 8 years May be confused with an unstable fracture or ligament injury Excessive sagittal plane motion of the C2-C3 and C3-C4 segments, seen on flexion and extension radiographs in infants; is also a common finding attributed to normal ligamentous laxity
C2-C3 Articulations		
Ball-and-socket articulation[5,7]	2-23	Anomalous pronglike projection of the C3 articular process articulates with a concavity within the C2 articular process
Pseudofusion of C2-C3 apophyseal joints[18]	2-24	Normal orientation of the C2-C3 apophyseal joint surfaces often results in the appearance of joint ankylosis on lateral radiographs
Synostosis and other anomalies[5-7]	2-25; 2-31	Developmental segmentation defects, frequently resulting in block vertebrae at the C2-C3 level; these synostoses are often accompanied by other anomalies

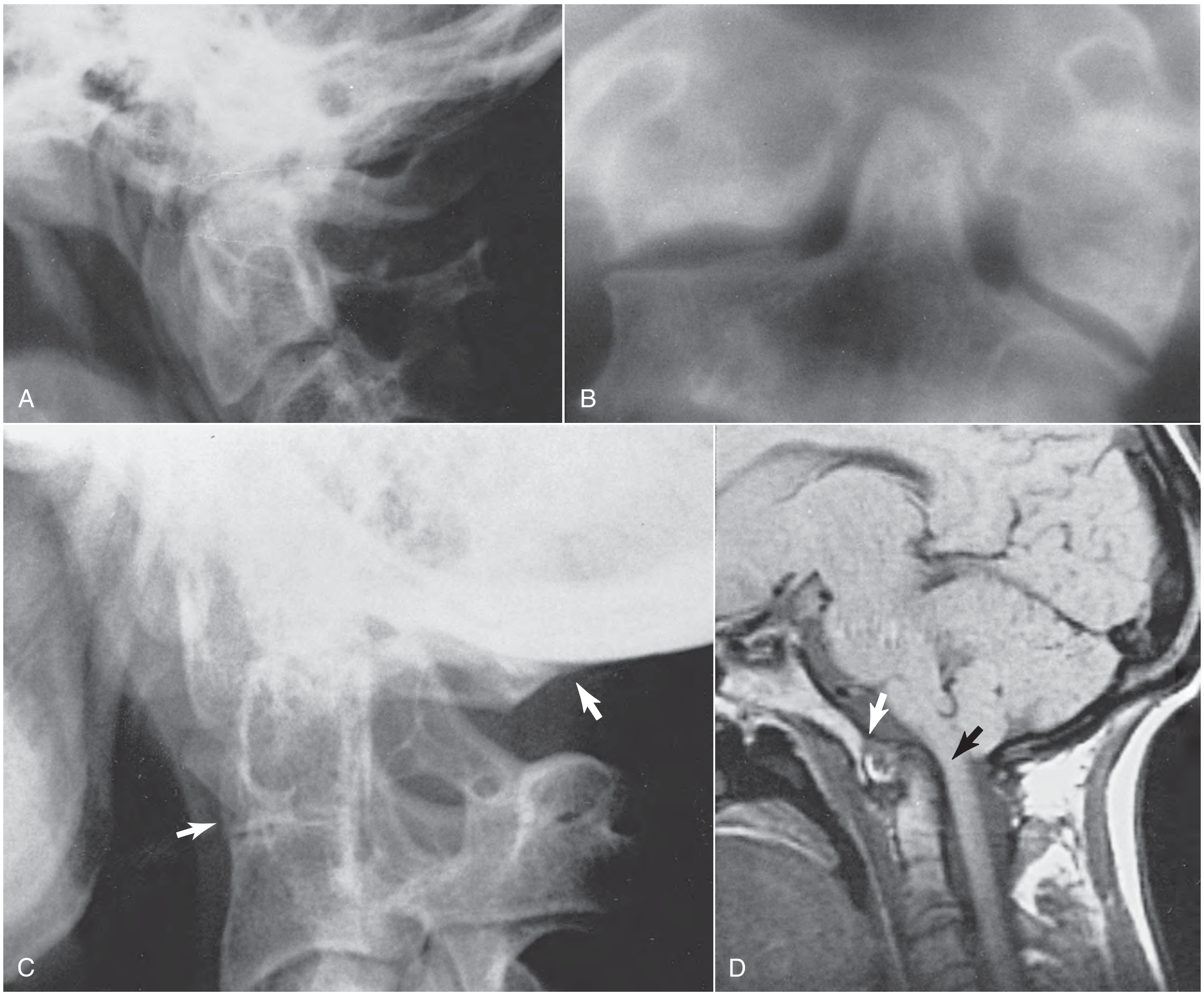

FIGURE 2–4 **Atlanto-occipital assimilation (occipitalization).**[4] **A-B,** Lateral radiograph **(A)** and frontal conventional tomogram **(B)** demonstrate fusion of the occipital condyle with the lateral mass of C1 on the right side and, to a lesser extent, on the left. **C-D,** Another patient: 27-year-old woman with stuttering and loss of memory after a motor vehicle accident. Lateral radiograph **(C)** shows assimilation of the atlas with the base of the occiput *(right arrow)*, synostosis (block vertebrae) of C2-C3 *(left arrow)*, and mild basilar impression. Sagittal T1-weighted (TR/TE, 800/25) spin echo MR image **(D)** reveals slight kinking of the spinomedullary junction *(black arrow)* and an unusually high position of the odontoid process within the foramen magnum. The anterior arch of atlas abuts on the clivus *(white arrow)*. (***C-D,*** *Courtesy T. Wei, DC, Portland, Ore.)*

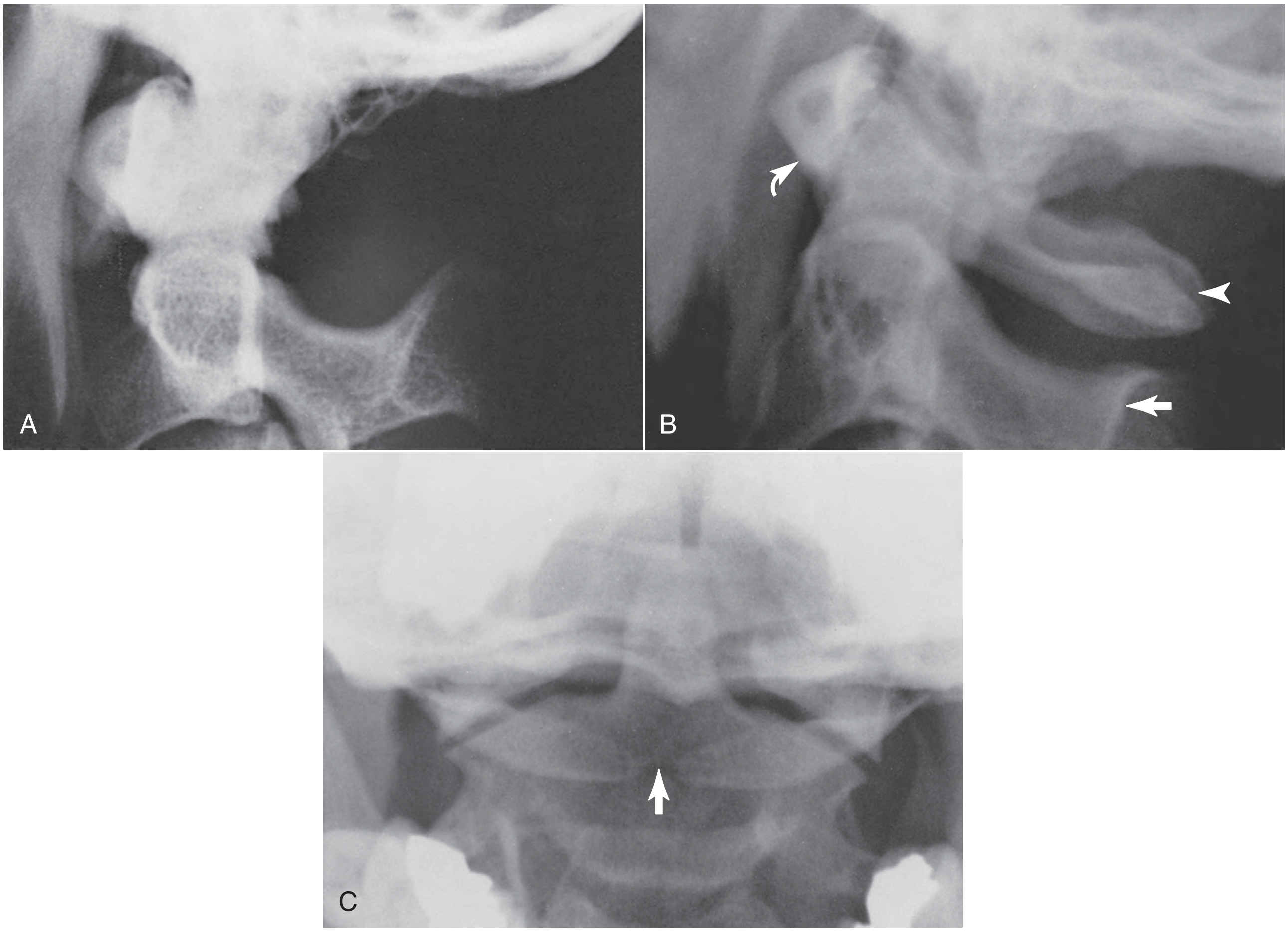

FIGURE 2–5 Agenesis of the posterior arch of C1.[4-8] **A,** Complete agenesis. The posterior arch of the atlas remains unossified. **B-C,** Partial agenesis (spondyloschisis). Lateral radiograph **(B)** shows a radiolucent cleft *(arrowhead)* and absence of the spinolaminar junction line. (Note the spinolaminar junction line identified at C2 by a straight arrow.) The anterior arch is hypertrophied and sclerotic *(curved arrow).* Frontal radiograph **(C)** demonstrates a median cleft in the posterior arch *(arrow).*

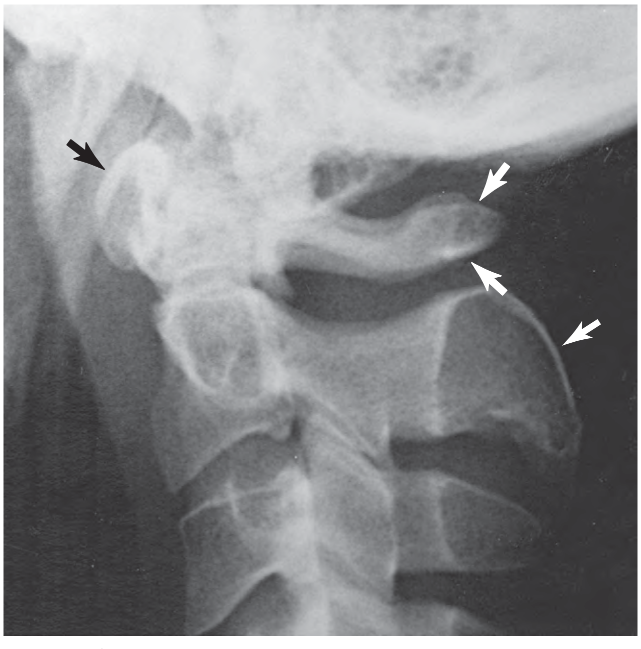

FIGURE 2–6 Anomalous atlantoaxial region.[4-8] The spinolaminar junction line at the posterior arch of the atlas is incomplete *(upper two arrows),* indicating partial agenesis or spondyloschisis of the posterior arch of C1. The anterior arch of the atlas is hypertrophic and sclerotic *(black arrow),* and the C2 spinous process is enlarged and unusually shaped *(lower arrow).* Hypertrophy and sclerosis of the anterior arch are commonly seen in patients with upper cervical spine anomalies, especially C1 spondyloschisis, agenesis of the posterior arch, and os odontoideum.

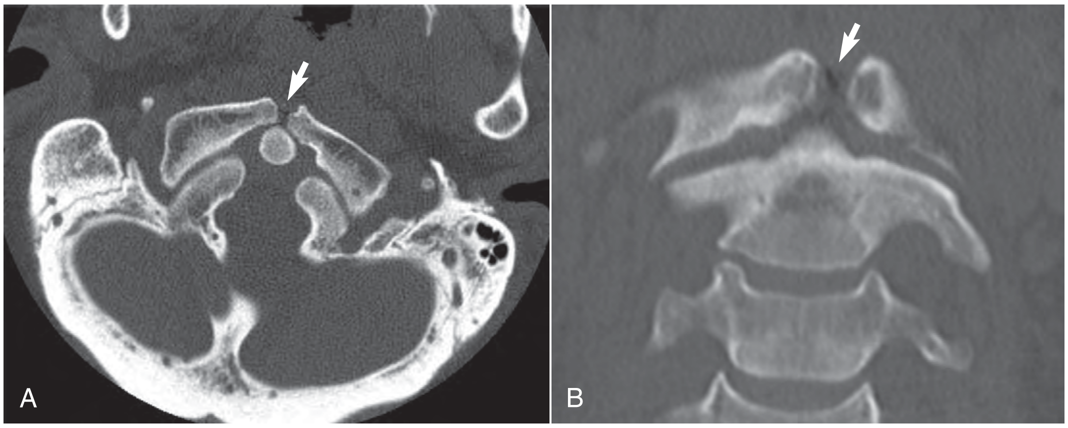

FIGURE 2–7 **Agenesis of the anterior arch of C1.**[4-7] **A,** Transaxial CT bone window through the occipito-atlanto-axial region of this 36-year-old woman reveals a midline radiolucency *(arrow)* representing failure of complete ossification of the anterior tubercle of atlas. This anomaly is termed *anterior spondyloschisis* and is extremely rare. Since nearly all patients with anterior spondyloschisis have nonfusion of the posterior arch of the atlas, an alternative cause could be a stress fracture of the anterior arch of C1 secondary to loss of hoop strength. **B,** Coronal CT bone window image in another patient reveals a similar finding *(arrow). (**B,** Courtesy B.A. Howard, MD, Charlotte, NC.)*

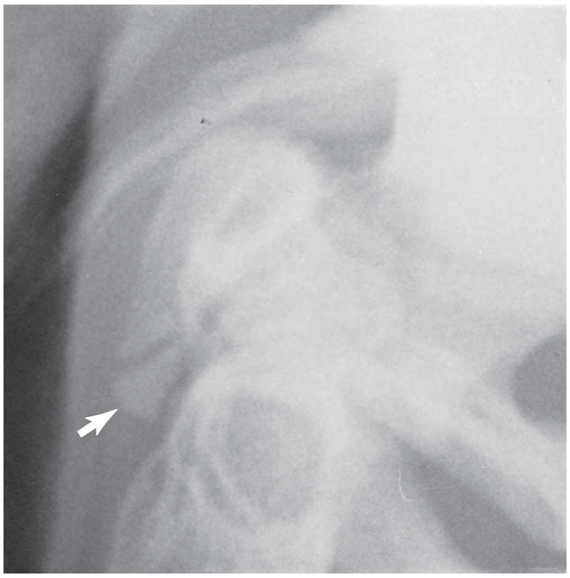

FIGURE 2–8 **Accessory ossicle.**[9] Observe the tiny ossicle of bone situated at the inferior aspect of the anterior arch of C1 *(arrow).* This painless normal variant should not be confused with an anterior arch fracture, hydroxyapatite crystal deposition within the longus colli tendon, or a degenerative osteophyte or enthesophyte.

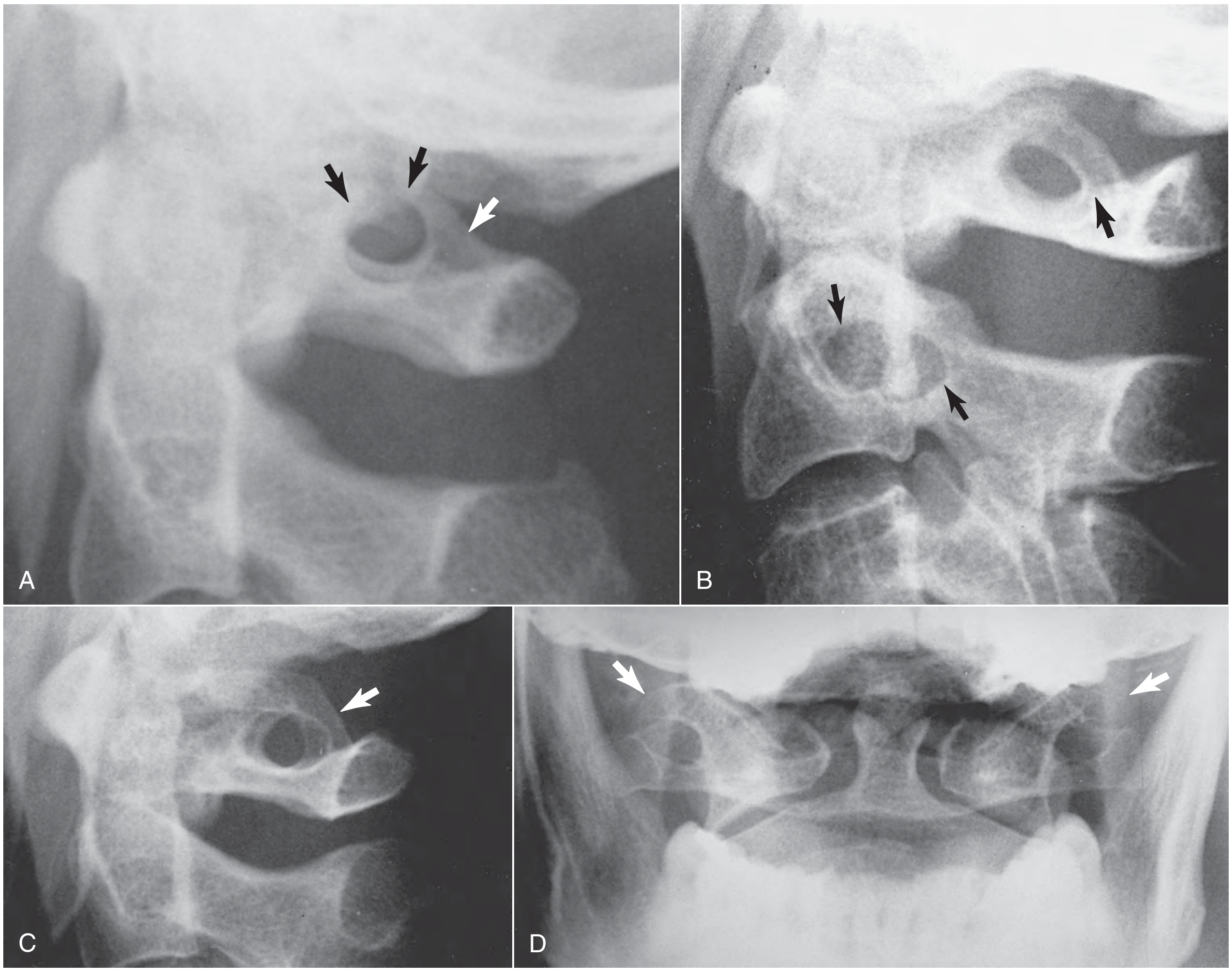

FIGURE 2–9 **Posterior ponticulus (arcuate foramen).**[5-7] **A,** This curvilinear osseous bridge is best visualized on the lateral radiograph *(arrows).* The osseous bridge joins the posterior arch with the lateral mass of C1 and forms a circular opening (arcuate foramen) for the passage of the vertebral artery and the C1 nerve. **B,** In this slightly rotated lateral radiograph from another patient with a posterior ponticulus anomaly *(uppermost arrow),* two circular radiolucent shadows overlying the C2 vertebral body also are present *(arrows).* These represent the normal foramina transversaria within the transverse processes of the axis. **C-D,** Another patient. In **C,** curvilinear osseous bridges extending from the superior aspect of the lateral masses of the atlas to the posterior arches of the atlas are evident on the lateral radiograph *(arrow).* In **D,** the open-mouth radiograph reveals that the osseous arches are continuous with the lateral masses *(arrows).*

FIGURE 2–10 **Sclerotic anterior tubercle.**[6] The anterior arch of the atlas appears sclerotic *(arrow).* A partial posterior ponticulus also is present. Sclerosis, with or without hypertrophy, often occurs in conjunction with posterior arch agenesis, os odontoideum, and other anomalies of the atlantoaxial region.

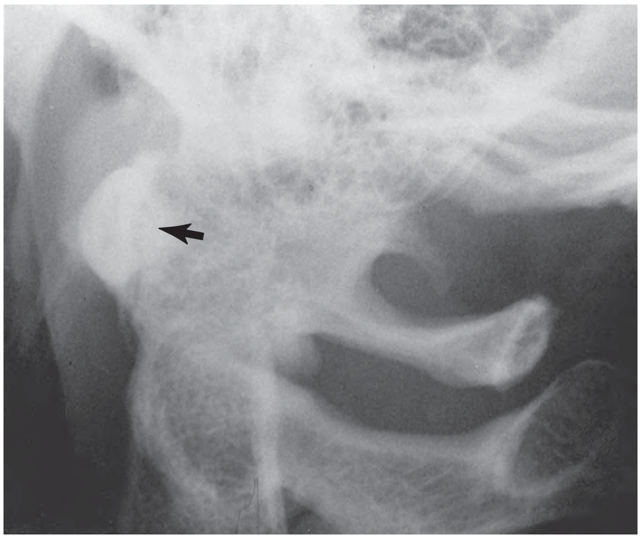

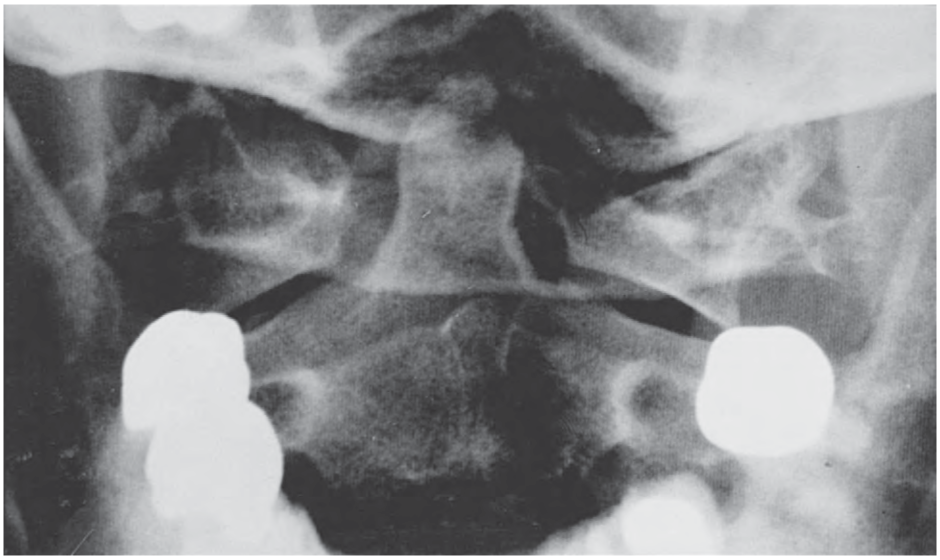

FIGURE 2–11 **Asymmetric atlas.**[7] The atlas has developed asymmetrically, simulating a compression fracture of the left lateral mass. Vertebral asymmetry is a common finding, especially at the transitional regions of the spine. *(Courtesy A.L. Anderson, DC, Portland, Ore.)*

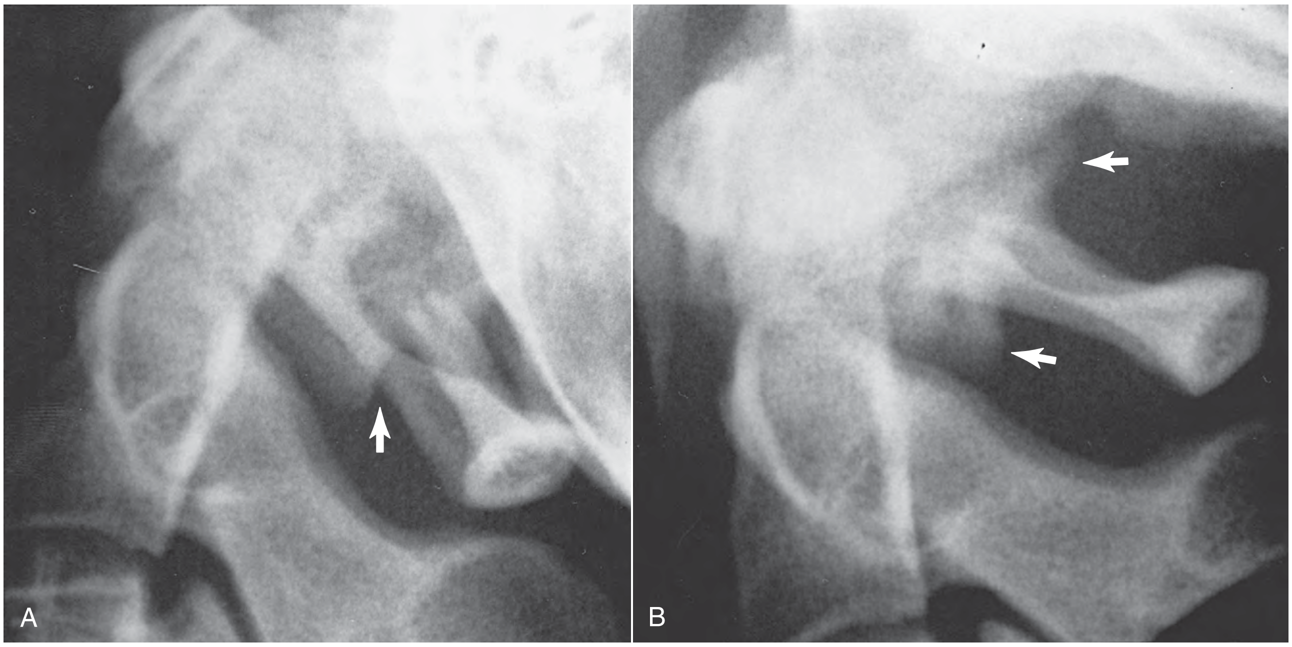

FIGURE 2–12 **Simulated fracture produced by rotation.**[5,7] **A,** Lateral radiograph taken in extension shows an apparent fracture of the posterior arch of the atlas with offset of the fragments *(arrow).* **B,** Neutral lateral film with normal alignment demonstrates that it is the overlying lateral masses of the atlas *(arrows)* that create the false appearance of a fracture.

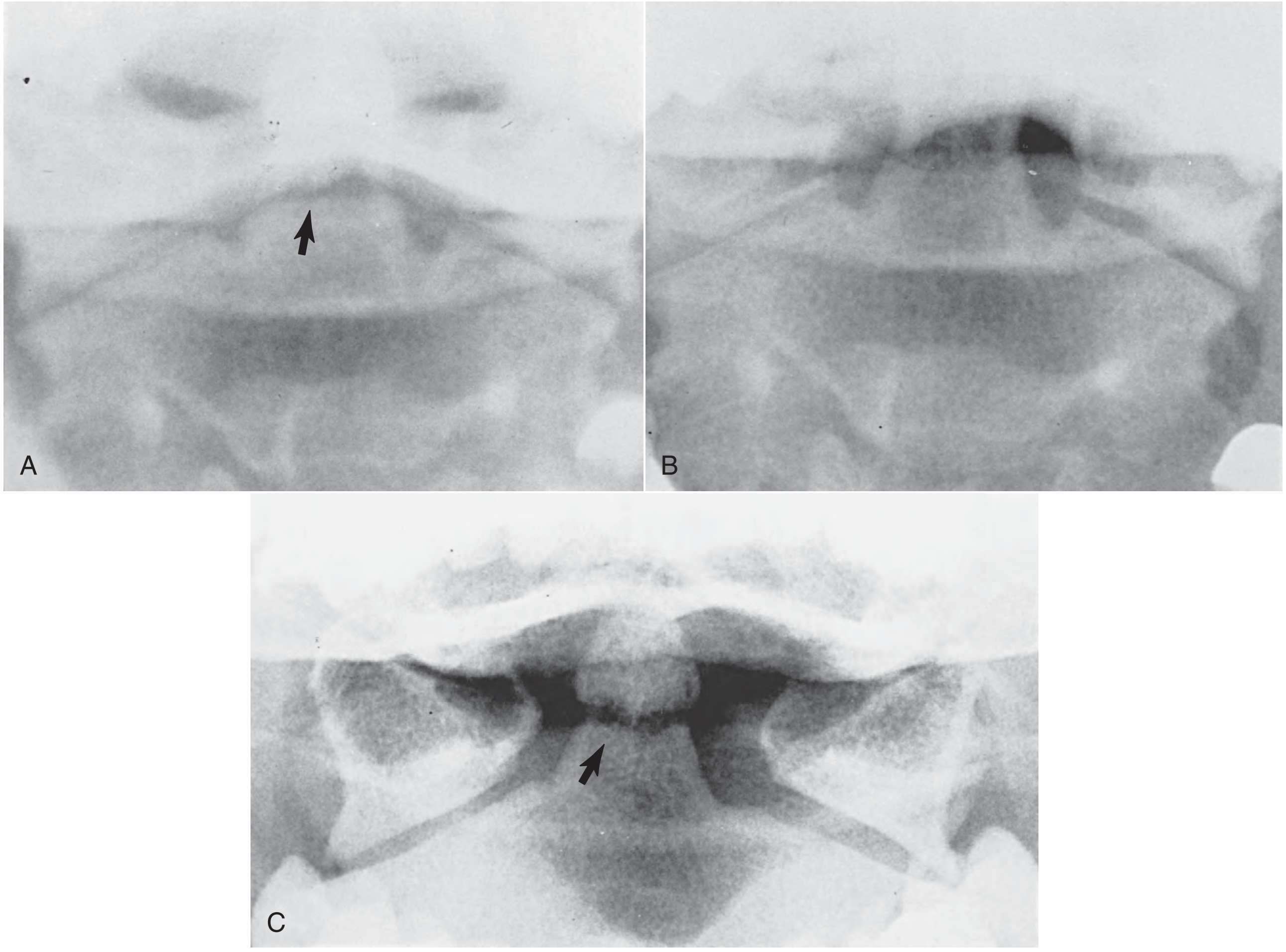

FIGURE 2–13 **Mach band effect.**[10] **A-B,** This 37-year-old woman complained of pain and stiffness after a motor vehicle collision. Initial radiograph **(A)** shows a transverse radiolucent defect across the base of the odontoid process *(arrow)* resembling a type II odontoid fracture. A second radiograph **(B)** taken moments later with slightly different head position reveals that the base of the odontoid is intact. In this case, on the initial radiograph, the base of the occiput overlies the top of the odontoid, and the posterior arch of C1 overlies the lower odontoid and C2 vertebral body. The intervening portion of the odontoid has no overlying density and therefore appears remarkably radiolucent—the Mach band effect. **C,** In a second patient, a transverse radiolucent line across the odontoid process *(arrow)* is created by the space between the anterior and posterior arches of the atlas and should not be misinterpreted as an odontoid fracture.

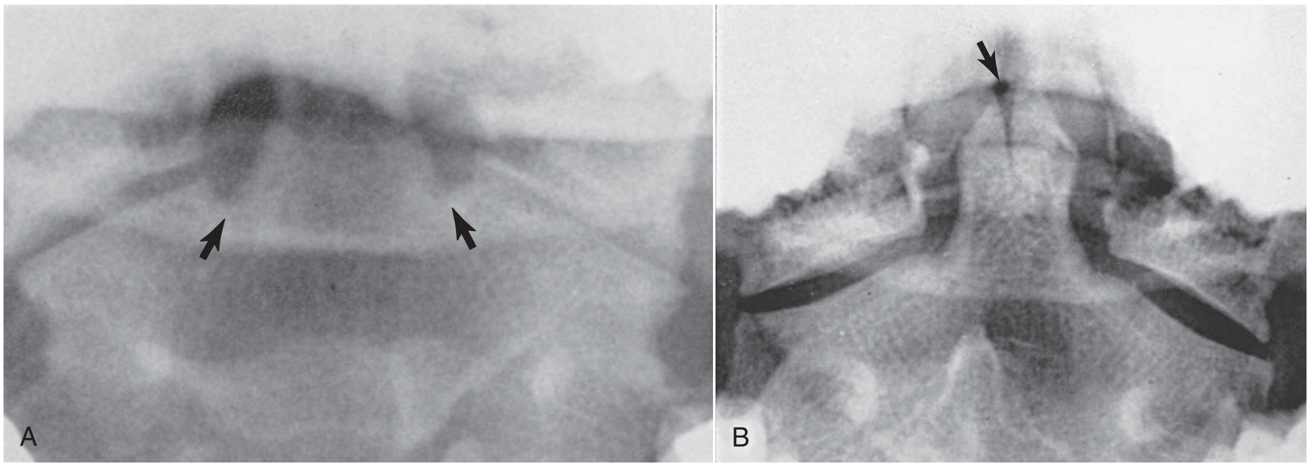

FIGURE 2–14 **Normal anatomy simulating fractures.**[5,7] **A,** Paraodontoid notches. Bilaterally symmetric notches adjacent to the base of the odontoid *(arrows)* are normal variants of no clinical consequence that may simulate fractures. **B,** Overlying incisors. A vertical radiolucent shadow overlying the odontoid process *(arrow)* results from the space between the two overlying central incisors and should not be mistaken for a split odontoid or a fracture.

TABLE 2-3 Some Causes of Atlantoaxial Instability and Subluxation*[6,19]

Common	Uncommon
Developmental Anomalies and Dysplasias	
Atlanto-occipital assimilation	Morquio syndrome
Down syndrome (trisomy 21)	Hurler syndrome
Os odontoideum	Spondyloepiphyseal dysplasia
Odontoid agenesis	Marfan syndrome
Odontoid hypoplasia	Metaphyseal dysplasia
Inflammatory Arthropathies and Connective Tissue Diseases	
Rheumatoid arthritis	Systemic lupus erythematosus
Ankylosing spondylitis	Behçet's syndrome
Psoriatic arthritis	Dialysis spondyloarthropathy
Reiter syndrome	Rheumatic fever
Juvenile idiopathic arthritis	Multicentric reticulohistiocytosis Calcium pyrophosphate dihydrate crystal deposition disease
Physical Injury	
Odontoid fracture	Some Jefferson fractures
	Rotatory atlantoaxial subluxation
	Transverse ligament rupture
Infection	
Retropharyngeal abscess (Grisel syndrome)	

* Atlantoaxial instability and subluxation are present or should be questioned when the atlantodental interspace exceeds 5 mm in children and 3 mm in adults on neutral lateral or flexion radiographs, or when the interspace distance changes between flexion and extension.

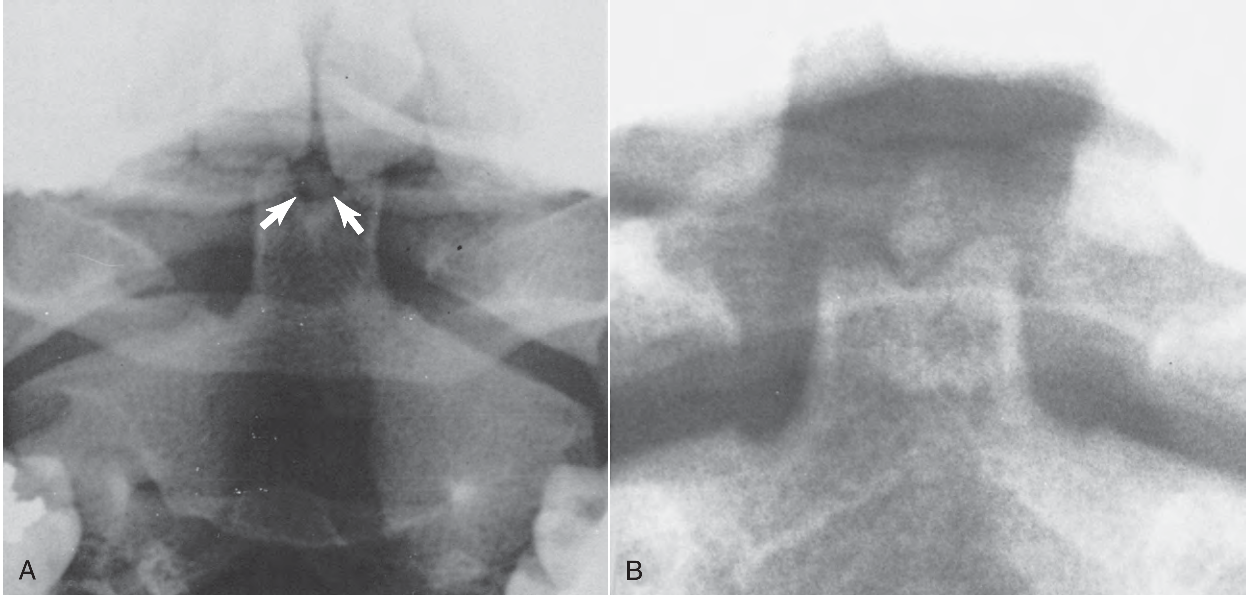

FIGURE 2–15 **Os terminale of Bergmann.**[5,7] **A,** Observe the small circular ossification center within the triangular or V-shaped radiolucent indentation *(arrows)*. **B,** In another patient, a more clearly defined diamond-shaped ossification center is present. The os terminale of Bergmann represents a persistent, ununited secondary growth center at the tip of the odontoid in a patient older than 12 years of age. This is of no clinical significance but must be differentiated from a type 1 odontoid fracture or an os odontoideum.

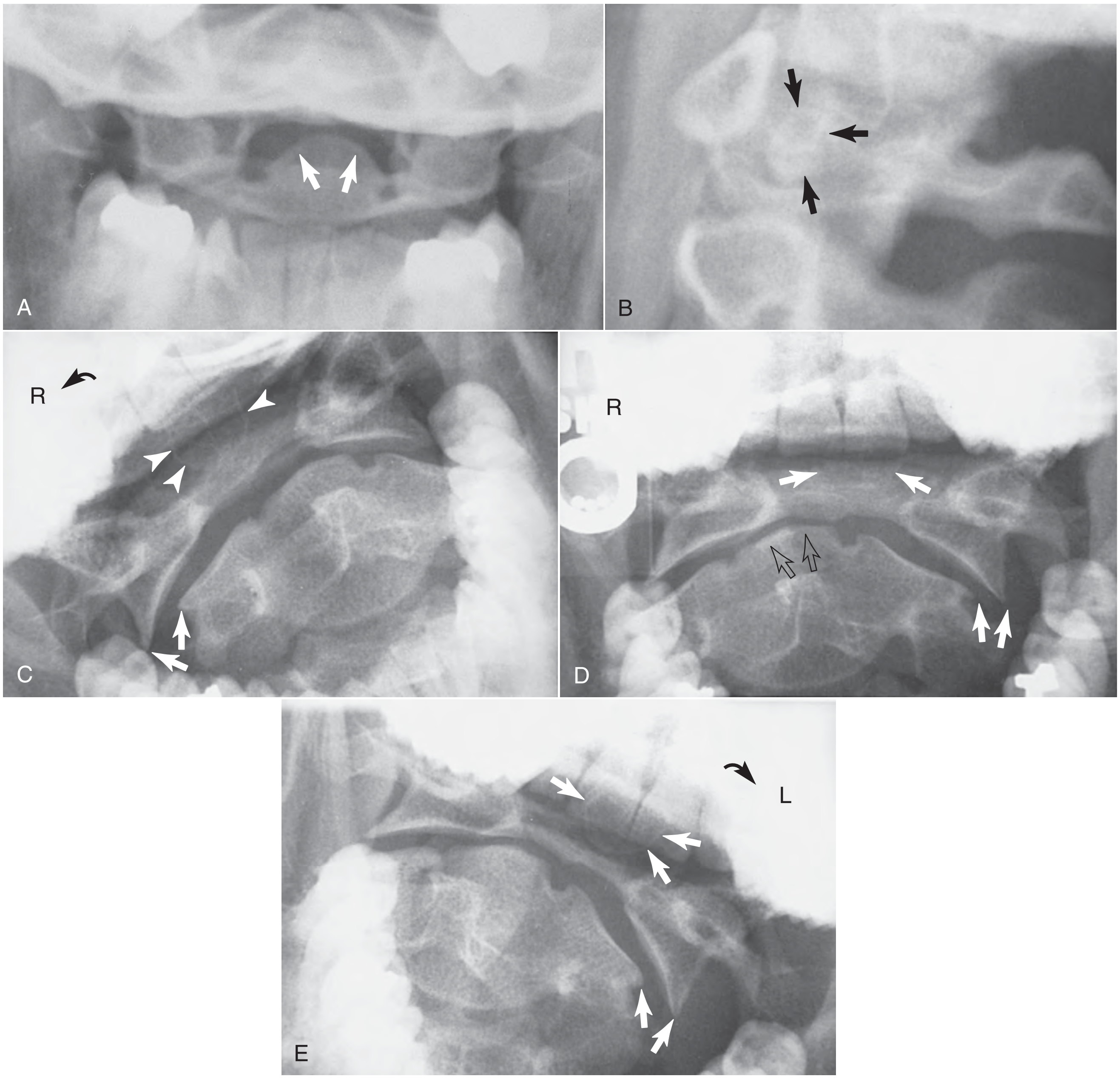

FIGURE 2–16 **Os odontoideum.**[4,7,11] **A,** Anteroposterior open-mouth view reveals an amputated appearance of the odontoid *(arrows),* and the ossicle is not visible. **B,** Lateral radiograph reveals an incompletely developed ossicle *(arrows)* that is not fused to the C2 vertebral body. The anterior arch of the atlas is sclerotic and hypertrophic, and the atlas is displaced posteriorly, indicating sagittal plane instability. **C-E,** Coronal plane instability in another patient. Frontal open-mouth radiographs obtained in active right lateral flexion **(C),** neutral posture **(D),** and active left lateral flexion **(E)** reveal a smooth cortical margin along the upper surface of the short odontoid *(open arrows)* and a separate, barely perceptible, dysplastic ossicle of bone above *(arrowheads).* Lateral translation of the lateral masses of the atlas in relation to C2 measured 16 mm, indicating coronal plane instability. (***C-E,*** *From Ramos LS, Taylor JAM, Lackey G, et al: Os odontoideum with sagittal and coronal plane instability: a report of three cases. Top Diagn Radiol Adv Imaging 3:5, 1996.)*

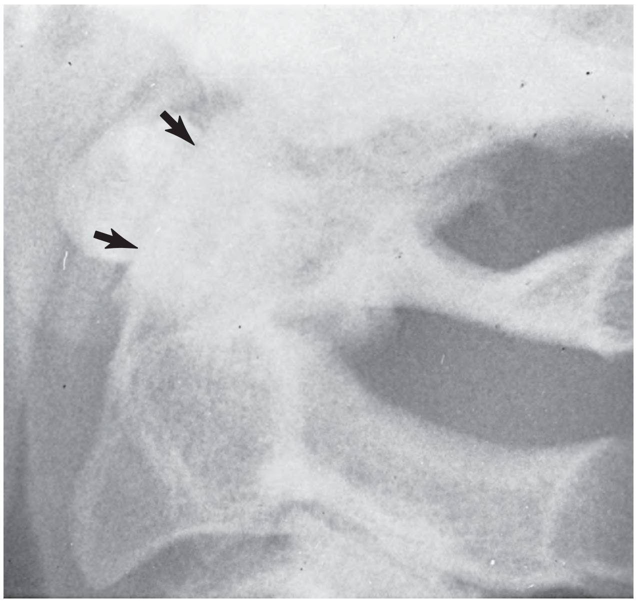

FIGURE 2–17 **Posterior inclination of the odontoid.**[12] The odontoid is tilted posteriorly *(arrows)* in this patient with no history of trauma. This peculiar posterior inclination is a variation of normal that may simulate a fracture. In cases of trauma, such a finding should lead to a careful search for an associated odontoid fracture. *(Courtesy E.E. Bonic, DC, St. Louis, Missouri.)*

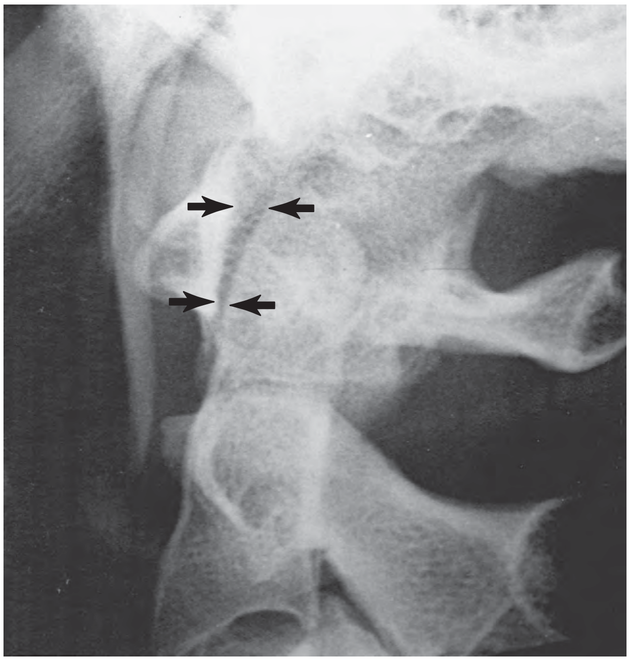

FIGURE 2–18 **V-shaped predens space.**[13,160] Observe the triangular atlantodental interspace in this patient (*arrows*). Such a V-shaped configuration is a variant of normal, and it should not automatically be considered an example of atlantoaxial instability. Bohrer and associates[13] postulate that this appearance may be due to increased flexion mobility at the atlantoaxial articulation, with developmental elongation or laxity of the cranial fibers of the transverse ligament or the posterior ligamentous complex, or both. In cases of suspected instability, flexion and extension radiographs should be obtained. The atlantodental interspace measured in the neutral, flexion, or extension position should be no more than 3 mm in adults or 5 mm in children. The measurement should be obtained at the central portion of this articulation.

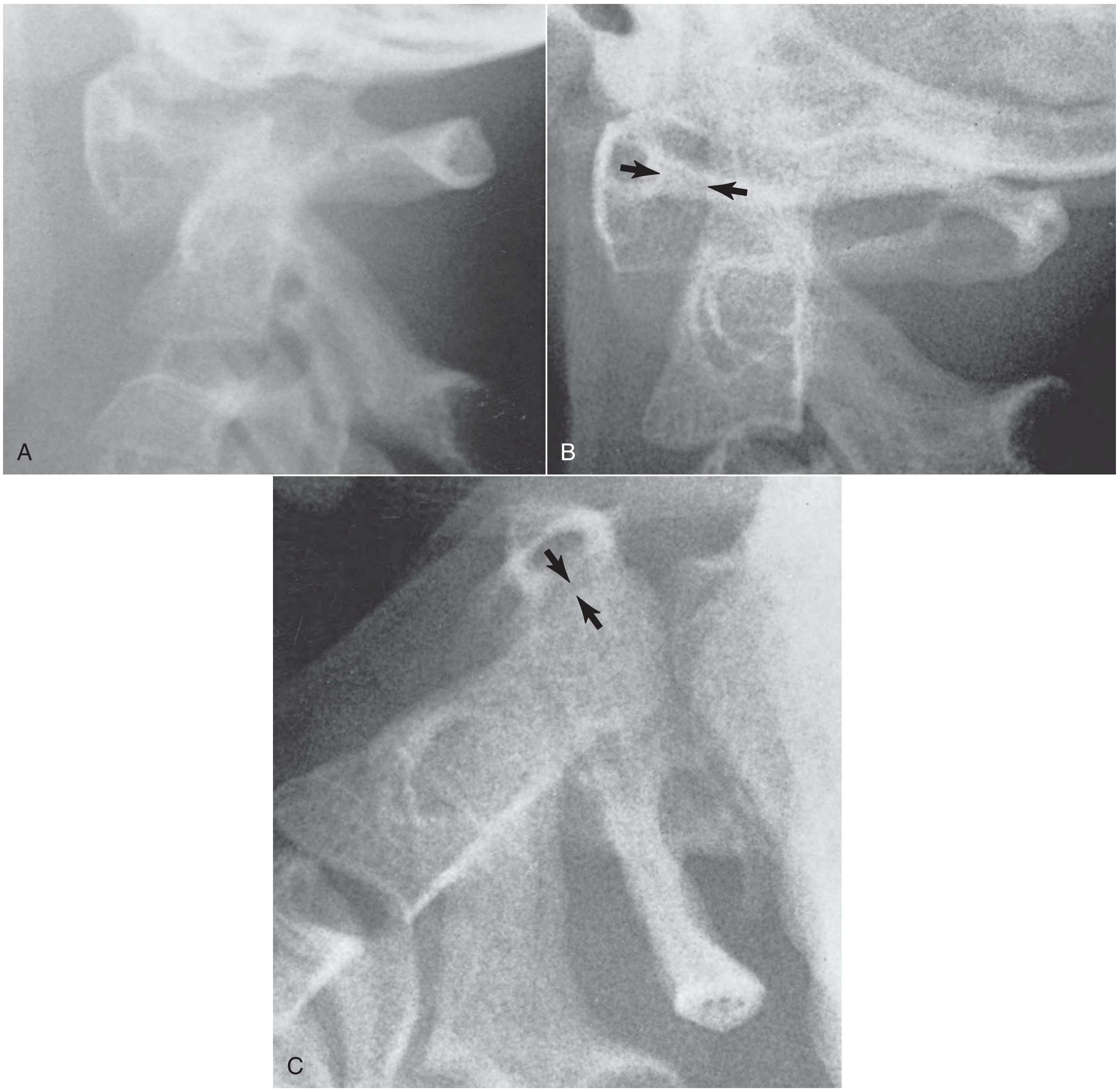

FIGURE 2–19 **Trisomy 21 (Down syndrome).**[14] **A,** Observe the increased atlantodental interspace in this child with Down syndrome. **B-C,** In another child, 9 years old, the flexion radiograph **(B)** reveals widening of the atlantodental interspace *(arrows)* and rotation of the atlas. On extension **(C),** the subluxation reduces, and the atlantodental interspace appears normal *(arrows). (Courtesy B.L. Harger, DC, Portland, Ore.)*

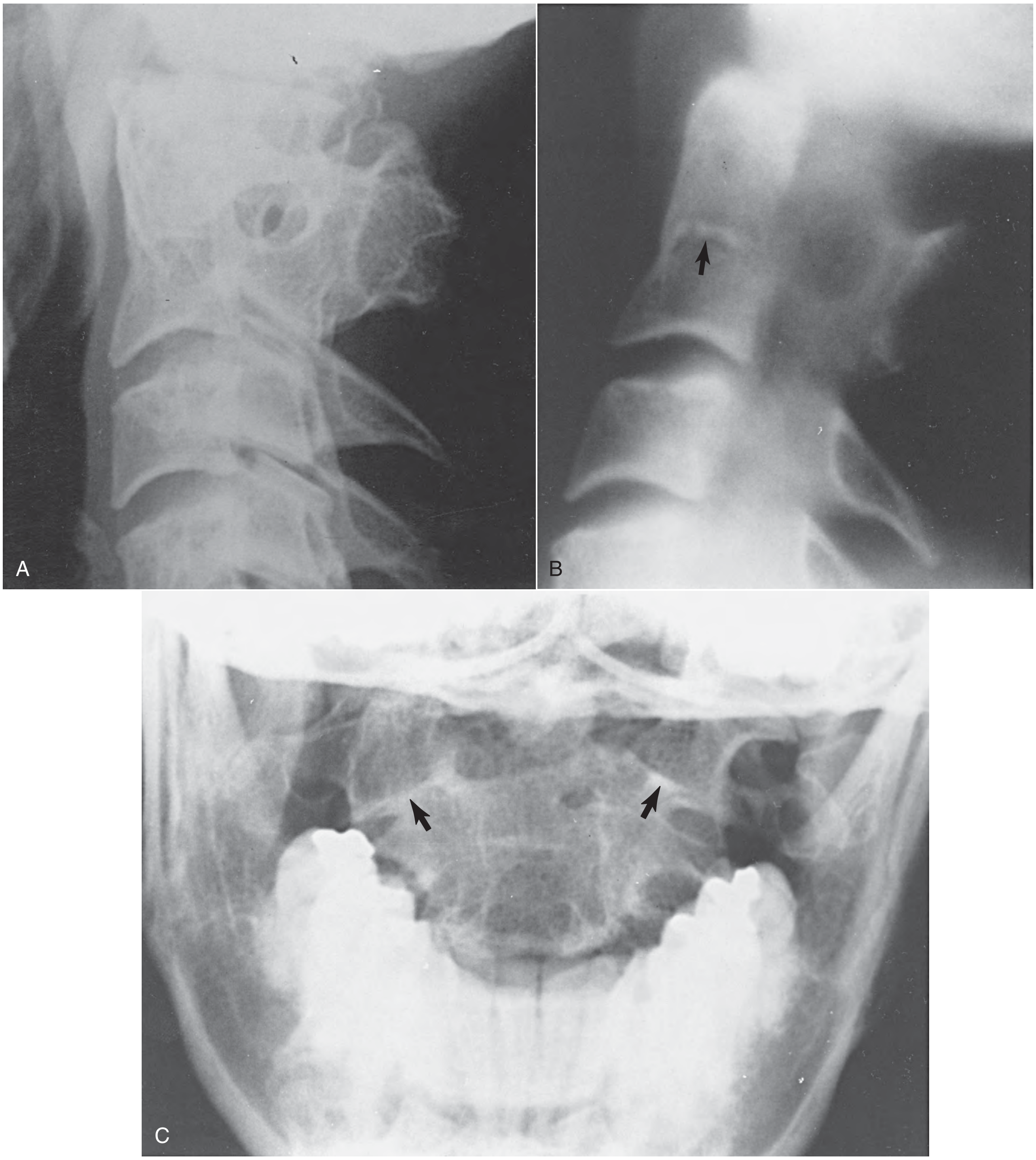

FIGURE 2–20 C1-C2 anomalies.[5,7] **A-C,** Synostosis. **A,** Lateral radiograph reveals that the articulation between the atlas and axis is not visualized. The posterior arch of C1 is fused to the C2 spinous process and lamina, and an anomalous foramen is present between the C1 and C2 segments, resembling an intervertebral foramen. **B,** Lateral conventional tomogram illustrates a partially calcified synchondrosis between the C2 vertebral body and odontoid process *(arrow)* with a waistlike narrowing at this junction. **C,** Anteroposterior open-mouth radiograph reveals fusion of the C1-C2 apophyseal joints *(arrows).*

Continued

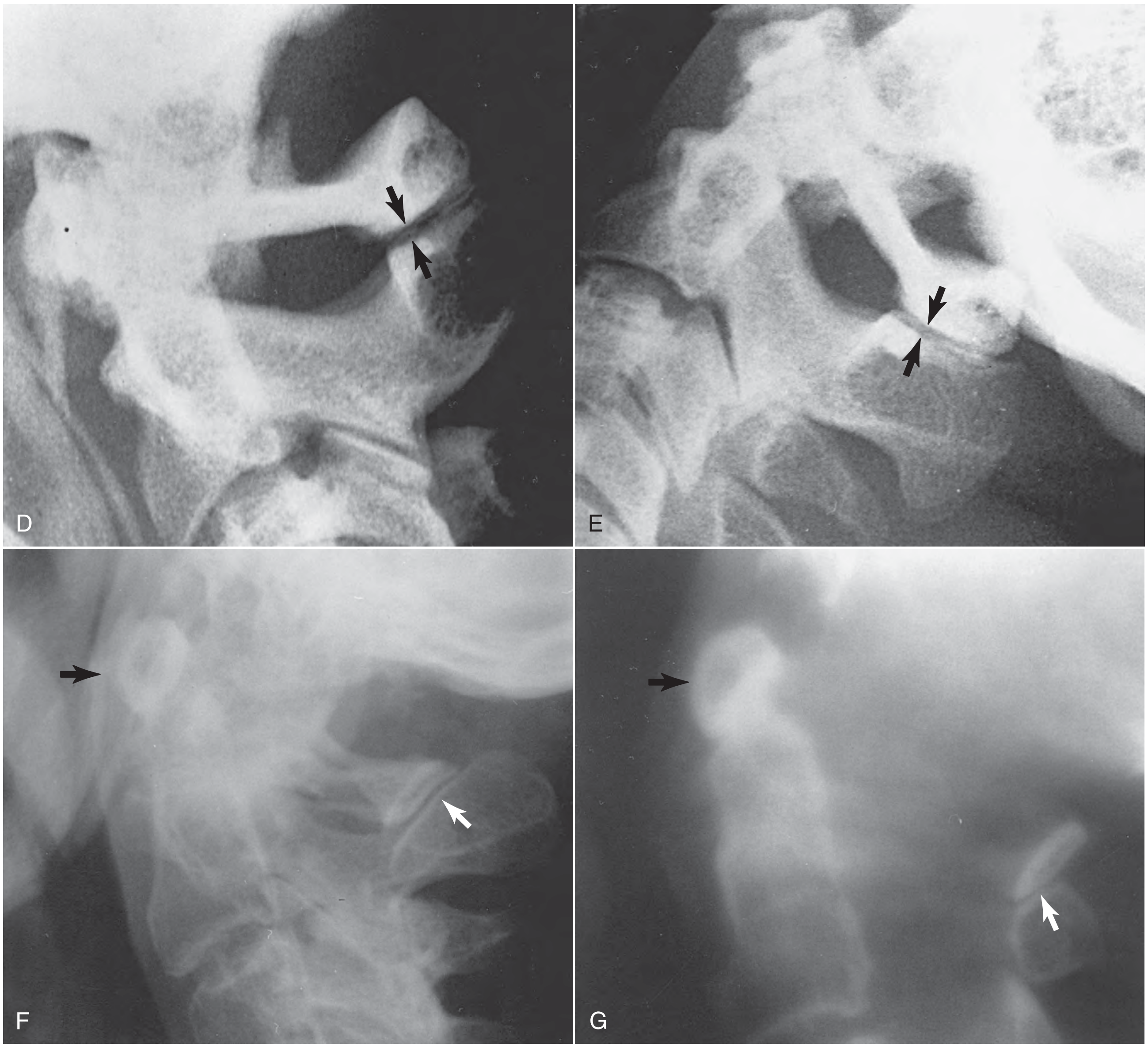

FIGURE 2–20, cont'd **D-E,** Anomalous articulation. In another patient, observe the unusual articulation between the posterior arch of the atlas and the spinous process of the axis. Only minimal separation of the posterior elements *(arrows)* is evident in flexion **(D)** and extension **(E)** radiographs. **F-G,** Complex atlantoaxial anomalies in an 87-year-old man with restriction of cervical flexion, extension, and rotation. Lateral radiograph **(F)** and conventional tomogram **(G)** reveal an anomalous tapered odontoid, high riding anterior arch of C1 *(black arrows),* and an apparent pseudoarticulation between the posterior arch of C1 and the spinous process of C2 *(white arrows).*

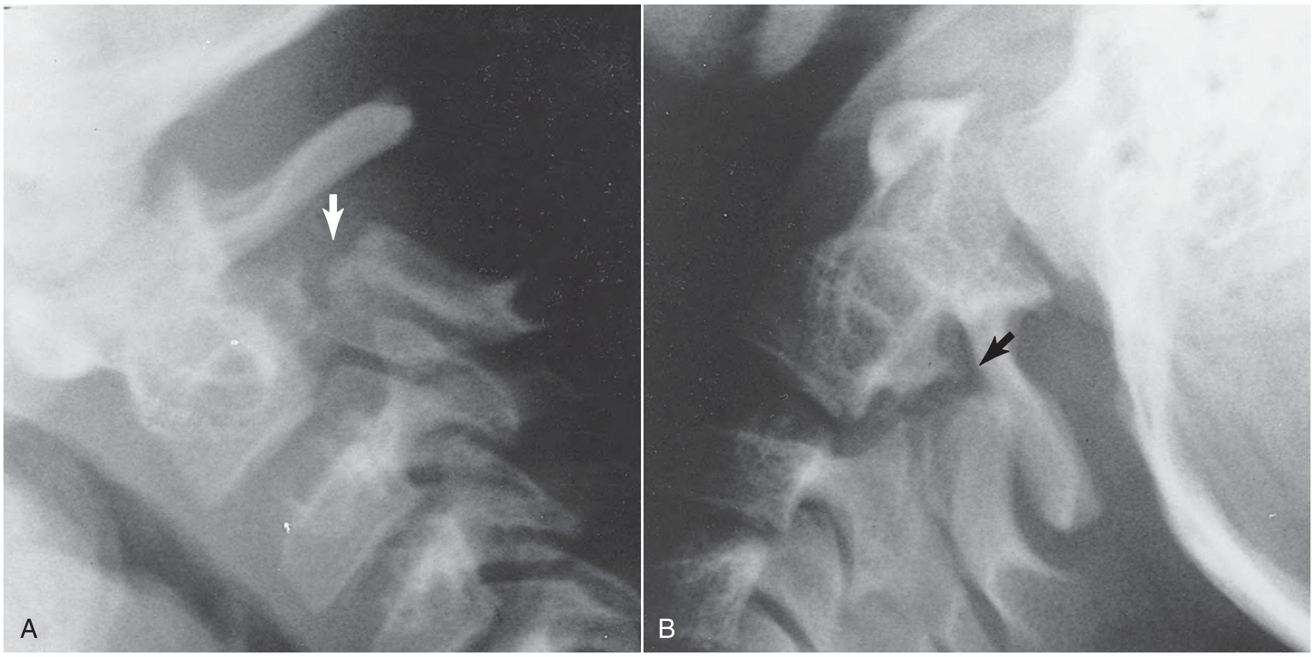

FIGURE 2–21 **C2 spondylolysis.**[15] This 9-year-old boy sustained mild head trauma. Flexion **(A)** and extension **(B)** films taken 1 week after the injury, when the patient was asymptomatic, show a radiolucent cleft in the neural arch of C2 *(arrows)* simulating a hangman's fracture. The flexion and extension films reveal no evidence of instability. Spondyloschisis and hypertrophy of the anterior arch also are present at C1. The diagnosis of fracture was excluded on the basis of absence of both symptoms and instability. This entity represents congenital spondylolysis of C2. Cervical spondylolysis and spondylolisthesis occur most commonly at C6 but also have been described at C2, as in this patient.

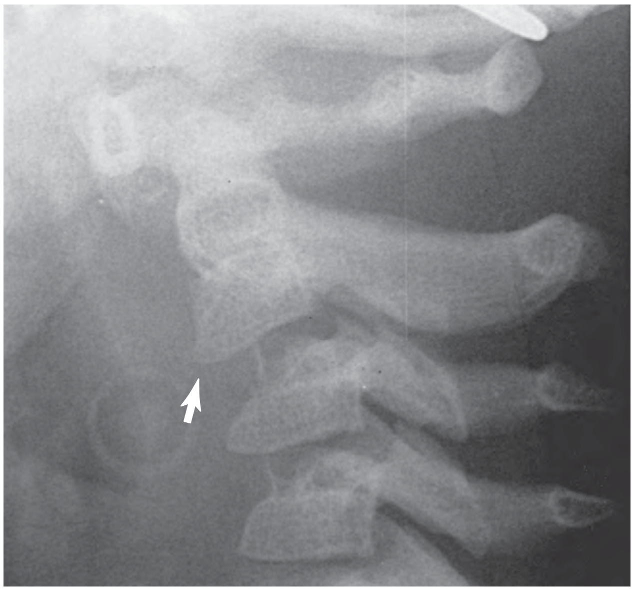

FIGURE 2–22 **C2 pseudosubluxation.**[16,17,135] Observe the anterior displacement of the C2 vertebral body *(arrow)* in relation to that of C3 in this 5-year-old child. This normal variant, seen in up to 24% of infants and children up to the age of 8 years, is termed *pseudosubluxation*. It should not be confused with an unstable fracture or ligament injury. Excessive sagittal plane movement of the C2-C3 and C3-C4 motion segments, seen on flexion and extension radiographs in infants, also is a common finding attributed to normal ligamentous laxity. Note additionally an atlantodental interspace that measures 5 mm in this child. This measurement is at the upper limits of normal in children and does not represent atlantoaxial instability.

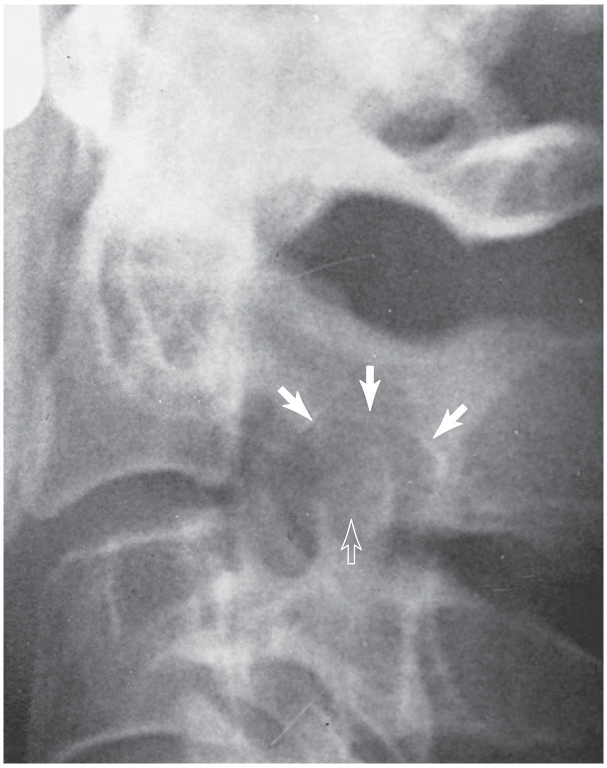

FIGURE 2–23 **Anomalous C2-C3 facet articulation.**[5,7] An unusually bulbous superior articular process of C3 *(open arrow)* articulates with a concave inferior articular process of C2 *(arrows)* in a ball-and-socket fashion. This anomaly has no known clinical significance. Note also the posterior ponticulus of the atlas. *(Courtesy D. McCallum, DC, Abbotsford, B.C., Canada.)*

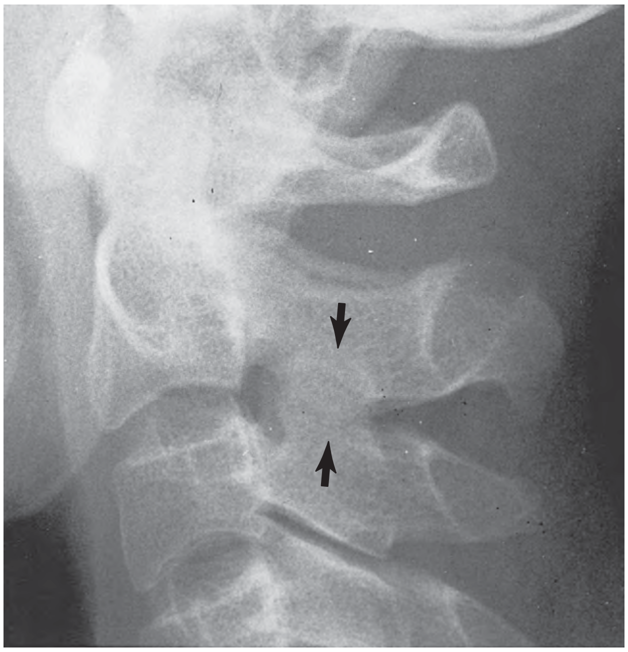

FIGURE 2–24 **C2-C3 facet joint "pseudofusion.**[18]**"** Observe the apparent ankylosis of the C2-C3 facet articulation *(arrows)*. This appearance, common at this level, results from the angulated orientation of the facet joints. As a result, the x-ray beam is not tangent to the articular surfaces, and therefore it fails to reveal the radiolucent joint space. In such cases, frontal open mouth and oblique radiographs typically reveal a normal joint space. This should not be confused with developmental or acquired synostosis. *(Courtesy E.E. Bonic, DC, St. Louis, Missouri.)*

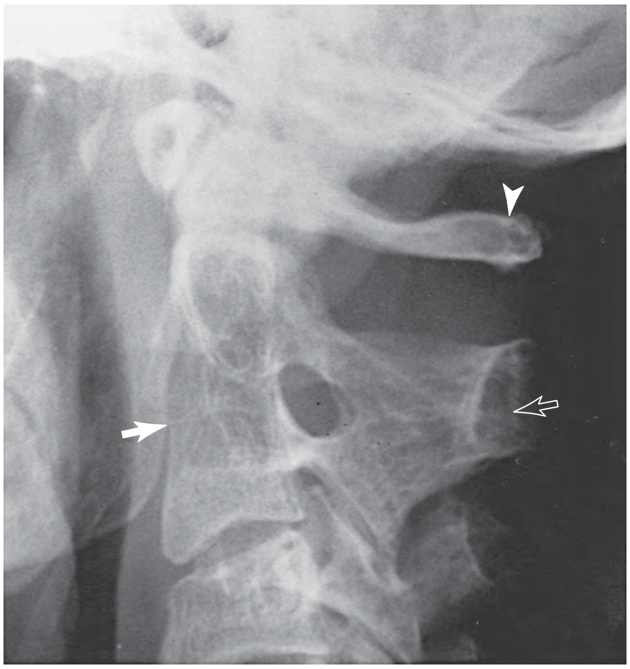

FIGURE 2–25 **Upper cervical spine anomalies.**[5-8] Lateral radiograph reveals absence of the spinolaminar junction line at C1, signifying spondyloschisis (nonunion of the posterior arch) *(arrowhead)*. Congenital synostosis (block vertebra) of the C2-C3 level also is present with absence of the intervertebral disc space *(arrow)* and nonsegmentation of the lamina, articular processes, and spinous processes (*open arrow*). Observe the prominent intervertebral foramen at this level. Approximately 50% of congenital block vertebrae also include nonsegmentation of the posterior elements.

TABLE 2-4 Some Developmental Anomalies, Anatomic Variants, and Sources of Diagnostic Error Affecting the Lower Cervical Spine (C3-C7)*

Entity	Figure(s), Table(s)	Characteristics
Normal ring apophyses[2]	2-26	Normal vertebral body ring apophyses may resemble tiny fractures
Nuclear impressions[2,7]	2-27	Normal curvilinear concave depressions on the undersurface of vertebral bodies are believed to be notochordal remnants; developmental variant unrelated to osteopenia or mechanical stress on the spine Differential diagnosis: Schmorl cartilaginous nodes, compression fractures, biconcave (fish vertebrae) deformities in osteoporosis, and H vertebrae characteristic of sickle cell anemia
Vertebra plana[7]	2-28	A change occurring in midcervical to lower cervical vertebral bodies in which the vertical height is diminished, resembling acute or pathologic collapse; characteristic of eosinophilic granuloma or normal variant
Elongated transverse processes[20,21]	2-29	Developmental overgrowth and anomalous articulation of the anterior tubercles of two adjacent transverse processes May cause anterolateral neck pain and decreased range of motion
Notching of the articular processes[22]	2-30	Normal variant characterized by a smooth, well-corticated, curvilinear depression of the superior aspect of the articular facet that may resemble a pillar fracture or erosion Most common at C5-C7
Synostosis (block vertebra)[5-7,23]	2-31	Developmental failure of segmentation of vertebral segments, most frequently present at C5-C6 and C2-C3 Often results in premature degenerative disease at adjacent vertebral levels owing to excessive intervertebral motion above and below the synostosis ***Imaging findings*** Waistlike constriction at the level of the intervertebral disc Disc space completely absent, or may be represented by a rudimentary, irregularly calcified structure Total height of the block vertebra less than expected from the number of segments involved Fusion of the posterior elements (50% of cases) ***Differential diagnosis*** Fusion from surgery or inflammatory arthropathy
Developmental (congenital) spinal stenosis[6]	2-32	Developmental narrowing of the spinal canal is uncommon and may be seen as an isolated phenomenon or associated with achondroplasia Sagittal diameter of the cervical canal should never measure less than 12 mm or less than 80% of the midvertebral body width Acquired (degenerative) stenosis is much more common than the congenital form and results from osteophyte proliferation into the spinal canal or nerve root canals
Klippel-Feil syndrome[24]	2-33 Table 2-5	Multiple segmentation defects and other anomalies
Pedicle agenesis[6,169]	2-34	Developmental absence of a pedicle Often results in sclerosis and hypertrophy of contralateral or adjacent pedicles May be associated with congenital spondylolisthesis and other anomalies This anomaly has been identified in a medieval archeological skeleton in England
Spina bifida occulta[5,7]	2-34	Midline defect within the neural arch in which the two laminae fail to fuse centrally at the spinolaminar junction, resulting in a radiolucent cleft or absent spinous process Seen as an isolated anomaly or in conjunction with other entities, such as congenital spondylolisthesis, cleidocranial dysplasia, or Klippel-Feil syndrome Osseous spina bifida rarely is associated with meningomyelocele (spina bifida vera), which represents protrusion of the meninges or spinal cord with consequent severe neurologic abnormalities
Congenital spondylolisthesis[25]	2-34	Most common at C6 Combination of anomalies, including spina bifida occulta, neural arch defect (such as pedicle agenesis), and anterolisthesis of the vertebral body

* See also Table 1-1.

Continued

TABLE 2-4 Some Developmental Anomalies, Anatomic Variants, and Sources of Diagnostic Error Affecting the Lower Cervical Spine (C3-C7)—cont'd

Entity	Figure(s), Table(s)	Characteristics
Persistent unfused ossification centers[7]	2-1, *E*, 2-35	Any vertebral secondary ossification center may fail to fuse and may persist into adulthood, usually with no clinical consequences May simulate fractures At the corner of a vertebral body, they often are called *limbus vertebrae*, and may be associated with displacement of disc material underneath the ring apophysis
Cervical ribs and elongated C7 transverse processes[26]	2-36	Transverse processes of C7 typically are shorter than those of T1 Both elongated transverse processes and cervical ribs may contribute to neurovascular compression of the thoracic outlet Cervical ribs are present in 10%-15% of patients with the Klippel-Feil syndrome
Tracheal cartilage calcification[6]	2-37	Normal physiologic calcification of cartilaginous tracheal rings
Hair artifact[5]	2-38	Streaklike artifacts from unusual hairstyles or wet hair
Lymph node calcification[6,27]	2-39	Lobulated calcific collections in prevertebral and paravertebral locations Cervical lymph node calcification may be evidence of previous tuberculosis or other granulomatous disease, or, less likely, lymphoma or metastatic disease
Ossification of the stylohyoid ligaments[28]	2-40	Diffuse elongation and ossification or calcification of the stylohyoid ligaments May possess one or more articulations Usually an incidental finding, but fracture may occur and, in a condition termed *Eagle syndrome*, there may be symptoms of pain, dysphagia, and a sensation of a lump in the throat More common in patients with mucopolysaccharidoses and diffuse idiopathic skeletal hyperostosis (DISH)

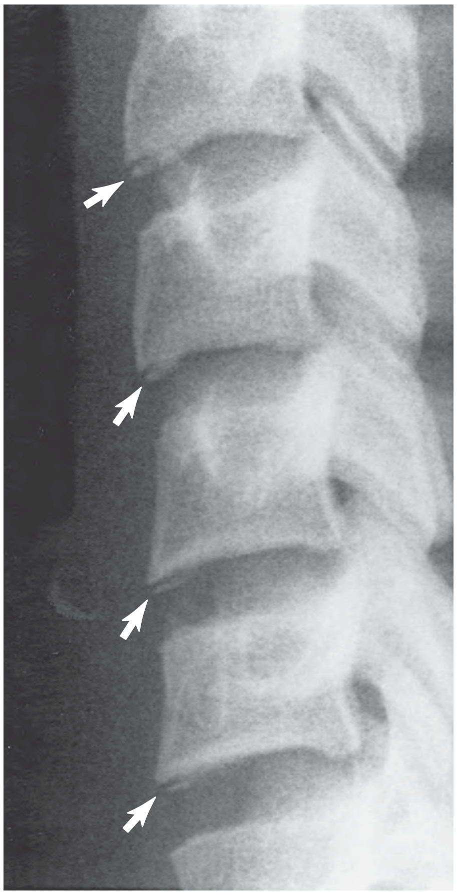

FIGURE 2–26 **Normal ring apophyses.**[2] Observe the tiny, linear, partially ossified secondary ossification centers *(arrows)* adjacent to the inferior vertebral endplates of C2-C6 on this radiograph of a 16-year-old boy.

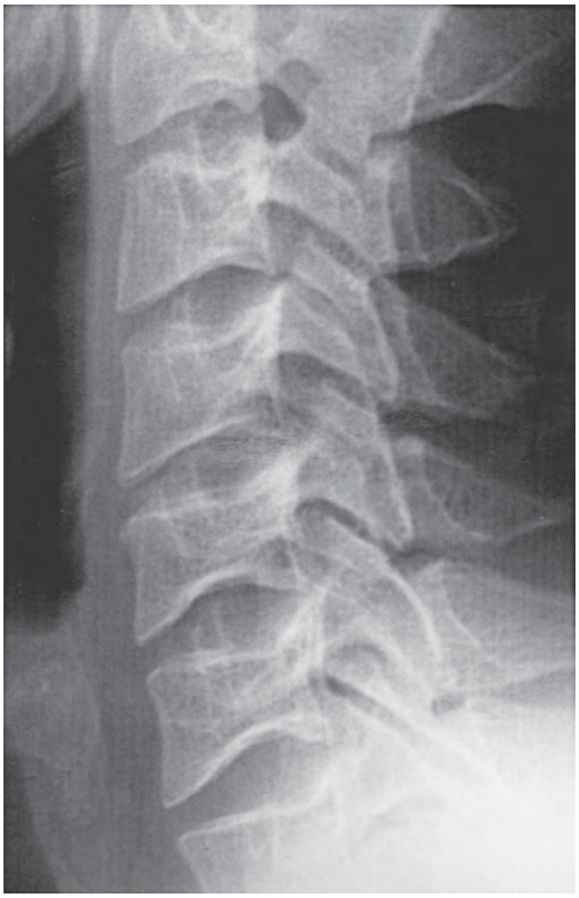

FIGURE 2–27 **Nuclear impressions.**[2,7] Lateral radiograph reveals prominent, broad-based, curvilinear depressions of the superior and inferior vertebral endplates. These indentations, which are believed to be related to notochordal remnants, represent a developmental variant and are unrelated to osteoporosis or mechanical stress on the spine.

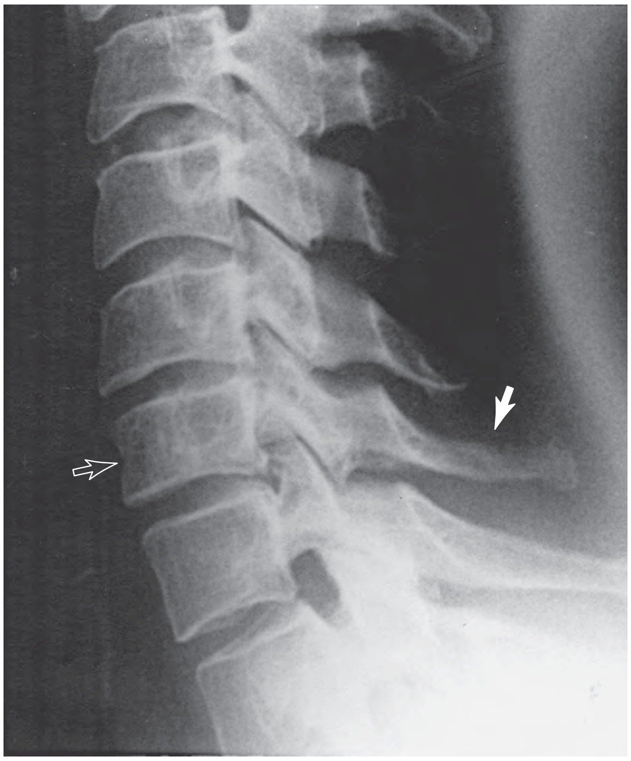

FIGURE 2–28 **Anomalous development of C6.**[7] The C6 vertebral body appears flattened *(open arrow),* and the spinous process is thin and attenuated *(arrow)*. A radionuclide bone scan was normal, favoring the diagnosis of an isolated anomaly.

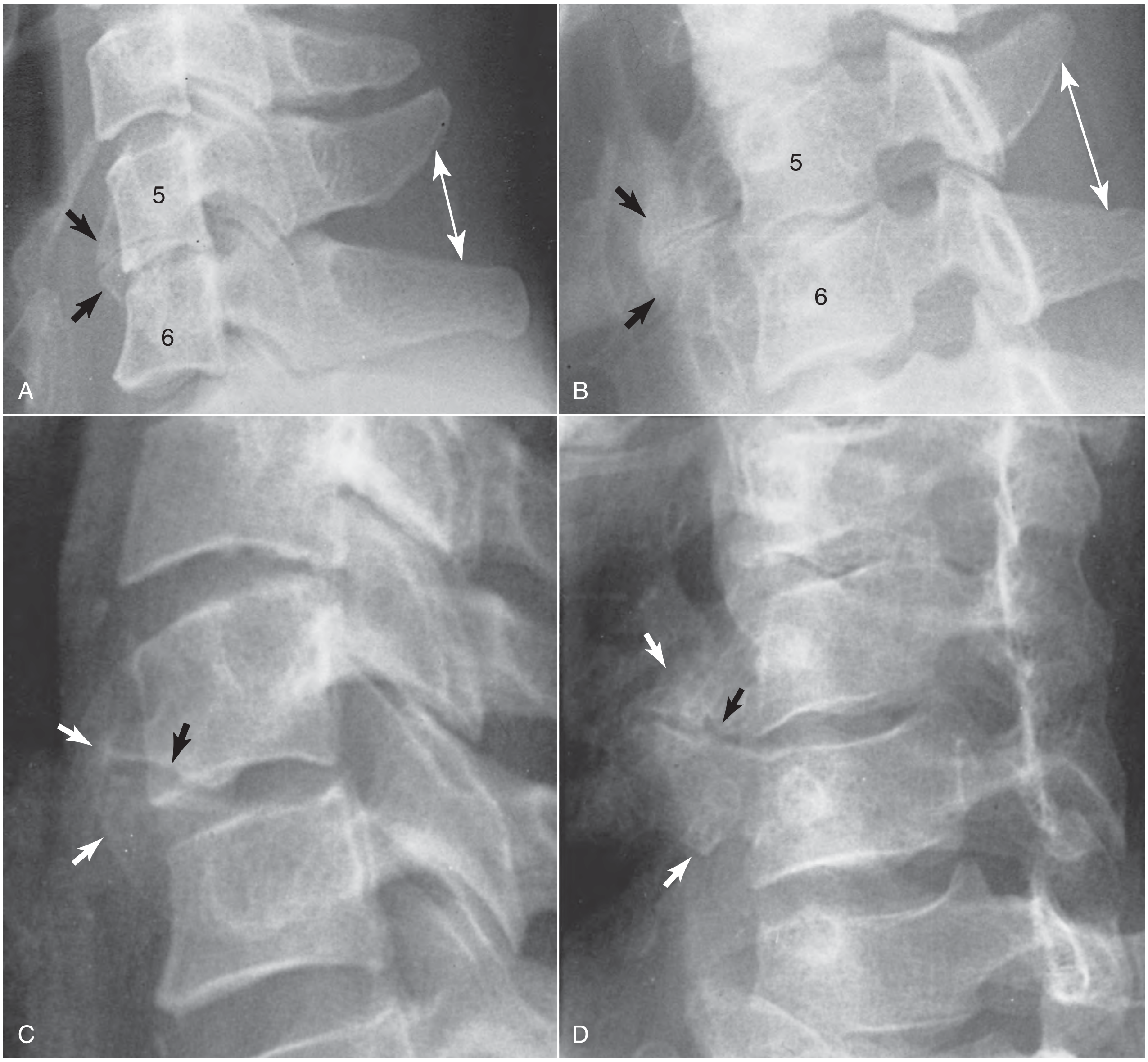

FIGURE 2–29 **Elongated anterior tubercles of the transverse processes.**[20,21] **A,** Lateral radiograph shows hypoplastic C5 and C6 vertebral bodies, narrowed disc space, and flaring of the spinous processes *(double-headed white arrow).* A thin projection of bone (*black arrows*) with a horizontal radiolucency is seen anterior to the disc space. **B,** Oblique radiograph reveals that the bone projection *(black arrows)* represents elongated anterior tubercles of the C5 and C6 transverse processes that form an anomalous articulation. These elongated transverse processes with accompanying pseudarthrosis may be a source of anterolateral neck pain and limitation of motion. **C-D,** In another patient, lateral **(C)** and oblique **(D)** radiographs show elongation of the anterior tubercles of the C5-C6 transverse processes *(white arrows)* with an anomalous articulation *(black arrows).*

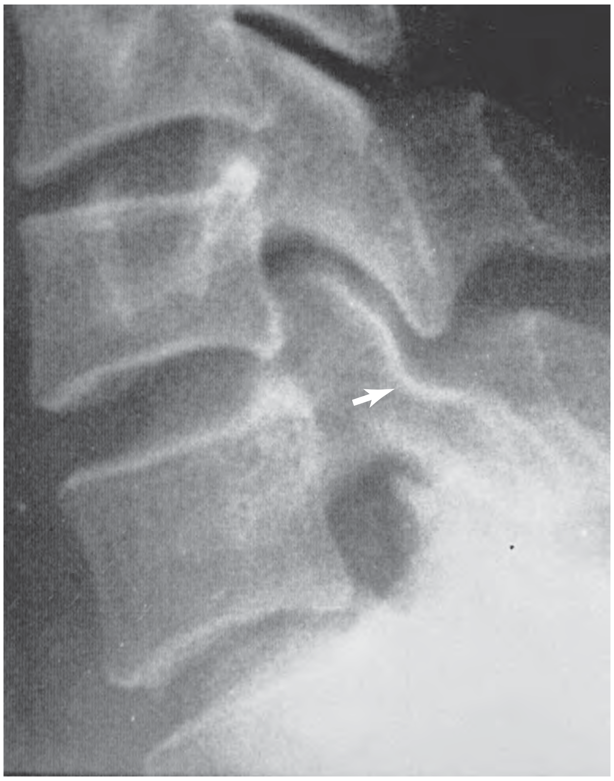

FIGURE 2–30 **Articular process notching.**[22] Notching of the superior apophyseal joint surface of C7 *(arrow)* represents a normal variation that may simulate an erosion or a fracture. Observe the well-corticated margin of the notch, characteristic of this normal variant. *(Courtesy R. Cormack, DC, Abbotsford, B.C., Canada.)*

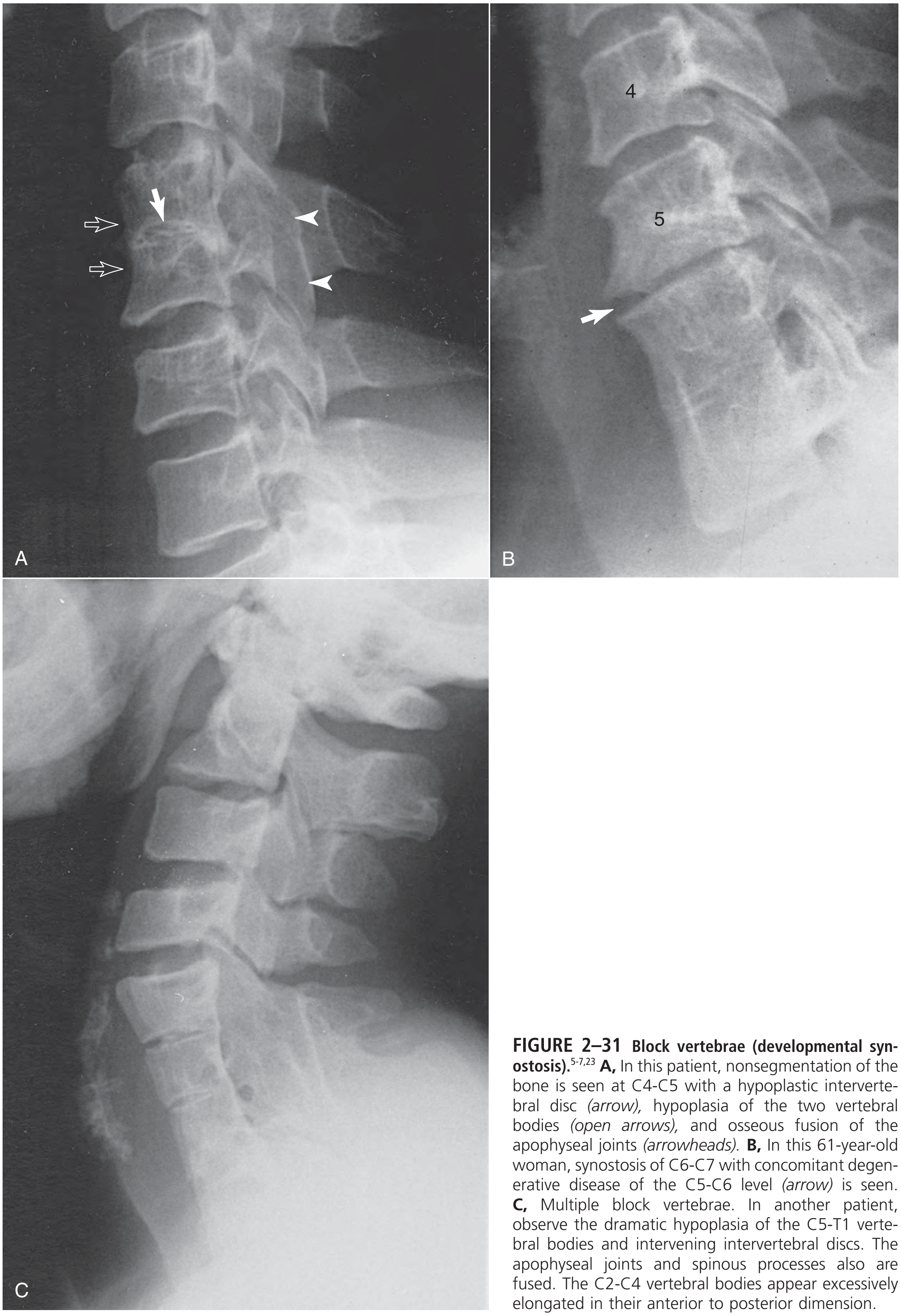

FIGURE 2–31 Block vertebrae (developmental synostosis).[5-7,23] **A,** In this patient, nonsegmentation of the bone is seen at C4-C5 with a hypoplastic intervertebral disc *(arrow),* hypoplasia of the two vertebral bodies *(open arrows),* and osseous fusion of the apophyseal joints *(arrowheads).* **B,** In this 61-year-old woman, synostosis of C6-C7 with concomitant degenerative disease of the C5-C6 level *(arrow)* is seen. **C,** Multiple block vertebrae. In another patient, observe the dramatic hypoplasia of the C5-T1 vertebral bodies and intervening intervertebral discs. The apophyseal joints and spinous processes also are fused. The C2-C4 vertebral bodies appear excessively elongated in their anterior to posterior dimension.

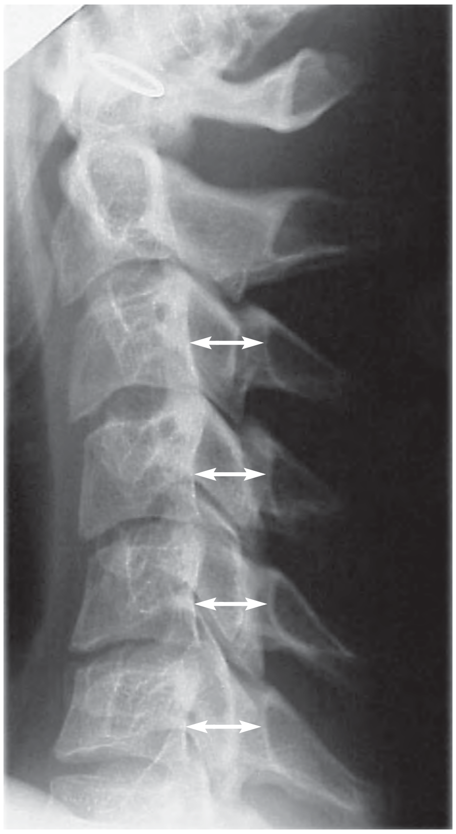

FIGURE 2–32 **Developmental (congenital) spinal stenosis.**[6] Lateral cervical radiograph in this 18-year-old male who presented with upper extremity hyperesthesia reveals narrowing of the of the spinal canal *(double arrows)*. The sagittal dimension of the cervical spine canal should never measure less than 12 mm, or less than 80% of the midvertebral body width.

TABLE 2-5 Klippel-Feil Syndrome[24] (Figure 2-33)

Entity	Characteristics and Prevalence
Malformations	
Clinical appearance: short neck, low posterior hairline, limitation of cervical spine motion	Classic clinical triad present in about 50% of cases
Multiple congenital synostoses (fusions) of cervical vertebrae	Most consistent osseous finding May involve any level, including upper thoracic vertebrae Fusions may be continuous or interrupted May result in extensive degenerative changes at adjacent spinal levels
Sprengel deformity	20%-25% of cases Unilateral or bilateral elevation of scapula
Omovertebral bone	Found in 30%-40% of fixed elevated scapulae
Cervical ribs	10%-15% of cases Women > men
Hemivertebrae	15%-20% of cases Usually contributes to congenital scoliosis
Spina bifida occulta	May be present at one or more levels in patients with cervical fusions
Other anomalies	Kyphosis, scoliosis, spinal stenosis, and rib, cranial, brain, and visceral anomalies
Complications	
Spinal cord compression Nerve root compression Cord transection Central stenosis Foraminal stenosis Fractures	These neurologic sequelae may develop spontaneously or with minor or major trauma as a result of instability, degenerative changes, or osseous abnormalities

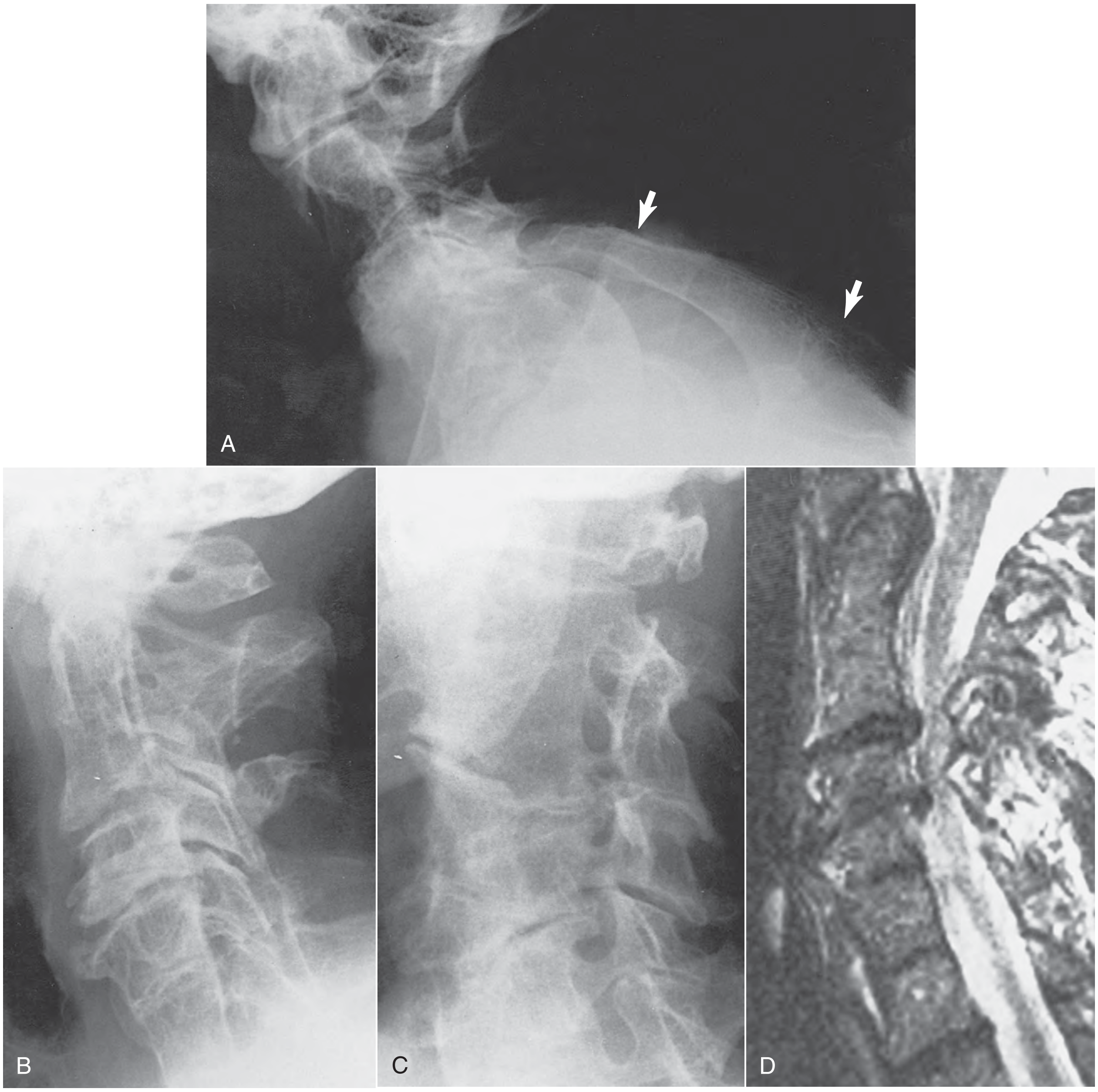

FIGURE 2–33 **Klippel-Feil syndrome.**[24] **A,** Congenital synostosis (block vertebrae) at multiple levels is evident in this 88-year-old man. An omovertebral bone also is seen *(arrows).* **B-D,** Fifty-eight-year-old man with radiculopathy after an injury. Lateral radiograph **(B)** reveals synostosis of C2-C3 and C5-C7 with extensive associated degenerative disease. Oblique radiograph **(C)** reveals extensive foraminal encroachment from uncovertebral and facet joint osteophytes. A parasagittal T2-weighted (TR/TE, 4000/100) spin echo MR image **(D)** shows disc protrusions and hypertrophic bone proliferation arising from the apophyseal joints and resulting in severe spinal canal stenosis at the C3-C4 and C4-C5 levels. Table 2-5 lists some of the malformations and complications commonly associated with Klippel-Feil syndrome. *(**B-D,** Courtesy S. Maskall, DC, Grand Forks, B.C.,Canada.)*

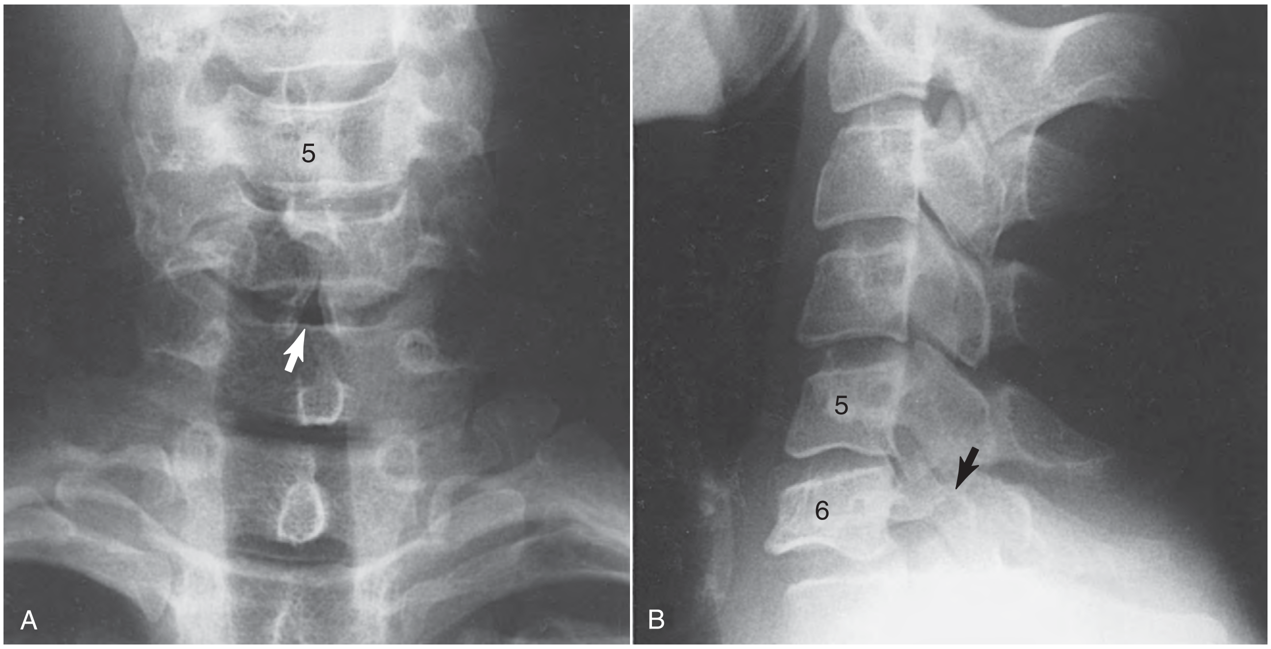

FIGURE 2–34 **Congenital spondylolisthesis.**[25] **A,** An anteroposterior radiograph reveals spina bifida occulta at C6 *(arrow).* **B,** Lateral radiograph shows minimal anterior displacement of C6 in relation to C7 and a neural arch defect consisting of incomplete ossification of the pedicles and articular processes of C6 *(arrow).* In addition, the C6 vertebral body is hypoplastic. *(Courtesy E.E. Bonic, DC, St. Louis, Missouri.)*

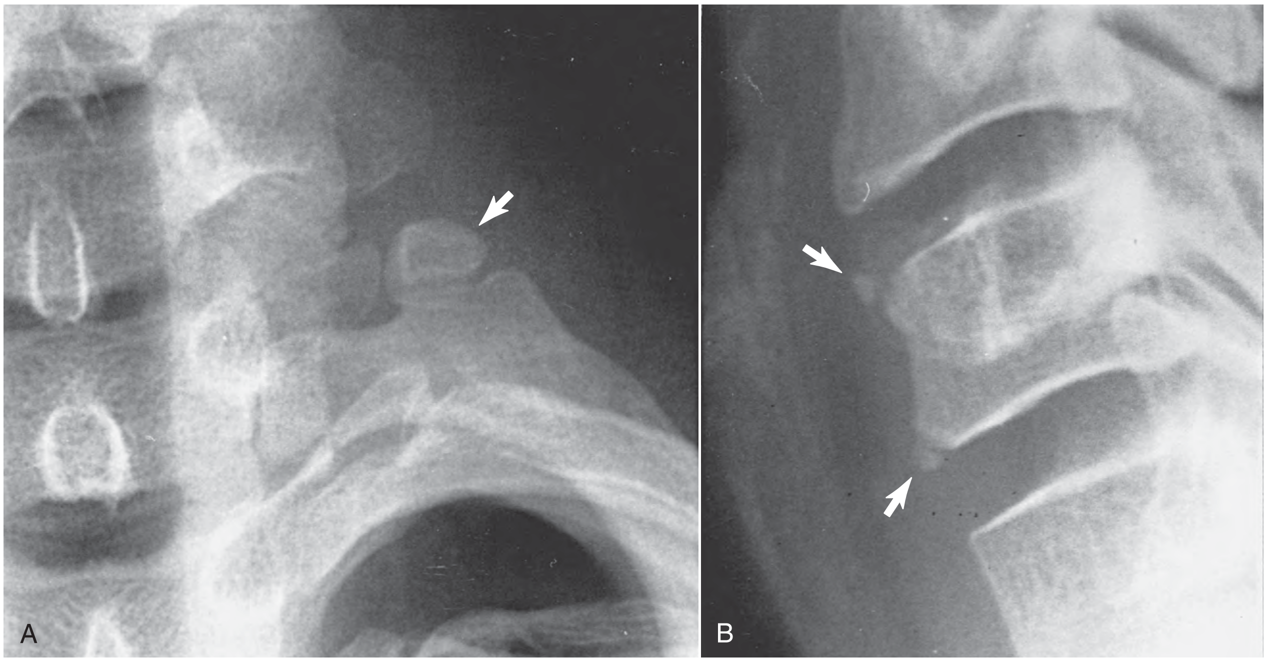

FIGURE 2–35 **Persistent (ununited) secondary ossification centers.**[7] **A,** An anomalous ossicle is present adjacent to the tip of the T1 transverse process and first rib *(arrow).* This probably represents failure of fusion of the secondary ossification center at the tip of the transverse process, a structure that usually fuses by the age of 25 years. **B,** In this 40-year-old man, two small triangular opacities are evident adjacent to the anterior corners of the C6 vertebral body *(arrows).* These ossification centers, which usually fuse to the vertebral body by the age of 17 or 18 years, may fail to fuse and persist into adulthood. These "limbus vertebrae" are variations of normal that may simulate a fracture.

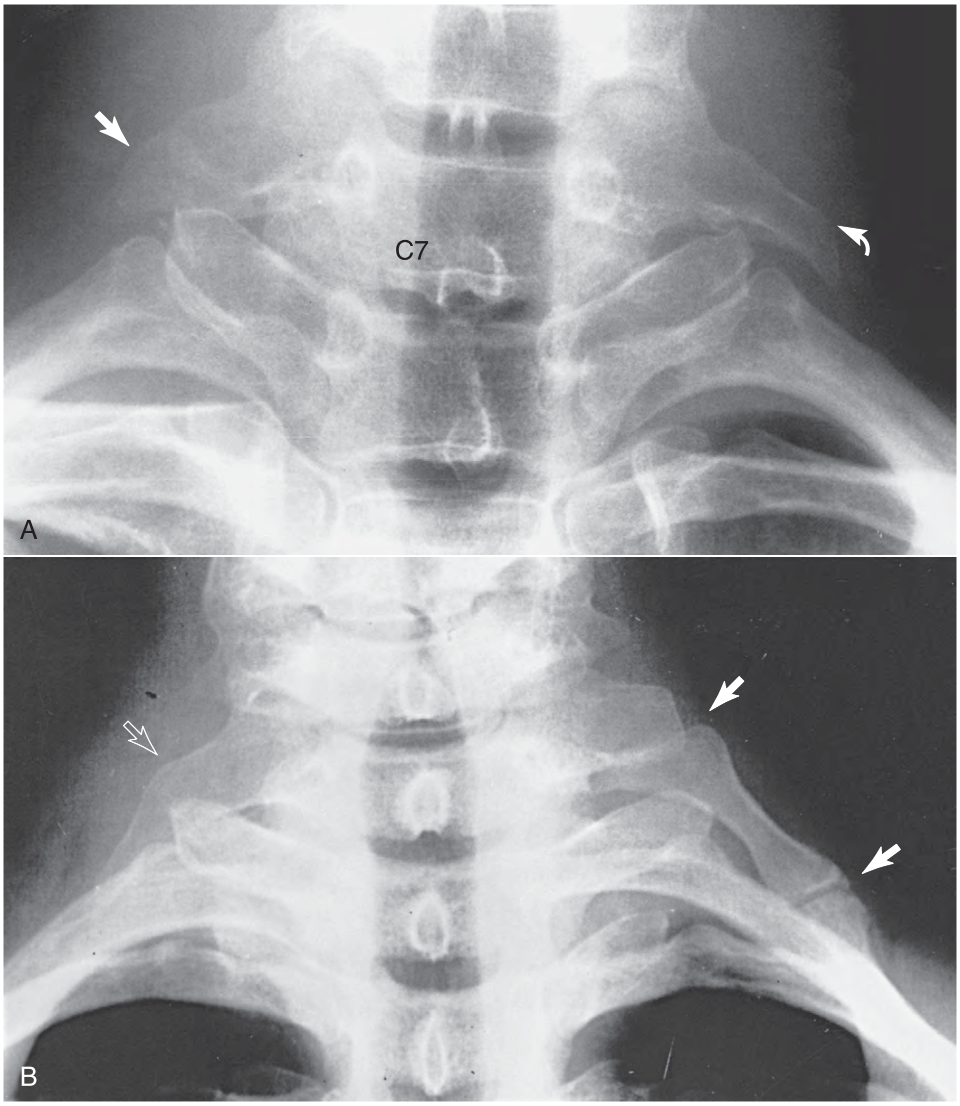

FIGURE 2–36 **Cervical rib and elongated C7 transverse process.**[26] **A,** The left C7 transverse process is elongated and has a tapered, sharpened appearance *(curved arrow).* A small, articulating cervical rib is evident on the right *(arrow).* **B,** In another patient, the right C7 transverse process is elongated and tapered *(open arrow),* and a cervical rib with two articulations *(arrows)* is present on the left.

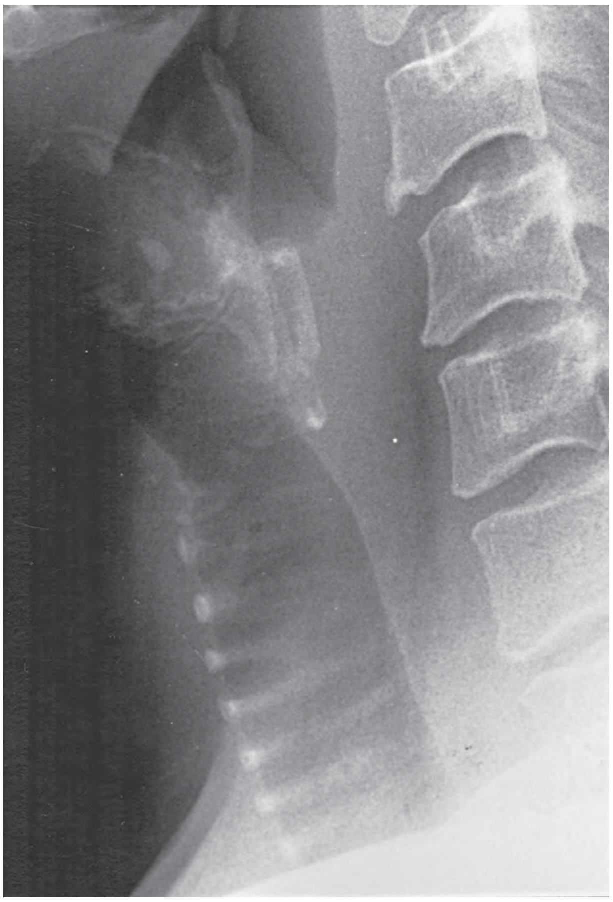

FIGURE 2–37 **Tracheal ring calcification.**[6] Prominent ringlike calcification of the tracheal cartilage is evident on a lateral radiograph of this 50-year-old woman. Such calcification is common in the elderly, is clinically asymptomatic, and is of no significance. *(Courtesy E.E. Bonic, DC, St. Louis, Missouri.)*

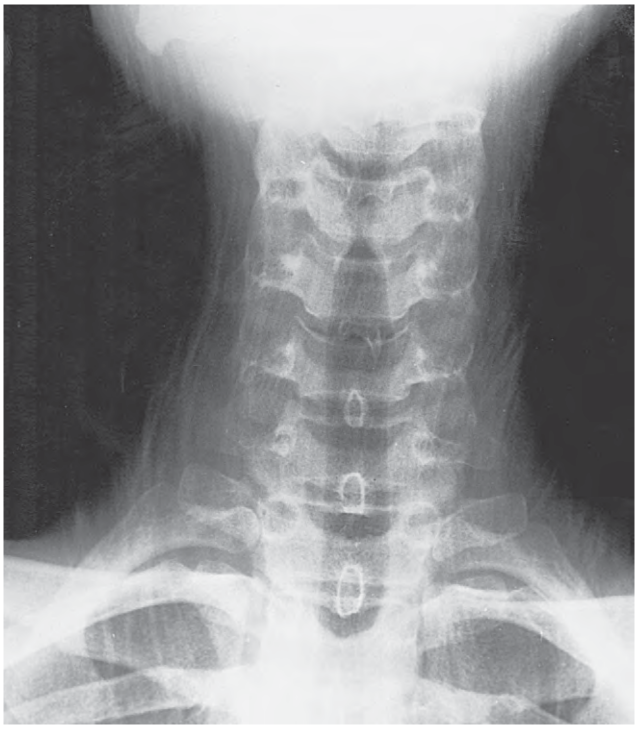

FIGURE 2–38 **Hair artifact.**[5] Streaky, vertically oriented opacities are seen over the cervical spine and soft tissues of the neck. This commonly encountered artifact results from overlying strands of hair. *(Courtesy E.E. Bonic, DC, Portland, Ore.)*

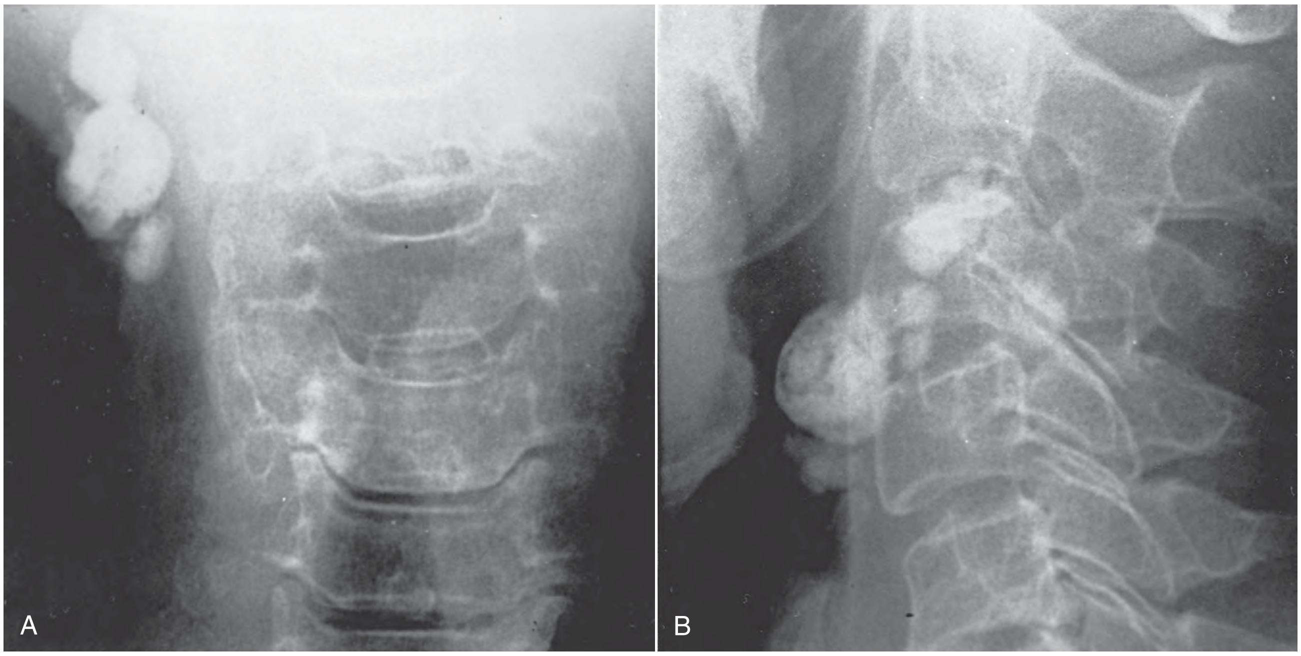

FIGURE 2–39 **Cervical lymph node calcification.**[6,27] Lobulated accumulations of calcification **(A-B)** are evident within the paraspinal soft tissues of the neck. These calcifications are consistent with lymph node calcification and should not be confused with the periarticular calcifications seen in connective tissue and crystal deposition diseases. *(Courtesy S. Maskall, DC, Grand Forks, B.C., Canada.)*

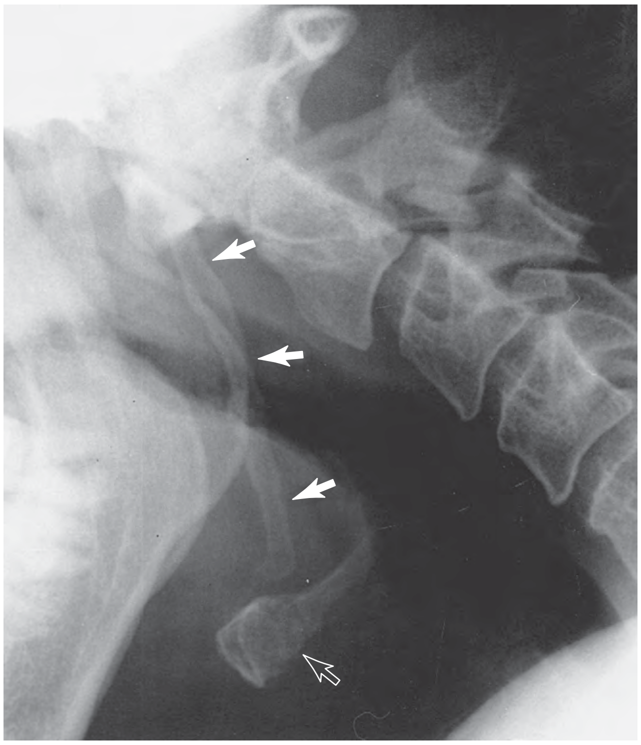

FIGURE 2–40 Ossification of the stylohyoid ligament.[28] In this lateral radiograph obtained in flexion, observe the vertical, linear ossified structure *(arrows)* overlying the prevertebral structures superior to the hyoid bone *(open arrow).* This represents ossification and elongation of the stylohyoid ligament, which usually is an incidental finding. This structure may possess one or more articulations, it may fracture, and, in a condition termed *Eagle syndrome*, it may cause symptoms of pain, dysphagia, and a sensation of a lump in the throat. The prevalence of ossified stylohyoid ligaments is higher in patients with mucopolysaccharidoses and diffuse idiopathic skeletal hyperostosis (DISH).

TABLE 2-6 Skeletal Dysplasias and Other Congenital Diseases Affecting the Cervical Spine*

Entity	Figure(s)	Characteristics in the Cervical Spine
Achondroplasia[29]		Brain stem compression by narrow foramen magnum Spinal stenosis with posterior scalloping of vertebral bodies Vertebral bodies may be flattened
Spondyloepiphyseal dysplasia congenita[30]	2-41	Hypoplasia of the odontoid with atlantoaxial instability Platyspondyly
Mucopolysaccharidoses (MPS)[31,32]	2-42	***MPS I-H (Hurler syndrome)*** Atlantoaxial instability may be present Rounded anterior vertebral margins with inferior beaking Posterior scalloping of vertebral bodies ***MPS IV (Morquio syndrome)*** Hypoplastic or absent odontoid with atlantoaxial instability Platyspondyly Posterior scalloping of vertebral bodies
Fibrodysplasia ossificans progressiva[33]		Sheetlike ossification within soft tissues of neck Hypoplastic vertebral bodies and intervertebral discs Apophyseal joint ankylosis
Osteopetrosis[34,35,141]	2-43	Patterns of osteosclerosis: diffuse osteosclerosis, bone-within-bone appearance, sandwich vertebrae
Osteopoikilosis[36]		Infrequently affects the spine Multiple punctate circular foci of osteosclerosis
Marfan syndrome[37]		Scoliosis in 40%-60% of persons Posterior vertebral body scalloping from dural ectasia Atlantoaxial instability may be present

* See also Table 1-2.

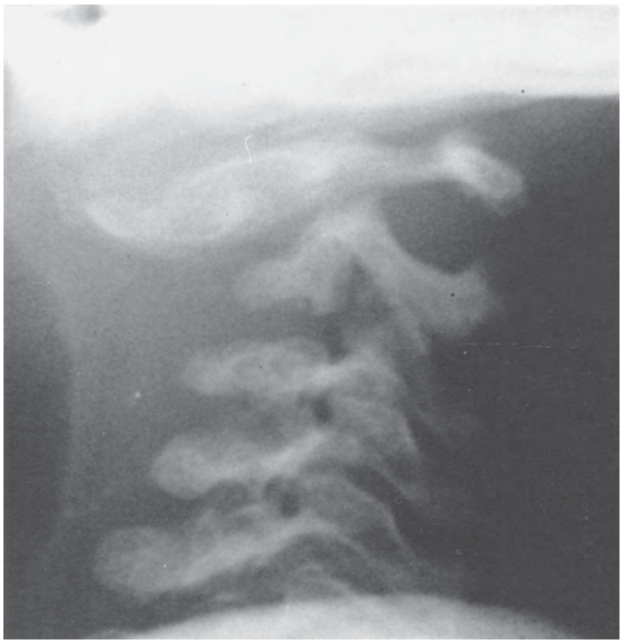

FIGURE 2–41 **Spondyloepiphyseal dysplasia congenita.**[30] This 5-year-old boy has platyspondyly, a hypoplastic odontoid process with atlantoaxial subluxation, instability, and craniocervical canal stenosis. Respiratory and visual complications may be severe, and a rare lethal form exists termed *hypochondrogenesis*.

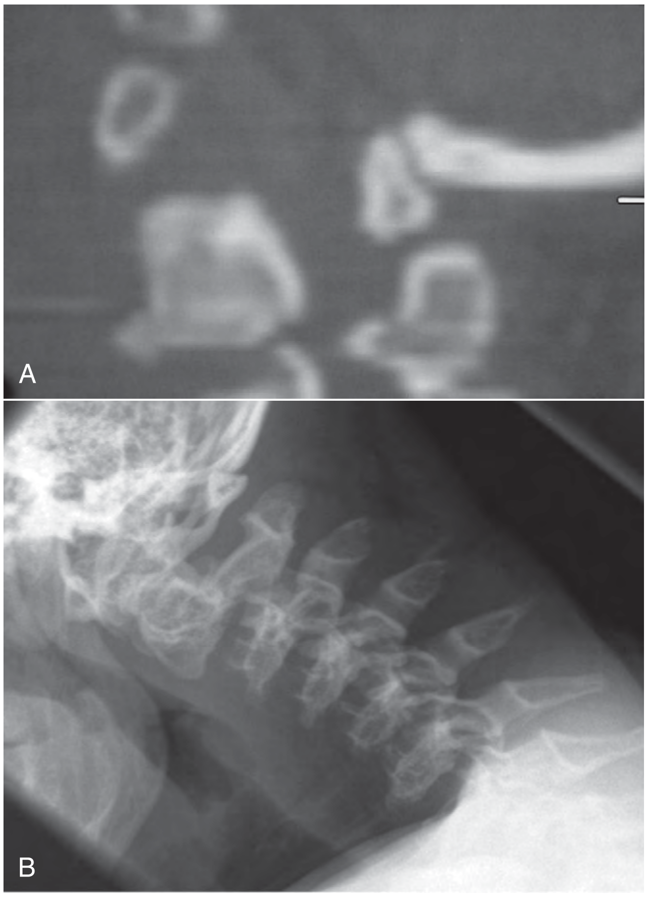

FIGURE 2–42 **Mucopolysaccharidoses: MPS IV (Morquio syndrome).**[31,32] **A,** Sagittal reformatted CT image of the upper cervical region of a young child reveals agenesis of the odontoid, an important cause of atlantoaxial instability in patients with MPS IV. **B,** Flexion radiograph of a 28-year-old man with MPS IV demonstrating the typical platyspondyly configuration of the vertebral bodies.

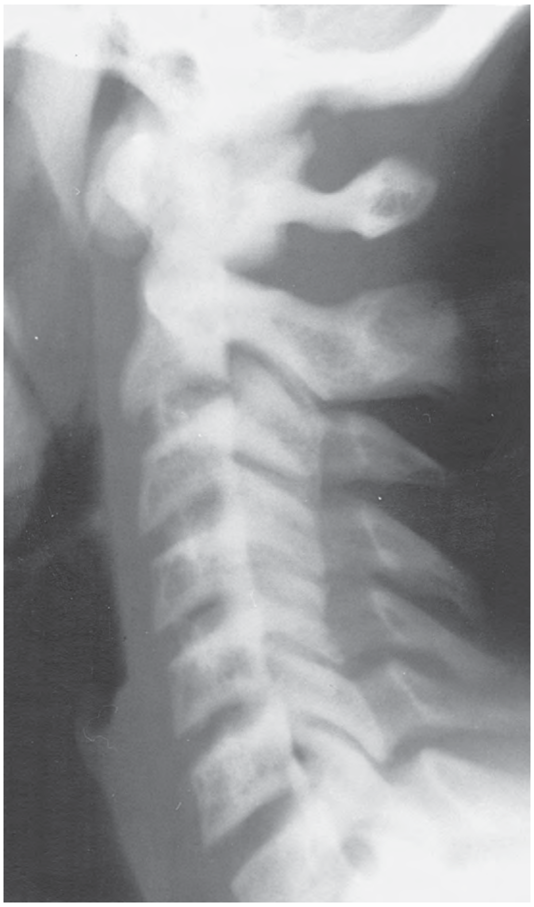

FIGURE 2–43 **Osteopetrosis.**[34,35,141] Diffuse sclerosis predominates at the vertebral endplates of the cervical spine in this 15-year-old boy with osteopetrosis. The radiographic pattern in the spine may be diffusely sclerotic, or osteopetrosis may be manifest as "sandwich vertebrae" or as a "bone-within-bone" appearance. Generalized osteosclerosis in osteopetrosis results from an increased amount of bone, not from an increase in the percentage of mineralized bone per unit volume of tissue.

TABLE 2-7 Cervical Spine Injuries: The Canadian C-Spine Rule. A Decision Rule to Determine Which Patients Require Diagnostic Imaging After Sustaining Cervical Spine Trauma[158]

Discussion

The Canadian C-spine rule can be applied to determine the need for diagnostic imaging in alert and stable patients sustaining cervical spine trauma and who are in stable condition. Criteria are listed as follows:

High-Risk Criteria Requiring Imaging

- Age ≥ 65
- Dangerous mechanism of injury
- Fall from 1 meter (5 stairs)
- Axial load to the head (i.e., diving)
- Motor vehicle collision at high speed ≥ 60 miles (100 km) per hour
- Rollover or ejection
- Motorized recreational vehicles
- Bicycle collision
- Presence of paresthesia in extremities

Low-Risk Criteria

Presence of any one of these in the absence of a high-risk criterion allows clinical assessment of active range of motion:

- Simple rear-end motor vehicle collision (this excludes being pushed into oncoming traffic, being hit by a bus or large truck, rollover, hit by a high-speed vehicle)
- Sitting position in the emergency department
- Ambulatory at any time
- Delayed onset of neck pain (i.e., not immediate onset of neck pain)
- Absence of midline cervical spine tenderness

TABLE 2-8 Canadian C-Spine Rule Algorithm*

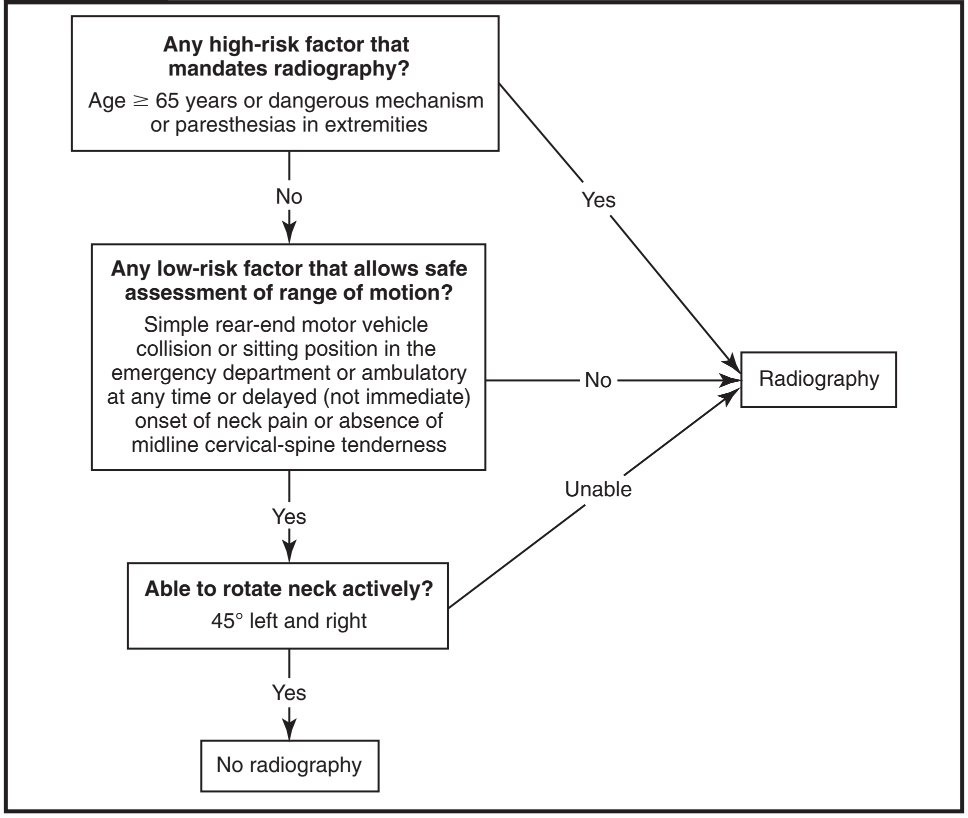
Any high-risk factor that mandates radiography?
Age ≥ 65 years or dangerous mechanism or paresthesias in extremities
No
Yes
Any low-risk factor that allows safe assessment of range of motion?
Simple rear-end motor vehicle collision or sitting position in the emergency department or ambulatory at any time or delayed (not immediate) onset of neck pain or absence of midline cervical-spine tenderness
No
Radiography
Unable
Yes
Able to rotate neck actively?
45° left and right
Yes
No radiography

* Reprinted with permission from Stiell IG, Clement CM, McKnight D, et al: The Canadian C-spine rule versus the NEXUS low-risk criteria in patients with trauma. N Engl J Med 349:2512, 2003.

TABLE 2-9 Cervical Spine Injuries With Stratification Based on Stability*

Fracture	Stability
Ruptured transverse ligament of the atlas	Least
Type II odontoid fracture	
Burst fracture with posterior ligamentous disruption	
Bilateral facet dislocation	
Burst fracture without posterior ligamentous disruption	
Hyperextension fracture dislocation	
C2 hangman's fracture	
Extension teardrop fracture (stable in flexion)	
Compression fracture of C1 (Jefferson burst fracture)	
Unilateral facet dislocation	
Anterior subluxation	
Simple wedge compression fracture without posterior disruption	
Pillar fracture	
Fracture of the posterior arch of C1	↓
Isolated spinous process fracture not involving the lamina (clay shoveler's fracture)	Most

* Modified from Trafton PG: Spinal cord injuries. Surg Clin North Am 62:61, 1982.

TABLE 2-10 Upper Cervical Spine Injuries*

Entity	Figure(s), Table(s)	Stability[†]	Mechanism	Characteristics
Atlas Injuries				
Atlanto-occipital dislocation[38,39]	2-44	Unstable	Hyperextension-shearing and distraction	Rare injury; almost always fatal Occurs with or without associated fracture Cranium usually is displaced anteriorly relative to the cervical spine Distance between the odontoid and basion is increased
Traumatic transverse ligament disruption[40,160,166]	2-45	Unstable	Poorly understood mechanism	Rupture of the transverse ligament with or without associated fractures Atlantoaxial instability invariable: atlantodental interspace more than 3 mm in adults and 5 mm in children *Rare:* only 1% of all cervical injuries Transverse ligament damage (partial tears) from whiplash trauma can be detected on high-resolution proton-weighted MR images, but the reliability still needs improvement. Nontraumatic causes of transverse ligament rupture much more frequent and include inflammatory arthritis, Down syndrome, anomalies, and infection
Rotatory atlantoaxial fixation[41-43,147,154,155]	2-46 Table 2-11	Variable	Hyper-rotation	Persistent pathologic fixation of the atlantoaxial joints in a rotated position such that the atlas and axis move as a unit rather than independently Patient typically has a persistent painful torticollis Occurs after rotational trauma, but also may occur after an inflammatory condition of the pharynx or upper respiratory tract, such as in Grisel syndrome Dynamic or functional CT is useful in identifying the presence and precise type of atlantoaxial rotatory fixation
Burst (Jefferson) fracture[44,147]	2-47 Table 2-11	Variable Deemed unstable when the transverse ligament is ruptured or avulsed	Axial compression	May be unilateral or bilateral Axial compressive loading causes compression of the lateral masses of C1 between the occipital condyles and the C2 articular processes, resulting in two, three, or four fracture fragments of the atlas ring (classic Jefferson fracture is four-part) Unilateral or bilateral displacement of lateral masses on open mouth view Normal lateral offset (pseudospread) of the atlas is common in normal children and may measure 4-6 mm Jefferson fracture should be suspected in patients with 3 mm or more of total lateral displacement, and transverse ligament damage should be suspected in patients with more than 7 mm of total lateral displacement seen on the anteroposterior view Permanent neurologic injury is uncommon with classic four-part Jefferson fractures
Posterior arch fracture[45,147]	2-48	Stable	Compressive hyperextension	Most common fracture of the atlas Results from compression of the atlas between the basiocciput and the posterior arch of C2 during hyperextension injury 90% are bilateral; 10% are unilateral Heals slowly, pseudarthroses are common

Anterior arch fracture[46,147]		Usually stable	Disruptive hyperextension	Horizontal fracture seen on lateral radiograph produced by avulsion of the tubercle of the anterior arch by the superior oblique portion of the longus colli muscle and the anterior longitudinal ligament Often associated with fractures of C1 posterior arch and odontoid
Isolated lateral mass fracture[46,147]		Usually stable	Axial compression or lateral hyperflexion	Extremely rare injury Fracture of the medial aspect of the lateral mass may result from avulsion by the transverse ligament
Isolated transverse process fracture[46,147]		Usually stable	Lateral hyperflexion	Extremely rare injury at C1 level Potential vertebral artery injury
Axis Injuries				
Odontoid fracture[47,48,147]			Complex and poorly understood mechanism including combinations of extreme flexion, extension, rotation, and shearing	*Most common axis fracture:* 55% of C2 fractures; 7%-13% of all cervical spine injuries Up to 90% of affected patients are intact neurologically at time of injury but may develop late-onset neurologic deficit Fracture-dislocation may complicate odontoid fractures Anterior odontoid displacement from flexion forces Lateral odontoid displacement from lateral flexion or rotational forces Three types of odontoid fracture based on fracture location
Type I	2-49	Stable		*Least common type:* believed to be caused by alar ligament avulsion Unilateral oblique fracture through the tip of the odontoid above the transverse ligament Nonunion and displacement rare
Type II	2-50	Unstable		Most common type Fracture occurs through the base of the odontoid at its junction with the C2 body; frequently disrupts the blood supply Nonunion occurs in more than 25% of cases Displacement (more than 60% of cases) and angulation (more than 25%) increase likelihood of nonunion Popular theory holds that os odontoideum actually represents a chronic nonunion type II odontoid fracture rather than a developmental anomaly
Type III	2-51	Stable		Horizontal or oblique fracture line extends from the base of the odontoid into the cancellous bone of the vertebral body, typically exiting through the articular process of C2 into the C1-C2 articulation Anterior displacement occurs in 58% of cases and lateral tilting of the odontoid greater than 5 degrees is present in about 66% of cases Nonunion occurs in less than 13% of cases

* From references 46, 50, 51, 147, 158, 159.

† Clinical instability here is defined as the inability to maintain vertebral relationships in such a way that spinal cord and nerve root damage are avoided and subsequent deformity and excessive pain do not develop. From White AA, Southwick WO, Panjabi MM: Clinical instability in the lower cervical spine. Clin Orthop 109:85, 1975.

Continued

TABLE 2-10 Upper Cervical Spine Injuries—cont'd

Entity	Figure(s), Table(s)	Stability[†]	Mechanism	Characteristics
Odontoid fracture with distraction	2-52	Highly unstable	Distraction	Rare fracture of odontoid (usually type II) with wide separation at fracture site
Hangman's fracture[47-49]	2-53	Varies according to type	Varies according to type	Four to 23% of all cervical spine fractures Sometimes termed *traumatic spondylolisthesis* of C2 Bilateral avulsion fractures of the neural arches from the C2 vertebral body Fractures occur through the pars interarticularis or adjacent portion of the articular processes Extension into the vertebral body occurs in as many as 18% of cases Neurologic damage occurs in less than 13% of cases but infrequently is permanent
Three types:				
Type I		Stable	Hyperextension	Nonangulated, nondisplaced (<2 mm), and normal C2-C3 disc
Type II		Unstable	Hyperextension or flexion-distraction	Anterior displacement or angulation with C2-C3 disc injury
Type III		Unstable	Hyperflexion	Anterior displacement or angulation with bilateral facet dislocation
Extension teardrop fracture[46]		Unstable	Disruptive hyperextension	Avulsion fracture of a triangular fragment of the anteroinferior margin of the body by the anterior longitudinal ligament Most common at C2, but may occur at any level Fragment may be displaced, distracted, or rotated More common in elderly persons with osteoporosis and spondylosis Usually not associated with neurologic deficit
Avulsion fracture of C2 body from hyperextension dislocation[46]		Unstable	Disruptive hyperextension	*Severe injury:* avulsion fracture of anteroinferior corner of vertebral body mediated through Sharpey fibers Usually occurs in lower cervical spine, but also seen at C2-C3 Frequently associated with acute cervical central cord syndrome
Oblique fracture of body[46]		Variable	Combinations of axial compression and rotation	Oblique fracture through the C2 vertebral body below the odontoid and articular processes Results in widened anteroposterior diameter of the C2 vertebral body: "fat C2 sign"
Isolated process fracture[46]		Usually stable	Hyperextension, rotation, hyperflexion, or direct trauma	Unilateral pedicle, lateral mass, or lamina Spinous process

TABLE 2-11 **Some Causes of Asymmetric Lateral Atlantodental Space**[43]
Two- to 5-mm discrepancy in this space has been documented in normal persons
Correlation with other radiographic evidence is necessary to determine the significance of this measurement
Normal Range of Cervical Motion and No Fixed Deformity
Congenital variation of odontoid shape
Slanting of odontoid process
Contour variations of C1 lateral articular masses
Restriction of Cervical Motion or Fixed Deformity
Rotatory atlantoaxial fixation (see Figure 2-46)
Jefferson fracture (see Figure 2-47)

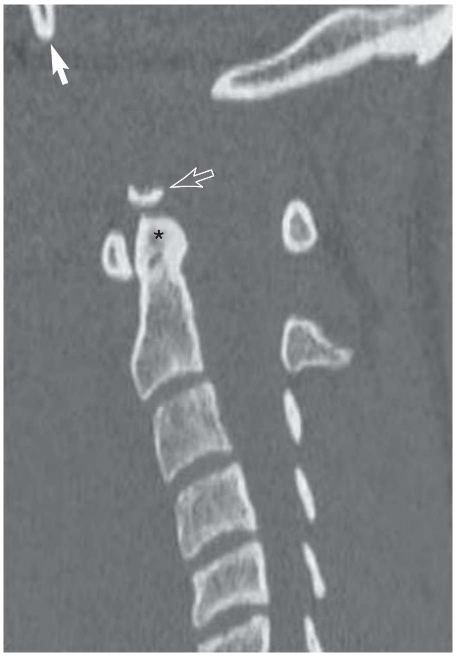

FIGURE 2–44 **Atlanto-occipital dislocation.**[38,39] This 28-year-old man was involved in a serious motor vehicle crash. Observe the increased distance between the odontoid *(*)* and basion *(arrow)* and the associated bone fragment *(open arrow)* from a fractured occipital condyle superior to the tip of the odontoid. Although this injury is usually immediately fatal, this patient survived for a short period of time.

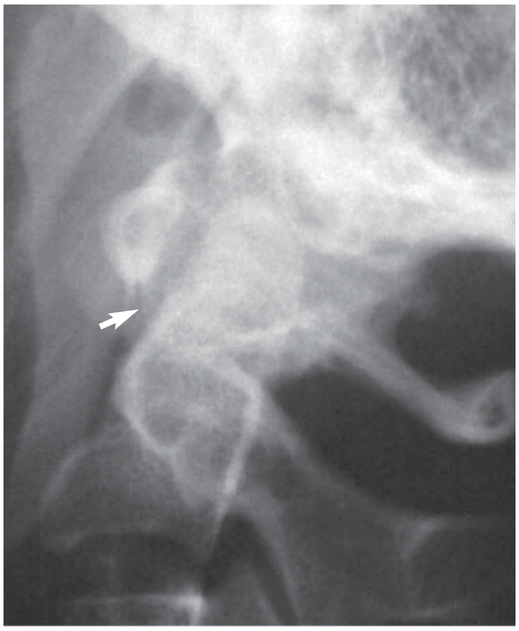

FIGURE 2–45 **Traumatic transverse ligament rupture.**[40,160,166] The atlantodental interspace is widened *(arrow)* in this 19-year-old female patient with traumatic transverse ligament disruption. This interspace should not exceed 3 mm in adults and 5 mm in children.

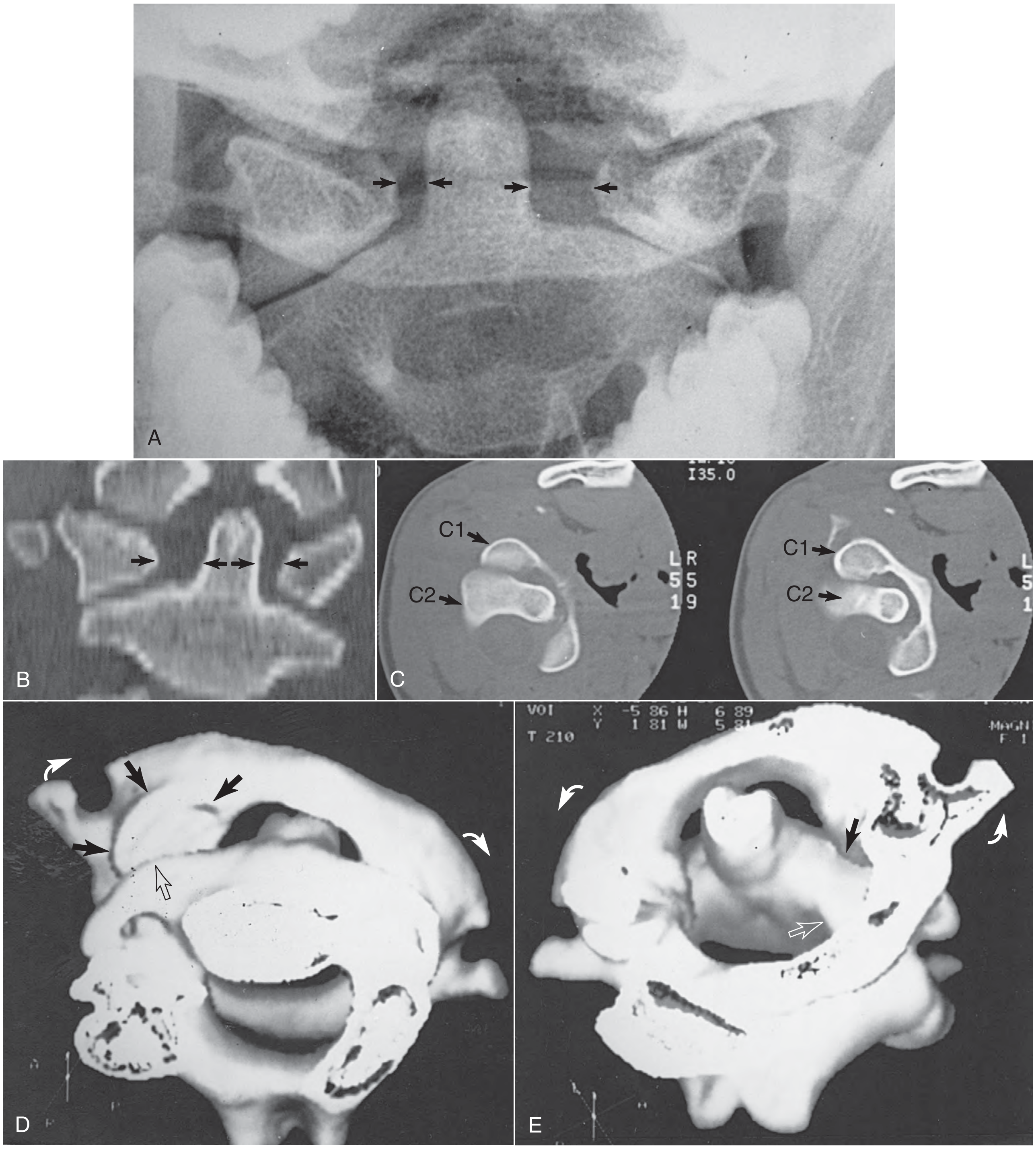

FIGURE 2–46 Rotatory atlantoaxial fixation.[41-43,154,155] **A,** Conventional radiographic findings. Observe the asymmetric space between the odontoid process and the medial aspect of the lateral masses of the atlas *(arrows)*. **B-E,** CT imaging findings. **B,** Coronal reformation. In another patient, asymmetric alignment of atlas and axis *(arrows)* is evident on this coronal CT image. **C,** Transaxial images obtained with the patient's head and neck in full left rotation show the anterior displacement of the right lateral mass of atlas *(C1)* relative to the articulating facet of axis *(C2)*. **D-E,** Three-dimensional CT reconstruction in a third patient shows the direction of rotation of the atlas *(curved arrows)*. In the first image, viewed from below **(D),** the right lateral mass of the atlas *(arrows)* is clearly situated anterior to the articulating surface of the C2 facet *(open arrow)*. Viewed from above **(E),** the articulating surface of the right lateral mass of the atlas *(arrow)* is displaced anteriorly in relation to the axis articular surface *(open arrow),* and the facet joints are locked in this position. (*Curved arrows* in **D** indicate direction of rotation of atlas.) (***B-E,*** *Courtesy B.A. Howard, MD, Charlotte, NC.)*

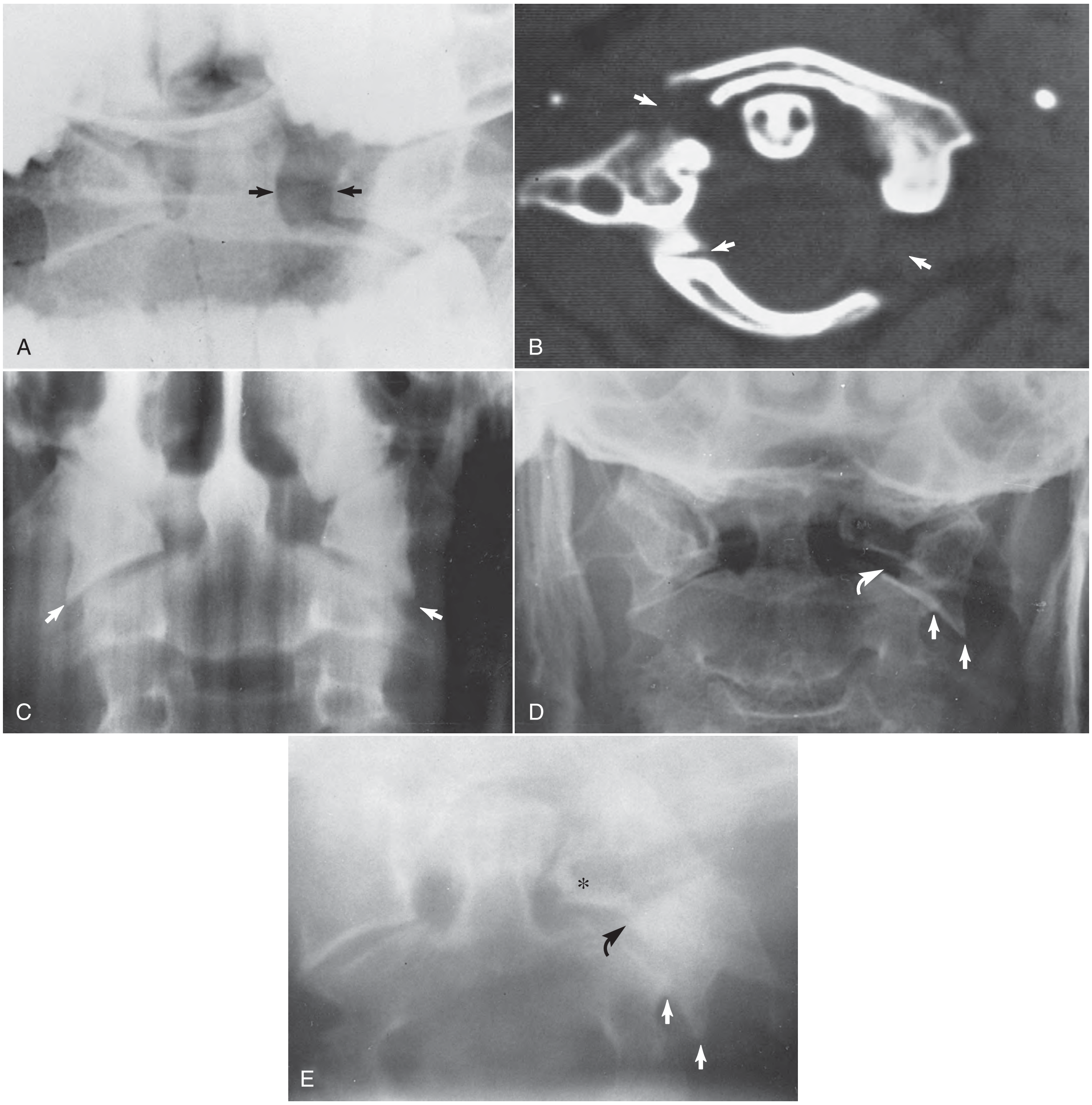

FIGURE 2–47 **Jefferson fracture: Burst fracture of the atlas.**[44] **A,** Anteroposterior open-mouth radiograph shows lateral offset of the atlas relative to the axis, seen as asymmetry of the paraodontoid spaces with marked widening on the left *(arrows)*. **B,** Transaxial CT scan shows a three-part fracture involving both posterior arches and the right anterior arch *(arrows)*. **C,** In another patient, a coronal conventional tomogram clearly shows the lateral displacement of the lateral masses of the atlas relative to the lateral aspect of C2 *(arrows)*. **D-E,** Frontal radiograph **(D)** and conventional tomogram **(E)** demonstrate lateral offset of the left lateral mass of the atlas in relation to the lateral margin of the axis *(arrows)*. The left paraodontoid space is not widened because the lateral mass of C1 is fractured *(curved arrows)*, and the medial fragment (*) is displaced toward the midline. Complete evaluation of such fractures requires analysis of multiple contiguous transaxial CT scans or conventional tomographic images.

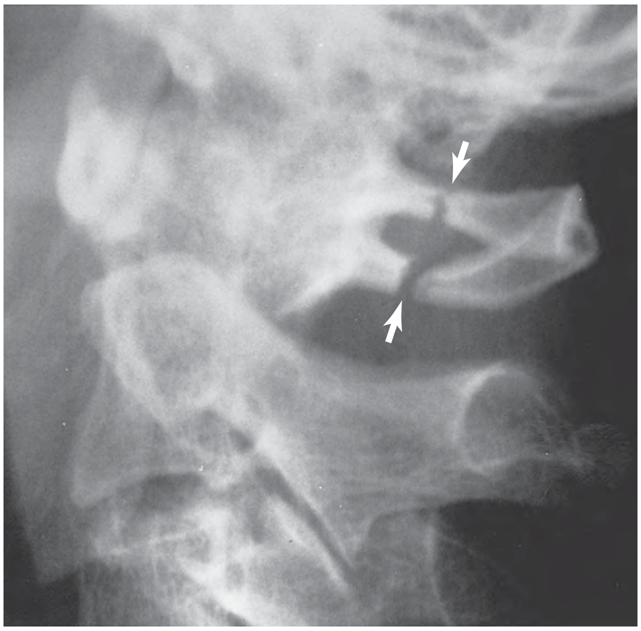

FIGURE 2–48 **Posterior arch fracture.**[45] Lateral radiograph shows bilateral fractures of the posterior arch of C1 that occurred after a hyperextension injury.

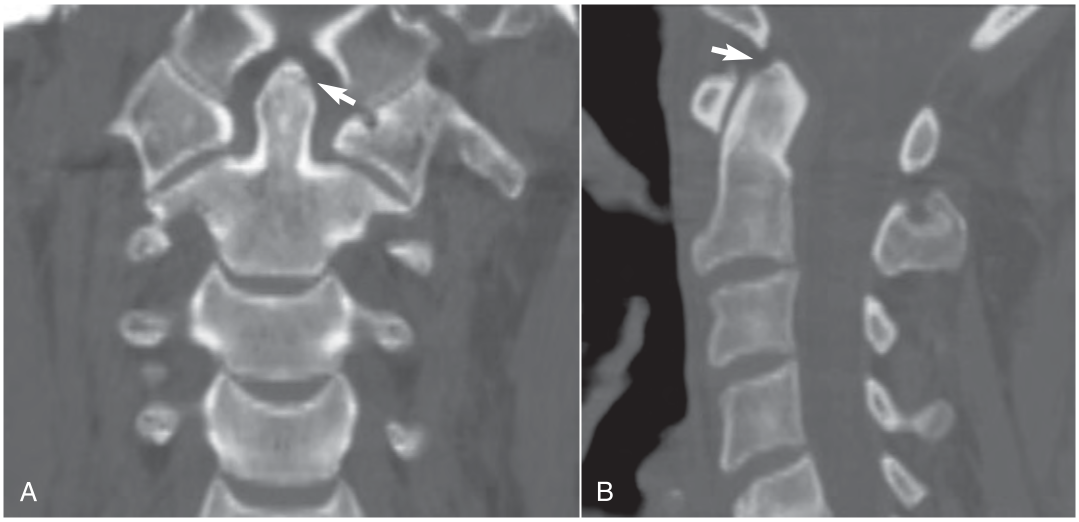

FIGURE 2–49 **Odontoid fracture: Type I.**[47,48,147] Coronal **(A)** and sagittal **(B)** reformatted CT bone window images in a 54-year-old man reveal a subtle fracture of the tip of the odontoid process *(arrows)*. This stable fracture is believed to be caused by alar ligament avulsion. Type I is the least common odontoid fracture and rarely results in complication.

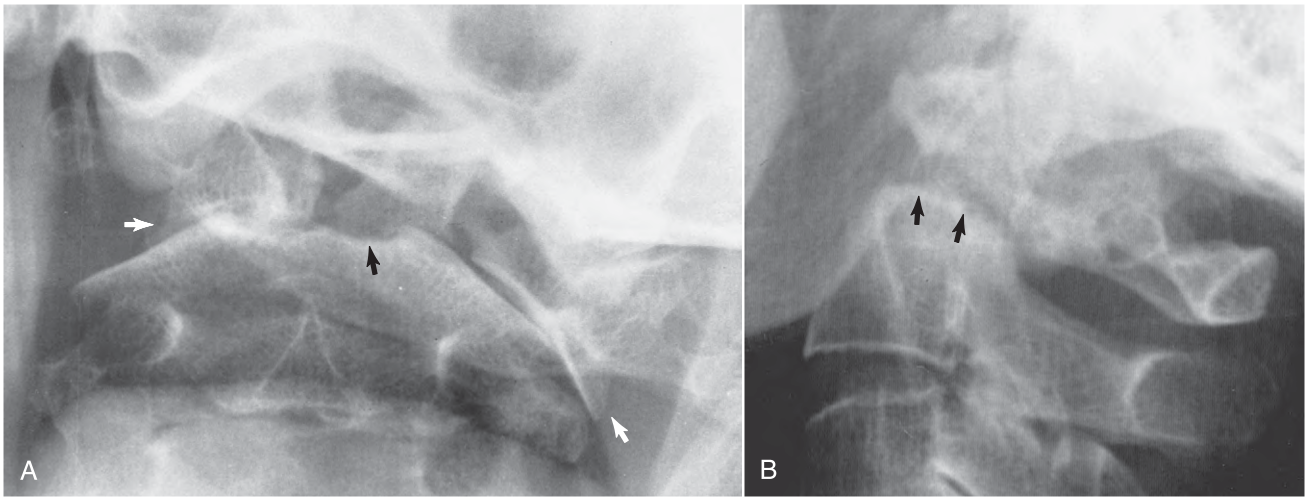

FIGURE 2–50 **Odontoid fracture: type II.**[47,48,147] This 84-year-old man fell on his face, injuring his cervical spine. **A,** Anteroposterior open-mouth radiograph demonstrates a radiolucent fracture cleft at the base of the laterally displaced odontoid process *(black arrow).* In addition, the lateral masses of the atlas are significantly displaced to the left *(white arrows).* **B,** Lateral radiograph also shows the fracture line *(arrows)* and posterior displacement of the odontoid and the atlas in relation to the body of axis. The type II odontoid fracture, occurring at the junction of the C2 body and the dens, is the most common type of odontoid fracture, is considered unstable, and frequently results in nonunion.

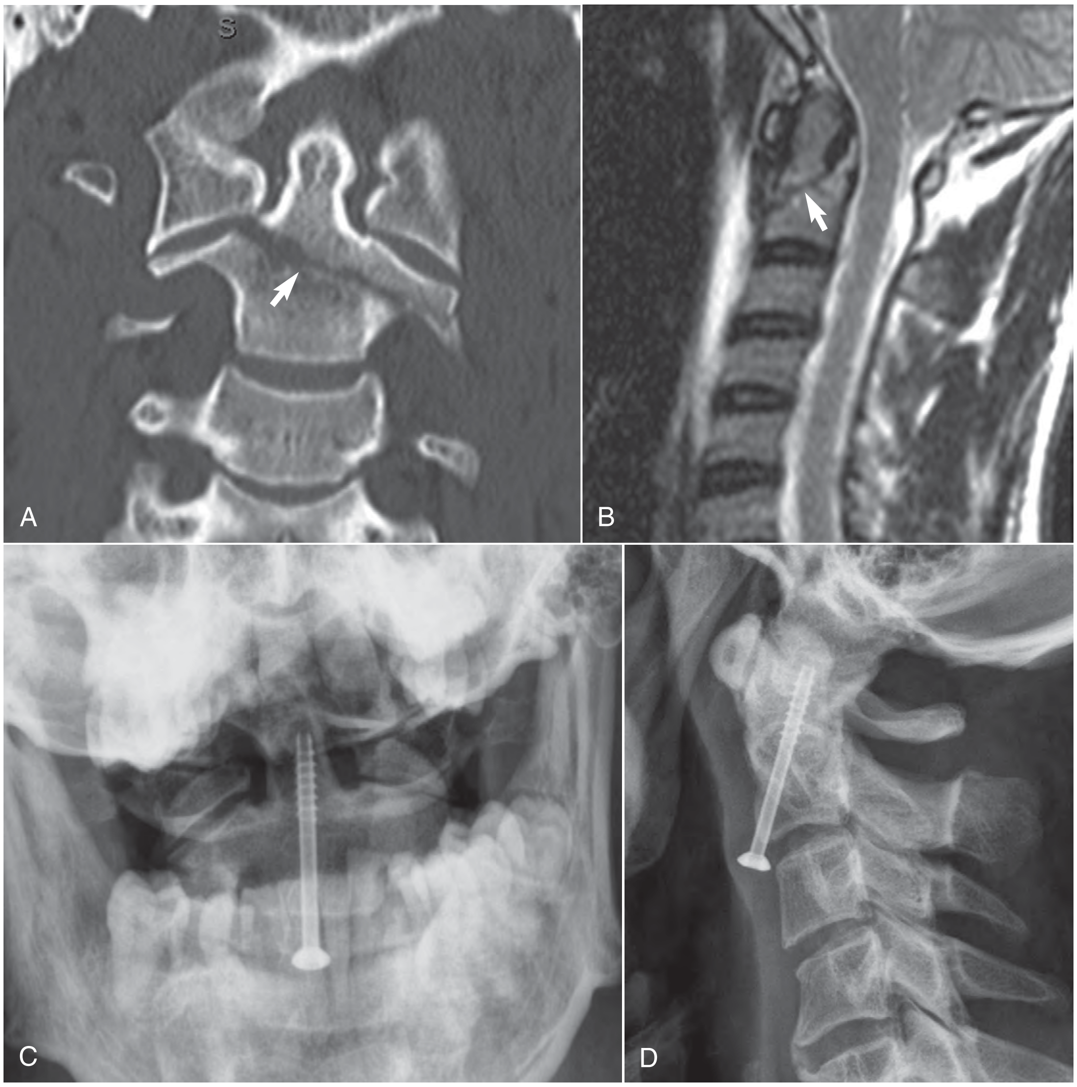

FIGURE 2–51 **Odontoid fracture: type III.**[47,48,147] Coronal reformatted CT scan **(A)** and sagittal T2-weighted MR image **(B)** reveal a slightly displaced oblique fracture *(arrow)* that extends from the base of the odontoid on the right and courses obliquely and inferiorly through the C2 vertebral body. The fracture passes through the articular surface of the right C2 lateral mass. In another patient who has sustained a type III odontoid fracture, anteroposterior and lateral radiographs **(C-D)** reveal surgical fixation with a cannulated screw extending from the anteroinferior C2 vertebral body superiorly into the odontoid. (***A-B,*** *Courtesy B.A. Howard, MD, Charlotte, NC;* ***C-D,*** *Courtesy K. Brown, DC, Syracuse, NY.)*

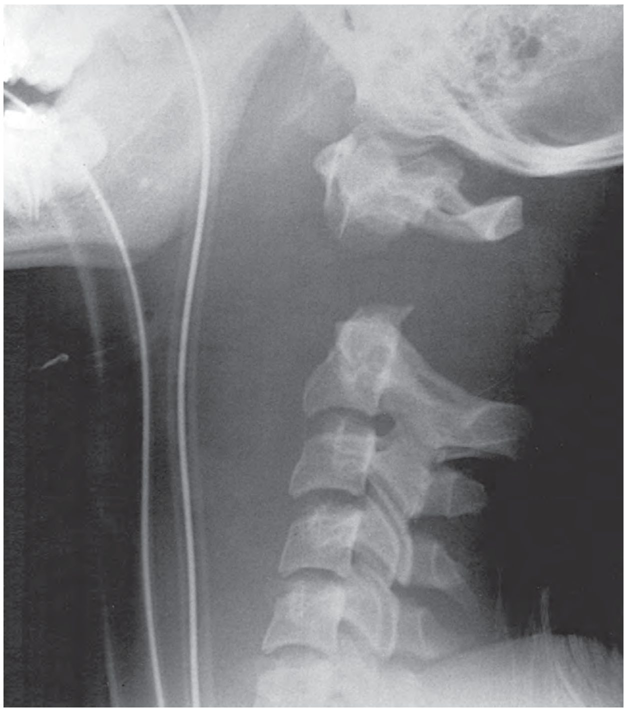

FIGURE 2–52 Odontoid fracture with severe distraction dislocation.[46,147] Observe the fracture through the base of the odontoid process. Dramatic prevertebral soft tissue swelling and hemorrhage also are evident. This rare type of odontoid fracture with severe distractive dislocation is secondary to massive trauma with predominantly distractive forces. Such injuries usually result in death. *(Courtesy W. Pogue, MD, San Diego, Calif.)*

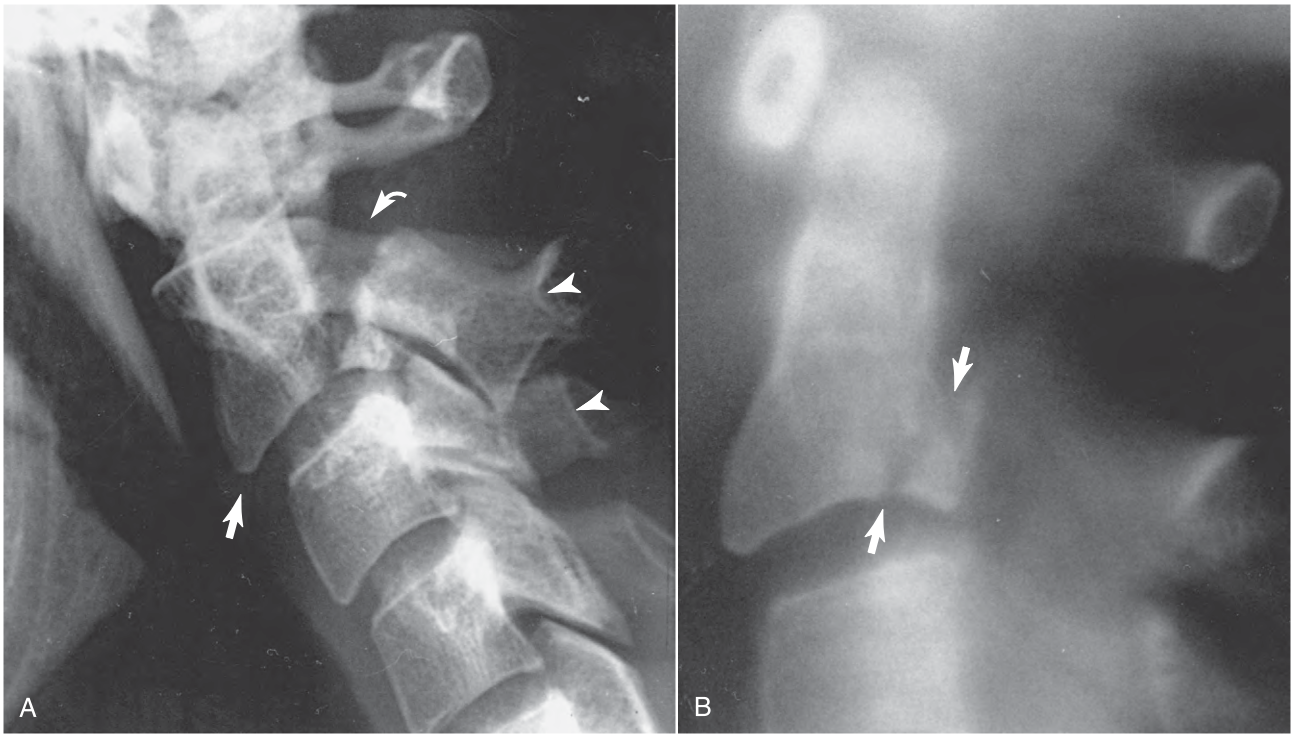

FIGURE 2–53 Hangman's fracture (Type II).[47-49] This 28-year-old man was involved in a high-speed motor vehicle accident in which his face struck the windshield and his neck was forced into hyperextension. **A,** Lateral radiograph shows fractures through both pedicles of the axis *(curved arrow)* with anterior displacement of the C2 vertebral body *(arrow).* In this injury, the spinolaminar junction line remains in normal alignment *(arrowheads).* **B,** Lateral conventional tomogram reveals more clearly the triangular fracture fragment of the posterior portion of the vertebral body *(arrows).*

TABLE 2-12 Lower Cervical Spine Injuries*

Entity	Figure(s), Table(s)	Stability†	Mechanism	Characteristics
Hyperflexion sprain[52,160,167]	2-54 Table 2-13	Unstable	Hyperflexion	*Acute disruption of ligaments in the following order of injury:* supraspinous, interspinous, ligamentum flavum, facet joint capsule; in severe cases, the posterior longitudinal ligament and posterior aspect of the anulus fibrosus also are disrupted C2-C3 and C3-C4 levels most frequent in children; lower cervical levels most frequent in adults Neurologic deficit usually mild and reversible Progressive kyphosis and delayed spinal instability develop in up to 33% of patients treated conservatively Partial ligament disruptions respond well to conservative care, but complete ligament ruptures typically require anterior or posterior cervical fusion Operative fixation should be performed early with kyphosis exceeding 20 degrees in children and 10 degrees in adults Initial radiographs frequently appear normal despite clinically evident cord injury
Bilateral apophyseal joint dislocation[53]	2-55	Unstable	Hyperflexion	Bilateral facet joint dislocation: highly unstable injury associated with neurologic deficit (75% of cases), disc herniations (as many as 50% of cases), and fractures Rupture of the posterior portion of the anulus fibrosus, posterior longitudinal ligament, and the capsular, interspinous, and supraspinous ligaments Inferior articular processes of the vertebra above dislocate and become perched (locked) in front of the superior articular processes of the vertebra below, resulting in spinal canal and foraminal stenosis Anterior vertebral body displacement typically is more than half the width of the vertebral body; this displacement increases during flexion but fails to reduce during extension Computed tomography (CT) and MR imaging are useful in assessing such injuries Flexion and extension radiographs in patients with severe cervical spine trauma should be obtained only under careful observation by a clinician and only in alert, cooperative patients who are able to actively perform these movements
Unilateral apophyseal joint dislocation[54-56]	2-56	Stable unless associated with facet fractures and neurologic deficit	Hyperflexion with rotation	In unilateral facet lock (dislocation), rupture of the interspinous ligament and capsule of the apophyseal joint allows the ipsilateral inferior facet of one vertebra to pivot, dislocate, and come to rest in the neural foramen anterior to the superior facet of the vertebra below Frequently accompanied by articular process fractures and bilateral damage of the rotated vertebra These injuries contribute to rotational instability and require specific internal fixation based on a precise delineation of all injuries Neurologic deficits, including radiculopathy, are relatively uncommon CT with parasagittal reformation is valuable in evaluating injuries in these patients

---

* From references 46, 60, 61, 158, 159, 167.

† Clinical instability here is defined as the inability to maintain vertebral relationships in such a way that spinal cord and nerve root damage are avoided and subsequent deformity and excessive pain do not develop. From White AA, Southwick WO, Panjabi MM: Clinical instability in the lower cervical spine. Clin Orthop 109:85, 1975. See also Table 2-14.

Continued

TABLE 2-12 Lower Cervical Spine Injuries—cont'd

Entity	Figure(s), Table(s)	Stability[†]	Mechanism	Characteristics
Spinous process fractures	2-57	Stable		Spinous process fractures generally are stable and do not result in neurologic injury Careful observation for evidence of other fractures or dislocations is essential
Two major types:				
Clay-shoveler's fracture[57]			Hyperflexion	*Most common type:* avulsion fracture of spinous process of C6-T2 levels Avulsed fragment typically is displaced inferiorly
Hyperextension type[46]			Hyperextension	*Less common type:* impaction injury of spinous processes Fracture from direct contact with adjacent spinous processes
Vertebral body compression fracture[46,51]		Usually stable	Compressive hyperflexion	Wedgelike compression of vertebral body Usually spares the posterior ligaments and results in simple compression fractures of the anterior vertebral column Considered benign because these fractures do not compromise the spinal canal, and they result in uncomplicated healing
Flexion teardrop fracture[58]	2-58	Unstable	Compressive hyperflexion	Highly unstable comminuted fracture of the vertebral body that results in severe neurologic injury in almost 90% of patients Injury occurs most frequently in diving and motor vehicle collisions Owing to the risk of neurologic injury related to instability, the lateral radiograph should be evaluated fully before flexion radiographs are obtained
Avulsion of the ring apophysis[46]		Stable	Hyperextension or, rarely, hyperflexion	Occurs in the vertebral body of the immature spine Usually not associated with neurologic damage, prevertebral soft tissue swelling, or other osseous injury Heals with an osseous excrescence at the inferior vertebral margin related to fusion of the avulsed apophysis with the vertebral body
Extension teardrop fracture[59]		Variable	Hyperextension	Avulsion fracture of a triangular fragment of the anteroinferior margin of the body by the anterior longitudinal ligament Most common at C2 but may occur at any level Fragment may be displaced, distracted, or rotated More common in elderly persons with osteoporosis and spondylosis Usually not associated with any neurologic deficit
Posttraumatic discovertebral injury: lucent annular cleft sign[60]	2-59	May represent instability	Hyperextension most common, but also seen with hyperflexion	Lucent cleft sign, often seen after hyperextension injuries, is believed to represent nitrogen gas accumulating within a traumatic avulsion of the anulus fibrosus from its attachment to the anterior cartilaginous endplate Gas-filled cleft often is accentuated on radiographs taken in extension, can be associated with disc space widening, and may persist for as long as 5 years after trauma Posttraumatic vacuum cleft should not be confused with the more common intradiscal vacuum associated with degenerative disc disease, a condition that usually is accompanied by disc space narrowing, osteophyte formation, and a more extensive and irregular collection of gas

TABLE 2-12 Lower Cervical Spine Injuries—cont'd

Entity	Figure(s), Table(s)	Stability†	Mechanism	Characteristics
Hyperextension fracture-dislocation[46,167]		Unstable	Hyperextension	Injury usually ruptures the anterior longitudinal ligament or intervertebral disc, or, in as many as 65% of patients, may result in avulsion of the anteroinferior corner of the vertebral body Severe hyperextension dislocation produces minimal radiographic findings but profound neurologic deficits In as many as 30% of cases, the only radiographic finding is prevertebral hematoma; in some cases, retrolisthesis is evident Disc space widening can occur, but may be evident only during traction or extension Extension radiographs also may reveal radiolucent annular clefts C5-C6 and C4-C5 most common levels of involvement
Hyperextension sprain[61,62]	2-60, 2-61	Generally considered stable	Hyperextension	Momentary dislocation that does not result in significant disruption of the spinal ligaments, osseous structures, or discs Neurologic damage is sustained, but stability usually is maintained May be impossible to differentiate sprain from reduced dislocation on radiographs Risk of neurologic injury is greater in patients with cervical spondylosis (because of acquired stenosis from osteophytes) and in patients with congenital spinal stenosis Typical neurologic injury is the central cord syndrome caused by hemorrhage in the central gray matter of the cervical cord
Pillar fractures[63,64]	2-62	Stable	Hyperextension and rotation	Unilateral (or, infrequently, bilateral) vertical, oblique, or crushing fracture of the articular process, most common at the C6 and C7 levels Represent 3%-11% of all cervical spine fractures and result in radiculopathy in 6%-39% of patients Special oblique or pillar views often are helpful, but CT or conventional tomography is definitive Normal bilateral asymmetry in the height of the articular pillars may be as great as 3 mm in about 40% of normal persons, and this asymmetric configuration may simulate a fracture
Other vertebral arch fractures[46]		Variable	Compressive hyperextension	Fractures of the pedicles or laminae
C3-C7 burst fracture[65]	2-63	Variable	Axial compression combined with flexion	Comminuted fracture of the vertebral body, usually sustained in motor vehicle accidents and diving injuries Most common at C5, C6, and C7 Vertebral body usually is comminuted; injury often is not associated with cervical kyphosis, interspinous fanning, or facet joint dislocation or subluxation Sagittal fracture line, seen on the anteroposterior view, may be difficult to detect Ligaments usually remain intact Neurologic deficits present in as many as 85% of patients owing to stretching of the cord across the posterior aspect of the vertebral body or compression of the cord by retropulsed fragments

Continued

TABLE 2-12 Lower Cervical Spine Injuries—cont'd

Entity	Figure(s), Table(s)	Stability†	Mechanism	Characteristics
Isolated sagittal fracture of the vertebral body[66]	2-64	Unstable	Axial compression	In this rare type of injury, routine radiography may be unreliable, failing to reveal the vertical fracture even though the patient may be quadriplegic CT is essential in such cases, reliably demonstrating fractures of the vertebral body, and, in most patients, associated posterior element fractures MR imaging is more useful for demonstrating spinal cord injury in these patients
Transverse process fracture[67]	2-65	Stable	Lateral hyperflexion	Uncommon
Uncinate process fracture[67]		Stable	Lateral hyperflexion	Uncommon
Nerve root or brachial plexus avulsion[67]		Variable	Lateral hyperflexion	Uncommon injury, most likely caused by motorcycle accidents and birth trauma Often associated with cervical fracture, dislocation, or both Myelography and CT myelography currently are superior to MR imaging for identifying nerve root avulsions
Lateral wedgelike compression of vertebral body[67]		Stable	Lateral hyperflexion	Uncommon Lateral wedging of vertebral body and its associated lateral mass
Microtrabecular bone injury (bone bruise or contusion)[179,180]		Stable	Variable	Typically invisible on radiographs Detected in 41.8% of spinal injury patients as vertebral body high signal on fluid-sensitive MR images May be observed in the vertebral bodies of contiguous or noncontiguous fractures or other vertebral injuries Some authorities recommend that in patients undergoing MR imaging of an injured spinal segment are better assessed by MR imaging of the entire spine

TABLE 2-13 Radiographic Findings in Hyperflexion Sprain With Posterior Ligament Disruption and Instability[46,160,167] (Figure 2-54)

Finding	Characteristics
Interspinous widening	Widening that is more than 2 mm greater than the interspinous width at both adjacent levels is indicative of instability; definite anterior cervical dislocation is present when the interspinous distance is more than 1.5 times that of both adjacent levels
Localized kyphosis	Focally exaggerated kyphosis is required to make the diagnosis of hyperflexion sprain Kyphosis at a single level measuring more than 11 degrees with persistent lordosis at adjacent levels is indicative of hyperflexion sprain and indicates posterior ligament damage
Posterior disc space widening	Widening of the posterior aspect of the disc space suggests annular disruption
Anterior vertebral displacement	Anterior rotation, or 1-3 mm anterior displacement of the superior vertebra, may be present with posterior ligament disruption
Abnormal movement or alignment on flexion and extension views	If this injury is suspected, clinician-supervised flexion and extension radiographs should be obtained only in alert, cooperative patients who are able to perform these motions actively Abnormal alignment is exaggerated with neck flexion and corrected with neck extension

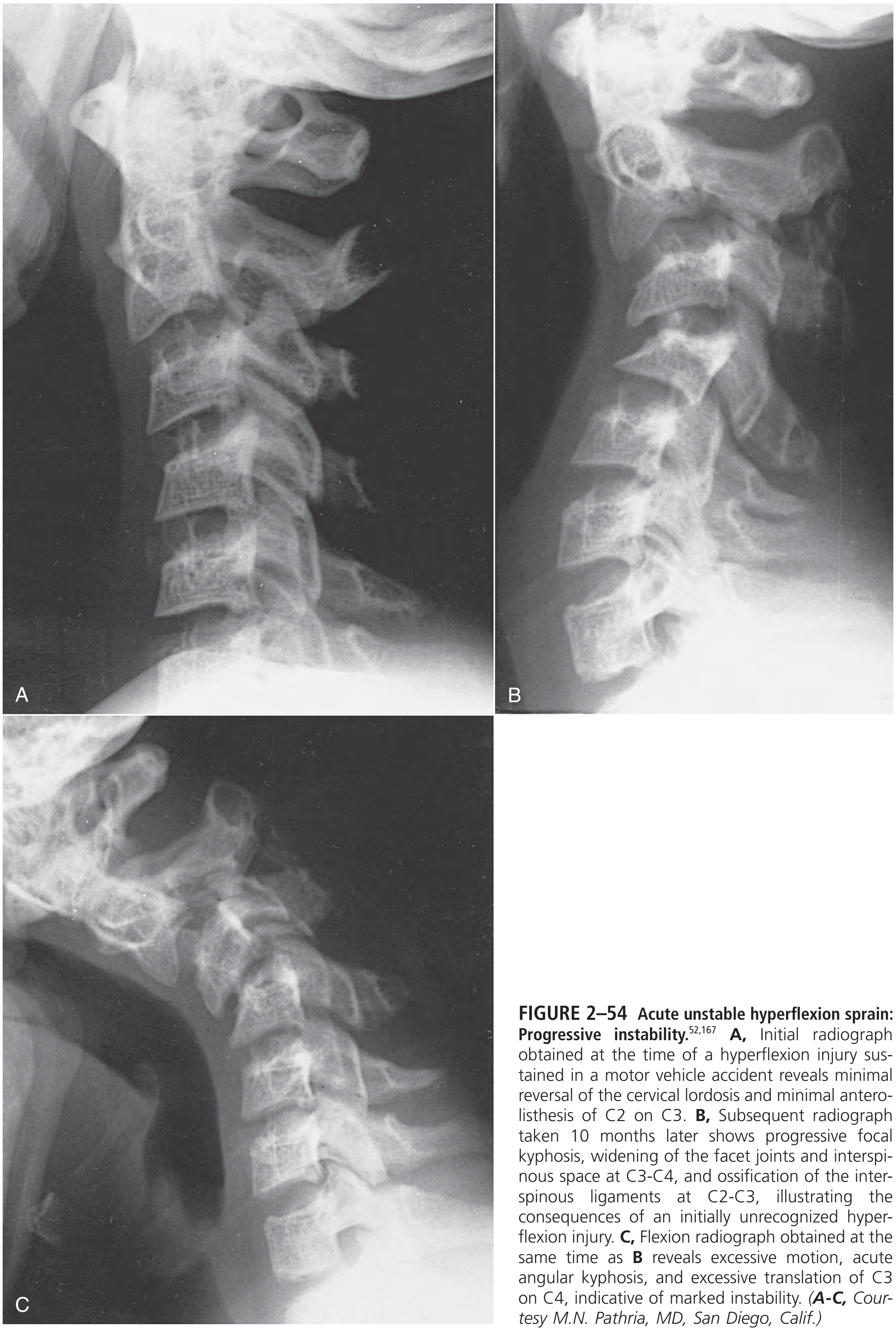

FIGURE 2–54 **Acute unstable hyperflexion sprain: Progressive instability.**[52,167] **A,** Initial radiograph obtained at the time of a hyperflexion injury sustained in a motor vehicle accident reveals minimal reversal of the cervical lordosis and minimal anterolisthesis of C2 on C3. **B,** Subsequent radiograph taken 10 months later shows progressive focal kyphosis, widening of the facet joints and interspinous space at C3-C4, and ossification of the interspinous ligaments at C2-C3, illustrating the consequences of an initially unrecognized hyperflexion injury. **C,** Flexion radiograph obtained at the same time as **B** reveals excessive motion, acute angular kyphosis, and excessive translation of C3 on C4, indicative of marked instability. (***A-C,*** *Courtesy M.N. Pathria, MD, San Diego, Calif.)*

TABLE 2-14 Checklist for the Diagnosis of Clinical Instability in the Middle and Lower Cervical Spine (C3-C7)[172]

Element	Point Value
Anterior elements destroyed or unable to function	2
Posterior elements destroyed or unable to function	2
Positive stretch test	2
Radiographic criteria	4
1. Flexion-extension radiographs a. Sagittal plane translation >3.5 mm or 20% (2 points) b. Sagittal plane rotation >20 degrees (2 points)	
OR	
1. Resting radiographs a. Sagittal plane translation >3.5 mm or 20% (2 points) b. Sagittal plane rotation >20 degrees (2 points)	
Developmentally narrow spinal canal (Sagittal diameter <13 mm or Pavlov's ratio <0.8)	1
Abnormal disc narrowing	1
Spinal cord damage	2
Nerve root damage	1
Dangerous loading anticipated	1

From White AA, Panjabi MM. Clinical Biomechanics of the Spine, 2nd ed. Philadelphia, Lippincott, 1990.
Total of 5 or more = unstable.

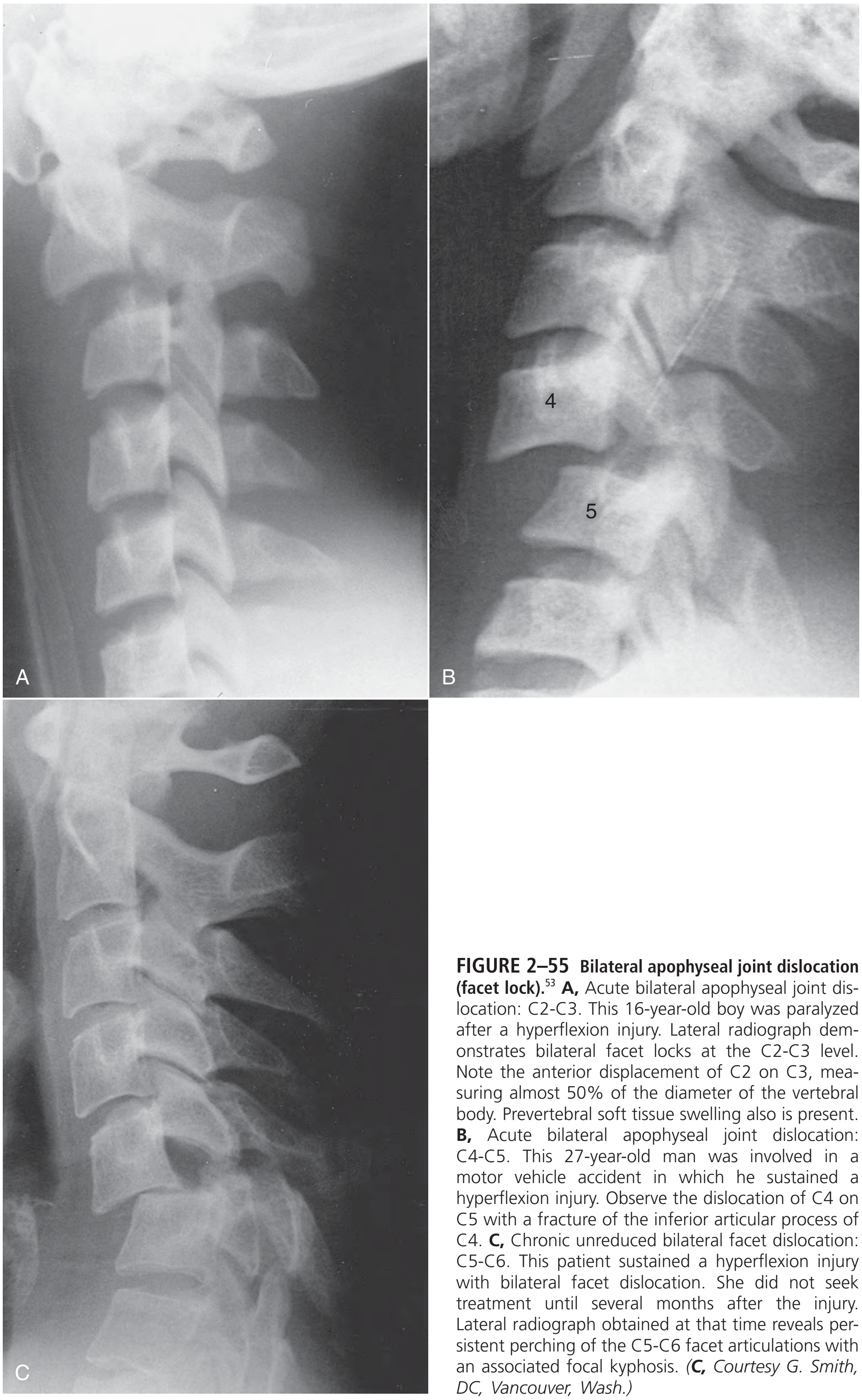

FIGURE 2–55 **Bilateral apophyseal joint dislocation (facet lock).**[53] **A,** Acute bilateral apophyseal joint dislocation: C2-C3. This 16-year-old boy was paralyzed after a hyperflexion injury. Lateral radiograph demonstrates bilateral facet locks at the C2-C3 level. Note the anterior displacement of C2 on C3, measuring almost 50% of the diameter of the vertebral body. Prevertebral soft tissue swelling also is present. **B,** Acute bilateral apophyseal joint dislocation: C4-C5. This 27-year-old man was involved in a motor vehicle accident in which he sustained a hyperflexion injury. Observe the dislocation of C4 on C5 with a fracture of the inferior articular process of C4. **C,** Chronic unreduced bilateral facet dislocation: C5-C6. This patient sustained a hyperflexion injury with bilateral facet dislocation. She did not seek treatment until several months after the injury. Lateral radiograph obtained at that time reveals persistent perching of the C5-C6 facet articulations with an associated focal kyphosis. (***C,** Courtesy G. Smith, DC, Vancouver, Wash.)*

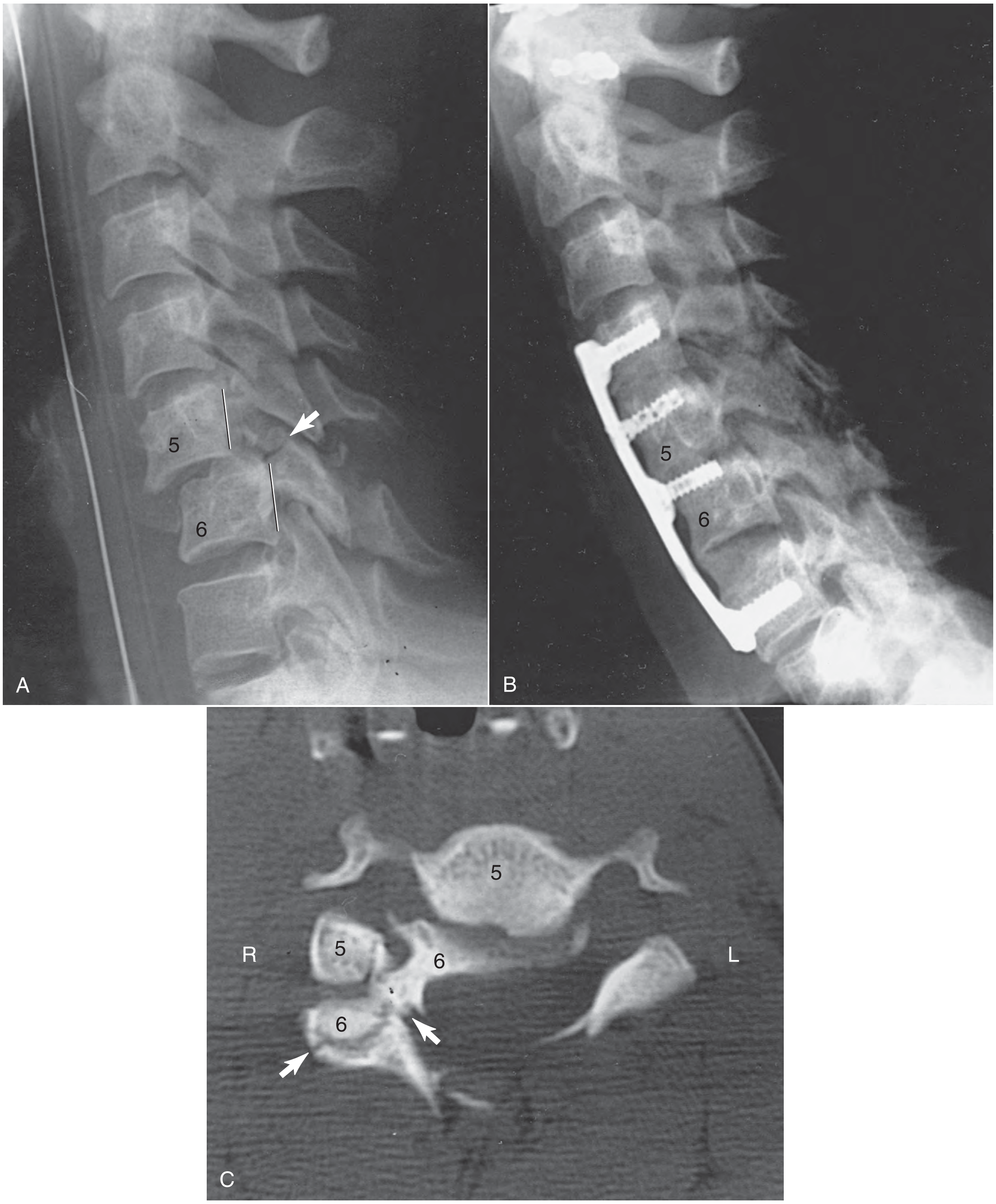

FIGURE 2–56 Unilateral apophyseal joint dislocation with articular process fracture.[54-56] **A,** Lateral radiograph obtained immediately after injury shows 7-mm anterior displacement of C5 on C6, malalignment of the C5-C6 facet joints, and a fracture *(arrow)* of the C6 superior articular process. **B,** Lateral radiograph obtained after surgery demonstrates improved alignment and anterior cervical fusion with a fixation plate and cannulated screws. **C,** Transaxial preoperative CT image shows the abnormal anatomic relationship of C5 and C6. The right C6 facet is seen dislocated in a position posterior to the C5 facet, which is perched (locked) anterior to its C6 counterpart. The body of C5 is rotated anteriorly on the right relative to the body of C6. A complex fracture of the C6 articular process *(arrows)* also is evident. *(Courtesy M.N. Pathria, MD, San Diego, Calif.)*

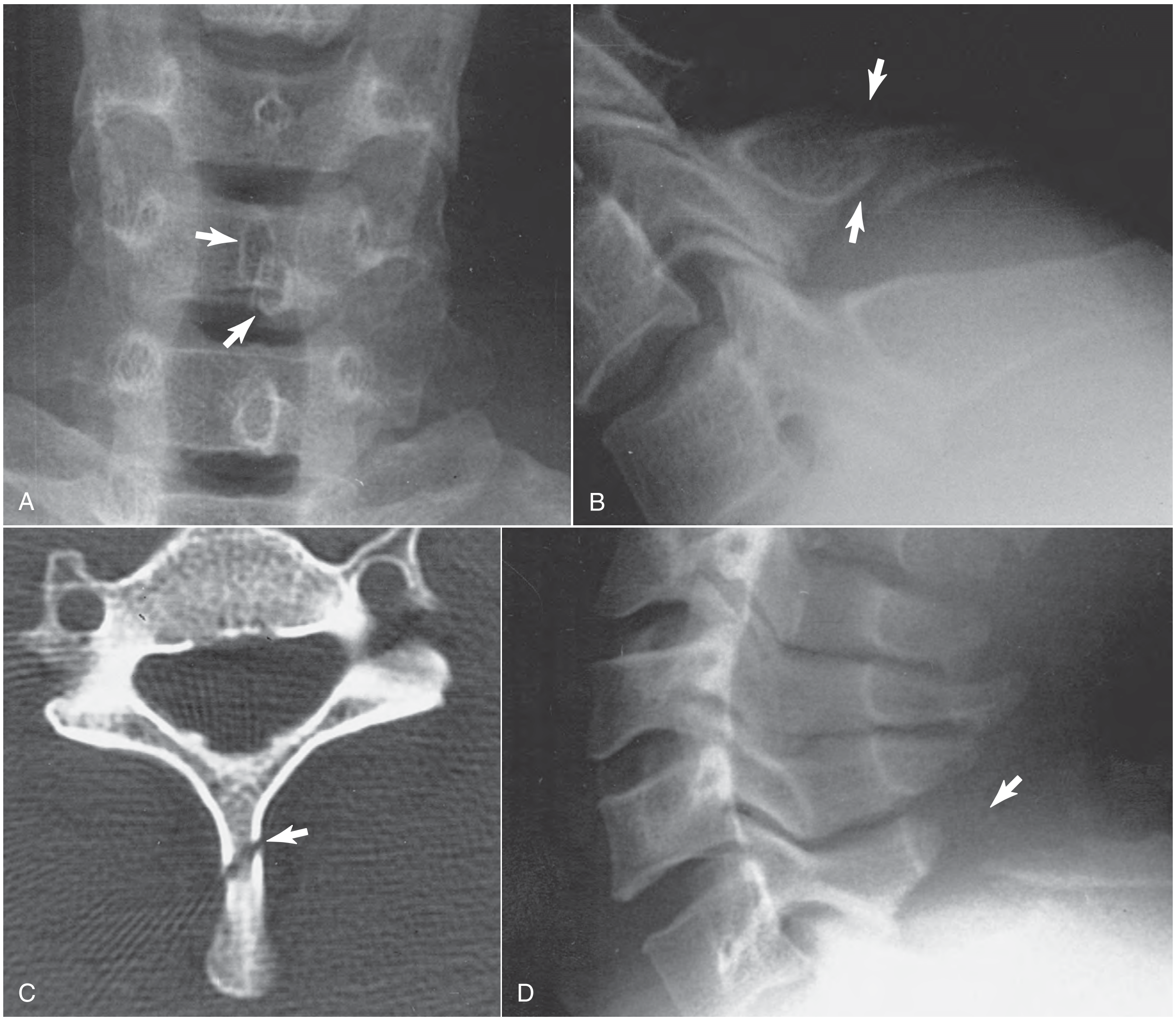

FIGURE 2–57 **Spinous process fractures.**[46,57] **A-C,** This 24-year-old man had a hyperflexion injury (clay-shoveler's fracture). **A,** Anteroposterior radiograph shows a double spinous process sign, which relates to simultaneous visualization of the fractured base and the caudally displaced tip of the spinous process *(arrows).* **B,** Lateral radiograph shows an oblique fracture of the tip of the C7 spinous process *(arrows)* with characteristic inferior displacement of the fracture fragment. **C,** Transaxial CT image shows the fracture confined to the spinous process *(arrow),* with minimal displacement and an otherwise intact neural arch. **D,** Hyperextension injury. This 22-year-old man suffered a hyperextension injury. Observe the fracture of the C7 spinous process *(arrow)* caused by forceful impaction of the posterior elements.

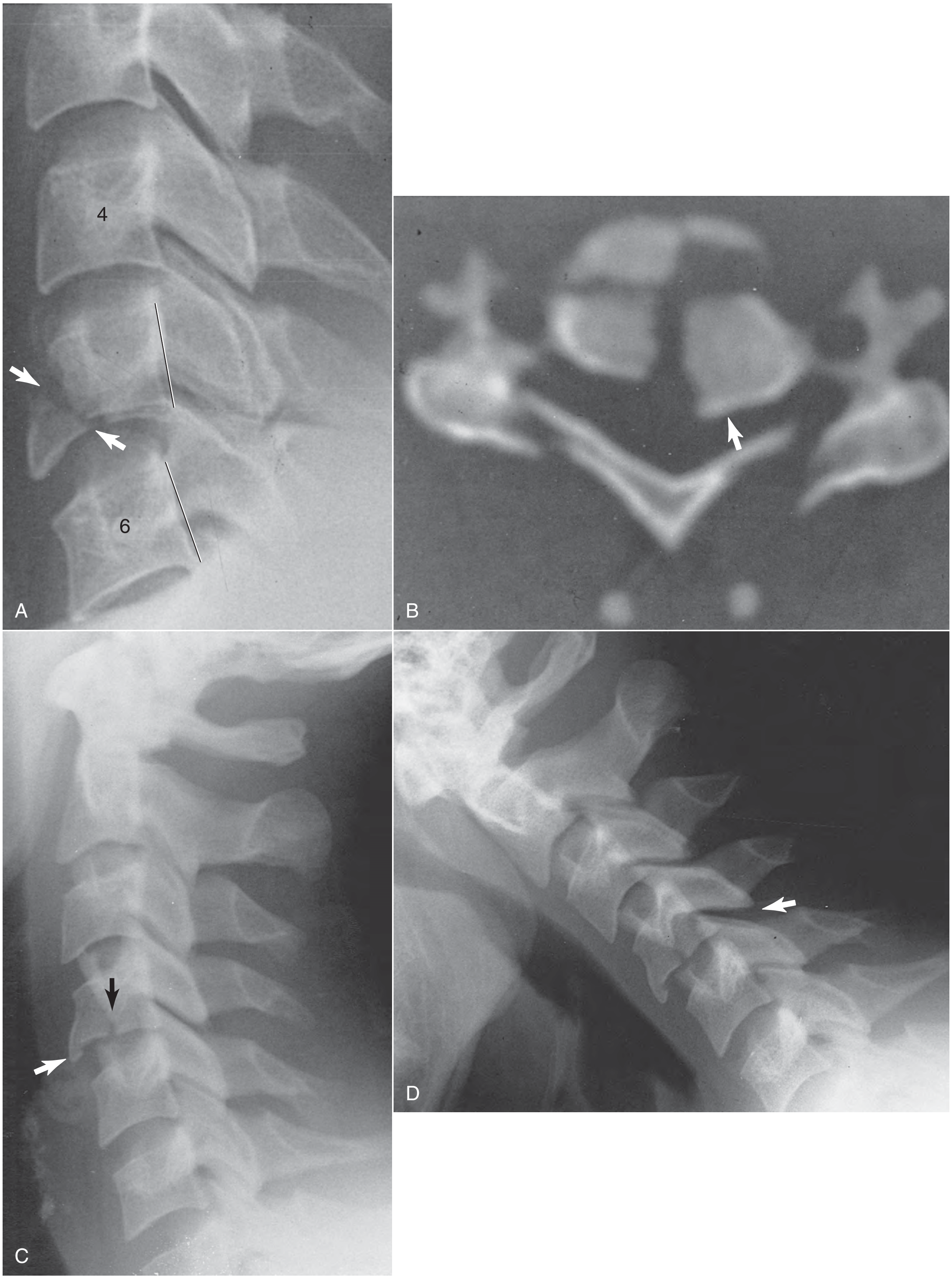

FIGURE 2–58 Flexion teardrop fractures.[58] **A-B,** Lateral cervical radiograph **(A)** shows a triangular fracture of the anteroinferior margin of the C5 vertebral body *(arrows).* Slight retrolisthesis of C5 also is seen (note the posterior body lines of C5 and C6). Transaxial CT image **(B)** reveals comminution of the C5 vertebral body. The principal injury seen on the CT scan is a stellate, vertical fracture with coronal and sagittal components. Retropulsion of one of the osseous fragments *(arrow)* resulting in central stenosis is evident on the CT image but is imperceptible on the radiograph. **C-D,** In another patient, the routine lateral cervical radiograph **(C)** shows a triangular fracture of the anteroinferior margin of the C5 vertebral body *(white arrow)* and a vertical fracture of the vertebral body *(black arrow).* A flexion radiograph **(D)** obtained before full evaluation of the neutral lateral radiograph shows excessive facet gapping *(white arrow)* and an increase in the interspinous space, both of which indicate ligamentous instability.

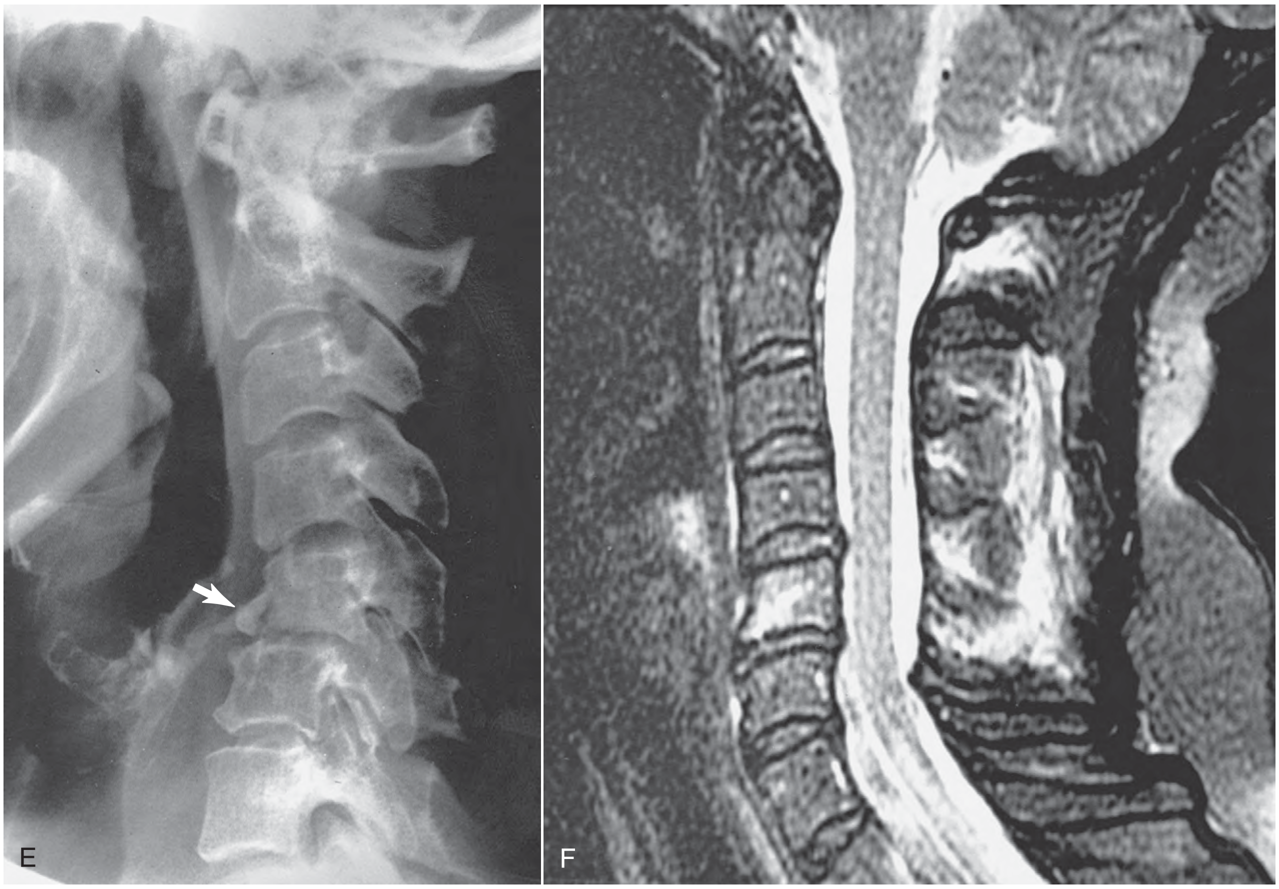

FIGURE 2–58, cont'd **E-F,** This 57-year-old woman was involved in a motor vehicle accident. In **E,** a lateral radiograph shows a triangular fracture of the anteroinferior corner of the C5 vertebral body *(arrow).* Acute angular kyphosis, posterior body displacement, and a suggestion of widened facet joints are evident. In **F,** a sagittal T2-weighted (TR/TE, 2857/96 Ef) fast spin echo MR image demonstrates high signal intensity within the vertebral body and the spinal ligaments posteriorly, consistent with edema or hemorrhage, or both. *(**A-D,** Courtesy M.N. Pathria, MD, San Diego; **E-F,** Courtesy D. Goodwin, MD, Hanover, NH.)*

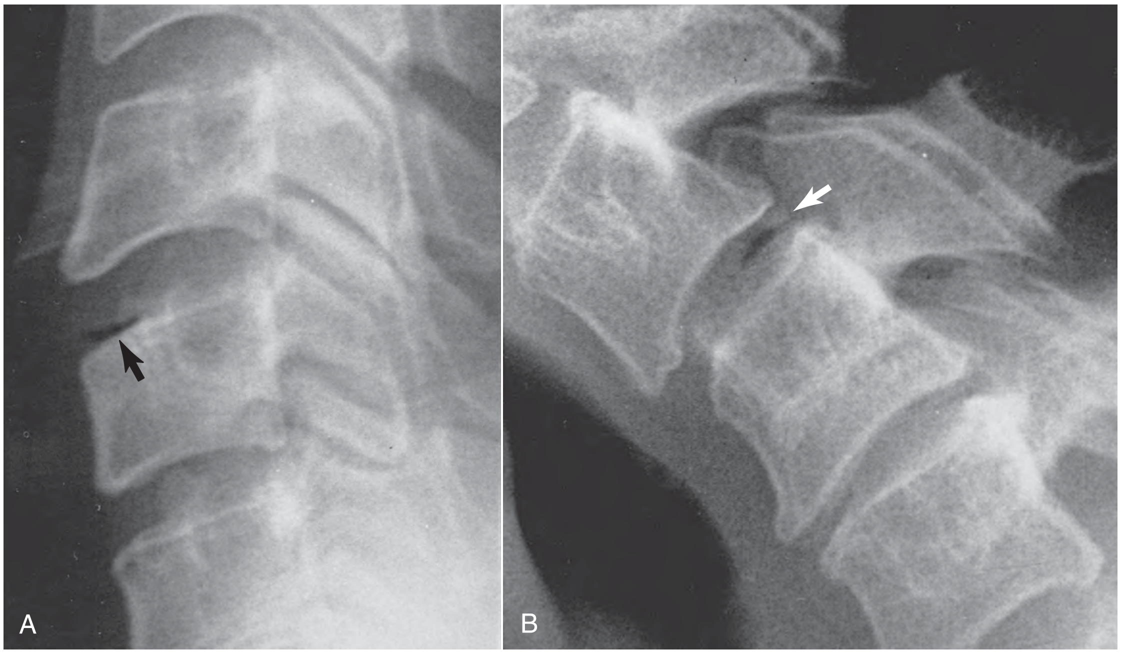

FIGURE 2–59 **Posttraumatic discovertebral injury: lucent annular cleft sign.**[60] **A,** Hyperextension injury. Lateral radiograph shows a linear collection of gas within the annular fibers of the intervertebral disc adjacent to the vertebral endplate. The lucent cleft sign *(arrow),* often seen after hyperextension injuries, is believed to represent traumatic avulsion of the anulus fibrosus from its attachment to the anterior cartilaginous endplate. **B,** Hyperflexion injury. Observe the gas density within the posterior portion of the C4-C5 disc *(arrow)* on this lateral radiograph obtained in flexion. This patient was recently involved in a rear-end impact motor vehicle collision and had severe neck pain. *(Courtesy M.N. Pathria, MD, San Diego, Calif.)*

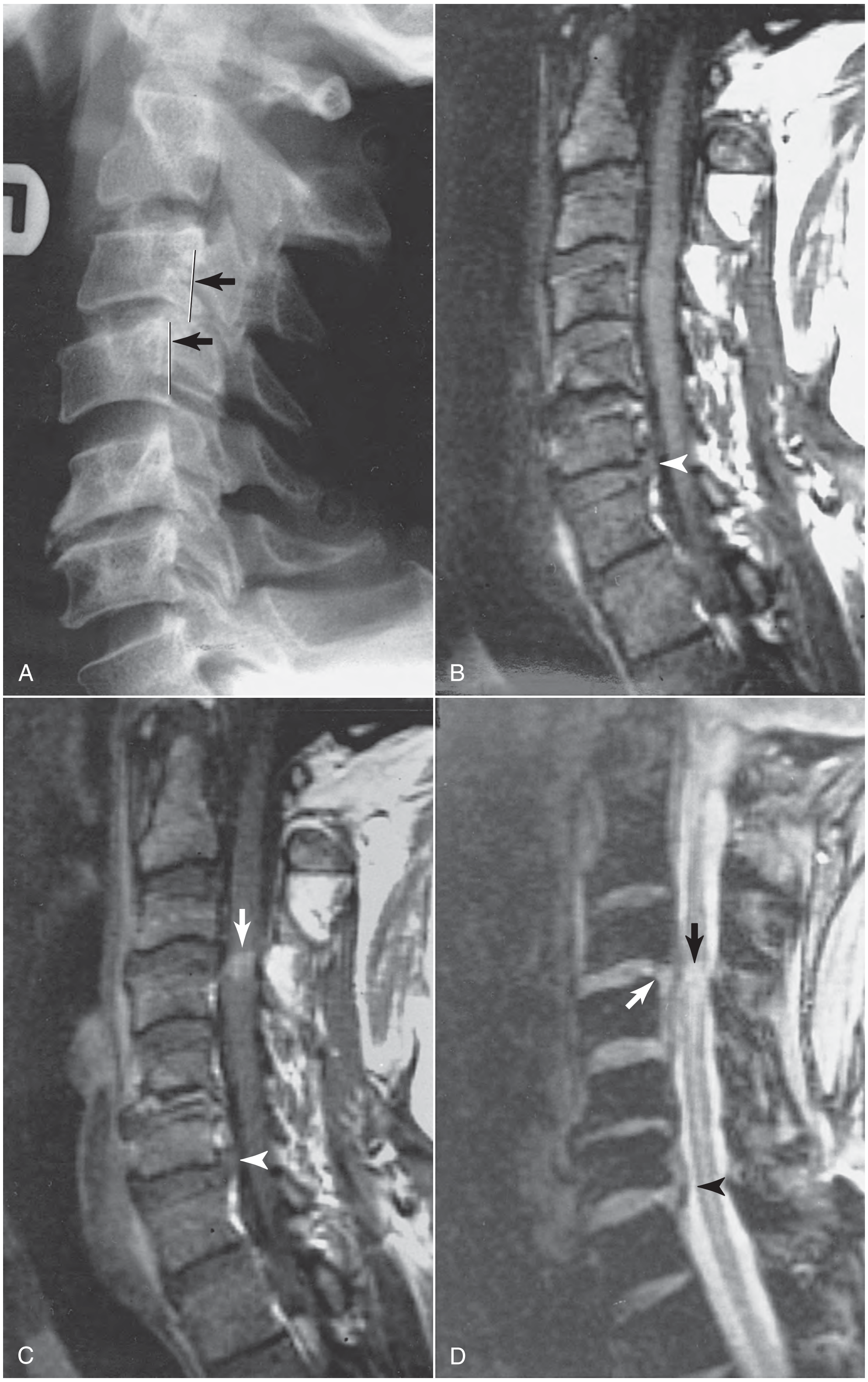

FIGURE 2–60 **Acute hyperextension sprain.**[61,62] This 51-year-old man sustained a hyperextension injury in a motor vehicle collision. He developed persistent neurologic signs and symptoms. **A,** Lateral radiograph. Observe the 5 mm of retrolisthesis of the C3 vertebral body relative to that of C4 *(arrows)*. C5-C6 degenerative spondylosis also is seen. **B-C,** Sagittal T1-weighted (TR/TE, 600/20) fat-suppressed spin echo MR images before **(B)** and after **(C)** intravenous gadolinium administration. The postgadolinium image shows enhancement (high signal intensity) of the injured spinal cord at the C3-C4 level *(white arrow)* not seen on the pregadolinium image. **D,** Sagittal (TR/TE, 600/17) gradient echo MR image also demonstrates a high signal intensity focus representing spinal cord contusion *(black arrow)*. Disc herniations are seen at C6-C7 *(arrowheads)* on all MR imaging sequences and at C3-C4 on the gradient echo image **(D)** *(small white arrow)*. *(Courtesy M.N. Pathria, MD, San Diego, Calif.)*

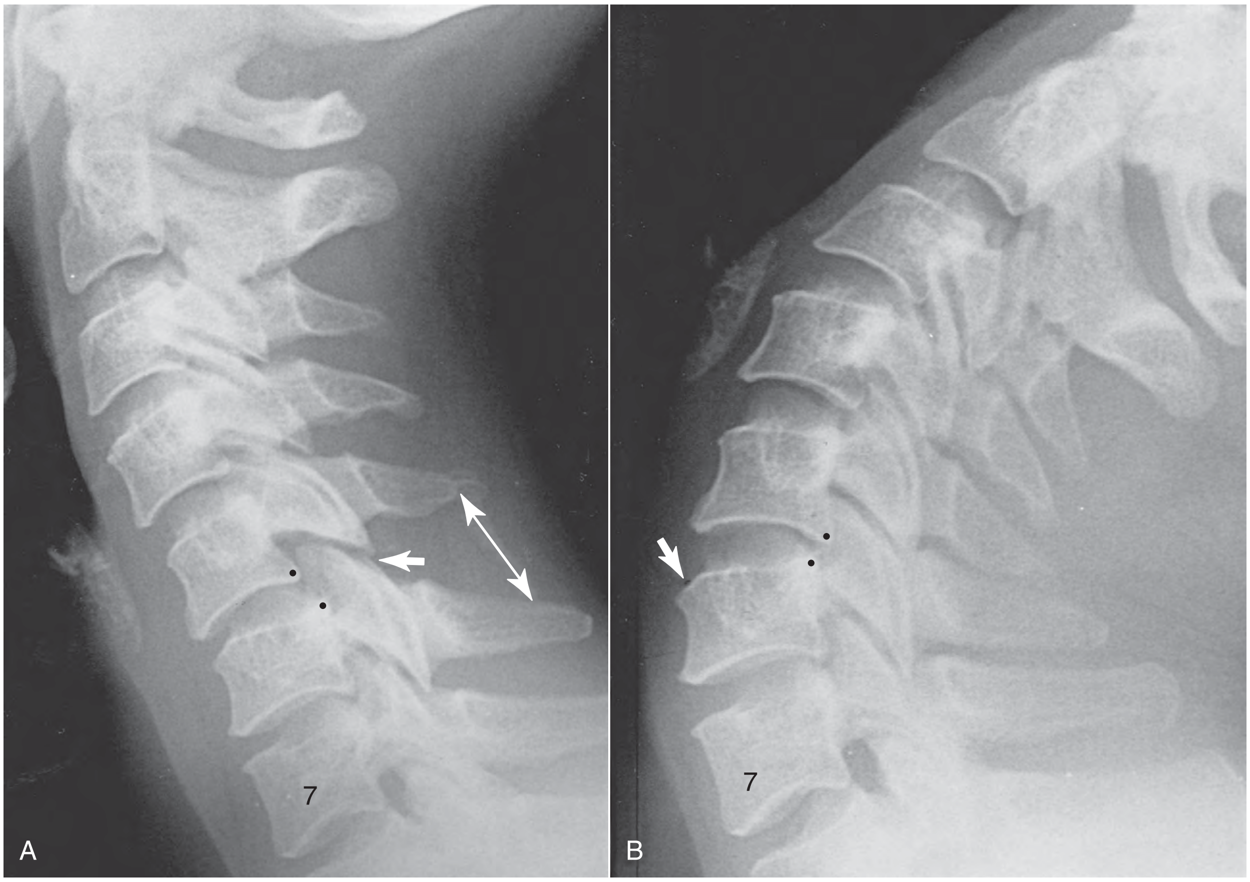

FIGURE 2–61 **Hyperflexion-hyperextension sprain: Segmental instability.**[61,62] This 26-year-old woman had severe neck and radiating arm pain after a rear-end automobile collision. **A,** Neutral lateral radiograph shows a reversal of the normal cervical lordosis, separation of the spinous processes *(double-headed arrow)* and facet joints *(small arrow),* and widening of the posterior C5-C6 intervertebral disc space *(black dots).* **B,** Lateral radiograph obtained during neck extension reveals 5 mm of posterior translation of the C5 vertebral body in relation to the C6 vertebral body *(black dots).* A small radiolucent vacuum cleft *(white arrow),* not well visualized on this reproduction, is present within the anterior fibers of the C5-C6 intervertebral disc. Excessive intersegmental motion and intradiscal vacuum cleft are indicative of segmental instability.

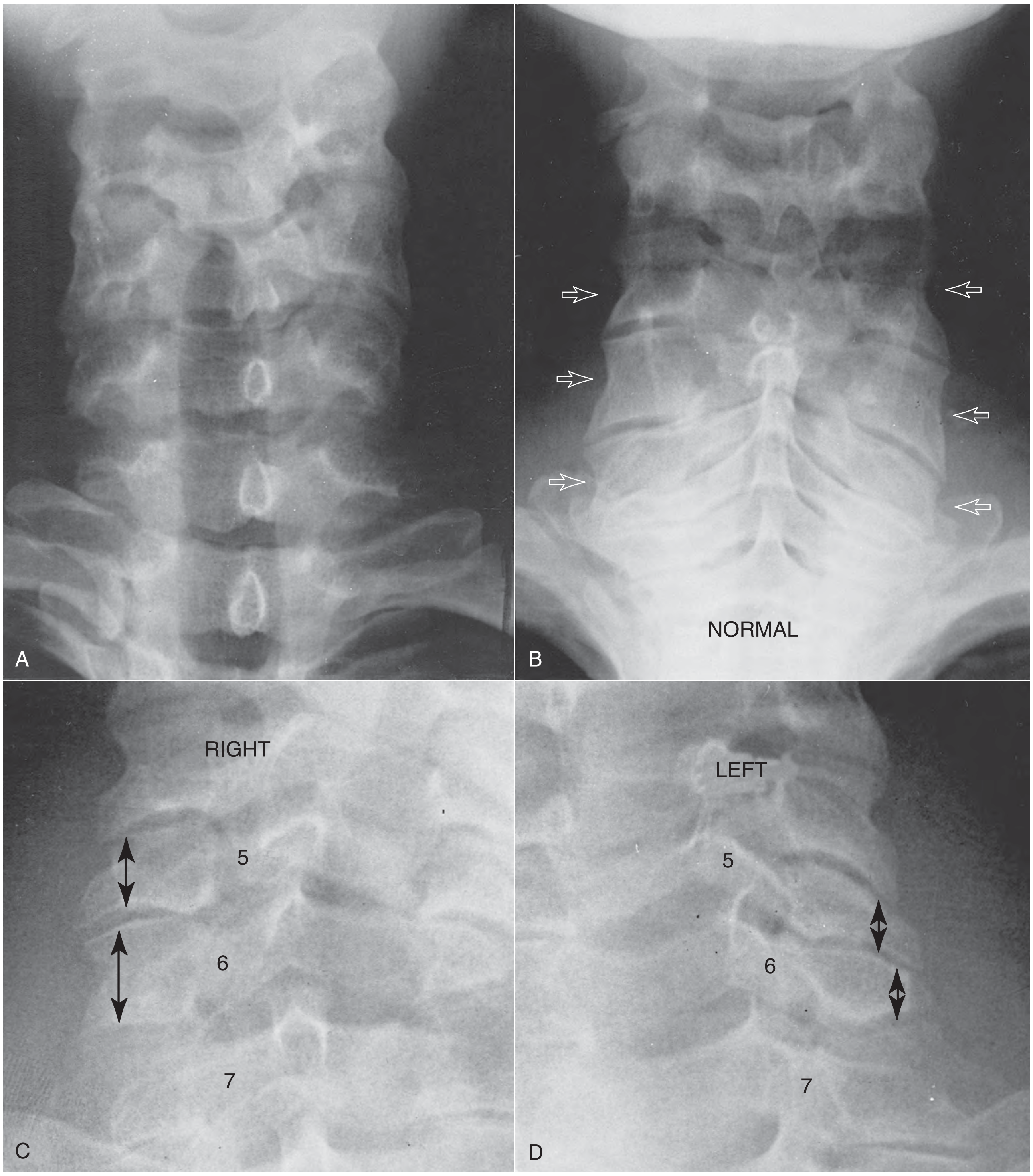

FIGURE 2–62 Pillar fracture: value of pillar views.[63,64] **A,** Normal anteroposterior projection. The articular processes are not well visualized. **B,** Normal anteroposterior pillar projection. The pillar radiograph is obtained using caudal tube angulation such that the beam is oriented along the plane of the facet joint, usually about 35 degrees caudally. Observe the symmetric and aligned articular processes, one on top of the other *(open arrows)*. **C-D,** This patient sustained a hyperextension-rotation injury compressing the left articular pillars. In **C,** the frontal pillar radiograph taken with left rotation. In **D,** the frontal pillar radiograph taken with right rotation. These radiographs reveal vertical compression of the left C5 and C6 articular processes *(double-headed arrows)*.

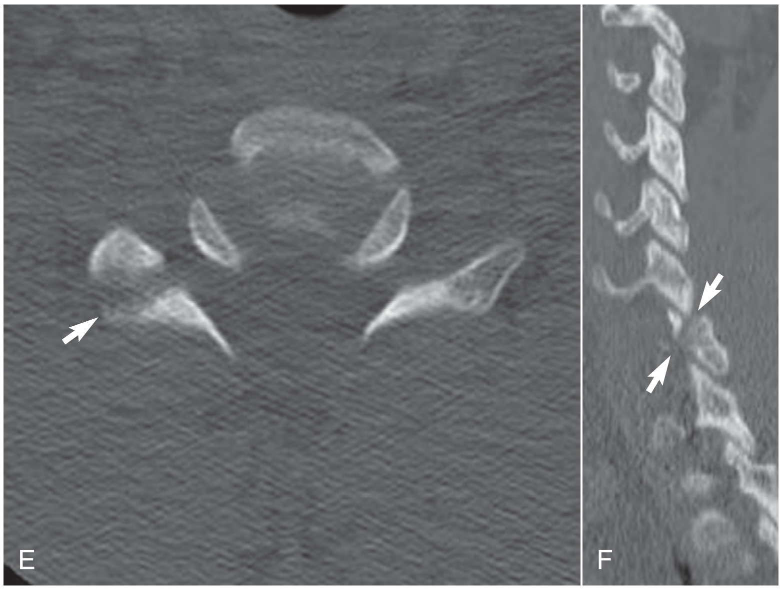

FIGURE 2–62, cont'd CT examination in the axial **(E)** and sagittal **(F)** planes clearly depicts a pillar fracture of the right C7 articular process (*arrows*) in another patient. The majority of pillar fractures occur at C4 through C7, with C6 involved in approximately 40% of cases. It should be noted that 2 to 3 mm of asymmetry in height of the articular processes is present in over 45% of normal persons and may lead to false-positive diagnoses. *(**C-D,** Courtesy T. Hall, DC, Central Point, Ore.)*

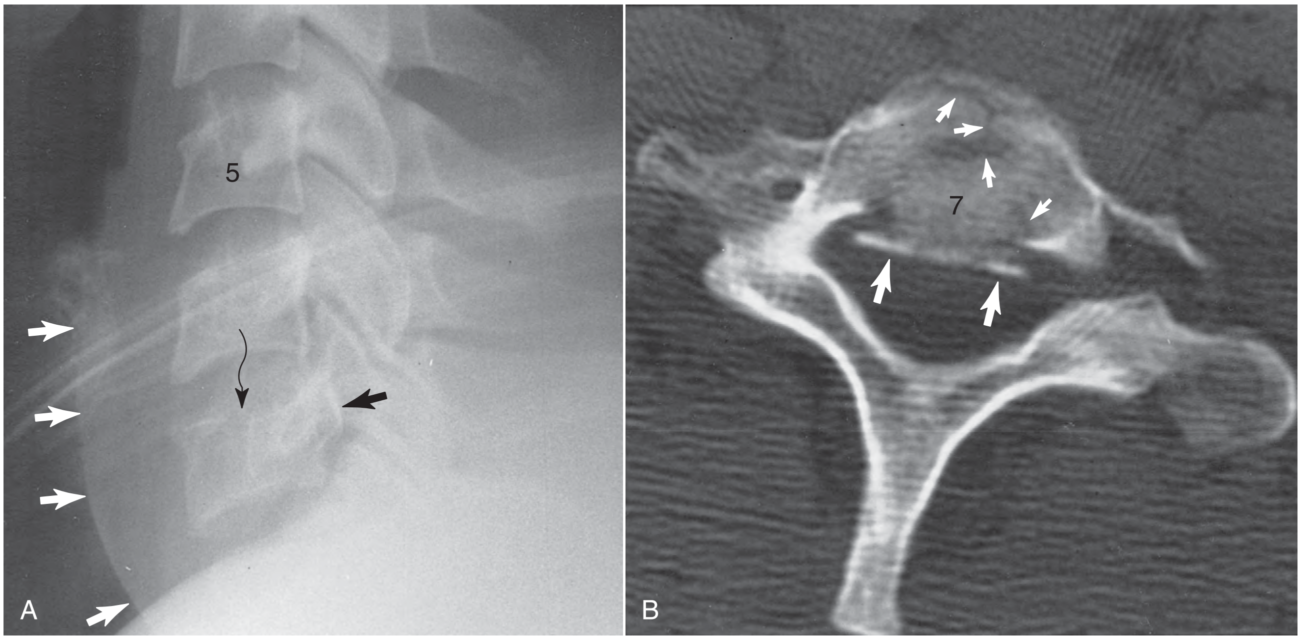

FIGURE 2–63 **Burst fracture.**[65] This 22-year-old man dove into a shallow pool. **A,** Lateral radiograph shows loss of height of the C7 vertebral body, retropulsion of the posterior body margin into the spinal canal *(black arrow),* a vertical fracture through the endplate *(wavy arrow),* and prevertebral soft tissue swelling *(white arrows).* **B,** Transaxial CT image through the C7 vertebral body shows the retropulsed bone fragment *(large white arrows),* resulting in canal stenosis. Comminution of the vertebral body also is noted *(small white arrows).* Burst fractures of the cervical spine typically are sustained in motor vehicle collisions and diving injuries and result in neurologic deficits in about 85% of patients. *(Courtesy M.N. Pathria, MD, San Diego, Calif.)*

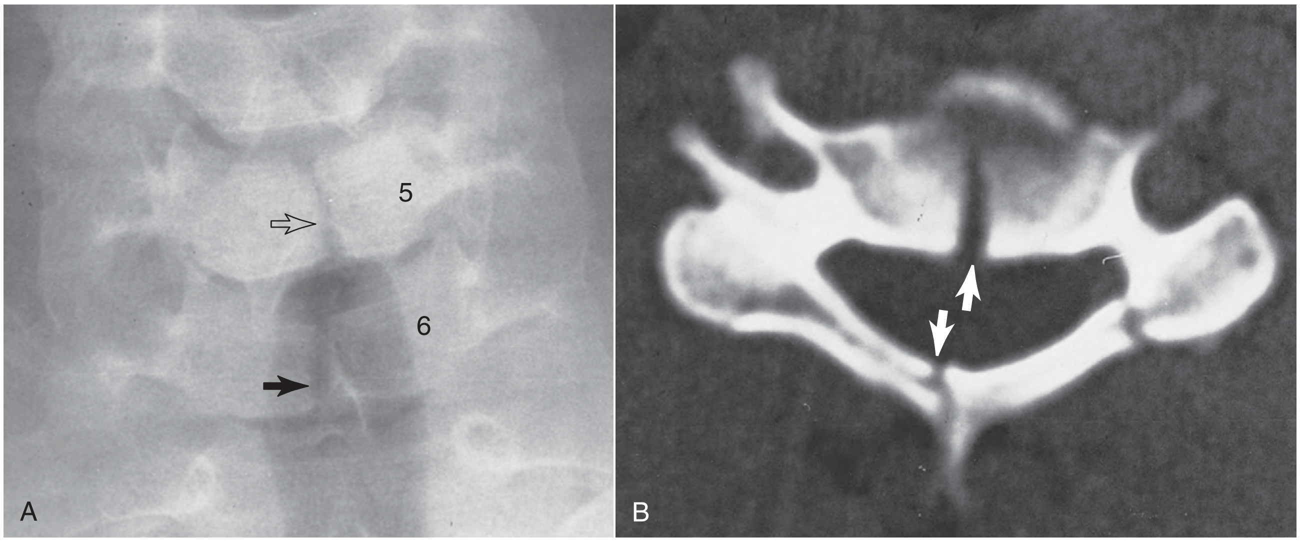

FIGURE 2–64 **Axial compression injury: sagittal fracture of C6 vertebral body.**[66] This 23-year-old man dove into shallow water. Although he was quadriplegic immediately after the injury, he regained motor function of his arms and left leg, but pain and temperature sensation deficit persisted on his left side. Vibration and position sense remained intact. **A,** Routine anteroposterior radiograph shows minimal compression and a vertical split in the vertebral body of C6 *(arrow).* The radiolucent vertical line *(open arrow)* through the C5 vertebral body represents the normal contracted larynx. **B,** Transaxial CT scan shows the vertical fracture extending through the vertebral body and the neural arch *(arrows).*

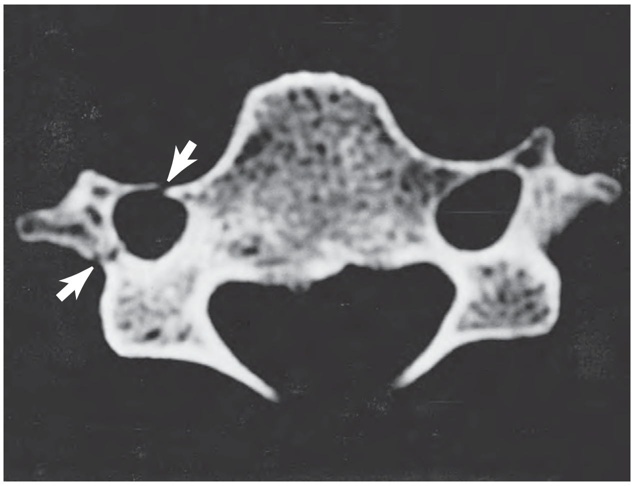

FIGURE 2–65 **Isolated transverse process fracture.**[67] This 34-year-old man was involved in a side-impact motor vehicle collision. He experienced anterolateral neck pain that failed to respond to conservative care. Routine radiographs (not shown) were normal. Transaxial CT image reveals a nondisplaced fracture across the transverse foramen and through both the anterior and posterior tubercles of the right transverse process of C4 *(arrows).* The patient experienced no signs or symptoms related to vertebral artery injury, and he had an uneventful recovery. *(Courtesy M.A. Hubka, DC, San Diego, Calif.)*

TABLE 2-15 Cervical Spine: Articular Disorders*

			Target Sites of Involvement			
Entity	**Figure(s) Table(s)**	**Characteristics**	**Occiput, C1, C2**	**C2-C7 Discovertebral Joints**	**C2-C7 Apophyseal Joints**	**C3-C7 Uncovertebral Joints**
Degenerative and Related Disorders						
Degenerative disc disease[6,68-70,173]	2-66, 2-67, Table 2-20	***Spondylosis deformans*** Osteophytes and osseous ridging Subchondral bone sclerosis		++		
		Intervertebral osteochondrosis Disc space narrowing Intradiscal vacuum phenomenon Disc calcification (rare) Frequently contributes to foraminal stenosis		++		
Osteoarthrosis or arthrosis[71-73,173]	2-67, 2-68	***Uncovertebral joint arthrosis*** Sclerosis, hypertrophy, and joint space narrowing				++
	2-69, 2-70	***Apophyseal (facet) joint osteoarthrosis*** Sclerosis, hypertrophy, and joint space narrowing Subluxation, capsular laxity, and synovial cysts may be present	++		++	
	2-71	***Degenerative spondylolisthesis*** Nonspondylolytic spondylolisthesis complicating degenerative disease Involves midcervical to lower cervical segments		+	+	
Idiopathic childhood disc calcification[74]	2-72	Cause unknown Boys = girls; 6-10 years of age Disc calcification may be associated with disc displacement C4-C7 levels involved most frequently; multiple discs affected in about 33% of cases Symptoms (including pain, stiffness, limitation of motion, dysphagia, torticollis) present in 75% of affected children and resolve within a few days to weeks Calcification usually disappears within months May lead to neurologic findings		++		
Diffuse idiopathic skeletal hyperostosis (DISH)[75]	2-73	*Flowing anterior hyperostosis:* prominent sheet of ossification on anterior aspect of spine High rate of occurrence of ossification of the posterior longitudinal ligament		++		

---

* See also Tables 1-7 to 1-11 and Table 1-19.

Continued

TABLE 2-15 Cervical Spine: Articular Disorders—cont'd

			Target Sites of Involvement			
Entity	**Figure(s) Table(s)**	**Characteristics**	**Occiput, C1, C2**	**C2-C7 Discovertebral Joints**	**C2-C7 Apophyseal Joints**	**C3-C7 Uncovertebral Joints**
Ossification of the posterior longitudinal ligament (OPLL)[76,151,152]	2-74	Occurs with increased frequency in patients with DISH Male:female, 2 : 1; most common in persons older than 50 years of age ***Clinical findings*** May be asymptomatic or may exhibit paresthesia, weakness, incoordination, incontinence, or loss of libido Cord signs (56% of symptomatic patients) Segmental signs (16% of cases) Neck, arm, shoulder pain (28% of cases) Symptoms vary according to thickness of ossification ***Imaging findings*** Segmental or continuous vertical sheet of ossification, as much as 1-5 mm thick, extending along the posterior margins of the vertebral bodies and discs within the spinal canal				
Inflammatory Disorders						
Rheumatoid arthritis (adult)[78,79,161-163]	2-75 2-76	Cervical spine involvement occurs in more than half of patients with rheumatoid arthritis ***Upper cervical spine findings*** Atlantoaxial instability and subluxation seen in 20%-25% of patients; associated potential spinal cord compression exacerbated on flexion Odontoid erosion and fracture Apophyseal joint erosion, sclerosis, and fusion ***Lower cervical spine findings*** Subaxial subluxation Apophyseal joint erosion, sclerosis, and fusion Intervertebral disc space narrowing Erosion and sclerosis of vertebral body margins Spinous process erosion Osteoporosis Absence of osteophytes and other osseous outgrowths	++ Instability	++	++	++

Juvenile idiopathic arthritis (juvenile chronic arthritis or juvenile rheumatoid arthritis)[80,81,145,146,153]	2-77, 2-78	Widespread discovertebral erosions and disc space narrowing Joint laxity with subluxation Odontoid erosions Diffuse apophyseal joint ankylosis Hypoplastic vertebral bodies at levels of apophyseal joint ankylosis Discs may be hypoplastic and calcified Higher incidence of atlantoaxial instability, facet joint ankylosis observed in patients with arthritis mutilans of hands	++ Instability Evident in up to 28% of patients[153]	++	++	++
Ankylosing spondylitis and enteropathic arthropathy[82,83,148-150,181,182]	2-79, 2-80	Widespread marginal syndesmophytes, osteitis, disc calcification, osteoporosis, squaring of vertebral bodies, and disc ballooning Discovertebral and apophyseal joint erosion and eventual ankylosis Ossification of ligaments, joint capsules, and outer annular fibers Odontoid erosions and atlantoaxial instability Cervical spine in ankylosing spondylitis is especially susceptible to fractures that may result in neurologic injury and even death; these typically affect the lower cervical spine and occur chiefly as a result of hyperextension injuries Ulcerative colitis and regional ileitis are the most common inflammatory bowel diseases to result in enteropathic arthropathy; identical skeletal findings as those in ankylosing spondylitis	++ Instability in 1%-2% of patients	++	++	++
Psoriatic spondyloarthropathy and reactive arthritis[84,85,181,182]	2-81, 2-82, 2-83	Nonmarginal paravertebral ossification Apophyseal joint narrowing, sclerosis, bony ankylosis, atlantoaxial subluxation Cervical spine changes more common in psoriasis than in reactive arthritis (Reiter syndrome)	++ Instability	++	++	

Continued

TABLE 2-15 Cervical Spine: Articular Disorders—cont'd

			Target Sites of Involvement			
Entity	**Figure(s) Table(s)**	**Characteristics**	**Occiput, C1, C2**	**C2-C7 Discovertebral Joints**	**C2-C7 Apophyseal Joints**	**C3-C7 Uncovertebral Joints**
SAPHO syndrome[176,177,181]		***Clinical findings*** Syndrome consists of (S) synovitis, (A) acne, (P) pustulosis, (H) hyperostosis, and (O) osteitis Some authorities include sternocostoclavicular syndrome and recurrent multifocal osteomyelitis as part of the SAPHO syndrome ***Imaging findings*** Vertebral body osteosclerosis, hyperostosis Paravertebral ossification Discovertebral lesions Osseous outgrowths resembling nonmarginal syndesmophytes Vertebral collapse May simulate infection, malignancy, or other spondyloarthropathies		++		
Crystal Deposition Disorders						
Calcium pyrophosphate dihydrate crystal deposition disease[86,87]	2-84	Widespread secondary degenerative disease Disc space narrowing and chondrocalcinosis of the anulus fibrosus, joint capsules, apophyseal joints, and articular cartilage	++ Instability	++	+	
Retropharyngeal calcific tendinitis (calcium hydroxyapatite crystal deposition)[88,136,144]	2-85	*Calcific tendinitis:* amorphous collection of calcification within the longus colli muscle and tendon seen anterior to the C2 vertebral body May be asymptomatic or result in painful swallowing, fever, occipital pain, and neck rigidity Symptoms are self-limited, usually resolving within 2 weeks Infrequently, such crystals are deposited in ligamentum flavum in older patients				
Gout[89,156]	2-86	Rare involvement of spine Prominent disc space narrowing and erosion of subchondral endplate May involve posterior elements and facet joints Tophaceous involvement may result in erosions that may calcify	+	+		

Alkaptonuria[90]	2-87	Widespread and severe disc space narrowing and diffuse anulus fibrosus calcification Intradiscal vacuum phenomenon Osseous bridging may resemble marginal syndesmophytes Eventual progression to bamboo spine	++			
Miscellaneous Disorders						
Neuropathic osteoarthropathy[77]		Widespread discovertebral and zygapophyseal joint destruction May resemble infectious spondylodiscitis Joint collapse, bone fragmentation, and kyphosis Syringomyelia, diabetes mellitus, and tabes dorsalis often affect the spine; most frequently affects the thoracolumbar region		++	+	
Pyogenic spondylodiscitis[91-93,138,170,174]	2-88, 2-89 Table 2-16	Up to 21-day latent period before radiographic changes appear Initially involves disc and adjacent vertebral body Severe monoarticular disc space narrowing that eventually may spread to adjacent levels Obliteration of vertebral endplate and vertebral collapse in late stages Paravertebral soft tissue mass or abscess	+ Instability	++	+ (late)	+
Tuberculous spondylodiscitis[94,174]	2-90	Usually involves thoracolumbar region Typically begins in the anterior vertebral body and spreads to the disc Rare involvement of neural arch Slower process than pyogenic infection	++ Instability	++	+	+
Dialysis spondyloarthropathy[95,165]	2-91	Seen in patients on long-standing hemodialysis May be related to amyloid deposition or, less commonly, calcium hydroxyapatite or calcium oxalate crystal deposition in disc Discovertebral joint erosions resembling those of infectious spondylodiscitis, neuropathic osteoarthropathy, and calcium pyrophosphate dihydrate crystal deposition disease on radiographs and MR imaging Disc space narrowing, erosion, and sclerosis of vertebral endplates Progression most influenced by duration of hemodialysis		++		

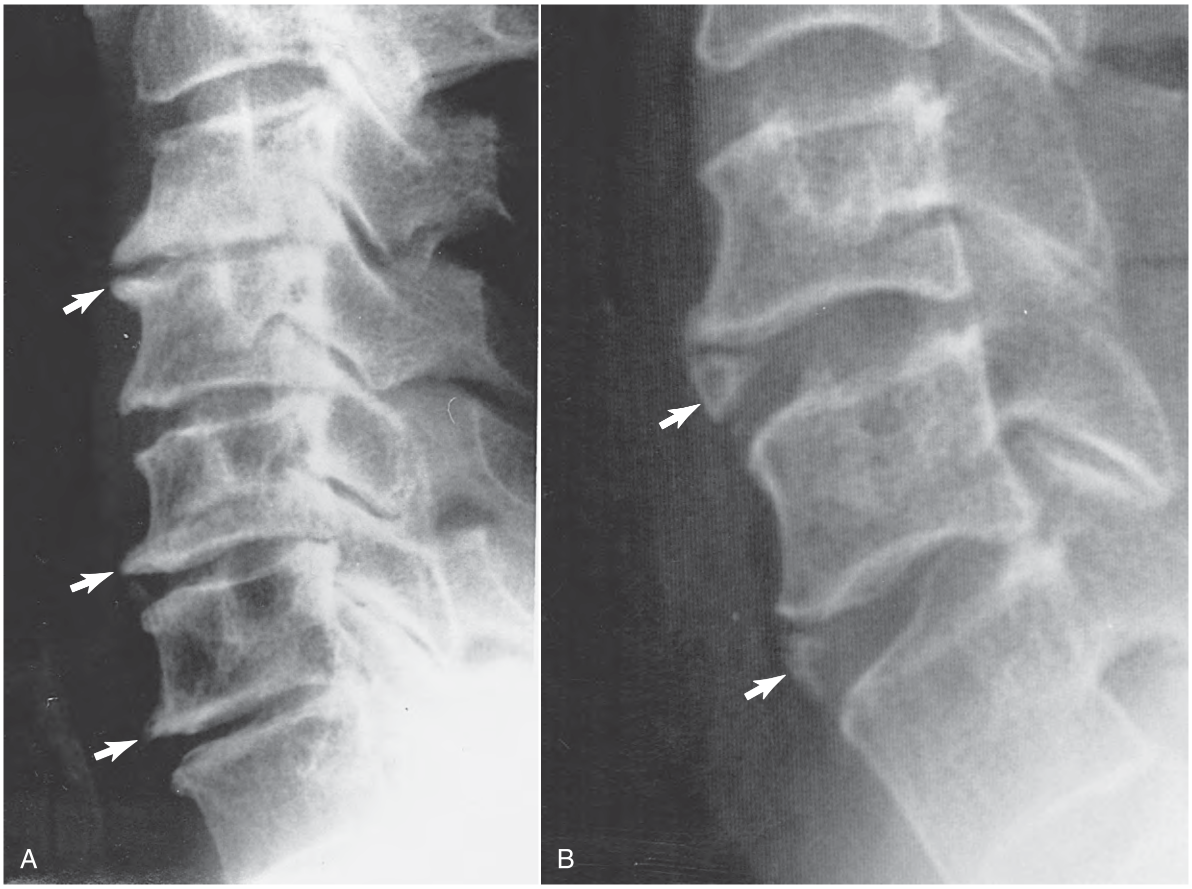

FIGURE 2–66 **Degenerative spine disease.**[6,68-70,157,173] **A,** Widespread disc space narrowing is associated with prominent osteophytes *(arrows)* and vertebral endplate sclerosis. Observe also the narrowing of the apophyseal joints and sclerosis of the articular facet surfaces. **B,** In another patient, small, triangular, well-corticated osseous densities are present within the anterior annular fibers *(arrows).* These ossicles have been termed *intercalary bones* and are a manifestation of degenerative disc disease. Intercalary bones differ from unossified secondary growth centers (limbus vertebrae) in that there is no corresponding wedge-shaped defect of the adjacent vertebral body corner.

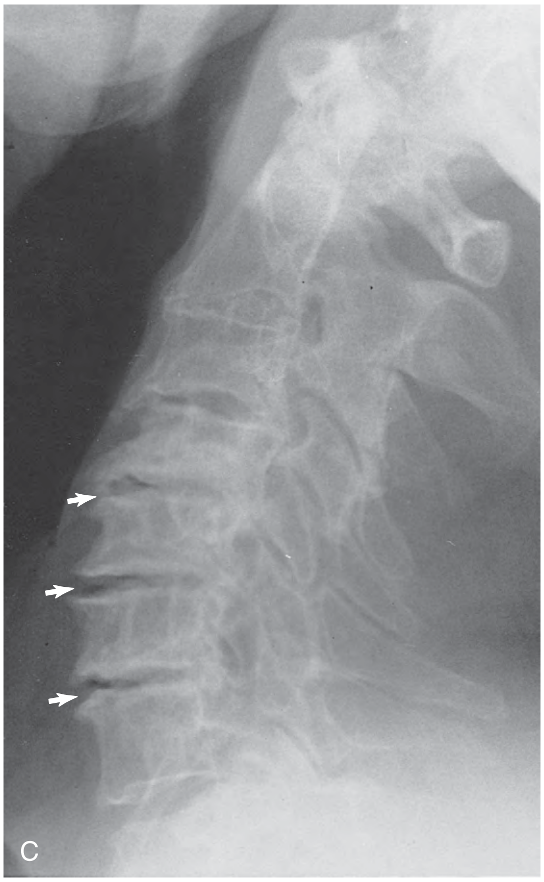

FIGURE 2–66, cont'd C, Advanced changes. Diffuse disc space narrowing, vacuum phenomena *(arrows),* well-defined sclerotic vertebral margins, osteophyte formation, facet joint arthrosis, and uncovertebral arthrosis are all present in this 75-year-old man. Congenital synostosis of C2-C3 with facet joint ankylosis and a rudimentary disc space also is evident.

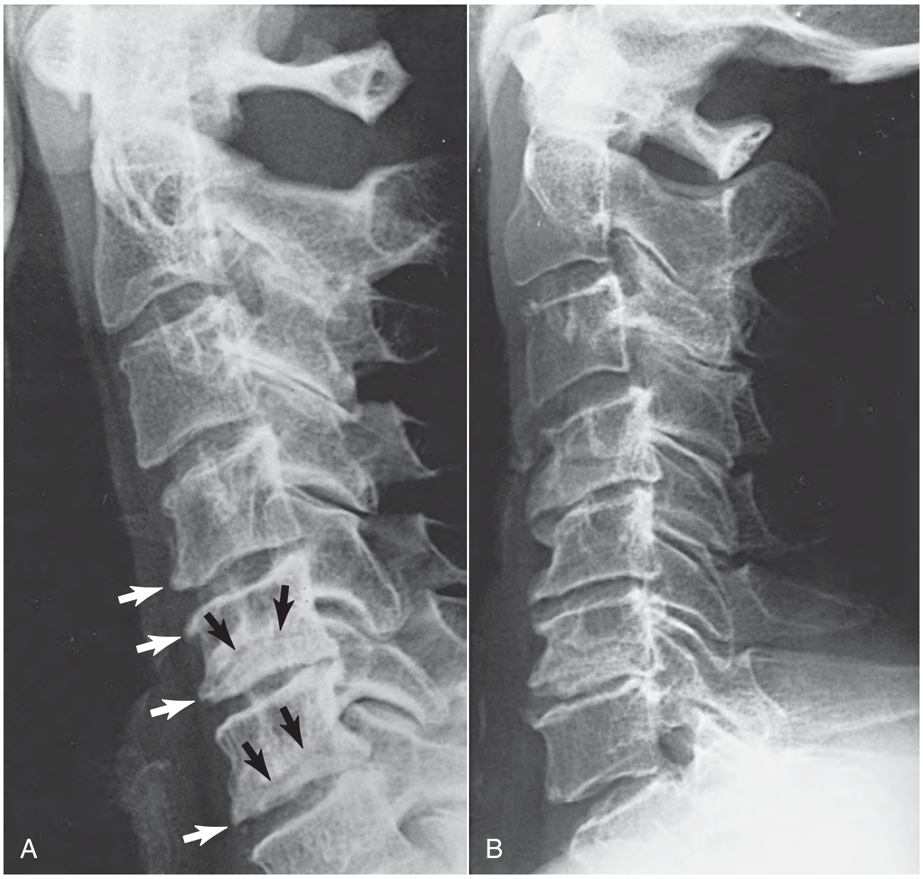

FIGURE 2–67 Degenerative spine disease.[71-73,157,173] **A,** Lateral cervical radiograph of a 71-year-old man shows extensive osteoarthrosis of the apophyseal joints characterized by joint space narrowing and subchondral sclerosis. Narrowing of the C4-C5, C5-C6, and C6-C7 intervertebral disc spaces and osteophytes *(white arrows)* arising from the vertebral body margins are evidence of degeneration. Uncovertebral joint arthrosis appears as hypertrophy of the uncinate processes with horizontal clefts across the C5 and C6 vertebral bodies *(black arrows),* a phenomenon termed *pseudofracture*. **B,** In another patient, similar findings are seen. The lordosis is reversed, and alignment abnormalities are seen involving C3 (anterolisthesis) and C4 (retrolisthesis). *(Courtesy F.G. Bauer, DC, Sydney, Australia.)*

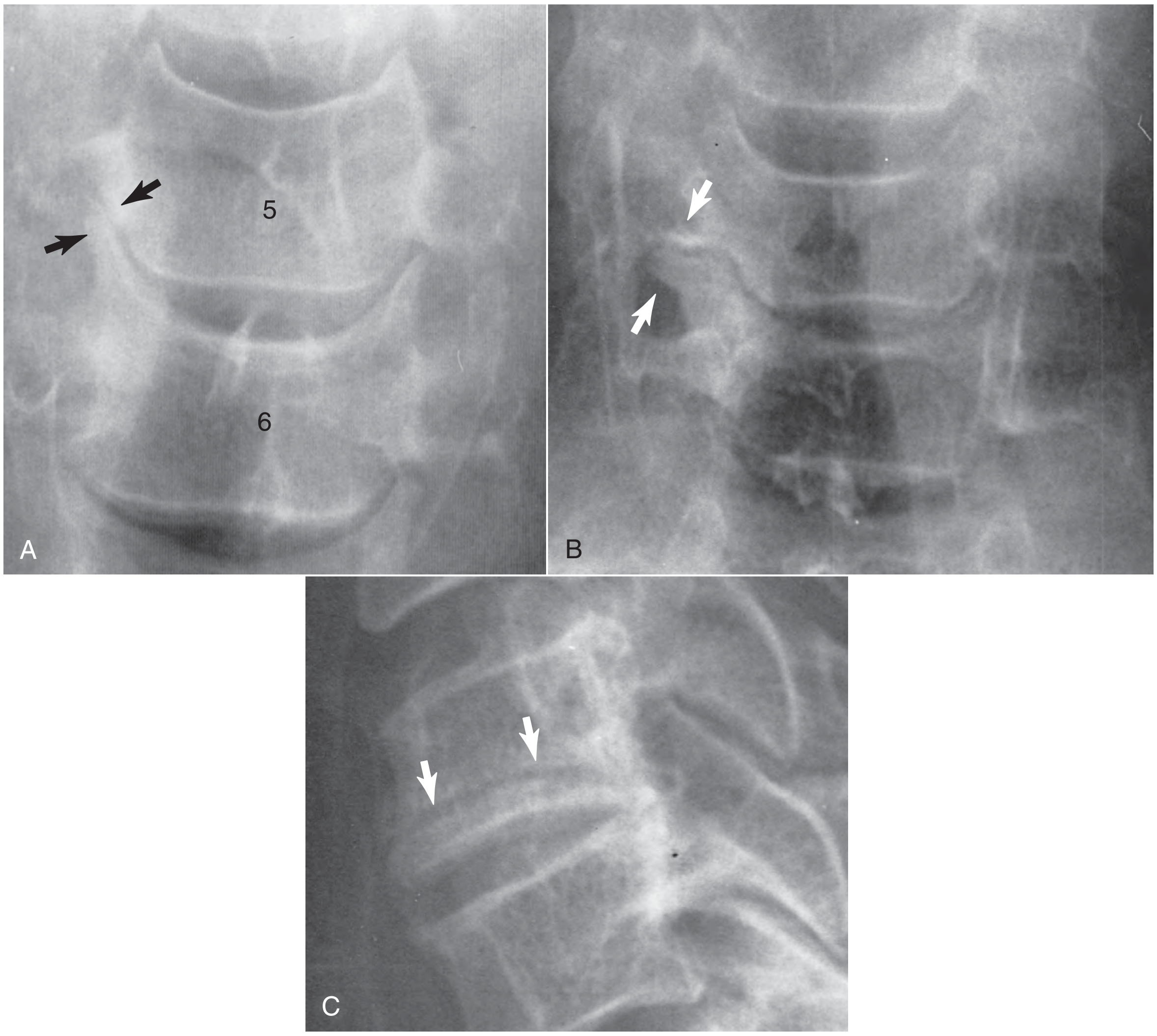

FIGURE 2–68 **Uncovertebral joint osteoarthrosis.**[71-73] **A,** Frontal radiograph of the cervical spine reveals the presence of hypertrophy and sclerosis of the C6 uncinate processes and corresponding narrowing of the uncovertebral articulation *(arrows)*. **B-C,** In another patient a frontal radiograph **(B)** shows prominent hypertrophy and osteophyte formation of the C6 uncinate processes and narrowing of the C5-C6 uncovertebral joint *(arrows)*. Lateral radiograph **(C)** shows a horizontal radiolucent region *(arrows)* through the inferior aspect of the C5 vertebral body, which represents the joint line of the degenerated uncovertebral joint (pseudofracture effect).

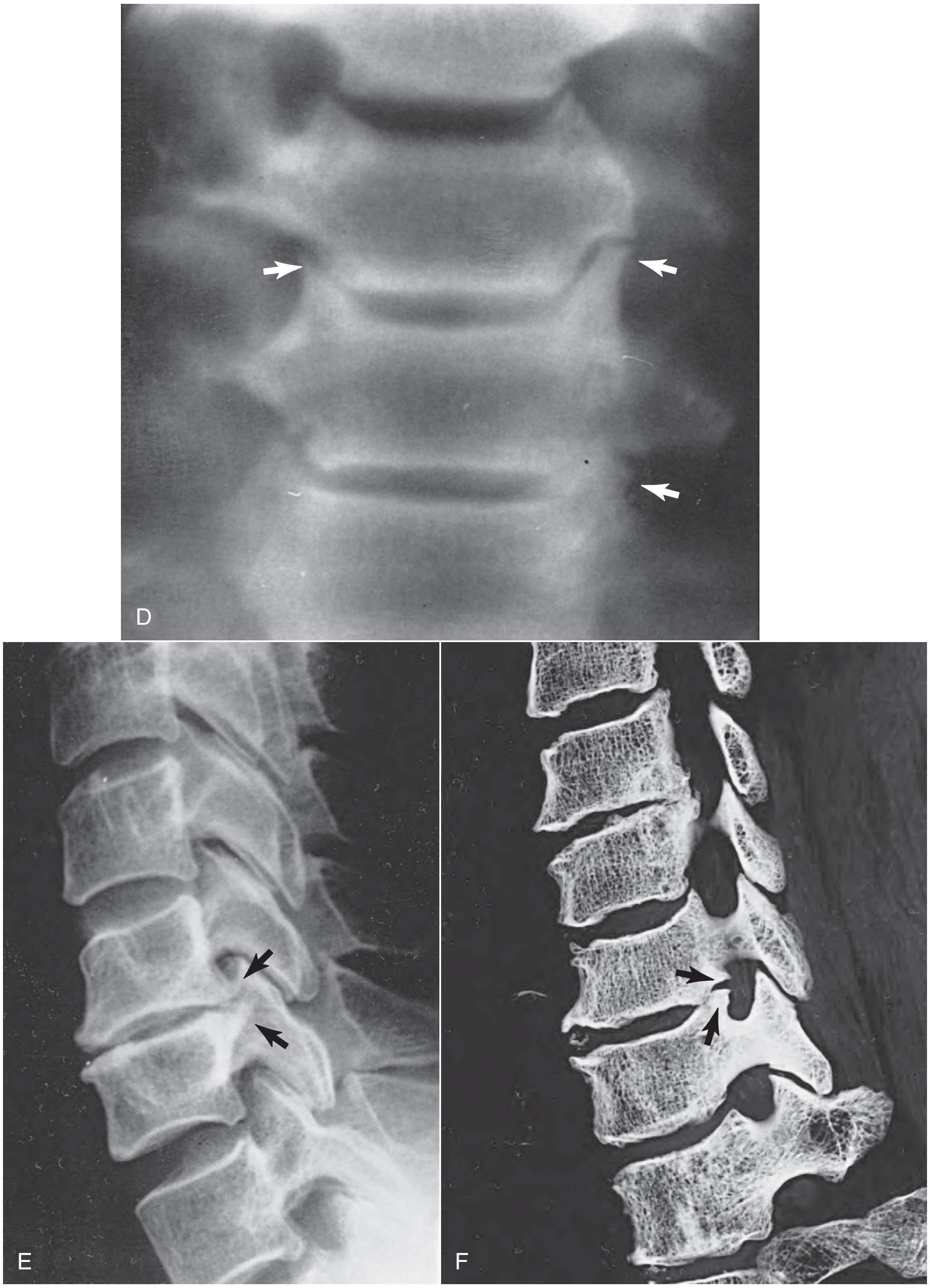

FIGURE 2–68, cont'd **D,** Frontal conventional tomogram clearly illustrates the sclerosis, hypertrophy, and osteophytes arising from the uncinate processes *(arrows),* and the associated narrowing of the uncovertebral articulations. **E,** Lateral cervical radiograph reveals disc space narrowing and marginal osteophytes arising from the discovertebral and uncovertebral margins. Large posterior osteophytes are evident *(arrows).* **F,** Oblique radiograph of a cadaveric specimen demonstrates the stenotic effect of posterolateral uncovertebral osteophytes (*arrows*) on the neural foramen. Such osteophytes represent a significant factor in foraminal stenosis and may be a source of nerve root compression and radiculopathy.

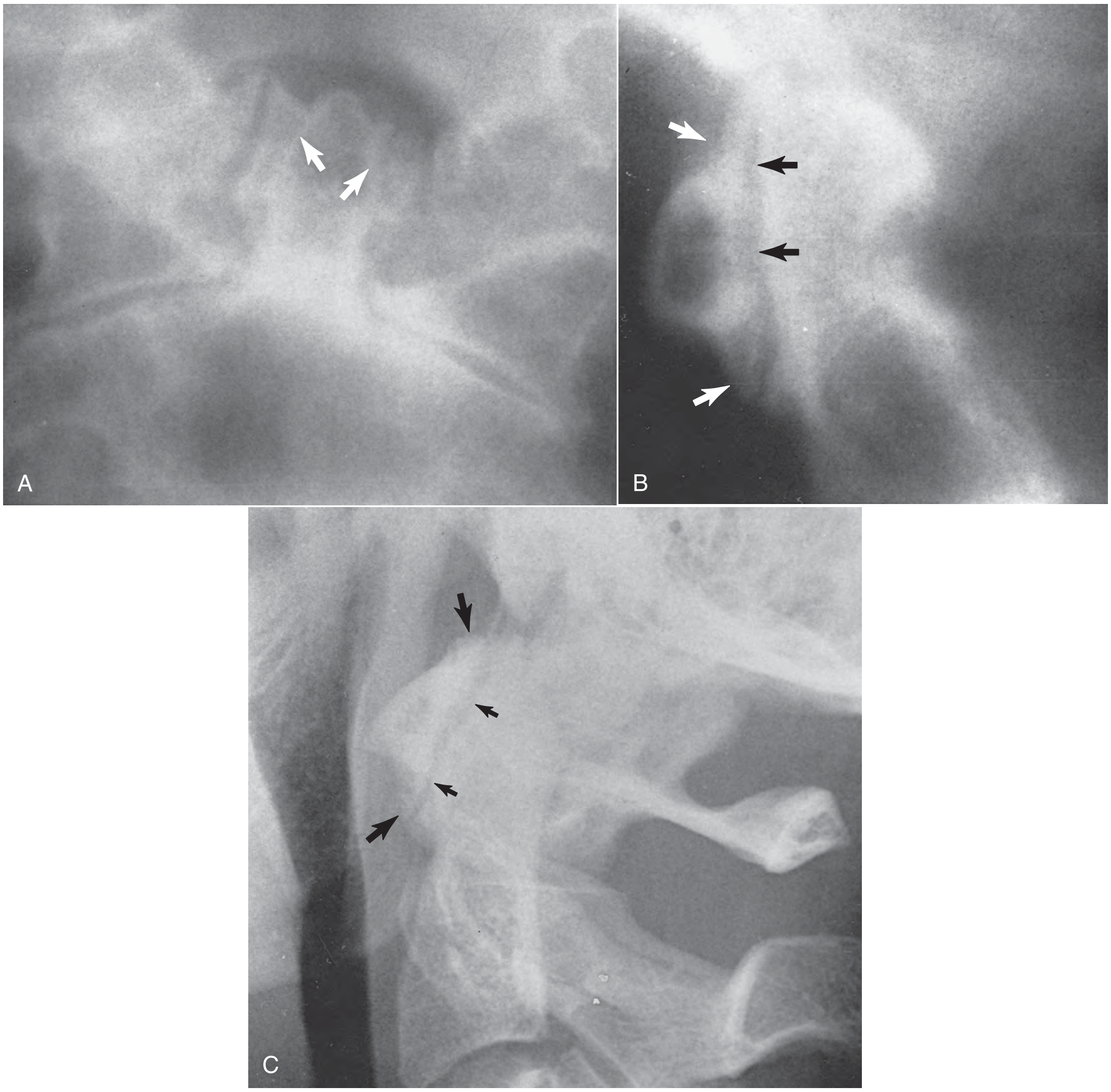

FIGURE 2–69 **Osteoarthrosis: C1-C2 articulations.**[71-73] **A-B,** Conventional tomogram in the frontal plane **(A)** shows narrowing of the lateral atlantoaxial synovial articulations and considerable bone proliferation about the odontoid process *(arrows).* Lateral conventional tomogram **(B)** demonstrates marked narrowing of the anterior median atlantoaxial articulation *(black arrows).* Prominent osteophytes also are seen arising from the inferior and superior margins of the anterior arch of the atlas *(white arrows).* **C,** Another case reveals narrowing of the atlantodental interspace *(small arrows),* sclerosis, and osteophytes *(large arrows).*

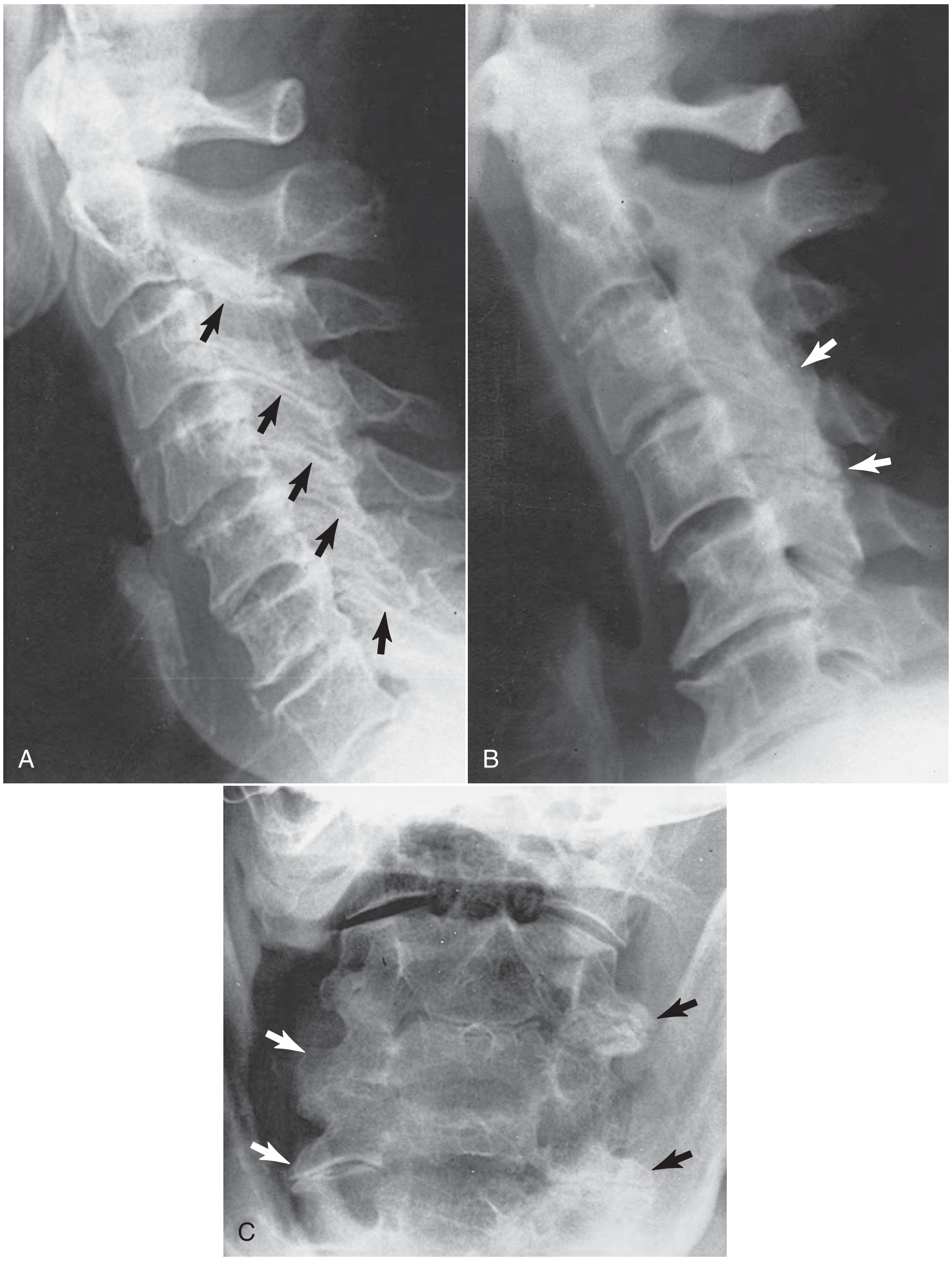

FIGURE 2–70 **Osteoarthrosis (degenerative joint disease): apophyseal joints.**[71-73,173] **A,** In this 77-year-old man, apophyseal joint space narrowing, osteophyte formation, and sclerosis are noted throughout the cervical spine *(arrows).* **B,** This 79-year-old man complained of progressive cervical spine stiffness and pain. Lateral radiograph reveals extensive sclerosis of the articular processes of C2 to C5 combined with dramatic joint space narrowing of the apophyseal joints *(arrows).* Marked degenerative disc disease also is present at the C5-C6 and C6-C7 levels. **C,** Frontal open-mouth radiograph from this elderly patient reveals dramatic osteophyte formation arising from the facet articulations throughout the cervical spine *(arrows). (C, Courtesy L. Hoffman, DC, Portland, Ore.)*

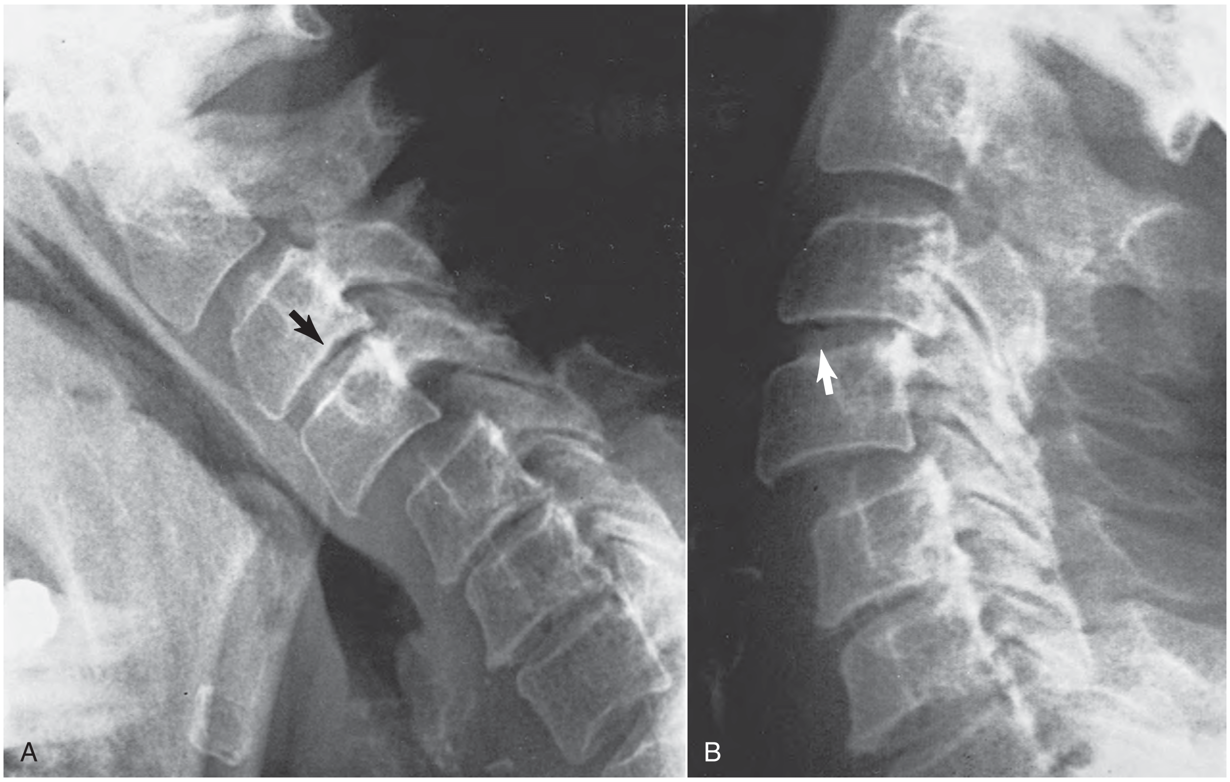

FIGURE 2–71 **Degenerative spondylolisthesis.**[71-73,173] This 73-year-old woman had neck pain and stiffness. Lateral radiographs taken in flexion **(A)** and extension **(B)** reveal extensive apophyseal joint space narrowing and sclerosis with anterolisthesis of C4 on C5. Minimal translation is present at C4-C5 between flexion and extension. At the C3-C4 level, however, disc space narrowing and a vacuum phenomenon *(arrows)* are present, and approximately 4 mm of translation is evident, suggesting instability. *(Courtesy W. Longstaffe, DC, Vancouver, B.C., Canada.)*

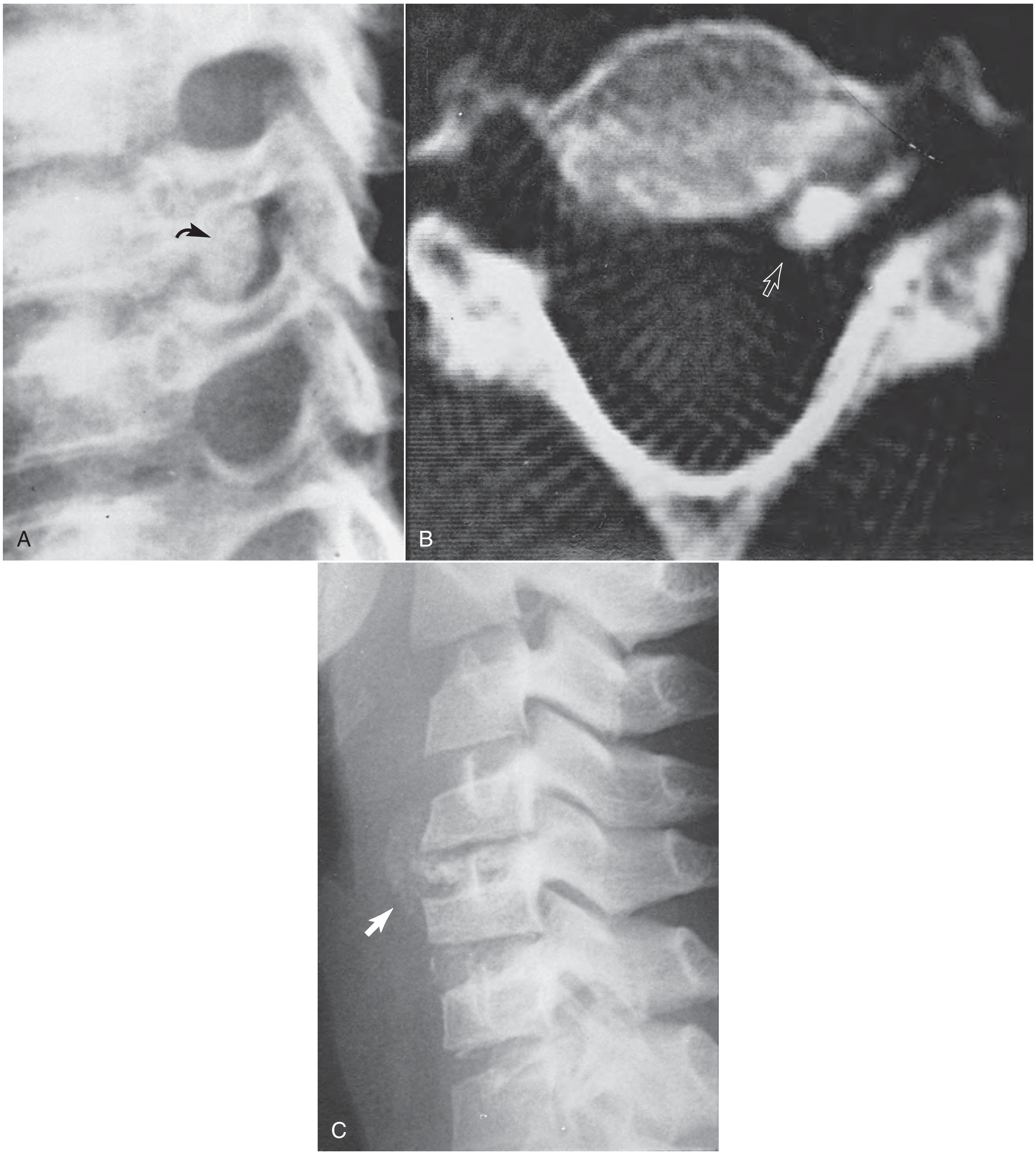

FIGURE 2–72 **Idiopathic intervertebral disc calcification.**[74] **A,** In this child, a calcified mass is seen in the neural foramen on the oblique radiograph *(curved arrow).* **B,** Transaxial CT scan reveals a calcified extruded intervertebral disc extending into the neural foramen *(open arrow).* **C,** In another child, anterior extrusion and extensive calcification of the C4-C5 intervertebral disc are seen *(arrow).* *(**A-B,** Courtesy M. Alcaraz, MD, Madrid, Spain; **C,** Courtesy P. Wilson, MD, Eugene, Ore.)*

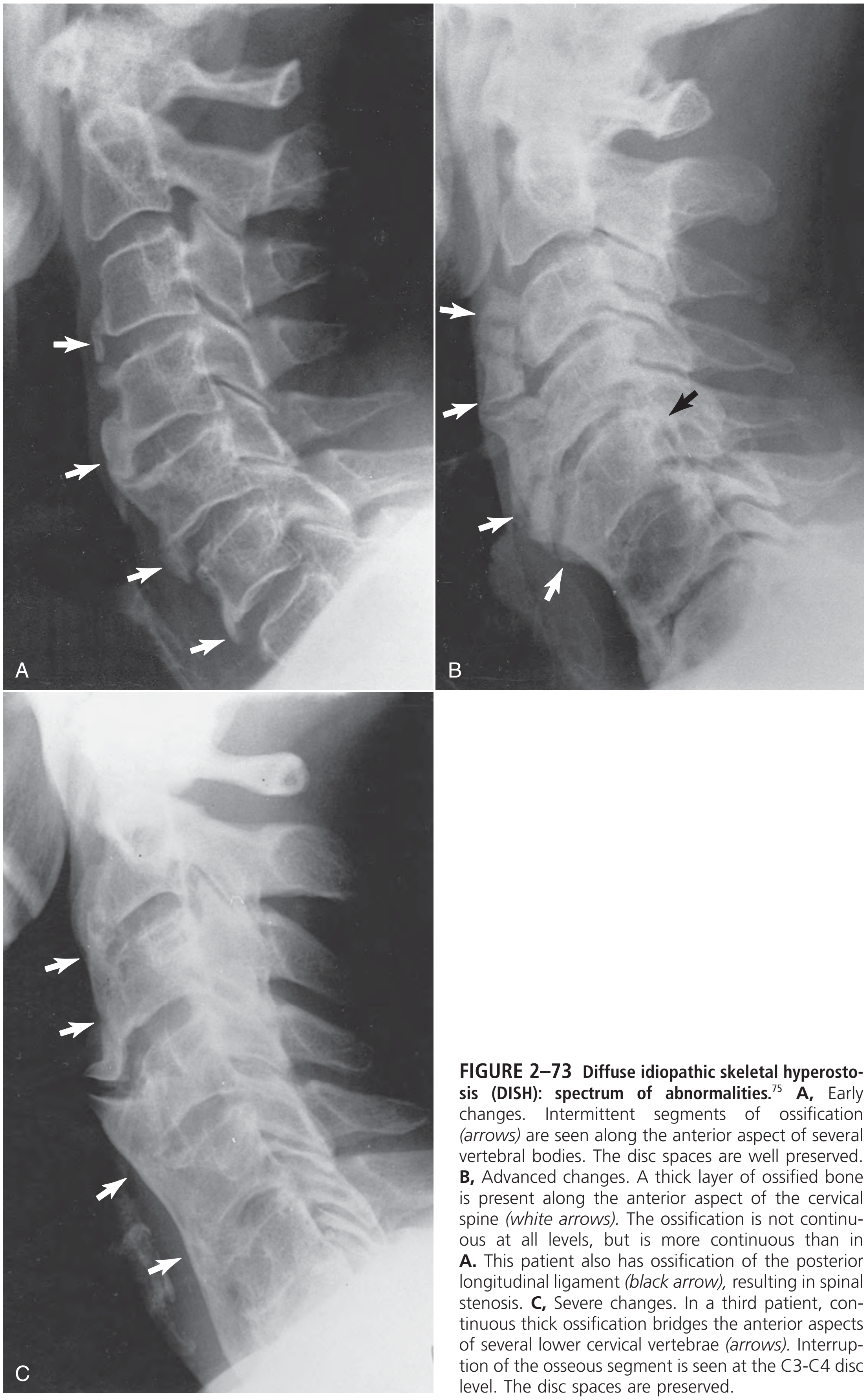

FIGURE 2–73 Diffuse idiopathic skeletal hyperostosis (DISH): spectrum of abnormalities.[75] **A,** Early changes. Intermittent segments of ossification *(arrows)* are seen along the anterior aspect of several vertebral bodies. The disc spaces are well preserved. **B,** Advanced changes. A thick layer of ossified bone is present along the anterior aspect of the cervical spine *(white arrows).* The ossification is not continuous at all levels, but is more continuous than in **A.** This patient also has ossification of the posterior longitudinal ligament *(black arrow),* resulting in spinal stenosis. **C,** Severe changes. In a third patient, continuous thick ossification bridges the anterior aspects of several lower cervical vertebrae *(arrows).* Interruption of the osseous segment is seen at the C3-C4 disc level. The disc spaces are preserved.

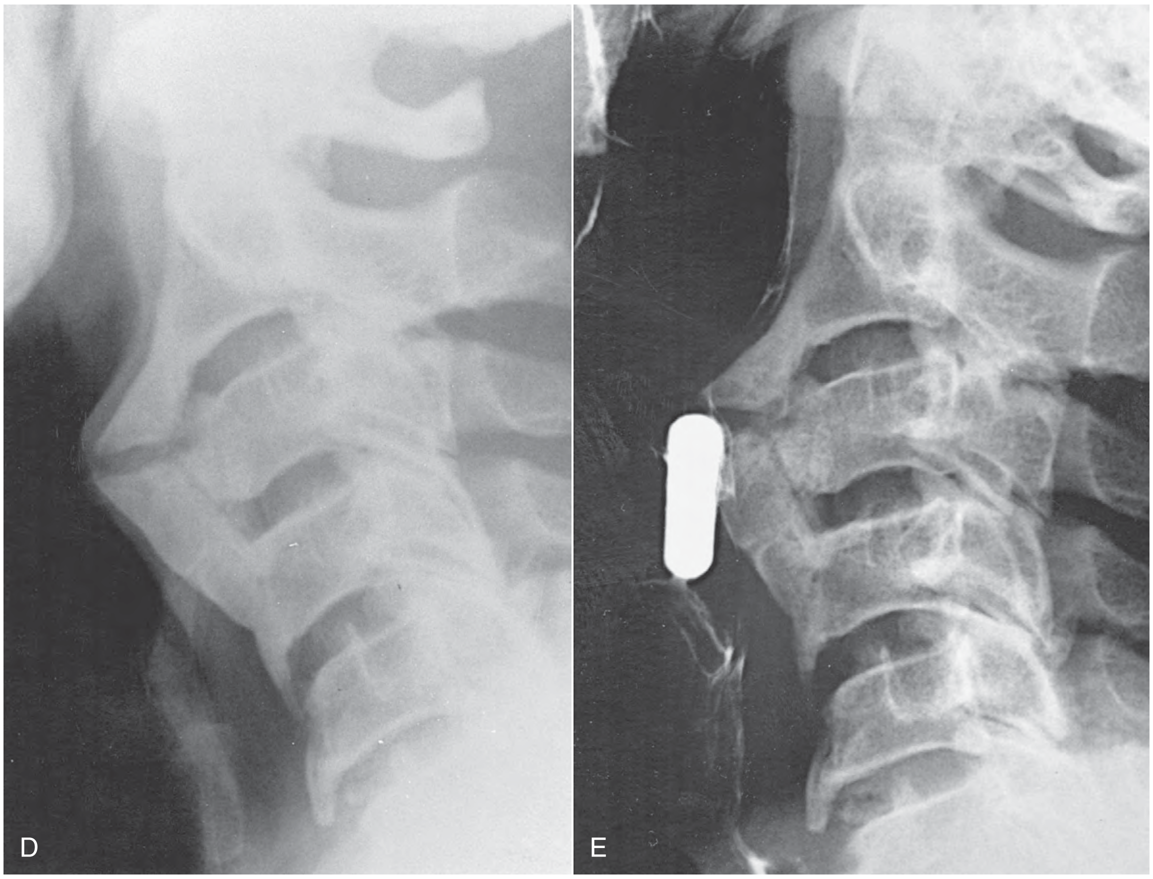

FIGURE 2–73, cont'd **D-E,** Severe changes. This patient had dysphagia. Routine radiograph **(D)** shows dramatic protuberant ossification. The radiograph obtained while the patient was swallowing a barium contrast tablet **(E)** documents esophageal obstruction at the site of osseous protrusion. *(**C,** Courtesy L. Bogle, MD, San Diego, Calif.; **D-E,** Courtesy C. Cortes, MD, Santiago, Chile.)*

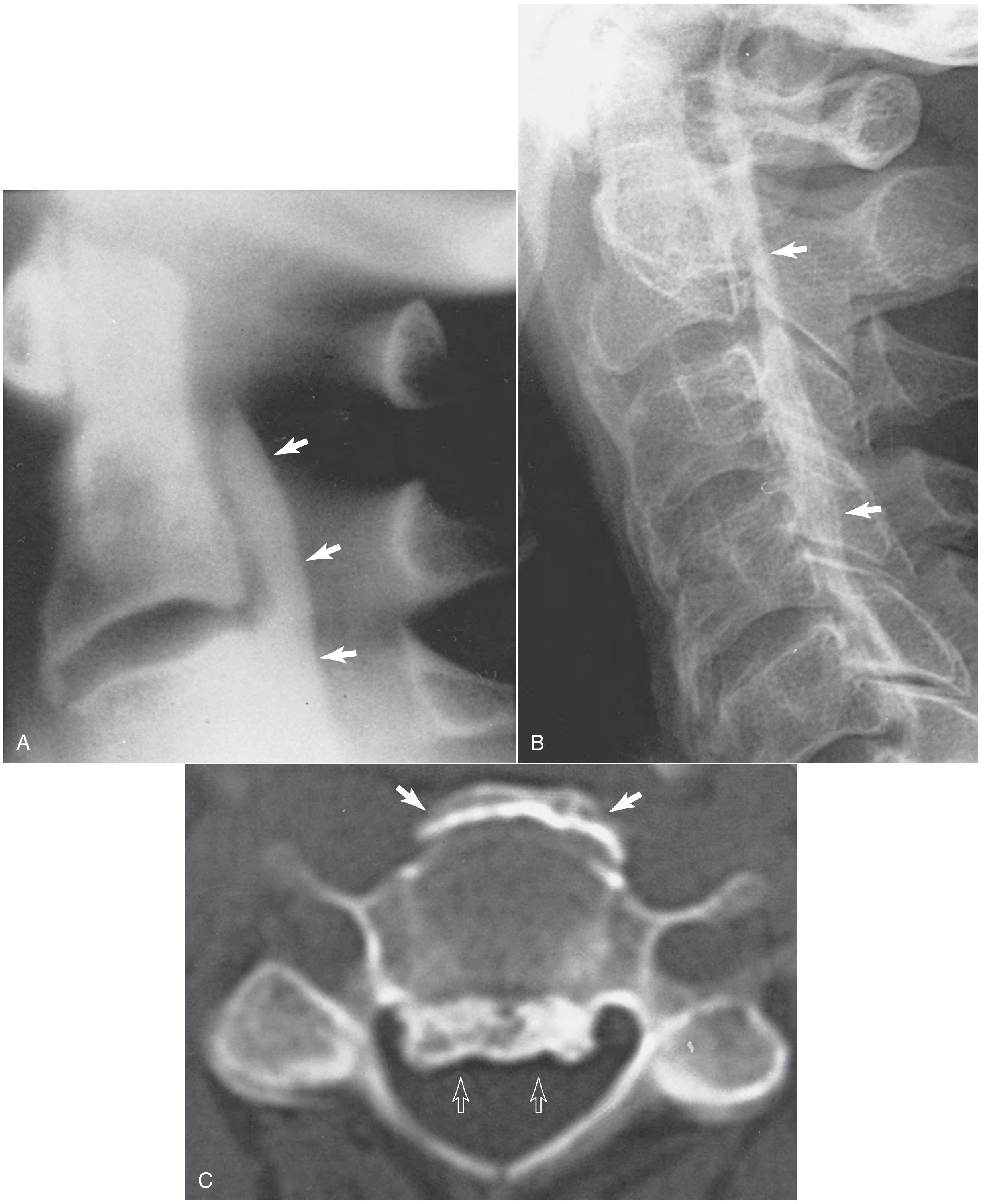

FIGURE 2–74 Ossification of the posterior longitudinal ligament in diffuse idiopathic skeletal hyperostosis (DISH).[76,151,152] **A,** A thick, vertical, linear band of ossification *(arrows)* is seen in the spinal canal of the upper cervical spine in this conventional tomogram of a patient with DISH. **B-C,** A 57-year-old man with neck pain. In **B,** a linear sheet of ossification within the spinal canal extending from C1 to C5 *(arrows)* is evident in this patient with DISH. In **C,** a transaxial CT scan at the C3 level reveals a thick layer of ossification *(open arrows)* occupying approximately 30% of the sagittal canal diameter. Observe also the ossification anterior to the vertebral bodies *(arrows)*. (***A,*** *Courtesy J. Mink, MD, Los Angeles;* ***B-C,*** *Courtesy E. Bosch, MD, Santiago, Chile.)*

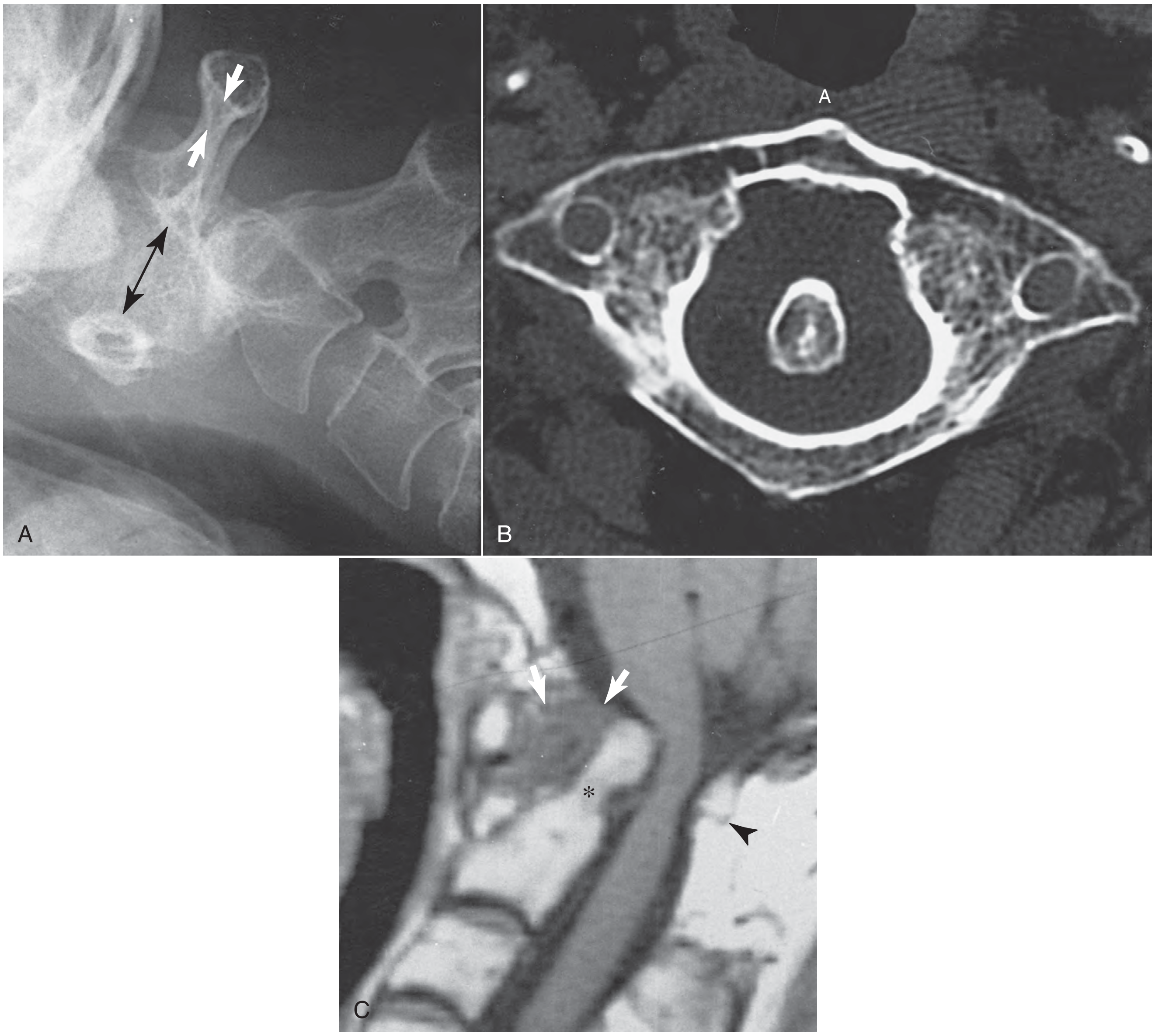

FIGURE 2–75 **Rheumatoid arthritis: atlantoaxial abnormalities.**[78,79,161-163] **A-C,** Atlantoaxial instability in a 55-year-old woman with no neurologic deficit. In **A,** a lateral radiograph obtained in flexion shows dramatic anterior displacement of the atlas in relation to the axis. The atlantodental interspace (predens space) measures 15 mm *(black double-headed arrow).* The sagittal canal diameter, measured between the posterior aspect of the odontoid and the spinolaminar junction line *(white arrows),* measures only 8 mm. In **B,** a transaxial CT scan confirms the atlantoaxial instability revealing that the odontoid process is situated posterior to the midline of the spinal canal rather than anteriorly adjacent to the anterior arch. The spinal cord is being compressed between the odontoid and the posterior arch. (*A,* Anterior.) In **C,** compression of the spinomedullary junction by the odontoid process anteriorly and the posterior arch of the atlas posteriorly *(arrowhead)* is clearly evident on this sagittal T1-weighted (TR/TE, 600/12) spin echo MR image. The atlantodental interspace is widened and contains low signal intensity pannus *(arrows).* It is the inflammatory synovial pannus that results in disruption of the transverse ligament and consequent erosion of the base of the odontoid (*).

Continued

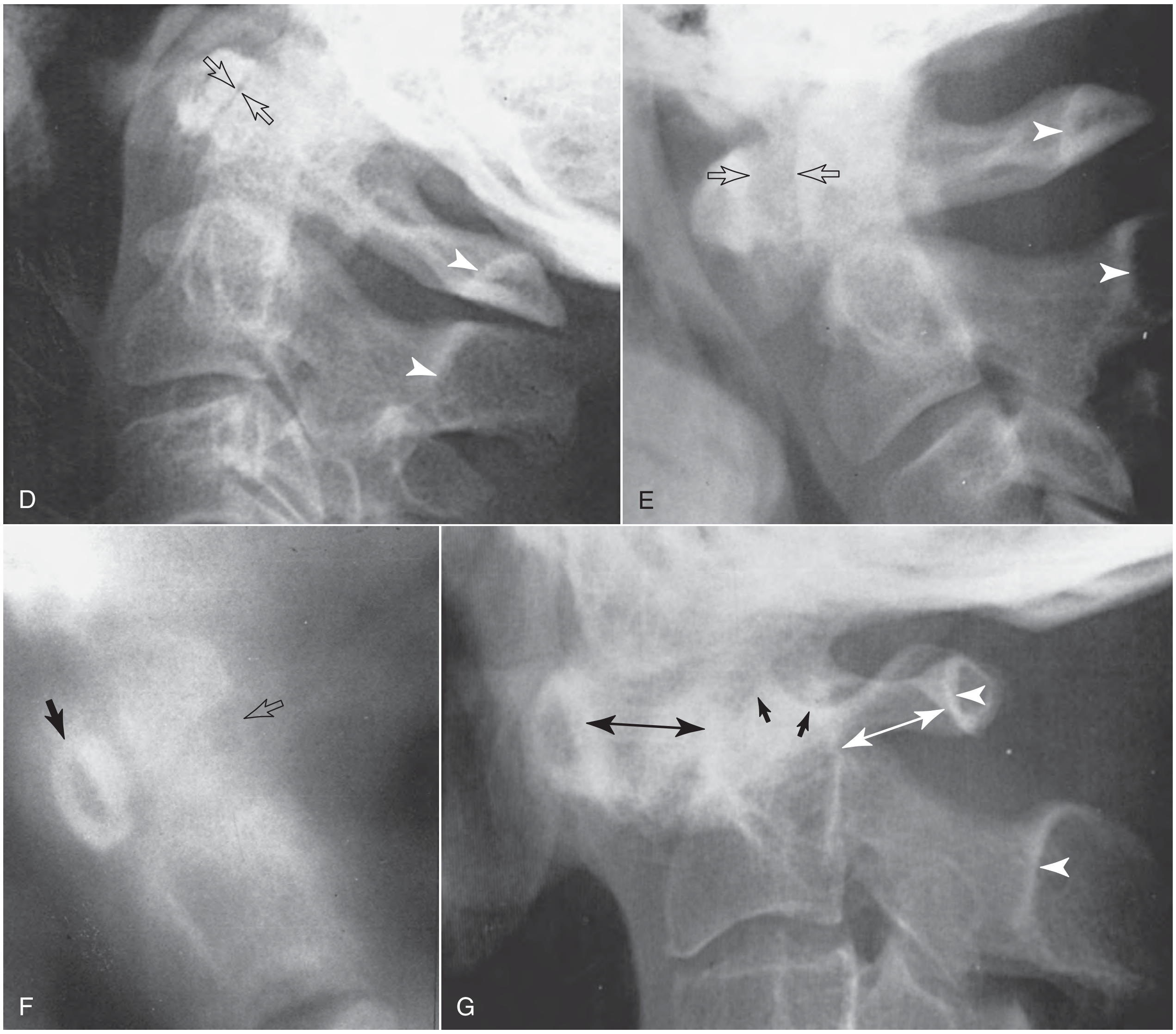

FIGURE 2–75, cont'd **D-E,** Atlantoaxial instability: Value of functional radiographs. In **D,** a lateral radiograph obtained in extension shows a normal atlantodental interspace *(open arrows)* and normal alignment of the C1 and C2 spinolaminar junctions *(arrowheads).* In **E,** a lateral radiograph obtained in flexion reveals widening of the atlantodental interspace *(open arrows)* and anterior displacement of the C1 spinolaminar junction line in relation to that of C2 *(arrowheads),* documenting atlantoaxial instability. Atlantoaxial instability exists when the atlantodental interspace exceeds 3 mm in adults and 5 mm in children. **F,** In another patient, a lateral conventional tomogram shows erosion of the posterior aspect of the odontoid at the point of contact with the synovial compartment of the transverse ligament *(open arrow).* Also evident is inferior subluxation of the atlas relative to the odontoid *(arrow),* a condition termed *cranial settling*. **G,** Cranial settling, anterior subluxation, and extensive odontoid erosions resulting in an amputated appearance *(arrows)* are observed in a male patient with chronic rheumatoid arthritis. Observe the displacement of the spinolaminar junction line between C1 and C2 *(arrowheads),* widening of the atlantodental interspace (*double-headed black arrow*), and the severely compromised sagittal canal diameter and space available for the cord *(double-headed white arrow).* (***A-C,*** *Courtesy M.N. Pathria, MD, San Diego, Calif.)*

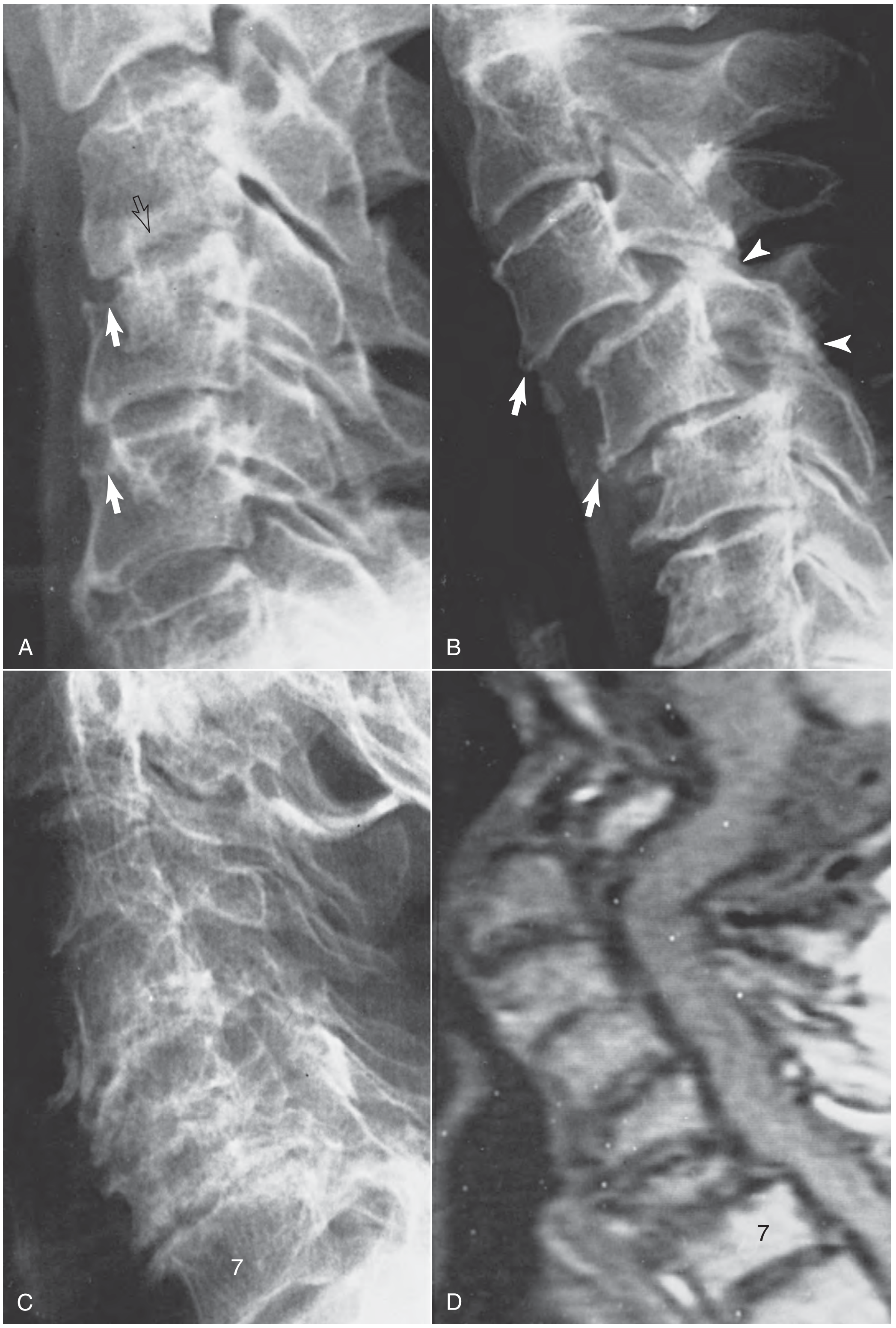

FIGURE 2–76 **Rheumatoid arthritis: midcervical and lower cervical spine abnormalities.**[78,79,161-163] **A,** Discovertebral joint changes. In this patient with early erosive changes, multiple intervertebral discs are narrowed and the vertebral endplates at C3-C4 are indistinct *(open arrow)*. Discovertebral erosions are evident at the anterosuperior vertebral body margins *(arrows)*. In the absence of osteophytes and subchondral sclerosis, such findings are highly suggestive of an inflammatory arthropathy. **B,** Subaxial joint subluxation: advanced changes. In this patient with advanced rheumatoid arthritis, dramatic anterior subluxation of C3 on C4 and C4 on C5 is seen *(arrow)*. Several disc spaces are narrowed, and osteophytes are small and poorly developed. Apophyseal joint narrowing, sclerosis, and subluxation also are present *(arrowheads)*. **C-D,** Advanced changes in a 66-year-old man. In **C,** severe disc space narrowing, indistinct and irregular endplates, and apophyseal joint erosion, narrowing, and subluxation are evident. Atlantoaxial instability with posterior dislocation of the atlas is also present. In **D,** a sagittal proton density-weighted (TR/TE, 1200/20) spin echo MR image reveals dramatic subluxation at C1-C2 and at C6-C7. Discovertebral junction erosions are prominent. The odontoid process appears to be eroded or fractured, and the spinal cord at C2-C3 appears kinked.

FIGURE 2–77 Juvenile idiopathic arthritis: upper cervical spine.[80,81,145,146] (Also known as *juvenile rheumatoid or juvenile chronic arthritis*.) Severe atlantoaxial instability with posterior dislocation of the atlas is seen in this 27-year-old woman with long-standing juvenile idiopathic arthritis. The anterior arch of the atlas (*) is dislocated in a posterior position with respect to the eroded odontoid process *(black arrows)* of C2 (2). Posterior dislocation of the atlas also is indicated by the malalignment of the spinolaminar junction lines of C1 and C2 *(white arrows)*. The vertebral bodies of C2 (2) and C3 (3) reveal abnormal translation. *(Courtesy J. Bramble, MD, Kansas City, Missouri, and M. Murphy, MD, Washington, DC.)*

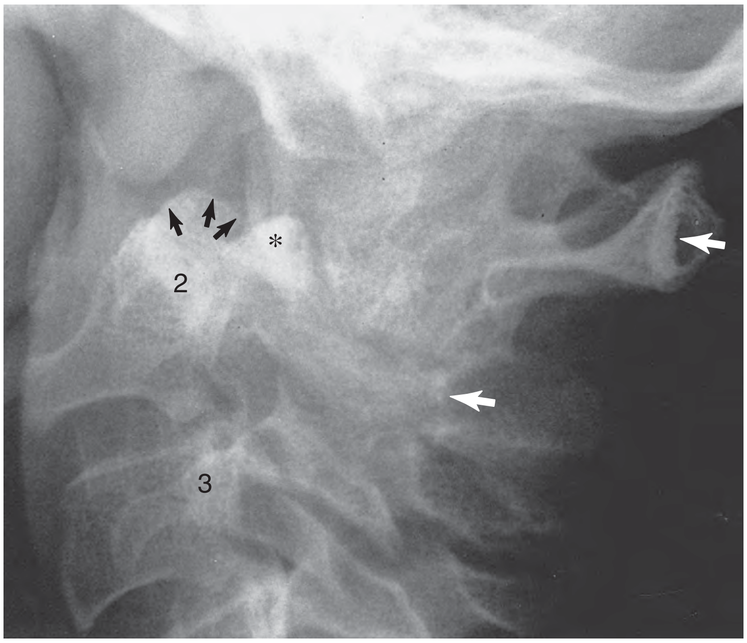

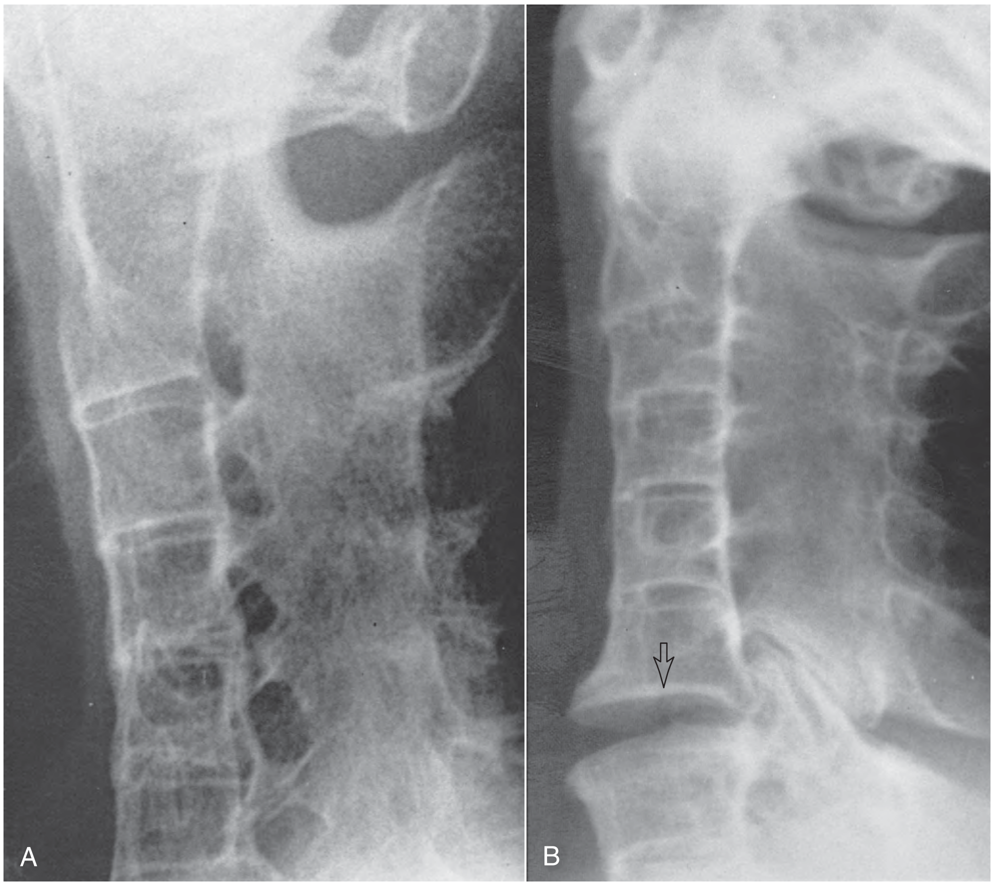

FIGURE 2–78 Juvenile idiopathic arthritis: upper cervical spine.[80,81,145,146] (Also known as *juvenile rheumatoid* or *juvenile chronic arthritis*.) **A,** Observe the widespread apophyseal joint ankylosis, disc space narrowing, and hypoplasia of the vertebral bodies in this 6-year-old girl with severe juvenile idiopathic arthritis. **B,** Widespread ankylosis, disc space narrowing, and hypoplasia of the vertebral bodies are seen in a 25-year-old woman. Atlantoaxial instability also is present. The C6-C7 interspace is not ankylosed *(open arrow)*, and in the presence of such widespread ankylosis of the adjacent segments, it may be a source of excessive motion and potential instability. The differential diagnosis in such cases includes juvenile-onset ankylosing spondylitis and Klippel-Feil syndrome. (***A,*** *Courtesy V. Vint, MD, San Diego, Calif;* ***B,*** *Courtesy C. Pineda, MD, Mexico City, Mexico.)*

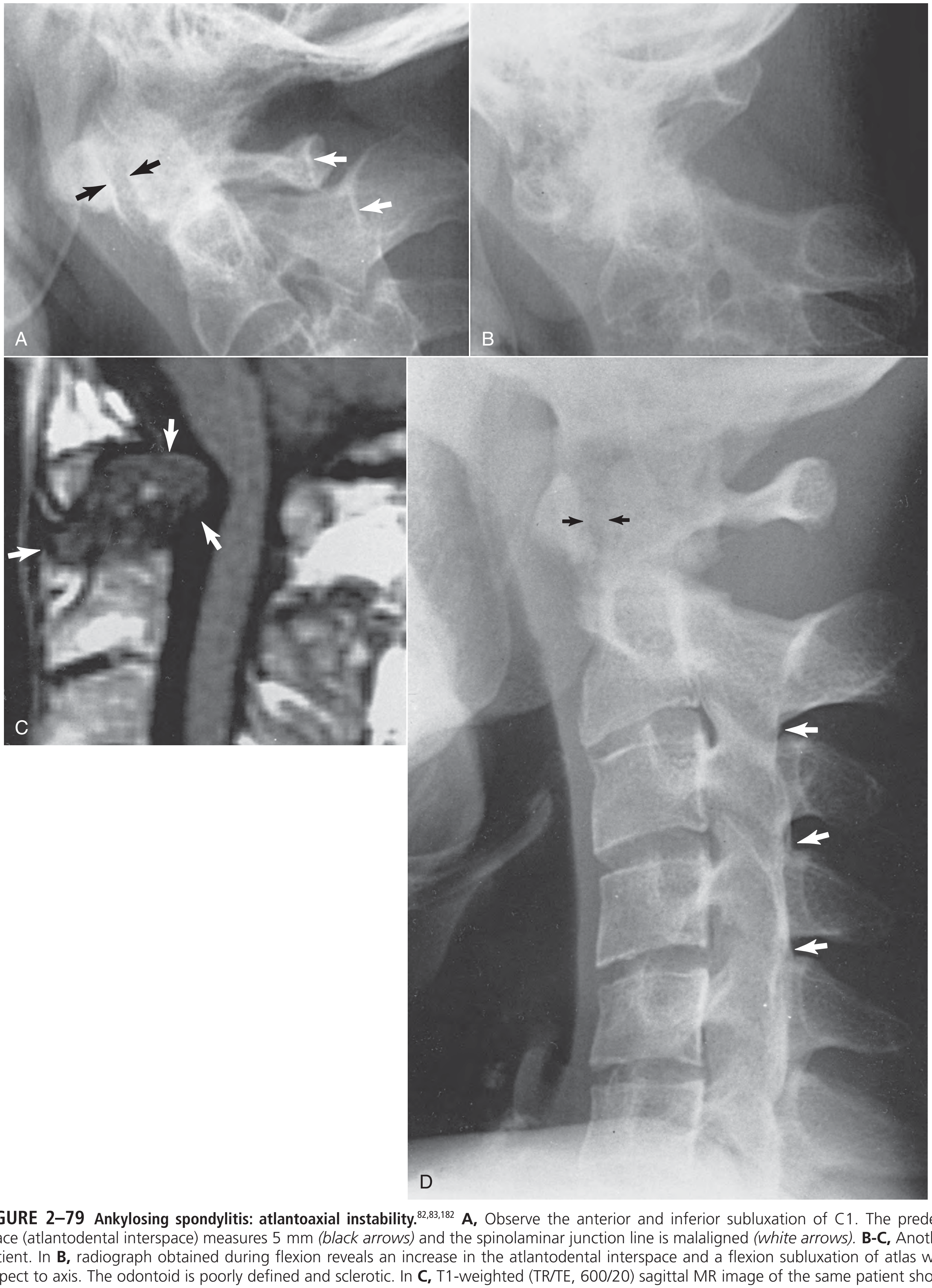

FIGURE 2–79 **Ankylosing spondylitis: atlantoaxial instability.**[82,83,182] **A,** Observe the anterior and inferior subluxation of C1. The predens space (atlantodental interspace) measures 5 mm *(black arrows)* and the spinolaminar junction line is malaligned *(white arrows)*. **B-C,** Another patient. In **B,** radiograph obtained during flexion reveals an increase in the atlantodental interspace and a flexion subluxation of atlas with respect to axis. The odontoid is poorly defined and sclerotic. In **C,** T1-weighted (TR/TE, 600/20) sagittal MR image of the same patient shows pannus of low signal intensity *(arrows)* eroding the odontoid process and impinging on the spinomedullary junction. **D,** Juvenile onset. This 20-year-old man had a 4-year history of arthritis. Radiograph obtained in flexion shows atlantoaxial instability *(black arrows)* and diffuse apophyseal joint ankylosis *(white arrows)*. He had no evidence of hypoplasia of the vertebral bodies, an important feature in differentiating this condition from juvenile idiopathic (chronic or rheumatoid) arthritis.

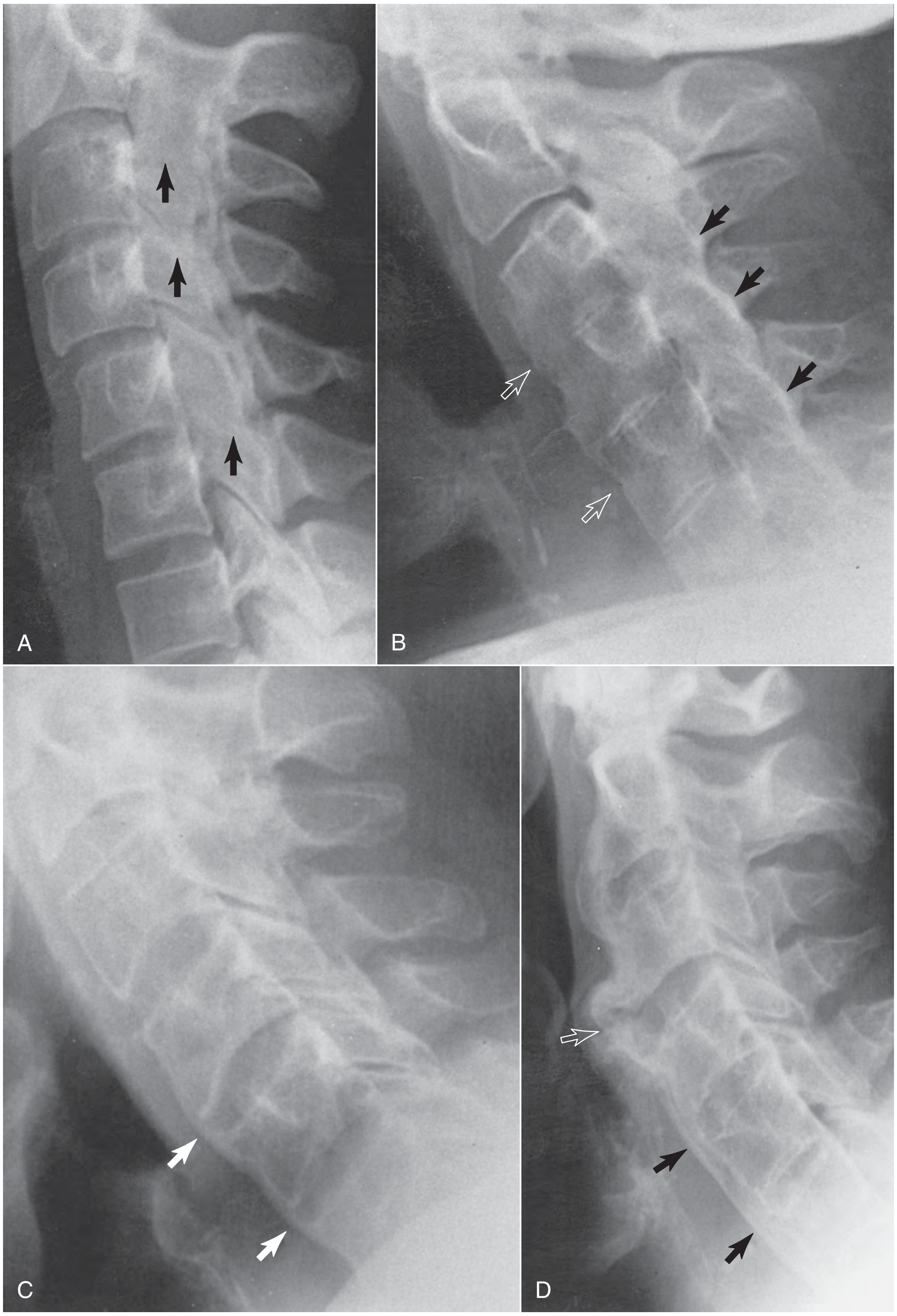

FIGURE 2–80 **Ankylosing spondylitis: spectrum of radiographic abnormalities.**[82,83,148-150,182] **A,** Lateral radiograph of this 38-year-old woman reveals extensive ankylosis of the apophyseal joints *(arrows)* with no evidence of syndesmophyte formation. **B,** In another patient, diffuse apophyseal joint ankylosis *(arrows),* disc space narrowing, and anterior vertebral body ankylosis *(open arrows)* are noted. An abnormal posture, in which the head is thrust forward, is also a frequent finding in ankylosing spondylitis. **C,** In a third patient, marginal syndesmophytes predominate in the lower cervical spine *(arrows).* The apophyseal joints appear somewhat irregular, but no ankylosis is evident. **D,** This patient has diffuse syndesmophyte formation at several levels and more prominent osteophyte formation at the C3-C4 level *(arrows),* perhaps secondary to excessive motion *(open arrow).*

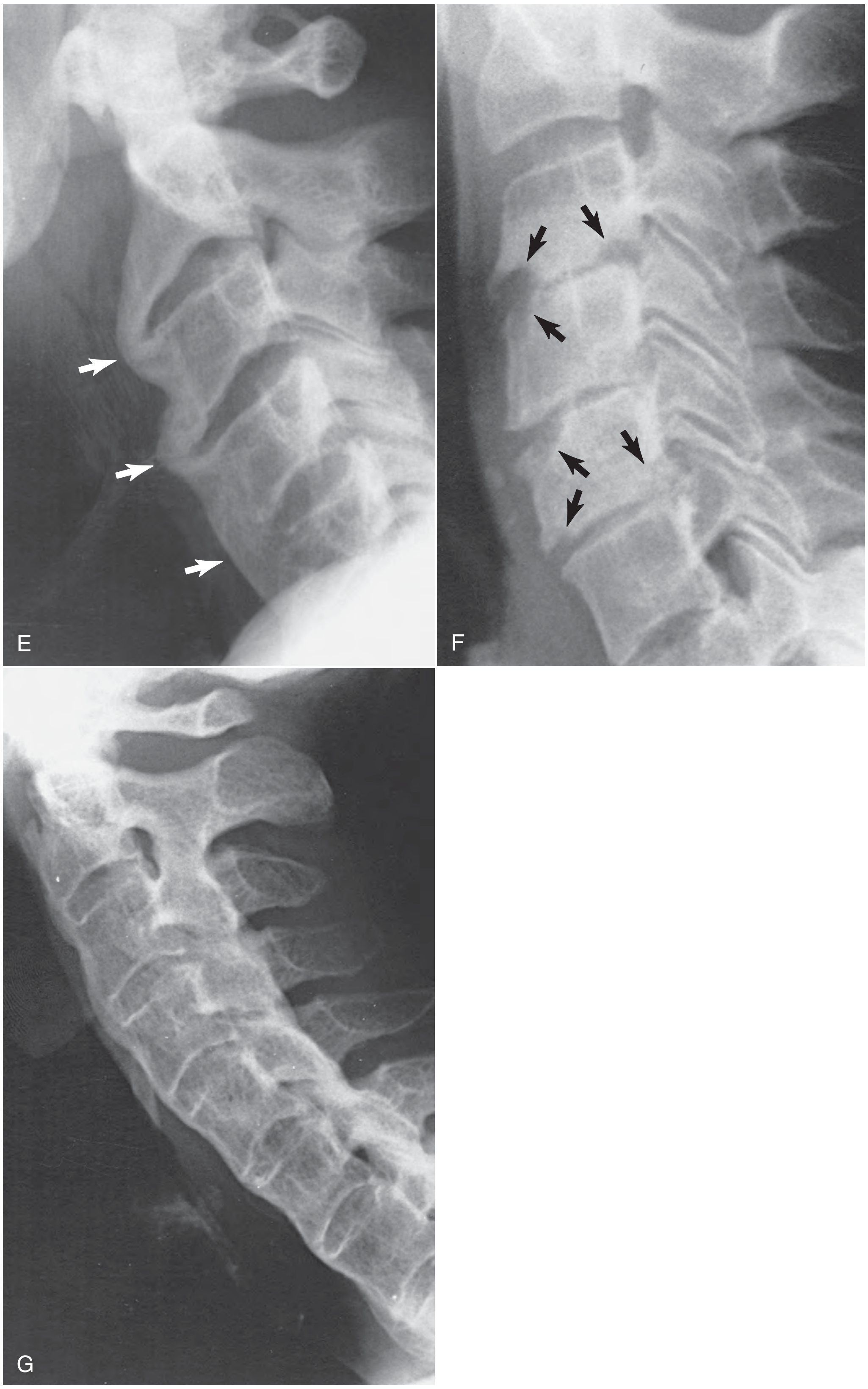

FIGURE 2–80, cont'd **E,** An atypical presentation of thick DISH-like flowing hyperostosis *(arrows)* is evident in this 49-year-old man with positive HLA-B27 and classic lumbar spine and sacroiliac changes of ankylosing spondylitis. **F,** Prominent disc space narrowing, peripheral endplate erosions *(arrows),* and osteitis of the vertebral bodies predominate in another patient with early ankylosing spondylitis. **G,** Advanced disease is characterized by diffuse ankylosis of the apophyseal joints, diffuse syndesmophyte formation, and ballooning of the discs.

Continued

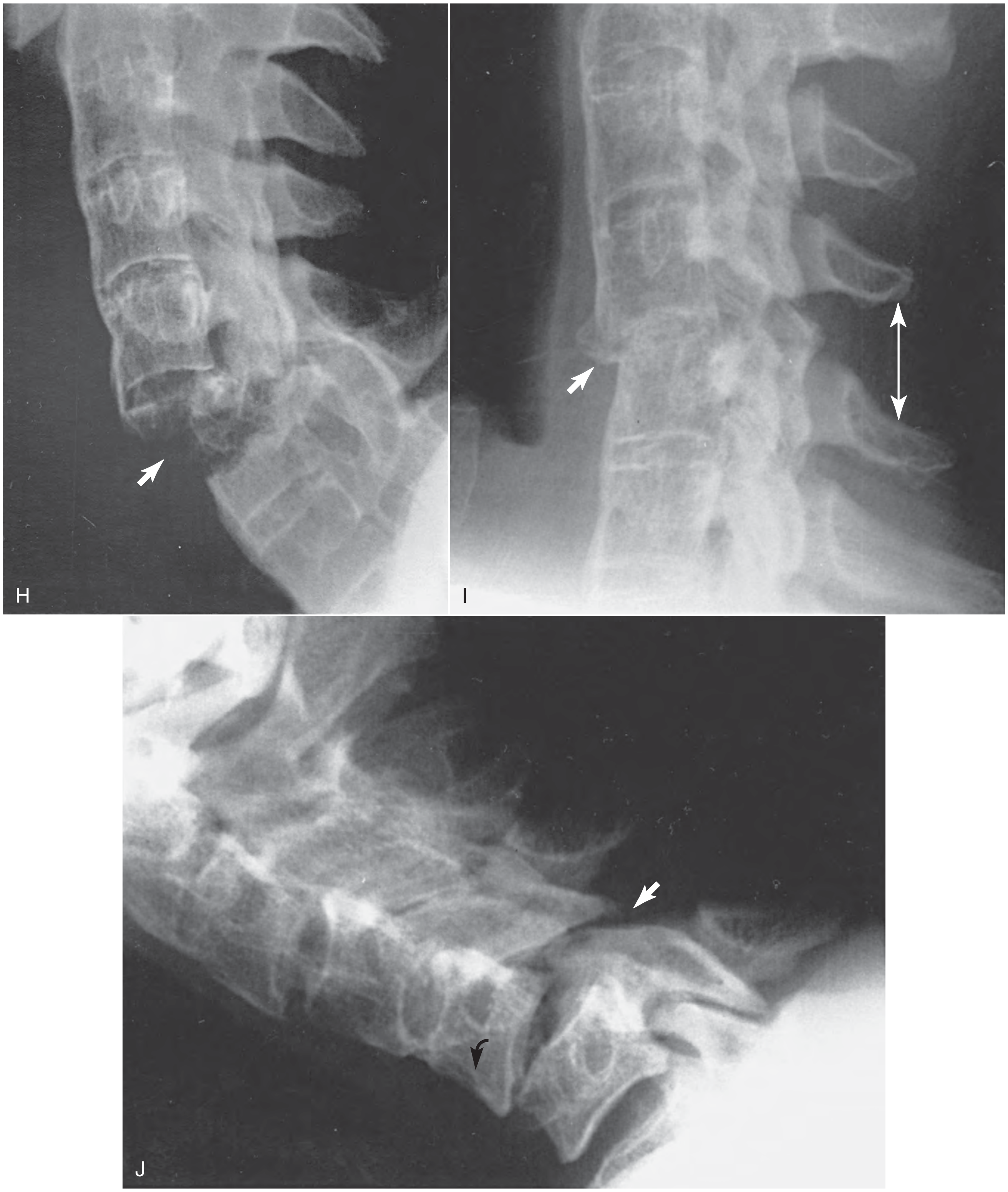

FIGURE 2–80, cont'd Fractures. In **H,** the patient had a fall that resulted in a fracture of his ankylosed C6 vertebral body *(arrow)* and apophyseal joints. In **I,** another patient, a lateral radiograph reveals a fracture of the ankylosed cervical spine at C4-C5. The fracture extends through the apophyseal joints and results in anterior displacement of C4 *(arrow)* and divergence of the C4-C5 spinous processes *(double-headed arrow)* with instability. **J,** Hyperflexion sprain. This 42-year-old man with ankylosing spondylitis sustained a cervical spine hyperflexion injury in a motor vehicle collision. A flexion radiograph reveals facet gapping *(arrow),* anterior C5 vertebral body subluxation *(curved arrow),* and disc space wedging at the C5-C6 level. (***J,*** *Courtesy D. Goodwin, MD, Lebanon, NH.)*

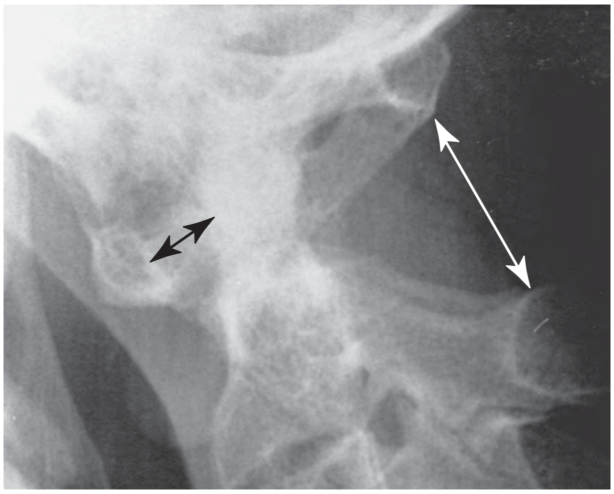

FIGURE 2–81 **Psoriatic arthropathy: atlantoaxial instability.**[84,181,182] Lateral radiograph obtained during flexion shows dramatic atlantoaxial subluxation in which the anterior arch of atlas has translated anteriorly *(black double-headed arrow)* and inferiorly in relation to the odontoid process. The space between the posterior arch of atlas and the C2 spinous process is widened *(white double-headed arrow).*

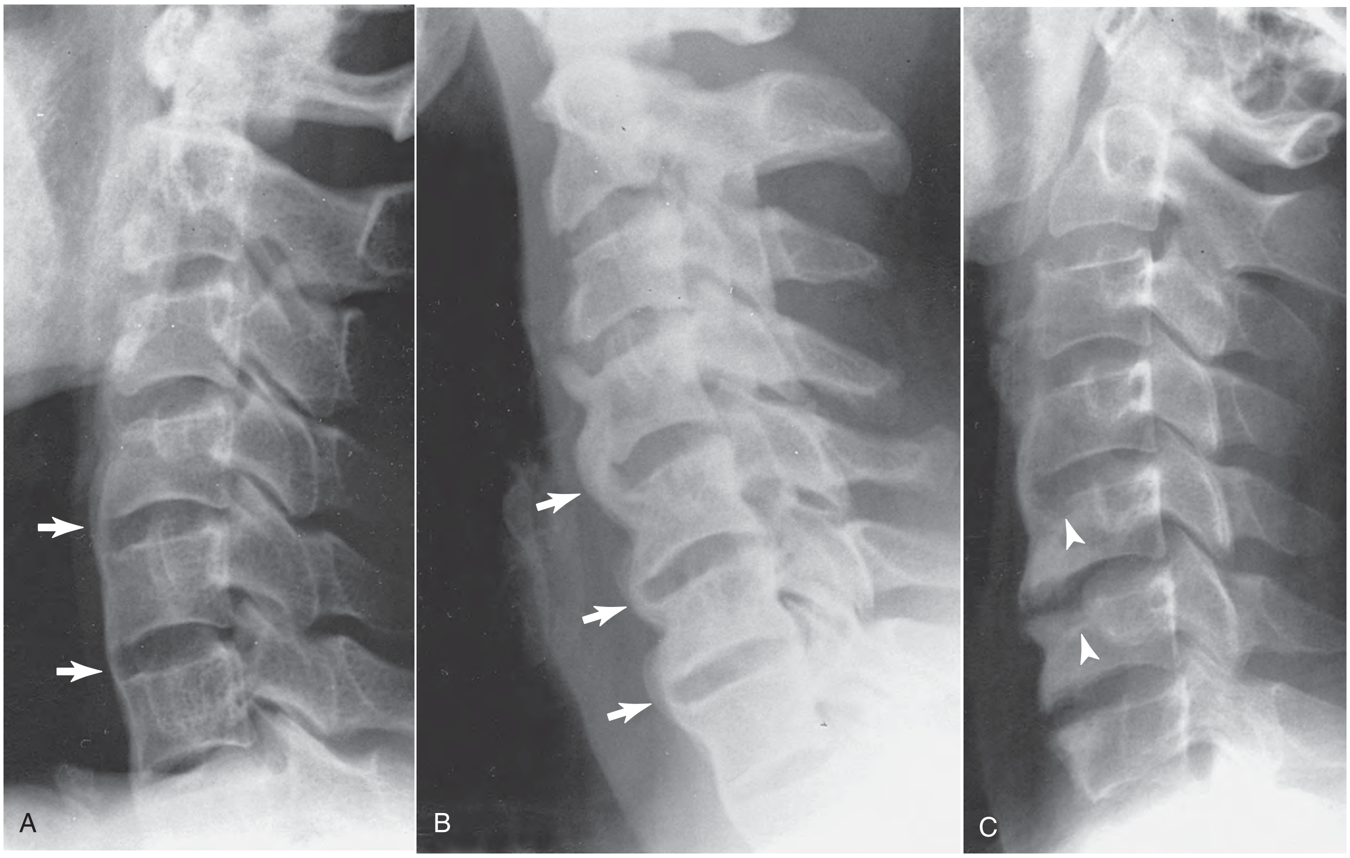

FIGURE 2–82 **Psoriatic arthropathy.**[84,181,182] **A,** A thin sheet of paravertebral ossification is seen spanning the anterior aspect of the lower cervical spine *(arrows).* The disc spaces and apophyseal joints are well preserved. **B,** In another patient, a thicker, more prominent pattern of ossification is present *(arrows).* The spinal outgrowths are nonmarginal, arising from the central portion of the anterior aspect of the vertebral body. The disc spaces are preserved. **C,** Acne conglobata. In a patient with this rare skin disease, the osseous outgrowths are seen as hyperostosis and sheetlike proliferations similar to findings seen in classic psoriatic arthritis. The disc and apophyseal joint spaces are intact, but erosions of the C5 and C6 vertebral endplates are evident *(arrowheads).* (*C, Courtesy N. Kinnis, MD, Chicago.)*

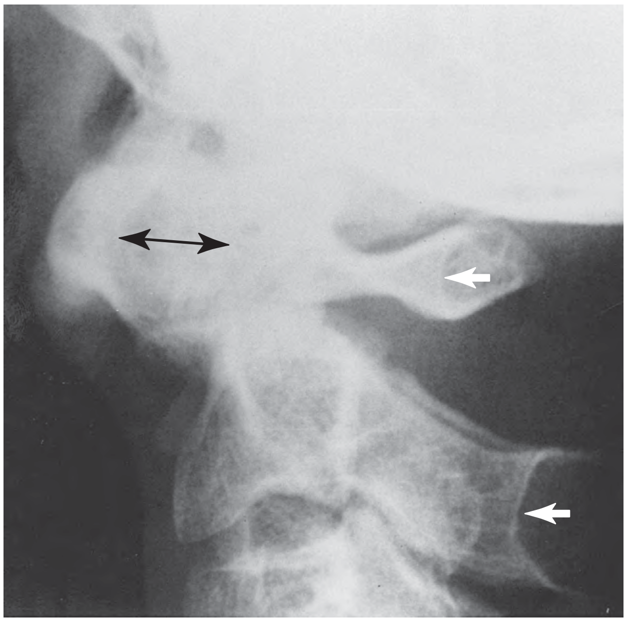

FIGURE 2–83 Reactive arthritis: atlantoaxial instability.[85] In this patient with long-standing Reiter syndrome, observe the anterior translation of C1 in relation to C2. The atlantodental interspace measures 14 mm *(black double-headed arrow),* and the C1 spinolaminar junction line is significantly displaced in relation to that of C2 *(white arrows).*

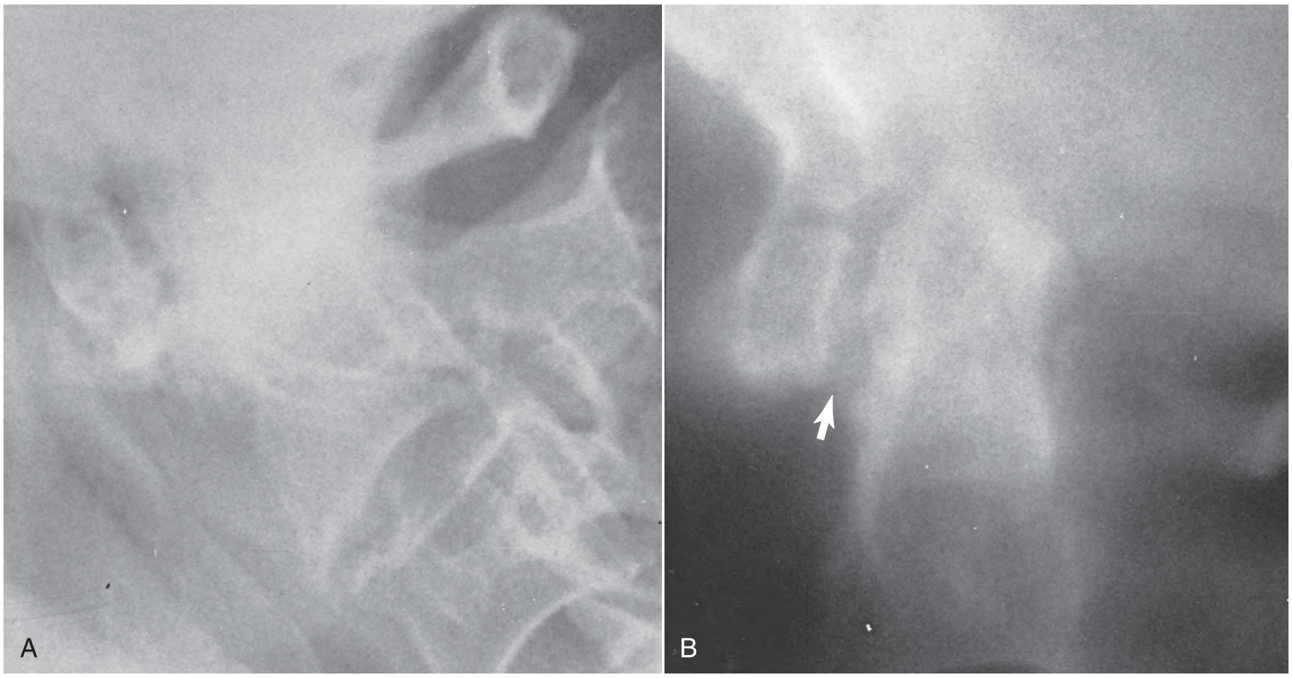

FIGURE 2–84 Calcium pyrophosphate dihydrate (CPPD) crystal deposition disease.[86,87] **A,** In a 76-year-old man, a lateral radiograph obtained in flexion reveals erosion and sclerosis of the atlantoaxial articulation. **B,** Lateral conventional tomogram reveals atlantoaxial instability *(arrow)* and irregularity of the articular surfaces.

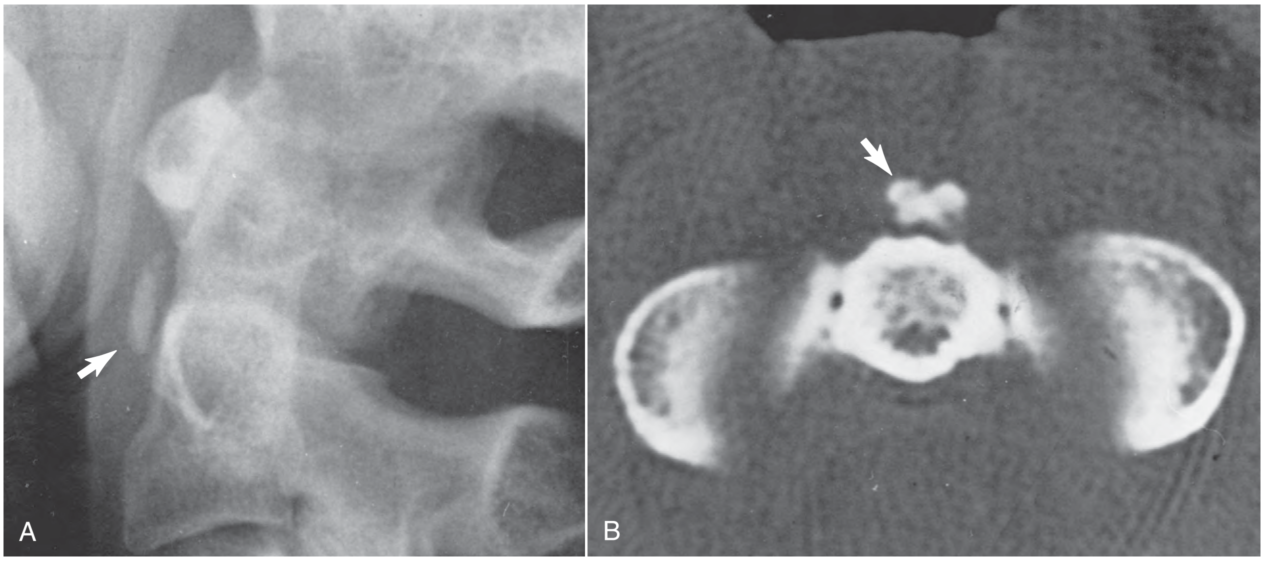

FIGURE 2–85 **Retropharyngeal calcific tendinitis: calcium hydroxyapatite crystal deposition disease (HADD)**[88,136,144] **A,** In this 46-year-old woman with neck pain, fever, and limitation of motion, a globular collection of calcification is seen within the soft tissues adjacent to the anterior aspect of the C2 vertebral body *(arrow).* **B,** In a 28-year-old man, a transaxial CT scan reveals that the calcification is located within the longus colli muscle and tendon *(arrow)* anterior to the base of the odontoid and posterior to the pharynx. Calcific tendinitis at this site is a self-limited condition that typically affects middle-aged persons. It may be asymptomatic or result in acute neck pain, torticollis, occipital pain, nuchal rigidity, and dysphagia. (***A-B,*** *Courtesy G. Greenway, MD, Dallas.)*

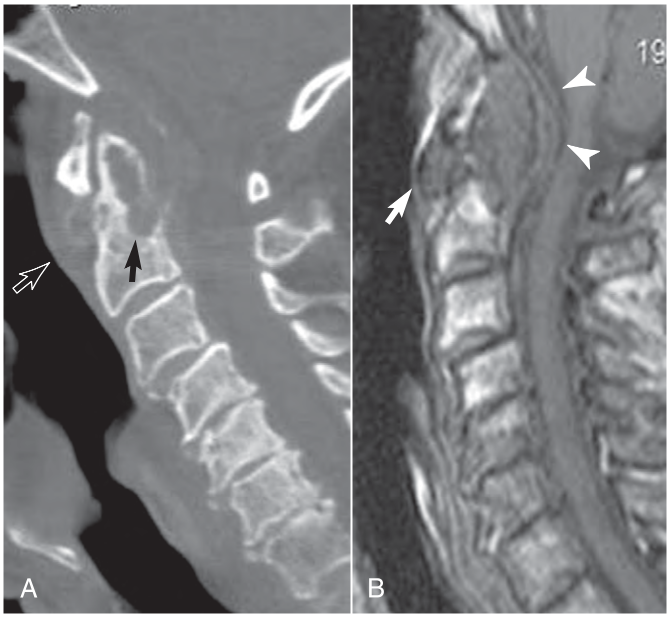

FIGURE 2–86 **Tophaceous gout.**[89,156] This 65-year-old man suffered from chronic tophaceous gout. Sagittal reformatted CT **(A)** image demonstrates extensive osteolytic destruction and cortical disruption *(arrow)* of the odontoid and prevertebral soft tissue prominence *(open arrow).* A sagittal T1-weighted MR **(B)** image shows extensive tophus eroding the odontoid with prevertebral *(arrow)* and epidural *(arrowheads)* extension of the tophaceous material.

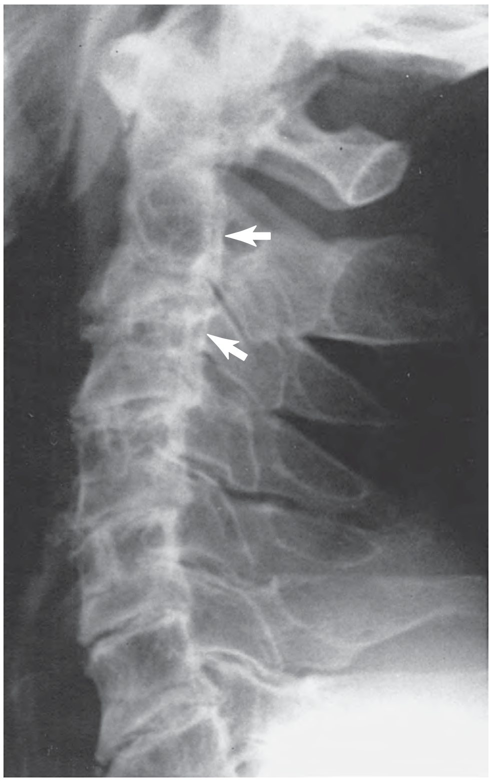

FIGURE 2–87 **Alkaptonuria.**[90] Prominent intervertebral disc narrowing, calcification, and ossification are evident in this patient with long-standing ochronosis. Note also the presence of vertebral endplate sclerosis. A vertical linear radiodense band within the spinal canal at the C2-C3 level *(arrows)* represents ossification of the posterior longitudinal ligament, a complication that may result in spinal stenosis.

TABLE 2-16 **MR Imaging Findings in Vertebral Osteomyelitis***

Loss of endplate definition (95%)

Contrast enhancement of both disc and vertebral body (94%)

Signal intensity changes of both the vertebral body on T1-weighted images and of the disc on T1-weighted and T2-weighted images (85%)

Signal intensity changes of both vertebral body and disc on T1-weighted and T2-weighted images (46%)

Ring enhancement with abscess

Homogeneous enhancement with phlegmon

Signal Change	Imaging Protocol	Site	Percent
Decreased	T1-weighted	Vertebral body	91
Increased	T2-weighted	Vertebral body	56
Increased	T2-weighted	Disc	95

Modified from Dagirmanjian A, Schils J, McHenry M, et al: MR imaging of vertebral osteomyelitis revisited. AJR 167:1539, 1996.

* N = 37 patients, 41 vertebral levels.

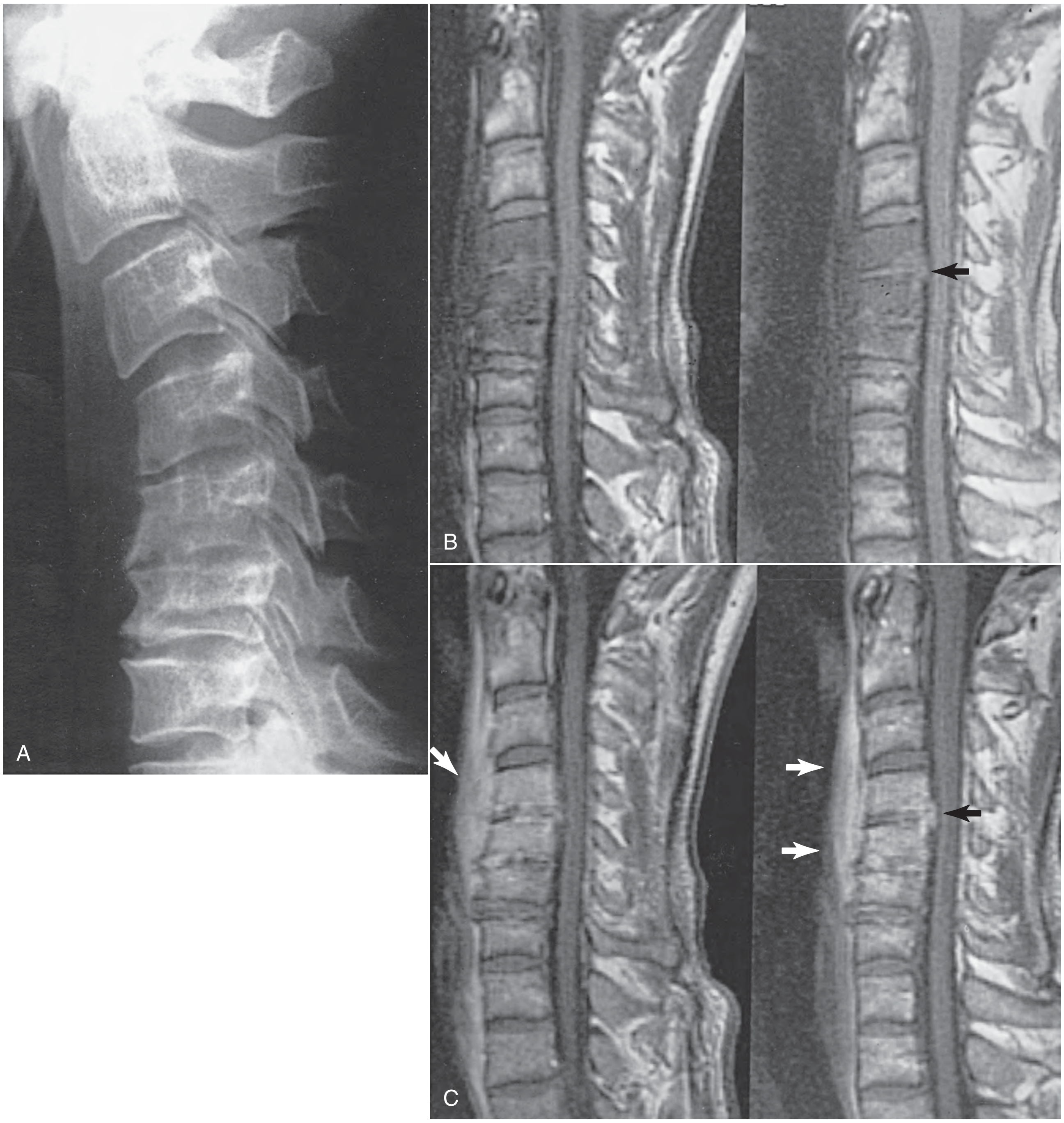

FIGURE 2–88 Infectious (pyogenic) spondylodiscitis: direct implantation.[91-93,138,170,174] This 40-year-old man had persistent neck pain after a discogram. **A,** Lateral radiograph reveals a kyphotic posture and marked disc space narrowing at C4-C5 and C5-C6. **B,** The routine sagittal T1-weighted (TR/TE, 450/20) spin echo MR images demonstrate low signal intensity in the marrow of the C4, C5, and C6 vertebral bodies. The intervertebral disc spaces are narrowed and erosions of the vertebral endplates are evident. **C,** Sagittal T1-weighted (TR/TE, 450/20) spin echo MR images obtained after intravenous gadolinium administration demonstrate marked enhancement within the vertebral bodies, prevertebral soft tissues *(white arrows),* and a small epidural abscess that extends into the spinal canal at the C4-C5 level *(black arrow). Staphylococcus aureus* was cultured, and the patient was treated with antibiotics.

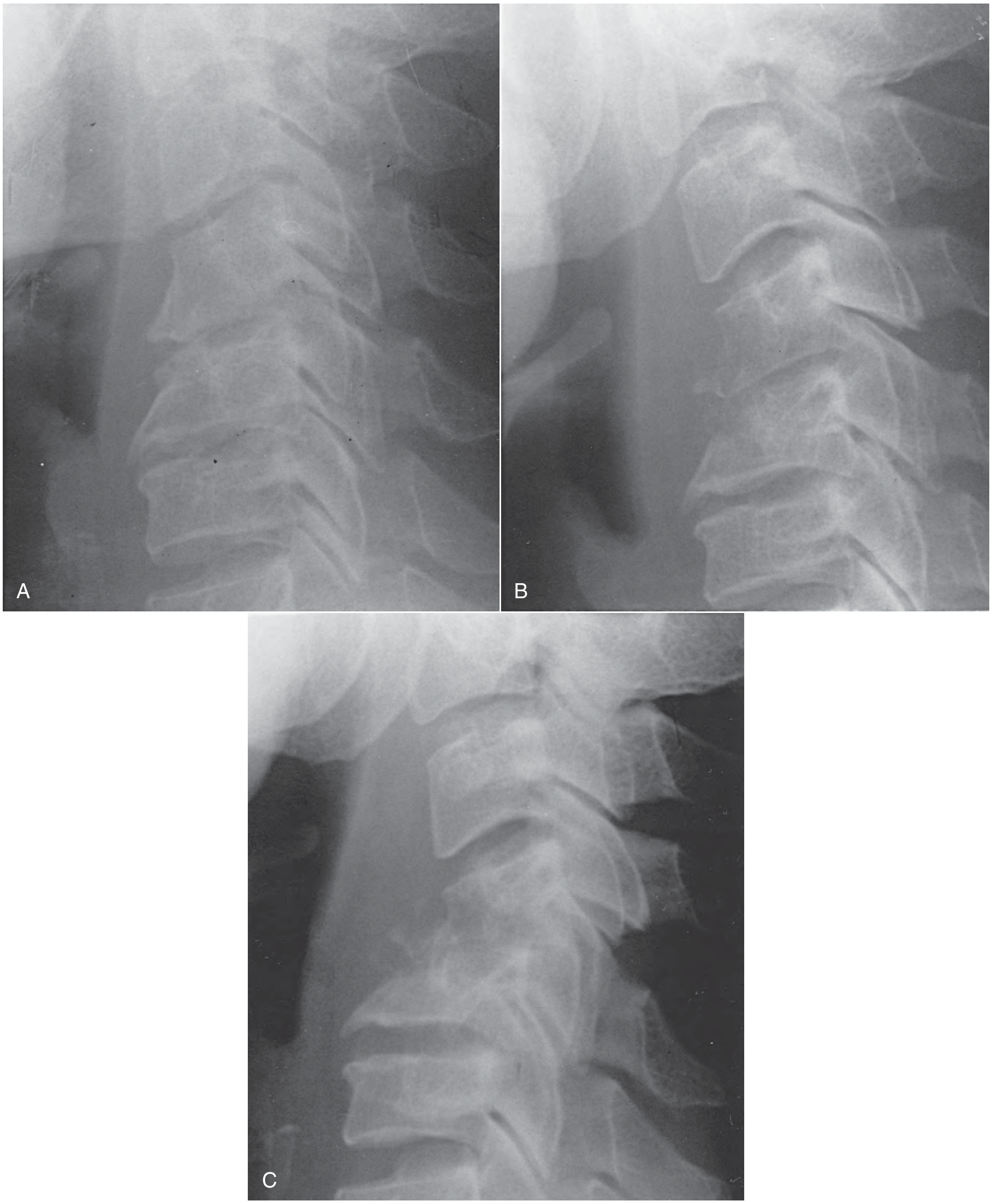

FIGURE 2–89 **Infectious (pyogenic) spondylodiscitis.**[91-93,138,170,174] Serial radiographs from this 40-year-old male heroin addict taken initially **(A)** and 3 weeks **(B)** and 6 weeks **(C)** later reveal rapid destruction of the C4-C5 discovertebral junctions. Observe the progressive obliteration of the cortical margins of the vertebral endplates and eventual pathologic vertebral collapse, resulting in dramatic subluxation. The organism cultured was *Klebsiella pneumoniae,* an extremely rare cause of musculoskeletal infection, usually found only in patients with diminished resistance.

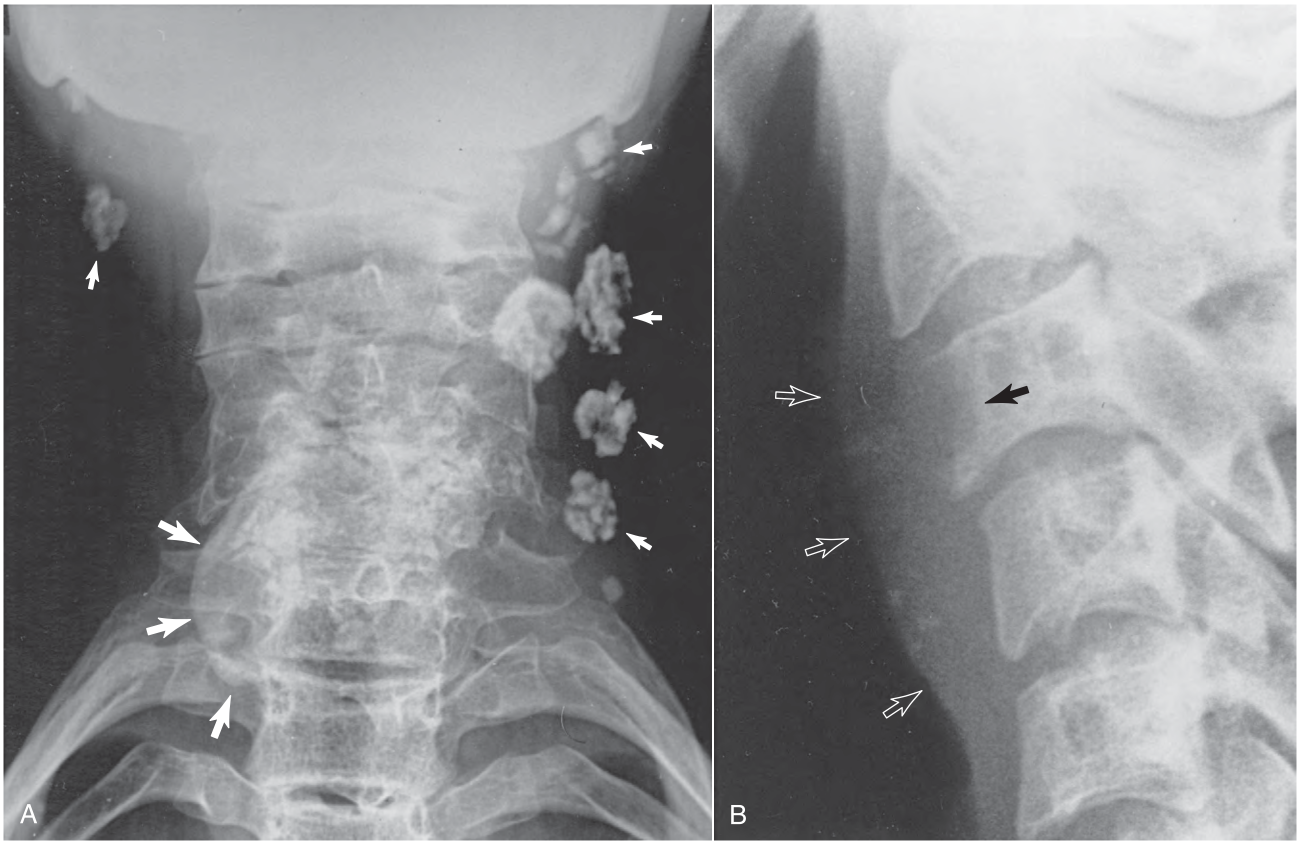

FIGURE 2–90 **Tuberculous spondylodiscitis.**[94,174] **A,** Calcified paravertebral abscess. Observe a diffuse curvilinear zone of calcification overlying the cervicothoracic region, representing a tuberculous abscess *(large arrows).* Extensive popcornlike calcifications also are noted in the paravertebral lymph nodes *(small arrows).* Extension of tuberculosis from vertebral and discal sites to the adjacent ligaments and soft tissues is frequent. Extension usually is anterolateral, but it may occur posteriorly into the peridural space. **B,** Prevertebral abscess. Prevertebral soft tissue swelling *(open arrows)* indicates extraspinal extension of an abscess in this patient. Note also the erosion of the third cervical vertebral body *(black arrow).* (***A-B,*** *Courtesy A. D'Abreu, MD, Porto Alegre, Brazil.)*

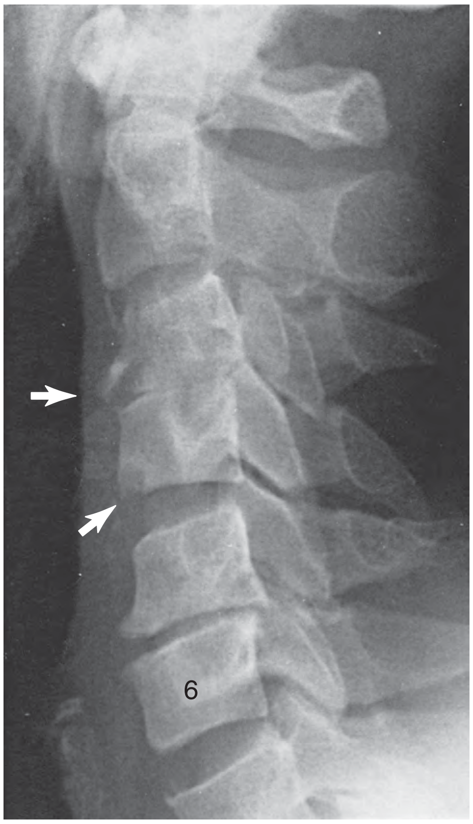

FIGURE 2–91 **Dialysis spondyloarthropathy.**[95,165] A radiograph from this hemodialysis patient demonstrates disc space destruction, vertebral endplate erosion, and vertebral body collapse at the C3-C4 level *(upper arrow).* A small erosion is seen at the inferior aspect of the C4 vertebral body *(lower arrow),* and early C5-C6 disc space narrowing also is evident. This peculiar type of destructive spondyloarthropathy, well recognized in patients undergoing hemodialysis for a period of years, must be differentiated from spinal infection, neuropathic osteoarthropathy, and calcium pyrophosphate dihydrate or calcium hydroxyapatite crystal deposition disease.

TABLE 2-17 Tumors and Tumorlike Lesions Affecting the Cervical Spine*

Entity	Figure(s), Table(s)	Characteristics
Malignant		
Skeletal metastasis[96]	2-92	75% osteolytic; 25% osteoblastic or mixed pattern Usually multiple sites of involvement Pathologic vertebral collapse, pedicle destruction, or ivory vertebra
Primary malignant neoplasms of bone		
Osteosarcoma (conventional)[97,183]		*Very rare occurrence in the spine:* only 4% of osteosarcomas arise from the spine Vertebral body involvement often leads to vertebral collapse Readily metastasizes to other bones and lung
Osteoblastoma (aggressive)[98]	2-93	23% of aggressive osteoblastomas affect the spine Expansile osteolytic lesion of the neural arch that may be partially ossified or contain calcium
Chondrosarcoma (conventional)[99]		*Extremely rare:* only 6% affect the spine Often contain calcification
Giant cell tumor (aggressive)[100]		Eccentric osteolytic lesion, rare in the spine
Fibrosarcoma[101]		Extremely rare in the spine
Ewing sarcoma[102]		Extremely rare in the cervical spine
Chordoma[103]	2-94	75% of all chordomas affect the spine; some of these involve the axis *Most common pattern:* central osteolytic, expansile destruction of the vertebral body; infrequently, osteosclerotic or mixed; soft tissue mass
Myeloproliferative Disorders		
Plasma cell myeloma[104,139,140]		Common malignancy of the spine
Multiple myeloma (75% of all plasma cell myeloma)	2-95	75% of patients have spinal lesions *Early:* Normal radiographs or diffuse osteopenia *Later:* Multiple well-circumscribed osteolytic lesions Pathologic vertebral collapse False-negative bone scans common
Solitary plasmacytoma (25% of all plasma cell myeloma)[178]		50% of plasmacytomas affect the spine Solitary, geographic, expansile, osteolytic lesion that frequently results in pathologic collapse 70% eventually develop into multiple myeloma Low signal intensity curvilinear areas within vertebra on T1-w spin echo MR imaging
Hodgkin disease[105,137]		43% of all skeletal lesions in Hodgkin disease affect the spine More than 60% of patients have multiple sites of involvement 75% of lesions are osteolytic; 25% are osteosclerotic
Primary lymphoma (non-Hodgkin)[106,107,137]	2-96	Spinal involvement in 13% of patients with non-Hodgkin lymphoma May result in multiple moth-eaten or permeative osteolytic lesions, with pathologic vertebral collapse Common cause of pathologic fracture Diffuse or localized sclerotic lesions are rare
Leukemia[108]		Osteoporosis, compression fractures, and radiolucent bands adjacent to the endplates
Benign		
Primary benign neoplasms of bone		
Enostosis[109]		Only 2% affect the spine Painless, circular zone of osteosclerosis May be normal or warm on bone scan
Osteoid osteoma[110]	2-97	6% of osteoid osteomas affect the spine Reactive sclerosis of the pedicle or other part of the neural arch Central radiolucent nidus usually is less than 1 cm in diameter and often is not visible on routine radiographs

* See also Tables 1-12 to 1-14.

TABLE 2-17 Tumors and Tumorlike Lesions Affecting the Cervical Spine—cont'd

Entity	Figure(s), Table(s)	Characteristics
Osteoblastoma (conventional)[184]	2-98	30% of osteoblastomas affect the spine Approximately 95% of osteoblastomas are benign Expansile lesion of neural arch, usually purely osteolytic with a predilection for C4, C5, and C6
Osteochondroma (solitary)[111,112]	2-99	Only 2% occur in the spine Pedunculated or sessile cartilage-covered osseous excrescence arising from the surface of a lamina, transverse process, or spinous process
Hereditary multiple exostosis[113]		*Infrequently involves spine:* multiple lesions, each with same appearance as solitary osteochondroma
Giant cell tumor (benign)[114]	2-100	Only 7% affect the cervical spine Eccentric osteolytic neoplasm 90%-95% of all giant cell tumors are benign
Hemangioma (solitary)[115,164,171]	2-101	25% affect the spine Corduroy cloth appearance of vertebral body related to accentuated vertical striations Extraosseous hemangiomas may occur and can result in cord compression and myelopathic signs and symptoms.
Aneurysmal bone cyst[116,117]	2-102	14% of all lesions affect the spine Eccentric, expansile osteolytic lesion arising from the neural arch; isolated involvement of the vertebral body is uncommon and usually is associated with simultaneous involvement of the posterior elements Typically more expansile than osteoblastoma
Tumorlike Lesions		
Paget disease[118,119,142,143,168]	2-103	Predilection for upper cervical segments, but may affect any level Usually polyostotic and expansile, and is one cause of ivory vertebrae Coarsened trabeculae and endplates may create picture-frame vertebrae Vertebral enlargement common Spinal involvement may be osteolytic, osteosclerotic, or mixed Contiguous vertebrae may be involved, obliterating the disc spaces and resembling developmental synostosis
Neurofibromatosis type I (von Recklinghausen disease)[120,121]	2-104 Tables 1-14, 2-18	50% of patients develop skeletal lesions Posterior vertebral scalloping and enlargement of the neural foramina Associated with short, angular kyphoscoliosis (50% of cases) and dramatic cervical kyphosis
Fibrous dysplasia[122] Monostotic (70%-80%) Polyostotic (20%-30%)	2-105	Monostotic and polyostotic forms Monostotic spinal involvement extremely rare (less than 1% of lesions) 21% of patients with polyostotic fibrous dysplasia have spine involvement Thick rim of sclerosis surrounding a radiolucent lesion within multiple vertebral bodies with or without pathologic collapse
Langerhans cell histiocytosis[123,124]	2-106	6% of all lesions affect the spine Flattened vertebral bodies or, less commonly, bubbly, lytic, or expansile lesions without vertebral body collapse With healing, the height of the pathologically collapsed vertebral body may be reconstituted, a finding more common in younger persons Thoracic and lumbar lesions are more common than cervical spine lesions

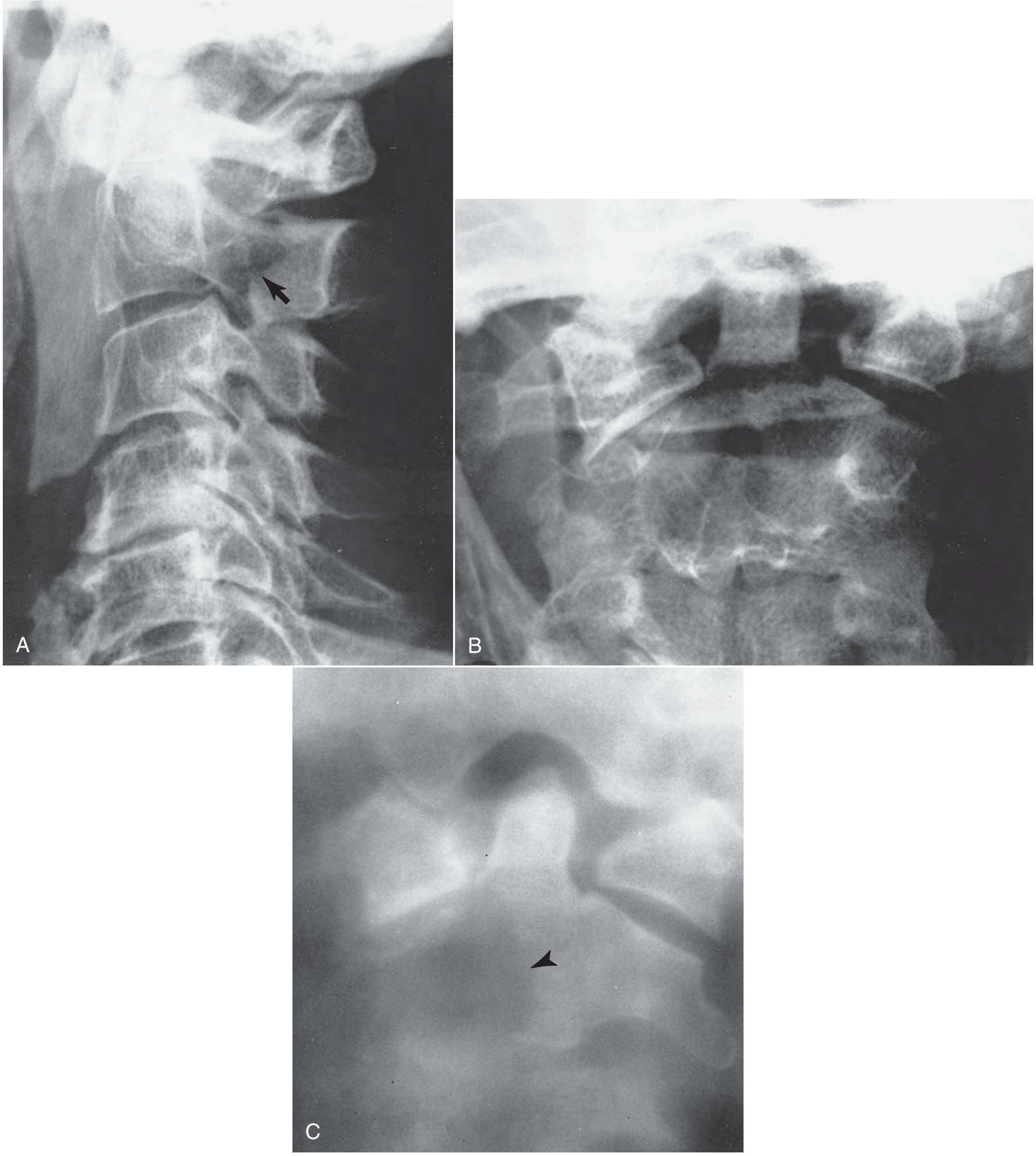

FIGURE 2–92 **Skeletal metastasis.**[96] Bronchogenic carcinoma: Osteolytic pattern. This 67-year-old man with lung cancer developed neck pain. **A-B,** Lateral cervical spine **(A)** and anteroposterior open mouth upper cervical **(B)** radiographs reveal barely perceptible osteolytic destruction and collapse of the second cervical vertebral body. In **A,** a fracture is seen through the neural arch *(arrow),* and severe lateral offset of the atlas in relation to the axis is present. **C,** Conventional tomogram more clearly defines the size and location of osteolytic destruction *(arrowhead).*

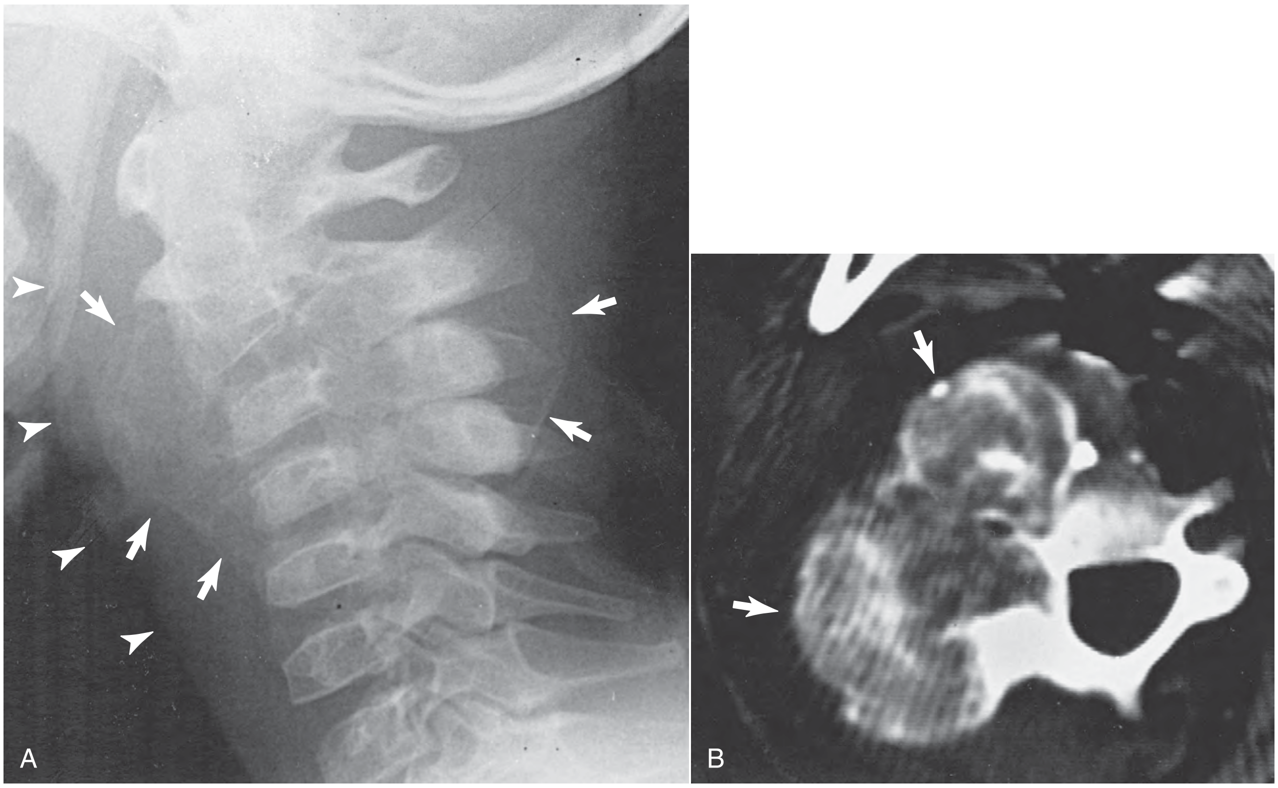

FIGURE 2–93 **Aggressive osteoblastoma.**[98] **A,** Lateral cervical spine radiograph of this 6-year-old boy shows a large, expansile lesion overlying the C2 to C5 cervical vertebrae *(arrows).* The articular processes of C2 and C3 appear radiolucent. Observe the prominent prevertebral soft tissues caused by swelling and extraosseous tumor extension *(arrowheads).* **B,** Transaxial CT scan through the C3 vertebral body documents the location, extent of osseous expansion, and partially calcified osteolytic matrix of the tumor.

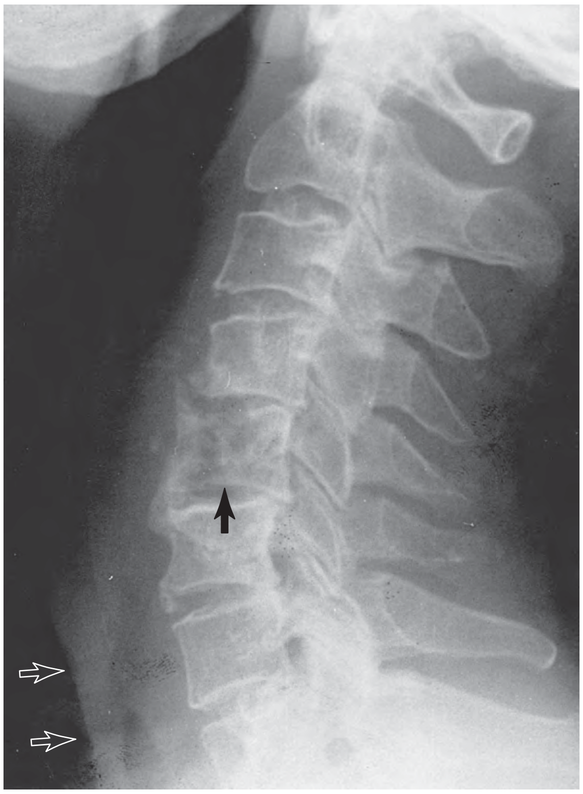

FIGURE 2–94 **Chordoma.**[103] A large, permeative, osteolytic lesion of the C5 vertebral body is seen *(arrow).* Note the osteolysis of the C5 vertebral endplates. Observe also the prominent prevertebral soft tissues, indicating swelling or neoplastic extension *(open arrows).*

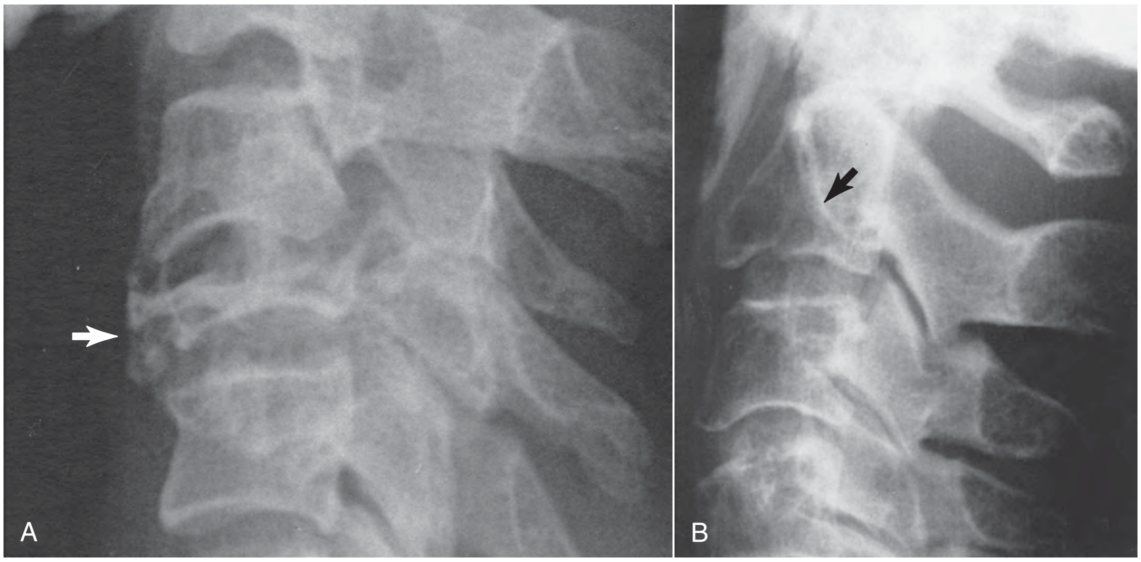

FIGURE 2–95 **Plasma cell myeloma.**[104,139,140] **A,** Complete collapse of the fourth cervical vertebral body *(arrow)* is seen in this 40-year-old man. **B,** In another patient, an osteolytic lesion within the vertebral body of C2 is seen *(arrow).* Diffuse osteopenia of the entire cervical spine is also present.

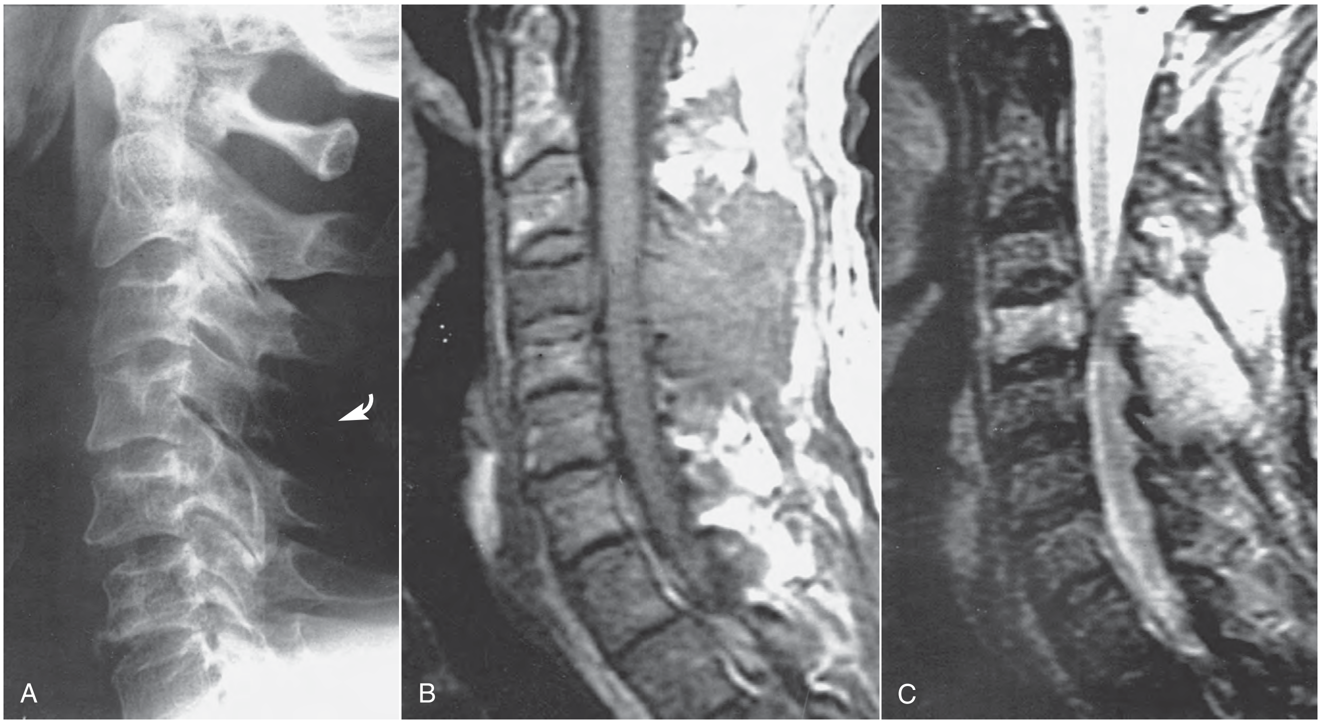

FIGURE 2–96 **Non-Hodgkin lymphoma: large cell type.**[106,107,137] Spinal involvement in a 65-year-old man. **A,** Routine radiograph reveals diffuse osteopenia and focal osteolysis of the fourth cervical spinous process *(curved arrow).* Sagittal T1-weighted (TR/TE, 600/11) **(B)** and T2-weighted (TR/TE, 2000/70) **(C)** spin echo MR images reveal destruction of this spinous process and a soft tissue mass that results in spinal canal stenosis. The high signal intensity in the C4 vertebral body on the T2-weighted image represents bone marrow edema or tumor infiltration.

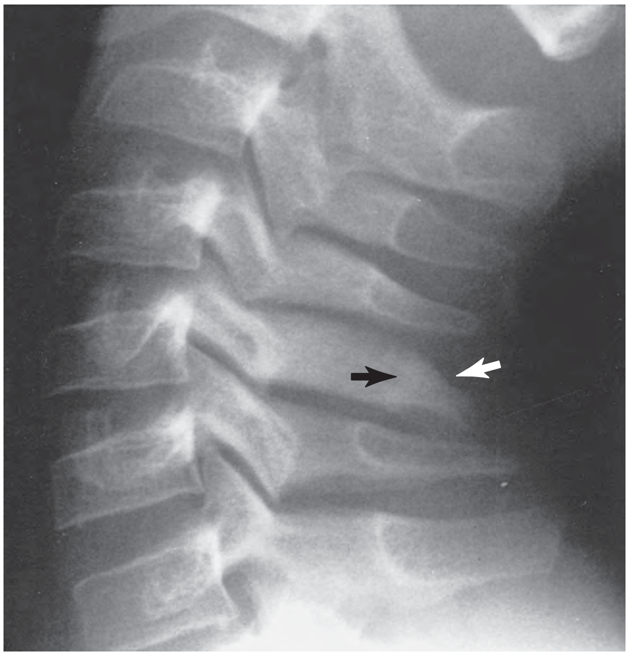

FIGURE 2–97 **Osteoid osteoma.**[110] In this 12-year-old boy with severe neck pain and rigidity, the spinous process of C5 appears sclerotic *(white arrow).* The spinolaminar junction line is obliterated, and a tiny circular radiolucent nidus is seen *(black arrow).* A biopsy revealed osteoid osteoma, and the lesion was surgically resected.

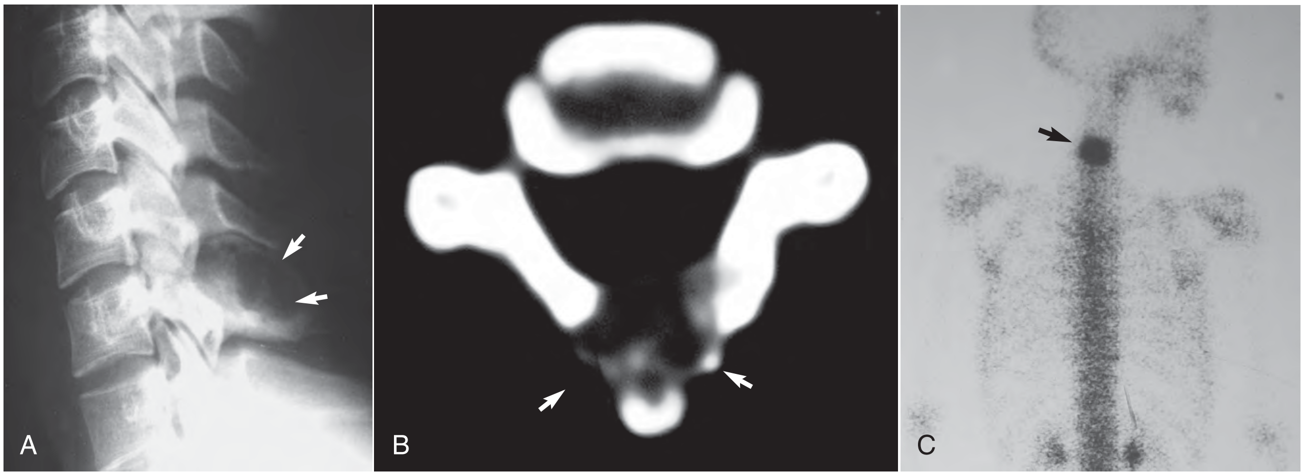

FIGURE 2–98 **Osteoblastoma (conventional).**[184] A lateral radiograph of the cervical spine **(A)** reveals an osteolytic expansile lesion involving the spinous process of C6 *(arrows).* An axial CT scan, soft tissue window **(B)** reveals the extent of the osteolytic process *(arrows)* and a bone scan **(C)** clearly demonstrates a focal zone of intense uptake *(arrow)* within the lower cervical spine. This lesion proved to be an osteoblastoma on pathologic examination.

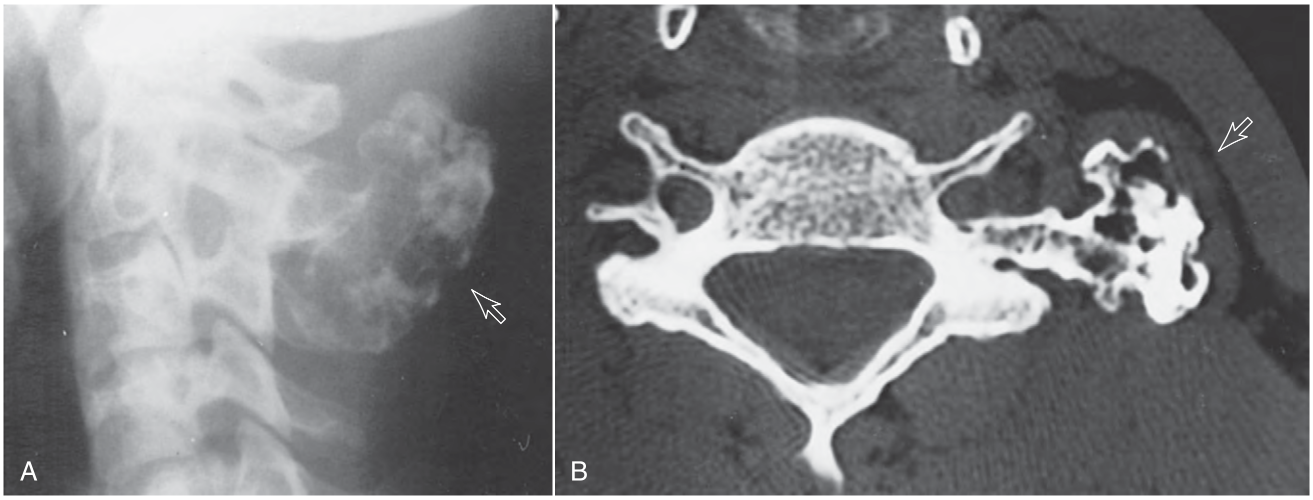

FIGURE 2–99 **Solitary osteochondroma.**[111,112] **A,** Oblique cervical spine radiograph from this 7-year-old child reveals an irregular, pedunculated osseous exostosis arising from the spinous process of C2 *(open arrow).* **B,** In another patient, a transaxial CT image reveals a large osteocartilaginous lesion. Observe that the cortex and medulla of the tumor are continuous with those of the posterior tubercle of the transverse process. The cartilaginous cap displaces the soft tissues of the anterolateral neck *(open arrow). (**B,** Courtesy G.D. Schultz, DC, Portland, Ore.)*

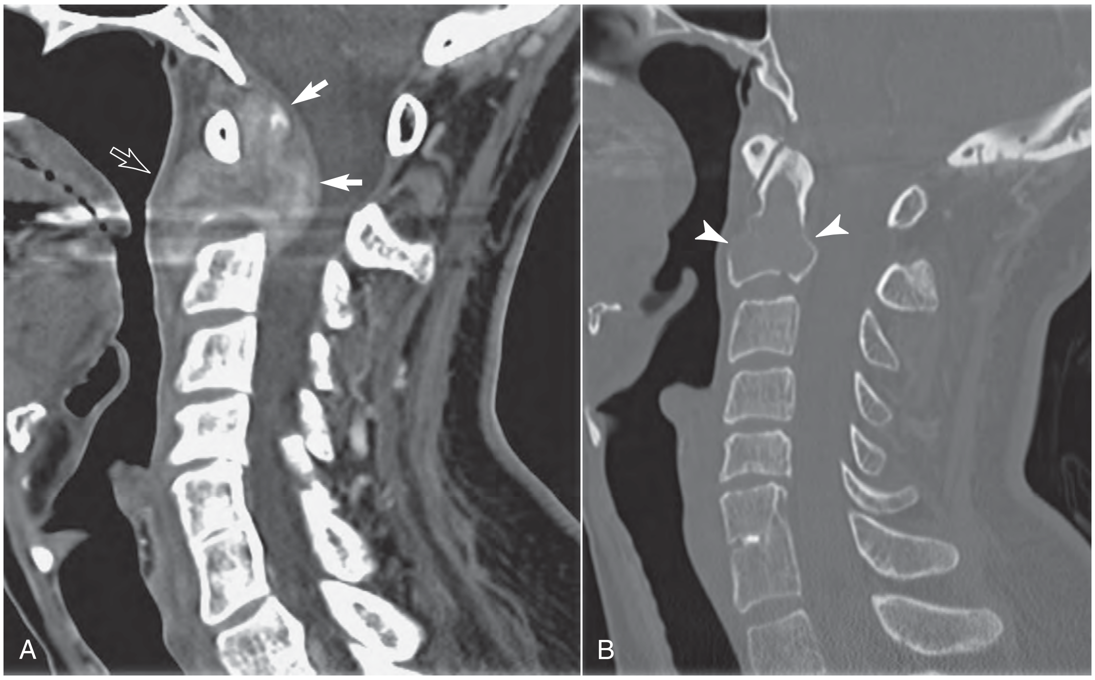

FIGURE 2–100 **Giant cell tumor (benign).**[114] This 50-year-old female had severe neck pain and neurologic signs that proved to be the result of a giant cell tumor involving the C2 vertebra. Reformatted sagittal soft tissue window **(A)** and bone window **(B)** CT images reveal extensive osteolytic destruction of the C2 vertebral body and odontoid *(arrowheads)* along with a large soft tissue mass extending into the prevertebral soft tissues *(open arrow)* and epidural space *(arrows)* resulting in significant stenosis. Of incidental note is the presence of a congenital synostosis (block vertebrae) of C6-C7. *(Courtesy B.A. Howard, MD, Charlotte, NC.)*

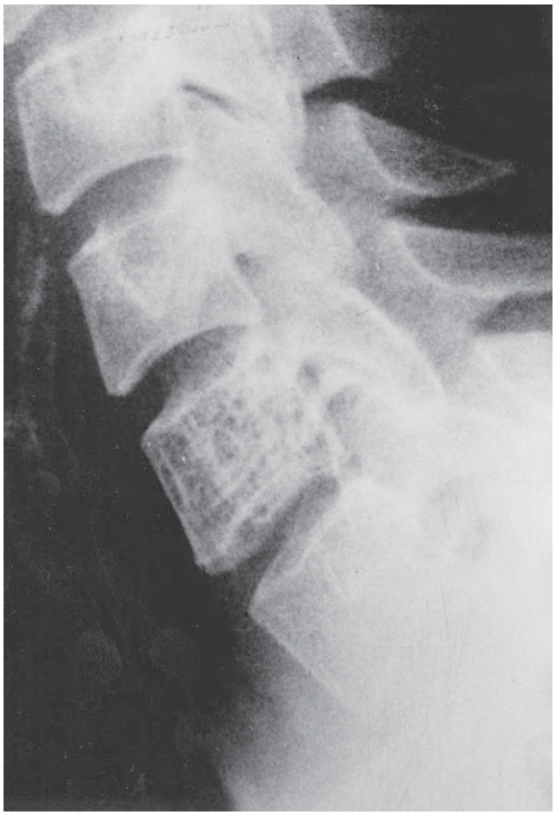

FIGURE 2–101 Hemangioma.[115,164,171] Observe the striated, lacelike trabeculae within the C6 vertebral body. The cortex and vertebral endplates are intact, and there is no evidence of vertebral body expansion. Hemangiomas may occasionally extend from the vertebral body into the neural arch, but not in this case. *(Courtesy A.L. Anderson, DC, Portland, Ore.)*

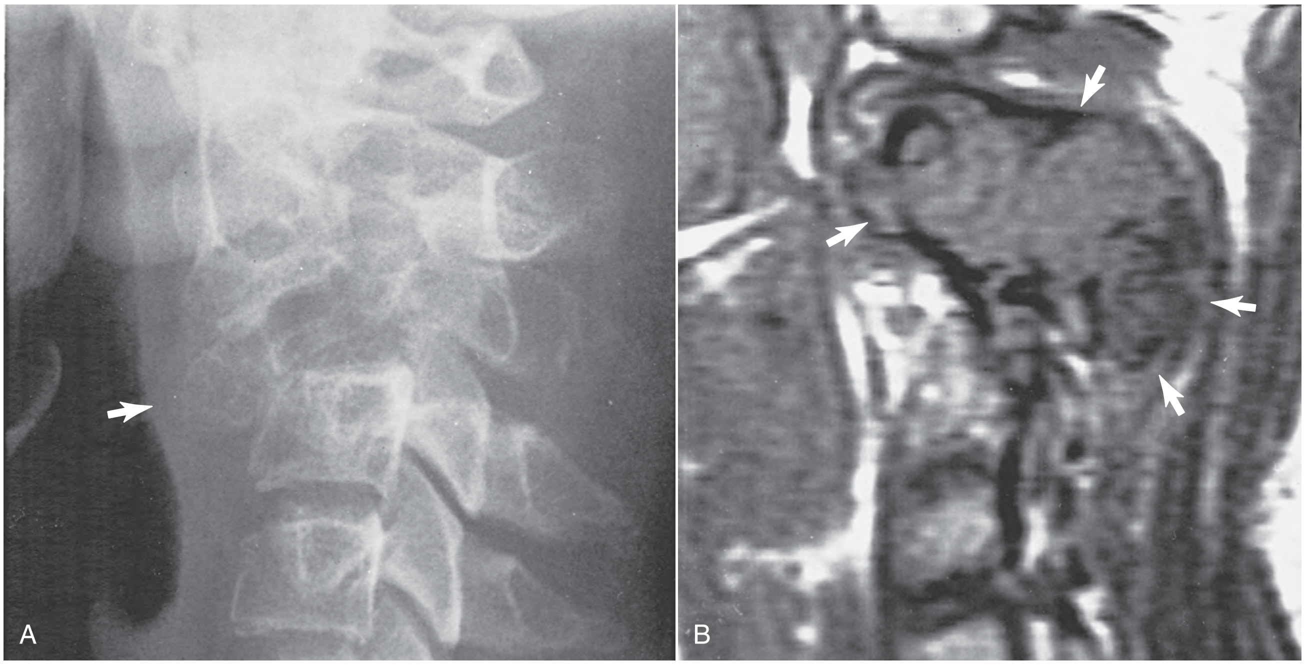

FIGURE 2–102 Aneurysmal bone cyst.[116,117] In this 10-year-old child, a routine lateral cervical radiograph **(A)** reveals an expansile osteolytic lesion of the C3 vertebral body and neural arch *(arrow)*. Sagittal T1-weighted (TR/TE, 700/20) spin echo MR image **(B)** more clearly defines the extent *(arrows)* and nature of the tumor as well as its widespread destruction and soft tissue infiltration. The lesion was biopsied and the histologic diagnosis was aneurysmal bone cyst. *(Courtesy L. Pinckney, MD, San Diego, Calif.)*

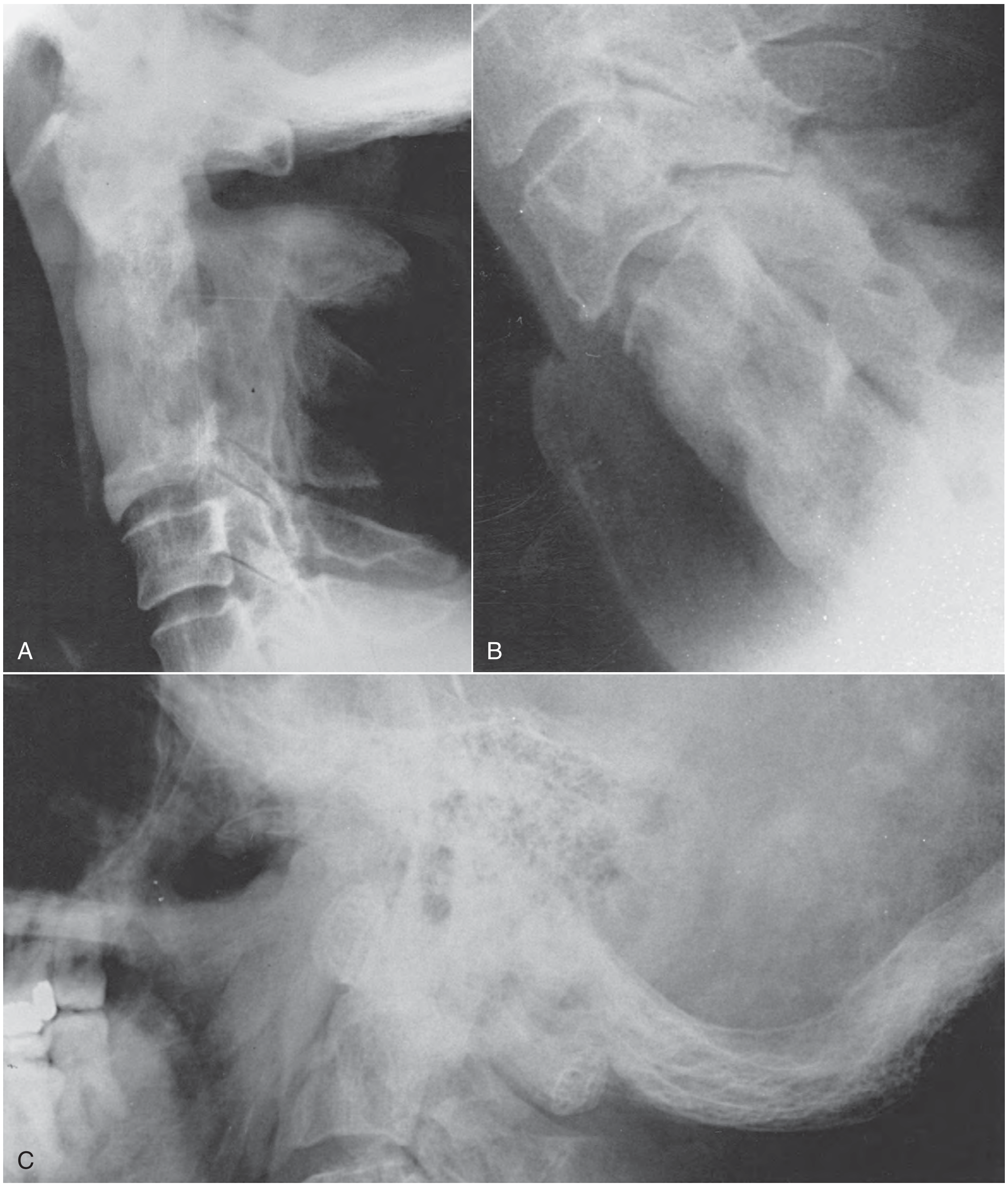

FIGURE 2–103 Paget disease.[118,119,142,143,168] **A,** Observe the expansion, fusion, and trabecular thickening involving the C2-C4 vertebrae in this patient with polyostotic Paget disease. **B,** In another patient, observe a similar pattern of osseous fusion affecting the C5-C7 levels. **C,** In a third patient, extensive upper cervical spine changes typical of Paget disease are evident. The base of the skull exhibits characteristic calvarial thickening and basilar invagination, complicating features of this bone-softening disease.

TABLE 2-18 Some Causes of Enlarged Cervical Intervertebral Foramen[6,19]

Neural Causes	Vertebral Artery Abnormalities
Neurofibroma* (Figure 2-104)	Vertebral artery tortuosity
Meningioma	Vertebral artery aneurysm (see Figure 2-118)
Meningocele	Arteriovenous malformation
Bone Neoplasms	Pseudoaneurysm
Aneurysmal bone cyst	Aortic coarctation
Skeletal metastasis	Subclavian steal syndrome
Osteoblastoma	Carotid artery obstruction
	Anomalous arterial loop
	Congenital
	Pedicle agenesis

* Most common cause.

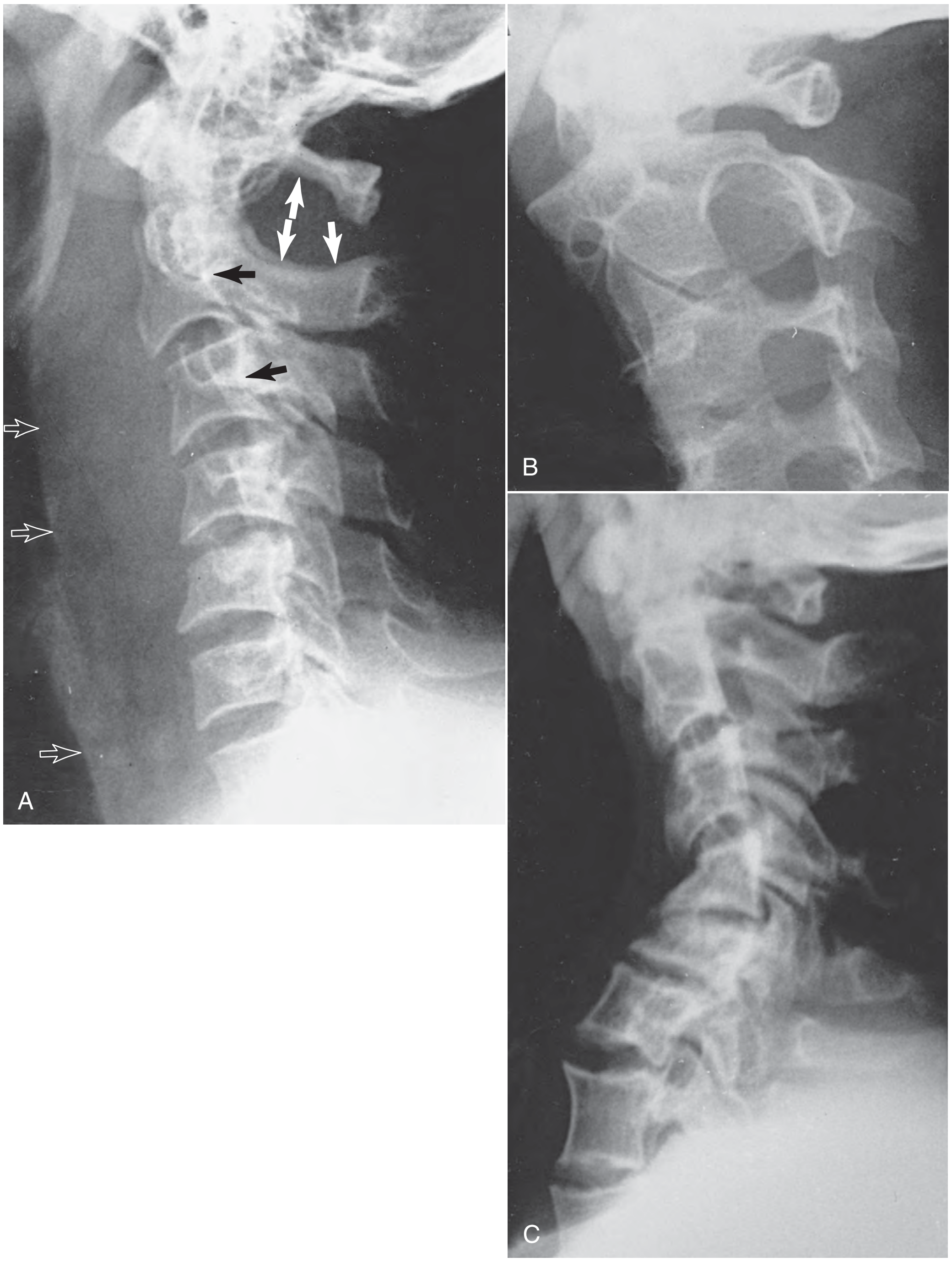

FIGURE 2–104 Neurofibromatosis type I (von Recklinghausen disease).[120,121] **A,** Note the posterior scalloping of the C2 and C3 vertebral bodies *(black arrows),* erosion of the C1 and C2 neural arches *(white arrows),* and dramatic prevertebral soft tissue widening *(open arrows)* caused by neurofibromas in the soft tissues. **B,** In another patient, an oblique cervical spine radiograph reveals characteristic enlargement of the neural foramina of C2-C3 owing to gradual scalloped erosion of the posterior vertebral bodies and adjacent pedicles. **C,** In a third patient, a severe kyphotic deformity with vertebral wedging is noted.

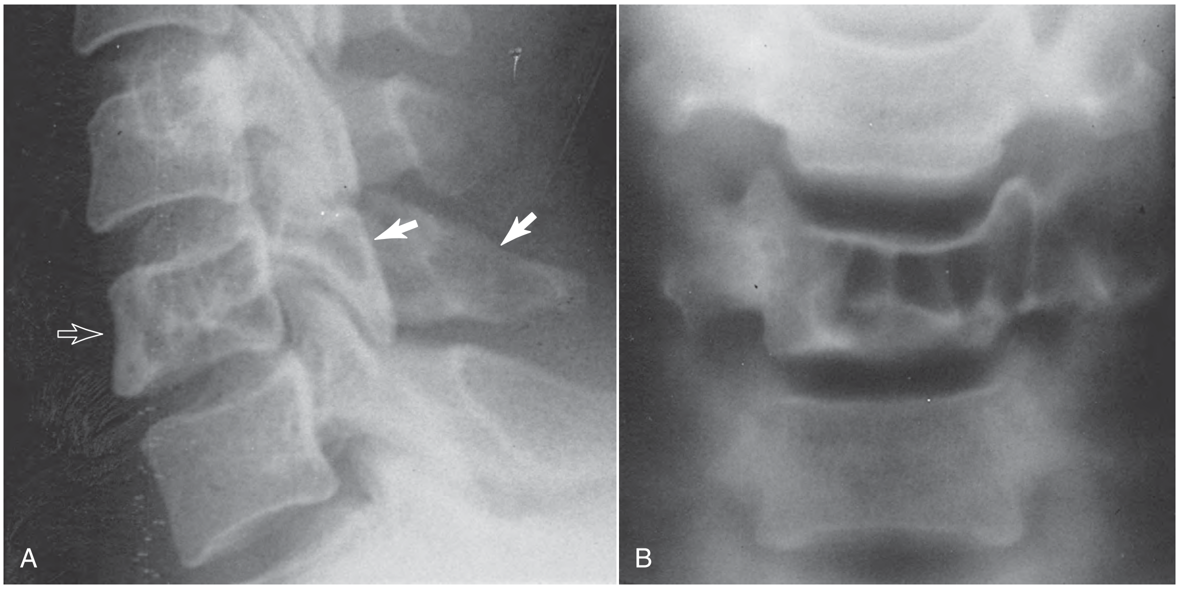

FIGURE 2–105 Fibrous dysplasia.[122] **A,** Lateral radiograph demonstrates trabecular alterations of the C6 vertebral body *(open arrow)* and neural arch *(arrows),* with areas of osteolysis and osteosclerosis. **B,** Frontal conventional tomogram more clearly delineates the osteolytic, multilocular appearance of the lesion. Pathologic collapse has occurred. Spinal involvement is infrequent in polyostotic fibrous dysplasia, and it is even more rare in monostotic disease.

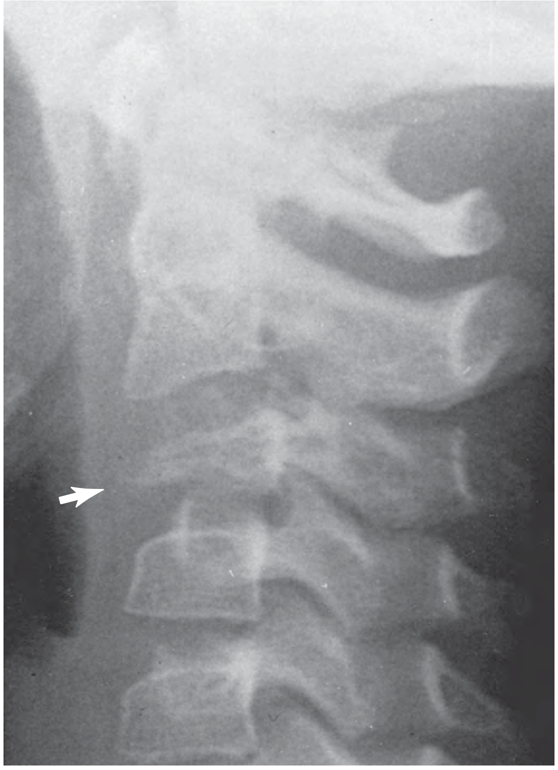

FIGURE 2–106 Langerhans cell histiocytosis: eosinophilic granuloma.[123,124] In this 6-year-old girl, a characteristic flattened C3 vertebral body (vertebra plana) is observed *(arrow)*. *(Courtesy L. Danzig, MD, Santa Ana, Calif.)*

TABLE 2-19 Metabolic Disorders Affecting the Cervical Spine*

Entity	Figure(s)	Characteristics
Generalized osteoporosis[125,126]	2-107	Uniform decrease in radiodensity, thinning of vertebral endplates, accentuation of vertical trabeculae, and fish vertebrae Most vertebral fractures occur in the thoracolumbar spine Routine radiographs may suggest the presence of osteoporosis, but bone densitometry is necessary for accurate assessment of the presence and extent of diminished bone mineral content See Chapters 1, 3, and 7 for more extensive discussions of osteoporosis
Osteomalacia[127]		Diminished radiodensity and prominent coarsened trabeculae Vertebral body fractures
Hyperparathyroidism and renal osteodystrophy[127]		Subchondral resorption at discovertebral junctions *Rugger-jersey spine:* bandlike sclerosis adjacent to superior and inferior surfaces of the vertebral body Vertebral fracture with biconcave deformities (more prominent in thoracolumbar spine)
Acromegaly[128]	2-108	Elongation and widening of the vertebral bodies, less common in the cervical than in the thoracic and lumbar regions Ossification of the anterior portion of the disc and posterior scalloping of vertebral bodies occur infrequently
Fluorosis[129]	2-109	Diffuse osteosclerosis and ossification of the posterior longitudinal ligament are the predominant spinal findings Prominent osteophytosis and periostitis also may be encountered Differential diagnosis includes DISH, osteopetrosis, skeletal metastasis, and other causes of diffuse osteosclerosis

* See also Table 1-15.

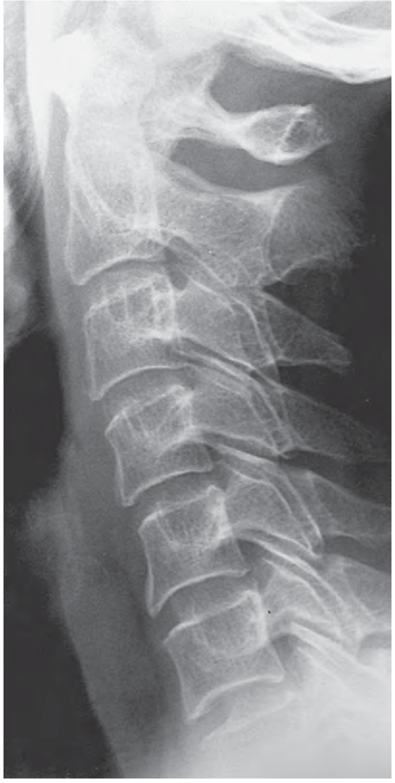

FIGURE 2–107 Generalized osteoporosis.[125,126] Marked thinning of the cortical margins and increased radiolucency of the vertebral bodies and posterior elements are seen in this 55-year-old postmenopausal woman. Although radiographs are relatively insensitive to changes in bone density, they may suggest the presence of osteopenia.

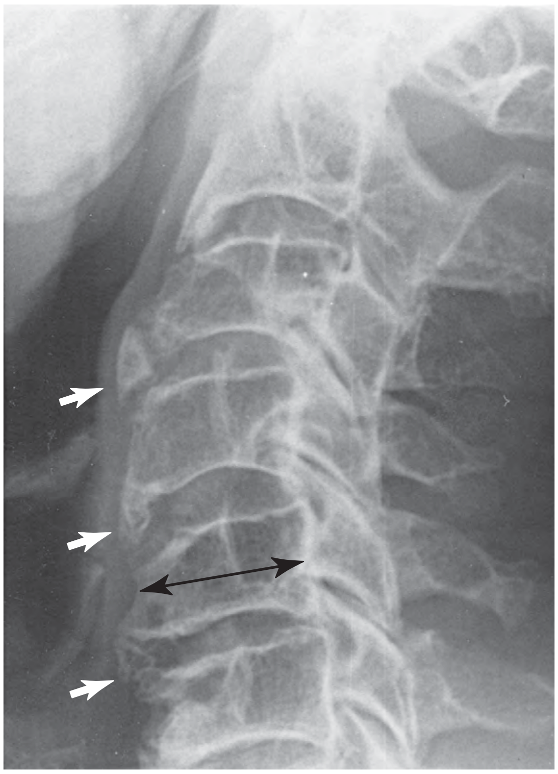

FIGURE 2–108 Acromegaly.[128] Elongation of the vertebral bodies *(double-headed arrow)* with prominent bone proliferation *(arrows)* is characteristic of acromegaly.

FIGURE 2–109 Fluorosis.[129] Observe the extensive ossification of the paraspinal ligaments and the generalized increased radiodensity of the spine in this patient with fluoride poisoning. *(Courtesy G. Beauregard, Montreal, Quebec, Canada.)*

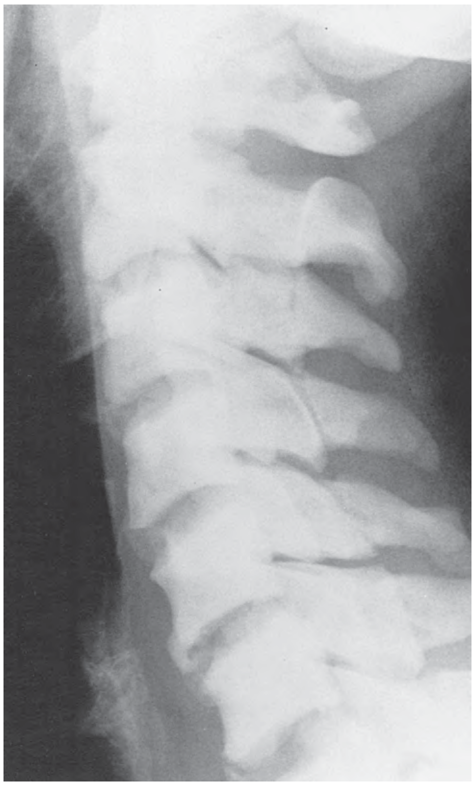

TABLE 2-20 Cervical Spine Intervertebral Disc Abnormalities

Entity	Figure(s), Table(s)	Characteristics
Acute disc herniation[130]	2-110	Peak prevalence is in the third and fourth decades of life Patients may have radiculopathy, neck pain, or myelopathy Most frequent sites are C6-C7 (60%-75%) and C5-C6 (20%-30%) Uncalcified (soft) disc herniations are not visible on plain radiographs; best imaged using MR imaging, computed tomography (CT), or CT myelography *Two major types identified:* Central (median) and foraminal (paramedian) ***Central disc herniation*** Central disc herniations may be compressive or noncompressive. Often those that compress the thecal sac may be as large as 3-5 mm without causing significant symptoms, such as radiculopathy Larger central herniations may compress the thecal sac and nerve roots, contributing to significant stenosis and resulting in radiculopathy or even myelopathy ***Foraminal disc herniation*** Lateral protrusions of disc material Owing to limited space within the nerve root canal, these herniations more frequently result in nerve root compression and radiculopathy than do central lesions Foraminal herniations may be more difficult to visualize than central lesions on MR images because of volume averaging and decreased conspicuousness within the nerve root canal Differentiation of disc herniations from degenerative osteophytes arising from the posterior discovertebral margins and uncovertebral joints may be difficult on MR imaging and myelography
Chronic cervical spondylosis[68-73]	2-116	See also earlier discussion (degenerative diseases) Degenerative disc disease (spondylosis) is very common in elderly patients and is often asymptomatic Chronic degeneration leading to posterior discovertebral, apophyseal, and uncovertebral marginal osteophytes may result in spinal stenosis, foraminal encroachment, and compression of cervical nerve roots (radiculopathy) or cord (myelopathy) Patients with degenerative (or congenital) stenosis are much more likely to develop myelopathy and are more susceptible to cord or nerve root damage from minor trauma The higher discs are more frequently involved in younger patients, whereas in older patients the lower discs are more frequently involved and the process of degeneration becomes more generalized MR imaging interpretation tends to overestimate the degree of foraminal stenosis

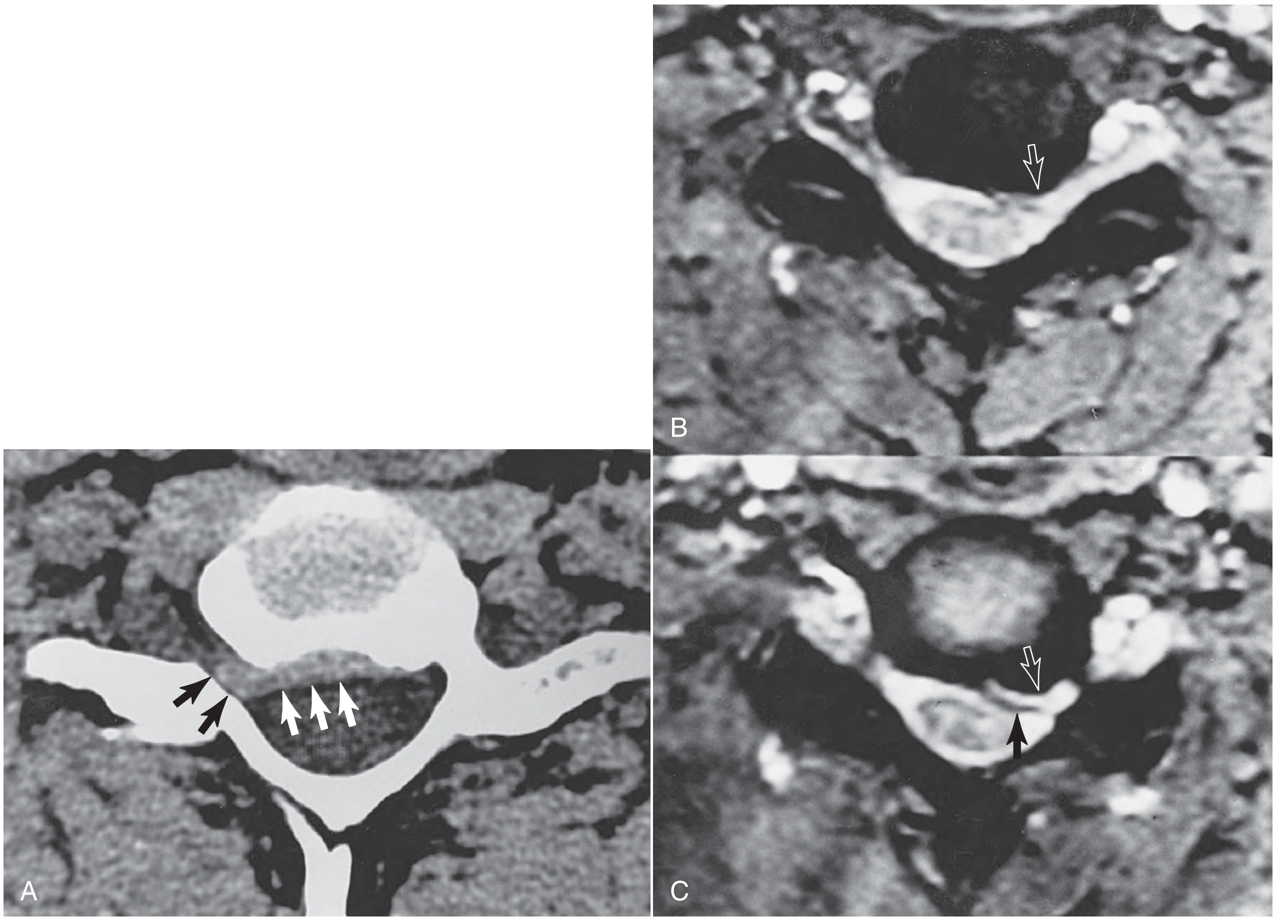

FIGURE 2–110 Intervertebral disc herniation.[130] **A,** Computed tomographic (CT) abnormalities: Transaxial soft tissue window computed tomographic (CT) image shows a right paramedian foraminal disc protrusion *(white arrows)* with herniation of disc material into the right nerve root canal *(black arrows)*. With the advent of MR imaging, CT scanning has taken on a secondary role in the evaluation of disc protrusions. **B-C,** Magnetic resonance (MR) imaging abnormalities. This 40-year-old man developed left upper-extremity weakness and radiculopathy. Transaxial gradient echo T2-weighted (TR/TE/flip angle, 500/20/30 degrees) MR images reveal a left C5-C6 posterolateral disc herniation. This lesion displaces the posterior longitudinal ligament *(arrow),* compresses and displaces the thecal sac, and obliterates the nerve root canal. Uncovertebral joint osteophytes are evident *(open arrows)* and contributed, with the disc herniation, to foraminal stenosis. Subsequent discectomy and fusion resulted in complete recovery. (***A,*** *Courtesy J. Haller, MD, Vienna, Austria;* ***B,*** *Courtesy B. Carson, DC, Kamloops, B.C., Canada.)*

TABLE 2-21 Cervical Spine Surgery*

Entity	Figure(s)	Indications	Complications
Spinal fusion (arthrodesis)[131,132,175]	2-111, 2-112	*Disc pathology:* often performed in conjunction with discectomy Fracture with instability Atlantoaxial instability Unstable developmental anomalies	Spinal cord compression Thecal sac encroachment Screw malpositioning Fracture or displacement of screw, plate, or wire Graft extrusion Osteomyelitis Postoperative kyphosis Failed interbody plug fusion Pseudarthrosis Postoperative prevertebral swelling Epidural hematoma Cerebrospinal fluid leak
Decompression[133,175]			
Laminectomy	2-113	Decompression for spinal stenosis Bilateral resection of neural arch	Postlaminectomy instability Postlaminectomy kyphosis
Laminoplasty	2-113	Decompression for spinal stenosis in which only one side of the neural arch is opened and the other side remains to act as a hinge	Complications not as frequent or severe as total laminectomy

* Modified from Pathria MN, Garfin SR: Imaging after spine surgery. In Resnick D (editor): Diagnosis of bone and joint disorders. 4th ed. Philadelphia, Saunders, 2002; Karasick D, Schweitzer ME, Vaccaro AR: Complications of cervical spine fusion: Imaging features. AJR 169:869, 1997.

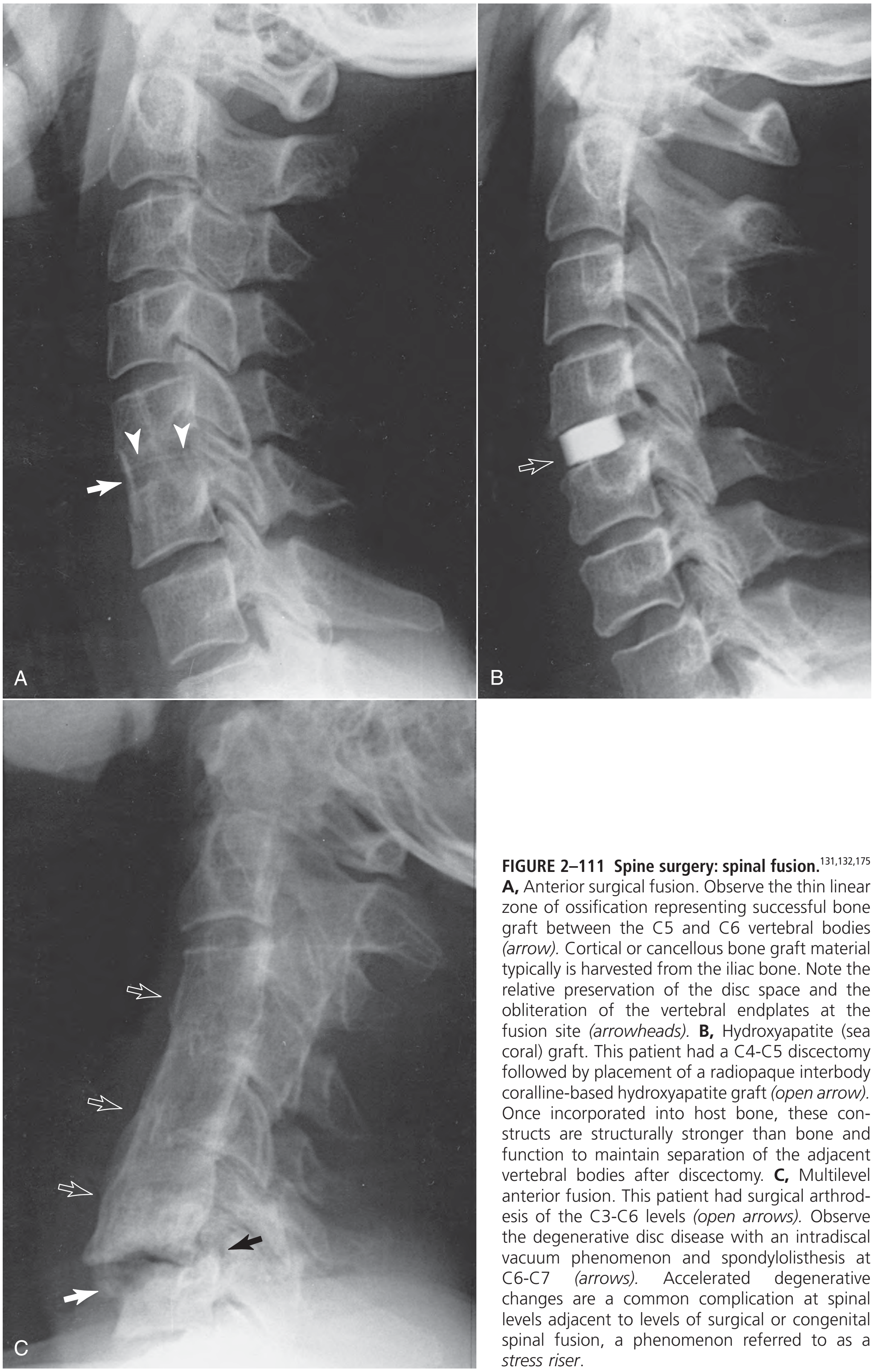

FIGURE 2–111 Spine surgery: spinal fusion.[131,132,175] **A,** Anterior surgical fusion. Observe the thin linear zone of ossification representing successful bone graft between the C5 and C6 vertebral bodies *(arrow).* Cortical or cancellous bone graft material typically is harvested from the iliac bone. Note the relative preservation of the disc space and the obliteration of the vertebral endplates at the fusion site *(arrowheads).* **B,** Hydroxyapatite (sea coral) graft. This patient had a C4-C5 discectomy followed by placement of a radiopaque interbody coralline-based hydroxyapatite graft *(open arrow).* Once incorporated into host bone, these constructs are structurally stronger than bone and function to maintain separation of the adjacent vertebral bodies after discectomy. **C,** Multilevel anterior fusion. This patient had surgical arthrodesis of the C3-C6 levels *(open arrows).* Observe the degenerative disc disease with an intradiscal vacuum phenomenon and spondylolisthesis at C6-C7 *(arrows).* Accelerated degenerative changes are a common complication at spinal levels adjacent to levels of surgical or congenital spinal fusion, a phenomenon referred to as a *stress riser*.

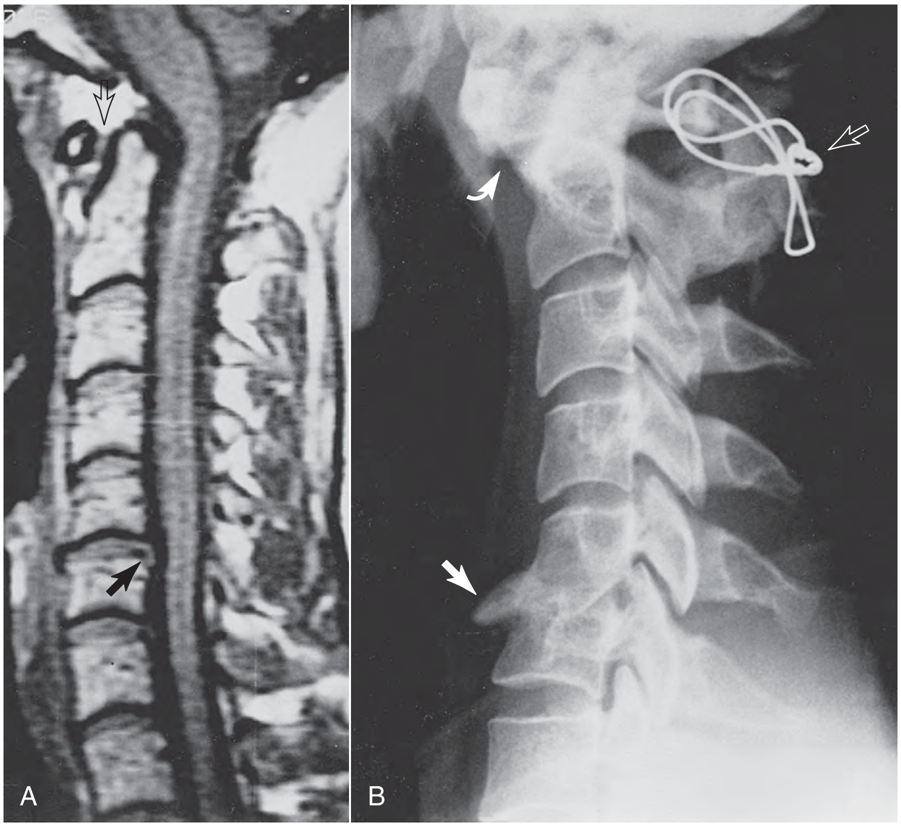

FIGURE 2–112 Spine surgery: atlantoaxial fusion and C5-C6 discectomy.[131,175] **A-B,** This 39-year-old man injured his neck while launching his boat, and he immediately developed upper extremity radiculopathy. Initial radiographs (not shown) revealed atlantoaxial subluxation and C5-C6 disc space narrowing secondary to disc degeneration. The atlantoaxial subluxation was determined to be related to a chronic tear of the transverse ligament that occurred many years earlier. In **A,** a sagittal T1-weighted (TR/TE, 600/20) spin echo MR image reveals wide separation of the atlantodental interspace *(open arrow)* and a C5-C6 disc herniation *(arrow).* This patient subsequently underwent two separate surgeries: C5-C6 discectomy and atlantoaxial stabilization. In **B,** a postoperative radiograph shows the bone graft and wires from a Gallie procedure used to stabilize the atlantoaxial articulation *(open arrow).* The atlantodental interspace remains widened *(curved arrow).* In addition, graft material in the C5-C6 disc space has become dislodged anteriorly *(arrow),* which necessitated another surgical procedure to repair this complication. *(Courtesy J. Upton, DC, Victoria, B.C., Canada.)*

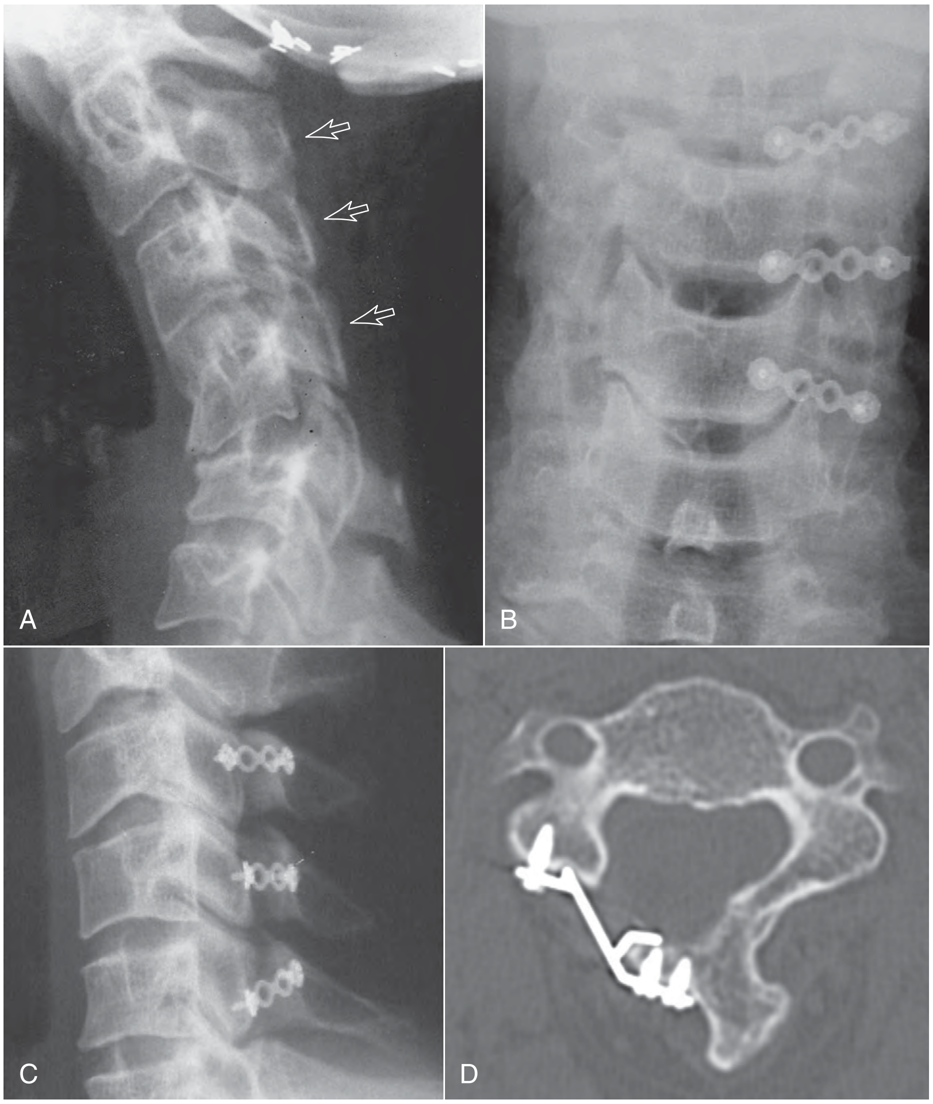

FIGURE 2–113 Decompressive surgery. A, Postlaminectomy kyphosis: Swan-neck deformity.[133,175] This 28-year-old woman developed a severe kyphosis after multiple-level cervical spine laminectomies. The operation was performed to remove a benign intraspinal tumor that extended from the brainstem into the lower cervical spinal canal. The spinous processes and laminae of C2-C5 have been excised *(open arrows),* and an acute angular kyphosis is present at the C4-C5 level. This swan-neck deformity, which is seen in patients with multilevel laminectomies, presumably results from loss of posterior ligamentous and osseous stability as well as muscle weakness. **B-C,** Laminoplasty.[133,175] This 42-year-old man underwent a unilateral left laminoplasty at C3, C4, and C5 for spinal stenosis. Observe the orthopedic instrumentation spanning the gap between the lateral masses and the spinous process unilaterally. **D,** In another patient, a transaxial CT bone window image reveals laminoplasty instrumentation spanning the laminotomy defect extending from the right articular process to the spinous process. Unilateral laminoplasty procedures are less likely than bilateral laminectomies to lead to postsurgical instability. *(**A,** Courtesy B.F. Dickson, DC, Vancouver, B.C., Canada; **D,** Courtesy B.A. Howard, MD, Charlotte, NC.)*

TABLE 2-22 Surgical Instrumentation and Bone Grafts*

Entity	Figure(s)	Characteristics
Plates	2-114	Stainless steel or titanium plates used primarily in anterior spinal fusions Maintain interbody grafts Used in conjunction with screws
Screws		Stabilize implant constructs and fractures Stainless steel or titanium Several types
Locking plate screws	2-114	Anchor plates in anterior spinal fusions
Lateral mass screws	2-114	May be used in conjunction with plates and longitudinal rods for posterior spinal fusions
Cannulated screws	2-51	Hangman's and odontoid fracture fixation Atlantoaxial instability fixation
Intervertebral disc replacements		Used in discectomy with fusion to restore disc space
Hydroxyapatite interbody graft	2-111	Graft material coralline-based (sea coral) hydroxyapatite
Autograft	2-114	Strut graft material harvested from patient's own fibula or iliac crest
Interbody cage	2-115	Metallic or synthetic polyetheretherketone (PEEK) spacer that holds in place a combination of bone graft and bone morphogenic protein (BMP) until it incorporates into adjacent bone
Disc prosthesis	2-115	Degenerative disc disease Alternative to spinal fusion Shock absorber and allows motion Titanium, calcium phosphate, cobalt chromium, and polyethylene
Expandable cages	2-116	Used to replace vertebral bodies, distract the vertebrae and constrain graft material until it fuses to adjacent spinal segments after corpectomy Also to provide stability in areas that have undergone decompression
Gallie fusion wires	2-112	Posterior fusion for atlantoaxial instability Gallie wire tied around bone graft material, C1 posterior arch, and C2 spinous process

* Modified from Pathria MN, Garfin SR: Imaging after spine surgery. In Resnick D (editor): Diagnosis of bone and joint disorders. 4th ed. Philadelphia, Saunders, 2002; Karasick D, Schweitzer ME, Vaccaro AR: Complications of cervical spine fusion: Imaging features. AJR 169:869, 1997.

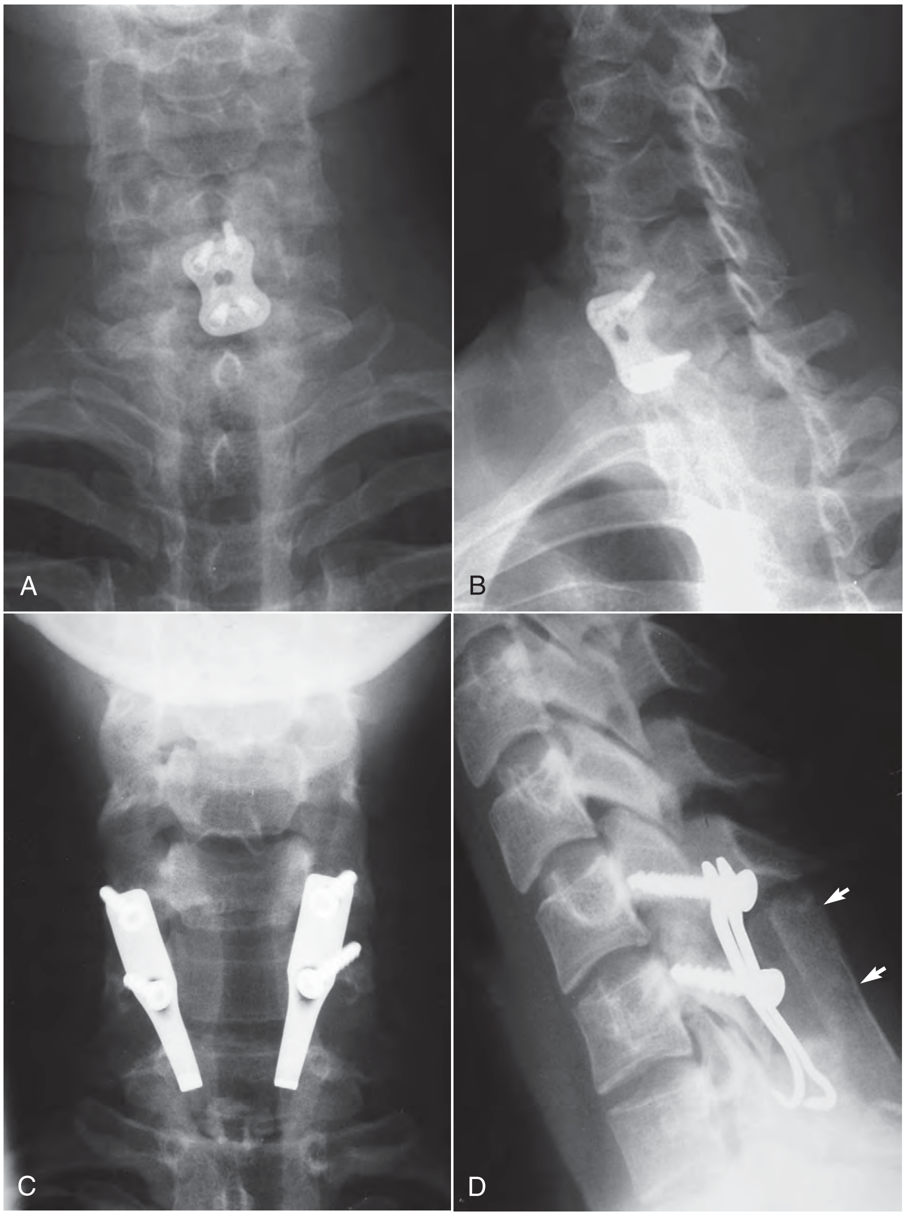

FIGURE 2–114 Spinal fusion surgery.[131,132,175] **A-B,** Anterior plates and screws. Anteroposterior and oblique radiographs demonstrate an H-shaped AO plate and four locking screws used in anterior fusion of C6-C7. **C-D,** In this patient who underwent a laminectomy for an osteoblastoma, posterior fusion is accomplished with four lateral mass screws implanted within the articular processes of C5 and C6 with bilateral connecting plates. In addition, a fibular strut is grafted to the spinous processes and laminae of C6, C7, and T1 *(arrows).* Spinal fusion is performed after discectomy and in cases of instability.

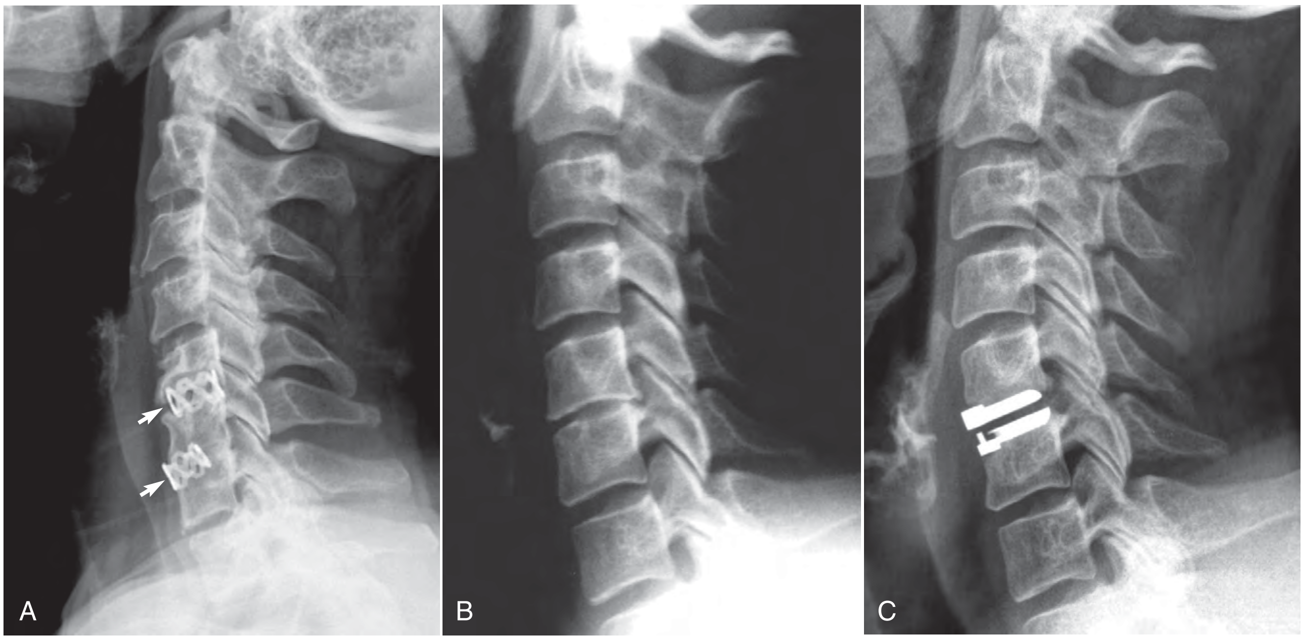

FIGURE 2–115 Intervertebral disc replacement surgery.[175] **A,** Interbody cages. One cage inserted in the C5-C6 disc space is properly aligned *(upper arrow)*, whereas the cage inserted in the C6-7 disc space is malpositioned-having displaced anteriorly *(lower arrow)*. **B-C,** Intervertebral disc prosthesis. A preoperative radiograph **(B)** depicts severe C5-C6 degenerative disc space narrowing. A disc prosthesis has been surgically implanted **(C)** following discectomy surgery. Note that the prosthetic device has incorporated with the vertebral endplates and has restored the disc height.

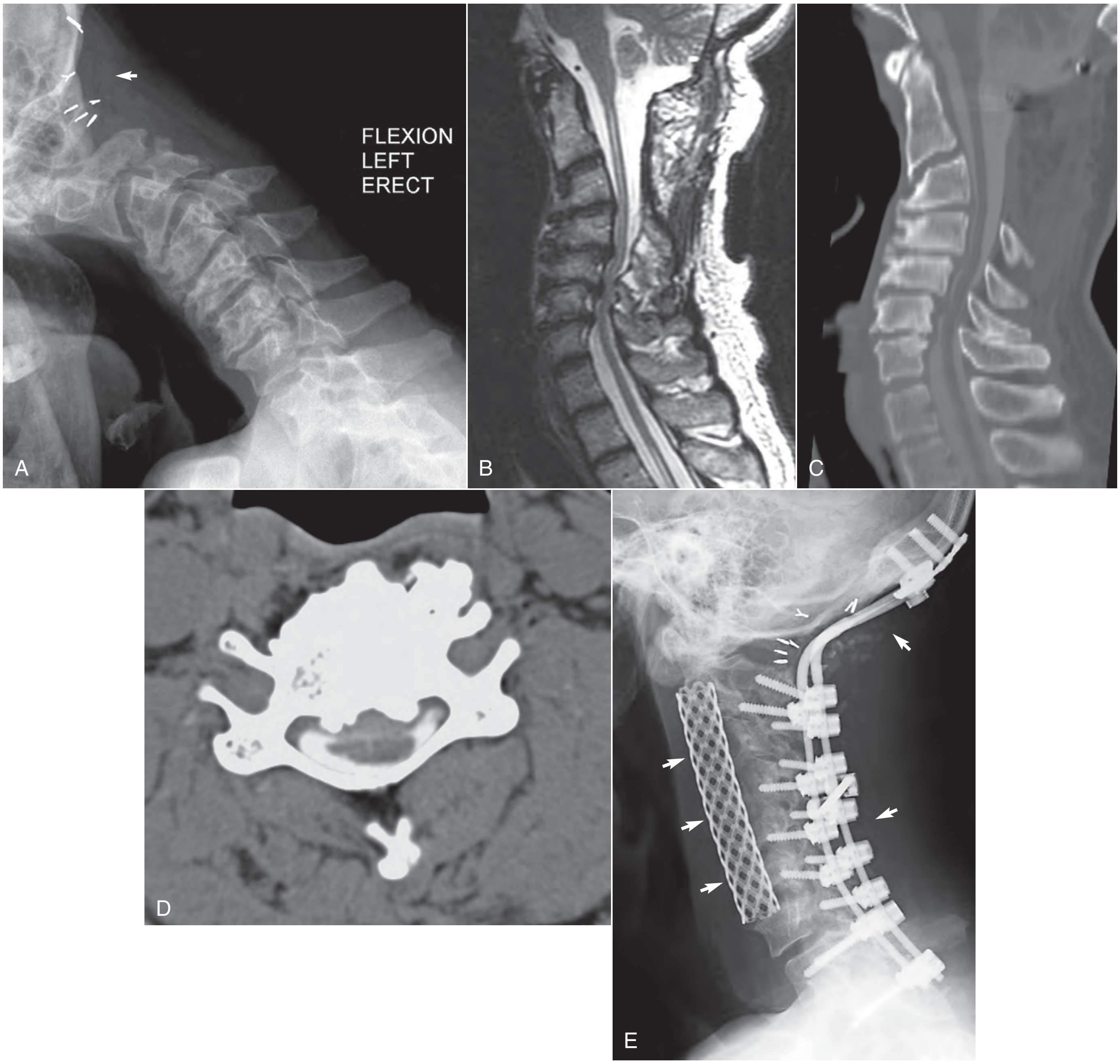

FIGURE 2–116 Extensive occipito-cervical fusion surgery.[175] This 53-year-old male suffering with chronic cervical spondylotic myelopathy had severe neurologic deficits and instability. **A,** A flexion radiograph reveals evidence of severe degenerative changes and previous laminectomies at C1-C3 and decompression of the foramen magnum *(arrow).* A T2-weighted sagittal MR image **(B),** sagittal **(C),** and axial **(D)** CT-myelography images show a reversal of the lordosis with severe stenosis and compression of the cervical cord. A postoperative radiograph **(E)** reveals extensive surgical instrumentation fusing the entire cervical spine from occiput to T1. Corpectomies have been performed from C2 to C6 and repaired with an expandable cage *(anterior arrows).* Paired lateral mass screws anchoring bilateral connecting plates are also visible posteriorly (*posterior arrows*). *(Courtesy B.A. Howard, MD, Charlotte, NC.)*

TABLE 2-23 Vascular Disorders Affecting the Cervical Spine

Entity	Figure(s)	Characteristics
Carotid artery atherosclerosis[6]	2-117	Mottled calcification of the carotid arteries visible on frontal radiographs lateral to the spine Most common site is at the bifurcation of the carotid artery
Tortuous vertebral artery[134]		Tortuosity of the vertebral artery can occur in elderly persons as a result of aging and may result in erosion of the posterior arch of atlas, pedicles, intervertebral foramina, or foramen transversarium of axis May result in vertebrobasilar insufficiency MR angiography is helpful in the evaluation of the vertebral arteries
Vertebral artery aneurysm[6]	2-118	*Rare occurrence in the vertebral artery:* vessel dilation and possible dissection May be congenital or occur secondary to atherosclerosis, infection (mycotic aneurysm), poststenotic dilation, syphilis, or arteritis May result in vertebrobasilar insufficiency MR angiography is helpful in the evaluation of the vertebral arteries

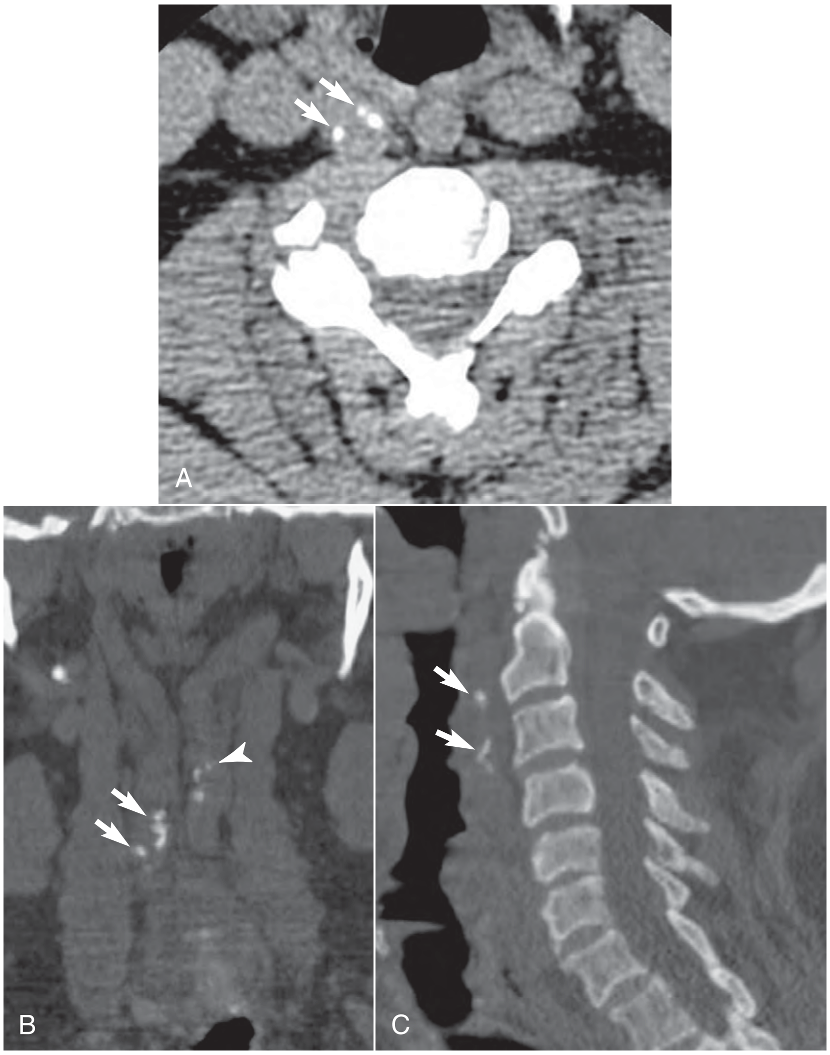

FIGURE 2–117 Carotid artery atherosclerosis: computed tomography.[6] This 74-year-old man complained of neck pain, dizziness and light-headedness. Transaxial bone window **(A),** coronal soft tissue window **(B),** and sagittal midline bone window **(C)** images reveal calcified atherosclerotic plaque within the wall of the right internal carotid artery *(arrows)* and to a lesser extent within the left *(arrowhead).* Note also the prevertebral location of the carotids due to their tortuosity. Surgeons need to be alerted to this abnormal location of the carotids before any cervical spine surgery.

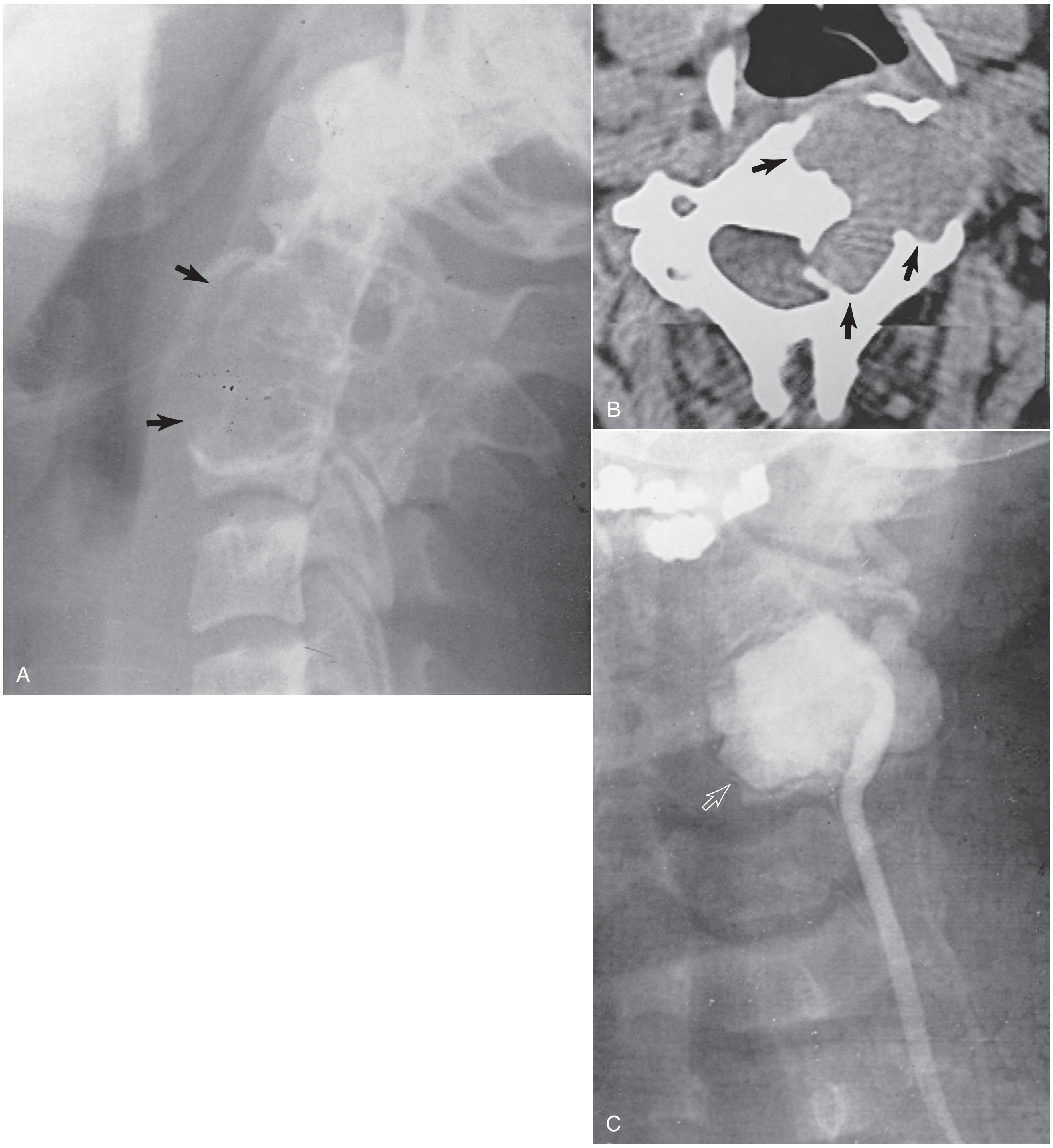

FIGURE 2–118 Vertebral artery aneurysm.[6] A 17-year-old woman with a mycotic vertebral artery aneurysm. **A,** A large, expansile, destructive lesion involving the C2 and C3 vertebral bodies is evident on this lateral radiograph *(arrows).* **B,** A transaxial computed tomographic (CT) image reveals destruction of approximately one half of the vertebral body *(arrows)* with extension into the spinal canal. **C,** A vertebral artery angiogram demonstrates a large lobulated collection of contrast material in the aneurysm *(open arrow)* that erodes the C2 and C3 vertebrae. This rare condition occurs most frequently at the C1-C2 region. It often results in erosion of adjacent osseous structures, including the pedicle, transverse process, and vertebral body. Other causes of vertebral erosion are listed in Table 2-18. *(Courtesy B.A. Howard, MD, Charlotte, NC.)*

CHAPTER 3

Thoracic Spine

NORMAL DEVELOPMENTAL ANATOMY

Accurate interpretation of pediatric thoracic spine radiographs requires a thorough understanding of normal developmental anatomy. Table 3-1 outlines the age of appearance and fusion of the primary and secondary ossification centers. Figures 3-1 and 3-2 demonstrate the radiographic appearance of many important developmental landmarks at selected ages from birth to skeletal maturity.

DEVELOPMENTAL ANOMALIES, ANATOMIC VARIANTS, AND SOURCES OF DIAGNOSTIC ERROR

Many anomalies, normal variations, and other sources of diagnostic error encountered in the thoracic spine may simulate disease processes (Table 3-2) and result in misdiagnosis. This chapter describes most of the more common processes, which are shown in Figures 3-3 to 3-8.

SKELETAL DYSPLASIAS AND OTHER CONGENITAL DISEASES

Table 3-3 lists a number of dysplastic and congenital disorders that affect the thoracic spine, and Figures 3-9 to 3-13 illustrate some of these manifestations.

ALIGNMENT ABNORMALITIES

A wide spectrum of alignment abnormalities may be encountered in the thoracic spine. These include alterations of the normal kyphotic curve (Table 3-4) and several types of scoliosis (Table 3-5). Many of these conditions are illustrated in Figures 3-14 to 3-24. Table 3-6 lists the main indications for further imaging in scoliosis patients.

PHYSICAL INJURY

Fractures, dislocations, and soft tissue injuries involving the thoracic spine are frequent, and often they are associated with serious clinical manifestations. Table 3-7 outlines the more important injuries of the upper, middle, and lower portions of the thoracic spine. The injuries are classified according to their most typical anatomic location and to their presumed mechanisms of injury. The differential diagnosis of acute versus chronic compression fractures is detailed in Table 3-8. In addition, Figures 3-25 to 3-33 demonstrate the most characteristic imaging manifestations of common thoracic spine injuries. Table 3-9 is a checklist for the diagnosis of clinical instability in the thoracic and thoracolumbar spine.

ARTICULAR DISORDERS

The thoracic spine is a frequent target site of involvement for many forms of degenerative, inflammatory, crystal-induced, and infectious spondyloarthropathies and other articular disorders. Table 3-10 lists these diseases, and Figures 3-34 to 3-51 illustrate the characteristic radiographic manifestations. Tables 3-11 and 3-12 describe osseous outgrowths of the spine and terminology applied to ankylosing spondylitis, respectively.

BONE TUMORS

A wide variety of malignant, benign, and tumorlike lesions affect the spine. Table 3-13 lists the neoplasms illustrated in this chapter in Figures 3-52 to 3-67. A more complete description of bone neoplasms is found in Tables 1-12 to 1-14.

METABOLIC AND HEMATOLOGIC DISORDERS

A number of metabolic disorders may manifest in the thoracic spine and are outlined in Table 3-14 and illustrated in Figures 3-68 to 3-75.

THORACIC SPINE SURGERY

Table 3-15 discusses vertebral augmentation for painful compression fractures and Figure 3-76 provides examples of balloon kyphoplasty, one of these surgical procedures.

TABLE 3-1 Thoracic Spine: Approximate Age of Appearance and Fusion of Ossification Centers*[1-3] (Figures 3-1 and 3-2)

Ossification	Primary or Secondary	No. of Centers	Age of Appearance (Years)	Age of Fusion (Years)	Comments
Neural arches (laminae)	P	2	Birth	1-1.5	Fuse together in midline in ascending order from T12 to T1
Vertebral body	P	1	Birth	4-5	Fuse to laminae
Spinous process	S	1	11-16	17-25	
Transverse processes	S	2	11-16	17-25	
Articular processes	S	4	11-16	17-25	
Endplate ring apophyses	S	2	11-16	17-25	Fuse to body

P, Primary; *S*, secondary.

* Ages of appearance and fusion of ossification centers in girls typically precede those of boys. Ethnic differences also exist.

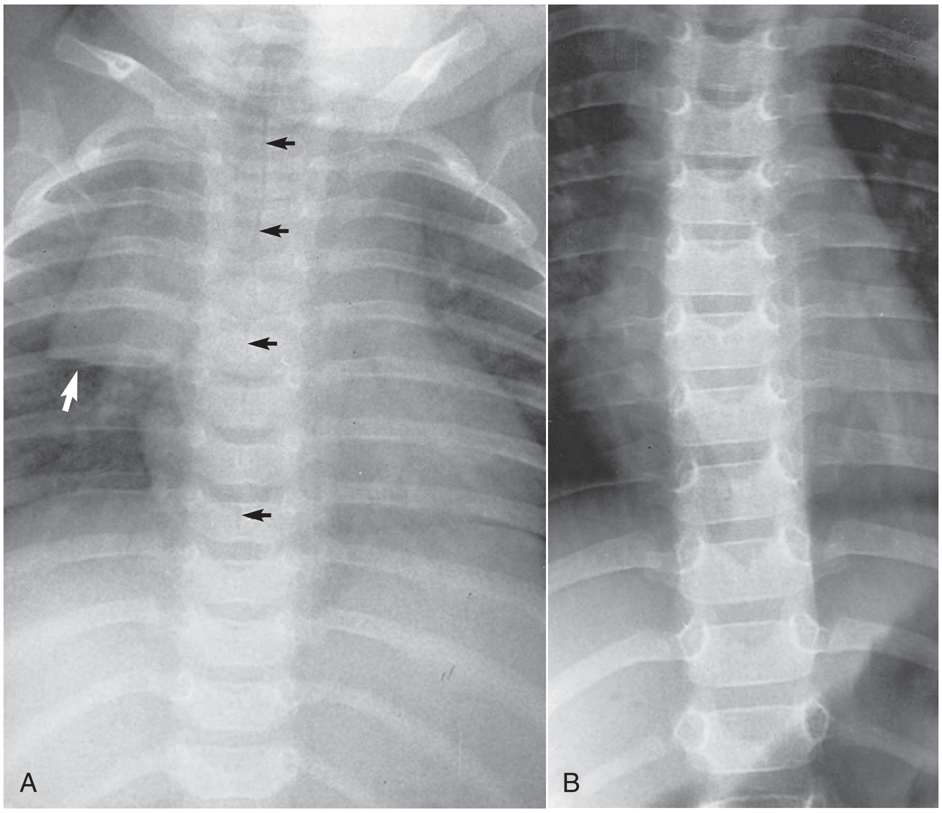

FIGURE 3–1 Skeletal maturation and normal development: anteroposterior thoracic spine radiographs.[1-3] **A,** A 5-month-old boy. Observe the multiple midline radiolucent areas *(black arrows)* representing the unfused primary ossification centers of the neural arches. The neural arches usually start to fuse within the first year, beginning with T12 and progressing to T1 within the next 6 months. In this child, the lower thoracic centers have fused somewhat prematurely. The spinal canal appears proportionately wide, and a prominent thymus (sail sign) is evident *(white arrow)*. **B,** A 3-year-old girl.

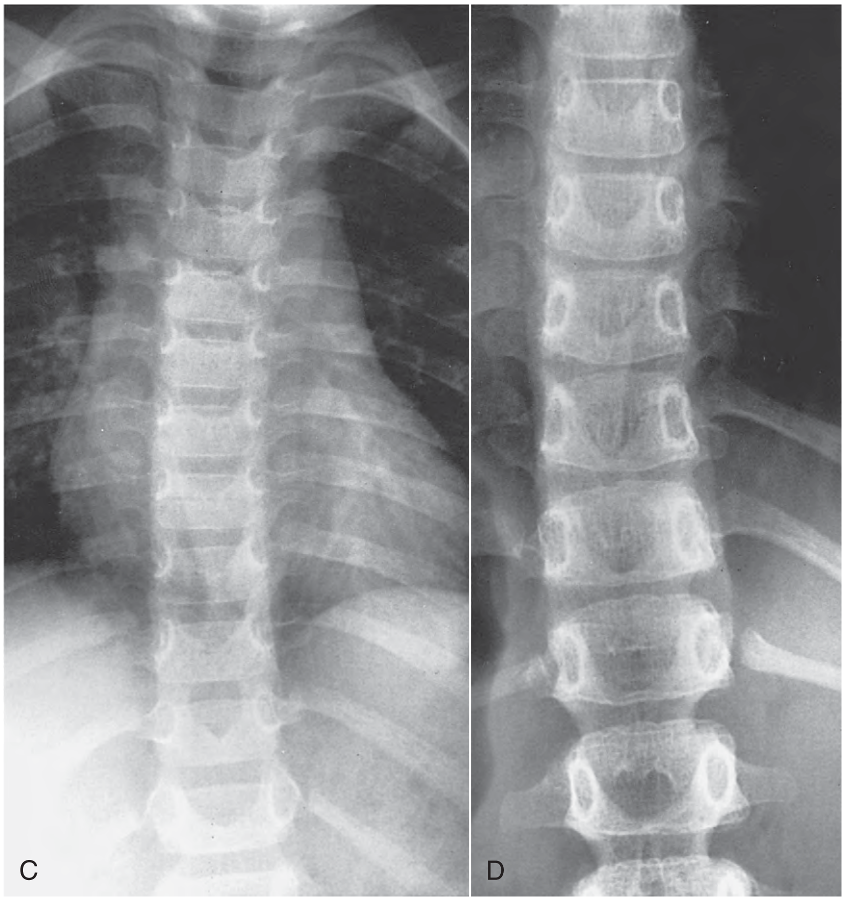

FIGURE 3–1, cont'd **C,** A 5-year-old boy. **D,** A 6-year-old girl. Irregularity of the superior and inferior vertebral body margins is common just before appearance of the secondary ring apophyses. The vertebral bodies are somewhat oval.

Continued

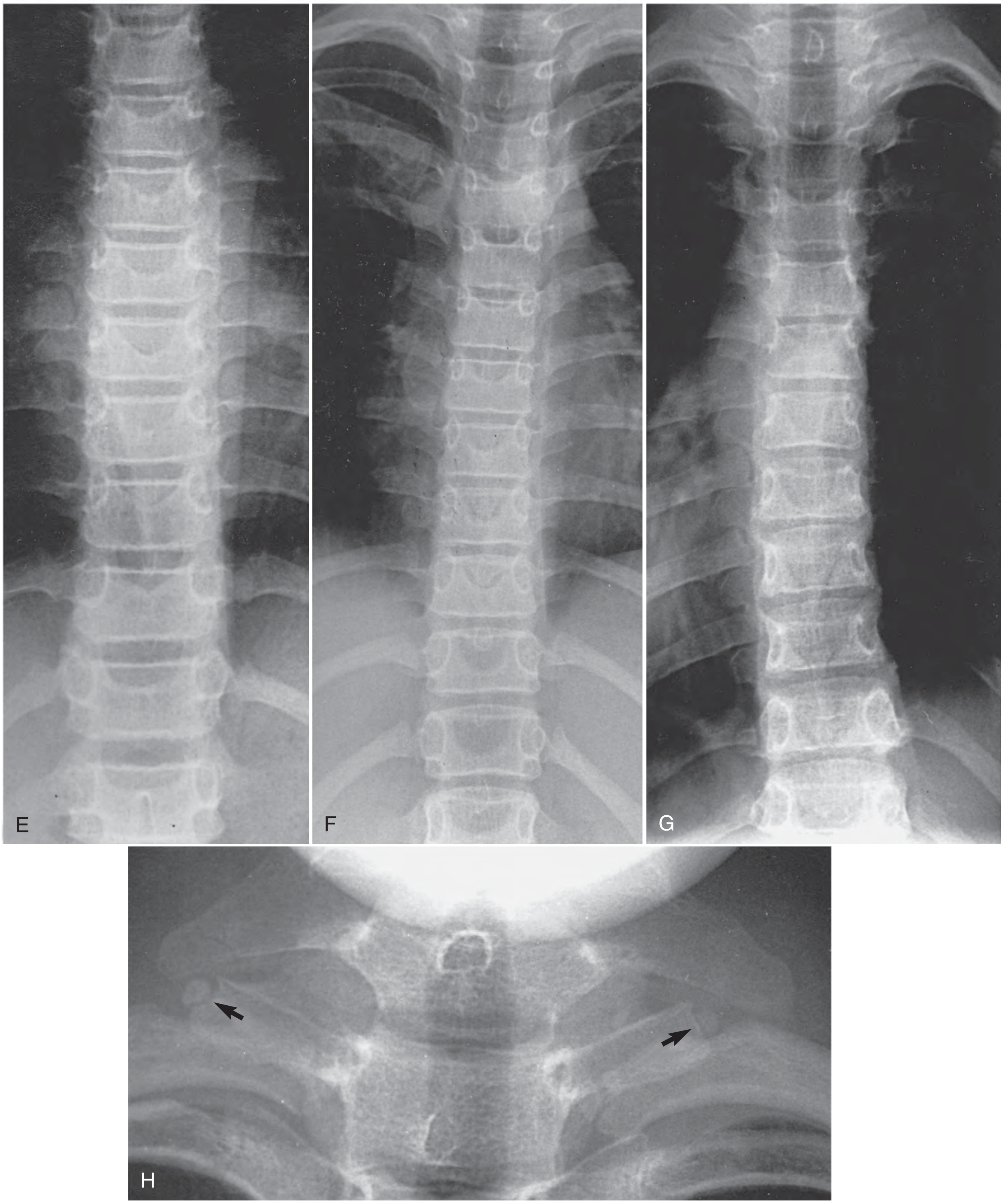

FIGURE 3–1, cont'd **E,** A 10-year-old boy. **F,** An 11-year-old girl. The vertebrae exhibit an adult configuration. **G,** A 13-year-old boy. The spine has an adult appearance. **H,** A 13-year-old girl. Observe the circular secondary ossification centers ("os cervicalis" if unfused in adult) at the tips of the transverse processes of T1 *(arrows)*. The ossification centers of the neural arches typically fuse to the vertebral bodies about the age of 1.5 years. The transverse processes of C7 are markedly elongated, a common developmental anomaly.

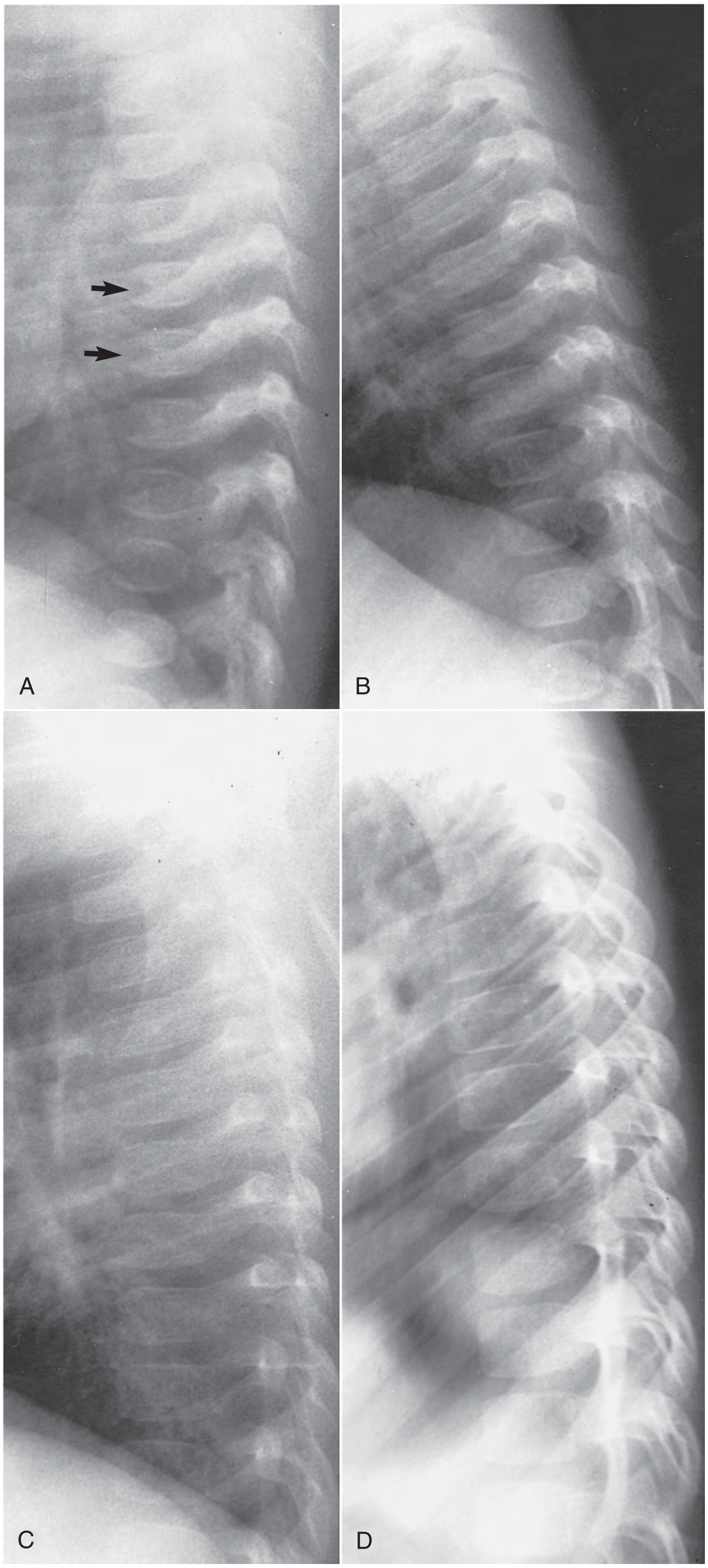

FIGURE 3–2 Skeletal maturation and normal development: lateral thoracic spine and chest radiographs.[1-3] **A,** A 2-month-old boy. The vertebral bodies are oval, and prominent vascular notches (Hahn venous channels) are present within the anterior margins *(arrows)*. The neural arches have not fused to the vertebral bodies, and the spinal canal appears proportionately wide. **B,** A 5-month-old boy. The neural arches have not yet completely fused to the vertebral bodies. **C,** A 13-month-old girl. **D,** A 3-year-old girl.

Continued

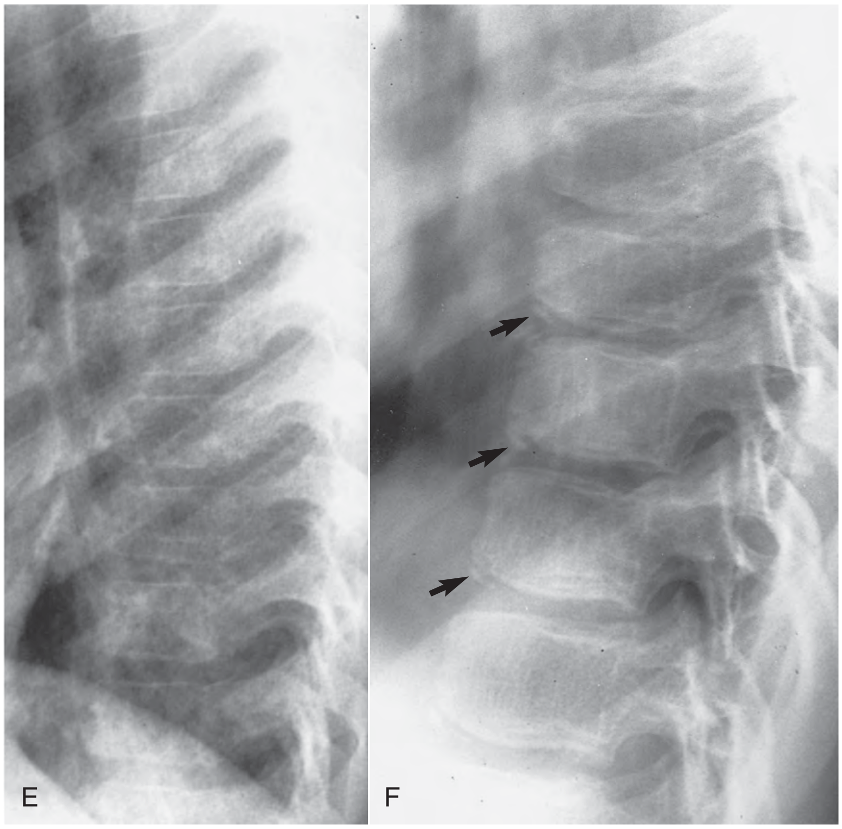

FIGURE 3–2, cont'd **E,** A 5-year-old boy. The vertebral body margins appear more square. The neural arches have fused to the vertebral bodies, a process that normally occurs between the ages of 4 and 6 years. **F,** A 13-year-old boy. The vertebral bodies are more rectangular. The secondary ring apophyses of the vertebral bodies have begun to appear *(arrows)*. These typically begin to ossify at puberty, although such ossification may be apparent as early as 7 years of age. These secondary ring apophyses usually fuse to the vertebral bodies between the ages of 17 and 25 years.

TABLE 3-2 Developmental Anomalies, Anatomic Variants, and Sources of Diagnostic Error Affecting the Thoracic Spine*

Entity	Figure(s)	Characteristics
Normal ring apophyses[4]	3-1 to 3-3	Normal vertebral body ring apophyses may resemble fractures or limbus vertebrae
Hahn venous channels[5]	3-4	*Normal anatomy:* a central horizontal vascular groove or channel that traverses the vertebral body These channels are quite prominent beginning with the first year of life but tend to disappear with age; even when they persist into adulthood, they are of no clinical significance
Spina bifida occulta[6]	3-5	Extremely common developmental anomaly consisting of a midline defect within the neural arch in which the two laminae fail to fuse centrally at the spinolaminar junction Spina bifida occulta results in a radiolucent cleft, or an absent spinous process, or both; it occurs most frequently at the L5-S1 and T11-T12 levels Seen as an isolated anomaly or in conjunction with other entities, such as congenital spondylolisthesis, cleidocranial dysplasia, or Klippel-Feil syndrome Cleft usually is occupied by strong cartilage and fibrous tissue and generally is of no clinical consequence Spina bifida may infrequently be associated with meningomyelocele, which represents protrusion of the meninges or spinal cord, or both; meningomyelocele may result in severe neurologic abnormalities
Hemivertebra[7,8]	3-6; see 3-17	Vertebral body originally develops from paired chondral centers, which at a later stage form a single ossification focus that is separated transiently by the notochordal remnant into anterior and posterior centers *Lateral hemivertebra* results from failure of development of one of the paired chondral centers Lateral hemivertebra might involve a normally occurring vertebra or it might be supernumerary; one pedicle may be normal or enlarged and its counterpart at the same level may be absent or hypoplastic; the incomplete segment may articulate with or be fused to the adjacent vertebra Frequently results in congenital scoliosis and may be associated with segmentation anomalies *Dorsal and ventral hemivertebrae* result from agenesis of either the anterior or posterior portion of the growth center, respectively; these occur much less frequently than lateral hemivertebrae
Butterfly vertebra[8]	3-7	Incomplete fusion of the two lateral chondral centers of the vertebral body results in a central sagittal constriction of the vertebral body, which is seen on a frontal radiograph and is considered a variant of enchondral ossification Interpedicle distance of the butterfly vertebra may be widened, and the adjacent vertebrae usually remodel to conform to the shape of the butterfly vertebra
Synostosis (block vertebra)[8]	2-31, 4-6	Developmental failure of segmentation of vertebral somites with subsequent fusion of adjacent vertebrae Often results in premature degenerative disease at adjacent vertebral levels owing to excessive intervertebral motion above and below the synostosis Findings include waistlike constriction at the level of the intervertebral disc; complete absence of disc space or a disc represented by a rudimentary, irregularly calcified structure; total height of the block vertebra is less than expected from the number of segments involved; fusion of the posterior elements (50% of cases) *Differential diagnosis:* surgical fusion or ankylosis from inflammatory arthropathy or previous infection
Tracheal cartilage calcification[7]	3-8	Normal physiologic calcification of cartilaginous tracheal rings; no clinical significance

* See also Table 1-1.

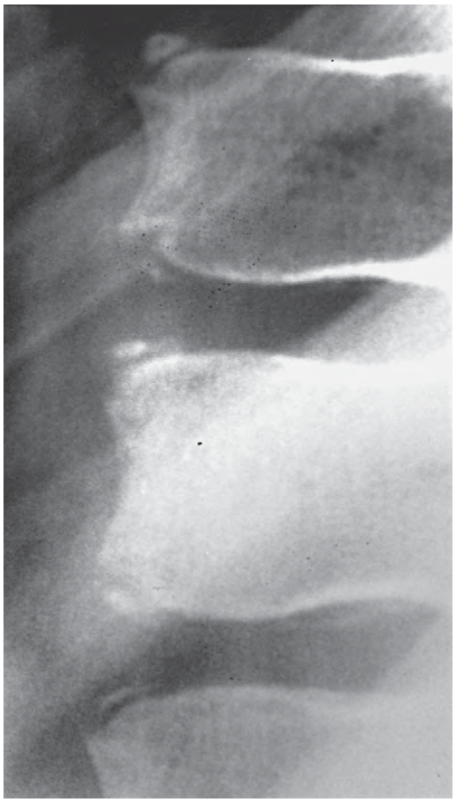

FIGURE 3–3 **Normal ring apophyses.**[4] Small triangular ossification centers are present at the anterosuperior and anteroinferior corners of the vertebral bodies in this 15-year-old boy. Notching and rounding of the adjacent corners of the vertebral bodies also are evident. This appearance of the normal vertebral body ossification centers should not be confused with fractures or limbus vertebrae.

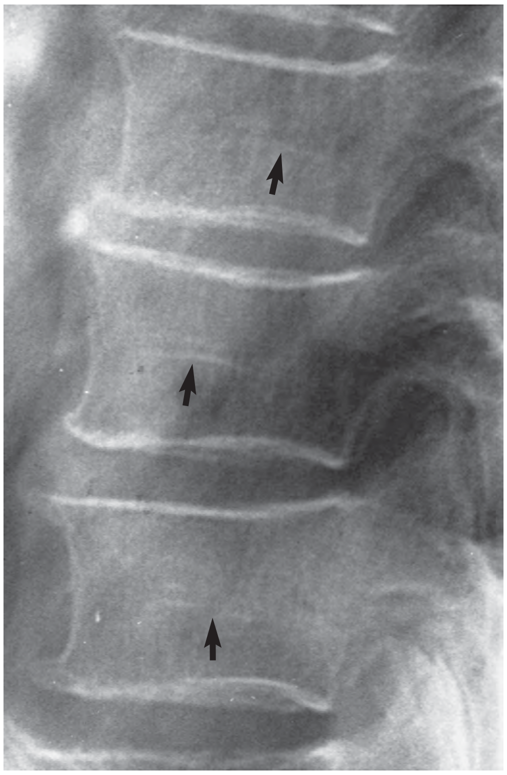

FIGURE 3–4 **Hahn venous channels.**[5] Horizontal radiolucent grooves through the central portion of the vertebral bodies *(arrows)* are seen most frequently in the lower thoracic spine and represent residual venous sinus channels that accommodate vertebral veins.

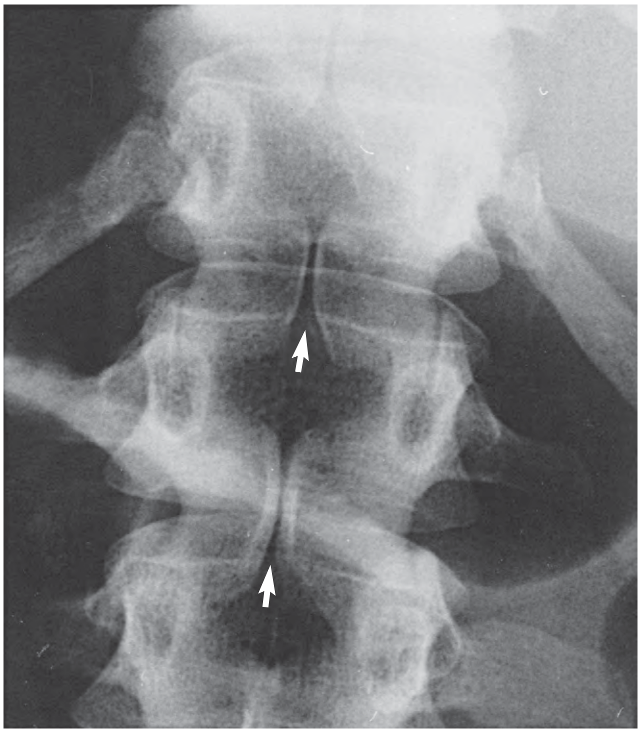

FIGURE 3–5 **Spina bifida occulta.**[6] Midline vertical radiolucent clefts in the thoracolumbar region *(arrows)* represent failure of union of the paired ossification centers of the neural arches.

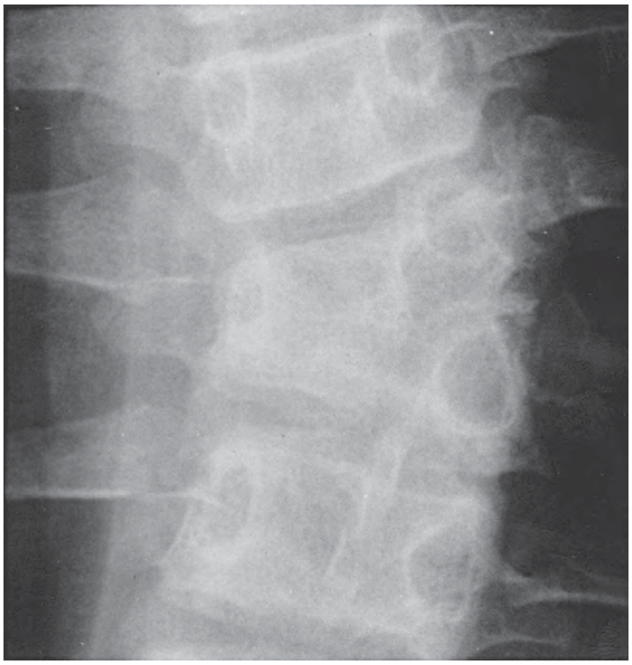

FIGURE 3–6 **Lateral hemivertebra.**[7,8] Observe the triangular appearance of the vertebral body in the lower thoracic spine. The anomalous vertebra possesses two pedicles and costovertebral articulations on the left and one pedicle and costovertebral articulation on the right, resulting in a congenital scoliosis. *(Courtesy A. Manne, DC, Minneapolis.)*

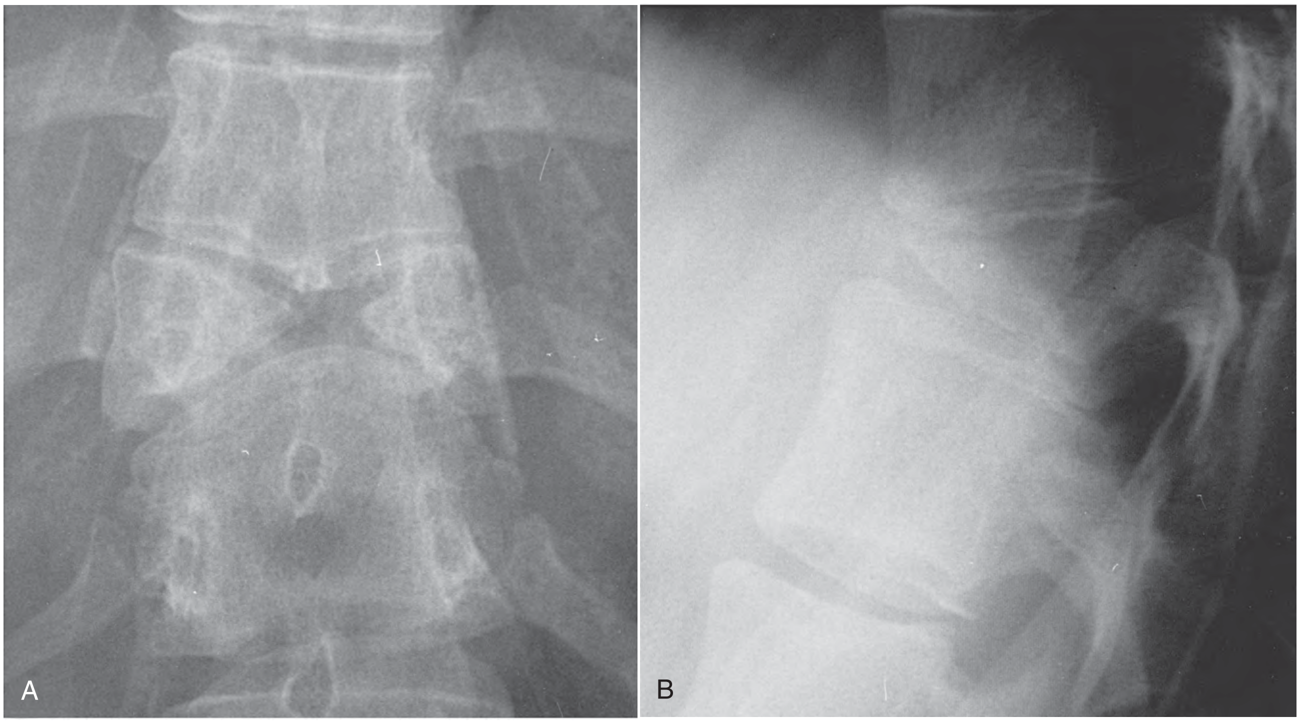

FIGURE 3–7 **Butterfly vertebra.**[8] Frontal **(A)** radiograph demonstrates a classic butterfly vertebra. The interpedicle distance is widened. A midline, vertically oriented sagittal defect in the vertebral body appears to divide the vertebra into two triangular segments, resembling a butterfly. The adjacent vertebral bodies have remodeled such that they appear to fit into the sagittal cleft defect, much like the pieces of a jigsaw puzzle. This feature helps to distinguish butterfly vertebrae from vertebral body fractures. Lateral radiograph **(B)** reveals a tapered appearance of the vertebral body anteriorly.

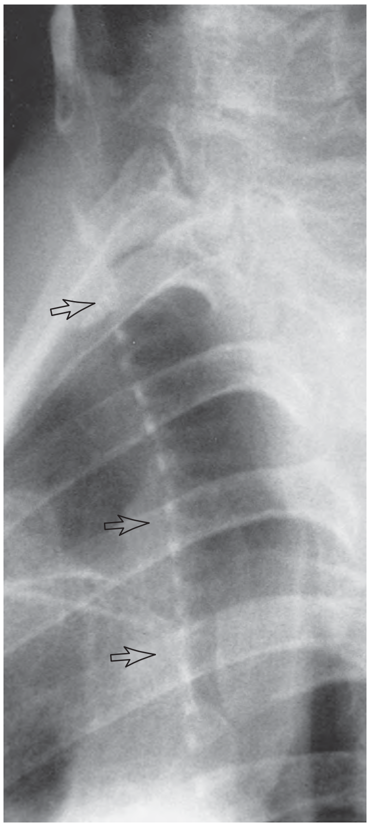

FIGURE 3–8 **Tracheal cartilage calcification.**[7] Extensive ringlike calcification of the tracheal cartilage *(open arrows)* is evident on an oblique radiograph from this 58-year-old woman. Such calcification is common in the elderly, is asymptomatic, and is of no clinical significance.

TABLE 3-3 Skeletal Dysplasias and Other Congenital Diseases Affecting the Thoracic Spine*

Entity	Figure(s)	Characteristics
Achondroplasia[9]		Spinal stenosis Vertebral bodies may be flattened and may demonstrate posterior scalloping
Spondyloepiphyseal dysplasia congenita[10]	3-9	Platyspondyly in adulthood and the "pear-shaped" vertebral appearance during infancy
Mucopolysaccharidoses (MPS)[11,12,115]	3-10	Two types most frequently affect the thoracic spine: ***MPS I-H (Hurler syndrome)*** Thoracolumbar gibbus deformity and posterior scalloping of vertebral bodies Rounded anterior vertebral body margins with inferior beaking ***MPS IV (Morquio syndrome)*** Platyspondyly Posterior vertebral body scalloping and kyphoscoliosis
Osteopetrosis[13,14,101]	3-11	*Patterns of osteosclerosis:* diffuse osteosclerosis; bone-within-bone appearance; sandwich vertebrae Bones are brittle and fracture easily
Osteopoikilosis[15]		Infrequently affects the spine Multiple punctate circular foci of osteosclerosis
Marfan syndrome[16,97,128]		Kyphoscoliosis in 40%-60% of persons Posterior vertebral body scalloping from dural ectasia; however, many patients may appear normal Significant osteopenia independent from body mass index
Osteogenesis imperfecta[17]	3-12	Osteoporosis and bone fragility Multiple compression fractures and severe kyphoscoliosis common
Chondrodysplasia punctata[18]	3-13	Stippled calcification of vertebral bodies Coronal clefts are present within the vertebral bodies of patients with the rhizomelic form

* See also Table 1-2.

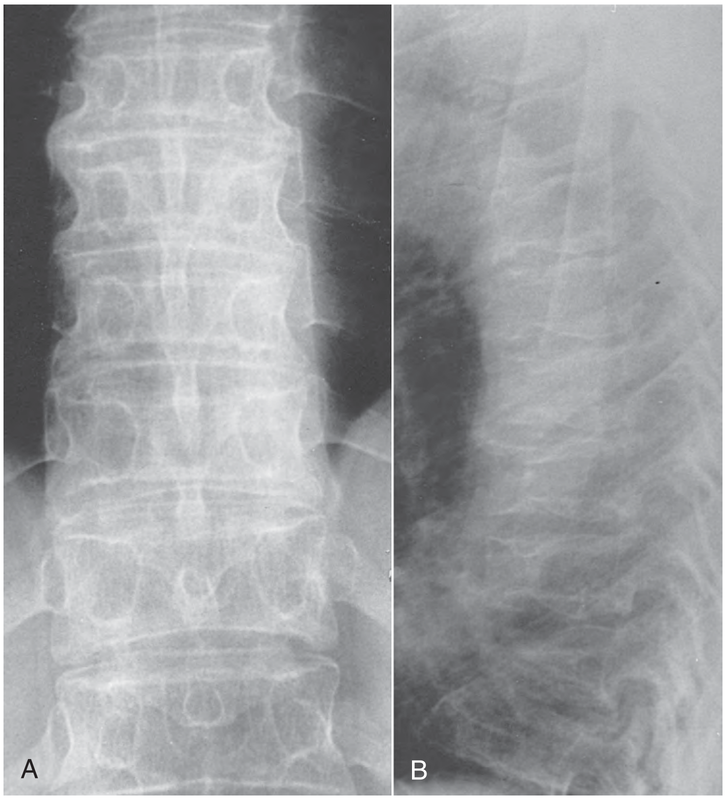

FIGURE 3–9 Spondyloepiphyseal dysplasia congenita.[10] Frontal **(A)** and lateral **(B)** routine radiographs reveal intervertebral disc spaces that appear narrow posteriorly and wide anteriorly owing to osseous humps that arise from the central and posterior portions of the vertebral endplates. This vertebral body shape is sometimes referred to as the *heaped-up appearance*. On the frontal view **(A),** the vertebral bodies appear flattened. These patients often have associated thoracic disc herniations.

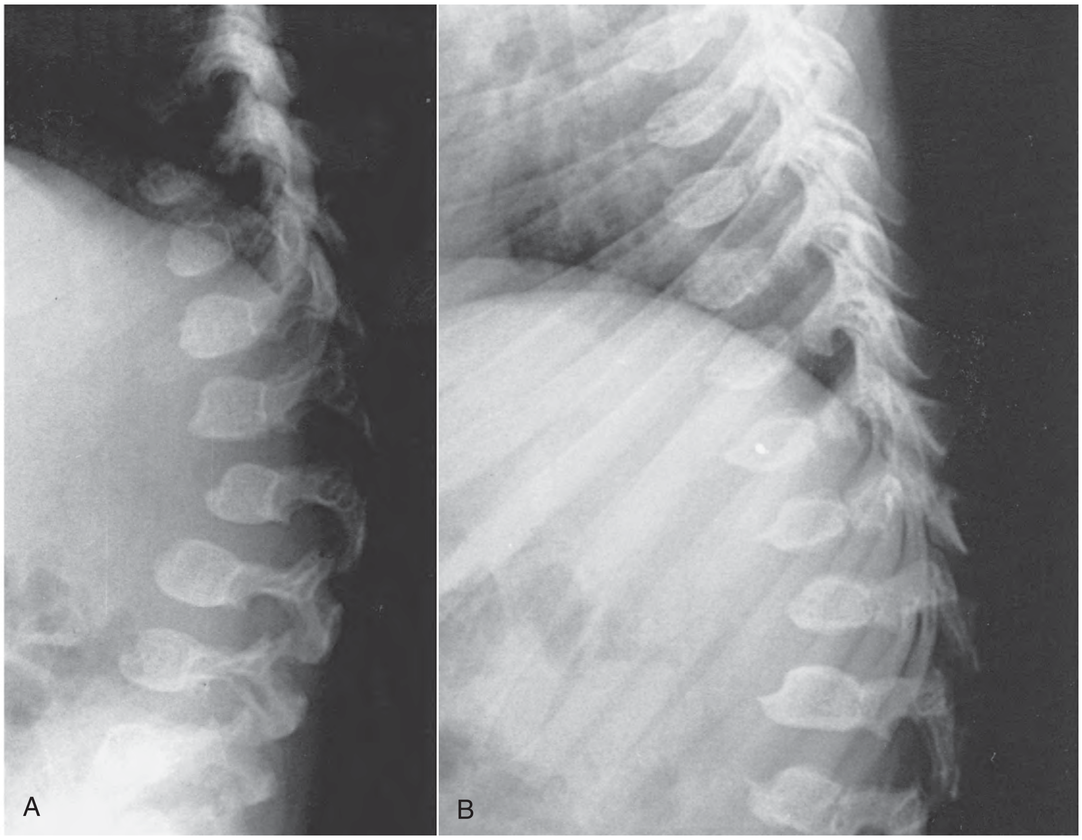

FIGURE 3–10 **Mucopolysaccharidoses (MPS).**[11,12,115] **A,** Hurler syndrome (MPS 1-H). In this 3-year-old child, beaklike projections are noted arising from the anteroinferior vertebral bodies. A thoracolumbar gibbus deformity also is present. These two findings are characteristic of this rare autosomal recessive mucopolysaccharidosis. **B,** Morquio syndrome (MPS IV). This child is of short stature and has a thoracolumbar kyphoscoliosis. Characteristic central tonguelike anterior beaking and rounding of the vertebral bodies are observed. In adults, the vertebrae typically appear flat and rectangular, with irregular margins.

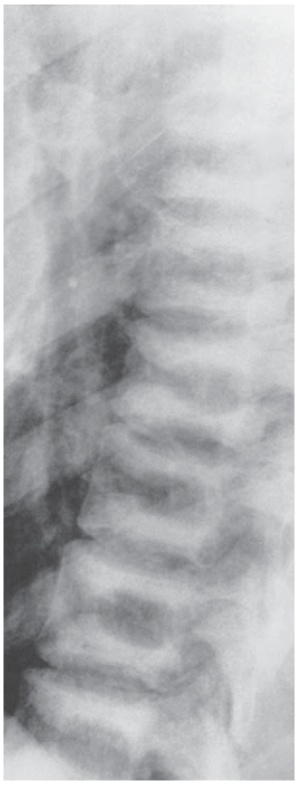

FIGURE 3–11 **Osteopetrosis.**[13,14,101] Dense osteosclerosis is noted adjacent to the superior and inferior vertebral endplates of the thoracic spine in this patient. This pattern of vertebral sclerosis is described as "sandwich" vertebrae; however, diffuse sclerosis and the "bone-within-bone" appearance also may be encountered.

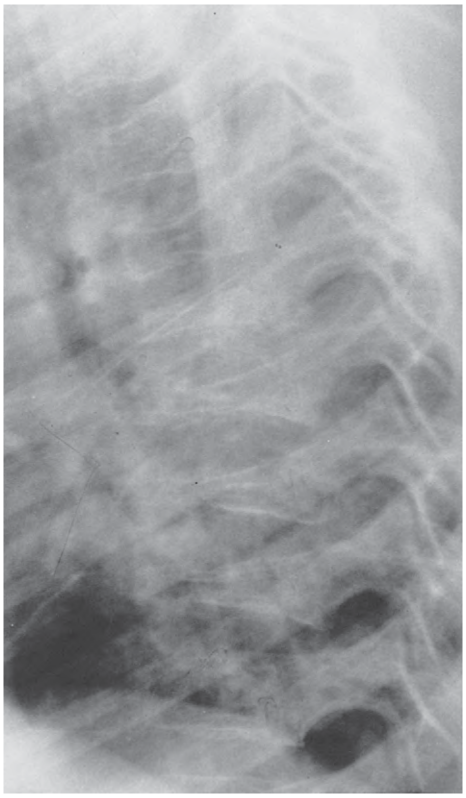

FIGURE 3–12 **Osteogenesis imperfecta.**[17] Routine radiograph from this 7-year-old patient reveals dramatic osteopenia and multiple wedge-shaped compression fractures.

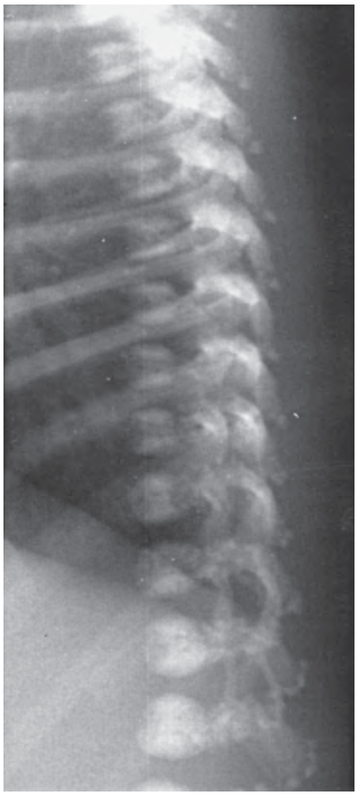

FIGURE 3–13 **Chondrodysplasia punctata.**[18] Radiograph from this 2-day-old infant shows the characteristic finding of stippled calcification of the thoracic vertebral bodies and neural arches. Several different forms of this rare multiple epiphyseal dysplasia have been identified.

TABLE 3-4 Alterations of Kyphosis

Entity	Figure(s)	Characteristics
Normal kyphosis[7,19,114]	3-14, *A-B*	Modified Cobb method is used to measure the thoracic kyphosis Normal maximum kyphosis ranges from 36-56 degrees in women and 40-66 degrees in men; measurements tend to increase with age and advancing osteoporosis
Congenital kyphosis[8]		Agenesis or underdevelopment of the anterior portion of the vertebral body ossification center results in a dorsal hemivertebra and subsequent kyphotic deformity; less likely to be caused by failure of segmentation of the anterior portion of two adjacent vertebral bodies, forming a congenital bar
Senile kyphosis[19]	3-14, *C*	Kyphosis secondary to severe degeneration of the anulus fibrosis Occurs mostly in nonosteoporotic persons who are in their seventh and eighth decades Men > women
Osteoporotic kyphosis[19,104,111]	3-14, *D*, 3-64	In older persons, generalized osteoporosis results in wedging or collapse of the anterior aspect of the vertebral bodies, especially the T6 and T7 levels Women > men May also occur in Cushing disease and other secondary causes of osteoporosis
Tuberculous spondylodiscitis[20]	3-49, 3-50	Thoracolumbar vertebral body collapse results in accentuated gibbus deformity and is seen in advanced tuberculous spondylodiscitis (Pott disease)
Ankylosing spondylitis[19,109]		Advanced ankylosis and syndesmophyte formation result in exaggerated thoracic kyphosis and flattening of the lumbar lordosis
Thoracolumbar injury[21]	3-27	Thoracolumbar compression fractures, burst fractures, or other hyperflexion-distraction or hyperflexion-shearing injuries may result in accentuation of the thoracic kyphosis
Straight back syndrome[7,22]	3-14, *E*	Flattening or reversal of the thoracic curve, which may alter intracardiac blood flow dynamics and be manifested as a functional cardiac murmur
Scheuermann disease[23,123]	3-15, *B* 3-14, *B*	Common form of osteochondrosis that usually begins between the ages of 13 and 17 years, and affects 4%-8% of the adolescent population, with a slight predilection for male patients Radiographic criteria include greater than 5 degrees of anterior wedging of at least three contiguous vertebral bodies, multiple Schmorl nodes, undulating surfaces of the vertebral endplates, narrowing of intervertebral disc spaces, and anteroposterior elongation of the apical vertebral bodies Increased thoracic kyphosis is present in 75% of patients; kyphosis may initially be correctable but may become progressively more fixed in position with age; other postural findings include increased lumbar lordosis or thoracolumbar kyphosis Many patients are asymptomatic; others may experience fatigue, aching back pain, stiffness, and discomfort usually occurring around the time of puberty; an increased prevalence of scoliosis and disc displacement also has been noted Multiple Schmorl nodes frequently are seen in patients with Scheuermann disease, although the precise cause is unclear; factors that appear to play a role in some cases of Scheuermann disease include: 1. Stress-induced intraosseous disc, displacements through congenitally or traumatically weakened portions of cartilaginous endplate 2. Osteoporosis during growth spurts 3. Genetic factors 4. Athletic activity
Gibbus deformity	3-10, 3-29, 3-30, 3-49, 3-50, 3-68	Acute angular kyphosis, typically affecting the thoracolumbar region, found in tuberculous spondylitis, hypothyroidism, achondroplasia, mucopolysaccharidoses, various other bone dysplasias, and some severe thoracolumbar flexion injuries

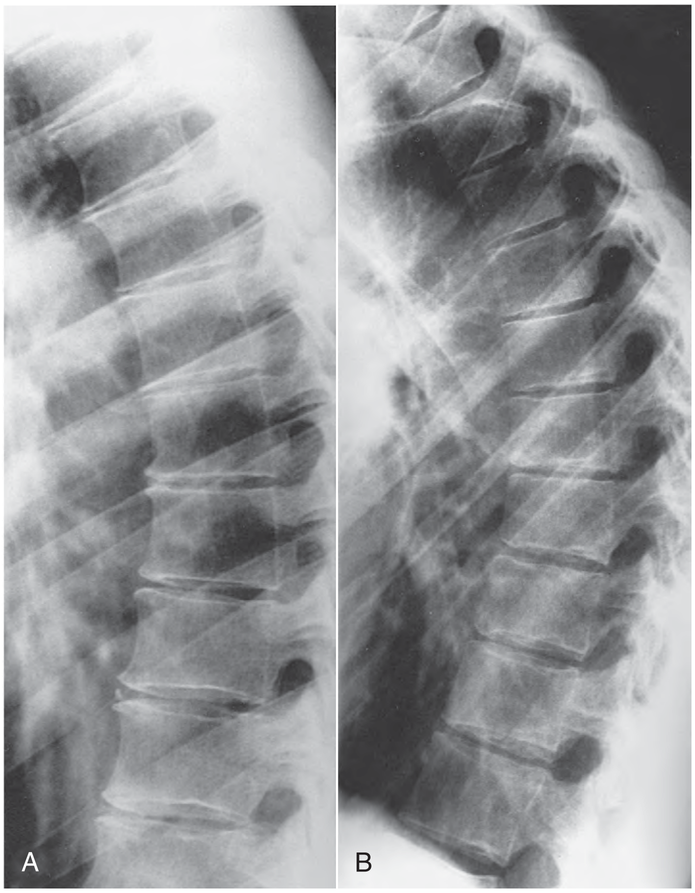

FIGURE 3–14 Thoracic kyphosis: normal and abnormal appearance. A, Normal kyphosis.[23,114] In a 37-year-old man, observe the normal thoracic kyphosis. In addition, early degenerative disc disease is noted, characterized by disc space narrowing, osteophytes, and calcification of the anterior annular fibers. **B,** Scheuermann kyphosis.[7,19,123] In another patient, observe a slightly exaggerated thoracic kyphosis. Mild irregularity of the vertebral endplates represents Schmorl cartilaginous nodes, and the findings are compatible with Scheuermann disease.

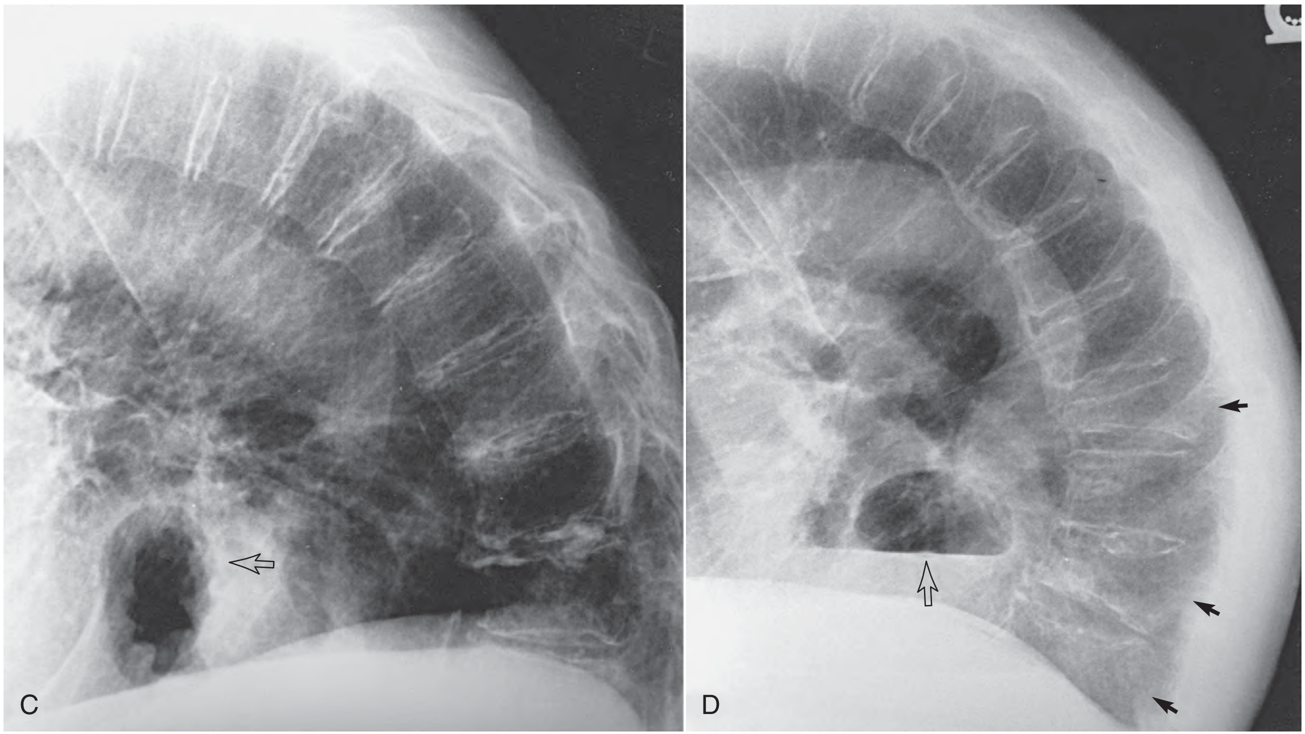

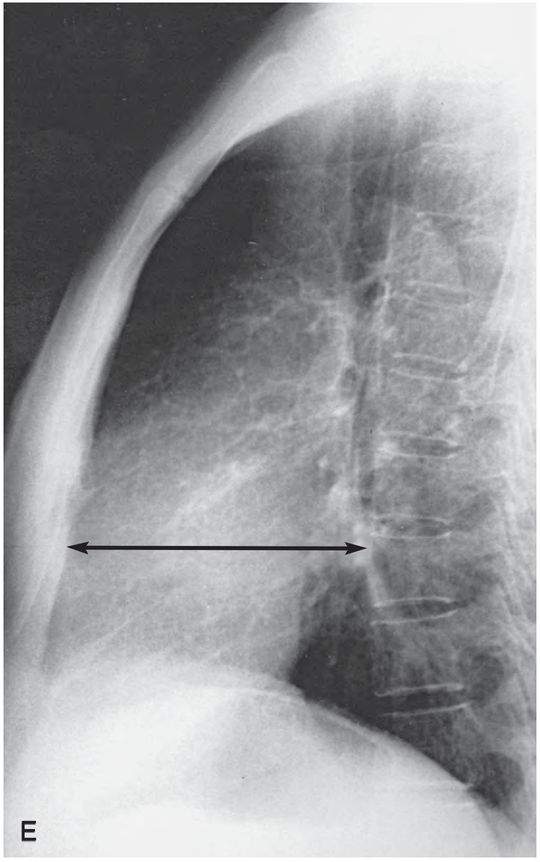

FIGURE 3–14, cont'd **C,** Senile kyphosis.[19] This 73-year-old woman with advanced postmenopausal osteoporosis and concomitant degenerative disc disease with intervertebral disc calcification has dramatic kyphosis measuring 102 degrees. Although mild anterior vertebral body wedging is noted at several levels, no frank compression fractures are present. The air density in the mediastinum *(open arrow)* represents a hiatal hernia. **D,** Osteoporotic kyphosis.[19,104,130] Severe kyphosis, anterior vertebral body ossification, and multiple compression fractures *(arrows)* are evident in this 82-year-old woman. She also has osteoporosis and a hiatal hernia *(open arrow)*. **E,** Reversed kyphosis or lordosis.[7,22] The thoracic spine of this 36-year-old woman has a lordotic, reversed kyphotic curve. This flattening of the thoracic kyphosis and the anteroposterior diameter of the chest may lead to a condition termed the *straight back syndrome*. In this syndrome, the sagittal dimension of the thoracic cage *(double-headed arrow)* measures less than 13 cm in men and 11 cm in women (on a 72-inch source-image receptor distance [SID] chest radiograph). Cardiac compression and a functional cardiac murmur have been identified in patients with this syndrome.

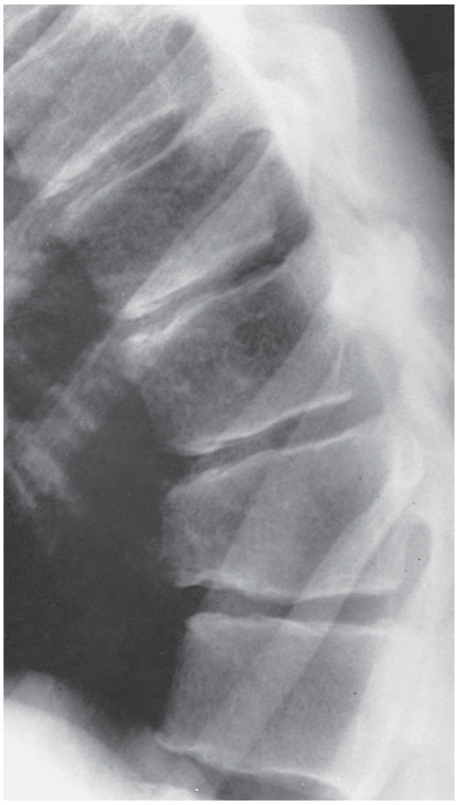

FIGURE 3–15 **Scheuermann disease.**[23,123] In a 22-year-old man with back pain, abnormalities include kyphosis, multiple endplate irregularities, disc space narrowing, and wedge-shaped vertebral bodies, which are characteristic of this disease. Schmorl nodes and limbus vertebrae, not prominent in this case, also occur in Scheuermann disease.

TABLE 3-5 Scoliosis

Entity	Figure(s)	Characteristics
Idiopathic Scoliosis		
Infantile-onset[8,123,124]		*Onset:* children younger than 4 years of age; not present at birth, but develops within first 6 months of life Rare in the United States; more common in the United Kingdom Resolution occurs in 74% of patients; progression mainly occurs with curves >50 degrees
Juvenile-onset[8,116,123,124]		*Onset:* 4-9 years of age 13% of all cases of scoliosis are detected in this age range Boys > girls before age of 6 years; girls > boys from ages 7-9 years Almost invariably progresses with growth MR imaging is useful in evaluating juvenile-onset scoliosis
Adolescent-onset[4,24,116,123,124]	3-16	*Onset:* 10 years of age to skeletal maturity Most common type of idiopathic scoliosis Girls:boys, 4:1 to 8:1 The use of MR imaging as a screening modality for all children with scoliosis is still controversial and further studies are needed to evaluate if the examination adds or changes the treatment of these patients.
Congenital Scoliosis		
Secondary to osseous developmental anomalies[25,116,123,124]	3-17; see 3-6	Failure of segmentation (unilateral block vertebra, pedicle bar, or neural arch fusion), partial duplication (supernumerary hemivertebra), or failure of formation (hemivertebra) results in structural lateral curvatures of the spine Progression is seen in 75% of cases Associated findings: rib, genitourinary tract, and thumb anomalies, congenital heart disease, and undescended scapula MR imaging is frequently recommended to evaluate children with congenital scoliosis or juvenile-onset idiopathic scoliosis.
Neurofibromatosis type I (von Recklinghausen disease)[26,116,123,124]	3-18; see 3-65	Classified as dystrophic Often appears initially as an acute scoliotic angulation and associated kyphosis; it also may resemble a smooth idiopathic curve May be associated with posterior scalloping of vertebral bodies and enlarged neural foramina Associated intraspinal abnormalities include dural ectasia, pseudomeningocele, and neurofibromas—intraspinal or neuroforaminal
Marfan syndrome[16,97,124,128]		Scoliosis occurs in 40%-60% of patients Male = female Smooth, long, sweeping curve resembles that of idiopathic scoliosis In young people the curve progresses more rapidly than in idiopathic scoliosis Thoracic scoliosis may be associated with posterior scalloping of vertebral bodies from dural ectasia
Diastematomyelia[8]	3-19	Two thirds of patients have scoliosis; diastematomyelia occurs in 15% of all patients with congenital scoliosis; often associated with other vertebral anomalies and short angular kyphosis Girls:boys, 2:1 Congenital longitudinal diastasis of the spinal canal and spinal cord with increased interpedicle distance Septum (ossified or unossified) divides the cord in 50%-75% of affected persons

Continued

TABLE 3-5 Scoliosis—cont'd

Entity	Figure(s)	Characteristics
Neuromuscular Scoliosis		In general, scoliotic curves in neuromuscular diseases tend to be long, sweeping, and C-shaped
Neuropathic[8]		*Cerebral palsy:* most common cause of neuromuscular scoliosis *Syringomyelia:* up to 70% of patients have scoliosis *Traumatic paraplegia and quadriplegia:* result in neuromuscular scoliosis, especially when injury occurs before skeletal maturation *Poliomyelitis:* no longer a common cause of neuropathic scoliosis
Myopathic[27]	3-20	Duchenne muscular dystrophy frequently results in proximal muscle weakness and incapacitation by adolescence Spinal deformity, including kyphosis and scoliosis, occurs in 60%-95% of children older than age 10 years who are confined to a wheelchair; may be complicated by respiratory failure, pneumonia, and eventual cardiac failure, which may be fatal, commonly by the third decade of life Asymmetric hip contractures, muscle weakness, and pelvic obliquity contribute to the scoliosis
Trauma		
Fracture[8]		Fractures may result in an antalgic curve convex to the side of injury
Back pain[8]		Antalgic muscle splinting often results from low back pain owing to disc displacements and other causes of mechanical pain; may result in self-limited lumbar and thoracic scoliosis
Radiation[28]	3-21	Radiation therapy for tumors of the kidney, thorax, or retroperitoneum causes asymmetric growth of vertebral structures within the radiation field; frequently results in scoliosis Scoliosis complicating radiation treatment is seen in 70% of patients with Wilms tumor and 76% of 5-year survivors of neuroblastoma
Neoplasms		
Bone tumors[29,129]	3-22; 3-61	Osteoid osteoma and osteoblastoma often result in painful scoliosis These tumors generally are seen on the concave side of the scoliosis at or near the apex of the curve
Spinal cord tumors[30]		10% of intraspinal tumors are associated with scoliosis May be associated with pedicle erosion, spinal canal widening, or paravertebral masses
Other Disorders		
Ossified disc fragment[31]	3-23	Thoracic disc herniations may calcify or ossify and result in a compensatory antalgic scoliosis
Secondary to leg length inequality[32]		Functional lumbar curve convex to the side of the shorter leg; compensatory thoracic curve in the opposite direction
Treatment for Scoliosis		
Spinal instrumentation[33]	3-24	Many different surgical methods used to treat severe scoliosis

TABLE 3-6 Main Indications for Further Imaging in Scoliosis[*]

A. Congenital scoliosis
B. Dysraphic states
C. Developmental causes (neurofibromatosis)
D. Painful deformity
E. Idiopathic scoliosis[†]
  1. Clinical
    - Age (<10 years)
    - Headache
    - Neurologic signs/symptoms
    - Neck symptoms
    - Foot deformity
    - Rapid progression
  2. Radiographic
    - Atypical curves (i.e., left thoracic)
    - Increased kyphosis
    - Wide spinal canal
    - Thin pedicle(s)
F. Abnormal somatosensory evoked potential (SEP) study
G. Preoperative
H. Postoperative

[*] From Cassar-Pullicino VN, Eisenstein SM: Imaging in scoliosis: what, why and how? Clin Radiol 57:543, 2002.

[†] Indications for MRI in “idiopathic” scoliosis.

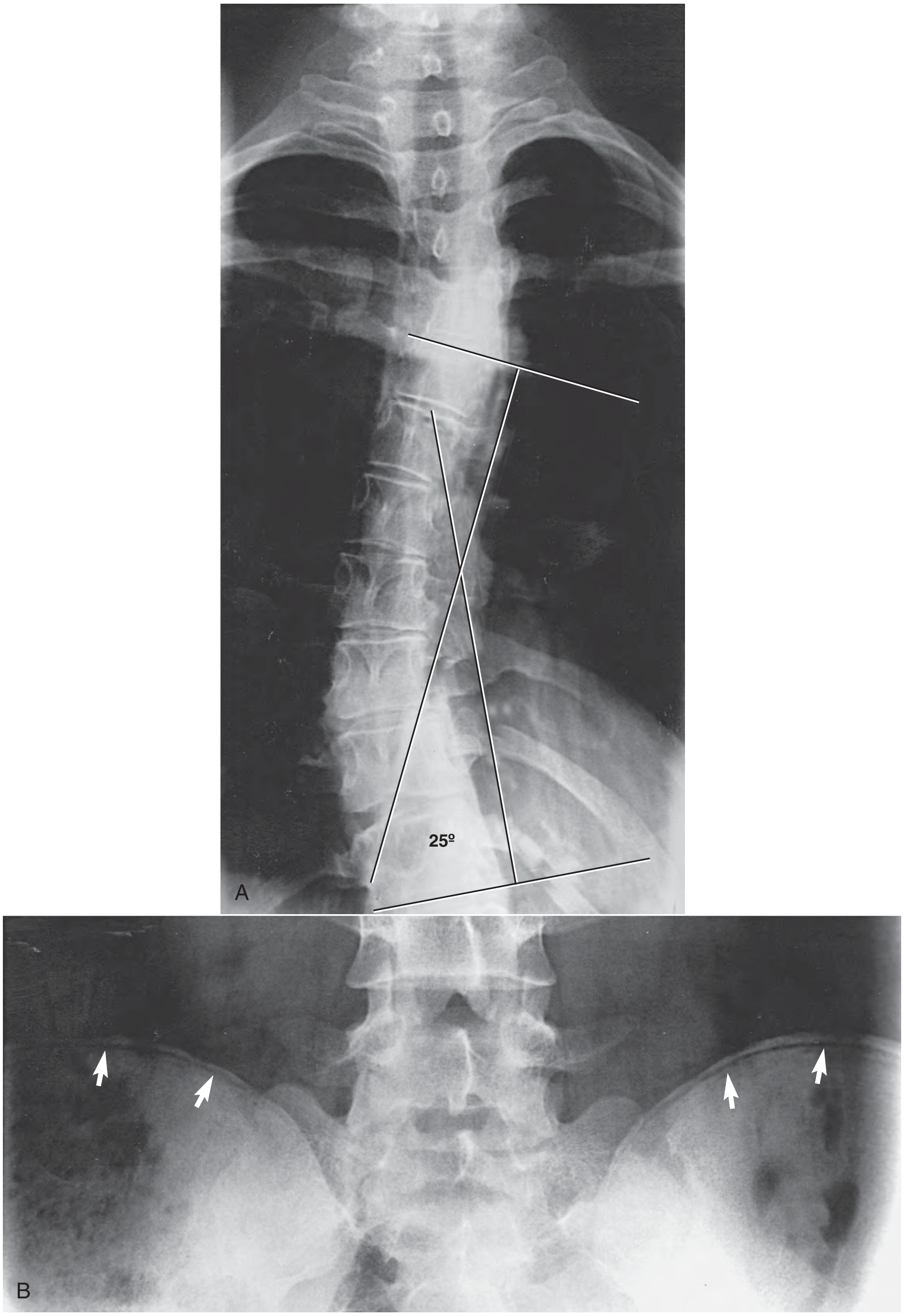

FIGURE 3–16 **Adolescent idiopathic scoliosis.**[4,24,116,123,124] **A,** This 26-year-old woman was diagnosed as having idiopathic adolescent scoliosis at the age of 13 years. A right convex curve extending from T5 to T11 measures 25 degrees using the Cobb method. A smaller left convex curve extends from T1 to T5. **B,** Determination of skeletal maturity: Risser sign. The normal iliac apophysis just before fusion in this 19-year-old man appears as a curvilinear ossified rim along each iliac crest *(arrows)*. The iliac apophyses begin to appear between the ages of 12 and 15 years, typically at the time of menarche in women. They may ossify multicentrically and appear rippled. Fusion of the apophysis to the iliac crest takes place between the ages of 21 and 25 years, a feature helpful in the determination of skeletal maturity in scoliotic patients (Risser sign).

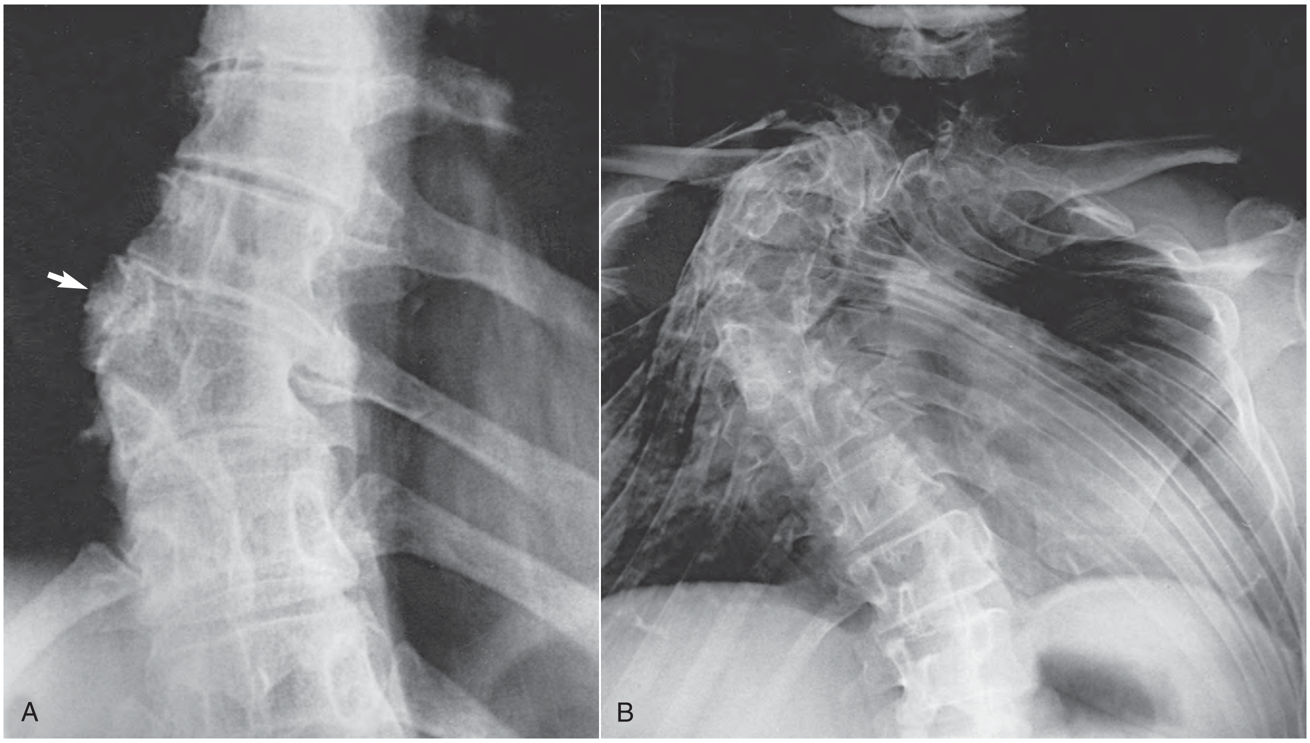

FIGURE 3–17 **Congenital scoliosis.**[25,116,123,124] **A,** Lateral hemivertebra. A frontal radiograph from this 25-year-old woman demonstrates short, angular lower thoracic scoliosis. A small incomplete triangular vertebral body (incarcerated vertebra) and its associated pedicle *(arrow)* are interposed between two relatively normal vertebrae on the right side. **B,** Severe thoracic scoliosis with crowding of the ribs, thoracic cage deformity, and numerous cervicothoracic anomalies is seen in another patient. Clinical note: MR imaging is frequently recommended to evaluate children with congenital scoliosis or juvenile-onset idiopathic scoliosis. *(**A,** Courtesy S. O'Connor, DC, Toronto, Ontario, Canada; **B,** Courtesy R.D. Stonebrink, DC, Portland, Oregon.)*

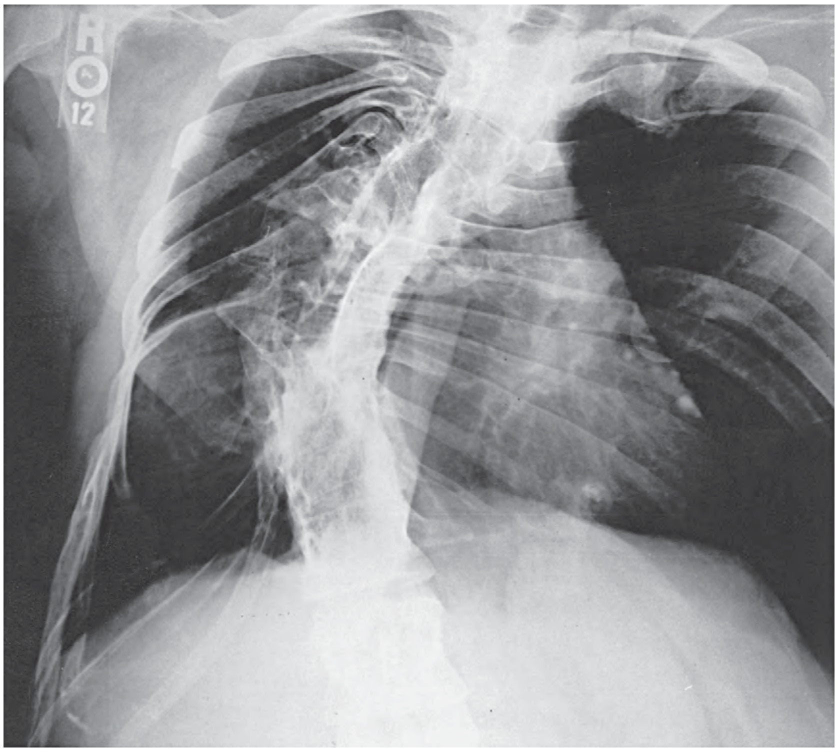

FIGURE 3–18 **Scoliosis: neurofibromatosis type I (von Recklinghausen disease).**[26,116,123,124] A severe S-shaped scoliosis with multiple rib deformities and ribbonlike ribs are seen. Scoliosis (with or without kyphosis) is the most common spinal manifestation of neurofibromatosis. The scoliosis associated with this disease can take one of two forms: the first resembles an ordinary idiopathic scoliosis with a long sweeping curve; the second is dysplastic, may be rapidly progressive, and is a sharply angulated, short-segment kyphoscoliosis. This latter type commonly involves fewer than six middle or lower thoracic vertebral segments. *(Courtesy S.K. Brahme, MD, San Diego.)*

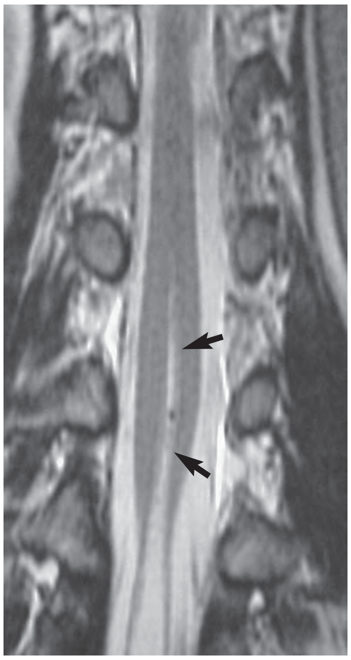

FIGURE 3–19 Diastematomyelia.[8] This 11-year-old girl with a left convex thoracic scoliosis (not shown) underwent MR examination including this coronal T2-weighted image of the lumbar spine. A midline longitudinal diastasis of the spinal cord is evident *(arrows)*. The low signal dot positioned between the dysraphic cord is a fibrous or osseous bar. This spinal dysraphism occurs twice as commonly in girls and may present as an atypical scoliosis.

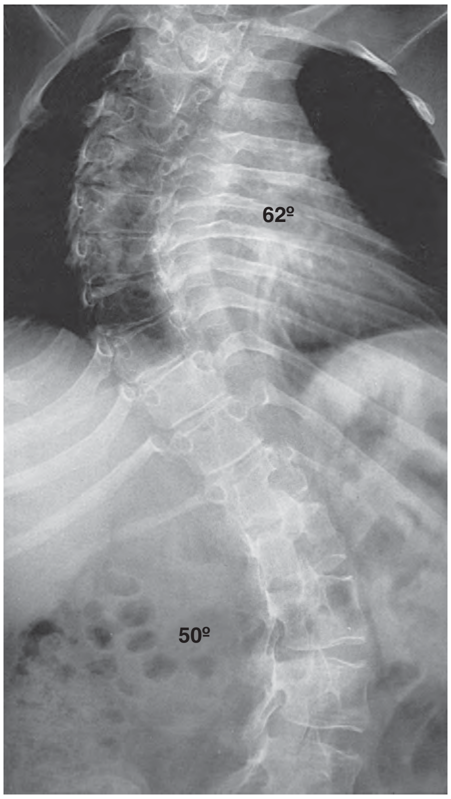

FIGURE 3–20 Scoliosis: neuromuscular disease-myopathic.[27,116,123,124] Frontal radiograph from this 15-year-old boy with Duchenne muscular dystrophy reveals severe scoliosis. The thoracic curve measures 62 degrees, and the lumbar curve measures 50 degrees.

FIGURE 3–21 Scoliosis: radiation therapy.[8] **A-B,** This 15-year-old boy underwent surgery and subsequent radiation therapy for a Wilms tumor. The radiation therapy results in growth abnormalities in the developing spine leading to scoliosis. The vertebral bodies on the right are decreased in height and the pedicles on the right are smaller than those on the left side. Multiple metallic surgical staples are also evident.

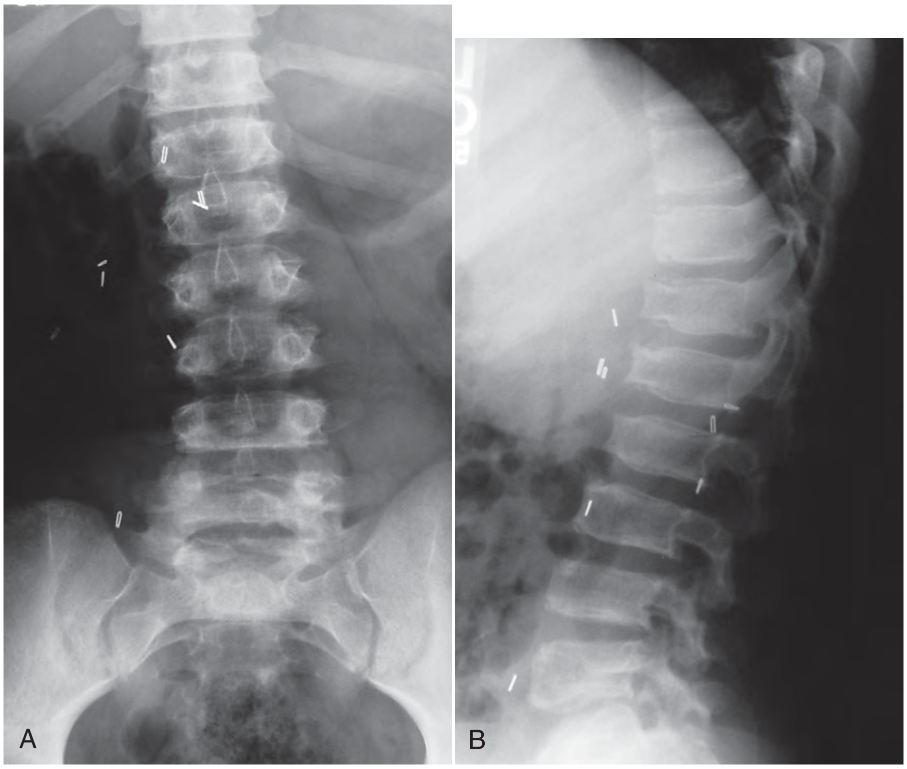

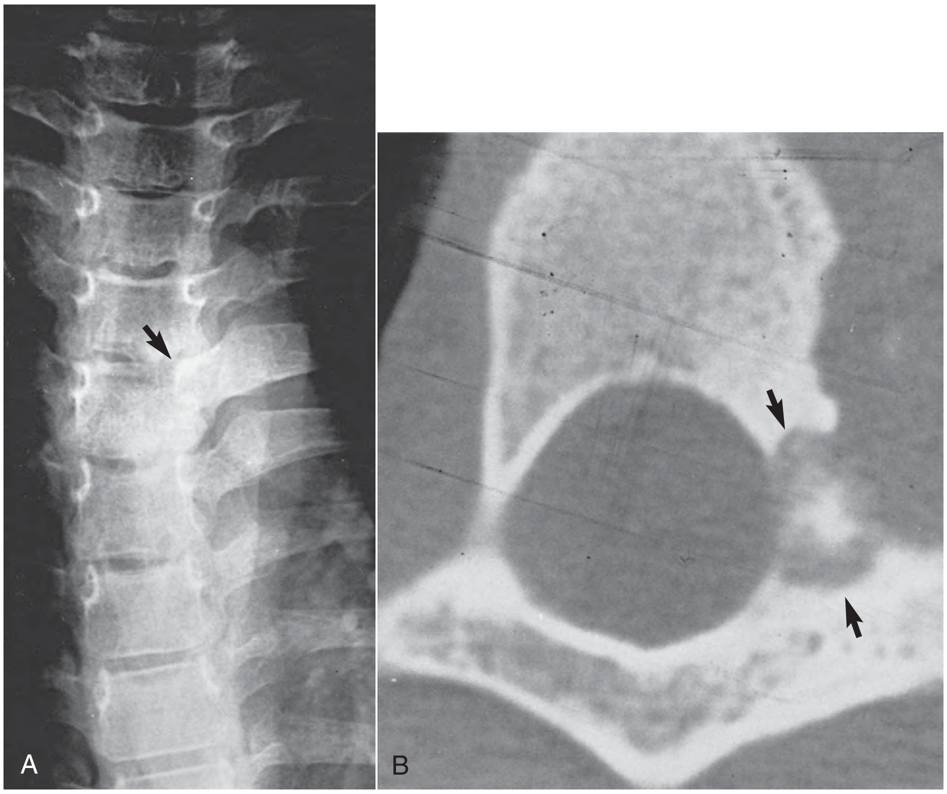

FIGURE 3–22 Scoliosis: osteoid osteoma.[29,129] This 9-year-old girl has painful scoliosis. Routine radiograph **(A)** shows scoliosis and sclerosis within the left T5 pedicle *(arrow)*. Transaxial CT image **(B)** demonstrates the radiolucent nidus *(arrows)* and central calcification surrounded by reactive sclerosis within the left pedicle and lamina.

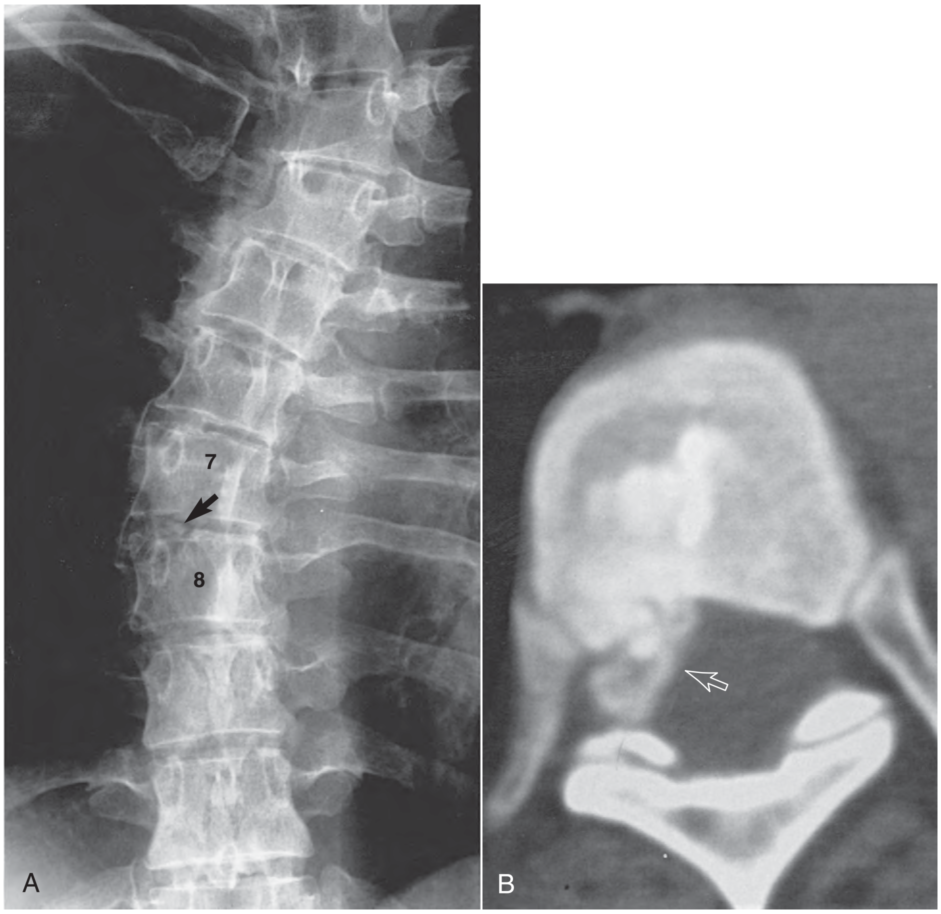

FIGURE 3–23 Scoliosis: extradural mass from ossified disc herniation.[31,124] This 40-year-old woman has persistent thoracic spine pain and an antalgic scoliosis. **A,** Frontal radiograph reveals a left cervicothoracic and right thoracic scoliosis. A small focus of calcification *(arrow)* is seen within the right T7-T8 disc space. **B,** Transaxial CT scan shows extensive calcification within both the T7-T8 disc and herniated disc fragment *(open arrow)*, the latter displacing the thecal sac. Thoracic disc herniations frequently calcify or ossify. *(Courtesy M. Gallagher, MD, Billings, Montana.)*

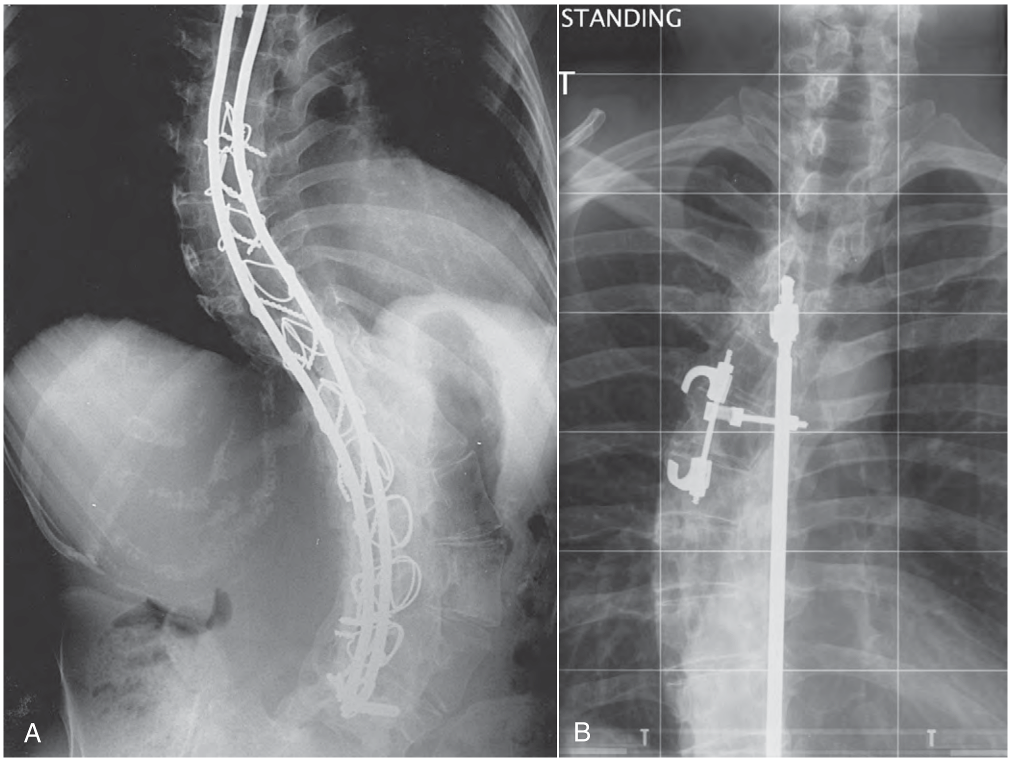

FIGURE 3–24 **Scoliosis: management with spinal instrumentation.**[33,123,124] **A,** This patient with severe scoliosis has Luque L-shaped rods implanted to help correct the deformity and stop progression of the scoliosis. **B,** An anteroposterior radiograph illustrates a threaded Harrington rod on the left that applies traction, and a shorter compression rod on the right that is attached to transverse processes with hooks in a patient with idiopathic scoliosis. These are only two of many surgical procedures used for fixation and derotation of scoliosis and are usually supplemented with bone grafting to obtain solid fusion.

TABLE 3-7 Fractures and Dislocations of the Thoracic Spine

Entity	Figure(s)	Characteristics
Upper Thoracic Spine (T1-T4)		
Vertebral body compression fractures[34,111,112]		Rare site for this injury; high likelihood of associated neurologic deficit More frequent in younger people *Mechanisms:* electric shock, seizures, motor vehicle accidents, motorcycle accidents, direct trauma, athletic injuries When compression fractures occur in the upper thoracic spine, the possibility of pathologic fracture secondary to tumor should be considered Many osteoporotic compression fractures are identified incidentally on multidetector computed tomography (MDCT) of the chest
Midthoracic Spine (T5-T9)		
Vertebral body compression fracture[35,111,112]	3-25	Frequent occurrence in osteoporotic persons Low prevalence of neurologic deficit *Mechanism:* single incident of trivial trauma, repeated minor trauma, or slow bone remodeling resulting from ongoing chronic microfractures
Schmorl cartilaginous nodes[36,110]	3-26	Displacement of intervertebral disc material through the cartilaginous endplate and subchondral bone plate Isolated Schmorl nodes may occur with acute trauma, degenerative disc disease, osteoporosis, osteomalacia, Paget disease, hyperparathyroidism, infection, and neoplasm May be painful, but usually have no neurologic complication Gadolinium-enhanced MR images reveal that larger Schmorl nodes are often vascularized, frequently are associated with bone marrow edema, and are more common in symptomatic patients than in asymptomatic patients Presence of multiple Schmorl nodes in an adolescent thoracic spine suggests the diagnosis of Scheuermann disease
Thoracolumbar Spine (T10-L2)*		
Vertebral body compression fracture[35,37-39,111,112,130]	3-25, 3-27, 3-28	Most common thoracolumbar spine injury Very common in elderly persons Low prevalence of neurologic deficit Affects only the anterior column *Mechanism:* trivial trauma, repeated minor trauma, or slow bone remodeling resulting from ongoing chronic microfractures, or hyperflexion-compression injury
Burst fracture[40]	3-29	14% of all thoracolumbar spine injuries; discussed in depth in Chapter 4
Thoracolumbar flexion injury: seat belt fracture[41-44,125,126]	3-30, 3-31	Most common in younger persons T12 (25.5%), L1 (38.2%), and L2 (14.5%) are most frequent sites Affects middle and posterior (and occasionally anterior) columns and often results in thoracolumbar facet instability Approximately 15% of patients have neurologic deficits and 40% have abdominal visceral injuries *Mechanism:* flexion-distraction over a fulcrum, such as that occurring in motor vehicle accidents in persons wearing a lap belt Occurs frequently in children restrained by lap belts in motor vehicle accidents ***Injury patterns*** 1. Disruption of posterior and middle column ligaments, compression fracture of anterior body, intact anterior ligaments 2. Disruption of anterior, middle, and posterior ligaments 3. Classic osseous Chance-type fracture: horizontal fracture through the body, pedicles, pars interarticularis, and spinous and transverse processes (Figure 3-30) 4. Up to 48% of cases have an associated burst-type fracture component involving buckling or retropulsion of the posterior vertebral body cortex.
Fracture-dislocation[34]	3-32	10%-20% of all thoracolumbar spine injuries; may also occur at the T3 to T8 region Complete disruption of three columns 53%-93% of patients develop permanent neurologic deficit *Mechanisms:* compression (anterior column); rotation, shear, and distraction (middle and anterior columns) Often severe injuries, usually with polytrauma
Any Region of Thoracic Spine		
Abused child syndrome[45]	3-33	Spine trauma is rare in child abuse Injuries include compression fractures of the vertebral body, acute disc displacement, avulsion of the posterior elements, and thoracolumbar fracture-dislocation

* From Denis F: The three column spine and its significance in the classification of acute thoracolumbar spinal injuries. Spine 8:817, 1983.

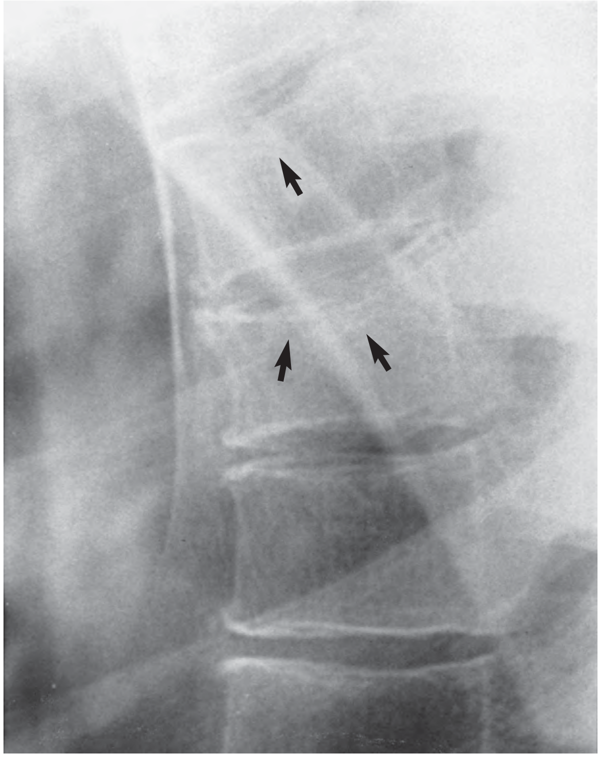

FIGURE 3–25 Compression fractures.[34,35,130] Routine lateral radiograph from this 73-year-old man demonstrates anterior wedge-shaped compression fractures of the fourth and fifth thoracic vertebral bodies. Observe the anterior and central endplate depressions *(arrows)*.

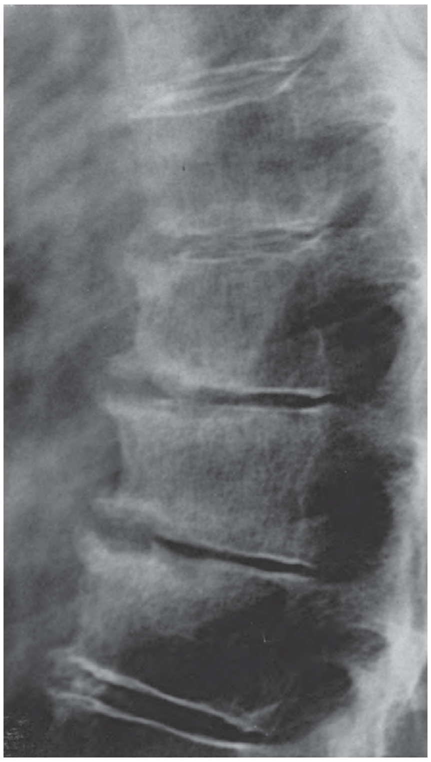

FIGURE 3–26 Schmorl (cartilaginous) nodes.[36,110] Irregularity of the vertebral endplates, lucent areas, and adjacent sclerosis typical of cartilaginous nodes throughout the thoracic spine is seen in this elderly patient.

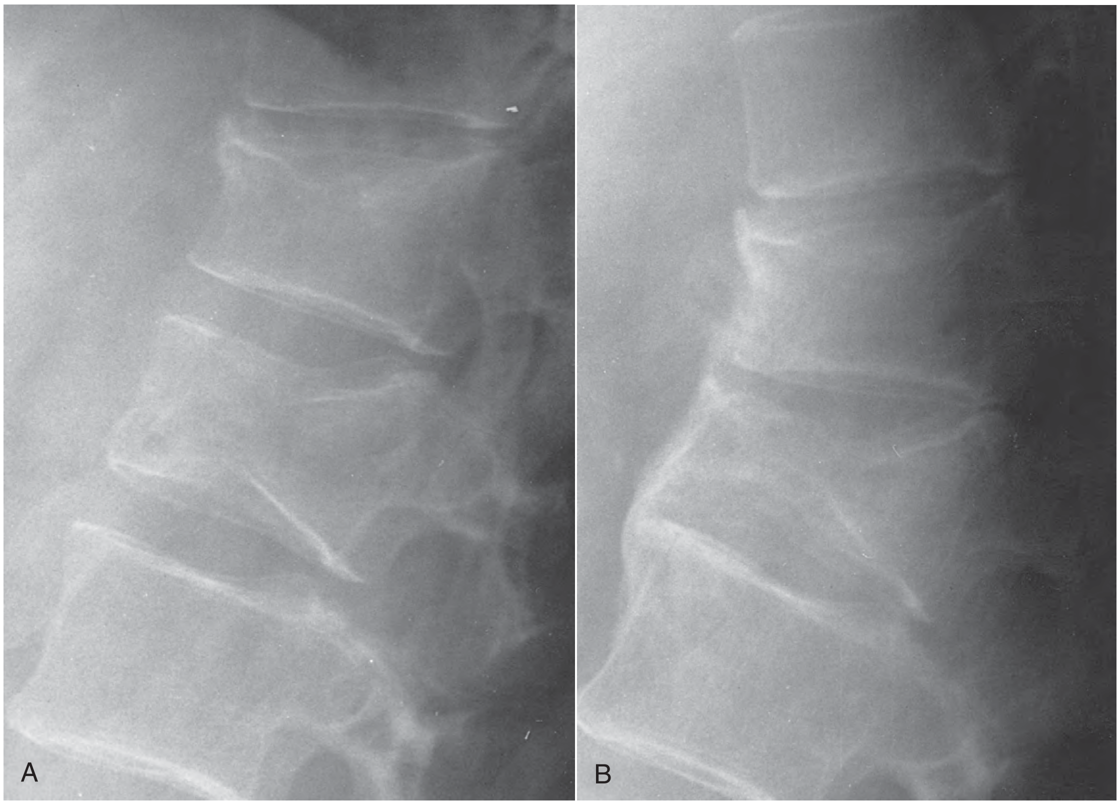

FIGURE 3–27 Compression fractures: natural history.[35,37-39,130] **A,** Initial radiograph taken at the time of injury shows generalized osteopenia and central endplate depressions of the T12 and L1 vertebral bodies. **B,** Radiograph obtained 2 years later reveals extensive osseous bridging of the anterior aspects of the compressed vertebrae and more advanced collapse of the L1 vertebral body. The presence of secondary degenerative ossification, as seen in this patient, is a reliable sign that the fracture occurred at least 18 months earlier (Table 3-7).

TABLE 3-8 Differential Diagnosis: Acute Versus Chronic Compression Fractures[7]

Features	Acute (Recent) Fracture (Within Last 2 Months)	Chronic (Remote) Fracture (Before Last 2 Months)
Vertebral body wedging	Present	Present; may progress with time
Step defect	Present	Absent
Sclerotic zone of impaction	Present	Absent
Disc space narrowing	Absent	Often present owing to degenerative disc disease
Paravertebral soft tissue hemorrhage	Present (variable)	Absent
Scintigraphy	Positive	Positive up to 18-24 months after fracture
MR imaging characteristics		
T1-weighted	Low signal intensity	Isointense to normal vertebral bodies
T1-weighted with gadolinium	High signal intensity	Isointense to normal vertebral bodies
T2-weighted	High signal intensity	Isointense to normal vertebral bodies

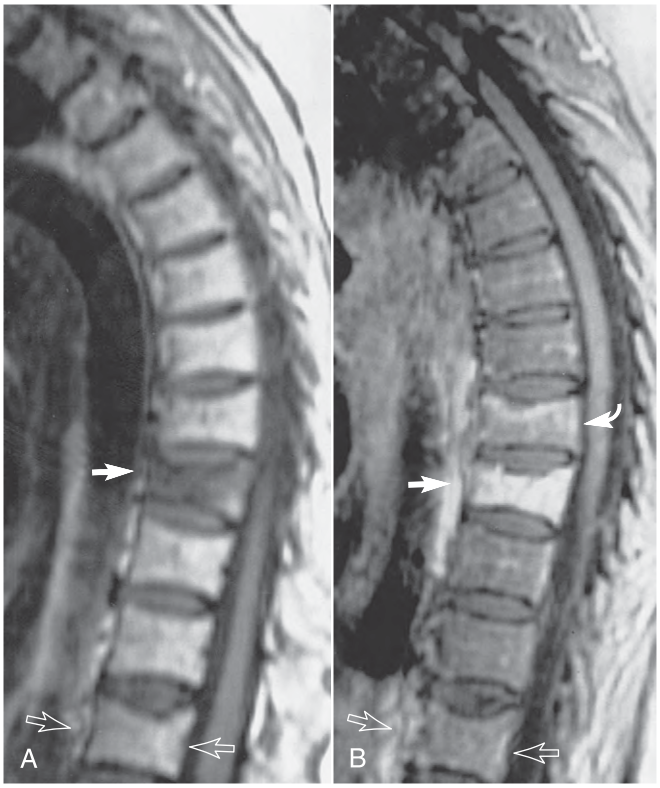

FIGURE 3–28 **Acute compression fracture: magnetic resonance (MR) imaging abnormalities.**[35,37-39] **A** and **B,** Sixty-three-year-old woman with severe kyphosis and acute thoracic spinal pain. Sagittal T1-weighted spin echo MR images obtained before (TR/TE, 500/12) **(A)** and after (TR/TE, 800/12) **(B)** intravenous administration of gadolinium contrast agent reveal a wedge-shaped compression deformity of T10 vertebral body *(arrow)*. Low signal intensity is seen in the pregadolinium image **(A)** and high signal intensity in the postgadolinium image **(B),** characteristic of a recently fractured vertebra. Compare the findings of the acute fracture in T10 to those of a remote, healed fracture of L1 *(open arrows)*. In the remote fracture, the signal intensity of the L1 vertebral body is the same as that of the adjacent vertebral bodies before **(A)** and after **(B)** contrast agent administration. A subacute fracture of T9 also is evident *(curved arrow)* in which the signal is less intense than that of the acute fracture on the postgadolinium image **(B).** Note high signal intensity in the prevertebral soft tissues in **B.** Compression fractures are common, especially in older women. MR imaging can be useful in differentiating between recent (acute) and long-standing (chronic) spine fractures and is well suited for assessing spinal cord and soft tissue injury (Table 3-7). However, differentiating between benign compression fractures and neoplastic, pathologic fractures can be difficult. The finding on MR images of a fluid collection within a collapsed vertebral body may represent osteonecrosis secondary to vertebral collapse. *(Courtesy M.N. Pathria, MD, San Diego.)*

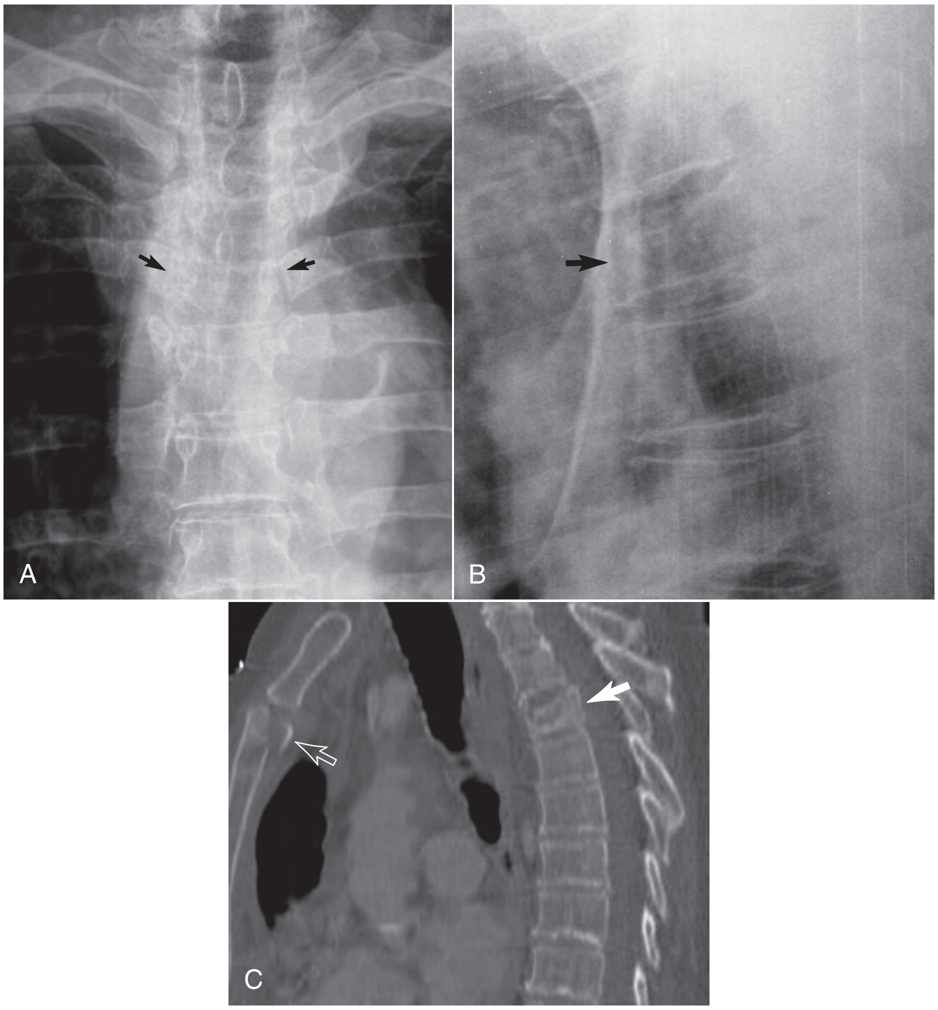

FIGURE 3–29 **Burst fracture.**[40] This 68-year-old man was involved in a severe rollover car crash and sustained a T4 burst fracture. Anteroposterior **(A)** and lateral **(B)** radiographs show some compression of the T4 vertebral body *(arrows)*, but the sagittal reformatted CT bone window **(C)** clearly reveals retropulsion of the vertebral body into the spinal canal in addition to compression *(white arrow)*. A fracture of the body of the sternum *(open arrow)* just below the manubriosternal junction is also present.

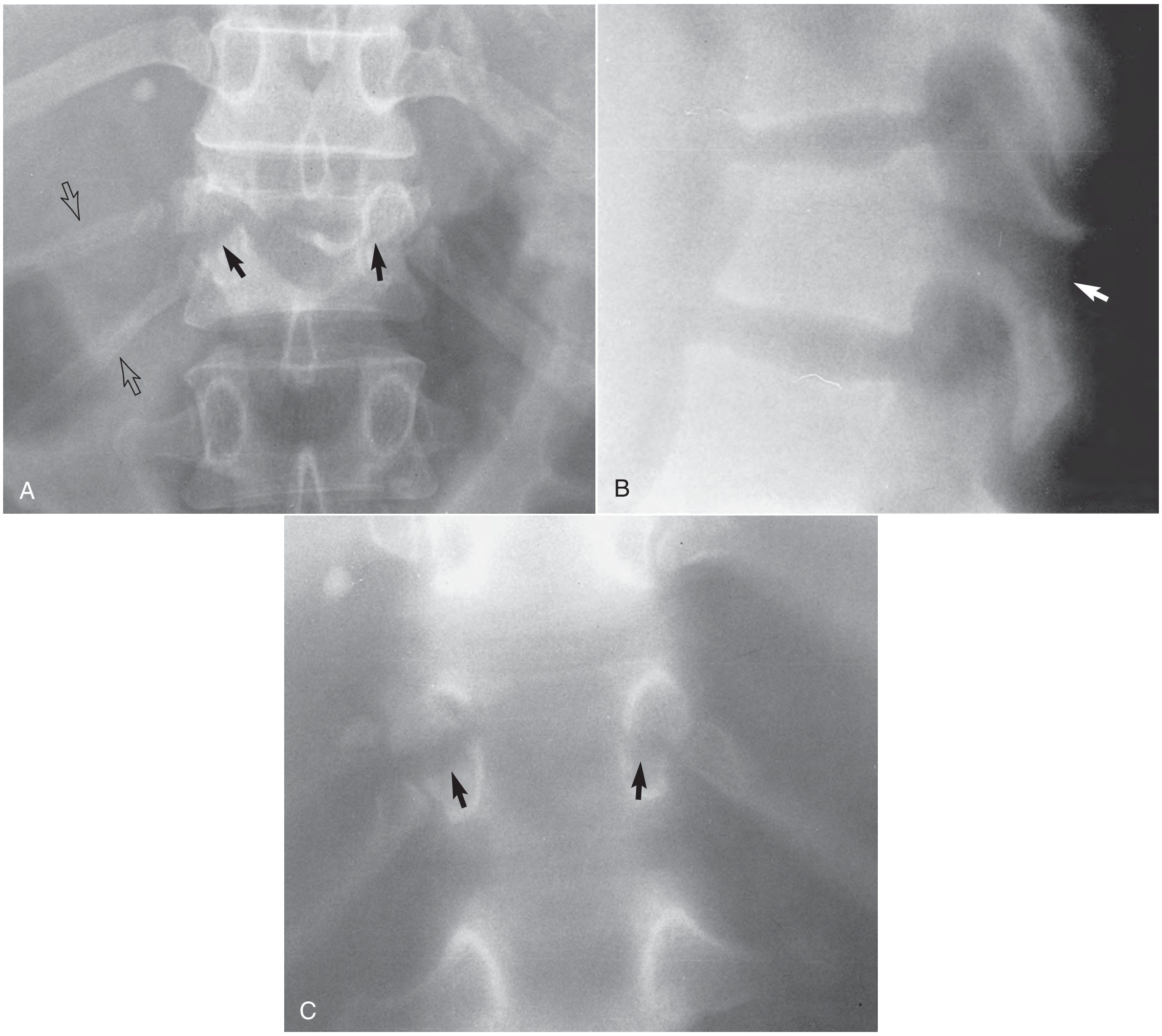

FIGURE 3–30 **Thoracolumbar flexion instability: seat belt fracture.**[41-44,125-127] **A** and **B,** Anteroposterior radiograph **(A)** and lateral **(B)** conventional tomogram reveal anterior vertebral body wedging and a horizontal fracture through the vertebral body and neural arch *(arrows)*. The twelfth rib is also split horizontally *(open arrows)*. This represents a horizontal fracture of the rib. **C,** Frontal conventional tomogram confirms the horizontal split through the pedicles *(arrows)*. The seat belt (or lap belt) injury of the thoracolumbar spine is caused by tensile failure of the spine, which results from a combination of forced hyperflexion and distraction over a fulcrum. This is the most common type of flexion-distraction injury and results in a horizontal splitting of the posterior osseous elements from distraction and minimal compression of the anterior portion of the vertebral body. When the fulcrum is anterior to the vertebral body, the injury becomes one purely of distraction termed a *Chance fracture*.

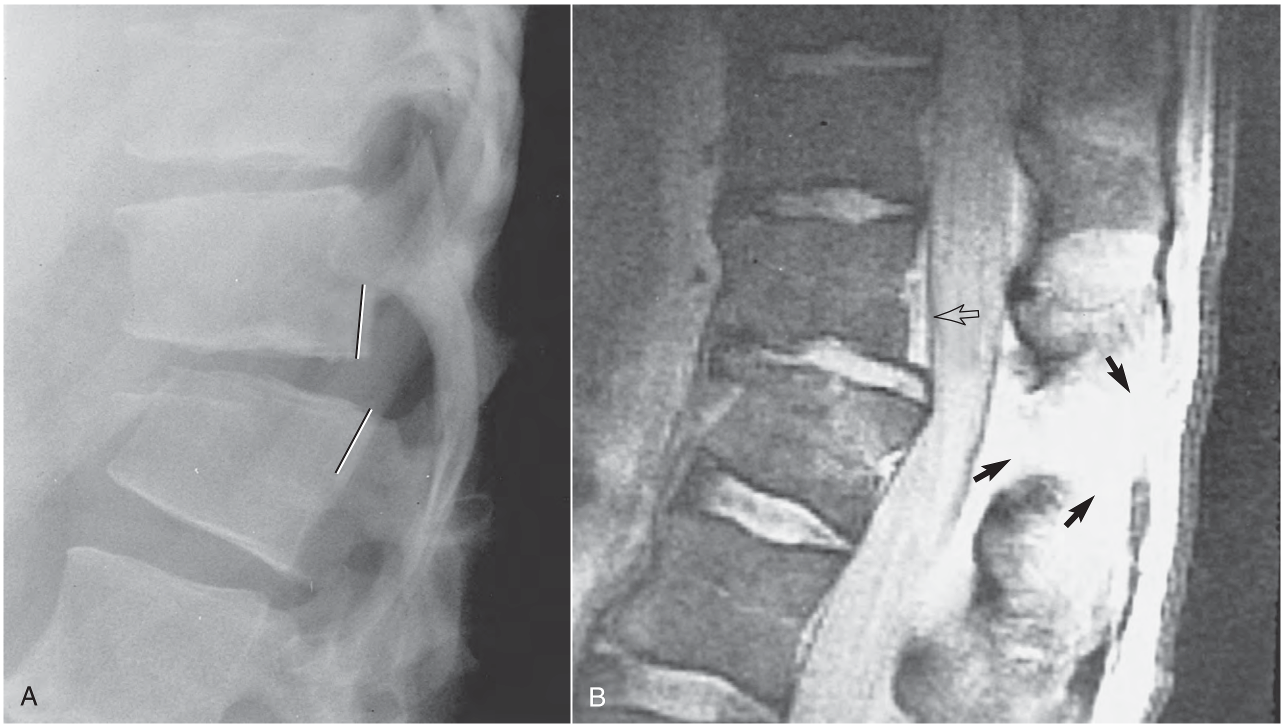

FIGURE 3–31 **Thoracolumbar flexion instability: ligament disruption.**[41-44,125-127] **A,** Lateral radiograph shows compression of the anterior aspect of the L1 vertebral body, anterior translation of the T12 vertebral body (vertical lines show displacement), and separation of the posterior elements, suggesting the possibility of an acute facet lock. **B,** Sagittal T2-weighted (TR/TE, 2700/60) spin echo MR image demonstrates disruption of the supraspinous and interspinous ligaments *(arrows)*. High signal intensity within these ligaments and the L1 vertebral body is characteristic of hemorrhage or edema. In addition, the posterior longitudinal ligament is stripped from the displaced T12 vertebral body *(open arrow)*, and the thecal sac is kinked and compressed. *(Courtesy M.N. Pathria, MD, San Diego.)*

FIGURE 3–32 **Fracture-dislocation.**[34] Frontal radiograph shows widening of the mediastinum *(arrows)* consistent with the presence of hematoma or aortic arch injury in this patient with a T3-T4 fracture-dislocation. The vertical lines demarcate the inner margins of the pedicles of T3 and T4 and illustrate the extent of lateral dislocation. These severe, unstable injuries are associated with an extremely high rate of neurologic injury, most commonly complete paraplegia. They occur most frequently at the T3 to T8 levels. Widening of the mediastinum should raise suspicion also of aortic arch injury.

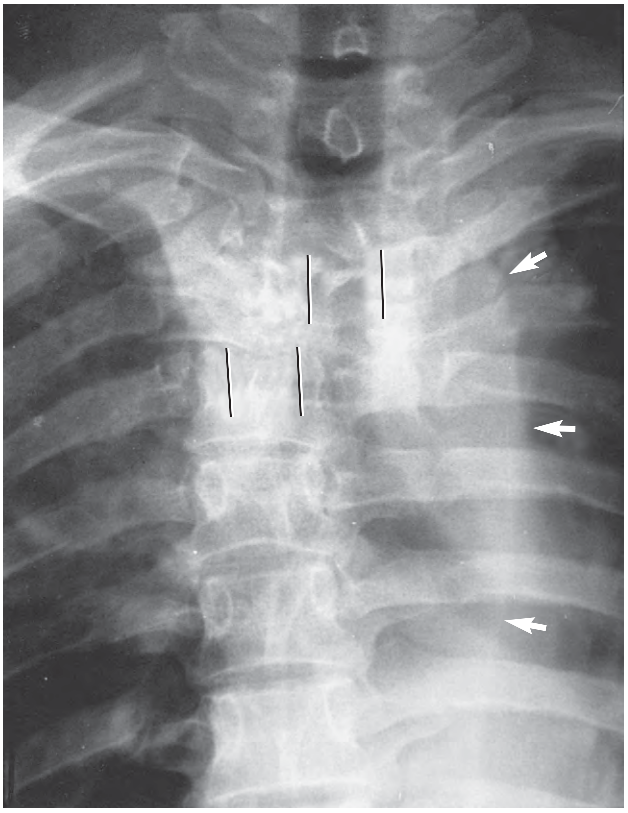

TABLE 3-9 Checklist for the Diagnosis of Clinical Instability in the Thoracic and Thoracolumbar Spine[125,126]

Element	Point Value
Anterior elements destroyed or unable to function	2
Posterior elements destroyed or unable to function	2
Disruptions of costovertebral articulations	1
Radiographic criteria	4
1. Sagittal plane translation >2.5 mm (2 points) 2. Relative sagittal plane angulations >5 degrees (2 points)	
Spinal cord or cauda equine damage	1
Dangerous loading anticipated	1

From White AA, Panjabi MM: Clinical biomechanics of the spine, 2nd Ed. Philadelphia, Lippincott, 1990.
Total of 5 or more = unstable.

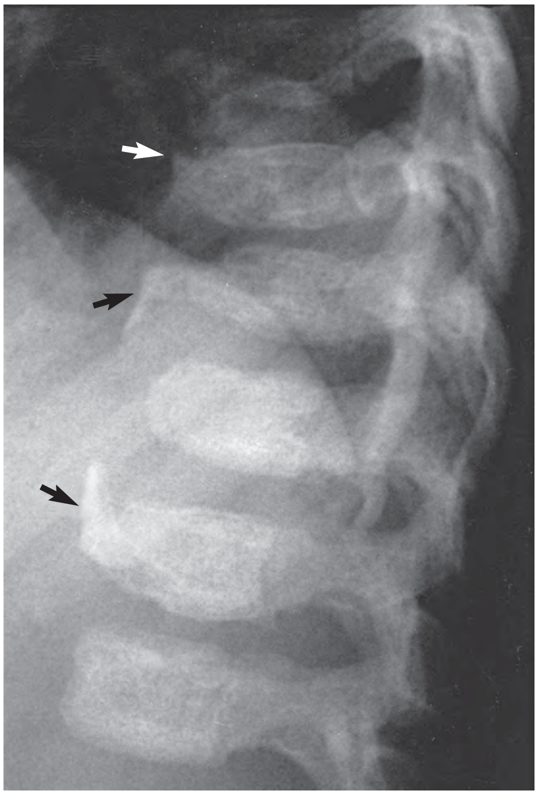

FIGURE 3–33 Abused child syndrome.[45] This 3-year-old girl was repeatedly subjected to physical abuse. Observe the multiple thoracolumbar spine fractures at different stages of healing. Flattening of several vertebral bodies and associated anterior tonguelike projections of bone proliferation are evident *(arrows)*.

TABLE 3-10 Thoracic Spine: Articular Disorders*

Entity	Figure(s), Table(s)	Characteristics
Degenerative and Related Disorders		
Degenerative disc disease[46,110,113]	3-34 Table 3-11	***Spondylosis deformans*** Osteophytes and osseous ridging Subchondral bone sclerosis ***Intervertebral osteochondrosis*** Disc space narrowing Intradiscal vacuum phenomenon Disc calcification (rare)
Costovertebral osteoarthrosis[46]	3-35	Sclerosis and hypertrophy of costotransverse and costovertebral articulations secondary to degeneration Osteophytes may be prominent Ipsilateral rib hypertrophy may be present May be painful and result in limitation of motion CT scanning is the best imaging technique, but it is seldom used because of its expense and the benign nature of costovertebral osteoarthrosis
Degenerative disc calcification[47]	3-36, *A*	Chronic degenerative calcific deposits occur primarily in the anulus fibrosus; affects older persons and may be asymptomatic Men > women It is unclear what proportion of these patients is symptomatic Calcification predominates in the midthoracic and upper lumbar intervertebral discs
Idiopathic childhood disc calcification[96]	3-36, *B-D*	Disc calcification in children, often associated with disc displacements, is symptomatic in 75% of cases Symptoms and signs include pain, stiffness, limitation of motion, and torticollis; fever, leukocytosis, and elevated erythrocyte sedimentation rate Symptoms generally resolve within a few days to weeks; calcification typically disappears within a few weeks to months Boys = girls
Ossified disc displacement[31]	3-37	Ossification of a disc herniation or fragment Calcification or ossification of thoracic discs in adults May be asymptomatic or may cause chronic or acute symptoms secondary to compression of the thecal sac
Diffuse idiopathic skeletal hyperostosis (DISH)[48-51]	3-38, 3-39 Table 3-11	Flowing anterior hyperostosis: prominent vertical sheet of ossification along the anterior vertebral bodies and anulus fibrosus Relative absence of degenerative changes and preservation of disc height Involvement of at least four contiguous segments Relatively normal apophyseal and sacroiliac joints T7-T11 most frequent sites of involvement
Ossification of the posterior longitudinal ligament (OPLL)[52]	3-40	Segmental or continuous vertical sheet of ossification of the posterior longitudinal ligament, up to 5 mm thick; extends along the posterior margins of the vertebral bodies and discs within the spinal canal Often accompanies DISH and may contribute to central stenosis with or without symptoms
Neuropathic osteoarthropathy[53]		Infrequently involves the upper and middle thoracic spine, but syringomyelia, diabetes mellitus, and tabes dorsalis may affect the thoracolumbar region Widespread discovertebral and zygapophyseal joint destruction, collapse, bone fragmentation, and kyphosis May resemble infectious spondylodiscitis

* See also Tables 1-7 to 1-10 and Table 1-19.

TABLE 3-10 Thoracic Spine: Articular Disorders*—cont'd

Entity	Figure(s), Table(s)	Characteristics
Inflammatory Disorders		
Ankylosing spondylitis and enteropathic arthropathy[54,55,109]	3-41, 3-42 Tables 3-11, 3-12	Widespread marginal syndesmophytes, osteitis, disc calcification, osteoporosis, squaring of vertebral bodies, and disc ballooning Erosion and eventual ankylosing of discovertebral junctions and apophyseal joints Ossification of ligaments, joint capsules, and outer annular fibers *Enteropathic arthropathy:* patients with ulcerative colitis and regional ileitis may develop identical imaging findings to those of ankylosing spondylitis Thoracic spine in ankylosing spondylitis is susceptible to fractures and pseudarthrosis, both of which can result in neurologic injury MR imaging is useful in identifying acute and chronic changes of sacroiliitis, osteitis, discovertebral erosive lesions, disc calcification and ossification, and rare complications such as fracture and cauda equine syndrome
Psoriatic spondyloarthropathy and reactive arthritis associated with Reiter syndrome[56,57]	3-43, 3-44 Table 3-11	Unilateral or bilateral, asymmetric, nonmarginal, comma-shaped paravertebral ossification about the lower thoracic and upper lumbar spine in 10%-15% of patients with psoriasis Apophyseal joint narrowing, sclerosis, and bony ankylosis
Progressive systemic sclerosis (scleroderma)[58]	3-45	Paraspinal calcific deposits are composed predominantly of calcium hydroxyapatite crystals
Dermatomyositis and polymyositis[59]	3-46	Subcutaneous and intermuscular calcification frequently involves the chest wall; may be evident on thoracic spine radiographs
Crystal Deposition Disorders		
Calcium pyrophosphate dihydrate crystal deposition disease[60,61]	3-47	May result in widespread secondary degenerative disease with disc space narrowing and chondrocalcinosis of the anulus fibrosus, joint capsules, apophyseal joints, and articular cartilage
Alkaptonuria[62]	3-48 Table 3-11	Widespread, severe disc space narrowing, diffuse anulus fibrosus calcification, and intradiscal vacuum phenomena Osteoporosis Osseous bridging may resemble marginal syndesmophytes Eventual progression to bamboo spine
Infection		
Pyogenic spondylodiscitis[63,98,107]	3-49	Up to 21-day latent period before radiographic changes appear Infection initially involves disc and adjacent vertebral body Severe one-level disc space narrowing that eventually may spread to adjacent levels, obliterating vertebral endplates and resulting in vertebral collapse in later stages Paravertebral soft tissue mass or abscess
Tuberculous spondylodiscitis[64,65]	3-50, 3-51	25%-60% of cases of skeletal tuberculosis affect the spine, principally the thoracolumbar region Anterior vertebral destruction and collapse often results in an acute, angular gibbus deformity Classically, vertebral bodies and disc are involved; posterior elements are affected infrequently Slower progression compared with that of pyogenic spondylodiscitis Paravertebral abscess is common

TABLE 3-11 Osseous Outgrowths of the Spine

Entity	Figure(s)	Definition	Representative Disorders	Appearance
Osteophyte	3-34	Hypertrophic proliferation of bone at the attachment of the annular fibers to the vertebral body	Degenerative disc disease (spondylosis deformans)	Triangular outgrowth located several millimeters from edge of the vertebral body; may be claw-shaped and may bridge the discovertebral joint in advanced disease
Marginal syndesmophyte	3-41	Ossification of the anulus fibrosus	Ankylosing spondylitis Alkaptonuria	Thin, symmetric, vertical outgrowth extending from the corner of one vertebral body margin to the next; results in the bamboo spine appearance
Flowing anterior hyperostosis	3-38, 3-39	Ossification of the intervertebral disc, anterior longitudinal ligament, and paravertebral connective tissue	Diffuse idiopathic skeletal hyperostosis (DISH)	Thick undulating outgrowth along the anterior aspect of the spine; may be intermittently separated from vertebral bodies by a radiolucent cleft
Nonmarginal paravertebral ossification	3-43, 3-44	Ossification of paravertebral connective tissue	Psoriatic arthropathy Reiter syndrome	Poorly defined or well-defined, asymmetric outgrowth that may be comma-shaped; separated from the edge of the vertebral body and intervertebral disc

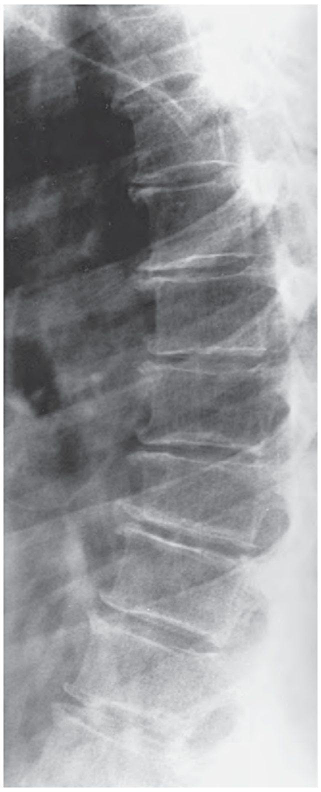

FIGURE 3–34 Degenerative disc disease.[46] Disc space narrowing, vertebral endplate sclerosis, and osteophyte formation are evident in this 41-year-old woman.

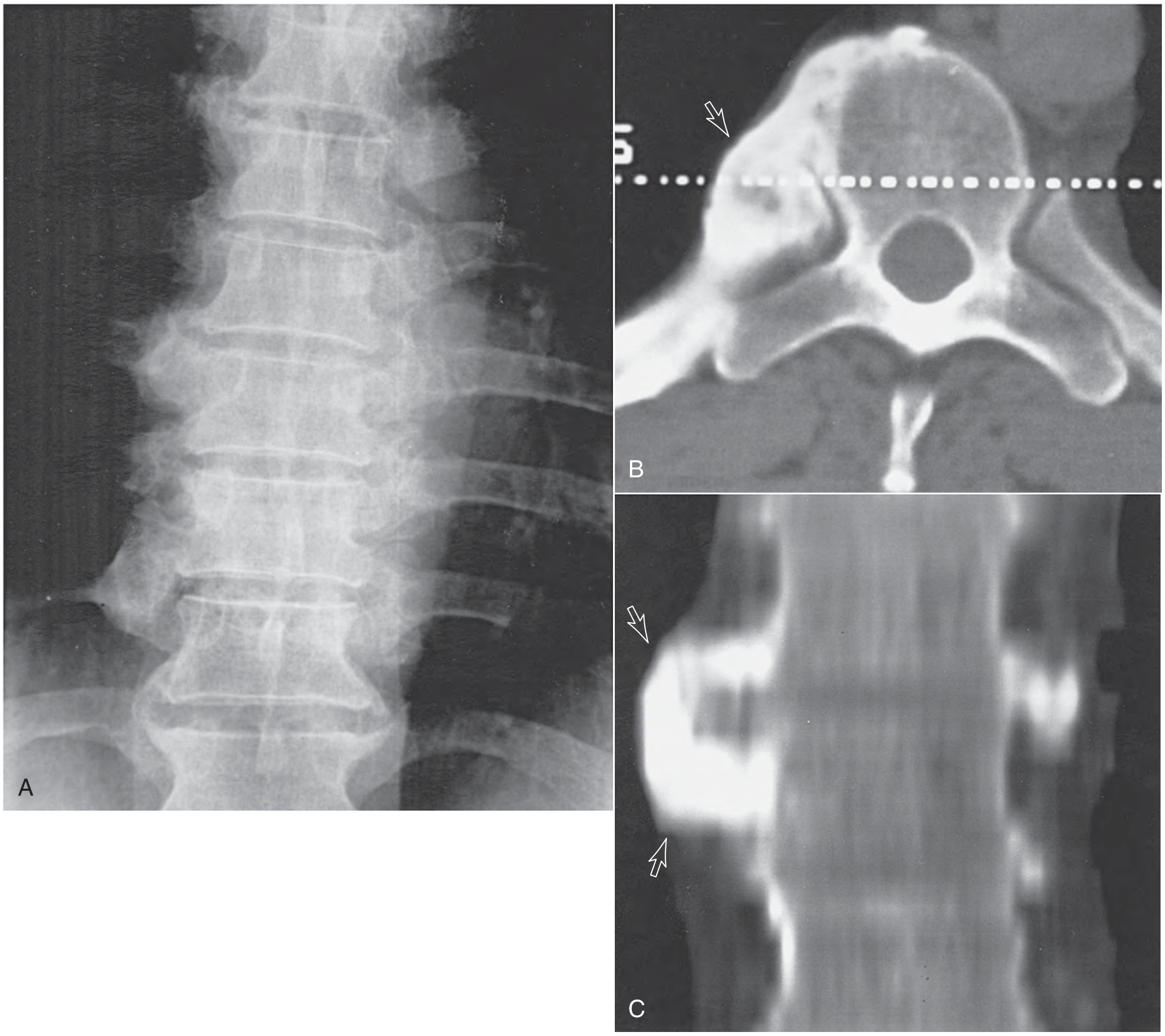

FIGURE 3–35 **Costovertebral osteoarthrosis.**[46] **A,** Frontal radiograph of the thoracic spine in this 52-year-old man shows extensive hyperostosis of the costovertebral articulations, resulting in a bulbous appearance. **B** and **C,** Transaxial **(B)** and coronal reformatted **(C)** CT images from another patient show marked hypertrophic bone arising from the costovertebral and costotransverse articulations *(open arrows)*. Note the enlarged, dense rib in **B,** consistent with stress hypertrophy.

Continued

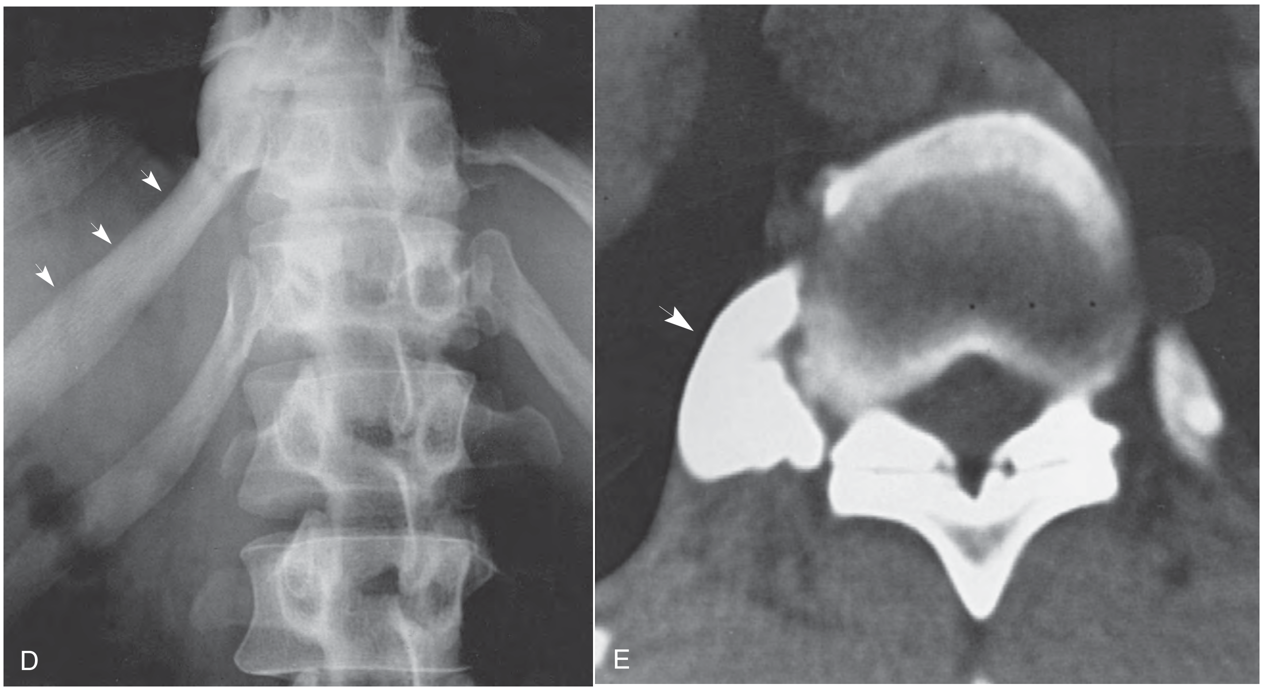

FIGURE 3–35, cont'd **D-E,** In another patient, a thoracolumbar radiograph **(D)** reveals extensive rib hyperostosis *(arrows)* and enlargement and sclerosis of the costovertebral joint *(open arrow)*. These findings are demonstrated *(arrow)* on the transaxial CT scan **(E).** Costovertebral joint degenerative disease tends to predominate on the right side of the spine. Cortical thickening and hyperostosis of the posterior portion of the ribs simulating Paget disease **(D-E)** also may occur in ankylosing spondylitis, diffuse idiopathic skeletal hyperostosis, and psoriatic spondyloarthropathy. *(**B-C,** Courtesy J. Haller, MD, Vienna, Austria.)*

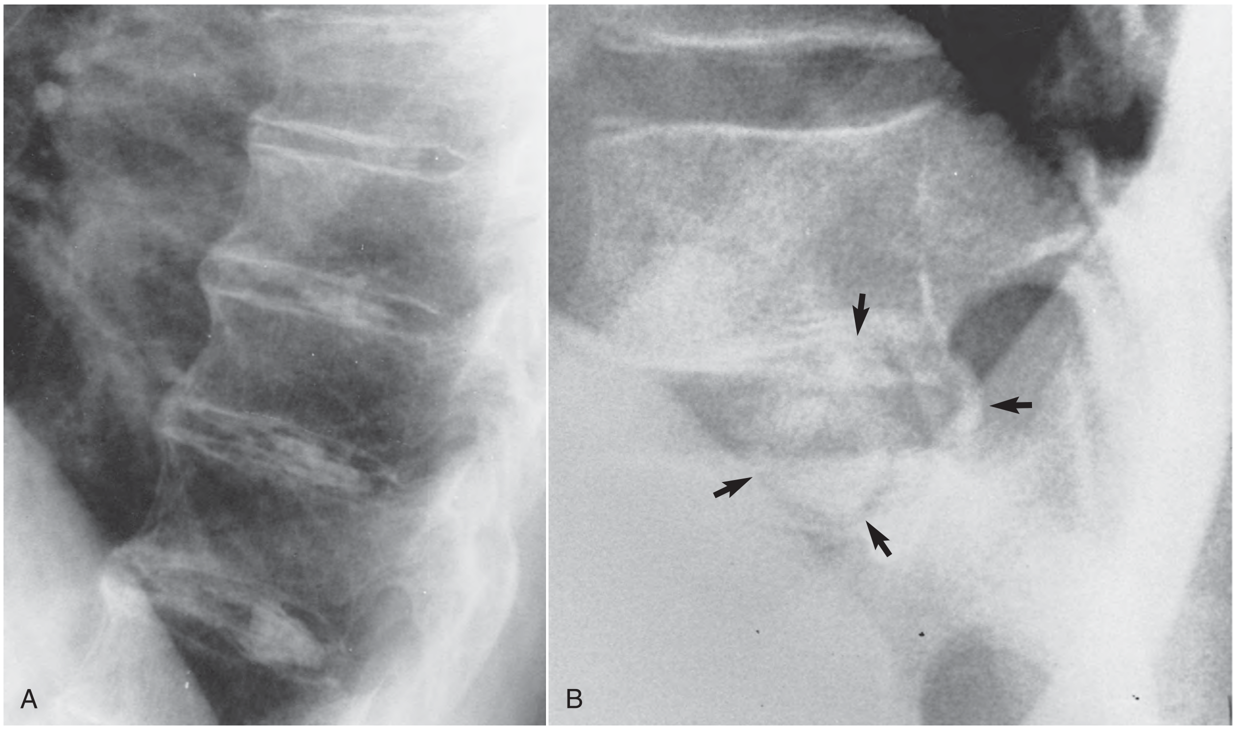

FIGURE 3–36 **Disc calcification. A,** Degenerative disc calcification: Adult.[47] A 60-year-old woman had lower thoracic spine pain. Lateral radiograph shows calcification of multiple thoracic intervertebral discs. **B-D,** Idiopathic childhood disc calcification.[96] This 11-year-old girl with back pain had a bone scan that was normal. In **B,** a lateral radiograph shows cloudy calcification overlying the T11-T12 disc space *(arrows)* with associated erosion of the inferior vertebral endplate of T11.

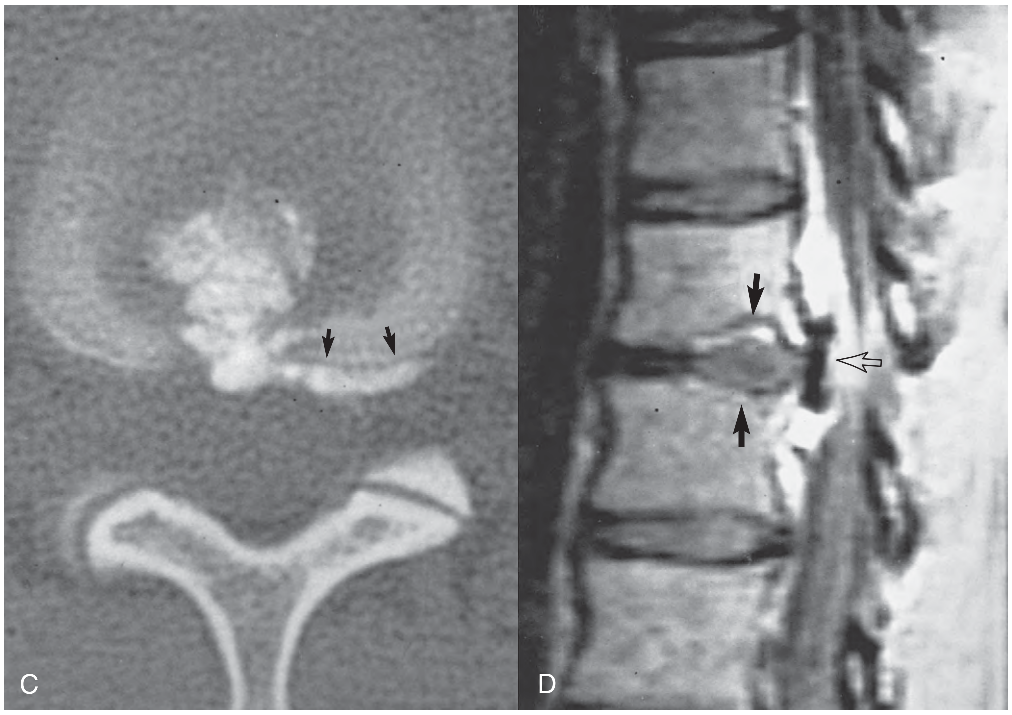

FIGURE 3–36, cont'd In **C,** a transaxial CT scan shows extensive circumferential calcification of the nucleus pulposus with posterior extension of calcified disc material extending posterolaterally into the left neural foramen *(arrows)*. In **D,** a sagittal T1-weighted (TR/TE, 700/15) spin echo MR image obtained after administration of intravenous gadolinium contrast agent reveals a large mass of intermediate signal intensity within the posterior aspect of the disc that erodes the adjacent vertebral bodies. The zone of high signal enhancement *(arrows)* probably represents edema. An additional low signal intensity mass corresponding to the posteriorly displaced calcified disc material and surrounding high signal intensity edema indent and displace the thecal sac *(open arrow)*. (***B-D,** Courtesy K. Koeller, MD, Washington, D.C.)*

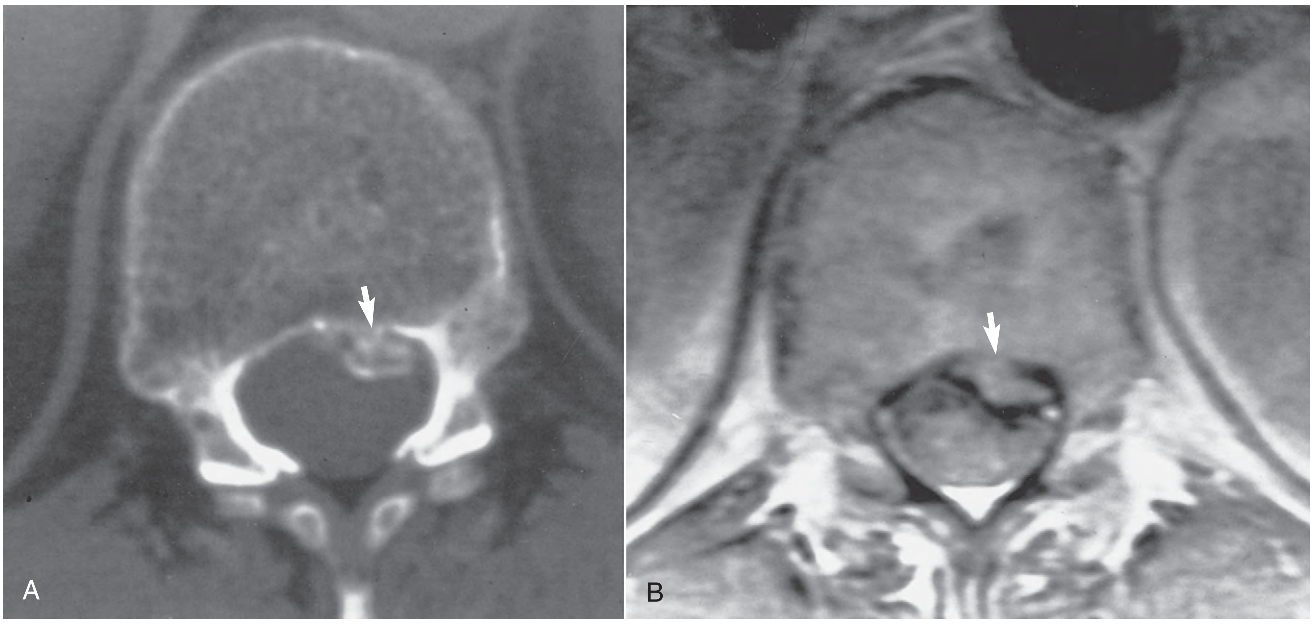

FIGURE 3–37 Ossification of a displaced disc fragment.[31] **A** and **B,** Seventy-five-year-old woman. In **A,** a transaxial CT image shows an area of high attenuation within the displaced T11-T12 intervertebral disc fragment *(arrow)*. In **B,** a corresponding transaxial fast spin echo (TR/TE, 2200/20) MR image shows the mass *(arrow)* to be composed of cortical and medullary bone that is displacing and compressing the thecal sac.

Continued

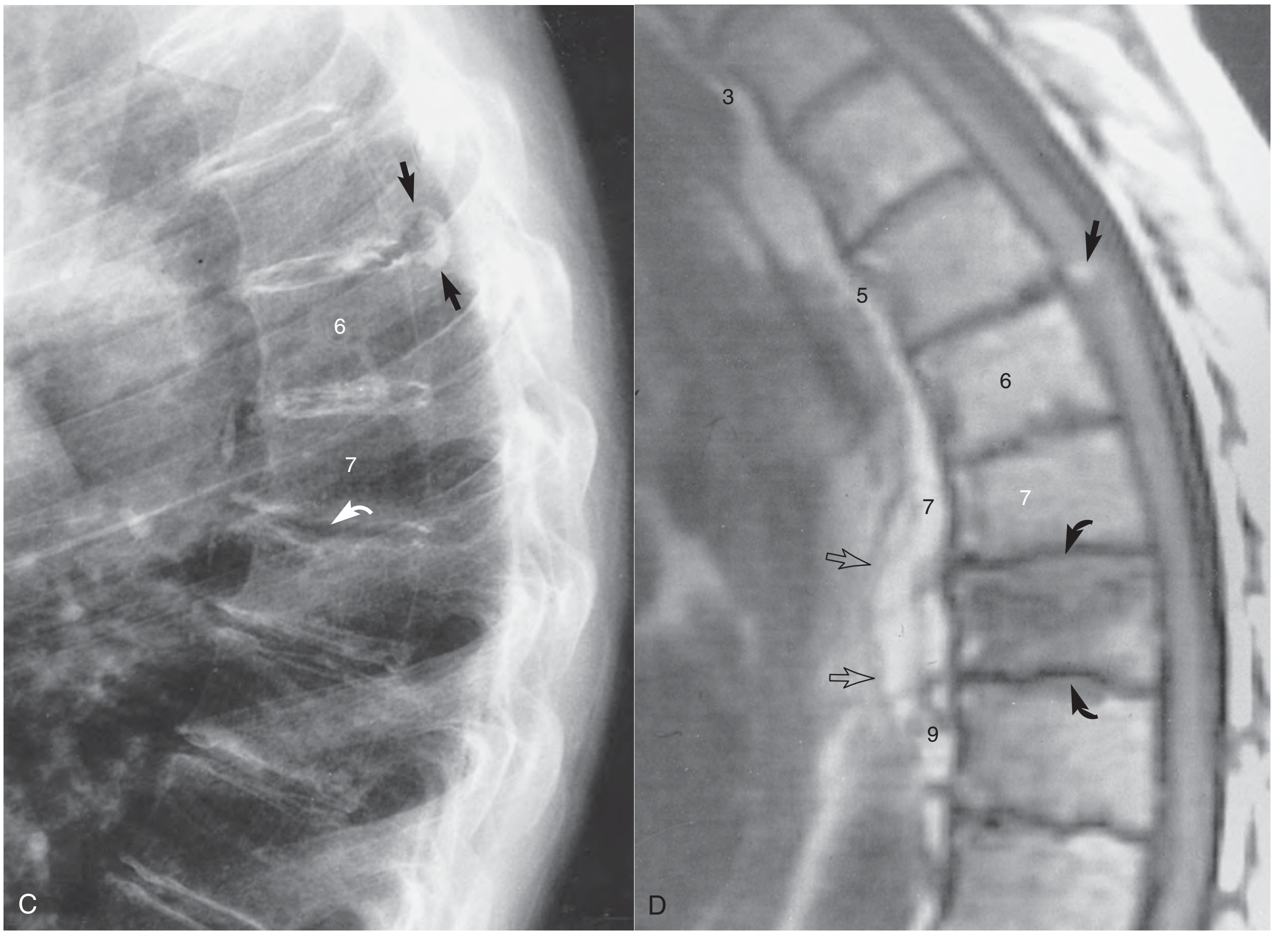

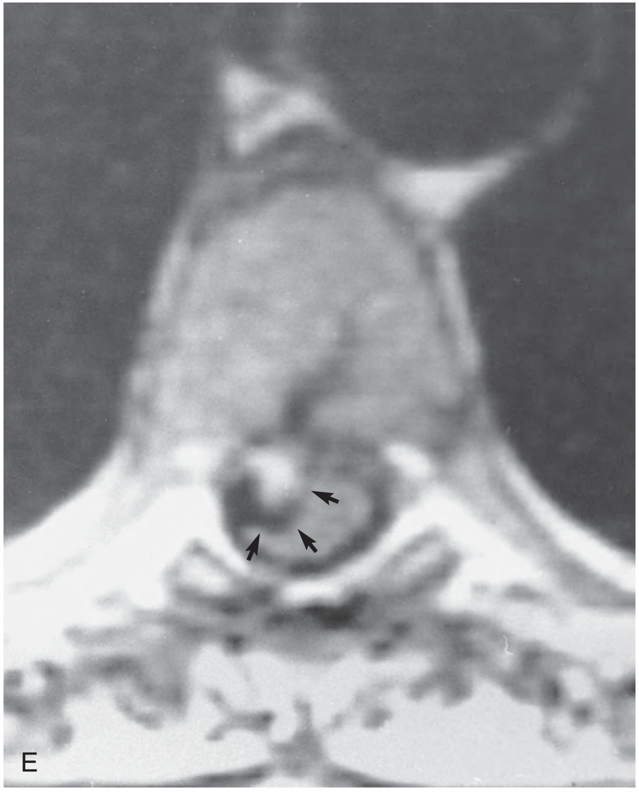

FIGURE 3–37, cont'd **C-E,** This 73-year-old woman had an acute osteoporotic compression fracture at T8. She also complained of long-standing upper thoracic and intercostal pain, which had been present since an acute injury 12 years earlier. In **C,** a lateral radiograph reveals a lobulated calcified or ossified mass arising from the posterior aspect of the T5-T6 disc space *(arrows)*. An acute compression fracture of T8 *(curved arrow)* is associated with extensive degenerative disc disease and calcification. In **D,** a sagittal T1-weighted (TR/TE, 500/12) spin echo MR image reveals a small focus of high signal intensity within the spinal cord at the T5-T6 level *(arrow)*. The low signal intensity of the T8 vertebral body *(curved arrows)* is associated with a paraspinal mass *(open arrows)*, consistent with the appearance of edema or hemorrhage. In **E,** a transaxial T1-weighted (TR/TE, 800/20) spin echo MR image shows a large mass *(arrows)* indenting and displacing the cord at the T5-T6 level. The mass exhibits a rim of low signal intensity corresponding to ossification and a central zone of high signal consistent with fatty replacement within a chronic disc herniation. *(**A-B,** Courtesy S. Eilenberg, MD, San Diego; **C-E,** Courtesy C. Cummins, D.C., Portland, Oregon.)*

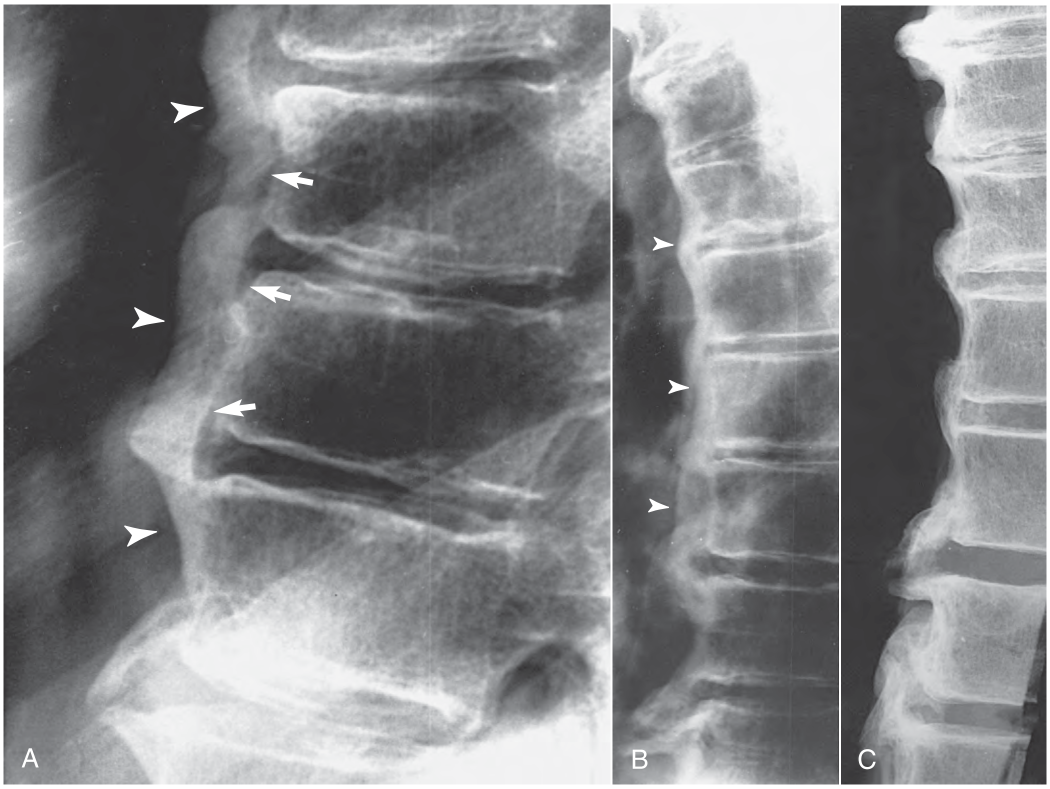

FIGURE 3–38 **Diffuse idiopathic skeletal hyperostosis (DISH).**[48-51] **A,** Lateral radiograph demonstrates the characteristic flowing hyperostosis of DISH anterior to several contiguous vertebral bodies *(arrowheads)*. Relative preservation of the disc spaces and the intermittent radiolucent zone between the ossification and the vertebral bodies *(arrows)* are well-recognized findings in this disease. **B,** In another patient, undulating ossification anterior to the thoracic spine *(arrowheads)* is evident. **C,** A specimen radiograph clearly reveals the flowing ossification typical of DISH. Observe the thick, bulky, undulating excrescences and normal disc spaces.

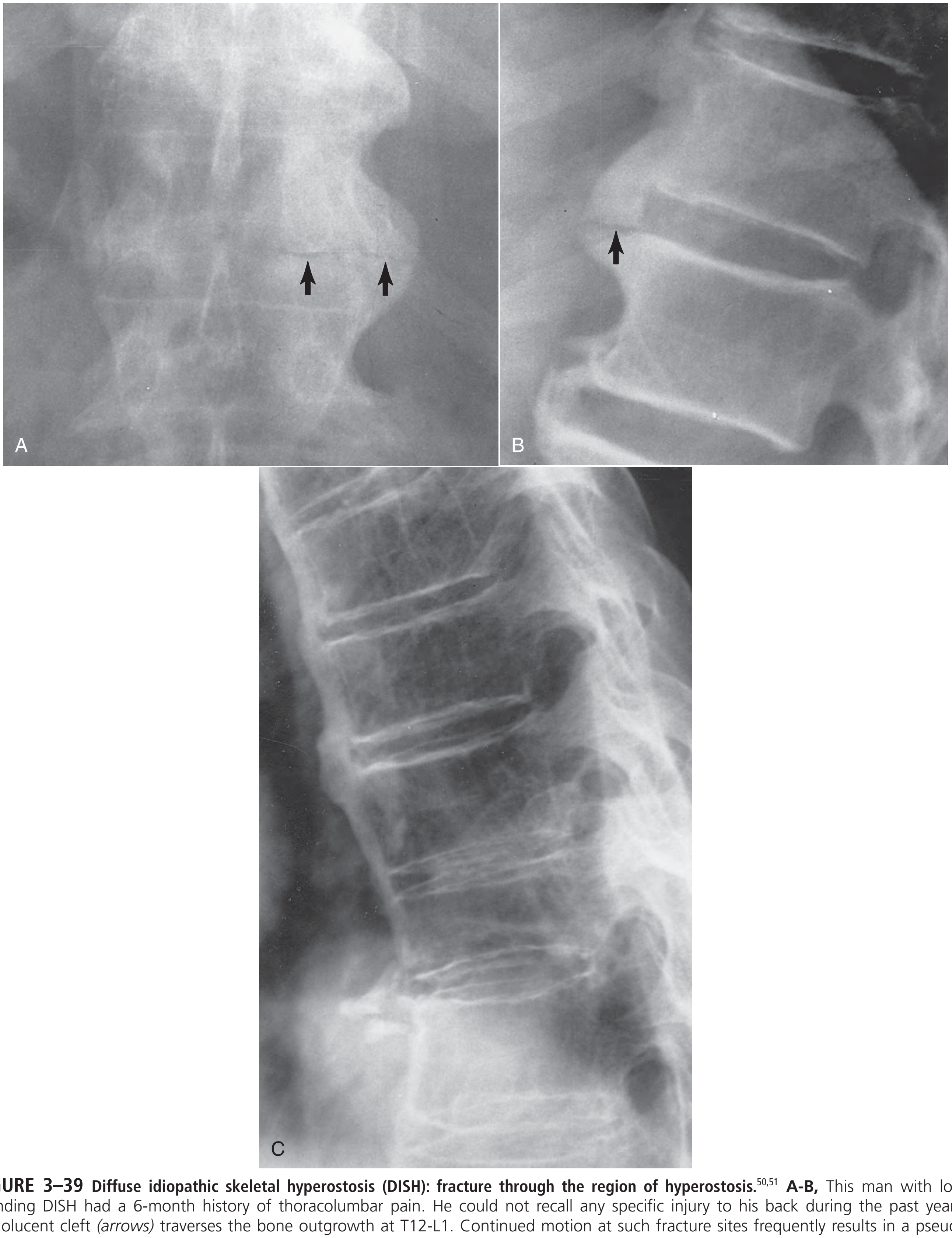

FIGURE 3–39 Diffuse idiopathic skeletal hyperostosis (DISH): fracture through the region of hyperostosis.[50,51] **A-B,** This man with longstanding DISH had a 6-month history of thoracolumbar pain. He could not recall any specific injury to his back during the past year. A radiolucent cleft *(arrows)* traverses the bone outgrowth at T12-L1. Continued motion at such fracture sites frequently results in a pseudarthrosis. **C,** In another patient with advanced DISH, a fracture has occurred through the region of hyperostosis, and the adjacent vertebral body is slightly diminished in height.

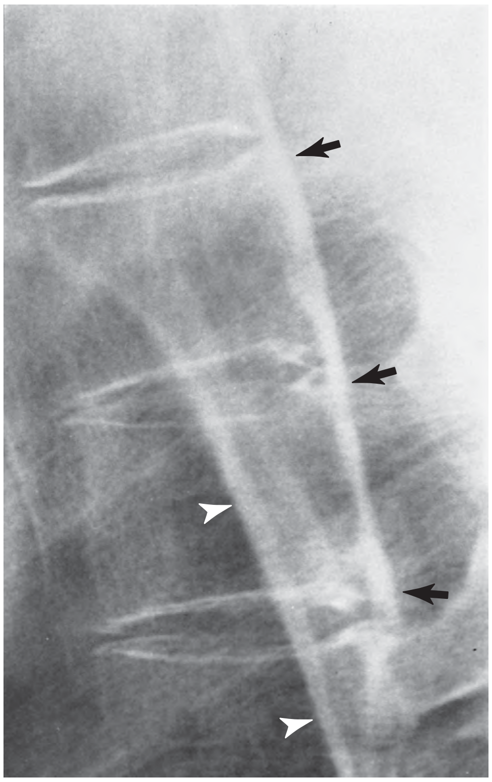

FIGURE 3–40 Ossification of the posterior longitudinal ligament (OPLL).[52] A thin linear sheet of ossification is observed within the spinal canal immediately posterior to the upper thoracic vertebral bodies *(arrows)*. The overlying scapular margin *(arrowheads)* should not be confused with abnormal ossification. *(Courtesy M. Mitchell, MD, Halifax, Nova Scotia, Canada.)*

TABLE 3-12 Terminology Commonly Applied to Spinal Abnormalities in Ankylosing Spondylitis

Term	Definition
Osteitis	Enthesopathy occurring at discovertebral junction and associated with erosion, sclerosis, and syndesmophytes
"Shiny corner" sign	Increased radiodensity of the corners of the vertebral body related to "osteitis"
Squaring	Loss of normal anterior vertebral body concavity related to erosion and resulting in a flattened or convex anterior margin of the vertebral body
Syndesmophyte	Ossification of the outer fibers of the anulus fibrosus leading to thin, vertical spinal outgrowths
Bamboo spine	Undulating vertebral contour due to extensive syndesmophytosis
Discitis	"Erosive" abnormalities of the discovertebral junction
Disc ballooning	Biconcave shape of the intervertebral disc space related to osteoporotic deformity and central flattening or collapse of the vertebral body
"Trolley track" sign	Three vertical radiodense lines on frontal radiographs related to ossification of the supraspinous and interspinous ligaments and the apophyseal joint capsules
Dagger sign	Single central radiodense line on frontal radiographs related to ossification of the supraspinous and interspinous ligaments

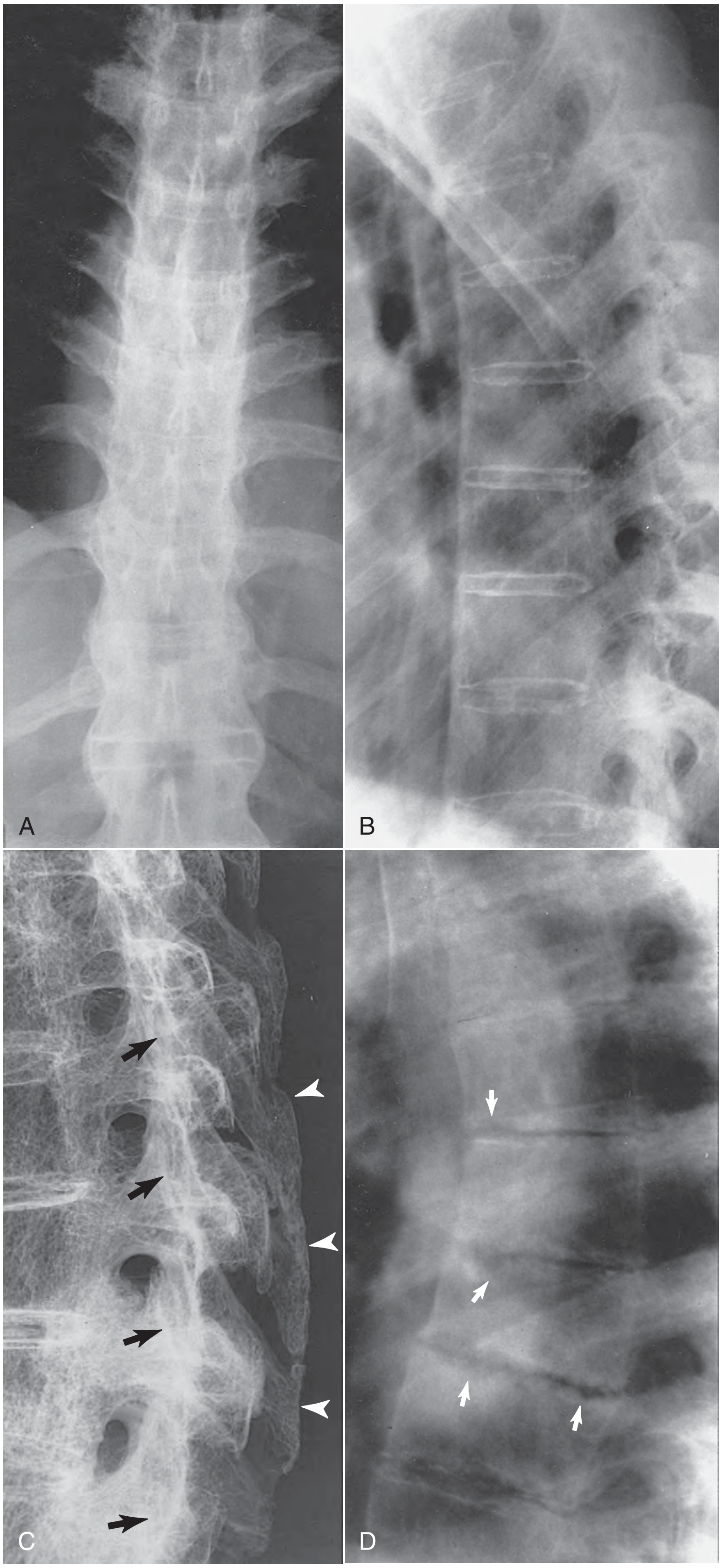

FIGURE 3–41 **Ankylosing spondylitis: spectrum of abnormalities.**[54,55,109] **A-B,** A 75-year-old man with long-standing ankylosing spondylitis. In **A,** a frontal radiograph reveals extensive ankylosis of the apophyseal joints, marginal syndesmophytes, and hyperostosis of the costovertebral joints. In **B,** a lateral radiograph clearly demonstrates continuous syndesmophyte formation and ankylosis of the apophyseal joints. **C,** Ossification of the supraspinous ligament *(arrowheads)* and widespread apophyseal joint ankylosis *(arrows)* are seen throughout the thoracic spine in this specimen radiograph. **D,** Erosive changes. In another patient, observe the diffuse disc space narrowing and vertebral endplate erosions *(arrows)*.

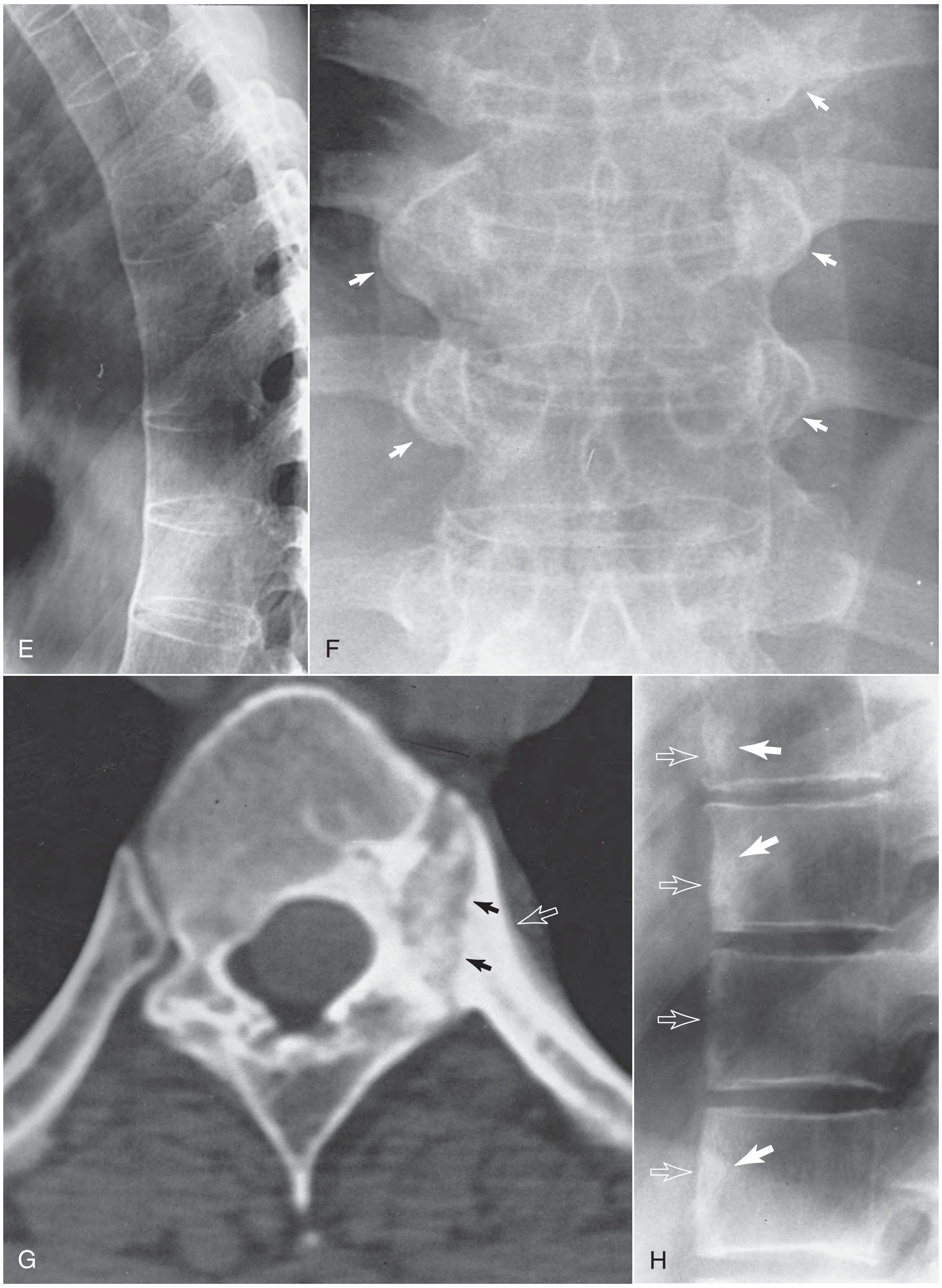

FIGURE 3–41, cont'd **E,** In a 57-year-old man with advanced disease, observe the extensive syndesmophyte production, osteopenia, ballooning of the disc spaces, and marked kyphosis. **F-G,** Costovertebral involvement. In **F,** a frontal radiograph shows prominent, bulbous enlargement of several costovertebral articulations *(arrows)*. In **G,** a transaxial CT scan in another patient demonstrates costovertebral joint space obliteration, subchondral bone erosion *(arrows)*, and cortical thickening of the adjacent rib *(open arrow)* and vertebral body. **H,** Osteitis. Squaring *(open arrows)* and sclerosis *(arrows)* of the anterior margins of vertebral bodies ("shiny corner" sign) are characteristic signs of osteitis typically seen in early ankylosing spondylitis. (***A-B,*** *Courtesy D. Goodwin, MD, Lebanon, NH.)*

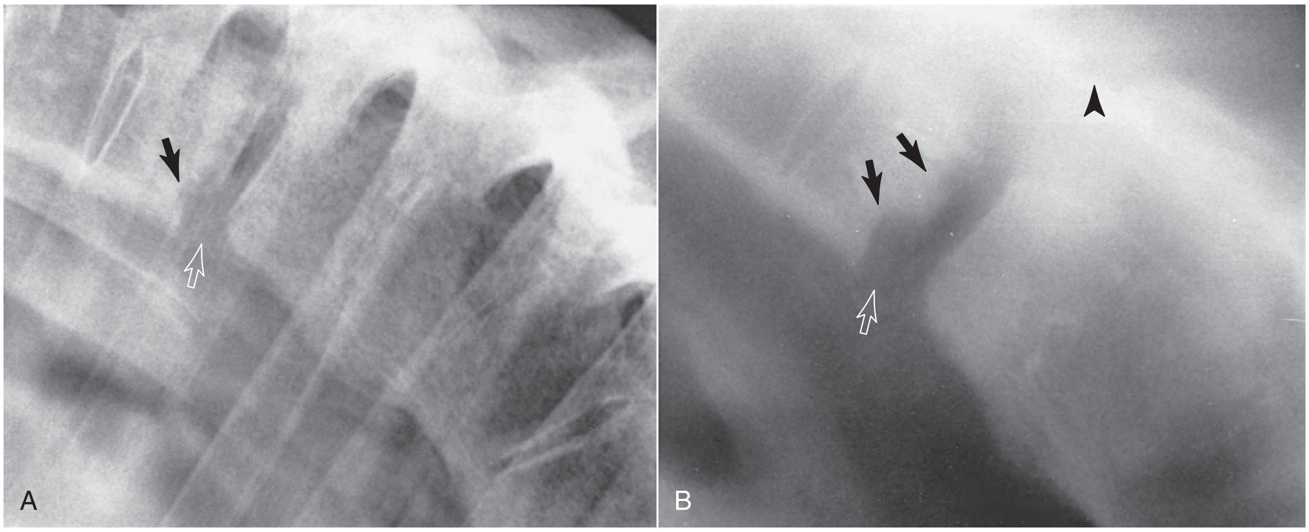

FIGURE 3–42 Ankylosing spondylitis: pseudarthrosis.[55,109] Lateral radiograph **(A)** and sagittal conventional tomogram **(B)** from a 59-year-old man with advanced ankylosing spondylitis who gradually developed signs and symptoms of cord compression. Observe the absence of ankylosis at one level *(open arrows)* and extensive osseous resorption, sclerosis, and erosions *(arrows)* of the discovertebral junctions characteristic of a pseudarthrosis. The tomogram confirms presence of a fracture through the posterior elements *(arrowhead)*. Pseudarthrosis may simulate spinal infection. Note also the widespread syndesmophyte formation, ankylosis, and kyphosis throughout the remainder of the spine.

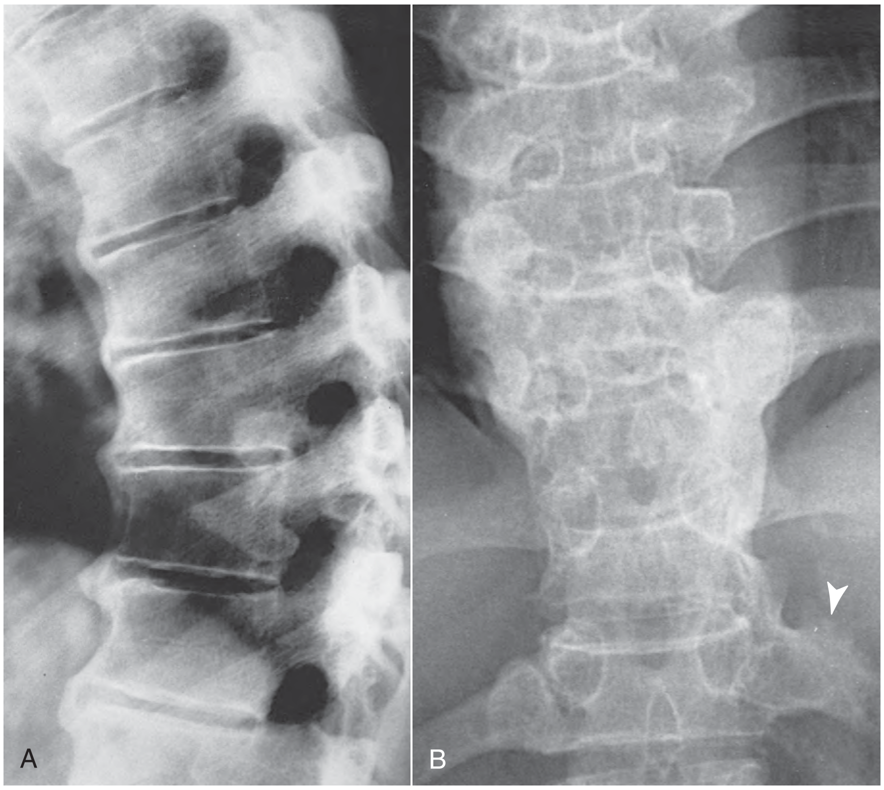

FIGURE 3–43 Psoriatic spondyloarthropathy.[56] **A,** The paravertebral ossification in this patient with polyarticular psoriatic spondyloarthropathy and dermopathy resembles the flowing hyperostosis of diffuse idiopathic skeletal hyperostosis (DISH). **B,** Prominent bulky paravertebral ossification is seen throughout the thoracic spine in this 28-year-old patient with long-standing psoriatic skin lesions and polyarticular arthropathy. Fluffy periostitis involving the twelfth rib *(arrowhead)*, a finding characteristic of the seronegative spondyloarthropathies, also is evident.

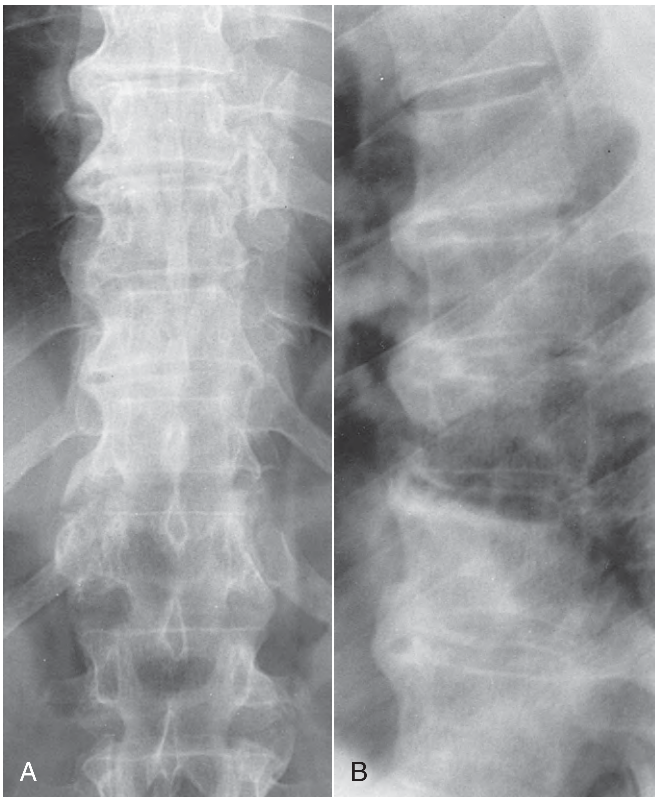

FIGURE 3–44 Reactive arthritis associated with Reiter syndrome.[57] Frontal **(A)** and lateral **(B)** radiographs of the thoracic spine in this 62-year-old man reveal paravertebral ossification in an asymmetric distribution. The characteristic pattern of ossification is that of comma-shaped, nonmarginal outgrowths. In this patient, some of the excrescences resemble the bridging osteophytes of degenerative disc disease and the flowing hyperostosis characteristic of diffuse idiopathic skeletal hyperostosis (DISH).

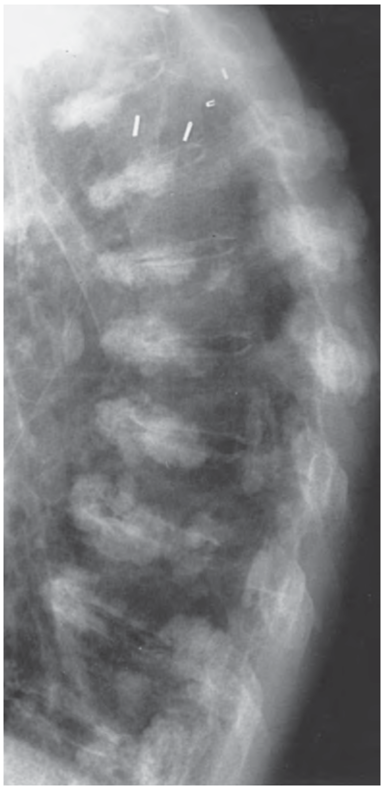

FIGURE 3–45 Progressive systemic sclerosis (scleroderma).[58] Extensive globular soft tissue calcification is seen adjacent to the intervertebral disc spaces and costovertebral joints. *(Courtesy A. Nemcek, MD, Chicago, and L. Rogers, Winston-Salem, NC.)*

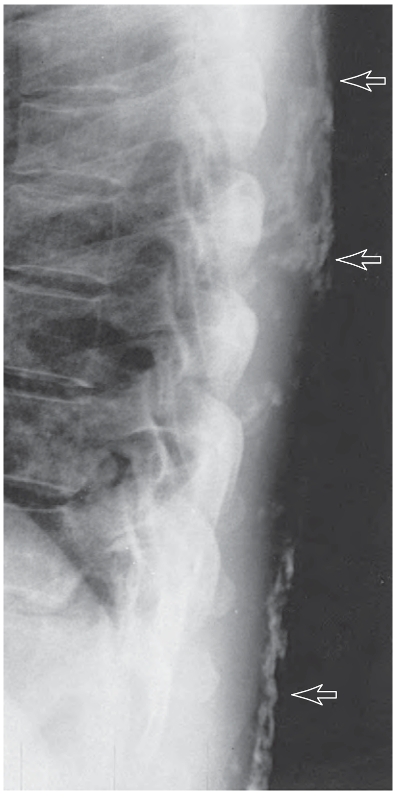

FIGURE 3–46 Dermatomyositis-polymyositis.[59] Diffuse subcutaneous calcification is seen in the paraspinal region posterior to the spine *(open arrows)*. *(Courtesy C. Pineda, MD, Mexico City, Mexico.)*

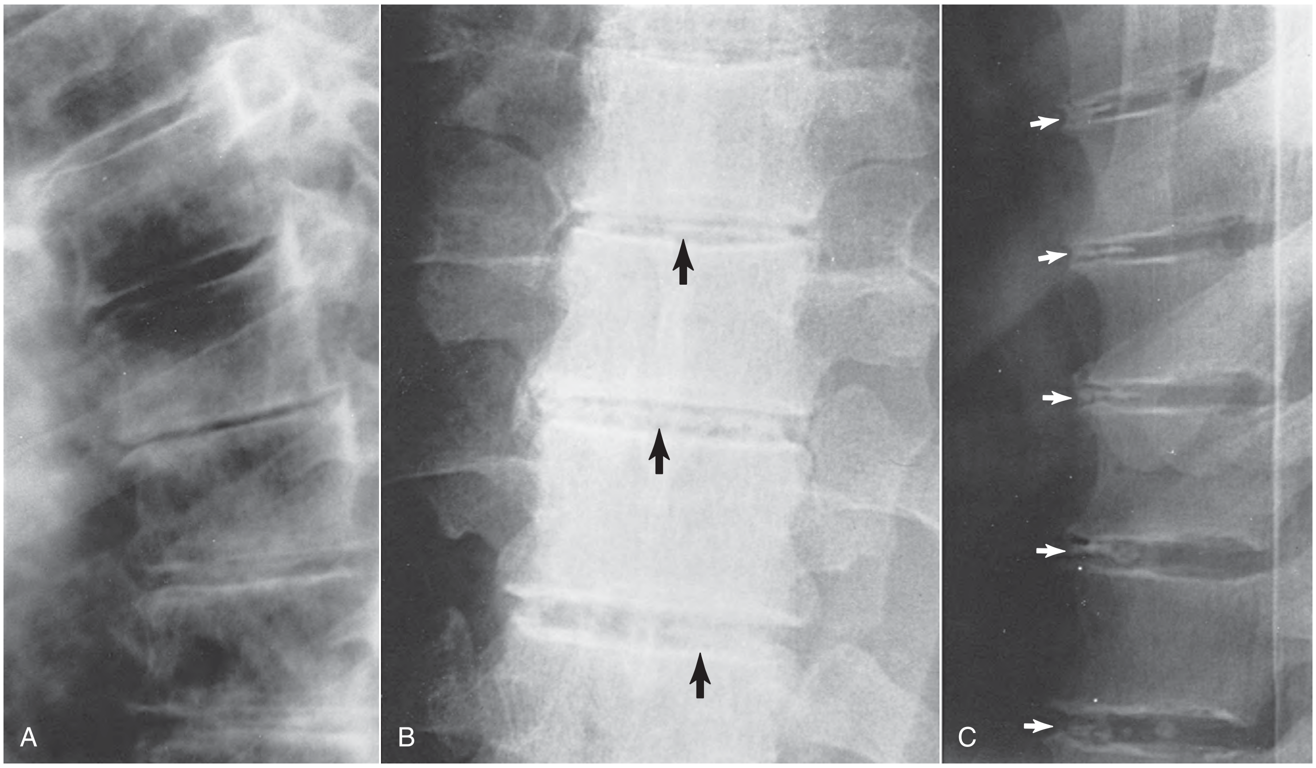

FIGURE 3–47 **Calcium pyrophosphate dihydrate (CPPD) crystal deposition disease.**[60,61] **A,** Severe disc space narrowing, calcification, and vacuum phenomena are accompanied by sclerosis of the vertebral endplates in this 77-year-old man. **B-C,** Frontal **(B)** and lateral **(C)** radiographs from this 46-year-old man show extensive intervertebral disc calcification *(arrows)* and narrowing throughout the thoracic spine.

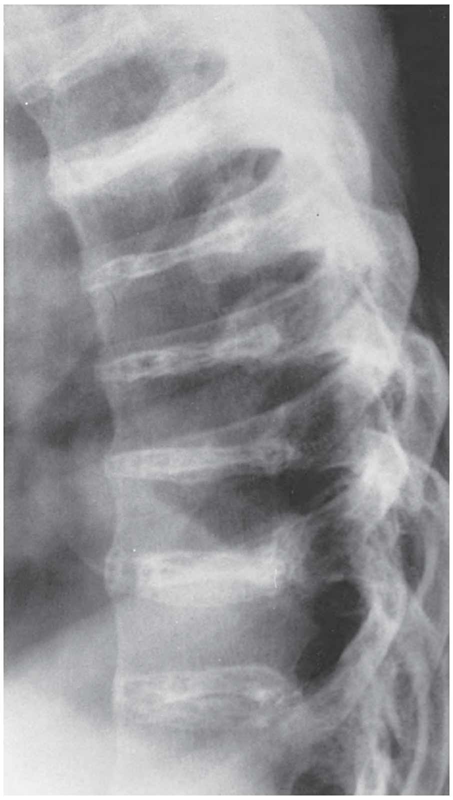

FIGURE 3–48 **Alkaptonuria.**[62] Diffuse disc space narrowing, calcification, and ossification, vertebral body osteoporosis, and small osteophytes are present in this patient.

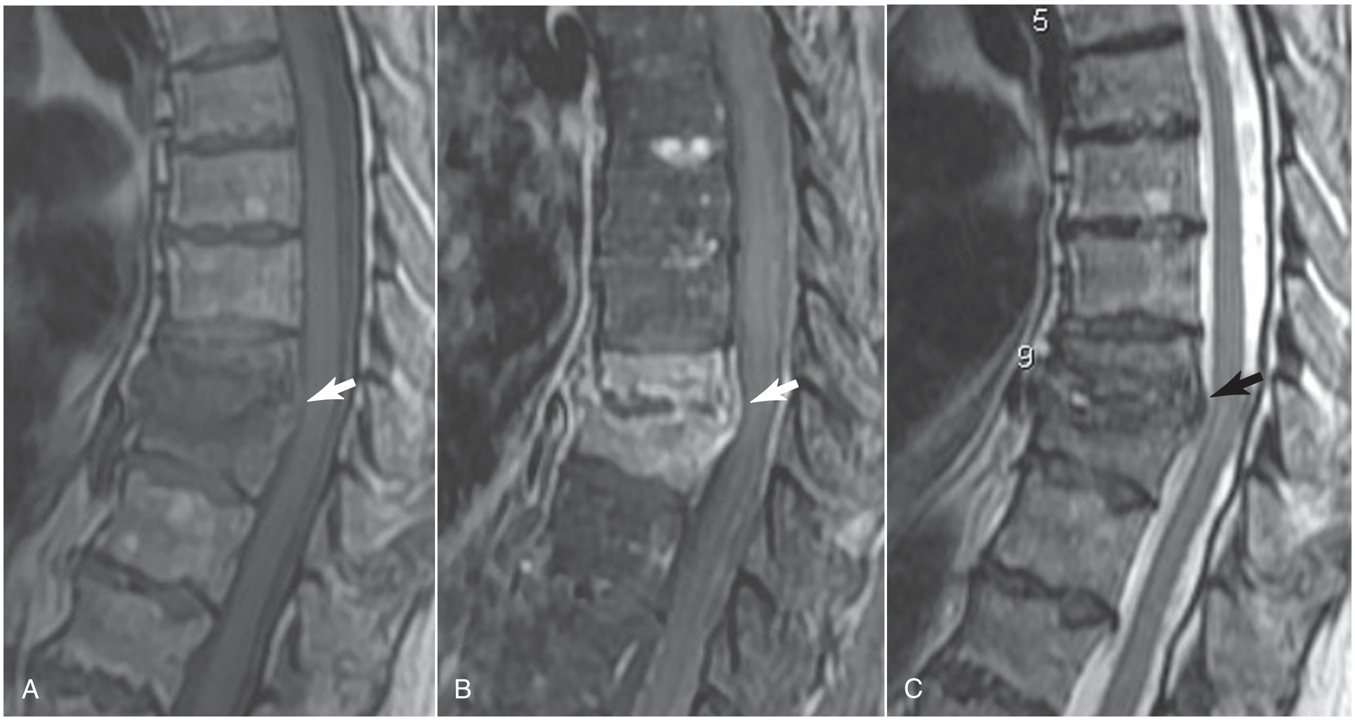

FIGURE 3–49 **Pyogenic spondylodiscitis.**[63,98,107] This 76-year-old female with fever and acute back pain underwent an MR imaging examination. Sagittal images including T1-weighted **(A),** T1-weighted fat suppression following gadolinium injection **(B),** and T2-weighted **(C)** sequences reveal vertebral endplate destruction with 30% to 50% vertebral body collapse of T9 and T10, obliteration of the intervening disc, and intense enhancement with cord compression resulting from epidural abscess *(arrows)*.

FIGURE 3–50 **Tuberculous spondylitis: paraspinal and epidural abscess.**[64,65] **A,** Routine radiography. On this anteroposterior thoracic radiograph, the paraspinal tissues are distended, displacing the paraspinal line *(white arrows)*. Narrowing of the intervertebral disc space also is demonstrated *(black arrows)*. **B-C,** MR imaging. Midsagittal **(B)** and parasagittal **(C)** T2-weighted (TR/TE 3500/112) fast-spin echo MR images reveal pathologic collapse of the T2 vertebral body and a large paraspinal and epidural abscess of high signal intensity. The inhomogeneous abscess *(white open arrows)* extends anteriorly throughout the prevertebral soft tissues into the cervical region. The epidural extension of the abscess displaces and compresses the thoracic spinal cord *(black arrow)*. Paraspinal subligamentous extension of tuberculous abscesses from vertebral and discal sites to the adjacent ligaments and soft tissues is frequent. Extension usually is anterolateral but may occur posteriorly into the peridural space, as in this case. (**B-C,** *Courtesy of T. Broderick, MD, Orange, Calif.)*

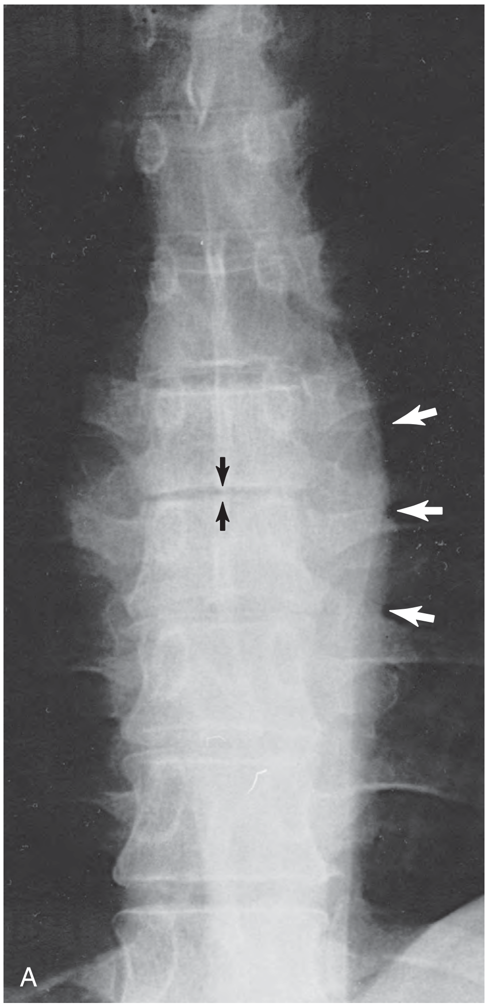

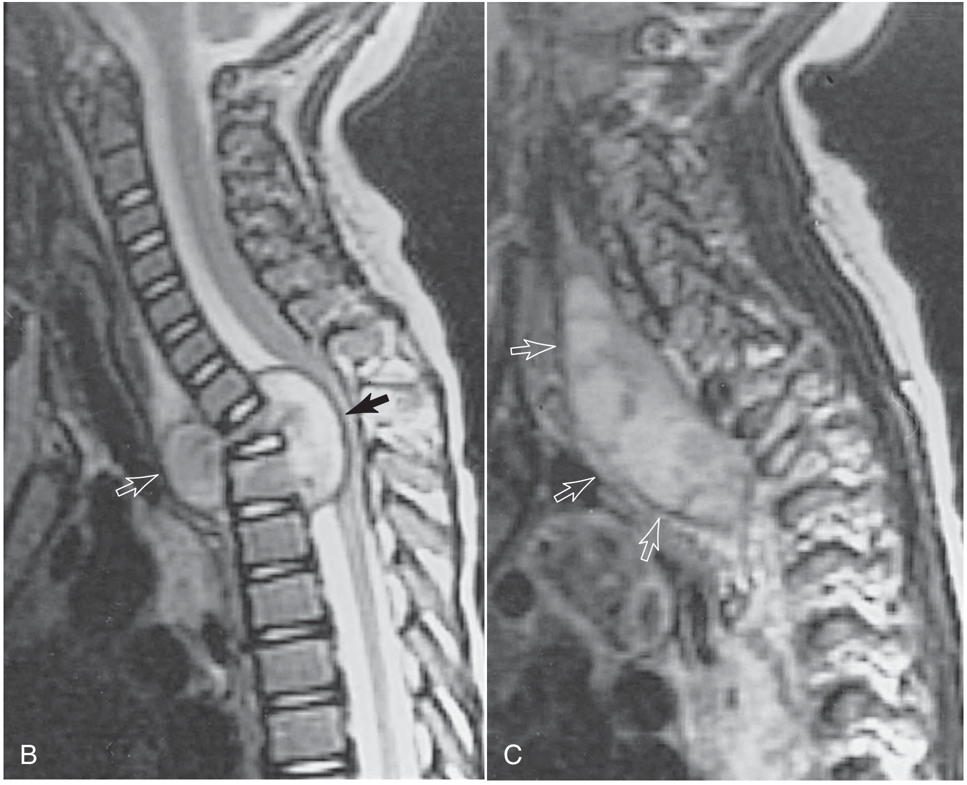

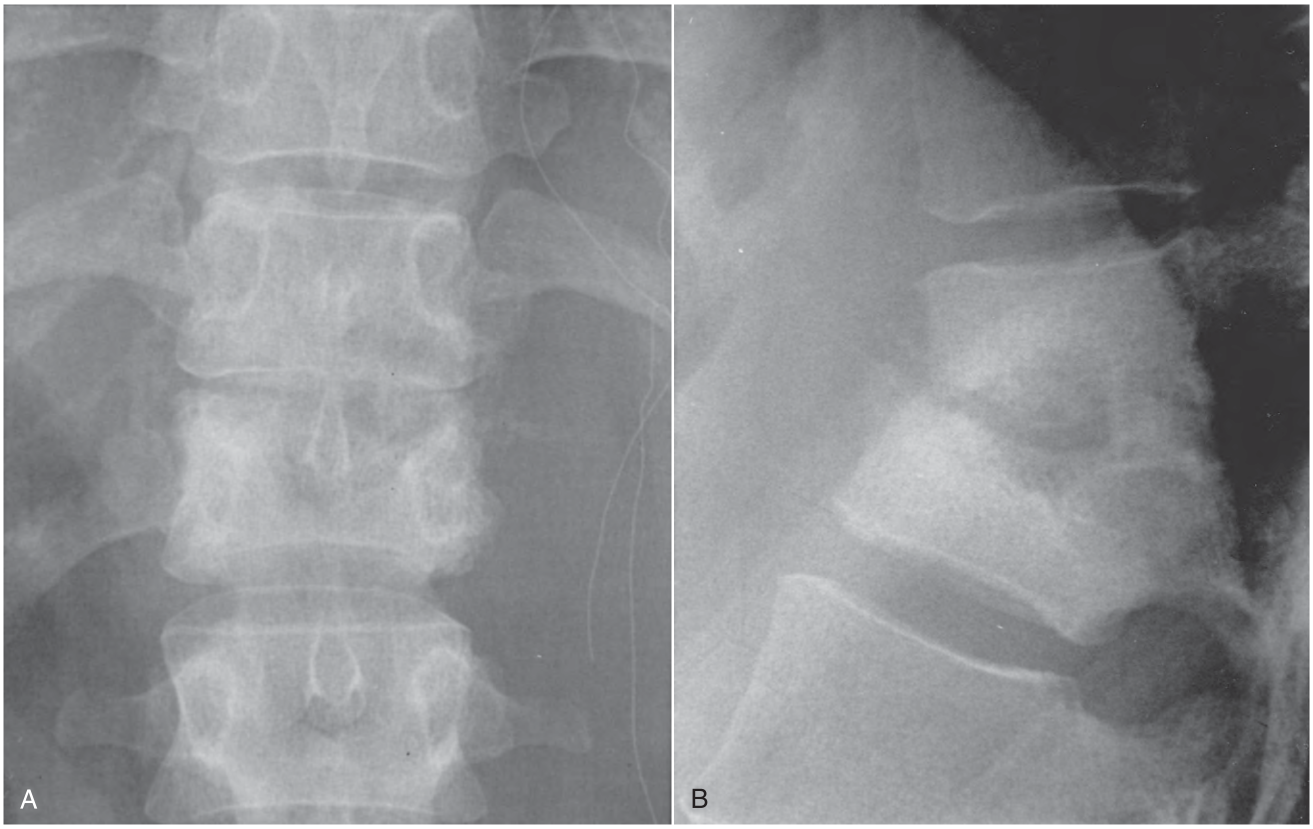

FIGURE 3–51 **Tuberculous spondylodiscitis.**[64,65] Observe the marked erosion and destruction of the vertebral endplates with adjacent reactive sclerosis, obliteration of the intervening disc space, and pathologic collapse of the vertebral bodies of T11 and T12 in this 33-year-old woman with known pulmonary tuberculosis. The left twelfth rib had been removed surgically.

TABLE 3-13 Tumors and Tumorlike Lesions Affecting the Thoracic Spine*

Entity	Figure(s)
Malignant Neoplasms	
Skeletal metastasis[66-68]	3-52 to 3-54
Primary malignant neoplasms of bone	
Osteosarcoma (conventional)[69,131]	3-55
Myeloproliferative disorders	
Plasma cell myeloma[70,71,99,100]	3-56
Myelofibrosis[72]	3-57
Hodgkin disease[73]	3-58
Leukemia[74]	3-59
Benign Neoplasms	
Enostosis[75]	3-60
Osteoid osteoma[76,129]	3-22, 3-61
Giant cell tumor (benign)[77]	3-62
Hemangioma (solitary)[78,108]	3-63
Tumorlike Lesions	
Paget disease[79,80,102,103,106]	3-64
Neurofibromatosis type I (von Recklinghausen disease)[81,82]	3-65
Fibrous dysplasia[83,84]	3-66
Langerhans cell histiocytosis[85,86]	3-67

* This table lists only the neoplasms illustrated in this chapter; for a more complete discussion of neoplasms, see Tables 1-12 to 1-14 and Table 2-17.

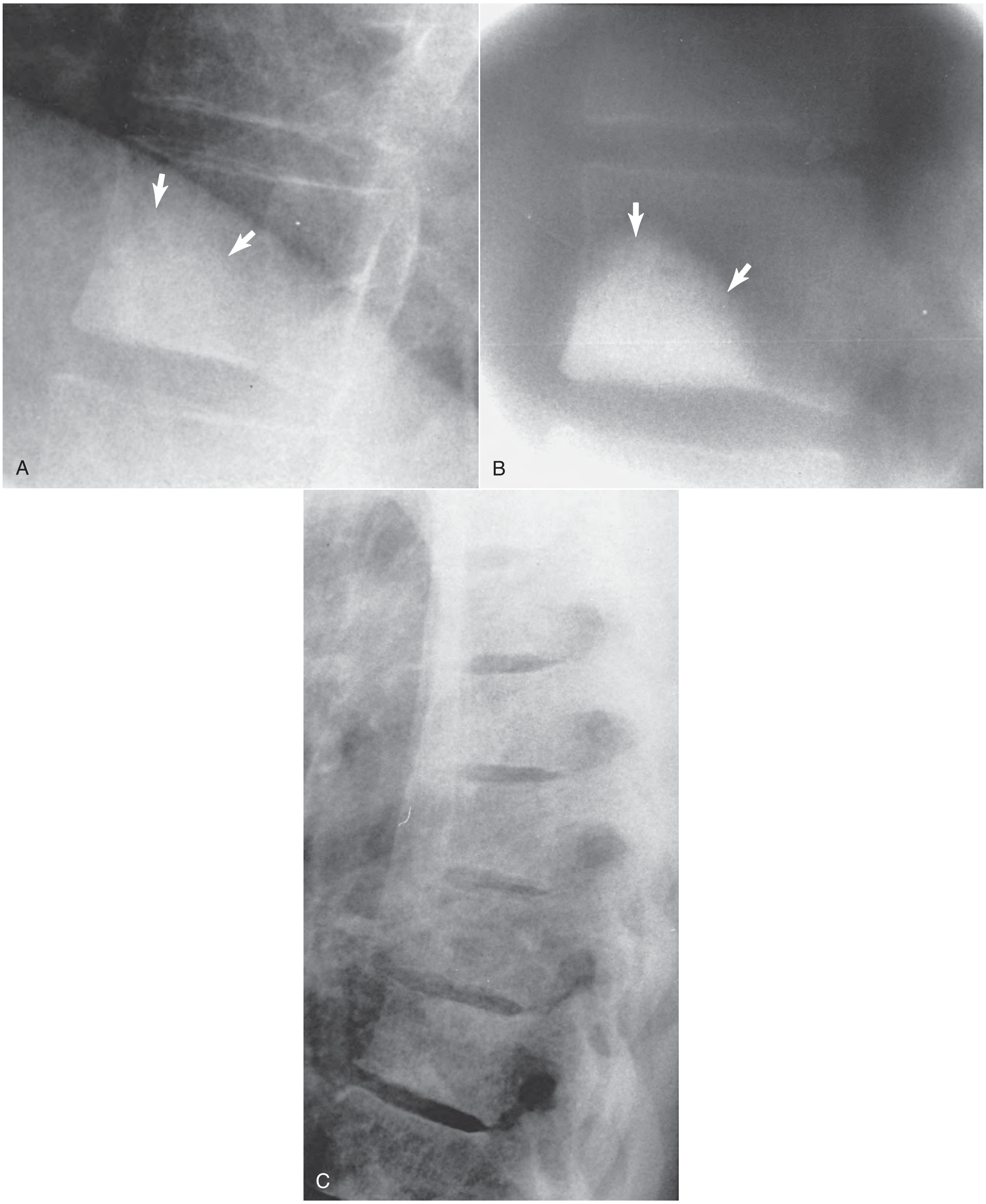

FIGURE 3–52 Skeletal metastasis: carcinoma of the prostate-osteoblastic pattern.[66,67] **A-B,** This 54-year-old man had been diagnosed as having carcinoma of the prostate several years before this radiographic examination. Lateral thoracic radiograph **(A)** shows osteosclerosis of the T11 vertebral body *(arrows)*. Conventional tomogram **(B)** clearly shows the osteosclerotic reaction of bone provoked by tumor infiltration *(arrows)*. This appearance resembles that of idiopathic hemispherical segmental sclerosis of the vertebral body. **C,** In another patient, a lateral thoracic radiograph shows a diffuse osteosclerotic pattern of metastatic disease uniformly involving all vertebrae. No evidence is seen of bone expansion, scalloping, or coarsened trabeculae, features that are helpful in differentiating osteoblastic metastatic disease from Hodgkin disease or Paget disease.

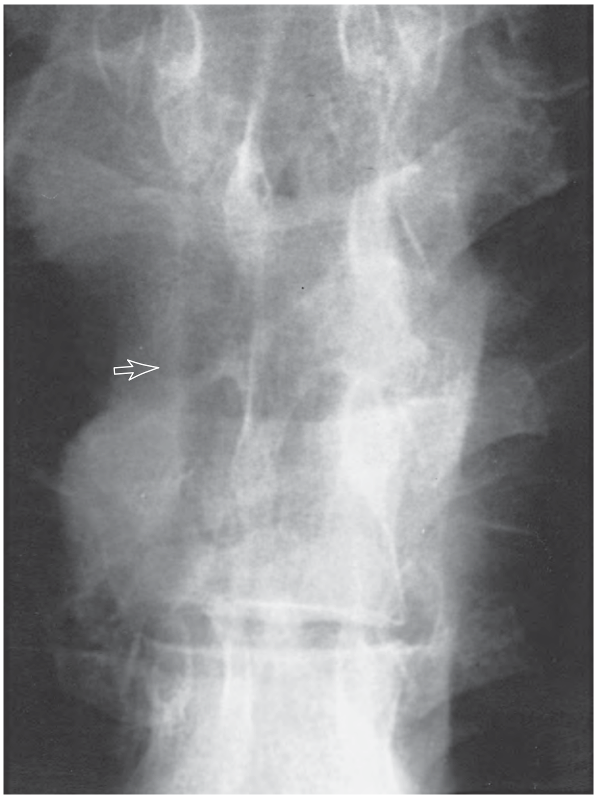

FIGURE 3–53 **Skeletal metastasis: missing pedicle sign.**[66-68] In this patient with lung carcinoma, destruction of the pedicle and lateral portion of the vertebral body is seen on the frontal radiograph *(open arrow)*. Osteolytic skeletal metastasis is the most common cause of a missing pedicle.

FIGURE 3–54 **Skeletal metastasis: Pancoast tumor.**[68] **A,** Routine radiograph reveals extensive destruction of the laminae, pedicles, and transverse processes of the first and second thoracic vertebrae *(arrows)*. The left first and second ribs also appear osteolytic. **B,** Transaxial CT scan from another patient reveals extensive vertebral body and costovertebral destruction *(arrows)* and a huge soft tissue mass *(open arrow)* from tumor extension and lymphadenopathy. **C,** Lower CT image reveals the Pancoast tumor that envelops the trachea and occupies a significant portion of the superior sulcus of the lung *(arrows)*. In Pancoast tumor, carcinoma of the apex of the lung most often invades adjacent ribs or cervicothoracic vertebrae via direct extension; or, less frequently, it spreads via hematogenous or lymphatic dissemination. *(Courtesy B.A. Howard, MD, Charlotte, NC.)*

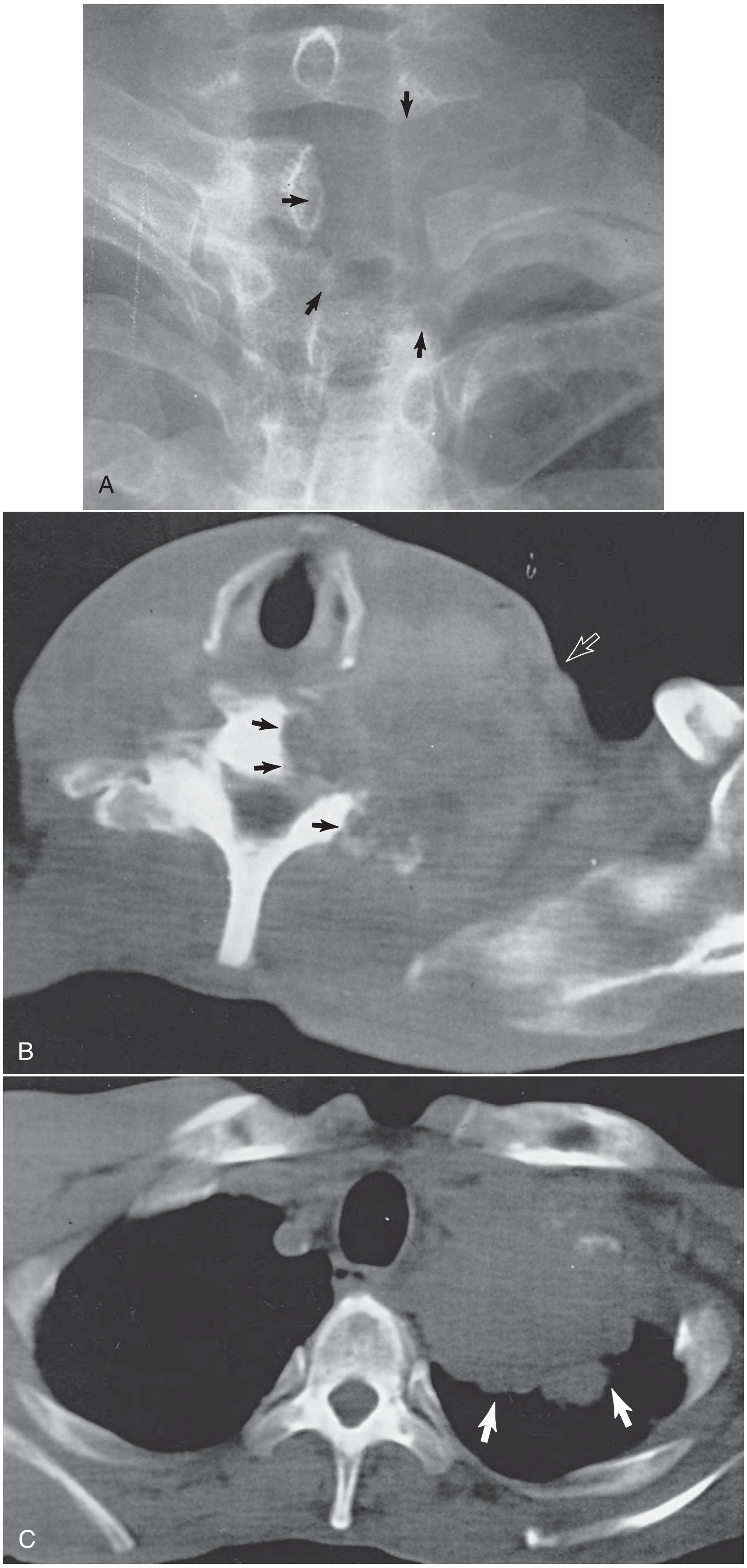

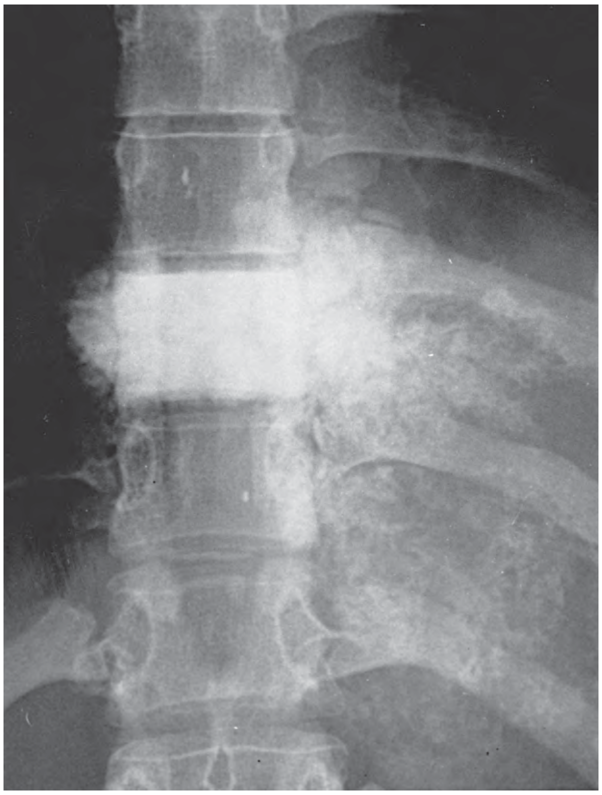

FIGURE 3–55 **Osteosarcoma: ivory vertebra.**[69,131] Frontal radiograph of the spine in this 21-year-old woman demonstrates an osteosclerotic (ivory) vertebra with extraordinary proliferative ossification of the paraspinal soft tissues. Note the laminectomy defects from previous decompression surgery.

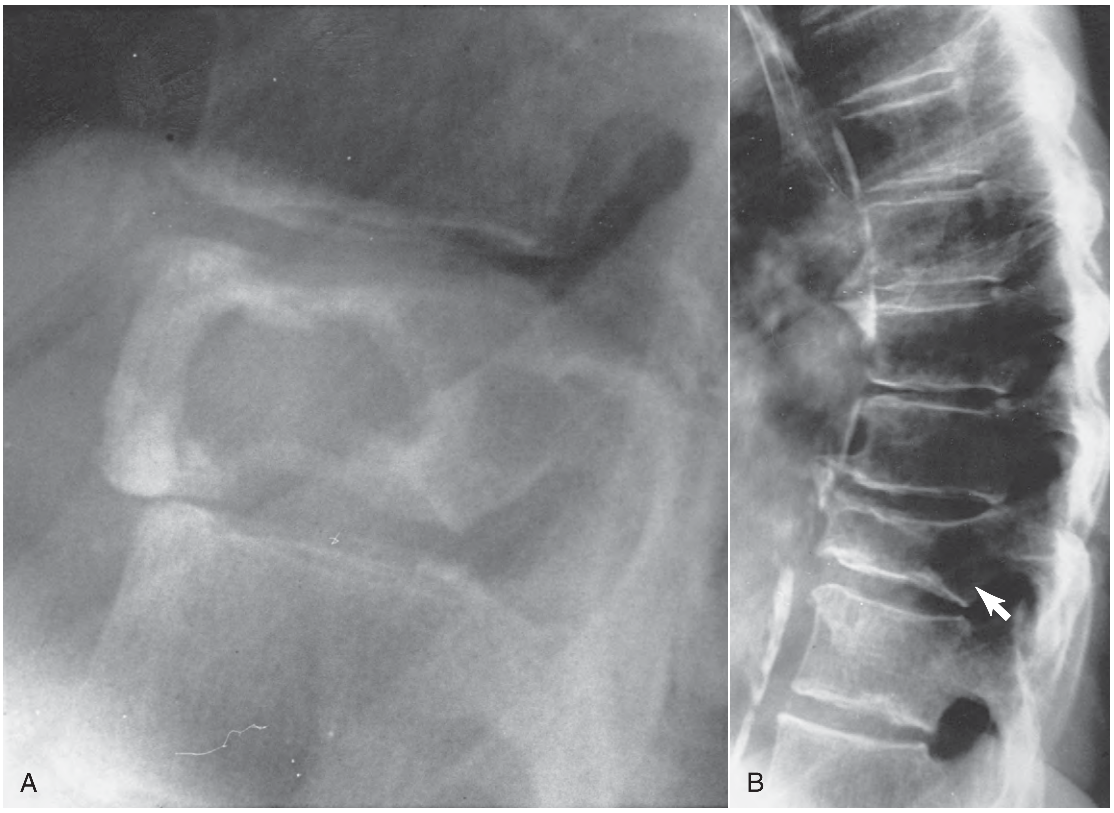

FIGURE 3–56 **Plasma cell myeloma: solitary plasmacytoma and multiple myeloma.**[70,71,99,100] **A,** Routine radiograph from a 39-year-old woman with plasmacytoma shows a central radiolucent lesion within a partially collapsed lower thoracic vertebral body. A thick rim of sclerosis, a finding that resembles fibrous dysplasia, surrounds the radiolucent region. Plasmacytoma refers generally to solitary lesions of plasma cell myeloma. **B,** Multiple myeloma. The prominent radiographic finding in this patient is diffuse osteopenia of the vertebral bodies. A pathologic vertebral compression fracture of T11 has occurred *(arrow)*. Extensive vascular calcification within the posterior wall of the thoracic aorta also can be seen. Plasma cell (multiple) myeloma is the most common primary malignant disease of bone. Infiltration of plasma cells occurs in patients 60 to 70 years of age and is particularly common in black persons.

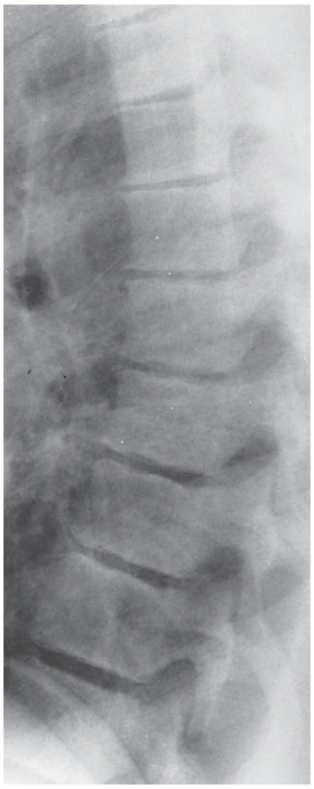

FIGURE 3–57 **Myelofibrosis.**[72] Diffuse osteosclerosis of the thoracic vertebrae is present in this patient. Myelofibrosis is an uncommon disease of middle-aged and elderly men and women. It is characterized by fibrotic or sclerotic bone marrow and extramedullary hematopoiesis. The main radiographic finding is osteosclerosis, but osteolysis or osteopenia also may occur occasionally. Patients usually have splenomegaly. *(Courtesy M.N. Pathria, MD, San Diego.)*

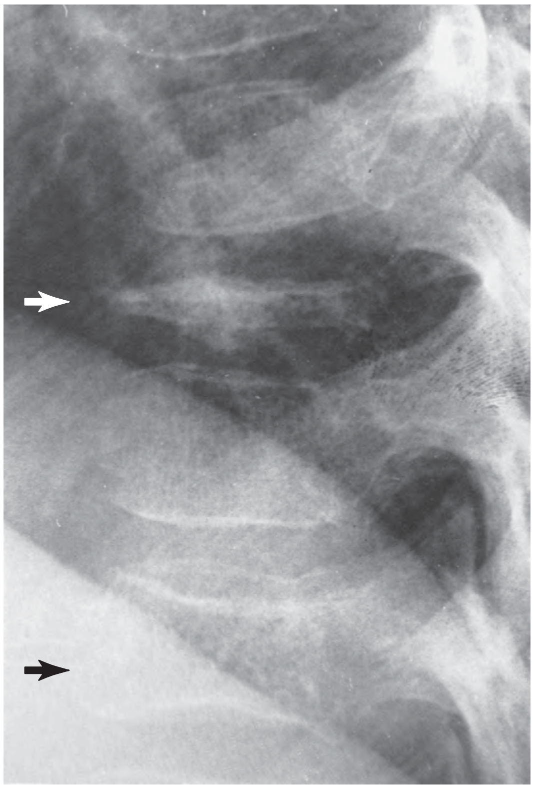

FIGURE 3–58 **Hodgkin disease.**[73] Lateral radiograph of the spine in this child with Hodgkin disease shows diffuse osteopenia. In addition, multiple collapsed vertebrae characterized by biconcave endplate deformities *(black arrow)* and vertebra plana *(white arrow)* are evident. Hodgkin disease may result in osteosclerosis, osteolysis, or a combination of the two.

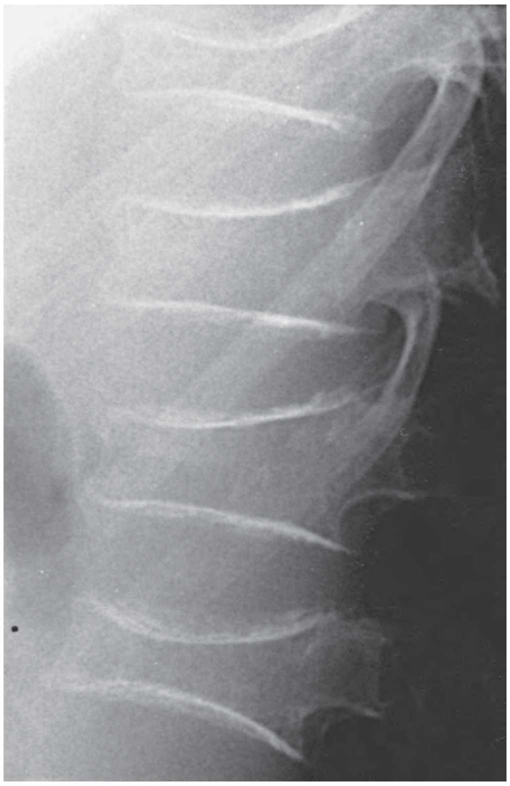

FIGURE 3–59 **Acute childhood leukemia.**[74] Multiple wedge-shaped and biconcave compression fractures are evident in this child.

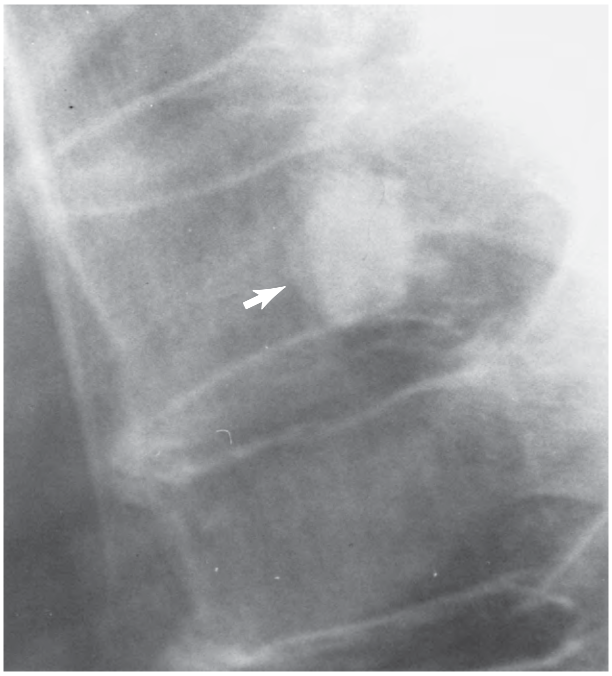

FIGURE 3–60 Bone island (enostosis).[75] A solitary, osteosclerotic lesion is seen in the vertebral body *(arrow)*. Enostoses are solitary (or infrequently multiple) discrete foci of osteosclerosis within the spongiosa of bone. They may be round, ovoid, or oblong; may possess a brush border; and tend to be aligned with the long axis of trabecular architecture. Giant bone islands have been reported to reach proportions of 4 × 4 cm in diameter. Additionally, enostoses may increase or decrease in size and may even be positive on bone scans, particularly in large and growing lesions. Enostoses should be differentiated from other osteosclerotic processes, such as osteoblastic metastasis, osteomas, osteoid osteomas, enchondromas, bone infarcts, fibrous dysplasia, and osteopoikilosis.

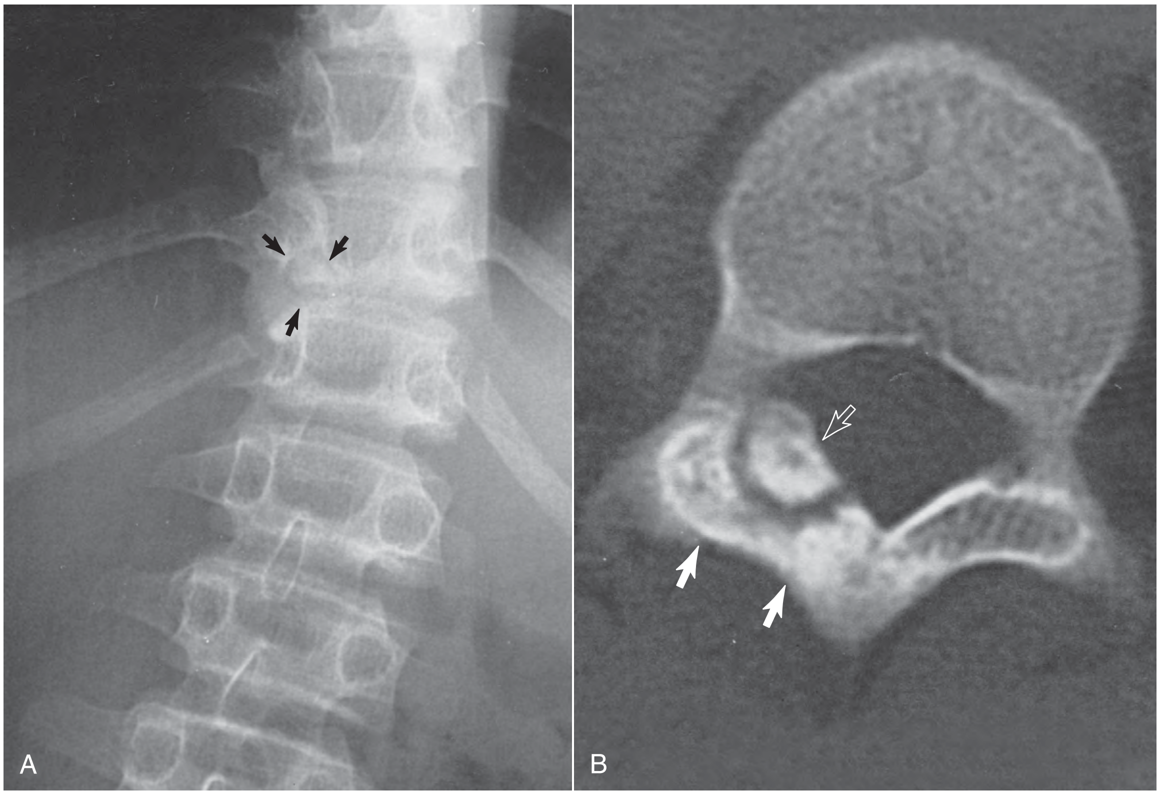

FIGURE 3–61 Osteoid osteoma.[76,124,129] A 13-year-old boy with painful scoliosis. **A,** Routine radiograph demonstrates an antalgic left thoracolumbar scoliosis. A circular radiolucent area with a central zone of calcification (nidus) is faintly visible within the right neural arch of T11 *(arrows)*. **B,** Transaxial CT image clearly shows the lesion localized to the right lamina of T11. A central zone of sclerosis representing the partially calcified nidus *(open arrow)* and reactive sclerosis of the adjacent bone *(arrows)* are evident.

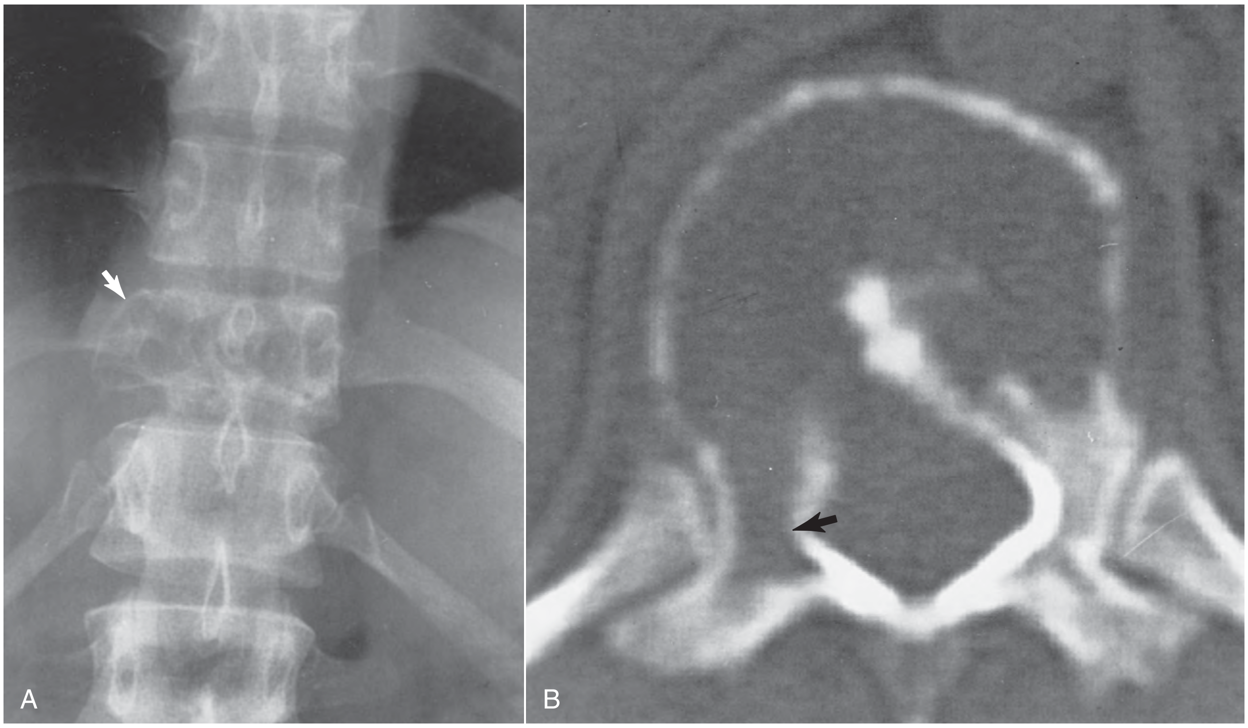

FIGURE 3–62 **Giant cell tumor.**[77] Radiographic investigation of back pain in this 29-year-old woman revealed an eccentric, expansile osteolytic lesion of the neural arch and partially collapsed vertebral body of T11. This is seen on the routine anteroposterior radiograph **(A)** *(arrow)* and is illustrated much more clearly on the transaxial CT image **(B).** The CT scan reveals that the lesion has destroyed the majority of the vertebral body and extends into the right pedicle and neural arch *(arrow)*. Fewer than 10% of all giant cell tumors affect the spine, and about 5% to 10% of all giant cell tumors are malignant. *(Courtesy C. Kusnick, MD, Irvine, Calif.)*

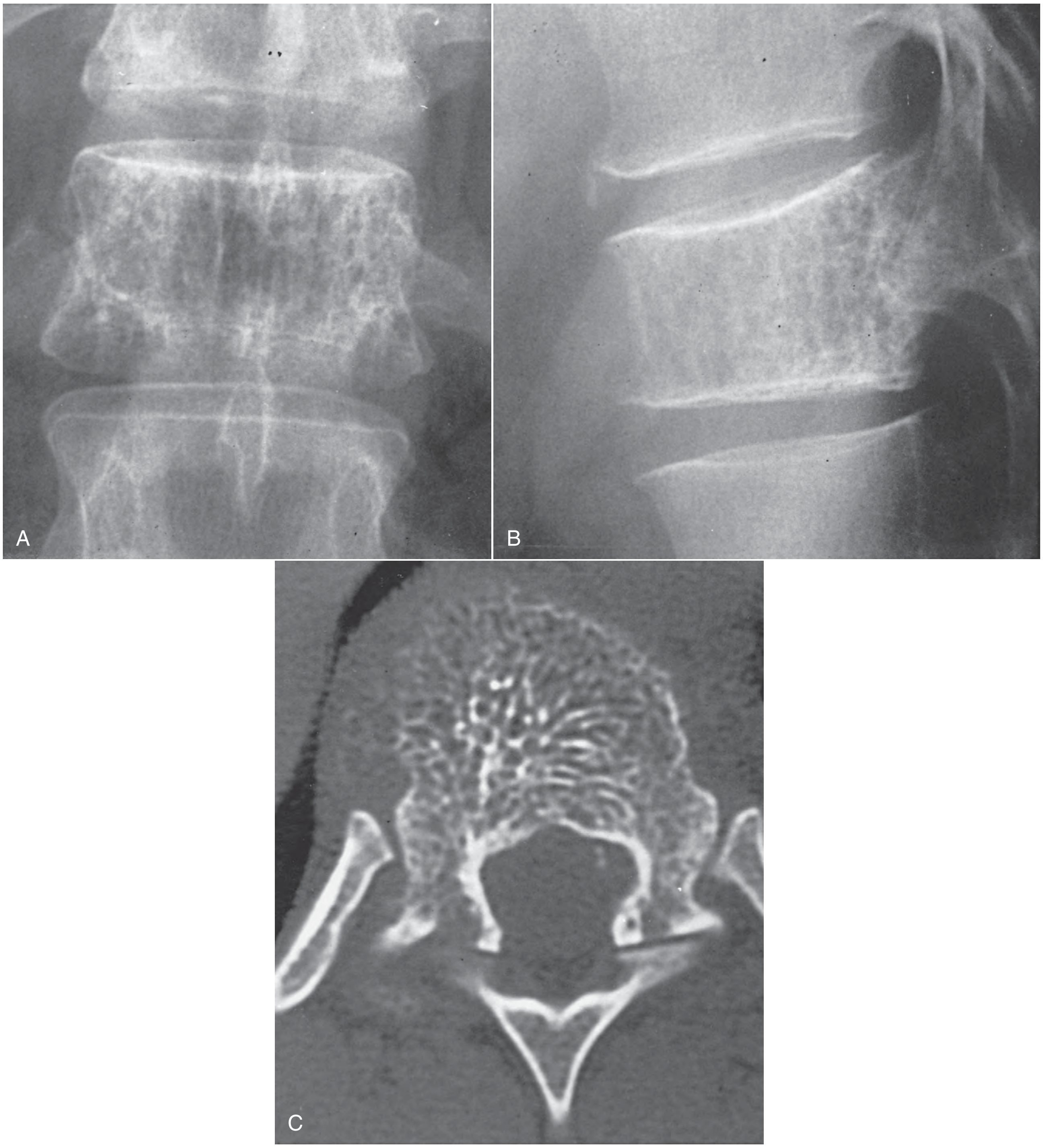

FIGURE 3–63 **Hemangioma.**[78,108] **A-B,** A man in his late 30s had thoracolumbar pain. Frontal **(A)** and lateral **(B)** radiographs show a radiolucent vertebral body, accentuated vertical trabeculae (the "corduroy cloth" appearance), and a wedge-shaped compression fracture of the T12 vertebral body. This is an infrequent complication of benign hemangiomas. Pathologic fractures may cause spinal cord compression as a result of epidural extension of tumor, osseous displacement, or epidural hemorrhage. **C,** In another patient, without a compression fracture, a transaxial CT scan of a thoracic vertebral hemangioma shows discrete columns of radiodense bone interspersed among the relatively osteopenic spongiosa of the vertebral body (polka-dot sign). Hemangiomas are considered the most common benign neoplasm of the spine. *(**A-B,** Courtesy P.H. VanderStoep, MD, St Cloud, Minn.)*

FIGURE 3–64 **Paget disease.**[79,80,102,103,106] Pagetic involvement of the thoracic spine is characterized by osseous enlargement and coarsening of trabeculae involving several vertebral bodies. Minimal collapse of the T11 vertebral body *(arrows)* also is present.

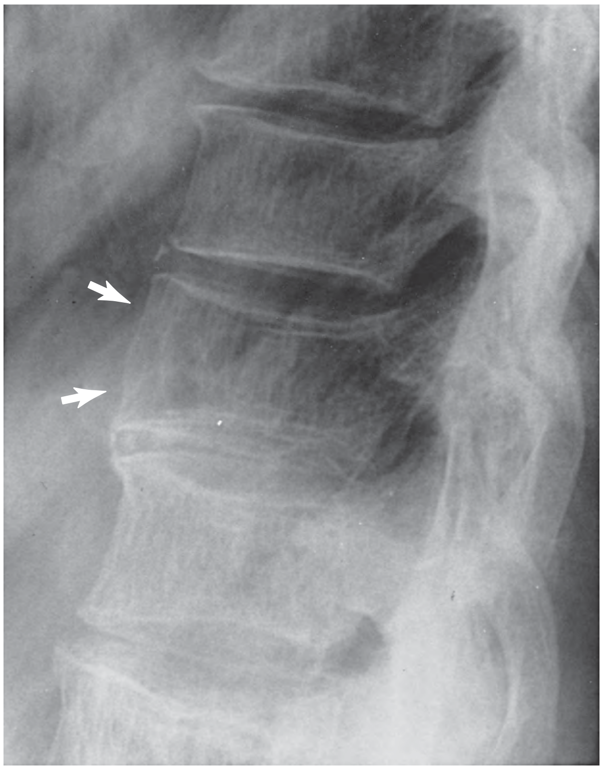

FIGURE 3–65 **Neurofibromatosis type I (von Recklinghausen disease).**[81,82] Coronal CT localizer image from this 31-year-old man shows characteristic scoliosis and elevated skin lesions (fibroma molluscum) *(arrows)*.

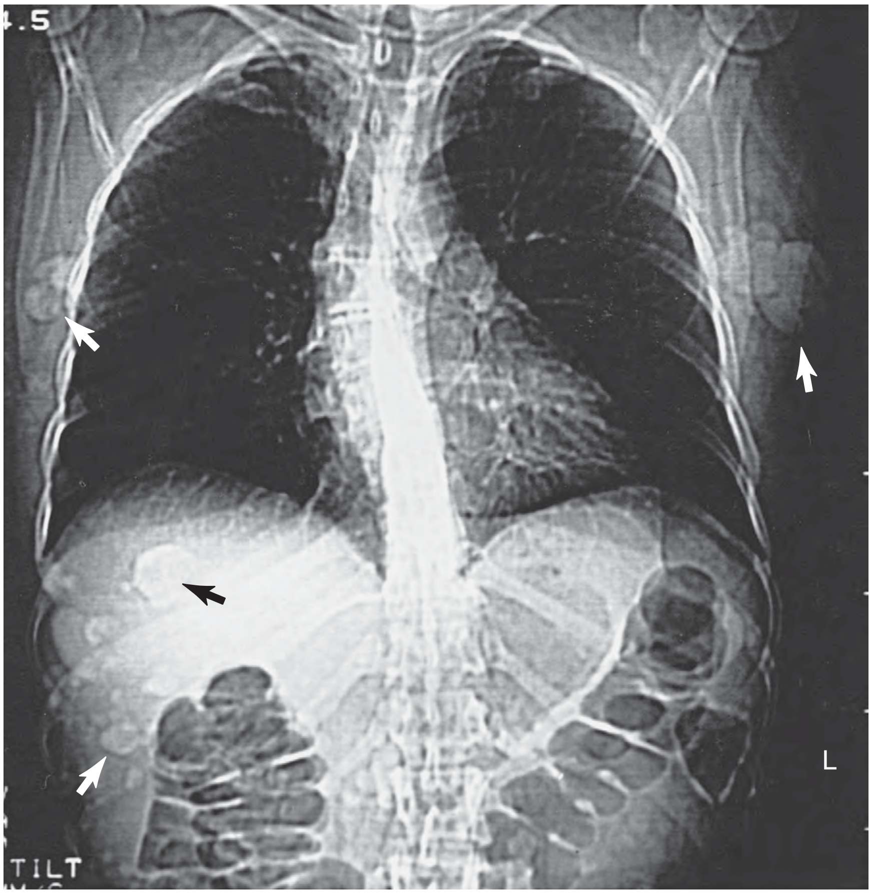

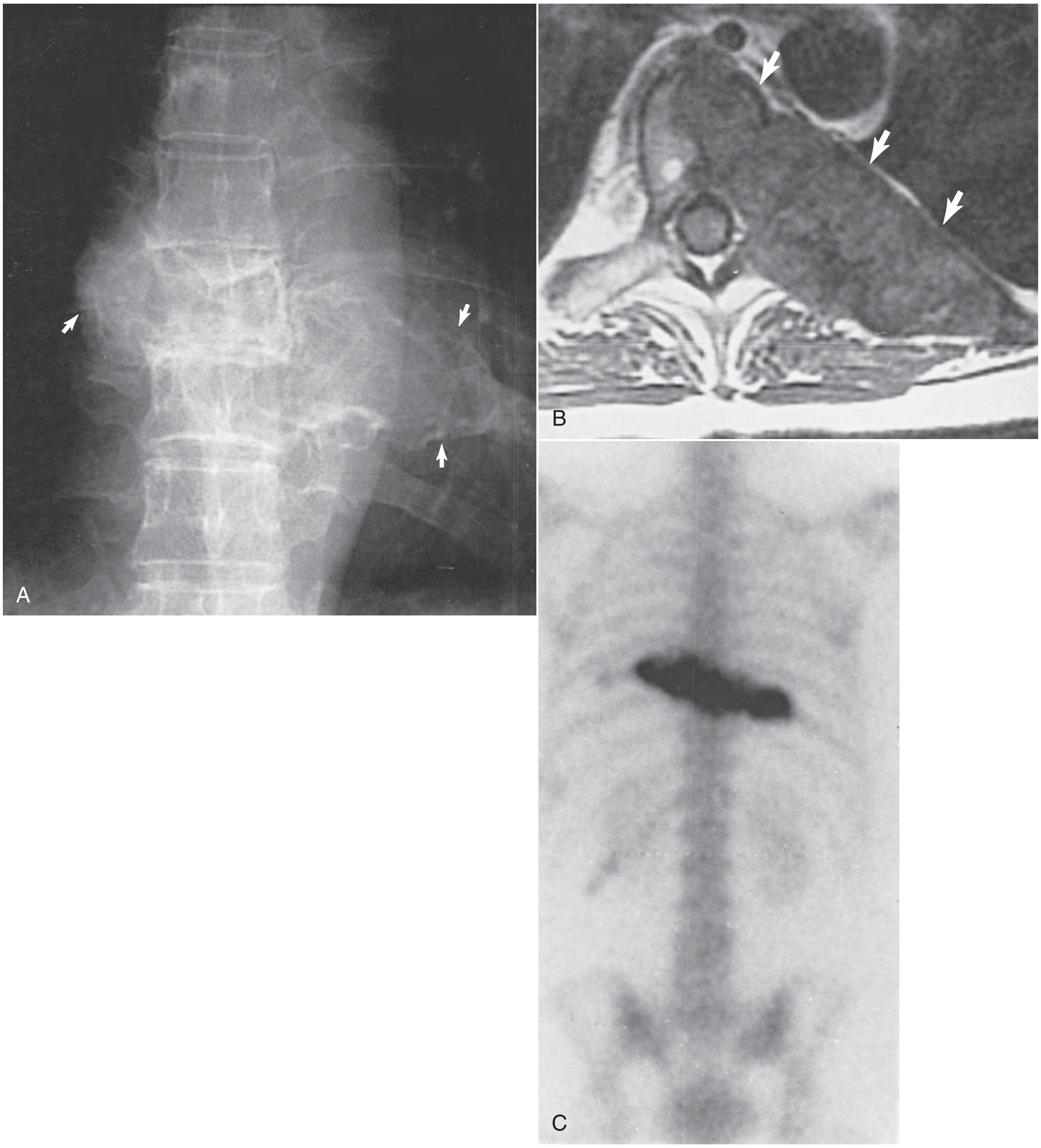

FIGURE 3–66 **Fibrous dysplasia.**[83,84] **A,** Frontal radiograph of the spine in this 55-year-old woman reveals irregular expansion and osteolytic destruction of two contiguous thoracic vertebrae and adjacent ribs *(arrows)*. **B,** Transaxial T1-weighted (TR/TE, 800/20) spin echo MR image shows the expansile nature and extent of this low signal intensity inhomogeneous lesion *(arrows)* involving the vertebral body and rib. **C,** A ^{99m}Tc-methylene diphosphonate bone scan shows intense concentration of the radionuclide in the distribution of the lesion.

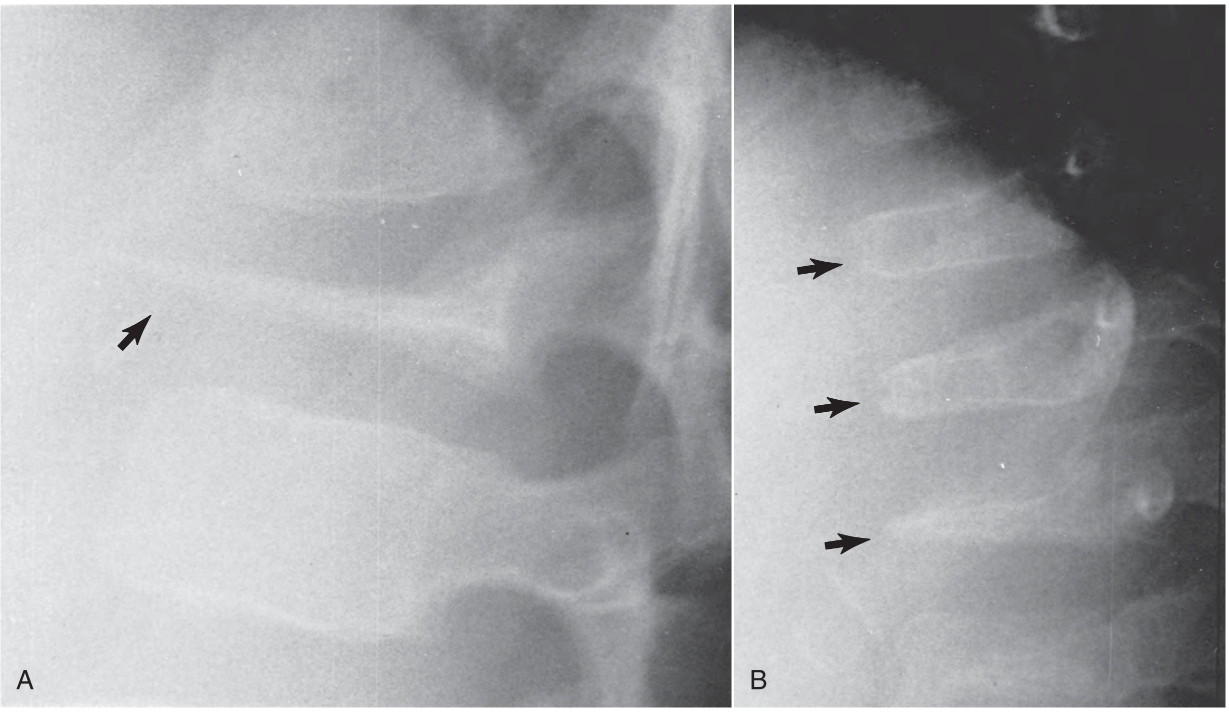

FIGURE 3–67 **Langerhans cell histiocytosis.**[85,86] **A,** Eosinophilic granuloma. Observe vertebra plana involving a single vertebral body *(arrow)*. **B,** Letterer-Siwe disease. Vertebra plana involving multiple thoracic vertebral bodies *(arrows)* is seen in a patient with extensive bone involvement. Eosinophilic granuloma of bone is the most frequently encountered form of Langerhans cell histiocytosis, a disease characterized by histiocytic infiltration of tissues. In addition to flattened vertebral bodies, bubbly, lytic, or expansile lesions without collapse may occur. With healing, the height of the vertebral body may be reconstituted, a finding more common in younger persons. Letterer-Siwe disease is the least common and most acute form of Langerhans cell histiocytosis, usually affects children under the age of 3 years, and has the poorest clinical prognosis. It is characterized by histiocytic infiltration in multiple visceral organs. The intermediate form of Langerhans cell histiocytosis—Hand-Schüller-Christian disease—is not illustrated.

TABLE 3-14 Metabolic and Hematologic Disorders Affecting the Thoracic Spine*

Entity	Figure(s)	Characteristics
Generalized osteoporosis[87,104,111,112,130]	3-68	Uniform decrease in radiodensity, thinning of vertebral endplates, accentuation of vertical trabeculae Thoracolumbar region of the spine is the most frequent site of osteoporotic compression fractures; many fractures are identified incidentally on multidetector computed tomography (MDCT) of the chest. Wedge-shaped vertebral deformities are most common in thoracic spine compression fractures; vertebra plana deformities are more likely to be related to pathologic fracture caused by plasma cell myeloma or skeletal metastasis Bone densitometry is necessary for accurate assessment of the presence and extent of diminished bone mineral content See Chapters 1 and 7 for more extensive discussions of osteoporosis See also Table 3-13
Osteomalacia[88]	3-69	Diminished radiodensity and prominent coarsened trabeculae Compression deformities of vertebral bodies
Hypothyroidism[89]	3-70	Bullet vertebrae, thoracolumbar gibbus deformity, osteoporosis, delayed development, ossification of the apophyses, and widened disc spaces
Renal osteodystrophy and hyperparathyroidism[90,91]	3-71	Findings are most prominent in the thoracolumbar spine Subchondral resorption at discovertebral junctions *Rugger-jersey spine:* bandlike osteosclerosis on the superior and inferior surfaces of the vertebral body in secondary form Vertebral fracture results in biconcave endplate deformities, more prominent in thoracolumbar spine
Acromegaly[92]	3-72	Elongation and widening of the vertebral bodies Ossification of the anterior portion of the disc; posterior scalloping of vertebral bodies occurs infrequently
Fluorosis[93]	3-73	Predominant spinal findings include diffuse osteosclerosis and ossification of the posterior longitudinal ligament (OPLL), prominent osteophytosis, and periostitis Differential diagnosis includes diffuse idiopathic skeletal hyperostosis (DISH), osteopetrosis, skeletal metastasis, and other causes of diffuse osteosclerosis
Sickle cell anemia[94,105]	3-74	Diffuse osteopenia and H-shaped vertebra H-shaped vertebral body indentations may simulate Schmorl nodes or biconcave (fish) vertebrae associated with osteoporosis
Osteonecrosis of the vertebral body[95,113,117]	3-75	Intravertebral vacuum phenomenon with pathologic vertebral body collapse Frequently associated with corticosteroid use Some authorities suggest that the term *osteonecrosis* used to designate intravertebral vacuum phenomenon may be inappropriate. They cite several cases where the gas in the body communicates with gas in the adjacent disc—the intervertebral disc vacuum phenomenon associated with degenerative disc disease. Others have raised the possibility that the intravertebral vacuum is a sign of fracture nonunion.

* See also Tables 1-15 to 1-18.

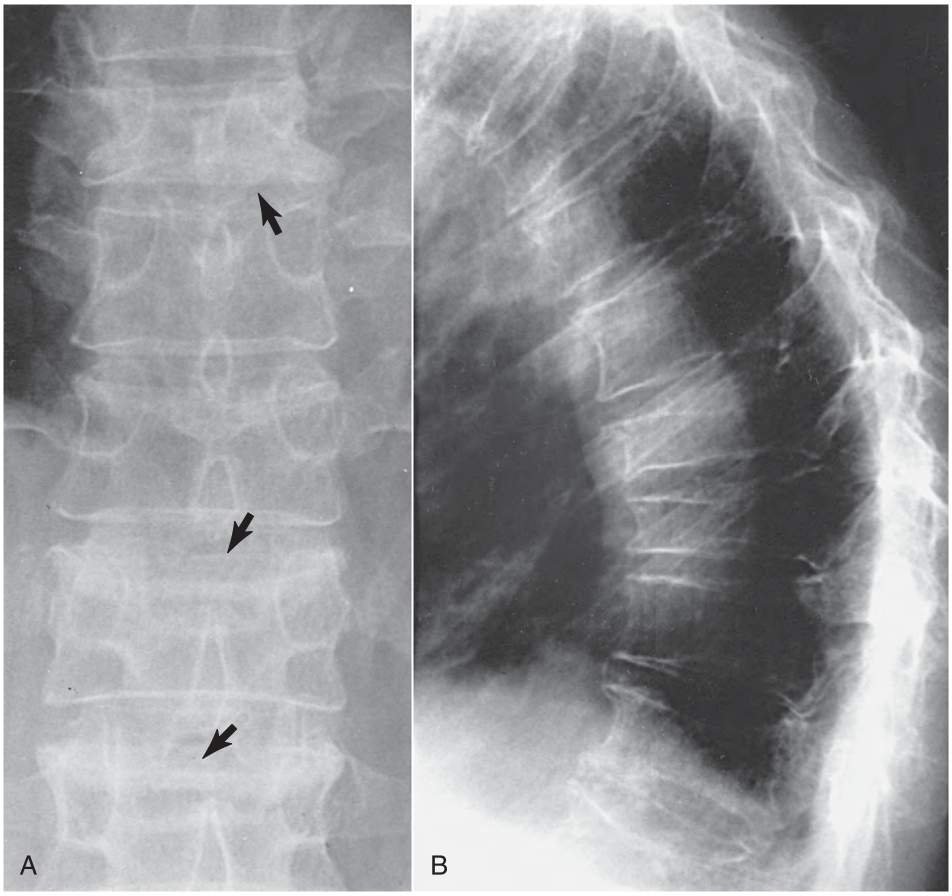

FIGURE 3–68 **Osteoporosis: spinal fractures.**[87,104,111] **A,** Frontal radiograph of the spine in this 59-year-old man with severe senile osteoporosis reveals fractures of several thoracolumbar vertebral bodies *(arrows)*. **B,** In a 61-year-old man with severe osteoporosis and multiple wedge-shaped vertebral body compression fractures, a dramatic kyphosis that measures greater than 100 degrees are observed. This kyphosis resulted in an insufficiency fracture of the sternum (not shown).

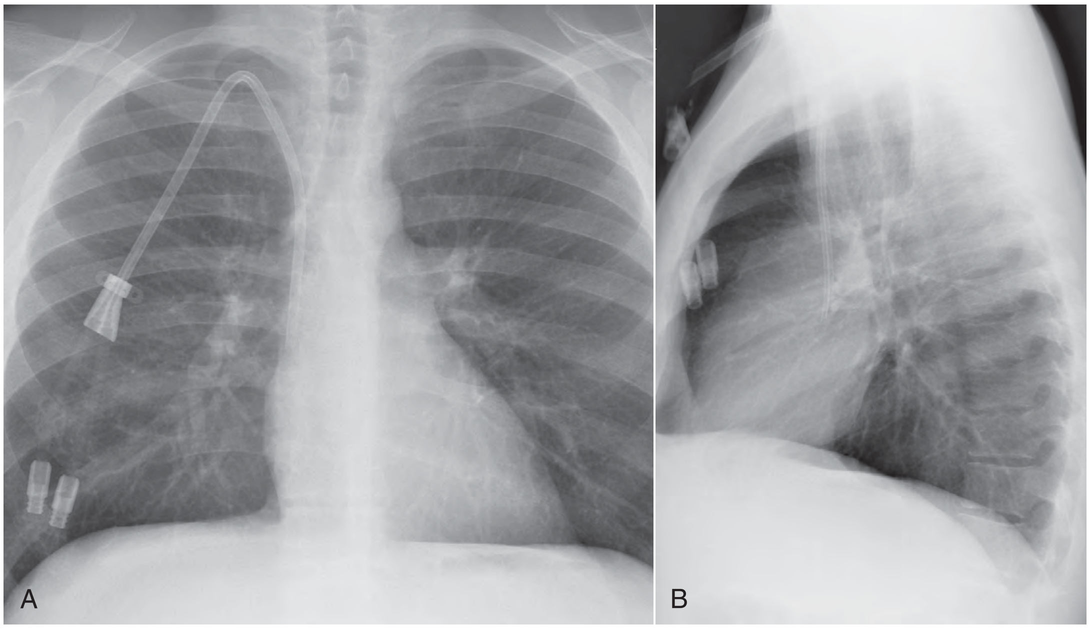

FIGURE 3–69 **Osteomalacia.**[88] This 34-year-old woman had longstanding osteomalacia and renal osteodystrophy. **A,** Posteroanterior and **(B)** lateral chest radiographs reveal a dialysis dual lumen tunneled internal jugular central venous catheter. Note on the lateral radiograph, the ill-defined margins to the vertebral bodies, one of the key radiographic features in separating osteomalacia from osteoporosis.

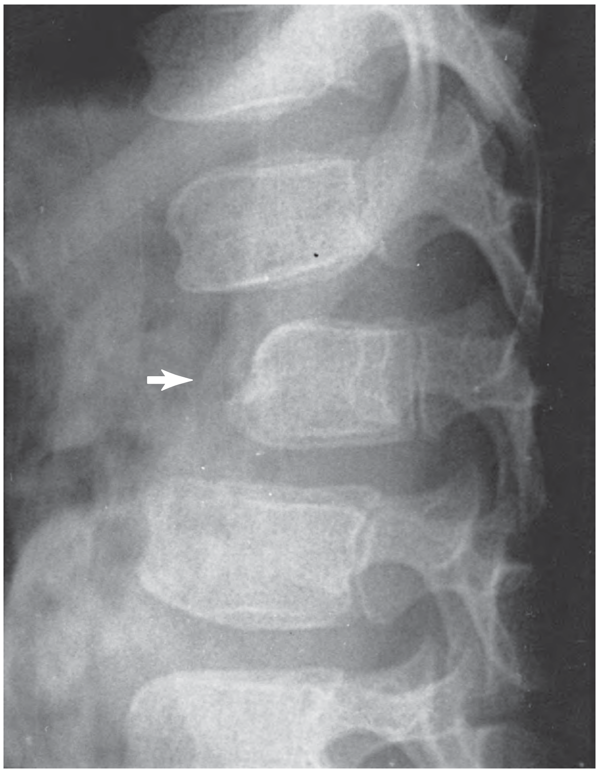

FIGURE 3–70 Hypothyroidism: bullet vertebra.[89] A characteristic finding in cretinism is thoracolumbar bullet-shaped vertebrae *(arrow)*.

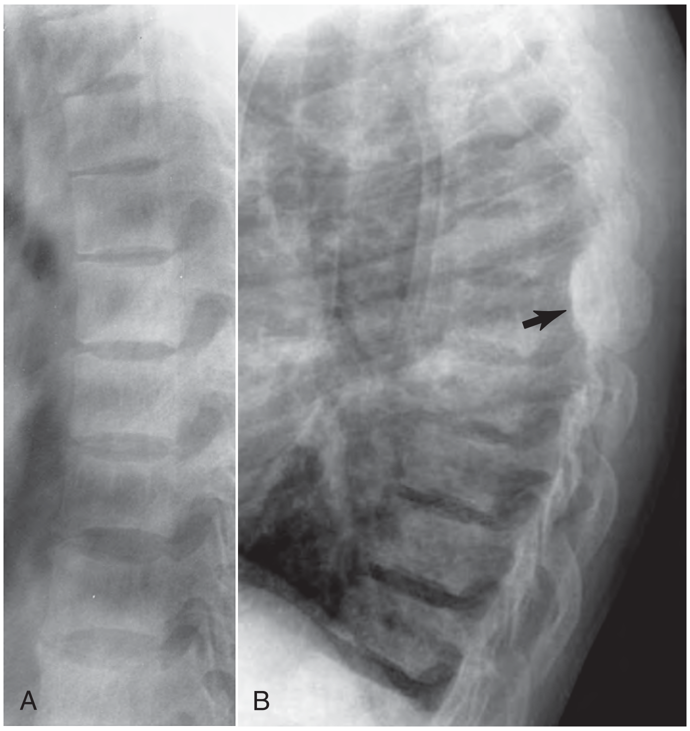

FIGURE 3–71 Rugger-jersey spine: renal osteodystrophy and hyperparathyroidism.[90,91] **A,** Horizontal linear bands of osteosclerosis within the superior and inferior aspects of the vertebral bodies are characteristic of the rugger-jersey spine appearance of renal osteodystrophy. This vertebral sclerosis may be accompanied by osteopenia of the intervening central portion of the vertebral body and may be associated with varying degrees of osseous collapse. The vertebral sclerosis may disappear after successful treatment. **B,** A lateral radiograph of this 30-year-old female with long-standing hyperparathyroidism reveals increased radiodensity of the vertebral bodies, specifically in a horizontal pattern along the superior and inferior portions of the vertebral bodies. This patient also had multiple brown tumors affecting the ribs, one of which is visible *(arrows)*.

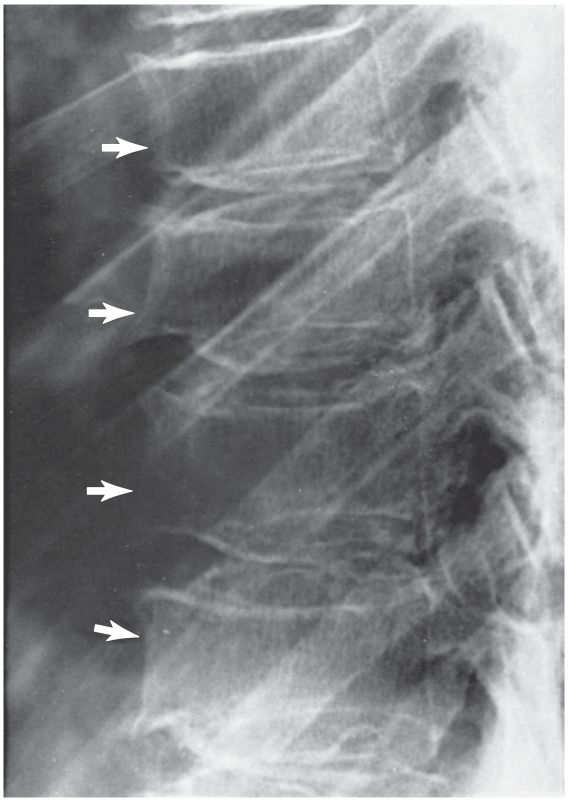

FIGURE 3–72 **Acromegaly.**[92] Observe the prominent flangelike bone formation and elongation of the vertebral bodies *(arrows)* in this 53-year-old man with long-standing acromegaly secondary to a pituitary adenoma.

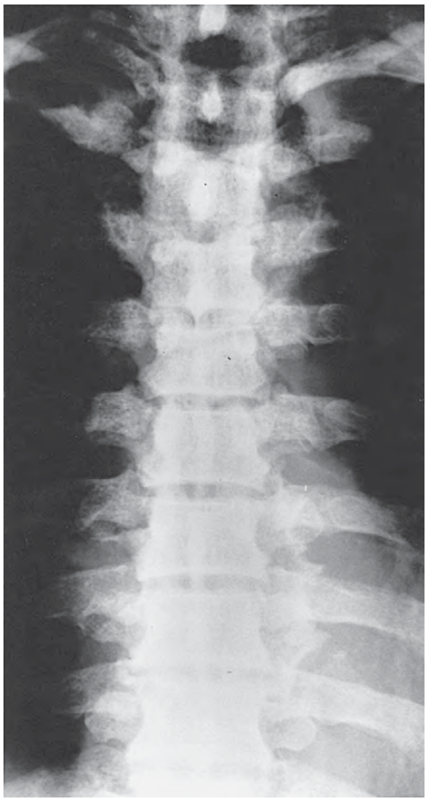

FIGURE 3–73 **Fluorosis.**[93] Observe the extensive ossification of the paraspinal ligaments and the generalized increased radiodensity of the spine in this patient with fluoride poisoning. *(Courtesy G. Beauregard, Montreal, Quebec, Canada.)*

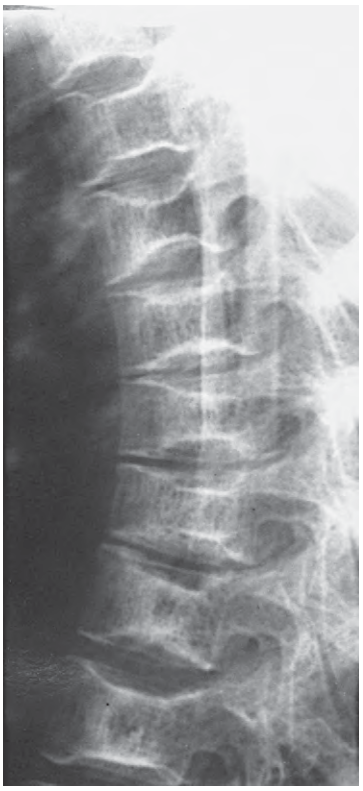

FIGURE 3–74 **Sickle cell anemia.**[94,105] H-shaped central endplate depressions are evident throughout the vertebral bodies of the thoracic spine. Such indentations are characteristic of sickle cell anemia and other hemoglobinopathies.

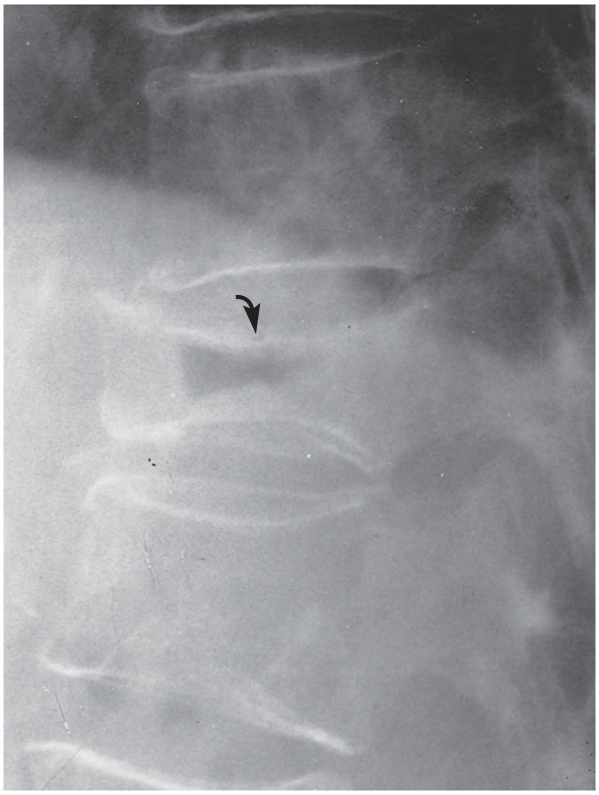

FIGURE 3–75 Steroid-induced osteonecrosis: vertebral collapse.[95,117] This 90-year-old woman on long-term corticosteroid medication had acute back pain. Lateral radiograph reveals diffuse osteopenia. A radiolucent collection of gas is present within the collapsed lower thoracic vertebral body *(curved arrow)*. This is termed the *intravertebral vacuum cleft*, and often it is a sign of vertebral osteonecrosis, frequently associated with the use of corticosteroid medication. *(Courtesy P. Kindynis, MD, Geneva, Switzerland.)*

TABLE 3-15 Percutaneous Vertebral Body Augmentation Surgery for Painful Compression Fractures

Procedure	Figure(s)	Characteristics	Complications
General considerations[121,130]		Indicated in patients with one or more osteoporotic compression fractures and severe, persistent, and often incapacitating focal back pain that is not responding to standard conservative medical therapy Indications for fractured vertebral bodies other than benign osteoporosis: Benign tumors such as hemangioma Malignancies such as metastasis and melanoma	
Vertebroplasty[118-120]		***Clinical Considerations*** Typically an outpatient procedure Fluoroscopically- or CT-guided transpedicular or posterolateral extrapedicular needle and sheath placement followed by injection of polymethylmethacrylate (PMMA) cement and barium into fractured vertebral body Pain relief is attributed to fracture stabilization, but thermal and chemical ablation of nerve endings in the vertebral body may also contribute to pain relief. Clinical success rates in terms of pain relief and functional improvement have been reported between 78% and 90% for vertebral compression fractures ***Imaging Findings*** One or two radiodense collections of cement seen bilaterally in the vertebral body Some restoration of body height is typically seen postoperatively Low signal intensity in vertebral body on both T1-w and T2-w MR images Careful examination for abnormal cement extravasation is essential	Overall complication rates reported at less than 5% Associated with increased risks of adjacent level fractures (controversial association) Cement extravasation 1. Posteriorly into spinal canal or neuroforamina 2. Anterolaterally into paraspinal soft tissues 3. Central venous filling may lead to pulmonary embolization of cement 4. Superiorly or inferiorly into adjacent intervertebral disc Postoperative infection Worsening of pain Recurrence of pain (with possible new fracture at a different level)
Kyphoplasty (Balloon tamp reduction)[121,122]	3-76	Similar to vertebroplasty with an additional step of percutaneous insertion of a balloon tamp through the pedicle into the fractured vertebral body The balloon is then inflated to achieve compaction of surrounding cancellous bone and to provide varying degrees of restoration of elevation of the involved vertebral body Balloon inflation is followed by cement injection as in vertebroplasty Advantages in comparison to vertebroplasty: 1. Improved kyphotic deformity correction especially if treated within 3 months of the actual fracture 2. Decreased potential for cement leakage 3. Equivalent pain relief and functional improvement to vertebroplasty	Significant complications rarely occur (only 0.7% per level treated) and include: Hypoxia Epidural hematoma Paraparesis Anterior cord syndrome Cement extravasation (less common than in vertebroplasty) Kyphoplasty does not appear to effect the survival of patients with vertebral compression fractures

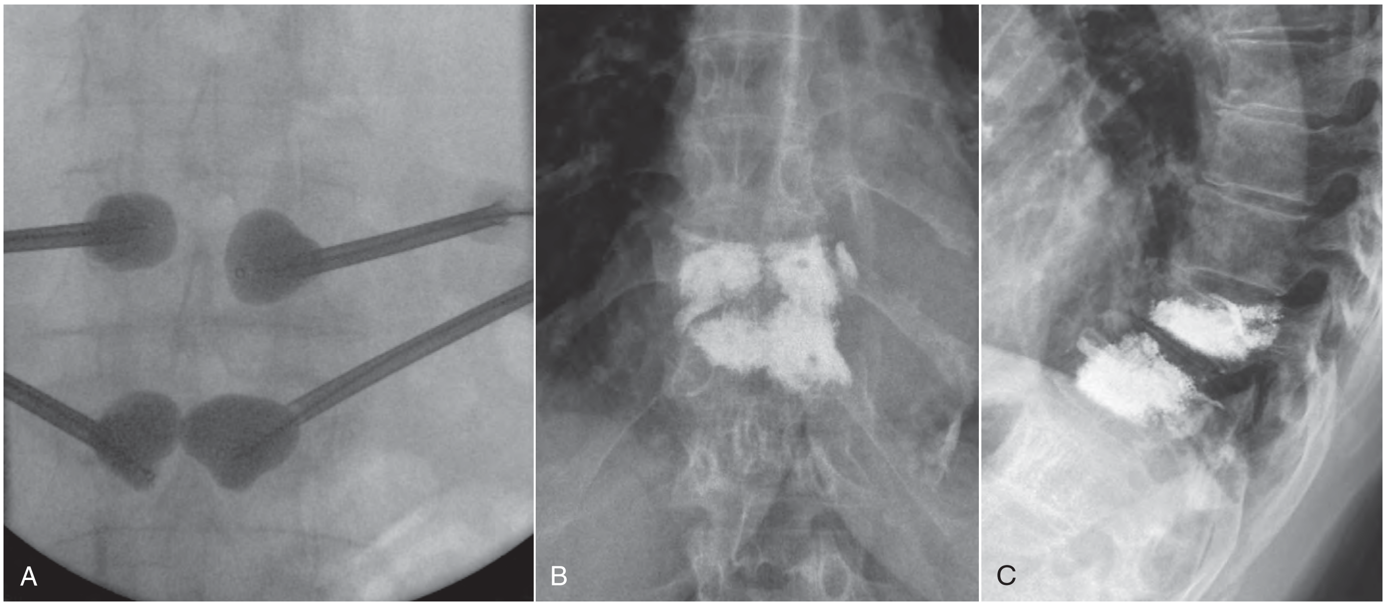

FIGURE 3–76 **Percutaneous vertebral body augmentation surgery for painful compression fractures: balloon kyphoplasty.**[121,122] **A,** Intraoperative fluoroscopic spot film reveals insertion and deployment of four balloons into two vertebral bodies through the pedicles. Once deployed and removed, cement is injected into the cavity created by the balloon to restore vertebral height and relieve pain. Anteroposterior **(B)** and lateral **(C)** radiographs in an 80-year-old woman with two thoracolumbar compression fractures shows the presence of radiopaque cement in the vertebral bodies. This procedure successfully achieved approximately 75% restoration of vertebral body height and the patient reported significant pain reduction postoperatively. *(**B-C,** Courtesy K. Brown, DC, Syracuse, NY.)*

CHAPTER 4

Lumbar Spine

NORMAL DEVELOPMENTAL ANATOMY

Accurate interpretation of pediatric lumbar spine radiographs requires a thorough understanding of normal developmental anatomy. Table 4-1 lists the age of appearance and fusion of the primary and secondary ossification centers. Figures 4-1 and 4-2 demonstrate the radiographic appearance of many important ossification centers and other developmental landmarks at selected ages from birth to skeletal maturity.

DEVELOPMENTAL ANOMALIES, ANATOMIC VARIANTS, AND SOURCES OF DIAGNOSTIC ERROR

The lumbar spine is a frequent site of anomalies, normal variations, and other sources of diagnostic error, many of which may simulate disease and result in misdiagnosis. Table 4-2 and Figures 4-3 to 4-16 are intended to familiarize the reader with the more common processes.

SKELETAL DYSPLASIAS AND OTHER CONGENITAL DISORDERS

Table 4-3 outlines a number of dysplastic and congenital disorders that affect the lumbar spine, and Table 4-4 lists some of the leading causes of vertebral scalloping. Figures 4-17 to 4-24 illustrate the radiographic manifestations of some of these disorders.

SPONDYLOLYSIS AND SPONDYLOLISTHESIS

Spondylolysis (defects of the pars interarticularis) and spondylolisthesis (vertebral slippage) are encountered frequently on imaging studies of the lumbar spine. Table 4-5 lists the types of such disorders, Table 4-6 describes a measurement technique used in evaluation, and Figures 4-25 to 4-35 show radiographic examples. Table 4-7 details a grading system for stress fractures of the pars interarticularis.

LUMBAR SCOLIOSIS

The topic of scoliosis is discussed in more detail in Chapter 3 (see Table 3-5 and Figures 3-16 to 3-24). Scoliosis also exhibits important manifestations in the lumbar spine. Table 4-8 lists some types of scoliosis that affect the lumbar spine in addition to those listed in Chapter 3. Figures 4-36 to 4-39 illustrate the radiographic findings.

PHYSICAL INJURY

Fractures, dislocations, and soft tissue injuries involving the lumbar spine are common, many of which result in serious clinical manifestations. Table 4-9 lists the important injuries of the lumbar spine and their characteristics. Table 4-10 addresses instability in burst fractures. In addition, Figures 4-40 to 4-46 represent examples of the most characteristic imaging manifestations of common lumbar spine injuries. Table 4-11 represents a checklist for the diagnosis of clinical instability in the lumbar spine.

INTERVERTEBRAL DISC DISORDERS

Table 4-12 lists several conditions involving lumbar intervertebral discs. Tables 4-13 to 4-17 deal with specific manifestations of disc disease. Figures 4-47 to 4-67 represent examples of imaging of intervertebral disc disorders.

ARTICULAR DISORDERS

The lumbar spine is a frequent target site of involvement for many forms of degenerative, inflammatory, crystal-induced, and infectious spondyloarthropathies and other articular disorders. Table 4-18 outlines these diseases and their characteristics, and Figures 4-68 to 4-84 illustrate the characteristic radiographic manifestations. Additionally, Chapter 3 provides discussions of osseous outgrowths of the spine (see Table 3-11) and terminology applied to ankylosing spondylitis (see Table 3-12).

BONE TUMORS

A wide variety of malignant and benign tumors and tumorlike lesions affect the spine. Those neoplasms illustrated in this chapter are described in Table 4-19; examples are illustrated in Figures 4-85 to 4-100. More complete lists of neoplasms are found in Chapter 1 (Tables 1-12 to 1-14). Table 4-20 lists the characteristics of several disorders that cause vertebral osteosclerosis.

METABOLIC AND HEMATOLOGIC DISORDERS

A number of metabolic disorders involve the lumbar spine. These are outlined in Table 4-21 and illustrated in Figures 4-101 to 4-114. Table 4-22 details the World Health Organization definitions of osteoporosis and osteopenia.

LUMBAR SPINE SURGERY

Surgical procedures for pathologic disc conditions, spinal stenosis, and other disorders are numerous. Table 4-23 lists a few of these procedures and their associated complications, whereas surgical instrumentation and various types of bone grafts are discussed in Table 4-24. Figures 4-115 to 4-122 illustrate the characteristic imaging findings of some surgical procedures.

VASCULAR DISORDERS

Aneurysms of the abdominal aorta and iliac arteries may be manifested clinically as low back pain, often simulating bone and joint disorders of the spine. A brief description of these aneurysms is provided in Table 4-25, and representative examples are shown in Figures 4-123 and 4-124.

TABLE 4-1 Lumbar Spine: Approximate Age of Appearance and Fusion of Ossification Centers*[1-3] (Figures 4-1, 4-2)

Ossification Center	Primary or Secondary	No. of Centers	Age of Appearance (Years)	Age of Fusion (Years)	Comments
L1-L4					
Neural arches (laminae)	P	2	Birth	1	Fuse together in order from L4 to L1
Vertebral body	P	1	Birth	5-6	Fuse to laminae
Spinous process	S	1	11-16	17-25	
Transverse processes	S	2	11-16	17-25	
Articular processes	S	4	11-16	17-25	
Mamillary processes	S	2	11-16	17-25	
Ring apophyses	S	2	11-16	17-25	Fuse to body
L5					
Neural arches (laminae)	P	2	Birth	5	Fuse together
Vertebral body	P	1	Birth	6	Fuse to laminae
Spinous process	S	1	11-16	17-25	
Transverse processes	S	2	11-16	17-25	
Articular processes	S	4	11-16	17-25	
Mamillary processes	S	2	11-16	17-25	
Ring apophyses	S	2	11-16	17-25	Fuse to body

P, Primary; *S*, secondary.

* Ages of appearance and fusion of ossification centers in girls typically precede those of boys. Ethnic differences also exist.

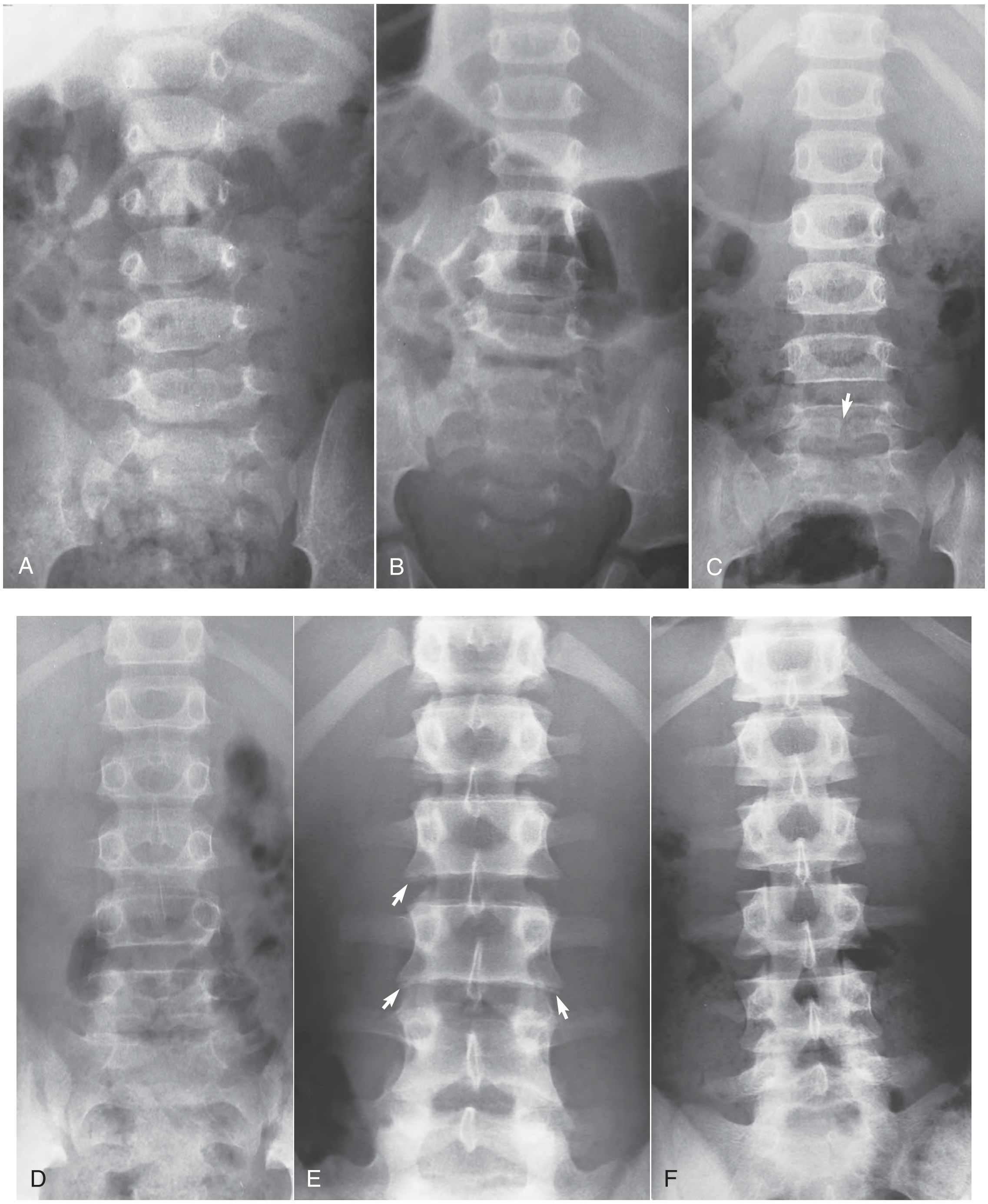

FIGURE 4–1 **Skeletal maturation and normal development: anteroposterior lumbar spine radiographs.**[1-3] **A,** A 14-month-old girl. The spinal canal appears proportionately wide in relation to the vertebral bodies. The laminae are thin and the interlaminar spaces are wide. **B,** A 2-year-old boy. **C,** An 8-year-old boy. The neural arch of L5 usually fuses between the ages of 5 and 6 years, but it has not yet fused in this patient *(arrow)*. Failure of fusion in adults (spina bifida occulta) at this level is a common developmental anomaly. Some of the vertebral endplates are jagged or serrated, a finding that often persists until complete fusion of the secondary ring apophysis to the vertebral body has occurred. **D,** A 10-year-old boy. The spinal canal remains disproportionately wide, and the superior vertebral endplates have a serrated appearance. **E,** A 13-year-old boy. The secondary ring apophyses have begun to ossify and are readily visible, especially adjacent to the inferior endplates *(arrows)*. Note also the serrated margins of the superior vertebral endplates. **F,** A 16-year-old boy. The vertebral bodies are more rectangular and the size of the spinal canal has begun to resemble that of the adult.

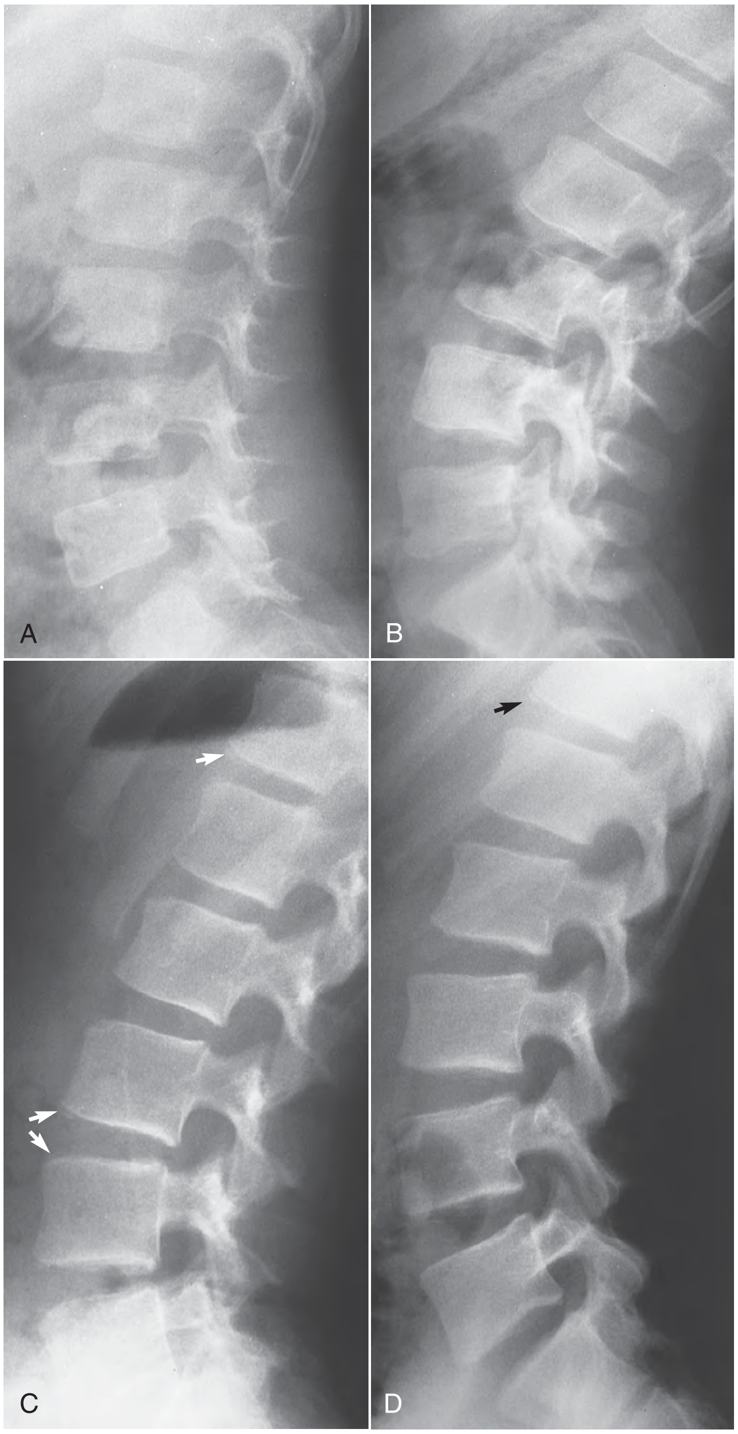

FIGURE 4–2 **Skeletal maturation and normal development: lateral lumbar spine radiographs.**[1-3] **A,** A 30-month-old girl. The vertebral body contours are rounded and the spinal canal appears disproportionately wide in relation to the vertebral body width. In some children at this age, the anterior vascular notches may be prominent and the vertebral bodies may show anterior beaking (neither of which are present in this child). **B,** A 9-year-old girl. The posterior vertebral bodies exhibit normal physiologic scalloping, an appearance that may begin as early as the age of 2 years. The overall shape of the vertebral body is rectangular, but the corners remain rounded because the ring apophyses are not yet ossified. **C,** An 11-year-old girl. The secondary ring apophyses are seen adjacent to the notched anterior vertebral body margins *(arrows)*. These ossification centers typically appear near the age of puberty but may appear as early as the age of 7 years. They fuse to the vertebral body between 17 and 25 years of age. **D,** A 13-year-old boy. The ring apophyses are visible at the thoracolumbar region *(arrow)*. The posterior vertebral body contours remain scalloped.

Continued

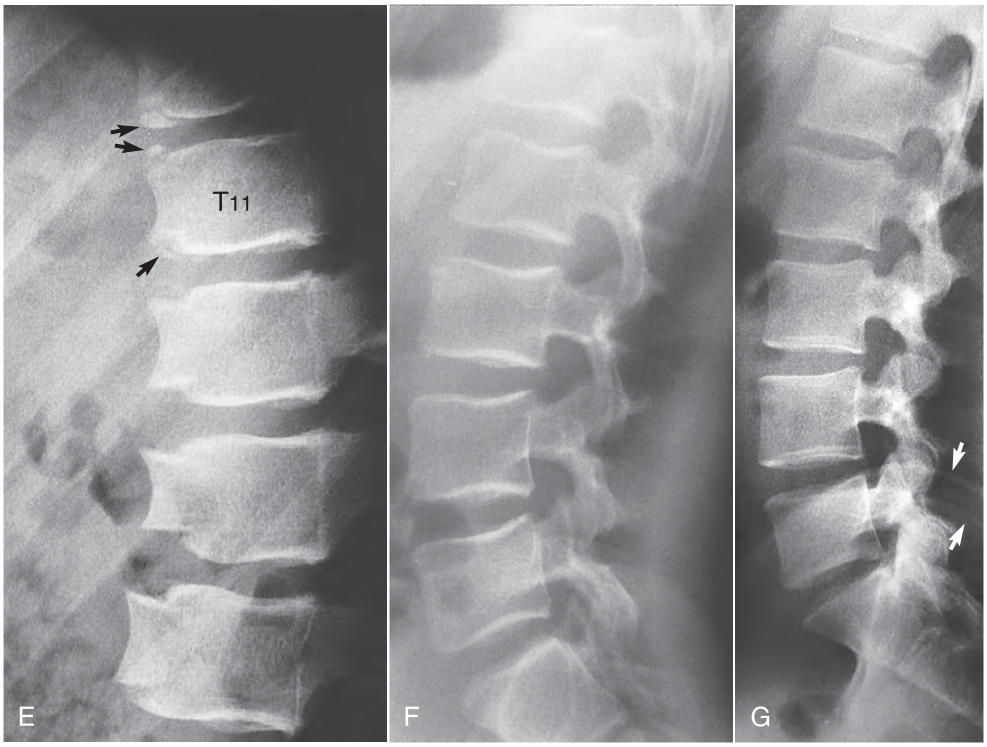

FIGURE 4–2, cont'd **E,** A 15-year-old boy. Observe the prominent notchlike defects of the vertebral bodies of T12, L1, and L2. These notches are normal in the juvenile spine and represent the space occupied by the unossified secondary ossification centers. Ossification of the ring apophyses is evident at the T10 and T11 levels *(arrows)*. **F,** A 15-year-old boy. In another patient, the notches are less prominent and the ring apophyses are ossified. Note the normal curvilinear appearance of the inferior vertebral body surfaces. The ring apophyses typically fuse to the vertebral endplates at about the age of 19 years in male adolescents and 16 years in female adolescents. Fusion may occur as late as the age of 25 years. **G,** Adult: 22-year-old man. All secondary ossification centers have fused to the vertebral bodies. The vertebral bodies are more rectangular, the posterior margin of each vertebral body is not scalloped, and the vertebral endplates have a less exaggerated curvilinear appearance. The secondary ossification centers of the iliac crests have yet to fuse to the ilium *(arrows)*. (***E,*** *Courtesy G.D. Schultz, DC, Portland, Ore.*)

TABLE 4-2 Some Developmental Anomalies, Anatomic Variants, and Sources of Diagnostic Error Affecting the Lumbar Spine*

Entity	Figure(s)	Figure(s)
Normal ring apophyses[4]	4-2, *C-F*	Normal vertebral body ring apophyses may resemble fractures or limbus vertebrae
Hahn venous channels[5]	4-3	*Normal anatomy:* a central horizontal vascular groove or channel that traverses the vertebral body; evident on radiographs, CT scans, and MR images These channels are quite prominent beginning with the first year of life, but they tend to disappear with age; they are of no clinical significance even when they persist into adulthood
Nuclear impressions[5,10]	4-4	Broad-based curvilinear indentations of the lower lumbar vertebral endplates seen on lateral radiographs; represent a variation of normal May be related to notochordal remnants or the Cupid bow contour seen on frontal radiographs *Differential diagnosis:* Schmorl cartilaginous nodes, compression fractures with biconcave deformities (fish vertebrae), and H vertebrae characteristic of hemoglobinopathy
Cupid bow contour[10]	4-5	Paramedian curvilinear indentations, generally of the inferior vertebral endplates, seen on frontal radiographs, which represent a normal variation closely related to nuclear impressions Most common at L4 and L5 Unrelated to osteoporosis fracture, or mechanical stress on the spine
Synostosis (block vertebrae)[11]	4-6	Developmental failure of segmentation of vertebral somites with subsequent fusion of adjacent vertebral bodies Most common lumbar sites are T12-L1 and L4-L5 Often results in premature degenerative disease at adjacent vertebral levels owing to excessive intervertebral motion above and below the synostosis ***Imaging findings*** 1. Waistlike constriction at the level of the intervertebral disc 2. Completely absent or rudimentary disc space, with or without irregular calcification 3. Total height of the block vertebra is less than expected from the number of segments that are involved 4. Fusion (nonsegmentation) of the posterior elements (50% of cases) *Differential diagnosis:* surgical fusion or ankylosis from inflammatory arthropathy or infectious discitis
Lumbar ribs[4]	4-7	Anomalous supernumerary ribs articulating with the transverse processes of the first lumbar vertebra Normal variant or developmental anomaly of no clinical significance
Spina bifida occulta[6,12,141]	4-8	Extremely common developmental anomaly consisting of a midline defect within the neural arch resulting from failure of the two laminae to fuse centrally at the spinolaminar junction Radiolucent cleft, absent spinous process, or failure of fusion at the spinolaminar junction; most frequent at L5 and S1 Isolated anomaly, or occurring in conjunction with other entities, such as cleidocranial dysplasia or clasp-knife syndrome Strong cartilage and fibrous tissues fill the cleft; the anomaly generally is of no clinical consequence Spina bifida may infrequently be associated with meningocele or meningomyelocele, which represents protrusion of the meninges or spinal cord, or both; may result in severe neurologic abnormalities Higher prevalence of spondylolysis and spondylolisthesis is associated with L5 spina bifida occulta
Clasp-knife syndrome[13]	4-9	Spina bifida occulta of S1 and elongation of the L5 spinous process During trunk extension, the L5 spinous process may impinge on the spinal canal, irritating pain-sensitive structures

* See also Table 1-1.

Continued

TABLE 4-2 Some Developmental Anomalies, Anatomic Variants, and Sources of Diagnostic Error Affecting the Lumbar Spine—cont'd

Entity	Figure(s)	Figure(s)
Developmental spinal stenosis[2,4,7]	4-10; see Figure 4-17	Congenital narrowing or hypoplasia of the spinal canal Common finding in achondroplasia Developmental stenosis may be complicated in later life by other diseases, such as degenerative stenosis ***Lumbar spine radiographic measurements*** 1. *Eisenstein method for sagittal canal measurement:* Lower limits of normal 15 mm: suggests stenosis 12 mm: unequivocal evidence of stenosis 2. *Interpedicle method for coronal canal measurement:* Lower limits of normal 20 mm at any lumbar level: suggests stenosis Measurements of stenosis on routine radiographs may be misleading; cross-sectional CT or MR imaging and clinical correlation are necessary to fully evaluate patients with suspected stenosis 3. *CT or MR imaging:* Measurements of cross-sectional area more accurate than radiographic measurements
Hemivertebra[7,8]	4-11	Vertebral body originally develops from paired chondral centers; at a later stage, a single ossification focus forms; this focus then separates transiently by the notochordal remnant into anterior and posterior centers *Lateral hemivertebra* results from failure of development of one of the paired chondral centers *Lateral hemivertebra* might involve a normally occurring vertebra or it might be supernumerary; one pedicle may be normal or enlarged and its counterpart at the same level may be absent or hypoplastic; the incomplete segment may articulate with or be fused to the adjacent vertebrae Frequently results in congenital scoliosis and may be associated with segmentation anomalies *Dorsal and ventral hemivertebrae* are much less frequent than lateral hemivertebrae and result from agenesis of either the anterior or posterior portion of the growth center, respectively
Butterfly vertebra[8,9]		Incomplete fusion of the two lateral chondral centers of the vertebral body results in a central sagittal constriction of the vertebral body, which is seen on a frontal radiograph and is considered a variant of enchondral ossification Interpedicle distance of the butterfly vertebra may be widened, and the adjacent vertebrae usually remodel to conform to the shape of the butterfly vertebra
Facet tropism[2,4,7]	4-12	Asymmetric orientation of left and right lumbosacral facet joint of the same level Most common at L4-L5 and L5-S1 L1-L2 to L4-L5 facet joints usually are oriented predominantly in the sagittal plane; L5-S1 facet joints usually are oriented in the coronal plane; tropism is a variation in this orientation, usually visualized on frontal radiographs; cross-sectional imaging (CT or MR) best demonstrates exact orientation of the articular surfaces *Clinical significance is controversial:* Preponderance of evidence does not support a relationship between facet tropism and degenerative disc disease May result in pedicle sclerosis
Ununited ossification center of the articular process[2]	4-13	Failure of fusion of the secondary ossification center of the inferior articular process, also termed *Oppenheimer ossicle* *Most common sites:* L3 and L4 inferior articular processes Smooth, nondisplaced, well-corticated fragment involving lower aspect of articular process Usually asymptomatic and of no clinical significance *Differential diagnosis:* fracture

TABLE 4-2 Some Developmental Anomalies, Anatomic Variants, and Sources of Diagnostic Error Affecting the Lumbar Spine—cont'd

Figure(s)	Figure(s)	Figure(s)
Articular process agenesis[14]	4-14	Rare, stable anomaly that usually is asymptomatic and an incidental finding *Most common site:* L5 inferior articular process Nonossified, cartilaginous, or fibrous analogue is present *Differential diagnosis:* pathologic destruction
Transitional lumbosacral segment[15-17,207,208]	4-15	Several different patterns of anomalous lumbosacral segmentation are referred to as "transitional vertebrae" and often are associated with other anomalies, such as spina bifida and neural arch defects; present in 5% to 8% of the population *Three typical patterns:* 1. Bilateral symmetric assimilation of the fifth lumbar and first sacral segments (sacralization), resulting in four mobile lumbar type vertebrae and elongation of the vertical height of the sacrum; assimilation can include complete osseous synostosis or incomplete synostosis in which a hyperplastic (spatulated) L5 transverse process forms an articulation with the sacral ala and may articulate with the ilium, forming the superior portion of the sacroiliac joint; lumbosacral disc space is decreased in height or absent 2. Bilateral symmetric segmentation of the first and second sacral segments (lumbarization), resulting in six mobile lumbar type of vertebrae and a decreased vertical height of the sacrum; the lowest mobile vertebra may resemble a normally formed lumbar vertebra with either a completely formed or rudimentary disc articulating with the sacrum 3. Unilateral or bilateral asymmetric variations of assimilation or nonsegmentation; a spatulated transverse process of the lowest lumbar vertebra may articulate with the sacral ala; this tendency toward assimilation may eventually lead to complete synostosis with the sacrum; sclerosis of the articulating surfaces might reflect uneven distribution of mechanical stress The iliolumbar ligament, readily identifiable on axial lumbar MR images, always arises from the L5 transverse process and can be used to confidently assign lumbar levels *Literature on the relationship of transitional vertebrae to signs and symptoms is confusing and sometimes contradictory:* Disproportionate degenerative changes often are encountered at articulations of transitional segments Patients with six lumbar type vertebrae appear to be predisposed to disc protrusions[4] Sclerosis of articulating surfaces may be associated with pain and tenderness over the anomaly[4] Weight gain, trauma, and even pregnancy may exacerbate symptoms[4] Patients with spondylolisthesis and four lumbar type vertebrae have greater slippage of their spondylolisthesis than patients with five lumbar type vertebrae[16] Other reviews have found no relationship between transitional vertebrae and back pain[17]
Diastematomyelia[18]	4-16	Congenital longitudinal diastasis of the thoracic or lumbar spinal canal and spinal cord with increased interpedicle distance Present in 15% of all patients with congenital scoliosis; two thirds of patients with diastematomyelia have scoliosis Often associated with other vertebral anomalies, short angular kyphosis, and tethering of the spinal cord Female : male, 2 : 1 50% to 75% of persons have a septum (ossified or unossified) dividing the cord Plain film radiography often is inadequate to recognize a septum even when it is present, and MR imaging or CT with or without myelographic contrast is indicated when this condition is suspected

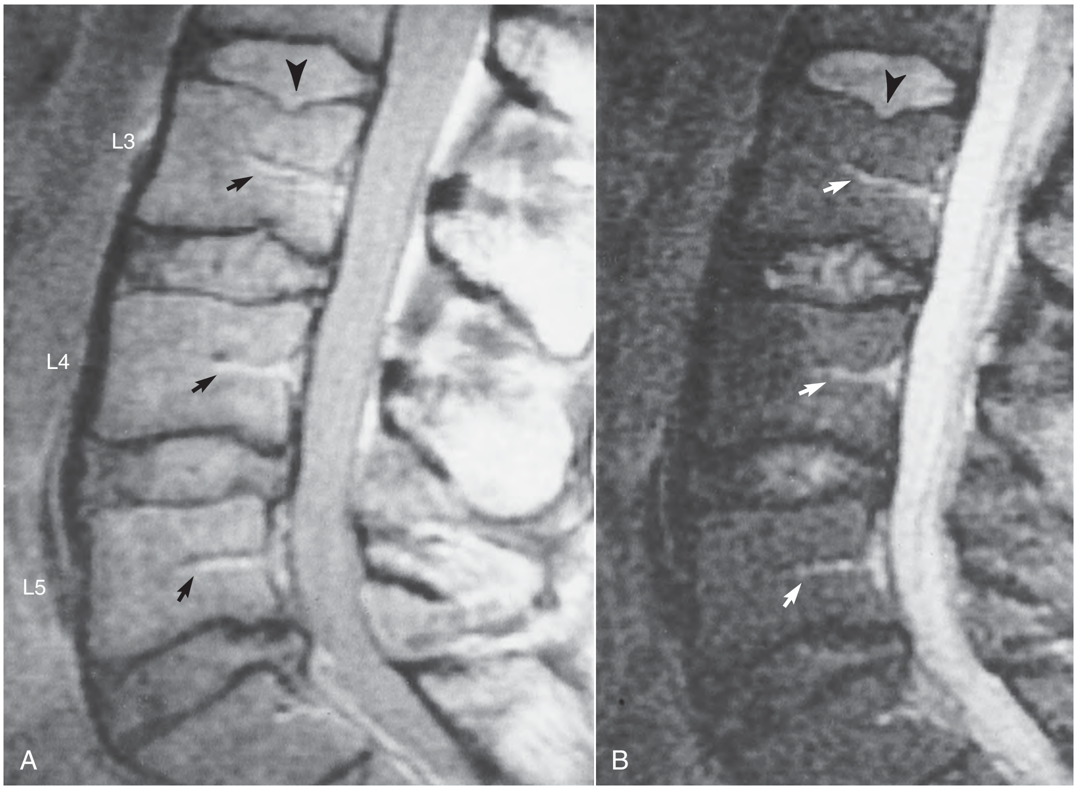

FIGURE 4–3 **Hahn venous channels: magnetic resonance (MR) imaging.**[4] Normal high signal intensity horizontal fissures *(arrows)* are seen within several vertebral bodies on proton density-weighted **(A)** and T2-weighted **(B)** sagittal spin echo MR images. These channels represent perforations for the vertebral veins and communicate posteriorly with the epidural venous plexus; therefore, they should not be misinterpreted as fractures. **A,** Schmorl node is present in the L3 superior endplate *(arrowheads)*.

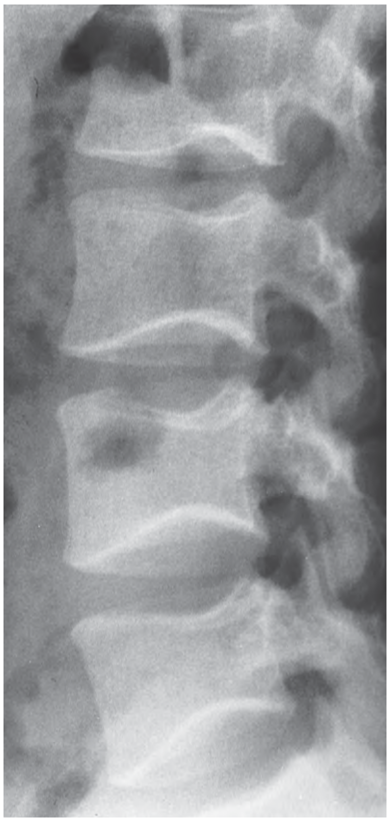

FIGURE 4–4 **Nuclear impressions.**[5,10] Lateral lumbar radiograph from this 26-year-old man demonstrates prominent, broad-based, curvilinear depressions of the vertebral endplates. These nuclear impressions, usually more prominent at the inferior endplate, represent a normal variation of vertebral contour and should not be confused with fracture, Schmorl nodes, or pathologic destruction.

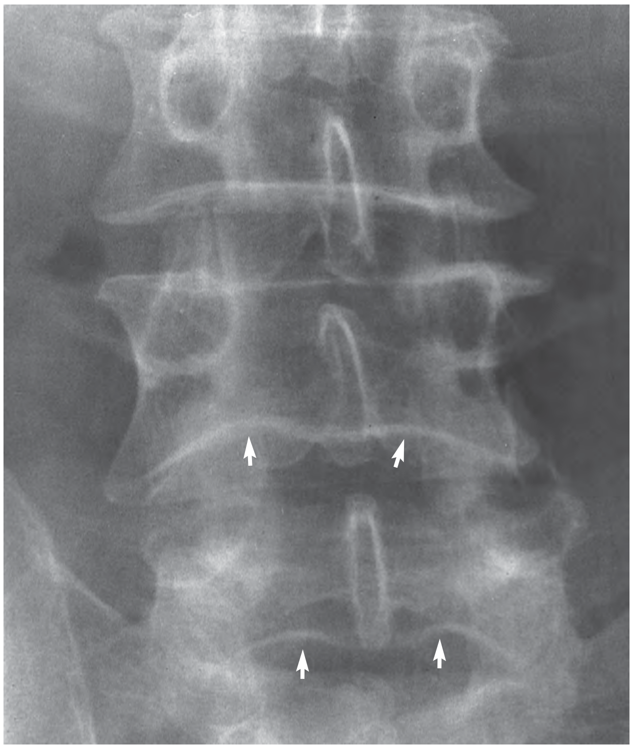

FIGURE 4–5 Cupid bow contour.[10] Frontal radiograph reveals normal paramedian curvilinear impressions of the inferior endplates of the L4 and L5 vertebral bodies (*arrows)*.

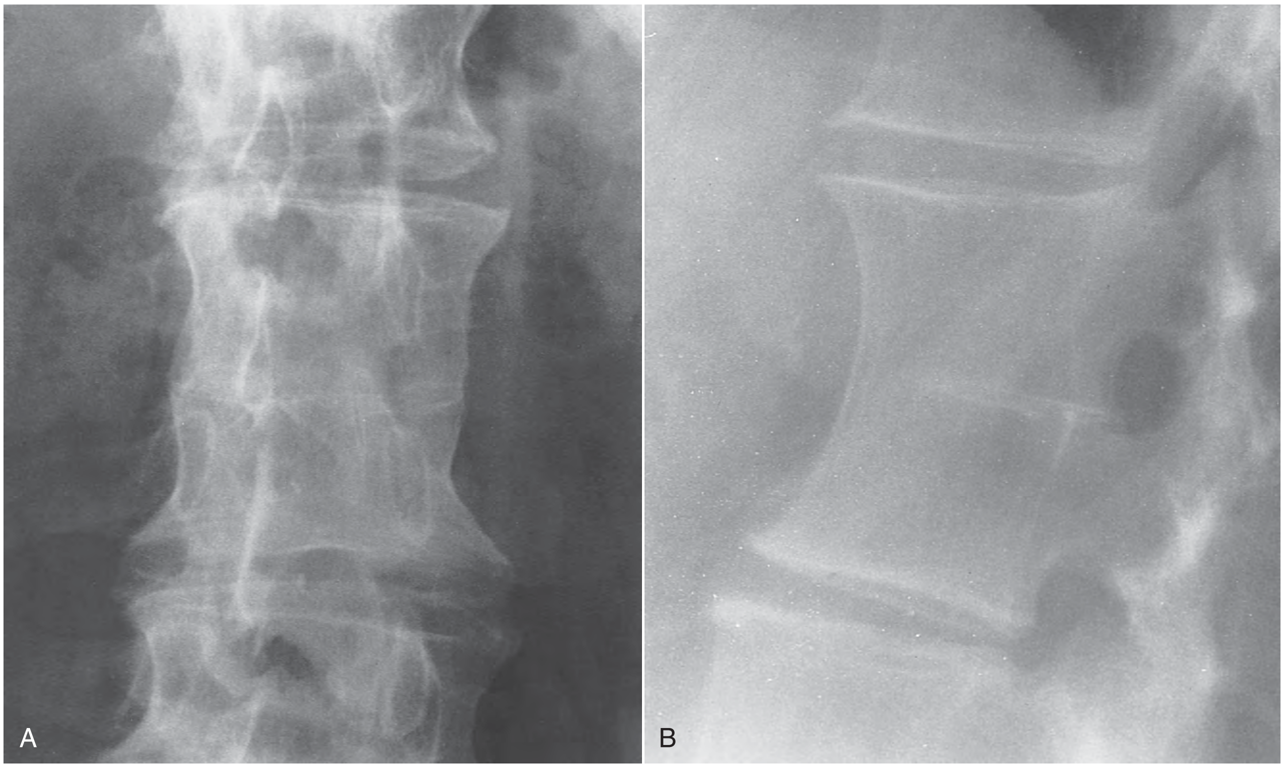

FIGURE 4–6 Developmental synostosis (block vertebrae).[11] Frontal **(A)** and lateral **(B)** radiographs demonstrate failure of segmentation of two contiguous vertebral segments. The intervening rudimentary intervertebral disc is calcified. The central portion of the vertebrae are hypoplastic (wasp-waist constriction). The degenerative intervertebral disc space narrowing and osteophyte formation, seen at adjacent levels, are frequent complications of block vertebrae. This degeneration occurs secondary to compensatory excessive motion at segments adjacent to block vertebrae.

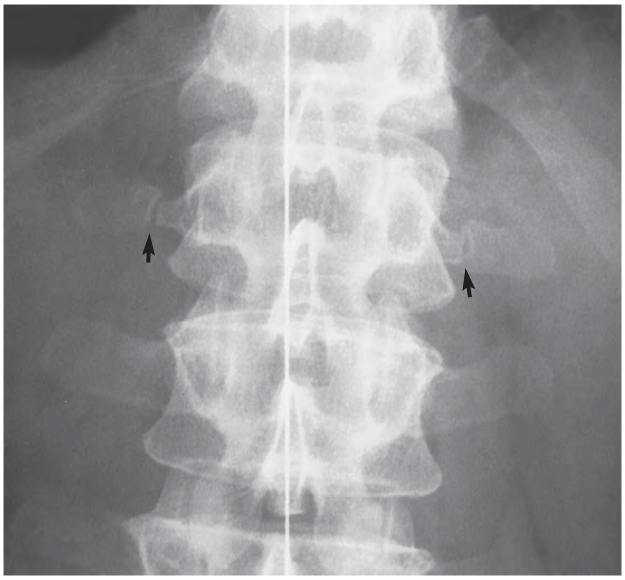

FIGURE 4–7 **Lumbar ribs.**[4] Small, hypoplastic transverse processes of L1 articulate with rudimentary anomalous ribs (*arrows*). This anomaly usually is an incidental finding of no clinical significance.

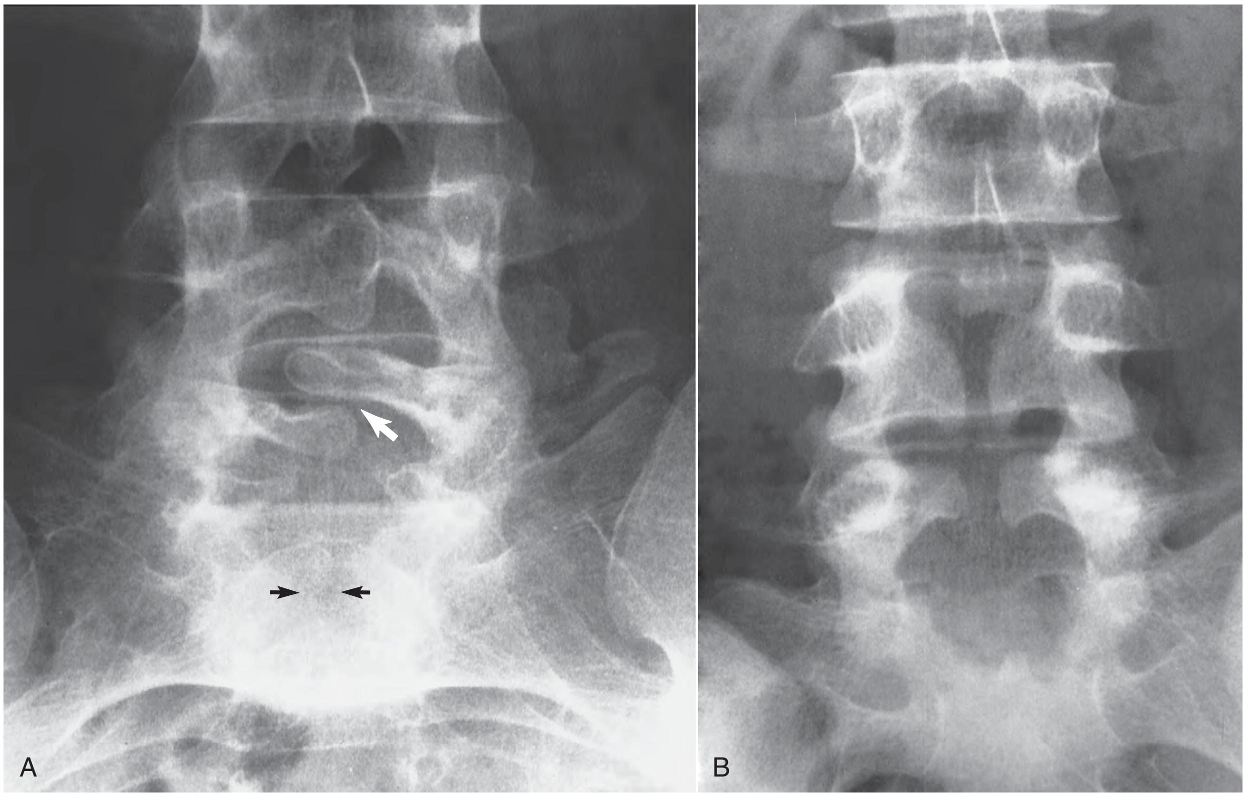

FIGURE 4–8 **Spina bifida occulta.**[6,12,141] **A,** In this 26-year-old man with a grade I spondylolytic spondylolisthesis, nonunion of the anomalous L5 laminae, seen as a radiolucent defect *(white arrow),* results in incomplete development of the spinous process. A small midline defect also is present at S1 *(black arrows),* representing another site of spina bifida occulta. **B,** In another patient, midline radiolucent defects represent incomplete formation of the spinous processes of L4 and L5 as well as the first sacral tubercle.

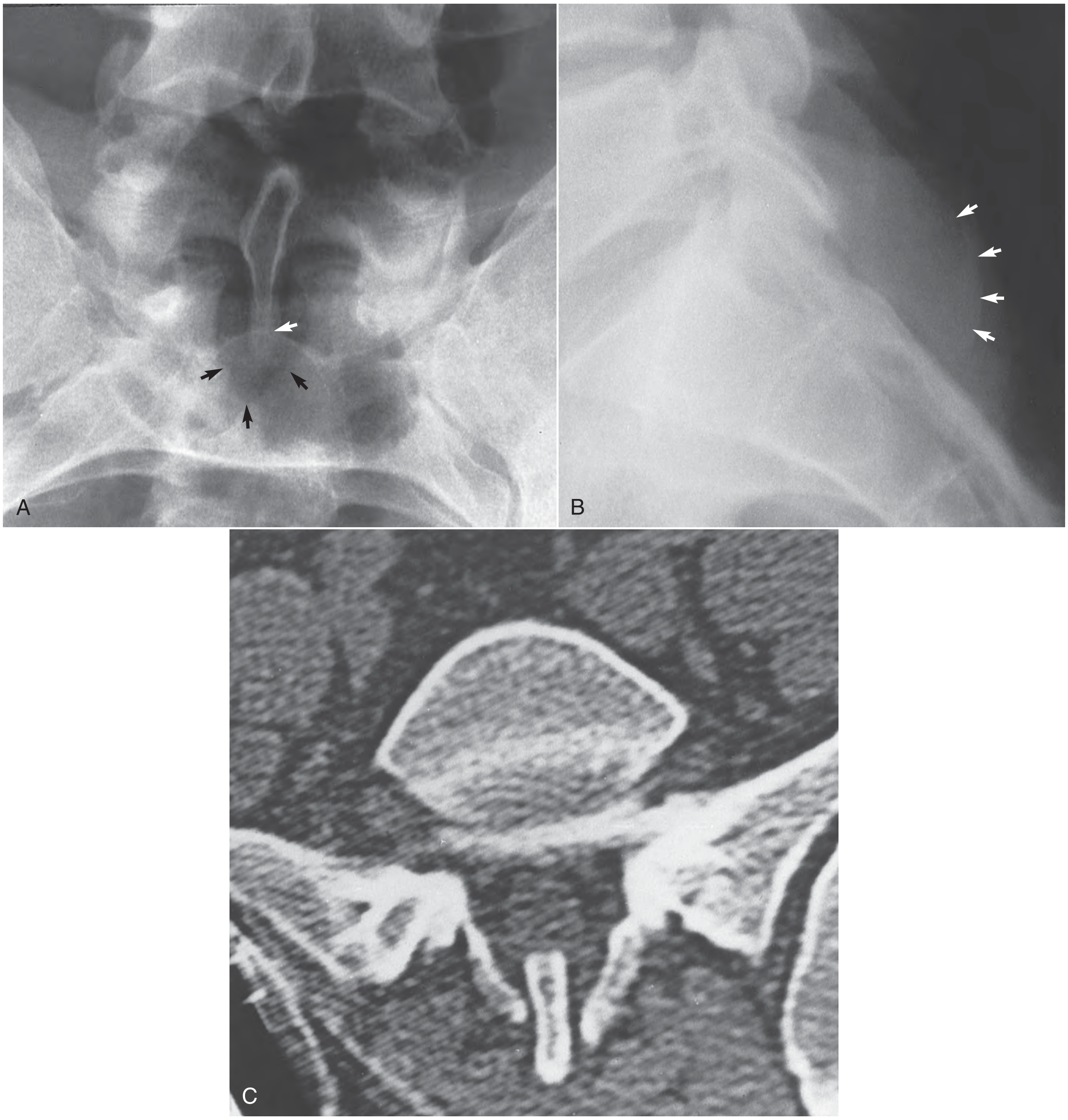

FIGURE 4–9 **Clasp-knife deformity.**[13] Frontal **(A)** and lateral **(B)** radiographs of the lumbar spine in a manual laborer with back pain exacerbated by trunk extension. Clasp-knife deformity involves inferior sloping and elongation of the L5 spinous process *(white arrows)* in conjunction with spina bifida occulta of S1 *(black arrows)*. A transaxial CT scan **(C)** obtained during trunk extension in another patient shows the L5 spinous process penetrating the S1 spina bifida and contacting the thecal sac. During extension, the L5 spinous process may impinge on the spinal canal, irritating pain-sensitive structures.

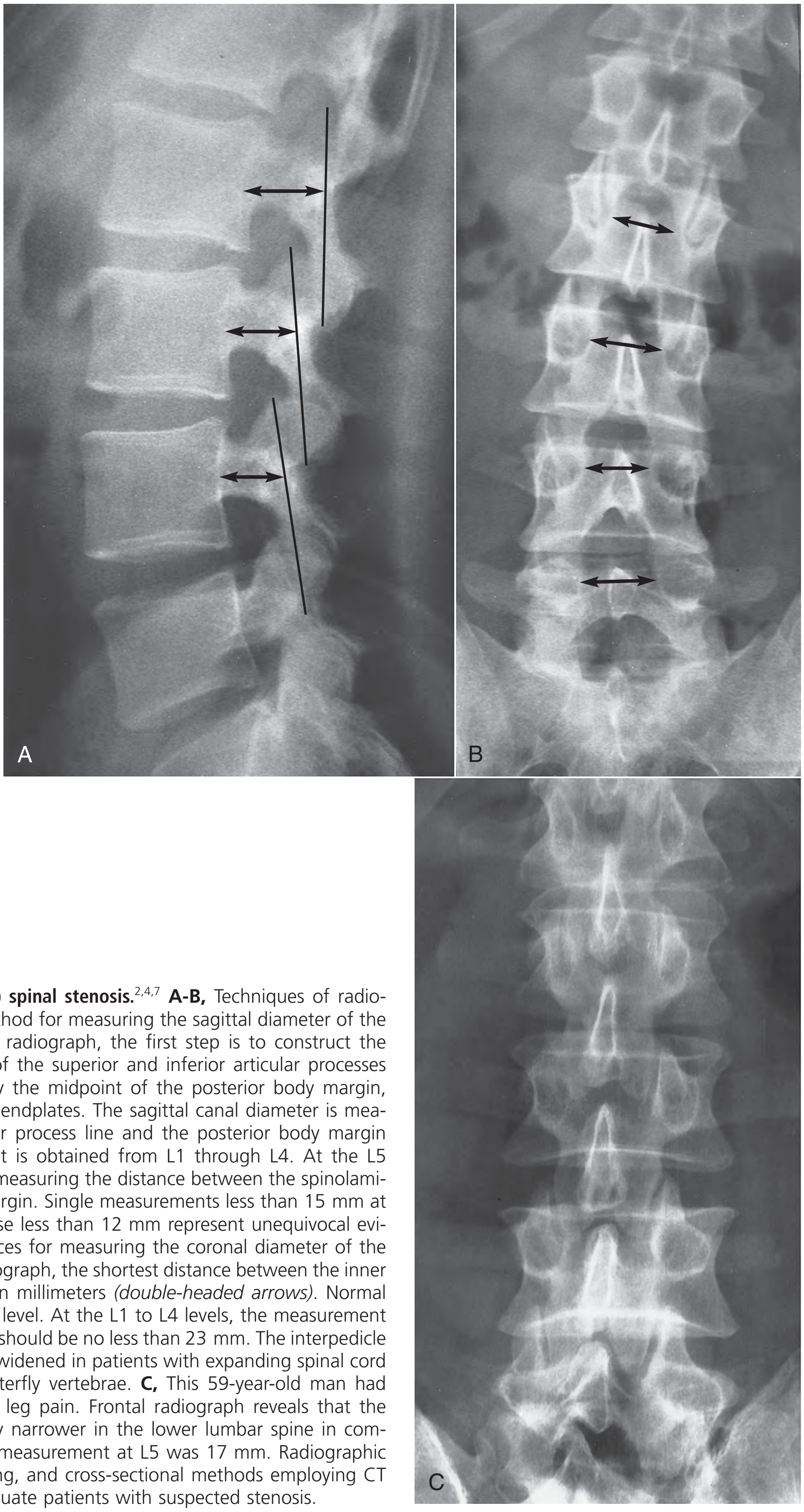

FIGURE 4–10 **Developmental (congenital) spinal stenosis.**[2,4,7] **A-B,** Techniques of radiographic measurement.[7] In **A,** Eisenstein method for measuring the sagittal diameter of the spinal canal is demonstrated. On a lateral radiograph, the first step is to construct the articular process line connecting the tips of the superior and inferior articular processes *(straight lines)*. The next step is to identify the midpoint of the posterior body margin, midway between the superior and inferior endplates. The sagittal canal diameter is measured (in millimeters) between the articular process line and the posterior body margin (*double-headed arrows)*. This measurement is obtained from L1 through L4. At the L5 segment, the measurement is obtained by measuring the distance between the spinolaminar junction line and the posterior body margin. Single measurements less than 15 mm at any lumbar level suggest stenosis, and those less than 12 mm represent unequivocal evidence of stenosis. In **B,** interpedicle distances for measuring the coronal diameter of the spinal canal are described. On a frontal radiograph, the shortest distance between the inner surfaces of the two pedicles is measured in millimeters *(double-headed arrows)*. Normal measurements vary according to the spinal level. At the L1 to L4 levels, the measurement should be no less than 21 mm, and at L5, it should be no less than 23 mm. The interpedicle distance is narrowed in spinal stenosis and widened in patients with expanding spinal cord tumors as well as burst fractures and butterfly vertebrae. **C,** This 59-year-old man had long-standing low back pain and bilateral leg pain. Frontal radiograph reveals that the interpedicle distances become progressively narrower in the lower lumbar spine in comparison with the upper lumbar spine. The measurement at L5 was 17 mm. Radiographic measurements of stenosis can be misleading, and cross-sectional methods employing CT or MR imaging should be used to fully evaluate patients with suspected stenosis.

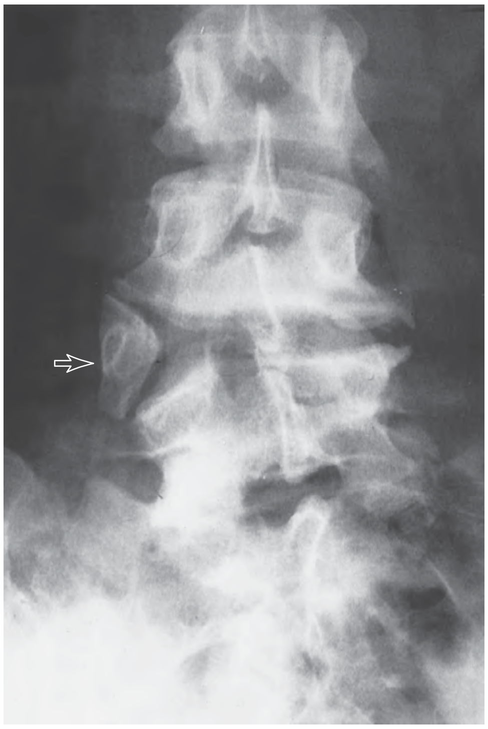

FIGURE 4–11 Lateral hemivertebra.[7,8] An incomplete, triangular vertebral body and corresponding pedicle is incorporated *(open arrow)* within the L4-L5 intervertebral disc space. Compensatory remodeling of the adjacent vertebral bodies and asymmetric degenerative disc disease also are seen at this level. Hemivertebrae frequently result in congenital scoliosis.

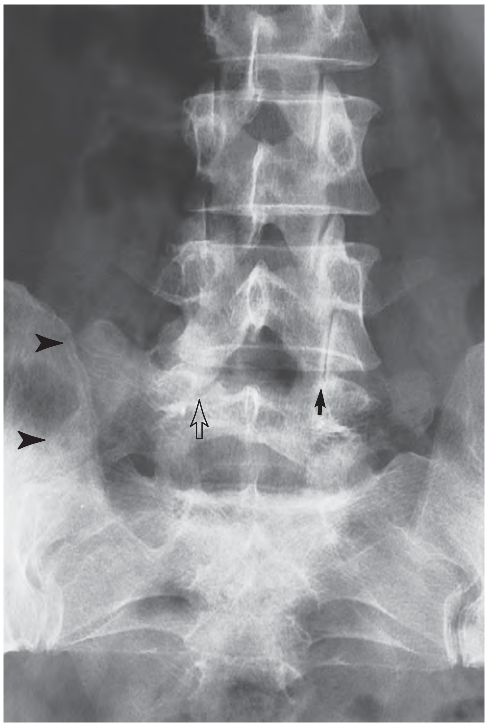

FIGURE 4–12 Facet tropism.[2,4,7] Observe the asymmetry of the lumbosacral apophyseal joint orientation: The left apophyseal joint is oriented in the sagittal plane *(solid arrow),* and the right apophyseal joint is oriented predominantly in the coronal plane *(open arrow)*. CT or MR imaging is necessary to determine the precise facet joint orientation, but such sophisticated techniques usually are not warranted. Note also that the right transverse process of the lowest lumbar type of vertebra is spatulated *(arrowheads)* and appears to articulate with the sacral ala. The lumbosacral region is a common site for multiple developmental anomalies. *(Courtesy F.G. Bauer, DC, Sydney, New South Wales, Australia.)*

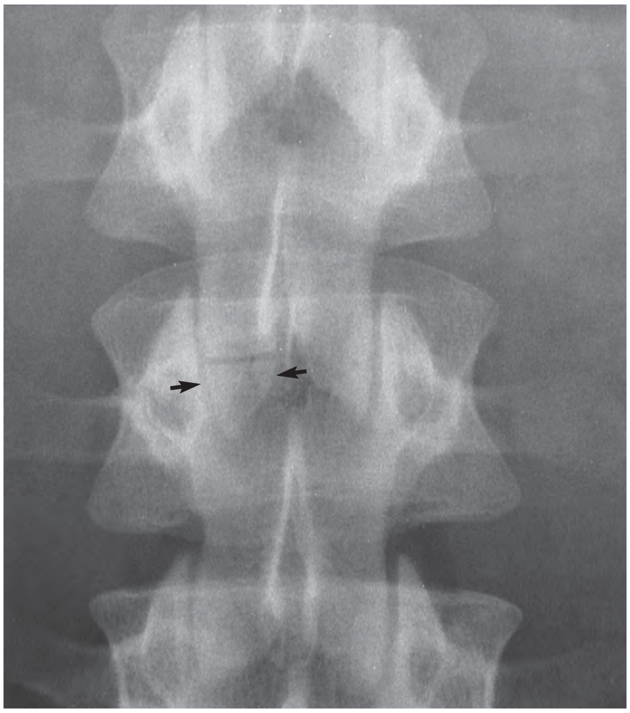

FIGURE 4–13 Ununited secondary ossification center of the articular process.[2] Failure of union of the secondary ossification center of the inferior articular process *(arrows)* is seen most frequently at L3 and L4 and has been referred to as *Oppenheimer ossicle*. This anomaly must be differentiated from a fracture.

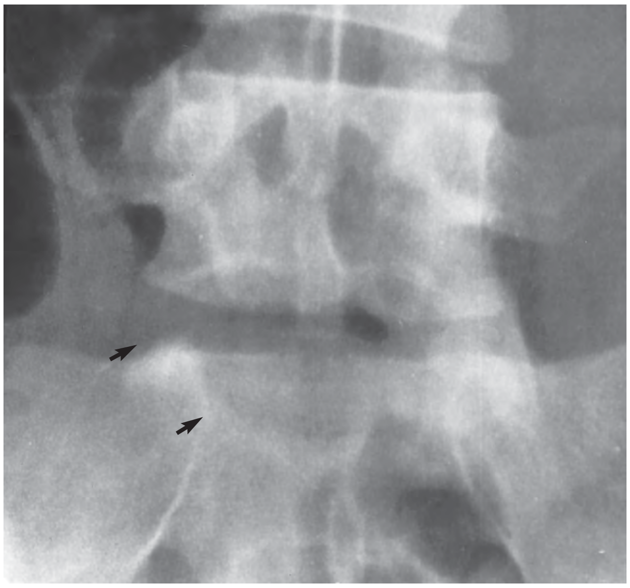

FIGURE 4–14 Agenesis of lumbosacral articular process.[14] Observe the absence of the right inferior articular process of L5 *(arrows)*. In this rare, stable, and often asymptomatic anomaly, a nonossified, cartilaginous, or fibrous analogue is present. This anomaly frequently is identified as an incidental finding, but it may resemble pathologic destruction such as that seen in skeletal metastasis. *(From Mitchell R: Congenital absence of a lumbosacral facet. Top Diagn Radiol Adv Imaging 1:3, 1993.)*

FIGURE 4–15 Transitional lumbosacral segment.[15-17,194,195] **A,** Frontal radiograph demonstrates a large, spatulated left L5 transverse process that articulates with the sacral ala *(arrow)*. **B,** In a second patient, both L5 transverse processes are enlarged and spatulated and articulate with the sacral alae. On the lateral lumbar spine radiograph (not shown), only four movable lumbar type of vertebrae were present, a condition termed *sacralization*. **C,** Observe the asymmetric growth of the transitional segment on this angulated radiograph. The left transverse process of the fifth lumbar vertebra is spatulated and forms an anomalous articulation with the first sacral segment and ilium, creating a portion of the sacroiliac joint *(arrows)*. The right L5 transverse process is of normal size *(arrowhead)* and does not articulate with the sacrum or ilium.

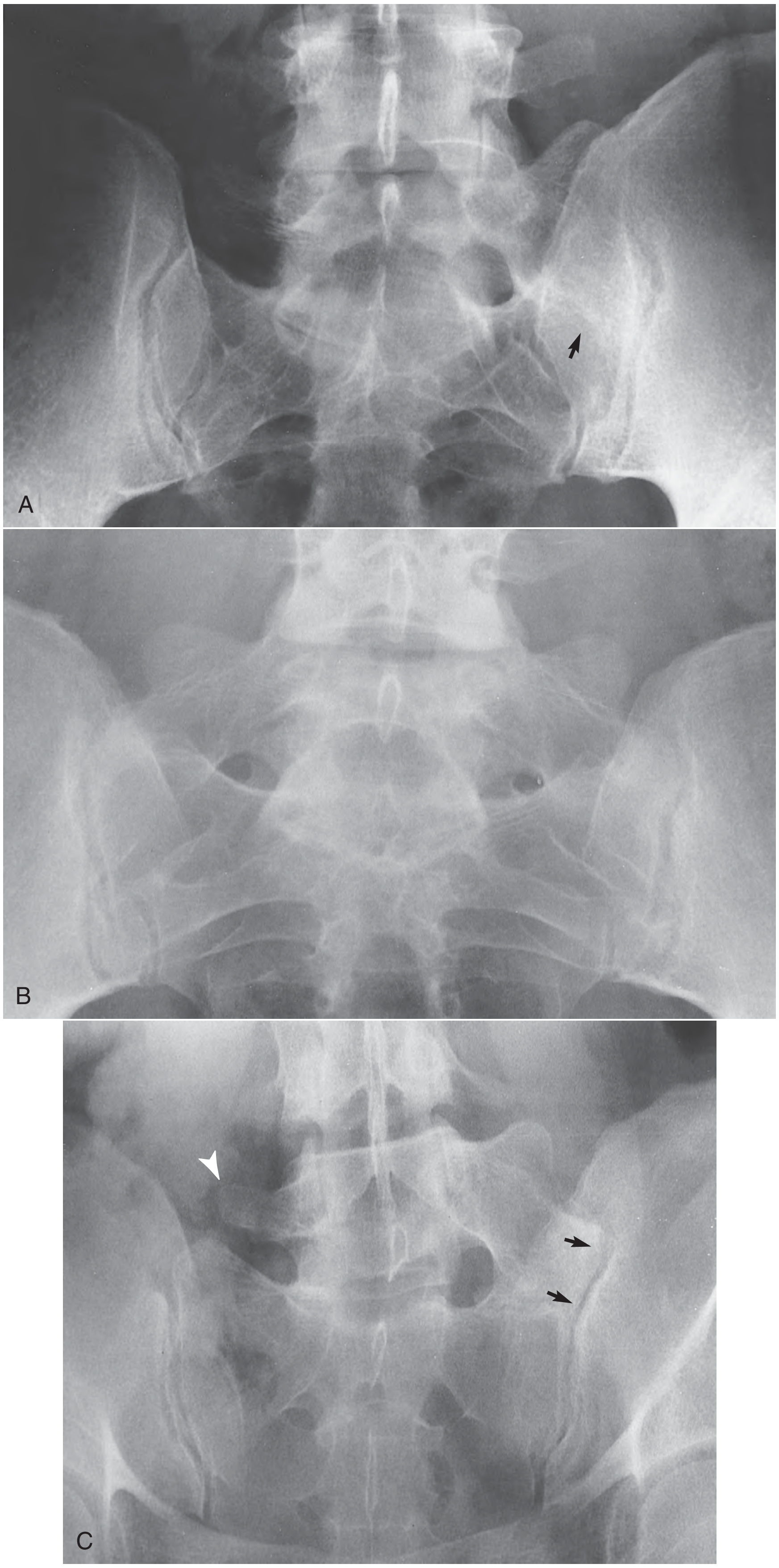

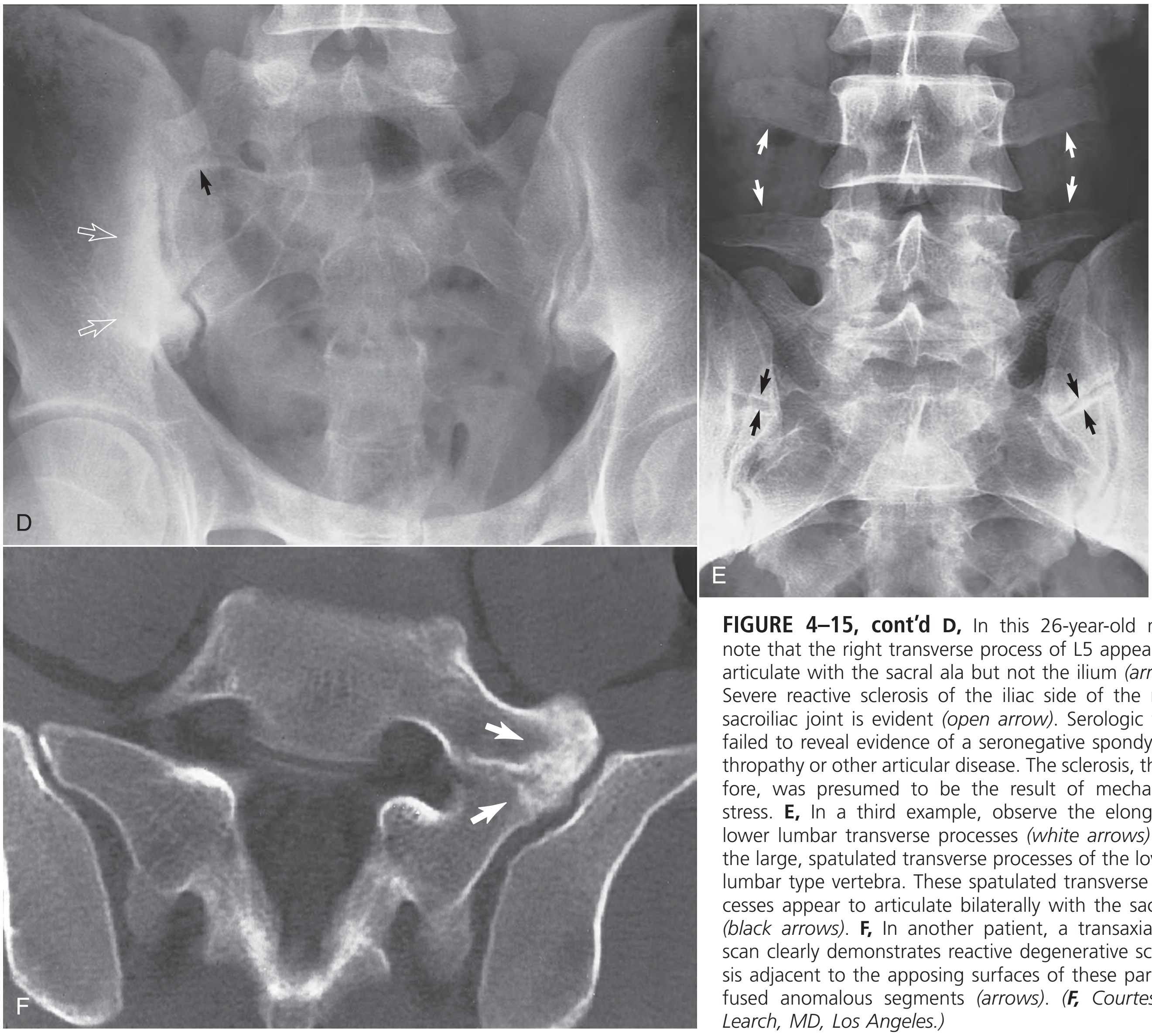

FIGURE 4–15, cont'd D, In this 26-year-old man, note that the right transverse process of L5 appears to articulate with the sacral ala but not the ilium *(arrow)*. Severe reactive sclerosis of the iliac side of the right sacroiliac joint is evident *(open arrow)*. Serologic tests failed to reveal evidence of a seronegative spondyloarthropathy or other articular disease. The sclerosis, therefore, was presumed to be the result of mechanical stress. **E,** In a third example, observe the elongated lower lumbar transverse processes *(white arrows)* and the large, spatulated transverse processes of the lowest lumbar type vertebra. These spatulated transverse processes appear to articulate bilaterally with the sacrum *(black arrows)*. **F,** In another patient, a transaxial CT scan clearly demonstrates reactive degenerative sclerosis adjacent to the apposing surfaces of these partially fused anomalous segments *(arrows)*. *(**F,** Courtesy T. Learch, MD, Los Angeles.)*

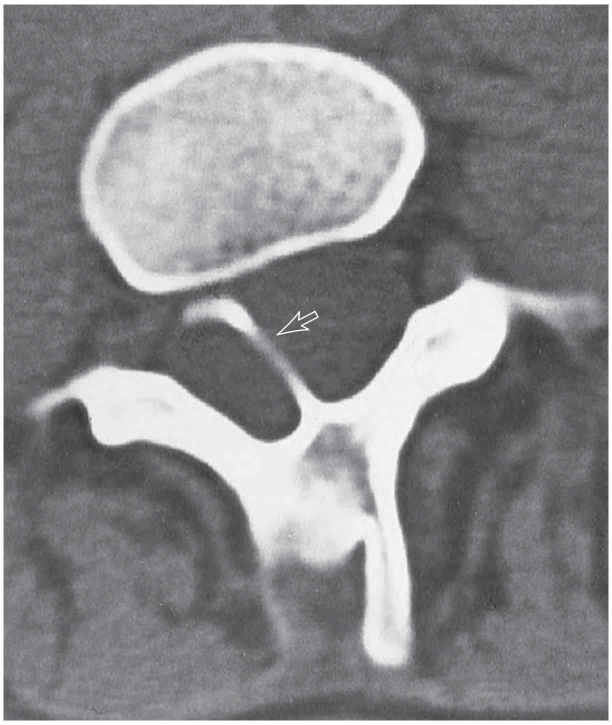

FIGURE 4–16 Diastematomyelia: CT scan.[18] A sagittally oriented vertical osseous bar *(open arrow)* divides the L3 thecal sac in this 22-year-old woman. Plain film radiography often is inadequate in the demonstration of this osseous or fibrous septum even when it is present. MR imaging or CT scanning with or without myelographic contrast is indicated when this condition is suspected. *(Courtesy B.L. Harger, DC, Portland, Oregon.)*

TABLE 4-3 Skeletal Dysplasias and Other Congenital Disorders Affecting the Lumbar Spine*

Entity	Figure(s), Table(s)	Characteristics
Achondroplasia[19]	4-17	***Imaging findings*** Spinal stenosis Thoracolumbar bullet vertebrae Posterior scalloping and flattening of vertebral bodies
Spondyloepiphyseal dysplasia congenita[20]		Platyspondyly and the "pear-shaped" vertebral body appearance
Mucopolysaccharidoses (MPS)[21,22]	4-18	*Two types most frequently affect the lumbar spine:* ***MPS I-H (Hurler syndrome)*** Thoracolumbar gibbous deformity and posterior scalloping of vertebral bodies Rounded anterior vertebral body margins with inferior breaking ***MPS IV (Morquio syndrome)*** Platyspondyly Posterior vertebral body scalloping and kyphoscoliosis
Osteopetrosis[23,24,157]	4-19; see Figure 4-31	*Patterns of osteosclerosis:* diffuse osteosclerosis; "bone-within-bone" appearance, "sandwich vertebrae" Bones are brittle and fracture easily
Osteopoikilosis[25,26]	4-20	Asymptomatic sclerosing dysplasia Multiple 2- to 3-mm circular foci of osteosclerosis Infrequently affects the spine; lumbar spinal stenosis has been reported as a rare complication of this dysplasia
Marfan syndrome[27,28]	4-21; see Figure 4-39 Table 4-4	Kyphoscoliosis in as many as 65% of persons Posterior vertebral body scalloping secondary to dural ectasia Tall, elongated vertebral bodies with exaggerated biconcavity; long transverse processes; 18% of patients have a lumbosacral transitional vertebra
Ehlers-Danlos syndrome[29]	4-22 Table 4-4	Posterior scalloping of vertebral bodies Platyspondyly and kyphoscoliosis
Osteogenesis imperfecta[30]		Osteoporosis and bone fragility Multiple compression fractures and severe kyphoscoliosis common
Chondrodysplasia punctata[31]	4-23	Stippled calcification of vertebral bodies Coronal clefts may be present within the vertebral bodies in the rhizomelic form
Diastrophic dysplasia[32]	4-24	Short stature, progressive scoliosis, kyphosis, and other abnormalities

* See also Table 1-2.

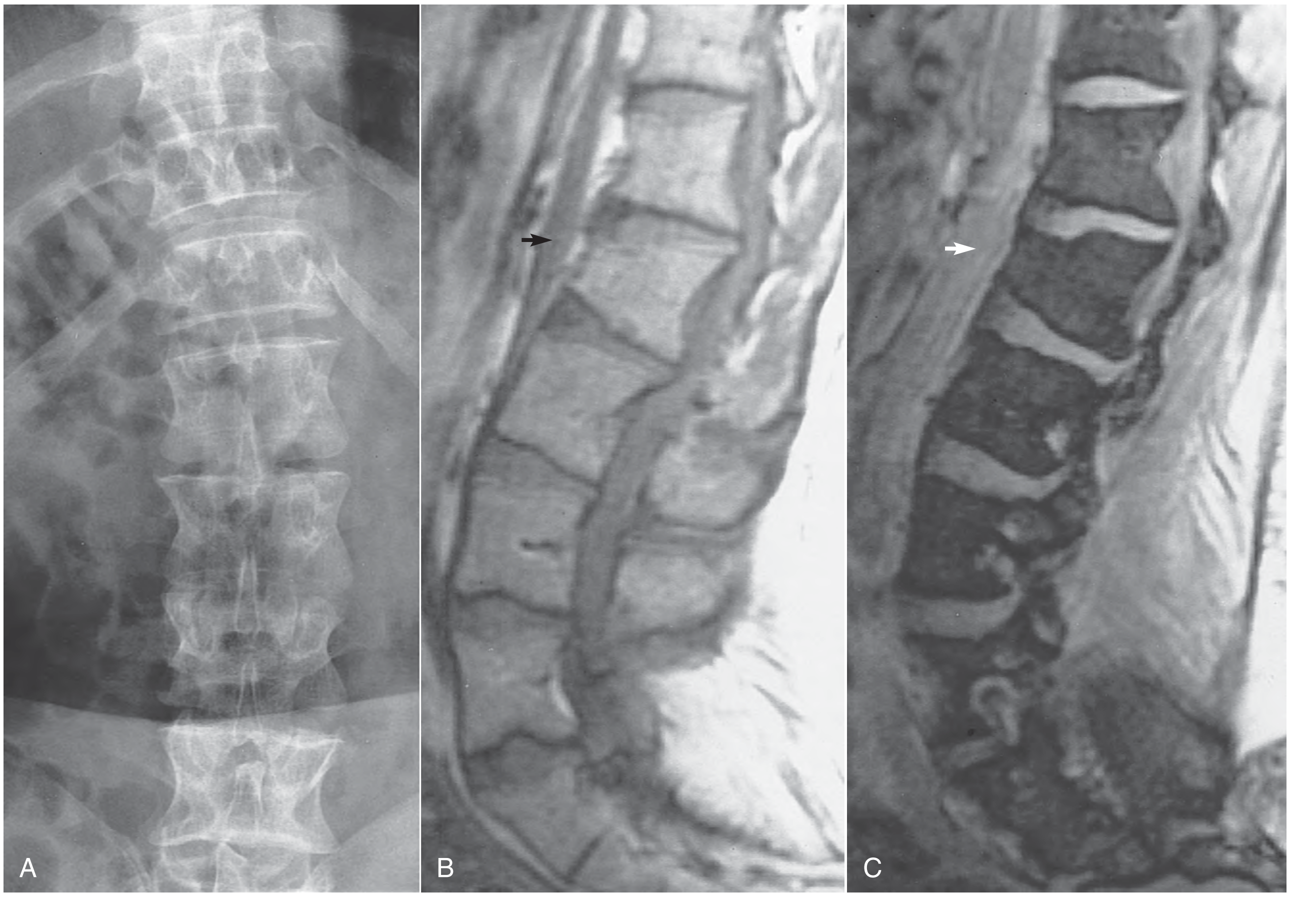

FIGURE 4–17 **Achondroplasia.**[19] Routine frontal radiograph **(A)** from this patient with heterozygous achondroplasia shows progressive narrowing of the lower lumbar interpedicle distances. Parasagittal T1-weighted (TR/TE, 600/20) spin echo **(B)** and multiplanar gradient recalled (MPGR) (TR/TE, 400/15; flip angle, 20 degrees) **(C)** MR images reveal severe central stenosis, scalloping of the posterior vertebral body margins, and a bullet-shaped thoracolumbar vertebra (*arrow*).

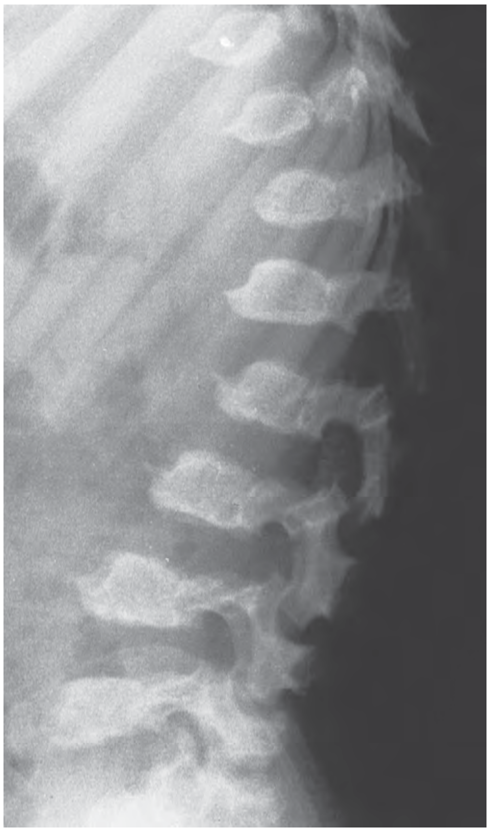

FIGURE 4–18 **Morquio syndrome (mucopolysaccharidosis [MPS] IV).**[21,22] This child with MPS IV has short stature and a thoracolumbar kyphoscoliosis. The central, tonguelike, anterior beaking and rounding of the vertebral bodies are typically seen in young patients with this syndrome. In adults, the vertebrae usually appear flat and rectangular, with irregular margins.

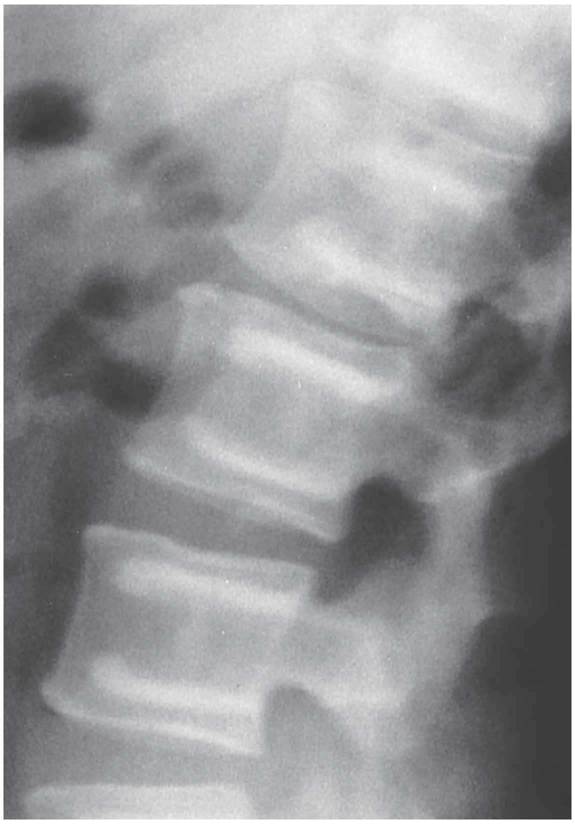

FIGURE 4–19 **Osteopetrosis tarda.**[23,24,147] The peculiar pattern of sclerosis observed in this patient is termed the *bone-within-bone appearance* because it resembles smaller vertebral bodies within normal vertebral bodies. The radiographic pattern of osteopetrosis in the spine may also be that of diffuse sclerosis, or it may be manifest as horizontal bands of sclerosis adjacent to the vertebral endplates ("sandwich vertebrae"). *(Courtesy R.B. Phillips, DC, Pocatello, Idaho.)*

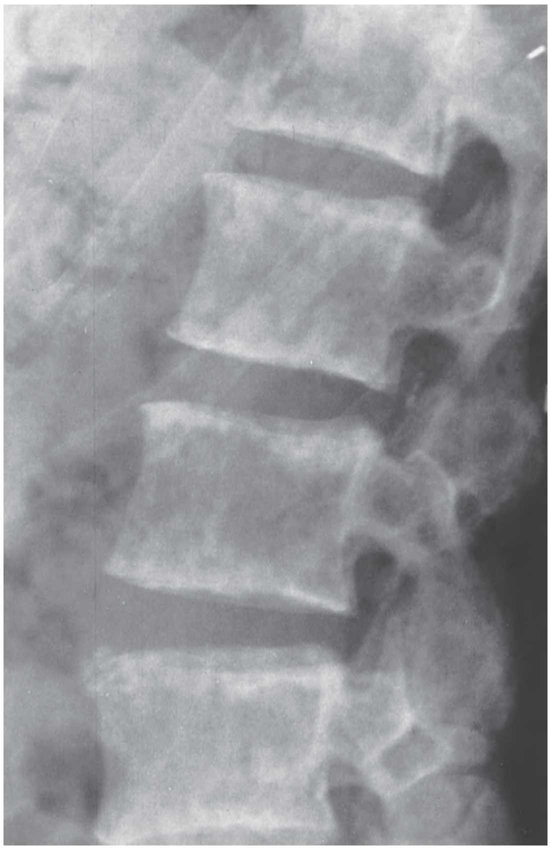

FIGURE 4–20 **Osteopoikilosis.**[25,26] Note the symmetric, circular, and ovoid osteosclerotic foci within the vertebral bodies and posterior elements. This sclerosing dysplasia is asymptomatic and of no clinical significance.

TABLE 4-4 Some Causes of Scalloped Vertebrae*

Posterior Vertebral Body Scalloping	Congenital disorders
Increased intraspinal pressure	Achondroplasia (Figure 4-17)
Intradural neoplasms	Morquio disease (Figure 4-18)
Intraspinal cysts	Hurler syndrome
Syringomyelia and hydromyelia	Physiologic scalloping (Figures 4-2, *B-D*)
Communicating hydrocephalus	**Anterior vertebral body scalloping**
Dural ectasia	Lymphoma (Figure 4-92, *C*)
Marfan syndrome (Figure 4-21)	Abdominal aortic aneurysm (Figure 4-123, *D*)
Ehlers-Danlos syndrome (Figure 4-22)	Lymphadenopathy
Neurofibromatosis (Figure 4-91)	Tuberculosis
Bone resorption	
Acromegaly	

* Adapted from Mitchell GE, Lourie H, Berne AS: The various causes of scalloped vertebrae with notes on their pathogenesis. Radiology 89:67, 1967.

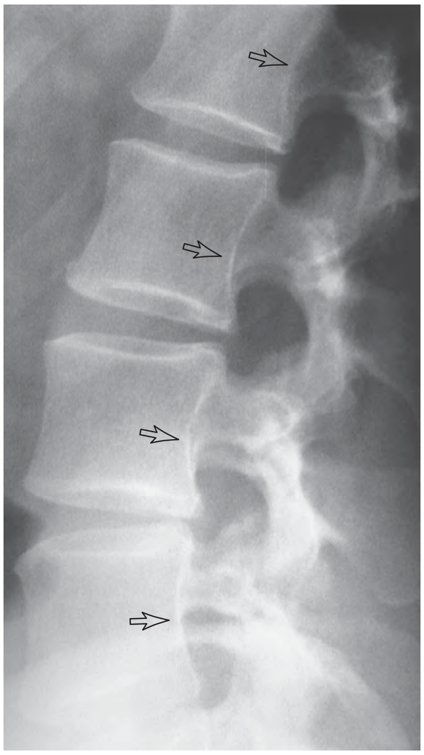

FIGURE 4–21 **Marfan syndrome.**[27,28] In this 39-year-old man with Marfan syndrome, posterior scalloping secondary to dural ectasia *(open arrows)* is evident in the tall and slender vertebral bodies.

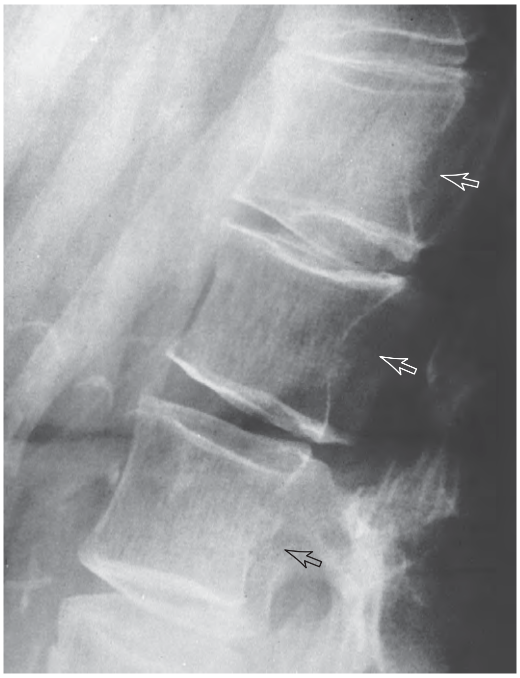

FIGURE 4–22 **Ehlers-Danlos syndrome.**[29] Lateral view of the lumbar spine reveals prominent scalloping of the posterior vertebral bodies *(open arrows)*. Platyspondyly and thoracolumbar scoliosis (not evident in this patient) also may be seen in patients with Ehlers-Danlos syndrome.

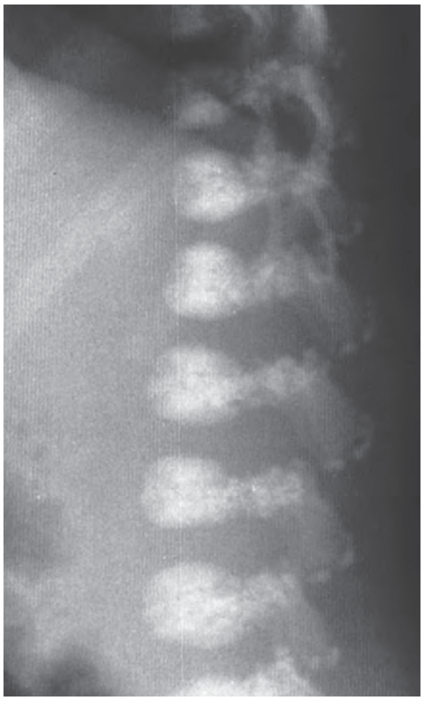

FIGURE 4–23 **Chondrodysplasia punctata.**[31] In this 2-day-old infant, the radiograph shows the characteristic stippled calcification of the lumbar vertebral bodies and neural arches.

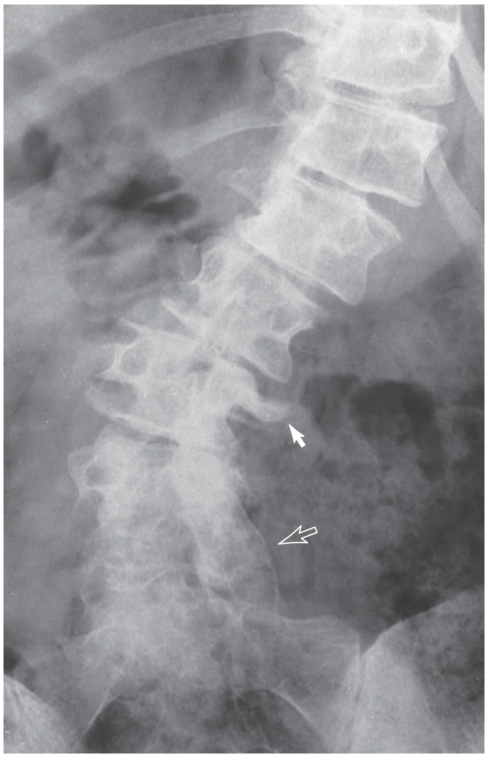

FIGURE 4–24 **Diastrophic dysplasia.**[32] A lumbar scoliosis is seen in this adult patient with diastrophic dysplasia. Observe the large degenerative osteophyte at the L2-L3 level *(solid arrow)*. A lumbar laminectomy and spinal fusion also have been performed *(open arrow)*.

TABLE 4-5 Spondylolysis and Spondylolisthesis

Entity	Type*	Figure(s)	Characteristics
Dysplastic spondylolisthesis[7,33,176,177]	I	4-25	Developmental anomaly of the neural arch of L4 or L5 or of the sacrum, resulting in anterior displacement of the L4 or L5 segment Rare cause of spondylolisthesis
Spondylolytic (isthmic) spondylolisthesis[7,34-36,169,176,177]	IIA	4-26, 4-27, 4-28	Fatigue (stress) fracture of the pars interarticularis (spondylolysis) with anterior vertebral body displacement (spondylolisthesis) Most common form of spondylolisthesis in persons under the age of 50 years 90% of spondylolyses occur at L5, followed in frequency by L4 and L3 Spondylolysis present in approximately 7% of Caucasians and as many as 16% of athletes Most progression of displacement usually occurs by age 10 years, with progression almost never occurring after age 18 years Instability uncommon: measured by functional radiography—flexion-extension and compression-traction radiographs As many as 50% of patients with spondylolysis or spondylolisthesis remain asymptomatic; patients with translation (instability) on functional radiographs have a higher prevalence of associated pain than those without translation; in patients without translation on functional radiographs, no relationship exists between pain and the amount of slippage Differentiation from acute isthmic fracture (type II C) requires clinical history, single photon emission computed tomographic (SPECT) imaging, or MR imaging
Spondylolisthesis from elongated intact pars interarticularis[7,33,176,177]	II B		Elongation of an intact pars interarticularis is extremely rare Believed to result from repetitive minor trabecular stress fractures of the pars interarticularis with consequent healing, sclerosis, hypertrophy, and elongation of this structure With progressive displacement, the pars interarticularis may fracture and separate becoming a type II A spondylolytic spondylolisthesis
Acute spondylolysis[37,38,176,177]	II C	4-29	Acute fracture of the pars interarticularis is an extremely rare cause of spondylolysis and spondylolisthesis Hyperextension injuries are believed to be the most common cause of acute pars interarticularis fracture in young athletes Associated with disabling low back pain Acute fractures are seldom bilateral and symmetric, the fracture margins are not well corticated, and progression of spondylolisthesis is rare Diagnosed by identifying increased radiopharmaceutical uptake on SPECT imaging or bone marrow edema on MR imaging; such positive SPECT and MR imaging findings correlate well with acute pain Most authorities recommend immobilization in a back brace for the management of this acute form of fracture
Degenerative spondylolisthesis[39,70,176,177,187,188]	III	4-30	Anterior vertebral displacement of one segment on another secondary to apophyseal joint degeneration without defects of the pars interarticularis *Synonyms:* pseudospondylolisthesis, nonspondylolytic spondylolisthesis, articular spondylolisthesis Most common at L4 in women who are older than 50 years of age; more common in black persons and in patients with transitional lumbosacral segments (synostosis of L5-S1); a higher prevalence is noted in patients with diabetes mellitus ***Clinical findings:*** Patients may be asymptomatic or may have back pain, sciatica, nerve root compression, intermittent claudication of the cauda equina; symptoms may be related to stenosis, disc herniation, or both; patients with progressive slippage are more likely to have pain; generally not associated with disability or long-term symptoms ***Prevalence:*** 28% in women who have borne children 16.7% in nulliparous women 7.5% in men

* Classification After Wiltse LL, Newman PH, MacNab I: Classification of spondylosis and spondylolysis. Clin Orthop 117:13, 1976.

TABLE 4-5 Spondylolysis and Spondylolisthesis—cont'd

Entity	Type*	Figure(s)	Characteristics
			Imaging findings Anterior vertebral displacement, apophyseal joint space narrowing, sclerosis, and osteophytes, remodeling of the neural arch, disc space narrowing, vacuum phenomenon, and hyperlordosis (variable) Flexion and extension radiographs are used to identify excessive translation and angulation indicative of segmental instability Forward slippage of the L4 vertebral body usually is less than 20% of the anteroposterior diameter of the L5 vertebral body (grade I)
Traumatic spondylolysis[7,33,176,177]	IV		Acute, severe injury resulting in fracture of the neural arch at a site other than the pars interarticularis Example: C2 hangman's fracture; rare in thoracic and lumbar spine
Pathologic spondylolysis[33,40,176,177]	V	4-31	Spondylolysis through pathologic bone, with or without spondylolisthesis Some disorders include skeletal metastasis, osteopetrosis, and Paget disease
Iatrogenic spondylolisthesis[176,177]	VI	See Figure 4-117	Excessive removal of bone following spine decompression surgery
Unilateral spondylolysis[7,41]		4-32	Unilateral pars interarticularis defect may occur as a result of a fatigue fracture (type II A) or an acute fracture (type II C) Sclerosis of the opposite pedicle is believed to be secondary to redistribution of weight-bearing forces through the contralateral pedicle and neural arch
Unstable spondylolisthesis[42-44]		4-33	Instability is a rare complication of most types of spondylolisthesis Clinical utility of functional lateral radiographs—compression-traction and flexion-extension radiographs—is controversial, and the evidence is somewhat contradictory Compression-traction radiographs may be useful in revealing instability of motion segments in patients with spondylolytic spondylolisthesis[44] In patients with clinically suspected lumbar instability of all causes, flexion-extension radiographs obtained with the patient standing more frequently reveal signs of instability than traction-compression radiographs[43] Flexion-extension radiographs obtained in the lateral decubitus position reveal even more motion than those obtained in the standing position[42] Translational instability: total anterior to posterior intersegmental motion in excess of 4 mm or 8% of the sagittal diameter of the vertebral body Angular instability: total intersegmental angular motion in excess of 12 degrees[42] or 20 degrees[43]
Progressive spondylolisthesis[45]		4-34	Progression occurs before 18 years of age in most cases of progressive spondylolytic spondylolisthesis Infrequently, new vertebral displacement or progression of an existing displacement may occur in adult spondylolysis and isthmic spondylolisthesis of L5 without evidence of trauma Thick L5 transverse processes and iliolumbar ligaments tend to protect against further slippage of L5
High grade spondylolisthesis[160]		4-35, *A*	Grade III or IV spondylolisthesis (i.e., anterior slippage greater than 50% of L5 over S1) *Often associated with:* Dystrophic changes of inferior L5 endplate: posterior bony outgrowth (osteophyte); sclerosis and necrosis of endplate Dystrophic changes of superior S1 endplate: posterior osseous hook; sclerosis, necrosis, and curved convex superior surface of endplate Severe L5-S1 disc degeneration
Spondyloptosis[161]		4-35, *B*	*Grade 5 spondylolisthesis:* rare occurrence Precise factors leading to such severe progression remain unknown but proximal sacral endplate damage postulated as a possible cause The posterior margin of the L5 vertebral body translates anteriorly beyond the anterior margin of the S1 vertebral body Dystrophic convex rounding of superior endplate of S1 present in 100% of cases; pars defects (89%); facet dysplasia (59%); spina bifida occulta (89%); disc degeneration (93%); trapezoidal shape of L5 vertebral body (74%)

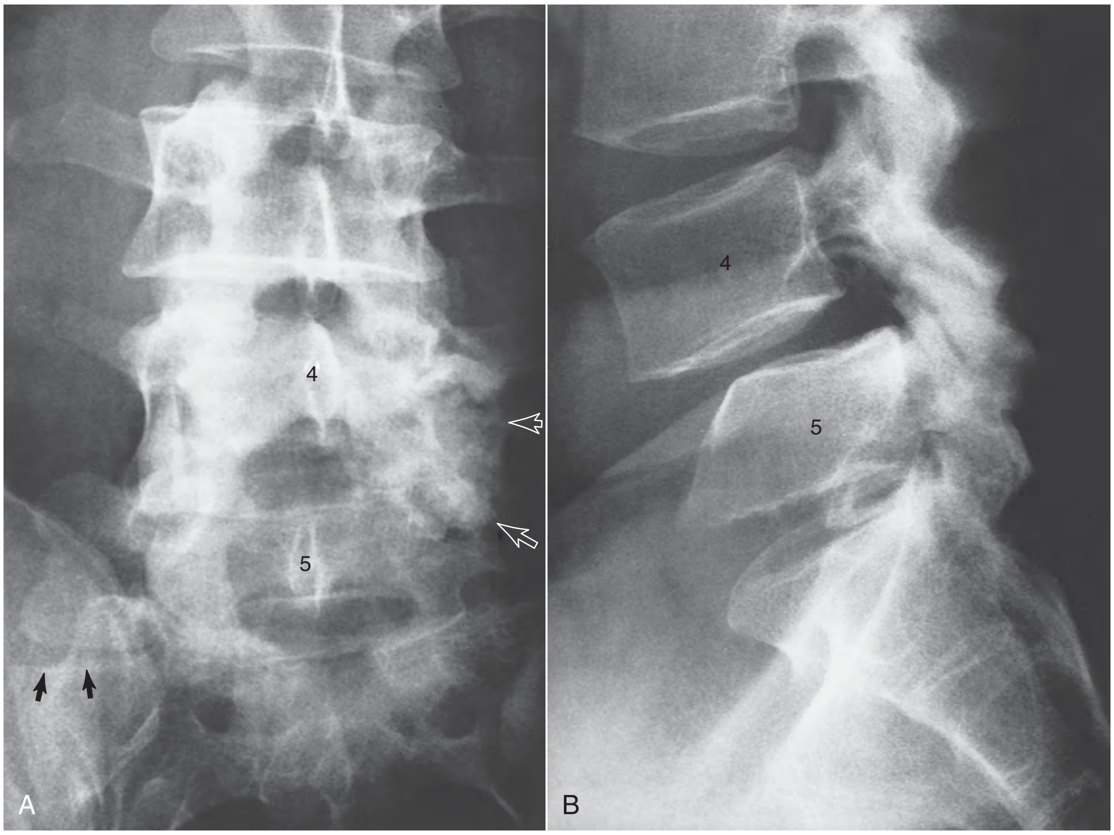

FIGURE 4–25 **Dysplastic spondylolisthesis.**[7,33] This 29-year-old manual laborer had chronic low back pain. **A,** Frontal radiograph reveals a transitional lumbosacral segment with a spatulated transverse process on the right that articulates with the sacrum *(solid arrows)*. Extensive osteophyte formation and bone proliferation of the contralateral L4-L5 apophyseal articulation are also seen *(open arrows)*. **B,** Lateral radiograph shows a wedge-shaped, dysplastic appearance of the anterosuperior margin of the L5 vertebral body and short L5 pedicles. The L4 vertebral body exhibits marked anterior translation and angulation in relation to L5, and the neural arch is elongated and sclerotic. Dramatic apophyseal joint degeneration also is evident, especially at the L4-L5 level. This patient has a combination of dysplastic (type I) and degenerative (type III) spondylolisthesis. *(Courtesy G. Murdoch, DC, Smithers, B.C., Canada.)*

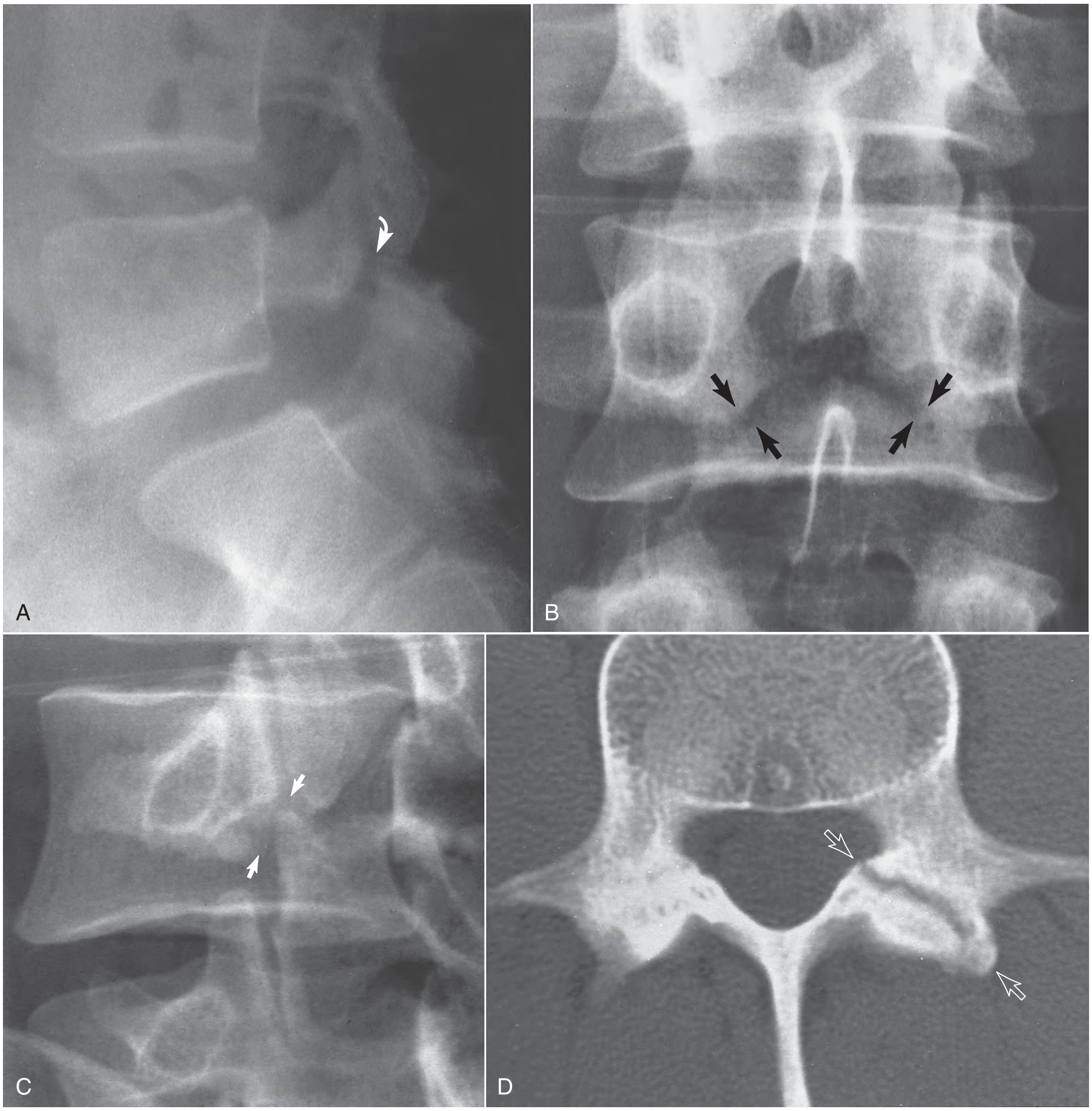

FIGURE 4–26 **Spondylolysis.**[7,33,159] **A,** Spondylolysis at L5. This 10-year-old girl complained of back pain after gymnastics. A radiolucent pars interarticularis defect (spondylolysis) is apparent at L5 *(curved arrow)*. Spondylolisthesis is minimal and the vertebral body morphology is normal. **B-C,** Spondylolysis. Frontal radiograph **(B)** shows the pars interarticularis defects *(arrows)*. These defects are best demonstrated on lateral and oblique **(C)** radiographs *(arrows)*. **D,** Spondylolysis at L4: CT abnormalities. Transaxial CT bone window shows a unilateral radiolucent defect through the pars interarticularis of L4 *(open arrows)*. Sclerosis and hypertrophic bone formation (callus) suggest that the fracture is healing. (***A,** Courtesy M.N. Pathria, MD, San Diego. **D,** Courtesy J. Amberg, MD, San Diego.)*

TABLE 4-6 Myerding Method of Measuring Spondylolisthesis[34]

Grade	Degree of Displacement
I	<25%
II	26%-50%
III	51%-75% (high-grade)
IV	76%-100% (high-grade)
V	>100% (spondyloptosis)

* Myerding method measures the amount of displacement of the posterior margin of the L5 vertebral body in relation to S1 on lateral radiographs (Figure 4-27).

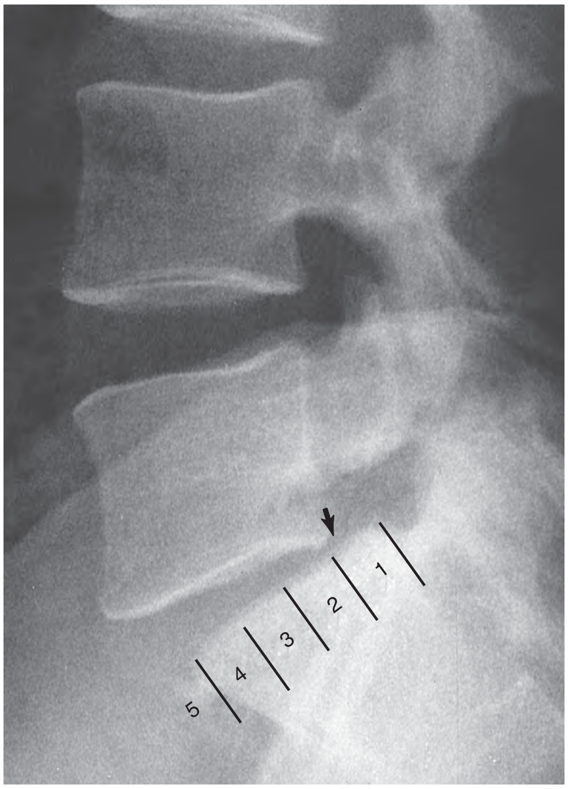

FIGURE 4–27 **Measurement of spondylolisthesis: Myerding method.**[34] On the lateral radiograph, a line constructed along the sacral base divides the sacrum into four equal parts. Another line drawn along the posterior vertebral body of L5 *(arrow)* is extended inferiorly to intersect one of these quadrants. The extent of L5 vertebral body displacement is graded (into grades 1 through 4) according to the quadrant intersected. In cases in which the L5 body translates beyond the sacral promontory, the spondylolisthesis is termed *grade V* and is called *spondyloptosis*. In this case, the spondylolisthesis is grade I (Table 4-6).

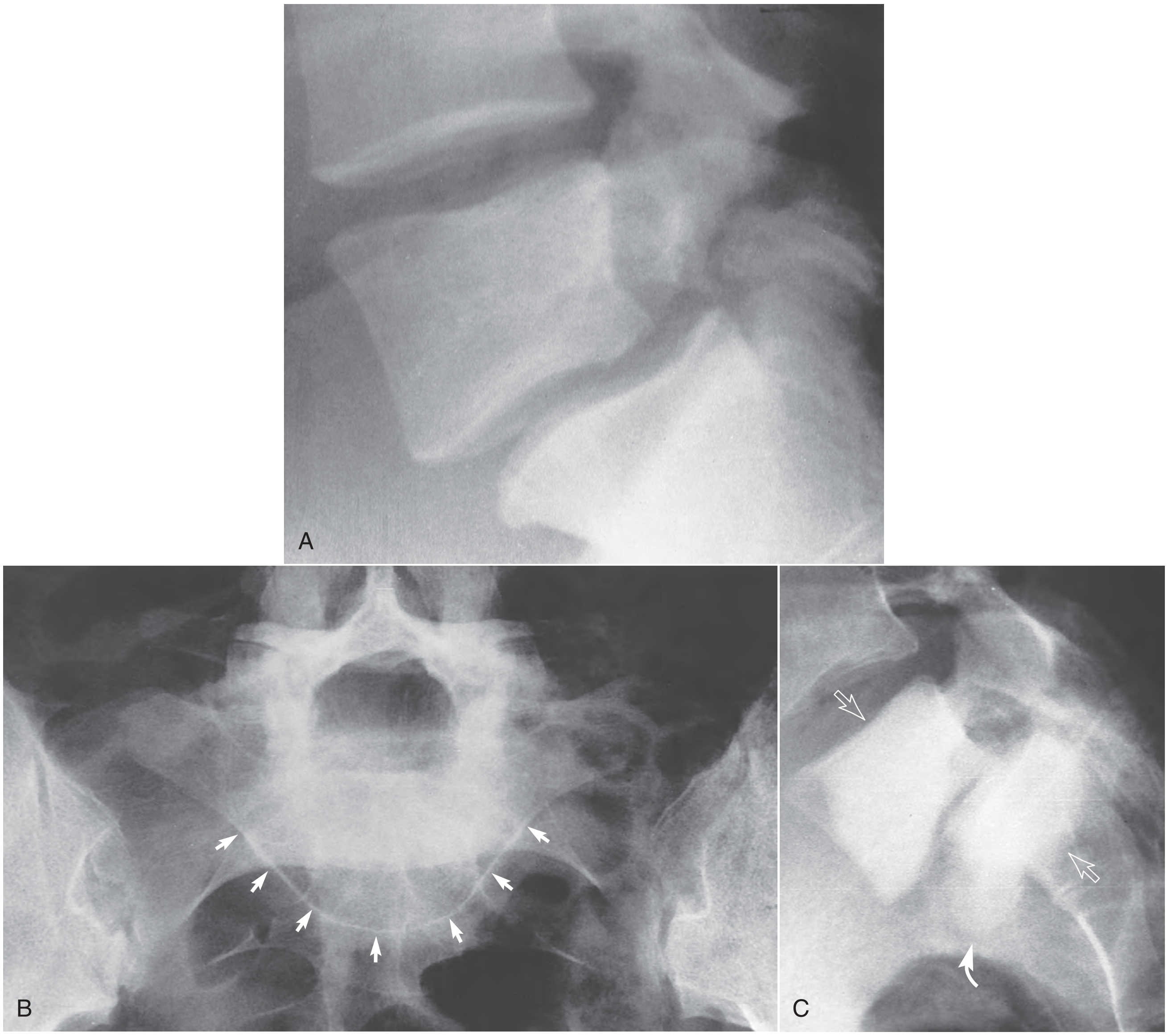

FIGURE 4–28 **Spondylolytic (isthmic) spondylolisthesis.**[35,36] **A,** Spondylolisthesis at L5. Lateral radiograph shows a grade 1 anterolisthesis of L5 and a pars interarticularis defect. Note the trapezoidal shape of the L5 vertebral body, a finding that may represent a normal contour and may also be exaggerated by bone remodeling in long-standing spondylolisthesis. **B,** The "inverted Napoleon hat" sign. Frontal radiograph demonstrates the "inverted Napoleon hat" sign or "bowline of Brailsford" sign characteristic of grades 3 to 5 spondylolisthesis. In these cases, the L5 vertebral body is translated anteriorly, such that on the frontal radiograph, it is seen in the axial plane rather than in the conventional coronal plane. The arrows indicate the anterior aspect of the L5 vertebral body. **C,** Degenerative sclerosis. Extensive sclerosis is observed in the L5 and S1 vertebral bodies *(open arrows)* in this 50-year-old man with a long-standing grade II spondylolytic spondylolisthesis. Observe also the presence of buttressing at the anterior aspect of the sacrum *(curved arrow)*. Sclerosis and buttressing are believed to be compensatory responses to mechanical stress from abnormal motion.

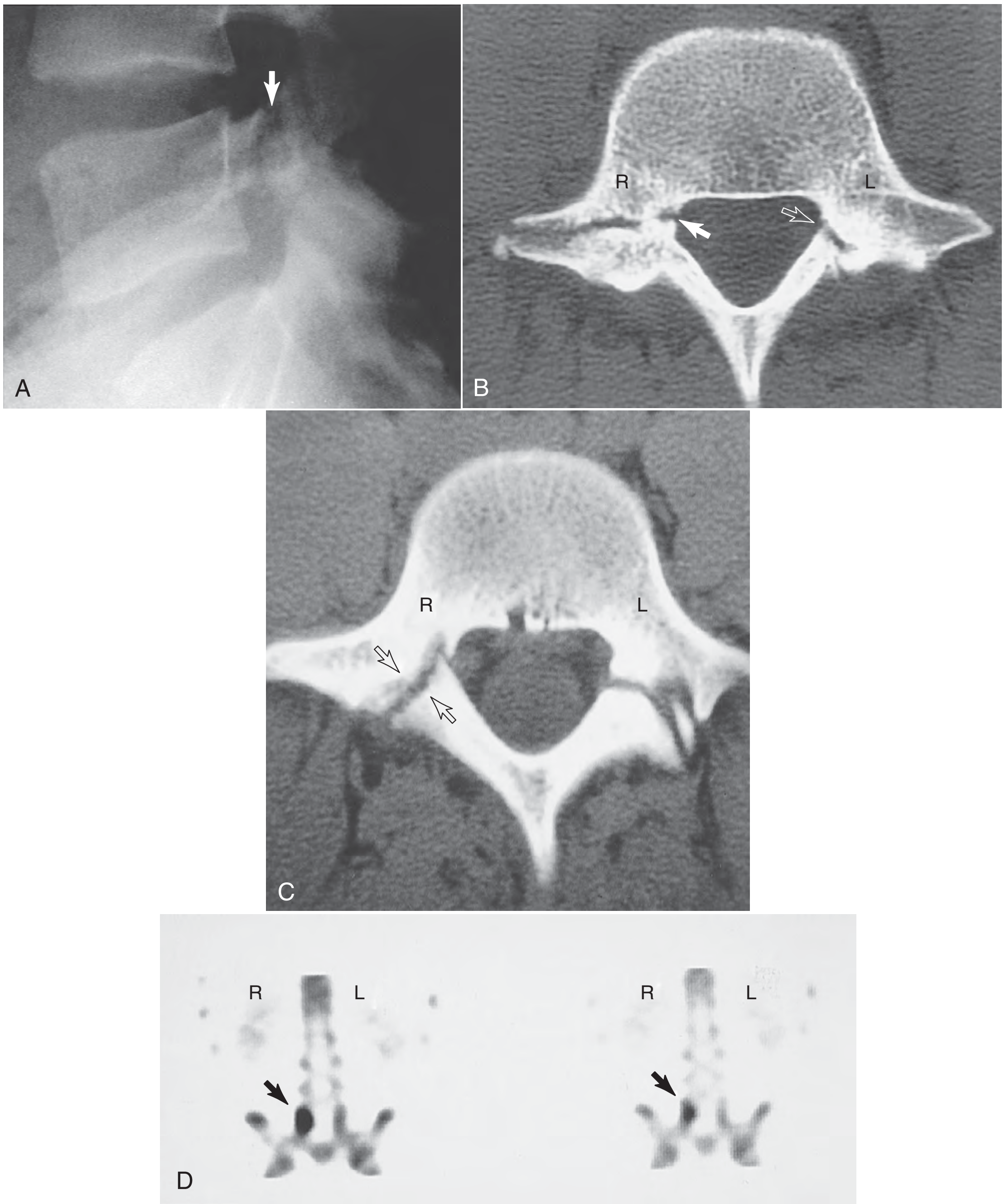

FIGURE 4–29 **Acute spondylolysis.**[37,38,179] **A-B,** Acute neural arch fracture in a 17-year-old boy who sustained a fall of 15 feet. Lateral radiograph **(A)** and transaxial CT scan **(B)** demonstrate a coronally oriented vertical fracture line through the right transverse process *(solid arrows)* and an oblique fracture line through the left pedicle-lamina junction of L5 *(open arrow)*. No anterior displacement of the vertebral body is seen. **C-D,** Acute pars interarticularis fracture in a 16-year-old high school football player. Routine radiographs (not shown) revealed bilateral spondylolysis but no evidence of spondylolisthesis. In **C,** a transaxial CT scan obtained 9 months after the initial onset of pain shows bilateral defects of the pars interarticularis. The fracture margins on the left are sclerotic and well-defined; the fracture margins on the right *(open arrows)* are less sclerotic and more poorly defined with significant resorption of the apposing bone surfaces. These findings suggest that the fracture on the right is more acute than the fracture on the left. In **D,** images from a coronal single photon emission computed tomographic (SPECT) bone scan obtained at the same time as the CT scan **(C)** reveal intense uptake of the radiopharmaceutical agent in the right pars interarticularis *(arrows)* and only moderate uptake on the left side. These findings confirm the acute nature of the right pars fracture and the more chronic nature of the left pars defect. Acute traumatic fractures of the neural arch are rare, painful lesions that are best imaged with SPECT imaging. CT and MR imaging also may be helpful in such cases. *(**C-D,** Courtesy S. Thorpe, DC, St. Petersburg, Fla.)*

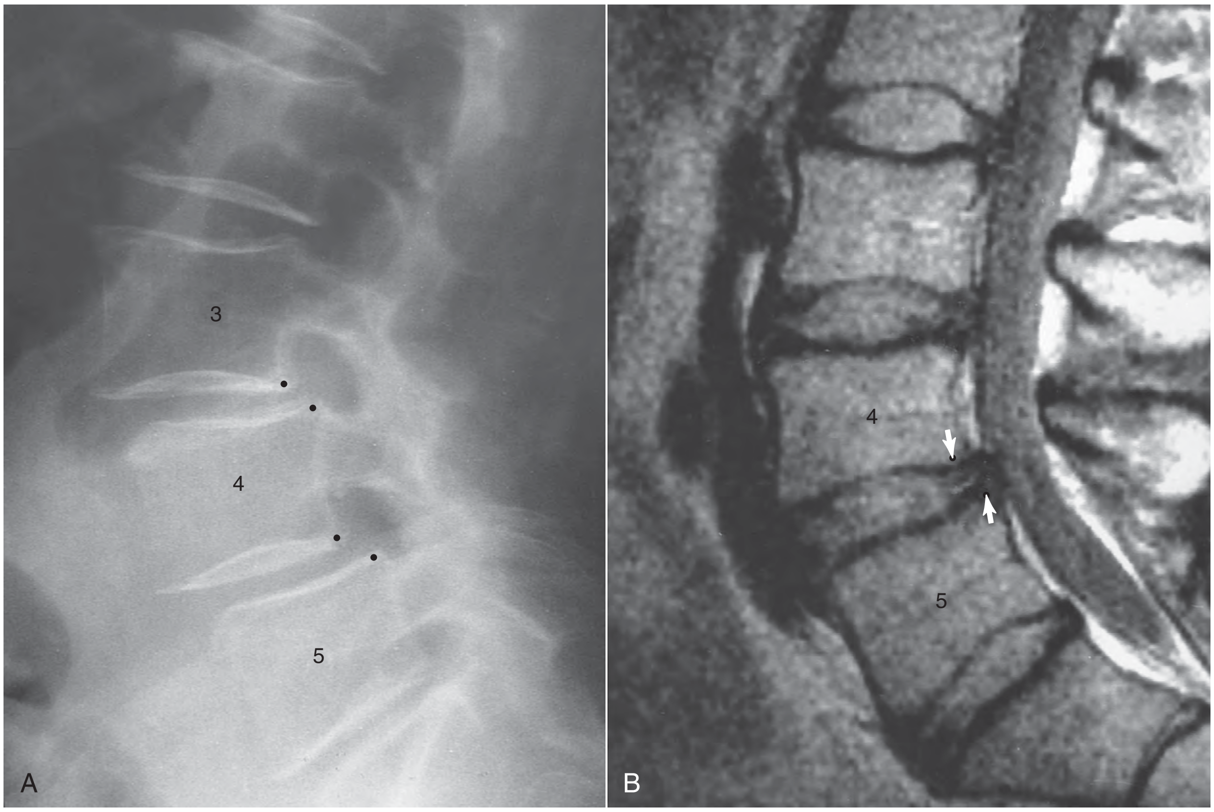

FIGURE 4–30 **Degenerative spondylolisthesis.**[39,70,165,187,189] **A,** Lateral radiograph from a 74-year-old woman with chronic low back pain reveals severe apophyseal joint osteoarthrosis and anterior displacement of both L3 and L4 *(dots)*. **B,** Midsagittal T1-weighted (TR/TE, 400/17) spin echo MR image from another patient shows degenerative spondylolisthesis of L4 *(arrows)* and consequent spinal stenosis and thecal sac compression.

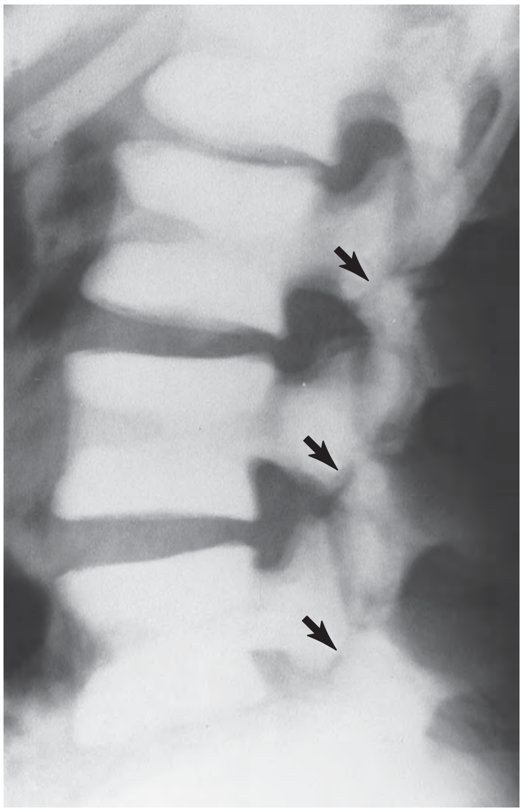

FIGURE 4–31 **Pathologic spondylolysis: osteopetrosis.**[33,40,147] In this 26-year-old man with episodic low back pain, the vertebral bodies appear diffusely sclerotic with an intervening central band of normal bone density (“sandwich vertebra”). The neural arches also are diffusely sclerotic, and pars interarticularis fractures are evident at three vertebral levels (*arrows*). These pathologic fractures of the pars interarticularis presumably occur as a result of brittle bones. *(From Khanchandani BA: Albers-Schonberg disease with multiple-level lumbar spondylolysis: a case report. Eur J Chiropr 37:5, 1989.)*

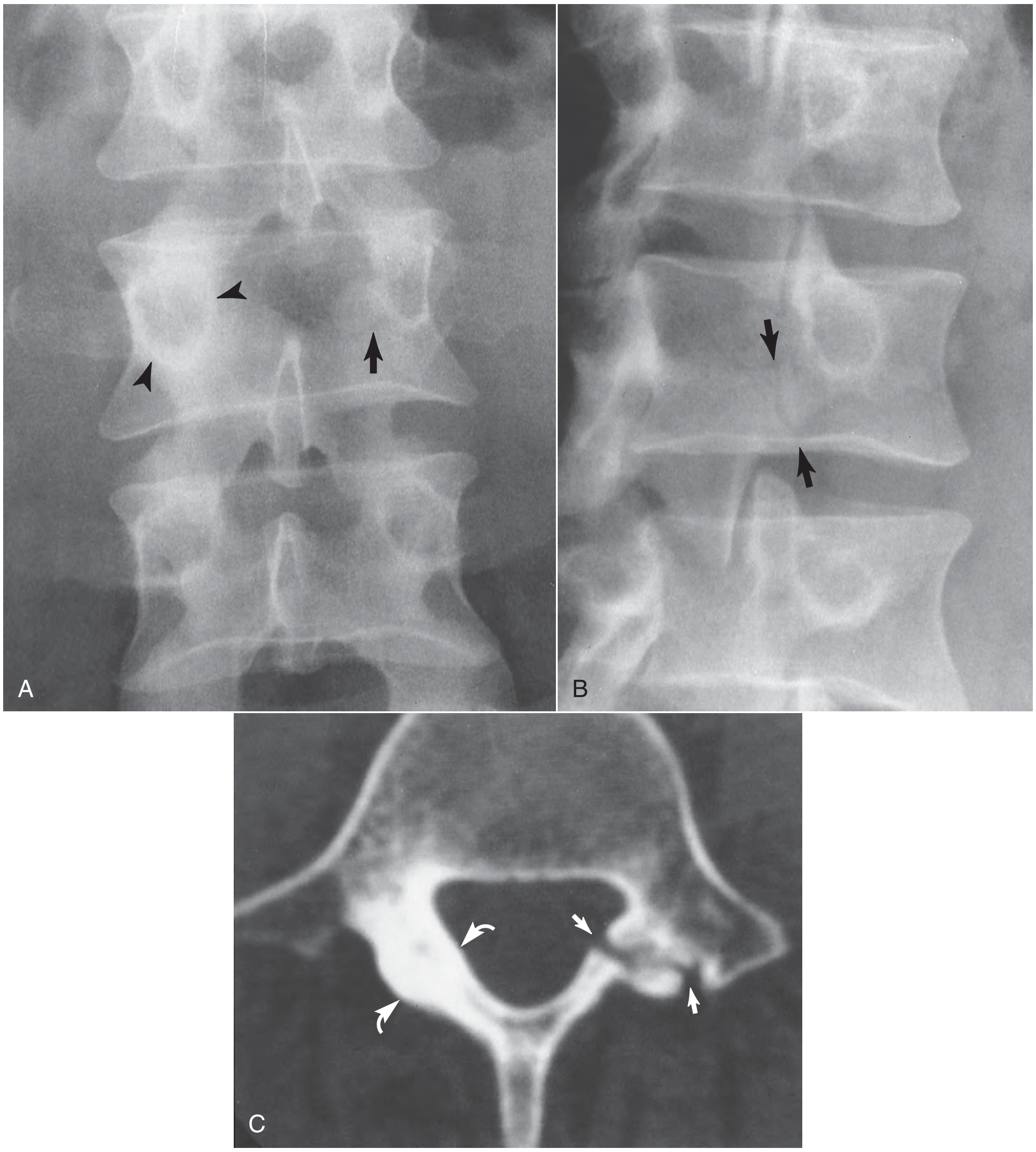

FIGURE 4–32 **Unilateral spondylolysis.**[7,41] **A,** Frontal radiograph shows a hypertrophic and sclerotic pedicle *(arrowheads)* and a poorly visualized pars interarticularis defect on the contralateral side *(arrows)*. **B,** Oblique radiograph shows a unilateral pars interarticularis defect *(arrows)*. **C,** Transaxial CT image from another patient illustrates a unilateral pars defect *(arrows)* with a contralateral sclerotic pedicle *(curved arrows)*. *(**A-B,** Courtesy J. Grilliot, DC, Toledo, Ohio.)*

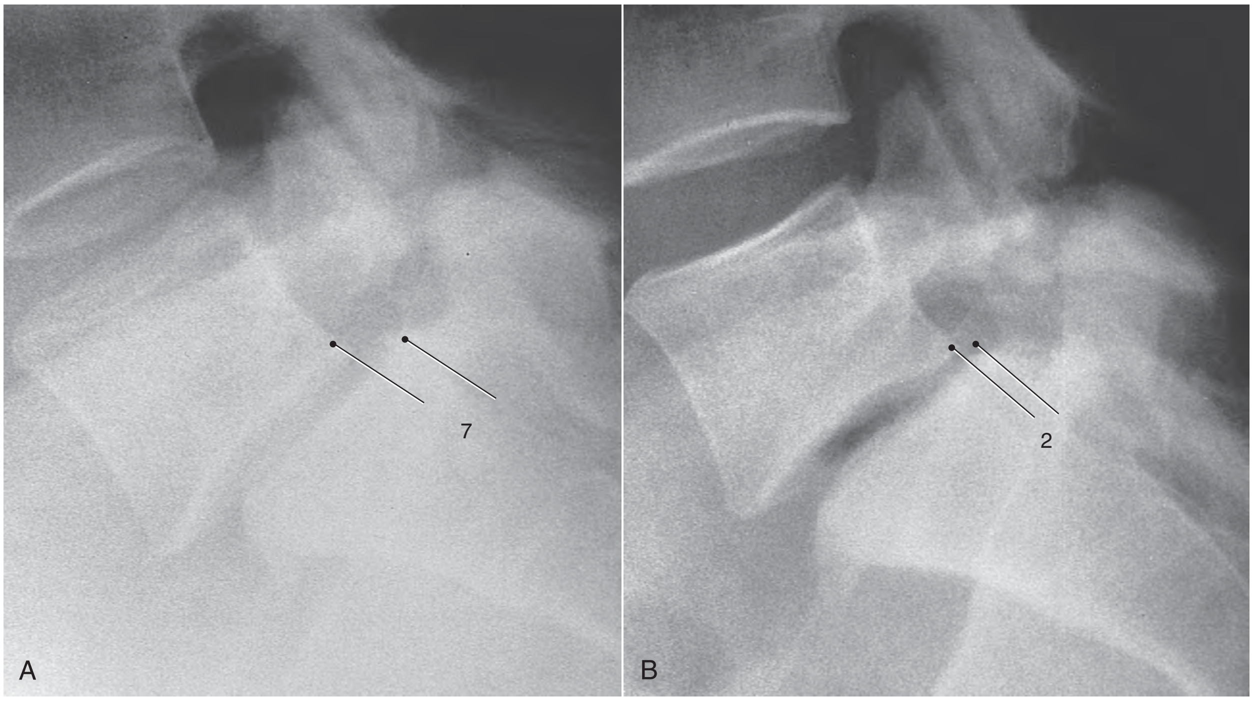

FIGURE 4–33 **Spondylolisthesis: instability evaluation with functional radiography.**[42-44,186] **A,** Radiograph obtained with compression shows 7 mm of anterior translation of L5 on S1 *(vertical lines with dots)*. **B,** Film obtained with traction reveals a reduction of the anterolisthesis to 2 mm *(vertical lines with dots)*. In addition, the disc space has widened, and intradiscal gas (vacuum phenomenon) is evident. Sagittal translation on functional radiographs in excess of 4 mm indicates instability and implies a higher probability of progression of the spondylolisthesis.

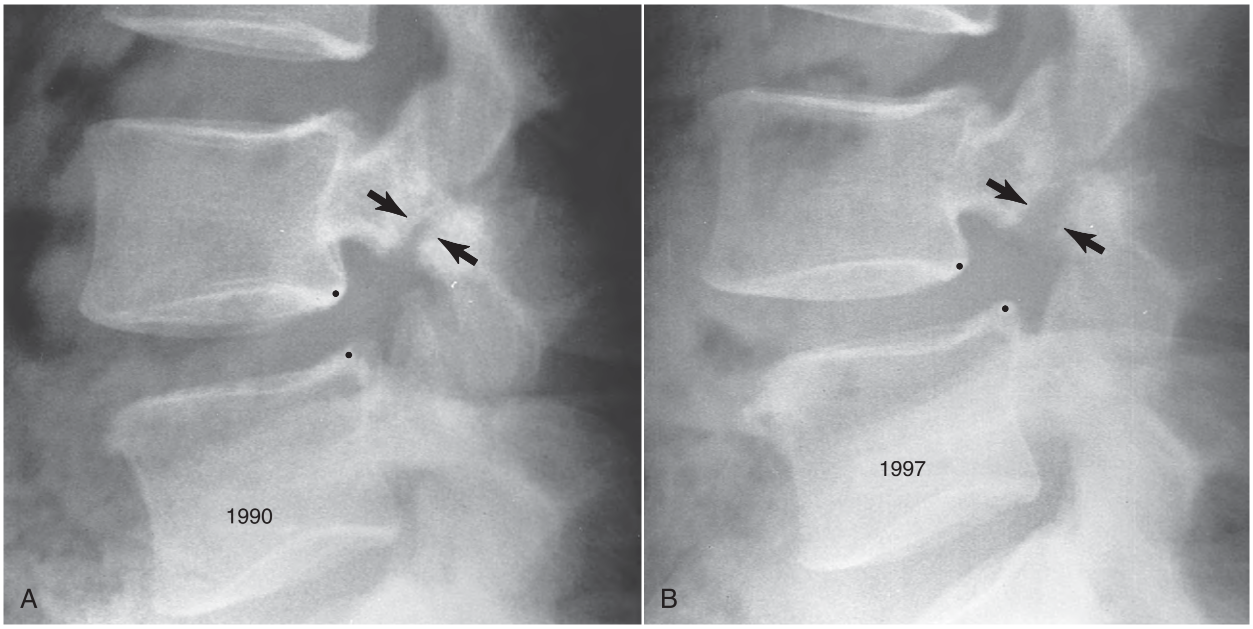

FIGURE 4–34 **Spondylolytic spondylolisthesis: serial progression in an adult.**[45,186] **A,** Upright (standing) spinal radiograph of a 42-year-old man obtained in 1990 reveals a spondylolysis of L4 with only minimal anterior displacement of L4 on L5. The pars interarticularis defects *(arrows)* are well visualized and the apposing margins appear sclerotic. **B,** Another upright spinal radiograph of the same patient obtained 7 years later, after a motor vehicle collision, reveals separation of the pars interarticularis defects *(arrows)* and a 5-mm progression of anterior translation of L4. The apposing margins of the pars defect appear less sclerotic and distinct and suggest the presence of resorption at this site. In this case, it is impossible to determine if there is a causal relationship between the motor vehicle collision and progression of the spondylolisthesis. With spondylolytic spondylolisthesis, progression usually occurs before 16 to 18 years of age. In adults, however, new vertebral displacement or progression of an existing displacement of an L5 isthmic spondylolisthesis may rarely occur with no history of trauma. *(Courtesy G.C. Stirling, DC, Kelowna, B.C., Canada.)*

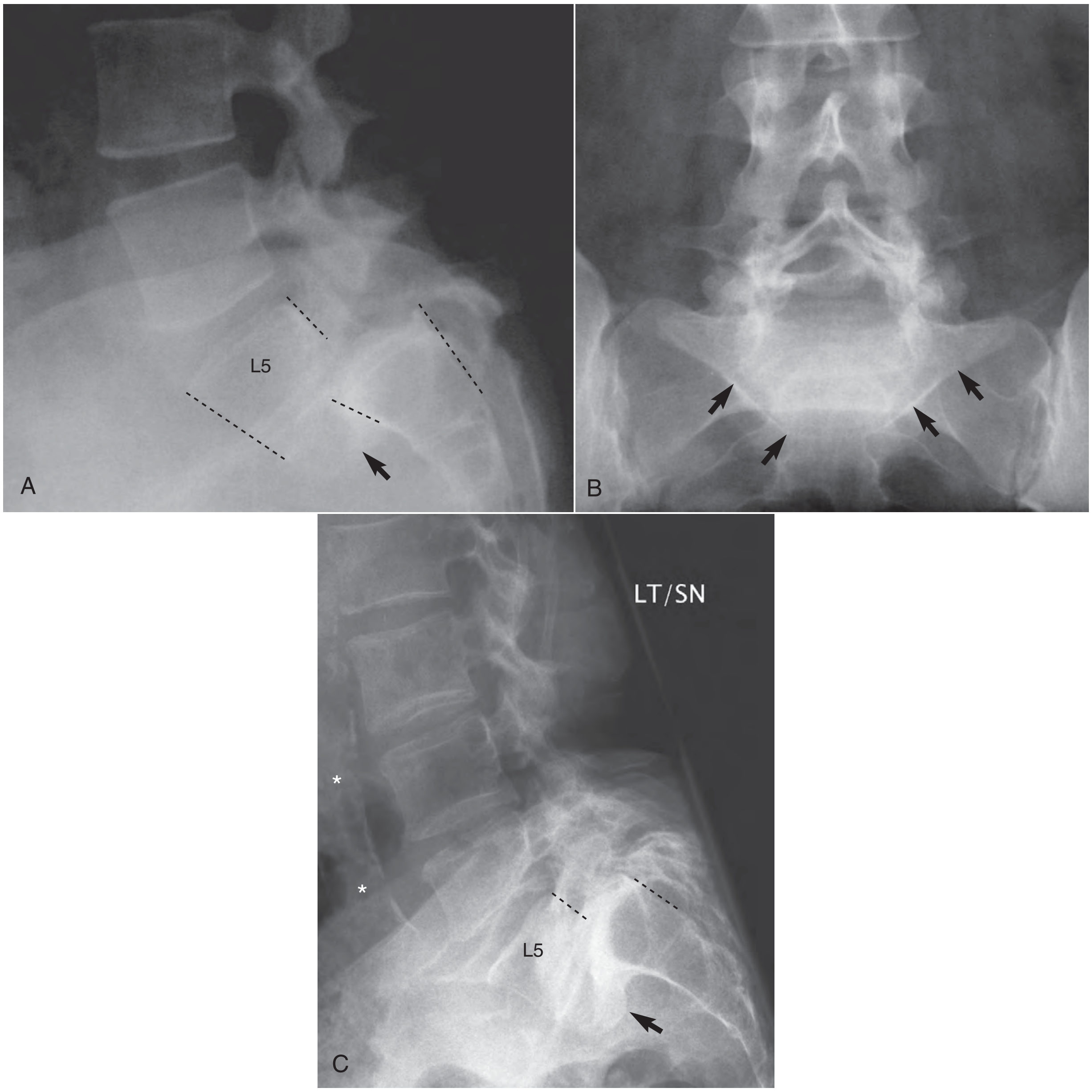

FIGURE 4–35 High grade spondylolisthesis: grades III and IV.[160,161] **A-B,** In this 20-year-old woman, 75% slippage (grade III anterolisthesis) of L5 is seen on the lateral radiograph **(A)** (dotted lines indicate anterior and posterior vertebral body margins of L5 and S1). The L5 vertebral body is trapezoidal in shape and early degenerative buttressing is evident at S1. The frontal radiograph **(B)** of this same patient reveals the characteristic inverted Napolean hat sign in which the L5 vertebra is visualized from an axial perspective owing to its extreme rotation (flexion) in the sagittal plane (arrows indicate the anterior margin of L5 vertebral body and the base of the transverse processes). **C,** In this 72-year-old man, grade IV spondylolisthesis of L5 has occurred in which the L5 vertebral body has slipped forward about 90% with respect to S1. Marked degenerative changes including a prominent buttress at S1 *(arrow),* and severe disc space narrowing and subchondral sclerosis at L5-S1 are also present. Abdominal aortic and iliac artery atherosclerosis is incidentally noted (*).

TABLE 4-7 Magnetic Resonance (MR) Imaging Grading System for Stress Fractures of the Pars Interarticularis*

Grade	Description	MR Imaging Features
0	Normal	Normal marrow signal Intact cortical margins
1	Stress reaction	Marrow edema Intact cortical margins
2	Incomplete fracture	Marrow edema Cortical fracture incompletely extends through pars
3	Complete active fracture	Marrow edema Fracture completely extends through pars
4	Fracture nonunion	No marrow edema Fracture completely extends through pars

* From Dunn AJ, Campbell RSD, Mayor PE, et al: Radiological findings and healing patterns of incomplete stress fractures of the pars interarticularis. Skeletal Radiol 37:443, 2008.

TABLE 4-8 Lumbar Scoliosis*

Entity	Figure(s), Table(s)	Characteristics
Idiopathic adolescent scoliosis[46]	4-36	Most common type of idiopathic scoliosis *Typical pattern:* right thoracic, left lumbar *Onset:* 10 years of age to skeletal maturity Girls : boys, 4 : 1 to 8 : 1
Degenerative scoliosis[47]	4-37 Table 4-17	Scoliosis in elderly persons is associated with advanced degenerative disease
Scoliosis secondary to limb length inequality[48]	4-38	Functional lumbar curve convex to the side of the shorter limb Compensatory thoracic curve in the opposite direction Functional curves typically are flexible in younger persons, but become more rigid and structural with advancing age through long-term changes from contracture or growth Sacral tilt also may result from pelvic asymmetry rather than limb length discrepancy
Marfan syndrome[27,49]	4-39	Scoliosis occurs in as many as 65% of patients No female predominance Smooth, long sweeping curve resembles that of idiopathic scoliosis In young people, the curve progresses more rapidly than in idiopathic scoliosis Thoracic scoliosis often is associated with posterior vertebral body scalloping from dural ectasia

* Only the types of scoliosis illustrated in this chapter are listed; for a more complete discussion of scoliosis, see Table 3-5.

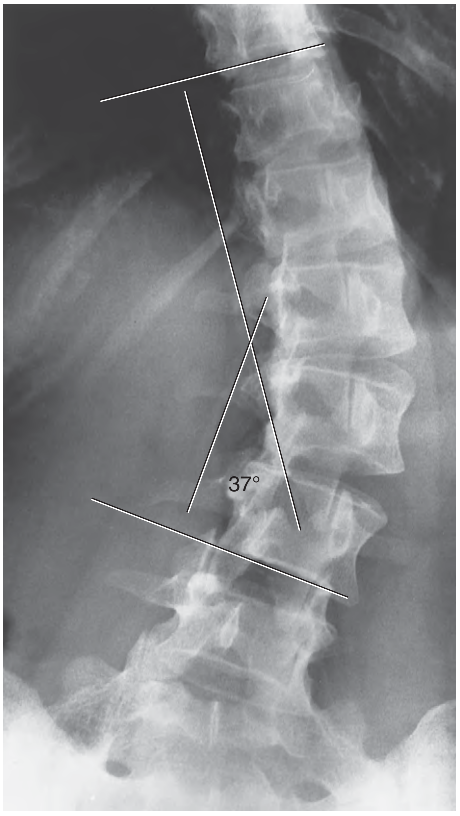

FIGURE 4–36 **Idiopathic scoliosis.**[46] This 26-year-old woman has idiopathic adolescent scoliosis that was diagnosed at 13 years of age. Using the Cobb measurement method, this left lumbar scoliosis measures 37 degrees. Marked vertebral body rotation also is noted.

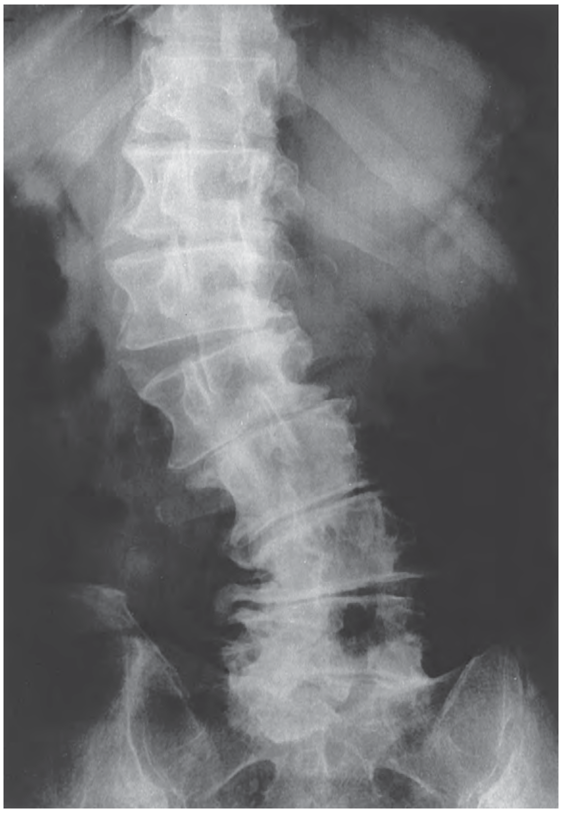

FIGURE 4–37 **Degenerative scoliosis.**[47] Right thoracolumbar and left lumbar idiopathic scoliosis in this 78-year-old man have been present since adolescence. Severe degenerative changes of the discs and apophyseal joints are evident on the concave aspects of the curves. Despite these severe degenerative changes, this patient had only occasional back pain and aching.

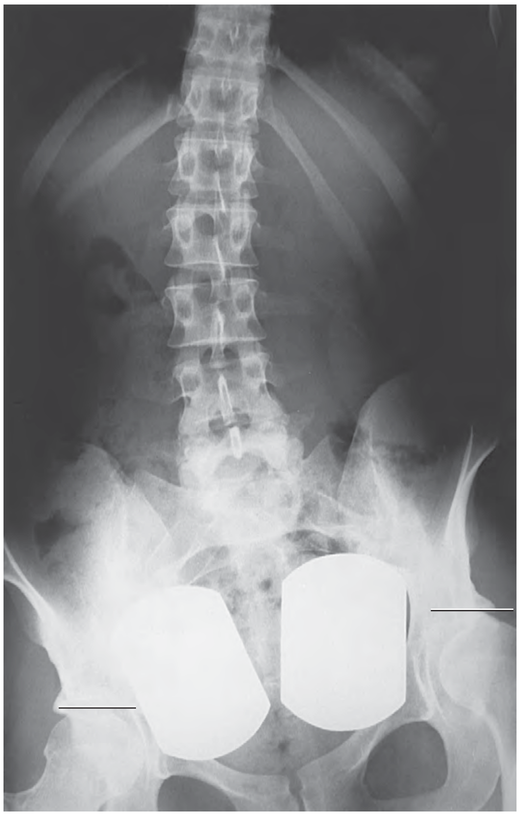

FIGURE 4–38 **Scoliosis secondary to limb length discrepancy.**[48] This patient sustained fractures of both the femur and the tibia during a motorcycle accident. After reduction and fixation, the right lower limb remained 8 cm short, resulting in prominent pelvic distortion and scoliosis seen on this upright radiograph. (Horizontal lines demonstrate the variation in height of the femoral heads.)

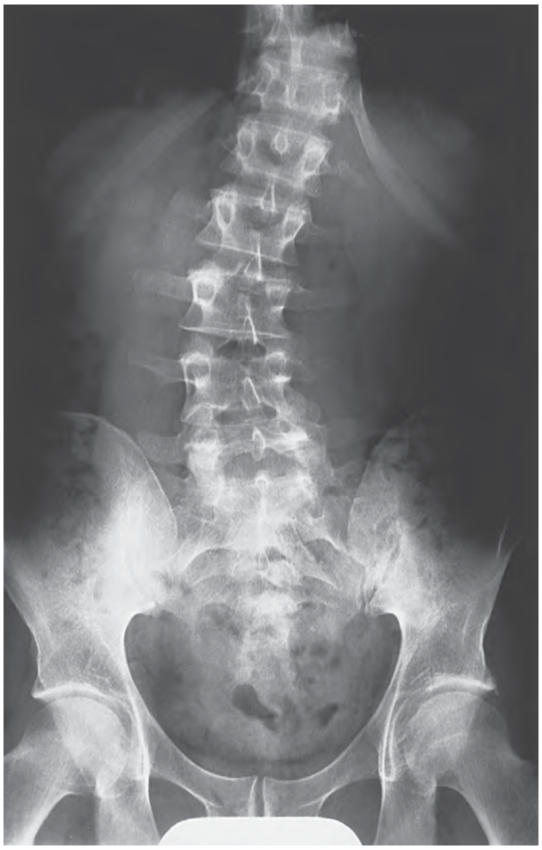

FIGURE 4–39 **Scoliosis: Marfan syndrome.**[27,49] A lumbar scoliosis is seen in this 29-year-old man with Marfan syndrome. Scoliosis is evident in up to 65% of patients with Marfan syndrome and exhibits a pattern similar to that of idiopathic scoliosis. In Marfan syndrome patients, however, the scoliosis typically begins earlier in life and progresses more rapidly.

TABLE 4-9 Fractures and Dislocations of the Lumbar Spine

Entity	Figure(s), Table(s)	Characteristics
Vertebral body compression fracture[50]	4-40	Usually upper lumbar region Frequent occurrence in osteoporotic persons ***Mechanisms*** Acute fracture from accidental, athletic, or occupational hyperflexion-compression injury; alternatively, trivial trauma, repeated minor trauma, or slow bone remodeling resulting from ongoing chronic microfractures Biconcave endplate deformities are common in the lumbar spine May be quite painful, but the middle column (posterior vertebral body) generally remains intact, and, therefore, these fractures are considered stable, infrequently resulting in neurologic deficit Unstable fractures or ligament injuries may be misinterpreted as stable compression fractures; all radiographs should be examined closely for evidence of retropulsion of the posterior margin of the vertebral body, as seen in burst fractures, or disruption of the posterior elements, as seen in seat belt fractures, both of which are unstable injuries
Burst fracture[51,52]	4-41 Table 4-10	More common in younger persons Most common in the thoracolumbar spine ***Mechanisms*** Predominantly axial compression during motor vehicle accident Comminution of vertebral body, widened interpedicle distance, retropulsion of vertebral body fragments Fractures of anterior and middle columns Up to 50% of patients have neurologic deficit May be unstable
Transverse process fracture[53,54]	4-42, 4-43	***Mechanisms*** Direct blow or lateral flexion 13.6% of all thoracolumbar spine injuries Often multiple transverse process fractures occur Abdominal visceral injury, including that to ureter and kidney in as many as 20% of patients Heterotopic ossification related to associated hematoma may result in a vertical osseous bridge spanning adjacent transverse processes
Fracture-dislocation[55,56,188]	4-44, 4-45	Rare injury of thoracolumbar or, less commonly, lumbosacral regions Highly unstable injury; results in complete disruption of all three columns Permanent neurologic deficit, usually complete paraplegia, in more than 90% of cases Occasional L5-S1 unilateral facet dislocation reported as a result of flexion and rotation mechanism ***Mechanisms*** Compression (anterior column), rotation, shear, and distraction (middle and posterior columns) Often severe injuries associated with polytrauma
Thoracolumbar flexion-distraction injury (Chance-type seat belt fracture)[55,182]	3-27, 3-28 Tables 3-7 and 3-9	See Tables 3-7 and 3-9
Acute pars interarticularis fracture[37,38,159]	4-29 Tables 4-5 and 4-7	Very uncommon form of spondylolisthesis
Apophyseal ring fracture (posterior limbus fracture)[57,58]	4-46	Avulsion of the posterior vertebral ring apophysis; usually associated with disc protrusion L4 and L5 most common sites CT best for delineating osseous fragment; MR imaging best for evaluating disc, thecal sac, and surrounding soft tissues Frequent radiculopathy and other neurologic signs
Abused child syndrome[137]	3-33	Spine trauma is rare in child abuse Injuries include compression fractures of the vertebral body, acute disc displacement, avulsion of the posterior elements, and thoracolumbar fracture dislocation

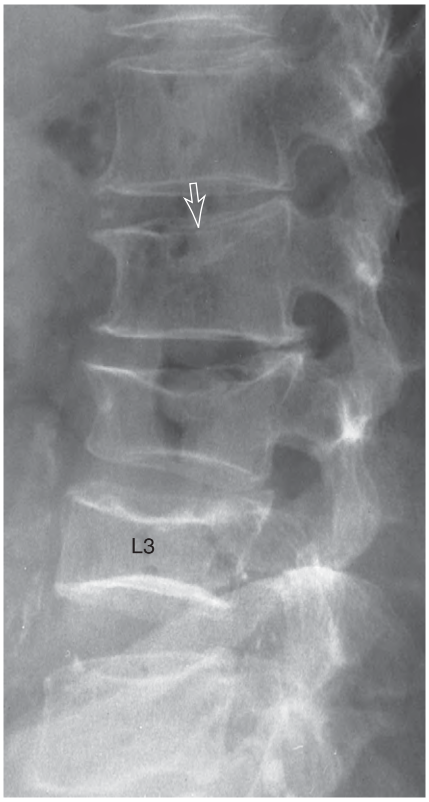

FIGURE 4–40 **Acute vertebral body compression fractures.**[50] Routine lateral radiograph from a 51-year-old man shows an anterior wedge-shaped deformity of the L2 vertebral body and a superior endplate depression of L1 *(open arrow)* and biconcave endplate deformities of L3.

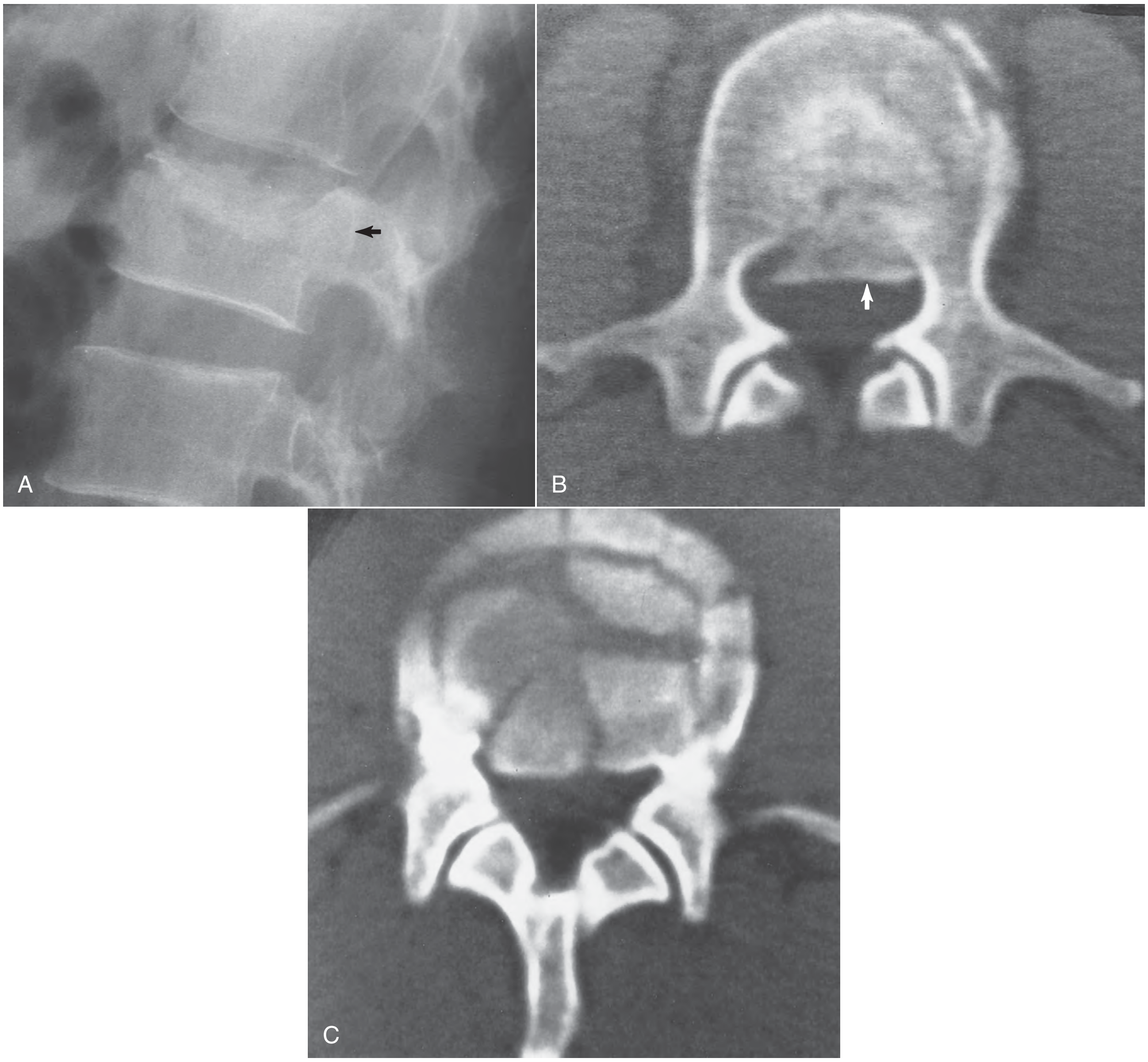

FIGURE 4–41 **Burst fracture.**[51,52] **A-B,** Lateral radiograph **(A)** and transaxial CT scan **(B)** of a 38-year-old man, which were taken after he had jumped from a 20-foot bridge, demonstrate a burst fracture of L2 with superior endplate disruption, vertebral-body comminution, and retropulsion of bone fragments into the spinal canal *(arrows)*. **C,** In another patient with a burst fracture of L3, a transaxial CT image shows severe comminution and retropulsion of the vertebral body.

TABLE 4-10 **Instability in Thoracolumbar Burst Fractures***

General Features of Unstable Burst Fractures

1. As many as 50% of burst fractures are unstable
2. 40% of cases involve disruption of the posterior ligament complex:
   - Supraspinous ligament
   - Interspinous ligament
   - Ligamenta flava
   - Facet joint capsule

Findings Indicating Instability in Burst Fractures

1. Progressive neurologic deficit
2. Posterior element disruption
3. Kyphosis that progresses 20 degrees or more in the presence of a neurologic deficit
4. Loss of height of the vertebral body of more than 50%, with associated facet joint subluxation
5. Retropulsed bone fragments detectable on CT scans in the presence of an incomplete neurologic injury

* Adapted from McAfee PC, Hansen AY, Lasda NA: The unstable burst fracture. Spine 7:365, 1982.

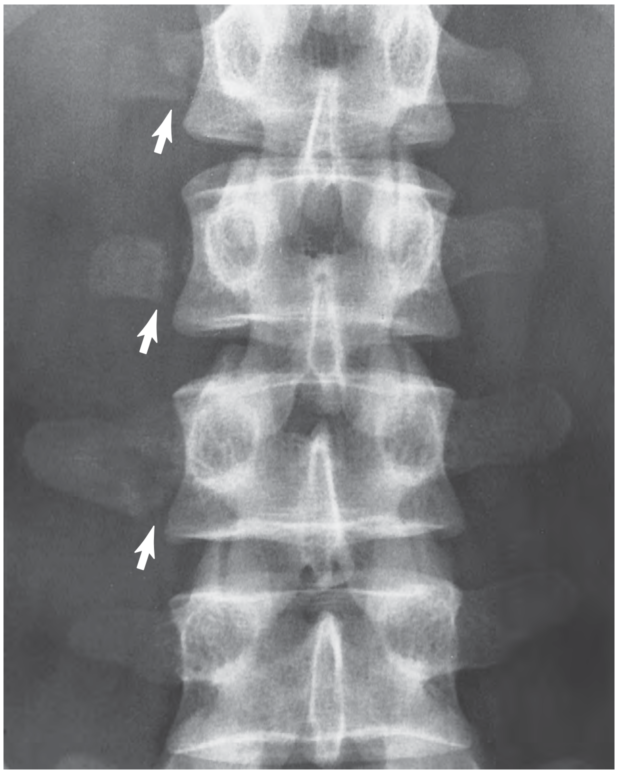

FIGURE 4–42 **Transverse process fractures.**[53,54] This 18-year-old man was in a motor vehicle accident in which he suffered a direct blow from a door handle to the paraspinal region. Minimally displaced fractures of the L1, L2, and L3 transverse processes are seen *(arrows)*. A scoliosis, convex to the side of the fractures, frequently accompanies this injury. Transverse process fractures are complicated by injury to the abdominal viscera, especially the kidney and ureter, in up to 20% of cases. The patient should be questioned about the presence of hematuria, and intravenous urography or CT scanning may be indicated if abdominal injuries are suspected.

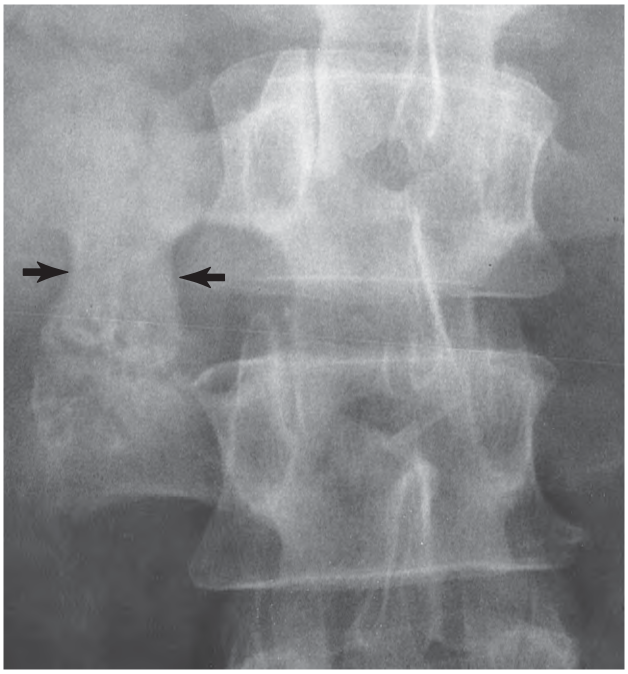

FIGURE 4–43 **Osseous bridging of the transverse processes.**[54] A unilateral, vertically oriented sheet of ossification is seen spanning the transverse processes of the lumbar spine *(arrows)*. This finding is usually the result of ossification of a hematoma resulting from a previous injury. Osseous bars spanning the transverse processes may also be developmental. Although similar in appearance, these anomalies are rare.

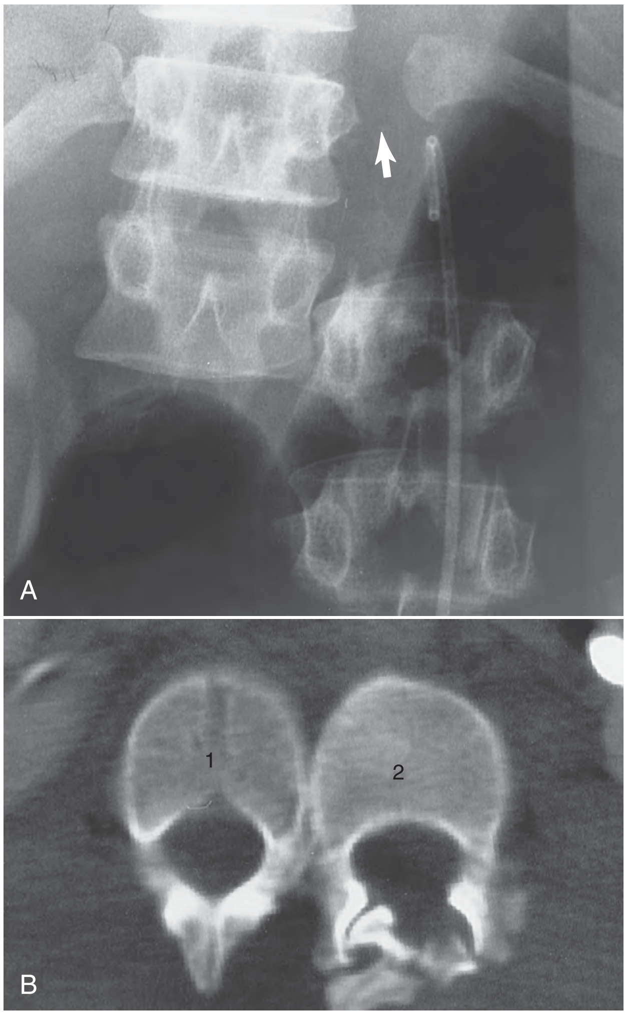

FIGURE 4–44 Fracture-dislocation.[55] A 28-year-old hearing-impaired man was struck by a train while walking on train tracks. **A,** Routine radiograph demonstrates a complete fracture-dislocation at the L1-L2 vertebral level. The left twelfth costovertebral joint is dislocated *(arrow)*. **B,** In a CT scan, the dislocated first *(1)* and second *(2)* lumbar vertebral bodies are seen side-by-side on one transaxial slice. *(Courtesy A. Nemcek, MD, Chicago.)*

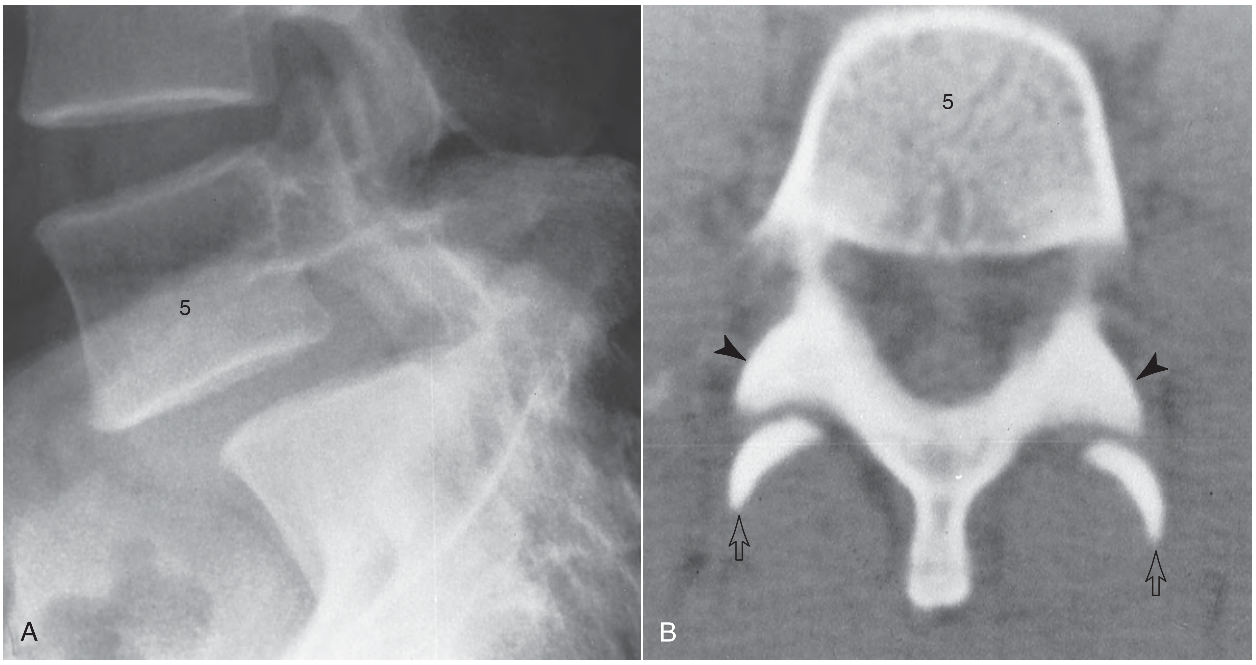

FIGURE 4–45 Lumbosacral apophyseal joint dislocation and facet lock.[56,188] **A,** Routine radiograph shows abnormal alignment of the L5-S1 facet articulations. **B,** The interlocked and dislocated position of the lumbosacral articular processes is better defined on a transaxial CT image. The L5 inferior articular processes *(arrowheads)* are situated anterior to the S1 superior articular processes *(open arrows)*. This rare injury usually results from severe trauma involving a complex mechanism that includes compressive hyperflexion and rotational or shear forces. It often is associated with fractures of the sacrum and lower lumbar spine.

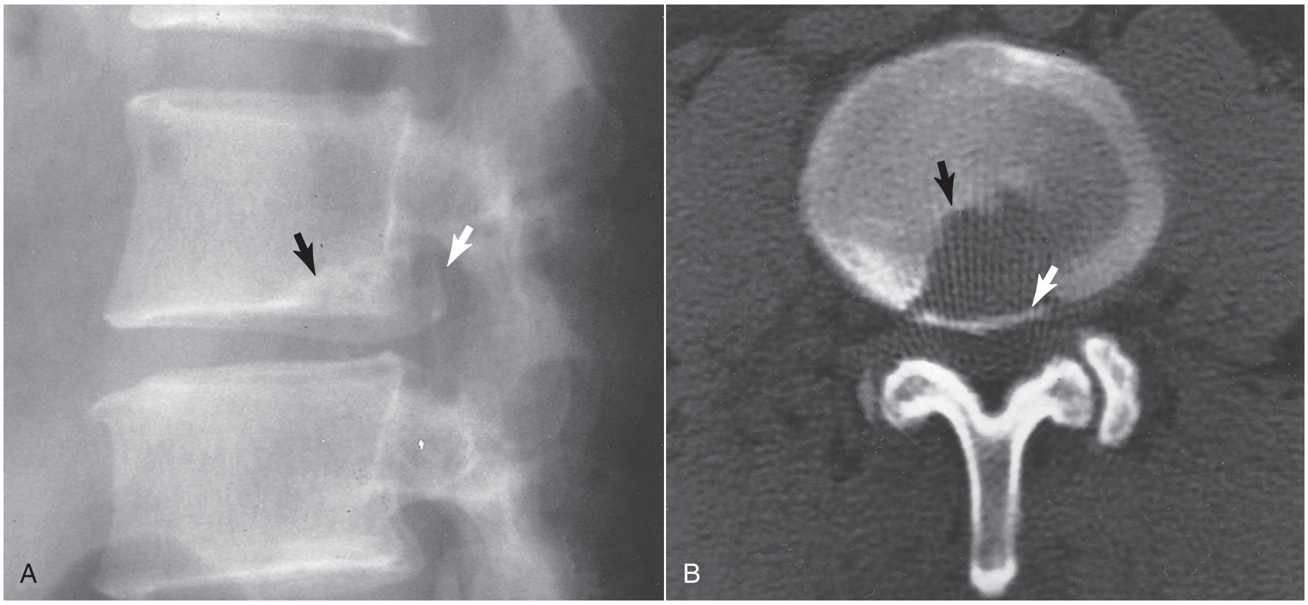

FIGURE 4–46 Posterior apophyseal ring avulsion fracture.[57,58] **A,** Lateral radiograph of this 35-year-old man shows a posterior fragment of bone projecting from the vertebral body into the spinal canal *(white arrow)*. Observe also the triangular defect in the vertebral body *(black arrow)*. **B,** Transaxial CT image shows a curvilinear rim of avulsed bone projecting into the spinal canal *(white arrow)* and a radiolucent Schmorl node in the posterior vertebral body *(black arrow)*. Posterior apophyseal ring avulsion fractures are often secondary to trauma that results in disc herniation and associated avulsion of the adjacent unfused ring apophysis. CT scanning is excellent for assessing the osseous components, and MR imaging is best suited to the evaluation of the soft tissue abnormalities.

TABLE 4-11 Checklist for the Diagnosis of Clinical Instability in the Lumbar Spine

Element	Point Value
Anterior elements destroyed or unable to function	2
Posterior elements destroyed or unable to function	2
Radiographic criteria	4
Flexion-extension radiographs 1. Sagittal plane translation >4.5 mm or 15% (2 points) 2. Sagittal plane rotation a. >15 degrees at L1-L2, L2-L3, and L3-L4 (2 points) b. >20 degrees at L4-L5 (2 points) c. >25 degrees at L5-S1 (2 points)	
OR 1. Resting radiographs a. Sagittal plane displacement >4.5 mm or 15% (2 points) b. Relative sagittal plane angulation >22 degrees (2 points)	
Cauda equina damage	3
Dangerous loading anticipated	1

Total of 5 or more = unstable.
From White AA, Panjabi MM: Clinical biomechanics of the spine, ed 2, Philadelphia, Lippincott, 1990.

TABLE 4-12 Lumbar Intervertebral Disc Disorders

Entity	Figure(s)	Table(s)	Characteristics
Degenerative disc disease[47,59-62,199]	4-47,		***Spondylosis Deformans***
	4-48,	3-11	Osteophytes and osseous ridging
	4-49	4-14	Subchondral bone sclerosis
			Intervertebral Osteochondrosis
		4-14	Disc space narrowing
		4-13	Intradiscal vacuum phenomenon
			Disc calcification is rare
		4-15	MR imaging signal changes in vertebral body bone marrow
		4-17	Degenerative diseases of the lumbar spine may result in several complications
Annular bulge[60,199]	4-49		Broad-based circumferential bulging of discal material beyond the margins of the vertebral body
			Present in 81% of asymptomatic persons
			Degenerative disc bulges: very common in older persons; often are associated with extensive osteophyte formation, disc space narrowing, and loss of T2-weighted MR imaging signal intensity in the disc secondary to degeneration
Disc herniation			Displaced nucleus pulposus extends through some or all of the fibers of the anulus fibrosus; associated with annular tears
			Anular tears present in 56% of asymptomatic persons
			Three types of herniation relate to increasing stages of severity: protrusion, extrusion, and sequestration
1. Protrusion[60,63,199]	4-50		Displaced nucleus pulposus extends focally through a defect in the annular fibers but still is confined by the intact outermost annular fibers: contained herniation
			Infrequently results in direct nerve root compression
			This type of herniation maintains contact with the disc of origin by a bridge as wide as or wider than any diameter of the displaced material
			Present in approximately 33% of asymptomatic persons
2. Extrusion[63-65,199]	4-51		A larger pattern of disc herniation in which the displaced nucleus pulposus penetrates all of the annular fibers and lies anterior or posterior to the longitudinal ligament: noncontained subligamentous herniation
			The extrusion remains attached to the parent disc and forms a focal extradural mass causing root sleeve or thecal sac impression
			The diameter of the disc material beyond the interspace is wider than the bridge, if any, that connects it to the disc of origin
			Usually associated with symptoms but only infrequently results in cauda equina compression or permanent neurologic deficit
3. Sequestration[64,65,199]	4-52		Free (sequestered) disc fragment is an extrusion that is no longer contiguous with the parent disc
			Displaced nucleus pulposus penetrates or extends around the posterior longitudinal ligament and lies within the epidural space; alternatively, the displaced nucleus, although not extending through this ligament, migrates for a considerable distance cephalad or caudad as a fragment that is separate from the remaining portion of the intervertebral disc: noncontained herniation
			Usually associated with symptoms and commonly results in cauda equina compression or permanent neurologic deficit
Tears of the annulus fibrosus[138,198,199]	4-53		Internal disruption and alteration of the anulus fibrosus in which radial or concentric tears in the anulus fibrosus are detected by MR imaging or discography
			T2-weighted MR imaging sequences show a high-intensity zone (HIZ) in the posterior anular fibers that may enhance further after intravenous gadolinium administration
			Discography reveals contrast coursing to the peripheral portions of the anulus through the annular tears
			May be related to "discogenic pain": in patients without nerve root compression, back pain may be secondary to irritation of the nerve endings of pain fibers in the peripheral portion of the anulus fibrosus from fibrosis or edema within an annular tear

TABLE 4-12 Lumbar Intervertebral Disc Disorders—cont'd

Entity	Figure(s)	Table(s)	Characteristics
Schmorl cartilaginous nodes[66,170-172]	4-54		Intravertebral disc herniation superiorly or inferiorly through the cartilaginous and osseous vertebral endplates, penetrating the spongiosa of the vertebral body Well-defined or poorly defined, punctate contour defect in vertebral endplate, often associated with surrounding osteosclerosis Occasionally painful, but these nodes usually are not associated with neurologic complications Isolated Schmorl nodes may occur with acute trauma, degenerative disc disease, osteoporosis, osteomalacia, Paget disease, hyperparathyroidism, infection, and neoplasm Gadolinium-enhanced MR images reveal that larger Schmorl nodes are often vascularized, are frequently associated with bone marrow edema, and are more common in symptomatic than in nonsymptomatic patients Presence of multiple Schmorl nodes in an adolescent thoracic spine suggests the diagnosis of Scheuermann disease Giant cystic Schmorl nodes and giant fatty Schmorl nodes have been reported and may resemble intravertebral pneumatocysts or fluid-filled cysts Edematous Schmorl nodes also occur, the majority of which do not change over time; occasionally these evolve in size over a short period of time.
Limbus vertebra[67]	4-55		Intravertebral herniation of disc material extending beneath the vertebral ring apophyseal ossification center, separating it from the vertebral body Disc material also may dissect underneath the anterior longitudinal ligament, causing pressure erosions of the body or displacing the ligament anteriorly along with the attached apophyseal ring fragment Often the limbus fragment fails to fuse to the vertebral body and persists into older age, frequently resulting in extensive degenerative change, especially osteophyte formation Most limbus vertebrae occur anteriorly, but posterior limbus vertebrae also may occur, often resulting in severe nerve root compression with neurologic deficit
Apophyseal ring fracture (posterior limbus vertebra)[57,58]	4-46 Table 4-9		Avulsion fracture of the posterior aspect of the ring apophysis associated with disc protrusion
Juvenile lumbar osteochondrosis[68]	4-56		Usually begins in adolescents and young adults and is more common in competitive athletes and in persons from rural communities Men > women Closely resembles Scheuermann disease but usually is localized to the thoracolumbar and lower lumbar regions and may not be associated with thoracic kyphosis Multiple Schmorl nodes, limbus vertebrae, undulating vertebral endplate surfaces, and posterior disc displacements Many cases are asymptomatic but others are associated with low back pain, sciatica, and intermittent nonvascular claudication in the lower extremities *Possible pathogenesis:* repeated axial compression of the spine with injury to the cartilaginous endplates
Juvenile degenerative disc disease[192]			Extremely rare condition in which patients under the age of 21 years have chronic low back pain with degenerative disc disease identified on MR imaging May have concomitant developmental (congenital) spinal stenosis
Epidural hematoma[174,175]	4-57		Epidural hematoma (EDH) may resemble a disc protrusion, extrusion, or sequestration and should be considered in the differential diagnosis Spontaneous EDH frequently associated with disc protrusion and acute events, such as sneezing and coughing MR imaging can reliably identify EDH and distinguish between EDH and disc protrusion, extrusion, or sequestration Most cases resolve without surgery

TABLE 4-13 Vertebral Gas Collections: Vacuum Phenomena[59,129,163,164]

Location	Causes
Intervertebral disc	Degenerative disc disease Extrusion of a disc fragment Vertebral collapse Trauma
Vertebral body	*Steroid-induced ischemia:* osteonecrosis Posttraumatic vertebral collapse of Kümmel Intraosseous pneumatocyst Intraosseous disc displacement: Schmorl node
Apophyseal joints	Degenerative joint disease Juxtafacet synovial cyst
Spinal canal	Idiopathic Synovial cyst
Soft tissues	Surgery

TABLE 4-14 Intervertebral Disc Space Narrowing and Adjacent Sclerosis

Entity	Figure(s)	Mechanism	Radiographic Appearance	Vacuum Phenomena
Degenerative disc disease	4-47, 4-48, 4-49	Degeneration of disc and cartilaginous endplate Schmorl nodes	Disc space narrowing Well-defined sclerotic vertebral margins	Present
Trauma	4-47, 4-48, 4-49	Disc injury and degeneration Schmorl nodes	Disc space narrowing Well-defined sclerotic vertebral margins Fracture Soft tissue mass	Variable
Neuropathic osteoarthropathy	See Figure 4-120	Loss of sensation and proprioception with repetitive trauma	Disc space narrowing Extensive vertebral body sclerosis Osteophytosis Fragmentation Malalignment	Prominent
Rheumatoid arthritis	See Figure 4-73	Apophyseal joint instability with recurrent discovertebral trauma or Inflammatory tissue extending from neighboring articulations	Disc space narrowing Poorly defined or well-defined sclerotic vertebral margins Subluxation Apophyseal joint abnormalities (Usually confined to the cervical spine)	Absent
Calcium pyrophosphate dihydrate crystal deposition disease	See Figure 4-79	Crystal deposition in cartilaginous endplate and intervertebral disc with degeneration	Disc space narrowing Calcification Poorly defined or well-defined sclerotic vertebral margins Fragmentation Subluxation	Variable
Alkaptonuria	See Figure 4-80	Crystal deposition in cartilaginous endplate and intervertebral disc with degeneration	Disc space narrowing Well-defined sclerotic vertebral margins Extensive disc calcification	Prominent
Infectious spondylodiscitis	See Figures 4-82, 4-83	Pyogenic or tuberculous osteomyelitis and spondylodiscitis	Disc space narrowing Poorly defined sclerotic vertebral margins Soft tissue abscess	Absent

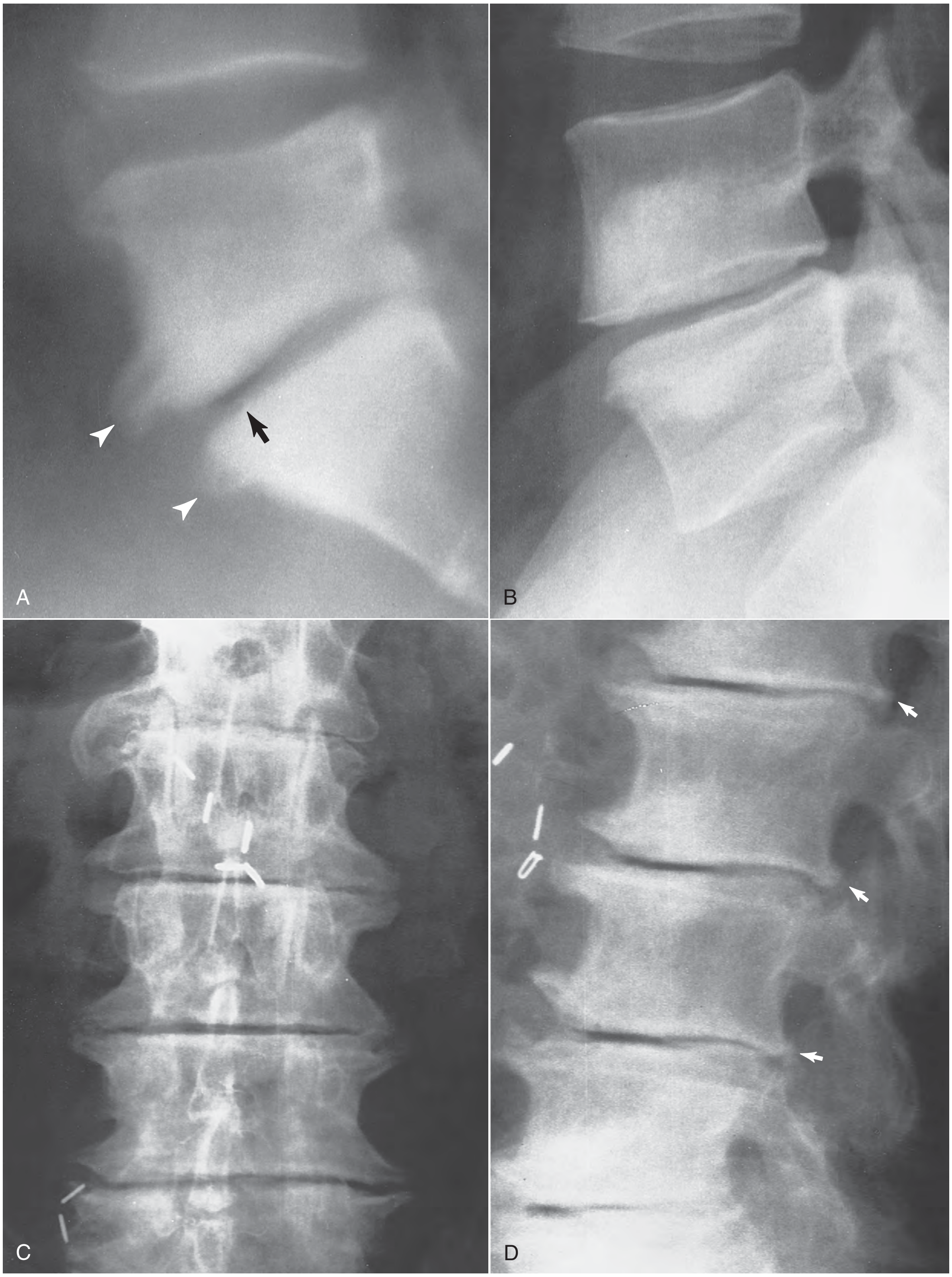

FIGURE 4–47 Degenerative disc disease.[47,59-61] **A,** Lateral conventional tomogram demonstrates disc space narrowing, intradiscal gas (vacuum phenomenon) *(arrow),* osteophytes *(arrowheads),* and sclerosis of the adjacent vertebral bodies. **B,** Observe the disc space narrowing and vertebral body sclerosis at the L4-L5 level in this 47-year-old woman. This pattern of vertebral body sclerosis, especially when it is an isolated finding, is termed *idiopathic segmental sclerosis* or *hemispheric spondylosclerosis* and may simulate osteoblastic skeletal metastasis. **C-D,** In this 68-year-old man, extensive disc space narrowing, osteophytes, vacuum phenomena, and vertebral body sclerosis are evident. Observe also the posterior osteophytes *(arrows)* that may contribute to foraminal and central canal stenosis.

Continued

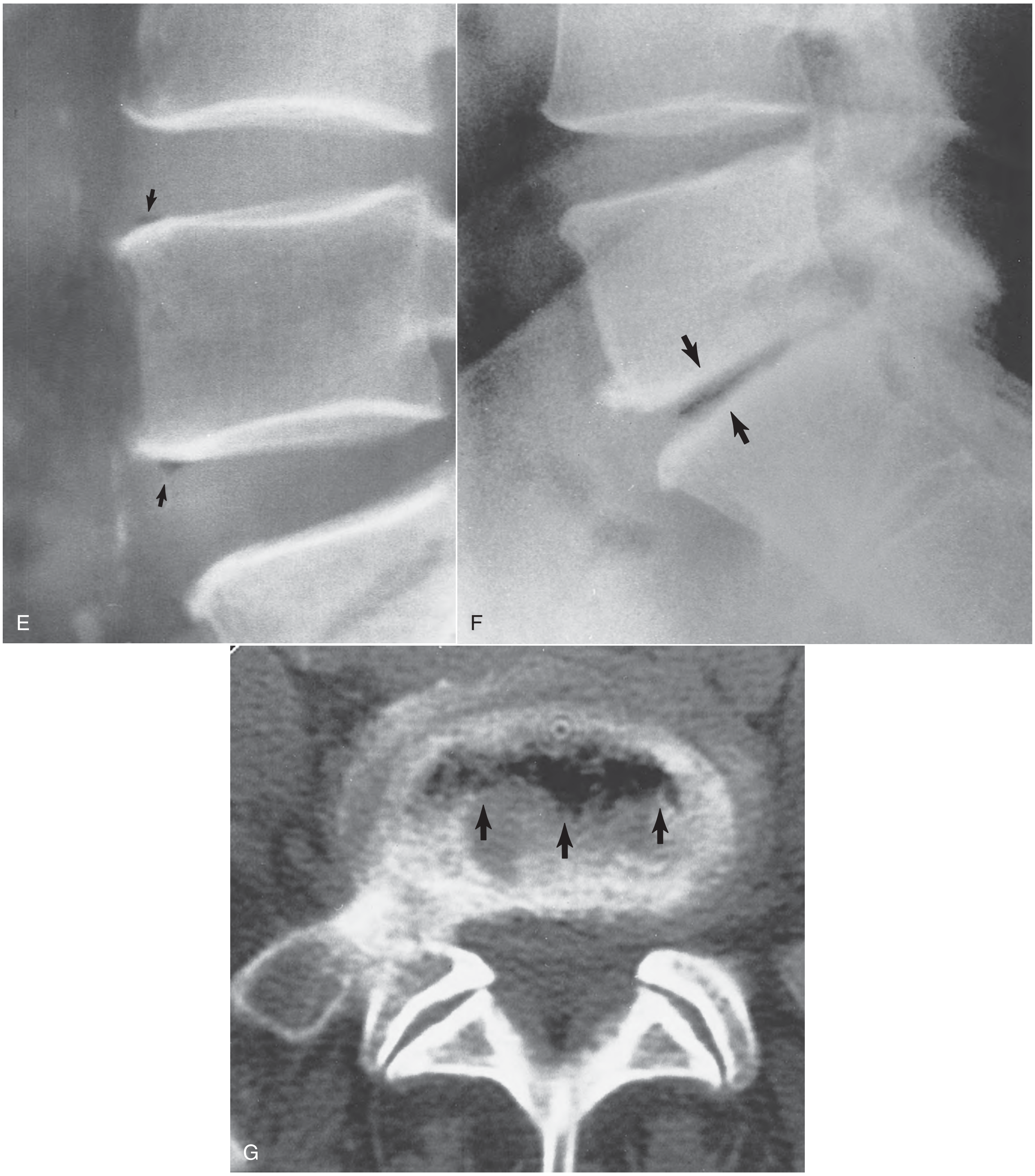

FIGURE 4–47, cont'd **E,** In another patient, small collections of gas within the disc are localized to the discovertebral junctions adjacent to the L4 vertebral body *(arrows)*. These focal vacuum phenomena probably are the result of annular degeneration. In the presence of acute trauma, especially in the cervical spine, these tiny "annular vacuum clefts" represent acute injuries of the annular fibers. **F,** Lumbosacral degenerative disc disease is evident in a 58-year-old man with severe disc space narrowing, vacuum phenomenon *(arrows),* traction osteophytes, and subchondral sclerosis. **G,** Vacuum phenomenon: CT scan findings. Transaxial CT scan shows a collection of gas *(arrows)* within the degenerated L5-S1 intervertebral disc. On routine lateral radiographs, a posterior disc height of the lumbosacral junction measuring less than 5.4 mm reliably indicates degenerative disc disease. Conversely, L5 posterior disc height measurements of more than 7.7 mm indicate the absence of degenerative disc disease. *(**F,** Reprinted with permission from Taylor JAM, Hoffman LE: The geriatric patient: diagnostic imaging of common musculoskeletal disorders. Top Clin Chiropr 3:23, 1996.)*

TABLE 4-15 Magnetic Resonance (MR) Imaging of Vertebral Body Bone Marrow in Degenerative Disc Disease*

		MR Imaging Signal Changes		
Type	**Figure(s)**	**T1-Weighted**	**T2-Weighted**	**Characteristics**
I	4-48, *A-B*	Decreased	Increased	Fibrovascular marrow changes 4%† May enhance with gadolinium contrast agent administration
II	4-48, *C-D*	Increased	Isointense or increased	*Fatty marrow changes:* conversion of hematopoietic to fatty marrow 16%†
III		Decreased	Decreased	*Sclerotic marrow changes:* absence of bone marrow in regions of osteosclerosis Associated with considerable sclerosis on radiographs

* Adapted from Modic MT, Steinberg PM, Ross JS, et al: Degenerative disc disease: assessment of changes in vertebral body marrow with MR imaging. Radiology 166:193, 1988. See also ref 186.

† Percentage of patients undergoing MR imaging examination for lumbar disc disease who exhibit these findings.

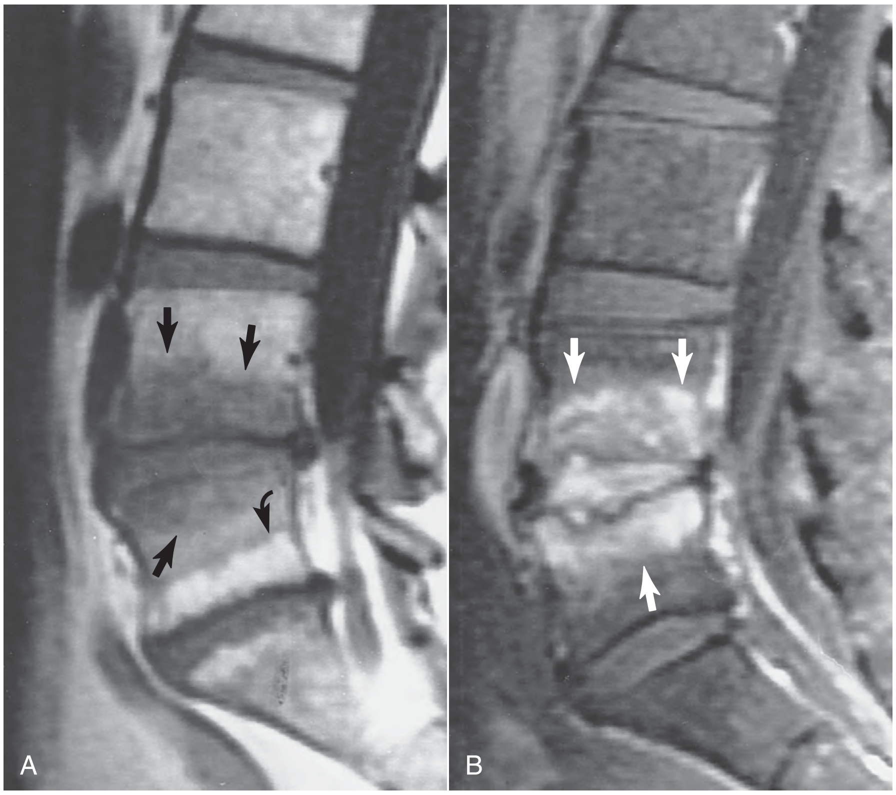

FIGURE 4–48 Degenerative disc disease: magnetic resonance (MR) imaging of marrow changes within the vertebral body.[62,165,173] **A-B,** Type I changes. In **A,** a sagittal T1-weighted (TR/TE, 600/20) spin echo MR image demonstrates degenerative disc narrowing at the L4-L5 level with decreased signal intensity *(straight arrows)* of the adjacent subchondral bone. Fat is seen within the subchondral marrow adjacent to the L5-S1 disc *(curved arrow)*. In **B,** another sagittal T1-weighted spin echo MR image obtained with fat suppression after administration of gadolinium contrast agent demonstrates increased signal intensity of the adjacent subchondral bone *(arrows)*.

Continued

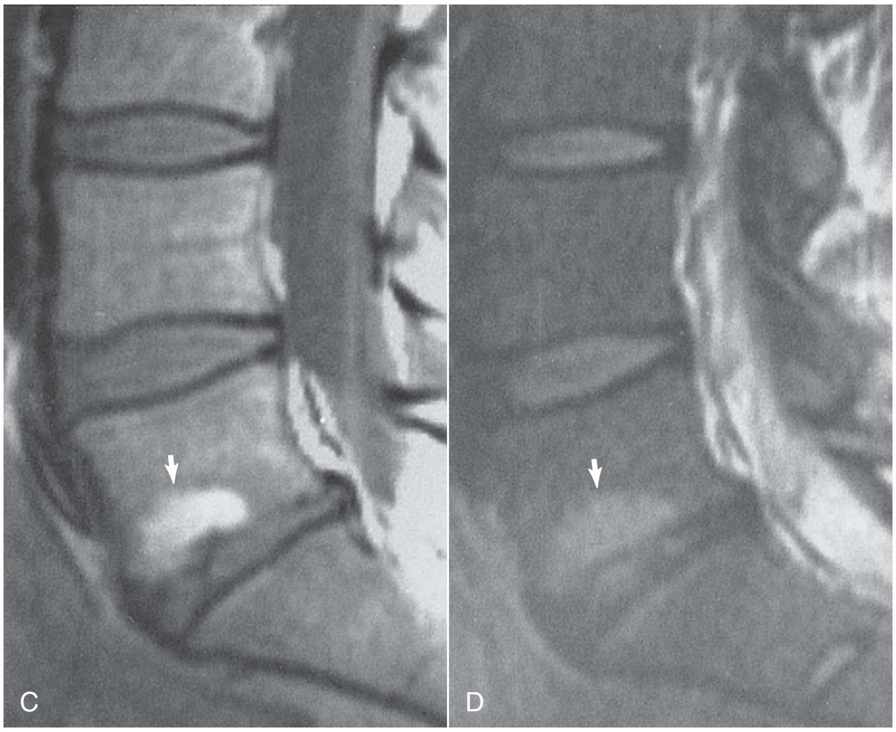

FIGURE 4–48, cont'd **C-D,** Type II changes in a 34-year-old woman with low back pain. In **C,** a sagittal proton density-weighted (TR/TE, 1000/20) spin echo MR image demonstrates degenerative disc narrowing at the L5-S1 level with a focus of increased signal intensity within the adjacent subchondral bone of the L5 vertebral body *(arrow)*. In **D,** a T2-weighted (TR/TE, 1000/90) spin echo MR image also exhibits increased signal intensity within the vertebral body *(arrow)* (Table 4-15). Endplate marrow signal intensity changes are also present in the lumbar spine of some asymptomatic subjects.

TABLE 4-16 **Prevalence of Disc Abnormalities on Magnetic Resonance Imaging in Asymptomatic Subjects***

Study, Year	Age Range (mean) Years	Number of Subjects	HNP	Bulging Disc	Degenerated Disc	HIZ	Other
Weishaupt, 1998[201]	20-50 (35)	60	60%	20%	72%	33%	NR contact or deviation 26%; NR compression, 2%
Stadnik, 1998[202]	17-71 (42)	36	33%	81%	72%	56%	
Boos, 1995[203]	20-50 (36)	46	76%	51% of discs	85%	14%	No sequestered disc; NR contact or deviation, 22%; disc bulge, protrusion, or extension, 64%
Jensen, 1994[204]	20-80 (42)	98	28%	52%			
Boden, 1990[205]	<60	53	22%	54%	46%		
	>60	14	36%	79%	93%		
Weinreb, 1989[206]	19-34 (28) females	86	9%	44%			

HNP, Herniated nucleus pulposus; *HIZ,* high-intensity zone; *NR,* nerve root.

* Adapted with permission from McCall I: Degenerative disorders of the spine. In: Pope TL, Bloem HL, Beltran J, et al (ed): Imaging of the musculoskeletal system. Philadelphia, Saunders Elsevier, 2008, p 1074.

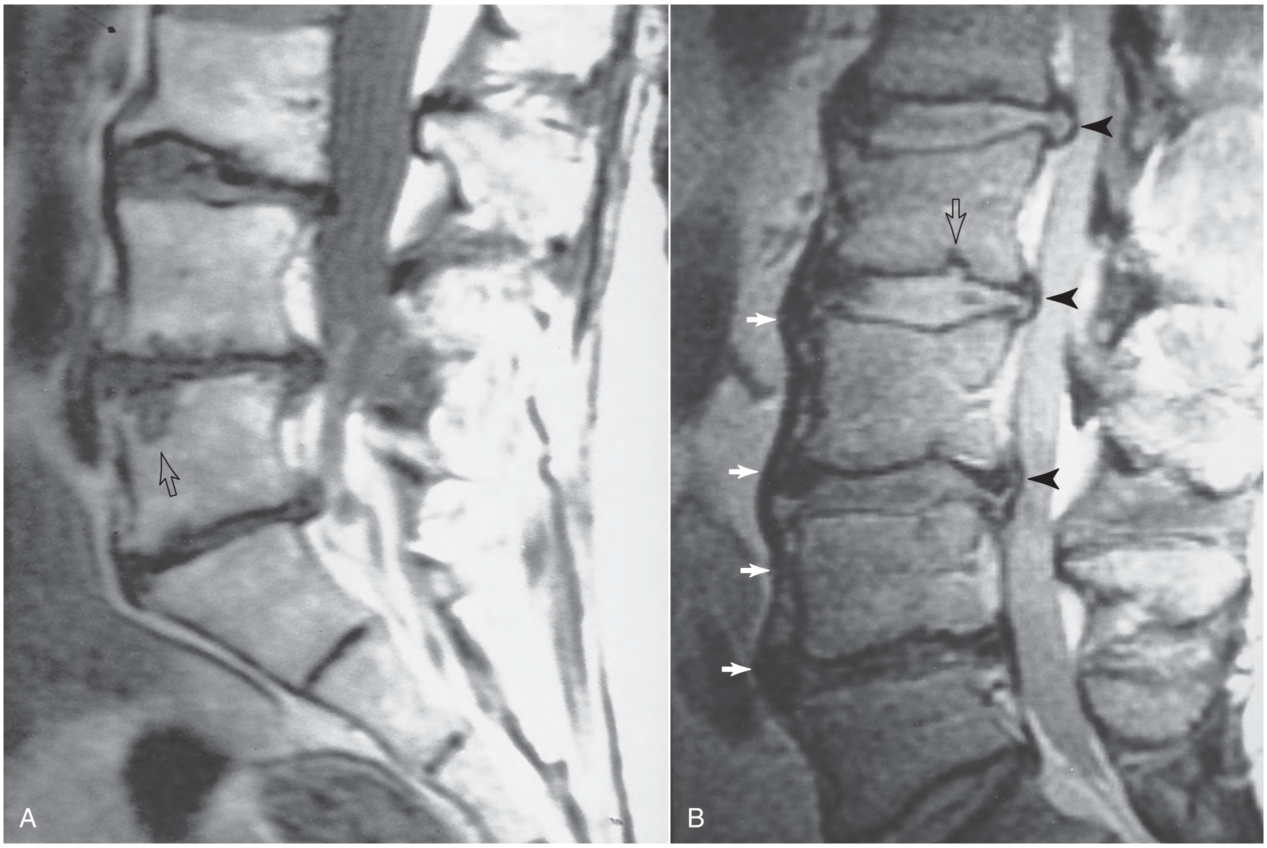

FIGURE 4–49 **Degenerative disc disease and annular bulges: magnetic resonance (MR) imaging abnormalities.**[60] **A,** Sagittal T1-weighted (TR/TE, 733/16) fast spin echo MR image of this 75-year-old woman shows extensive disc space narrowing and degenerative disc bulges at several levels. **A,** Schmorl (cartilaginous) node representing intravertebral disc displacement also is present *(open arrow)*. **B,** Midsagittal proton density-weighted (TR/TE, 2500/30) spin echo MR image reveals decreased signal intensity of the L3-L4, L4-L5, and L5-S1 lumbar discs and posterior degenerative disc bulges at the L1-L2, L2-L3, and L3-L4 levels *(arrowheads)*. **A,** Schmorl node is evident in the L2 inferior endplate *(open arrow)*. In addition, the anterior longitudinal ligament is stripped away from the vertebral bodies by anterior disc bulges and osteophytes *(white arrows)*.

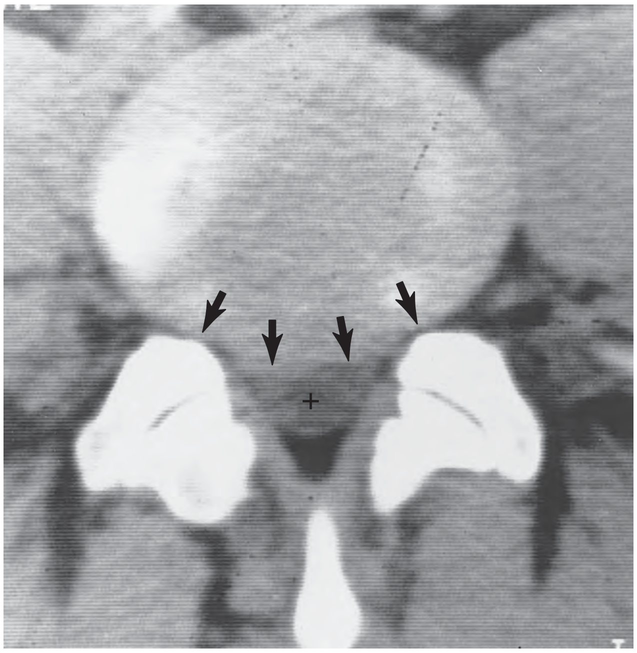

FIGURE 4–50 **Intervertebral disc protrusion: CT scan abnormalities.**[60,63] Transaxial CT image shows a broad-based central disc protrusion *(black arrows)* that displaces the thecal sac (+) and virtually obliterates the nerve root canals.

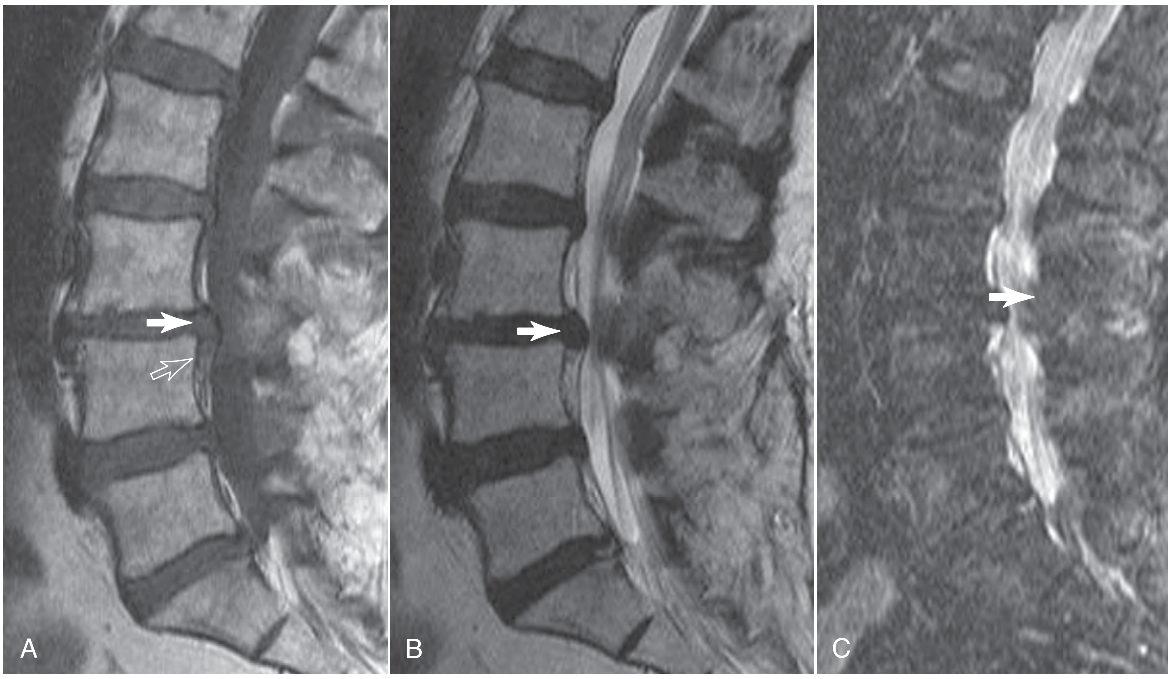

FIGURE 4–51 **Intervertebral disc extrusion: magnetic resonance (MR) imaging.**[64,65] This 69-year-old woman presented with severe back pain and lower extremity radiculopathy. Sagittal T1-weighted **(A),** T2-weighted **(B),** and STIR **(C)** MR images reveal a large extruded L3-L4 disc extrusion *(arrows)*. The T1-weighted image **(A)** reveals that the extruded disc material displaces inferiorly underneath the posterior longitudinal ligament *(open arrow)*. The extruded material results in significant thecal sac compression, but it is still contiguous with the parent disc.

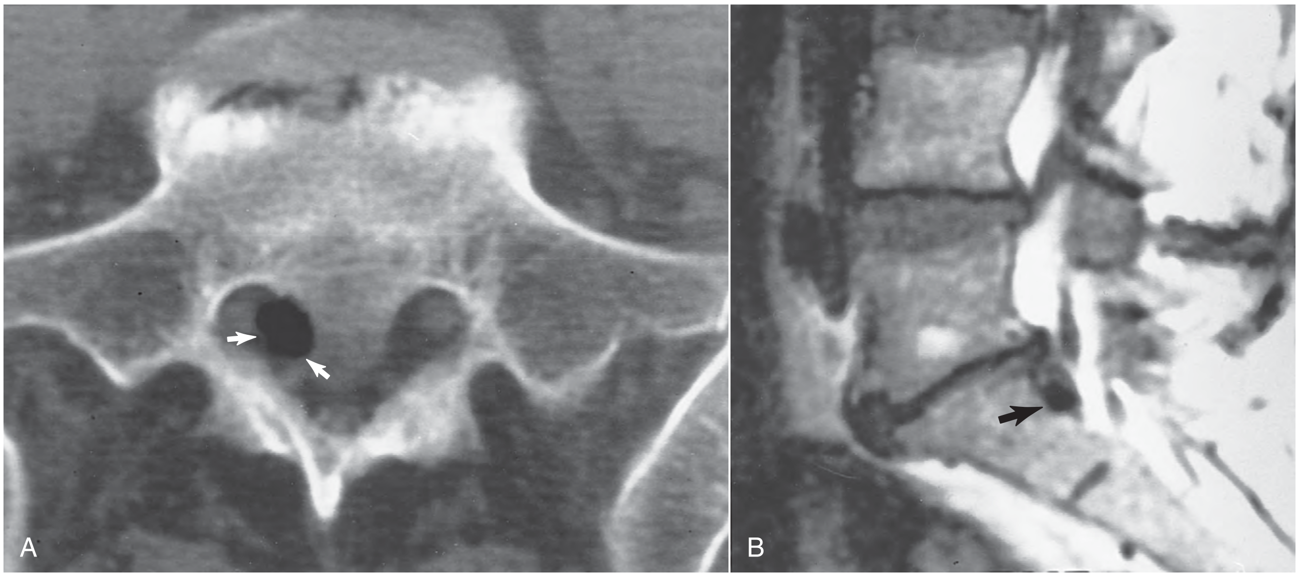

FIGURE 4–52 **Intervertebral disc sequestration.**[64,65] **A-B,** Sequestrated fragment with intradiscal vacuum phenomenon. In **A,** a transaxial CT image at the S1 level reveals an intradiscal vacuum phenomenon seen as a radiolucent collection of gas *(arrows)* within a large noncontained L5-S1 disc sequestration. In **B,** a sagittal T1-weighted (TR/TE, 400/17) spin echo MR image of the same patient shows a focal area of signal void corresponding to the gas collection within the disc fragment *(arrow)*. The L5-S1 disc is narrowed and the L4-L5 disc bulges posteriorly. A focal collection of fat is evident in the fifth lumbar vertebral body.

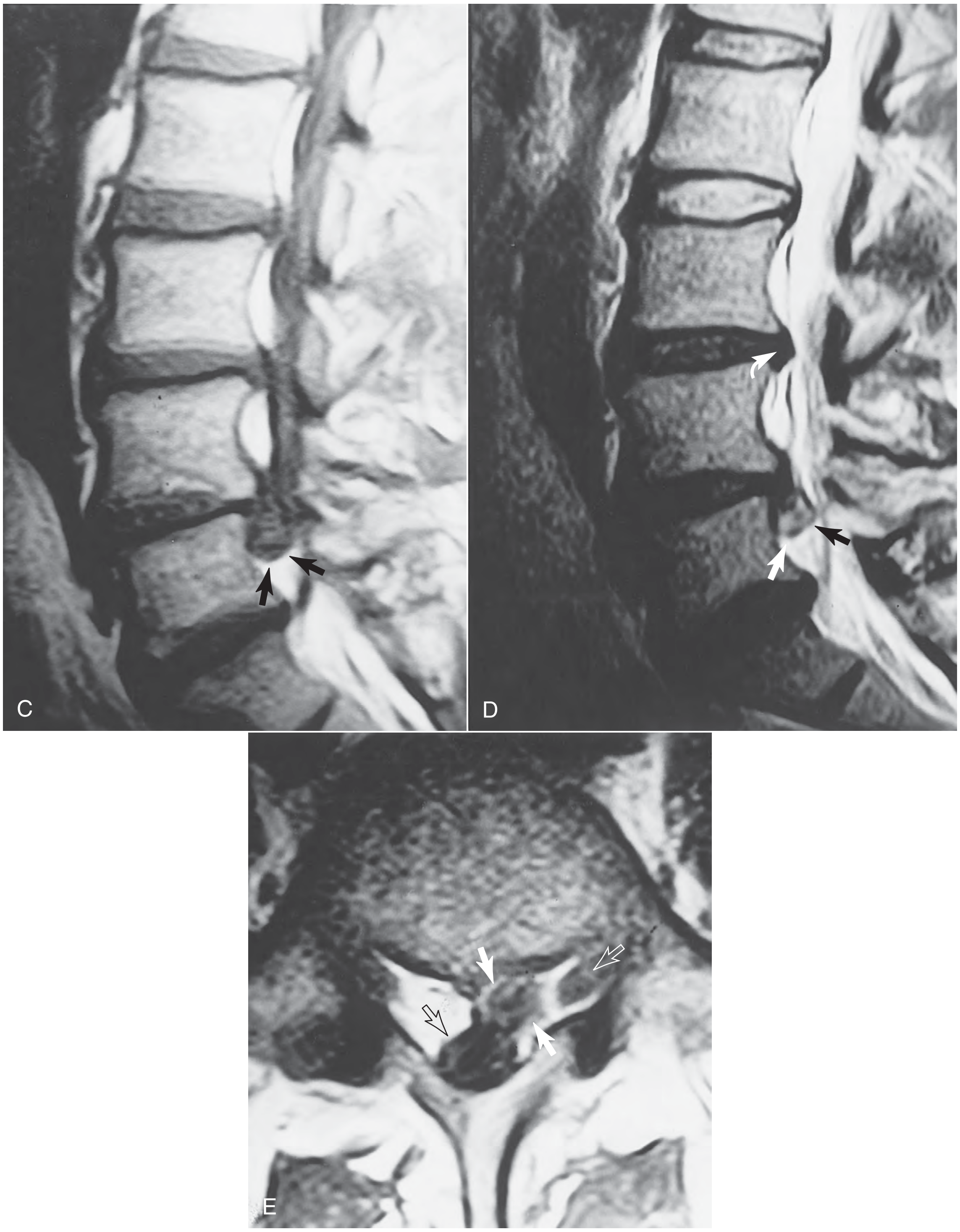

FIGURE 4–52, cont'd **C-E,** MR images from another patient with severe low back pain and radiculopathy. In **C,** a sagittal T1-weighted (TR/TE, 457/20) spin echo MR image reveals a lobulated mass of intermediate to low signal intensity *(arrows)* within the spinal canal posterior to the L5 vertebral body and adjacent to a severely degenerated L4-L5 disc. In **D,** the sagittal T2-weighted (TR/TE, 3000/96) fast spin echo MR image reveals heterogeneous signal intensity within the noncontained mass *(arrows)*. A contained L3-L4 disc protrusion also is present *(curved arrow)*. In **E,** a transaxial T1-weighted (TR/TE, 744/20) spin echo MR image through the lesion at the level of the L5 lateral recess shows the sequestrated fragment *(arrows)* displacing the thecal sac posteriorly *(black open arrow)* and abutting on the nerve root *(white open arrow)*. (***A-B,*** *Courtesy S. Eilenberg, San Diego;* ***C-E,*** *Courtesy L. Ramos, DC, Berlin, NH.)*

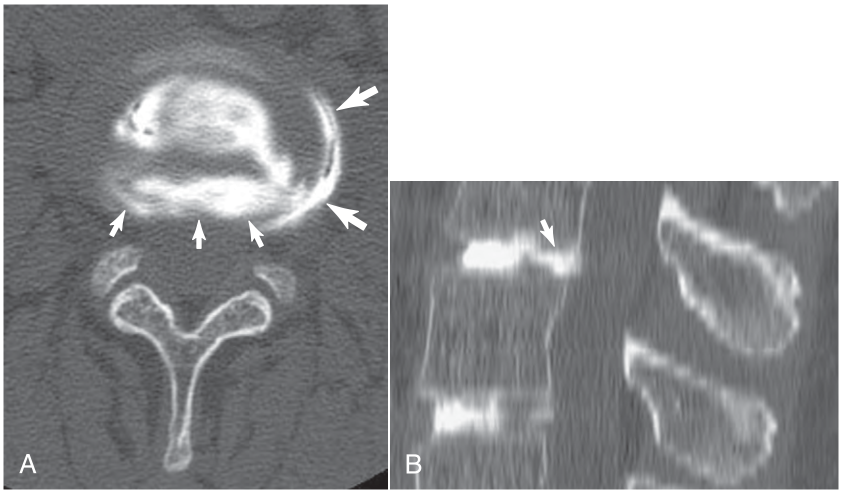

FIGURE 4–53 **Tears of the annulus fibrosus (internal disc derangement): CT-discography.**[198,199] This 50-year-old woman with discogenic back pain had radiopaque contrast material injected into the nucleus pulposus of L3-4 and L4-5 followed by CT scanning. An axial image at the L3-L4 level **(A)** and a reformatted sagittal image of the L3-L4 and L4-L5 levels **(B)** reveal extravasation of contrast material into tears in the posterior annular fibers *(thin arrows)* and in a concentric pattern in the peripheral lateral annular fibers *(thick arrows)*. Discography is often used as a provocative test to determine the anatomic origin of discogenic pain.

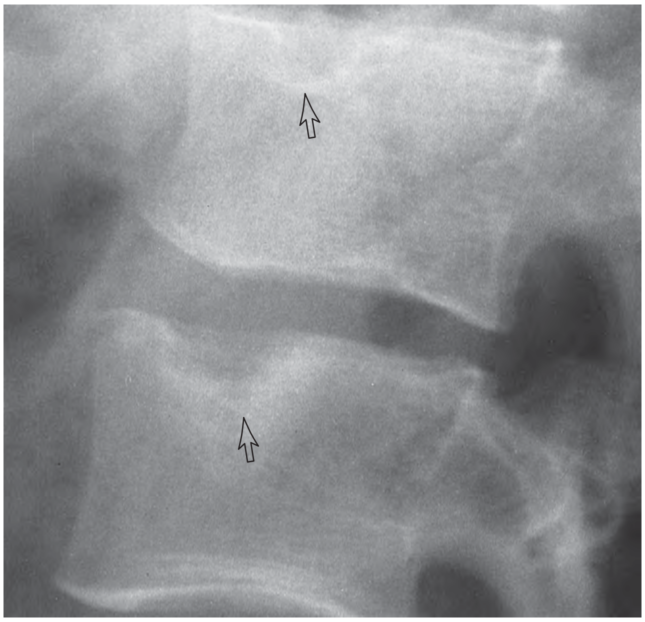

FIGURE 4–54 **Schmorl (cartilaginous) nodes.**[66,170-172] Schmorl nodes are evident in two adjacent vertebral bodies in this patient with Scheuermann disease. Observe both the irregularity of the vertebral endplate surfaces and focal radiolucent depressions with adjacent sclerotic margins (*open arrows)*. Schmorl nodes represent displacements of intervertebral disc tissue into the vertebral body and are caused by an abnormality of the discovertebral junction.

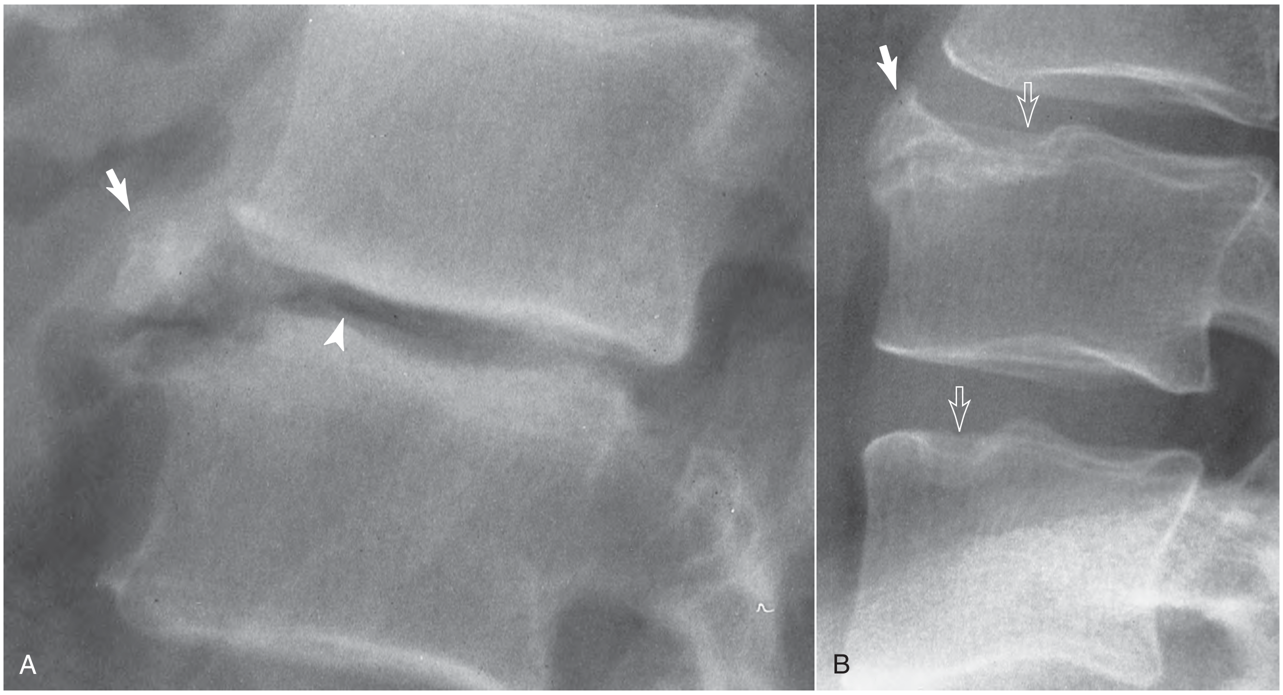

FIGURE 4–55 Limbus vertebra.[67] **A,** A triangular, sclerotic bone fragment *(arrow)* is seen adjacent to the anterosuperior margin of the vertebral body. Note the radiolucent cleft separating the fragment from the vertebral body. Significant degenerative disease with a vacuum disc phenomenon also is present *(arrowhead)*. **B,** Lateral radiograph of a 38-year-old man demonstrates anterior Schmorl nodes *(open arrows)* within the superior vertebral endplates of L4 and L5. At L4, the triangular osseous fragment, or limbus vertebra *(arrow)*, represents the residual apophyseal ring that was separated from the vertebral body during adolescence. Associated degenerative changes also are apparent.

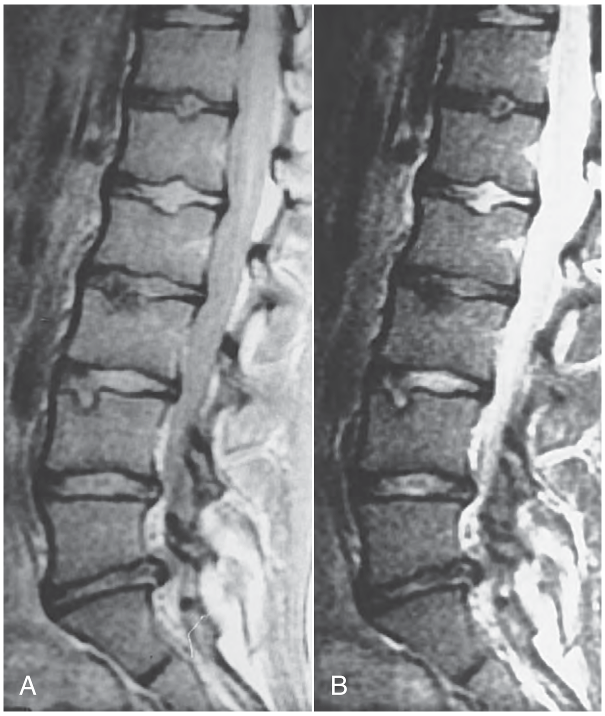

FIGURE 4–56 Juvenile lumbar osteochondrosis (lumbar Scheuermann disease).[68] **A-B,** Sagittal proton density-weighted (TR/TE, 2500/30) **(A)** and T2-weighted (TR/TE, 2500/70) **(B)** spin echo MR images from this 15-year-old boy demonstrate Schmorl nodes, endplate irregularities, and intervertebral disc calcification. Low signal intensity of the L2-L3 and L5-S1 discs and posterior disc displacement at the L4-L5 and L5-S1 levels also are evident. *(Courtesy C. Gundry, MD, Minneapolis, Minn.)*

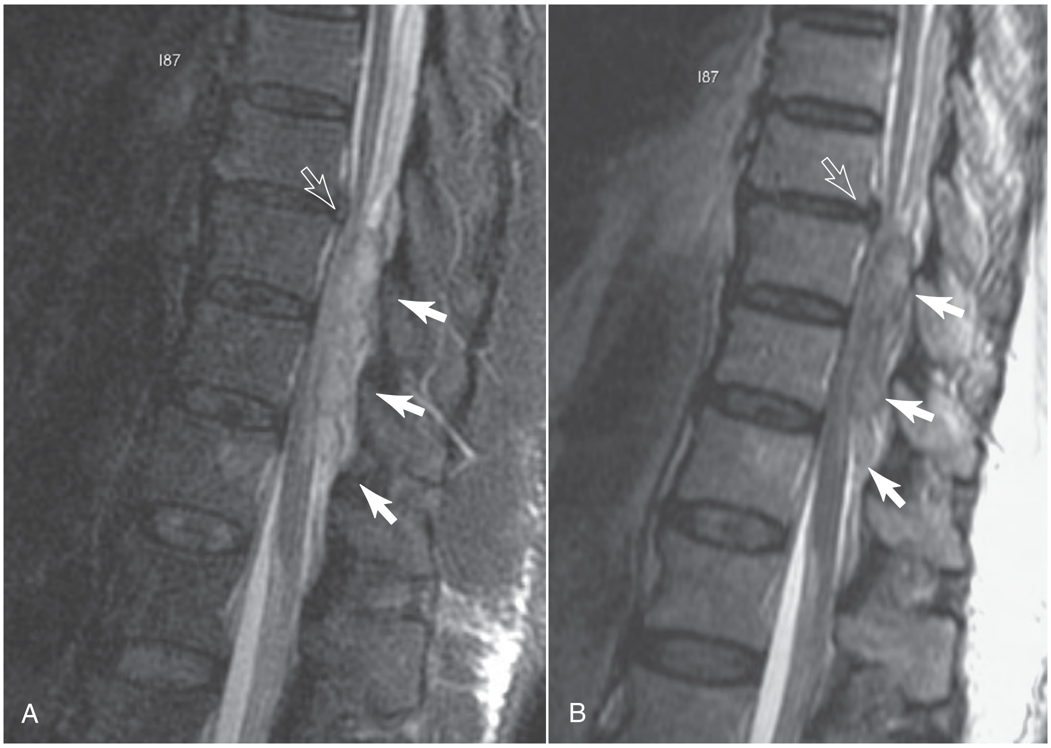

FIGURE 4–57 Spontaneous epidural hematoma.[174,175] This 70-year-old woman has neurologic deficits. Sagittal T2-weighted images with **(A)** and without **(B)** fat suppression reveal an elongated lobulated mass occupying over 75% of the spinal canal at the lower thoracic region (*arrows),* resulting in significant compression of the cord. Note the adjacent disc protrusion (*open arrows).* Epidural hematomas are not common, but when they occur they are often associated with disc protrusion and acute events, such as sneezing and coughing. MR imaging can reliably identify EDH and distinguish between EDH and disc protrusion, extrusion, or sequestration.

TABLE 4-17 Complications of Degenerative Disease of the Lumbar Spine

Entity	Figure(s)	Characteristics
Alignment Abnormalities		
Segmental instability[43,44,69,165,166]	4-58	Excessive or abnormal motion associated with degenerative disease of the lumbar spine ***Findings suggestive of lumbar instability*** Static radiographic findings: Gas within disc Traction osteophytes Radial fissure in disc during discography Retrolisthesis Degenerative or spondylolytic (isthmic) spondylolisthesis Functional radiographic findings on flexion-extension radiographs: Forward or backward displacement of one vertebra on another in excess of 3 to 4 mm Narrowing of intervertebral foramina Loss of disc height Disc wedging in excess of 12 to 20 degrees *Possible causes:* trauma, spondylolisthesis, other pathologic processes, and spine surgery
Degenerative spondylolisthesis[39,70-72,165,187]	4-59	See Table 4-5
Degenerative retrolisthesis[39,165,189]	4-60	Posterior vertebral displacement of one segment on another secondary to degenerative disc disease Decreased height of intervertebral disc, closer approximation of vertebral bodies, and gliding or telescoping of the corresponding articular processes ***Imaging findings*** Vacuum phenomenon, disc space narrowing, vertebral body marginal sclerosis, osteophytes, apophyseal joint instability and subluxation with posteroinferior displacement of the inferior articular processes of the upper vertebra in relation to the subjacent level L2 on L3 affected most commonly, but also occurs above and below this level Clinical findings are variable and include the following: pain, difficulty with trunk flexion or extension, spinal rigidity, and neurologic abnormalities related to stenosis and cord compression
Degenerative lumbar scoliosis[47,71,72]	4-61	Scoliosis in elderly persons that is associated with extensive degenerative changes; the scoliosis often precedes the degenerative changes, and the curve may progress slowly with continued degeneration ***Imaging findings*** Eccentric disc space narrowing, vertebral body sclerosis, osteophytes, vacuum phenomena, and apophyseal joint degeneration predominating on the concave side of the curve Clinical findings vary from asymptomatic cases to disabling low back and lower extremity pain, weakness, and neurogenic claudication *Far-out syndrome:* impingement of the fifth lumbar spinal nerve between the L5 transverse process and the sacrum; complication of degenerative lumbar scoliosis
Degenerative lumbar kyphosis[47,184]		Marked loss or even reversal of the lumbar lordosis in patients with extensive degenerative spine disease ***Imaging findings*** Loss of sacral base inclination, narrowing of disc spaces, decreased height of anterior portion of lumbar vertebral bodies ***MR imaging findings*** Lumbar paraspinal muscles have smaller cross-sectional area and higher proportion of fat deposits than controls ***Differential diagnosis*** Acquired lumbar kyphosis[179] caused by primary paraspinal tardive myopathy; Also termed *bent spine syndrome* (BSS); results in major functional disability and pain that worsens over time
Baastrup disease[47,194]	4-62	Degenerative changes of the spinous processes and intervening interspinous soft tissues characterized by enlarged spinous processes with flattened, sclerotic superior and inferior margins that approximate each other during trunk extension May develop interspinous bursae Often painful on trunk extension

Continued

TABLE 4-17 Complications of Degenerative Disease of the Lumbar Spine—cont'd

Entity	Figure(s)	Characteristics
Intervertebral Disc Displacement		
Anterior, posterior, superior, or inferior disc displacement		See Table 4-12
Vertebral Body Sclerosis		
Segmental sclerosis of vertebral bodies[73,165]	4-63	Osteosclerosis of the vertebral body, which may occur alone or adjacent to a degenerative disc, associated with loss of disc height and vacuum phenomena Predilection for L3 and L4 anteroinferior vertebral bodies; may affect two adjacent vertebral bodies *Magnetic resonance (MR) imaging:* decreased signal on T1-weighted images; increased signal on T2-weighted images (resembling type I marrow changes and infectious spondylodiscitis) *Synonyms:* hemispherical spondylosclerosis, pseudoinfection of the disc, nonneoplastic sclerosis of the vertebral body, idiopathic segmental sclerosis of the vertebral body, traumatic lesion of the discovertebral junction Also prominent in association with Schmorl cartilaginous nodes Differential diagnosis of vertebral sclerosis includes infection, neoplasm, Paget disease, osteopetrosis, and renal osteodystrophy (Tables 4-14 and 4-20)
Intervertebral Disc Calcification and Ossification		
Calcification[47,185]	4-64	Chronic degenerative calcific deposits in older persons occur primarily in the anulus fibrosus of elderly persons Men > women Prevalence increases with age and extent of disc space narrowing Unclear what proportion of these patients have symptoms Calcification predominates in the midthoracic and upper lumbar intervertebral discs and may be associated with disc displacement
Ossification[47]		Disc degeneration or trauma may lead to proliferation of both fibrous tissue and blood vessels through clefts in the cartilaginous endplate; hypervascularity stimulates ossification within the intervertebral discs Ossified tissue possesses trabeculae, may simulate osteophytes, and may lead to decreased mobility
Spinal Stenosis		
General concepts[167,193]		Three types based on anatomic site of involvement: central, lateral recess, and foraminal stenosis Degenerative stenosis predominates in the lower lumbar segments and further complicates existing developmental stenosis Osteophytes, posterior or posterolateral disc displacements, apophyseal joint hypertrophy and subluxation, enlarged laminae, and buckling or hypertrophy of the ligamenta flava may all contribute to spinal canal narrowing Measurements of stenosis on routine radiographs may be misleading; cross-sectional CT or MR imaging and clinical correlation are necessary to fully evaluate patients with suspected stenosis Axial loading increases the severity of lumbar canal stenosis; the effect of axial loading on MR imaging examination is greatest at the L4-5 and L5-S1 levels.
Central stenosis[74,157,162,165]	4-65	***Imaging findings*** Distortion of normal canal configuration by hypertrophic changes Compression of thecal sac in an anteroposterior direction Obliteration of adjacent epidural fat ***Lumbar spine radiographic measurements*** 1. Eisenstein method for sagittal canal measurement Lower limits of normal 15 mm: suggests stenosis 12 mm: unequivocal evidence of stenosis 2. Interpedicle method coronal canal measurement: Lower limits of normal 20 mm at any lumbar level: suggests stenosis

TABLE 4-17 Complications of Degenerative Disease of the Lumbar Spine—cont'd

Entity	Figure(s)	Characteristics
		CT and MR imaging measurements *Lower limits of normal:* 11.5-mm midsagittal diameter 16-mm coronal diameter (interpedicle distance) Patients with a cross-sectional area of the lumbar spinal canal below 70 mm^2 have significantly greater functional disability than patients with larger cross-sectional areas.
Lateral (subarticular) recess stenosis[47,74,165]	4-66, 4-67	Bone hypertrophy about the superior articular process may result in lateral recess stenosis with compression or displacement of the nerve root or epidural and perineural fat ***Borders of the lateral recess*** *Anterior:* posterior surface of vertebral body *Posterior:* superior articular process and pars interarticularis *Lateral:* medial margin of pedicle ***CT and MR imaging measurements*** Anteroposterior dimension is measured at the superior aspect of the pedicle *4-5 mm:* highly suggestive of lateral recess stenosis *Less than 3 mm:* definite lateral recess stenosis
Foraminal stenosis[47,74,178]	4-65, 4-66	Nerve root occupies the uppermost region of the foramen directly beneath the pedicle of the upper vertebra; stenosis of this region is more significant than stenosis of the lower portion of the foramen ***Borders of the intervertebral foramen*** *Anterior:* posterior aspect of vertebral bodies and disc *Superior:* pedicle of upper vertebra *Inferior:* pedicle of lower vertebra *Posterior:* superior articular process and pars interarticularis Foraminal stenosis may be caused by posterolateral disc displacements, osseous ridges or osteophytes arising from the posterior aspect of the vertebral body, synovial cysts, or postoperative fibrosis Radiography may show foraminal stenosis from osteophytes, but it is insensitive to soft tissue findings and correlates poorly with clinical findings CT and MR imaging reveal displacement or distortion of the exiting nerve root and the surrounding epidural or perineural fat
Degenerative Cysts[183,189]		Some cysts are incidental findings whereas others may produce acute or chronic symptoms Most occur within the central spinal canal or less frequently within the neural foramen or perispinal tissues and may compress neural structures or result in erosion of adjacent osseous vertebral structures Identified on MR imaging as fluid-filled epidural masses
Synovial juxtafacet joint cysts	4-67	Most common type of intraspinal degenerative cyst and occur with facet joint osteoarthrosis or trauma L4-L5 most common site lateral epidural space; more common in females Often synovial lined and communicate with the facet joint articulation
Ligamentum flavum cysts		Nonsynovial lined Occur in relation to ligamentous pseudocystic degeneration or hemorrhage adjacent to the ligamentum flavum
Disc cysts		Pseudocystic foci that communicate with and develop adjacent to disc protrusions usually in the ventrolateral epidural space May evolve from a previous epidural hematoma or softening and fluid production in a degenerated and herniated disc resulting in external spillage of fluid that is subsequently encapsulated by a pseudomembrane
Ganglion cysts of the posterior longitudinal ligament		Rare manifestation of ligamentous degeneration, and is presumed to be related to mechanical stress Occur mostly in young men
Cysts associated with Baastrup disease		Cystic extensions from interspinous bursae that may project into the posterior epidural space, into perispinal tissues, or within the interspinous space itself

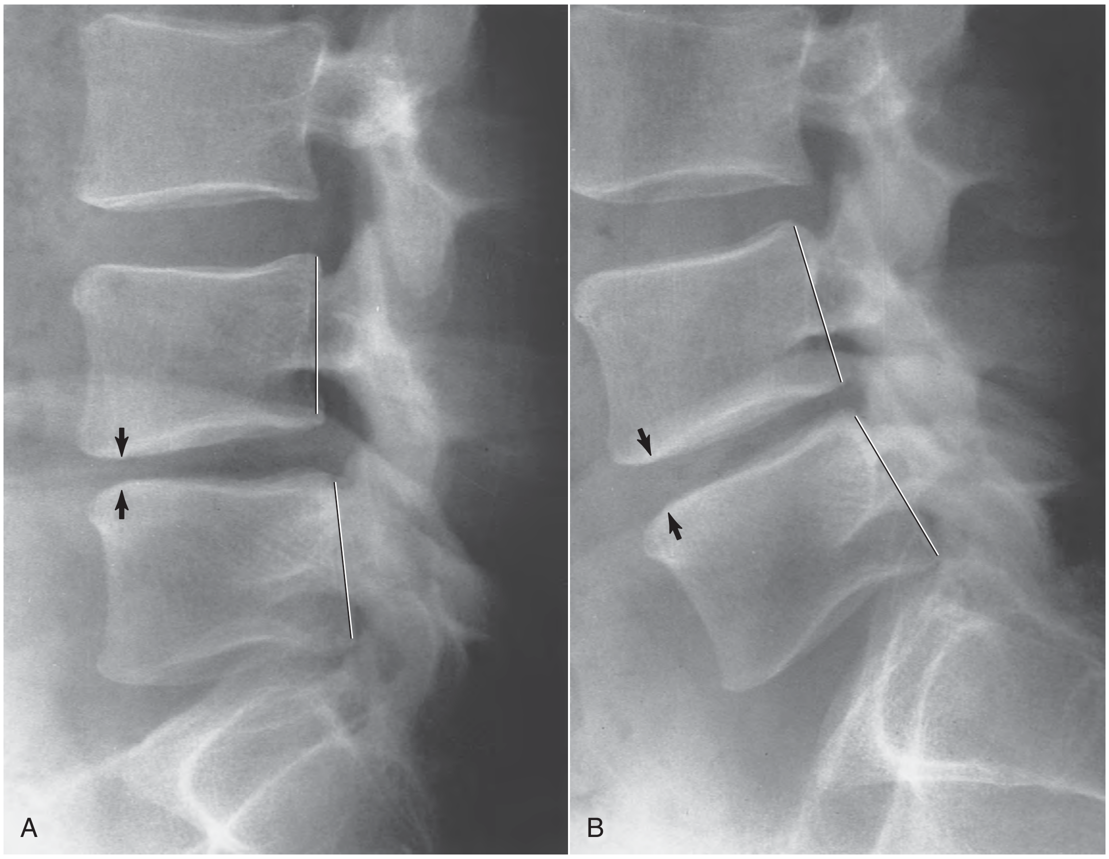

FIGURE 4–58 **Segmental instability: abnormal intersegmental motion.**[43,44,69,156,186] Lateral lumbar radiographs obtained in flexion **(A)** and extension **(B)** reveal narrowing of the L4-L5 disc. The disc angle changes dramatically between flexion and extension *(arrows),* and the L4 vertebral body translates anteriorly with respect to L5 during flexion. This translation is illustrated by the change in position of the vertical lines along the posterior vertebral body margins. Segmental instability may be a complication of trauma, spondylolisthesis, spinal surgery, degenerative disease, or other causes.

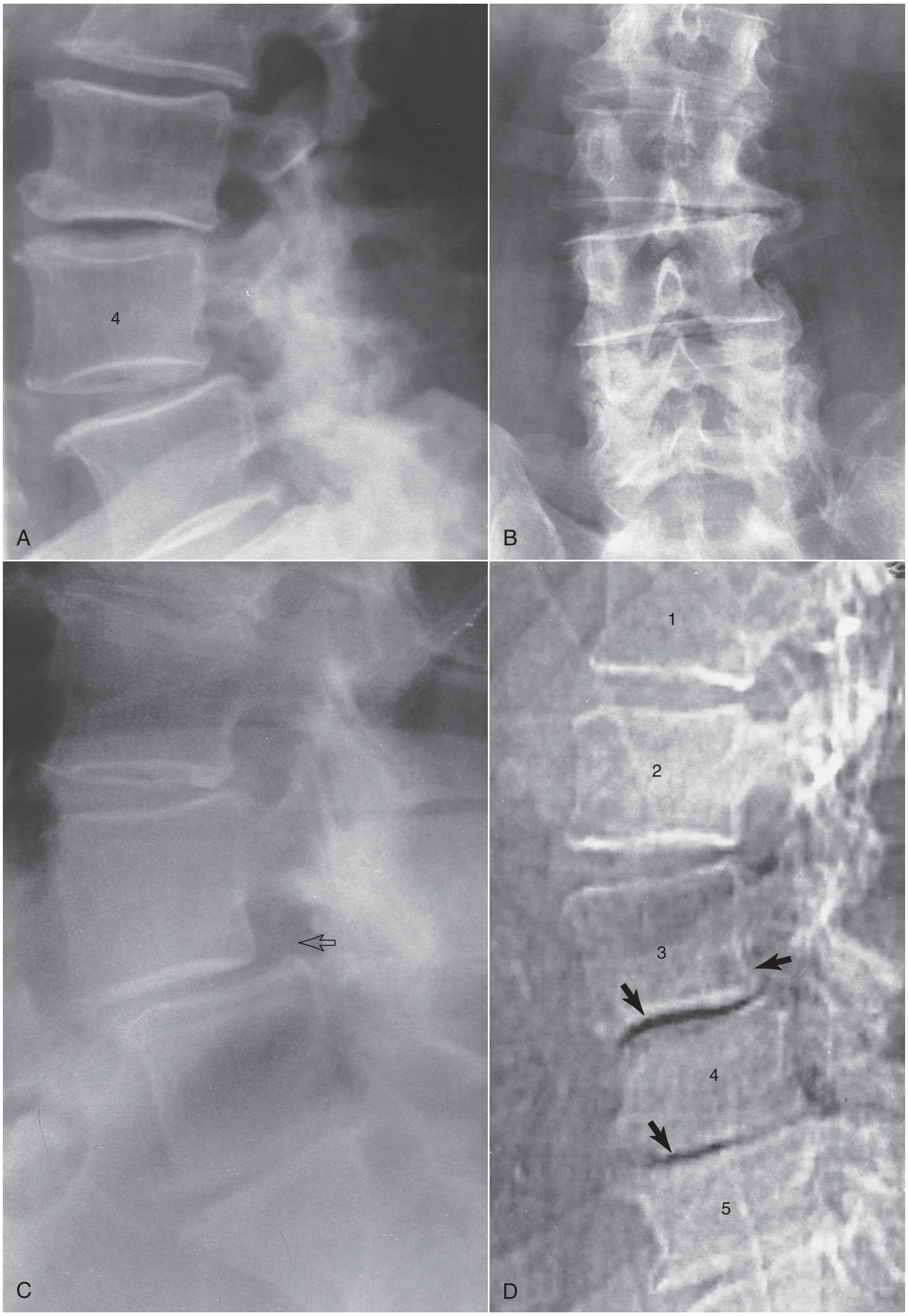

FIGURE 4–59 **Degenerative disease-alignment abnormalities.**[39,70-72,165,189] **A-B,** A 79-year-old man. Lateral **(A)** and frontal **(B)** radiographs demonstrate extensive degenerative disc disease, vacuum disc phenomenon, apophyseal joint osteoarthrosis, and degenerative scoliosis. Degenerative spondylolisthesis is seen at L4 with anterior displacement relative to L5. Degenerative retrolistheses are evident at the L2-L3 and L3-L4 levels. **C,** Degenerative spondylolisthesis of L4 *(open arrow)* is evident in another patient with severe apophyseal joint osteoarthrosis. **D,** In a third patient, sagittal CT reconstruction reveals advanced L3-L4, L4-L5, and L5-S1 disc degeneration with intradiscal gas *(left arrows)* and L3 degenerative spondylolisthesis *(right arrow)*.

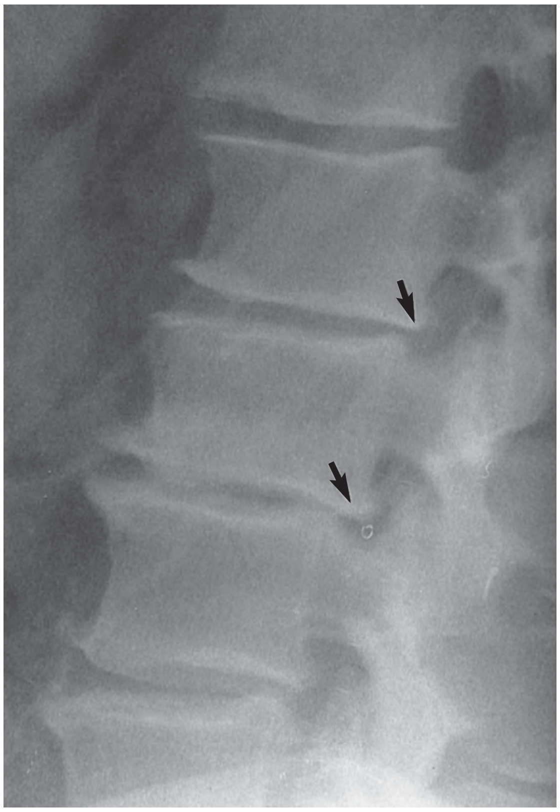

FIGURE 4–60 Degenerative retrolisthesis.[39,165,187] Degenerative retrolistheses at L2-L3 and L3-L4 *(arrows)* are associated with marked disc degeneration, apophyseal joint osteoarthrosis, and foraminal narrowing in this elderly patient.

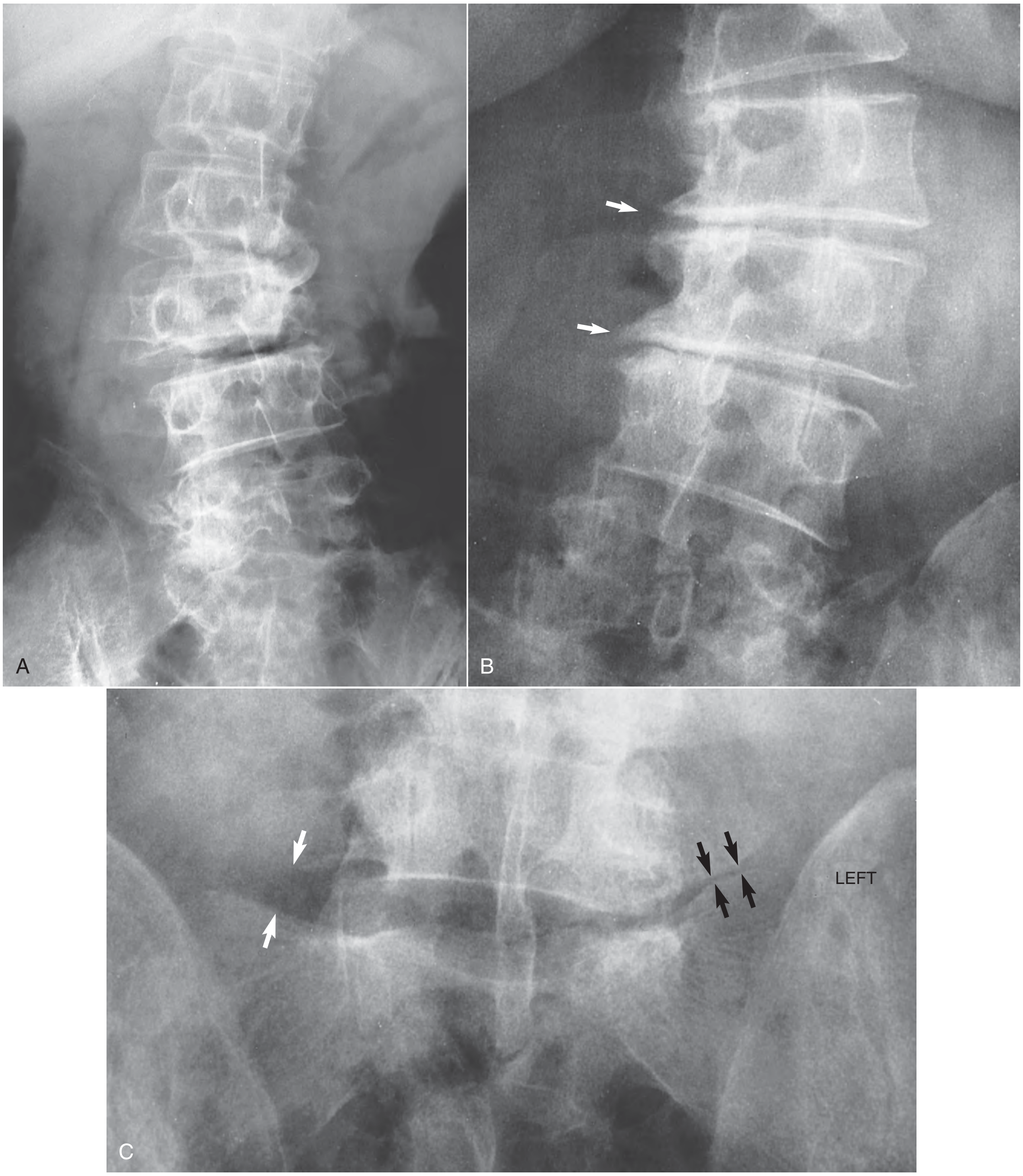

FIGURE 4–61 **Degenerative scoliosis.**[47,71,72] **A,** This lumbar scoliosis is associated with asymmetric disc degeneration and extensive osteophytosis on the concave side of the curve. A prominent vacuum phenomenon is seen in the L3-L4 intervertebral disc. **B-C,** The "far-out" syndrome in an 81-year-old woman with persistent back pain and left buttock pain. In **B,** a routine frontal radiograph shows severe scoliosis, asymmetric disc space narrowing, prominent osteophytosis, and bone sclerosis predominating on the concave side of the curve *(white arrows)*. In **C,** an angulated frontal radiograph shows lateral flexion of the L5 vertebra with asymmetric disc space narrowing. The right L5 transverse process and sacral ala are normally spaced *(white arrows),* but impaction of the left L5 transverse process on the ipsilateral sacral ala is evident *(black arrows)*. This abnormal alignment and impaction may result in entrapment of the L5 spinal nerve as it passes through this anatomic space, a condition termed the *far-out syndrome*. Surgery may be necessary to decompress the L5 nerve. (***B-C,*** *Reprinted with permission from Taylor JAM, Hoffman LE: The geriatric patient: diagnostic imaging of common musculoskeletal disorders. Top Clin Chiropr 3:23, 1996.)*

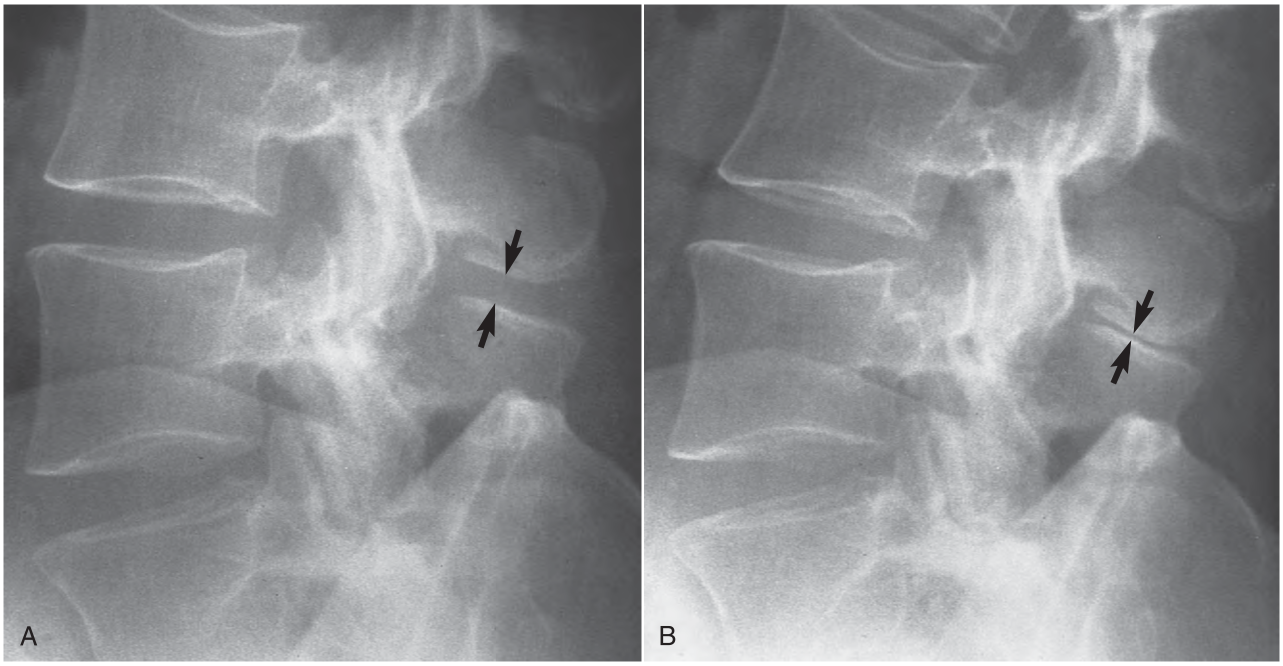

FIGURE 4–62 **Baastrup disease.**[47] Lateral radiographs obtained in the neutral position **(A)** and in extension **(B)** reveal enlarged spinous processes with flattened, sclerotic superior and inferior margins *(arrows)*. The spinous processes abnormally approximate on extension, often causing pain.

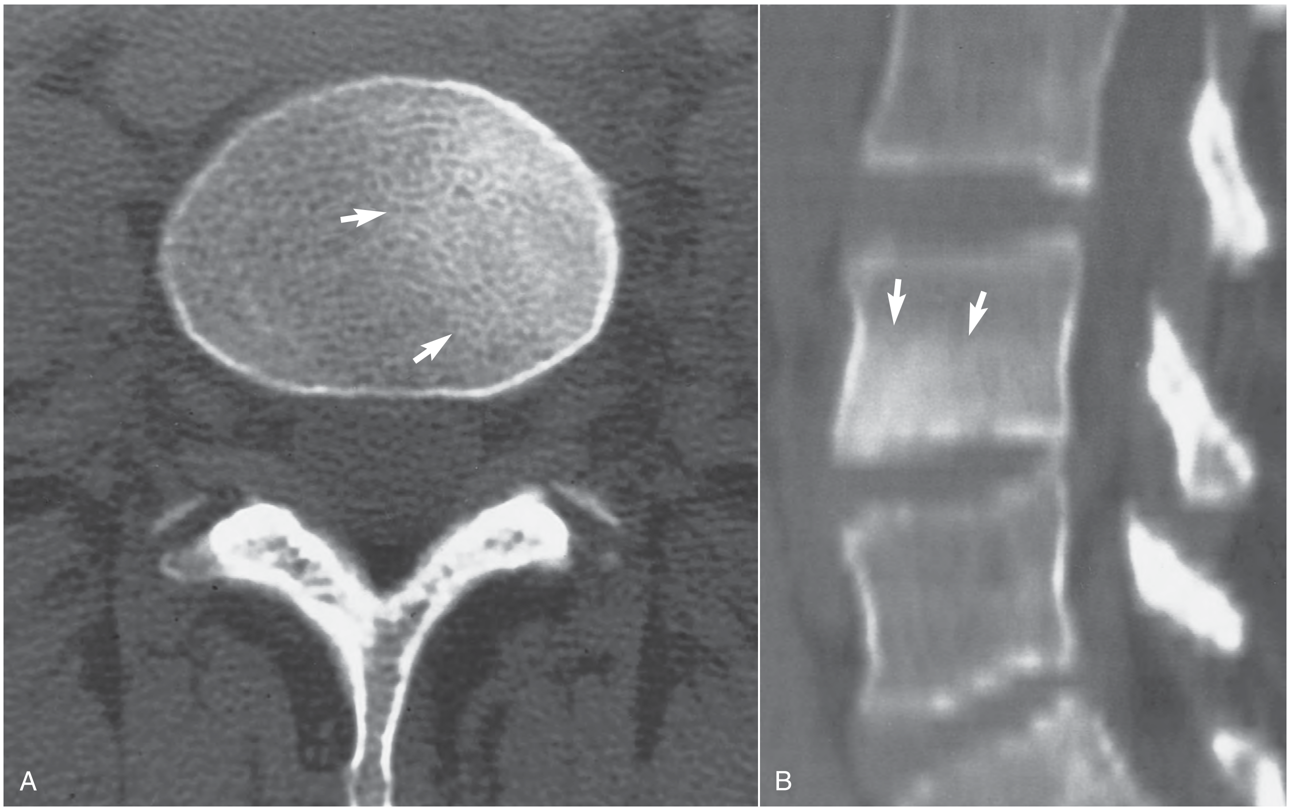

FIGURE 4–63 Segmental sclerosis of the vertebral body: Hemispheric spondylosclerosis.[73] Transaxial **(A)** and reconstructed sagittal **(B)** CT images show eccentric osteosclerosis of the L4 vertebral body *(arrows)* adjacent to the intervertebral disc. The differential diagnosis includes osteoblastic skeletal metastasis and other osteosclerotic lesions of bone. *(Courtesy M.N. Pathria, MD, San Diego.)*

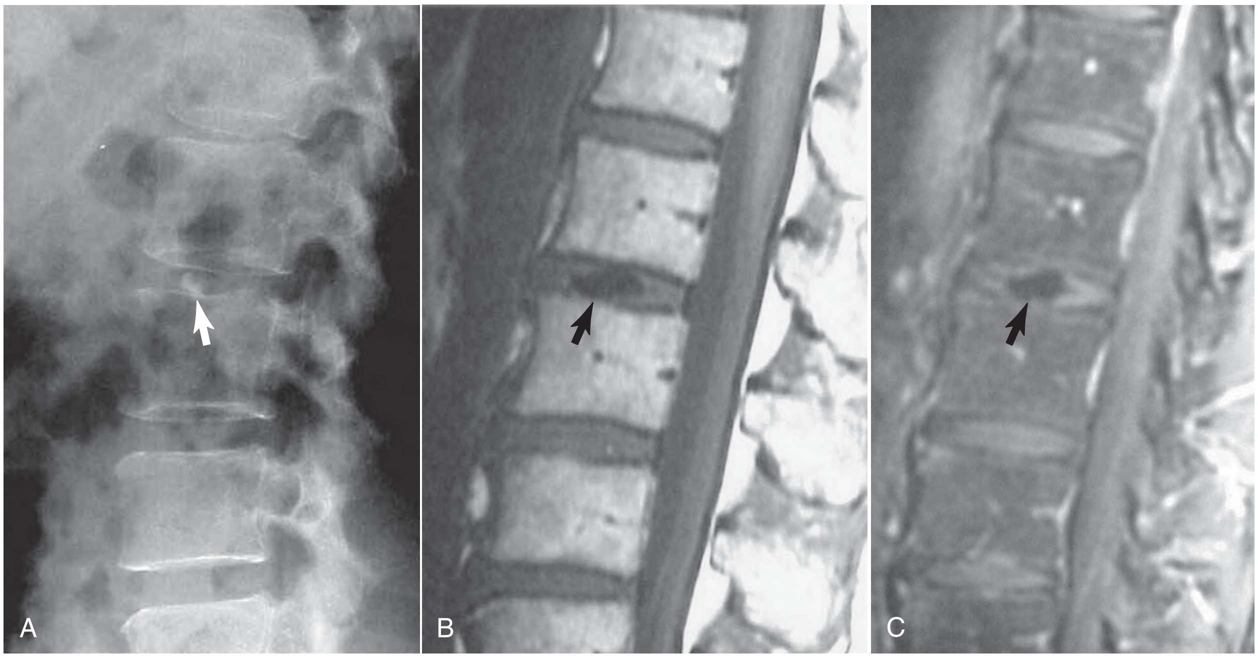

FIGURE 4–64 **Intervertebral disc calcification.**[47,185] This 59-year-old man presented with chronic upper lumbar spine pain. A lateral radiograph **(A)** reveals faint calcification within the L1-L2 disc space *(arrow)*. Sagittal T1-weighted spin echo MR images before **(B)** and after **(C)** intravenous administration of gadolinium and fat suppression reveal a more well-defined ovoid focus of low signal intensity in the region of the nucleus pulposus *(arrows)*.

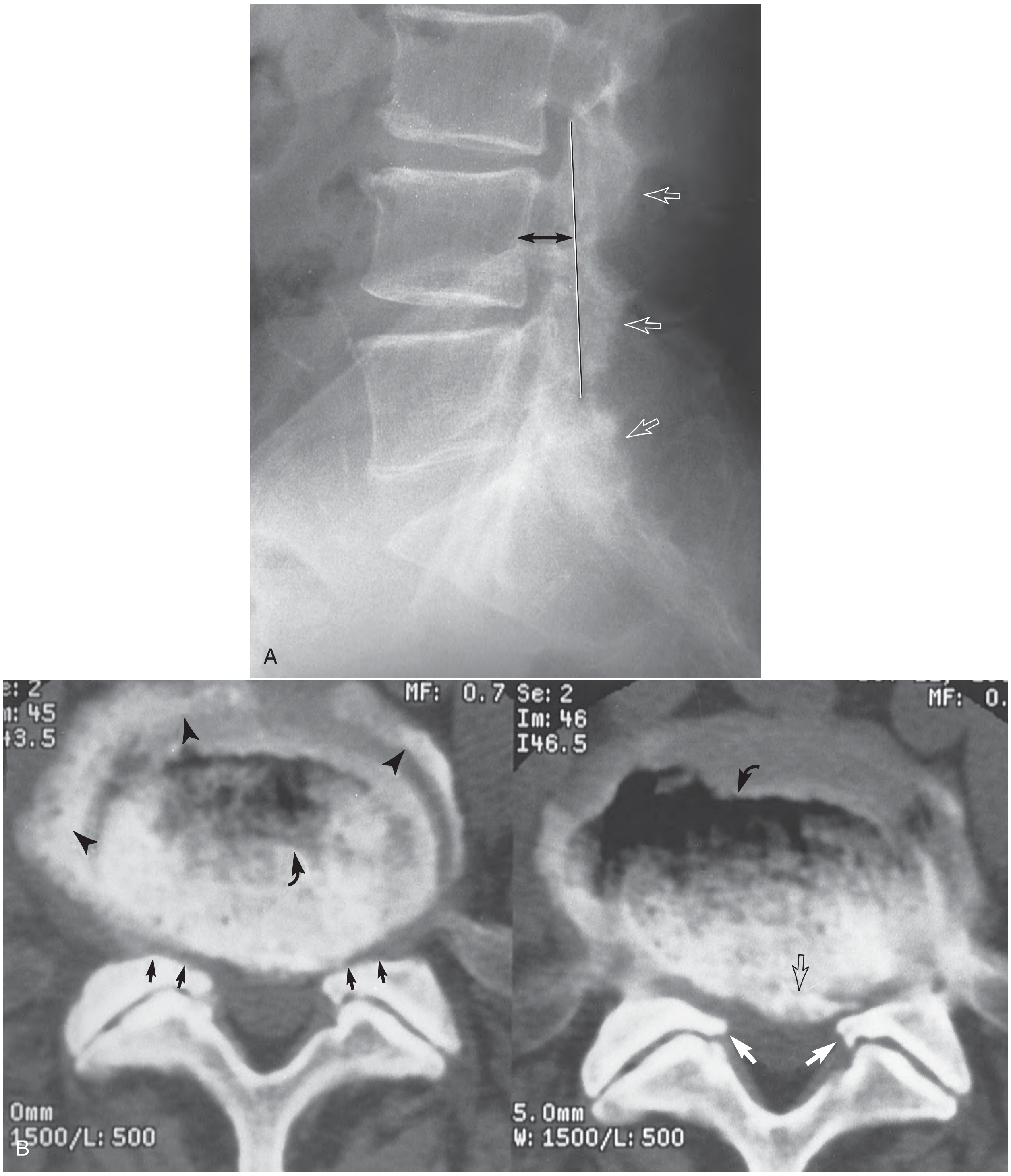

FIGURE 4–65 **Degenerative disease-spinal stenosis.**[74,157,162,165,189,193] **A,** Lateral radiograph shows extensive sclerosis and osteophyte proliferation of the posterior facet articulations in the lower lumbar region *(open arrows)*. The sagittal diameter of the spinal canal is narrowed *(double-headed arrow)*. Measurements of spinal canal diameter obtained on routine radiographs may suggest the possibility of spinal stenosis, but they tend to be inaccurate and have poor correlation with signs and symptoms. **B,** In another patient, two contiguous transaxial CT images reveal hypertrophic osteophytes arising from the articular processes *(white arrows)* and discovertebral junctions *(arrowheads),* vacuum disc phenomenon *(curved arrows),* and ossification of the posterior longitudinal ligament *(open arrow)*. The neural foramina are narrowed *(small black arrows),* and the thecal sac is compressed and displaced.

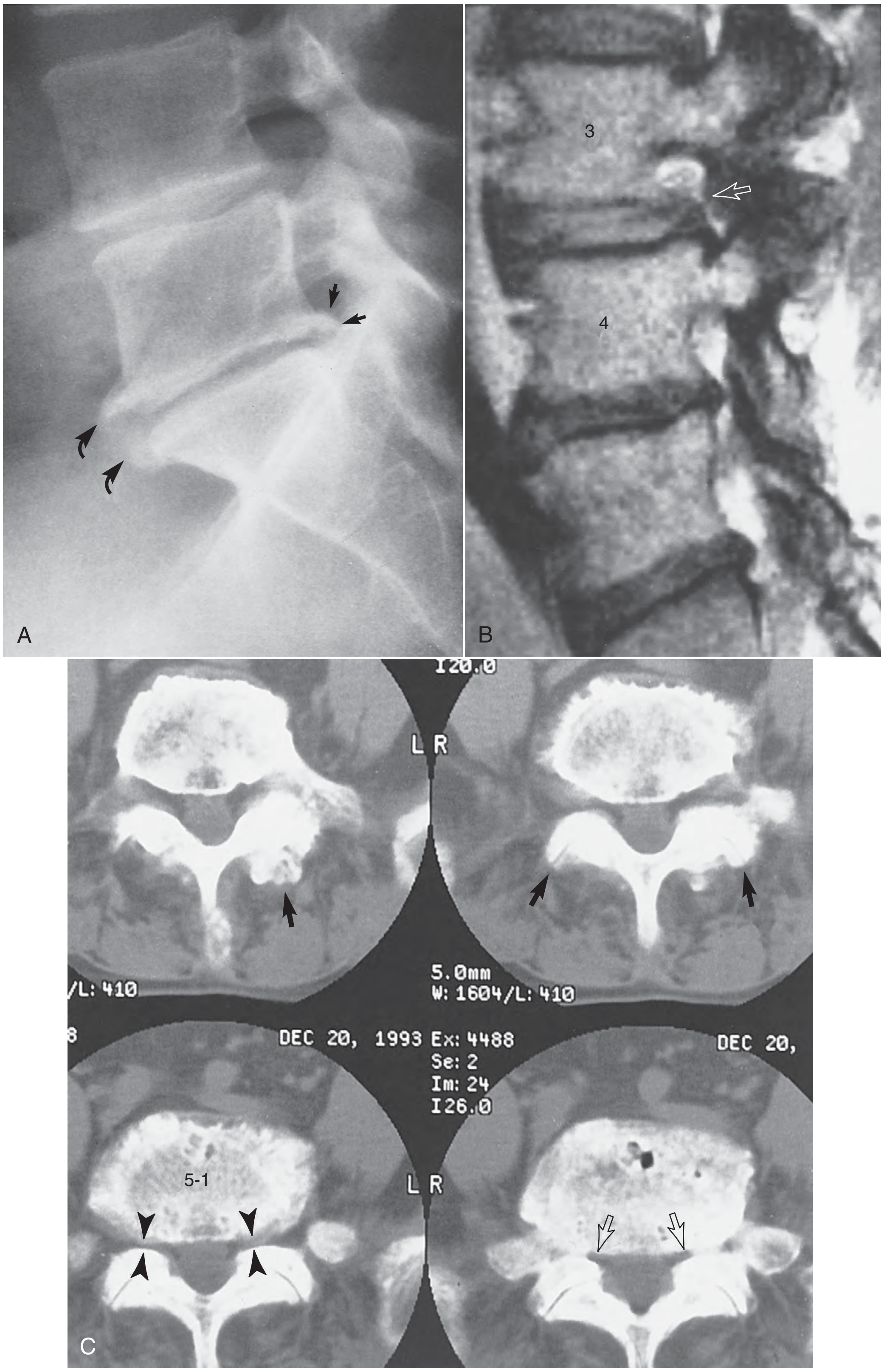

FIGURE 4–66 **Degenerative disease: foraminal and lateral recess stenosis.**[47,74,165,189,193] **A,** Anterior *(curved arrows)* and posterior *(arrows)* osteophytes are prominent in this patient with severe L4-L5 and L5-S1 degenerative disc space narrowing. The posterior osteophytes contribute to foraminal stenosis. **B,** Parasagittal T2-weighted MR image of a patient with L3 degenerative spondylolisthesis shows narrowing and distortion of the L3-L4 intervertebral foramen by the hypertrophic and anteriorly subluxated apophyseal joints *(open arrow)*. **C,** Four transaxial CT images from a 71-year-old woman with bilateral neurogenic claudication and a clinical diagnosis of degenerative spinal stenosis demonstrate severe hypertrophy of the articular processes *(large arrows)* and osseous encroachment of the intervertebral foramina (*arrowheads),* and lateral recesses *(open arrows*). (***A,*** *Reprinted with permission from Taylor JAM, Hoffman LE: The geriatric patient: diagnostic imaging of common musculoskeletal disorders. Top Clin Chiropr 3:23,1996;* ***C,*** *Courtesy D. Peterson, DC, Portland, Oregon.)*

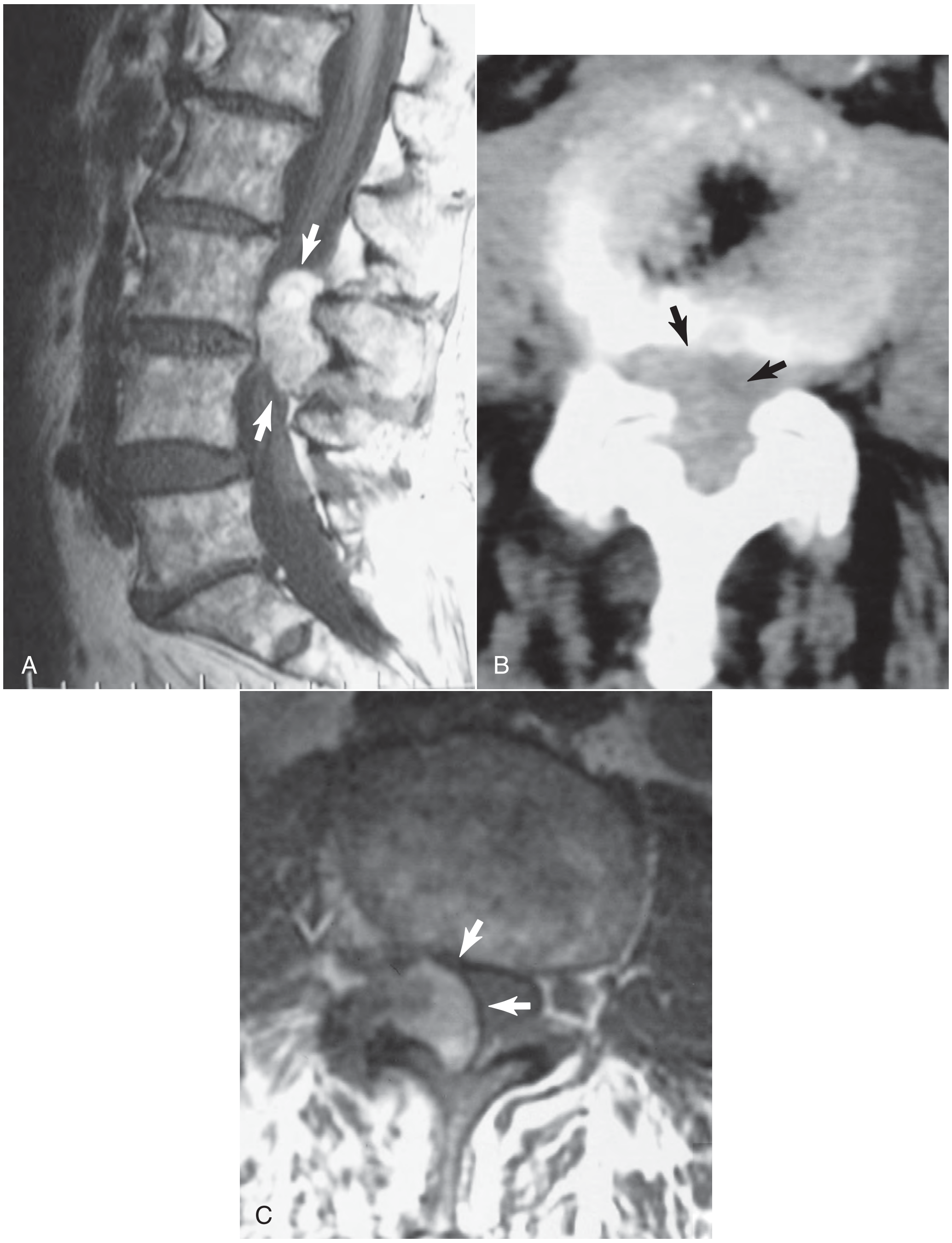

FIGURE 4–67 **Synovial juxtafacet cyst.**[183,189] This 84-year-old who has gradual onset of low back pain and progressive neurologic deficit underwent CT scanning and MR imaging examinations. A sagittal T1-weighted spin echo MR image **(A)** shows a lobulated ovoid mass that occupies the majority of the sagittal diameter of the spinal canal at the L3-L4 level *(arrows)*. The mass appears to arise from the posterior aspect of the canal and results in significant compression of the cauda equina. A transverse CT soft tissue window at the L3-L4 disc level **(B)** reveals severe osseous hypertrophy adjacent to the facet joints, worse on the right. A large mass *(arrows)* arises from the right facet joint and protrudes into the spinal canal occupying more than 50% of the transverse diameter and compressing and displacing the thecal sac. Degenerative vacuum phenomenon of the disc is also evident. On a transaxial T1-weighted spin echo MR image **(C)** obtained at approximately the same level as the transverse CT scan **(B),** the mass and its compressive effect upon the thecal sac *(arrows)* is much more conspicuous. On T1-weighted imaging, the mass contains material that is hyperintense to the thecal sac but slightly hypointense to intramuscular fat, likely due to condensed proteinaceous fluid. These common synovial-lined cysts arise from degenerative facet joints and are seen more frequently in women.

TABLE 4-18 Lumbar Spine: Articular Disorders*

Entity	Figure(s), Table(s)	Characteristics
Degenerative and Related Disorders		
Degenerative spine disease[47,58-62,75,165,189]	4-47 to 4-49, 4-68	***Spondylosis deformans*** Osteophytes and osseous ridging (Table 3-11) Subchondral bone sclerosis ***Intervertebral osteochondrosis*** Disc space narrowing Intradiscal vacuum phenomenon Disc calcification is rare ***Apophyseal joint osteoarthrosis*** Subchondral bone sclerosis Articular process hypertrophy Joint space narrowing Synovial cysts in some cases Degenerative diseases of the lumbar spine may result in several complications (Table 4-17)
Diffuse idiopathic skeletal hyperostosis (DISH)[76]	4-69	***Imaging findings*** 1. *Flowing anterior hyperostosis:* prominent vertical sheet of ossification along the anterior vertebral bodies and anulus fibrosus (Table 3-11) 2. Relative absence of degenerative changes and preservation of disc height 3. Involvement of at least four contiguous segments 4. Relatively normal apophyseal joints Fifty percent of patients with DISH have associated ossification of the posterior longitudinal ligament (OPLL)
Ossification of the posterior longitudinal ligament (OPLL)[76]	4-70	Segmental or continuous vertical sheet of ossification of the posterior longitudinal ligament, up to 5 mm thick; extends along the posterior margins of the vertebral bodies and discs within the spinal canal Often accompanies DISH (more than 40% of OPLL patients have DISH) L1 and L2 are the most common lumbar levels of involvement Frequently contributes to central stenosis with or without symptoms
Ossification and calcification of other spinal ligaments[77]	4-71	Ossification of the following spinal ligaments has been described in association with degenerative disease and DISH: Iliolumbar ligament Ligamenta flava Supraspinous ligament
Neuropathic osteoarthropathy[78]	4-72	Syringomyelia, tabes dorsalis, and diabetes mellitus may result in neuropathic osteoarthropathy affecting the thoracolumbar region Widespread discovertebral and zygapophyseal joint destruction, collapse, bone fragmentation, and kyphosis
Inflammatory Disorders		
Rheumatoid arthritis[79]	4-73	Lumbar spine involvement rare Apophyseal joint erosion, sclerosis, and subluxation Intervertebral disc space narrowing Spinous process erosion Osteoporosis Absence of osteophytes and other osseous outgrowths
Ankylosing spondylitis and enteropathic arthropathy[80,81,155]	4-74, 4-75 Tables 3-11, 3-12	Widespread marginal syndesmophytes, osteitis, disc calcification, osteoporosis, squaring of vertebral bodies, and disc ballooning Erosion and eventual ankylosis of discovertebral junctions and apophyseal joints Ossification of ligaments, joint capsules, and outer anular fibers (syndesmophytes) Ulcerative colitis and regional ileitis are the most common inflammatory bowel diseases to result in radiographic findings identical to those of ankylosing spondylitis Arachnoid diverticula also may complicate long-standing ankylosing spondylitis; can be associated with the cauda equina syndrome

* See also Tables 1-7 to 1-10 and Table 1-19.

TABLE 4-18 Lumbar Spine: Articular Disorders—cont'd

Entity	Figure(s), Table(s)	Characteristics
Psoriatic spondyloarthropathy and reactive arthritis[82,142]	4-76, 4-77	Unilateral or bilateral, asymmetric, nonmarginal, comma-shaped paravertebral ossification about the thoracolumbar spine in 10% to 15% of patients with psoriasis Paravertebral ossification—found in both psoriasis and reactive arthritis (Reiter syndrome)—may resemble the osseous outgrowths seen in other diseases (Table 3-11) Apophyseal joint narrowing, sclerosis, and bony ankylosis
Neurologic Injury[83]	4-78	Patients with paraplegia and quadriplegia may develop spine changes identical to those of neuropathic osteoarthropathy, DISH, ankylosing spondylitis, psoriatic spondyloarthropathy, Reiter syndrome, and degenerative disease Pseudarthrosis may occur as a result of improper fracture healing and may be accompanied by dramatic hypertrophic bone formation
Crystal Deposition Disorders		
Calcium pyrophosphate dihydrate crystal deposition disease[84,85]	4-79	May result in widespread secondary degenerative disease (pyrophosphate arthropathy) with disc space narrowing and chondrocalcinosis of the anulus fibrosus, joint capsules, apophyseal joints, and articular cartilage
Alkaptonuria[86,87]	4-80	Widespread, severe disc space narrowing, diffuse anulus fibrosus calcification, intradiscal vacuum phenomenon Osteoporosis and loss of lumbar lordosis Osseous bridging may resemble marginal syndesmophytes (Table 3-11) Eventual progression to complete ankylosis
Gouty arthropathy[88,191]	4-81	Spine involvement is extremely uncommon Osteophytosis and tophaceous erosive abnormalities of the apophyseal joints; discovertebral erosions may resemble those seen in infectious spondylodiscitis, septic arthritis, and degenerative disc disease Paraspinal calcification may be seen
Infection		
Pyogenic spondylodiscitis[89,90,143,153]	4-82 Table 2-16	Latent period of as long as 21 days before radiographic changes appear Infection initially involves disc and adjacent vertebral body Severe disc space narrowing at one level that eventually may spread to adjacent levels, obliterating vertebral endplates and resulting in vertebral collapse in later stages Paravertebral soft tissue mass or abscess
Tuberculous spondylodiscitis[91,92]	4-83	Spine involvement in 25% to 60% of cases of skeletal tuberculosis Thoracolumbar region is the most frequent site of infection Anterior vertebral destruction and collapse often result in an acute, angular gibbus deformity Classically, the vertebral bodies and disc are involved; the posterior elements are affected infrequently Paravertebral abscesses are common
Septic arthritis of facet joints[178]	4-84	Uncommon cause of back pain and reduced range of motion Time to diagnosis ranges from 21 to 90 days Laboratory tests reveal inflammation: elevated C-reactive protein, erythrocyte sedimentation rate, neutrophil count Widened joint space secondary to destructive lesions, marginal joint erosions, intraarticular effusion, synovitis and spread to adjacent soft tissues may be seen on CT or MR imaging

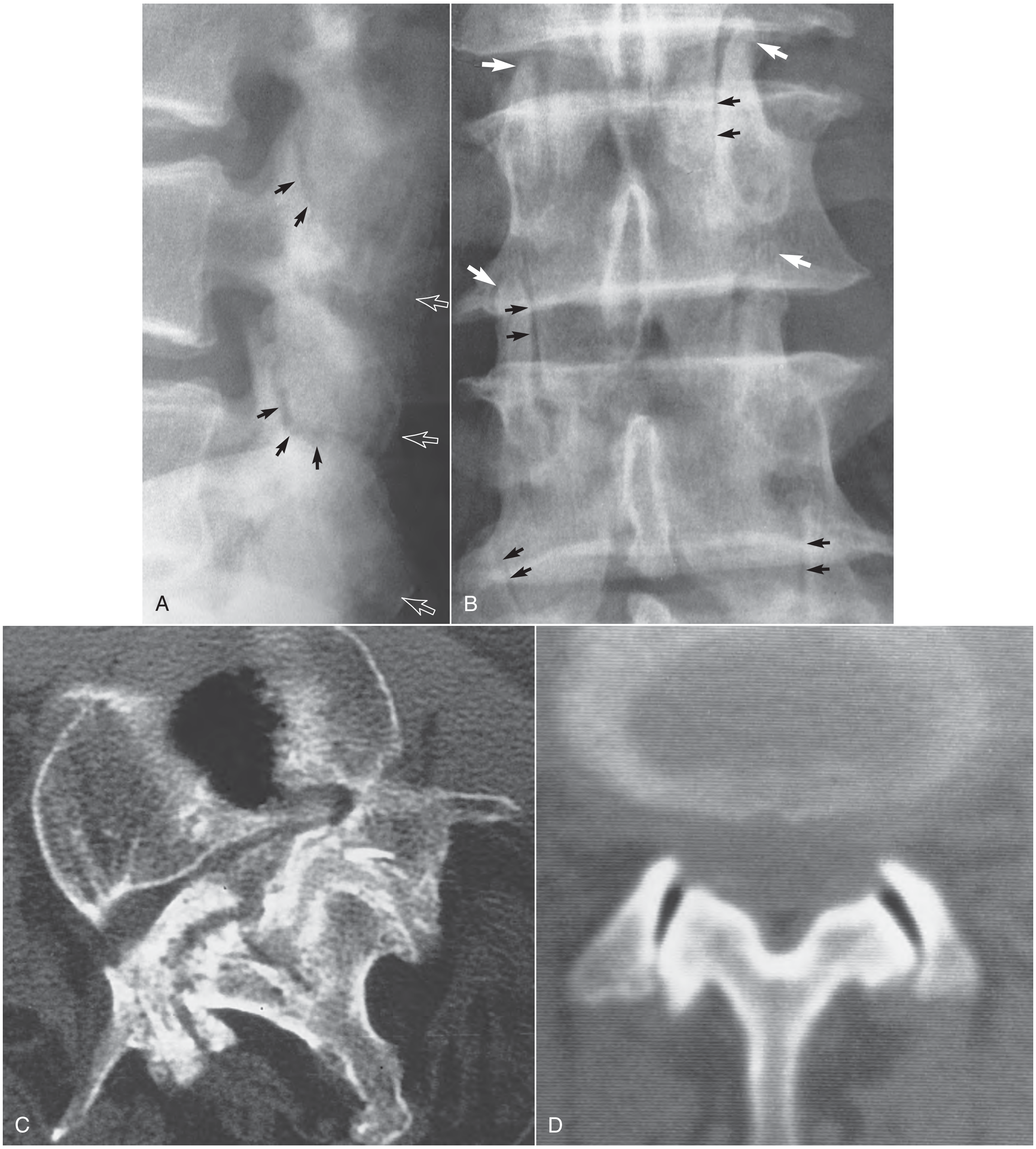

FIGURE 4–68 Apophyseal joint osteoarthrosis.[75] **A,** Lateral radiograph reveals extensive bone proliferation, sclerosis *(open arrows),* and irregularity *(arrows)* of the apophyseal joints. **B,** Anteroposterior radiograph shows joint space narrowing *(black arrows),* sclerosis, and hypertrophy of the superior articular processes *(white arrows)*. **C,** CT imaging abnormalities in a patient with severe, long-standing idiopathic scoliosis. Transaxial CT image obtained after administration of myelographic contrast material shows extensive degeneration of the L3-L4 apophyseal joints. The findings include hypertrophy and sclerosis of the articular processes, osteophyte formation, apophyseal joint space narrowing with intraarticular gas (vacuum phenomenon), and dramatic central canal stenosis. **D,** In another patient, a transaxial CT image reveals extensive intraarticular gas and subchondral sclerosis of the articular processes. *(**A-B,** Courtesy E.E. Bonic, DC, Portland, Ore; **C,** Courtesy W. Peck, MD, Orange, Calif.)*

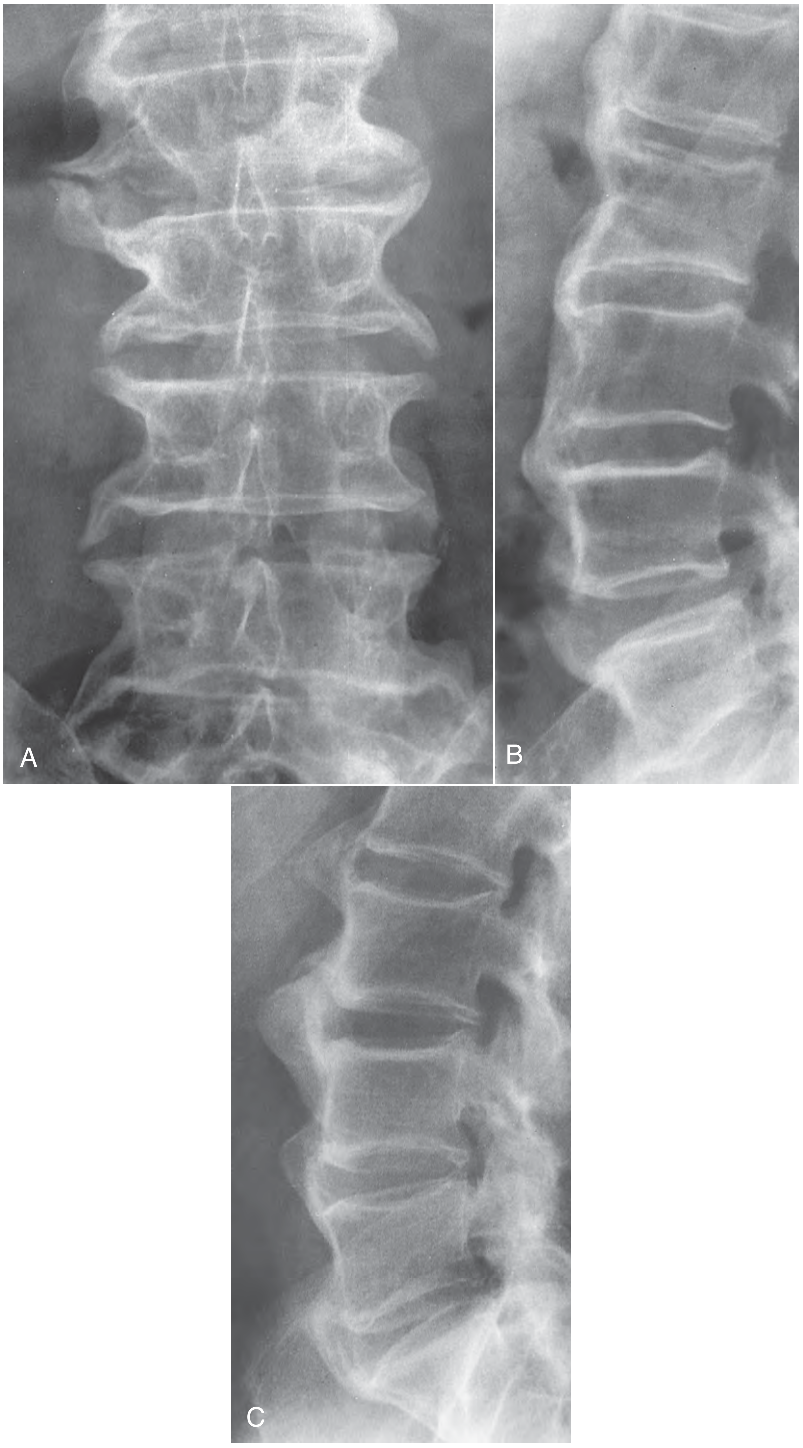

FIGURE 4–69 Diffuse idiopathic skeletal hyperostosis (DISH).[76] **A,** Prominent flowing hyperostosis is seen arising from the central portion of the vertebral bodies on this anteroposterior radiograph. The disc spaces are preserved. **B,** In another patient, the thick layer of ossification spans several vertebral levels, and the widths of the disc spaces are relatively well maintained. **C,** Similar findings are evident in a third patient.

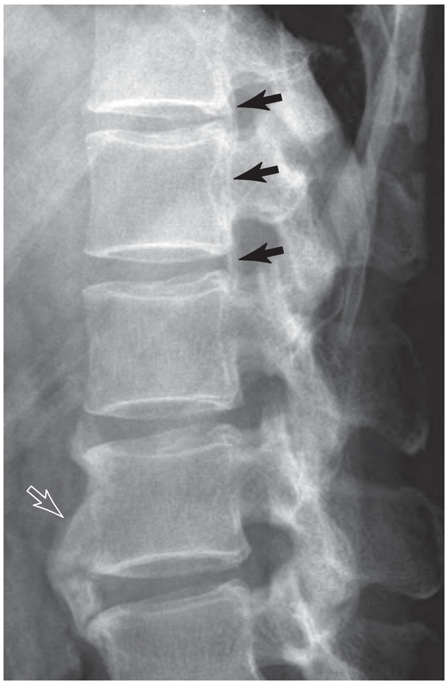

FIGURE 4–70 Ossification of the posterior longitudinal ligament (OPLL).[76] A thin vertical sheet of ossification is evident within the spinal canal just posterior to the upper lumbar vertebral bodies and intervening discs *(arrows)*. Note also the flowing hyperostosis anteriorly *(open arrow),* characteristic of DISH. OPLL and DISH commonly coexist.

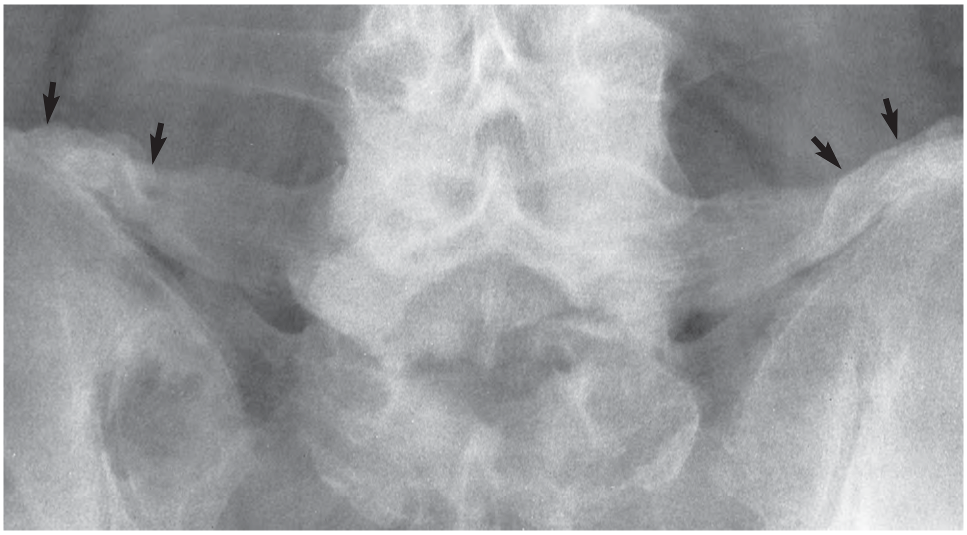

FIGURE 4–71 Iliolumbar ligament ossification.[77] Diffuse ossification of the iliolumbar ligaments *(arrows)* is a finding common to both degenerative disease and diffuse idiopathic skeletal hyperostosis (DISH). Deep palpation of the ossified iliolumbar ligaments may elicit pain.

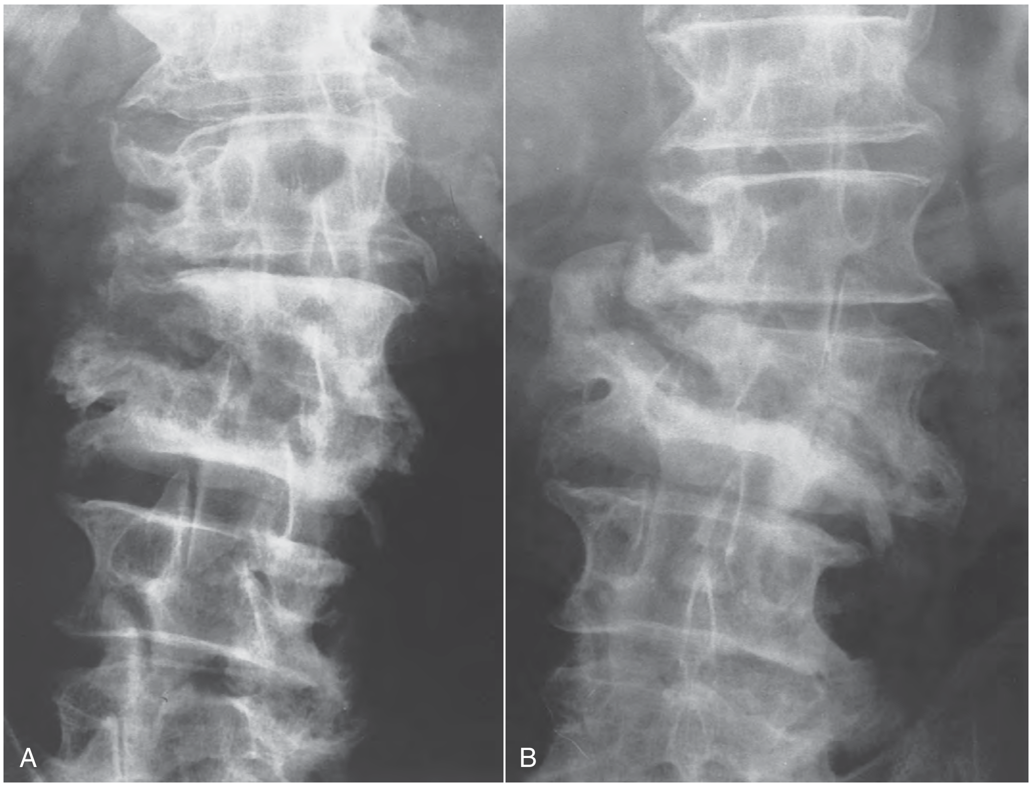

FIGURE 4–72 **Neuropathic osteoarthropathy (Charcot spine): neurosyphilis.**[78] This patient is a 65-year-old man with long-standing syphilis. **A,** Initial radiograph shows extensive destruction and disorganization of the L2 and L3 vertebral bodies. Osteophyte formation and sclerosis also are apparent. **B,** Radiograph obtained 2 years later shows progression of the destructive changes, marked sclerosis, and bulky osteophyte formation. This appearance resembles the improper fracture healing or pseudarthrosis seen in paralyzed patients.

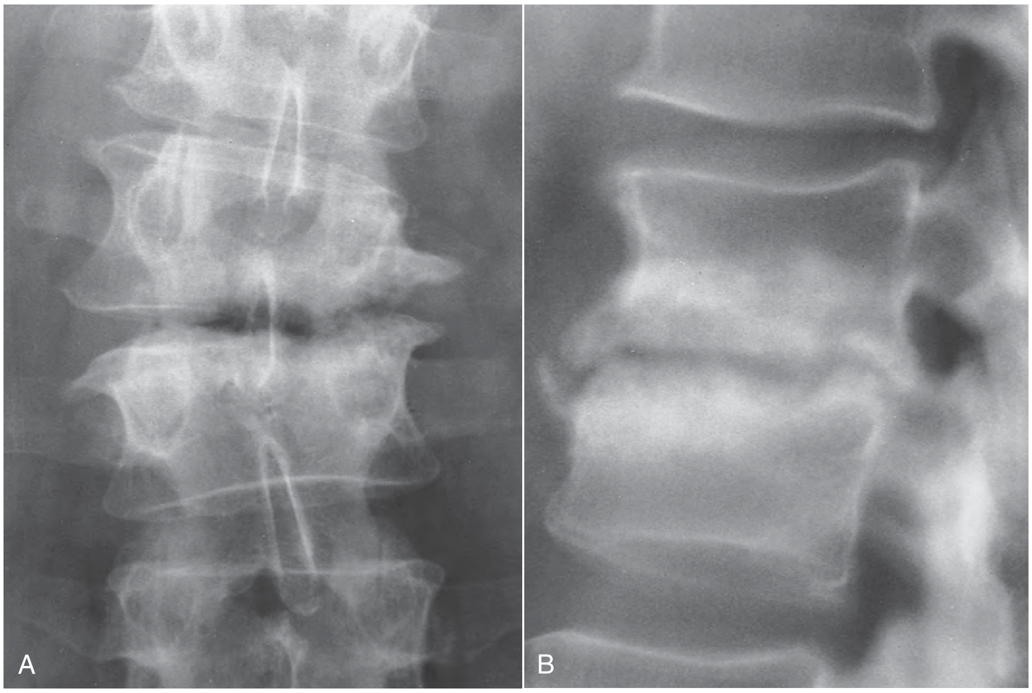

FIGURE 4–73 **Rheumatoid arthritis.**[79] In this 53-year-old patient with rheumatoid arthritis, a routine frontal radiograph **(A)** and a lateral conventional tomogram **(B)** reveal disc space narrowing, poorly defined osseous erosions, and sclerosis. These findings resemble those of infection, degenerative disc disease, and neuropathic joint disease. The presence of intradiscal gas and osteophytes is characteristic of degenerative disc disease. The indistinct vertebral endplates, however, are more typical of an inflammatory process. Although these joint changes may occasionally be found in patients with rheumatoid arthritis, their pathogenesis is debated.

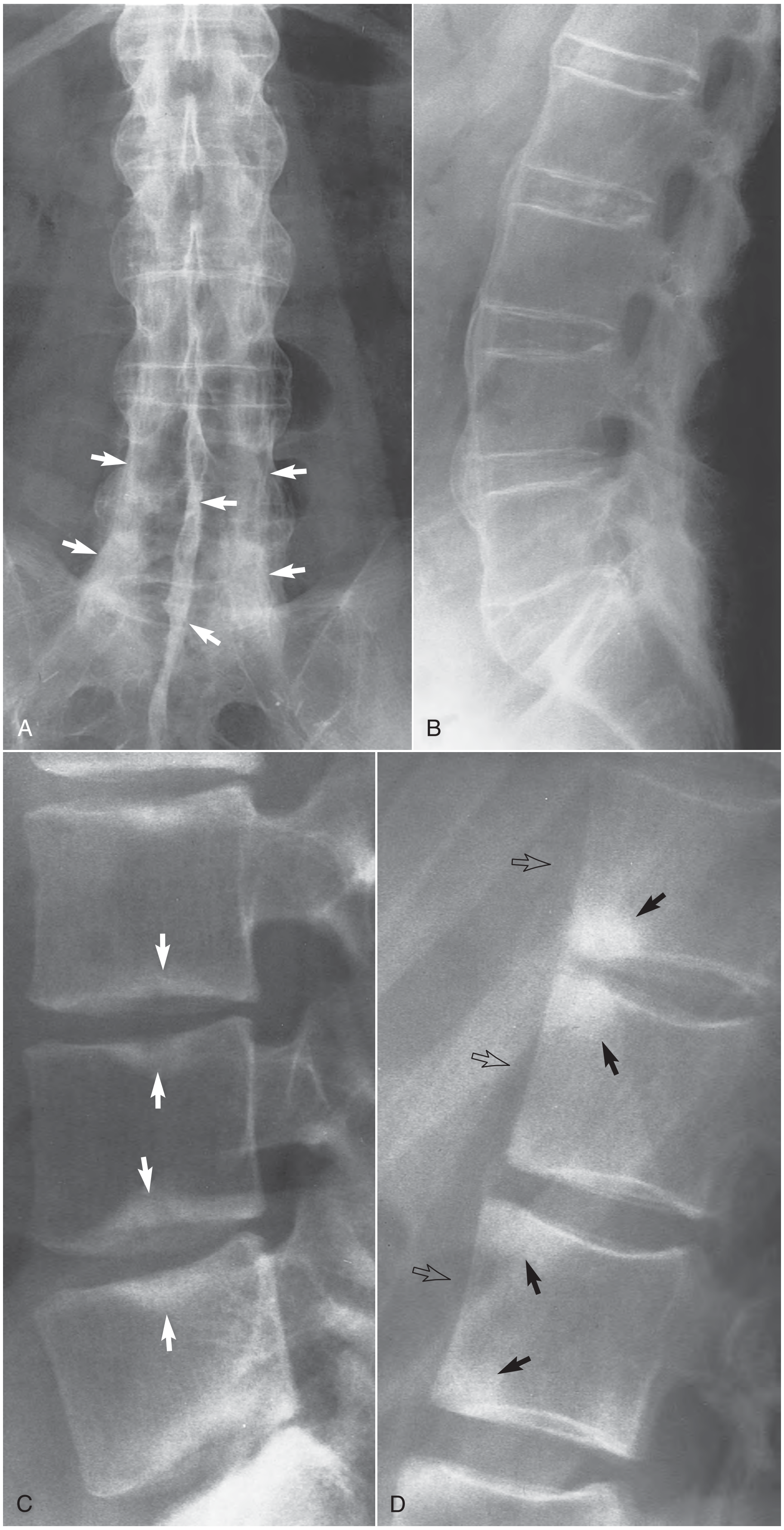

FIGURE 4–74 Ankylosing spondylitis: spectrum of abnormalities.[80,155] **A-B,** A 75-year-old man with long-standing ankylosing spondylitis. In **A,** a frontal radiograph reveals undulating syndesmophytes (bamboo spine). The presence of ossification and ankylosis of the apophyseal joints and supraspinous ligaments *(arrows)* is termed the *trolley track sign*. In **B,** a lateral radiograph demonstrates the continuous marginal syndesmophyte formation, ankylosis of the apophyseal joints, and discal calcification. **C,** Central discovertebral erosions. Observe the presence of multiple central discovertebral erosions throughout the lumbar spine *(arrows)*. The erosions have an associated sclerotic margin and somewhat resemble Schmorl nodes. This patient shows no evidence of syndesmophyte formation. **D,** "Shiny corner" sign. Osseous erosion and osteitis at the anterior aspects of the vertebral bodies adjacent to the discovertebral margin have resulted in sclerosis, which is referred to as the "shiny corner" sign *(arrows)*. The loss of the normal anterior concavity of the vertebral bodies is a frequent finding termed *squaring (open arrows)*.

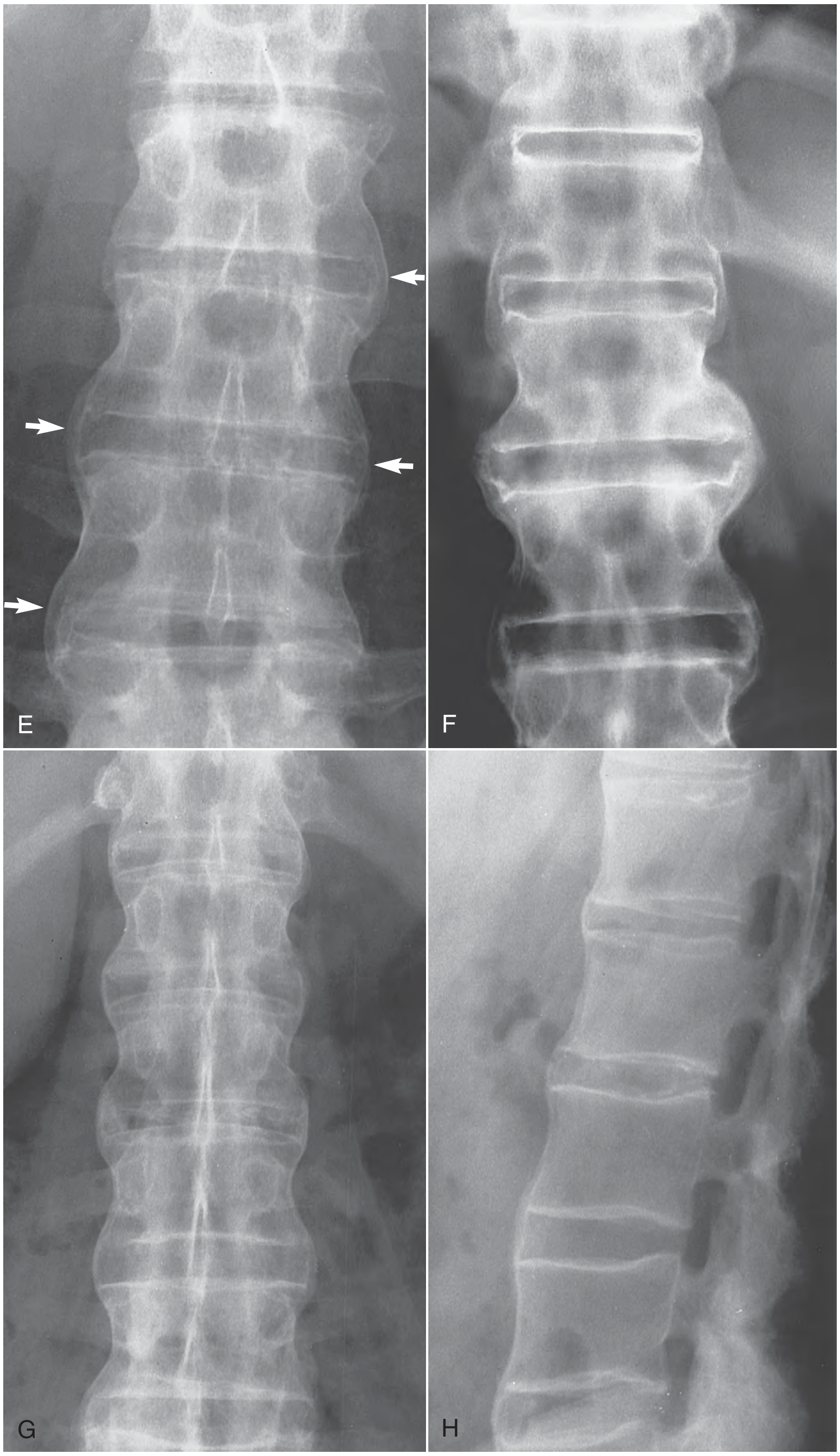

FIGURE 4–74, cont'd **E,** Syndesmophytes. A routine radiograph demonstrates the characteristic thin, curvilinear, marginal syndesmophytes arising from the corners of the vertebral bodies throughout the lumbar spine *(arrows)*. This appearance is sometimes referred to as the *bamboo spine* appearance. **F,** In another patient, conventional tomography more clearly shows the slender marginal syndesmophytes. **G-H,** In another patient with ankylosing spondylitis, radiographs show extensive syndesmophyte formation. See also Table 3-12 for terminology applied to ankylosing spondylitis. *(**A-B,** Courtesy D. Goodwin, MD, Lebanon, NH; **C,** Courtesy J. Amberg, MD, San Diego; **D,** Courtesy A. Brower, MD, Norfolk, Va; **F,** Courtesy T. Broderick, MD, Orange, Calif.)*

FIGURE 4–75 Ankylosing spondylitis: arachnoid diverticulae.[81,155] Observe the scalloped erosions of the neural arch *(open arrows)* on this CT scan from a patient with long-standing ankylosing spondylitis. Arachnoid diverticula are a rare complication of ankylosing spondylitis.

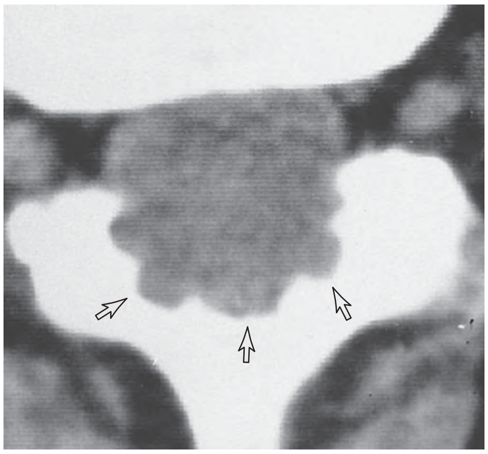

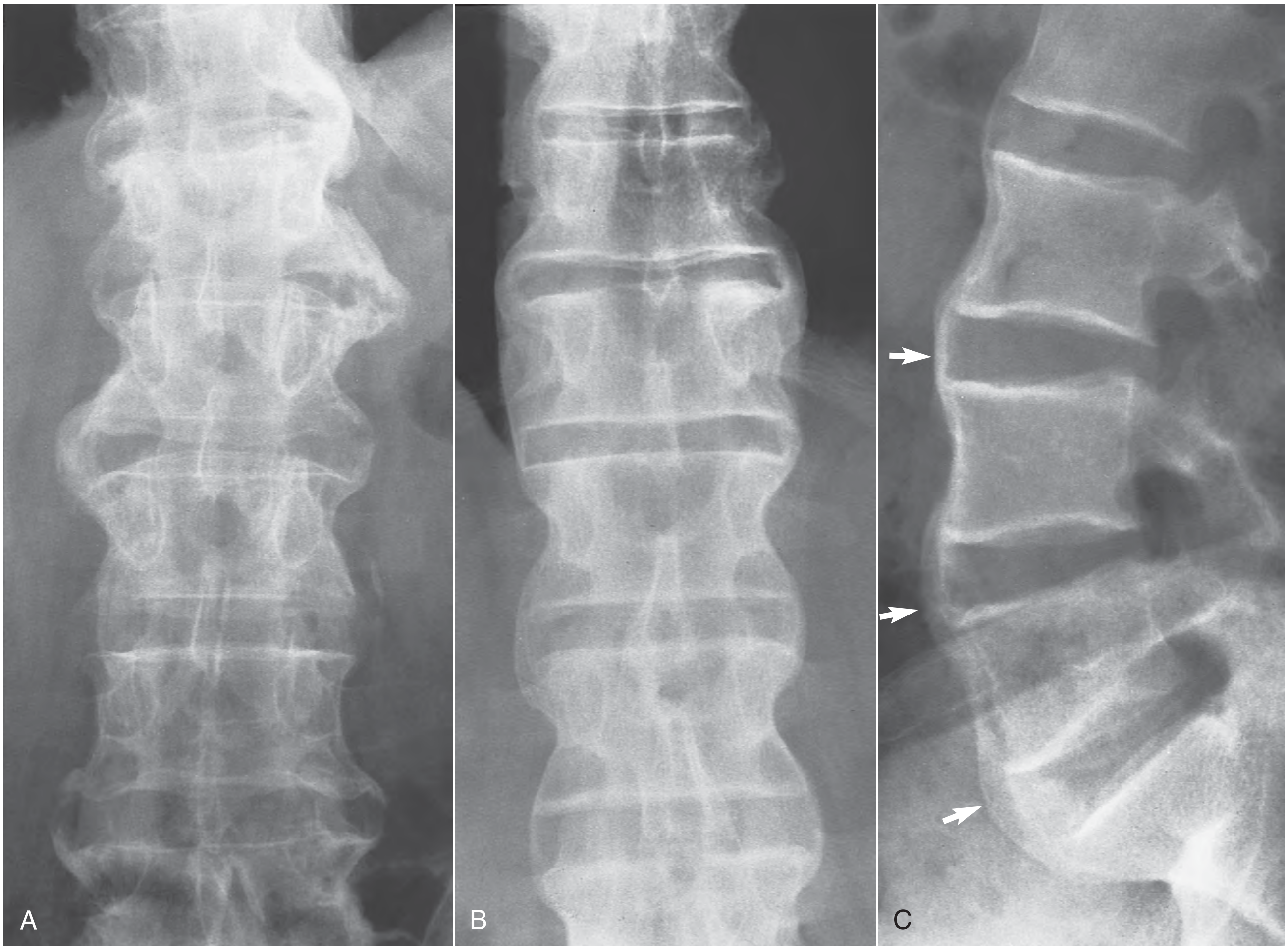

FIGURE 4–76 Psoriatic spondyloarthropathy.[82,142] **A,** Asymmetric bulky osseous projections are seen arising several millimeters from the corners of the vertebral bodies and bridging several intervertebral discs. This asymmetric paravertebral ossification is characteristic of the spondyloarthropathy of psoriasis and Reiter syndrome. **B-C,** A 69-year-old man with long-standing psoriatic skin lesions and polyarticular joint disease. In **B,** an anteroposterior radiograph reveals prominent undulating paravertebral ossification throughout the lumbar spine. The continuous symmetric pattern of ossification in this patient is somewhat atypical of psoriatic spondyloarthropathy, resembling instead the more classic syndesmophytes of ankylosing spondylitis. In **C,** a lateral radiograph shows the characteristic undulating osseous outgrowths that span the anterior aspect of the lumbar vertebrae and disc spaces *(arrows)*. The disc spaces are well preserved.

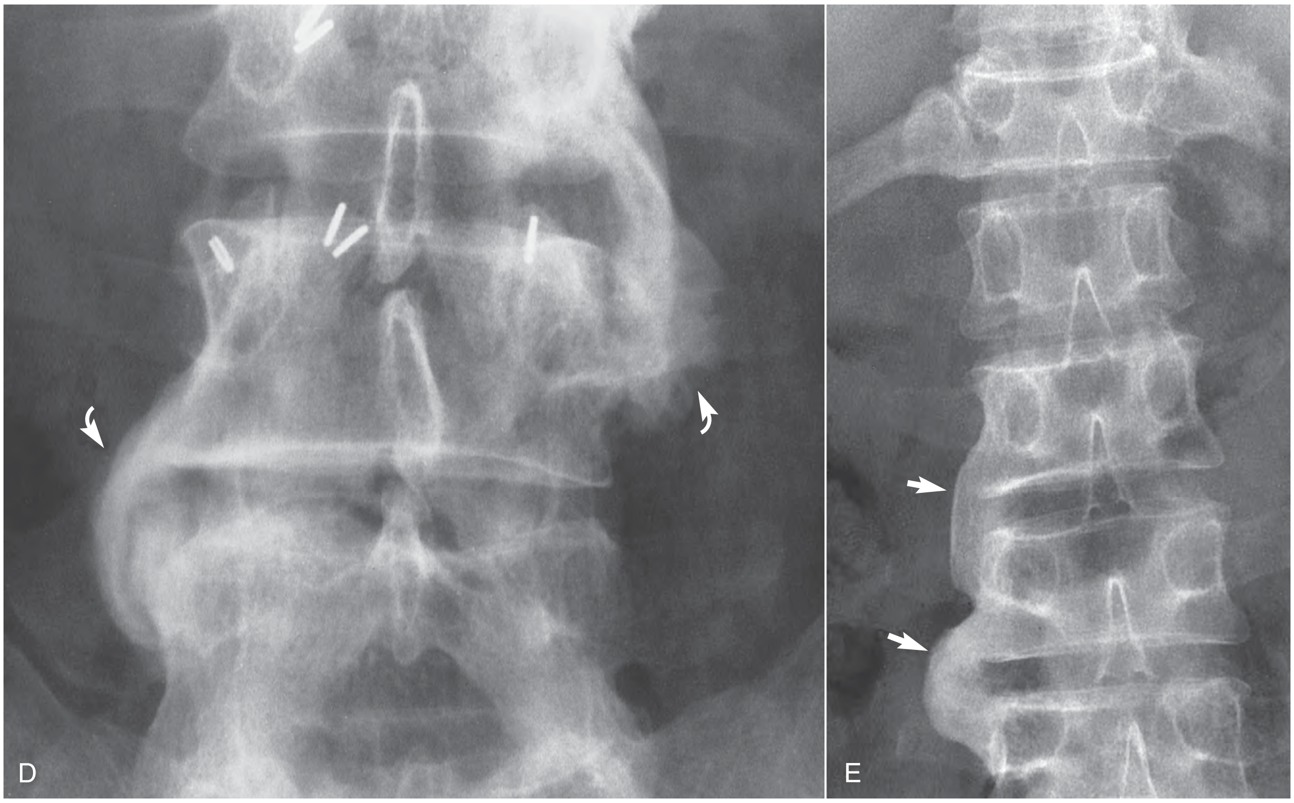

FIGURE 4–76, cont'd **D,** In another patient, bulky asymmetric paravertebral ossification of the lumbosacral region is seen *(curved arrows)*. **E,** In a fourth patient, unilateral ossification spans the L2-L3 and L3-L4 intervertebral disc spaces *(arrows)*. Unilateral or bilateral asymmetric paravertebral ossification of the lower thoracic and upper lumbar spine is evident radiographically in 10% to 15% of patients with psoriasis. The paravertebral ossification, characteristic of both psoriatic spondyloarthropathy and Reiter syndrome, may resemble the marginal syndesmophytes seen in ankylosing spondylitis, the flowing hyperostosis of diffuse idiopathic skeletal hyperostosis (DISH), or the osteophytes of degenerative disc disease. In psoriatic spondyloarthropathy and Reiter syndrome, however, the excrescences may be large, bulky, or fluffy and often parallel the lateral surfaces of the vertebral bodies and intervertebral discs. The characteristic radiographic and clinical features usually allow differentiation of psoriatic spondyloarthropathy and Reiter syndrome from these other conditions.

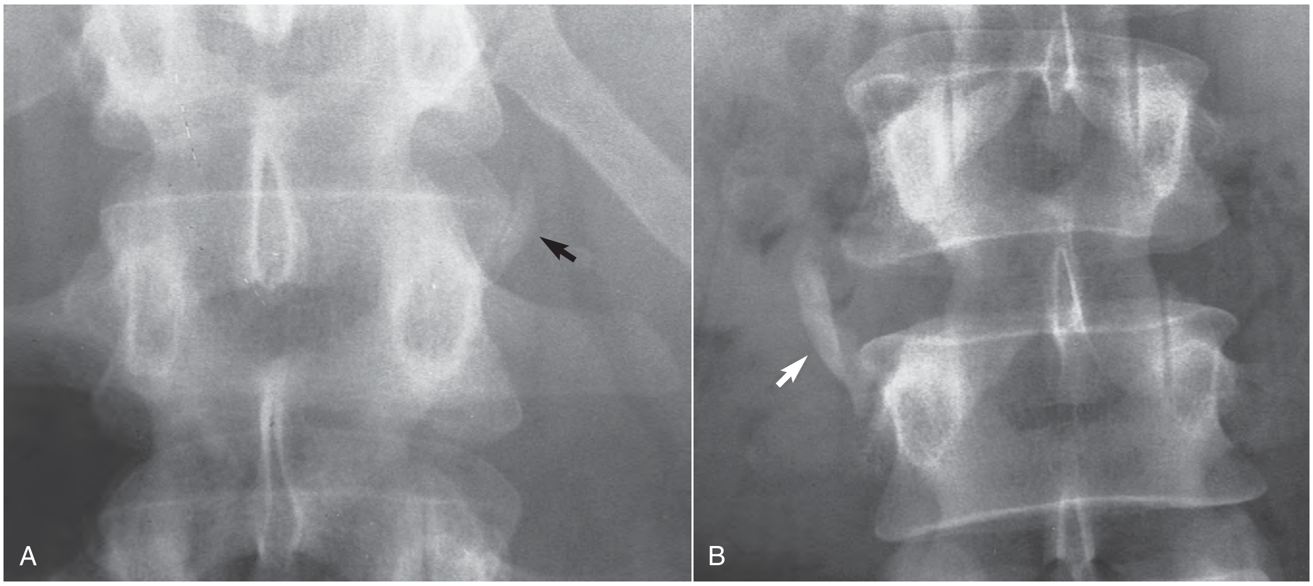

FIGURE 4–77 **Reactive arthritis (Reiter syndrome): paravertebral ossification.**[82,142] **A,** Observe the comma-shaped osseous excrescence arising from the lateral aspect of the vertebral body of L1 *(arrow)*. This pattern is characteristic of seronegative spondyloarthropathies, such as Reiter syndrome and psoriatic spondyloarthropathy. **B,** In another patient, a characteristic nonmarginal paravertebral excrescence is seen spanning two adjacent lumbar vertebrae *(arrow)*.

FIGURE 4–78 **Neurologic injury: spinal abnormalities.**[83] **A-B,** Neuropathic osteoarthropathy: Spine changes in a paraplegic man (Charcot spine). In **A,** a routine radiograph shows intradiscal gas (vacuum phenomena) and vertebral body sclerosis. In **B,** a sagittal T1-weighted (TR/TE, 600/20) spin echo MR image reveals low signal intensity within both the disc and the sclerotic portions of the adjacent vertebral bodies. **C-D,** In a different patient with paralysis, frontal **(C)** and lateral **(D)** radiographs demonstrate thick, flowing hyperostosis and relative preservation of disc spaces, a pattern resembling the changes of diffuse idiopathic skeletal hyperostosis (DISH).

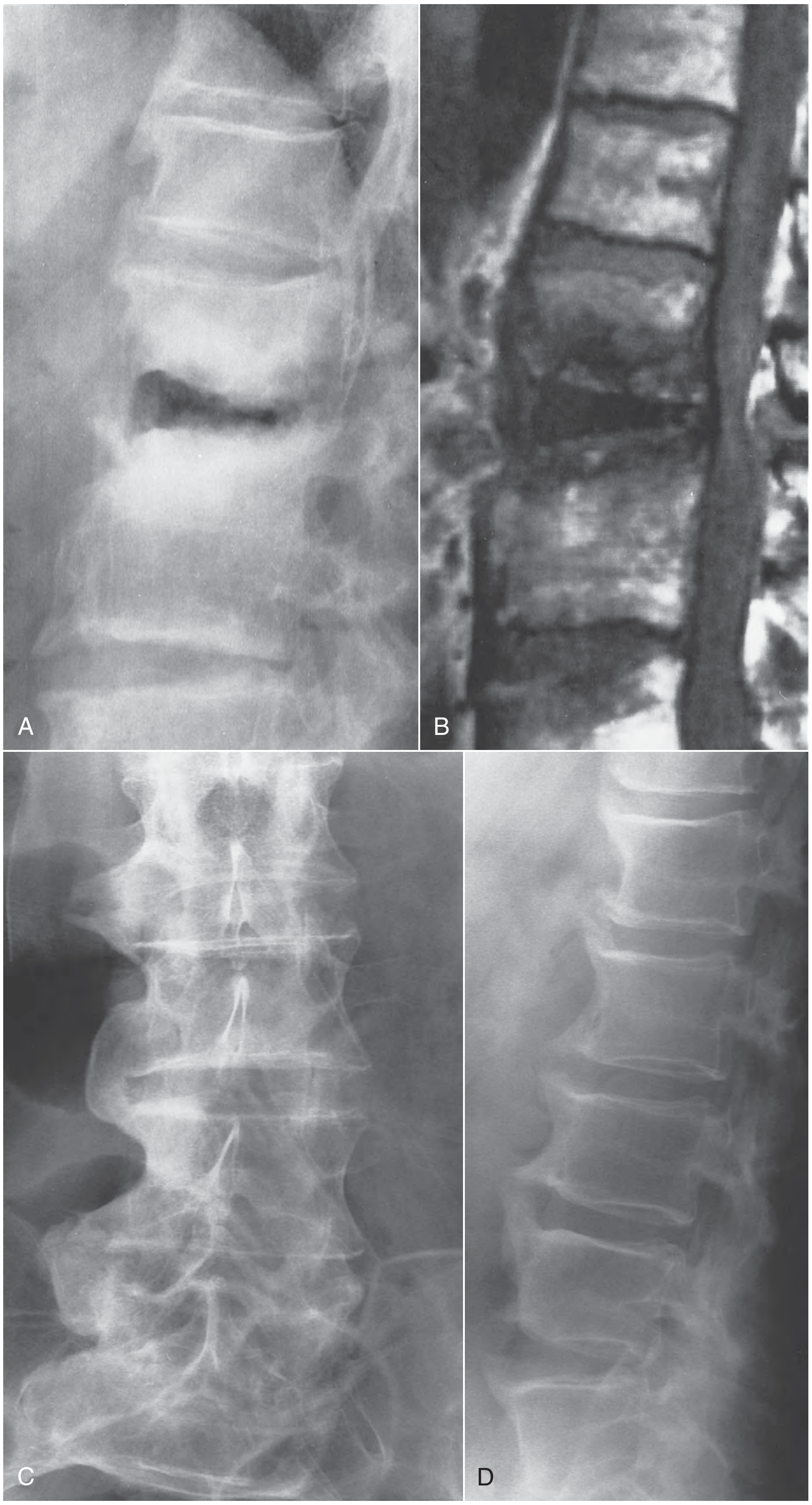

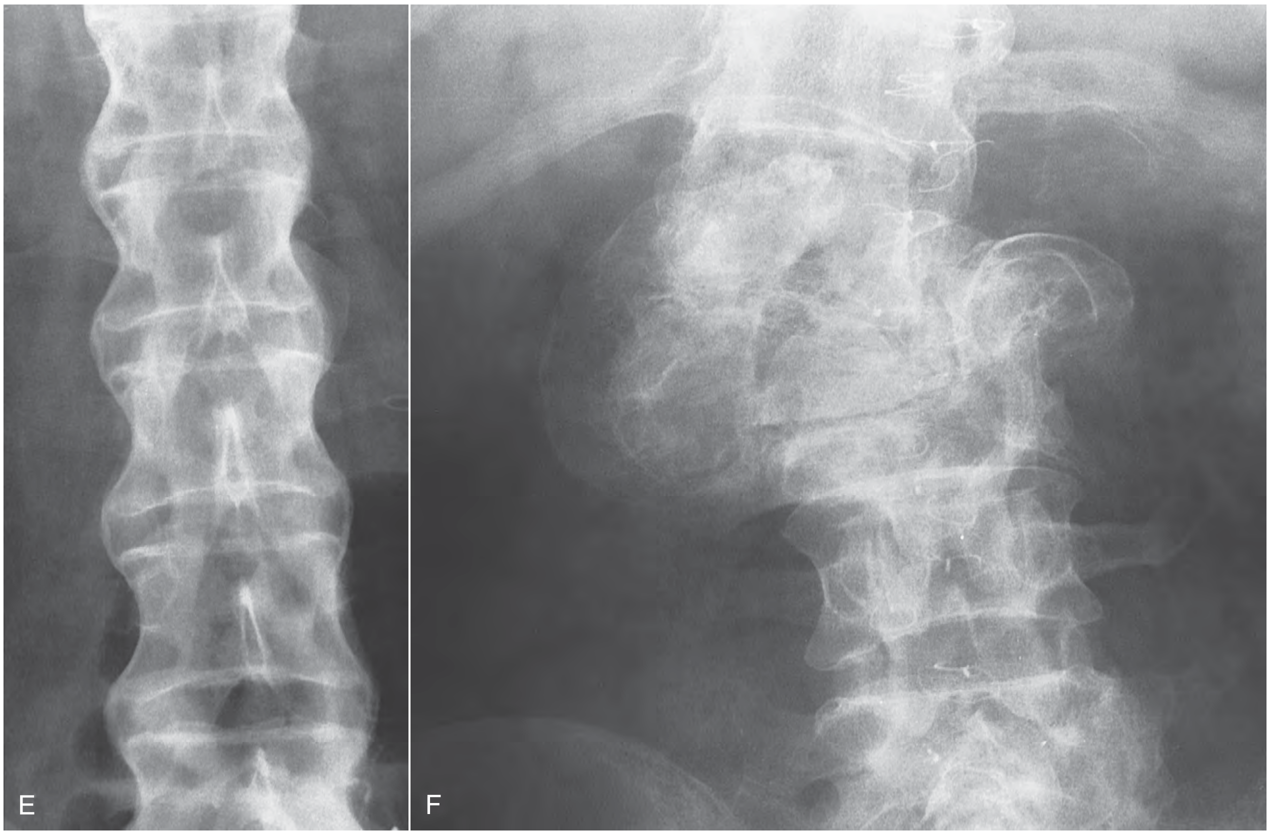

FIGURE 4–78, cont'd **E,** In this quadriplegic man, the diffuse syndesmophyte formation is more typical of ankylosing spondylitis. **F,** In another patient, a pseudarthrosis with bizarre hypertrophic bone formation is characteristic of improper fracture healing, a pattern occasionally seen in paralyzed patients. *(From Park Y-H, Huang G-S, Taylor JAM, et al: Patterns of vertebral ossification and pelvic abnormalities in paralysis: a study of 200 patients. Radiology 188:561, 1993.)*

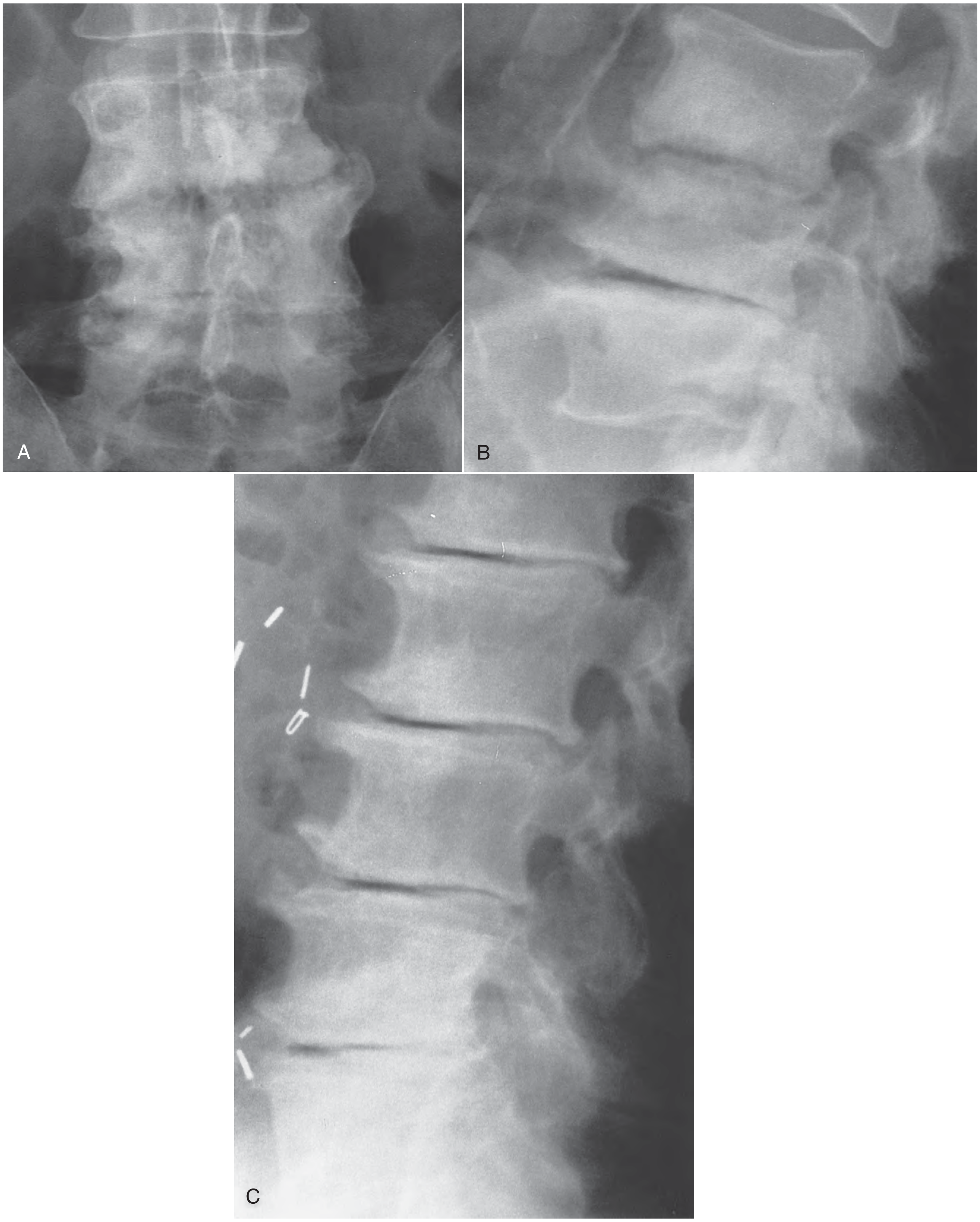

FIGURE 4–79 Calcium pyrophosphate dihydrate (CPPD) crystal deposition disease.[84,85] **A-B,** In this 60-year-old man, marked disc space narrowing, intradiscal gas, and vertebral body sclerosis is seen. The eroded, indistinct vertebral endplates and severe disc space narrowing resemble the changes of infectious spondylodiscitis. **C,** In a 68-year-old man, severe disc space loss, osteophytes, vertebral body sclerosis, and intradiscal vacuum phenomena are seen.

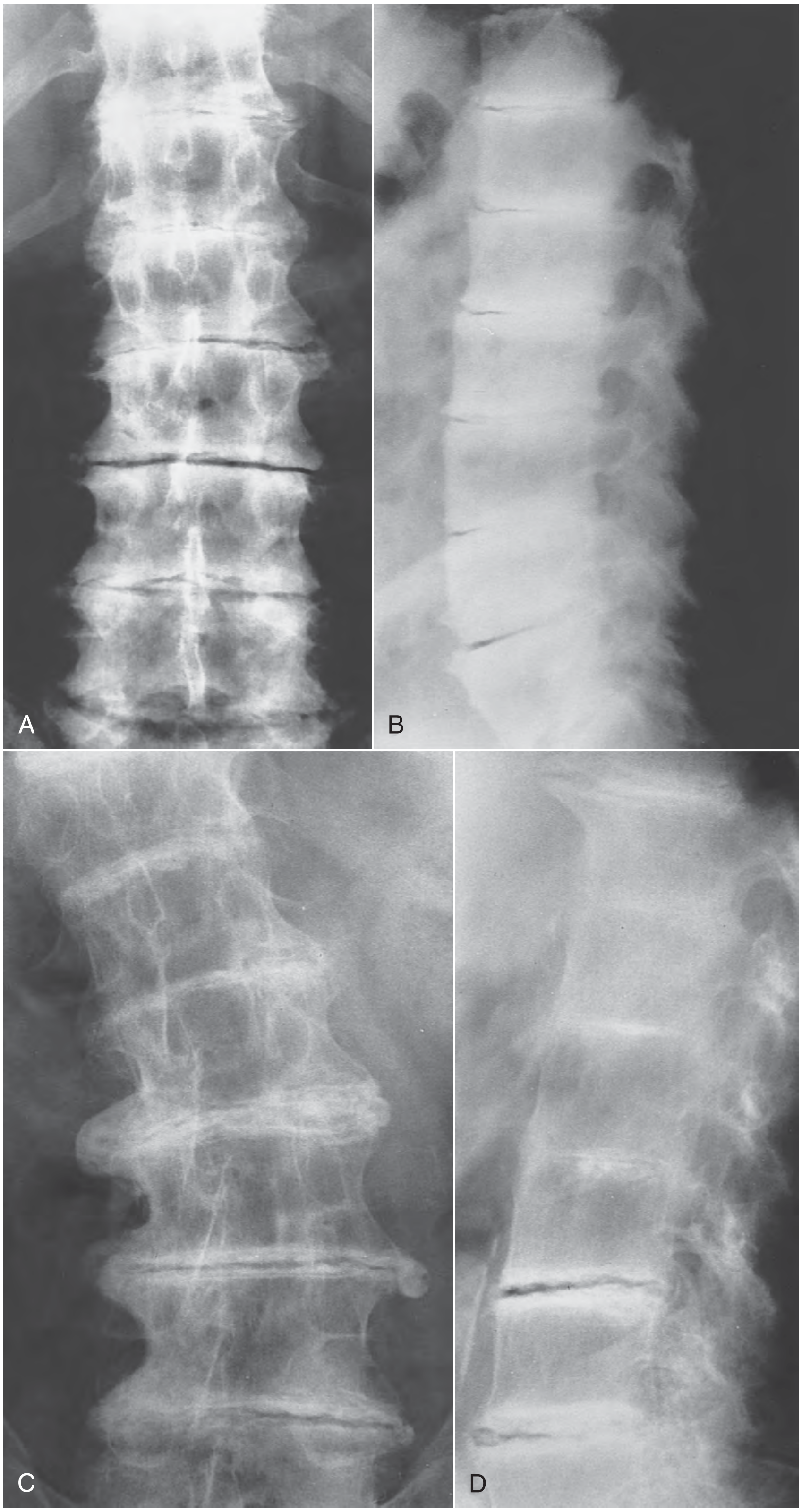

FIGURE 4–80 **Alkaptonuria (ochronotic arthropathy).**[86,87] **A-B,** Radiographs of this 42-year-old man exhibit severe, diffuse disc space narrowing, vacuum phenomena, and adjacent subchondral sclerosis. Disc calcification is not prominent in this patient. **C,** In another patient, observe the widespread disc space narrowing and calcification, vertebral endplate sclerosis, and prominent osteophytosis. This patient also has scoliosis. **D,** In a third patient, widespread ossification of spinal ligaments and intervertebral discs results in ankylosis of several lumbar segments. Intradiscal gas is present within two lower lumbar intervertebral discs. *(**A-B,** Courtesy P. Katzenstein, MD, Houston; **C,** Courtesy G. Marques, MD, São Paulo, Brazil.)*

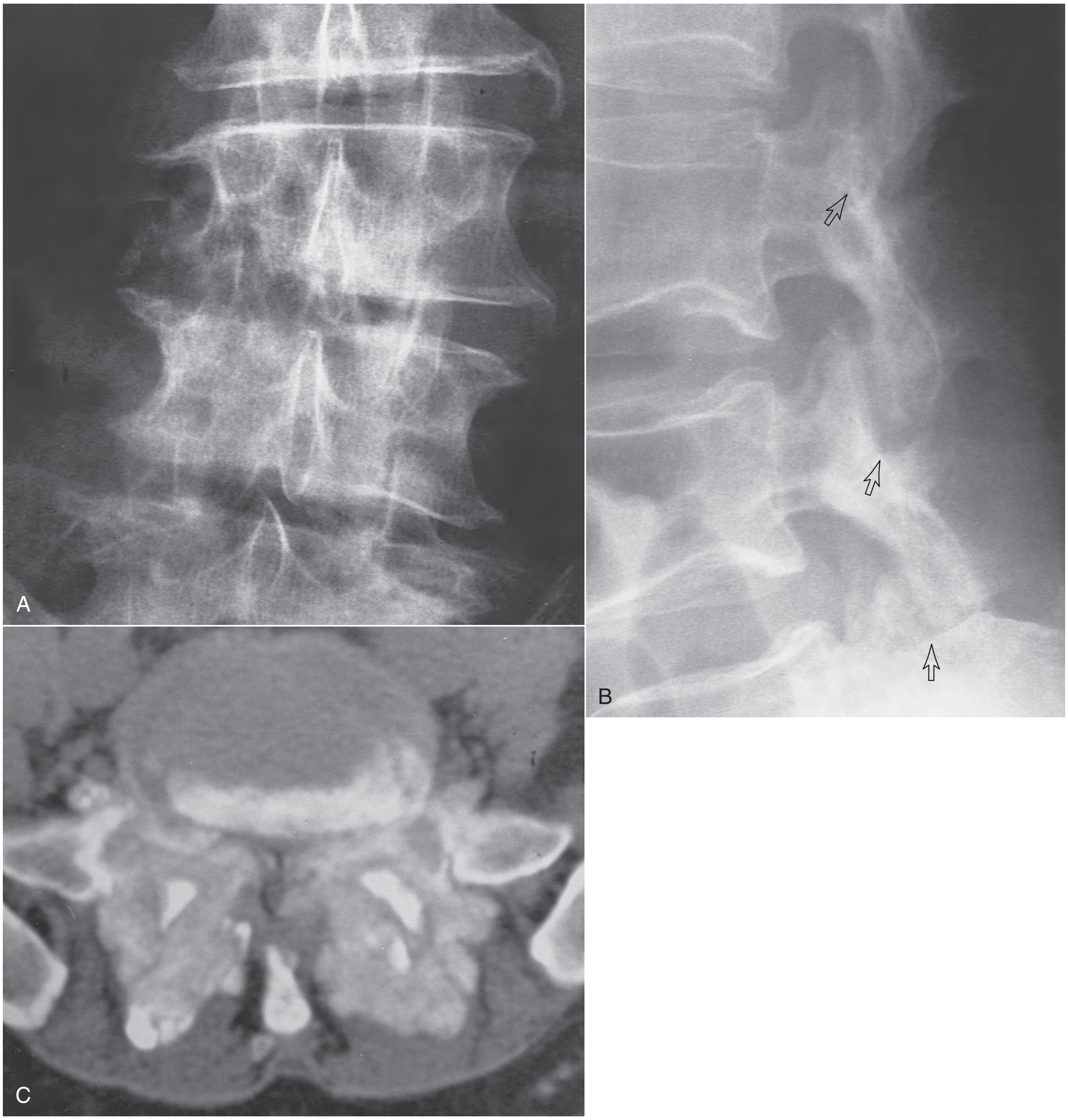

FIGURE 4–81 **Gouty arthropathy.**[88,191] **A,** Asymmetric discovertebral erosion is evident in this patient with long-standing gout. **B-C,** A 53-year-old man with low back pain and symptoms of spinal stenosis has chronic tophaceous gout, gouty nephritis, and chronic renal insufficiency. In **B,** a lateral radiograph reveals erosion of the apophyseal articulations *(open arrows)*. In **C,** a transaxial CT image shows bizarre accumulations of calcified tophaceous material adjacent to the eroded laminae and apophyseal joints. This has resulted in severe spinal canal stenosis. Spinal involvement is rare in gout. *(**A,** Courtesy B. A. Howard, MD, Charlotte, NC; **B-C,** Courtesy C. Chen, MD, Taipei, Taiwan, Republic of China.)*

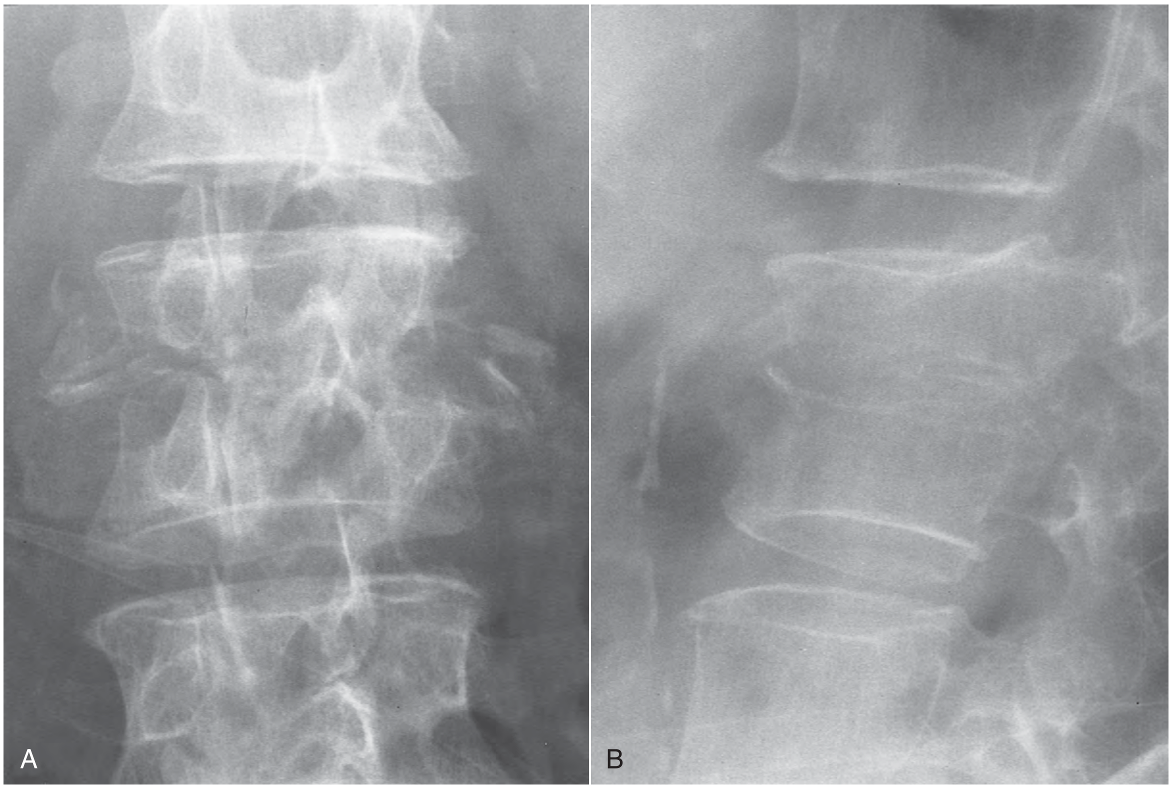

FIGURE 4–82 **Pyogenic spondylodiscitis.**[89,90,143,153] **A-B,** Obliteration of the L2-L3 intervertebral disc space and destruction of the adjacent vertebral endplates and bodies are evident. Osseous debris is noted in the paraspinal region. Complete vertebral body collapse is imminent. Infectious spondylodiscitis occurs in up to 3.7% of patients undergoing lumbar discectomy. Prophylactic antibiotic therapy is effective in preventing such postoperative infection. Refer also to Table 2-16 for MR imaging findings in spinal osteomyelitis.

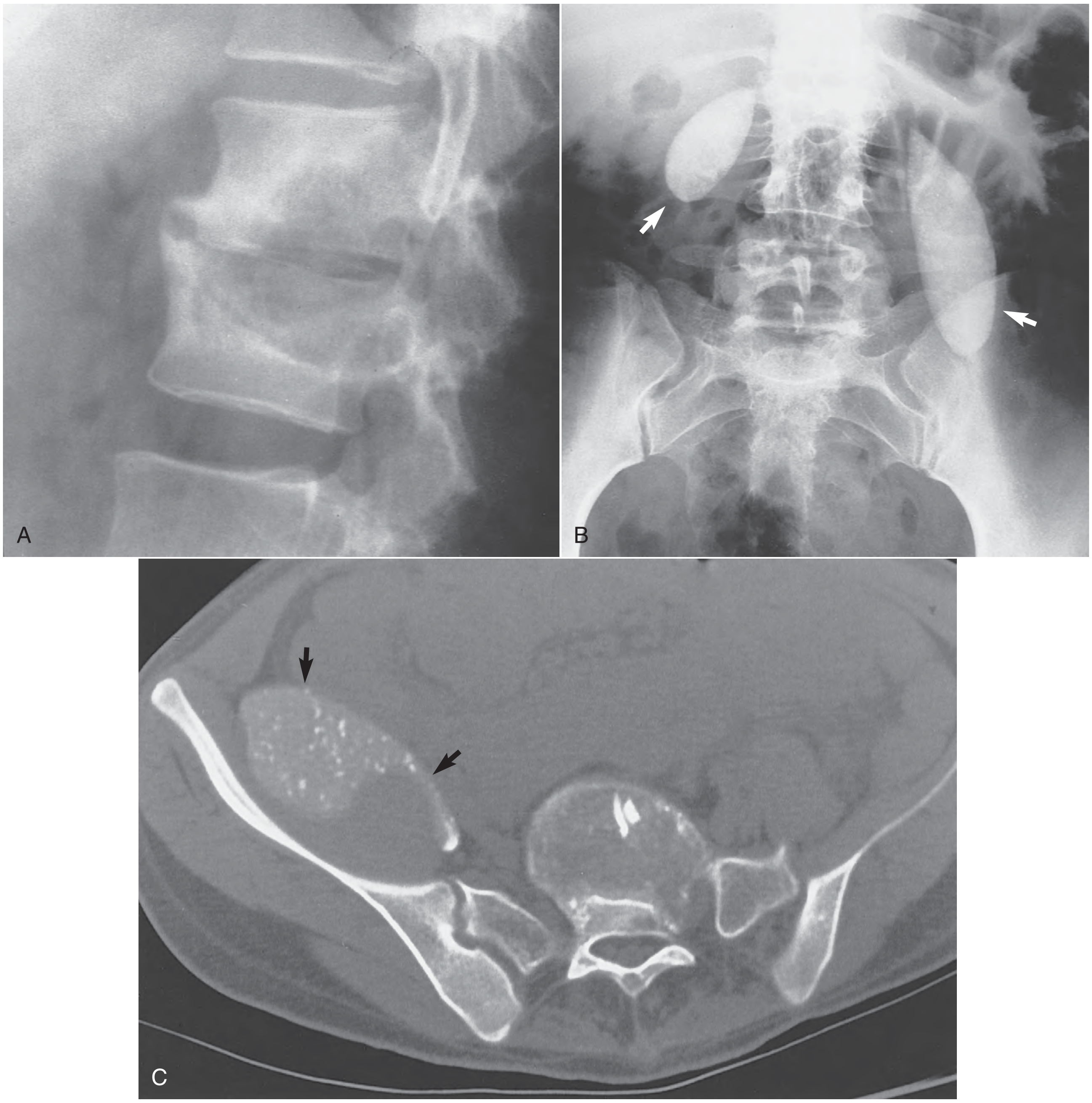

FIGURE 4–83 **Tuberculous spondylitis.**[91,92] **A,** Observe the loss of definition of the vertebral endplate, marked narrowing of the intervening disc space, and large scalloped erosions of the two adjacent vertebral bodies. **B-C,** Psoas abscess. In **B,** a routine radiograph of a patient with spinal tuberculosis shows extensive calcification within bilateral psoas abscesses *(arrows)*. In **C,** a transaxial CT image of a 13-year-old girl with long-standing tuberculosis shows a soft tissue mass in the vicinity of the iliopsoas muscle *(arrows)*. Observe the punctate calcification within this tuberculous abscess about the L5-S1 disc. The spine is affected in 25% to 60% of patients with skeletal tuberculosis. The vertebral bodies and disc typically are involved, although the posterior elements also may be affected. *(**C,** Courtesy M.N. Pathria, MD, San Diego.)*

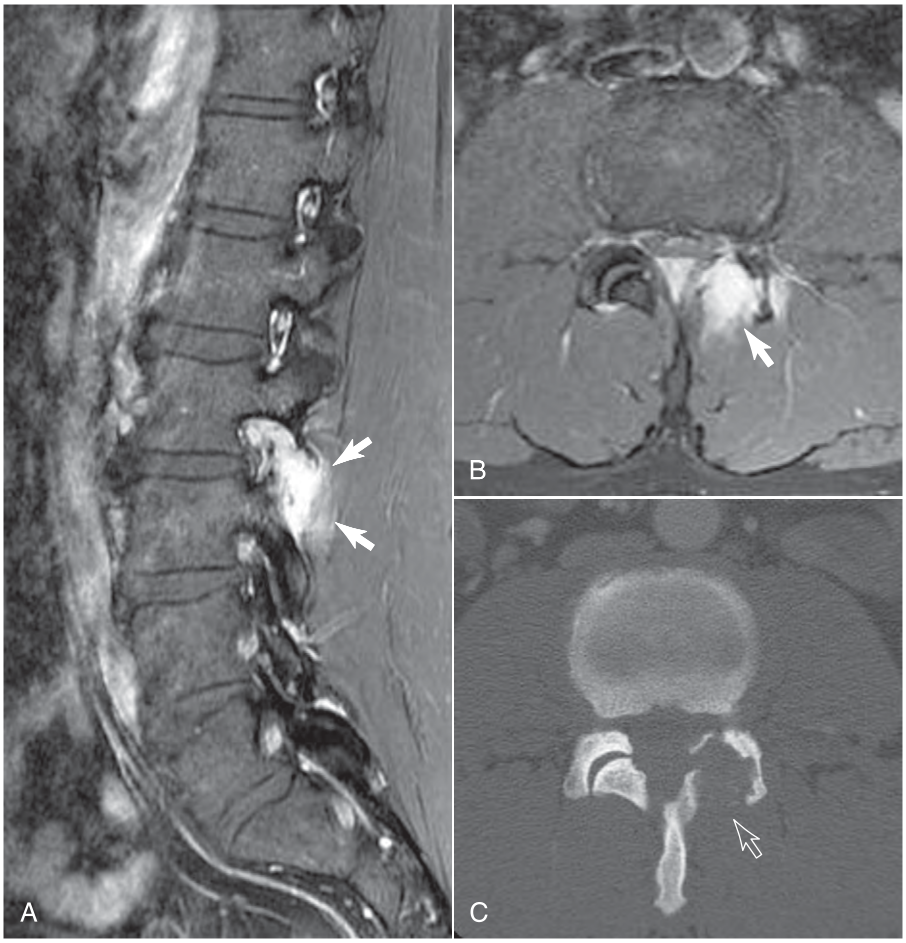

FIGURE 4–84 **Septic arthritis of a facet joint.**[178] This 40-year-old man presenting with back pain and fever underwent MR and CT imaging examinations. Sagittal **(A)** and transaxial **(B)** T1-weighted fat-suppressed spin echo images after intravenous administration of gadolinium shows destruction of the left L2 and L3 articular processes with marked hyperintensity in the intervening facet joint and soft tissues consistent with edema and abscess material *(arrows)*. A corresponding transaxial CT bone window at the L2-L3 disc level **(C)** clearly depicts extensive destruction of the articular processes and significant widening of the left facet joint *(open arrow)*. The joint aspirate yielded granulomatous material that cultured *Coccidioidomycosis* fungus.

TABLE 4-19 Tumors and Tumorlike Lesions Affecting the Lumbar Spine*

Entity	Figure(s)
Malignant Neoplasms	
Skeletal metastasis[93-96]	4-85, 4-86, 4-87
Primary malignant neoplasms of bone	
Chordoma[97]	4-88
Osteosarcoma (conventional)[98,190]	4-89
Myeloproliferative disorders	
Plasma cell myeloma[99,100,144,145]	4-90
Plasmacytoma[99,144]	4-91
Hodgkin disease[95,101,140,146]	4-92
Leukemia[102]	4-93
Benign Neoplasms	
Primary benign neoplasms	
Enostosis[103]	4-94
Osteochondroma[104,105]	4-95
Aneurysmal bone cyst[106,107]	4-96
Hemangioma[108,154]	4-97
Tumorlike lesions	
Paget disease[109,110,148,149,152]	4-98
Neurofibromatosis type I (von Recklinghausen disease)[111]	4-99
Langerhans cell histiocytosis[112,113]	4-100

* This table lists only the neoplasms illustrated in this chapter; for a more complete discussion of neoplasms see Tables 1-12 to 1-14 and Table 2-17.

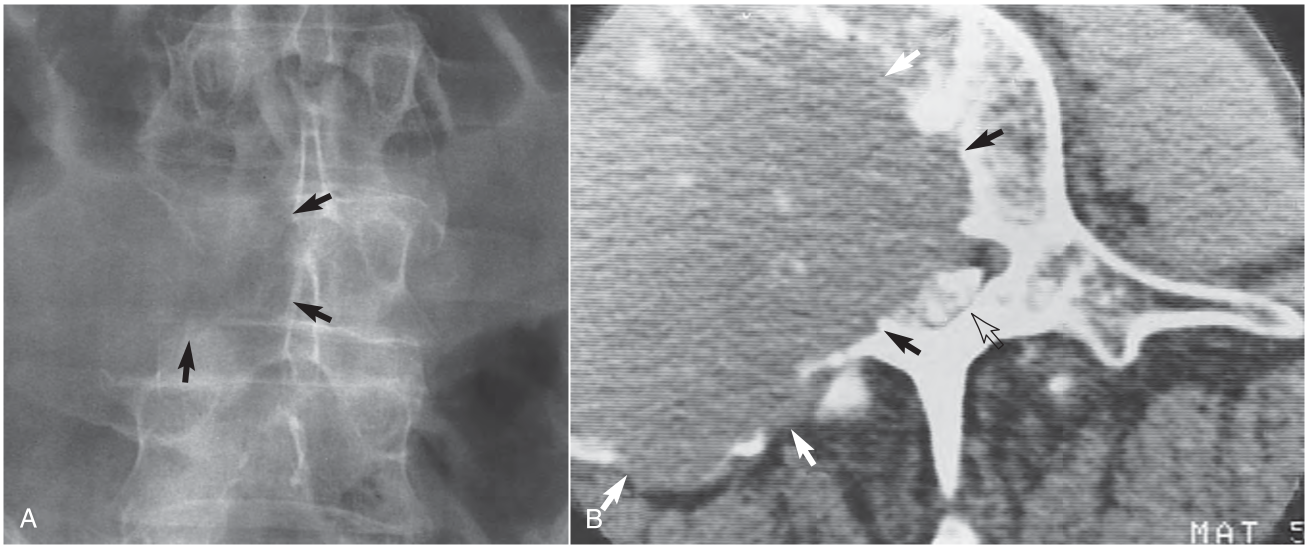

FIGURE 4–85 Skeletal metastasis: vertebral destruction.[93] This 60-year-old man with known renal cell carcinoma developed back pain. **A,** Frontal radiograph shows osteolytic destruction of the right L3 pedicle and vertebral body *(arrows)*. **B,** Transaxial CT-myelographic image shows widespread destruction of the vertebral body, pedicle, and lamina *(black arrows)*. A huge soft tissue mass *(white arrows)* displaces the thecal sac, compressing it against the left lamina *(open arrow)*. Unilateral pedicle destruction is termed the *winking owl sign*, and bilateral pedicle destruction has been referred to as the *blind vertebra sign*. Skeletal metastasis is the most common cause of a missing pedicle. CT, MR imaging, and scintigraphy play an essential role in the evaluation of patients with skeletal metastasis.

TABLE 4-20 Vertebral Osteosclerosis

Representative Disorders or Causes	Characteristics
Ivory Vertebra and Other Sclerotic Lesions of Vertebral Bodies	
Paget disease[109,110,148,149,152]	Older patient, expansion, coarse trabeculae, picture frame vertebrae
Hodgkin disease[95,101,140,146]	Younger patient, occasional anterior vertebral body scalloping
Osteoblastic metastasis[94-96]	Solitary, patchy, or diffuse sclerosis, history of primary carcinoma
Enostosis[103]	Giant bone island
Chordoma[97]	Solitary, rare cause of sclerotic vertebra
Infection[89,90]	Rare cause of sclerotic vertebra, associated disc destruction
Hemangioma[108,154]	Striated corduroy cloth vertebra, usually solitary, rarely expansile
Osteopetrosis[23,24,147]	Diffuse sclerosis, "sandwich vertebrae," or "bone-within-bone" appearance
Osteopoikilosis[15]	Rare in spine, multiple circular sclerotic lesions of uniform size
Fluorosis[122]	Diffuse osteosclerosis and osteophytosis
Sclerotic Pedicle[41]	
Osteoblastic metastasis	Solitary lesions rare; bone scan usually reveals more lesions
Osteoid osteoma	Sclerosis, hypertrophy, small radiolucent nidus, severe pain
Osteoblastoma	Expansile lesions
Enostosis	Bone island within or overlying pedicle
Unilateral spondylolysis	Stress hypertrophy from contralateral pars interarticularis defect
Spina bifida occulta	Variable appearance, stress hypertrophy
Facet tropism	Stress hypertrophy
Laminectomy	Contralateral stress hypertrophy
Spinal fusion	Reactive sclerosis or graft bone
Agenesis or hypoplasia of contralateral pedicle or neural arch	Stress hypertrophy from absence of contralateral pedicle, lamina, or articular process

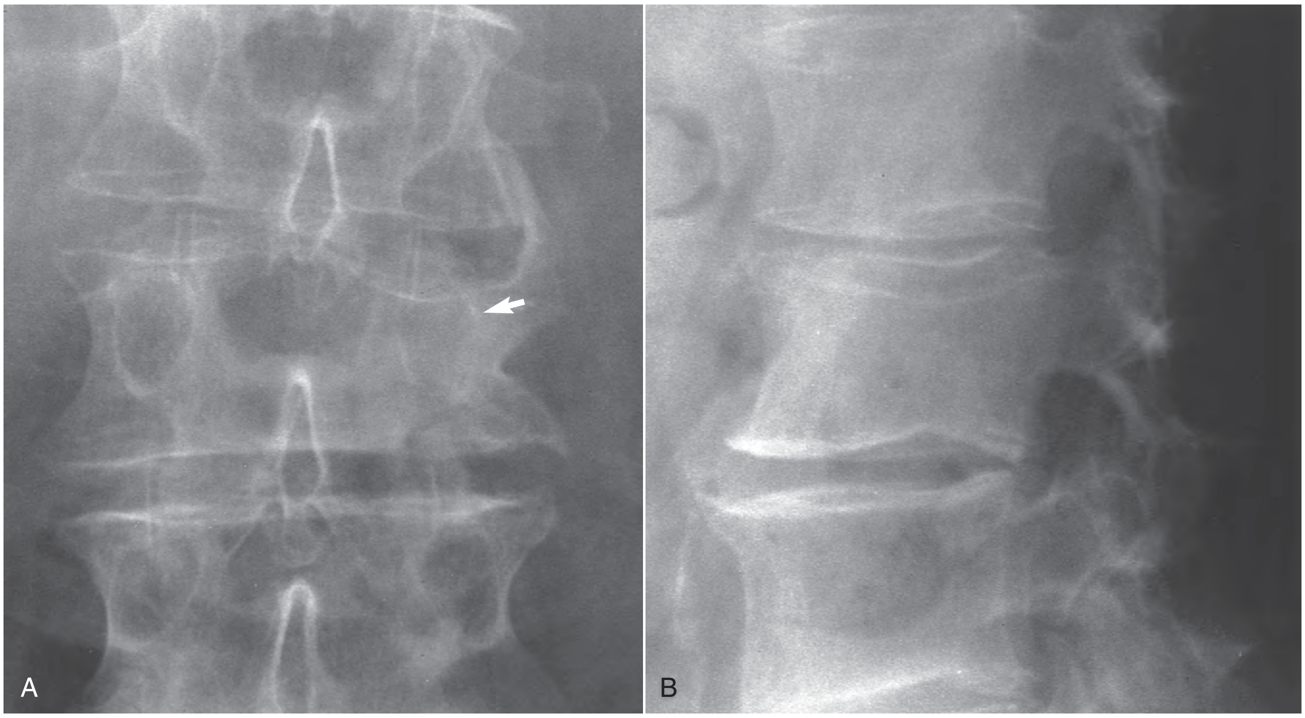

FIGURE 4–86 **Skeletal metastasis[94,95]: prostate carcinoma-variable presentations. A-B,** An 83-year-old man with prostate carcinoma. Routine frontal **(A)** and lateral **(B)** radiographs of the lumbar spine show extensive osteolytic destruction of the L2 vertebral body. Collapse of the vertebral endplate and osteolysis of the left pedicle also are evident *(arrow)*.

Continued

FIGURE 4–86, cont'd **C,** Osteoblastic pattern. Lateral radiograph shows a diffuse osteosclerotic pattern of metastatic disease. No evidence is present of bone expansion, scalloping, or coarsened trabeculae. **D-E,** In another man with prostate carcinoma, the radiographic appearance **(D)** of the L1 vertebral body is osteoblastic. The involved vertebral body has undergone pathologic collapse. A bone scan from this patient **(E)** reveals increased accumulation of the radiopharmaceutical agent localized to the L1 vertebra *(arrows)*. In skeletal metastasis secondary to prostate carcinoma, the osteoblastic pattern is seen in approximately 80% of cases, and the osteolytic or mixed patterns constitute the remaining 20% of cases.

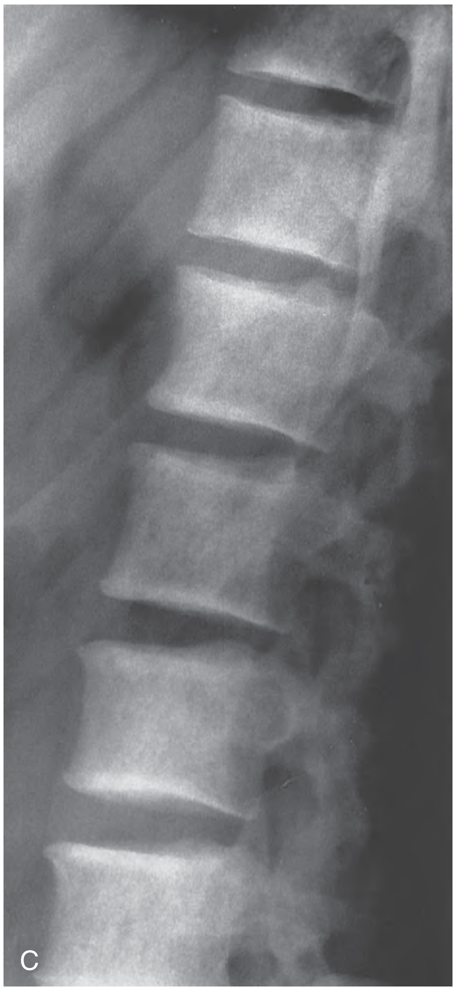

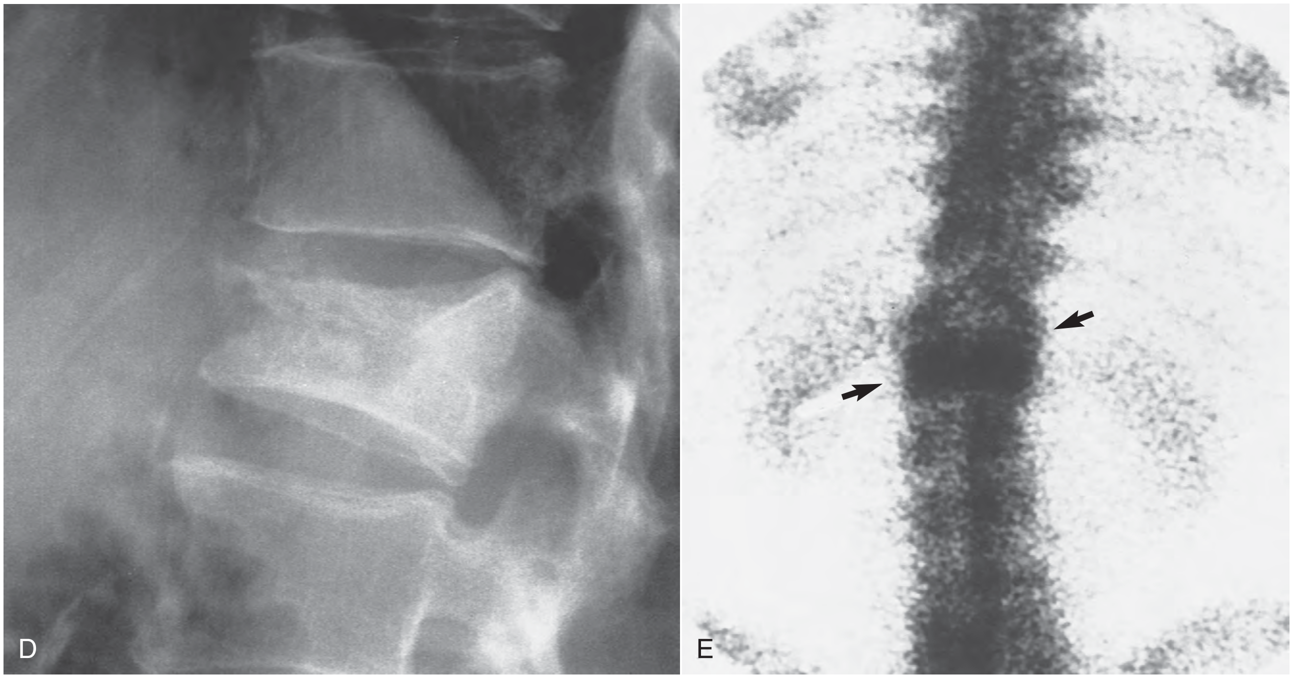

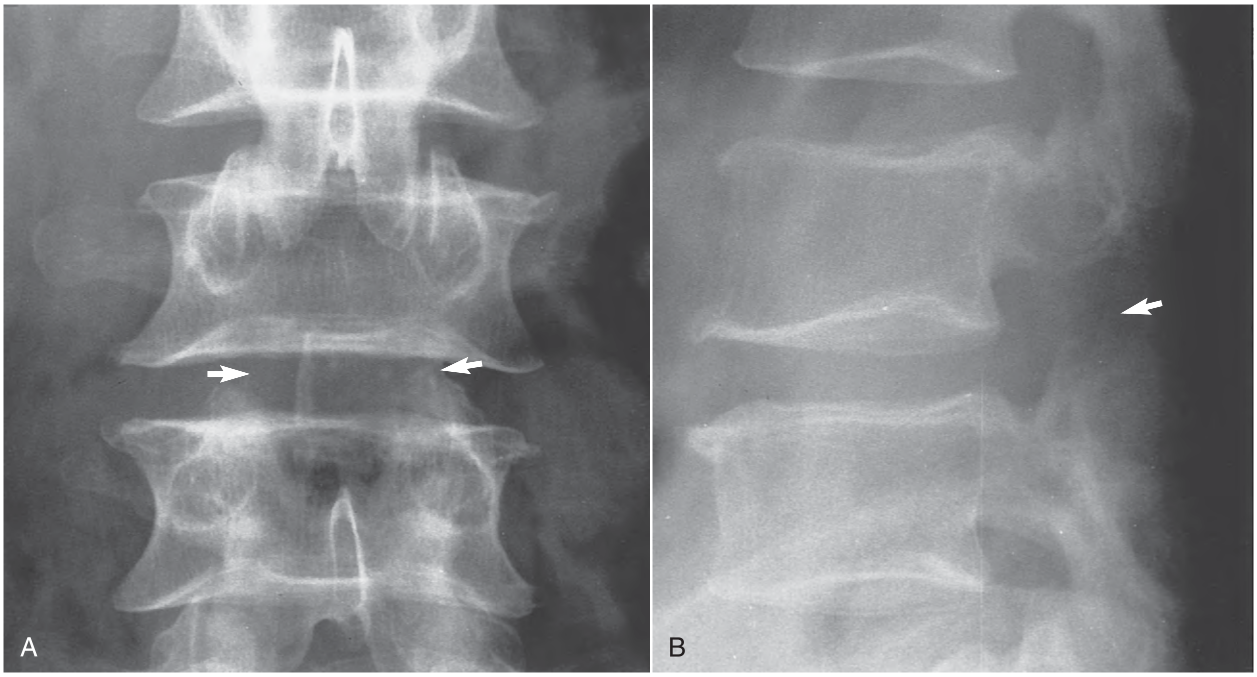

FIGURE 4–87 **Skeletal metastasis: osteolytic pattern.**[96] In this patient, frontal **(A)** and lateral **(B)** radiographs demonstrate osseous destruction of the inferior articular processes *(arrows),* portions of the pedicles, the entire laminae, and the spinous process of the L3 vertebra.

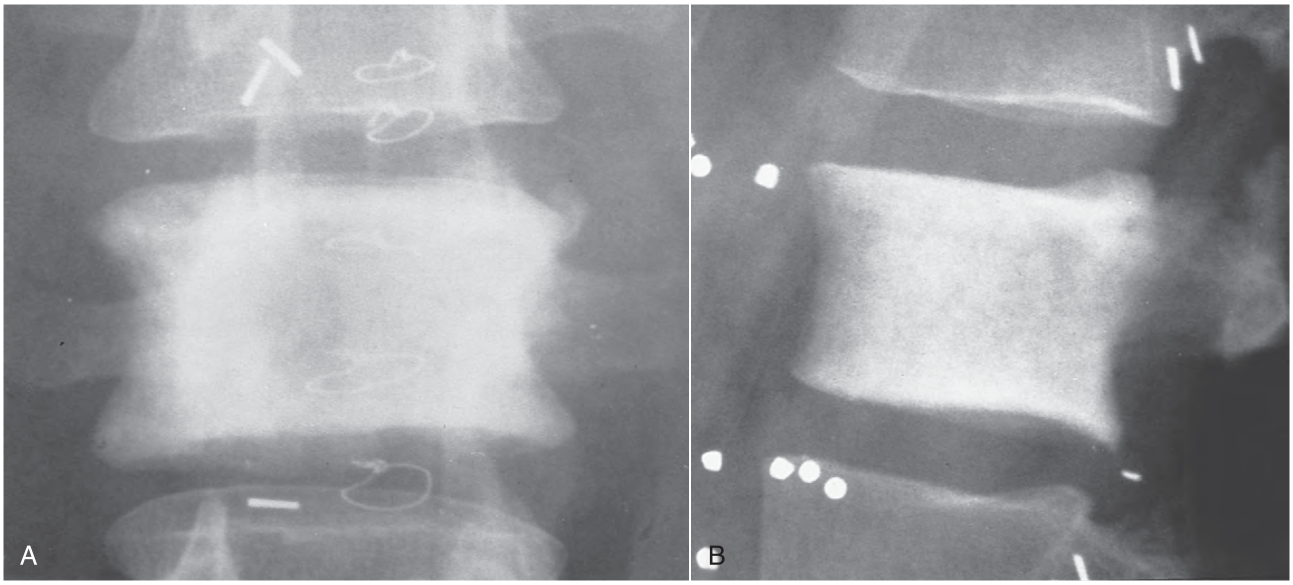

FIGURE 4–88 **Chordoma: ivory vertebra.**[97] Frontal **(A)** and lateral **(B)** radiographs show osteosclerosis of the L2 vertebra of this 38-year-old man with chordoma. He developed neurologic signs and symptoms secondary to an epidural soft tissue mass and subsequently underwent a three-level laminectomy to decompress the spinal canal. Of incidental note are metal buckshot artifacts from an old hunting accident. Approximately 75% of all reported chordomas occur in the vertebral column, sacrum, and coccyx.

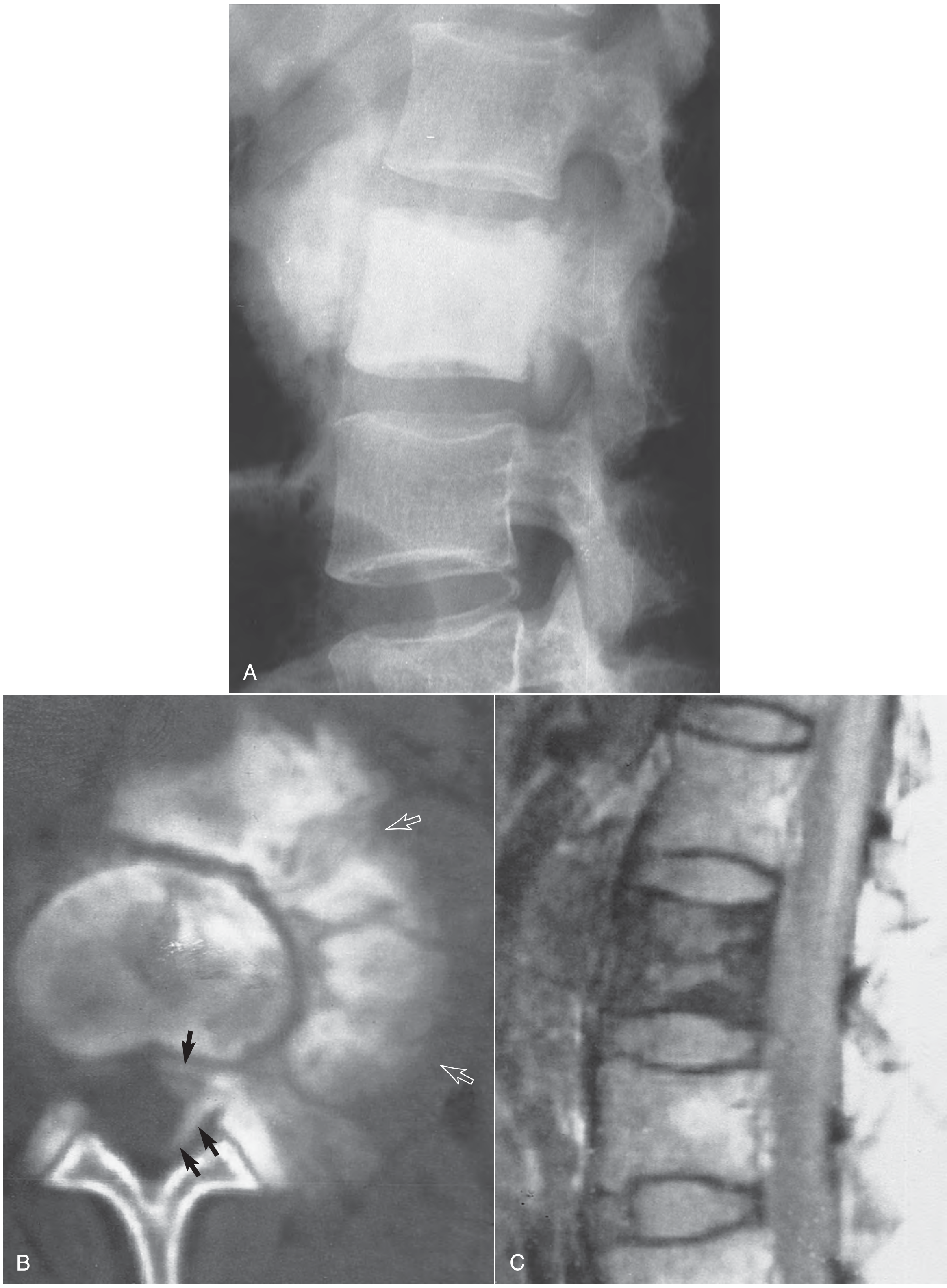

FIGURE 4–89 **Osteosarcoma.**[98,190] A 44-year-old woman had low back and leg pain. **A,** Lateral radiograph reveals an osteosclerotic (ivory) vertebra and an associated radiodense mass in the soft tissues. **B,** Transaxial CT scan shows the increased radiodensity of the vertebral body, and paraspinal *(open arrows)* and epidural *(arrows)* extension of the neoplasm. **C,** Sagittal T1-weighted (TR/TE, 700/20) spin echo MR image demonstrates low signal intensity of the involved vertebral body. The histologic diagnosis was osteosarcoma. Osteosarcoma is a common primary malignant tumor of bone, but spinal osteosarcomas occur infrequently. Conventional osteosarcoma occurs most frequently in persons between the ages of 10 and 25 years, although it also affects older and younger patients. It is twice as common in men. The tumor may be osteoblastic, osteolytic, or more frequently a mixed appearance with both osteoblastic and osteolytic components. Only 4% of osteosarcomas arise from the vertebral column. *(Courtesy A. Deutsch, MD, Los Angeles.)*

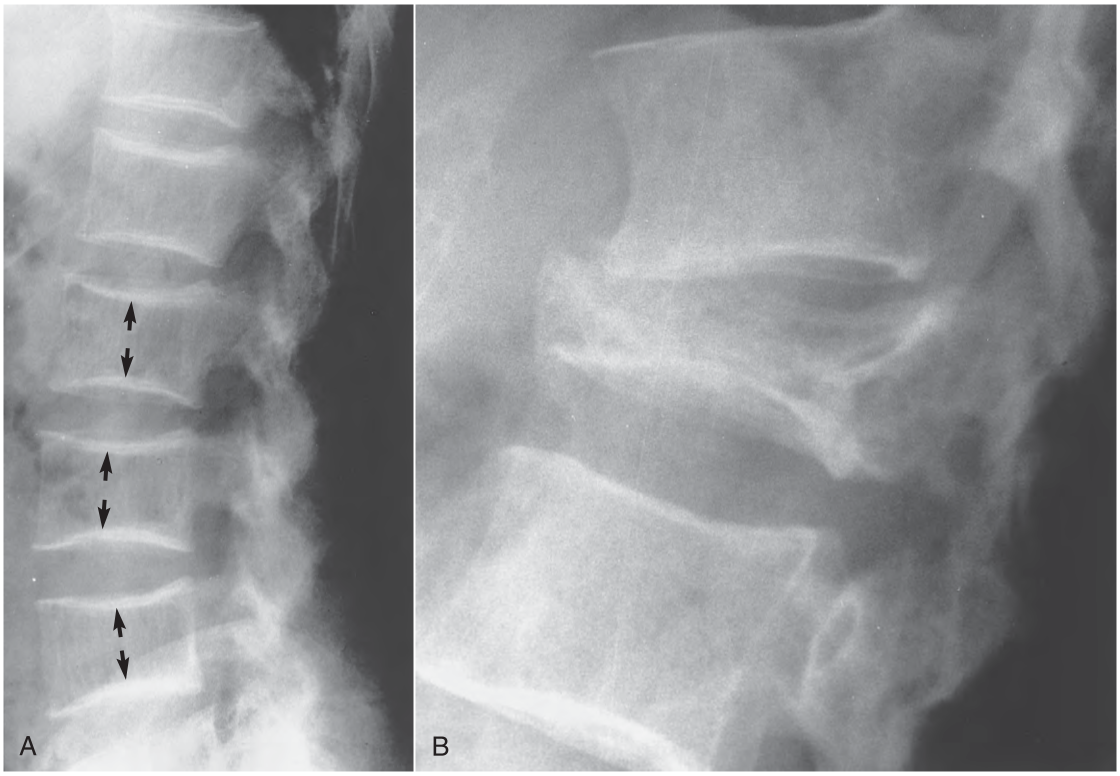

FIGURE 4–90 **Plasma cell myeloma.**[99,100,144,145] **A,** Diffuse osteopenia with increased radiolucency of the medullary portion of the vertebral bodies and early biconcave (fish) deformities *(arrows)* are seen in this patient with diffuse myeloma throughout the spine. The early changes of myeloma, as in this patient, are radiographically indistinguishable from the generalized osteoporosis of aging. **B,** In this 40-year-old man, the L2 vertebra has undergone pathologic collapse. Plasma cell (multiple) myeloma is a common malignant disease of plasma cells that typically affects patients who are 60 to 70 years of age. It is particularly common in black persons. Clinically, these patients have bone pain, particularly in the back and chest, weakness, fatigue, fever, weight loss, bleeding, neurologic signs, and many other signs and symptoms. Serum electrophoresis is positive in 80% to 90% of patients, and Bence-Jones proteinuria is apparent in 40% to 60% of patients with this disease. Classically, myeloma is first manifested as widespread osteolytic lesions with discrete margins, which appear uniform in size. Alternatively, diffuse osteopenia may be the only radiographic finding.

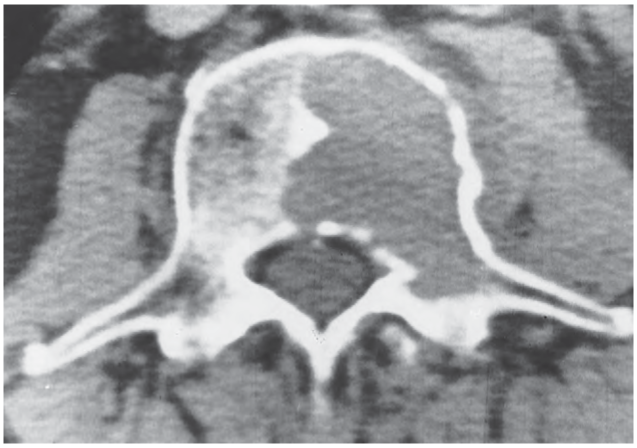

FIGURE 4–91 **Plasmacytoma.**[99,144] Transaxial CT scan of the lumbar spine in a patient with plasmacytoma shows medullary osteolysis of the left side of the lumbar vertebral body and a portion of the pedicle. Solitary plasmacytoma (solitary plasma cell myeloma), in comparison with multiple myeloma, is rare, affects younger patients (average age 50 years), can simulate giant cell tumor, and often results in neurologic manifestations. The lesion may be expansile and multicystic with thickened trabeculae, or it may be purely osteolytic. The spine is the most common site of involvement. Serum electrophoresis and Bence-Jones proteinuria tests are not as reliable as they are in multiple myeloma.

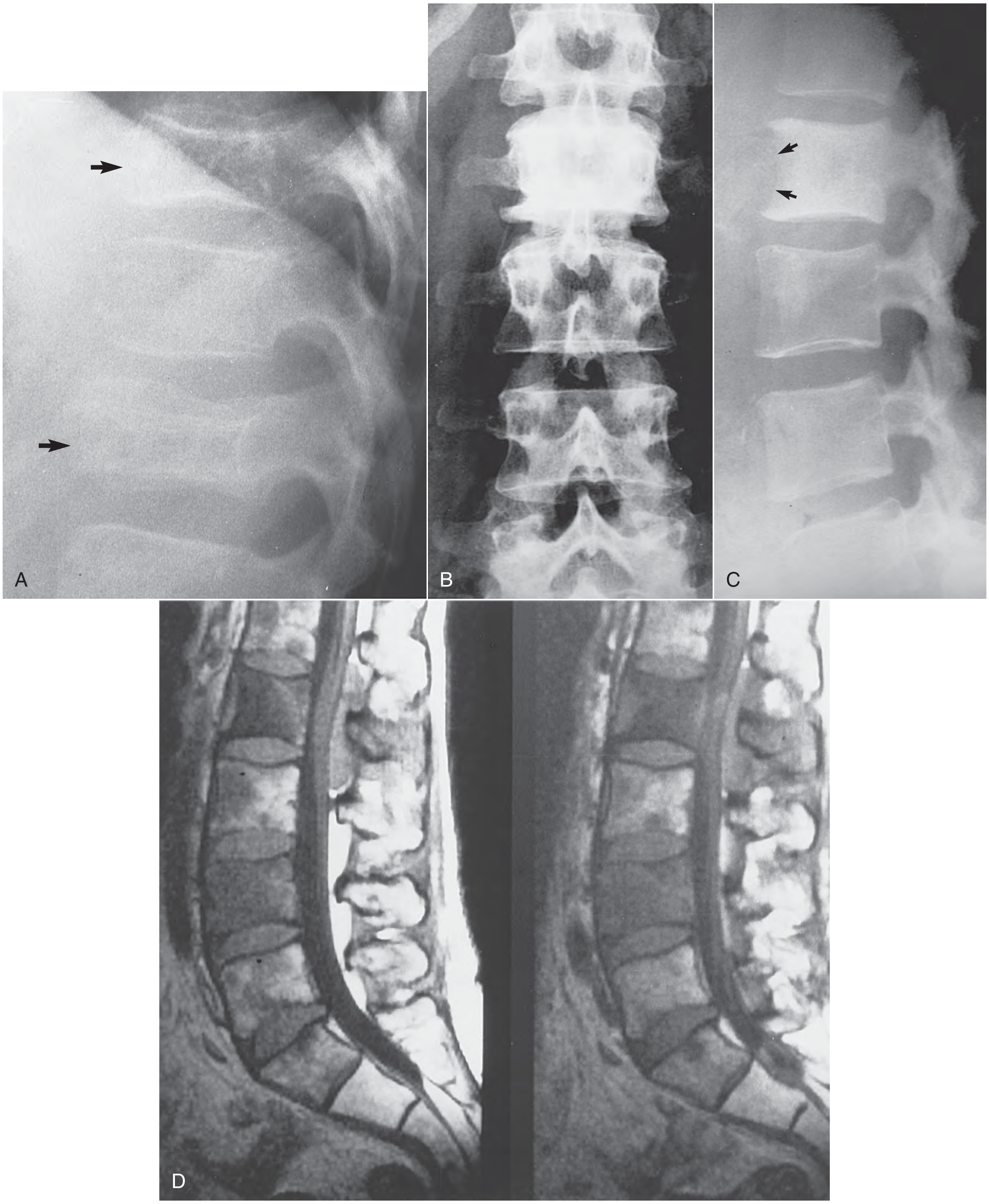

FIGURE 4–92 Hodgkin disease.[95,101,140,146] **A,** Osteolytic pattern. Lateral radiograph of this child with Hodgkin disease shows diffuse osteopenia and multiple biconcave collapsed vertebrae *(arrows)*. **B-D,** Osteosclerotic pattern: ivory vertebra. In a 38-year-old man, frontal **(B)** and lateral **(C)** radiographs reveal a diffusely sclerotic L2 vertebral body (ivory vertebra) *(arrows)*. Mild anterior scalloping of the L2 vertebral body is evident on the lateral radiograph *(arrows)*. Two contiguous sagittal T1-weighted (TR/TE, 560/19) spin echo MR images **(D)** reveal inhomogeneous signal intensity of the bone marrow throughout the lumbar spine, indicating disseminated marrow infiltration with neoplastic lymphomatous cells.

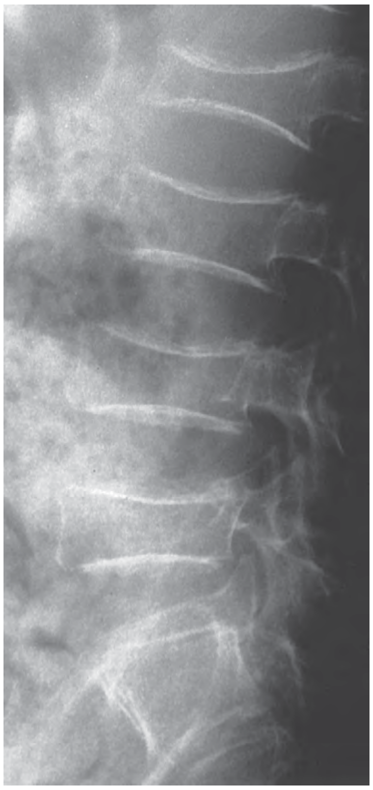

FIGURE 4–93 Acute childhood leukemia.[102] Multiple wedge-shaped and biconcave (fish vertebrae) compression fractures are apparent in this child with acute leukemia. Radiographic skeletal changes occur in up to 70% of persons with acute childhood leukemia. These findings include diffuse osteopenia, osteolytic lesions, and, rarely, osteomyelitis.

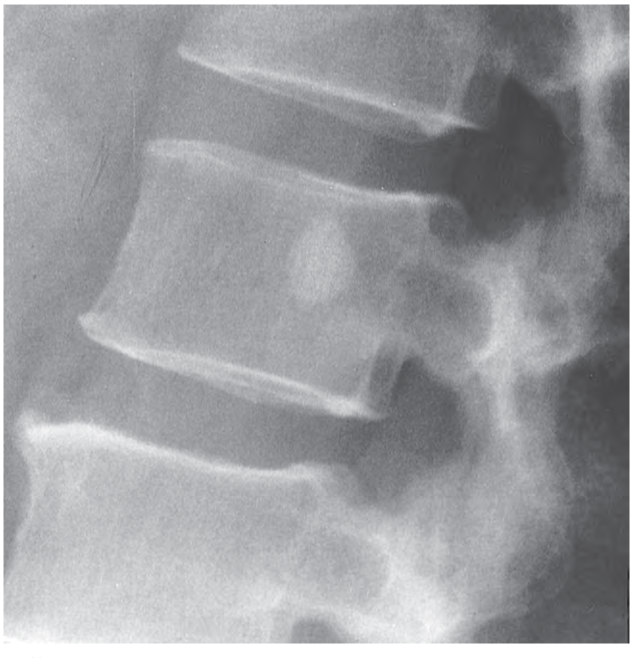

FIGURE 4–94 Enostosis (bone island).[103] Conventional radiograph shows a solitary, circular, osteosclerotic lesion in the L3 vertebral body of this 58-year-old man. A bone scan (not shown) revealed a slight increase in uptake of the bone-seeking radiopharmaceutical agent at the site of the lesion. Enostoses are solitary (or rarely multiple) discrete foci of osteosclerosis within the spongiosa of bone. They may be round, ovoid, or oblong and tend to be aligned with the long axis of the trabecular architecture. They often have a brush border consisting of radiating osseous spicules that intermingle with the surrounding trabeculae of the spongiosa.

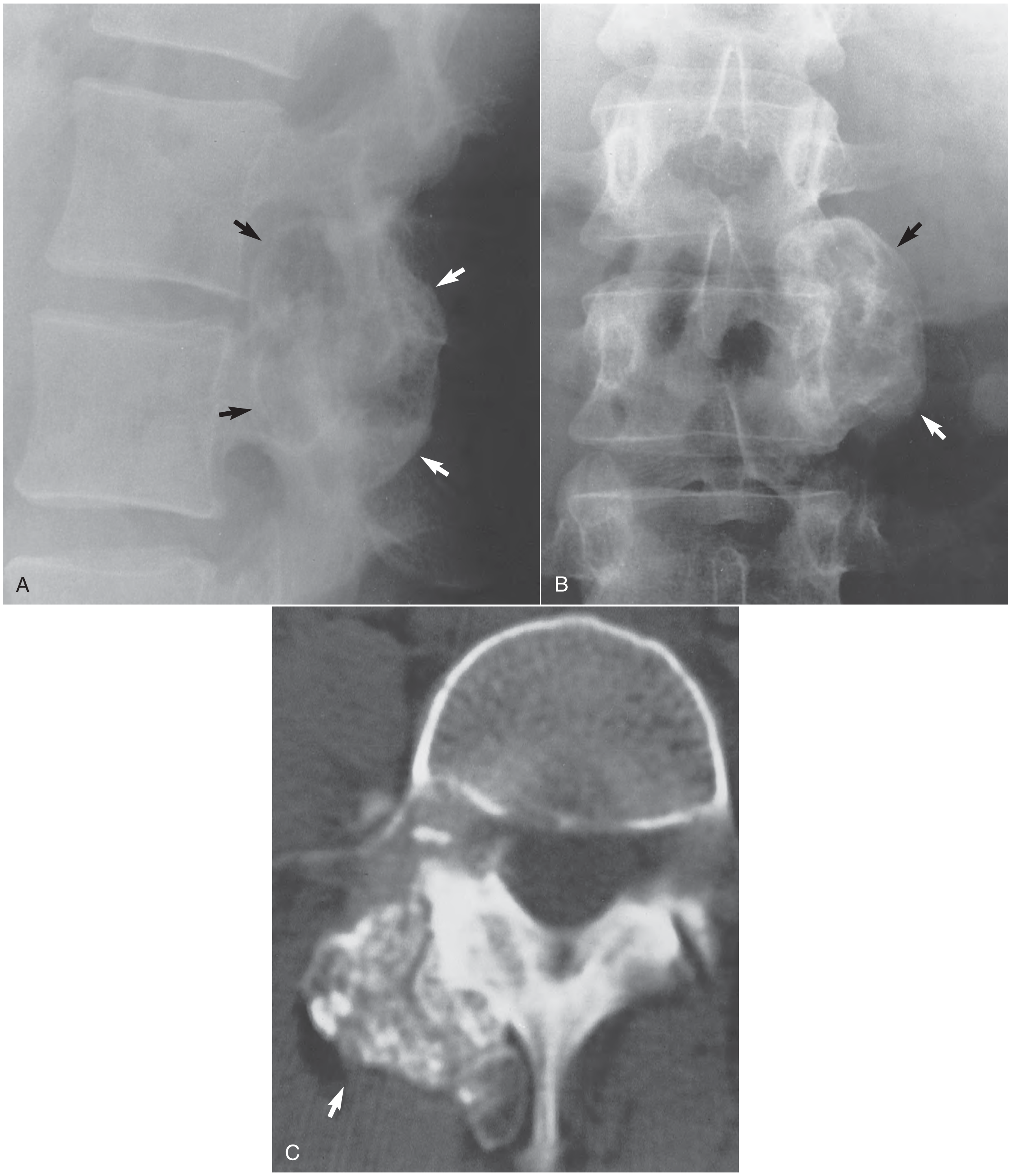

FIGURE 4–95 **Spinal osteochondroma.**[104,105] Anteroposterior **(A)** and lateral **(B)** radiographs reveal a large ovoid osteochondroma arising from the L3 neural arch (*arrows*). **C,** In another patient, a transaxial CT bone window reveals a large broad-based osteocartilaginous mass arising from the right lamina and transverse process of the third lumbar vertebra *(arrow)*. Spinal osteochondromas arise predominantly from the posterior elements and account for only about 2% of all osteochondromas. These benign neoplasms are cartilage-covered osseous excrescences that arise from the surface of bones. They may be solitary or multiple (hereditary multiple exostoses). They may occur spontaneously or after accidental or iatrogenic injury or irradiation. Over 70% of these painless, slow-growing masses occur in patients younger than 20 years of age. Symptoms and signs may occur after fracture, compression of adjacent neurovascular structures, or malignant transformation, a complication occurring in less than 1% of solitary lesions as well as in up to 25% of hereditary multiple exostoses. Rapid growth of an osteochondroma, although not pathognomonic of malignant transformation, is an ominous sign necessitating surgical removal of the lesion. (***A-B,*** *Courtesy R. Kerr, MD, Los Angeles;* ***C,*** *Courtesy L. White, MD, Toronto.)*

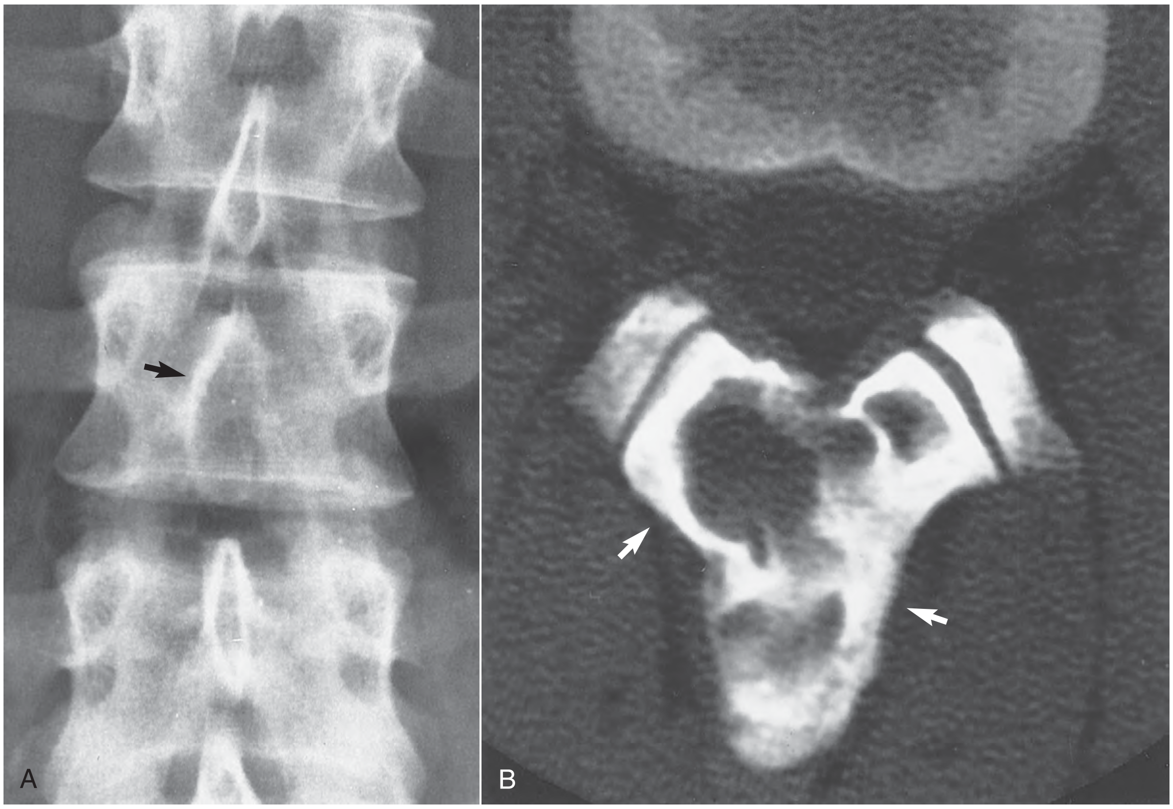

FIGURE 4–96 **Aneurysmal bone cyst.**[106,107] An 18-year-old man had back pain. An anteroposterior radiograph **(A)** reveals subtle expansion and radiolucency of the L3 spinous process *(arrow)*. A transaxial CT bone window image **(B)** more accurately shows the osseous expansion, osteosclerosis, and multiseptate osteolytic foci *(arrows)*. Approximately 14% of aneurysmal bone cysts occur in the spine, primarily in the posterior elements. This benign tumor is a thin-walled, expansile lesion containing blood-filled cystic cavities. Most aneurysmal bone cysts are discovered in patients younger than 20 years of age (age range, 3 to 70 years). Clinical findings include local pain and tenderness and, occasionally, neurologic symptoms. Acute, severe pain may accompany pathologic fracture of aneurysmal bone cysts. Ten percent of spinal aneurysmal bone cysts recur within 6 months of surgery. *(Courtesy P. Kindynis, MD, Geneva.)*

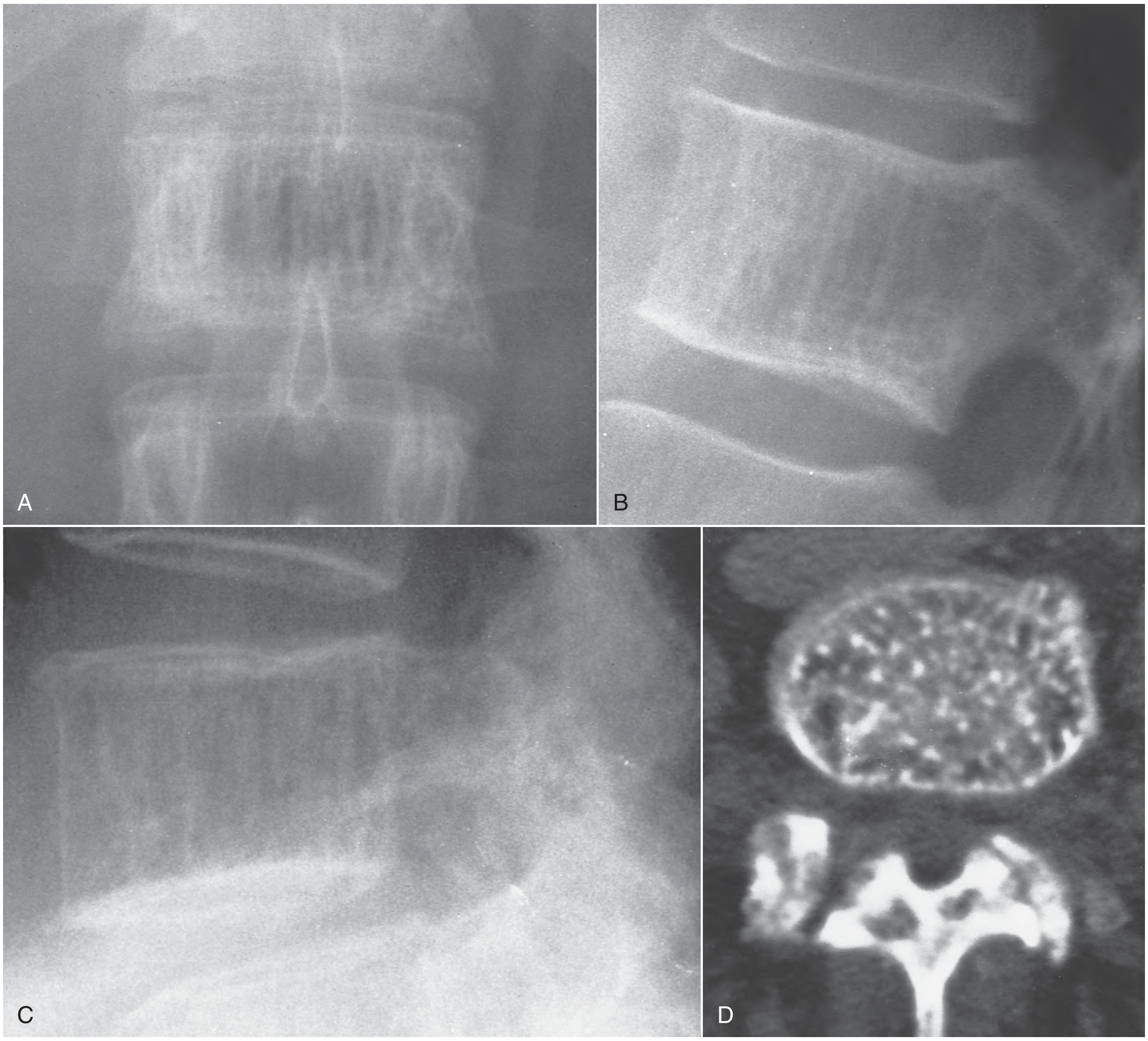

FIGURE 4–97 **Hemangioma.**[108,154] **A-B,** A 53-year-old man. Anteroposterior **(A)** and lateral **(B)** radiographs show the characteristic "corduroy cloth" appearance of a hemangioma affecting the L1 vertebral body. This appearance is produced by the coarse vertical radiodense striations that are interspersed among the relatively osteopenic spongiosa of the vertebral body. **C-D,** This 77-year-old woman had multiple spinal hemangiomas. Lateral radiograph **(C)** demonstrates coarse vertical trabeculae within the osteopenic vertebral body and pedicle of L4. Transaxial CT image through L4 **(D)** demonstrates the radiodense vertical trabeculae within the osteopenic spongiosa of the vertebral body ("polka-dot" sign) and posterior elements. Approximately 25% of hemangiomas occur in the spine, and as such, are considered the most common benign neoplasm of the spine. *(**C-D,** Courtesy V. Vint, MD, San Diego.)*

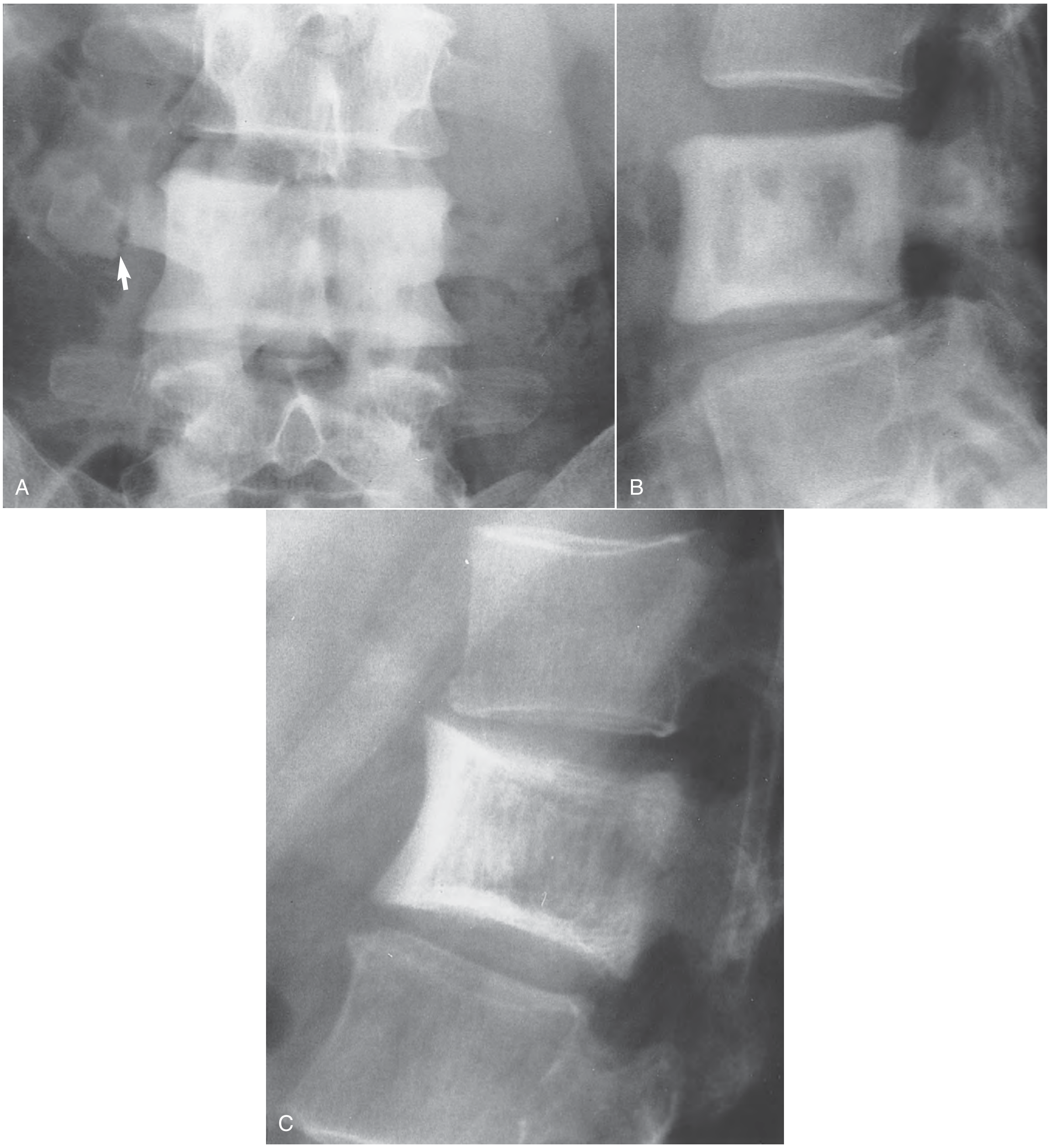

FIGURE 4–98 Paget disease: radiographic appearance.[109,110,148,149,152] **A-B,** Picture-frame vertebra. Frontal **(A)** and lateral **(B)** radiographs show sclerosis of the vertebral body and cortical thickening of its periphery. This pattern is best seen on the lateral film and is referred to as the *picture frame vertebral body*. A pathologic fracture of the transverse process is also seen *(arrow)*. **C,** In another patient, observe the characteristic picture-frame appearance with significant osseous enlargement of the vertebral body.

Continued

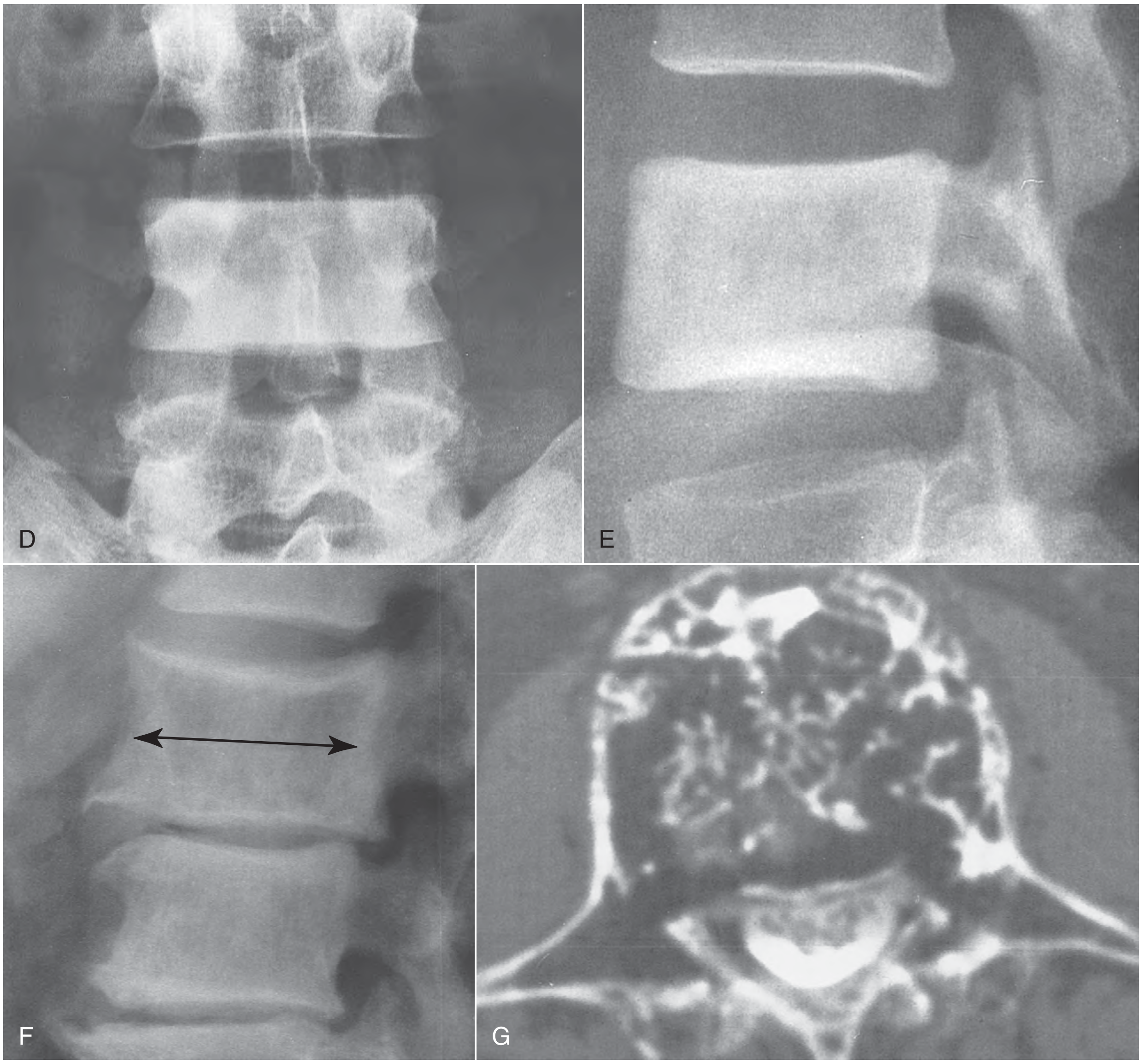

FIGURE 4–98, cont'd **D-E,** Ivory vertebra. In a third patient, observe the diffuse sclerosis of the L4 vertebral body. The sclerosis dominates at the periphery of the vertebral body. Paget disease is one cause of an ivory vertebra. **F,** Vertebral enlargement. Observe the localized osseous expansion of the L2 vertebral body *(double-headed arrow)*. **G,** CT imaging findings. Transaxial CT-myelographic image shows the typical coarsened trabecular pattern, intervening radiolucency of medullary bone, and enlarged osseous contour typical of Paget disease.

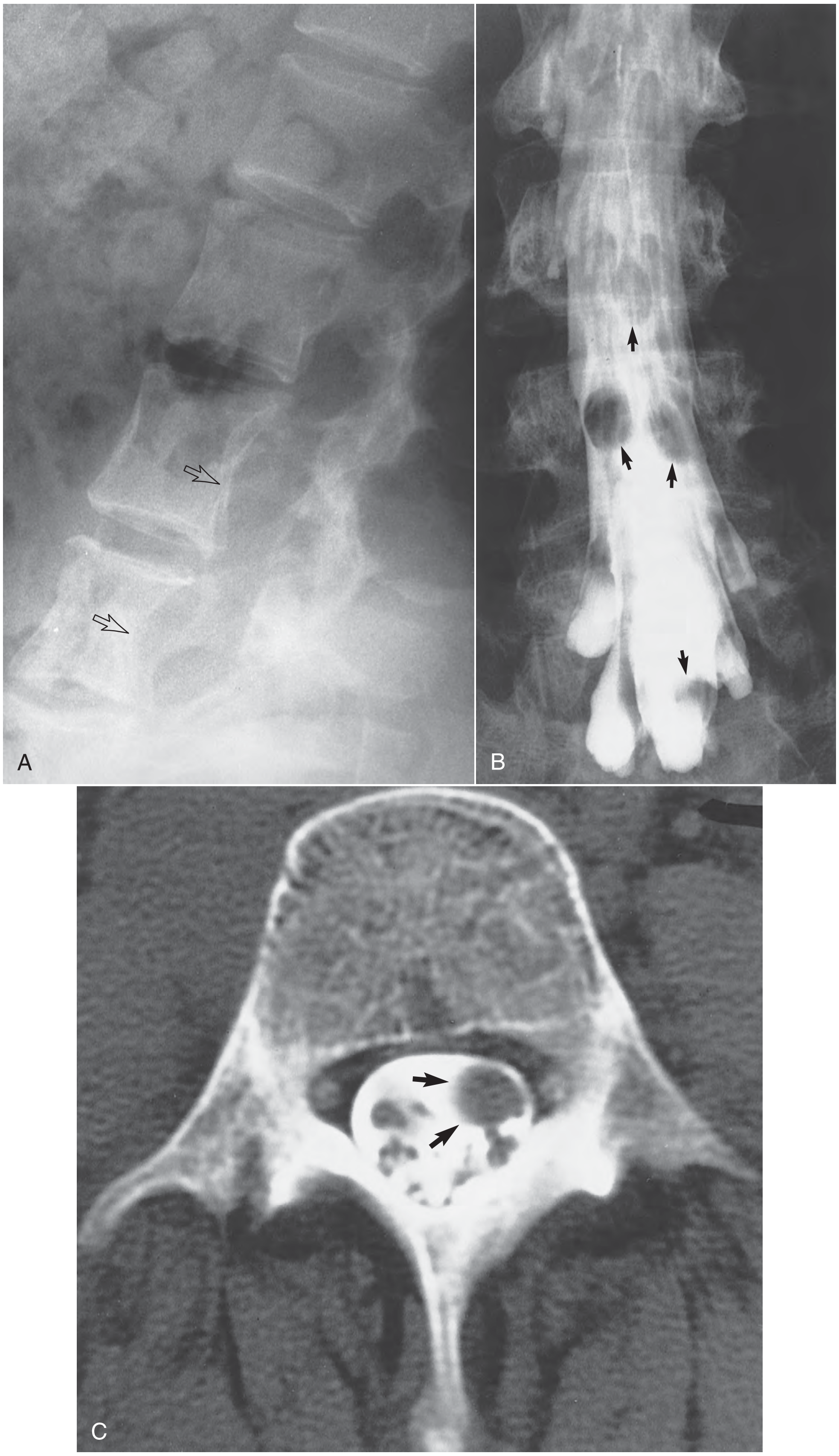

FIGURE 4–99 **Neurofibromatosis type I (von Recklinghausen disease).**[111] **A,** Lateral radiograph shows posterior vertebral body scalloping and expansion primarily of the L3 and L4 neural foramina *(open arrows)*. Scalloping results from intrinsic dysplastic changes in the bone or from neighboring dural ectasia rather than from mechanical pressure exerted by a local neurofibroma. **B-C,** 23-year-old woman. Routine radiograph **(B)** and transaxial CT scan **(C)** after metrizamide myelography show lobulated intrathecal neurofibromas of varying size *(arrows)*. (***A,** Courtesy G. Koors, DC, Eugene, Ore, and G. Smith, DC, Portland, Ore.)*

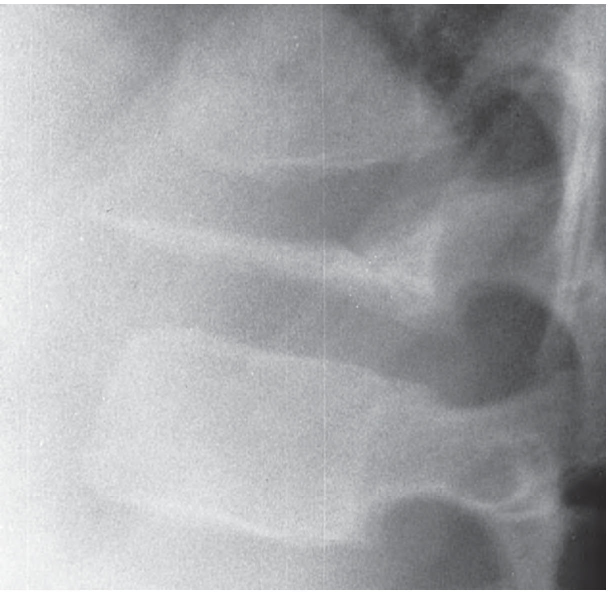

FIGURE 4–100 **Langerhans cell histiocytosis: Eosinophilic granuloma.**[112,113] Observe vertebra plana involving a thoracolumbar vertebral body. Eosinophilic granuloma of bone is the most frequent and mildest form of Langerhans cell histiocytosis, a disease characterized by histiocytic infiltration of tissues. In addition to flattened vertebral bodies, eosinophilic granuloma may appear as bubbly, lytic, or expansile lesions without collapse. With healing, the height of the vertebral body may be reconstituted, a finding more common in younger persons.

TABLE 4-21 Metabolic and Hematologic Disorders Affecting the Lumbar Spine*

Entity	Figure(s)	Characteristics
Generalized osteoporosis[114-117]	4-101, 4-102, 4-103, 4-104	Uniform decrease in radiodensity, thinning of vertebral endplates, accentuation of vertical trabeculae Thoracolumbar region of the spine is the most frequent site of osteoporotic compression fractures Wedge-shaped vertebral deformities due to compression fractures are most common in thoracic spine; biconcave deformities are more common in the lumbar spine; vertebra plana deformities are more likely to be related to pathologic fracture due to plasma cell myeloma, skeletal metastasis, or other destructive process
	Table 4-22	Quantitative bone mineral analysis (densitometry) is necessary for accurate assessment of the presence and extent of diminished bone mineral content Dual energy x-ray absorptiometry is the most widely used method to assess bone mineral density owing to its ease of use, high precision, and low radiation exposure to patients[180-182]
Osteomalacia[118]	4-105	Diminished radiodensity and prominent coarsened trabeculae Vertebral compression fractures
Hypothyroidism[119]	4-106	Bullet-shaped vertebra, thoracolumbar gibbus deformity, osteopenia, delayed development, and widened disc spaces
Hyperparathyroidism and renal osteodystrophy[120]	4-107	Findings are most prominent in the thoracolumbar spine and include subchondral resorption at discovertebral junctions and the rugger-jersey spine—bandlike osteosclerosis adjacent to the superior and inferior surfaces of the vertebral body Vertebral fracture typically results in biconcave thoracolumbar endplate deformities
Acromegaly[121]	4-108	Elongation and widening of the vertebral bodies; ossification of the anterior portion of the disc; posterior scalloping of vertebral bodies occurs infrequently; increased disc height; premature degenerative disease, exuberant osteophytosis
Fluorosis[122]	4-109	Diffuse osteosclerosis and ossification of the posterior longitudinal ligament, prominent osteophytosis, and periostitis Differential diagnosis includes osteopetrosis, skeletal metastasis, other causes of diffuse osteosclerosis, and diffuse idiopathic skeletal hyperostosis (DISH) (Table 4-20)
Mastocytosis[123]	4-110	Spinal skeletal changes include combinations of diffuse or focal osteosclerosis, osteopenia, or osteolysis
Gaucher disease[124,151]	4-111	Vertebral changes include diffuse vertebral body collapse and, infrequently, H-shaped, steplike defects in the vertebral bodies
Sickle cell[150] anemia[125-127]	4-112	Diffuse osteopenia and H-shaped vertebra Compensatory vertical growth of adjacent vertebral bodies results in "tower vertebrae"
β-thalassemia[128,139]	4-113	Findings similar to those of sickle cell anemia with osteopenia, lacelike trabecular pattern, and, infrequently, H-shaped vertebral bodies
Osteonecrosis of the vertebral body[129]	4-114	Intravertebral vacuum phenomenon with pathologic vertebral body collapse Frequently associated with corticosteroid use

* See also Tables 1-15 to 1-17.

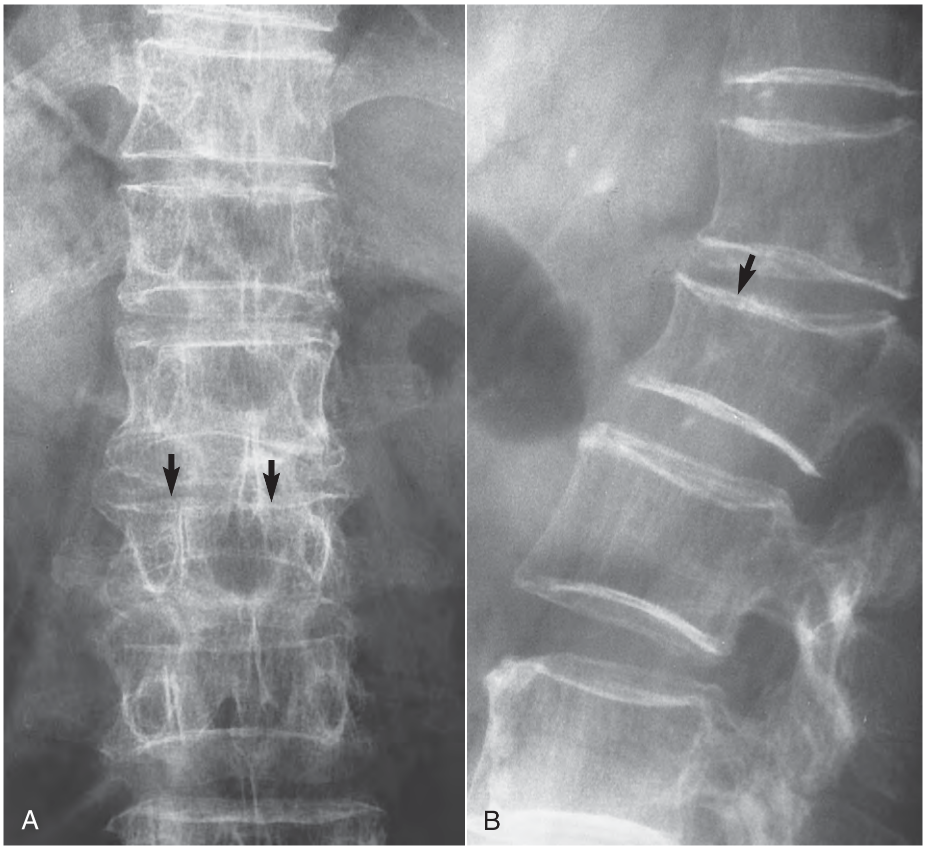

FIGURE 4–101 Generalized osteoporosis.[114,115] Frontal **(A)** and lateral **(B)** radiographs in a 73-year-old woman who had acute thoracolumbar pain after a minor fall. Observe the thinning of the cortices, increased radiolucency of medullary bone, and apparent accentuation of the vertical trabeculae. A wedge-shaped compression fracture of the L2 vertebral body is also seen *(arrows)*. Routine radiographs may suggest the presence of osteoporosis and reveal fractures; however, bone densitometry is necessary for accurate quantification of the presence and extent of diminished bone mineral content.

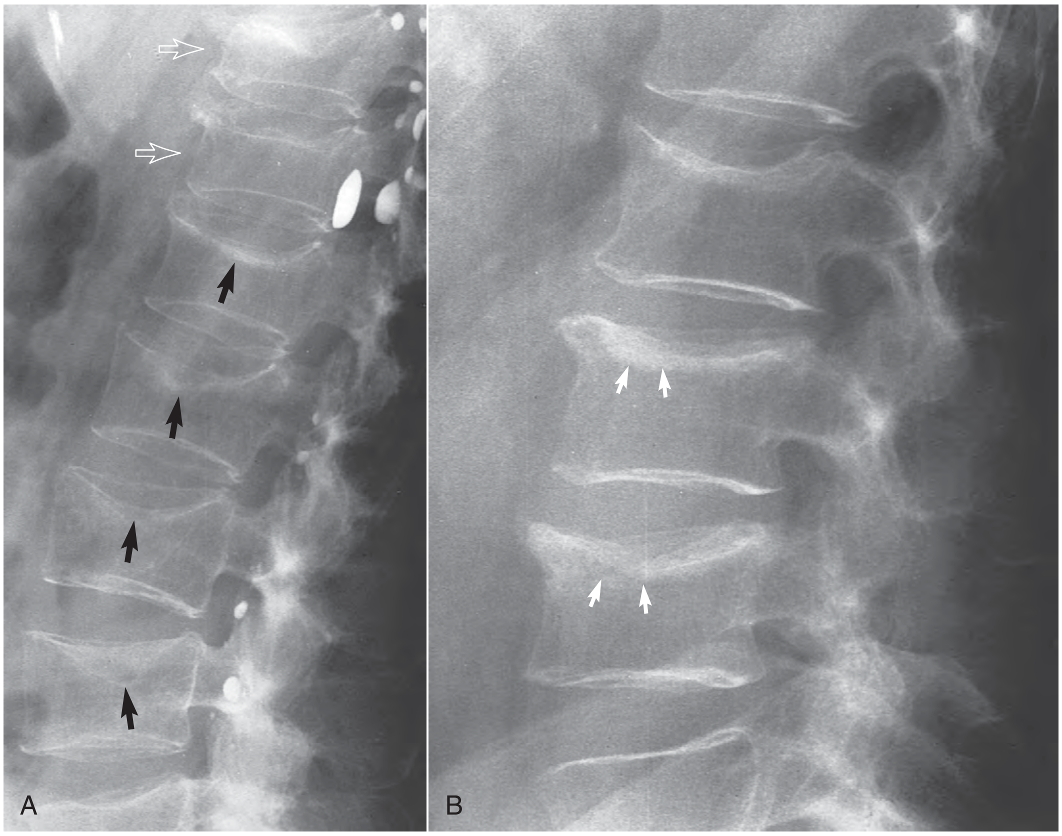

FIGURE 4–102 Osteoporosis: spinal fractures.[114] **A,** Senile osteoporosis. In this 68-year-old patient, observe the central endplate deformities of all lumbar vertebral bodies (*arrows)* and wedge-shaped deformities of T11 and T12 *(open arrow)*. Residual myelographic contrast material is incidentally seen within the spinal canal. **B,** Corticosteroid-induced osteoporosis. This 67-year-old asthmatic man on long-term corticosteroid medication developed back pain but could not recall injuring his back. A radiograph shows diffuse, severe osteopenia, multiple biconcave vertebral body deformities, and a distinct zone of sclerosis along the superior endplates of L3 and L4 *(arrows)*. This band of increased density is commonly encountered in steroid-induced vertebral fractures and may relate to abundant callus formation.

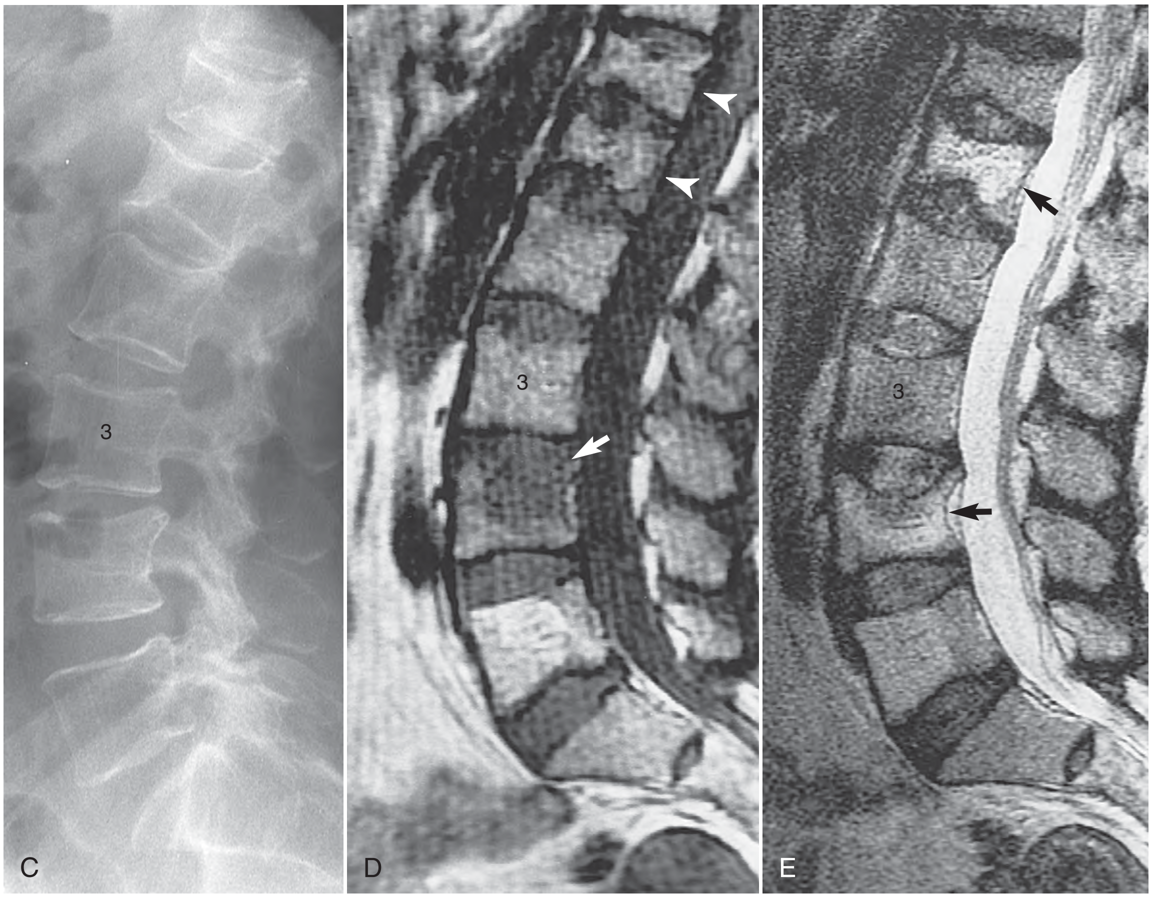

FIGURE 4–102, cont'd C-E, Magnetic resonance (MR) imaging evaluation. A 49-year-old woman with acute back pain. In **C,** a routine radiograph shows diffuse osteopenia and vertebral endplate fractures at T12, L1, and to a lesser extent, L4. In **D,** a sagittal T1-weighted (TR/TE, 800/16) fast spin echo MR image shows low signal intensity of the L4 marrow *(arrow)* and intermediate signal intensity of the T12 and L1 vertebral bodies *(arrowheads)*. **E,** A sagittal T2-weighted (TR/TE, 3800/102) fast spin echo MR image reveals high signal intensity in the L1 and L4 bodies *(arrows)*, indicating that these two fractures are probably acute. The T12 vertebral body shows no hyperintensity, indicating that it most likely occurred at an earlier time. Of incidental note is a focus of high signal intensity in the L5 vertebral body on both T1- and T2-weighted images, characteristic of a hemangioma.

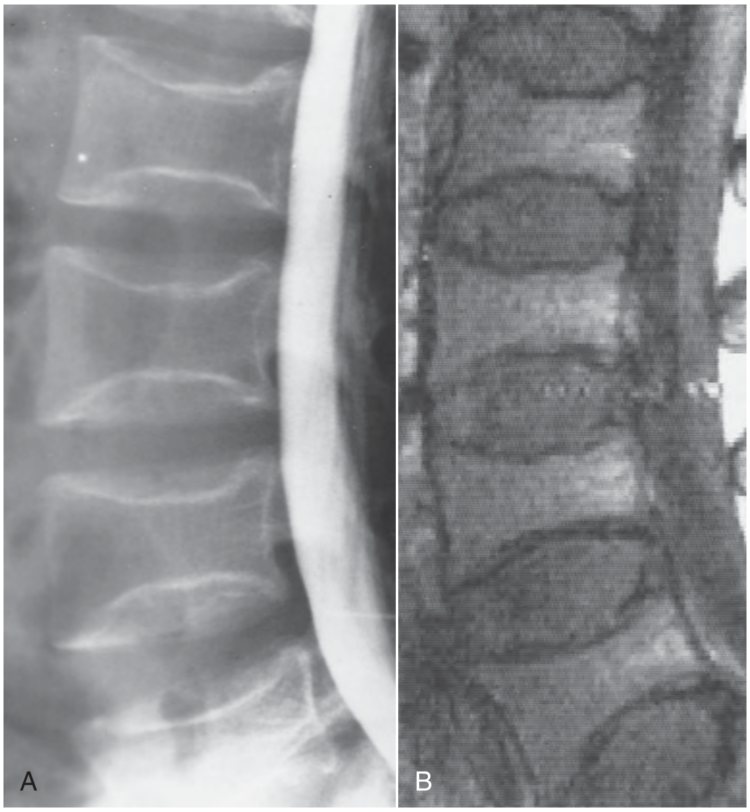

FIGURE 4–103 **Corticosteroid-induced osteoporosis: vertebral collapse.**[116] This 22-year-old woman received long-term corticosteroid medication as a child. **A,** Lateral radiograph obtained during a myelographic examination shows diffuse osteopenia and widespread biconcave vertebral endplate deformities. **B,** Sagittal T1-weighted (TR/TE, 200/26) spin echo MR image reveals the compressed vertebral bodies. Biconcave vertebral fractures often are termed *fish vertebrae* because they resemble the shape of normal vertebrae in fish. Osteoporosis and fractures may occur as a result of excessive exogenous corticosteroid administration or endogenous corticosteroid secretion, such as in Cushing disease. *(Courtesy G. Greenway, MD, Dallas.)*

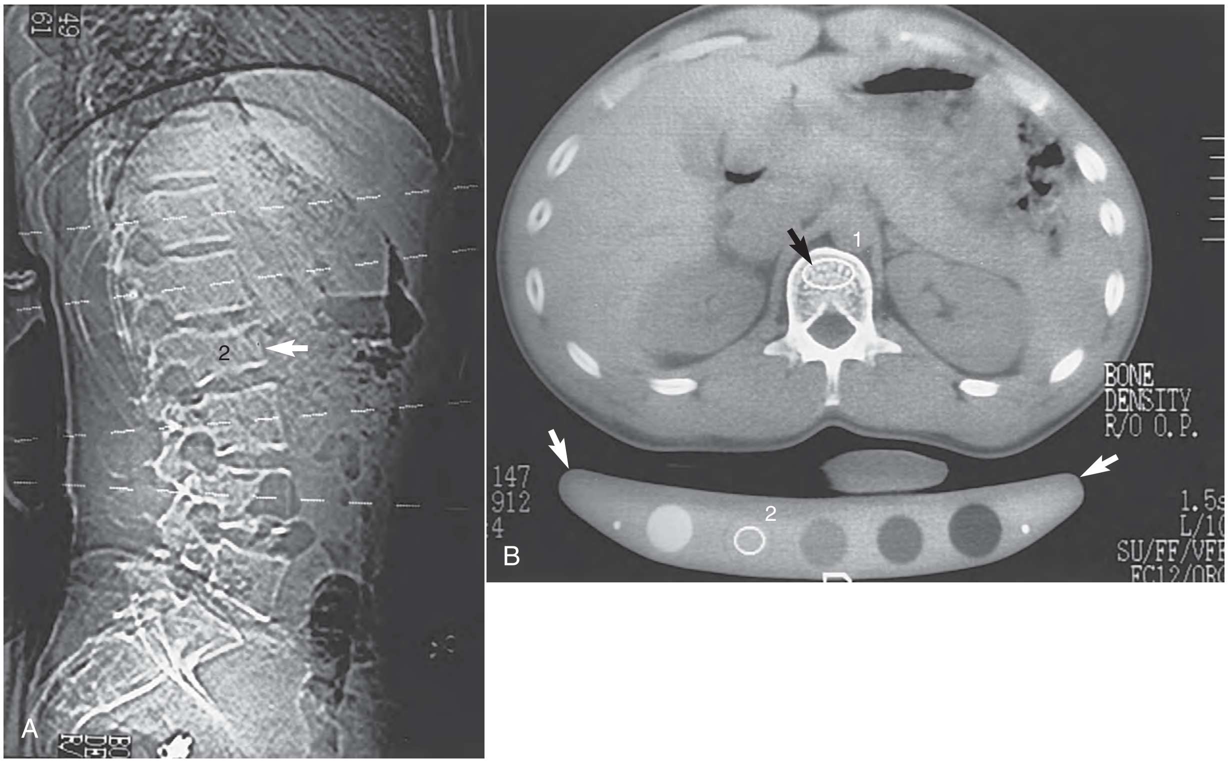

FIGURE 4–104 **Quantitative bone mineral analysis (densitometry).**[115,117,158,167-169] **A-B,** Quantitative computed tomography (QCT). In **A,** a lateral scout view localizes the midplane of four vertebral bodies to be sampled. A compression fracture of the L2 vertebral body is seen *(arrow)*. In **B,** an 8- to 10-mm thick transaxial section is obtained at each level to be sampled. An oval cursor *(black arrow)* is positioned anteriorly within the spongiosa portion of the vertebral body that contains purely trabecular bone. During acquisition of the sections, the patient lies supine on a calibration phantom device with compartments containing solutions of K_2HPO_4 of predetermined densities *(white arrows)*. The precise bone mineral density within the trabecular bone of the vertebral body is then computed by comparing it with these calibrated densities.

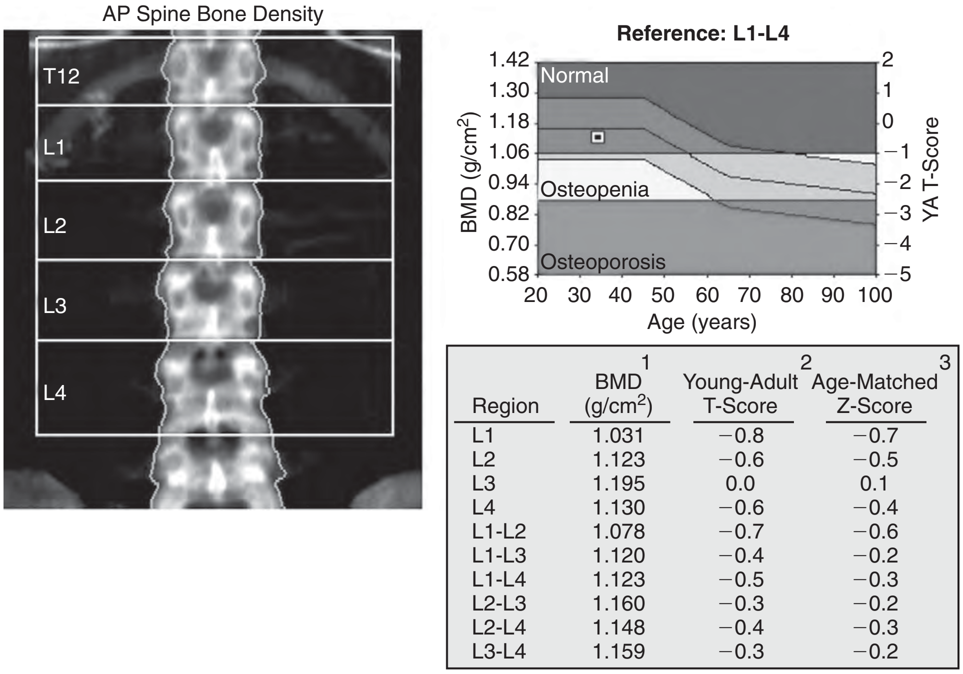
AP Spine Bone Density
T12
L1
L2
L3
L4
Reference: L1-L4
1.42
1.30
1.18
1.06
0.94
0.82
0.70
0.58
BMD (g/cm2)
2
1
0
−1
−2
−3
−4
−5
YA T-Score
Normal
Osteopenia
Osteoporosis
20 30 40 50 60 70 80 90 100
Age (years)

Region	BMD (g/cm^2) 1	Young-Adult T-Score 2	Age-Matched Z-Score 3
L1	1.031	−0.8	−0.7
L2	1.123	−0.6	−0.5
L3	1.195	0.0	0.1
L4	1.130	−0.6	−0.4
L1-L2	1.078	−0.7	−0.6
L1-L3	1.120	−0.4	−0.2
L1-L4	1.123	−0.5	−0.3
L2-L3	1.160	−0.3	−0.2
L2-L4	1.148	−0.4	−0.3
L3-L4	1.159	−0.3	−0.2

FIGURE 4–104, cont'd **C,** Dual energy x-ray absorptiometry (DXA). **C** shows a normal lumbar spine as depicted on a DXA display and printout. Measured sites include the L1 to L4 vertebral bodies. For each region of interest, areal bone mineral density (g/cm^2) is computed. The printout and graph on the right compares the patient's bone mineral density with normal peak bone mass in young adults (T-score) and an age, sex, weight, and ethnicity-matched control population (Z-score), both of which are predetermined in a reference database. With both QCT and DXA, the patient's bone mineral density is expressed in terms of standard deviations from the normal—information that can be applied to management, prognosis, and estimation of fracture risk. (See Table 4-22).

TABLE 4-22 World Health Organization (WHO) Definitions of Osteoporosis and Osteopenia[167-169]

Terminology	T-Score Definitions*
Normal	T ≥ –1.0
Osteopenia	T between –2.5 and –1.0
Osteoporosis	T ≤ –2.5
Established osteoporosis	T ≤ –2.5 in the presence of one or more fragility fractures

* Used to interpret spine, hip, and forearm dual-energy x-ray absorptiometry (DXA) scan results in postmenopausal white women.

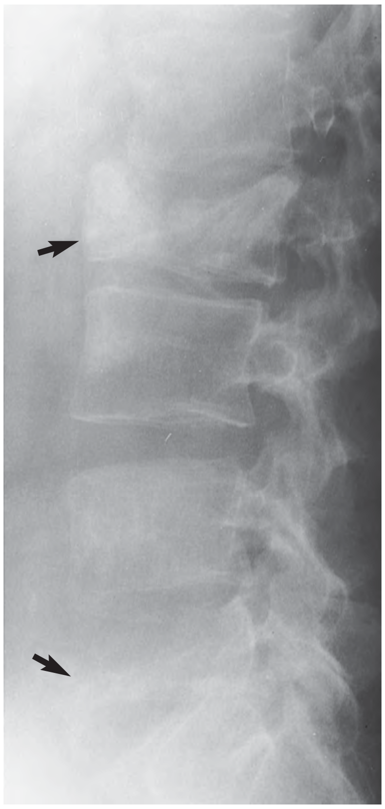

FIGURE 4–105 **Osteomalacia: spine fractures.**[118] This young man with epilepsy had been on long-term phenytoin (Dilantin) therapy. He sustained compression fractures of the L2 and L5 vertebral bodies *(arrows)*. Observe the diffuse osteopenia and abundant sclerosis associated with the L2 vertebral body. *(Courtesy P. Fenton, MD, Kingston, Ontario, Canada.)*

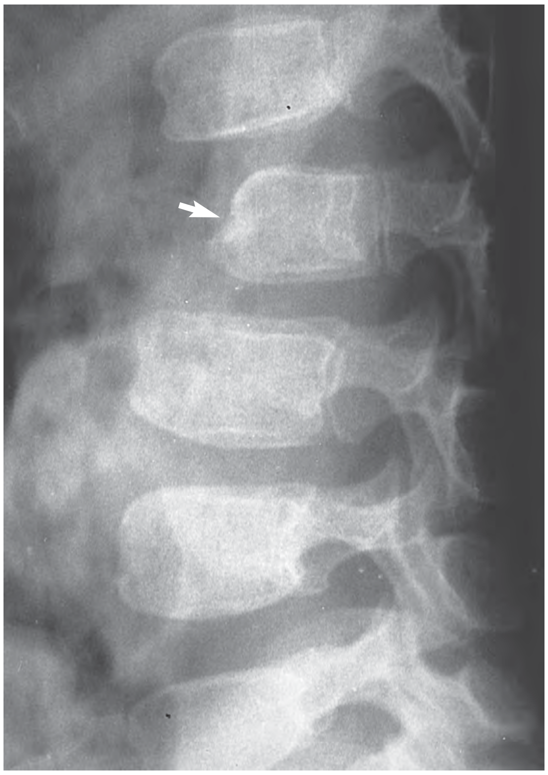

FIGURE 4–106 **Hypothyroidism: bullet vertebra.**[119] A characteristic finding in cretinism is the thoracolumbar bullet-shaped vertebra *(arrow)*. Additional spinal changes observed in hypothyroidism include gibbus deformity, osteoporosis, delayed epiphyseal development and ossification, and widened disc spaces.

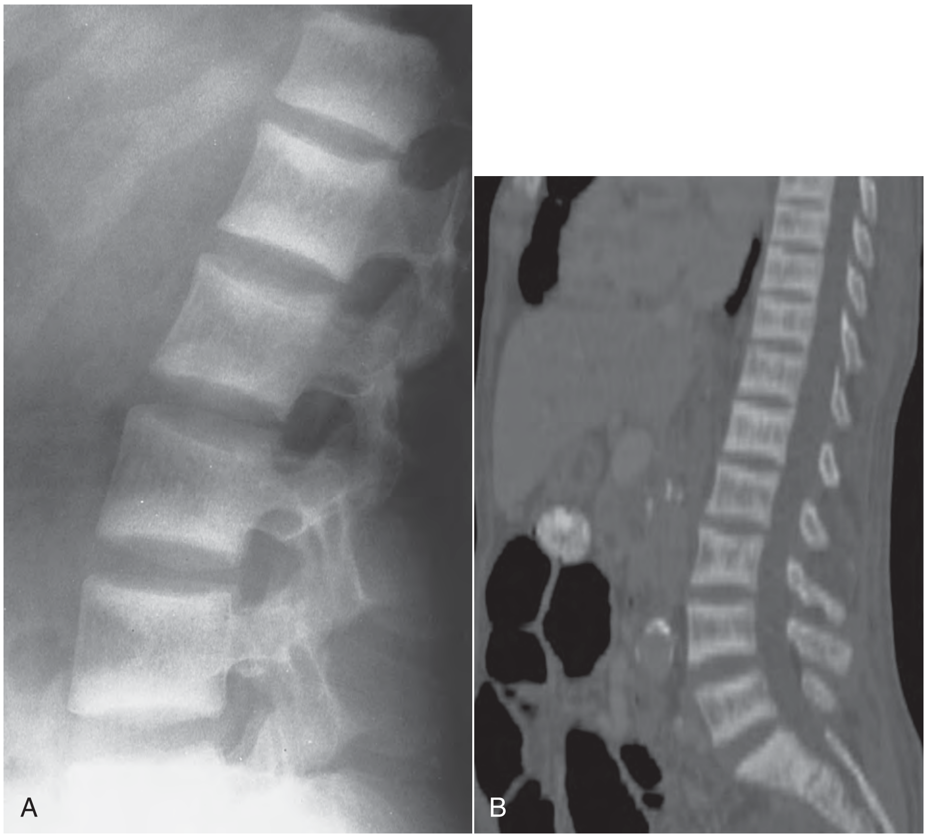

FIGURE 4–107 Rugger-jersey spine.[120] **A,** Hyperparathyroidism. Observe the horizontal bands of osteosclerosis affecting the superior and inferior aspects of the lumbar vertebral bodies. This sclerosis may disappear after treatment. Additional vertebral manifestations of hyperparathyroidism include diffuse osteopenia or osteosclerosis. **B,** Renal osteodystrophy in a patient with chronic renal failure. A sagittal reformatted CT bone window depicts the characteristic horizontal bands of sclerosis (rugger-jersey appearance) typical of longstanding renal osteodystrophy.

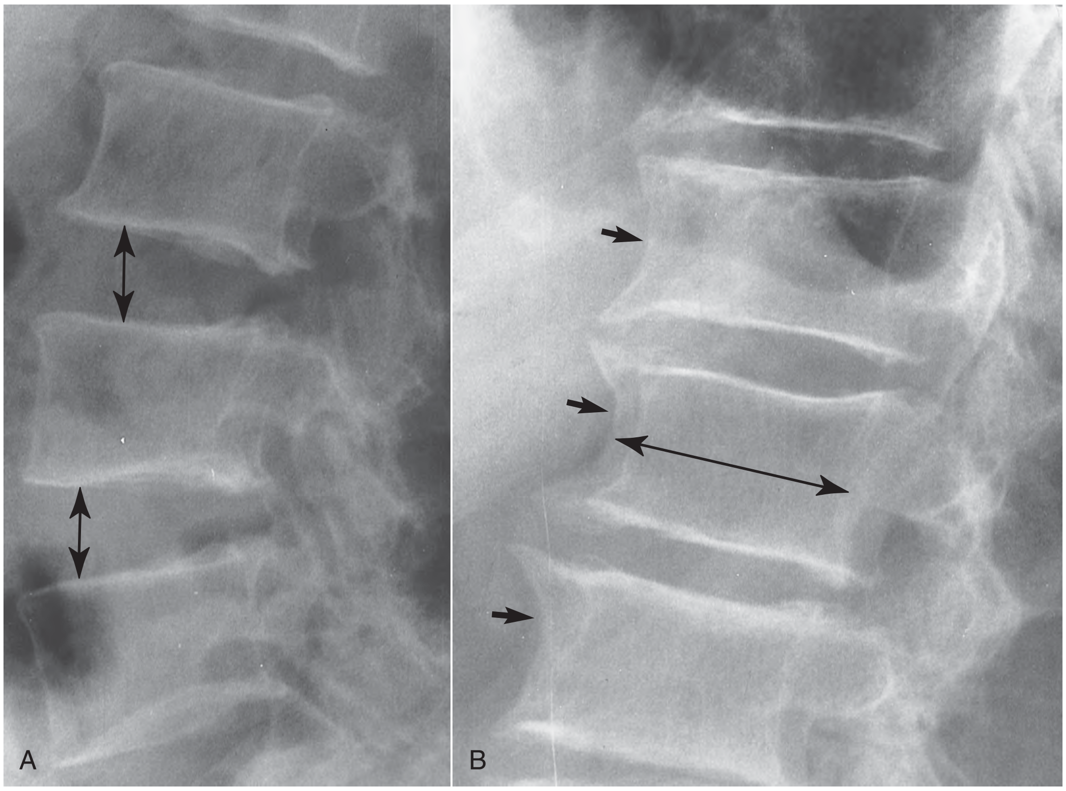

FIGURE 4–108 Acromegaly.[121] **A,** Prominent disc space widening *(double-headed arrows)* is seen throughout the lumbar spine in this 53-year-old man with long-standing acromegaly. **B,** In another patient, a 72-year-old man, thick flange-like bone proliferation at the anterior aspects of the vertebral bodies *(arrows)* contributes to an increased sagittal diameter of each vertebral body *(double-headed arrow)*. Hypersecretion of growth hormone (somatotropin) from pituitary adenomas or hyperplasia in adults results in radiographic changes that relate to overgrowth of bone and soft tissues.

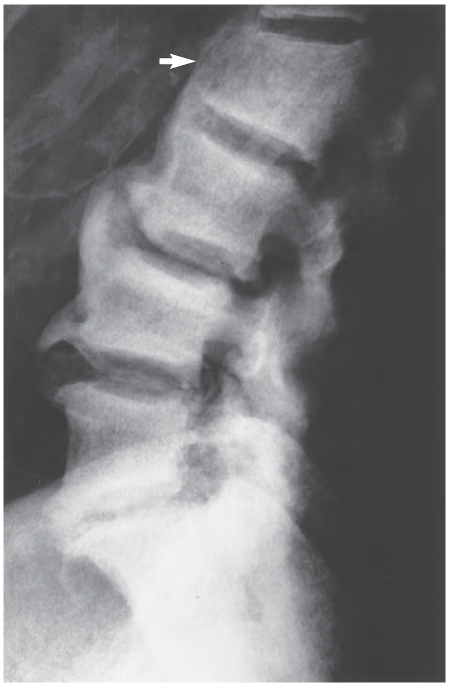

FIGURE 4–109 **Iatrogenic fluorosis.**[122] Long-term sodium fluoride was administered to this 80-year-old woman for treatment of osteoporosis. Extensive ossification of the paraspinal ligaments and generalized increased radiodensity of the spine are seen. A compression fracture of the L2 vertebral body *(arrow)* occurred before the fluoride treatment.

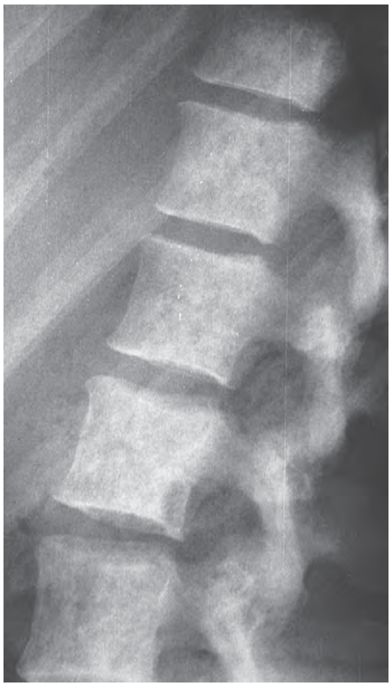

FIGURE 4–110 **Mastocytosis.**[123] Widespread, patchy osteosclerosis throughout the lumbar spine is evident in this 38-year-old woman with systemic mastocytosis. *(Courtesy B. Holtan, MD, Rock Springs, Wyo.)*

FIGURE 4–111 **Gaucher disease.**[124,151] Observe the multiple collapsed vertebrae *(arrows)* in this patient with Gaucher disease. *(Courtesy A. Brower, MD, Norfolk, Va.)*

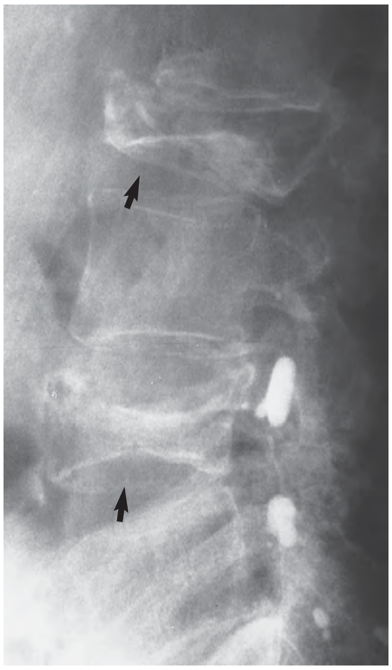

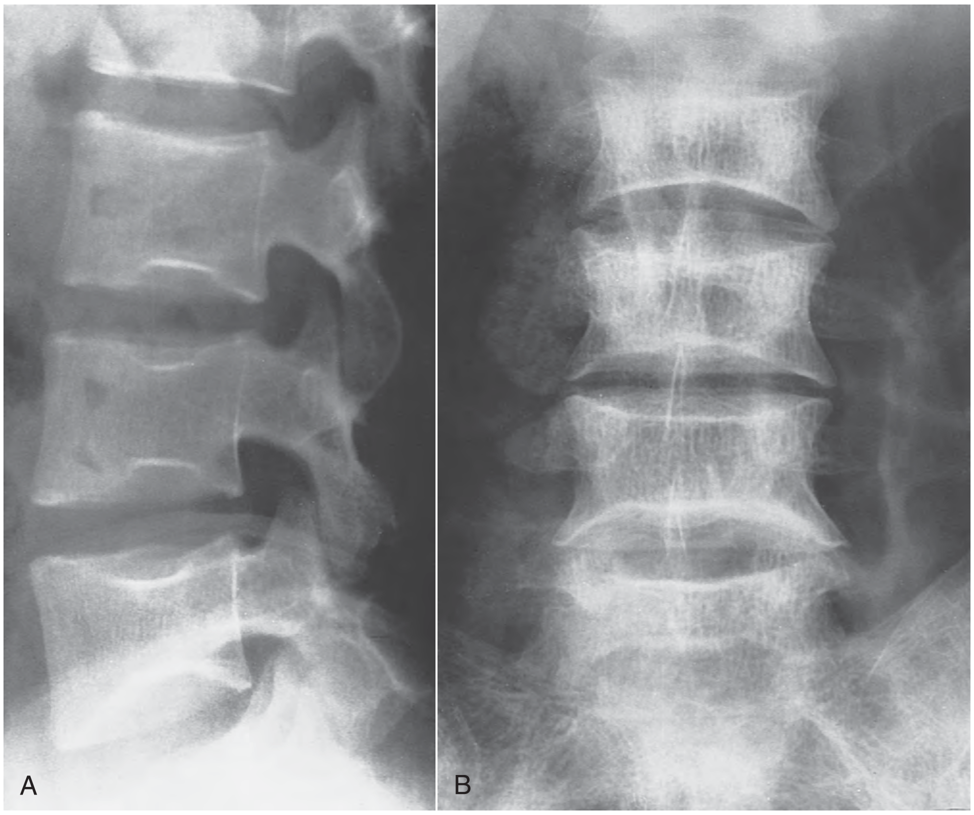

FIGURE 4–112 **Sickle cell anemia.**[125-127,150] **A,** Radiograph from this 21-year-old man with anemia reveals several central indentations of osteopenic vertebral bodies. **B,** Sickle cell hemoglobin C disease. In this 24-year-old man, the lumbar spine is osteosclerotic, the trabeculae are prominent, and the vertebral bodies exhibit H-shaped central endplate depressions.

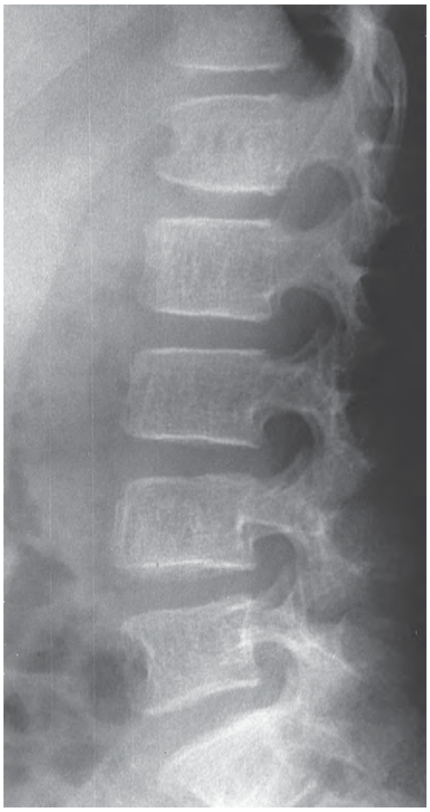

FIGURE 4–113 **β-thalassemia.**[128,139] In this 11-year-old boy, marked osteopenia and lacelike trabeculae are observed throughout the lumbar spine.

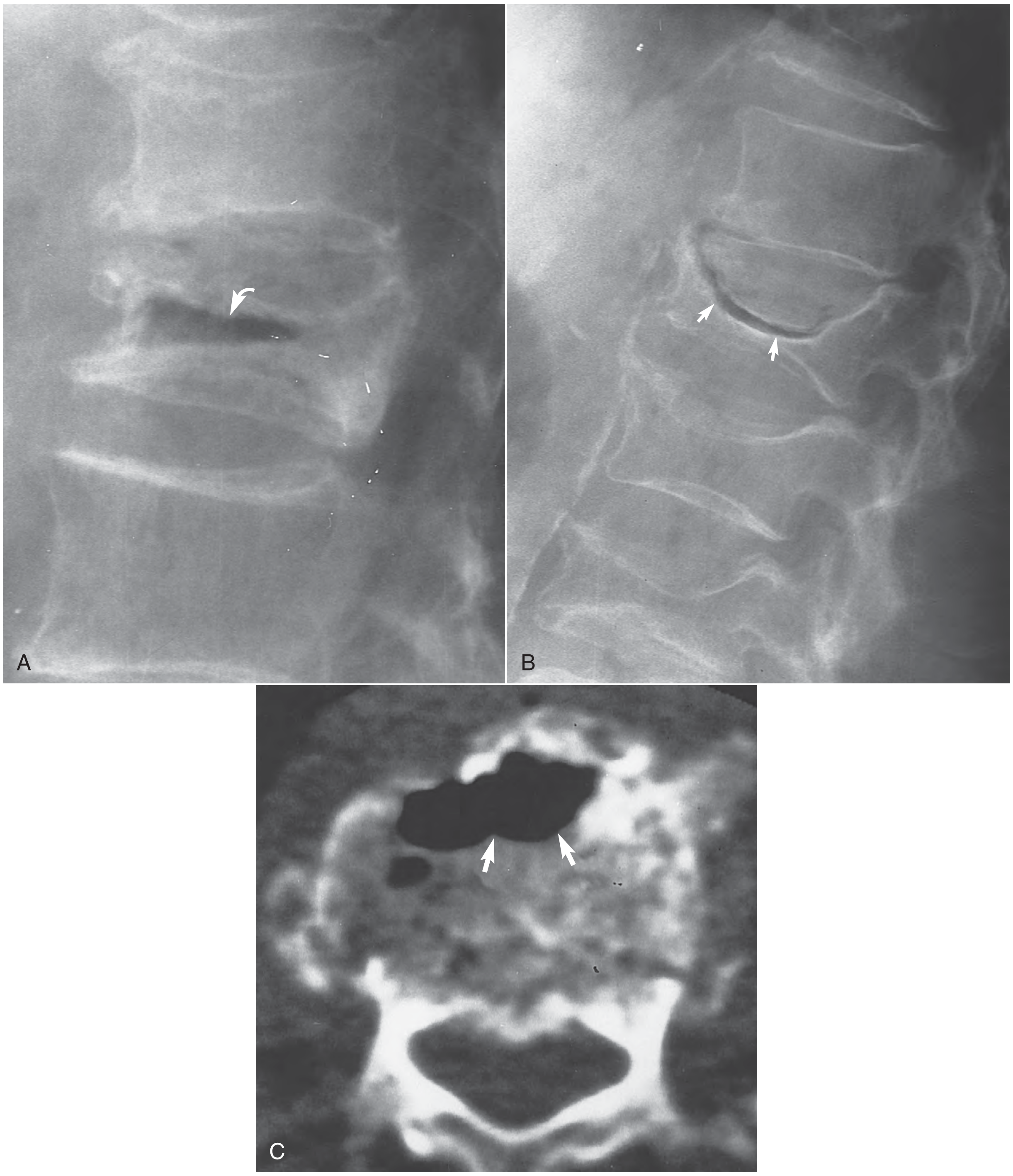

FIGURE 4–114 **Corticosteroid-induced osteonecrosis and vertebral collapse.**[129] **A,** This 79-year-old woman on long-term corticosteroid medication had acute low back pain. A lateral radiograph reveals diffuse osteopenia. Upper lumbar vertebral collapse is associated with a radiolucent collection of gas within the fractured body *(curved arrow)*. Gas within the vertebral body is termed the *intravertebral vacuum cleft* and is a sign of vertebral osteonecrosis, often associated with the use of corticosteroid medication. **B,** In another patient, diffuse osteopenia and multiple biconcave compression fractures are seen. A prominent intravertebral vacuum cleft is present *(arrows)*. This finding should not be confused with intradiscal gas characteristically seen with degenerative disc disease. **C,** In a third patient, the gas collection within the vertebral body *(arrows)* is depicted on this transaxial CT image. (***A,*** *Courtesy P. Kindynis, MD, Geneva.* ***C,*** *Courtesy G. Greenway, MD, Dallas.)*

TABLE 4-23 Lumbar Spine Surgery*

Type of Surgery	Figure(s)	Indications	Complications
Spinal fusion[130] (arthrodesis)	4-115	Pathologic disc processes Instability	Spinal cord compression Thecal sac encroachment Screw malpositioning Fracture, displacement, or malposition of screw, plate, or wire Osteomyelitis Failed interbody plug fusion Pseudarthrosis Epidural hematoma Cerebrospinal fluid leak
Laminectomy and facetectomy[131-133]	4-116, 4-117, 4-118	Decompression for spinal stenosis	Postlaminectomy instability Postlaminectomy kyphosis Epidural hematoma Osteomyelitis Neural arch stress fractures

* Adapted from Pathria MN, Garfin SR: Imaging after spine surgery. In Resnick D (ed): Diagnosis of bone and joint disorders. 4th Ed. Philadelphia, Saunders, 2002, p 521.

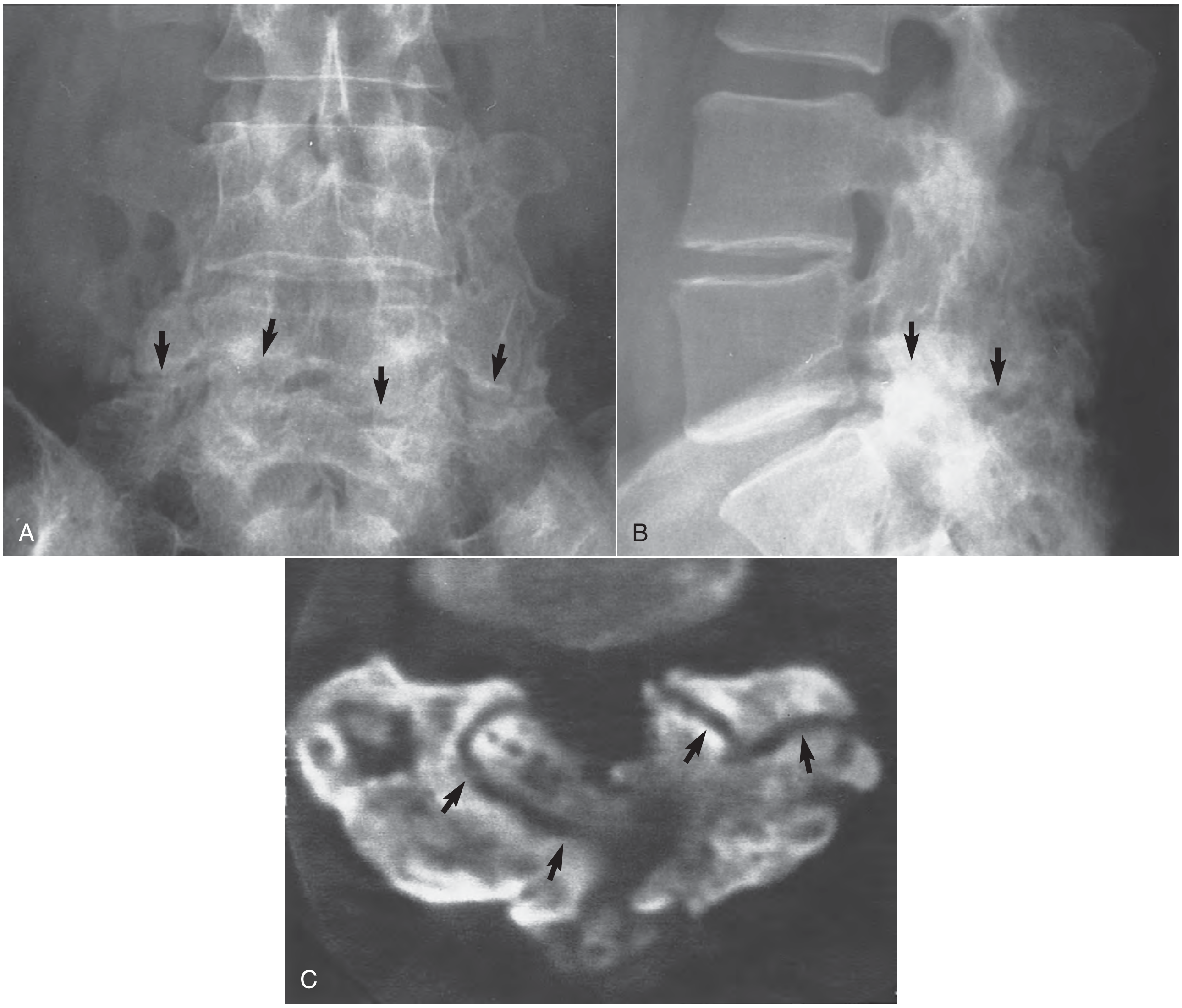

FIGURE 4–115 **Spine surgery: failed spinal fusion.**[130] This 42-year-old patient had persistent pain 18 months after posterior L4-L5 and L5-S1 fusion. **A-B,** Frontal **(A)** and lateral **(B)** radiographs show extensive bilateral intertransverse bone grafts at the L4-L5 and L5-S1 levels. A radiolucent defect *(arrows)* is seen at the L5-S1 segment and suggests both nonincorporation and nonunion of the graft. **C,** Transaxial CT scan obtained at the L5-S1 level shows a radiolucent discontinuity *(arrows)* in the graft material, confirming the presence of nonunion and pseudarthrosis.

FIGURE 4–116 **Spine surgery: laminectomy and facetectomy.**[131] Trans-axial CT-myelogram image reveals a complete L5 laminectomy and right facetectomy in this 31-year-old woman. The left articular processes and facet joint *(arrow)* are intact, whereas the spinous process, right lamina, and articular processes are absent. This procedure is employed for the treatment of symptomatic lumbar stenosis. Such extensive surgeries with complete resection of the laminae and articular processes frequently result in instability unless accompanied by arthrodesis.

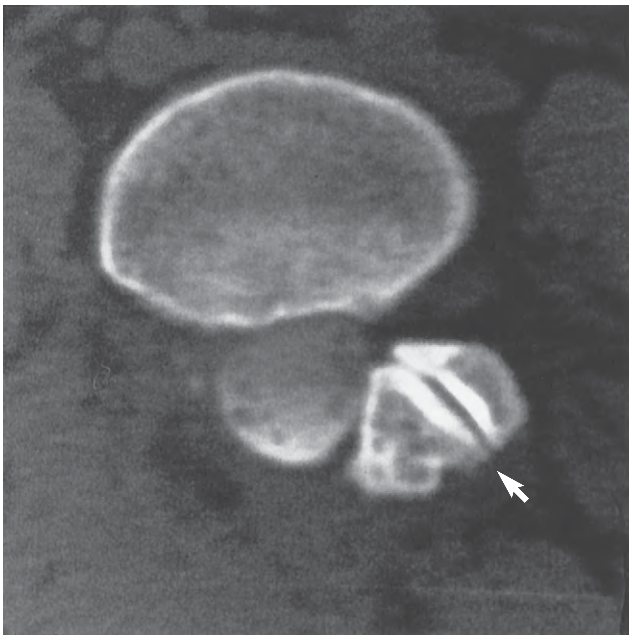

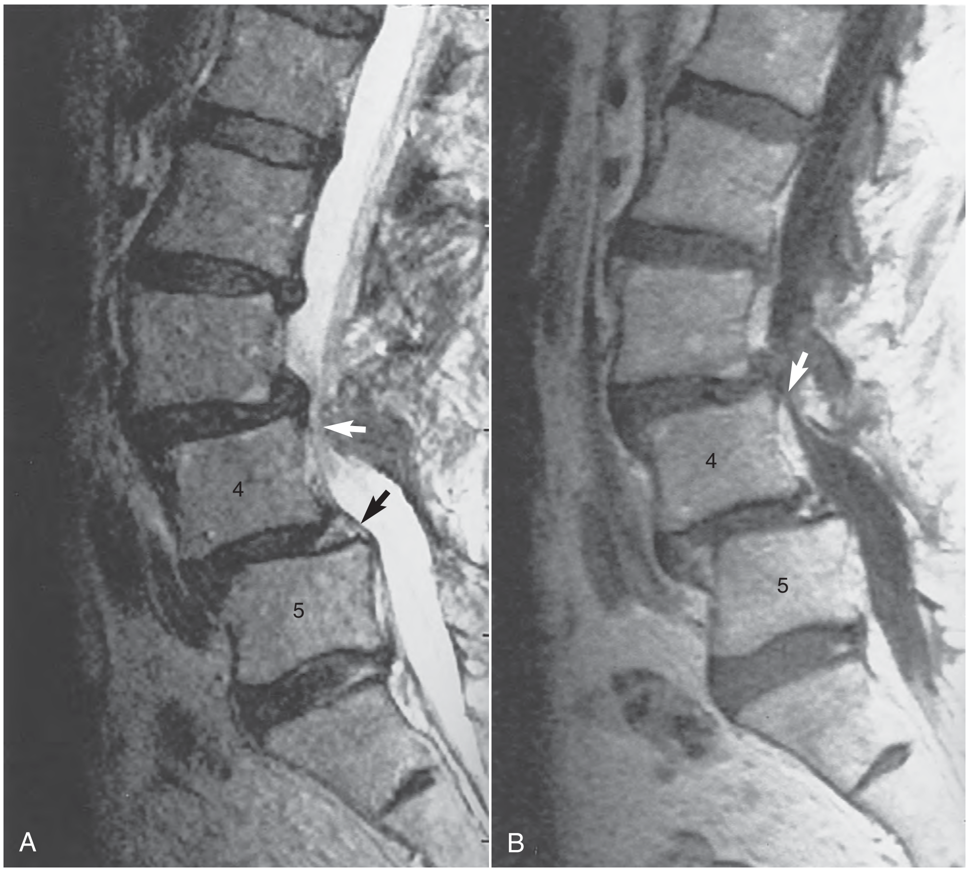

FIGURE 4–117 **Postsurgical spine instability: magnetic resonance (MR) imaging.**[132,156] This 73-year-old woman underwent multilevel decompressive laminectomies for spinal stenosis. She had persistent postsurgical pain and disability and was sent for MR imaging. Parasagittal T2-weighted (TR/TE, 4000/100) **(A)** and postgadolinium T1-weighted (TR/TE, 650/15) **(B)** spin echo MR images reveal widespread disc degeneration with degenerative anterolisthesis of L3 and L4. The sagittal diameter of the spinal canal is severely narrowed at the L3-L4 level *(white arrows)*. Disc protrusions are apparent at L2-L3 and L3-L4. The posterior longitudinal ligament is tethered over the posterior aspect of the L4 and L5 vertebral bodies *(black arrow)*. Postoperative segmental instability, as demonstrated in this patient, is the most common complication encountered in patients after extensive decompressive surgery of the thoracic or lumbar region. Postoperative instability also occurs in up to 65% of elderly women with preexisting degenerative spondylolisthesis. *(Courtesy R. Lutz, DC, Prince Rupert, B.C., Canada.)*

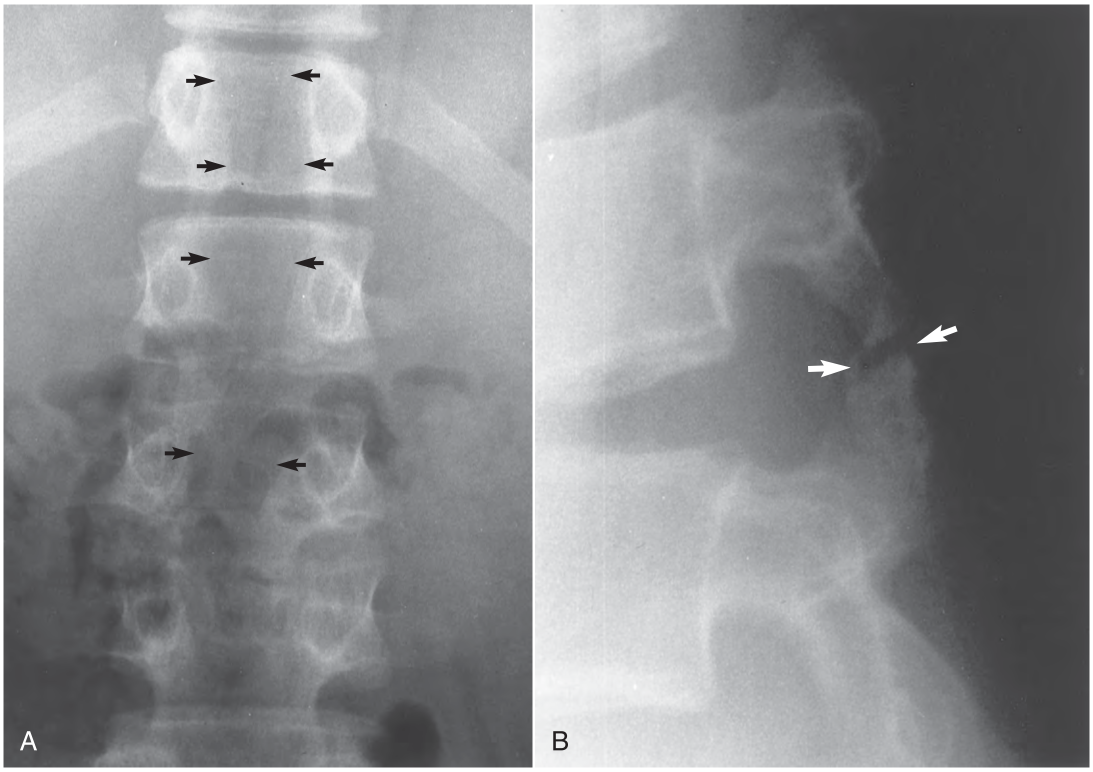

FIGURE 4–118 **Stress (fatigue) fracture, postsurgical.**[133] This 17-year-old male patient underwent a laminectomy extending from the T11 to L3 levels. **A,** Frontal radiograph reveals the multilevel laminectomy *(arrows)*. **B,** Lateral radiograph shows a fracture through the L2 inferior articular process *(arrows)* and an associated flexion deformity. Fatigue fracture of the articular process is a well-recognized complication of extensive laminectomy surgery. *(Courtesy J.A. Amberg, MD, San Diego, Calif.)*

TABLE 4-24 **Surgical Instrumentation and Bone Grafts***

Entity	Figure(s)	Characteristics
Direct current stimulators[134]	4-119	Implanted subcutaneously to apply electrical current to stimulate bone growth in graft material
Rod fixation systems[197]	4-120	*Treatment of scoliosis:* Apply traction and compression for derotation and fusion usually in conjunction with bone grafting (i.e., Harrington rod and various other types).
Pedicle screw fixation systems[197]	4-121	To stabilize spines after laminectomy, painful spondylolisthesis, symptomatic degenerative instability, postfracture deformity, scoliosis, and prevention or treatment of pseudarthrosis May be connected to rods or plates to stabilize a multiple level segment of the spine Often used in conjunction with bone grafting, prostheses, or cages
Intervertebral disc replacements[197]		Used in discectomy with fusion to restore disc space
Autograft		Strut graft material harvested from patient's own fibula or iliac crest
Interbody cage	4-122	Metallic spacer that incorporates into adjacent bone
Disc prostheses	4-122	Degenerative disc disease Alternative to spinal fusion Shock absorber and allows motion Titanium, calcium phosphate, cobalt chromium, and polyethylene
Expandable cages[197]		Used to replace vertebral bodies and to fuse spinal segments after corpectomy Also to provide stability in areas that have undergone decompression

* Adapted from Pathria MN, Garfin SR: Imaging after spine surgery. In Resnick D (ed): Diagnosis of bone and joint disorders. 4th Ed. Philadelphia, Saunders, 2002, p 521.

FIGURE 4–119 Direct current electrical stimulation.[134] An electrical stimulator and its electrodes have been implanted subcutaneously in the paraspinal tissues to enhance osseous incorporation of a bone graft at the L4-L5 and L5-S1 levels. *(Courtesy F.G. Bauer, DC, Sydney, New South Wales, Australia.)*

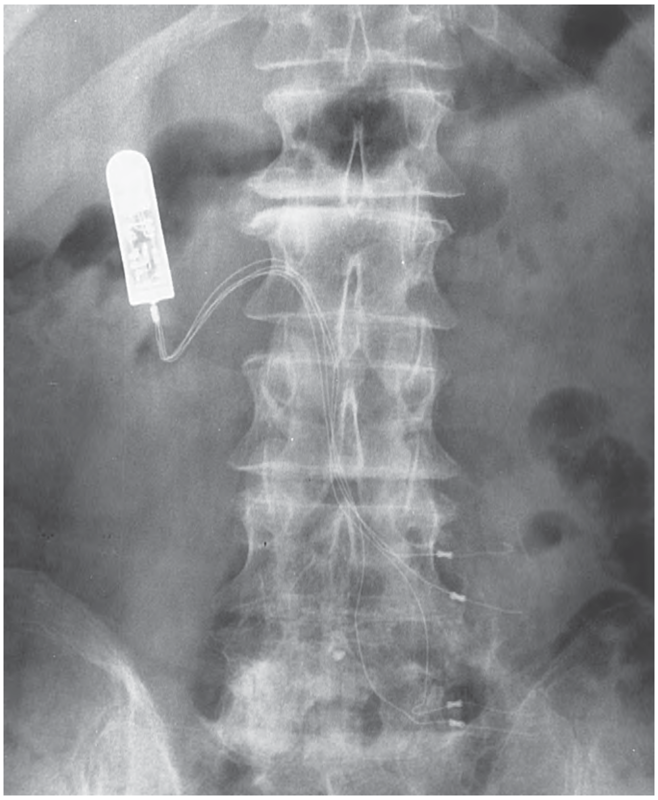

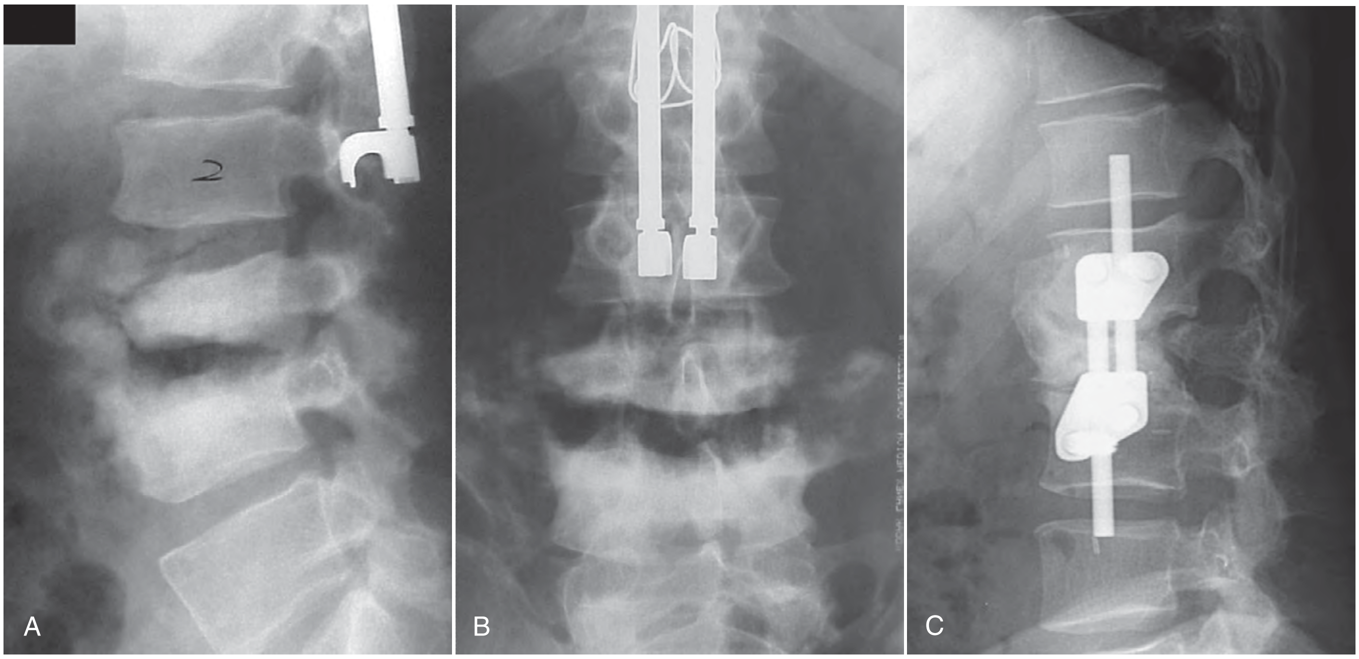

FIGURE 4–120 Rod fixation systems.[197] **A-B,** A 34-year-old man with a spinal injury and paralysis, who had Harrington rods surgically inserted 15 years earlier to stabilize his spine. Neuropathic osteoarthropathy with a stress riser pseudarthrosis has developed below the end of the rod and is characterized by partial collapse of L3 and L4 with incomplete healing, gas in the disc space, sclerosis in the adjacent vertebral bodies, and osseous debris in the soft tissues. **C,** Another patient who sustained a burst fracture of the second lumbar vertebral body has undergone surgical stabilization with two plates anchored into the L1 and L3 vertebral bodies with screws, and linked together with connecting rods, achieving fusion and stabilization of the three segments.

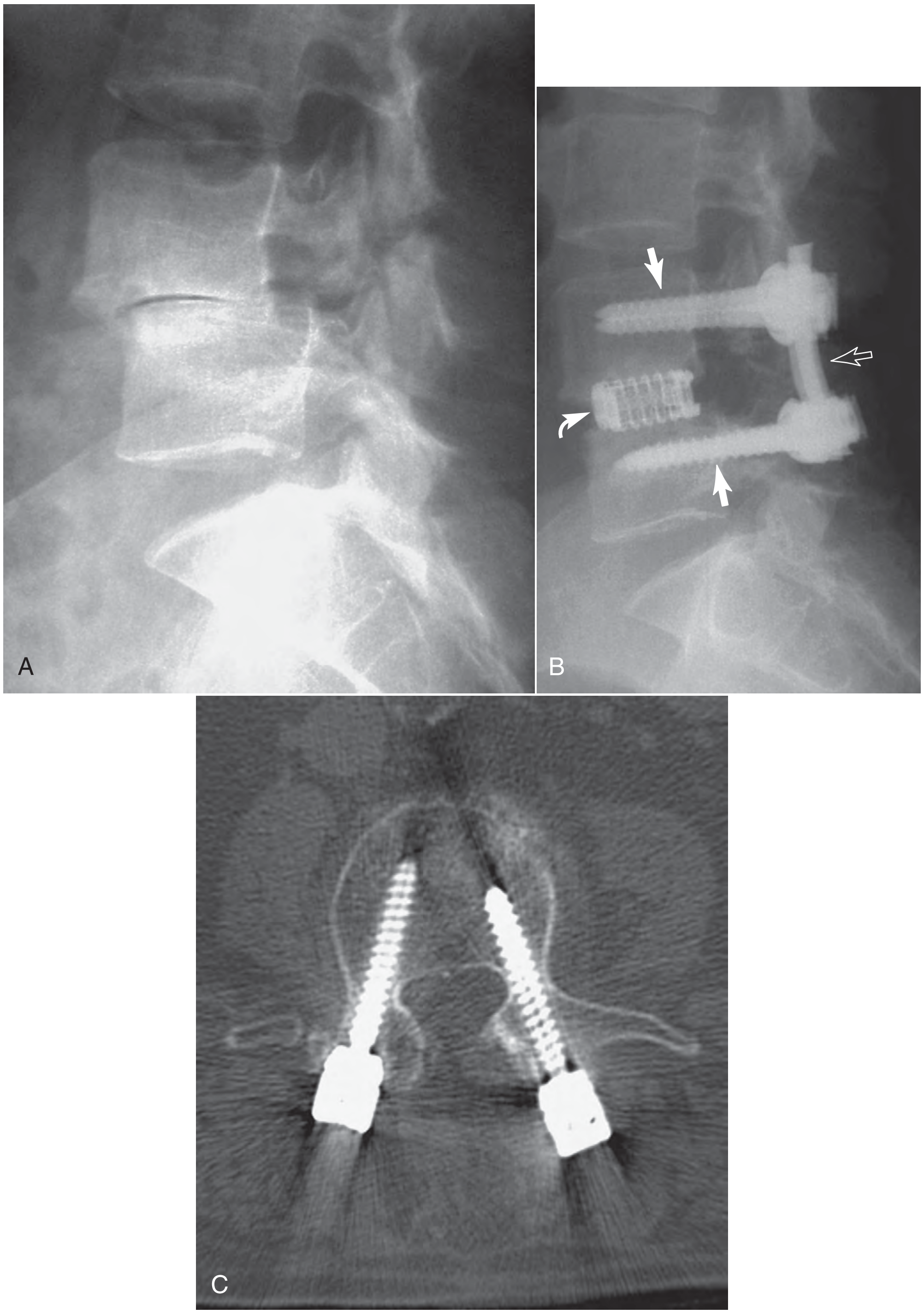

FIGURE 4–121 Pedicle screw fixation system.[197] **A,** A preoperative radiograph reveals L4 spondylolysis with a grade II anterolisthesis. **B,** The postoperative radiograph shows restoration of normal alignment, placement of bilateral pedicle screws *(arrows)* at L4 and L5 with intervening bilateral connecting rods *(open arrow)*, and insertion of two intervertebral disc replacement cages *(bent arrow)* with posterior spinal canal decompression. **C,** Normal placement of bilateral pedicle screws is clearly depicted on a CT bone window scan. (*C, Courtesy B. A. Howard, MD, Charlotte, NC.)*

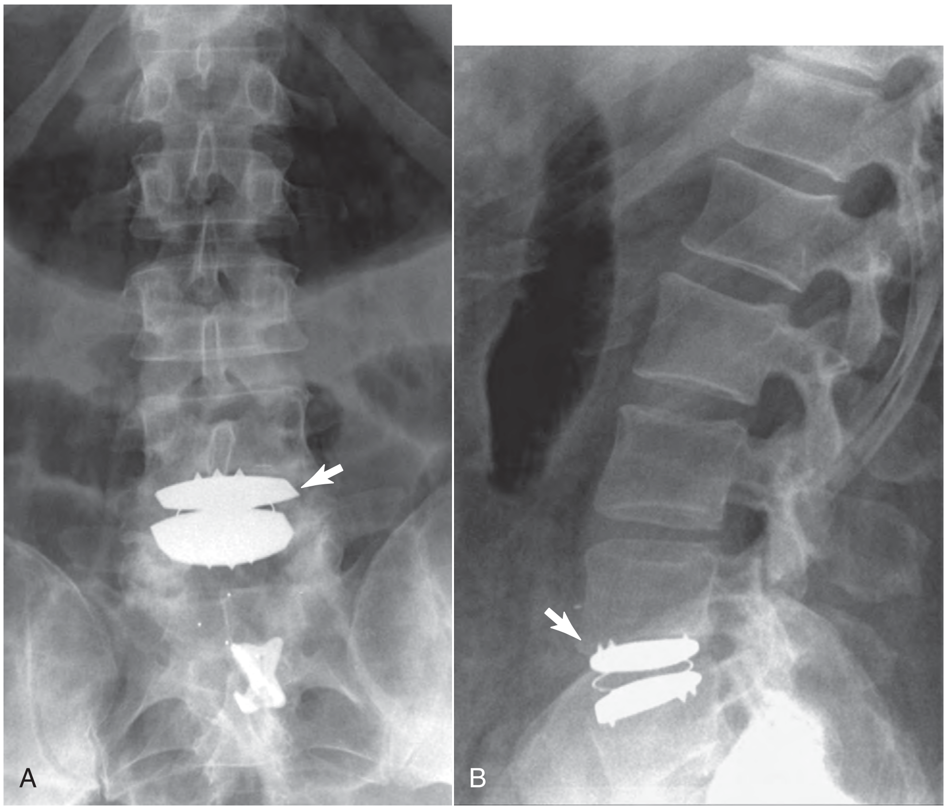

FIGURE 4–122 Intervertebral disc replacement: disc prosthesis.[197] This patient had a disc prosthesis implanted *(arrows)* after an L4-L5 discectomy.

TABLE 4-25 Vascular Disorders Affecting the Lumbar Spine

Entity	Figure(s)	Characteristics
Abdominal aortic aneurysm (AAA)[135,136,180,196]	4-123	Patients frequently have low back pain, but 50% are asymptomatic Prevalence of AAA in persons older than the age of 50 years varies from as low as 1.4% in women to as high as 8.2% in men Aorta is considered aneurysmal if diameter exceeds 3.8 cm; those greater than 6 cm are associated with a rupture rate of 75%; surgery usually indicated in aneurysms over 5 cm Ruptured AAA accounts for 1.3% of the deaths in men older than 65 years of age; risk of death as a consequence of rupture is three times that of elective surgery for repair of aneurysm *Risk factors for AAA:* male sex, age older than 75 years, white race, previous vascular disease, cigarette smoking, family history, and hypercholesterolemia ***Diagnosis:*** *Physical examination:* often inadequate in the diagnosis of AAA *Radiography:* calcification of vessel wall visible in about 75% of cases; may be seen initially on abdominal or lumbar spine radiographs *Diagnostic ultrasonography:* method of choice for screening (98% accuracy). *CT scan:* also accurate in the diagnosis of AAA but more expensive and with greater radiation exposure than ultrasonography The United States Preventive Services Task Force recommends routine diagnostic ultrasound screening for AAA in men aged 65 to 75 years who have ever smoked but recommends against such screening in women Scalloping or erosion of the anterior aspect of adjacent vertebral bodies is extremely rare and has been referred to as Oppenheimer erosions.
Iliac artery aneurysm[135,136]	4-124	Less common than AAA, but risk factors are the same Dilation of calcified vessel wall overlying lower lumbar or sacroiliac region

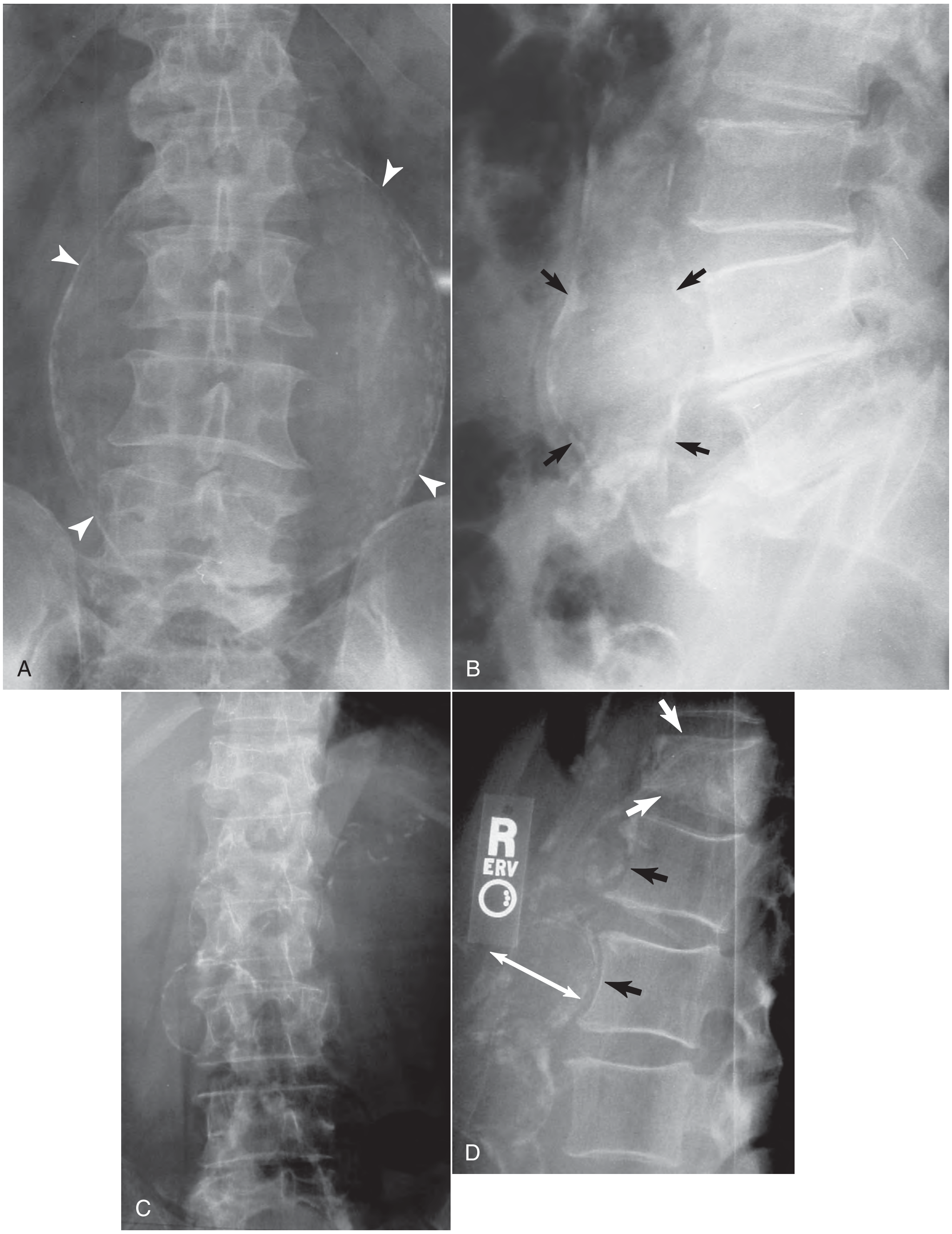

FIGURE 4–123 Abdominal aortic aneurysm.[135,136,180,196] **A,** This 74-year-old man had diffuse low back pain. Frontal radiograph shows a huge, oval, dilated abdominal aortic aneurysm (AAA). The aneurysm shows characteristic linear, plaquelike calcification *(arrowheads),* and measures 14.5 cm at its maximum transverse diameter. **B,** In another patient, a large, atherosclerotic AAA is evident on the lateral radiograph *(arrows)*. The curvilinear plaquelike calcification allows visualization of this life-threatening condition. **C-D,** In a third patient, a 77-year-old female, anterior vertebral body scalloping as a result of erosion from a longstanding aneurysm is present *(thick black arrows)*. This finding is best depicted on the lateral radiograph **(D).** The double-headed white arrow depicts the sagittal diameter of the aneurysm at the L2 vertebral body level. A T12 vertebral compression fracture is also present *(small white arrows)*. (*__B,__ Reprinted with permission from Taylor JAM, Hoffman LE: The geriatric patient: diagnostic imaging of common musculoskeletal disorders. Top Clin Chiropr 3:23, 1996.)*

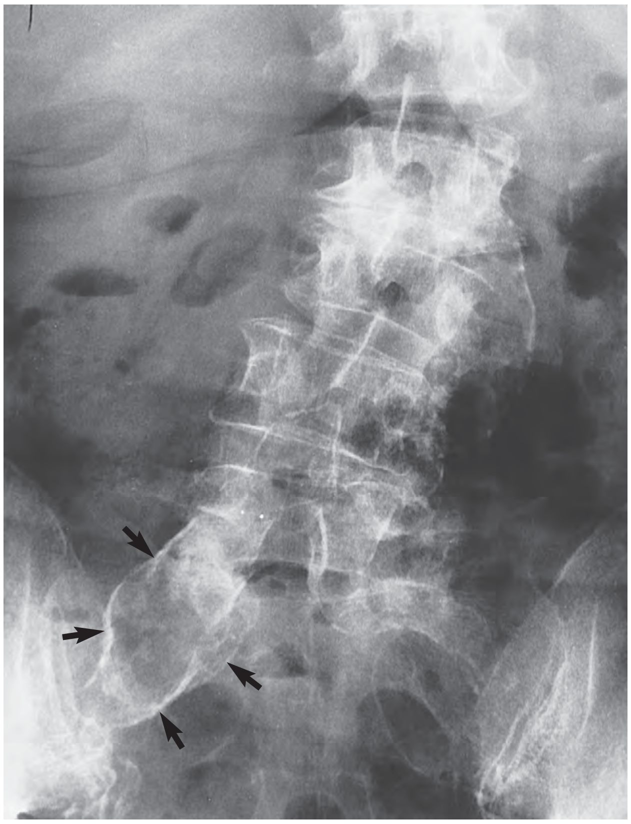

FIGURE 4–124 Iliac artery aneurysm.[135,136] Observe the aneurysm of the atherosclerotic common iliac artery *(arrows)*. This 81-year-old patient also has degenerative scoliosis. *(Reprinted with permission from Taylor JAM, Hoffman LE: The geriatric patient: diagnostic imaging of common musculoskeletal disorders. Top Clin Chiropr 3:23, 1996.)*

CHAPTER 5

Sacrococcygeal Spine and Sacroiliac Joints

NORMAL DEVELOPMENTAL ANATOMY

The accurate assessment of pediatric radiographs of the sacrum, coccyx, and sacroiliac joints requires a thorough knowledge of normal developmental anatomy. Table 5-1 outlines the age of appearance and fusion of the primary and secondary ossification centers. Figures 5-1 and 5-2 demonstrate the radiographic appearance of many important ossification centers and other developmental landmarks at selected ages from birth to skeletal maturity.

DEVELOPMENTAL ANOMALIES, VARIANTS, AND SKELETAL DYSPLASIAS

Interpretation of radiographs of the sacrum, coccyx, and sacroiliac joint region is frequently complicated by the presence of anomalies or normal variations and occasionally by skeletal dysplasias. Many of these entities have already been presented in Chapter 4. Table 5-2 and Figures 5-3 to 5-7 illustrate additional examples of these commonly encountered processes.

When considering vertebral anomalies, it is helpful to remember some general rules:

1. Most anomalies occur at transitional areas, such as the lumbosacral and sacrococcygeal regions.
2. When one anomaly is identified, always search for more: anomalies may be multiple.
3. Anomalies may occur in isolation or be associated with more diffuse abnormalities as part of a syndrome.
4. Osseous anomalies may be associated with underlying or distant neurologic or visceral anomalies.

PHYSICAL INJURY

Physical injury, including fractures and joint trauma, may involve the sacrum, coccyx, or sacroiliac joints alone, in combination with each other, or in combination with other spinal, pelvic, and abdominal visceral injuries. Some combined injuries are discussed in more detail in Chapter 6 in association with pelvic trauma. Table 5-3 lists the important injuries in this region and discusses their characteristics. Many examples are illustrated in Figures 5-8 to 5-12.

ARTICULAR DISORDERS

The sacroiliac joints are a frequent target site of involvement for degenerative, inflammatory, metabolic, and infectious spondyloarthropathies. Table 5-4 outlines these diseases and their characteristics, and Table 5-5 describes their anatomic distribution. Figures 5-13 to 5-24 provide examples of characteristic radiographic manifestations.

BONE TUMORS

Many different malignant tumors, benign tumors, and tumorlike lesions affect the sacrum, and, to a lesser extent, the coccyx. Table 5-6 lists only those neoplasms illustrated in Figures 5-25 to 5-32. A more complete list of vertebral column neoplasms—including sacrococcygeal lesions—is found in Chapter 2 (Table 2-17).

TABLE 5-1 Sacrum and Coccyx: Approximate Age of Appearance and Fusion of Ossification Centers[1-4] (Figures 5-1, 5-2)

Ossification Center	Primary or Secondary	No. of Centers	Age of Appearance (Years)*†	Age of Fusion* (Years)†	Comments
Sacrum					
Bodies	P	5	Birth	18-30	Fuse together in order from S5-S1
Neural arches	P	10	Birth	5	Fuse in order: S2, S1, S4, S3
Costal processes	P	4	Birth	5-18	S1-S4
Anterior costal apophyses	S	8	1-25	18-25	S1-S4
Posterior costal apophyses	S	4	1-22	18-25	S1-S2
Transverse process apophyses	S	8 or 10	1-19	5-18	Lateral sacral crest
Spinous process apophyses	S	3	5-22	5-22	S1-S3
Endplate ring apophyses	S	10	1-21	13-17	S1-S5
Mamillary process apophyses	S	2	1-4	1-18	S1
Coccyx					
Bodies	P	4	1-18	No fusion	Variable number
Neural arch or cornua	P	2	1-6	No fusion	Present at first coccygeal segment only
Transverse process apophyses	S	2		No fusion	Present at first coccygeal segment only

† Adapted from Broome DR, Hayman LA, Herrick RC, et al: Postnatal maturation of the sacrum and coccyx: MR imaging, helical CT, and conventional radiography. AJR 170:1061, 1998. In this study, ossification centers typically were evident on CT and MR imaging long before they appeared radiographically.

P, Primary; *S,* secondary.

* Ages of appearance and fusion of ossification centers in girls typically precede those of boys. Ethnic differences also exist.

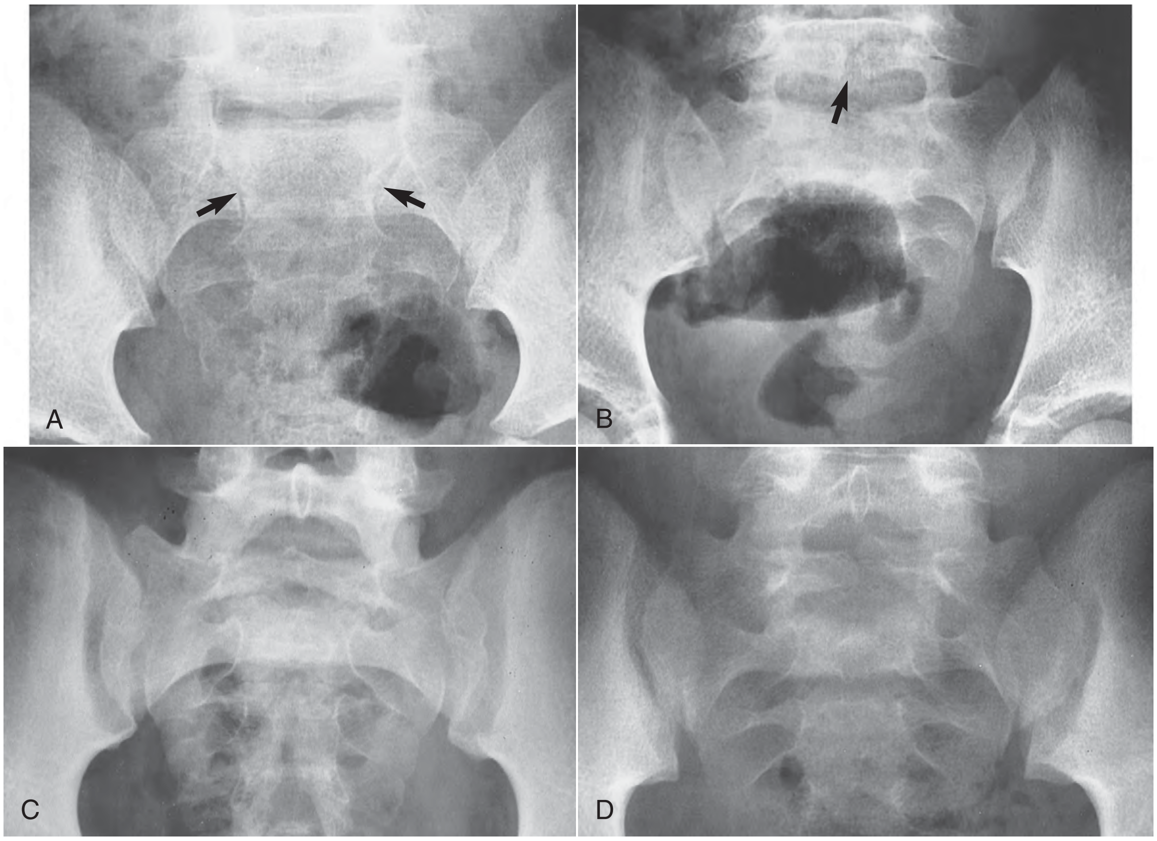

FIGURE 5–1 Skeletal maturation and normal development: frontal sacrococcygeal radiographs.[1-5,45] **A,** A 4-year-old boy. The primary ossification centers are unfused and appear as vertical radiolucent shadows *(arrows)*. **B,** An 8-year-old boy. The sacroiliac joints are wide, and the L5 neural arch has not yet fused *(arrow)*. Portions of the sacrum are obscured by bowel gas. **C,** Observe the apparent widening of the sacroiliac joints in this 9-year-old boy. **D,** In an 11-year-old child, the S1 neural arch remains unfused.

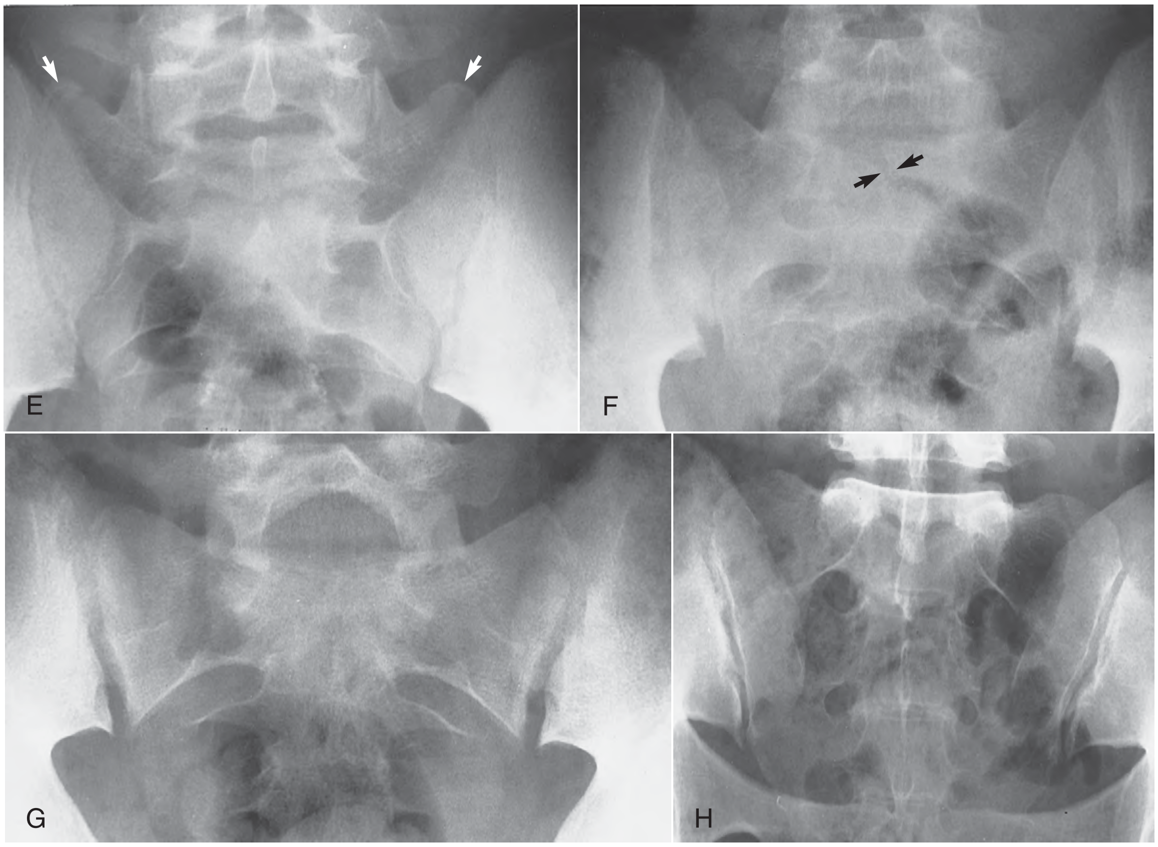

FIGURE 5–1, cont'd **E,** A 13-year-old boy. The sacroiliac joints have a more adult configuration in this child compared with the more juvenile appearance of the sacroiliac joints in the patient in **F.** Observe the bilateral ossification centers of the sacral alae *(arrows)*. **F,** Another 13-year-old boy. The ossification center of the S1 neural arch, which typically fuses by the age of 5 years, remains unfused in this child *(arrows),* a condition termed *spina bifida occulta*. This developmental anomaly is common at that level and usually is of no clinical significance. **G,** A 14-year-old girl. Posteroanterior radiograph obtained with caudad tube tilt. The sacroiliac joints are wide, and bilateral ossification centers are present at the sacral alae. The widening of the sacroiliac joints, seen in many of these children, is associated with blurred and poorly defined articular margins. These findings relate to the presence of thick articular cartilage and incomplete subchondral ossification. Occasionally, they are accompanied by normal subchondral sclerosis, not to be confused with the findings of sacroiliitis. **H,** Adult configuration. In this 30-year-old man, observe the well-defined subchondral bone, uniform joint space, and the absence of adjacent sclerosis. The angulated frontal projection of the sacroiliac joints is ideal for clearly visualizing the sacroiliac joints. This projection is obtained as a posteroanterior view with 20 to 30 degrees of caudal tube angulation or as an anteroposterior view with 20 to 30 degrees of cephalad tube angulation.

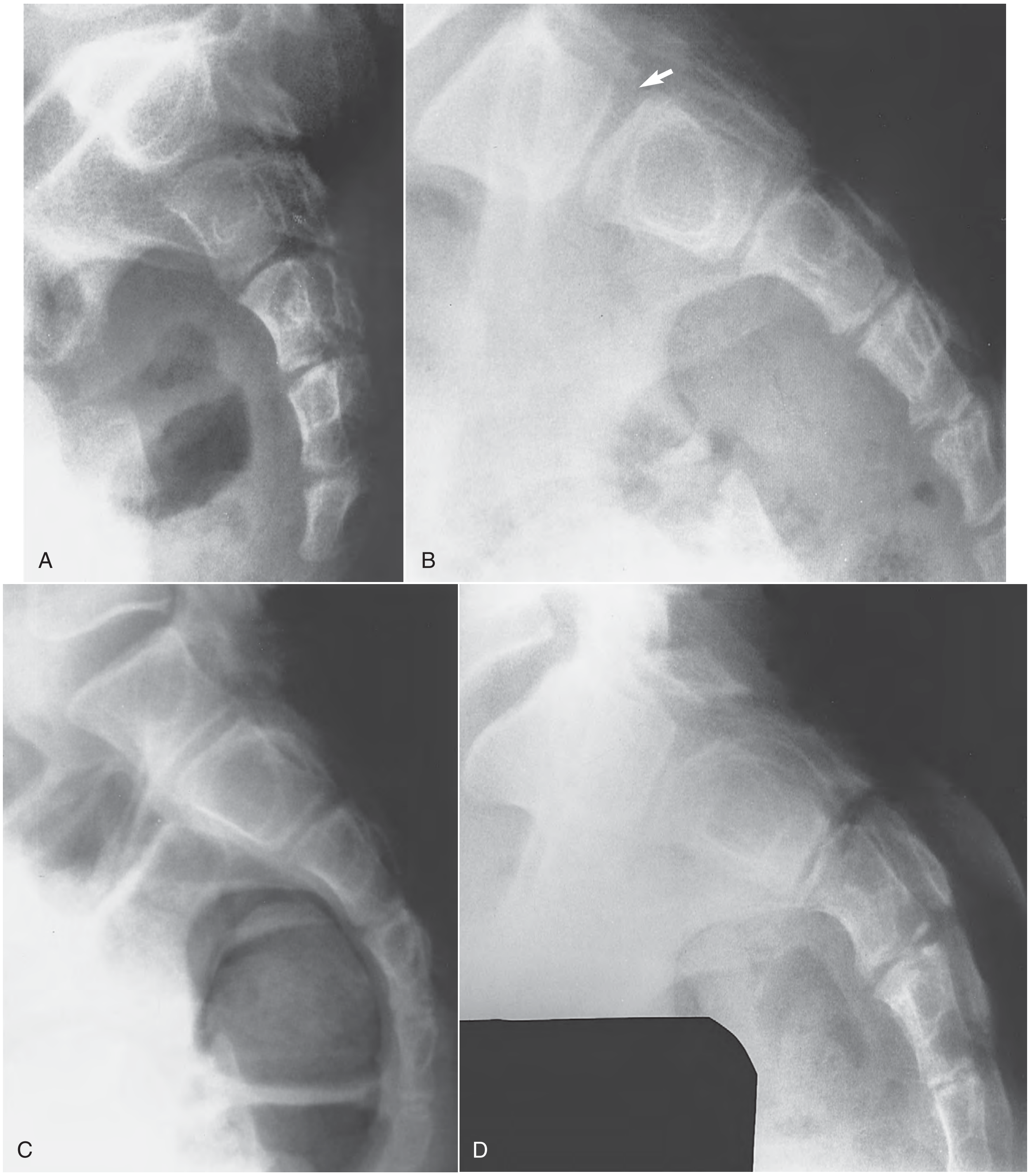

FIGURE 5–2 Skeletal maturation and normal development: lateral sacrococcygeal radiographs.[1-4] **A,** A 7-year-old boy. Each individual sacral segment is well visualized. **B,** A 10-year-old boy. The radiolucent growth center at S1-S2 often is wedge-shaped *(arrow)* and may create the false appearance of spondylolisthesis at S1-S2. **C,** A 13-year-old boy. The individual sacral segments remain unfused. **D,** A 14-year-old boy. The body segments appear better defined and are beginning to fuse. These body segments usually fuse completely between the ages of 18 and 30 years, beginning at S5 and ending at S1.

TABLE 5-2 Developmental Anomalies, Anatomic Variants, and Skeletal Dysplasias Affecting the Sacrum and Coccyx*

Entity	Figure(s), Table(s)	Characteristics
Pseudonarrowing of sacroiliac joint[6]	5-3	Positional rotation of the patient in which the radiographic beam is not tangent to the joint, simulating the appearance of joint space narrowing Repositioning the patient usually results in a more adequate radiograph and corrects this potential source of misinterpretation
Sacral wing fossa[7]	5-4	Well-circumscribed circular radiolucent zone within the sacral wing, or ala, simulating an osteolytic lesion Normal variant of no clinical significance
Accessory sacroiliac articulations[8]	5-5; see 5-13, *D*	Accessory articulation between the sacrum and the ilium; usually between the posterior superior iliac spine or iliac tuberosity of the ilium and the posterolateral aspect of the sacrum Present in as much as 30% of the population In some cases, it may represent only a contact point rather than a true articulation True articulation may undergo degenerative changes
Spina bifida occulta[9,10]	5-6	Extremely common developmental anomaly consisting of a midline defect within the neural arch in which the paired sacral arches fail to fuse in the midline Radiolucent cleft occurring most frequently at L5 and S1 segments Sacral hiatus present in 1% to 7% of persons; failure of ossification of all sacral arches; no clinical significance Strong cartilage and fibrous tissues fill the cleft; anomaly generally is of no clinical consequence Isolated anomaly or occurring in conjunction with other entities, such as cleidocranial dysplasia or clasp-knife syndrome *Spina bifida infrequently associated with meningomyelocele:* protrusion of the meninges or spinal cord, or both; meningomyelocele may result in severe neurologic abnormalities
Clasp-knife syndrome[12]	4-9	Spina bifida occulta of S1 and elongation of the L5 spinous process During trunk extension, the L5 spinous process may impinge on the spinal canal, irritating pain-sensitive structures
Sacral agenesis[11]	5-7	Complete or partial sacral agenesis present in 0.1% to 0.2% of all infants of diabetic mothers Also seen as a component of the VATER syndrome complex (vertebral, anorectal, tracheal, esophageal, renal anomalies), and may be associated with other gastrointestinal and genitourinary anomalies, or meningomyelocele Frequently accompanied by developmental acetabular dysplasia with congenital hip dislocation Flexion and extension radiographs can be performed to evaluate spinal stability
Paraglenoid sulcus[3,5]	5-14, 5-15	Focal zone of bone resorption occurring in response to increased stress at the site of attachment of the inferior sacroiliac ligament, seen almost exclusively in women Bilateral grooves in inferior ilium just lateral to the sacroiliac joints Deep grooves occur only in parous women Increased prevalence is found in persons with hyperlordosis and, questionably, with osteitis condensans ilii No clinical significance
Sacrococcygeal synostosis[6]		First coccygeal segment often is fused to the lowest sacral segment, and the lower coccygeal vertebrae may be fused together; no clinical significance
Facet tropism[5,7,10]	4-12 Table 4-2	Asymmetric orientation of left and right lumbosacral facet joints
Transitional lumbosacral segment[12]	4-15 Table 4-3	

---

* See also Tables 1-1 and 1-2.

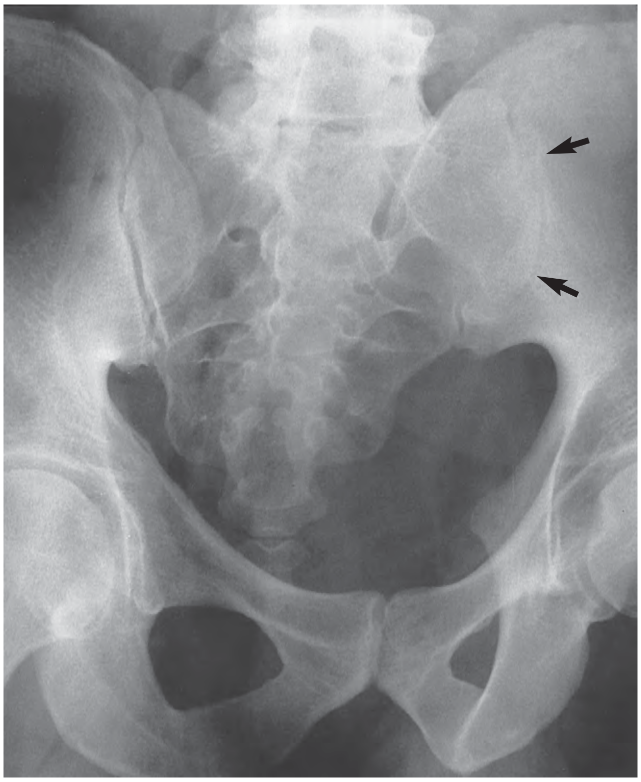

FIGURE 5–3 **Pseudonarrowing of the sacroiliac joints from patient obliquity on imaging.**[6] This incorrectly positioned frontal radiograph was taken with the patient rotated relative to the film. Such obliquity results in a false appearance of unilateral sacroiliac joint narrowing, ankylosis, or obliteration *(arrows)*.

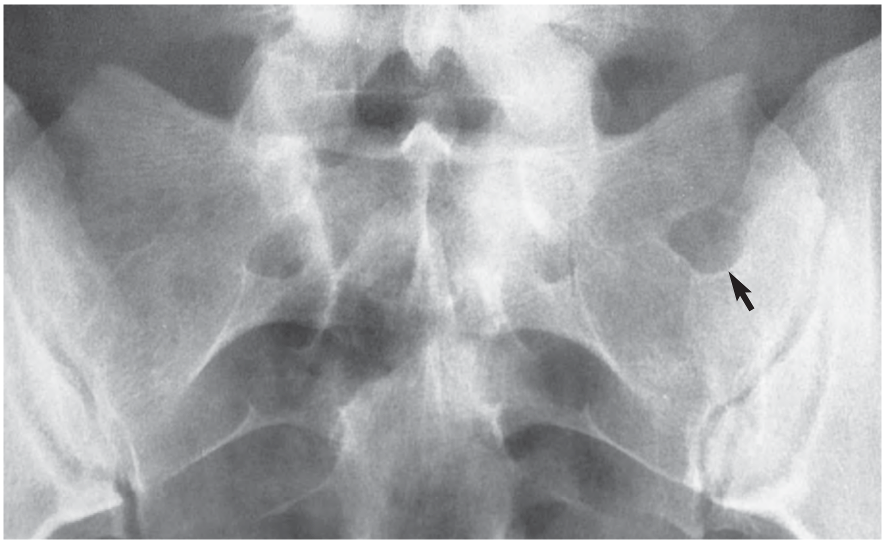

FIGURE 5–4 **Sacral wing fossa.**[7] Observe the well-circumscribed radiolucent shadow in the sacral wing simulating an osteolytic lesion *(arrow)*. Such fossae are normal variants that are of no clinical significance. *(Courtesy D. McCallum, DC, Abbotsford, B.C., Canada.)*

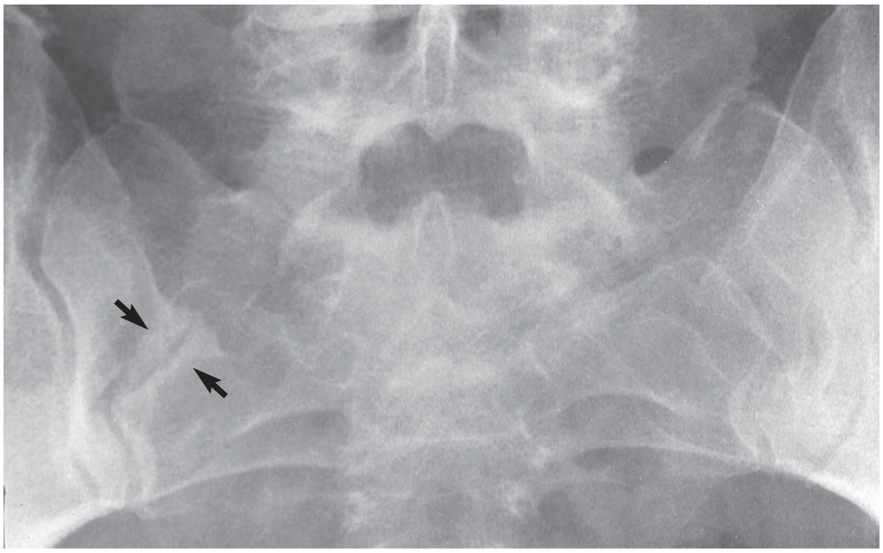

FIGURE 5–5 Accessory sacroiliac articulation.[8] An anomalous articulation between the ilium and sacrum is seen adjacent to the posterior superior iliac spine *(arrows)*.

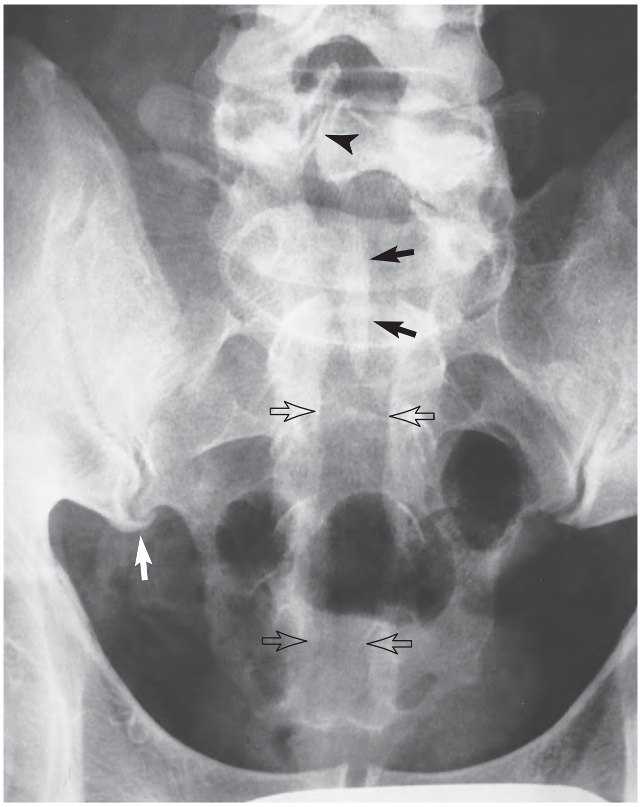

FIGURE 5–6 Spina bifida occulta.[9,10] A long midline defect is present throughout every sacral segment *(open arrows)*. This defect, which represents failure of ossification of all the sacral arches and has been termed a *sacral hiatus*, is a harmless variation found in 1% to 7% of the normal population. A vertical zone of incomplete ossification is evident within the midline cleft at the S1 level *(black arrows)*. The neural arches of L5 also are anomalous, touching in the midline, but with no evidence of fusion *(arrowhead)*. An osteophyte spans the lower sacroiliac joint *(white arrow)*.

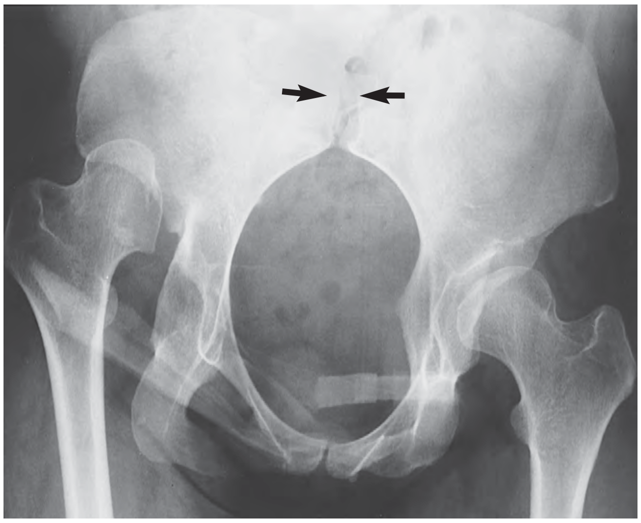

FIGURE 5–7 Sacral agenesis.[11] Frontal radiograph from a 26-year-old woman reveals complete absence of the sacrum with both ilia articulating in the midline *(arrows)*. Acetabular dysplasia with congenital hip dislocation, present in this patient, frequently accompanies sacral agenesis.

TABLE 5-3 **Injuries of the Sacrococcygeal Spine and Sacroiliac Joint***

Entity	Figure(s)	Characteristics
Fracture of the sacrum[13,14,46]	5-8, 5-9	Isolated transverse fractures of the sacrum are rare but usually stable; easily overlooked on routine radiographs Vertical fractures more likely to be associated with other osseous and ligamentous injuries Associated unstable (type III) pelvic fractures and sacroiliac injury are common (see Chapter 6) *Complications:* 30% to 40% of unstable type III injuries result in injury of the urethra or other pelvic viscera; neurologic injury of sacral nerve roots also may occur
Insufficiency fracture of the sacrum[15-17,47]	5-10	*Risk factors:* osteoporosis (most common), rheumatoid arthritis, prolonged corticosteroid medication, pelvic irradiation Sclerotic appearance with osteolysis simulating malignancy; often misdiagnosed or overlooked on routine radiographs; classic H-shaped pattern on scintigraphy may not always be present; CT and MR imaging also useful Often bilateral involvement *Complications:* delayed union, refracture, and additional fractures
Stress (fatigue) fracture of the sacrum[48]	5-11	Rare occurrence in long-distance runners May mimic sciatica from lumbosacral disc disease May be bilateral or unilateral MR imaging: Vertical linear abnormal signal paralleling the sacroiliac joint: high signal on T2-w and low signal on T1-w images *CT imaging:* Vertical linear sclerosis and cortical disruption paralleling the sacroiliac joint Bone scintigraphy: Vertical linear increased uptake paralleling the sacroiliac joint
Fracture of the coccyx or sacrococcygeal dislocation[14]		Women > men *Mechanism:* fall on buttocks in seated position Best seen on lateral radiograph Stable injury usually with minimal complications; occasional chronic coccygodynia
Diastasis of the sacroiliac joint[14]	5-12	Isolated fractures near or diastasis of the sacroiliac joint are rare occurrences that usually result from direct trauma Isolated injury stable; diastasis combined with pelvic ring fracture is unstable (see Chapter 6)
Abused child syndrome[18]		Sacrococcygeal trauma rare in child abuse Injuries may include fracture or dislocation

* See also Tables 1-4 and 1-5.

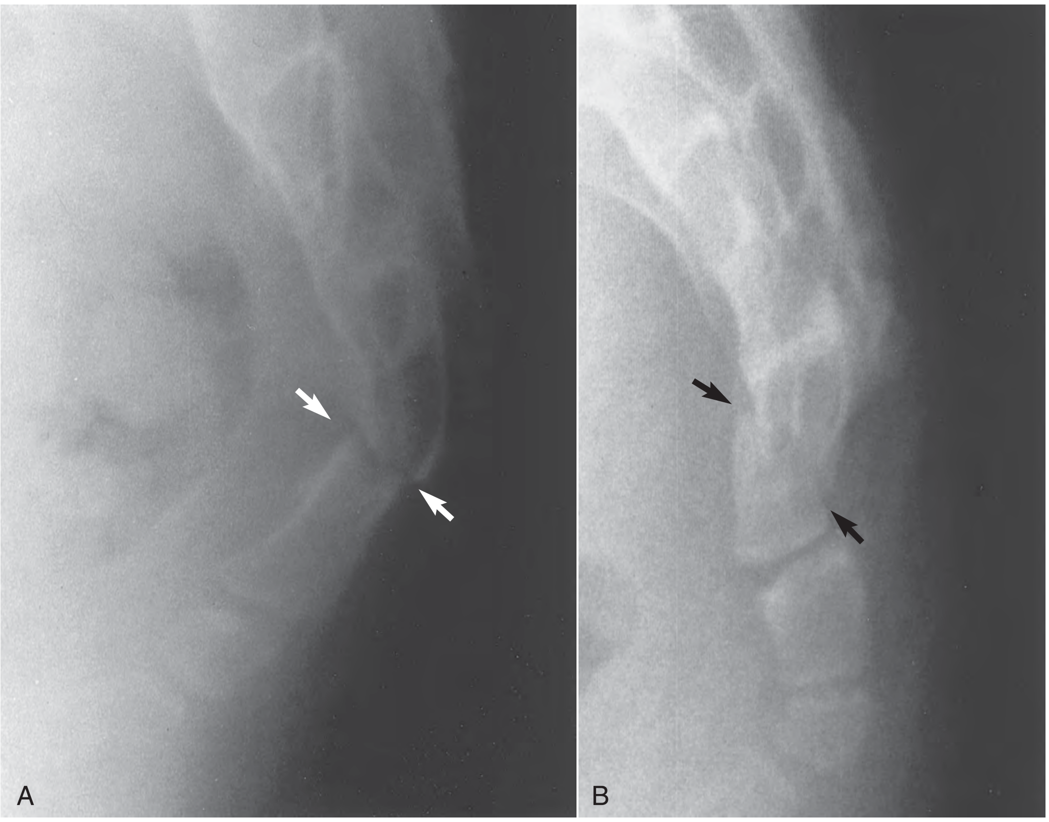

FIGURE 5–8 **Sacral fractures.**[13,14,46] **A,** Observe the transverse, horizontal fracture of the sacrum with anterior displacement just above the sacrococcygeal articulation *(arrows)*. **B,** Distal sacral fracture. This 28-year-old woman fell on her buttocks. Observe the oblique, minimally displaced fracture of the distal sacrum *(arrows)* on this lateral sacrococcygeal radiograph. Isolated transverse fractures of the sacrum are rare and easily overlooked on routine radiographs. Identification of such a fracture, as with other types of sacral fracture, should prompt a careful search for associated fractures of the spine and pelvis. CT imaging and scintigraphy may be helpful in evaluating sacral fractures.

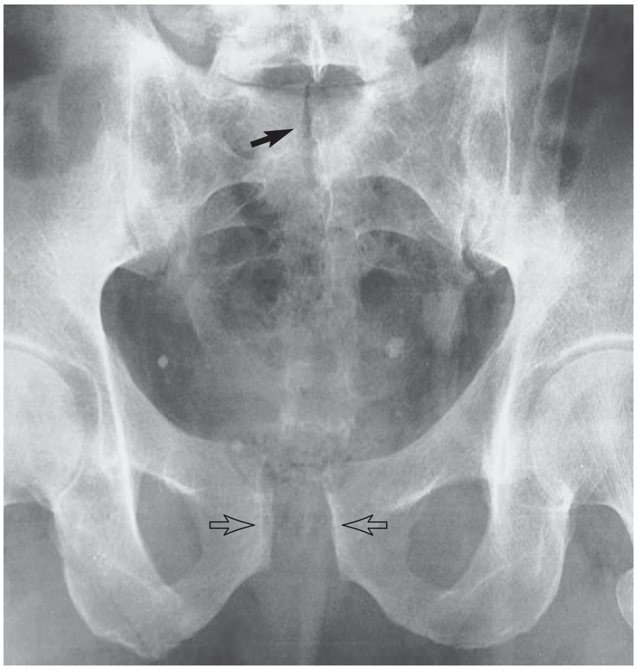

FIGURE 5–9 **Sacral fracture with associated pubic diastasis.**[13,14,46] A frontal radiograph reveals a vertical fracture through the sacrum *(arrow)* and an associated diastasis of the pubic symphysis *(open arrows)*. Injuries with double breaks (fractures or diastases) of the pelvic ring (type III injuries) are highly unstable. Type III pelvic injuries frequently are associated with injuries to the urethra or other visceral organs.

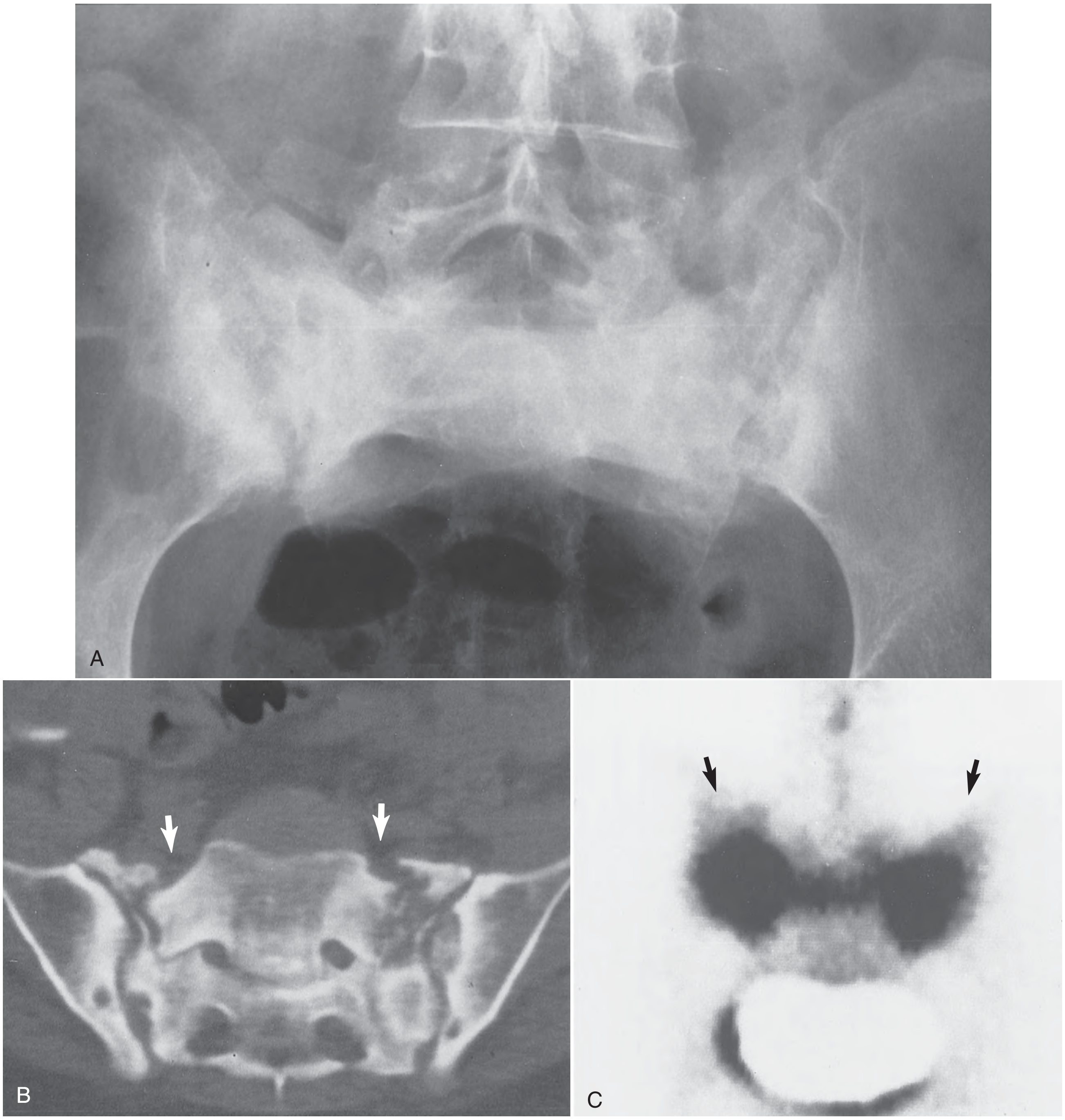

FIGURE 5–10 **Insufficiency fracture: 65-year-old woman with osteoporosis.**[15-17,47] **A,** A frontal radiograph reveals diffuse osteosclerosis and fragmentation of the sacrum and adjacent subchondral bone of the ilium. **B,** Transverse CT image shows bilateral fractures *(arrows)* and adjacent sclerosis involving the sacrum and both iliac bones. **C,** Scintigraphy clearly demonstrates the classic H-shaped pattern of increased radionuclide activity *(arrows)*. Sacral insufficiency fractures occur in about 20% of patients undergoing pelvic radiation therapy. *(Courtesy G. Greenway, MD, Dallas.)*

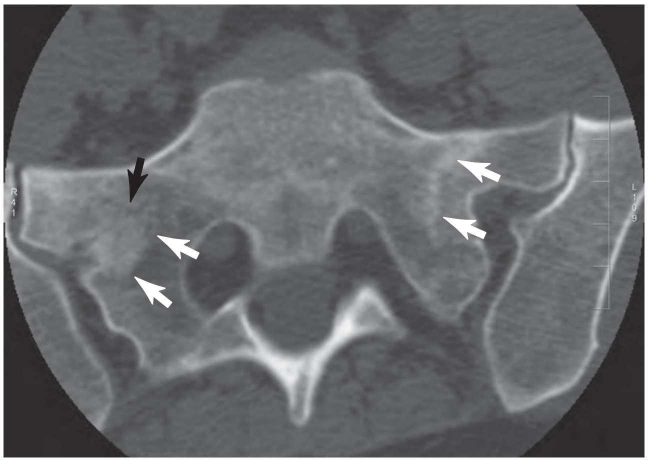

Figure 5–11 **Stress (fatigue) fracture of the sacrum.** This 39-year-old postpartum woman developed gradual onset of low back pain. A transaxial CT bone window through the first sacral segment reveals bilateral coronally oriented zones of increased density *(white arrows)*. A radiolucent fracture line is also visible within the sclerotic region on the right *(black arrow)*. It is believed that this stress fracture may be an insufficiency fracture secondary to pregnancy and breastfeeding.

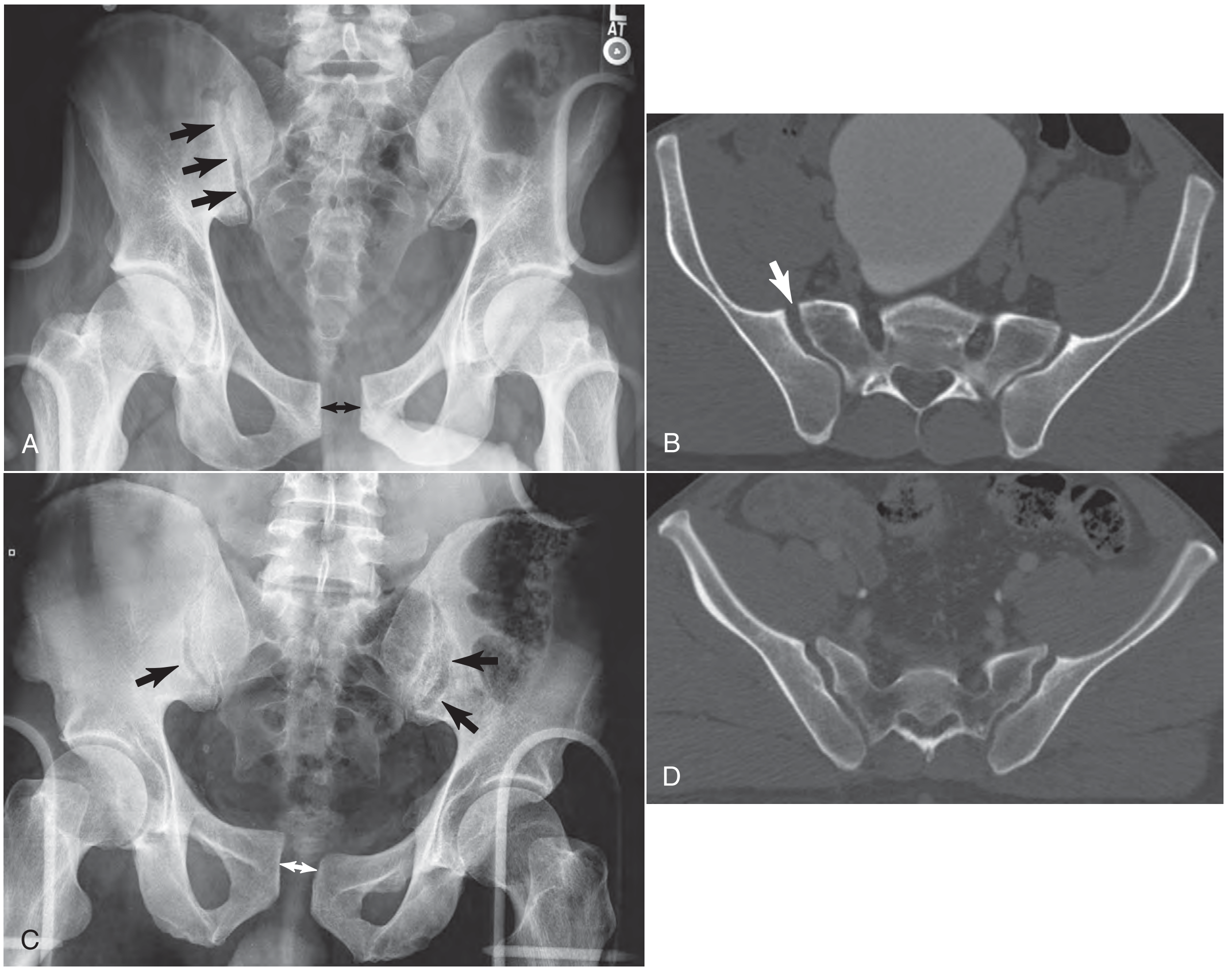

Figure 5–12 **Diastasis of the sacroiliac joint. A-B,** Unilateral involvement. Radiograph **(A)** and transaxial CT bone window **(B)** reveal widening of the right sacroiliac joint *(arrows)* in this 26-year-old man after trauma. Note also the associated pubic symphysis diastasis *(double arrow),* an injury that frequently accompanies sacroiliac joint diastasis. **C-D,** Bilateral involvement. This 49-year-old male pedestrian was struck by a vehicle at an intersection. The radiograph **(C)** clearly depicts widening of the symphysis pubis *(double arrow)* and left sacroiliac joint *(arrows),* but the right sacroiliac joint is not as clearly visualized and widening of the joint space was equivocal *(left arrow)*. The transaxial CT bone window **(C),** however, clearly demonstrates bilateral sacroiliac joint diastasis *(arrows)*.

TABLE 5-4 Sacroiliac Joint: Articular Disorders*

Entity	Figure(s)	Characteristics
Degenerative and Related Disorders		
Degenerative joint disease[19,20,49]	5-13	Accompanies aging and is accelerated by previous injury and lumbosacral transitional segments Men > women Narrowed articular space Osteophytes (may simulate osteoblastic pelvic lesions) Subchondral bone sclerosis Vacuum phenomenon
Ligament calcification and ossification[19]	5-14	Calcification or ossification of the sacroiliac, sacrotuberous, or sacrospinous ligaments occurs in degenerative disease, diffuse idiopathic skeletal hyperostosis (DISH), fluorosis, or as an idiopathic phenomenon
Osteitis condensans ilii[5,21,49]	5-15	Well-defined triangular sclerosis of the iliac side of the sacroiliac joints Most frequently bilateral and relatively symmetric process; occasionally unilateral Affects primarily women and frequently is associated with paraglenoid sulci Cause not clear; predominant theory suggests that the condition is secondary to mechanical stress across the joint coupled with increased vascularity during pregnancy Postulated theories include associations with urinary tract infections and ankylosing spondylitis, but these do not have widespread support Radiographic appearance may simulate that of ankylosing spondylitis and other seronegative spondyloarthropathies
DISH[22]	5-16	Enthesopathy of ligaments and paraarticular bone excrescences predominate at the anterior, anterosuperior, or anteroinferior articular margins and tend to bridge the joint rather than cause true intraarticular ankylosis or sacroiliitis Bridging ossification may span the inferior sacroiliac joint or the upper ligamentous portion of the joint
Inflammatory Disorders		
Rheumatoid arthritis[23]	5-17	Sacroiliac joint involvement rare and findings are mild compared with those in ankylosing spondylitis Unilateral or bilateral Sclerosis and erosions Osteoporosis Absence of osteophytes and other osseous outgrowths
Ankylosing spondylitis[24,25,44,45,49]	5-18	Sacroiliitis is the hallmark of ankylosing spondylitis Occurs early in the disease Usually bilateral and symmetric in distribution Initial joint space widening from erosions Eventually results in osseous ankylosis ***MR and CT imaging*** MR imaging is reliable in visualization of joint erosions and bone marrow edema in early seronegative spondyloarthropathy and allows for differentiation between active and chronic sacroiliitis CT scanning is also useful at identifying erosions, subchondral sclerosis, and later ankylosis
Enteropathic arthropathy[26]	5-19	Changes identical to those of ankylosing spondylitis Sacroiliitis and spondylitis account for about 20% to 30% of articular involvement in ulcerative colitis, whereas peripheral involvement constitutes as much as 60%
Psoriatic spondyloarthropathy[27,42,44,49]	5-20	Sacroiliac joint changes are found on radiographs of approximately 10% to 25% of patients with moderate or severe psoriatic skin disease Unilateral or bilateral asymmetric pattern of sacroiliitis is typical
Reactive arthritis associated with Reiter syndrome[28,42,44]	5-21	Associated with sacroiliac joint changes in about 50% of cases Unilateral or bilateral asymmetric pattern of sacroiliitis is typical Associated with urethritis and conjunctivitis

* See also Tables 1-7 to 1-10 and Table 1-19.

TABLE 5-4 Sacroiliac Joint: Articular Disorders—cont'd

Entity	Figure(s)	Characteristics
Metabolic Disorders		
Hyperparathyroidism[29,30]	5-22	Bilateral, symmetric subchondral bone resorption predominates on the iliac side and results in widening of the sacroiliac joints Minimal adjacent subchondral sclerosis
Renal osteodystrophy[30,31]	5-23	Sacroiliac changes identical to those in hyperparathyroidism
Infection		
Pyogenic septic arthritis[32]	5-24	Septic arthritis results in unilateral sacroiliac joint widening and destruction Paravertebral soft tissue mass or abscess variable; osseous ankylosis rare Tuberculous infection of the sacroiliac joint occurs only infrequently

TABLE 5-5 Distribution of Sacroiliac Joint Articular Disorders

		Sacroiliac Joint Involvement				
Entity	**Figure(s)**	**Pathology**	**Intraarticular Ankylosis**	**Bilateral Symmetric***	**Bilateral Asymmetric***	**Unilateral***
Degenerative and Related Disorders						
Degenerative disease	5-13	Joint degeneration	Absent	+	++	+
Osteitis condensans ilii	5-15	Iliac sclerosis	Absent	++	+	+
Diffuse idiopathic skeletal hyperostosis (DISH)	5-16	Enthesopathy	Absent	++		
Inflammatory Disorders						
Rheumatoid arthritis	5-17	Erosion, minor sclerosis	Absent		+	+
Ankylosing spondylitis	5-18	Erosion, sacroiliitis, iliac sclerosis	Common	++		
Enteropathic arthropathy	5-19	Erosion, sacroiliitis, iliac sclerosis	Common	++		
Psoriatic spondyloarthropathy	5-20	Erosion, sacroiliitis, iliac sclerosis	Uncommon	+	++	+
Reiter syndrome	5-21	Erosion, sacroiliitis, iliac sclerosis	Uncommon	+	++	+
Metabolic Disorders						
Hyperparathyroidism	5-22	Subchondral resorption, minimal sclerosis	Absent	++		
Renal osteodystrophy	5-23	Subchondral resorption, minimal sclerosis	Absent	++		
Infection						
Pyogenic septic arthritis	5-24	Septic arthritis with joint destruction	Uncommon			++

* +, Occasional pattern of distribution; ++, predominant pattern of distribution.

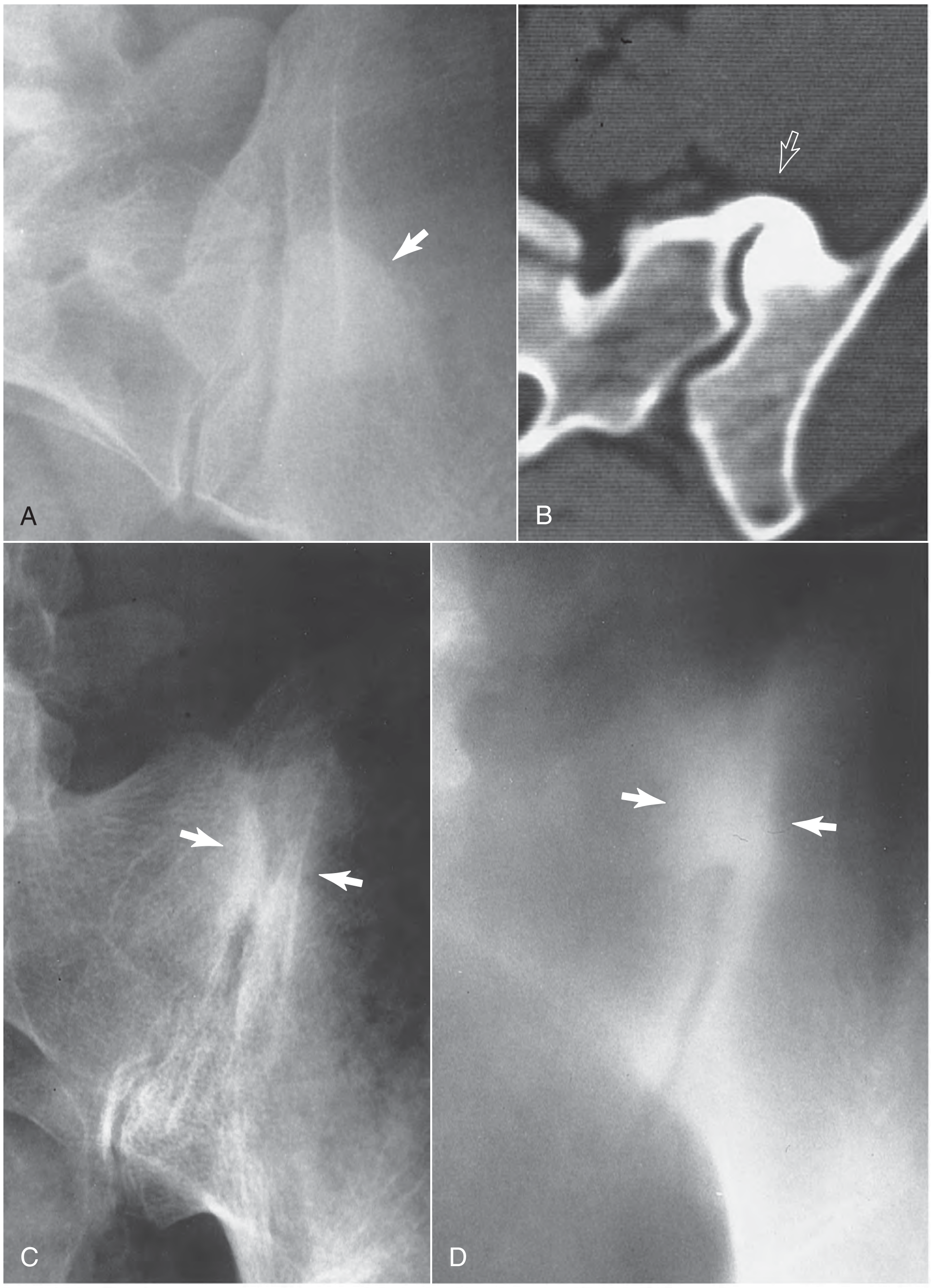

FIGURE 5–13 **Degenerative joint disease.**[19,20,49] **A-B,** This 39-year-old man had injured his sacroiliac joint. In **A,** a radiograph obtained 15 years later reveals an area of increased density overlying the left sacroiliac joint *(arrow)*. In **B,** a transaxial CT scan more clearly defines the nature of this osteophyte bridging the anterior portion of the sacroiliac joint *(open arrow)*. **C-D,** Another patient, a 41-year-old man. In **C,** the routine radiograph shows sclerosis overlying the right sacroiliac joint *(arrows)*. In **D,** conventional tomography reveals an osteophyte spanning the joint *(arrows)*. Sacroiliac joint osteophytes may simulate osteoblastic lesions of bone.

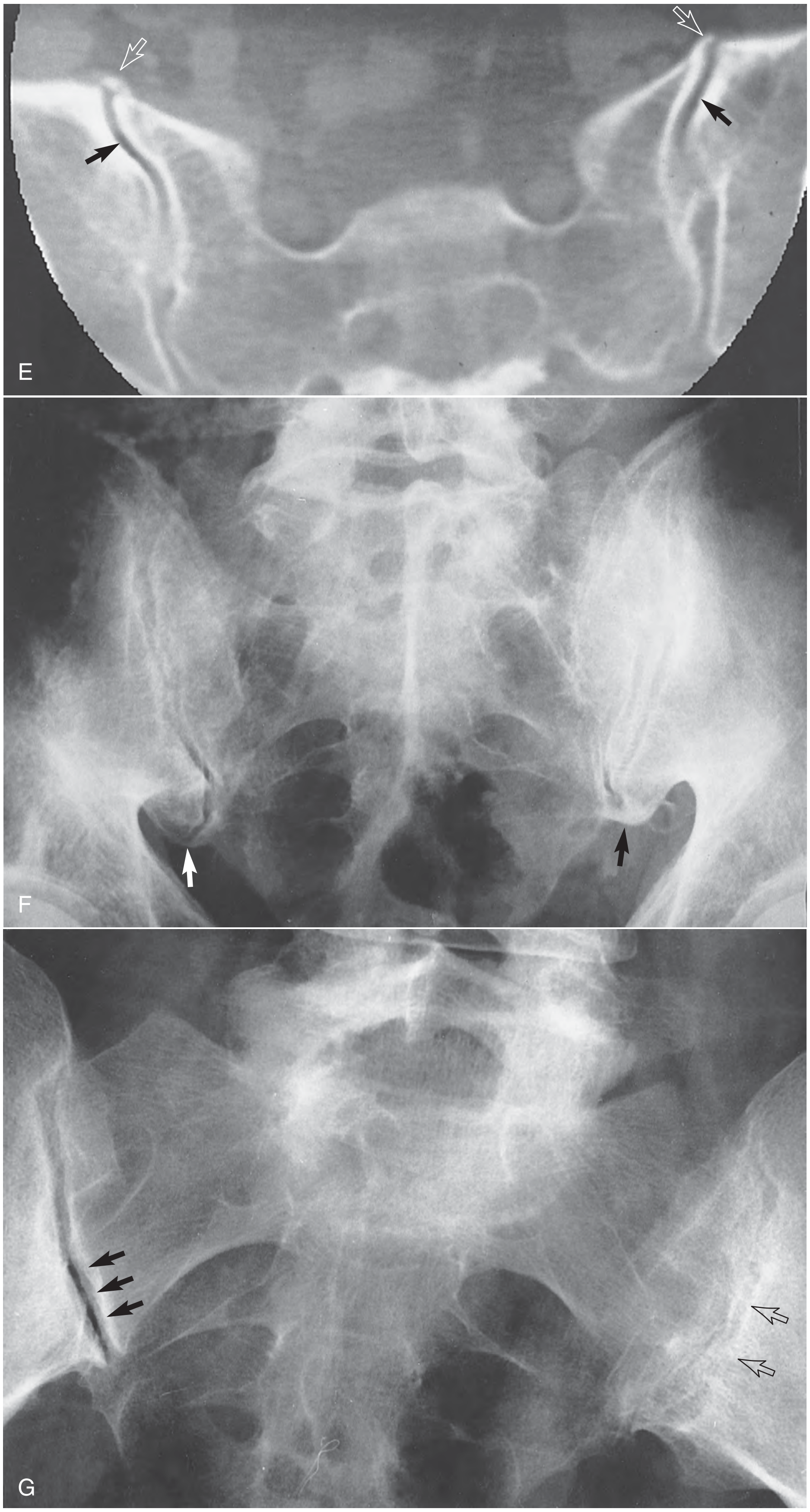

FIGURE 5–13, cont'd **E,** In a third patient, a transaxial CT scan reveals bilateral subchondral sclerosis, small anterior osteophytes *(open arrows),* and intra-articular gas *(arrows)*. **F,** This 73-year-old man had back pain and stiffness. Radiograph shows bridging osteophytes spanning the inferior aspect of both sacroiliac joints *(arrows)*. Subtle sclerosis also is seen adjacent to the middle regions of the sacroiliac joints. **G,** In another patient, a vacuum phenomenon is evident on one side *(arrows),* whereas sclerosis and joint-space narrowing predominate on the other side *(open arrows)*. (***C-D,*** *Courtesy P. Wilson, M.D., Eugene, Ore.;* ***F-G,*** *Reprinted with permission from Taylor JAM, Hoffman LE: The geriatric patient: diagnostic imaging of common musculoskeletal disorders. Top Clin Chiropr 3:23, 1996.)*

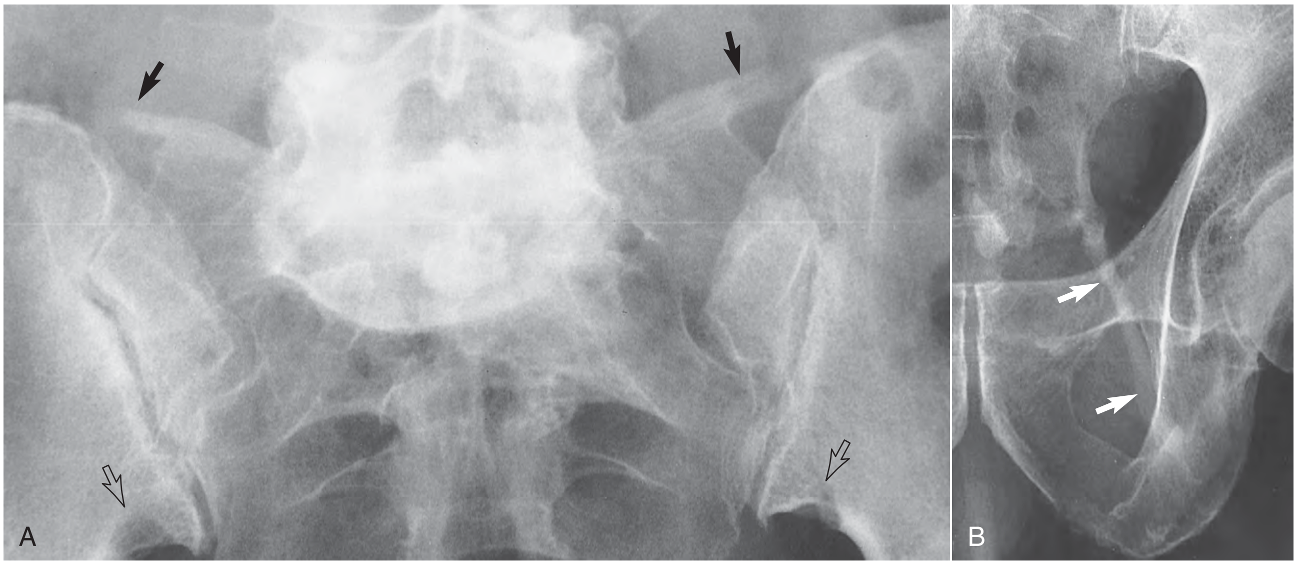

FIGURE 5–14 Ligament calcification and ossification.[19] **A,** Observe the enthesopathic proliferation involving the superior sacroiliac ligaments *(arrows)*. Minimal degenerative disease of the sacroiliac joints, characterized by bilateral subchondral bone sclerosis and a vacuum phenomenon within the right sacroiliac joint, also is evident. Bilateral notches within the inferior ilium adjacent to the sacroiliac joints are termed *paraglenoid sulci (open arrows)*. These grooves represent a normal variant found almost exclusively in women and occur after pregnancy, likely because of the gravid uterus compressing the superior gluteal artery against the ilium. **B,** Sacrotuberous ligament ossification is seen in this 79-year-old patient *(arrows)*. Ligament ossification may be idiopathic or associated with degenerative disease, fluorosis, or diffuse idiopathic skeletal hyperostosis (DISH).

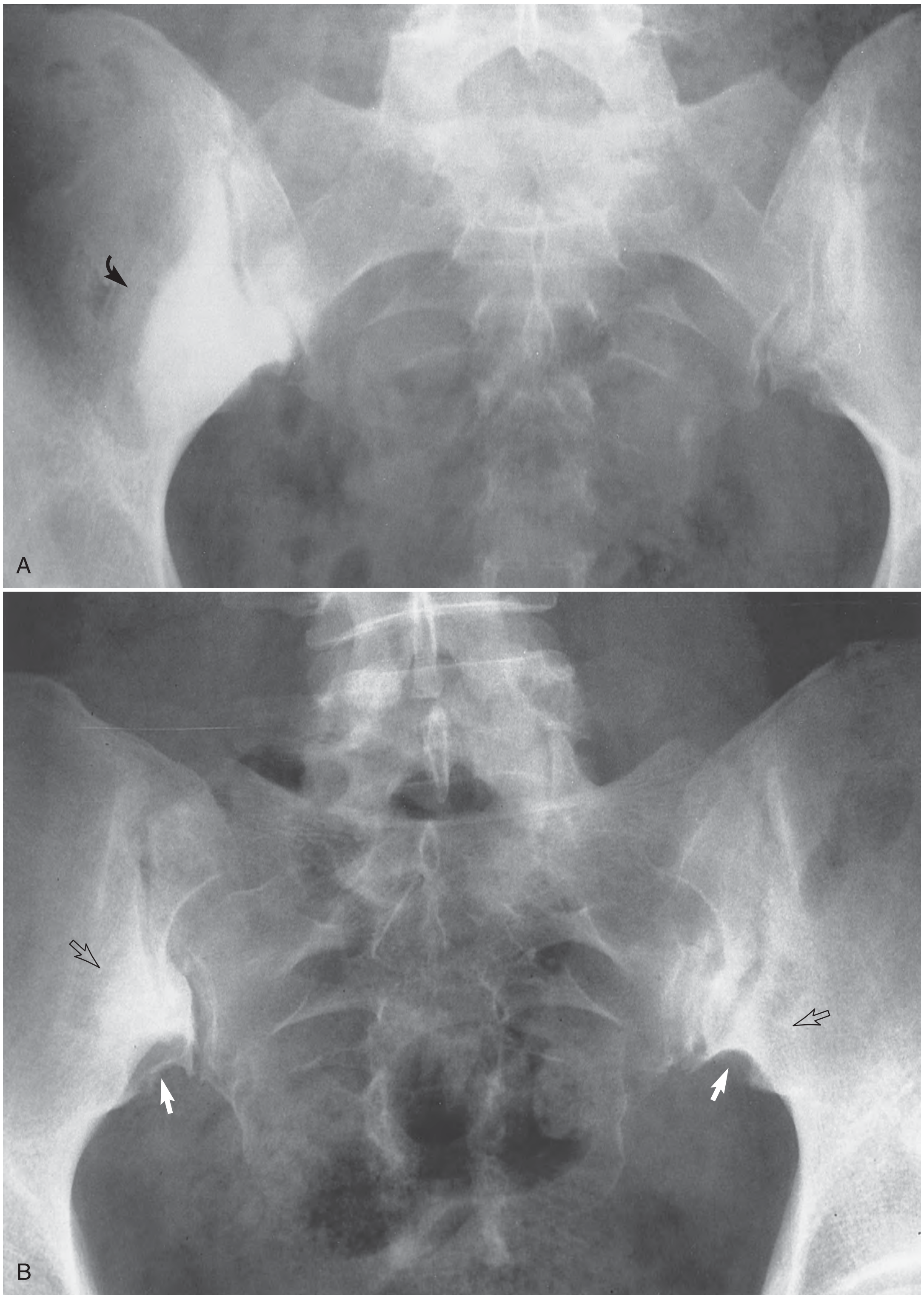

FIGURE 5–15 **Osteitis condensans ilii.**[21,49] **A,** Unilateral triangular hyperostosis is seen *(curved arrow)* in the ilium of this postpartum woman. **B,** In another patient, observe the triangular areas of ossification adjacent to the inferior portions of the sacroiliac joints *(open arrows)*. Also noted are bilateral paraglenoid fossae *(arrows)*.

Continued

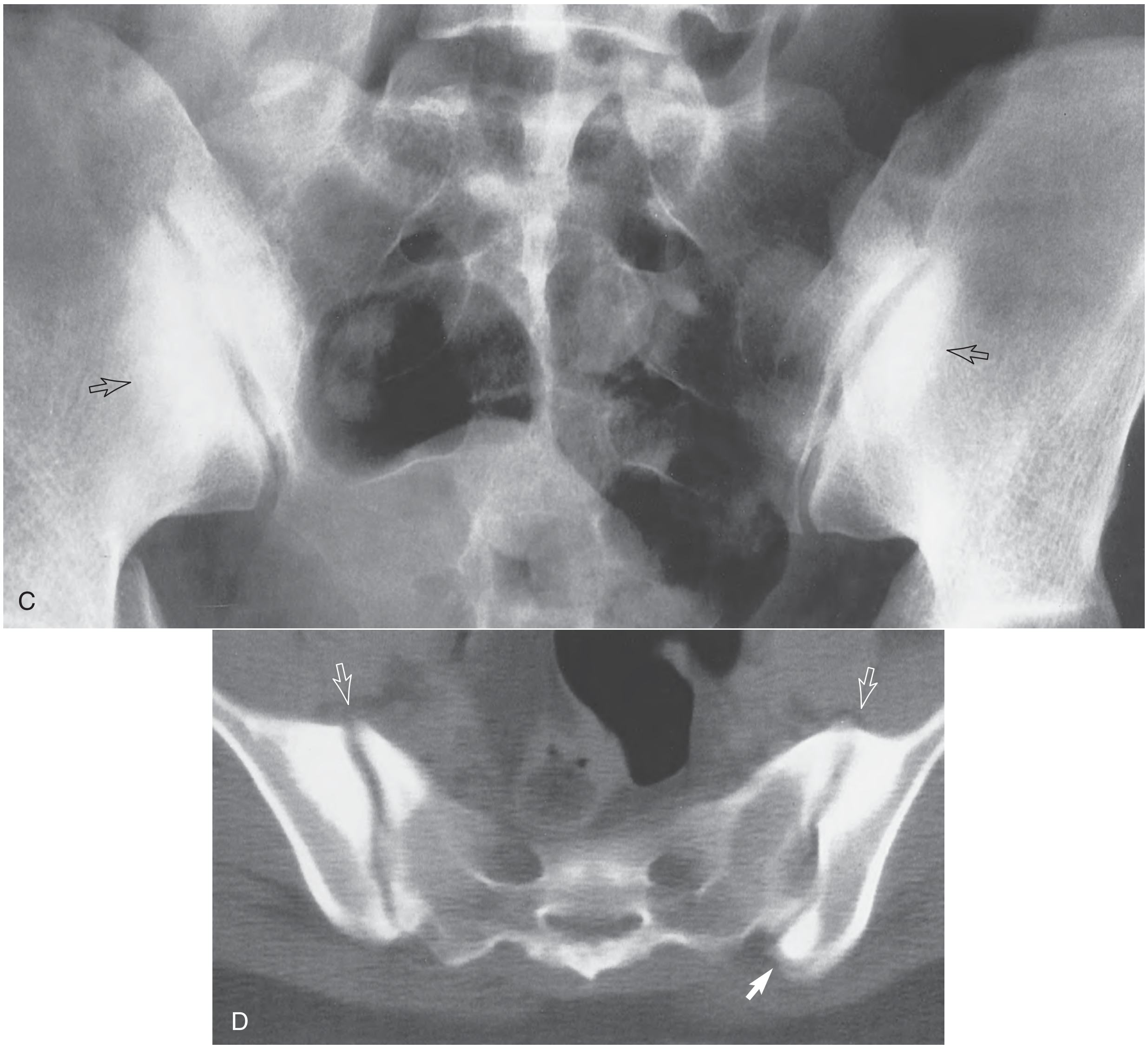

FIGURE 5–15, cont'd **C-D,** This 23-year-old woman was involved in a motor vehicle accident and fractured her right ischium and pubis. In **C**, a radiograph reveals, as an incidental finding, bilateral, well-defined osteosclerosis *(open arrows)* predominating on the iliac side of the articulations. The joint spaces are well maintained and the joint margins are sharply defined. In **D,** a transaxial CT scan clearly delineates the sclerosis involving both the iliac and sacral aspects of the joint *(open arrows)*. A small focal zone of sclerosis also is noted adjacent to an accessory sacroiliac articulation *(arrow)*.

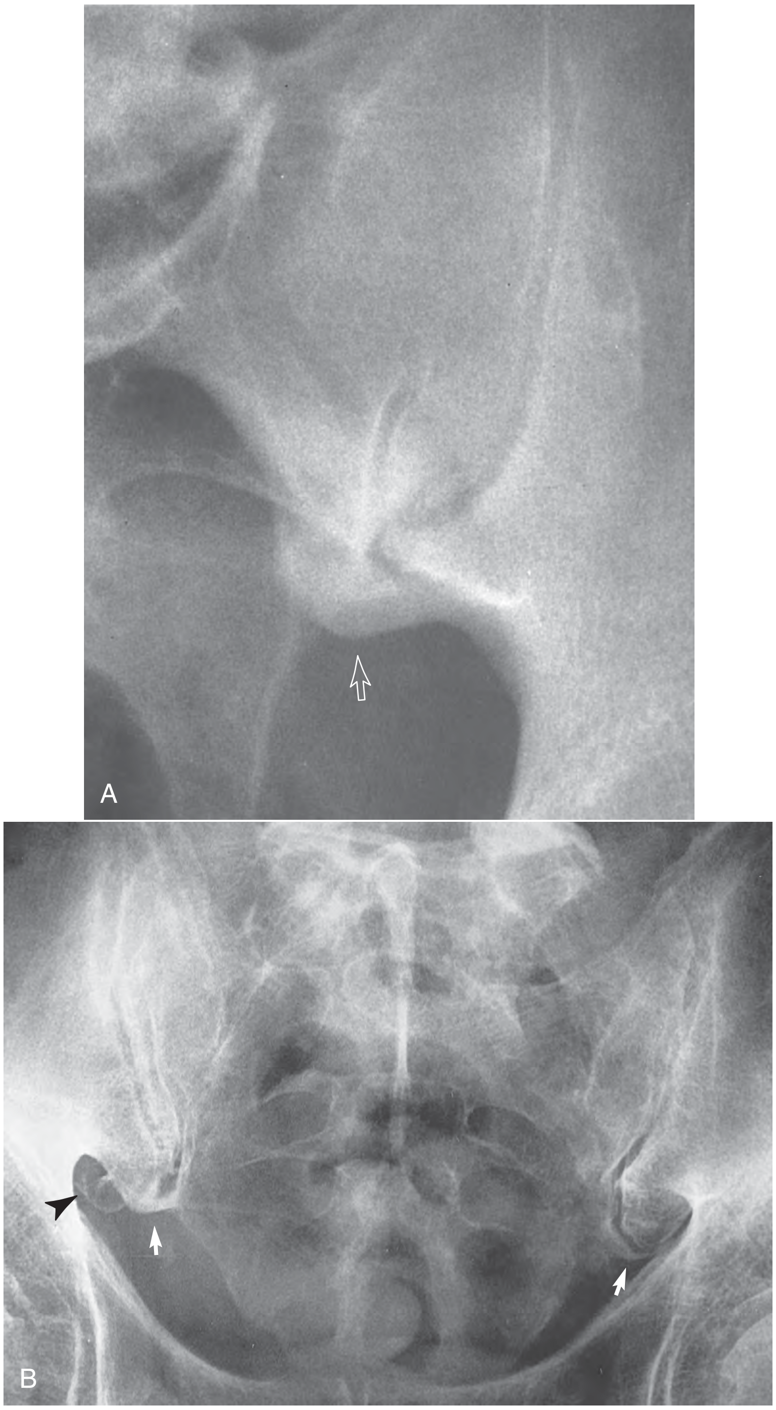

FIGURE 5–16 **Diffuse idiopathic skeletal hyperostosis (DISH).**[22] **A,** Bridging ossification is seen at the inferior aspect of the sacroiliac joint *(open arrow)* in this patient with long-standing DISH. The sacroiliac joint is otherwise normal. **B,** In another patient, bilateral osseous bridging *(arrows)* and vascular calcification *(arrowhead)* are evident.

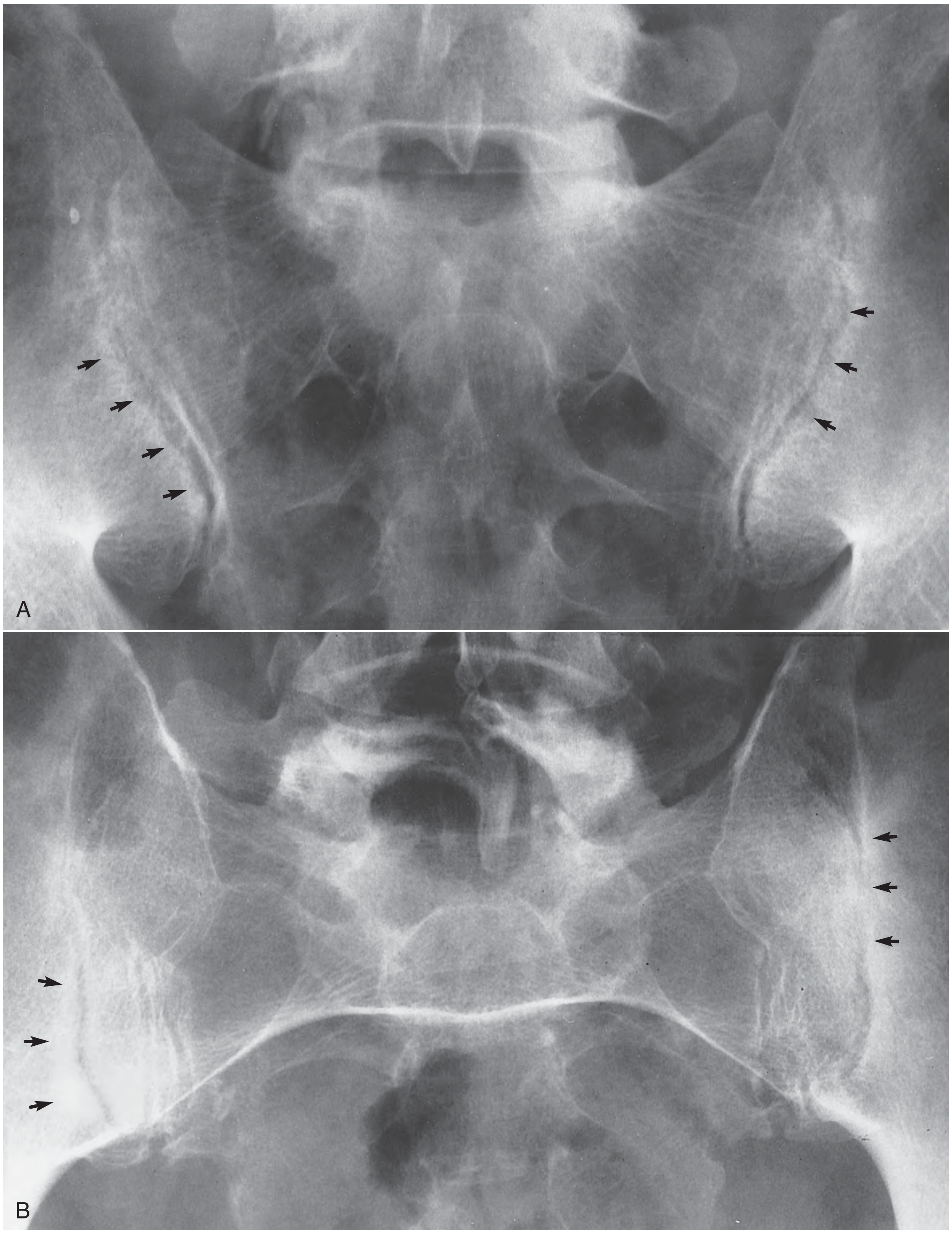

FIGURE 5–17 **Rheumatoid arthritis.**[23] **A,** Subtle subchondral bone erosion mainly on the iliac side of the joints *(arrows)* and minimal sclerosis are seen in this patient. **B,** In another patient with rheumatoid arthritis, mild erosive changes and minimal sclerosis involving the lower right and middle left portions of the articulations are evident *(arrows)*.

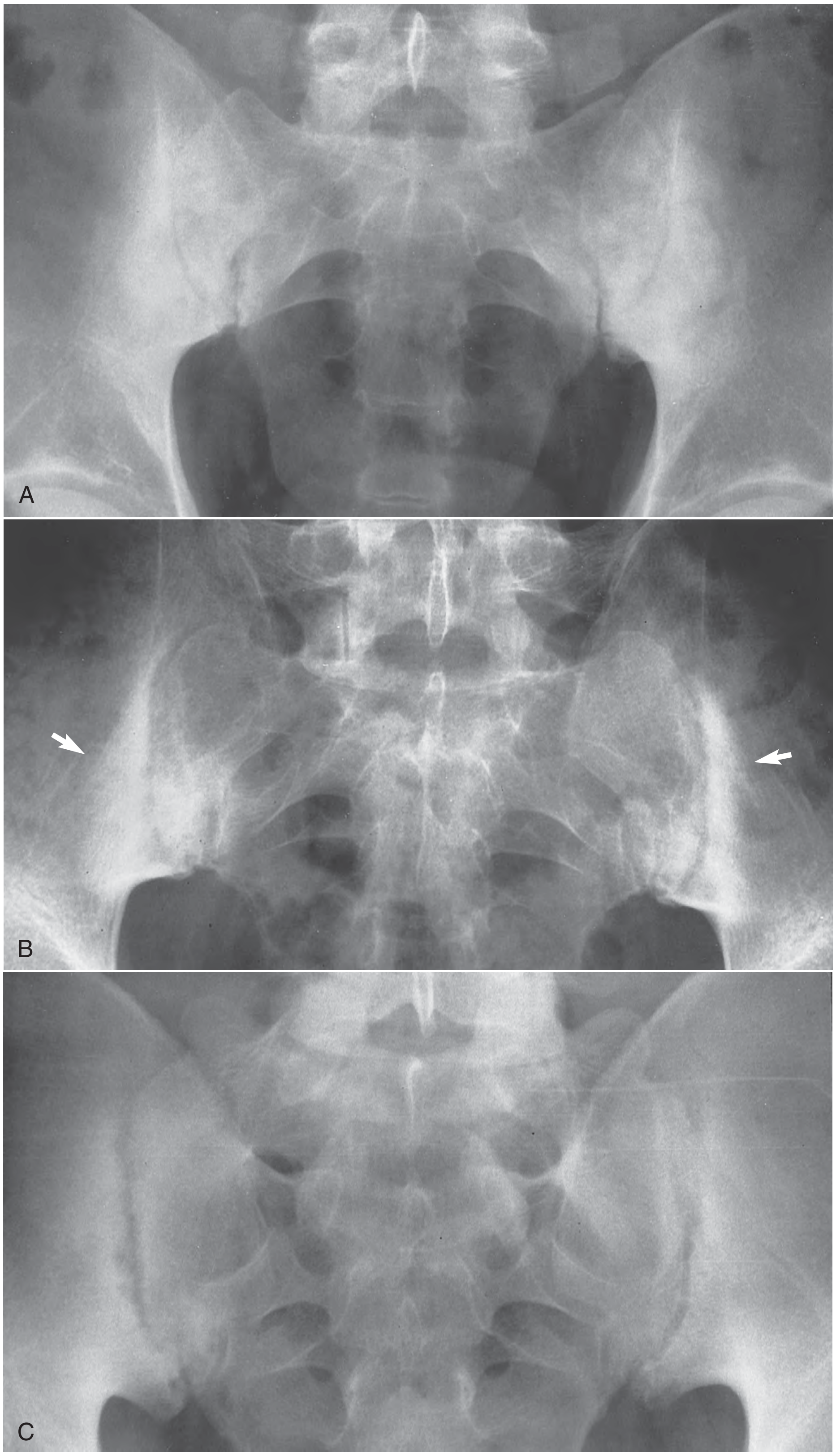

FIGURE 5–18 **Ankylosing spondylitis.**[24,25,44,45,49] **A,** Bilateral sacroiliitis. Blurring of the sacroiliac joint margins is associated with subchondral sclerosis, predominating on the iliac side of the sacroiliac joints in this 40-year-old man with long-standing ankylosing spondylitis. **B,** In another patient, marked sclerosis *(arrows)* and blurring of the subchondral bone are noted. **C,** In a third patient, sacroiliitis with sclerosis and subchondral bone erosion are apparent.

Continued

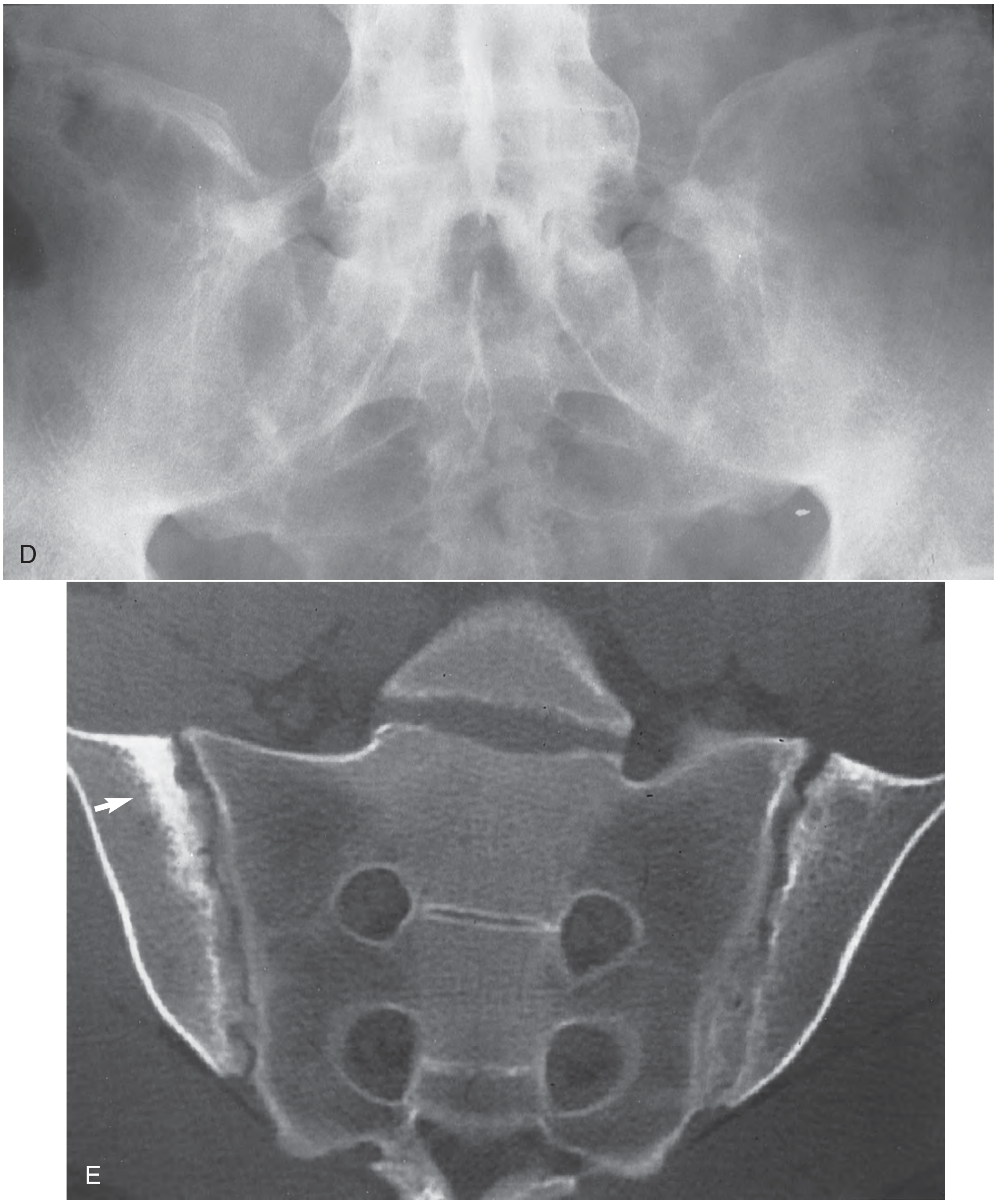

FIGURE 5–18, cont'd **D,** Ankylosis. In a 65-year-old man with advanced ankylosing spondylitis, the sacroiliac joint margins are completely obliterated by osseous ankylosis. Observe the enthesopathy of the L5 transverse processes and the characteristic syndesmophytes in the lumbosacral spine. **E,** CT abnormalities. CT scan shows bilateral erosion of subchondral bone with asymmetric sclerosis of the iliac side of the joints, especially on the right *(arrow)*. (***E,*** *Courtesy T. Learch, MD, Los Angeles.)*

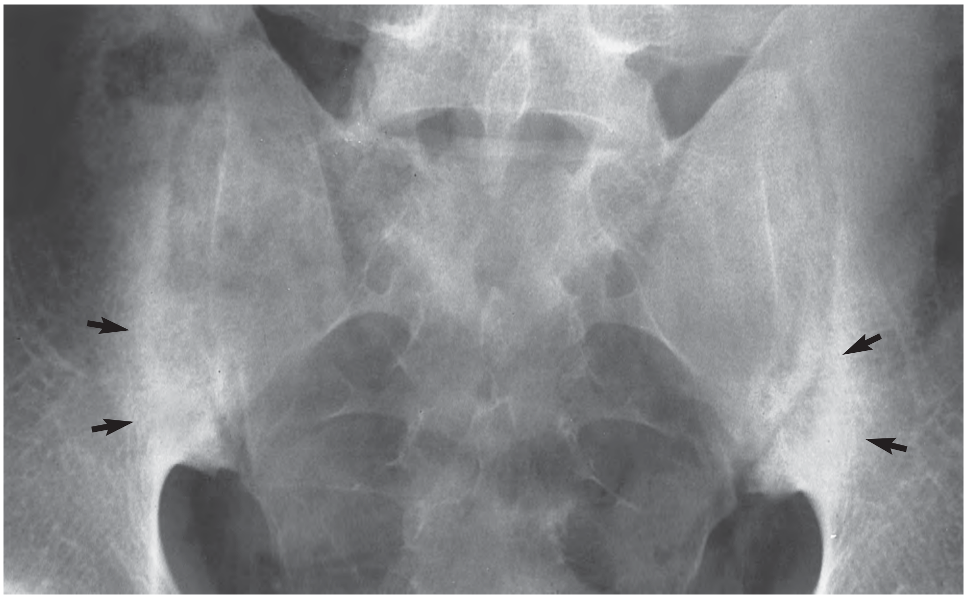

FIGURE 5–19 **Ulcerative colitis: enteropathic arthropathy.**[26,44] Bilateral, symmetric sacroiliitis is characterized by joint-space narrowing, subarticular erosions, and subchondral bone sclerosis involving the lower synovial portion of the articulations *(arrows)*.

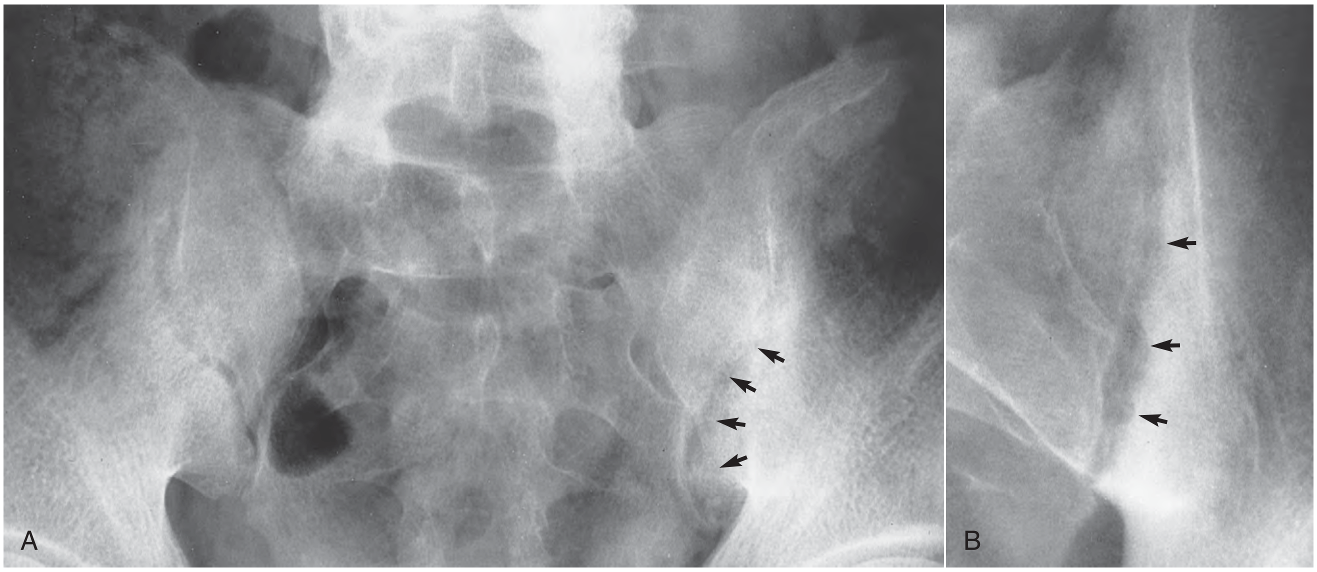

FIGURE 5–20 **Psoriatic spondyloarthropathy.**[27,42,44,49] **A,** Asymmetric sacroiliac joint changes including loss of definition of the lower portion of the left sacroiliac joint *(arrows)* and subchondral sclerosis are characteristic of sacroiliitis. The margins of the right sacroiliac joint are slightly indistinct. **B,** In another patient, subchondral scalloped erosions *(arrows)* are accompanied by sclerosis of the iliac side of the joint. The subarticular joint surface is indistinct.

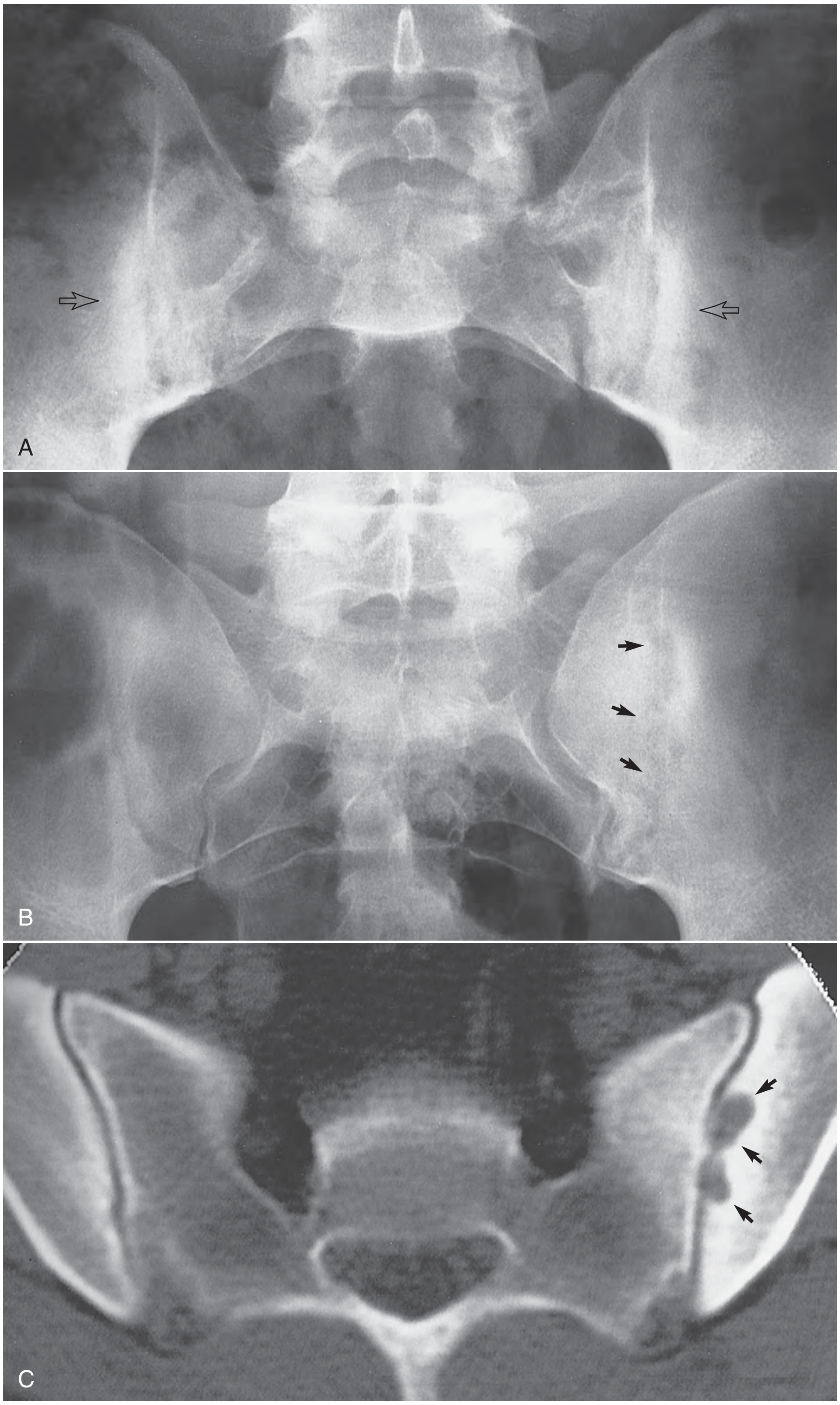

FIGURE 5–21 **Reactive arthritis associated with Reiter syndrome.**[28,42,44,49] **A,** Bilateral symmetric sacroiliitis is evident in this 35-year-old man with urethritis, conjunctivitis, and back pain. The radiographic findings include sclerosis predominating on the iliac side of the joints *(open arrows)* and indistinct subchondral joint margins. A lumbosacral transitional segment with enlargement of the left L5 transverse process, which has an anomalous articulation with the sacrum, also is present. **B,** In another patient, the findings, predominating on the left side, include asymmetric sclerosis and indistinct joint margins *(arrows)*. **C,** In a third patient, a transaxial CT image reveals unilateral sacroiliitis with subchondral erosions *(arrows)* and prominent sclerosis, especially on the iliac side of the articulation.

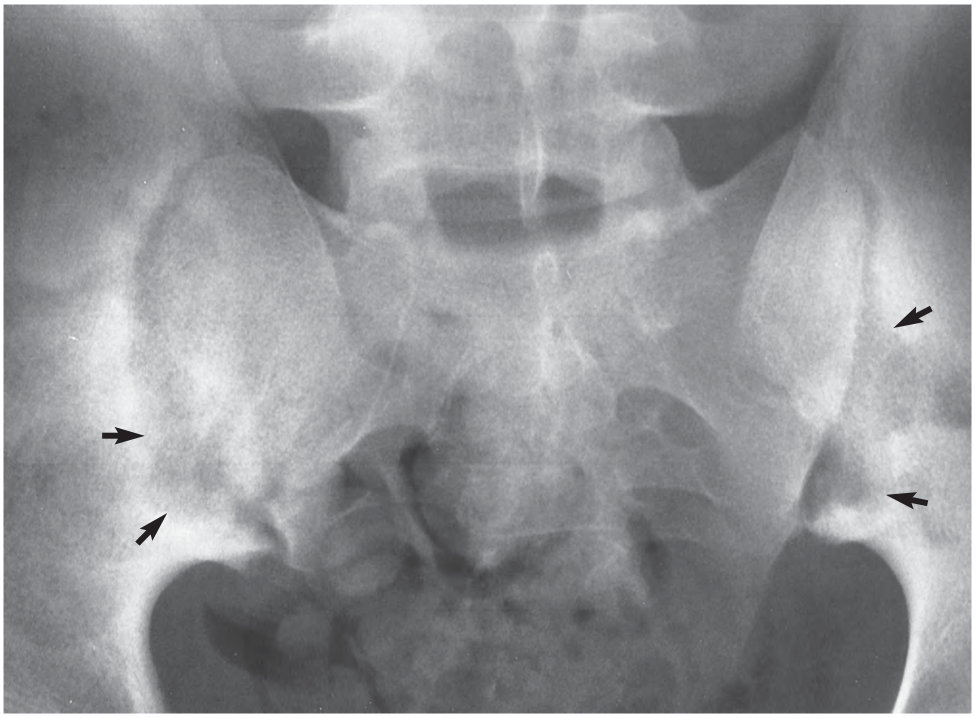

FIGURE 5–22 Hyperparathyroidism: subchondral resorption.[29,30] Extensive resorption of the subarticular bone is seen adjacent to the sacroiliac joints *(arrows)* in this 28-year-old man with renal failure and secondary hyperparathyroidism.

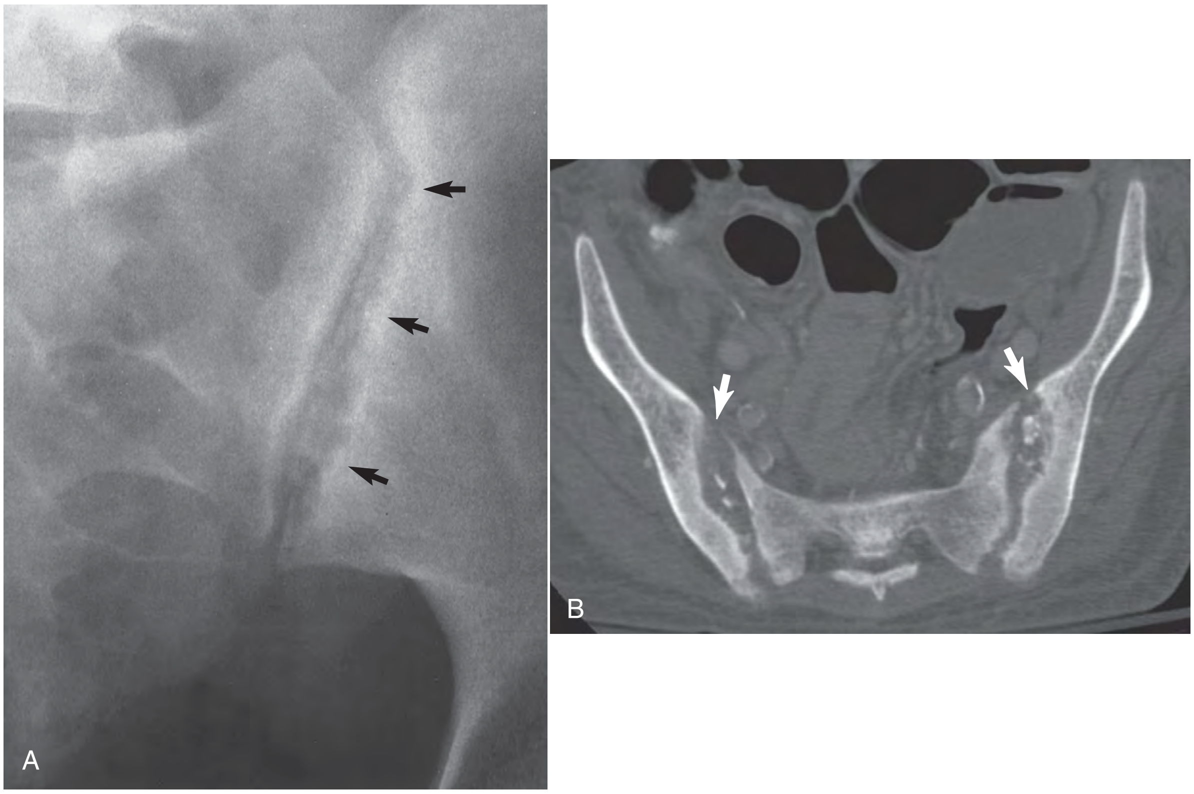

FIGURE 5–23 Renal osteodystrophy: subchondral resorption.[30,31] **A,** Observe the widening and indistinct margins of the subchondral bone adjacent to the sacroiliac joint *(arrows)* in this patient with chronic renal disease, renal osteodystrophy, and secondary hyperparathyroidism. Notable resorption of bone is present, but the amount of subchondral bone sclerosis is minimal. **B,** A transaxial CT bone window image in another patient, a 54-year-old man with chronic renal osteodystrophy, demonstrates bilateral widened sacroiliac joints containing detritic osseous debris resulting from extensive subchondral resorption *(black arrows)*. Vascular calcification is also present within the iliac arteries bilaterally *(white arrows)*. *(Courtesy J.T. Knudsen, DC, and C. Yomtob, DC, Los Angeles, Calif.)*

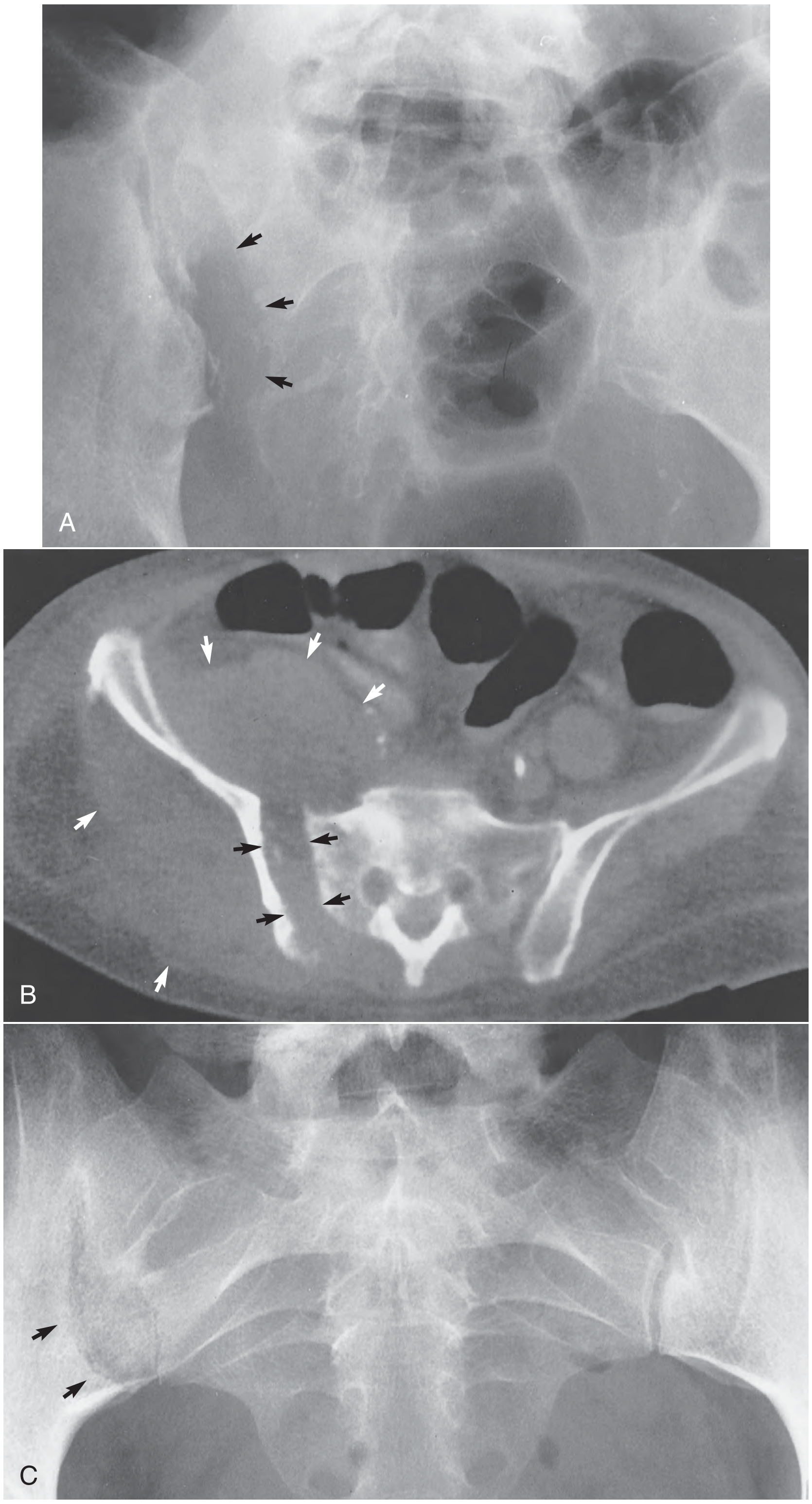

FIGURE 5–24 **Pyogenic septic arthritis.**[32] **A-B,** Abscess formation. This 58-year-old woman had low back pain. In **A,** the routine radiograph demonstrates unilateral destruction of the subchondral bone of the sacrum adjacent to the lower sacroiliac joint *(arrows)*. The subchondral bone of the ilium is not well visualized on this radiograph, but it also appears eroded. In **B,** the transaxial CT image shows joint-space widening and extensive erosion of the adjacent subchondral surfaces of bone *(black arrows)*. A huge soft tissue abscess extending from the articulation into the pelvic basin and gluteal region is seen *(white arrows)*. **C,** In another patient, a 28-year-old heroin addict, a routine radiograph demonstrates unilateral sacroiliitis with joint widening and obliteration of the sharp margin of the subchondral surface of the articulation *(arrows)*. *Pseudomonas aeruginosa* was cultured from a bone biopsy specimen. Intravenous drug abusers are especially predisposed to sacroiliac joint infections. The sacroiliitis of pyogenic infection usually is monoarticular and may result in eventual osseous ankylosis.

TABLE 5-6 Sacrococcygeal Spine Neoplasms*

Entity	Figure(s)
Malignant Neoplasms[50,52]	
Skeletal metastasis	
Osteolytic metastasis[33,34]	5-25
Osteoblastic metastasis[33,34]	5-26
Primary malignant neoplasms of bone	
Chordoma[35,50-52]	5-27
Chondrosarcoma[50]	
Ewing sarcoma and primitive neuroectodermal tumor[50]	
Osteosarcoma[50]	
Myeloproliferative disorders	
Multiple myeloma[50]	
Plasmacytoma[36,52]	5-28
Benign Neoplasms[50,52]	
Primary benign neoplasms	
Enostosis[37]	5-29
Giant cell tumor[38]	5-30
Aneurysmal bone cyst[50]	
Osteoblastoma[50]	
Hemangioma[50]	
Tumorlike lesions	
Paget disease[39,40,43]	5-31
Neurofibromatosis type I (von Recklinghausen disease)[41]	5-32

* For a more complete discussion of neoplasms see Tables 1-12 to 1-14 and 2-17.

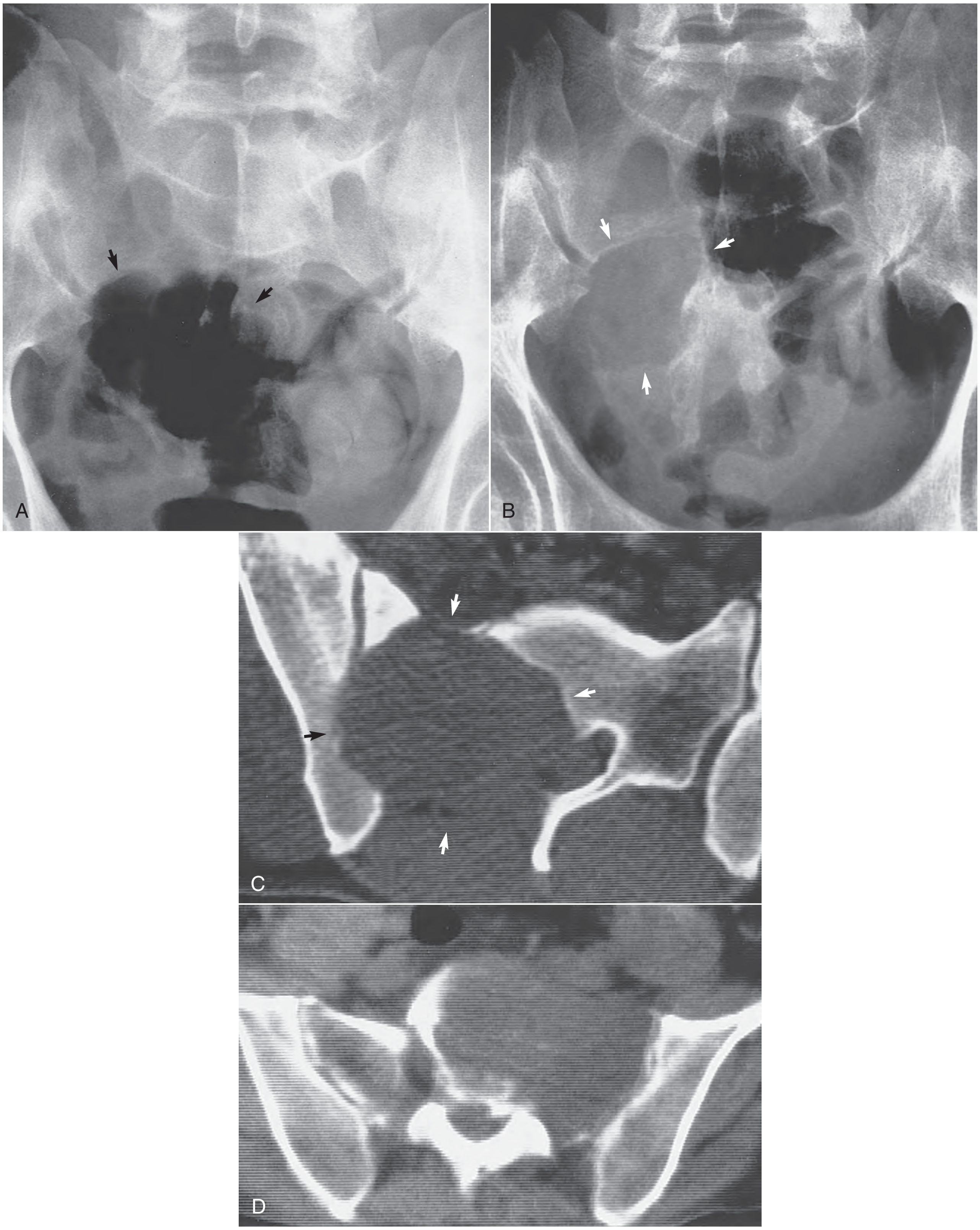

FIGURE 5–25 **Skeletal metastasis: osteolytic pattern.**[33,34] This 42-year-old man had a 6-month history of severe right leg pain. **A,** On the initial radiograph, the lower sacrum is obscured by overlying bowel gas *(arrows)*. **B,** Radiograph obtained the next day reveals a large osteolytic lesion in this region *(arrows)*. **C,** Striking osteolysis of the sacrum and ilium is evident on the transaxial CT display *(arrows)*. The histologic diagnosis proved to be skeletal metastasis secondary to renal cell carcinoma. **D,** In another patient, a transaxial CT scan through the sacrum delineates the extent of osteolytic destruction in this patient with skeletal metastasis. The lesion does not cross the sacroiliac joint, remaining confined to the sacrum. *(**A-C,** Courtesy G. Greenway, MD, Dallas.)*

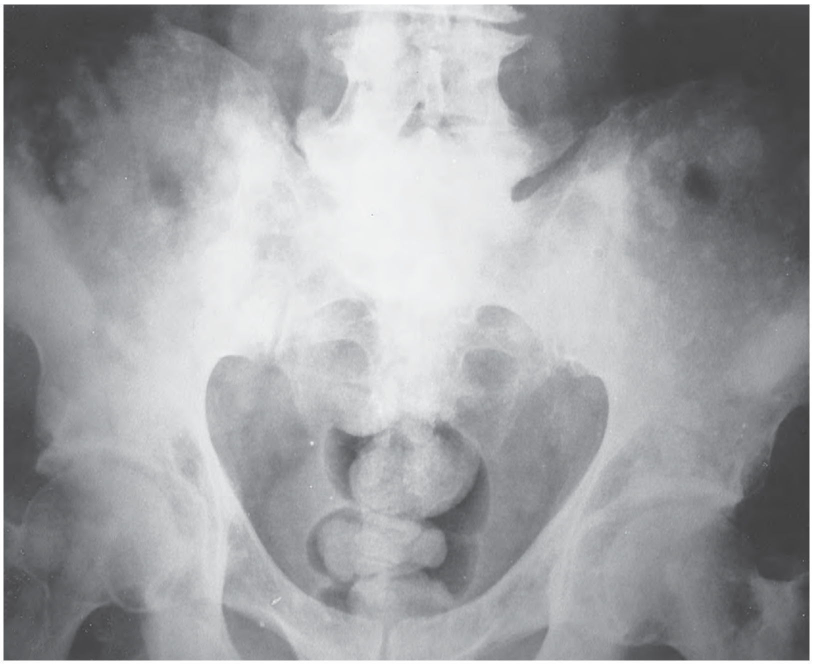

FIGURE 5–26 **Skeletal metastasis: osteosclerotic pattern.**[33,34] In this 82-year-old patient with advanced prostate carcinoma, diffuse osteoblastic skeletal metastasis is evident throughout the pelvis, sacrum, and lumbar spine. Prostate carcinoma is manifested as purely osteosclerotic metastases in approximately 80% of cases.

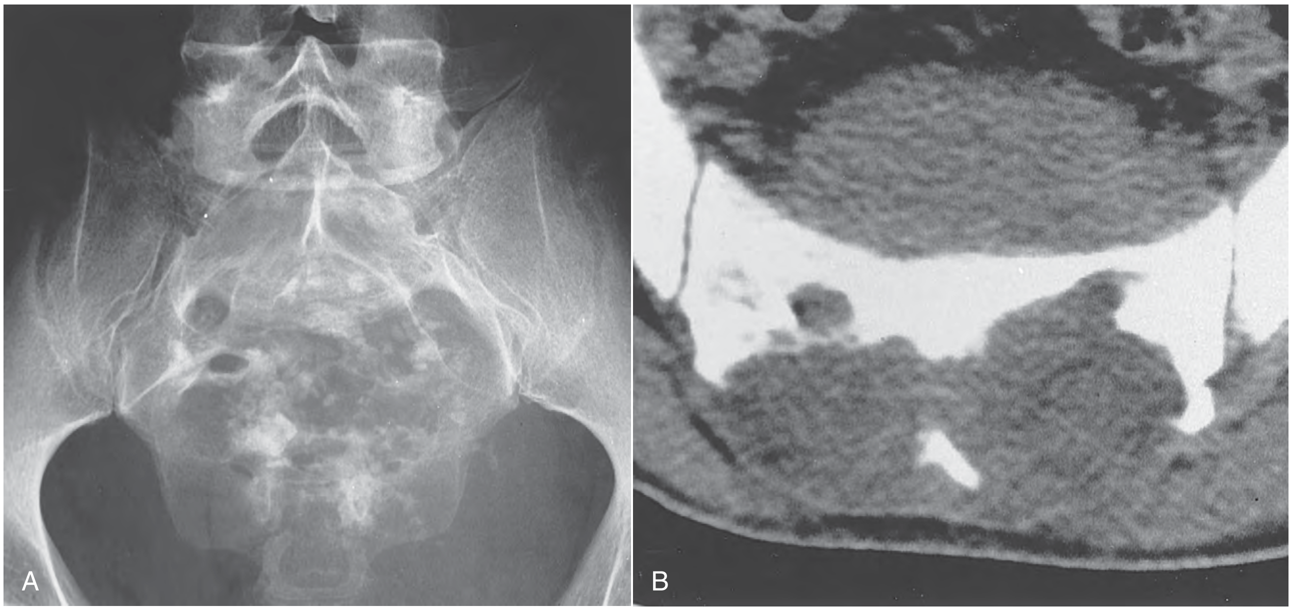

FIGURE 5–27 **Chordoma.**[35,51] **A,** This large sacral chordoma is predominantly osteolytic with prominent punctate calcification within its matrix, a feature seen in 50% to 70% of sacrococcygeal chordomas. **B,** In another patient, radiographs from this 29-year-old man (not shown) revealed osteolytic destruction of the sacrum. The transaxial CT image shows a large destructive lesion of the sacrum with soft tissue extension. Approximately 50% of all chordomas are sacrococcygeal in location. In addition to chordoma, the differential diagnosis of sacral tumors includes giant cell tumor, plasmacytoma, chondrosarcoma, neurogenic tumor, meningocele, and skeletal metastasis. *(**B,** Courtesy K. Kortman, MD, San Diego.)*

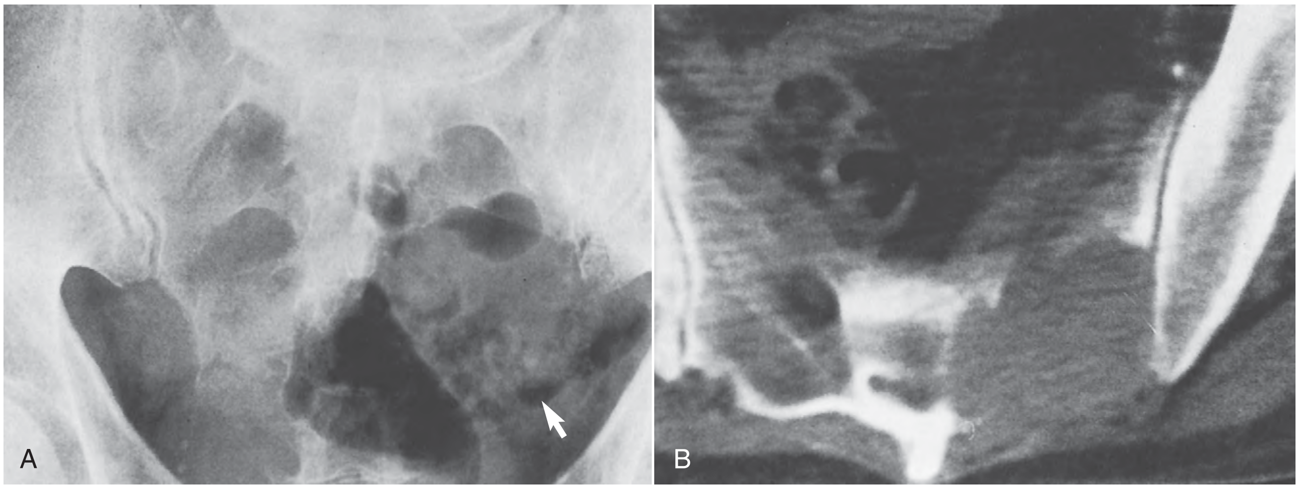

FIGURE 5–28 **Plasmacytoma.**[36,52] A 74-year-old man developed progressive pain in the lower back and left buttock over a 6-week period. The pain radiated to the left thigh and calf and was intensified when the leg was raised. The subtle osteolytic lesion in the sacrum *(arrow),* demonstrable on the plain radiograph **(A),** is readily evident on a transaxial CT image **(B).** A closed biopsy of the lesion confirmed the presence of a plasmacytoma. *(From Resnick D: Diagnosis of bone and joint disorders. 4th Ed. Philadelphia, Saunders, 2002, p. 2207.)*

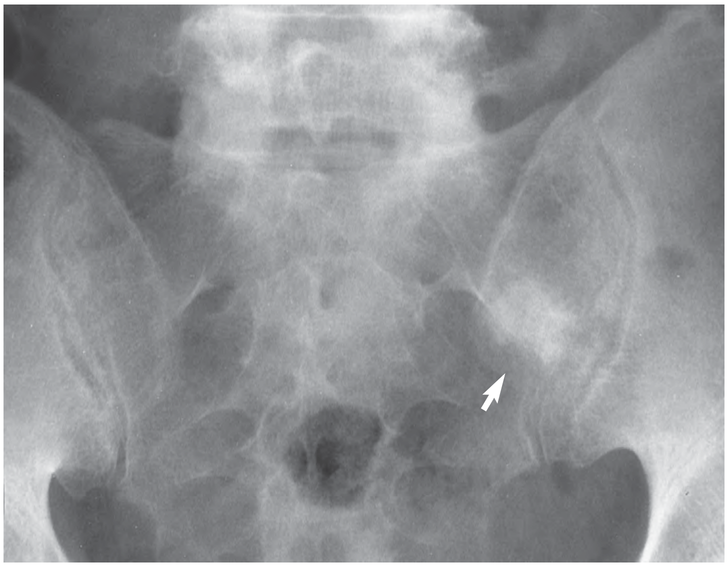

FIGURE 5–29 **Enostosis (bone island).**[37] Observe the solitary, circular, osteosclerotic lesion in the sacrum *(arrow)*. The sacrum is one of the most common sites for bone islands. It is usually a solitary, discrete focus of osteosclerosis within the spongiosa of bone. It may be round, ovoid, or oblong. It often has a brush border composed of radiating osseous spicules that intermingle with the surrounding trabeculae of the spongiosa. Additionally, enostoses may increase or decrease in size and may even be positive on bone scans, especially in large or growing lesions. Enostoses in the sacrum must be differentiated from other osteosclerotic processes, such as osteoblastic metastasis, osteoma, osteoid osteoma, enchondroma, bone infarct, fibrous dysplasia, and osteopoikilosis.

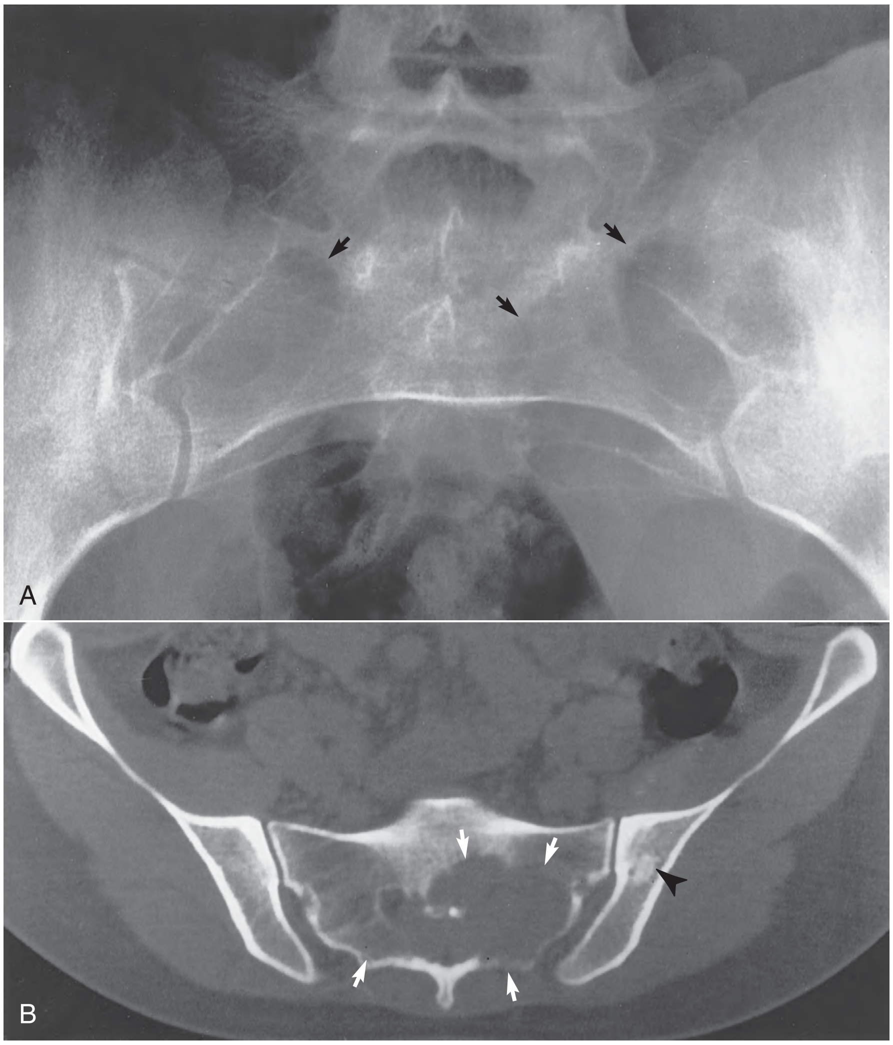

FIGURE 5–30 **Giant cell tumor.**[38] This 27-year-old woman had sacral pain. The anteroposterior radiograph **(A)** shows poorly defined radiolucency involving both sides of the sacrum *(arrows)*. A transaxial CT image **(B)** more clearly delineates the extent of involvement of the large, eccentric, purely radiolucent lesion *(white arrows)*. Fewer than 10% of all giant cell tumors affect the spine, but the sacrum is the most common spinal site of involvement. About 5% to 10% of giant cell tumors are malignant. Of incidental note is an enostosis (bone island) within the ilium *(arrowhead)*.

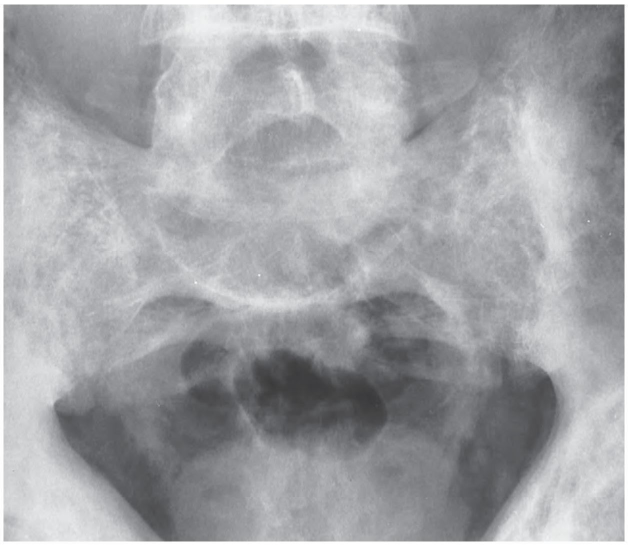

FIGURE 5–31 Paget disease.[39,40,43] Routine radiograph from this patient reveals diffuse sclerosis of the sacrum with accentuation of trabeculae and poorly defined bone expansion. The sacrum is a frequent site of involvement in Paget disease.

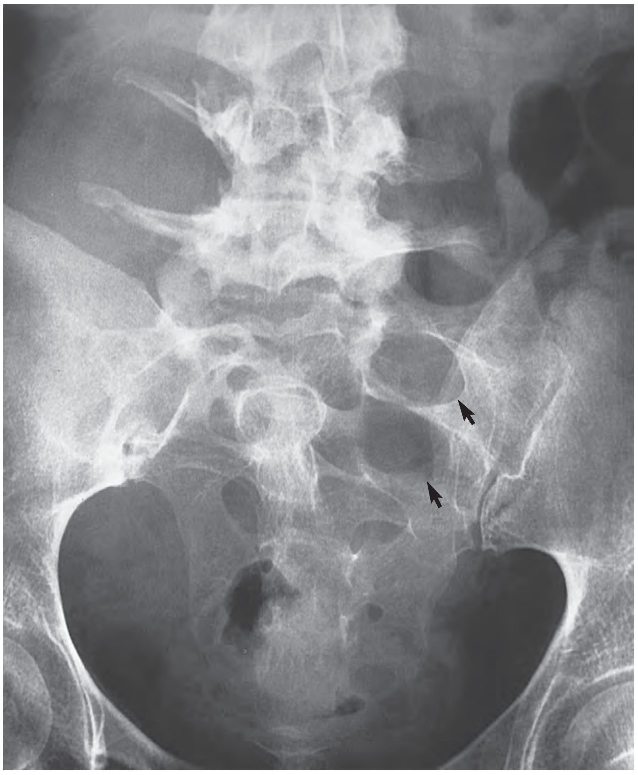

FIGURE 5–32 Neurofibromatosis type I (von Recklinghausen disease).[41] Observe the enlarged sacral foramina in this patient with neurofibromatosis *(arrows)*. The transverse processes of the lower lumbar vertebrae are dysplastic and attenuated. *(Courtesy G. Koors, DC, Eugene, Ore, and G. Smith, DC, Vancouver, Wash.)*

PART III

Pelvis and Lower Extremities

CHAPTER 6

Pelvis and Symphysis Pubis

NORMAL DEVELOPMENTAL ANATOMY

Accurate interpretation of pediatric pelvic radiographs requires a thorough understanding of normal developmental anatomy. Table 6-1 outlines the age of appearance and fusion of the primary and secondary ossification centers. Figures 6-1 through Figures 6-5 demonstrate the radiographic appearance of many important ossification centers and other developmental landmarks at selected ages from birth to skeletal maturity.

DEVELOPMENTAL ANOMALIES, ANATOMIC VARIANTS, AND SOURCES OF DIAGNOSTIC ERROR

The pelvis is an important site of anomalies, normal variants, and other sources of diagnostic error that may simulate disease and result in misdiagnosis. Table 6-2 and Figures 6-6 to 6-11 have been selected as examples of some of the more common of these processes.

SKELETAL DYSPLASIAS AND OTHER CONGENITAL DISEASES

Table 6-3 outlines a number of the skeletal dysplasias and congenital disorders that affect the pelvis and symphysis pubis. Figures 6-12 to 6-18 illustrate the radiographic manifestations of some of these disorders.

PHYSICAL INJURY

Fractures, dislocations, and soft tissue injuries involving the pelvis and symphysis pubis are often associated with serious clinical manifestations. Table 6-4 lists the more important injuries of the pelvis and their characteristics. Figures 6-19 to 6-27 represent examples of frequently encountered pelvic injuries. Tables 6-5 and 6-6 address traumatic abnormalities involving the pubic bones and symphysis pubis articulation.

ARTICULAR DISORDERS

The symphysis pubis, a fibrous joint, is a site of involvement for a variety of degenerative, inflammatory, crystal-induced, and infectious articular disorders. Table 6-7 outlines these diseases and their characteristics, and Figures 6-28 to 6-39 illustrate their typical radiographic manifestations.

NEOPLASMS

The bones of the pelvis are a frequent site of involvement for several malignant and benign tumors and tumorlike lesions. Table 6-8 lists and characterizes the neoplasms that typically involve the pelvis. Many of these disorders are illustrated in Figures 6-40 to 6-57.

METABOLIC, HEMATOLOGIC, AND INFECTIOUS DISORDERS

Many metabolic, hematologic, and infectious disorders exhibit radiographic changes in the bones of the pelvis. Table 6-9 outlines these disorders, and Figures 6-58 to 6-67 illustrate some of the more common examples.

TABLE 6-1 Pelvis: Approximate Age of Appearance and Fusion of Ossification Centers[1-5] (Figures 6–1 to 6–5)

Ossification Center	Primary or Secondary	No. of Centers	Age of Appearance* (Years)	Age of Fusion* (Years)	Comments
Ilium	P	2	Birth	14 14	Fuses with ischium Fuses with pubis
Ischium	P	2	Birth	4-8 14	Fuses with pubis Fuses with ilium
Pubis	P	2	Birth	4-8 14	Fuses with ischium Fuses with ilium
Iliac crest apophysis	S	2	14-16	18-25	
Iliac spine	S	2	16	18-25	
Pubic symphysis	S	2	16	18-25	
Ischial tuberosity apophysis	S	2	16	18-25	

P, Primary; *S,* secondary.

* Ages of appearance and fusion of ossification centers in girls typically precede those of boys. Ethnic differences also exist.

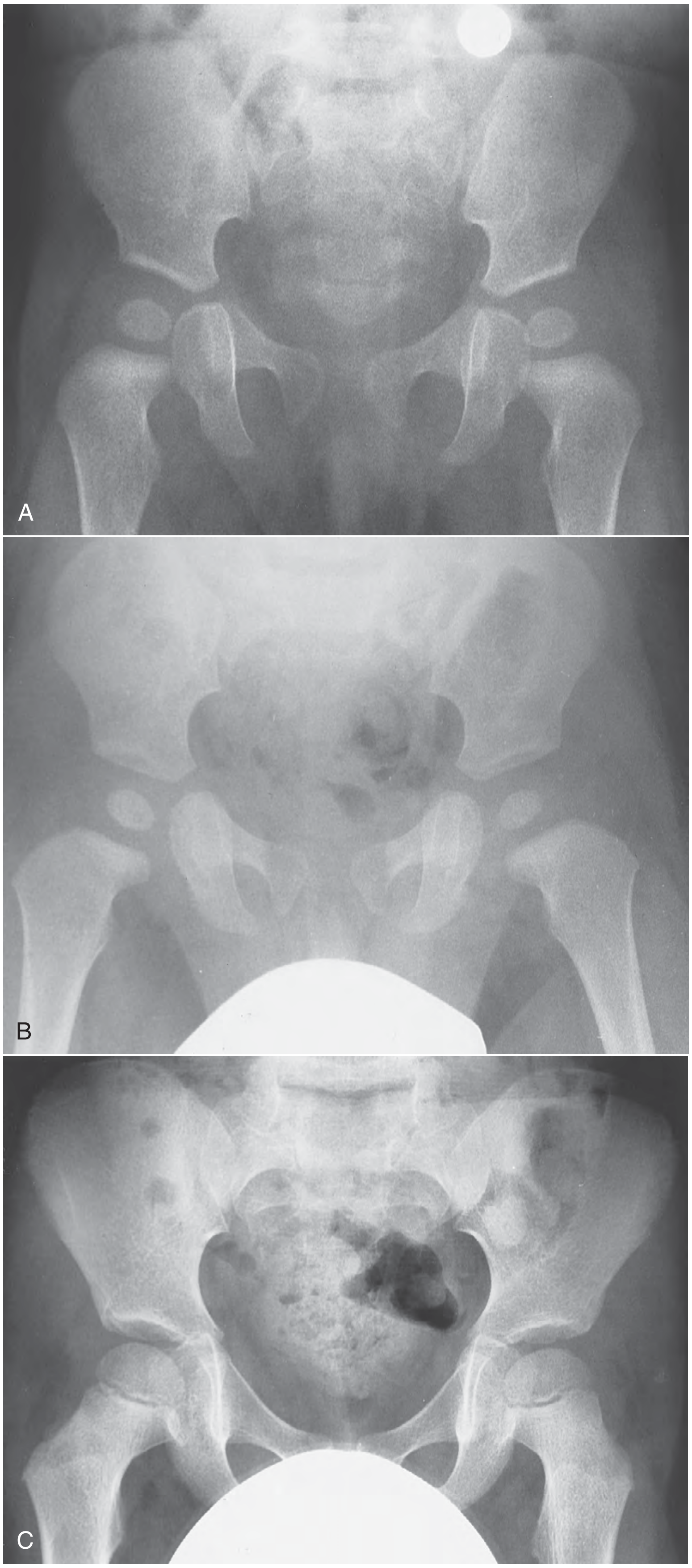

FIGURE 6–1 Skeletal maturation and normal development: frontal pelvic radiographs.[1-4] **A,** A 6-month-old girl. The triradiate cartilages and ischiopubic synchondroses are not fused. The capital femoral epiphyses, which usually begin to ossify between the ages of 1 and 8 months, are present. At this stage, the capital femoral epiphyses are circular and small, and the iliac bones are proportionately small. **B,** An 8-month-old boy. Skeletal development approximates that of the 6-month-old girl **(A). C,** A 4-year-old boy. The iliac bones are proportionately larger, and the triradiate cartilages are diminishing in size before fusion. The femoral capital epiphyses are larger, and the physeal growth center is thinner, more linear, and conforms to the shape of the femoral necks.

Continued

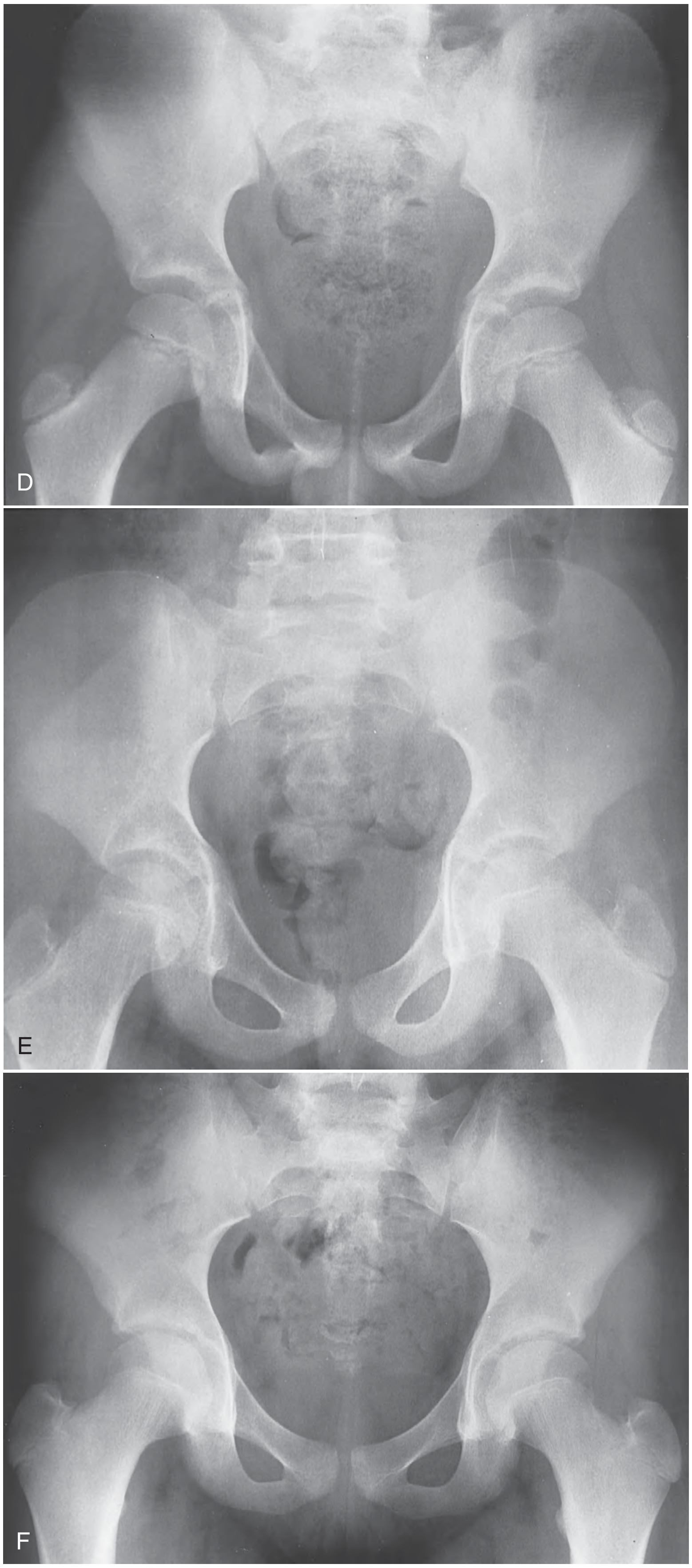

FIGURE 6–1, cont'd **D,** A 7-year-old boy. The triradiate cartilages remain unfused, but the ischiopubic synchondroses are fusing in an asymmetric pattern. The ossified apophyses of the greater trochanters are developing. Observe the presence of normal physiologic acetabular protrusion. This phenomenon persists until about 13 years of age in girls and 16 years of age in boys, when the pelvis adopts the adult configuration. **E,** A 9-year-old girl. The apophyses of the lesser trochanters are beginning to ossify. The femoral capital epiphyses and greater trochanter apophyses are taking on adult proportions but remain unfused. Physiologic protrusio acetabuli persists. **F,** A 13-year-old girl. The pelvis is adopting adult proportions. The greater and lesser trochanters and the femoral capital epiphyses are fusing to the femur. The triradiate cartilages and ischiopubic synchondroses are fused. The apophyses of the ischium and iliac crests have not yet appeared.

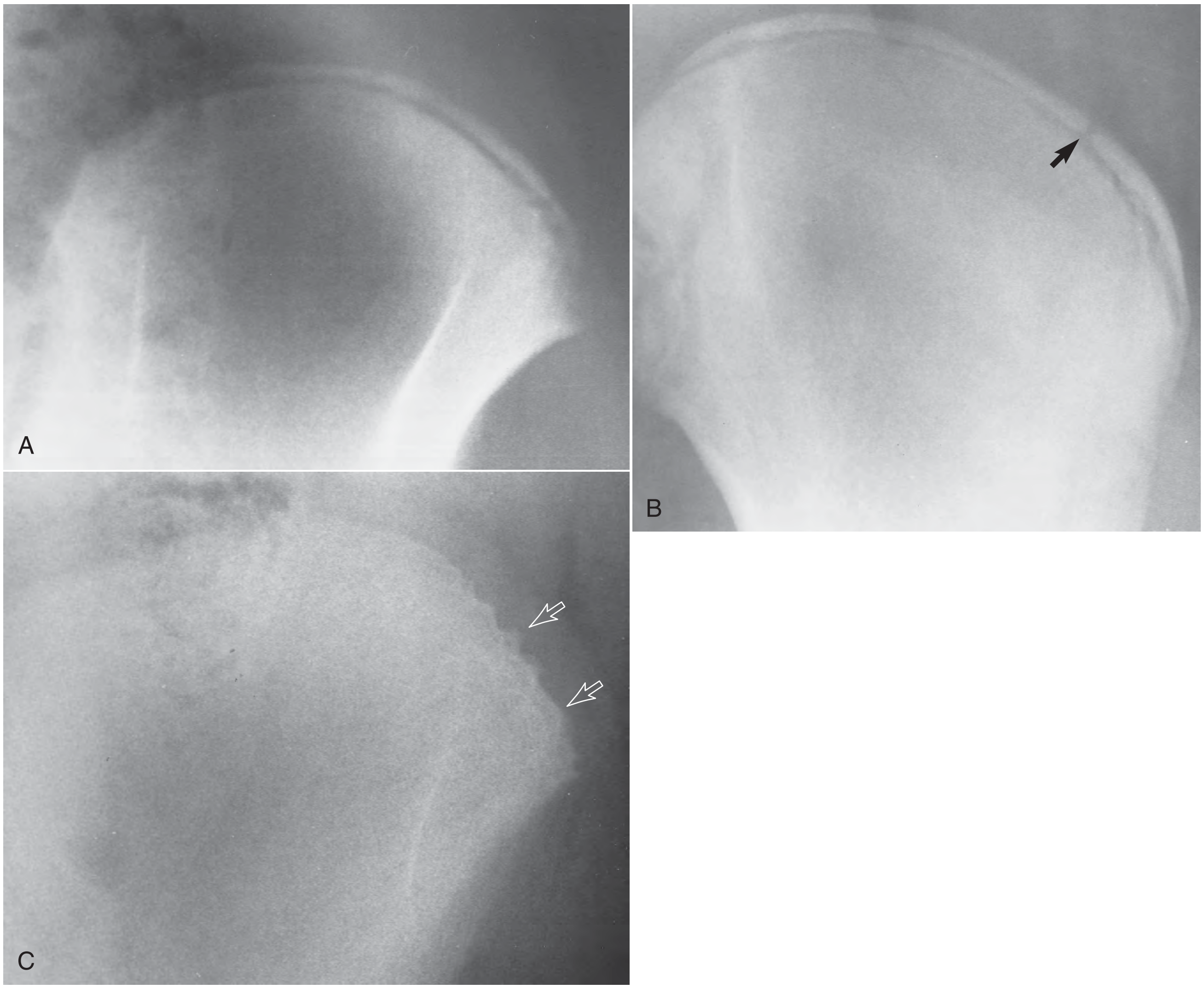

FIGURE 6–2 **Skeletal maturation and normal development of the iliac crest apophysis.**[1-5] **A,** A 13-year-old girl. Approximately 60% of the iliac apophysis is ossified. **B,** A 14-year-old girl. The apophysis is almost completely ossified, but it has not yet fused to the ilium. Note the superolateral radiolucent disruption of the apophysis *(arrow)*. This fragmentation is a variation of normal and is of no clinical significance. **C,** A 15-year-old boy. The superolateral margin of the iliac crest appears serrated *(open arrows),* a finding that is typical just before and during ossification of the iliac apophysis. The iliac crest apophysis has not begun to ossify in this 15-year-old boy, illustrating that between boys and girls there is variability in the onset of puberty and skeletal maturity, with boys typically showing a lag.

Continued

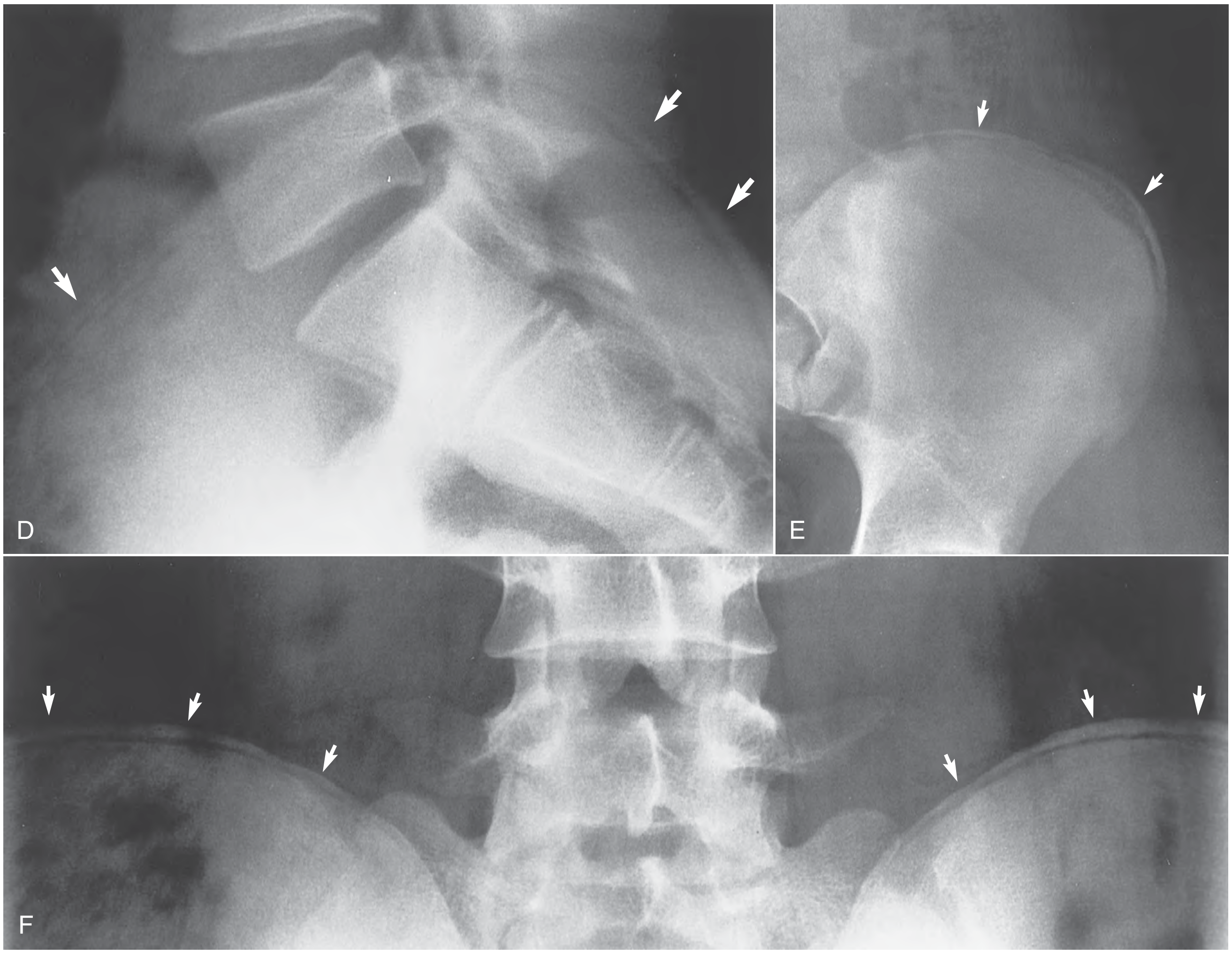

FIGURE 6–2, cont'd **D,** A 13-year-old boy. A lateral radiograph reveals advanced ossification of the iliac crest apophysis *(arrows)*. **E,** In another 14-year-old girl, observe the thin curvilinear ossifying growth center *(arrows)* adjacent to the iliac crest. Although the growth center is almost completely ossified, it has not fused with the ilium, indicating incomplete skeletal maturation. **F,** Normal iliac apophysis just before fusion in a 19-year-old man. Note the curvilinear ossified rim along the iliac crest *(arrows)*. The iliac crest apophysis begins to ossify at or about the onset of puberty, beginning laterally at the anterosuperior iliac spine and progressing medially toward the posterosuperior iliac spine. When the apophysis is fully ossified and fused to the ilium—usually between the ages of 20 and 25 years—it indicates that the patient is skeletally mature. This indicator, sometimes referred to as the *Risser sign*, is useful in the management of scoliosis.

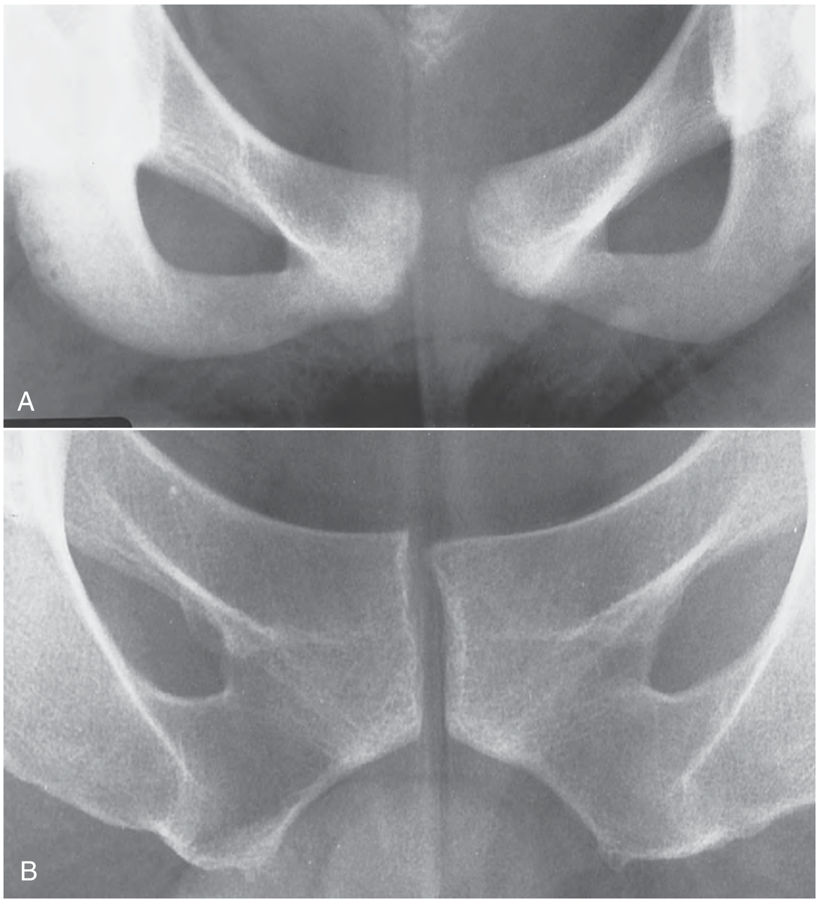

FIGURE 6–3 Skeletal maturation and normal development: symphysis pubis.[1-4] **A,** A 13-year-old girl. Observe the rounded appearance of the articular surfaces of the symphysis pubis. Paired secondary ossification centers typically appear about the age of 16 years and fuse to the pubic bones by the age of 20 to 25 years. **B,** A 35-year-old man. In the adult, a flat, parallel configuration of the apposing joint surfaces is evident. Slight offset of the superior aspect is common and is usually of no clinical significance.

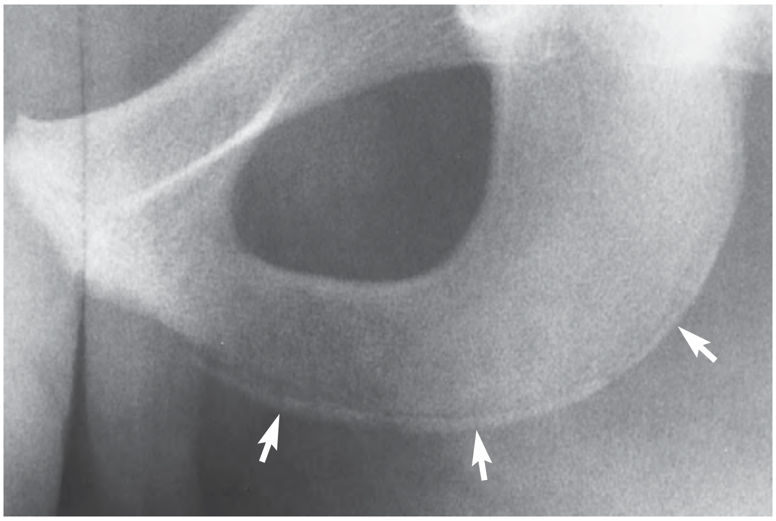

FIGURE 6–4 Skeletal maturation and normal development: ischial apophysis.[1-4] In this 15-year-old boy, observe the linear zone of ossification adjacent to the inferior aspect of the ischium *(arrows)*. This secondary ossification center first appears in adolescence about the age of 15 years and fuses to the ischial bone between the ages of 20 and 25 years.

TABLE 6-2 **Developmental Anomalies, Anatomic Variants, and Sources of Diagnostic Error Affecting the Pelvis***

Entity	Figure(s)	Characteristics
Unfused ischiopubic synchondroses[6]	6-5, *B*	Failure of fusion of the synchondrosis joining the ischium and pubis No clinical significance Frequently confused with fracture These synchondroses normally fuse between the ages of 4 and 8 years and may appear bulbous and expansile, simulating callus surrounding a healing fracture May not close synchronously and may even reappear after initial closure
Pelvic digit[7]	6-6	Anomalous, elongated, riblike or digitlike structure within the pelvis Also called *pelvic rib* or *ectopic lumbar rib* May have one or more articulations and a pseudarthrotic attachment to the ilium No clinical significance
Os acetabuli marginalis superior[4]	6-7	Large or small triangular ossicle with well-corticated margins adjacent to the superior acetabular rim Present in about 5% of normal persons No clinical significance but may simulate acetabular rim fracture
Grooves in ilium for nutrient artery[4,6]	6-8	V-shaped or Y-shaped groove in iliac wing for nutrient artery Normal anatomy of no clinical significance
Pelvic phleboliths[8]	6-9	Pelvic vein calcification appears as multiple circular radiodense areas overlying the lower pelvic basin and the pubic rami No clinical significance
Calcification of the pectineal ligament[4]	6-10	Characteristic curvilinear rim of calcification parallels the superior margins of the pubic bones Normally, an aponeurotic extension of the lacunar ligament extends laterally to the iliopectineal line Calcification of this ligament is a normal variant frequently found in elderly patients *Differential diagnosis:* periosteal proliferation, Paget disease Cephalad angulation of the x-ray beam also may produce a double contour of the upper margin of the pubic bone simulating this appearance
Penile implant[8]	6-11	Penile implants used for impotency overlie the lower pubic region within the penis

* See also Table 1-1.

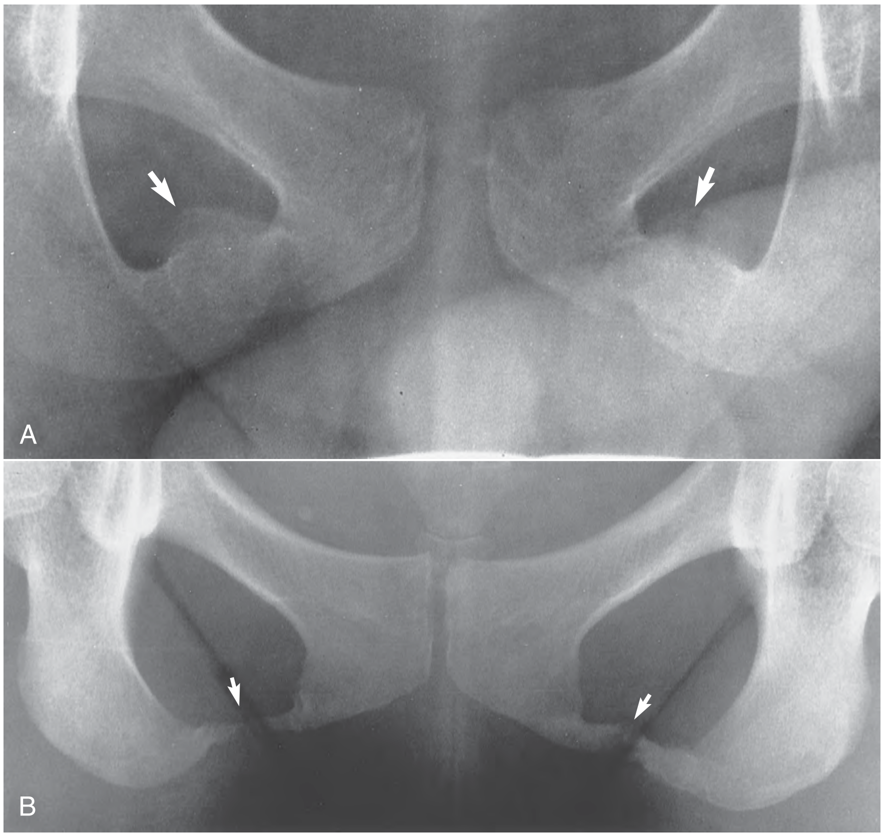

FIGURE 6–5 Ischiopubic synchondroses.[6] **A,** Observe the bulbous osseous expansion at the site of the ischiopubic synchondroses *(arrows)*. This finding is a variation of normal, is present in adolescence, may be asymmetric, and represents normal hyperostosis at the site of fusion of the ischiopubic synchondrosis. These expansile areas should not be confused with healing fractures or osteochondroses. **B,** Unfused ischiopubic synchondrosis. This 38-year-old woman with low back pain had radiographs taken of her lumbosacral spine and pelvis. The frontal radiograph incidentally reveals radiolucent defects in the region of the ischiopubic junctions, with a tapered appearance of the adjacent pubis and ischium. This anatomic variation is of no clinical significance.

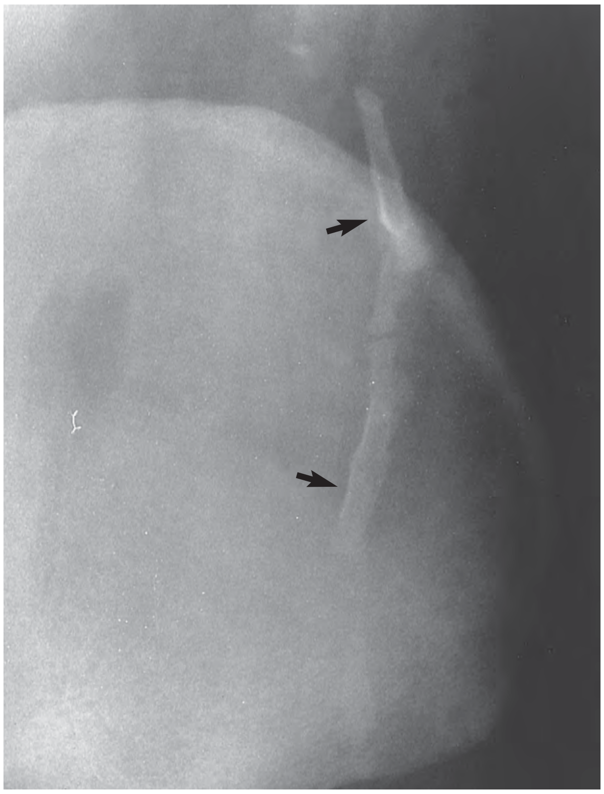

FIGURE 6–6 **Pelvic digit.**[7] This anomaly, also called a *pelvic rib* or *ectopic lumbar rib*, is seen as an elongated, two-part, riblike, or digitlike, structure with a pseudarthrotic attachment overlying the ilium *(arrows)*.

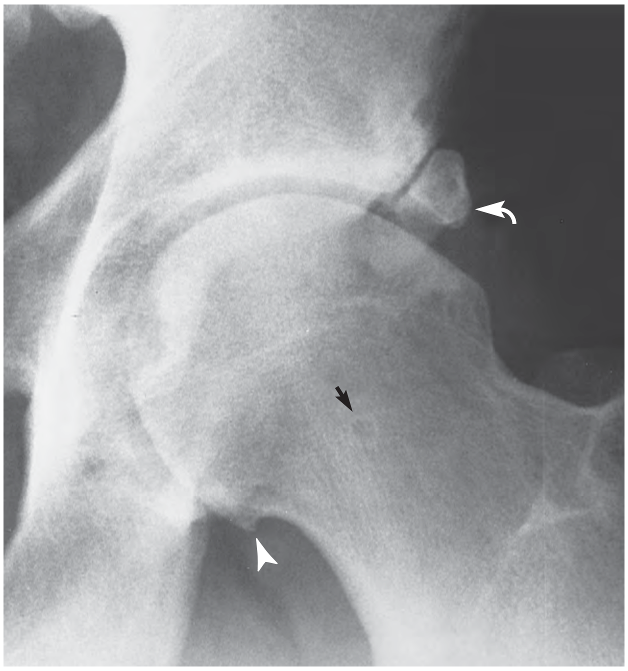

FIGURE 6–7 **Os acetabuli.**[4] A 27-year-old man had bilateral prominent os acetabuli. These triangular ossicles with well-corticated margins adjacent to the superior acetabular rim *(curved arrow)* are present in about 5% of the population. Note also the presence of a small herniation pit *(arrow)* and an osteophyte surrounding the femoral head-neck junction *(arrowhead)*. *(From Taylor JAM, Harger BL, Resnick D: Diagnostic imaging of common hip disorders: A pictorial review. Top Clin Chiropr 1:8, 1994.)*

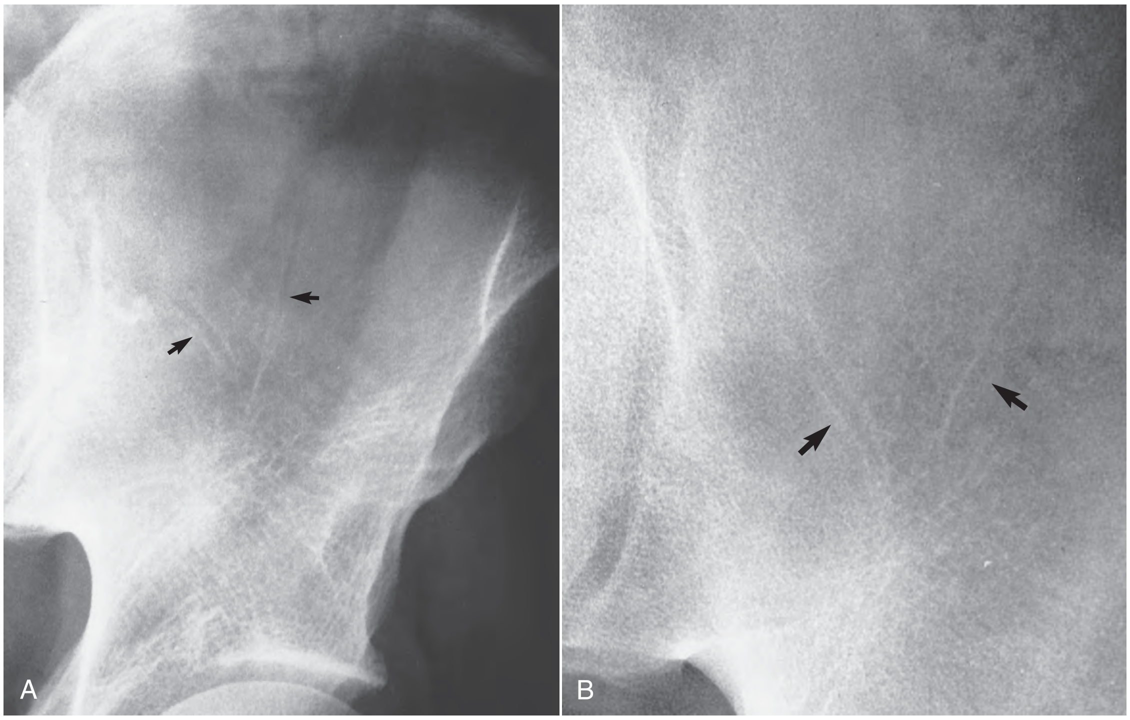

FIGURE 6–8 **Grooves for the nutrient arteries of the ilium.**[4,6] **A,** The typical Y- or V-shaped groove for the nutrient arteries in the iliac wing *(arrows)* is evident. **B,** A similar groove *(arrows)* is seen in the ilium of another patient. This commonly encountered normal vascular channel may be prominent and should not be mistaken for a stellate fracture.

FIGURE 6–9 Pelvic phleboliths.[8] Observe the circular radiodense shadows overlying the lower pelvic basin and pubic ramus in three separate patients. These opacities, which represent calcification in pelvic veins, may contain a central radiolucent region. They are of no clinical significance.

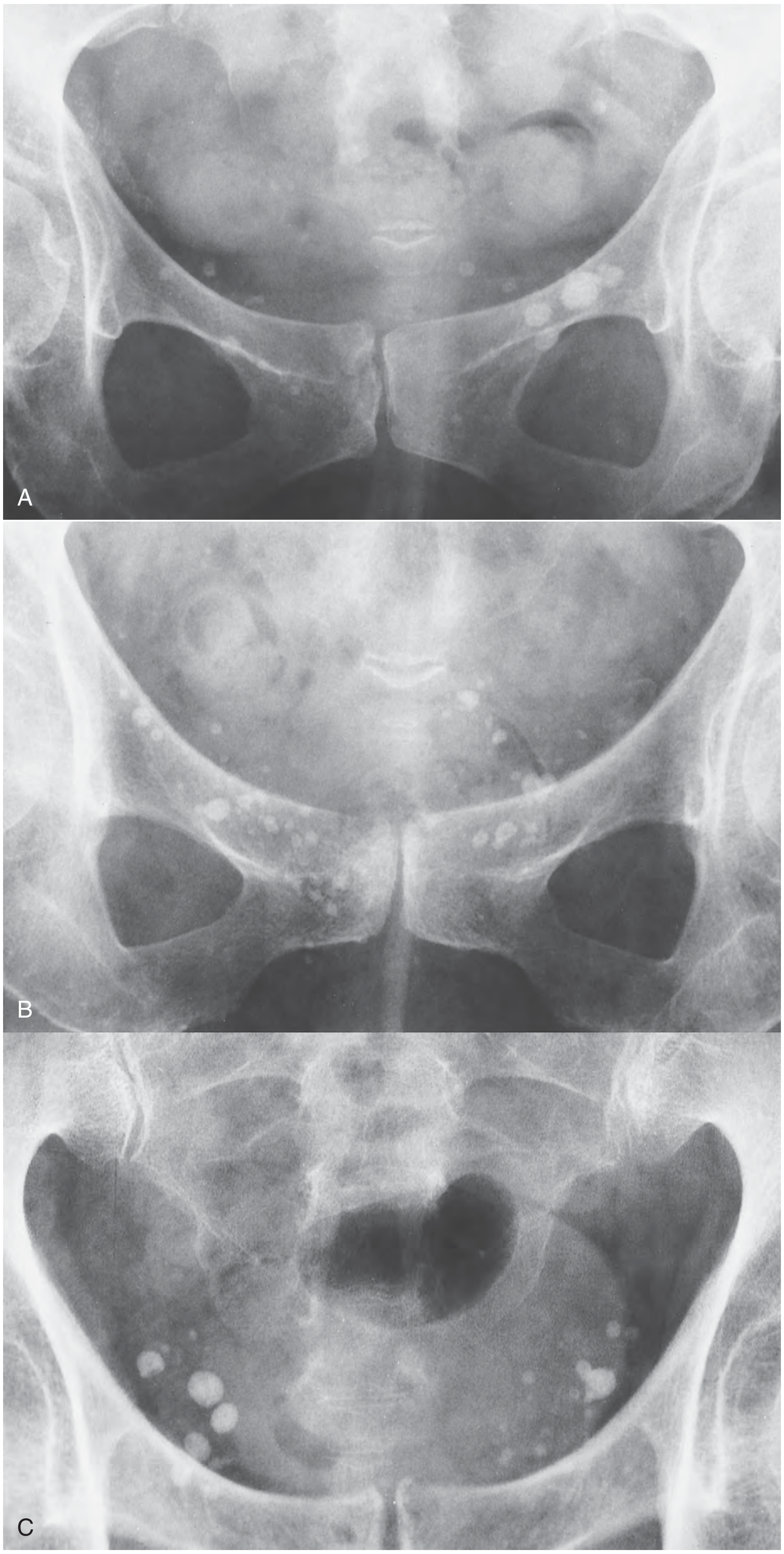

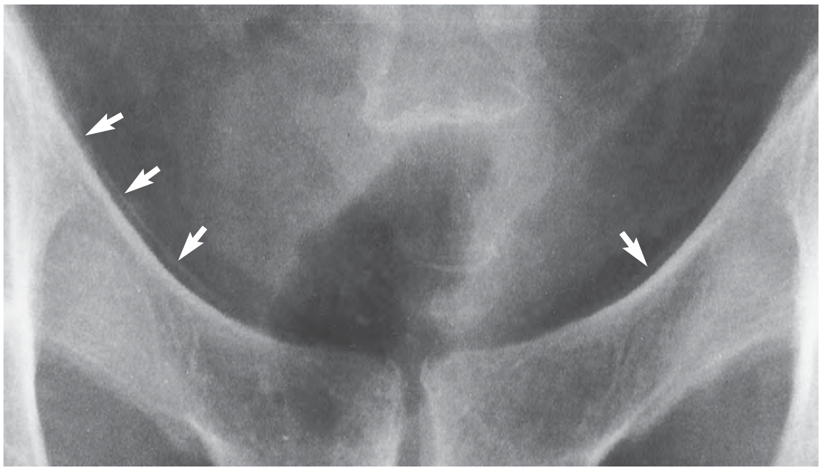

FIGURE 6–10 **Calcification of the pectineal ligament.**[4] In this 75-year-old man, characteristic bilateral curvilinear rims of calcification *(arrows)* parallel the superior margins of the pubic bones and extend laterally to the iliopectineal lines.

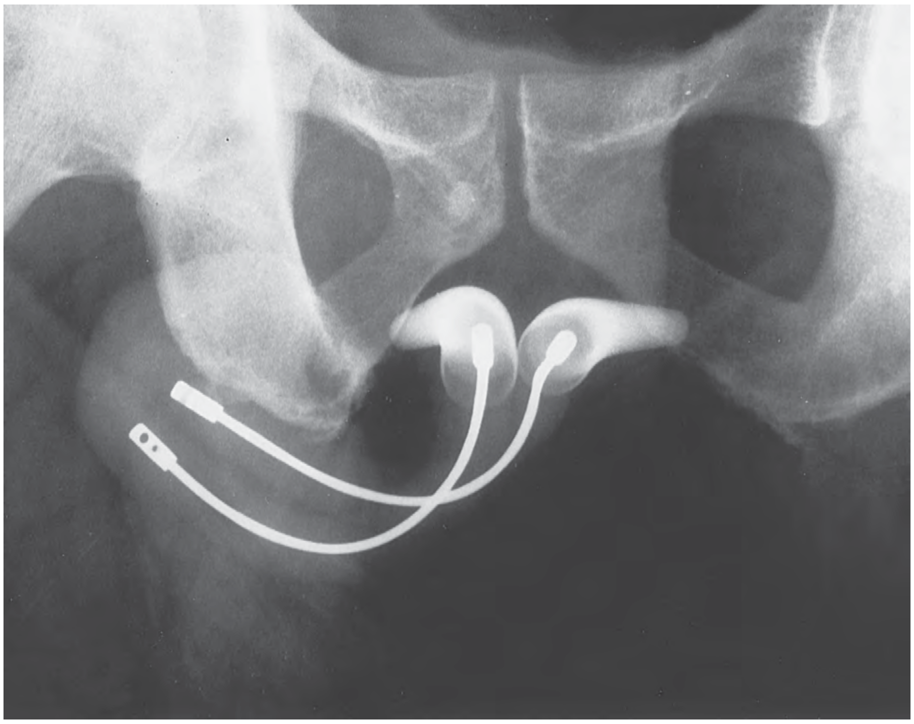

FIGURE 6–11 **Penile implant[8] (metallic) in a patient being treated for impotence.**

TABLE 6-3 Skeletal Dysplasias and Other Congenital Diseases Affecting the Pelvis*

Entity	Figure(s)	Characteristics
Achondroplasia[9,115]	6-12	*"Champagne glass" pelvis:* flattened pelvic opening Square appearance of iliac bones Small sacrosciatic notches Flattened acetabular angles Short femoral necks and coxa vara deformities Bilateral "sagging rope" sign representing a circumferential overhang of the femoral heads over the femoral necks
Down syndrome (trisomy 21)[10]	6-13	Flaring of iliac wings Flattening of acetabular roofs Decreased iliac angle Developmental hip dysplasia (40% of affected persons)
Osteopetrosis[11,92]	6-14, *A*	May appear as diffuse osteosclerosis or bone-within-bone appearance of ilium Bones are brittle and fracture easily
Osteopoikilosis[12]	6-14, *B*	Multiple 2- to 3-mm circular foci of osteosclerosis Symmetric periarticular lesions predominate about the hip joints and at the periphery of the pelvic bones
Mucopolysaccharidoses (MPS)[13]	6-15	**MPS I-H (Hurler syndrome)** Pseudoenlargement of acetabular region Wide femoral necks Coxa valga **MPS IV (Morquio syndrome)** Flaring of the iliac wings Underdevelopment of acetabular roofs Coxa valga Dysplasia of femoral capital epiphyses
Osteogenesis imperfecta[14]	6-16	Severe osteopenia Thin cortices Multiple fractures Narrow pelvis with protrusio acetabuli Bone remodeling Altered trabecular architecture
Cleidocranial dysplasia[15]	6-17	Incomplete ossification of the pubic bones May simulate pubic diastasis or destructive osseous lesions
Hereditary osteo-onychodysostosis (HOOD syndrome)[16]	6-18	Bilateral iliac horns that arise from the posterior surface of the iliac wing and project into the buttocks Unilateral iliac horns can also be an isolated finding unassociated with other skeletal abnormalities

* See also Table 1-2.

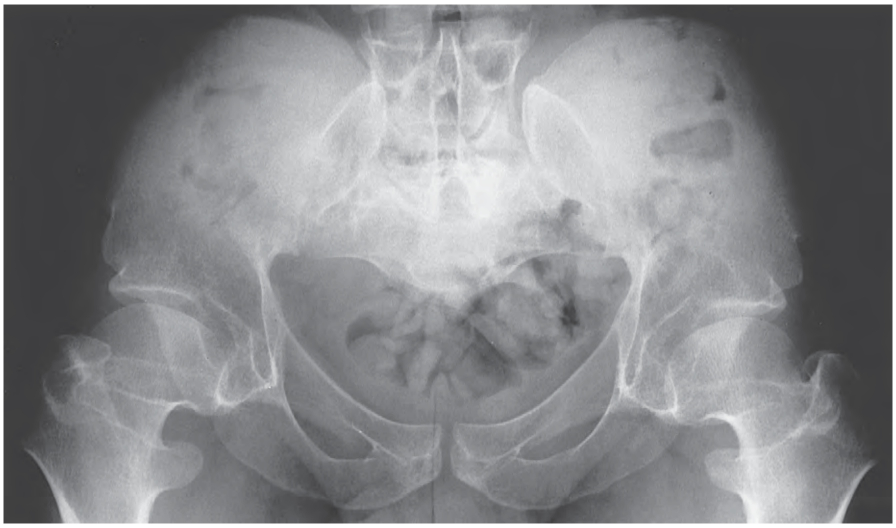

FIGURE 6–12 **Achondroplasia.**[9,115] In this adult patient, the pelvic opening is flattened, creating the "champagne glass" appearance. The iliac bones are squared and have small sacrosciatic notches and flat acetabular angles. The femoral necks are short, and coxa varus deformities are present bilaterally. Note also the bilateral "sagging rope" sign representing a circumferential overhang of the femoral heads over the femoral necks.

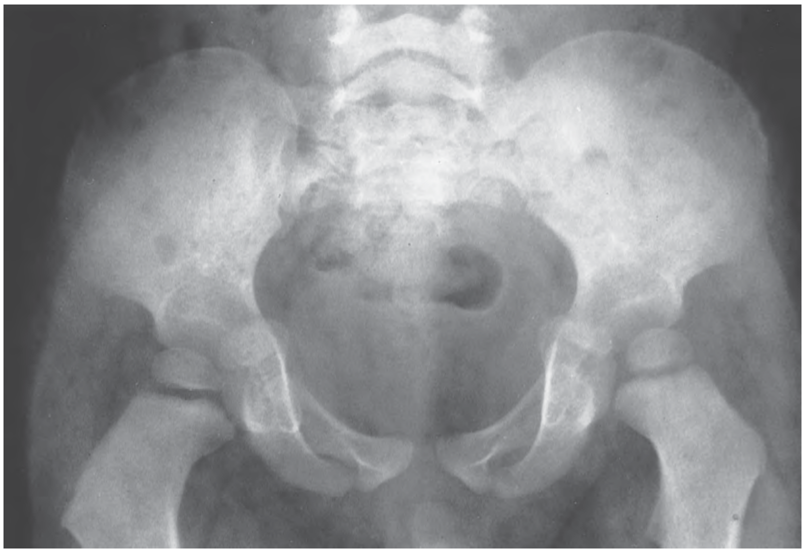

FIGURE 6–13 **Down syndrome (trisomy 21).**[10] Observe flaring of the iliac wings, flattening of the acetabular roofs, and decreased iliac angles in this child with Down syndrome. Developmental hip dysplasia, although absent in this patient, is present in about 40% of affected persons with Down syndrome. The iliac flaring may persist into adulthood.

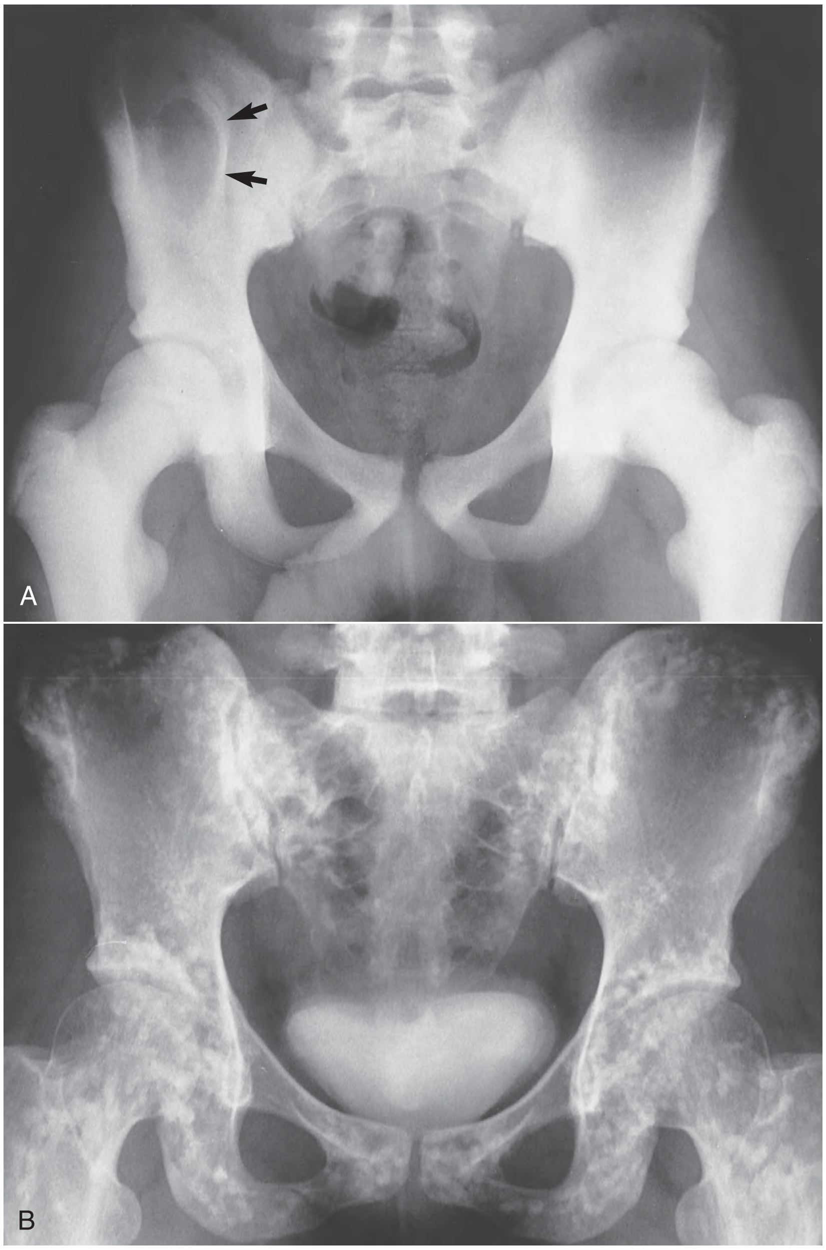

FIGURE 6–14 **Sclerosing dysplasias.**[11,12,92] **A,** Osteopetrosis. A routine radiograph of the pelvis in this 15-year-old boy exhibits diffuse osteosclerosis of the pelvic bones. The curvilinear opacity within the right ilium *(arrows)* is referred to as the "*bone-within-bone*" appearance. **B,** Osteopoikilosis. Circular and ovoid osteosclerotic foci are localized in a periarticular pattern about the hip joints and at the periphery of the pelvic bones. The symmetric, periarticular distribution is characteristic of this fairly common sclerosing dysplasia. Although the epiphysis may be affected, most lesions predominate in the metaphysis. Osteopoikilosis was an incidental, asymptomatic finding in this patient who was undergoing a cystogram (note contrast in the bladder).

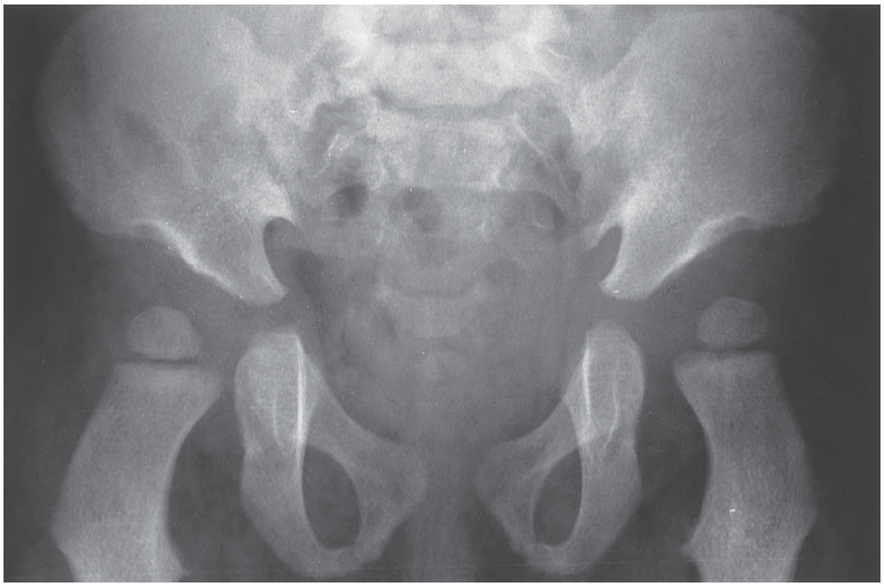

FIGURE 6–15 **Hurler syndrome (MPS 1-H).**[13] Characteristic hypoplasia of the superior acetabular region, wide femoral necks, and coxa valga deformities are seen in the pelvis of this 3-year-old girl with Hurler syndrome.

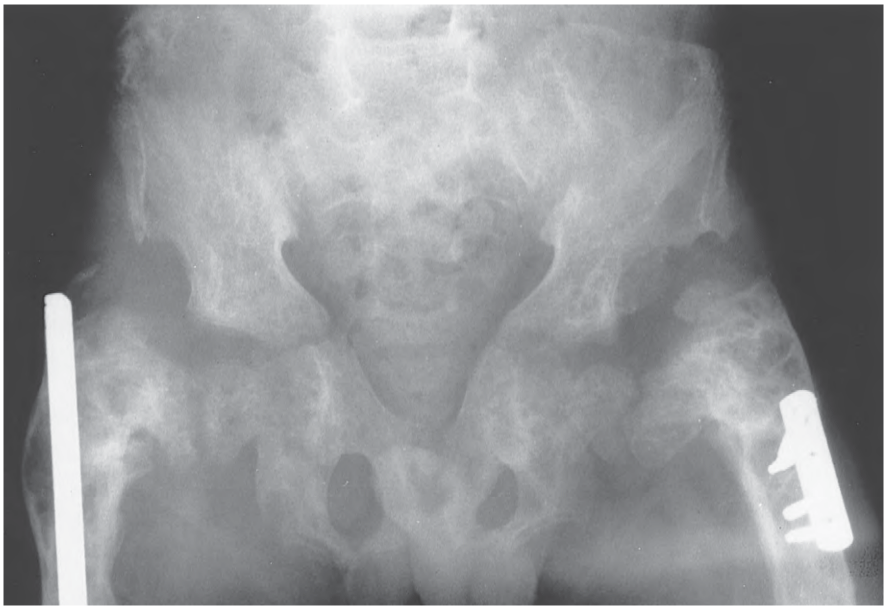

FIGURE 6–16 Osteogenesis imperfecta.[14] Routine radiograph from this 7-year-old patient reveals remodeling of bone, altered trabecular architecture, bilateral protrusio acetabuli, and coxa vara deformities. The pelvis demonstrates a triradiate shape. Femoral fixation devices are also seen.

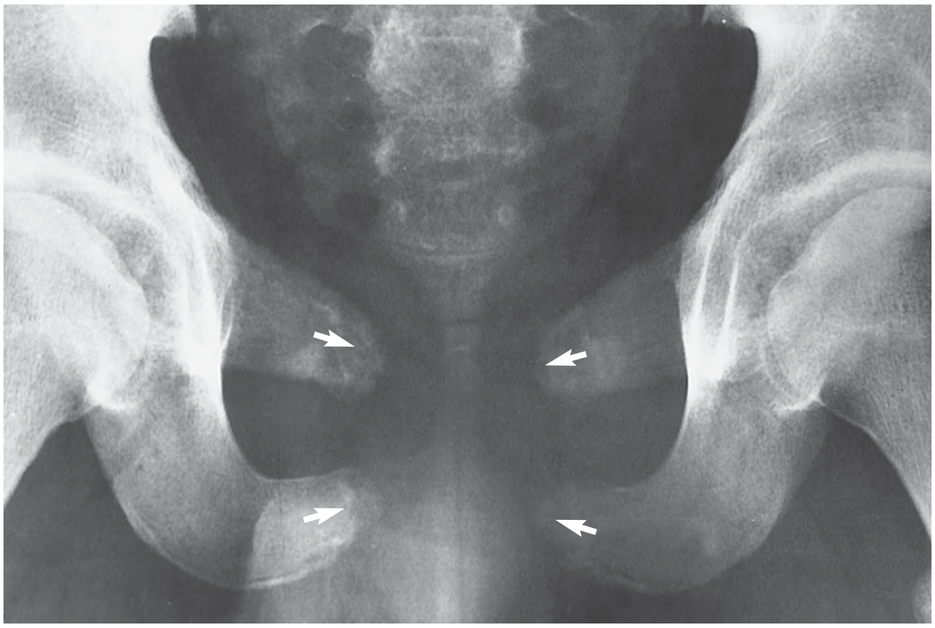

FIGURE 6–17 Cleidocranial dysplasia.[15] Incomplete ossification of the pubic bones *(arrows)* in this disorder may simulate destructive lesions. *(Courtesy A.G. Bergman, MD, Stanford, Calif.)*

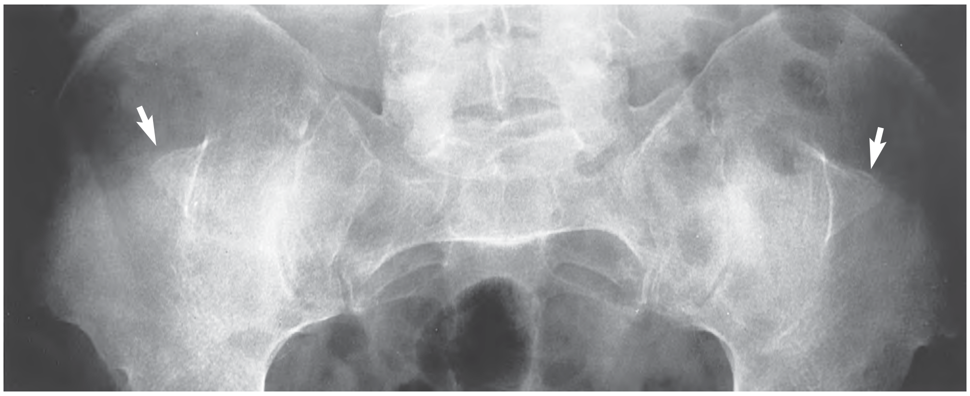

FIGURE 6–18 Hereditary osteo–onychodysostosis (HOOD) syndrome.[16] Observe the characteristic bilateral outgrowths arising from the posterior iliac wings *(arrows)*. The presence of these iliac horns, which occasionally are capped by an epiphysis, is virtually pathognomonic of the HOOD syndrome. This patient also had associated hypoplasia and splitting of the nails of the fingers and toes, absence of the patellae, and dislocation of the radial heads.

TABLE 6-4 Injuries of the Bony Pelvis*

Entity	Figure(s)	Characteristics
Type I: Injuries Without Disruption of the Pelvic Ring		30% of all pelvic fractures
Acute pelvic avulsion fracture[17,97,107]	6-19	Prevalent in adolescent athletes involved in high level sporting activities Stable avulsion fracture of bone at muscular and tendinous insertion The most common sites, the most likely involved muscle or tendon, and two or three most common related activities: 1. *Ischial tuberosity:* hamstring muscles; gymnastics, soccer, fencing 2. *Anterior inferior iliac spine:* rectus femoris muscle; soccer, athletics, tennis 3. *Anterior superior iliac spine:* sartorius or tensor fasciae femoris muscle; soccer, athletics, gymnastics 4. *Superior corner of symphysis pubis:* adductor muscles; soccer, fencing 5. *Iliac crest:* abdominal muscles; soccer, gymnastics, tennis *Complication:* bizarre skeletal overgrowth or deformity simulating neoplasm (rider's bone)
Fracture of the pubis or ischium[18,106]		Unilateral stable fractures of a single ramus are common in the following situations: 1. *Elderly patients:* after a fall or hip surgery 2. *Young athletes:* as a stress fracture Subsequent osteolysis may simulate a neoplasm
Fracture of the iliac wing[18,106]	6-20	Duverney fracture is a fracture of the iliac wing that occurs as a result of direct injury Stable and infrequently displaced
Fracture of the sacrum[19-22,106]	See Figures 5-8, 5-9	See Chapter 5 for discussion and illustrations Isolated transverse fracture of the sacrum is stable and occurs only infrequently
Fracture or dislocation of the coccyx[18]		See Chapter 5 for discussion
Type II: Injuries with Single Break in the Pelvic Ring		25% of all pelvic fractures
Fractures of two ipsilateral rami[18,106]		Unilateral straddle fracture Unilateral stable fractures of superior and inferior ischiopubic rami Associated fractures or ligamentous disruptions common
Single fracture near, or diastasis of, the symphysis pubis[18,23,106,113]	6-21, *A, B*	Isolated stable fractures of the pubic ramus or pubic diastasis are rare occurrences The greater the degree of diastasis, the more likely is the occurrence of a second break in the pelvic ring and visceral injury Pubic diastasis exceeding 25 mm suggests a high likelihood of sacrospinous and anterior sacroiliac ligament disruption Intrapartum and postpartum diastasis Known rare complication of pregnancy related to increased elasticity of the pubic ligaments Reported incidence varies between 1 in 300 to 1 in 5000 deliveries Usually limited to 7 mm or less In most cases it is self-limited, gradually reducing over a period of months
Single fracture near, or diastasis of, the sacroiliac joint[24]		Rare occurrence that usually results from direct trauma Stable injury
Type III: Injuries with Double Breaks in the Pelvic Ring		
Double vertical fractures of the ischiopubic ring or dislocations of the pubis[18,25]	6-22	Straddle fracture: 20% of all pelvic fractures Bilateral vertical fractures of both pubic rami or unilateral fractures of the superior and inferior pubic rami combined with symphyseal diastasis Unstable ***Complications*** Urethral or visceral damage in 30% to 40% of cases Hemorrhage and peripheral nerve injury common Associated spine and other remote fractures 10% mortality rate with all pelvic fractures

---

* See also Tables 1-4 to 1-6.

TABLE 6-4 Injuries of the Bony Pelvis—cont'd

Entity	Figure(s)	Characteristics
Double vertical fractures or dislocations of the pelvis[25]	6-23, 6-24	Malgaigne fracture: 15% of all pelvic fractures ***Types*** 1. Vertical fracture of both pubic rami combined with either a sacroiliac joint dislocation or a fracture of the ilium or sacrum 2. Symphyseal dislocation combined with either a sacroiliac joint dislocation or a fracture of the ilium or sacrum Sacroiliac joint dislocation is twice as common as paraarticular fracture Unstable fractures Hemorrhage, urinary tract injury, peripheral nerve injury common Associated spine and other remote fractures
Type IV: Injuries of the Acetabulum[26-28,111]	6-25	Four important bony landmarks 1. Anterior acetabular rim 2. Posterior acetabular rim 3. Iliopubic (anterior) column 4. Ilioischial (posterior) column Fractures result from impact of the femoral head against the acetabulum May involve one or two columns Classified as wall fractures, column fractures, and transverse fractures Fracture types may overlap, fitting into more than one classification ***Complications*** Intraarticular osseous fragments Associated fractures of the bony pelvis Triradiate cartilage damage in children Degenerative joint disease Protrusio acetabuli Ischemic necrosis (usually associated with posterior hip dislocation) Heterotopic ossification Pelvic visceral, nerve, and vascular injury common
Stress Injuries of the Pelvis		
Stress (fatigue) fractures[29,96,110]	6-26	Pregnant women, joggers, long-distance runners, and patients with hip osteoarthrosis or hip arthroplasty are predisposed to parasymphyseal and pelvic ring fatigue fractures Acetabular fatigue fractures are rare, but occur in endurance athletes and military recruits; two types identified: a. Acetabular roof stress fractures b. Anterior column, often occurring simultaneously with inferior pubic ramus fracture ***Complications*** Osteolysis simulating malignancy Delayed union Refracture ***Imaging*** CT, MR imaging and scintigraphy reveal these fractures
Insufficiency fractures[20-22,30,109]	6-27	Sites include parasymphyseal, sacral, and paraacetabular regions Predisposing factors include osteoporosis, radiation therapy, advanced age, arthroplasty, skeletal metastasis, corticosteroid therapy, rheumatoid arthritis, and vitamin D deficiency Osteolysis simulating malignancy ***Complications*** Delayed union Refracture Additional pelvic fractures

Adapted from Kane WJ: Fractures of the pelvis. In Rockwood CA Jr, Green DP (eds): Fractures in adults. 2nd Ed. Philadelphia, JB Lippincott, 1984, p 1112.

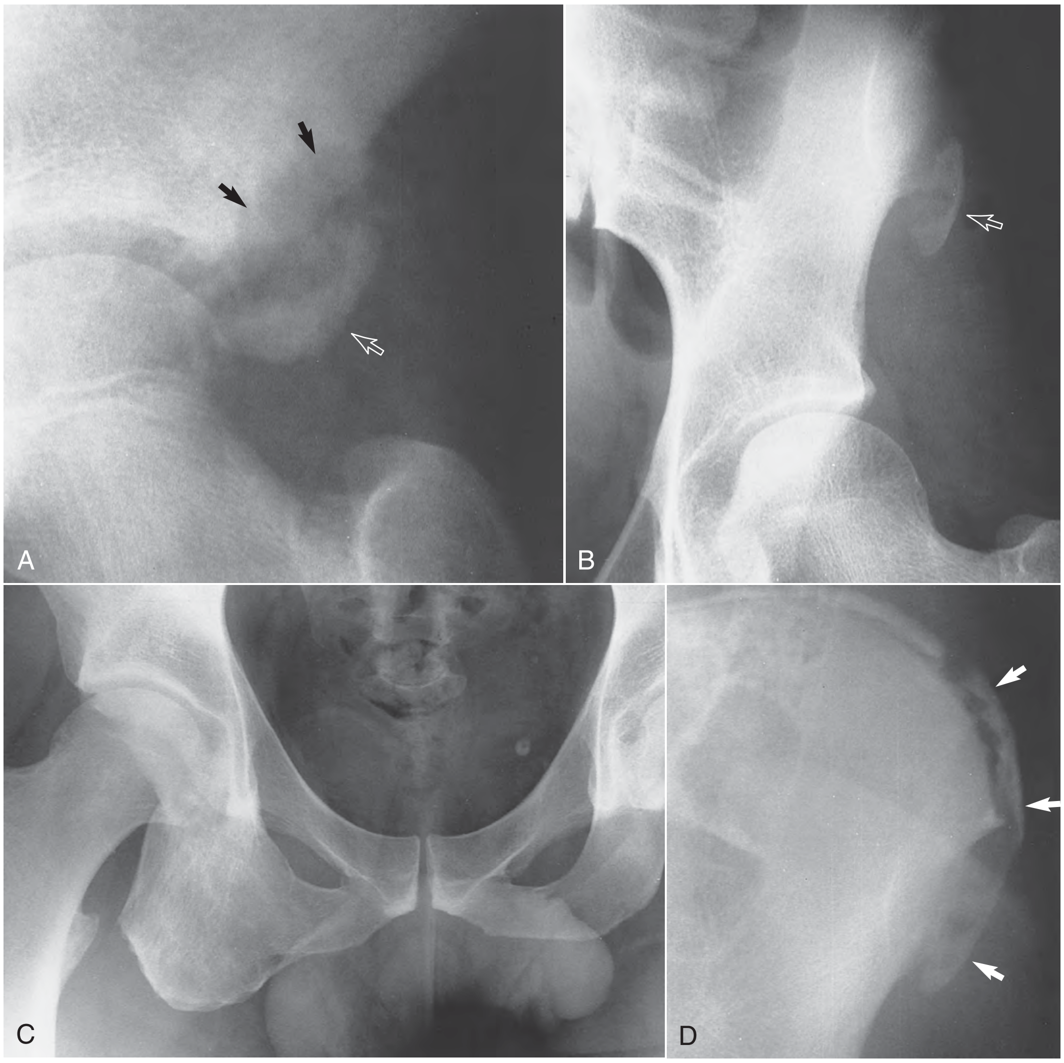

FIGURE 6–19 **Pelvic avulsion injuries.**[17,97] **A,** Anteroinferior iliac spine. The avulsed fragment *(open arrow)* is related to muscular pull at the attachment of the rectus femoris muscle. Note the radiolucent defect adjacent to the acetabular rim *(arrows)*. **B,** Anterosuperior iliac spine. Routine radiograph shows avulsion of the anterosuperior iliac spine, the attachment site of the sartorius muscle *(open arrow)*. **C,** Ischial tuberosity. This 30-year-old man had an old avulsion fracture of the ischial tuberosity at the site of attachment of the hamstring tendons. The fracture has healed with dramatic osseous enlargement a finding often termed "*rider's bone.*" **D,** Iliac apophysis. This 14-year-old girl felt something pop in the anterior thigh during a fight. Observe the separation of the iliac apophysis, the site of attachment of the abdominal muscles *(arrows)*. (***B,*** *Courtesy W. Ewing, MD, Pueblo, Colo.)*

FIGURE 6–20 **Type I injury: Duverney fracture.**[18] Observe the solitary fracture of the iliac wing after a direct injury in this teenager. These fractures represent about 30% of all pelvic fractures. They do not disrupt the pelvic ring, and therefore are considered stable.

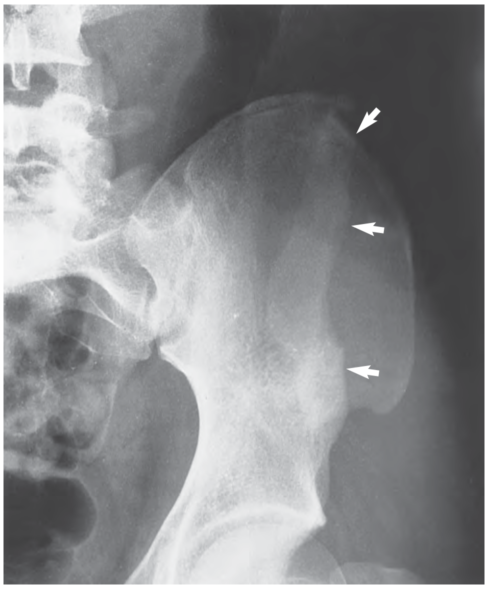

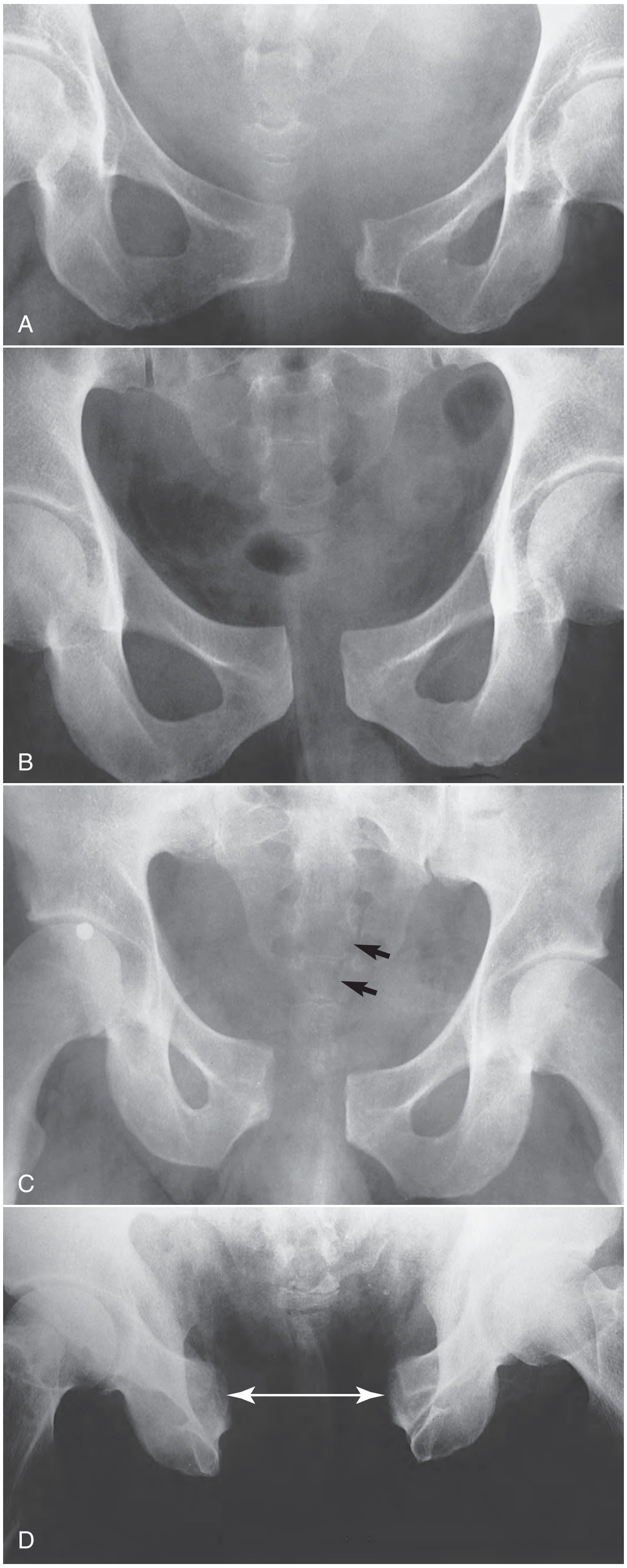

FIGURE 6–21 **Diastasis of the pubic symphysis.**[18,23,113] **A,** Postpartum diastasis. This 38-year-old woman had persistent pain and tenderness in the pubic region after an uncomplicated vaginal delivery. Widening of the symphysis pubis measuring 20 mm is evident. This is a self-limited condition related to increased elasticity of the pubic ligaments during pregnancy. **B,** Type II injury. This man was involved in a motorcycle accident. The articulation measures 15 mm, and no associated sacral fractures or sacroiliac diastases were found. **C,** Type III injury. A 35-mm pubic diastasis is associated with a vertical fracture of the sacrum *(arrows)*. Diastasis of the left sacroiliac joint also was present. **D,** Type III injury. Dramatic separation of the symphysis pubis is evident *(double-headed arrow)* in this patient, who has sustained a type III unstable pelvic injury in a motorcycle accident. A sacral fracture was also evident (not shown). This injury resulted in associated rectal laceration and denervation of the lower extremity. *(**A-C,** Courtesy B.A. Howard, MD, Charlotte, NC; **D,** Courtesy F.G. Bauer, DC, Sydney, New South Wales, Australia.)*

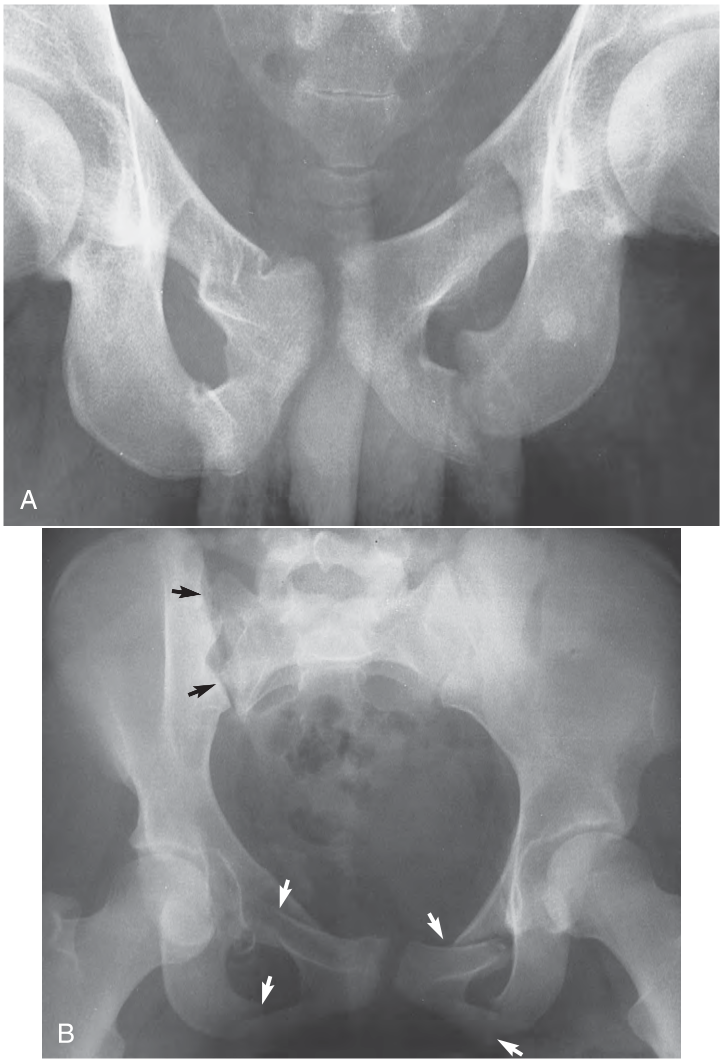

FIGURE 6–22 **Type III pelvic injuries.**[18] **A,** Straddle fracture. Observe the bilateral vertical fractures of the pubic rami in this 18-year old boy. **B,** In another patient, a 17-year-old girl, bilateral fractures of the ischiopubic rami *(white arrows)* are combined with diastasis of the right sacroiliac joint *(black arrows)*.

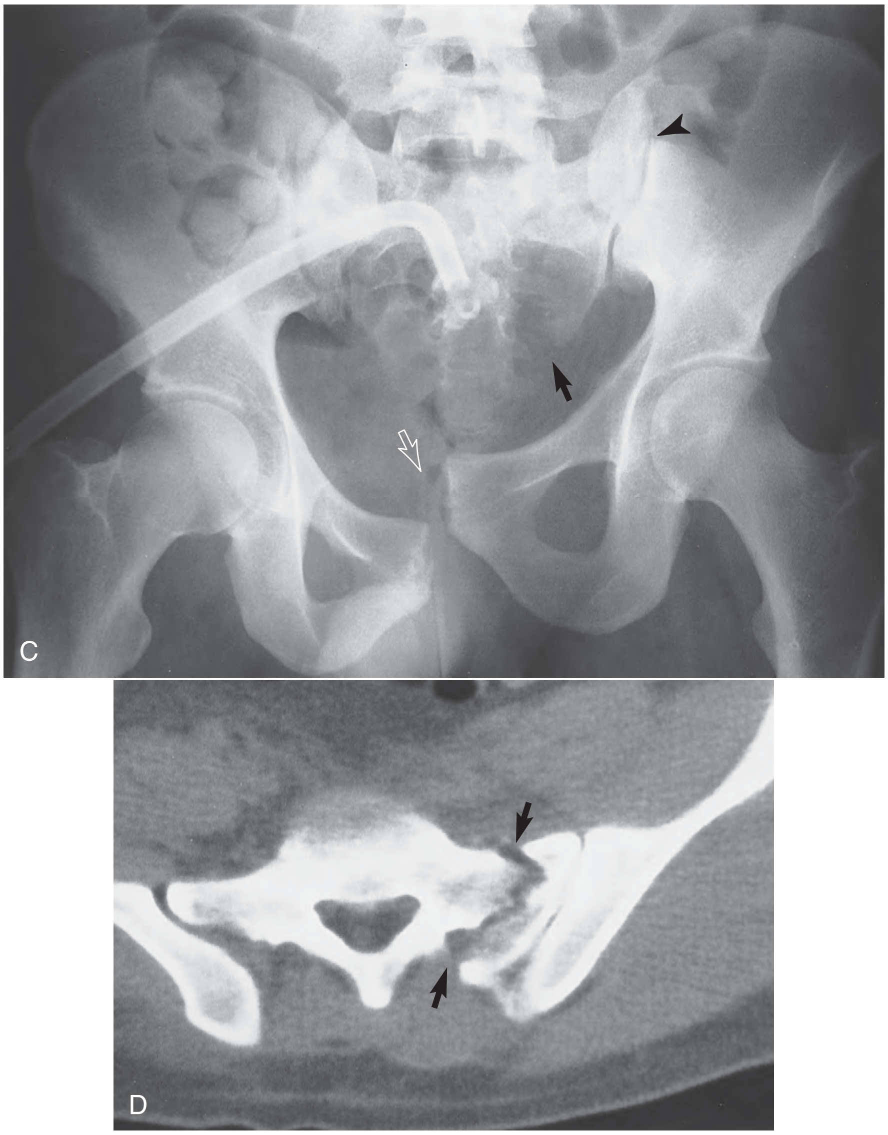

FIGURE 6–22, cont'd **C-D,** Complex pelvic injury in another patient. In **C,** an anteroposterior radiograph of the pelvis reveals a fracture of the sacrum *(black arrow),* sacroiliac joint diastasis *(arrowhead),* and pubic diastasis *(open arrow)*. A suprapubic catheter is in place. In **D,** a transaxial CT scan from the same patient as in **C** demonstrates the extent of the sacral fracture *(arrows)*. Intraarticular gas within the right sacroiliac joint suggests the presence of diastasis.

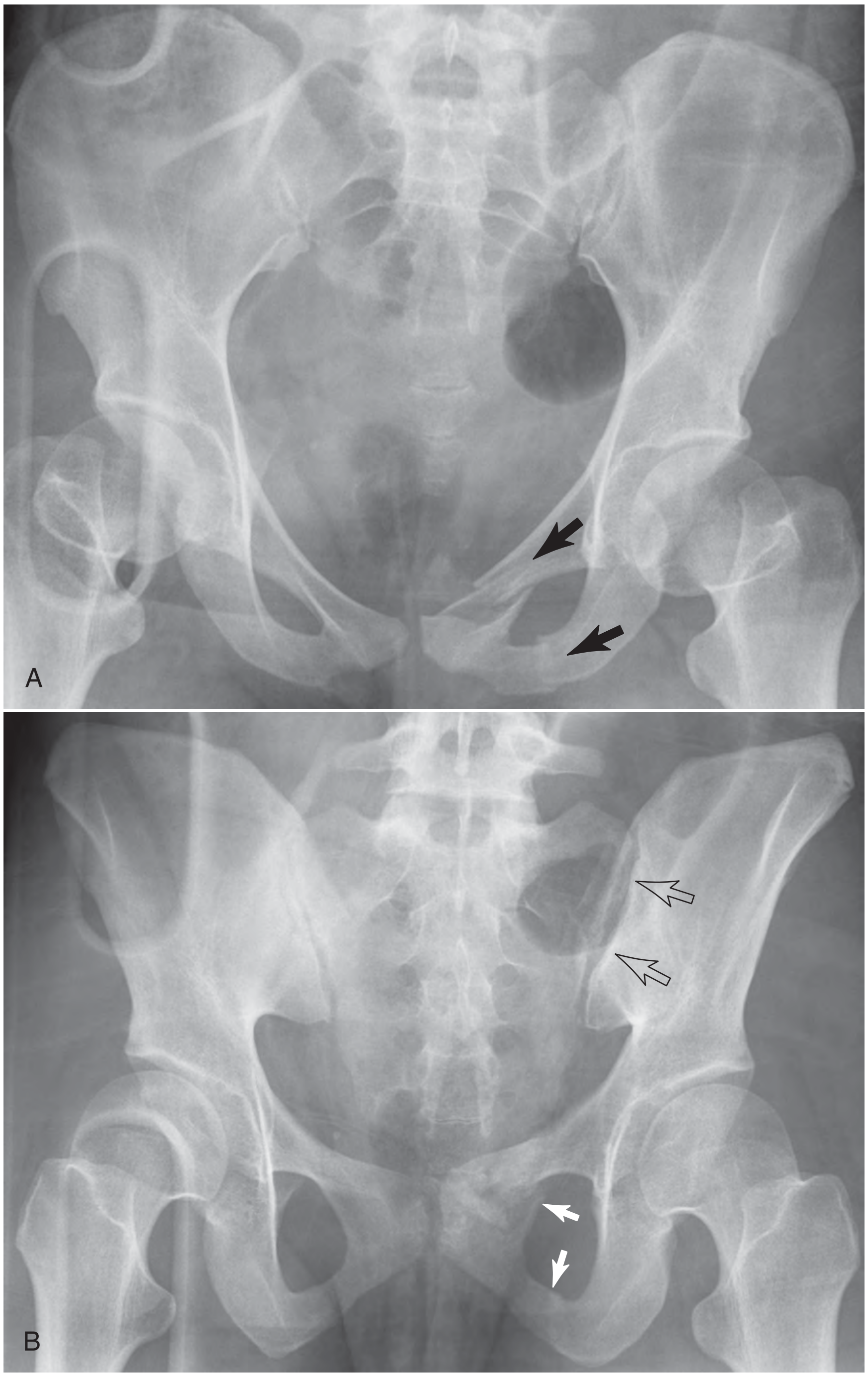

FIGURE 6–23 **Type III injury: Malgaigne fracture-dislocation.**[25] **A,** An anteroposterior inlet projection of the pelvis of this 22-year-old man reveals minimally displaced vertical fractures *(arrows)* of both the left superior pubic ramus and the left ischiopubic ramus. On this view, the sacrum, ilium, and sacroiliac joints appear normal. **B,** On the anteroposterior outlet view, diastasis of the left sacroiliac joint becomes obvious *(open arrows),* whereas the ischiopubic fractures are not as conspicuous *(arrows)*. With any traumatic disruption of the pelvic ring, it is important to conduct a thorough search for additional fractures or dislocations.

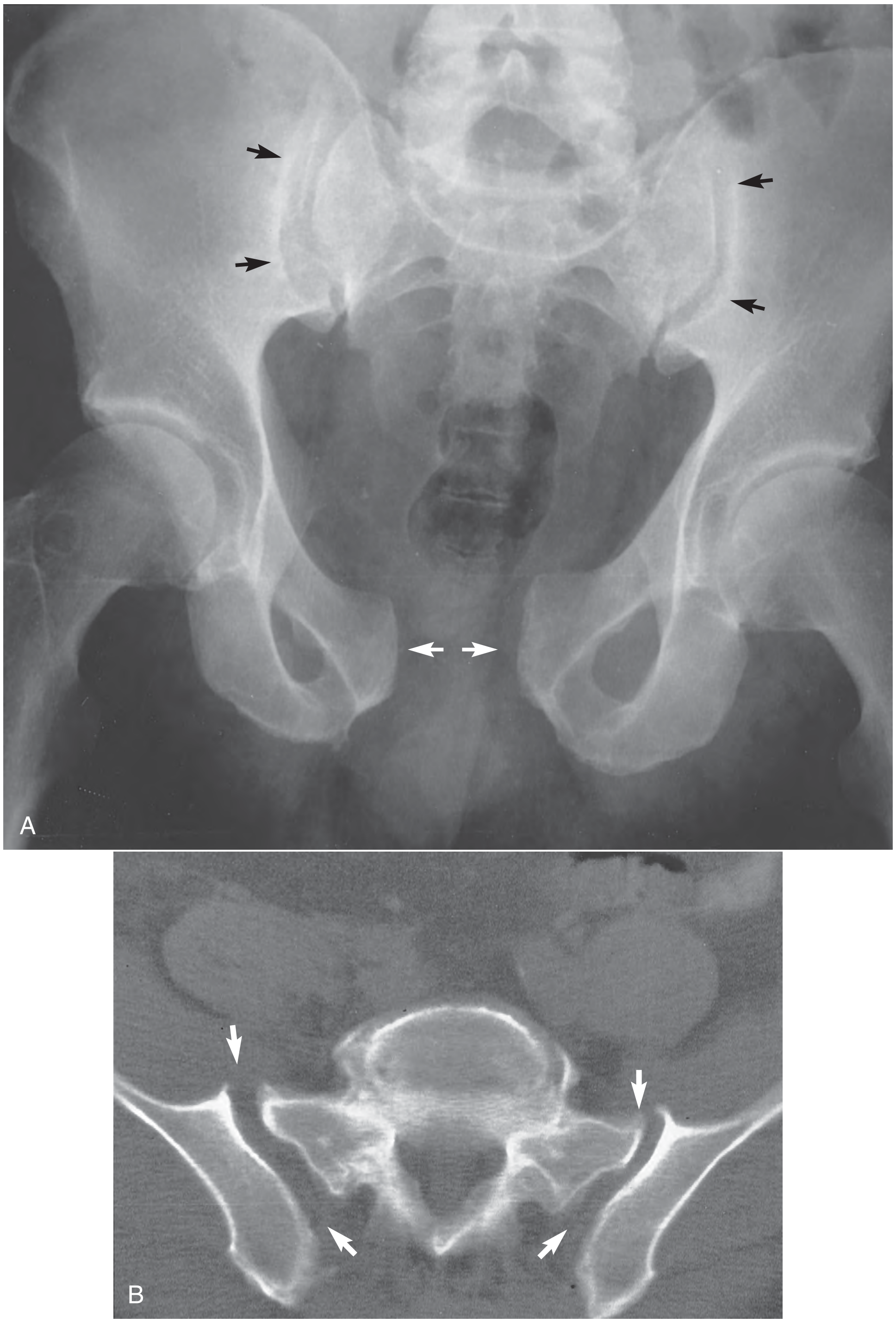

FIGURE 6–24 Complex pelvic injury: sprung pelvis.[25] Routine radiograph **(A)** shows wide diastasis of the symphysis pubis *(white arrows)* and less obvious sacroiliac joint widening *(black arrows)*. Transaxial CT scan **(B)** demonstrates the bilateral sacroiliac joint diastasis *(arrows)* more clearly. The sprung pelvis occurs as a result of massive crushing injuries and, as with other pelvic injuries, may be complicated by hemorrhage, urinary tract injury, peripheral nerve injury, and remote injuries.

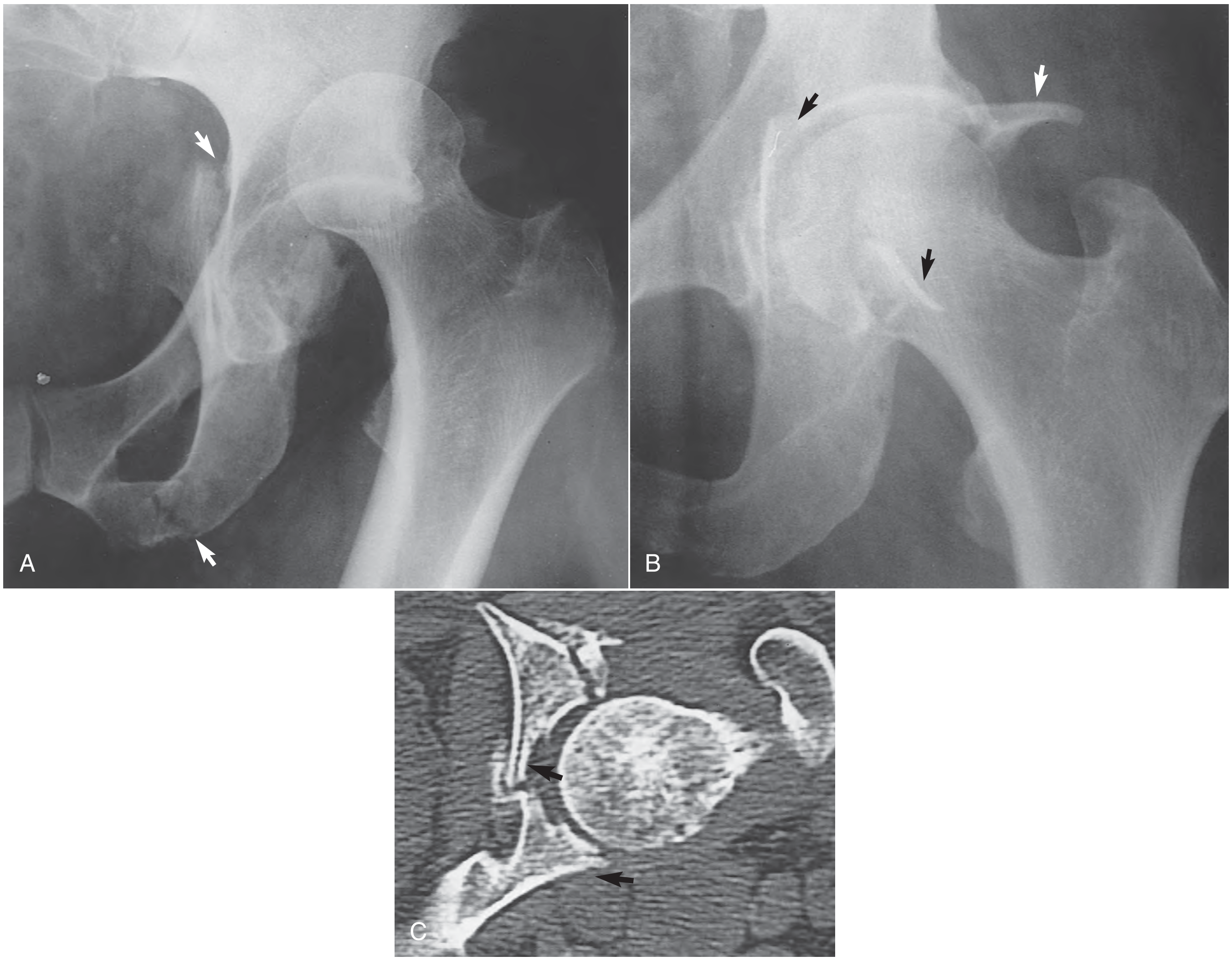

FIGURE 6–25 Acetabular fracture.[26-28] **A-C,** This 29-year-old man sustained a posterior hip dislocation in a motor vehicle accident. In **A,** a prereduction radiograph shows the posterior hip dislocation and associated fracture of the acetabulum and ischium *(arrows)*. In **B,** a postreduction radiograph shows the associated fracture fragments *(arrows)*. **C,** Postreduction, transaxial CT scan shows the extensive comminution of the acetabulum *(arrows)*.

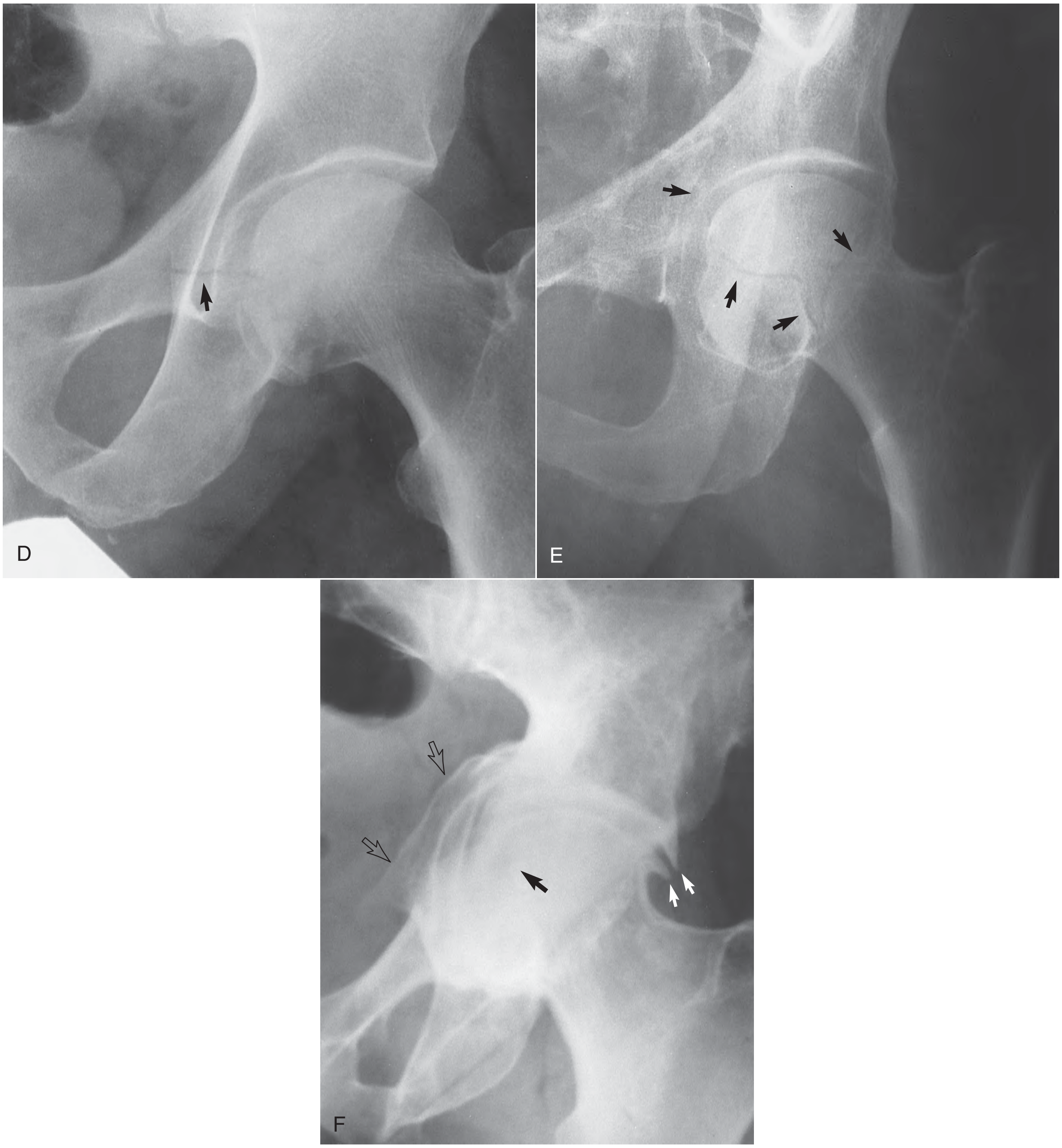

FIGURE 6–25, cont'd **D** and **E,** Value of oblique projections. In another patient, routine frontal radiograph **(D)** reveals only one fracture line *(arrow)*. In **E,** a 45-degree oblique (Judet) projection demonstrates more clearly the comminuted fractures of the central acetabular region and posterior acetabular rim fractures superimposed on the femoral head *(arrows)*. **F,** Postinjury complications. In a third patient, several years after sustaining an acetabular fracture, osteophytes *(white arrows)* and axial joint space narrowing *(black arrow)* characteristic of degenerative joint disease can be observed. Persistent acetabular protrusion can also be observed *(open arrows)*. CT imaging is indicated in most cases of pelvic trauma because it provides a cross-sectional display of the bony pelvis, identification of intraarticular fracture fragments, and evidence of hemorrhage and other soft tissue or visceral injury. Magnetic resonance (MR) imaging is useful in detecting subclinical injury of the sciatic nerve and occult injuries of the femoral head not readily visible on CT scans. MR imaging, however, is not as accurate as CT in identifying intraarticular fragments. *(**F,** From Taylor JAM, Harger BL, Resnick D: Diagnostic imaging of common hip disorders: A pictorial review. Top Clin Chiropr 1:8, 1994. Reprinted with permission.)*

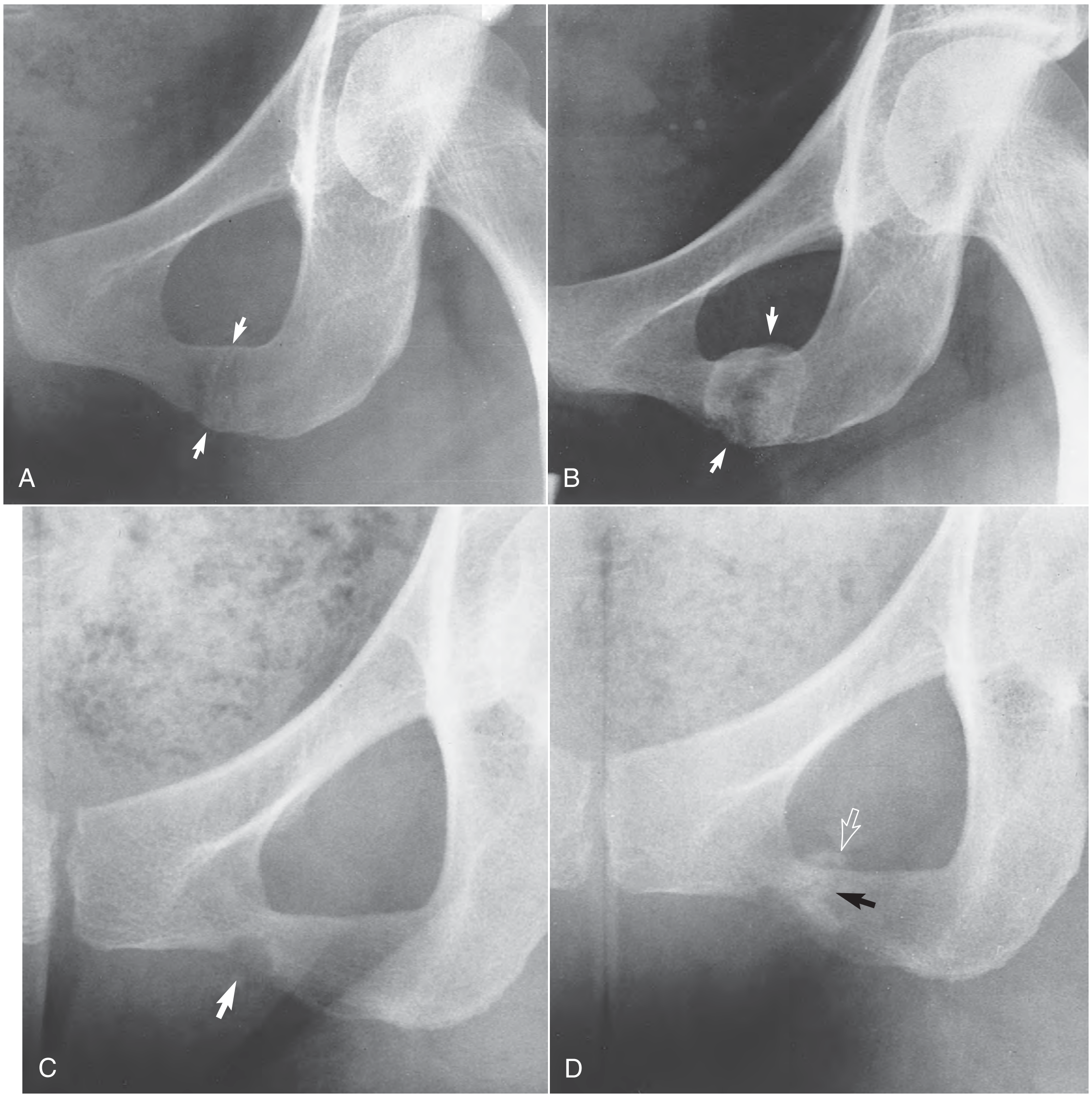

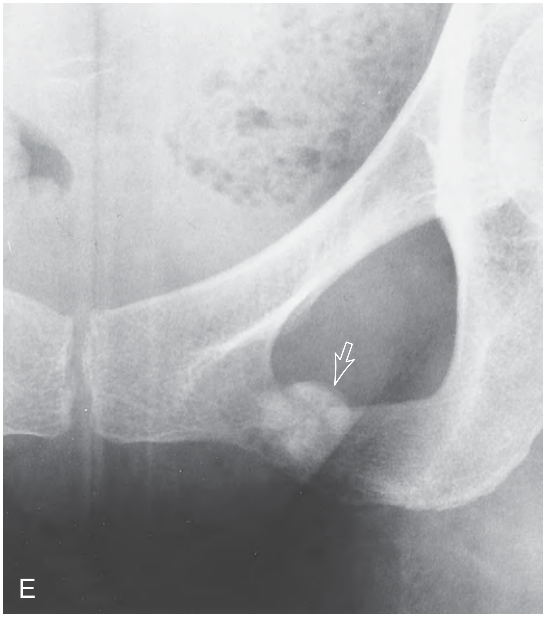

FIGURE 6–26 Stress (fatigue) fracture.[29,30,110] **A-B,** A 35-year-old female runner had a 4-week history of left hip pain. In **A,** an initial radiograph reveals a transverse radiolucent shadow through the inferior ischiopubic ramus *(arrows)*. In **B,** a serial radiograph obtained 7 months later demonstrates bulbous callus formation at the fracture site, indicating adequate healing. **C-E,** This 25-year-old woman began an aggressive exercise regimen, including distance running. In **C,** the initial radiograph taken at the time of onset of pain shows a small, circular, osteolytic cortical lesion in the pubic ramus *(arrow)*. In **D,** a serial radiograph taken 1 month later reveals evidence of a fracture line *(arrow)* and early callus formation *(open arrow)*. In **E,** a third radiograph taken 3 months after the initial film **(C)** reveals abundant callus *(open arrow)*. Fatigue fractures of the pubic ramus affect normal bone primarily in pregnant women, joggers, long-distance runners, and marathoners. (***C-E,*** *Courtesy S. Standish, DC, and C. Russell, DC, Calgary, Alberta, Canada.)*

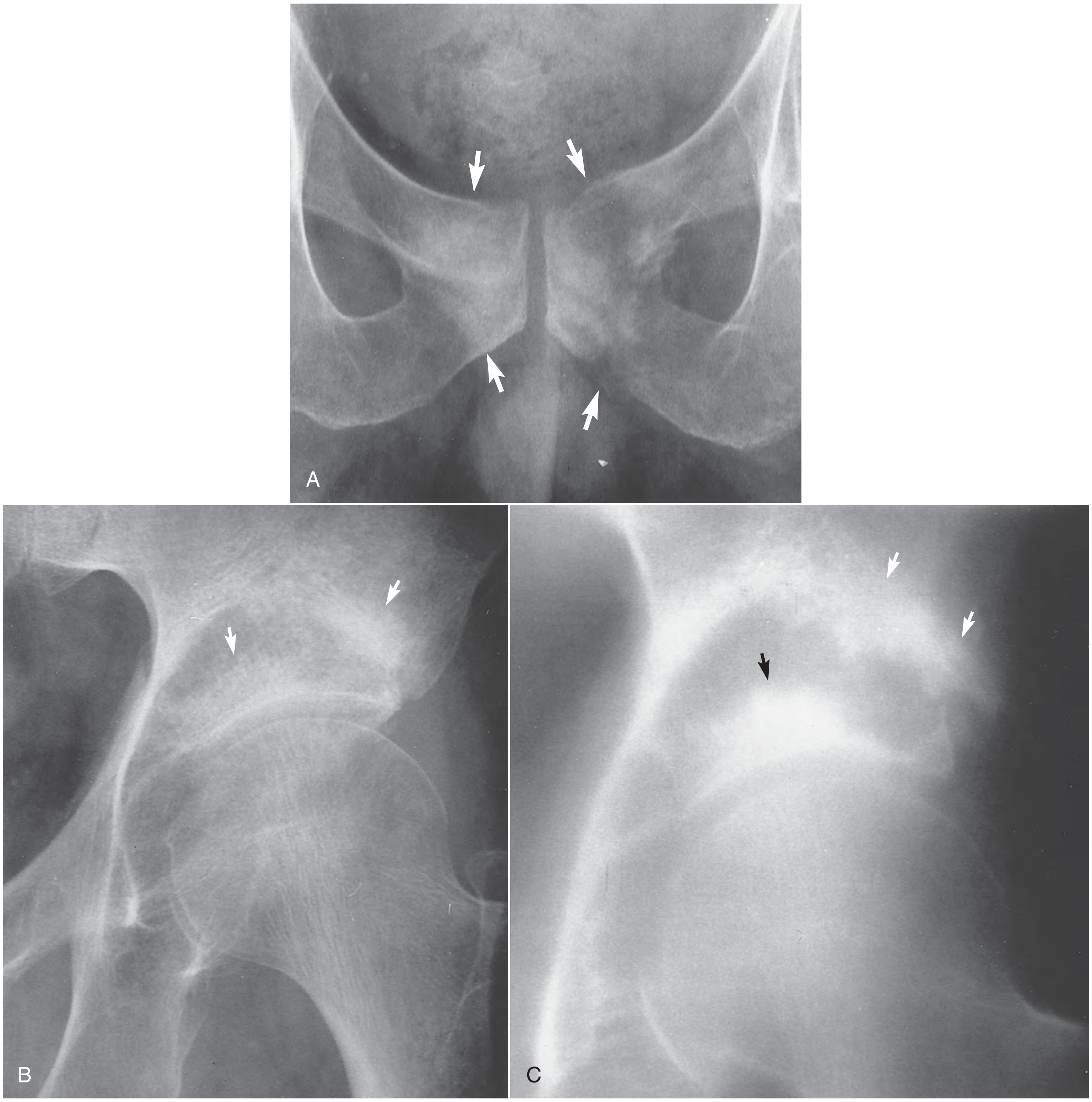

FIGURE 6–27 **Insufficiency fracture.**[20-22,30,109] **A,** Parasymphyseal location. Frontal radiograph of this 61-year-old man shows bilateral insufficiency fractures of bone adjacent to the pubic symphysis *(arrows)*. The findings include osteolysis, osteosclerosis, and bone fragmentation, resembling an aggressive destructive process. **B-C,** Supraacetabular location. In a 76-year-old man with carcinoma of the prostate, zones of increased density are seen on the frontal radiograph **(B)** *(arrows)*. Conventional tomography **(C)** performed 2 weeks after the radiograph was obtained shows areas of increased radiolucency and sclerosis *(arrows),* typical of an insufficiency fracture. Parasymphyseal and supraacetabular insufficiency fractures occur after radiation therapy or hip arthroplasty and in patients with osteoporosis, osteoarthrosis, or rheumatoid arthritis of the hip.

TABLE 6-5 Spectrum of Clinical Athletic Pubalgia Syndromes: Differential Diagnosis[98,101-104]

Entity	Figure(s)	Characteristics
General considerations[98,101,108]		Frequently encountered and often overlapping syndromes resulting from a wide variety of athletic activities that represent a spectrum of entities centered about the pubic symphysis and its tendinous attachments The term *sports hernia* is frequently used by lay persons and sportscasting media, but its true definition remains uncertain, and therefore use of the term should be discouraged
Osteitis pubis[98,104]	Table 6-7	***Imaging findings*** Bilateral symmetric subchondral bone sclerosis, irregularity, resorption, osteolysis Restoration of the osseous surface and disappearance of sclerosis may be associated with bony ankylosis of the joint ***MR imaging findings*** Bone marrow edema involving subchondral margin on both sides of symphysis pubis ***Symphyseal cleft injection (symphysography)*** Anesthetic injection performed under fluoroscopic guidance with nonionic contrast material has been advocated as a diagnostic symptom provocation test and as a therapeutic maneuver for short-term treatment and symptom relief in patients with osteitis pubis Abnormal extravasation of contrast material indicates coexistent avulsion injury or insertional injury to adjacent muscles and tendons Osteitis pubis may be isolated or in conjunction with rectus abdominus and thigh adductor tendon pathology
Stress (fatigue) fracture[98,110]	6-26 Table 6-4	Chronic repetitive stress, classically in long distance running and military activities, results in fatigue type of stress fracture about the pubis Traction from muscle and tendon attachments such as the adductor magnus on the inferior pubic ramus ***MR imaging findings*** Focal bone marrow edema; fracture line; periosteal edema; callus formation; surrounding soft tissue edema
Rectus abdominus insertional tendinopathy[98,101]		Rectus abdominus tendon attaches to the anteroinferior pubis just lateral to the pubic symphysis over a span of approximately 2 cm Often treated surgically ***MR imaging findings*** High signal intensity on fluid-sensitive images at site of attachment of rectus abdominus tendon; Some insertional injuries involve frank rupture, but many more are subtle injuries May be confused with or combined with inguinal hernias and adductor longus and brevis insertional injuries
Adductor syndromes[98,101]		*Syndromes include:* frank avulsions; hypoxic tendinosis; calcific tendinitis; and myotendinous strains Many are treated conservatively *Tendon involvement:* pectineus; adductor longus; adductor brevis ***MR imaging findings*** High signal intensity on fluid-sensitive images at site of attachment of specific tendon
Inguinal hernias[98,100,108]		Direct, indirect, or even spigelian hernias may result in athletic pubalgia Careful clinical examination and MR imaging obtained during Valsalva maneuver are often useful Herniography has been recommended to evaluate athletes in which the cause of groin pain is unclear or ambiguous
Remote muscle strains[98,101]		Strains and myotendinous injuries at sites remote from the pubic symphysis may result in pubalgia: sartorius, gracilis, obturator internus, tensor fascia lata, gluteus medius
Sacroiliitis[98]	Tables 5-4, 5-5	Remote sacroiliac joint pathology, such as septic arthritis or seronegative spondyloarthropathy, may refer pain simulating athletic pubalgia
Apophysitis[98]	Table 6-4	Acute or repetitive trauma to childhood or adolescent apophyses can result in avulsion fractures or apophysitis ***MR imaging findings*** Asymmetrical abnormal hyperintensity on fluid-sensitive images at site of apophysis with possible periosteal reaction and periapophyseal fluid signal; fragmentation or frank avulsion may also be observed
Visceral pelvis pathology[98]		Visceral lesions presenting as clinical athletic pubalgia are more common in women. Pathologies include cysts, endometriosis, fibroid, and other uterine masses, femoral hernias
Soft tissue masses[98]		Benign and malignant soft tissue neoplasms may mimic athletic pubalgia
Intrinsic hip joint pathology[98]		Articular pathologies, labral tears, osteoarthrosis, osteochondral lesions, primary synovial processes all may result in pubalgia-like referred pain

TABLE 6-6 Classification and Grading of Abnormalities in the Pubic Bone and Symphysis[99]

Grade	Changes	Criteria
0	No changes	
1	Slight changes	a. Cortical irregularity with erosions <1 mm b. Absence of cysts or cysts <1 mm c. Bony proliferation, beaking <1 mm (cancellous sclerosis and hyperostosis may also occur)
2	Intermediate changes	a. Increased subchondral irregularity with erosions from 1 to 3 mm b. Cysts <5 mm c. Beaking <2 mm (moderately increased cancellous sclerosis and hyperostosis may also occur)
3	Advanced changes	a. Erosions >5 mm b. Increased appearance of cysts c. Increased beaking

Adapted from reference 99.

TABLE 6-7 Symphysis Pubis and Pelvis: Articular Disorders*

Entity	Figure(s)	Characteristics
Degenerative and Related Disorders		
Degenerative disease[31]	6-28	*Pelvis:* Degenerative enthesopathy of the pelvis is common in aging persons *Symphysis pubis:* Accompanies aging and is accelerated by childbirth and trauma Osteophytes, subchondral sclerosis, vacuum phenomenon May resemble infection and inflammatory spondyloarthropathies
Diffuse idiopathic skeletal hyperostosis (DISH)[31-33]	6-29	*Pelvis:* Extensive enthesopathy and ligament ossification
	6-30	*Symphysis pubis:* Osseous bridging of the symphysis pubis
Osteitis pubis[34,35]	6-31 Table 6-5	Painful, self-limited condition Women: after childbirth or pelvic surgery Men: after prostate or bladder surgery Athletes: as a result of chronic stress across the articulation or as a result of acute avulsion of muscle attachments adjacent to the joint Other injuries and low-grade infections may also precipitate these changes ***Radiographic findings*** Bilateral symmetric subchondral bone sclerosis, irregularity, resorption, osteolysis Restoration of the osseous surface and disappearance of sclerosis may be associated with bony ankylosis of the joint
Inflammatory Disorders		
Rheumatoid arthritis[36]		Rare involvement of symphysis pubis: is usually clinically silent Subchondral erosion, mild sclerosis, joint space narrowing
Ankylosing spondylitis[37,114]	6-32	Symphysis pubis involved in 16% to 23% of patients with ankylosing spondylitis Erosions, sclerosis, blurring of subchondral surfaces, joint space narrowing, and eventual ankylosis of symphysis pubis More severe changes identified in patients who suffer from the disease for prolonged time periods (i.e., more than 15 years)
Psoriatic spondyloarthropathy and reactive arthritis associated with Reiter syndrome[37]	6-33	Symphysis pubis findings similar to those of ankylosing spondylitis, but less frequently involved
Dermatomyositis and polymyositis[38]	6-34	Diffuse sheetlike calcification in soft tissues surrounding pelvis

* See also Tables 1-7 to 1-11 and Table 1-19.

Continued

TABLE 6-7 Symphysis Pubis and Pelvis: Articular Disorders—cont'd

Entity	Figure(s)	Characteristics
Crystal Deposition and Metabolic Disorders		
Calcium pyrophosphate dihydrate (CPPD) crystal deposition disease[39,40,89]	6-35	Articular space narrowing, sclerosis, chondrocalcinosis within joint, and in some cases, considerable bone fragmentation
Hemochromatosis[41]	6-36	Findings identical to those of CPPD crystal deposition disease
Alkaptonuria[42]	6-37	Accelerated degenerative disease, chondrocalcinosis, joint space narrowing, sclerosis, fragmentation, and osseous bridging
Renal osteodystrophy[43,44]	6-38	Subchondral resorption results in indistinct subchondral bone margins and widening of the symphysis pubis and sacroiliac joint
Infection		
Infective osteitis pubis[35,45]	6-39	Occasionally, osteitis pubis is associated with a low-grade infection Predisposing factors: intravenous drug abuse and pelvic surgery More aggressive course than "sterile" osteitis *pubis* Antibiotics usually provide relief of symptoms

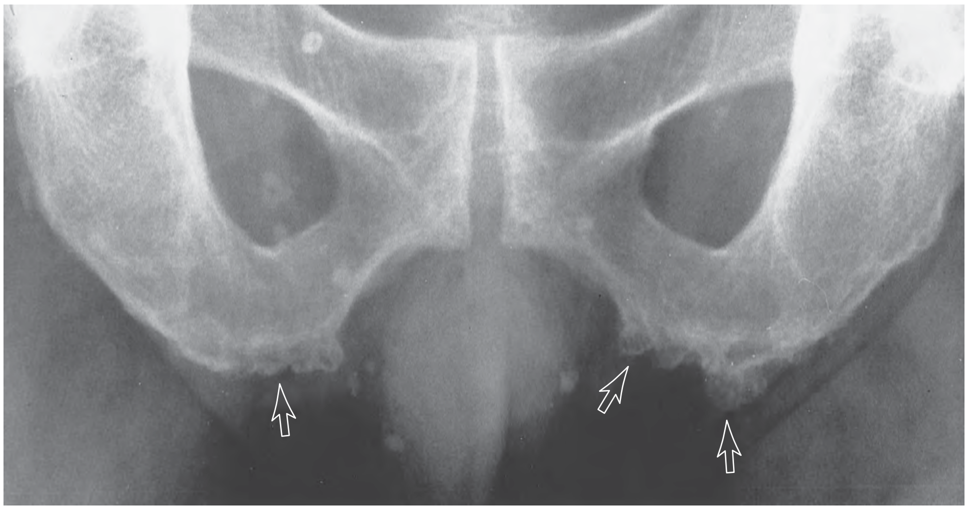

FIGURE 6–28 Degenerative enthesopathy.[31] Observe the irregular whiskerlike projections of bone arising from the ischiopubic region *(open arrows)*. Enthesophytes are bony projections at the site of attachment of ligaments and tendons, in this case where the hamstring muscles are attached to the pelvis. Such enthesophytes are seen as a result of degeneration or in patients with diffuse idiopathic skeletal hyperostosis or seronegative spondyloarthropathies. The small, circular opaque shadows represent incidental pelvic phleboliths.

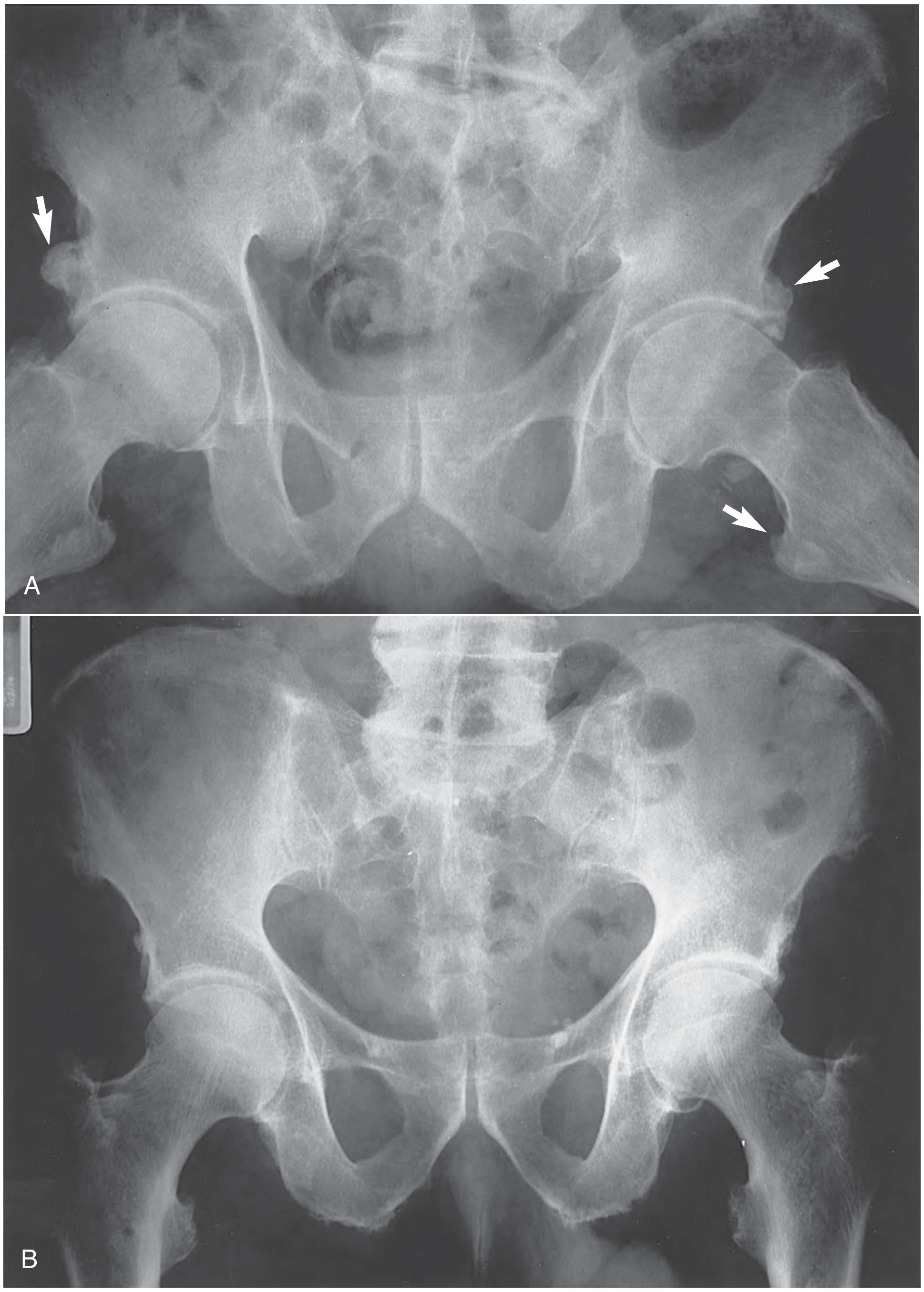

FIGURE 6–29 Diffuse idiopathic skeletal hyperostosis (DISH).[31,32] **A,** Pelvic enthesopathy. Prominent osseous excrescences are present at several characteristic sites in the pelvis *(arrows)*. **B,** In another patient, enthesopathy is seen at multiple sites of tendinous attachment.

Continued

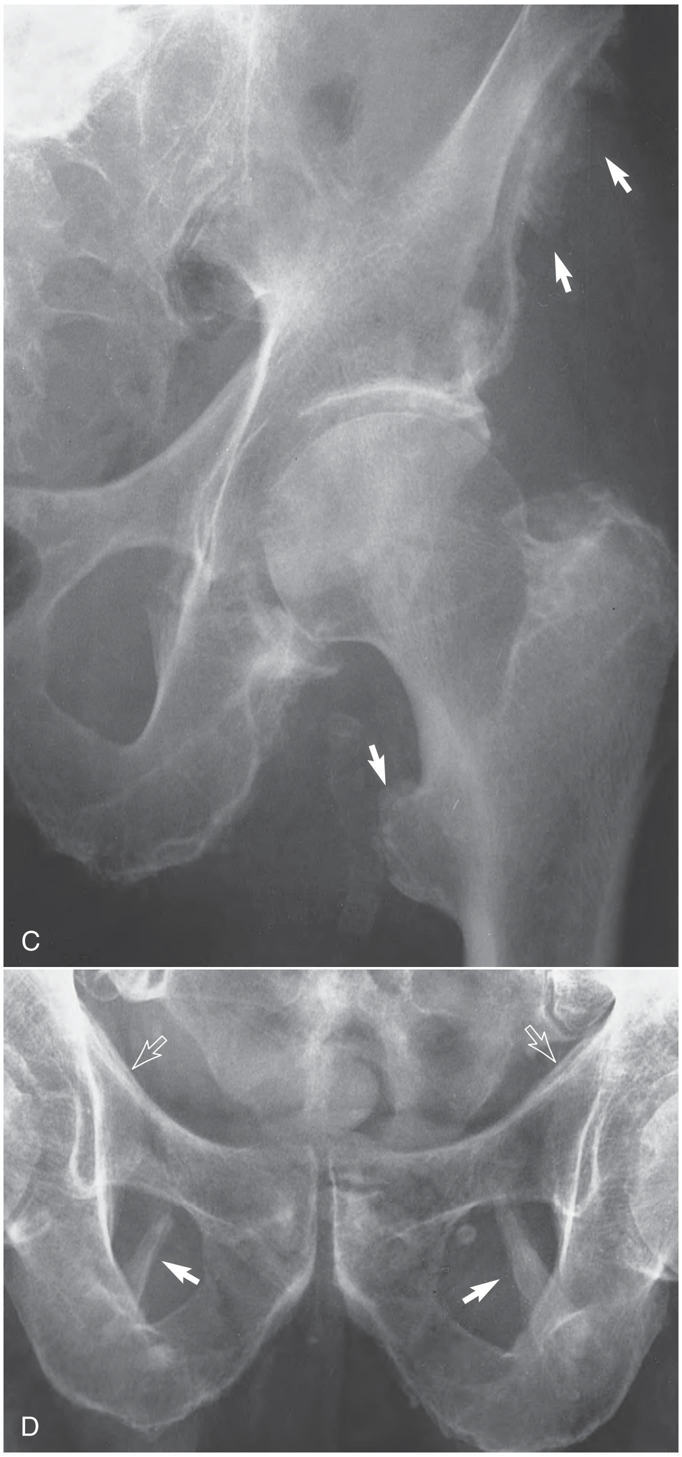

FIGURE 6–29, cont'd **C,** In a third patient, ossification and para-articular osseous excrescences (whiskering) project from several sites along the margin of the innominate bones and lesser trochanter *(arrows)*. **D,** Ligament ossification. In this 73-year-old man with DISH, observe the extensive ossification of the sacrotuberous ligaments *(arrows)*. Note also pectineal ligament calcification *(open arrows)*.

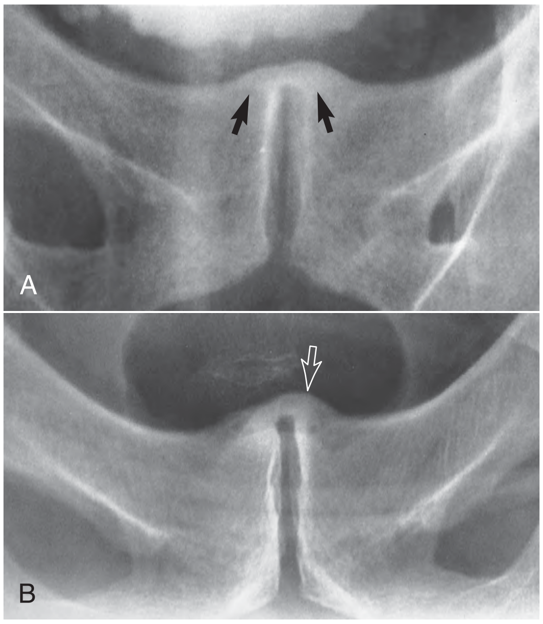

FIGURE 6–30 **Diffuse idiopathic skeletal hyperostosis (DISH): Symphysis pubis abnormalities.**[33] **A,** On this intravenous urogram, observe the osseous bridging spanning the superior aspect of the symphysis pubis *(arrows)*. **B,** In a 78-year-old man, similar osseous bridging of the symphysis pubis is evident *(open arrow)*.

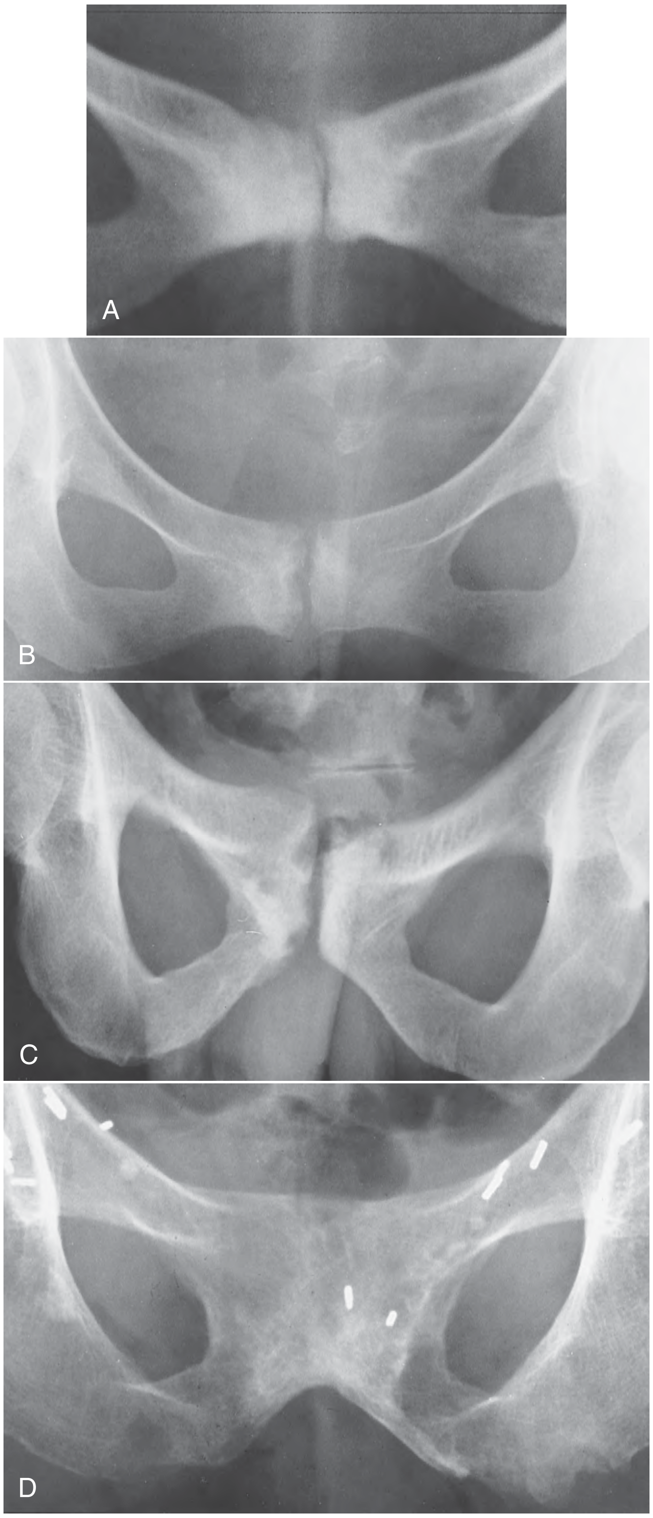

FIGURE 6–31 **Osteitis pubis.**[34,35] **A,** This 30-year-old woman had localized pubic pain for several months after childbirth. The radiograph reveals bilateral subchondral bone sclerosis and narrowing of the joint space. **B,** A 27-year-old woman initially developed pubic pain during the third trimester of pregnancy. The radiographic findings include diffuse sclerosis of the apposing surfaces of the pubic symphysis and irregularity of the articular surfaces. Her symptoms eventually resolved and the sclerosis disappeared. **C,** A 32-year-old man. Posttraumatic sclerotic changes and irregularity of the joint surfaces are seen adjacent to the pubic symphysis on the frontal radiograph. Offset of the adjacent pubic bones is a frequent finding, which is attributed to pelvic obliquity or instability and is not necessarily related to osteitis pubis. **D,** Ankylosis. This patient underwent a transurethral prostatectomy and developed osteitis pubis. This radiograph, obtained 2 years later, reveals complete osseous ankylosis. *(**B,** Courtesy V. Vint, MD, La Jolla, Calif.)*

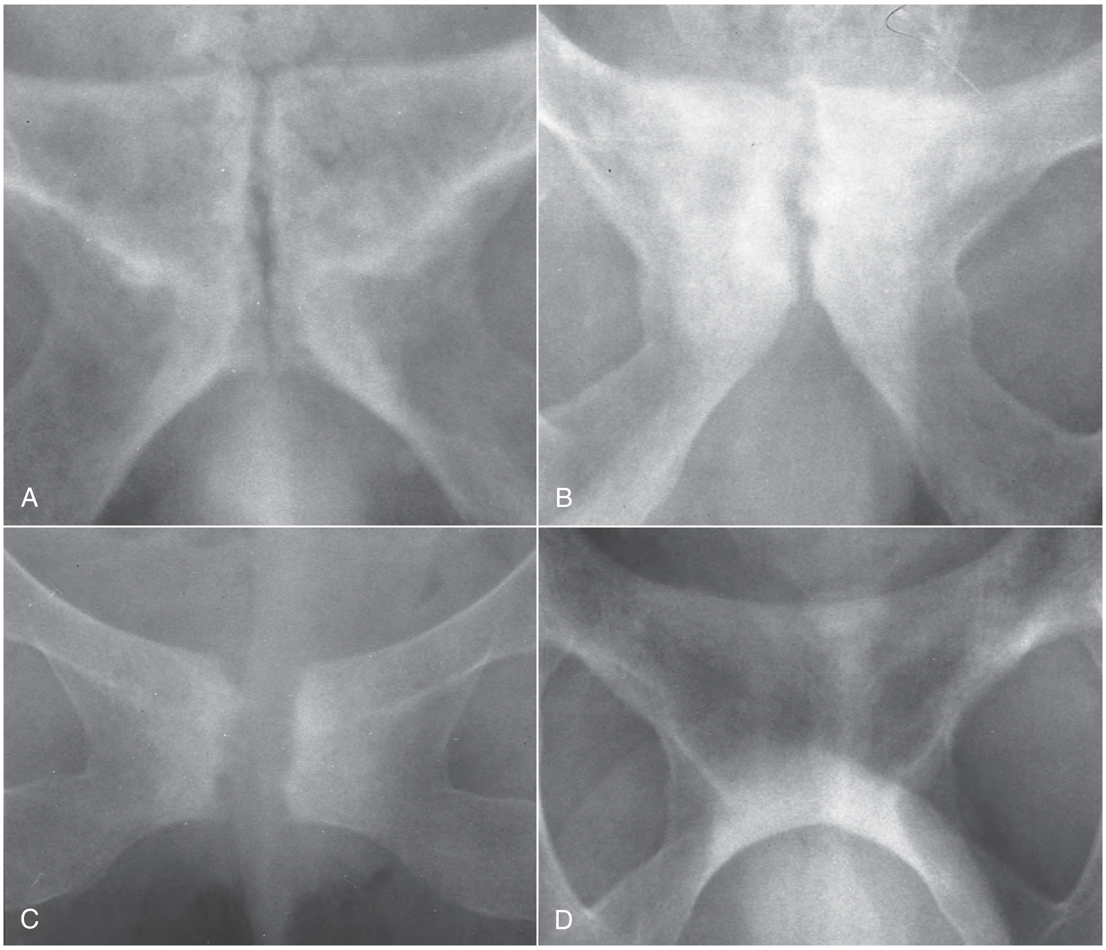

FIGURE 6–32 **Ankylosing spondylitis: spectrum of abnormalities.**[37,114] **A,** Observe the narrowing of the symphysis pubis and indistinct margin of the parasymphyseal subchondral bone surface. **B,** In another patient, the joint space is narrowed and the joint surfaces are indistinct and irregular. Additionally, the subchondral bone is sclerotic. **C,** In a 61-year-old woman with severe ankylosing spondylitis, the symphysis pubis is markedly widened, and the articular margins are indistinct and mildly sclerotic, an appearance resembling that of septic arthritis or hyperparathyroidism. **D,** Complete ankylosis of the symphysis pubis is present in this 38-year-old man with advanced ankylosing spondylitis.

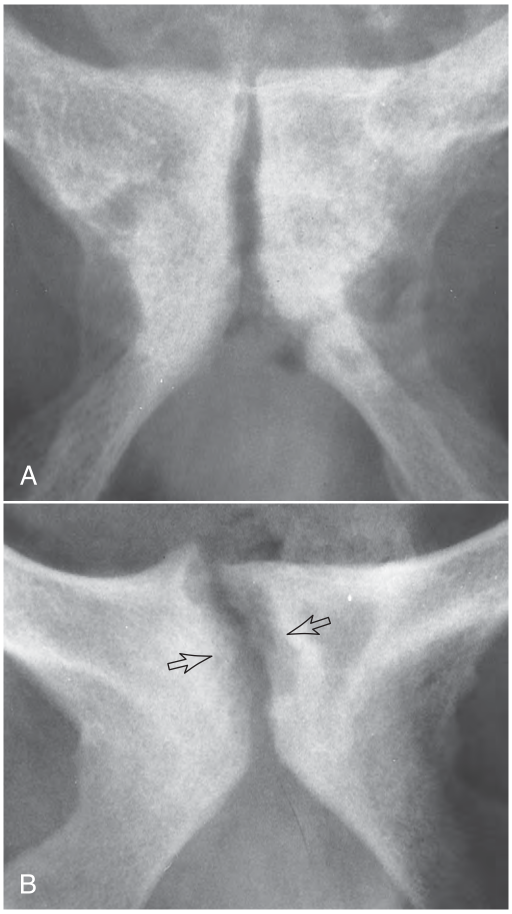

FIGURE 6–33 **Psoriatic arthropathy: pubic symphysis.**[37] **A,** The parasymphyseal subchondral bone appears sclerotic, and the articular surfaces are indistinct. **B,** In another patient, subchondral erosions *(open arrows)* and parasymphyseal sclerosis are seen.

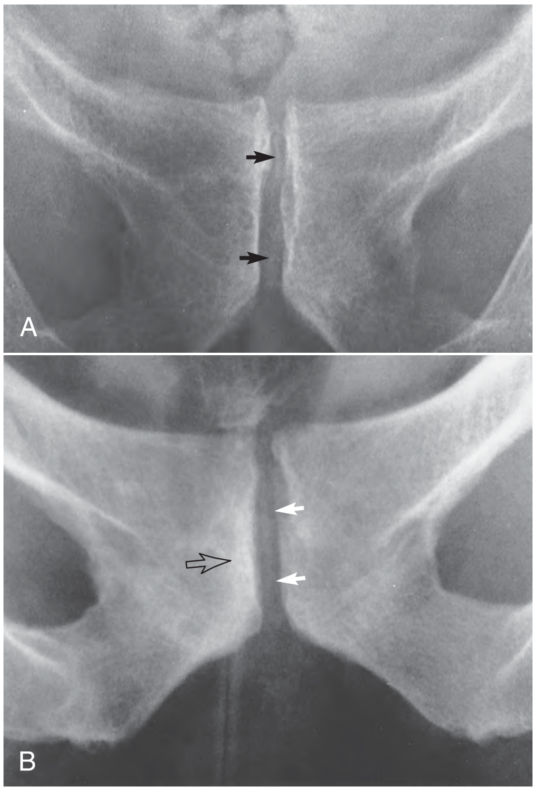

FIGURE 6–35 **Calcium pyrophosphate dihydrate (CPPD) crystal deposition disease.**[39,40,89] **A,** Observe the linear band of chondrocalcinosis within the symphysis pubis *(arrows)*. **B,** In another patient, chondrocalcinosis *(arrows)* and subchondral sclerosis *(open arrow)* are evident.

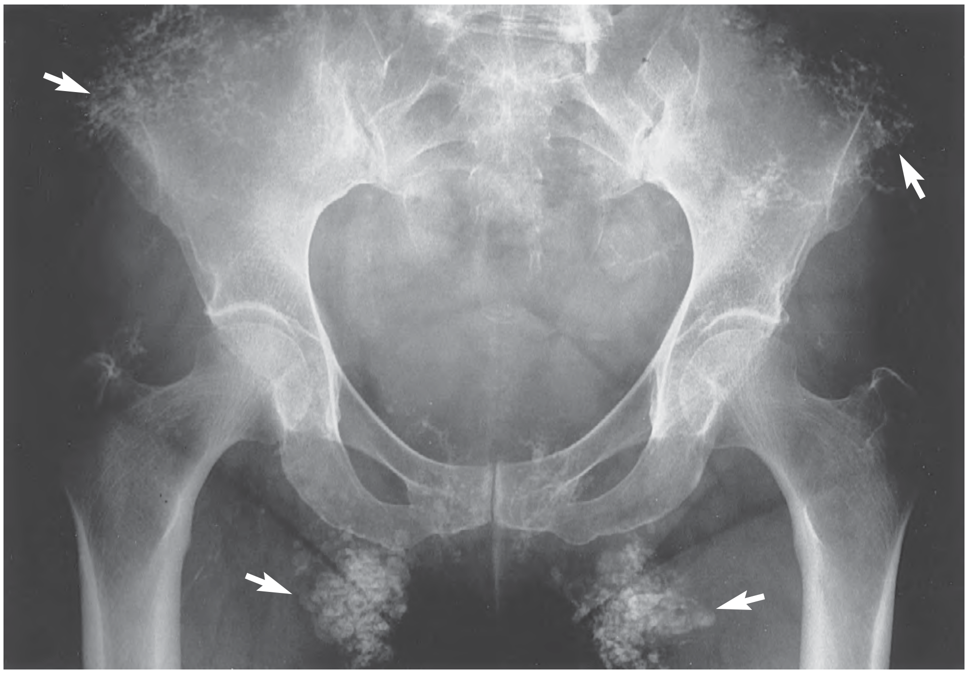

FIGURE 6–34 **Dermatomyositis.**[38] Multiple areas of sheetlike calcification are seen within the soft tissues of the pelvis *(arrows)* in this 57-year-old woman with dermatomyositis.

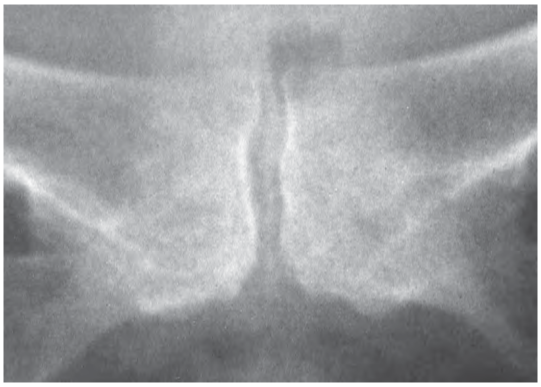

FIGURE 6–36 **Hemochromatosis.**[41] Observe the linear calcification within the symphysis pubis. The radiographic findings of hemochromatosis resemble those of calcium pyrophosphate dihydrate (CPPD) crystal deposition disease. *(Courtesy G. Greenway, MD, Dallas.)*

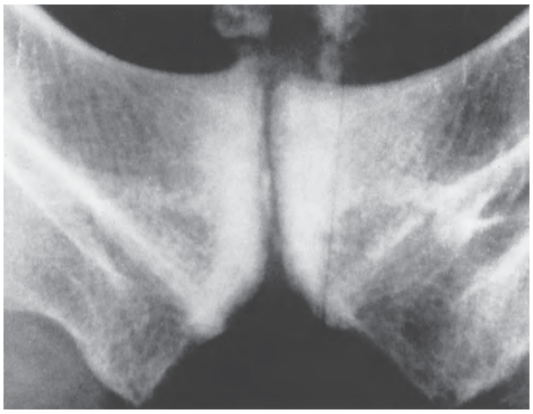

FIGURE 6–37 **Alkaptonuria: symphysis pubis.**[42] Radiograph reveals severe joint space narrowing, osteophytosis, and extensive subchondral sclerosis characteristic of alkaptonuria. *(Courtesy J. Goobar, MD, Ostersund, Sweden.)*

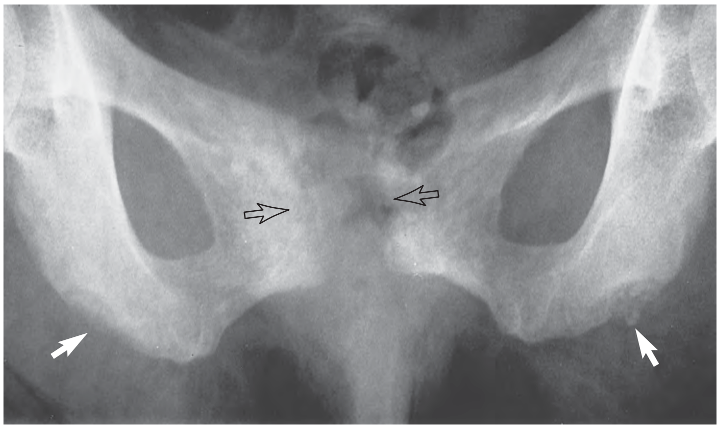

FIGURE 6–38 **Renal osteodystrophy: subchondral resorption.**[43,44] Observe the widening and indistinct margins of the subchondral bone adjacent to the symphysis pubis *(open arrows)* in this patient with chronic renal disease, renal osteodystrophy, and secondary hyperparathyroidism. Also evident is subtendinous resorption of the ischial tuberosities *(arrows)*. *(Courtesy J.T. Knudsen, DC, and C. Yomtob, DC, Los Angeles.)*

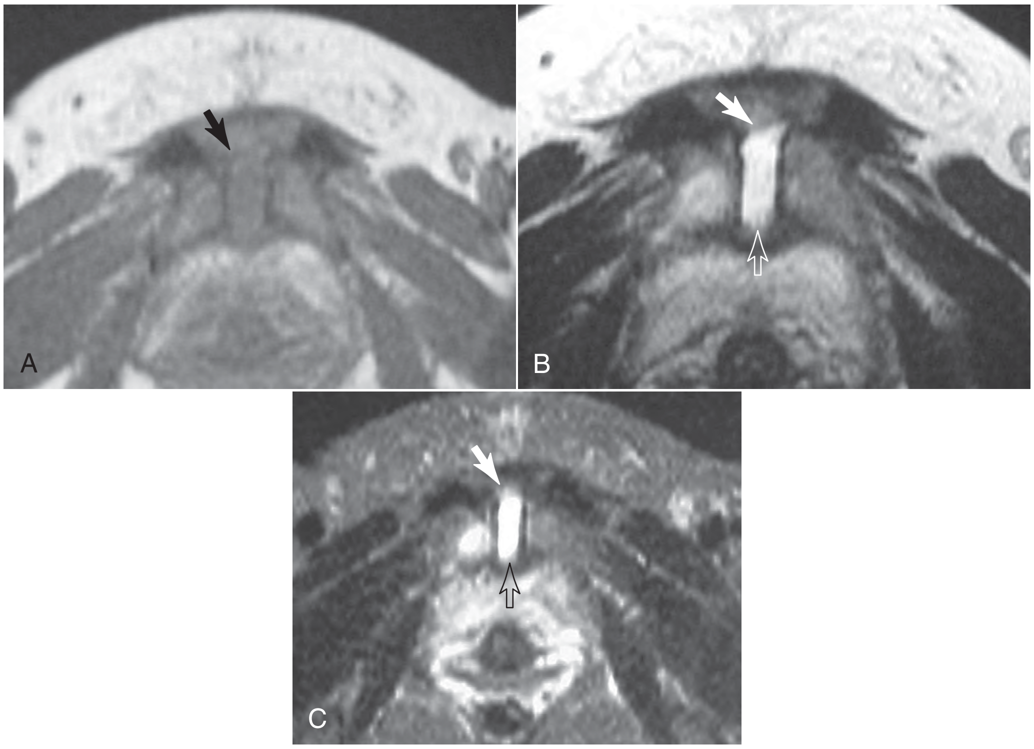

FIGURE 6–39 **Infective osteitis pubis.**[35,45] This 32-year-old female developed persistent symphyseal pain and fever after a normal pregnancy and a natural delivery. Widening of the symphysis pubis is evident *(arrows)* on transaxial T1-weighted **(A),** T2-weighted **(B),** and fat-suppressed T2-weighted (STIR) **(C),** MR images. High signal intensity within the symphysis pubis is seen *(open arrows)* on both T2-weighted sequences, a finding that proved to be a result of infectious arthritis. A circular focus of high signal intensity in the body of the right pubis is evident in image **C.**

TABLE 6-8 **Tumors and Tumorlike Lesions Affecting the Pelvis***

Entity	Figure(s)	Characteristics
Malignant Neoplasms		
Skeletal Metastasis[46,47,112]	6-40	15% of skeletal metastatic lesions affect pelvic bones A diagnosis of avulsion fracture of the pelvis in an adult without appropriate history of substantial trauma must raise the suspicion of an underlying malignancy and may require additional imaging evaluation and even biopsy
Primary Malignant Neoplasms of Bone		
Osteosarcoma[48,93]	6-41	7% of osteosarcomas affect the pelvic bones May be osteoblastic, osteolytic, or mixed Many different types
Osteoblastoma (aggressive)[49]		13% of aggressive osteoblastomas affect the pelvic bones Expansile osteolytic lesion that may be partially ossified or contain calcium
Chondrosarcoma (conventional)[50,51]	6-42	24% of chondrosarcomas affect the pelvic bones Peripheral chondrosarcomas arise from preexisting osteochondromas, or infrequently manifests as juxtacortical lesions arising from the periosteal membrane Central chondrosarcomas may contain a bulky cartilaginous cap Tend to be osteolytic lesions frequently containing calcifications Soft tissue masses common in pelvic lesions
Giant cell tumor (aggressive)[52]		Only 4% of aggressive giant cell tumors involve the pelvis Eccentrically located osteolytic lesion
Fibrosarcoma[53]	6-43	10% of fibrosarcomas affect the pelvic bones Purely osteolytic destruction with no associated sclerotic reaction or periostitis
Ewing sarcoma[54]	6-44	18% of Ewing sarcomas affect the pelvic bones Aggressive permeative or moth-eaten pattern of bone destruction

* See also Tables 1-12 to 1-14.

Continued

TABLE 6-8 Tumors and Tumorlike Lesions Affecting the Pelvis—cont'd

Entity	Figure(s)	Characteristics
Myeloproliferative Disorders		
Plasma cell (multiple) myeloma[55]	6-45	75% of all patients with plasma cell myeloma have the multiple form 27% of patients with myeloma have pelvic bone involvement
Solitary plasmacytoma[55]	6-46	25% of all patients with plasma cell myeloma have the solitary form; 70% of these eventually develop into multiple myeloma 13% of solitary plasmacytomas affect the bones of the pelvis
Hodgkin disease[56]		11% of lesions in Hodgkin disease occur in the pelvic bones
Primary lymphoma (non-Hodgkin)[57,58,91]		18% of bone lesions in non-Hodgkin lymphoma occur in the pelvic bones
Leukemia[59]	6-47	Occasional pelvic involvement
Benign Neoplasms		
Primary Benign Neoplasms of Bone		
Enostosis[60]	6-48	25% of enostoses (bone islands) occur in the pelvic bones, especially about the acetabulum
Osteoid osteoma[61]	6-49	Only 2% of osteoid osteomas occur in the pelvic bones
Osteoblastoma (conventional)[62]		Rare involvement of pelvic bones (2%)
Enchondroma (solitary)[51,63]		Only 3% of solitary enchondromas affect the pelvic bones
Enchondromatosis (Ollier disease)[63]		Lesions of Ollier disease resemble multiple enchondromas and frequently occur in the pelvis
Maffucci syndrome[63]		More than 20% of lesions in Maffucci syndrome occur in the pelvis Multiple enchondromas and soft tissue hemangiomas
Osteochondroma (solitary)[51,64]	6-50	Only 5% of solitary osteochondromas arise from the bones of the pelvis
Hereditary multiple exostosis[51,65]		The multiple osteochondroma-like lesions occasionally involve pelvic bones, but femoral necks are more frequently affected
Giant cell tumor (benign)[66]	6-51	Fewer than 5% of benign giant cell tumors are located in the pelvic bones
Simple bone cyst[67]	6-52	2% of simple bone cysts occur in the pelvis; multiloculated and eccentric
Aneurysmal bone cyst[68]	6-53	Almost 10% of aneurysmal bone cysts involve the pelvic bones Eccentric, thin-walled, expansile, multiloculated osteolytic lesion
Tumorlike Lesions		
Paget disease[69-71,94,95]	6-54, 6-55	Predilection for pelvic bones Usually polyostotic and may have unilateral involvement of one hemipelvis May result in protrusio acetabuli and osteoarthrosis of the hip Fewer than 2% undergo malignant transformation
Neurofibromatosis 1[72]		Formerly designated *von Recklinghausen disease* Occasional pelvic bone involvement Dysplastic appearance with deformity and remodeling of bone and circumscribed osteolytic lesions
Monostotic fibrous dysplasia[73]	6-56, *A-B*	*Monostotic pelvic involvement rare:* 7% of all monostotic lesions affect the pelvis Malignant transformation rare
Polyostotic fibrous dysplasia[73]	6-56, *C*	Pelvic bone involvement is seen in 78% of cases of polyostotic fibrous dysplasia Unilateral or bilateral, asymmetric involvement of the innominate bones usually associated with concomitant disease in the proximal portion of the femur Lesions contain thick rim of sclerosis surrounding a radiolucent lesion; ground-glass appearance of matrix Acetabular protrusion may occur
Langerhans cell, histiocytosis[74,75]	6-57	20% of lesions affect the pelvic bones, most frequently eosinophilic granuloma Malignant transformation rare, but more common than in solitary fibrous dysplasia

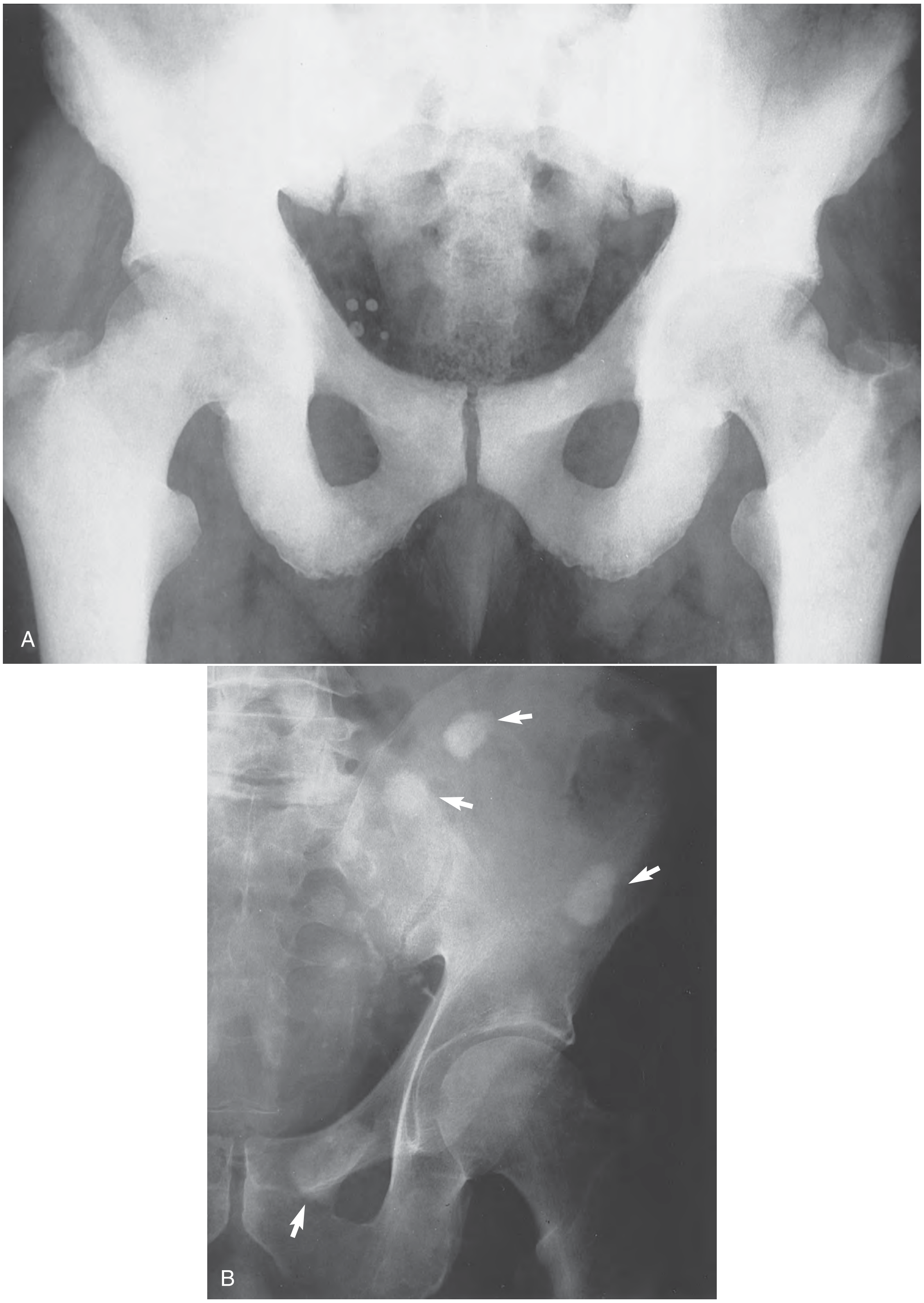

FIGURE 6–40 **Skeletal metastasis: spectrum of abnormalities.**[46,47] **A,** Diffuse osteosclerotic pattern. Frontal pelvic radiograph of this man with prostate carcinoma shows uniform, diffuse osteosclerosis of the pelvis, sacrum, and proximal portions of the femora. **B,** Patchy osteosclerotic pattern. In another patient with prostate carcinoma, observe the distinct, asymmetric, circular, and oval osteoblastic lesions *(arrows)* throughout the bones of the pelvis.

Continued

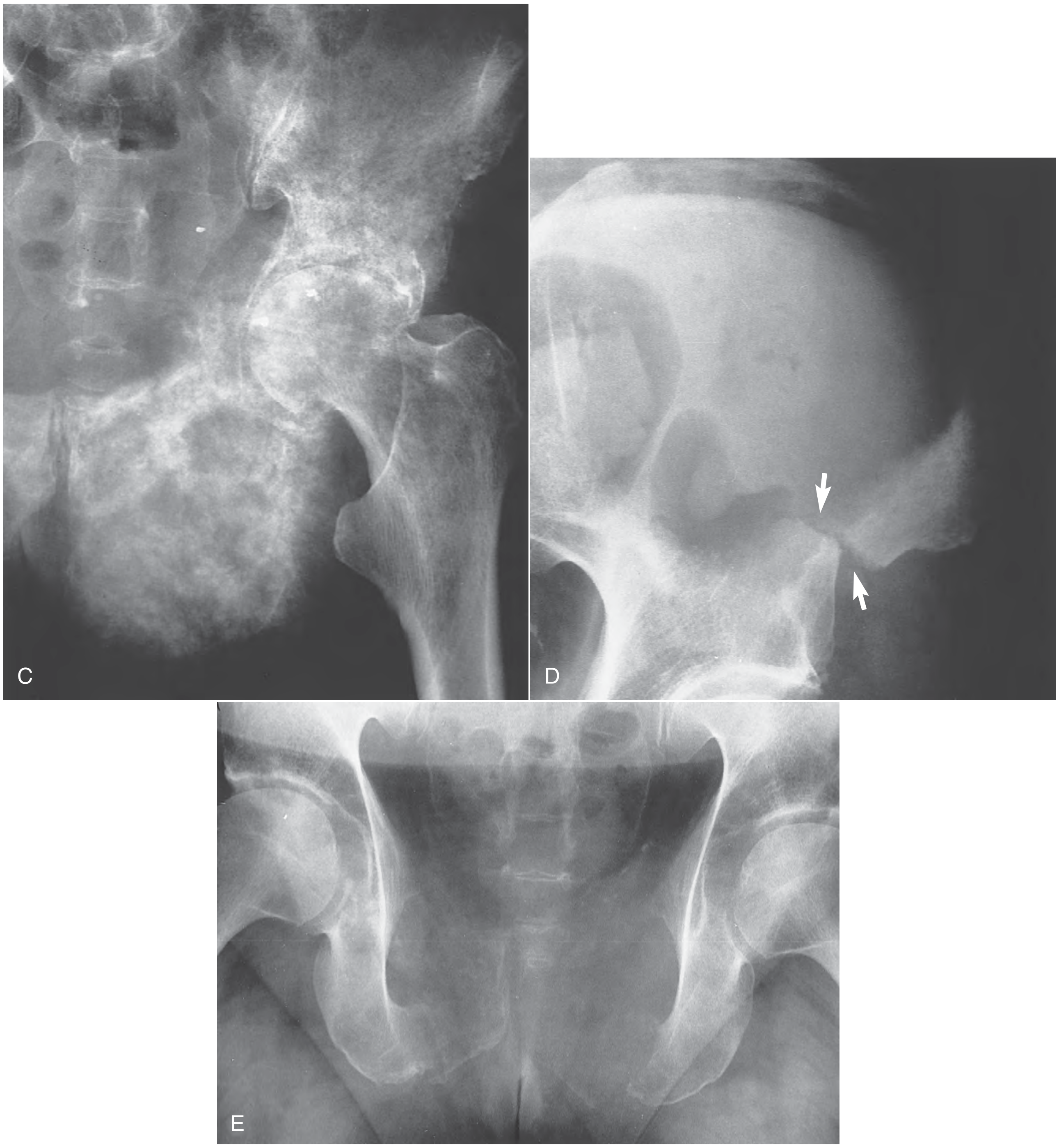

FIGURE 6–40, cont'd **C,** Expansile pattern. A radiograph of the pelvis of this patient with primary bronchogenic carcinoma shows a bizarre, expansile, mixed pattern of osteolysis and osteosclerosis. The cortical margins are poorly defined, and acetabular protrusion is evident. Skeletal metastases secondary to primary carcinoma of the kidney, thyroid, and lung often exhibit a blow-out pattern of severe osteolytic destruction. **D,** Pathologic fracture. A huge osteolytic metastatic lesion of the ilium is associated with a transverse pathologic fracture *(arrows)* secondary to osseous weakening. Breast metastasis is the leading cause of pathologic fracture in skeletal metastasis. **E,** Osteolytic pattern. Widespread destruction of both pubic rami is evident in this patient with skeletal metastasis from bronchogenic carcinoma.

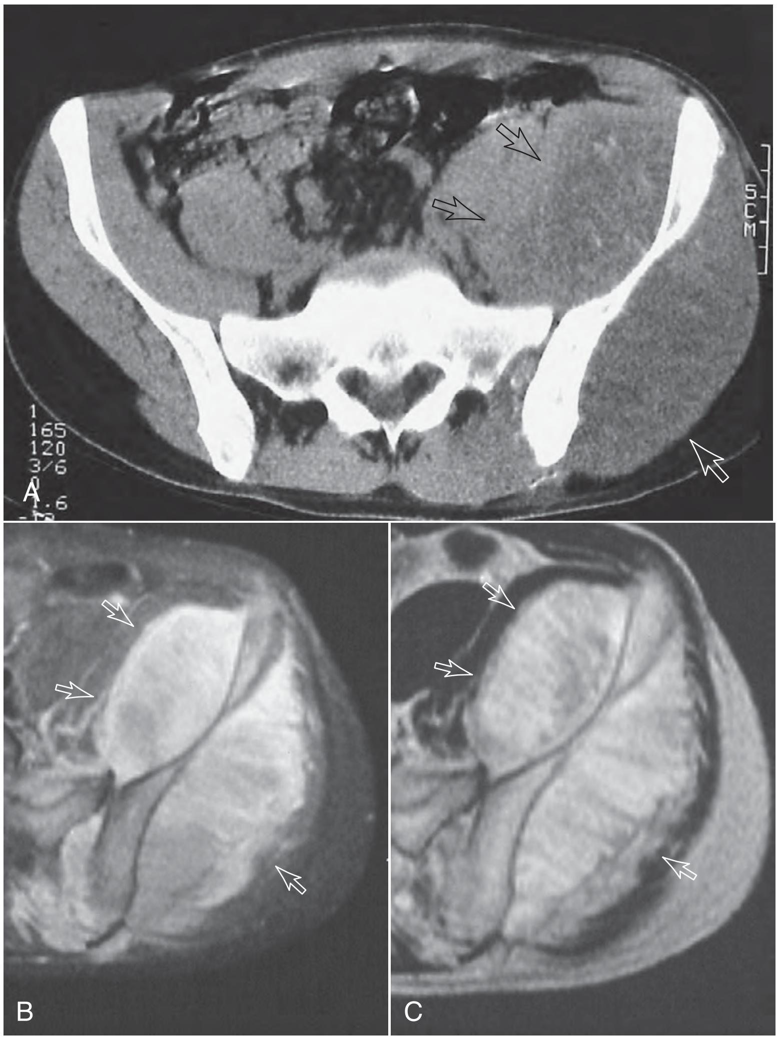

FIGURE 6–41 Osteosarcoma.[48,93] This 16-year-old boy had persistent left hip and buttock pain. A transaxial CT scan **(A)** shows a large, low attenuation mass containing calcification located anterior and posterior to the iliac wing *(arrows)*. A transaxial T1-weighted MR image **(B)** obtained after intravenous administration of gadolinium shows intense enhancement of a huge inhomogeneous mass on both sides of the ilium that contains linear low intensity streaking. A similar appearance is seen on a T2-weighted axial image **(C).** The linear streaking within the matrix of the mass represents a spiculated or sunburst periosteal reaction. The pathologic diagnosis in this case was chondroblastic high-grade osteosarcoma.

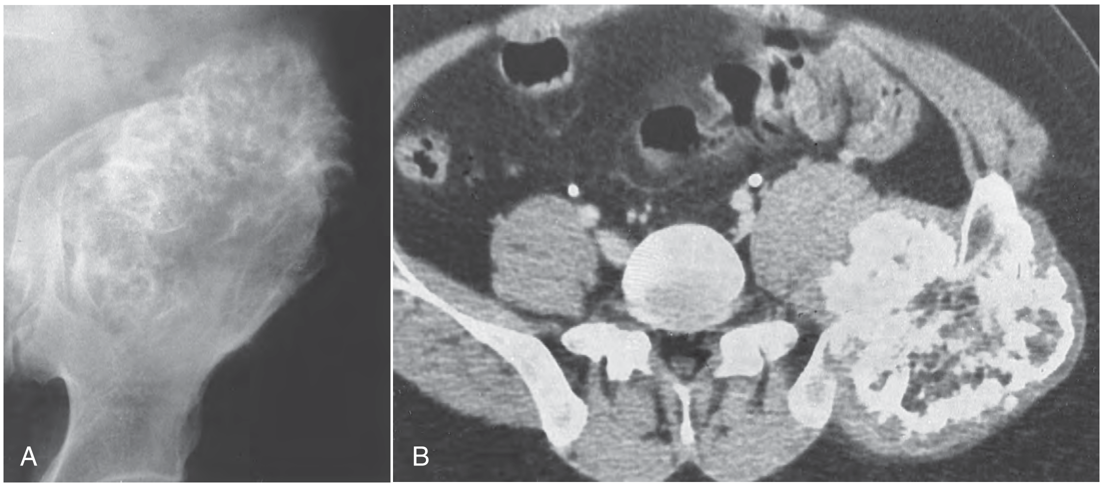

FIGURE 6–42 Chondrosarcoma.[50,51] This 25-year-old man complained of a painful lump in the gluteal region. **A,** The routine radiograph shows a bizarre, irregular, calcified excrescence resembling a cauliflower arising from the ilium. **B,** Transaxial CT image depicts the lesion clearly. Observe the tumor expanding into the pelvis, displacing pelvic structures, and expanding into the buttock, displacing the gluteal musculature. These findings are visible on the CT scan, but are not well seen on the radiograph. *(Courtesy T. Mattson, MD, Riyadh, Saudi Arabia.)*

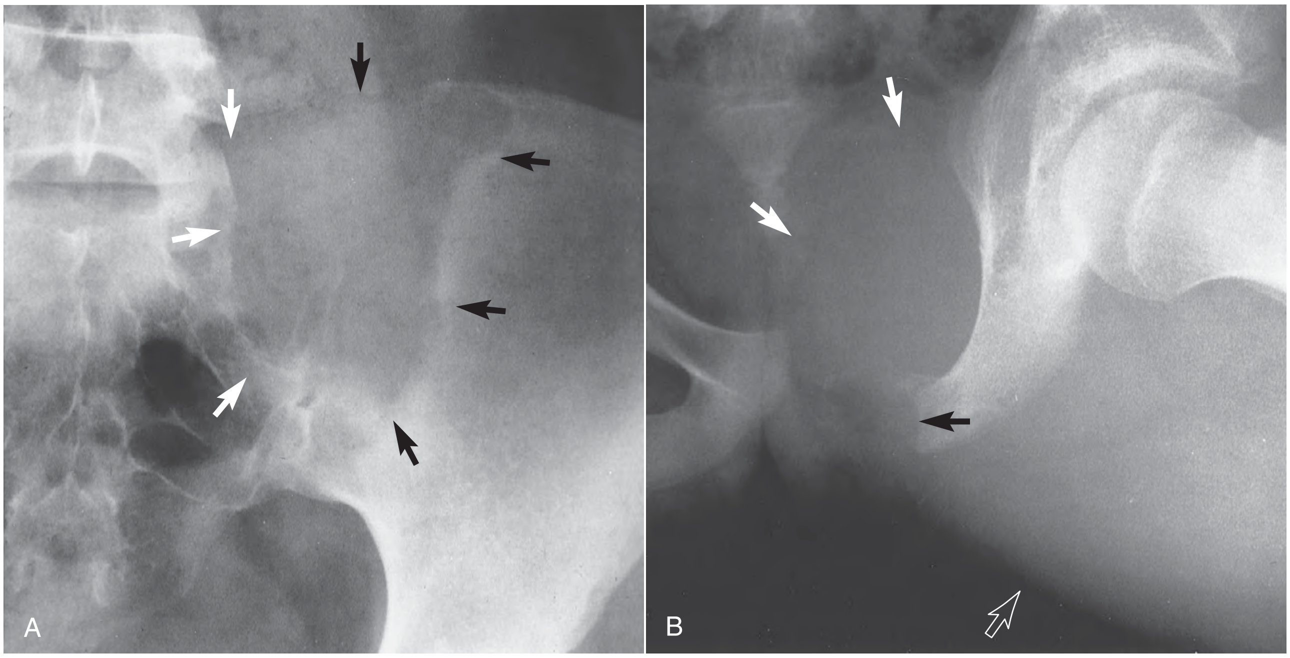

FIGURE 6–43 **Fibrosarcoma.**[53] **A,** A purely osteolytic lesion involving both the ilium *(black arrows)* and the sacrum *(white arrows)* is seen. No reactive sclerosis is identified. **B,** In a 13-year-old boy, complete osteolytic destruction of the pubic bone *(arrows)* is seen. No evidence of calcification or ossification is present within the lesion. Marked soft tissue swelling or a soft tissue mass is seen *(open arrow)*. The histologic diagnosis based on biopsy results was fibrosarcoma.

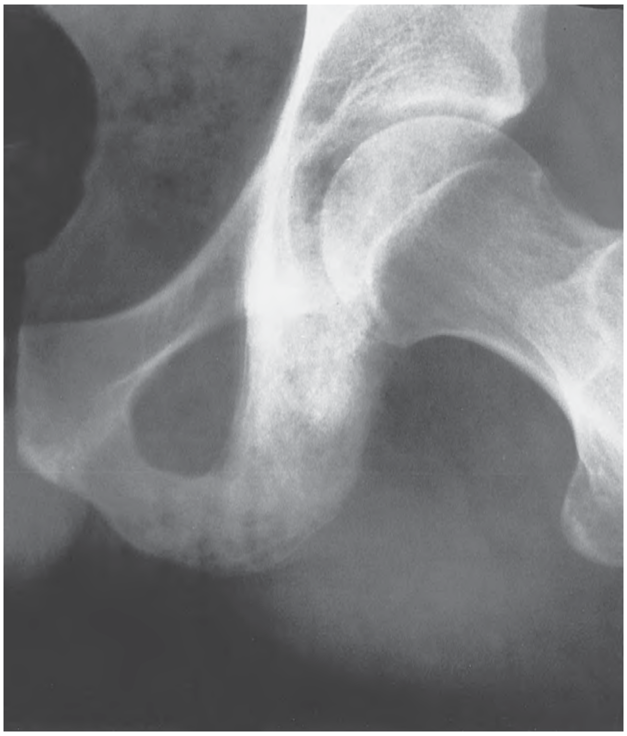

FIGURE 6–44 **Ewing sarcoma.**[54] A permeative pattern of bone destruction combined with sclerosis is evident in this aggressive lesion of the ischium in a 17-year-old male patient. A laminated periosteal response is evident along the medial aspect of the ischium.

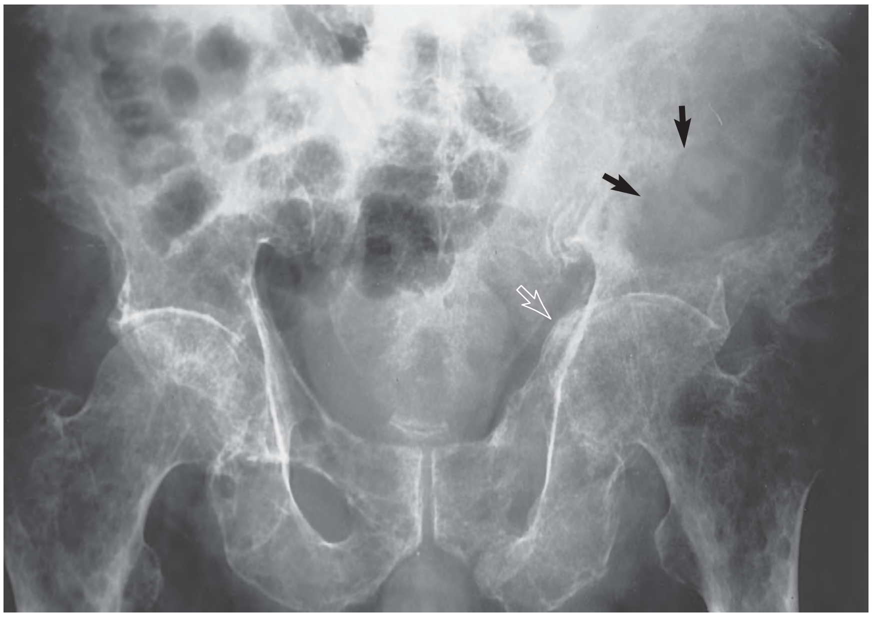

FIGURE 6–45 **Plasma cell (multiple) myeloma.**[55] Diffuse osteopenia and numerous osteolytic lesions permeate the bones of the pelvis and proximal femora. Pathologic collapse of the left acetabulum has resulted in acetabular protrusion *(open arrow)*. A large zone of osteolytic destruction is seen in the left ilium *(arrows)*.

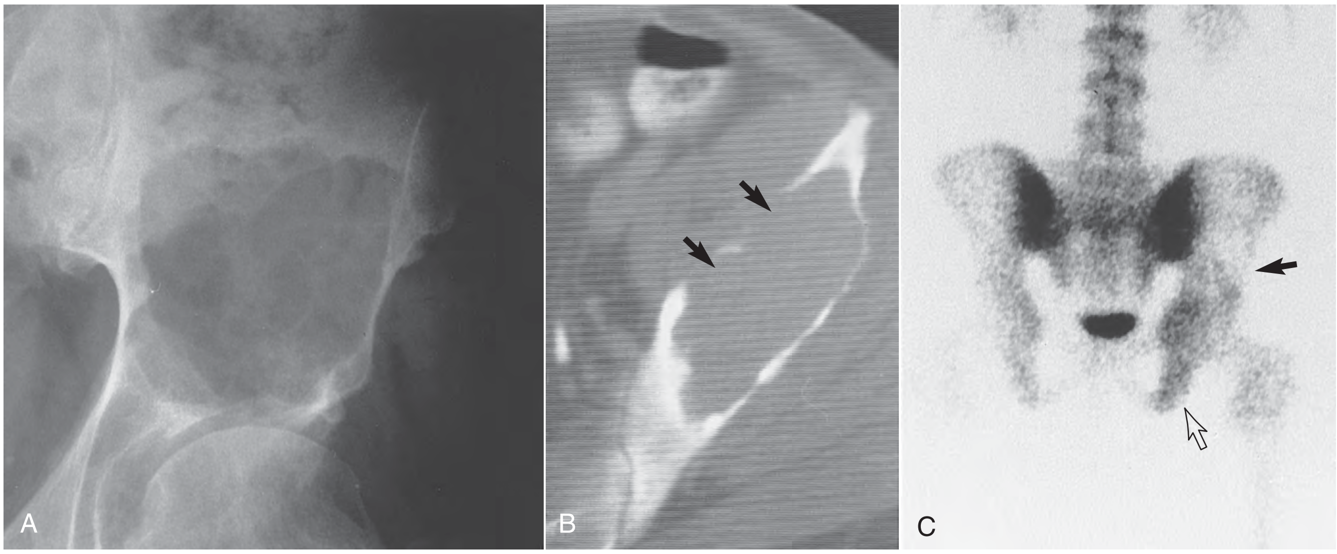

FIGURE 6–46 **Solitary plasmacytoma.**[55] The patient is a 44-year-old man with back and buttock pain. **A,** Routine radiograph shows a large, multiloculated, osteolytic lesion of the ilium. **B,** Transaxial CT scan demonstrates the slightly expansile nature of the lesion and confirms the presence of cortical perforation *(arrows)*. **C,** Scintigraphy: Mildly decreased uptake of the radiopharmaceutical agent is seen at the site of the lesion *(arrow)* on the bone scan, with mildly increased uptake in the adjacent bone of the ischiopubic ramus *(open arrow)*. These are findings that may relate to additional stress at this site. False-negative results on bone scans are common in plasma cell myeloma, and these scans should not be relied on to exclude the diagnosis.

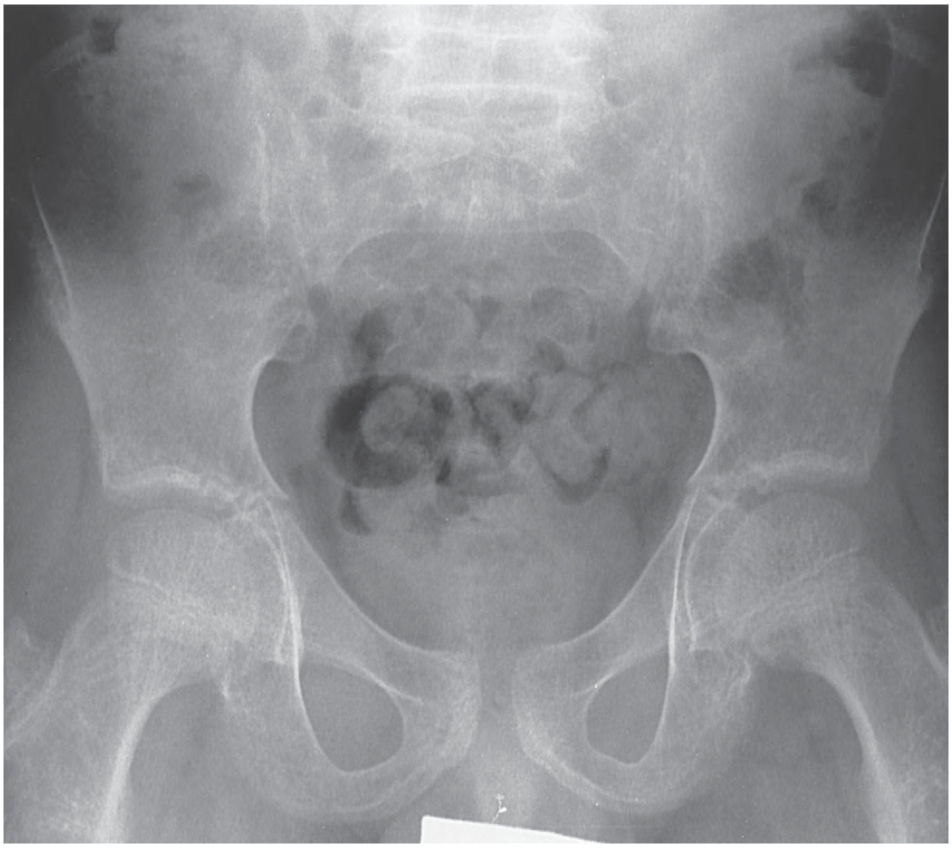

FIGURE 6–47 Acute childhood leukemia.[59] This 11-year-old boy has generalized osteopenia throughout the bones of the pelvis and proximal ends of the femora. Growth recovery lines are seen about the symphysis pubis.

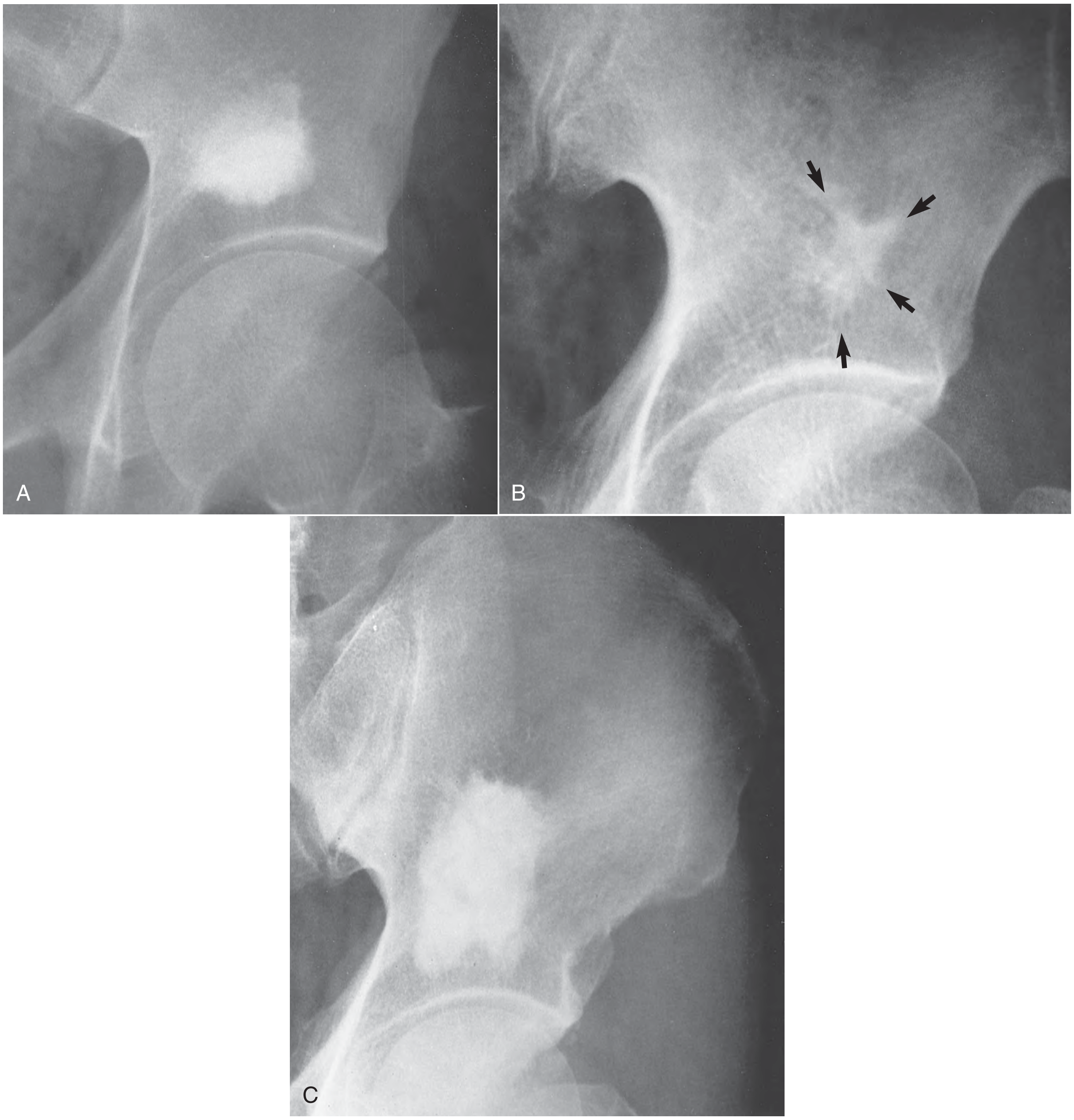

FIGURE 6–48 **Enostosis (bone island).**[60] **A,** A large, solitary, circular, osteosclerotic lesion is located in the supraacetabular region, a common site of bone islands. **B,** This enostosis has prominent radiating spicules along its margin *(arrows)*. **C,** Giant bone island. In another patient, observe the huge osteosclerotic lesion with a spiculated margin in the supraacetabular region. (***B,** From Taylor JAM, Harger BL, Resnick D: Diagnostic imaging of common hip disorders: A pictorial review. Top Clin Chiropr 1:8, 1994.)*

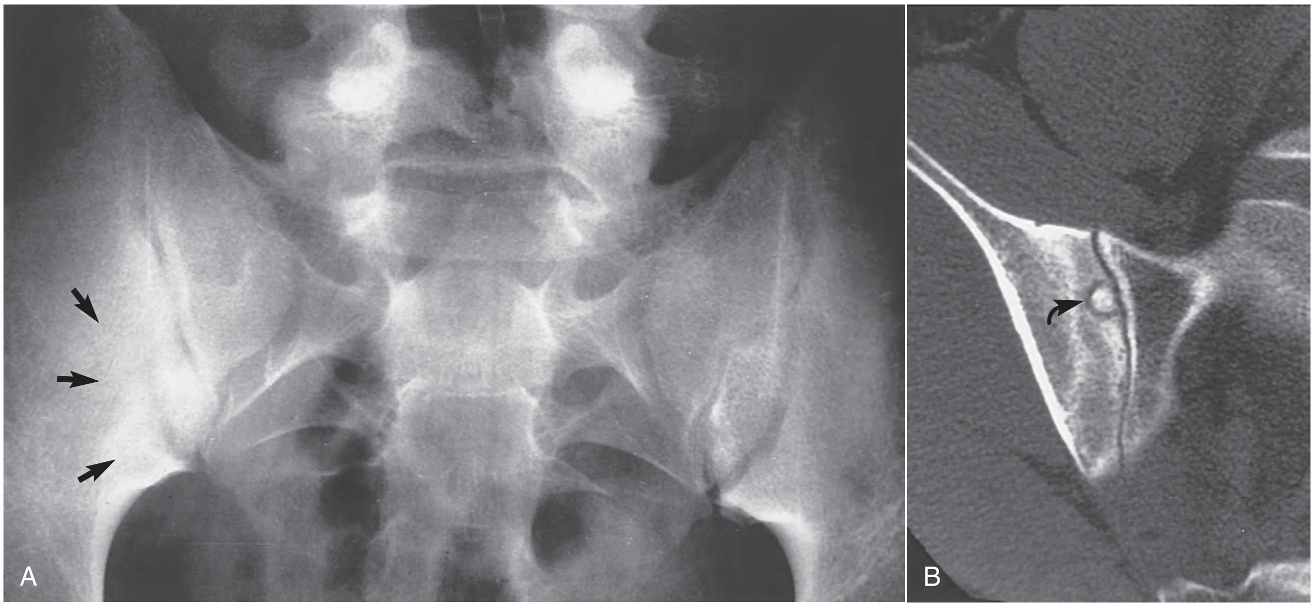

FIGURE 6–49 **Osteoid osteoma.**[61] **A,** Frontal radiograph reveals nonspecific sclerosis of the right ilium adjacent to the sacroiliac joint *(arrows)*. The nidus of the tumor is not visible on the plain radiograph. **B,** Transaxial CT scan shows, in exquisite detail, the partially calcified nidus *(curved arrow)* surrounded by reactive sclerosis, a classic appearance of osteoid osteoma. *(Courtesy A. D'Abreu, MD, Porto Alegre, Brazil[JT4].)*

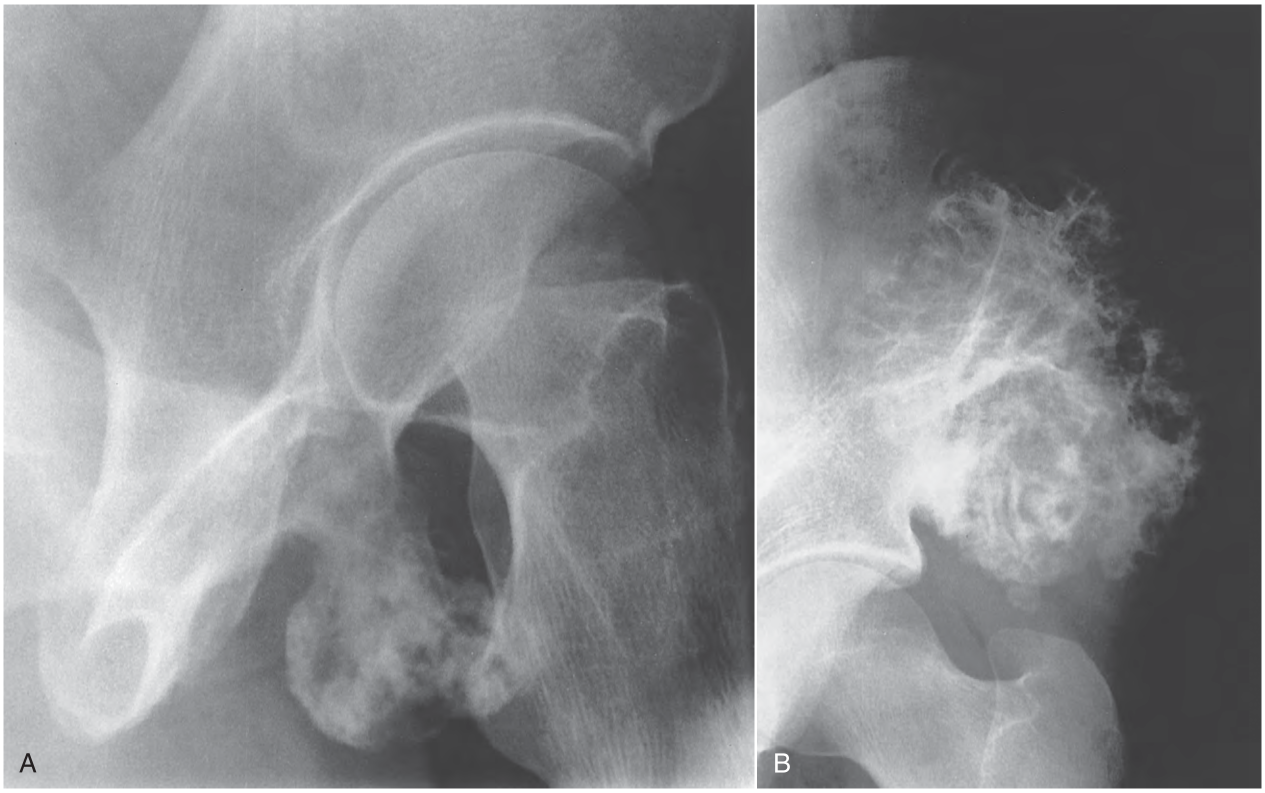

FIGURE 6–50 **Solitary osteochondroma.**[51,64] **A,** *Ischium:* A large, pedunculated, osseous outgrowth is seen arising from the ischium and projecting toward the lesser trochanter of the femur. The mass is bulbous, and the cortical margin is well defined. Small areas of radiolucency are seen within the substance of the lesion, most likely representing zones of unossified cartilage. **B,** *Ilium:* Possible malignant transformation to chondrosarcoma. A cauliflower-like osseous lesion arising from the ilium appears irregular and has multiple areas of radiolucency throughout its matrix. This lesion became painful, and was growing rapidly. The biopsy result was equivocal, indicating possible transformation to chondrosarcoma.

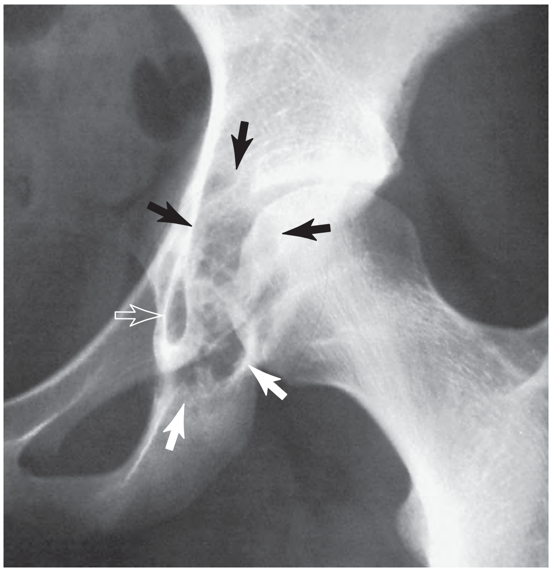

Figure 6–51 **Giant cell tumor: acetabulum.**[66] This anteroposterior view in a 21-year-old woman reveals a multiloculated, geographic, osteolytic lesion involving the medial wall of the acetabulum *(arrows)* and Kohler teardrop *(open arrow)*. The lesion is slightly expansile, and is partially visualized through the overlying femoral head. It does not appear to have provoked a periosteal reaction or produced cortical destruction. The pathologic diagnosis was a giant cell tumor.

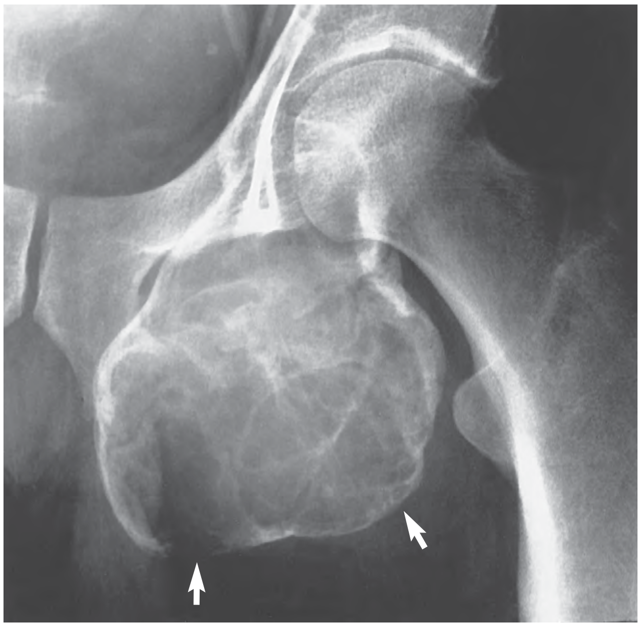

FIGURE 6–53 **Aneurysmal bone cyst.**[68] An expansile, multiseptated osteolytic lesion arises from the ischiopubic ramus of this 40-year-old man *(arrows)*. The sclerotic margins are well defined. (The apparent cortical lucent shadow in the lower margin of the tumor is an artifact of photographic reproduction.) The histologic diagnosis was an aneurysmal bone cyst. *(Courtesy R. Stiles, MD, Atlanta.)*

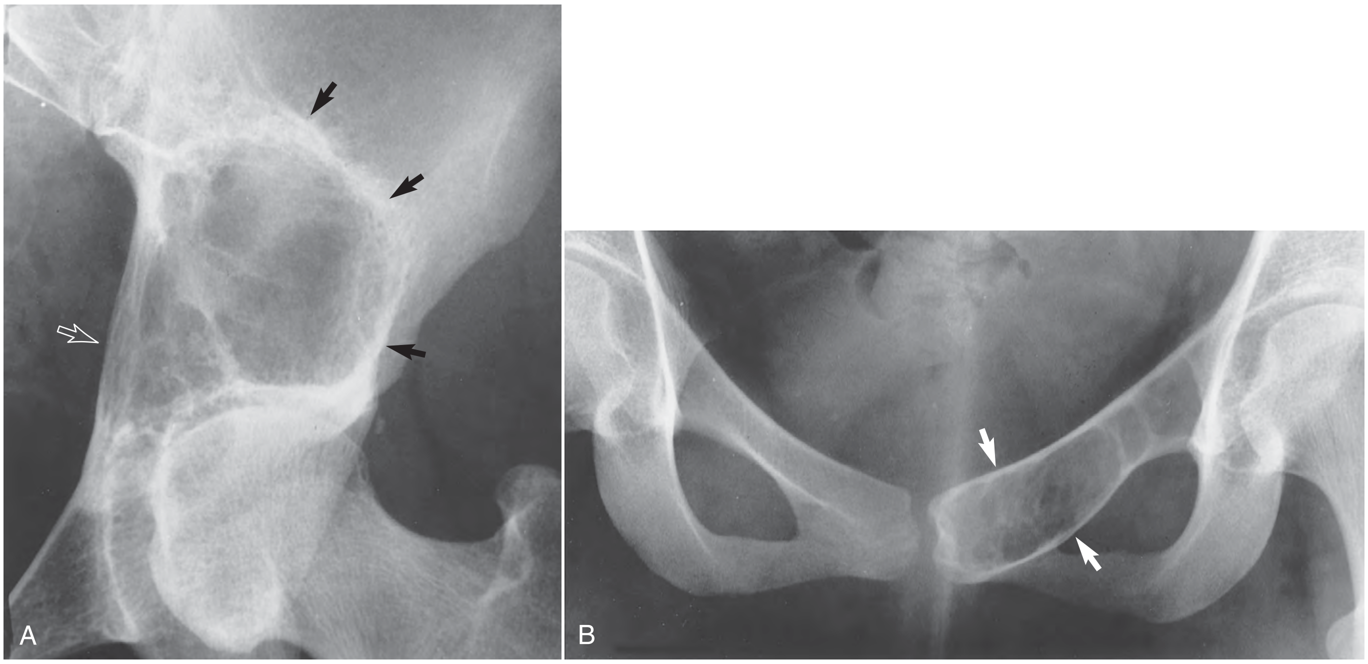

FIGURE 6–52 **Simple bone cyst.**[67] **A,** This 21-year-old woman has a biopsy-proved simple bone cyst in the acetabulum, which was found incidentally on pelvic radiographs performed for trauma. Frontal radiograph reveals a geographic, radiolucent, multiloculated lesion with cortical thinning medially *(open arrow)* and a thin sclerotic margin surrounding its periphery *(arrows)*. This simple bone cyst resembles fibrous dysplasia and giant cell tumor. **B,** Simple bone cyst. Radiographs obtained from a 20-year-old woman after a fall demonstrate a radiolucent lesion within the pubic ramus. It is a centrally located, geographic, expansile, multiloculated lesion. Cortical thinning and a thin sclerotic margin *(arrows)* are evident. The patient had no pain over this area before the fall.

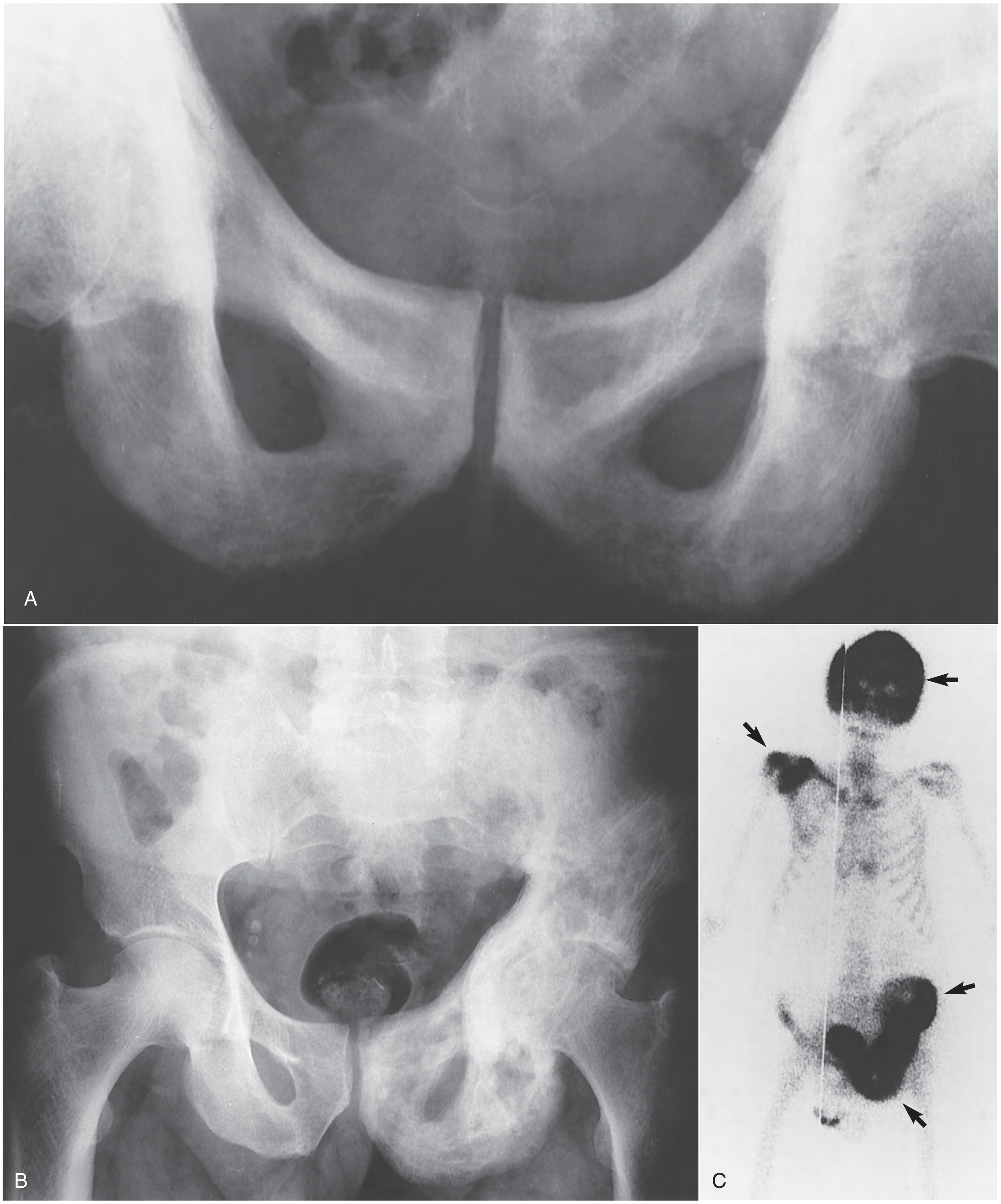

FIGURE 6–54 **Paget disease.**[69,70,94,95] **A,** Osteosclerotic pattern. In this patient with long-standing Paget disease, generalized osteosclerosis and trabecular thickening are evident. **B** and **C,** Hemipelvis involvement in another patient. In **B,** diffuse osteosclerosis, trabecular and cortical bone thickening, bone enlargement, and acetabular protrusion involve only the left hemipelvis. In **C,** intense scintigraphic activity is evident in the left hemipelvis, skull, and right scapula *(arrows)*.

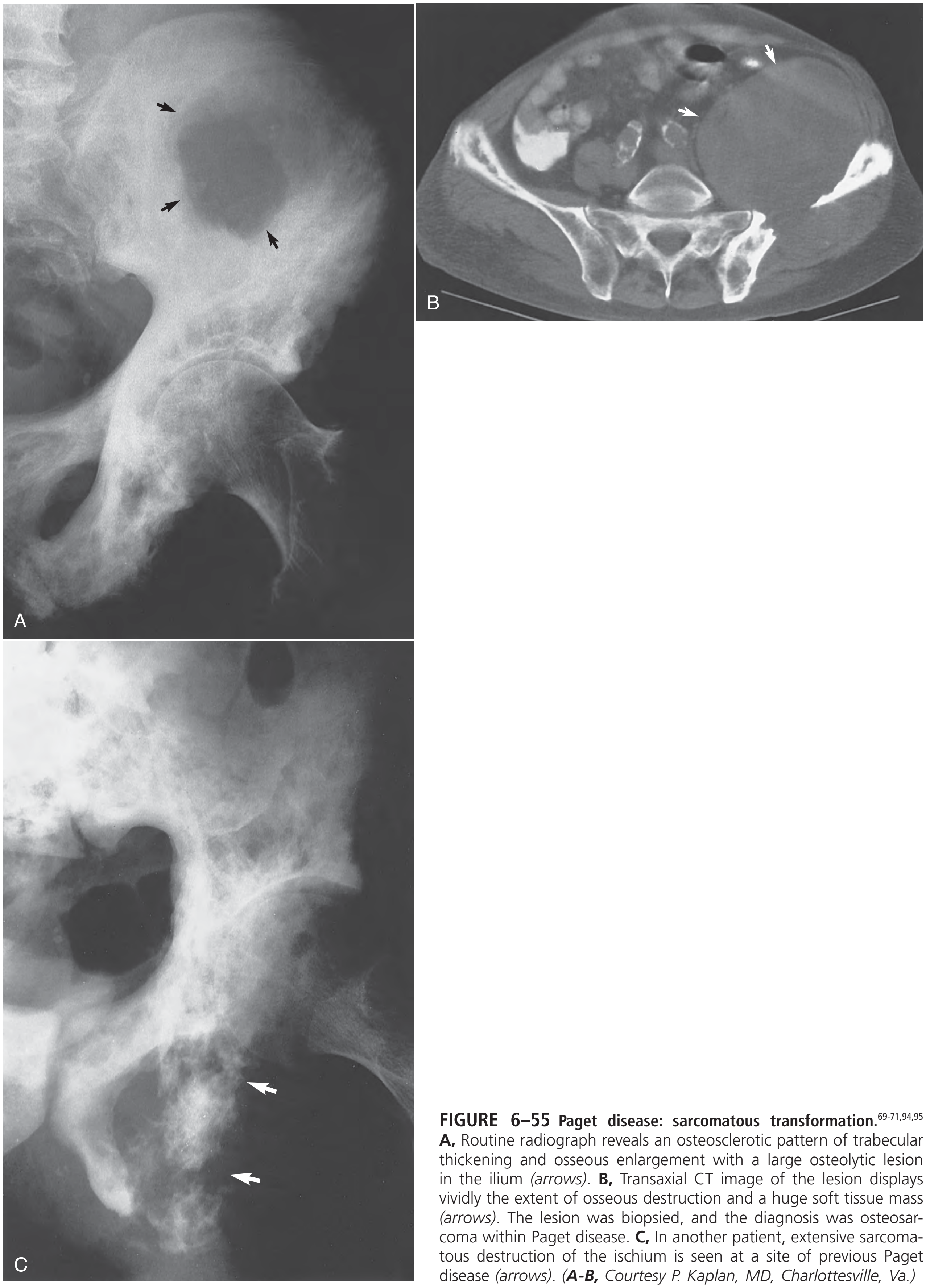

FIGURE 6–55 Paget disease: sarcomatous transformation.[69-71,94,95] **A,** Routine radiograph reveals an osteosclerotic pattern of trabecular thickening and osseous enlargement with a large osteolytic lesion in the ilium *(arrows)*. **B,** Transaxial CT image of the lesion displays vividly the extent of osseous destruction and a huge soft tissue mass *(arrows)*. The lesion was biopsied, and the diagnosis was osteosarcoma within Paget disease. **C,** In another patient, extensive sarcomatous destruction of the ischium is seen at a site of previous Paget disease *(arrows)*. *(**A-B,** Courtesy P. Kaplan, MD, Charlottesville, Va.)*

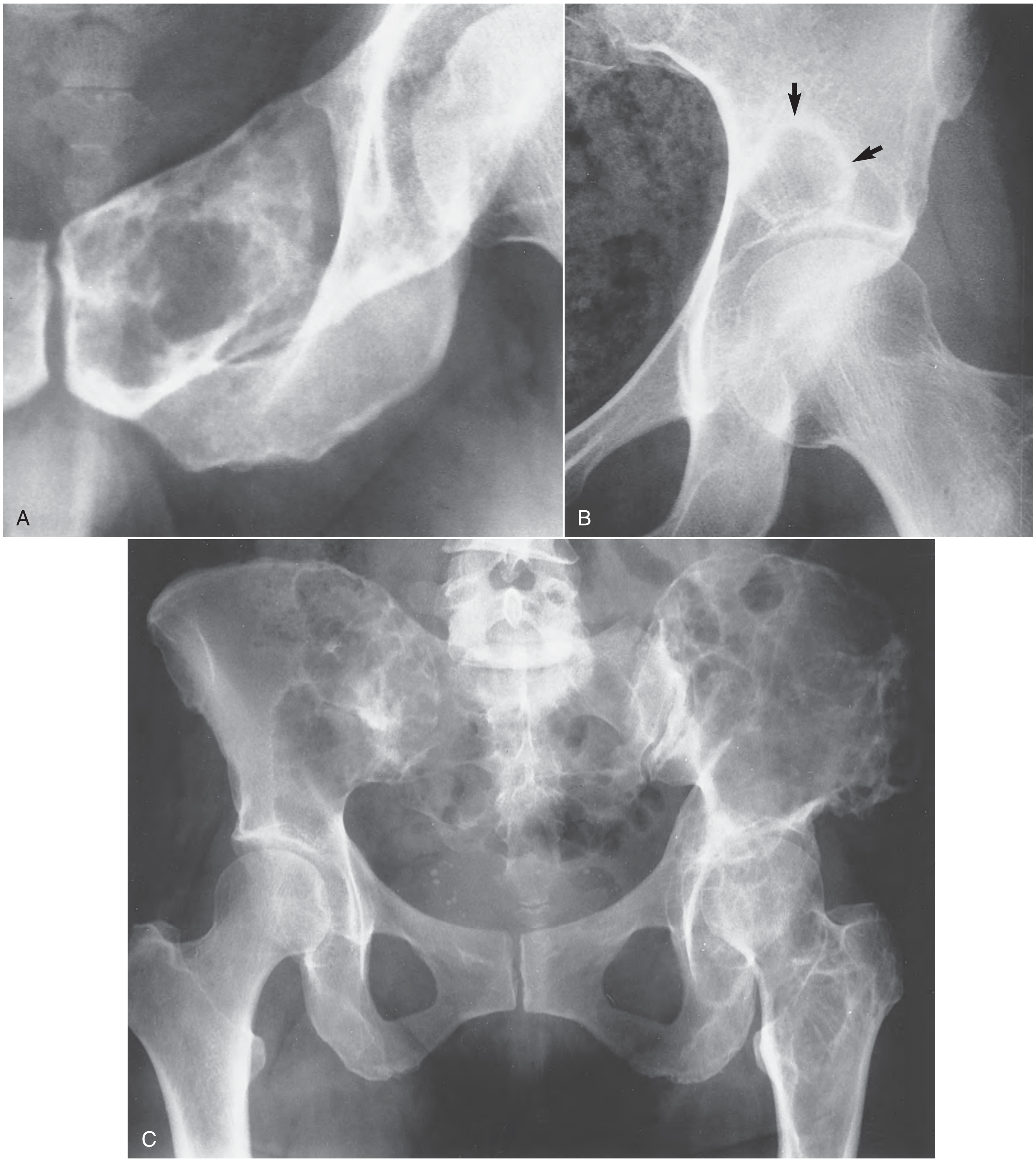

FIGURE 6–56 **Fibrous dysplasia.**[73] **A,** Monostotic form. In this 54-year-old man, an expansile, multiloculated lesion in the pubic ramus demonstrates the characteristic ground-glass appearance of fibrous dysplasia. **B,** This 49-year-old woman with monostotic fibrous dysplasia has a well-defined supraacetabular lesion with a sclerotic margin *(arrows)*. **C,** Polyostotic form: pelvis and femur. Observe the multiloculated, osteolytic, slightly expansile lesions throughout the pelvis and left femur of this 55-year-old woman. The lesions are surrounded by continuous curvilinear sclerotic margins, and the tumor matrix appears smoky or hazy, a finding termed the *ground-glass appearance*. *(**B,** Courtesy G. Greenway, MD, Dallas.)*

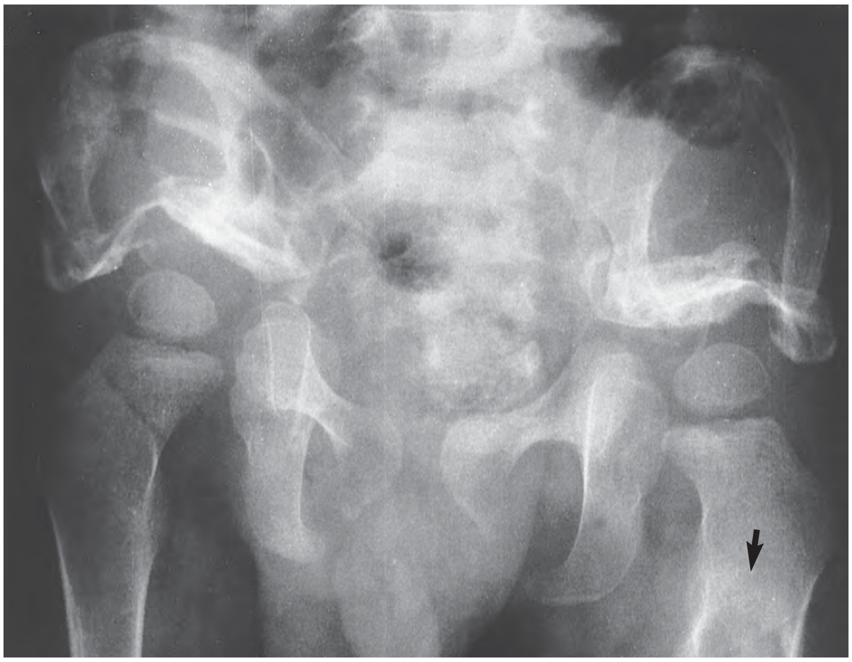

FIGURE 6–57 Langerhans cell histiocytosis: eosinophilic granuloma.[74,75] Observe the large osteolytic lesions involving both ilia and proximal portion of the femur *(arrow)*. Prominent acetabular remodeling and collapse are also evident.

TABLE 6-9 Metabolic, Hematologic, and Infectious Disorders Affecting the Pelvis*

Entity	Figure(s)	Characteristics
Generalized osteoporosis[76]		Uniform decrease in radiodensity, thinning of cortices, accentuation of weight-bearing trabeculae May result in parasymphyseal and supraacetabular insufficiency fractures
Osteomalacia[77]	6-58	Diminished radiodensity and prominent coarsened trabeculae Transverse "pseudofractures" common in osteomalacia
Hyperparathyroidism and renal osteodystrophy[78]	6-59	*Brown tumor:* solitary or multiple expansile osteolytic lesions containing fibrous tissue and giant cells; may disappear after treatment for hyperparathyroidism Subchondral resorption about symphysis pubis and sacroiliac joints
Hypoparathyroidism[79]	6-60	Prominent enthesopathy and bone proliferation arising from pelvic bones: resembles changes of diffuse idiopathic skeletal hyperostosis (DISH) Osteosclerosis (as many as 23% of patients) Painless subcutaneous calcification
Mastocytosis[80]	6-61	Resembles lymphoma and leukemia; combinations of diffuse or focal osteosclerosis or, less likely, osteopenia or osteolysis
Sickle cell anemia[81,82]	6-62	Diffuse osteopenia or osteosclerosis and osteonecrosis
β-thalassemia[82,90]	6-63	Diffuse osteopenia with lacelike trabecular pattern Marrow hyperplasia, growth disturbances, fractures, crystal deposition, extramedullary hematopoiesis
Hemophilia[83,84]	6-64	*Hemophilic pseudotumor:* geographic osteolytic lesions with internal trabeculation and multiloculated appearance
Osteomyelitis[85,105]	6-65	Poorly defined permeative bone destruction Periostitis; usually single layer or solid Osteomyelitis of the ischiopubic synchondrosis in children has been reported
Poliomyelitis[86]	6-66	Bone atrophy results in asymmetric hypoplasia and osteopenia of the hemipelvis and femur May result in scoliosis and mechanical disorders of the spine and lower extremity
Radiation changes[87,88]	6-67	***Adults*** Insufficiency fractures, osteomyelitis, bone infarcts, and radiation-induced neoplasms: osteosarcoma, malignant fibrous histiocytoma, chondrosarcoma ***Children*** Asymmetric hypoplasia of the pelvis and spine with scoliosis, and radiation-induced neoplasms: osteochondroma (common), enchondroma (rare), and osteoblastoma

* See also Tables 1-15, 1-16, and 1-19.

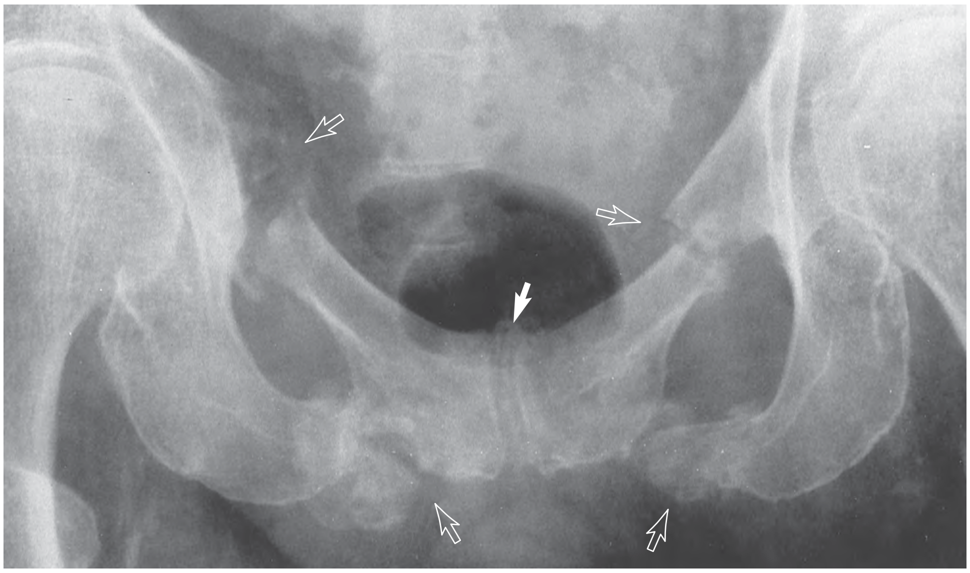

FIGURE 6–58 **Osteomalacia.**[77] Bilateral insufficiency fractures of the superior and inferior pubic rami *(open arrows)* are seen in this 85-year-old woman. The fractures occurred several months earlier, and healing appears to be delayed, with evidence of osteolysis and incomplete callus formation. Chondrocalcinosis of the symphysis pubis *(arrow),* related to calcium pyrophosphate dihydrate (CPPD) crystal deposition, is also evident.

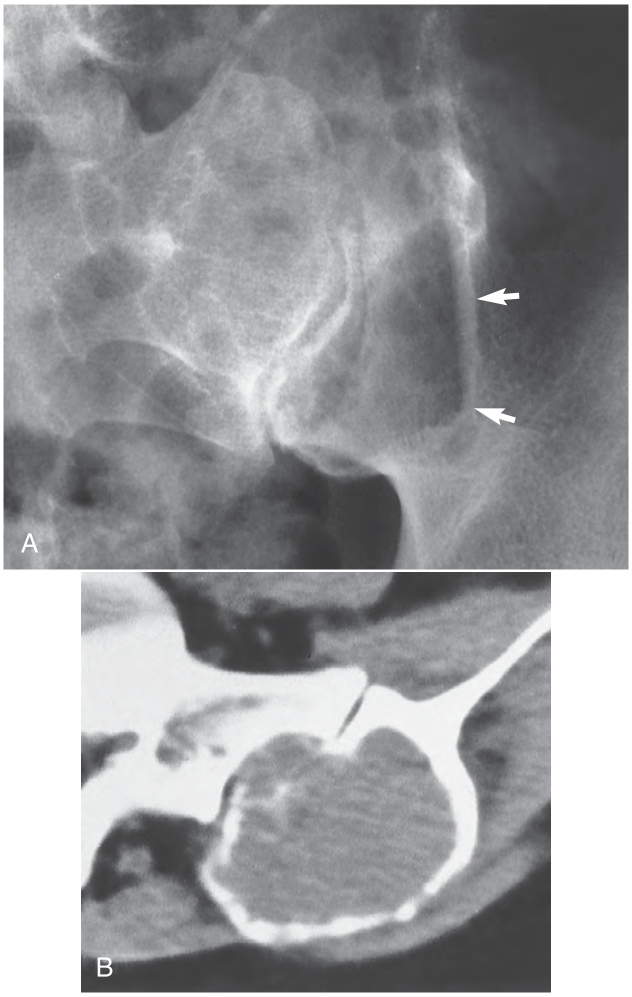

FIGURE 6–59 **Renal osteodystrophy: hyperparathyroidism with brown tumors.**[78] **A,** Routine radiograph shows an expansile osteolytic lesion with a thick sclerotic margin *(arrows)* in the subchondral region of the ilium adjacent to the sacroiliac joint. **B,** CT scan taken with a transaxial soft tissue window clearly displays the expansile nature of this lesion with a well-corticated margin. *(Courtesy A. Newberg, MD, Boston.)*

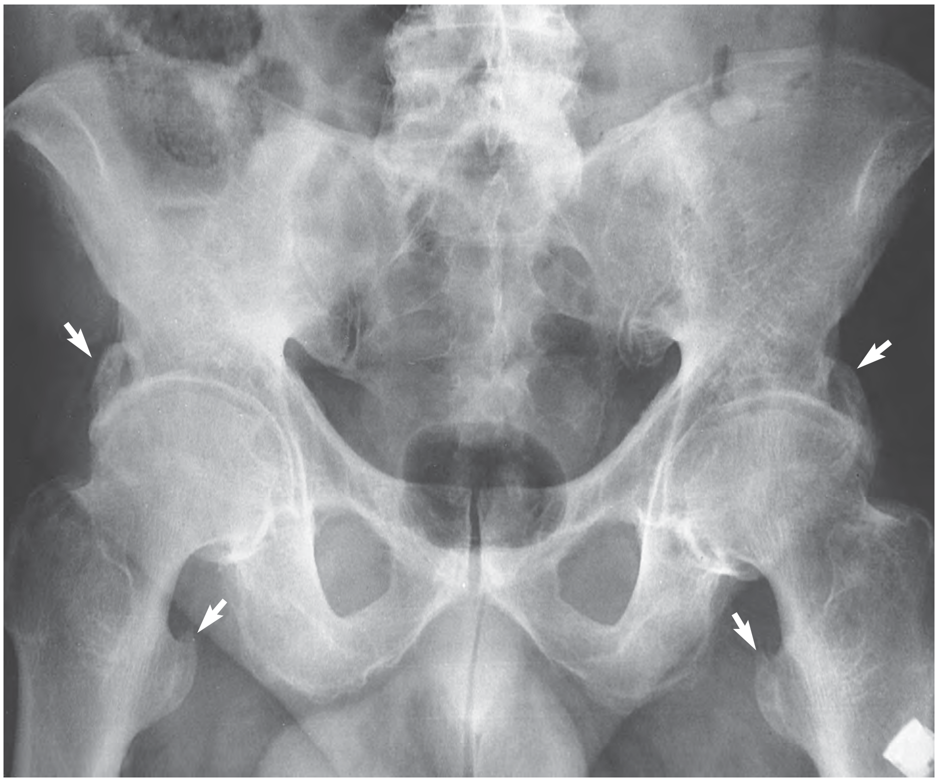

FIGURE 6–60 **Hypoparathyroidism: enthesopathy.**[79] Observe the bone proliferation adjacent to the acetabulum and other surfaces of the pelvic bones *(arrows)* in this 49-year-old man. These changes resemble those of diffuse idiopathic skeletal hyperostosis (DISH). *(Courtesy V. Wing, MD, Walnut Creek, Calif.)*

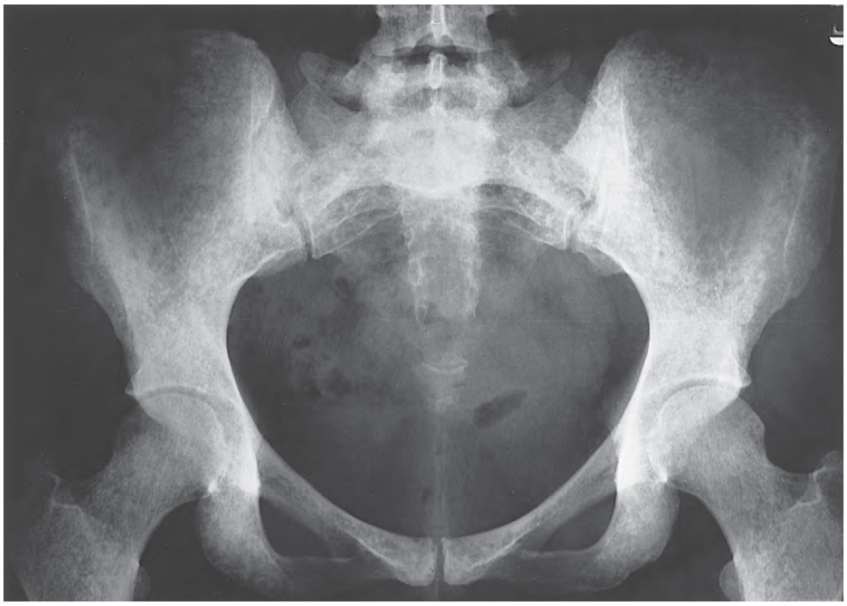

FIGURE 6–61 **Mastocytosis.**[80] Observe the widespread, patchy osteosclerosis throughout the pelvic bones of this 38-year-old woman. *(Courtesy B. Holtan, MD, Rock Springs, Wyo.)*

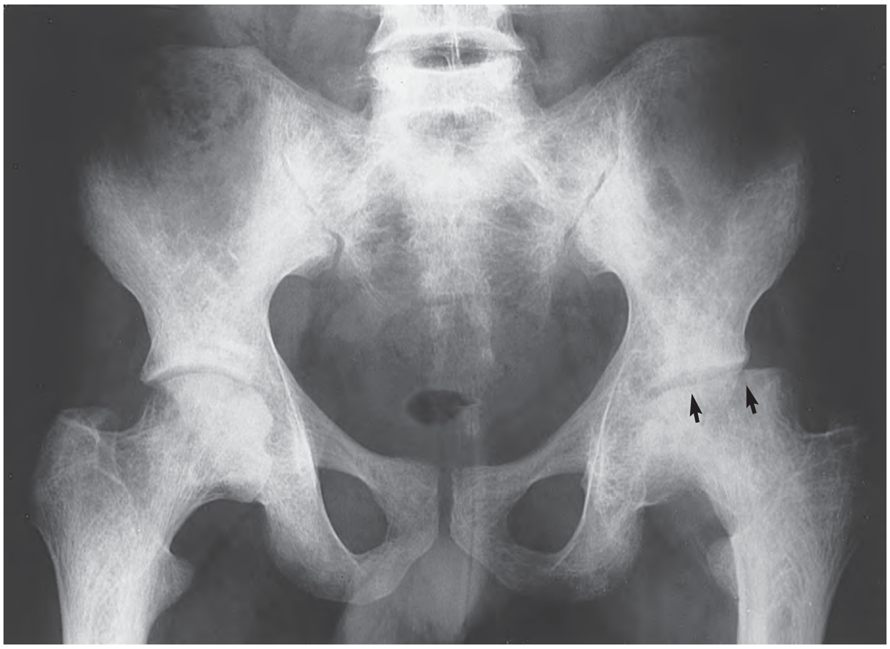

FIGURE 6–62 **Sickle cell-hemoglobin C disease.**[81] In this 24-year-old man, the bones are sclerotic, the trabeculae are coarsened, and the femoral heads are osteonecrotic. The left femoral head is significantly collapsed *(arrows)*. Note deformity of the lower lumbar vertebral bodies.

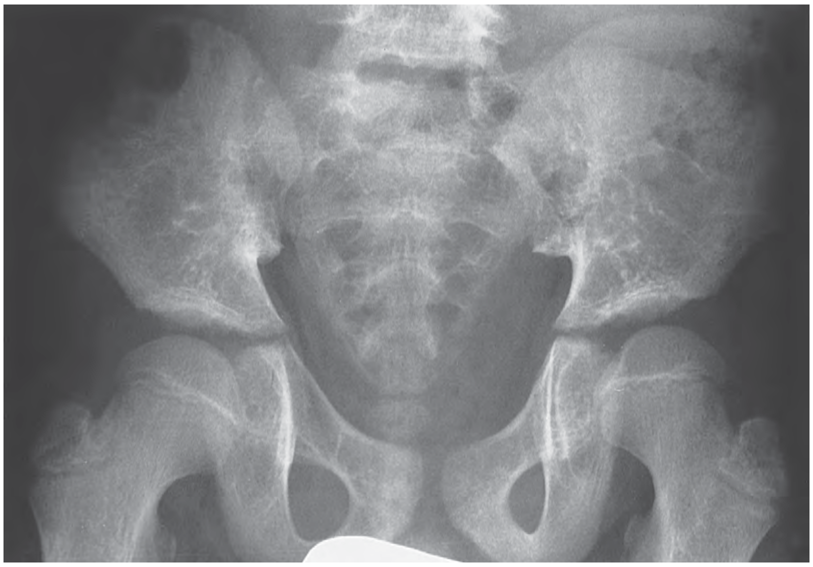

FIGURE 6–63 **ß-thalassemia.**[82,90] Observe the lacy trabecular pattern, osteoporosis, and extreme thinning of cortical bone in the pelvis of this 11-year-old girl with thalassemia.

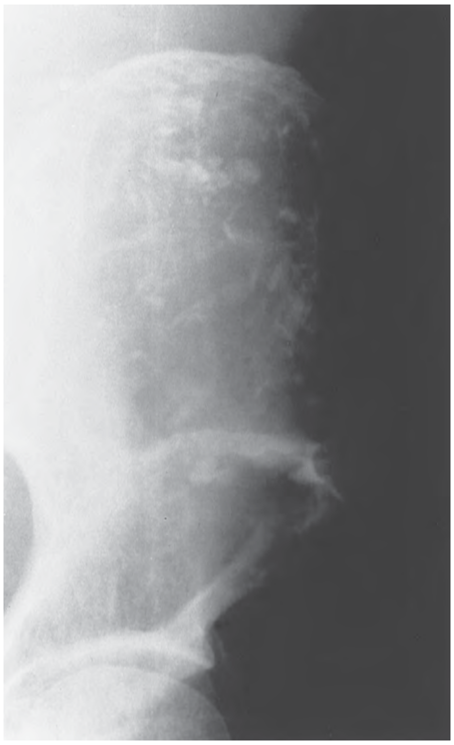

FIGURE 6–64 **Hemophilia: pseudotumor.**[83,84] A large, slightly expansile, osteolytic lesion located in the ilium is seen in this 37-year-old man with long-standing hemophilia. Osseous debris is present within the matrix of the lesion. The hemophilic pseudotumor results from intraosseous or subperiosteal hemorrhage.

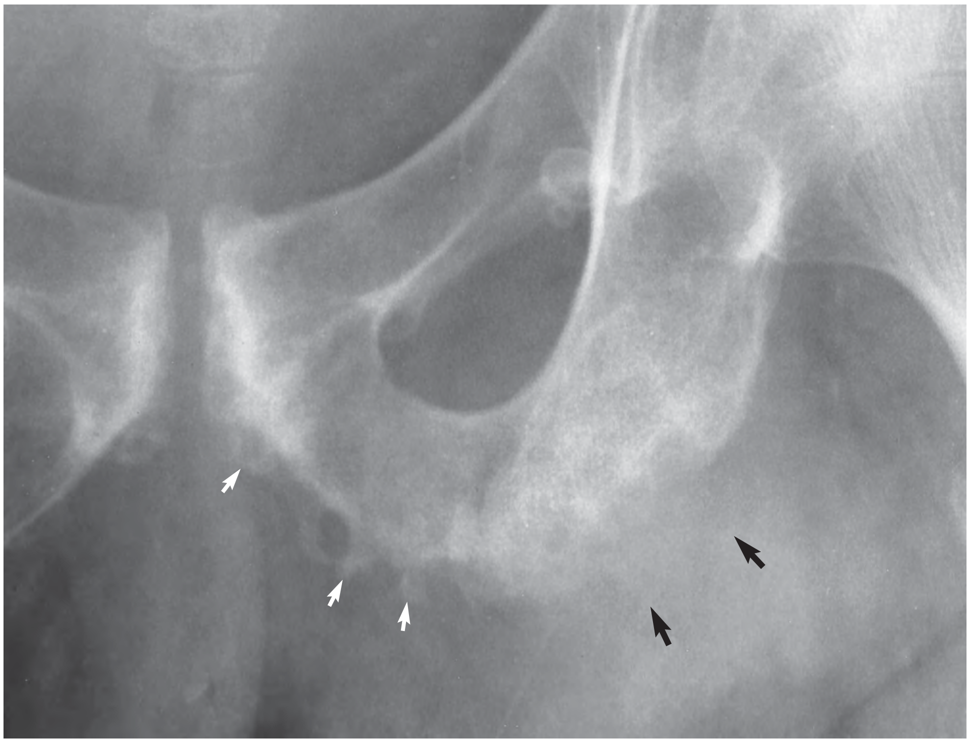

FIGURE 6–65 **Osteomyelitis: actinomycosis.**[85] This 72-year-old man has a sinus draining to his buttock. Diffuse soft tissue swelling and a large erosion of the ischial tuberosity are seen *(black arrows)*. Osseous outgrowths arising from the pubic bone *(white arrows)* probably represent degenerative enthesopathy. Actinomycosis is a noncontagious, suppurative infection that is caused by anaerobic organisms normally found in the mouth.

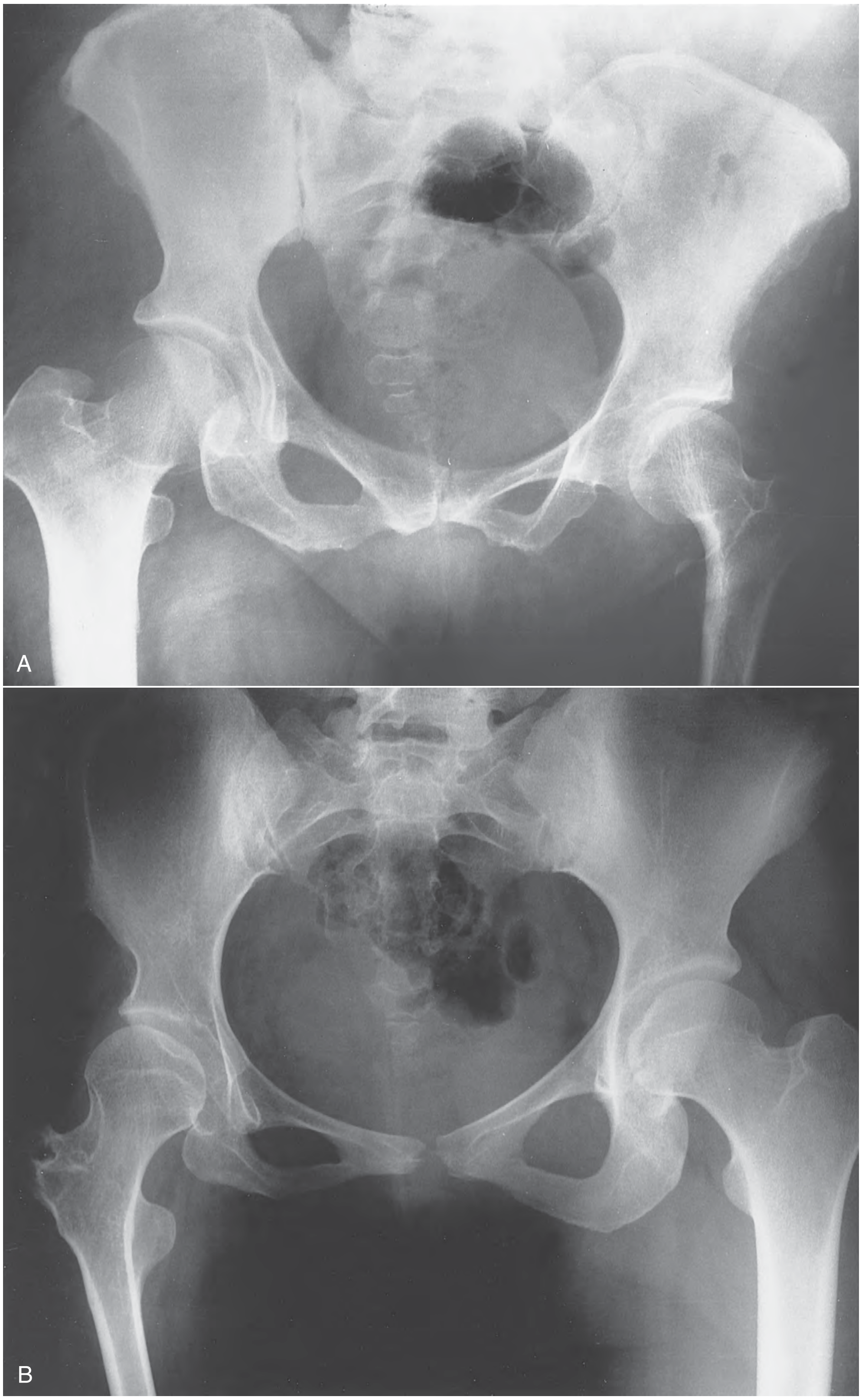

FIGURE 6–66 Poliomyelitis: bone atrophy.[86] **A,** Observe the coxa valga deformity, hypoplasia, and osteopenia of the left hemipelvis, sacrum, and proximal portion of the femur in this 53-year-old woman with poliomyelitis. **B,** In another patient, right-sided atrophy of the hemipelvis and proximal portion of the femur are associated with unilateral osteopenia.

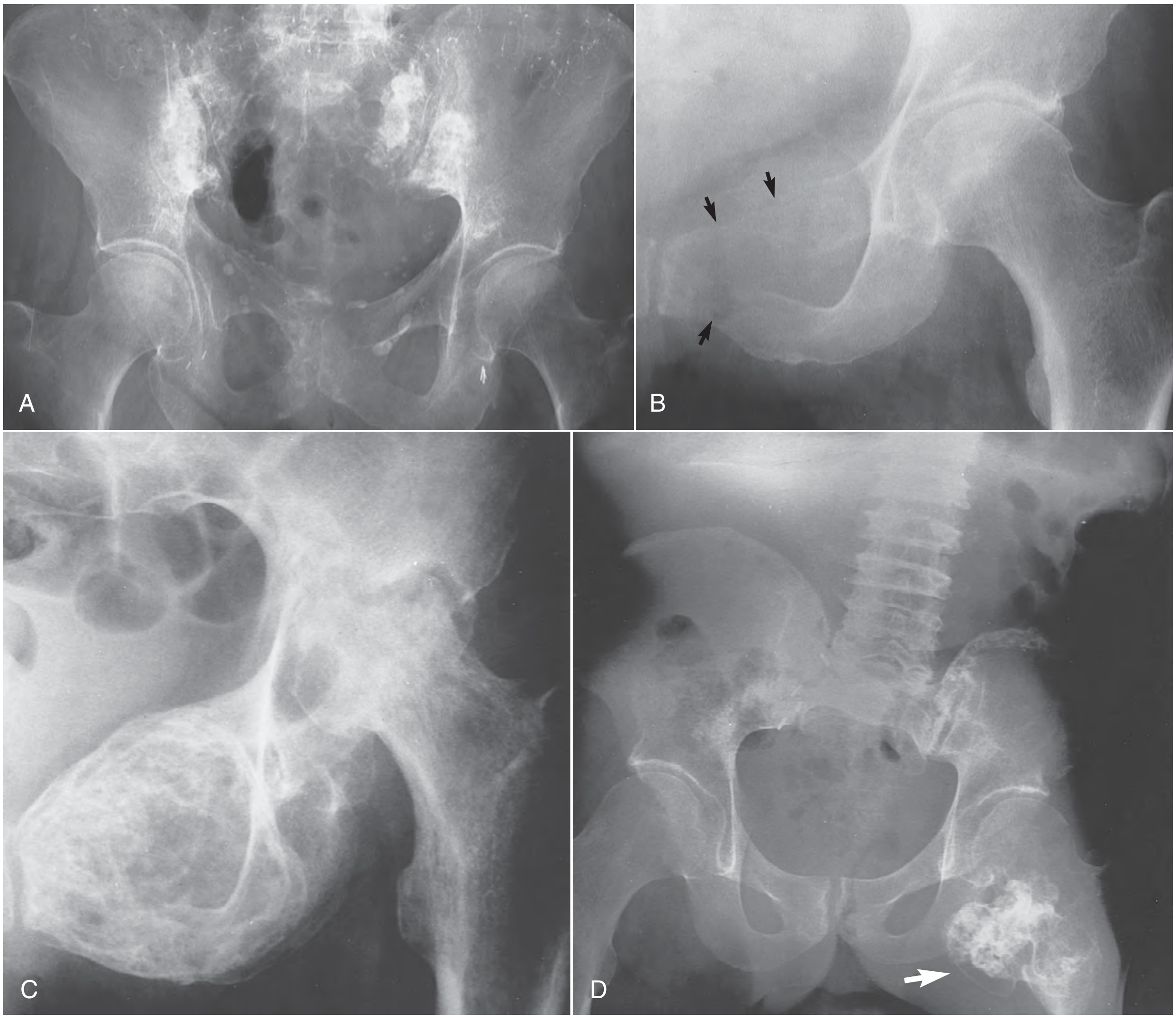

FIGURE 6–67 Radiation changes.[87,88] **A,** Insufficiency fractures. This 80-year-old woman underwent radiation therapy for carcinoma of the uterine cervix. Observe the multiple osteosclerotic insufficiency fractures involving the sacrum, ilia, and parasymphyseal region. Differentiation among radiation changes, skeletal metastasis, and chondrosarcoma may be difficult in such cases. **B-C,** 55-year-old woman with endometrial carcinoma. In **B,** a frontal pelvic radiograph shows osteolytic metastasis involving the left pubic ramus *(arrows)*. In **C,** another radiograph taken 30 months after a course of radiation therapy shows osteonecrosis of the femoral head and acetabulum. Mature ossification of the ischiopubic ramus is indicative of healing. **D,** Effects on the immature skeleton. This young patient underwent radiation therapy for Wilms' tumor. Observe the radiation-induced osteochondroma arising from the femur *(arrow),* platyspondyly, and unilateral hypoplasia of the left innominate bone. *(**B-C,** Courtesy H. Kroon, MD, Leiden, Netherlands.)*

CHAPTER 7

Hip

NORMAL DEVELOPMENTAL ANATOMY

Accurate interpretation of radiographs of the pediatric hip requires a thorough understanding of normal developmental anatomy. Table 7-1 outlines the age of appearance and fusion of the primary and secondary ossification centers. Figures 7-1 and 7-2 demonstrate the radiographic appearance of many important ossification centers and other developmental landmarks at selected ages from birth to skeletal maturity.

DEVELOPMENTAL ANOMALIES, ANATOMIC VARIANTS, AND SOURCES OF DIAGNOSTIC ERROR

The hip joint and proximal portion of the femur are sites of anomalies, anatomic variations, and other sources of diagnostic error that may simulate disease and potentially result in misdiagnosis. Table 7-2 and Figures 7-3 to 7-5 represent selected examples of some of the more common processes.

HIP DEFORMITIES

The proximal portion of the femur and the acetabulum are frequent sites for deformities such as coxa vara, coxa valga, and acetabular protrusion. Table 7-3 lists the major causes of such deformities. Figures 7-6 to 7-8 illustrate some selected examples of these deformities. Other examples are displayed throughout the chapter as they are manifested in several other diseases.

DEVELOPMENTAL DYSPLASIA OF THE HIP

Developmental dysplasia of the hip with associated instability, subluxation, and dislocation are important pediatric disorders that are described in Table 7-4. Some of the more useful radiographic measurements and their normal values are listed in Table 7-5. Figures 7-9 to 7-14 illustrate the imaging manifestations and radiographic measurements of developmental dysplasia.

PHYSICAL INJURY

Physical injury to the hip region may result in a wide variety of fractures of the proximal portion of the femur and acetabulum as well as dislocations of the hip joint itself. Table 7-6 outlines three types of hip dislocation, two of which are illustrated in Figure 7-15. Table 7-7 lists the most common types of fracture in this area. (Figures 7-16 to 7-24.) Table 7-8 describes the specific classifications of fractures of the proximal portion of the femur, and Table 7-9 lists their associated complications.

Several examples of these fractures are illustrated in Figures 7-18 to 7-20. Acetabular fractures were discussed and illustrated in Chapter 6 (Figure 6-25).

INTERNAL DERANGEMENTS

The soft tissues within and around the hip are complex and may be affected by a variety of developmental and acquired disorders. Table 7-10 describes internal derangements of the synovial structures within the hip joint and soft tissue disorders about the region of the hip. Figures 7-25 to 7-29 illustrate many features of these conditions, with an emphasis on MR imaging findings.

ARTICULAR DISORDERS

The hip joint is a frequent target site of involvement for many degenerative, inflammatory, crystal-induced, and infectious disorders of articulations. Table 7-11 outlines these diseases and their characteristics, and Table 7-12 identifies the patterns of joint space narrowing typical of these disorders. Figures 7-30 to 7-52 illustrate the typical radiographic manifestations of the most common articular disorders affecting the hip.

METABOLIC DISORDERS

Several metabolic disorders affect the hip joint as well as the surrounding osseous and soft tissue structures. Table 7-13 lists some of the more common disorders and discusses their characteristics. Table 7-14 describes the

Singh index, a radiographic method of analysis used in assessing bone density of the proximal portion of the femur. Figures 7-53 to 7-64 illustrate the typical imaging findings of many metabolic diseases.

OSTEONECROSIS OF THE FEMORAL HEAD

The femoral head is the most common site of involvement for osteonecrosis, an ischemic condition of bone. Additionally, Legg-Calvé-Perthes disease (osteonecrosis of the immature femoral head ossification center) is a relatively common condition that results in important clinical consequences. Table 7-15 lists the most important characteristics of osteonecrosis of the femoral head. Tables 7-16 and 7-17 outline the staging of Legg-Calvé-Perthes disease and adult osteonecrosis, respectively. Several examples of these disorders are illustrated in Figures 7-65 to 7-68.

TABLE 7-1 **Hip: Approximate Age of Appearance and Fusion of Ossification Centers[1-4] (Figures 7–1 and 7–2)**

Ossification Center	Primary or Secondary	No. of Centers Per Hip	Age of Appearance*	Age of Fusion* (Years)	Comments
Femoral capital epiphysis	P	1	1-8 months	16-20	Fuses with femoral neck
Greater trochanter	S	1	18-54 months	16-19	Fuses with femur
Lesser trochanter	S	1	9-13 years	16-18	Fuses with femur
Acetabulum	S	1	16 years	25	May persist as os acetabuli marginalis superior in adults

P, Primary; *S,* secondary.

* Ages of appearance and fusion of ossification centers in girls typically precede those of boys. Ethnic differences also exist.

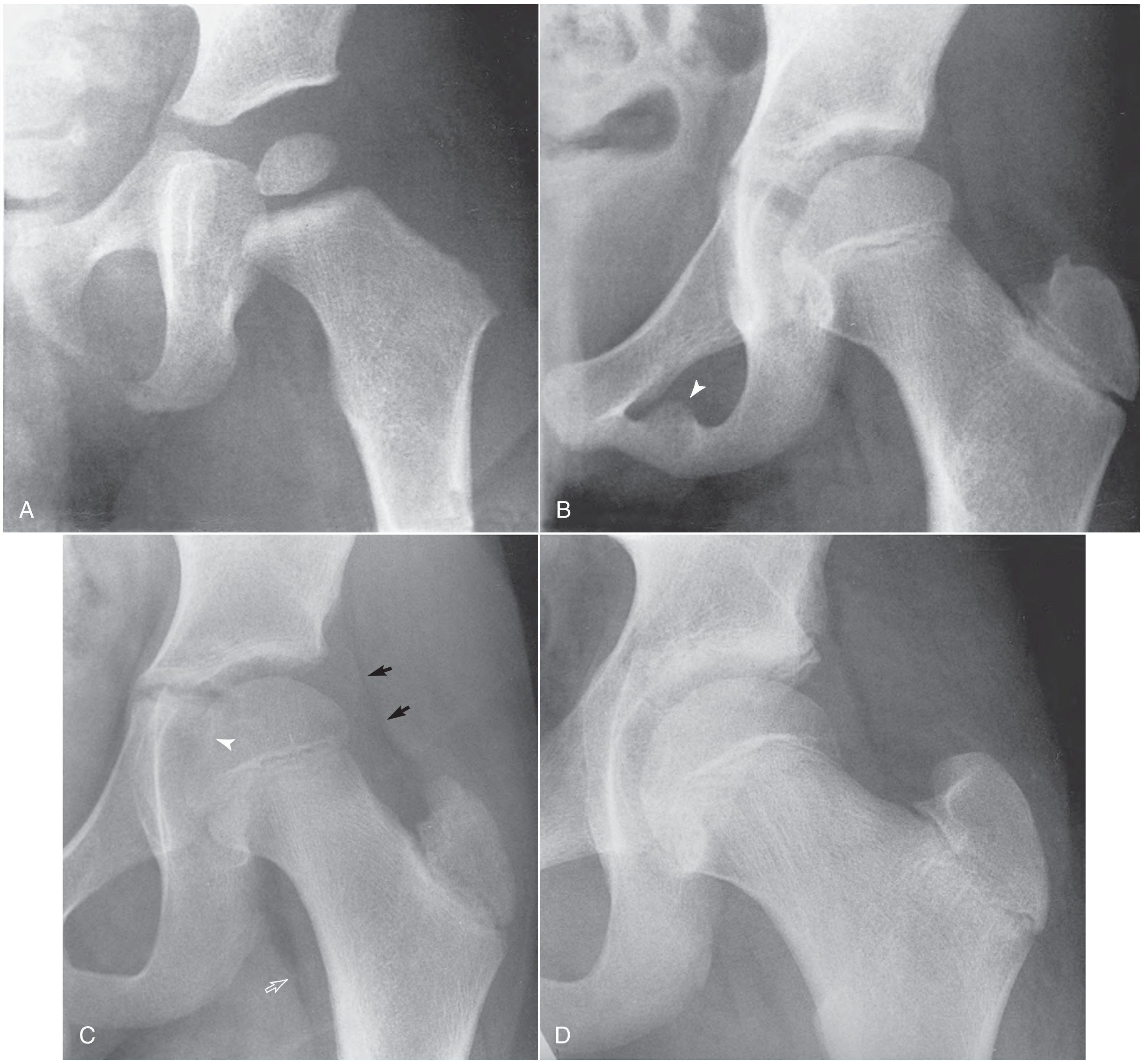

FIGURE 7–1 **Skeletal maturation and normal development of the hip.**[1-4] Anteroposterior radiographs. **A,** In a 2-year-old boy, the femoral capital epiphysis is round and small. The triradiate cartilage and ischiopubic synchondrosis are not yet fused. The femoral capital epiphysis generally begins to appear between the first and eighth months of life, allowing radiographic assessment of developmental dysplasia of the hip. **B,** In a 7-year-old girl, the greater trochanter ossification center is ossified and well developed. The ischiopubic synchondrosis has fused and is seen as a normal bulbous, calluslike protrusion *(arrowhead)*. The femoral capital epiphysis is approaching adult proportions, and the physeal growth center is thinner, more linear, and conforms to the shape of the femoral neck. **C,** In an 11-year-old boy, anatomic proportions approximate those of the adult, but the apophyses of the lesser trochanter and ischium have not yet appeared. Minimal physiologic acetabular protrusion is evident, and the fossa of the fovea capitus is apparent *(arrowhead)*. The gluteal *(arrows)* and iliopsoas *(open arrow)* fat planes are clearly visualized. **D,** In a 15-year-old boy, secondary ossification centers for the lesser trochanter and acetabulum are visible. Acetabular protrusion is not as evident as in the previous example **(C).** The femoral capital epiphysis and greater trochanter apophysis are about to fuse to the femur.

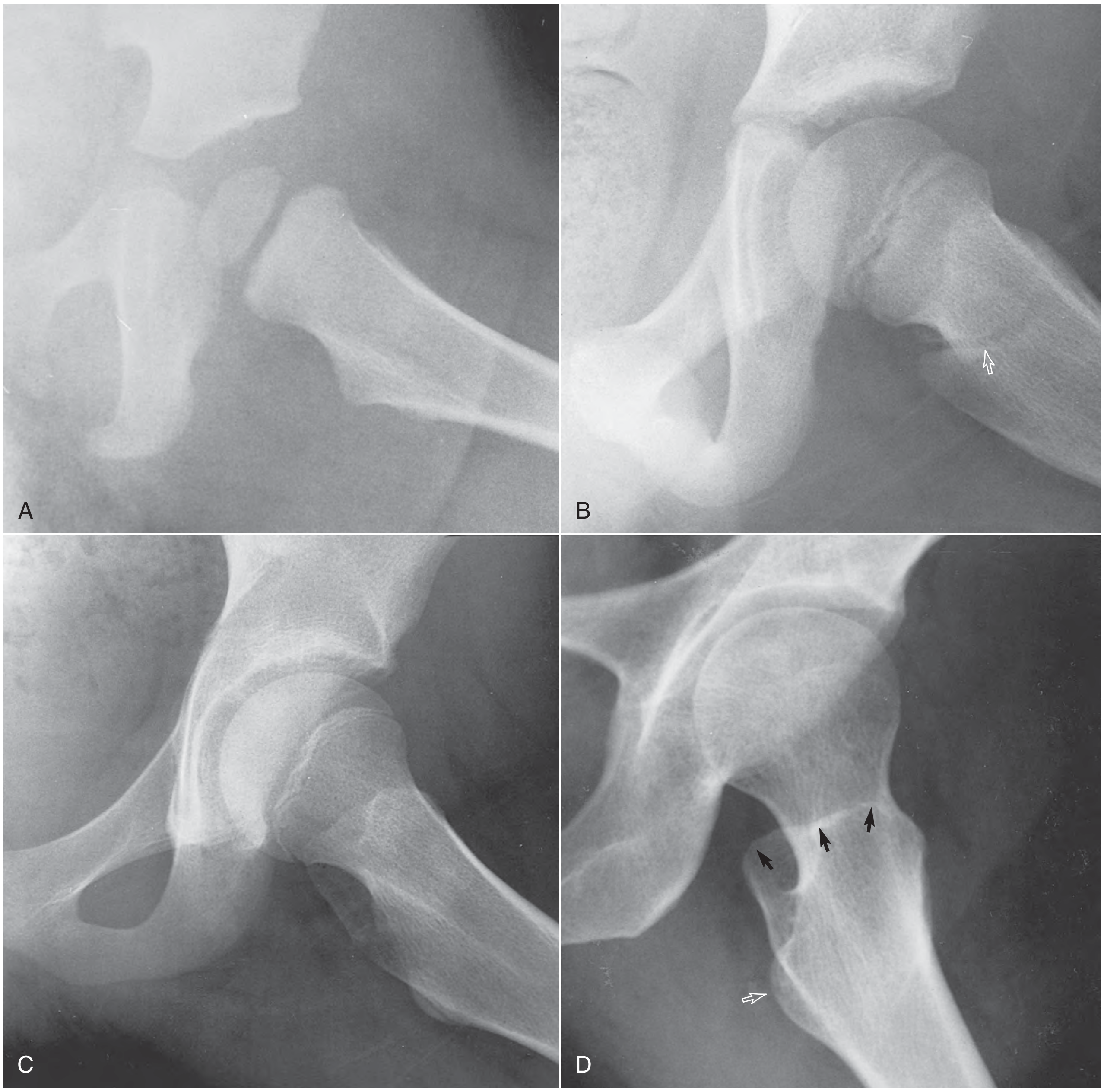

FIGURE 7–2 Skeletal maturation and normal development of the hip. Frog-leg (lateral) radiographs.[1-4] **A,** A 2-year-old boy. **B,** A 7-year-old boy. The radiolucent line represents the unfused lesser trochanter *(open arrow)*. **C,** A 13-year-old girl. Observe the lesser trochanter apophysis. The femoral capital epiphysis appears sclerotic owing to its position overlying the acetabular margin, and this finding should not be mistaken for osteonecrosis or other osteosclerotic processes. **D,** Adult. The apophyses of the greater *(arrows)* and lesser *(open arrow)* trochanters are fully fused.

TABLE 7-2 Developmental Anomalies, Anatomic Variants, and Sources of Diagnostic Error Affecting the Hip*

Entity	Figure(s)	Characteristics
Synovial herniation pits[5,6]	6-7, 7-3	Also termed *Pitt's pits* Small, round, radiolucent area surrounded by a well-defined sclerotic margin, located in the anterior surface of the femoral neck Unilateral or bilateral ingrowth of fibrous and cartilaginous elements through a cortical perforation Occasionally painful but usually asymptomatic May enlarge and are usually negative on bone scan
Os acetabuli marginalis superior[4,7]	6-7	Large or small triangular ossicle with well-corticated margins adjacent to the superior acetabular rim Present in about 5% of normal persons No clinical significance but may simulate acetabular rim fracture
Fovea capitis[4,7]	7-4	Normal notch in the medial aspect of the articular surface of the femoral head that accommodates the ligamentum teres femoris and its associated blood vessels Should not be mistaken for an erosion of the articular surface
Positional variations of the femoral neck[4,7,8]	7-5	Frontal radiographs of the hip or pelvis should be obtained with internal rotation of the femur, a position that results in an elongated appearance of the femoral neck Radiographs taken with external rotation result in a shortened appearance of the femoral neck with superimposition of the greater trochanter and femoral neck

* See also Table 1-1.

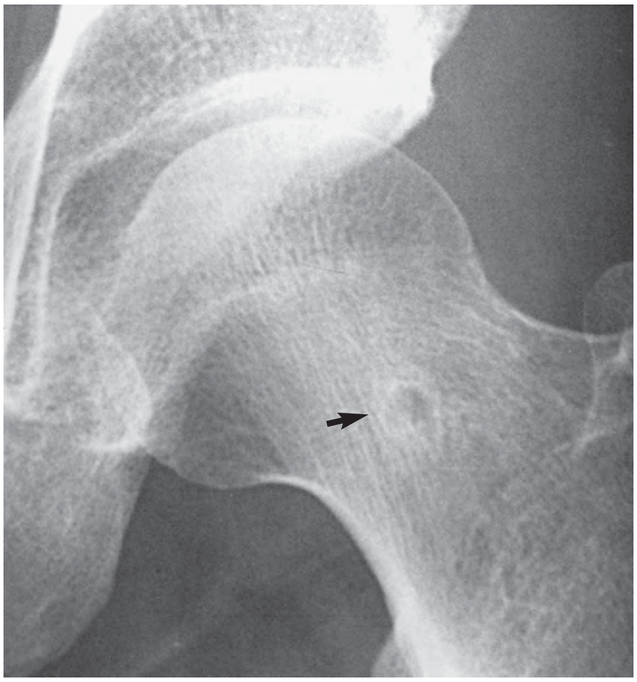

FIGURE 7–3 Synovial herniation pit.[5,6] This variation of normal appears as a solitary, circular, well-circumscribed radiolucent lesion in the femoral neck *(arrow)*. It represents a benign in-growth of fibrous and cartilaginous elements through a perforation of the cortex in the anterior surface of the femoral neck. Such lesions may enlarge and are occasionally painful.

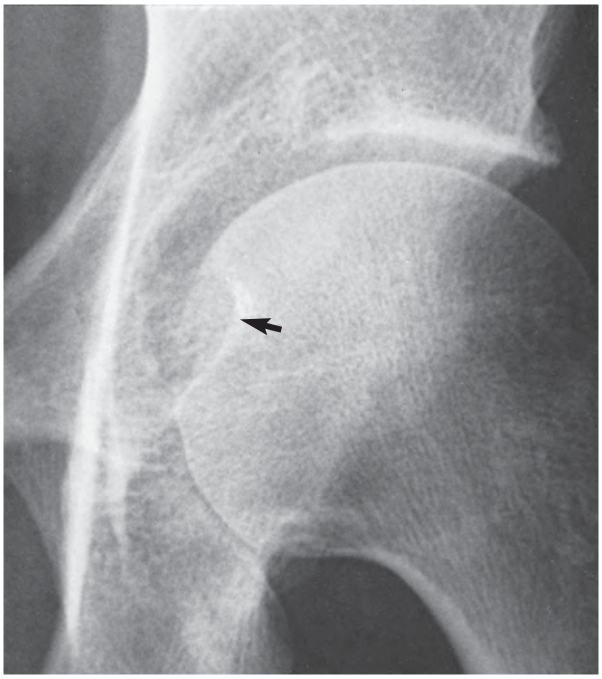

FIGURE 7–4 **Fovea capitis.**[4,7] The normal notch in the medial articular surface of the femoral head *(arrow)* represents the site of attachment of the ligamentum teres femoris and should not be misdiagnosed as an erosion.

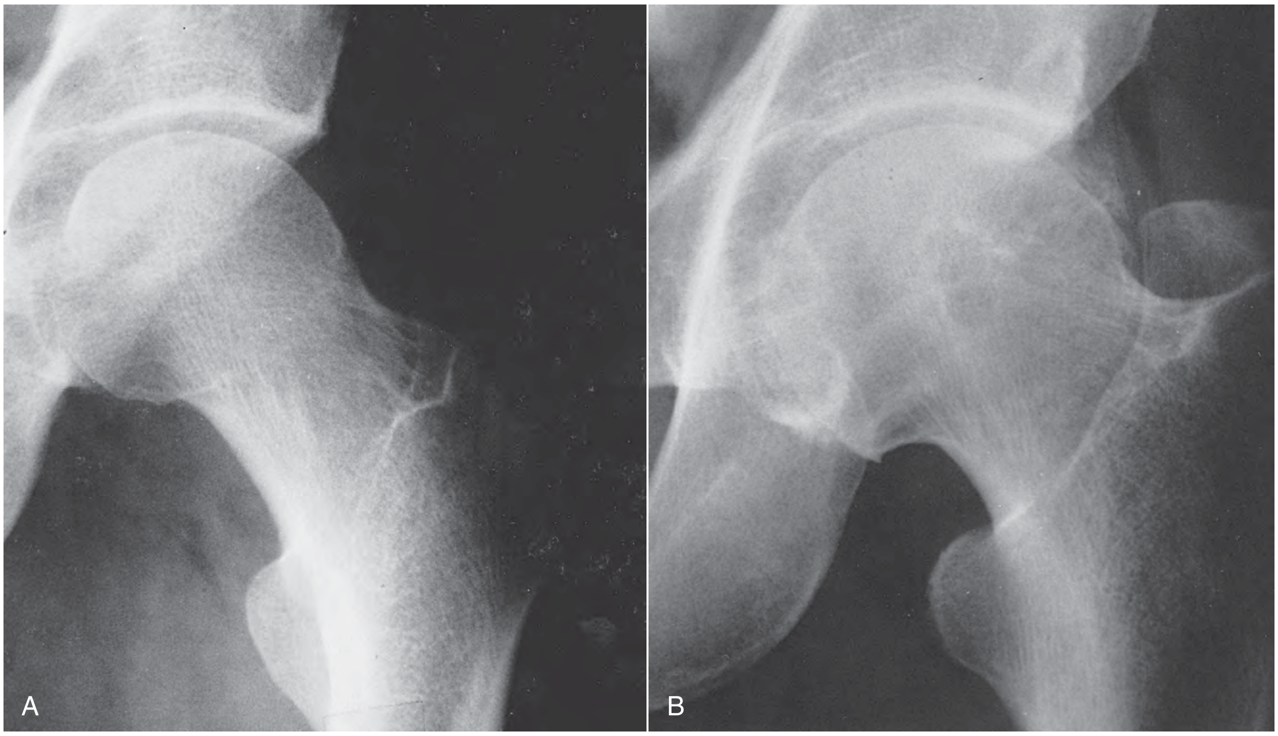

FIGURE 7–5 **Positional variations of the femoral neck.**[4,7,8] **A,** Routine anteroposterior radiograph obtained with 15 degrees of internal rotation of the thigh. The femoral neck has an elongated appearance because it is more parallel to the film. **B,** Improper positioning of the patient with external rotation of the thigh results in superimposition of the greater trochanter and the femoral neck. In this position, the femoral neck is more perpendicular to the film, creating a shortened appearance and making it difficult or impossible to evaluate. This patient has calcium pyrophosphate dihydrate (CPPD) crystal deposition disease.

TABLE 7-3 Hip Deformities[8-14,99]

Entity	Figure(s)
Coxa Vara	
Legg-Calvé-Perthes disease	7-6, *B*; see Figure 7-65
Infantile (developmental) coxa vara	7-7
Paget disease	7-8, *C*
Slipped capital femoral epiphysis	See Figures 7-16, 7-46
Femoral neck fracture	See Figures 7-17, 7-22
Rickets	See Figure 7-59
Cleidocranial dysplasia	
Developmental dysplasia of the hip	7-9, 7-13
Meningomyelocele	
Multiple epiphyseal dysplasia	
Osteogenesis imperfecta	
Renal osteodystrophy	
Neuromuscular disorders	
Rheumatoid arthritis	
Osteonecrosis	
Coxa Valga	
Idiopathic	7-6, *C*
Poliomyelitis	7-6, *D*
Femoral neck fracture	See Figure 7-18
Abductor muscle weakness	
Hereditary multiple exostosis	
Cleidocranial dysplasia	
Hunter syndrome	
Meningomyelocele	
Juvenile chronic arthritis	
Ollier disease	
Neuromuscular disorders	
Diastrophic dysplasia	
Protrusio Acetabuli	
Acetabular fracture	6-25
Rheumatoid arthritis	7-8, *A-B*
Paget disease	7-8, *C*
Primary protrusio acetabuli (Otto pelvis)	7-8, *D*
Skeletal metastasis	7-8, *E*
Ankylosing spondylitis	See Figure 7-34
Psoriatic arthropathy	See Figure 7-35
Collagen vascular diseases	See Figure 7-38
Calcium pyrophosphate dihydrate (CPPD) crystal deposition disease	See Figure 7-30
Alkaptonuria	See Figure 7-44
Idiopathic chondrolysis	See Figure 7-50
Osteomalacia and rickets	See Figure 7-58, 7-59
Sickle cell anemia	See Figure 7-64
Osteoarthrosis	
Radiation	
Marfan syndrome	

Adapted from Swischuk LE: Differential diagnosis in pediatric radiology, Baltimore, Williams & Wilkins, 1984; and Chapman S, Nakielny R: Aids to radiological differential diagnosis. 4th Ed. Philadelphia, Saunders, 2003.

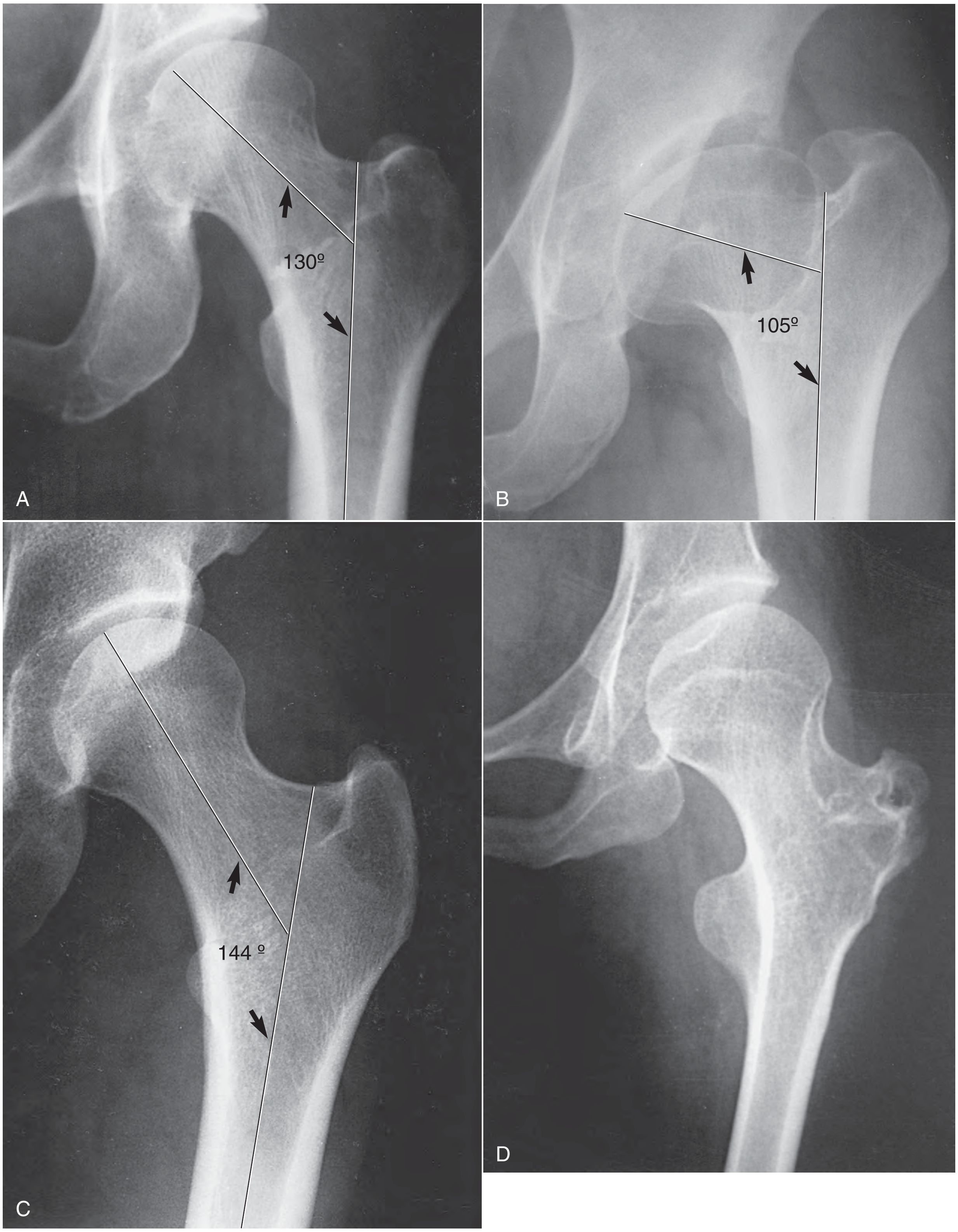

FIGURE 7–6 **Hip deformities: coxa vara and coxa valga.**[8-10] **A,** Normal femoral angle. In the normal situation, the femoral angle should measure between 120 and 130 degrees. The angle is determined by drawing lines through the femoral shaft and the femoral neck, parallel to the midaxis of each structure. The angle is 130 degrees in this patient. **B,** Coxa vara. In this adult patient who had had Legg-Calvé-Perthes disease as a child, a decreased femoral angle measures 105 degrees. Note also the flattening and deformity of the femoral head and shortening of the femoral neck. **C,** Coxa valga deformity. In another adult with idiopathic coxa valga, the femoral angle measures 144 degrees. **D,** Coxa valga deformity: poliomyelitis. Observe the valgus deformity of the proximal femur associated with hypoplasia of the femoral shaft. Many different conditions result in coxa valga and vara deformities (Table 7-3). *Technical note:* Accurate femoral angle measurements can be calculated only on frontal radiographs obtained with the femur internally rotated 15 degrees.

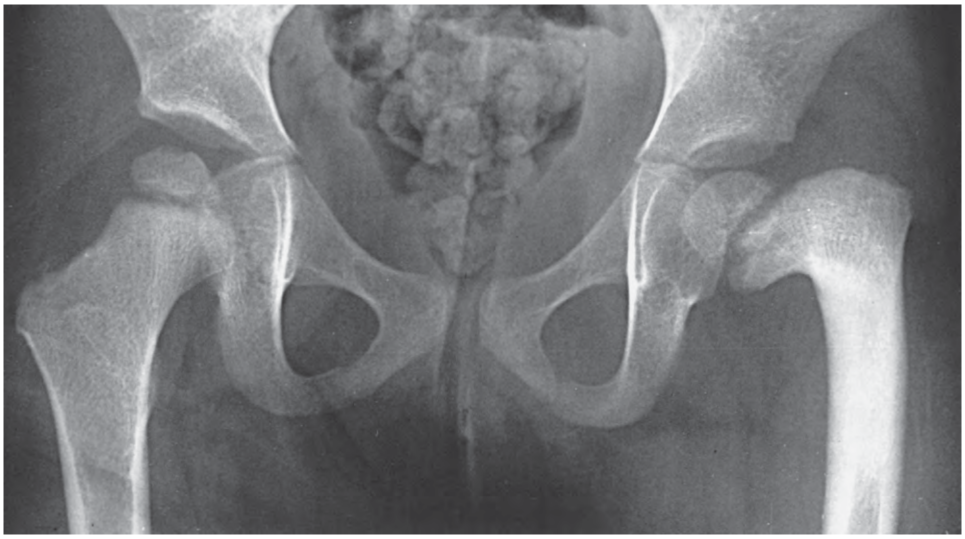

FIGURE 7–7 Infantile (developmental) coxa vara.[11] Observe the sharply angulated unilateral varus deformity of the femoral neck in relation to the femoral shaft. The infantile or developmental form of coxa vara usually becomes apparent in the first few years of life, especially as the child first begins to walk. It is unilateral in 60% to 75% of cases, and the child has a lurching or "duck-waddle" gait. Radiographically, the neck-shaft angle is less than 120 degrees, the proximal femoral physis is vertically oriented, and the femoral head appears dramatically depressed relative to the greater trochanter. Differential diagnosis includes other causes of coxa vara (Table 7-3). *(Courtesy M. N. Pathria, MD, San Diego.)*

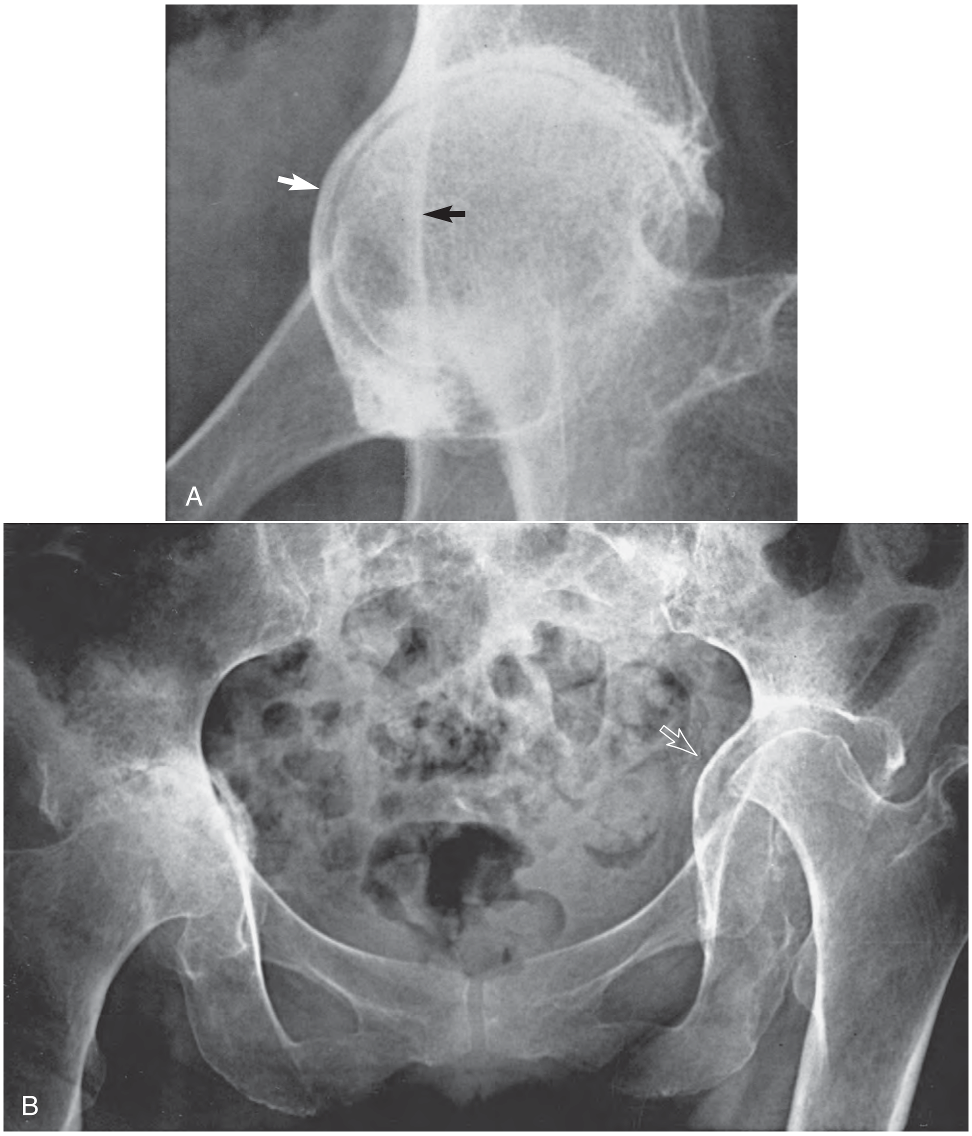

FIGURE 7–8 Protrusio acetabuli.[8-10,12-14] **A,** Measurement. A protrusio acetabuli deformity is present when the acetabular line *(white arrow)* projects medially to the ilioischial line *(black arrow)* by 3 mm or more in men and by 6 mm or more in women. **B,** Rheumatoid arthritis. This 69-year-old woman with rheumatoid arthritis has asymmetric bilateral acetabular protrusion. The left femoral head is severely eroded, and the acetabulum is dramatically remodeled *(open arrow)*. The right femoral head is not as severely damaged, but the joint space is uniformly narrowed and the acetabulum is protruding medially. Illustration continued on following page.

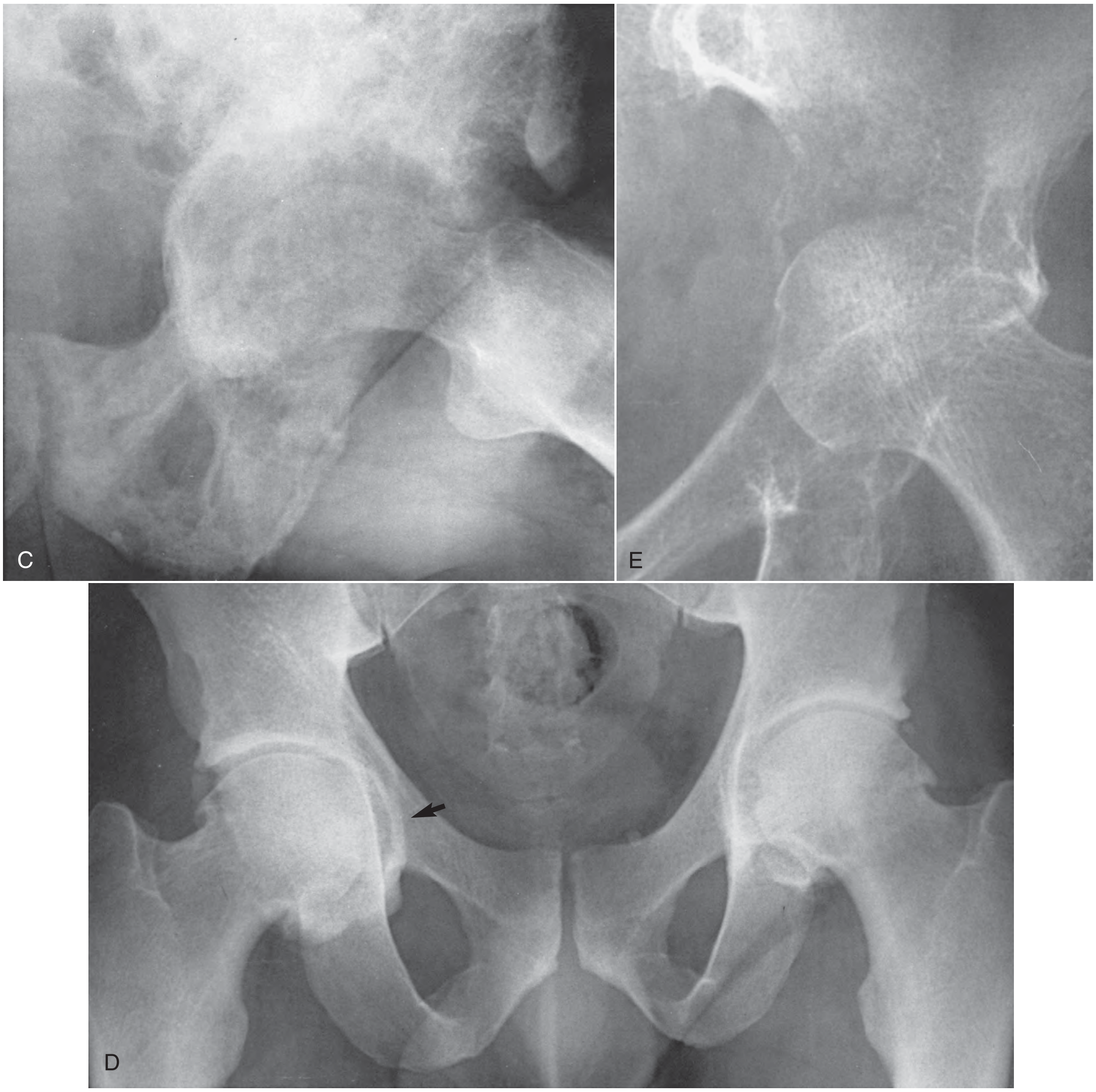

FIGURE 7–8, cont'd **C,** Paget disease. Observe the extensive acetabular protrusion in this patient with severe Paget disease. **D,** Primary protrusio acetabuli (Otto pelvis). A frontal pelvic radiograph of this 26-year-old man shows bilateral symmetric concentric loss of joint space with axial and medial migration of the femoral heads. This results in mild bilateral acetabular protrusion, more severe on the right *(arrow)*. Degenerative osteophytes are also seen arising from both femoral heads and acetabula. Primary protrusio acetabuli is a familial, idiopathic condition that may lead to premature secondary degenerative joint disease of the hips. It is usually bilateral and symmetric, and is much more frequent in women than in men. This condition may resemble idiopathic chondrolysis of the hip. **E,** Skeletal metastasis: Periarticular bone involvement. This 65-year-old woman developed a destructive lesion of the left hemipelvis secondary to metastasis (or direct invasion) from a clear cell carcinoma of the uterus. The loss of acetabular support has allowed inward protrusion of the femoral head. (See Table 7-3.) *(**D,** Courtesy R. Taketa, MD, Long Beach, Calif.)*

TABLE 7-4 Developmental Dysplasia of the Hip[15-18,99,101]

Entity	Figure(s)	Characteristics
Terminology		
Developmental dysplasia of the hip (DDH)		Deformity of the acetabulum in which the head of the femur may be properly located or partially or completely displaced Hips that are subluxatable, dislocatable, subluxated, or dislocated Results in continuously deforming acetabular cartilage
Instability		Type I hip dysplasia pattern Subluxatable and dislocatable hips Pliable labrum may be slightly deformed
Subluxation		Type II hip dysplasia pattern Protrusion of the femoral head beyond the acetabulum with contact still maintained Fibrocartilaginous superior acetabular labrum may be everted or inverted
Dislocation		Type III hip dysplasia pattern Loss of contact between femoral head and acetabulum Frequently results in inversion and hypertrophy of the acetabular labrum, which causes an impediment to reduction
Etiology and Predisposing Factors		
Mechanical factors		Results from restricted space in utero with limitation of fetal motion Oligohydramnios Among newborn infants with DDH, 60% are firstborns Breech presentation (30% of DDH patients) Associated with torticollis (20% of cases) Associated with clubfoot and metatarsus varus (2% of cases) Also associated with generalized joint laxity, scoliosis, cardiac and renal anomalies, and multiple syndromes
Functional factors		Elevated estrogen levels (more common in newborn infants with DDH) block collagen maturation
Epidemiology		
Prevalence		*DDH:* 2-6 live newborn infants per 1000 births *Complete dislocation:* 1 per 1000 births Four to eight times more common in girls than boys Familial incidence in 20% of patients Left hip involved in 80% of patients Bilateral in 25% of cases
		Risk of DDH 1. *Female fetus in breech presentation:* 1 in 15 2. *Female fetus in nonbreech presentation:* 1 in 25 3. *Newborn infant with affected sibling:* 6% 4. *Newborn infant with one affected parent:* 12% 5. *Newborn infant with two affected parents:* 36%
		Ethnicity *Native Americans and Lapps:* 25-50 per 1000 live newborn infants *Chinese and black Africans:* negligible prevalence rate
Detection and Evaluation		
Physical examination		Ortolani reduction maneuver and Barlow dislocation maneuver 1% missed diagnosis based on these tests These tests are more accurate in cases of frank dislocation Long-standing dislocations with muscle spasm or formation of a pseudoacetabulum may result in false-negative tests

TABLE 7-4 Developmental Dysplasia of the Hip[15-18,99,101]—cont'd

Entity	Figure(s)	Characteristics
Routine radiography	7-9 to 7-11	Earliest radiographic signs appear at 6 weeks of age Radiographs are most useful after 2 to 8 months of age, when the cartilaginous femoral head begins to ossify Frontal views are preferred over frog-leg views because dislocations may reduce in the frog-leg position Femoral head ossification center usually is much smaller or absent in the dysplastic hip Several lines and angles are used to measure the relationship of the femur to the acetabulum (Table 7-5) ***Limitations of Radiography*** Cartilaginous femoral head is not visible on radiographs in the first few months of life, the most critical time in the diagnosis of DDH Frontal projections do not show anteroposterior displacement Patient positioning is demanding and often results in pelvic rotation or tilting that interferes with accurate measurements Risk of ionizing radiation
Ultrasonography	7-12	More sensitive than physical examination and far superior to radiography in the first few months of life Should be performed at 4-6 weeks in infants with any risk factor or abnormal physical findings with a stable hip; should be performed within 2 weeks in patients with abnormal physical examination results and unstable hip Measurements can be obtained for acetabular angle, acetabular coverage of the femoral head, acetabular cartilage thickness, and lateral head distance
Computed tomography (CT)	7-13	CT scanning may be used to document the adequacy of a reduction in DDH, especially in the transverse plane, revealing anterior or posterior displacement Also useful in measuring acetabular anteversion and other preoperative and postoperative morphologic changes
Magnetic resonance (MR) imaging	7-14	Reserved for complicated cases of DDH in which initial treatment has been unsuccessful

Adapted from Gerscovich EO: A radiologist's guide to imaging in the diagnosis and treatment of developmental dysplasia of the hip. I and II. Skeletal Radiol 26:386, 447, 1997.

TABLE 7-5 Radiographic Measurements in Developmental Dysplasia of the Hip[16,100]

		Normal Values (Degrees)	
Method	**Age**	**Female**	**Male**
Acetabular index (AI)	Newborn infant	28.8 ± 4.8	26.4 ± 4.4
	3 months	25.0 ± 3.5	22.0 ± 4
	6 months	23.2 ± 4	20.3 ± 3.7
	1 year	21.2 ± 3.8	19.8 ± 3.6
	2 years	18.0 ± 4	19.0 ± 3.6
		A value >30-32 is abnormal at any age	
Center-edge (C-E) angle	3 months	18-20	
	2 years	30	
		Lowest limit of normal	
	5-8 years	19	
	9-12 years	25	
	13-20 years	26-30	
Medial joint space (MJS)	6 months to 11 years	5-12 mm	
		Difference between the two hips: <1.5 mm	

Adapted from Gerscovich EO: A radiologist's guide to imaging in the diagnosis and treatment of developmental dysplasia of the hip. I. General considerations, physical examination as applied to real-time sonography and radiography. Skeletal Radiol 26:386, 1997.

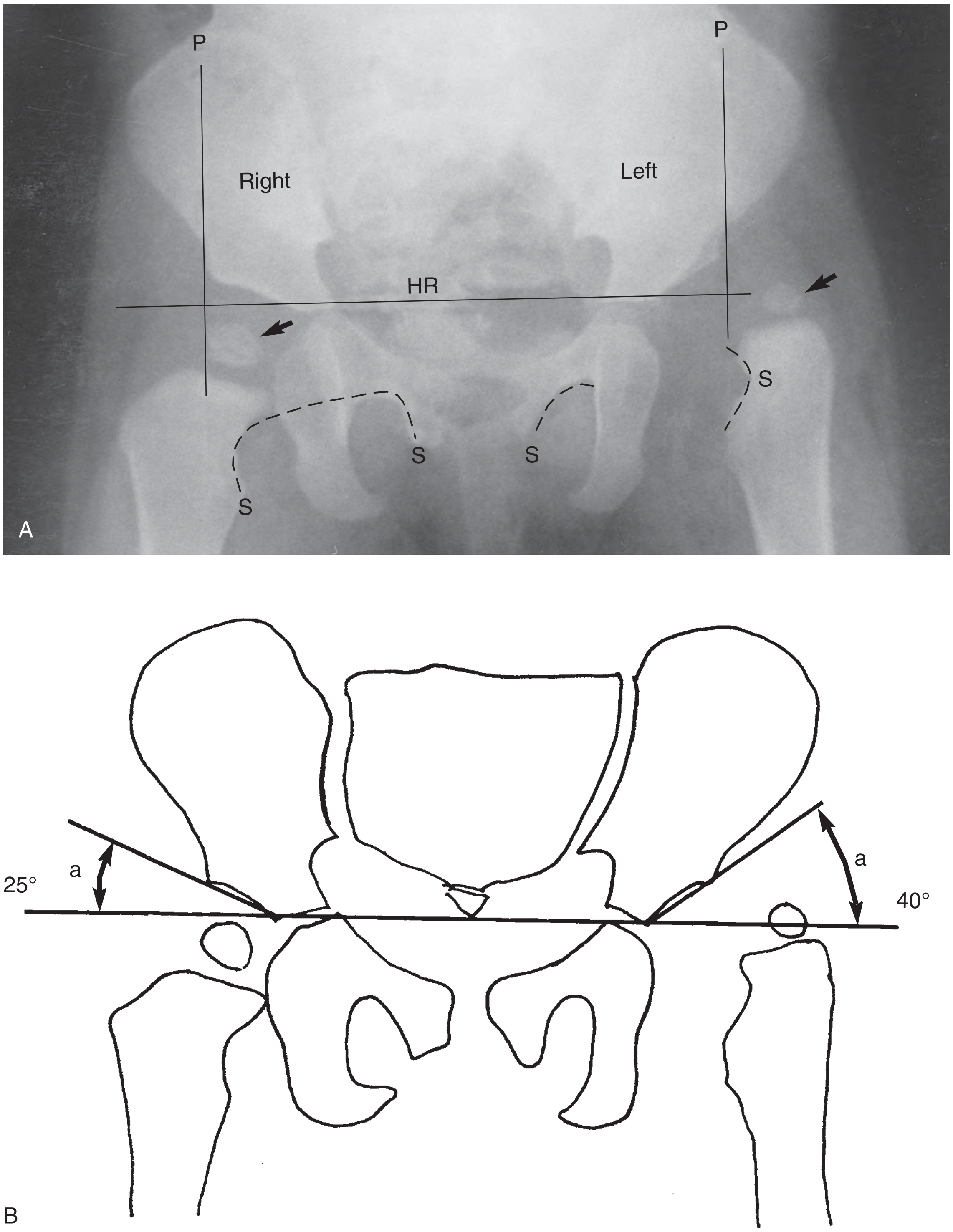

FIGURE 7–9 **Developmental dysplasia of the hip (DDH): Radiographic measurements.**[15,16] (See Table 7-5 for normal values.) **A,** Hilgenreiner line, Perkin line, and Shenton line. Pelvic radiograph from an 8-month-old girl with left acetabular dysplasia and hip dislocation. Hilgenreiner line (HR) is a transverse line intersecting the top of both triradiate cartilages. Perkin's line (P) is a vertical line perpendicular to Hilgenreiner line that intersects the lateral acetabular margin. Normally, the femoral head ossification centers *(arrows)* and the upper medial corner of the femoral metaphyses should project in the lower medial quadrant of the intersection of the Hilgenreiner line and Perkin line. The left femoral head is dislocated superiorly and laterally, and the right femoral head is located in the normal position. Shenton line (S) is a smooth, continuous arc extending from the medial aspect of the femoral neck to the lower margin of the superior pubic ramus. In this patient, Shenton line on the right is normal and continuous; on the left, the line is disrupted owing to superolateral dislocation of the hip. **B,** Acetabular index. A schematic diagram illustrates the angle (a) formed between Hilgenreiner line and the acetabular roof line. In this example, the left acetabular index measures 40 degrees in the dysplastic hip and 25 degrees in the normal right hip. In normal newborn infants, this measurement is less than 30 to 32 degrees and becomes progressively smaller in older infants.

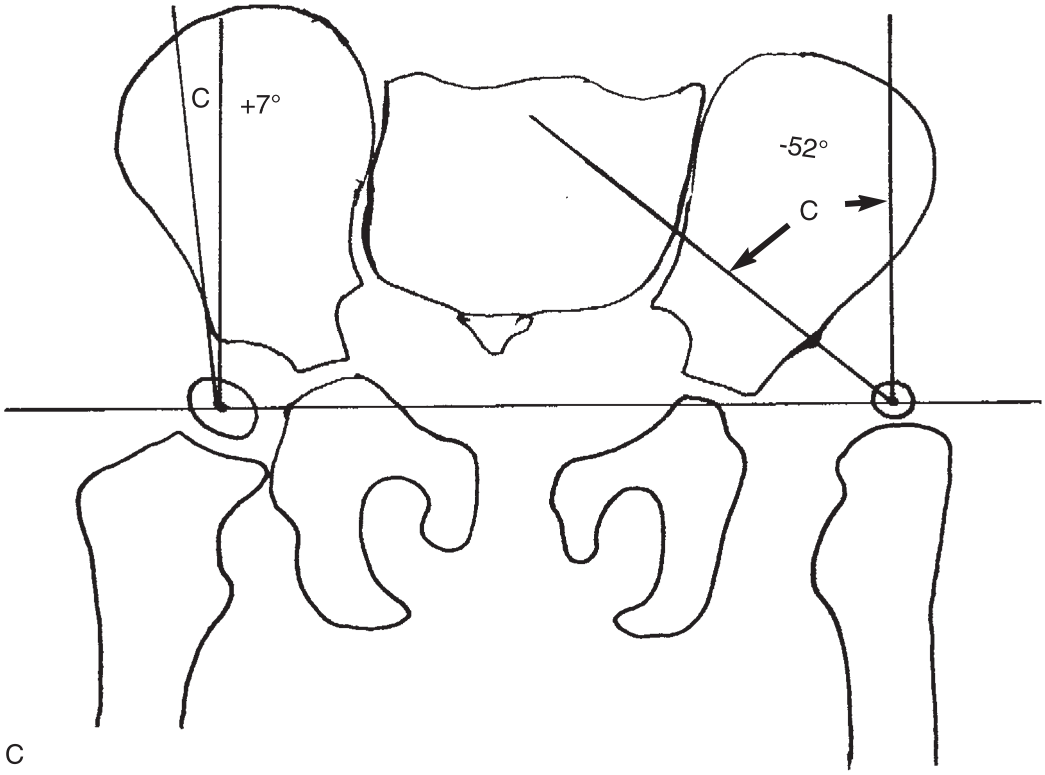

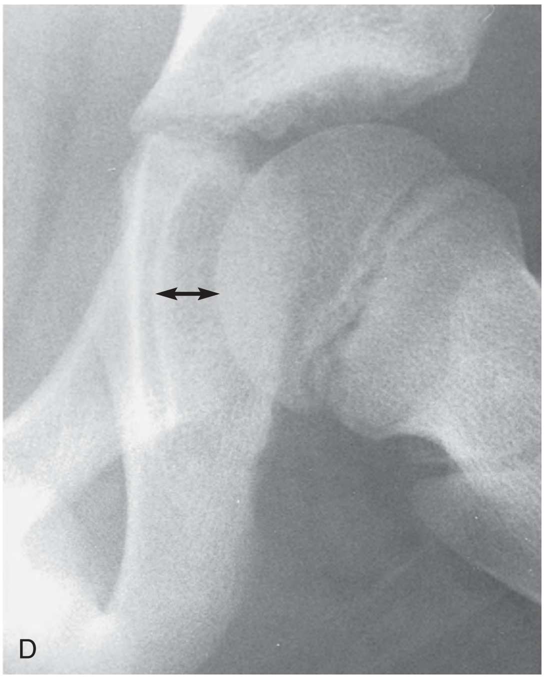

FIGURE 7–9, cont'd **C,** Center-edge (C-E) angle. A line intersecting the centers of both femoral epiphyses is constructed. A vertical line perpendicular to the initial line is then drawn from the center of the epiphysis. A third line is drawn superiorly from the center of the epiphysis to the lateral acetabular margin. The C-E angle represents the angle between the last two lines and is measured bilaterally. In this example, the angle is +7 degrees in the normal right hip and –52 degrees in the dislocated left hip. **D,** Medial joint space (MJS) width. The MJS width is the distance between the lateral aspect of the acetabular wall and the medial aspect of the ossification center of the femoral head at its widest portion *(double-headed arrow)*. If the femoral head is not ossified, the line is drawn to the medial aspect of the metaphysis. In children aged 6 months to 11 years, this measurement should range from 5 to 12 mm, and the difference between the two hips should not exceed 1.5 mm.

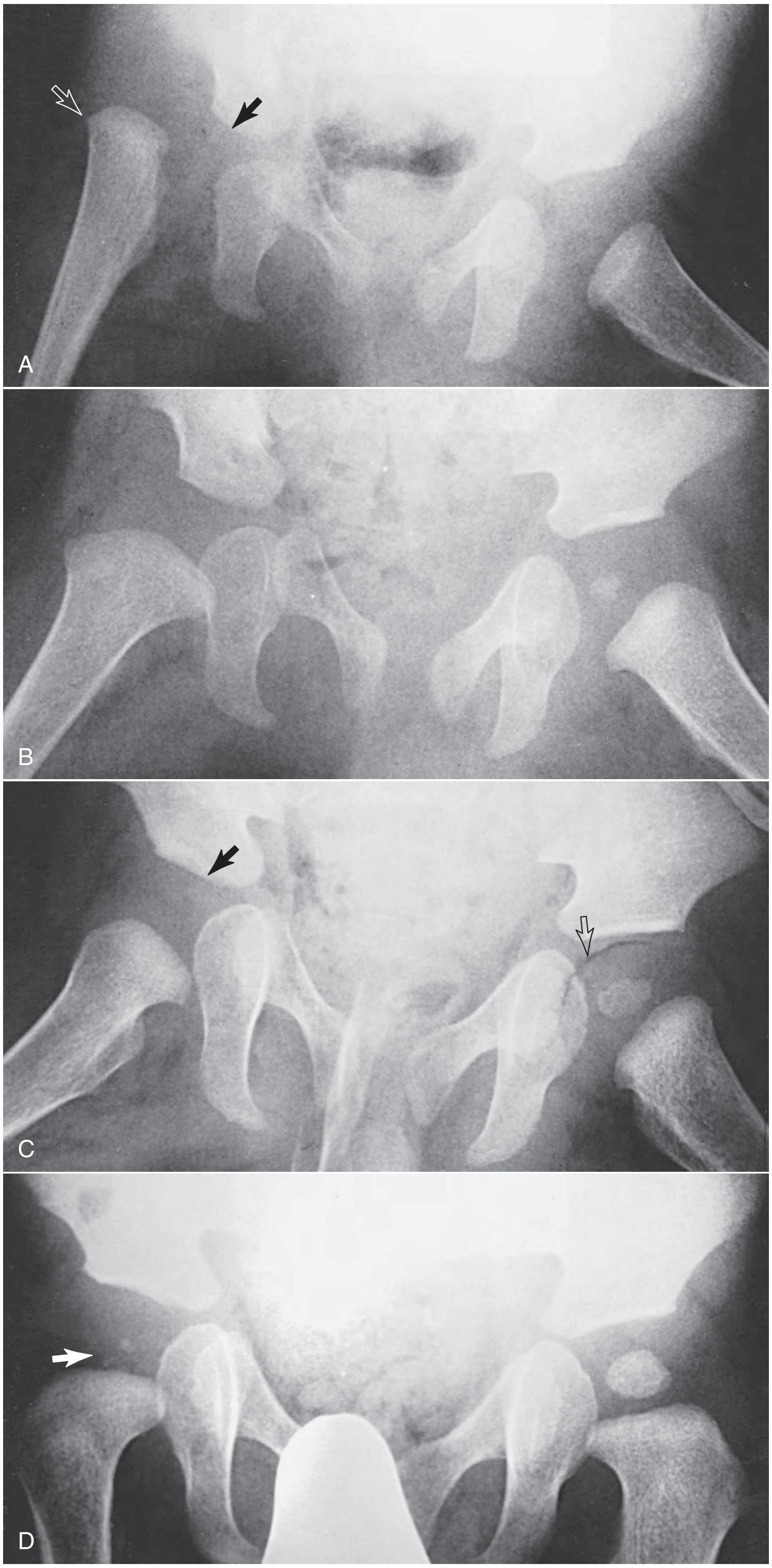

FIGURE 7–10 Developmental dysplasia of the hip (DDH).[15,16] Serial radiographs of a boy with a clicking right hip and positive Barlow and Ortolani tests. **A,** 5 months of age. The right acetabulum is shallow and poorly developed *(arrow)*. The right femur is dislocated superiorly and laterally *(open arrow)*. The femoral head epiphyses have not yet begun to ossify. **B,** Nine months of age, after treatment in a harness. The left femoral head has begun to ossify normally, but the right remains unossified. The right femur is positioned more adequately than in the earlier radiograph **(A). C,** Eleven months of age, with continued treatment in a harness. The right femoral head remains unossified, and the right acetabulum remains underdeveloped *(arrow)*. The femur was not displaced at the time the radiograph was obtained. Intraarticular gas outlines the cartilaginous epiphysis of the left hip (*open arrow)* in this frog-leg view, a normal finding that is often present during traction of the thigh. **D,** Eighteen months of age. The right femoral head has begun to ossify *(arrow)* and is well positioned in relation to the acetabulum. *(Courtesy B.A. Howard, MD, Charlotte, NC.)*

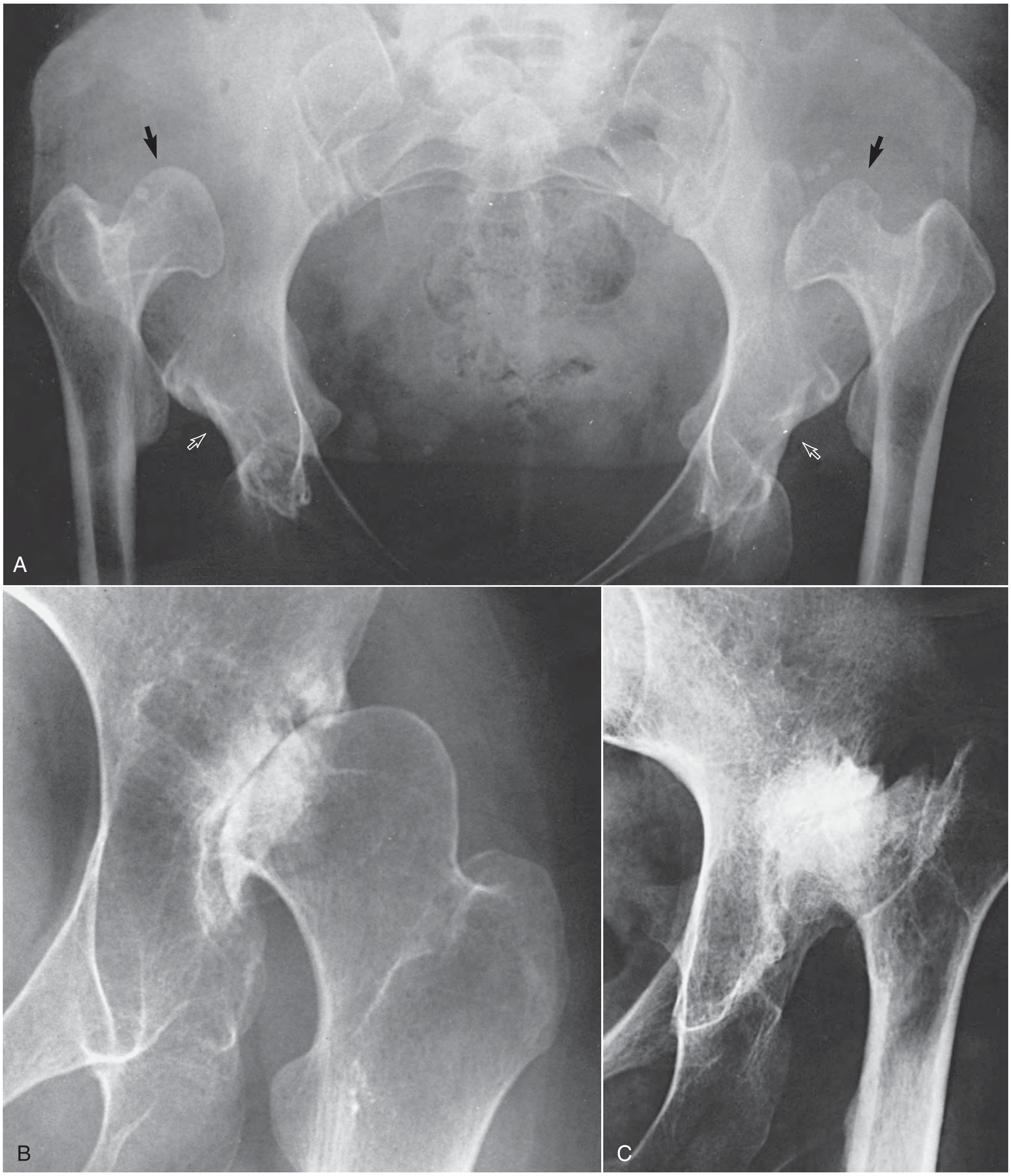

FIGURE 7–11 **Developmental dysplasia of the hip (DDH) in the adult.**[15,99] **A,** Bilateral hip dislocations are evident on this frontal radiograph of an adult patient who had untreated type III DDH as a child. Symmetric acetabular hypoplasia *(open arrows)* and abnormal articulation of the femoral heads with the posterior iliac fossae are seen *(arrows)*. **B,** Osteoarthrosis, secondary to DDH.[114] Observe the subchondral sclerosis, cyst formation, joint space narrowing, and osteophytes in this 32-year-old woman with long-standing type III DDH. A pseudoacetabulum has developed in a position superior to the normal location of the acetabulum, and the femoral head is only partially covered by the acetabulum. **C,** In a third patient, a 35-year-old man, severe degenerative changes, including sclerosis and joint space obliteration, remodeling of the femoral head, and formation of a pseudoacetabulum on the superolateral aspect of the ilium, are evident. Early detection of hip dysplasia is essential for appropriate management. *(**C,** From Taylor JAM, Harger BL, Resnick D: Diagnostic imaging of common hip disorders: A pictorial review. Top Clin Chiropr 1:8, 1994. Reprinted with permission.)*

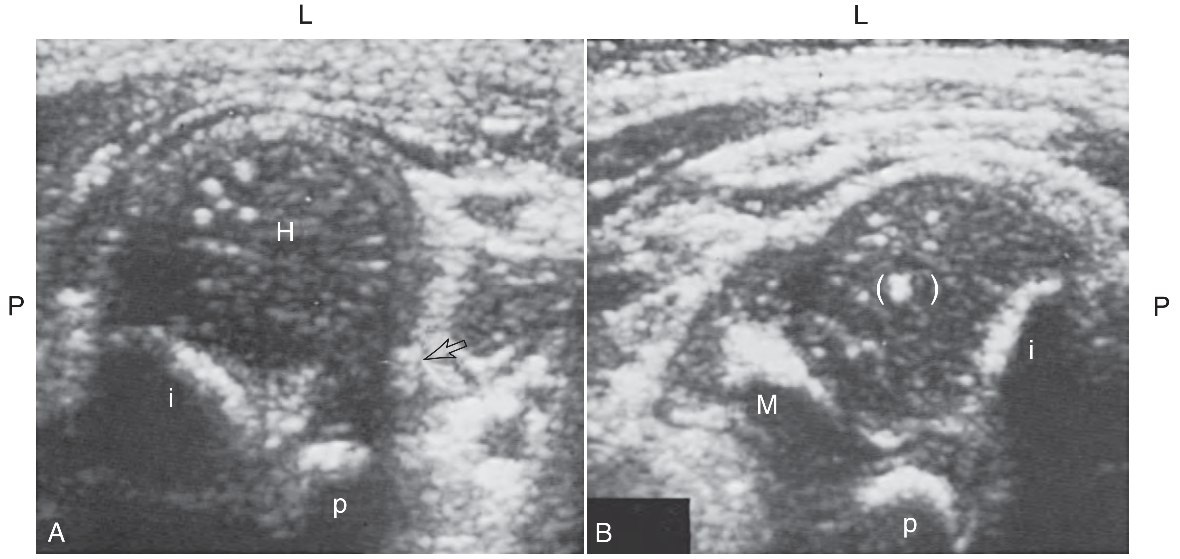

FIGURE 7–12 Developmental dysplasia of the hip (DDH): ultrasonography.[16,17] **A,** Transaxial image of right subluxatable hip after stress. The femoral head (H) has subluxated posteriorly and laterally with respect to the acetabulum. **B,** Contralateral normal left hip for comparison. More advanced maturation of the femoral head ossific nucleus (parentheses) is evident. *I,* Ischium; *p,* pubis; *L,* lateral; *P,* posterior; *M,* femoral metaphysis. *(From Resnick D, Kang SK: Internal derangements of joints. Philadelphia, Saunders, 1997, p. 538.)*

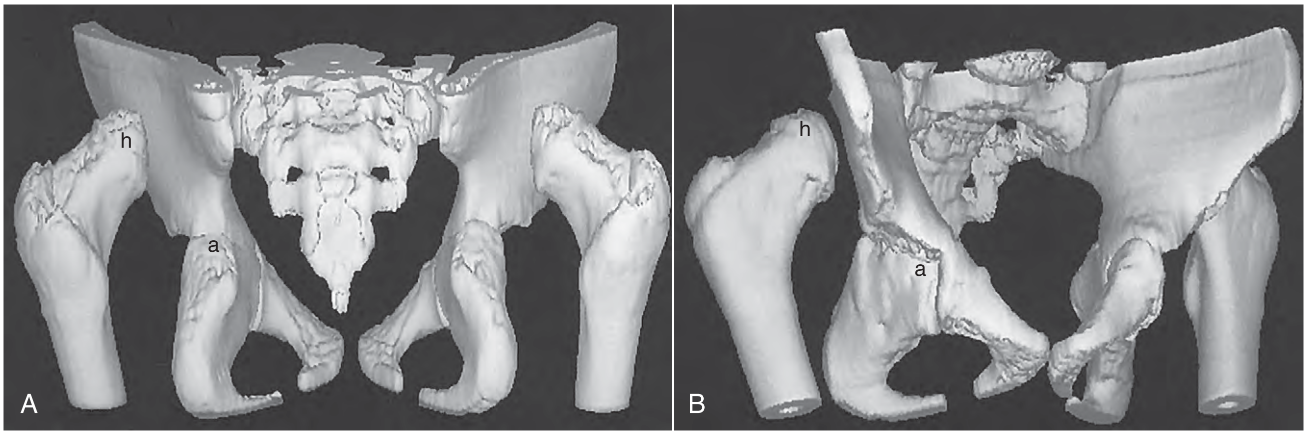

FIGURE 7–13 Developmental dysplasia of the hip (DDH): CT.[18,99] Three-dimensional reformatted CT scan of untreated DDH. Posterior **(A)** and right anterior oblique **(B)** images reveal an aspheric, superiorly dislocated femoral head (h), and the shallow, featureless acetabulum (a). *(From Dwek JR, Chung CB, Sartoris DJ. In: Resnick D (ed.), Diagnosis of bone and joint disorders. 4th Ed. Philadelphia, Saunders, 2002, p. 4371.)*

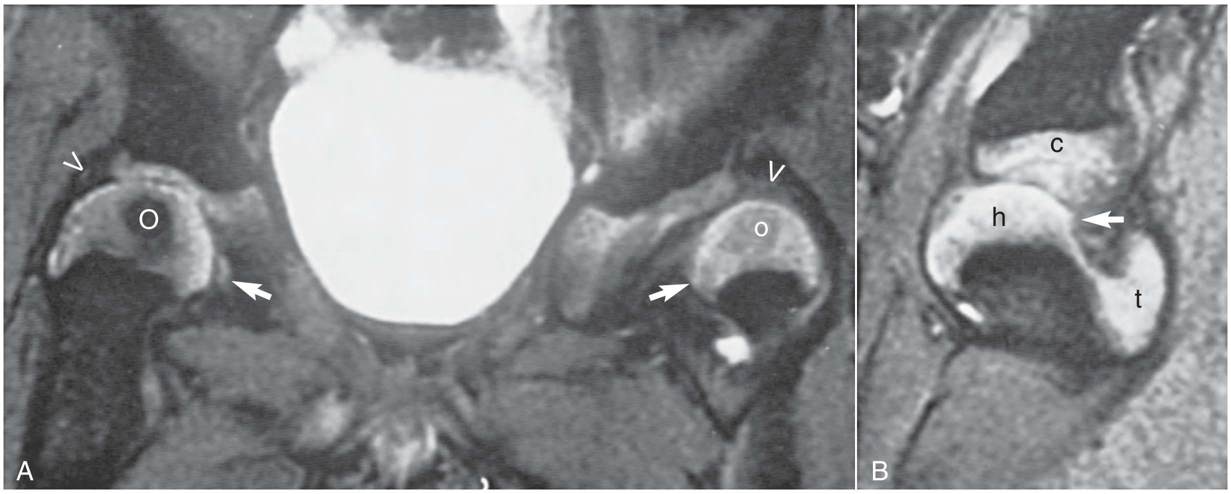

FIGURE 7–14 Developmental dysplasia of the hip (DDH): magnetic resonance (MR) imaging.[18,99] **A,** Coronal gradient echo (TR/TE, 100/25) MR image reveals lateral subluxation of the left femoral head *(arrow)* and presence of a secondary ossification center that is delayed in development (O > o). Both acetabular labra are in the normal everted position *(arrowheads)*. **B,** Sagittal MR image (TR/TE, 100/25) demonstrates mild anterior subluxation of the femoral head *(arrow)*. Note the continuity between the cartilaginous femoral head (h) and the greater trochanter (t), triradiate cartilage (c). *(From Resnick D, Kang SK: Internal derangements of joints. Philadelphia, Saunders, 1997, p. 539.)*

TABLE 7-6 Traumatic Dislocations of the Hip*

Entity	Figure(s)	Characteristics	Complications and Related Injuries
Posterior hip dislocation[19,77]	7-15	80%-85% of all hip dislocations Usually result from dashboard injury in which the flexed knee strikes the dashboard during a head-on automobile collision Motorcycle accidents are also a common cause of this injury Dislocated femoral head is seen on frontal radiograph at or above the level of the acetabulum, displaced superolaterally with the femur adducted and internally rotated	Associated trauma and fractures to the knee, femur, and acetabulum Shear fractures of femoral head (7%-10% of cases) Compression fractures of femoral head (13%-60% of cases) Osteonecrosis (25% of cases) Acetabular labral tears Sciatic nerve injury Periarticular soft tissue calcification and ossification Secondary degenerative joint disease Entrapment of acetabular labrum or osseous fragment Occasional recurrence
Anterior hip dislocation[19]	7-15	10% to 11% of all hip dislocations Results from forced abduction and external rotation of the thigh Two types of anterior dislocation: ***1. Inferior (obturator) dislocation:*** 90% of anterior dislocations Anterior and inferomedial femoral head displacement is seen on the frontal radiograph with the femur abducted and externally rotated ***2. Superior dislocation:*** 10% of anterior dislocations Femoral head dislocates superiorly May be confused for a posterior dislocation	Associated impaction fractures of the femoral head or other fractures of the acetabular rim, greater trochanter, or femoral neck Osteonecrosis (4% of cases) Vascular injury (1% of cases) Occasional recurrence
Central acetabular fracture-dislocation[20,21]	See Figure 6-25	Rare injury Results from forces applied to the lateral side of the greater trochanter and pelvis, with forces transmitted through the femoral head	Central acetabular fracture Hemorrhage into pelvis Secondary degenerative joint disease Associated visceral injury and other musculoskeletal injuries

* See also Tables 1-4 to 1-6.

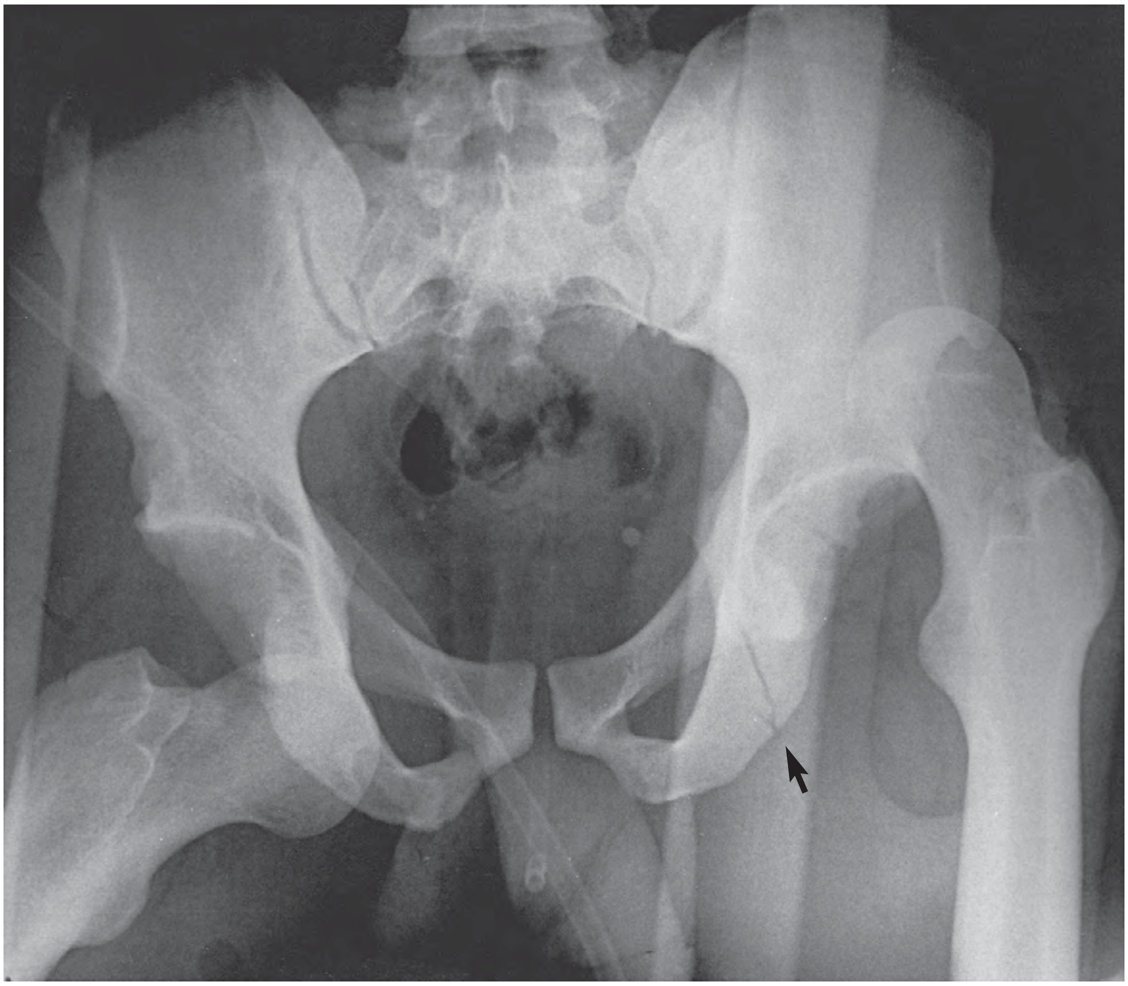

FIGURE 7–15 Bilateral hip dislocation with associated pelvic fractures.[19,104] This patient was involved in a motorcycle accident. Note the presence of both anterior and posterior hip dislocations with associated fractures of the acetabular margin and ischium *(arrow)*. *(Courtesy T. Martin, MD, and J. Spaeth, MD, Albuquerque, NM.)*

TABLE 7-7 Fractures and Physeal Injuries About the Hip*

Entity	Figure(s), Table(s)	Characteristics
Acetabular fractures[20,21]	6-25 Table 6-4	See Chapter 6
Slipped capital femoral epiphysis[22,118]	7-16; 7-46	Salter-Harris type I growth plate injury More common in boys, African Americans, and obese children *Boys:* aged 10-17 years, twice as frequent on the left side *Girls:* aged 8-15 years, both sides affected equally 20%-35% of patients have bilateral involvement History of injury in fewer than 50% of cases *Predisposing factors:* adolescent growth spurt, hormonal influences, obesity, and increased levels of physical activity Infrequently found in younger children with severe trauma, malnutrition, developmental acetabular dysplasia, Legg-Calvé-Perthes disease, tuberculosis ***Imaging findings*** Decreased height of involved epiphysis in relation to contralateral side on frontal radiograph Blurring and widening of the physis Lateral cortical line of the femoral neck (Klein line) does not intersect a portion of the epiphysis—most evident on the frog-leg projection Typical epiphyseal slippage is posteromedioinferior Varus deformity ***Complications*** Shortening and broadening of the femoral neck Osteonecrosis (6%-15% of cases) Chondrolysis (as many as 40% of cases) Degenerative joint disease Persistent varus deformity
Stress (fatigue) fracture of the femoral neck[23,24]	7-17	Activity-related onset of pain *Young athletes:* common activities include long-distance running, ballet dancing, gymnastics, and marching May become complete fractures with displacement ***Transverse type*** More frequent in older patients Radiolucent area in the superior aspect of the femoral neck ***Compression type*** More common in younger patients Stable in most cases Appears as haze of callus surrounding the inferior aspect of the neck
Insufficiency fracture of the femoral neck[25]	7-18	Most common in elderly patients, especially women *Predisposing factors:* osteoporosis, rheumatoid arthritis, corticosteroid medication, malignancy, radiation therapy History of minor trauma is often elicited Fractures tend to course horizontally across the femoral neck at angles almost perpendicular to the trabeculae
Subchondral insufficiency fracture of the femoral head[117]	7-19	Occurs in elderly patients, especially females with osteoporosis No history of antecedent trauma MR imaging characteristically demonstrates a low-intensity band on T1-weighted images that corresponds to a linear subchondral fracture and its associated repair tissue; the subchondral portion of the lesion appears as an area of homogenously high signal intensity on T2-weighted images. *Differential diagnosis:* osteonecrosis of the femoral head, a condition that occurs in a younger middle-aged population with risk factors such as corticosteroid or alcohol use
Avulsion fracture of the lesser trochanter[116]	7-20	Uncommon sports-related injury occurring most often in adolescent soccer players before closure of the apophyseal growth plate Forceful contraction of iliopsoas muscle while the thigh is fixed in an extended position In adults, avulsion of the lesser trochanter may be an insufficiency fracture occurring as a result of malignancy
Acute fractures of the proximal portion of the femur	7-21 Tables 7-8, 7-9	

* See also Tables 1-4 and 1-5.

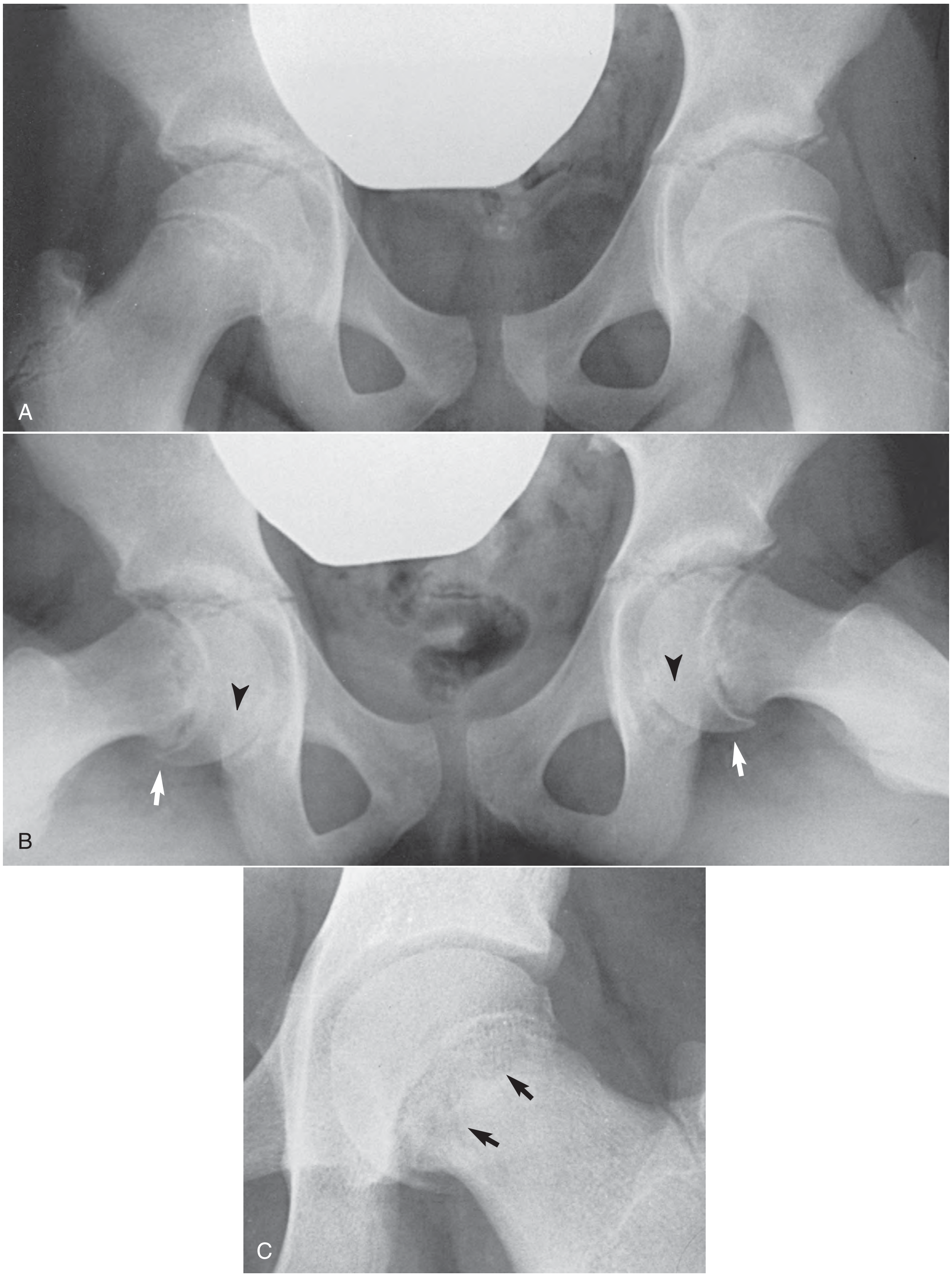

FIGURE 7–16 **Slipped capital femoral epiphysis.**[22,118] **A-B,** Bilateral involvement. Frontal **(A)** and frog-leg **(B)** projections of this 11-year-old girl show posteromedial displacement of both proximal femoral epiphyses *(white arrows)*. The arrowheads indicate the direction of displacement. The growth plates appear widened, and the osseous margins are blurred and indistinct. **C,** In another patient, a frontal radiograph shows subphyseal radiolucency *(arrows),* widening of the physis, and minimal slippage of the femoral capital epiphysis.

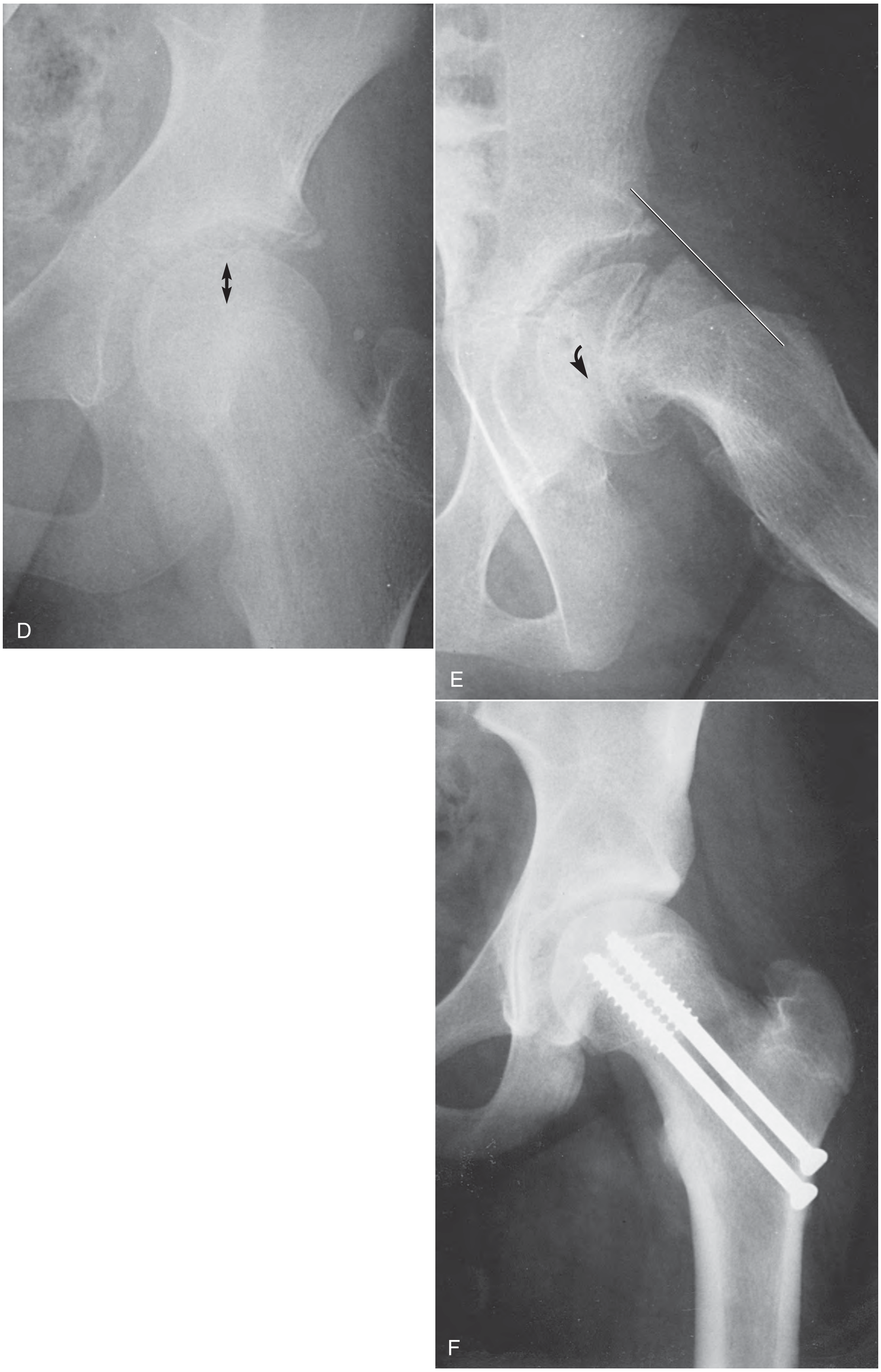

FIGURE 7–16, cont'd **D-E,** This 9-year-old girl had knee pain and a limp. In **D,** a frontal radiograph reveals a decrease in the vertical height of the capital femoral epiphysis *(double-headed arrow)* but no visible misalignment because the displacement occurred predominantly in a posterior direction. In **E,** a lateral frog-leg projection rotates the femur, revealing medial and posterior migration of the epiphysis in the direction of the curved arrow. A line constructed along the outer margin of the femoral neck (Klein line) should intersect the epiphysis. In this case, the line does not intersect the epiphysis. **F,** In a fourth patient, orthopedic lag screws have been inserted in an attempt to facilitate fusion of the epiphysis to the metaphysis and to avoid further slippage. *(**C,** Courtesy B. Howard, MD, Charlotte, NC.; **D-F,** From Taylor JAM, Harger BL, Resnick D: Diagnostic imaging of common hip disorders: A pictorial review. Top Clin Chiropr 1:8, 1994.)*

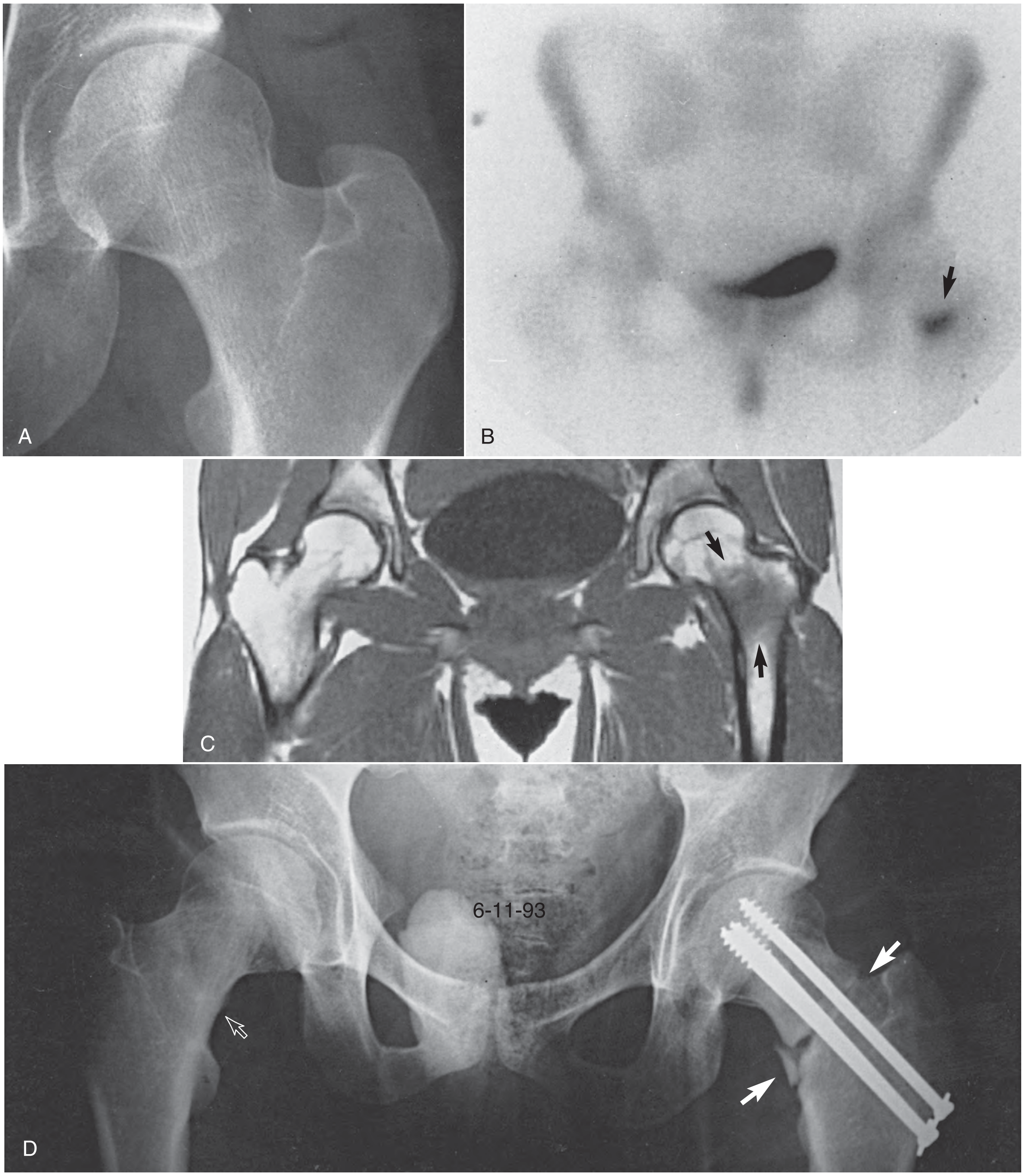

FIGURE 7–17 **Stress (fatigue) fracture: femoral neck.**[23,24] **A-C,** This runner developed hip pain. In **A,** a frontal radiograph shows a radiodense line across the medial aspect of the femoral neck. In **B,** a bone scan obtained at the same time as the radiograph shows a zone of increased uptake of radionuclide corresponding to the fracture site *(arrow)*. **C,** A coronal T1-weighted (TR/TE, 500/15) spin echo MR image demonstrates low signal intensity at the fracture site due to compression of bone and surrounding marrow edema *(arrows)*. **D,** Another patient. This military recruit developed bilateral stress fractures from repeated marching. The problem went undiagnosed, resulting in a complete fracture through the left femoral neck *(arrows)*. The fracture was repaired with lag screws. A zone of sclerosis *(open arrow)* in the contralateral femoral neck represents the other stress fracture. *(**D,** From Taylor JAM, Harger BL, Resnick D: Diagnostic imaging of common hip disorders: A pictorial review. Top Clin Chiropr 1:8, 1994. D, Courtesy G. S. Huang, MD, Taipei, Taiwan.)*

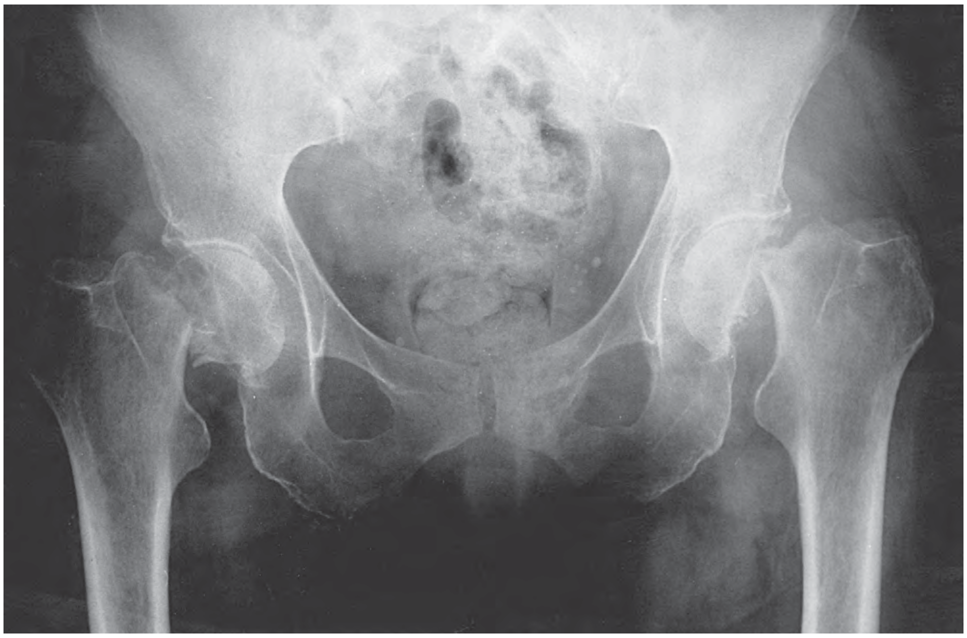

FIGURE 7–18 **Stress (insufficiency) fractures.**[25,117] In this 62-year-old woman with long-standing rheumatoid arthritis, bilateral insufficiency fractures have resulted in displacement and varus deformities. *(Courtesy V. Vint, MD, La Jolla, Calif.)*

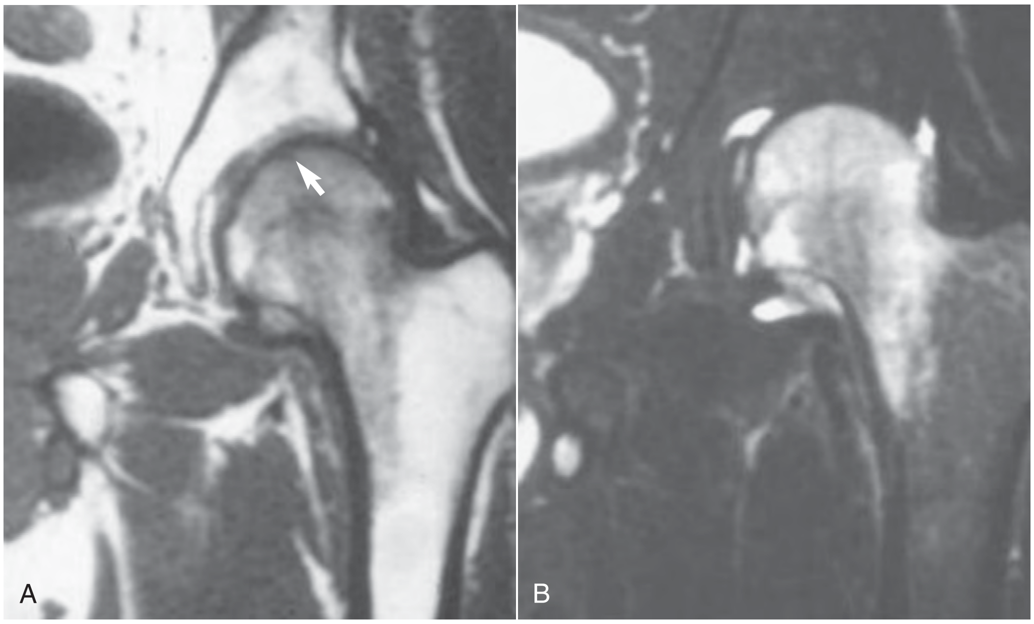

FIGURE 7–19 **Subchondral insufficiency fracture of the femoral head.**[117] This obese elderly female patient with osteoporosis presented with hip pain, but could remember no antecedent trauma. A coronal T1-weighted MR image **(A)** shows diffuse low signal intensity of the femoral head and neck whereas the T2-weighted fat suppressed image **(B)** reveals high signal intensity characteristic of bone marrow edema. The insufficiency fracture line itself is not well visualized in these images (*arrow* in **A**).

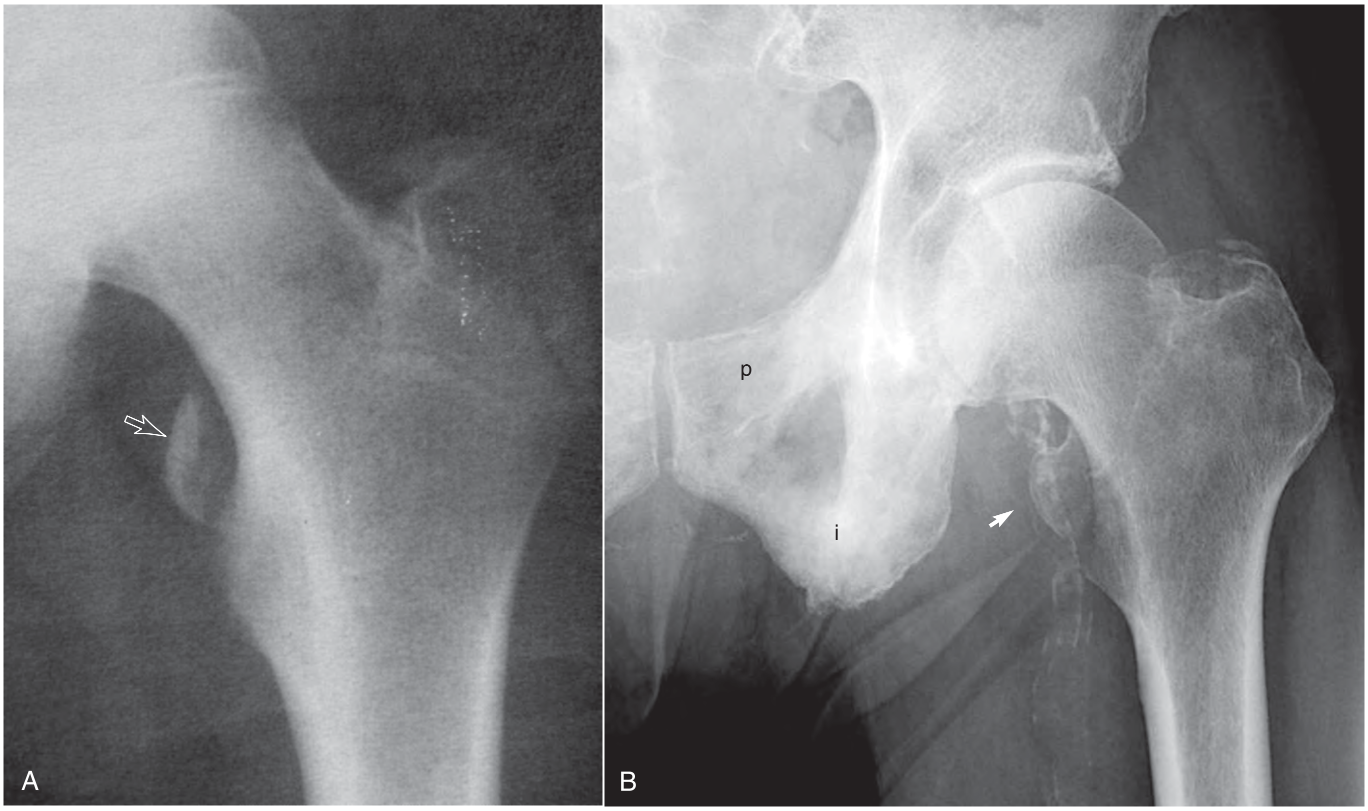

FIGURE 7–20 **Avulsion fractures of the lesser trochanter.**[116] **A,** This 13-year-old boy felt something pop and experienced sudden excruciating groin pain while playing soccer. The radiograph reveals avulsion and slight superior displacement of the lesser trochanter *(open arrow),* the insertion of the iliopsoas tendon. **B,** This 70-year-old man with skeletal metastasis from prostate carcinoma developed groin pain. The avulsed bone fragment is displaced superiorly *(arrow)* and is partially obscured by overlying vascular calcification. Observe the osteoblastic deposition from skeletal metastasis within the ischium (i) and pubis (p). While both patients have lesser trochanter avulsions, traumatic avulsion is the inciting factor in the teenager, whereas pathologic (insufficiency) fracture through an area of metastatic infiltration is the mechanism in the elderly patient.

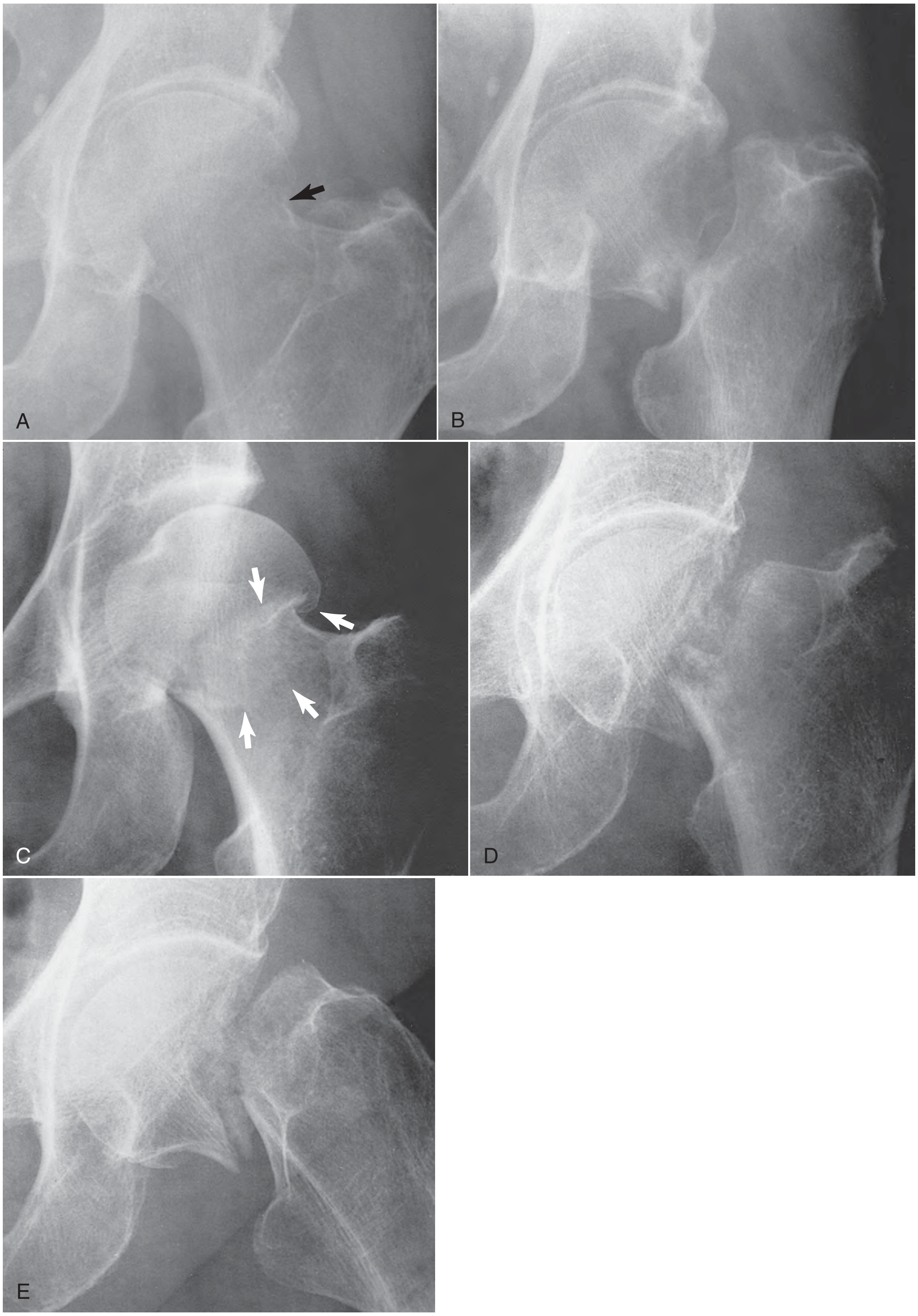

FIGURE 7–21 **Intracapsular fractures of the femoral neck: radiologic diagnosis.**[26,27,80,104] **A-B,** This 74-year-old osteoporotic woman sustained a minor fall. In **A,** a radiograph obtained on the day of injury reveals a subtle offset of the subcapital cortex at the head-neck junction *(arrow)* that was initially overlooked. In **B,** a radiograph obtained 3 weeks later shows a complete intracapsular fracture, extensive resorption and rotation at the fracture site, and marked varus deformity. **C,** In another patient, a 51-year-old woman, observe the impaction and valgus deformity at the site of this subcapital fracture *(arrows)*. Slight offset in the cortex and cortical bone impaction are often difficult to see on routine radiographs. **D-E,** An 87-year-old woman. Frontal **(D)** and frog-leg **(E)** projections reveal a displaced intracapsular fracture. Magnetic resonance (MR) imaging, CT, and scintigraphy often are helpful in the early diagnosis of occult hip fractures.[110] The radiographic appearance of subcapital fractures of the femoral neck unrelated to neoplasm often is similar to that of pathologic fractures. This appearance is caused primarily by rotation of the fracture fragments, and the finding is accentuated by displacement.

TABLE 7-8 Classification of Fractures of the Proximal Portion of the Femur

Entity	Characteristics
A. Classified According to Fracture Type[79,104]	
Major trauma	Major direct forces along the shaft of the femur with or without a rotational component
Insufficiency fracture	Most common in elderly patients, especially women, with osteoporosis
Pathologic fracture	Uncommon Patients with skeletal metastasis, Paget disease, and other pathologic disorders of bone
Fatigue fracture	Uncommon Young athletes
B. Classified According to Anatomic Location[79,104]	
Intracapsular fractures	Twice as common as extracapsular fractures
Subcapital	Immediately beneath the articular surface of the femoral head at the head-neck junction (Figure 7-21)
Transcervical	Across the middle of the femoral neck
Basicervical	Across the base of the femoral neck
Extracapsular fractures	
Intertrochanteric	Across a line between the greater and lesser trochanters
Subtrochanteric	Distal to the intertrochanteric line
C. Classified According to Degree of Displacement, Instability, or Extent of Fracture	
Intracapsular fractures[80,104]	***Garden system*** Classified according to displacement
Type I	Incomplete or impacted fracture
Type II	Complete fracture without osseous displacement
Type III	Complete fracture with partial displacement of fracture fragments commonly associated with shortening and external rotation of the distal fragments
Type IV	Complete fracture with total displacement of the fragments
Intertrochanteric fractures[81,104]	***Evans system*** Classified according to the presence or absence of stability and ease of fracture reduction
Type I	Stable fractures (50%) Absence of comminution of medial cortices of the proximal and distal fragments and absence of displacement of the lesser trochanter
Type II	Unstable fractures (50%) 1. Fractures with reversed obliquity and marked tendency toward medial displacement of the femoral shaft due to adductor muscle pull or to comminution of the greater trochanter and adjacent posterolateral surface of the shaft 2. Fractures in which there is absence of contact between the proximal and distal fragments due to comminution or medial and posterior displacement of fracture fragments
Subtrochanteric fractures[82,104]	***Seinsheimer system*** Classified according to the extent of the fracture and the configuration of fracture lines
Type I	Nondisplaced fracture
Type II	Two-part fracture
Type III	Three-part fracture
Type IV	Comminuted fracture with four or more fragments
Type V	Combined subtrochanteric and intertrochanteric fractures

* See also Tables 1-4 and 1-5.

TABLE 7-9 Complications of Fractures of the Proximal Portion of the Femur*

Entity	Figure(s)	Complications	Characteristic
Intracapsular fractures[80,104]	7-22	Delayed union	Under normal circumstances, these fractures show evidence of healing in the first 6 months, and fractures that remain ununited beyond that time are considered delayed union
		Nonunion	Fractures that do not unite after 12 months are considered nonunion fractures 5%-25% of cases ***Predisposing factors for delayed union and nonunion*** Advancing age Osteoporosis Posterior comminution of fracture Inadequate reduction Poor internal fixation technique
		Osteonecrosis	10%-30% of cases ***Predisposing factors for osteonecrosis*** Moderate or severe displacement of fracture fragments Persistent motion with inadequate stabilization Increased intracapsular pressure from hemarthrosis Vascular injury to femoral head during trauma or attempts at reduction
		Thromboembolism	
		Postoperative infection	
Intertrochanteric fractures[81,104]	7-23	Varus deformity	Nonsurgical and occurring after failed internal fixation
		Secondary subcapital fracture	Occurring after internal fixation of intertrochanteric fracture
		Vessel injury	Laceration of adjacent vessels
		Nonunion	Uncommon
		Osteonecrosis	Uncommon Fewer than 1% of cases
Subtrochanteric fractures[82,104]	7-24	Delayed union	
		Nonunion	
		Implant failure	

* See also Tables 1-4 to 1-6.

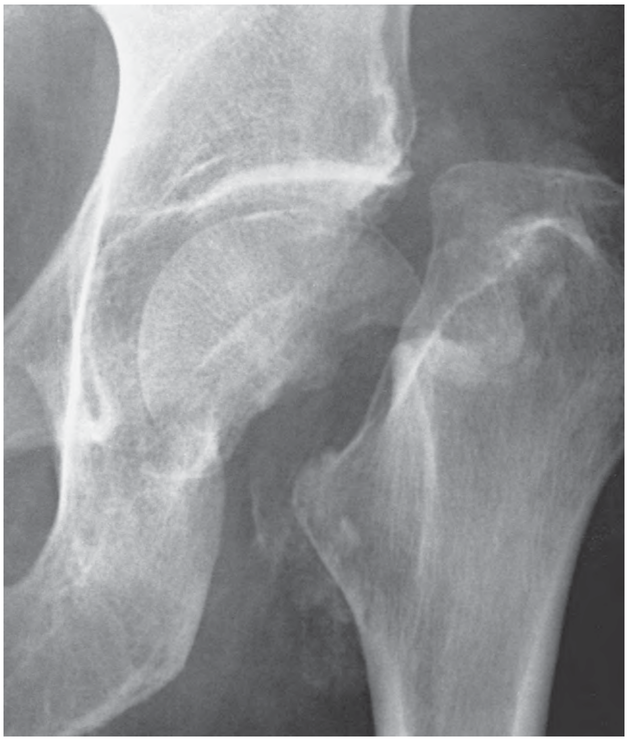

FIGURE 7–22 Intracapsular femoral neck fracture with nonunion and osteolysis.[28,104] Observe osteolysis of the femoral neck in this 71-year-old man with an ununited subcapital fracture. Osseous debris is seen within and around the fracture cleft, and rotation is evident at the fracture site.

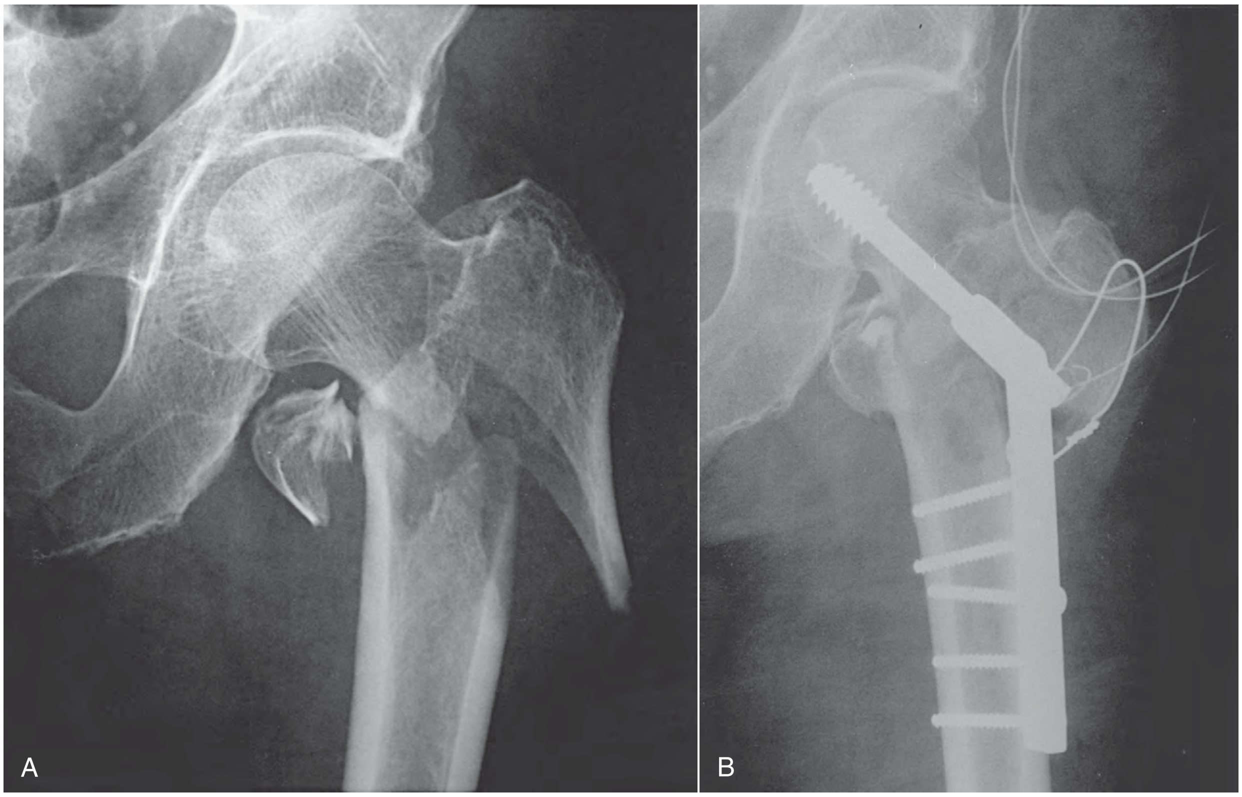

FIGURE 7–23 **Intertrochanteric fracture: surgical repair.**[29,104] **A,** An unstable type II comminuted intertrochanteric fracture is seen in this 69-year-old man. Marked displacement of both trochanters is evident. **B,** A dynamic (sliding) compression screw has been used to provide fixation while allowing impaction to occur at the fracture during healing and weight-bearing. Intertrochanteric fractures predominate in elderly patients and usually result from falls.

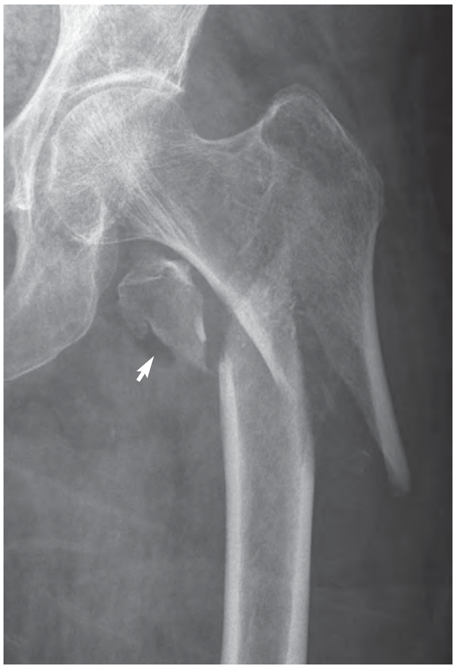

FIGURE 7–24 **Sub/pertrochanteric fracture.**[104] A extraarticular fracture through the subtrochanteric region of the femur in an 87-year-old woman is characterized by avulsion of the lesser trochanter *(arrow)*, poor apposition, and significant varus deformity.

TABLE 7-10 Internal Derangements of the Hip Joint[98,112]

Entity	Figure(s)	Characteristics
Acetabular labrum abnormalities[111,112]		The acetabular labrum is best imaged by MR arthrography in which intraarticular gadolinium is injected to distend the joint to provide optimum contrast Labral abnormalities predispose to osteoarthrosis Most abnormalities involve the anterior and superior labra; posterosuperior abnormalities more common in younger patients
Labral detachment and tears	7-25	Detachments are more common than tears ***MR arthrography findings*** Presence of contrast at the junction of the labrum and its attachment to the acetabular rim with or without displacement
Intrasubstance tears and cystic degeneration		***MR arthrography findings*** Presence of intrasubstance contrast material within the labrum
Perilabral ganglion cysts	7-26	Association with labral pathology, especially detachments Increased incidence in patients with developmental acetabular dysplasia Begin as extraarticular soft tissue collections, and may eventually erode into adjacent acetabulum
Femoroacetabular impingement[90-97,112]		Morphologic abnormalities about the hip joint result in early degenerative changes predominantly in young male patient populations ***Clinical findings*** Hip pain on flexion and internal rotation and disproportionate loss of range of motion during internal rotation Two types have been identified
A. Pincer-type[112]	7-27	Morphologic abnormalities in the acetabular side of the joint predominantly in older female patients Redundant acetabulum leads to excessive coverage of the femoral head and during hip flexion pincer impingement leads to abnormal linear contact between acetabular rim and femoral head-neck junction ***MR imaging findings*** Primarily labral damage and only minimal cartilage damage along the acetabular rim Coxa profunda, acetabular retroversion, protrusion, trauma, and labral ossification
B. Cam-type[112]	7-28	Morphologic abnormalities in the femoral side of the joint Offset of the femoral head-neck junction termed pistol-grip deformity results in abnormal compression and stress between the acetabular labrocartilaginous complex and the prominent femoral head-neck junction during hip flexion ***MR imaging findings*** Combinations of acetabular cartilage tear, labral tear, abnormal head-neck morphology and fibrocystic changes in the femoral neck representing early manifestations of osteoarthrosis
Greater trochanteric pain syndrome[105-107]	7-29	***Clinical findings*** Clinical condition characterized by pain and point tenderness on the lateral aspect of the hip when lying on the hip or using the extremity Related to peritrochanteric bursitis or tears of the abductor (gluteus medius and minimus) muscles or tendons ***MR imaging findings*** Hyperintensity surrounding the greater trochanter on T2-weighted images Hyperintensity can be feathery, crescentic, or round in shape and can be seen in several locations such as: Subtendinous Intratendinous (tendinopathy) Subfascia lata Superficial to fascia lata Partial tears of the gluteus medius or minimus may be evident
Synovial abnormalities[18]		MR imaging is useful in identifying synovial abnormalities such as synovitis, synovial cysts, and iliopsoas bursitis

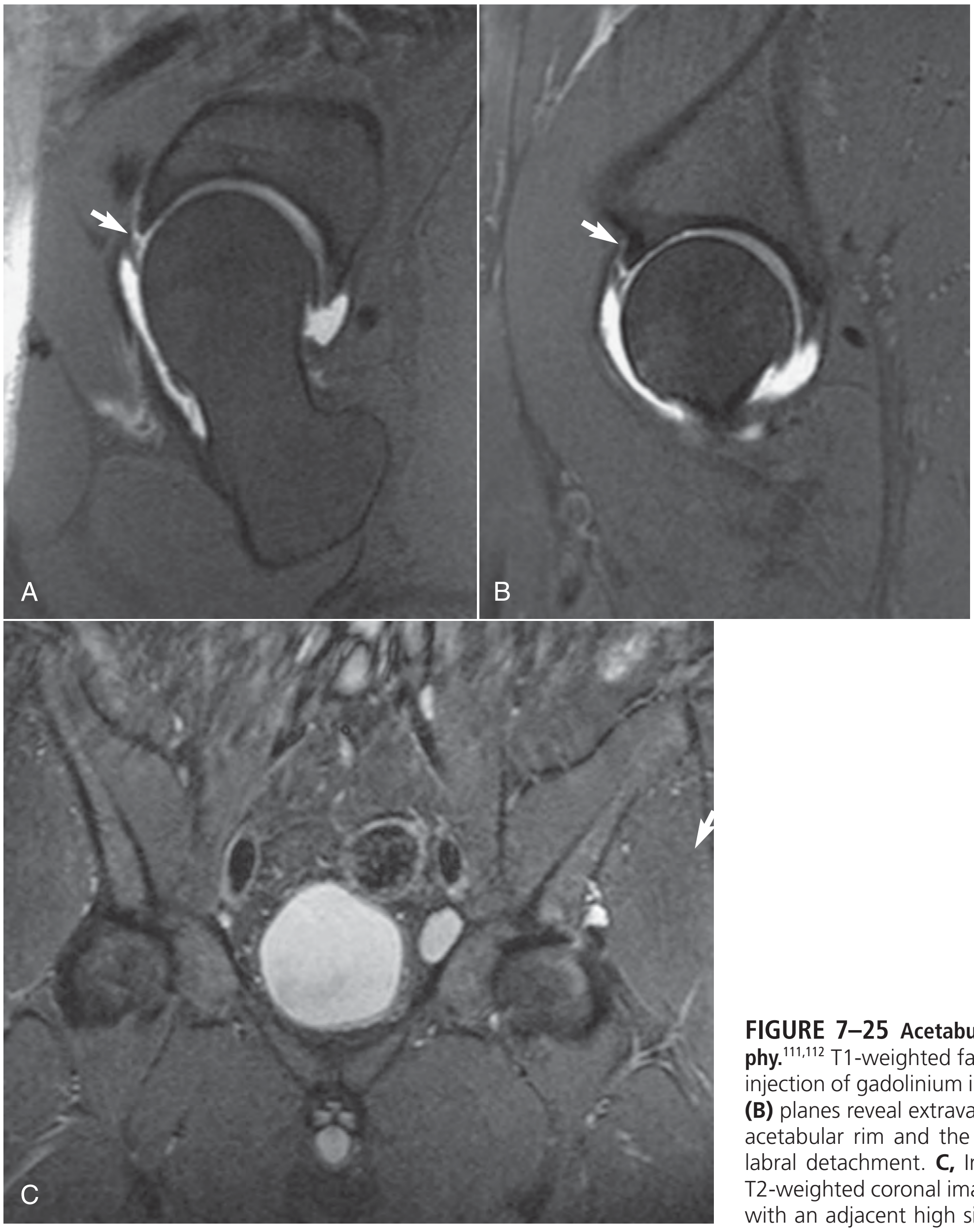

FIGURE 7–25 Acetabular labrum detachment: MR arthrography.[111,112] T1-weighted fat suppressed images after intraarticular injection of gadolinium in the transaxial oblique **(A)** and sagittal **(B)** planes reveal extravasation of contrast *(arrow)* between the acetabular rim and the anterior labrum depicting an anterior labral detachment. **C,** In a 38-year-old man, a fat-suppressed T2-weighted coronal image shows an anterosuperior labral tear with an adjacent high signal intensity perilabral cyst *(arrow)*.

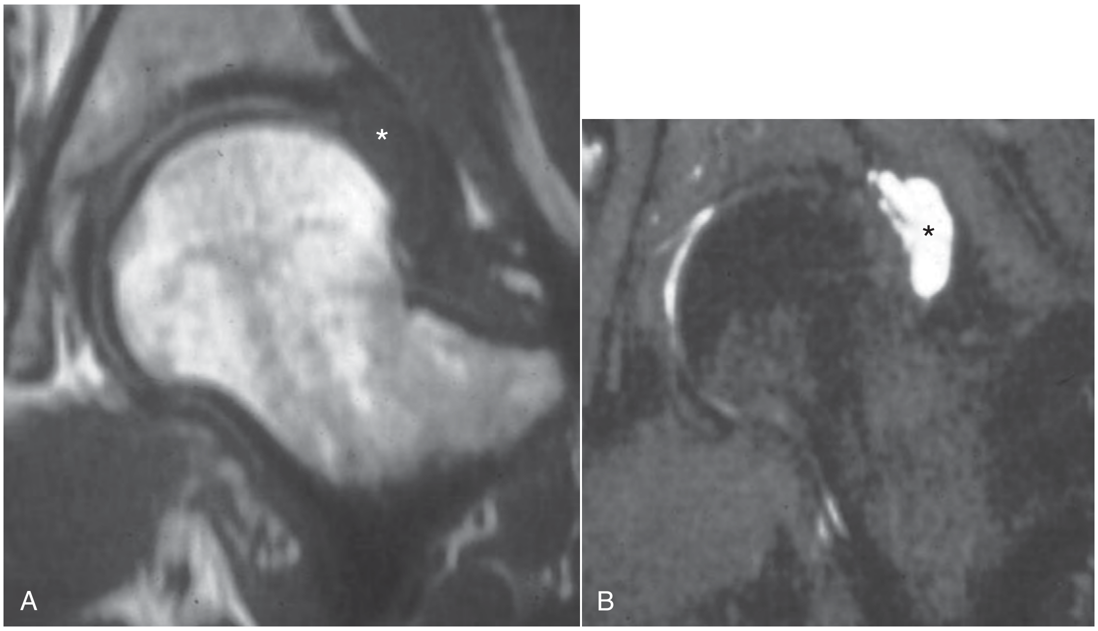

FIGURE 7–26 Perilabral ganglion cysts.[111,112] Coronal T1-weighted **(A)** and STIR **(B)** MR images show a large cystic fluid collection adjacent to the lateral aspect of the femoral head and acetabulum (*) consistent with the appearance of a perilabral ganglion cyst. These cysts, which are high signal intensity on fluid-sensitive images, may be associated with dysplastic acetabuli, labral tears, or with both findings.

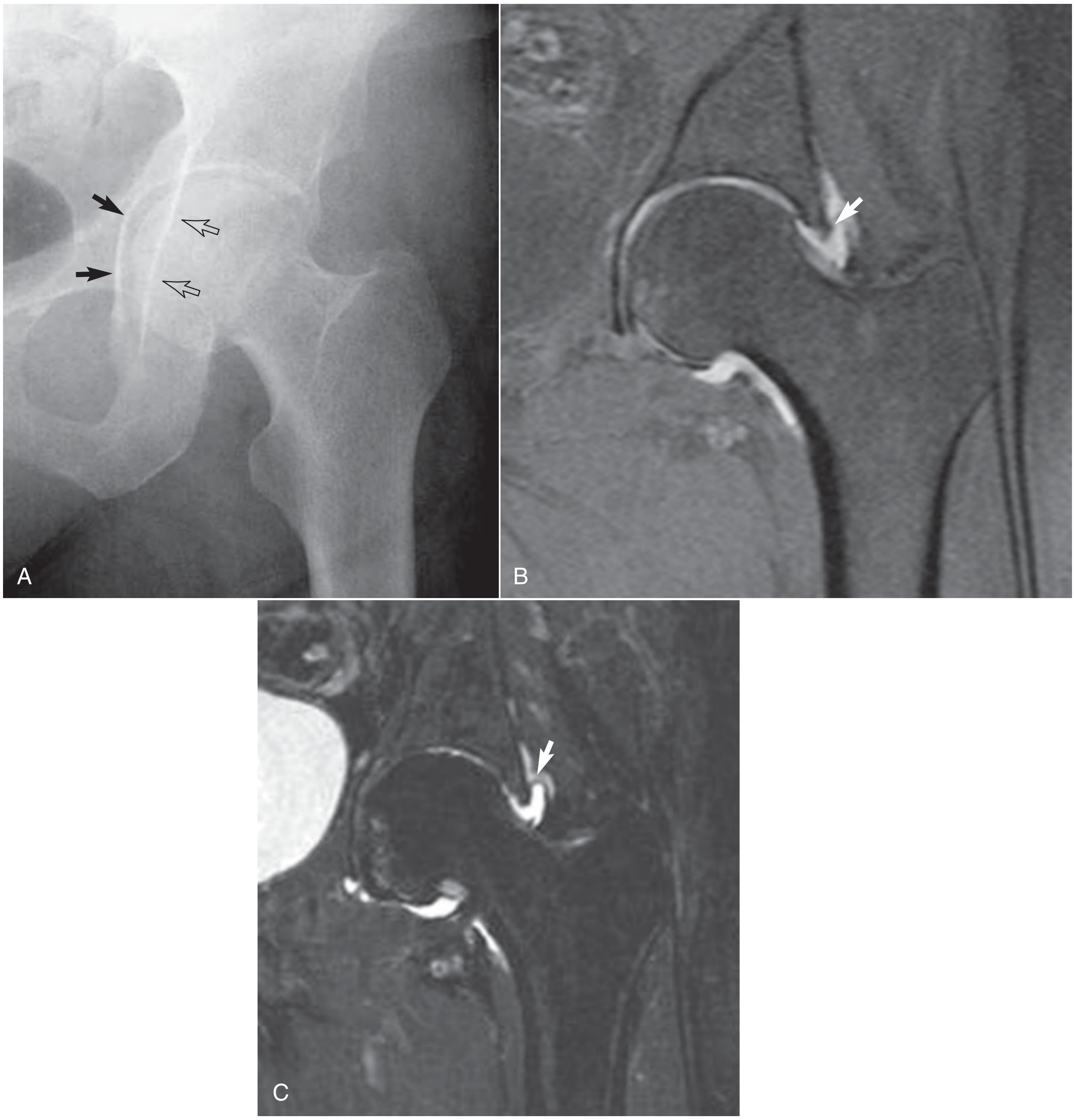

FIGURE 7–27 **Femoroacetabular impingement: pincer type.**[92-97] This 54-year-old female presented with left hip pain. The anteroposterior radiograph **(A)** demonstrates concentric joint space narrowing and acetabular protrusion evidenced by the medial floor of the acetabulum *(arrows)* protruding in toward the pelvic brim; the medial floor of the acetabulum also lies medial to the ilioischial line *(open arrows),* which is superimposed over the femoral head. Coronal fat-suppressed T1-weighted **(B)** and T2-weighted **(C)** images obtained after intraarticular gadolinium administration demonstrate the exaggerated depth of the acetabulum and the apparent elongation of the superior acetabulum and labrum *(arrows)*. This situation leads to a "pincer" effect involving abnormal contact between the acetabular labrum and femoral neck.

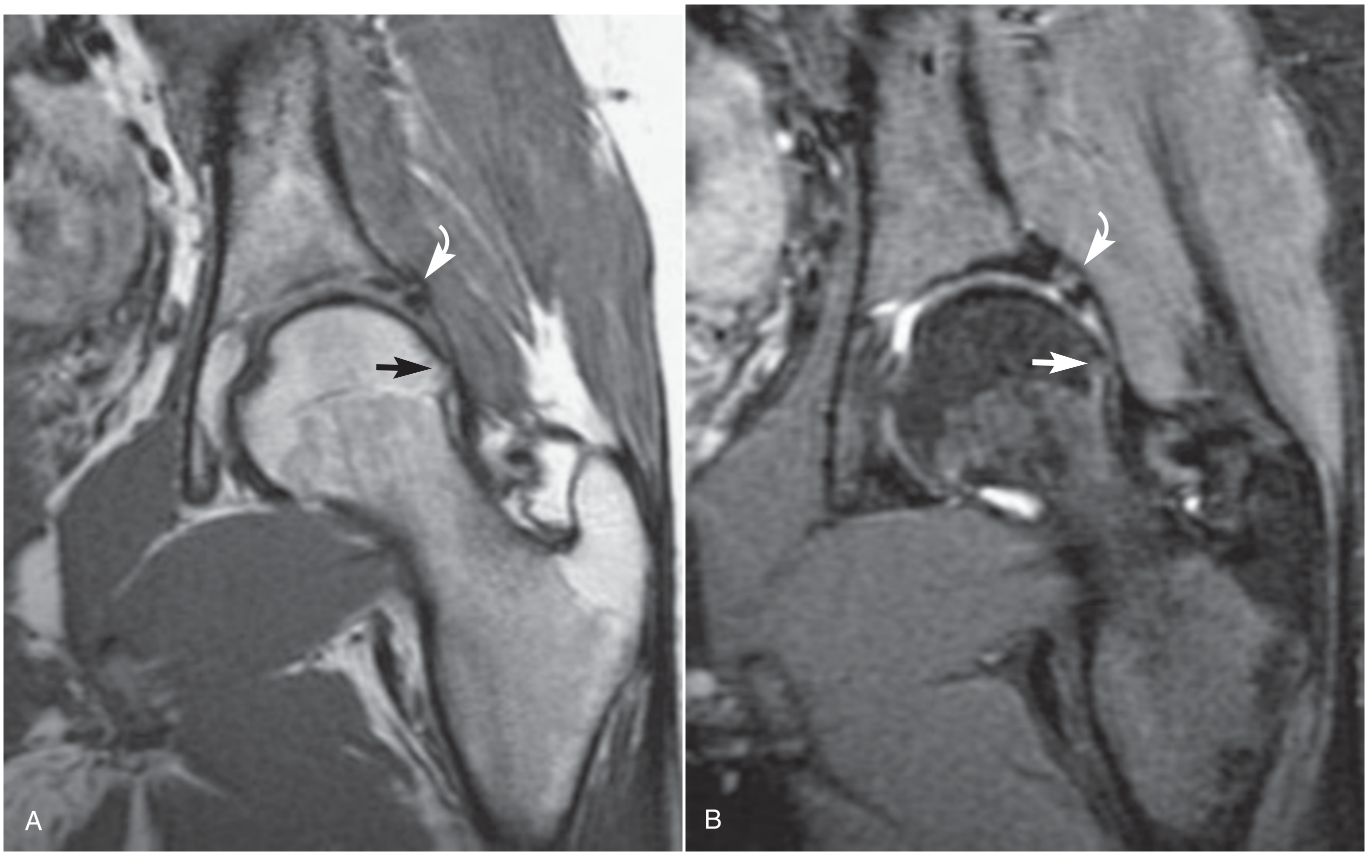

FIGURE 7–28 Femoroacetabular impingement: cam-type.[92-97] In this 21-year-old woman with hip pain, coronal T1-weighted **(A)** and T2-weighted fat suppressed **(B)** MR images show a labral tear, *(bent arrows)* an abnormal osseous bump formation at the head-neck junction *(arrows)* and a reduced transverse diameter of the femoral neck, part of which may be due to slice selection. CAM type femoroacetabular impingement frequently occurs in young physically active individuals and often results in premature degenerative disease and labral pathology.

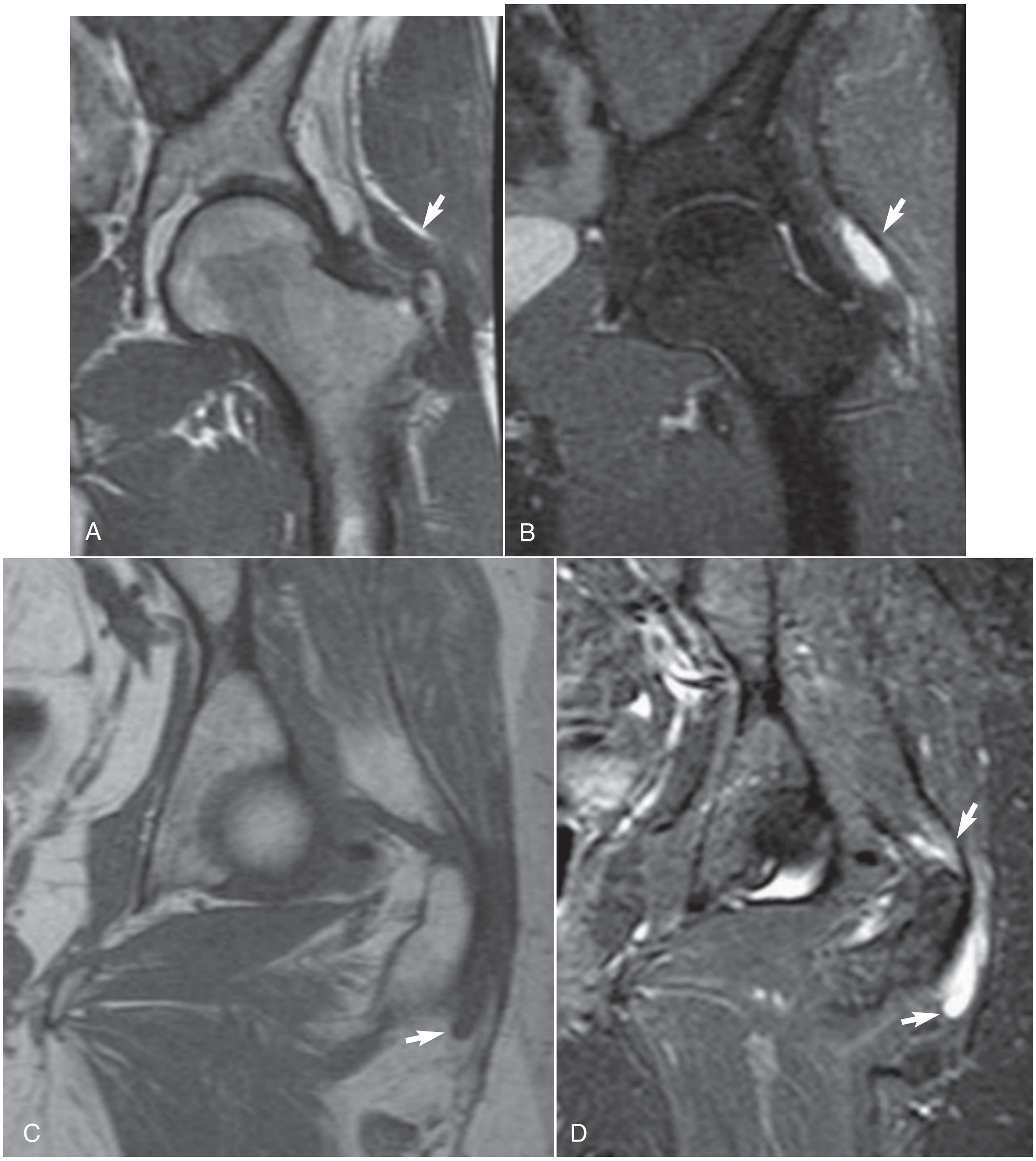

FIGURE 7–29 Greater trochanteric pain syndrome.[105-107] **A-B,** Gluteus minimus partial tear and subgluteus minimus bursitis lead to decreased signal intensity on a T1-weighted coronal spin echo MR image and increased signal intensity on a STIR coronal MR image just superior to the greater trochanter *(arrows)*. **C-D,** Trochanteric bursitis reveals similar signal characteristics located lateral to the greater trochanter *(arrows)*. The greater trochanteric pain syndrome is typically related to peritrochanteric bursitis or tears of the abductor (gluteus medius and minimus) muscles or tendons, all of which are usually detectable on MR imaging.

TABLE 7-11 Articular Disorders Affecting the Hip*

Entity	Figure(s)	Characteristics
Degenerative and Related Disorders		
Osteoarthrosis[30-32,108,114]	7-30	***Imaging findings*** *Osteophytes:* circumferential (collar) osteophytes may simulate fracture of the femoral neck Subchondral sclerosis Subchondral cysts Subluxation Buttressing *Intraarticular bodies:* infrequently secondary synovial osteochondromatosis Causes of secondary osteoarthrosis of the hip: trauma, Legg-Calvé-Perthes disease, developmental dysplasia, shallow acetabulum, congenital hip dislocation, slipped capital femoral epiphysis *See also* Table 1-7
Diffuse idiopathic skeletal hyperostosis (DISH)[33]	7-31	Enthesopathy and ligament ossification about the acetabulum, ischiopubic region, and lesser trochanters DISH typically does not result in joint space narrowing of the hip
Inflammatory Disorders		
Rheumatoid arthritis[34,35]	7-32, 7-33	Hip involvement common in rheumatoid arthritis ***Imaging findings*** Bilateral symmetric, concentric joint space narrowing with axial migration of femoral head Subchondral erosion Absent or mild sclerosis Periarticular osteoporosis Synovial cysts
Juvenile idiopathic arthritis[34]		*AKA:* Juvenile chronic arthritis or juvenile rheumatoid arthritis Diffuse joint space loss with concentric narrowing, periarticular osteoporosis, and erosions of the femoral head and acetabulum
Ankylosing spondylitis[36]	7-34	Bilateral symmetric, concentric joint space narrowing with axial migration of the femoral heads Osteophytosis about the superolateral aspect of the femoral head may lead to a collar surrounding the head-neck junction Acetabular and femoral cysts, periarticular osteoporosis, mild acetabular protrusion; may eventually result in partial or complete intraarticular osseous ankylosis
Psoriatic arthropathy and reactive arthritis[37]	7-35	Hip involvement similar to but less frequent than in ankylosing spondylitis
Dermatomyositis and polymyositis[38]	7-36	Widespread sheetlike calcification in soft tissues surrounding pelvis and hip region
Progressive systemic sclerosis (scleroderma)[39]	7-37	Globular accumulations of periarticular soft tissue calcinosis
Systemic lupus erythematosus (SLE)[40]	7-38, See Figure 7-68	Osteonecrosis of the femoral head occurs in SLE patients treated with corticosteroid therapy; also occurs in SLE patients not treated with steroid medication, possibly because of vasculitis
Mixed connective tissue disease[40]	7-38	Mixed connective tissue diseases and overlap syndromes Diseases include combinations of rheumatoid arthritis, dermatomyositis, scleroderma, systemic lupus erythematosus, or scleroderma Radiographic features variable; may result in diffuse joint space narrowing, erosions, soft tissue calcinosis, and acetabular protrusion

* See also Tables 1-7 to 1-10 and Table 1-19.

TABLE 7-11 Articular Disorders Affecting the Hip—cont'd

Entity	Figure(s)	Characteristics
Crystal Deposition and Metabolic Disorders		
Calcium pyrophosphate dihydrate (CPPD)[41,42]	7-39	Articular space narrowing, sclerosis, cyst formation, osteophytes, and intraarticular and periarticular chondrocalcinosis Acetabular protrusion and considerable femoral head destruction and fragmentation resembling neuropathic osteoarthropathy may occur in severe cases
Calcific bursitis and tendinitis[43]	7-40	Calcium hydroxyapatite crystal deposition in tendons and bursae about the hip Single or multiple cloudlike linear, triangular, or circular soft tissue calcifications at the gluteal insertions in the greater trochanter and surrounding bursae; also adjacent to acetabular margin, lesser trochanter, and proximal portion of femur Occasionally, large tumorlike accumulations of calcification will also be seen about the hip in patients with chronic renal disease or collagen vascular disorders
Rapidly destructive hip disease[44,78,109]	7-41	Cause is unclear; believed to be related to a generalized process such as osteonecrosis or intraarticular deposition of calcium hydroxyapatite crystals Severe, rapid atrophic destruction of femoral head resembling septic arthritis
Gouty arthropathy[45]	7-42	Rare hip involvement Periarticular erosions predominate; soft tissue tophi may be identified
Hemochromatosis[46]	7-43	Rare disorder exhibiting findings identical to those of CPPD crystal deposition disease with prominent chondrocalcinosis
Alkaptonuria[47]	7-44	Rare hip joint involvement Accelerated degenerative disease, chondrocalcinosis, diffuse joint space narrowing, sclerosis, fragmentation, osteophytosis, mild acetabular protrusion, and eventual femoral head remodeling
Infection		
Pyogenic septic arthritis[48,49,83,84]	7-45, 7-46	***Imaging findings in adult septic arthritis of the hip*** Rapid concentric loss of joint space Periarticular osteoporosis Loss of definition and destruction of subchondral bone Capsular distention Erosions ***Imaging findings in neonatal and childhood septic arthritis of the hip*** Soft tissue swelling or capsular distention Pathologic subluxation or dislocation: lateral displacement of ossification center Slipped capital femoral epiphysis Metaphyseal osteomyelitis Concentric loss of joint space
Iliopsoas bursal abscess[120]	7-47, 7-48	Abscesses in the iliopsoas muscle tendon or bursae can develop as a primary process or more commonly secondary to infection elsewhere. *Staphylococcus aureus* and *Mycobacterium tuberculosis* are the most common organisms
Tuberculous arthritis[50]	7-48	*Phemister triad:* juxtaarticular osteoporosis, peripherally located erosions, gradual joint space narrowing Various degrees of soft tissue swelling Subchondral erosions Periarticular abscess

Continued

TABLE 7-11 Articular Disorders Affecting the Hip—cont'd

Entity	Figure(s)	Characteristics
Miscellaneous Disorders		
Neurologic injury: heterotopic ossification[51,52]	7-49	Periarticular soft tissue ossification in paraplegic and quadriplegic patients Begins as poorly defined opaque areas; typically progresses to large accumulations possessing trabeculae and often results in complete osseous ankylosis
Idiopathic chondrolysis of the hip[53]	7-50	Idiopathic monoarticular disorder seen mainly in adolescents, especially African Americans; also seen in children with slipped capital femoral epiphysis ***Clinical findings*** Pain, restriction of motion, stiffness, absence of trauma history, aspiration fails to reveal presence of effusion or organisms ***Imaging findings*** Osteoporosis, diffuse joint space narrowing, erosion of subchondral bone
Pigmented villonodular synovitis[54,55,85]	7-51	Cystic erosions on both sides of the joint Hemorrhagic joint effusion Eventual osteoporosis Well preserved joint space until late in the disease Extraarticular process termed giant cell tumor of the tendon sheath may be related to pigmented villonodular synovitis
Idiopathic synovial osteochondromatosis[56-58]	7-52	Multiple intraarticular or periarticular collections of calcification or ossification of variable size and density Erosion of adjacent bone Secondary osteoarthrosis Noncalcified bodies are best demonstrated with arthrography or MR imaging Secondary synovial osteochondromatosis may occur as a result of degenerative joint disease

TABLE 7-12 Hip Joint Disorders: Typical Patterns of Joint Space Narrowing

	Joint Compartment			Symmetry		
Entity	Superior	Medial	Axial	Unilateral	Bilateral Asymmetric	Bilateral Symmetric
Osteoarthrosis	+	Rare		+	+	
Calcium pyrophosphate dihydrate (CPPD) crystal deposition disease	Rare		+		+	+
Rheumatoid arthritis	Rare		+			+
Juvenile chronic arthritis	Rare		+			+
Osteonecrosis (late in disease process)	+		+	+	+	
Ankylosing spondylitis	Rare		+			+
Psoriatic arthropathy and Reiter syndrome			+		+	
Neuropathic osteoarthropathy	Rare	+	+	+	+	
Septic arthritis			+	+		
Idiopathic chondrolysis of the hip			+	+		
Alkaptonuria			+		+	+
Hemophilia			+		+	+
Osteomalacia		+	+			+
Paget disease with secondary joint degeneration	+	+	+	+	+	

+, Predominant pattern(s); *Rare*, less common patterns.

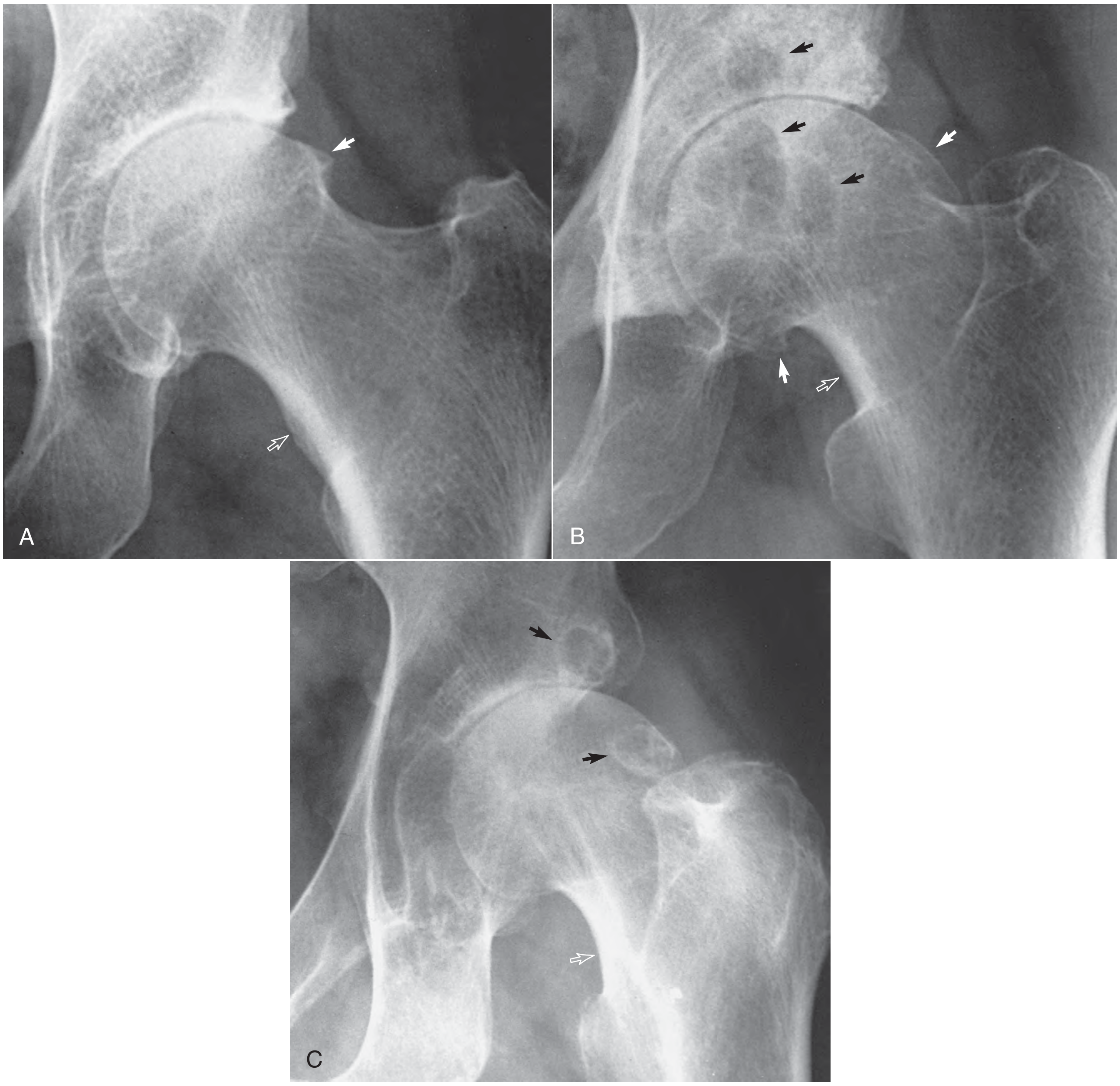

FIGURE 7–30 **Osteoarthrosis: spectrum of abnormalities.**[30-32,108,114] **A-D,** Radiographic changes of hip joint osteoarthrosis include joint space narrowing (predominantly in the superior compartment), osteophytes *(white arrows),* subchondral cysts *(black arrows),* subchondral sclerosis, and buttressing of the medial femoral neck *(open arrows)*. In **A,** mild changes are evident. In **B,** moderate changes include more severe joint space narrowing and circumferential (collar) osteophytes at the head-neck junction *(white arrows),* buttressing of the femoral neck, and subchondral cysts. All of these changes are more prominent in this patient with advanced disease. In **C,** moderate changes in another patient consist of subchondral cysts, which are a prominent feature on this radiograph.

Continued

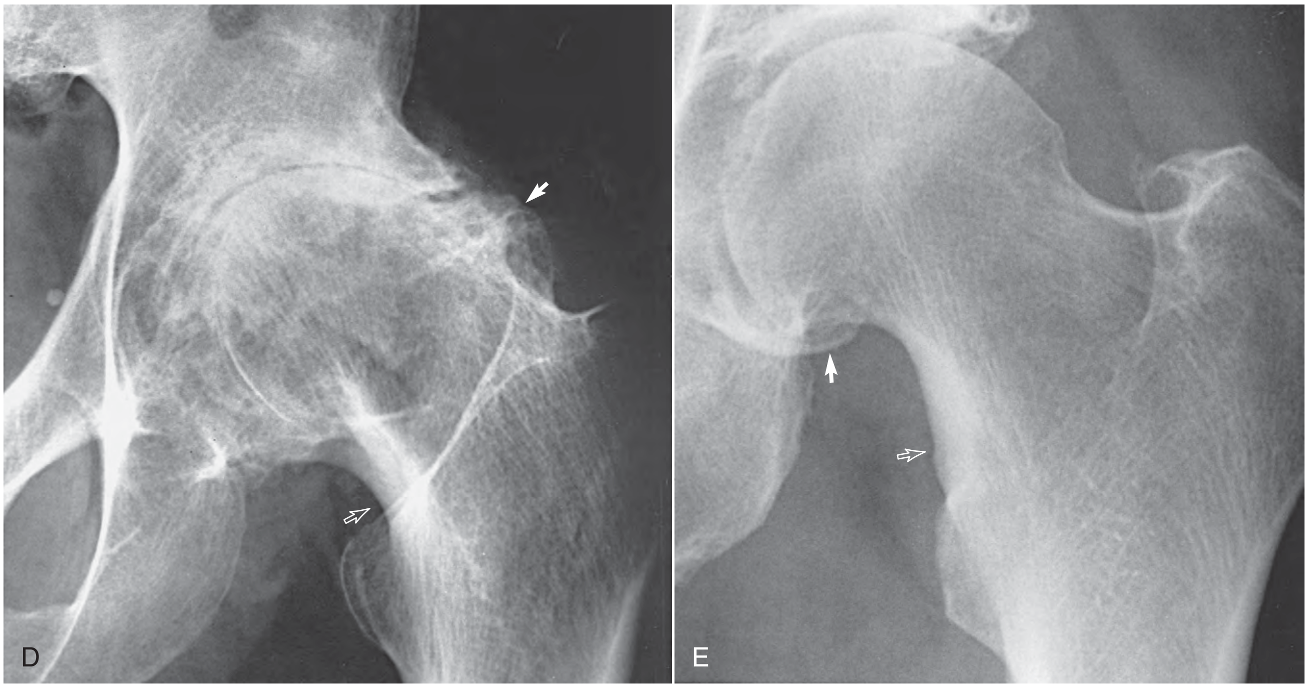

FIGURE 7–30, cont'd D, Severe changes. Severe sclerosis, osteophyte formation, joint space obliteration, and medial buttressing are evident. **E,** Buttressing. Observe the prominent sclerosis and hypertrophy of the medial cortex of the femoral neck *(open arrow),* a finding that most frequently accompanies degenerative joint disease. Buttressing may also be apparent in osteonecrosis, developmental acetabular dysplasia, rheumatoid arthritis, and ankylosing spondylitis. It likewise may be seen adjacent to an osteoid osteoma. An osteophytic rim is evident surrounding the acetabulum *(arrow)*.

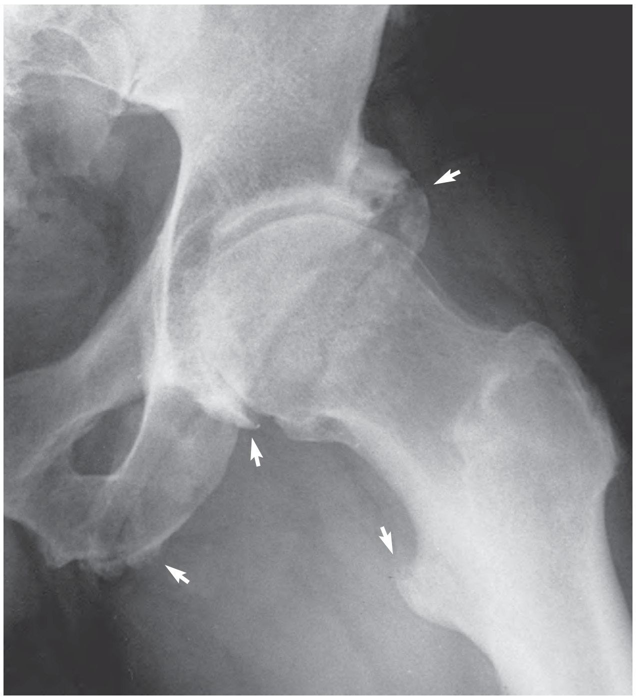

FIGURE 7–31 Diffuse idiopathic skeletal hyperostosis (DISH).[33] Observe the hypertrophic periarticular enthesopathy *(arrows)* affecting the acetabular, ischiopubic, and lesser trochanteric regions in this patient with long-standing DISH. Evidence of degenerative joint disease is also present.

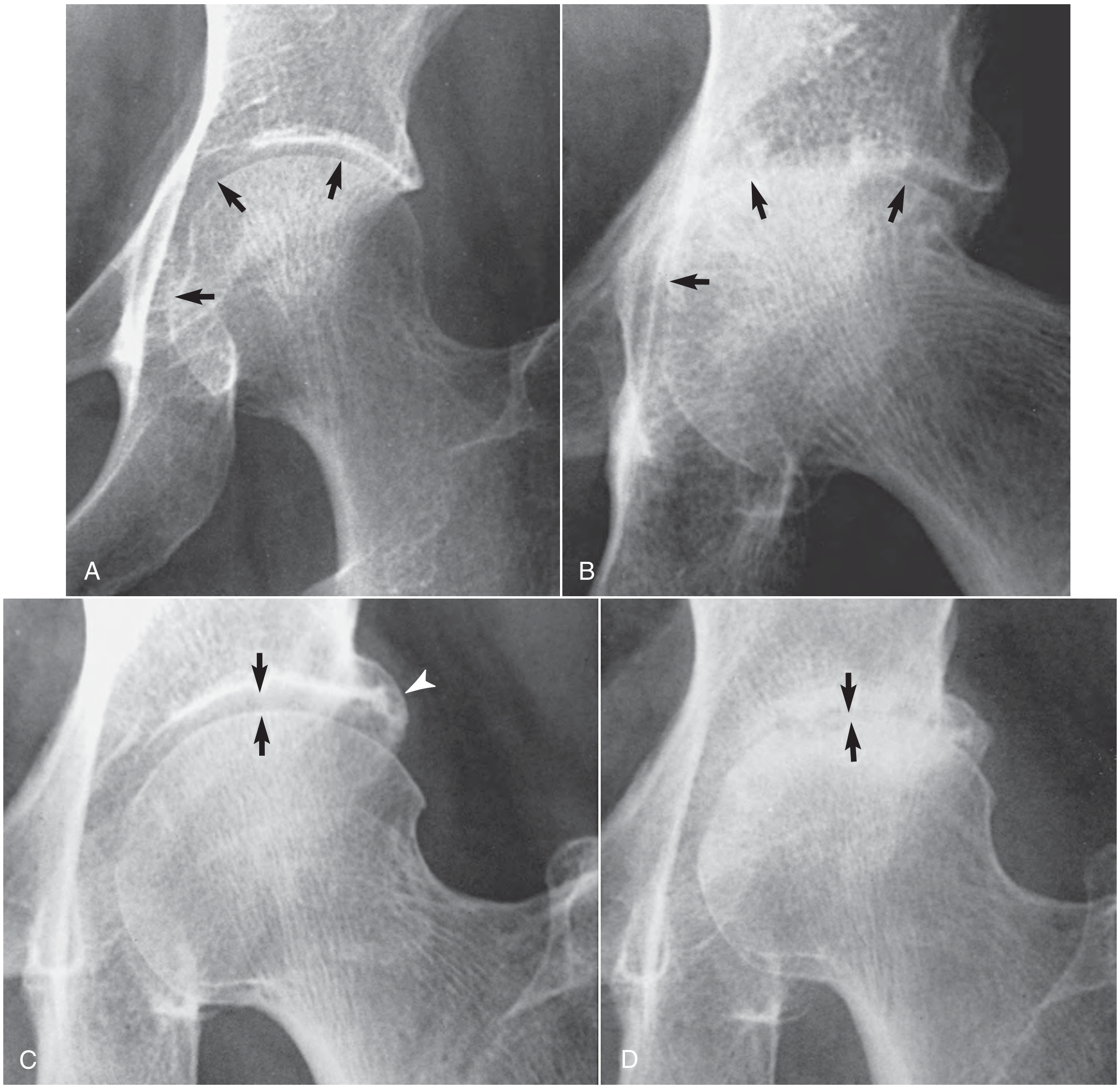

FIGURE 7–32 **Rheumatoid arthritis: hip abnormalities.**[34] **A,** Early changes. Uniform (concentric) joint space narrowing has resulted in axial migration of the femoral head in relation to the acetabulum *(arrows)*. These changes were bilateral and symmetric. This is the most characteristic pattern of joint space narrowing in the hip in patients with rheumatoid arthritis. **B,** Advanced changes. This man with rheumatoid arthritis had bilateral symmetric involvement (opposite hip not shown) with severe axial migration and joint space obliteration *(arrows)*. Periarticular osteopenia and absence of productive changes, such as osteophytes and sclerosis, are characteristic signs of this inflammatory synovial process. **C-D,** Progressive changes: Serial radiographs. In **C,** an initial radiograph shows early uniform joint space narrowing *(arrows)*. An acetabular osteophyte *(arrowhead)* relates to superimposed degenerative joint disease. In **D,** a radiograph taken 5 years later demonstrates progressive joint space narrowing *(arrows),* subchondral erosions, and sclerosis.

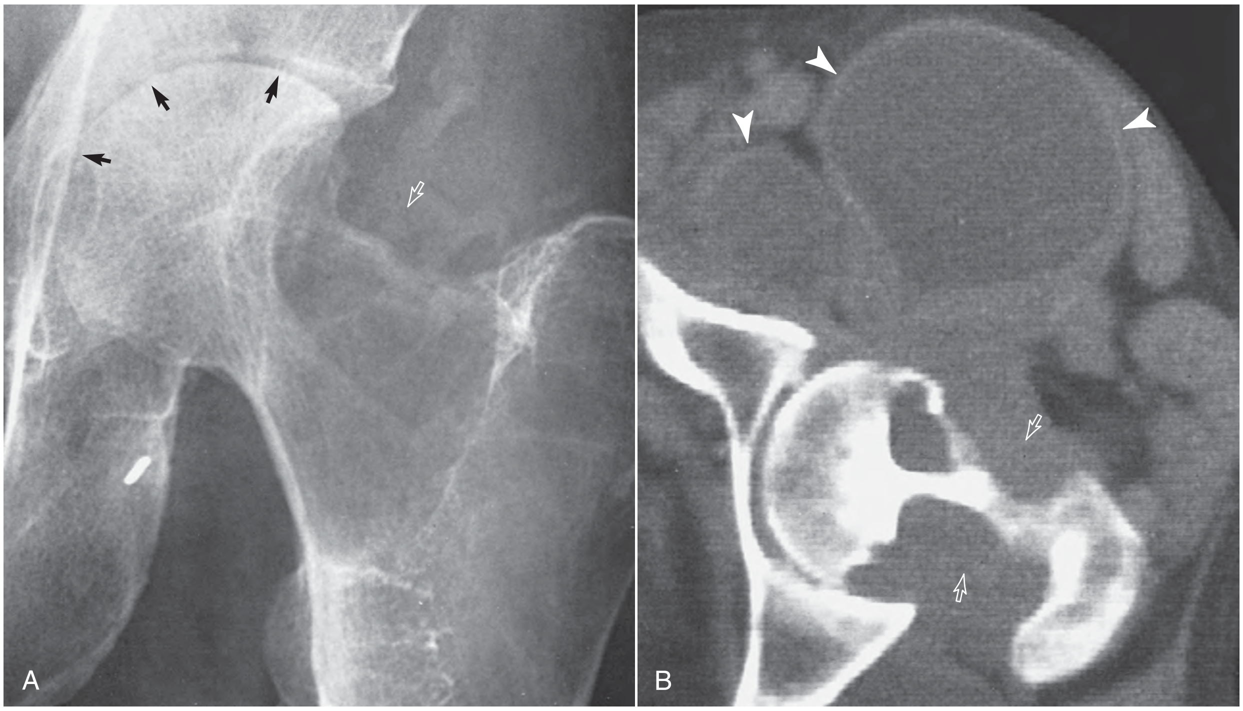

FIGURE 7–33 **Rheumatoid arthritis: synovial cyst.**[35] A 54-year-old man with long-standing rheumatoid arthritis and a mass in the groin. **A,** Anteroposterior radiograph shows extensive scalloped osteolytic destruction of the femoral neck *(open arrow)*. Uniform loss of joint space with axial migration of the femoral head is also present *(arrows)*. **B,** Transaxial CT scan at the level of the femoral neck reveals a synovial cyst that is seen as two circular fluid-filled outpouchings *(arrowheads)* anterior to the femur. Osseous destruction of the femoral neck *(open arrows)* and diffuse joint space narrowing are also evident. *(Courtesy J. Scavulli, MD, San Diego.)*

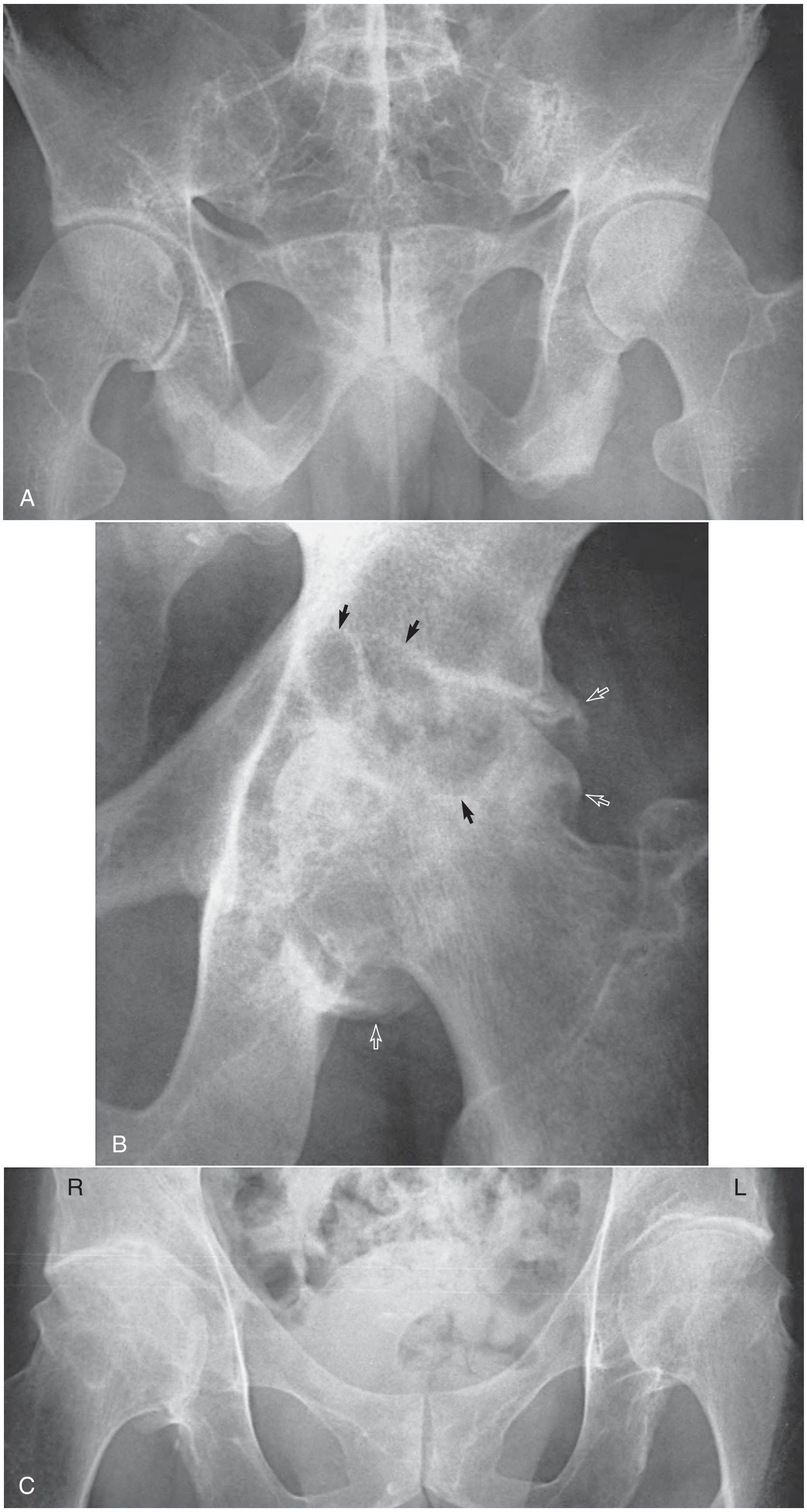

FIGURE 7–34 **Ankylosing spondylitis.**[36] **A,** A pelvic radiograph from this 36-year-old man with long-standing ankylosing spondylitis reveals bilateral concentric narrowing of the hip joint spaces. Observe also the presence of enthesopathy adjacent to both ischial tuberosities. The sacroiliac joints are ankylosed. **B,** In another patient with concentric loss of joint space and prominent osteophytes *(open arrows),* large subchondral cysts are present in the femoral head and acetabulum *(arrows).* **C,** Bilateral, relatively symmetric involvement of both hips in a 47-year-old man with a 20-year history of ankylosing spondylitis. Observe the concentric decrease of joint space, osteophyte formation, and subchondral cyst formation that predominate on the right side. Hip involvement in ankylosing spondylitis is common and exhibits a bilateral symmetric pattern in more than 75% of cases. *(**A,** Courtesy M.N. Pathria, MD, San Diego.)*

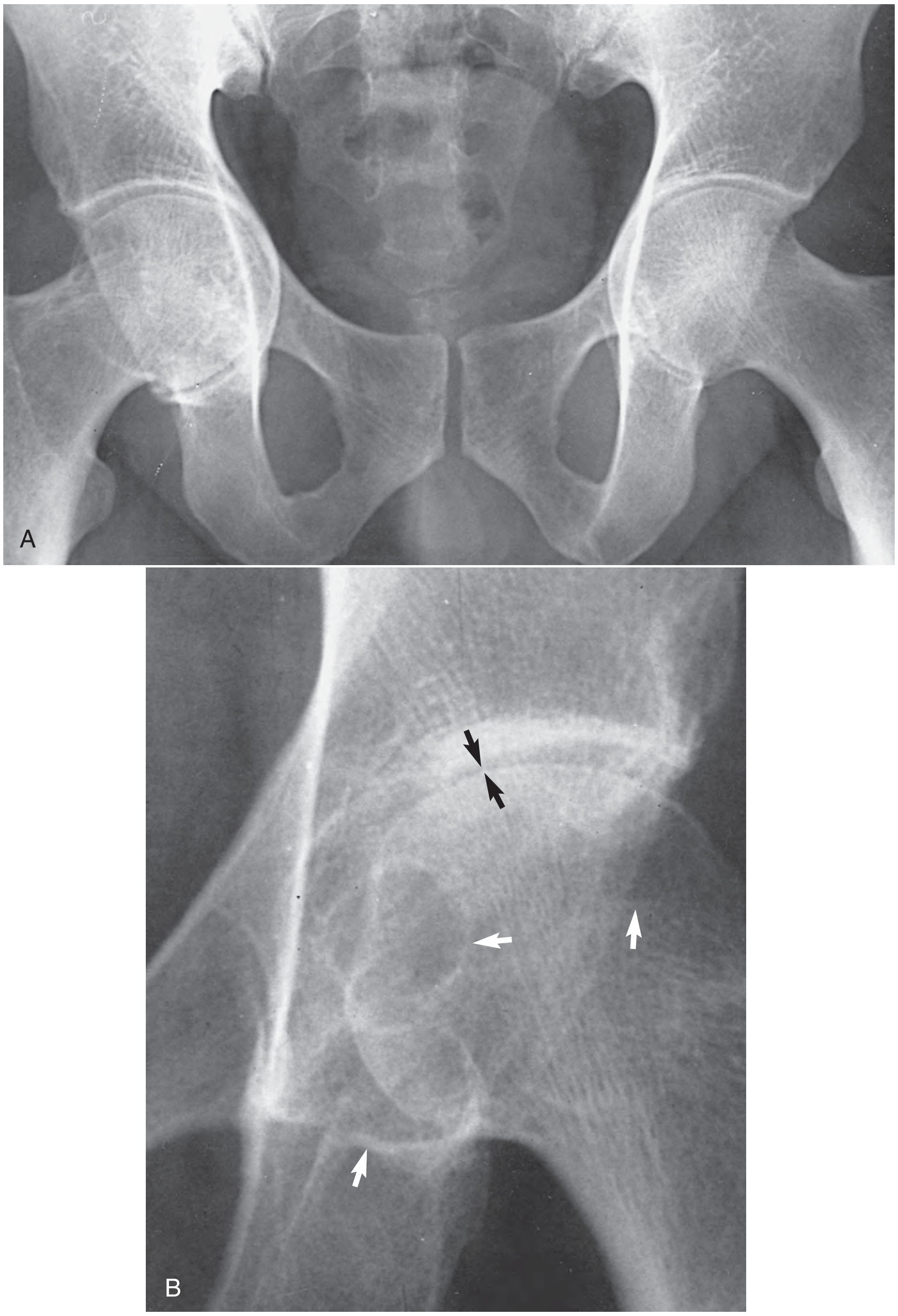

FIGURE 7–35 **Psoriatic arthropathy.**[37] **A,** This patient with psoriatic skin lesions and polyarticular inflammatory disease of long duration demonstrates axial migration of the femoral heads and early acetabular protrusion. **B,** Diffuse axial loss of joint space *(black arrows)* and large subchondral cysts *(white arrows)* are present in this patient with chronic psoriasis of the skin and joints.

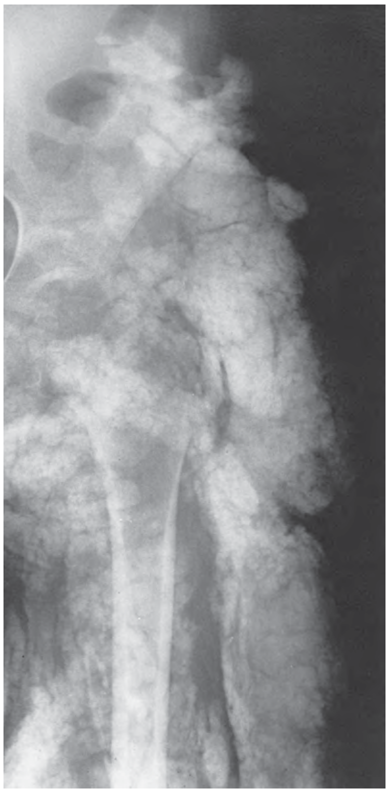

FIGURE 7–36 Dermatomyositis-polymyositis.[38] Bizarre globular calcification is present within the muscles and subcutaneous tissues of the upper thigh and hip region in this 9-year-old boy with dermatomyositis-polymyositis. *(Courtesy T. Broderick, MD, Orange, Calif.)*

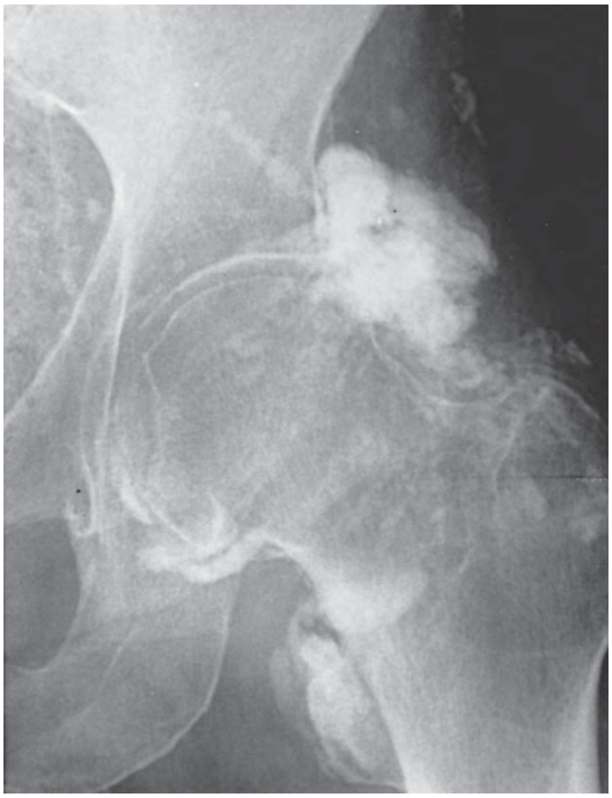

FIGURE 7–37 Progressive systemic sclerosis (scleroderma).[39] Extensive globular accumulations of periarticular soft tissue calcification are seen adjacent to the hip joint. Concentric joint space narrowing is evident. *(Courtesy A. Nemcek, MD, Chicago, and L. Rogers, Winston-Salem, NC.)*

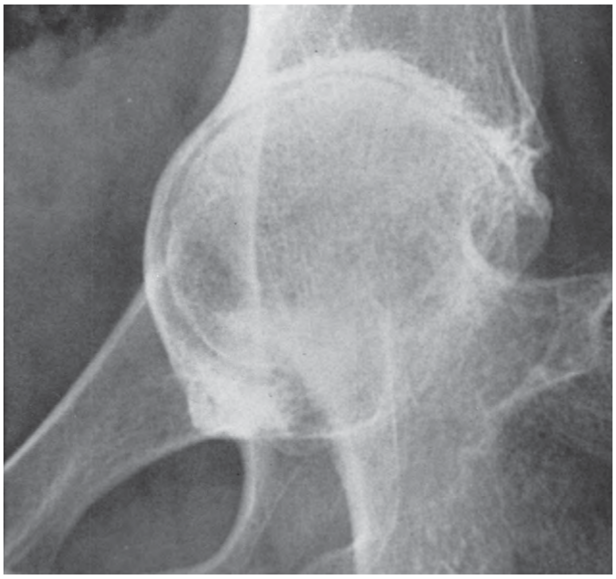

FIGURE 7–38 Collagen vascular disease: overlap syndrome.[40] A patient with juvenile idiopathic (rheumatoid) arthritis subsequently developed classic systemic lupus erythematosus as an adult. Observe the symmetric joint space narrowing typical of inflammatory arthritis. Protrusio acetabuli is also seen. *(Courtesy V. Vint, MD, San Diego.)*

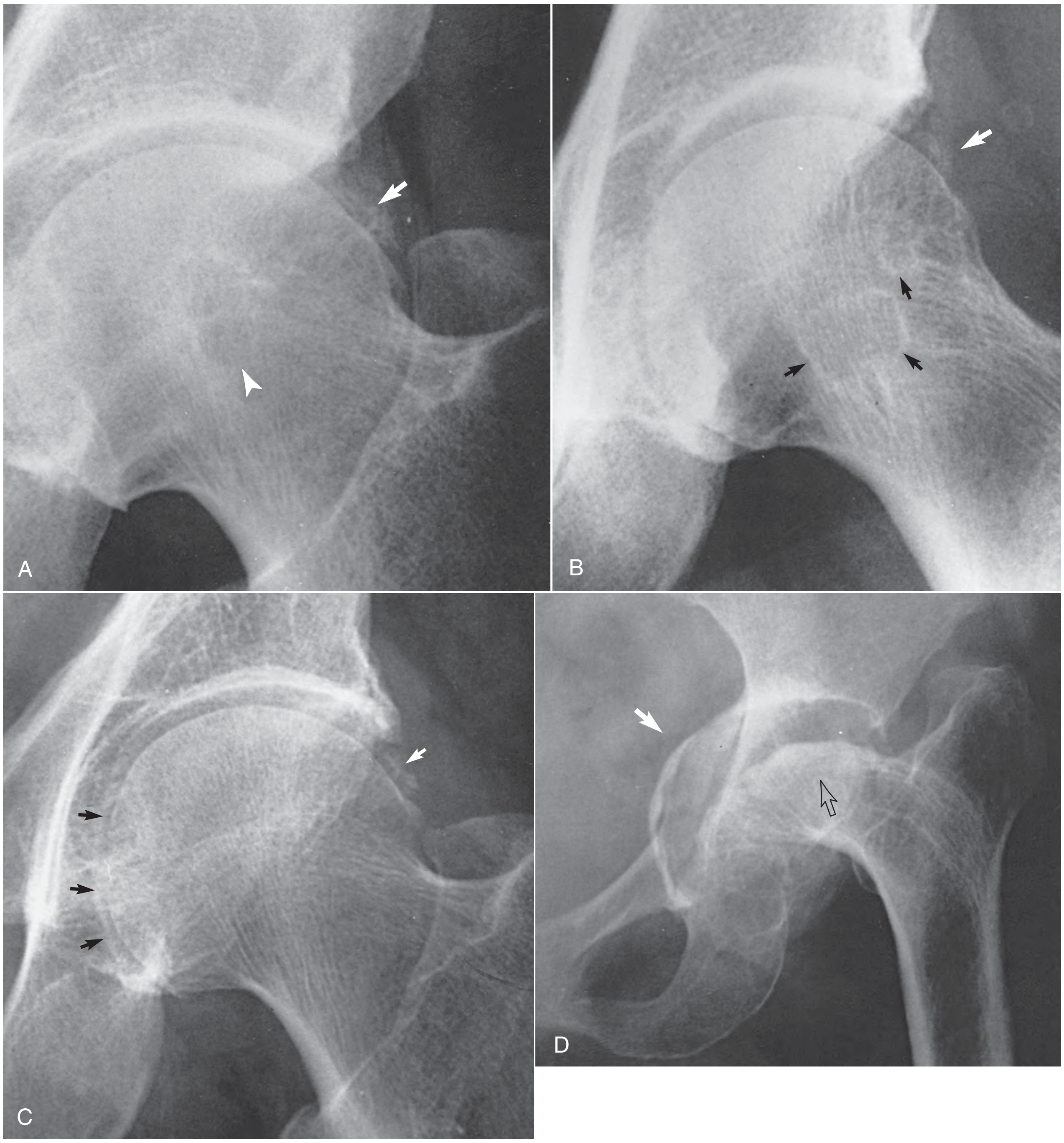

FIGURE 7–39 Calcium pyrophosphate dihydrate (CPPD) crystal deposition disease.[41,42] **A,** Chondrocalcinosis of the hyaline cartilage of the hip *(arrow),* as in this patient, is found in about 45% of patients with CPPD crystal deposition disease. Observe also the subchondral cyst in the femoral head *(arrowhead)* and the joint space narrowing. **B,** In another patient, subtle chondrocalcinosis *(white arrow)* and subchondral cysts *(black arrows)* are apparent. **C,** In a 76-year-old man, chondrocalcinosis is evident *(arrows)*. Medial and axial joint space narrowing is noted. **D,** This 80-year-old woman has severe acetabular protrusion *(arrow)* and dramatic femoral head destruction *(open arrow)* secondary to pyrophosphate arthropathy. (***B,** Courtesy G. Greenway, MD, Dallas.)*

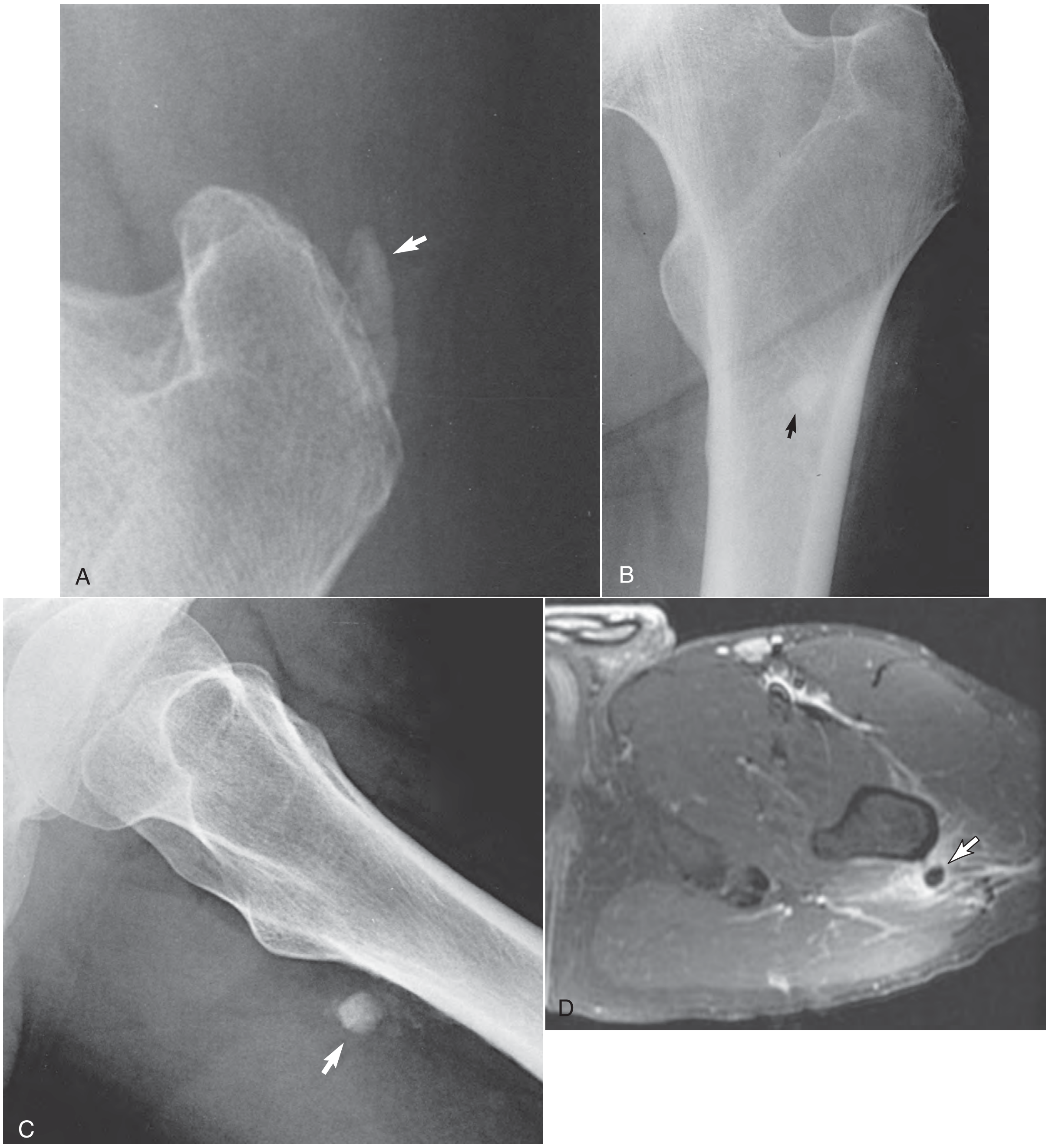

FIGURE 7–40 **Calcium hydroxyapatite crystal deposition.**[43] **A,** Calcific bursitis: In this 50-year-old woman with hip pain, observe the cloudlike accumulation of calcification overlying the greater trochanter *(arrow)*, representing calcific trochanteric bursitis. **B-C,** Calcific tendinitis. Two radiographs reveal calcification at the site of attachment *(arrows)* of the gluteus maximus tendon. **D,** In a third patient, a 42-year-old man, an axial proton density fat-suppressed spin echo MR image reveals a low signal intensity collection of calcification *(arrow)* within the gluteus maximus muscle adjacent to the greater trochanter surrounded by high signal intensity intermuscular and intramuscular edema.

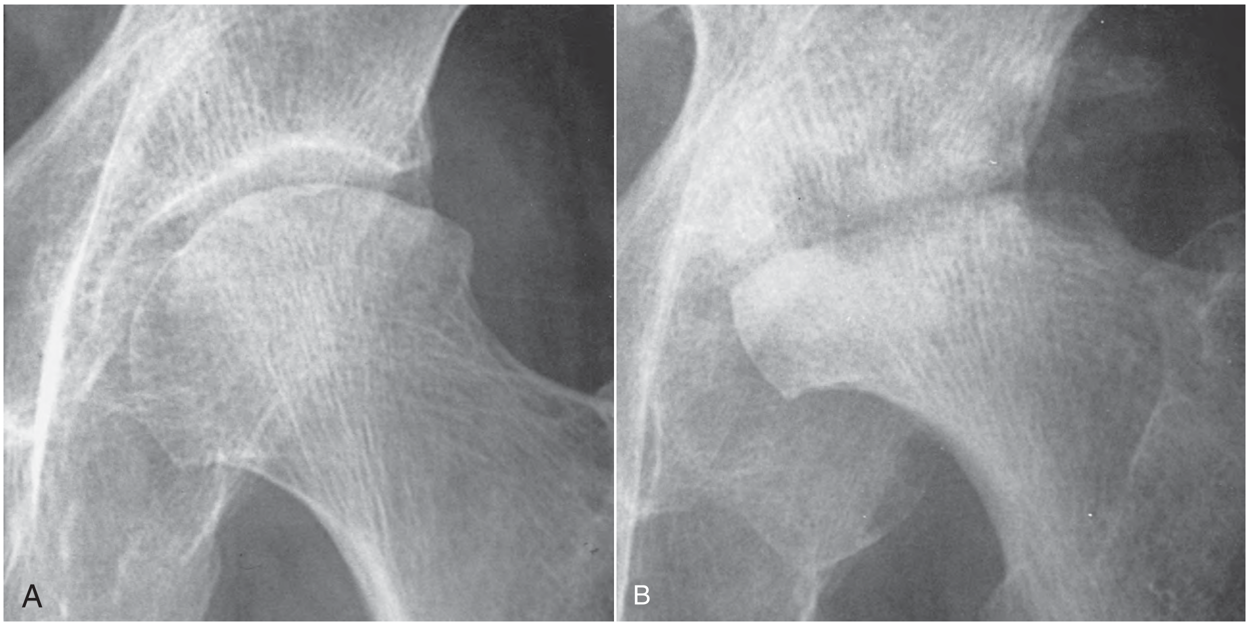

FIGURE 7–41 Rapidly destructive hip disease.[44,78,109] This 74-year-old man had rapid onset of hip pain and limp. **A,** Initial radiograph shows minimal joint space narrowing and irregularity of the femoral articular surface. **B,** Radiograph obtained 5 months later shows dramatic dissolution and atrophic destruction of the femoral head and loss of definition of the acetabulum. Joint aspiration failed to reveal infectious organisms. The cause of these abnormalities is unclear, but they are believed to be related to a generalized process such as intraarticular deposition of calcium hydroxyapatite crystals.

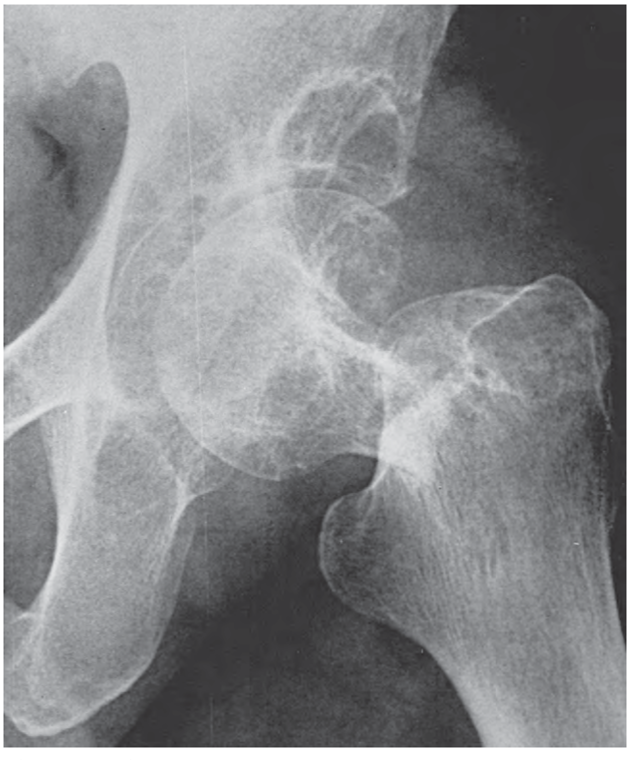

FIGURE 7–42 Gouty arthritis and coexistent chronic renal insufficiency.[45] A 53-year-old man with chronic tophaceous gout, gouty nephritis, and chronic renal insufficiency had acute onset of severe hip pain. A pathologic fracture of the femoral neck with varus angulation is evident on the frontal radiograph. Extensive periarticular erosion of the femoral neck with an overhanging margin is present. Multiple subchondral cystlike erosions also are seen in the acetabulum. The erosive changes likely result from tophaceous deposits or deposition of amyloid secondary to chronic renal disease. *(Courtesy C. Chen, MD, Taipei, Taiwan, Republic of China.)*

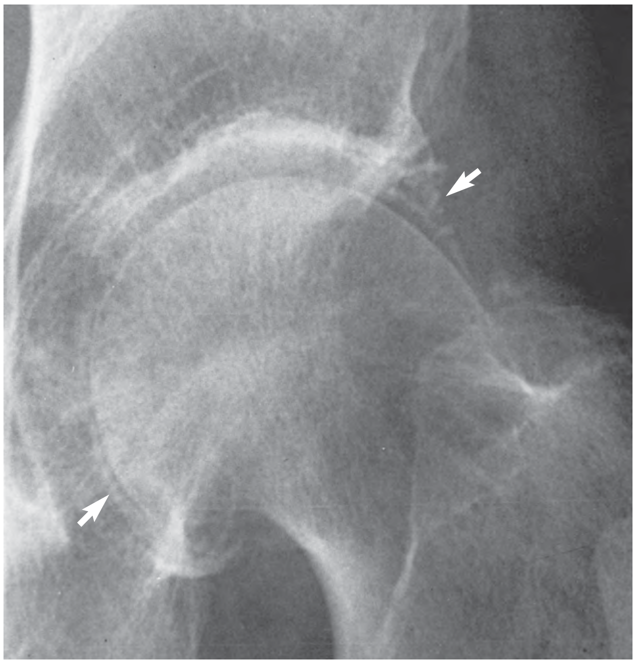

FIGURE 7–43 Hemochromatosis: chondrocalcinosis.[46] Observe the linear calcification within the hyaline cartilage paralleling the femoral head and also within the acetabular labrum *(arrows)*. Articular changes in hemochromatosis are indistinguishable from those of idiopathic calcium pyrophosphate dihydrate (CPPD) crystal deposition disease.

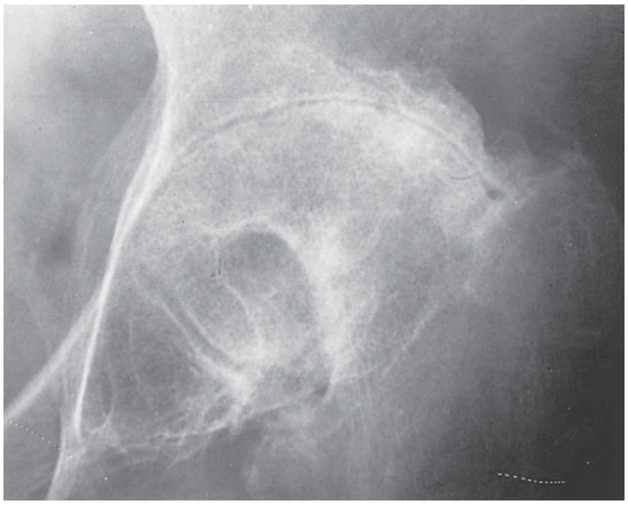

FIGURE 7–44 **Alkaptonuria.**[47] The radiographic changes of severe ochronotic arthropathy include diffuse joint space narrowing, osteophytosis, mild acetabular protrusion, and femoral head remodeling.

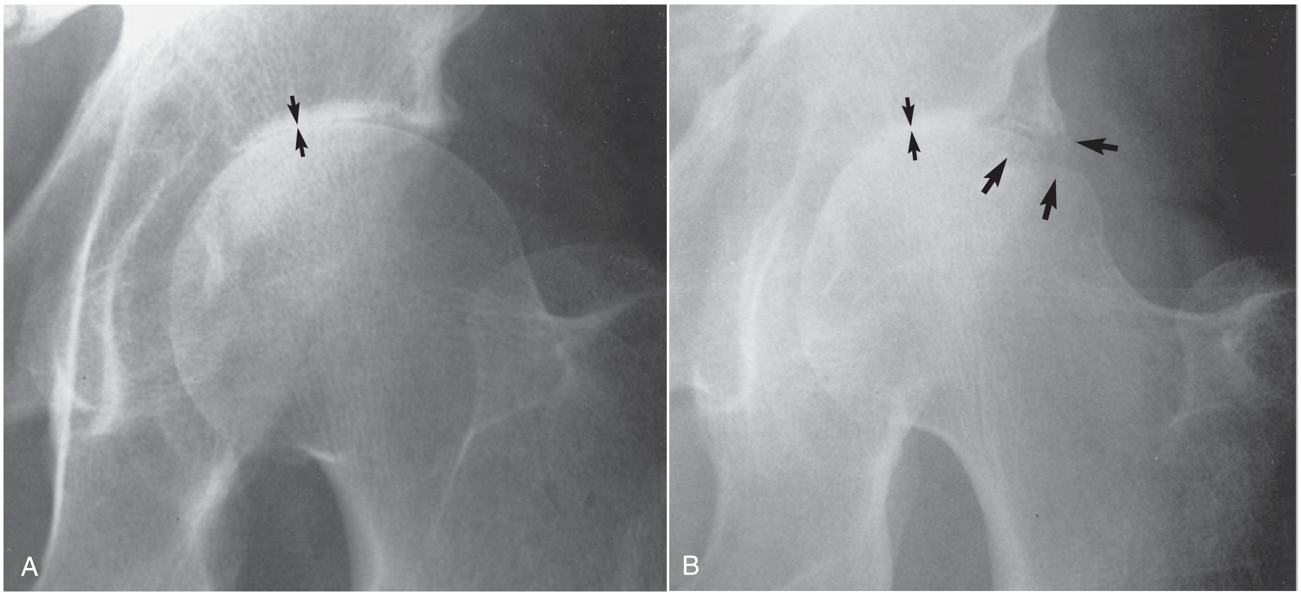

FIGURE 7–45 **Septic arthritis and osteomyelitis.**[48,83] **A-B,** This 47-year-old man had hip pain and fever. Routine radiographs taken at initial presentation **(A)** and 11 days later **(B)** show the rapid, destructive nature of infectious arthritis. Observe the concentric loss of joint space *(small arrows),* periarticular osteopenia, and destruction of the femoral head and acetabulum *(large arrows)*. The causative organism in this case was ß-hemolytic streptococcus.

Continued

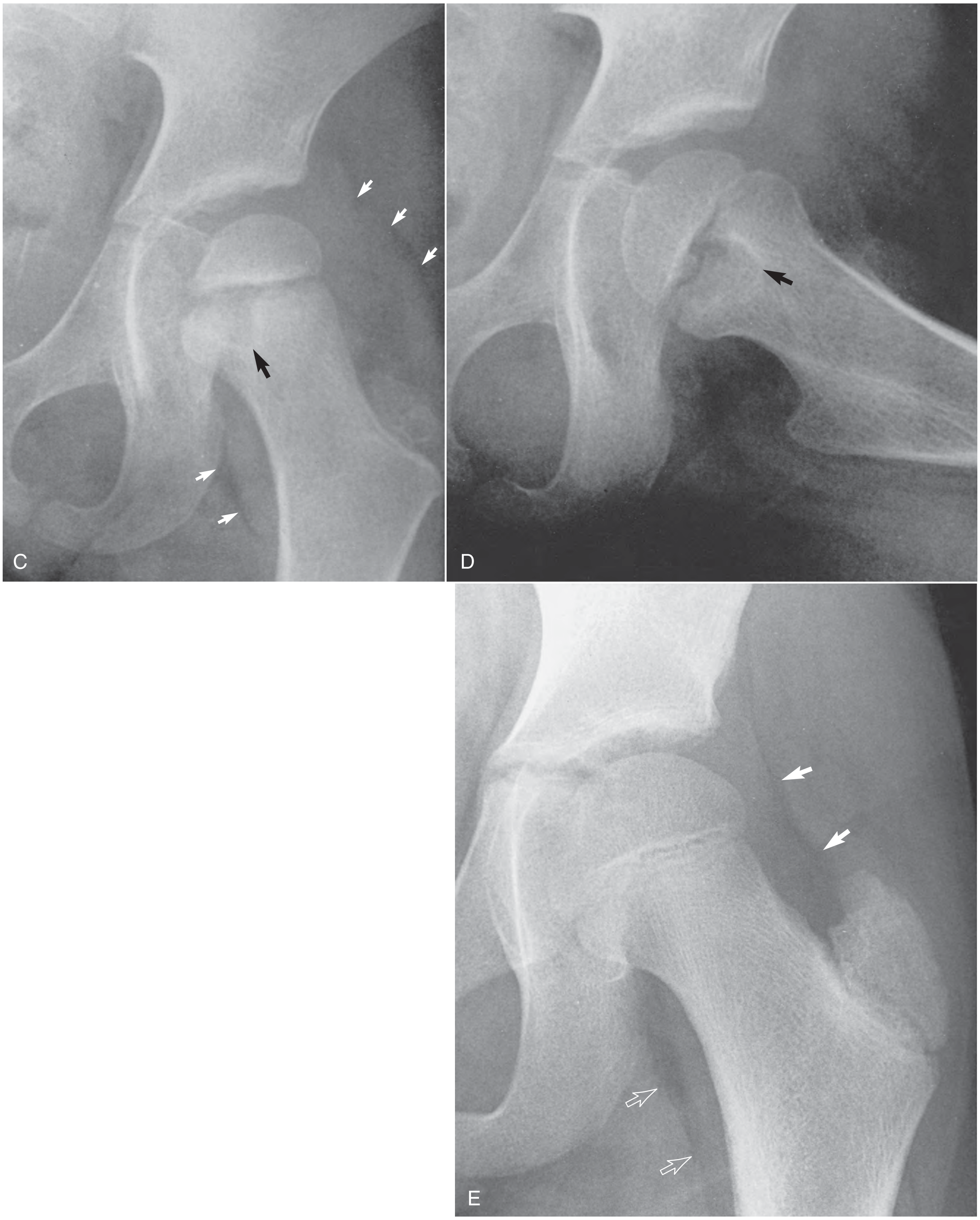

FIGURE 7–45, cont'd **C-D,** Osteomyelitis with large joint effusion. Anteroposterior **(C)** and frog-leg **(D)** projections of this 3-year-old girl illustrate a well-defined osteolytic lesion within the proximal femoral metaphysis abutting on the physis *(black arrows)*. Displacement of the capsular, iliopsoas, and gluteal fat planes of the hip joint *(white arrows)* in **C** indicates a prominent joint effusion. Metaphyseal osteomyelitis in the proximal portion of the femur may spread to the contiguous joint, resulting in septic arthritis. **E,** Normal fat planes adjacent to the hip. For comparison in a normal child, the gluteal *(arrows)* and iliopsoas *(open arrows)* fat planes are seen. Note that the fat planes are curved inward, toward the joint, rather than bulged out as in **C.** The soft tissue findings indicative of intraarticular fluid may be more helpful in this age group than in adults. *(**C-D,** Courtesy P. H. VanderStoep, MD, St Cloud, Minn.)*

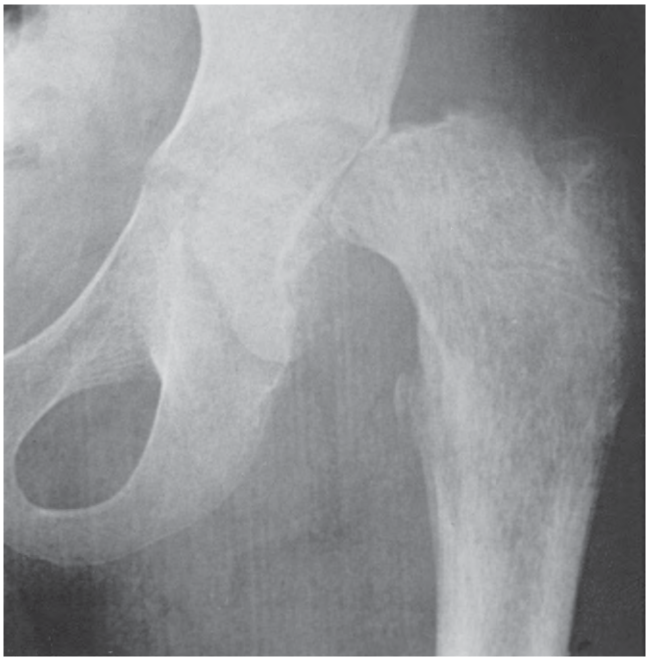

FIGURE 7–46 **Septic arthritis with epiphysiolysis.**[49,83,84] This young patient with pyogenic arthritis of the hip developed a slipped capital femoral epiphysis secondary to physeal destruction by infection. Note the superior displacement of the femoral neck in relation to the femoral head. *(Courtesy B. Howard, MD, Charlotte, NC.)*

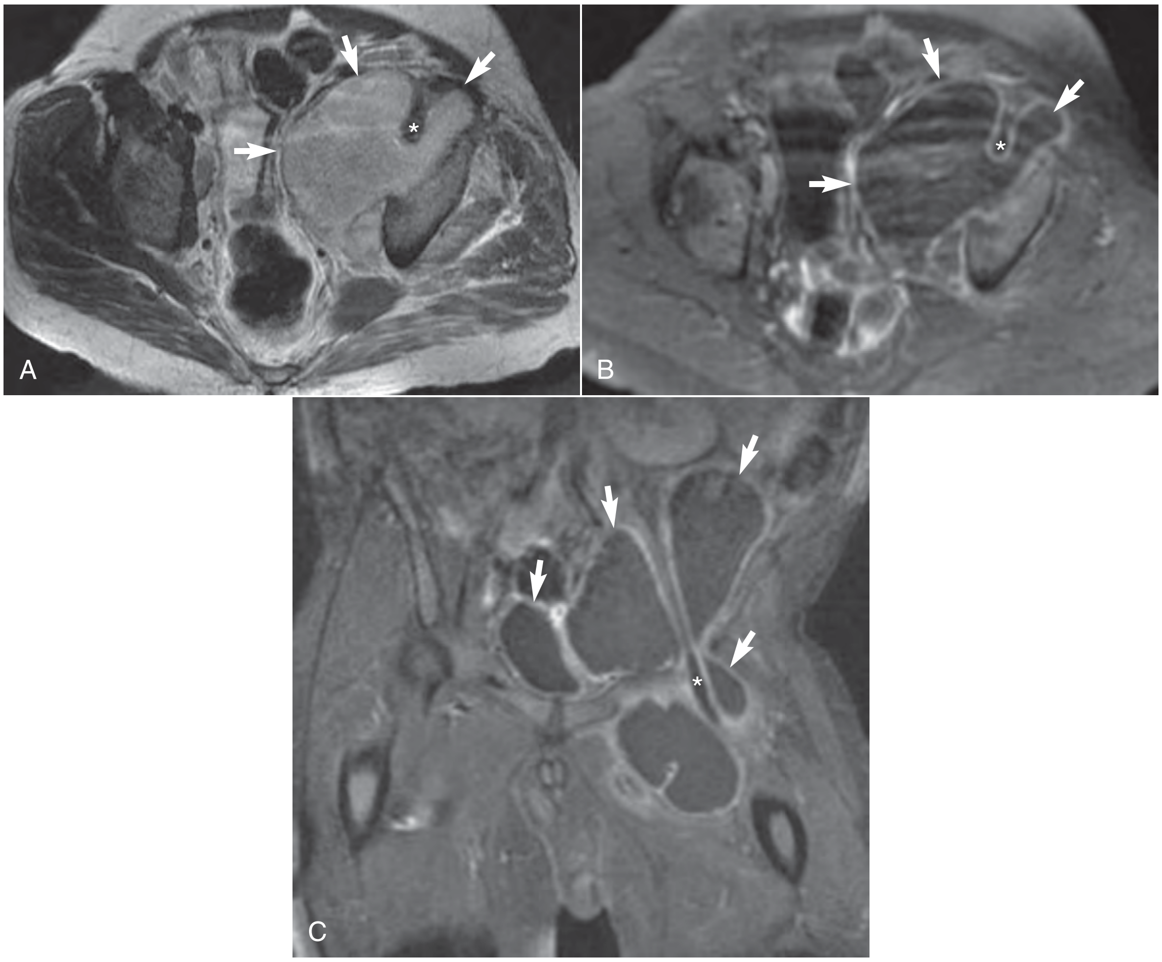

FIGURE 7–47 **Infectious iliopsoas bursitis.**[120] **A,** In this transaxial T2-weighted MR image through the pelvis, a large intermediate signal mass *(arrows)* adjacent to the anterior aspect of the left iliac wing displaces the abdominal organs. Transaxial **(B)** and coronal **(C)** T1-weighted fat-suppressed MR images obtained after the intravenous administration of gadolinium show that the extensive abscess *(arrows)* is infolded by the iliopsoas tendon (*) and exhibits high signal intensity rim enhancement. *Staphylococcus aureus* was cultured from the aspirate. Some atrophy and apparent fatty infiltration of the left gluteus maximus muscle is seen in image **A.**

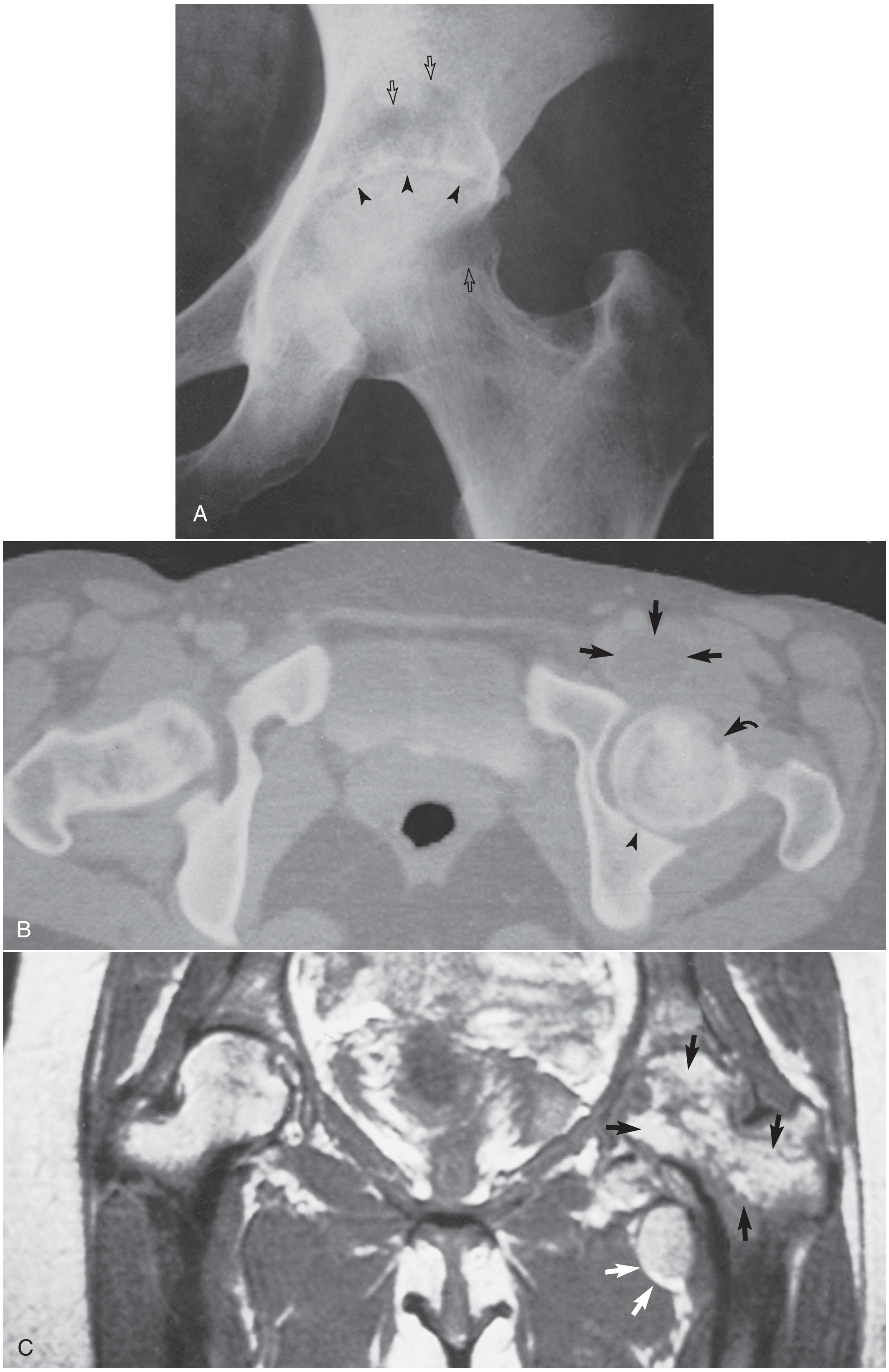

FIGURE 7–48 Tuberculous arthritis: psoas abscess.[50] This 40-year-old woman with a history of pulmonary tuberculosis had hip pain of 2 months' duration. **A,** Anteroposterior radiograph shows concentric joint space narrowing *(arrowheads)* and patchy areas of periarticular osteopenia *(open arrows)*. **B,** Transaxial CT image reveals narrowing of the joint posteriorly *(arrowhead)* and a large infected synovial cyst or abscess arising from the anterior portion of the joint *(straight arrows)*. A small erosion also is seen within the anterior cortex of the femoral head *(curved arrow)*. **C,** A coronal (TR/TE, 2000/30) proton-density-weighted spin echo MR image reveals the high signal intensity of an abscess or infected cyst in the vicinity of the iliopsoas tendon attachment *(white arrows)* and areas of mixed signal intensity within the marrow of the proximal portion of the femur *(black arrows)*. *Mycobacterium tuberculosis* was cultured from the abscess and joint aspirate. *(From Taylor JAM, Harger BL, Resnick D: Diagnostic imaging of common hip disorders: A pictorial review. Top Clin Chiropr 1:8, 1994. Courtesy G. S. Huang, Taipei, Taiwan.)*

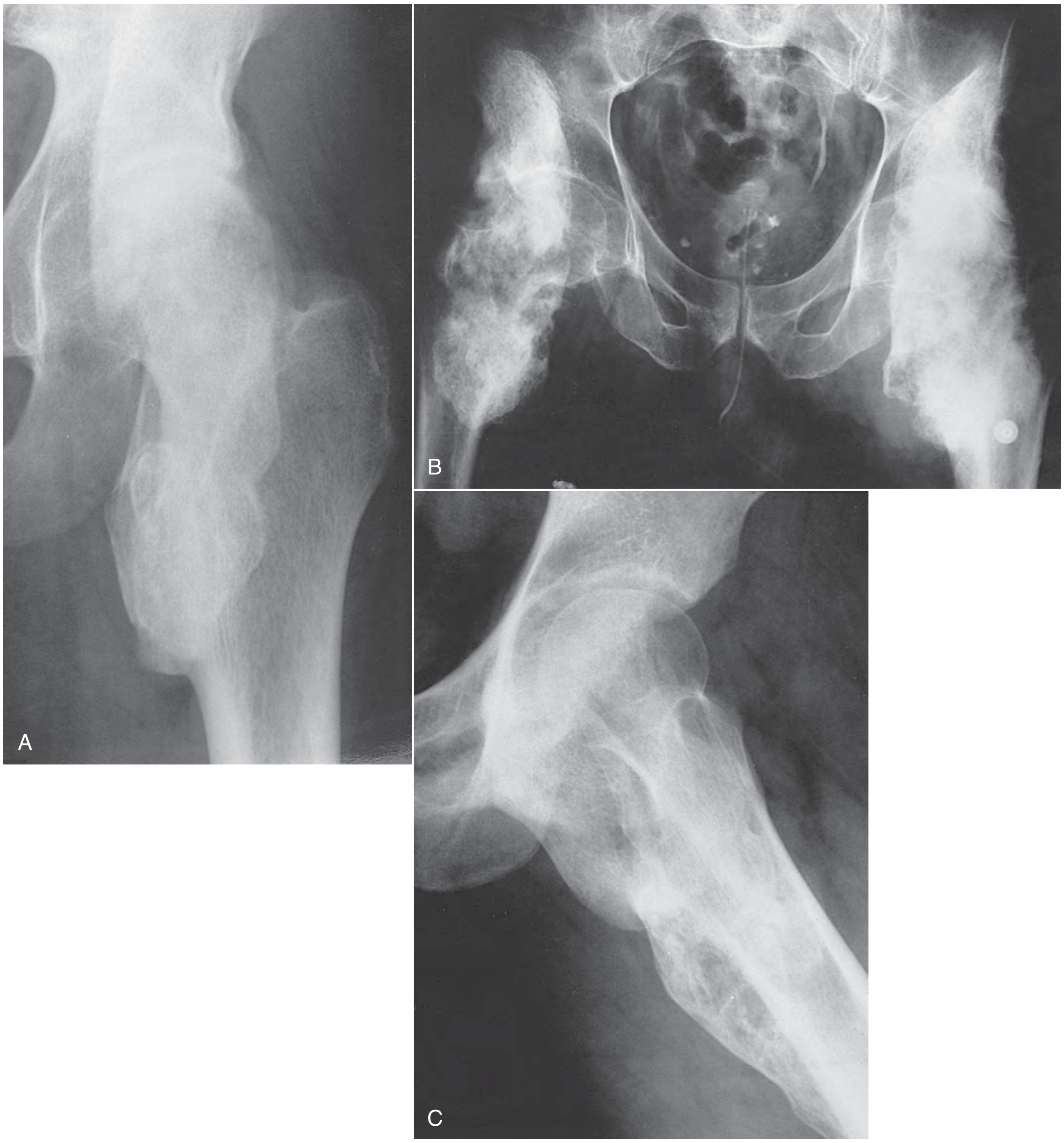

FIGURE 7–49 Neurologic injury: heterotopic ossification.[51,52] **A,** A radiograph of this 17-year-old paralyzed patient shows extensive deposition of soft tissue ossification about the hip joint. **B,** In another paraplegic patient, diffuse prolific heterotopic ossification is seen surrounding both hip joints. A Foley catheter is in place for a neurogenic bladder. **C,** This 24-year-old man sustained a brain injury in a motor vehicle accident and was comatose for 2 weeks. Observe the extensive ossification surrounding the hip joint, which has resulted in complete osseous ankylosis.

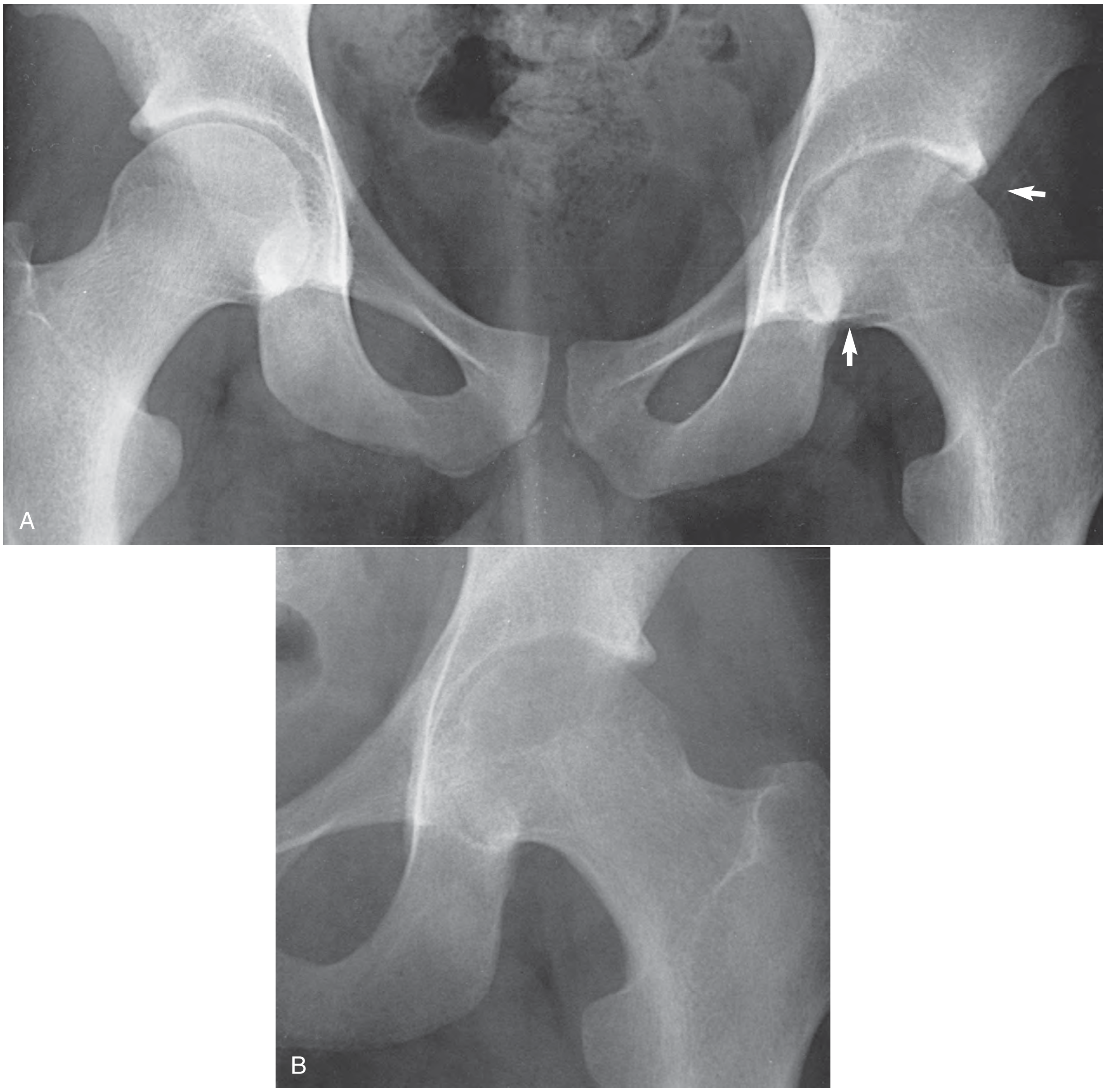

FIGURE 7–50 **Idiopathic chondrolysis of the hip.**[53] **A,** Observe the unilateral osteoporosis and uniform joint space narrowing of the left hip *(arrows)* in this young man. The opposite hip appears normal. **B,** Another frontal radiograph of the involved hip taken 3 weeks later shows advancing osteopenia, concentric loss of joint space, and indistinct subchondral bone surfaces. Aspiration of the joint did not reveal evidence of septic arthritis, a major diagnostic consideration.

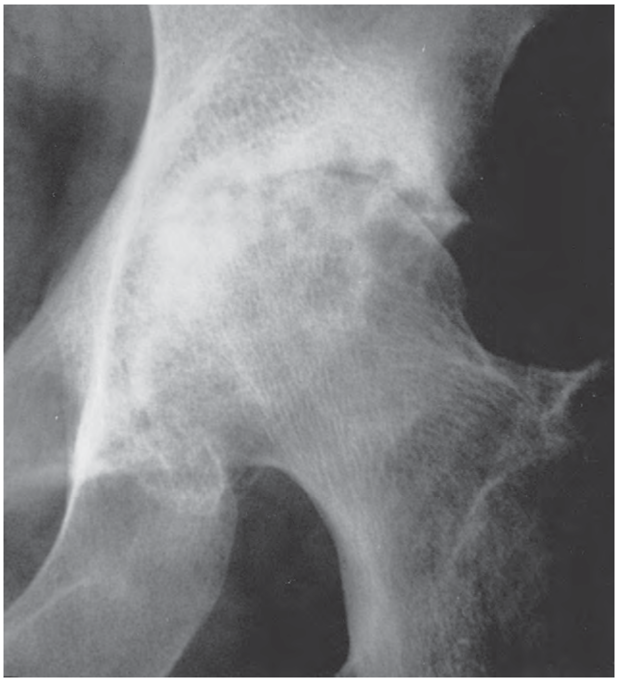

FIGURE 7–51 Pigmented villonodular synovitis.[54,55,85] A 34-year-old man had groin and hip pain. Several erosions within the subchondral bone of the femoral head and acetabulum are noted. The joint space is diffusely narrowed, an inconsistent finding in this disease. Osteopenia is not prominent.

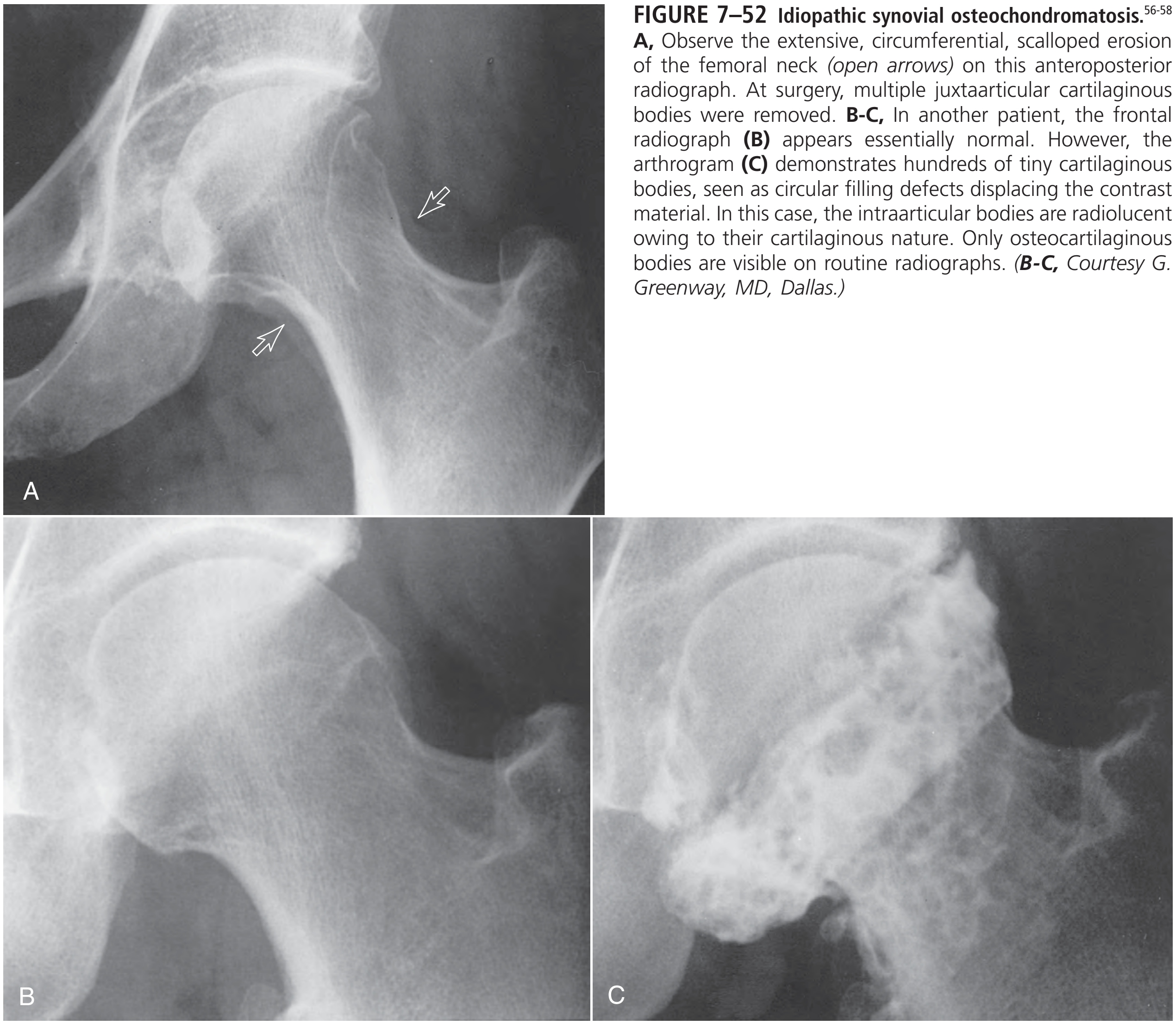

FIGURE 7–52 Idiopathic synovial osteochondromatosis.[56-58] **A,** Observe the extensive, circumferential, scalloped erosion of the femoral neck *(open arrows)* on this anteroposterior radiograph. At surgery, multiple juxtaarticular cartilaginous bodies were removed. **B-C,** In another patient, the frontal radiograph **(B)** appears essentially normal. However, the arthrogram **(C)** demonstrates hundreds of tiny cartilaginous bodies, seen as circular filling defects displacing the contrast material. In this case, the intraarticular bodies are radiolucent owing to their cartilaginous nature. Only osteocartilaginous bodies are visible on routine radiographs. *(**B-C,** Courtesy G. Greenway, MD, Dallas.)*

TABLE 7-13 Metabolic and Hematologic Disorders Affecting the Hip*

Entity	Figure(s)	Characteristics
Generalized osteoporosis[59-62,86,102,103]	7-53, 7-54, 7-55	*Singh index:* predictable pattern of trabecular bone loss in the proximal portion of the femur (Table 7-14) Quantitative bone mineral analysis (densitometry) is necessary to assess the presence and extent of diminished bone mineral content accurately Dual energy x-ray absorptiometry (DXA) is the most widely used method to assess bone mineral density owing to its ease of use, high precision, and low radiation exposure to patients *Major complication:* fractures of the proximal portion of the femur in 17.5% of women older than age 50 years and in 6% of men older than age 50 years
Transient osteoporosis of the hip[63,64,86]	7-56	***Clinical findings*** Young and middle-aged adults typically with no history of trauma or infection Hip pain, antalgic limp, limitation of movement Unilateral, although opposite hip may occasionally be involved later *Self-limited:* full recovery in 2 to 6 months ***Imaging findings*** Progressive, rapid, regional osteoporosis of the femoral head several weeks after onset of pain Acetabulum and femoral neck involved less extensively Positive bone scan Magnetic resonance (MR) imaging signal: decreased on T1-weighted, increased on T2-weighted images typical of bone marrow edema Joint effusion on T2-weighted images Bone density on radiographs and MR imaging signal return to normal in 1 year
Transient migratory bone marrow edema[87,119]	7-57	Initially designated transient regional osteoporosis but now believed to be identical syndromes ***Clinical findings*** Migratory arthralgia of weight-bearing joints of lower limb especially the femoral head and neck; proximal to distal is typical May resemble transient osteoporosis of the hip Associated with systemic osteoporosis Self-limiting ***Imaging findings*** *Radiography:* osteopenia often subtle and nondetectable *Bone densitometry:* osteopenia or osteoporosis *Bone scintigraphy:* increased radionuclide uptake *MR imaging:* bone marrow edema in symptomatic region that is usually transient and migratory from one femoral head and neck to the other
Osteomalacia and rickets[65]	7-58 7-59	***Osteomalacia*** Axial and appendicular skeleton Osteopenia Decreased trabeculae; remaining trabeculae appear prominent and coarsened Looser zones or pseudofractures (i.e., insufficiency fractures) ***Rickets*** Findings are most prominent in the appendicular skeleton Metaphyseal demineralization: frayed metaphysis, widened physis Bowing of bones Osteopenia
Hypothyroidism[66]	7-60	Slipped capital femoral epiphysis may be the presenting feature of the disease Delayed skeletal maturation, linear sclerosis in metaphysis, irregularity of ossification of the greater trochanter, femoral head (i.e., epiphyseal dysgenesis)

* See also Tables 1-15 and 1-16.

TABLE 7-13 Metabolic and Hematologic Disorders Affecting the Hip—cont'd

Entity	Figure(s)	Characteristics
Hyperparathyroidism[67]	7-61	Subperiosteal, subchondral, subligamentous, intracortical, and endosteal bone resorption Occasional bone sclerosis (more common with renal osteodystrophy) Chondrocalcinosis (calcium pyrophosphate dihydrate [CPPD] crystal deposition) Brown tumors Severe bone remodeling with osteitis fibrosa cystica (now infrequently encountered) Acetabular protrusion in advanced cases Soft tissue calcification
Renal osteodystrophy[67,68]	7-62	Osteosclerosis or osteopenia Similar findings to those of hyperparathyroidism, osteomalacia, and rickets Pathologic fractures Soft tissue calcification
Acromegaly[69]	7-63	*Initially:* cartilage hypertrophy results in hip joint space widening *Later:* premature degenerative disease with subchondral cysts and exuberant osteophytosis surrounding femoral head-neck junction
Sickle cell anemia[70,88]	7-64	Diffuse osteopenia, protrusio acetabuli, and osteonecrosis may be encountered in severe cases of sickle cell anemia and other hemoglobinopathies
Gaucher disease[76,89]	7-68	Osteonecrosis of femoral head

TABLE 7-14 Osteoporosis of the Proximal Portion of the Femur: The Singh Index*[59]

Grade	Radiographic Appearance of Trabeculae in the Proximal Portion of the Femur	Grade	Radiographic Appearance of Trabeculae in the Proximal Portion of the Femur
6	***No evidence of osteoporosis*** All normal trabecular groups visible Proximal portion of the femur appears to be completely occupied by cancellous bone	3	***Suggests definite osteoporosis*** Break in continuity of principal tensile trabeculae opposite greater trochanter
5	***Subtle evidence of osteoporosis*** Principal tensile and compressive trabeculae accentuated Ward triangle is prominent	2	***Marked osteoporosis*** Only the principal compressive trabeculae are seen No tensile trabeculae visible
4	***Equivocal evidence of osteoporosis*** Principal tensile trabeculae reduced in number but continue to extend from lateral cortex to the femoral neck	1	***Severe osteoporosis*** Marked reduction even in number of principal compressive trabeculae

* Adapted from Taylor JAM, Resnick D: Radiographic-pathologic correlation. In Sartoris DJ: Osteoporosis: Diagnosis and management. New York, Marcel Dekker, 1996, p 157.

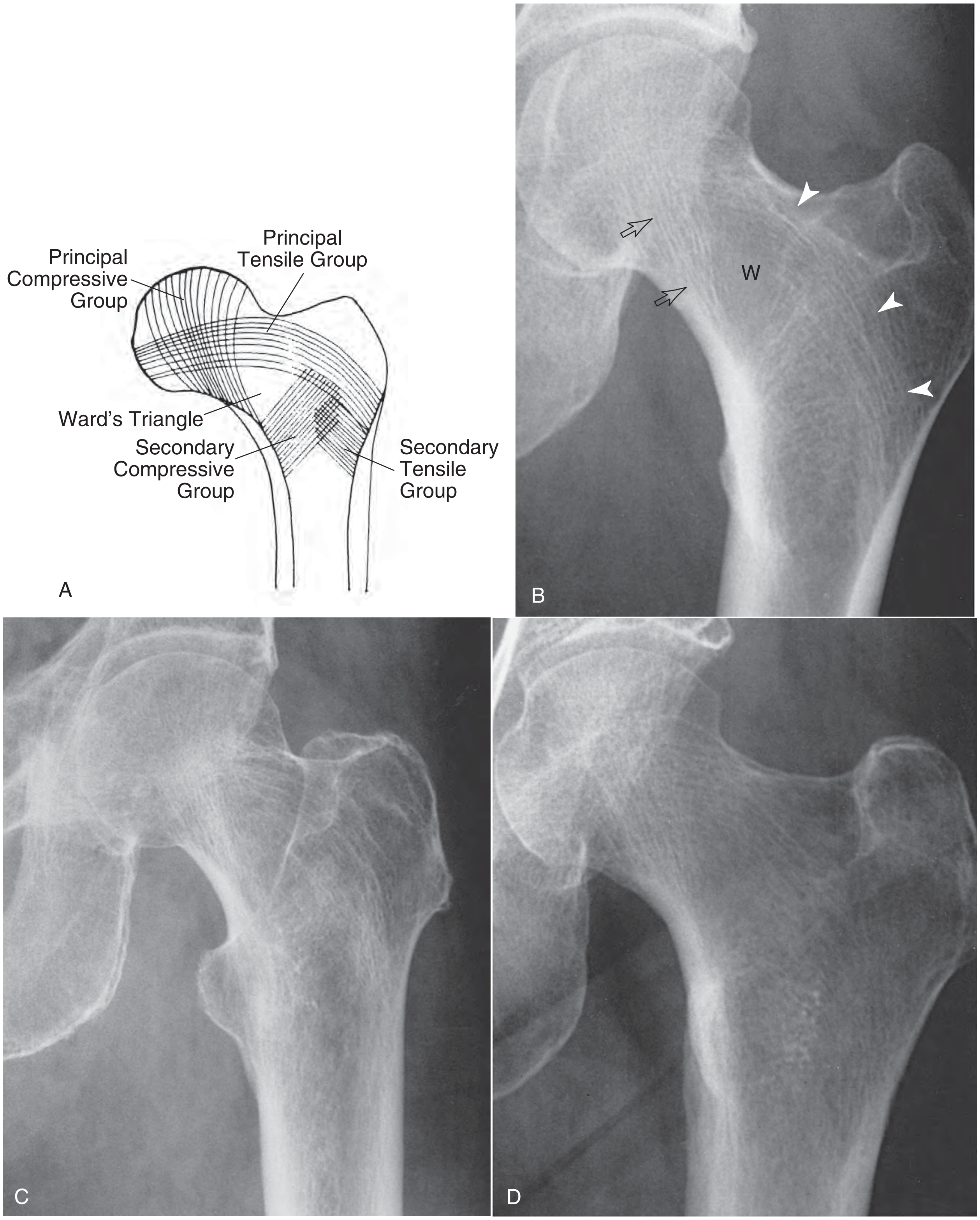

FIGURE 7–53 Osteoporosis[59-61,86] **A,** Normal trabecular pattern, proximal portion of femur. Four of the anatomic groups of trabeculae are indicated in this schematic drawing. Ward triangle lies within the neutral axis, wherein compressive and tensile forces balance one another, and contains thin, widely spaced trabeculae. Analysis of these trabeculae may be used as a radiographic index (i.e., Singh index) of osteoporosis in this region (Table 7-14). **B,** Normal trabecular pattern: Radiographic appearance in a patient with minimal osteoporosis. Ward triangle (W) is a relatively radiolucent zone located between the principal tensile *(arrowheads)* and principal compressive *(open arrows)* groups of trabeculae. **C,** Osteoporosis. In this 79-year-old woman with severe corticosteroid-induced osteoporosis, note the increased radiolucency, cortical thinning, and paucity of trabeculae within the proximal portion of the femur. The osteopenia is especially prevalent within the greater and lesser trochanters and in Ward triangle. **D,** Mild osteoporosis secondary to hemiplegia occurring after a cerebrovascular accident. Note the increased radiolucency combined with relative loss of the primary tensile trabeculae. *(**A,** From Resnick D: Diagnosis of bone and joint disorders. Philadelphia, Saunders, 1995, p. 1824.)*

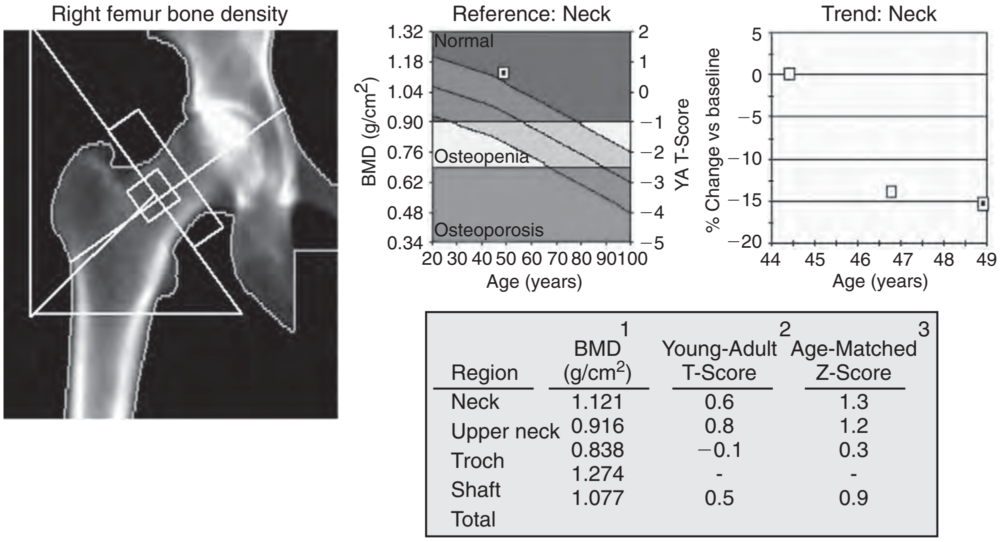
Right femur bone density
Reference: Neck
1.32
1.18
1.04
0.90
0.76
0.62
0.48
0.34
BMD (g/cm²)
Normal
Osteopenia
Osteoporosis
2
1
0
−1
−2
−3
−4
−5
YA T-Score
20 30 40 50 60 70 80 90 100
Age (years)
Trend: Neck
5
0
−5
−10
−15
−20
% Change vs baseline
44 45 46 47 48 49
Age (years)

Region	1 BMD (g/cm^2)	2 Young-Adult T-Score	3 Age-Matched Z-Score
Neck	1.121	0.6	1.3
Upper neck	0.916	0.8	1.2
Troch	0.838	−0.1	0.3
Shaft	1.274	-	-
Total	1.077	0.5	0.9

FIGURE 7–54 **Quantitative bone mineral analysis (densitometry).**[62,102,103] Dual energy x-ray absorptiometry (DXA) in a 34-year-old female with normal bone mineral density. Data are shown as depicted on a DXA display and printout for a scan of the left proximal portion of the femur. Regions of interest (ROI) include the femoral neck, upper femoral neck, greater trochanter, and femoral shaft. For each ROI, the area (cm^2), bone mineral content (g), and areal bone mineral density (g/cm^2) are computed. Further evaluation includes comparing the patient's bone mineral density with normal peak bone mass (T-score) and age, sex, weight, and ethnicity matched (Z-score) control populations, both of which are predetermined in a reference database. With DXA, the patient's bone mineral density is expressed in terms of standard deviations from normal, information that can be applied to management, prognosis, and estimation of fracture risk. (See Table 4-22)

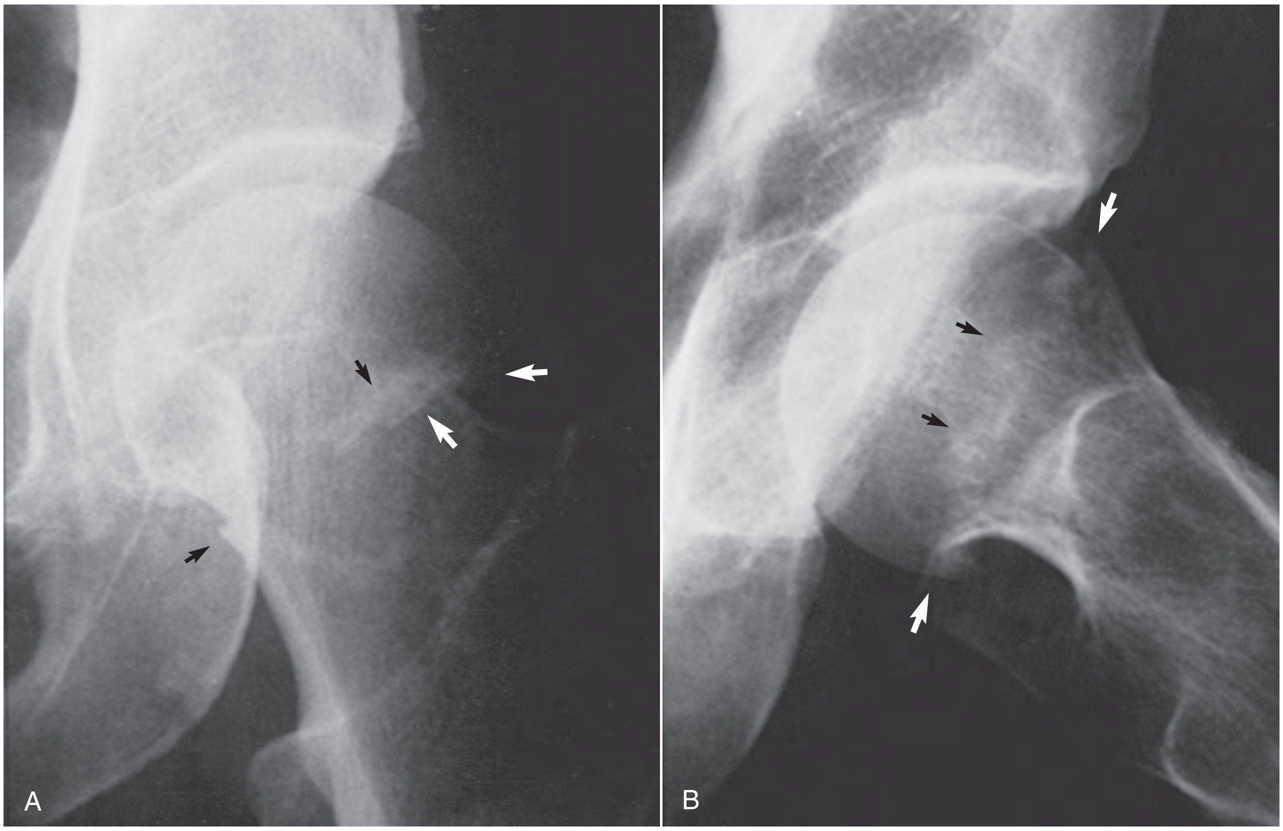

FIGURE 7–55 **Osteoporosis: complicated by subcapital fracture.**[60,86,104] This 62-year-old osteoporotic woman slipped on an icy sidewalk and fractured her hip. Anteroposterior **(A)** and frog-leg **(B)** projections reveal cortical offset and slight compaction of the femoral neck at the subcapital region *(arrows)*. Intracapsular fractures are frequent complications of osteoporosis. *(From Taylor JAM, Harger BL, Resnick D: Diagnostic imaging of common hip disorders: A pictorial review. Top Clin Chiropr 1:8, 1994. Reprinted with permission. Courtesy T. Wei, DC, Portland, Ore.)*

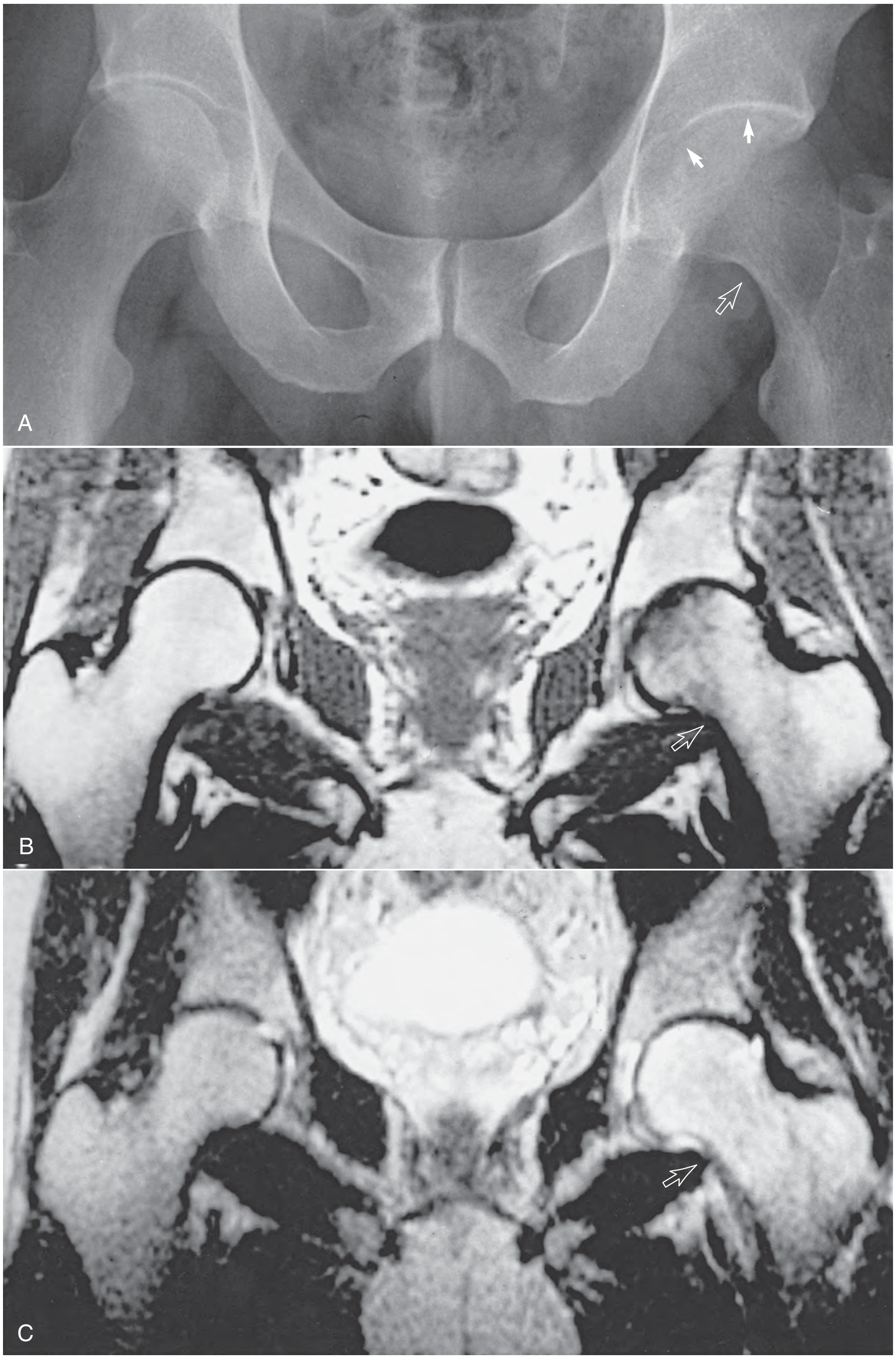

FIGURE 7–56 Transient osteoporosis of the hip.[63,64,86] **A-C,** A 40-year-old man with left hip pain. In **A,** initial radiograph shows diffuse osteopenia of the proximal portion of the left femur *(open arrow)*. In addition, the subarticular cortex is rather indistinct *(arrows)*. In **B,** a coronal T1-weighted (TR/TE, 418/15) spin echo MR image reveals intermediate signal intensity *(open arrow)* of the bone marrow in the left femoral head and neck. In **C,** a coronal T2-weighted (TR/TE, 2000/110) spin echo MR image demonstrates high signal intensity *(open arrow)* within the bone marrow of the left femoral head and neck.

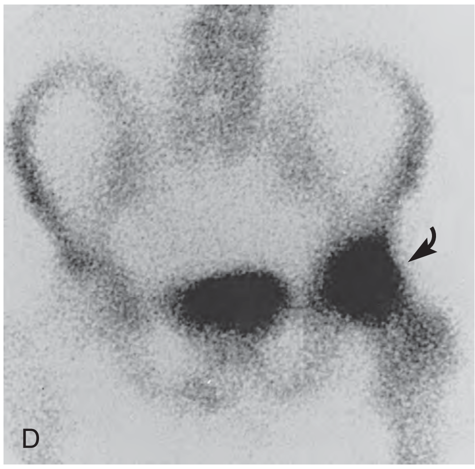

FIGURE 7–56, cont'd **D,** Bone scan in another patient shows increased isotope uptake localized to the left femoral head *(curved arrow),* a characteristic feature of this disease. The findings illustrated in these patients are consistent with bone marrow edema characteristic of transient osteoporosis of the hip and are thought to be secondary to insufficiency fractures. Bone marrow edema may also be observed in cases of osteonecrosis, trauma, infection, and infiltrative neoplasms. *(**A-C,** Courtesy E. Bosch, MD, Santiago, Chile.)*

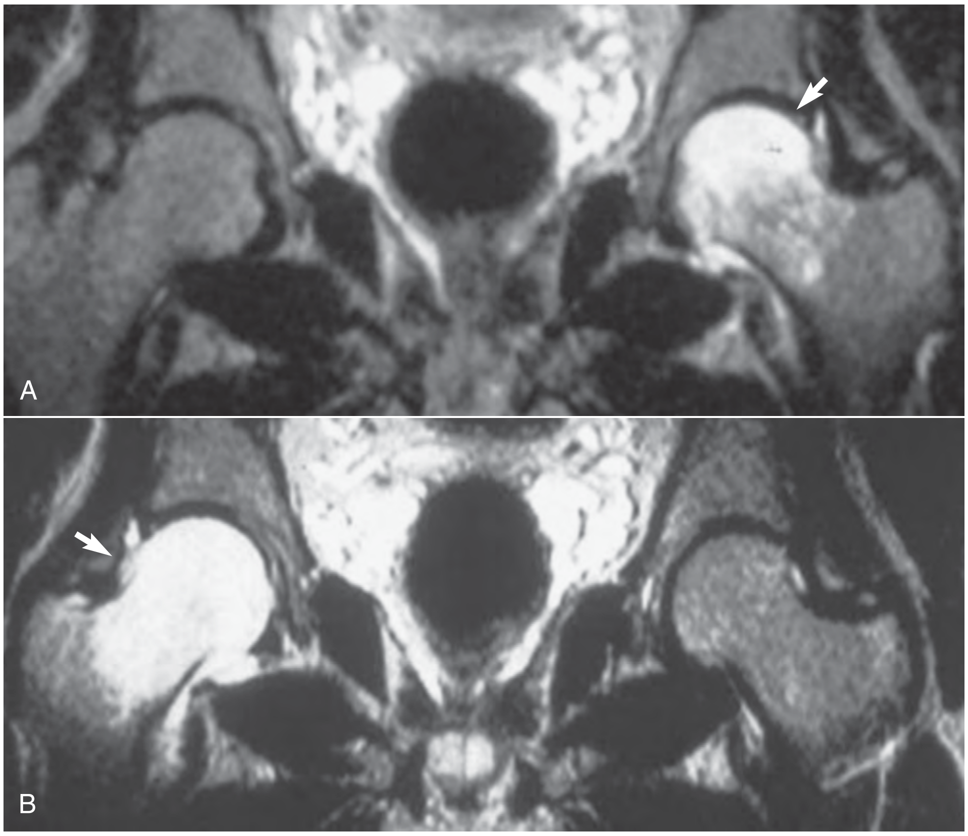

FIGURE 7–57 **Transient migratory bone marrow edema.**[87,119] This man initially presented with left hip pain and a limp. A T2-weighted fat-suppressed coronal image **(A)** reveals dramatic high signal intensity involving the left femoral head and portions of the neck *(arrow),* consistent with bone marrow edema. As the symptoms subsided on the left side, similar pain began to develop in the right hip. Images obtained with identical pulse sequences 7 months later **(B)** show resolution of the initially edematous left femoral head and neck and even more intense involvement on the right *(arrow)*. This pattern of transient migratory bone marrow edema is identical to the syndrome initially designated regional migratory osteoporosis, although osteoporosis may be subtle and not detectable on conventional radiographs and is now thought to be due to sequential subchondral (occult) insuffiency fractures.

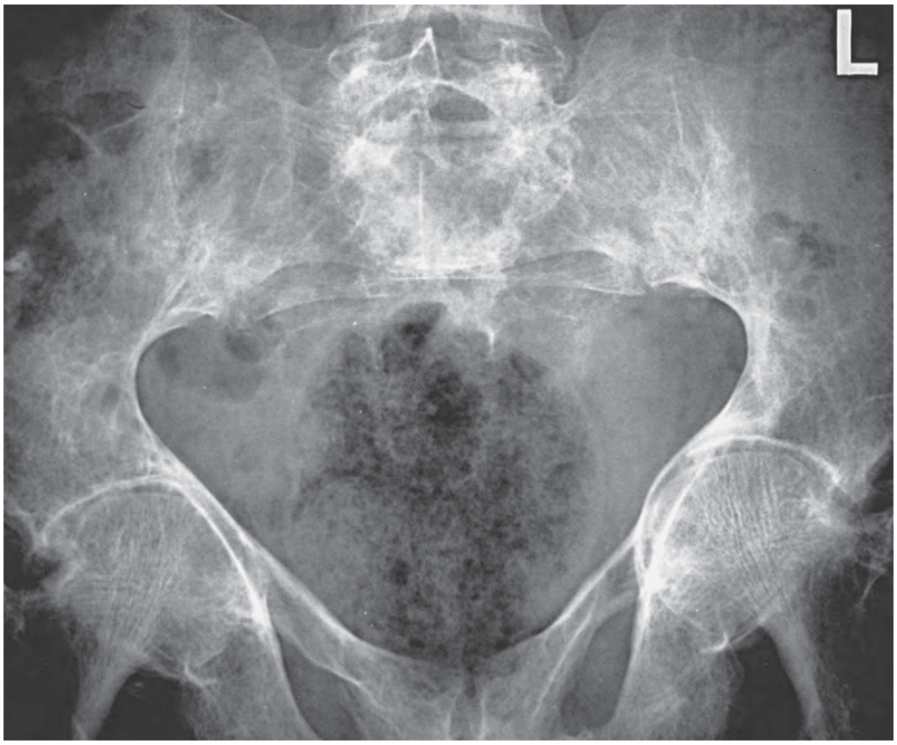

FIGURE 7–58 **Osteomalacia and hyperparathyroidism.**[65] In this 60-year-old woman, observe the marked osteopenia and acetabular deformity, worse on the left.

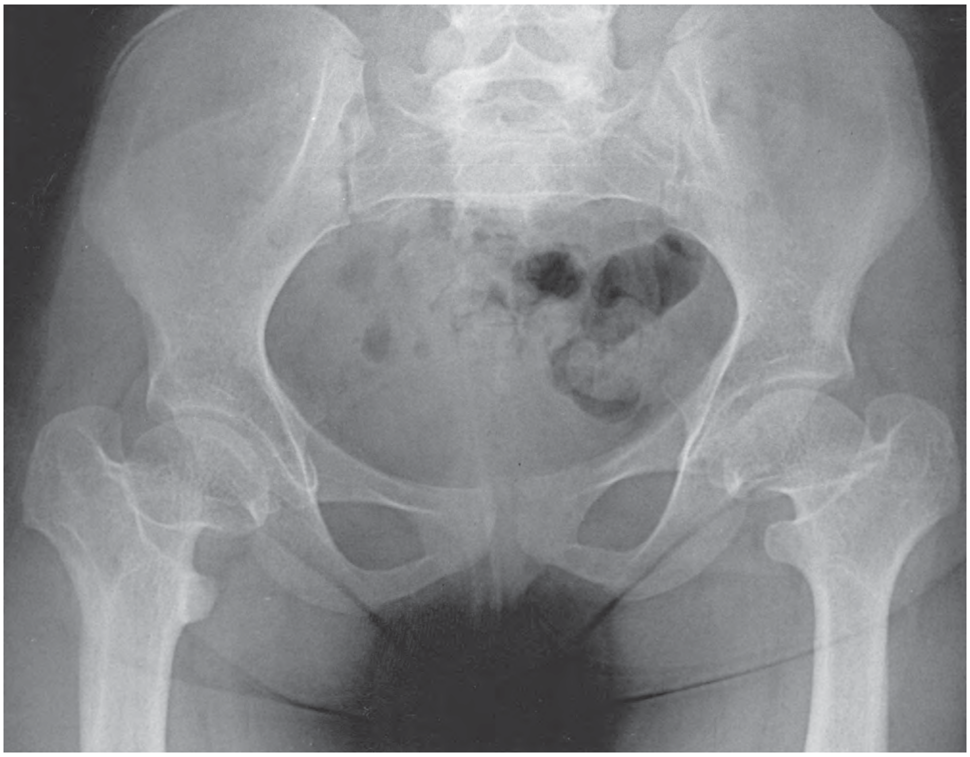

FIGURE 7–59 **Rickets: coxa vara deformities.**[65] In this 15-year-old girl with long-standing vitamin D-resistant rickets, bilateral varus deformities of the hip are associated with shortening of the femoral necks.

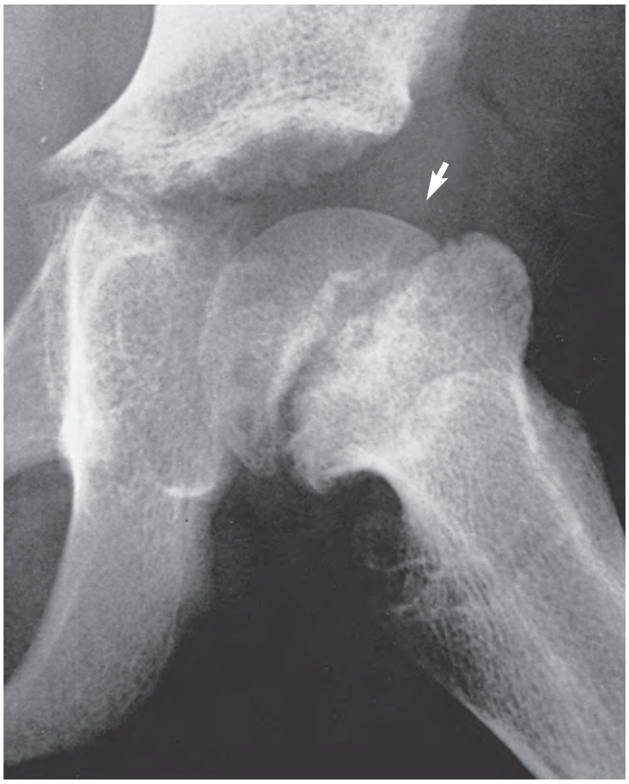

FIGURE 7–60 **Hypothyroidism.**[66] This 13-year-old girl had bilateral hip pain that developed over a period of 1 year. Radiographs revealed a slipped capital femoral epiphysis *(arrow),* which was bilateral (other hip not shown). The patient also had delayed bone age. Slipped capital femoral epiphysis, an important manifestation of hypothyroidism, can be bilateral or unilateral, and it may be the initially apparent feature of this disease. *(Courtesy G. Greenway, MD, Dallas.)*

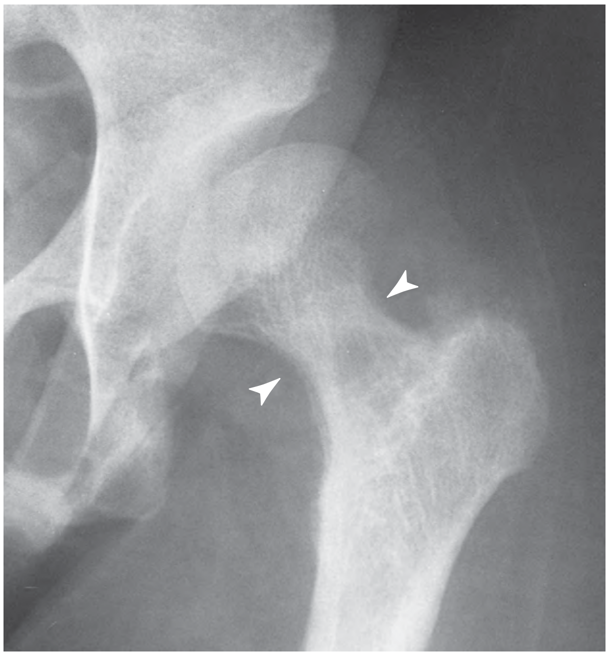

FIGURE 7–61 **Hyperparathyroidism.**[67,68] A radiograph of the proximal portion of the femur in this 18-year-old woman with chronic renal failure shows subperiosteal bone resorption of the femoral neck *(arrowheads).*

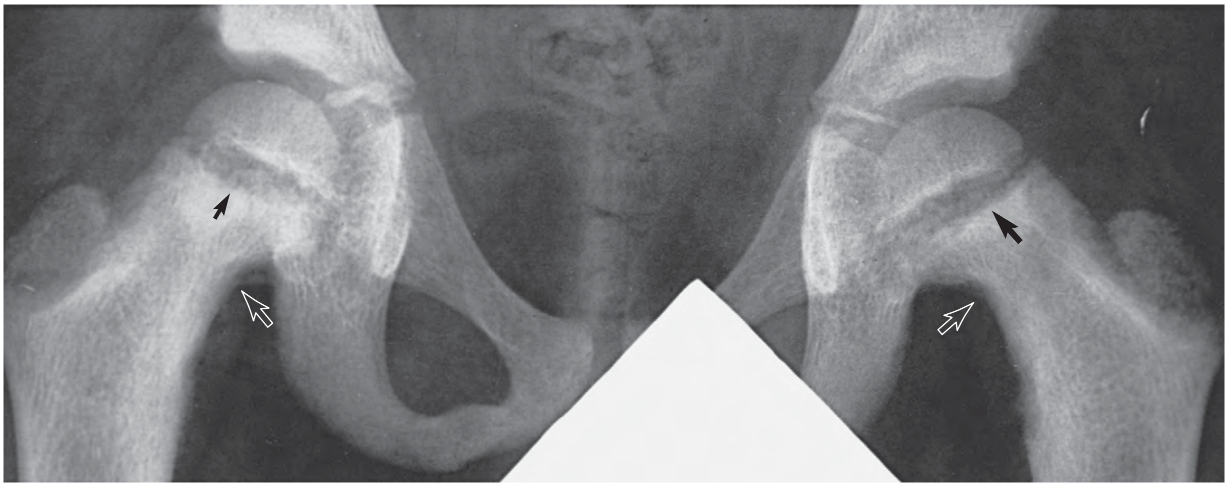

FIGURE 7–62 **Renal osteodystrophy.**[67,68] Observe the generalized dense sclerosis, subchondral resorption adjacent to the femoral physes *(arrows),* and cortical resorption at the medial aspects of the femoral necks *(open arrows)* in this child with long-standing renal insufficiency. *(Courtesy B. L. Harger, DC, Portland, Ore.)*

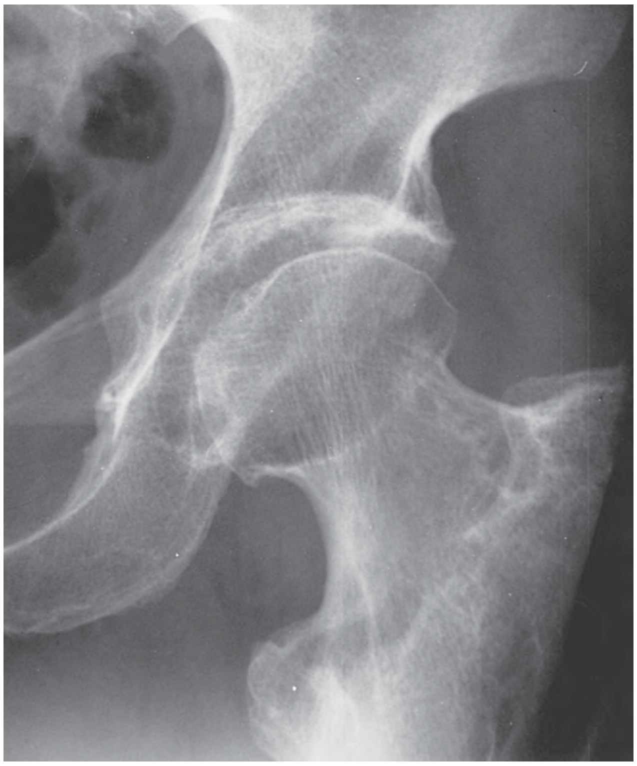

FIGURE 7–63 **Acromegaly.**[69] Widening of the hip joint space, prominent osteophyte formation, and irregularity of the articular surfaces are characteristic of acromegalic arthropathy. The pathogenesis of this arthropathy relates to proliferation of chondrocytes with secondary degeneration of the abnormally proliferated cartilage.

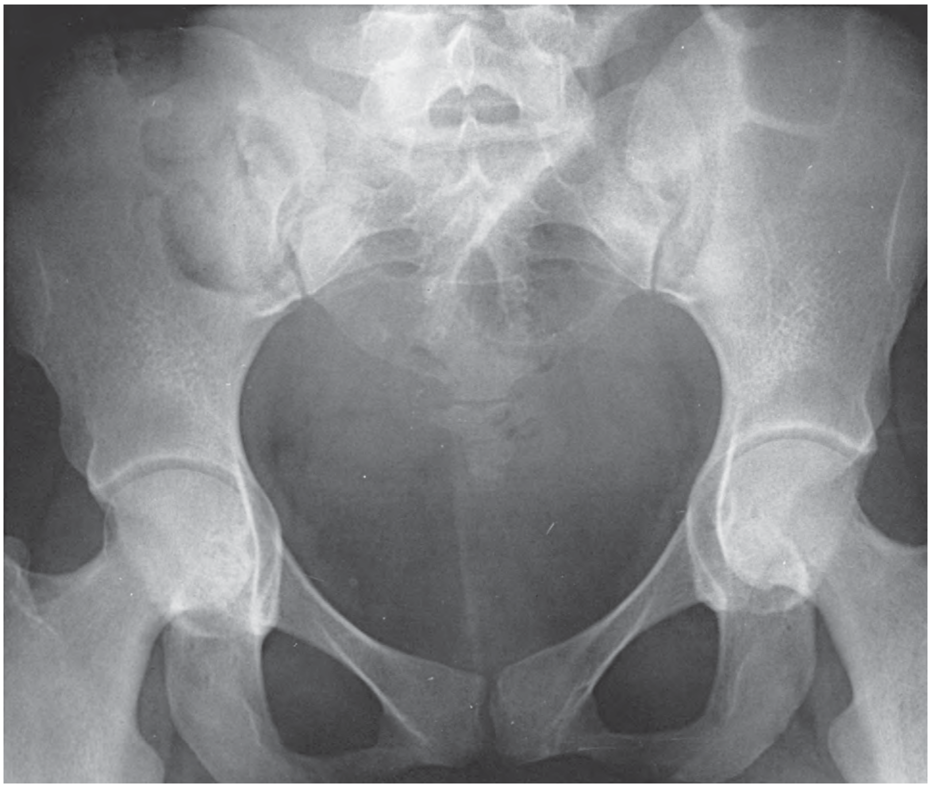

FIGURE 7–64 **Sickle cell anemia: acetabular protrusion.**[7,88] Protrusio acetabuli is present in up to 20% of patients with sickle cell anemia. The cause is unclear, but it may be related to acetabular ischemia from vascular occlusion. Epiphyseal osteonecrosis (not seen in this patient) is a frequent complication of sickle cell anemia and other hemoglobinopathies.

TABLE 7-15 **Osteonecrosis of the Femoral Head***

Entity	Figure(s)	Characteristics
Legg-Calvé-Perthes Disease[71,113]	7-65	
Definition		Osteonecrosis of the immature femoral capital epiphysis
Distribution		Bilateral in 10% to 20% of patients
Typical age of onset		3-12 years of age; in most patients onset is between the ages of 4 and 8 years
Gender		Male : female, 4 or 5 : 1
Factors associated with increased incidence		Breech presentation, later-born children within the family, lower socioeconomic status, older parental age, urban living environment
Radiographic findings		*Catterall classification:* grades I-IV (Table 7-16) Epiphyseal flattening, deformity, fragmentation, and osteosclerosis Crescent sign with or without subchondral collapse and sequestered bone fragments Metaphyseal sclerosis and cyst formation Eventual degenerative joint disease and mushroom appearance of femoral head Shortening of femoral neck from failure of normal growth Magnetic resonance (MR) imaging may be used to determine the extent of epiphyseal involvement and to document the presence and extent of deformity
Prognosis		Almost always remodels and heals, but may result in residual deformity in the shape of the femoral head
Differential diagnosis		Femoral head irregularity and collapse in children: Legg-Calvé-Perthes, Meyer dysplasia, hypothyroidism, epiphyseal dysplasia, spondyloepiphyseal dysplasia, sickle cell anemia, Gaucher disease, infection, and hemophilia
Osteonecrosis of the Adult Femoral Head[72-76,115]	7-66 to 7-68	
Synonyms		Ischemic necrosis, avascular necrosis, aseptic necrosis
Distribution		Bilateral in 50% of patients
Typical age of onset		20-40 years
Gender		Male = female
Imaging findings		Stages 0-V (Table 7-17)
		Radiographic findings May be negative Bone sclerosis Cysts Subchondral collapse (crescent sign) May be focal or "segmental" area of involvement Joint space narrowing in advanced cases
		Scintigraphic findings Increased radionuclide uptake in femoral head Often focal in superior portion With or without photopenic areas
		CT findings Increased density area often is wedge-shaped, corresponding to segmental region of involvement Articular collapse
		MR imaging findings Focal abnormalities of femoral head Surrounding margin of low signal in T1-weighted images with central higher signal zone consistent with fat; may exhibit high signal with acute bleeding Variable signal in T2-weighted images Diffuse abnormalities of femoral head and neck related to bone marrow edema
Prognosis		Variable, but progressive in 75% of cases Often necessitates operative intervention

---

* See also Tables 1-17 and 1-18.

TABLE 7-16 Grades of Femoral Involvement in Legg-Calvé-Perthes Disease (Catterall Classification)[113]

	Grade			
	I	II	III	IV
Anterior part of epiphysis involved	+	+	–	–
Majority of epiphysis involved	–	–	+	–
Whole epiphysis involved	–	–	–	+
Sequestrum	–	+	+	+
Anterior crescent sign	–	+	–	–
Anterior crescent sign extends posteriorly	–	–	+	–
Anterior and posterior crescent sign	–	–	–	+
Articular collapse	–	+	+	+
Localized metaphyseal abnormalities	–	+	–	–
Diffuse metaphyseal abnormalities	–	–	+	+

+, Present; –, absent.

TABLE 7-17 Staging of Osteonecrosis in the Adult Femoral Head

	Stage of Osteonecrosis					
Characteristics	0	I	II	III	IV	V
Clinical Assessment						
Suspected necrosis	+	+	+	+	+	+
Clinical findings	–	+	+	+	+	+
Advanced Imaging						
Bone scan	–	+	+	+	+	+
Magnetic resonance (MR) imaging	–	+	+	+	+	+
Radiographic Findings						
Osteopenia	–	–	+	+	+	+
Cystic areas	–	–	+	+	+	+
Bone sclerosis	–	–	+	+	+	+
Crescent sign	–	–	–	+	+	+
Subchondral collapse	–	–	–	–	+	+
Flattening of femoral head	–	–	–	–	+	+
Joint space narrowing	–	–	–	–	–	+
Acetabular abnormalities	–	–	–	–	–	+

+, Present; –, absent.

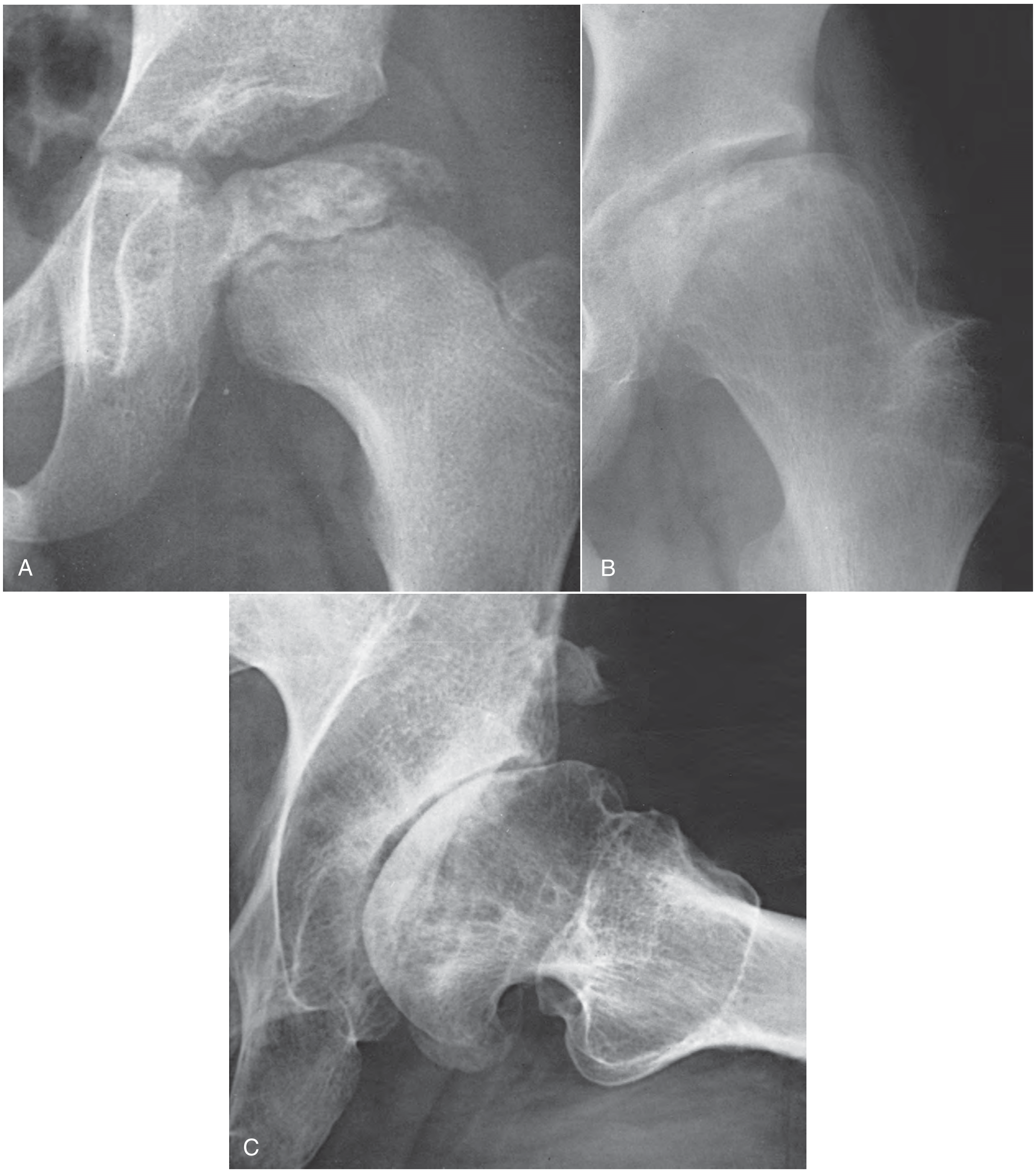

FIGURE 7–65 **Legg-Calvé-Perthes disease.**[71,113] **A,** Sclerosis, flattening, fragmentation, and deformity of the proximal femoral epiphysis are noted in this 8-year-old boy. **B,** In a 16-year-old boy with long-standing Legg-Calvé-Perthes disease, observe the flattening of the femoral head, osseous fragmentation of the subchondral bone, overall widening of the femoral neck, and deformity of the acetabulum. **C,** In a 60-year-old man who had Legg-Calvé-Perthes disease as a child, observe the nonuniform joint space narrowing, subchondral sclerosis, subchondral cysts, and osteophytes indicative of secondary degeneration, a frequent complication of this childhood disease. The mushroom-shaped femoral head is characteristic. (See also Figure 7–6, *B*.) (***A,** Courtesy P. VanderStoep, MD, St Cloud, Minn.)*

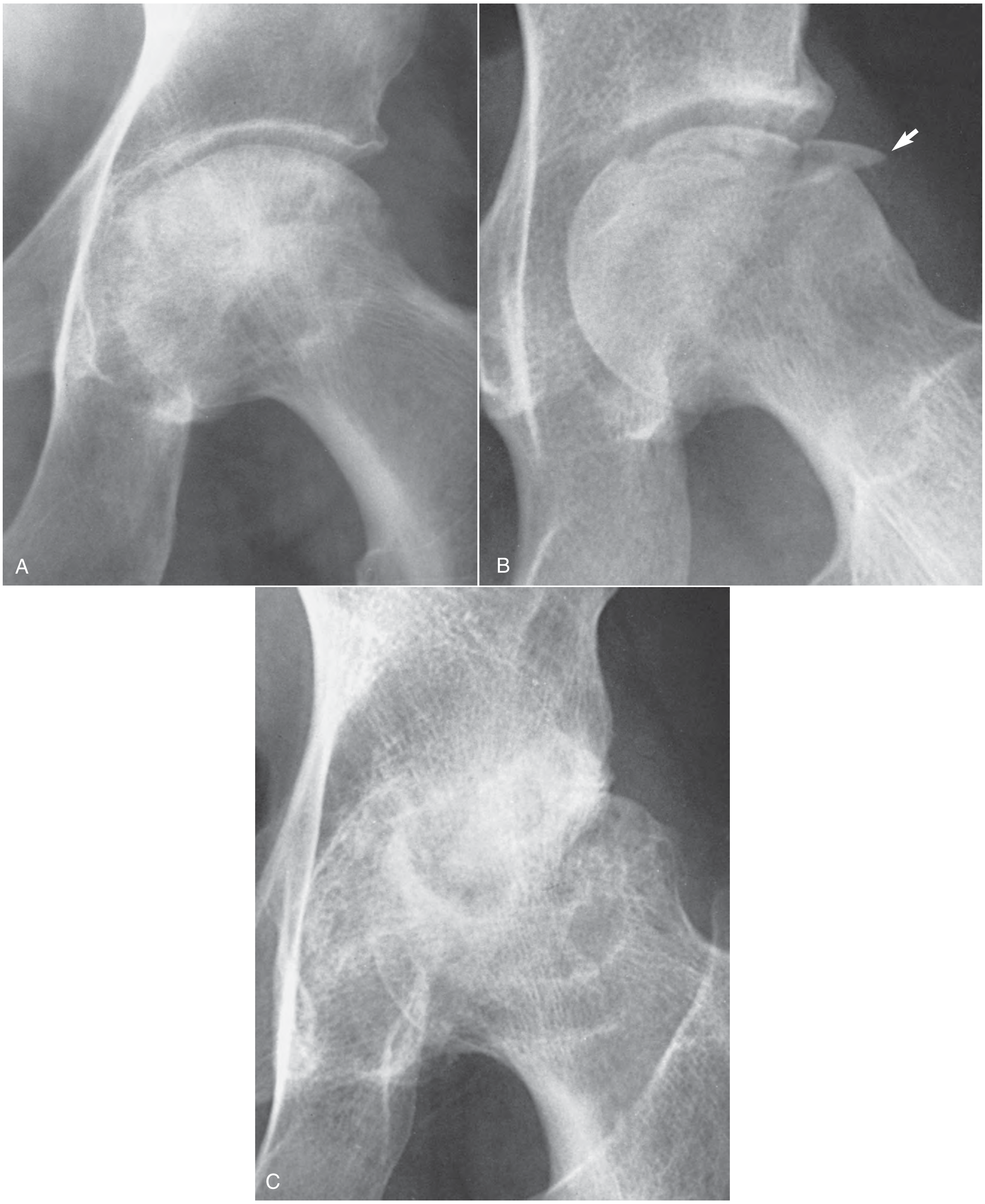

FIGURE 7–66 **Osteonecrosis: routine radiography.**[72,73] **A,** Early involvement (stage II). Subchondral cystlike lucent areas and sclerosis are seen in the femoral head of this 47-year-old man. Note the relative preservation of joint space, a feature typical of early osteonecrosis. **B,** Moderate disease (stage IV). In a 27-year-old intravenous drug abuser, a radiograph reveals notable subchondral collapse, femoral head flattening, and a displaced osseous fragment *(arrow)*. **C,** Advanced disease (stage V). This 52-year-old man worked in a decompression chamber. Observe the marked collapse of the femoral head, cystlike femoral and acetabular radiolucent areas, patchy sclerosis, and joint space narrowing. This patient eventually developed bilateral involvement.

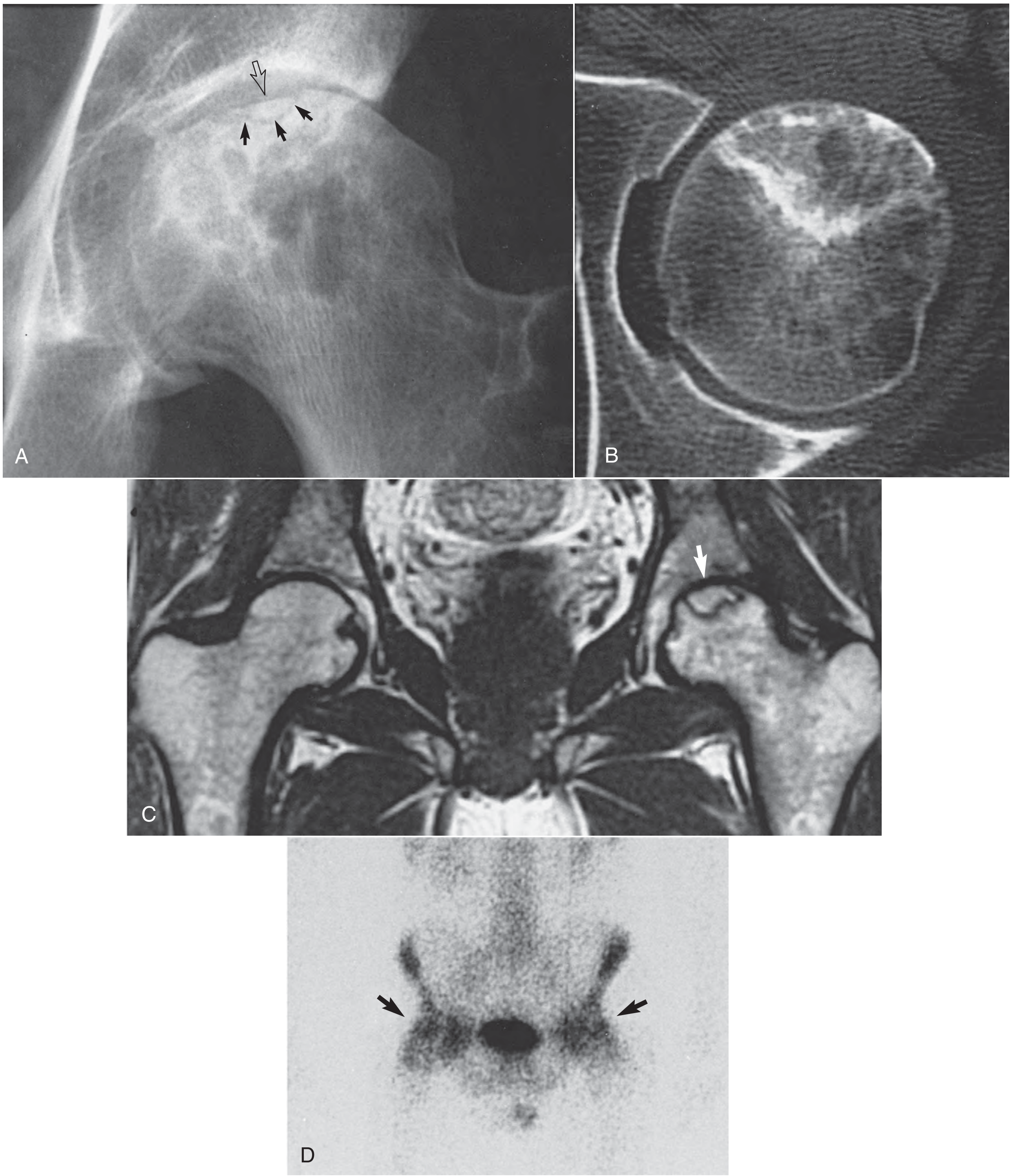

FIGURE 7–67 **Osteonecrosis: imaging abnormalities.**[72,73,115] **A,** The classic radiographic findings of stage V osteonecrosis include a subchondral radiolucent line (crescent sign) *(arrows),* collapse and flattening of the femoral head articular surface *(open arrow),* large subchondral radiolucent areas surrounded by sclerosis, and the absence of osteophytes. This patient exhibits some superolateral joint space narrowing and sclerosis, indicating that this is a long-standing process. **B,** CT. In another patient, a transaxial CT scan shows a well-localized focus of osteonecrosis confined to the anterior aspect of the femoral head, a pattern termed segmental osteonecrosis. The cystlike radiolucent areas are bordered by a well-defined zone of osteosclerosis. **C,** MR imaging. In a third patient, a coronal T1-weighted (TR/TE, 600/20) spin echo MR image shows a curvilinear zone of low signal intensity surrounding a zone of intermediate signal intensity within the left femoral head *(arrow)*. MR imaging is ideal for evaluating osteonecrosis and is more sensitive to early changes than routine radiography. **D,** Bone scan. In a fourth patient with bilateral osteonecrosis, increased uptake is seen in both femoral heads *(arrows)*.

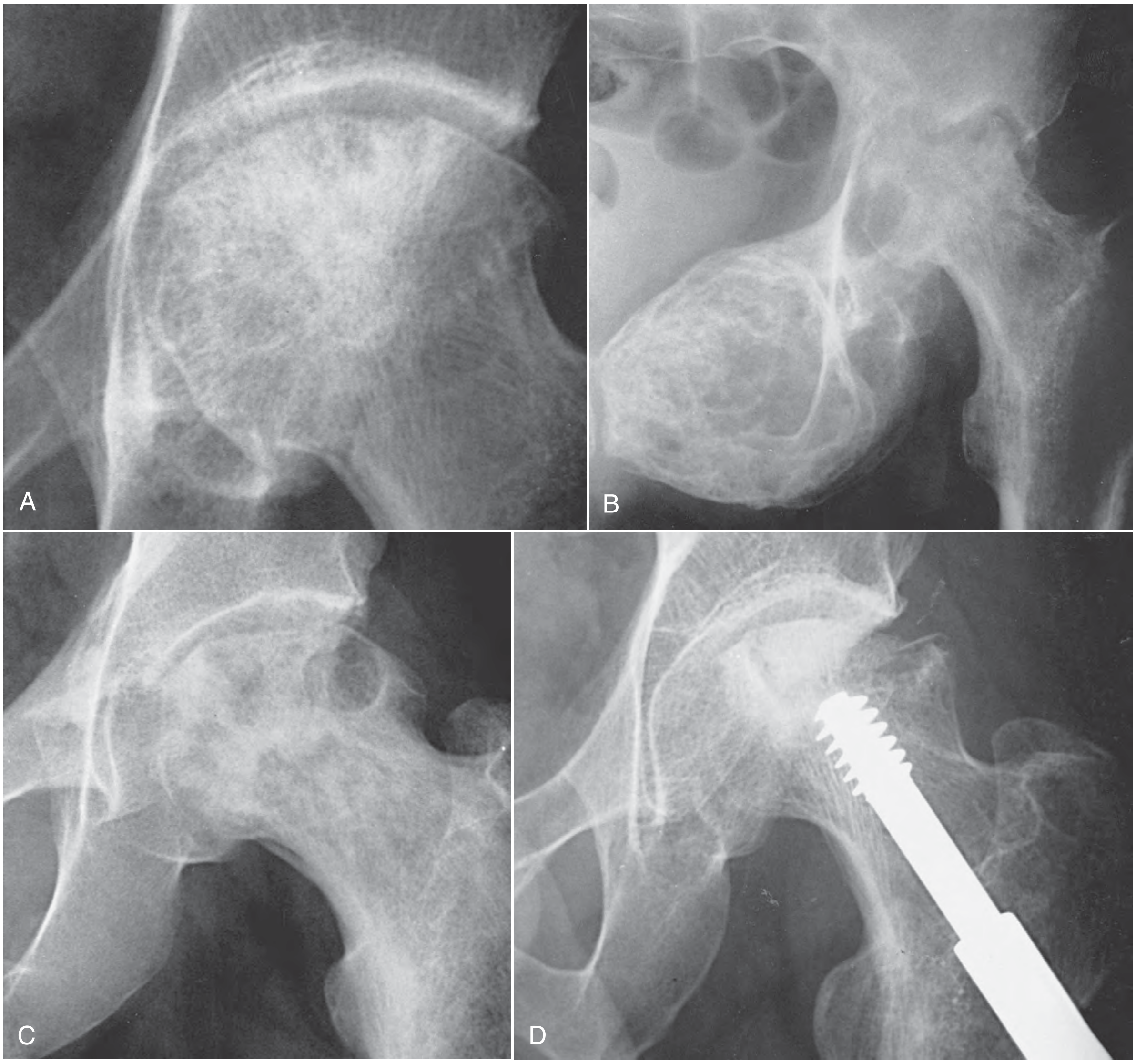

FIGURE 7–68 Osteonecrosis: some associated disorders.[74-76] **A,** Systemic lupus erythematosus. This 35-year-old woman had been taking corticosteroid medication for 5 years for long-standing systemic lupus erythematosus. Articular collapse of the femoral head is associated with cystlike radiolucent areas and surrounding sclerosis typical of osteonecrosis. Secondary degenerative changes are also evident. The osteonecrosis was bilateral. The femoral head is the most common site of osteonecrosis in patients with systemic lupus erythematosus. **B,** Radiation-induced osteonecrosis. In this 55-year-old woman with endometrial carcinoma, a radiograph obtained after a course of radiation therapy shows osteonecrosis of the femoral head, destruction of the acetabulum, joint space loss, and a large sclerotic metastatic lesion involving the ischiopubic ramus. **C,** Gaucher disease.[89] Observe the multiple cystic subchondral lesions, articular collapse, and punctate sclerosis in the femoral head and neck of this patient with Gaucher disease complicated by osteonecrosis. **D,** Postsurgical osteonecrosis. In this patient with a previous intertrochanteric fracture treated with a dynamic hip screw, evidence of type IV osteonecrosis is seen. This complication is less frequent in intertrochanteric fractures than in subcapital fractures. Femoral head osteonecrosis has been reported in HIV-infected patients receiving highly active antiretroviral treatment (HAART). *(**B,** Courtesy H. Kroon, MD, Leiden, Netherlands; C, Courtesy V. Vint, MD, La Jolla, Calif. **D,** From Taylor JAM, Harger BL, Resnick D: Diagnostic imaging of common hip disorders: A pictorial review. Top Clin Chiropr 1:8, 1994.)*

CHAPTER 8

Femur

DEVELOPMENTAL ANOMALIES, ANATOMIC VARIANTS, SKELETAL DYSPLASIAS, AND OTHER CONGENITAL DISEASES

A wide variety of developmental anomalies, anatomic variants, skeletal dysplasias, and other congenital conditions affect the femur and its surrounding structures. Table 8-1 and Figures 8-1 through 8-6 represent selected examples of some of the more common of such processes.

PHYSICAL INJURY

The femoral diaphysis may be a site of acute fracture, fatigue fracture, or insufficiency fracture. Additionally, the muscles of the thigh are a frequent site of posttraumatic heterotopic ossification. These conditions are described in Table 8-2 and are illustrated in Figures 8-7 through 8-12. Injuries to the proximal and distal portions of the femur are discussed in Chapters 7 and 9, respectively.

BONE TUMORS

The femur is the bone most frequently affected by malignant and benign neoplasms and tumorlike processes. Tables 8-3 through 8-5 list some of the characteristics of these disorders. Their radiographic manifestations are illustrated in Figures 8-13 through 8-43.

METABOLIC, HEMATOLOGIC, AND INFECTIOUS DISORDERS

Several metabolic, hematologic, and infectious disorders involve the femur. Table 8-6 lists some of the more common disorders and describes their characteristics. The radiographic features of these disorders are illustrated in Figures 8-44 through 8-54. Additional manifestations of the disorders within the proximal and distal portions of the femur are discussed in Chapters 7 and 9, respectively.

TABLE 8-1 Developmental Anomalies, Anatomic Variants, Skeletal Dysplasias, and Other Congenital Diseases Affecting the Femur*

Entity	Figure(s)	Characteristics
Limb length inequality[1-3]	8-1	*Synonyms:* anisomelia, leg length discrepancy, short leg syndrome ***Etiology*** Congenital disorders, paralysis, infection, trauma, neoplasm, joint replacement surgery Accurate assessment aids in treatment planning Three imaging techniques are used for measuring the length of the femur and tibia: 1. *Orthoradiograph:* single exposure of entire length of both lower extremities on a long film; may be obtained supine or standing 2. *Scanogram:* three separate exposures are obtained of the hips, knees, and ankles; the patient is immobilized in a supine position, and the x-ray tube and cassette are moved to expose all three anatomic regions on one film 3. *CT scanogram:* an anteroposterior scout scanogram of both lower extremities is obtained; cursors are placed at the superior tip of the capital femoral epiphysis and the most distal portion of the lateral femoral condyle and measurements are obtained; tibial length is determined in a similar manner; lateral views of the femur also may be obtained and measured to account for limb flexion CT scanograms are accurate and result in less radiation exposure than radiographic techniques; this is particularly useful in patients with joint contractures
Proximal femoral focal deficiency (PFFD)[4]	8-2	Spectrum of conditions characterized by partial absence and shortening of the proximal portion of the femur Disorder is congenital but not inherited Usually PFFD is an isolated anomaly, unilateral in 90% of affected patients ***Imaging findings*** Femoral head may be present or absent; may be just a small ossicle *Acetabulum:* variable degree of dysplasia *Femoral shaft:* short, often deformed Sometimes no connection exists between femur and acetabulum
Osteopetrosis[5,77]	8-3	Diffuse osteosclerosis results in brittle bones and predisposition to pathologic fracture of femur Erlenmeyer flask deformity
Osteopoikilosis[6]	8-4	Multiple 2- to 3-mm circular foci of osteosclerosis Symmetric periarticular lesions resembling bone islands predominate about hip and knee articulations
Osteopathia striata[7]	8-5	Regular, linear, vertically oriented bands of osteosclerosis extending from the metaphysis for variable distances into the diaphysis Longest lesions are frequently found in the femur Metaphyseal flaring of the femur also may be seen with osteopathia striata
Melorheostosis[8,9]	8-6	*Usual pattern:* hemimelic involvement of a single femur Peripherally located cortical hyperostosis resembling "flowing candle wax" on the surface of bones Paraarticular soft tissue calcification and ossification may occur and may even lead to joint ankylosis May be positive on bone scans
Mixed sclerosing bone dystrophy[10]	8-4, *B*	Combinations of various sclerosing dysplasias including osteopoikilosis, osteopetrosis, osteopathia striata and melorheostosis

* See also Tables 1-1 and 1-2.

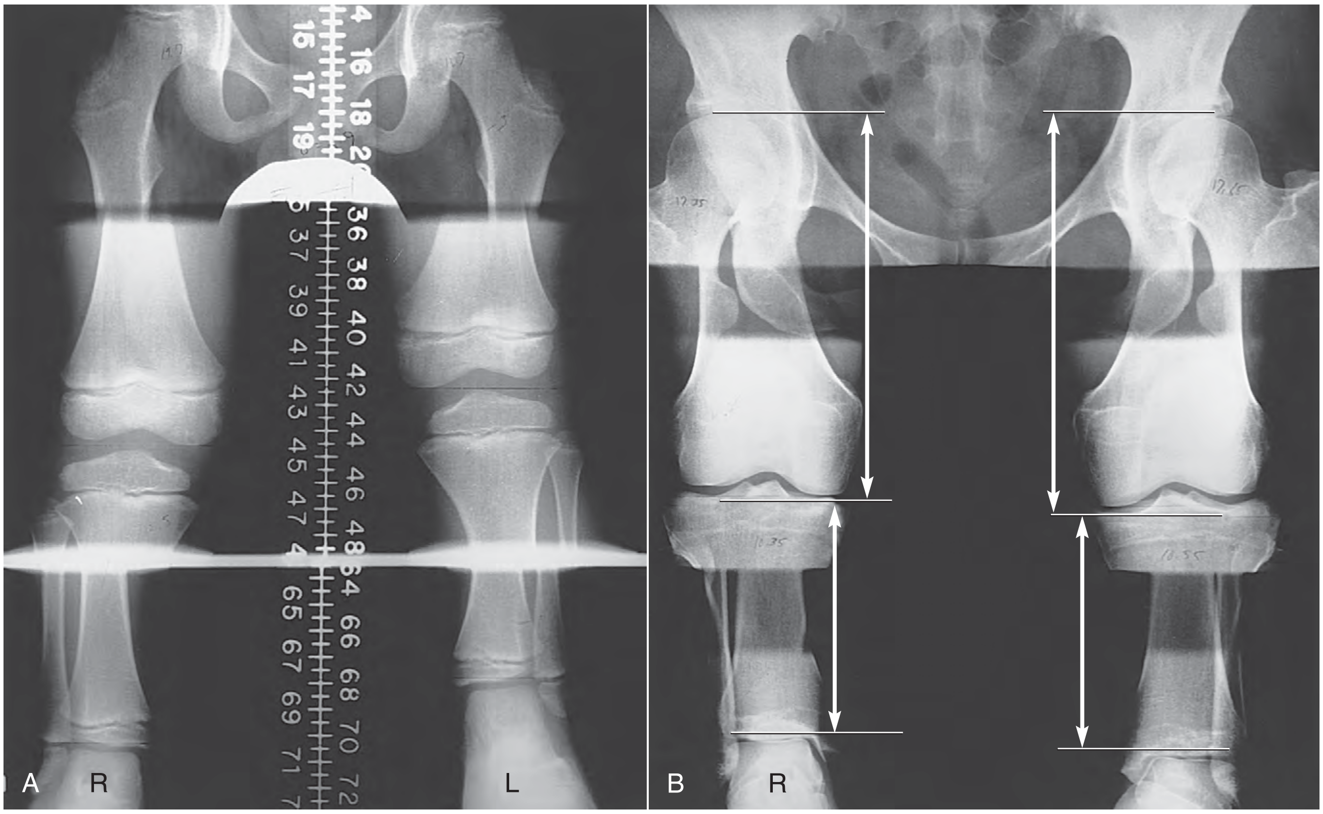

FIGURE 8–1 Limb length inequality: measurement techniques.[1-3] **A-B,** Radiographic scanogram. In **A,** a scanogram from a 12-year-old child with a noticeable limp and short leg reveals a 3-cm deficiency of the left femur and a 0.2-cm deficiency of the left tibia. In **B,** an adult patient, the landmarks for the measurements of the tibia and fibula are illustrated. In this example, the right femur had a 0.3-cm deficiency and the right tibia had a 0.2-cm deficiency. In this procedure, the patient remains stationary in a supine position on the radiographic table, and three separate exposures of the hips, knees, and ankles are taken on one film. The accurate measurement of the length of the femur and tibia assists in management planning.

Continued

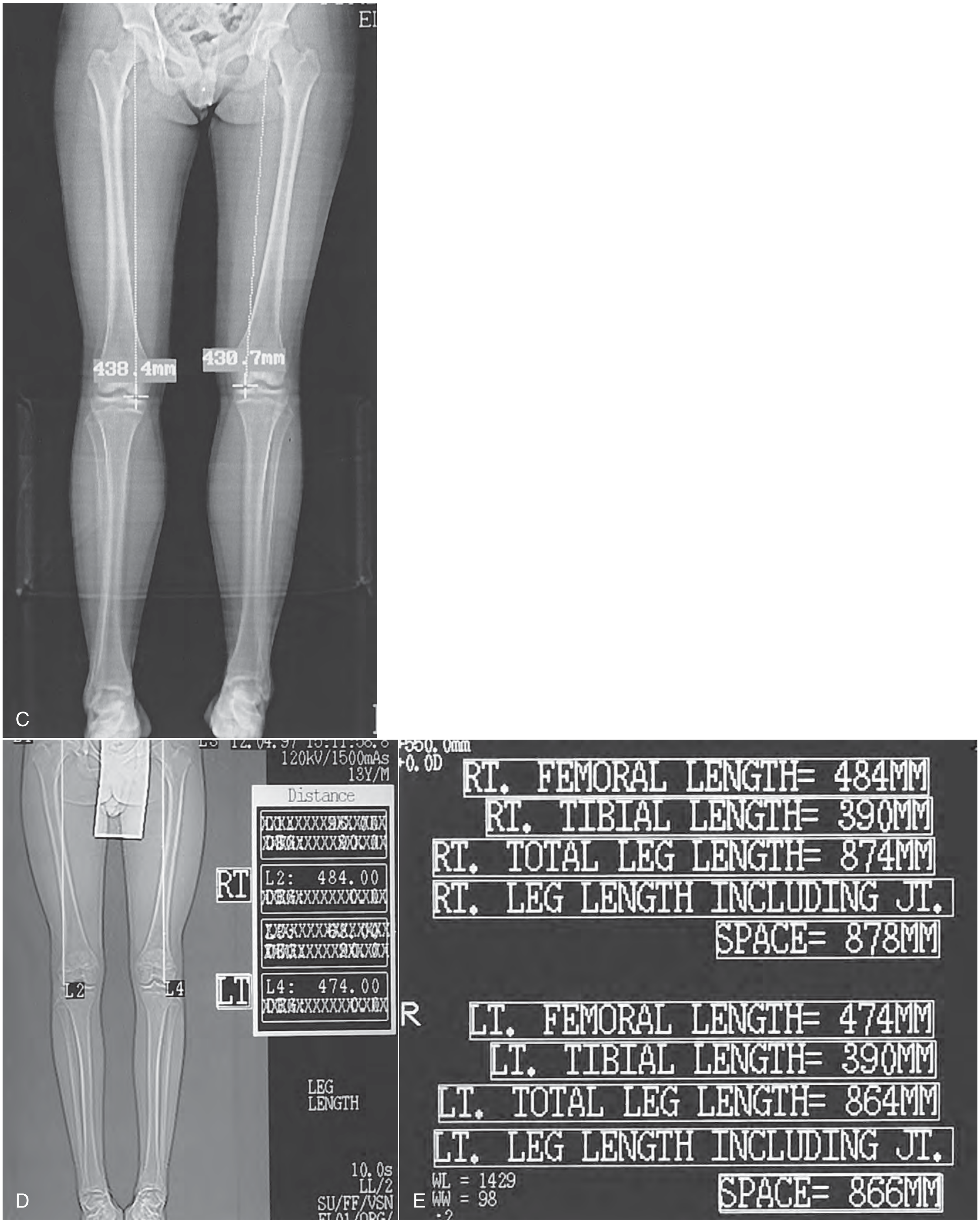
C
438.4mm
430.7mm
D
L3 12.04.97 15:11:58.8
120kV/1500mAs
13Y/M
Distance
RT
L2: 484.00
LT
L4: 474.00
L2
L4
LEG
LENGTH
10.0s
LL/2
SU/FF/VSN
E
+550.0mm
+0.0D
R
WL = 1429
WW = 98

RT. FEMORAL LENGTH= 484MM
RT. TIBIAL LENGTH= 390MM
RT. TOTAL LEG LENGTH= 874MM
RT. LEG LENGTH INCLUDING JT.
SPACE= 878MM

LT. FEMORAL LENGTH= 474MM
LT. TIBIAL LENGTH= 390MM
LT. TOTAL LEG LENGTH= 864MM
LT. LEG LENGTH INCLUDING JT.
SPACE= 866MM

FIGURE 8–1, cont'd **C-E**, CT scanogram. In **C,** a frontal CT image of the entire lower extremities is obtained with the patient in the supine position, and precise anatomic measurements of each extremity are made. In this patient, the left femur is 7.7 mm shorter than the right. Similar measurements of the tibiae are also obtained, and an overall leg length is determined. In **D,** another patient, the left femur (474 mm) is 10 mm shorter than the right (484 mm). In **E,** a computerized display of the same patient as in **D** shows the precise length of tibia, femur, and total lower extremity bilaterally.

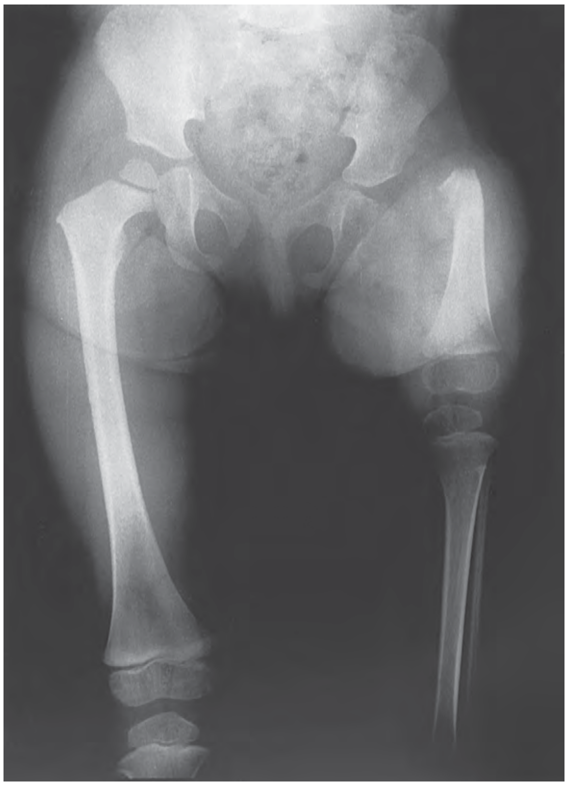

FIGURE 8–2 **Proximal femoral focal deficiency (PFFD).**[4] In this 4-year-old girl, the proximal portion of the left femur is shortened and tapered. No evidence of ossification of the proximal femoral epiphysis is present, and unilateral hip dislocation is evident. *(Courtesy J. Spaeth, MD, Albuquerque, NM.)*

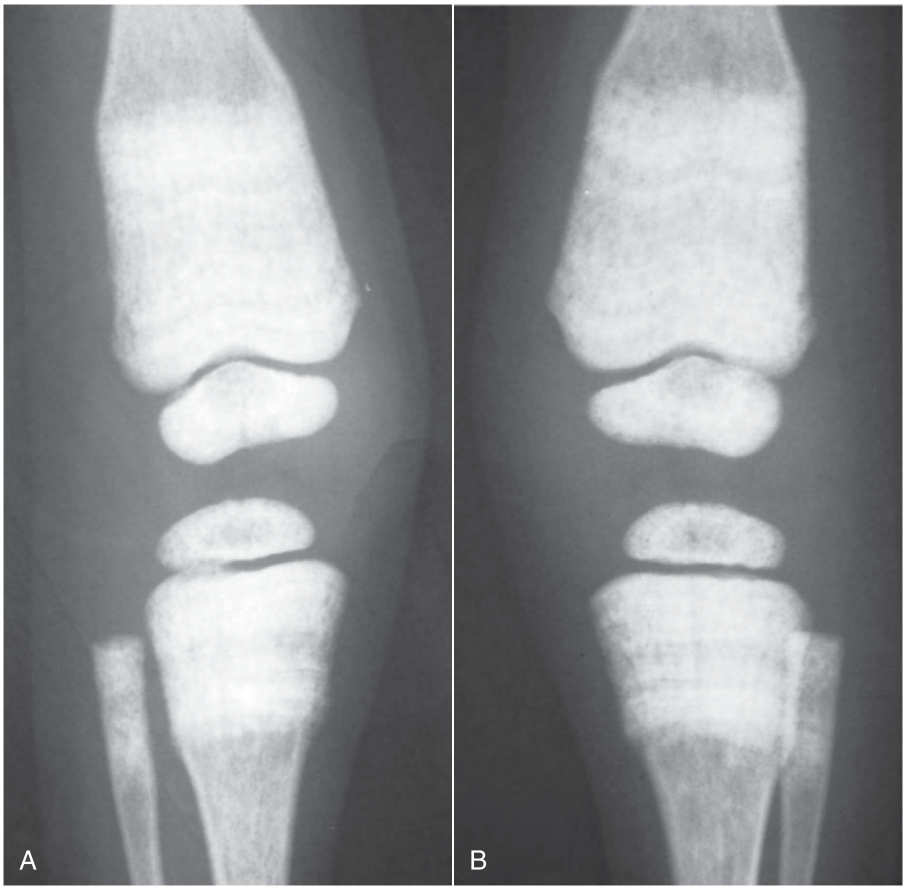

FIGURE 8–3 **Osteopetrosis.**[5,77] Bilateral frontal radiographs of the knees in this 5-year-old boy reveal marked radiodensity of the metaphyseal and epiphyseal regions of the femora and tibiae and the metaphyses of the fibulae. Close examination of the radiodense regions reveals that it is composed of transverse striations. Note also the widening of the metaphyses, a finding that results from undertubulation of growing bone termed *Erlenmeyer flask deformity.*

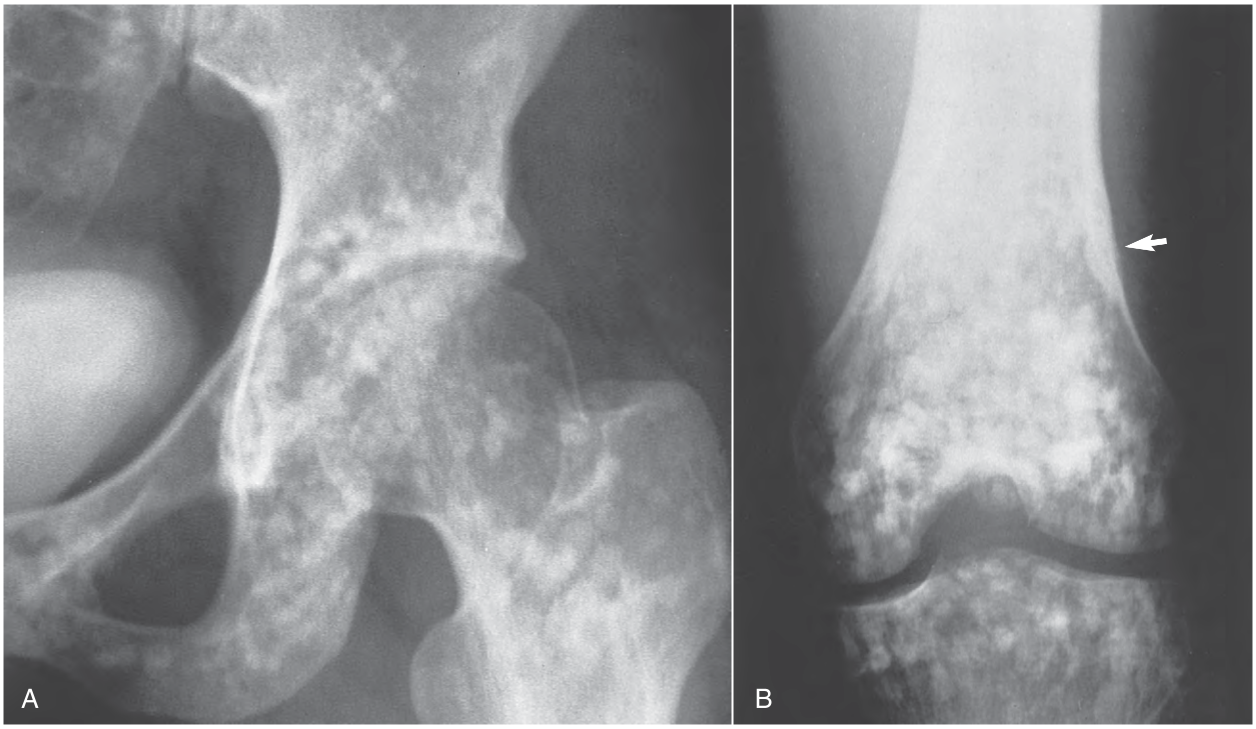

FIGURE 8–4 **Osteopoikilosis.**[6] **A,** Note the circular and ovoid osteosclerotic foci localized in a periarticular distribution within the femur and pelvic bones. The symmetric, periarticular distribution is characteristic of this fairly common sclerosing dysplasia. Although the epiphysis may be affected, most lesions predominate in the metaphysis. Osteopoikilosis was an incidental asymptomatic finding in this patient, who was undergoing cystography (note contrast agent in the bladder). **B,** Mixed sclerosing bone dystrophy.[10] Evidence of both punctate zones of sclerosis (typical of osteopoikilosis), and linear hyperostosis (characteristic of melorheostosis) *(arrow)* is seen in the distal end of the femur and proximal portion of the tibia in this patient. Mixed sclerosing bone dystrophy is a condition characterized by radiologic features of more than one of the sclerosing dysplasias, including osteopoikilosis, osteopathia striata, and melorheostosis. *(**B,** Courtesy C. Resnik, MD, Baltimore, Md.)*

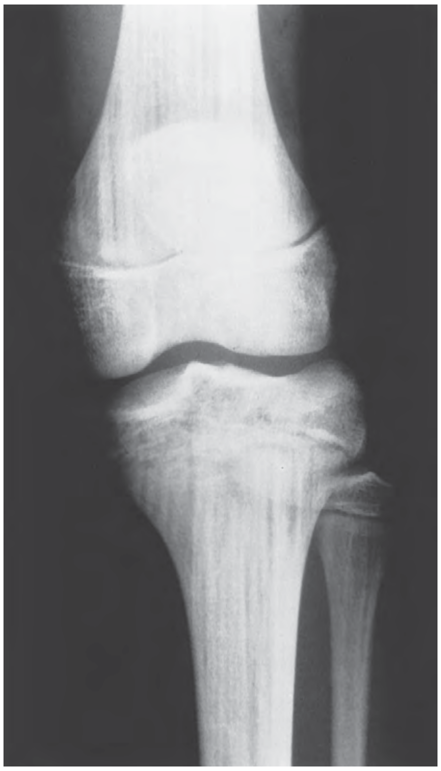

FIGURE 8–5 **Osteopathia striata.**[7] Linear regular bands of increased radiodensity are seen extending vertically from the metaphyses into the diaphyses of the femur, tibia, and fibula. The skeletal manifestations of this rare sclerosing dysplasia are usually bilateral.

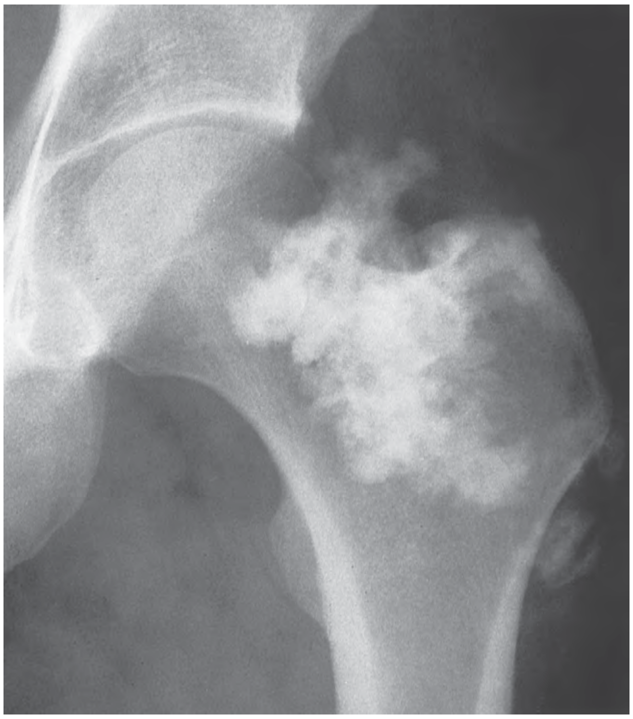

FIGURE 8–6 **Melorheostosis.**[8,9] A cloudlike accumulation of ossification is seen adjacent to the proximal portion of the femur. The characteristic radiographic abnormalities of melorheostosis include asymmetric hyperostosis simulating flowing candle wax, which typically affects only one side of an extremity. *(Courtesy A. Newberg, MD, Boston.)*

TABLE 8-2 Fractures of the Femoral Diaphysis and Soft Tissue Injury*

Entity	Figure(s)	Characteristics	Complications and Related Injuries
Acute Fractures of the Femoral Diaphysis[11]			
Any level		Major trauma with associated injuries of tibia, patella, acetabulum, hip, or knee Open or closed Spiral, oblique, or transverse fracture with possible butterfly fragment and comminution	Refracture Peroneal nerve injury Thrombophlebitis Nonunion (1% of cases), malunion, or delayed union Infection Fat embolization (10% of cases)
Proximal	8-7	Less common than midshaft fractures Commonly extend into subtrochanteric region	Malalignment Nonunion
Middle	8-8	Most common site Transverse fracture at this location is most typical	Malalignment Nonunion
Distal and supracondylar	8-9	Less common than midshaft fractures	Malalignment Arterial injury
Stress Fractures of the Femoral Diaphysis			
Stress (fatigue) fractures[12,13,84-86]	8-10	Ballet and long-distance running Often inconspicuous on radiographs Scintigraphy, CT, and MR imaging useful	May result in complete fracture with or without displacement
Stress (insufficiency) fractures[87]		Rare type of injury often resulting in longitudinal pattern of stress injury Often inconspicuous on radiographs Scintigraphy, CT, and MR imaging useful	*Systemic risk factors include:* Osteoporosis, osteomalacia, hyperparathyroidism, osteopetrosis, fluoride treatment, corticosteroids, and rheumatoid arthritis *Local risk factors include:* Internal fixation, osteotomy, osteoarthrosis, Paget disease, fibrous dysplasia, and radiation therapy
Adductor Insertion Avulsion Syndrome (Thigh Splints)[89,90]	8-11	Painful stress-related changes affecting the proximal to mid femoral shaft at the insertion of the adductor muscles of the thigh Pain in hip, thigh, or groin Usually unilateral, but may be bilateral	***Radiographic findings*** Often normal ***MR imaging findings*** 4-9 cm longitudinal thin rim of high signal intensity along the medial periosteum of the femoral shaft on fluid sensitive images Associated high signal in adjacent marrow and cortex consistent with appearance of developing fatigue fracture
Posttraumatic Heterotopic Ossification[14]	8-12	Also termed *myositis ossificans posttraumatica* Ossifying hematoma in muscle after direct trauma such as "charley horse" injury Faint calcific intermuscular or intramuscular shadow may appear within 2-6 weeks of injury Well-defined region of ossification aligned parallel to the long axis of the femur may be evident within 6-8 weeks *Most frequent location:* quadriceps muscle Associated periostitis may relate to subperiosteal hemorrhage	Limitation of motion May result in abnormal hip or knee biomechanics and lead to premature joint degeneration May resemble aggressive neoplasms, such as osteosarcoma or Ewing sarcoma
Calcific tendinitis with osseous involvement[88]		Calcific tendinitis (calcium hydroxyapatite crystal deposition) with associated bone involvement is seen most commonly in the femur *Locations:* Posterior and subtrochanteric along the linea aspera at the level of or within 6 cm of the lesser trochanter Rarely distal femoral condyle adjacent to the medial femoral condyle	***Imaging findings*** Cortical erosion (most common manifestation) Solid appearing concretions near tendon attachment to bone Marrow edema on MR imaging and increased radionuclide uptake on scintigraphy Periosteal reaction may be evident May be confused for malignancy

* See also Tables 1-4 to 1-6.

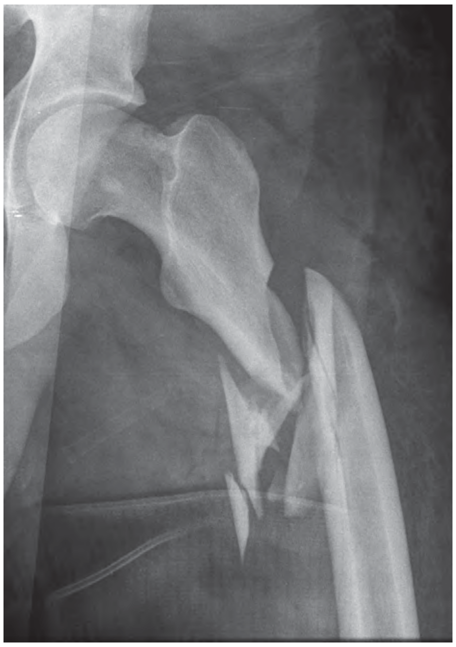

FIGURE 8–7 Acute fracture of the proximal end of the femoral diaphysis.[11] This 20-year-old man was involved in a motorcycle crash. Observe the multiple fracture fragments with poor apposition and resultant varus deformity. The large triangular piece of bone on the medial aspect is designated a *butterfly fragment,* a common finding in comminuted femoral fractures.

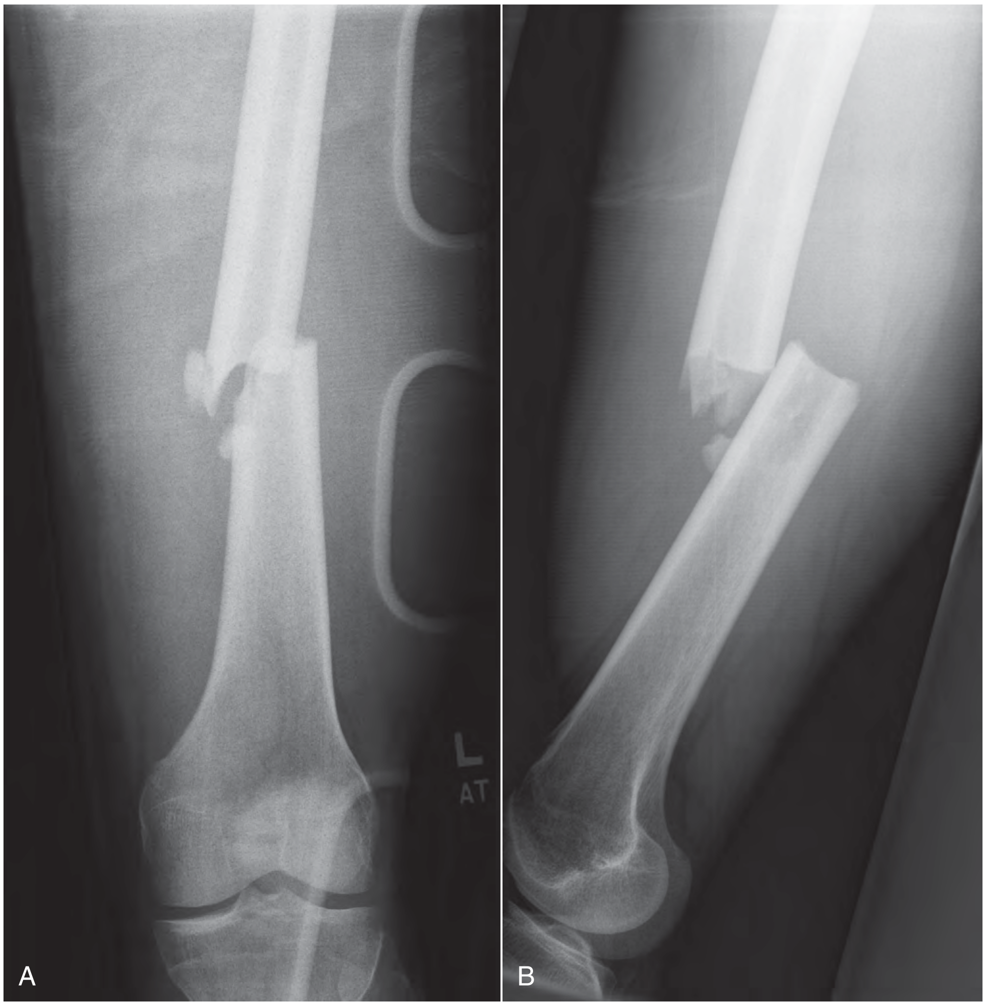

FIGURE 8–8 Acute fractures of the midshaft of the femoral diaphysis.[11] **A-B,** This 25-year-old pedestrian was struck by a fast-moving motor vehicle. He sustained a transverse fracture of the midshaft of the femur that is complicated by bayonet apposition and posterior angulation of the fracture apex.

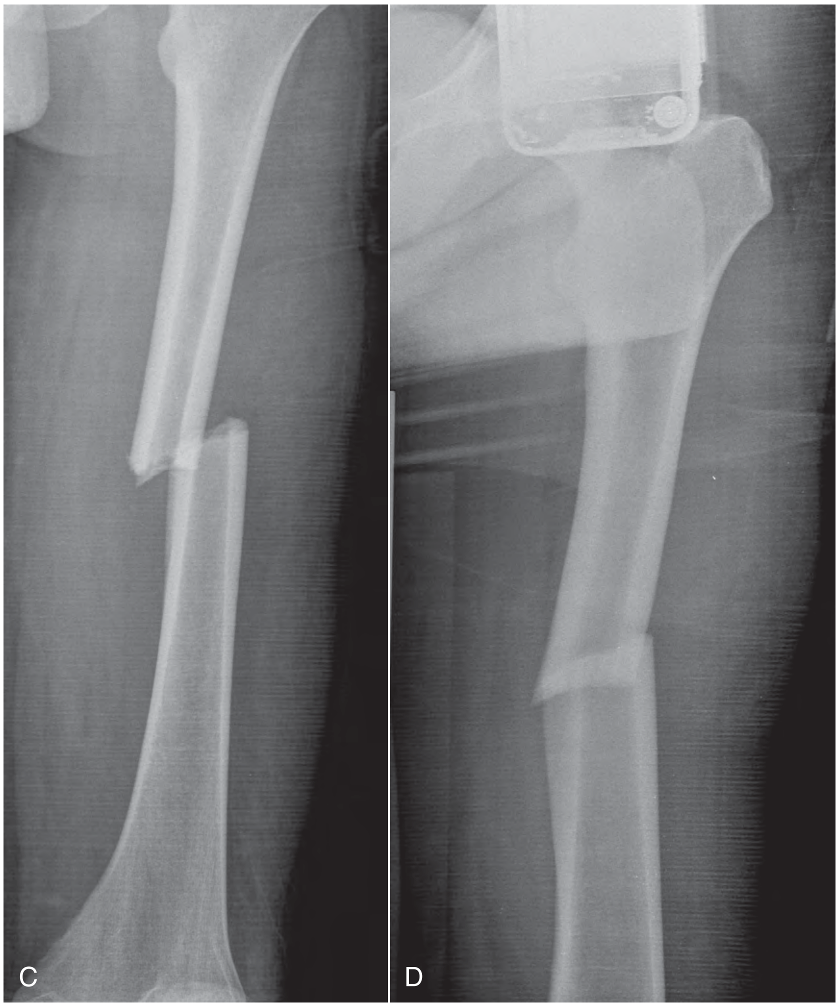

FIGURE 8–8, cont'd **C-D,** In a 20-year-old male, a transverse midshaft fracture of the femur is markedly displaced with bayonet apposition. The malalignment and true apposition is not as well depicted on the lateral radiograph **(D).** Fractures with a transverse orientation, or butterfly fragment, tend to involve high-velocity mechanisms of injury and direct trauma to the affected area.

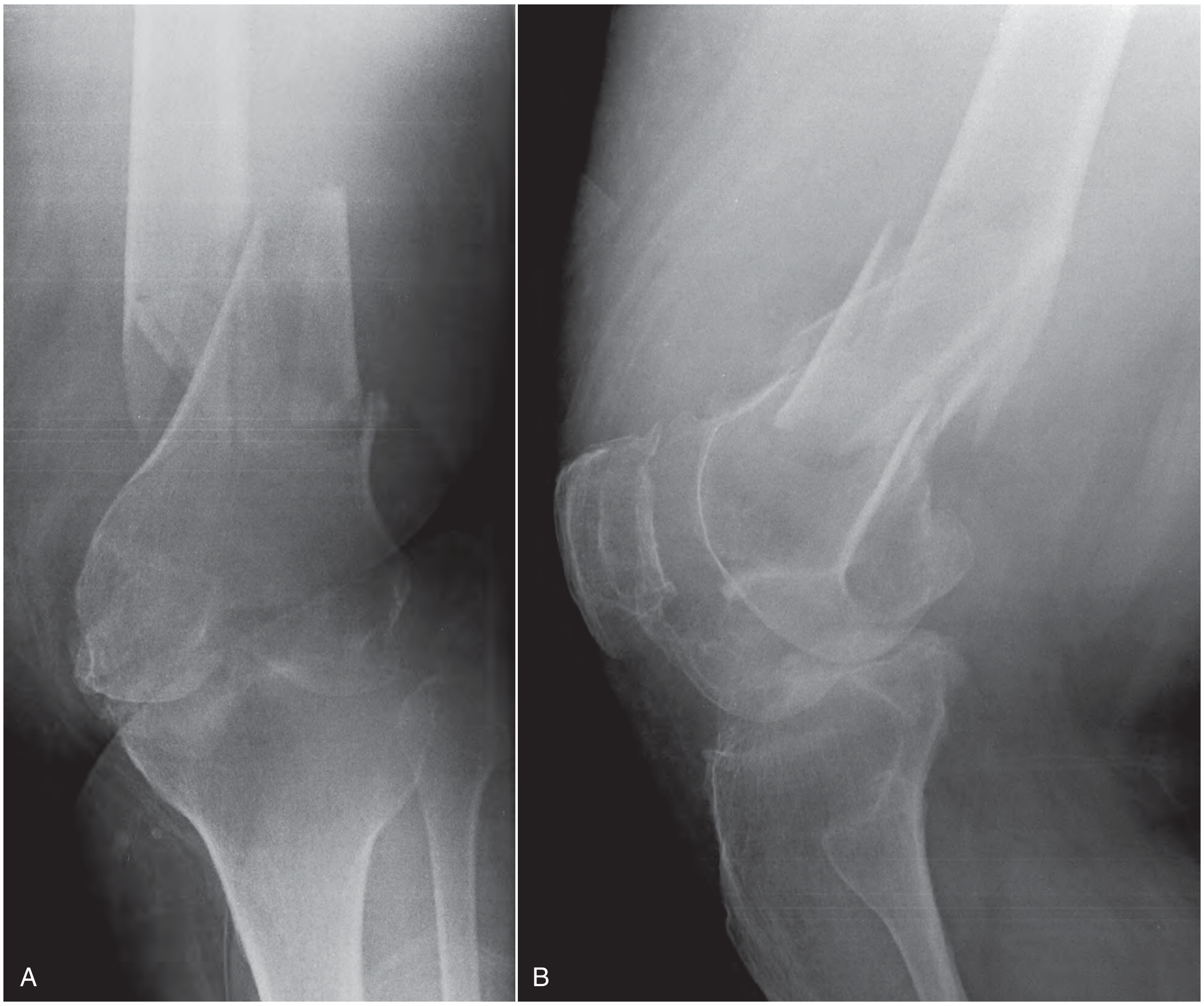

FIGURE 8–9 Acute fracture of the distal end of the femoral diaphysis and supracondylar region.[11] This 59-year-old woman was struck by a moving vehicle as she was crossing the road at an intersection. Anteroposterior **(A)** and lateral **(B)** radiographs reveal osteopenia and a comminuted fracture of the supracondylar region of the femur. Note the poor alignment and bayonet apposition of the main fracture fragments. Although this was an acute injury, the decreased bone mineral density probably contributed to the fragility of the bone, resulting in a more complex injury.

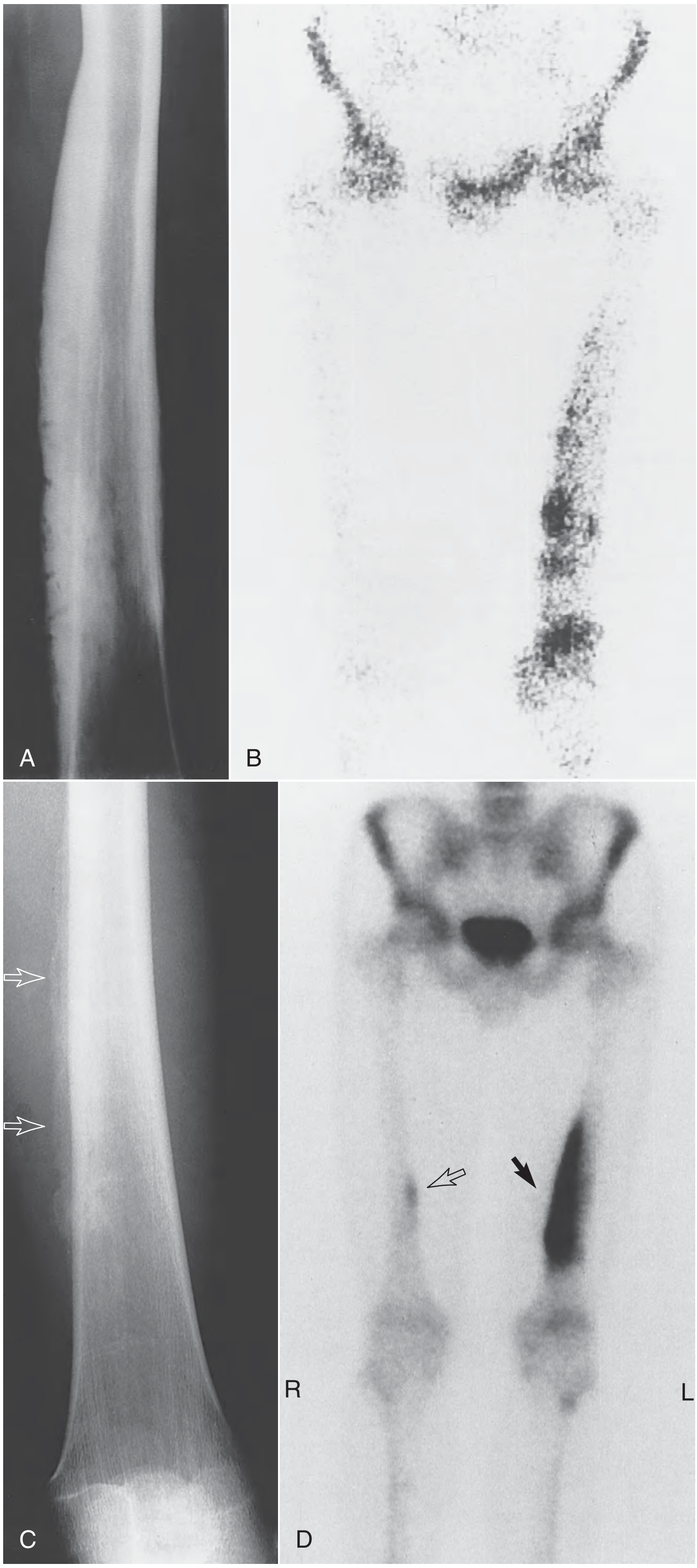

FIGURE 8–10 **Stress (fatigue) fracture of femoral diaphysis.**[12,13,84-86] **A-B,** A 53-year-old woman. In **A,** a routine radiograph shows notable periosteal and endosteal new bone formation with thickening and hyperostosis of the shaft of the femur. Multiple irregular, transverse, radiolucent striations are evident. In **B,** a bone scan shows increased uptake throughout the medial shaft of the femur corresponding to the zones of hyperostosis and radiolucent striations. **C-D,** This 19-year-old marine recruit had bilateral thigh pain, worse on the left. In **C,** a frontal radiograph shows thick periostitis along the medial aspect of the femoral diaphysis *(open arrows)*. In **D,** scintigraphic examination reveals prominent radionuclide activity at the medial aspect of the left femur *(arrow)*. Mild increased focal uptake in the right femoral shaft *(open arrow)* represents an early stress reaction. Scintigraphy and MR imaging often are helpful in the early diagnosis of stress reactions and fractures in bone. *(**A-B,** Courtesy A. Newberg, MD, Boston.)*

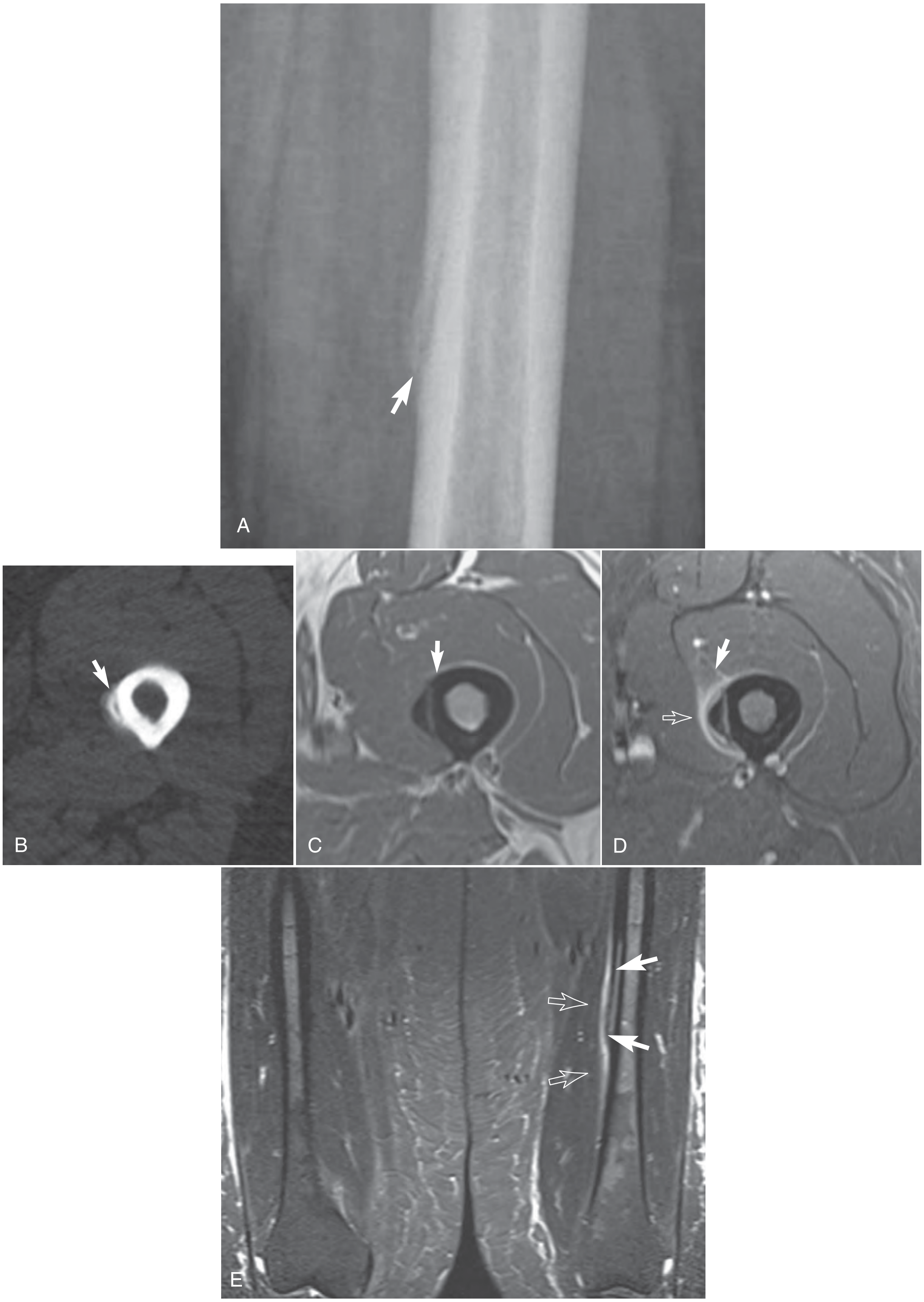

FIGURE 8–11 **Adductor insertion avulsion syndrome: thigh splints.**[89,90] This 50-year-old woman has left hip pain. **A,** A frontal radiograph of the thigh reveals an oblique radiolucent linear defect within the medial cortex of the femur *(arrow)*. A transaxial bone window CT scan **(B)** reveals the linear defect more clearly. T1-weighted transaxial **(C)** and fat-suppressed proton density-weighted transaxial **(D)** and coronal MR images **(E)** also reveal the linear fracture site *(arrows)*. Periosteal edema is noted *(open arrows)* overlying the linear fracture site on the fluid-sensitive sequences **(D-E).** The coronal image **(E)** demonstrates that the linear fracture is approximately 10 cm in length. This case illustrates the typical appearance of periosteal edema and linear cortical stress fracture at the adductor longus and brevis femoral insertion site. This syndrome has been designated "thigh splints" because it closely resembles the pathophysiology and appearance of the more well-known phenomenon of "shin splints."

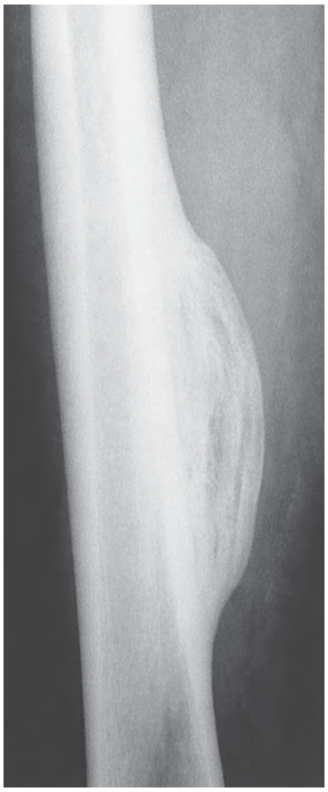

FIGURE 8–12 **Heterotopic ossification: posttraumatic myositis ossificans.**[14] This 56-year-old man had sustained an injury 2 months earlier. A radiograph shows a zone of well-organized ossification arising from the surface of the femur. *(Courtesy G. Scher, MD, San Diego.)*

TABLE 8-3 Malignant Tumors Affecting the Femur*

Entity	Figure(s)	Characteristics
Skeletal Metastasis[15-17]	8-13 to 8-15	Fewer than 10% of skeletal metastatic lesions affect the femur 75% permeative or moth-eaten osteolysis 25% diffuse or patchy osteosclerosis or mixed pattern of lysis and sclerosis Usually multiple sites of involvement Pathologic fracture Predilection for the lesser trochanter ***Cortical metastasis*** Prevalent in the long bones of patients with metastasis, especially from bronchogenic carcinoma Small radiolucent, eccentric, saucer-shaped, scalloped erosions are referred to as *cookie-bite* lesions
Primary Malignant Tumors of Bone		
Osteosarcoma (conventional)[18,73,78,79]	8-16	50%-75% of osteosarcomas occur in the femur and tibia about the knee Osteolytic, osteosclerotic, or mixed patterns of medullary and cortical destruction Prominent periosteal reaction common Preferential involvement of the metaphysis High-grade surface osteosarcoma, a rare subtype that resembles conventional osteosarcoma, will more frequently affect the diaphysis
Osteosarcoma (parosteal)[19,78,79]	8-17	64% of parosteal osteosarcomas occur in the femur *Most common site:* posterior surface of distal end of the femur Osteosclerotic surface lesion of bone Large radiodense, oval, sessile mass with smooth or irregular margins Peripheral portion of lesion may have plane separating it from the femur Ossification begins centrally and progresses outwardly as opposed to heterotopic bone formation (myositis ossification)

* See also Table 1-12.

Continued

TABLE 8-3 Malignant Tumors Affecting the Femur—cont'd

Entity	Figure(s)	Characteristics
Osteoblastoma (aggressive)[20]		11% of aggressive osteoblastomas occur in the femur Expansile osteolytic lesion that may be partially ossified or contain calcium Metaphyseal location Aggressive osteoblastomas have histologic and imaging characteristics suggestive of malignancy and can be difficult to differentiate from osteosarcoma
Chondrosarcoma (conventional)[21,22]	8-18	24% of chondrosarcomas occur in the femur Tend to be osteolytic lesions, sometimes containing a bulky cartilaginous cap and frequently contain calcifications May have a soft tissue mass
Giant cell tumor (aggressive)[23]	8-19	More than 40% of aggressive giant cell tumors occur in the femur Involve the knee and less commonly the hip Eccentrically located, subarticular osteolytic lesion extending into the metaphysis Cortical destruction and soft tissue mass are variable findings Radiographic appearance is an inaccurate guide to determining malignancy of lesion; biopsy necessary
Fibrosarcoma[24]		39% of fibrosarcomas involve the femur Purely osteolytic destruction with no associated sclerotic reaction or periostitis Most common in distal portion of the femur
Malignant fibrous histiocytoma[24]	8-20	44% of malignant fibrous histiocytomas involve the femur Pathologic fracture in 30%-50% of cases Metaphyseal location with frequent spread to epiphysis and diaphysis Moth-eaten or permeative osteolysis, frequently resembling fibrosarcoma
Ewing sarcoma[25]	8-21	22% of Ewing sarcomas occur in the femur Permeative or moth-eaten osteolysis, aggressive cortical erosion or violation, laminated or spiculated periostitis and soft tissue masses Most lesions central and diametaphyseal in location
Myeloproliferative Disorders		
Multiple myeloma[26,94]	8-22	16% of multiple myeloma lesions occur in the femur *Early:* normal radiographs or diffuse osteopenia *Later:* widespread well-circumscribed osteolytic lesions with discrete margins, which appear uniform in size 97% osteolytic; 3% osteosclerotic False-negative bone scans common
Solitary plasmacytoma[26]	8-23	18% of solitary plasmacytomas occur in the femur Solitary, geographic, expansile, osteolytic lesion that frequently results in pathologic fracture 70% of cases eventually develop into multiple myeloma
Hodgkin disease[27,72]	8-24	10% of osseous involvement occurs in the femur 75% of lesions are osteolytic—permeative, or moth-eaten osteolysis 25% of lesions are osteosclerotic More than 60% of patients have multiple sites of involvement
Primary lymphoma (non-Hodgkin)[28,29,72,76]	8-25	Approximately 24% of lesions in primary lymphoma occur in the femur Multiple moth-eaten or permeative osteolytic lesions Diffuse or localized sclerotic lesions are rare Common cause of pathologic fracture
Leukemia[30]	8-26	Diffuse osteopenia, radiolucent or radiodense transverse metaphyseal bands, osteolytic lesions, periostitis, and infrequently, osteosclerosis Radiodense metaphyses more frequently in patients undergoing chemotherapy for leukemia; may resemble lead poisoning

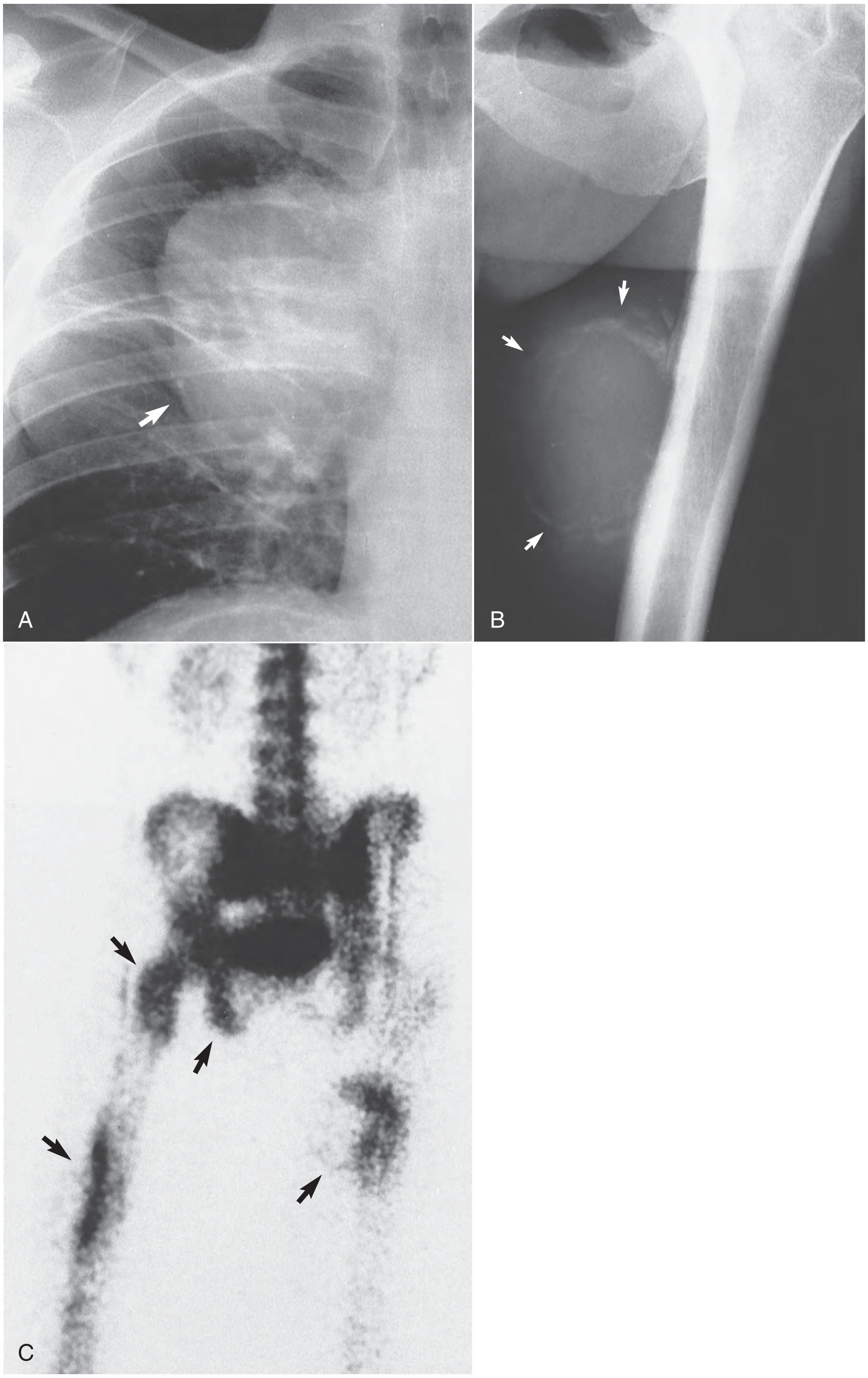

FIGURE 8–13 Skeletal metastasis: Osteolytic pattern.[15] This 40-year-old man with bronchogenic carcinoma had widespread metastasis throughout his skeleton. **A,** Posteroanterior chest radiograph demonstrates a large pulmonary mass representing the primary tumor *(arrow)*. **B,** Frontal radiograph of the femur shows an osteolytic cortical lesion with a thin-shelled, calcified soft tissue mass *(arrows)*. **C,** Bone scan shows several sites of increased uptake of radionuclide *(arrows)* and specifically outlines the osseous shell surrounding the soft tissue mass.

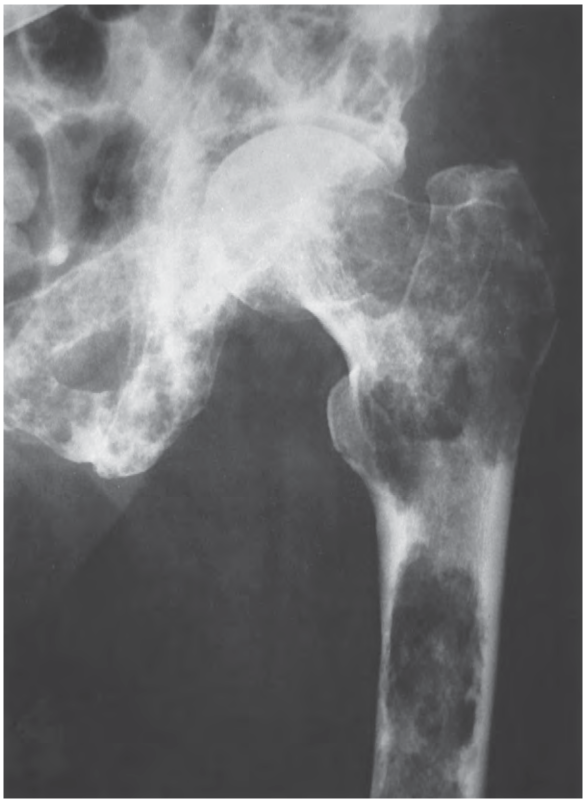

FIGURE 8–14 **Skeletal metastasis: mixed pattern.**[16] This 56-year-old woman had a history of breast carcinoma and diffuse bone pain. A combined pattern of osteolytic destruction and osteosclerosis is evident throughout the proximal portion of the femur and pelvis. *(From Taylor AM, Harger BL, Resnick D: Diagnostic imaging of common hip disorders: A pictorial review. Top Clin Chiropr 1:8, 1994; Courtesy F.G. Bauer, Sydney, Australia.)*

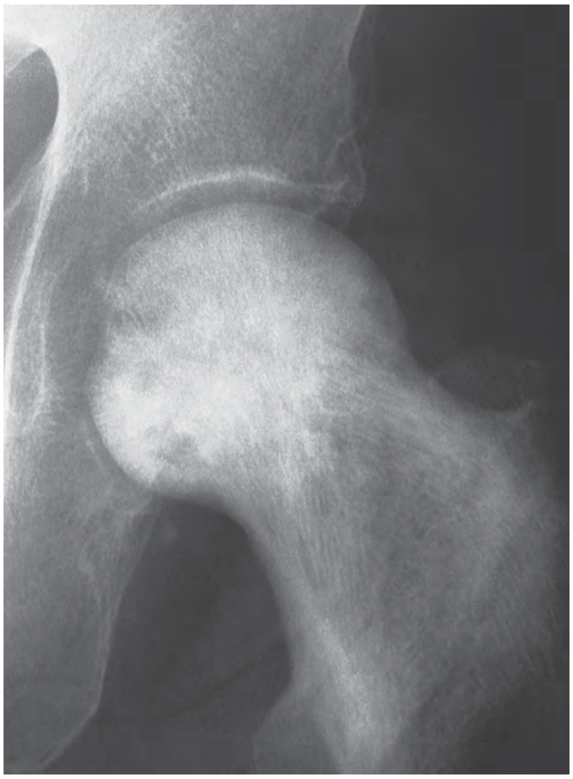

FIGURE 8–15 **Skeletal metastasis: osteoblastic pattern.**[17] This patient with prostate carcinoma developed metastasis to the bone. Radiographs show a diffuse pattern of osteosclerosis that extends to the subarticular region of the femoral head. Sclerosis and prominence of the primary weight-bearing trabeculae as well as subarticular involvement resemble the changes of Paget disease.

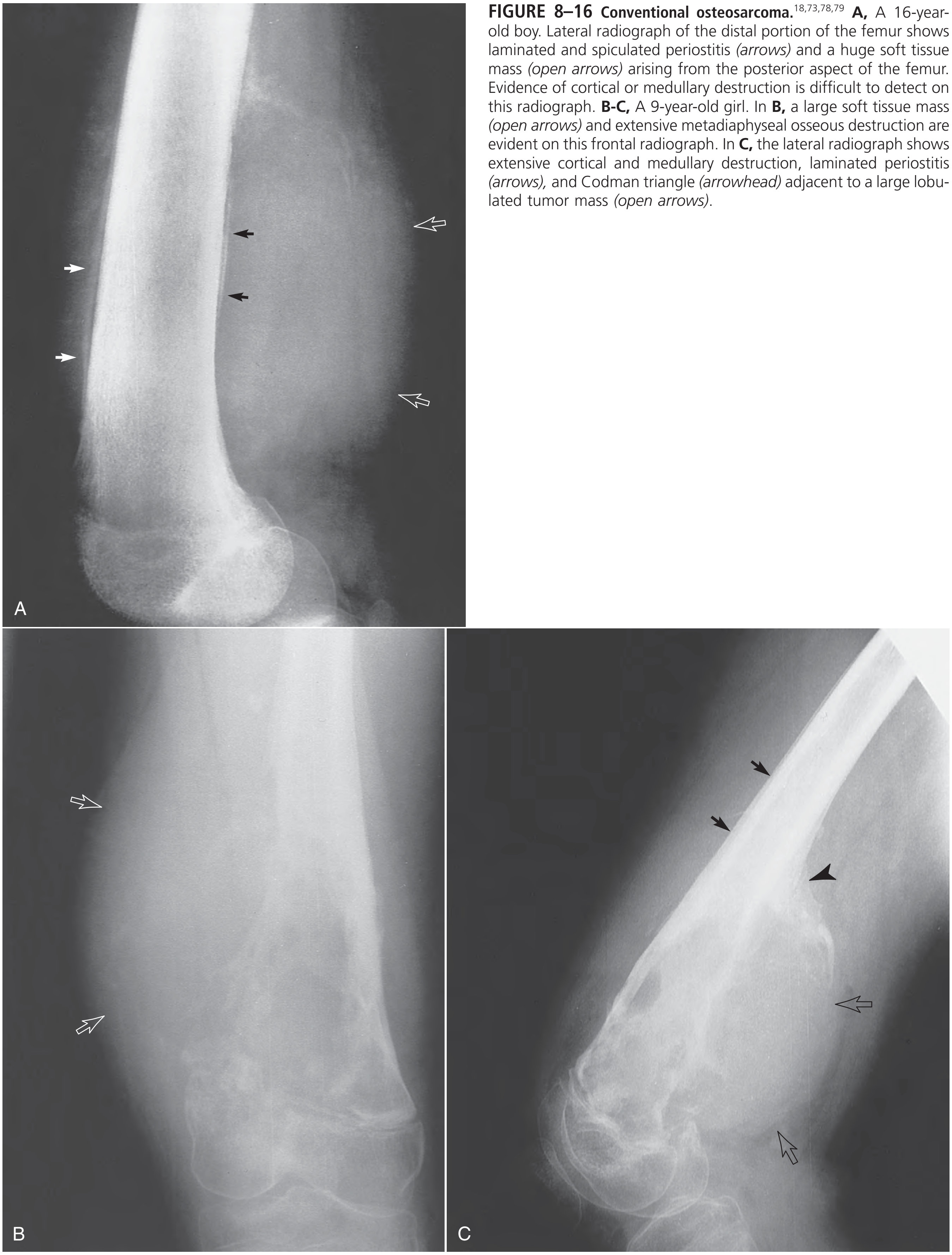

FIGURE 8–16 Conventional osteosarcoma.[18,73,78,79] **A,** A 16-year-old boy. Lateral radiograph of the distal portion of the femur shows laminated and spiculated periostitis *(arrows)* and a huge soft tissue mass *(open arrows)* arising from the posterior aspect of the femur. Evidence of cortical or medullary destruction is difficult to detect on this radiograph. **B-C,** A 9-year-old girl. In **B,** a large soft tissue mass *(open arrows)* and extensive metadiaphyseal osseous destruction are evident on this frontal radiograph. In **C,** the lateral radiograph shows extensive cortical and medullary destruction, laminated periostitis *(arrows),* and Codman triangle *(arrowhead)* adjacent to a large lobulated tumor mass *(open arrows)*.

Continued

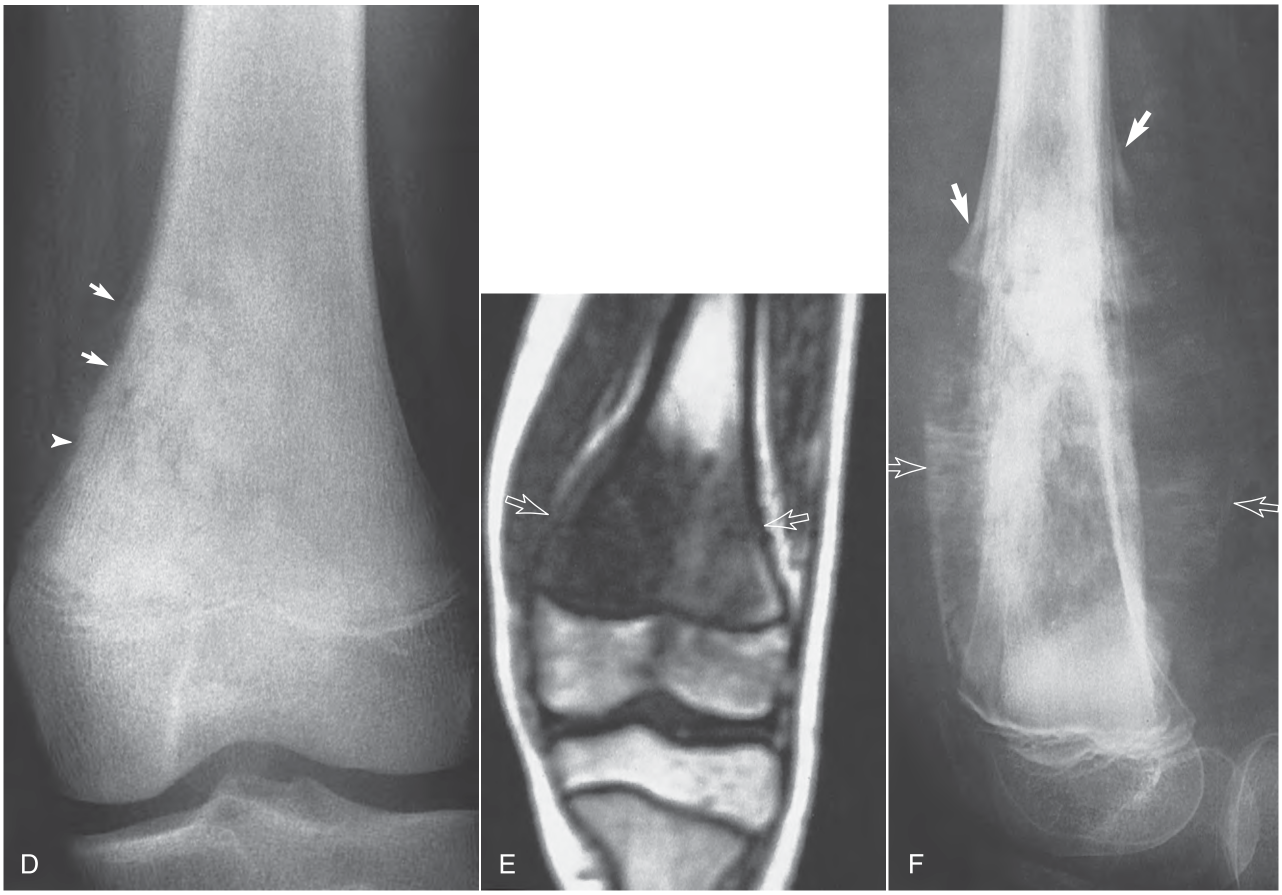

FIGURE 8–16, cont'd **D-E,** A 12-year-old girl with leg pain. In **D,** an anteroposterior radiograph shows an osteosclerotic metaphyseal lesion. The cortical margin of the medial aspect of the metaphysis is indistinct *(arrows)*. A barely perceptible periosteal reaction is also seen *(arrowhead)*. In **E,** a coronal T1-weighted (TR/TE, 600/20) spin echo MR image shows an area of low signal intensity corresponding to the metaphyseal region of osteosclerosis *(open arrows)*. **F,** Periosteal reaction patterns. Radiograph of another patient with osteosarcoma demonstrates typical patterns of aggressive periosteal reaction. Codman triangle is seen as a triangular buttress appearing to arise from the surface of bone at the tumor margins *(arrows)*. The spiculated periosteal reaction is evident as a series of parallel horizontal spicules emanating from the underlying bone (hair-on-end pattern) at the site of the tumor *(open arrows)*.

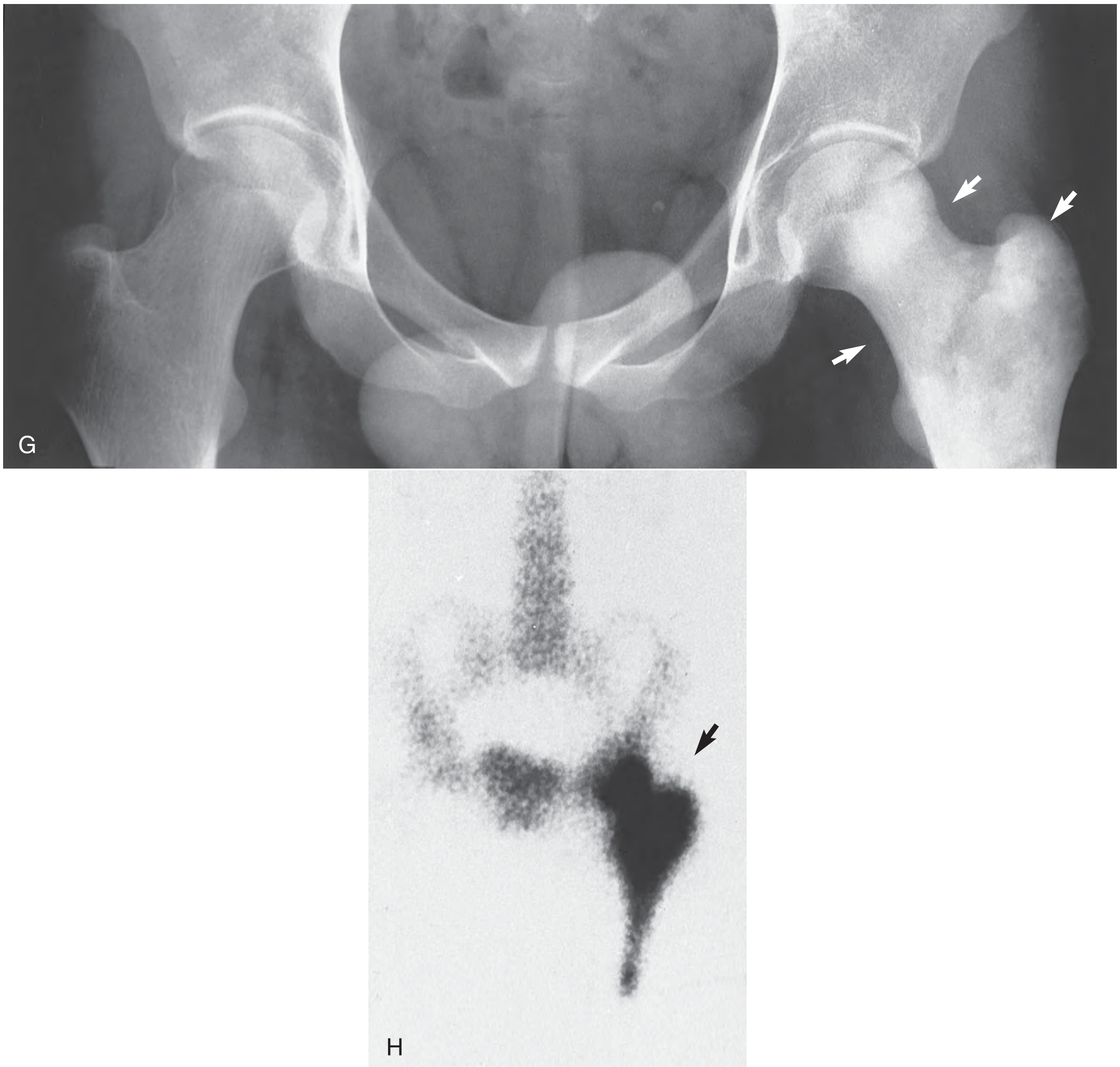

FIGURE 8–16, cont'd **G-H,** Conventional osteosarcoma in a 19-year-old man: Osteoblastic pattern. In **G,** a frontal pelvic radiograph reveals patchy osteosclerosis in the proximal portion of the left femur *(arrows)*. In **H,** a bone scan obtained the same day shows intense increased uptake of the bone-seeking radiopharmaceutical agent at the site of the lesion *(arrow)*. (***B-C,*** *Courtesy A.L. Anderson, DC, Portland, Ore;* ***D-E,*** *Courtesy R. Kerr, MD, Los Angeles;* ***G-H,*** *Courtesy T. Broderick, MD, Orange, Calif.)*

FIGURE 8–17 **Parosteal osteosarcoma**[19,78,79] A large osteosclerotic parosteal osteosarcoma is seen arising from the surface of the femoral diaphysis. The pedunculated attachment to the surface of the femur is helpful in differentiating this malignant neoplasm from more benign processes, such as posttraumatic myositis ossificans.

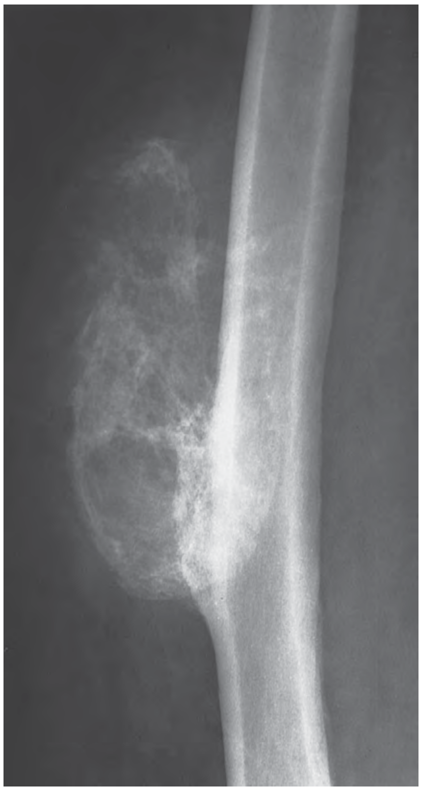

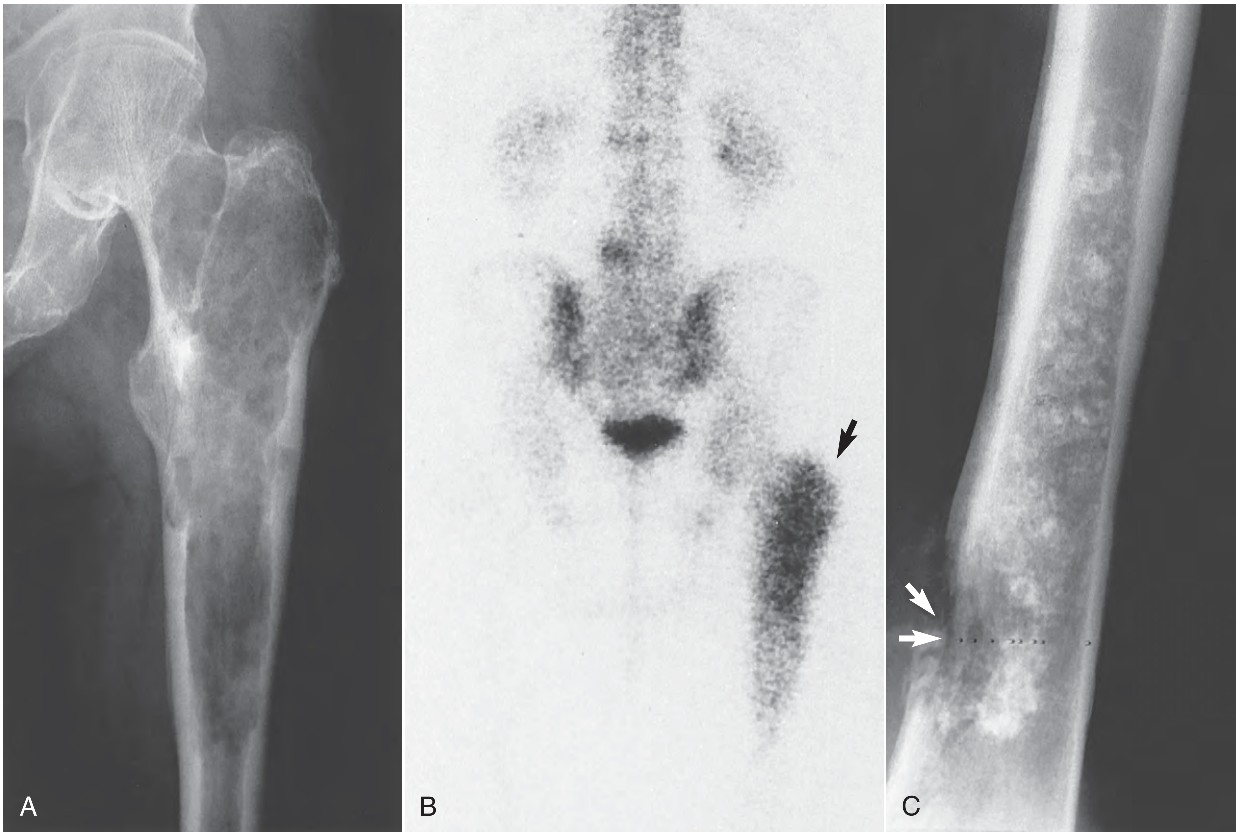

FIGURE 8–18 **Conventional chondrosarcoma**[21,22] **A,** Routine frontal radiograph of a 63-year-old male patient, demonstrates a moth-eaten destructive appearance of the proximal portion of the femur extending from the femoral neck into the middiaphysis. Extensive endosteal scalloping is noted. **B,** Radionuclide bone scan reveals intense homogeneous increased uptake at the site of the lesion *(arrow)*. **C,** Routine radiograph of the femur in another patient shows a long metadiaphyseal lesion with extensive stippled calcification, endosteal scalloping, and cortical perforation *(arrows)*. *(Courtesy J. Schils, MD, Cleveland, Ohio.)*

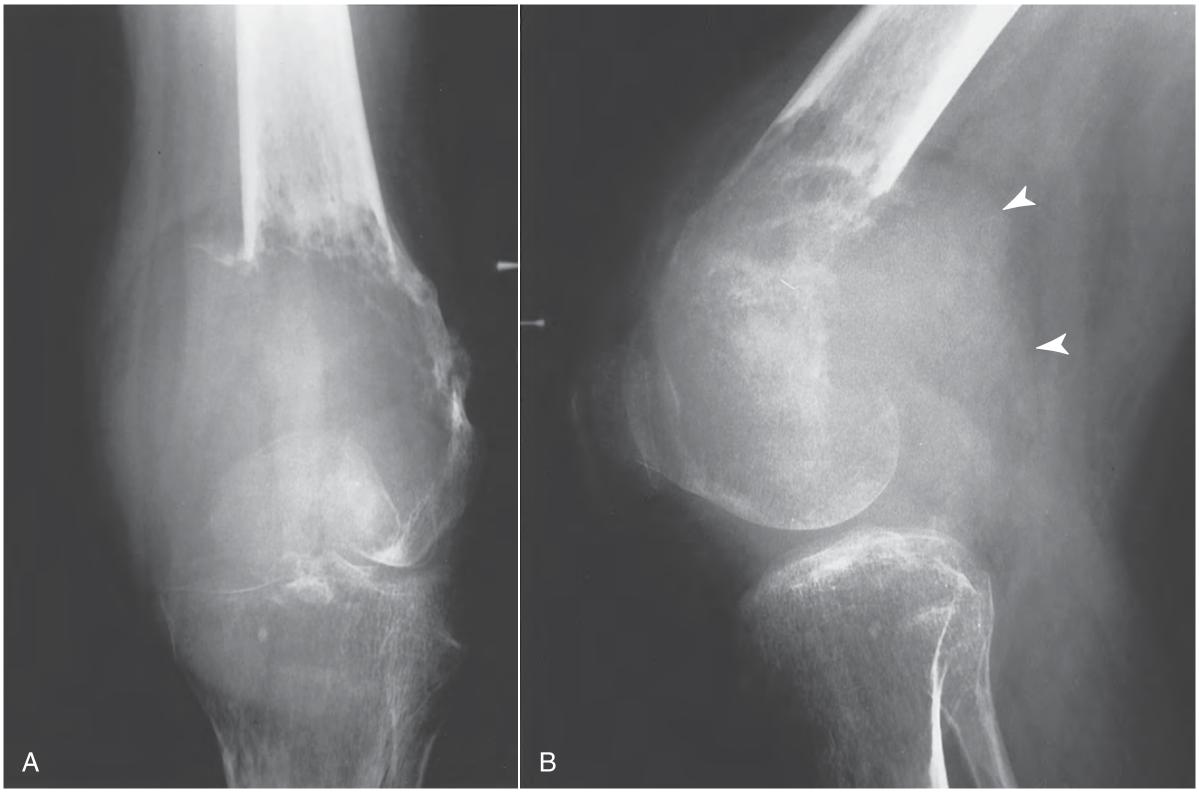

FIGURE 8–19 Aggressive giant cell tumor.[23] This 33-year-old man had a history of several months' duration of an increasingly painful, expanding mass near his knee. **A,** Frontal radiograph. **B,** Lateral radiograph. A highly destructive osteolytic lesion obliterates the cortical and medullary bone of the entire metaphysis and subchondral region of the distal portion of the femur. The matrix of the lesion is purely osteolytic, and a pathologic fracture with angulation is seen on the lateral view. A large soft tissue mass is evident *(arrowheads)*. Marked osteopenia secondary to disuse is seen in the proximal portions of the tibia and fibula. The tumor was biopsied, analyzed, and reported to be a malignant (aggressive) giant cell tumor.

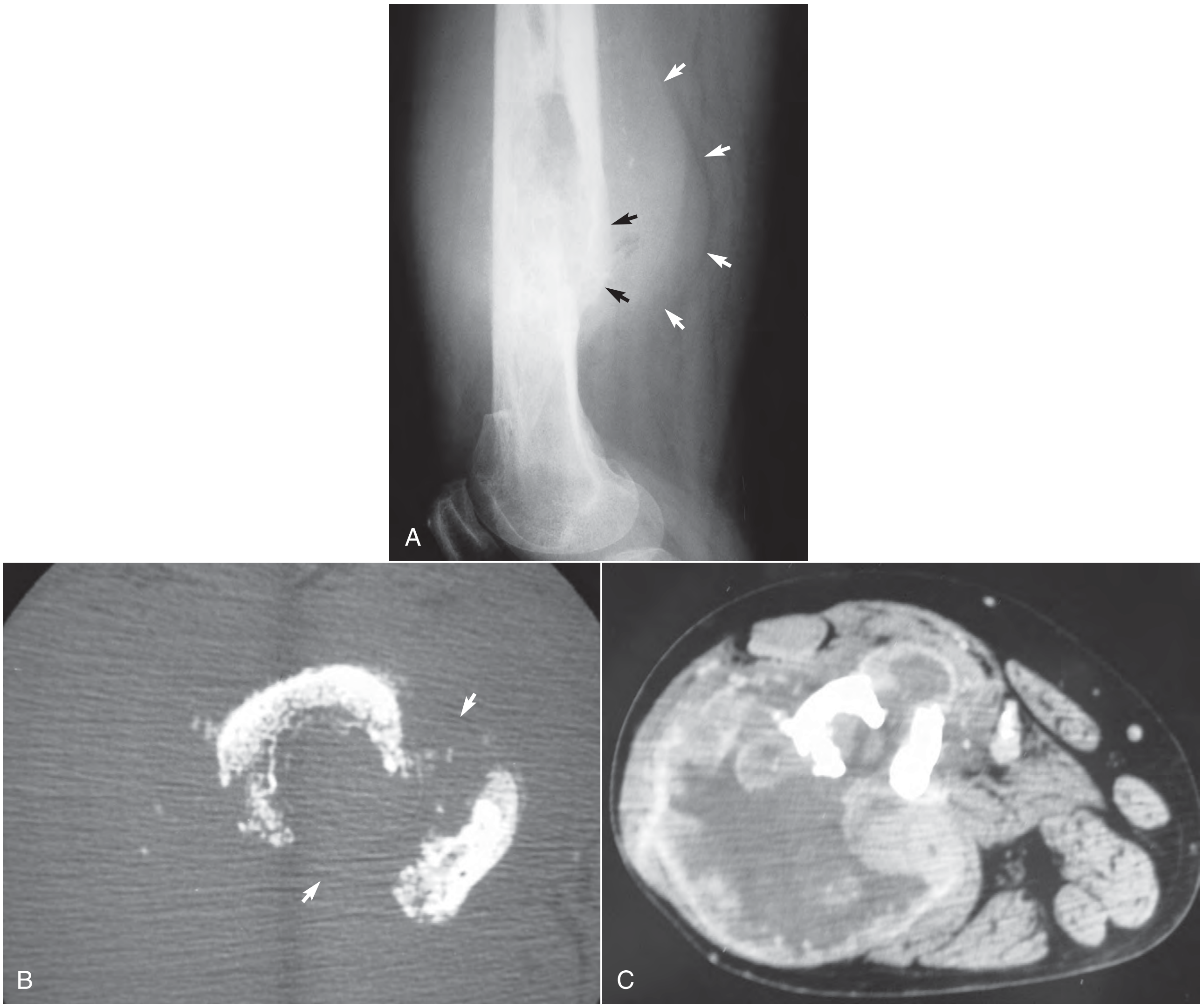

FIGURE 8–20 **Malignant fibrous histiocytoma: bone and soft tissue involvement.**[24] A lateral radiograph **(A)** reveals a large soft tissue mass in the posterior thigh *(white arrows)* with a pathologic fracture *(black arrows)* involving the midshaft of the femur. A transaxial CT scan bone window **(B)** clearly shows the extent of bone destruction and separation of the anterior cortex from the posterior cortex *(arrows)* due to the pathologic fracture. Osseous debris is scattered throughout the soft tissues. Another transaxial CT scan, with a soft tissue window obtained after intravenous contrast administration **(C)** reveals a mixed attenuation within the soft tissues of the posterior thigh and communication of the large mass with the marrow cavity of the femur. Peripheral contrast enhancement is seen within the soft tissue mass.

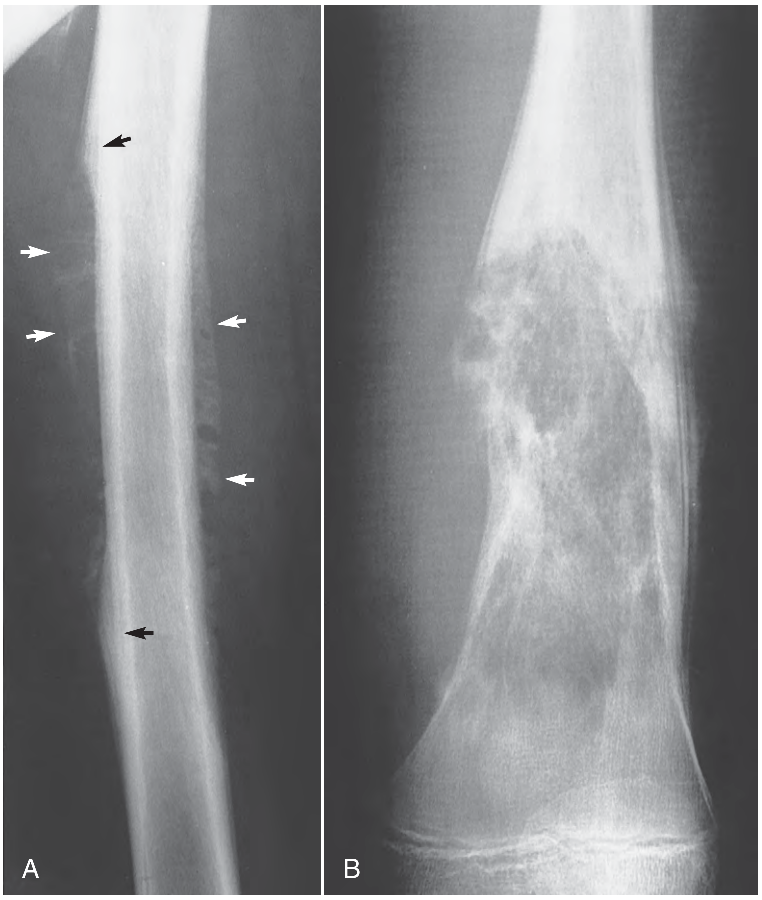

FIGURE 8–21 **Ewing sarcoma.**[25] **A,** Routine radiograph of this 12-year-old boy with biopsy-proven Ewing sarcoma demonstrates spiculated periostitis *(white arrows)* and Codman triangles *(black arrows)* involving the femoral diaphysis. **B,** In this 9-year-old boy, permeative osteolytic destruction of the metadiaphysis of the distal end of the femur is associated with aggressive, laminated periostitis and cortical destruction. *(**B,** Courtesy T. Broderick, MD, Orange, Calif.)*

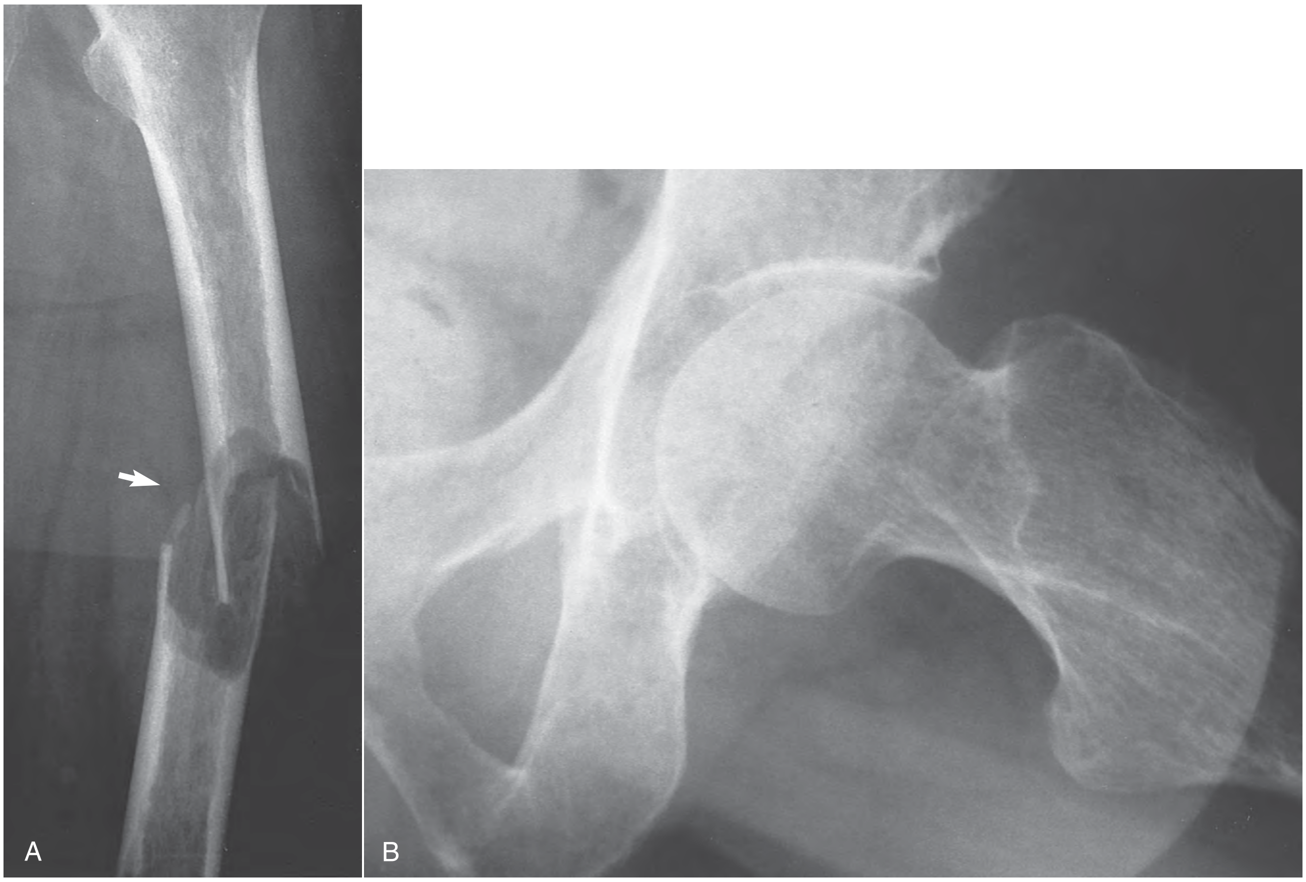

FIGURE 8–22 **Plasma cell (multiple) myeloma.**[26,94] **A,** Pathologic fracture has occurred through a large osteolytic lesion in the middiaphysis of the femur *(arrow)* in this patient with a histologic diagnosis of multiple myeloma. **B,** In another patient with multiple myeloma, a permeative pattern of diffuse osteopenia is the only radiographic manifestation. *(**A,** Courtesy V. Wing, MD, Danville, Calif.; **B,** From Taylor JAM, Harger BL, Resnick D: Diagnostic imaging of common hip disorders: A pictorial review. Top Clin Chiropr 1:8, 1994.)*

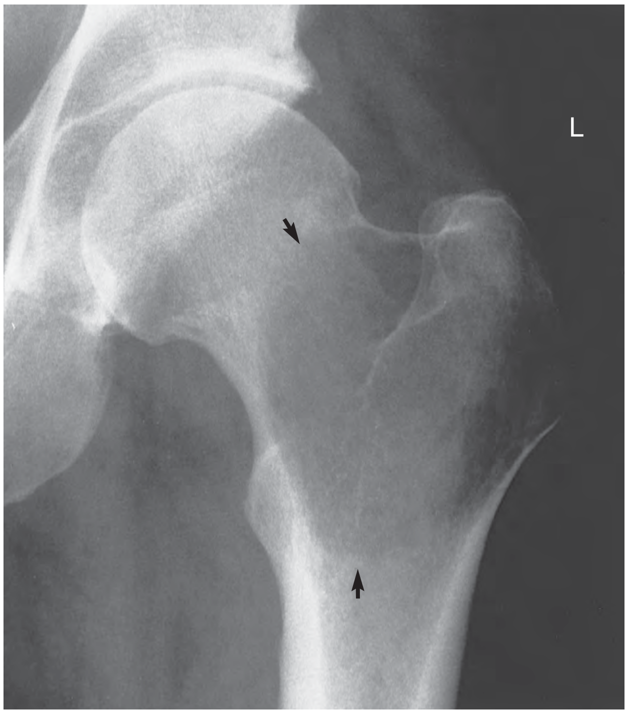

FIGURE 8–23 **Solitary plasmacytoma.**[26] This 37-year-old man had a 4-month history of hip pain and a limp. A large, solitary osteolytic lesion *(arrows)* is evident in the intertrochanteric region of the proximal portion of the femur. *(Courtesy G. Greenway, MD, Dallas, Texas.)*

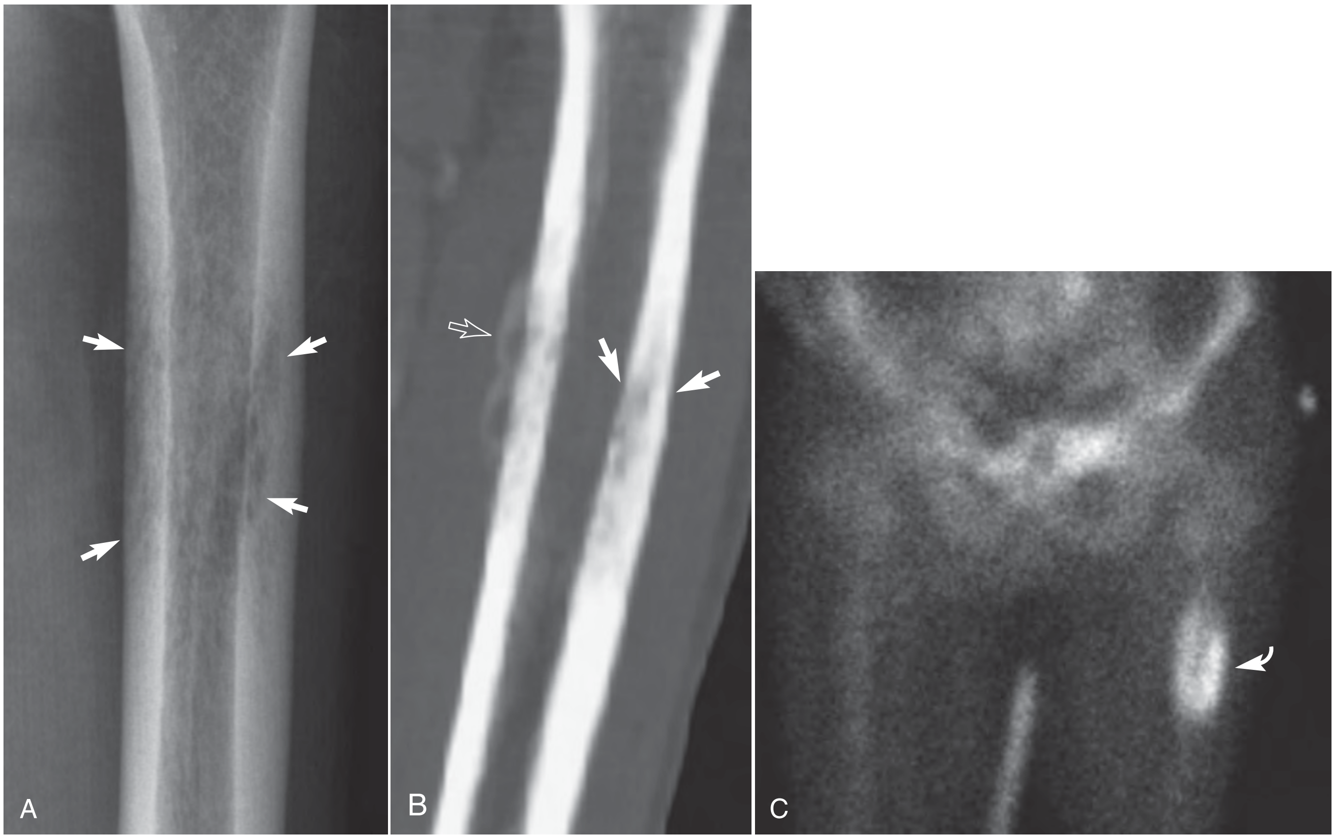

FIGURE 8–24 **Hodgkin disease.**[27,72] This 57-year-old man with AIDS developed deep aching thigh pain. The radiograph **(A)** shows moth-eaten destruction of cortical and cancellous bone in the midshaft of the femur *(arrows)*. **(B)** A reformatted coronal CT bone window also reveals the moth-eaten destruction *(arrows)* and periosteal reaction along the medial aspect of the femoral cortex *(open arrow)*. The bone scan **(C)** shows intense increased accumulation of radionuclide within the femoral diaphysis *(curved arrow)*.

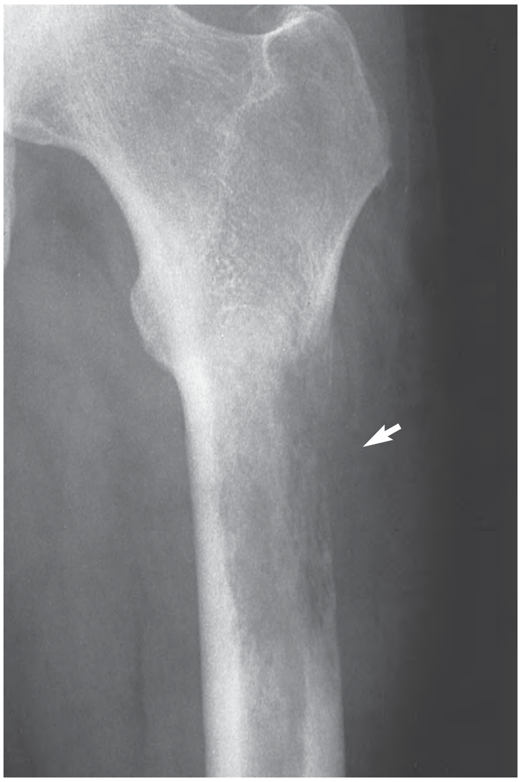

FIGURE 8–25 **Non-Hodgkin lymphoma: histiocytic type.**[28,29,72,76] Observe the eccentric moth-eaten osteolysis and cortical penetration *(arrow)* of the femoral diaphysis in this 47-year-old man.

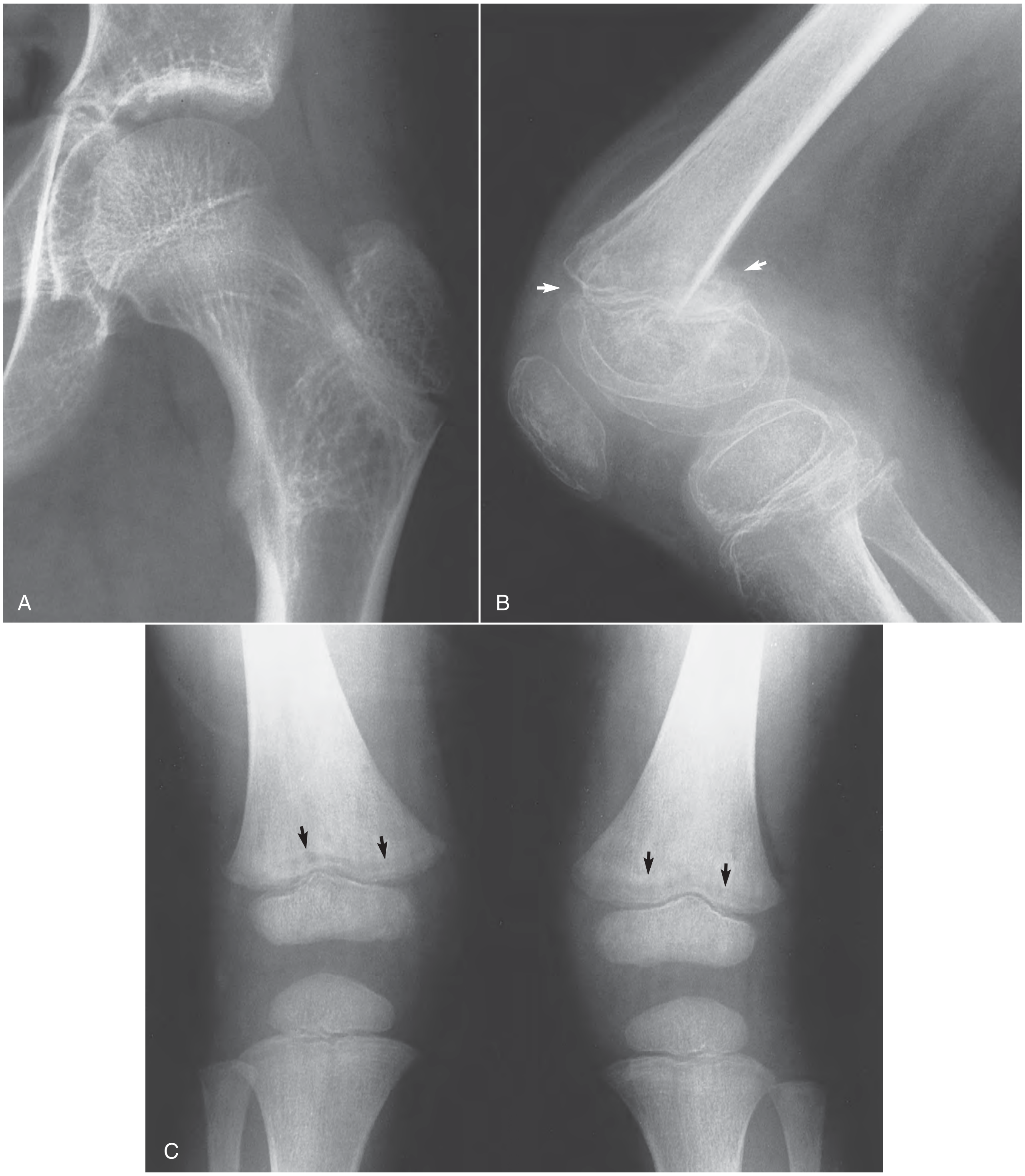

FIGURE 8–26 **Leukemia.**[30] **A-C,** Acute lymphocytic leukemia. In a 14-year-old boy **(A-B),** a radiograph **(A)** of the proximal portion of the femur demonstrates diffuse osteopenia and apparent trabecular accentuation. Observe the increased radiolucency and prominence of the primary weight-bearing trabeculae. In **B,** diffuse osteopenia and a displaced pathologic fracture through the distal femoral physis *(arrows)* are evident. Excessive radiolucency is seen in the epiphyses and metaphyses. **C,** In another patient, observe the bilateral radiolucent metaphyseal bands involving the distal portions of the femora *(arrows)*.

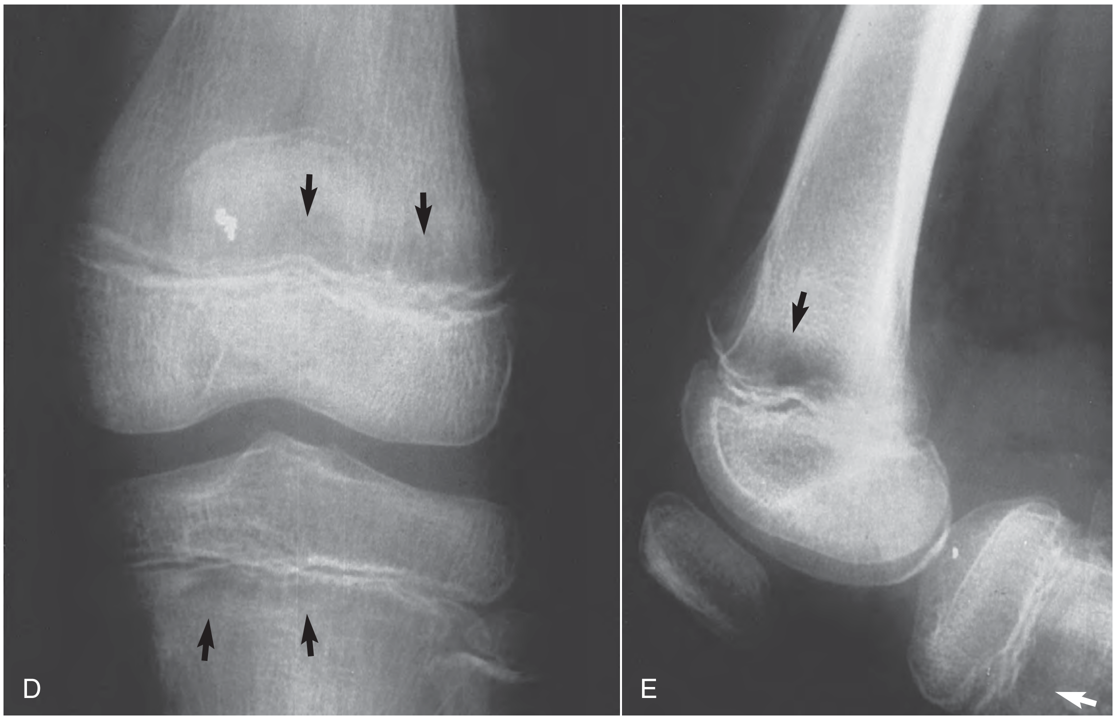

FIGURE 8–26, cont'd **D-E,** Acute childhood leukemia. Anteroposterior and lateral radiographs of the knee in this 8-year-old girl with acute leukemia reveal transverse radiolucent bands in the metaphyses of the femur and tibia *(arrows)*.

TABLE 8-4 Benign Tumors Affecting the Femur*

Entity	Figure(s)	Characteristics
Enostosis[31]	8-27	25% of enostoses (bone islands) occur in the femur Solitary, painless, infrequently multiple, discrete focus of osteosclerosis within the spongiosa of bone Round, ovoid, or oblong with brush border composed of radiating osseous spicules that interdigitate with the surrounding trabeculae of the spongiosa
Osteoid osteoma[32-34,91]	8-28	32% of osteoid osteomas occur in the femur Solitary cortical or subperiosteal lesion with reactive sclerosis surrounding central radiolucent nidus Nidus is less than 1 cm in diameter and usually not visible on routine radiographs: CT remains the investigation of choice for identifying the nidus; MR imaging also useful Intracapsular lesions provoke less reactive sclerosis and are more likely to cause joint pain
Osteoblastoma (conventional)[35]	8-29	Fewer than 15% of conventional osteoblastomas involve the femur Osteolytic, osteosclerotic, or both Solitary expansile lesion that may be subperiosteal Partially calcified matrix in many cases Cortical thinning Often resembles large osteoid osteoma
Enchondroma (solitary)[36]	8-30	Approximately 10% of solitary enchondromas involve the femur Central or eccentric medullary osteolytic lesion Lobulated endosteal scalloping Approximately 50% of lesions have stippled calcification within the matrix
Enchondromatosis (Ollier disease)[36]		Multiple enchondromas; frequently involve the femur
Maffucci syndrome[36]		More than 50% of cases involve the femur Multiple enchondromas and soft tissue hemangiomas Unilateral distribution in 50% of cases

---

* See also Table 1-13.

Continued

TABLE 8-4 Benign Tumors Affecting the Femur—cont'd

Entity	Figure(s)	Characteristics
Chondroblastoma[37,38,70]	8-31	Approximately one third of chondroblastomas affect the femur Solitary, circular osteolytic lesion affecting femoral capital epiphyses, trochanteric apophyses, and distal femoral epiphyses May exhibit calcification in matrix Occasionally periosteal reaction and edema may be seen on MR imaging
Chondromyxoid fibroma[39]		17% of chondromyxoid fibromas occur in the femur Solitary, eccentric, elongated metaphyseal lesion 2-10 cm in length Cortical expansion, coarse trabeculation, endosteal sclerosis Calcification is rare (5%-27% of cases) May appear aggressive with large "bite" lesion penetrating cortex
Osteochondroma (solitary)[40,41,93]	8-32	More than 30% of solitary osteochondromas arise from the femur Pedunculated or sessile cartilage-covered osseous excrescence arising from the surface of the metaphysis of the distal or proximal portion of the femur Cortex and medulla are continuous with the host bone Typically, grow away from the adjacent joint Pedunculated lesions can fracture, potentially resulting in pain and neurovascular compromise
Hereditary multiple exostosis[42-44]	8-33	Multiple osteochondromas, sometimes numbering in the hundreds Femoral neck frequently involved; also occur about the knee May result in valgus deformity of hip and widening of the femoral neck
Nonossifying fibroma and fibrous cortical defect[45]	8-34	Almost 40% of nonossifying fibromas and fibrous cortical defects involve the femur Solitary eccentric, multiloculated osteolytic lesion arising from the metaphyseal cortex Resembles a well-circumscribed blisterlike shell of bone arising from the cortex Cortical thinning is often present
Giant cell tumor (benign)[46]	8-35	Approximately one third of benign giant cell tumors occur in the femur; most commonly in the distal portion of the femur; also found at the proximal region near the hip Solitary eccentric osteolytic neoplasm with a predilection for the subarticular region Often multiloculated and expansile Radiographs are inaccurate in distinguishing benign from aggressive giant cell tumors
Intraosseous lipoma[47,71]	8-36	15% of intraosseous lipomas occur in the femur Intertrochanteric region and femoral neck are common sites of involvement Solitary osteolytic lesion surrounded by a thin, well-defined sclerotic border Occasional central calcified or ossified nidus Osseous expansion occurs infrequently Cortical destruction and periostitis absent
Simple bone cyst[48]	8-37	Approximately 25% of all simple bone cysts occur in the femur Mildly expansile, solitary osteolytic lesion within medullary cavity of proximal portion of femur May be multiloculated
Aneurysmal bone cyst[49]	8-38	Approximately 15% of aneurysmal bone cysts occur in the femur Eccentric, thin-walled, expansile osteolytic lesion of the metaphysis Thin trabeculation with multiloculated appearance Buttressing at edge of lesion Typically more expansile than osteoblastoma Fluid levels may be seen with CT scan or MR imaging

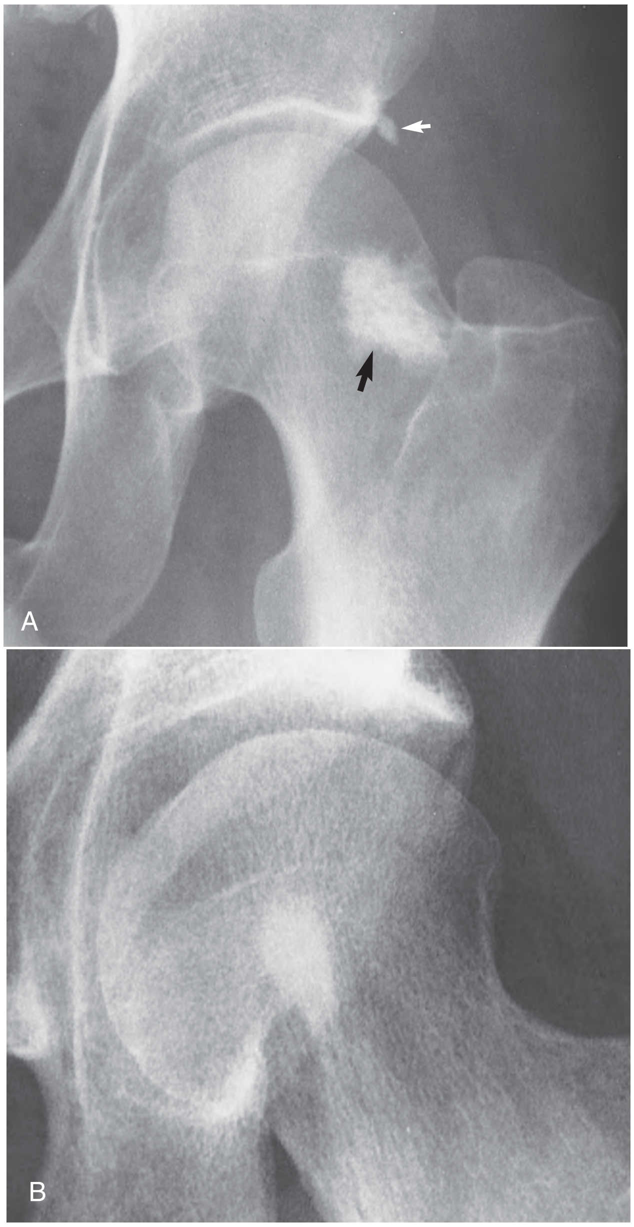

FIGURE 8–27 **Enostosis (bone island).**[31] **A,** Observe the solitary, circular osteosclerotic lesion that is aligned with the long axis of trabecular architecture in the femoral neck *(black arrow)*. Note the irregular margins of the lesion. Incidentally, a small os acetabuli *(white arrow)* is present. **B,** In another patient, note that the enostosis is oriented along the long axis of the principal compressive trabeculae.

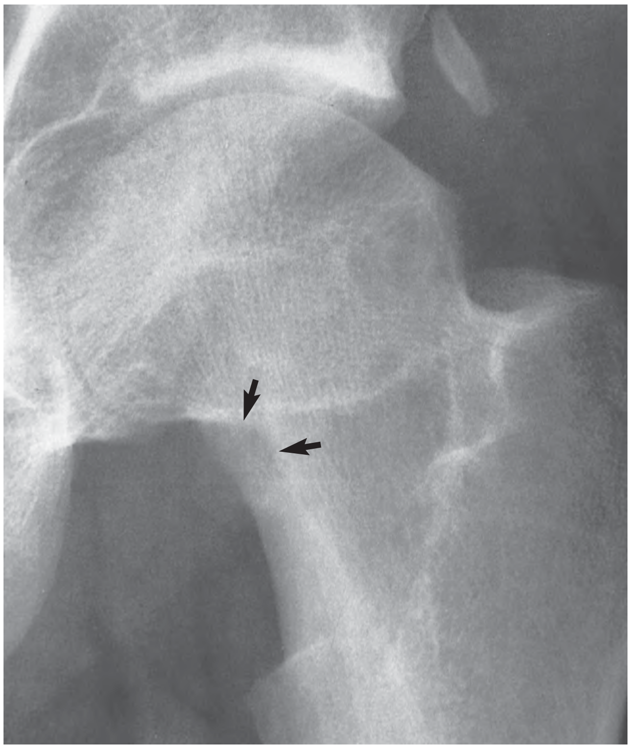

FIGURE 8–28 **Osteoid osteoma.**[32-34,91] A painful intracapsular osteoid osteoma in this 22-year-old man is seen as a circular radiolucent area within the cortex of the medial femoral neck *(arrows)*. In addition, this patient has findings consistent with degenerative disease of the hip joint. The femur is the bone that is affected most commonly by osteoid osteoma (32% occur in the femur), although epiphyseal or intracapsular lesions such as in this patient are rare. Intracapsular osteoid osteomas do not characteristically provoke severe reactive sclerosis.

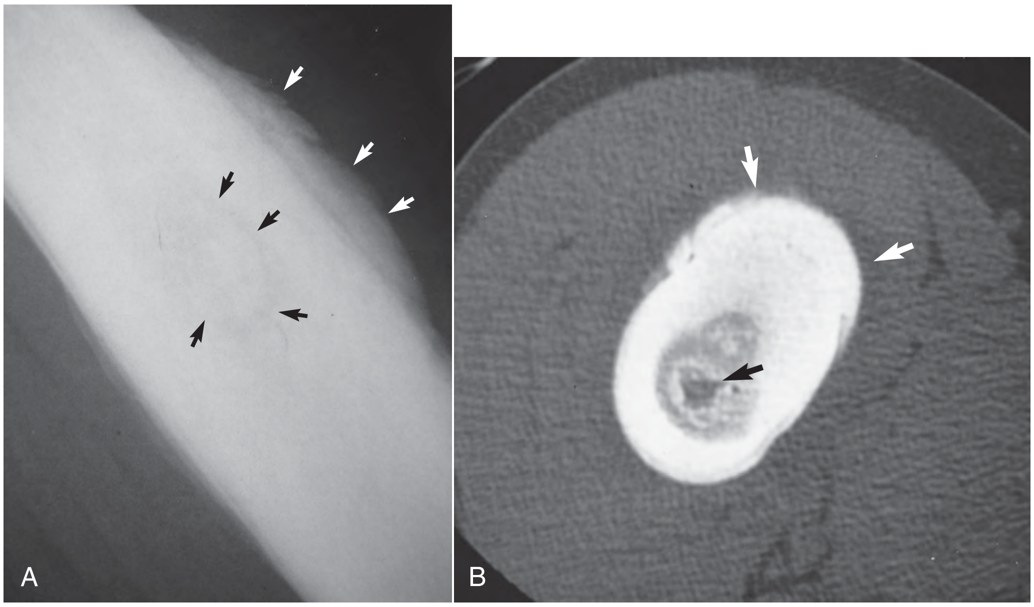

FIGURE 8–29 Osteoblastoma.[35] This 11-year-old developed thigh pain. A magnified radiograph of the femoral diaphysis **(A)** shows a very faint ovoid radiolucency *(black arrows)* surrounded by dense sclerosis, widening of the bone, and a solid periosteal reaction enveloping the diaphysis *(white arrows)*. A transaxial CT image **(B)** through the center of the lesion reveals that the widening of the bone is due to eccentric subperiosteal new bone formation (periosteal reaction) *(white arrows)*. The matrix of the lesion appears to contain amorphous calcification and a focus of low attenuation similar to the density of fat *(black arrow)*. Osteoid osteoma would be a reasonable alternative diagnosis, but the nidus of the osteoid osteoma is typically much smaller than the radiolucent focus seen in this case.

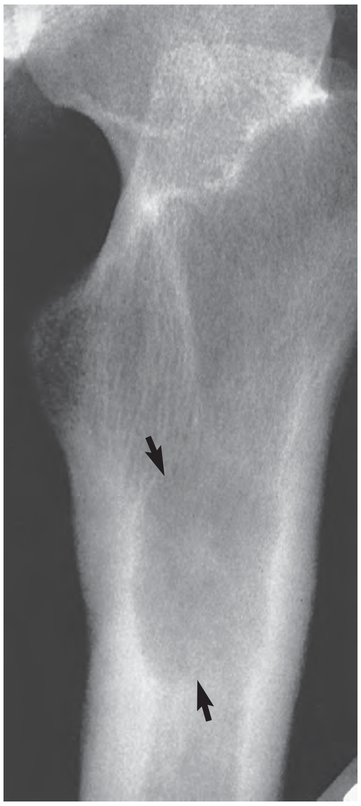

FIGURE 8–30 Enchondroma.[22,36] This painless, oval, geographic osteolytic lesion has resulted in minimal endosteal scalloping of the proximal femoral diaphysis *(arrows)*. *(Courtesy R. Kerr, MD, Los Angeles.)*

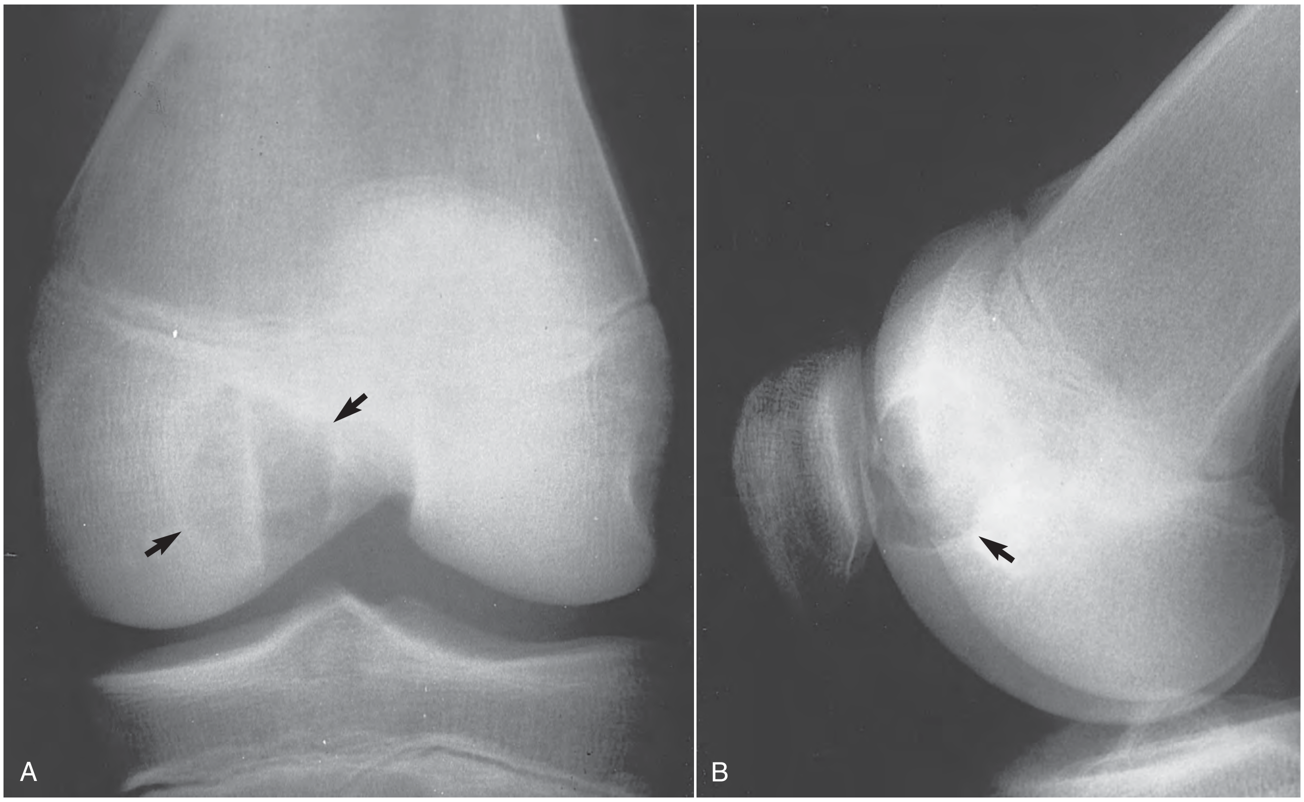

FIGURE 8–31 **Chondroblastoma.**[37,38,70] This 16-year-old boy had knee pain for 4 months. Anteroposterior **(A)** and lateral **(B)** radiographs show a well-defined, geographic osteolytic lesion involving the distal femoral epiphysis *(arrows)*. Tissue biopsy is necessary to differentiate chondroblastoma from clear cell chondrosarcoma. *(Courtesy G. Greenway, MD, Dallas, Texas.)*

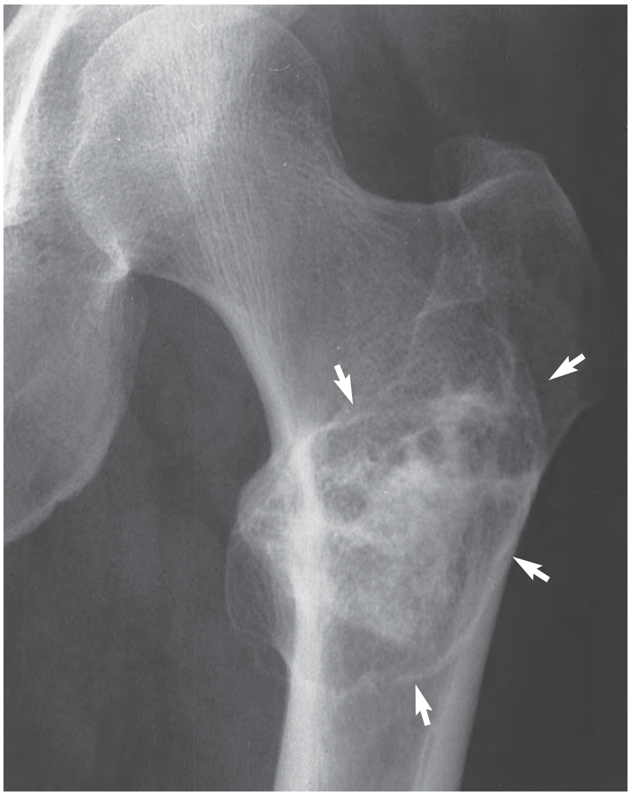

FIGURE 8–32 **Solitary osteochondroma.**[40,41,93] A large osteochondroma arising from the intertrochanteric region of the femur is seen *en face (arrows),* with zones of increased and decreased radiodensity. In this location, fibrous dysplasia and intraosseous lipoma should be considered in the differential diagnosis.

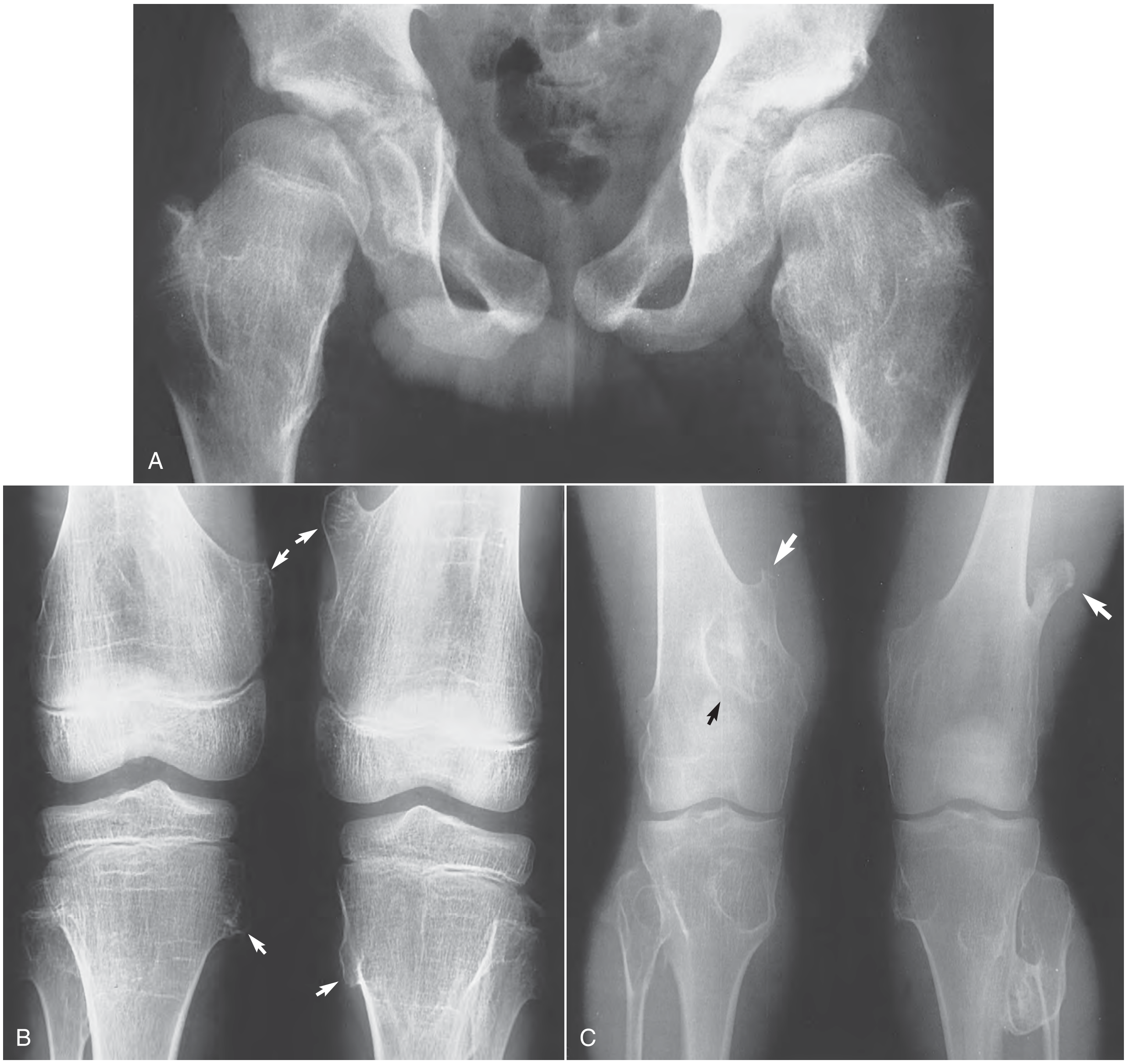

FIGURE 8–33 **Hereditary multiple exostoses.**[42-44] **A,** Marked deformity and expansion of the femoral necks are apparent in this 14-year-old boy with hereditary multiple exostosis. **B,** Observe the pedunculated exostoses *(arrows)* involving the distal end of the femora and proximal portion of the tibiae in this 11-year-old boy. **C,** In a third patient, large bilateral pedunculated and sessile osseous outgrowths are seen arising from the metaphyses of the femora *(arrows),* tibiae, and fibulae.

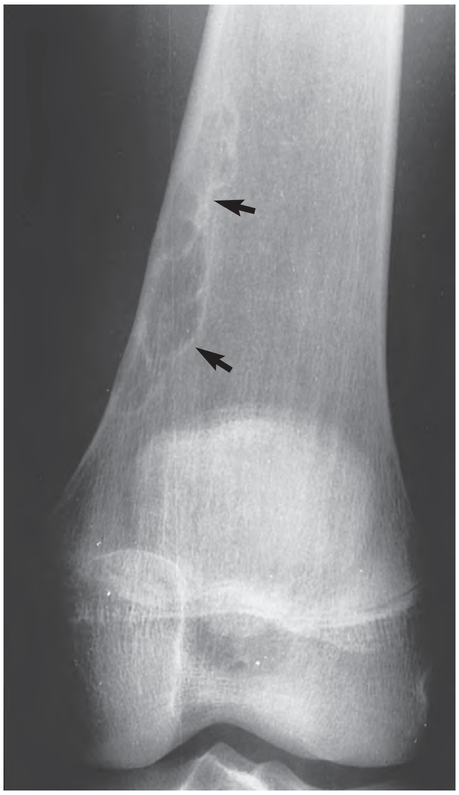

FIGURE 8–34 **Nonossifying fibroma.**[45] Routine radiograph shows an eccentric, multiloculated geographic lesion *(arrows)* in the metadiaphysis of the distal portion of the femur. The cortical margin appears lobulated, and evidence of cortical thinning is present.

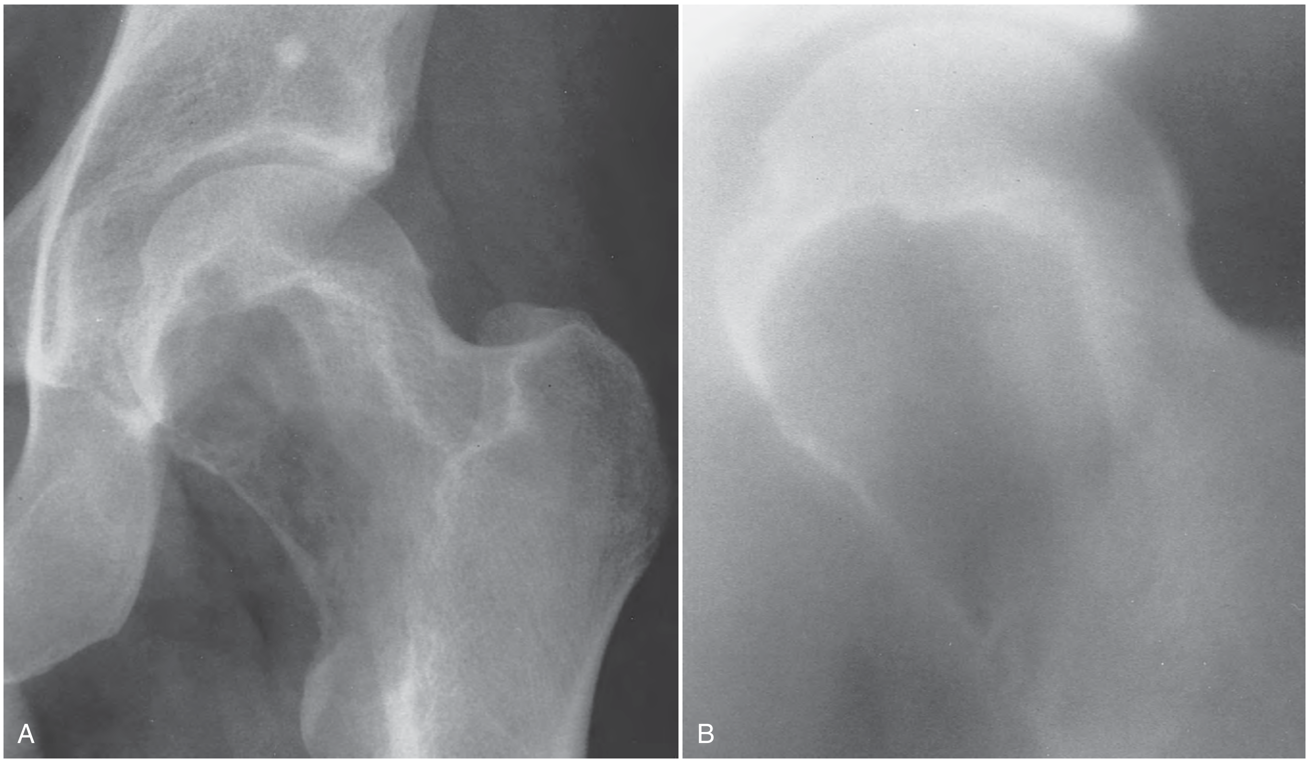

FIGURE 8–35 **Giant cell tumor.**[46] Frontal radiograph **(A)** and conventional tomogram **(B)** of the proximal end of the femur reveal an eccentric, osteolytic geographic lesion extending into the subchondral region of the femoral head, resulting in cortical thinning and minimal expansion. *(Courtesy G. Greenway, MD, Dallas, Texas.)*

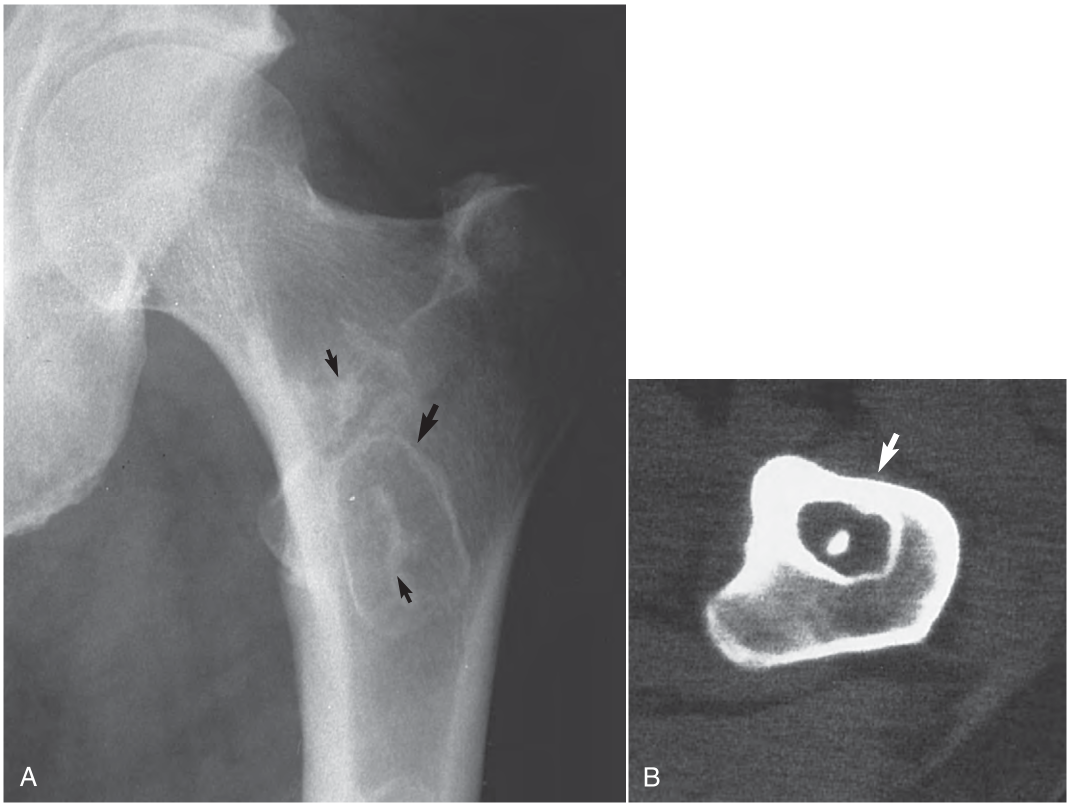

FIGURE 8–36 **Intraosseous lipoma.**[47,71] **A,** Routine frontal radiograph of this 57-year-old man reveals a geographic lesion with a faint rim of sclerosis *(large arrow)* and two foci of sclerosis *(small arrows)* in the femoral metaphysis. **B,** Transaxial CT image confirms the fatty nature of the lesion by measurements of attenuation values derived from CT data. Lipomas of bone often possess a small, central, radiodense focus *(arrow)* called a *target sequestrum*.

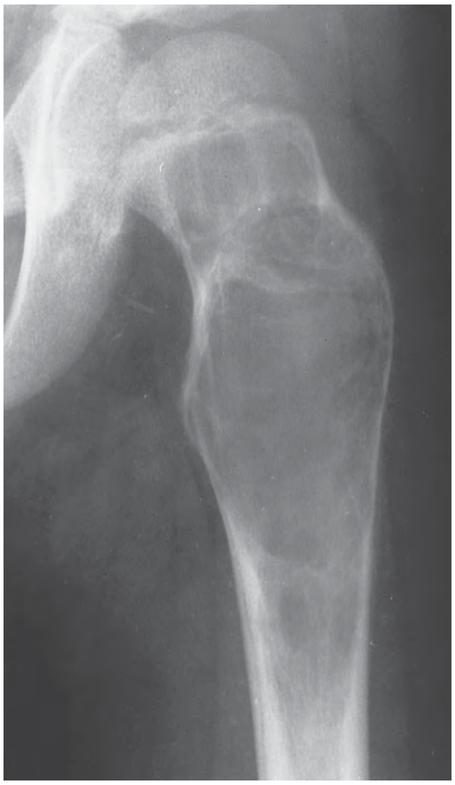

FIGURE 8–37 **Simple bone cyst.**[48] Routine radiograph of the proximal portion of the femur in this child reveals a centrally located, geographic, multiloculated metadiaphyseal lesion. Cortical thinning, a thin sclerotic margin, and mild osseous expansion are evident.

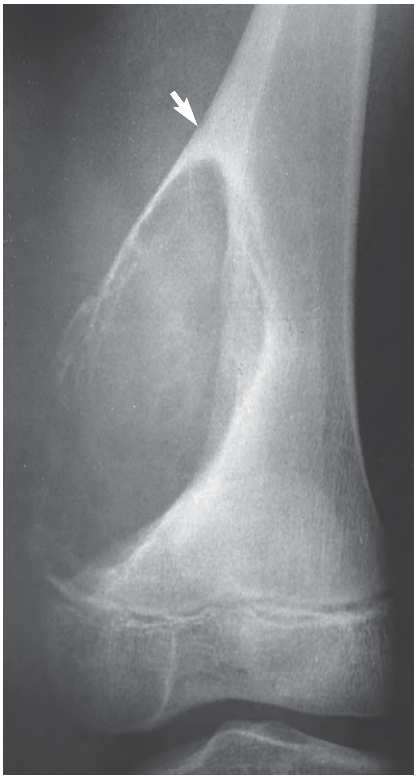

FIGURE 8–38 **Aneurysmal bone cyst.**[49] This aneurysmal bone cyst was found in the distal portion of the femur in a 10-year-old boy. Observe the eccentric, expansile appearance of the lesion. Evidence of buttressing is seen at the margin of the lesion *(arrow),* a feature characteristic of aneurysmal bone cysts. The matrix often contains fine trabeculation. *(Courtesy A. Newberg, MD, Boston.)*

TABLE 8-5 Tumorlike Lesions Affecting the Femur*

Entity	Figure(s)	Characteristics
Paget disease[50,51,80,81]	8-39	Femur is one of the most commonly involved bones Usually polyostotic and may be unilateral Coarsened trabeculae and bone enlargement Stages of involvement: osteolytic (50%), osteosclerotic (25%), mixed (25%), and malignant transformation (less than 2%) Pathologic fracture, coxa vara (shepherd's crook) deformities, insufficiency fractures in convex surface of bowed bones, acetabular protrusion
Neurofibromatosis 1[52]	8-40	Formerly designated *von Recklinghausen disease* Femur involved only occasionally Dysplastic appearance of femur with overconstriction, deformity, remodeling of bone, and circumscribed osteolytic lesions Soft tissue involvement may predominate
Monostotic fibrous dysplasia[53,92]	8-41	15% of monostotic lesions affect the femur Predilection for the intertrochanteric region Thick rim of sclerosis surrounding radiolucent lesion Ground-glass appearance of fibrous matrix Acetabular protrusion may occur
Polyostotic fibrous dysplasia[53,92]	8-42	92% of patients have femoral lesions Unilateral or bilateral, asymmetric femoral involvement Usually associated with concomitant disease in the innominate bone Lesions appear the same as those in monostotic form but are frequently larger, more expansile, and more multiloculated than monostotic lesions
Langerhans cell histiocytosis[54,55]	8-43	Femur is involved in 15% of cases Osteolytic lesions may be multiloculated and expansile

* See also Table 1-14.

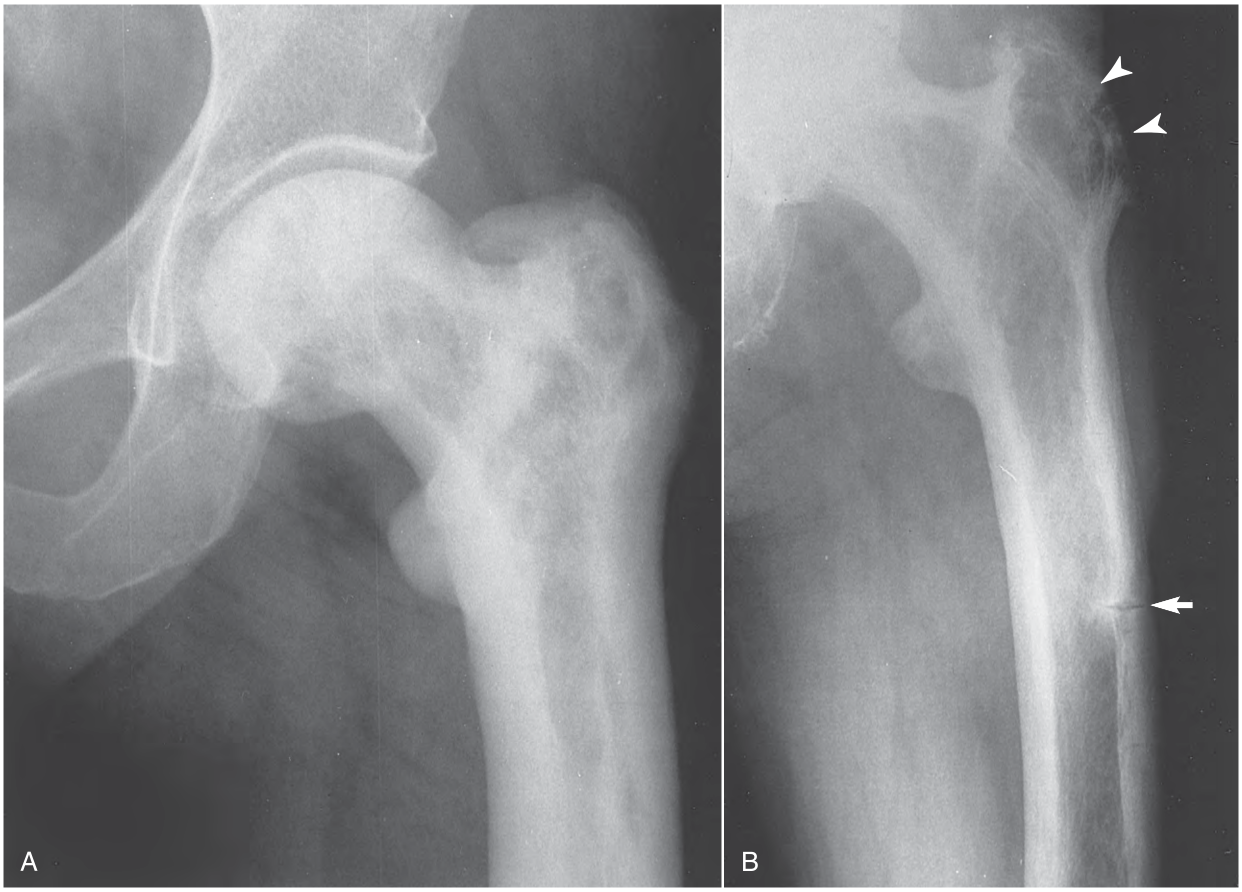

FIGURE 8–39 **Paget disease.**[50,51,80,81] **A,** The osteosclerotic pattern of Paget disease is seen involving the proximal portion of the femur. Observe the characteristic subarticular distribution and the coarsened, thickened, and sclerotic appearance of the cortex and trabeculae. **B,** In another patient, diaphyseal involvement predominates. An area of osteolysis is seen involving the greater trochanteric region *(arrowheads)*. An insufficiency fracture *(arrow)* and minimal bowing of the femur accompany the characteristic findings of thickened cortex and coarsened trabeculae. In Paget disease, such incomplete fractures usually appear on the convex side of the bone and may progress to extend across the entire bone to become complete fractures.

FIGURE 8–40 **Neurofibromatosis 1.**[52] This 24-year-old male with known neurofibromatosis 1 underwent MR imaging to evaluate a popliteal mass that had been enlarging for 6 months. Sagittal T1-weighted **(A)** and T2-weighted **(B)** fat-suppressed MR images reveal multiple round and ovoid mixed signal intensity lobulated masses within the intermuscular fat (“bag of worms” appearance) of the posterior thigh *(arrows)*. The masses coincide with the course of the femoral nerve and are consistent with the appearance of plexiform neurofibromas.

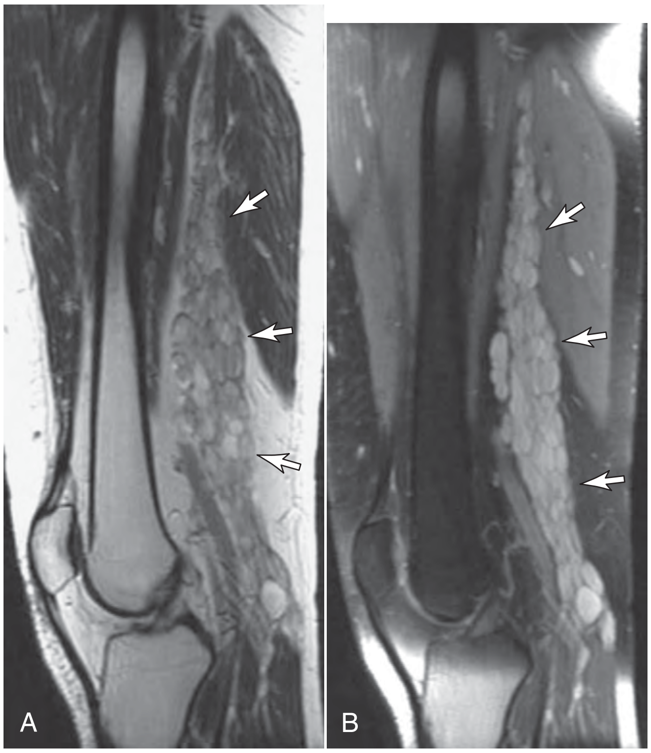

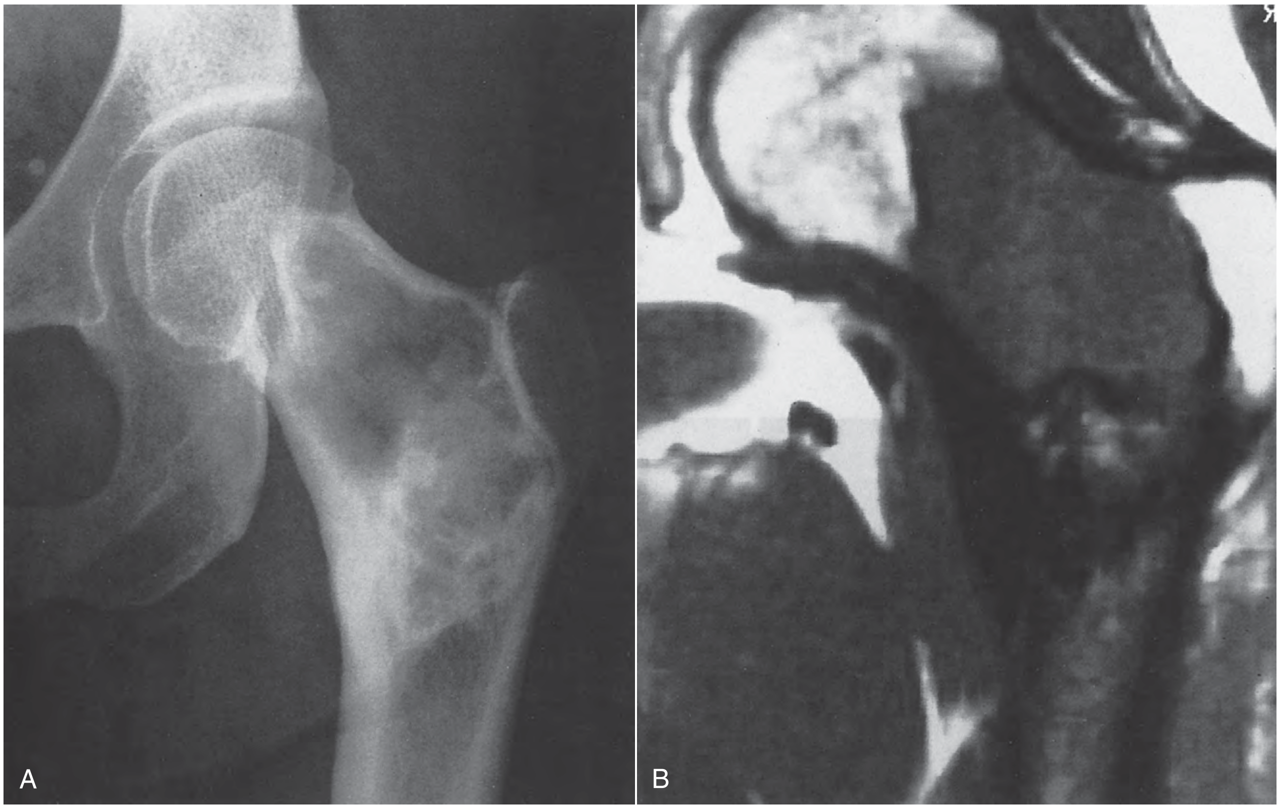

FIGURE 8–41 **Monostotic fibrous dysplasia.**[53,92] **A,** In a 50-year-old woman, a routine radiograph **(A)** demonstrates an osteolytic lesion occupying a large portion of the femoral neck and intertrochanteric region. The predominantly osteolytic lesion has a sclerotic margin and a ground-glass matrix. In **B,** a coronal T1-weighted (TR/TE, 500/15) spin echo MR image reveals low signal intensity within the lesion. *(Courtesy J. Kramer, MD, Vienna.)*

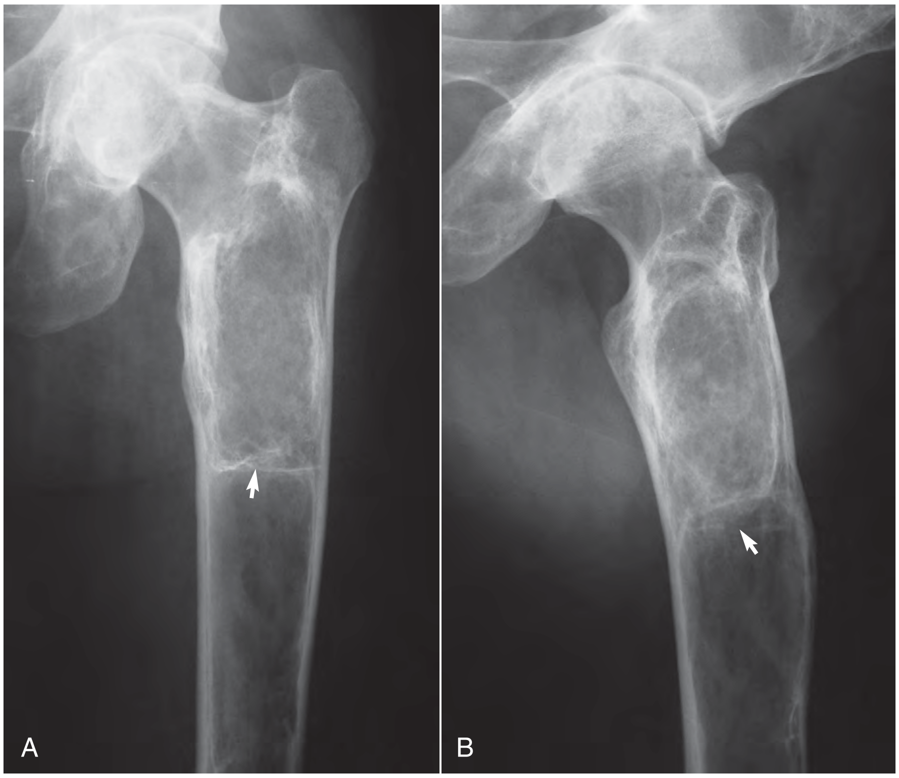

FIGURE 8–42 **Polyostotic fibrous dysplasia.**[53,92] Anteroposterior **(A)** and lateral **(B)** radiographs of the femur show mild expansion of the diameter of the femur with cortical thinning, and a large multiloculated osteolytic lesion within the neck, intertrochanteric region, metaphysis, and diaphysis of the femur *(arrows)*. A large part of the metaphyseal portion of the lesion is surrounded by a thick rind of sclerosis and the matrix within the medullary cavity exhibits a ground glass appearance, typical of fibrous dysplasia. Similar lesions were found in the adjacent ischium and bilaterally involving many bones.

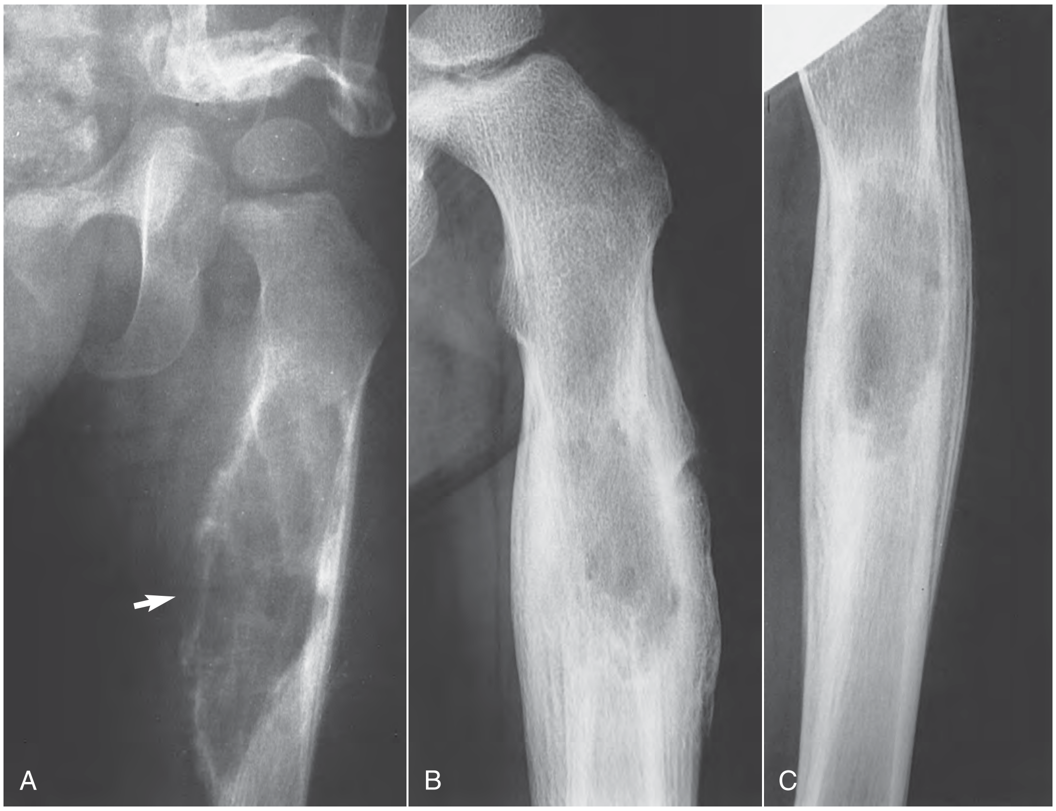

FIGURE 8–43 **Langerhans cell histiocytosis: Eosinophilic granuloma.**[54,55] **A,** Observe the large, multilocular osteolytic lesion *(arrow)* involving the femoral diaphysis with acetabular remodeling and collapse. Extensive involvement of the innominate bones was also present. **B-C,** Frontal **(B)** and lateral **(C)** radiographs of the proximal portion of the femur show a geographic lesion with prominent, laminated, organized periostitis. Eosinophilic granuloma of bone is the most frequent and mildest form of Langerhans cell histiocytosis, a disease characterized by histiocytic infiltration of tissues. *(**B-C,** Courtesy U. Mayer, MD, Klagenfurt, Austria.)*

TABLE 8-6 Metabolic, Hematologic, and Infectious Disorders Affecting the Femur*

Entity	Figure(s)	Characteristics
Generalized osteoporosis[56]	7-53 to 7-55	Uniform decrease in radiodensity, thinning of cortices, accentuation of weight-bearing trabeculae May result in insufficiency fractures of the femoral neck See Chapter 7
Osteogenesis imperfecta[68]	8-44	Osteoporosis and bone fragility Thin, gracile appearance of entire skeleton Severe deformities and fractures commonly affect the femur
Osteomalacia and rickets[69,82]	8-45	***Osteomalacia*** Diffuse osteopenia Decreased trabeculae; remaining trabeculae appear prominent and coarsened Looser zones (pseudofractures) ***Rickets*** Findings are most prominent in the appendicular skeleton Metaphyseal demineralization resulting in frayed metaphyses Bowing deformities Osteopenia Looser zones
Hyperparathyroidism and renal osteodystrophy[57]	8-46	*Brown tumor*: solitary or multiple expansile osteolytic lesions containing fibrous tissue and giant cells; may disappear after treatment for hyperparathyroidism Osteosclerosis more common in renal osteodystrophy
Gaucher disease[58,83]	8-47	Marrow infiltration results in osteopenia, osteolytic lesions, cortical diminution, and medullary widening Osseous weakening results in pathologic fractures *Modeling deformities:* Erlenmeyer flask deformity (widening of the distal diametaphysis of the femur) Osteonecrosis of the femoral head
Myelofibrosis[59,60]	8-48	Chief radiographic finding: osteosclerosis Occasional periosteal bone apposition or periostitis, osteolysis, or osteopenia
Secondary hypertrophic osteoarthropathy[61]	8-49	Syndrome characterized by digital clubbing, arthritis, and bilateral symmetric periostitis of femur and other tubular bones Complication of many diseases including bronchogenic carcinoma, mesothelioma, and other intrathoracic and intraabdominal diseases
Hypovitaminosis C (scurvy)[62]	8-50	Radiographic evidence of skeletal changes in scurvy is seen only in advanced longstanding disease ***Infantile scurvy*** Periostitis secondary to subperiosteal hemorrhage Transverse radiodense zone of provisional calcification (white line of Frankel) Transverse radiolucent metaphyseal line (scurvy line, Trümmerfeldzone) Beaklike metaphyseal excrescences (corner or angle sign or Pelken spurs) Radiodense shell surrounding radiolucent epiphyses (Wimberger sign of scurvy) Healing scurvy may result in increased radiodensity of the metaphyses and epiphyses
Meningomyelocele[63]	8-51	Prominent bilateral periosteal new bone formation Epiphyseal fragmentation and physeal widening
Growth resumption (Harris) lines[64]	8-52	Transverse radiodense lines representing a sign of new or increased growth in children, presumably after a period of inhibited bone growth from a previous episode of trauma, infection, malnutrition, or other chronic disease state Occasionally seen in normal children without episodes of trauma or disease
Osteomyelitis[65,74,75]	8-53	Acute pyogenic osteomyelitis frequently involves the metaphysis in children Poorly defined permeative bone destruction Chronic osteomyelitis most frequently involves the femur: poorly defined areas of sclerosis and osteolysis, thin linear periostitis, and sequestration
Chronic recurrent multifocal osteomyelitis (CRMO)[66]		Occurs mainly in children and adolescents Initial lytic destruction of metaphysis adjacent to growth plate with no periosteal bone formation or sequestration
Collagen vascular disease: soft tissue calcification[67]	8-54	Dermatomyositis, polymyositis, scleroderma, and other collagen vascular diseases may result in soft tissue calcinosis in the thigh *Differential diagnosis:* hyperparathyroidism, neurologic injury, melorheostosis, posttraumatic heterotopic ossification, soft tissue neoplasms

* See also Tables 1-15, 1-16, and 1-19.

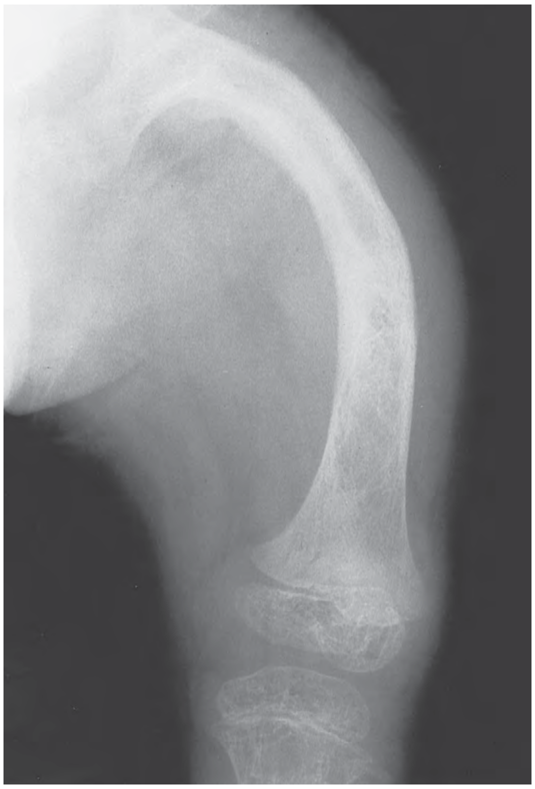

FIGURE 8–44 **Osteogenesis imperfecta.**[68] Dramatic bowing and coxa vara deformity involving the femur are seen in this young patient. Generalized osteopenia was observed throughout the skeleton, but this appearance is masked by increased density from cortical thickening as a result of bowing deformities and previous trauma.

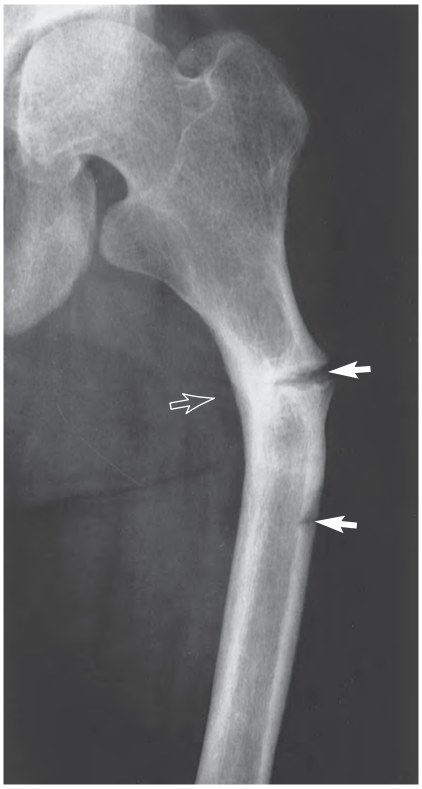

FIGURE 8–45 **Hypophosphatemic rickets.**[69,82] In this patient with long-standing hypophosphatemia, diffuse osteopenia, two incomplete transverse fractures *(arrows),* and bowing deformity *(open arrow)* involving the femoral diaphysis are present. *(Courtesy C. Pineda, MD, Mexico City.)*

FIGURE 8–46 **Hyperparathyroidism: Brown tumors.**[57] **A-B,** Bilateral radiographs of this 5-year-old girl with secondary hyperparathyroidism reveal multiple septated, osteolytic brown tumors in the femoral shafts. Marked femoral bowing is also present. *(Courtesy T. Broderick, MD, Orange, Calif.)*

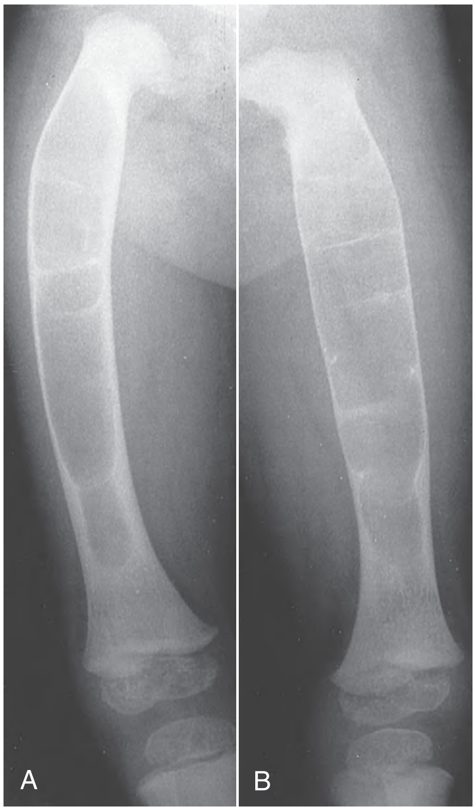

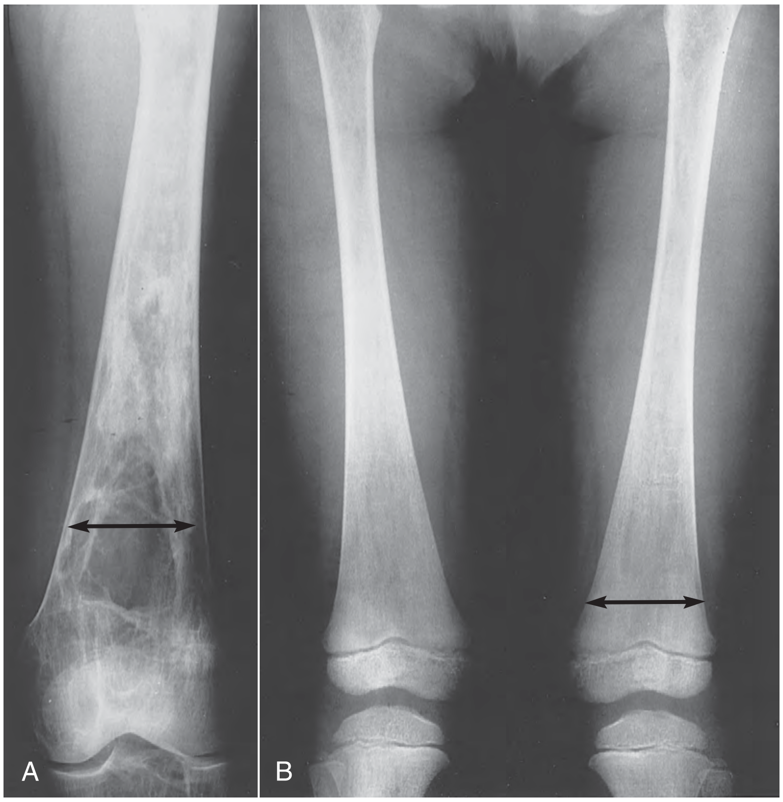

FIGURE 8–47 Gaucher disease.[58,83] **A,** Radiograph of this 26-year-old man with Gaucher disease demonstrates large septated osteolytic lesions due to extensive marrow replacement. Observe also the presence of undertubulation (Erlenmeyer flask deformity) *(double-headed arrow)* and osteosclerotic intraosseous infarcts throughout the diaphysis. **B,** In a child, bilateral femoral undertubulation is seen as widening of the metaphyses *(double-headed arrow)*. Severe cortical thinning also is evident. Gaucher disease additionally may be characterized by osteopenia, osteonecrosis, cortical erosion, and coarsened trabecular pattern.

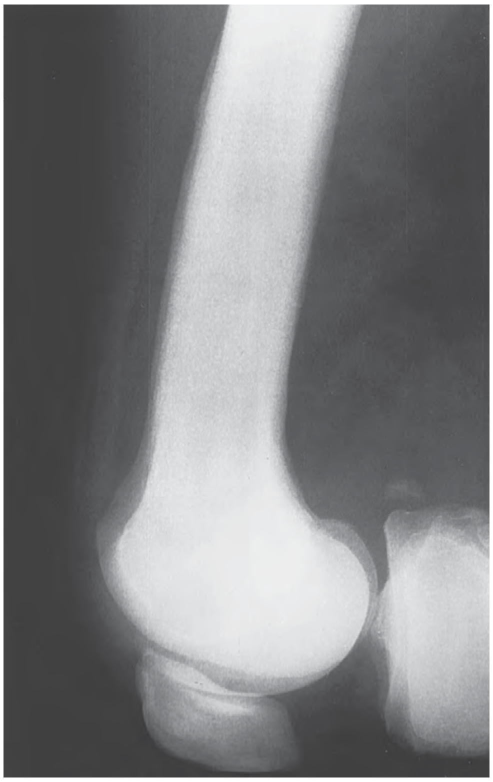

FIGURE 8–48 Myelofibrosis.[59,60] Diffuse osteosclerosis involving the entire femur is characteristic of myelofibrosis. *(Courtesy G. Greenway, MD, Dallas, Texas.)*

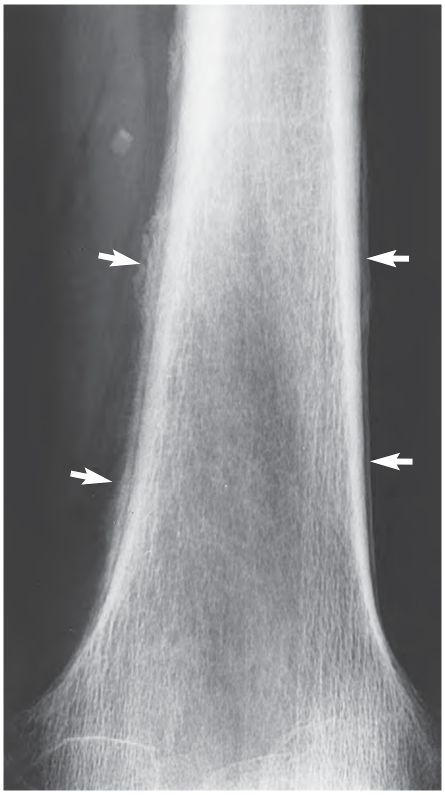

FIGURE 8–49 **Secondary hypertrophic osteoarthropathy.**[61] Bilateral symmetric periostitis involving the distal portion of the femur *(arrows)* was present in this patient with bronchogenic carcinoma. Observe the thick solid layer of new bone formation characteristic of hypertrophic osteoarthropathy. *(Courtesy U. Mayer, MD, Klagenfurt, Austria.)*

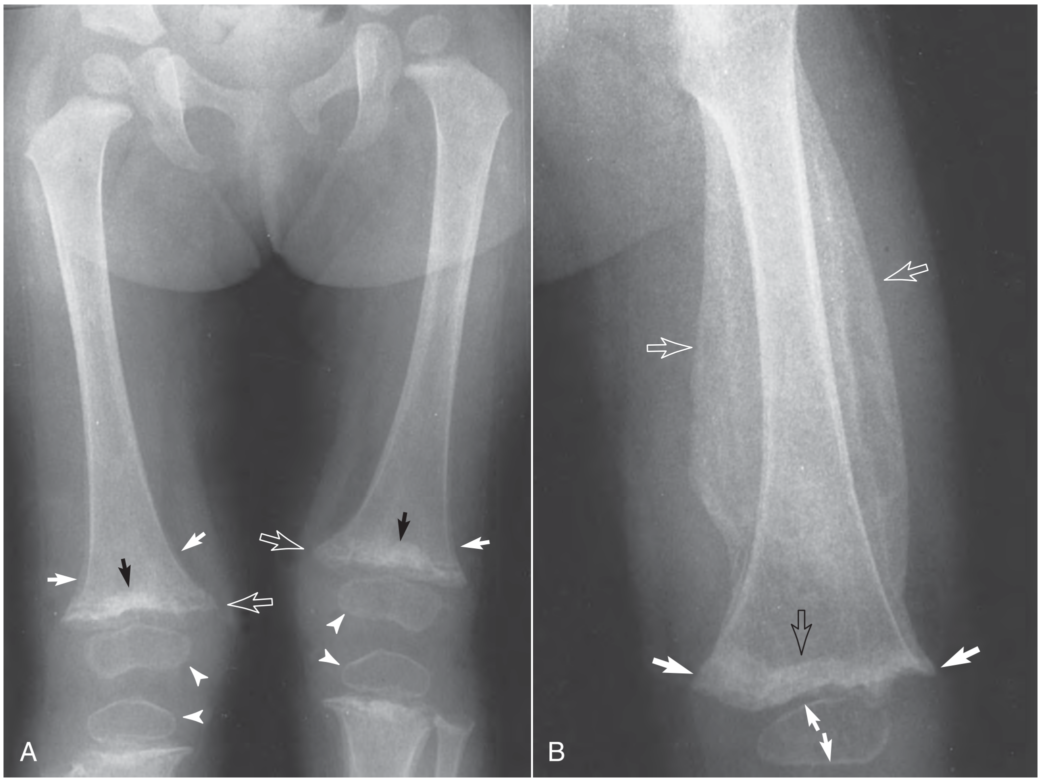

FIGURE 8–50 **Hypovitaminosis C (scurvy).**[62] **A,** In this infant, bilateral femoral radiographs demonstrate subtle periostitis caused by subperiosteal hemorrhage *(white arrows)*. In addition, thick, sclerotic metaphyseal lines *(black arrows),* beaklike excrescences (Pelken spurs) *(open arrows),* and radiodense shells around the radiolucent epiphyses (Wimberger ring) *(arrowheads)* are seen. These findings are all consistent with long-standing scurvy. **B,** This patient exhibits classic radiographic findings of chronic ascorbic acid deficiency, including thick periostitis from subperiosteal hemorrhage *(white open arrows),* a sclerotic metaphyseal line *(black open arrow),* Pelken spurs *(large arrows),* radiolucent epiphysis surrounded by a sclerotic shell (Wimberger ring) *(small arrows),* and generalized osteopenia.

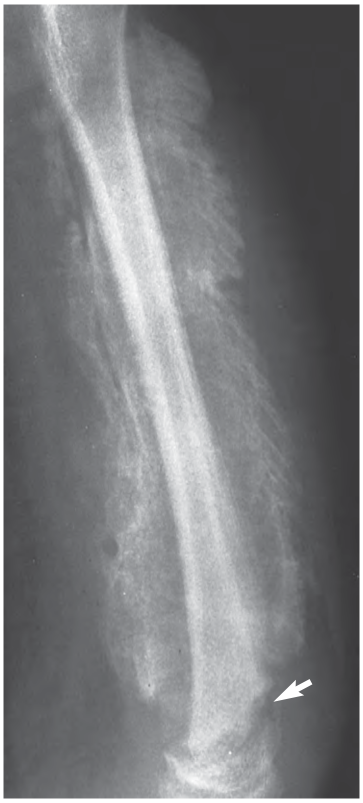

FIGURE 8–51 **Meningomyelocele.**[63] In this 6-year-old boy born with a meningomyelocele, exuberant periosteal new bone formation was present bilaterally. Widened, fragmented distal femoral growth plates also are evident *(arrow)*. *(Courtesy J.E.L. Desautels, MD, Calgary, Alberta, Canada.)*

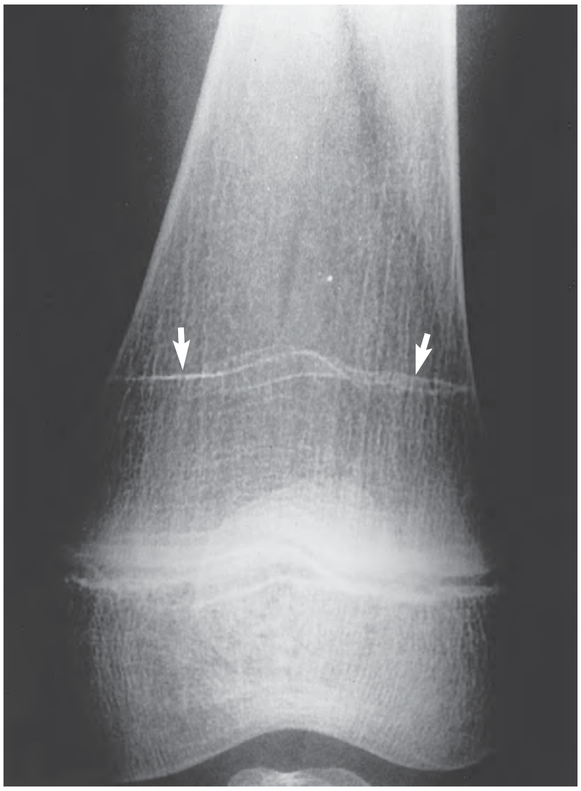

FIGURE 8–52 **Growth resumption (Harris) lines.**[64] In this chronically ill 6-year-old child with juvenile idiopathic arthritis, prominent transverse sclerotic bands are seen in the distal femoral metaphysis *(arrows)*.

FIGURE 8–53 **Pyogenic osteomyelitis: *Staphylococcus aureus.***[65,74,75] This 23-year-old man had pain of 4 months duration. Frontal **(A)** and lateral **(B)** radiographs demonstrate a large elongated radiolucent lesion with endosteal scalloping of the medullary cavity of the femoral diaphysis *(black arrows)*. A thin layer of periosteal reaction is seen on the frontal view *(white arrows)*. A more aggressive zone of permeative destruction is present at the superior aspect of the lesion *(curved arrows)*. A well-defined radiolucent channel was evident at the bottom of the lesion, typical of infection, but it is not well seen in these photographs. *(Courtesy G. Greenway, MD, Dallas, Texas.)*

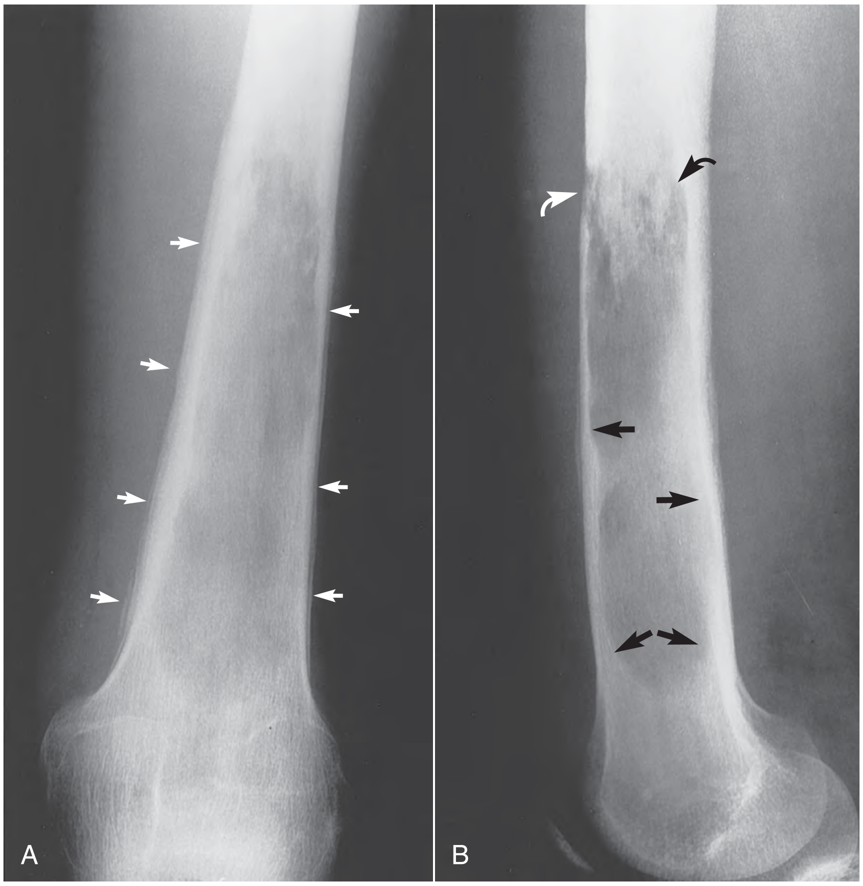

FIGURE 8–54 **Collagen vascular disease: dermatomyositis and polymyositis.**[67] Observe the globular, sheetlike, and amorphous calcification within the muscles and subcutaneous tissues adjacent to the femur in this 16-year-old girl with dermatomyositis-polymyositis. Dermatomyositis and polymyositis are diseases of striated muscle that are characterized by diffuse, nonsuppurative inflammation and degeneration. Dermatomyositis affects skin and muscle, and polymyositis affects only muscle. The cause is unknown, and patients of all ages are affected. About one third of patients also have Raynaud phenomenon, and up to 50% have arthralgia. *(Courtesy C. Van Lom, MD, San Diego.)*

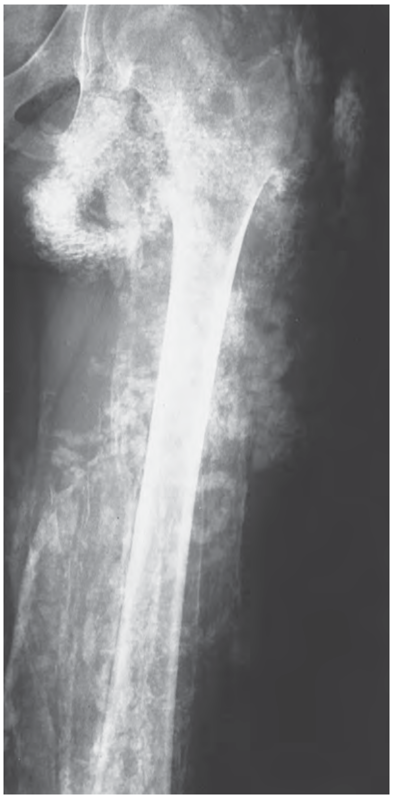

CHAPTER 9

Knee

NORMAL DEVELOPMENTAL ANATOMY

Accurate interpretation of radiographs of the pediatric knee requires a thorough understanding of normal developmental anatomy. Table 9-1 outlines the age of appearance and fusion of the primary and secondary ossification centers. Figures 9-1 and 9-2 demonstrate the radiographic appearance of many important ossification centers and other developmental landmarks at selected ages from birth to skeletal maturity.

DEVELOPMENTAL ANOMALIES, ANATOMIC VARIANTS, AND SOURCES OF DIAGNOSTIC ERROR

The knee and patella are sites of anomalies, anatomic variations, and other sources of diagnostic error that may simulate disease and potentially result in misdiagnosis. Table 9-2 and Figures 9-3 to 9-5 address some of the more common processes.

SKELETAL DYSPLASIAS AND OTHER CONGENITAL DISEASES

Table 9-3 outlines a number of skeletal dysplasias and congenital disorders that affect the knee and patella. Figures 9-6 to 9-8 illustrate the radiographic manifestations of some of these disorders.

ALIGNMENT ABNORMALITIES

Several alignment abnormalities affect the knee and patella. Tables 9-4 and 9-5 outline a number of potential causes of genu valgum, genu varum, genu recurvatum, patella alta, patella baja, and lateral patellar displacement. These malalignments are illustrated throughout this chapter as they are manifested in many disorders.

PHYSICAL INJURY

Physical injury to the knee results in a wide variety of fractures and dislocations. Table 9-6 describes fractures of the distal portion of the femur, proximal end of the tibia, and the patella. Dislocations of the knee joint itself, the patella, and the proximal tibiofibular articulation are described in Table 9-7. These conditions are illustrated in Figures 9-9 to 9-27. Fractures of the diaphyses of the femur, the tibia, and the fibula are described and illustrated in Chapters 8 and 10, respectively.

INTERNAL DERANGEMENTS AND SOFT TISSUE DISORDERS

The soft tissues within and around the knee are complex and may be involved in a variety of inherited and acquired disorders. This section describes internal derangements and soft tissue disorders of the synovial structures (Table 9-8), the menisci (Tables 9-9 and 9-10), the ligaments and tendons (Table 9-11), and the patellofemoral articulation (Table 9-12). Figures 9-28 to 9-54 illustrate many features of these conditions, with an emphasis on radiographic and MR imaging findings.

ARTICULAR DISORDERS

The knee is a frequent target site of involvement for many degenerative, inflammatory, crystal-induced, and infectious articular disorders. Table 9-13 outlines these diseases and their chief characteristics. Table 9-14 provides a compartmental analysis emphasizing the pattern of joint space narrowing typical of these disorders. Figures 9-55 to 9-70 illustrate the typical imaging manifestations of the most common articular disorders affecting the knee.

NEOPLASMS

The patella and the knee joint itself are infrequent sites of involvement for malignant and benign tumors and tumorlike lesions. Table 9-15 lists and characterizes the neoplasms that typically involve the patella. Figure 9-71 illustrates an example of skeletal metastasis invading the articulation and its surrounding bones. Many of the more common patellar tumors are illustrated in Figures 9-72 to 9-75.

METABOLIC, HEMATOLOGIC, AND VASCULAR DISORDERS

Several metabolic, hematologic, and vascular disorders affect the knee and the surrounding osseous and soft tissue structures. Table 9-16 lists some of the more common disorders and describes their characteristics. Figures 9-76 to 9-84 illustrate the typical imaging findings of several of these disorders.

TABLE 9-1 Knee: Approximate Age of Appearance and Fusion of Ossification Centers[1-4] (Figures 9-1 and 9-2)

Ossification Center	Primary or Secondary	No. of Centers Per Knee	Age of Appearance* (Years)	Age of Fusion* (Years)
Patella	P	1	Girls: 1.5-3.5 Boys: 3-5	
Distal femoral epiphysis	S	1	Birth	19-22
Proximal tibial epiphysis	S	1	Birth	18-23
Proximal fibular epiphysis	S	1	2-5	21-24
Tibial tubercle apophysis	S	1	10-13	18-24

P, Primary; *S*, secondary.

* Ages of appearance and fusion of ossification centers in girls typically precede those of boys. Ethnic differences also exist.

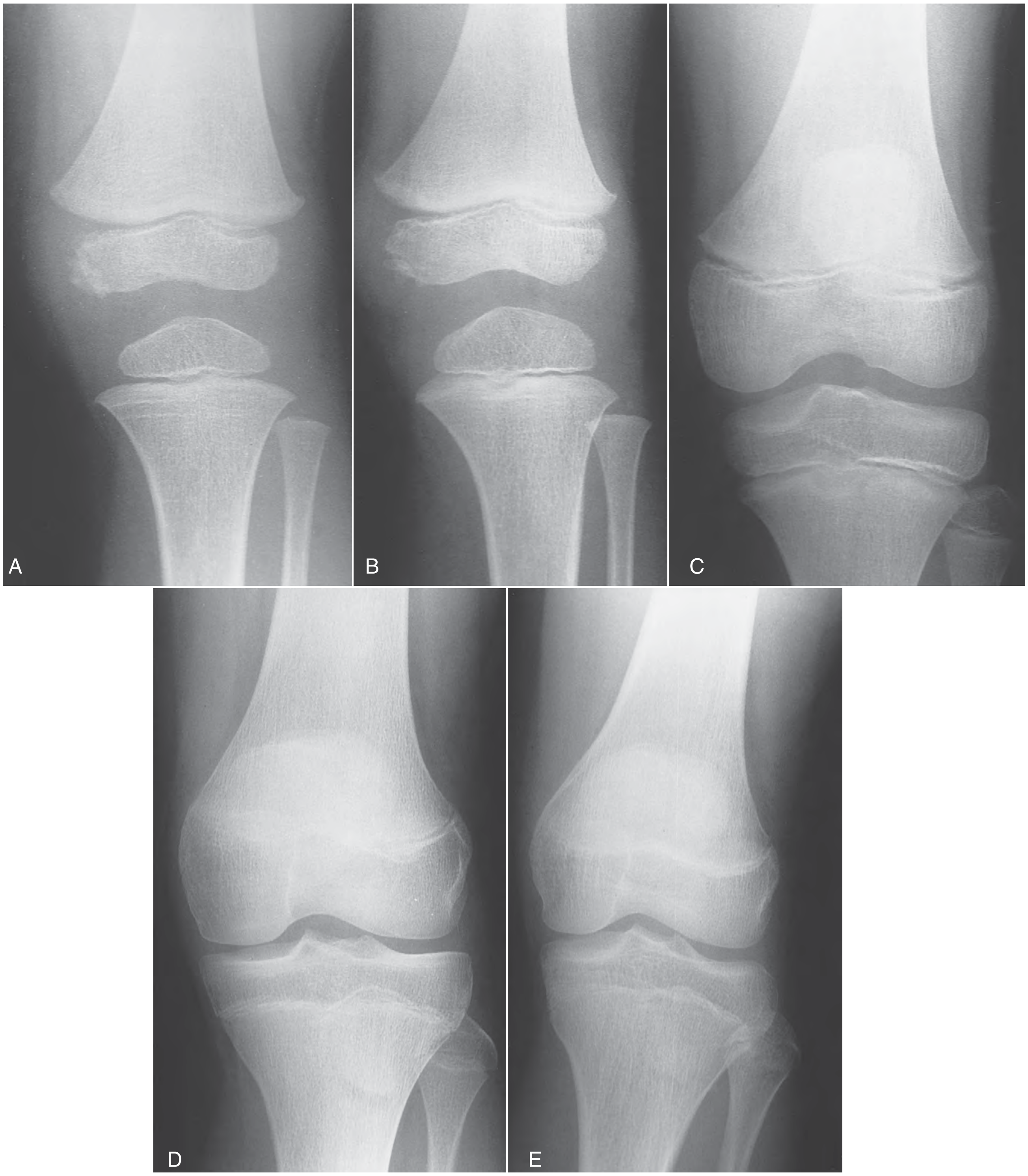

FIGURE 9–1 **Skeletal maturation and normal development: anteroposterior knee radiographs.**[1-4] **A,** A 2-year-old girl. The secondary ossification center of the proximal end of the fibula is barely visible, typically appearing between the ages of 18 months and 5 years. The proximal tibial epiphysis is ossified, but it is much smaller than the metaphysis. A normal, irregular, serrated appearance of the medial aspect of the distal femoral epiphysis is evident. The zones of provisional calcification are radiodense. Beaking of the distal femoral metaphysis is prominent laterally. **B,** A 4-year-old boy. The tibial and femoral epiphyses are approaching the size of the metaphyses. The medial aspect of the femoral epiphysis remains irregular, and the proximal fibular epiphysis is barely visible. The zones of provisional calcification remain sclerotic. Beaking of the distal lateral femoral metaphysis persists. **C,** A 10-year-old boy. The widths of the tibial and femoral epiphyses have exceeded the widths of the adjacent metaphyses. The fibular epiphyses and patella are well developed and resemble the adult configuration. **D,** A 13-year-old girl. The distal femoral and proximal tibial epiphysis are fusing to their adjacent metaphyses. The patella has adopted adult proportions. **E,** A 15-year-old girl. The femoral, tibial, and fibular epiphyses have fused to their respective metaphyses, but the physeal lines are still clearly visible.

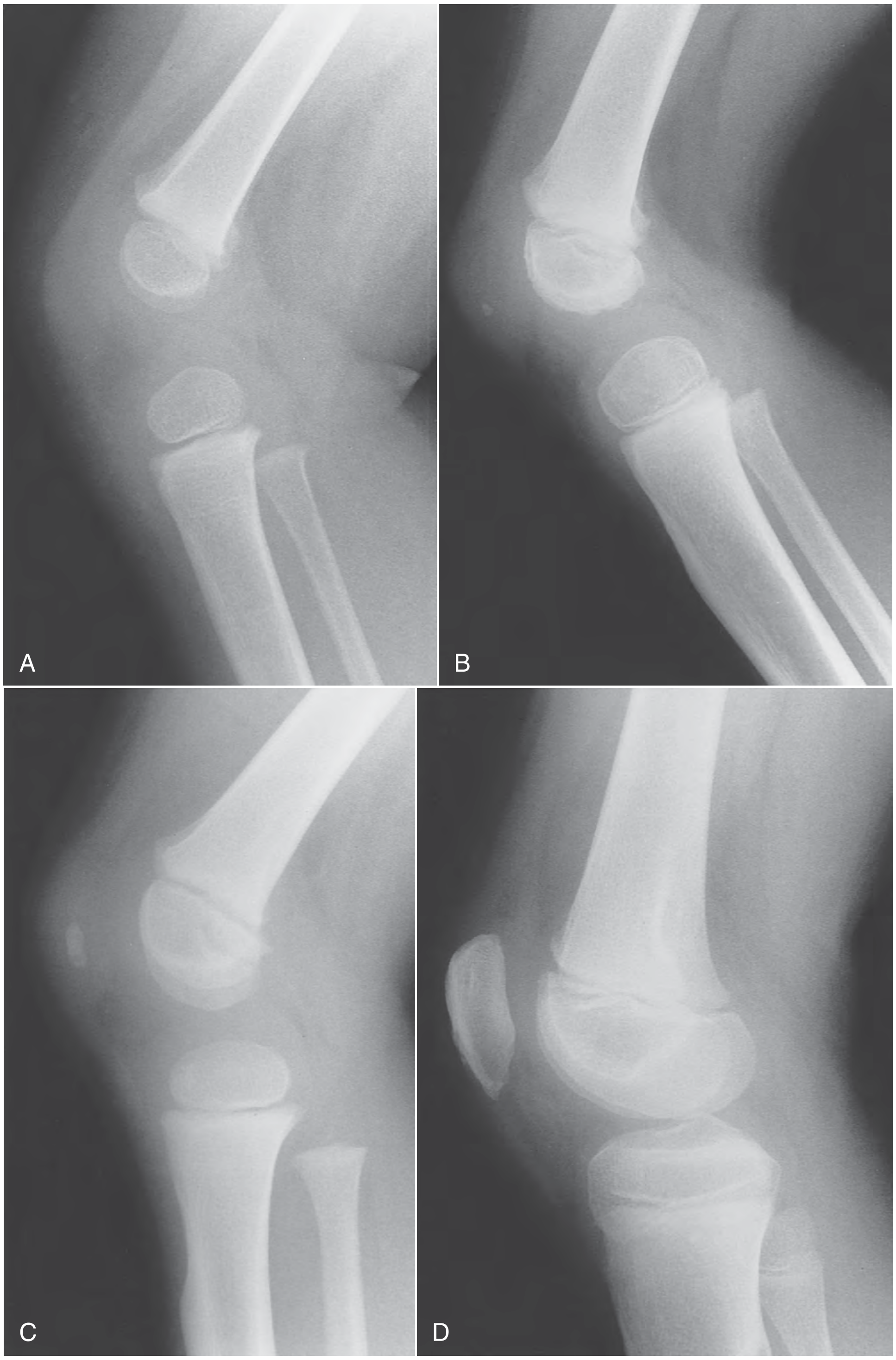

FIGURE 9–2 Skeletal maturation and normal development: lateral knee radiographs.[1-4] **A,** An 18-month-old boy. The patellar and fibular head ossification centers have not ossified. The femoral and tibial epiphyses are ossified and round, and the zones of provisional calcification are radiodense. **B,** A 4-year-old boy. The primary center of ossification for the patella has begun to ossify. The femoral epiphysis is irregular. **C,** A 5-year-old boy. The patellar ossification center is more prominent, and a normal pronounced indentation is evident at the anterior portion of the tibia at the eventual site of the tibial tubercle. The fibular epiphyseal center is barely visible. **D,** A 9-year-old boy. The patella and the epiphyses are more fully ossified and have grown in size.

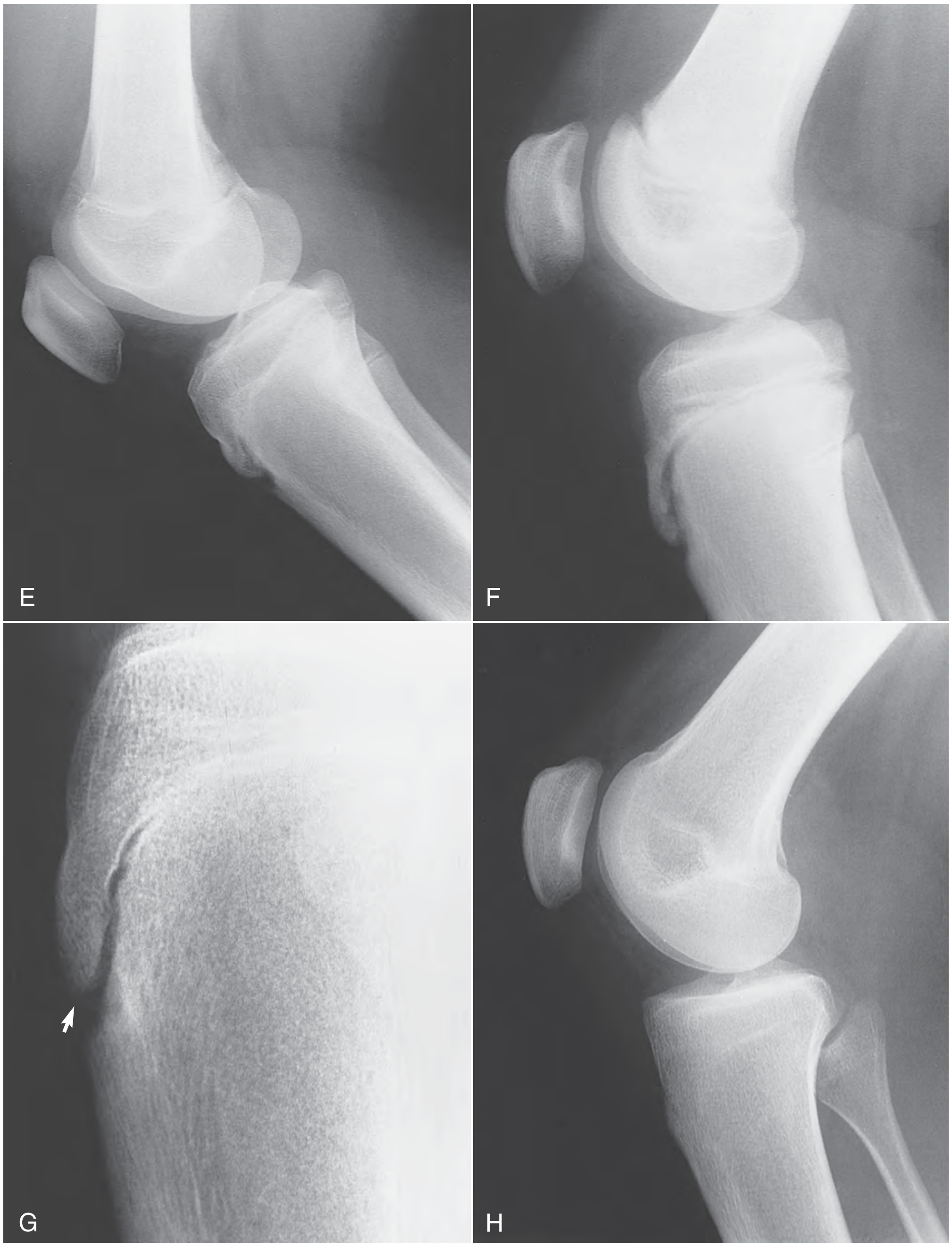

FIGURE 9–2, cont'd **E,** A 12-year-old girl. The zones of provisional calcification are not as radiodense. The patella is approaching adult proportions, and the epiphyses of the femur, tibia, and fibula are conforming to the shape of their respective metaphyses and are beginning to fuse. The tibial tubercle, arising from the anterior aspect of the proximal tibial epiphysis, is undergoing ossification and projects inferiorly along the shaft of the tibia. **F,** A 14-year-old boy. The tibial tubercle, now quite prominent, remains separated from the tibial shaft by a radiolucent cartilaginous cleft. Fusion of the epiphyses of the femur, the tibia, and the fibula lags behind that in the 12-year-old girl **(E),** a typical occurrence around this age. **G,** A 14-year-old girl. A close-up radiograph shows the normal appearance of the apophysis of the tibial tubercle before fusion *(arrow)*. **H,** A 15-year-old girl. The tibial tubercle apophysis has been incorporated into the tibial shaft. All epiphyses have fused, and the physeal lines remain barely visible.

TABLE 9-2 Developmental Anomalies, Anatomic Variants, and Sources of Diagnostic Error Affecting the Knee*

Entity	Figure(s)	Characteristics
Accessory ossification centers[5,6]		Accessory ossification centers in the inferior pole of the patella may simulate fractures or Sinding-Larsen-Johansson disease Usually asymptomatic
Bipartite patella[5-8,138]	9-3	Developmental anomaly in which the ossification center of the patella may be fragmented or fail to unite Present in approximately 2% of the population M:F, 9:1 Bilateral in 80% of cases and may occasionally be accompanied by mild pain Bipartite fragment located at superolateral aspect of patella at the attachment of the vastus lateralis muscle Bone edges are smoothly corticated and not displaced from the parent bone Fragment usually is connected to the patella by fibrous tissue Two separate pieces of bone—bipartite patella; three pieces of bone—tripartite patella; more than 3 pieces—multipartite patella Typical location, absence of severe pain, and characteristic appearance allow differentiation from acute fractures, which usually are horizontal (transverse) or stellate and possess jagged, irregular edges ***MR imaging findings of bipartite patella*** Bone marrow edema in superolateral bipartite fragment and associated soft tissues may be present
Dorsal defect of the patella[9]	9-4, *A-B*	Variant in ossification Circular radiolucent defect in superolateral pole of patella May simulate a neoplasm May be related to bipartite patella Usually a self-limited, incidental finding in children
Juxtacortical desmoid[10,11]	9-5	Also termed *periosteal desmoid, avulsive cortical irregularity, cortical irregularity syndrome, cortical desmoid,* and *distal metaphyseal femoral defect* Normal variant believed to be a benign reaction to stress or trauma occurring at the musculotendinous insertion site of the adductor magnus muscle or, less commonly, of the medial head of the gastrocnemius muscle Occurs only in children, adolescents, or young adults Male > female Histologic and imaging findings simulate malignancy Usually asymptomatic ***Radiographic findings*** Irregular periosteal new bone formation Cortical irregularity and scalloping Soft tissue swelling is often seen in this condition ***MR imaging findings*** Low signal intensity on T1-weighted images High signal intensity on T2-weighted images Surrounding rim of low signal intensity on all sequences
Hypoplastic or aplastic patellae[5]	9-6	Rare condition usually seen in association with hereditary osteo-onychodysostosis (nail-patella syndrome) and other congenital syndromes
Patellar duplication[12]		Coronal cleft between two separate patellae has been referred to as *double patella*, a rare anomaly that may be associated with multiple epiphyseal dysplasia Transverse cleft may separate the patella into two separate pieces; usually associated with trauma or cerebral palsy
Lateral dystopia of the patella[5]		Lateral malposition of patella, hypoplasia of lateral femoral condyle, prominent medial femoral condyle, small patella with flattened ridge between medial and lateral facets Frequently associated with congenital patellar dislocation with habitual patellar dislocation—"slipping patella"

* See also Table 1-1.

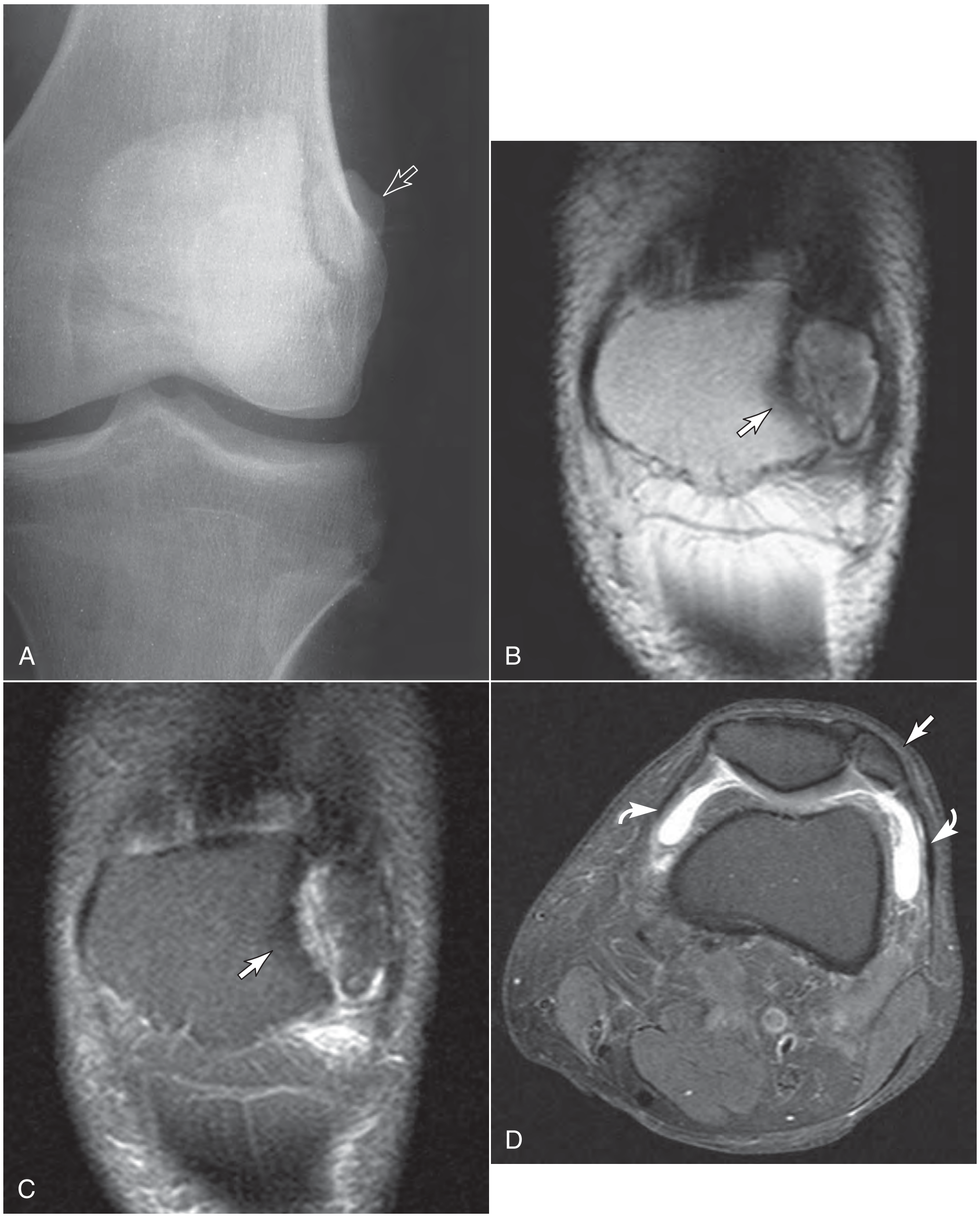

FIGURE 9–3 **Bipartite patella.**[5-8,138] **A,** Observe the characteristic radiolucency separating a circular ossified region at the superolateral aspect of the patella *(open arrow)*. **B-D,** MR imaging appearance in another patient. T1-weighted coronal **(B)** and proton–density-weighted fat suppressed coronal **(C)** and transaxial **(D)** images show the lateral location of the nondisplaced bipartite patella *(arrows)*. Some high signal intensity is seen between the two pieces of the patella on the fluid-sensitive image **(C),** probably representing edema. The characteristic location and smooth, rounded, nondisplaced edges indicate that this is not an acute fracture, despite the edema and a large high signal intensity joint effusion seen on the axial image *(curved arrows)*.

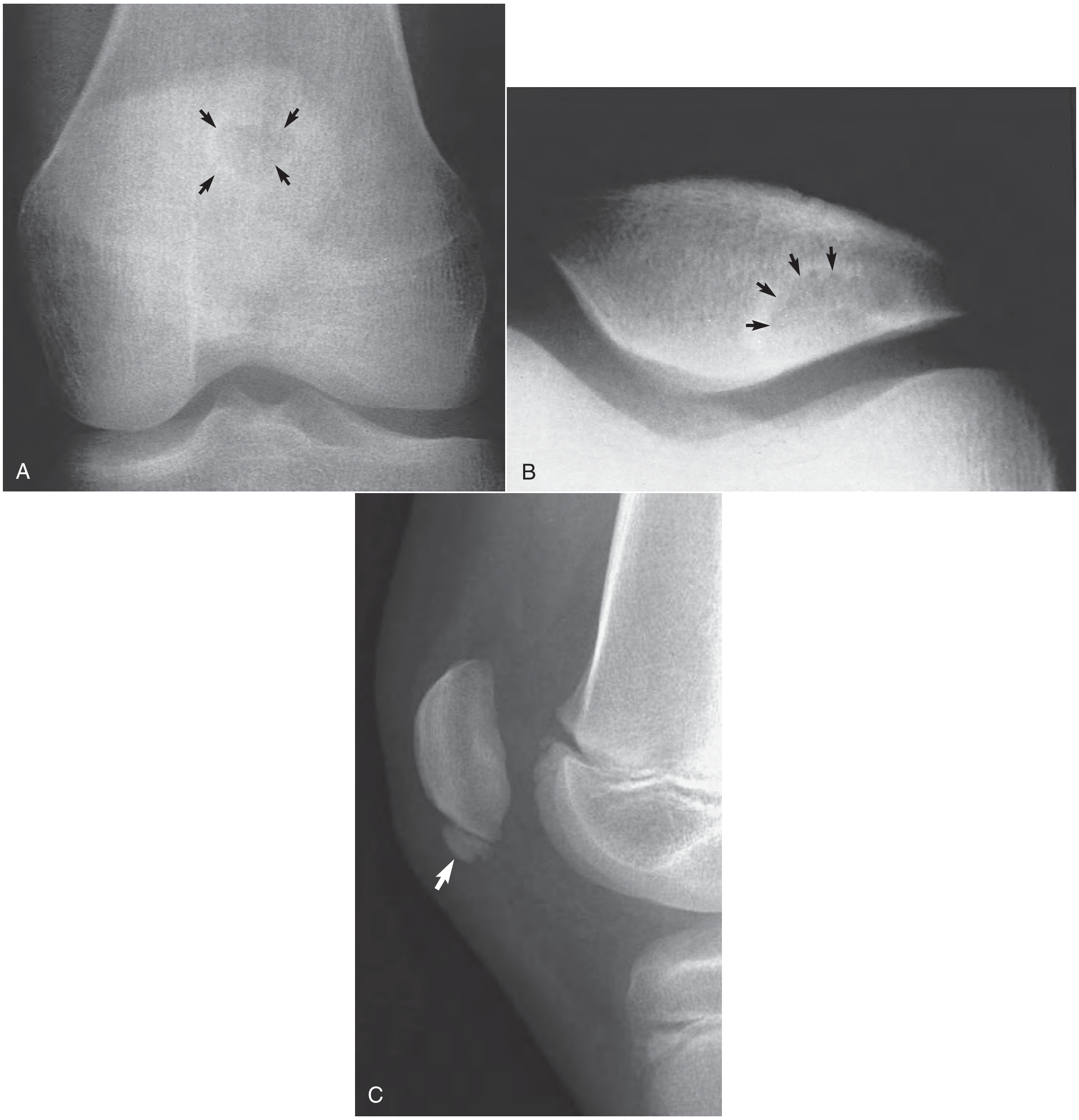

FIGURE 9–4 Patellar variants.[9] **A-B,** Dorsal defect of the patella. A well-circumscribed radiolucent defect *(arrows)* is seen on frontal **(A)** and tangential **(B)** radiographs in the superior pole on the dorsal surface of the patella. **C,** Patellar ossicle. In another patient, a small triangular ossicle is present adjacent to the inferior pole of the patella *(arrow)*. Both these variations in ossification are usually self-limited, incidental findings in children or adults. *(**C,** Courtesy J.R. Thompson, DC and E.C. Fritsch, DC, Houston, Texas.)*

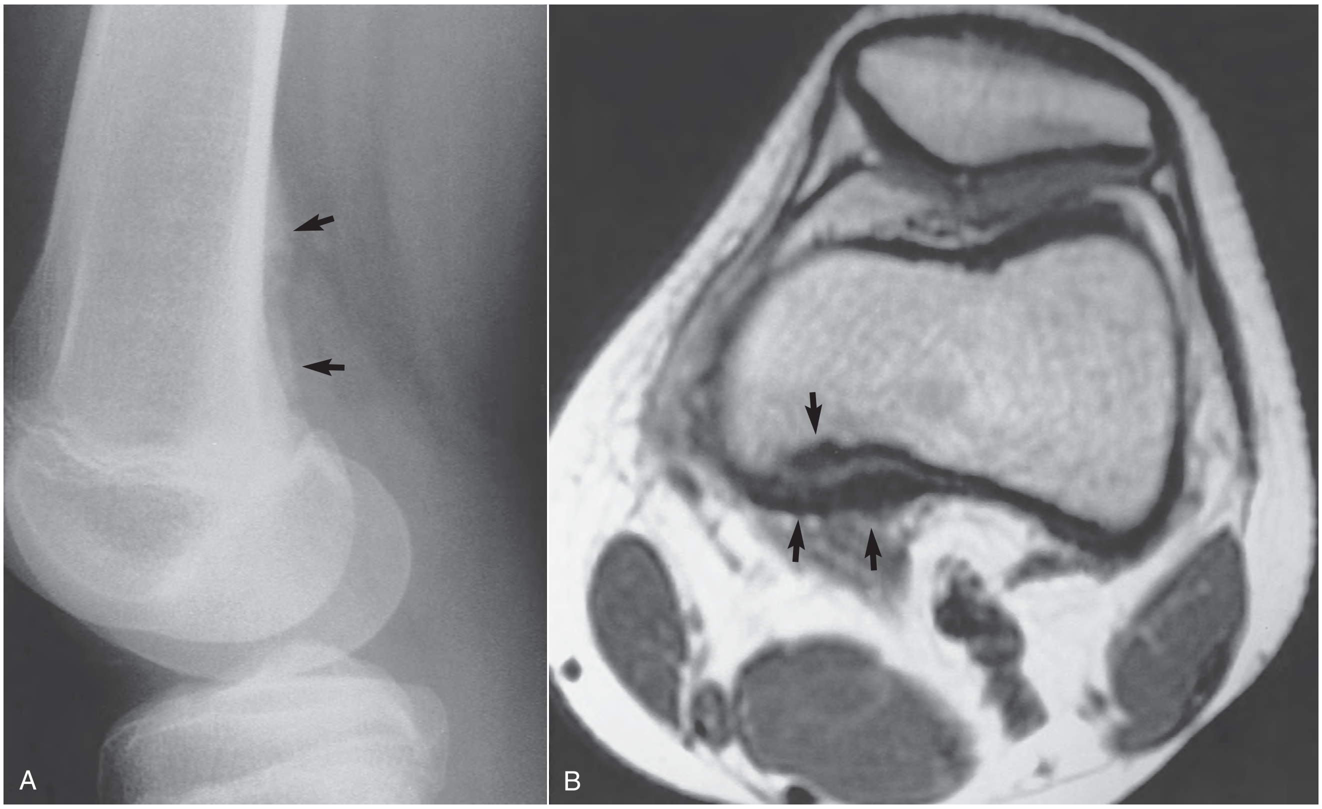

FIGURE 9–5 **Juxtacortical desmoid (avulsive cortical irregularity).**[10,11] This 12-year-old swimmer had knee pain. A lateral radiograph **(A)** and a transaxial T1-weighted (TR/TE, 400/20) spin echo MR image **(B)** show irregular periosteal new bone formation and cortical irregularity along a segment of the posteromedial cortex *(arrows)*. The MR image localizes the lesion precisely. This classic location and appearance allow differentiation from a malignant process such as osteosarcoma. *(Courtesy D. Witte, MD, Memphis, Tenn.)*

TABLE 9-3 **Skeletal Dysplasias and Other Congenital Diseases Affecting the Knee***

Entity	Figure(s)	Characteristics
Hereditary osteo-onychodysostosis[13]	9-6	Absent or hypoplastic patellae
Dysplasia epiphysealis hemimelica[14,15] (Treavor disease)	9-7	Asymmetric cartilaginous overgrowth in one or more epiphyses Radiographically resembles large eccentric osteochondroma arising from tibial or femoral epiphyses Bulky irregular ossification extending into soft tissues
Ehlers-Danlos syndrome[16]		Genu recurvatum Joint laxity Soft tissue hemangiomas appear as phleboliths on radiographs
Chondrodysplasia punctata[17]	9-8	Rare condition Stippled calcification in the immature cartilaginous skeleton: epiphyses of the femur and tibia and within the patella

* See also Table 1-2.

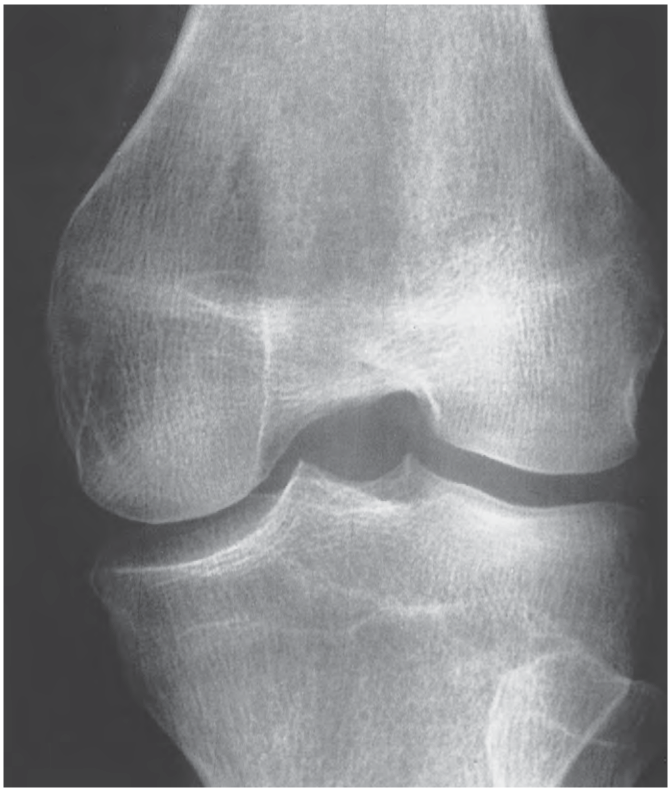

FIGURE 9–6 **Hereditary osteo-onychodysostosis (HOOD or nail-patella syndrome).**[13] Observe the characteristic absence of the patella.

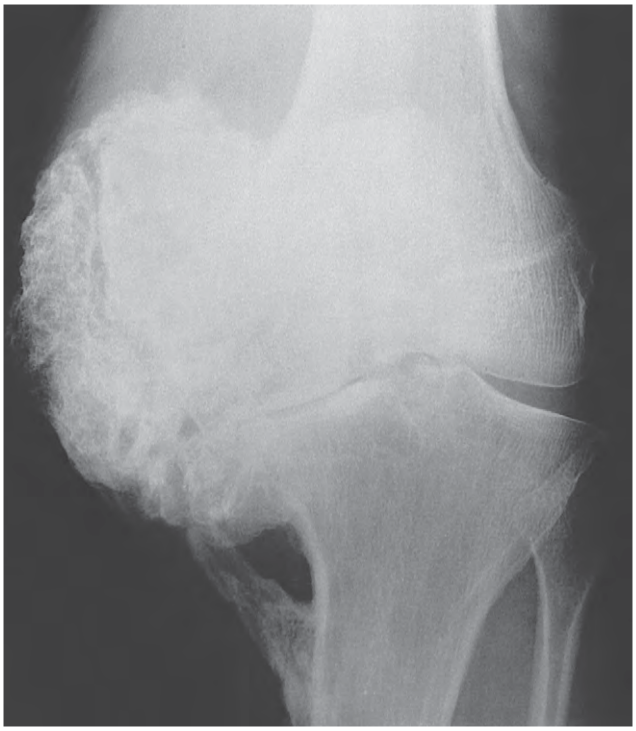

FIGURE 9–7 **Dysplasia epiphysealis hemimelica (Trevor disease).**[14,15] A huge cloudlike accumulation of ossification is seen arising from the medial aspect of the tibia and femur, spanning the medial aspect of the knee. A small osseous bridge also connects the mass to the proximal tibial shaft. These changes have resulted in a mild varus deformity. *(Courtesy J. Schils, MD, Cleveland, Ohio.)*

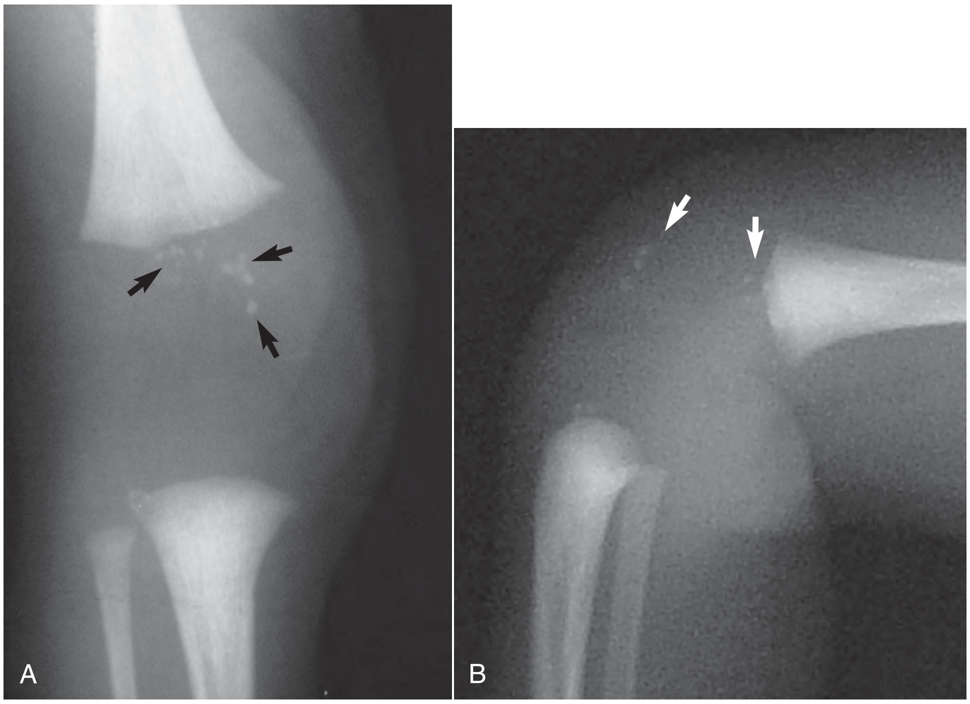

FIGURE 9–8 **Chondrodysplasia punctata.**[17] **A-B,** Radiographs of this 2-day-old girl with the rhizomelic autosomal recessive form of chondrodysplasia punctata reveal stippled ossification within the distal femoral epiphysis *(arrows)*. This stippled calcification is usually bilateral and may occur in the immature cartilaginous portions of the epiphyses of the femur, tibia, and patella. Since the patella and tibial epiphyses are not yet ossified in this patient, involvement of those bones is not yet evident.

TABLE 9-4 Alignment Abnormalities: Knee

Entity	Figure(s)
Genu Valgum (Knock-Knees)	
Osteo-onychodysostosis	9-6
Tibial plateau fracture	9-15
Medial collateral ligament tear	9-44
Rheumatoid arthritis	9-57
Flatfeet (pronation)	
Neuromuscular disease	
Achondroplasia	
Osteoarthrosis	
Multiple epiphyseal dysplasia	
Neurofibromatosis	
Osteogenesis imperfecta	
Homocystinuria	
Proximal tibial metaphyseal fracture	
Genu Varum (Bowlegs)	
Dysplasia epiphysealis hemimelica	9-7
Osteoarthrosis	9-55
Rheumatoid arthritis	9-57
Neuropathic osteoarthropathy	9-70
Rickets	9-77
Idiopathic	
Physiologic prenatal bowing	
Tibia vara (Blount disease)	10-2
Achondroplasia	
Premature partial growth arrest	
Multiple epiphyseal dysplasia	
Genu Recurvatum (Hyperextended Knees)	
Osgood-Schlatter disease	9-22
Knee dislocation	9-25
Neuropathic osteoarthropathy	9-70
Ehlers-Danlos syndrome	
Premature partial growth arrest	
Posterior cruciate ligament tear	
Neuromuscular disease	

TABLE 9-5 Alignment Abnormalities: Patella

Entity	Figure(s)
Patella Baja (Inferiorly Displaced Patella)	
Neuromuscular disease	9-14
Osgood-Schlatter disease	9-22
Quadriceps tendon tear	9-51
Achondroplasia	
Surgery involving transfer of tibial tubercle	
Patella alta (Superiorly Displaced Patella)	
Joint effusion	9-23, 9-27
Patellar tendon tear	9-50, 9-61
Chondromalacia patella	9-54
Patellar subluxation and dislocation	
Osgood-Schlatter disease	
Neuromuscular disease	
Homocystinuria	
Patellar sleeve fracture	9-13
Sinding-Larsen-Johansson disease	
Lateral Patellar Displacement	
Patellar dislocation	9-26
Patellofemoral instability	9-53
Developmental lateral dystopia	

See also Table 9-12.

TABLE 9-6 Fractures About the Knee[139]*

Entity	Figure(s)	Characteristics	Complications and Related Injuries
Fractures of the Distal Portion of the Femur			
All types[18,19]		Most injuries result from axial loading combined with varus, valgus, or rotational stress	Ligament disruption Patellar fracture Other associated fractures
Supracondylar[18,19]	9-9	Extraarticular, transverse, or slightly oblique orientation May be displaced, comminuted, impacted, open, or closed	Displaced fragments Popliteal artery injury
Intercondylar[18,19]		Intraarticular extension Supracondylar fracture combined with vertical component Y or T configuration	Incongruity of femorotibial or patellofemoral articular surfaces Degenerative joint disease Patellofemoral tracking disorders
Condylar[20]	9-10	Sagittal or coronal fracture lines isolated to the region of a single condyle	
Patellar Fractures			
All types[21,22]		Direct injury from fall or direct blow or indirect injury related to contraction of the quadriceps mechanism Unilateral injuries predominate	Osteochondral fracture Displaced fragments Ischemic necrosis involving proximal fragment 1-3 months after injury
Transverse[21,22]	9-11, *A*	50%-80% of cases Indirect force most common mechanism	
Longitudinal[21]	9-11, *B*	25% of cases Direct injury such as striking knee on dashboard of car	

* See Tables 1-4 and 1-5.

TABLE 9-6 Fractures About the Knee—cont'd

Entity	Figure(s)	Characteristics	Complications and Related Injuries
Stellate or comminuted[21]	9-11, *C, D*	20%-35% of cases	
Stress (fatigue) fracture[22]	9-12	Rare occurrence of spontaneous displaced or nondisplaced fracture Usually transverse fracture of middle or distal third of patella Occur most frequently in young athletes	
Patellar sleeve avulsion fracture[23,134]	9-13	Rare cartilaginous avulsion from the lower pole of the patella in children Results from hyperextension injuries with eccentric contraction of quadriceps on flexed knee ***Radiographic findings*** Radiographs may be normal Avulsed fragment from inferior pole of patella Joint effusion with patella alta ***MR imaging findings*** Marrow edema in patella Peripatellar soft tissue edema Osteochondral fracture through cartilage-bone interface Joint effusion or lipohemarthrosis Thickening of patellar tendon with edema	Severity of avulsion often underestimated on routine radiography Fracture separation and displacement may be identified with diagnostic ultrasound
Spastic paralysis[24]	9-14	Fragmentation or separation of the inferior pole of the patella Seen in patients with cerebral palsy and other causes of spastic paralysis Related to a traction phenomenon with contusion or tendinitis in the proximal attachment of the patellar tendon with subsequent calcification or ossification May also represent an avulsion injury	
Fractures of the Proximal Portion of the Tibia			
Tibial plateau fractures			
All types[25-27]	9-15	Vertical compression, valgus, varus, and rotational forces May be intraarticular or extraarticular	Cruciate and collateral ligament injuries and avulsion fractures Meniscal injuries Depression of plateau Lipohemarthrosis Peroneal nerve or artery injury Degenerative joint disease
Isolated lateral plateau[25-27]	9-15	75%-80% of all plateau fractures Valgus stress predominates ***Type I*** Wedge-shaped pure cleavage or fracture that splits the lateral plateau ***Type II*** Combined cleavage and compression fracture ***Type III*** Pure compression fracture	Valgus deformity Fibular head and neck fractures

Continued

TABLE 9-6 Fractures About the Knee—cont'd

Entity	Figure(s)	Characteristics	Complications and Related Injuries
Isolated medial plateau[25-27]		5%-10% of all plateau fractures Varus forces predominate ***Type IV*** May be split, wedge-shaped, or depressed and comminuted; may involve associated fractures of tibial eminences	
Combined medial and lateral plateau[25-27]		10%-15% of all plateau fractures ***Type V*** Bicondylar fracture	Fibular head and neck fractures
Fractures of the Tibial Intercondylar Eminences[28,129]	9-16	Result from violent twisting, abduction-adduction injury, or direct contact with the femoral condyle Avulsion from cruciate ligament Intraarticular fracture fragment may be undisplaced, hinged, detached, or detached and inverted More common in children than adults	Associated cruciate ligament injury Intraarticular fracture fragment
Segond Injury[29]	9-17	*Segond fracture:* avulsion fracture of the proximal portion of the tibia at the attachment of the lateral joint capsule Occurs as a result of internal rotation of the tibia with the knee in flexion Acute avulsion appears as thin, vertically oriented sliver of bone just distal to the joint line on the lateral tibia Fracture fragment eventually merges with the lateral tibial margin, producing an outgrowth that simulates an osteophyte	Anterior cruciate ligament disruption (75%-100% of cases) Meniscal tears (more than 60% of cases)
Fractures of the Proximal Portion of the Fibula[19]	10-14	Fractures of fibular head or neck result from direct or indirect forces:	Contusion or traction of the biceps tendon Peroneal nerve injury
		Direct blows	Anterior tibial artery rupture
		Varus forces associated with avulsion of proximal pole or styloid process	Associated collateral ligament injury and lateral tibial plateau fracture
		Valgus force associated with lateral plateau fracture	Avulsion of fibular head with possible intraarticular entrapment
		Twisting forces at ankle may cause high fibular fracture (Maisonneuve fracture)	Associated ankle injuries
Child abuse[30,31,123]	9-18	Most frequent in children 1-4 years of age Metaphyseal corner fractures of femur and tibia Physeal injuries Fractures in various stages of healing Acute fractures of the tibia and femur Subperiosteal hemorrhage with periosteal reaction	Associated injuries elsewhere
Growth plate injuries			
Distal femoral physis[32]	9-19	1.2% of growth plate injuries Type II and III injuries common *Most common age:* 10-15 years Trauma from birth, athletic, or automobile injuries Child catches legs between spokes of a wagon or bicycle wheel Clipping injury in adolescent football	Shortening and angulation of the femur Prognosis guarded

TABLE 9-6 Fractures About the Knee—cont'd

Entity	Figure(s)	Characteristics	Complications and Related Injuries
Proximal tibial physis[32]	9-20	Proximal tibial physis injuries are rare Type III lesions predominate	Approximately 20% of patients develop partial or complete growth arrest Popliteal artery injury
Tibial tubercle apophysis[33,34]	9-21	Rare injury Violent avulsion at patellar tendon attachment Fracture may extend vertically into proximal tibial epiphysis	Disruption of quadriceps mechanism
Posttraumatic Osteochondroses			
Osgood-Schlatter disease[5,35,140]	9-22	Acute or chronic repetitive trauma resulting in various degrees of avulsion of the apophysis of the tibial tubercle at the distal attachment of the patellar tendon ***Clinical findings*** Local pain, tenderness, swelling, and palpable mass over tibial tubercle Symptoms aggravated with activity and alleviated with rest Most frequently appears initially between the ages of 10 and 17 years Male > female (3:1 to 10:1 ratio) Related to participation in sports that involve kicking, jumping, and squatting Usually self-limited with symptoms resolving when the tibial apophysis fuses between 18 and 24 years of age Bilateral in as many as 60% of cases ***Soft tissue radiographic findings*** Swelling and irregularity of the soft tissues anterior to tibial tubercle Thickening of the patellar tendon Loss of sharpness or obliteration of the inferior angle of the infrapatellar fat pad Widening of soft tissues bordering the anterior articular surface of the tibia ***Osseous radiographic findings*** Inconsistent and unreliable Irregularity, fragmentation, and displacement of the tibial tubercle ossification center Ossicles may persist into adulthood ***MR imaging findings*** MR useful in revealing early and progressive changes Edema surrounding the tibial tuberosity Partial avulsion and partial proximal displacement of the secondary ossification center, which may lead to complete separation Damaged ossification center may progress to the formation of an ossicle	Normal ossification of the tibial tubercle apophysis may resemble Osgood-Schlatter disease with amorphous calcification, fragmentation, rarefaction, and sclerosis
Sinding-Larsen-Johansson disease[5]		Painful fragmentation or avulsion of the inferior pole of the patella Self-limited condition that may result in permanent irregularity of patellar margin Pathogenesis disputed: may represent traction apophysitis or posttraumatic osteonecrosis	

Continued

TABLE 9-6 Fractures About the Knee—cont'd

Entity	Figure(s)	Characteristics	Complications and Related Injuries
Osteochondral Fracture[36,37]	9-23	Momentary, persistent, or recurrent dislocations and subluxations of the patella may result in injury to the patella or lateral femoral condyle or both Acute injury to the articular surface can result in cartilaginous or osteocartilaginous fracture fragments within the joint	Associated with painful joint effusion or hemarthrosis, joint locking, clicking, and limitation of motion
Osteochondritis Dissecans[38-41]	9-24	Fragmentation and possible separation of a portion of the articular surface Adolescent onset most frequent, but occurs from childhood to middle age Symptoms and signs usually begin between 15 and 20 years of age Men > women Significant history of trauma in only 50% of cases Femoral condyles are the most typical location: medial condyle 85% of cases and lateral condyle 15% of cases MR arthrography and CT arthrography are the most useful imaging techniques Patellar involvement is rare	Painful or painless joint effusion Joint locking, clicking, and limitation of motion

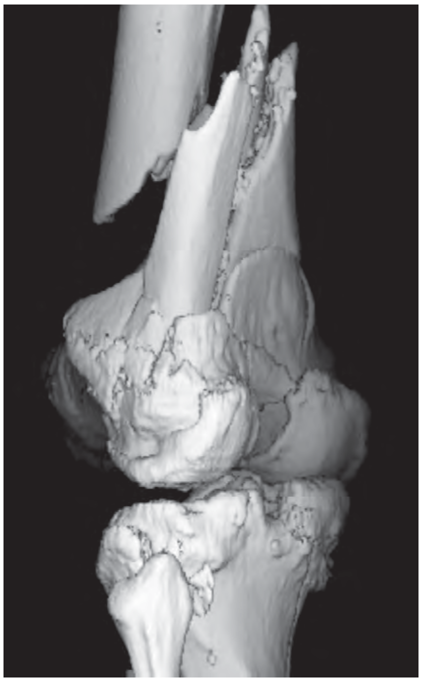

FIGURE 9–9 Supracondylar femoral fracture.[18,19] A 3-dimensional surface rendered CT image of the knee in this 46-year-old man demonstrates a comminuted fracture of the supracondylar region of the femur. Comminuted fragments of an associated proximal tibial fracture are not as well seen on this image.

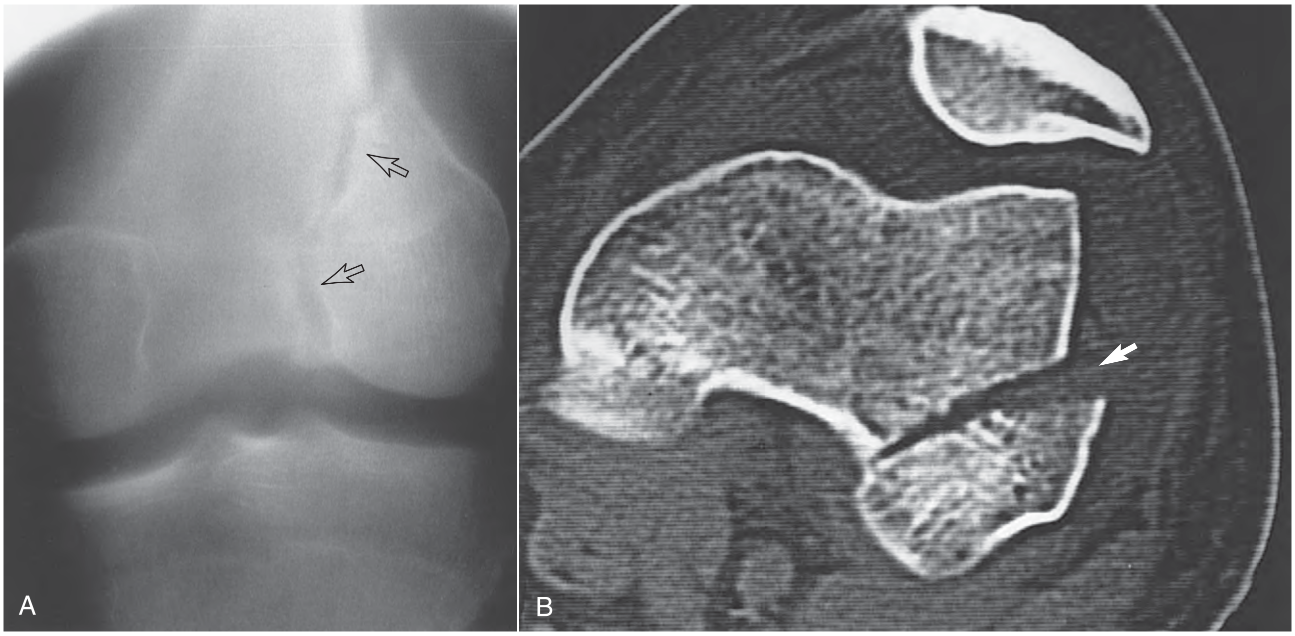

FIGURE 9–10 **Fracture of the lateral femoral condyle.**[20] **A,** Coronal conventional tomogram shows a sagittally oriented vertical intraarticular fracture involving the lateral femoral condyle *(open arrows)*. **B,** Transaxial CT scan shows minimal displacement of the fracture fragment *(arrow)*. Condylar fractures, in which sagittal fracture lines are isolated to a single condyle, may be difficult to detect on routine radiographs and often, as in this case, require conventional tomography or CT.

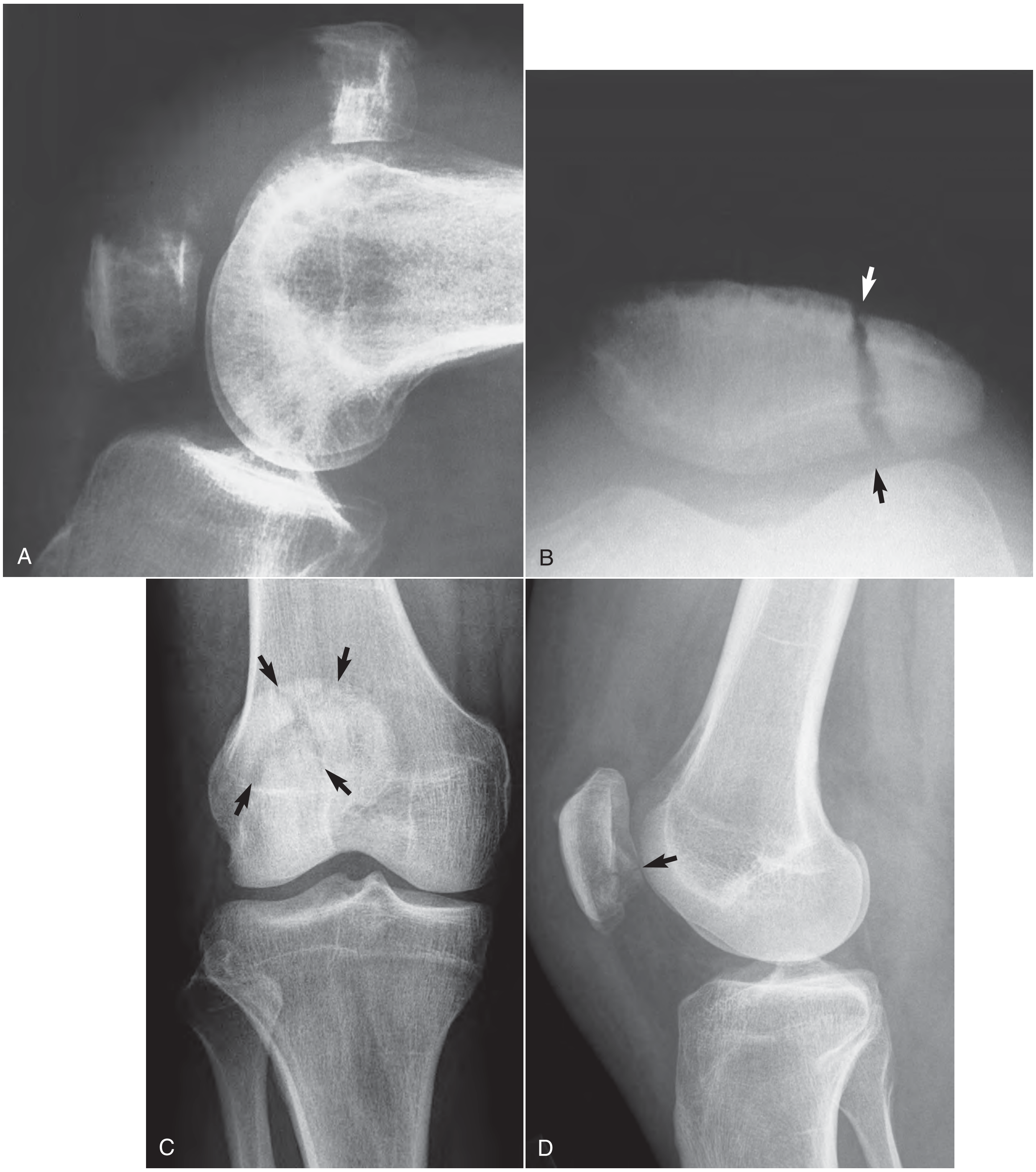

FIGURE 9–11 Patellar fracture.[21,22] **A,** Transverse fracture of the patella with wide displacement of the fracture fragments. **B,** Tangential radiography from another patient shows a jagged, minimally displaced longitudinal fracture of the patella *(arrows)*. **C-D,** This 27-year-old man fell directly on his patella, causing a stellate comminuted fracture *(arrows)*.

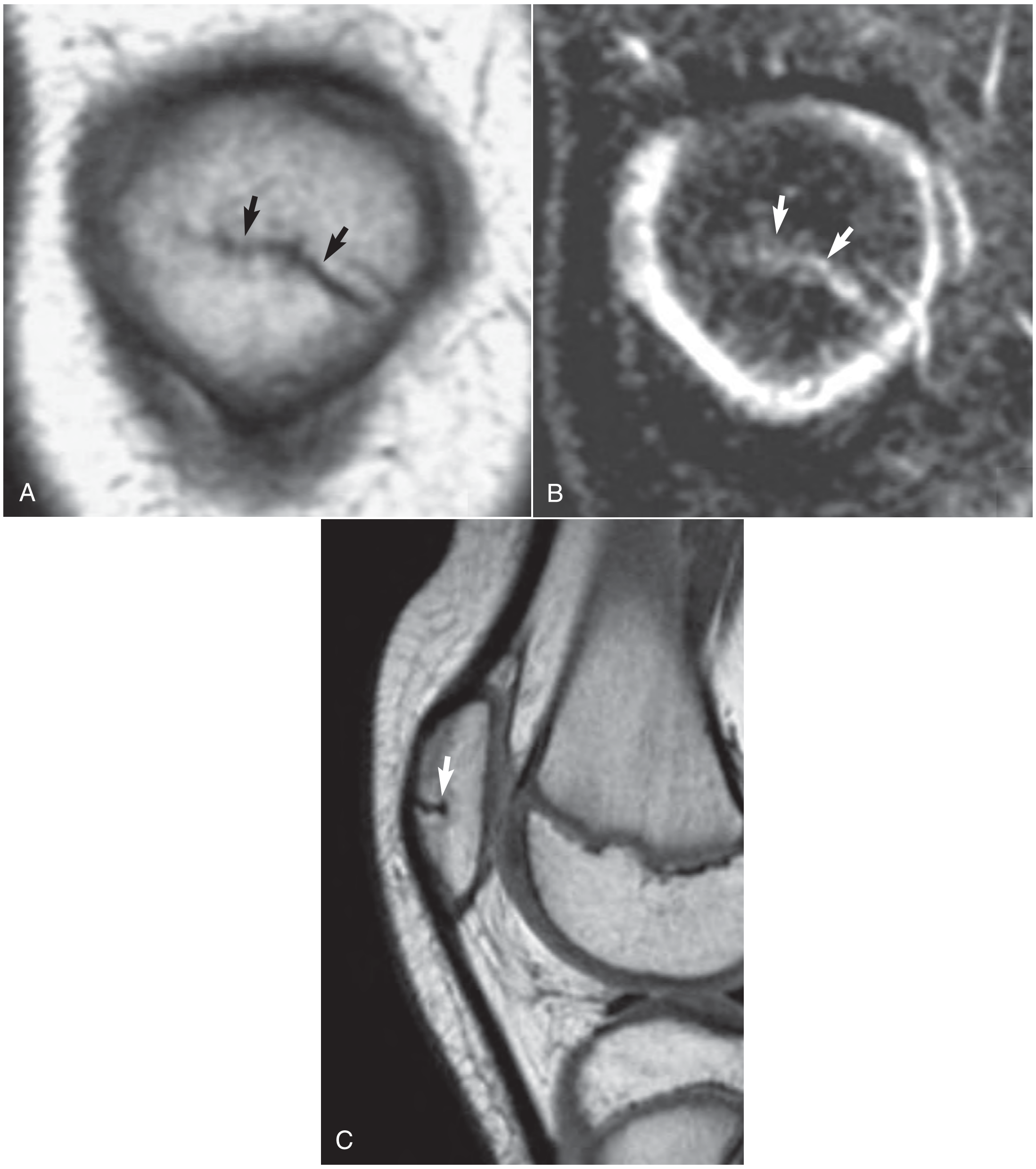

FIGURE 9–12 **Stress (fatigue) fracture of the patella.**[22] This 9-year-old ballerina developed gradual onset of anterior knee pain but could not recall any single traumatic event such as a fall or a direct blow. Coronal T1-weighted **(A)** and proton-density MR images in the coronal **(B)** and sagittal **(C)** planes clearly reveal a nondisplaced, noncomminuted transverse fatigue fracture through the patella *(arrows)*.

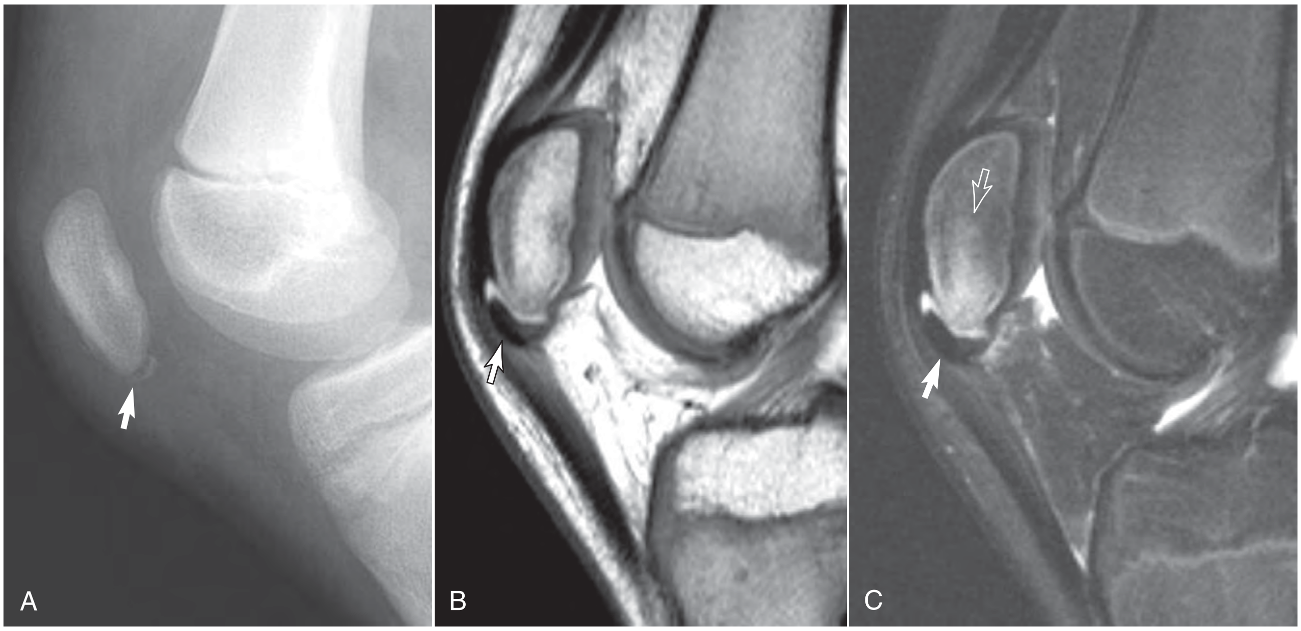

FIGURE 9–13 Acute patellar sleeve avulsion fracture.[23,134] This 11-year-old male developed anterior knee pain. **A,** The lateral radiograph shows a crescent-shaped flake of bone representing an osteochondral avulsion of the inferior pole of the patella *(arrow)*. The patellar position appears normal. The sagittal proton–density-weighted MR image **(B)** shows the bone fragment *(arrow)* separated from the inferior pole of the patella by a thin zone of high signal intensity edema. The quadriceps and patellar tendons are intact, but the patellar tendon demonstrates high signal intensity near its attachment to the avulsed fracture fragment. Additionally, a sagittal proton–density-weighted image obtained with fat suppression **(C),** shows high signal intensity within the patella *(open arrow)* indicative of bone marrow edema (bone contusion).

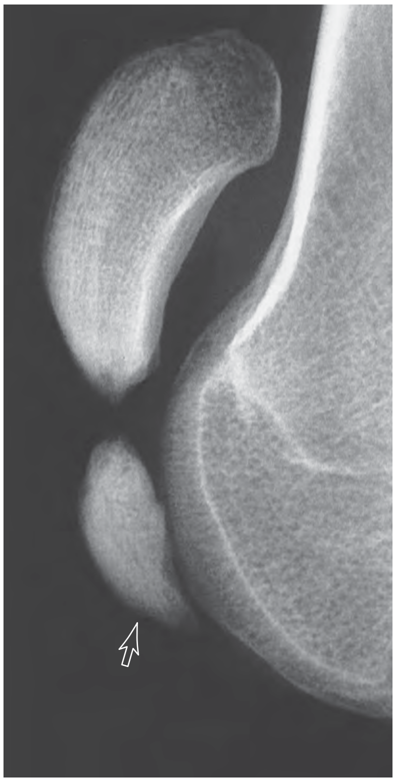

FIGURE 9–14 Spastic paralysis: patella.[24] Observe the fragmentation of the inferior pole of the patella *(open arrow)* in this 17-year-old patient with cerebral palsy. The lesion, frequently associated with spastic paralysis, probably is related to a traction phenomenon.

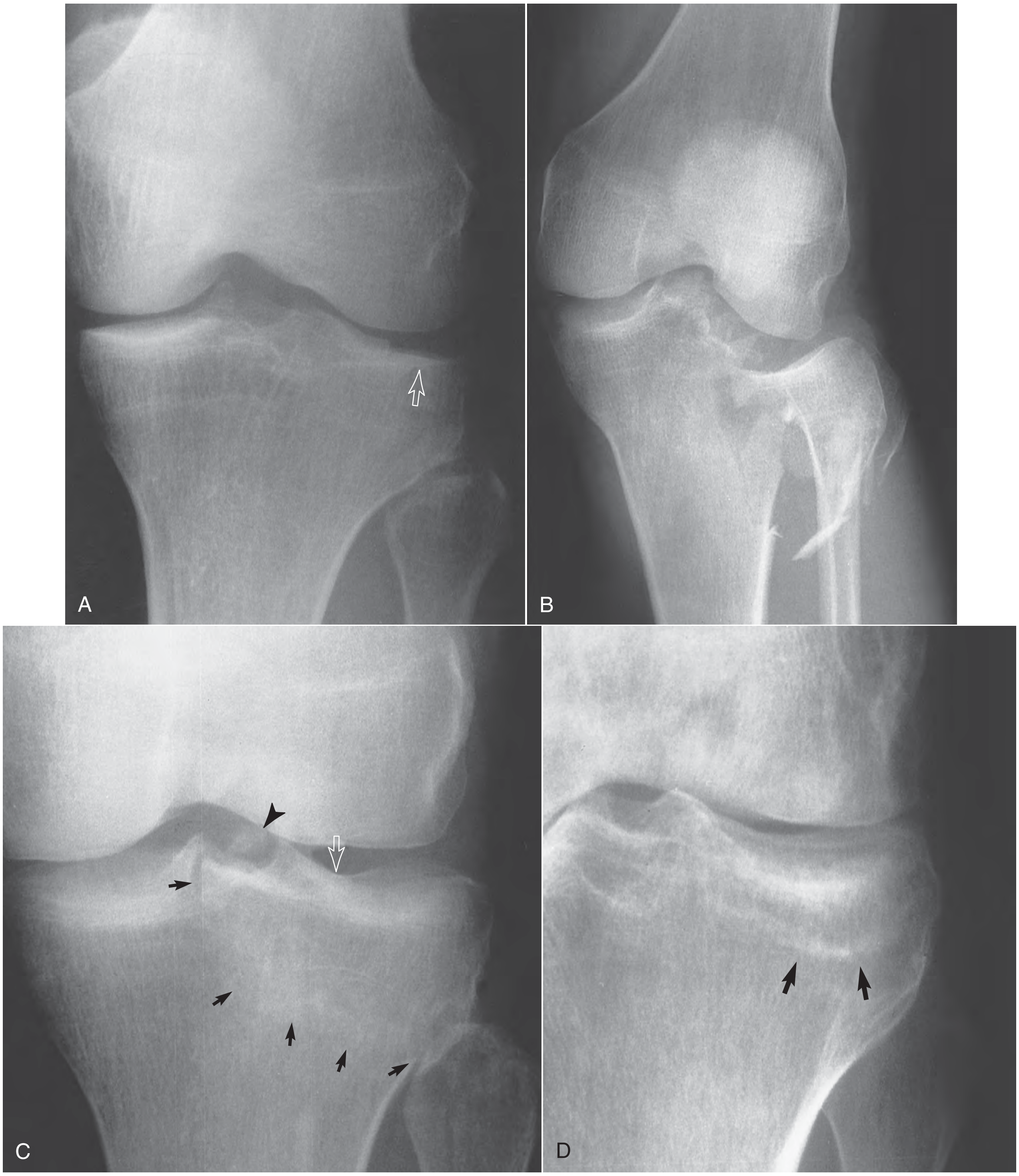

FIGURE 9–15 **Tibial plateau fracture.**[25-27] **A,** Acute fracture: Type III. A 47-year-old man was involved in a motor vehicle collision. Frontal radiograph reveals minimal depression of the lateral tibial plateau *(open arrow)*. **B,** Acute comminuted fracture: Type II. In another patient, observe the severely comminuted lateral plateau and lateral displacement of the proximal tibiofibular articulation. **C,** In another patient with a type III fracture, the radiograph shows depression of the lateral tibial articular surface *(open arrow)* and compaction of the fracture fragments *(arrows)*. An intraarticular fragment also is seen *(arrowhead)*. **D,** Stress (fatigue) fracture. This 50-year-old woman developed pain after embarking on a rigorous program of running after years of inactivity. Observe the transverse zone of sclerosis *(arrows)* characteristic of a fatigue fracture of the lateral tibial plateau *(arrows)*.

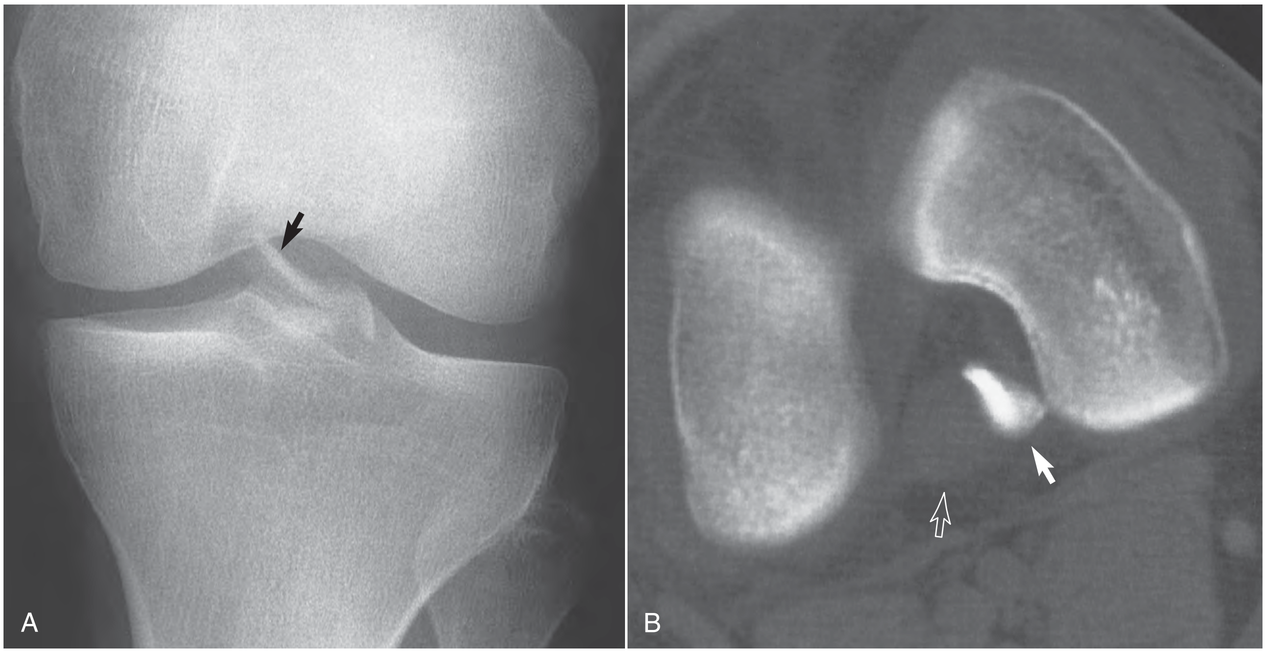

FIGURE 9–16 **Avulsion fracture of the tibial eminence.**[28,129] **A,** Frontal radiograph of this 18-year-old boy reveals a displaced bone fragment *(arrow)* within the knee joint related to an avulsion of the tibial eminence. **B,** Axial CT scan shows the osseous fragment *(arrow)* attached to the circular posterior cruciate ligament *(open arrow)*.

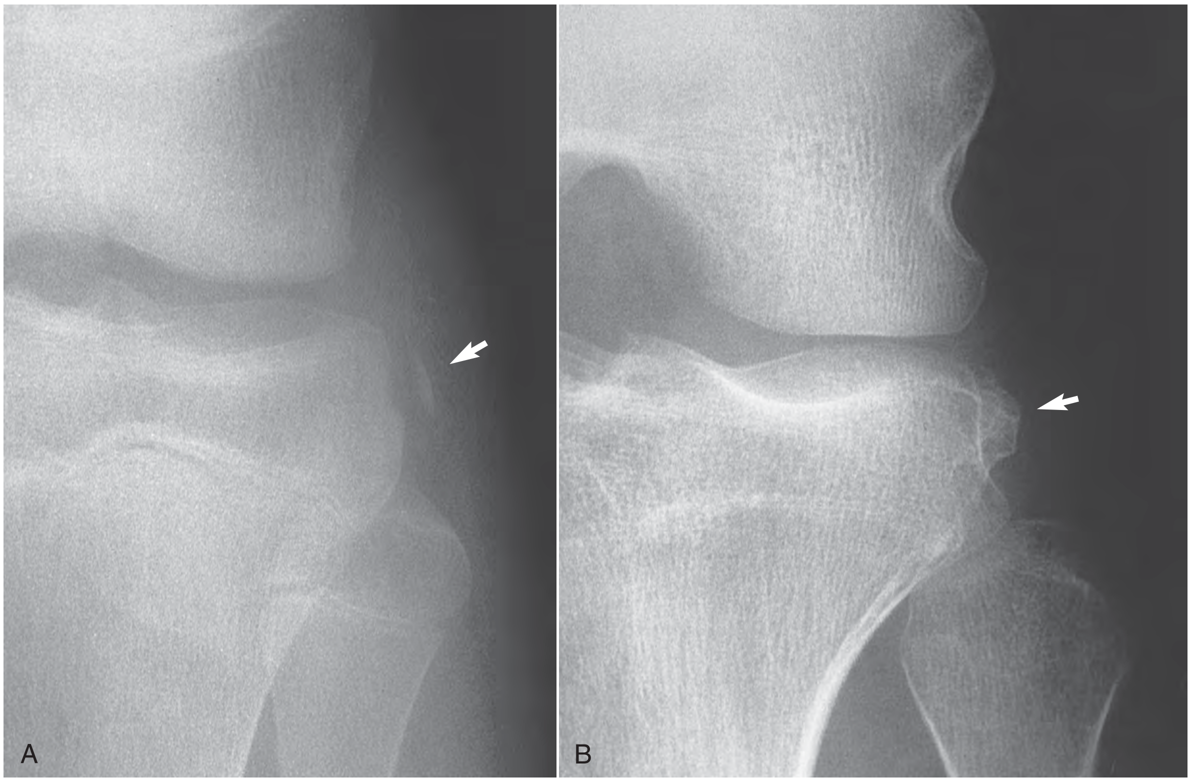

FIGURE 9–17 **Segond injury: lateral capsular avulsion.**[29] **A,** Acute situation. A thin, vertically oriented linear avulsion fracture is seen at the superolateral aspect of the lateral tibial condyle. **B,** Chronic situation. Anteroposterior intercondylar view in a 33-year-old man shows a well-defined bony excrescence arising from the lateral tibial rim proximal to the head of the fibula *(arrow)*. This appearance of an irregular outgrowth of bone is typical of a healed Segond injury, indicating a previous avulsion and disruption of the lateral joint capsule.

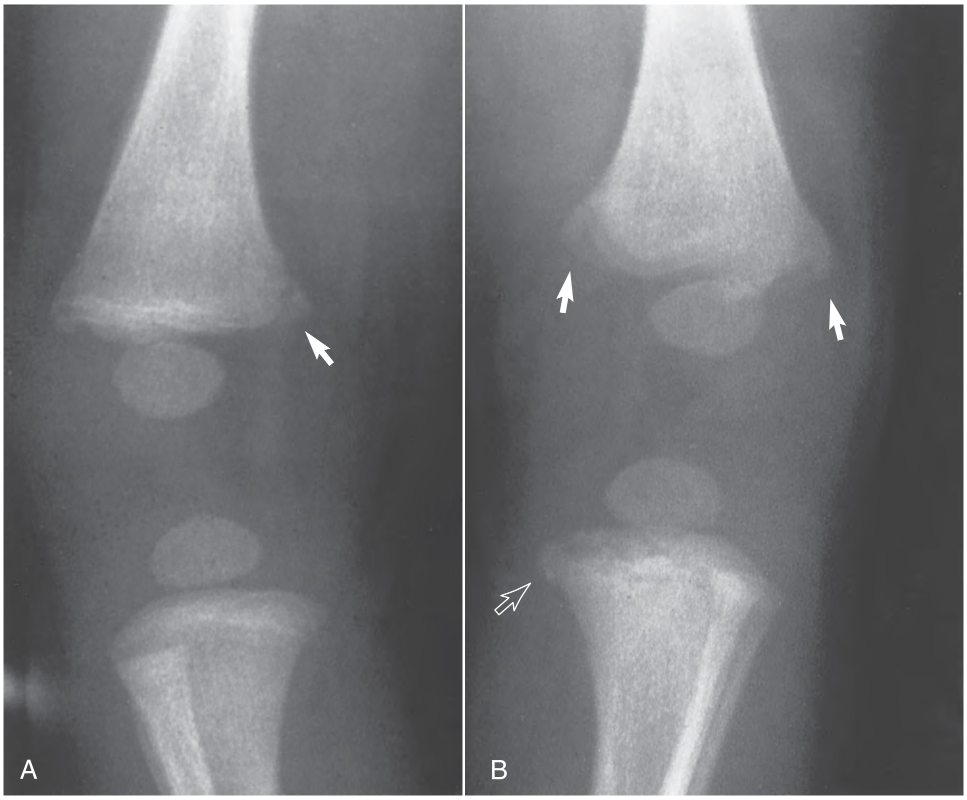

FIGURE 9–18 **Child abuse.**[30,31,123] **A-B,** Observe the irregularities and corner fractures of the proximal tibial metaphyseal margin *(open arrow)* and both distal femoral metaphyseal margins *(arrows)*. Metaphyseal lesions of child abuse classically involve the knee. These fractures tend to be less conspicuous when they are acute, and become more visible with healing. *(Courtesy D. Edwards, MD, San Diego.)*

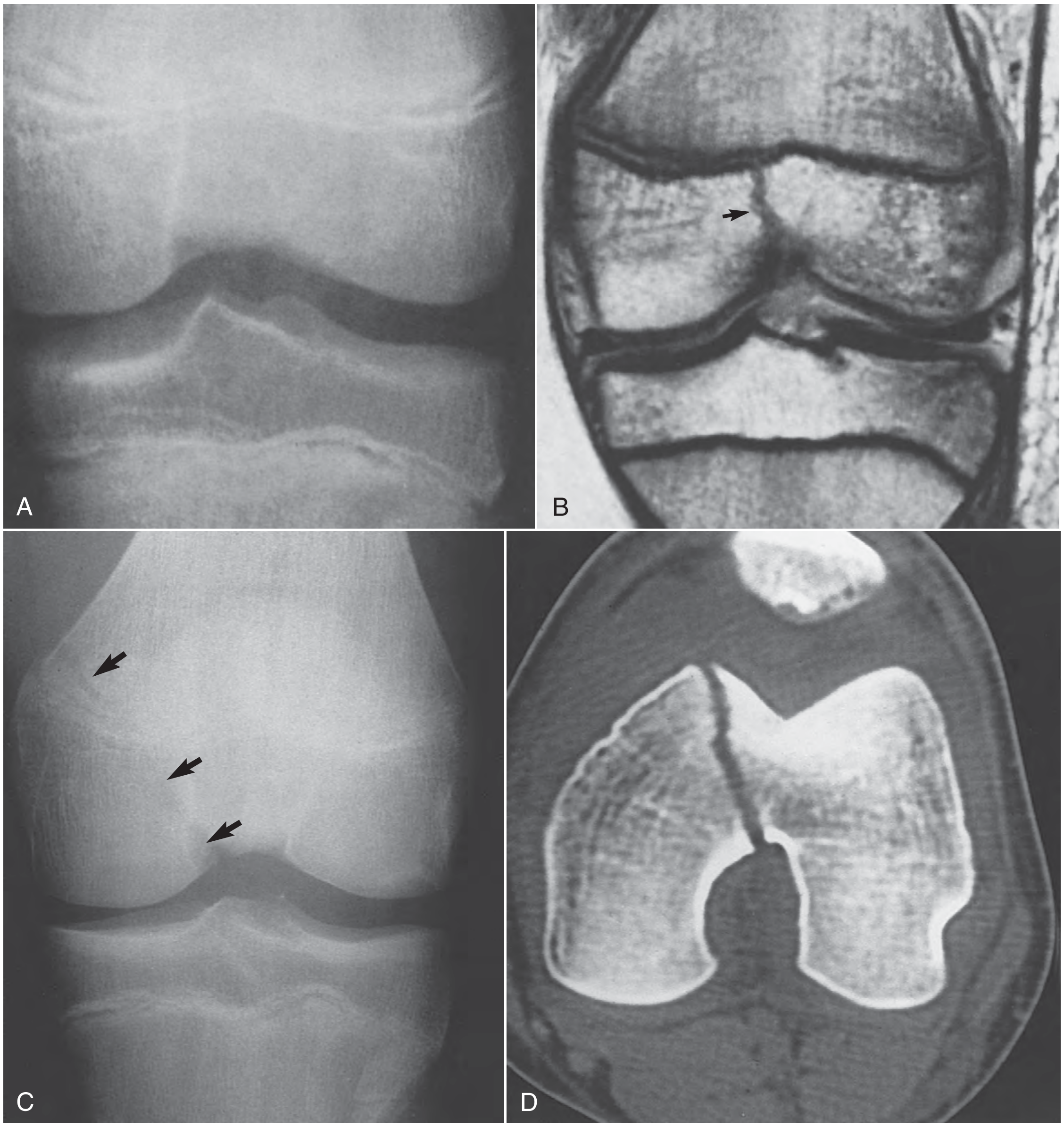

FIGURE 9–19 **Growth plate injuries: magnetic resonance (MR) imaging-distal portion of the femur.**[32] **A-B,** In a 13-year-old boy, a frontal radiograph **(A)** reveals no significant abnormality. A coronal T1-weighted (TR/TE, 800/20) spin echo MR image **(B)** shows a vertical fracture line *(arrow)* in the distal femoral epiphysis, indicative of a Salter-Harris type III growth plate injury. Bone contusions appear as regions of diminished signal intensity in the metaphysis and epiphysis of the distal portion of the femur and in the epiphysis of the proximal end of the tibia. **C-D,** Salter-Harris type IV injury. In **C,** a routine radiograph of a 15-year-old boy shows an intercondylar fracture through the medial condylar growth plate and the metaphysis and epiphysis of the distal portion of the femur *(arrows)*. In **D,** a transaxial CT scan shows the extent of the complete nondisplaced fracture. *(**A-B,** From Resnick D [ed]: Diagnosis of bone and joint disorders. 4th Ed. Philadelphia, Saunders, 2002, p. 2728.) **C-D,** Courtesy G. Greenway, MD, Dallas, Texas.)*

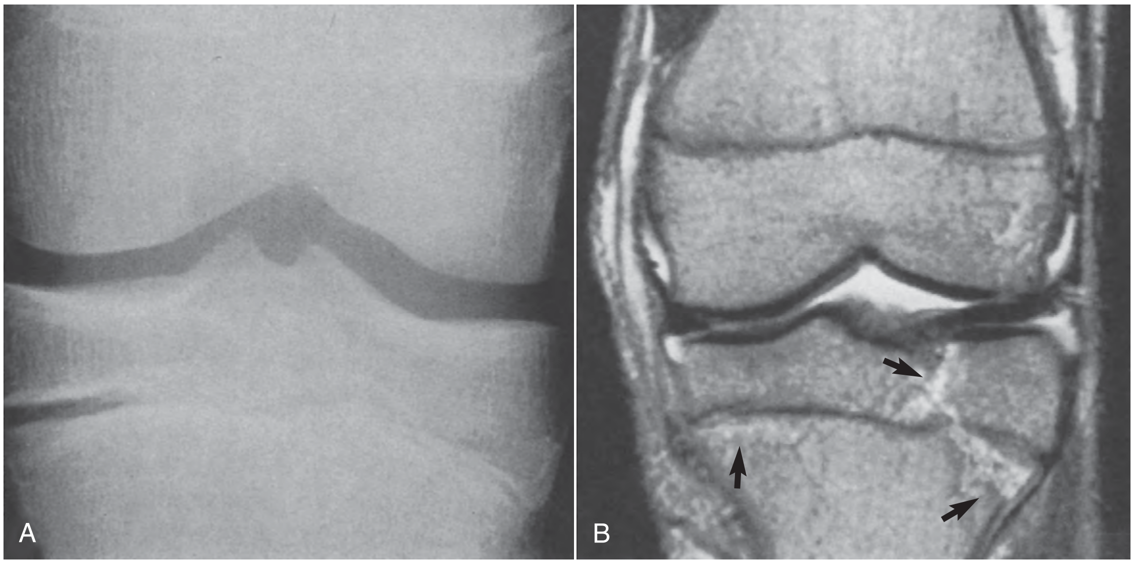

FIGURE 9–20 **Growth plate injuries: magnetic resonance (MR) imaging-proximal portion of the tibia.**[32] This young boy suffered an injury to the knee while playing soccer. **A,** Routine radiograph shows widening of the medial portion of the proximal tibial physis, suggesting a Salter-Harris type I injury. **B,** Coronal T2-weighted (TR/TE, 2000/80) spin echo MR image reveals high signal intensity *(arrows)* in the tibial epiphysis and metaphysis, consistent with a Salter-Harris type IV injury. High signal intensity also is seen in a bone contusion of the lateral portion of the distal femoral epiphysis and in and about the medial collateral ligament, indicating ligament disruption and soft tissue edema. A joint effusion is present. *(From Resnick D [ed]: Diagnosis of bone and joint disorders. 4th Ed. Philadelphia, Saunders, 2002.)*

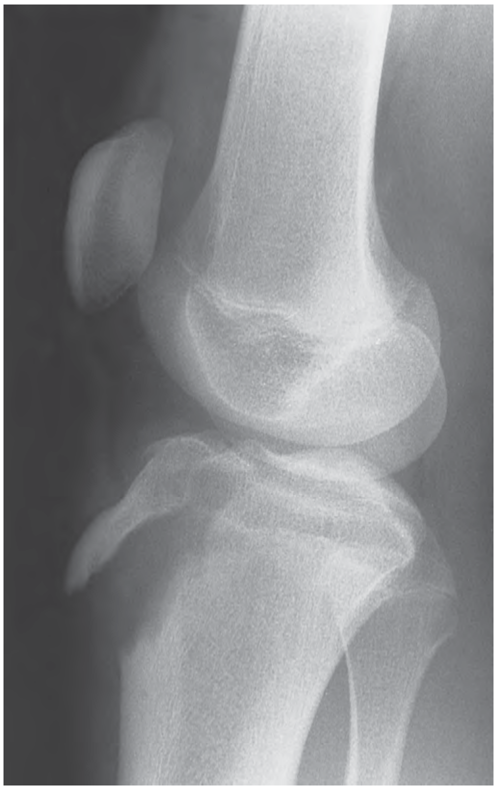

FIGURE 9–21 **Avulsion fracture: tibial tubercle apophysis.**[33,34] A lateral radiograph of the knee in this 14-year-old boy shows an extensive avulsion of a large segment of the tibial tubercle at the attachment of the patellar tendon. The fracture extends through the proximal tibial epiphysis into the articulation.

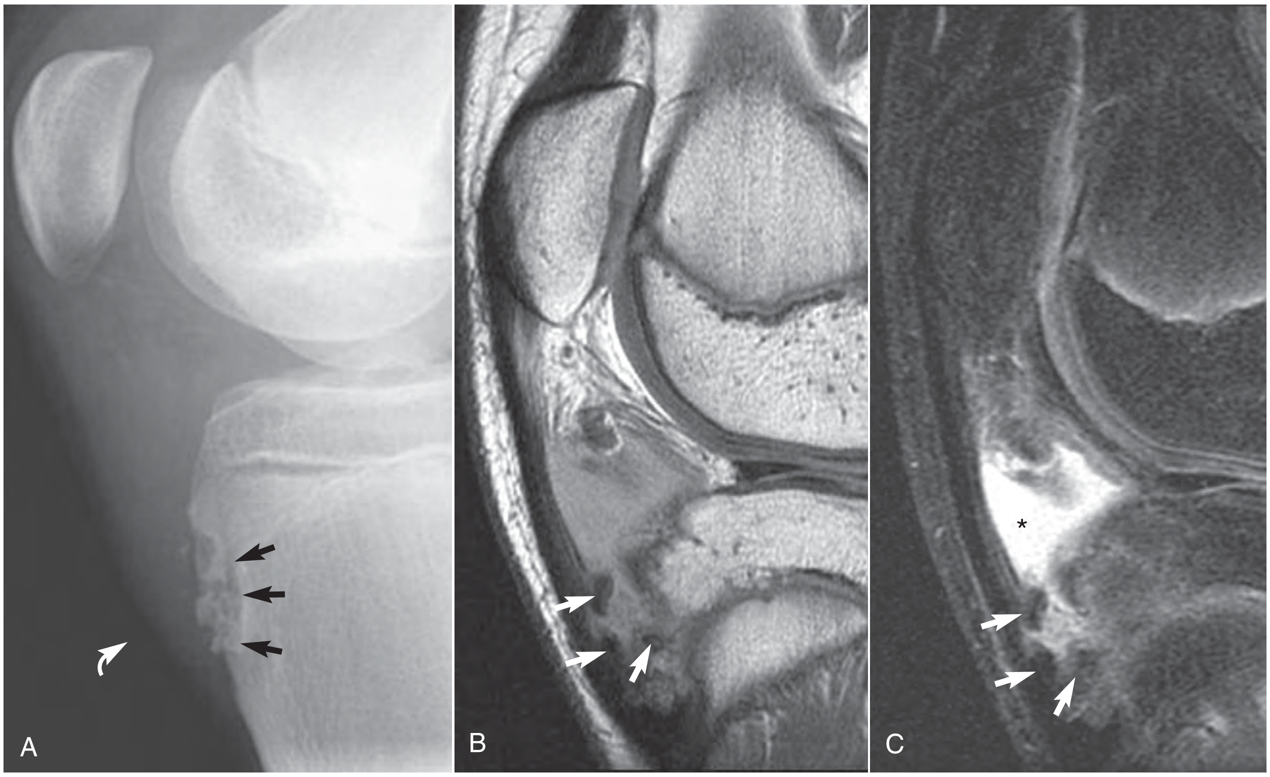

FIGURE 9–22 **Osgood-Schlatter disease.**[35,140] This 13-year-old physically active basketball player complained of right knee pain for several months. He was diagnosed clinically with Osgood-Schlatter disease. The lateral radiograph **(A),** obtained to help confirm the diagnosis and to exclude other causes of pain, reveals irregularity and fragmentation *(arrows)* of the tibial tubercle and soft tissue swelling *(curved arrow)*. A sagittal proton–density-weighted MR image **(B)** shows fragmentation of the tibial tuberosity *(arrows)* just proximal to the attachment of the thickened patellar tendon. A sagittal proton–density-weighted MR image with fat suppression **(C)** also shows high signal intensity edema surrounding the fragmentation *(arrows)* and within the Hoffa fat pad (*).

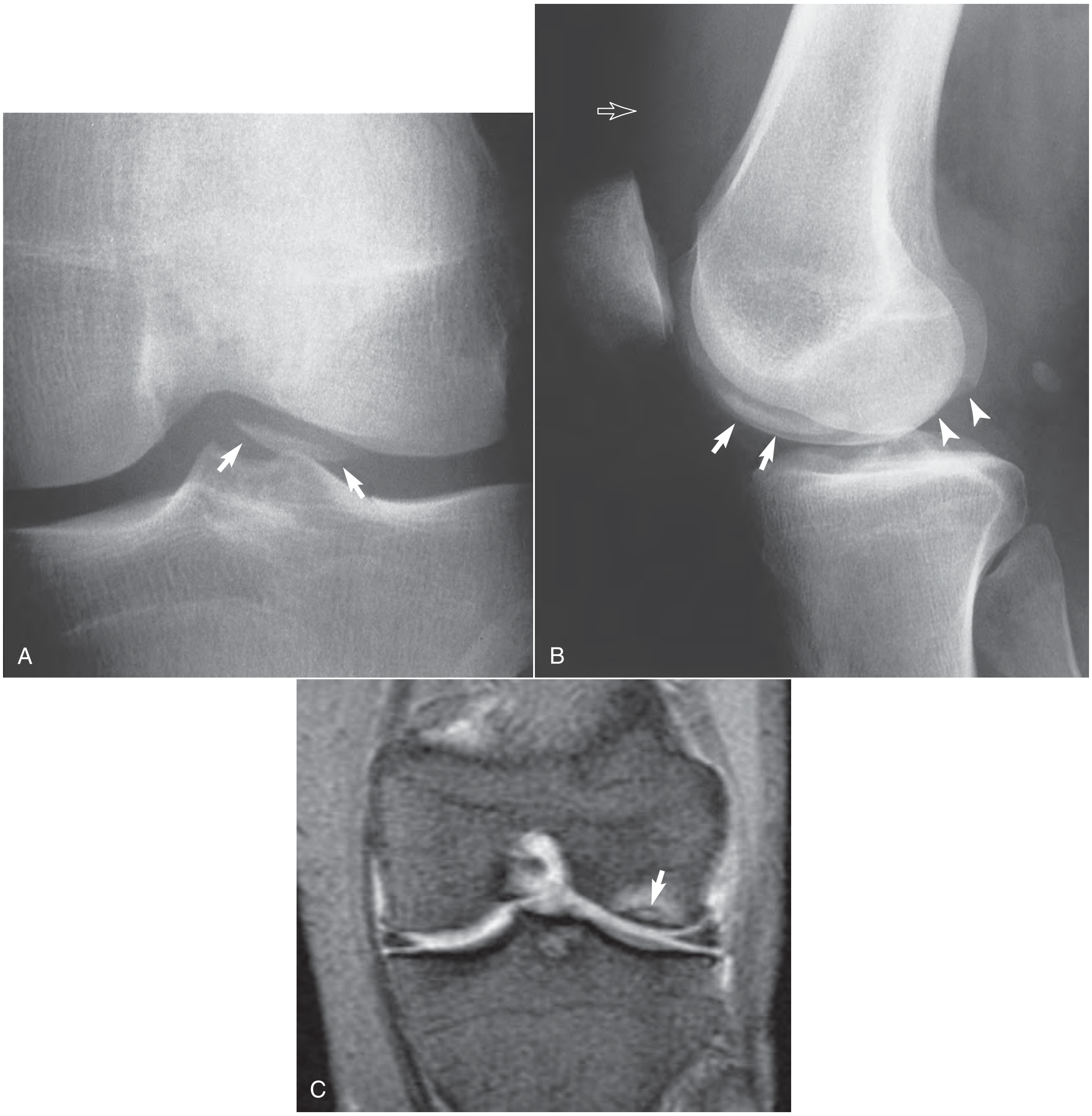

FIGURE 9–23 **Osteochondral fracture.**[36,37] Frontal **(A)** and lateral **(B)** radiographs of this 23-year-old man show a crescent-shaped osseous fragment *(arrows)* and a corresponding radiolucent defect in the posterior aspect of the lateral femoral condyle *(arrowheads)*. A large joint effusion *(open arrow)* displaces the superior portion of the patella. **(C)** A coronal proton–density-weighted fat-suppressed MR image in this 72-year-old woman with an acute anterior cruciate ligament tear (note the empty lateral aspect of the intercondylar notch) has a corresponding osteochondral fracture of the lateral femoral condyle, from impaction of the posterolateral tibial plateau at the time of the ACL tear. This is seen as a broad zone of high signal intensity bone marrow edema in the subchondral surface of the bone, and a small arc of low signal intensity corresponding to the trabecular fracture line *(arrow)*.

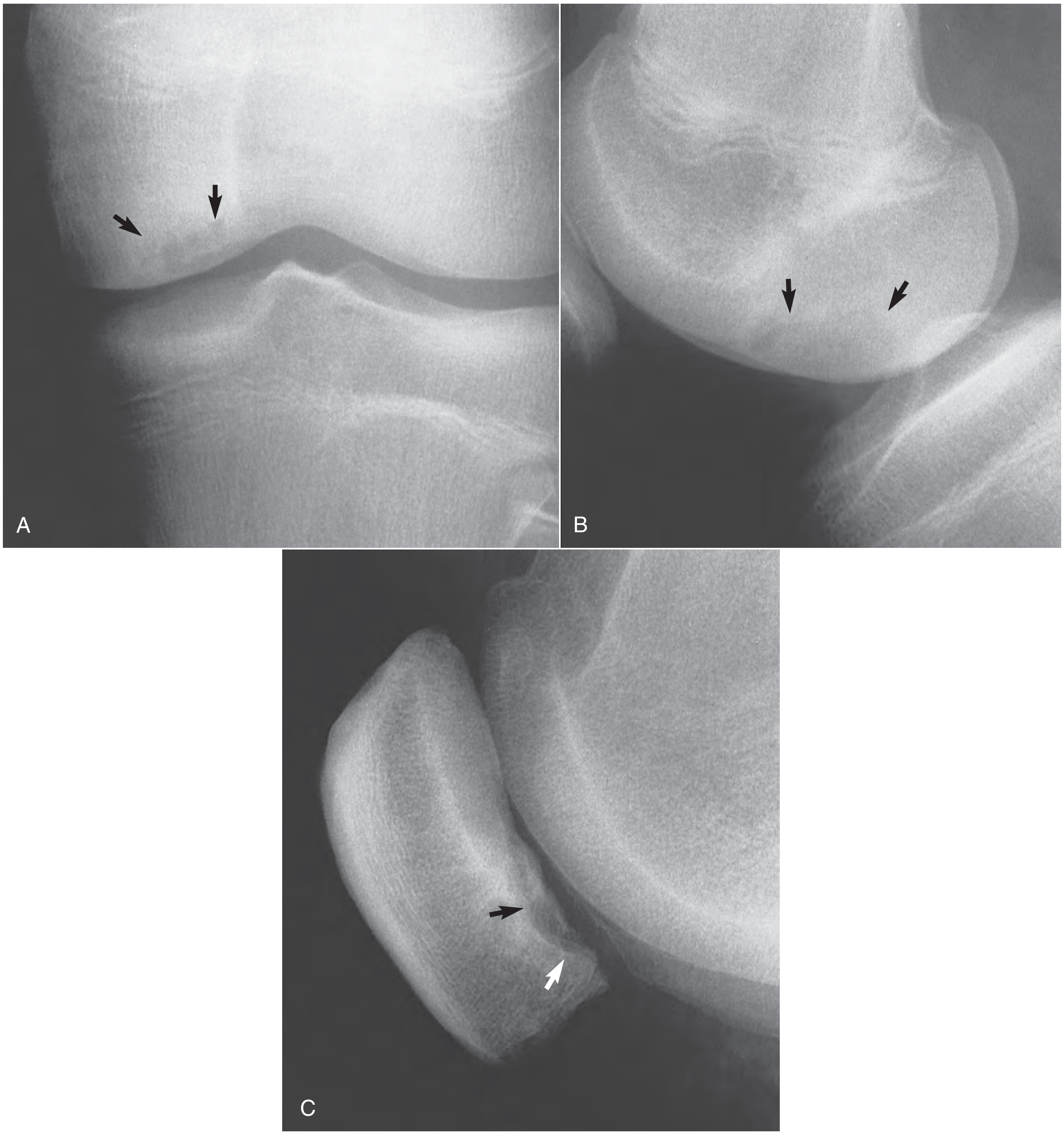

FIGURE 9–24 Osteochondritis dissecans.[38-41] **A-B,** Distal portion of the femur. Frontal **(A)** and lateral **(B)** radiographs of this 15-year-old patient show a classic subchondral radiolucent defect in the lateral aspect of the medial femoral condyle *(arrows)*. Eighty-five percent of cases of osteochondritis dissecans affect the medial femoral condyle, most commonly at the lateral aspect. **C,** Patella. Lateral radiograph shows a radiolucent defect in the articular surface of the patella *(arrows)*. Degenerative changes are also noted in the superior aspect of the patellofemoral joint. The patella is an uncommon site for osteochondritis dissecans. The medial patellar facet is involved most frequently.

TABLE 9-7 Dislocations About the Knee139*

Entity	Figure(s)	Characteristics	Complications and Related Injuries
Femorotibial Dislocation			Associated fractures
All types		Rare but serious injury High-energy trauma from automobile collisions, industrial injuries, or falls from a considerable height Occasionally occurs with sports injuries Closed injuries more common than open injuries	Visceral and head injuries Popliteal artery laceration or thrombosis (25%-50% of cases) Popliteal vein and peroneal nerve injury Capsular, meniscal, and ligamentous injury Disruption of four major knee ligaments or both cruciate ligaments implies that a dislocation has occurred
Anterior	9-25	30%-50% of all knee dislocations Hyperextension injury Tearing of posterior capsule, posterior cruciate ligament, and anterior cruciate ligament	
Posterior		Next in frequency to anterior dislocations Crushing blows to the anterior surface of the proximal end of the tibia	Injury of extensor mechanism of knee
Lateral, medial, and rotary		Uncommon Valgus, varus, or torsional injury	Collateral ligament damage
Patellar Dislocation[44,136]	9-26	Direct blow or exaggerated contraction of quadriceps mechanism Lateral displacement predominates Patellar subluxation or dislocation is often a transient, recurrent problem Spontaneous reduction usually occurs ***Predisposing factors*** Patella alta Deficient height of lateral femoral condyle Shallowness of the patellofemoral groove Genu valgum or genu recurvatum Lateral insertion of patellar tendon Muscular weakness (vastus medialis muscle) Excessive tibial torsion	Osteochondral fracture of medial patellar facet and lateral femoral condyle Patellar tracking disorders Retinacular injury of femoral or patellar site of attachment (76% of cases) Contusions of femoral condyle and patella
Proximal Tibiofibular Joint Sprain and Dislocation[19,137]	9-27	Dislocation is a rare injury Seen in parachuting and horseback riding injuries Adduction of the knee in the flexed position Anterior dislocation twice as common as posterior dislocation Subtle radiographic findings of anterior dislocation include anterior and lateral fibular displacement MR imaging demonstrates ligamentous sprain	Common peroneal nerve injury

* See also Table 1-6.

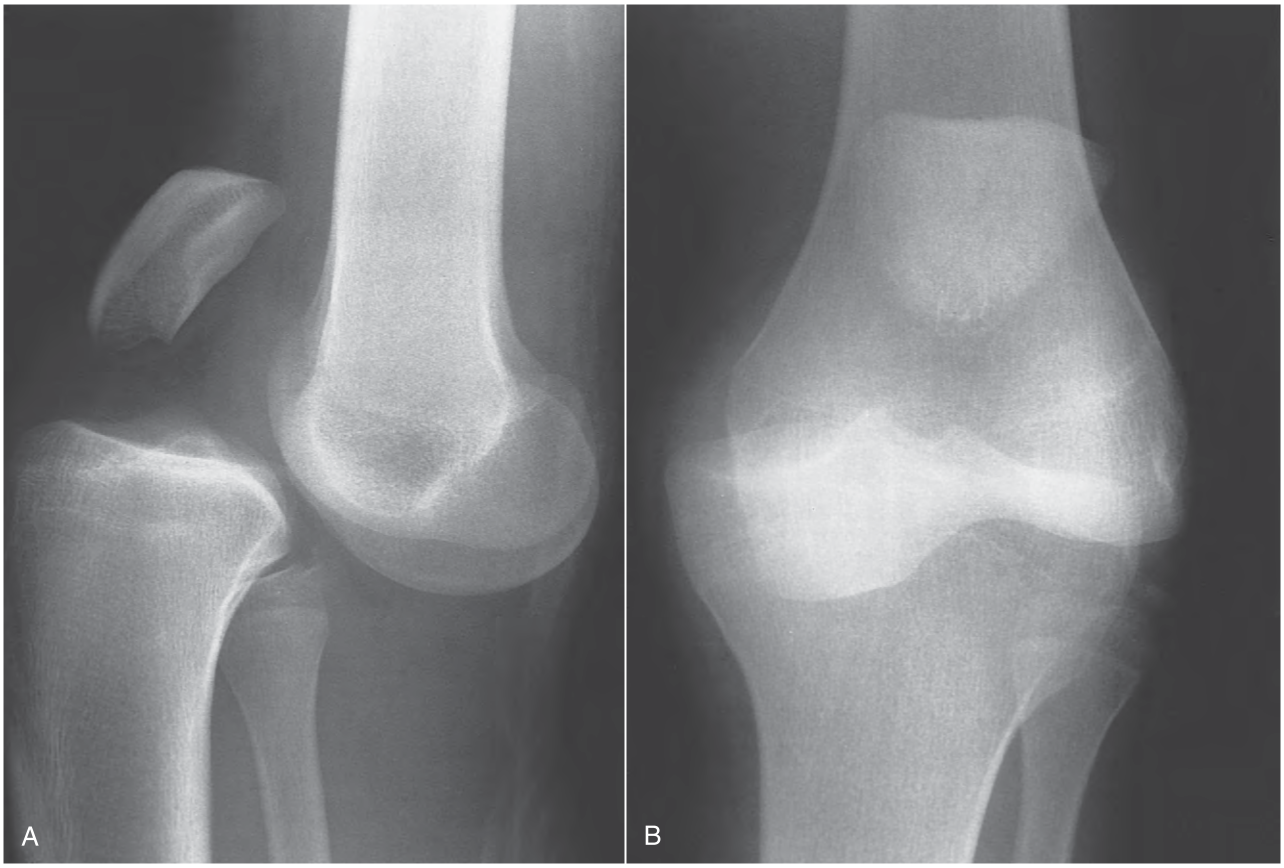

FIGURE 9–25 **Acute anterior femorotibial dislocation.**[42,43] **A,** Lateral radiograph of the knee in this 18-year-old man shows anterior dislocation of the tibia and fibula. **B,** Anteroposterior radiograph shows marked overlap of the tibia and femur and medial dislocation of the tibia with respect to the femur. Nearly all cases of such dislocation result in complete disruption of the cruciate ligaments, and many also result in injury to the menisci, collateral ligaments, peroneal tendon, and popliteal artery.

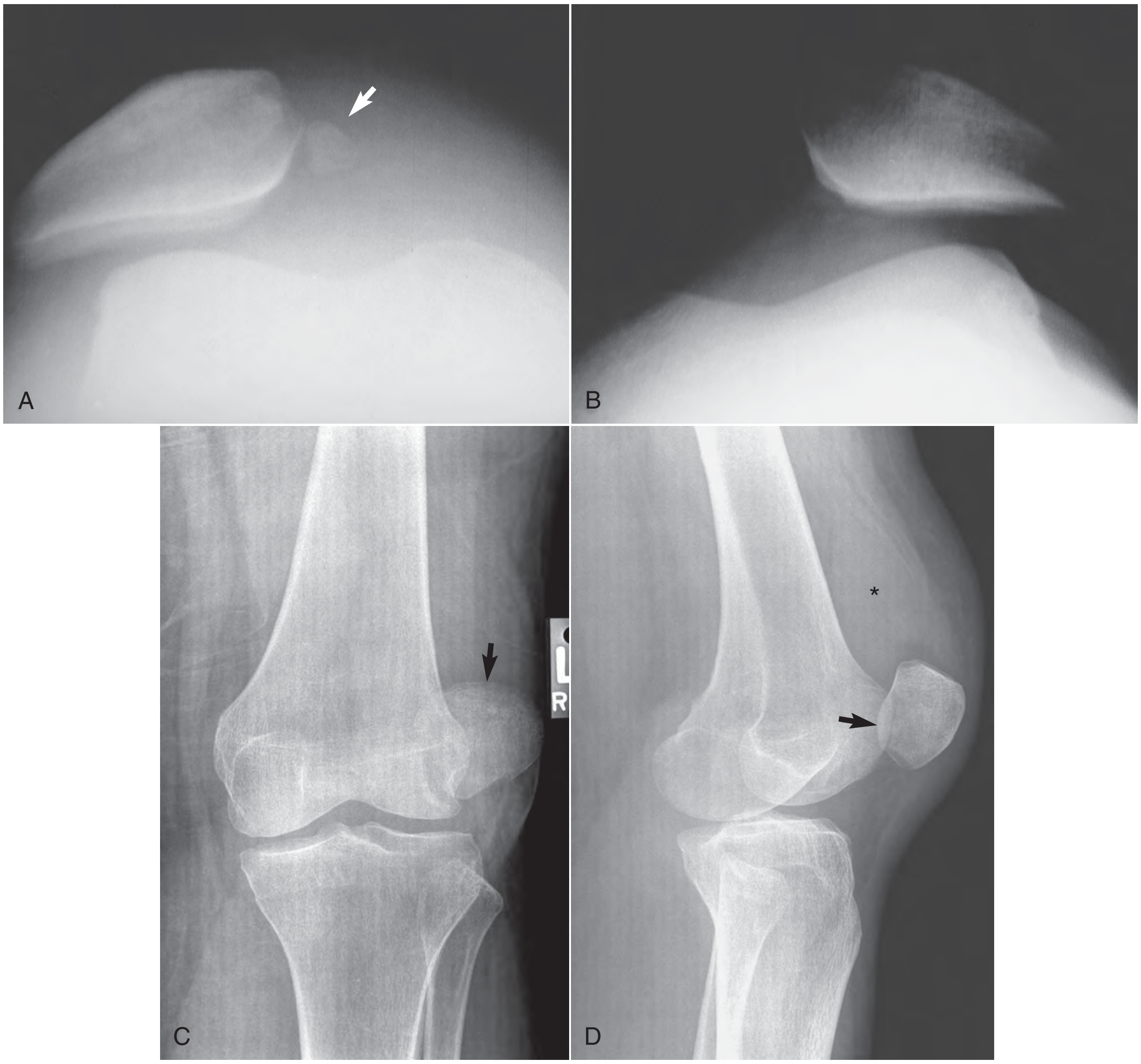

FIGURE 9–26 **Patellar subluxation and dislocation.**[44] **A-B,** Bilateral dislocation. Axial radiographs of the knee in this 25-year-old woman reveal bilateral lateral patellar dislocations. Observe the fracture of the right medial patellar facet resulting from avulsion at the site of attachment of the medial retinaculum *(arrow)*. Note also the straight line appearance of the lateral patellar facet and the gentle slope of the lateral femoral condyle, both of which predispose to patellofemoral instability with subluxation and dislocation. Lateral patellar dislocation often is a transient phenomenon, with spontaneous reduction. **C-D,** Unilateral dislocation. In a 42-year-old woman with a history of recurrent dislocations, anteroposterior and oblique radiographs show significant lateral dislocation of the patella. Severe prepatellar soft tissue swelling and intraarticular effusion (*) are also evident.

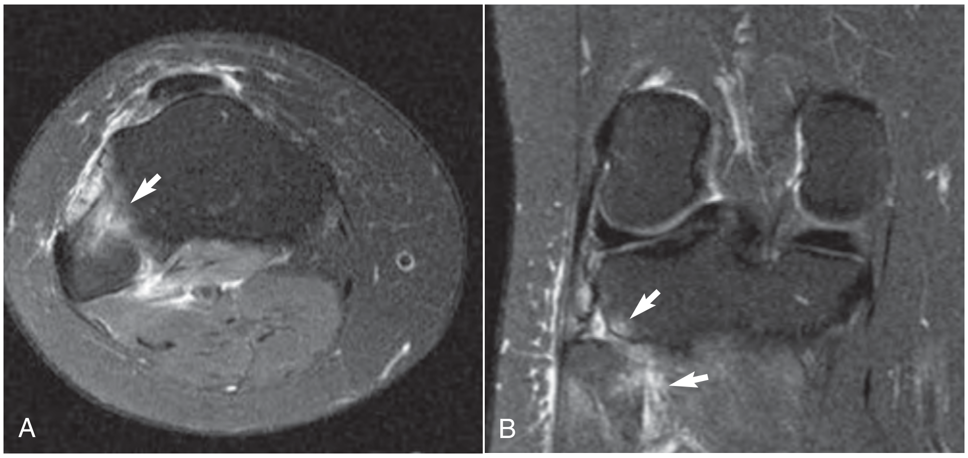

FIGURE 9–27 **Superior tibiofibular joint: ligament sprain and bone contusion.** This 48-year-old woman fell 4 weeks before the MR examination was performed. Axial **(A)** and coronal **(B)** proton-density fat-suppressed MR imaging reveals significant high signal intensity *(arrows)* within the fibular head and corresponding region of the lateral tibial condyle and within the ligaments and the superior tibiofibular joint itself. No actual fracture or dislocation is observed.

TABLE 9-8 Internal Derangements—Synovial Disorders and Bone Contusions*

Entity	Figure(s), Table(s)	Characteristics	Complications and Related Disorders
Joint effusion[45,46]	9-28, 9-20, 9-23, 9-35, 9-46, *B*, 9-55, *C*, 9-58, *D*, 9-64, *D*, 9-71, 9-74, 9-80, *B*	Accumulation of excessive synovial fluid within joint Enlargement of the suprapatellar recess seen on lateral radiographs, CT, MR and ultrasonogram ***MR imaging findings*** Low signal intensity on T1-weighted and high signal intensity on T2-weighted spin echo MR images	Bland effusion associated with acute injury or internal joint derangement Differential diagnosis: pyarthrosis, hemarthrosis, or effusion associated with proliferative synovitis Absence of effusion with severe trauma may indicate capsular rupture of such a degree that fluid extravasates into the soft tissues surrounding the knee
Hemarthrosis[47]	9-68, *E, F,* 9-71, 9-80, *B*	Accumulation of blood within joint Hemarthroses usually result in joint effusion within the first few hours after injury As many as 75% of acute traumatic hemarthroses are associated with anterior cruciate ligament injuries With MR imaging, single fluid level may be seen in acute stage and hemosiderin deposition of low signal intensity in the chronic stage	
Lipohemarthrosis[48-50]	9-29	Accumulation of blood and lipid material within synovial fluid Fat-blood interface seen on cross-table, horizontal beam lateral radiographs and transaxial and sagittal MR images Double fluid-fluid levels on MR images are more specific for lipohemarthrosis than a single fluid-fluid level	Usually related to acute intraarticular fracture May accompany fractures of the tibial plateau, fibula, patella, or distal portion of femur and injury to cartilage, ligaments, fat pads, or synovium
Synovial cysts[51,52]	9-30	Most common in popliteal region Also termed *Baker cysts* Communication between the synovial cavities and bursae Enlarged palpable mass with or without pain Ruptures can simulate thrombophlebitis MR, CT, ultrasonography, or arthrography will demonstrate synovial cysts	Any inflammatory, degenerative, traumatic or neoplastic condition that produces knee effusion may lead to synovial cysts: rheumatoid arthritis, degenerative joint disease, gout, villonodular synovitis, synovial osteochondromatosis, and other articular diseases
Periarticular ganglion cysts[53]		Loculated or septated cysts containing jellylike viscous fluid Adjacent to fibular head or proximal tibiofibular joint May also occur at the tibial insertion of the pes anserinus tendons, where it has been referred to as *pes anserinus bursitis*	May lead to common peroneal nerve compression May rarely result in anterior compartment syndrome
Intraarticular ganglion cysts[54]	9-31	Infrequent Arise adjacent to the infrapatellar fat bodies and the cruciate ligaments	May result in knee pain similar to that of meniscal tears

* See also Tables 1-6 and 1-10.

TABLE 9-8 Internal Derangements—Synovial Disorders and Bone Contusions—cont'd

Entity	Figure(s), Table(s)	Characteristics	Complications and Related Disorders
Synovial plicae[55]	9-32	Remnants of embryonic synovial tissue that divided the joint into three separate compartments during early development May be a normal finding in adults Occasionally these membranes become pathologically thickened, leading to symptoms referred to as the *plica syndrome* *Three most common plicae:* infrapatellar, suprapatellar, and medial patellar	Symptoms may mimic those of arthritis, meniscal injury, and other internal derangements of the knee Occasional flexion contractures of the knee
Bursitis[56]	9-33	Any bursa about the knee may become inflamed Prepatellar bursitis (housemaid's knee), deep or superficial infrapatellar bursitis, pes anserinus bursitis, and suprapatellar bursitis Ultrasonography and MR imaging are best techniques for evaluating bursitis High signal intensity on T2-weighted images	Prepatellar bursitis may develop from chronic stress with prolonged kneeling Other causes of bursitis include infection, synovial inflammatory disease, and gouty arthropathy
Pigmented villonodular synovitis[57,58,127]	9-34 Table 1-10	Knee is most frequent site of involvement ***Imaging findings*** Cystic erosions on both sides of the joint Hemorrhagic joint effusion Eventual osteoporosis Well-preserved joint space until late in the disease	
Idiopathic synovial osteochondromatosis[59]	9-35, 9-36 Table 1-10	***Imaging findings*** Multiple intraarticular or periarticular collections of calcification of variable size and density Erosion of adjacent bone Noncalcified bodies are best demonstrated with arthrography or MR imaging	Primary idiopathic synovial osteochondromatosis leads to secondary osteoarthrosis and, infrequently, to malignant transformation (fewer than 5% of cases) Secondary synovial osteochondromatosis may occur as a result of osteoarthrosis
Bone contusion (bruise)[130,131]	9-37	Posttraumatic bone marrow changes demonstrated on MR imaging from a combination of hemorrhage, infarction, edema and microtrabecular compression fractures Radiographically invisible ***MR imaging findings*** *T1-weighted images:* Geographic nonlinear areas of signal loss *T2-weighted fat suppression images:* High signal intensity areas Usually in a subchondral location adjacent to acute soft tissue injury	Often accompanies acute ligament, tendon, and meniscal injuries May resemble nontraumatic marrow edema syndromes: differential diagnosis based on clinical history

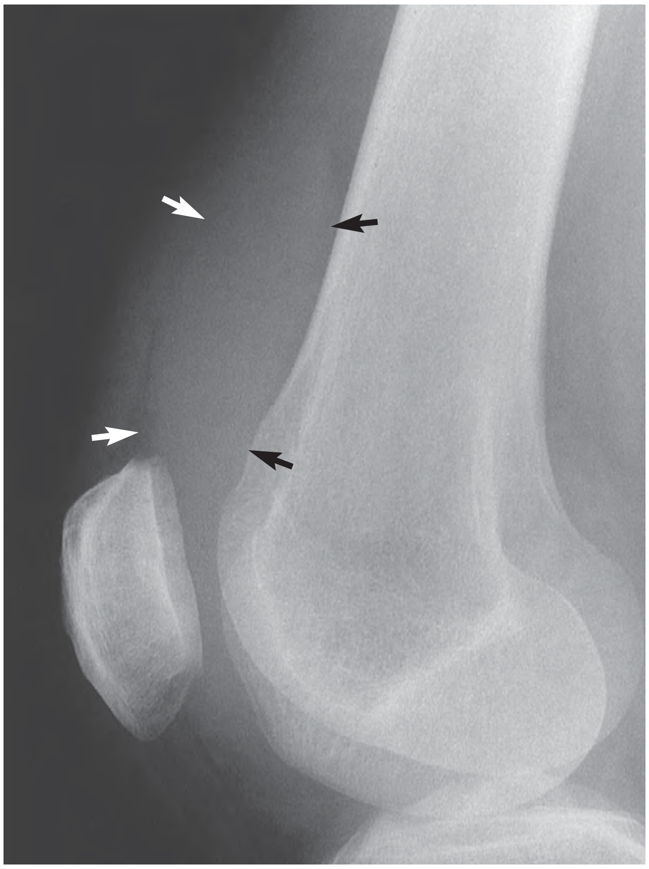

FIGURE 9–28 Joint effusion.[45,46] Observe the distention of the suprapatellar pouch *(arrows)* in this patient with an injury to the knee. Bloody effusions (hemarthroses) generally appear within the first few hours after injury, and nonbloody effusions usually appear 12 to 24 hours after injury.

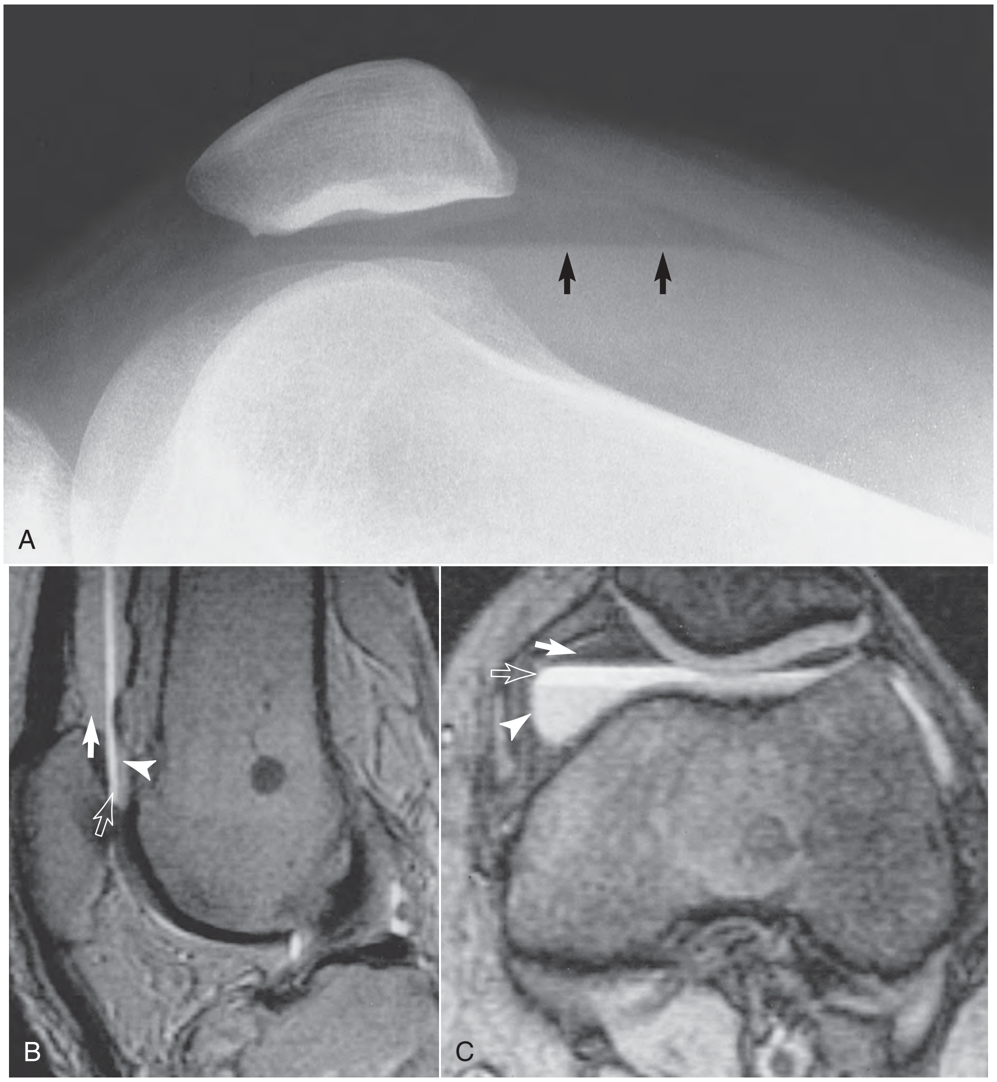

FIGURE 9–29 **Lipohemarthrosis.**[48-50] **A,** Routine radiography. This cross-table, horizontal-beam lateral radiograph shows a straight, radiodense fluid line at a fat-blood interface *(arrows)*. This finding strongly suggests an intraarticular fracture, the fat and blood being released from bone marrow after cortical fracture. **B-C,** MR imaging. In **B,** a different patient, a sagittal T2-weighted (TR/TE, 2000/70) spin echo MR image shows three distinct layers. The uppermost layer *(solid arrow)* represents fat, the middle layer *(open arrow)* contains serum, and the lowest layer *(arrowhead)* contains erythrocytes. A band representing chemical shift artifact at the interface of serum and fat is difficult to identify. In **C,** a transaxial multiplanar gradient recalled (MPGR) (TR/E, 500/11; flip angle, 15 degrees) MR image reveals these same layers *(solid* and *open arrows, arrowhead)* and a band representing chemical shift artifact. *(**B-C,** From Resnick D, Kang HS, Pretterklieber ML: Internal derangements of joints. 2nd Ed. Philadelphia, Saunders, 2006, p. 1579.)*

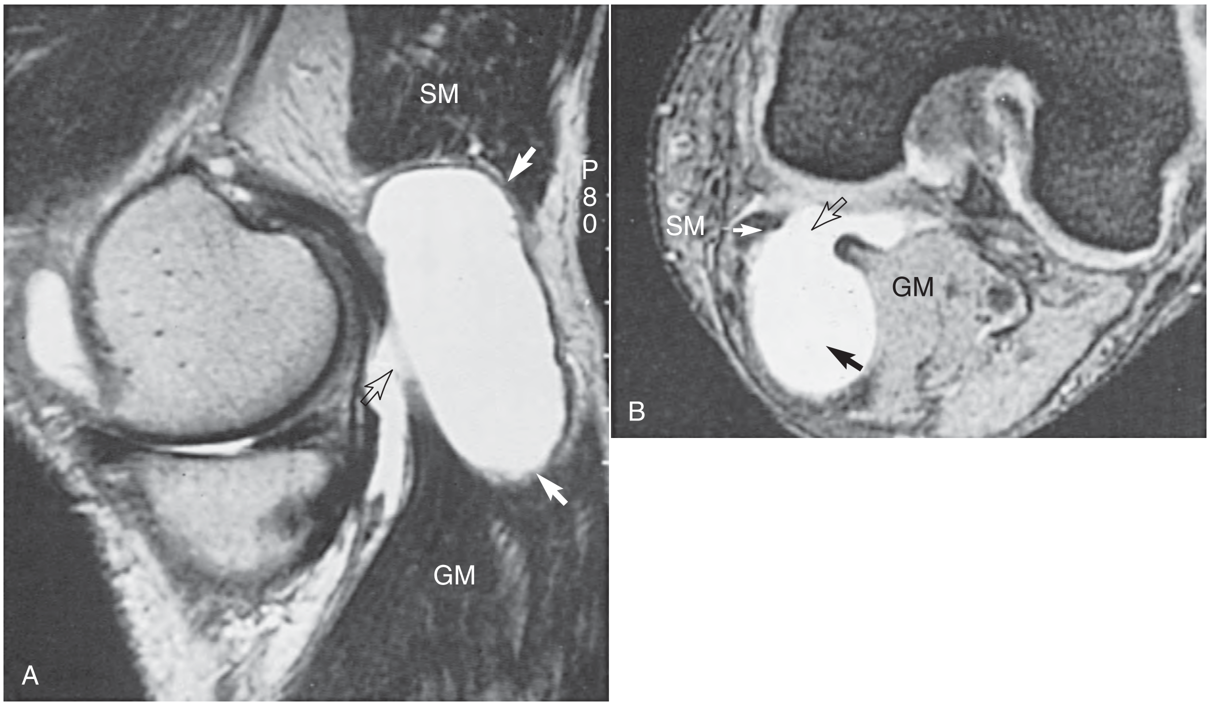

FIGURE 9–30 **Synovial cysts: MR imaging.**[51,52] **A,** Sagittal T2-weighted (TR/TE, 4000/76) fast spin echo MR image shows a channel *(open arrow)* leading from the joint into a large synovial cyst *(solid arrows)* located between the semimembranosus muscle (SM) and the medial head of the gastrocnemius muscle (GM). **B,** Transaxial MPGR (TR/E, 500/11; flip angle, 15 degrees) MR image shows the communicating channel *(open arrow)* and the synovial cyst *(solid black arrow)* located between the semimembranosus muscle (SM) and the medial head of the gastrocnemius muscle (GM). *(From Resnick D, Kang HS, Pretterklieber ML: Internal derangements of joints. 2nd Ed. Philadelphia, Saunders, 2006, p. 1591.)*

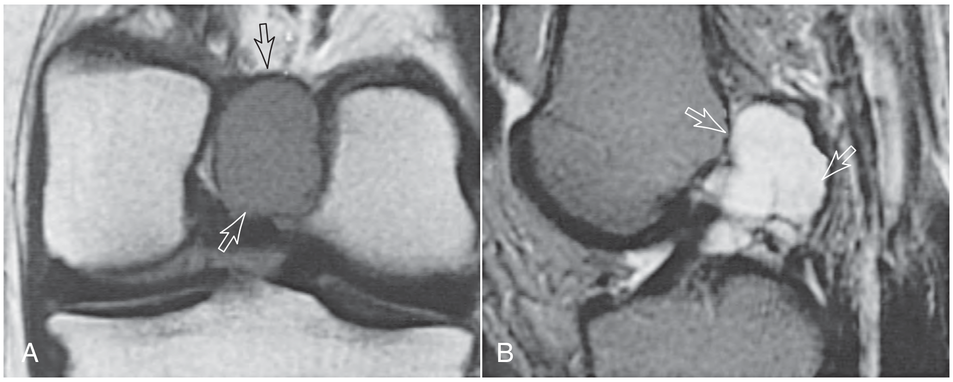

FIGURE 9–31 **Intraarticular ganglion cysts: MR imaging-posterior cruciate ligament.**[54] Coronal T1-weighted (TR/TE, 800/25) spin echo MR image **(A)** and sagittal T2-weighted (TR/TE, 2000/80) spin echo MR image **(B)** show the large ganglion cyst *(open arrows)* adjacent to the posterior cruciate ligament. *(From Resnick D, Kang HS, Pretterklieber ML: Internal derangements of joints. 2nd Ed. Philadelphia, Saunders, 2006, p. 1596.)*

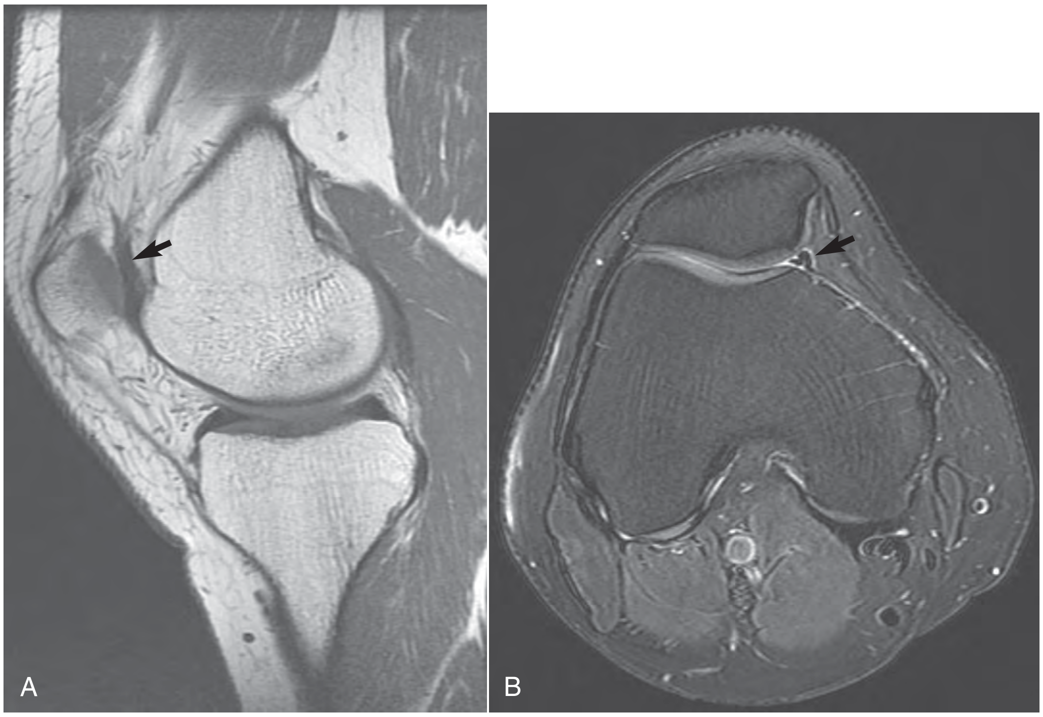

FIGURE 9–32 **Synovial plica.**[55] This 27-year-old man developed knee pain and locking. Sagittal proton-density **(A)** and axial proton-density fat suppressed **(B)** MR images show a linear low signal structure within the medial patellofemoral joint representing a thickened medial synovial plica *(arrows)*.

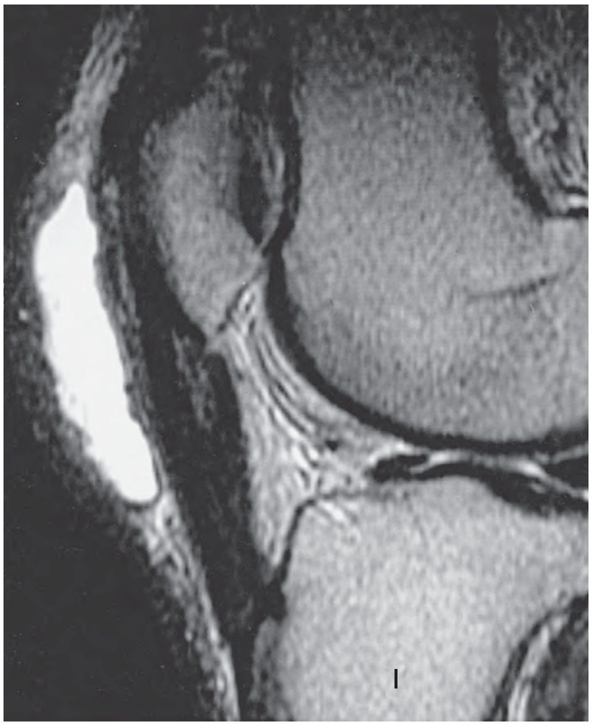

FIGURE 9–33 **Prepatellar bursitis (housemaid's knee): magnetic resonance (MR) imaging.**[56] Sagittal T2-weighted (TR/TE, 2200/80) spin echo MR image shows the fluid-filled bursa and a thickened, partially torn patellar tendon. *(From Resnick D, Kang HS, Pretterklieber ML: Internal derangements of joints. 2nd Ed. Philadelphia, Saunders, 2006, p. 1606.)*

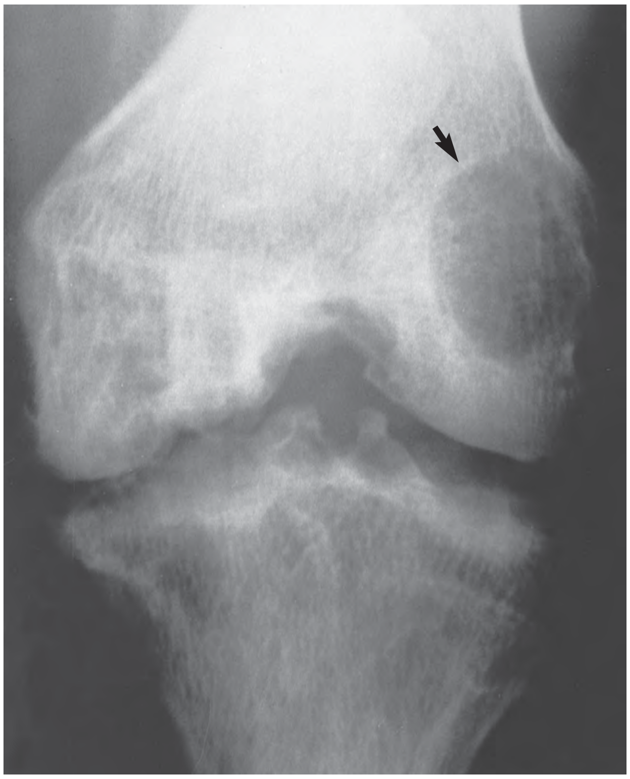

FIGURE 9–34 **Pigmented villonodular synovitis.**[57,58,127] Multiple erosions are seen within the subchondral bone of the femur and the tibia, creating an irregular appearance of the articular surfaces. A large cyst is present in the lateral femoral condyle *(arrow)*. The knee is the most common articulation to be affected in pigmented villonodular synovitis. *(Courtesy H. Griffiths, MD, Minneapolis, Minn.)*

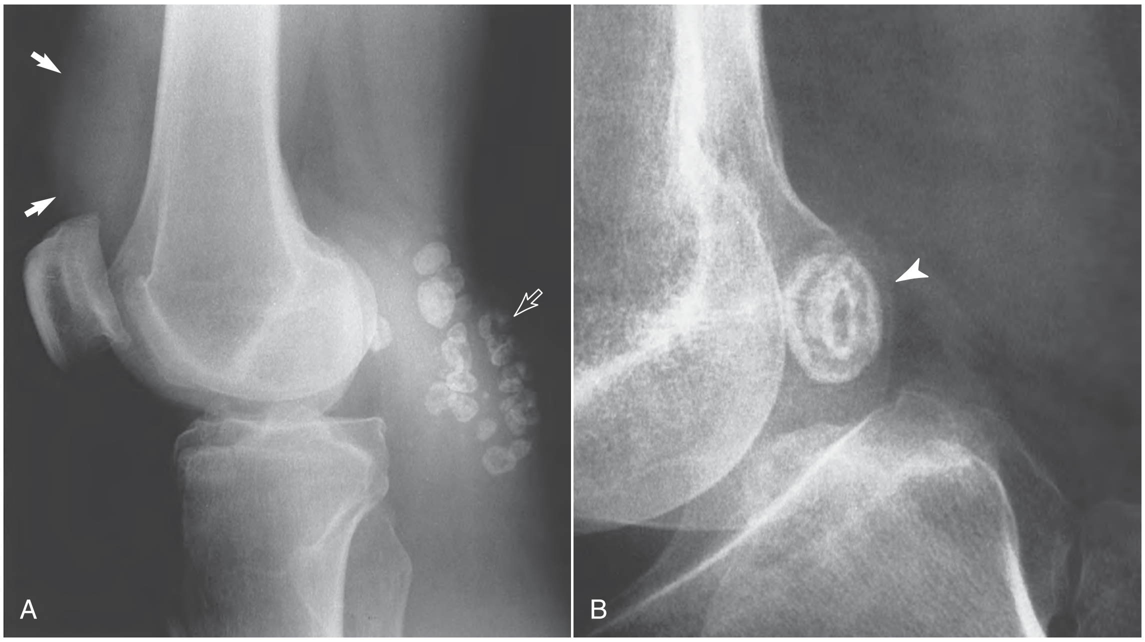

FIGURE 9–35 **Secondary synovial osteochondromatosis: intraarticular osteochondral bodies.**[59] **A,** Multiple round and ovoid osseous bodies *(open arrow)* are evident posterior to the knee within a synovial (Baker) cyst. The bodies have a somewhat stippled or laminated appearance. Degenerative changes and a large joint effusion *(arrows)* are also present. **B,** In another patient, a solitary oval, laminated intraarticular body is seen *(arrowhead)*. These osteochondral bodies are usually degenerative or posttraumatic. A primary idiopathic form of synovial osteochondromatosis also occurs in which cartilage is formed by the synovium.

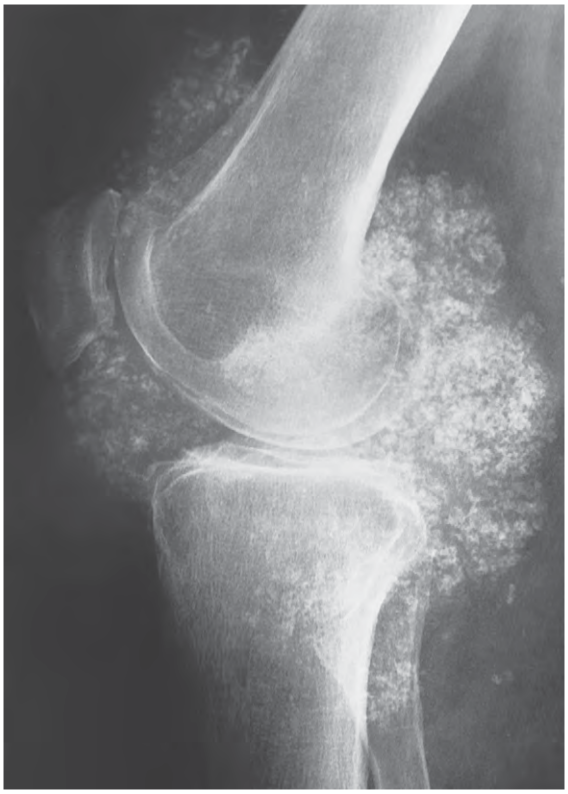

FIGURE 9–36 **Recurrent primary idiopathic synovial osteochondromatosis.**[59] Observe the multiple juxtaarticular radiodense, osteocartilaginous bodies within the joint cavity, especially in the infrapatellar, suprapatellar, and popliteal regions. This patient already has had two operations to remove osteocartilaginous bodies. Idiopathic synovial osteochondromatosis represents metaplastic or neoplastic proliferation of cartilaginous bodies by the synovial membrane. Noncalcified lesions are best evaluated by arthrography. *(Courtesy A.G. Bergman, MD, Stanford, Calif.)*

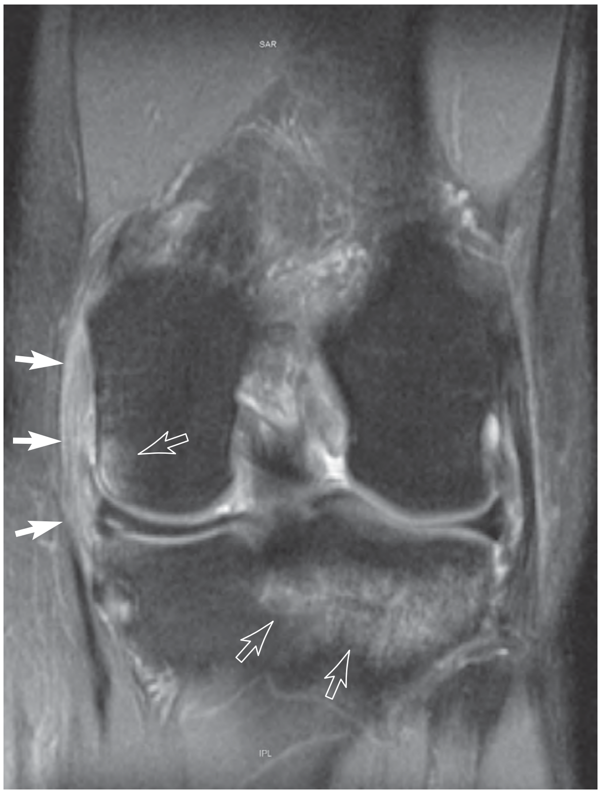

FIGURE 9–37 **Bone contusion.**[130,131] This 28-year-old man sustained a valgus injury to his knee. A coronal proton-density fat suppressed MR image reveals a medial collateral ligament tear *(arrows)* and high signal intensity bone marrow edema underneath the articular surface of the lateral tibial plateau and in the medial aspect of the femoral condyle *(open arrows)*. Bone contusions represent trabecular microfracture from bone impaction often occurring in conjunction with ligament, tendon, or articular cartilage injury.

TABLE 9-9 Internal Derangements—Meniscal Disorders

Entity	Figure(s)	Characteristics	Complications and Related Disorders
Meniscal degeneration[60]		Encountered in elderly patients Mucinous or eosinophilic degeneration ***Radiographic findings (rare)*** Intrameniscal gas Meniscal chondrocalcinosis: calcium hydroxyapatite or calcium pyrophosphate dihydrate crystal deposition ***MR imaging findings*** Increased signal intensity on MR images Areas of grade 1 and 2 intrameniscal signal intensity that do not communicate with the articular surface of the meniscus Often difficult to differentiate from meniscal tear	Age-related changes aggravated or precipitated by the following: Physical injury Osteoarthrosis Intrameniscal crystal deposition Association with meniscal tears is unclear
Discoid meniscus[61]	9-38	Broad, disclike meniscus lacking the normal semilunar appearance Lateral >> medial Found in up to 2.7% of population Most patients presenting with torn meniscus are between 15 and 35 years of age ***Classified according to shape*** *Slab:* flat, circular *Biconcave:* biconcave disc thinner in its central portion *Wedge:* large but normally tapered *Anterior:* enlarged anterior horn *Forme fruste:* slightly enlarged *Grossly torn:* too deformed for accurate classification ***MR imaging*** Visualization of bowtie appearance on at least three contiguous 5 mm sagittal sections, or an abnormally thickened bowtie appearance Discoid appearance rather than wedge-shaped appearance on coronal images	High prevalence of associated meniscal tear
Meniscal cysts[62]	9-39	Multiloculated collections of mucinous material that occur at the periphery of the meniscus Found in 1% of meniscectomies Three to seven times more frequent adjacent to the lateral meniscus May be discovered as a focal mass or swelling at the joint line Also referred to as *ganglion cysts* Usually high signal intensity on T2-weighted images	Frequently associated with myxoid degeneration and horizontal cleavage tears of the adjacent meniscus Irritation of the common peroneal nerve may occur
Meniscal ossicles[63,64]	9-40	Abnormal foci of ossification within the menisci *Most common site:* posterior horn of medial meniscus *Cause unclear:* represent either vestigial structures or acquired after trauma May be asymptomatic or associated with local pain	Meniscus is usually normal, but associated findings include tears of discoid meniscus
Meniscal tears[65-68]	9-41 to 9-43	See Table 9-10	

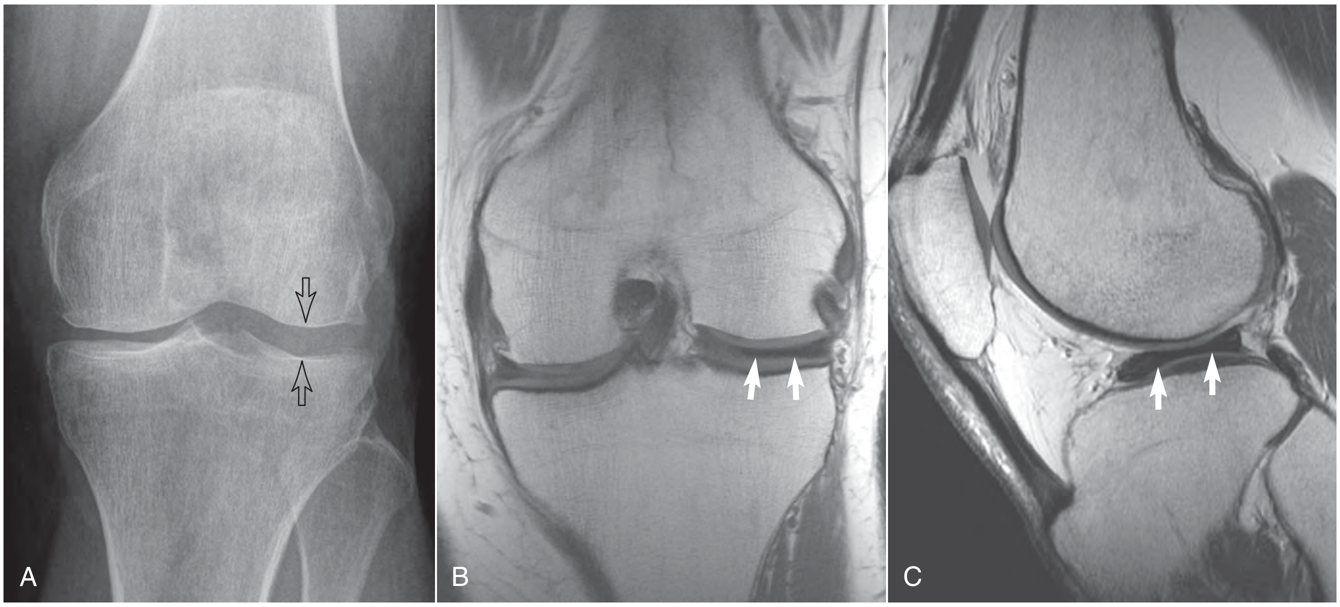

FIGURE 9–38 **Discoid lateral meniscus.**[61] This 57-year-old woman had chronic knee pain ever since she was a teenager. An anteroposterior radiograph **(A)** reveals osteophyte formation and widening of the lateral joint space *(apposing arrows)* with slight hypoplasia of the lateral femoral condyle. The medial joint space is relatively well preserved. Coronal T1-weighted **(B)** and sagittal proton-density **(C)** MR images reveal an abnormally shaped lateral meniscus that appears more disclike *(arrows)* than the normal triangular or wedge-shaped meniscus. The abnormally thickened bow-tie appearance in which the anterior and posterior horns of the lateral meniscus are connected was evident on five contiguous 3 mm sagittal sections. In this case, the discoid lateral meniscus is not torn, and the medial meniscus appeared normal in signal intensity and configuration.

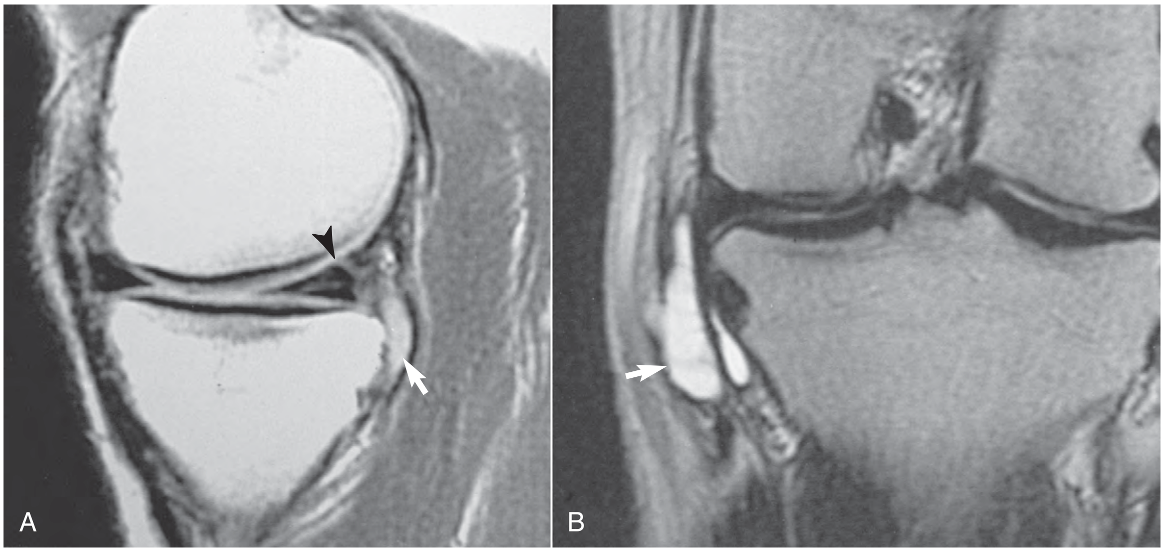

FIGURE 9–39 **Meniscal cysts: MR imaging-medial meniscus.**[62] A large meniscal cyst *(arrows)* associated with a tear *(arrowhead)* of the posterior horn of the medial meniscus is well demonstrated on sagittal proton density-weighted (TR/TE, 2000/32) spin echo **(A)** and coronal fast spin echo (TR/TE, 3300/100) **(B)** MR images. Observe the intimate relationship between the cyst and the superficial portion of the medial collateral ligament in **B.** *(From Resnick D, Kang HS: Internal derangements of joints. Philadelphia, Saunders, 1997, p. 626.)*

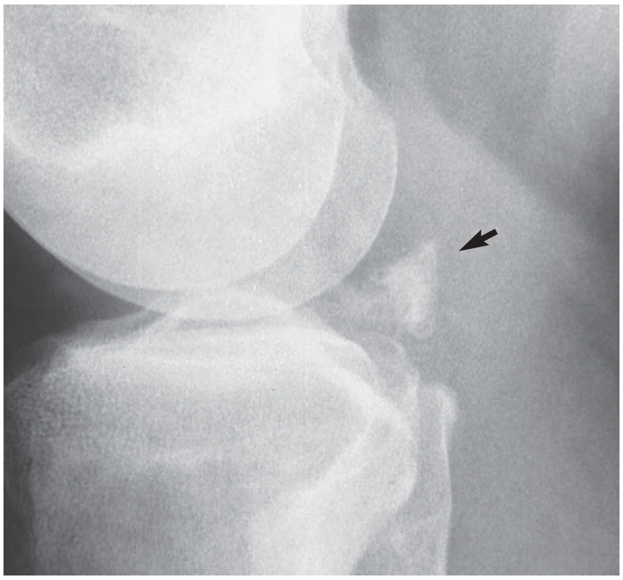

FIGURE 9–40 **Meniscal ossicle.**[63,64] On a lateral radiograph, observe the triangular ossification in the posterior horn of the meniscus *(arrow)* in this 51-year-old man.

TABLE 9-10 Internal Derangements—Meniscal Tears[65-68]

Entity	Figure(s)	Characteristics
Pathogenesis		*Traumatic:* acute injuries in young persons *Degenerative:* more in older patients in association with osteoarthrosis
Clinical findings		*Symptoms:* pain and tenderness overlying affected meniscus, effusion, joint locking *Signs:* positive McMurray test with snapping or popping
Classification	9-41	Longitudinal and radial Longitudinal tears are vertical or horizontal
General		Medial tears more common than lateral tears
Longitudinal tears		90%-95% of all meniscal tears ***Vertical longitudinal tears*** Three times more common in medial than lateral meniscus Peripheral or central Posterior horn, midportion, anterior horn, or combinations *Bucket handle tear:* inner portion displaced into the central portion of the joint ***Horizontal longitudinal tears*** Cleavage lesions common in degenerated menisci in older patients May be oblique and extend to superior or inferior surface Medial, lateral, or both Often associated with meniscal cyst
Radial tears		5%-10% of all meniscal tears Vertical tear of the inner margin of the meniscus Most frequently involves middle third of lateral meniscus Parrot beak or flap tears extend anterolaterally or posterolaterally Extensive radial tears may divide the meniscus into anterior and posterior portions
MR imaging features	9-42, 9-43	Sagittal T1-weighted and proton density-weighted spin echo MR images most useful for detecting high signal intensity characteristic of tears Coronal, transaxial, and T2-weighted images not as valuable in detecting tears Sensitivity, specificity, and accuracy of MR imaging for meniscal tears: 85%-90% Tears of the posterior horn of the lateral meniscus and small tears of the inner edge of each meniscus are often overlooked on MR imaging studies
MR Imaging Grading System	9-42, 9-43	Classified according to changes in signal intensity and changes of morphology: grades 0 through 3
Grade 0		*Normal:* uniform low signal intensity
Grade 1		Indicative of degenerative changes One or several punctate regions of intermediate signal intensity not contiguous with an articular surface of the meniscus (capsular margin not considered an articular surface)
Grade 2		Indicative of more advanced degenerative changes Linear regions of intermediate signal intensity without extension to the articular surface of the meniscus
Grade 3		Indicative of fibrocartilaginous tear Regions of intermediate signal intensity with extension to the articular surface of the meniscus When grade 3 signal is seen on only one image, it should be designated “possible tear” as opposed to “definite tear”

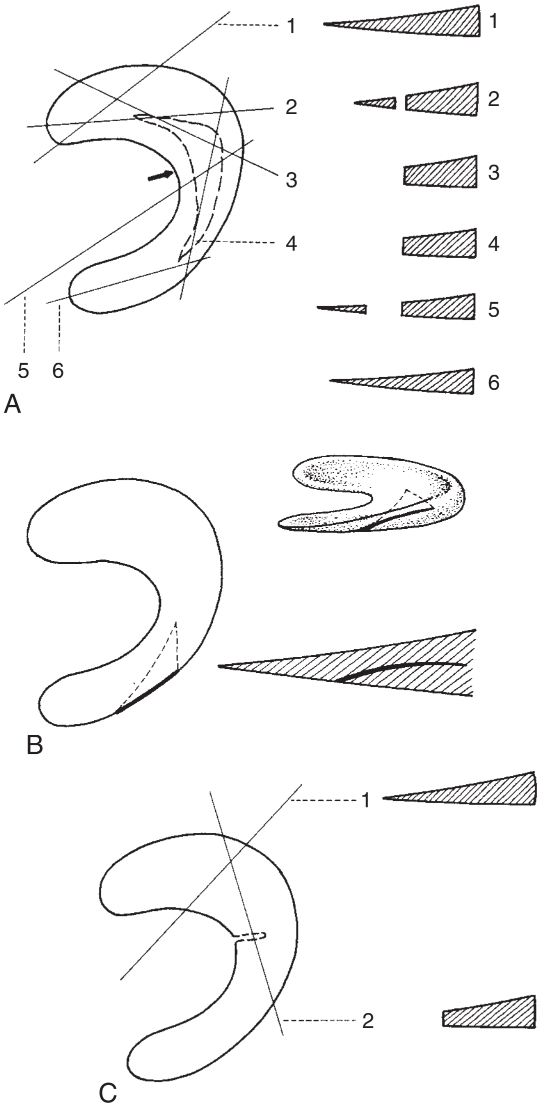

FIGURE 9–41 **Meniscal tears: classification.**[65,66] **A,** Longitudinal vertical tears (with displacement). The medial meniscus is viewed from above with the posterior horn located superiorly. The longitudinal vertical tear can be seen, and the inner fragment is displaced centrally *(arrow)*. The appearance in radial sections obtained with MR imaging depends on the specific site of the tear. A view of the posterior aspect of the meniscus (position 1) is normal. Slightly more anteriorly (position 2), a vertical tear is apparent with minimal displacement of the fragment. At positions 3 and 4, an amputated meniscal morphology can be seen. At position 5, significant displacement of the inner fragment is observed. The anterior horn of the meniscus (position 6) appears normal. **B,** Longitudinal horizontal tears. The medial meniscus is viewed from above *(left),* in front *(top right),* and in longitudinal section *(bottom right)*. The extent and appearance of the tear can be appreciated. Such cleavage lesions tend to occur more in older patients with meniscal degeneration. **C,** Radial tear. The medial meniscus is viewed from above, with its posterior horn located superiorly. A radial tear is evident on the inner contour of the meniscus. Some radial sections provided by MR imaging will appear normal (position 1), whereas others passing through the tear (position 2) will reveal a blunted or truncated inner meniscal contour. *(From Resnick D, Kang HS: Internal derangements of joints. Philadelphia, Saunders, 1997, p. 610.)*

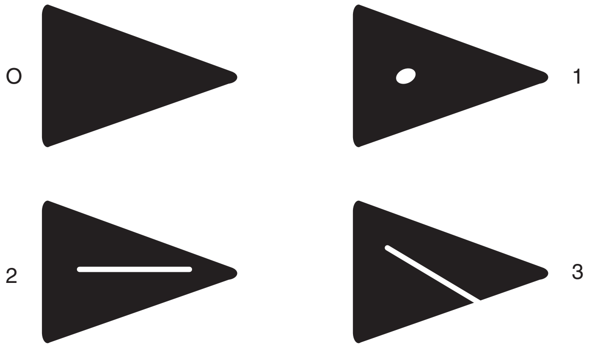

FIGURE 9–42 **Grades of intrameniscal signal intensity: MR imaging.**[65] Grade 0: The normal meniscus appears as uniform low signal intensity. Grade 1: The meniscus may contain one or several circular foci of intermediate signal intensity. Grade 2: The meniscus may contain a linear region of intermediate signal intensity that does not extend to an articular surface of the meniscus. Grade 3: The meniscus may contain linear or irregular regions of intermediate signal intensity that extend to one or both articular surfaces. *(From Resnick D, Kang HS, Pretterklieber ML: Internal derangements of joints. 2nd Ed. Philadelphia, Saunders, 2006, p. 1645.)*

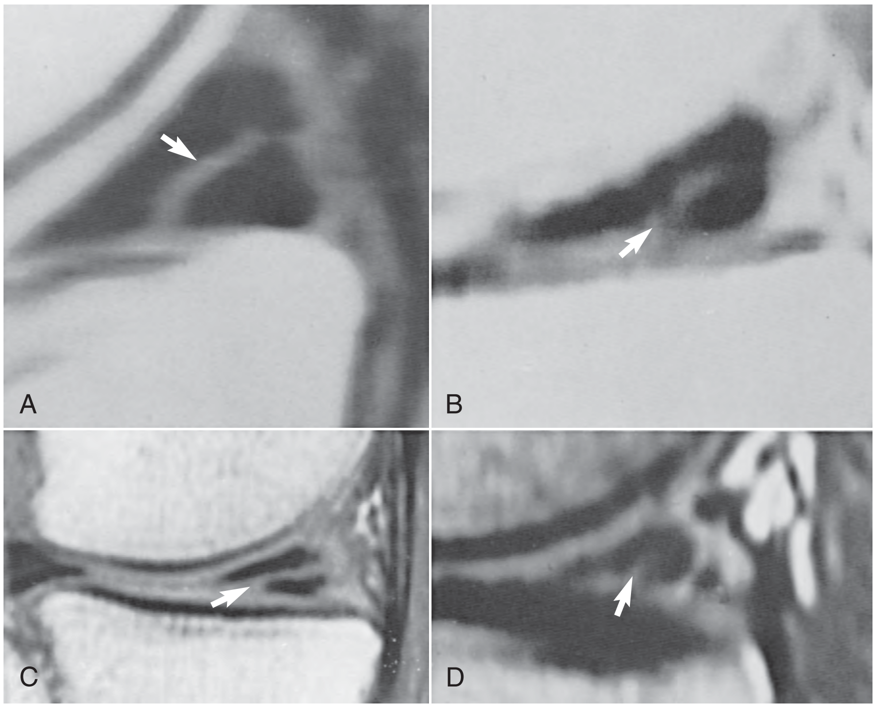

FIGURE 9–43 **Meniscal tears: abnormalities of intrameniscal signal intensity and meniscal morphology.**[65-68] Sagittal proton–density-weighted (TR/TE, 2000/20) spin echo MR images. **A,** Posterior horn of the medial meniscus. A grade 3 pattern of intrameniscal signal intensity *(arrow)* that communicates with the inferior articular surface of the meniscus is evident. **B,** Posterior horn of the medial meniscus. A grade 3 pattern of intrameniscal signal intensity *(arrow)* and irregularity of the inferior meniscal surface are seen. **C,** Posterior horn of the medial meniscus. A grade 3 pattern of increased signal intensity *(arrow)* and altered meniscal morphology are evident. **D,** Posterior horn of the lateral meniscus. A grade 3 pattern of intrameniscal signal intensity *(arrow)* and an irregular inferior and inner meniscal surface are seen. *(From Resnick D, Kang HS, Pretterklieber ML: Internal derangements of joints. 2nd Ed. Philadelphia, Saunders, 2006, p. 1649.)*

TABLE 9-11 Internal Derangements—Ligament and Tendon Disorders*

Entity	Figure(s), Table(s)	Characteristics	Complications and Related Disorders
Ligament Abnormalities			
Medial collateral ligament (MCL) tears[69-71,141]	9-37, 9-44, 9-45	Valgus injuries	Lateral tibial plateau fracture Associated tears of the menisci, cruciate ligaments, or lateral collateral ligament
		Radiographic findings Joint effusion Rare avulsion fracture Medial joint space widening on valgus stress *Pellegrini-Stieda syndrome in chronic tears:* Ossification of proximal attachment of the MCL and the distal attachment of the adductor magnus tendon	
		Magnetic resonance (MR) imaging findings *Acute sprain:* subcutaneous edema, hemorrhage, joint effusion, and slight contour irregularity of MCL fibers *Acute partial tear:* same as sprain with discontinuity and increased signal intensity (T2-weighted images) of some MCL fibers *Acute complete tear:* same findings as partial tear, but also frank discontinuity of all fibers of the MCL *Chronic:* intraligamentous ossification (Pellegrini-Stieda syndrome)	Bone contusions of femoral condyles or tibial plateaus

* See also Table 1-6.

TABLE 9-11 Internal Derangements—Ligament and Tendon Disorders—cont'd

Entity	Figure(s), Table(s)	Characteristics	Complications and Related Disorders
Lateral collateral ligament tears[71]	9-46	Varus injuries ***Radiographic findings*** Focal soft tissue swelling and possible avulsion of fibular head and styloid process ***MR imaging findings*** Interruption or waviness of the lateral collateral ligament or tendon of the biceps femoris tendon; or regions of high signal intensity within or adjacent to these structures on T2-weighted images	Fibular head avulsion fracture Rupture of biceps femoris tendon Iliotibial tract rupture Lateral displacement of the lateral meniscus Popliteus muscle and tendon injuries Cruciate ligament injuries
Lateral capsular ligament avulsion fracture[29]	9-17 Table 9-6	Segond injury: avulsion fracture of lateral tibial rim	
Anterior cruciate ligament tears[72-75]	9-47	One of the most frequent sequelae of knee trauma ***Radiographic findings*** Avulsion fracture of anterior tibial eminence Segond fracture Posterior fracture of lateral tibial plateau Osteochondral fracture of lateral femoral condyle ***MR imaging findings*** Sensitivity, specificity, and accuracy from 90%-100% for tears of the anterior cruciate ligament Acute injuries: High signal intensity on T2-weighted spin echo images with inhomogeneous appearance on sagittal images Empty notch sign on coronal images from retraction of torn ligament Disruption or wavy contour of fibers *Chronic injuries:* alterations in angulation of ligament with scar tissue formation Many indirect signs also evident	*O'Donoghue triad:* simultaneous tears of the medial meniscus, anterior cruciate, and medial collateral ligaments Chronic instability of the anterior cruciate ligament predisposes to additional injuries such as meniscal tears ***Indirect signs*** Segond fractures Bone bruises Deep notch in lateral femoral condyle Buckling of posterior cruciate ligament (PCL) Posterior PCL line Coronal PCL line Coronal fibular collateral ligament (FCL) sign Buckling of patellar tendon Anterior translation of tibia (drawer sign) Shearing of infrapatellar fat body
Posterior cruciate ligament (PCL) tears[76]	9-48	Less common than anterior cruciate ligament tears Force applied to the anterior aspect of the proximal portion of the tibia with the knee flexed Extreme flexion, extension, rotation, or valgus forces may also result in this injury Usually occurs during a fall or from striking the knee against the dashboard during a motor vehicle collision ***Radiographic findings*** Joint effusion Rare avulsion fracture of tibial site of insertion Radiography usually not helpful in diagnosis ***MR imaging findings*** Tears usually occur in the midsubstance, but occasionally at distal or proximal end *Acute or subacute:* high signal intensity on T2-weighted images Discontinuity of fibers	Isolated injury (30% of cases) Combined with other injuries (70% of cases) Complete tear (45% of cases) Partial tear (47% of cases) Bone avulsions (8% of cases) Associated ligament injuries (38% of cases) Associated meniscal injuries (47% of cases) Bone contusions or fractures (36% of cases)

Continued

TABLE 9-11 Internal Derangements—Ligament and Tendon Disorders—cont'd

Entity	Figure(s), Table(s)	Characteristics	Complications and Related Disorders
Tendon Abnormalities			
Patellar tendinosis[77,78,135,136]	9-49	Jumper's knee Overuse syndrome related to sudden and repetitive extension of the knee Most common in athletes: running, kicking, jumping ***Radiographic findings*** Usually normal, but may show thickening of the patellar tendon and obscuration of portions of the infrapatellar fat body ***MR imaging findings*** Sagittal images are most useful Thickening and indistinct posterior margin of the tendon Increased signal intensity at inferior or superior end of tendon indicative of superimposed tear	May result in patellofemoral pain, patellar tracking disorders, or complete patellar tendon rupture
Tears of the Quadriceps Mechanism		***General*** Indirect forces applied to the extensor mechanism may result in ruptures of the patellar or quadriceps tendons (or fractures of the patella)	
Patellar tendon tear[79,94,135]	9-50	Failure occurs at the junction with the patella or, less commonly, the tibial tubercle ***Radiographic findings*** Complete tears result in patella alta Incomplete tears are associated with normal patellar position Prominent soft tissue swelling ***MR imaging findings*** Thickening and complete or incomplete disruption of the tendon In recent tears, high signal intensity of the tendon and its surrounding structures is evident on T2-weighted spin echo, certain gradient echo, and short-τ inversion-recovery (STIR) images	May occur spontaneously or after vigorous exercise in patients with chronic patellar tendinosis Rheumatoid arthritis, chronic renal disease, corticosteroid use, and systemic lupus erythematosus all may predispose to rupture
Quadriceps tendon tear[79,80]	9-51	Partial or complete tears result from injury involving a direct blow to the tendon or forceful flexion of the knee ***Imaging findings*** Patella baja position in complete tears Soft tissue swelling, distortion of soft tissue planes above the patella, avulsed patellar fragment, and buckled or undulating appearance of patellar tendon ***MR imaging findings*** Partial or complete discontinuity of the tendon Undulating or buckled appearance of patellar tendon In acute tears, hemorrhage and edema result in high signal intensity on T2-weighted spin echo and some gradient echo images	Rheumatoid arthritis, chronic renal disease, corticosteroid use, and systemic lupus erythematosus all may predispose to rupture

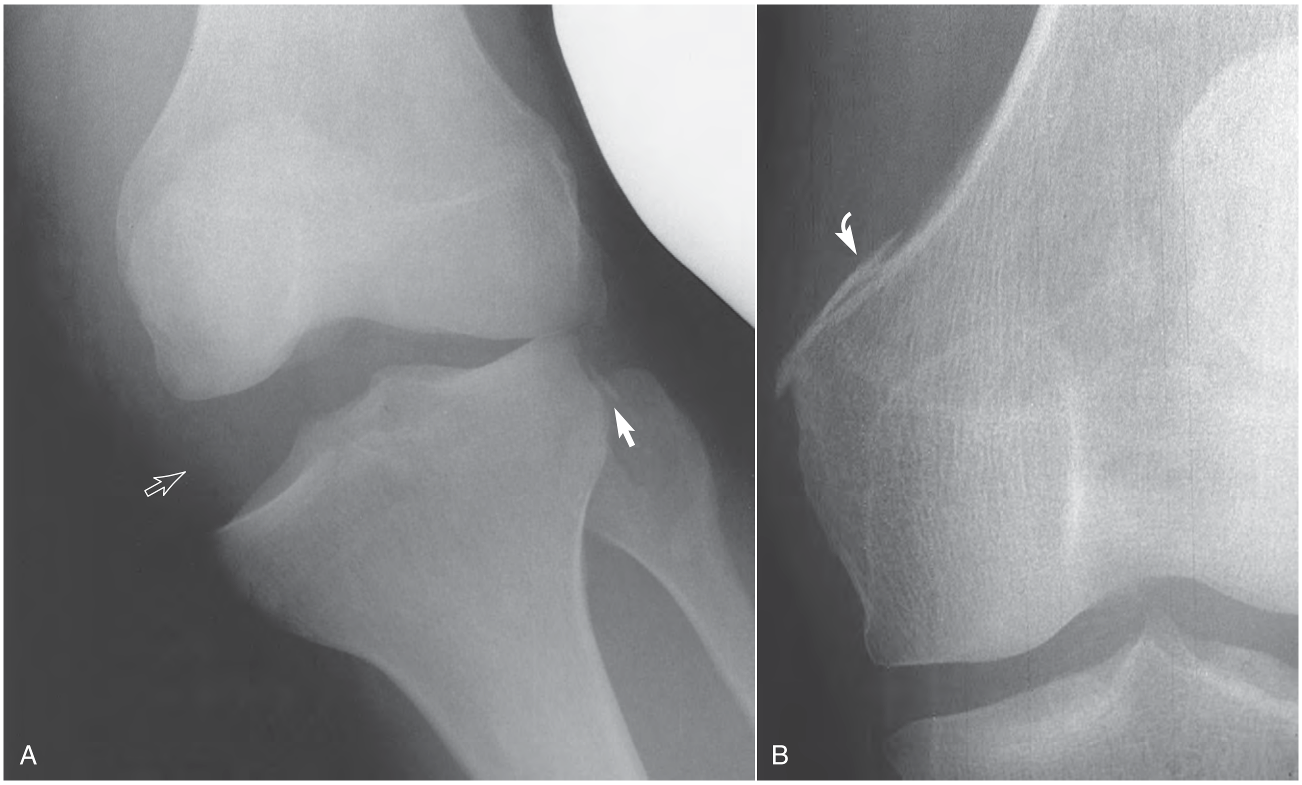

FIGURE 9–44 **Medial collateral ligament injury. Acute and chronic radiographic appearance.**[69,70,141] **A,** Acute injury. Valgus stress radiograph shows severe widening of the medial joint compartment *(open arrow)* in this 24-year-old man with complete (grade III) rupture of the medial collateral ligament. A bone fragment related to avulsion of the lateral capsular ligament is shown *(arrow)*. Isolated injuries of the medial collateral ligament are rare and are usually accompanied by associated internal derangements, which should be evaluated by MR imaging. **B,** Chronic injury: Pellegrini-Stieda syndrome. Observe the thin layer of ossification or calcification *(curved arrow)* characteristic of a long-standing injury at the proximal attachment of the medial collateral ligament. Such ossification has also been demonstrated to occur in the distal attachment of the adductor magnus tendon.

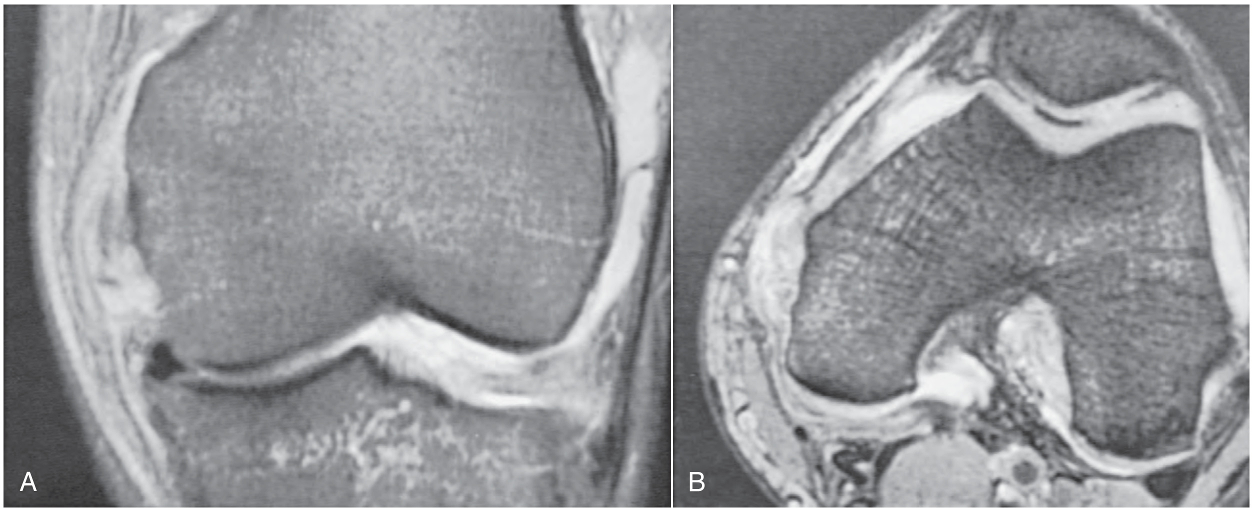

FIGURE 9–45 **Complete tear of the medial collateral ligament: magnetic resonance (MR) imaging.**[69-71] **A,** Coronal fast spin echo (TR/TE, 4000/18) MR image. **B,** Transaxial MPGR (TR/TE, 400/16; flip angle, 30 degrees) MR image. A poorly demarcated, elongated area of high signal intensity adjacent to the medial femoral condyle is consistent with an acute tear of the medial collateral ligament. The anterior portion of the medial patellar retinaculum appears intact. *(From Resnick D, Kang HS: Internal derangements of joints. Philadelphia, Saunders, 1997, p. 644.)*

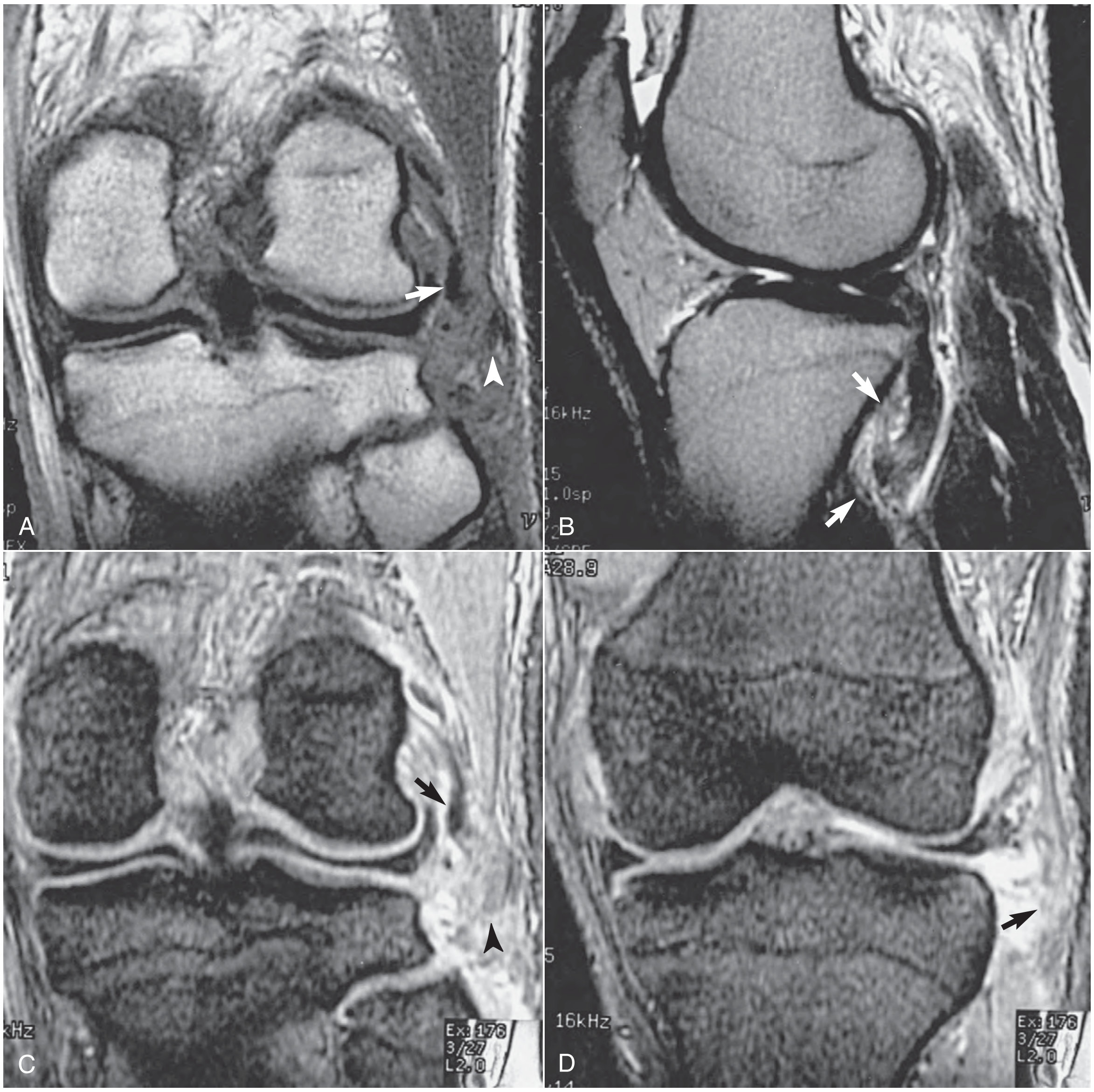

FIGURE 9–46 **Injuries of the lateral collateral ligament, biceps femoris muscle and tendon, iliotibial tract, and popliteus muscle: MR imaging.**[71] This 21-year-old man developed severe knee instability after a recent injury. Although not shown on these images, the anterior cruciate ligament was also disrupted. **A,** The coronal T1-weighted (TR/TE, 749/18) spin echo MR image shows avulsion of the biceps femoris tendon *(arrowhead)* and waviness of the lateral collateral ligament *(arrow)*. **B,** On a sagittal fast spin echo (TR/TE, 4466/90) MR image, note abnormal signal intensity and morphology of the popliteus muscle *(arrows),* joint effusion, and soft tissue edema. **C,** Coronal MPGR (TR/TE, 500/15; flip angle, 25 degrees) MR image of the posterior aspect of the joint again shows avulsion of the biceps femoris tendon *(arrowhead)* and an abnormal lateral collateral ligament *(arrow)*. Note the high signal intensity of the adjacent soft tissues. **D,** More anteriorly, a coronal MPGR (TR/TE, 500/15; flip angle 25 degrees) MR image shows disruption of the iliotibial tract *(arrow),* lateral displacement of the lateral meniscus, and, to a lesser extent, medial soft tissue edema. The anterior cruciate ligament appears abnormal, although this was more evident in other images. *(From Resnick D, Kang HS, Pretterklieber ML: Internal derangements of joints. 2nd Ed. Philadelphia, Saunders, 2006, p. 1783.)*

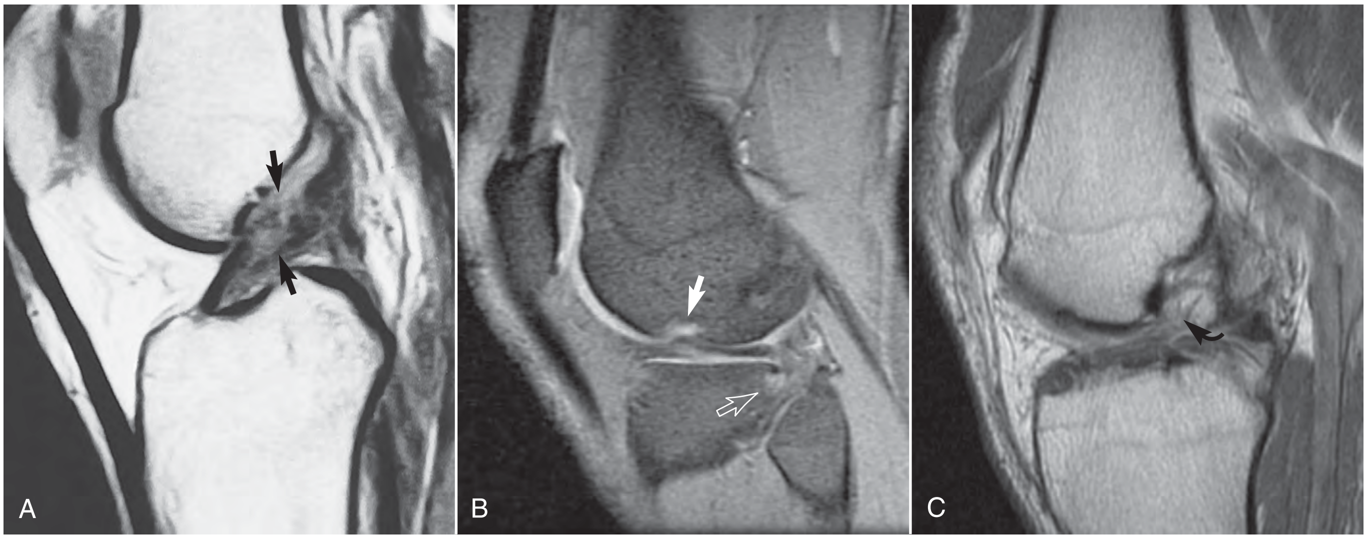

FIGURE 9–47 **Acute anterior cruciate ligament tear.**[72-75] **A,** This 31-year-old woman injured her knee while running. A sagittal proton–density-weighted (TR/TE, 1100/25) spin echo MR image reveals discontinuity and inhomogeneous intermediate signal intensity within the midportion of the anterior cruciate ligament *(arrows)*. The patellar tendon is intact and shows no evidence of buckling. **B-C,** Sagittal proton-density MR images with **(B)** and without **(C)** fat suppression in another patient, a 38-year-old man who severely twisted his knee playing soccer 3 months previously. The midline sagittal image **(C)** shows the absence of an ACL *(curved arrow),* and the lateral parasagittal fat suppressed image **(B)** shows the osteochondral impaction fracture of the lateral femoral condyle *(straight arrow)* and the corresponding edema of the lateral tibial plateau *(open arrow)*. (***A,*** *Courtesy L. Beinekis, D.C., Portland, Ore.)*

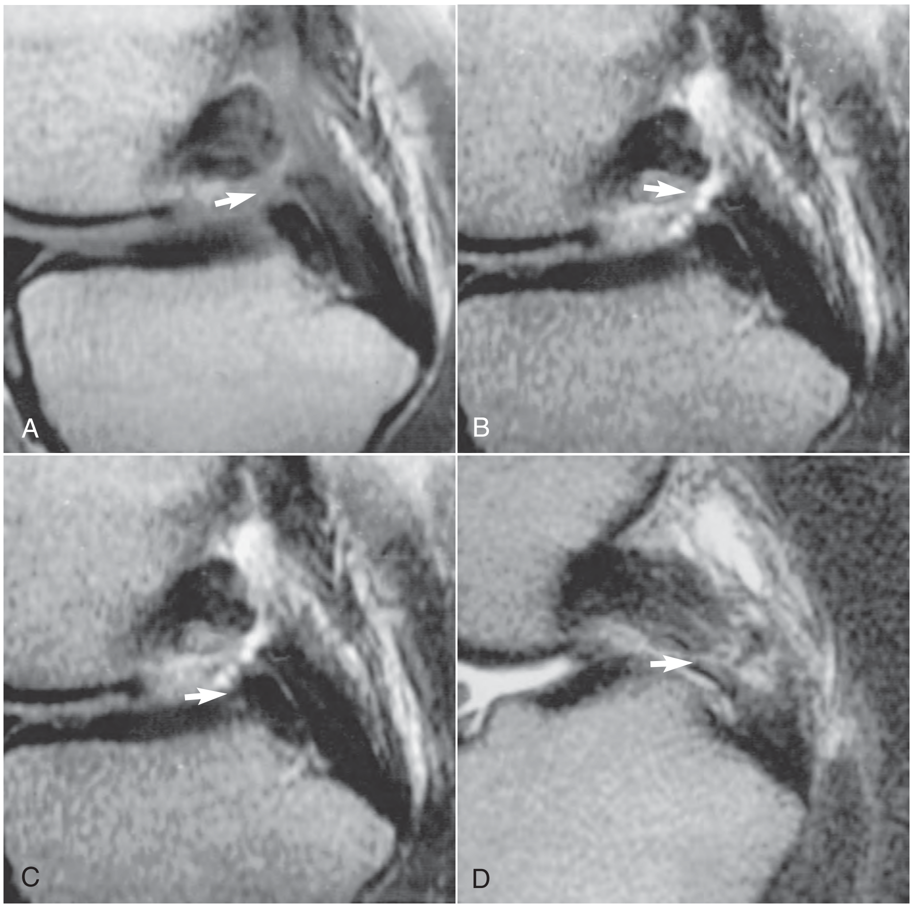

FIGURE 9–48 **Acute complete posterior cruciate ligament tears: MR imaging.**[76] **A-B,** Sagittal proton–density-weighted (TR/TE, 2000/30) **(A)** and T2-weighted (TR/TE, 2000/80) **(B)** spin echo MR images reveal complete disruption *(arrows)* of the posterior cruciate ligament, with an increase in signal intensity in **B. C-D,** Sagittal proton–density-weighted (TR/TE, 2200/20) **(C)** and T2-weighted (TR/TE, 2200/80) **(D)** spin echo MR images in a second patient again show complete disruption *(arrows)* of the posterior cruciate ligament, with an increase in signal intensity in **D.** *(From Resnick D, Kang HS, Pretterklieber ML: Internal derangements of joints. 2nd Ed. Philadelphia, Saunders, 2006, p. 1871.)*

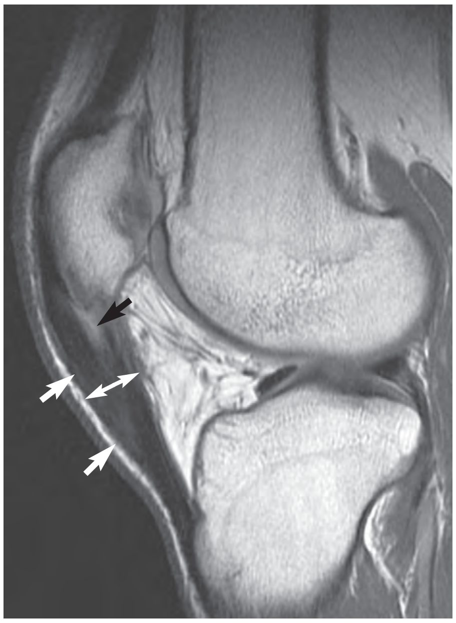

FIGURE 9–49 **Patellar tendinosis: jumper's knee.**[77,78,135,136] A sagittal proton–density-weighted MR image in this basketball player with anterior knee pain shows high signal intensity *(black arrow)* within a swollen patellar tendon *(white arrows)* at its attachment to the inferior pole of the patella.

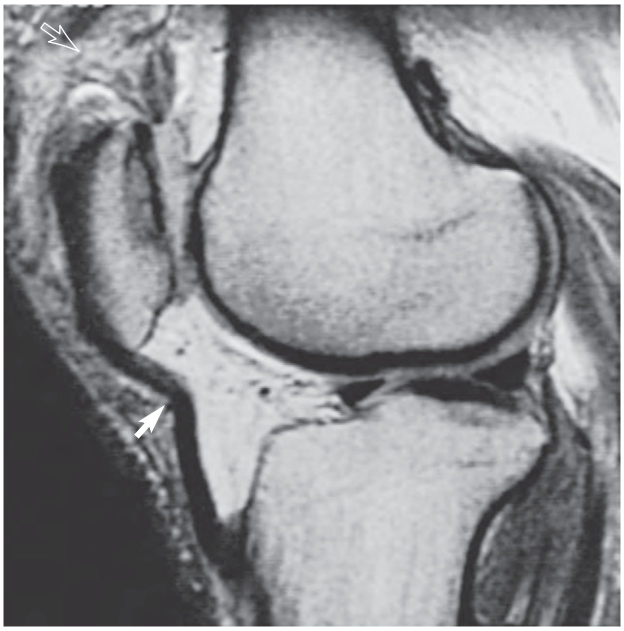

FIGURE 9–51 **Complete tear of the quadriceps tendon: MR imaging.**[79,80] Sagittal proton–density-weighted (TR/TE, 2000/20) spin echo MR image demonstrates an abnormal buckled or wrinkled contour of the patellar tendon *(solid arrow)* related to a complete rupture *(open arrow)* of the quadriceps tendon. *(From Resnick D, Kang HS: Internal derangements of joints. Philadelphia, Saunders, 1997, p. 670.)*

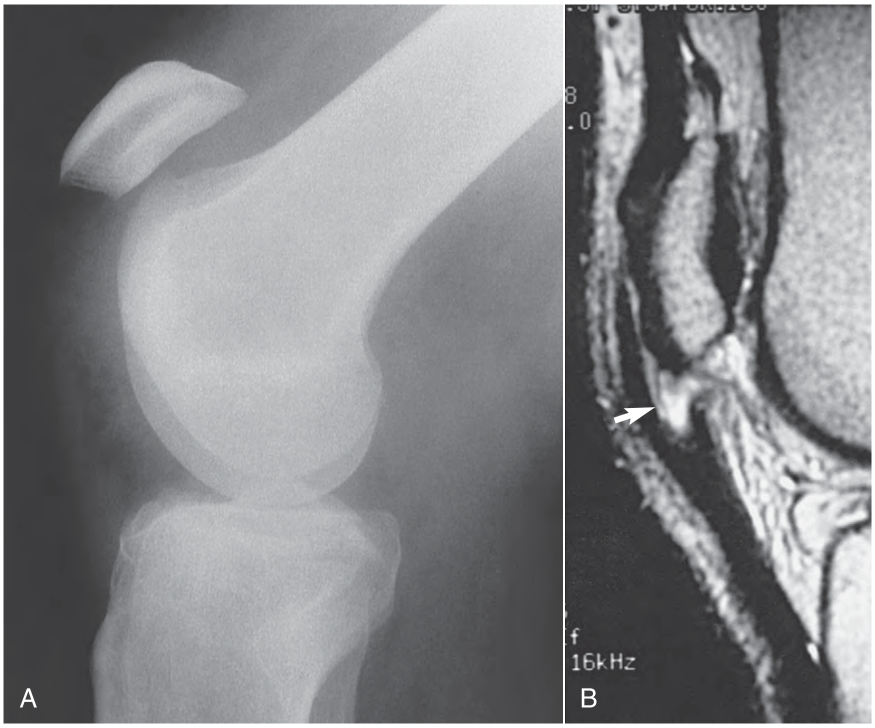

FIGURE 9–50 **Patellar tendon tears.**[78,79,135] **A,** Radiographic features. Observe the superior displacement of the patella (patella alta) in this patient with a complete tear of the patellar tendon. **B,** Magnetic resonance (MR) imaging features. In another patient, a sagittal T2-weighted (TR/TE, 4466/90) spin echo MR image clearly displays the site of tendon disruption *(arrow)*. Observe the high signal intensity within the ruptured tendon. *(**A** From Siweck CW, Rao JP: Ruptures of the extensor mechanism of the knee joint. J Bone Joint Surg [Am] 63:932, 1981. **B,** From Resnick D, Kang HS: Internal derangements of joints. Philadelphia, Saunders, 1997, p. 665.)*

TABLE 9-12 Internal Derangements—Patellofemoral Disorders[136]

Entity	Figure(s), Table(s)	Characteristics	Complications and Related Disorders
Patella alta[81]	9-52 Table 9-5	Superior patellar position best seen on lateral radiographs *Insall-Salvati ratio:* measurement method Height of the patella and length of patellar tendon are determined on lateral radiograph; ratio of these measurements should be approximately 1:1; in patella alta, the patellar tendon is longer than the height of the patella	Associated with patellar tendon rupture, recurrent lateral patellar subluxation or dislocation, Sinding-Larsen-Johansson disease, and joint effusions
Patella baja[81]	9-52 Table 9-5	Inferior patellar position best seen on lateral radiographs *Insall-Salvati ratio is abnormal:* the patellar height is longer than the length of the patellar tendon	Associated with neuromuscular disorders and achondroplasia; also may be present after surgery involving transfer of the tibial tubercle
Patellofemoral instability[82,83]	9-53	Patellofemoral tracking disorder in which the patella moves abnormally with respect to the femur during flexion and extension Radiography, CT, MR, and kinematic MR imaging are all used to assess the patellofemoral relationship Patellofemoral tracking is affected by the configuration of the trochlea, the patellar shape, and the relationship of the patella to the femur Excessive lateral pressure syndrome: abnormal lateral tilt of the patella with respect to the femur; this leads to patellofemoral pain	Transient, recurrent, lateral subluxation or dislocation of the patella Excessive lateral pressure syndrome Chondromalacia patellae Osteochondral fractures Avulsion fractures Medial retinacular injury
Chondromalacia patellae[84,85]	9-54	*Synonym:* patellofemoral pain syndrome Cartilage loss involving one or more portions of the patella; this leads to patellofemoral pain, crepitus, and synovitis Imaging techniques generally are inadequate to assess cartilage loss CT arthrography can be useful in cases with advanced cartilage loss	*Cause is unclear:* may be related to single or recurrent episodes of acute trauma, as in excessive lateral pressure syndrome, patellofemoral instability, and anatomic variations in bone morphology

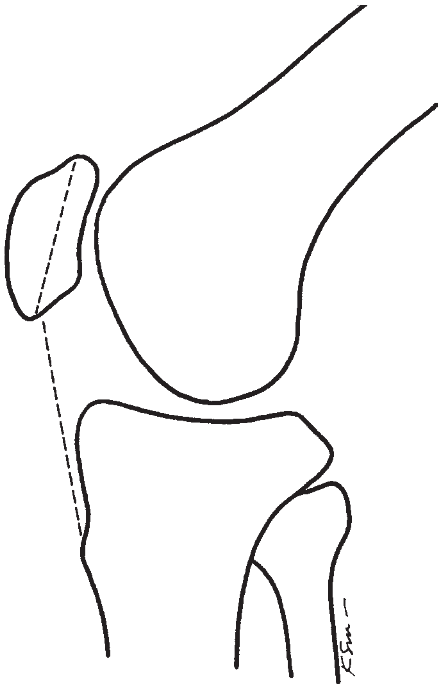

FIGURE 9–52 Patellar position: Insall-Salvati method.[81] The ratio of patellar tendon length to the greatest diagonal length of the patella should be approximately 1:1. This method may be used to diagnose patella alta and patella baja. In patella alta, the patellar tendon length exceeds that of the patellar length; in patella baja, the length of the patella exceeds that of the tendon. *(From Resnick D, Kang HS, Pretterklieber ML: Internal derangements of joints. 2nd Ed. Philadelphia, Saunders, 2006, p. 1901.)*

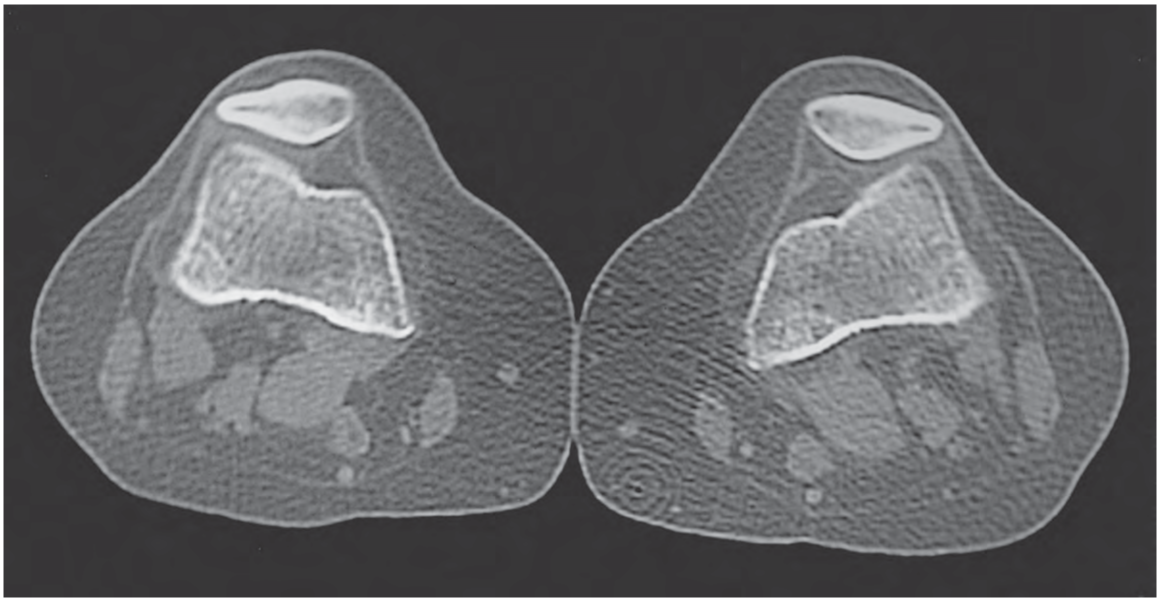

FIGURE 9–53 **Patellofemoral instability: CT scanning.**[82-84] Transaxial CT scan, obtained with the knees flexed 20 degrees, shows lateral subluxation of both patellae. *(From Resnick D, Kang HS, Pretterklieber ML: Internal derangements of joints. 2nd Ed. Philadelphia, Saunders, 2006, p. 1903.)*

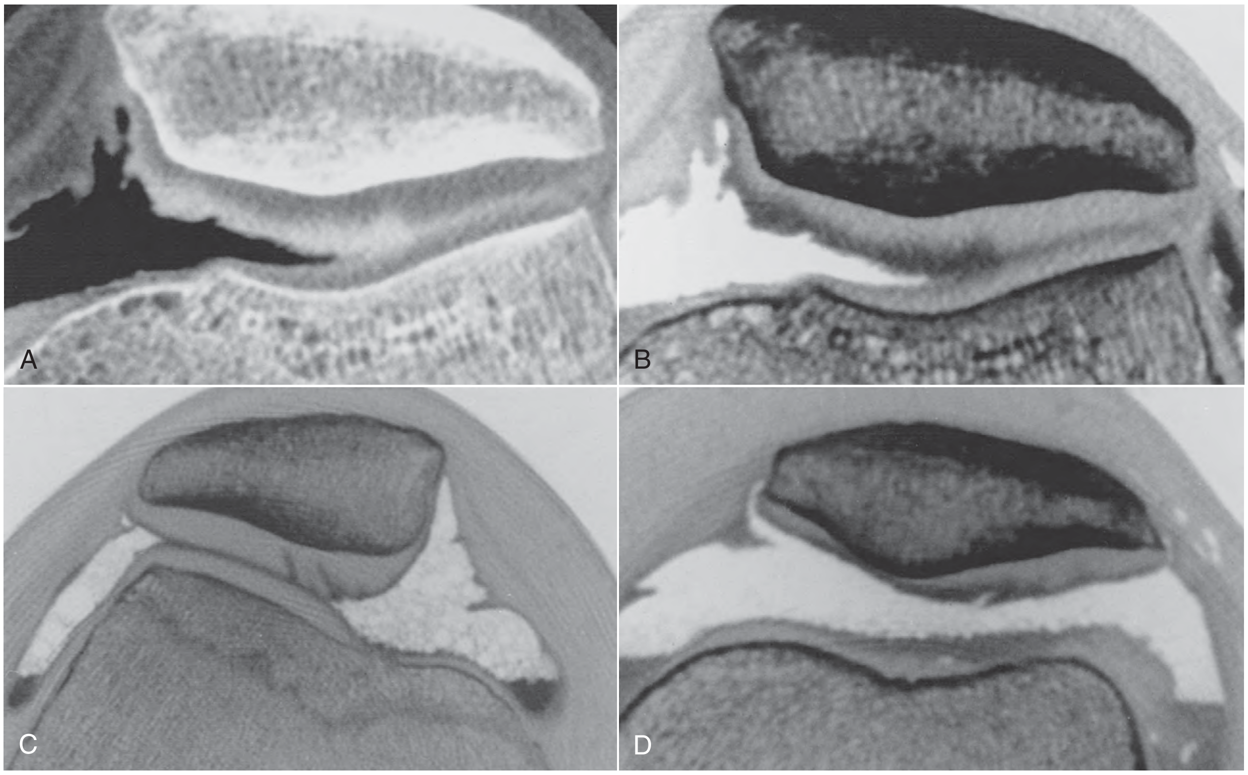

FIGURE 9–54 **Chondromalacia patellae: CT arthrography.**[85] **A-B,** Transaxial CT arthrographic images (using double-contrast technique) filmed without **(A)** and with **(B)** subtraction technique show imbibition of radiopaque contrast material and cartilage fibrillation and ulceration. **C-D,** Two additional subtracted CT arthrographic images of other patients reveal cartilage fissuring and contrast material imbibition. *(From Resnick D, Kang HS, Pretterklieber ML: Internal derangements of joints. 2nd Ed. Philadelphia, Saunders, 2006, p. 1906. Courtesy A. D'Abreau, MD, Porto Alegre, Brazil.)*

TABLE 9-13 Articular Disorders Affecting the Knee*

Entity	Figure(s)	Characteristics
Degenerative and Related Disorders		
Osteoarthrosis[86,87,132,133,137]	9-55	Findings predominate in the medial femorotibial compartment in men; distribution more variable in women Involvement of proximal tibiofibular joint is less common than tibiofemoral involvement Marginal osteophytes are the most sensitive radiographic feature of osteoarthrosis of the femorotibial joint Subchondral sclerosis and subchondral cysts are less sensitive radiographic features and rarely occur in the absence of osteophyte formation Subluxation *Intraarticular bodies:* infrequently, secondary synovial osteochondromatosis *Joint space narrowing:* PA view with 15 degrees of knee flexion is able to detect joint-space narrowing accurately and to achieve optimum alignment of the medial tibial plateau
Diffuse idiopathic skeletal hyperostosis (DISH)[88]	9-56	Occasional knee involvement with enthesopathy and ligament ossification about the knee
Inflammatory Disorders		
Rheumatoid arthritis[89]	9-57	Knee involvement common in rheumatoid arthritis Bilateral symmetric, concentric joint space narrowing of medial and lateral joint spaces and of patellofemoral joint Subchondral erosion Absent or mild sclerosis Periarticular osteoporosis
Juvenile idiopathic arthritis[90-91]	9-58	Knee involvement common Soft tissue swelling and joint effusion Epiphyseal overgrowth (ballooning) Squaring of inferior pole of patella Widening of the intercondylar notch Diffuse, bilateral symmetric joint space loss Periarticular osteoporosis Erosions of the femoral condyles and tibial surfaces Closely resembles findings in hemophilic arthropathy
Ankylosing spondylitis[92]	9-59	Bilateral symmetric, joint space narrowing of all three compartments Erosions Joint effusion Enthesopathy of quadriceps and patellar tendons at the anterior aspect of the patellae Rarely, may eventually result in partial or complete intraarticular osseous ankylosis
Psoriatic arthropathy and reactive arthritis	9-60	Knee involvement similar to but less frequent than ankylosing spondylitis
Systemic lupus erythematosus (SLE)[94]	9-61	Osteonecrosis of the femoral condyles in SLE patients treated with or without corticosteroid therapy Patellar and quadriceps tendon ruptures
Dermatomyositis and polymyositis[95]	9-62	Widespread sheetlike calcification in skin and muscle about the knee
Mixed connective tissue disease[96,97]	9-63	Radiographic features variable; may result in diffuse joint space narrowing, erosions, and soft tissue calcinosis

* See also Tables 1-7 to 1-10 and Table 1-19.

Continued

TABLE 9-13 Articular Disorders Affecting the Knee—cont'd

Entity	Figure(s)	Characteristics
Crystal Deposition and Metabolic Disorders		
Calcium pyrophosphate dihydrate (CPPD) crystal deposition disease[98-100,124,129]	9-64	Knee is most commonly involved articulation Differs from osteoarthrosis in its prominent involvement of the patellofemoral and lateral tibiofemoral joint compartments and its high rate of chondrocalcinosis ***Imaging findings*** Prominent joint effusion during acute episode Articular space narrowing, sclerosis, cyst formation, and osteophytes. Intraarticular and periarticular chondrocalcinosis of hyaline cartilage and fibrocartilage, calcification of capsule and synovium *Advanced, severe disease:* considerable osseous destruction and fragmentation resembling neuropathic osteoarthropathy
Gouty arthropathy[101]	9-65	Rare knee involvement Periarticular erosions Soft tissue tophi and joint effusions Intraosseous tophi result in osteolytic cystlike lesions in patella
Hemochromatosis[102]	9-66	Arthropathy identical to that of calcium pyrophosphate dihydrate (CPPD) crystal deposition disease Prominent chondrocalcinosis
Acromegalic arthropathy[89]	9-67	Hyperostosis and ossification of the patellar attachments of the quadriceps and patellar tendons Cartilage hypertrophy may initially result in joint space widening Degenerative joint disease later results in cartilage thinning, sclerosis, and osteophytes
Hemophilic arthropathy[103,125]	9-68	Knee is the joint most commonly affected in hemophilia *Typical pattern:* bilateral symmetric joint involvement Findings closely resemble the changes in juvenile idiopathic arthritis ***Imaging findings*** Dense joint effusions *Periarticular osteoporosis:* radiolucent epiphyses Articular surface irregularity and flattening Subchondral cysts Overgrowth of epiphyses (ballooning) Widening of the intercondylar notch Squaring of inferior pole of patella Fixed flexion deformity
Infection		
Pyogenic septic arthritis[104,126]		Rapid loss of joint space usually begins in femorotibial compartments; may eventually involve patellofemoral joint Periarticular osteoporosis Loss of definition and destruction of subchondral bone Capsular distention Erosion May disseminate from site of metaphyseal osteomyelitis
Tuberculous arthritis[105]	9-69	Various degrees of soft tissue swelling Gradual joint space narrowing Periarticular osteoporosis Peripherally located erosions Subchondral erosions Periarticular abscess Patellar involvement: osteolytic lesions with sequestrum
Miscellaneous Disorder		
Neuropathic osteoarthropathy[89]	9-70	*Most frequent causes of knee involvement:* tabes dorsalis and diabetes mellitus; less common causes are amyloidosis and congenital indifference to pain ***Imaging findings*** Large joint effusions Joint space narrowing and obliteration Joint subluxation, disorganization, and destruction Bone fragmentation, destruction, and sclerosis

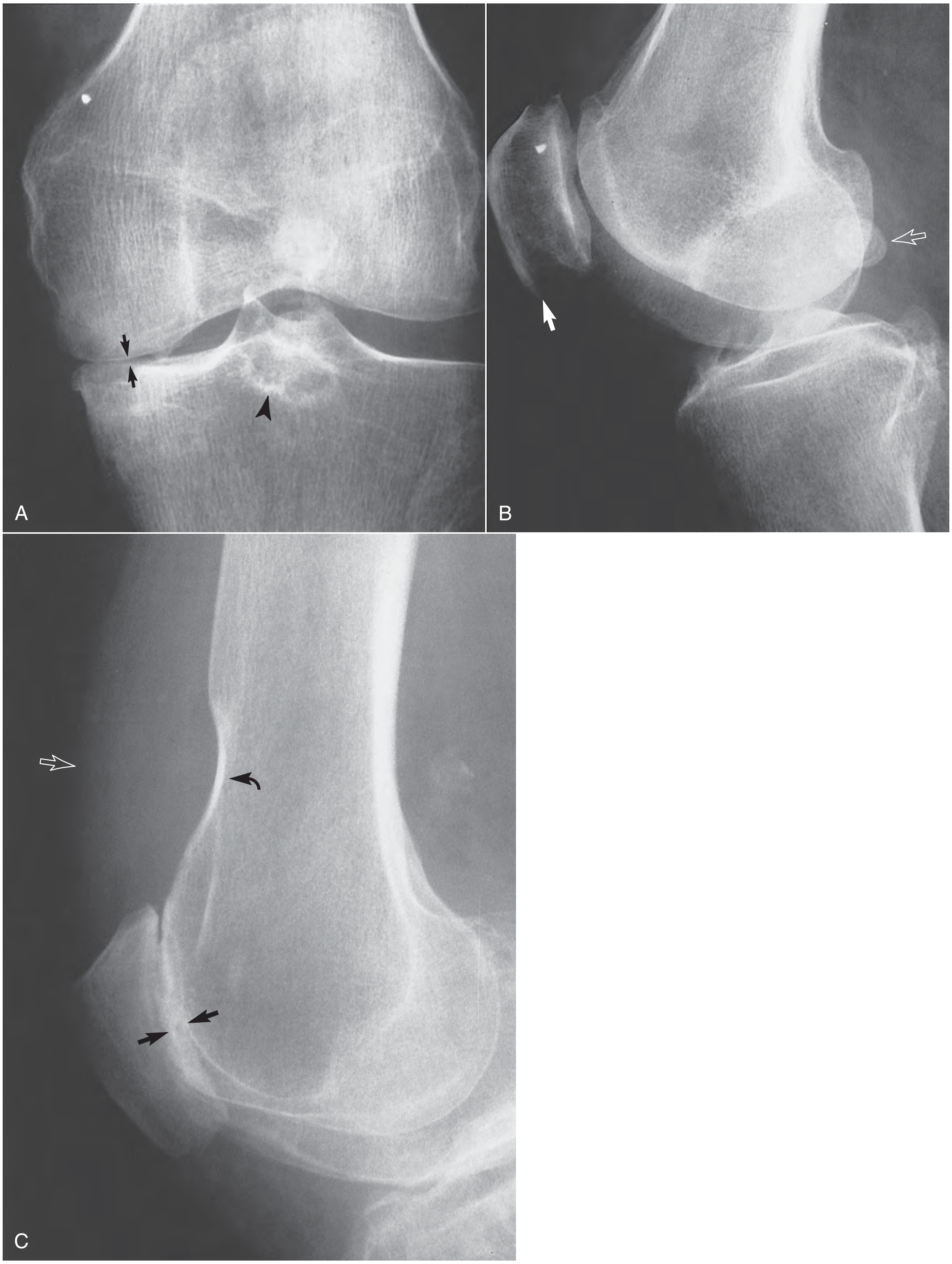

FIGURE 9–55 **Osteoarthrosis (degenerative joint disease).**[86,87,132,133] **A-B,** Frontal **(A)** and lateral **(B)** radiographs show medial femorotibial joint space narrowing *(black arrows),* patellar enthesophyte *(white arrow),* subchondral cyst formation *(arrowhead),* and a large laminated intraarticular osseous body *(open arrow).* **C,** In another patient, patellofemoral joint abnormalities predominate. Extensive narrowing of the patellofemoral compartment *(arrows)* and a joint effusion *(open arrow)* are present. Anterior scalloping of the distal portion of the femur *(curved arrow)* is a result of mechanical irritation from repeated contact with the patella. Similar scalloped defects may be observed in hyperparathyroidism and calcium pyrophosphate dihydrate (CPPD) crystal deposition disease.

Continued

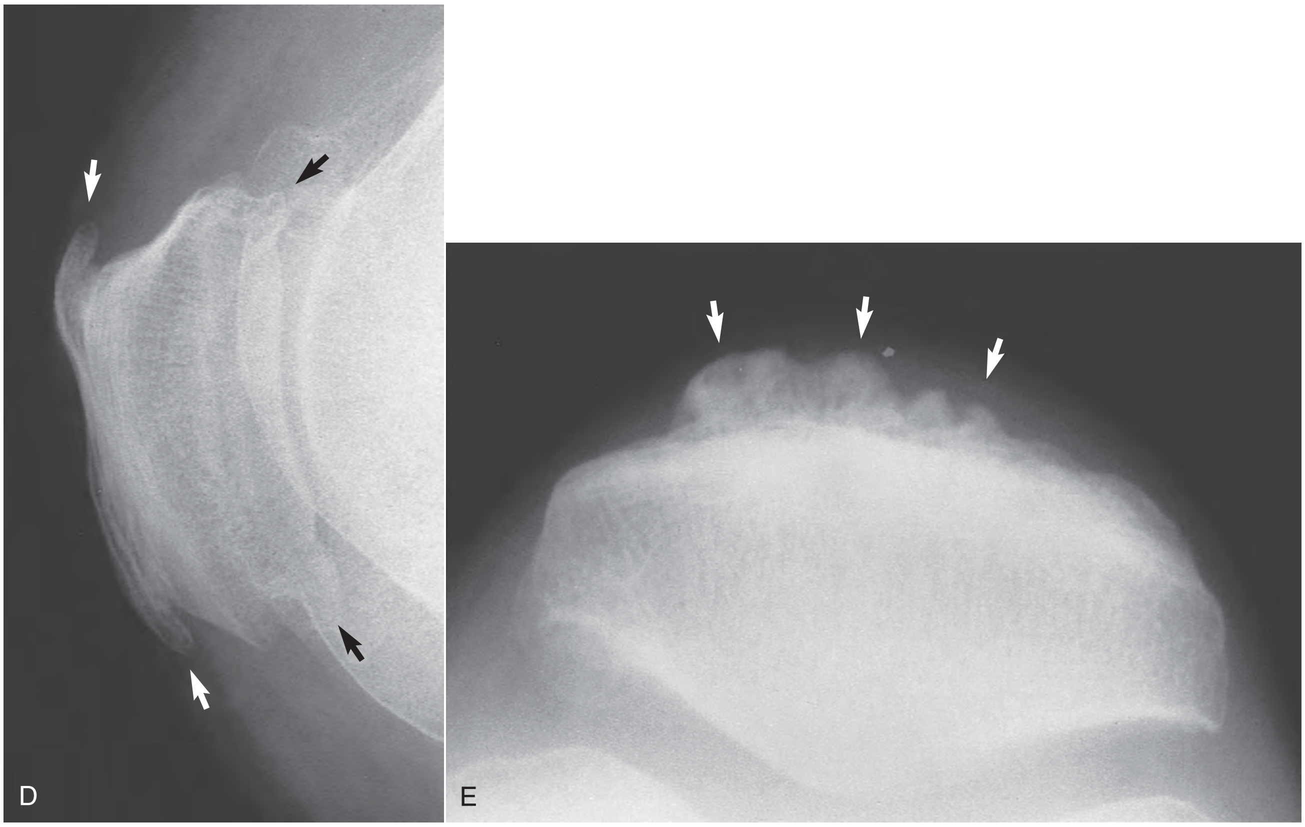

FIGURE 9–55, cont'd **D-E,** Patellar enthesopathy. In **D,** bony excrescences (enthesophytes) arising from the anterior aspect of the patella *(white arrows)* at the site of attachment of the quadriceps mechanism are evident on this lateral radiograph. Note also the patellofemoral joint space narrowing and osteophytes *(black arrows)* arising from the posterior margins of the patella. **E,** On this tangential radiograph, observe the typical toothlike osseous excrescences at the quadriceps attachment to the anterior surface of the patella *(arrows),* a finding sometimes referred to as the *patellar tooth sign*. Enthesophytes are probably related to abnormal stress at the ligamentous or tendinous connection of the quadriceps mechanism to the bone and are not a manifestation of osteoarthrosis. Such enthesopathy is common in elderly patients and in patients with diffuse idiopathic skeletal hyperostosis.

FIGURE 9–56 **Diffuse idiopathic skeletal hyperostosis (DISH).**[88] Radiograph of this 69-year-old man with long-standing DISH reveals prominent, thick patellar enthesopathy *(open arrow),* a feature characteristic in the peripheral skeleton. A small osteophyte *(arrow),* probably related to degenerative disease, is also present. Knee involvement is seen in about 29% of DISH patients.

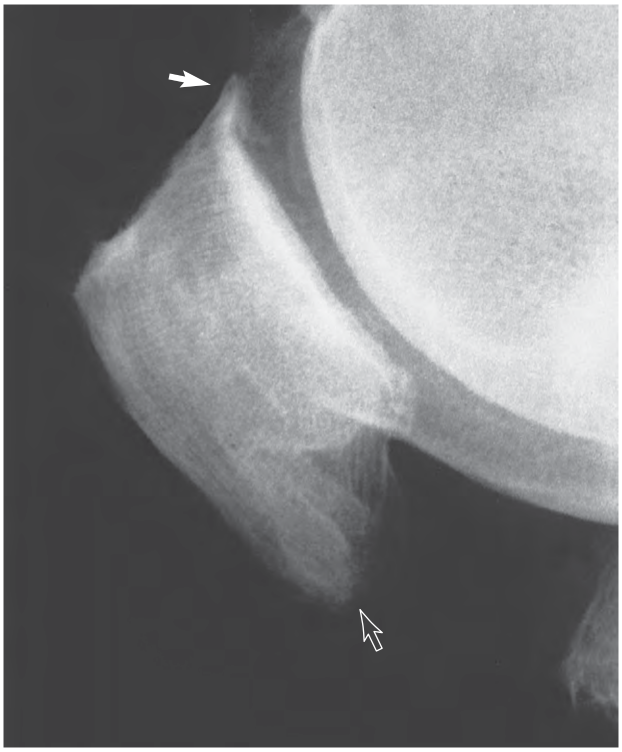

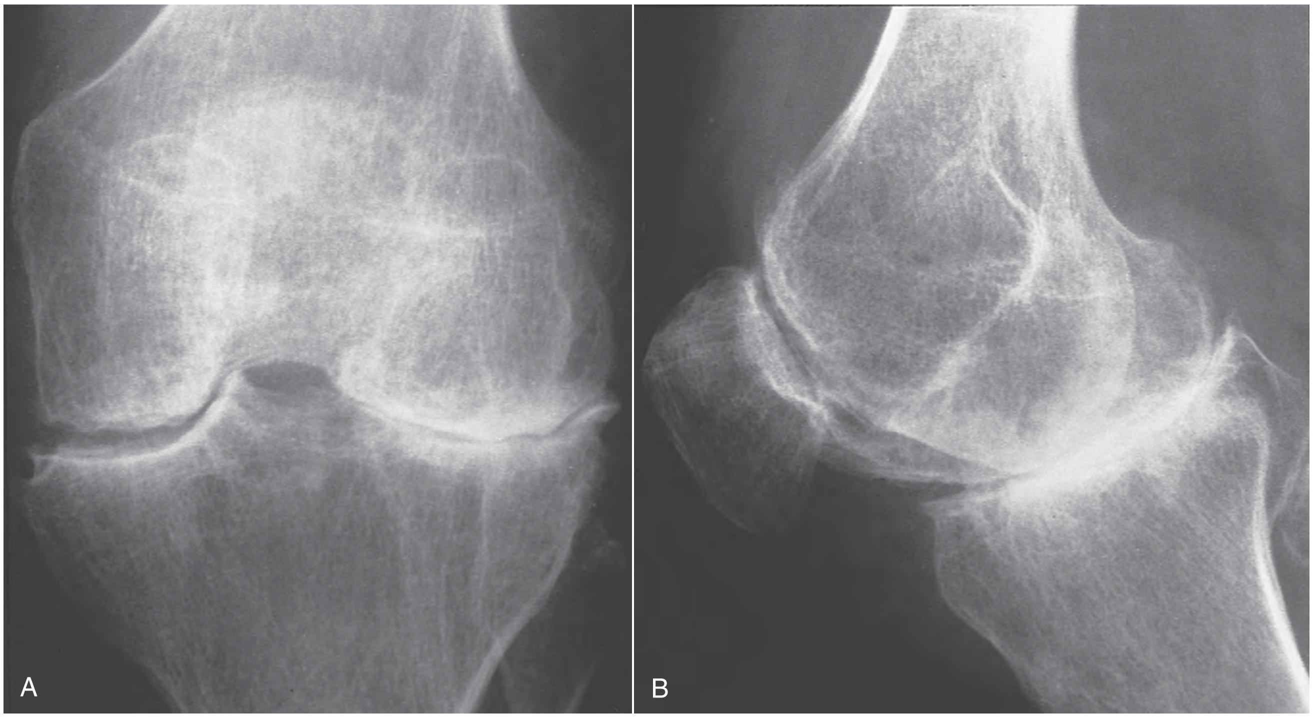

FIGURE 9–57 **Rheumatoid arthritis.**[89] **A,** A 59-year-old woman with early-onset, adult type of rheumatoid arthritis. Frontal **(A)** and lateral **(B)** radiographs show signs of both inflammatory disease and degenerative disease. The uniform loss of the patellofemoral and the medial and lateral joint spaces, along with relative absence of osteophytes, is characteristic of rheumatoid arthritis. The other knee (not shown) was equally affected. The subchondral sclerosis and lateral tibial osteophyte are characteristic of superimposed degenerative joint disease.

TABLE 9-14 **Articular Disorders of the Knee: Compartmental Analysis**

Entity	Figure(s)	Femorotibial Compartments	Patellofemoral Compartment
Osteoarthrosis	9-55	Medial > lateral	Commonly involved in conjunction with medial or lateral femorotibial disease
Rheumatoid arthritis	9-57	Medial = lateral	Commonly involved in conjunction with medial or lateral femorotibial disease
Calcium pyrophosphate dihydrate (CPPD) crystal deposition disease	9-64	Medial < lateral	Commonly involved alone or in conjunction with medial or lateral femorotibial disease
Infectious arthritis	9-69	Medial = lateral	May involve any compartment, but more frequent in femorotibial joints
Hyperparathyroidism	9-80	Medial = lateral	Subchondral resorption, crystal-induced arthropathies, or unknown mechanism

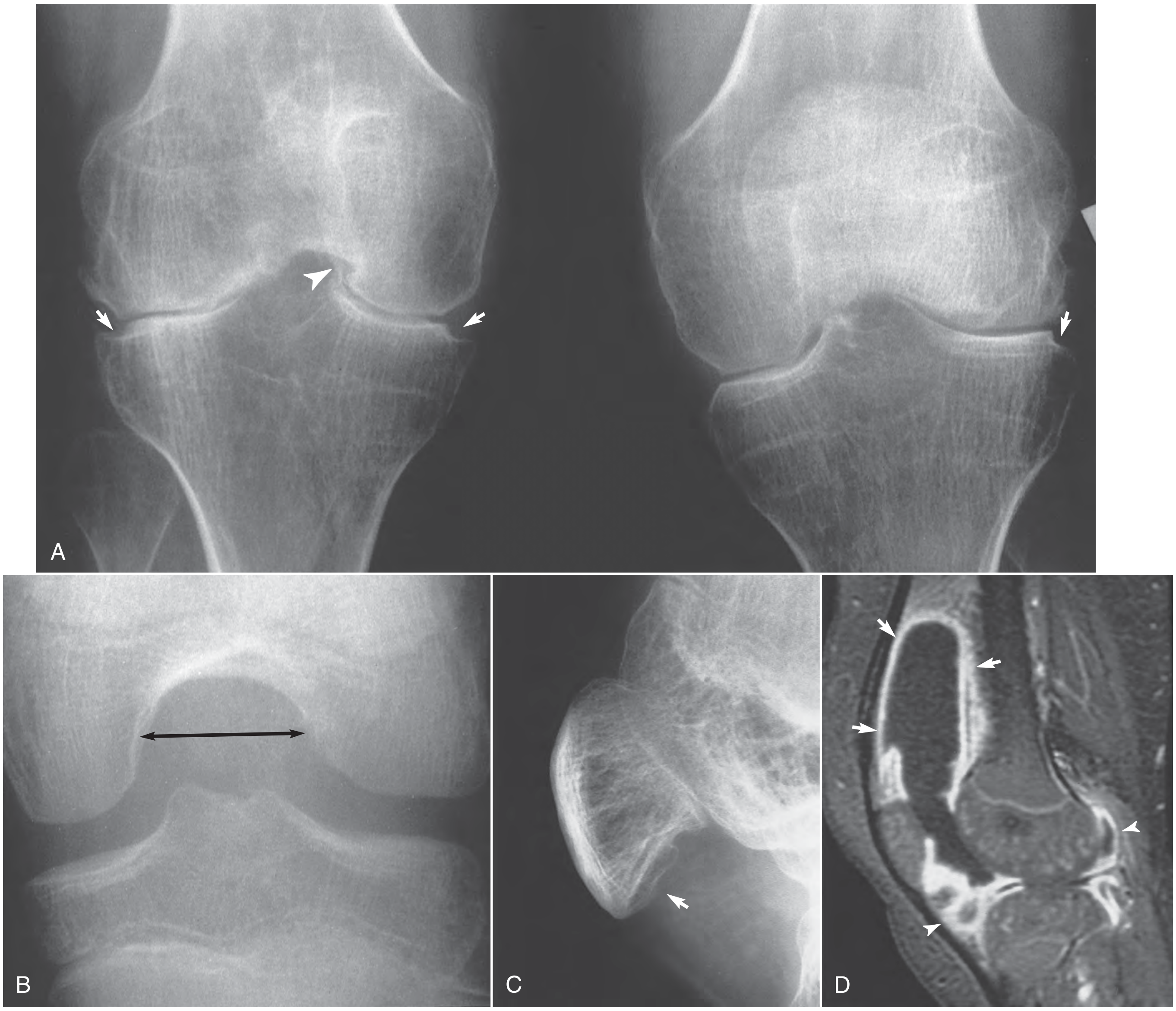

FIGURE 9–58 **Juvenile idiopathic arthritis: knee abnormalities.**[90,91] **A,** Osteoporosis, marginal erosions *(arrows),* bilateral symmetric joint space narrowing, widening of the intercondylar notch *(arrowhead),* and overgrowth of the medial femoral condyles are evident in this 22-year-old woman with long-standing juvenile rheumatoid arthritis. **B,** Widening of the intercondylar notch *(double-headed arrow)* is a common finding in juvenile chronic arthritis, illustrated on this routine frontal radiograph of another patient. **C,** Flattening of the inferior portion of the patella results in a characteristic squared patellar configuration *(arrow)*. **D,** A sagittal T1-weighted (TR/TE, 550/11) spin echo MR image after administration of gadolinium contrast agent shows a large, low signal intensity suprapatellar joint effusion surrounded by an enhancing zone of high signal intensity characteristic of inflamed, hypertrophic synovial membrane *(arrows)*. Similar synovial changes are observed in the posterior and infrapatellar synovial compartments *(arrowheads)*. The radiographic findings of juvenile idiopathic arthritis closely resemble those of hemophilia. *(**D,** Courtesy B. Coley, MD, Columbus, Ohio.)*

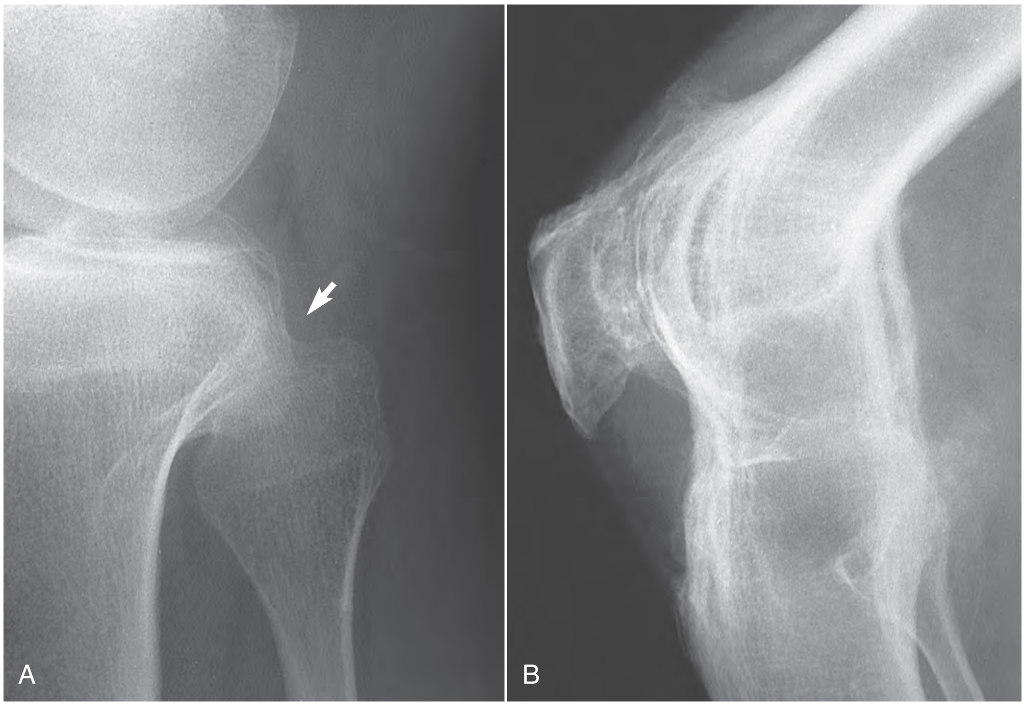

FIGURE 9–59 **Ankylosing spondylitis.**[92] **A,** This 20-year-old man had a 4-year history of juvenile onset ankylosing spondylitis. Observe partial osseous ankylosis of the proximal tibiofibular joint *(arrow)*. **B,** In another patient, a 67-year-old man with a 40-year history of adult-onset ankylosing spondylitis, observe the osseous ankylosis of the femorotibial joint, diffuse muscle atrophy, and patellofemoral joint space narrowing. Radiographic abnormalities in the knees are found in about 30% of persons with severe ankylosing spondylitis.

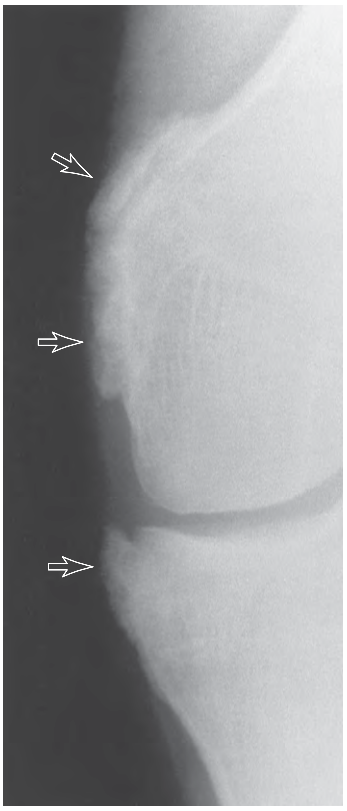

FIGURE 9–60 **Reactive arthritis.**[93] In this 24-year-old man with Reiter syndrome and HLA B27 antigen, observe the prominent, irregular periarticular osseous proliferation arising from the medial tibia and femur *(open arrows)*. Such fluffy enthesopathy is characteristic of the seronegative spondyloarthropathies. *(Courtesy R. Shapiro, MD, Sacramento, Calif.)*

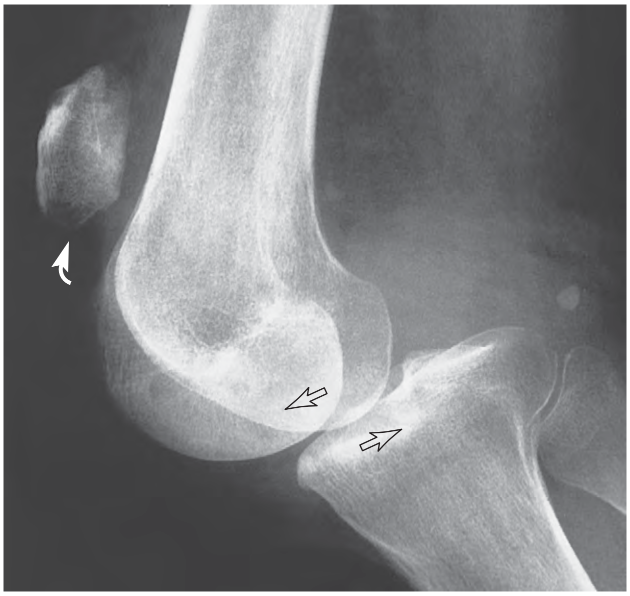

FIGURE 9–61 **Systemic lupus erythematosus.**[94] Lateral radiograph of the knee reveals superior patellar displacement (patella alta) as a result of spontaneous rupture of the patellar tendon *(curved arrow)*. Posterior subluxation of the tibia in relation to the femur also is present *(open arrows)*. Spontaneous tendon rupture in systemic lupus erythematosus is almost invariably associated with corticosteroid administration. *(Courtesy A.G. Bergman, MD, Stanford, Calif.)*

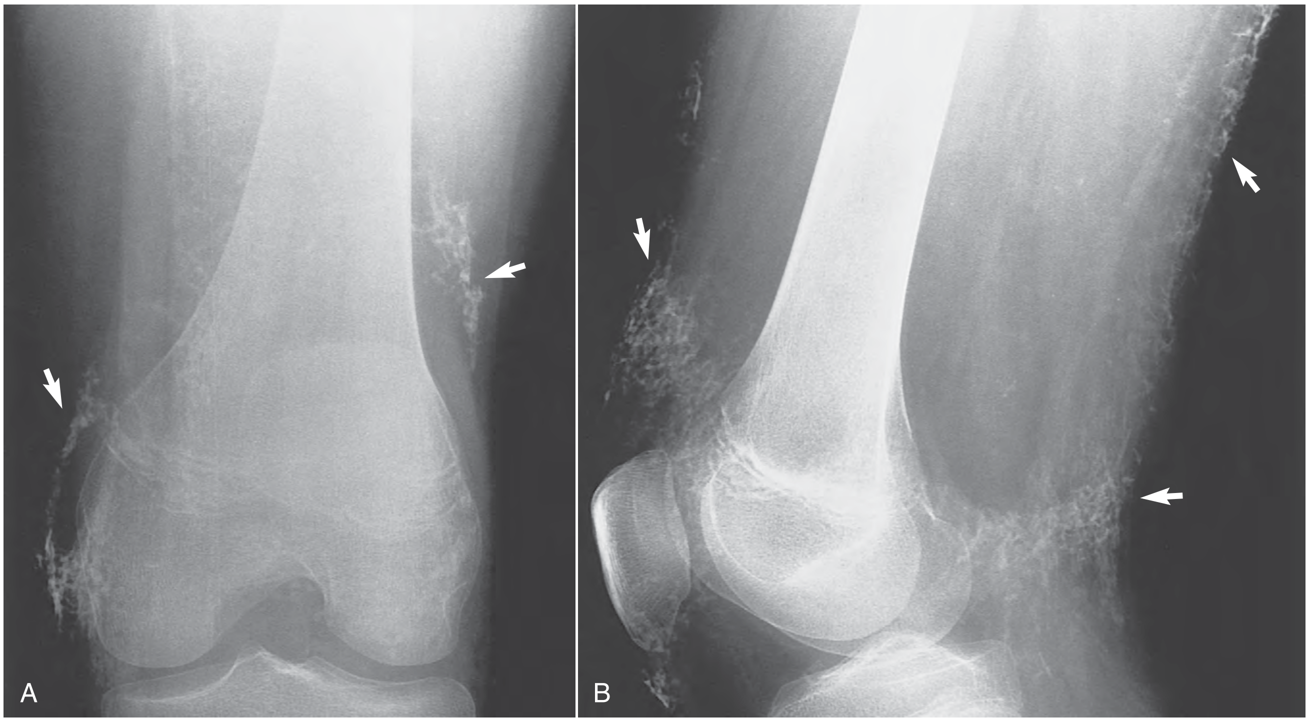

FIGURE 9–62 Dermatomyositis and polymyositis.[95] Frontal **(A)** and lateral **(B)** radiographs of this 13-year-old girl reveal a characteristic sheetlike calcinosis within the subcutaneous tissues about the knee and thigh *(arrows)*.

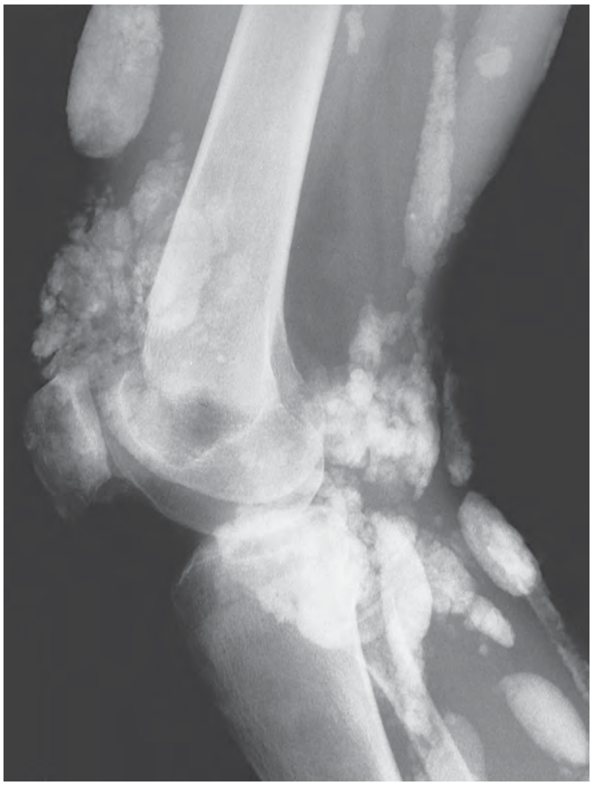

FIGURE 9–63 Mixed connective tissue disease.[96,97] This patient with bizarre globular accumulations of periarticular calcification exhibits clinical and radiographic findings of combined dermatomyositis, scleroderma, and systemic lupus erythematosus.

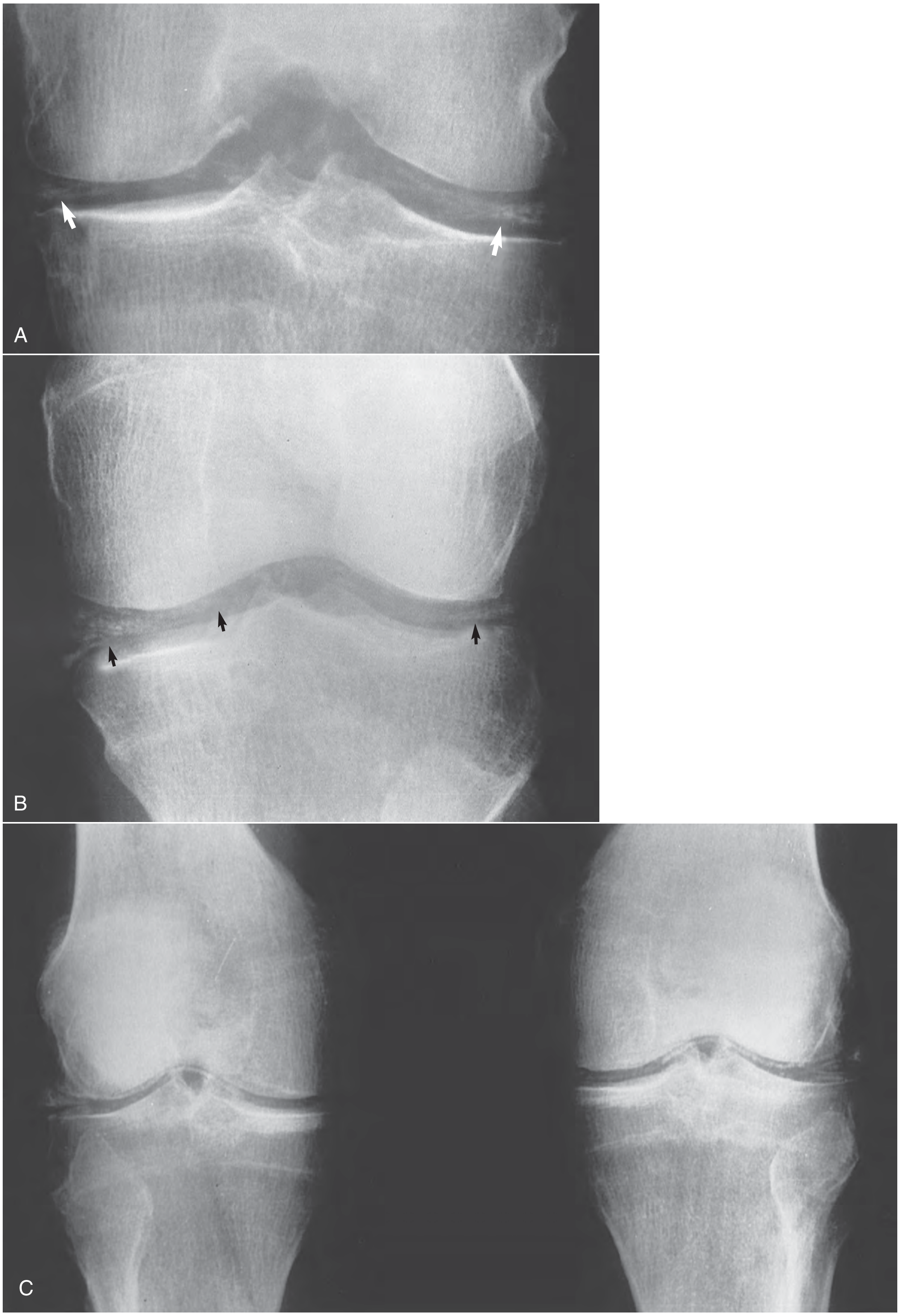

FIGURE 9–64 Calcium pyrophosphate dihydrate (CPPD) crystal deposition disease.[98-100,124,129] **A,** In this 75-year-old man, observe chondrocalcinosis within the hyaline cartilage lining the tibial and femoral articular surfaces and the meniscal fibrocartilage *(arrows)*. **B,** In another patient, linear calcification is seen in the meniscal fibrocartilage and hyaline cartilage of the tibiofemoral articulation *(arrows)*. **C,** Bilateral narrowing of the medial and lateral compartments, as well as extensive chondrocalcinosis, is characteristic of CPPD crystal deposition disease.

Continued

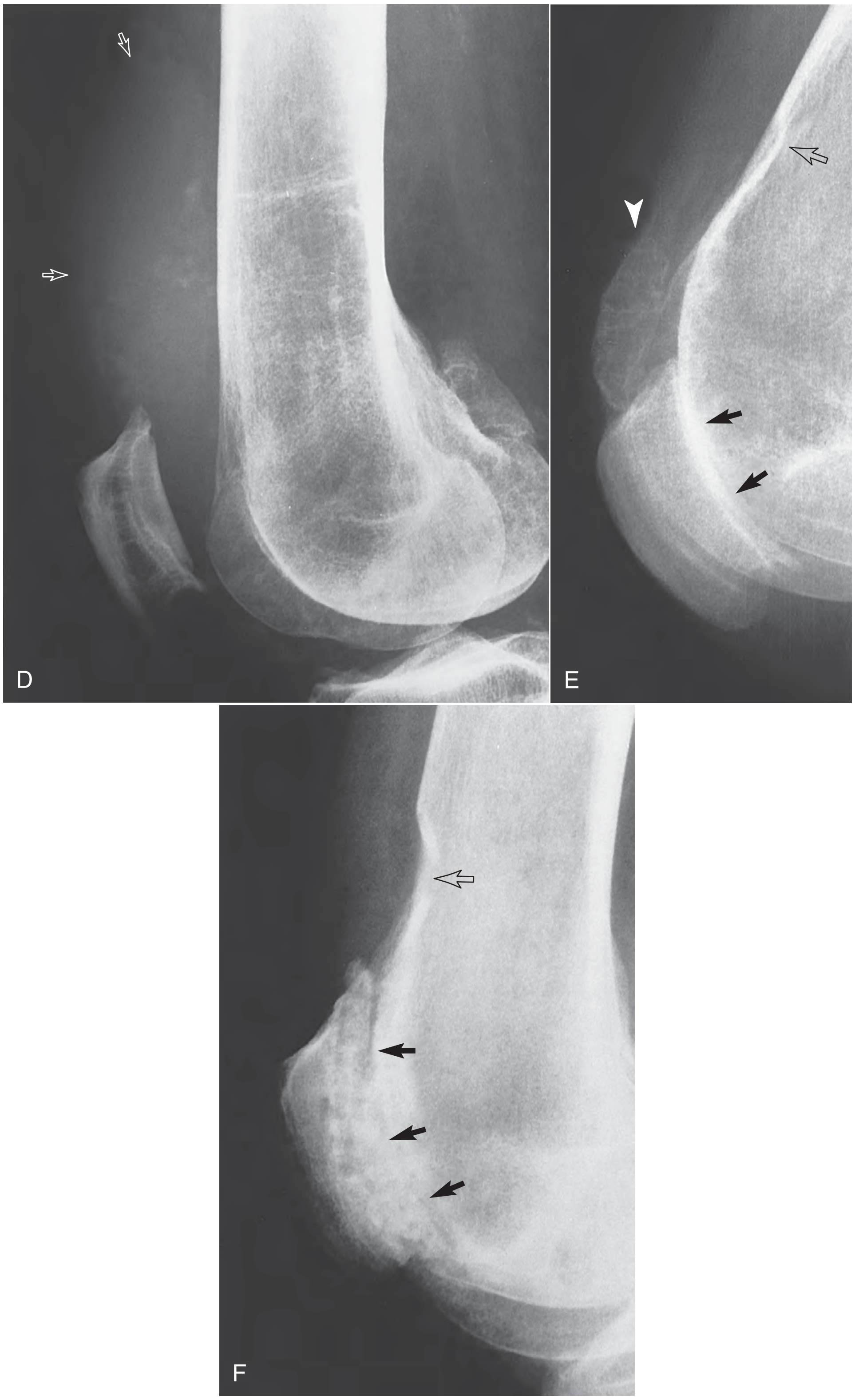

FIGURE 9–64, cont'd **D,** Radiograph taken during an acute episode of pseudogout reveals anterior displacement of the patella caused by a huge suprapatellar effusion *(open arrows)*. Synovial calcification is also evident. **E,** Patellofemoral joint involvement predominates in this patient. Findings include extensive compartmental narrowing *(arrows)* and a suprapatellar femoral erosion *(open arrow)*. An intraarticular body within the suprapatellar pouch *(arrowhead)* is also apparent. **F,** In another patient, destructive patellofemoral arthropathy with joint space narrowing *(arrows)* and femoral erosion *(open arrow)* are seen.

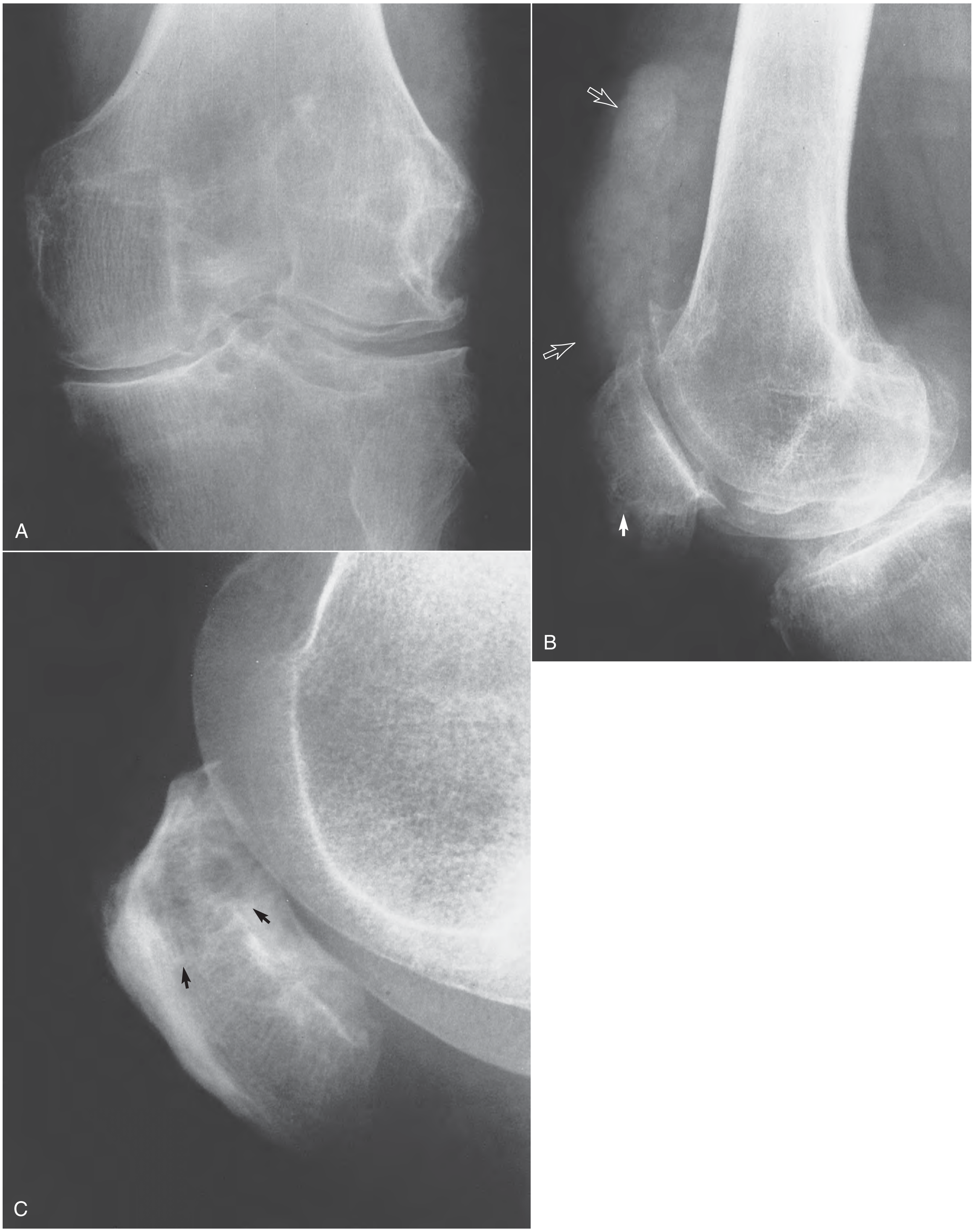

FIGURE 9–65 **Gouty arthropathy.**[101] **A-B,** Articular abnormalities in a 54-year-old man who had had long-standing gout. In **A,** a frontal radiograph shows a large periarticular marginal erosion of the lateral femoral condyle. Multiple cystlike lesions are also seen in the subarticular regions of bone, and prominent osteophytes simulate chondrocalcinosis. In **B,** a lateral radiograph reveals a large radiodense suprapatellar effusion *(open arrows)*. The opacity may represent tophaceous deposits in the suprapatellar bursa. A characteristic intraosseous erosion is present within the patella *(arrow)*. Patellofemoral joint space narrowing and osteophytes probably are related to coexistent osteoarthrosis. **C,** Patellar abnormalities. In another patient, cystic erosion of the patella is evident *(arrows)*. Such osteolytic lesions in gout typically occur within the superolateral aspect of the patella and are often accompanied by an associated calcified soft tissue mass.

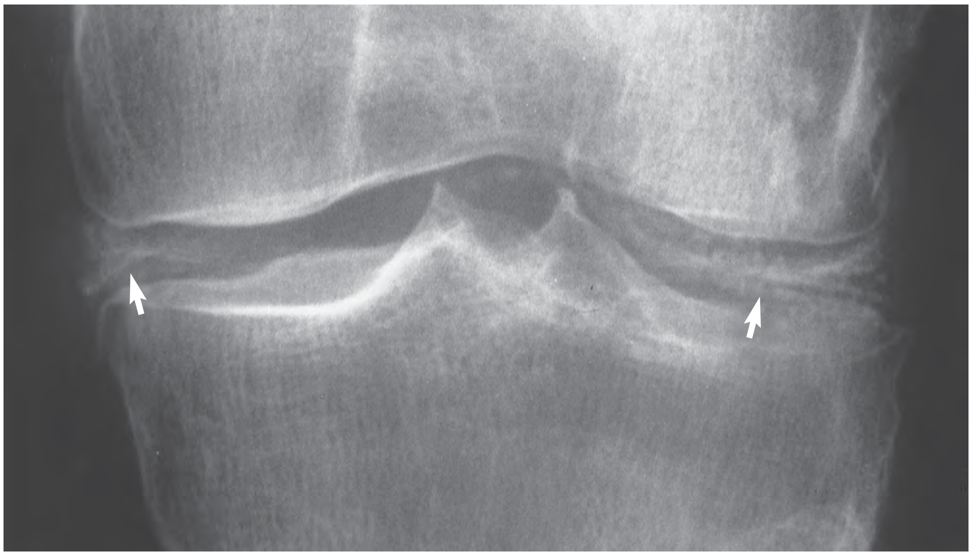

FIGURE 9–66 **Hemochromatosis: chondrocalcinosis.**102 Observe the linear calcification within the fibrocartilage of the medial and lateral menisci *(arrows)*.

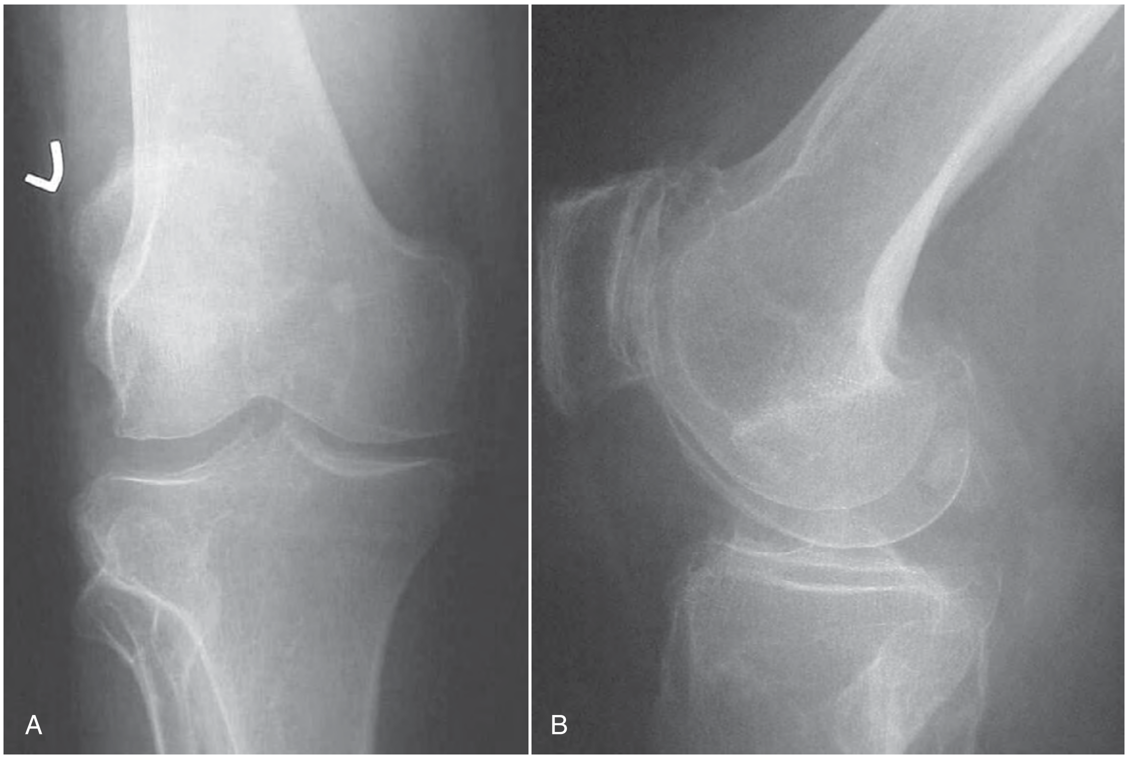

FIGURE 9–67 **Acromegalic arthropathy.**89 **A-B,** Radiographs of this patient with a pituitary adenoma and longstanding acromegaly reveal hyperostosis and ossification (enthesopathy) of the patellar attachments of the quadriceps and patellar tendons, lateral joint space widening (as a result of cartilage hypertrophy), and degenerative changes such as patellofemoral and medial joint space narrowing, subchondral sclerosis and marginal osteophytes. Hypertrophy of the fabella is the result of excessive bone formation.

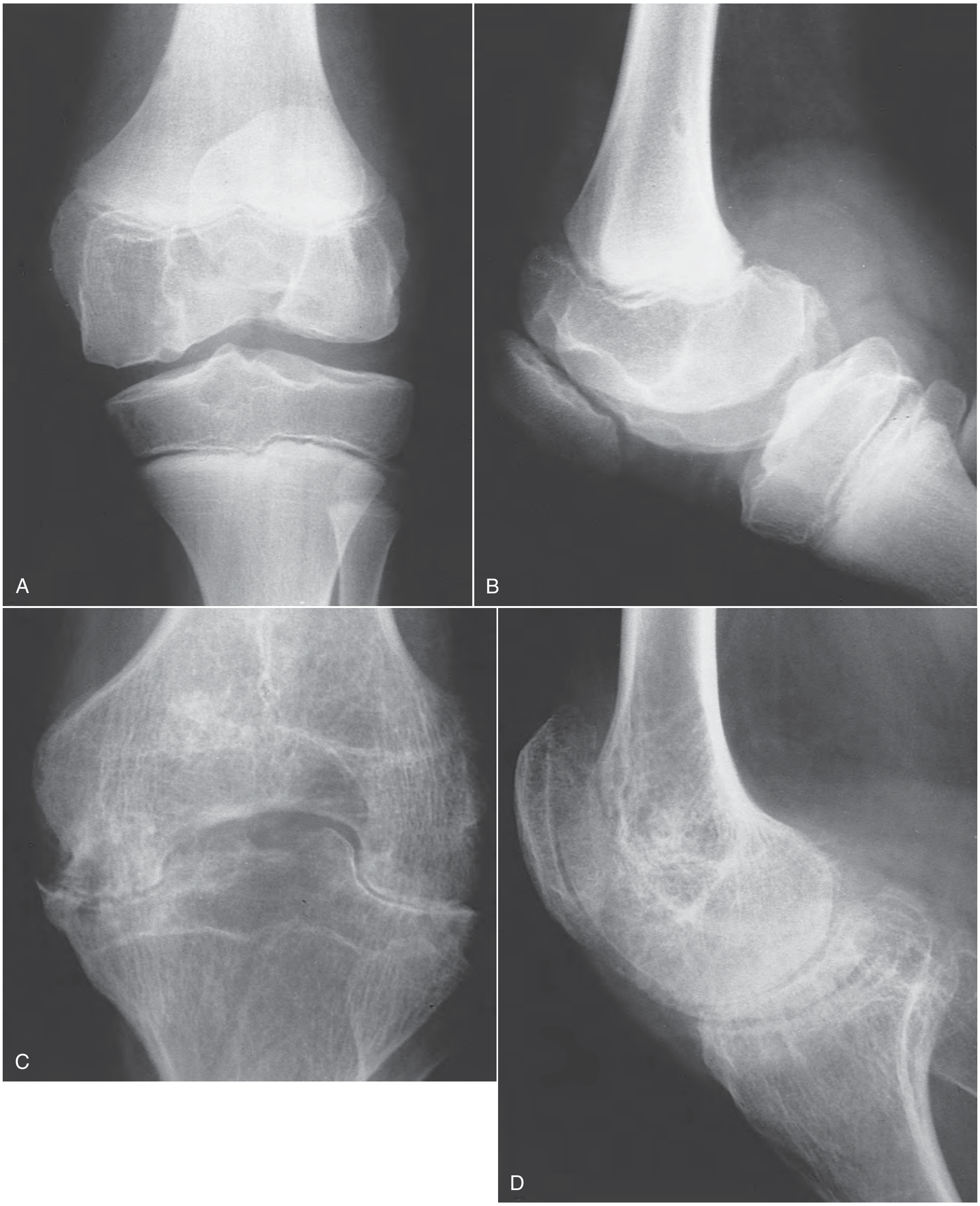

FIGURE 9–68 **Hemophilic arthropathy: radiographic abnormalities.**[103,125] **A-B,** Frontal **(A)** and lateral **(B)** radiographs of this boy with hemophilia reveal well-defined subchondral erosions resulting in an undulating appearance of the joint surfaces. Epiphyseal hyperplasia, squaring of the distal end of the femur, patellofemoral joint space narrowing, and a radiodense joint effusion are also evident. **C-D,** In another patient, a 40-year-old man, frontal **(C),** and lateral **(D)** radiographs reveal the characteristic widening of the intercondylar notch, osteopenia, enlargement and ballooning of the epiphyses, dramatic joint space narrowing, and flattening of the articular surfaces of bone. The patella is eroded and the patellofemoral joint is obliterated.

Continued

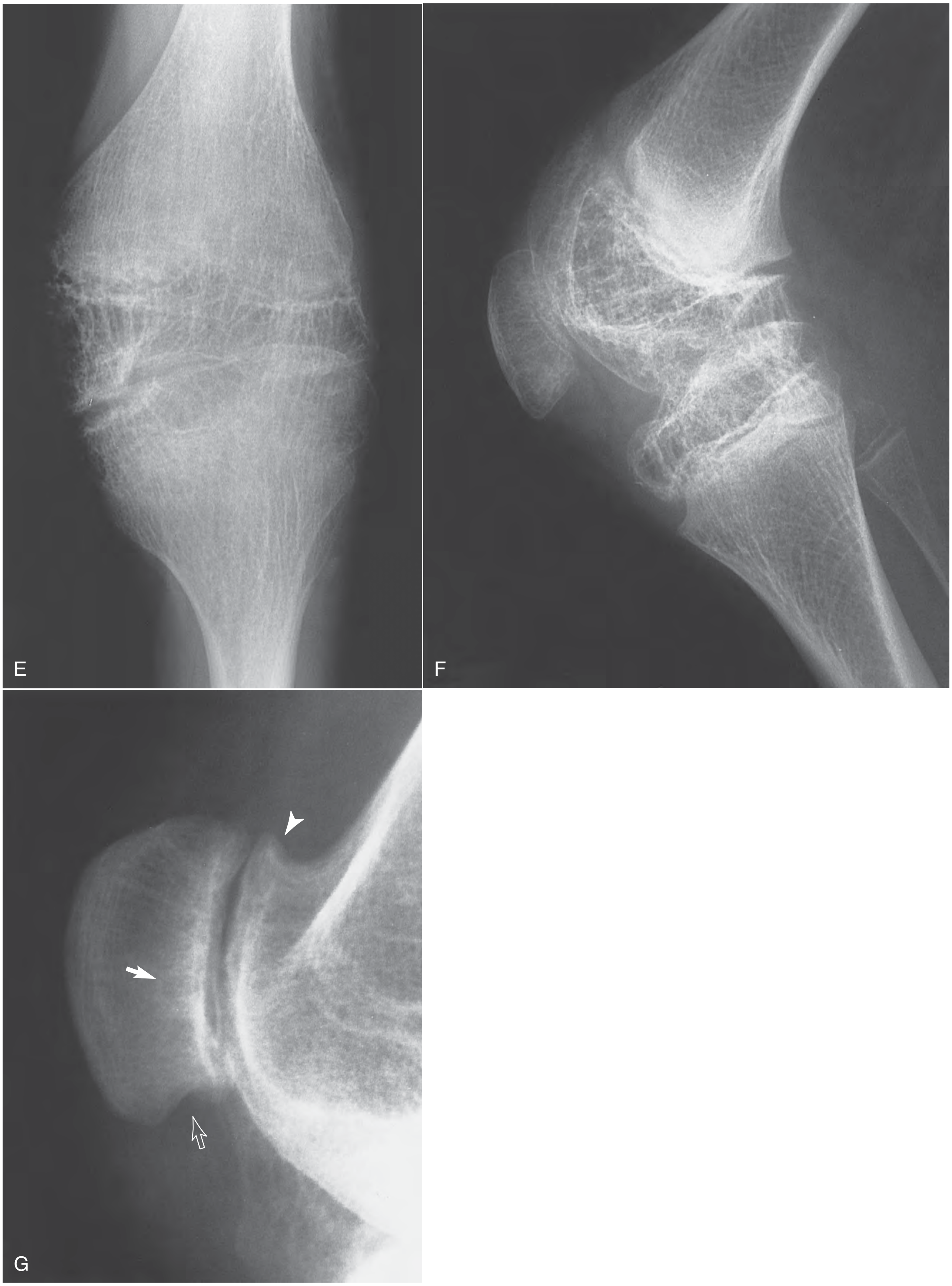

FIGURE 9–68, cont'd **E-F,** This 17-year-old boy has had long-standing hemophilia and has sustained several episodes of hemarthrosis involving several joints. Frontal **(E)** and lateral **(F)** radiographs reveal severe articular destruction, advanced diffuse osteopenia, enlargement of the medial femoral condyle, squaring of the inferior aspect of the patella, and severe muscle atrophy. **G,** In a fourth patient, patellofemoral changes include joint space narrowing, osteophytes *(arrowhead),* cyst formation *(arrow),* and prominent squaring of the inferior margin of the patella *(open arrow).*

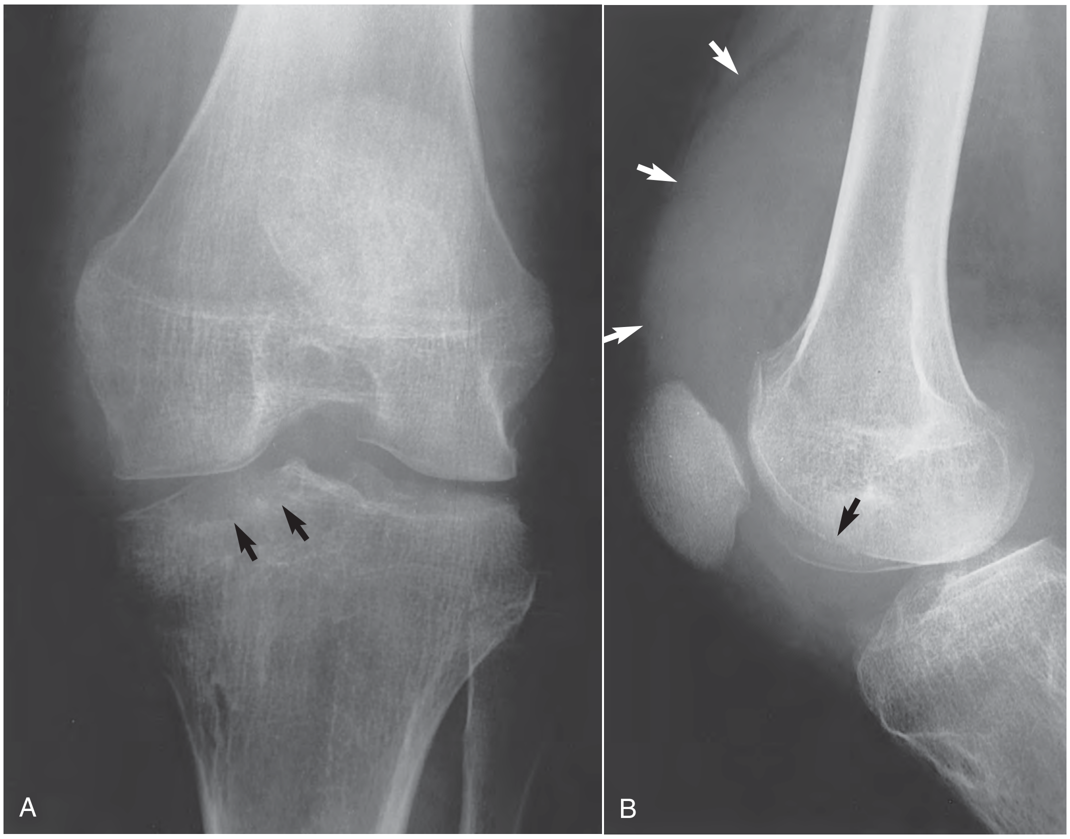

FIGURE 9–69 **Tuberculous arthritis.**[105] Routine frontal **(A)** and lateral **(B)** radiographs of the knee in this 19-year-old patient reveal the characteristic findings of joint infection. Marginal and central erosions *(black arrows),* minimal periarticular osteoporosis, and a huge joint effusion distending the suprapatellar bursa and displacing the patella *(white arrows)* are evident. *Mycobacterium tuberculosis* was cultured from the joint aspirate.

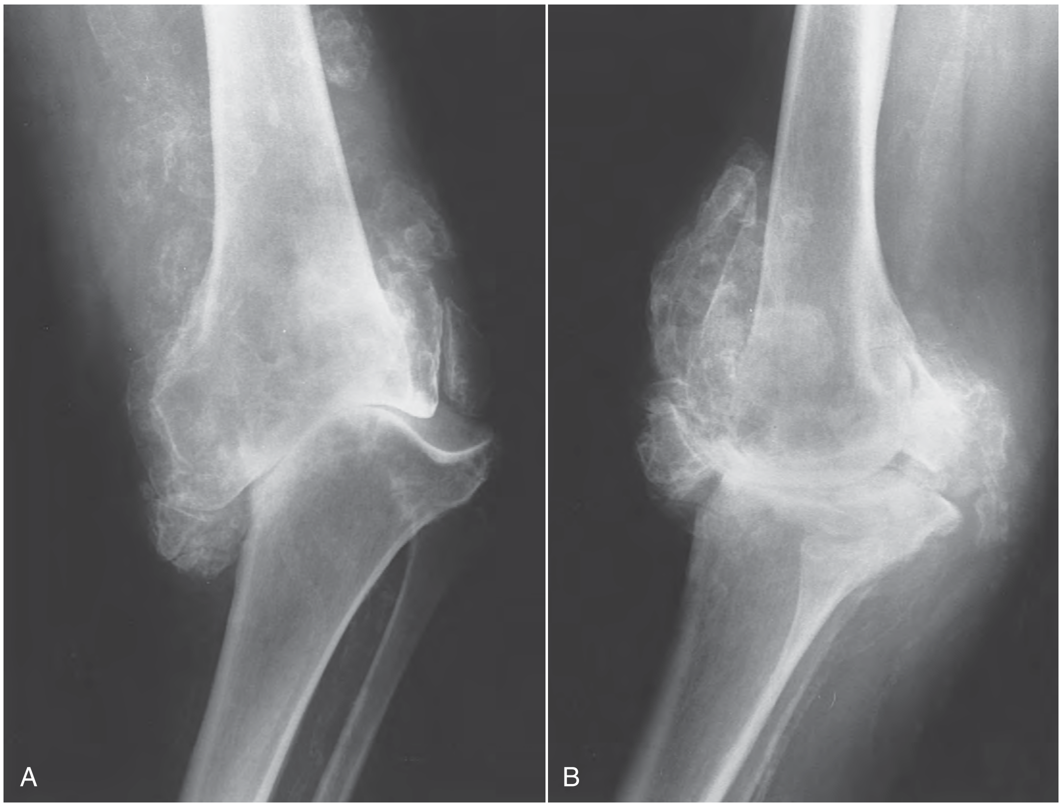

FIGURE 9–70 **Neuropathic osteoarthropathy: neurosyphilis.**[89] This 67-year-old man with long-standing syphilis had no pain in his knees but complained of deformities, unsteadiness while walking, and limitation of motion. **A,** Frontal radiograph of the left knee reveals a striking pattern of exuberant new bone formation, fragmentation, varus angulation, subluxation, destruction, and remodeling of the joint surfaces. **B,** Lateral radiograph of the opposite knee shows marked genu recurvatum and changes similar to those on the left side. Note also the extensive vascular calcification. *(**A,** Courtesy P. VanderStoep, MD, St Cloud, Minn.)*

TABLE 9-15 Bone Tumors and Other Lesions Affecting the Knee and Patella*

Entity	Figure(s)	Characteristics
Malignant		
Skeletal Metastasis[106]	9-71	Most common in the axial skeleton; rare occurrence about the knee 75% of cases exhibit permeative or moth-eaten osteolysis *Articular involvement:* may involve both sides of the articulation with widespread destruction
Myeloproliferative disorder		
Plasma cell (multiple) myeloma[107,142]	9-72	Bones about the knee are an uncommon site for multiple myeloma Early diffuse osteopenia or later widespread well-circumscribed osteolytic lesions with discrete margins, which appear uniform in size
Benign		
Chondroblastoma[108,109]	9-73	*Predilection for the epiphyses and apophyses:* the patella is an "epiphyseal equivalent" structure Circular osteolytic lesion less than 5 or 6 mm in diameter May exhibit calcification in matrix Occasionally periosteal reaction in adjacent metaphysis with corresponding marrow edema seen on MR images
Giant cell tumor[89]	8-35	Eccentric osteolytic neoplasm with a predilection for the subarticular region Often multiloculated expansile lesion Radiographs are inaccurate in distinguishing benign from aggressive giant cell tumors
Aneurysmal bone cyst[110]	9-74	Eccentric, thin-walled, expansile osteolytic lesion Thin trabeculation with multiloculated appearance
Tumorlike lesions		
Paget disease[111 112]	9-75	Usually polyostotic and may have unilateral involvement Coarsened trabeculae and bone enlargement *Patterns of involvement:* osteolytic (50%), osteosclerotic (25%), and mixed (25%)
Other patellar lesions		
Hemangioma		Osteolytic, prominent trabeculae
Lipoma		Osteolytic
Enchondroma		Osteolytic, matrix calcification
Plasmacytoma		Osteolytic, expansile
Aggressive giant cell tumor		Osteolytic, cortical destruction
Primary lymphoma		Osteolytic or osteosclerotic
Osteosarcoma		Osteolytic or osteosclerotic
Chondrosarcoma		Osteolytic, soft tissue mass, matrix calcification
Degenerative cyst		Osteolytic, associated degenerative changes
Brodie abscess		Osteolytic, sclerotic margin
Intraosseous ganglion		Osteolytic

* See also Tables 1-12 to 1-14.

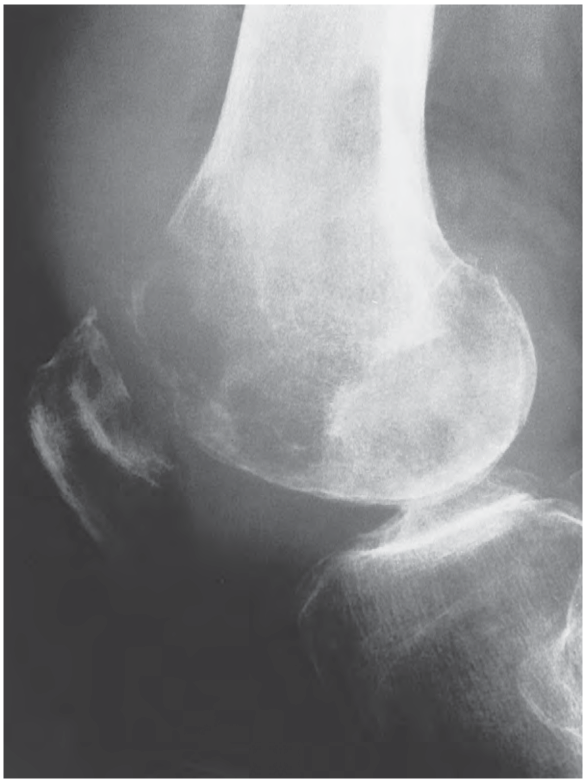

FIGURE 9–71 **Skeletal metastasis. Articular involvement.**[106] In this patient with skeletal metastasis from an unknown primary source, a large osteolytic pattern of destruction involving the distal end of the femur is evident. A large suprapatellar joint effusion or mass is also present. Biopsy indicated anaplastic carcinoma involving bone and extending into the articular cavity with hemarthrosis. *(Courtesy V. Vint, MD, La Jolla, Calif.)*

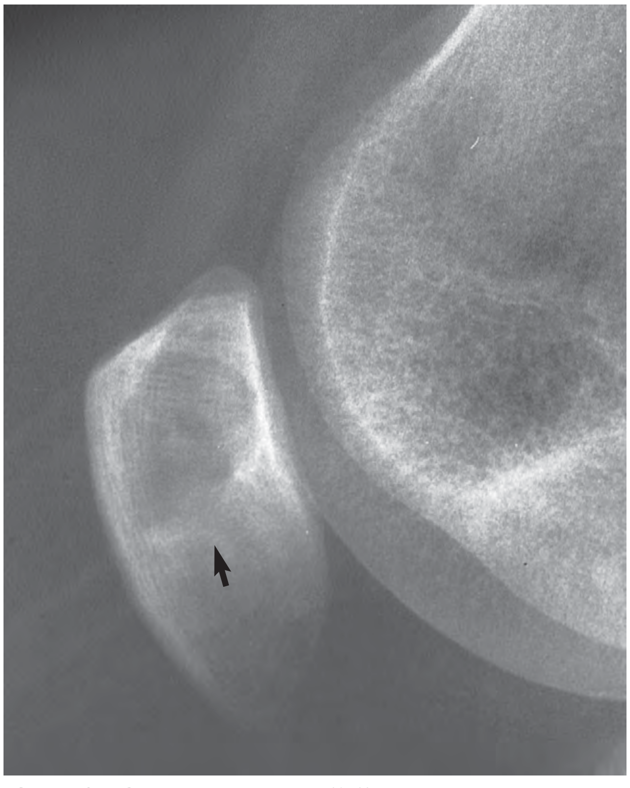

FIGURE 9–73 **Chondroblastoma.**[108,109] This 19-year-old man with a 6-month history of patellar pain had a solitary radiolucent lesion within the patella *(arrow)*. The lesion is well defined, possesses a sclerotic margin, and is associated with extensive soft tissue swelling overlying the patella.

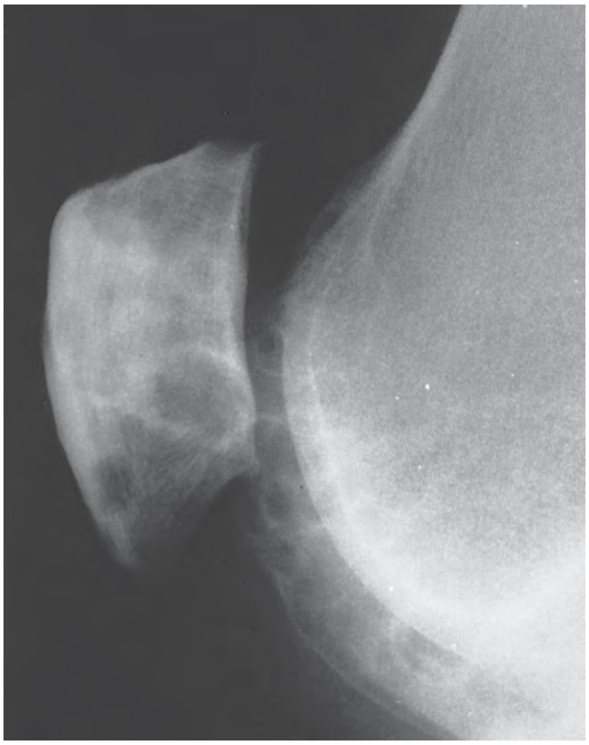

FIGURE 9–72 **Plasma cell (multiple) myeloma.**[107,142] Multiple geographic lesions are evident in the patella and the femoral condyles in this patient with multiple myeloma. Classically, myeloma is first manifested as widespread osteolytic lesions with discrete margins, which appear uniform in size. Alternatively, diffuse osteopenia may be the only radiographic finding.

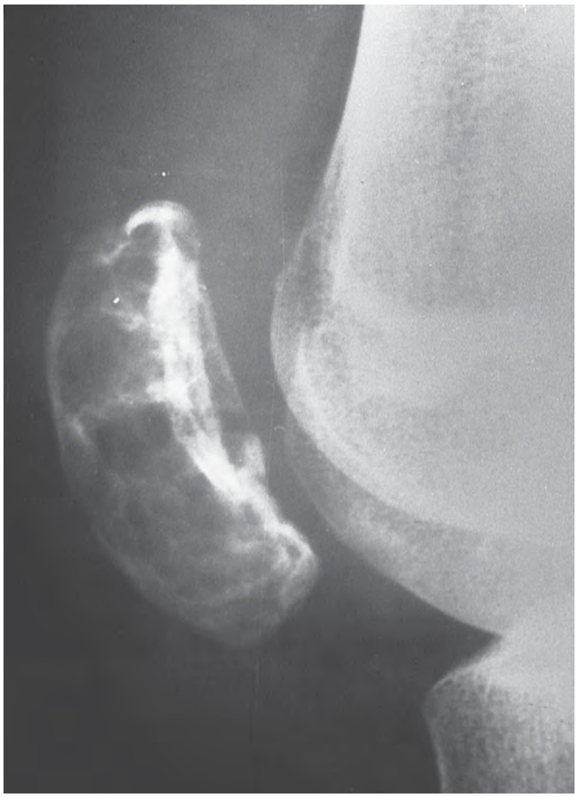

FIGURE 9–74 **Aneurysmal bone cyst.**[110] An expansile osteolytic lesion is seen involving the patella. The radiographic appearance of a multiseptated osteolytic lesion in the patella is nonspecific, and biopsy was required to confirm the diagnosis of aneurysmal bone cyst in this patient. A joint effusion is also present, displacing the superior pole of the patella anteriorly. *(Courtesy R. Stiles, MD, Atlanta.)*

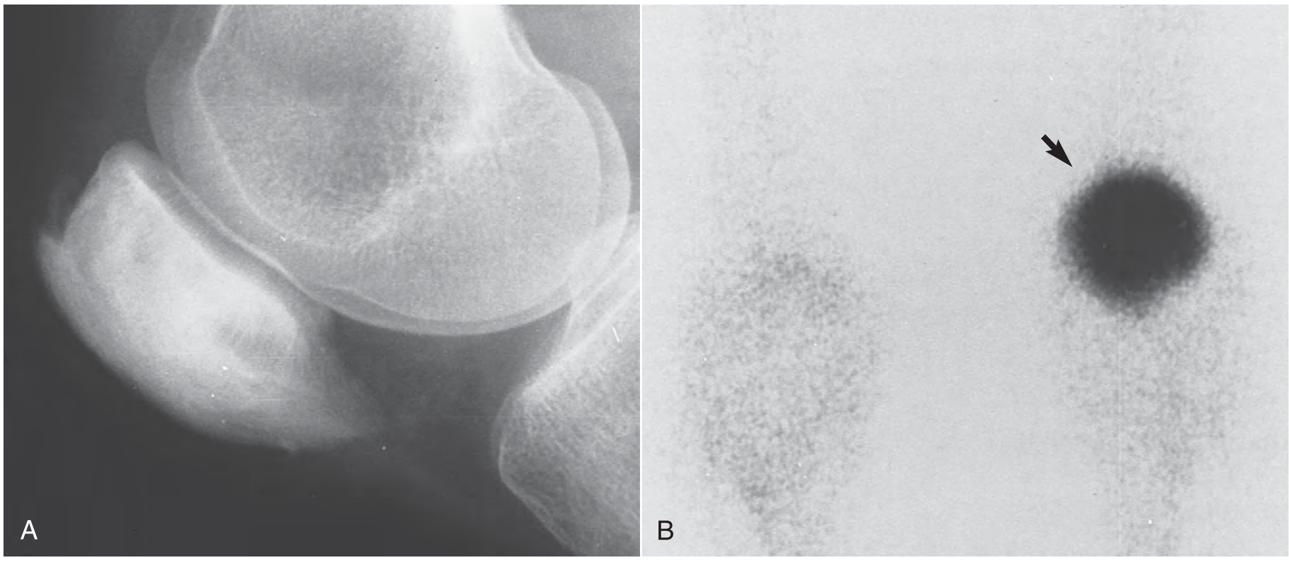

FIGURE 9–75 **Paget disease.**[111,112] **A,** Lateral radiograph reveals coarsely trabeculated osteoblastic involvement of the patella. **B,** Bone scan reveals intensely increased uptake of bone-seeking radiopharmaceutical agent *(arrow).*

TABLE 9-16 Metabolic, Hematologic, and Vascular Disorders*

Entity	Figure(s)	Characteristics
Generalized osteoporosis[89]	9-76	Increased radiolucency Trabecular accentuation
Rickets[113]	9-77	Metaphyseal demineralization: frayed metaphysis Bowing of bones Osteopenia
Primary hypertrophic osteoarthropathy[114]	9-78	*Pachydermoperiostosis:* primary form (3%-5% of all cases) of hypertrophic osteoarthropathy Rare autosomal dominant disease characterized by enlargement of the hands and feet, digital clubbing, convexity of the nails, cutaneous abnormalities, and joint pains Bilateral symmetric periostitis of the long tubular bones
Hypovitaminosis C (scurvy)[115]		Radiographic evidence of skeletal changes in scurvy is seen only in advanced long-standing disease Periostitis secondary to subperiosteal hemorrhage Sclerotic metaphyseal lines Beaklike metaphyseal excrescences Radiodense shell surrounding epiphyses Healing scurvy may result in increased radiodensity of the metaphyses and epiphyses
Hyperparathyroidism[116-119]	9-79	Subperiosteal bone resorption of medial tibial metaphysis Occasional bone sclerosis (more common with renal osteodystrophy) Chondrocalcinosis ([calcium pyrophosphate dihydrate] CPPD crystal deposition) Brown tumors Severe bone remodeling with osteitis fibrosa cystica (now infrequently encountered) Soft tissue calcification
Renal osteodystrophy[116-119]	9-80, 9-81	Similar findings to those in hyperparathyroidism, osteomalacia, and rickets Pathologic fractures

TABLE 9-16 Metabolic, Hematologic, and Vascular Disorders*—cont'd

Entity	Figure(s)	Characteristics
Osteonecrosis[120,121]	9-81 to 9-83	Secondary epiphyseal osteonecrosis and medullary osteonecrosis See Table 1-17 for predisposing causes and associations Spontaneous osteonecrosis Idiopathic osteonecrosis may occur spontaneously in the absence of any risk factors; most common in women older than 60 years of age; sudden onset of localized tenderness, stiffness, effusion, and restriction of motion; usually unilateral; most frequently affects the weight-bearing surface of the medial femoral condyle; initial radiographs frequently normal Bone sclerosis, subchondral cysts, subchondral collapse Subchondral collapse and associated meniscal and articular cartilage abnormalities
Popliteal artery aneurysm[52,122]	9-84	May appear as a pulsatile mass in the popliteal fossa Often posttraumatic Complications include leaking, embolism, and thrombus

* See also Tables 1-15 to 1-17.

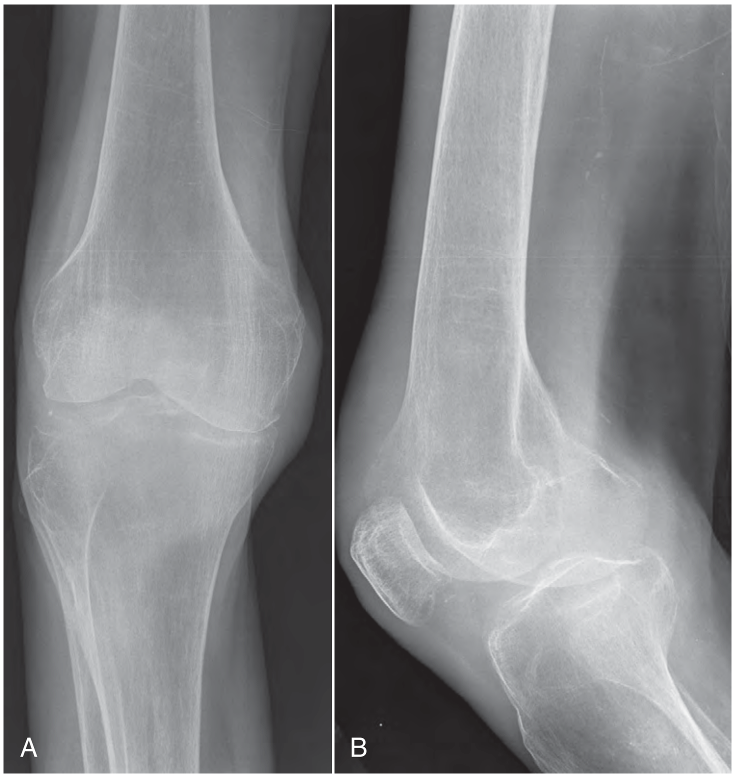

FIGURE 9–76 **Generalized osteoporosis.**[89] Anteroposterior **(A)** and lateral **(B)** radiographs of the knee in this 93-year-old man reveal severely decreased radiodensity of the medullary cavities and thinning of the cortices. While radiographs are inaccurate at quantifying bone mineral density, comparison of the relative radiographic densities of osseous and soft tissue structures provide at least a qualitative estimate of decreased bone mineral content. Note also the atrophy of the anterior and posterior thigh muscles.

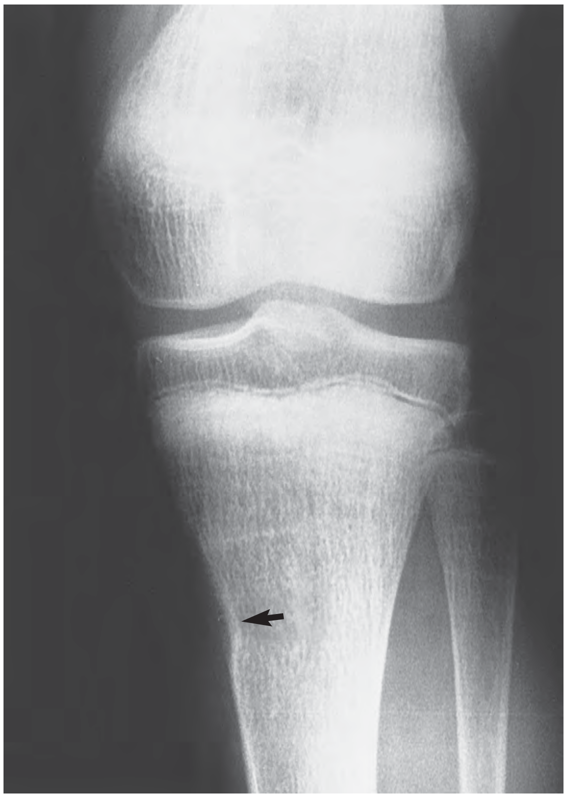

FIGURE 9–77 **Renal rickets.**[113] A knee radiograph of this 19-year-old woman with rickets and chronic renal disease shows metaphyseal sclerosis and erosion of the medial tibial metaphysis *(arrow),* characteristic of renal rickets.

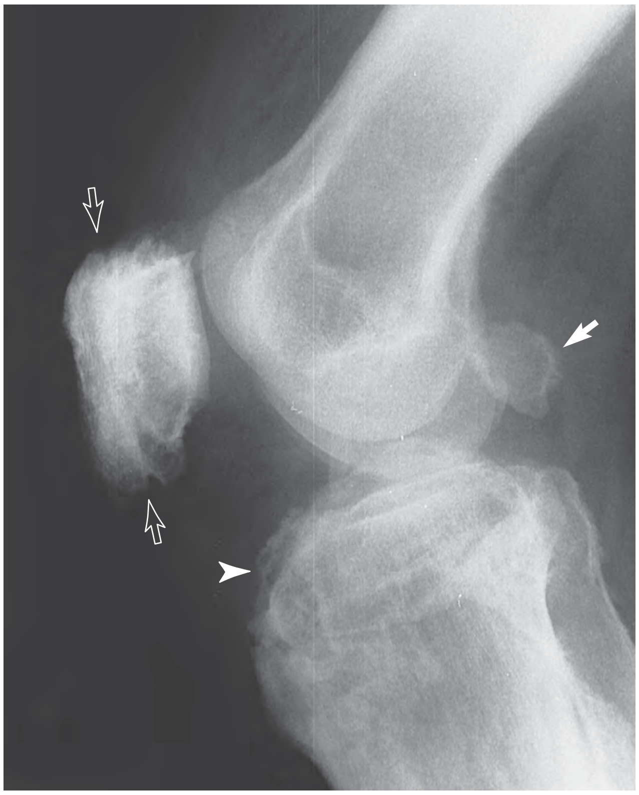

FIGURE 9–78 **Primary hypertrophic osteoarthropathy: pachydermoperiostosis.**[114] Observe the widespread prominent enthesophytes arising from the patella *(open arrows),* fabella *(arrow),* and anterior surface of the tibia *(arrowhead)*. The findings in this patient were bilateral and symmetric and affected several bones throughout the skeleton. *(Courtesy C. Chen, MD, Kaohsiung, Taiwan.)*

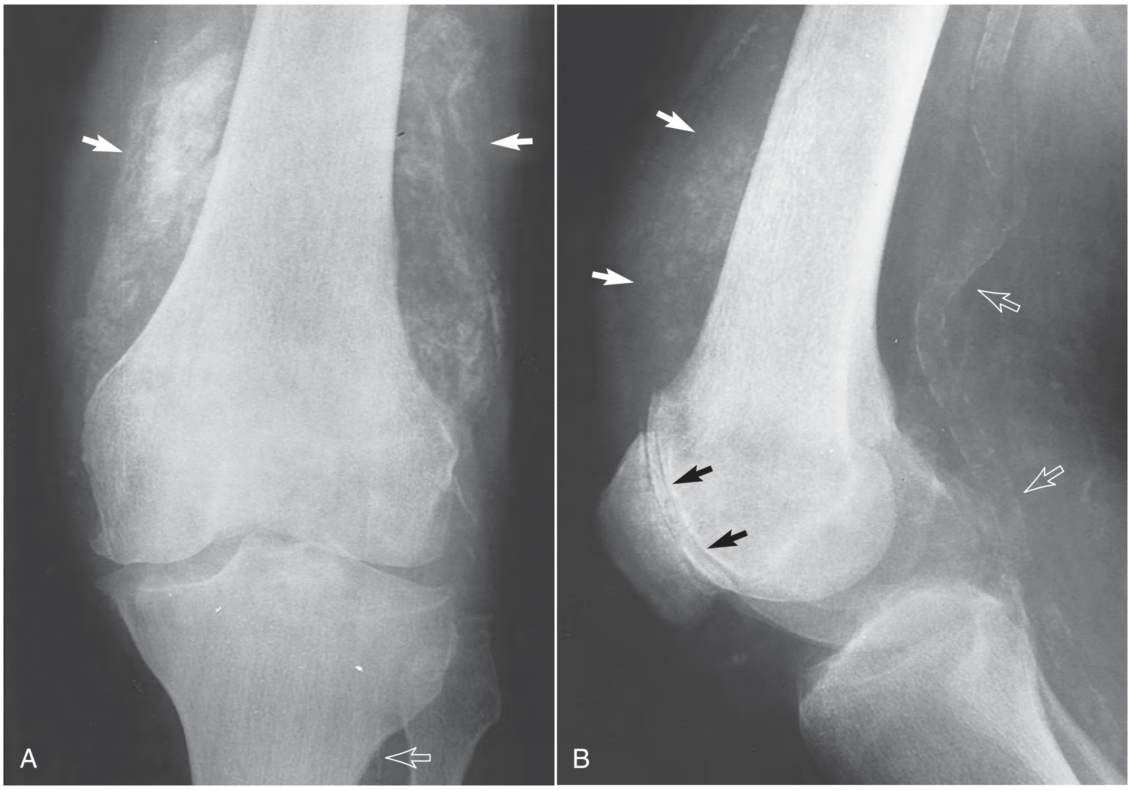

FIGURE 9–79 **Hyperparathyroidism.**[116,117] Frontal **(A)** and lateral **(B)** radiographs show extensive intraarticular soft tissue calcification involving the synovium, suprapatellar bursa *(white arrows),* and vasculature *(open arrows)* about the knee. Observe also the dramatic erosion and deformity of the posterior surface of the patella *(black arrows)*.

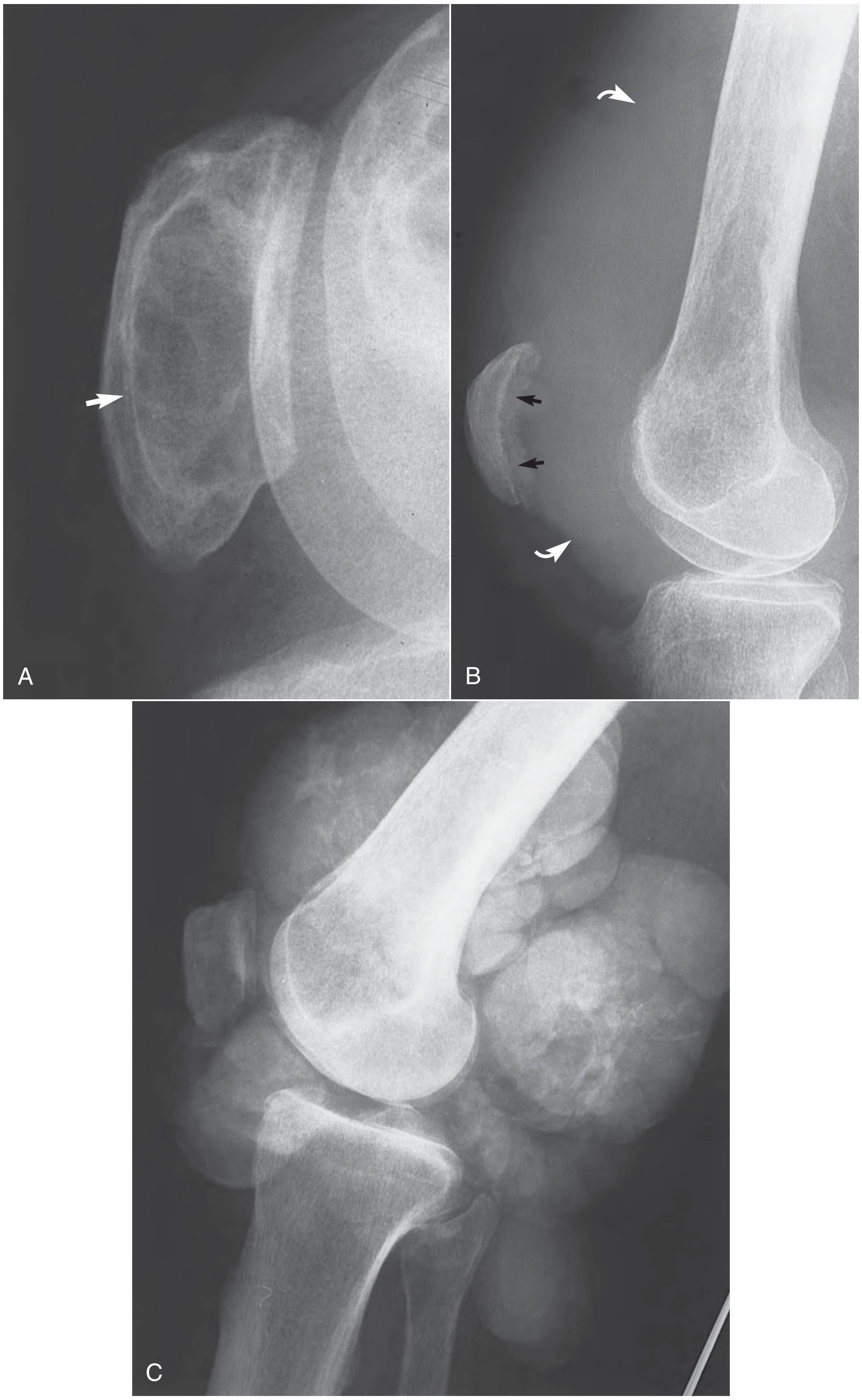

FIGURE 9–80 Renal osteodystrophy: radiographic abnormalities.[116-120] **A,** Brown tumor. Routine radiograph reveals an osteolytic lesion affecting the patella *(arrow)* in this patient with chronic renal failure and secondary hyperparathyroidism. Brown tumors represent localized accumulations of fibrous tissue and giant cells, which can replace bone and may produce expansion. They may be single or multiple and may disappear after treatment of the underlying cause of hyperparathyroidism. **B,** Patellofemoral erosion and hemarthrosis. In a 68-year-old woman, observe the presence of a large suprapatellar effusion *(curved arrows)* and subchondral erosion and deformity of the undersurface of the patella *(small arrows)*. **C,** In a third patient with secondary hyperparathyroidism, observe the presence of intraarticular and intrabursal tumoral calcification. (***C,*** *Courtesy J. Goobar, MD, Ostersund, Sweden.)*

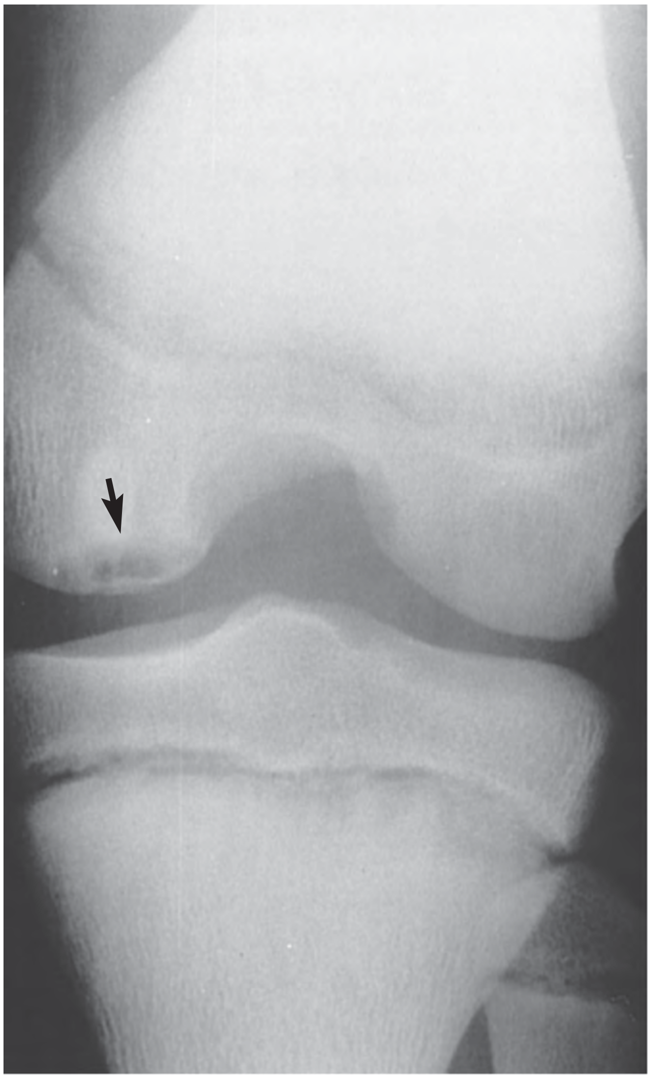

FIGURE 9–81 Osteonecrosis: chronic renal disease.[120,121] In a 15-year-old boy with renal osteodystrophy, observe the generalized osteosclerosis, physeal widening and irregularity, and evidence of osteonecrosis of the medial femoral condyle *(arrow)*. Osteonecrosis has been reported in patients with chronic renal failure treated with and without dialysis or transplantation.

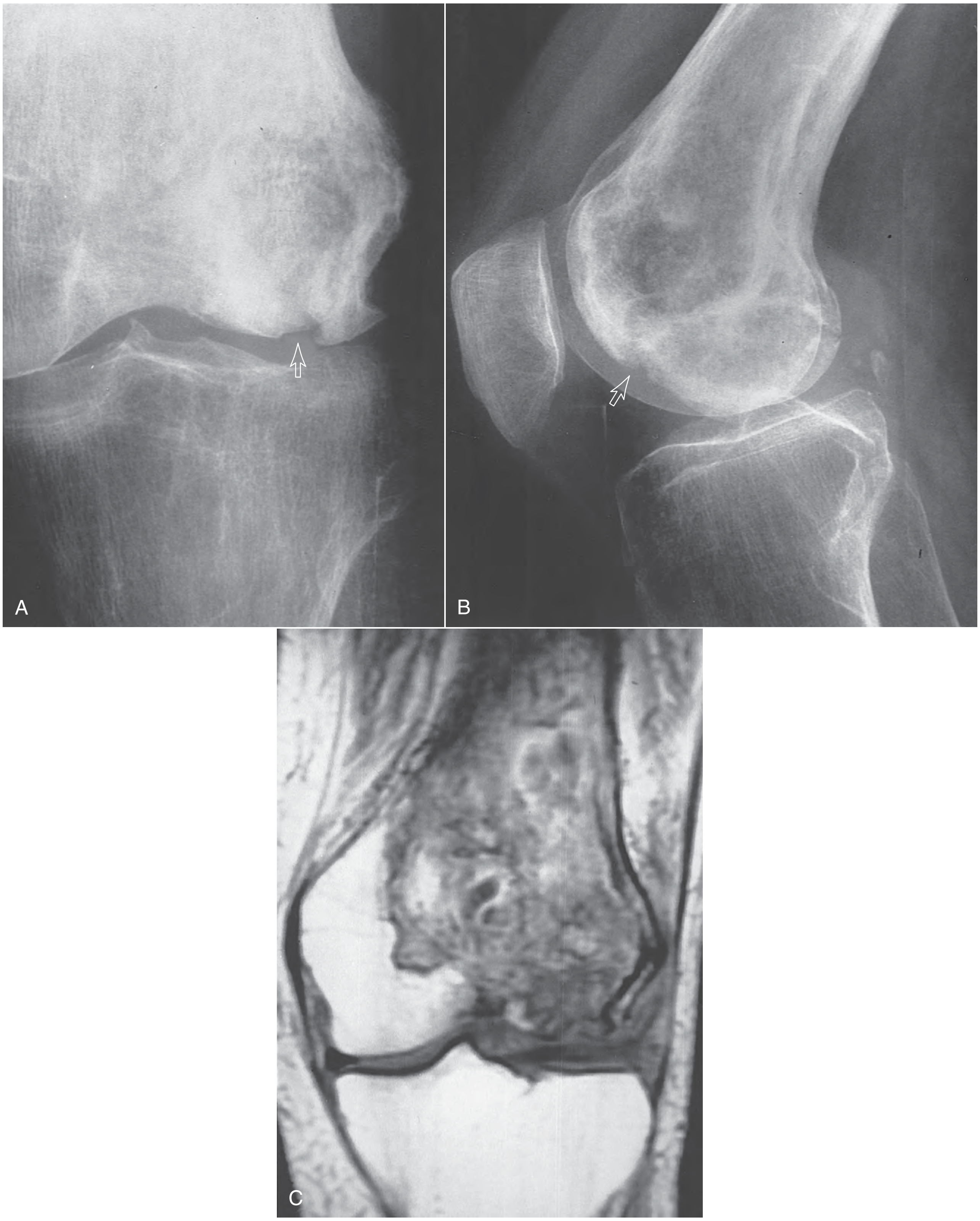

FIGURE 9–82 **Spontaneous osteonecrosis about the knee.**[120,121] This 73-year-old woman had no risk factors for osteonecrosis, and no underlying cause for these changes was found. **A,** Routine frontal radiograph shows increased density of the lateral femoral condyle. The articular surface has collapsed *(open arrow),* and areas of osteolysis also are seen. **B,** Lateral radiograph shows collapse of the articular surface of the lateral condyle *(open arrow)* combined with areas of osteolysis and osteosclerosis. **C,** Coronal T1-weighted (TR/TE, 600/22) spin echo MR image shows extensive mixed intermediate to low signal intensity characteristic of widespread osteonecrosis in the lateral femoral condyle and femoral metaphysis. MR imaging is ideally suited for evaluating osteonecrosis. *(Courtesy D. Artenian, MD, Fresno, Calif.)*

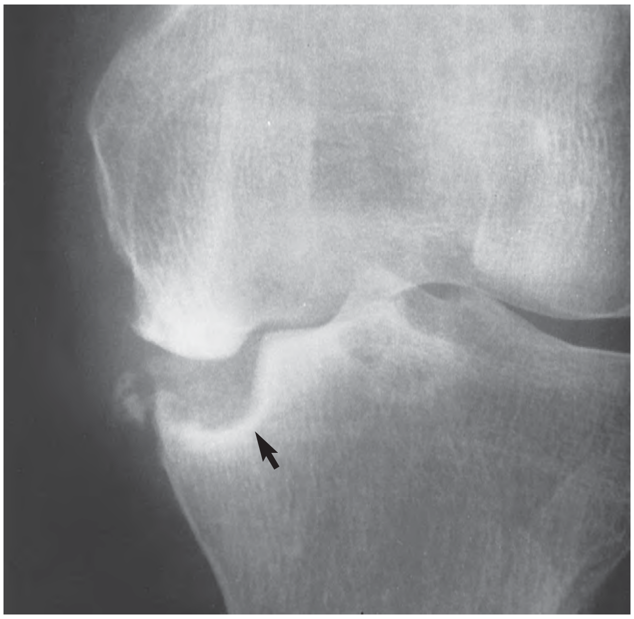

FIGURE 9–83 Corticosteroid-induced osteonecrosis.[121] Observe, in this patient on long-term corticosteroid therapy, joint space narrowing and collapse of the articular surface of the tibial plateau (bite sign) *(arrow)*. Typical radiographic features of osteonecrosis include subchondral curvilinear radiolucent shadows (crescent sign), osteopenia, osteosclerosis, bony collapse and fragmentation, and a relatively normal articular space early in the disease process. Osteonecrosis may occur as a result of either exogenous corticosteroid administration or excessive endogenous corticosteroid secretion.

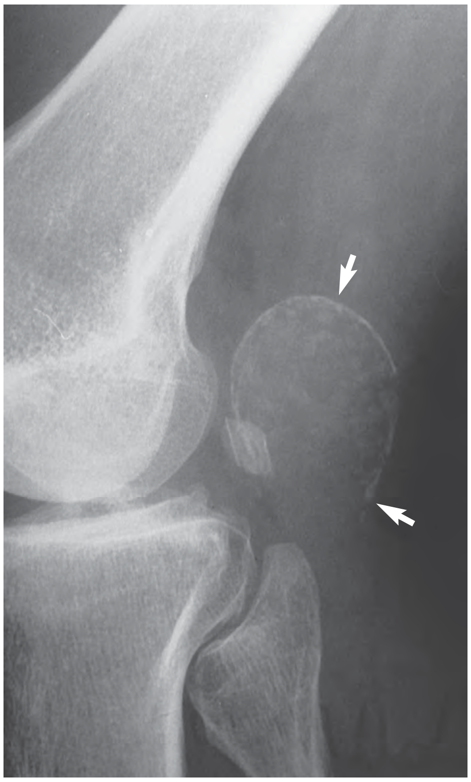

FIGURE 9–84 Posttraumatic popliteal artery aneurysm.[52,122] This 61-year-old man had a pulsatile mass in the popliteal fossa several months after fracturing the shaft of his femur. A large ovoid mass with a calcified rim is evident behind the knee *(arrows)*. The differential diagnosis includes synovial cyst, calcified soft tissue neoplasm, or popliteal vein aneurysm. *(Courtesy A. Orloff, MD, San Diego.)*

CHAPTER 10

Tibia and Fibula

ANATOMIC VARIANTS, SKELETAL DYSPLASIAS, AND OTHER CONGENITAL DISEASES

A number of anatomic variants, skeletal dysplasias, and other congenital conditions affect the tibia and its surrounding structures. Table 10-1 and Figures 10-1 to 10-9 represent selected examples of some of the more common processes.

PHYSICAL INJURY

The tibial and fibular diaphyses and metaphyses are sites of acute fracture, fatigue fracture, and insufficiency fracture. Additionally, the muscles of the leg are a frequent site for posttraumatic heterotopic ossification. These conditions and others are described in Table 10-2 and are illustrated in Figures 10-10 to 10-16. Injuries of the proximal and distal portions of the tibia and the fibula are discussed in Chapters 9 and 11, respectively.

NEOPLASMS

The tibia and the fibula are frequently affected by malignant and benign tumors and tumorlike processes. Tables 10-3 to 10-5 list some of the characteristics of these disorders. Their radiographic manifestations are illustrated in Figures 10-17 to 10-43.

METABOLIC AND HEMATOLOGIC DISORDERS

Several metabolic and hematologic disorders involve the tibia and fibula and their related soft tissues. Table 10-6 lists some of the more common disorders and describes their characteristics. Their radiographic features are illustrated in Figures 10-45 to 10-58. Further manifestations of these disorders within the proximal and distal portions of the tibia and the fibula are described in Chapters 9 and 11, respectively.

INFECTIOUS DISORDERS

The tibia is one of the most common sites of osteomyelitis. Table 10-7 lists some of the more typical forms of osteomyelitis that affect the tibia and fibula and describes their characteristics. The imaging features of these disorders are illustrated in Figures 10-59 to 10-65. Further manifestations of infection within the proximal and distal portions of the tibia and the fibula are described in Chapters 9 and 11, respectively.

TABLE 10-1 Anatomic Variants, Skeletal Dysplasias, and Other Congenital Diseases Affecting the Tibia and the Fibula*

Entity	Figure(s)	Characteristics
Limb length inequality[1-3]	10-1	*Synonyms:* anisomelia, leg length discrepancy, short leg syndrome *Etiology:* developmental, paralysis, infection, trauma, neoplasm, joint replacement surgery Accurate assessment aids in treatment planning Three imaging techniques may be used for measuring the length of the femur and tibia: 1. *Orthoradiograph:* single exposure of entire length of both lower extremities on a long film; may be obtained supine or standing 2. *Radiographic scanogram:* three separate exposures are obtained of the hips, knees, and ankles; the patient is immobilized in a supine position, and the x-ray tube and cassette are moved to expose all three anatomic regions on one film 3. *CT scanogram:* an anteroposterior scout scanogram of both lower extremities is obtained; cursors are placed at the superior tip of the capital femoral epiphysis and the most distal portion of the lateral femoral condyle and measurements are obtained; tibial length is determined in a similar manner by measuring from the tibial plateau to the tibial plafond; lateral views of the femur and tibia also may be obtained and measured to account for limb flexion; CT scanograms are accurate, result in less radiation exposure than radiographic techniques, and they are particularly useful in patients with joint contractures
Infantile tibia vara (Blount disease)[4]	10-2	Painless local disturbance of growth is usually first recognized between the ages of 1 and 3 years Less commonly, an adolescent type is encountered in which the deformity appears between the ages of 8 and 15 years Affects the medial aspect of the proximal portion of the tibia, resulting in tibial bowing within the first few years of life More common in black persons Believed to be more prevalent in children who begin to walk at an early age
Focal fibrocartilaginous dysplasia[95]	10-3	*Synonym:* focal fibrocartilaginous dysplasia associated with tibia vara Rare dysplasia involving fibrous and cartilaginous tissue at the pes anserinus insertion into the tibia Results in a unilateral deformity of the proximal end of the tibia with a prominent cortical defect within the medial proximal tibial metaphysis and varus deformity of the diametaphyseal portion of the tibia Deformity appears as early as 2 months of age and resembles the deformity of Blount disease
Osteopetrosis[5,104]	10-4	Diffuse osteosclerosis results in brittle bones and predisposition to pathologic fracture Erlenmeyer flask deformity
Osteopoikilosis[6]	10-5	Multiple 2- to 3-mm circular foci of osteosclerosis Symmetric periarticular lesions resembling bone islands predominate in the patellae and proximal and distal ends of the tubular bones about the knee
Osteopathia striata[7]		Regular, linear, vertically oriented bands of osteosclerosis extending from the metaphysis for variable distances into the diaphysis Long lesions are frequently found in the tibia Metaphyseal flaring of the tibia may also be seen with osteopathia striata
Melorheostosis[8,9]	10-6	Hemimelic distribution of peripherally located cortical hyperostosis resembling flowing candle wax on the surface of the tibia or fibula Paraarticular soft tissue calcification and ossification may occur and may even lead to joint ankylosis
Mixed sclerosing bone dystrophy[10]	10-7	Rare condition in which patients have imaging findings characteristic of more than one and occasionally all of the sclerosing dysplasias
Osteogenesis imperfecta[11]	10-8	Severe osteoporosis Pencil-thin cortices Multiple fractures Bowing of long bones Rare cystic form: ballooning of bone, metaphyseal flaring, and honeycombed appearance of thick trabeculae
Progressive diaphyseal dysplasia[12]	10-9	Camurati-Engelmann disease Bilateral fusiform thickening of the diaphyses of the tibia and fibula Cortical thickening and hyperostosis result in increased diaphyseal radiodensity

---

* See also Tables 1-1 and 1-2.

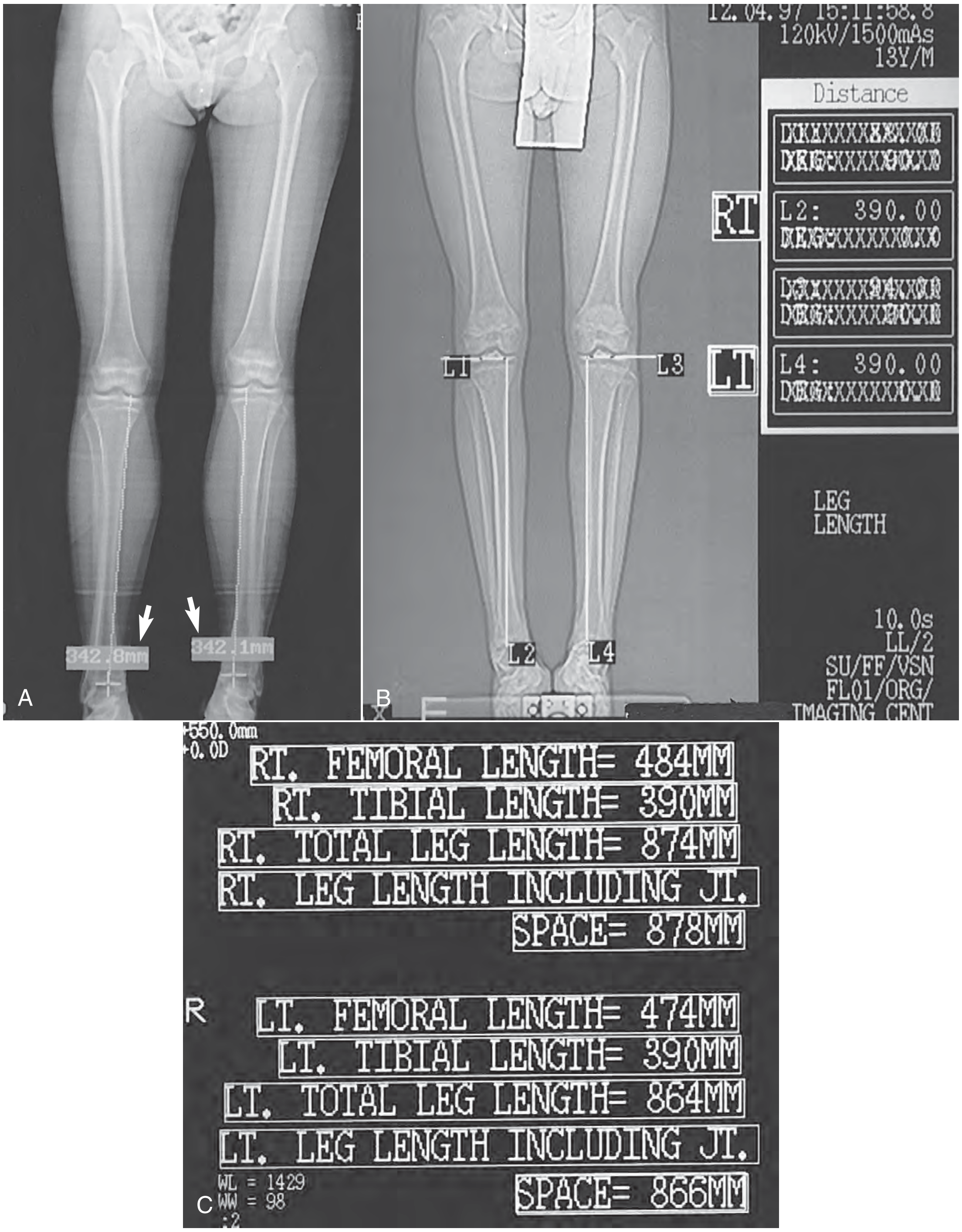
342.8mm
342.1mm
A
12.04.97 15:11:58.8
120kV/1500mAs
13Y/M
Distance
RT
L2: 390.00
LT
L4: 390.00
L1
L3
L2
L4
LEG
LENGTH
10.0s
LL/2
SU/FF/VSN
FL01/ORG/
IMAGING CENT
B
+550.0mm
+0.0D
RT. FEMORAL LENGTH= 484MM
RT. TIBIAL LENGTH= 390MM
RT. TOTAL LEG LENGTH= 874MM
RT. LEG LENGTH INCLUDING JT.
SPACE= 878MM
R
LT. FEMORAL LENGTH= 474MM
LT. TIBIAL LENGTH= 390MM
LT. TOTAL LEG LENGTH= 864MM
LT. LEG LENGTH INCLUDING JT.
SPACE= 866MM
WL = 1429
WW = 98
:2
C

FIGURE 10–1 **Limb length inequality: measurement with CT scanogram.**[1-3] In this procedure, both lower extremities are imaged in the supine position, and precise anatomic measurements of the tibiae and fibulae are made. **A,** In this patient, the left tibia measures 342.1 mm and the right tibia measures 342.8 mm *(arrows)*. The left tibia, therefore, is only 0.7 mm shorter than the right tibia. Similar measurements of the femur and entire lower extremity are also obtained. **B,** In another patient, the tibiae are equal in length (390 mm). **C,** A computerized display in the same patient **(B)** displays the precise length measurements of tibia, femur, and total leg bilaterally.

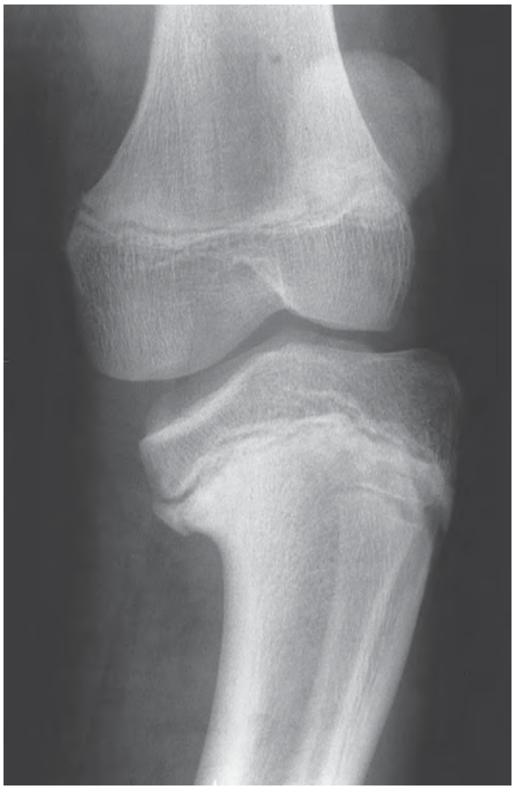

FIGURE 10–2 **Blount disease: infantile tibia vara.**[4] In this 11-year-old girl, observe the varus deformity of the tibia with epiphyseal deformity and prominence and sclerosis of the proximal medial tibial metaphyses. Prominent tibial torsion is also present.

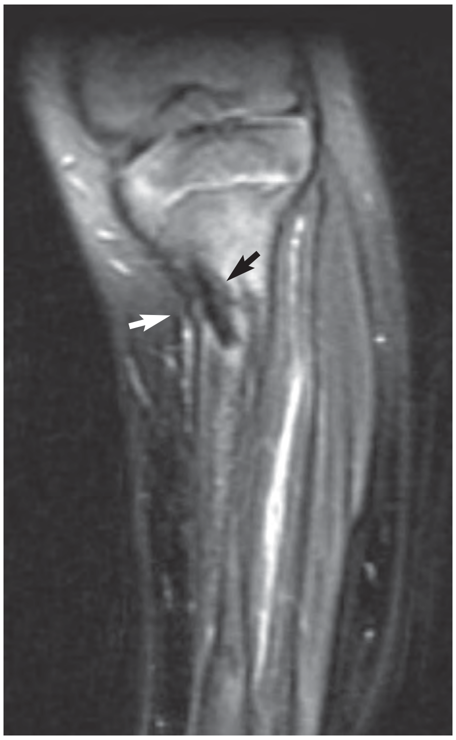

FIGURE 10–3 **Focal fibrocartilaginous dysplasia.**[95] A coronal proton–density-weighted fat-suppressed MR image of the tibia in this 2-year-old boy reveals a cortical defect with a prominent varus deformity of the diametaphyseal region of the tibia *(white arrow)*. A low signal intensity area within the medullary bone is also seen *(black arrow)*. This rare dysplasia that is usually unilateral and may resemble Blount disease involves fibrous and cartilaginous tissue at the pes anserine insertion into the tibia.

FIGURE 10–4 **Osteopetrosis.**[5,104] Bilateral anteroposterior radiographs of the right knee **(A)** and left leg **(B)** in this 5-year-old boy reveal transverse striations of radiodensity involving the metaphyseal and epiphyseal regions of the both ends of the tibiae and the metaphyses of both fibulae. An Erlenmeyer flask deformity, characterized by widening of the metaphysis *(double arrow)* is also present.

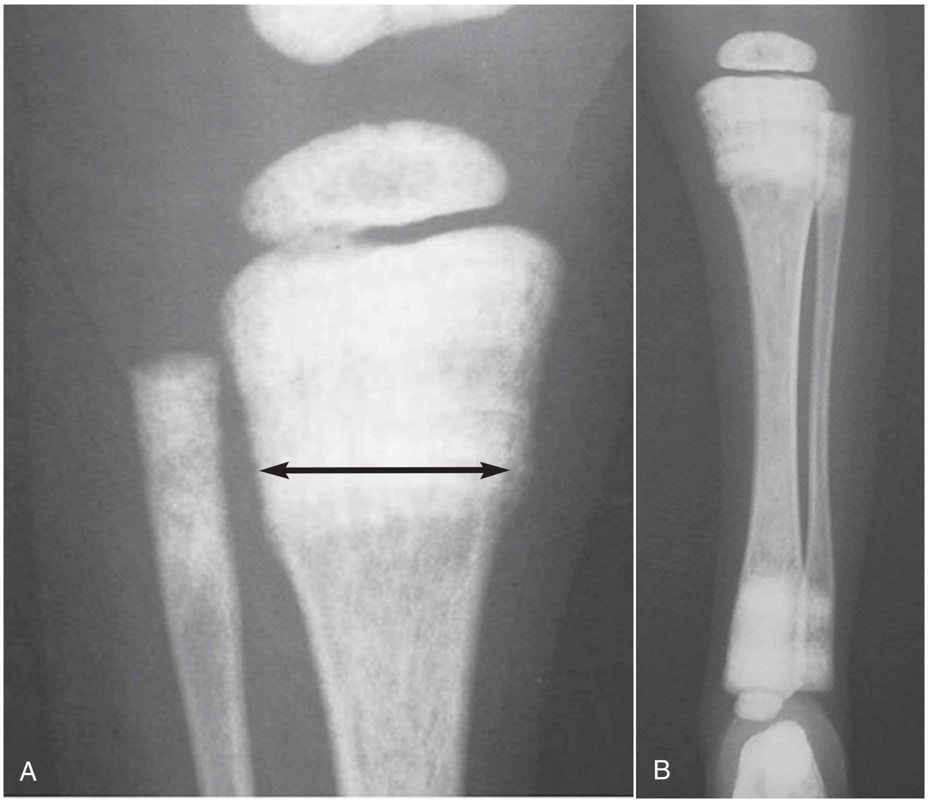

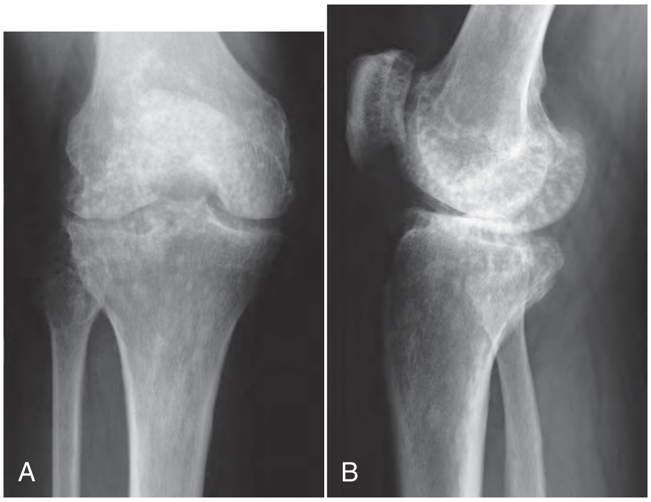

FIGURE 10–5 **Osteopoikilosis.**[6] Radiographs of the knee of this 59-year-old woman reveal numerous circular radiopacities involving the periarticular regions of all the bones about the knee, a process that was bilateral and symmetric and involved bones of the upper and lower extremity (other areas not shown).

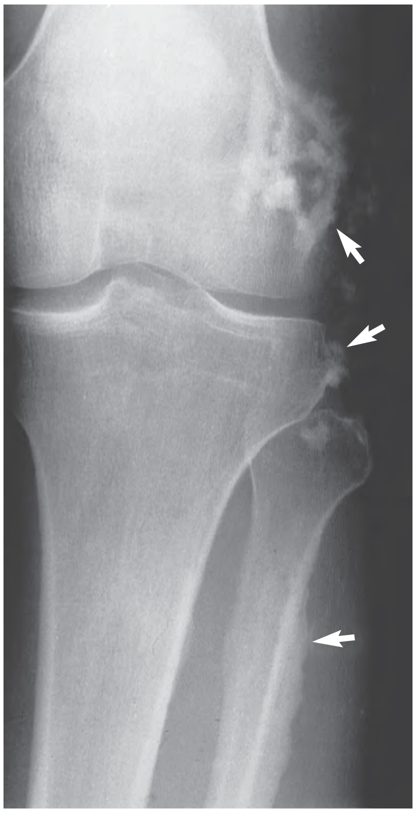

FIGURE 10–6 **Melorheostosis.**[8,9] Observe the characteristic radiographic abnormalities of asymmetric hyperostosis (simulating flowing candle wax) affecting the proximal portion of the fibula. Cloudlike accumulations of hyperostosis and soft tissue ossification also are seen adjacent to the distal portion of the femur and the proximal portion of the tibia *(arrows)*. *(Courtesy A. Newberg, MD, Boston.)*

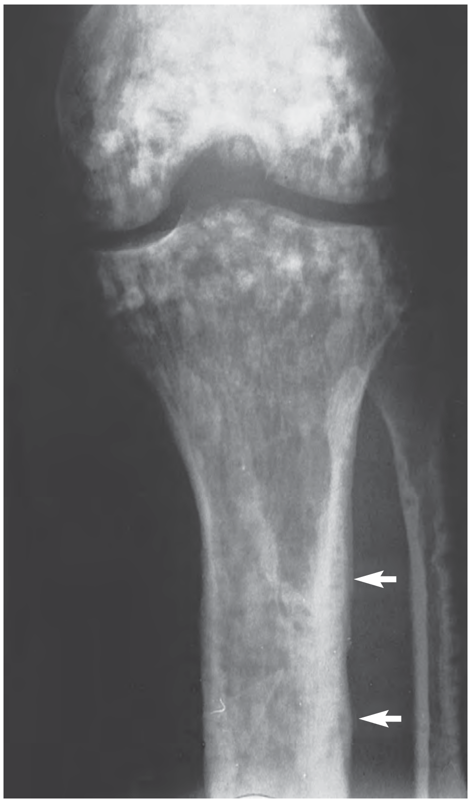

FIGURE 10–7 **Mixed sclerosing bone dystrophy.**[10] Evidence of both linear hyperostosis characteristic of melorheostosis *(arrows)* and punctate zones of sclerosis typical of osteopoikilosis are seen in the proximal part of the tibia and the distal end of the femur in this patient. *(Courtesy C. Resnik, MD, Baltimore, Md.)*

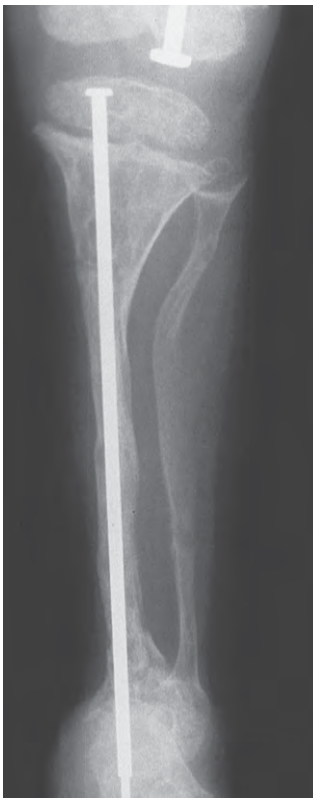

FIGURE 10–8 **Osteogenesis imperfecta.**[11] Characteristic radiographic findings in the tibia and the fibula include severe bowing of the osteoporotic, thin, and gracile bones. Multiple fractures in various stages of healing and intramedullary rods are seen.

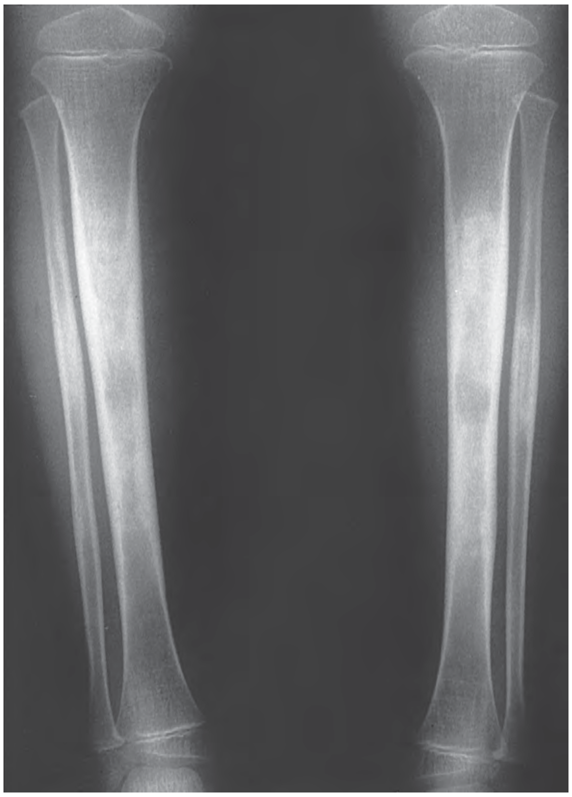

FIGURE 10–9 Progressive diaphyseal dysplasia (Camurati-Engelmann disease).[12] Observe the exuberant fusiform, hyperostotic bone formation and cortical thickening within the diaphyses of the tibiae and fibulae.

TABLE 10-2 Fractures of the Tibial and Fibular Diaphyses and Soft Tissue Injury*

Entity	Figure(s)	Characteristics	Complications and Related Injuries
Tibia			
Acute tibial fractures[13,14,117]	10-10	*Direct trauma:* transverse or comminuted fracture *Indirect trauma:* oblique, spiral, or segmental fractures Middle and distal thirds > proximal third Prognosis related to amount of displacement, degree of comminution, open or closed fracture, and infection Proximal metaphyseal fracture may be associated with genu valgum deformity in children Uncomplicated tibial shaft fractures should heal within 16-18 weeks in adults and more quickly in children	Associated fractures of the fibula, especially in direct and severe trauma Delayed union (5%-15% of cases) Nonunion (most common in distal third of tibia) Infection with or without nonunion Vascular injury (to anterior tibial artery or, less commonly, posterior tibial artery) Compartment syndrome (anterior > posterior or lateral compartment) Nerve injury (uncommon, peroneal and posterior tibial nerves) Refracture (especially in athletes) Leg shortening Complex regional pain syndrome Fat embolism
Acute childhood fractures[15]	10-11	*Toddler fracture:* nondisplaced spiral fracture in children 1-3 years of age May be occult on initial radiographs and may require bone scintigraphy or serial radiographs to reveal the fracture	

* See also Tables 1-4 and 1-6.

TABLE 10-2 Fractures of the Tibial and Fibular Diaphyses and Soft Tissue Injury—cont'd

Entity	Figure(s)	Characteristics	Complications and Related Injuries
Stress-related Bone Injuries of the Tibia			
Fatigue fractures[16-20,98,112-115]	10-12	Stress fractures of the proximal portion of the tibia are usually fatigue fractures and occur in children as a result of running activities Transverse and, less commonly, longitudinal fractures may be identified Fractures are often occult on radiographs MR imaging is the single best imaging technique in assessment of patients with suspected tibial stress injuries; in some patients with negative MR imaging findings, CT can depict osteopenia, which is the earliest finding of a fatigue cortical bone injury MR imaging of longitudinal fatigue fractures reveals eccentric bone marrow edema, vertical cleft on one or more axial images, eccentric periosteal reaction or soft tissue edema; tend to be in close proximity to the nutrient foramen	May result in complete fracture with or without displacement
Insufficiency fractures[21,22]	10-13	*Predisposing disorders:* osteoporosis, rheumatoid arthritis, osteomalacia, rickets, and other bone diseases	
Shin splints[96]		*Synonyms:* shin soreness, shin splint syndrome, medial tibial stress syndrome, soleus syndrome Usually related to athletic activity, especially running Pathophysiology is controversial—postulates include: 1. Fatigue damage in bone (atypical fatigue fracture) 2. Traction periostitis at origin of tibialis posterior muscle or insertion of crural fascia (soleus bridge) 3. Compartment syndrome Radiographs are usually normal Magnetic resonance (MR) imaging more useful in acute cases; may result in false negative results in patients with chronic symptoms Three-phase radionuclide bone scan may reveal abnormal linear longitudinal uptake	The relationship of shin splints and fatigue fractures is controversial, but both may represent fatigue damage to bone
Fibula			
Acute fibular fractures[23]	10-14	Isolated fractures related to direct injury are rare *Maisonneuve fracture:* fracture of the proximal portion of the fibula associated with severe ankle injuries; because of dramatic ankle symptoms, the proximal fibular fracture may be initially overlooked	Often associated with fractures of the tibia and injuries of the ankle
Stress-related Bone Injuries of the Fibula[116]	10-15	The majority of fibular stress (fatigue) fractures involve the lateral cortex of the distal fibula Sport activities include cross country, marathon and decathlon running, basketball, football, volleyball, soccer, and sprinting	
Posttraumatic Heterotopic Ossification[24]	10-16	Myositis ossificans posttraumatica Faint calcific intermuscular or intramuscular shadow may appear within 2-6 weeks of injury Well-defined region of ossification aligned parallel to the long axis of the tibia or fibula may be evident within 6-8 weeks Usually involves gastrocnemius and tibialis anterior muscles Associated periostitis may relate to subperiosteal hemorrhage	Limitation of motion Compartment syndromes May result in abnormal knee biomechanics and lead to premature degeneration May resemble aggressive neoplasms such as osteosarcoma or Ewing sarcoma

FIGURE 10–10 Tibial diaphysis fractures.[13,14] **A-B,** Frontal **(A)** and lateral **(B)** radiographs of this 10-year-old boy reveal a minimally displaced spiral fracture of the distal tibial diaphysis. **C,** In another patient, a 33-year-old man, spiral fractures of both the tibia and fibula are seen. **D,** In yet another patient with healing fractures of the middiaphyses of the tibia and fibula, evidence of callus formation, persistent malalignment, and limb shortening are seen. Spiral tibial (and fibular) fractures are generated by twisting forces applied during falls or sporting activities, such as skiing.

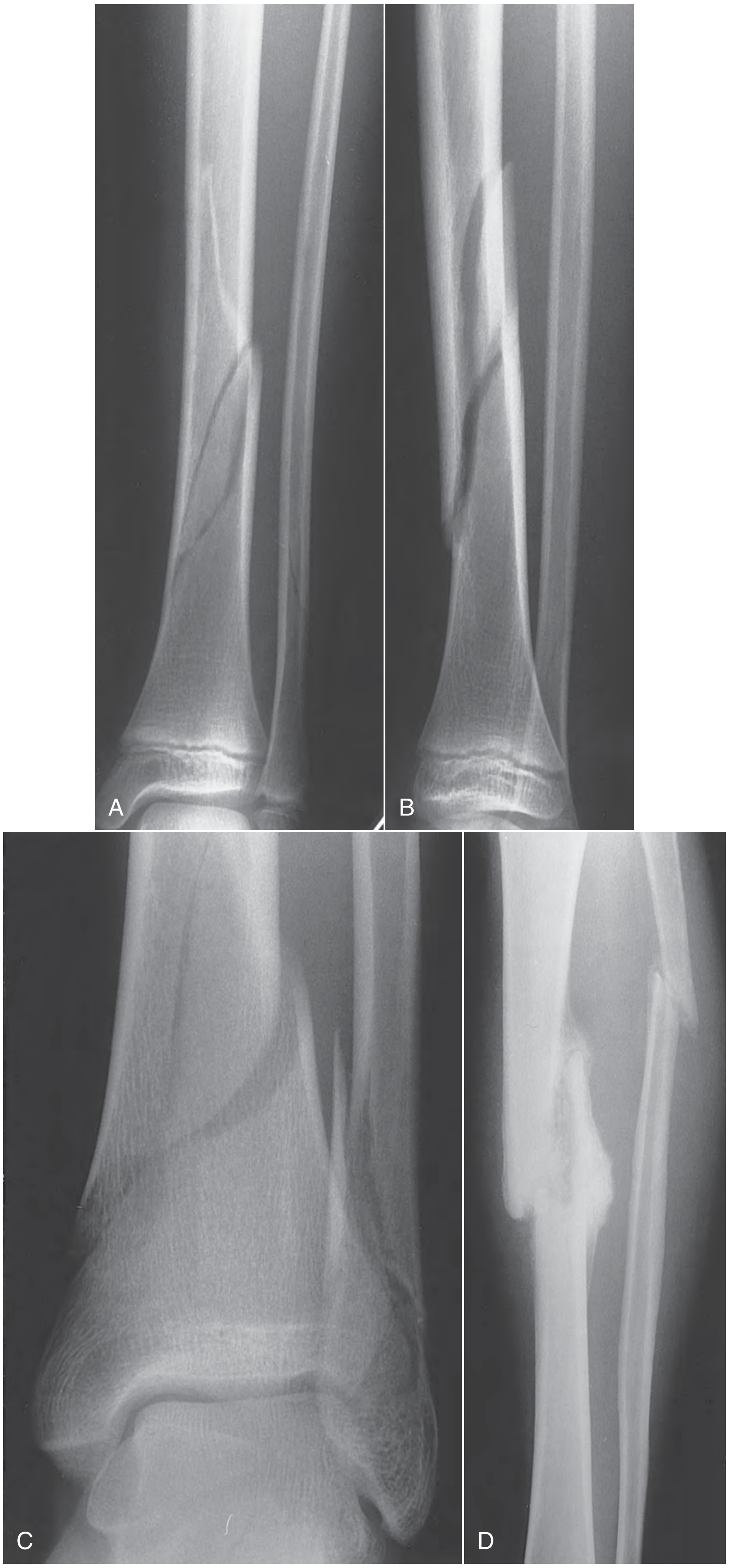

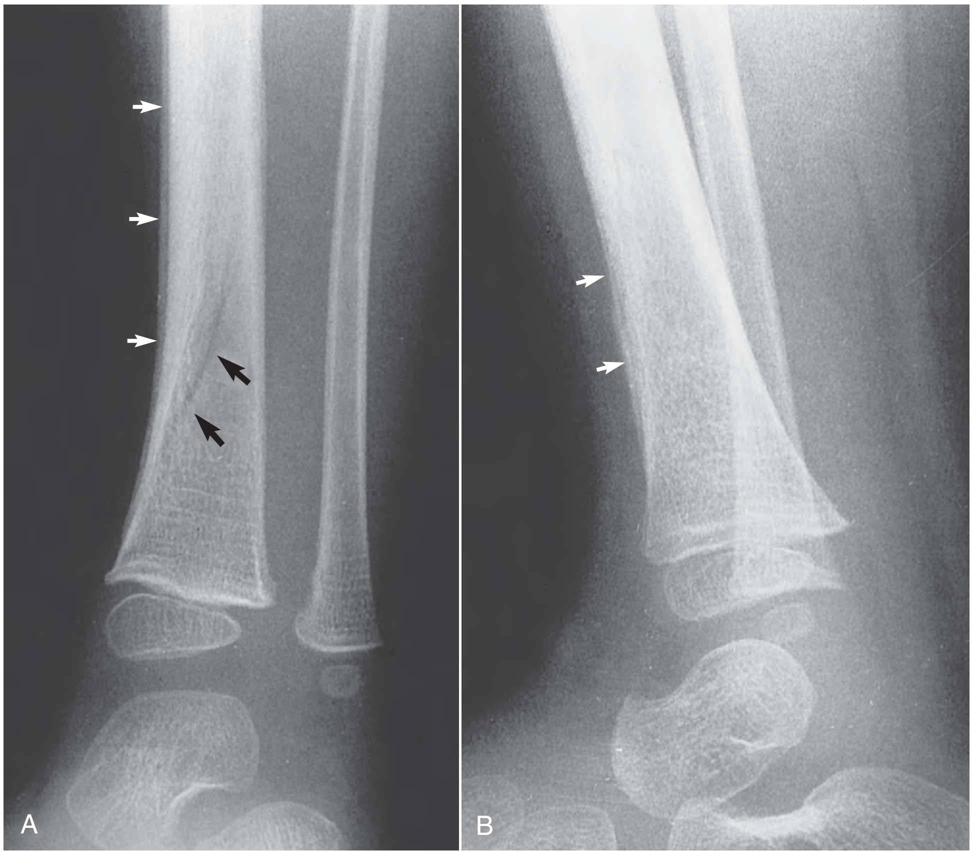

FIGURE 10–11 **Toddler's fracture.**[15] Two-year-old child with 10-day history of a painful limp. **A,** Nondisplaced oblique fracture of the distal end of the tibia is seen on this frontal radiograph *(black arrows)*. An extensive zone of periostitis *(white arrows)* indicates that healing is taking place. **B,** Lateral radiograph reveals periostitis *(arrows),* but the fracture line is not visible. *(Courtesy B.L. Harger, DC, Portland, Ore.)*

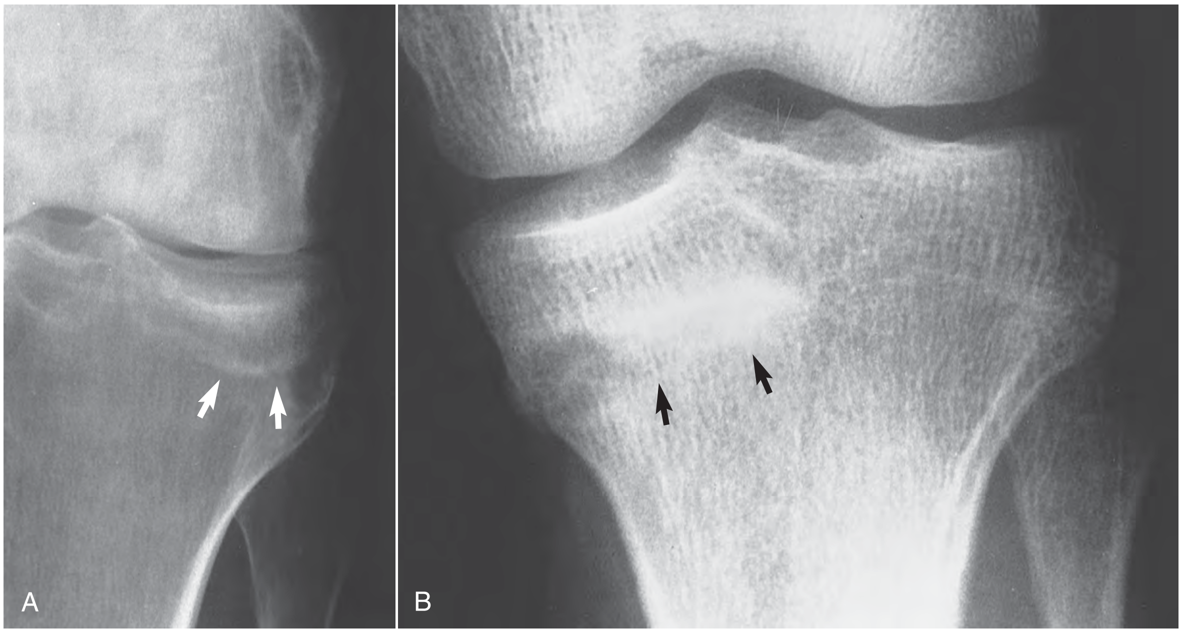

FIGURE 10–12 **Stress-related bone injury: fatigue fractures.**[16-20,98,112-115] **A,** This 27-year-old woman developed tibial pain after long-distance running. Observe the transverse zone of sclerosis within the tibial plateau *(arrows)* characteristic of a stress fracture. **B,** In this 58-year-old woman, a band of increased density *(arrows)* is apparent in the proximal tibial metaphysis.

Continued

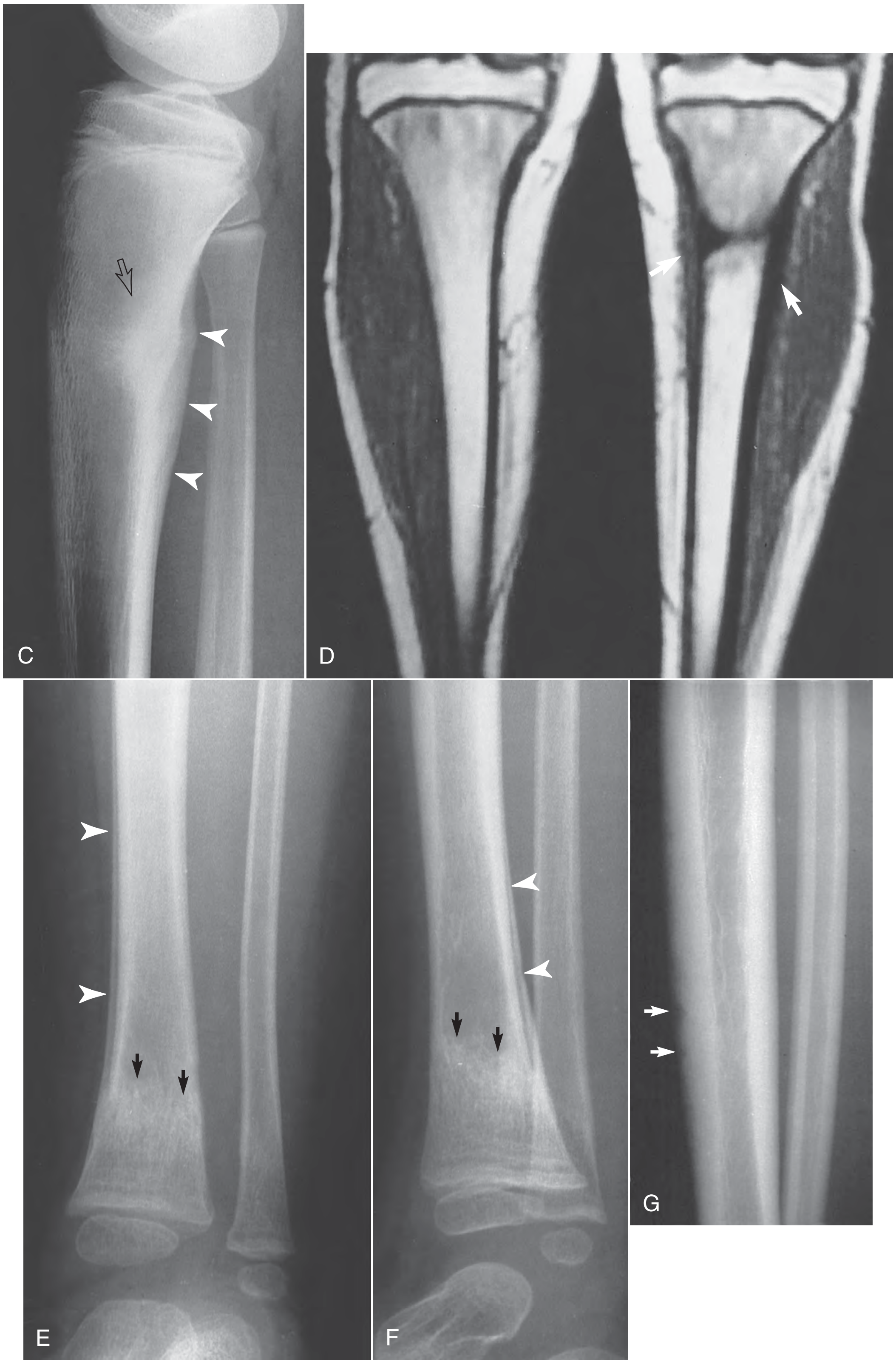

FIGURE 10–12, cont'd C-G, A 12-year-old boy. In **C,** a transverse zone of sclerosis *(open arrow)* with a collar of periostitis *(arrowheads)* is evident on a routine radiograph. In **D,** a transverse band of low signal intensity on a coronal T1-weighted (TR/TE, 617/20) spin echo MR image also is accompanied by diffuse periosteal new bone formation *(arrows)*. **E-F,** Radiographs of the distal portion of the tibia in this infant reveal a transverse zone of sclerosis *(arrows)* and extensive periostitis *(arrowheads)* typical of a fatigue fracture. **G,** Multiple diaphyseal stress fractures of the tibia. A lateral radiograph of the leg in this 13-year-old female gymnast reveals thickening of the anterior tibial cortex and several radiolucent, scalloped indentations *(arrows)*. (***C-D,*** *Courtesy K. Van Lom, MD, San Diego.)*

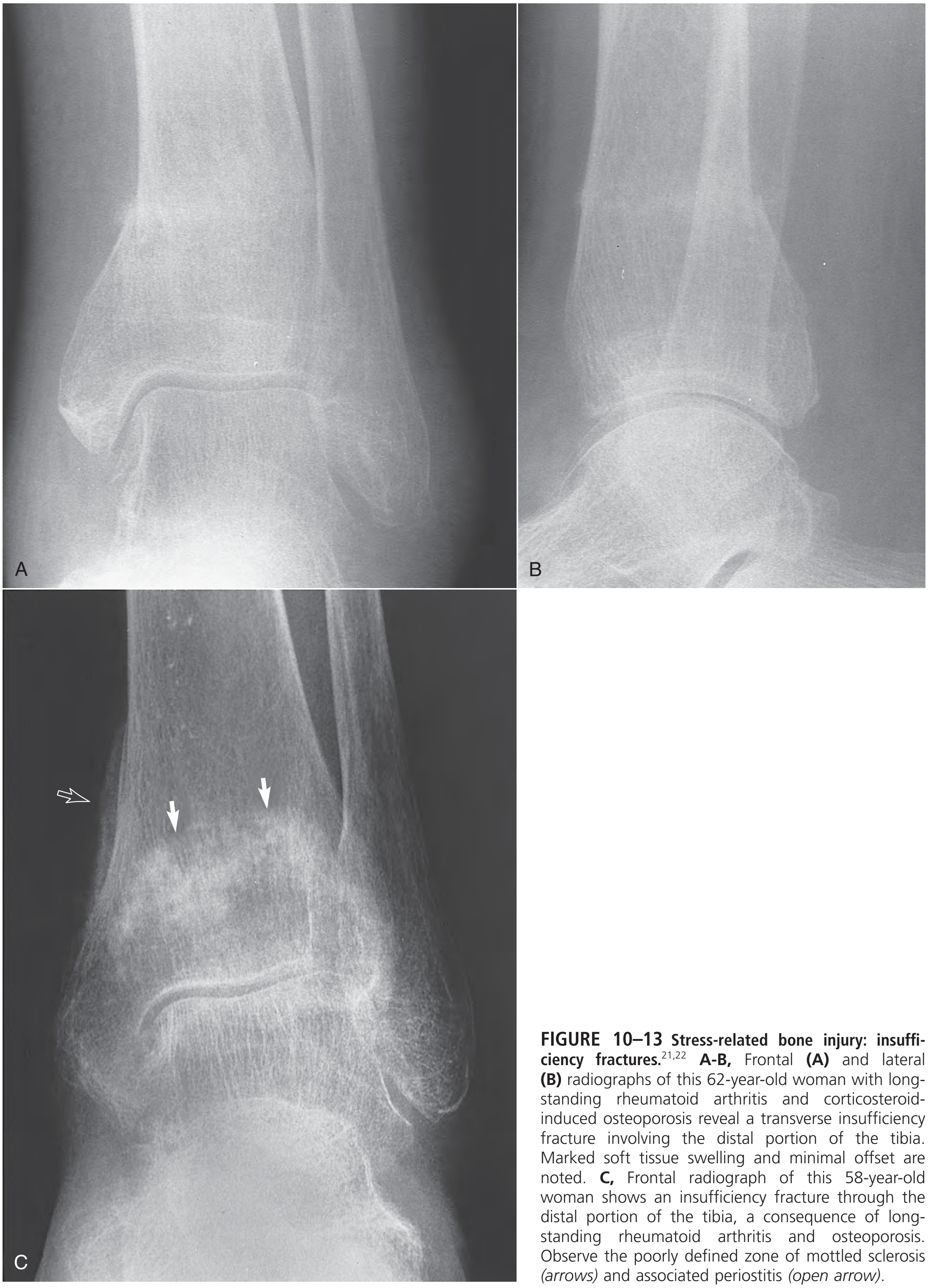

FIGURE 10–13 Stress-related bone injury: insufficiency fractures.[21,22] **A-B,** Frontal **(A)** and lateral **(B)** radiographs of this 62-year-old woman with long-standing rheumatoid arthritis and corticosteroid-induced osteoporosis reveal a transverse insufficiency fracture involving the distal portion of the tibia. Marked soft tissue swelling and minimal offset are noted. **C,** Frontal radiograph of this 58-year-old woman shows an insufficiency fracture through the distal portion of the tibia, a consequence of long-standing rheumatoid arthritis and osteoporosis. Observe the poorly defined zone of mottled sclerosis *(arrows)* and associated periostitis *(open arrow)*.

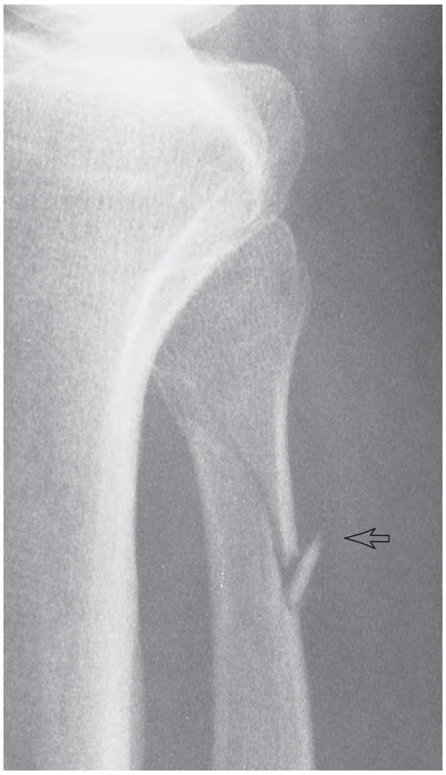

FIGURE 10–14 **Proximal fibular fracture: Maisonneuve fracture.**[23] This patient sustained a pronation-external rotation stage IV ankle injury rupturing the anterior talofibular ligament and fracturing the proximal portion of the fibula *(arrow)*. This fracture is referred to as a *Maisonneuve fracture* and usually is associated with severe ankle injuries. Because of the dramatic symptoms about the ankle, the proximal fibular fracture may initially be overlooked.

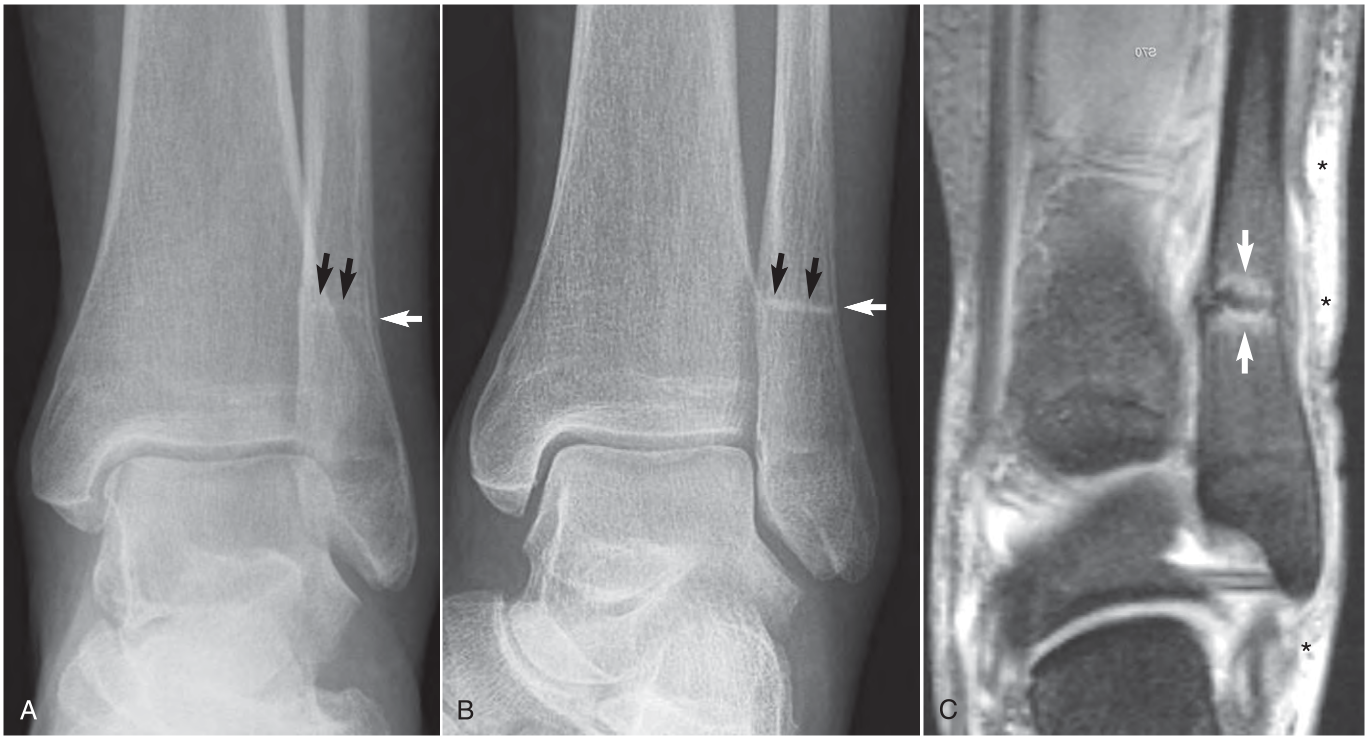

FIGURE 10–15 **Stress (fatigue) fracture of the fibula.**[116] This 61-year-old woman developed ankle pain and swelling just above the lateral malleolus. Radiographs **(A-B)** obtained several weeks after the onset of pain show an almost imperceptible angulation of the fibular metaphysis *(white arrows)* associated with a transverse zone of radiodensity *(black arrows),* a finding that probably represents new bone formation as a result of the initial healing response. **C,** A coronal proton-density fat suppressed MR image of the ankle clearly demonstrates the healing fracture with a low signal intensity transverse fracture line surrounded by high signal intensity bone marrow edema *(arrows)*. Slight angulation at the fracture site and high signal intensity of overlying subcutaneous edema (*) are also visible.

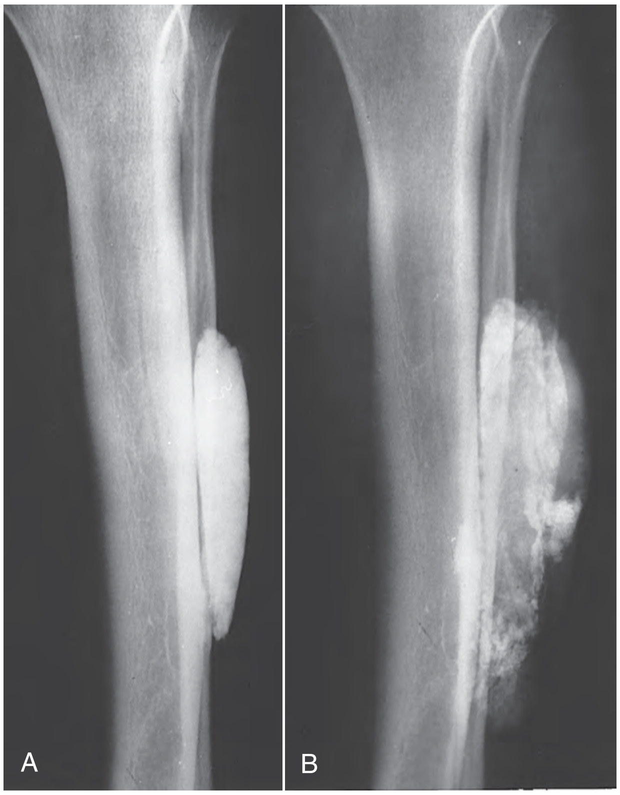

FIGURE 10–16 Posttraumatic heterotopic ossification: myositis ossificans.[24] Serial radiographs of a 46-year-old man with painful swelling of the leg and a history of repeated injuries. **A,** Initial radiograph reveals a homogeneous, densely sclerotic osseous mass with regular margins in the soft tissues adjacent to the lateral surface of the diaphyseal portion of the tibia, separated from the normal underlying bone by a radiolucent cleft. **B,** Radiograph taken 15 years later demonstrates that the lesion has grown and has become more irregular. Although the underlying bone is grossly normal, a suggestion of mild cortical bulging and endosteal thickening is evident. This case is unusual, because generally areas of myositis ossificans merge with the adjacent bone and decrease in size over a varying period of time. The differential diagnosis of myositis ossificans must include aggressive neoplasms, such as parosteal, periosteal, and soft tissue osteosarcoma and Ewing sarcoma.

TABLE 10-3 Malignant Tumors Affecting the Tibia and the Fibula*

Entity	Figure(s)	Characteristics
Skeletal Metastasis[25-27]		
Lung, prostate, breast, kidney, thyroid gland	10-17, 10-18	Fewer than 5% of metastatic lesions affect the tibia or fibula *Occasional site of cortical metastasis, especially in patients with bronchogenic carcinoma; small,* radiolucent, eccentric, saucer-shaped, scalloped cortical erosions are referred to as *"cookie-bite"* lesions
Primary Malignant Tumors of Bone		
Osteosarcoma (conventional)[28,105,106]	10-19	21% of osteosarcomas affect the tibia; 3% affect the fibula Preference for metaphyses Osteolytic, osteosclerotic, or mixed patterns of medullary and cortical destruction Laminated, spiculated, or Codman triangle periosteal reactions common
Osteosarcoma (parosteal)[29,105,106]	10-20	Approximately 10% of parosteal osteosarcomas affect the tibia; 3% affect the fibula Osteosclerotic surface lesion of bone Large radiodense, oval, sessile mass arising from the surface of bone; smooth or irregular margins Peripheral portion of lesion may have cleavage plane separating it from the tibia or fibula Ossification begins centrally and progresses outward, opposite that of benign heterotopic bone formation (myositis ossification)

---

* See also Table 1-10.

Continued

TABLE 10-3 Malignant Tumors Affecting the Tibia and the Fibula—cont'd

Entity	Figure(s)	Characteristics
Osteoblastoma (aggressive)[30]	10-21	Approximately 13% of aggressive osteoblastomas involve the tibia; 6% involve the fibula Expansile osteolytic metaphyseal lesion that may be partially ossified or contain calcium Difficult to differentiate from osteosarcoma or benign osteoblastoma
Chondrosarcoma (conventional)[31]		Fewer than 10% of chondrosarcomas affect the tibia and fibula Lesions tend to be osteolytic; sometimes have a bulky cartilaginous cap and frequently contain calcification May have soft tissue mass
Giant cell tumor (aggressive)[32]		Approximately 17% of aggressive giant cell tumors involve the tibia; 2% involve the fibula Eccentrically located, subarticular osteolytic lesion extending into the metaphysis Cortical destruction and soft tissue mass are variable findings
Fibrosarcoma[33,34]	10-22	About 16% of fibrosarcomas involve the tibia; 3% involve the fibula Purely osteolytic destruction, soft tissue mass, and no associated sclerotic reaction or periostitis
Malignant fibrous histiocytoma[34]		Approximately 20% affect the tibia; less than 2% affect the fibula Moth-eaten or permeative osteolysis of the metaphysis with frequent spread to epiphysis and diaphysis Pathologic fracture common
Adamantinoma[35]	10-23	Tibia is the site of involvement in more than 80% of adamantinomas; the fibula is a rare primary site, but it may be involved with adjacent tibial lesions Central or eccentric, multilocular, slightly expansile, sharply or poorly delineated osteolytic lesion with reactive bone sclerosis Periostitis rare May be related to osteofibrous dysplasia (ossifying fibroma) in children and adolescents
Ewing sarcoma[36]	10-24	Approximately 10% of Ewing sarcomas involve the tibia and another 10% involve the fibula Permeative or moth-eaten osteolysis, aggressive cortical erosion or violation, laminated or spiculated periostitis and soft tissue masses Most lesions are central and diametaphyseal
Myeloproliferative Disorders		
Plasma cell (multiple) myeloma[37,119]	10-25	Fewer than 5% of myeloma lesions occur in the tibia and fibula *Early:* normal radiographs or diffuse osteopenia *Later:* widespread, well-circumscribed osteolytic lesions with discrete margins, which usually appear uniform in size
Hodgkin disease[38,100]	10-26	Infrequent involvement of tibia and fibula 75% of lesions are osteolytic; 25% are osteosclerotic Permeative or moth-eaten osteolysis affecting multiple bones
Primary lymphoma (non-Hodgkin)[39,40,100,103]	10-26	Of all skeletal lesions in primary lymphoma, about 9% occur in the tibia, and about 2% occur in the fibula Multiple moth-eaten or permeative osteolytic lesions and pathologic fracture Diffuse or localized sclerotic lesions are rare
Leukemia[41]	10-27	Diffuse osteopenia, radiolucent or radiodense transverse metaphyseal bands, osteolytic lesions, periostitis, and infrequently, osteosclerosis Radiodense metaphyses found more frequently in patients undergoing chemotherapy for leukemia; may resemble lead poisoning

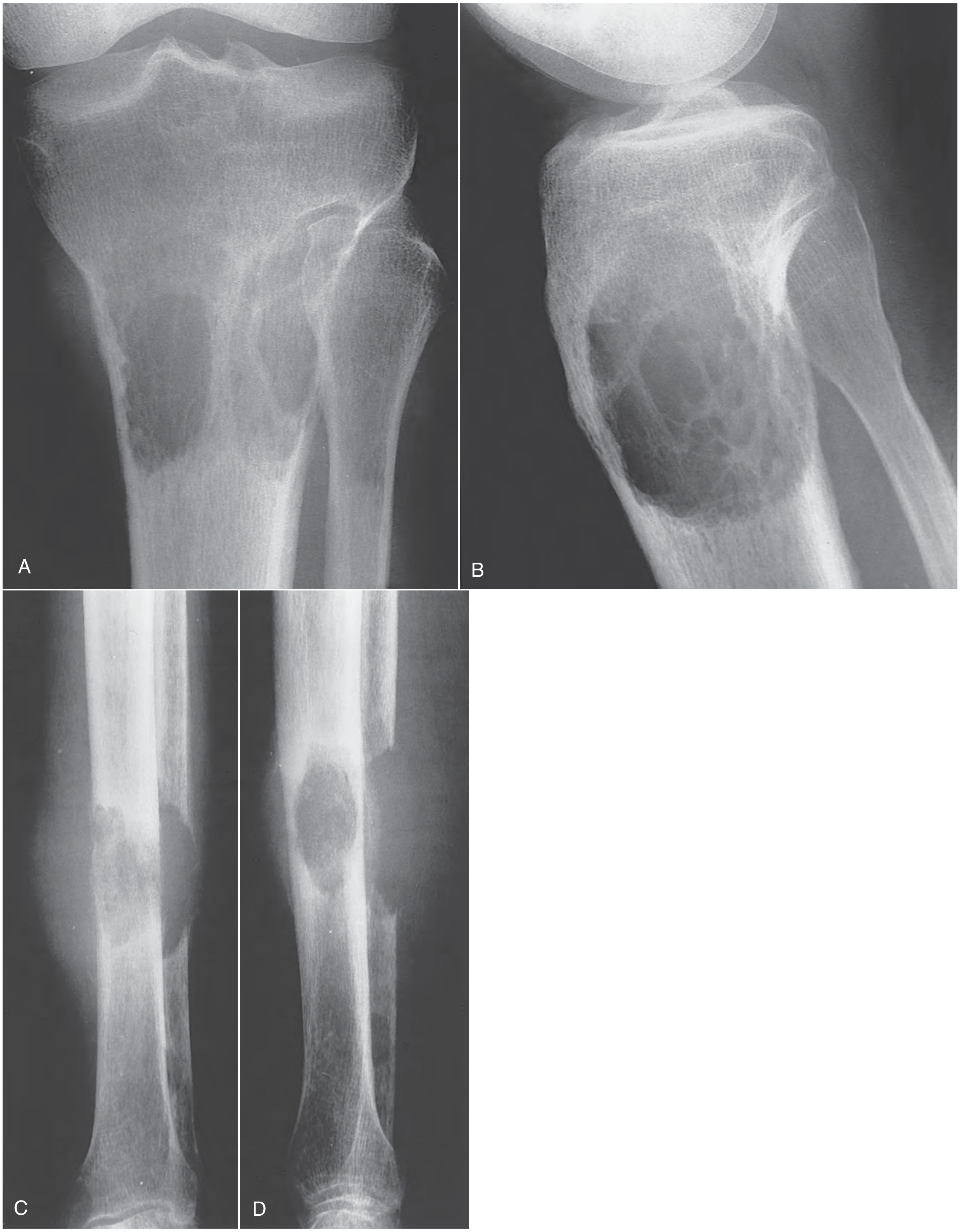

FIGURE 10–17 **Skeletal metastasis.**[25,26] **A-B,** Frontal **(A)** and lateral **(B)** radiographs of this man with renal cell carcinoma show a large, multiloculated, osteolytic lesion within the proximal tibial metadiaphysis. **C-D,** Cortical pattern of osteolytic destruction. This patient with primary ovarian carcinoma developed metastasis to bone. Frontal **(C)** and lateral **(D)** radiographs demonstrate scalloped erosions of the distal tibial and fibular cortices (cookie-bite lesions). Although cortical involvement with cookie-bite lesions is typically seen in bronchogenic metastasis, these lesions may also be found with other primary tumors. Ovarian cancer rarely metastasizes to bone. (***A-B,*** *Courtesy G. Greenway, MD, Dallas, Texas.* ***C-D,*** *Courtesy A. D'Abreu, MD, Porto Alegre, Brazil.)*

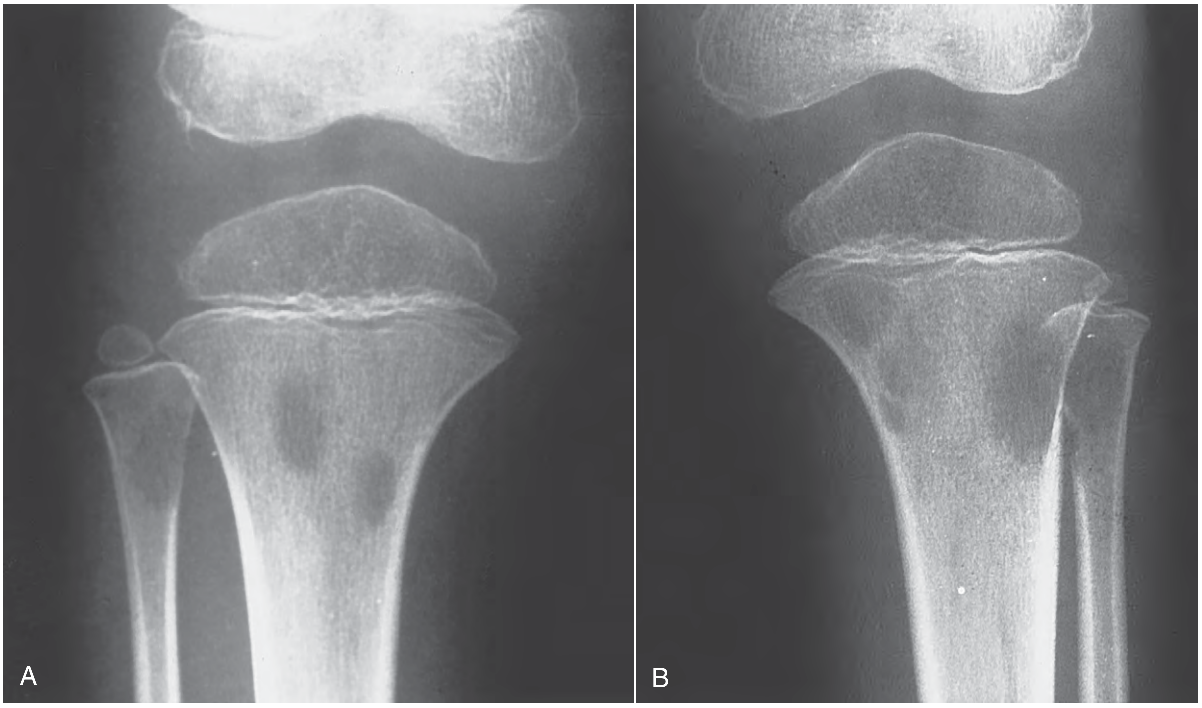

FIGURE 10–18 **A-B, Skeletal metastasis: Wilms tumor.**[27] This child developed bilateral leg pain. Bilateral frontal radiographs show multiple osteolytic metaphyseal lesions of the proximal portions of the tibiae and fibulae. Wilms tumor, or nephroblastoma, is the most common abdominal tumor of infancy and childhood. It metastasizes to the skeleton in fewer than 5% of cases, and in those cases it is usually osteolytic.

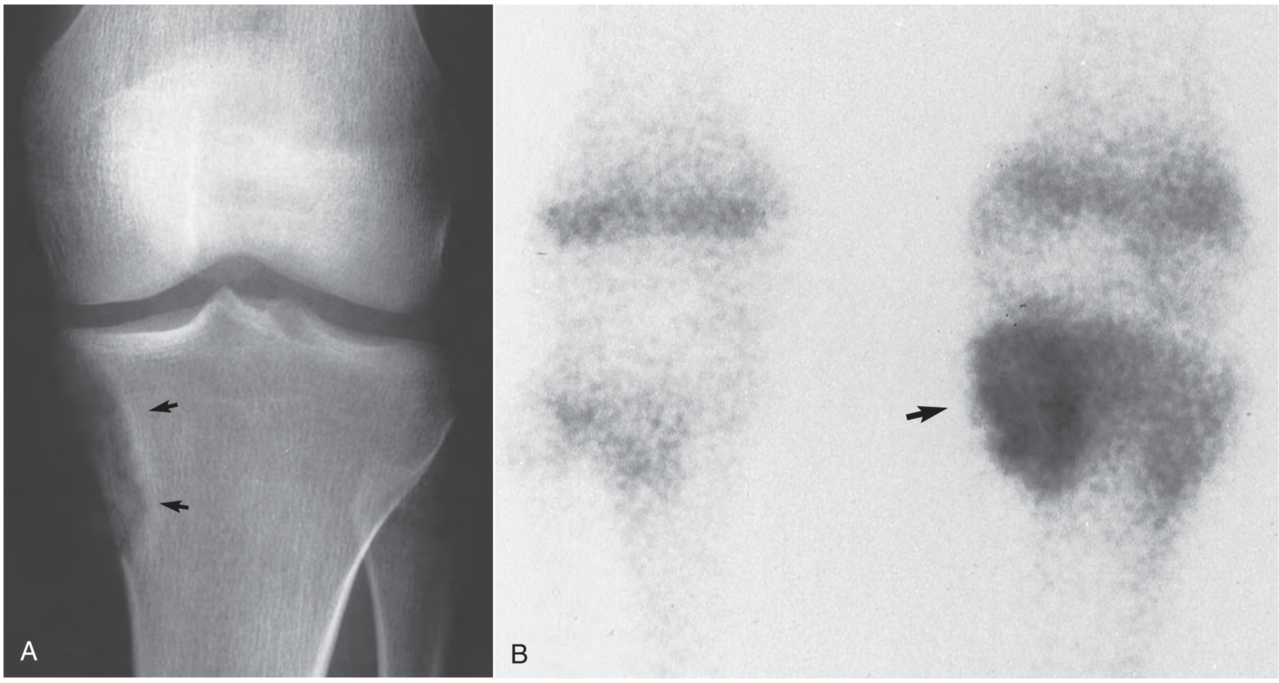

FIGURE 10–19 **Conventional osteosarcoma: osteolytic pattern.**[28,105,106] This 16-year-old girl complained of long-standing knee pain. **A,** Routine radiograph demonstrates aggressive osteolytic destruction of the proximal tibial metaphysis *(arrows)*. **B,** Bone scan reveals homogeneous, intense, increased uptake of the bone-seeking radionuclide at the site of the lesion *(arrow)* compared with the minimal uptake at the contralateral tibial growth centers.

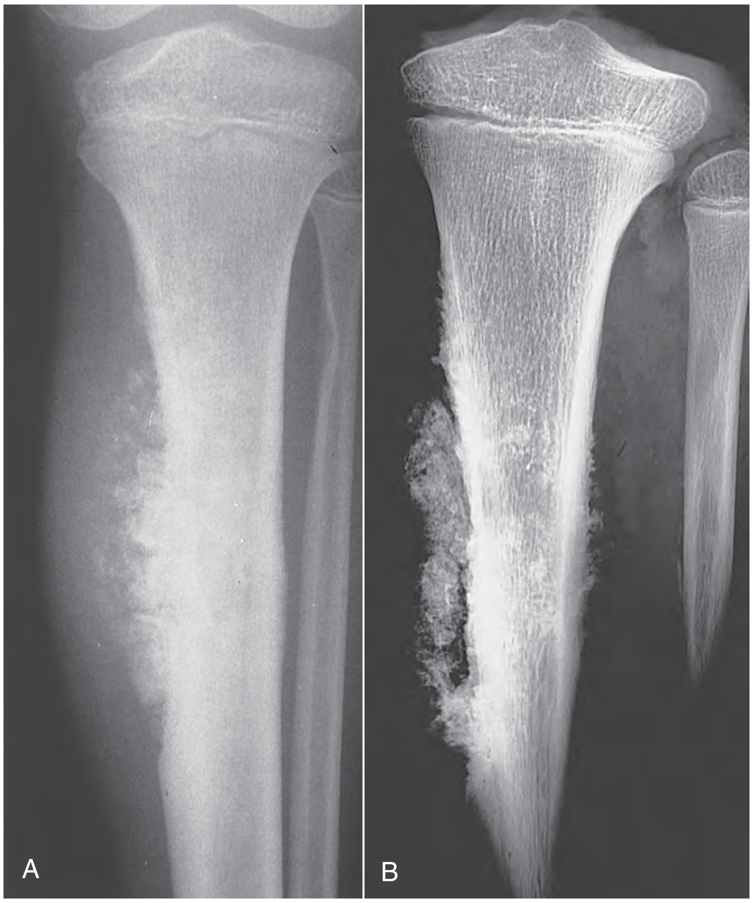

FIGURE 10–20 Parosteal osteosarcoma.[29,105,106] This 10-year-old boy underwent amputation for treatment of his sarcoma. **A,** Routine frontal radiograph of the knee shows an aggressive pattern of cortical thickening and radiating cloudlike osseous proliferation on the surface of the medial tibial cortex. A large soft tissue mass overlies the lesion. **B,** Section radiograph of the amputated segment shows similar findings in better detail.

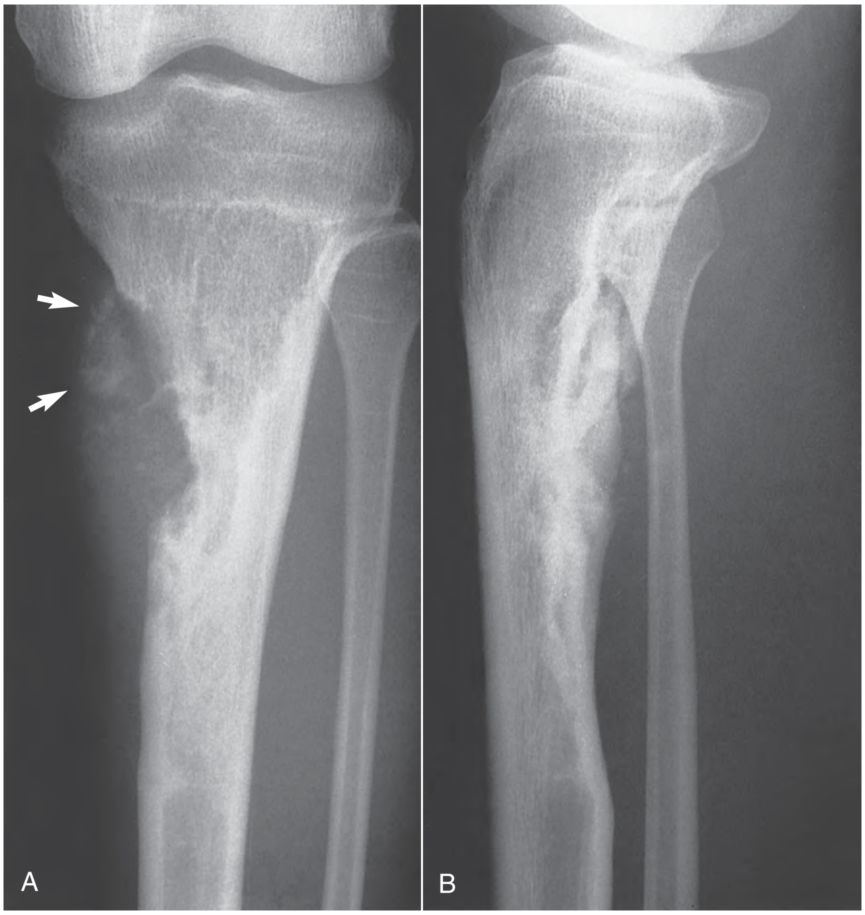

FIGURE 10–21 Aggressive (malignant) osteoblastoma.[30] This 25-year-old woman underwent multiple operations from the age of 16 years for recurrence of her biopsy-confirmed osteoblastoma. Frontal **(A)** and lateral **(B)** radiographs show an aggressive pattern of bone destruction involving the medial cortex of the proximal tibial metaphysis. Note the soft tissue extension of the tumor with extraosseous ossification *(arrows)*.

FIGURE 10–22 Fibrosarcoma.[33,34] An osteolytic lesion within the proximal tibial metaphysis has a deceptively benign appearance, exhibiting a sharp sclerotic zone of transition *(arrows)* between normal and abnormal bone. Minimal osseous expansion and cortical thinning are evident, but no obvious cortical destruction can be detected. Biopsy revealed a fibrosarcoma of bone. This case illustrates that aggressive malignant tumors can exhibit a relatively benign radiographic appearance.

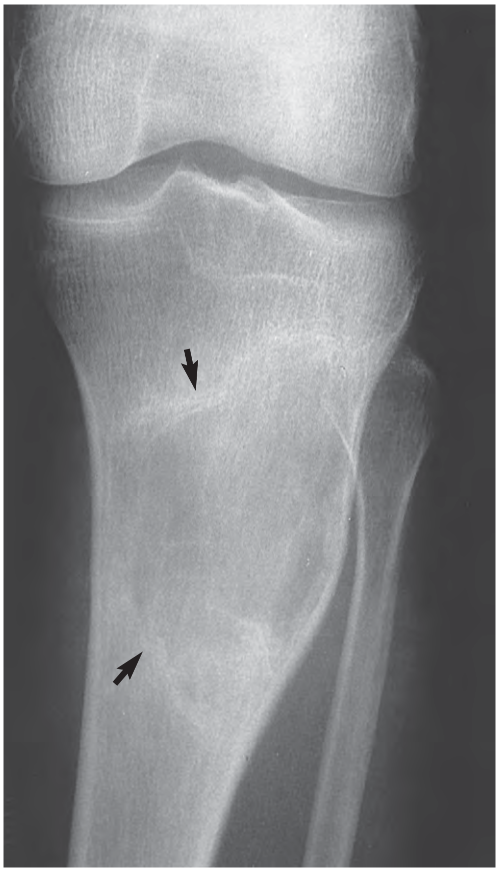

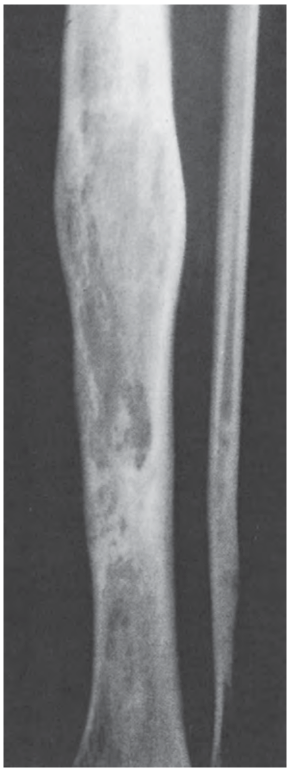

FIGURE 10–23 Adamantinoma.[35] Lesions accompanied by both sclerosis and osteolysis are evident in the tibia and the fibula. The tibial lesion is slightly expansile, and the margins are poorly defined. *(From Resnick D: Diagnosis of bone and joint disorders. 4th Ed. Philadelphia, Saunders, 2002, p. 4057. Courtesy R. Kerr, MD, Los Angeles.)*

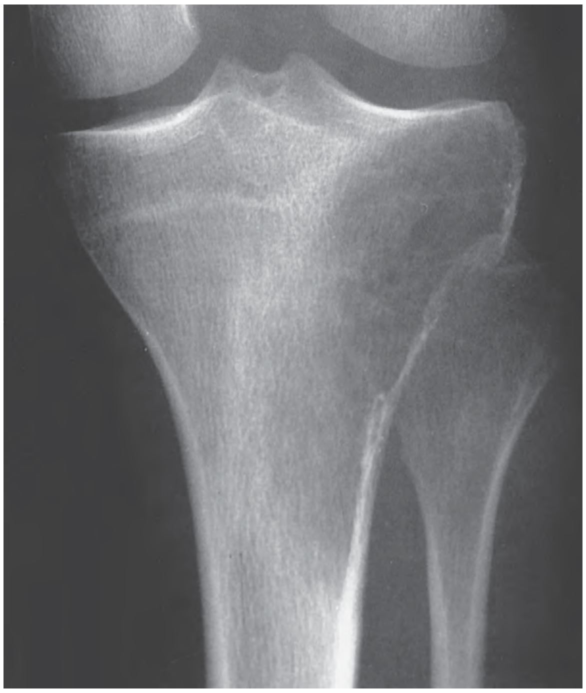

FIGURE 10–24 **Ewing sarcoma.**[36] Radiograph of the knee in this 18-year-old woman shows a permeative pattern of purely osteolytic destruction affecting the proximal tibial metaphysis. The lesion extends into the subchondral region and also erodes the cortex of the lateral tibia.

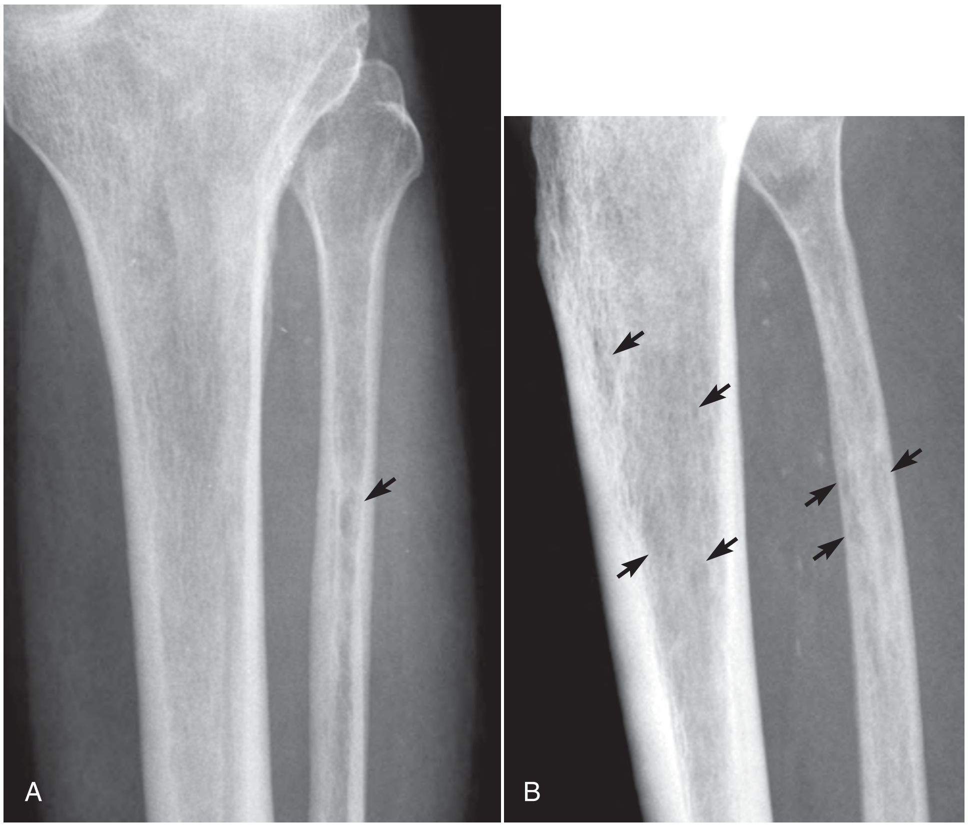

FIGURE 10–25 **Plasma cell (multiple) myeloma.**[37,119] Radiographs of the tibia and fibula in this 70-year-old man with bone pain and positive M-spike on serum electrophoresis show multiple circular osteolytic lesions within the tibia and fibula *(arrows)*. While these lesions are subtle, radiographs often appear normal or simply osteopenic.

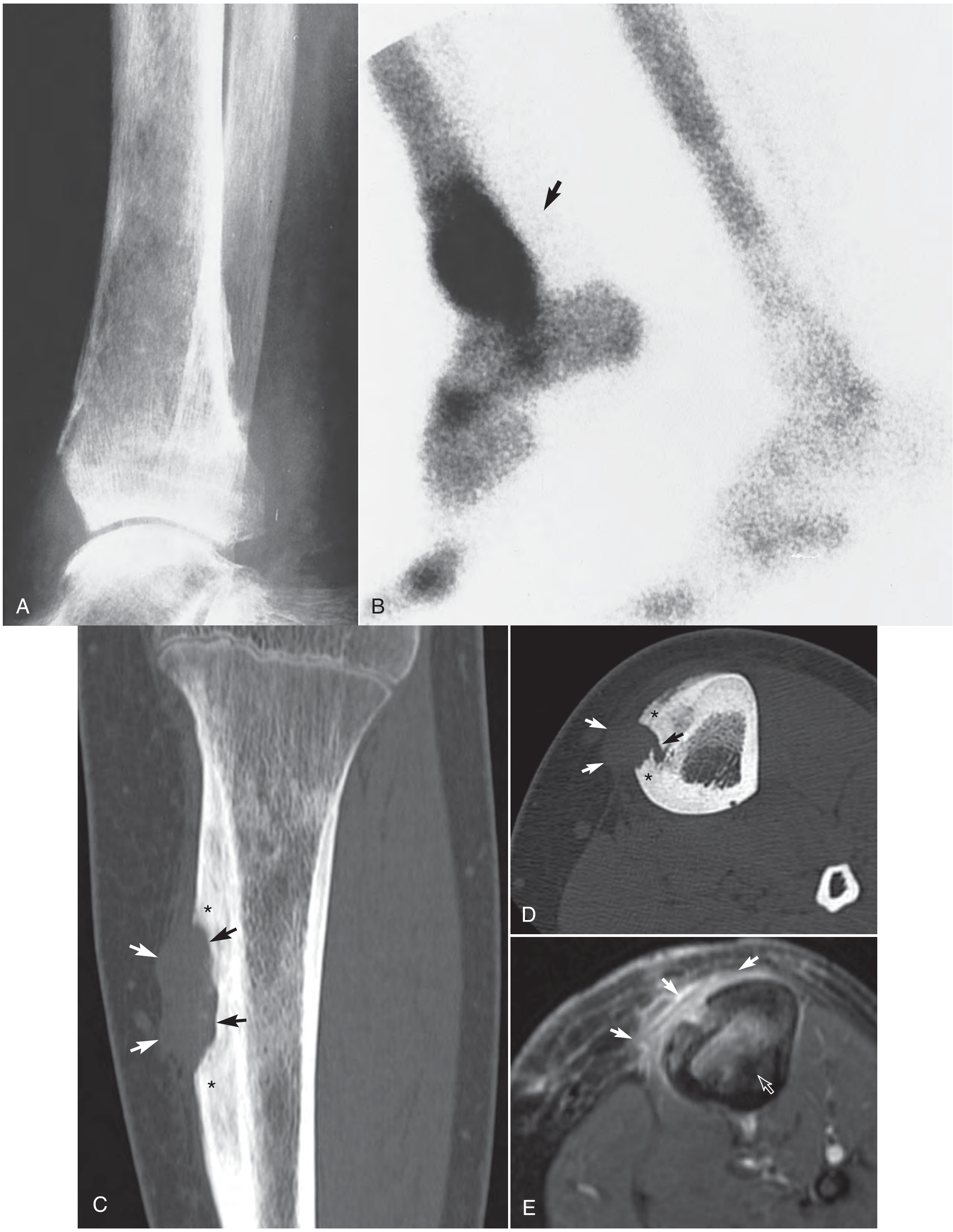

FIGURE 10–26 Lymphoma. A-B, Non-Hodgkin lymphoma: histiocytic type.[39,40,100,103] **A,** A radiograph of this 72-year-old woman reveals diffuse, permeative osteolysis and cortical destruction of the distal end of the tibia. **B,** Bone scan comparing both extremities reveals intense radionuclide accumulation at the involved site *(arrow)*. **C-E** Periosteal lymphoma: primary B cell type. This 13-year-old boy has tibial pain. Examination revealed lymphadenopathy and hepatosplenomegaly. CT bone window scans in the coronal **(C)** and transaxial **(D)** planes reveal cortical (subperiosteal) new bone formation in the form of Codman triangle (*), a central scalloped zone of cortical destruction *(black arrow),* and an ovoid soft tissue mass *(white arrows)*. **E,** A transaxial T1-weighted, fat-suppressed MR image obtained after intravenous administration of gadolinium reveals, once again, cortical destruction with high signal intensity edema within the soft tissue mass *(arrows)*. Some high signal intensity is also evident in the adjacent bone marrow *(open arrow)*. *(Courtesy G. Greenway, MD, Dallas, Texas.)*

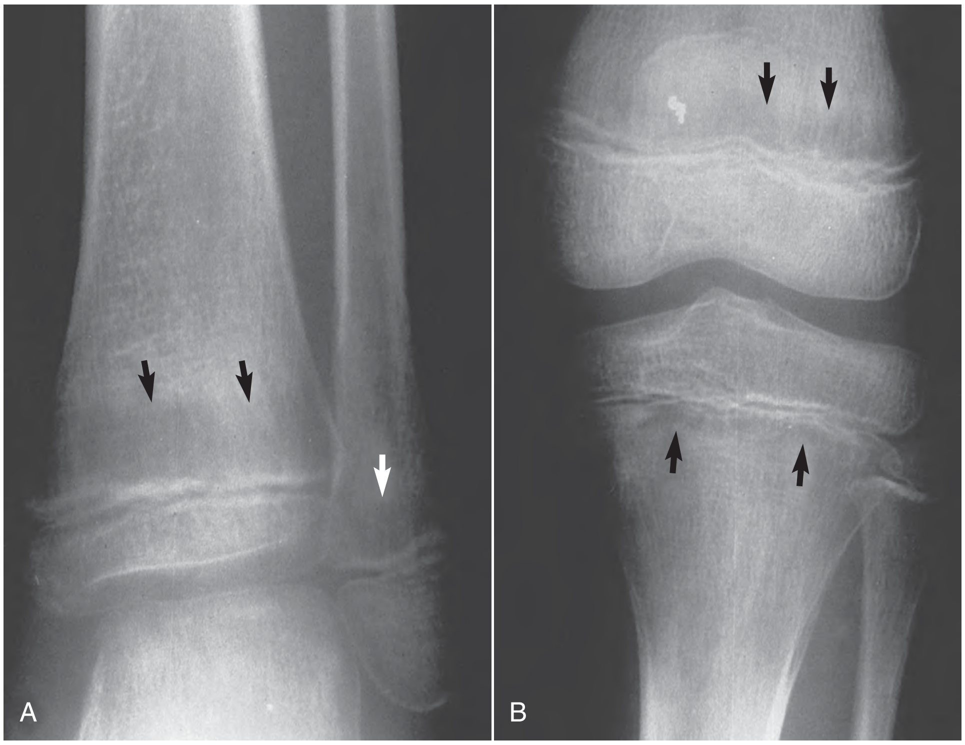

FIGURE 10–27 **Acute childhood leukemia.**[41] This 8-year-old girl was diagnosed with acute leukemia. **A,** Radiograph of the distal ends of the tibia and fibula reveals transverse radiolucent bands through the metaphyses *(arrows)*. **B,** Similar radiolucent bands *(arrows)* are seen in the distal femoral and the proximal tibial metaphyses.

TABLE 10-4 Primary Benign Tumors Affecting the Tibia and the Fibula*

Entity	Figure(s)	Characteristics
Enostosis[42,80,118]		Bone island Fewer than 10% of enostoses occur in the tibia and fibula Solitary or multiple circular or oblong discrete foci of mature osteosclerotic compact bone within the spongiosa portion of bone Usually asymptomatic, but giant painful bone islands in the tibia up to 10 cm in diameter have been reported Differential diagnosis includes osteoma, osteoid osteoma, osteoblastoma, enchondroma, bone infarction, fibrous dysplasia, healed nonossifying fibroma and osteosarcoma
Osteoid osteoma[43-45]	10-28	24% of osteoid osteomas occur in the tibia; 4% occur in the fibula Cortical or subperiosteal lesion; reactive sclerosis surrounding central radiolucent nidus Nidus usually less than 1 cm in diameter and often not visible on routine radiographs
Osteoblastoma (conventional)[46]		Approximately 15% of conventional osteoblastomas occur in the tibia and fibula Osteolytic, osteosclerotic, or both Expansile lesion with cortical thinning Partially calcified matrix in many cases Often resembles large osteoid osteoma May be subperiosteal
Osteofibrous dysplasia[35,47]	10-29	Also termed *ossifying fibroma* Rare fibro-osseous lesion of tubular bones occurs almost exclusively in the tibia (and, infrequently, the ipsilateral fibula) Long diaphyseal lesion with intracortical osteolysis clearly marginated by a band of osteosclerosis Hazy or ground-glass appearance reminiscent of fibrous dysplasia Occasionally purely osteosclerotic Osseous expansion Bowing, deformity, and pathologic fracture

* See also Table 1-13.

Continued

TABLE 10-4 Primary Benign Tumors Affecting the Tibia and the Fibula—cont'd

Entity	Figure(s)	Characteristics
Enchondroma (solitary)[48]	10-30	Tibia and fibula are infrequent sites of solitary enchondroma Solitary, central, or eccentric medullary osteolytic lesion with lobulated endosteal scalloping Stippled calcification (50% of lesions)
Enchondromatosis (Ollier)[48]	10-31	Multiple enchondromas Commonly affect the fibula and tibia
Maffucci syndrome[48]		Multiple enchondromas and soft tissue hemangiomas More than half of patients with Maffucci syndrome have tibial and fibular involvement Unilateral distribution in 50% of cases
Chondroblastoma[49,50,97]	10-32	Approximately 18% of chondroblastomas involve the tibia Circular osteolytic lesion affecting the proximal tibial epiphysis, or apophysis of the tibial tubercle May exhibit calcification in matrix Tissue biopsy is necessary to differentiate from clear cell chondrosarcoma
Chondromyxoid fibroma[51]	10-33	Approximately 40% of chondromyxoid fibromas involve the tibia; 8% involve the fibula Eccentric, elongated metaphyseal lesion 2-10 cm in length Cortical expansion, coarse trabeculation, endosteal sclerosis Calcification is rare (5%-27% of cases) May appear aggressive with large "bite" lesion penetrating cortex
Osteochondroma (solitary)[52,53]	10-34	Eighteen percent of solitary osteochondromas involve the tibia; 4% involve the fibula Pedunculated or sessile cartilage-covered osseous excrescence arising from the surface of the metaphysis of the proximal or distal portion of the tibia or fibula
Hereditary multiple exostosis[54]	10-35	Commonly involves tibia and fibula Multiple sessile and pedunculated osteochondromas
Nonossifying fibroma and fibrous cortical defect[55,56]	10-36	Forty-three percent occur in the tibia; 8% occur in the fibula Eccentric, multiloculated osteolytic lesion arising from the metaphyseal cortex Resembles a well-circumscribed blisterlike shell of bone arising from the metaphyseal cortex; often bilateral and symmetric May migrate away from the physis with longitudinal metaphyseal growth
Giant cell tumor (benign)[57]	10-37	More than 25% of benign giant cell tumors occur in the tibia; 4% occur in the fibula Eccentric osteolytic neoplasm with a predilection for the subarticular region of the proximal portion of the tibia Often multiloculated expansile lesion
Intraosseous lipoma[58,99]	10-38	Osteolytic lesion surrounded by a thin, well-defined sclerotic border Central calcified or ossified nidus is common Osseous expansion occasionally Cortical destruction and periostitis absent
Hemangioma (solitary)[59]		Rare in the tibia and fibula Radiolucent, slightly expansile intraosseous lesion Radiating, latticelike or weblike trabecular pattern Occasional cortical thinning Rarely periostitis, soft tissue mass, or osteosclerosis Intracortical and periosteal forms of hemangioma are extremely rare, but predominate in the tibia and fibula
Simple bone cyst[60]	10-39	Also termed *solitary,* or *unicameral, bone cyst* Six percent of simple bone cysts affect the tibia; 5% affect the fibula Mildly expansile solitary osteolytic lesion within medullary cavity of tibial or fibular metaphyses Multiloculated; may migrate away from the physis with normal longitudinal metaphyseal growth Fallen-fragment sign in patients with pathologic fracture
Aneurysmal bone cyst[61]	10-40	Fifteen percent of aneurysmal bone cysts involve the tibia; 7% involve the fibula Eccentric, thin-walled, expansile osteolytic lesion of the metaphysis; thin trabeculation with multiloculated appearance Buttressing at edge of lesion

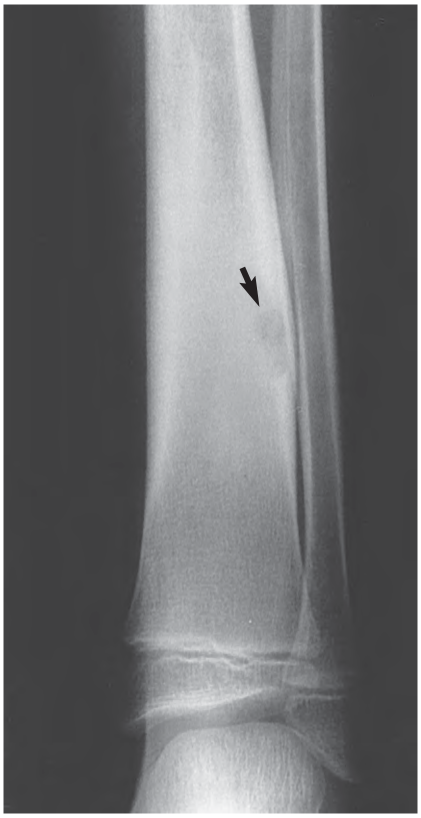

FIGURE 10–28 **Osteoid osteoma.**[43-45] This 7-year-old boy had a 1-year history of lower leg and ankle pain. The pain was present with activity, worse at night, and relieved by salicylates. Observe the diffuse reactive sclerosis and minimal bone expansion surrounding an eccentric, oval, radiolucent nidus *(arrow)* within the distal tibial diaphysis. *(Courtesy G. Greenway, MD, Dallas.)*

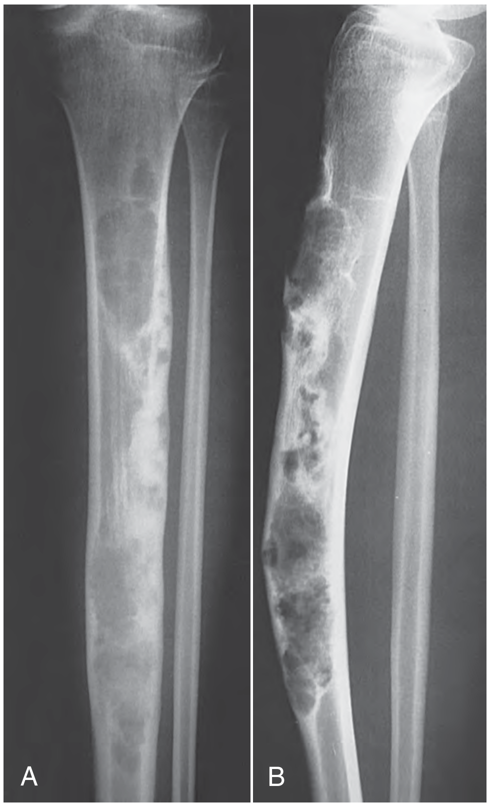

FIGURE 10–29 **Ossifying fibroma.**[47] Anteroposterior **(A)** and lateral **(B)** radiographs show a sharply marginated, multilocular, radiolucent lesion with associated bone sclerosis, bowing, and osseous expansion involving the tibial diaphysis. The lesions closely resemble those of polyostotic fibrous dysplasia.

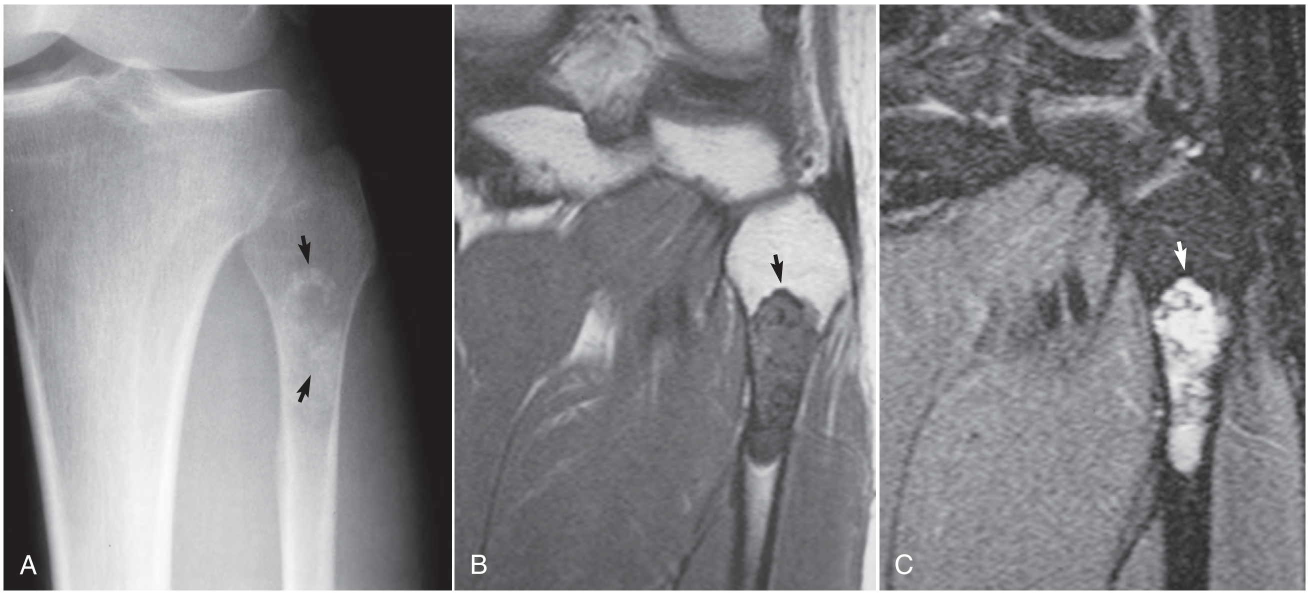

FIGURE 10–30 **Solitary enchondroma.**[48] This patient was being examined for an acute knee injury. The radiograph **(A)** reveals calcification within the medullary cavity of the fibular metaphysis *(arrows)*. A coronal T1-weighted MR image **(B)** shows an inhomogeneous intermediate to low signal intensity within the matrix of a geographic lesion *(arrow)*. The lesion is well-defined, predominantly medullary in location, and does not break the cortex of the fibula or extend into the adjacent soft tissues. A coronal proton-density fat suppressed MR image **(C)** exhibits a high signal intensity matrix *(arrow)* with small arclike zones of low signal intensity consistent with the appearance of a partially calcified cartilage-based tumor.

FIGURE 10–31 **Enchondromatosis (Ollier disease).**[48] Progressive changes are evident within the tibia and the fibula in a child from the ages of 2 years **(A)** to 12 years **(B).** Findings include metaphyseal expansion, stippled calcification, and osseous deformity. Alternatively, lesions may appear multiloculated with endosteal scalloping. *(From Resnick D: Diagnosis of bone and joint disorders. 4th Ed. Philadelphia, Saunders, 2002, p. 4503.)*

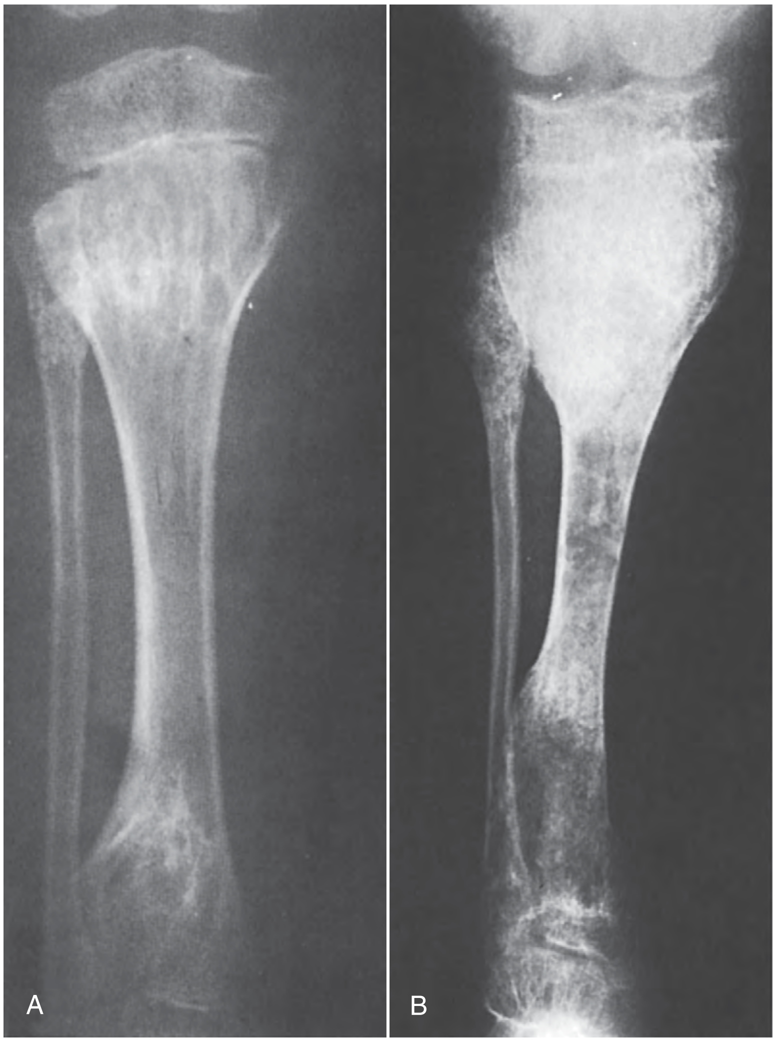

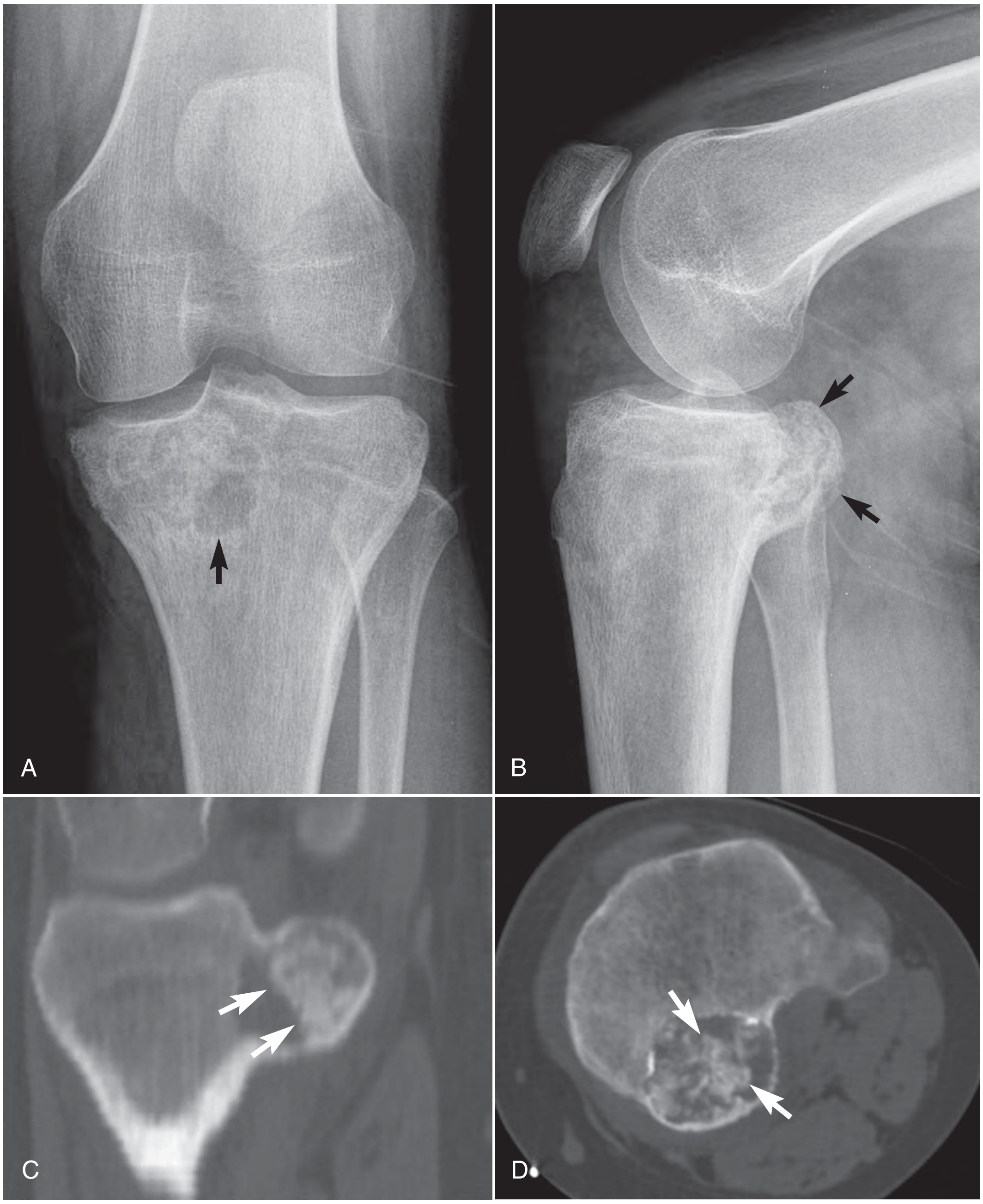

FIGURE 10–32 **Chondroblastoma.**[49,50,97] This 17-year-old female presented with knee pain. **A,** Anteroposterior radiograph reveals a circular geographic osteolytic lesion in the metaphysis of the tibia *(arrow)*. **B,** The lateral radiograph shows the lesion to be expansile and eccentric projecting off the posterior aspect of the subchondral and metaphyseal regions of the tibial plateau *(arrows)*. Additionally, there is evidence of calcification within the matrix. Sagittal reformatted **(C)** and transaxial **(D)** CT bone window images reveal the extensive calcification *(arrows)* within the osteolytic expansile lesion. No evidence of cortical destruction or adjacent soft tissue mass or swelling can be seen.

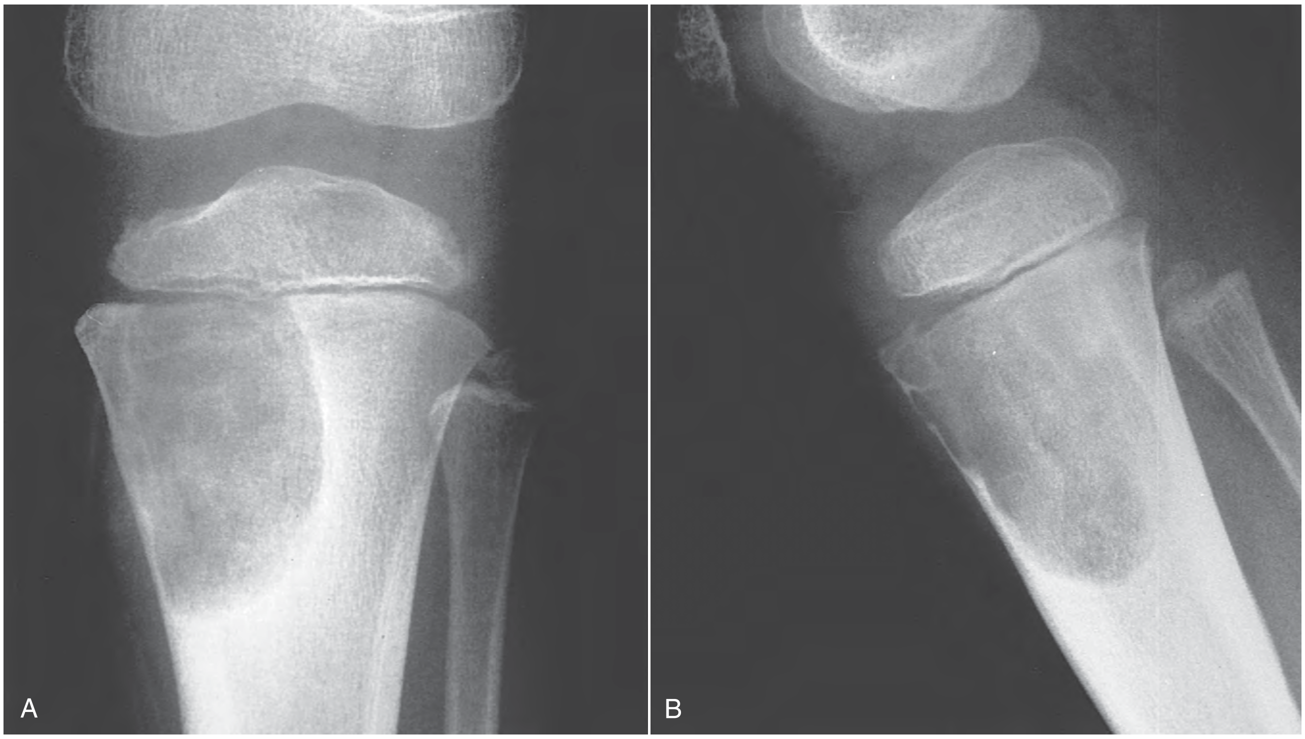

FIGURE 10–33 **Chondromyxoid fibroma.**[51] **A-B,** Radiographs of the knee in a 6-year-old boy show an eccentric, osteolytic lesion in the proximal tibial metaphysis. A well-defined, sclerotic margin is present. *(Courtesy D. Goodwin, MD, Lebanon, NH.)*

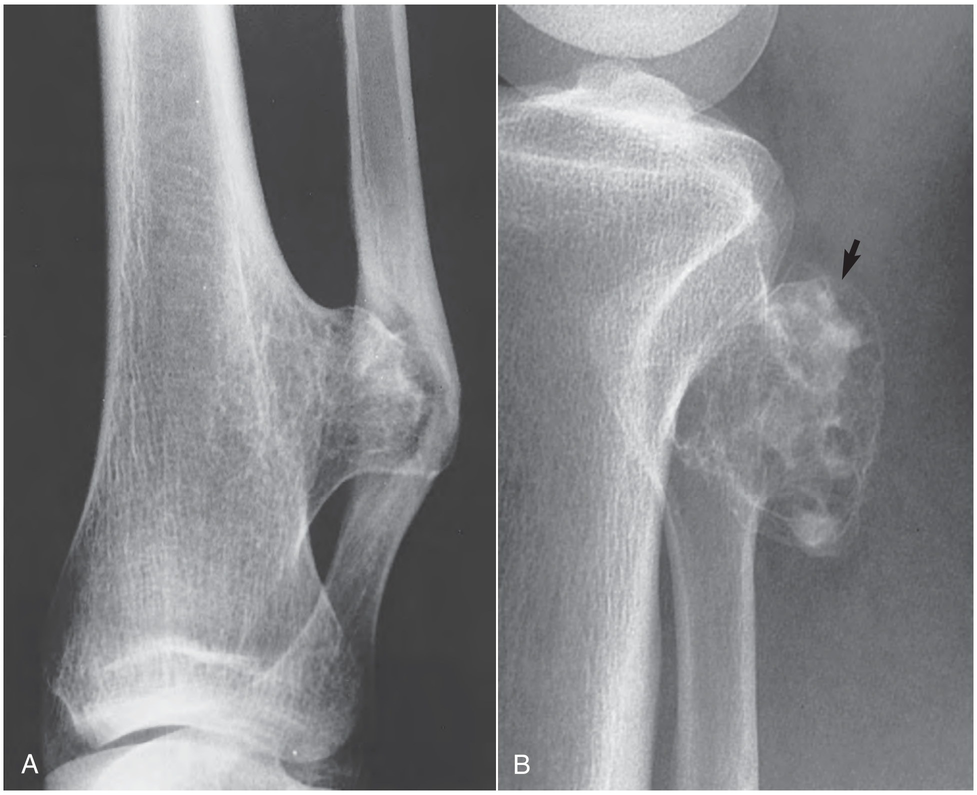

FIGURE 10–34 **Solitary osteochondroma.**[52,53] **A,** Tibia. A large pedunculated osteochondroma has resulted in dramatic fibular deformity and remodeling. Almost 20% of osteochondromas occur in the tibia. **B,** Fibula. Lateral radiograph of this 31-year-old man shows a large, expansile, cauliflower-shaped osteocartilaginous lesion arising from the proximal metaphysis of the fibula *(arrow)*. Fewer than 5% of osteochondromas arise from the fibula. (***A,*** *Courtesy J. Slivka, MD, San Diego;* ***B,*** *Courtesy R. Thomas, MD, Santa Ana, Calif.)*

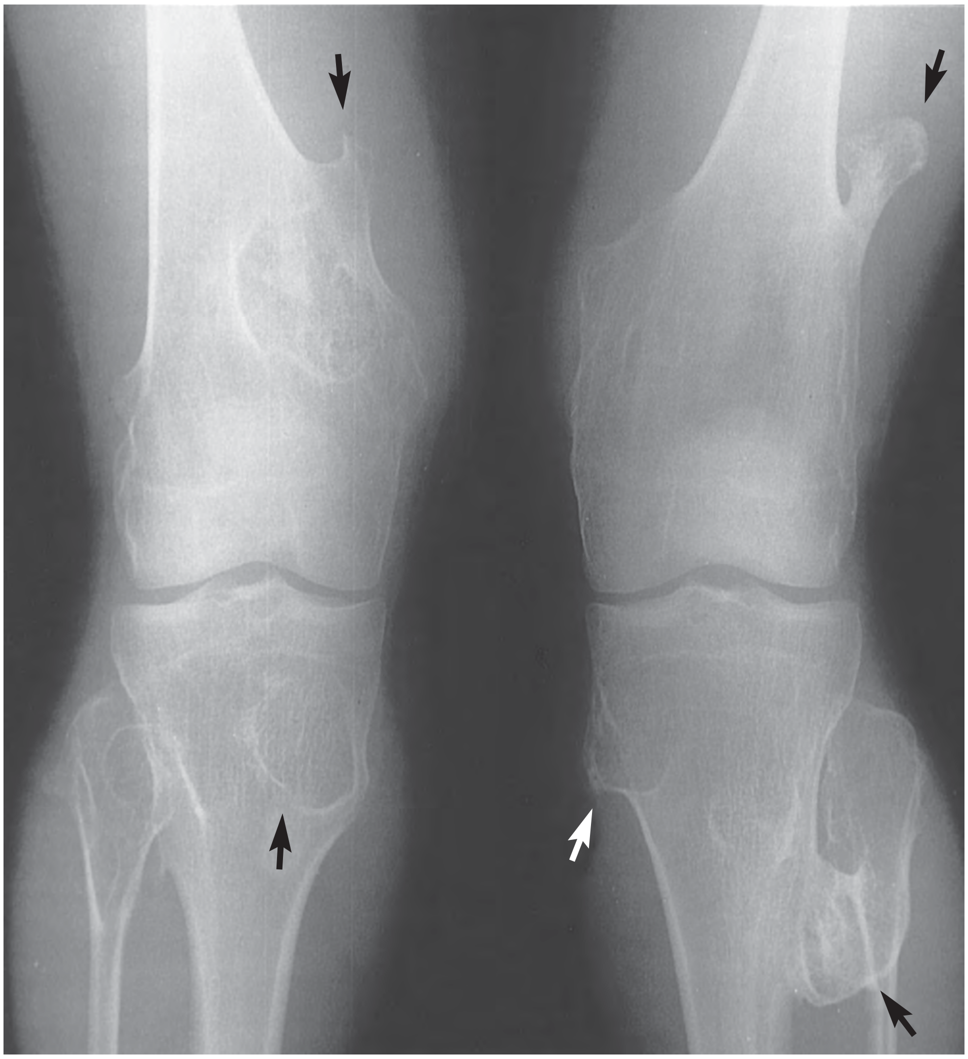

FIGURE 10–35 **Hereditary multiple exostosis.**[54] Large bilateral sessile and pedunculated osseous outgrowths are seen arising from the metaphyses of the femora, tibiae, and fibulae *(arrows)*.

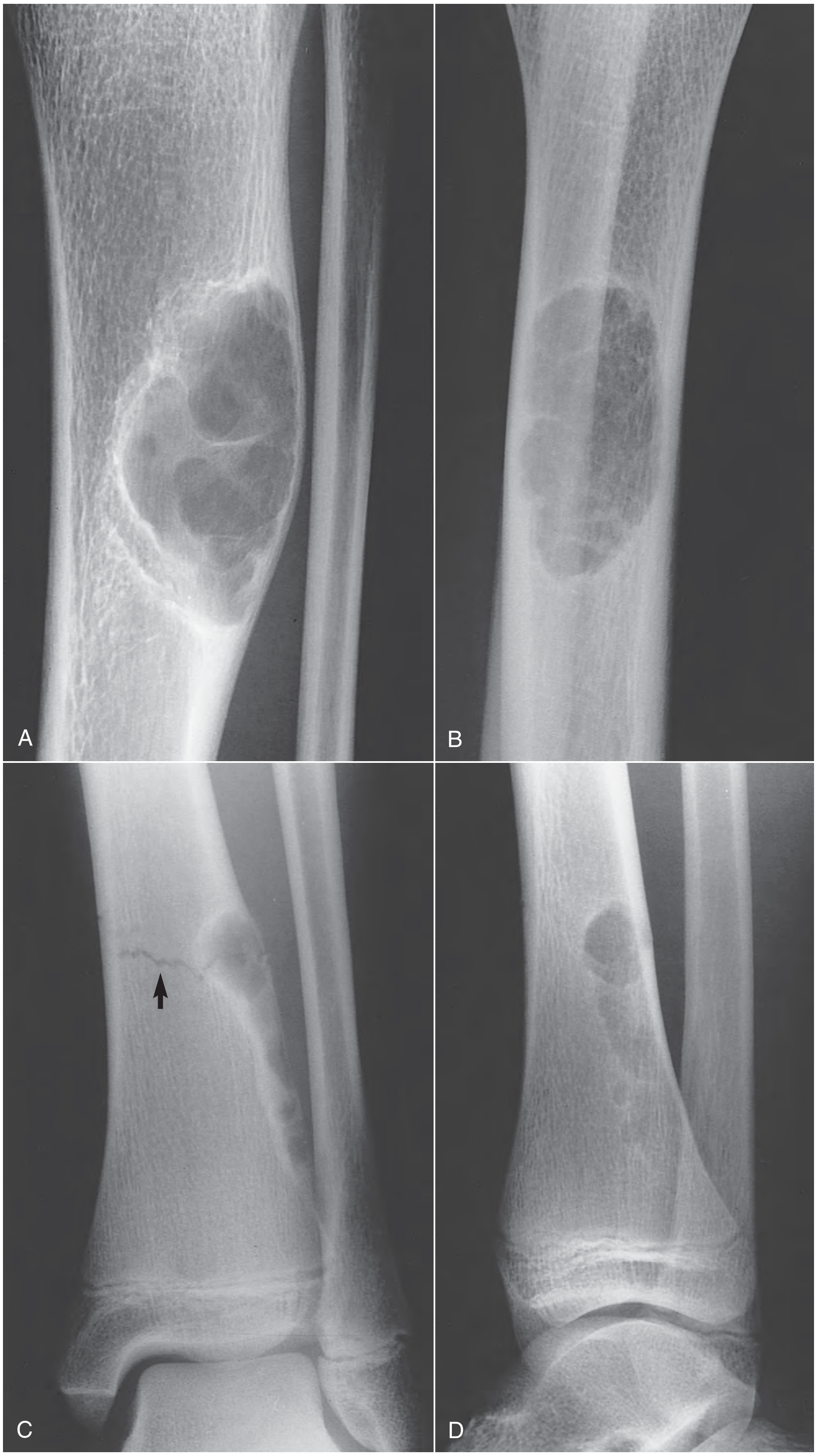

FIGURE 10–36 Nonossifying fibroma.[55,56] **A-B,** Anteroposterior **(A)** and lateral **(B)** magnification radiographs of the tibia show a large, eccentric, slightly expansile, multiloculated, geographic, osteolytic lesion. Observe the cortical thinning and endosteal scalloping. Routine frontal **(C)** and oblique **(D)** radiographs of another patient, a 15-year-old boy, show a typical metaphyseal nonossifying fibroma. A transverse pathologic fracture *(arrow)* is visible predominantly on the anteroposterior view **(C).** Observe the somewhat "blistered" appearance of the cortex, a common finding in this condition. *(**A-B,** Courtesy U. Mayer, MD, Klagenfurt, Austria.)*

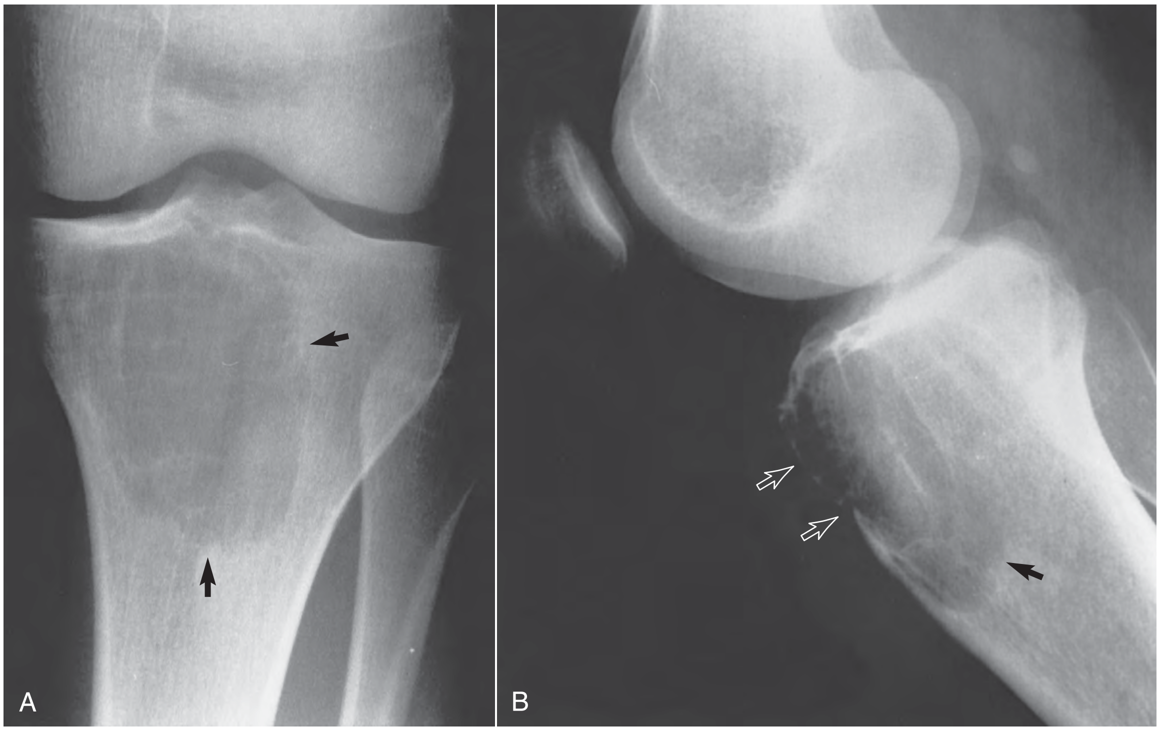

FIGURE 10–37 **Giant cell tumor.**[57] Frontal **(A)** and lateral **(B)** radiographs of the knee in a 19-year-old woman with a 2-year history of knee pain. An eccentric, osteolytic, geographic lesion extending into the subchondral region of the proximal portion of the tibia *(arrows)* is revealed. The tumor produces thinning and destruction of the anterior tibial cortex *(open arrows)*. Slight bone expansion is present, and the lesion possesses a delicate trabecular pattern. The radiographic appearance of the giant cell tumor is an inaccurate guide to the histologic composition and clinical behavior of the lesion: Benign lesions may appear aggressive and aggressive lesions may appear benign. *(Courtesy G. Greenway, MD, Dallas.)*

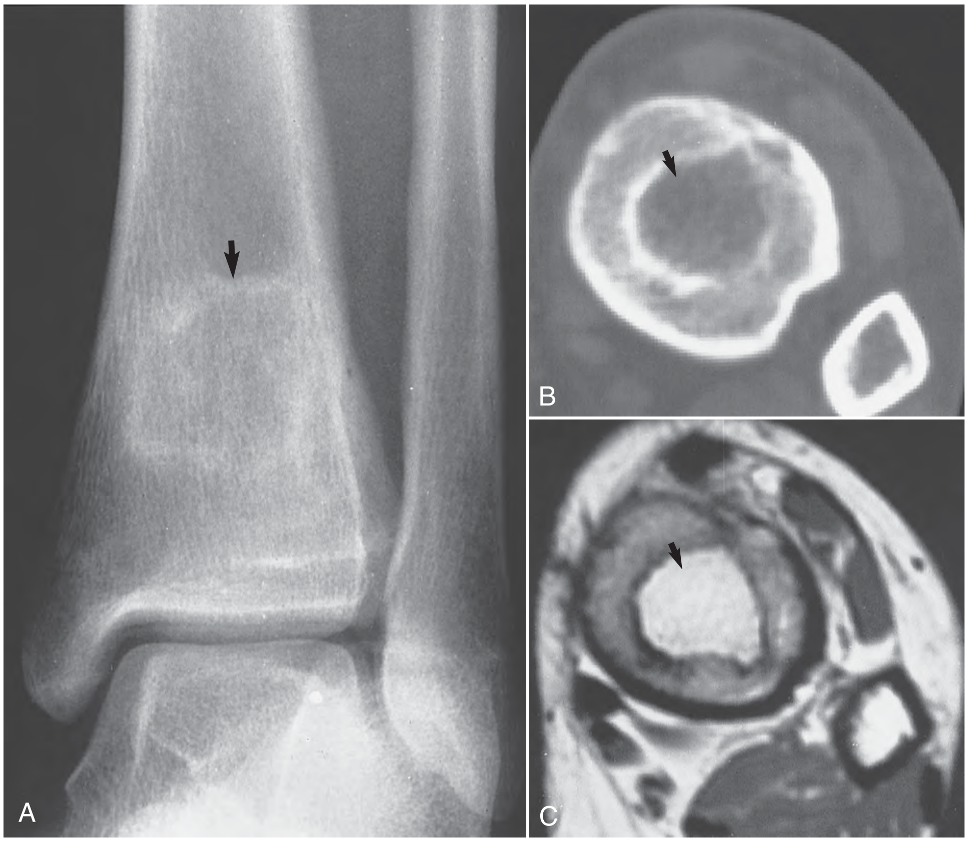

FIGURE 10–38 **Intraosseous lipoma.**[58,99] Patient is a 15-year-old girl. **A,** Routine radiograph. Observe the geographic osteolytic lesion with a faint rim of sclerosis involving the metaphyseal region of the distal portion of the tibia *(arrow)*. **B,** Transaxial CT scan confirms the location and fatty nature of the tumor *(arrow)* by measurements of attenuation values derived from CT data. **C,** Transaxial T1-weighted (TR/TE, 650/200) spin echo image. Observe the high signal intensity of the matrix of the lesion *(arrow),* characteristic of fat. *(Courtesy K. Gerber, MD, San Diego.)*

FIGURE 10–39 **Simple bone cyst.**[60] A 12-year-old girl noticed sudden leg pain after a minor fall. Frontal **(A)** and lateral **(B)** films of the fibula show a pathologic fracture through a cystlike, slightly expansile diaphyseal lesion. Endosteal scalloping is present, and periostitis, probably from fracture healing, is seen adjacent to the lesion. A "fallen fragment" is seen as a tiny piece of comminuted bone that is resting in a dependent position within the fluid-filled matrix *(arrow)*. *(Courtesy V. Vint, MD, La Jolla, Calif.)*

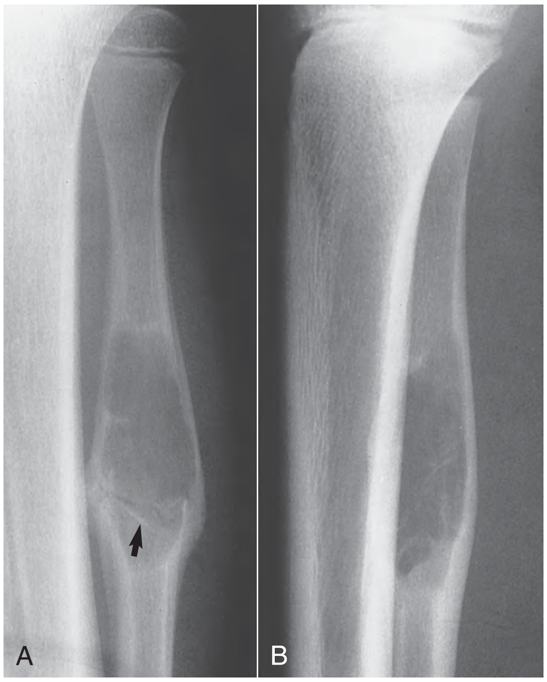

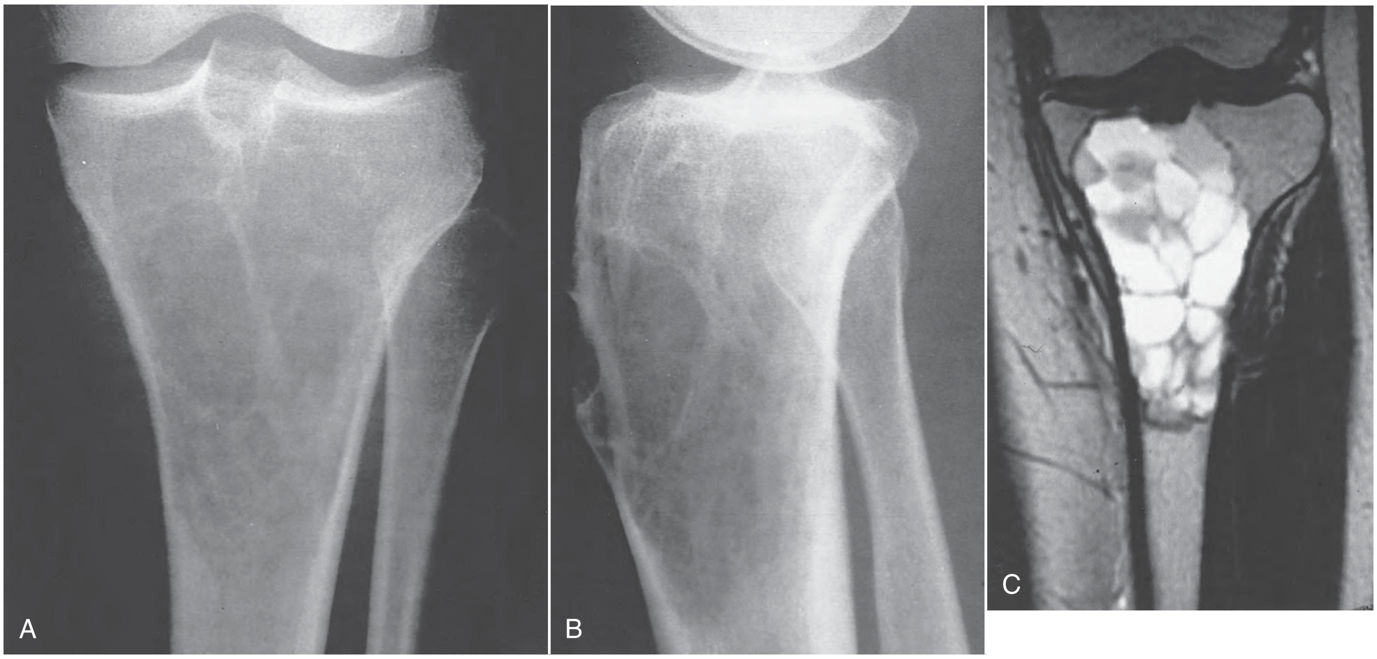

FIGURE 10–40 **Aneurysmal bone cyst.**[61] Routine frontal **(A)** and lateral **(B)** radiographs of the knee show an expansile, eccentrically located osteolytic metaphyseal lesion involving the proximal portion of the tibia. A coronal T2-weighted (TR/TE, 3000/104 Ef) fast spin echo MR image **(C)** reveals the multichambered, fluid-filled matrix. Transaxial MR images (not shown) demonstrated fluid-fluid levels within this aneurysmal bone cyst. *(Courtesy A. Newberg, MD, Boston.)*

TABLE 10-5	Tumorlike Lesions of Bone Affecting the Tibia and the Fibula*	
Entity	**Figure(s)**	**Characteristics**
Paget disease[62-64,107,108]	10-41	The tibia is the fourth most common site of involvement (after the pelvis and femur) The fibula is one of the least likely bones to be involved Usually polyostotic and may have unilateral involvement Coarsened trabeculae and bone enlargement Pathologic fracture Pseudofractures of convex surface of bowed bones Saber-shin deformity (anterior tibial bowing) Blade of grass appearance (flame-shaped advancing edge of osteolysis) common in tibia
Neurofibromatosis 1[65,66]	10-42	Formerly designated von Recklinghausen disease Tibia and fibula involvement common Dysplastic bones with overconstriction, deformity, and remodeling Circumscribed cystlike intraosseous lesions The tibia and fibula are common sites for pseudarthroses: deformed bones fracture and heal incompletely
Monostotic fibrous dysplasia[67]	10-43	Fewer than 10% of monostotic lesions involve the tibia; 2% involve the fibula Thick rim of sclerosis surrounding radiolucent lesion; hazy ground-glass appearance of matrix Tibial or fibular bowing may occur
Polyostotic fibrous dysplasia[67]	10-44	More than 80% of patients have tibial involvement; more than 60% have fibular involvement Polyostotic lesions tend to be more expansile and multiloculated than monostotic lesions Bowing is also more prominent in polyostotic form
Langerhans cell histiocytosis[68]		Tibial and fibular involvement is extremely uncommon Osteolytic lesions may be multiloculated and expansile

* See also Table 1-14.

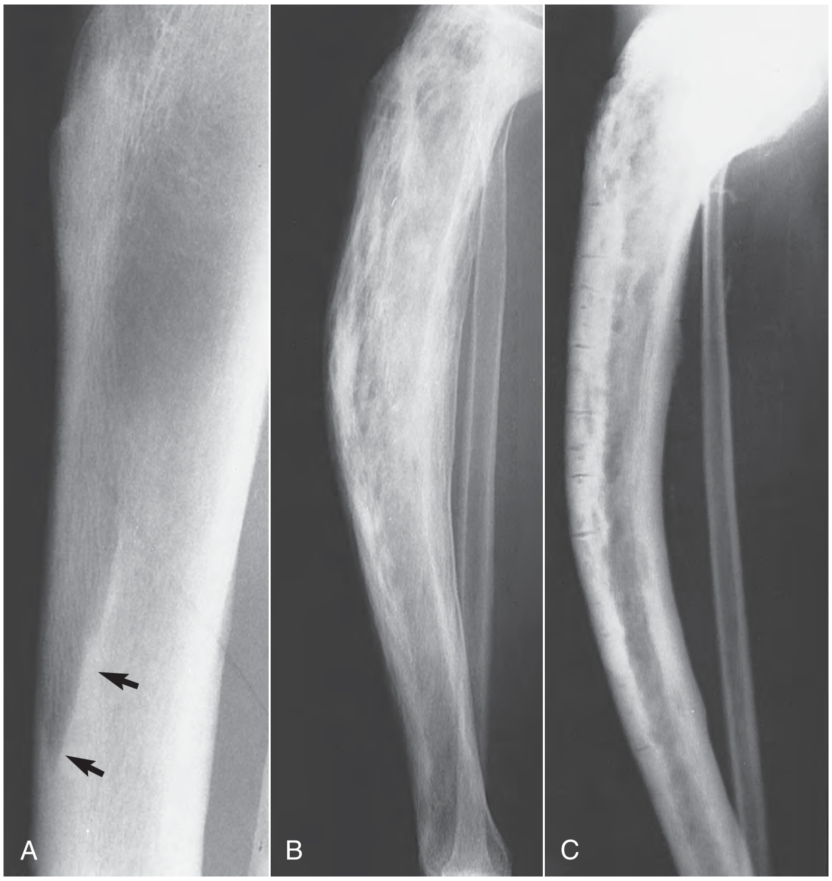

FIGURE 10–41 Paget disease.[62-64,107,108] **A,** Osteolytic pattern. Osteolytic destruction is seen as a wedge-shaped, radiolucent edge (blade-of-grass or flame-shaped appearance) within the tibial diaphysis *(arrows)*. **B,** Combined pattern. In another patient with long-standing Paget disease, the combined pattern of osteolytic and osteosclerotic disease predominates. Anterior bowing of the tibia is also evident, a complication termed *saber-shin deformity.* **C,** Osteosclerotic pattern. In a third patient, diffuse osteosclerosis, cortical thickening, pseudofractures, and anterior bowing are the predominant findings. The fibula, which is unaffected, is one of the bones least commonly involved in Paget disease.

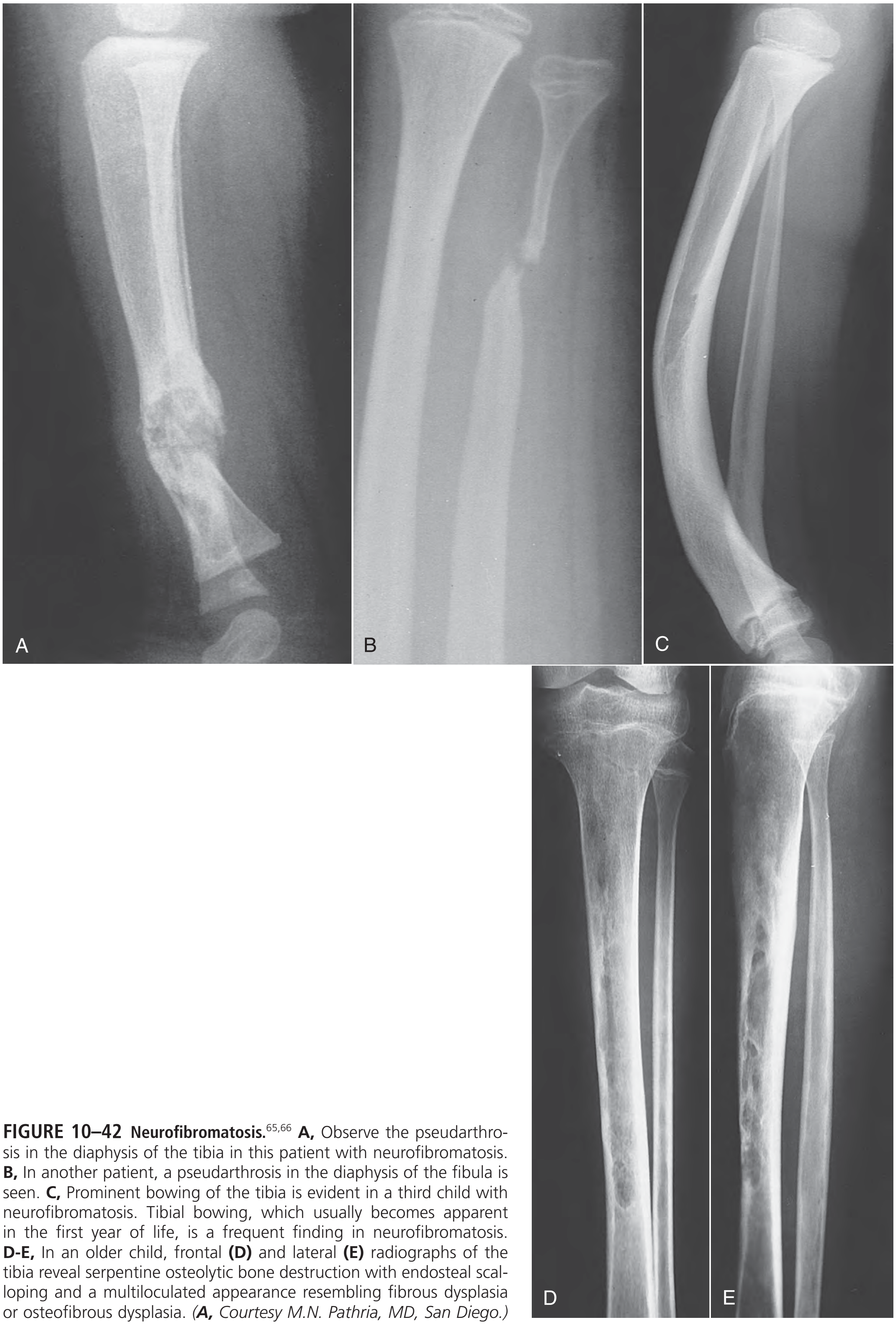

FIGURE 10–42 Neurofibromatosis.[65,66] **A,** Observe the pseudarthrosis in the diaphysis of the tibia in this patient with neurofibromatosis. **B,** In another patient, a pseudarthrosis in the diaphysis of the fibula is seen. **C,** Prominent bowing of the tibia is evident in a third child with neurofibromatosis. Tibial bowing, which usually becomes apparent in the first year of life, is a frequent finding in neurofibromatosis. **D-E,** In an older child, frontal **(D)** and lateral **(E)** radiographs of the tibia reveal serpentine osteolytic bone destruction with endosteal scalloping and a multiloculated appearance resembling fibrous dysplasia or osteofibrous dysplasia. (***A,*** *Courtesy M.N. Pathria, MD, San Diego.)*

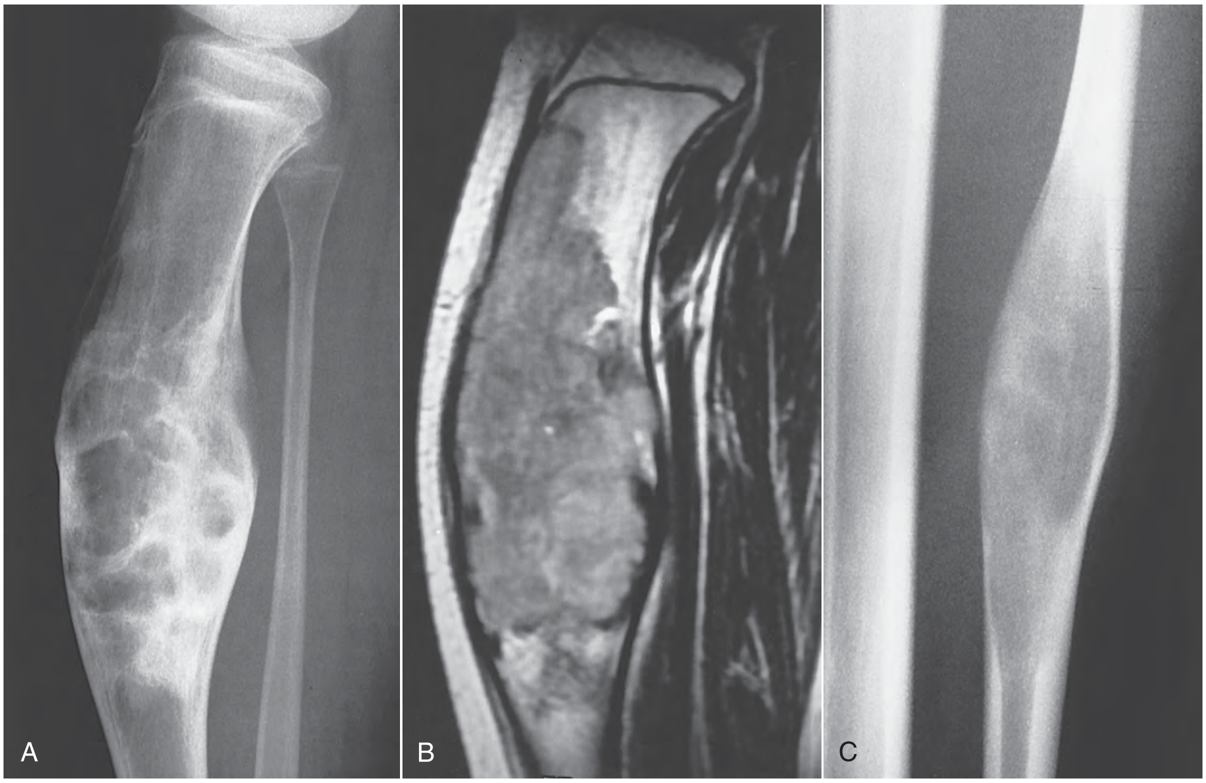

FIGURE 10–43 **Monostotic fibrous dysplasia.**[67] **A-B,** Tibial involvement in a 14-year-old boy. In **A,** a lateral radiograph of the tibia demonstrates an expansile, multilocular diaphyseal lesion. It is characterized by endosteal scalloping, undulating zones of sclerosis, and a hazy osteolytic matrix. Tibial bowing is also apparent. In **B,** a fast spin echo (TR/TE, 4,000/75) MR image shows an inhomogeneous intermediate intensity signal within the matrix. **C,** Fibula. A characteristic ground-glass appearance with cortical endosteal scalloping is seen in this lesion in the fibular diaphysis. The fibula is infrequently affected by fibrous dysplasia. (***A-B,*** *Courtesy B.Y. Yang, MD, Kaohsiune Hsien, Taiwan;* ***C,*** *Courtesy G. Greenway, MD, Dallas.)*

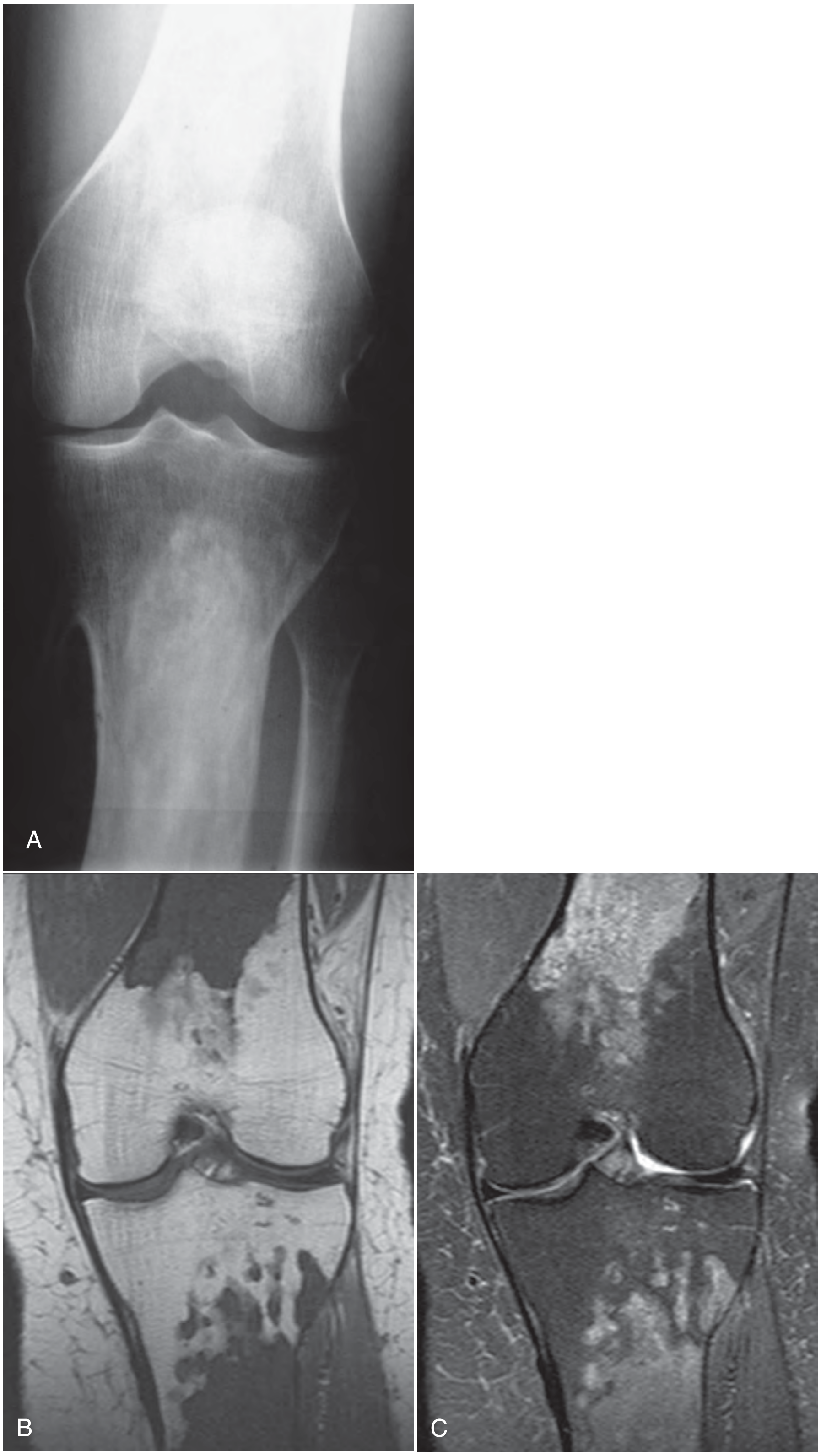

FIGURE 10–44 **Polyostotic fibrous dysplasia.**[67] The anteroposterior radiograph **(A)** shows slight widening, increased medullary bone density, and cortical thinning of the tibial metaphysis. Similar changes in the distal femur (not well seen on this image) were observed bilaterally. Coronal T1-weighted MR imaging **(B)** shows a dramatic pattern of lesions involving much of the medullary cavity of the femoral and tibial metaphyses. The signal is somewhat punctate at its peripheral regions and is isointense to muscle. A coronal proton-density fat suppressed image **(C)** shows signal intensity hyperintense to muscle and to normal marrow. There is no evidence of cortical destruction or soft tissue extension.

TABLE 10-6 Metabolic, Hematologic, and Vascular Disorders Affecting the Tibia and the Fibula*

Entity	Figure(s)	Characteristics
Generalized osteoporosis[69]		Uniform decrease in radiodensity, thinning of cortices, accentuation of weight-bearing trabeculae May occasionally result in insufficiency fractures of the tibia and fibula
Regional osteoporosis[69,70]	10-45	May occur as a result of disuse and immobilization after a fracture or other injury or in complex regional pain syndrome Findings may be more widespread in paralyzed patients Bandlike, patchy, spotty, or periarticular osteopenia Subperiosteal (rare) and intracortical bone resorption Subchondral and juxtaarticular cystlike lesions Occasional scalloping of tibia
Osteogenesis imperfecta[11]	10-8	See Table 10-1
Osteomalacia[71,109]	10-46	Osteopenia; decreased trabeculae; remaining trabeculae appear prominent and coarsened Looser zones (pseudofractures)
Rickets[71,109]	10-47	Metaphyseal demineralization: frayed metaphyses Bowing deformities Osteopenia Looser zones
Hyperparathyroidism and renal osteodystrophy[72-74]	10-48, 10-49	*Brown tumor:* solitary or multiple expansile osteolytic lesions containing fibrous tissue and giant cells; may disappear after treatment for hyperparathyroidism Occasionally severe tibial and fibular bowing occurs Osteosclerosis more common in renal osteodystrophy
Hypoparathyroidism[75,76]	10-50	Osteosclerosis Subcutaneous calcification Premature physeal fusion Periarticular bone proliferation—enthesopathy
Hypovitaminosis C (scurvy)[77,78]	10-51	Radiographic evidence of skeletal changes in scurvy is seen only in advanced, long-standing disease Periostitis secondary to subperiosteal hemorrhage Sclerotic metaphyseal lines Beaklike metaphyseal excrescences Radiodense shell surrounding epiphyses Healing scurvy may result in increased radiodensity of the metaphyses and epiphyses
Gaucher disease[79,110]	10-52	Osteopenia, septated osteolytic lesions, cortical diminution, and diametaphyseal widening from undertubulation (Erlenmeyer flask deformity) Osseous weakening may result in pathologic fractures Coarsened trabecular pattern
Venous insufficiency[80]	10-53	Thick, undulating periosteal reaction along the tibia and fibula seen in as many as 60% of patients with chronic disabling venous stasis Associated calcification and ossification in soft tissue
Primary hypertrophic osteoarthropathy[81]	10-54	Also termed *pachydermoperiostosis*: primary form of hypertrophic osteoarthropathy Only 3%-5% of all cases of hypertrophic osteoarthropathy Bilateral symmetric tibial and fibular periostitis
Secondary hypertrophic osteoarthropathy[81,82]	10-55	Syndrome characterized by digital clubbing, arthritis, and periostitis Complication of many diseases, including bronchogenic carcinoma, mesothelioma, and other intrathoracic and intraabdominal diseases Bilateral symmetric periostitis of tibiae and fibulae
Growth recovery (Harris) lines[83,111]	10-56	Transverse radiodense lines in the tubular bones of children representing a sign of new or increased growth; presumably after a period of inhibited bone growth from a previous episode of trauma, infection, malnutrition, or other chronic disease state
Collagen vascular disease: soft tissue calcification[84]	10-57	Dermatomyositis, polymyositis, scleroderma, and other collagen vascular diseases may result in soft tissue calcinosis in the leg or calf *Differential diagnosis:* hyperparathyroidism, neurologic injury, melorheostosis, posttraumatic heterotopic ossification, soft tissue neoplasms
Medullary osteonecrosis[85]	10-58	Also termed *intramedullary bone infarct* or *metadiaphyseal osteonecrosis* Patchy intramedullary sclerosis with areas of radiolucency Irregular calcific deposits Closely resembles appearance of enchondroma

* See also Tables 1-15 to 1-17.

FIGURE 10–45 Regional osteoporosis: complex regional pain syndrome.[69,70] After a minor foot injury, this patient developed progressive pain and disability. Observe the bandlike and patchy metaphyseal osteopenia *(arrowheads)* and the subarticular loss of bone density within the talus and distal end of the tibia. Spotty, patchy, and bandlike bone resorption is typical of rapid-onset osteoporosis, such as that seen in disuse, burns, frostbite, paralysis, or, as in this case, complex regional pain syndrome. Such an appearance may simulate that of an aggressive neoplasm.

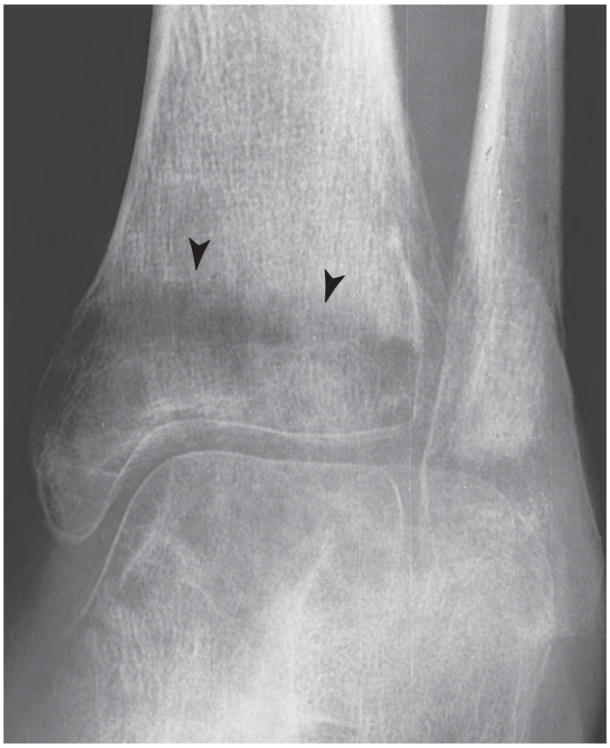

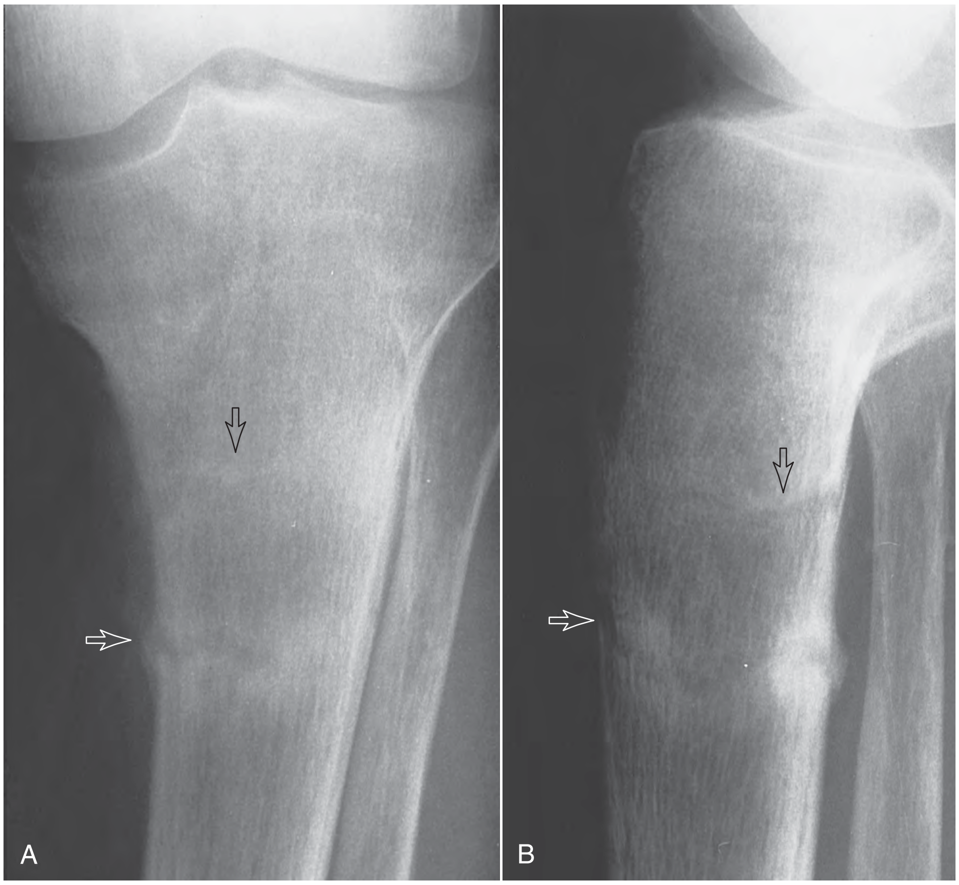

FIGURE 10–46 Osteomalacia.[71,109] Frontal **(A)** and lateral **(B)** radiographs of a 53-year-old man who had long-standing vitamin D-resistant osteomalacia. Diffuse osteopenia and two transverse insufficiency fractures are evident in the metadiaphysis of the tibia *(open arrows)*. A thin veil of callus is apparent at the margin of the lower fracture.

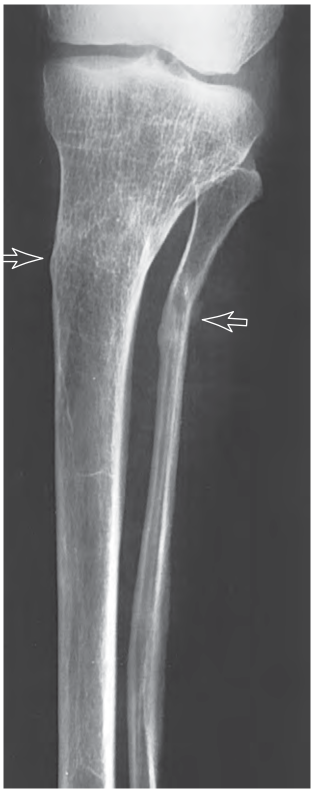

FIGURE 10–47 **Rickets (hypophosphatemic).**[71,109] In this patient with long-standing hypophosphatemia, diffuse osteopenia and bowing deformities of the tibia and fibula are present *(open arrows)*. *(Courtesy C. Pineda, MD, Mexico City.)*

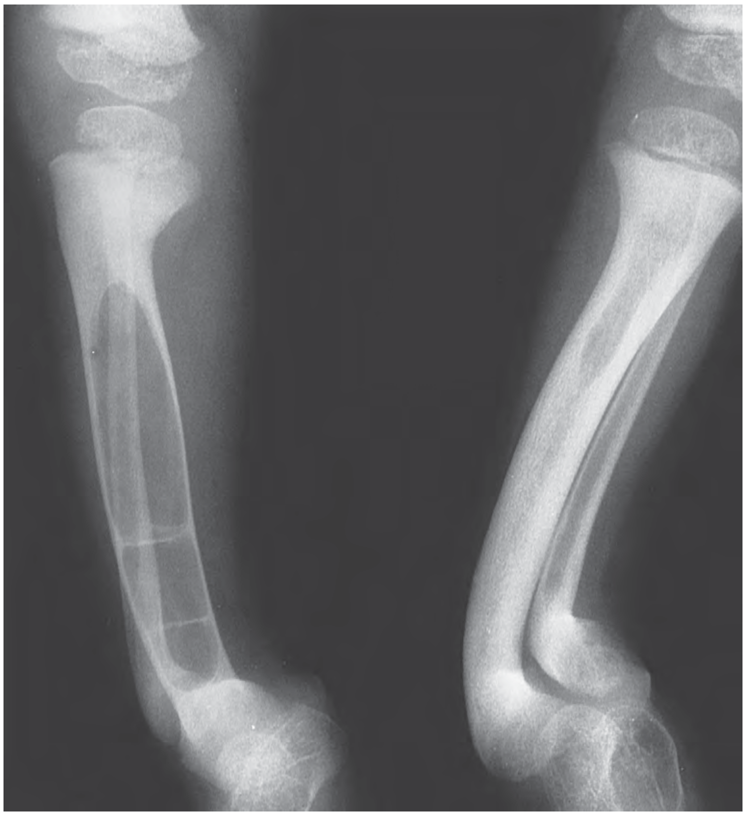

FIGURE 10–48 **Secondary hyperparathyroidism: Brown tumors.**[72] Observe the multiple, septated brown tumors in both tibiae of this 5-year-old girl with secondary hyperparathyroidism. Dramatic tibial bowing from bone softening is also present. Such severe skeletal involvement with brown tumors and deformities has been referred to as *osteitis fibrosa cystica*. *(Courtesy T. Broderick, MD, Orange, Calif.)*

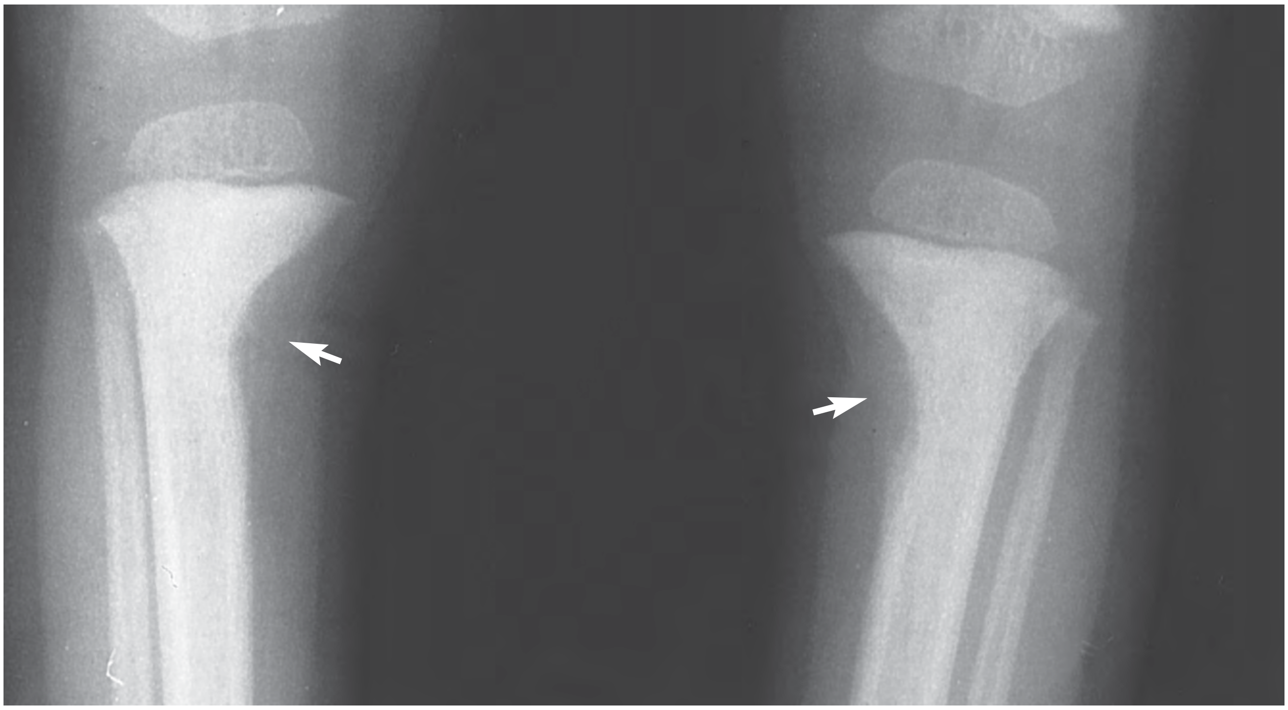

FIGURE 10–49 Renal osteodystrophy.[73,74] In a 4-year-old boy with secondary hyperparathyroidism, observe the generalized osteosclerosis and the characteristic subperiosteal resorption of the medial aspect of the proximal tibial metaphyses *(arrows)*.

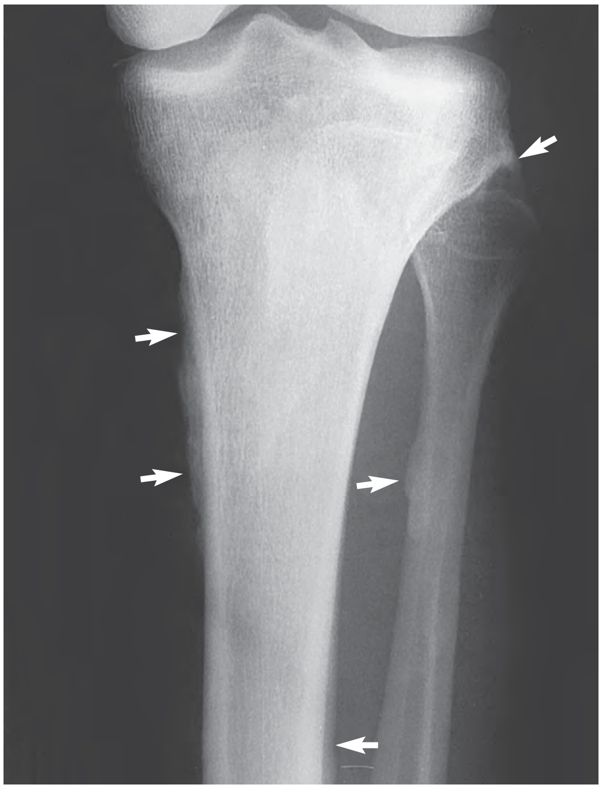

FIGURE 10–50 Hypoparathyroidism.[75,76] Osseous proliferation is seen as prominent excrescences in the proximal portion of the tibia *(arrows)* in this man with hypoparathyroidism.

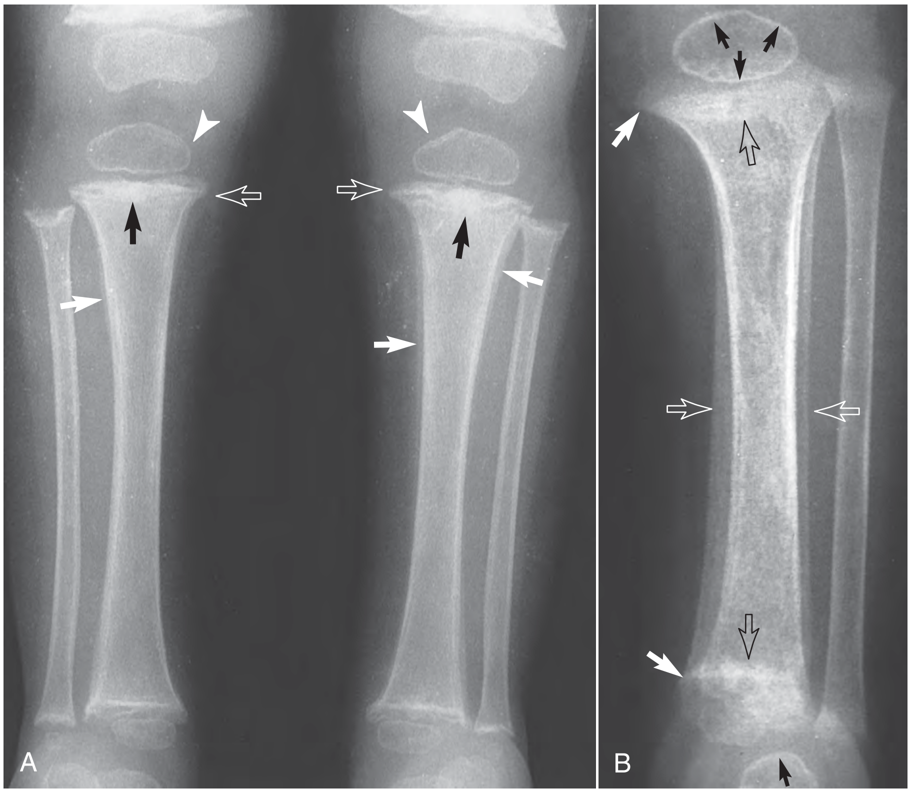

FIGURE 10–51 **Hypovitaminosis C (scurvy).**[77,78] **A,** In this infant, bilateral radiographs of the tibiae and fibulae demonstrate periostitis caused by subperiosteal hemorrhage *(white arrows),* thick sclerotic metaphyseal lines *(black arrows),* beaklike excrescences *(open arrows),* and radiodense shells around the epiphyses (Wimberger ring) *(arrowheads)*. These findings all are consistent with scurvy. **B,** In another child with chronic ascorbic acid deficiency, observe the thick periostitis from subperiosteal hemorrhage *(white open arrows),* sclerotic metaphyseal line *(black open arrows),* beaklike metaphyseal excrescences (Pelken spurs) *(white arrows),* radiolucent epiphysis surrounded by a sclerotic shell (Wimberger ring) *(black arrows),* and generalized osteopenia.

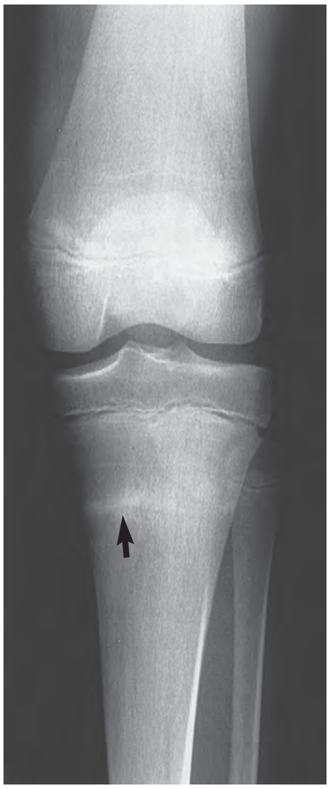

FIGURE 10–52 **Gaucher disease.**[79,110] Undertubulation (Erlenmeyer flask deformity) and cortical thinning are associated with an insufficiency fracture *(arrow)* of the tibia of this 13-year-old girl with Gaucher disease. *(Courtesy G. Greenway, MD, Dallas.)*

FIGURE 10–53 **Venous insufficiency: periosteal reaction.**[80] Frontal **(A)** and lateral **(B)** radiographs show a thick, undulating, single-layer periosteal reaction along the shafts of the tibia and the fibula in this patient with chronic venous stasis. Such changes predominate in the lower extremity and occur in 10% to 60% of patients with chronic disabling venous stasis.

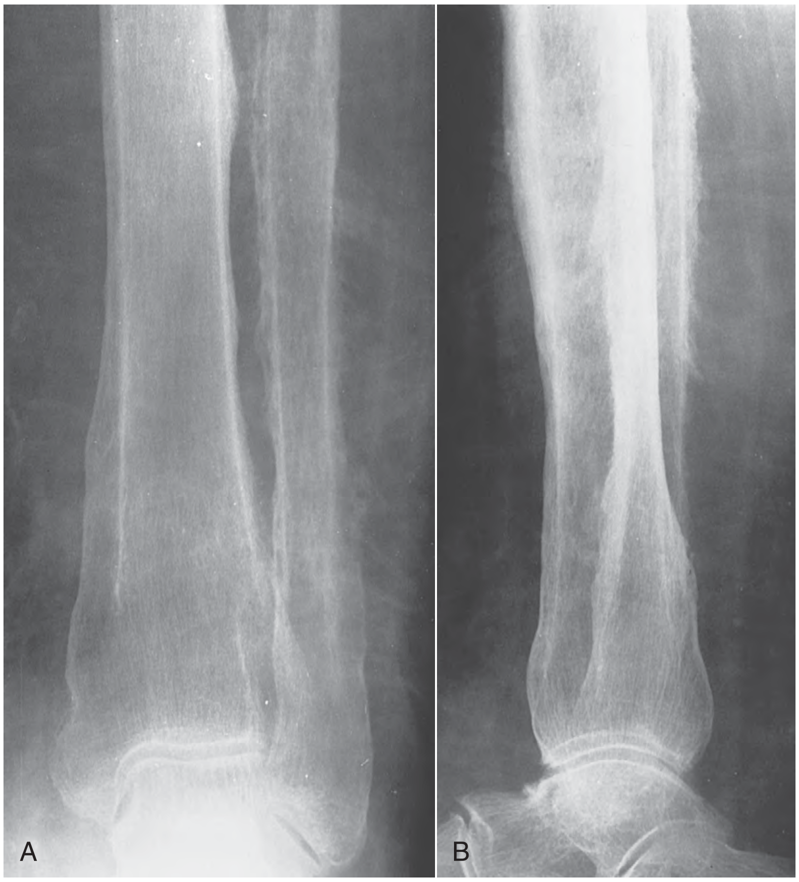

FIGURE 10–54 **Primary hypertrophic osteoarthropathy: pachydermoperiostosis.**[81] Observe the widespread prominent periostitis affecting the tibiae and fibulae. The findings in this patient were bilateral and symmetric and affected several tubular bones throughout the skeleton. *(Courtesy C. Chen, MD, Kaohsiung, Taiwan.)*

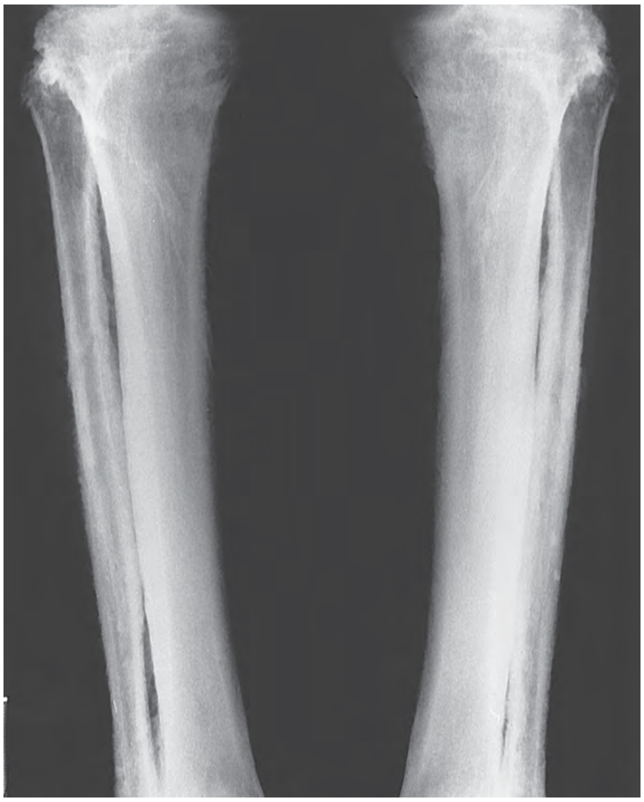

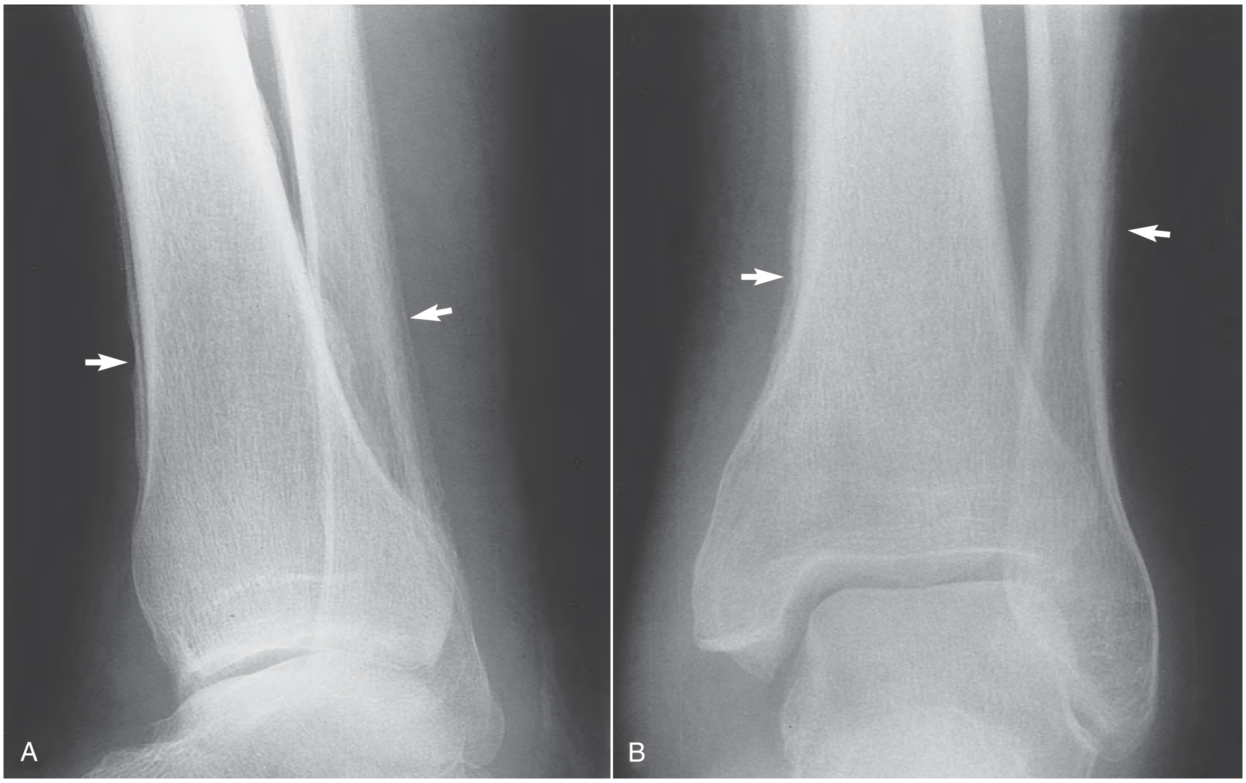

FIGURE 10–55 **Secondary hypertrophic osteoarthropathy.**[81,82] **A,** Periostitis of the tibia and the fibula is seen in this patient with bronchogenic carcinoma. **B,** Radiograph of the distal portions of the tibia and fibula *(arrows)* in this 60-year-old man with bronchogenic carcinoma reveals periostitis of the distal diaphysis and metaphysis of the tibia and fibula. Soft tissue swelling is also present. Both patients had bilateral symmetric periostitis.

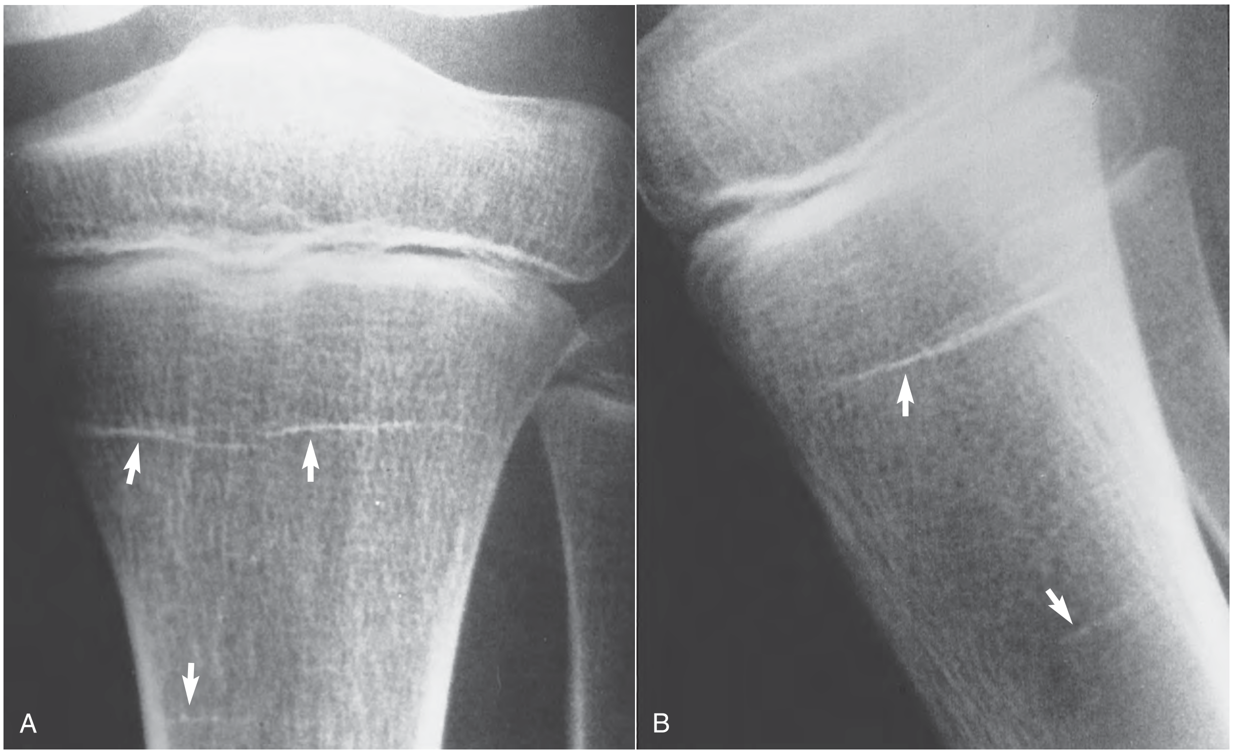

FIGURE 10–56 **Growth resumption (Harris) lines.**[83,111] **A-B,** In this chronically ill 6-year-old child with juvenile idiopathic arthritis, prominent transverse sclerotic bands are seen in the proximal tibial metaphysis and diaphysis *(arrows)*. These transverse radiodense lines represent a sign of new or increased growth, presumably after a period of inhibited bone growth.

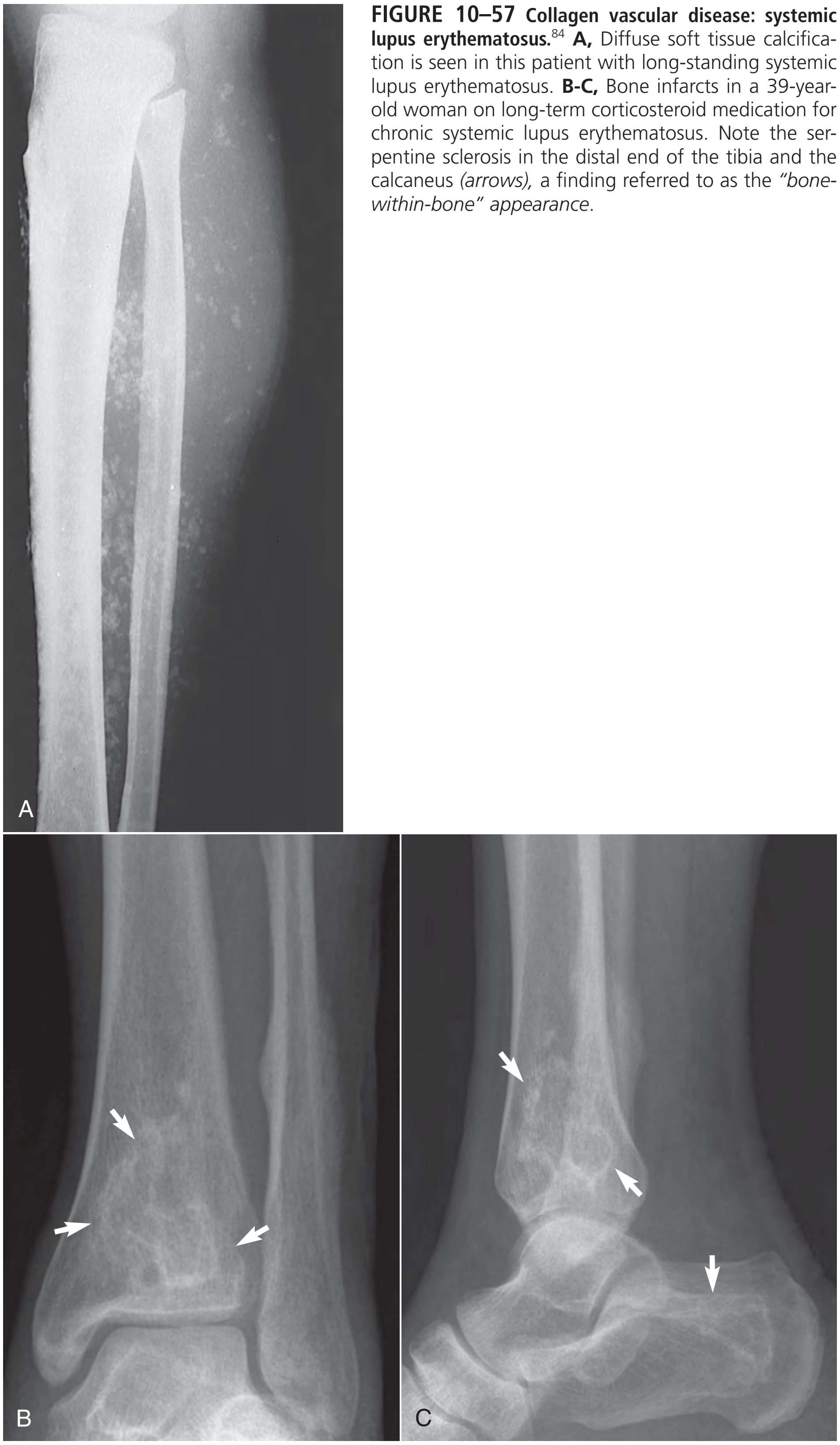

FIGURE 10–57 Collagen vascular disease: systemic lupus erythematosus.[84] **A,** Diffuse soft tissue calcification is seen in this patient with long-standing systemic lupus erythematosus. **B-C,** Bone infarcts in a 39-year-old woman on long-term corticosteroid medication for chronic systemic lupus erythematosus. Note the serpentine sclerosis in the distal end of the tibia and the calcaneus *(arrows),* a finding referred to as the *"bone-within-bone" appearance*.

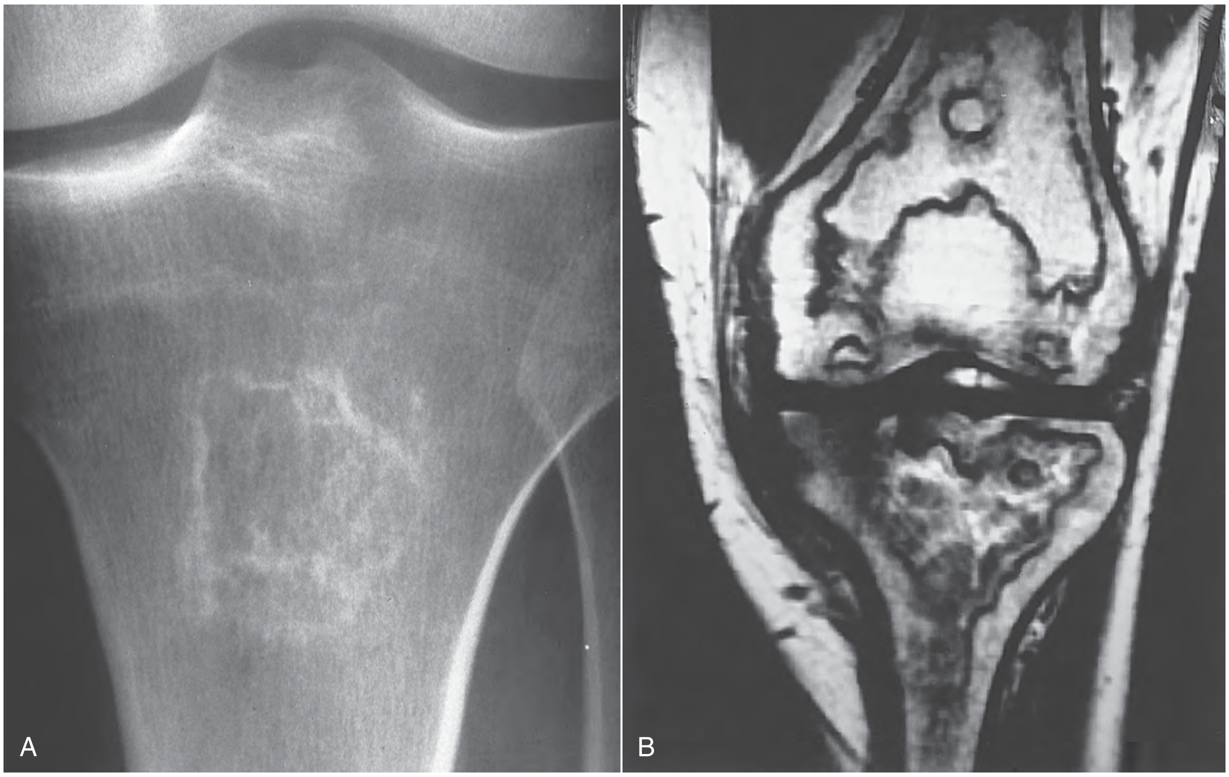

FIGURE 10–58 **Medullary osteonecrosis: bone infarct.**[85] **A,** This 46-year-old alcoholic man had bilateral osteonecrosis of the femoral heads. A radiograph of the knee reveals a circular zone of osteosclerosis in the proximal tibial metaphysis, characteristic of a medullary bone infarct. Differentiating these lesions radiographically from chondrogenic neoplasms, such as enchondroma and chondrosarcoma, is often difficult. **B,** In another patient, a coronal T1-weighted (TR/TE, 600/20) spin echo MR image reveals extensive replacement of normal marrow with mixed signal intensity surrounded by a well-defined undulating rim of low signal intensity in the subchondral region, metaphysis, and diaphysis of the proximal end of the tibia and the distal portion of the femur. This appearance is typical of medullary infarct. *(**B,** Courtesy L. Pertcheck, MD, Denver.)*

TABLE 10-7 **Infectious Disorders Affecting the Tibia and the Fibula***

Entity	Figure(s)	Characteristics
Acute pyogenic osteomyelitis[86,101,102]	10-59	Tibia is a frequent site of infection Metaphysis in children Also seen in intravenous drug abusers, diabetic persons, and immunocompromised patients Poorly defined permeative bone destruction
Chronic osteomyelitis[87,101,102]	10-60	Tibia is a frequent site Osteosclerosis and cortical thickening Thick, single layer periosteal bone proliferation Areas of osteolysis and poorly defined areas of sclerosis Sequestrum and involucrum Cloaca formation
Brodie abscess[88]	10-61	Most frequently found in children The tibia is the most common site of Brodie abscess Circular, geographic zone of osteolysis Sharply circumscribed sclerotic margin Metaphyseal location Radiolucent channel (i.e., tract sign) may communicate with growth plate, joint, or surface of bone

* See also Table 1-19.

Continued

TABLE 10-7 Infectious Disorders Affecting the Tibia and the Fibula—cont'd

Entity	Figure(s)	Characteristics
Chronic recurrent multifocal osteomyelitis (CRMO)[89,90]	10-62	Unknown cause Occurs mainly in children and adolescents Radiographic findings suggesting acute or subacute osteomyelitis Initial osteolytic destruction of metaphysis adjacent to growth plate with no periosteal bone formation or sequestration May be associated with pustular skin lesions
Tuberculous osteomyelitis[91]	10-63	Osteolytic lesions may be accompanied by surrounding sclerosis, periostitis, and sequestrum Intracortical lesions are rare *Cystic tuberculosis:* disseminated lesions throughout the skeleton (rare) Often begins in epiphysis and spreads to adjacent joint Metaphyseal lesions in children may violate the growth plate (helping to differentiate tuberculous osteomyelitis from pyogenic osteomyelitis)
Congenital syphilis[92,93]	10-64	Symmetric, transverse, radiolucent, metaphyseal bands or linear, longitudinal, alternating lucent and sclerotic bands ("celery stalk" appearance) Other osseous abnormalities include osteochondritis, diaphyseal osteomyelitis, and gumma formation
Leprous osteomyelitis[94]	10-65	Multiple osteolytic lesions surrounded by sclerosis

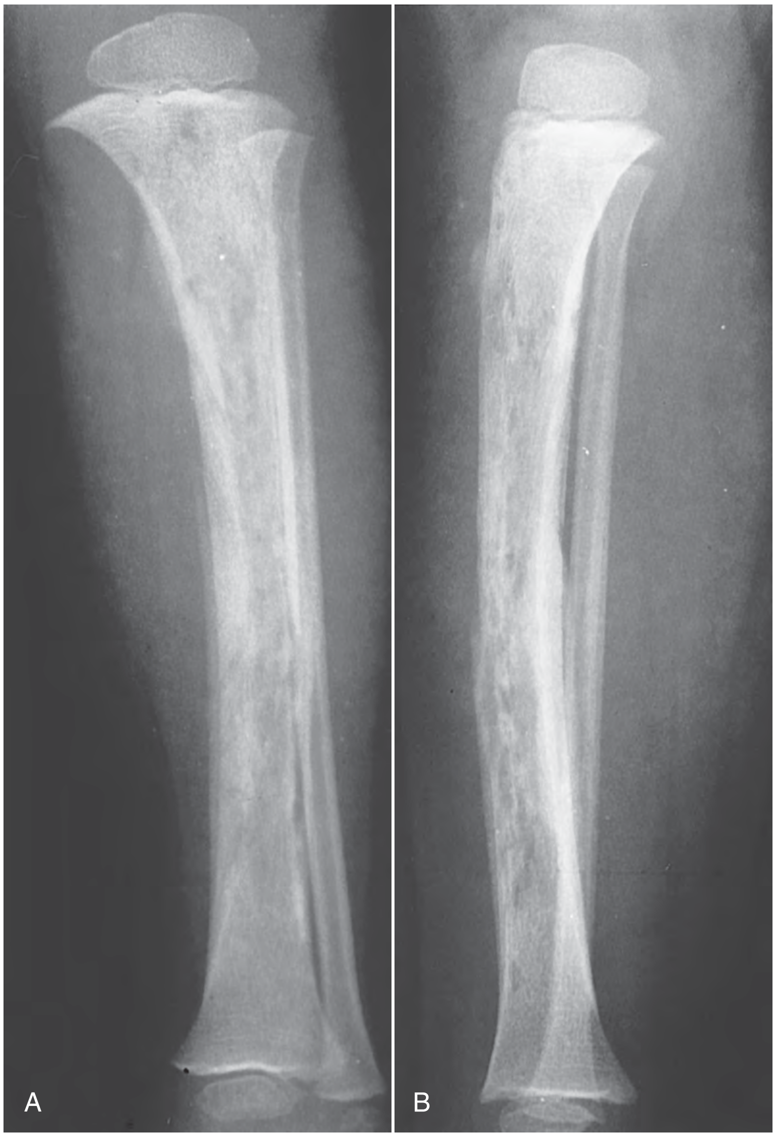

FIGURE 10–59 Acute staphylococcus osteomyelitis.[86,101,102] This young patient had a 2-week history of pain, warmth, and tenderness over the tibia. Frontal **(A)** and lateral **(B)** radiographs show poorly defined osteolysis throughout the diaphyses and proximal tibial metaphysis. Exuberant periosteal new bone formation appears as generalized increased radiodensity.

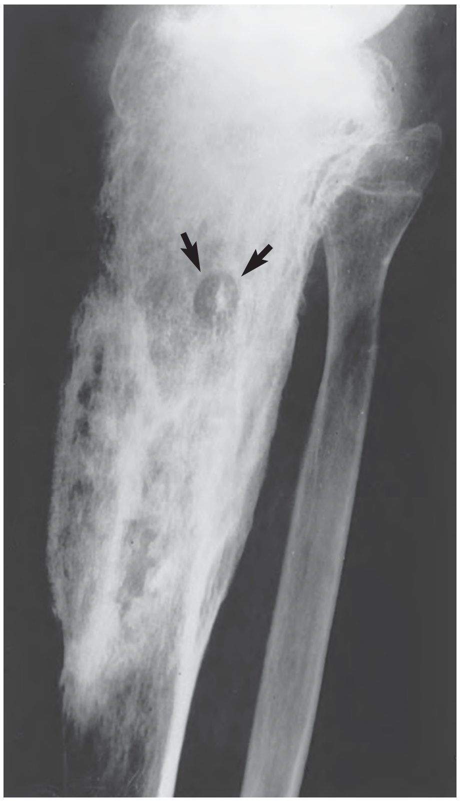

FIGURE 10–60 Chronic osteomyelitis: *Staphylococcus aureus*.[87,101,102] This patient with chronic osteomyelitis developed pain in the tibia. Widespread sclerosis, bone expansion from periosteal bone proliferation, and areas of osteolysis in the proximal portion of the tibia are characteristic of chronic osteomyelitis. A circular radiolucent cavity containing a sharply marginated, radiodense focus (sequestrum) *(arrows)*, one sign of activity in chronic osteomyelitis. *(Courtesy C. Pineda, MD, Mexico City.)*

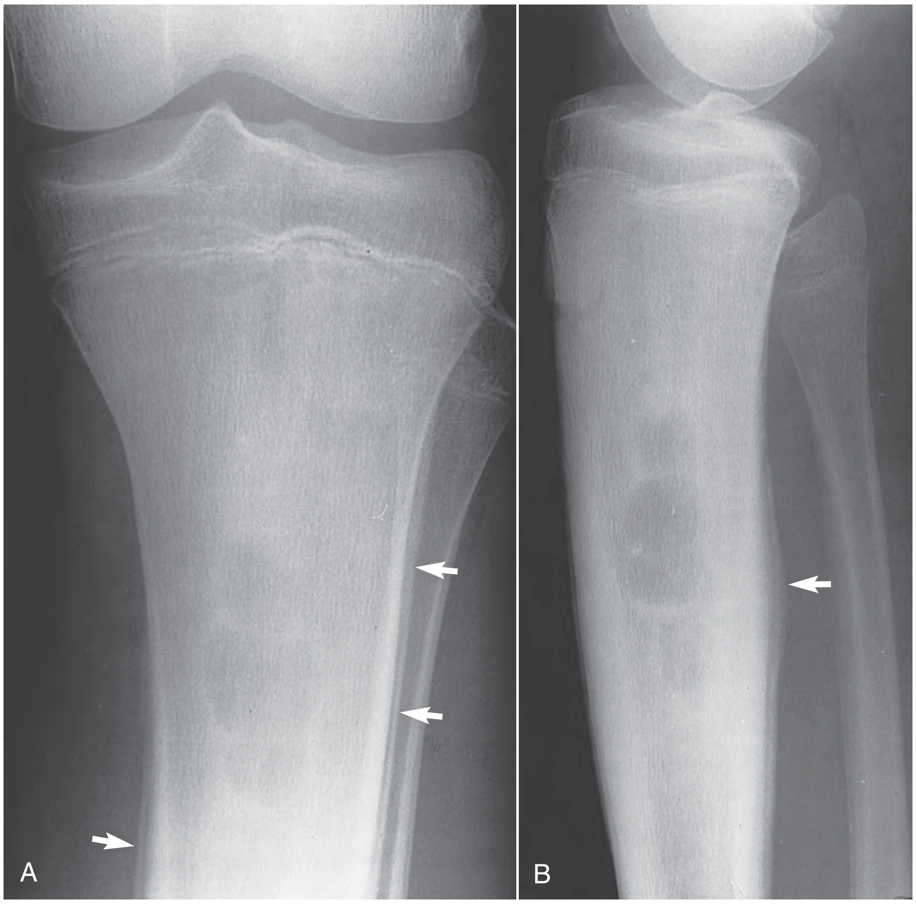

FIGURE 10–61 Brodie abscess: subacute osteomyelitis.[88] **A-B,** This 13-year-old girl complained of knee pain. Frontal **(A)** and lateral **(B)** radiographs of the tibia reveal a multiloculated, elongated, well-circumscribed osteolytic lesion with surrounding sclerosis involving the proximal diaphysis of the tibia. A single-layer periosteal reaction envelops the tibia *(arrows)*.

Continued

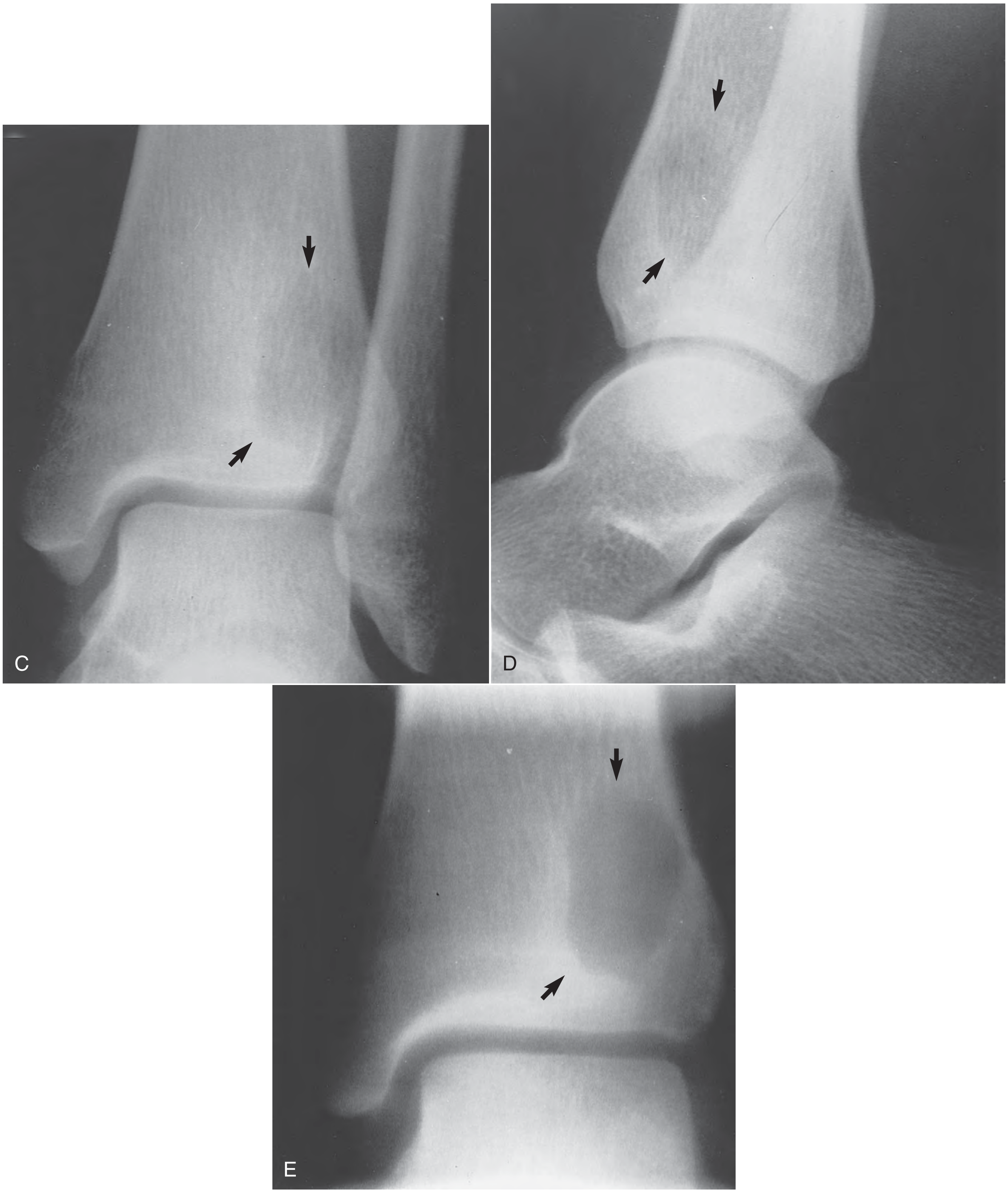

FIGURE 10–61, cont'd **C-E** This 16-year-old girl complained of persistent ankle pain. Frontal **(C)** and lateral **(D)** radiographs show a well-circumscribed, geographic osteolytic lesion surrounded by a sclerotic zone in the distal tibial metaphysis *(arrows)*. The lesion is delineated more clearly with conventional tomography **(E).** The causative organism in both patients was *Staphylococcus aureus.*

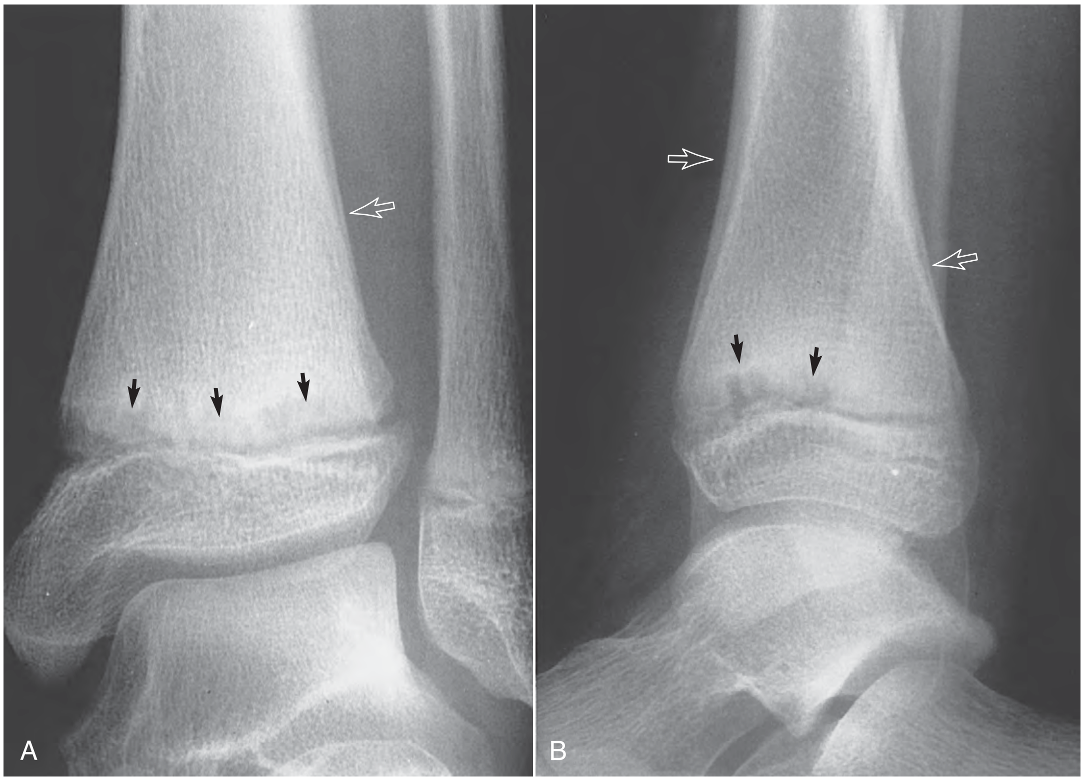

FIGURE 10–62 **Chronic recurrent multifocal osteomyelitis.**[89,90] This 12-year-old boy had unilateral ankle swelling and pain for 4 months. Eight months earlier, he had unilateral wrist pain and swelling. The erythrocyte sedimentation rate was slightly elevated, but all other serologic tests had normal results. Radiographs revealed similar changes at both sites. The findings on oblique **(A)** and lateral **(B)** radiographs include periostitis *(open arrows),* widening of the distal tibial physis, metaphyseal sclerosis, and subchondral osteolysis of the metaphysis adjacent to the growth plate *(arrows)*. This unusual entity is controversial, and it is not certain whether it is truly infectious in nature. It typically causes significant symptoms but regresses without residual change. The metaphyses of long tubular bones are the most frequent sites of involvement. *(Courtesy S. Cassell, MD, Eugene, Ore.)*

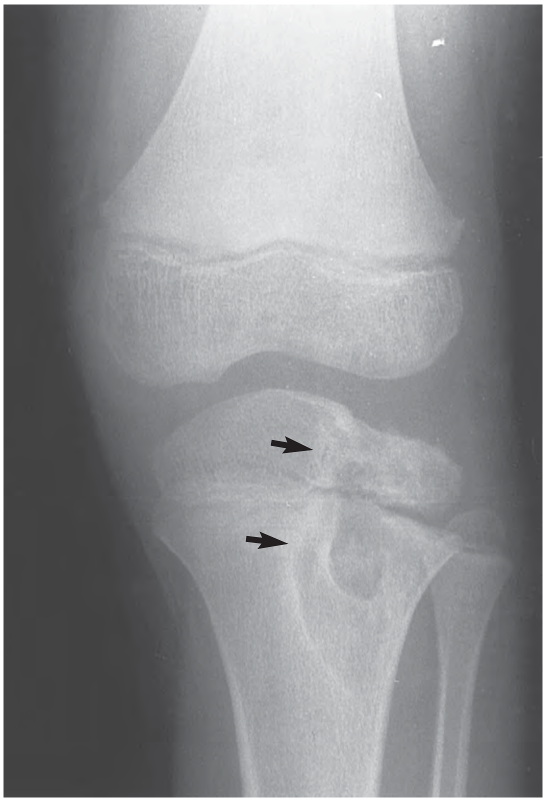

FIGURE 10–63 **Tuberculous osteomyelitis: transphyseal spread.**[91] This 6-year-old girl has an atypical presentation of tuberculous osteomyelitis. A large, well-circumscribed osteolytic lesion *(arrows)* beginning in the metaphysis has spread across the physis to involve the epiphysis.

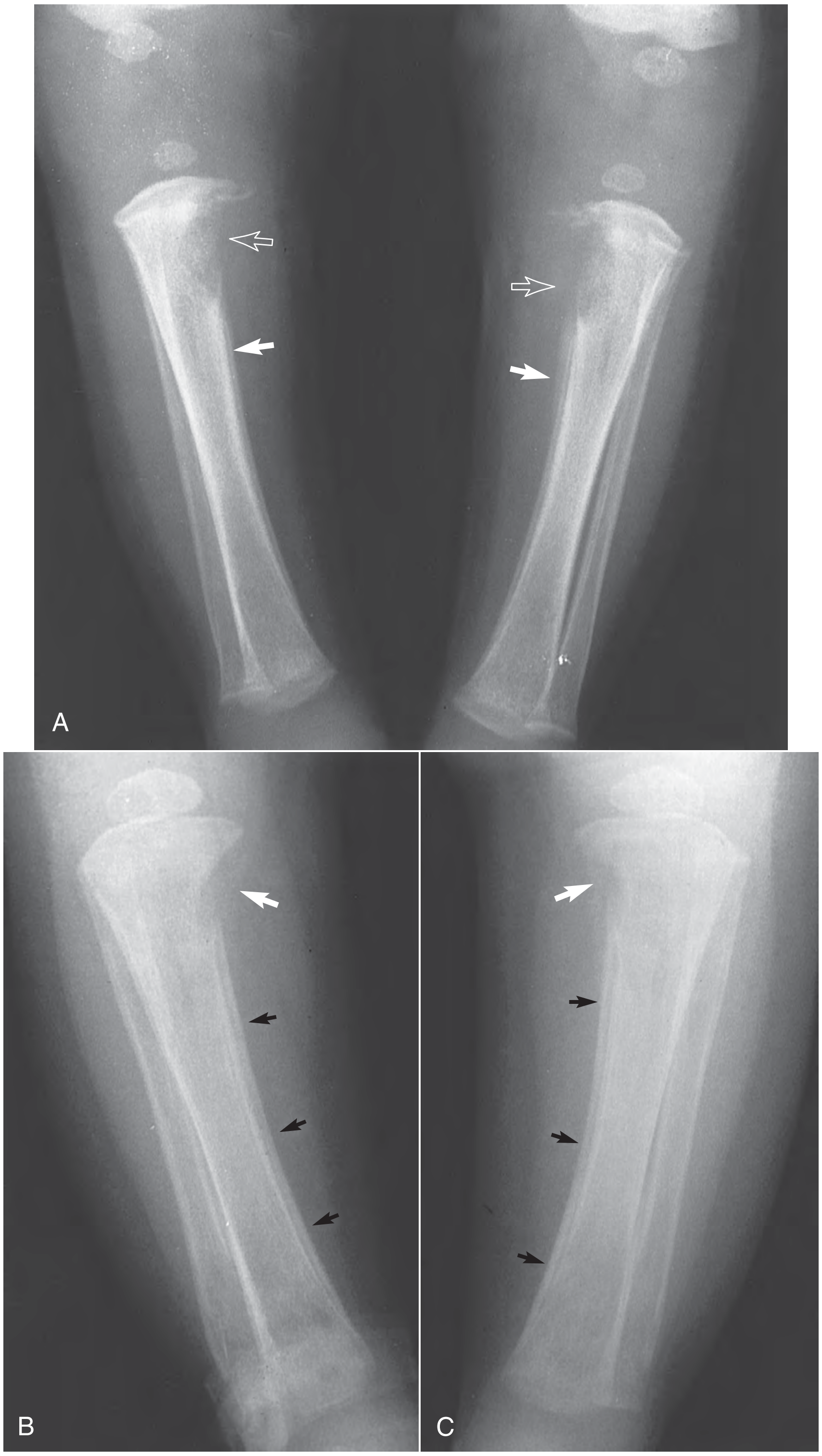

FIGURE 10–64 **Congenital syphilis.**[92,93] **A,** A radiograph of this 2-month-old baby demonstrates bilateral periostitis *(arrows)* and defects in the proximal medial tibial metaphyses (Wimberger sign) *(open arrows)*. **B-C,** In another patient, radiographs of the lower extremities reveal extensive bilateral periostitis *(black arrows)* and osseous erosions of the medial tibial metaphysis (Wimberger sign) *(white arrows)*.

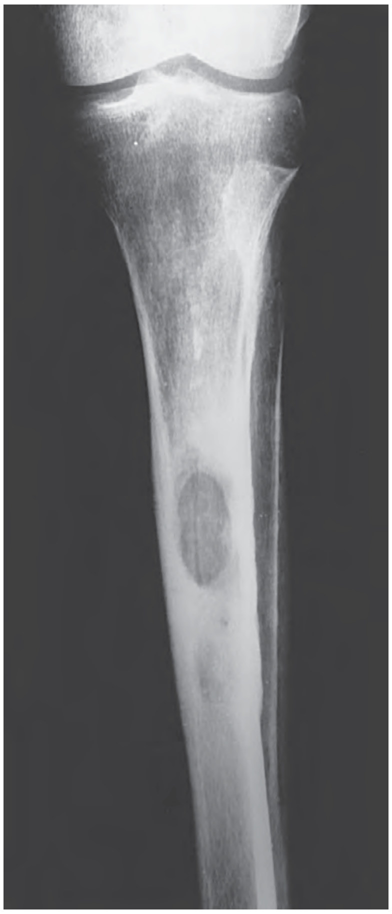

FIGURE 10–65 **Leprous osteomyelitis.**[94] In this patient with known leprosy, multiple osteolytic lesions surrounded by dense sclerosis were found to be related to hematogenous spread of infection, a rare manifestation of leprosy. The lesions were evident bilaterally. *(Courtesy J. Schils, MD, Cleveland.)*

CHAPTER 11

Ankle and Foot

NORMAL DEVELOPMENTAL ANATOMY

A thorough understanding of normal developmental anatomy is essential for accurate interpretation of radiographs of the pediatric ankle and foot. Table 11-1 outlines the age of appearance and fusion of the primary and secondary ossification centers. Figures 11-1 to 11-3 demonstrate the radiographic appearance of many important ossification centers and other developmental landmarks at selected ages from birth to skeletal maturity.

DEFORMITIES OF THE ANKLE AND FOOT

Several congenital and pathologic processes result in alignment deformities about the ankle and foot. Table 11-2 describes a number of these deformities, many of which are illustrated in Figures 11-4 to 11-13; others are illustrated throughout the chapter as they are manifested in many disorders.

DEVELOPMENTAL ANOMALIES, ANATOMIC VARIANTS, AND SOURCES OF DIAGNOSTIC ERROR

The ankle and foot are frequent sites of anomalies, anatomic variants, and other sources of diagnostic error that may simulate disease and potentially result in misdiagnosis. Table 11-3 and Figures 11-14 to 11-27 represent selected examples of some of the more common processes.

SKELETAL DYSPLASIAS AND OTHER CONGENITAL DISEASES

Table 11-4 outlines a number of the skeletal dysplasias and congenital disorders that affect the ankle and foot. Figures 11-28 to 11-31 illustrate the radiographic manifestations of some of these disorders.

PHYSICAL INJURY

Physical injury to the ankle and foot results in a wide variety of fractures and dislocations. Fractures and dislocations of the ankle (Tables 11-5 and 11-6), the tarsal bones (Table 11-7), and the metatarsals and phalanges (Table 11-8) are listed and discussed in this section. Specific features of stress fractures in the foot and ankle are presented in Table 11-9 and soft tissue injuries are described in Table 11-10. Many of these traumatic conditions are illustrated in Figures 11-32 to 11-63. Fractures of the diaphyses of the tibia and fibula are described and illustrated in Chapter 10.

ARTICULAR DISORDERS

The articulations of the ankle and foot are frequent target sites for degenerative, inflammatory, and crystal-induced disorders. Table 11-11 outlines these diseases and their radiographic characteristics. Table 11-12 represents a compartmental analysis emphasizing the target sites of joint involvement typical of some of the more common disorders. Table 11-13 outlines the differential diagnosis of articular disorders that result in calcaneal changes. Figures 11-64 to 11-81 illustrate the typical radiographic manifestations of the most common articular disorders affecting the ankle and foot.

INFECTIOUS DISORDERS

The soft tissues, bones, and joints of the ankle and foot are frequent sites of involvement for infectious disorders. Table 11-14 describes the major types of infection. These disorders are illustrated in Figures 11-82 to 11-86.

TUMORS AND TUMORLIKE LESIONS

Table 11-15 lists and characterizes the neoplasms that typically involve the ankle and foot, many of which are illustrated in Figures 11-87 to 11-106.

METABOLIC, HEMATOLOGIC, AND VASCULAR DISORDERS

Several metabolic, hematologic, and vascular disorders affect the bones of the foot and the surrounding soft tissue structures. Table 11-16 lists some of the more common disorders and describes their characteristics. Figures 11-107 to 11-114 illustrate the typical imaging findings of several of these disorders.

OSTEONECROSIS AND OSTEOCHONDROSES

Osteonecrosis of the bones about the ankle and foot may occur spontaneously or result from trauma or other predisposing factors. Furthermore, several epiphyseal disorders termed *osteochondroses* may involve the bones of the foot. Table 11-17 describes these disorders, and Figures 11-115 to 11-119 illustrate typical examples of their radiographic appearance.

TABLE 11-1 Ankle and Foot: Approximate Age of Appearance and Fusion of Ossification Centers[1-4] (Figures 11-1 to 11-3)

Ossification Center	Primary or Secondary	No. of Centers	Age of Appearance*	Age of Fusion* (Years)
Distal tibial epiphysis	S	1	2-3 years	14-18
Distal fibular epiphysis	S	1	2-3 years	14-18
Talus	P	1	Birth	
Calcaneus	P	1	Birth	
Calcaneal apophysis (girls)	S	1	7-9 years	14-18
Calcaneal apophysis (boys)	S	1	10-12 years	18-22
Cuboid bone	P	1	Birth	
Navicular bone	P	1	1.5-4 years	
Cuneiforms 1 and 2	P	1 each	3-4 years	
Cuneiform 3 (lateral)	P	1	5-6 months	
First phalangeal base	S	1	3-4 years	14-20
First metatarsal base	S	1	3-4 years	14-20
Second to fifth metatarsal heads	S	4	3-4 years	14-20

P, Primary; *S,* secondary.

* Ages of appearance and fusion of ossification centers in girls typically precede those of boys. Ethnic differences also exist.

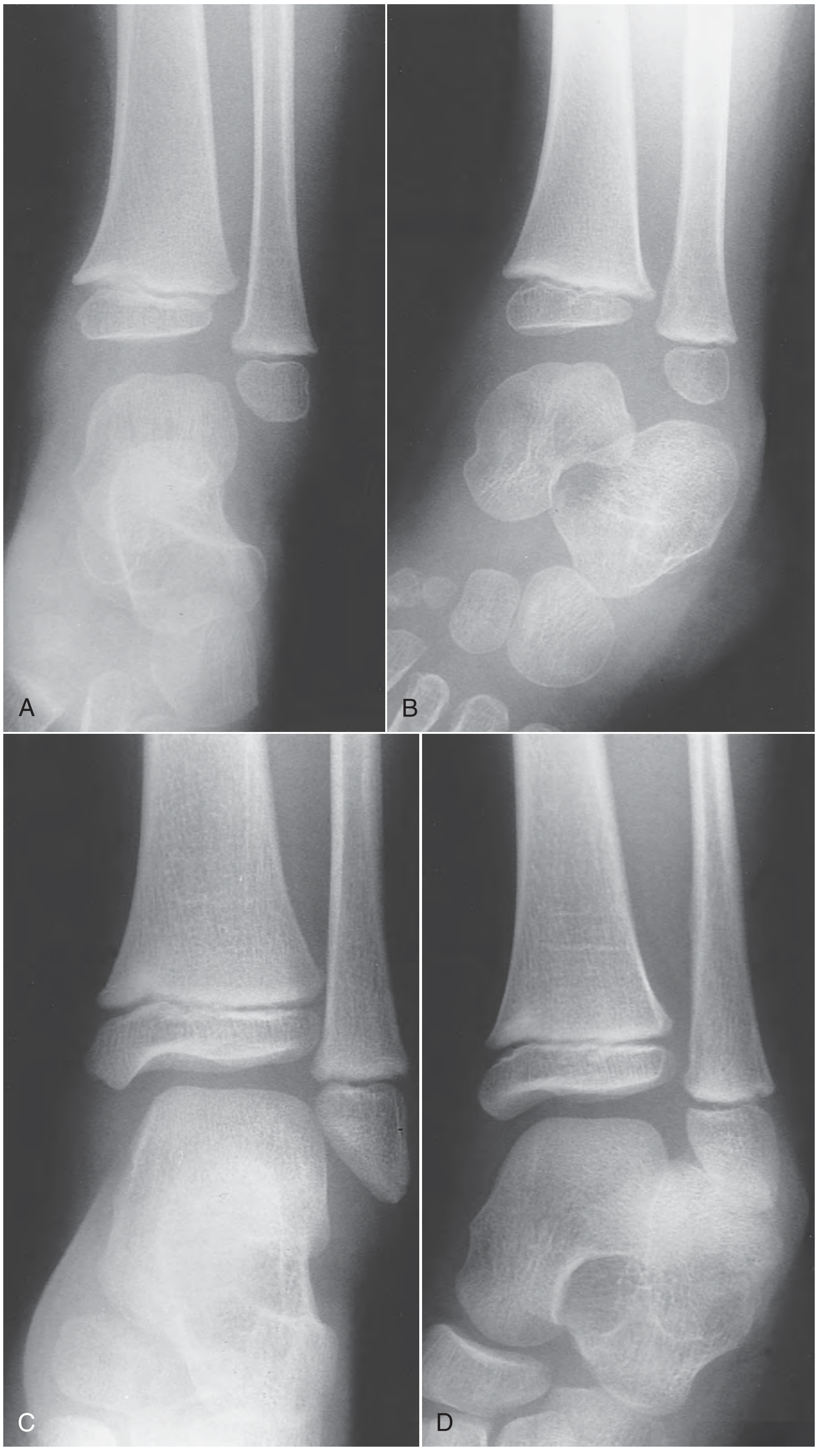

FIGURE 11–1 Skeletal maturation and normal development: anteroposterior and oblique ankle radiographs.[1-4] **A-B,** A 3-year-old boy. The tibial and fibular epiphyses are rounded and small in relation to the adjacent metaphyses. The talus is incompletely ossified, the superior margins are rounded and undulating, and the tibiotalar joint space appears wide. The zones of provisional calcification within the tibia and fibula are sclerotic, and the metaphyses are beaklike. **C-D,** A 7-year-old girl. The superior talar surface is flatter and the tibiotalar joint space is narrower. The tibial and fibular epiphyses conform to and approximate the width of the metaphyses. The zones of provisional calcification remain radiodense. Irregular ossification of the medial aspect of the tibial and fibular epiphyses is common during normal development.

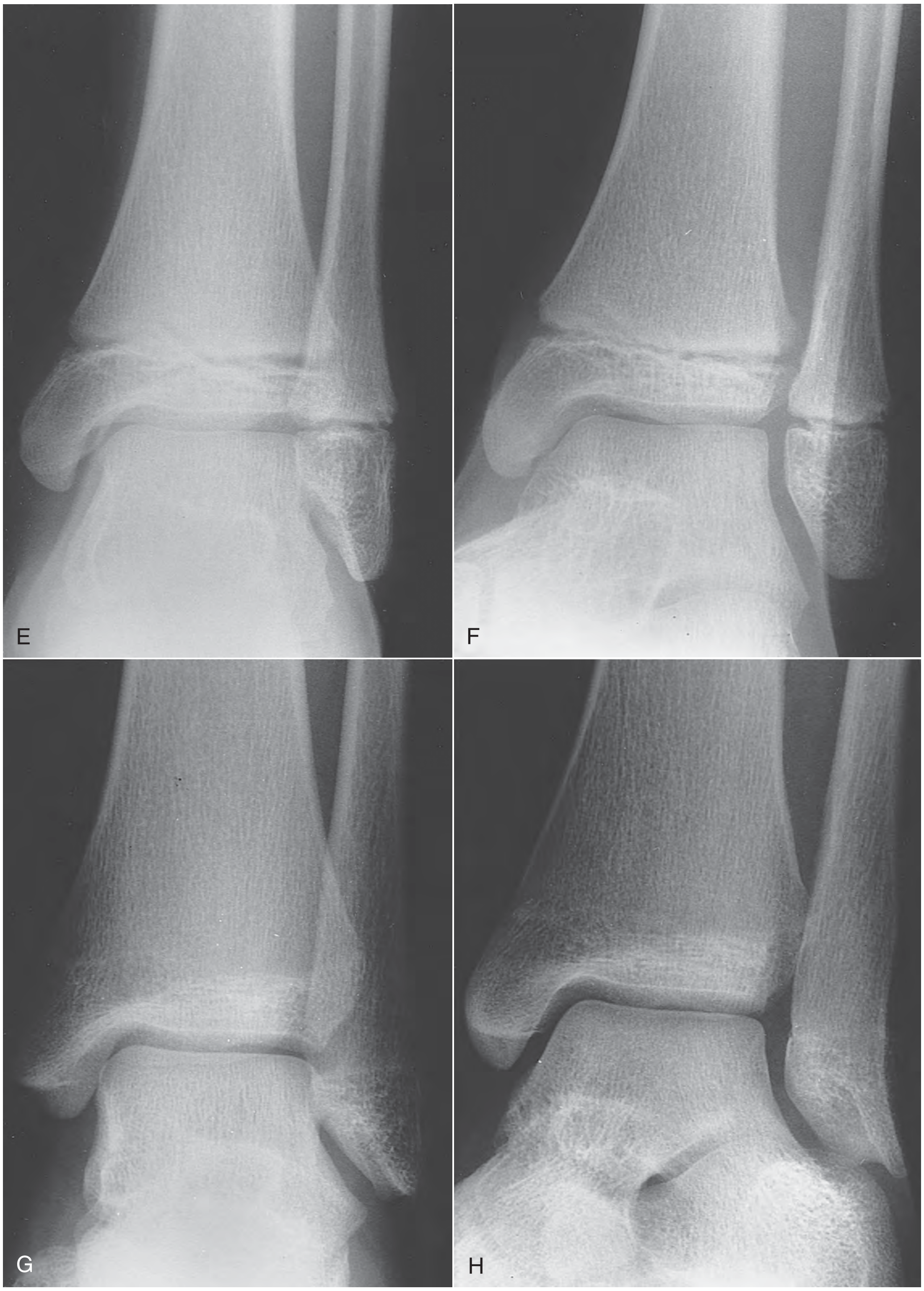

FIGURE 11–1, cont'd **E-F,** A 9-year-old girl. The tibial and fibular epiphyses are wider than their adjacent metaphyses. The physeal line is narrowed, and the zone of provisional calcification is less dense than previously observed. The talus and mortise joints exhibit an adult configuration. **G-H,** A 13-year-old girl. The epiphyses of the tibia and fibula have fused, and the physeal scars are barely visible.

Continued

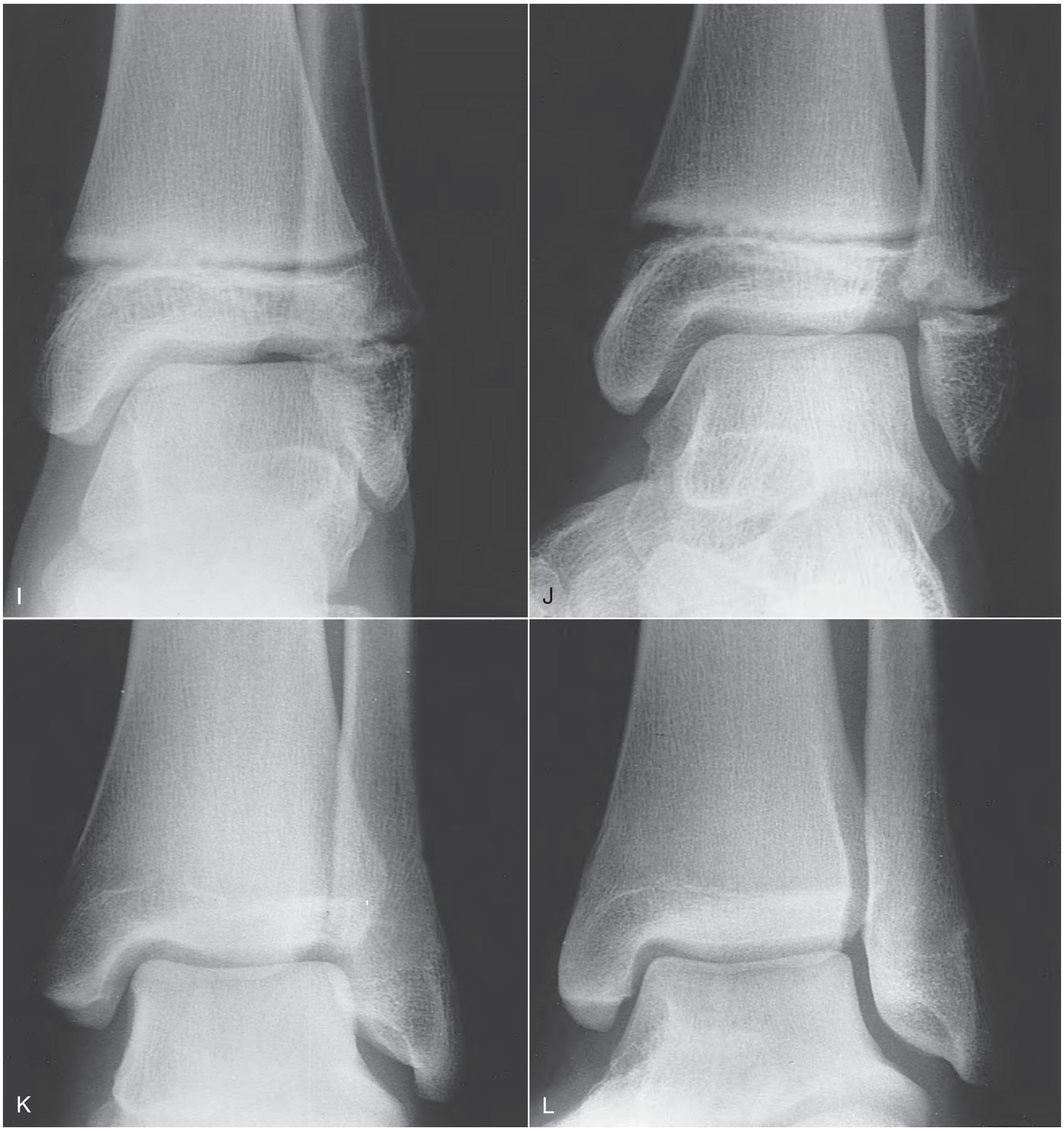

FIGURE 11–1, cont'd **I-J,** A 14-year-old boy. Development in the male skeleton lags behind that of the female (compare to **G-H**). In this case, the physes remain open, the zones of provisional calcification are radiodense, and the metaphyseal margins are irregular just before fusion. **K-L,** A 16-year-old boy. Complete epiphyseal fusion is evident. The physeal scars remain visible. Skeletal maturation in a boy of this age corresponds approximately to that of a 13-year-old girl **(G-H).**

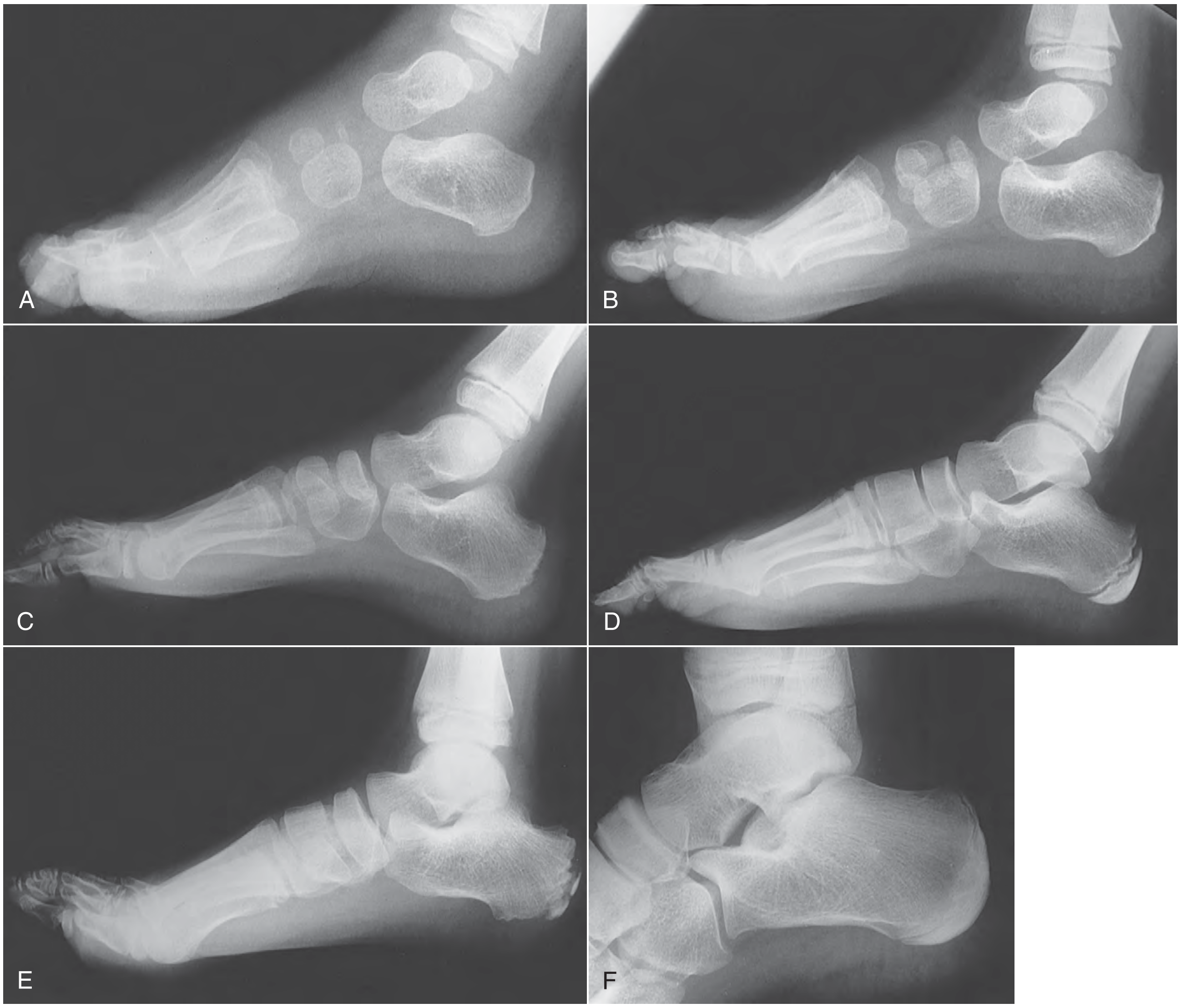

FIGURE 11–2 Skeletal maturation and normal development: Lateral radiographs of the foot and ankle.[1-4] **A,** A 2-year-old girl. The tibial and fibular epiphyses and the talus, calcaneus, cuboid, third cuneiform, and navicular bones are ossified. **B,** A 4-year-old boy. The first and second cuneiform bones are now also ossified. **C,** A 6-year-old boy. The tibial and fibular epiphyses are approaching the width of their respective metaphyses, and the zones of provisional calcification are radiodense. The posterior margin of the calcaneus is serrated. **D,** A 9-year-old girl. The tarsal bones have an adult configuration. The sclerotic calcaneal apophysis is evident, and the apposing margins are serrated. The zone of provisional calcification of the distal end of the tibia remains radiodense. **E,** An 11-year-old boy. The calcaneal apophysis is sclerotic and fragmented, and the adjacent calcaneus has a normal sawtooth appearance. Skeletal development in boys lags behind that of girls, as evidenced by comparison with the 9-year-old girl in **D. F,** A 15-year-old boy. The calcaneal apophysis is partially fused with the adjacent calcaneus. The tibial and fibular epiphyses are beginning to fuse, and the zones of provisional calcification are less sclerotic than previously.

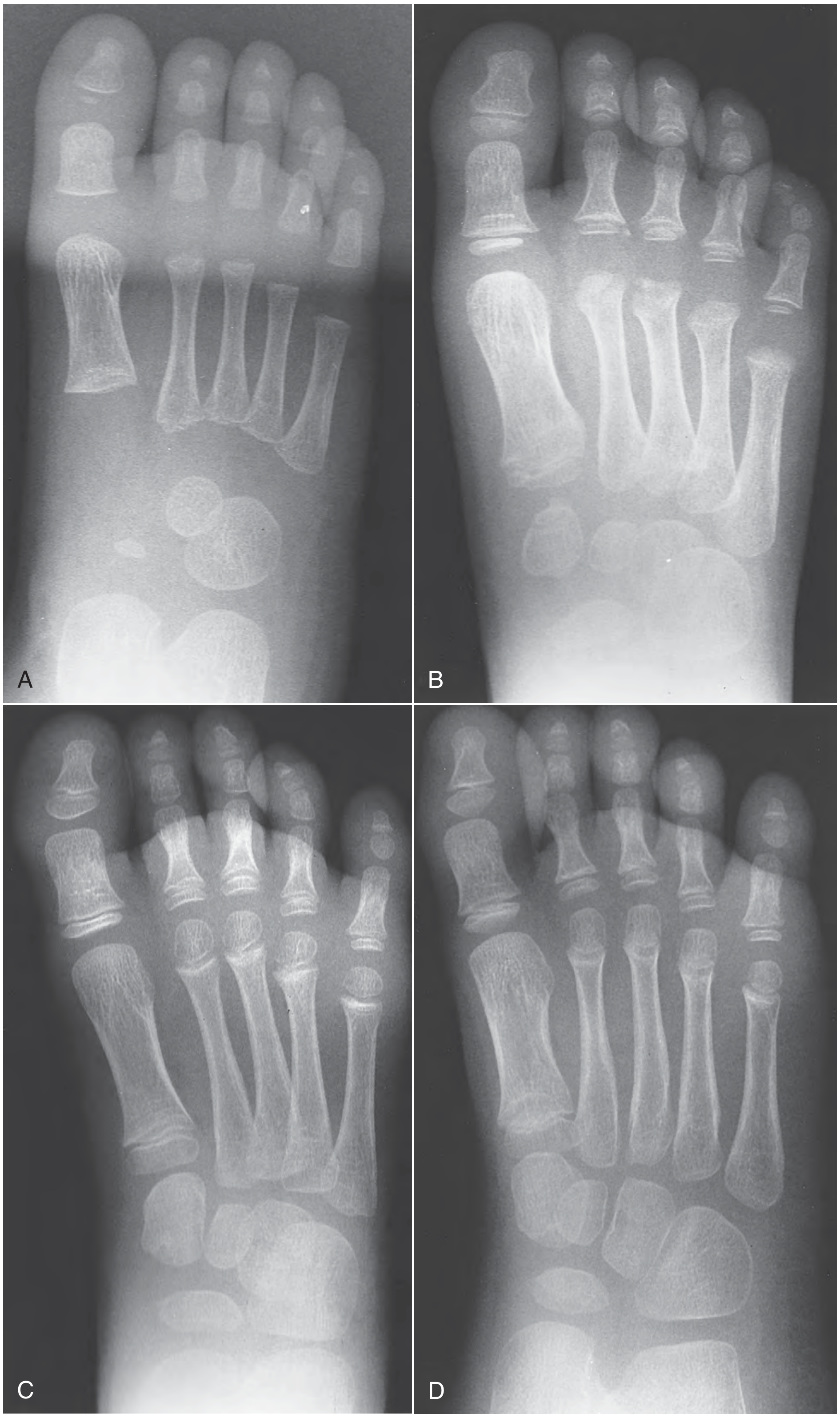

FIGURE 11–3 Skeletal maturation and normal development: radiographs of the forefoot.[1-4] **A,** A 21-month-old boy. The cuboid, third cuneiform, and navicular bones are ossified. The epiphysis of the first distal phalanx has appeared, but no other metatarsal or phalangeal epiphyses are visible. **B,** A 31-month-old girl. Ossification of the remaining two cuneiforms is evident, and the metatarsal and phalangeal epiphyses are beginning to appear. **C-D,** A 4-year-old girl. Epiphyseal development is progressing, especially in the metatarsal centers.

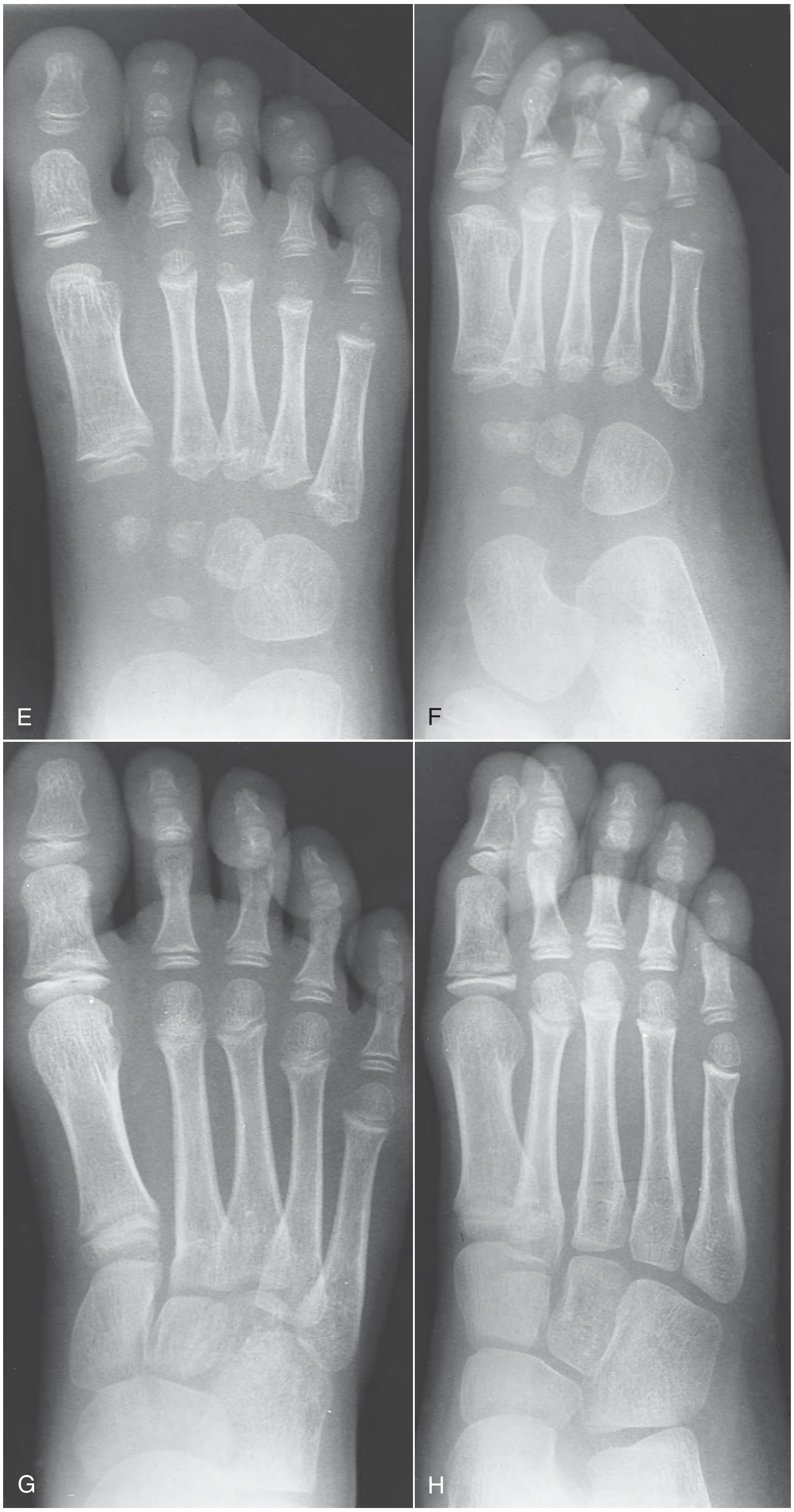

FIGURE 11–3, cont'd **E-F,** A 5-year-old boy. Epiphyseal development and ossification of the tarsal bones of this boy **(E-F)** lag behind those of the 4-year-old girl **(C-D). G-H,** A 7-year-old girl. The tarsal bones have approximated the adult configuration. The metatarsal and phalangeal epiphyseal centers have grown to adult proportions but have not yet fused.

Continued

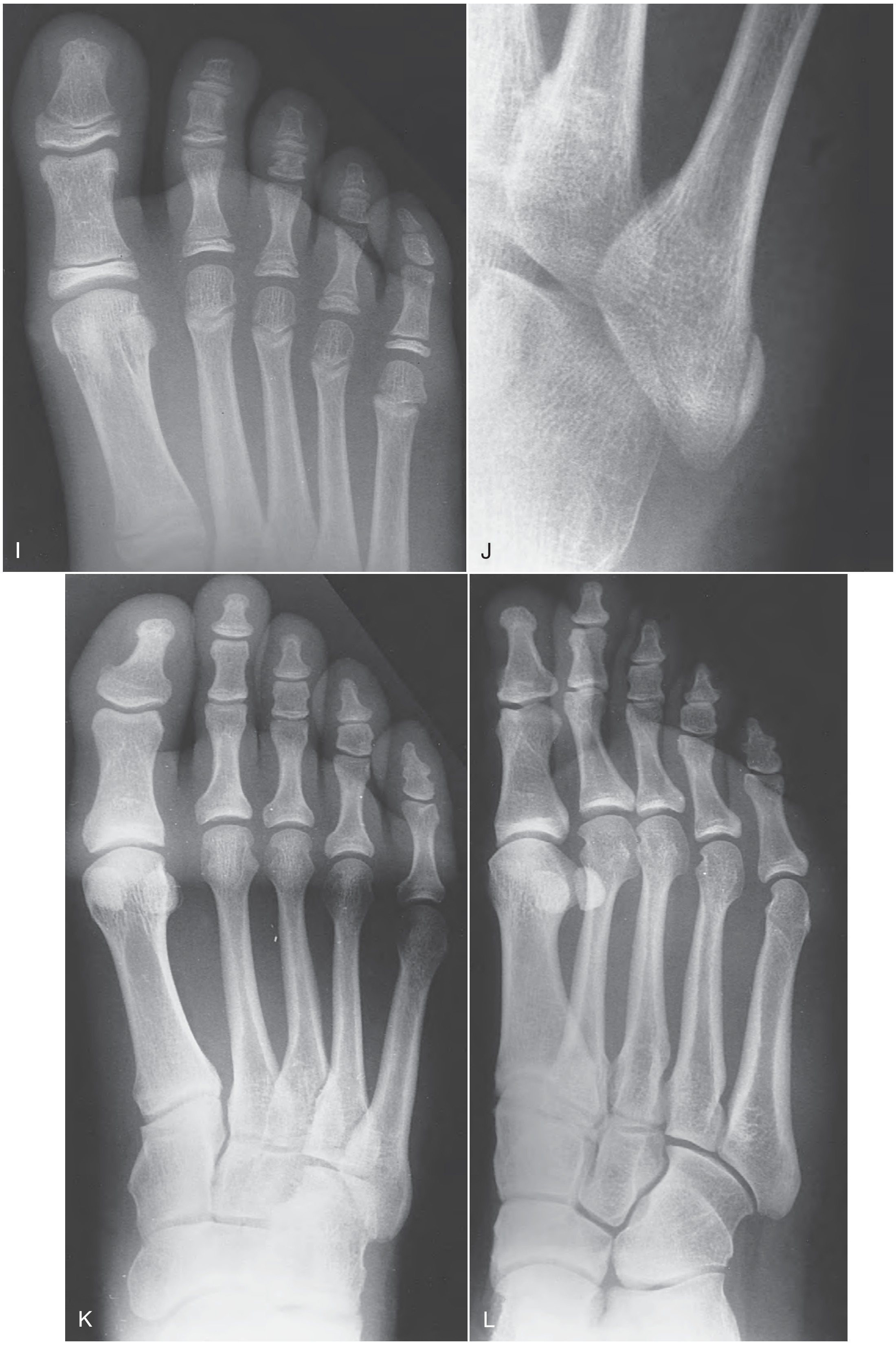

FIGURE 11–3, cont'd **I,** An 11-year-old boy. The radiodensity of the first and fifth proximal phalangeal epiphyseal centers is a normal finding just before fusion. The hallux sesamoid bones are ossified and clearly visible. **J,** A 13-year-old boy. Observe the longitudinal secondary ossification center of the fifth metatarsal styloid process. This should not be mistaken for a fracture. **K-L,** A 15-year-old girl. The metatarsal and phalangeal epiphyseal centers have all fused. The tarsal bones are well developed and their configuration resembles that of adults. Of incidental note is a synostosis of the fifth distal interphalangeal joint.

TABLE 11-2 Deformities of the Ankle and Foot

Entity	Figure(s)	Characteristics	Comments
Tibiotalar slant[5-6,154]	11-4; 11-67, *B*, 11-77, *B*	Angular joint surfaces of the tibial plafond and talar dome seen on anteroposterior views of the ankle	Improper radiographic positioning (pseudotibiotalar slant) Hemophilia Juvenile (idiopathic) arthritis Sickle cell anemia Multiple epiphyseal dysplasia Hereditary multiple exostoses
Ball-and-socket ankle joint[8,196]	11-5	Convex configuration of the proximal talar articular surface and associated concave configuration of the distal tibial articular surface	Talocalcaneal coalition Adaptation of joint to facilitate inversion and eversion motions that are restricted by talocalcaneal fusion
Varus deformity of foot[7]		Heel is inverted Forefoot is adducted and inverted	Usually developmental Often combined with other deformities
Valgus deformity of foot[7]		Heel is everted Forefoot is abducted and everted	Usually developmental Often combined with other deformities
Equinus deformity of foot[7]		Foot is plantar flexed Toes are lower than heel	Usually developmental Often combined with other deformities
Calcaneus deformity of foot[7]		Foot is dorsiflexed Toes are higher than heel	Usually developmental Often combined with other deformities
Talipes equinovarus[7]	11-6	Congenital clubfoot Plantar flexion of foot Hindfoot equinus Cavus deformity Parallel long axis of talus and calcaneus Metatarsus varus	Usually isolated abnormality May be associated with the following: Arthrogryposis Meningomyelocele Developmental acetabular dysplasia Tibial hypoplasia
Talipes calcaneovalgus[7]		Common disorder Usually bilateral Severe dorsiflexion of foot Calcaneus and valgus deformity of heel Abduction and planus deformity of forefoot	Developmental
Congenital vertical talus[7,168]	11-7	Rocker-bottom foot Rare rigid form of congenital flatfoot Talus oriented vertically and caudally Equinus deformity of heel Dorsiflexion and valgus deformity of forefoot Navicular bone dislocated dorsally Talus in varus position and only posterior portion articulates with tibia	Developmental Trisomy 13-15 or trisomy 18 80% of patients have associated disorders such as: Scoliosis Dysraphism Syndactyly Developmental hip dysplasia Congenital heart disease
Hereditary pes planus[4,7]	11-8	Flatfoot deformity Present in as much as 10% of population Foot functions normally and is flexible Talus may be plantar flexed (vertical talus) in severe cases	Hereditary variation of normal
Acquired pes planus[4,7,164]	11-9	Flatfoot deformity develops secondary to underlying disorder The C sign is specific, but not sensitive for a flatfoot deformity in patients with talocalcaneal coalition	Arthritis Neuropathic osteoarthropathy Posterior tibial tendon weakness or rupture Tarsal coalition Ehlers-Danlos syndrome Osteogenesis imperfecta
Pes planovalgus[4,7]		More severe form of flatfoot typically associated with underlying disorders	Neuromuscular disorders Posterior tibial tendon rupture

Continued

TABLE 11-2 Deformities of the Ankle and Foot—cont'd

Entity	Figure(s)	Characteristics	Comments
Cavus deformity[9]	11-10	Elevation of the longitudinal arch Occasional equinus deformity	Developmental Acquired: neurologic disorders
Metatarsus varus (adductus)[7]	11-11	Adduction and varus position of all metatarsals at the tarsometatarsal articulations Heel in normal position Fifty percent of cases are bilateral	Unknown cause Present at birth; usually detected during the second to third months of age Associated with stress fracture of the lateral metatarsal bones
Hallux valgus[10-12,182]	11-12	One of the most common toe deformities Lateral deviation (valgus deformity) of the first proximal phalanx in relation to the first metatarsal Often associated with lateral subluxation of the hallux sesamoid bones Women > men; bilateral asymmetric May be aggravated by advancing age, obesity, and physiologically inappropriate footwear	*Developmental:* often coexists with metatarsus varus and possible bunion formation Osteoarthrosis of the first MTP joint Inflammatory arthropathies Crystal deposition arthropathies Fibrodysplasia ossificans progressiva
Hallux rigidus[10,181]	11-64, *D*	Advanced osteoarthrosis with painful restriction of dorsiflexion at the first MTP joint	Hallux rigidus occurs more commonly in women and older age groups, and in patients with flat or chevron-shaped metatarsal head, longer proximal phalanx (with an increased sized base), increased hallux abductus interphalangeal angle, or a first metatarsal longer than the second metatarsal
Hallux varus[7]	11-66, *C*	Rare deformity Medial deviation (varus deformity) of the first proximal phalanx in relation to the first metatarsal	Developmental; often in conjunction with polydactyly and syndactyly Infrequent finding in rheumatoid arthritis
Hammer toe[4,7]	11-13	Dorsiflexion deformity of MTP joint with possible subluxation or dislocation of the proximal phalanx Plantar flexion of the PIP joint Dorsiflexion of DIP joint Most commonly involves second and fifth toes	Secondary to acquired or congenital foot deformities
Claw toe[4,7]		Dorsiflexion of MTP joint Plantar flexion of PIP and DIP joints dorsiflexed Proximal phalanx is oriented vertically	Secondary to acquired or congenital foot deformities
Mallet toe[4,7]		Plantar flexion of DIP joint	Secondary to acquired or congenital foot deformities
Curly toe[4,7]		No deformity of MTP joint Plantar flexion of PIP and DIP joints	Secondary to acquired or congenital foot deformities

DIP, Distal interphalangeal; *MTP,* metatarsophalangeal; *PIP,* proximal interphalangeal.

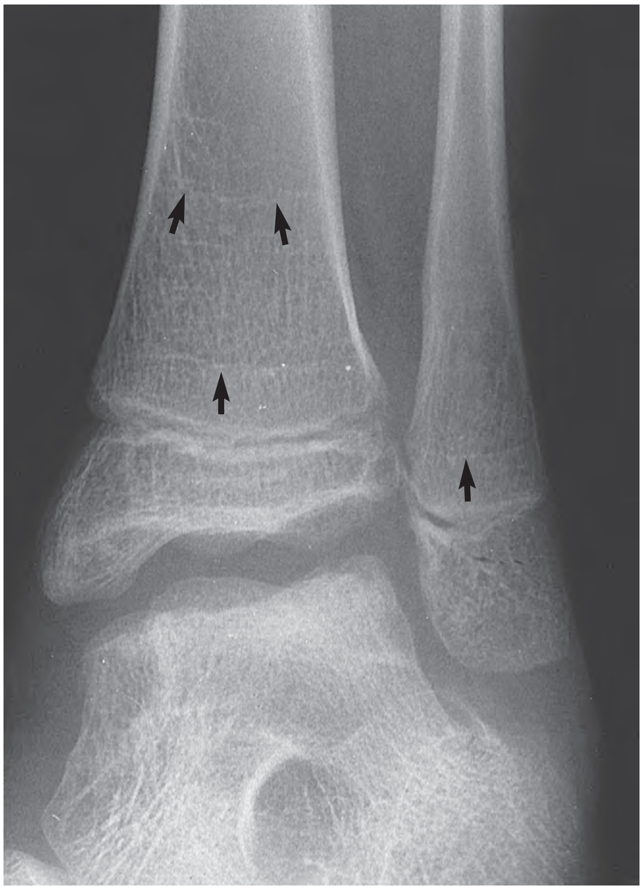

FIGURE 11–4 **Tibiotalar slant: hemophilic arthropathy.**[5,6,154] Oblique radiograph of the ankle in a 9-year-old boy with hemophilia reveals flattening and erosion of the superior surface of the talus with a characteristic tibiotalar slant. Prominent growth recovery lines *(arrows)* are also evident within the tibia and fibula. The joint space is relatively well preserved. Tibiotalar slant also occurs in juvenile idiopathic arthritis, Trevor disease, fibrous dysplasia, and many other disorders. Additionally, pseudotibiotalar slant may result from improper positioning of the patient.

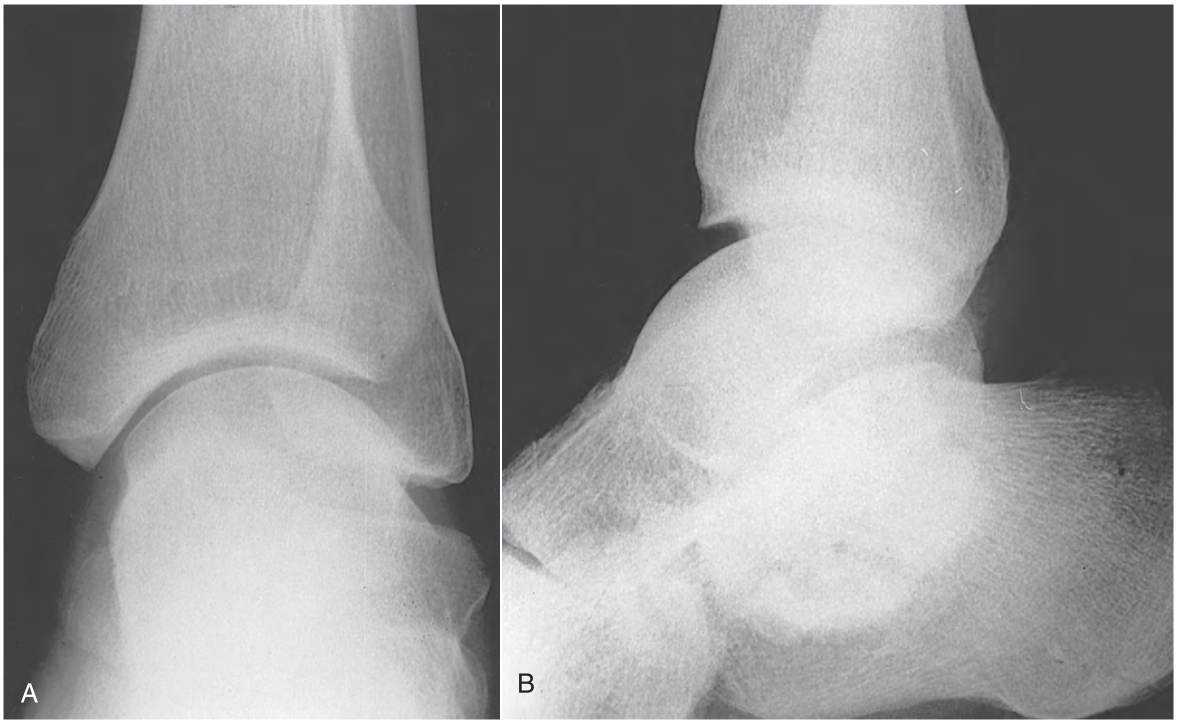

FIGURE 11–5 **Ball-and-socket ankle joint: talocalcaneal coalition.**[8,196] Frontal **(A)** and lateral **(B)** radiographs of the ankle in this patient with congenital talocalcaneal coalition reveal a rounded convex appearance of the proximal talar articular surface and a concave appearance of the distal end of the tibia. The ball-and-socket ankle joint presumably represents an adaptation of the tibiotalar joint to provide inversion and eversion motion, which is restricted owing to the talocalcaneal fusion.

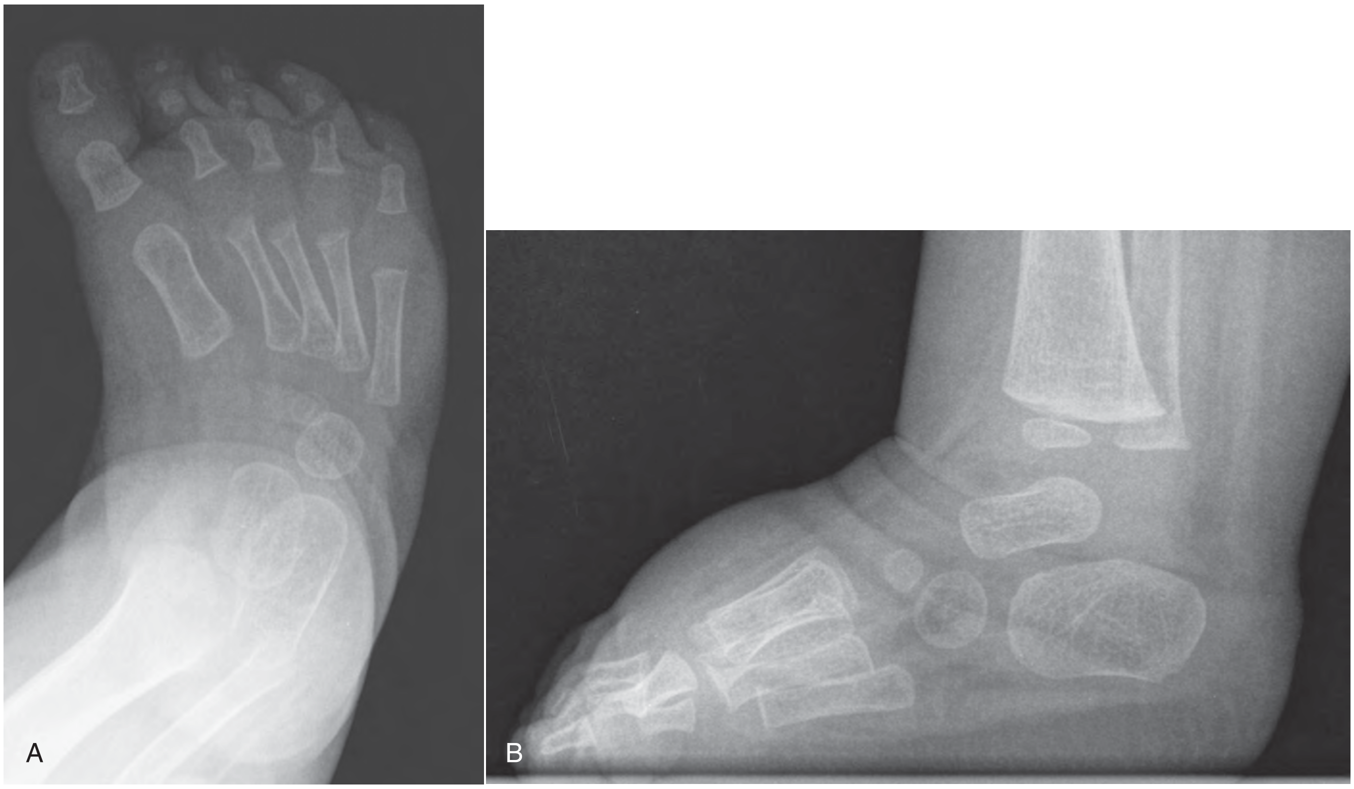

FIGURE 11–6 Talipes equinovarus (congenital clubfoot).[7] In a 1-year-old boy, anteroposterior **(A)** and lateral **(B)** radiographs show the characteristic findings including cavus deformity, parallel long axes of the talus and calcaneus, and metatarsus varus. The deformities were bilateral (other side not shown).

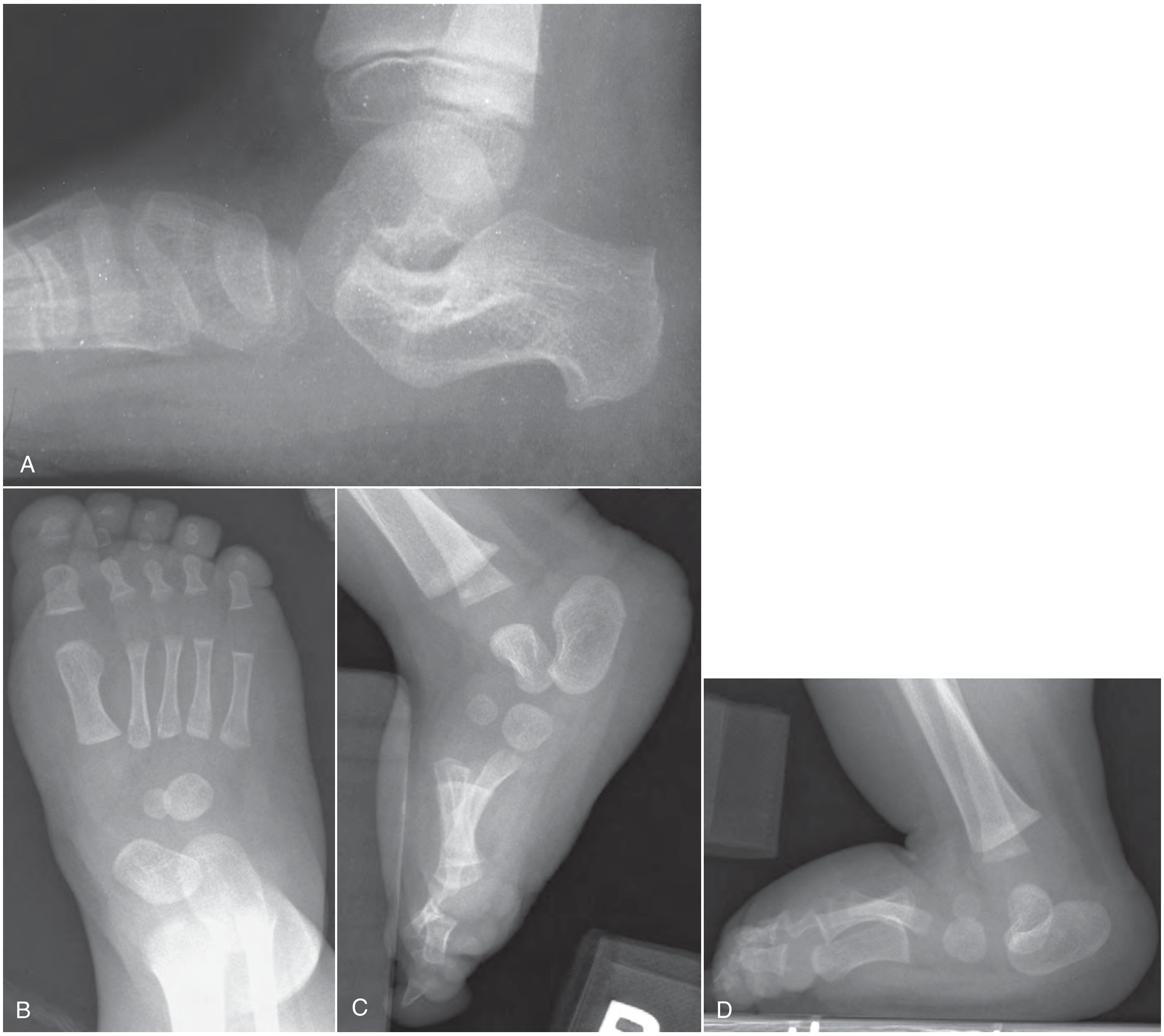

FIGURE 11–7 **Congenital vertical talus (rocker-bottom foot).**[7,168] **A,** The talus is vertically oriented on the lateral radiograph, and the longitudinal arch appears flattened. **B-D,** In another child, a 5-month-old girl, similar findings are evident. Lateral radiographs obtained in maximum plantar flexion **(C)** and maximum dorsiflexion **(D)** illustrate the persistent rocker-bottom appearance of the foot and limited range of motion. In this rare congenital deformity, the talonavicular joint is dislocated and the foot is rigid, creating a fixed deformity. More than 80% of affected children have associated abnormalities, such as congenital hip dislocation, scoliosis, dysraphism, ventricular septal defect, syndactyly, or one of the trisomy syndromes.

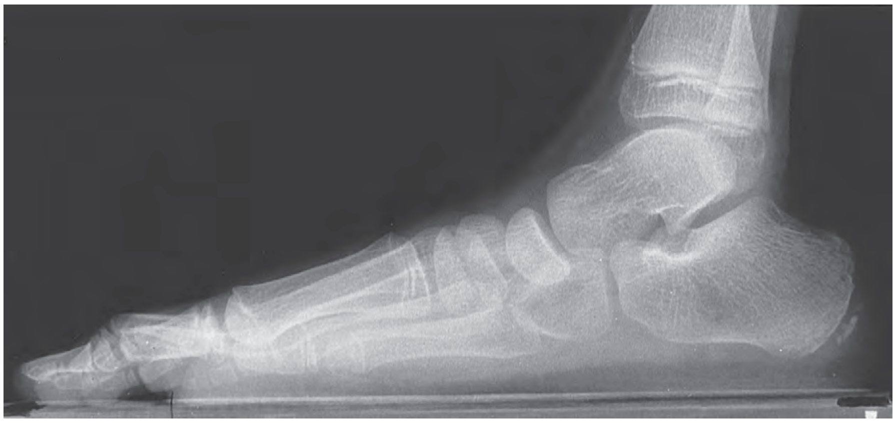

FIGURE 11–8 Pes planus (flatfoot deformity).[4,7] Standing radiograph of the foot in this 9-year-old boy shows a characteristic reduction in the height of the longitudinal arch. This hereditary form of flatfoot, present in about 10% of the population, is considered a variation of normal in which the foot functions normally and is flexible. A more severe form of flatfoot associated with neuromuscular disorders is termed *pes planovalgus*. Additionally, adults may develop flatfoot secondary to severe arthritis, neuropathic joint disease, or rupture of the posterior tibial tendon.

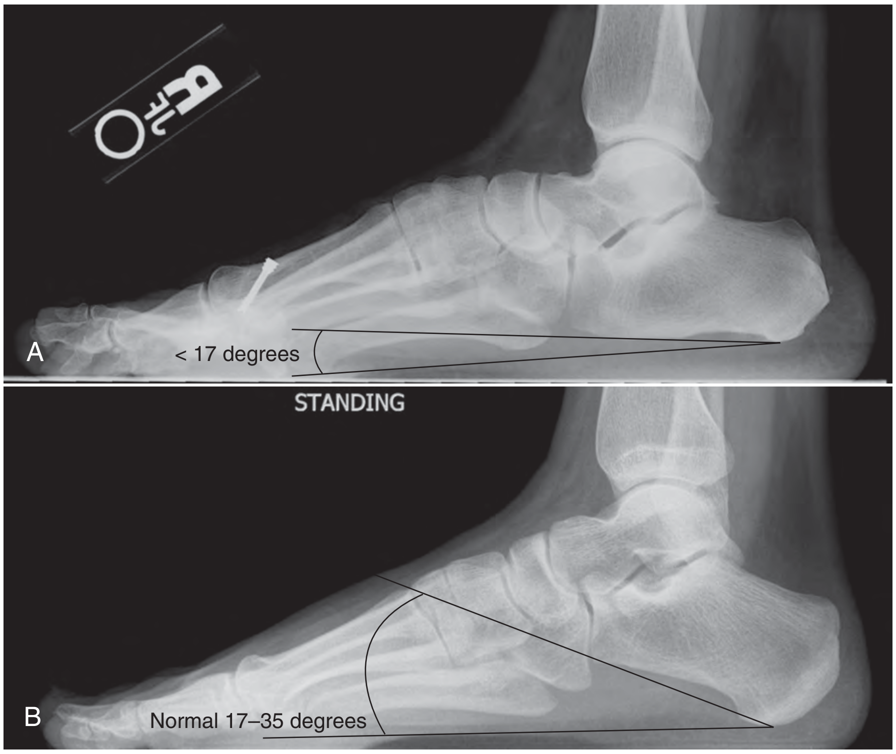

FIGURE 11–9 Acquired pes planus.[4,7,164] In this 68-year-old female, a flat longitudinal arch is evidenced by a calcaneal pitch of less than 17 degrees **(A).** The normal calcaneal pitch ranges from 17 to 35 degrees as seen in a normal patient **(B).**

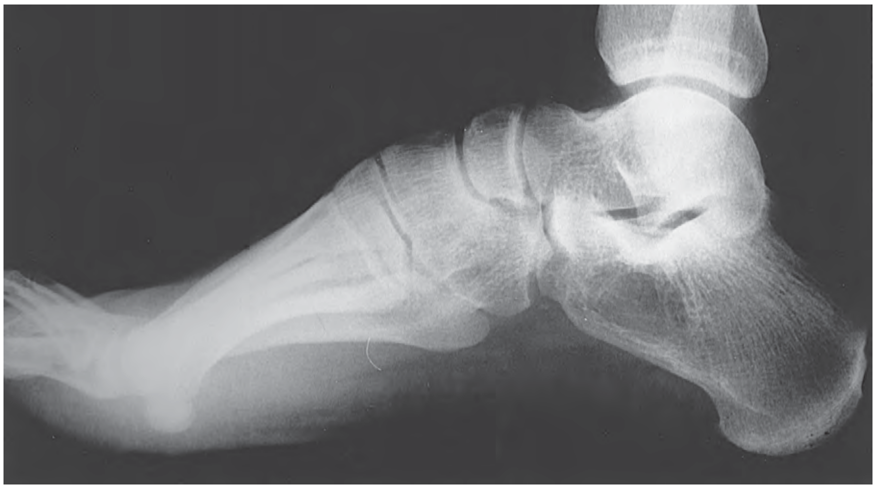

FIGURE 11–10 Cavus deformity.[9] Elevation of the longitudinal arch is seen in this radiograph of a 28-year-old man. This deformity, characterized by an unusually high longitudinal arch, may be congenital or acquired. Acquired cases are usually associated with a neurologic disorder. The calcaneal pitch measures more than 35 degrees in patients with cavus deformity.

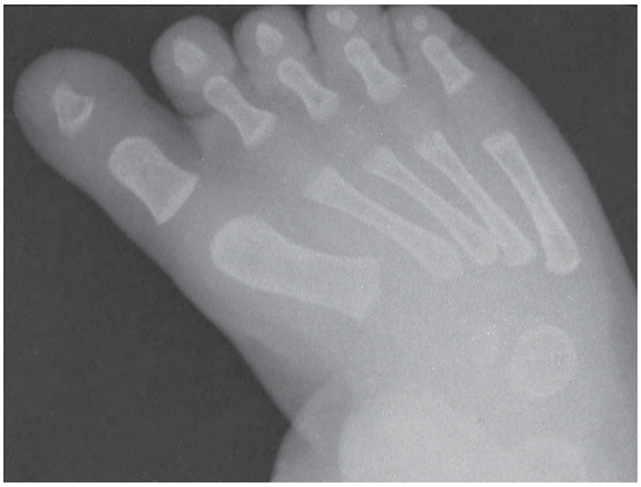

FIGURE 11–11 **Metatarsus varus (adductus) deformity.**[7] Observe the adduction and varus position of all the metatarsal bones at the tarsometatarsal articulations. The heel is typically in a normal position. This common deformity is of unknown cause.

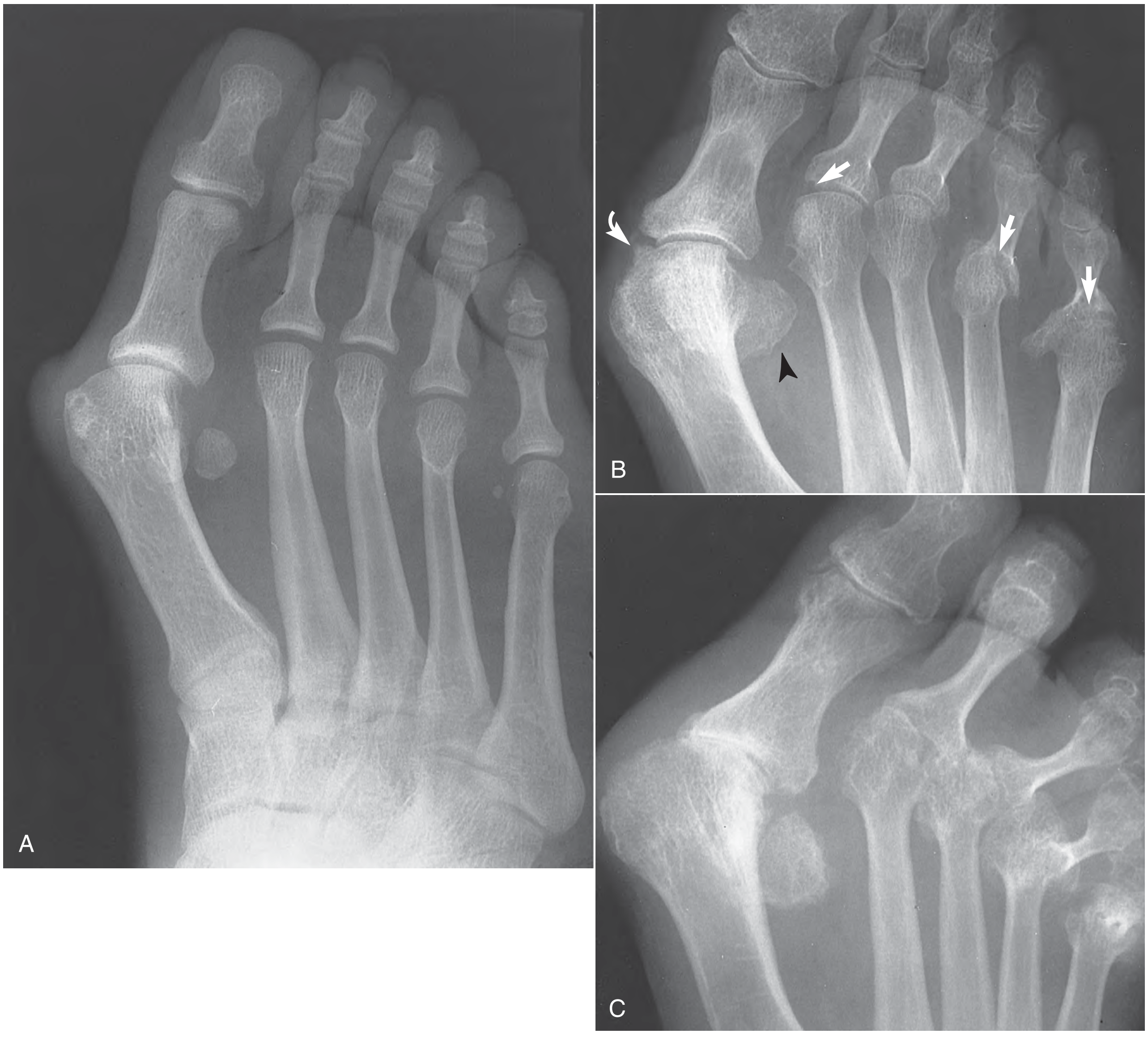

FIGURE 11–12 **Hallux valgus: differential diagnosis.**[10-12,182] **A,** Osteoarthrosis. Marked degenerative joint disease (osteoarthrosis) of the first metatarsophalangeal joint has resulted in severe valgus deformity with prominence of the soft tissues overlying the medial aspect of the articulation (bunion). Other findings include considerable nonuniform joint space narrowing, subchondral sclerosis, osteophyte formation, and osseous hypertrophy of the medial aspect of the metatarsal head. Note also the lateral subluxation of the sesamoid bones. **B,** Ankylosing spondylitis. Marked hallux valgus is associated with multiple juxtaarticular and intraarticular erosions *(arrows),* metatarsophalangeal joint space narrowing, fluffy periostitis *(curved arrow),* and sesamoid bone subluxation *(arrowhead)*. **C,** Rheumatoid arthritis. Striking valgus deformity of the great toe accompanies valgus deformities of the lateral four metatarsophalangeal joints. Observe the widespread periarticular erosions and the lateral subluxation of the hallux sesamoid bones.

Continued

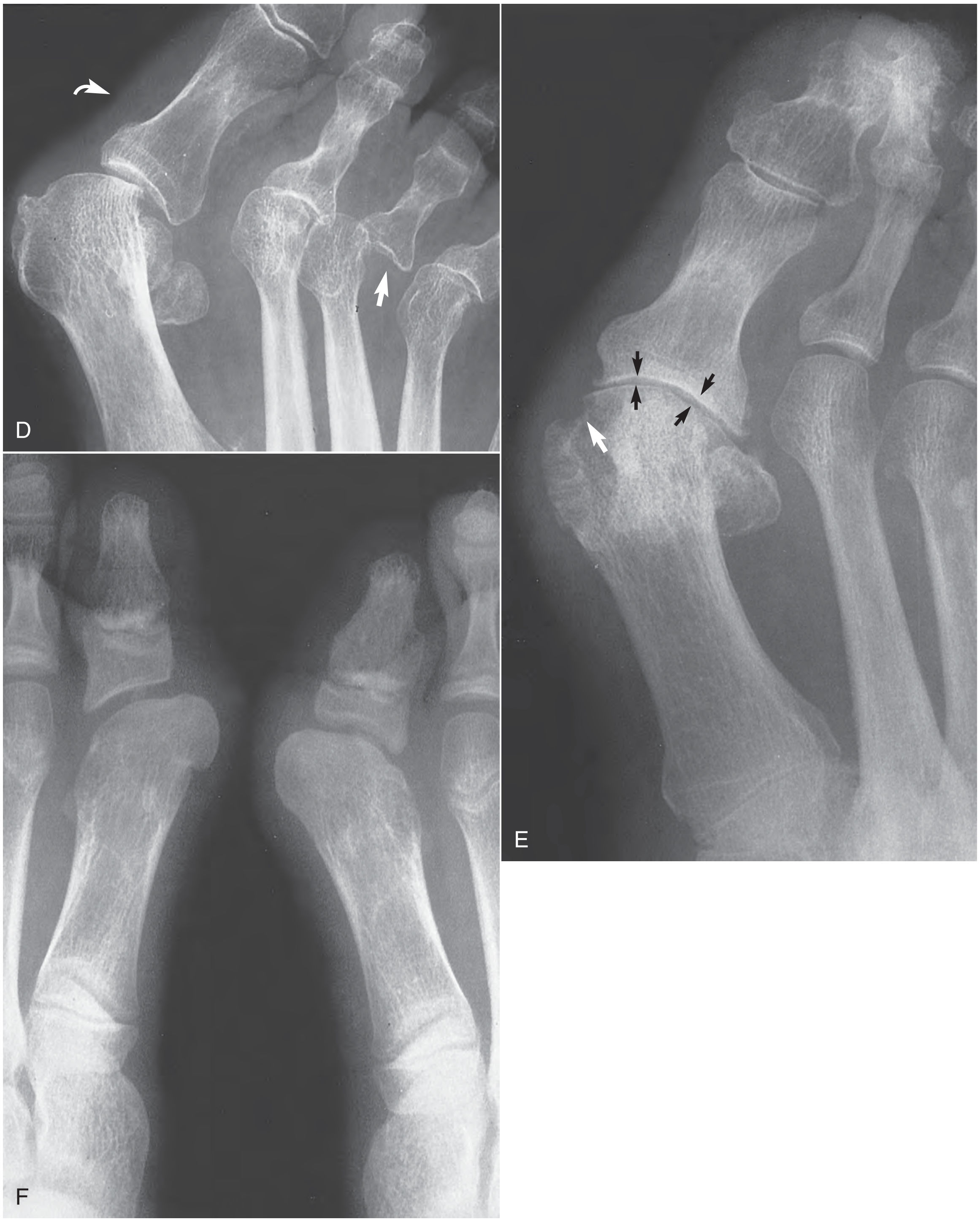

FIGURE 11–12, cont'd **D,** Calcium pyrophosphate dihydrate (CPPD) crystal deposition disease. Lateral deviation of the metatarsophalangeal joint *(curved arrow)* is associated with a dislocation of the third metatarsophalangeal joint *(arrow)* in this patient. **E,** Gout. Hallux valgus deformity, joint space narrowing *(black arrows),* soft tissue swelling, and erosions *(white arrow)* are seen in this man with long-standing gout. **F,** Fibrodysplasia (myositis) ossificans progressiva. Frontal radiograph of both feet shows bilateral hallux valgus deformities with angulation of the distal metatarsal articular surfaces, a characteristic finding in this ossifying diathesis. Note also the abnormal shortening of the first proximal phalanges.

FIGURE 11–13 **Hammer toe deformities.**[4,7] A 44-year-old man. The dorsoplantar radiograph **(A)** reveals subluxations of the four lateral metatarsophalangeal joints. The lateral radiograph **(B)** shows dorsiflexion deformities of the metatarsophalangeal joints and corresponding plantar flexion deformities of the proximal interphalangeal joints.

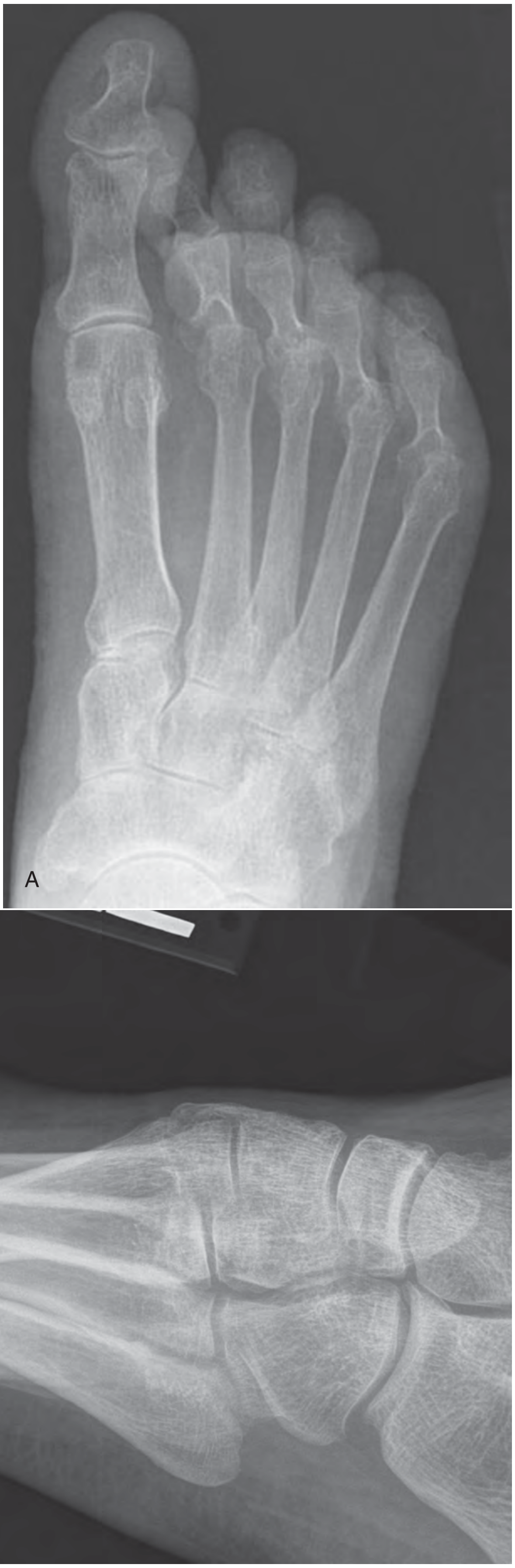

TABLE 11-3 Developmental Anomalies, Anatomic Variants, and Sources of Diagnostic Error Affecting the Ankle and Foot

Entity	Figure(s)	Characteristics
Tarsal Coalition **Developmental**[165,196]		Fibrous, cartilaginous, or osseous congenital fusion of two or more tarsal bones Ossification of fibrous or cartilaginous fusions occurs during the second decade and may lead to the onset of symptoms
1. Calcaneonavicular[13,14,165,196]	11-14	May represent 50% of all cases of tarsal coalition Occasionally bilateral Asymptomatic or associated with rigid flatfoot Best radiographic view: 45-degree oblique foot Fibrous and cartilaginous fusions not directly visible *Secondary signs:* Close approximation of the calcaneus and navicular Irregular cortical surfaces Hypoplastic head of talus Enlargement of anterior process of calcaneus ("anteater nose" sign)
2. Talocalcaneal[13-16,163,164,196]	11-5, 11-15	Approximately 35%-50% of all cases of tarsal coalition Twenty percent of cases are bilateral Signs and symptoms tend to be more severe than in calcaneonavicular coalition Best radiographic view: 45-degree axial view of calcaneus; CT and arthrography often diagnostic *Secondary signs seen on a lateral radiograph:* Talar break Widening of the lateral talar process Nonvisualization of middle subtalar joint *C-sign:* curvilinear radiopacity overlying the sustentaculum tali Asymmetric anterior subtalar joint May result in a ball-and-socket ankle joint CT scanning or MR imaging may be useful diagnostically
3. Talonavicular[13,165,196]		Rare form of coalition Best seen on dorsoplantar radiograph
4. Calcaneocuboid[13,165,196]		Infrequent form of coalition Readily visible on routine radiographs
5. Talocuboid[196]	11-16	Extremely rare form of coalition
Accessory ossicles[4,175,189,197]		Unfused ossicles (accessory bones) represent normal anatomic variants that are usually of no clinical significance (only the most commonly named ossicles are listed below) Rarely result in symptoms; frequently simulate fractures Typical location and smooth, well-corticated margins help to distinguish ossicles from fractures
1. Os trigonum[4,17,18]	11-17	Adjacent to posterior process of talus Best seen on lateral radiograph Simulates fracture of the posterior process of the talus May be associated with the os trigonum syndrome: painful condition in ballet dancers, aggravated by prolonged or repeated forced plantar flexion See posterior impingement syndrome, Table 11-10
2. Accessory talus[4]		Adjacent to the medial aspect of talus, just anterior to site of os trigonum Best seen on lateral radiograph
3. Calcaneus secondarium[4]	11-18	Adjacent to the anterior process of the calcaneus Round or triangular ossicle within the gap of the calcaneus, cuboid, talus, and navicular bones Best seen on oblique radiograph of midfoot
4. Os intermetatarseum[19]	11-19	Variable shaped ossicle located dorsally between the bases of the first and second metatarsals; may be elongated Best seen on oblique or dorsoplantar views of foot May be painful

TABLE 11-3 Developmental Anomalies, Anatomic Variants, and Sources of Diagnostic Error Affecting the Ankle and Foot—cont'd

Entity	Figure(s)	Characteristics
5. Os vesalianum[20]	11-20	Situated at the insertion of the peroneus brevis tendon at the base of the fifth metatarsal Often confused with an os peroneum May be painful
6. Os peroneum[4,197]	11-21	Situated within the peroneus longus tendon adjacent to the cuboid bone Often multicentric Typically located more proximally than the os vesalianum May be bipartite and may fracture or become displaced with rupture of the peroneus longus muscle or tendon
7. Os tibiale externum[21,22]	11-22	*Accessory navicular:* two types *Type I:* circular sesamoid bone embedded within posterior tibial tendon *Type II:* triangular ossicle adjacent to the medial aspect of the navicular bone at the navicular tubercle May be painful
8. Os supranaviculare[4]		Small triangular ossicle adjacent to the dorsal surface of the proximal portion of the navicular bone Should not be confused for avulsion fractures that usually involve the distal aspect of the dorsal surface of the navicular bone
9. Os subfibulare[4,198,199]	11-23	Circular ossicle adjacent to the inferior tip of the fibula There is some debate whether this represents a true sesamoid bone, an ossicle, or a nonunion of an old avulsion fracture of the tip of the fibula at the anterior talofibular ligament attachment
10. Os sustentaculi[176,200]	11-24	Rare small accessory bone bridged to the posterior aspect of the sustentaculum tali by a fibrocartilaginous union May be painful and develop degenerative sclerosis and cystic changes where it communicates or articulates with the sustentaculum tali of the calcaneus and the talus itself CT imaging demonstrates the osseous anatomy best, and MR imaging depicts any associated edematous changes
Sesamoid bones[175,189]		Smooth ossicles embedded within tendons on the plantar side of the foot, usually just proximal to the adjacent joint
1. Hallux sesamoids[23,195]	11-25, *A, B*; 11-54	Medial and lateral sesamoids are invariably present at the first MTP joint; congenital absence extremely rare; when absent, they usually have been surgically resected Situated within the flexor hallucis brevis tendons and are covered with hyaline cartilage Usually arise from a single ossification center; bipartite (4%), tripartite, and multipartite sesamoids arise from multiple centers and involve the medial sesamoid more commonly May fracture or dislocate (Table 11-8)
2. Other sesamoids[4]	11-25, *C*	Frequent locations of single or double sesamoids: second and fifth metatarsal heads *Infrequent locations:* third and fourth metatarsal heads, first proximal phalanx, and second middle phalanx
Normal pseudocystic radiolucent area in calcaneus[4,5]	11-26	Normal triangular radiolucent area frequently is seen within the calcaneus Represents an area relatively devoid of trabecular within the normal trabecular arrangement of the spongiosa portion of bone May simulate a simple bone cyst or intraosseous lipoma Presence of a nutrient foramen within the lucent area is useful in confirming a pseudocyst as opposed to a true cyst or tumor
Talar beak[24]		Osseous prominence on superior aspect of the anterior process of the talus Normal variant simulating degenerative osteophytes Also seen in osteoarthrosis and talocalcaneal coalition
Epiphyseal variations[25]		Normal metacarpal and phalangeal epiphyses may be radiodense, irregular, asymmetric, divided by a cleft, or cone-shaped

Continued

TABLE 11-3 Developmental Anomalies, Anatomic Variants, and Sources of Diagnostic Error Affecting the Ankle and Foot—cont'd

Entity	Figure(s)	Characteristics
Syndactyly[7]		Developmental lack of differentiation between two or more digits Fusion of two digits may be partial or complete Osseous or soft tissue involvement Occurs as an isolated anomaly or in association with a generalized syndrome Syndactyly of the second and third digits is most likely an isolated anomaly Nonsegmentation of the metatarsals is termed *synmetatarsalism*
Macrodactyly[26]		Localized overgrowth of both soft tissues and osseous elements of a digit Congenital form is present at birth Also associated with neurofibromatosis, soft tissue hemangiomas, macrodystrophia lipomatosa, and lymphangioma
Polydactyly[7,27,28]	11-27	Developmental duplication of a digit Most frequently an isolated anomaly but may be related to a generalized syndrome Duplication of a great toe (preaxial polydactyly) is more likely syndrome-related than duplication of the fifth toe (postaxial polydactyly)
Symphalangism[7]	11-3, *K, L*	Developmental lack of differentiation of one phalanx to another within the same digit, usually related to absence of ossification centers Fusion of middle and distal phalanges of the fifth toe is a common isolated anomaly; at other sites, it may be a component of a generalized syndrome

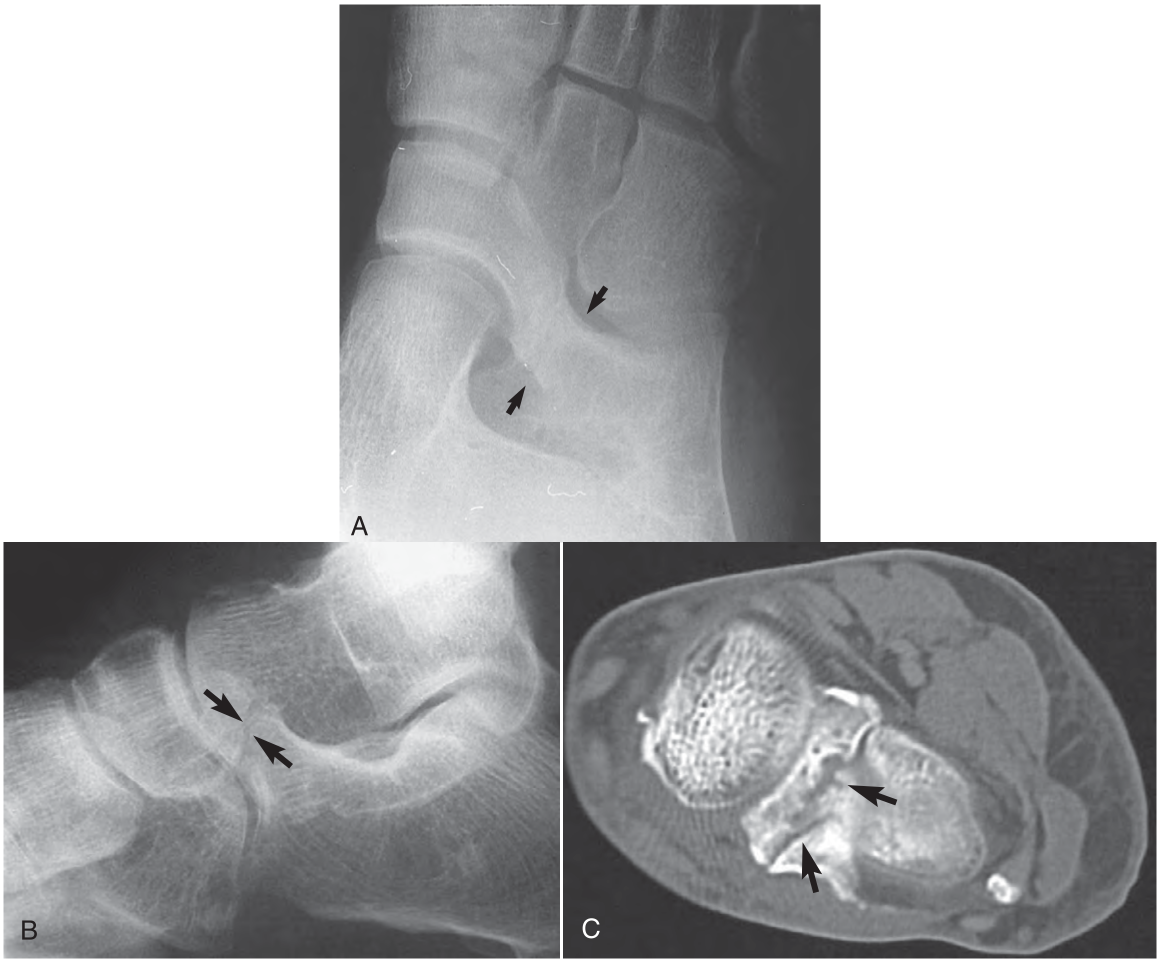

FIGURE 11–14 Tarsal coalition (fusion): calcaneonavicular articulation.[13,14,165,196] **A,** A 45-degree medial oblique radiograph of the foot in this 12-year-old boy demonstrates osseous coalition of the calcaneonavicular articulation *(arrows),* the most frequent site of tarsal coalition. **B-C,** In another patient, incomplete fusion representing a fibrous or cartilaginous coalition is evident *(arrows)* on a lateral radiograph **(B).** On an axial oblique CT bone window scan **(C),** the anomalous articulation *(arrows)* is irregular, somewhat sclerotic, and the adjacent subchondral bone is sclerotic and cystic in appearance, all suggestive of degenerative disease. The fusion is sometimes bilateral and may be either asymptomatic or associated with a rigid flatfoot deformity. The abnormality may be overlooked on frontal and lateral radiographs. The ankylosis can be osseous, fibrous, or cartilaginous.

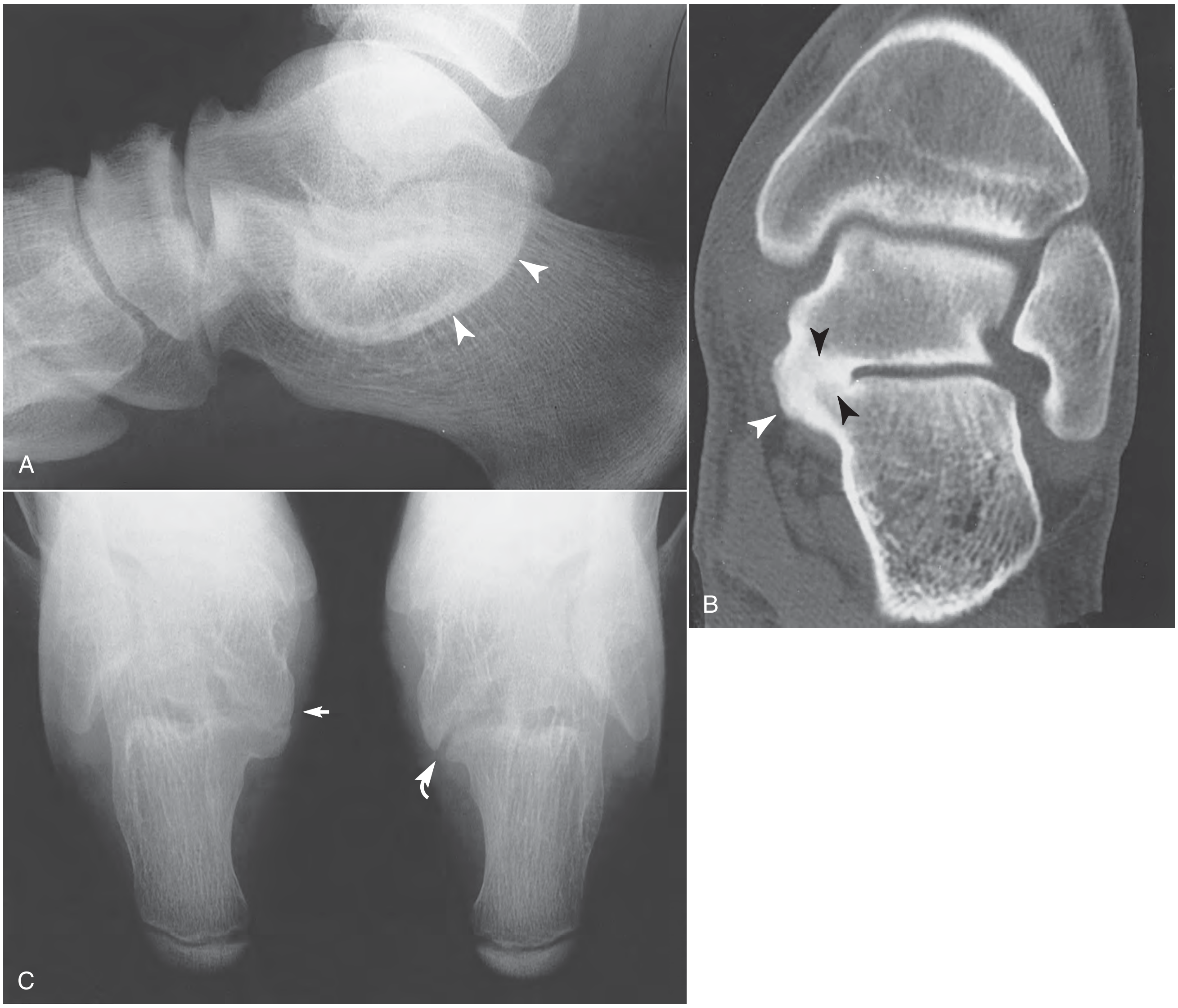

FIGURE 11–15 Tarsal coalition (fusion): talocalcaneal articulation.[13-16,163,164,196] **A-B,** A 36-year-old man. In **A,** a routine lateral radiograph reveals a curvilinear radiodensity overlying the sustentaculum tali (C-sign) *(arrowheads)*. In **B,** a coronal CT scan shows osseous fusion of the talocalcaneal articulation *(arrowheads)*. **C,** An 8-year-old girl. A fully penetrated axial radiograph (Harris-Beath projection) may be required in addition to routine frontal and lateral projections to visualize the middle facet ankylosis. On the right *(straight arrow),* almost complete osseous fusion is seen. On the left *(curved arrow),* the radiolucent joint space is seen, indicating incomplete fusion of the medial talocalcaneal articulation. The ankylosis typically occurs at the middle facet between the talus and the sustentaculum tali and is bilateral in 20% to 25% of affected persons. In many cases, CT **(B),** arthrography, or CT combined with arthrography is necessary to evaluate fibrous or osseous fusions adequately.

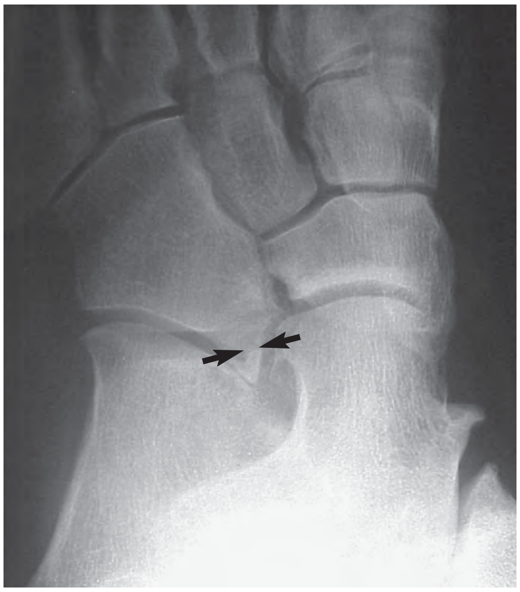

FIGURE 11–16 **Tarsal coalition (fusion): talocuboid articulation.**[196] A medial oblique radiograph of the midfoot in this 50-year-old man with foot pain reveals an anomalous fibrous coalition *(arrows)* between the talus and cuboid bones. This is an extremely rare site for coalition to occur.

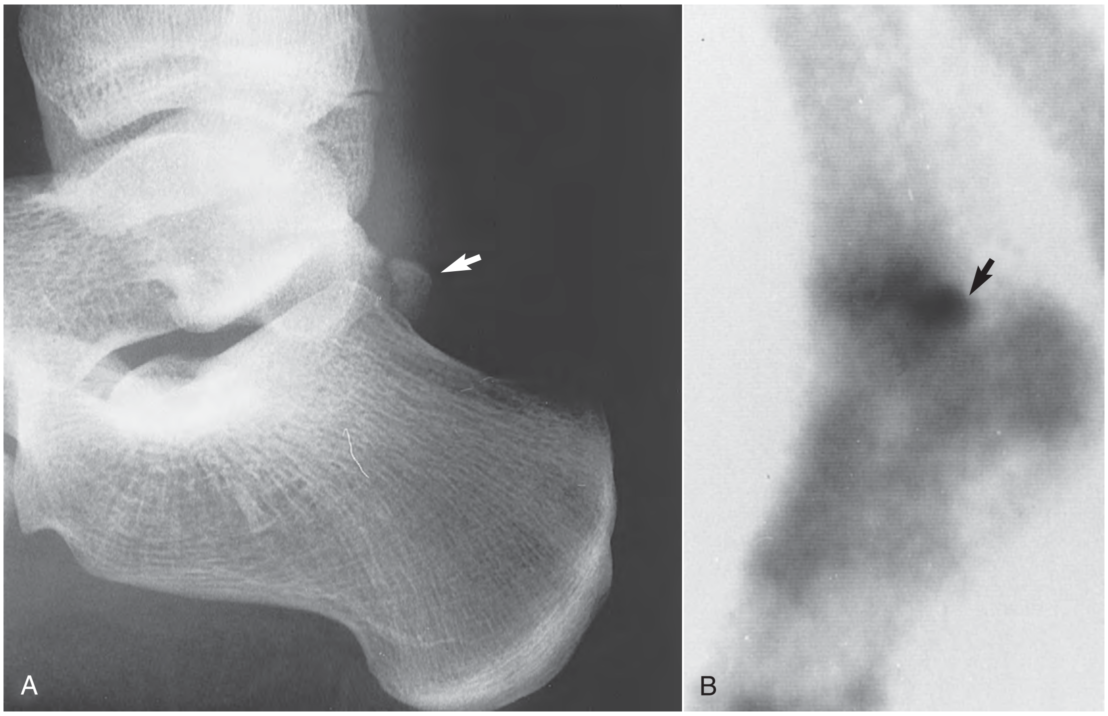

FIGURE 11–17 **Os trigonum syndrome: posterior ankle impingement syndrome.**[4,17,18] **A,** Radiograph of this 14-year-old ballet dance student reveals the presence of an os trigonum *(arrow)*. **B,** Scintigraphy shows marked increased uptake localized in the os trigonum *(arrow)* and mild uptake at the growing physes about the ankle and foot. Surgical excision of the os trigonum relieved the pain. This condition, more common in athletes such as professional ballet dancers, is aggravated by forced plantar flexion of the ankle.

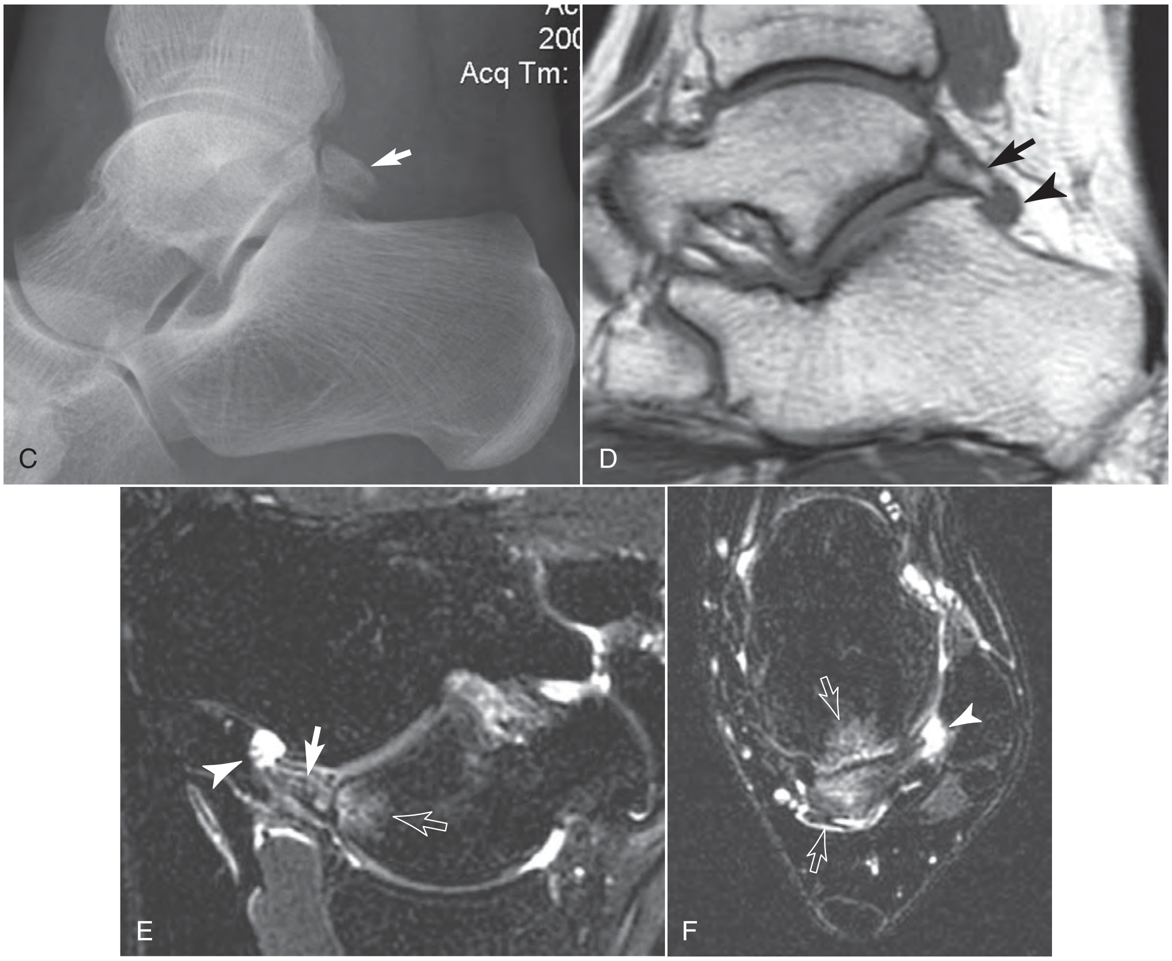

FIGURE 11–17, cont'd **C,** Another os trigonum is clearly evident in a second patient *(arrow)*. **D-F,** Os trigonum resulting in posterior ankle impingement syndrome in a 19-year-old man. A T1-weighted sagittal MR image **(D)** shows an ovoid ossicle *(arrow)* just posterior to the talocalcaneal articulation. Fat-suppressed proton–density-weighted images in the sagittal **(E)** and transaxial **(F)** planes reveal the ossicle *(arrow)* and abnormal high signal within the ossicle and the posterior talus *(open arrows)* representing bone marrow edema. A small secondary posterior joint effusion is also present *(arrowheads)*. *(Courtesy G. Greenway, MD, Dallas, Texas.)*

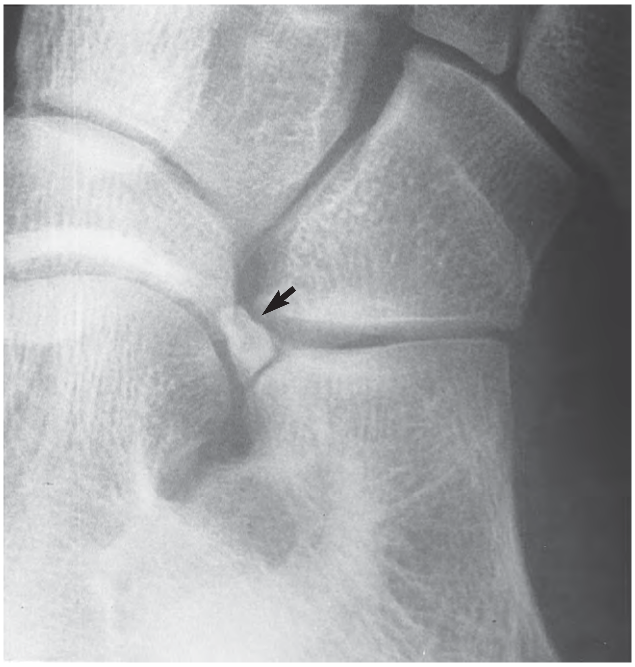

FIGURE 11–18 **Calcaneus secundarium.**[4] This ossicle *(arrow),* arising from the anterior process of the calcaneus and best seen on an oblique radiograph, should not be mistaken for an avulsion fracture.

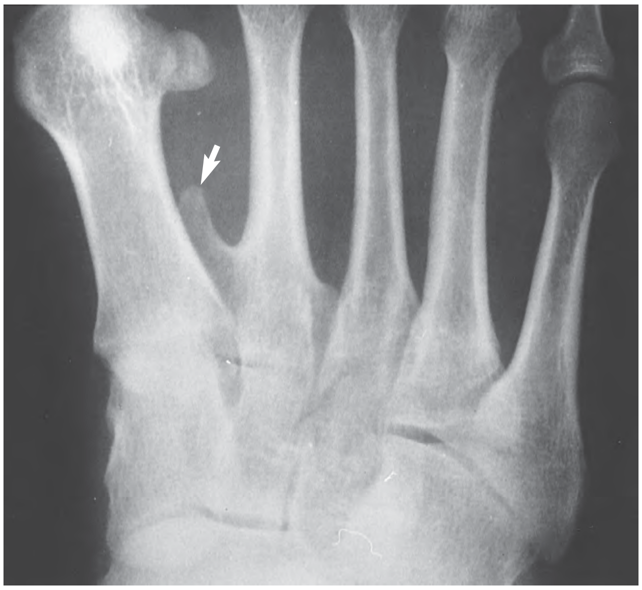

FIGURE 11–19 **Os intermetatarseum.**[19] A curvilinear flange of bone is seen arising from the base of the second metatarsal bone in the space between the first and second metatarsal bones *(arrow)*. The appearance of these ossicles is highly variable, and they may be painful.

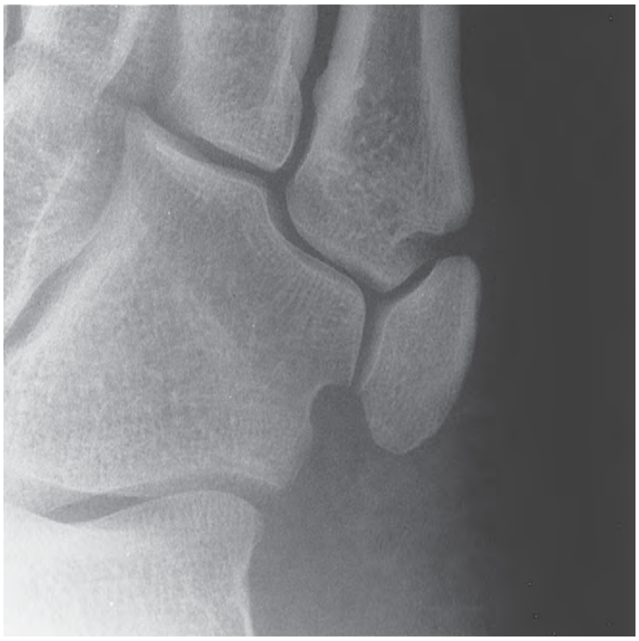

FIGURE 11–20 **Os vesalianum.**[20] This ossicle, situated adjacent to the base of the fifth metatarsal and cuboid bones, is widely separated from the bone and is completely corticated, with a smooth sclerotic margin. This normal variant may be painful and should not be confused with an ununited fracture.

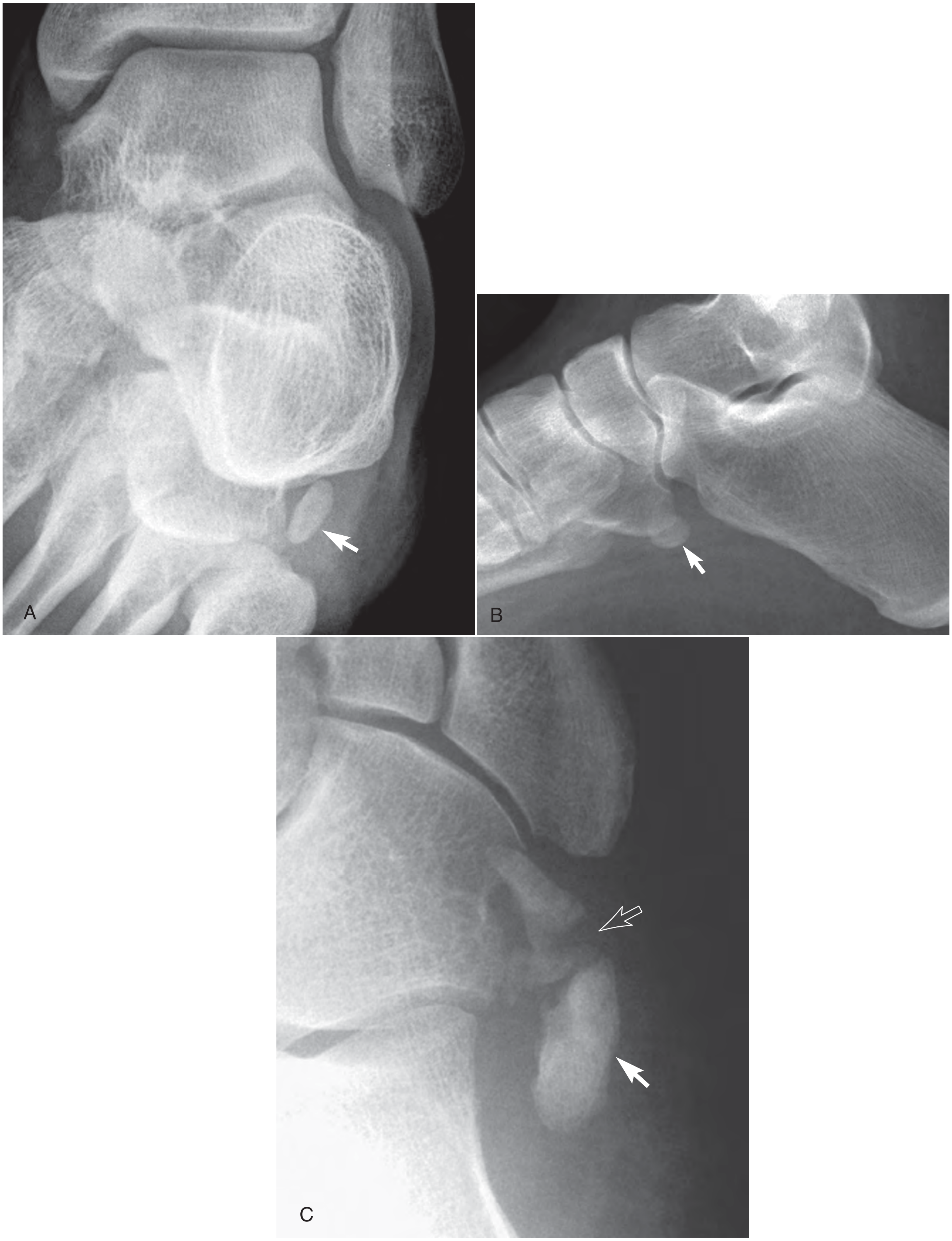

FIGURE 11–21 **Os peroneum.**[4,197] **A,** A medial oblique view of the ankle in a 21-year-old man shows an ovoid ossicle of bone *(arrow)* located proximal to the fifth metatarsal styloid process *(arrow)*. **B,** In another patient, the ossicle is clearly visible on a lateral radiograph *(arrow)*. **C,** This 51-year-old man twisted his ankle, felt an audible pop, and experienced immediate excruciating pain in the lateral aspect of his foot. The radiograph reveals a fracture and diastasis *(open arrow)* of a bipartite os peroneum. The proximal fragment is osteosclerotic *(arrow)*, perhaps a result of osteonecrosis. (***B,*** *Courtesy of J.R. Thomspon, DC, and E.C. Fritsch, DC, Houston;* ***C,*** *From Lee AH, Taylor JAM, Sherwood WH: Acute fracture and diastasis of a bipartite os peroneum: Case report. Topics in diagnostic radiology and advanced imaging; 11:4, 2007.)*

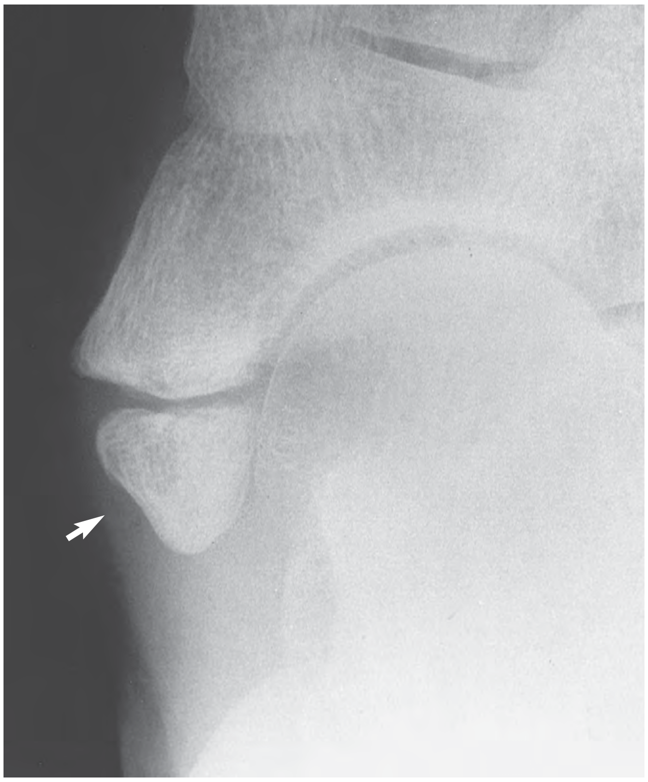

FIGURE 11–22 **Os tibialis externa (accessory navicular).**[21,22] A well-corticated triangular ossicle of bone *(arrow)* is clearly separated from the proximal portion of the medial aspect of the navicular bone (navicular tubercle). Two types of accessory navicular have been described: type I is a circular sesamoid bone embedded within the posterior tibial tendon; type II is a separate triangular ossification center at the navicular tubercle, as seen in this patient.

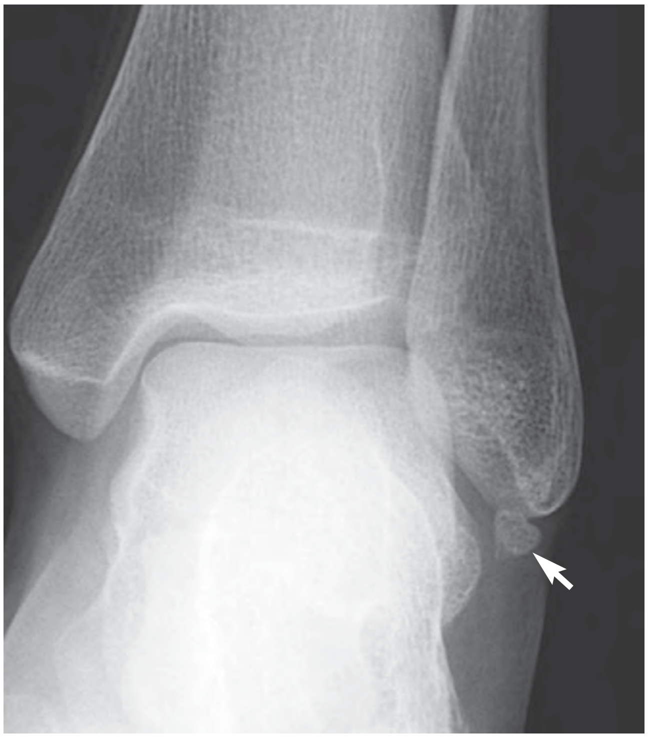

FIGURE 11–23 **Os subfibulare.**[4,198,199] An anteroposterior ankle radiograph in this 21-year-old man reveals a small round ossicle of bone with smooth corticated margins *(arrow)* just distal to the inferior tip of the fibula. Acute avulsion fractures of the distal end of the fibula have uneven margins that possess no cortex at the fracture site. It is often difficult, however, to differentiate os subfibulare from an old ununited fibular avulsion fracture due to a previous injury.

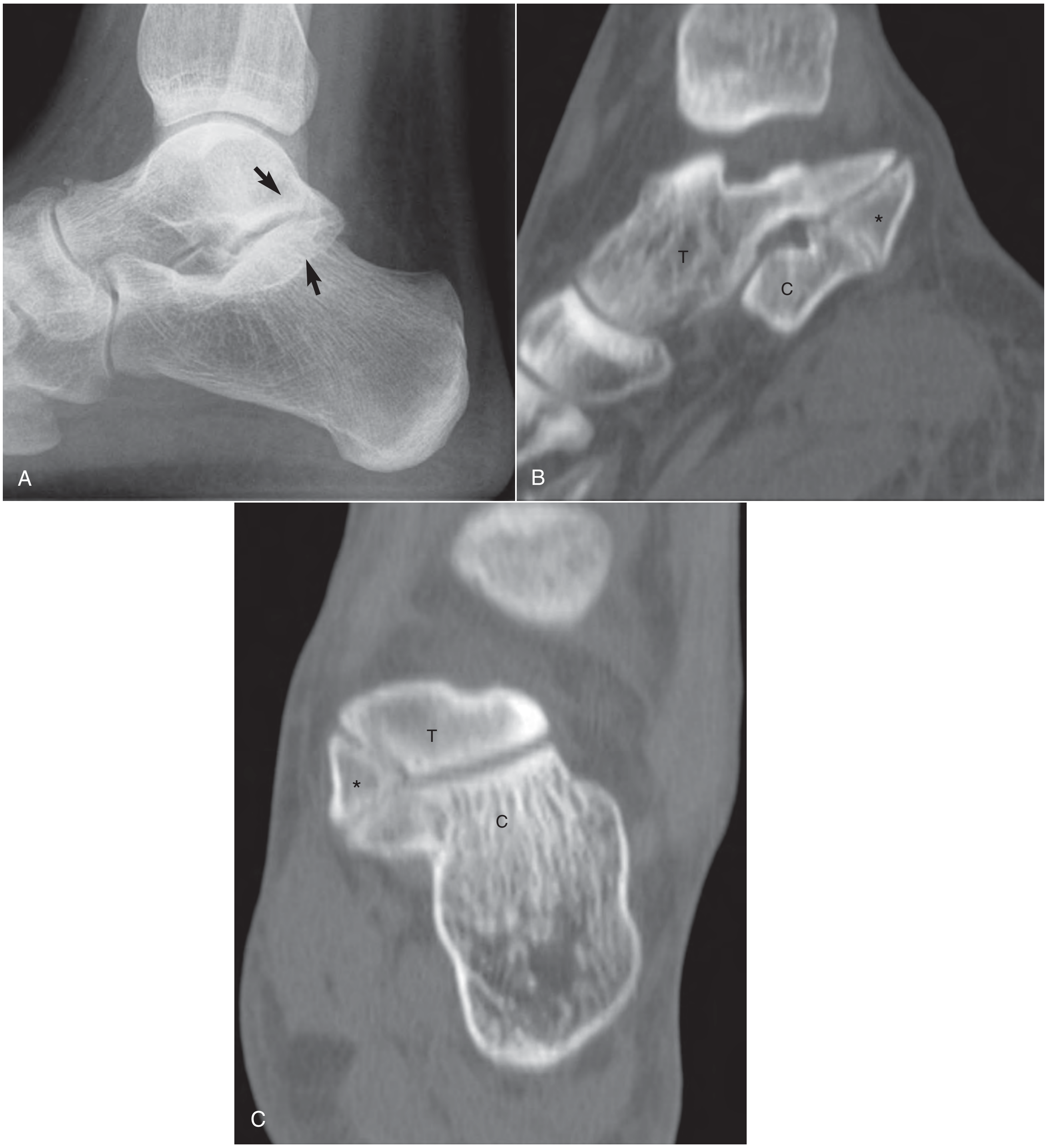

FIGURE 11–24 **Os sustentaculi.**[176,200] This 29-year-old female complained of chronic hindfoot pain. **A,** A lateral radiograph shows excessive subchondral sclerosis adjacent to the posterior talocalcaneal joint *(arrows)*. **B,** A sagittal CT bone window image shows an abnormal triangular ossicle (*) articulating with the calcaneus *(C)* and talus *(T)*. Similar findings are seen on a coronal CT bone window image **(C).**

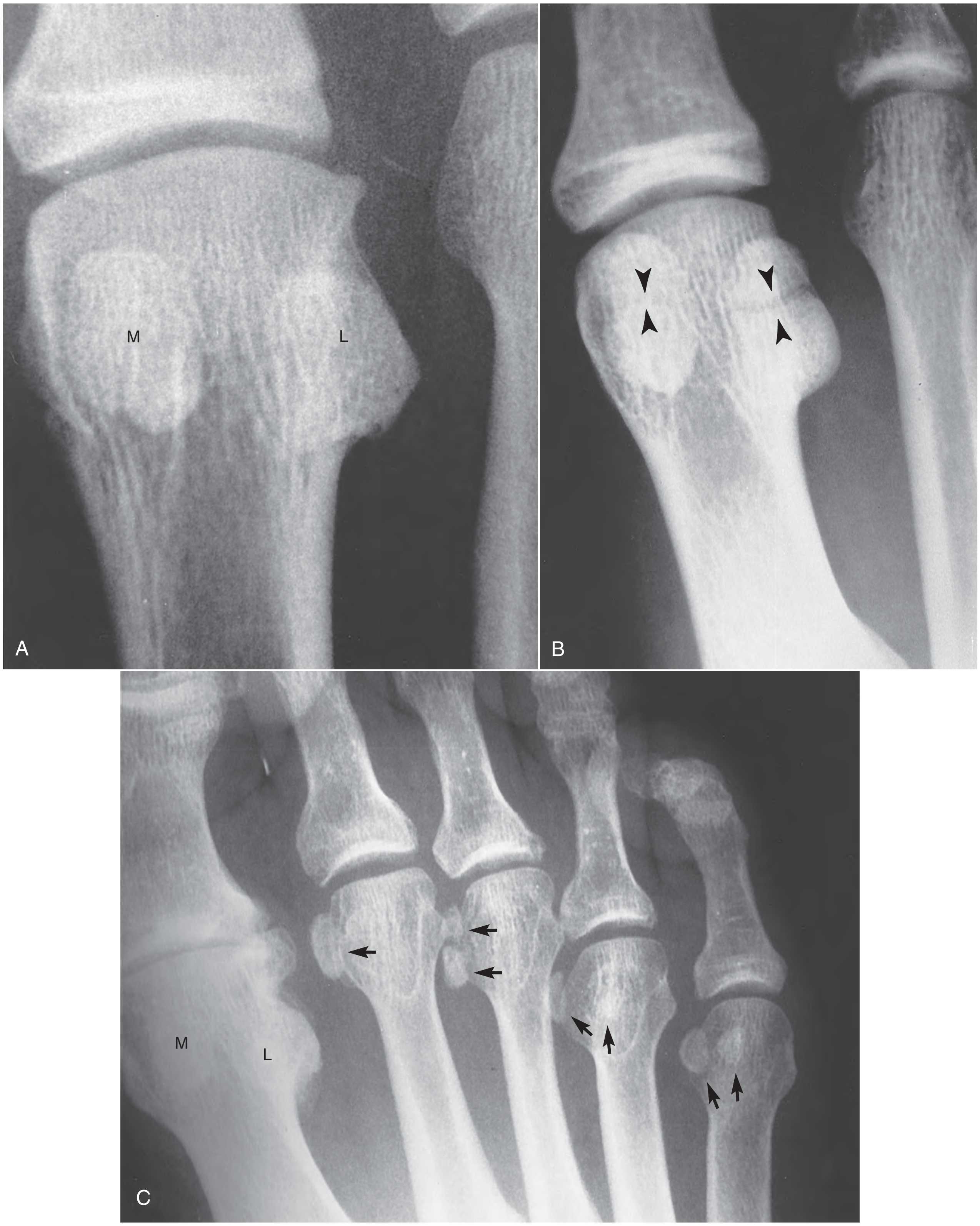

FIGURE 11–25 **Sesamoid bones: normal anatomy and anatomic variations.**[23,195] **A,** Normal hallux sesamoid bones. The medial (M) and lateral (L) hallux sesamoids are invariably present, embedded in the flexor hallucis brevis tendons of the great toe. **B,** Bipartite hallux sesamoid bones. Transverse radiolucent regions are evident through both medial and lateral hallux sesamoid bones *(arrowheads)*. Observe the smooth, well-corticated margins, a feature that allows differentiation from a fracture. **C,** Multiple sesamoid bones are seen adjacent to all metatarsal heads. Sesamoid bones adjacent to the second through fifth metatarsal heads *(arrows)* are variable in appearance. Marked degenerative changes are seen at the first metatarsophalangeal joint in this patient. *M,* medial; *L,* lateral. (***A,*** *Courtesy G. Bustin, DC, San Dimas, Calif.)*

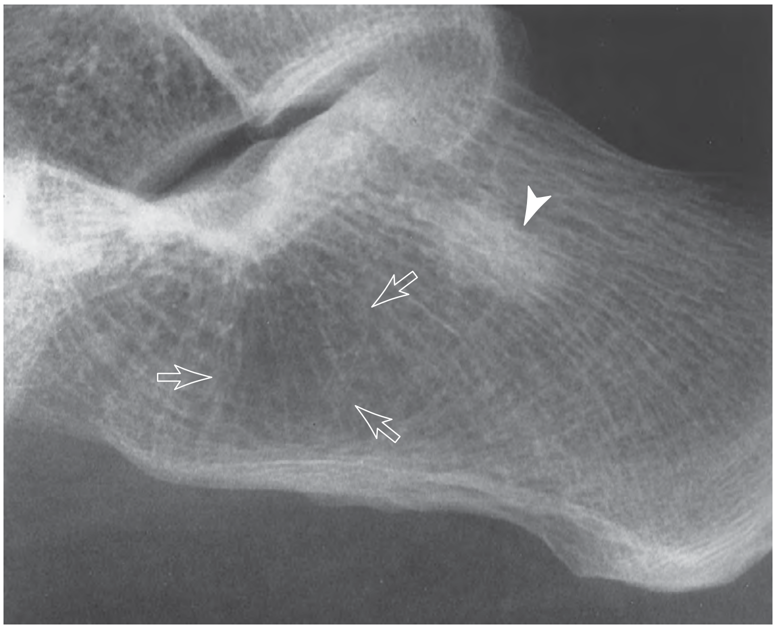

FIGURE 11–26 Normal pseudocystic radiolucency in calcaneus.[4,5] Observe the triangular region of radiolucency *(open arrows)* within the normal trabecular pattern of spongiosa bone. This area, relatively devoid of trabeculae, is clearly seen in some patients and is less conspicuous in others. It may simulate a simple bone cyst, lipoma, or other tumor. Note also the presence of a radiodense enostosis *(arrowhead)*.

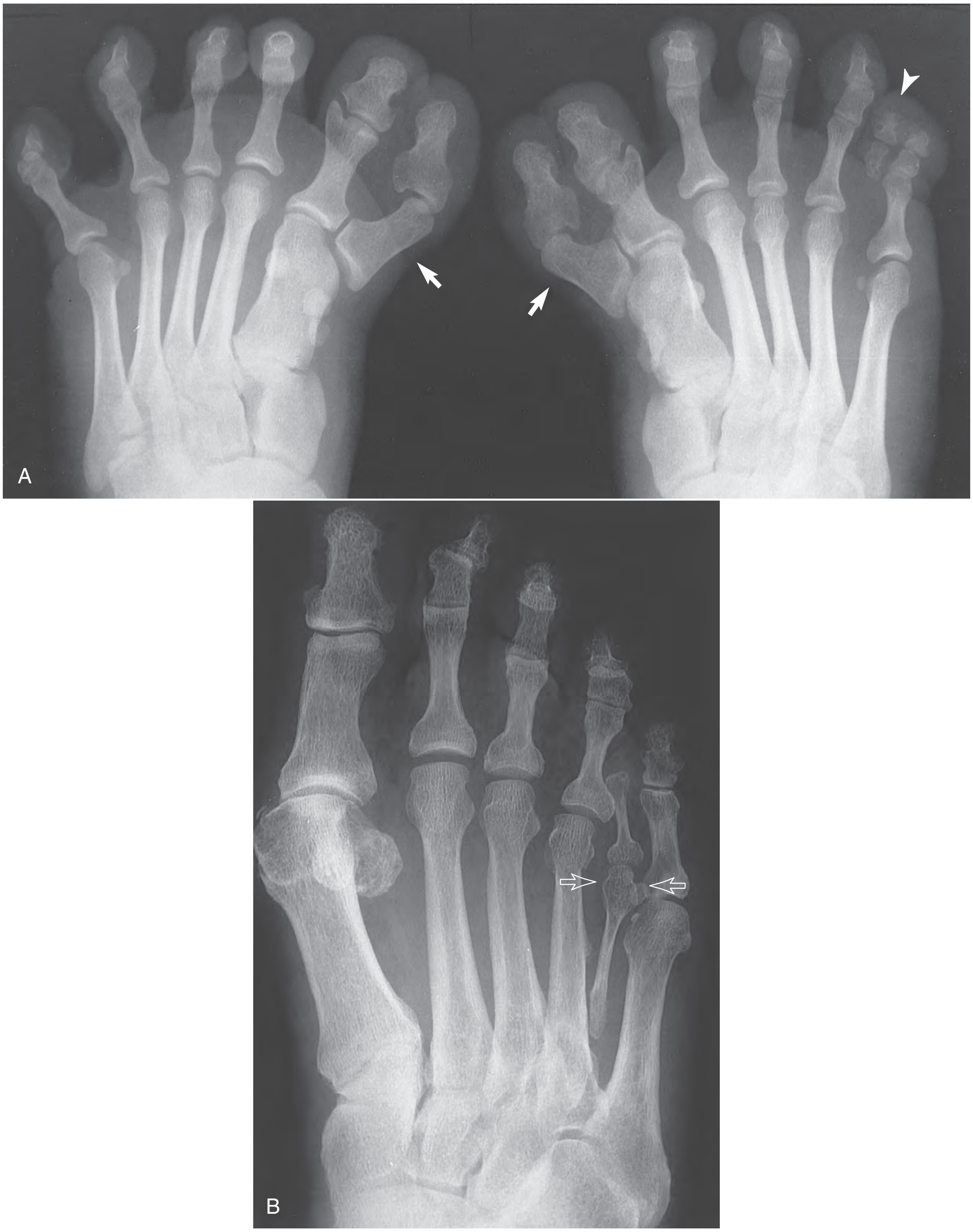

FIGURE 11–27 **Polydactyly.**[7,27,28] **A,** Supernumerary digits are seen medial to the great toes bilaterally *(arrows)* and between the fourth and fifth toes unilaterally *(arrowhead)*. Deformities of the adjacent phalanges and metatarsals also are present. **B,** In another patient, an extra digit is interposed between the two most lateral metatarsals and phalanges *(open arrows)*. Polydactyly in the foot usually involves the fifth digit and may be syndrome-related.

TABLE 11-4 Skeletal Dysplasias and Other Congenital Diseases Affecting the Ankle and Foot

Entity	Figure(s)	Characteristics
Fibrodysplasia (myositis) ossificans progressiva[12]	11-12, *F*	*Multiple congenital anomalies:* polydactyly, syndactyly, hypoplasia of great toe, hallux valgus, and symphalangism
Dysplasia epiphysealis hemimelica[29] (Trevor disease)	11-28	Asymmetric cartilaginous overgrowth in one or more epiphyses Radiographically resembles large eccentric osteochondroma arising from distal tibial epiphysis Bulky irregular ossification extending into soft tissues
Osteogenesis imperfecta[30]	11-29	Severe osteoporosis with pencil-thin cortices Multiple fractures and bowing *Rare cystic form:* ballooning of bone, metaphyseal flaring, and honeycombed appearance of thick trabeculae
Osteopoikilosis[31]	11-30	Predilection for tarsal bones Multiple round or oval radiodense foci within spongiosa bone
Melorheostosis[32,33]	11-31	Occasional involvement of feet Unilateral, hemimelic involvement is typical Cortical thickening and flowing hyperostosis resembling flowing candle wax
Marfan syndrome[34]		Arachnodactyly Hallux valgus Pes planus
Ehlers-Danlos syndrome[35]		Hallux valgus Pes planovalgus with joint laxity
Macrodystrophia lipomatosa[36]		Rare condition of unknown cause Bizarre digital overgrowth of fatty tissue within the soft tissues of the foot

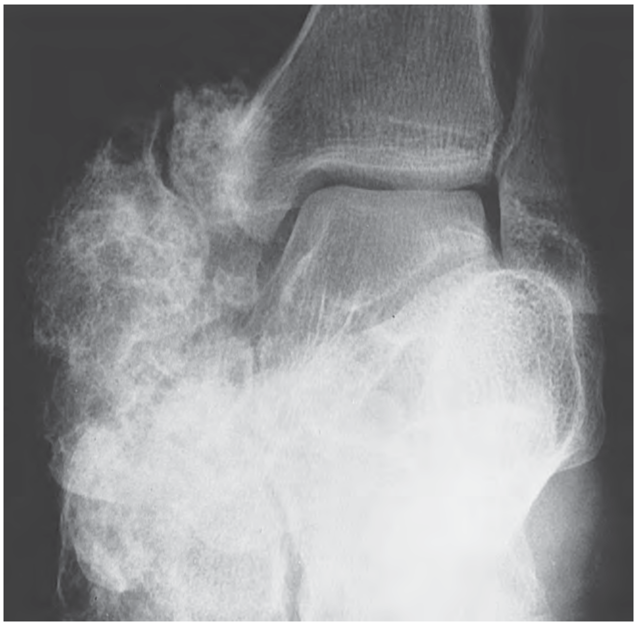

FIGURE 11–28 **Dysplasia epiphysealis hemimelica (Trevor disease).**[29] A large lobulated accumulation of ossification is seen arising from the medial aspect of the distal end of the tibia and tarsal bones spanning the medial aspect of the ankle. This uncommon developmental disorder characterized by asymmetric cartilaginous overgrowth in one or more epiphyses. Joint dysfunction, pain, limitation of motion, and a mass may accompany the disease. *(Courtesy J. Schils, MD, Cleveland.)*

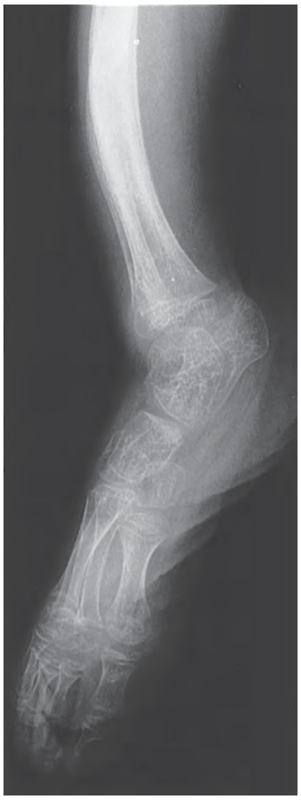

FIGURE 11–29 **Osteogenesis imperfecta.**[30] Severe osteopenia and thin gracile cortical bones are present in the foot and ankle in this infant with osteogenesis imperfecta. Bowing of the tibia is also evident. Pes planus deformities may be seen on weight-bearing radiographs (not shown).

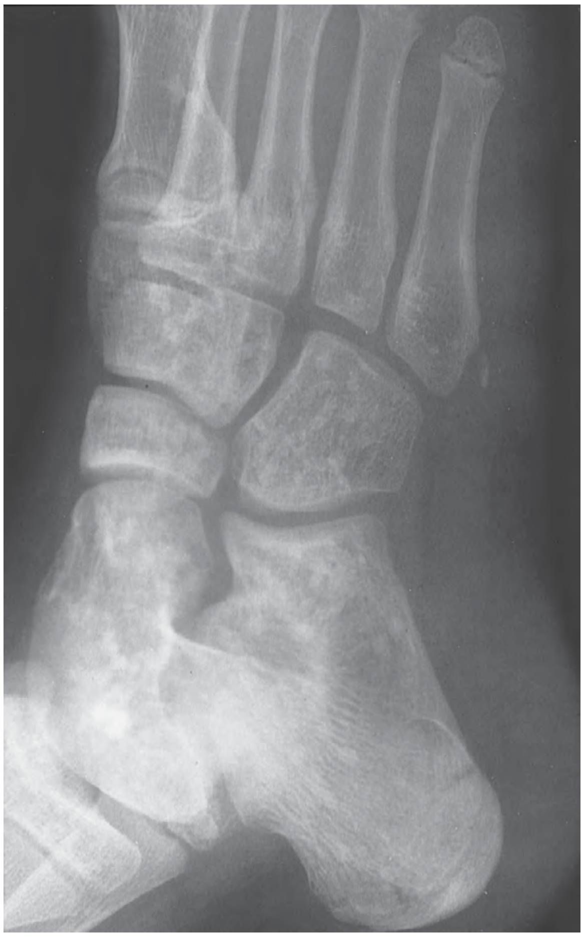

FIGURE 11–30 **Osteopoikilosis.**[31] Note the circular and ovoid osteosclerotic foci localized within a number of bones of the foot in a periarticular distribution.

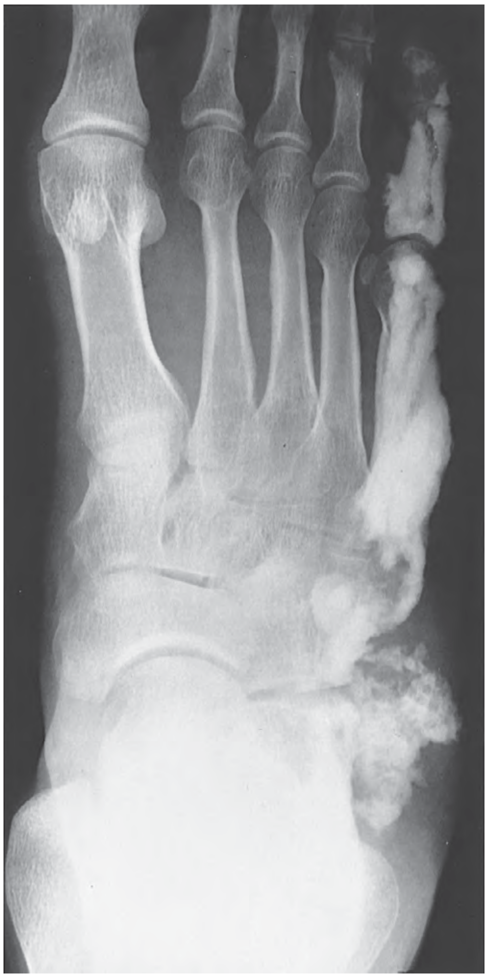

FIGURE 11–31 **Melorheostosis.**[32,33] Findings include prominent soft tissue ossification and the characteristic pattern of hemimelic hyperostosis involving the lateral aspect of the fifth metatarsal, phalanges, and lateral tarsal bones. Note the absence of involvement of the medial four digits of the foot. Melorheostosis is a sclerosing dysplasia of bone that can result in joint swelling and contracture, pain, restriction of motion, growth disturbances, muscle weakness and atrophy, and skin changes. It may be positive on bone scans.

TABLE 11-5 Acute Fractures About the Ankle: Lauge-Hansen Classification*

Fracture Type	Stage	Figure(s)	Characteristics
Supination—external rotation fractures (SER)[37,38]			Sixty percent of all fractures about the ankle Mechanism: external rotation of the supinated foot forces the talus against the fibula Progression of events occurs, beginning with stage I and continuing through stage IV with increasing severity of injury
	SER I		Rupture of anterior talofibular ligament or avulsion fracture of the anterior surface of the fibula or tibia (Tillaux fracture) Ligamentous injuries often not detected on radiographs
	SER II		Short oblique fracture of the distal end of the fibula within 1.5-2.5 cm from the tibiotalar joint
	SER III		Fracture of posterior aspect of the tibia
	SER IV	11-32	Fracture of medial malleolus or rupture of deltoid ligament Widening of the medial tibiotalar articulation with deltoid ligament rupture
Supination—adduction fractures (SAD)[37]			Twenty percent of all fractures about the ankle Mechanism: medially directed adduction forces acting upon the supinated foot Two stages are identified: Stage I resulting from less force than that sustained in a stage II injury
	SAD I	11-33, *A*	Rupture of the lateral ligaments or a transverse (traction or avulsion) fracture of the distal portion of the fibula adjacent to the tibiotalar articulation
	SAD II	11-33, *B*	Fracture of medial malleolus resulting from continued pressure from the medial displacement of the talus
Pronation—external rotation fractures (PER)[37,39-40]		11-34, 11-35	PER and PAB stages I and II are radiographically indistinguishable, and combined, represent 20% of all fractures about the ankle Mechanism: external rotation forces acting upon the pronated foot As forces increase, the injuries progress to higher stages
	PER I		Deltoid ligament rupture in 60% of cases Fracture of the medial malleolus in 40% of cases
	PER II		Rupture of the distal tibiofibular syndesmosis (interosseous ligament) or avulsion fracture of the anterior or posterior tubercle
	PER III	11-36	Injuries of stage I and II combined with a transverse supramalleolar fracture of the fibula >2.5 cm (usually 6-8 cm) above the tibiotalar articulation
	PER IV		Injuries of stage I-III combined with a fracture of the posterior tibial margin
Pronation-abduction fracture (PAB)[37]			Mechanism: abduction forces acting upon the pronated foot PER and PAB stages I and II are radiographically indistinguishable As forces increase, the injuries progress to higher stages
	PAB I		Deltoid ligament rupture (60% of cases) Fracture of the medial malleolus (40% of cases)
	PAB II		Rupture of the distal tibiofibular syndesmosis (interosseous ligament) or an avulsion fracture of the anterior or posterior tubercle
	PAB III		Injuries of stage I and II combined with a transverse supramalleolar fibular fracture
Pronation-dorsiflexion fracture (PDF)[37]			Pilon fracture Rare: less than 0.5% of all fractures about the ankle Mechanism: axial loading forces predominate Forced dorsiflexion on a pronated foot, often occurring in a fall from a height that drives the talus into the ankle mortise
	PDF I		Fracture of medial malleolus
	PDF II		Anterior tibial fracture
	PDF III		Supramalleolar fracture of the fibula
	PDF IV		Transverse fracture of the posterior aspect of the tibia, which communicates with the anterior tibial fracture

* The Lauge-Hansen classification system is based on the position of the foot (e.g., supination or pronation) relative to the body at the time of injury and the direction of talus displacement or rotation (e.g., abduction, external rotation) in relation to the ankle mortise.

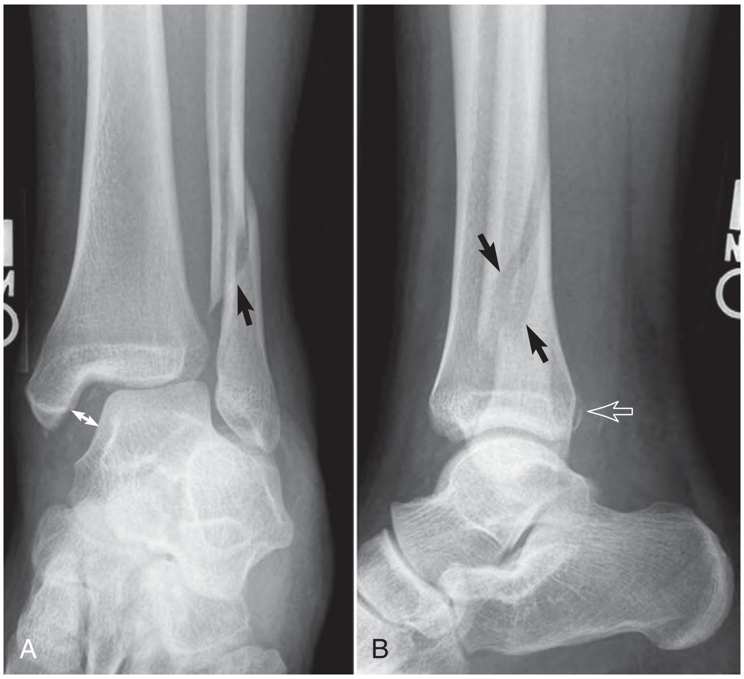

FIGURE 11–32 **Ankle fracture-dislocation: supination-external rotation (SER) fracture, stage IV.**[37,38] This anteroposterior radiograph **(A)** shows an oblique fracture of the distal portion of the fibula *(arrow)* and widening of the medial tibiotalar joint *(double arrow)* representing rupture of the deltoid ligament. The lateral radiograph **(B)** shows minimal displacement of the fibular fracture *(arrow)* and fracture of the posterior malleolus of the tibia *(open arrow)*. SER injuries account for about 60% of all ankle fractures.

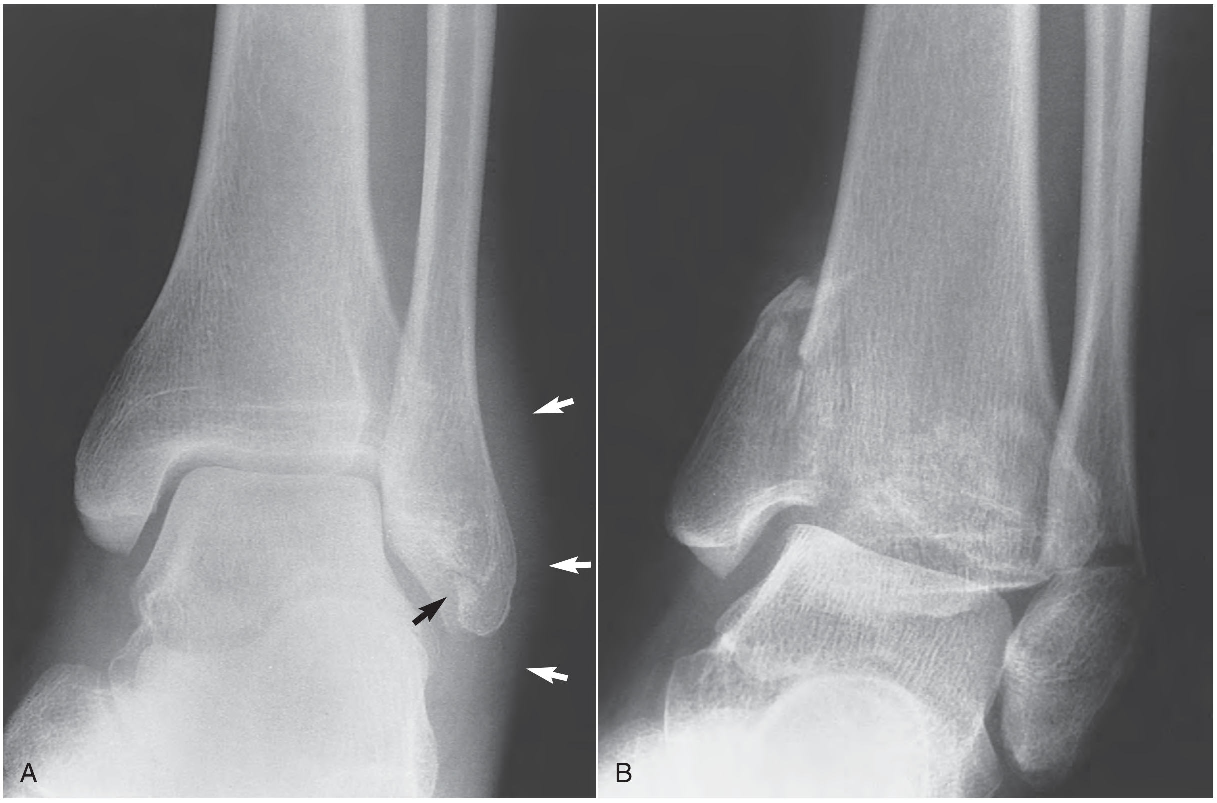

FIGURE 11–33 **Ankle injury: supination-adduction (SAD) fractures.**[37] **A,** Stage I injury. Note the simple nondisplaced avulsion fracture of the fibula *(black arrow)* and the associated soft tissue swelling *(white arrows)* over the lateral side of the ankle. **B,** Stage II injury. A bimalleolar fracture is evident on this radiograph.

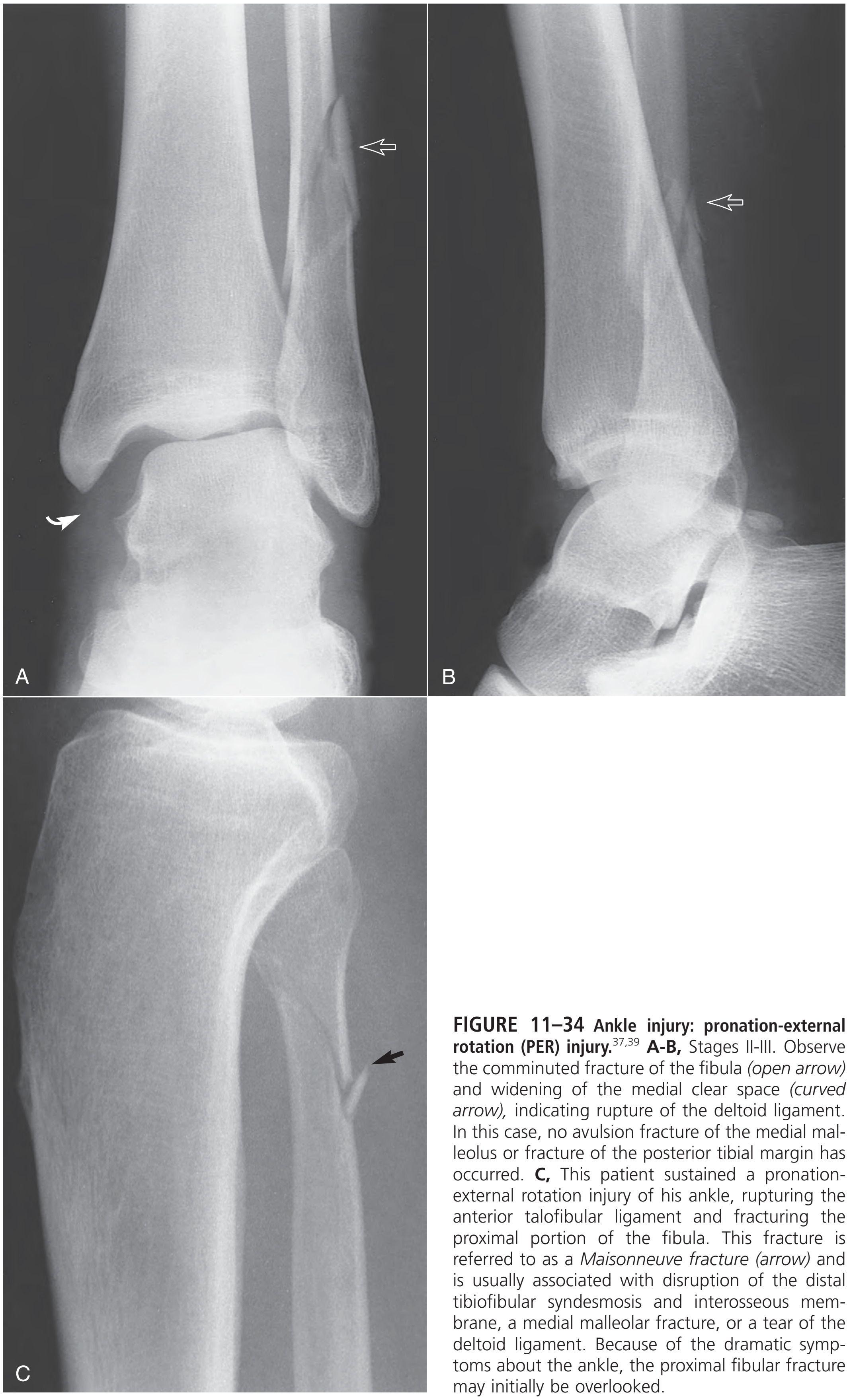

FIGURE 11–34 Ankle injury: pronation-external rotation (PER) injury.[37,39] **A-B,** Stages II-III. Observe the comminuted fracture of the fibula *(open arrow)* and widening of the medial clear space *(curved arrow),* indicating rupture of the deltoid ligament. In this case, no avulsion fracture of the medial malleolus or fracture of the posterior tibial margin has occurred. **C,** This patient sustained a pronation-external rotation injury of his ankle, rupturing the anterior talofibular ligament and fracturing the proximal portion of the fibula. This fracture is referred to as a *Maisonneuve fracture (arrow)* and is usually associated with disruption of the distal tibiofibular syndesmosis and interosseous membrane, a medial malleolar fracture, or a tear of the deltoid ligament. Because of the dramatic symptoms about the ankle, the proximal fibular fracture may initially be overlooked.

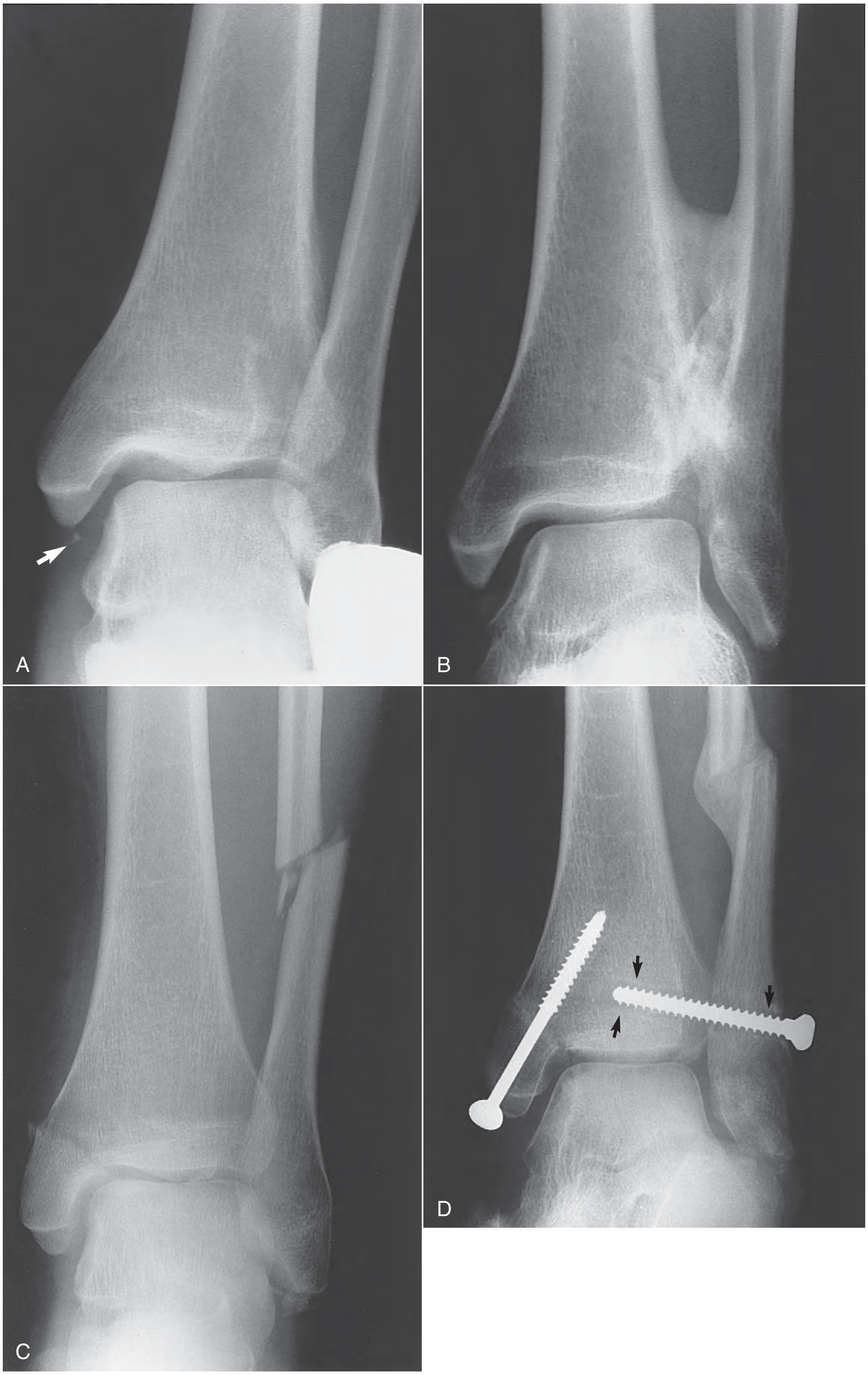

FIGURE 11–35 **Ankle injury: natural history and complications.**[40] **A-B,** This 36-year-old man sustained a pronation ankle injury. In **A,** an initial eversion stress radiograph obtained at the time of injury reveals widening of the medial clear space and a tiny flake of bone *(arrow)* representing an avulsion of the medial malleolus. In **B,** another radiograph obtained 2 years later demonstrates dramatic posttraumatic ossification of the interosseous membrane of the distal tibiofibular articulation. **C-D,** Surgical repair with complications. This 33-year-old woman sustained a pronation-external rotation type IV injury. In **C,** the initial radiograph shows a medial malleolar fracture and a displaced, comminuted oblique fracture of the fibula well above the ankle joint. In **D,** a radiograph taken 4 months postoperatively shows loosening of the cannulated screws used for interfragmentary compression and persistent deformity of the healed fibula. Loosening is seen as a radiolucent area surrounding the screws *(arrows)* and as pulling out of the screws.

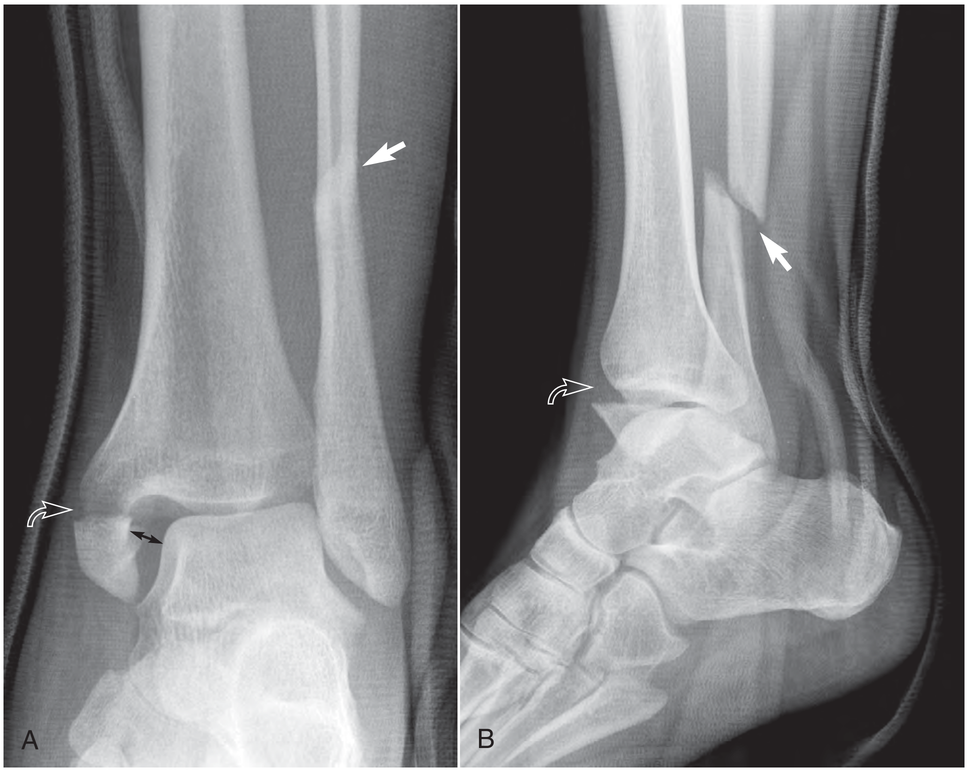

FIGURE 11–36 **Ankle injury: pronation-external rotation (PER) injury type III.**[37,39-40] A 35-year-old man. Anteroposterior **(A)** and lateral **(B)** radiographs taken through a cast show minimal widening of the medial aspect of the tibiotalar articulation *(double arrows),* transverse fracture of the medial malleolus *(curved arrows),* and a short oblique fracture of the fibula approximately 8 cm above the distal end *(arrows)*. The anterior and posterior malleoli of the tibia are not fractured.

TABLE 11-6 **Fractures and Dislocations About the Ankle**[159]

Entity	Stage	Figure(s)	Characteristics
Acute fractures about the ankle[37-40]		11-32 to 11-36	*See Table 11-5:* Lauge-Hansen classification Often associated with osteochondritis dissecans or osteochondral fracture of the talus (Table 11-7)
Distal portion of the tibia[40]			Isolated fractures rare; result from ankle injuries involving impaction of talus on tibial plafond
Intraarticular osteochondral bodies[41]		11-37	Osteochondral bodies within the ankle joint may arise from osteochondral fractures or osteochondritis dissecans *Best imaging methods:* CT arthrography and MR imaging Osteochondral bodies often migrate to the anterior or posterior recess, where they may become embedded in the synovial membrane *Differential diagnosis:* primary or secondary idiopathic synovial osteochondromatosis
Unclassified Fractures			
Isolated fracture of the posterior tibial margin[40]			Posterior malleolar fracture: Rare injury *Mechanism:* compression by the talar dome; may occur while kicking an object with the ankle in neutral or plantar flexed positions Lateral view with slight external rotation reveals the fracture

Continued

TABLE 11-6 Fractures and Dislocations About the Ankle[159]—cont'd

Entity	Stage	Figure(s)	Characteristics
Isolated fracture of the anterior tibial margin[40]			Rare injury *Two types:* 1. Compression forces from a dorsiflexed talus Comminuted fracture of anterior margin of distal end of the tibia 2. Fall on the calcaneus with the talus being forced upward and forward Large fragment of anterior margin is fractured
Child Abuse[42]		11-38	Most frequent in children 1-4 years of age Metaphyseal corner fractures of the distal end of the tibia Growth plate injuries Fractures in various stages of healing Acute fractures of the tibia and fibula Subperiosteal hemorrhage with periosteal reaction Associated injuries elsewhere
Growth Plate Injuries			
Distal portion of the tibia[43-45]		11-39	Eleven percent of all Salter-Harris fractures of the skeleton Most common between ages 9 and 14 years Salter-Harris type II injury most frequent at this site; types III, IV, and I also occur in order of decreasing frequency Primary mechanism appears to be external rotation or plantar flexion of the foot Ten to 12% of these injuries result in growth disturbances Type II injury may be complicated by anterior tibial neurovascular bundle interposition, preventing reduction, and compromising blood supply Two-plane fracture (Tillaux or Kleiger fracture) involves only the epiphysis Triplane fracture includes also a metaphyseal fracture, physeal injury, articular surface involvement, and transverse, sagittal, and coronal components and represents a variant of a type IV injury
Distal portion of the fibula[40]			Nine percent of all Salter-Harris fractures of the skeleton Salter-Harris types I and II are most frequent at this site Mechanism: supination-inversion Commonly results in a minimally displaced fracture of the distal fibular epiphysis
Stress-related Bone Injuries[190]			
Fatigue fracture[40]		See Figures 10-12, *E, F*	Distal end of the tibia: long-distance running in young athletes, golfing, and in persons with osteoarthritis Subtle fissure develops at the junction of the medial malleolus and medial tibial plafond Distal portion of the fibula: heavy-weight training, ballet dancing, and long-distance running; also secondary to traumatic tibiofibular synostosis
Insufficiency fracture[46]		11-40	Distal portion of the tibia or fibula Osteoporosis from rheumatoid arthritis or corticosteroid use in older patients
Dislocations			
Tibiotalar joint dislocation[47]		11-41	Medial dislocation of the talus is the most common type Anterior, posterior, and other displacements also occur in association with other injuries Often associated with fractures and ligamentous injuries about the ankle

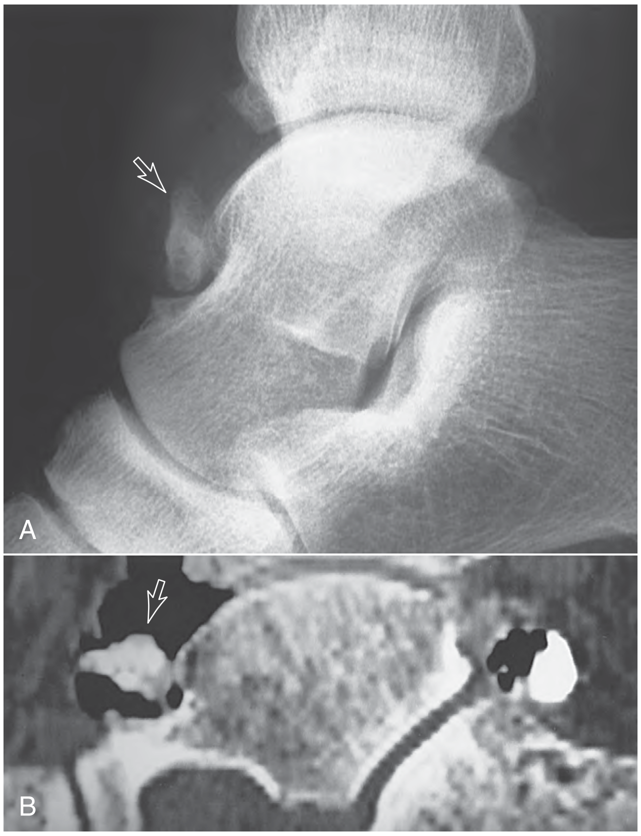

FIGURE 11–37 **Intraarticular osteochondral body.**[41] This 44-year-old woman has had chronic ankle pain for 4 years. **A,** Routine radiograph shows an osseous fragment anterior to the articular surface of the talus *(open arrow)*. **B,** CT arthrography. A reformatted sagittal CT scan after introduction of air and iodinated contrast material reveals an osteochondral body *(open arrow)* attached to the synovium of the anterior portion of the joint.

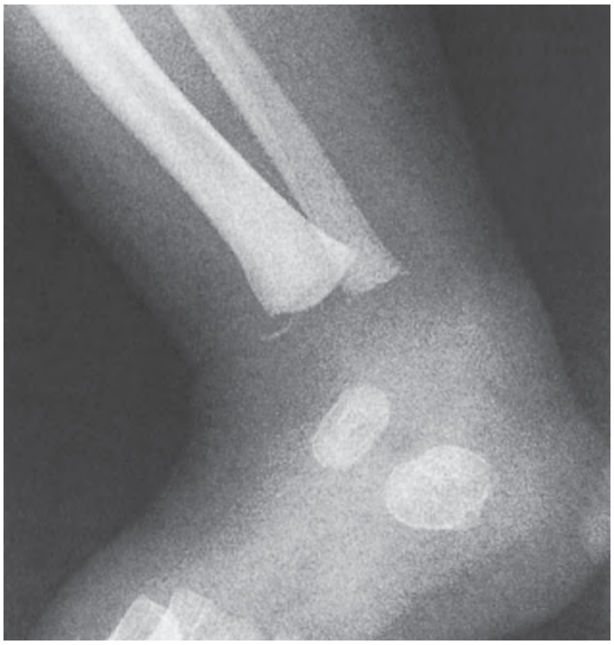

FIGURE 11–38 **Child abuse: metaphyseal injury.**[42] The lateral view of the ankle demonstrates metaphyseal injuries of the distal ends of the tibia and fibula. Observe the normal skeleton and the absence of periosteal new bone formation. Most of these fractures are unilateral and involve the left side, but they also may be bilateral. These fractures are less conspicuous when acute and more conspicuous when they begin to heal. *(From Hilton SVW, Edwards DK. Practical pediatric radiology. 2nd Ed. Philadelphia, Saunders, 1994, p. 398.)*

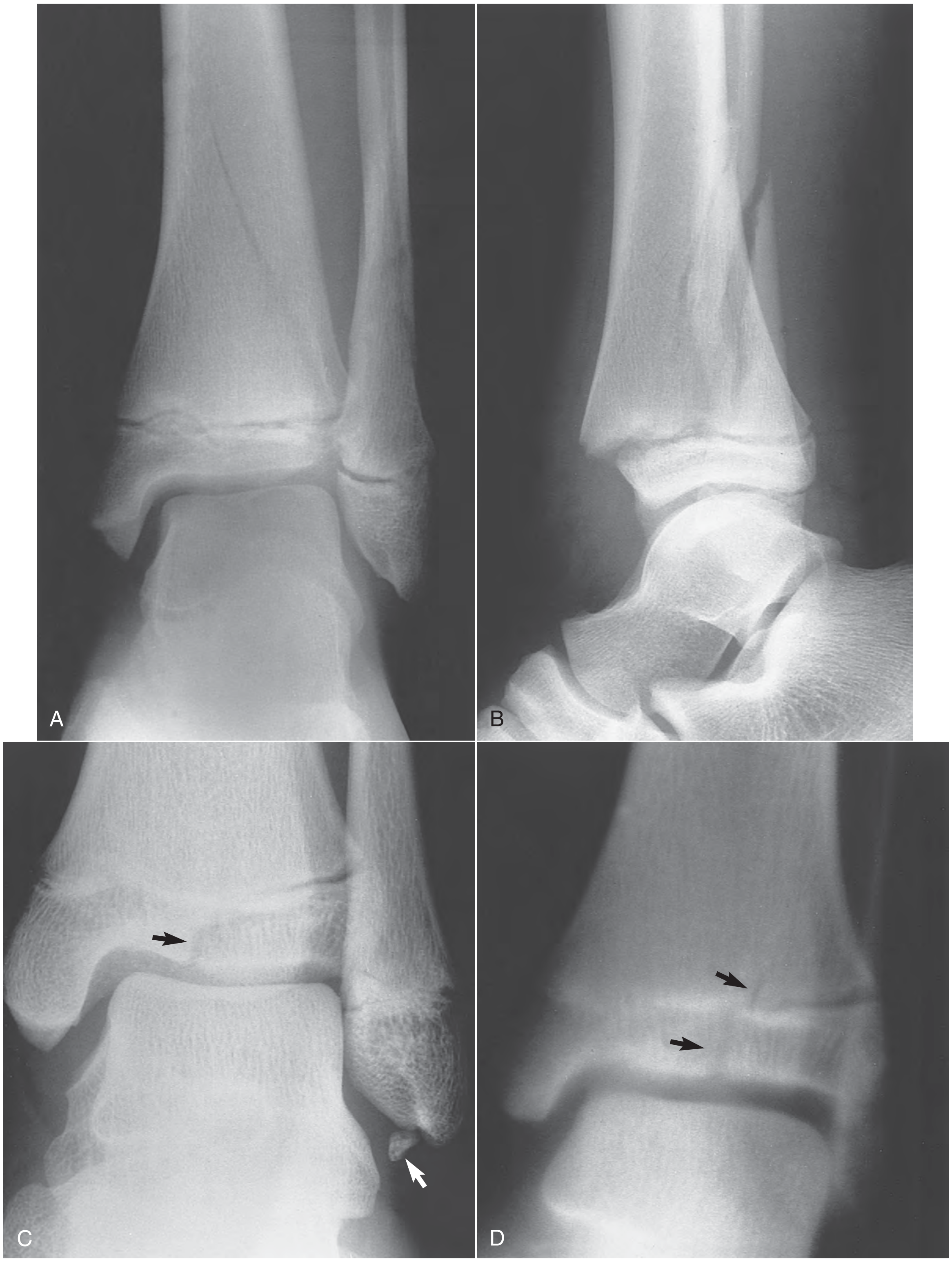

FIGURE 11–39 **Growth plate injuries.**[43-45] **A-B,** Type II physeal injury. Frontal **(A)** and lateral **(B)** radiographs of the ankle in this 14-year-old boy show a fracture through the distal tibial physeal plate and extending into the metaphysis. A large metaphyseal fragment, posterior displacement of the epiphysis, and an oblique fracture of the fibula are also present. **C-D,** Type IV physeal injury. Frontal radiograph **(C)** and conventional tomogram **(D)** of the ankle in a 13-year-old boy demonstrate fractures through the epiphysis, physis, and metaphysis *(black arrows)*. The radiograph does not show the metaphyseal component. An avulsion of the distal end of the fibula is also apparent *(white arrow)*. Growth plate injuries about the ankle are common, type II injuries being the most frequent. These injuries may be accompanied by neurovascular entrapment and growth disturbances, complications that occur in 10% to 12% of physeal injuries at this site.

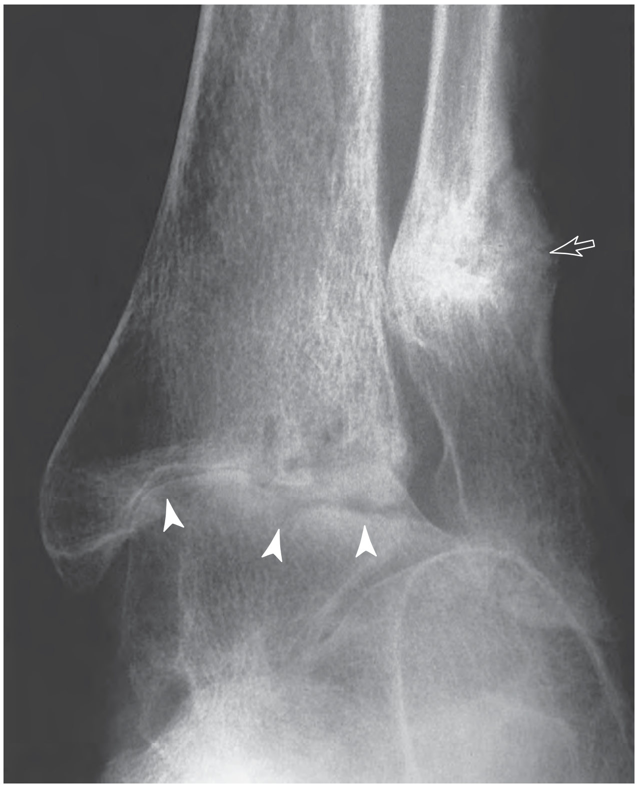

FIGURE 11–40 **Stress (insufficiency) fracture.**[46,190] This 62-year-old woman with long-standing rheumatoid arthritis and osteoporosis has sustained an insufficiency fracture through the distal portion of the fibula *(open arrow)*. The tibiotalar joint is diffusely narrowed and extensively eroded and deformed *(arrowheads)* as a result of rheumatoid arthritis. This patient had sustained a similar fracture of the opposite fibula several years earlier. *(Courtesy J. Rubinstein, MD, PhD, Reno, Nev.)*

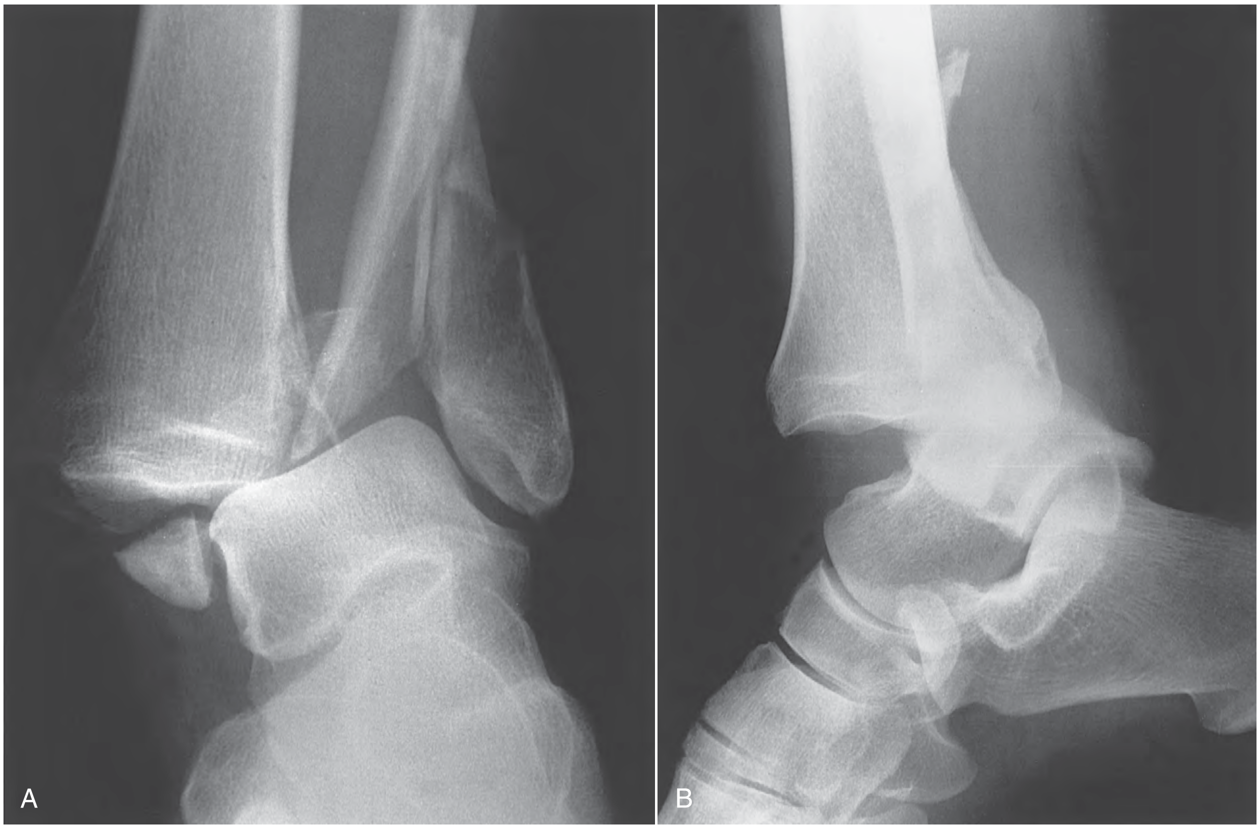

FIGURE 11–41 **Fracture-dislocation: tibiotalar joint.**[47] Frontal **(A)** and lateral **(B)** radiographs reveal fracture-dislocation of the tibiotalar joint. The posteriorly dislocated fibula was trapped behind the tibia, requiring open reduction. This rare injury typically results from severe external rotation of the foot and is termed the *Bosworth fracture-dislocation* of the ankle.

TABLE 11-7 Fractures and Dislocations of the Tarsal Bones

Entity	Figure(s)	Characteristics	Complications and Related Injuries
Fractures of the calcaneus[48-50]		Most frequent tarsal bone to fracture	
Extra-articular fracture[166]	11-42, *A, B*	25% of all calcaneus fractures Twisting forces are most important Fractures of any part of the bone, including: A. Avulsion of the calcaneal tuberosity B. Fracture of the anterior calcaneal process—2 mechanisms: i) *avulsion:* flexion-inversion and distraction of the bifurcate ligament leading to avulsion ii) *nutcracker:* rare impaction phenomenon with eversion and dorsiflexion of the midfoot	Usually uncomplicated Probable association with calcaneonavicular coalition and avulsion fracture of the anterior calcaneal process
Stress (fatigue) fracture	11-42, *C*	Common in military recruits	May become complete fracture
Stress (insufficiency) fracture	11-42, *D*	Rheumatoid arthritis, neurologic disorders, and other diseases	May become complete fracture
Intraarticular fracture	11-42, *E, F*	75% of all calcaneus fractures Poorer prognosis than for extra-articular fracture Comminution and rotation of the fragments are common and disrupt the subtalar joint Vertical falls in which the talus is driven into the cancellous bone of the calcaneus CT important in evaluation	Subtalar degenerative joint disease Malunion Peroneal tendon dislocation and entrapment Displaced fragments
Fractures of the talus[51,52,183]	11-43	Second most frequent tarsal bone to fracture AKA aviator's astragalus Avulsion fractures predominate: superior surface talar neck; lateral, medial and posterior aspects of the body	May be associated with dislocations of the tibiotalar or subtalar joints
Talar neck		Eversion stress causes avulsion at the site of attachment of deep fibers of the deltoid ligament to the body of the talus	Complications in up to 90% of displaced fractures include: delayed union, nonunion, infection, degenerative joint disease, ischemic necrosis especially of the proximal portion of the bone
Talar body[191]		Infrequent fracture resulting from severe dorsiflexion and external rotation impacts the body on the lateral malleolus Stress (fatigue) fractures of the talar body have been reported in elite female gymnasts; radiographs initially negative but become positive 4-6 weeks later; CT, MR imaging and scintigraphy may be useful	Ischemic necrosis, degenerative joint disease, and delayed union
Lateral process		*Rare:* Less than 2% of talar fractures Severe ankle dorsiflexion and pronation, observed most frequently during sport activities particularly snow boarding	Nonunion with pseudarthrosis, subtalar degenerative joint disease Immediate diagnosis results in better outcome and fewer complications than cases with delayed diagnosis
Posterior process		Severe plantar flexion of the foot causes compression of talus between tibia and calcaneus—nutcracker effect	Posterior process: may be confused with os trigonum and may result in posterior ankle impingement syndrome
Head of talus		Rare fracture related to longitudinal compression combined with plantar flexion of the foot	Associated injuries of tarsal navicular bone and talonavicular joint Osteonecrosis is infrequent

TABLE 11-7 Fractures and Dislocations of the Tarsal Bones—cont'd

Entity	Figure(s)	Characteristics	Complications and Related Injuries
Osteochondral lesion: Osteochondritis dissecans of the talus[53,192]	11-44	Osteochondritis dissecans and osteochondral fractures of the talar dome are common after ankle injury Osseous defect may be quite subtle or invisible on radiographs, and CT, arthrography, or MR imaging may be necessary to delineate the fracture site Men > women; Age 10-40 years Two major anatomic sites: *Medial talar dome:* believed to be related to a combination of plantar flexion of the foot with inversion, followed by rotation of the tibia on the talus Typically involves posterior third of medial border *Lateral talar dome:* results from inversion injuries of the ankle in which the lateral margin of the talus impacts upon the fibula Fragment may remain in place or it may displace Typically involves middle third of lateral border	Pain aggravated by motion, limitation of motion, clicking, locking and swelling
Dislocations of the talus[54]	11-45	Usually accompanied by fractures of bone but may be isolated injuries	
		Subtalar dislocation: disruption of the talocalcaneal and talonavicular articulations As many as 80% of cases are medial subtalar dislocations Forceful inversion of the foot, most typically a basketball injury	Ischemic necrosis
		Total talar dislocation: infrequent and serious injury	Ischemic necrosis and infection
Fractures of the navicular bone[55-58]	11-46, 11-47	Acute fractures occur infrequently Most likely sites: dorsal surface, tuberosity, and body	Often initially overlooked Associated fractures or dislocations
	11-48	*Stress (fatigue) fracture:* sagittally oriented fracture observed in physically active persons, especially basketball players and runners	Can result in complete fracture
Fractures of the cuboid and cuneiform bones[40,169,190]		Acute fractures infrequent Stress (fatigue and insufficiency) fractures also infrequently encountered	Often initially overlooked Associated fractures and dislocations
Tarsal dislocations[59,60,184,185]	11-49; 11-78, *C*	Lisfranc fracture-dislocation of the tarsometatarsal joints Direct or more commonly indirect high-energy trauma Mechanism includes plantar hyperflexion with forced supination or pronation resulting in fractures of the metatarsal bases and/or injury of the ligaments *Indirect:* violent abduction of the forefoot leads to lateral displacement of the four lateral metatarsal bones with or without a fracture of the base of the second metatarsal and cuboid bone; the first metatarsal bone may dislocate in the same (homolateral) or opposite (divergent) direction as the other metatarsals Routine radiographs useful in depicting obvious fractures MR imaging allows depiction of disruption of Lisfranc ligament and tarsal and metatarsal fractures Other tarsal subluxations and dislocations are rare	Degenerative joint disease Ankylosis Isolated joint malalignment in an asymptomatic patient with no ligamentous injury, no fracture and no bone marrow edema might reflect normal anatomic features and must be interpreted carefully

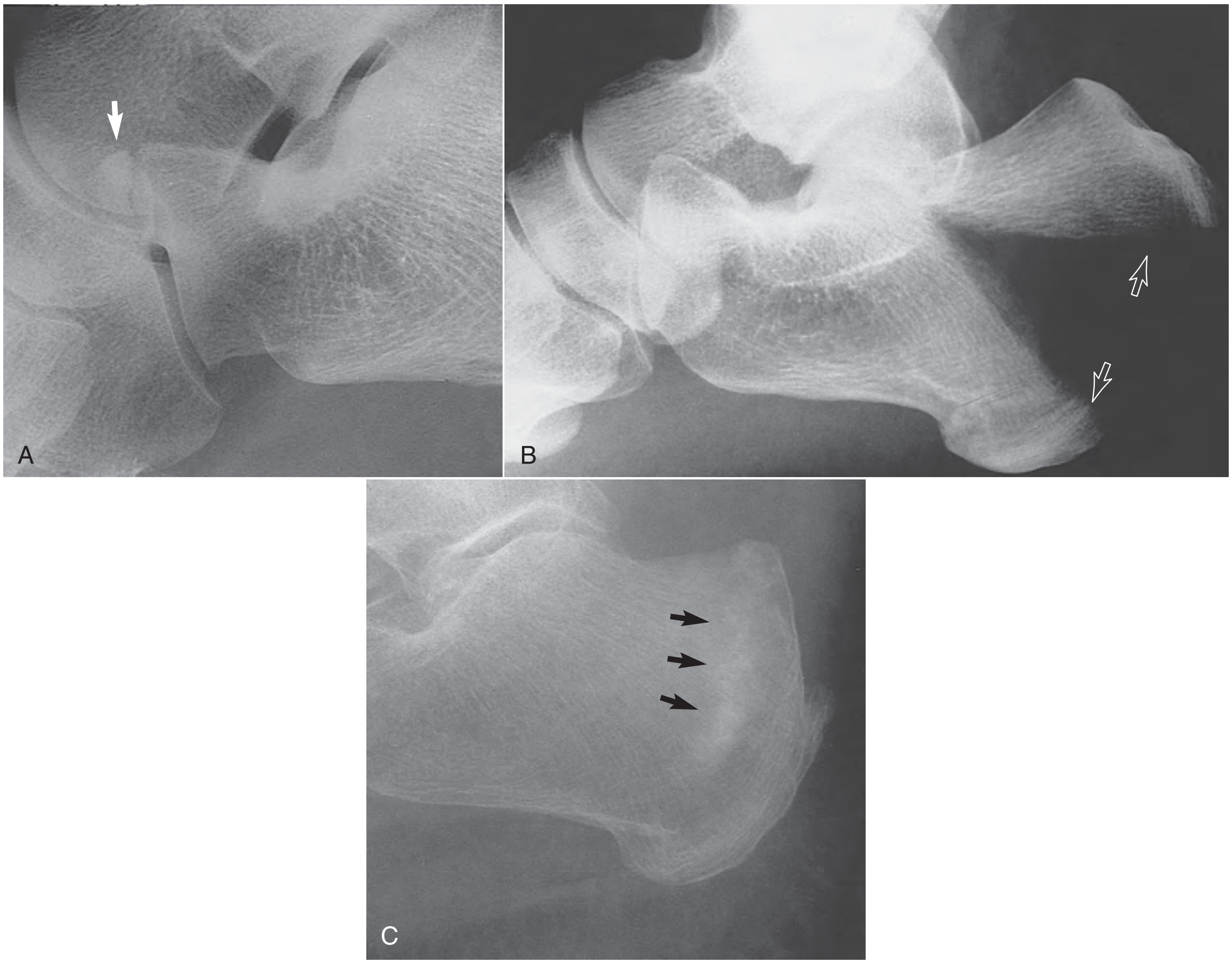

FIGURE 11–42 Fractures of the calcaneus.[48-50,150] **A,** Anterior process avulsion. A fracture of the anterior process of the calcaneus is seen *(arrow)*. This extraarticular fracture, which can be difficult to detect on routine radiographs, results most commonly from twisting injuries and occurs at the site of attachment of the ligamentum bifurcatum. It may resemble the calcaneus secundarium, a normal ossicle. **B,** Calcaneal tuberosity avulsion. Observe the superior displacement of the fracture fragment *(open arrows),* which has been avulsed by the Achilles tendon. **C,** Stress (fatigue) fracture. Observe the vertically oriented sclerotic zone *(arrows)* in the posterior aspect of the calcaneus. This radiographic appearance is characteristic of stress fractures. Calcaneal fatigue fractures have been reported after jumping, parachuting, prolonged standing, and recent immobilization. These fractures are common in military recruits.

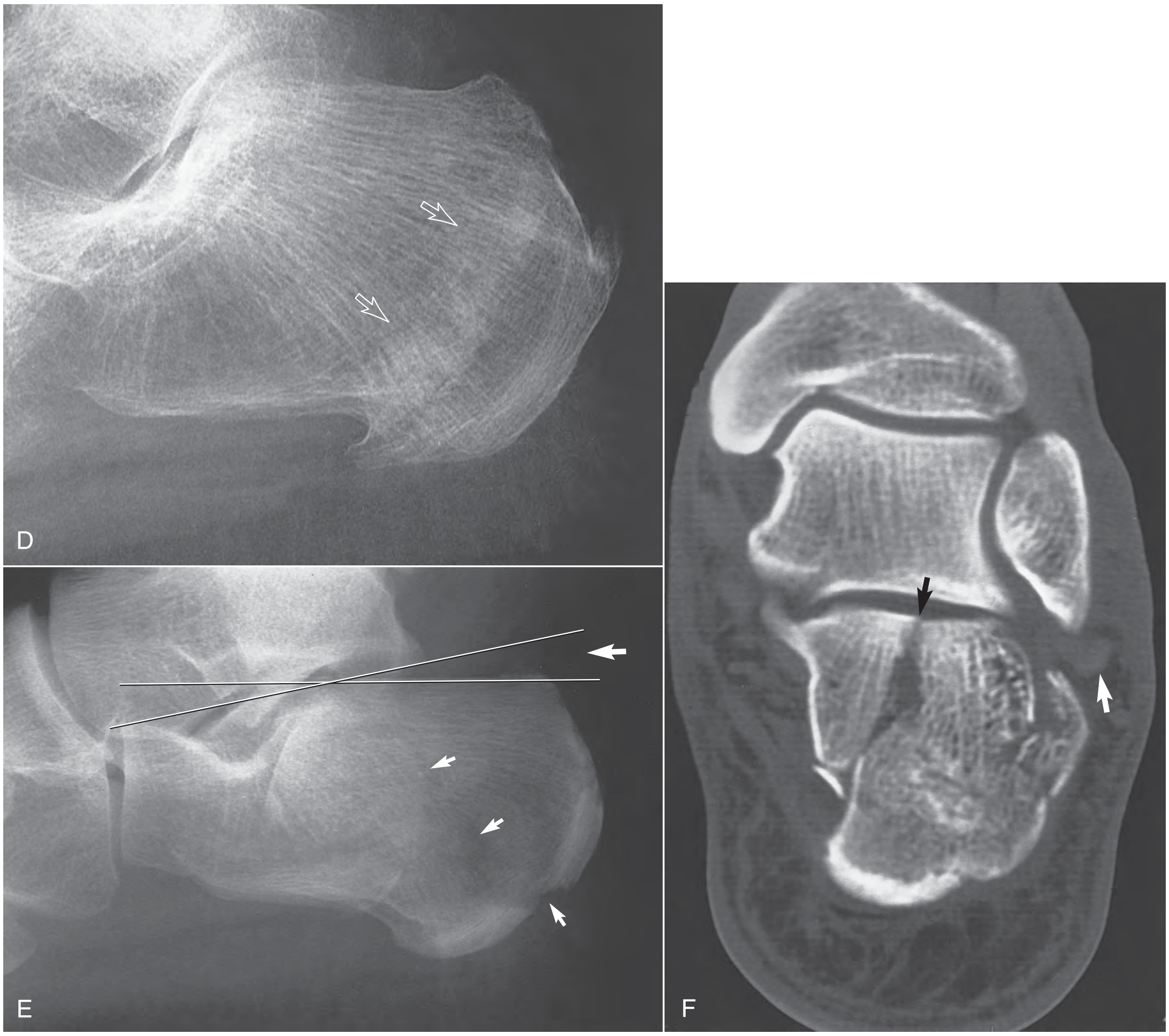

FIGURE 11–42, cont'd **D,** Stress (insufficiency) fracture. In a 58-year-old woman with rheumatoid arthritis, a vertically oriented zone of sclerosis is seen *(open arrows)*. This is a classic appearance of calcaneal insufficiency fracture, a frequent complication of rheumatoid arthritis. **E-F,** Intraarticular fracture: Böhler angle and CT examination. In **E,** a routine lateral radiograph shows a fracture of the calcaneus *(small arrows)*. A useful measurement is the Böhler angle, which is formed by the intersection of two lines. The first line is constructed between the highest point of the anterior process of the calcaneus and the highest point of the posterior articular surface; the second line is constructed between the latter point and the most superior part of the calcaneal tuberosity. In a normal calcaneus, Böhler angle measures between 25 and 40 degrees. In this patient, it measures 10 degrees *(large arrow)* owing to a complex intraarticular fracture. In **F,** a direct-acquisition coronal CT image shows the complexity of this comminuted, intraarticular fracture. Findings include marked lateral displacement of the lateral portion of the calcaneus, abutment of this region of the calcaneus, and the distal portion of the fibula, displacement of the peroneal tendons *(white arrow),* and communication of the fracture line with the subtalar joint *(black arrow)*. The calcaneus is the most common site of tarsal fracture. Fractures are bilateral in about 10% of cases and usually result from a vertical fall, such as a jump from a height. Many of these fractures may be seen on lateral radiographs as a decrease in the Böhler angle. Intraarticular fractures are more complex, are associated with a poorer prognosis, and are best evaluated with CT. *(**B, E,** and **F,** Courtesy M.N. Pathria, MD, San Diego.)*

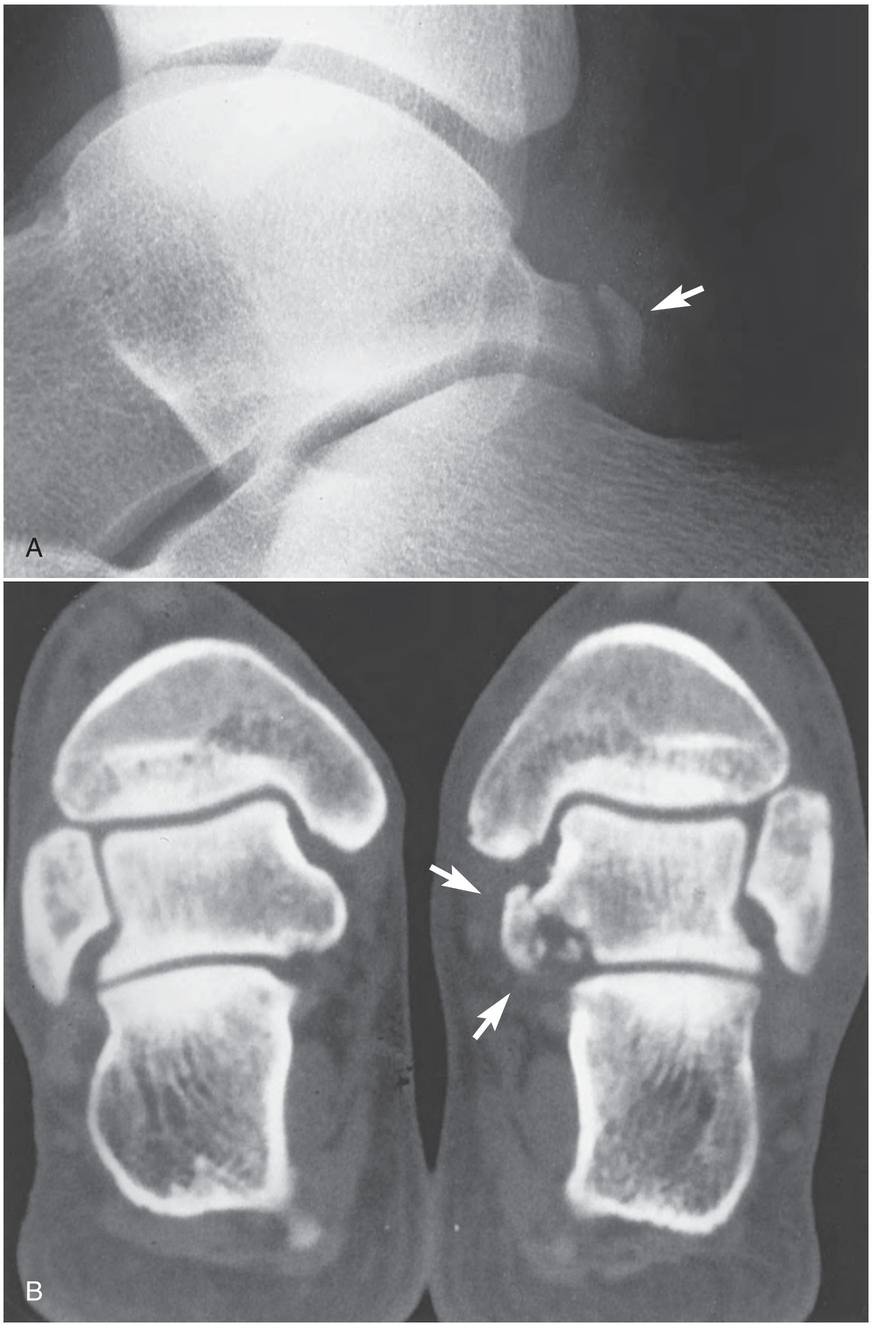

FIGURE 11–43 **Fractures of the talus.**[51,52,183] **A,** Posterior process *(arrow)*. This fracture usually occurs during severe plantar flexion of the foot, owing to compression between the posterior surface of the tibia and the calcaneus. The posterior process may be difficult to differentiate from an os trigonum, a normal ossicle that also may be painful. **B,** Talar body. Bilateral coronal CT scan accurately reveals an avulsion fracture of the medial portion of the left talus *(arrows)*. Observe the normal opposite talus. The routine radiograph (not shown) appeared normal in this 29-year-old man who injured his ankle in a jump from a 7-foot wall. Such fractures usually occur after eversion stress with osseous avulsion at the site of attachment of the deep fibers of the deltoid ligament. A frontal radiograph obtained with external rotation of the ankle (not shown) is the best projection for demonstrating fractures of the medial process of the talus. *(**B,** Courtesy G. Greenway, MD, Dallas, Texas.)*

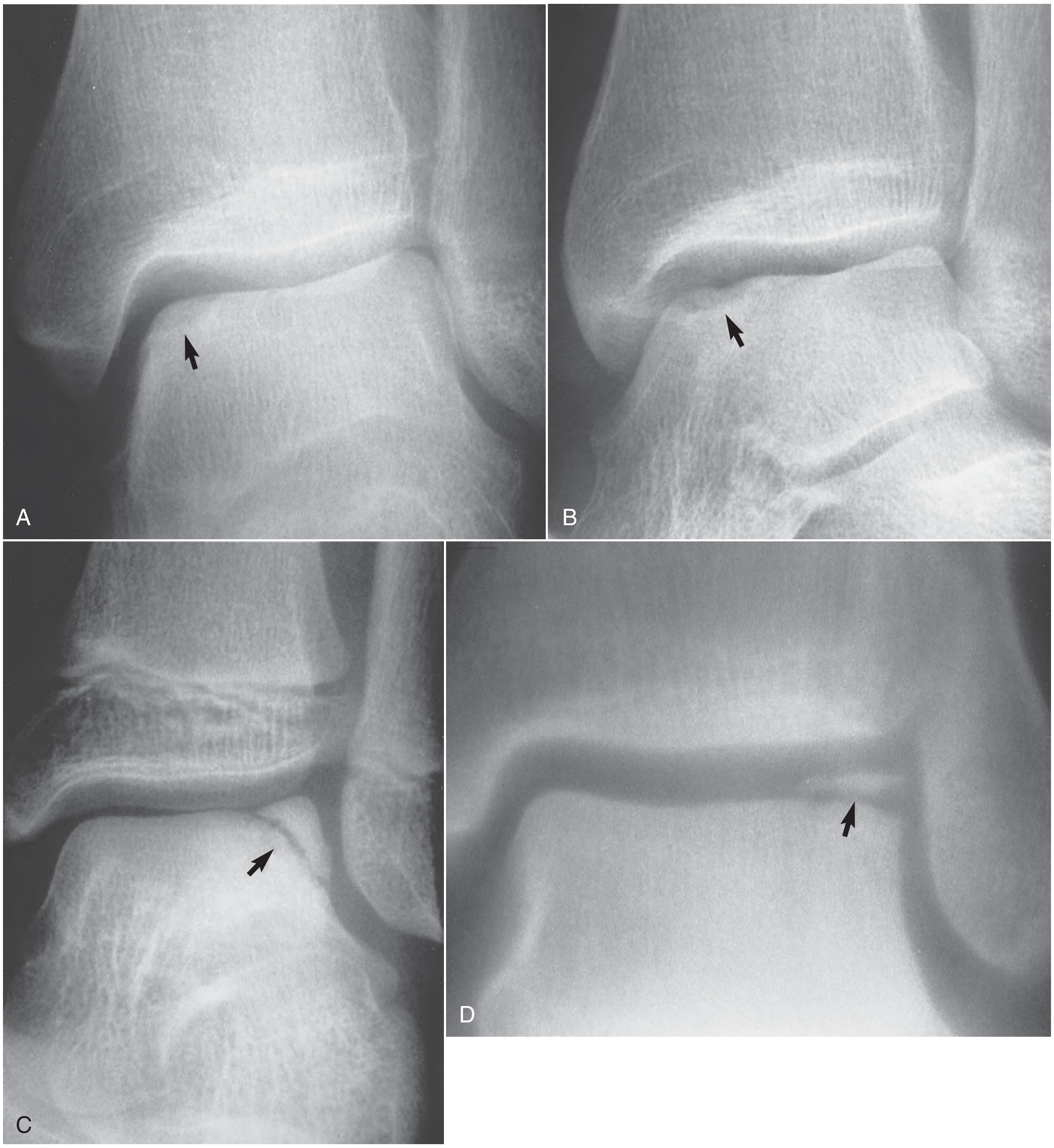

FIGURE 11–44 Osteochondral lesion: osteochondritis dissecans.[53,192] **A-B,** Medial talar dome. Anteroposterior **(A)** and medial oblique **(B)** radiographs show a radiolucent osteochondral defect on the medial talar dome *(arrows)*. No associated bone fragment is seen. Such osseous and osteocartilaginous bodies are better seen with computed arthrotomography or MR imaging. **C-D,** Lateral talar dome. In **C,** a 10-year-old female gymnast, observe the osteosclerotic, triangular osseous fragment adjacent to the lateral articulating surface of the talar dome *(arrows)*. The underlying bone also appears osteosclerotic. The lesions were bilateral (other side not shown). In **D,** another patient, a conventional coronal tomogram clearly identifies an osseous fragment separated from a similar location on the talar dome. (***A-B,*** *Courtesy R. Kerr, MD, Los Angeles;* ***C,*** *Courtesy G. Greenway, MD, Dallas, Texas.)*

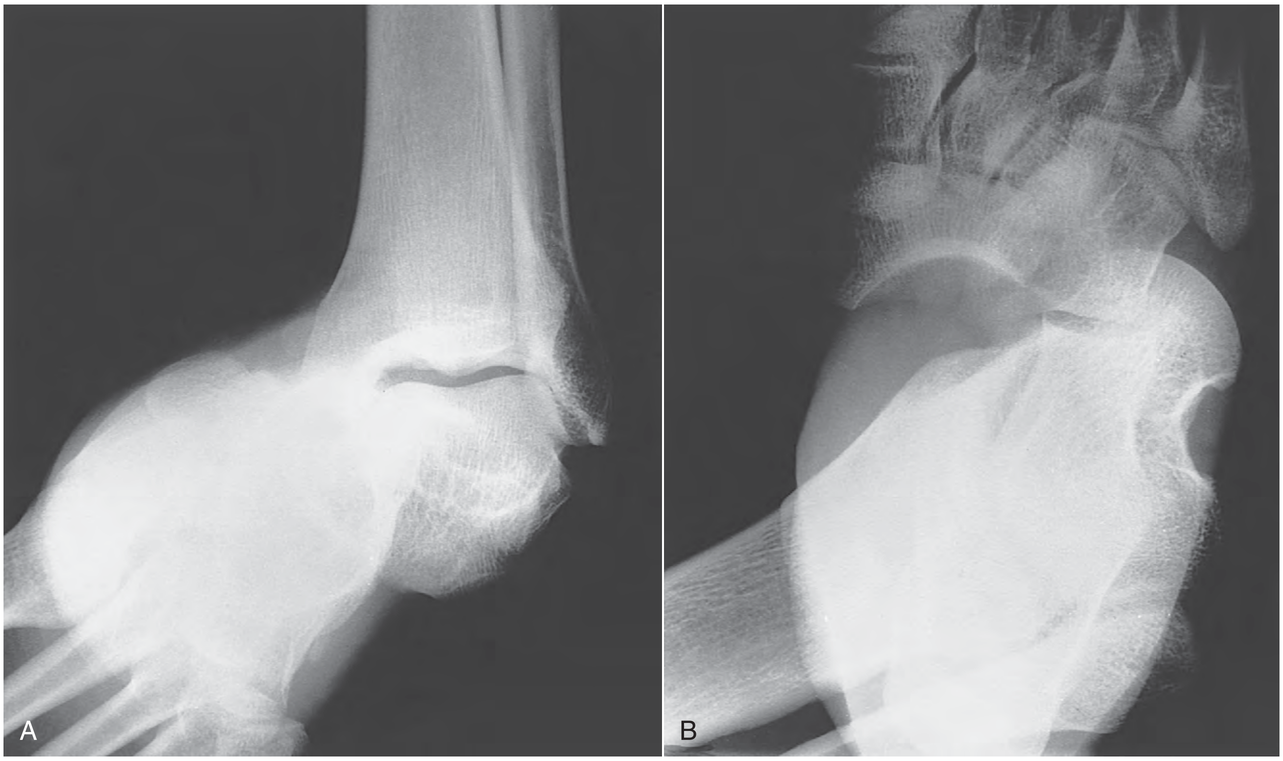

FIGURE 11–45 **Medial subtalar dislocation.**[54] **A-B,** Note the dislocation of the anterior talocalcaneonavicular and posterior subtalar joints and a relatively normal alignment of the calcaneocuboid joint. *(From Resnick D: Diagnosis of bone and joint disorders. 4th Ed. Philadelphia, Saunders, 2005, p 2899.)*

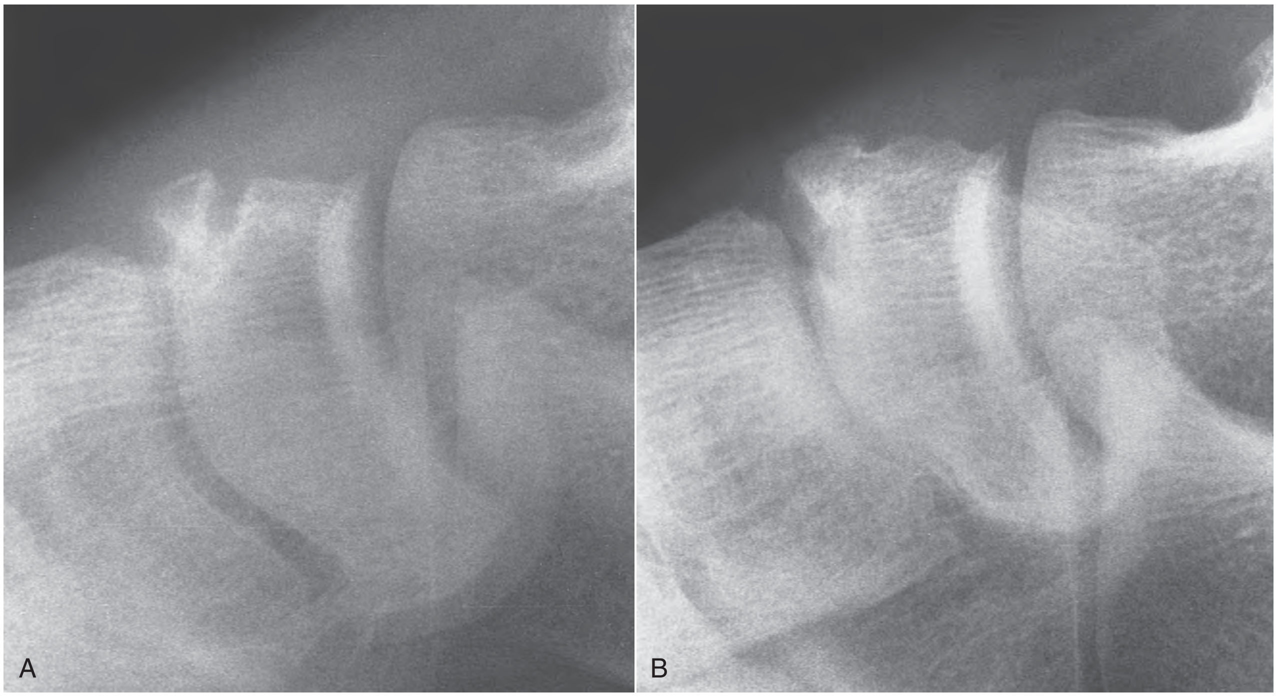

FIGURE 11–46 **Healing navicular fracture.**[55] This 18-year-old woman had pain on the dorsum of the foot after a soccer injury. The initial diagnosis was a painful os supranaviculare, seen on a radiograph taken several months after the injury **(A).** The pain persisted and another radiograph was obtained 1 year later **(B),** which showed fusion of the triangular fracture fragment.

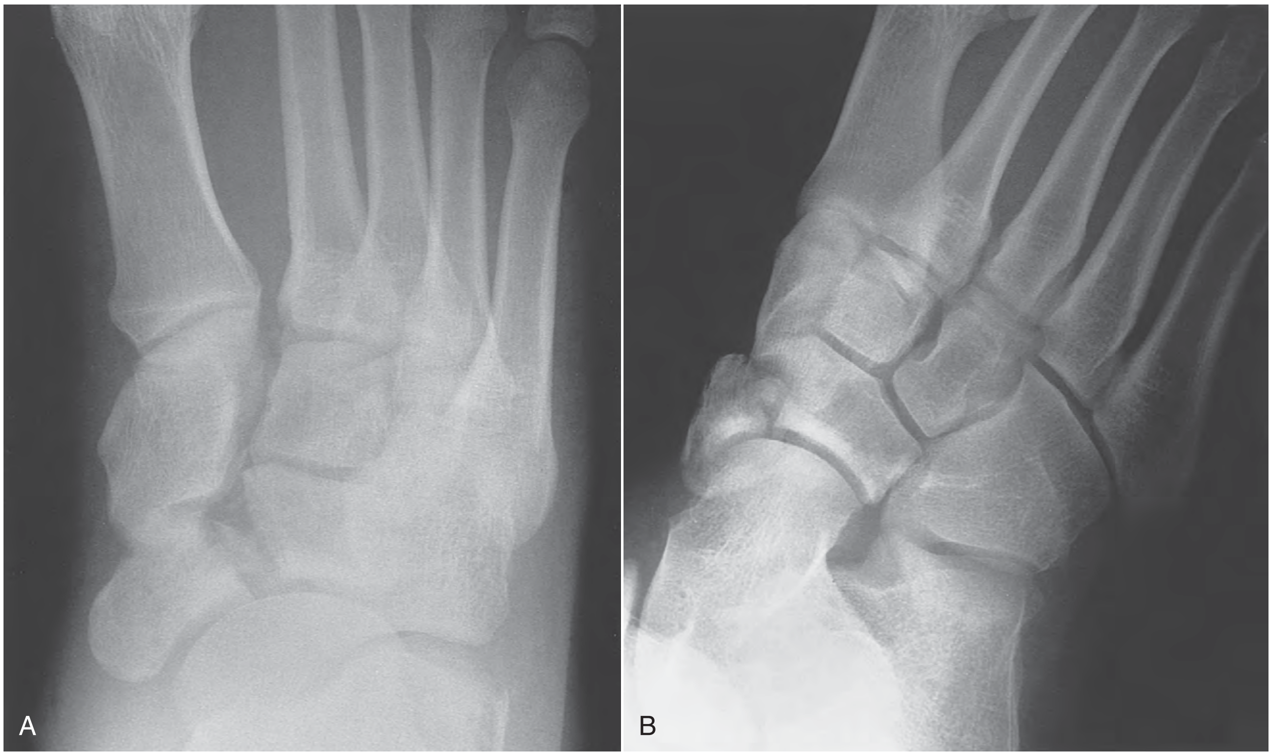

FIGURE 11–47 **Navicular fracture with dissociation of medial and intermediate cuneiform bones.**[56] **A-B,** This 21-year-old man was involved in a motorcycle accident. Radiographs reveal a longitudinal fracture of the navicular bone, which is aligned with the widened space between the medial and intermediate cuneiform bones. This is an unstable injury requiring surgical reduction.

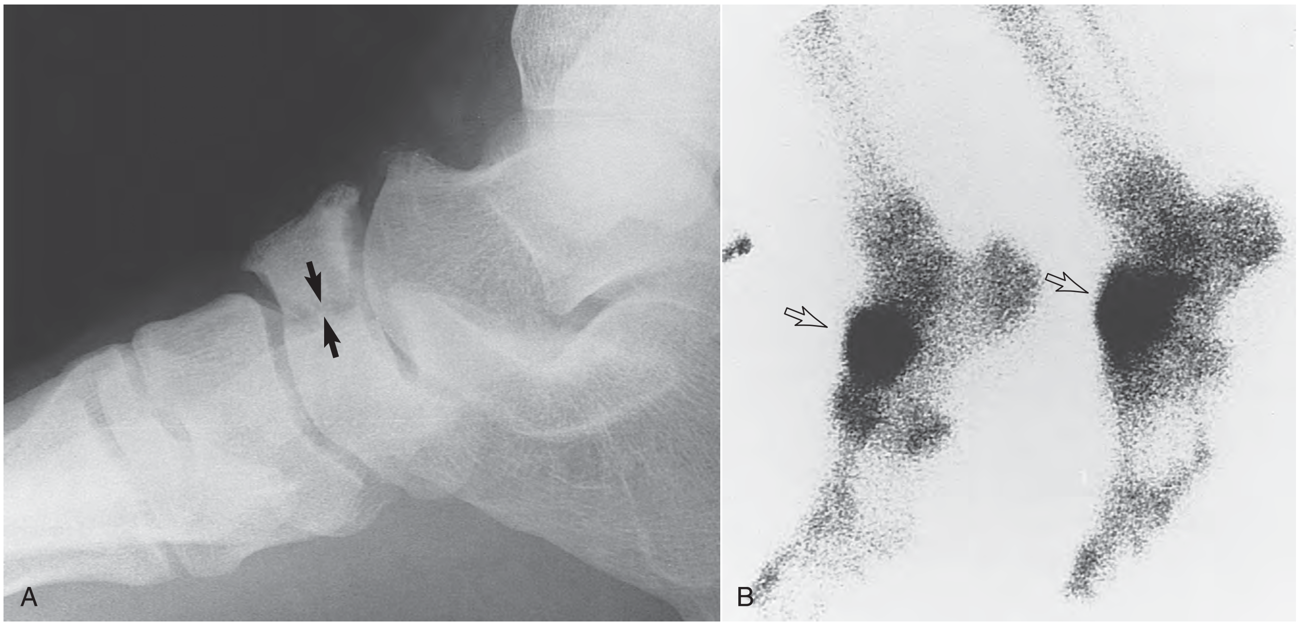

FIGURE 11–48 **Stress (fatigue) fracture of tarsal navicular.**[57,58,150,190] **A,** Lateral radiograph of this 21-year-old female physical education student shows a linear sagittal lucent area surrounded by marginal sclerosis within the navicular bone *(arrows)*. **B,** Bone scan demonstrates bilateral increased uptake of the bone-seeking pharmaceutical agent, revealing stress fractures of both navicular bones *(arrows)*. The first fracture apparently was undiagnosed until the time of this examination. Stress fractures of the navicular bone are associated with activities involving stomping on the ground, marching, and long-distance running. They are especially common in basketball players and runners. Such fractures are often not seen on conventional radiographs, and accurate diagnosis requires further evaluation by clinical examination, CT, scintigraphy, and magnetic resonance (MR) imaging. *(Courtesy M. Mitchell, MD, Halifax, Nova Scotia, Canada.)*

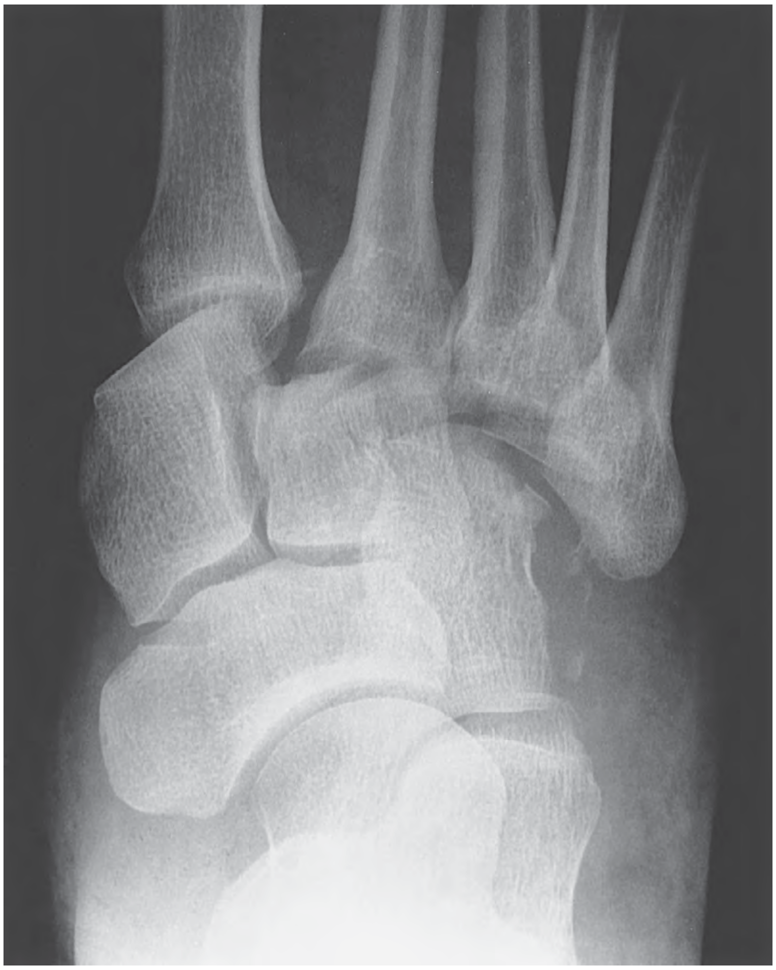

FIGURE 11–49 Lisfranc fracture-dislocation of the tarsometatarsal joints.[59,60,184] Observe the lateral dislocation of all the metatarsal bones. Fractures of the cuboid and bases of the metatarsal bones are also seen. In this case, all five metatarsals are dislocated laterally, a pattern described as homolateral. When the first metatarsal dislocates medially, in the opposite direction of the other four metatarsals, it is termed the *divergent pattern*.

TABLE 11-8 Fractures and Dislocations of the Metatarsals and Phalanges[159]

Entity	Figure(s)	Characteristics	Complications and Related Injuries
Acute metatarsal fracture[40,174,178]	11-50	Caused by direct and indirect forces Transverse, oblique, spiral, or comminuted *Shaft and neck:* heavy object falling on foot *Rare fractures:* first metatarsal bone and the metatarsal heads	
		Base of the fifth metatarsal: two types 1. *Avulsion of the tuberosity:* sudden inversion results in avulsion of a portion of the styloid process by the attachment of the short peroneal muscle or the lateral component of the plantar aponeurosis Transverse orientation of fracture helps to differentiate it from a normal longitudinal growth center	Fragment may enter cuboid-metatarsal joint space Routine radiographs of the foot may fail to reveal avulsion fractures of the base of the fifth metatarsal; an additional AP radiograph of the ankle that includes the base of the fifth metatarsal may depict the fracture to better advantage
		2. *Jones fracture:* transverse fracture of the proximal portion of the diaphysis	Frequently associated with delayed union, nonunion, and refracture
Metatarsal stress (fatigue) fracture[64-66,150,190]	11-51	Second and third metatarsal shafts (march fracture) or metatarsal bases are common sites of fatigue fractures, but any metatarsal can be affected Often caused by marching, ballet dancing, prolonged standing, foot deformities, and surgical resection of adjacent metatarsal bones. Stress fracture infrequently affects the metatarsal heads, simulating Freiberg infraction or diabetic neuropathic osteoarthropathy	May result in complete fracture Recurrence if the stressful activity is not discontinued
Phalangeal fracture[44,67,68]	11-52	Frequently occurring fractures Common mechanism is the stubbed toe	Osteomyelitis in children with physeal damage from nail bed injury
	11-53	Growth plate injuries in children	Residual deformity
Sesamoid bone fracture[23,195]	11-54	Hallux sesamoid bones fracture most frequently	Osteonecrosis Osteoarthrosis and hallux rigidus
Metatarsophalangeal (MTP) joint dislocation[69]		First MTP joint is commonly affected Can occur in any direction related to mechanism of injury *Turf toe:* Hyperextension of the first MTP joint with disruption of the plantar aspect of the joint and joint capsule, which tears away from the metatarsal head; may be associated with hallux sesamoid bone fracture	Complications of any type of hyperextension injury of the great toe: Chondromalacia of the first metatarsal head Hallux rigidus Hallux valgus Dorsal osteophytes Periarticular calcification
		Sesamoid bone dislocations, with or without intraarticular entrapment, may occur rarely, especially at the first toe	May interfere with closed reduction
Interphalangeal (IP) joint dislocation[69]	11-55	The first IP joint is commonly affected	Complications similar to those of MTP joint dislocations

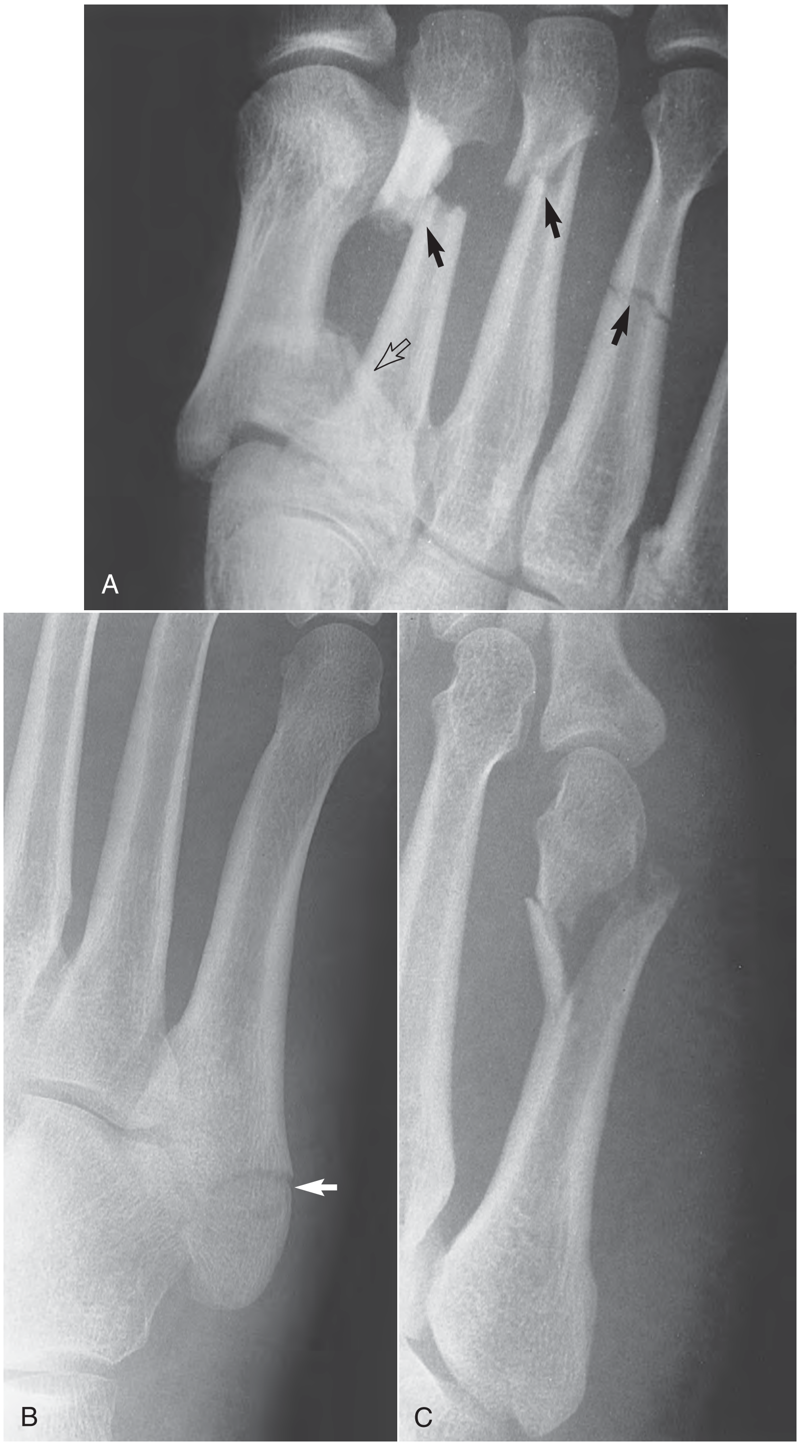

FIGURE 11–50 **Metatarsal fractures.**[40,61-63,174,178] **A,** Multiple metatarsal fractures *(arrows)* are seen on this oblique radiograph obtained after this man dropped a heavy object on his foot. Observe the medial displacement of the distal portions of the metatarsals. The base of the first metatarsal also appears fractured *(open arrow)*. **B,** This 32-year-old man sustained an inversion injury of the foot in a parachuting accident. Note the fracture of the fifth metatarsal base *(arrow)* that enters the cuboid-fifth metatarsal articulation. It is believed to be an avulsion injury at the attachment of the peroneus brevis tendon or the lateral cord of the plantar aponeurosis. This injury should not be confused with the Jones fracture, a transverse fracture that occurs more distally through the fifth metatarsal diaphysis. The Jones fracture frequently results in delayed union, nonunion, and refracture. **C,** In a third patient, a routine radiograph reveals a comminuted fracture of the distal portion of the fifth metatarsal, which is complicated by dorsomedial displacement.

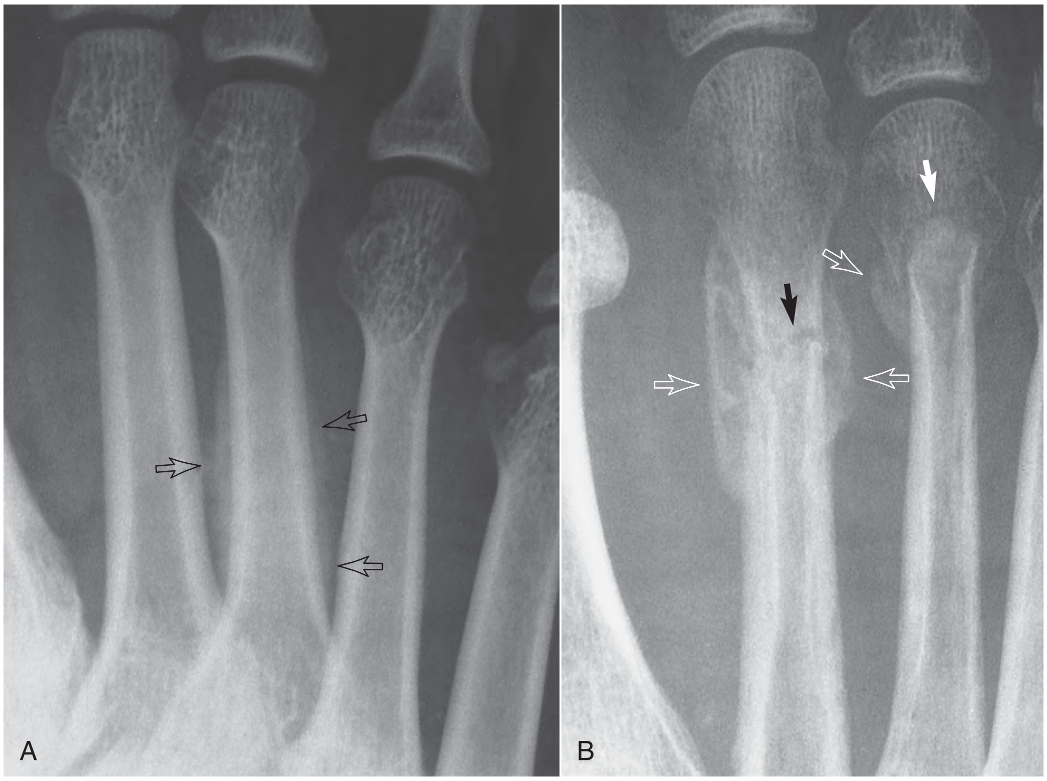

FIGURE 11–51 **Metatarsal stress (fatigue) fracture: March fracture.**[64-66,150,190] **A,** Early findings. In this patient with exercise-induced foot pain, periosteal new bone formation envelops the third metatarsal diaphysis *(open arrows)*. No fracture line is seen. **B,** Later findings. In this 34-year-old woman who recently began a jogging program, observe the fatigue fractures of the second and third metatarsal shafts. The findings include transverse radiolucent fracture lines *(arrows)* with surrounding periostitis *(open arrows)*. Stress fractures commonly affect the metatarsal bones and accompany marching, ballet dancing, prolonged standing, foot deformities, and foot surgery. The middle and distal portions of the second and third metatarsals are most commonly affected. Such fractures, referred to as *march fractures*, may be imperceptible radiographically in the early stages. Bone scans, MR images, or serial radiographs are often necessary to confirm the diagnosis. Stress fractures of the metatarsal heads are less common than those of the shaft and neck and are more frequently overlooked.

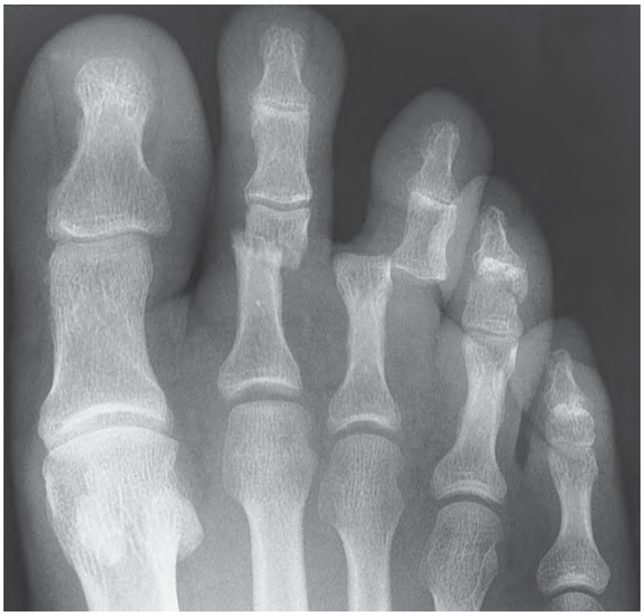

FIGURE 11–52 **Fracture-dislocation.**[67] Frontal radiograph reveals a fracture of the second proximal phalanx and a dislocation of the third proximal interphalangeal joint in this 37-year-old man who had dropped a heavy safe on his foot.

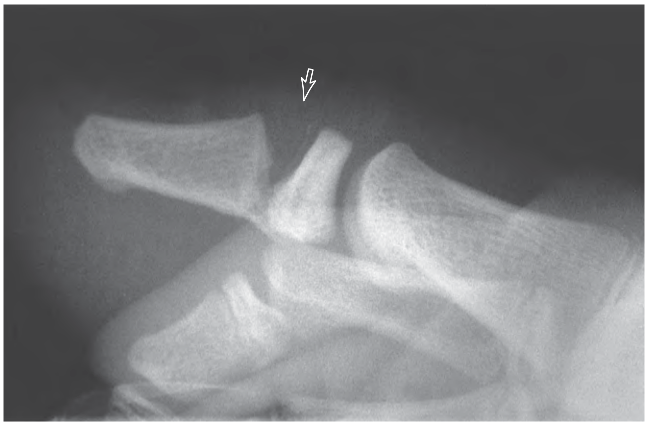

FIGURE 11–53 **Salter-Harris type I injury.**[44,68] Observe the wide separation of the distal phalangeal epiphysis and metaphysis in this child after he had stubbed his toe *(open arrow)*. Such injuries commonly violate the nail bed, creating an open injury and increasing the likelihood of osteomyelitis or septic arthritis.

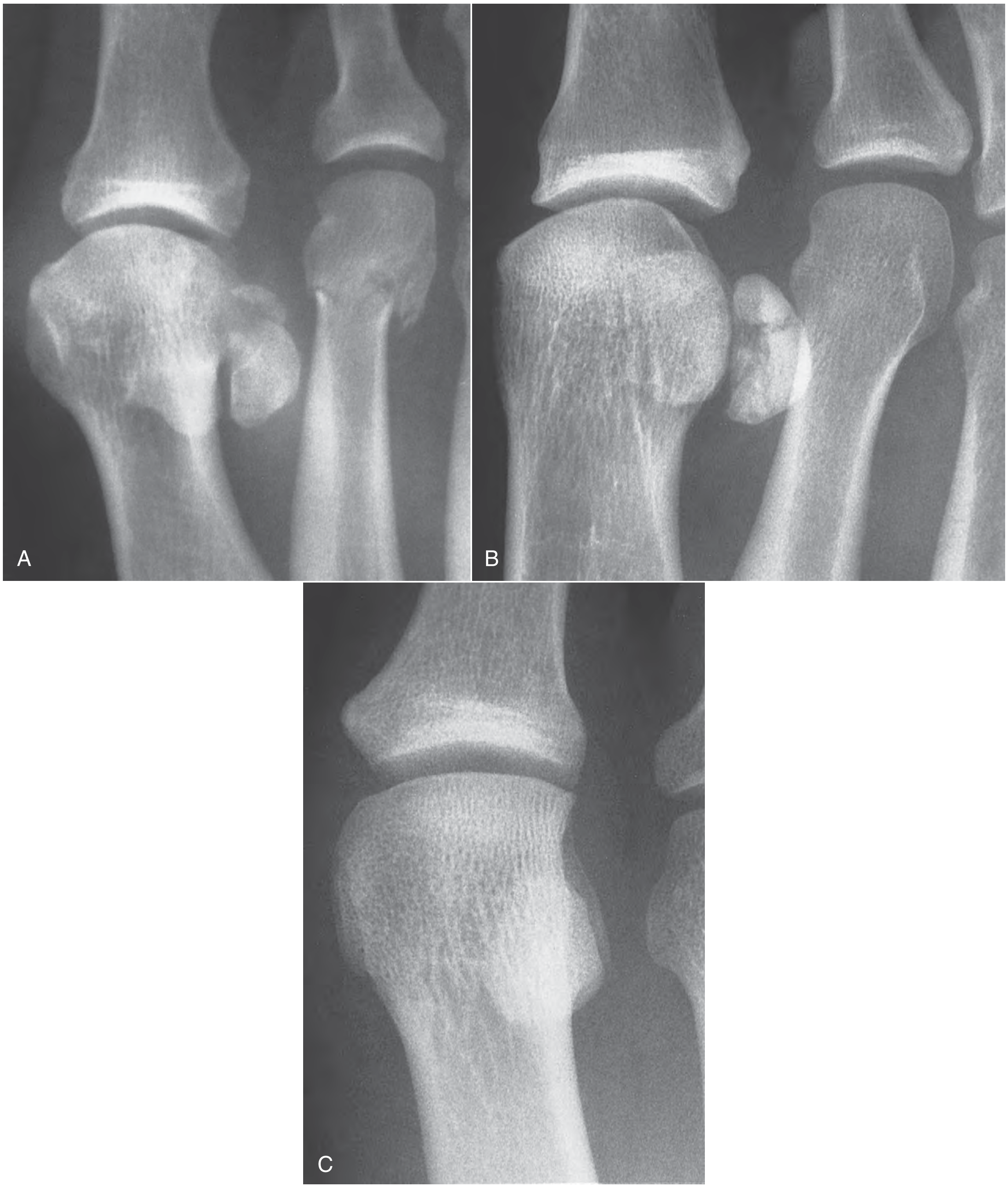

FIGURE 11–54 **Hallux sesamoid bone fracture.**[23,195] **A,** This patient's foot was run over by an automobile. Observe the fracture of the hallux sesamoid bone and a fracture of the second metatarsal bone. **B,** In another patient, the lateral hallux sesamoid bone is fractured. Fracture fragments typically have jagged edges, lack a corticated margin, and may be displaced. These features usually allow differentiation from painful bipartite sesamoid bones, which appear smooth, well-corticated, and nondisplaced. **C,** Sesamoidectomy. This patient had surgical removal of the medial hallux sesamoid after a fracture. Congenital absence of the hallux sesamoid bones occurs rarely. When one or both of these bones is absent, surgical removal is the most likely cause.

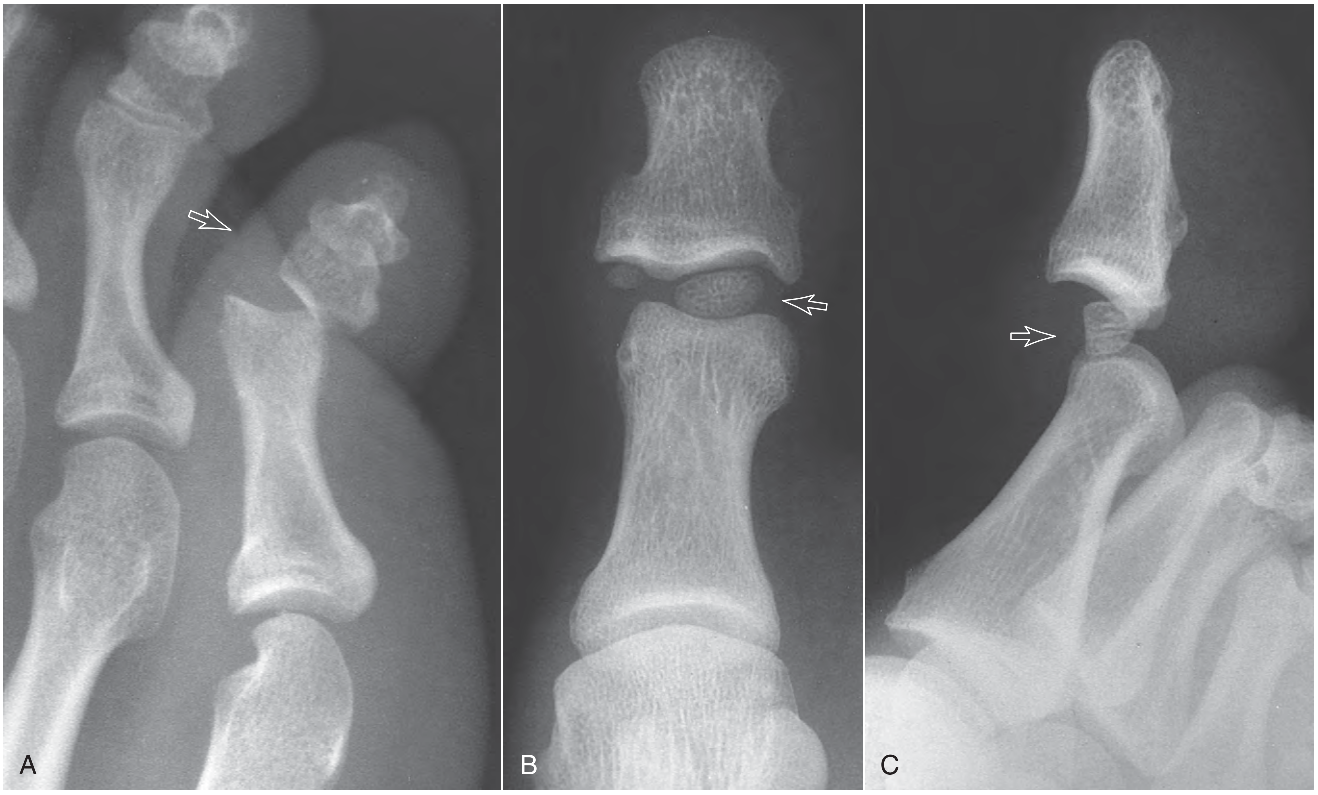

FIGURE 11–55 **Dislocation: interphalangeal joints.**[69] **A,** Observe the dislocation of the fifth proximal interphalangeal joint with lateral displacement of the middle phalanx *(open arrow)*. **B,** Dislocation of the interphalangeal joint of the great toe with intraarticular entrapment of the sesamoid bone *(open arrow)* is evident. **C,** In another patient, radiographs taken after attempts at reduction show persistent entrapment of the sesamoid bone *(open arrow),* necessitating open reduction.

TABLE 11-9 **Specific Features of Stress Fractures in Foot and Ankle***

Bone	Location	Mechanism of Injury	Complications
Sesamoids	Medial ossiculum; middle to distal	Traction injury at toe-off phase	Nonunion
First proximal phalanx	Medial	Avulsion injury by adductors at tiptoe position or sprint in place	
First metatarsal (uncommon)	Head		Sequential fracture
First metatarsal (uncommon)	Proximal		Sequential fracture
Second metatarsal	Base: medial and volar aspect	Most rigid part of the Lisfranc joint	Nonunion, sequential fracture
Second-third metatarsals	Distal	Concentration of shear forces at second metatarsal during propulsive phase	Nonunion, sequential fracture
Fifth metatarsal	Distal to tuberosity	Distraction forces when foot hits the ground	Delayed union, nonunion, refracture
Middle and lateral metatarsals	Distal	Gait change	Delayed union, nonunion
Cuneiforms	Middle	Compression	
Tarsal navicular	Central third, proximal to distal, complete or incomplete sagittal fractures	Maximum shear stress, especially during plantar flexion combined with pronation	Slow healing, complete fracture, delayed union, nonunion, osteonecrosis of lateral fragment, refracture
Cuboid		Compression	
Os peroneum		Avulsion injury	

* Reprinted with permission from Ref 190.

Continued

TABLE 11-9 Specific Features of Stress Fractures in Foot and Ankle—cont'd

Bone	Location	Mechanism of Injury	Complications
Os trigonum		Fracture, pseudarthrosis, impingement	
Talus	Usually neck, occasionally medial or posterior tubercle	Fulcrum effect at neck of talus at heel strike	Avascular necrosis
Calcaneus	Posterior dorsal (vertical coronal fracture)	Compression	Bilateral fractures
Distal fibula	Supramalleolar "runner's" fracture (linear transverse or horizontal oblique fracture)	Everted foot and calf muscle action pushing fibula forward	Peroneal tendon subluxation, associated with medial malleolar fracture in insufficiency
Medial malleolus	Supramalleolar (vertical or oblique fracture)	Internal rotation of talus against medial malleolus during heel strike	Associated with lateral supramalleolar fracture in insufficiency

TABLE 11-10 Soft Tissue Injuries About the Ankle and Foot

Entity	Figure(s)	Characteristics
Joint effusion[70,171]	11-56	Accumulation of excessive synovial fluid with joint Usually seen as a bulging of the anterior capsule on lateral radiographs but the overall accuracy of radiographs for the diagnosis of ankle effusions is quite low. Therefore, documentation of distention of the anterior recess on MR imaging is considered the gold standard. Bland effusion associated with acute injury, or internal joint derangement Proliferative effusion associated with synovial proliferation as in inflammatory arthropathy and villonodular synovitis *Pyarthrosis:* purulent material in joint from pyogenic septic arthritis *Hemarthrosis:* accumulation of blood within joint: hemophilia, villonodular synovitis
Ligament injuries[71]	11-57	Severe ligament injuries may result in chronic ankle instability Classified as acute, subacute, or chronic *Lateral complex:* most commonly injured; inversion sprains *Medial complex:* deltoid ligaments; eversion sprains *Tibiofibular complex:* tibiofibular syndesmosis; least commonly injured Radiographs obtained with the application of inversion stress, eversion stress, and anterior stress (anterior drawer) may reveal excessive motion indicating disruption of ligaments Magnetic resonance (MR) imaging also useful
Tendon injuries[72-75]	11-58 11-59 11-60 11-61	Achilles tendon Tibialis anterior tendon Tibialis posterior tendon Peroneus longus and brevis tendon *Spectrum of injuries:* *Tendinitis:* inflammation of a tendon (more proper term is tendinosis or tendinopathy, indicating degeneration rather than inflammation) *Tenosynovitis:* inflammation of a tendon sheath *Tendon rupture:* *Type I:* partial disruption with vertical splits and bulbous hypertrophy *Type II:* partial disruption with attenuation *Type III:* complete disruption and retraction of torn ends MR imaging is the most useful imaging study

TABLE 11-10 Soft Tissue Injuries About the Ankle and Foot—cont'd

Entity	Figure(s)	Characteristics
Ankle Impingement Syndromes		
Anterolateral ankle impingement[160,161,191]	11-62	Relatively uncommon cause of chronic lateral ankle pain produced by entrapment of abnormal soft tissue in the anterolateral gutter of the ankle. Thought to occur after relatively minor ankle inversion injuries (about 3% of ankle sprain injuries) *Clinical findings include:* anterolateral tenderness and swelling; pain with single leg squatting; pain with dorsiflexion and eversion MR arthrography of the tibiotalar joint is accurate in assessing the anterolateral recess of the ankle
Anterior ankle impingement[161,191]		Relatively common cause of chronic ankle pain especially in athletes subjected to repeated stress in dorsiflexion, typical in soccer players Beaklike osteophyte at the anterior rim of the tibial plafond associated with a corresponding osteophyte or zone of sclerosis over the opposed margin of the talus proximal to the talar neck within the anterior ankle joint capsule Osteophytes impinge on each other during dorsiflexion and the soft tissues become entrapped and painful Radiographs reveal osteophytes and impingement, MR imaging reveals resultant cartilage damage, bone marrow edema, and synovitis
Anteromedial ankle impingement[161,191]		Uncommon cause of chronic ankle pain that results in a meniscoid lesion, which is represented by a soft-tissue thickening anterior to the tibiotalar ligaments; may also be related to partially torn deltoid ligaments or thickened anterior tibiotalar ligament Most commonly related to an inversion mechanism of injury MR arthrography is the most effective imaging method to clearly depict the meniscoid lesion, thickened ligament and any osteochondral lesions
Posteromedial ankle impingement[161,191]	11-63	Uncommon syndrome occurring after severe ankle inversion sprains Involves contusion and crushing of the deep posterior fibers of the medial deltoid ligament between the medial wall of the talus and the medial malleolus MR imaging depicts the lesion, thickened soft tissues, and bone marrow edema
Posterior ankle impingement[161,162,191]	11-17	Repetitive or acute forced plantar flexion results in a nutcracker mechanism in which the posterior talus and associated soft tissues are compressed by the adjacent posterior tibia and the calcaneus Also referred to as the *os trigonum syndrome*, *talar compression syndrome*, and *posterior block of the ankle* Ballet and sporting activities *Common precipitating factors:* Os trigonum (See Table 11-3) Prominent elongated lateral tubercle of talus (Stieda process) Downward sloping posterior lip of tibia Prominent posterior process of calcaneus Intraarticular bodies Inflammation and edema of posterior ankle soft tissues: Synovitis of flexor hallucis longus tendon sheath or posterior synovial recess of the subtalar and tibiotalar joints and posterior intermalleolar ligament *Osseous injury:* Fracture, fragmentation, and pseudarthrosis of os trigonum or talar tubercle MR imaging reveals osseous anatomy and synovitis, osseous injury, and bone marrow edema

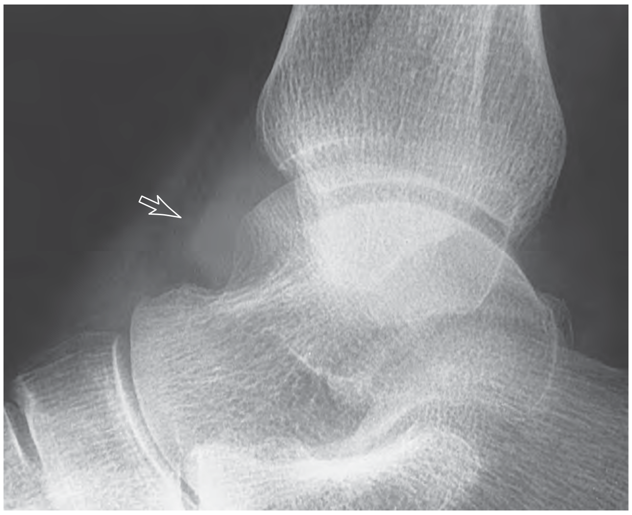

FIGURE 11–56 **Joint effusion.**[70,171] Observe the radiodense distention of the anterior capsule *(arrow),* indicative of a large effusion or hemarthrosis. Radiographically, it is impossible to differentiate between bloody effusions (hemarthroses), which generally appear within the first few hours of injury, and nonbloody effusions, which usually appear 12 to 24 hours after injury. Furthermore, the overall accuracy of radiographs for the diagnosis of ankle effusions is quite low. Documentation of distention of the anterior recess on MR imaging is considered the gold standard.

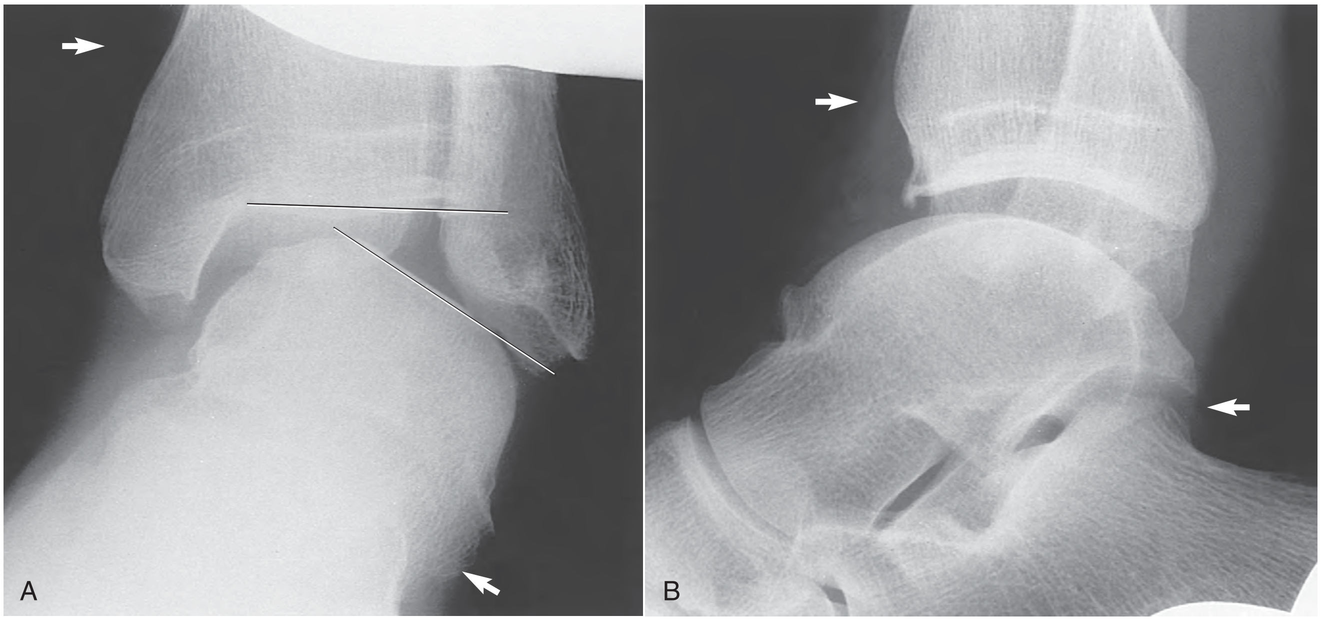

FIGURE 11–57 **Ankle ligament instability: stress radiography.**[71] **A,** Frontal varus (inversion) stress radiograph obtained with the ankle in the inverted position shows marked separation of the lateral portion of the talocrural joint, indicating some degree of lateral ligament disruption. The divergent lines along the tibial plafond and the superior talar articular surface illustrate the extent of displacement. The arrows demonstrate the direction of force applied by the examiner. **B,** Lateral radiograph obtained with the application of anterior stress to the calcaneus and posterior stress to the tibia *(arrows)*. This procedure, termed the *anterior drawer test*, shows anterior displacement of the talus on the tibia, indicative of lateral ligament injury.

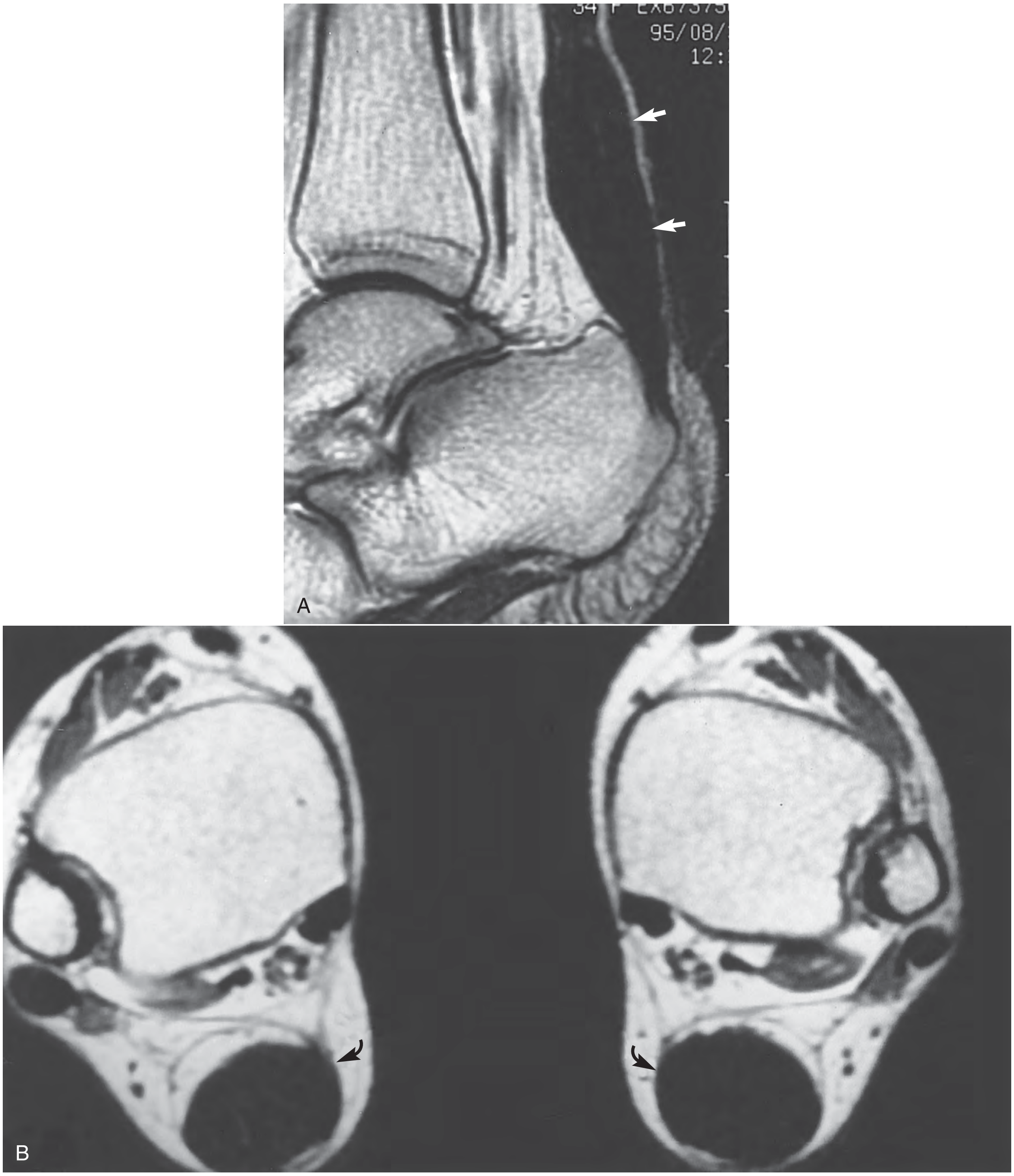

FIGURE 11–58 **Achilles tendinitis: bilateral.**[72] This 34-year-old woman had bilateral pain and swelling of the Achilles tendons. **A,** Sagittal (TR/TE, 3000/84) fast spin echo MR image shows bulbous hypertrophy of the distal aspect of the Achilles tendon *(arrows)*. **B,** Bilateral transaxial T1-weighted (TR/TE, 549/16) spin echo MR image reveals the extreme hypertrophy of both Achilles tendons immediately above their attachment to the calcaneus *(curved arrows)*. *(Courtesy B.Y. Yang, MD, Kaoshiung, Taiwan.)*

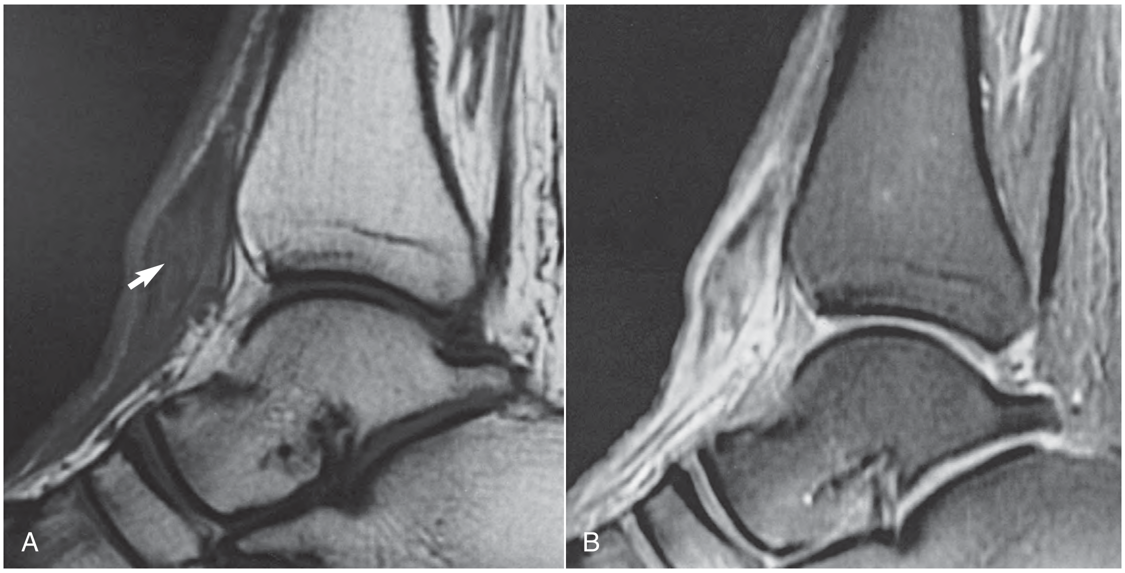

FIGURE 11–59 **Injuries of the tibialis anterior tendon: MR imaging—chronic partial tear.**[73] Sagittal T1-weighted (TR/TE, 750/15) spin echo MR image **(A)** shows an enlarged tendon *(arrow),* which is inhomogeneous in signal intensity. After intravenous injection of a gadolinium compound, a sagittal fat-suppressed T1-weighted (TR/TE, 550/15) spin echo MR image **(B)** reveals enhancement of signal intensity within and around the abnormal tendon. *(From Resnick D, Kang HS, Pretterklieber ML: Internal derangements of joints. 2nd Ed. Philadelphia, Saunders, 2006, p 2167.)*

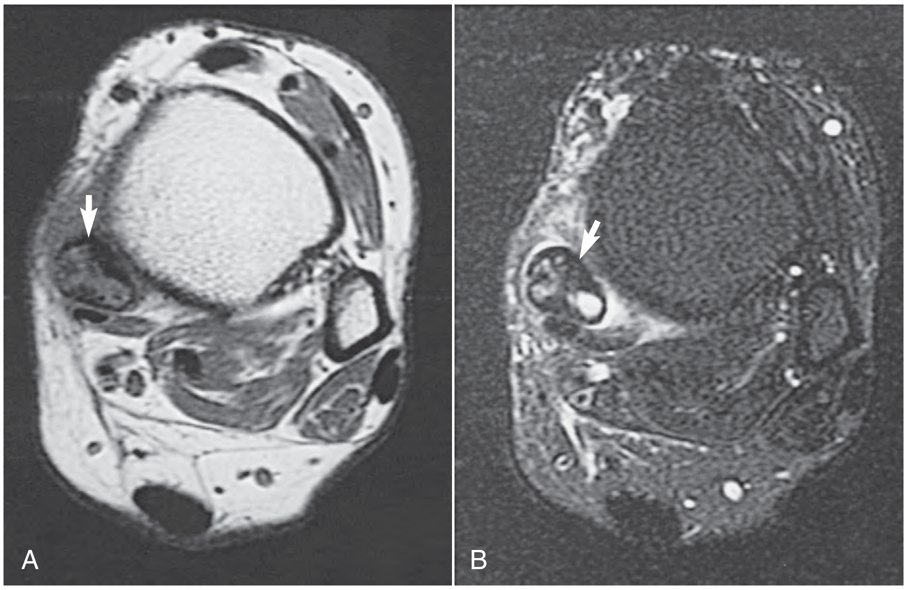

FIGURE 11–60 **Injuries of the tibialis posterior tendon: magnetic resonance (MR) imaging—chronic partial tear.**[74] **A,** Transaxial T1-weighted (TR/TE, 500/17) spin echo MR image shows an enlarged tibialis posterior tendon *(arrow),* which is inhomogeneous in signal intensity. **B,** Transaxial fat-suppressed fast spin echo MR image (TR/TE, 4500/114) reveals the hypertrophied tendon *(arrow)* containing longitudinal splits. Fluid is present in the surrounding tendon sheath, and soft tissue edema is also evident. *(From Resnick D, Kang HS, Pretterklieber ML: Internal derangements of joints. 2nd Ed. Philadelphia, Saunders, 2006, p 2153; Courtesy D. Goodwin, MD, Hanover, NH.)*

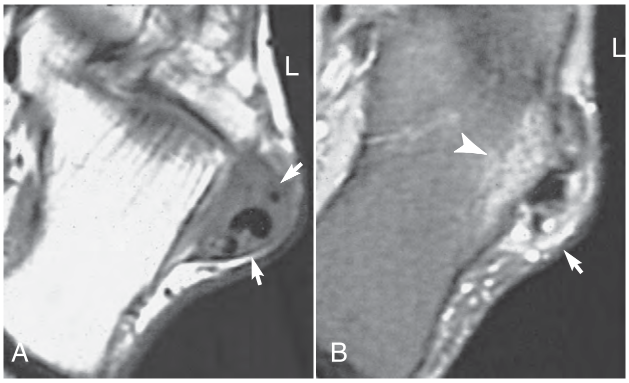

FIGURE 11–61 **Injuries of the peroneal tendon and sheath: peroneal tendinitis and tenosynovitis.**[75] Transaxial T1-weighted (TR/TE, 400/17) spin echo **(A)** and transaxial T2-weighted (TR/TE, 3300/100) fast spin echo **(B)** MR images show a fluid-filled mass *(arrows)* about the peroneus longus and peroneus brevis tendons. Note the reactive edema in the marrow of the calcaneus *(arrowhead)* in **B.** *(From Resnick D, Kang HS: Internal derangements of joints. Philadelphia, Saunders, 1997, p 874.)*

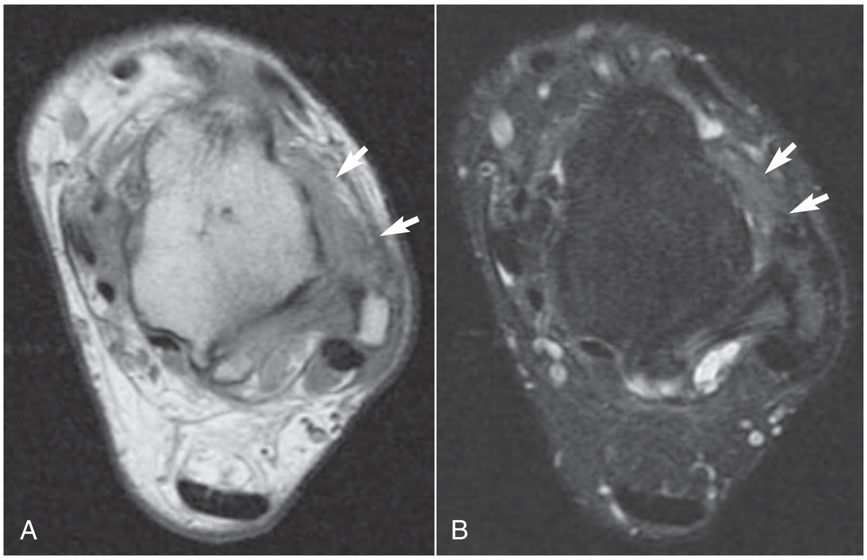

FIGURE 11–62 **Anterolateral ankle impingement syndrome.**[160,161,191] Transaxial T1-weighted **(A)** and T2-weighted fat suppressed **(B)** MR images in this 22-year-old man with chronic recurrent ankle sprains show a large collection of fibrotic scar tissue anterior to the fibula *(arrows)*. This scar tissue exhibits intermediate signal on T1- and T2-weighted images. Some edema is noted surrounding the abnormal tissue on the T2-weighted image. The pain and swelling associated with this syndrome is believed to be caused by entrapment of the abnormal scar tissue in the anterolateral recess of the ankle.

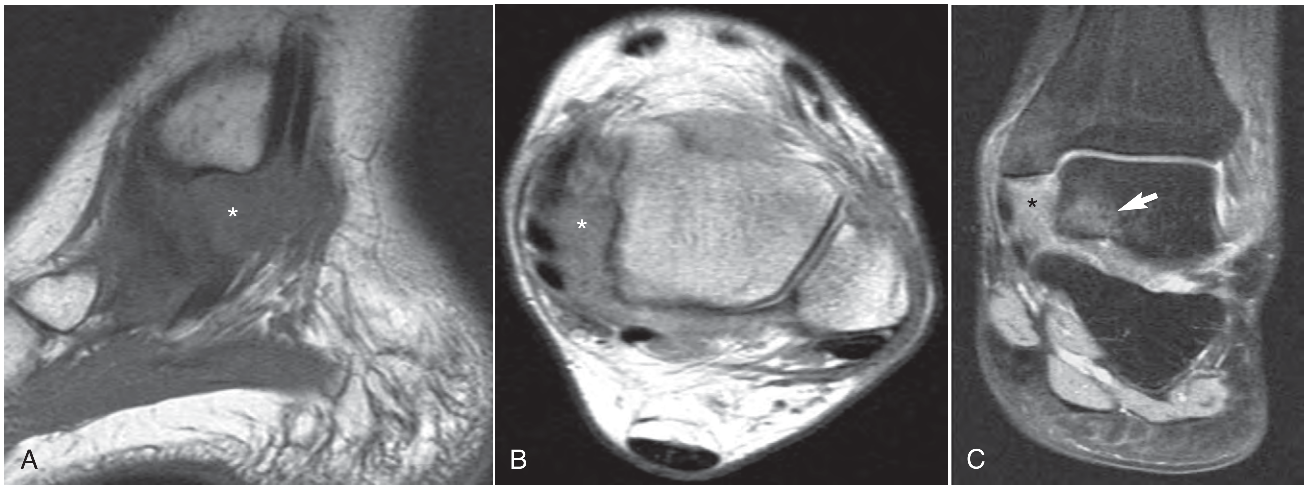

FIGURE 11–63 **Posteromedial ankle impingement syndrome.**[161,191] This 35-year-old woman developed chronic medial ankle pain after several ankle inversion injuries. A large mass (*) isointense to muscle is seen just below the medial malleolus, and appears to engulf and displace the posterior tibial and flexor digitorum longus tendons on sagittal **(A)** and axial **(B)** T1-weighted MR images. The coronal proton-density fat suppressed image **(C)** depicts this mass of thickened soft tissues as an intermediate signal (*) isointense to muscle as well as bone marrow edema within the medial aspect of the talus *(arrow)*. This syndrome is believed to involve contusion and crushing of the deep posterior fibers of the medial deltoid ligament between the medial wall of the talus and the medial malleolus.

TABLE 11-11 Articular Disorders of the Ankle and Foot

Entity	Figure(s)	Characteristics
Degenerative and Related Disorders		
Osteoarthrosis[76-78]	11-64	Predilection for first metatarsophalangeal (MTP) joint; progresses to hallux valgus and hallux rigidus Secondary osteoarthrosis may involve any joint previously injured
Erosive osteoarthritis[172]		Usually found in the hands of elderly women, but rare occurrences in the feet have been reported Involves the distal and proximal interphalangeal joints and may resemble psoriatic arthropathy
Diffuse idiopathic skeletal hyperostosis (DISH)[79]	11-65	*Enthesophytes:* osseous excrescences arise from the surfaces of the talus, navicular, and cuboid bones, the base of fifth metatarsal, and the posterior and plantar aspects of the calcaneus
Inflammatory Disorders		
Rheumatoid arthritis[80,81]	11-66	Bilateral symmetric, concentric joint space narrowing, erosion, and subluxation
Juvenile idiopathic arthritis[6,82,83]	11-67	Also termed *juvenile rheumatoid* or *juvenile chronic arthritis* Soft tissue swelling Diffuse, bilateral symmetric joint space loss and erosion Periarticular osteoporosis
Ankylosing spondylitis[83,84]	11-68	Approximately 15% of patients with ankylosing spondylitis develop abnormalities of the feet Calcaneal erosions and enthesopathy Erosions predominate at the MTP joints May eventually result in partial or complete intraarticular osseous ankylosis
Psoriatic arthropathy[77,85-87,153,180] and reactive arthritis associated with Reiter syndrome[77,88,153]	11-69, 11-70	Findings similar to those of ankylosing spondylitis *Ray pattern:* involvement of several joints within the same digit *Diffuse soft tissue swelling:* sausage digit Fluffy, poorly defined periarticular periostitis Prominent hindfoot involvement with fluffy calcaneal enthesopathy and erosions
Systemic lupus erythematosus[89]		Deforming nonerosive arthropathy Hallux valgus, MTP joint subluxation, widening of forefoot Rarely, osteonecrosis of tarsal bones
Dermatomyositis and polymyositis[90]	11-71	Diffuse soft tissue calcification
Scleroderma (progressive systemic sclerosis)[91]	11-72	Achilles tendon calcification Soft tissue, periarticular, and intra-articular calcification about the MTP joints Hallux valgus deformity
Crystal Deposition and Metabolic Diseases		
Calcium pyrophosphate dihydrate (CPPD) crystal deposition disease[92,93]	11-73	Periarticular and intra-articular calcification Arthropathy is rare; affects talonavicular joint
Calcium hydroxyapatite crystal deposition disease[94]	11-74	Calcific deposits within tendons and bursae occasionally seen about ankle, foot, and heel First MTP joint involvement may resemble gout

TABLE 11-11 Articular Disorders of the Ankle and Foot—cont'd

Entity	Figure(s)	Characteristics
Gouty arthropathy[95,148]	11-75	First MTP and IP joints most common sites but may involve any joint in ankle or foot Periarticular erosions and soft tissue tophi
Hemochromatosis[96]		Rare involvement of ankle and foot Findings resemble those of CPPD crystal deposition disease and predominate in the tibiotalar and MTP joints
Miscellaneous Disorders		
Idiopathic synovial osteochondromatosis[97,98]	11-76	Multiple intraarticular or periarticular collections of intracapsular osteochondral or chondral bodies of variable size and density within the tibiotalar joint May result in erosion of adjacent bone Idiopathic form more common than secondary form
Hemophilic arthropathy[6,99,154]	11-4, 11-77	Tibiotalar joint degeneration: joint space narrowing with bloody effusion (hemarthrosis) Subchondral sclerosis and collapse Tibiotalar slant from osseous overgrowth Growth recovery lines may be evident
Neuropathic osteoarthropathy[100-104,151,170]	11-78, 11-79	*Ankle involvement:* tabes dorsalis, amyloidosis, diabetes mellitus, and congenital indifference to pain *Foot involvement:* diabetes mellitus, leprosy, alcoholism, congenital insensitivity to pain, peripheral nerve injury ***Imaging findings*** Large joint effusions Joint space narrowing and obliteration Joint subluxation, disorganization, and destruction Bone fragmentation, destruction, and sclerosis
Frostbite[105]	11-80	Local tissue damage from cellular injury as a result of the freezing process itself or from the vascular insufficiency it produces Soft tissue swelling, osteoporosis, periostitis, secondary infection, arthritis secondary to cartilage injury, terminal tuft resorption, epiphyseal abnormalities, and premature physeal fusion in children
Silicone synovitis[106]	11-81	Complication of silastic arthroplasty Believed to be a reaction to shedded silicone particles embedded within the synovium with resultant synovial hypertrophy, and chronic inflammatory and giant cell infiltration of the synovial membrane Associated soft tissue swelling and preservation of cartilage spaces is often found

TABLE 11-12 **Distribution, Symmetry, and Preferential Target Sites of Articular Disorders of the Ankle and Foot**

	Distribution and Symmetry			Articular Compartments*									
Entity	***Bilateral Symmetric***	***Bilateral Asymmetric***	***Unilateral***	***TT***	***TCN***	***ST***	***CN***	***CC***	***TMT***	***First MTP***	***Second to Fifth MTP***	**First IP**	**Second to Fifth IP**
Osteoarthrosis		+	+						+	+			
Neuropathic osteoarthropathy		+				+	+	+	+		+		
Rheumatoid arthritis	+				+	+	+	+	+	+	+	+	
Gout	+	+		+	+	+	+	+	++	++	+	++	+

* *CC,* Calcaneocuboid; *CN,* cuneonavicular; *IP,* interphalangeal; *MTP,* metatarsophalangeal; *ST,* posterior subtalar; *TCN,* talocalcaneonavicular; *TMT,* tarsometatarsal; *TT,* tibiotalar.

TABLE 11-13 Differential Diagnosis: Calcaneal Involvement in Articular Disorders[77]

Entity	Figure(s)	Characteristics
Degenerative enthesopathy[186]	11-64, *E*	Well-defined, sharply marginated osseous excrescences (heel spurs) arising from: A. *Plantar enthesophytes:* Arise from several insertion sites on the plantar surface of the calcaneus: Abductor digiti minimi muscle Flexor digitorum brevis muscle Plantar fascia Short plantar ligament B. *Achilles enthesophytes:* Arise from the insertion of the Achilles tendon on the posterior surface of the calcaneus Controversial association with plantar heel pain and plantar fasciitis
Diffuse idiopathic skeletal hyperostosis (DISH)	11-65	Prominent, bilateral symmetric, well-defined enthesophyte proliferation at sites of attachment of the Achilles tendon and plantar aponeurosis
Rheumatoid arthritis		Well-defined posterior and plantar enthesophytes Retrocalcaneal bursitis results in unilateral or bilateral erosions of calcaneus Achilles tendinitis and soft tissue mass in pre-Achilles fat pad Minimal or no reactive sclerosis
Ankylosing spondylitis and psoriatic arthropathy	11-68, *D, E,* 11-69, *B*	Well-defined enthesophytes at the Achilles tendon attachment Poorly defined enthesophytes at plantar aspect of bone Retrocalcaneal bursitis results in erosions at posterosuperior aspect of calcaneus Erosions may be associated with reactive sclerosis Outgrowths more irregular and fuzzy than those in rheumatoid arthritis
Reiter syndrome	11-70, *B-D*	Poorly defined plantar and posterosuperior enthesophytes Retrocalcaneal bursitis results in unilateral or bilateral erosions on plantar and posterosuperior aspects of calcaneus Enthesophytes less well defined than in rheumatoid arthritis
CPPD crystal deposition disease		Bilateral or unilateral linear, calcific collections within the Achilles tendon and plantar aponeurosis
Calcium hydroxyapatite crystal deposition disease		Bilateral or unilateral linear, calcific collections within the Achilles tendon and plantar aponeurosis
Gout		Tophaceous nodules in and about the Achilles tendon may result in erosions of the posterior aspect of the calcaneus
Acromegaly	11-113	Prominent enthesophyte proliferation at attachments of the Achilles tendon and plantar aponeurosis Heel pad thickening (men > 23 mm; women > 21.5 mm)
Hyperparathyroidism		Bilateral, symmetric subligamentous erosions at attachment of plantar aponeurosis, or less commonly, at the posterosuperior aspect of the calcaneus

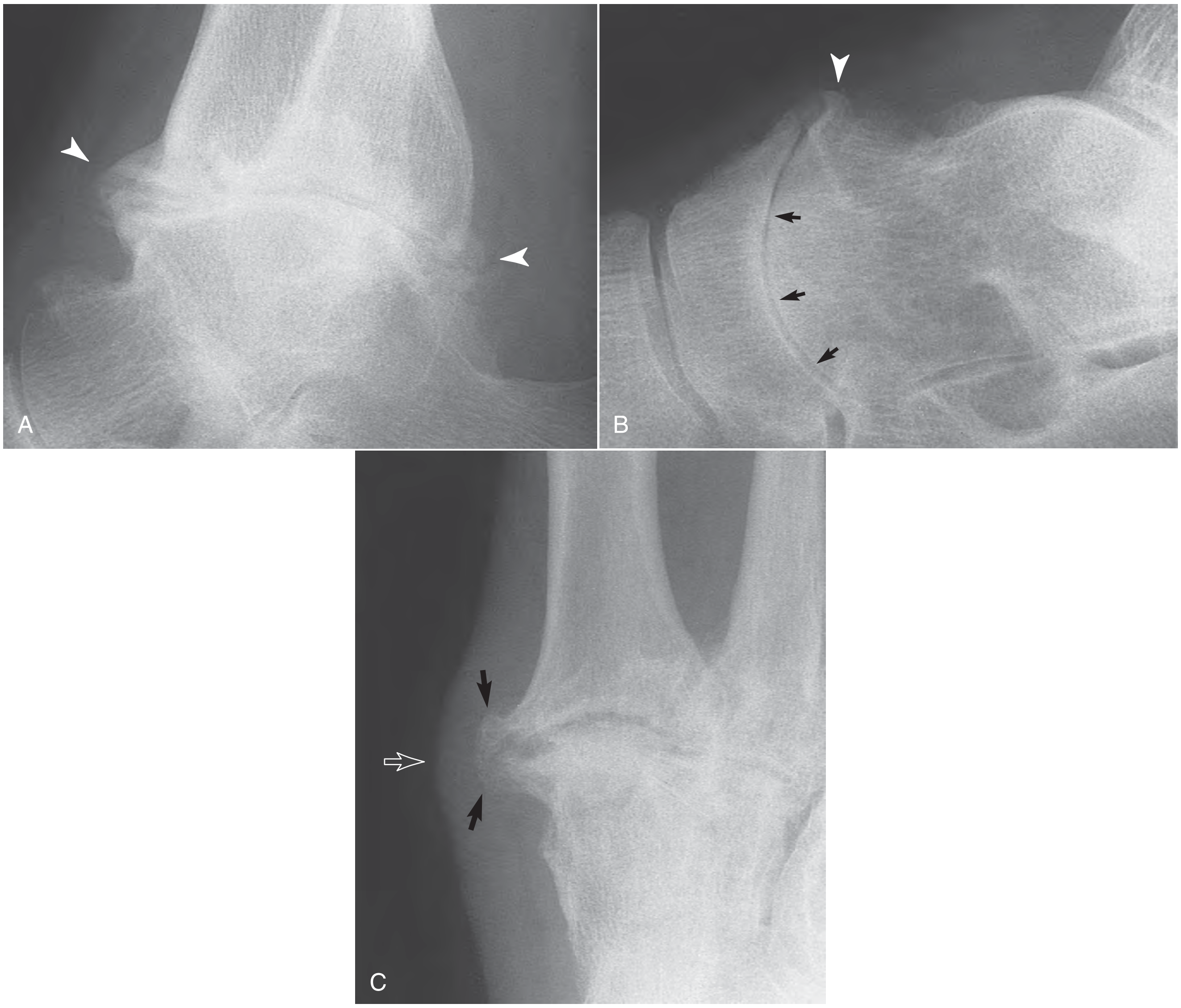

FIGURE 11–64 Osteoarthrosis.[76-78,181] **A,** Tibiotalar joint. Joint space narrowing, osteophyte formation *(arrowheads)* and subchondral sclerosis characterize this degenerative ankle joint. Degenerative disease of the ankle typically occurs after ligament injury, fracture, repetitive trauma, or sports injury. **B,** Talonavicular joint. Marked joint space narrowing *(arrows),* dorsal osteophyte formation *(arrowhead),* and subchondral bone sclerosis are evident in the talonavicular articulation of this 41-year-old man. **C,** First tarsometatarsal joint. Prominent osteophytes *(arrows),* subchondral sclerosis, and nonuniform joint space narrowing are signs of degenerative joint disease at this location in a 59-year-old man. Soft tissue prominence is also noted overlying the joint *(open arrow).*

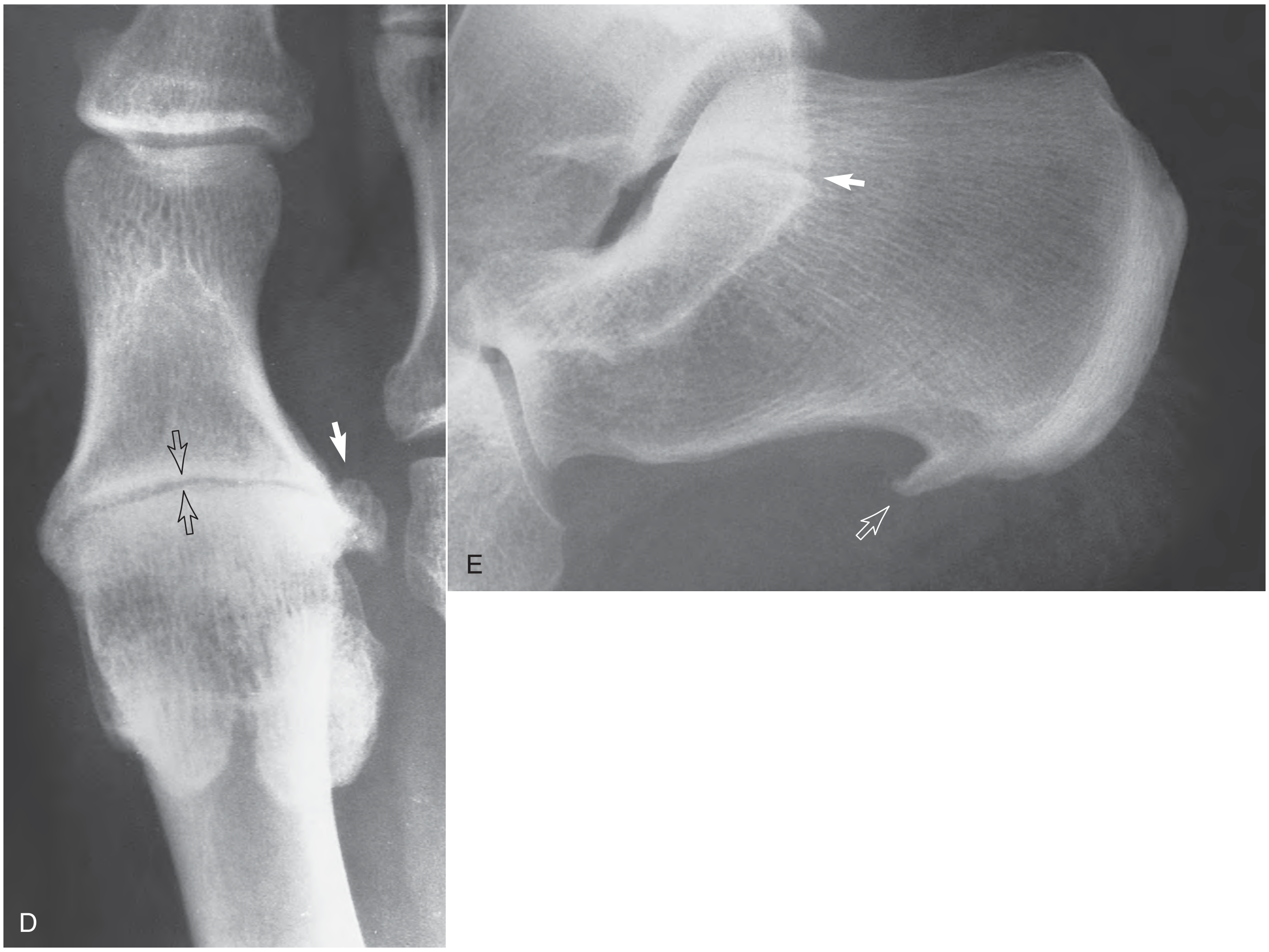

FIGURE 11–64, cont'd **D,** Hallux rigidus. Degenerative joint disease of the first metatarsophalangeal joint has resulted in joint space narrowing *(open arrows),* subchondral sclerosis, and osteophytes *(arrow)*. This condition often accompanies a hallux valgus deformity and bunion formation and is characterized by painful degenerative rigidity of the first metatarsophalangeal joint of the great toe. **E,** Degenerative plantar enthesophyte. Observe the well-defined, sharply marginated osseous excrescence arising from the site of attachment of the plantar aponeurosis on the calcaneus *(open arrow)* in this 53-year-old woman with plantar fasciitis. Such degenerative "heel spurs" often are painful. Of incidental note is the presence of talocalcaneal coalition *(white arrow)*.

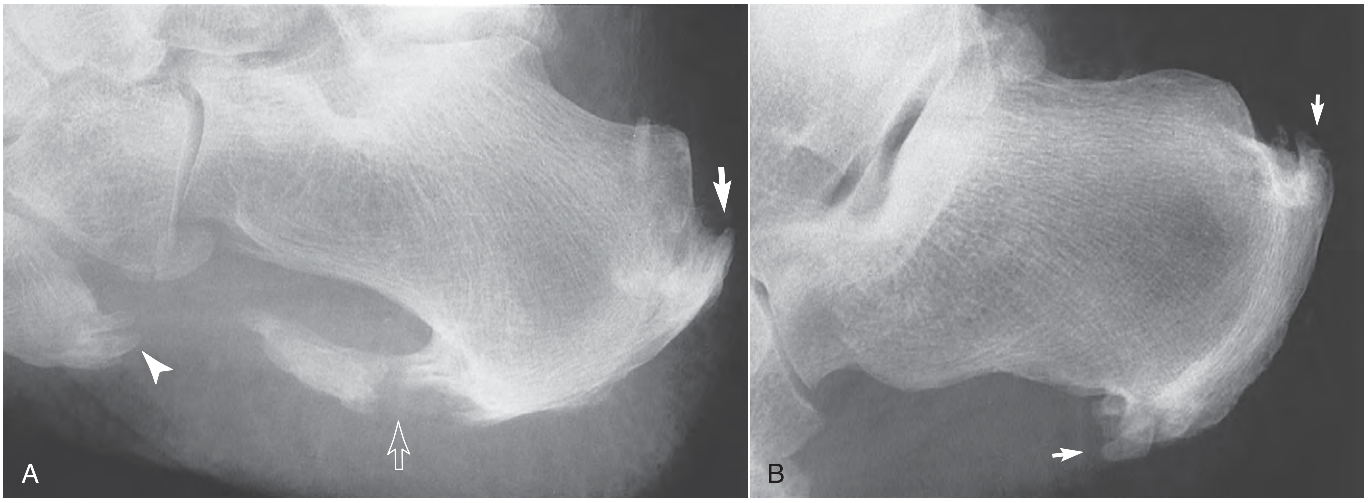

FIGURE 11–65 **Diffuse idiopathic skeletal hyperostosis (DISH): calcaneal enthesopathy.**[77,79] **A,** Prominent osseous excrescences arising from the sites of attachment of the Achilles tendon *(arrow),* plantar aponeurosis, and peroneus brevis tendon attachment *(arrowhead)* represent characteristic enthesophytes seen frequently in patients with DISH. The large plantar enthesophyte is fractured *(open arrow)*. **B,** In another patient, prominent enthesophytes at the attachments of the Achilles tendon and plantar aponeurosis are noted *(arrows)*. Enthesopathy of the calcaneus is present in about 76% of patients with DISH.

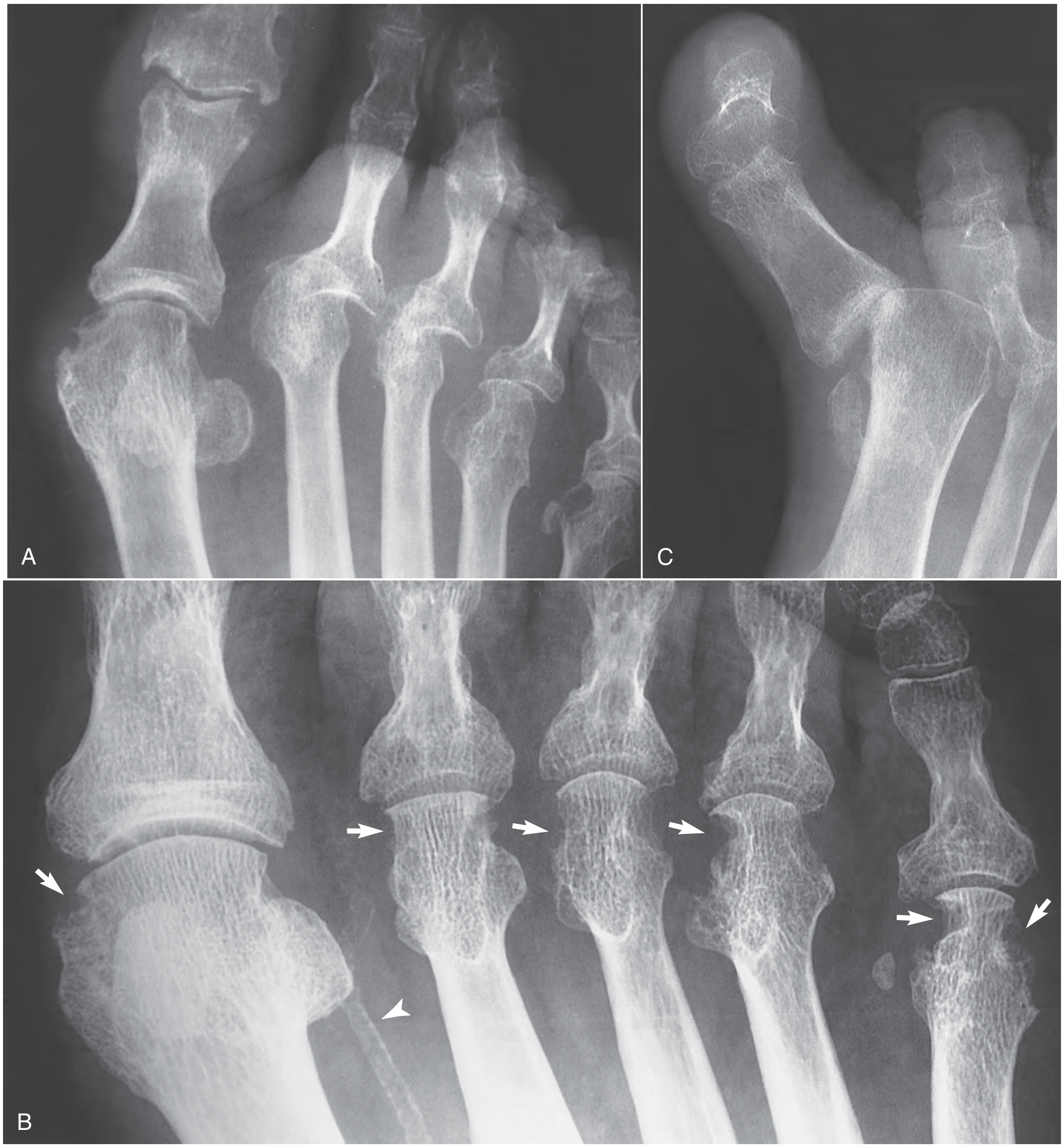

FIGURE 11–66 **Rheumatoid arthritis.**[80,81] Forefoot abnormalities. **A,** In a patient with advanced rheumatoid arthritis, the findings include marginal erosions adjacent to the metatarsophalangeal joints, joint dislocations, periarticular osteopenia, and soft tissue swelling. Involvement of the hallux interphalangeal joint is also present. **B,** In another patient, extensive rheumatoid erosions are seen in characteristic locations *(arrows)*. Vascular calcification is also clearly visualized *(arrowhead)*. **C,** Severe and unusual hallux varus deformity and subluxation are present at the first metatarsophalangeal joint. Periarticular osteopenia, sesamoid subluxation, and erosions are also present. Clinical abnormalities of the forefoot are present in up to 90% of patients with long-standing rheumatoid arthritis and represent the initial manifestation of the disease in 10% to 20% of patients.

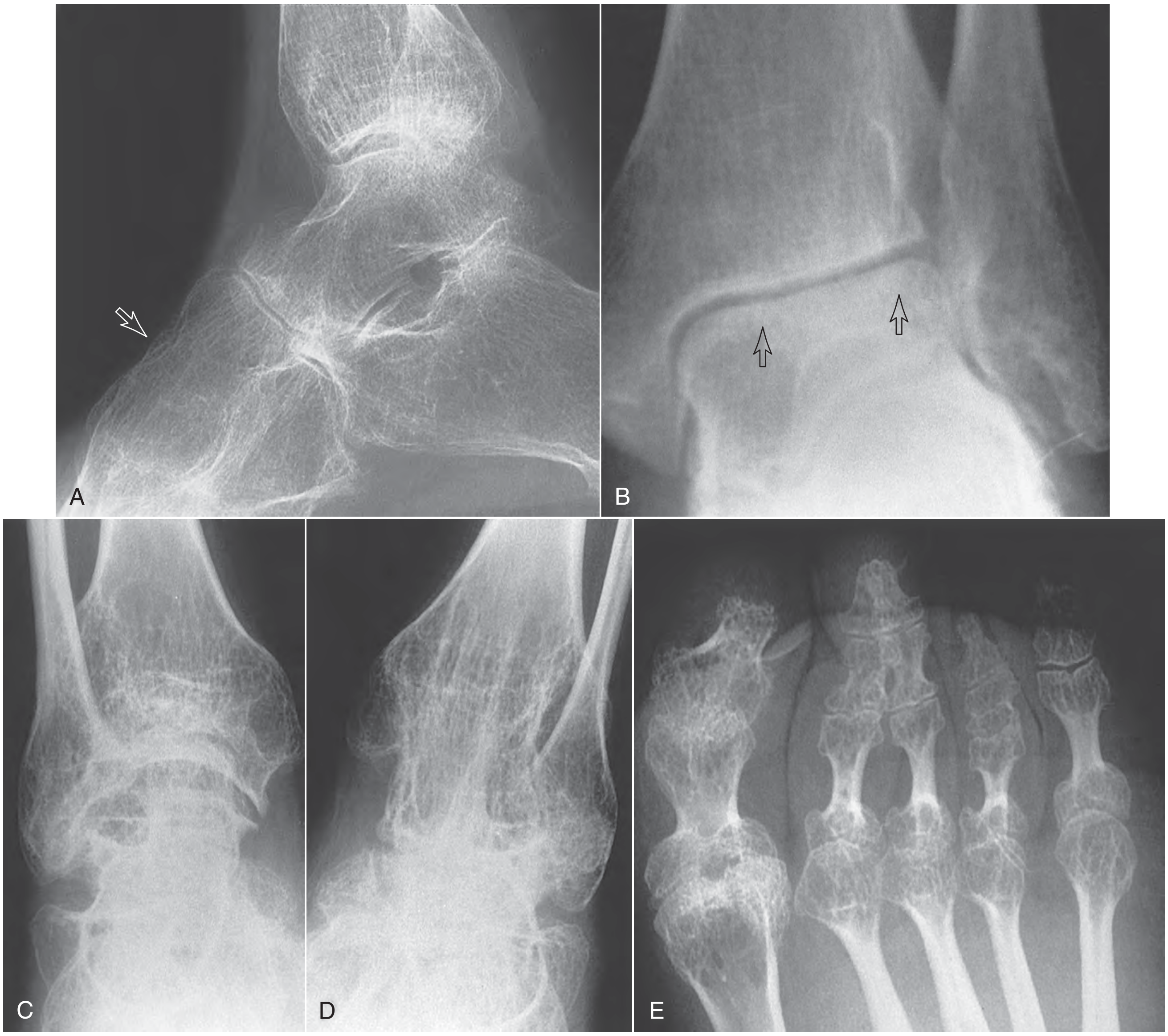

FIGURE 11–67 **Juvenile idiopathic (chronic or rheumatoid) arthritis.**[6,82,83] **A-B,** Ankle abnormalities. In **A,** osteoporosis, uniform joint space narrowing, widespread tarsal ankylosis *(open arrow),* and soft tissue atrophy are present in this 22-year-old woman with long-standing juvenile idiopathic arthritis. **B,** In another patient, observe the tibiotalar slant *(open arrows),* a sign found in juvenile idiopathic arthritis, hemophilia, Trevor disease, and many other conditions. **C-D,** Ankle abnormalities—advanced changes. Osteoporosis, epiphyseal overgrowth, joint space erosions, and ankylosis involve both ankles in a relatively symmetric pattern in this 36-year-old woman. **E,** Foot abnormalities-advanced changes. Osteoporosis, epiphyseal overgrowth, joint space erosions, and ankylosis appear in this 36-year-old woman. The findings were bilateral and symmetric. *(**B,** Courtesy A. Brower, MD, Norfolk, Va.* ***C-E,*** *Courtesy V. Vint, MD, San Diego.)*

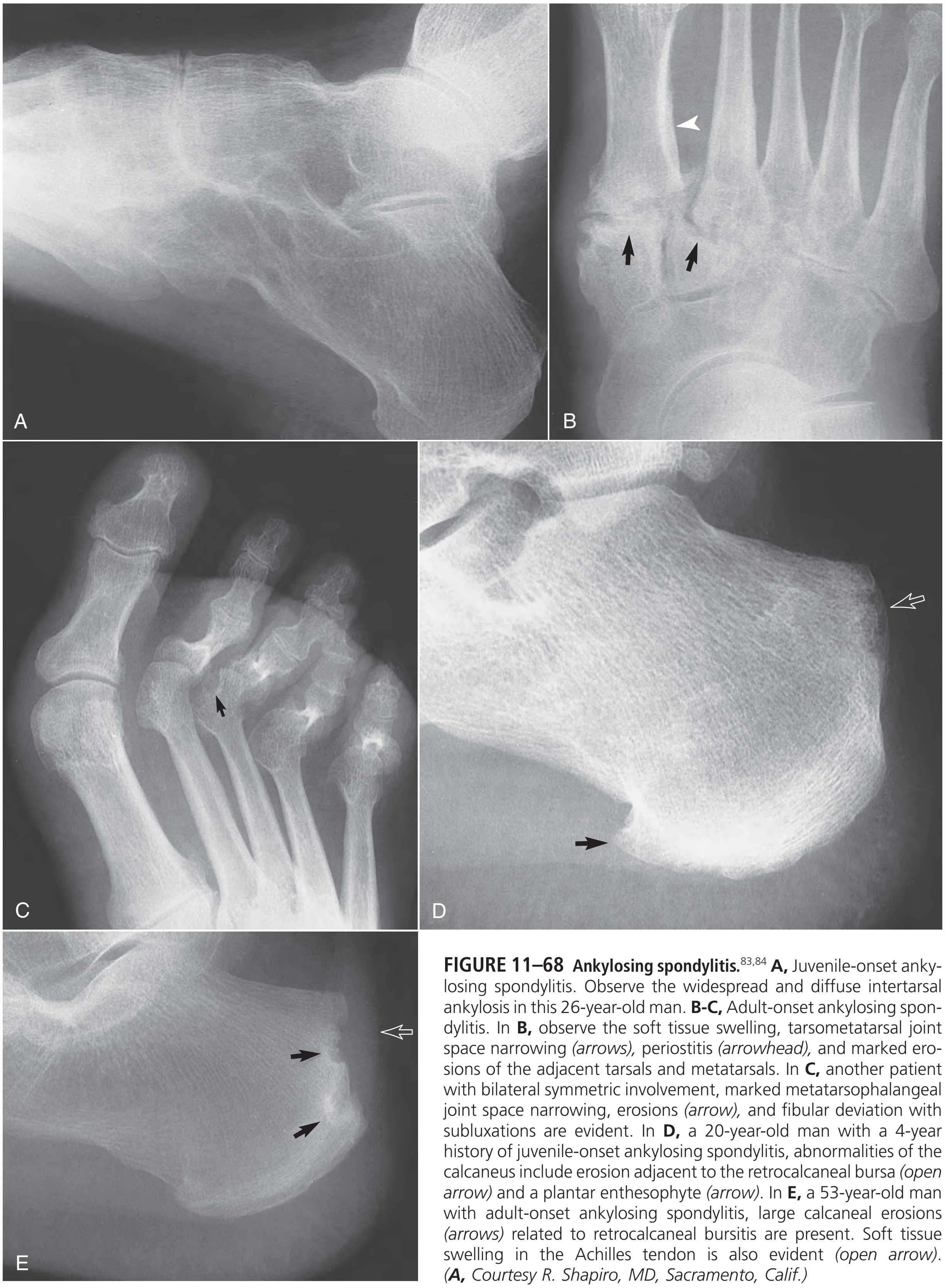

FIGURE 11–68 Ankylosing spondylitis.[83,84] **A,** Juvenile-onset ankylosing spondylitis. Observe the widespread and diffuse intertarsal ankylosis in this 26-year-old man. **B-C,** Adult-onset ankylosing spondylitis. In **B,** observe the soft tissue swelling, tarsometatarsal joint space narrowing *(arrows),* periostitis *(arrowhead),* and marked erosions of the adjacent tarsals and metatarsals. In **C,** another patient with bilateral symmetric involvement, marked metatarsophalangeal joint space narrowing, erosions *(arrow),* and fibular deviation with subluxations are evident. In **D,** a 20-year-old man with a 4-year history of juvenile-onset ankylosing spondylitis, abnormalities of the calcaneus include erosion adjacent to the retrocalcaneal bursa *(open arrow)* and a plantar enthesophyte *(arrow)*. In **E,** a 53-year-old man with adult-onset ankylosing spondylitis, large calcaneal erosions *(arrows)* related to retrocalcaneal bursitis are present. Soft tissue swelling in the Achilles tendon is also evident *(open arrow)*. *(**A,** Courtesy R. Shapiro, MD, Sacramento, Calif.)*

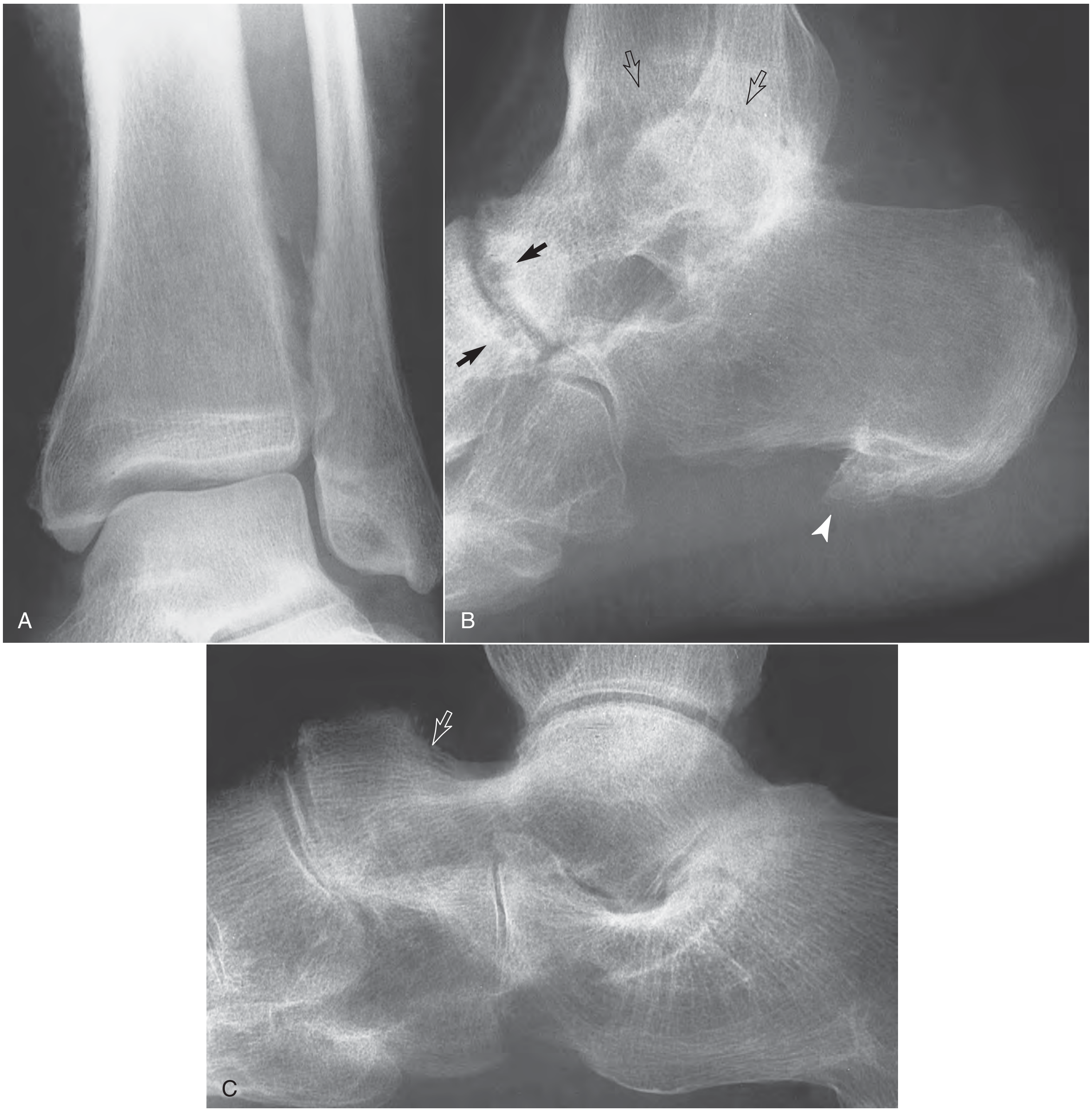

FIGURE 11–69 Psoriatic arthropathy.[77,85-87,153,180] **A,** Ankle involvement. Observe the exuberant fluffy periostitis arising from the distal ends of the tibia and fibula in this 47-year-old man with psoriasis. Although he has no evidence of joint space narrowing or erosions, typical psoriatic arthropathy was seen in the hand. Periarticular periostitis is frequently encountered in patients with seronegative spondyloarthropathies; however, special care should be taken to differentiate this from hypertrophic osteoarthropathy. **B,** Calcaneal involvement. In a 49-year-old man with psoriatic skin disease and polyarticular joint disease, a lateral ankle radiograph reveals a fluffy bony enthesophyte at the site of attachment of the plantar fascia on the calcaneus *(arrowhead)*. Erosive changes at the talonavicular joint *(arrows)* and bony ankylosis of the tibiotalar joint *(open arrows)* are seen. **C,** Midfoot involvement. Complete osseous ankylosis of the talonavicular joint *(open arrow)* is observed in this 61-year-old man with chronic psoriatic skin disease and polyarticular joint disease. Before ankylosis, a talonavicular dislocation had occurred, accounting for the inferior displacement of the talus in relation to the navicular bone. Of interest, a developmental talocalcaneal coalition is also noted.

Continued

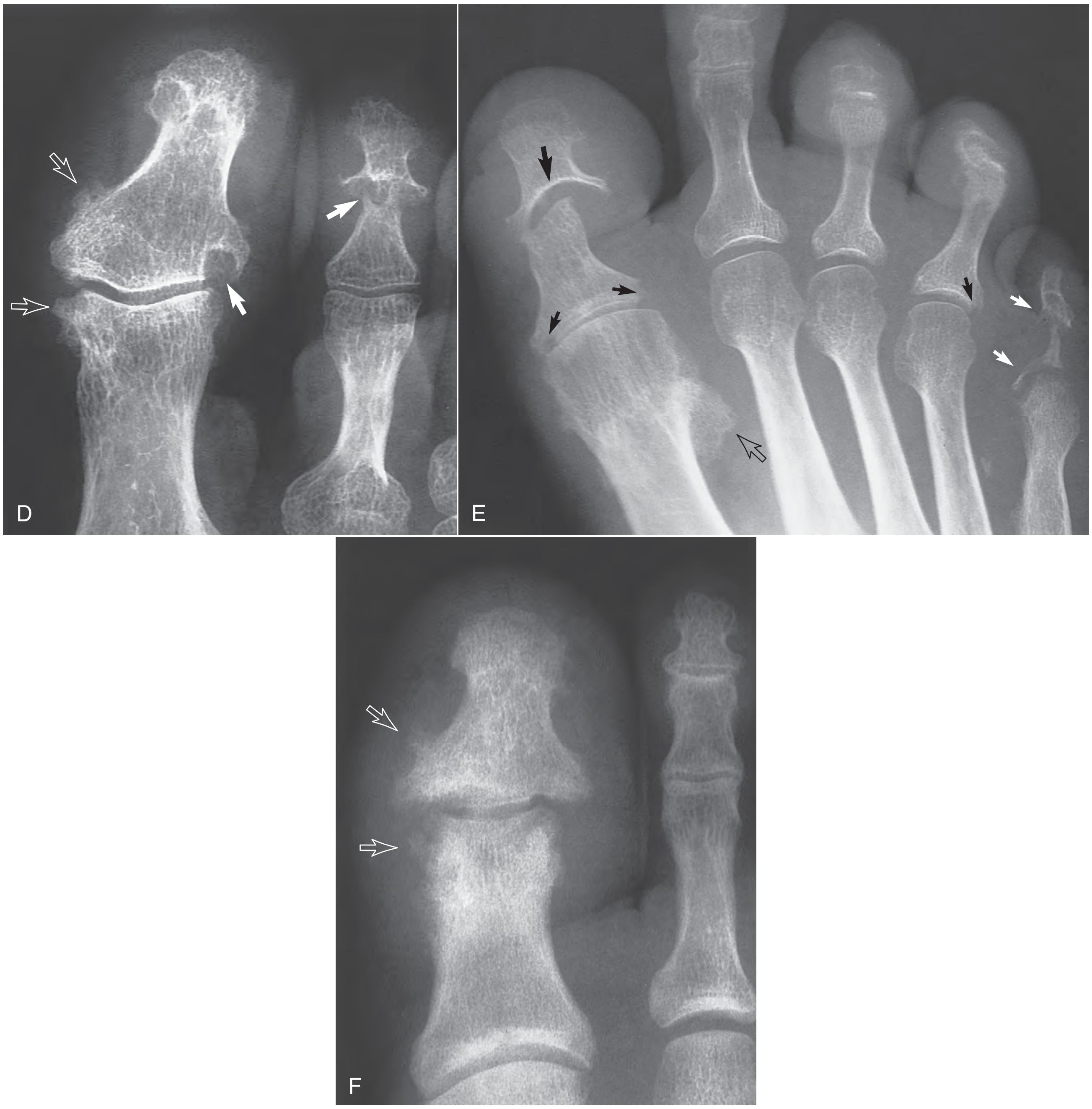

FIGURE 11–69, cont'd **D-F,** Forefoot involvement. In **D,** intraarticular erosions are seen at the terminal interphalangeal joints of the first and second digits *(arrows)*. Fluffy periostitis *(open arrows),* characteristic of seronegative spondyloarthropathies, also is present. In **E,** another patient, central erosions of the first and fifth terminal phalangeal articular surfaces and resorption of the distal end of the proximal phalanx and metatarsal bone are characteristic of inflammatory arthropathies, termed *pencil-and-cup erosions (large black arrow)*. Note also the dramatic soft tissue swelling, marginal erosions *(small black arrows),* and periostitis involving the hallux sesamoid bone *(open arrow)*. In **F,** a third patient, prominent soft tissue swelling, central erosions, "whiskering" or periostitis *(open arrows)*, and absence of periarticular osteoporosis are classic changes in psoriatic arthritis. The joints of the adjacent digit appear unaffected. *(**A,** Courtesy T. Marklund, MD, Linköping, Sweden.)*

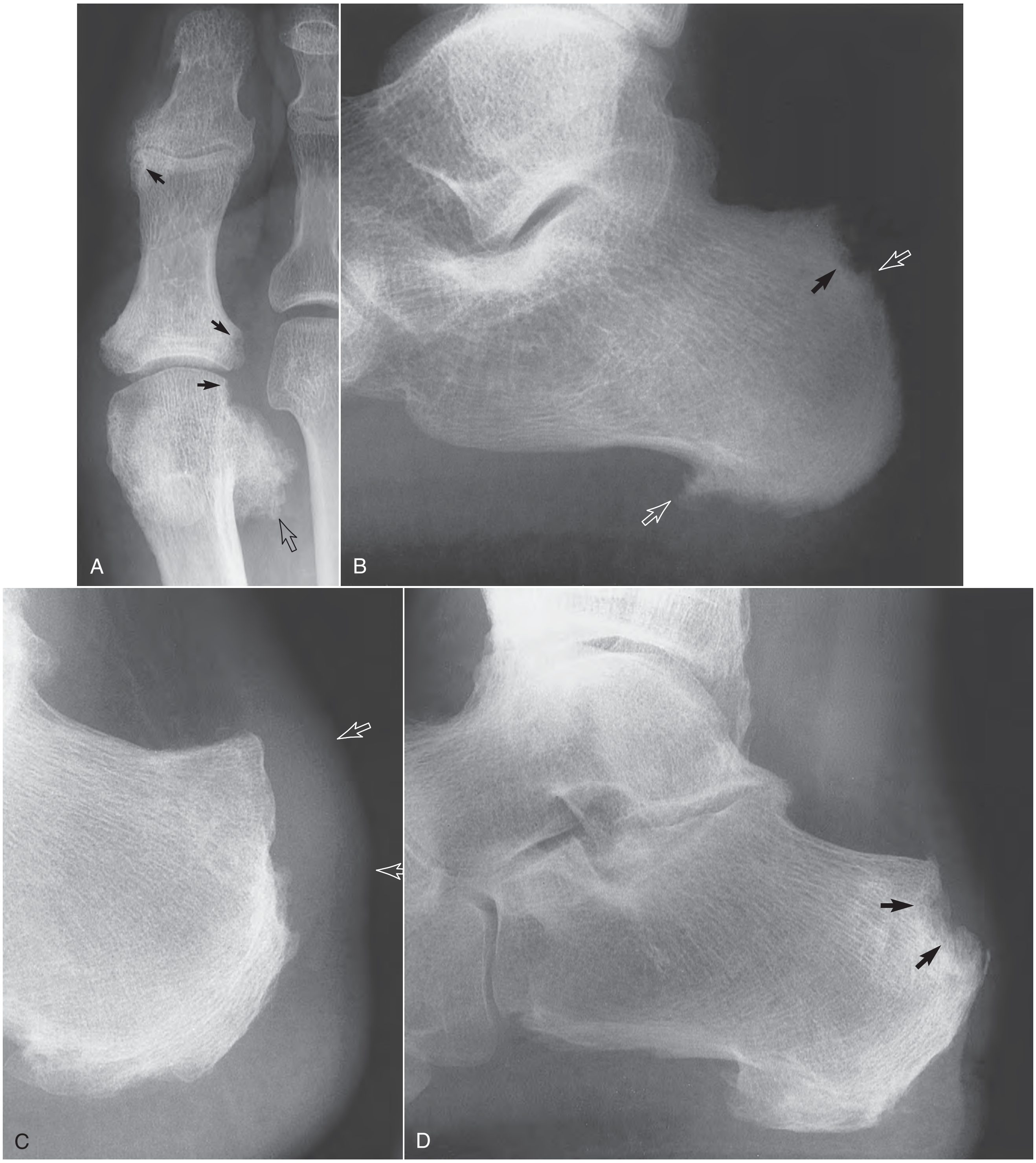

FIGURE 11–70 **Reiter syndrome.**[77,88,153] **A,** Forefoot abnormalities. Prominent fluffy bone proliferation with poorly defined osseous outlines is evident at the hallux sesamoid *(open arrow)* and adjacent to the articulations. Diffuse soft tissue swelling and marginal erosions *(arrows)* are also seen. **B-D,** Calcaneal abnormalities. In **B,** a fluffy pattern of enthesopathy is seen arising from the plantar and posterior aspects of the calcaneus *(open arrows)*. A prominent erosion is also seen adjacent to the retrocalcaneal bursa *(arrow)*. In **C,** another patient, osseous proliferation and soft tissue swelling of the Achilles tendon *(open arrows)* are evident. In **D,** advanced changes in a third patient include a posterior erosion *(arrows)* secondary to retrocalcaneal bursitis and prominent enthesopathy. Calcaneal changes are evident in 25% to 50% of patients with Reiter syndrome. *(**B,** Courtesy T.R. Yochum, DC, Denver, Colo.)*

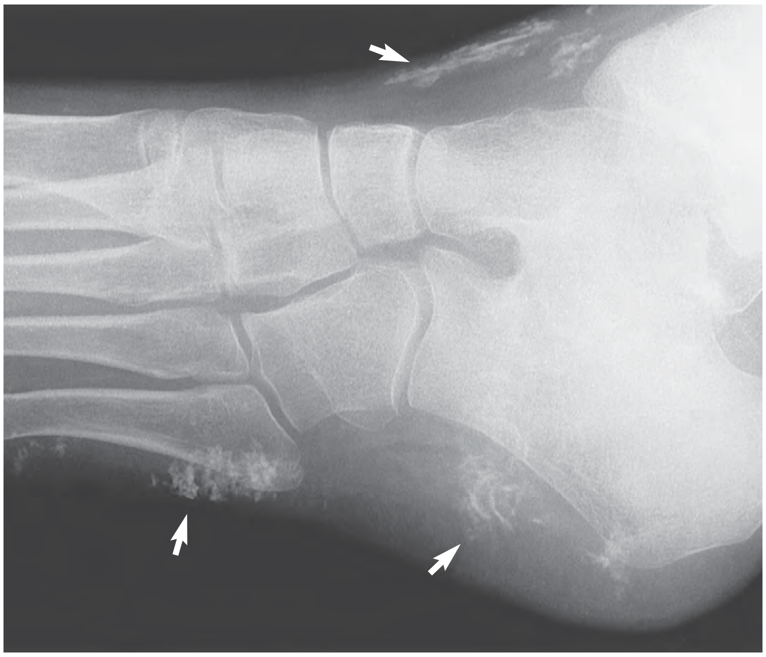

FIGURE 11–71 **Dermatomyositis and polymyositis.**[90] Observe the sheet-like subcutaneous calcinosis *(arrows)* in this 13-year-old girl with long-standing dermatomyositis.

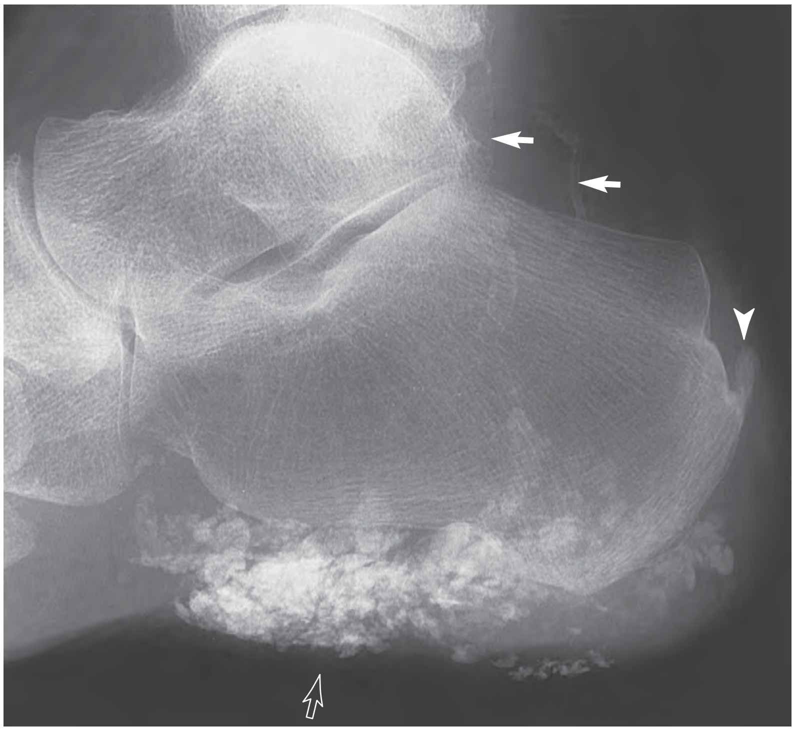

FIGURE 11–72 **Scleroderma (progressive systemic sclerosis).**[91] Extensive soft tissue calcification *(open arrow)* is seen in the heel pad of this patient with long-standing scleroderma. An Achilles tendon enthesophyte *(arrowhead)* and vascular calcification *(arrows)* are also evident.

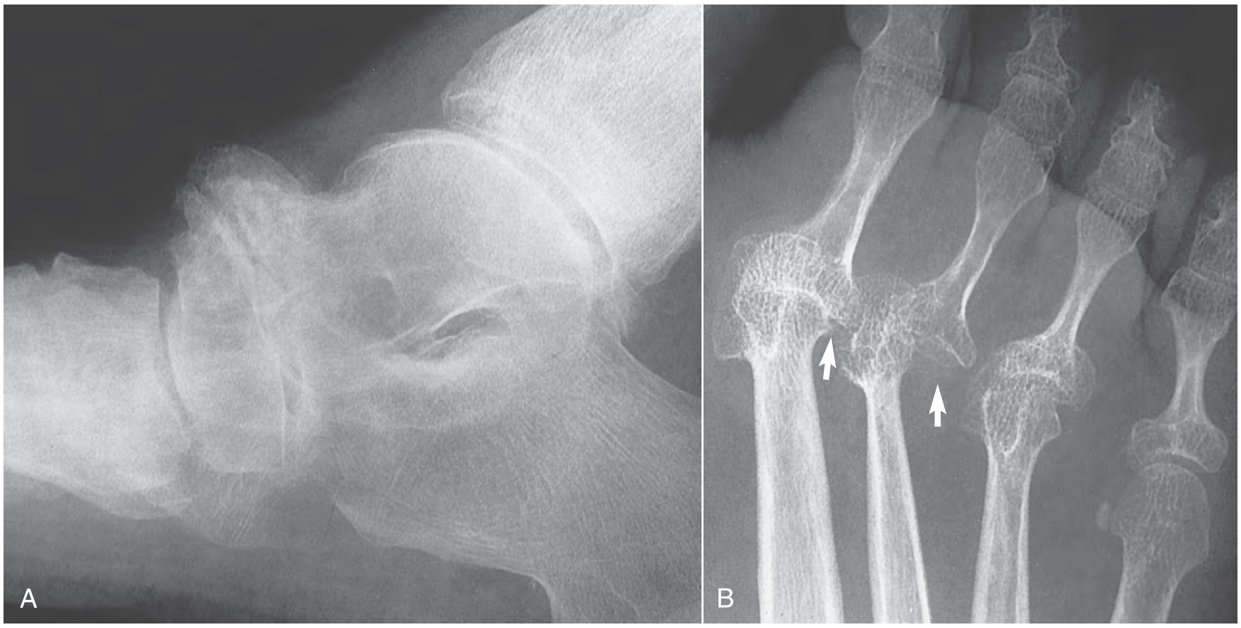

FIGURE 11–73 Calcium pyrophosphate dihydrate (CPPD) crystal deposition disease.[92,93] **A,** Midfoot and hindfoot involvement. Extensive hypertrophic osteophytes are seen about the talonavicular articulation in this 82-year-old man with CPPD crystal deposition disease. **B,** Forefoot involvement. Observe the dislocations of the second, third, and fourth metatarsophalangeal joints *(arrows)*.

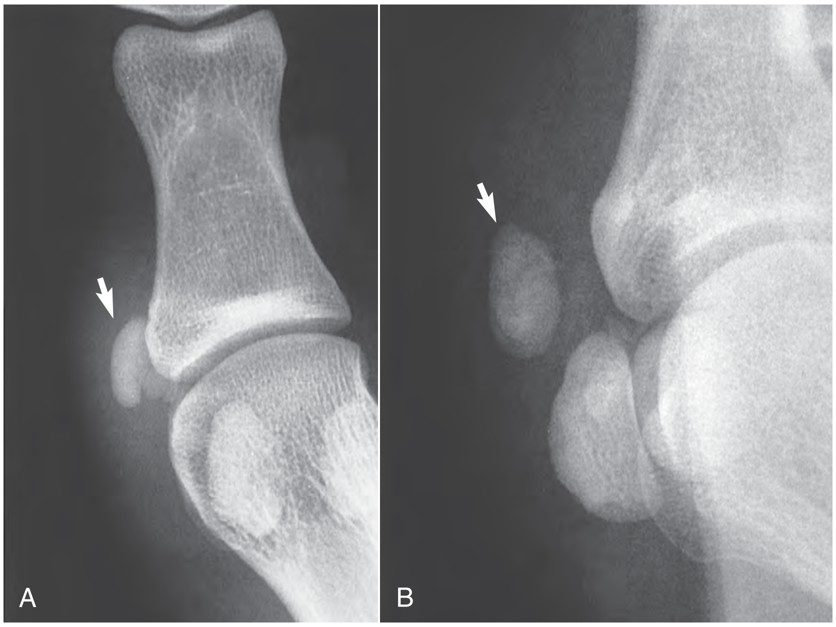

FIGURE 11–74 Calcific bursitis: calcium hydroxyapatite crystal deposition.[94] Frontal **(A)** and lateral **(B)** radiographs show cloudlike accumulations of calcification *(arrow)* overlying the first metatarsophalangeal joint. Periarticular hydroxyapatite crystals may be deposited in tendons, bursae, or soft tissues.

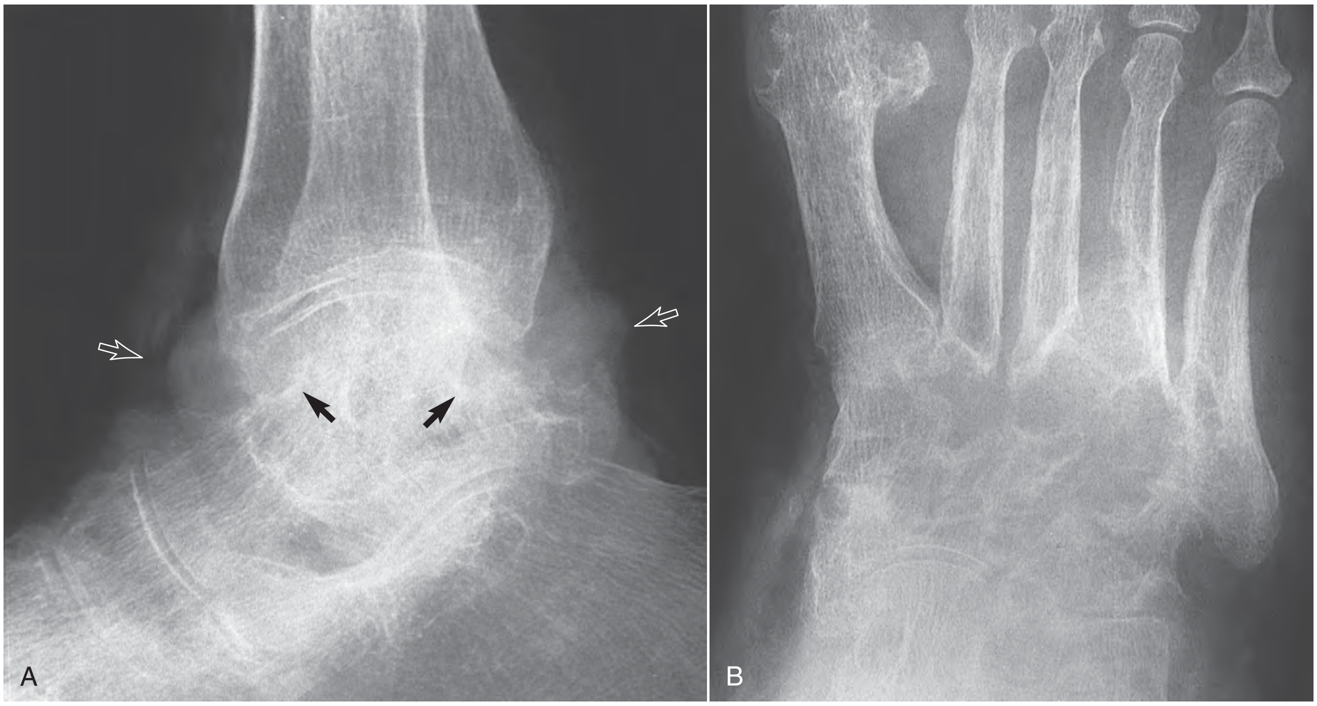

FIGURE 11–75 **Gouty arthropathy.**[95,148] **A,** Ankle involvement. Observe the radiodense joint effusion anterior and posterior to the ankle joint *(open arrows)* of this 65-year-old man with polyarticular gouty arthritis. Erosions of the talus exhibit an overhanging margin *(arrows)*. **B,** Midfoot abnormalities. Extensive erosions are seen about the tarsometatarsal articulations in this patient with long-standing gout.

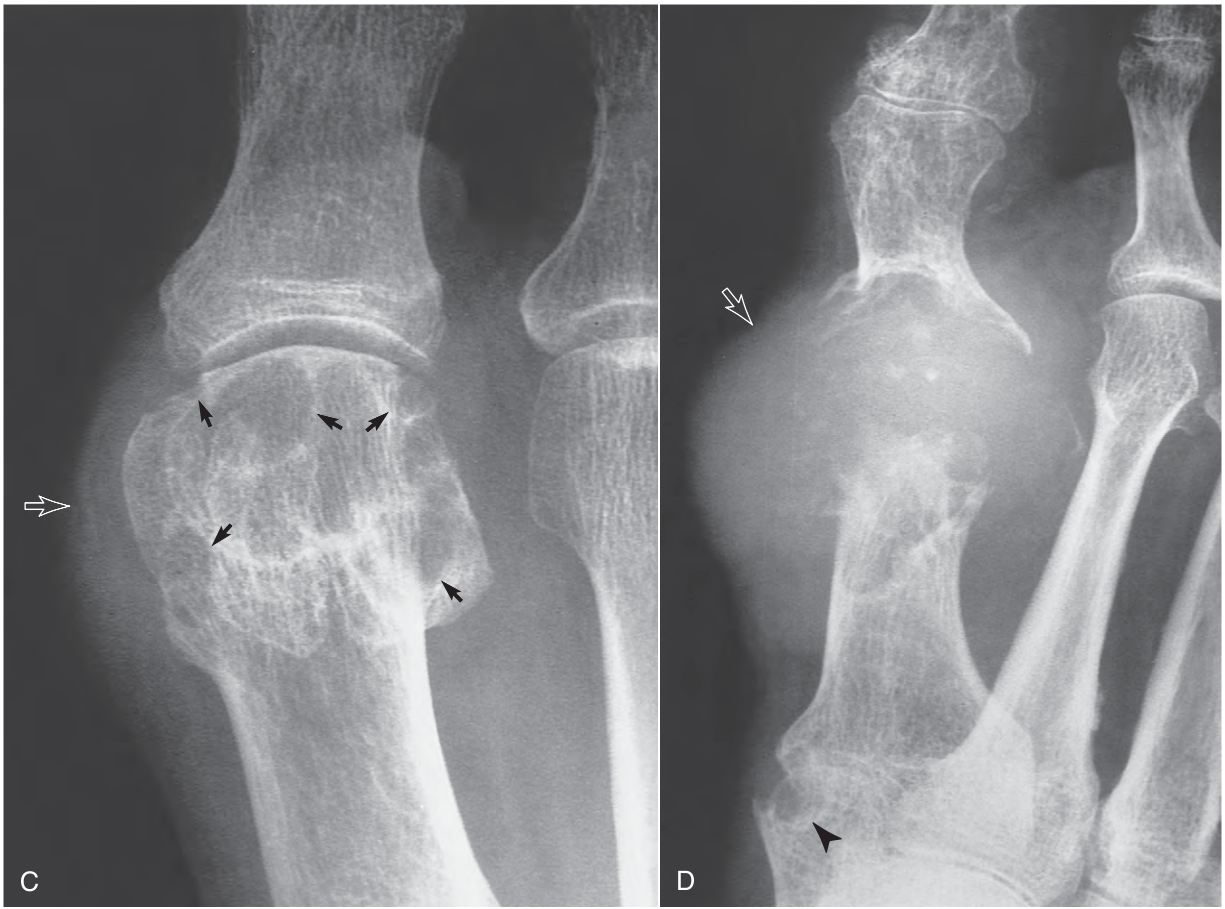

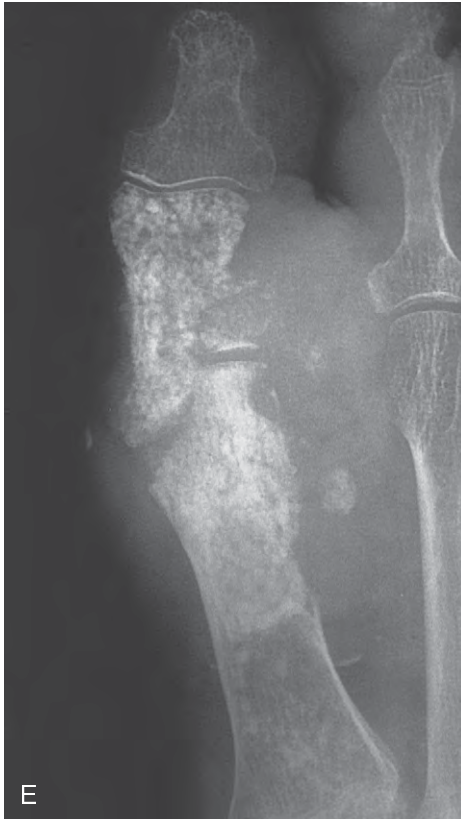

FIGURE 11–75, cont'd C-E, Forefoot abnormalities. In **C,** moderate changes are seen in a 72-year-old man with chronic gout, consisting of soft tissue swelling *(open arrow)* and cystlike subarticular erosions in the first metatarsal head and hallux sesamoid bones *(arrows)*. In **D,** advanced changes are evident in this patient with severe, chronic gout. Dramatic soft tissue swelling and tophus formation *(open arrow),* extensive subarticular bone destruction with overhanging margins, and intraarticular osseous debris are seen involving the first metatarsophalangeal joint. A small erosion also is seen at the first tarsometatarsal joint *(arrowhead)*. In **E,** intraosseous calcification is present. Severe gouty erosions, soft tissue swelling, joint destruction, and osseous debris are accompanied by intraosseous calcified tophaceous deposits within the first metatarsal bone and proximal phalanx. (See also Figure 11-104.) *(**C-E,** Courtesy T. Broderick, MD, Orange, Calif.)*

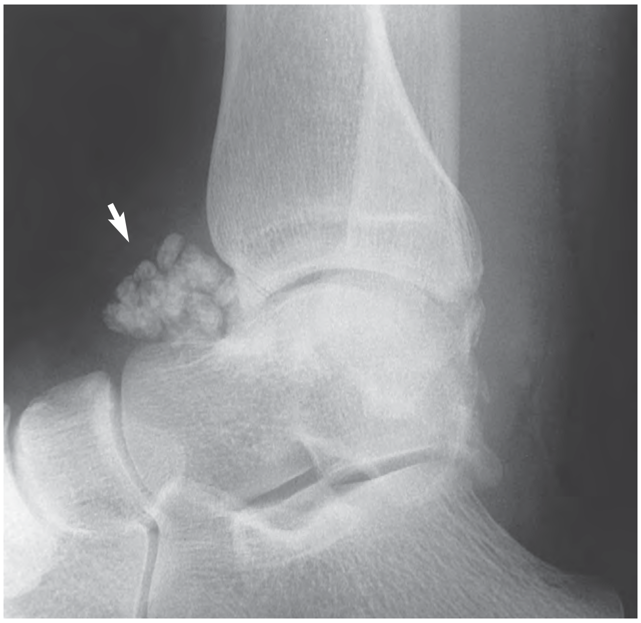

FIGURE 11–76 **Idiopathic synovial osteochondromatosis.**[97,98] Multiple intraarticular radiodense osteocartilaginous bodies have accumulated in the anterior recess of the joint capsule of the tibiotalar joint *(arrow)*. Idiopathic synovial osteochondromatosis represents metaplastic or neoplastic proliferation of cartilaginous bodies by the synovial membrane. Secondary synovial osteochondromatosis also may occur as a result of degenerative joint disease. Noncalcified lesions are best evaluated with arthrography.

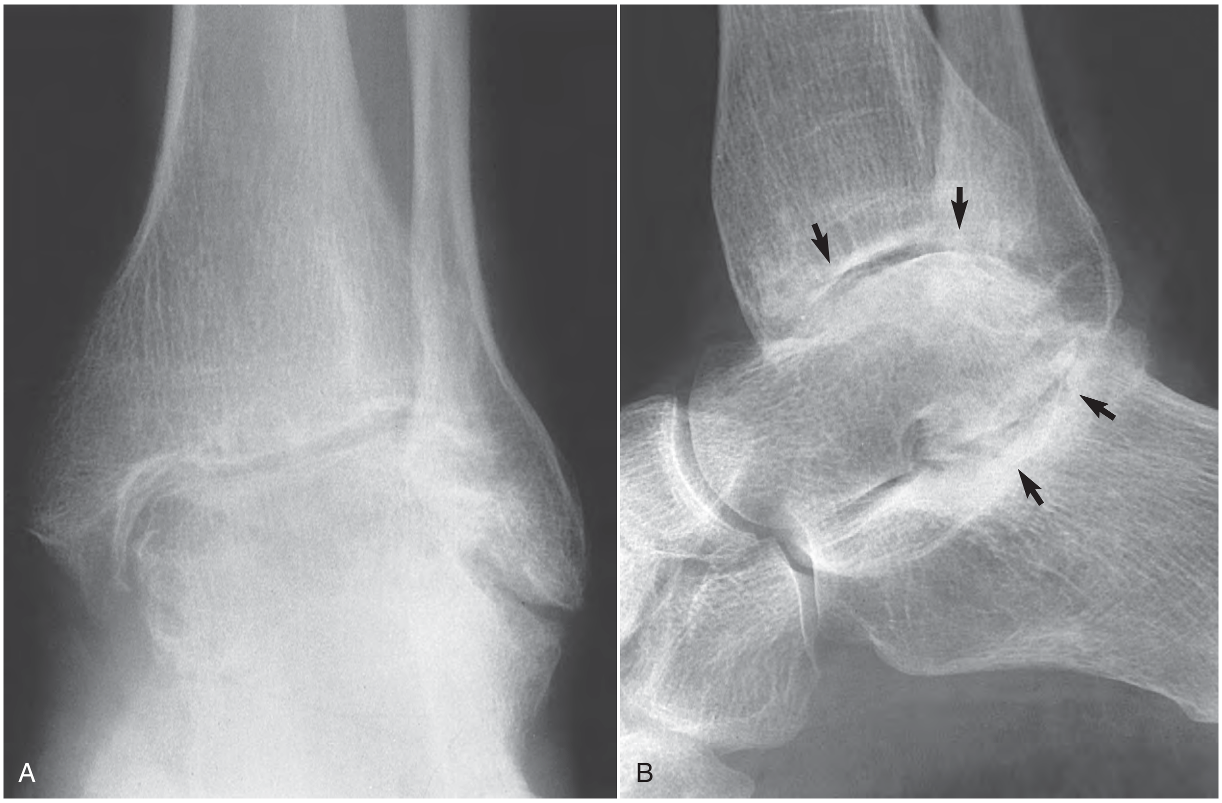

FIGURE 11–77 **Hemophilic arthropathy: ankle abnormalities.**[6,99,154] **A,** In a 28-year-old man, joint space narrowing, osteopenia, and tibiotalar slant from osseous overgrowth all are characteristic findings in this bleeding disorder. Growth recovery lines are also evident within the tibia. **B,** In a 31-year-old man, tibiotalar and subtalar joint space narrowing, sclerosis, and subchondral collapse are seen.

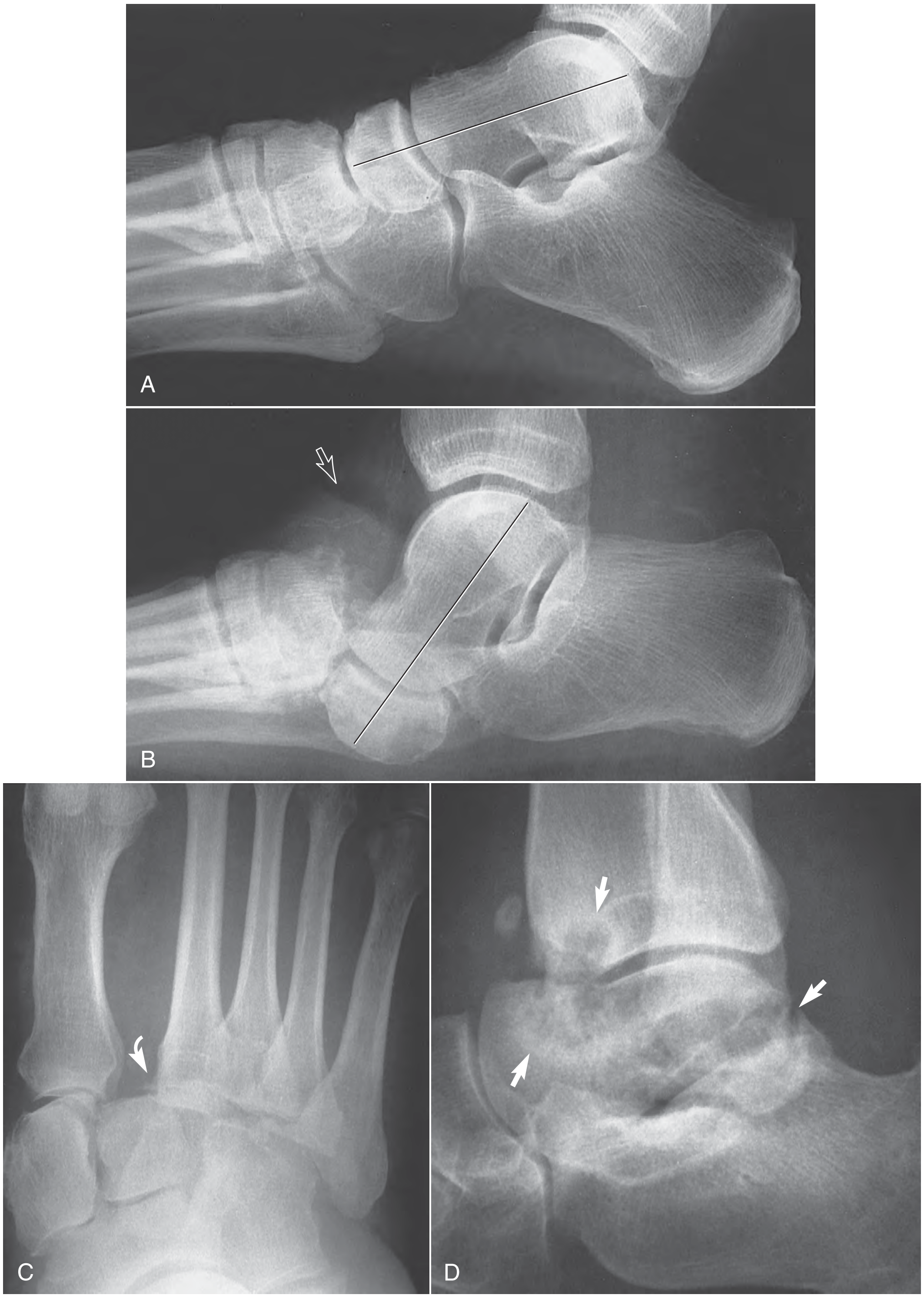

FIGURE 11–78 **Neuropathic osteoarthropathy.**[100,101,151,170] Diabetes mellitus. **A-B,** Serial progression in a patient with poorly controlled insulin-dependent diabetes. In **A,** an initial radiograph taken in a recumbent non—weight-bearing position is essentially normal. In **B,** a weight-bearing radiograph taken 5 years later reveals dramatic destruction of the midtarsal articulations with midfoot collapse *(open arrow)*. The naviculocuneiform joint is disarticulated, and the patient is bearing weight directly on the navicular bone. Osseous debris is also seen associated with these changes. The lines indicate the orientation of the long axis of the talus and navicular bones before and after the midfoot collapse. Such midfoot collapse in diabetic neuropathic joint disease is associated with rupture of the tibialis posterior tendon. **C,** In another patient, lateral dislocations of the tarsometatarsal joints *(curved arrow)* represent a neuropathic Lisfranc fracture-dislocation. Spontaneous fractures and dislocations occur frequently with diabetic neuroarthropathy, and the Lisfranc pattern is common. **D,** Juvenile-onset diabetes. An ankle radiograph of this 22-year-old patient with diabetes mellitus shows collapse of the talus with osteolytic erosive changes of the tibia and talus *(arrows)*. Aspiration of the joint revealed blood but no evidence of infectious organisms. *(**D,** Courtesy L. Danzig, MD, Santa Ana, Calif.)*

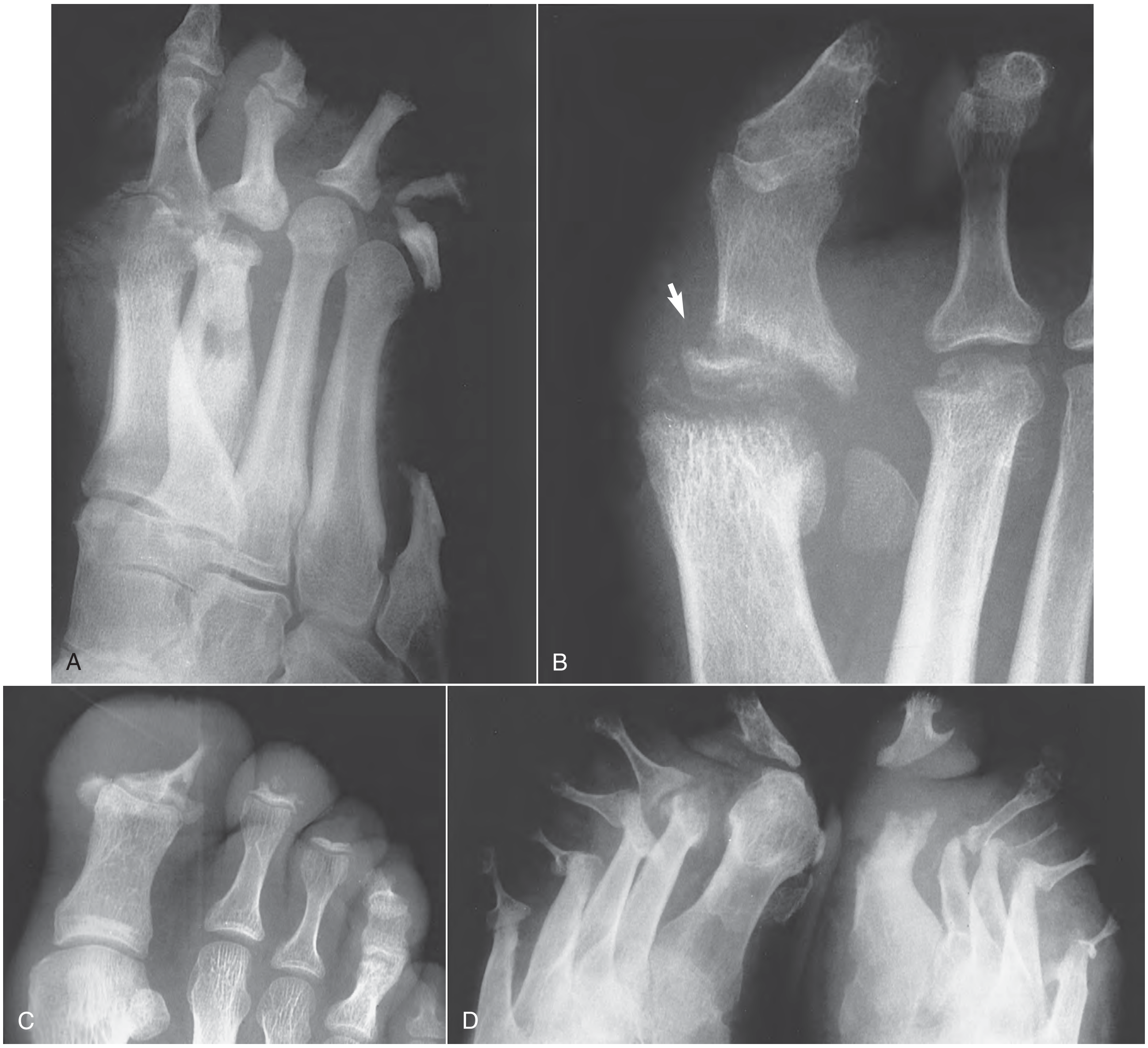

FIGURE 11–79 Neuropathic osteoarthropathy.[102-104,151] **A,** Congenital insensitivity to pain. Atrophic resorption and tapering of several metatarsal bones and phalanges are associated with periostitis, sclerosis, and fragmentation. In this case, neuropathic osteoarthropathy is probably complicated by osteomyelitis involving the second metatarsal. **B,** Alcoholism. A 35-year-old alcoholic man had increasing pain and swelling over the great toe. An oblique radiograph shows dissolution and fragmentation of the articular surfaces of the first metatarsal bone and proximal phalanx *(arrow)* with considerable soft tissue swelling and ulceration overlying the joint. Milder but similar changes are seen at the second metatarsophalangeal articulation. **C-D,** Leprosy. In **C,** acro-osteolysis is evident. Observe the tapered, atrophic resorption of the terminal phalanges of the first three digits in this patient with leprous acro-osteolysis. The soft tissues of the terminal tufts are foreshortened and swollen. In **D,** advanced changes in another patient consist of diffuse osteolysis, bone atrophy, and tapering involving several phalanges and metatarsal bones. Marked disorganization and soft tissue deformity are also seen. Bilateral symmetric involvement is characteristic in leprosy. Other musculoskeletal abnormalities associated with leprosy include periostitis, osteitis, osteomyelitis, leprous arthritis, and secondary infection. (***A,*** *Courtesy M. Pallayew, MD, Montreal, Quebec, Canada.* ***C,*** *Courtesy W. Coleman, DPM, Carville, La.;* ***D,*** *Courtesy of J. Haller, MD, Vienna, Austria.)*

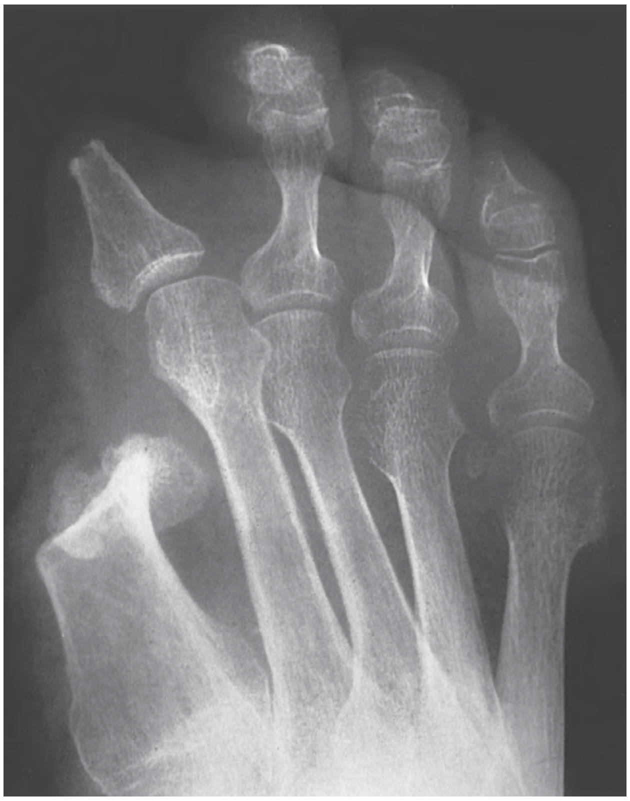

FIGURE 11–80 **Frostbite.**[105] This man sustained frostbite of his feet. Radiograph reveals osteoporosis, acro-osteolysis, and contractures of the toes. Amputation of the first and second toes is consistent with frostbite itself, surgical amputation, or both. *(Courtesy R. Fellows, MD, Fairbanks, Alaska.)*

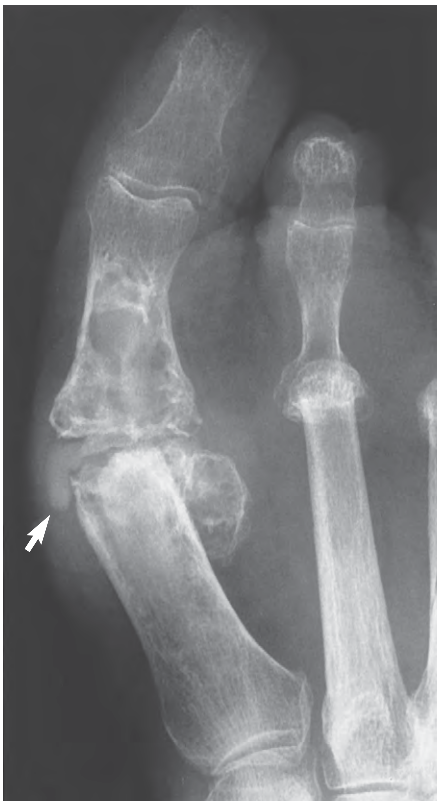

FIGURE 11–81 **Silicone synovitis.**[106] This patient with severe rheumatoid arthritis has a silastic prosthesis in the first metatarsophalangeal joint *(white arrow)*. Well-defined radiolucent defects and erosions are present in the adjacent bones, characteristic of silicone synovitis, a well-known complication of silicone arthroplasty. In this case, the prosthesis is also deformed.

TABLE 11-14 Infectious Disorders of the Ankle and Foot

Entity	Figure(s)	Characteristics
Cellulitis[107,170]	11-82	Soft tissue infection usually as a result of stasis ulcers and vascular insufficiency Frequent complication of diabetes mellitus, foreign bodies, puncture wounds, or skin ulceration *Cellulitis is a clinical diagnosis:* radiographs are not helpful, except in identifying gas in the soft tissues in gas-forming infections Gas-forming organisms include *Escherichia coli, Aerobacter aerogenes,* and *Bacteroides*; clostridial infection may result in extensive gas formation (gas gangrene), necessitating amputation *Pseudomonas aeruginosa* frequently cultured from puncture wounds Spread of infection typically occurs along the plantar compartments of the foot, leading to contamination of adjacent bones and joints
Pyogenic osteomyelitis and septic arthritis[108-111,154-157,170,193]	11-82, 11-83, 11-84	Pyogenic infection of bones and joints usually spreads from contiguous sources of cellulitis Especially prevalent in patients with diabetes mellitus Difficult to differentiate from neuropathic osteoarthropathy, a coexistent condition in many diabetic patients *Osteomyelitis:* soft tissue swelling, osteolytic destruction *Septic arthritis:* most joint infections begin as a monoarticular arthritis but frequently spread to adjacent bones and joints in the foot Rapid loss of joint space and destruction of subchondral bone Periarticular osteopenia, joint subluxation, and periostitis
Tuberculous osteomyelitis and arthritis[112]	11-85	Tuberculous infection is much less common than pyogenic infection in the ankle and foot; when it does occur, it has a predilection for the ankle joint Mild symptoms and indolent course *Most common organism: Mycobacterium tuberculosis* *Osteomyelitis:* usually begins in epiphysis as an osteolytic lesion; may spread to metaphysis and diaphysis as moth-eaten or permeative pattern of destruction; may involve several bones of the foot *Spina ventosa:* tuberculous dactylitis; soft tissue swelling, bone destruction, periostitis, and bone expansion involving one or several digits; children > adults *Arthritis:* Juxtaarticular osteoporosis, joint space narrowing, joint effusion, and periarticular erosions
Unusual and atypical infections[113,201]	11-86	*Coccidioidomycosis:* fungal disorder occurring in Mexico and southwestern United States; results in osteolytic lesions; may be disseminated; predilection for the calcaneus *Congenital syphilis: Treponema pallidum;* diametaphyseal gummas result in periostitis and aggressive bone destruction *Madura foot:* rare chronic granulomatous fungal disease due to *Madurella* and the actinomycetes; extensive soft tissue necrosis and widespread bone destruction

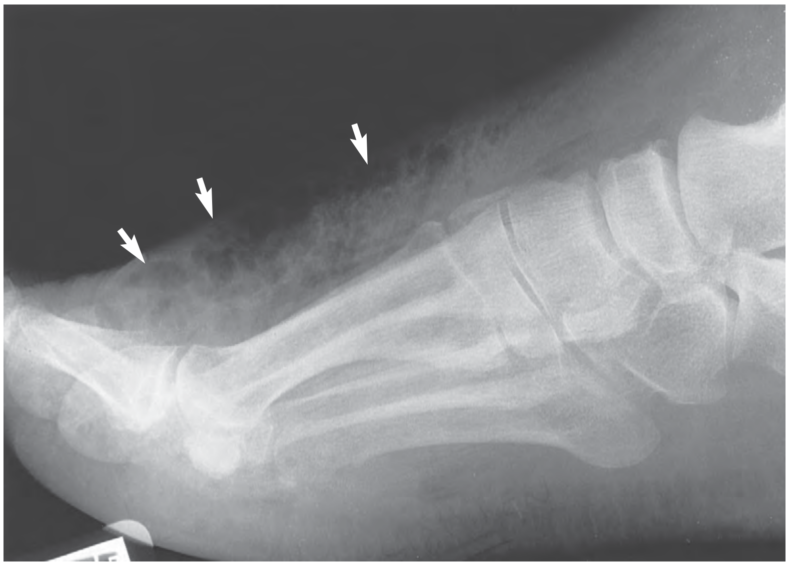

FIGURE 11–82 Cellulitis and osteomyelitis: gas gangrene.[107,155,157,170] This 56-year-old insulin-dependent diabetic patient developed an ulcer on her foot that drained pus for 2 weeks. Observe the diffuse soft tissue swelling and streaky soft tissue emphysema *(arrows)* from a gas-forming organism. Laboratory culture yielded ß-hemolytic and non-ß-hemolytic streptococcus and *Bacteroides* organisms. Most gas-producing organisms are anaerobes.

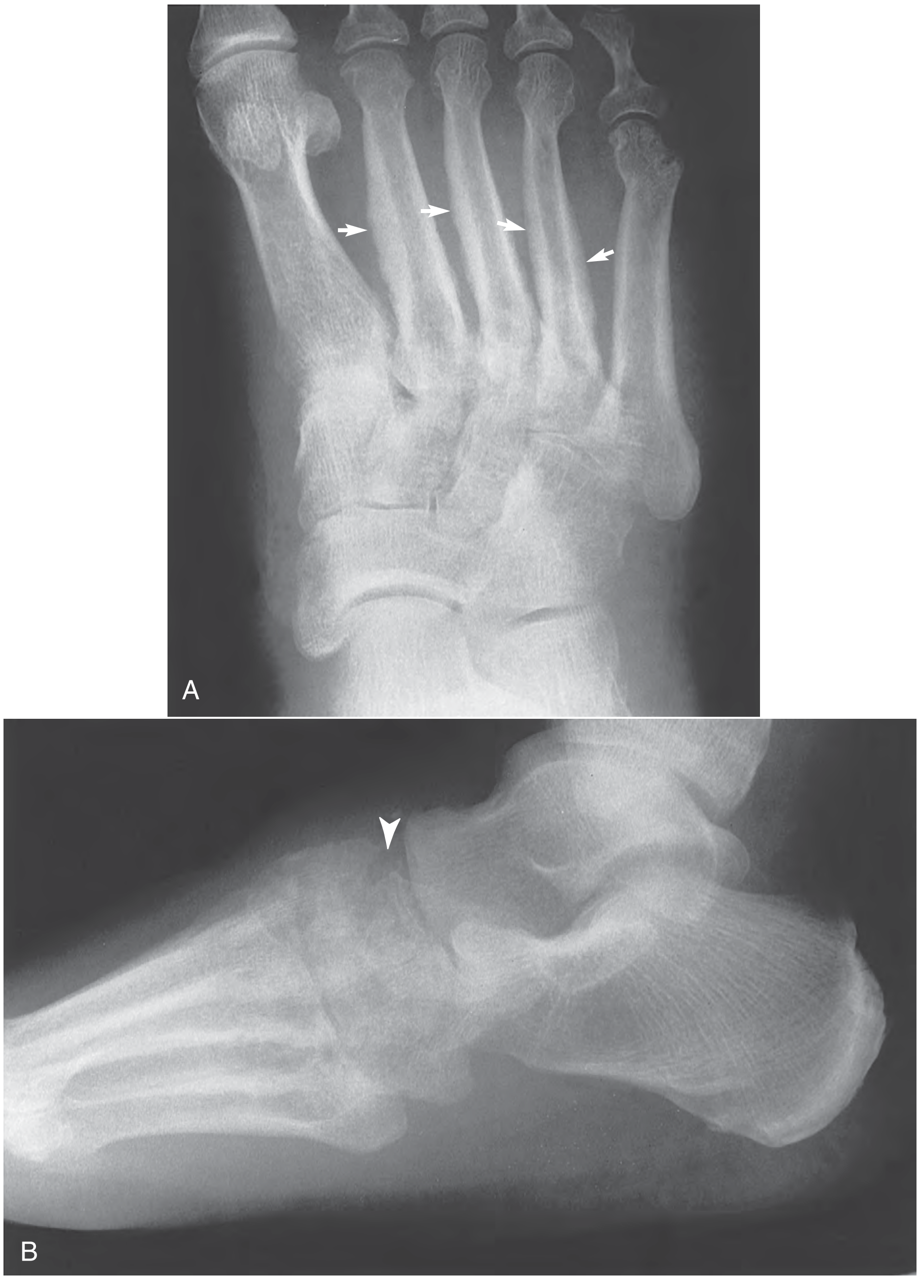

FIGURE 11–83 **Pyogenic osteomyelitis and septic arthritis: diabetes mellitus.**[108-111,154-157,193] **A-B,** A 41-year-old insulin-dependent diabetic patient. Frontal **(A)** and lateral **(B)** radiographs of the foot demonstrate diffuse osteolysis and indistinct cortical margins of the distal row of tarsal bones and metatarsal bases. A large erosion of the superior aspect of the navicular bone *(arrowhead)* and periosteal new bone formation in the shafts of the metatarsals *(arrows)* are well visualized. Joint space narrowing of several intertarsal and tarsometatarsal articulations is also seen.

Continued

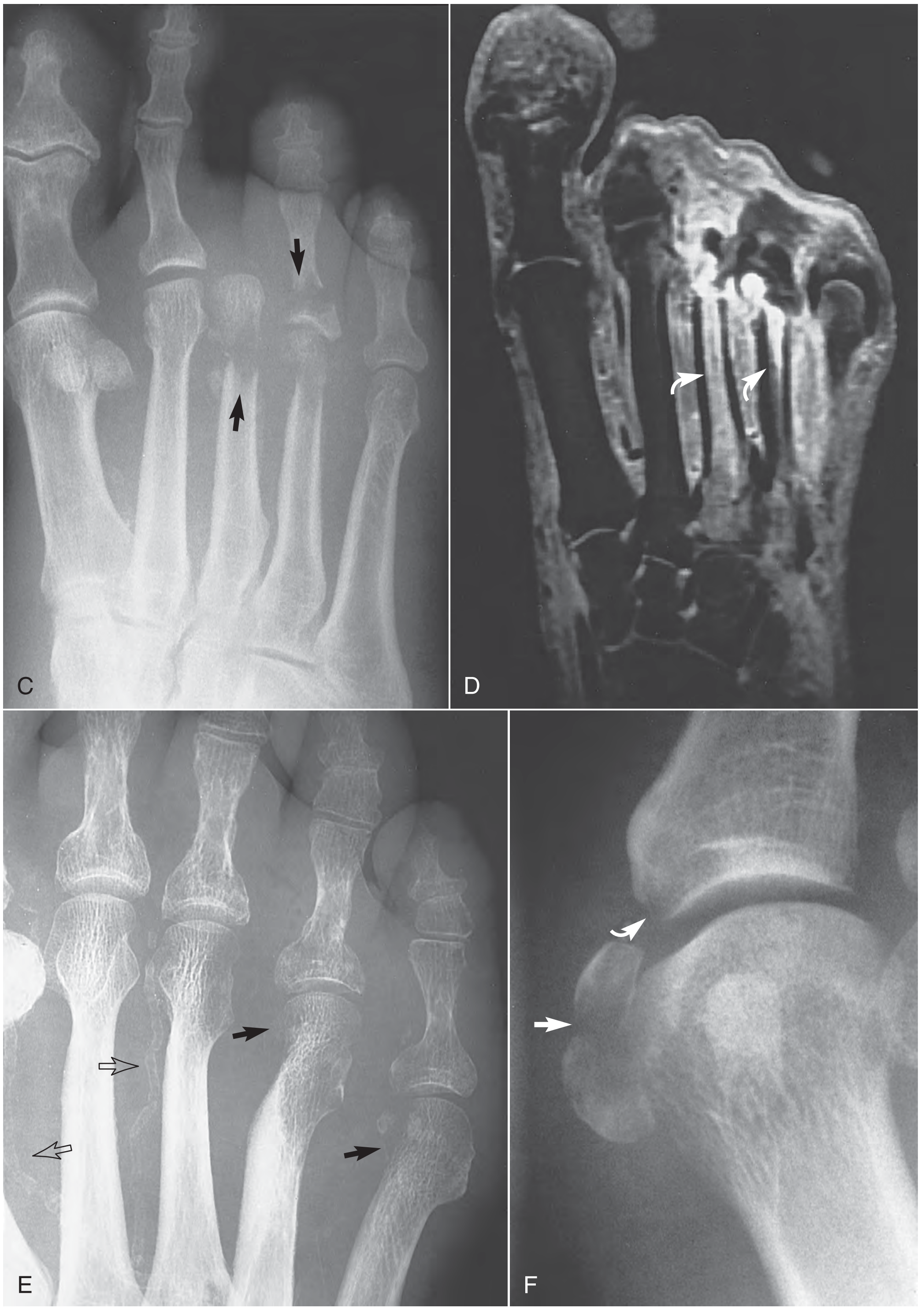

FIGURE 11–83, cont'd **C-D,** A 63-year-old man with poorly controlled diabetes. In **C,** a routine radiograph demonstrates previous surgical amputation of the phalanges of the third toe. Permeative osteolysis involving the three lateral metatarsals and phalanges is evident. In addition, pathologic fractures or zones of osteolysis are seen in the distal third metatarsal and fourth proximal phalanx *(arrows)*. Also observe the soft tissue swelling involving the fourth digit. In **D,** a coronal T1-weighted (TR/TE, 900/13) fat-suppressed MR image obtained after intravenous gadolinium contrast agent administration reveals high signal intensity within the marrow of the third and fourth metatarsal shafts *(curved arrows),* confirming the presence of osteomyelitis. High signal intensity in the surrounding soft tissues indicates hyperemia, edema, and possible soft tissue infection. **E,** In a third patient, a radiograph of the foot reveals diffuse periarticular osteopenia and erosions of the fourth and fifth metatarsal heads *(arrows)*. Note the diffuse vascular calcification *(open arrows)* typically encountered in the foot of the diabetic patient. **F,** This fourth patient developed pain about the first metatarsophalangeal joint. A radiograph demonstrates diffuse osteolysis and pathologic fracture *(arrow)* of the medial hallux sesamoid bone. Another erosion of the proximal phalanx is also evident *(curved arrow)*. A subsequent biopsy revealed evidence of *Staphylococcus aureus*.

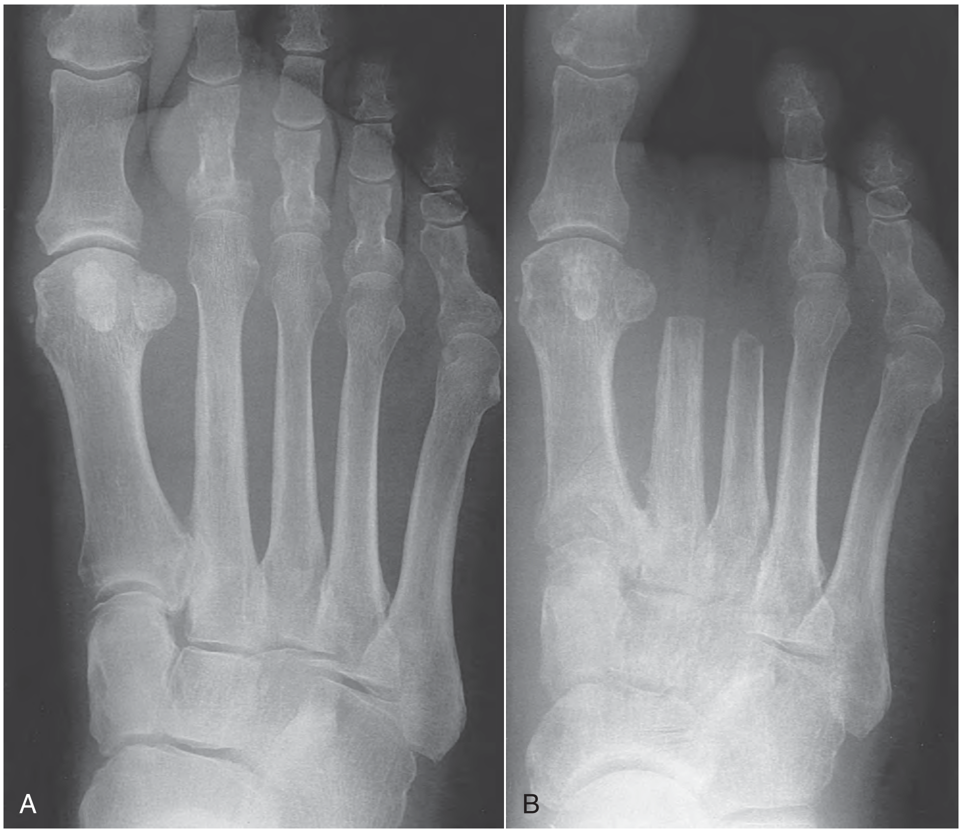

FIGURE 11–84 **Osteomyelitis and septic arthritis: tarsal involvement.**[108-111,155,156] Serial radiographs **(A-B,)** taken 4 months apart show rapidly progressive osteomyelitis of the tarsal bones and destruction of the intertarsal articulations by septic arthritis. The second and third phalanges and distal metatarsals have been surgically amputated in the interim for progressive infection.

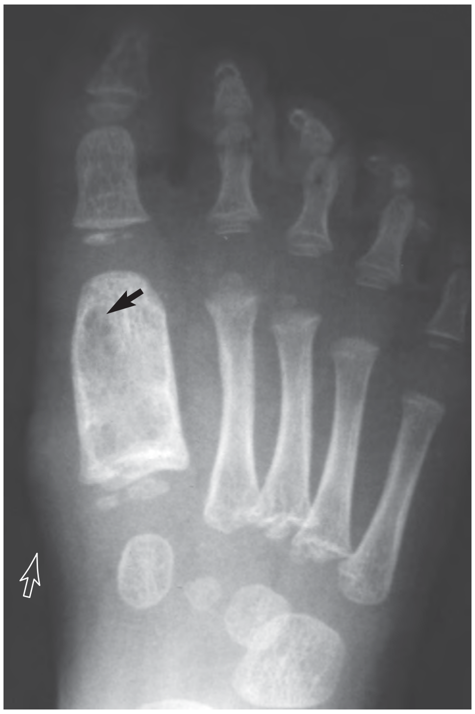

FIGURE 11–85 **Tuberculous dactylitis (spina ventosa).**[112] In this 2-year-old girl, marked widening and enlargement of the first metatarsal is evident. The bone appears more radiodense than normal, but on close examination, this increased density is combined with cystlike osteolytic destruction within the medullary cavity *(arrow)*. Soft tissue swelling is also prominent *(open arrow)*.

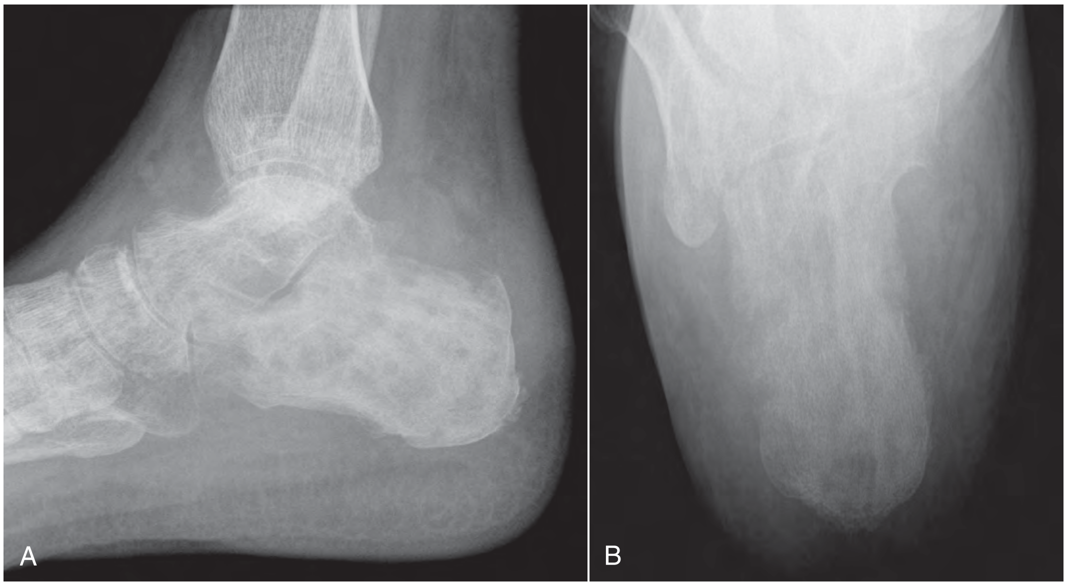

FIGURE 11–86 Maduromycosis: Madura foot. A 35-year-old female from middle America.[113,201] Soft tissue swelling and multiple foci of osteolytic destruction are present throughout the calcaneus and other tarsal bones. There is also some increased radiodensity intermixed with the osteolytic lesions obscuring the normal trabecular pattern of the calcaneus. Maduromycosis is a rare chronic granulomatous fungal infection particularly prevalent in India. Infection of the foot usually occurs as a result of posttraumatic soft tissue invasion by organisms that are normal inhabitants of the soil. This infection is notorious for severe bone, joint, and soft tissue destruction.

TABLE 11-15 Tumors and Tumorlike Lesions Affecting the Ankle and Foot[177]

Entity	Figure(s)	Characteristics
Malignant Tumors of Bone		
Secondary malignant tumors of bone		
Skeletal metastasis[114]	11-87	Fewer than 1% of metastatic lesions affect the bones of the foot Acral metastases most frequently occur in patients with carcinoma of the lung, bronchus and kidney
Primary malignant tumors of bone		
Osteoblastoma (aggressive)[115]		Eleven percent of aggressive osteoblastomas affect the bones of the foot Expansile osteolytic lesion that may be partially ossified or contain calcium
Fibrosarcoma[116]	11-88	Two percent of fibrosarcomas affect the bones of the foot Purely osteolytic destruction with no associated sclerotic reaction or periostitis
Ewing sarcoma[117,173]	11-89	Three percent of Ewing sarcomas affect the bones of the foot, most commonly the calcaneus, metatarsals, and phalanges Aggressive permeative or moth-eaten pattern of bone destruction Central diaphyseal lesions of the tubular bones predominate
Synovial cell sarcoma[118,149]	11-90, 11-106	Uncommon malignant neoplasms frequently found in the soft tissues in extraarticular locations More common in lower extremity Frequent recurrence and metastases, especially to the lung Poor prognosis Aggressive osteolytic destruction Approximately 20%-30% contain calcification
Myeloproliferative disorders of bone		
Plasma cell (multiple) myeloma[119]	11-91	Two percent of multiple myeloma lesions occur in the bones of the foot Diffuse osteopenia or discrete osteolytic lesions

* Information reproduced from reference 194.

TABLE 11-15 Tumors and Tumorlike Lesions Affecting the Ankle and Foot[177]—cont'd

Entity	Figure(s)	Characteristics
Benign Tumors of Bone		
Enostosis[120]	11-92	Five percent of enostoses affect the bones of the foot
Osteoid osteoma[121,187]	11-93	Eight to eleven percent of osteoid osteomas occur in the bones of the foot
Subungual exostosis[122,202]	11-94	Solitary osteochondroma-like lesion arising from the dorsal surface of the distal phalanx Pressure on the undersurface of the nail may cause severe pain Lesion possesses smooth continuation of cortical and medullary bone Most frequently affects great toe
Enchondroma (solitary)[123]	11-95	About 7% of solitary enchondromas affect the bones of the foot Lesions in the foot are more common in Ollier disease and Maffucci syndrome (>60% of patients with Maffucci syndrome)
Chondroblastoma[124,125,167]	11-96	Approximately 10% of chondroblastomas occur in the bones of the foot Eccentric osteolytic lesion that involves epiphyses, apophyses, or epiphyseal equivalents; predilection for talus and calcaneus
Giant cell tumor (benign)[126,179]	11-97	Fewer than 2% of benign giant cell tumors are located in the bones of the foot
Simple bone cyst[125]	11-98	Only 1% of simple bone cysts occur in the bones of the foot Multiloculated and eccentric lesion usually affecting the calcaneus
Intraosseous lipoma[128,152,188]	11-99	Approximately 32% of intraosseous lipomas occur in the calcaneus *Age range:* 12-66 years (average 42 years) Geographic osteolytic lesion ranging in size from 2-4 cm in diameter with: Sclerotic margins (61%) Central calcification (62%) Bone expansion (13%)
Aneurysmal bone cyst[129]	11-100	Approximately 8% of aneurysmal bone cysts involve the bones of the foot Eccentric, thin-walled, expansile, multiloculated osteolytic lesion Fluid levels seen with MR imaging
Tumorlike Lesions of Bone		
Paget disease[130,131,185]	11-101	Occasional involvement of the bones of the foot Usually polyostotic Calcaneus is the most frequent bone affected in the foot, but a very rare location for the monostotic form
Fibrous dysplasia[132]	11-102	Involvement of the bones of the foot is rare in the monostotic form but present in about 75% of patients with polyostotic disease
Soft Tissue Tumors and Masslike Lesions of the Ankle and Foot[194]*		Diagnostic ultrasound and MR imaging are frequently used to diagnose these conditions
Cystic tumorlike lesions		
Ganglia		*Benign:* Most common soft tissue mass in the foot and ankle representing 40% of suspected soft tissue masses *Palpable lesions:* most are around the tarsometatarsal joint Nonpalpable (clinically occult) ganglia are most commonly located in the sinus tarsi and tarsal canal
Synovial cysts		Benign synovial-lined, juxtaarticular fluid collections that form in response to effusions associated with internal joint derangement
Adventitial bursa		Benign bursae that form when abnormal friction develops between opposing rigid structures Can be painful when inflamed Common adjacent to the first metatarsophalangeal joint in patients with hallux rigidus and hallux valgus

Continued

TABLE 11-15 Tumors and Tumorlike Lesions Affecting the Ankle and Foot[177]—cont'd

Entity	Figure(s)	Characteristics
Noncystic tumorlike lesions		
Morton interdigital neuroma	11-103	Benign nontumorous lesion with neural degeneration and perineural reactive fibrosis most often located within the third and second digital interspaces One third are asymptomatic; remainder cause pain and numbness radiating to toes MR imaging shows a round intermediate signal soft tissue nodule outlined by adjacent fat in the interspace
Rheumatoid nodules		Benign foci of granulomatous tissue with central necrosis occurring in subcutaneous tissues of 20%-30% of patients with rheumatoid arthritis, especially women with advanced disease
Callus		Benign superficial soft tissue thickening overlying pressure points that develop in response to mechanical pressure May ulcerate and lead to deep infections in diabetic patients
Synovial-based processes		
Synovial chondromatosis		Benign, uncommon disorder characterized by multiple hyaline cartilage nodules that form within a joint, tendon sheath, or bursa M : F, 2 : 1 to 4 : 1; third or fourth decade Cartilaginous nodules not visible on radiographs unless calcified; MR imaging or MR arthrography are useful
Pigmented villonodular synovitis		Benign proliferation of synovium that grossly resembles a shaggy red beard *Synonym:* Diffuse-type giant cell tumor May be intraarticular and extraarticular and often results in bone erosion Frequency of involvement: Hindfoot > midfoot > forefoot
Gouty tophi	11-104	Benign focal urate crystal deposits that occur in advanced cases; as many as 40% of patients with recurrent episodes of tophaceous gout Calcified tophi may be radiodense on radiographs
Soft tissue tumors		
Plantar fibromatosis	11-105	Benign superficial fibroblastic tumor characterized by nodular fibrous proliferation arising in the plantar aponeurosis; may be very extensive Male > Female; 20%-50% bilateral; more common in epileptics, diabetics, and alcoholics with liver disease
Giant cell tumor of tendon sheath		Benign, localized form of giant cell tumor with proliferation of synovial-like tissue arising from the synovium of tendon sheaths Female > male; ages 30-50 years
Lipoma		Benign subcutaneous tumor comprised of mature adipocytes Most common mesenchymal soft tissue tumor in adults More common in obese patients between the ages of 40 and 60 years; multiple in 5% of patients Usually diagnosed clinically without the use of imaging
Soft tissue chondroma		Benign extraosseous and extrasynovial soft tissue tumor composed principally of mature hyaline cartilage Calcification may be seen on radiographs, but MR imaging is typically helpful in diagnosis Lesions may be large and confused for chondrosarcoma Rare malignant transformation to chondrosarcoma
Synovial sarcoma[118,149]	11-90, 11-106	Malignant mesenchymal spindle-cell tumors; resemble synovial cells, but do not actually derive from synovial cells Occur at any age but are slightly more common in young adult men Lobulated deep soft tissue masses that may erode adjacent bone One third of lesions are calcified; 10%-25% have fluid-fluid levels on MR imaging Forty percent metastasize to lungs, skeleton, or regional lymph nodes
Undifferentiated pleomorphic sarcoma		Malignant lesion previously termed *malignant fibrous histiocytoma* Most common type of sarcoma in patients older than 40 years; slight male predominance; more common in thigh than foot Five-year survival rate: 50%-60%
Leiomyosarcoma		Malignant smooth muscle tumor that only occasionally involves the foot and ankle Calcification seen in 15% of cases Local recurrence and distant metastasis can occur

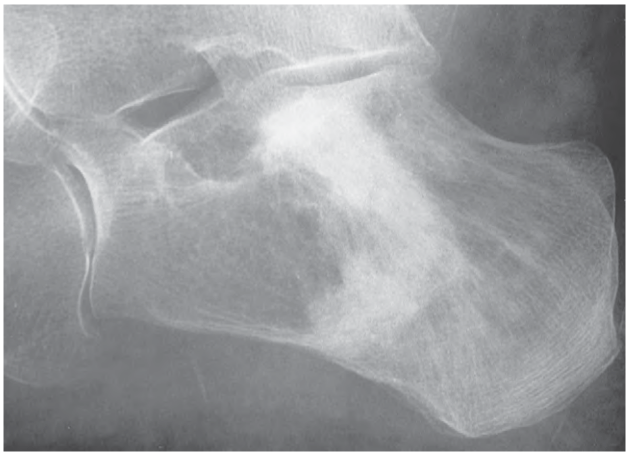

FIGURE 11–87 Skeletal metastasis.[114] Lateral radiograph of the calcaneus in this 76-year-old woman with a history of breast carcinoma reveals a mixed pattern of osteoblastic and osteolytic metastasis. Skeletal metastases from the breast may be manifested as lytic, blastic, or mixed lesions.

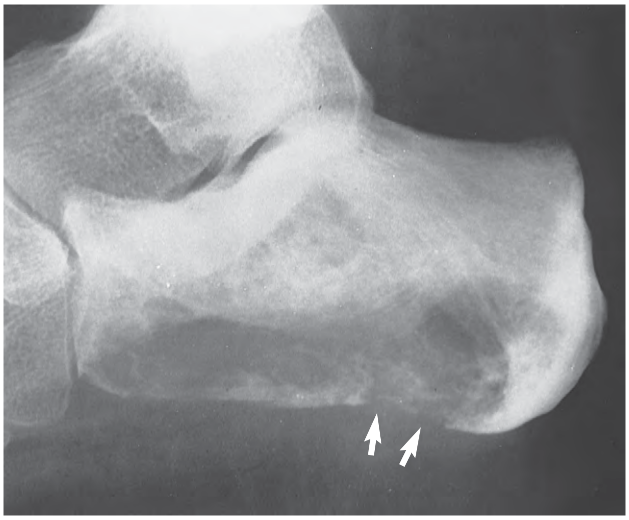

FIGURE 11–88 Fibrosarcoma.[116] A large, purely osteolytic lesion permeates the plantar aspect of the calcaneus in this 21-year-old woman. Minimal surrounding bone sclerosis is evident, but no periosteal reaction can be detected. Cortical perforation is seen *(arrows)*.

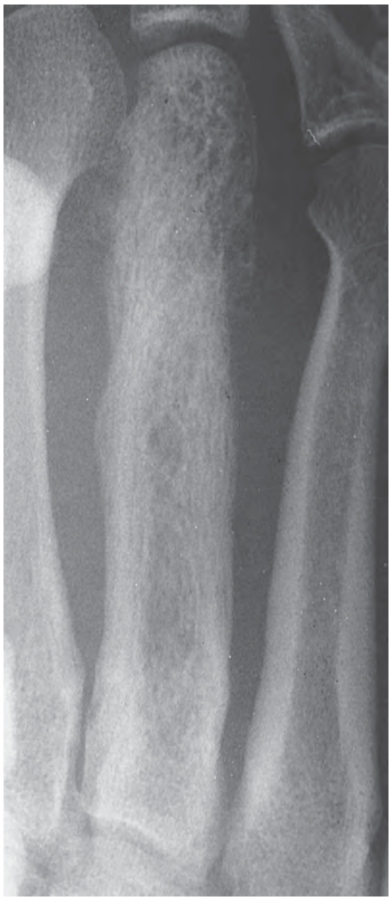

FIGURE 11–89 Ewing sarcoma.[117,173] A permeative pattern of osteolytic destruction with indistinct cortical margins is evident in the third metatarsal bone of this 21-year-old man. The lesion involves the full length of the bone.

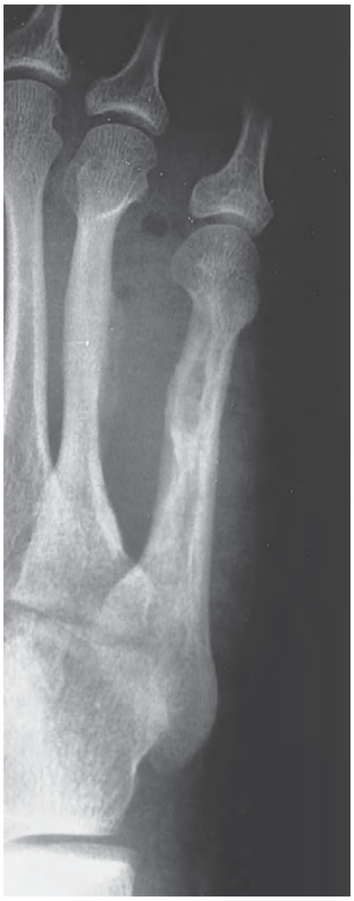

FIGURE 11–90 Synovial sarcoma.[118,149] This 23-year-old woman complained of a painful soft tissue mass on the lateral aspect of her foot. Permeative destruction involving the fifth metatarsal diaphysis with erosion of the adjacent fourth metatarsal bone is noted. The histologic diagnosis was synovial cell sarcoma. (See also Fig 11-106.)

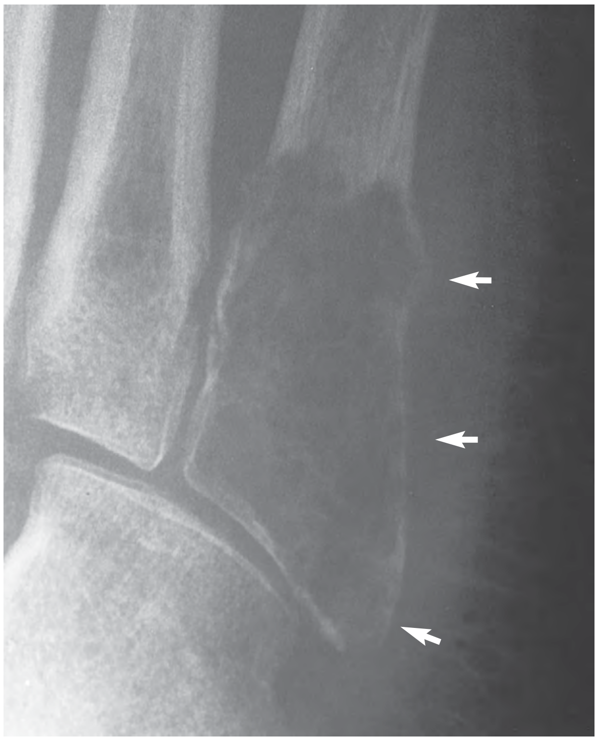

FIGURE 11–91 **Plasma cell (multiple) myeloma.**[119] A 48-year-old woman. Osteolytic destruction, cortical thinning, and disruption are all evident in the base of the fifth metatarsal bone *(arrows)*.

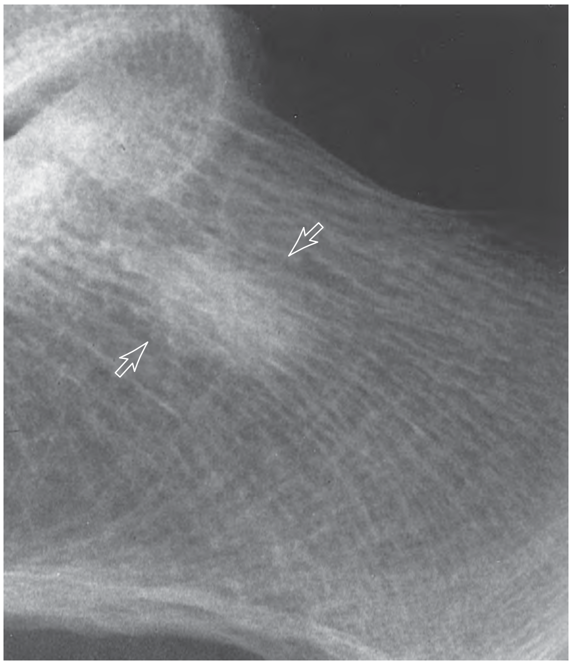

FIGURE 11–92 **Enostosis (bone island).**[120] An ovoid osteosclerotic focus *(open arrows)* is seen within the calcaneus. The long axis of the enostosis is oriented parallel to the axis of the major trabeculae.

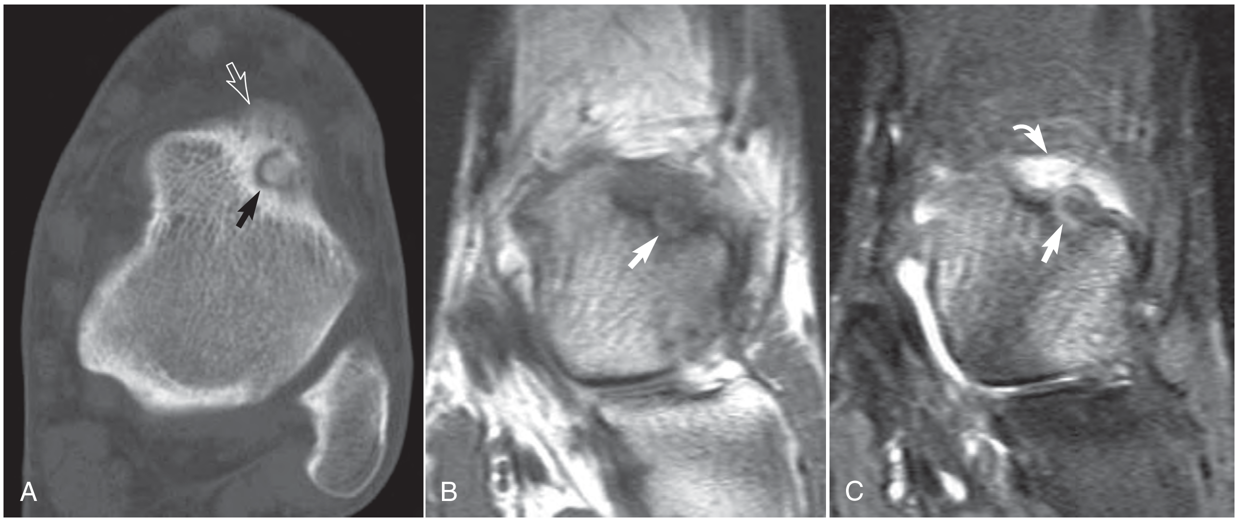

FIGURE 11–93 **Osteoid osteoma: talus.**[121,187] A 22-year-old man. **A,** A transaxial CT bone window image shows a circular 5-mm diameter radiolucent nidus *(arrow)* in the cortex of the anterior margin of the talus. Calcification is present within the matrix of the nidus, and reactive new bone formation surrounds the lesion *(open arrow)*. **B,** Coronal T1-weighted MR imaging shows mainly the low signal intensity of surrounding reactive sclerosis, with a slightly higher signal arising from the nidus itself *(arrow),* except for the calcified central portion of the nidus, which is also of low signal. **C,** The fluid-sensitive T2-weighted fat suppressed transaxial image shows high signal intensity soft tissue edema from synovitis *(curved arrow)* surrounding the lesion *(arrow)*.

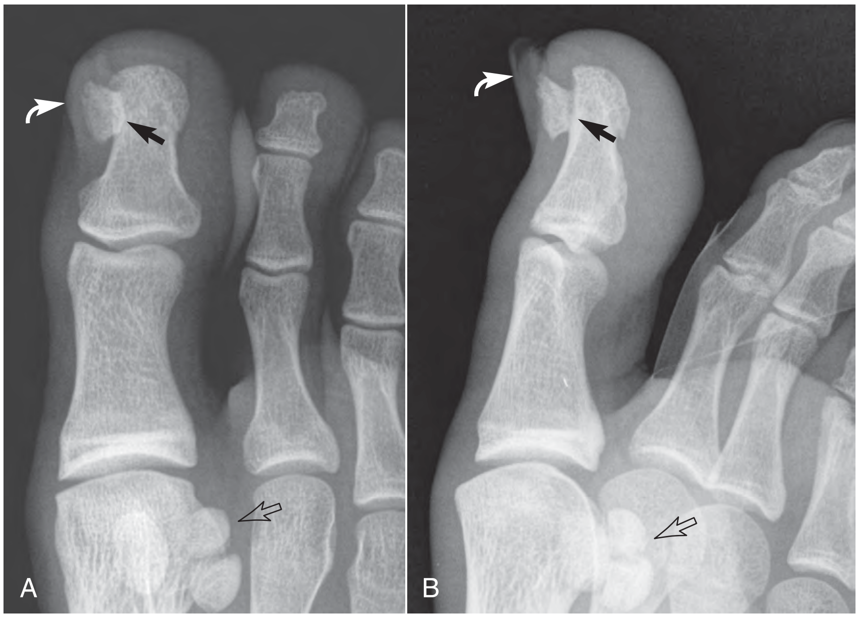

FIGURE 11–94 **Subungual exostosis.**[122,202] An outgrowth of mature bone *(black arrows)* arising from the dorsal surface of the terminal phalanx of the great toe displaces the overlying nail bed *(curved arrows)*. Up to 80% of these benign osseous exostoses occur at this site on the great toe. They are usually solitary and frequently result in pain, swelling, and ulcerations of the nail bed or surrounding tissue with secondary infection. Of incidental note is a bipartite fibular hallux sesamoid bone *(open arrows)*.

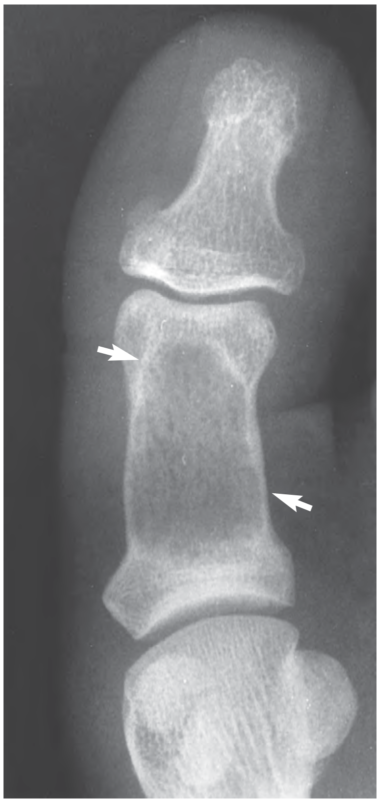

FIGURE 11–95 **Enchondroma.**[123] A large, purely osteolytic, geographic lesion with endosteal scalloping is seen in the metaphyses and diaphysis of the proximal phalanx of the great toe *(arrows)*. Solitary enchondroma is a benign neoplasm composed of hyaline cartilage that develops in the medullary cavity and is usually discovered in the third or fourth decade of life. Most lesions are painless, and the presence of painful lesions should arouse the suspicion of malignant transformation, a complication that occurs only rarely in solitary lesions and in as many as 20% to 30% of cases of multiple lesions (Ollier disease and Maffucci syndrome).

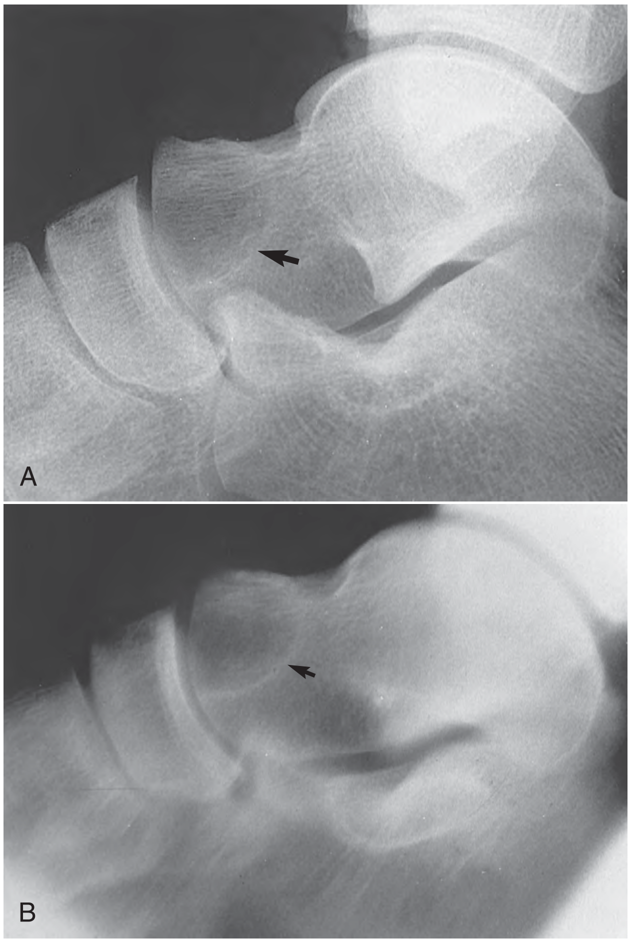

FIGURE 11–96 **Chondroblastoma.**[124,125,167] Twenty-year-old man with ankle pain. **A,** Lateral radiograph shows an osteolytic lesion in the talus. It is subchondral in location (an "epiphyseal equivalent" site) and geographic in appearance. **B,** Conventional tomography confirms the findings *(arrow)*. *(Courtesy T. Goergen, MD, San Diego.)*

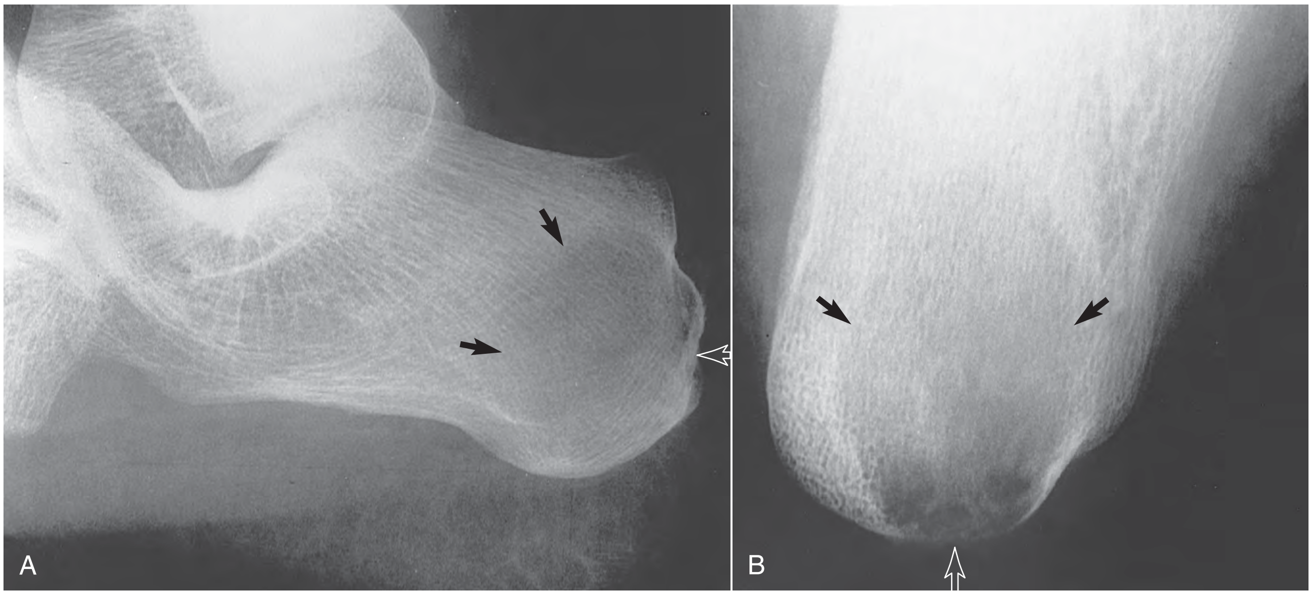

FIGURE 11–97 **Giant cell tumor.**[126,179] Lateral **(A)** and axial **(B)** radiographs of the calcaneus in this 33-year-old man show a circular, well-defined osteolytic lesion *(arrows),* which is eccentrically located, abutting on the posterior aspect of the calcaneus *(open arrows)*. The calcaneus is an infrequent site for giant cell tumor. *(Courtesy G. Greenway, MD, Dallas, Texas.)*

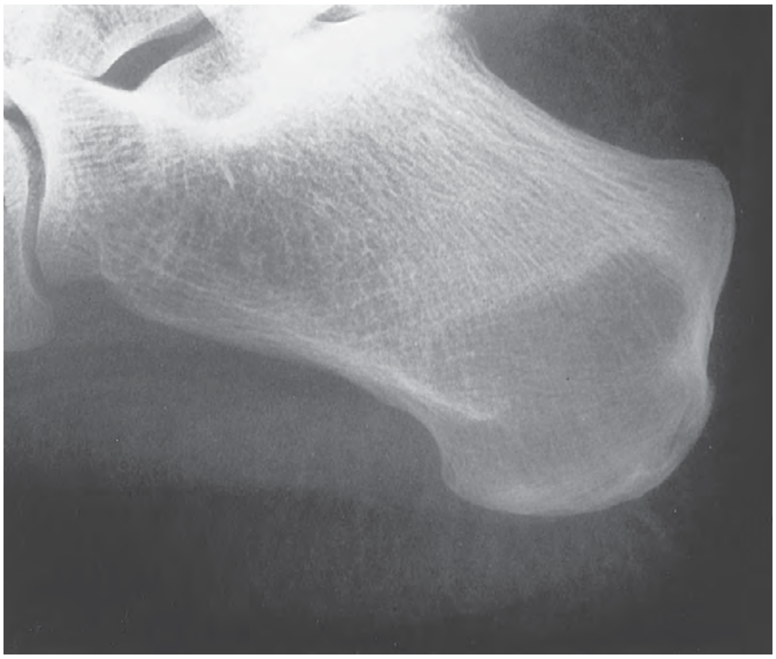

FIGURE 11–98 **Simple bone cyst.**[127] Lateral radiograph of the calcaneus in this 16-year-old woman with a biopsy-proven simple bone cyst reveals a geographic radiolucent lesion with a barely perceptible sclerotic margin. Approximately 3% of all simple bone cysts occur in the calcaneus. Typically, they are solitary, and they are asymptomatic unless a pathologic fracture has occurred. Simple bone cysts are usually found more anteriorly in the calcaneus. *(Courtesy R.J. Binden, MD, Oakland, Calif.)*

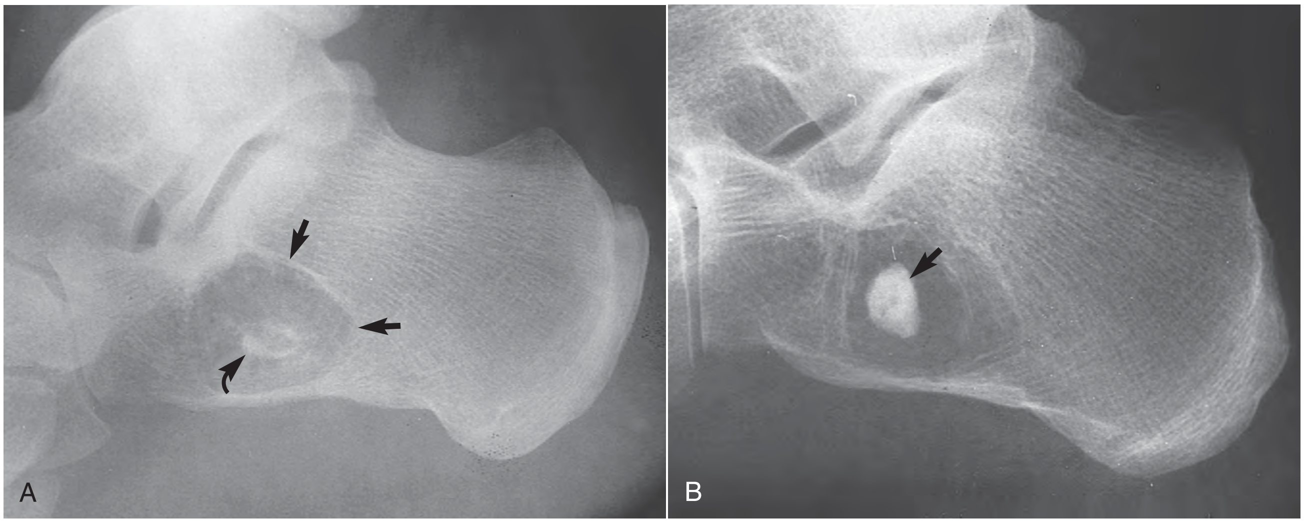

FIGURE 11–99 **Intraosseous lipoma.**[128,152,188] **A,** Observe the classic appearance of a large, circular, radiolucent calcaneal lesion *(arrows)* containing a central fleck of calcification *(curved arrow)*. **B,** In another patient, a lateral radiograph of the calcaneus shows the characteristic appearance of an intraosseous lipoma. Observe the localization of the lesion in the triangular area between the major trabecular groups at the junction of the anterior and middle thirds of the calcaneus. The lesion is geographic and contains a central sclerotic focus *(arrow)*. Simple bone cysts, which are also radiolucent, often occupy the same location in the calcaneus but rarely possess the central focus of calcification (see Figure 11-98). (***A,*** *Courtesy P.H. VanderStoep, MD, St Cloud, Minn.* ***B,*** *Courtesy A.H. Newberg, MD, Boston.)*

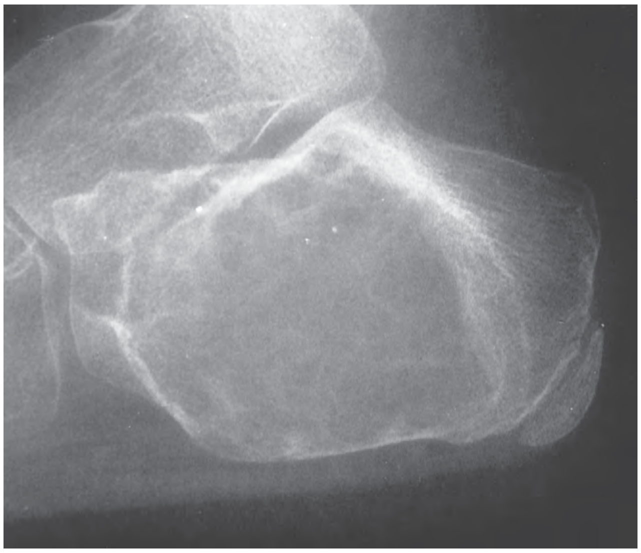

FIGURE 11–100 **Aneurysmal bone cyst.**[129] Lateral radiograph of the calcaneus in this 11-year-old boy shows osseous expansion of this osteolytic trabeculated lesion. The cortex is not disrupted. CT images (not shown) demonstrated the extent of the lesion. *(Courtesy T. Broderick, MD, Orange, Calif.)*

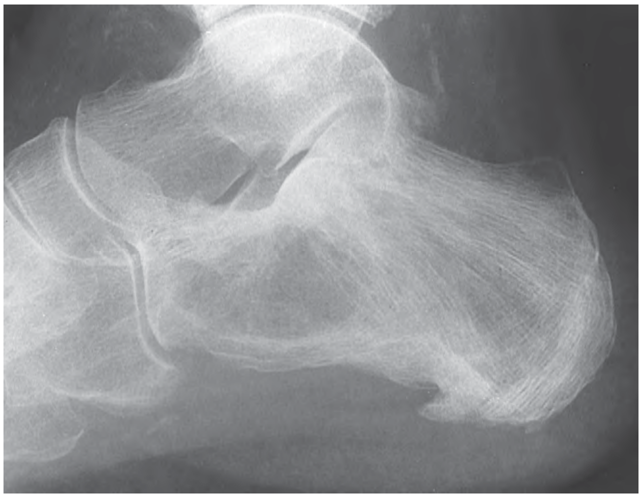

FIGURE 11–101 **Paget disease: calcaneus.**[130,131] In this patient with the combined osteolytic and osteosclerotic pattern of Paget disease, observe the areas of thickened, coarsely trabeculated bone with radiolucent regions of varying size. Minimal bone enlargement is also present. Paget disease only infrequently involves the bones of the foot, but the calcaneus is the most likely bone affected. Furthermore, the calcaneus is a more likely site for the polyostotic form, but a very rare location for the monostotic form of Paget disease.

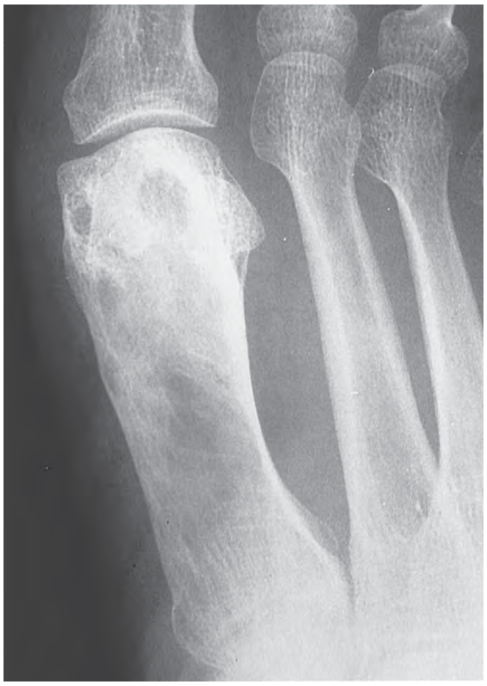

FIGURE 11–102 Fibrous dysplasia.[132] Observe the characteristic poorly defined trabeculae, hazy ground-glass appearance, and slight expansion of the first metatarsal bone in this radiograph of a 60-year-old man.

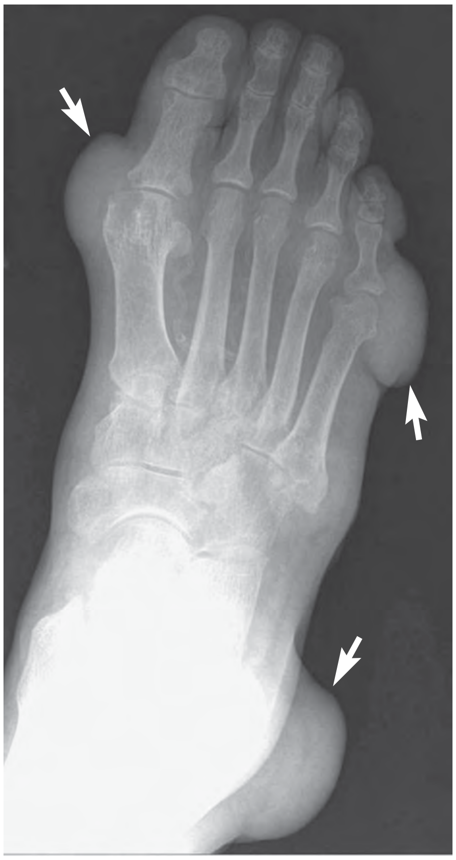

FIGURE 11–104 Gouty tophi.[194] In addition to the periarticular erosions, observe the large radiodense soft tissue masses *(arrows)* in this 44-year-old man with tophaceous gout. (See also Figure 11-75.)

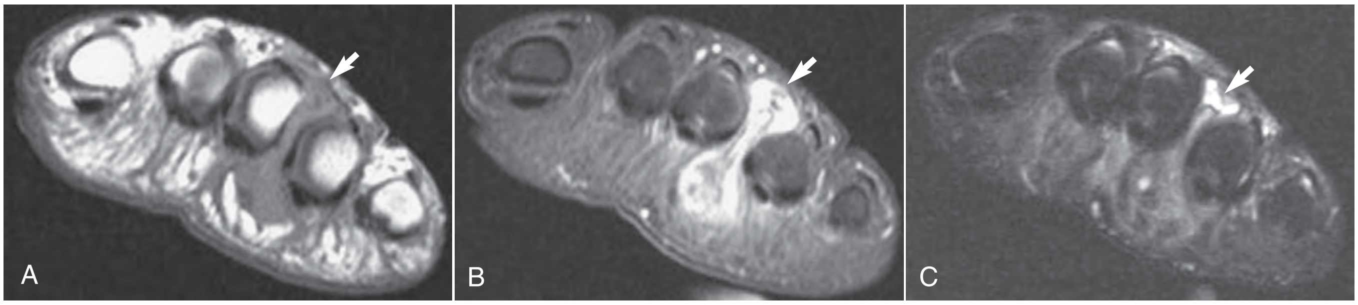

FIGURE 11–103 Morton interdigital neuroma.[194] Coronal MR imaging sequences through the metatarsals. **A,** T1-weighted; **B,** Fat-suppressed T1-weighted after intravenous administration of gadolinium; **C,** Fat-suppressed T2-weighted. A biconcave mass within the third intermetatarsal space *(arrows)* is low signal intensity on T1-weighting **(A),** brightly enhanced after gadolinium administration **(B),** and only slightly more intense than muscle on T2-weighting **(C).** The plantar enhancement is due to the neuroma, but the rim of dorsal enhancement is due to intermetatarsal bursitis that often accompanies the neuroma.

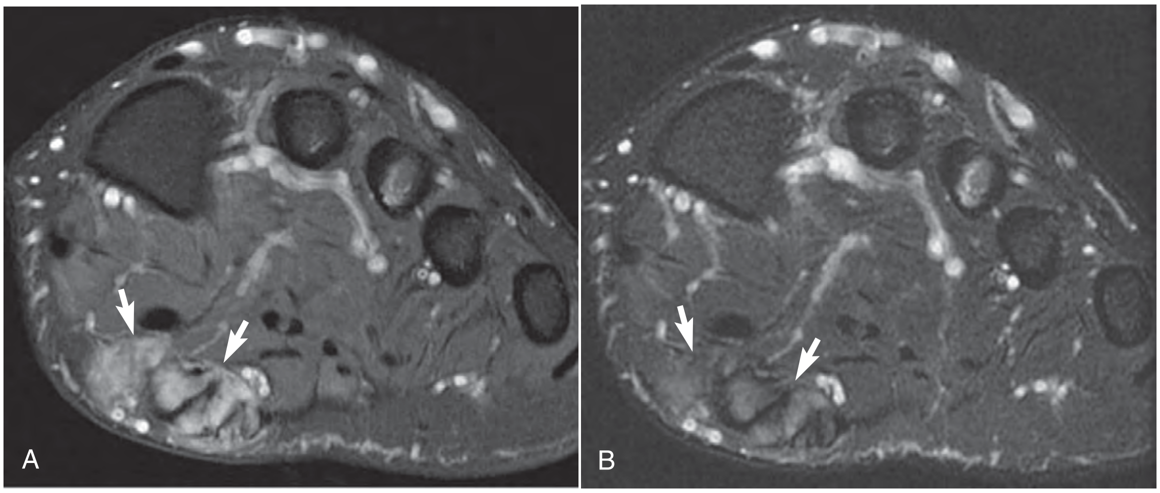

FIGURE 11–105 **Plantar fibroma.**[194] Coronal fat suppressed T1-weighted image obtained after intravenous gadolinium administration **(A)** and a coronal T2-weighted image **(B)** of the forefoot reveal a mixed signal mass on the plantar surface underlying the first metatarsal *(arrows)*. The mass appears to be lobulated and enhances with gadolinium. Plantar fibromatosis (also designated Ledderhose disease) is a common condition that is usually asymptomatic and is associated with fibrous proliferation of portions of the plantar aponeurosis. It occurs at any age, is more common in men, may be unilateral or bilateral, and either solitary or multiple.

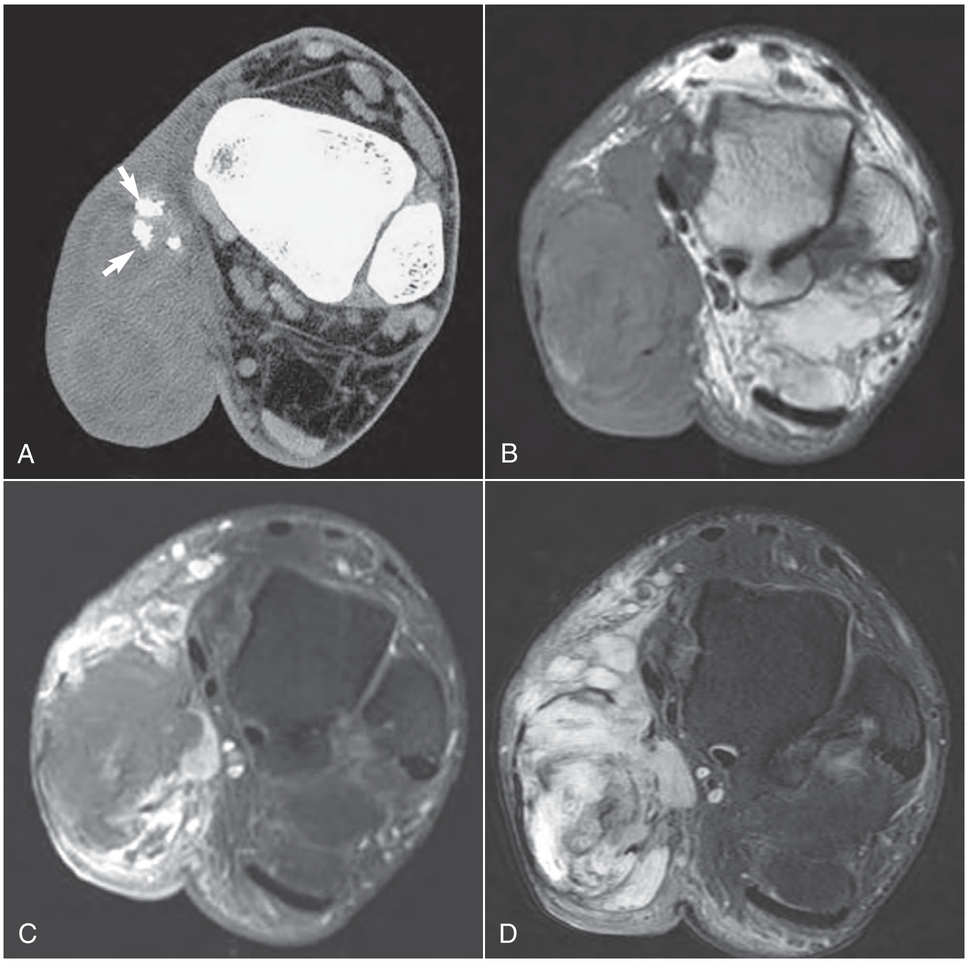

FIGURE 11–106 **Synovial sarcoma.**[118,149] A 25-year-old male with large painful mass arising from the medial side of the ankle. Cross-sectional transaxial imaging at the distal tibiofibular joint. A CT scan, soft tissue window **(A)** shows a large lobulated soft tissue mass with internal calcification *(arrows)*. A T1-weighted image without contrast **(B)** shows an intermediate signal intensity lesion. T1-weighted imaging after intravenous gadolinium administration **(C)** shows irregular peripheral enhancement of the lesion and the T2-weighted image **(D)** reveals an inhomogeneous septated high signal intensity mass with whirled interspersed strands of low signal intensity. The lesion compresses and displaces adjacent tendon sheaths, but does not appear to invade or destroy these structures or the neighboring bone.

TABLE 11-16 Metabolic, Hematologic, and Vascular Disorders Affecting the Ankle and Foot

Entity	Figure(s)	Characteristics
Generalized osteoporosis[133]	11-107	Uniform decrease in radiodensity, thinning of cortices May occasionally predispose to insufficiency fractures of the calcaneus and metatarsals
Regional osteoporosis[134]	11-108	May occur as a result of disuse and immobilization after a fracture or other injury; also seen in complex regional pain syndrome, burns, frostbite, and paralysis; may occur as an idiopathic painful condition that may later migrate to other locations Findings may be more widespread in paralyzed patients Bandlike, patchy, spotty, or periarticular osteopenia Subperiosteal and intracortical bone resorption Subchondral and juxtaarticular erosions
Poliomyelitis[135]	11-109	Diffuse bone and soft tissue atrophy Regional osteoporosis
Hyperparathyroidism and renal osteodystrophy[136,137]	11-110, 11-111	Brown tumors Subperiosteal resorption Metastatic soft tissue calcification
Vascular calcification[138]	11-112	Linear vessel wall calcification readily visible on routine radiographs Calcification within the tunica media of arterial walls occurs in patients with diabetes mellitus and hyperparathyroidism and is termed *Mönckeberg atherosclerosis* Frequently affects the tibialis anterior artery, dorsalis pedis artery, and smaller arteries of the foot The clinical significance of such atherosclerosis is unclear; regarded by some authorities as insignificant
Acromegaly[139,140]	11-113	*Soft tissue overgrowth:* heel pad thickening, joint space widening, and clubbing of toes *Osseous overgrowth:* enlargement of sesamoid bones and terminal tufts, periarticular excrescences Acromegalic arthropathy with eventual secondary osteoarthrosis
Gaucher disease[141]	11-114	Osteopenia, septated osteolytic lesions, cortical diminution, and diametaphyseal widening (Erlenmeyer flask deformity) Osseous weakening may result in pathologic fractures Coarsened trabecular pattern May result in osteonecrosis

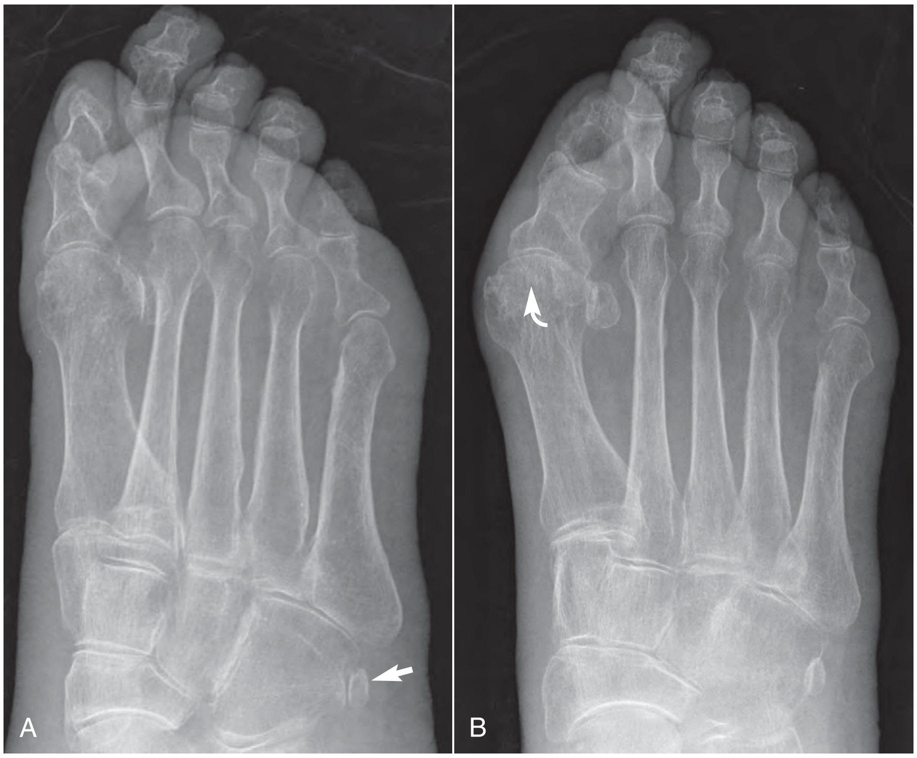

FIGURE 11–107 Generalized osteoporosis.[133] Severe osteopenia with decreased radiodensity and thinning of cortical margins is typical of generalized osteoporosis in this 84-year-old woman. Of incidental note are degenerative hallux valgus *(curved arrow)* and an os peroneum *(small arrow)*.

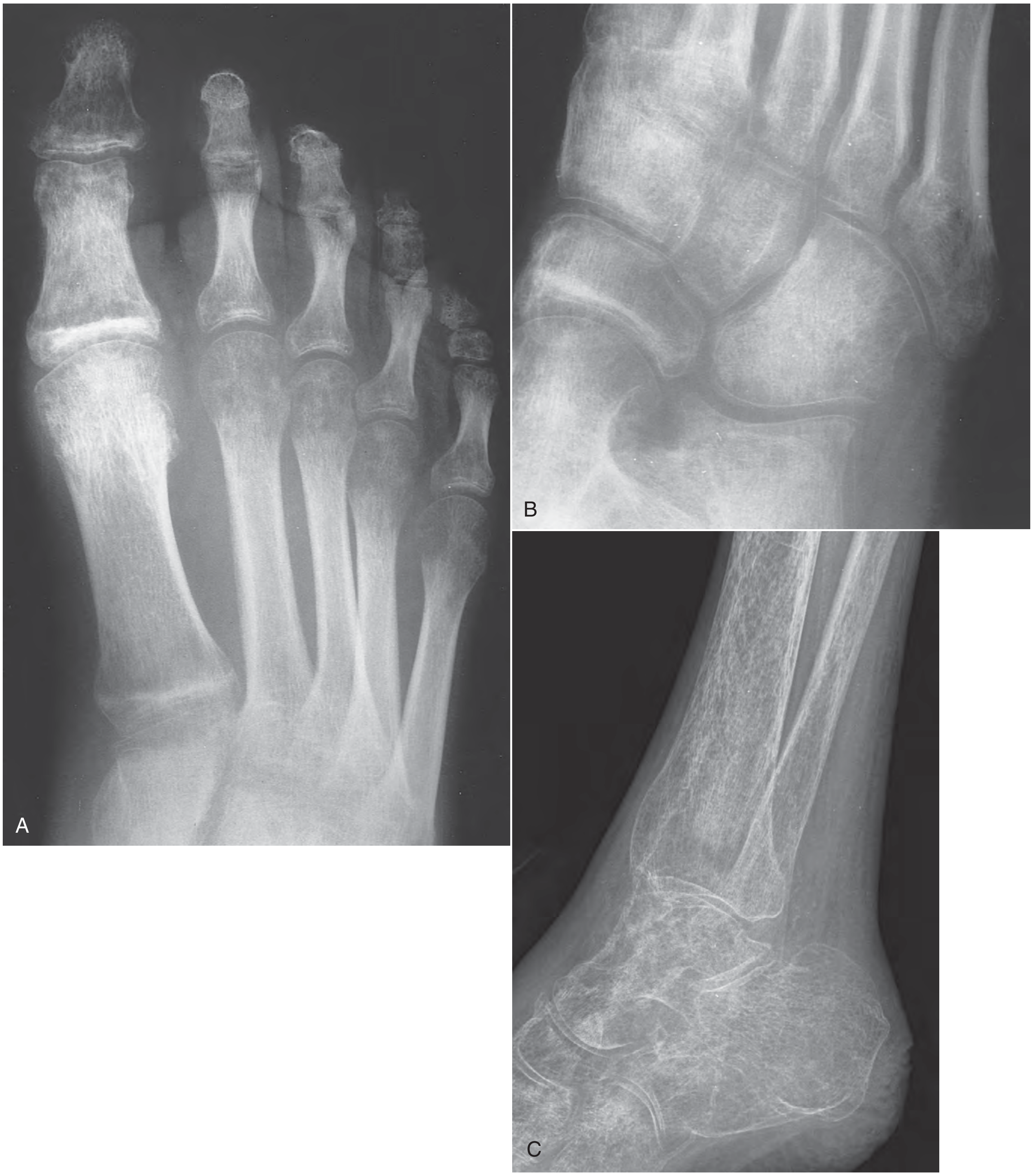

FIGURE 11–108 **Regional (disuse) osteoporosis.**[134] **A-B,** This 22-year-old man sustained a proximal tibial fracture and was immobilized in a cast for 8 weeks. In **A,** subcortical, periarticular, patchy, and spotty loss of bone density is evident throughout the tarsal and metatarsal bones and the phalanges, which is characteristic of the osteoporosis of immobilization. In **B,** an oblique radiograph of the midfoot in the same patient shows the patchy subarticular distribution typical of regional osteoporosis. **C,** In another patient, an 81-year-old paralyzed bedridden man, severe moth-eaten osteopenia is noted as a consequence of prolonged disuse. Spotty, patchy, and bandlike bone resorption is typical of rapid-onset osteoporosis, such as that seen in disuse, burns, frostbite, paralysis, or complex regional pain syndrome, an appearance that may simulate an aggressive neoplasm.

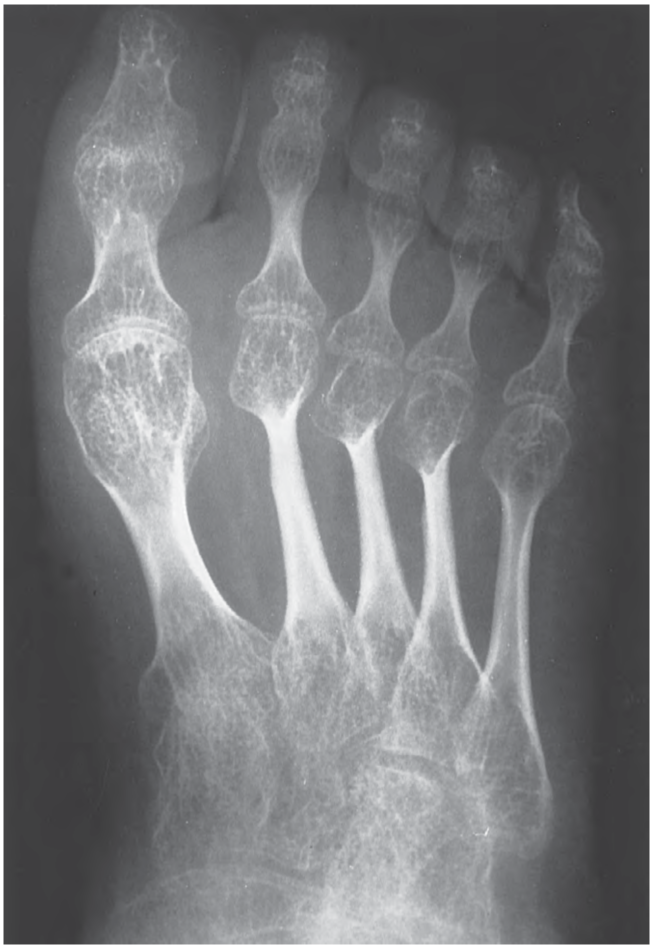

FIGURE 11–109 **Poliomyelitis.**[135] Observe the soft tissue atrophy, diffuse regional osteopenia, and atrophy of bone in this patient with long-standing poliomyelitis. The diaphyses of the long bones appear thin and atrophic, creating an expanded appearance of the distal ends of the bones.

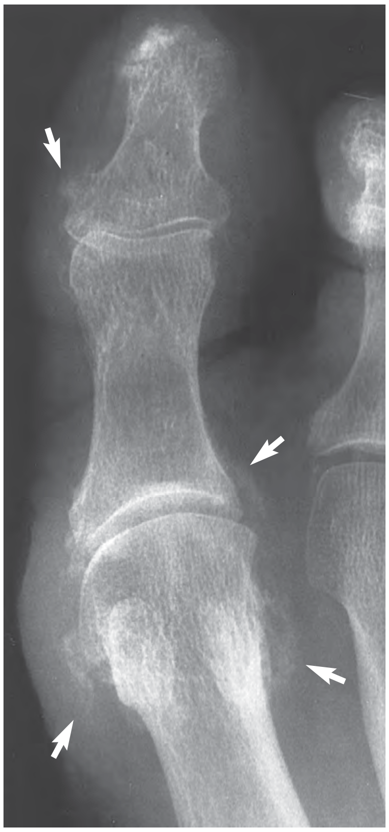

FIGURE 11–110 **Hyperparathyroidism.**[136,137] Observe the extensive periarticular calcification *(arrows)* in this 64-year-old woman with chronic renal failure. This form of metastatic soft tissue calcification is related to a disturbance in calcium or phosphorus metabolism and is seen in hyperparathyroidism and renal osteodystrophy. *(Courtesy T. Broderick, MD, Orange, Calif.)*

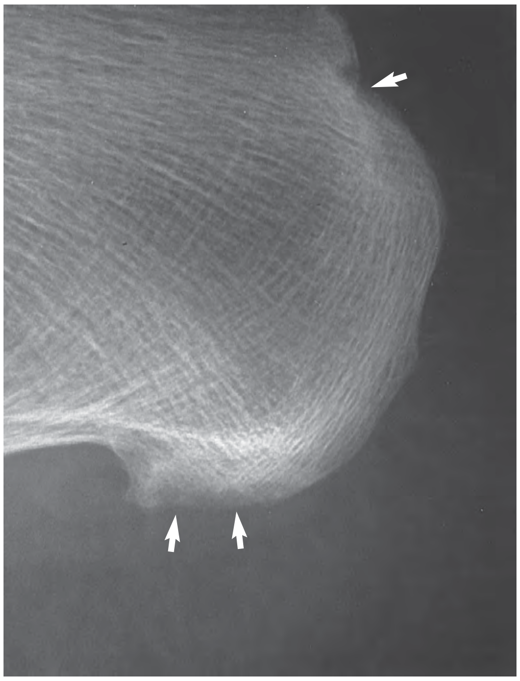

FIGURE 11–111 **Renal osteodystrophy.**[136,137] Indistinct cortical margins *(arrows)* represent subligamentous resorption of the calcaneus in a patient with renal osteodystrophy.

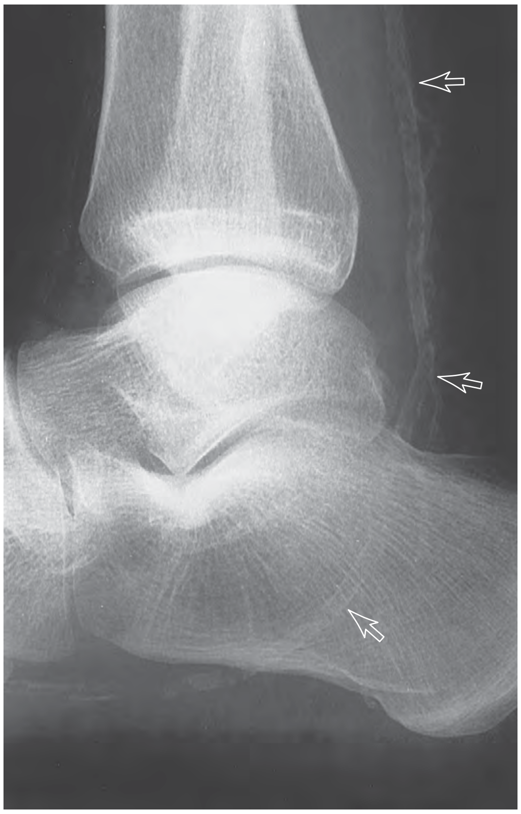

FIGURE 11–112 **Vascular calcification: diabetes mellitus.**[138] Extensive arterial wall calcification (Mönckeberg atherosclerosis) involving the posterior tibial artery *(open arrows)* is seen in this patient with long-standing diabetes mellitus. Calcification of the tunica media of the arteries is a well-recognized complication of diabetes mellitus.

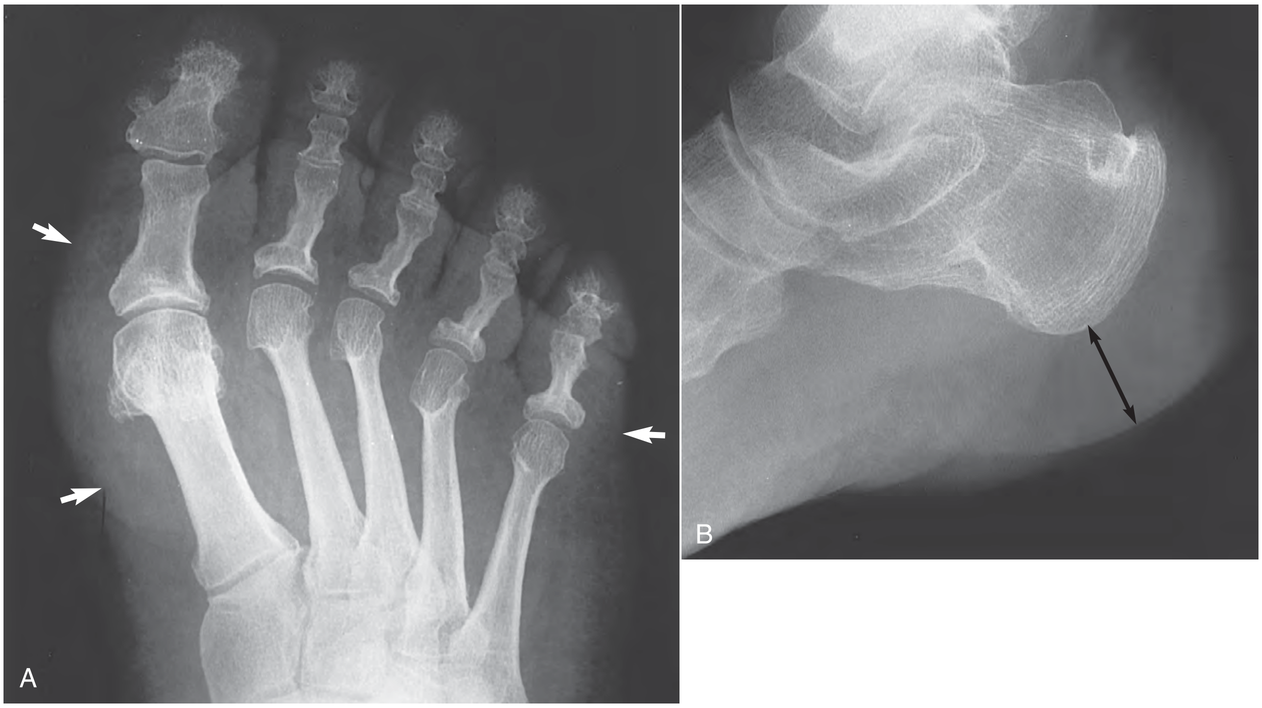

FIGURE 11–113 **Acromegaly.**[139,140] **A,** Acromegalic arthropathy. Prominent soft tissues *(arrows),* widened joint spaces, periarticular excrescences, and prominence of the terminal tufts are characteristic findings in this patient with acromegaly. **B,** Thickening of the heel pad. Normally, the heel pad thickness should be no more than 23 mm in men and 21.5 mm in women. The heel pad is considerably more prominent *(double-headed arrow)* in this patient with long-standing acromegaly.

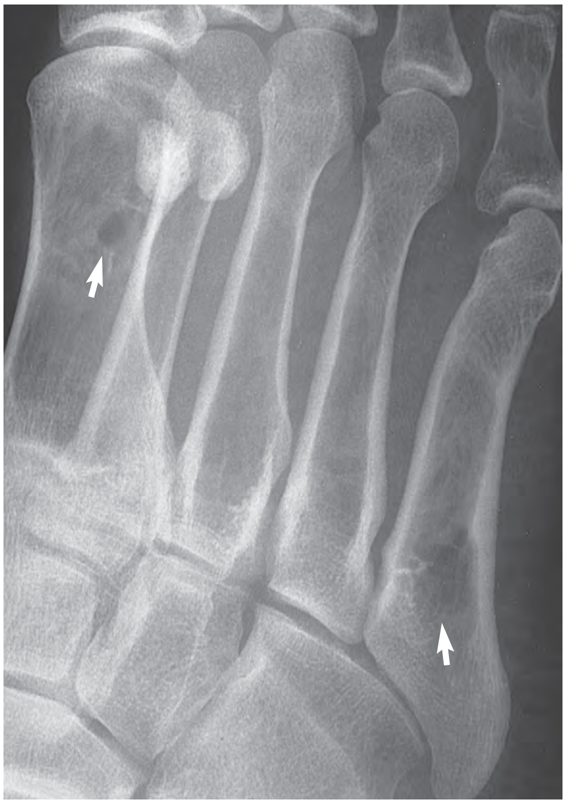

FIGURE 11–114 **Gaucher disease.**[141] Observe the multiple osteolytic lesions *(arrows)* within the metatarsal bones in this 51-year-old woman with extensive marrow infiltration. *(Courtesy M.N. Pathria, MD, San Diego.)*

TABLE 11-17 Osteonecrosis and Osteochondroses Affecting the Ankle and Foot

Entity	Figure(s)	Characteristics
Sickle cell anemia[142]	11-115	Hand-foot syndrome or sickle cell dactylitis Typically affects children between the ages of 6 months and 2 years Osteonecrosis of the small bones of the hand and foot results from vascular occlusion Affects 20%-50% of children with sickle cell anemia Soft tissue swelling, osteolysis, and diffuse periostitis
Osteonecrosis of the talus[143,144]	11-116	Disabling complication of corticosteroid use and fractures and dislocations of the talus Radiographic findings may not be present for 1-3 months: surrounding disuse osteopenia creates a relative increase in the density of the talar body that may be combined with collapse of the articular surface *Hawkins sign:* a subchondral radiolucent band seen in the dome of the talus on anteroposterior ankle radiographs 6-8 weeks after disuse or immobilization; radiolucent band results from active hyperemia of bone and is a reliable sign that the blood supply to the talar dome is preserved, and that ischemic necrosis will not likely occur Magnetic resonance (MR) imaging is useful in defining the extent of osteonecrosis
Köhler disease[145]	11-117, *A*	Fragmentation, flattening, irregularity, and sclerosis of the tarsal navicular bone in children Boys > girls; 3-7 years of age Local pain, tenderness, swelling, and limitation of motion Self-limited condition; over a period of 2-4 years, the bone may regain its normal size, density, and trabecular structure *Possible causes:* 1. Osteonecrosis secondary to mechanical forces 2. Manifestation of normal or altered ossification
Mueller-Weiss syndrome[146]	11-117 *B, C*	Painful spontaneous osteonecrosis of the tarsal navicular bone in adults Believed to be due to osteonecrosis related to previous injury or chronic stress
Freiberg infraction[147]	11-118	Abnormality of the metatarsal head secondary to osteonecrosis resulting from repeated trauma Second metatarsal bone most frequent site Women > men Patients wearing high-heeled shoes are predisposed to Freiberg infraction Articular surface fragmentation and collapse; initial joint space widening; eventual osteoarthrosis and sclerotic stress reaction of metatarsal
Normal calcaneal apophysis[4]	11-119	Calcaneal apophysis in children is normally sclerotic, may be fragmented, and is associated with a jagged appearance of the posterior margin of the calcaneus These widely variable normal findings should not be misdiagnosed as osteochondrosis, osteonecrosis, or fracture Frequently mislabeled as *Sever disease*

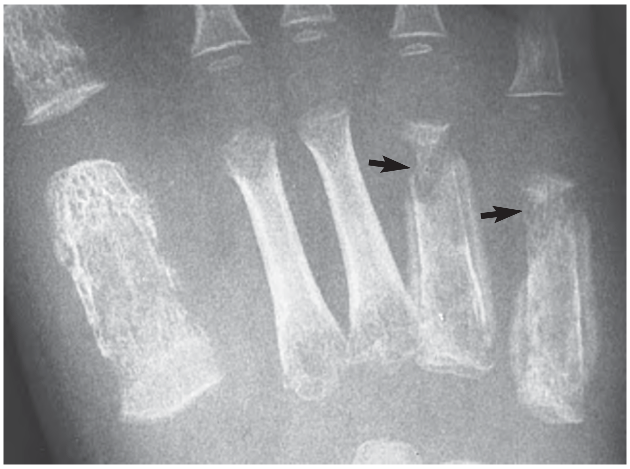

FIGURE 11–115 **Sickle cell anemia: sickle cell dactylitis.**[142] Soft tissue swelling, permeative destruction, large areas of osteolysis *(arrows),* and diffuse periostitis involving several metatarsal bones are evident in this patient with sickle cell dactylitis. *(Courtesy P. Kaplan, MD, Charlottesville, Va.)*

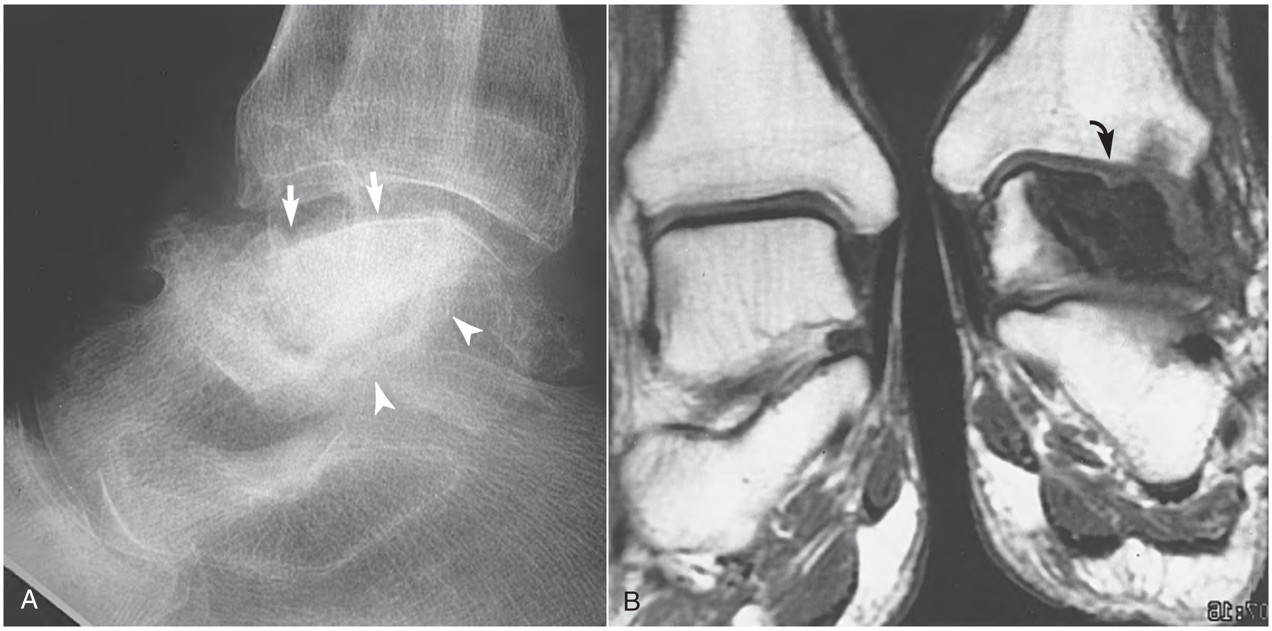

FIGURE 11–116 **Osteonecrosis: talus.**[143,144] Fifty-five-year-old man with ankle pain. **A,** Lateral radiograph shows central collapse *(arrows)* and increased density (*arrowheads)* of the talus. **B,** Coronal T1-weighted (TR/TE, 700/16) spin echo MR image of both ankles shows an abnormal left talus with a well-defined zone of decreased signal intensity and associated collapse of the articular surface (*curved arrow)*. Normal high signal intensity marrow is evident in the opposite talus.

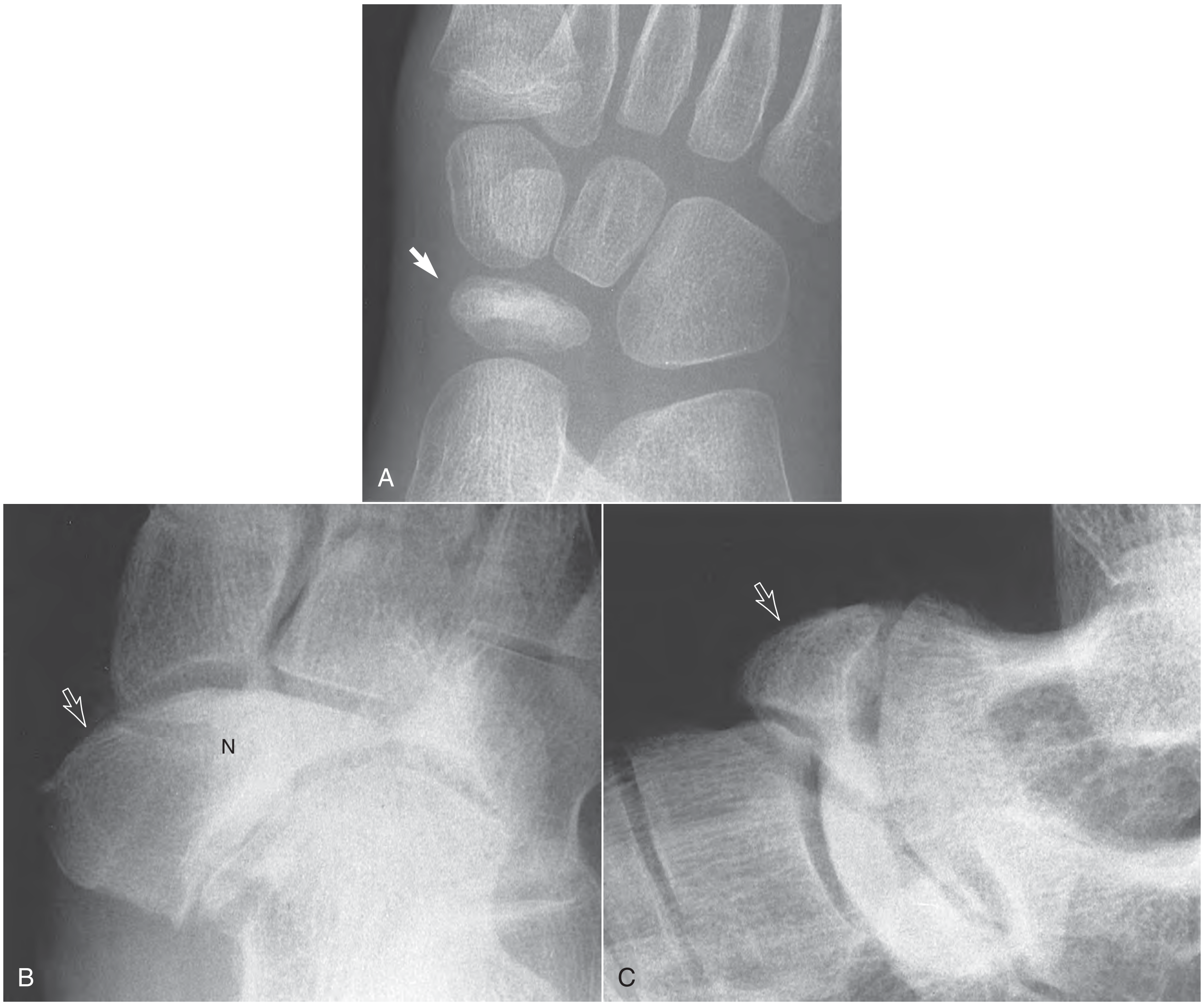

FIGURE 11–117 Osteonecrosis and osteochondrosis: tarsal navicular bone.[145,146] **A,** Köhler disease. An oblique radiograph of the foot in this 5-year-old boy with a painful limp demonstrates osteosclerosis and collapse of the tarsal navicular bone (*arrow*). The disease, more common in boys, usually occurs between the ages of 3 and 7 years, with an onset of local pain, tenderness, swelling, and limitation of motion. It is believed by some authorities that Köhler disease represents osteonecrosis possibly secondary to mechanical forces. Other investigators, however, regard the condition as a manifestation of normal or altered ossification. The disease is self-limited in that over a period of 2 to 4 years, the bone may become normal in size, density, and trabecular structure. **B-C,** Mueller-Weiss syndrome: Spontaneous osteonecrosis of the tarsal navicular bone. In **B,** a frontal radiograph shows a medially displaced *(open arrow),* comma-shaped navicular bone (N). The lateral portion of the bone is collapsed. In **C,** a lateral radiograph, the navicular bone appears triangular and is minimally displaced dorsally *(open arrow)*. The Mueller-Weiss syndrome is a painful condition in adults, more common in women, that is believed to be due to osteonecrosis related to previous injury or chronic stress. The differential diagnosis includes osteonecrosis associated with other conditions, such as systemic lupus erythematosus and corticosteroid use, fatigue fracture, or insufficiency fracture related to rheumatoid arthritis, chronic renal disease, or diabetes mellitus. *(**B-C,** Courtesy E. Bosch, MD, Santiago, Chile.)*

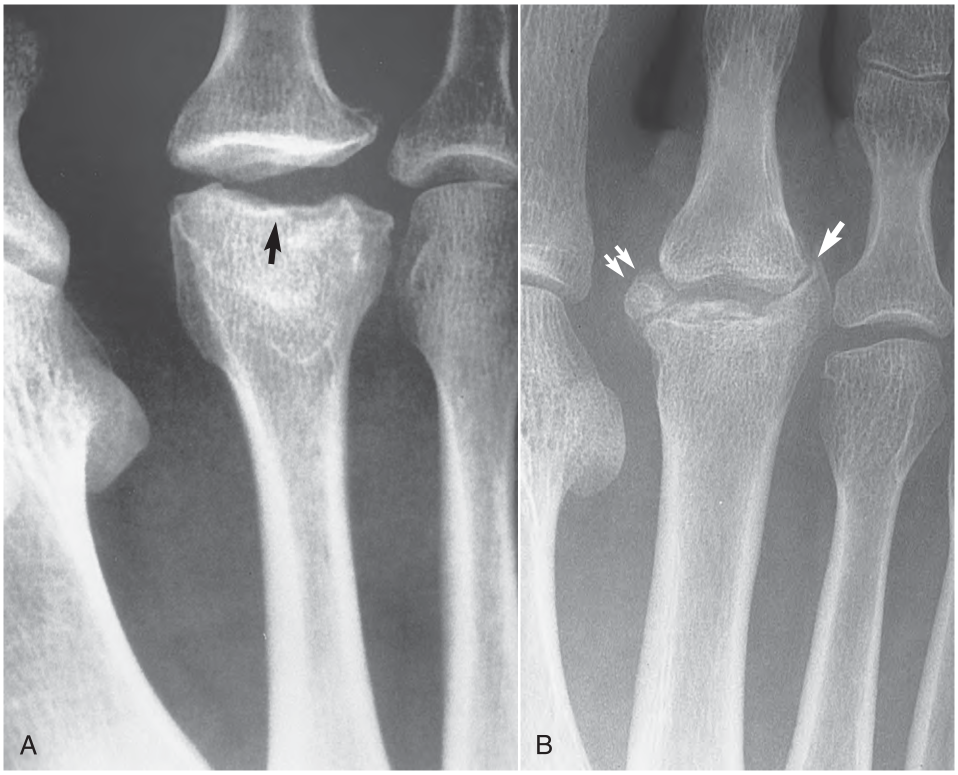

FIGURE 11–118 **Freiberg infraction.**[147] **A,** Flattening and deformity of the subchondral surface of the second metatarsal head is seen *(arrow)*. The metatarsophalangeal joint appears widened owing to collapse of the subchondral bone. Note the osteophytes adjacent to the articulation. **B,** In another patient, osteophytes *(arrow),* subarticular collapse, and intraarticular osseous bodies *(double arrows)* are noted, likewise involving the second metatarsal head. Observe also the widening and cortical thickening of the second metatarsal shaft. (***A,*** *Courtesy M.N. Pathria, MD, San Diego.)*

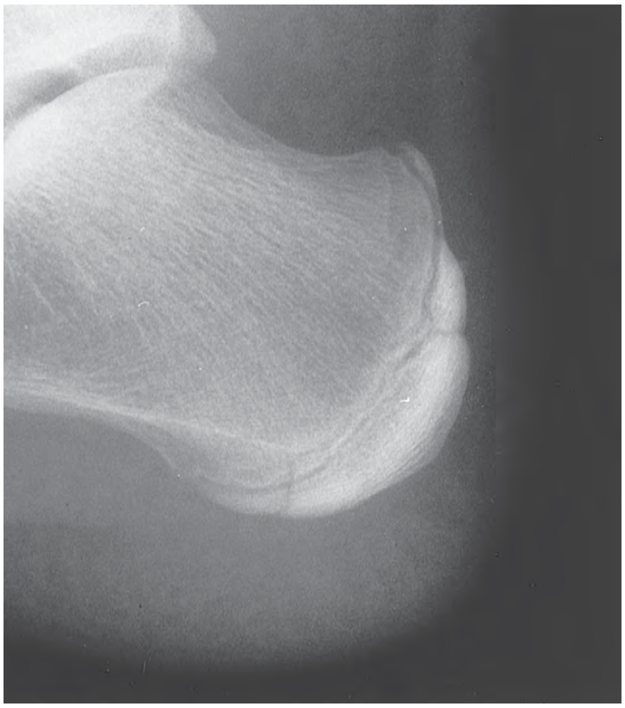

FIGURE 11–119 **Normal calcaneal apophysis.**[4] The calcaneal apophysis in this child is sclerotic and fragmented, and the posterior edge of the calcaneus is somewhat ragged in appearance. Sclerosis is often present as a result of weight-bearing in children who walk; the apparent fragmentation is a result of ossification occurring at multiple sites; and the posterior surface of the immature calcaneus frequently appears irregular. All of these findings are normal and should not be mistaken for osteochondrosis, osteonecrosis, or fracture. This finding has, in the past, been incorrectly designated Sever disease.

PART IV

Thoracic Cage and Upper Extremeties

CHAPTER 12

Ribs, Sternum, and Sternoclavicular Joints

NORMAL DEVELOPMENTAL ANATOMY

The accurate assessment of pediatric radiographs of the ribs, sternum, and sternoclavicular joints requires a thorough knowledge of normal developmental anatomy. Table 12-1 outlines the ages of appearance and fusion of the primary and secondary ossification centers. Figures 12-1 and 12-2 demonstrate the radiographic appearance of the development of the thoracic cage at different ages from infancy to skeletal maturity.

DEVELOPMENTAL ANOMALIES, ANATOMIC VARIANTS, AND SKELETAL DYSPLASIAS

Developmental anomalies, normal variations, and occasionally, skeletal dysplasias affect the ribs, sternum, and sternoclavicular joints. Table 12-2 and Figures 12-3 to 12-9 illustrate some of the more commonly encountered processes. Table 12-3 lists the major causes of rib notching and Figure 12-10 illustrates one example.

PHYSICAL INJURY

Physical injury, including fractures and joint trauma, may involve the ribs, sternum, and sternoclavicular joints alone, in combination with each other, or in combination with other spinal, pelvic, abdominal, and thoracic visceral injuries. Some combined injuries are discussed in more depth in Chapters 3 and 13 in association with the thoracic spine and shoulder, respectively. Table 12-4 lists the important injuries in this region and describes their characteristics. Many examples of these injuries are illustrated in Figures 12-11 to 12-19. Table 12-5 lists some of the causes of an extrapleural mass.

ARTICULAR DISORDERS

The sternoclavicular, costovertebral, manubriosternal, and sternocostal joints are target sites of involvement for degenerative, inflammatory, metabolic, and infectious arthropathies. Table 12-6 outlines these diseases and their characteristics, and Figures 12-20 to 12-26 provide examples of the typical imaging manifestations.

TUMORS AND TUMORLIKE LESIONS OF BONE AND SOFT TISSUES

Many different malignant, benign, and tumor-like lesions affect the ribs. The most common bone and soft tissue tumors and tumor-like lesions affecting the ribs, sternum and chest wall are listed in Table 12-7, many of which are illustrated in Figures 12-27 to 12-42.

METABOLIC, HEMATOLOGIC, AND INFECTIOUS DISORDERS

Table 12-8 describes a wide variety of metabolic, hematologic, and infectious disorders that may involve the ribs and sternum. The radiographic manifestations of many of these conditions are illustrated in Figures 12-43 to 12-49.

TABLE 12-1 **Ribs and Sternum: Approximate Age of Appearance and Fusion of Ossification Centers[1-3] (Figures 12-1 and 12-2)**

Ossification Center	Primary or Secondary	No. of Centers (Per Rib)	Age of Appearance* (Year)	Age of Fusion* (Year)	Comments
Ribs					
Body	P	1	Birth	22-25	Head and tubercle fuse to body
Head	S	1	14	22-25	Fuse to body
Tubercle	S	1 or 2	14	22-25	Fuse to body Ribs 1 to 10 only
Sternum					
Manubrium	P	1	Birth	No fusion	Infrequently fuses to body in old age
Body of first segment	P	1	Birth	8-25	Fuses to second segment
Body of second segment	P	1	Birth	8-25	Fuses to third segment
Body of third segment	P	1	Birth	4-8	Fuses to fourth segment
Body of fourth segment	P	1	Birth		
Xiphoid process	S	1	3-4	No fusion	Infrequently fuses to fourth segment in old age

P, Primary; *S,* secondary.

* Ages of appearance and fusion of ossification centers in girls typically precede those of boys. Ethnic differences also exist.

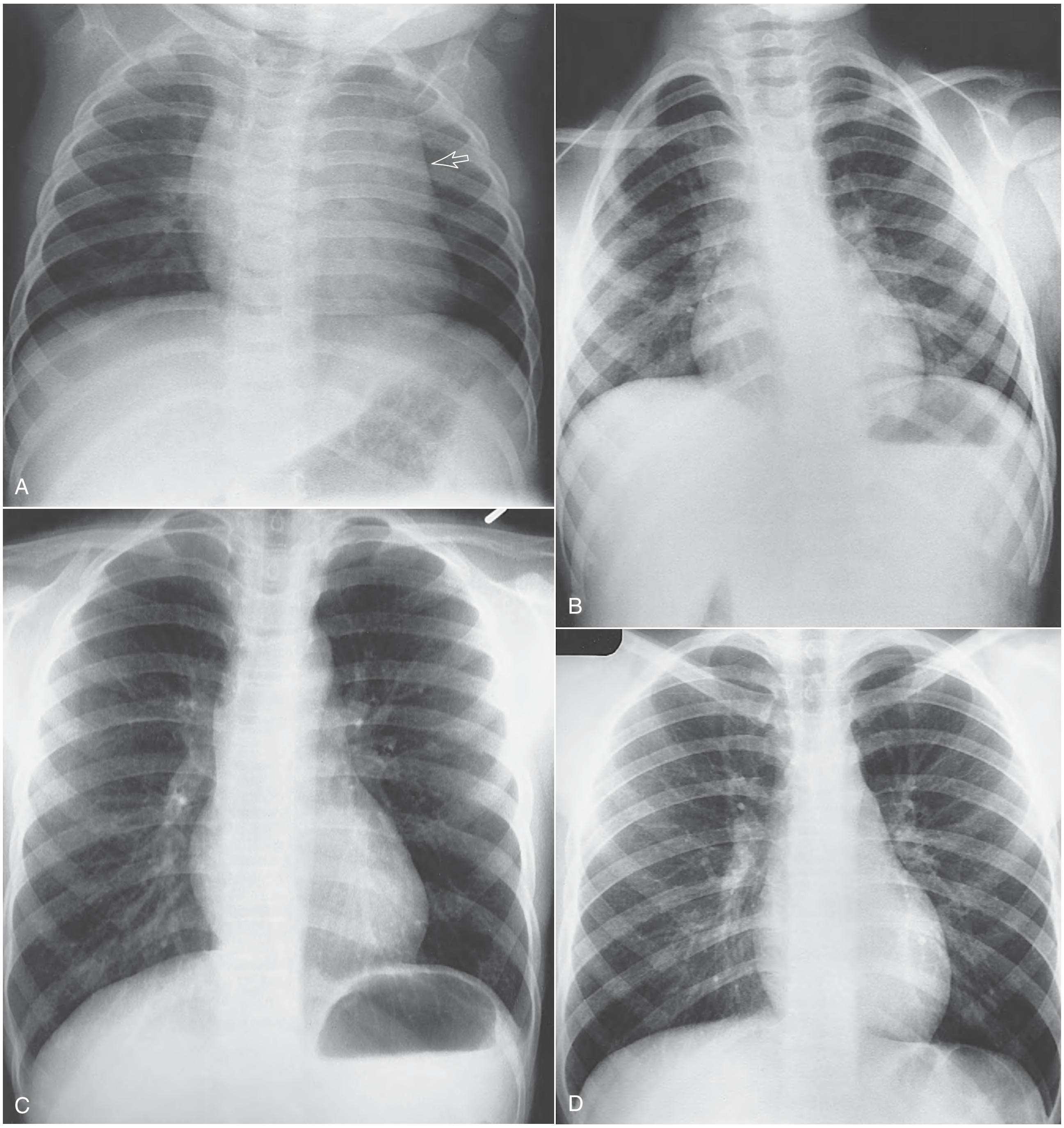

FIGURE 12–1 Skeletal maturation and normal development: frontal radiographs of the thoracic cage.[1-3] **A,** A 7-month-old girl. The cardiac silhouette is disproportionately large in relation to the size of the thoracic cage. A prominent thymus gland *(open arrow),* a normal finding in infants, is also apparent in this patient. **B,** A 3-year-old girl. **C,** An 8-year-old girl. **D,** A 14-year-old boy. The heart and mediastinum are of adult proportions. Secondary ossification centers of the rib heads and tubercles usually appear between the ages of 14 to 16 years and fuse to the body of the rib by the age of 25 years (not shown). Rib tubercles do not typically develop on the eleventh and twelfth ribs.

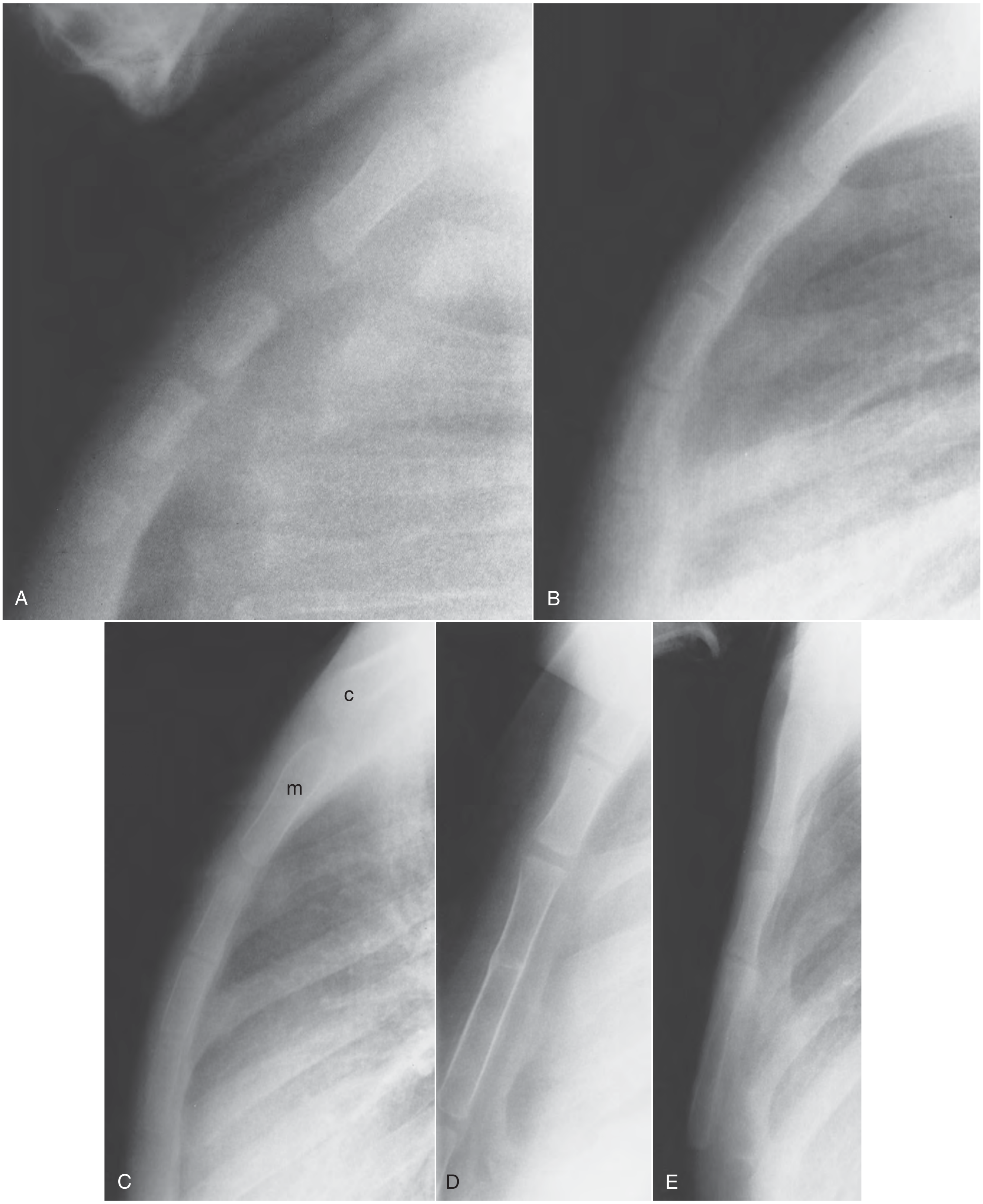

FIGURE 12–2 **Skeletal maturation and normal development: sternum.**[1-3] **A,** A 2-month-old boy. At this age, the sternum is ossified but large gaps, filled with cartilage, remain between the individual segments. **B,** A 3-year-old girl. As ossification proceeds, the intersegmental gaps become narrower. **C,** A 7-year-old boy. The first, second, and third segments of the sternal body are beginning to fuse. The normal clavicle *(c)* should not be confused with a dislocation of the manubrium *(m)*. **D,** A 12-year-old boy. The second and third segments have fused. **E,** A 14-year-old boy. The intersegmental centers have fused, but the manubriosternal junction remains open.

Continued

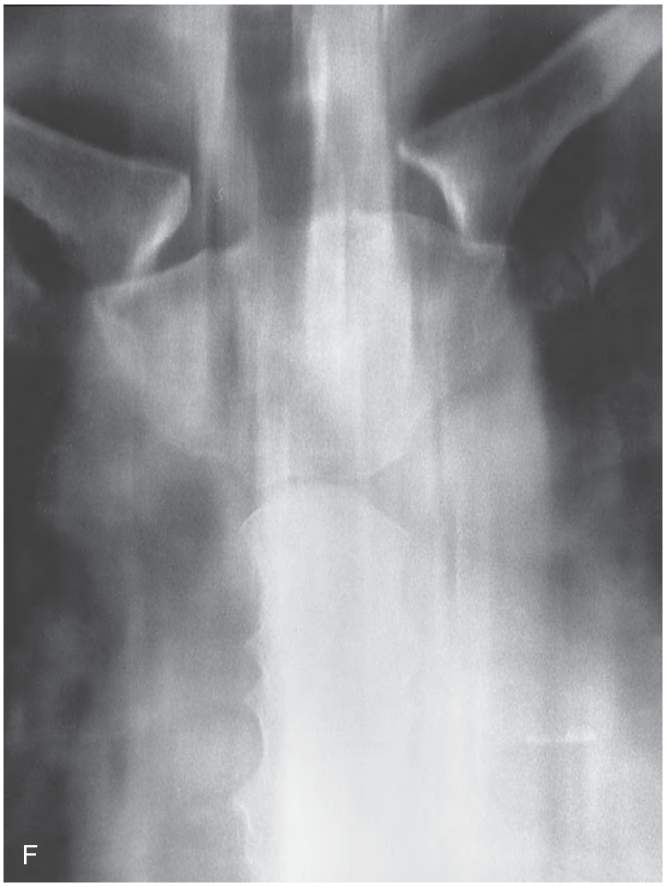

FIGURE 12–2, cont'd **F,** Adult: 35-year-old woman. This coronal conventional tomogram reveals the sternoclavicular joints and manubriosternal junction. Observe that the manubrium has not fused to the sternal body. The primary ossification centers of the manubrium and three or four segments of the sternal body typically are ossified at birth. The secondary ossification center of the xiphoid process first appears about the age of 15 years. The intersegmental centers of the sternal body fuse between the ages of 8 and 25 years. Fusion of the manubriosternal junction occurs only rarely. When it does, fusion occurs after the age of 30 years.

TABLE 12-2 Developmental Anomalies, Anatomic Variants, and Skeletal Dysplasias Affecting the Ribs and Sternum*

Entity	Figure(s)	Characteristics
Ribs		
Cervical rib[4-6]	See Figure 2-36	Transverse processes of C7 are typically shorter than those of T1 Both elongated C7 transverse processes and cervical ribs may contribute to neurovascular compression of the thoracic outlet Cervical ribs are present in 10% to 15% of patients with the Klippel-Feil syndrome (see Table 2-5)
Transitional rib anomalies[3,4]	See Figure 4-7 12-3	Wide variation of hypoplastic, hyperplastic, and unusually shaped ribs may occur at the thoracolumbar transitional region; usually of no clinical significance *Lumbar rib:* anomalous supernumerary ribs articulating with the transverse processes of the first lumbar vertebra Other entities include horizontal ribs, asymmetric ribs, and ribs associated with vertebral anomalies
Intrathoracic rib[7-9]	12-4	Extremely rare anomaly in which a rib protrudes within the thoracic cavity Usually unilateral and generally asymptomatic Occasionally, the intrathoracic rib may have a fibrous diaphragmatic attachment, which can disrupt respiration
Rib foramen[5]		Rare anomaly; radiolucent foramen may involve any rib; no clinical significance; may simulate an osteolytic lesion
Bifurcated rib[3,5]		Anomalous bifurcation in anterior aspect of rib near its costochondral junction; no clinical significance

* See also Tables 1-1 and 1-2.

TABLE 12-2 Developmental Anomalies, Anatomic Variants, and Skeletal Dysplasias Affecting the Ribs and Sternum—cont'd

Entity	Figure(s)	Characteristics
Rib synostosis[3,5]	12-5	Complete or incomplete anomalous fusion of two adjacent ribs, usually of no clinical significance *Srb's anomaly:* rare anomalous synostosis of the first and second ribs Osseous bridging of small segments of two adjacent ribs, with or without pseudarthrosis, has also been reported
Congenital pseudarthrosis[5]		Anomalous failure of ossification of the central portion of the first rib Margins are smooth and well-corticated but may have bulbous appearance Usually painless but may simulate fatigue fracture
Costochondral cartilage calcification or ossification[3,10]	12-6	Calcification or ossification of the costochondral cartilage may begin as early as age 20 years; appears to be a physiologic reaction to muscular contraction related to the relative rigidity of chest wall On frontal radiographs, the ossification appears forklike in men and tonguelike in women On lateral radiographs, large calcified masses may be seen overlying the sternum Especially prevalent in older individuals, and usually of no clinical significance Also found in children with hyperthyroidism
Achondroplasia[5]		Symmetric shortening of ribs; may not completely extend around the thorax
Osteopetrosis[5]	12-7	Diffuse sclerosis of ribs with predisposition to rib fracture
Sternum[98]		
Sternal foramen and cleft[11]		Vascular channel within the lower sternal body; occurs in as many as 20% of adults; asymptomatic variant of no clinical significance
Sternal fissure (bifid sternum)[3,12]		Rare anomalous failure of fusion of the sternal ridges resulting in a midline vertical split in any segment of the sternum Complete fissure often associated with anomalies of diaphragm, heart, and other organs Incomplete fissure not usually associated with other anomalies
Asymmetry of developing ossification centers[3,4]		Numerous anatomic variants and anomalies of development frequently result in asymmetric or unusual shape of the manubrium, body, and xiphoid process
Accessory ossicles[3]		Variant seen in as many as 4% of adults Os episternalia (or suprasternalia) located above the manubrium; often paired Os parasternalia located lateral to the manubrium in the cartilage of the first ribs
Absent xiphoid process[3,88]		Normal finding in 47% of women and in 9% of men
Pectus excavatum[3,13,88]	12-8	*Funnel chest:* common chest wall deformity; may be an isolated anomaly or it may accompany Marfan syndrome or Ehlers-Danlos syndrome Depression of sternum seen best on physical examination and on lateral radiographs; displacement of heart toward left hemithorax may result in obscuration of right heart border on frontal radiographs
Pectus carinatum[3,5,88]		*Pigeon breast:* deformity characterized by anterior displacement of the sternum; may be an isolated anomaly or may be associated with Morquio syndrome
Cleidocranial dysplasia[3,5]	12-9	Hypoplasia or aplasia of the sternoclavicular joint found in combination with clavicular abnormalities

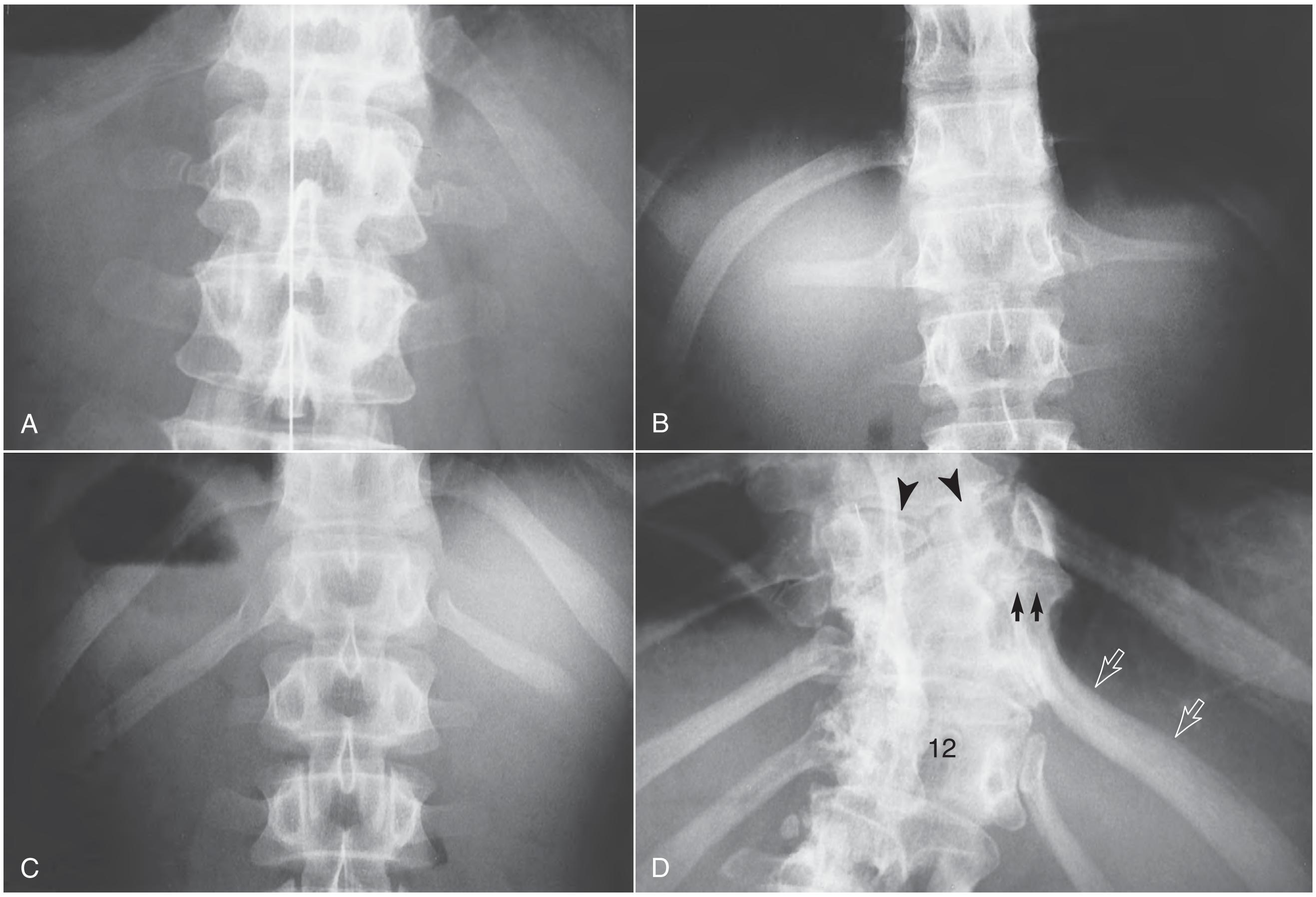

FIGURE 12–3 **Transitional rib anomalies and anatomic variations.**[3,4] **A,** Lumbar ribs. Observe the small articulating ribs arising from the L1 transverse processes. **B,** Horizontal twelfth ribs. The twelfth ribs are short, straight, and oriented horizontally. **C,** Asymmetric twelfth ribs. Observe the variation in the length of the two twelfth ribs. **D,** Anomalous ribs associated with spinal anomalies. A short, angular kyphosis is associated with a T10 butterfly vertebra *(arrowheads)*. The eleventh thoracic vertebra is wedge-shaped. The left eleventh rib has an abnormal costovertebral articulation *(arrows)* and exhibits stress-induced reactive sclerosis *(open arrows)*.

FIGURE 12–4 **Intrathoracic rib.**[7-9] An anomalous rib *(arrows)* arises from the posteroinferior margin of the right fourth rib and is projected over the inner portion of the lung field in this frontal projection. *(Courtesy S. Hilton, MD, San Diego.)*

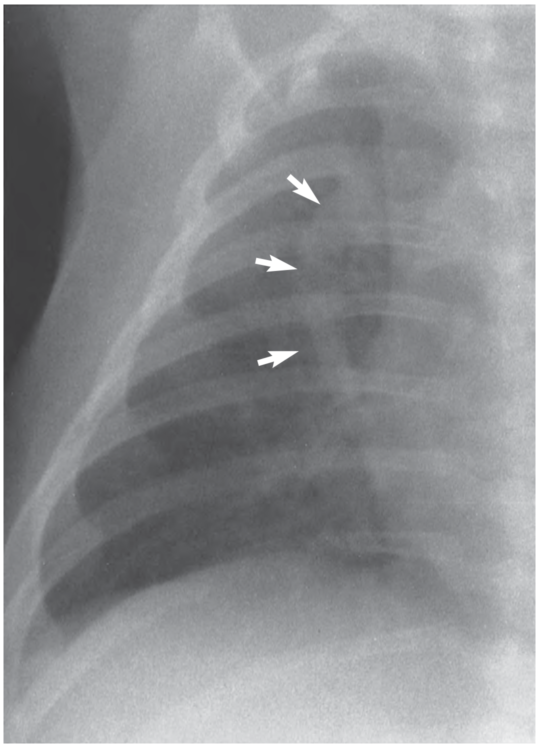

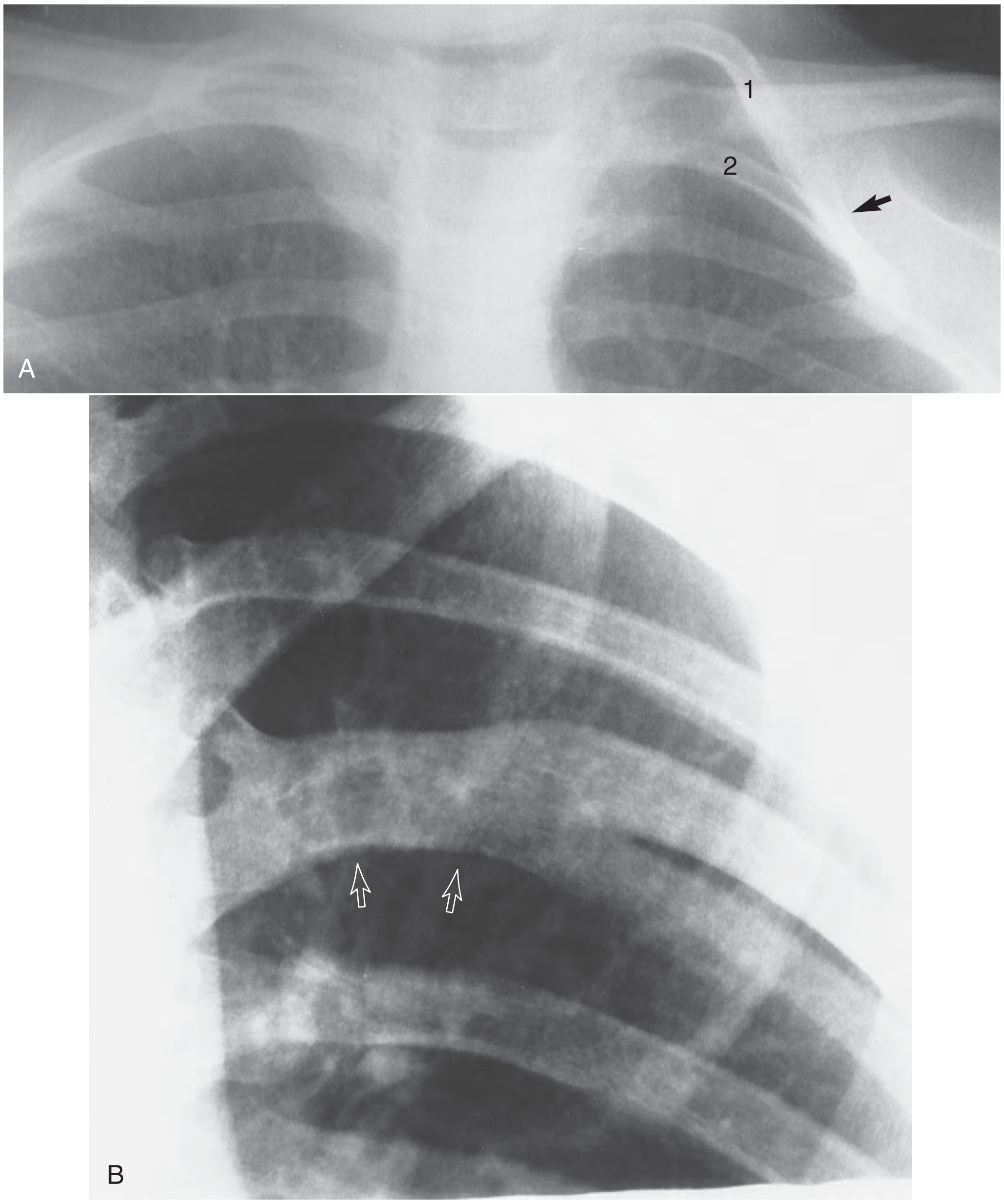

FIGURE 12–5 **Rib synostosis.**[3,5] **A,** Posteroanterior chest film in this 6-year-old child reveals anomalous fusion *(arrow)* of the left first (1) and second (2) ribs, resulting in an unusual depression of the left side of the thoracic cage. Such synostosis of the first and second ribs has been referred to as *Srb's anomaly*. **B,** Observe the fusion of the proximal portion of the fourth and fifth ribs *(open arrows)* in this patient. The synostosis was asymptomatic and was discovered as an incidental finding on an earlier chest radiograph.

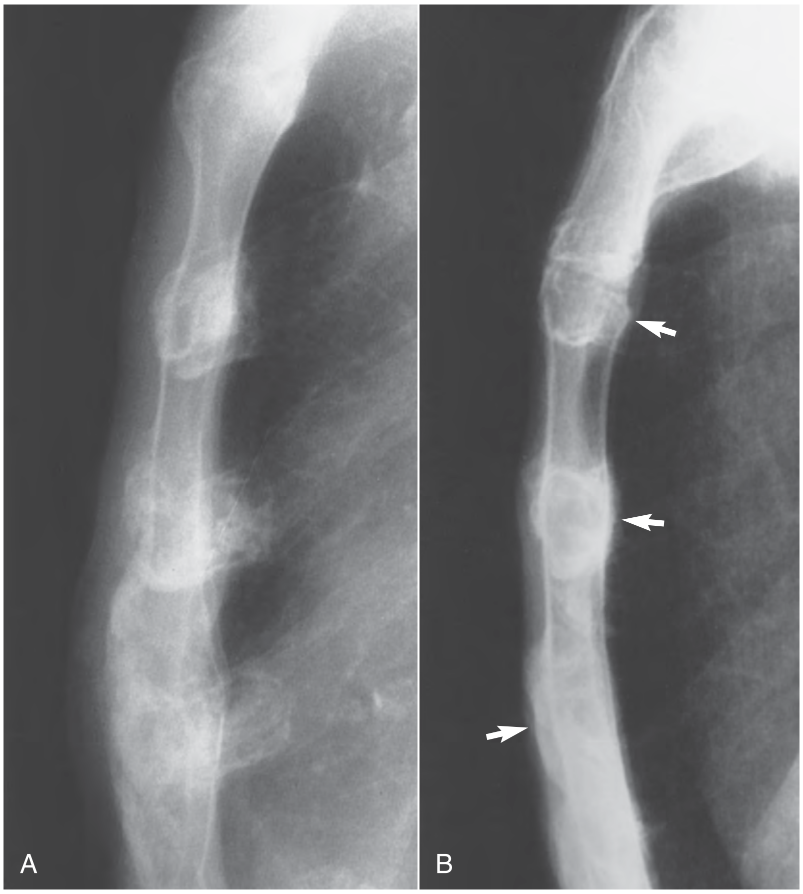

FIGURE 12–6 Costochondral calcification or ossification.[3,10] **A,** Lateral radiograph of the sternum reveals several bulbous zones of faintly calcified costal cartilage. **B,** In another patient, observe the prominent, expansile appearance of calcified costal cartilages *(arrows)*.

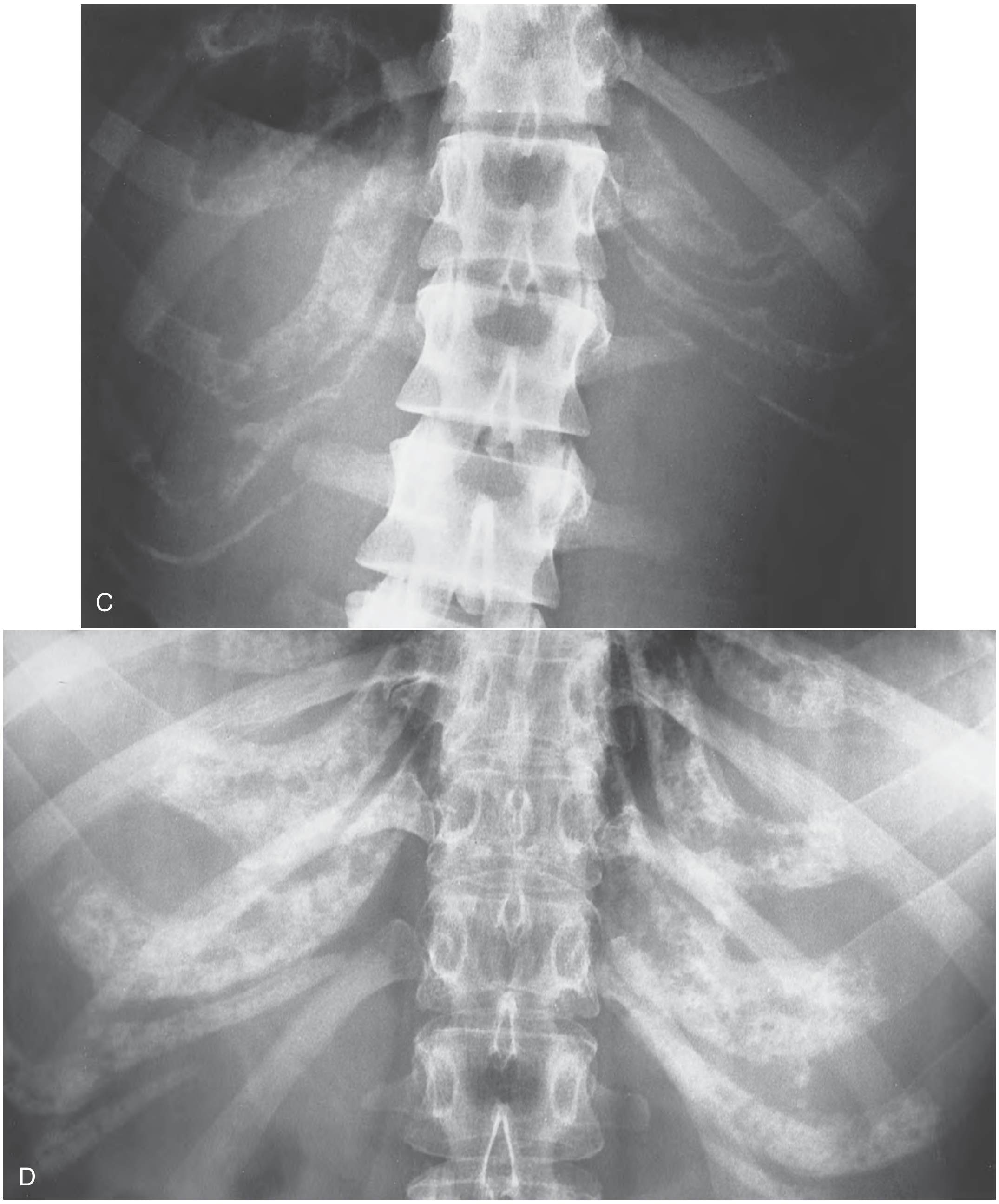

FIGURE 12–6, cont'd C-D, In two additional patients, observe the diffuse calcification of the costochondral cartilages on frontal radiographs.

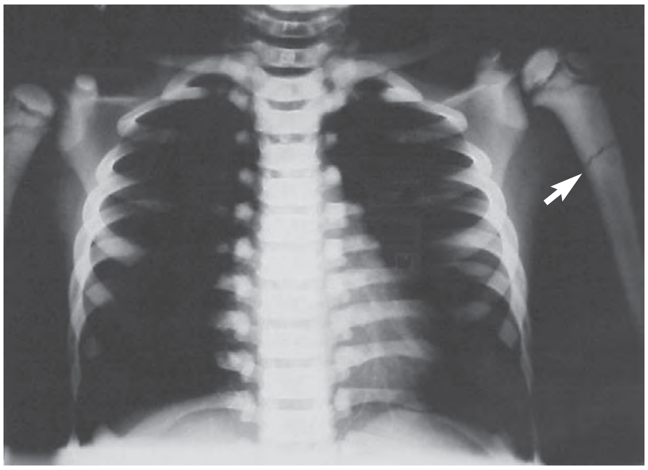

FIGURE 12–7 Osteopetrosis.[5] Observe the diffuse increased radiodensity of the ribs, spine, and humeri. A pathologic transverse fracture of the proximal humeral diaphysis is present *(arrow)*. Pathologic fracture is one of the leading complications of this disease owing to brittle bones.

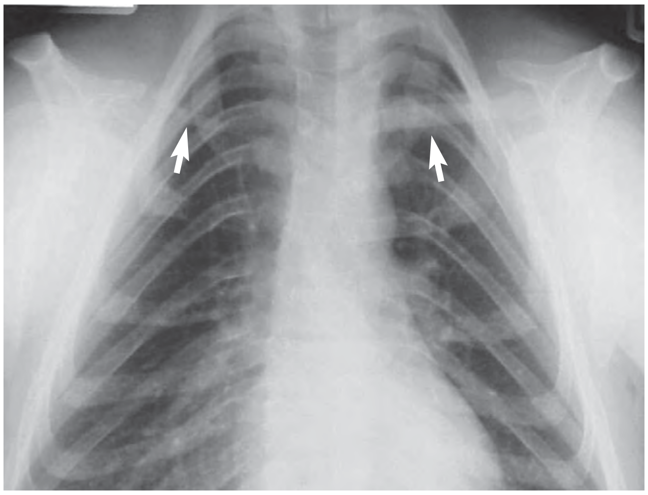

FIGURE 12–9 Cleidocranial dysplasia.[3,5] This 32-year-old man with drooping shoulders, born with cleidocranial dysplasia has hypoplastic clavicles *(arrows)* and a narrow bell-shaped thoracic cage. This autosomal dominant disease results in faulty intramembranous ossification.

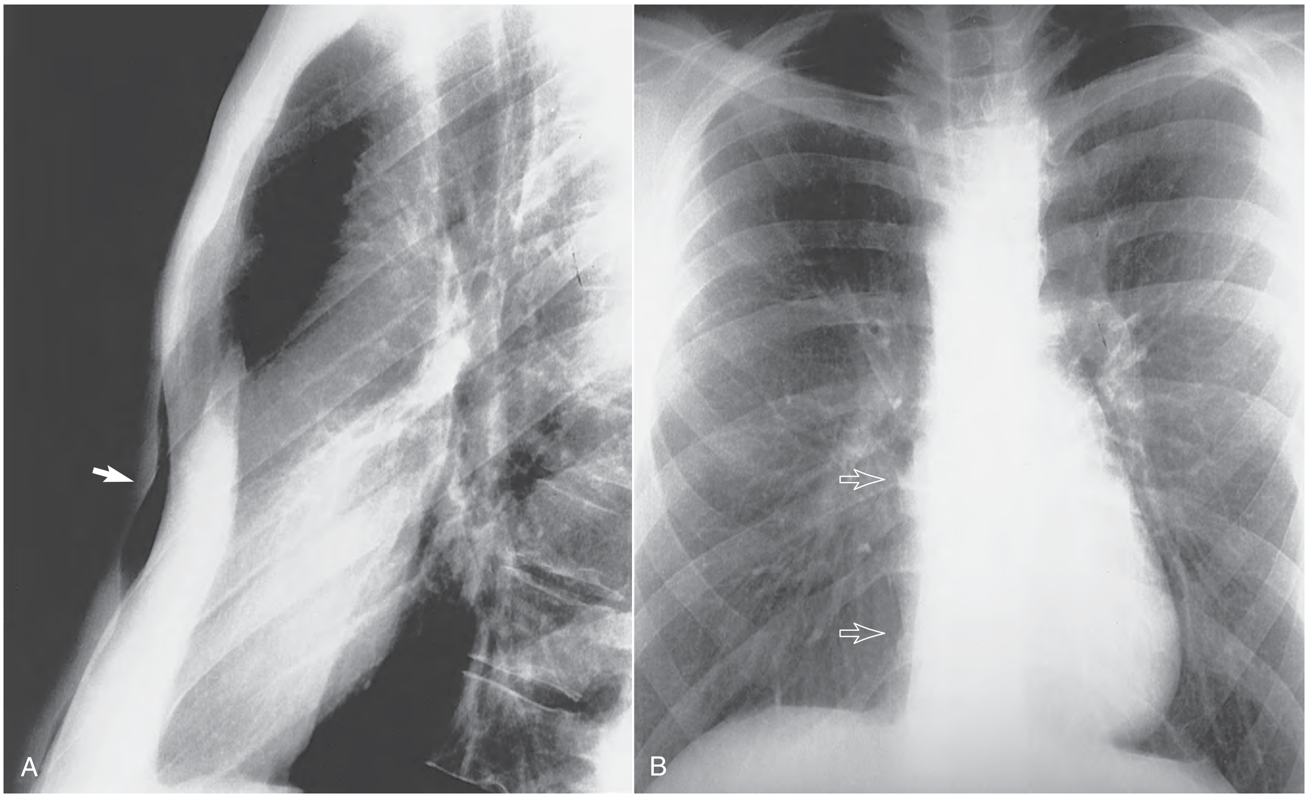

FIGURE 12–8 Pectus excavatum.[3,13,88] Lateral **(A)** and posteroanterior **(B)** chest radiographs of a 27-year-old man reveal depression of the sternum *(solid arrow)* and displacement of the right heart border toward the left hemithorax *(open arrows)*. This common chest wall deformity may be an isolated anomaly, or it may accompany Marfan syndrome or Ehlers-Danlos syndrome. *(Courtesy I. Roug, DC, Marietta, Ga.)*

TABLE 12-3 Rib Notching[14]

Category	Specific Entities	Figure(s)	Characteristics
Normal variant	Normal persons		Prominent groove within the inferior aspect of the rib that may resemble pathologic destruction or erosion
Normal aging phenomenon	Osteoporosis in elderly patients		Postmenopausal or senile osteoporosis may result in indistinct cortical margins
Collagen vascular disease	Rheumatoid arthritis Systemic lupus erythematosus Sjögren syndrome Scleroderma		Symmetric groovelike indentations along the superior costal margins of the second to fifth ribs
Neurogenic tumors	Neurofibromatosis Thoracic neuroblastoma	See Figure 12-40	Dysplastic bone formation contributes to twisted ribbonlike configuration of the ribs; superior and inferior erosions of adjacent ribs may also occur as a result of pressure from adjacent neurofibromas
Paralysis	Poliomyelitis Posttraumatic paralysis		Disuse osteoporosis may result in diminished mineralization of bone
Diminished muscle tone	Marfan syndrome		Thin ribs with superior and inferior defects
Subperiosteal resorption	Hyperparathyroidism Renal osteodystrophy		Subperiosteal resorption of cortical bone may resemble destructive osteolysis
Congenital heart disease and vascular disease	Coarctation of the aorta (Rösler sign) Venous dilation Tetralogy of Fallot Surgery for congenital heart disease	12-10	Symmetric inferior (and occasionally superior) erosion, usually of the posterior margin of the fourth to eighth ribs Pressure erosion from prominent collateral circulation

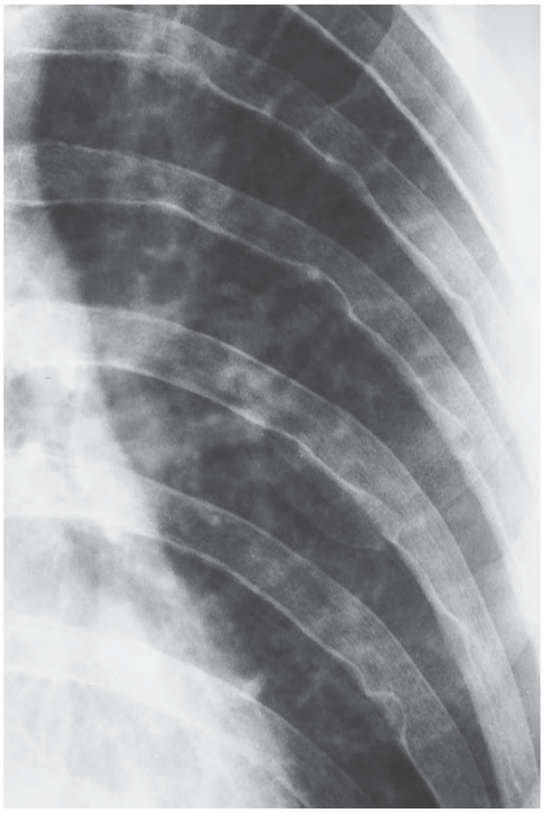

FIGURE 12–10 Coarctation of the aorta: rib notching (Rösler sign).[14] Observe the undulating inferior rib margins in this patient. The fourth through eighth ribs were involved bilaterally. The rib notching seen in patients with coarctation of the aorta has been referred to as the *Rösler sign*. *(Courtesy R. Arkless, MD, Seabeck, Wash.)*

TABLE 12-4 Injuries of the Ribs and Sternum*

Entity	Figure(s)	Characteristics	Complications and Related Disorders
Ribs			
Acute rib fracture[15-17]	12-11, 12-12	Direct injuries from falls or blows to the chest Multiple ribs are commonly fractured Crushing injuries may cause separation at the costochondral junctions or associated sternal fractures	Pneumothorax, hemothorax, lung contusion
		Fractures of first and second rib imply severe and unusual trauma	Vascular injury with fractures of upper two ribs
		Flail chest: two fractures in one rib, allowing that part of the thoracic cage to move independently of the remaining portion Rib fractures and associated soft tissue hematoma, edema, and hemothorax may also be evaluated using diagnostic ultrasonography	Impaired ventilation, pendulum breathing, ineffective cough, hypoxia, and pulmonary edema may complicate flail chest
Child abuse[18-20,83,84,89]	12-13	*Synonym:* nonaccidental injury Any of the following findings should raise suspicion of child abuse: 1. Single or multiple rib fractures in children, especially between the ages of 1 and 4 2. Fractures at different phases of healing 3. Fractures of the rib heads adjacent to the costovertebral joints 4. Bilateral rib fractures Fractures may not be visible on initial radiographs, but as healing progresses, callus formation and subperiosteal new bone formation become more evident	Multiple and unusual fractures and other signs elsewhere Child abuse may eventually result in repeated morbidity and even death if not detected and if abuse continues Oblique radiographs of the ribs should be included in the skeletal radiographic survey.
Stress (fatigue) fracture of ribs[21-24,94,95]	12-14 12-15	*Cough fracture:* repeated coughing in bronchitis or other pulmonary disease Fatigue fractures have also been linked to carrying heavy packs and to activities associated with golf, rowing, and tennis Chronic stress from costovertebral osteoarthrosis, adjacent vertebral fracture, or other articular disease may result in osteosclerotic reaction of rib	Difficulty breathing and impaired recuperation
Costovertebral joint dislocation[25]		Extremely rare, usually resulting from direct injury to the first, eleventh, or twelfth ribs Slipping rib syndrome: displacement of tenth rib at the costovertebral articulation caused by trauma; may result in upper abdominal or loin pain and may be accompanied by a snapping sensation and point tenderness	
Tietze syndrome (costosternal syndrome)[26]		Benign, self-limited, painful enlargement of the upper costal cartilages occurring insidiously or after minor trauma Seen in as many as 10% of patients with chest pain Radiographs usually normal but may reveal osteosclerosis of ribs and sternum	May simulate cardiogenic chest pain

* See also Tables 1-4 to 1-6.

TABLE 12-4 Injuries of the Ribs and Sternum—cont'd

Entity	Figure(s)	Characteristics	Complications and Related Disorders
Sternum			
Acute sternal fracture[27,88]	12-16	Direct trauma, such as chest-crushing injuries, result in fractures principally at the manubriosternal junction Direct blows to the upper region of the sternum may result in transverse fractures at the site of impact Indirect trauma rarely results in fracture of the sternum	Associated injury of ribs and costal cartilages Aortic, arterial, tracheal, cardiac, or pulmonary injuries may lead to death
Stress (insufficiency) fracture of the sternum[28,88]	12-17	Severe osteoporosis and chronic progressive thoracic kyphosis infrequently result in insufficiency fractures of the sternum Osteomalacia, plasma cell myeloma, and renal osteodystrophy may also result in insufficiency fractures by the same mechanism	Progressive kyphosis
Sternoclavicular joint dislocation[29,88,97]	12-18	Sternoclavicular dislocations are rare Best evaluated by CT-imaging	
		1. *Anterior dislocation:* far more common than posterior dislocation; results from major, indirect trauma transmitted along the long axis of the clavicle from an injury to the shoulder region	Anterior dislocation may be associated with fractures of the ribs, sternum, and clavicle
		2. *Posterior dislocation:* results from direct forces applied to the anteromedial aspect of the clavicle	Posterior dislocations may impinge on the trachea, esophagus, great vessels, or other mediastinal structures, leading to vascular injury, cough, dysphagia, dyspnea, or even death
Manubriosternal junction dislocation[30,88]	12-19	Usually results from direct trauma or crushing injuries of the chest	May be associated with spinal, rib, and clavicle fractures May be complicated by injury to the aorta, other arteries, trachea, heart, and lung

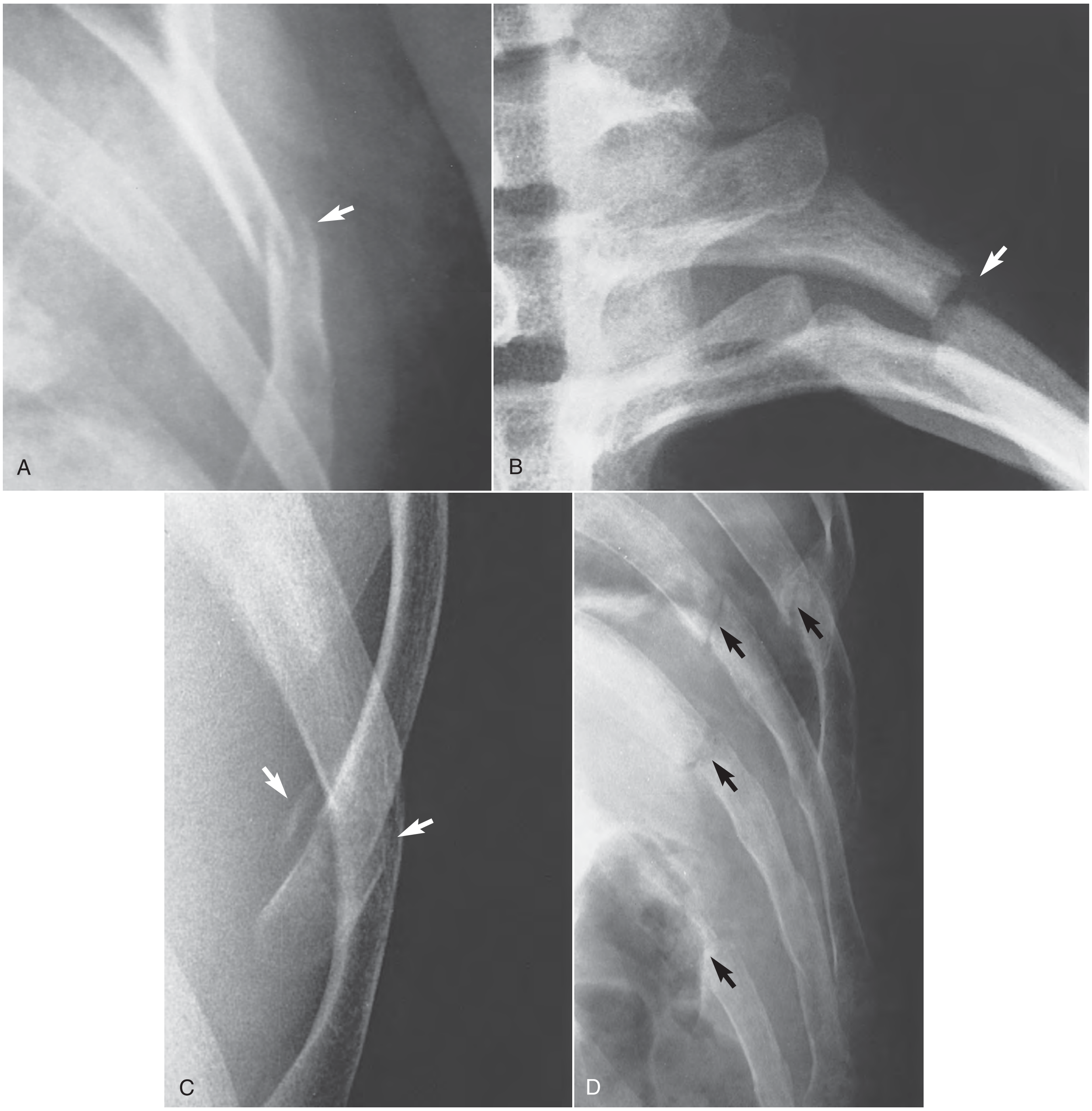

FIGURE 12–11 **Acute rib fractures.**[15-16] **A,** Acute fracture in a 70-year-old man after a car accident. Observe the cortical offset of the sixth rib adjacent to the fracture site *(arrow)*. **B,** Acute first rib fracture. Frontal radiograph of the ribs in this 19-year-old man obtained after a body surfing injury at a rock concert shows a slightly displaced fracture of the first rib *(arrow)*. Fractures of the first and second ribs generally occur with severe trauma and may be associated with vascular injury or other fractures of the shoulder girdle or spine. **C,** Minimally displaced fracture of the eighth rib is seen 14 days after trauma. A faint zone of callus is evident *(arrows)*. **D,** Radiograph of the ribs, obtained 2 weeks after this rodeo bull-rider was thrown from a bull, shows multiple lower rib fractures *(arrows)*.

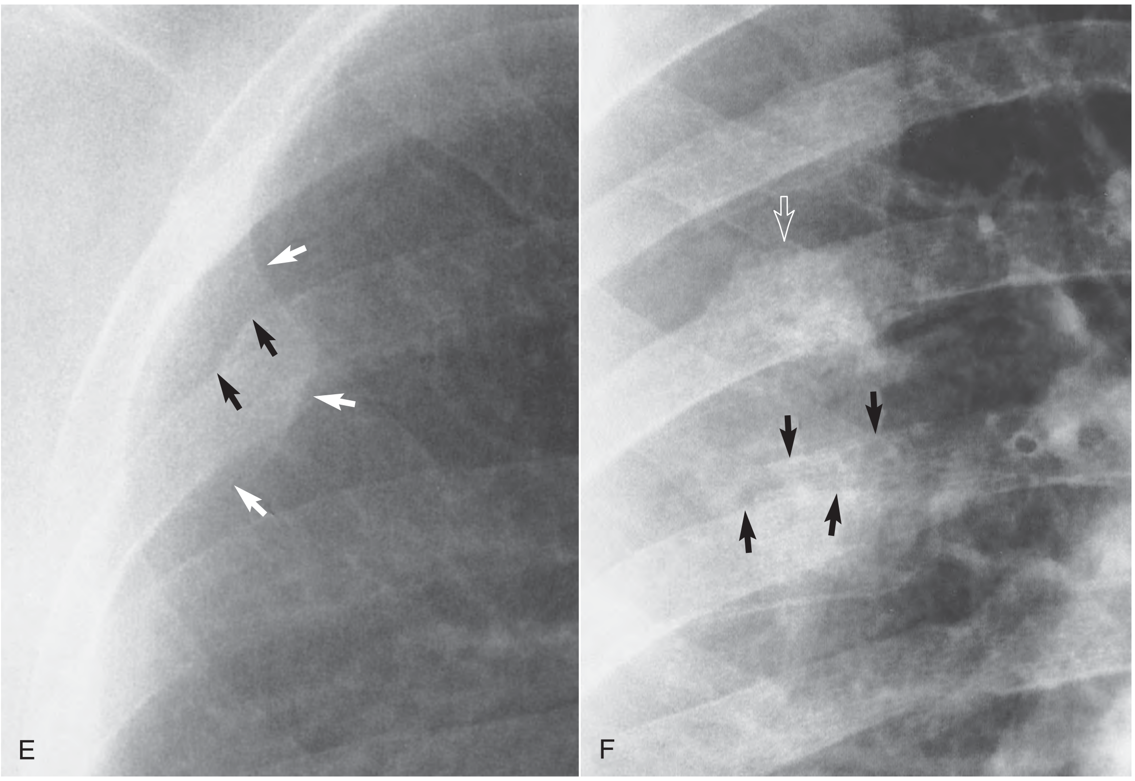

FIGURE 12–11, cont'd **E,** Healing rib fracture seen in profile reveals bony offset *(black arrows)*. A prominent extrapleural mass with tapering edges and a convex border protruding into the lung *(white arrows)* is also evident. **F,** Rib displacement *(arrows)* and early callus formation *(open arrow)* are evident in another patient with rib fractures. (***B*** *Courtesy E.E. Bonic, DC, St Louis, MO.)*

TABLE 12-5 Some Causes of an Extrapleural Mass[31,32]*

	Figure(s)
Common Causes	
Rib fracture	12-11
Skeletal metastasis	12-28
Plasma cell myeloma	12-33
Fibrous dysplasia	12-41
Osteosarcoma	12-29
Ewing sarcoma	12-32
Brown tumor	12-46
Chondrosarcoma	12-31
Mediastinal masses	
Rare Causes	
Hematoma	
Lipoma	
Neurofibroma	
Chest wall masses	
Postsurgical causes	
Chest wall infection	
Tuberculosis	
Subphrenic mass	

* An extrapleural mass is seen on chest radiographs as a radiodense area adjacent to the inner margin of the chest wall. The mass has a sharply convex margin that protrudes into and displaces the lung field. The upper and lower margins of the mass are tapered and may be concave toward the lung surface. This appearance has been termed the extrapleural sign.

FIGURE 12–12 Posttraumatic pneumothorax.[17] This 61-year-old man sustained multiple rib fractures in a motor vehicle collision. He had severe pain and shortness of breath. Observe the medially displaced edge of the pleural margin *(arrows),* absence of lung markings peripherally, and excessive opacification of the lung tissue. Blunting of the costophrenic sulcus and a fluid level *(open arrows)* indicate the presence of a pleural effusion. Pneumothorax and hemothorax are important complications of rib fractures and other thoracic cage injuries.

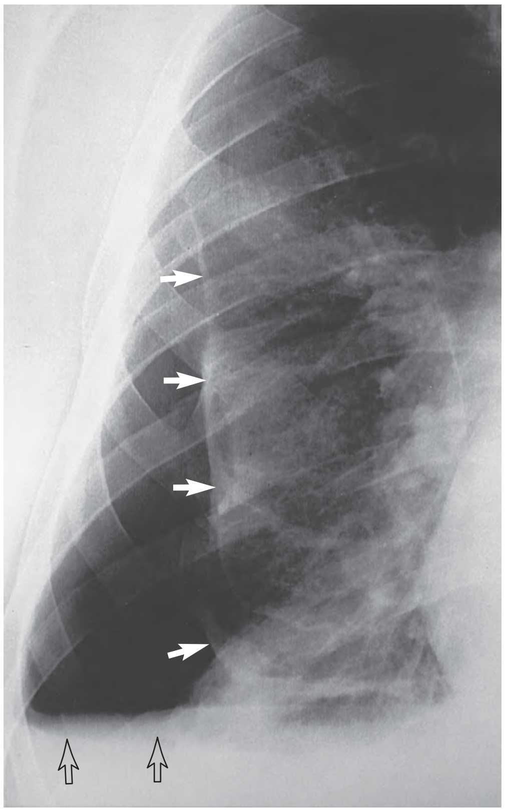

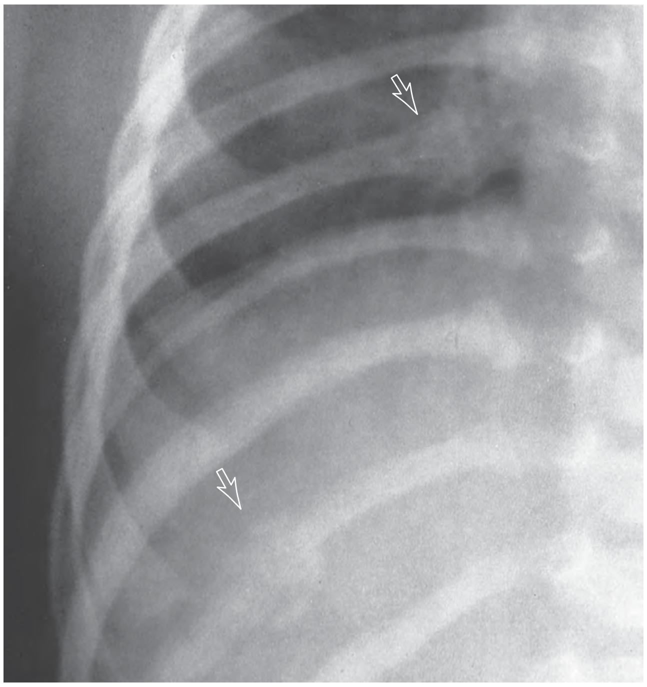

FIGURE 12–13 Child abuse.[18-20,83,84,89] Observe the multiple rib fractures *(open arrows),* a common finding in the abused child. Such fractures are often bilateral, are paravertebral, or involve the heads of the ribs. Oblique radiographs may reveal rib fractures not visible on frontal or lateral radiographs. *(Courtesy D. Edwards, MD, San Diego.)*

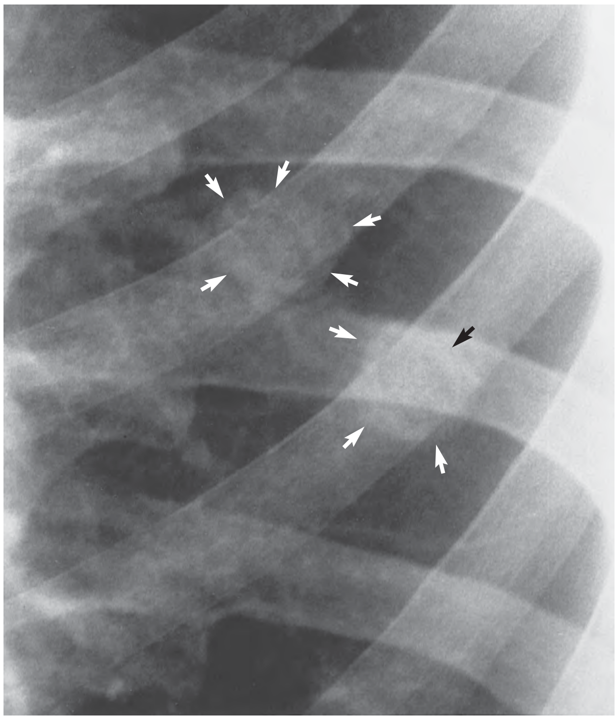

FIGURE 12–14 Stress (fatigue) fracture: healing cough fracture.[21-24,94,95] This 39-year-old man with severe bronchitis sustained fatigue fractures of two of his ribs (“cough fractures”). Observe the callus formation surrounding the fracture sites *(arrows)* in these radiographs obtained 6 weeks after the initial fractures. *(Courtesy G. Greenstein, DC, Bridgeport, Conn.)*

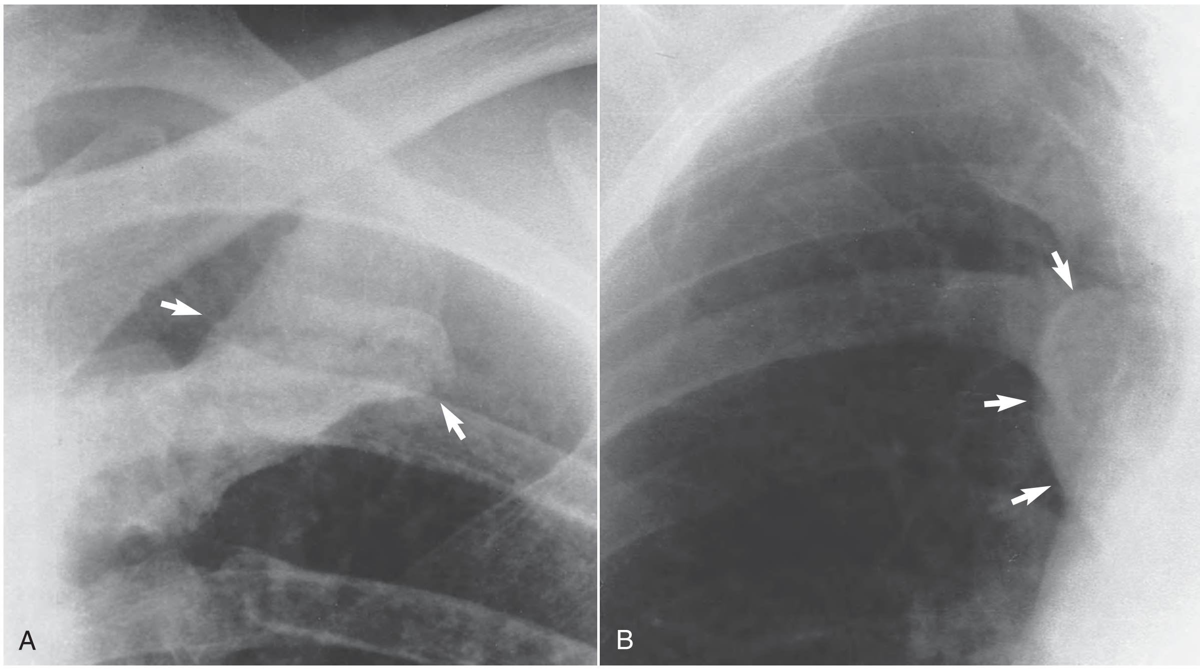

FIGURE 12–15 **Stress (fatigue) fracture and reaction to stress.**[21-24,95] **A,** Fatigue fracture. Transverse radiolucent line with surrounding sclerosis *(arrows)* represents a healing fatigue fracture of the first rib secondary to repeated throwing activity. Other causes of stress fracture of this rib include golfing, carrying a back pack, coughing, or other physical activities. **B,** Reactive stress changes. Observe the diffuse sclerosis involving the posterior aspect of the rib and the costovertebral joint osteophytes in this patient with diffuse idiopathic skeletal hyperostosis (DISH) *(arrows)*. This reactive sclerosis is seen in a variety of conditions, including costovertebral joint arthrosis, ankylosing spondylitis, and DISH. (***A,*** *Courtesy B. Groth, MD, Mosinee, Wis.)*

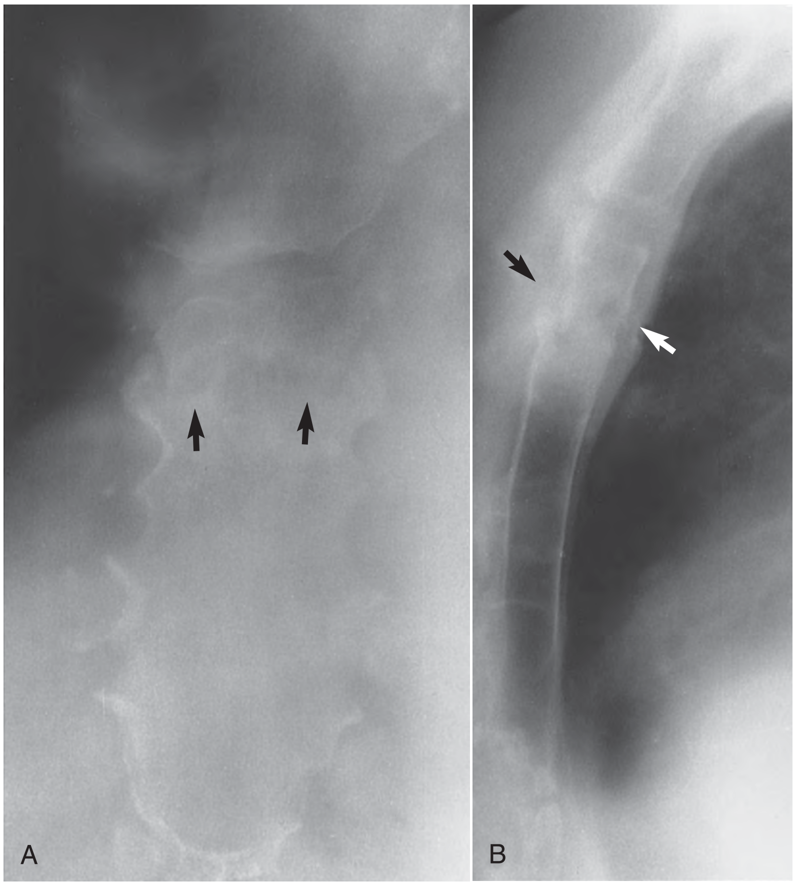

FIGURE 12–16 **Acute sternal fracture.**[27] Frontal **(A)** and lateral **(B)** radiographs show a transverse fracture of the sternal body, just below the manubrium *(arrows)*. Biopsy revealed a nonpathologic fracture.

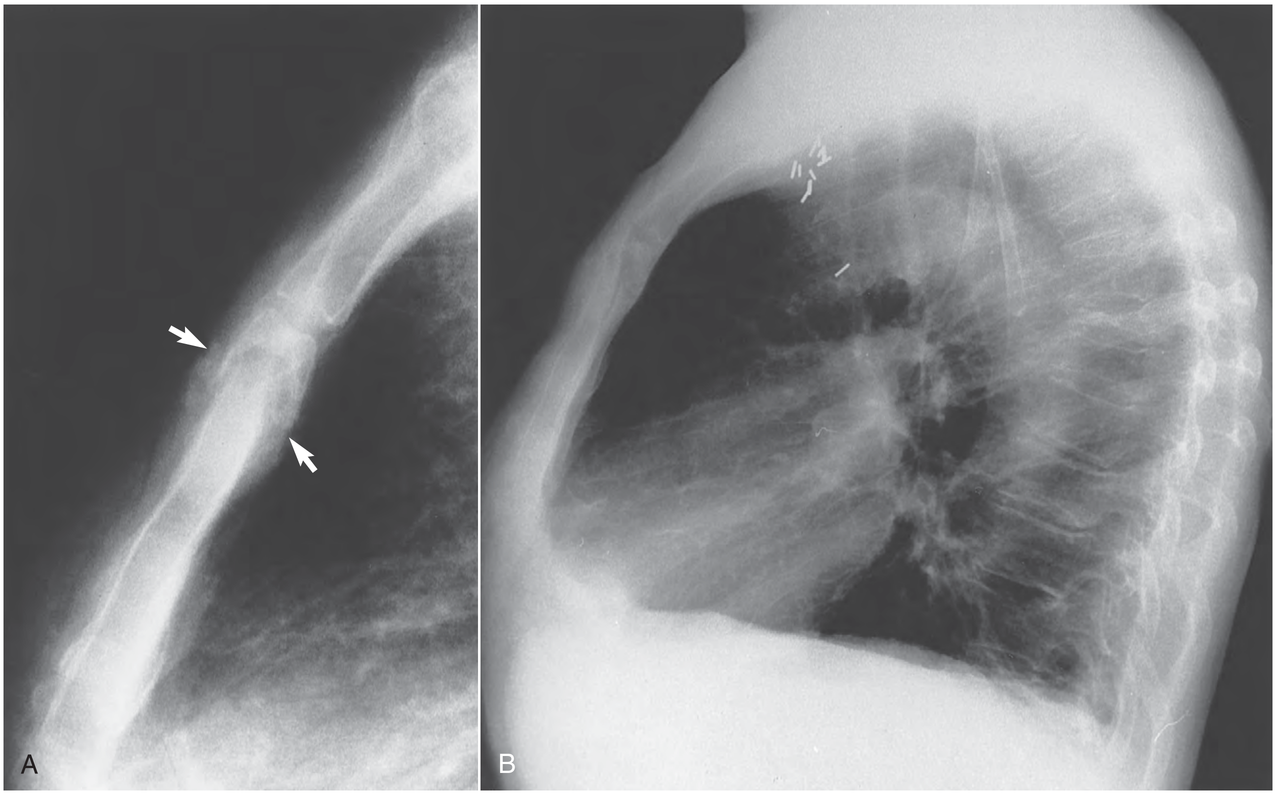

FIGURE 12–17 Stress (insufficiency) fracture of the sternum.[28,88] **A,** Observe the fracture of the sternum *(arrows)* seen in association with progressive kyphosis in this 63-year-old woman. **B,** Lateral chest radiograph in the same patient demonstrates osteoporosis, kyphosis, and multiple compression fractures. *(Courtesy R. Kerr, MD, Los Angeles.)*

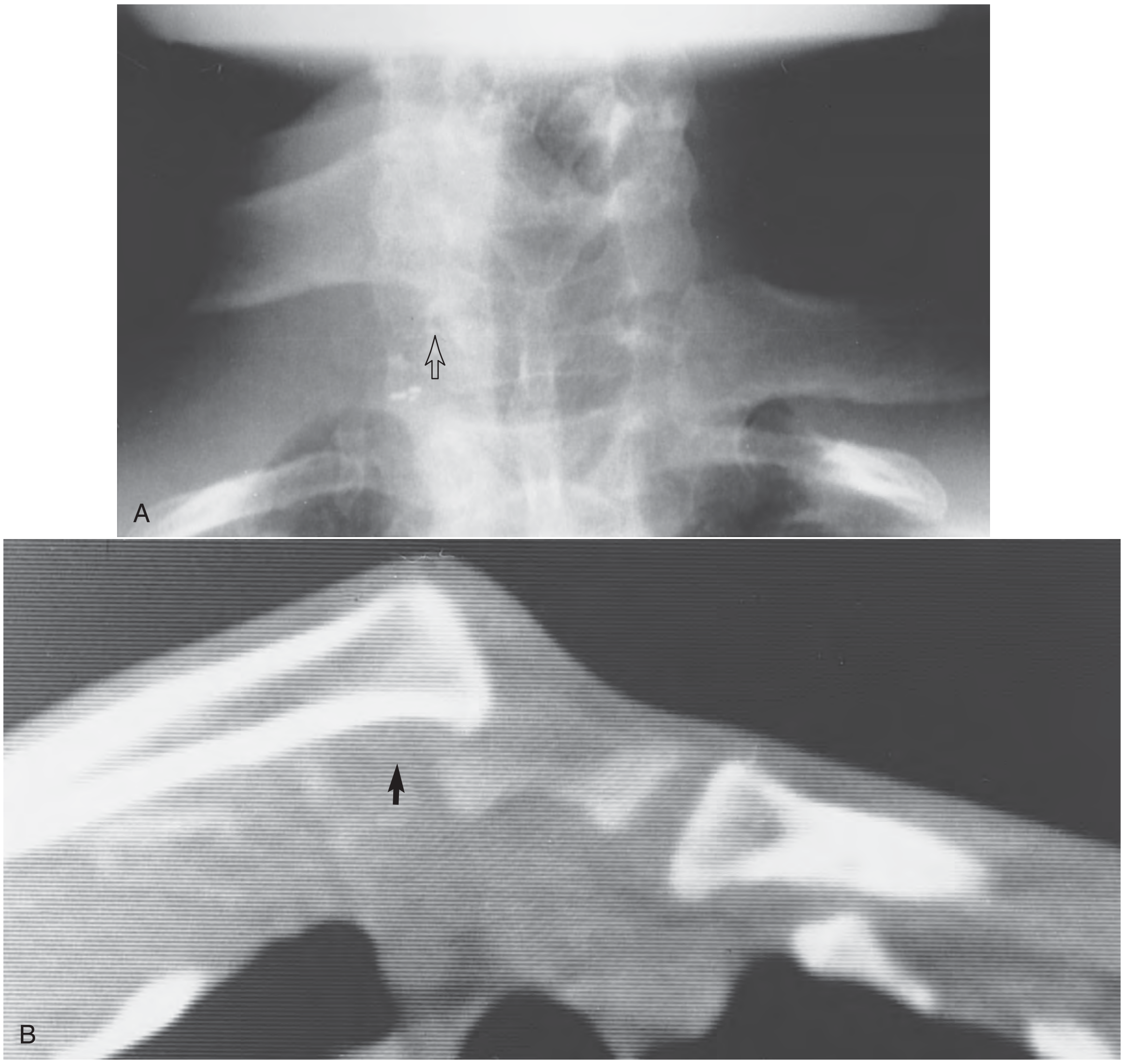

FIGURE 12–18 **Sternoclavicular joint: anterior dislocation.**[29,88,97] **A,** Frontal lordotic radiograph shows superior displacement of the right clavicle *(open arrow)* in relation to the opposite clavicle. **B,** In another patient, a transaxial CT scan clearly displays the anterior dislocation of the sternoclavicular joint *(arrow)*. Sternoclavicular joint dislocations are rare. Anterior dislocation, far more common than posterior dislocation, typically results from major, indirect trauma transmitted along the long axis of the clavicle from an injury to the shoulder region.

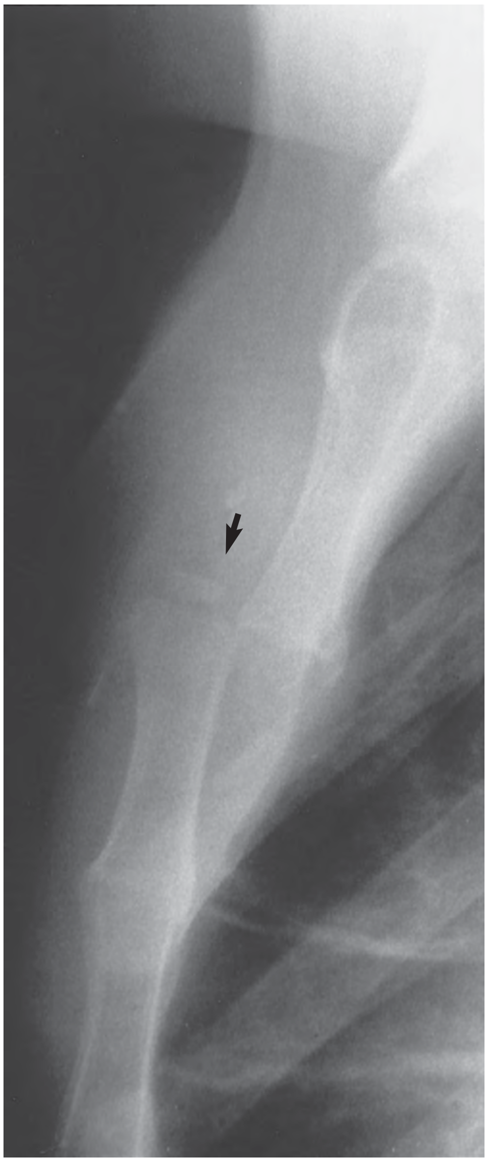

FIGURE 12–19 **Manubriosternal junction dislocation.**[30,88] Observe the anterior dislocation *(arrow)* of the body of the sternum at the manubriosternal junction. Sternal dislocations may be associated with spine, rib, and clavicle fractures and may be complicated by injury to the major arteries, trachea, heart, and lung.

TABLE 12-6 Articular Disorders Affecting the Joints of the Thoracic Cage*

Entity	Figure(s)	Characteristic Sites of Involvement	Characteristics
Degenerative and Related Disorders			
Osteoarthrosis[3,33,34,88]	See Figure 3-35 12-20	Costovertebral joint Sternoclavicular joint First sternocostal joint	Narrowed articular space Osteophytes (may simulate pulmonary lesions) Subchondral bone sclerosis
Inflammatory Disorders			
Rheumatoid arthritis[34-37]	12-21	Manubriosternal junction (30% to 70% of patients) Sternoclavicular joint (30% of patients)	Unilateral or bilateral subchondral erosions and, rarely, extensive osteolysis Absence of osteophytes and other osseous outgrowths
Ankylosing spondylitis[38-40]	12-22	Sternoclavicular joint	Bilateral or unilateral involvement Erosion, sclerosis, and, occasionally, ankylosis
Psoriatic arthritis[38,39]	12-23	Sternoclavicular joint Manubriosternal junction	Findings can be severe and may be associated with pain and soft tissue swelling Osteoporosis, subchondral erosion, hyperostosis, and synostosis May resemble rheumatoid arthritis or ankylosing spondylitis
Sternocostoclavicular hyperostosis[41,88]	12-24, *A-B*; See also Figure 13-74	Sternum Upper ribs Clavicle	Bilateral bone overgrowth and soft tissue ossification Associated with pustulosis palmaris et plantaris in 30% to 50% of patients (see SAPHO syndrome) Age 40-60 years; men > women *Clinical findings:* pain, swelling, tenderness, and local heat overlying the anterior upper chest wall
SAPHO syndrome[41,85,88]	12-24, *C-D*	Sternum Anterior portions of ribs Clavicle Sternoclavicular joint Manubriosternal junction	SAPHO is an acronym for the findings of synovitis (S), acne (A), pustulosis (P), hyperostosis (H), and osteitis (O) Arthro-osteitis associated with acne or pustulosis palmaris et plantaris; closely related to sternocostoclavicular hyperostosis, psoriasis, and chronic recurrent multifocal osteomyelitis Prominent hyperostosis and painful osteitis of the anterior chest wall and synovitis of the nearby joints
Reactive arthritis associated with Reiter syndrome[38,42]		Manubriosternal junction	Osseous erosion and bony proliferation Findings identical to those of psoriatic and rheumatoid arthritis Associated with urethritis and conjunctivitis
Dermatomyositis and polymyositis[43]	12-25	Muscles and subcutaneous tissues of chest wall	Diffuse subcutaneous, intermuscular, and intramuscular calcification of chest wall
Infection			
Pyogenic septic arthritis[44]	12-26	Sternoclavicular joint Manubriosternal junction Costosternal joint	Intravenous drug abusers predisposed to sternoclavicular joint infections Unilateral joint space widening and destruction Soft tissue mass or abscess variable Osseous ankylosis rare

* See also Tables 1-7 to 1-10.

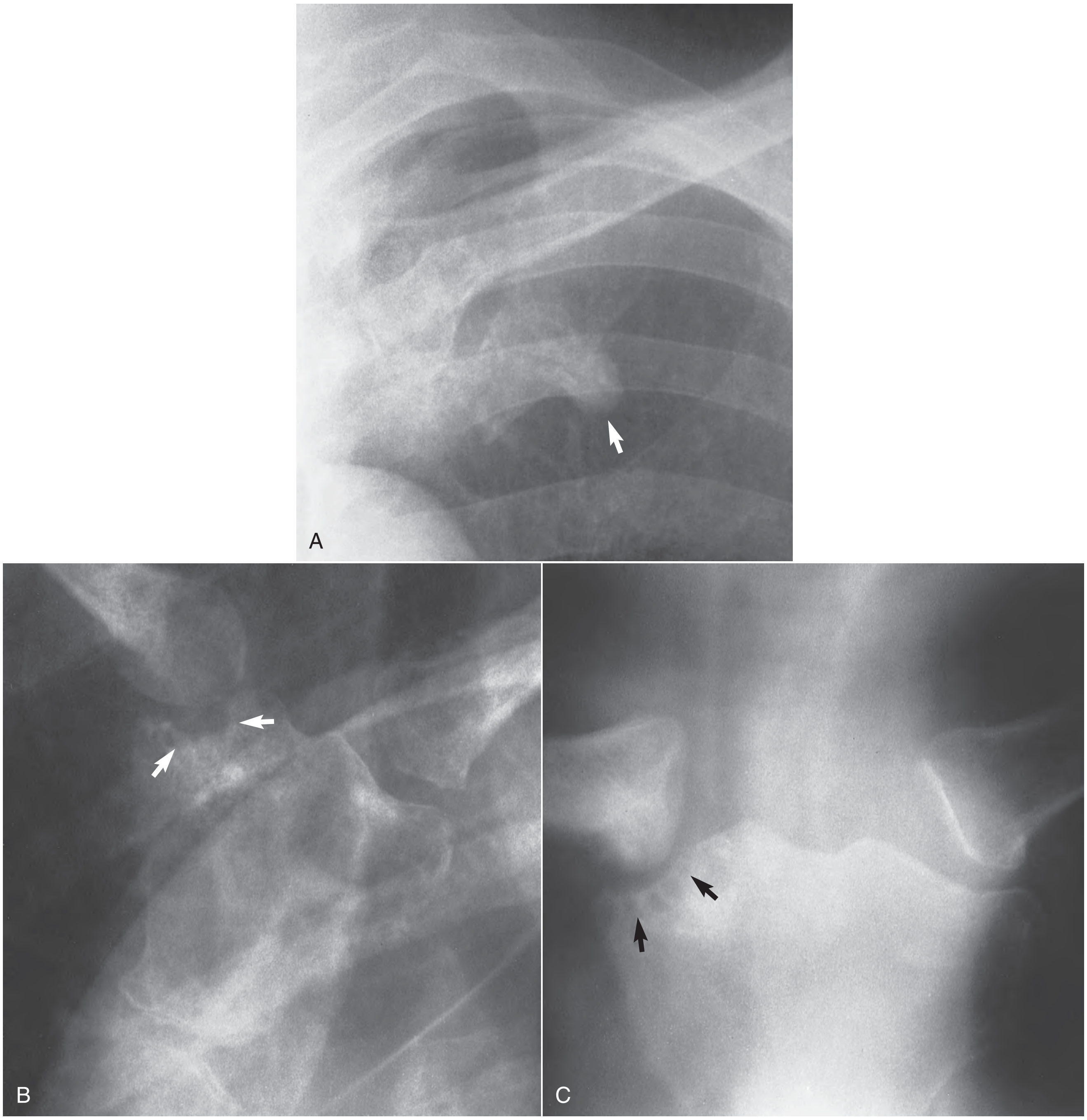

FIGURE 12–20 **Osteoarthrosis.**[3,33,34,88] **A,** First sternocostal joint. Observe the prominent osteophytes arising from the first sternocostal articulation *(arrow)*. Degenerative disease is a frequent finding at this site and may simulate a pulmonary mass. **B-C,** Sternoclavicular joint. This 69-year-old woman had undergone mediastinal surgery 1 year before these radiographs were taken. In **B,** an oblique radiograph shows the nonspecific finding of an indistinct subchondral margin of the manubrial surface of the right sternoclavicular joint *(arrows)*. In **C,** a coronal conventional tomogram more clearly shows the sclerosis, the poorly defined margin of the medial aspect of the clavicle, and subchondral cyst formation *(arrows)* within the manubrium adjacent to the joint.

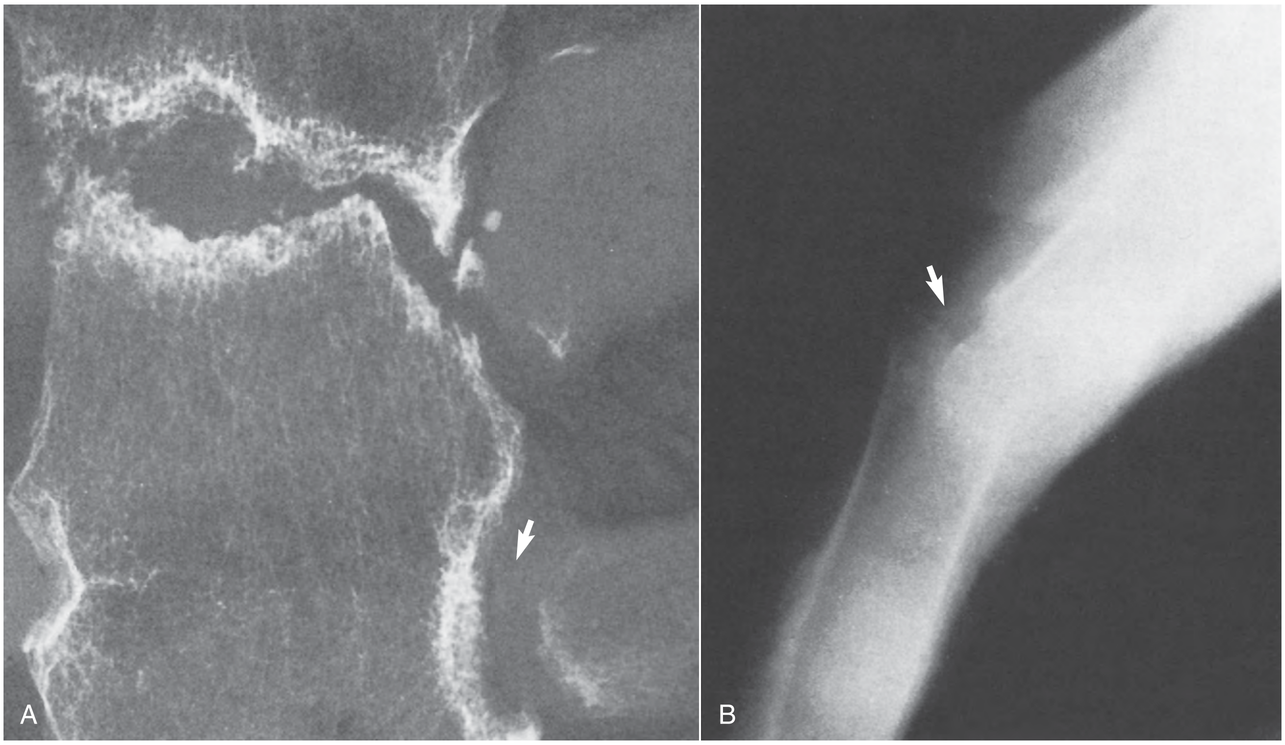

FIGURE 12–21 **Rheumatoid arthritis: manubriosternal junction.**[34-37] **A,** Radiographic abnormalities of the manubriosternal junction are illustrated in this coronal section of the sternum. They include osseous erosions and sclerosis. Also note irregularity of the sternocostal joints *(arrow)*. **B,** Lateral radiograph from another rheumatoid arthritis patient reveals spontaneous subluxation of the manubriosternal junction *(arrow)*. *(From Resnick D: Diagnosis of bone and joint disorders. 3rd Ed. Philadelphia, Saunders, 1995, p 906.)*

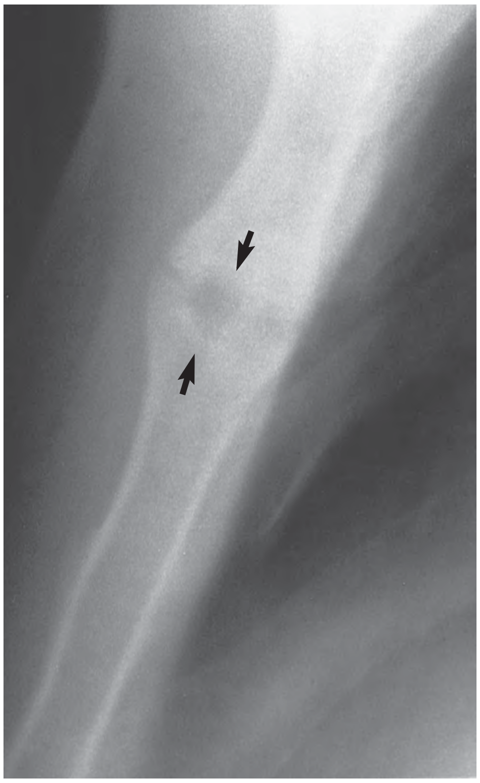

FIGURE 12–22 **Ankylosing spondylitis.**[38-40] The manubriosternal junction is narrowed and indistinct, and the subchondral bone is eroded *(arrows)* in this 49-year-old man with a 10-year history of ankylosing spondylitis.

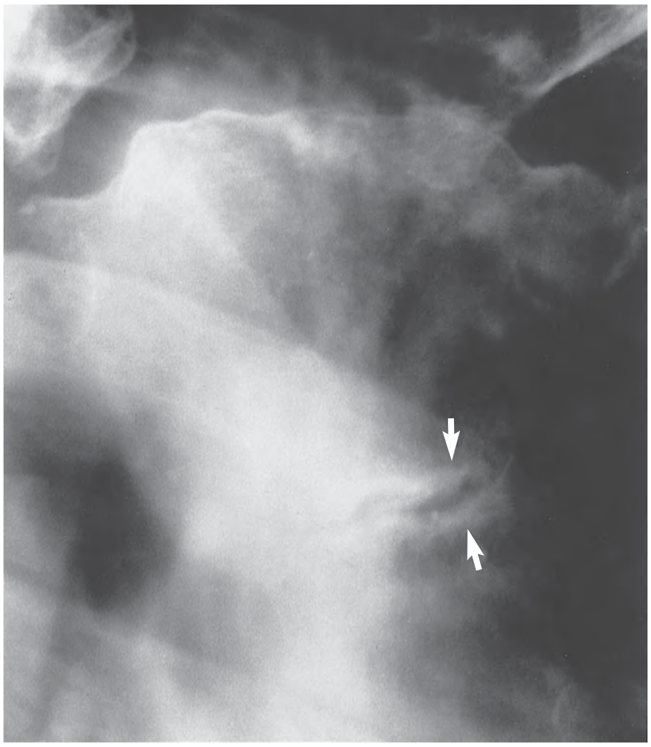

FIGURE 12–23 **Psoriatic arthropathy: manubriosternal junction.**[38,39] Observe the joint space irregularity and sclerosis of the manubriosternal junction *(arrows)* in this 53-year-old man with psoriatic skin lesions and foot involvement. Radiographic changes in psoriatic arthritis that affect the manubriosternal junction may resemble those seen in rheumatoid arthritis and ankylosing spondylitis and include osteoporosis, subchondral erosion, sclerosis, and synostosis.

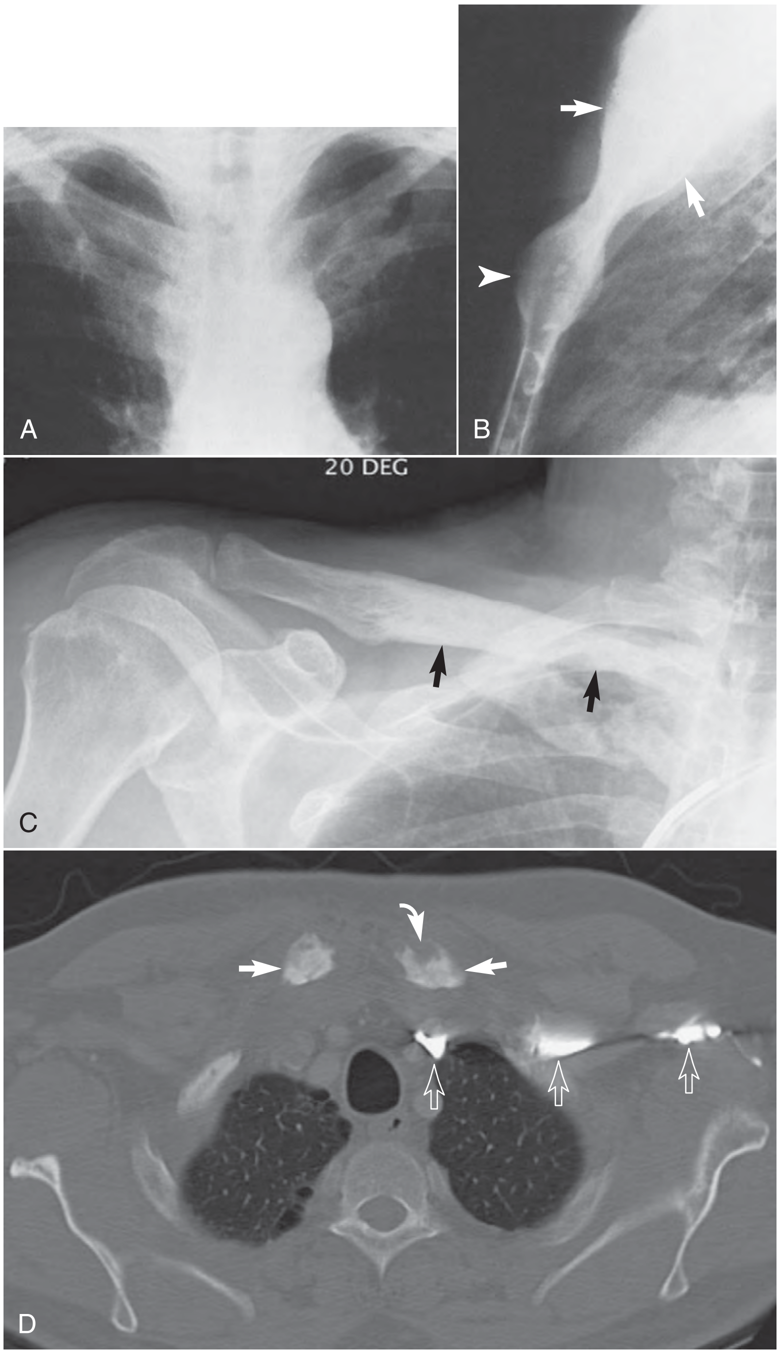

FIGURE 12–24 Osteosclerotic disorders associated with acne and pustulosis palmaris et plantaris.[41,85,88] **A-B,** Sternocostoclavicular hyperostosis.[41] Progressive soft tissue prominence developed in the upper anterior chest wall in this 53-year-old woman. **A,** Osseous mass is projected over the upper chest on both sides. Observe also the obliteration of the inferior aspects of the clavicles, the anterior margins of the first ribs, and the sternoclavicular joints. **B,** Lateral radiograph reveals the ossified mass *(arrows)* and ossification of the manubriosternal junction *(arrowhead)*. **C-D,** SAPHO syndrome.[41,85,88] **C,** A frontal radiograph in a 65-year old man with chronic pustulosis palmaris et plantaris reveals marked sclerosis of the proximal two thirds of the clavicle *(arrows)*. **D,** A transaxial CT scan in the same patient at the level of the proximal ends of the clavicles, following intravenous contrast administration reveals dense sclerosis of the proximal ends of both clavicles *(arrows)* and an erosion *(curved arrow)* within the anterior surface of the left clavicle. Contrast is evident within the central veins of the left arm *(open arrows)*. SAPHO is an acronym for the findings of synovitis (S), acne (A), pustulosis (P), hyperostosis (H), and osteitis (O). (***A-B,*** *From Resnick D: Diagnosis of bone and joint disorders. 3rd Ed. Philadelphia, Saunders, 1995, p 4454. Courtesy R. Kerr, MD, Los Angeles.)*

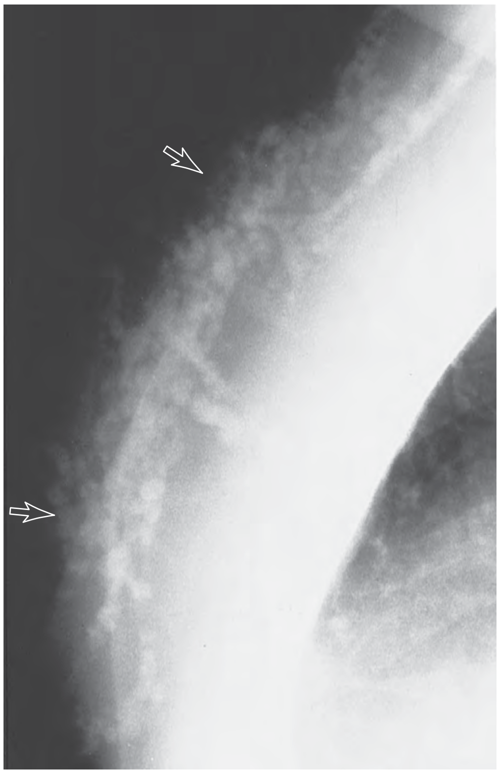

FIGURE 12–25 **Dermatomyositis and polymyositis: anterior chest wall.**[43] Diffuse soft tissue calcification is seen in the pectoral region anterior to the sternum *(open arrows)* in this patient with diffuse dermatomyositis and polymyositis. *(Courtesy C. Pineda, MD, Mexico City.)*

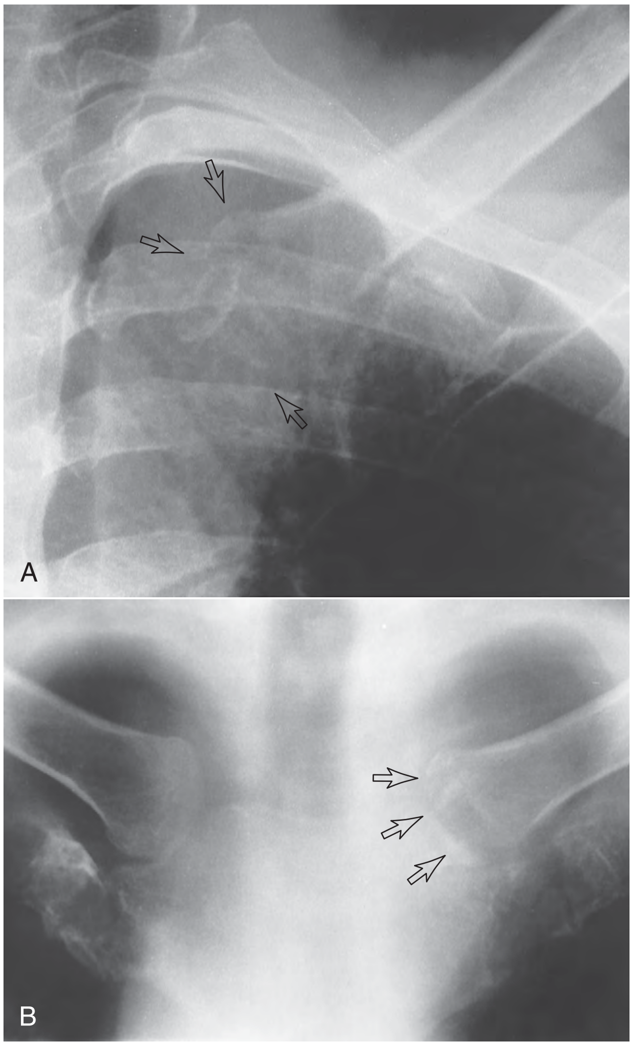

FIGURE 12–26 **Pyogenic septic arthritis: sternoclavicular joint.**[44,88] In a 53-year-old female intravenous drug addict, a frontal radiograph **(A)** and conventional tomogram **(B)** of the sternoclavicular joint show joint space narrowing, osteopenia, and erosions of the subchondral bone *(open arrows)*, typical of septic arthritis. *Staphylococcus aureus* was cultured from the joint.

TABLE 12-7 Tumors and Tumorlike Lesions Affecting the Ribs, Sternum, and Chest Wall*

Entity	Figure	Characteristics
Secondary Malignant Tumors of Bone		
Skeletal metastasis[45-47]	12-27 12-28	Ribs are commonly involved in skeletal metastasis; sternum infrequently involved *Pancoast tumor:* Bronchogenic carcinoma of the superior sulcus frequently invades and destroys the upper ribs and cervicothoracic spine by direct extension or by hematogenous or lymphatic dissemination; associated with apical lung mass; clinical findings of ptosis, myosis, and anhidrosis (Horner syndrome)
Primary Malignant Tumors of Bone		
Osteosarcoma[48-50,93]	12-29 12-30	Fewer than 3% of osteosarcomas affect the ribs Most rib osteosarcomas are secondary, arising from malignant transformation of Paget disease or irradiated bone Osteolytic, osteoblastic, and mixed patterns of bone destruction Pulmonary metastases from osteosarcoma may be seen on radiographs of the chest or thoracic spine: multiple ossified masses within the lung field
Osteoblastoma (aggressive)[51]		Two percent of aggressive osteoblastomas affect the ribs Expansile osteolytic lesion that may be partially ossified or contain calcium
Chondrosarcoma[52,53]	12-31	Approximately 20% of chondrosarcomas affect the ribs; 2% affect the sternum Most rib lesions are conventional or mesenchymal forms Tend to be osteolytic lesions, sometimes containing a bulky cartilaginous cap and frequently containing calcifications Soft tissue masses common
Ewing sarcoma[54]	12-32	Eight percent of Ewing sarcomas affect the ribs Aggressive permeative or moth-eaten pattern of bone destruction Central metadiaphyseal location and soft tissue mass are common
Myeloproliferative Disorders		
Plasma cell (multiple) myeloma[55]	12-33	Seventy-five percent of all plasma cell myeloma are the multiple form Twenty-five percent of myeloma patients with skeletal lesions have rib involvement; 15% have sternal involvement Diffuse osteopenia or punctate osteolytic lesions
Hodgkin disease[56]		Sixteen percent of skeletal lesions in Hodgkin disease occur in the ribs; 4% occur in the sternum
Primary lymphoma (non-Hodgkin)[57]	12-34	Approximately 2% of patients with primary non-Hodgkin lymphoma have rib involvement May result in multiple moth-eaten or permeative osteolytic lesions Diffuse or localized sclerotic lesions are rare
Primary Benign Tumors of Bone[90,91]		
Enostosis[58]		Twelve percent of enostoses occur in the ribs
Osteoid osteoma[59-61]	12-35	Fewer than 2% of osteoid osteomas occur in the ribs Central radiolucent nidus with surrounding reactive sclerosis
Osteoblastoma (conventional)[62]		Up to 12% of osteoblastomas involve the ribs
Enchondroma (solitary)[53,63]	12-36	Up to 8% of solitary enchondromas arise in the ribs Usually osteolytic and frequently are expansile and multiloculated Matrix may be calcified
Maffucci syndrome[53]		More than 30% of patients with Maffucci syndrome have rib involvement Soft tissue hemangiomas in addition to multiple enchondromas Higher risk of malignant transformation than with solitary enchondroma
Osteochondroma (solitary)[64]	12-37	Fewer than 5% of solitary osteochondromas occur in the ribs Often bulky cartilaginous lesions arising from the anterior aspect of the ribs adjacent to costal cartilage
Intraosseous lipoma[65]		Approximately 8% of lipomas occur in the ribs Radiolucent solitary lesions
Hemangioma[66]	12-38	Approximately 9% of hemangiomas occur in the ribs Osseous expansion and trabecular striation within lesions

* See also Tables 1-12 to 1-14.

TABLE 12-7 Tumors and Tumorlike Lesions Affecting the Ribs, Sternum, and Chest Wall—cont'd

Entity	Figure	Characteristics
Aneurysmal bone cyst[67]		Less than 3% of aneurysmal bone cysts involve the ribs Eccentric, thin-walled, expansile, multiloculated osteolytic lesion
Giant cell tumor[90-92]		Approximately 1% to 7.5% of giant cell tumors occur within the ribs Can be locally aggressive and about 30% to 50% recur after resection Eccentric, osteolytic, expansile, cortical thinning, soft tissue mass
Tumorlike Lesions		
Paget disease[68]	12-39	Rare involvement of ribs Usually polyostotic and may exhibit unilateral involvement
Neurofibromatosis 1[69]	12-40	Formerly designated von Recklinghausen disease Commonly affects ribs Mesodermal dysplasia (and occasionally pressure erosion) results in thin ribbonlike ribs with widened intercostal spaces Circumscribed osteolytic lesions occasionally appear
Monostotic fibrous dysplasia[70]	12-41, *A*	Approximately 28% of all monostotic lesions affect the ribs Most common benign lesion of the rib cage, representing 30% of primary benign chest wall lesions Thick rim of sclerosis surrounding a radiolucent lesion or radiodense lesion; ground-glass appearance of matrix; tends to affect entire rib; anterior end of rib may appear bulbous and expanded Most rib lesions, whether monostotic or polyostotic, are unilateral, assisting in the differentiation from lesions such as metastasis and hyperparathyroidism, diseases that are typically more widely disseminated
Polyostotic fibrous dysplasia[70,91]	12-41, *B-D*	Rib involvement is seen in more than 50% of cases of polyostotic fibrous dysplasia Unilateral (or infrequently, bilateral asymmetric) involvement of the ribs
Langerhans cell histiocytosis[71]		Five percent of lesions affect the ribs, most frequently eosinophilic granuloma Single or multiple osteolytic lesions often result in pathologic fracture
Soft Tissue Tumors and Masslike Lesions of the Chest Wall[96]		
Peripheral nerve tumors Schwannoma Neurofibroma Ganglioneuroma		Slow-growing lesions originating within a nerve sheath (schwannoma, neurilemoma), nerve (neurofibromas; plexiform or nonplexiform), or ganglia (ganglioneuroma) Most are benign, but schwannoma can be malignant
Fatty tumors Lipoma Liposarcoma		Relatively common Lipoma more common than liposarcoma
Hemangioma		Rare benign lesion composed of multiple dilated thin-walled tortuous vessels
Elastofibroma	12-42	Elastofibroma dorsi are muscular tumors of the posterior chest wall
Metastasis		Breast carcinoma recurrence rates in chest wall are 5% to 20%
Lymphoma		Rare; direct extension from mediastinum
Abscess		Most common in IV drug abusers and following trauma
Aggressive fibromatosis		Locally aggressive; recurrence rate up to 50%
Malignant fibrous histiocytoma (MFH)		Invasive tumors of older patients that spread readily; underlying bone involvement is common

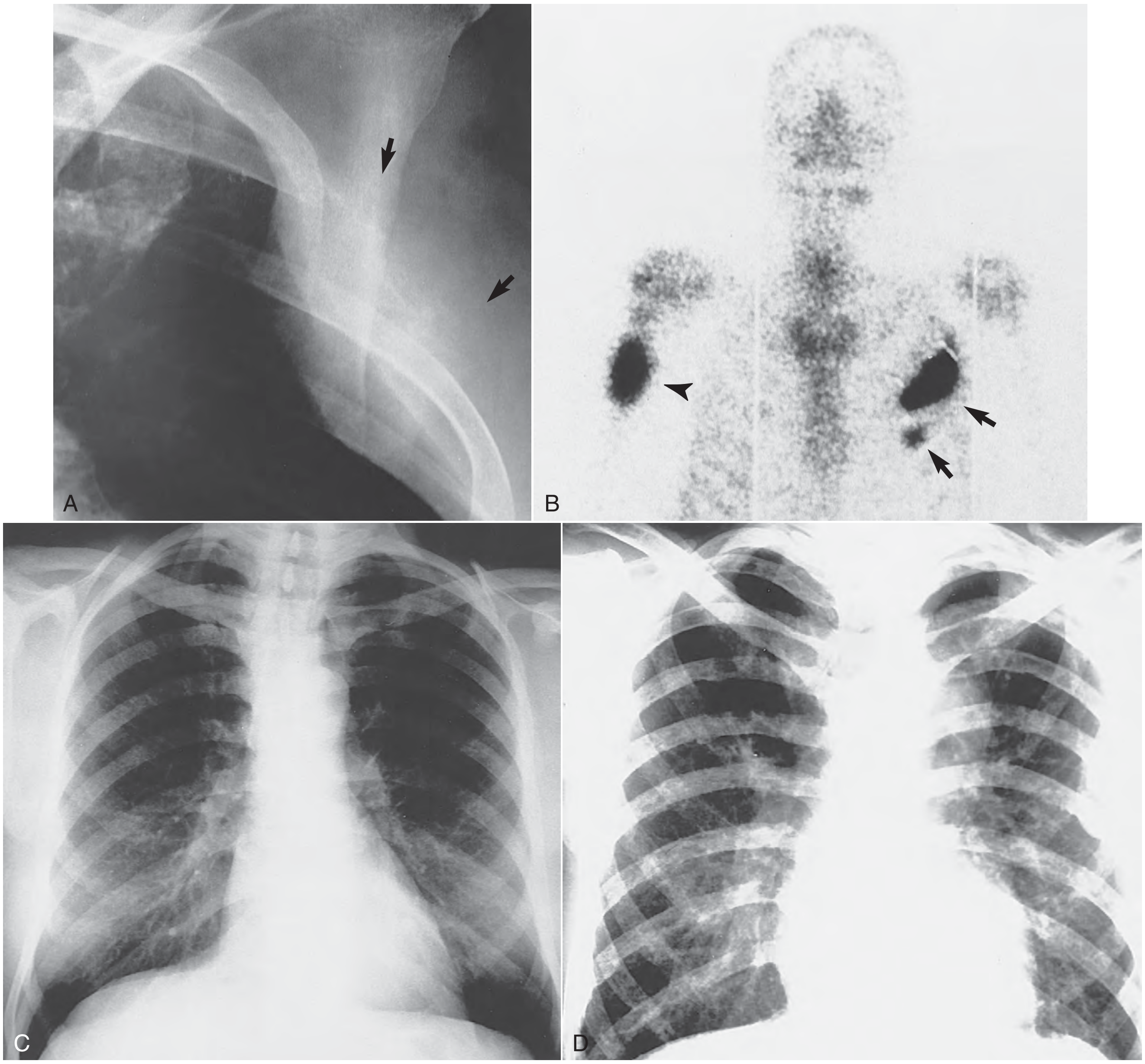

FIGURE 12–27 **Skeletal metastasis: ribs—various patterns.**[45-47] **A-B,** Osteolytic pattern. A 61-year-old man with known prostate carcinoma had rib pain. In **A,** an anteroposterior view of the rib shows widespread osteolytic destruction of the posterolateral aspect of the left third rib *(arrows)*. In **B,** a bone scan reveals increased accumulation of the bone-seeking radionuclide in the affected ribs *(arrows)* and in the contralateral humerus *(arrowhead)*. Several other sites (not shown), including the pelvis and spine, revealed widespread metastases. **C,** Osteoblastic pattern. Radiograph of the chest and thoracic cage in this man with prostate carcinoma shows a diffuse osteoblastic pattern of metastatic disease. No evidence of bone enlargement, scalloping, or coarsened trabeculae is seen. **D,** Mixed pattern. A 20-year-old man with a medulloblastoma metastatic to the skeleton complained of severe bone pain. His radiographs reveal a mixed pattern of metastasis with both osteolytic and osteoblastic lesions throughout the bones of the thoracic cage.

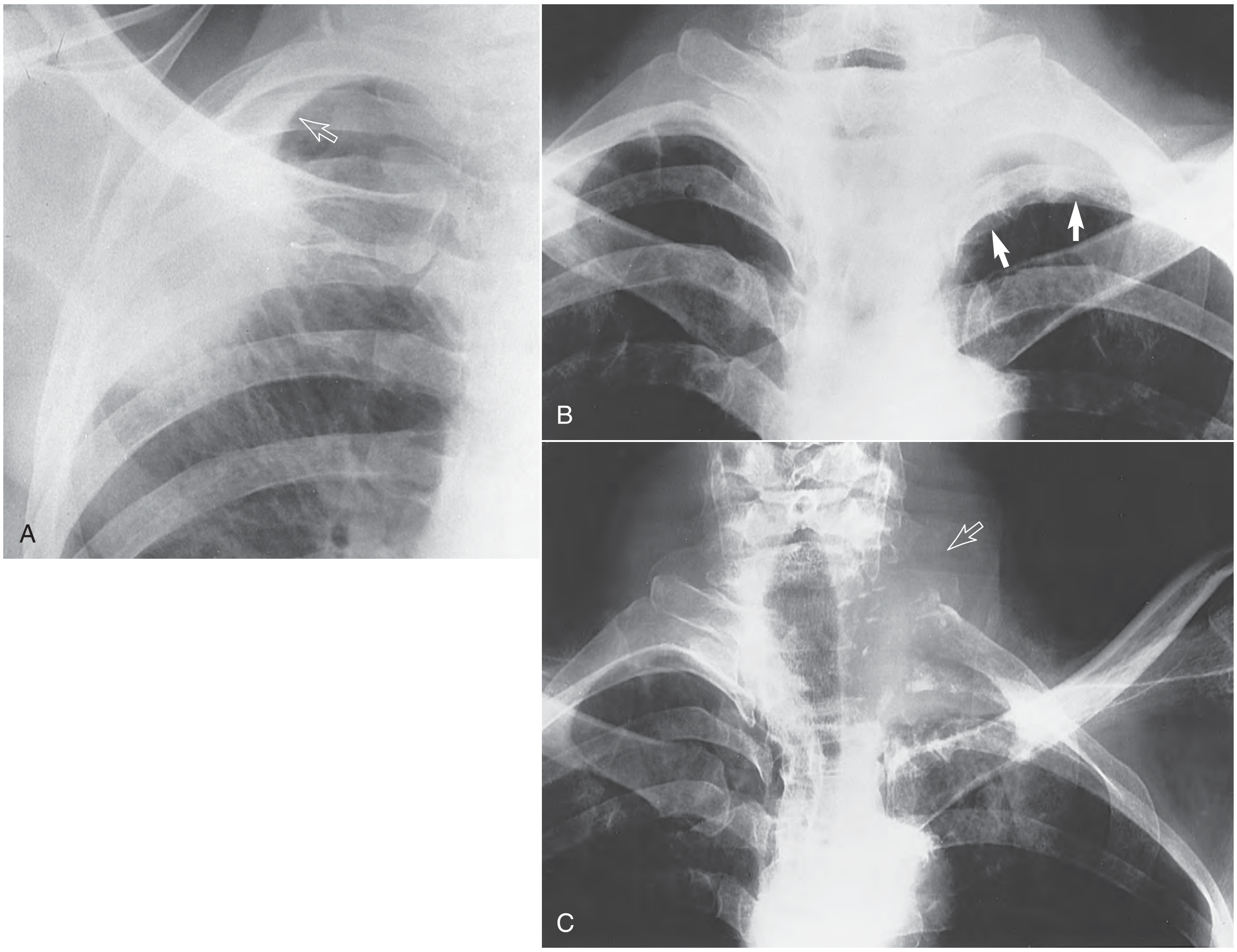

FIGURE 12–28 **Skeletal metastasis: Pancoast tumor.**[45-47] **A,** Large radiopaque soft tissue mass is present in the right lung apex in this patient with carcinoma of the lung. Underlying rib destruction, not well seen on this chest radiograph, is suggested by the tapering extrapleural sign at the edge of the lesion *(open arrow)*. **B,** In another patient with a Pancoast tumor, a subtle radiopaque area is noted in the left lung apex *(arrows)*. **C,** In a third patient, extensive osteolytic destruction of the upper ribs and thoracic vertebrae is evident *(open arrow)*. In Pancoast tumors, carcinoma of the apex of the lung invades adjacent ribs or cervicothoracic vertebrae by direct extension. In other cases, contiguous spread of tumor into the adjacent bone may result from hematogenous or lymphatic dissemination. *(Courtesy B.A. Howard, MD, Charlotte, NC.)*

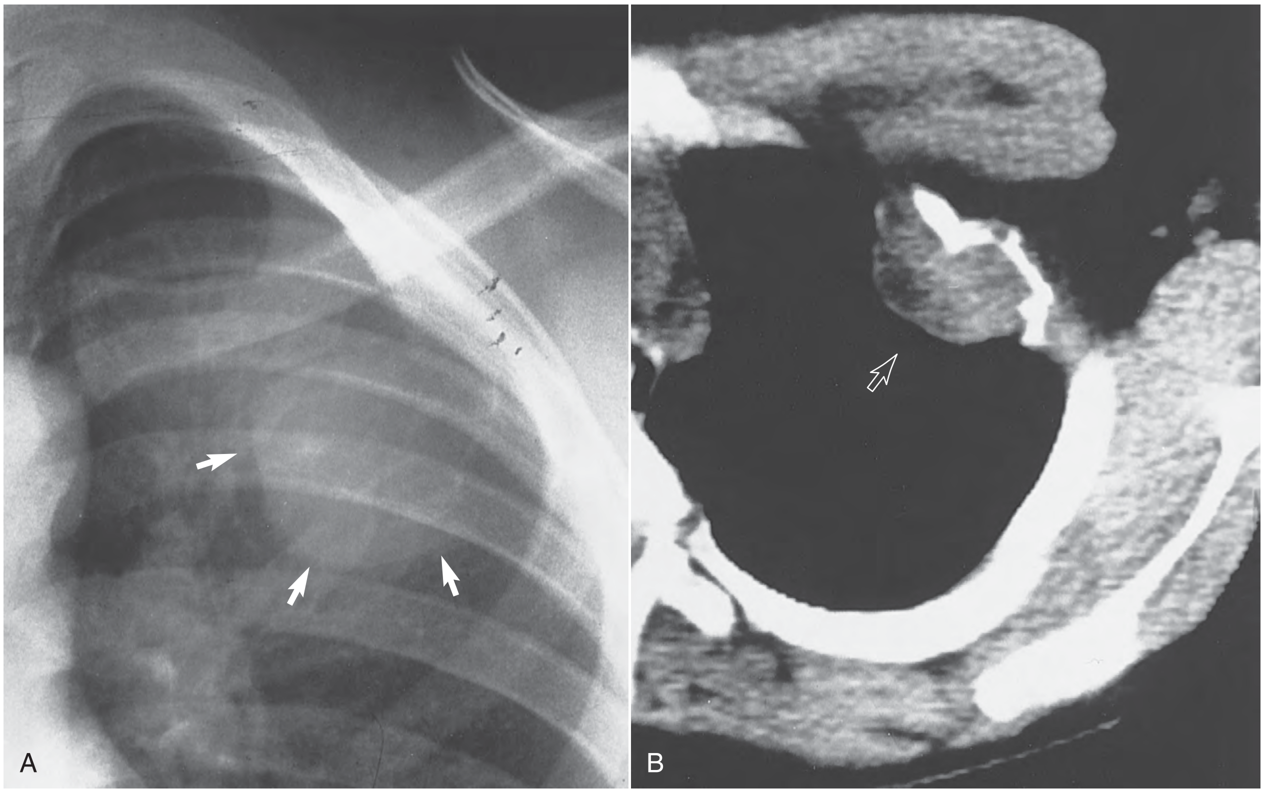

FIGURE 12–29 **Primary osteosarcoma.**[48-50,93] A 10-year-old boy had pain along the anterior aspect of the rib cage. **A,** Posteroanterior chest radiograph shows a large, lobulated extrapleural soft tissue mass overlying the upper lung field *(arrows)*. **B,** Transaxial CT scan localizes the lesion to the anterior aspect of the rib, revealing osseous destruction and a large associated soft tissue mass *(open arrow)*.

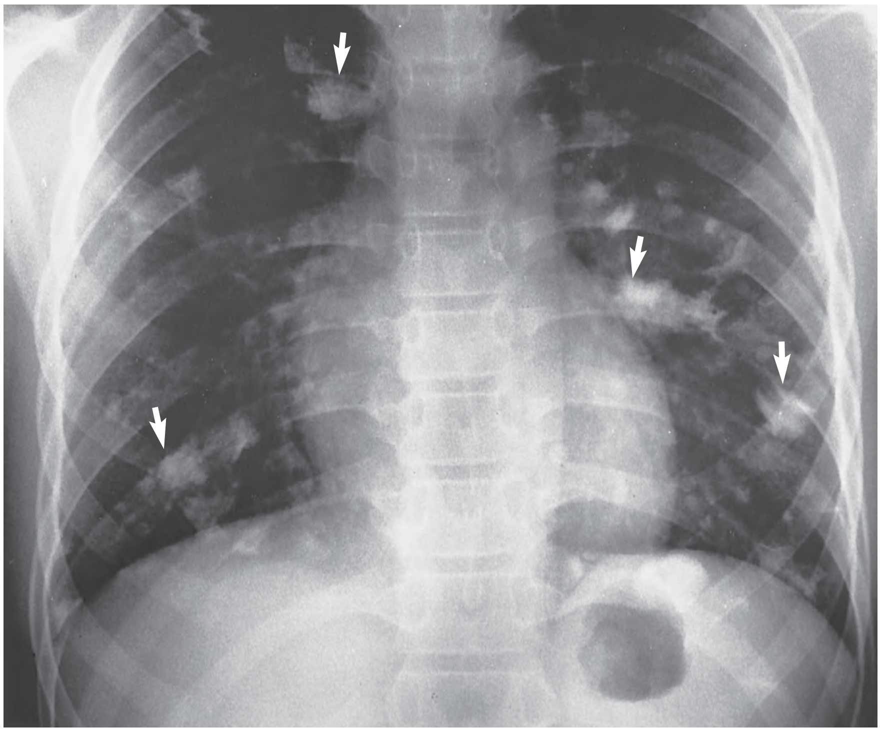

FIGURE 12–30 **Osteosarcoma: pulmonary metastasis.**[50,93] Posteroanterior chest radiograph of this 12-year-old boy with known osteosarcoma in the femur reveals multiple ossified masses throughout the lungs *(arrows)*.

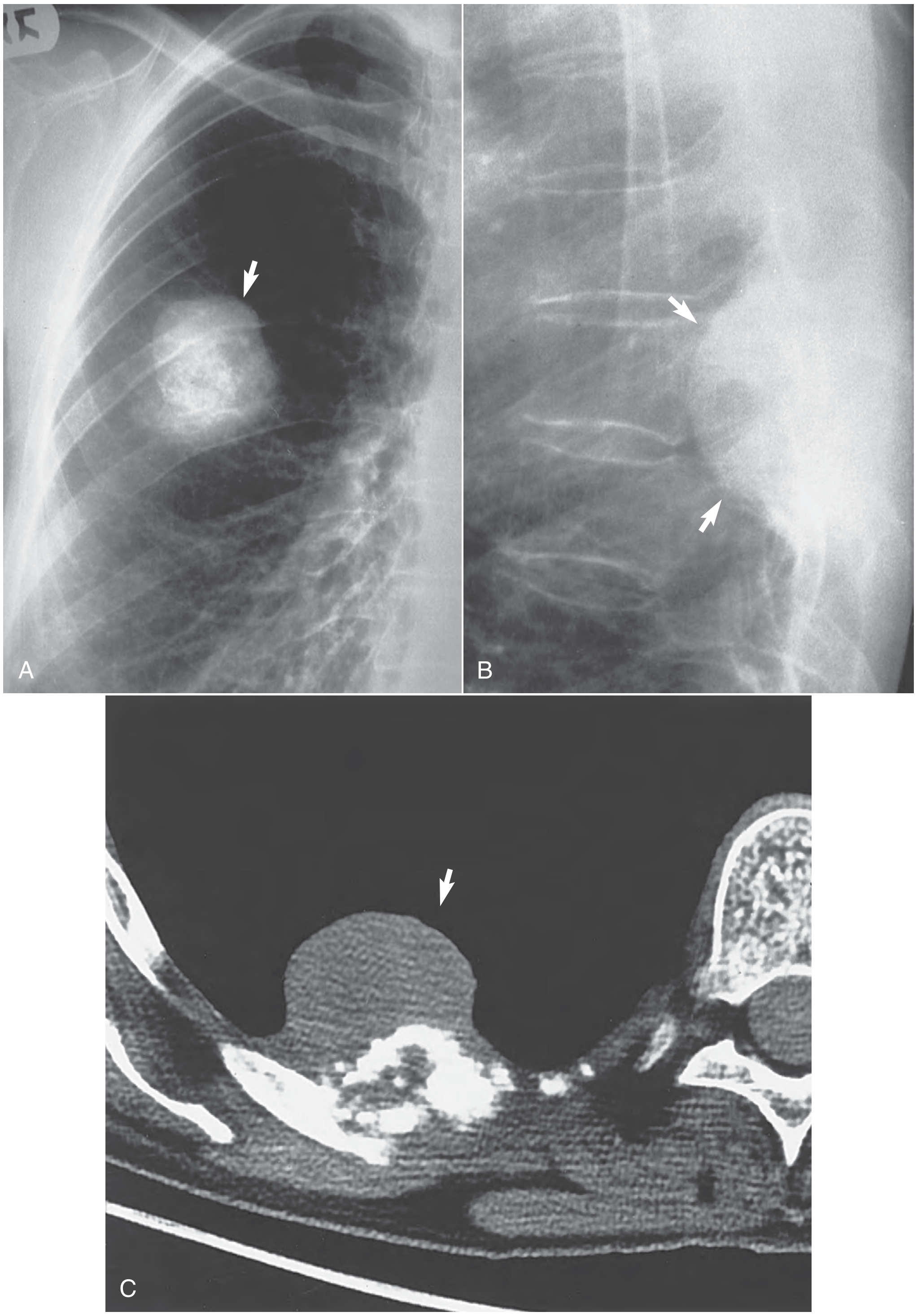

FIGURE 12–31 **Mesenchymal chondrosarcoma.**[52,53] This 51-year-old woman had a 1-month history of right posterior chest wall pain. **A-B,** The posteroanterior **(A)** and lateral **(B)** chest radiographs demonstrate a pleural-based mass in the periphery of the right hemithorax, adjacent to the eighth rib *(arrows)*. **C,** Transaxial CT scan shows a calcified mass arising from the anterior aspect of the posterolateral portion of the right eighth rib *(arrow)*. The lesion was resected and examined, and the histologic diagnosis was mesenchymal chondrosarcoma. Mesenchymal chondrosarcoma is a particularly aggressive form, characterized by a poor prognosis and a greater tendency to metastasize than conventional chondrosarcoma. *(Courtesy G. Greenway, MD, Dallas, Texas.)*

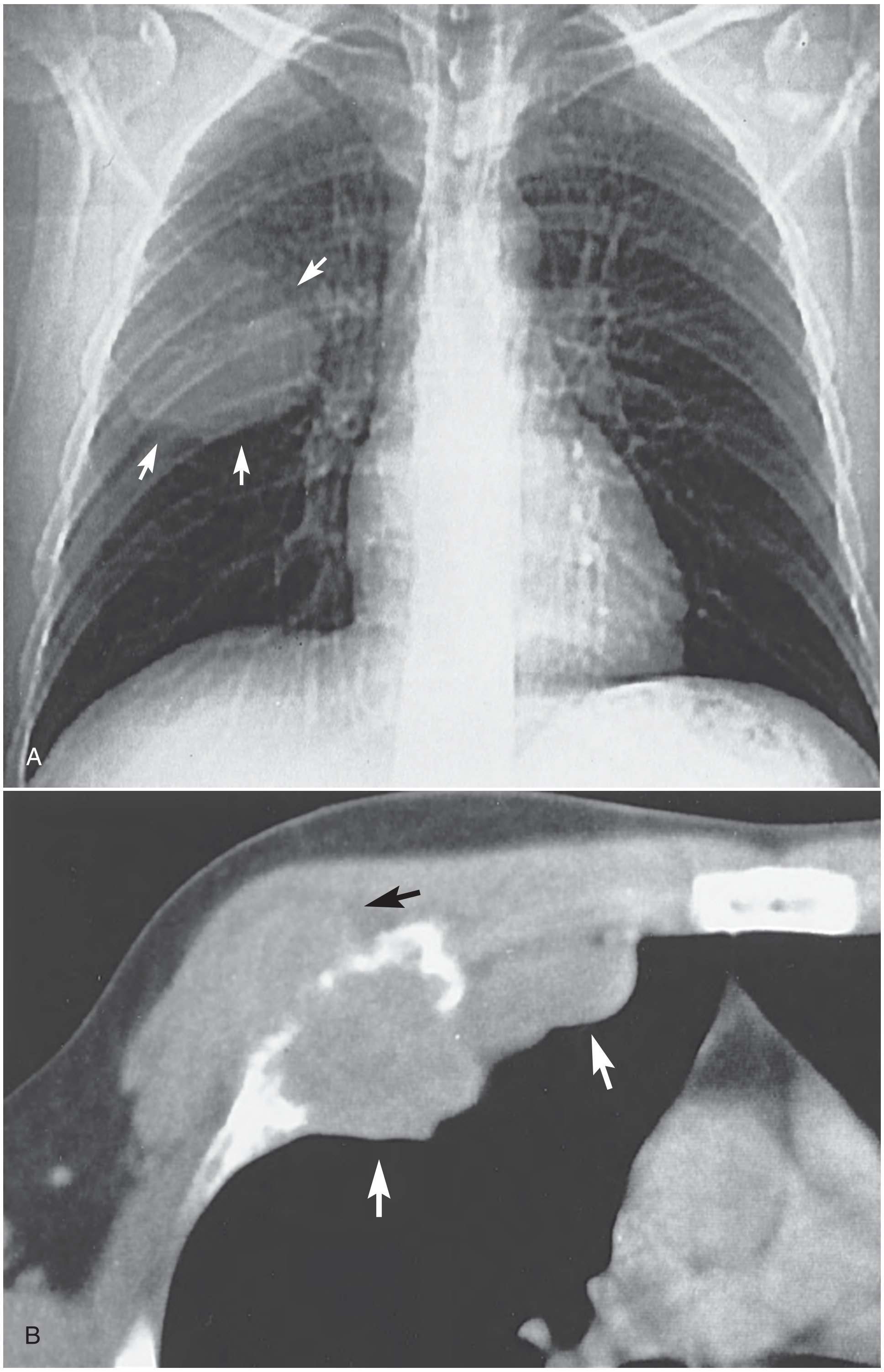

FIGURE 12–32 **Ewing sarcoma.**[54] This 28-year-old male patient had a painless, enlarging right upper chest wall mass. **A,** Frontal CT localizer scan shows a large extrapleural mass overlying the right lung field *(arrows)*. **B,** Transaxial CT scan delineates more clearly the extent and nature of this expansile lesion involving the anterior aspect of the third rib. The lesion, which destroys the bone, is also associated with a large soft tissue mass *(arrows)*. *(Courtesy G. Greenway, MD, Dallas, Texas.)*

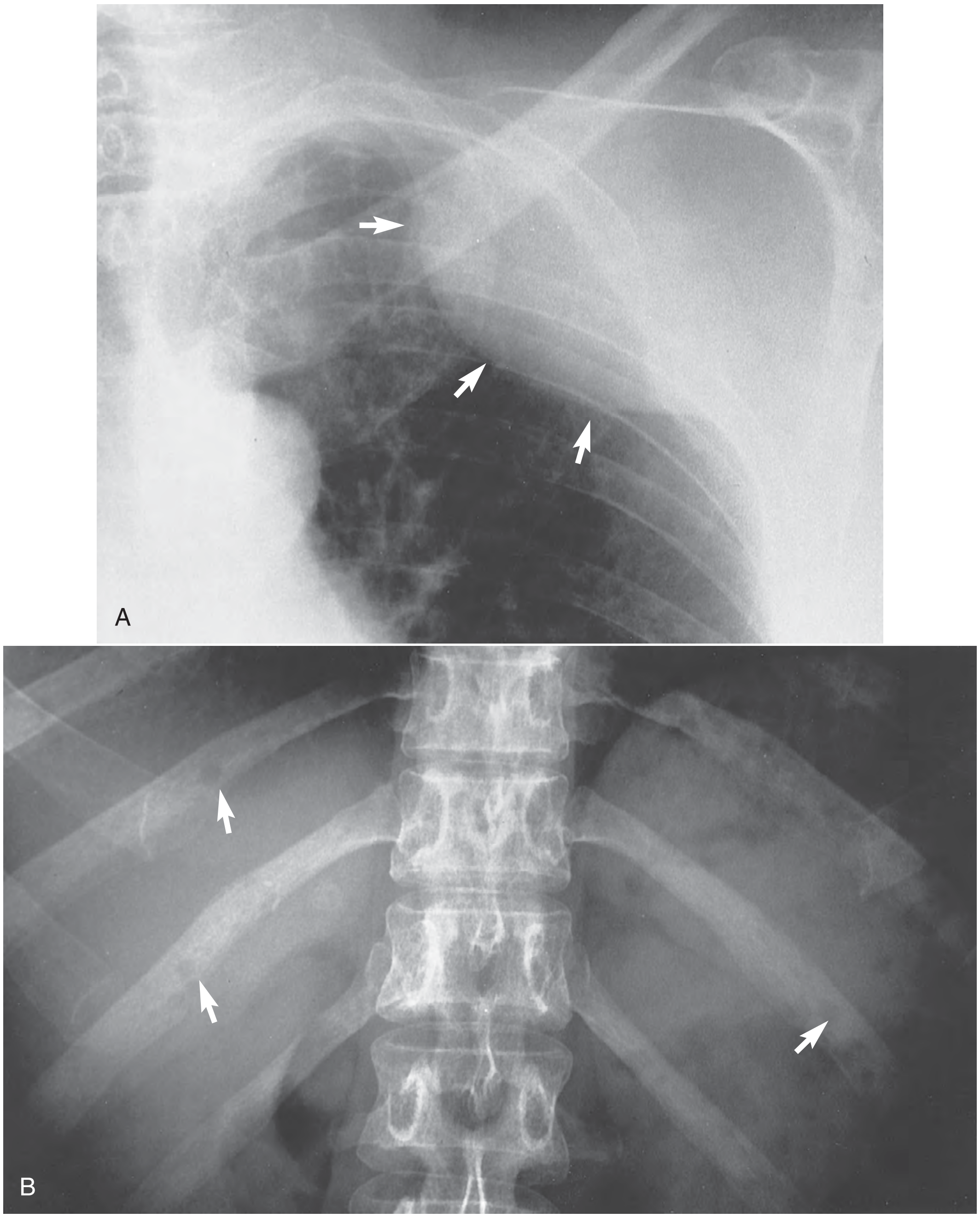

FIGURE 12–33 **Plasma cell myeloma.**[55] Variable presentation in two separate patients. **A,** This patient with multiple myeloma involving the rib exhibits an extrapleural sign documenting the presence of a pleural-based lesion *(arrows)*. **B,** In another patient with myeloma, the radiographic appearance is that of diffuse osteopenia with multiple well-defined, punched-out lesions within the ribs. A few of these lesions are identified by arrows. Some patients with plasma cell myeloma reveal only diffuse osteopenia on radiographs.

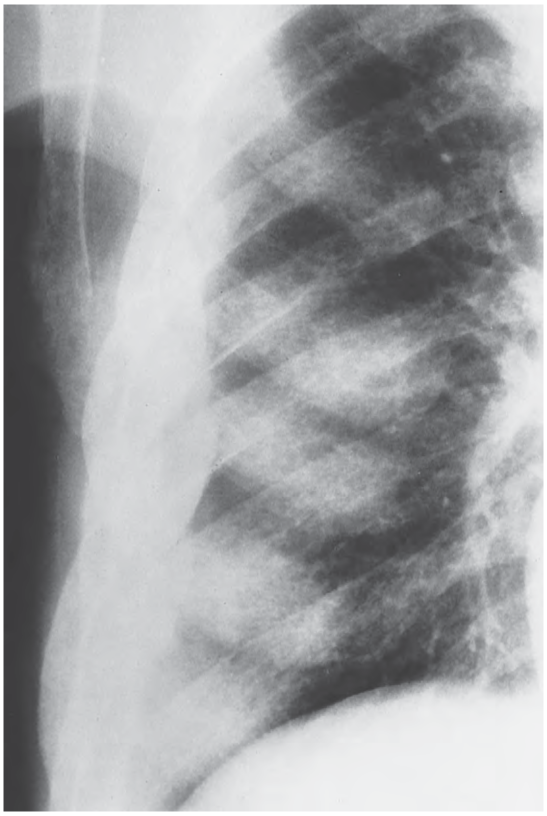

FIGURE 12–34 **Primary non-Hodgkin lymphoma.**[57] Observe the diffuse osteosclerotic, expansile appearance of the ribs in this 58-year-old man with long-standing, untreated primary lymphoma. Similar changes were evident throughout most of the skeleton. *(Courtesy R. Arkless, MD, Seabeck, Wash.)*

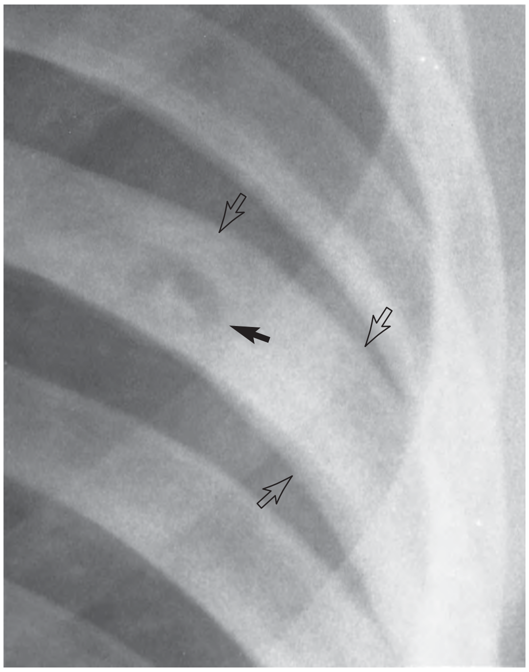

FIGURE 12–35 **Osteoid osteoma.**[59-61] An ovoid radiolucent area *(arrow)* containing a central opaque region is surrounded by bone sclerosis and hypertrophy *(open arrows)* within the rib of this young patient. The radiolucent area represents the nidus of the tumor, and the surrounding hyperostosis is a reactive phenomenon. *(Courtesy A. Brower, MD, Norfolk, Va.)*

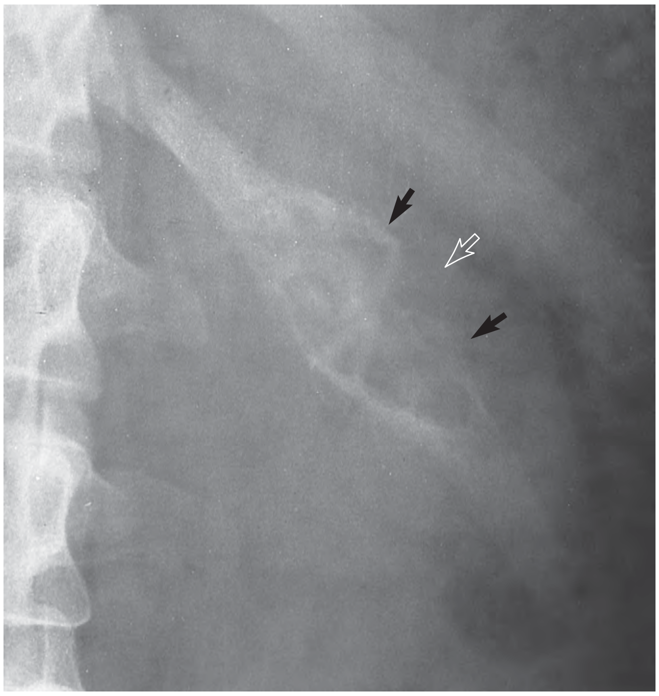

FIGURE 12–36 **Enchondroma.**[53,63] This lesion appears multiloculated *(black arrows),* demonstrates osseous expansion, and possesses a questionable area in which the cortex is difficult to visualize *(open arrow)*. Biopsy confirmed that the lesion was a benign enchondroma. More typically cartilage lesions develop at the costochondral junction.

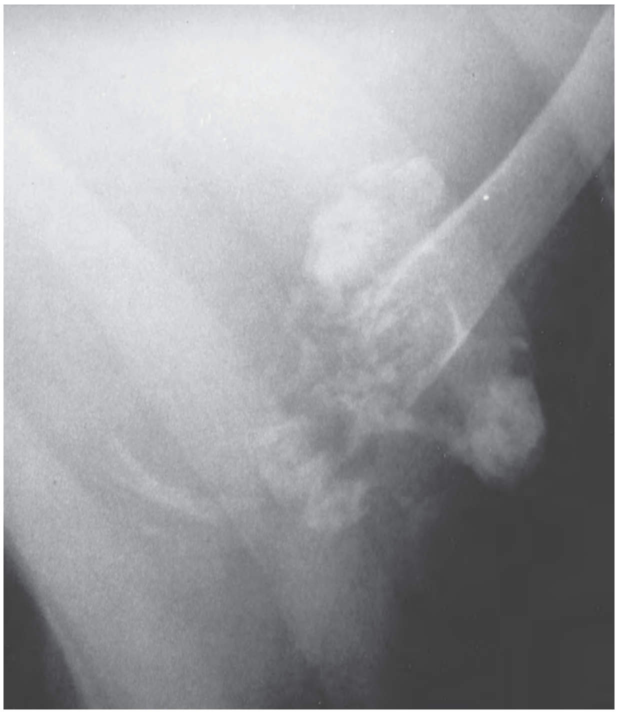

FIGURE 12–37 **Osteochondroma.**[64] A cauliflower-shaped ossified lesion arises from the costochondral junction of the seventh rib. The costochondral region is the most likely site for a rib osteochondroma owing to the presence in this area of normal cartilaginous tissue. *(Courtesy B.L. Harger, DC, Portland, Ore.)*

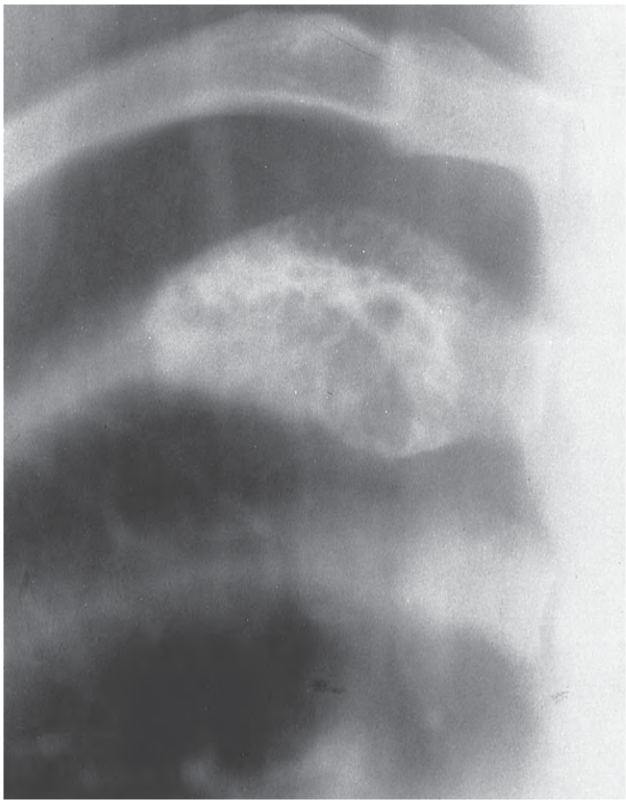

FIGURE 12–38 Hemangioma.[66] Conventional tomogram shows osseous expansion of this striated osteolytic rib lesion. About 9% of all hemangiomas occur in the ribs. Most lesions are asymptomatic.

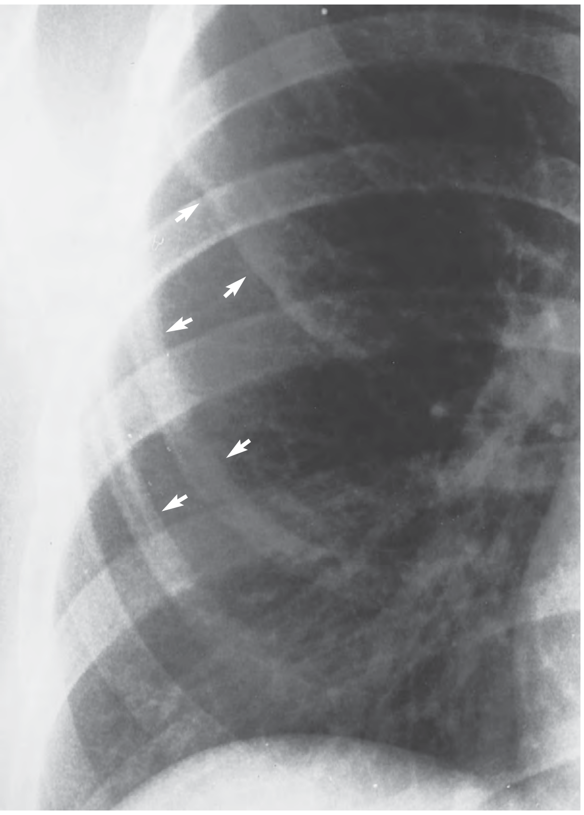

FIGURE 12–40 Neurofibromatosis: rib involvement.[69] In a 20-year-old woman, extensive narrowing and irregularity of the anterior portions of several ribs *(arrows)* are evident. This appearance reflects a generalized mesodermal dysplasia typical of neurofibromatosis. Pressure erosions of the ribs from neurofibromas (not evident in this patient) also may occur. *(Courtesy R. Arkless. MD, Seabeck, Wash.)*

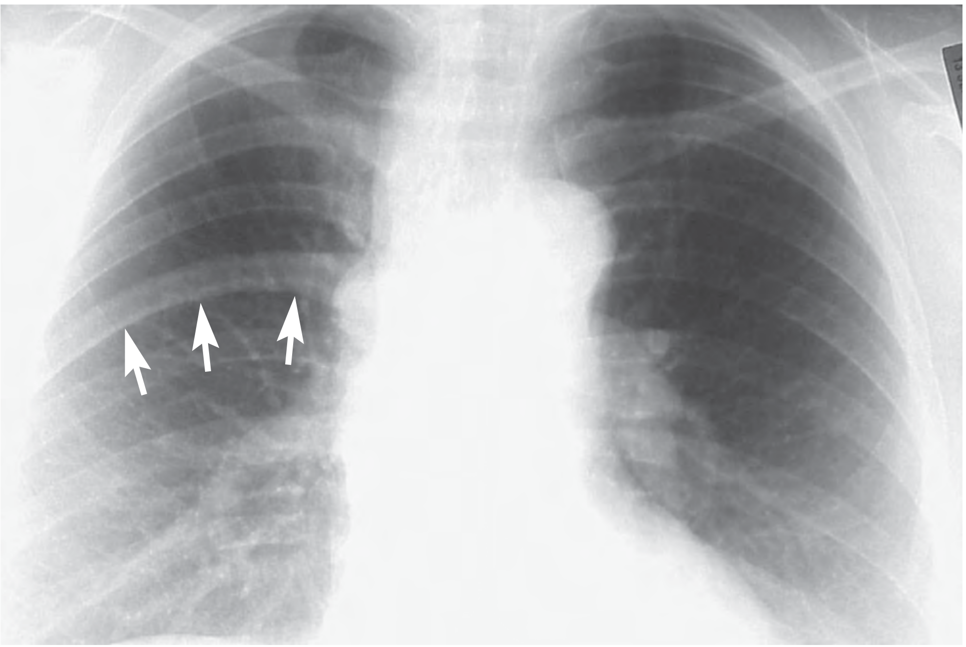

FIGURE 12–39 Paget disease: rib involvement.[68] This 68-year-old man with known polyostotic Paget disease had a routine chest radiograph that revealed a slightly enlarged osteosclerotic right seventh rib *(arrows)*.

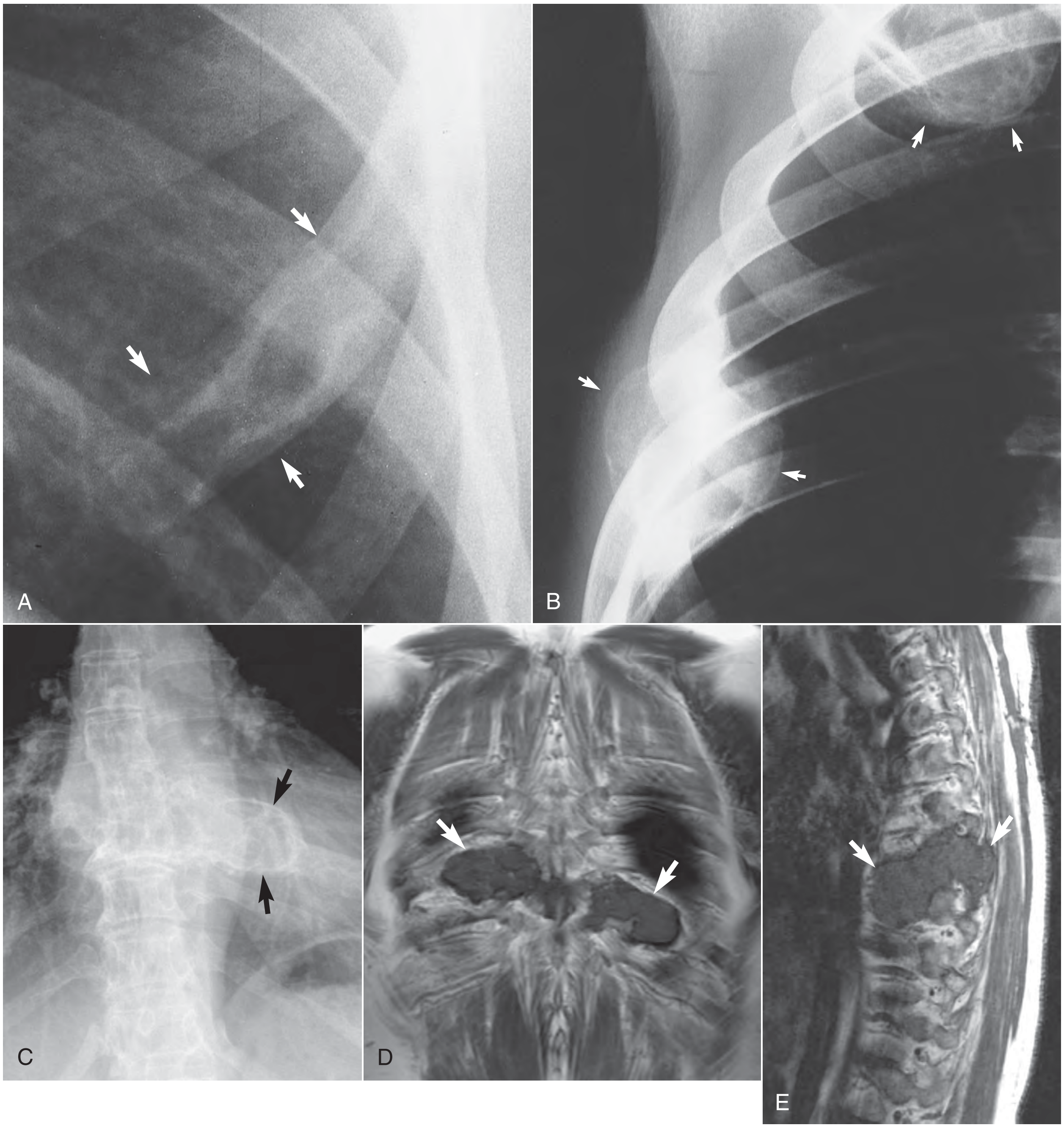

FIGURE 12–41 **Fibrous dysplasia.**[70] **A,** Monostotic form. An undulating sclerotic margin is seen adjacent to this slightly expansile, radiolucent rib lesion *(arrows)*. **B-E** Polyostotic form. **B,** In a second patient, expansile lesions of the first and fifth ribs are seen *(arrows)*. Observe the extrapleural sign associated with each lesion. **C-E,** A radiograph of this 70-year-old woman with longstanding polyostotic fibrous dysplasia depicts a large expansile lesion involving a lower left rib *(arrows)* and the spine **(C).** Coronal **(D)** and sagittal **(E)** T1-weighted MR images show low signal intensity expansile lesions involving the ribs bilaterally *(arrows)*.

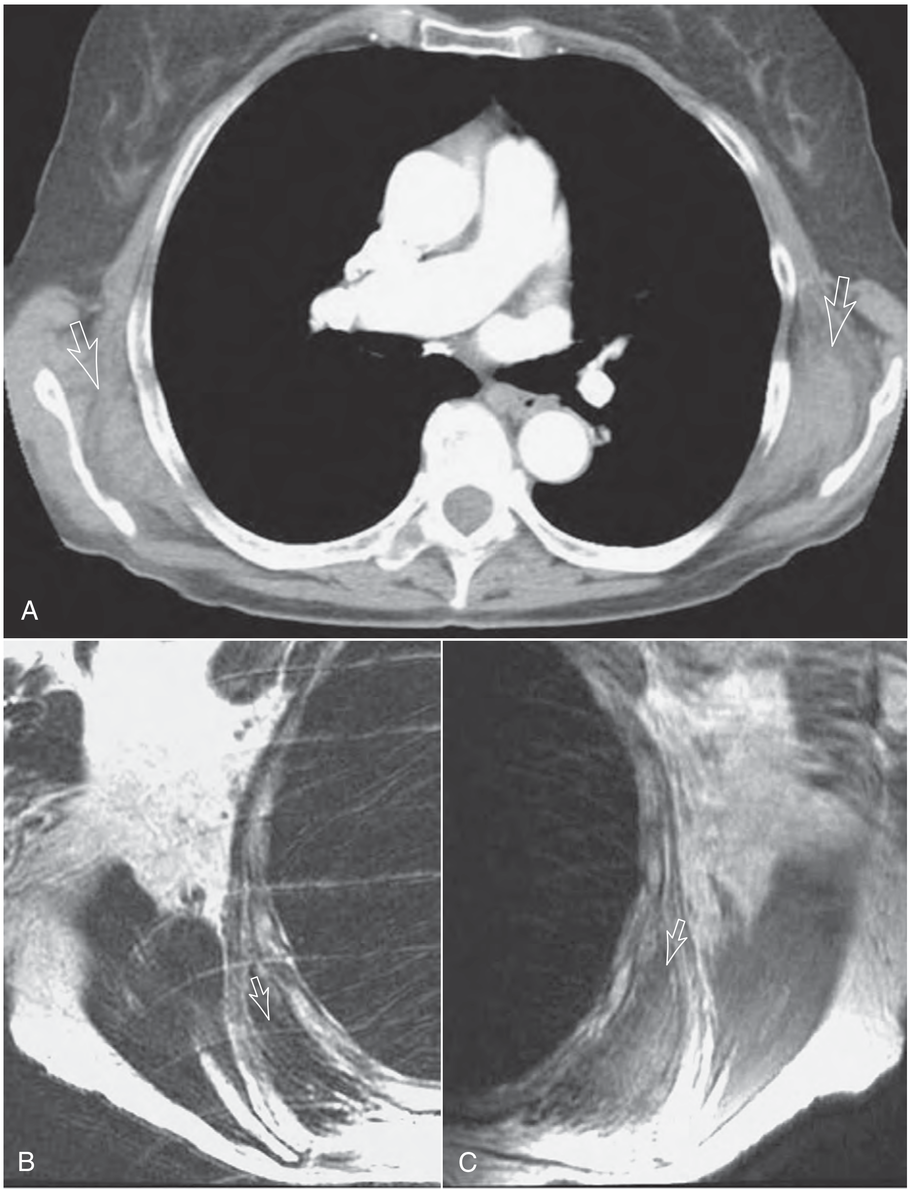

FIGURE 12–42 **Elastofibroma: chest wall involvement.**[96] This 76-year-old woman was examined for enlarging bilateral masses on her upper back. A transverse CT scan obtained after intravenous contrast **(A)** shows bilateral masses between the scapulae and chest wall *(open arrows)*. With contrast enhancement, the masses are essentially the same density as skeletal muscle. **B-C,** Bilateral transaxial T1-weighted MR images reveal that the masses *(open arrows)* are well defined, that they have the same signal intensity as muscle, and that there is no invasion of adjacent tissues.

TABLE 12-8 Metabolic, Hematologic, and Infectious Disorders Affecting the Ribs and Sternum*

Entity	Figure(s)	Characteristics
Generalized osteoporosis[72]	12-17	Uniform decrease in radiodensity, thinning of cortices, frequently results in insufficiency fractures of the ribs and, less frequently, the sternum Acute rib fractures may occur with minimal trauma in osteoporotic patients
Osteogenesis imperfecta[73]	12-43	Osteoporosis and bone fragility Thin, gracile appearance of ribs with pectus carinatum Severe rib deformities and multiple fractures common
Osteomalacia[74,86]	12-44	Diffuse osteopenia *Liberty Bell chest:* Bone softening results in a bell-shaped deformity of the thoracic cage Decreased trabeculae; remaining trabeculae appear prominent and coarsened *Looser zones (pseudofractures):* transverse fractures of ribs
Rickets[74,86]	12-45	*Rachitic rosary:* bulbous appearance of ribs adjacent to costochondral junction resulting from metaphyseal widening Osteopenia with rib fractures
Hyperparathyroidism and renal osteodystrophy[75]	12-46	*Brown tumor:* solitary or multiple expansile osteolytic lesions containing fibrous tissue and giant cells; may disappear after treatment for hyperparathyroidism Subperiosteal resorption may result in rib notching or erosion Osteosclerosis more common in renal osteodystrophy
Hemodialysis treatment[76,77]	12-47	Diffuse osteopenia and spontaneous rib fractures Amyloidosis of sternoclavicular joints
Thalassemia[78]	12-48	Marrow hyperplasia within ribs produces an expansile appearance of the proximal ends of the ribs adjacent to the costovertebral joints
Acromegaly[3]		Elongation of the inferior body of the rib with marginal sclerosis Widening of anterior costal end of rib and dentate costal cartilage interface
Myelofibrosis[79]		Diffuse osteosclerosis of bones of thoracic cage Occasional periosteal bone apposition or periostitis, osteolysis, or osteopenia
Infantile cortical hyperostosis (Caffey disease)[80]		Uncommon disease of infancy Cortical hyperostosis of the ribs in a monostotic, unilateral, or diffuse pattern Predilection for the lateral arches of the ribs Osseous bridging of ribs may occur with healing Pleural effusions ipsilateral to the side of involvement are common
Osteomyelitis[81,87,88]		Acute pyogenic osteomyelitis frequently involves the bones about the sternoclavicular region in intravenous drug abusers Sternal infections may occur after median sternotomy for open heart surgery Typical organisms in chest wall infections include staphylococcus, pseudomonas, actinomyces, aspergillus, coccidioides, brucella, mycobacterium *Atypical organisms: Rochalimaea* (*Bartonella) henselae* from cat scratch disease may result in osteomyelitis of a rib
Chronic recurrent multifocal osteomyelitis (CRMO)[82]	12-49	Occurs mainly in children and adolescents Involves the bones of the anterior chest wall and clavicle Initial lytic destruction of metaphysis adjacent to growth plate with no periosteal bone formation or sequestration Closely related to the SAPHO (synovitis, acne, pustulosis, hyperostosis, and osteitis) syndrome (Table 12-6)

* See also Tables 1-15 to 1-19.

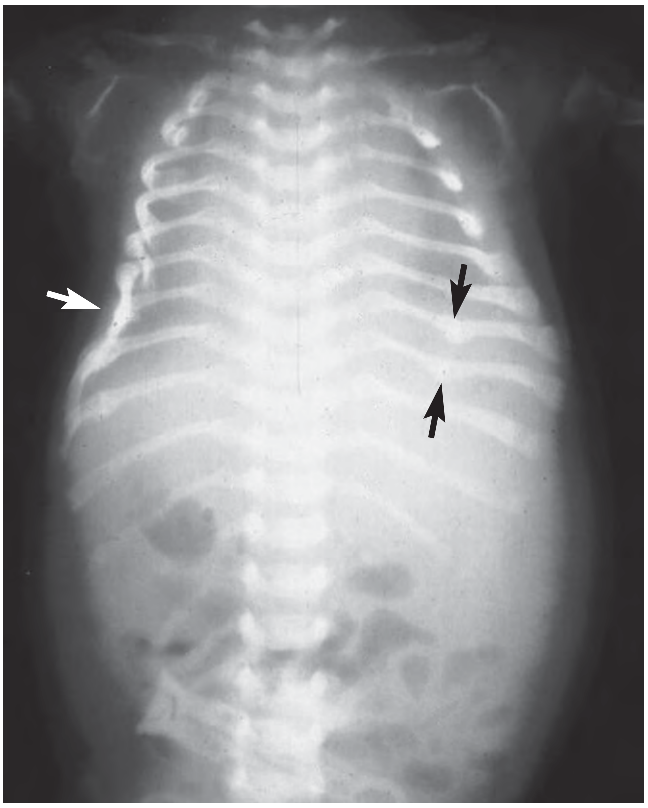

FIGURE 12–43 **Osteogenesis imperfecta.**[73] A frontal radiograph of the torso in this newborn shows many fractures *(arrows)* in the thin and gracile ribs. Patients with osteogenesis imperfecta have osteoporosis with abnormal skeletal fragility, blue sclerae, dentinogenesis imperfecta, and premature otosclerosis; presence of any two of these abnormalities confirms the diagnosis. Several different types and genetic mutations have been identified.

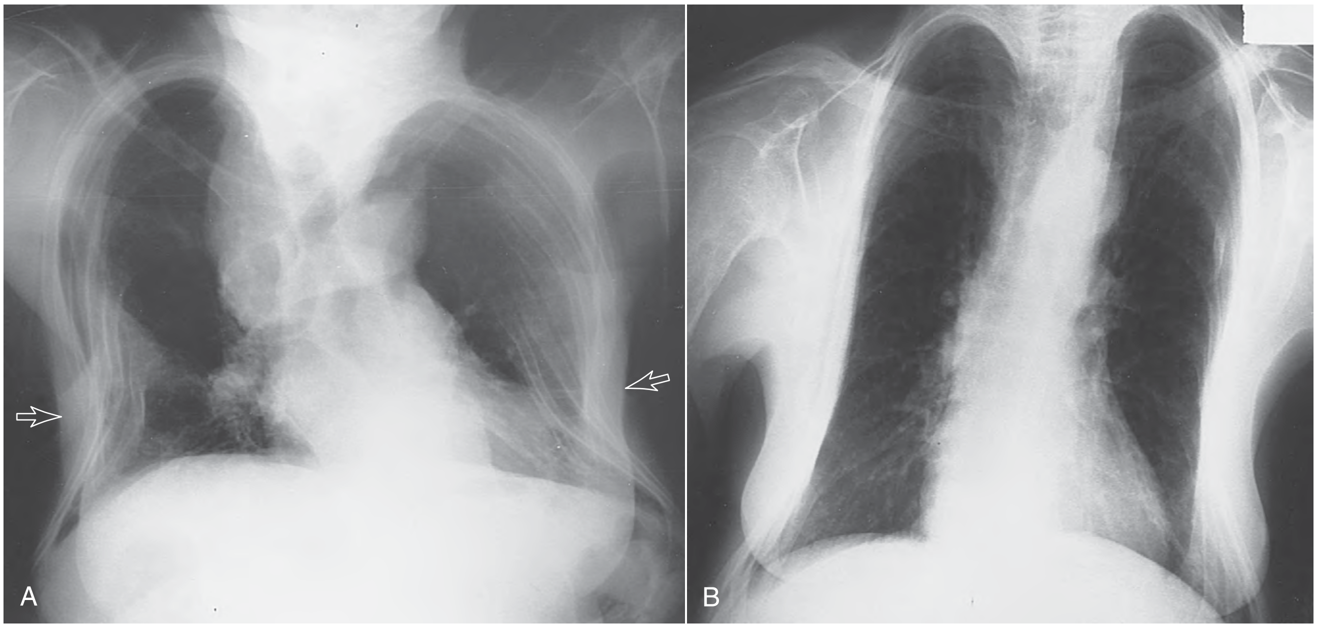

FIGURE 12–44 **Osteomalacia.**[74,86] **A,** Bone softening in this patient with osteomalacia secondary to gluten enteropathy has resulted in multiple rib deformities. The bilateral central indentation of the thoracic cage *(open arrows)* has been termed the *Liberty Bell* chest. Note also the diffuse osteopenia throughout the skeleton. **B,** In this 60-year-old woman with osteomalacia and hyperparathyroidism, similar findings are evident.

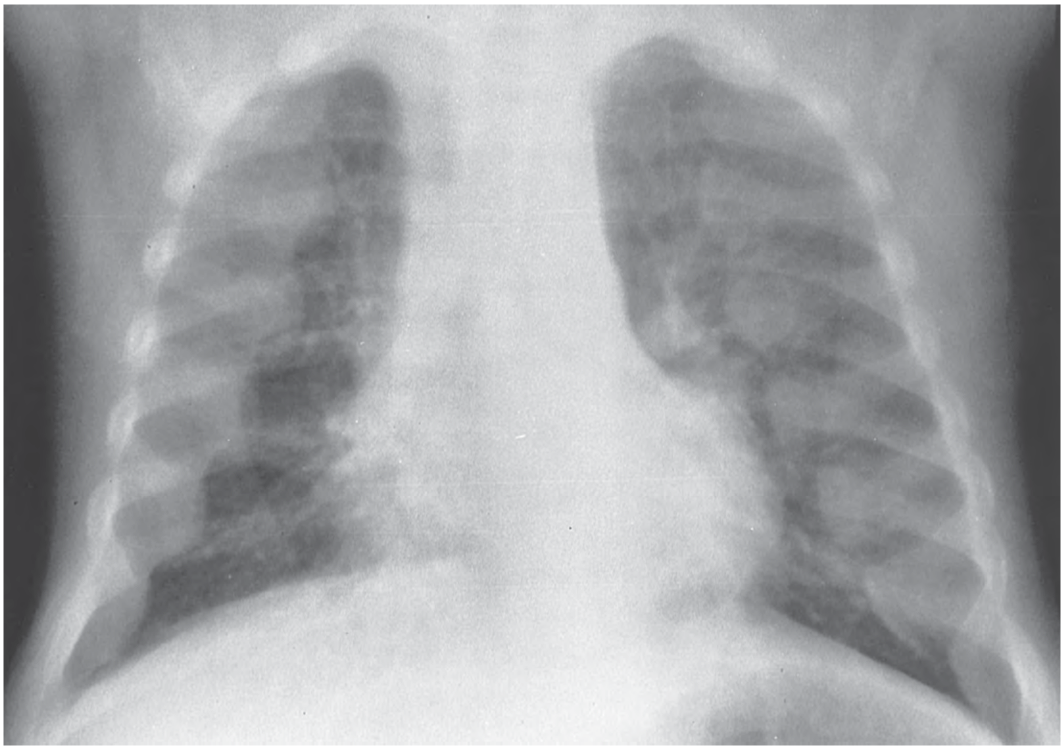

FIGURE 12–45 **Rickets: rachitic rosary.**[74,86] Bulbous expansion of the anterior aspect of the ribs at the costochondral junctions, the so-called *rachitic rosary*, is a classic finding in children with advanced rickets.

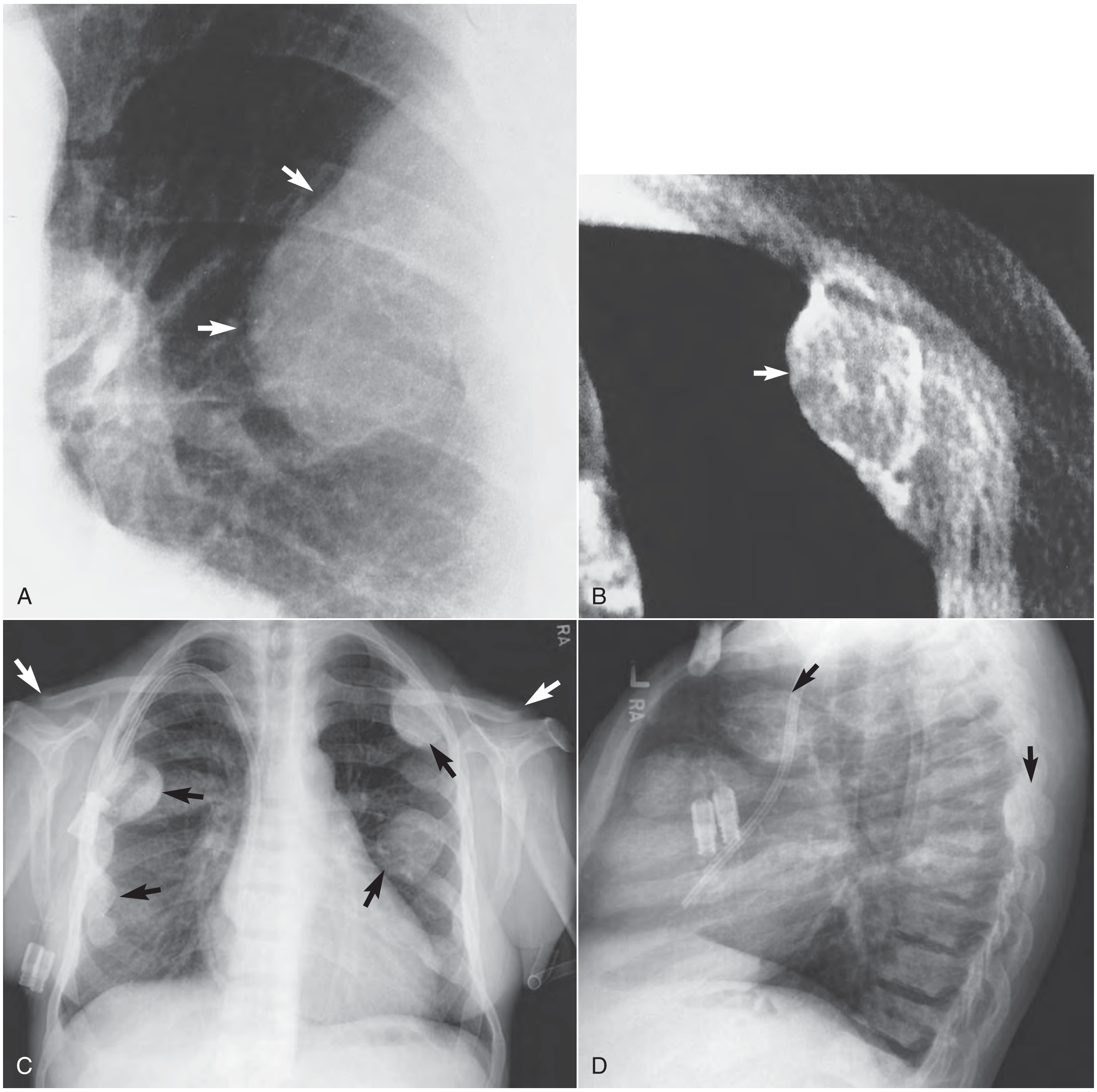

FIGURE 12–46 **Hyperparathyroidism: Brown tumors.**[75] Routine radiograph **(A)** and a transaxial CT scan **(B)** in a patient with primary hyperparathyroidism demonstrate a large expansile mass in the rib that causes an extrapleural sign *(arrows)*. The CT scan displays the lesion to best advantage. **C-D,** Chest radiographs in another patient, a 30-year-old woman with hyperparathyroidism, who has a tunneled right internal jugular double lumen dialysis catheter in situ, reveal multiple large expansile rib lesions that proved to be brown tumors *(black arrows)*. Subchondral resorption of the ends of the clavicles *(white arrows)* is also a complication of hyperparathyroidism. The rugger-jersey spine appearance is visible within the vertebral bodies in **D.**

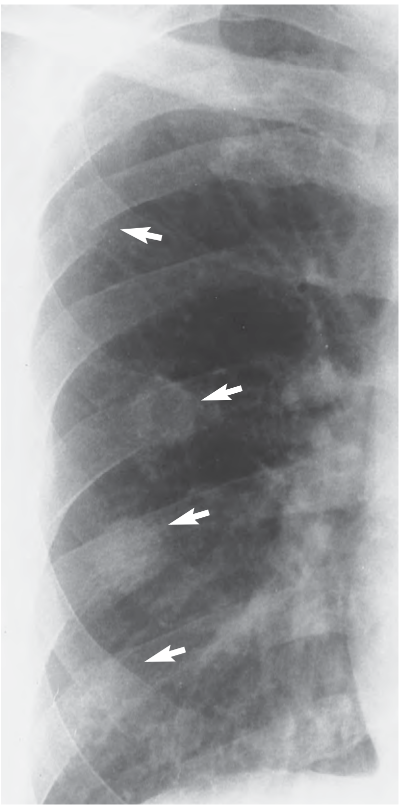

FIGURE 12–47 Hemodialysis treatment: spontaneous fractures.[76,77] Radiograph of this patient on long-term hemodialysis therapy for chronic renal failure demonstrates diffuse osteopenia and multiple healing rib fractures *(arrows)*. The ribs are the most frequent site of spontaneous fractures in a hemodialysis patient whose condition is poorly managed.

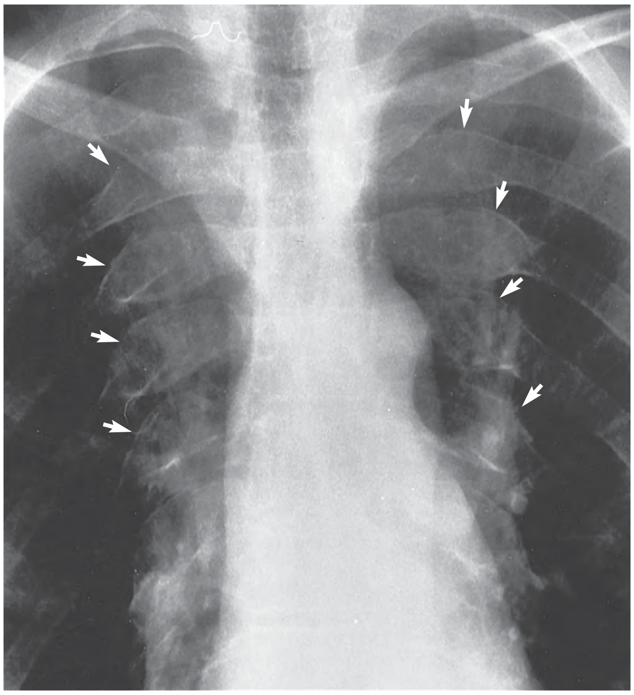

FIGURE 12–48 Thalassemia major.[78] Extensive expansion of the posterior aspect of the ribs *(arrows)* is seen as a manifestation of marrow hyperplasia in this 27-year-old man with thalassemia major.

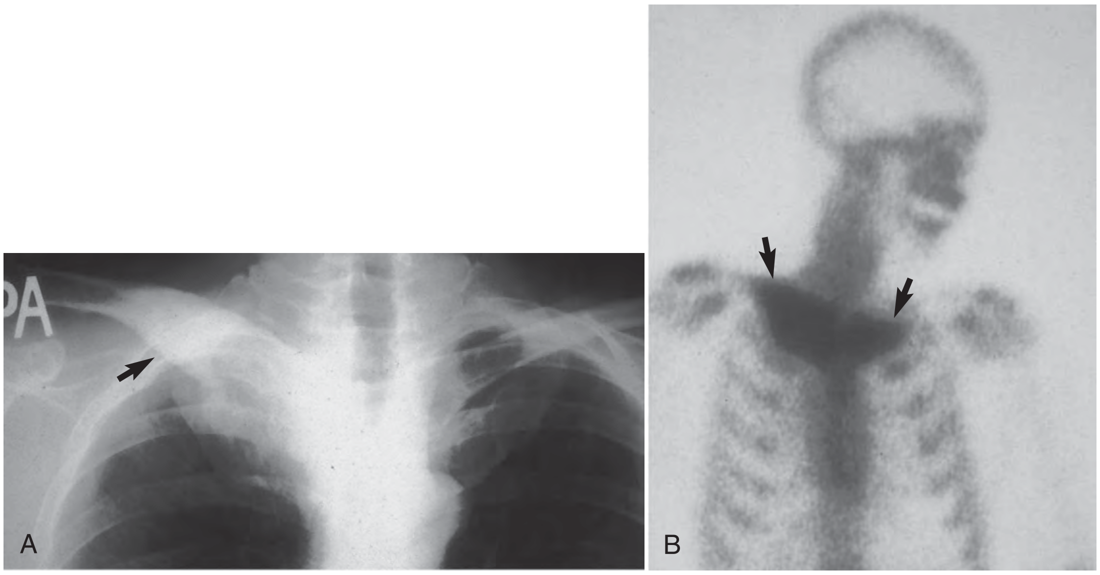

FIGURE 12–49 Chronic recurrent multifocal osteomyelitis.[82] A close-up of a frontal radiograph **(A)** shows extreme sclerosis and enlargement of the medial portion of the right clavicle *(arrows)*. The bone scan **(B)** reveals intense uptake of radiopharmaceutical in the right and left clavicle and sternoclavicular joints *(arrows)*.

CHAPTER 13

Clavicle, Scapula, and Shoulder

NORMAL DEVELOPMENTAL ANATOMY

Accurate interpretation of radiographs of the pediatric shoulder requires a thorough understanding of normal developmental anatomy. Table 13-1 outlines the age of appearance and fusion of the primary and secondary ossification centers. Figures 13-1 and 13-2 demonstrate the radiographic appearance of many important ossification centers and other developmental landmarks at selected ages from birth to skeletal maturity.

DEVELOPMENTAL ANOMALIES, ANATOMIC VARIANTS, AND SOURCES OF DIAGNOSTIC ERROR

The shoulder is a frequent site of anomalies, anatomic variations, and other sources of diagnostic error that may simulate disease and potentially result in misdiagnosis. Table 13-2 and Figures 13-3 to 13-13 represent selected examples of some of the more common processes affecting the clavicle, the scapula, and the proximal portion of the humerus.

SKELETAL DYSPLASIAS AND OTHER CONGENITAL DISEASES

The bones and joints about the shoulder are frequent sites of skeletal dysplasias and other congenital diseases. Table 13-3 lists some of the more frequently occurring conditions, and Figures 13-14 and 13-16 illustrate two examples of dysplasia.

PHYSICAL INJURY

Physical injury to the shoulder region results in a wide variety of fractures of the clavicle, the scapula, and the proximal portion of the humerus. Additionally, dislocations of the glenohumeral joint and the acromioclavicular joint are frequently encountered. Table 13-4 lists the most common types of fractures, and Table 13-5 outlines the various types of shoulder dislocation. Several examples of these injuries are illustrated in Figures 13-17 to 13-28. Injuries of the sternoclavicular joint are discussed in Chapter 12, and fractures of the humeral diaphysis are discussed and illustrated in Chapter 14.

INTERNAL JOINT DERANGEMENTS AND OTHER SOFT TISSUE INJURIES

The shoulder is second only to the knee in frequency of internal joint derangements. Common abnormalities of tendons, ligaments, joint capsules, labral structures, and other miscellaneous traumatic soft tissue disorders are listed in Table 13-6. Table 13-7 describes the main features of the complex topic of shoulder impingement syndromes. Figures 13-29 to 13-39 illustrate several examples of the conditions discussed in Tables 13-6 and 13-7.

ARTICULAR DISORDERS

The glenohumeral, acromioclavicular, and coracoclavicular joints are frequent target sites of involvement for many degenerative, inflammatory, crystal-induced, and infectious articular disorders. Table 13-8 outlines these diseases and their characteristics. Figures 13-40 to 13-57 illustrate the typical imaging manifestations of the most common articular disorders affecting the shoulder.

NEOPLASMS

The clavicle and the scapula are infrequent sites of involvement for benign, malignant, and tumorlike lesions of bone. Table 13-9 describes the range of such neoplasms, many of which are illustrated in Figures 13-58 to 13-67.

METABOLIC, HEMATOLOGIC, AND INFECTIOUS DISORDERS

Several metabolic, hematologic, and infectious disorders affect the bones and soft tissue structures about the shoulder region. Table 13-10 lists some of the more common disorders and discusses their characteristics. Figures 13-68 to 13-73 illustrate the typical imaging findings of many of these disorders.

MISCELLANEOUS DISORDERS RESULTING IN CLAVICULAR OSTEOSCLEROSIS, PERIOSTITIS, OR BONE ENLARGEMENT

Table 13-11 describes a variety of conditions that result in osteosclerosis, periostitis, or bone enlargement of the clavicle. Figures 13-74 to 13-77 illustrate some of the more common examples.

TABLE 13-1 **Shoulder: Approximate Age of Appearance and Fusion of Ossification Centers[1-4] (Figures 13-1 and 13-2)**

Ossification Center	Primary or Secondary	No. of Centers (Per Bone)	Age of Appearance* (Years)	Age of Fusion* (Years)	Comments
Clavicle					
Shaft	P	1	Birth		
Proximal epiphysis	S	1	16-20	22-25	Fuses with shaft
Scapula					
Body	P	1	Birth		
Coracoid process	S	1	Birth to 1	16-19	Fuses with body
Coracoid tip epiphysis	S	2	15-19	20-24	Fuses with coracoid process
Subcoracoid epiphysis	S	1	10	20-24	Fuses with coracoid process
Margin of glenoid	S	1	14-19	20-24	Fuses with body
Border and angle epiphyses	S	2	15-17	20-24	Fuses with body
Acromion process	S	2	14-17	19-22	Fuses with body
Proximal Portion of Humerus			**Months**		
Humeral head epiphysis	S	1	Birth to 1	4-6	Fuses with greater tuberosity
Greater tuberosity	S	1	3-27	4-6	Fuses with humeral head
Lesser tuberosity	S	1	3-27	20-23	Fuses with humeral head
Humeral metaphysis				20-23	Head and tuberosity fuse to metaphyses

P, Primary; *S,* secondary.

* Ages of appearance and fusion of ossification centers in girls typically precede those of boys. Ethnic differences also exist.

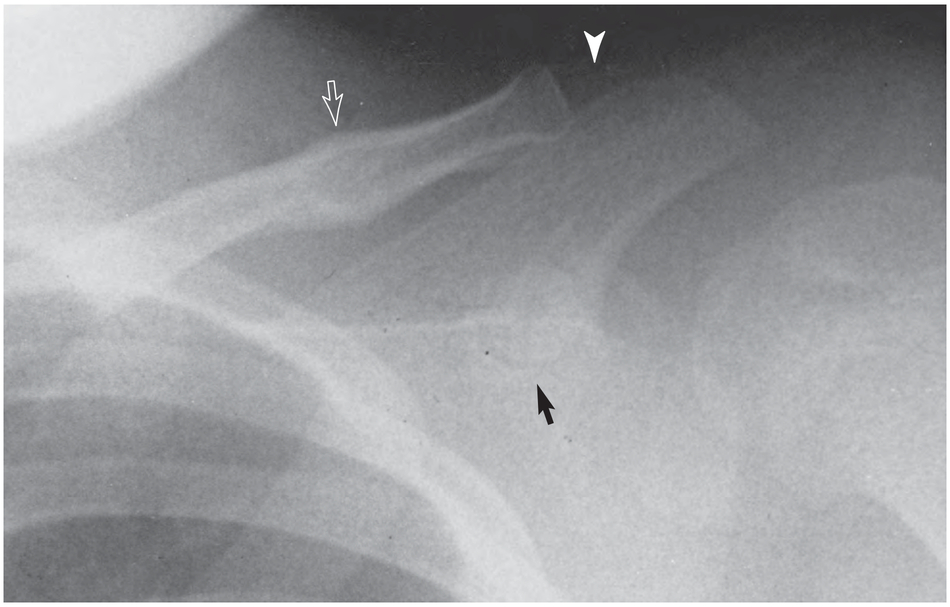

FIGURE 13–1 **Skeletal maturation and normal development: clavicle, young child.**[1-4] Frontal projection of the clavicle in this 2-year-old girl shows a normal expansion at the junction of the middle and distal thirds of the clavicle *(open arrow)* that is the result of its curved contour. Note the unfused ossification center of the coracoid process *(arrow)* and the wide acromioclavicular articulation *(arrowhead)*. The clavicle is the first bone of the body to ossify during fetal life. It ossifies from membrane with cartilage growth at the ends. An epiphyseal ossification center appears at the medial end of the clavicle between the ages of 16 and 20 years. The appearance of the clavicle is dependent on its position and, as a result, may appear bowed or twisted.

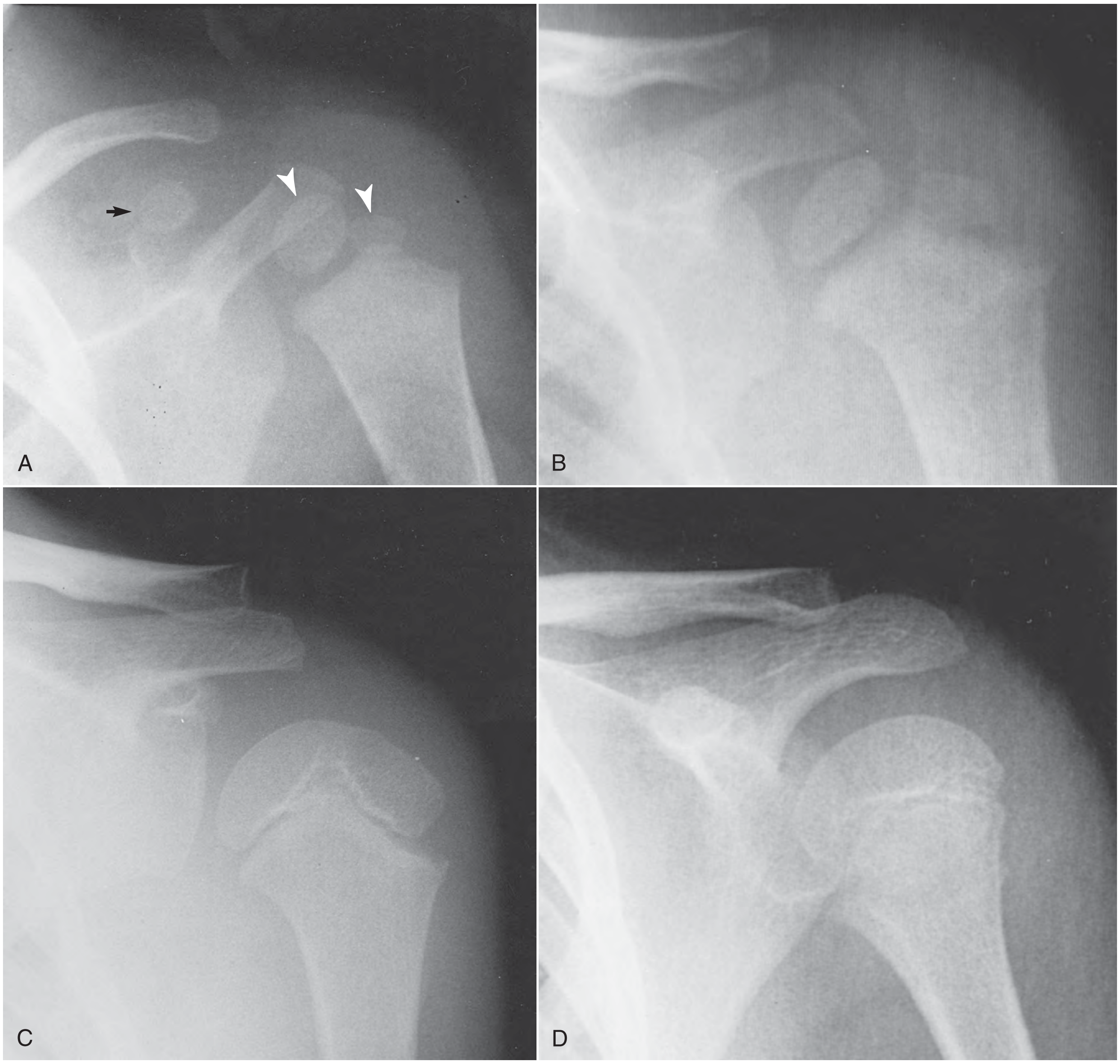

FIGURE 13–2 Skeletal maturation and normal development: shoulder.[1-4] **A,** A 16-month-old girl. Observe the paired proximal humeral capital epiphyses *(arrowheads)* and the adjacent radiodense area of the zone of provisional calcification. The secondary ossification center of the coracoid process is evident *(arrow)* and has not yet fused to the scapula. The acromioclavicular joint is characteristically wide. **B,** A 2-year-old boy. The humeral capital epiphyses are larger, and the zone of provisional calcification in the humeral metaphysis remains radiodense. **C,** A 5-year-old girl. The paired humeral capital epiphyses have fused together and conform to the chevron-shaped humeral metaphysis. **D,** An 8-year-old girl. The humeral capital epiphysis is now the same width as the adjacent metaphysis. The acromioclavicular joint remains wide.

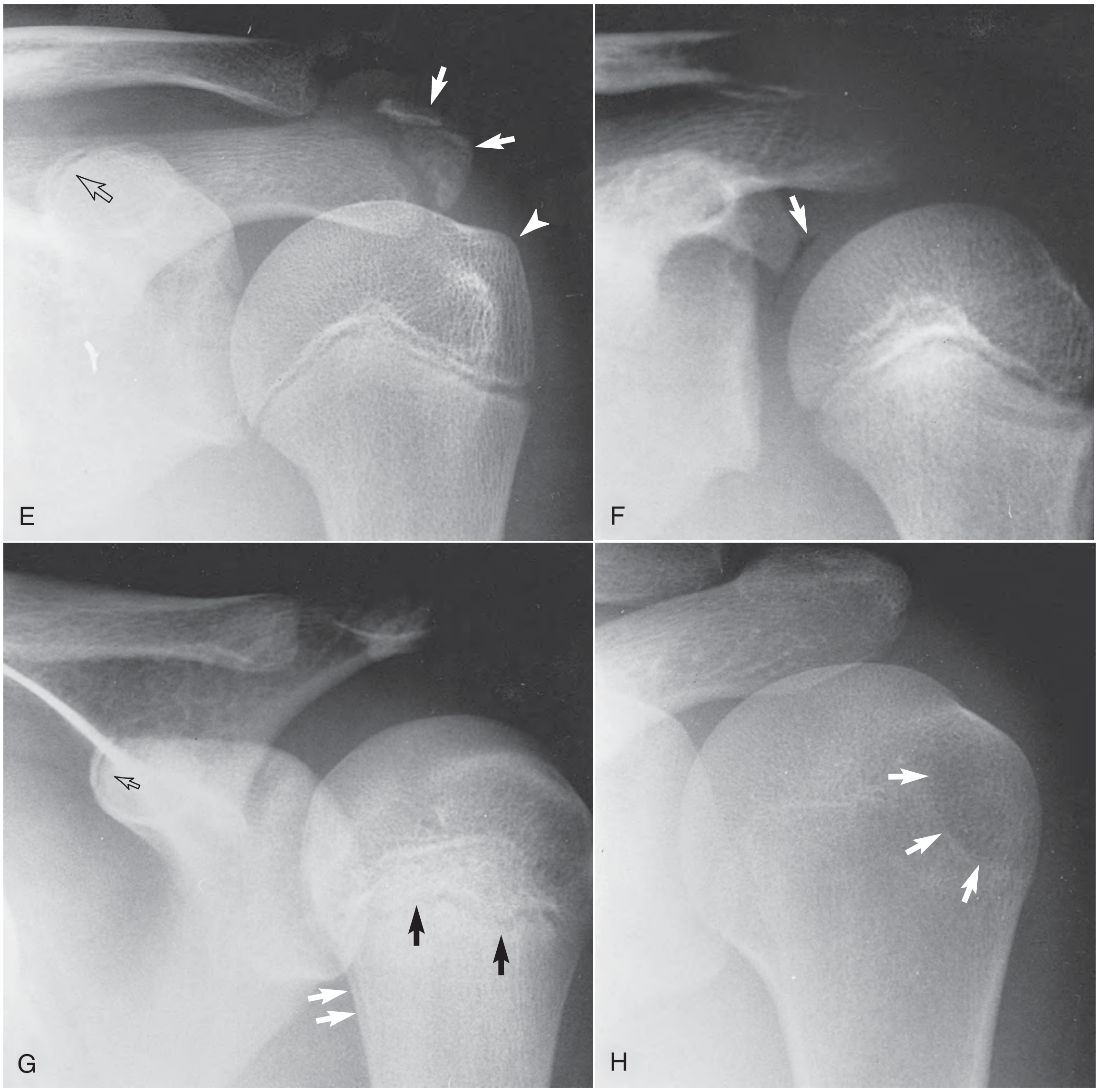

FIGURE 13–2, cont'd **E,** A 12-year-old girl. Secondary ossification centers for the acromion *(arrows)* and coracoid *(open arrow)* processes are apparent. The greater tuberosity is now distinctly visible *(arrowhead)*. **F,** A 12-year-old boy. A normal physiologic intraarticular vacuum phenomenon *(arrow)* is present, outlining the articular cartilage of the humeral head. **G,** A 14-year-old boy. On this internal rotation radiograph, the physeal line of the humeral capital epiphysis is seen as an irregular transverse line *(black arrows)* just before closure. This should not be confused with a fracture. The greater tuberosity forms a superimposed arc of radiodensity overlying the humeral head. A secondary ossification center is present at the coracoid process *(open arrow)*. Unusual projection of the cortex simulates periostitis of the humeral metaphysis *(white arrows)*. **H,** A 16-year-old girl. This radiograph reveals normal adult proportions and closure of all ossification centers. A small, normal humeral pseudocyst is present within the greater tuberosity *(arrows)*. The acromioclavicular joint is of normal adult width.

TABLE 13-2 Developmental Anomalies, Anatomic Variants, and Sources of Diagnostic Error Affecting the Shoulder

Entity	Figure(s)	Characteristics
Clavicle		
Fork deformity of the medial end of clavicle[5]	13-3	In young people, the medial articular surface of the clavicle appears fork-shaped before completion of development May persist into adulthood in otherwise normal persons and should not be mistaken for a disease process
Ununited ossification centers[5]	13-4	Ossification centers of the medial ends of the clavicles may persist into adulthood and simulate fractures
Rhomboid fossa[5,6]	13-5	Scalloped undersurface of the medial aspect of the clavicles at the attachment of the rhomboid ligament between the clavicle and first rib Often bilateral but not always symmetric Normal anatomic variant that may simulate destructive lesion of the clavicle or a cavitating lesion of the lung apex
Congenital pseudarthrosis[7]	13-6	Congenital pseudarthrosis affects the right clavicle almost exclusively; bilateral in 10% of cases; left side involvement frequently associated with dextrocardia Pseudarthrosis may occur as an isolated phenomenon or in association with neurofibromatosis and fibrous dysplasia
Clavicular companion shadow[8]	13-7	Normal radiodense area paralleling the superior aspect of the clavicle represents the normal soft tissue shadows, such as the platysma muscle, adjacent to the clavicle Should not be mistaken for an apical lung lesion, periostitis, or subperiosteal hemorrhage
Clavicle duplication[147]		*Extremely rare anomaly:* only six cases of duplicated clavicle have been reported (one with triplication of the coracoid process)
Coracoclavicular joint[9]	13-8	Anomalous osseous flange arising from the undersurface of the clavicle that articulates with the coracoid process Normal variant in the region of the coracoclavicular ligament; usually of no clinical significance Infrequently painful after trauma; surgical resection may relieve the pain Heterotopic ossification of coracoclavicular ligaments after acromioclavicular dislocation may simulate a coracoclavicular joint
Scapula		
Sprengel deformity[6,10]	13-9	Developmental anomaly involving elevation of the scapula Present in approximately 25% of patients with the Klippel-Feil syndrome May also be seen as an isolated anomaly
Omovertebral bone[6,10]	13-9	Anomalous bone, cartilage, or fibrous tissue extending from the superior angle of the scapula to the spinous process, lamina, or transverse process of the C5 or C6 vertebra Present in 30% to 40% of patients with Sprengel deformity
Hypoplasia of the glenoid neck[11,164]	13-10	Also termed *scapular dysplasia* and *dentated glenoid anomaly* *Findings:* scapular neck hypoplasia, notched articular surface of the glenoid cavity, and widening of the inferior aspect of the glenohumeral articular surface Usually bilateral and relatively symmetric Family history of similar abnormalities observed in some cases Many patients have pain and limited shoulder motion Approximately 25% have multidirectional glenohumeral instability
Ununited ossification centers[5]		Failure of ossification of several secondary ossification centers occurs about the acromion (os acromiale), coracoid process, glenoid, and inferior angle of the scapula (infrascapular bone)

TABLE 13-2 Developmental Anomalies, Anatomic Variants, and Sources of Diagnostic Error Affecting the Shoulder—cont'd

Entity	Figure(s)	Characteristics
Os acromiale[12,13,149]	13-11	Ossification center of the tip of the acromion usually fuses with the acromion before the person reaches 25 years of age; persists into adulthood in as many as 8% of persons Triangular shape; may simulate fracture May be associated with pain and an increased prevalence of external shoulder impingement syndrome and rotator cuff tears
Scapular duplication[155]		Extremely rare anomaly Usually associated with additional malformations
Prominent vascular channel[5]	13-12	Vascular channels within the wing of the scapula may be prominent and resemble fractures—often parallel the scapular spine
Proximal Portion of Humerus		
Humeral pseudocyst[14]	13-2, *H* 13-13	Zone of diminished trabeculae within the spongiosa bone of the greater tubercle of the humerus May simulate destructive neoplasm such as chondroblastoma

See also Table 1-1.

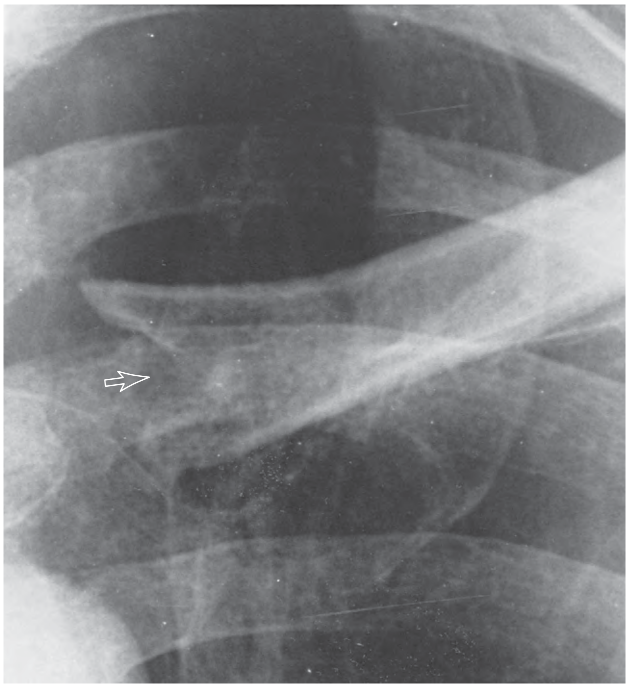

FIGURE 13–3 Fork deformity of the medial end of the clavicle.[5] In young people, the medial articular surface of the clavicle appears fork-shaped before completion of development. This appearance *(open arrow)* may persist into adulthood in otherwise normal persons and should not be mistaken for osseous destruction or other pathologic condition.

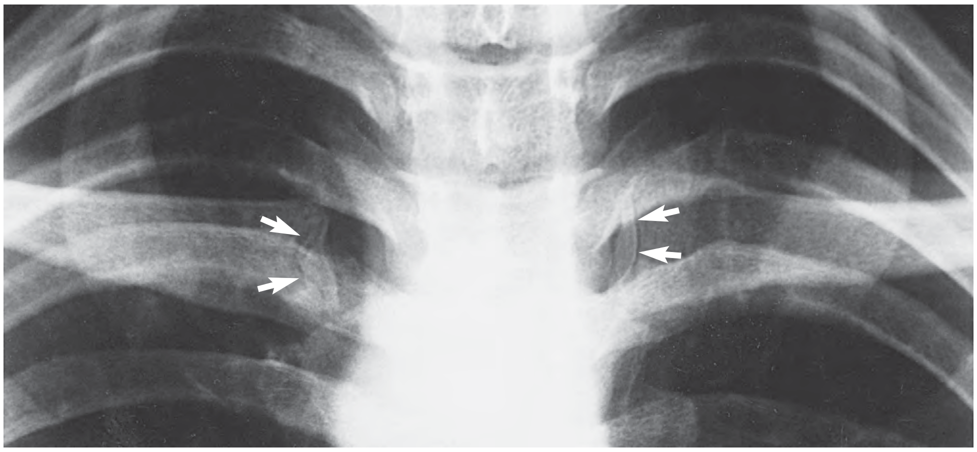

FIGURE 13–4 **Ununited ossification centers.**[5] Observe the failure of ossification of the secondary ossification centers of the medial ends of the clavicles *(arrows)* in this 30-year-old man. This ossification center typically begins to ossify between the ages of 16 and 20 years and fuses between the ages of 22 and 25 years.

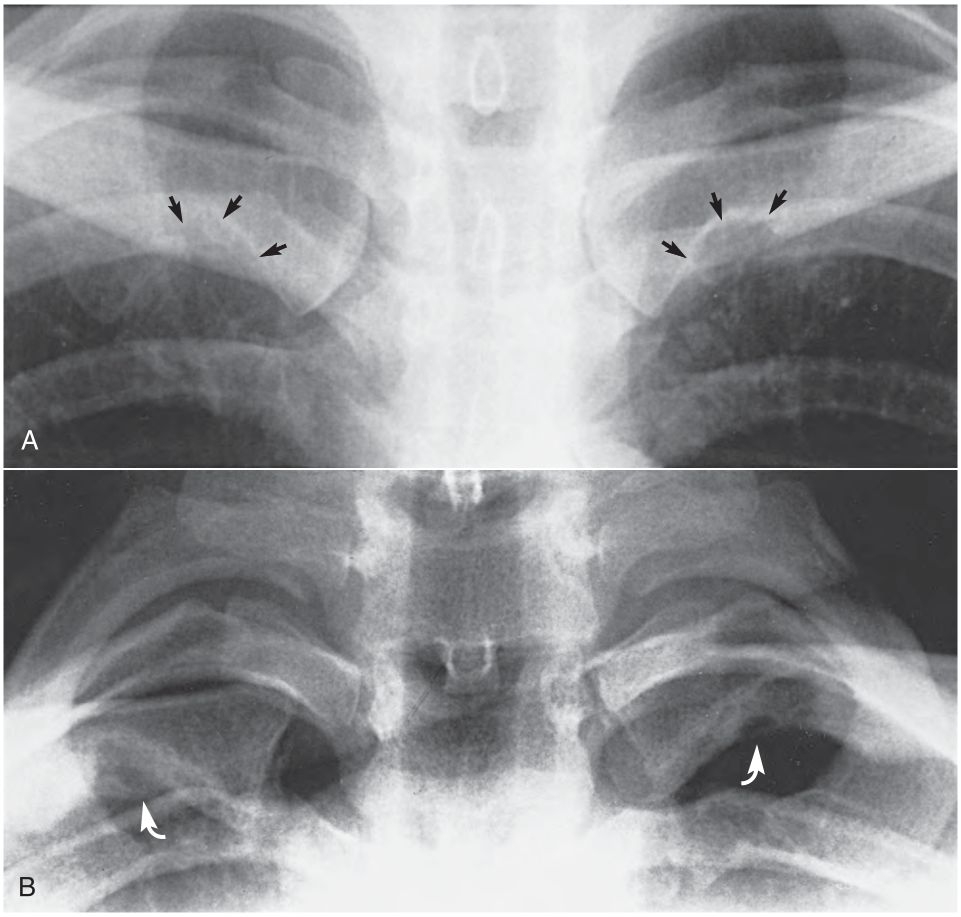

FIGURE 13–5 **Rhomboid fossae.**[5,6] **A,** Note the scalloped appearance of the undersurface of the medial aspect of both clavicles *(arrows)*. **B,** Another bilateral example in a 16-year-old boy *(curved arrows)*. Rhomboid fossae are normal anatomic variants that may simulate destructive lesions of the clavicle or cavitating lesions of the lung apex.

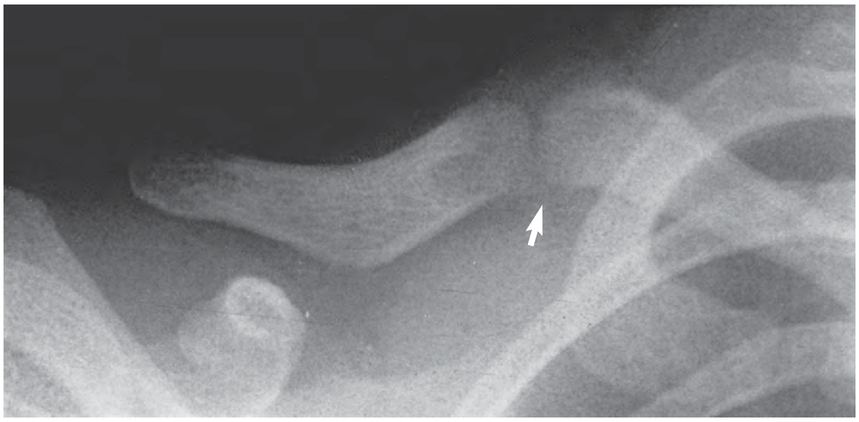

FIGURE 13–6 **Congenital pseudarthrosis of the clavicle.**[7] Observe the radiolucent defect in the middiaphysis of the clavicle in this infant *(arrow)*. Callus formation is absent, and the bone edges adjacent to the pseudarthrosis are rounded. *(Courtesy A. D' Abreu, MD, Porto Alegre, Brazil.)*

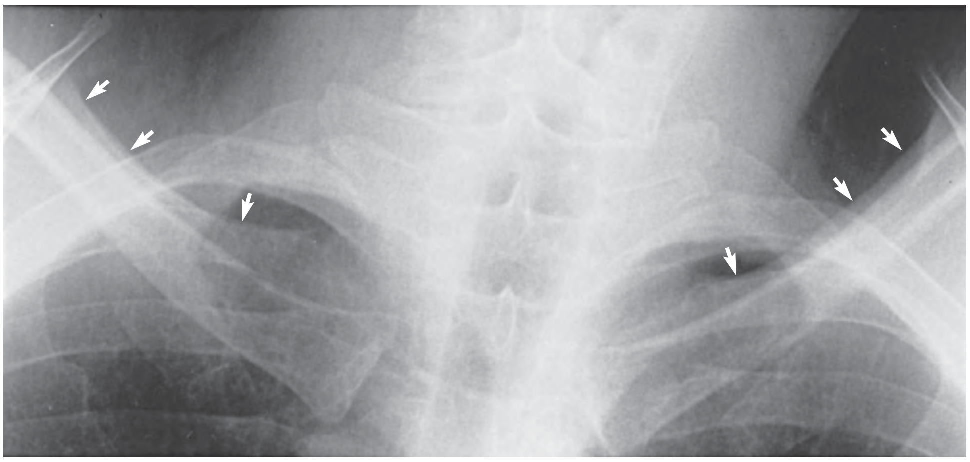

FIGURE 13–7 **Clavicular companion shadow.**[8] Observe the normal radiodense shadow paralleling the superior aspect of the clavicle *(arrows)*. This finding represents the normal subcutaneous soft tissues adjacent to the clavicle and should not be mistaken for an apical lung lesion, periostitis, or subperiosteal hemorrhage.

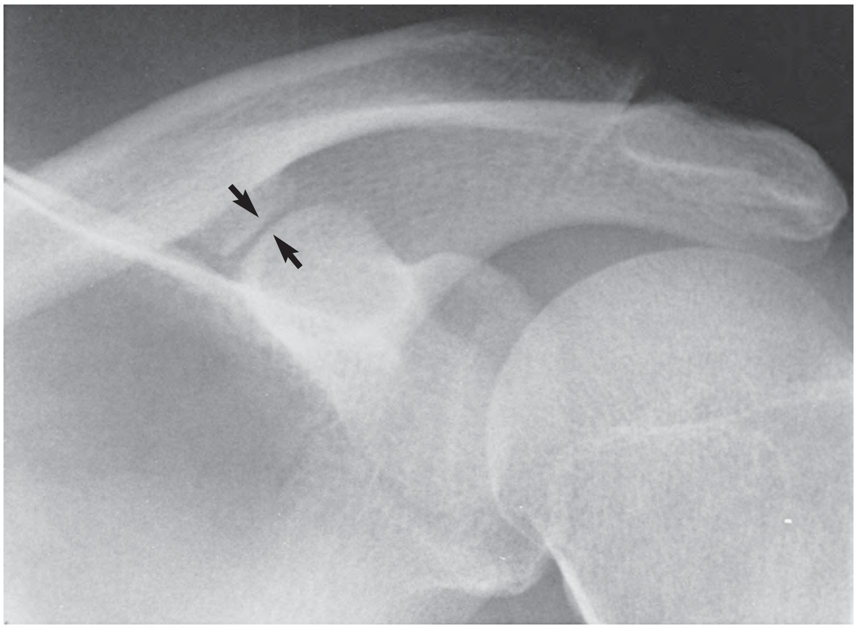

FIGURE 13–8 **Coracoclavicular joint.**[9] An anomalous osseous flange arising from the undersurface of the clavicle articulates with the coracoid process *(arrows)*. This normal variant in the region of the coracoclavicular ligament is usually of no clinical significance.

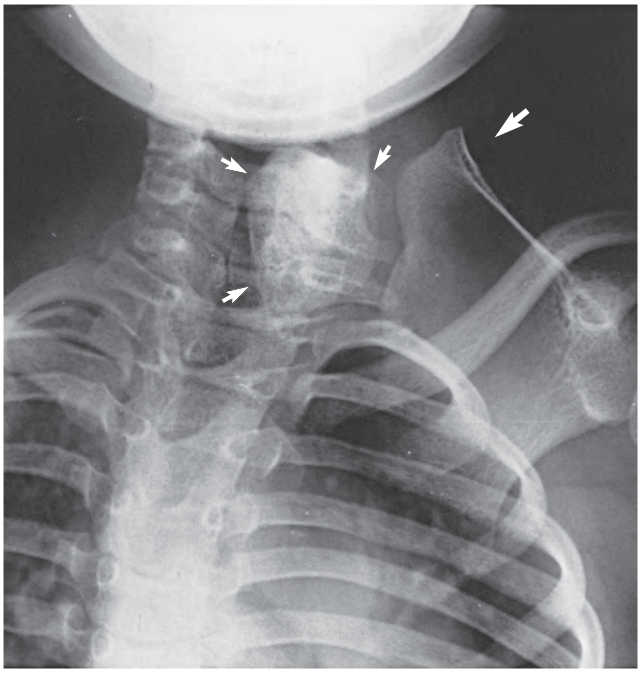

FIGURE 13–9 **Sprengel deformity and omovertebral bone: Klippel-Feil syndrome.**[6,10] Observe the elevation of the scapula (Sprengel deformity) *(large arrow),* omovertebral bone *(small arrows),* and multiple other cervical spine anomalies in this patient with Klippel-Feil syndrome. Sprengel deformity is present in about 25% of patients with Klippel-Feil syndrome.

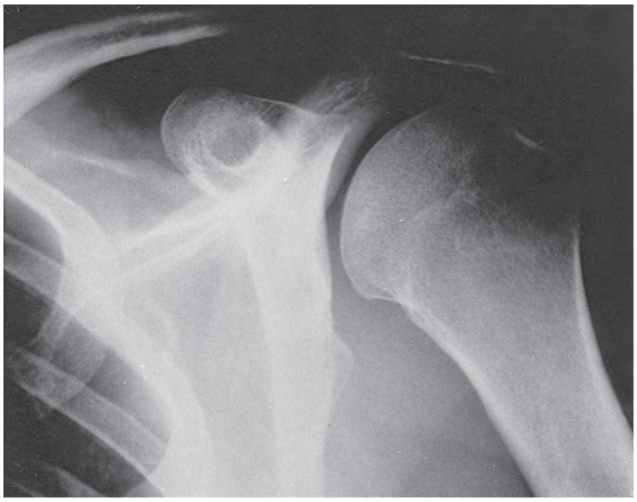

FIGURE 13–10 **Glenoid hypoplasia (scapular dysplasia).**[11,164] This patient exhibits typical findings, including scapular neck hypoplasia, notched articular surface of the glenoid, and widening of the inferior articular surface. *(Courtesy A. Brower, MD, Norfolk, Va.)*

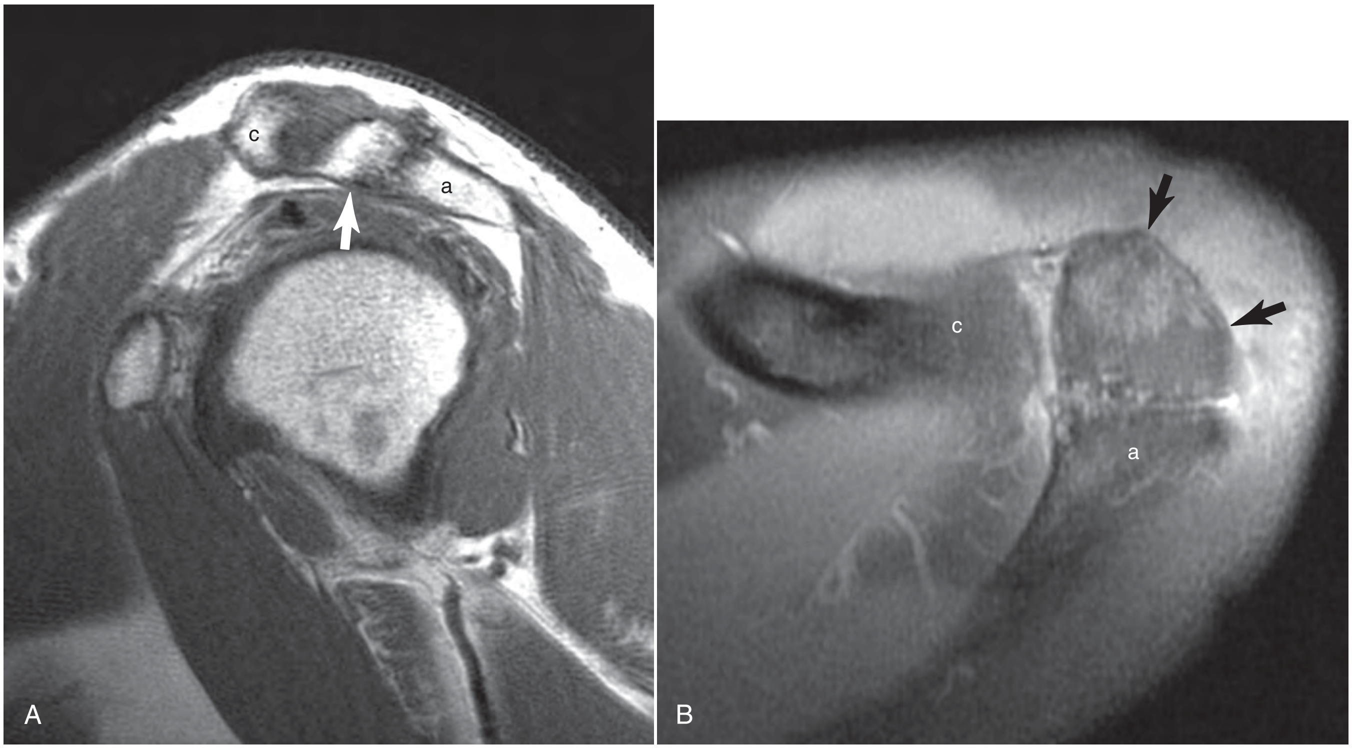

FIGURE 13–11 **Os acromiale.**[12,13,149] A 54-year-old man. **A,** A sagittal T1-weighted MR image shows an accessory ossicle of bone *(arrow)* between the clavicle (c) and acromion (a). **B,** Axial T1-weighted MR image reveals the triangular configuration of the os acromiale *(arrows)* and its smooth articulation with the clavicle (c) and somewhat irregular articulation with the acromion (a).

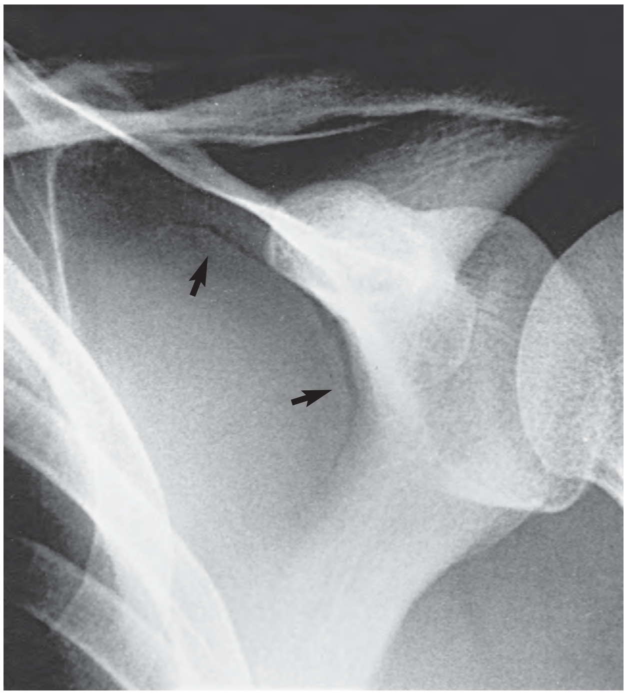

FIGURE 13–12 **Prominent vascular channel.**[5] A curvilinear radiolucent vascular groove in the wing of the scapula is seen *(arrows)*. Such vascular grooves may simulate fractures. *(Courtesy L. E. Hoffman, DC, Portland, Ore.)*

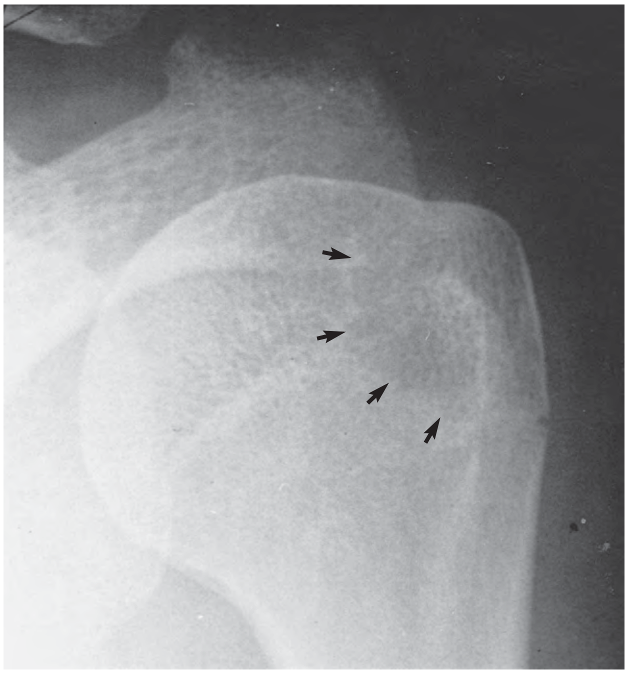

FIGURE 13–13 **Humeral pseudocyst.**[14] The circular area of radiolucency adjacent to and within the greater tuberosity *(arrows)* is a normal zone of trabecular diminution termed the humeral pseudocyst. The curvilinear inferior margin separates the relatively porous lateral region from the more densely compact spongiosa located medially.

TABLE 13-3 Skeletal Dysplasias and Other Congenital Diseases Affecting the Shoulder

Entity	Figure(s)	Characteristics
Achondroplasia[15]		Splaying of the proximal portion of the humerus Metaphyseal cupping
Infantile cortical hyperostosis (Caffey disease)[16,122]		Clinical triad: hyperirritability, palpable masses overlying affected bones, and soft tissue swelling Bilateral symmetric periosteal new bone formation along the clavicular shaft and, less commonly, the scapula May be associated with Erb-Duchenne palsy
Fibrodysplasia ossificans progressiva[17]	13-14	Extensive soft tissue ossification involving the shoulder girdle musculature, tendons, fascia, and ligaments
Osteopoikilosis[18]	13-15	Proximal portion of humerus and glenoid region frequently affected Multiple circular zones of osteosclerosis tend to accumulate in a periarticular distribution
Osteopetrosis[19]		Diffuse sclerosis of clavicle, scapula, and humerus Flared proximal humeral metaphysis May lead to pathologic fracture
Melorheostosis[20]		Hemimelic distribution of flowing hyperostosis along humeral shaft or scapula Occasional soft tissue ossification
Cleidocranial dysplasia[21]	13-16	Failure of ossification of the clavicular growth centers resulting in hypoplasia or complete absence (10% of cases) of clavicles Scapulae may be hypoplastic or deformed Marked shoulder hypermobility often leads to glenohumeral joint dislocations

See also Table 1-2.

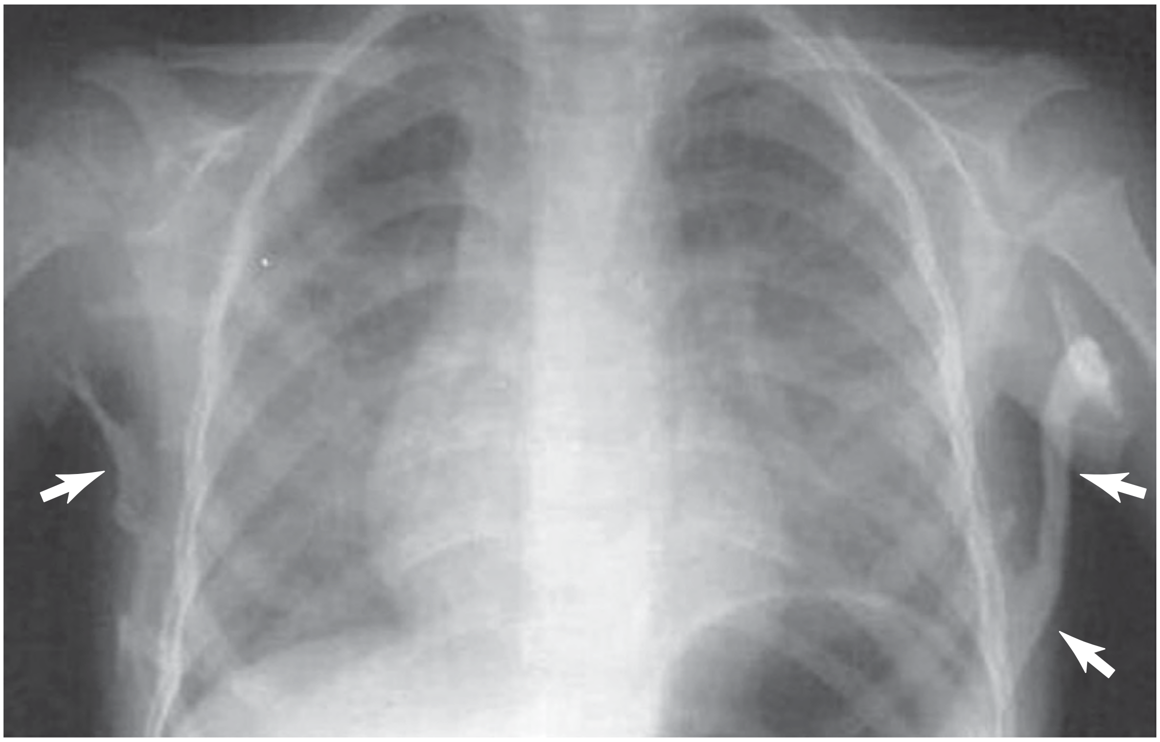

FIGURE 13–14 Fibrodysplasia ossificans progressiva.[17] A 3-year-old girl. Observe the large sheets of ossification *(arrows)* extending from the thoracic cage into the axillae and toward the humeri bilaterally.

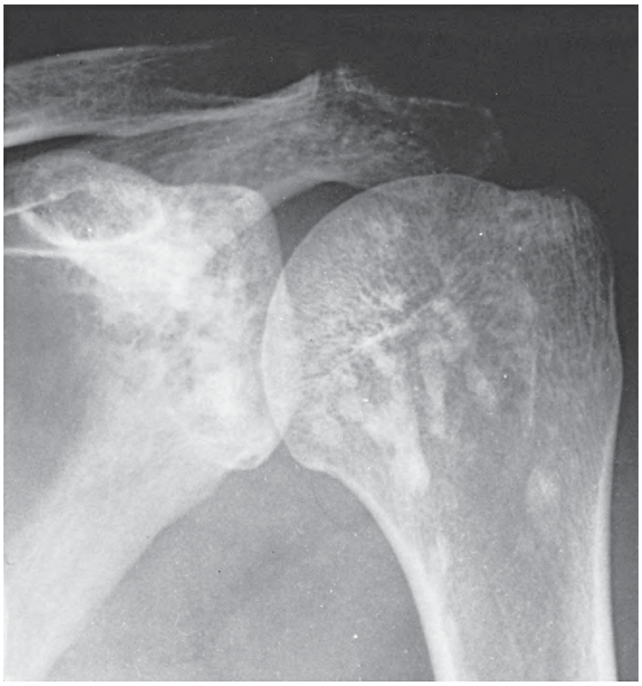

FIGURE 13–15 **Osteopoikilosis.**[18] Note the circular and ovoid osteosclerotic foci localized within the humerus and scapula. A symmetric periarticular distribution is characteristic of this sclerosing dysplasia. Although the epiphysis may be affected, lesions occur predominantly in the metaphysis. Osteopoikilosis is typically a process that affects several bones about the major joints.

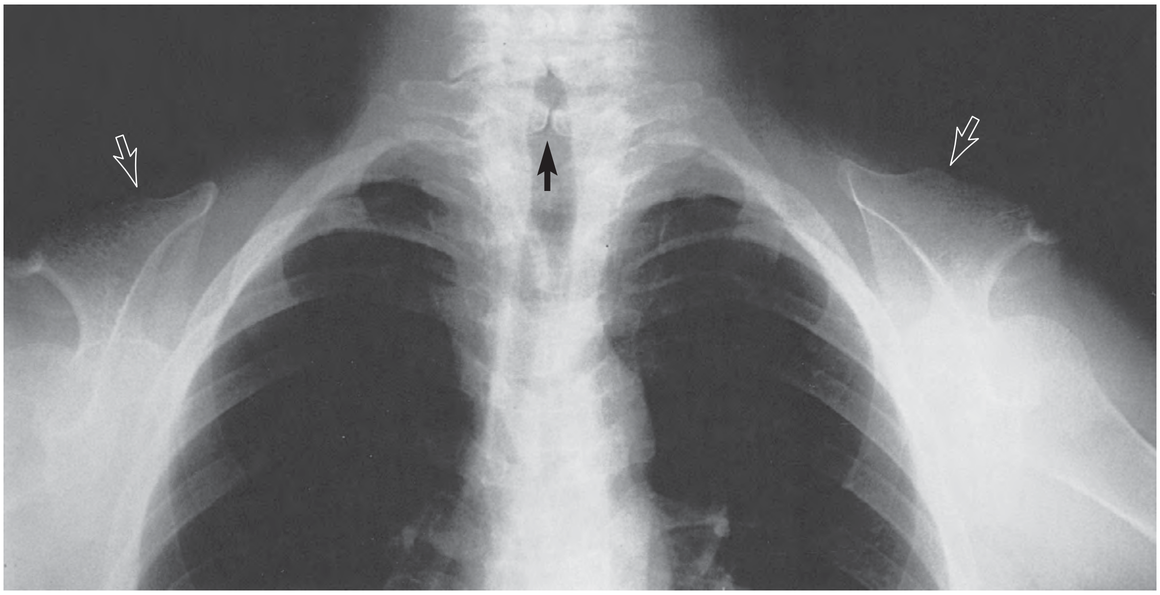

FIGURE 13–16 **Cleidocranial dysplasia.**[21] Complete absence of the clavicles, spina bifida occulta *(arrow),* and hypoplastic scapulae *(open arrows)* are evident. Involved patients have varying degrees of hypermobility and drooping of the shoulders. Any portion of the clavicle may be absent, but the middle and outer portions are affected most commonly. Total clavicular agenesis is evident in only 10% of cases. The scapula may be underdeveloped with a small glenoid cavity.

TABLE 13-4 Fractures About the Shoulder

Injury	Figure(s), Table(s)	Characteristics	Complications and Related Injuries
Fractures of the Proximal Portion of the Humerus			
Acute fractures in adults[22,23]	13-17	Middle-aged and elderly adults Osteoporosis significant predisposing factor Classified as one-part to four-part fractures based on the degree and the location of displacement among: Surgical neck Anatomic neck Greater and lesser tuberosities	May be associated with lipohemarthrosis, drooping shoulder, intraarticular bodies, degenerative disease, delayed union, heterotopic bone formation, rotator cuff injury, injury of brachial plexus and axillary artery, marked humeral head rotation, and osteonecrosis
Growth plate injuries in children[24,25]	13-18	*Type I physeal injury:* Slipped humeral epiphysis Boys aged 11 to 16 years *Little League shoulder syndrome:* epiphysiolysis of the humeral epiphysis	Limb shortening in 10% of patients
Fractures of the Clavicle[26,27,144]	13-19	Most common bone fractured during childbirth Frequent accidental injury in children Infrequent injury in child abuse Stress (fatigue) fracture of the medial end of the clavicle secondary to nervous tic, professional baseball, and radical neck dissection has been reported	*All types:* Nonunion uncommon (<1%) Posttraumatic pseudarthrosis also rare First rib fracture *Children:* clavicle fractures heal rapidly without significant deformity *Adults:* resultant deformity secondary to excessive callus formation may be observed
Intermediate segment	13-19, *A, E, F*	Seventy-five percent to 80% of clavicle fractures Fall on outstretched arm or fall on shoulder	Occasional cosmetic deformity Neurovascular compression by large callus (rare)
Distal (lateral) segment	13-19, *B, C*	Fifteen percent to 20% of clavicle fractures Downward forces on humerus and scapula	Delayed union or nonunion rarely Posttraumatic osteolysis of the clavicle Acromioclavicular and coracoclavicular joint injuries
Proximal (medial) segment	13-19, *D*	Five percent of clavicle fractures Direct trauma Intraarticular and transverse types	Degenerative joint disease with intraarticular type Sternoclavicular joint injuries

TABLE 13-4 Fractures About the Shoulder—cont'd

Injury	Figure(s), Table(s)	Characteristics	Complications and Related Injuries
Fractures of the Scapula[28-30,156,157]		Five percent to 7% of all fractures about the shoulder CT scanning with orthogonal reconstruction is the most useful imaging modality to detect and define the extent of scapular injury	*All types:* 95% associated with fractures of the clavicle, ribs, and skull or dislocation of the acromioclavicular joint
Scapular body	13-20, *A, B*	*Most frequent site:* 50% to 70% of scapular fractures Direct trauma from fall, motor vehicle collision or seizures	Associated fractures at other sites
Glenoid fossa and articular surface	13-20, *C*	Violent force is applied laterally that drives the humerus into the glenoid fossa Stress fracture: inferior margin of the glenoid in baseball pitchers (rare) Intraarticular	Instability Glenohumeral joint osteoarthrosis Labral injuries
Acromion process	13-20, *D*	Direct trauma or muscular traction Most common injury of the scapula in child abuse; partial avulsion or complete fracture; usually unilateral and left-sided	Significant neurologic injury to brachial plexus
Coracoid process	13-20, *E*	***Mechanisms*** 1. Direct injury from dislocating humeral head 2. Direct force on tip 3. Avulsion from traction of coracoclavicular ligament 4. Stress fracture in trapshooters	Significant neurologic injury to brachial plexus
Floating shoulder	13-20, *F*	Combined fractures of the scapular neck and ipsilateral clavicle Result in disruption of the stability of the suspensory structures of the shoulder effectively dissociating the upper extremity from the axial skeleton	Muscle forces and the weight of the arm typically pull the glenoid fragment distally and anteromedially
Scapular neck	13-21	Second most frequent site Direct blow	Labral injuries
Scapular spine	13-21	Rare injury Direct trauma	
Fractures of the First and Second Ribs[31]	12-11, *B*; Table 12-4	Major trauma to the thorax or shoulder Stress fracture from heavy backpacking and weightlifting	Rupture of the lung apex or subclavian artery, aneurysm of the aortic arch, tracheoesophageal fistula, pleurisy, hemothorax, cardiac alterations, neurologic injury, and other fractures, especially of cervicothoracic transverse processes

See also Tables 1-4 and 1-5.

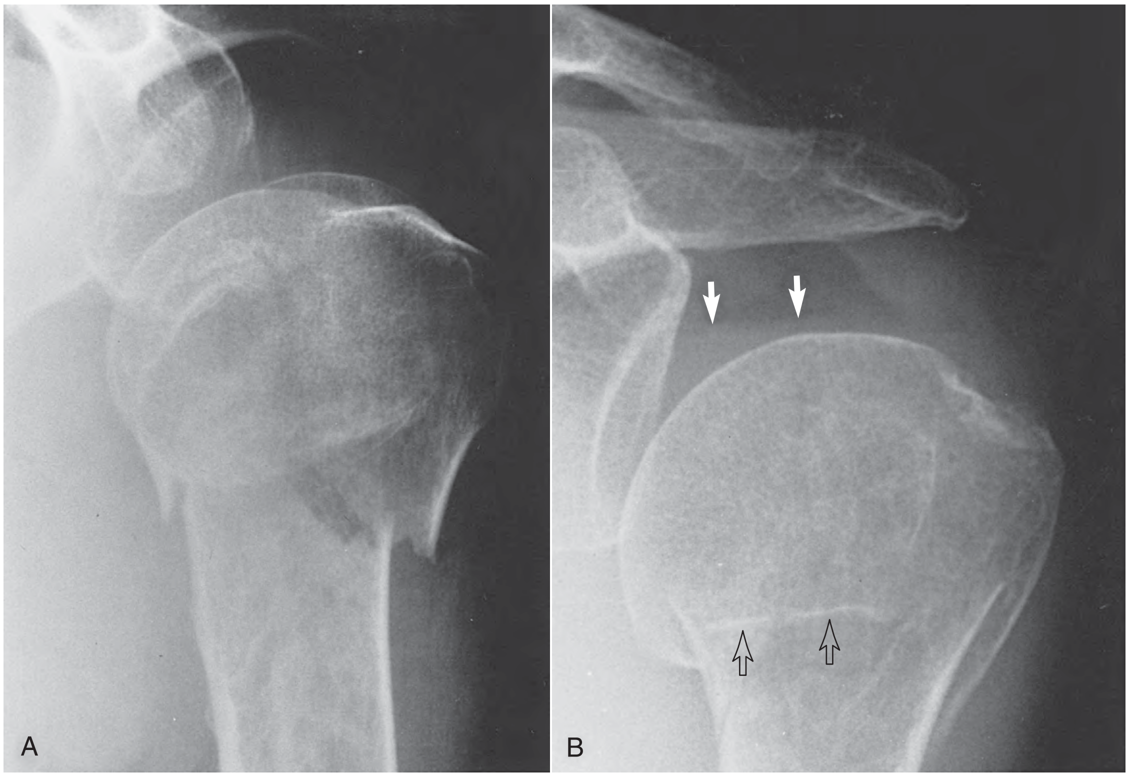

FIGURE 13–17 Fractures of the proximal portion of the humerus.[22,23] **A,** This 74-year-old osteoporotic man had fallen on his shoulder 3 weeks before this radiograph was obtained. The radiograph reveals a minimally displaced three-part fracture of the surgical neck and greater tuberosity of the humerus. A CT scan revealed that the lesser tuberosity was intact. **B,** In another patient, fracture of the surgical neck of the humerus *(open arrows)* is accompanied by a lipohemarthrosis, which is seen as a fat-fluid level *(arrows)* and represents release of fat from the bone marrow into the joint fluid. Observe also the inferior subluxation of the humeral head relative to the glenoid fossa, a condition that may be caused by a large joint effusion and is termed a *drooping shoulder*. Fractures of the proximal portion of the humerus occur most frequently in patients older than 45 years of age, especially osteoporotic persons. They are classified as one-part to four-part on the basis of the degree and the location of displacement among four regions of the humerus: head, shaft, greater tuberosity, and lesser tuberosity.

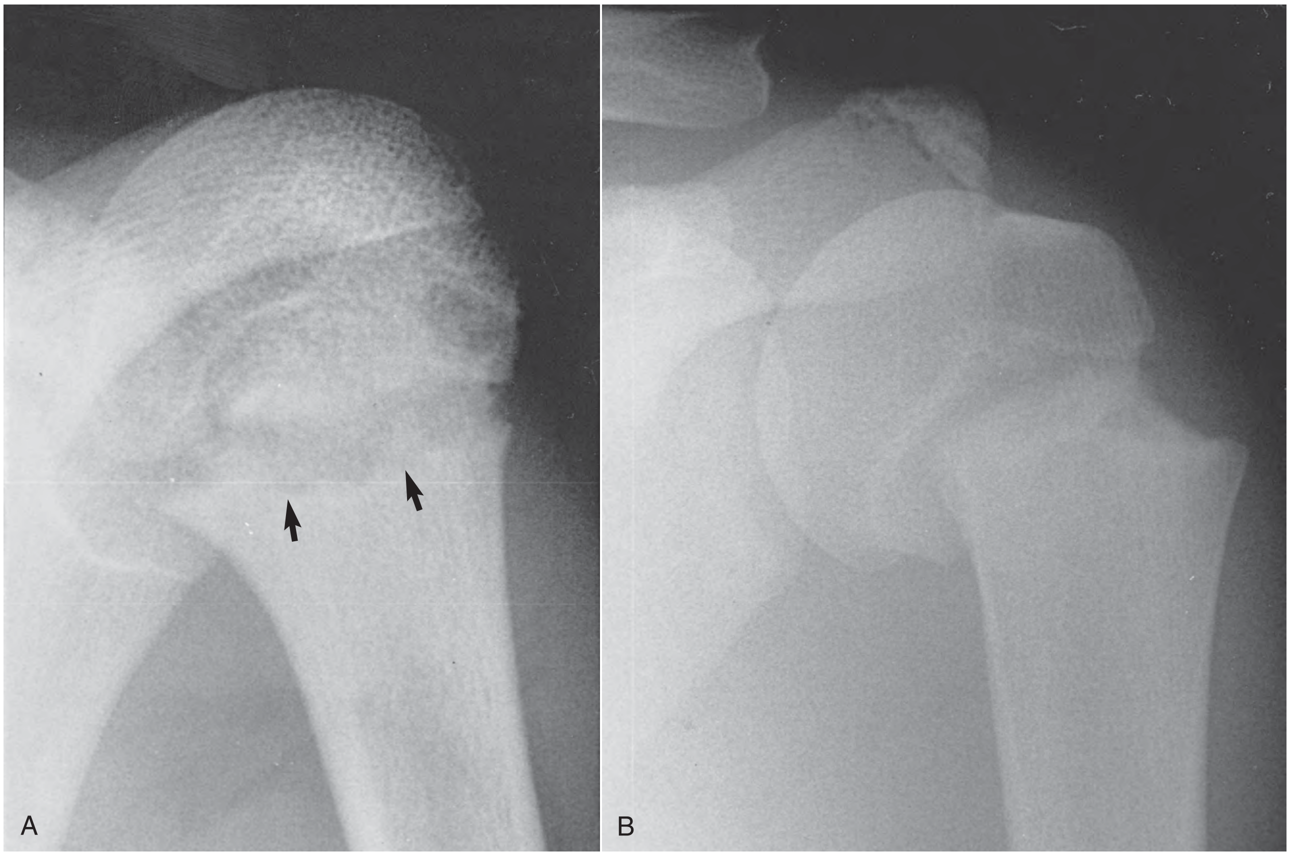

FIGURE 13–18 **Growth plate injury: Little League shoulder syndrome.**[24,25] **A,** This 13-year-old baseball pitcher developed progressive shoulder pain in his pitching arm. Observe the widening and irregularity of the humeral physis *(arrows)* and the sclerosis of the adjacent metaphyseal margin. **B,** A more severe example shows a fracture through the growth plate of the proximal end of the humerus in a 14-year-old baseball pitcher. Note the obvious displacement of the humeral epiphysis. Little League shoulder syndrome represents epiphysiolysis of the proximal humeral epiphysis in adolescent baseball pitchers. It is a Salter-Harris type I growth plate injury that may result in shortening of the limb. Such injuries may also occur as a result of a fall on an outstretched arm with the wrist and elbow fully extended. (***A,*** *Courtesy G. Greenway, MD, Dallas.)*

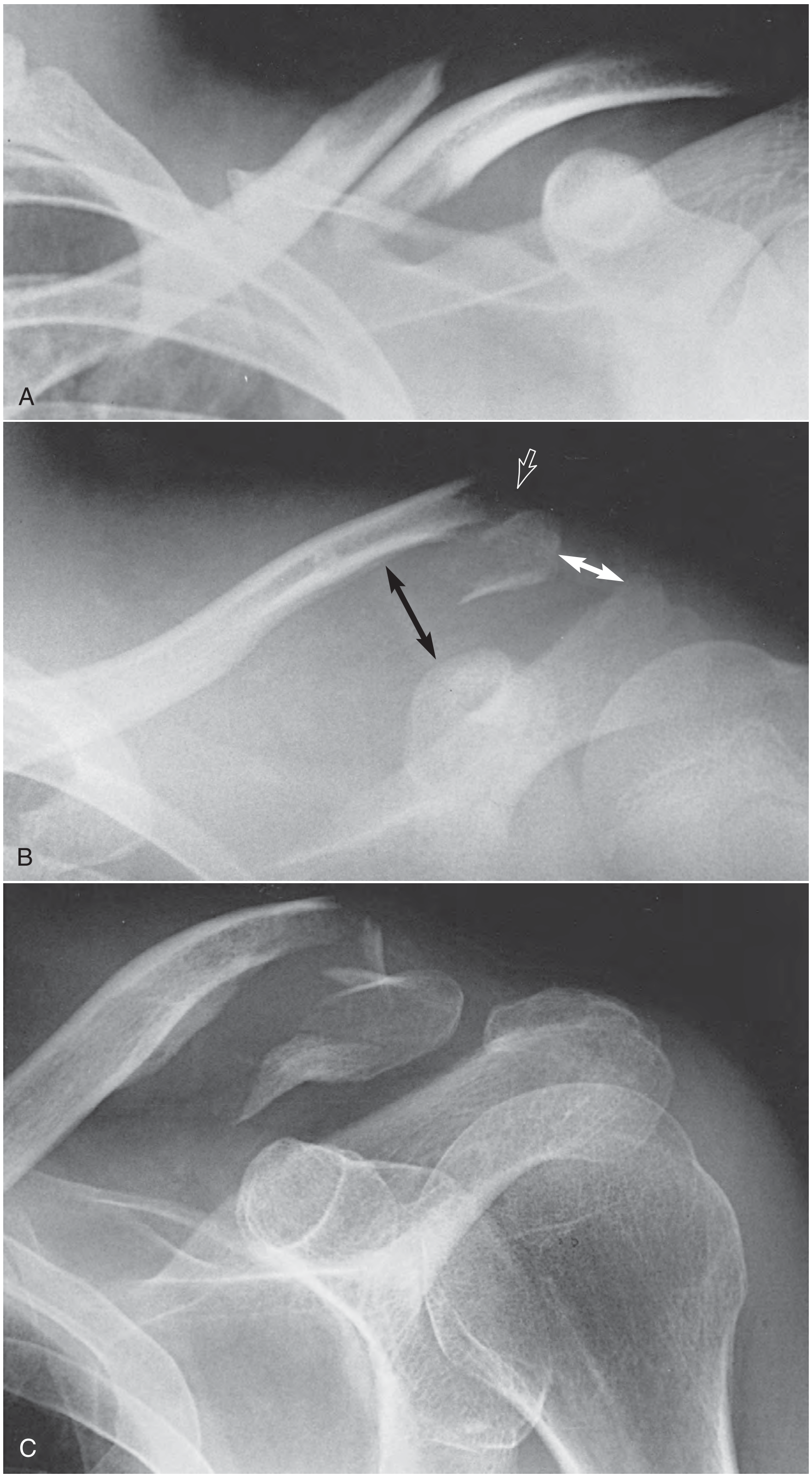

FIGURE 13–19 **Clavicle fractures.**[26,27,144] **A,** Intermediate segment. Note the fracture at the junction of the distal and intermediate thirds of the clavicle. The intermediate or middle segment of the clavicle is pulled upward by the sternocleidomastoid muscle, and the distal segment is pulled downward by the weight of the arm and inward by the pull of the pectoralis major and latissimus dorsi muscles on the scapula and the humerus. This parallel offset of the two fragments is termed *bayonet apposition*, a common finding in fractures of the intermediate segment. **B,** Lateral segment. A fracture of the distal end of the clavicle *(open arrow)* is associated with complete rupture of the coracoclavicular ligaments *(black double-headed arrow)* and acromioclavicular ligaments *(white double-headed arrow)* in a 13-year-old boy. Observe the widened coracoclavicular distance and superior displacement of the proximal portion of the clavicle. **C,** A similar fracture of the lateral segment is seen in an adult. Note the comminuted fragments and upward displacement of the medial portion of the clavicle.

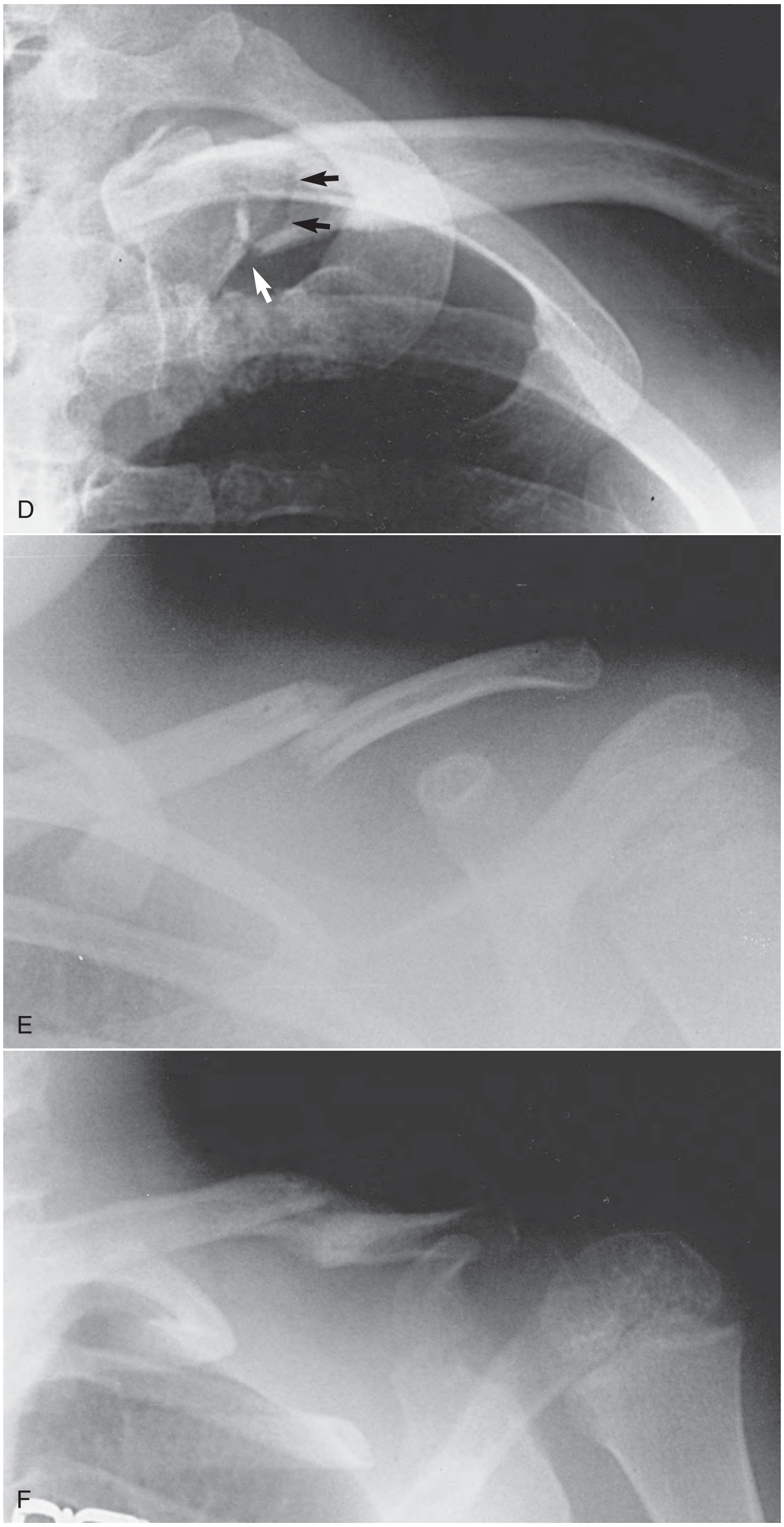

FIGURE 13–19, cont'd **D,** Medial segment. Observe the comminuted fracture of the medial segment of the clavicle *(arrows)*. **E-F,** Normal healing in a child. In this 5-year-old child, the initial radiograph **(E)** shows a fracture of the intermediate segment with bayonet apposition. The medial portion of the clavicle is pulled upward, and the lateral segment is pulled downward and toward the midline. A subsequent radiograph **(F),** obtained 65 days after injury, demonstrates solid bone fusion with abundant callus formation and remodeling despite poor apposition of fracture fragments. Stress fractures of the clavicle are rare; they occur either as fatigue fractures in athletes or as insufficiency fractures after radiation or surgery.

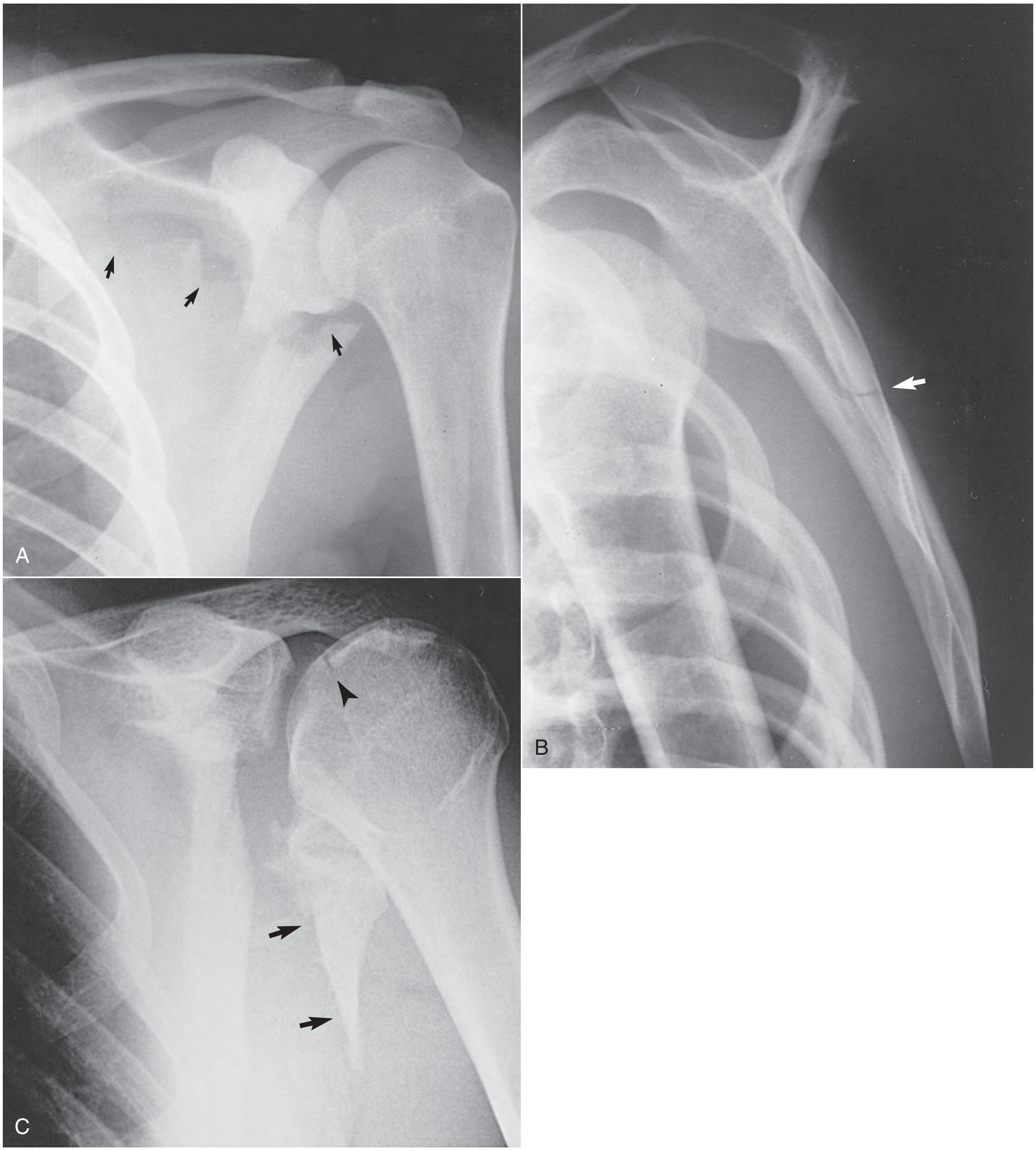

FIGURE 13–20 **Scapular fractures.**[28-30] **A,** Body of scapula. Observe the jagged transverse fracture through the entire body of the scapula *(arrows)*. About 50% to 70% of scapular fractures involve the body and result from direct force. **B,** Value of scapular Y projection. In another patient, the scapular Y view clearly demonstrates a fracture of the body of the scapula *(arrow)* associated with an anterior subcoracoid glenohumeral dislocation. **C,** Complex fracture of glenoid and body. In this patient, a comminuted intraarticular fracture of the glenoid and scapular body with severe inferior displacement of the fracture fragment is evident *(arrows)*. The greater tuberosity of the humerus is also fractured *(arrowhead)*.

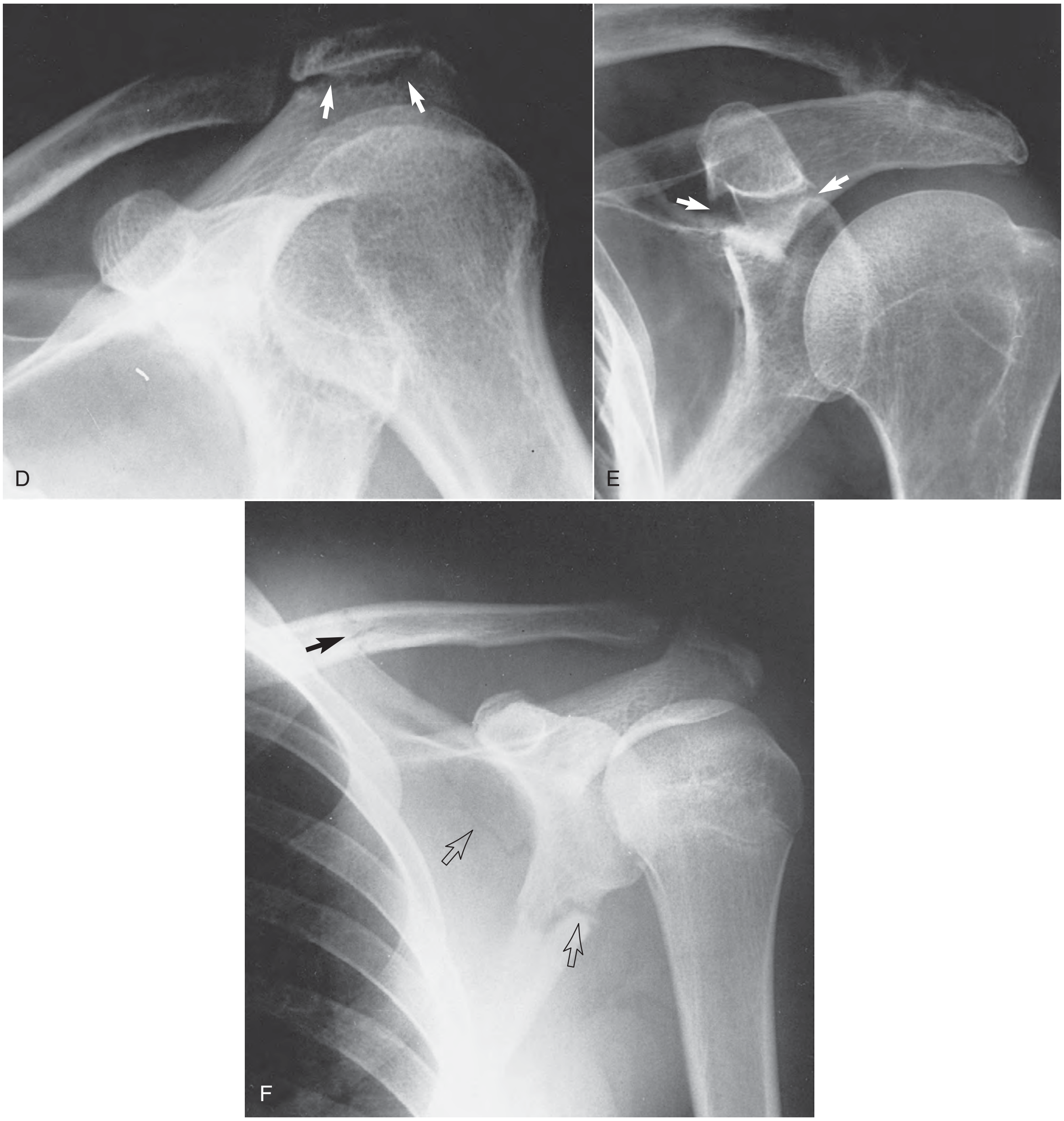

FIGURE 13–20, cont'd **D,** Acromion fracture. A transverse fracture line through the base of the acromion *(arrows)* is evident. Brachial plexus injury is a rare but well-recognized complication of acromion fractures. **E,** Coracoid process fracture. Observe the fracture through the coracoid process *(arrows)*. Fractures of the coracoid process usually result from direct trauma or from an avulsion of the coracoclavicular ligament, the short head of the biceps, or the coracobrachialis muscle. Patients with this type of fracture should be observed carefully for associated fractures and neurologic injury. **F,** Floating shoulder. Observe the transverse fractures through the body of the scapula *(open arrows)* and the intermediate segment of the clavicle *(arrow)*. Combined fractures of the scapular neck and ipsilateral clavicle disrupt the stability of the suspensory structures of the shoulder, a condition termed *floating shoulder*. Scapular fractures are often associated with pneumothorax and fractures of the ribs, clavicle, and skull. *(**C,** Courtesy R. Crokin, DC, Portland, Ore.)*

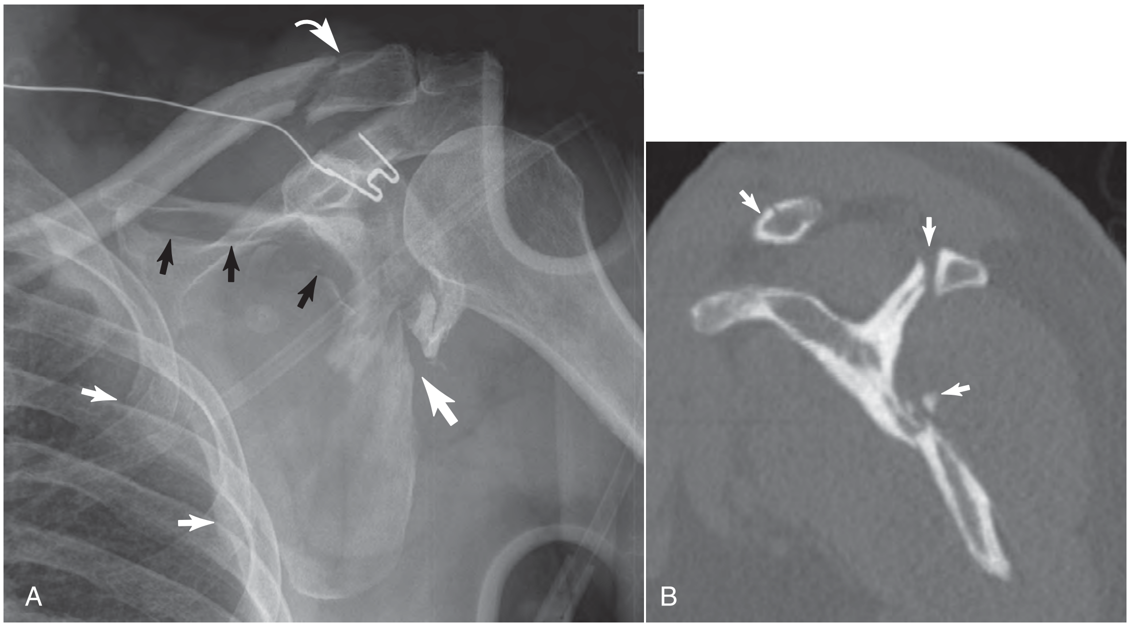

FIGURE 13–21 Fractures of the scapular neck and spine.[28-30,156,157] In this 67-year-old male after a major automobile collision, an anteroposterior radiograph **(A)** shows a comminuted fracture of the scapular neck *(large white arrow)* and along the base of the scapular spine *(black arrows)*. The distal end of the clavicle *(curved arrow)* and adjacent ribs *(small white arrows)* are also fractured. A sagittal CT scan **(B)** also depicts the fractures *(arrows)*. Combined fractures of the scapula and clavicle, as in this case, result in an unstable condition termed *floating shoulder*, in which the shoulder girdle essentially loses its osseous connection with the thoracic cage.

TABLE 13-5 Dislocations of the Shoulder*

Entity	Figure(s), Table(s)	Characteristics	Complications and Related Injuries
Glenohumeral Joint Dislocation		Eighty-eight percent of all shoulder dislocations	
Anterior dislocation[32-35,159]	13-22	Ninety-five percent of glenohumeral joint dislocations *Four types:* subcoracoid, subglenoid, subclavicular, intrathoracic ***Imaging findings*** Hill-Sachs fracture Bankart fracture Loss of normal half-moon overlap between glenoid and humeral head Disruption of scapulohumeral arch	Recurrence (40% of cases), Hill-Sachs lesion (50%-100% of recurrent cases), Bankart lesion (20% of cases), avulsion fracture of greater tuberosity, labral injury, brachial plexus injury, rotator cuff injury, rib fractures
Posterior dislocation[36,159]	13-23	Two percent to 4% of glenohumeral joint dislocations *Three major types:* subacromial, subglenoid, subspinous More than 50% initially unrecognized Often occurs as a result of electric shock or seizure ***Imaging findings*** Trough line or reverse Hill-Sachs fracture Reverse Bankart lesion Fracture of lesser tuberosity Positive rim sign Loss of normal half-moon overlap between glenoid and humeral head Humeral head appears in same position on internal and external AP projections because the patient is not able to externally rotate the arm	Secondary degenerative disease, disruption of posterior capsule, fracture of posterior glenoid rim, lesser tuberosity avulsion, subscapularis tendon injury
Superior dislocation[37]	13-24	Rare injury	Rotator cuff, capsule and biceps tendon injury, fractures of clavicle, acromion, coracoid process, and humeral tuberosities
Inferior dislocation (luxatio erecta)[38]	13-25	Rare injury The humeral head is dislocated inferiorly and the upper extremity is held in a hyperabducted position.	Fractures of greater tuberosity, acromion, coracoid process, clavicle, and inferior glenoid rim Axillary artery and brachial plexus injury, recurrent dislocations, and adhesive capsulitis
Drooping shoulder[39,142]	13-17, *B*, 13-26	*Rare occurrence:* in patients with fractures of the surgical neck of the humerus Cause unknown but may relate to atony of deltoid muscle or hemarthrosis Results in self-limited displacement that corrects in weeks Drooping shoulder has also been reported secondary to calcific tendinitis of the rotator cuff	Associated humeral fracture

* See also Table 1-5.

Continued

TABLE 13-5 Dislocations of the Shoulder—cont'd

Entity	Figure(s), Table(s)	Characteristics	Complications and Related Injuries
Acromioclavicular (AC) Joint Dislocation[40,41,128,140,151,154]	13-27	Ten percent of all shoulder dislocations Frequent injury between ages 16 and 40 years *Old terminology:* shoulder separation	*Complications of all types:* Premature degenerative disease CC ligament calcification or ossification Posttraumatic osteolysis of the clavicle Persistent instability
Type I injury		Mild sprain of AC ligament CC ligament intact Normal appearance on radiographs	
Type II injury		Moderate sprain AC ligament and joint capsule ruptured CC ligaments partially sprained but remain intact AC joint space widened on radiographs	
Type III injury		Severe sprain AC ligament and joint capsule completely ruptured CC ligaments completely ruptured Superior displacement of clavicle on radiographs and CC interspace is 25% to 100% greater than normal shoulder	Deltoid and trapezius muscles may be detached from distal end of clavicle
Type IV injury		Type III with avulsion of CC ligament from clavicle with posterior displacement of clavicle with penetration of clavicle through periosteal sleeve or displaced into or through the trapezius muscle Concurrent dislocation of sterno-clavicular joint	
Type V injury		Exaggerated Type III with a posterior dislocation of clavicle behind acromion CC interspace separated between 100% to 300%	
Type VI injury		Type III with inferolateral dislocation of lateral end of clavicle	
Sternoclavicular Joint Dislocation[42,154]	12-18; Table 12-4	*Rare:* only 2% to 3% of all shoulder dislocations Severe trauma	*Anterior dislocation:* Avulsion of inferior margin of clavicle, growth plate injury; more common than posterior dislocation *Posterior dislocation:* Injury to trachea, esophagus, great vessels, or nerves in the superior mediastinum; may lead to cough, dyspnea, dysphagia, and even death
Scapulothoracic Dissociation[156]	13-28	Complete disruption of the scapulothoracic articulation with lateral scapular displacement *High-energy mechanisms:* >50% motorcycle injuries; also pedestrian accidents and falls from height	Dislocations of sternoclavicular and acromioclavicular joints Clavicle and rib fractures Vascular and neurologic damage such as brachial plexus injury Visceral injuries (>85%) Avulsion of muscle attachments Death (11%)

AC, Acromioclavicular; *CC,* coracoclavicular.

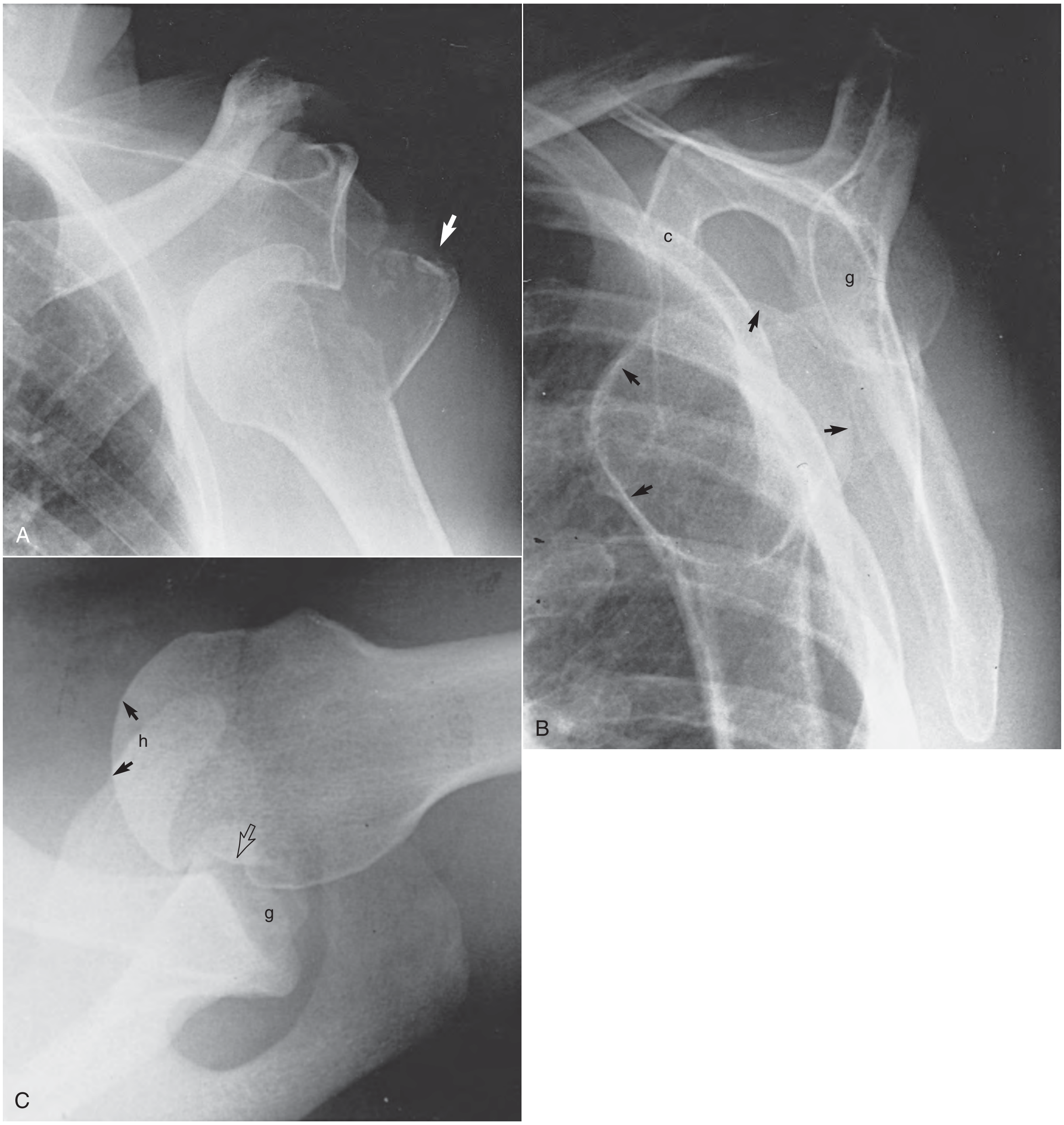

FIGURE 13–22 **Anterior glenohumeral joint dislocation: radiographic assessment and complications.**[32-35,159] **A-B,** Anterior glenohumeral joint dislocation with associated fracture. In **A,** a frontal radiograph shows an anterior dislocation of the humeral head with an associated displaced and comminuted greater tuberosity fracture *(arrow)*. In **B,** a tangential radiograph of the scapula, the scapular Y view, the anterior displacement of the humeral head *(arrows),* which lies anterior to the glenoid cavity (g) and inferior to the coracoid process (c), is clearly demonstrated. In addition to associated fractures, anterior glenohumeral joint dislocations may be complicated by brachial plexus and rotator cuff injuries. **C,** Axillary radiograph. This view clearly demonstrates the anterior dislocation of the humeral head articular surface (h) *(arrows)* with respect to the glenoid cavity (g). This projection is often difficult to obtain while the humeral head remains displaced. A Hill-Sachs impaction fracture of the humeral head also is seen *(open arrow)*.

Continued

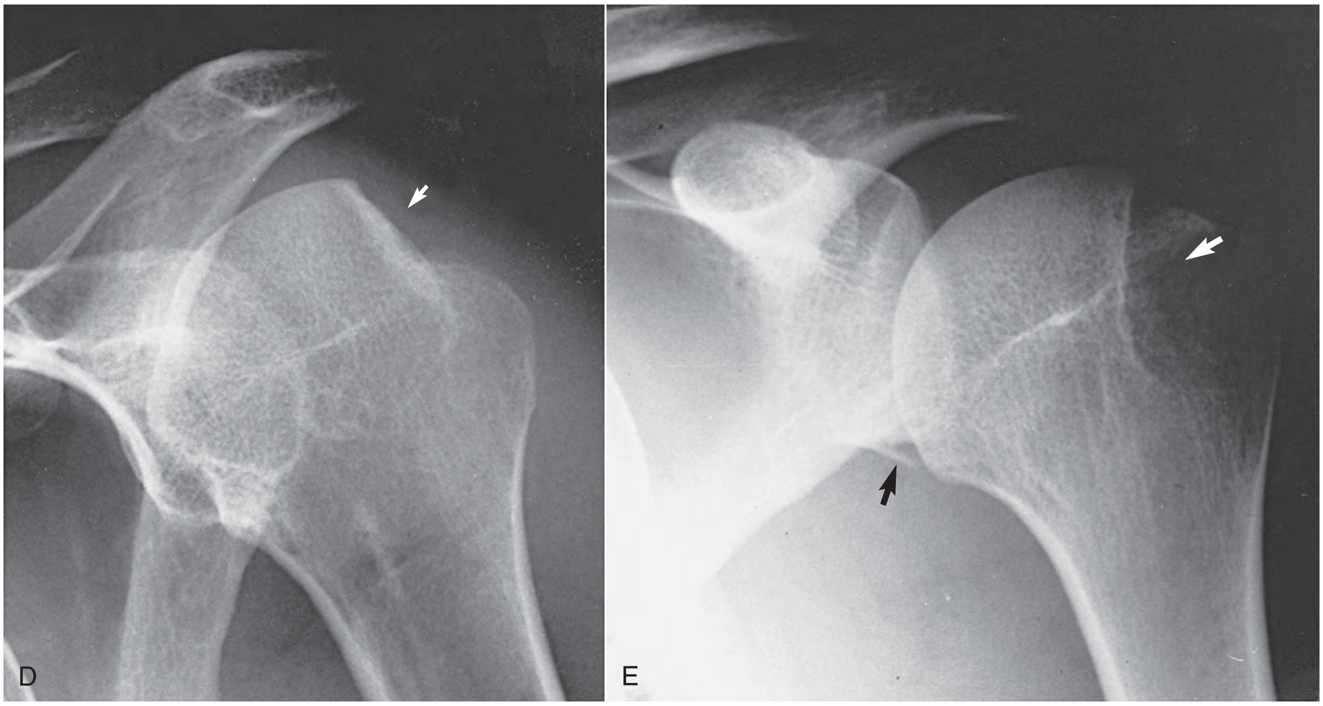

FIGURE 13–22, cont'd **D,** Hill-Sachs lesion. In a patient with recurrent anterior dislocation, observe the compression fracture of the posterolateral aspect of the humeral head *(arrow)*. **E,** Bankart and Hill-Sachs lesions. In a patient with recurrent dislocations and a Hill-Sachs fracture *(white arrow),* observe the bone fragment adjacent to the glenoid rim *(black arrow)*. The Hill-Sachs lesion is a compression fracture of the posterolateral aspect of the humeral head that is produced by impaction of the humerus against the anterior rim of the glenoid; it is reported to be present in 50% to 100% of recurrent dislocations. Bankart lesions are fractures of the anterior glenoid rim caused by impaction of the humeral head as it dislocates. Osseous lesions may be seen via routine radiography, but purely cartilaginous labral injuries require CT arthrography or MR imaging.

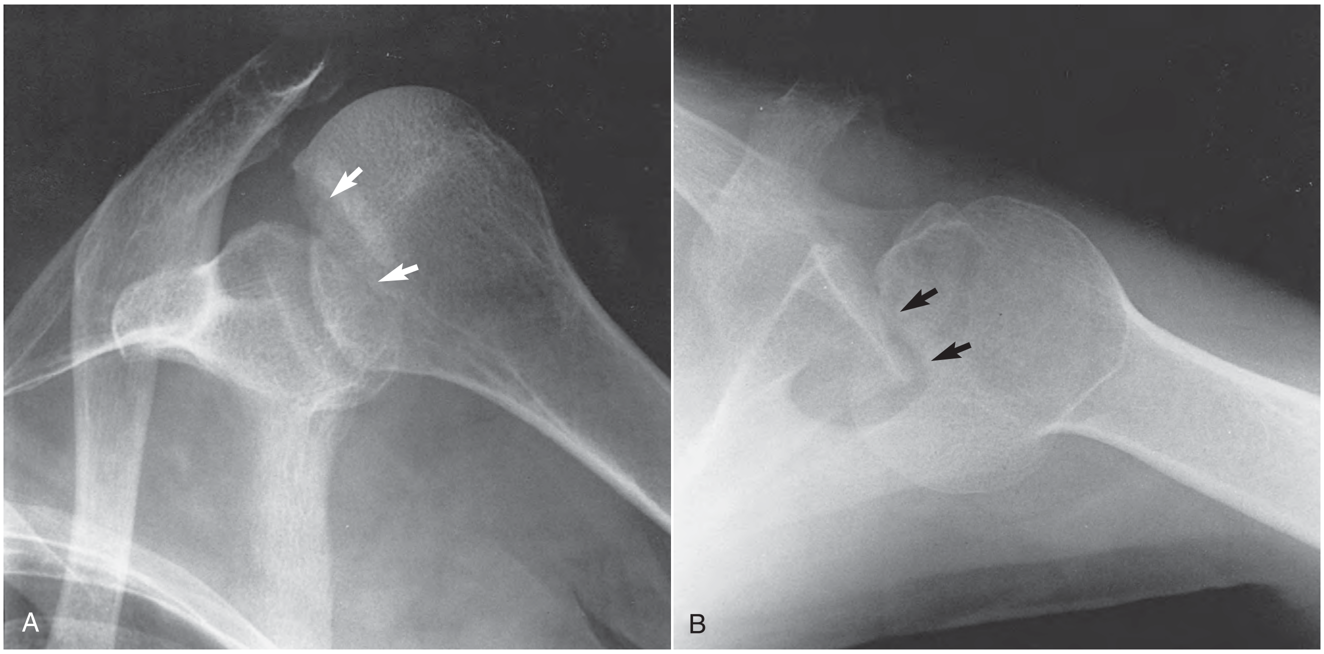

FIGURE 13–23 **Posterior glenohumeral joint dislocation.**[36,159] This 35-year-old man with a chronic irreducible posterior dislocation is unable to externally rotate the arm at the glenohumeral joint. **A,** Internal rotation radiograph shows the characteristic trough fracture *(arrows)* caused by impaction of the humeral head against the posterior rim of the glenoid. **B,** Axillary radiograph clearly shows the posteriorly dislocated humeral head in relation to the glenoid and trough fracture *(arrows)*. Posterior dislocations represent only 2% to 4% of all shoulder dislocations. More than half of these dislocations are unrecognized on initial evaluation. Bilateral posterior dislocations may be seen in patients after seizures and electrical shocks.

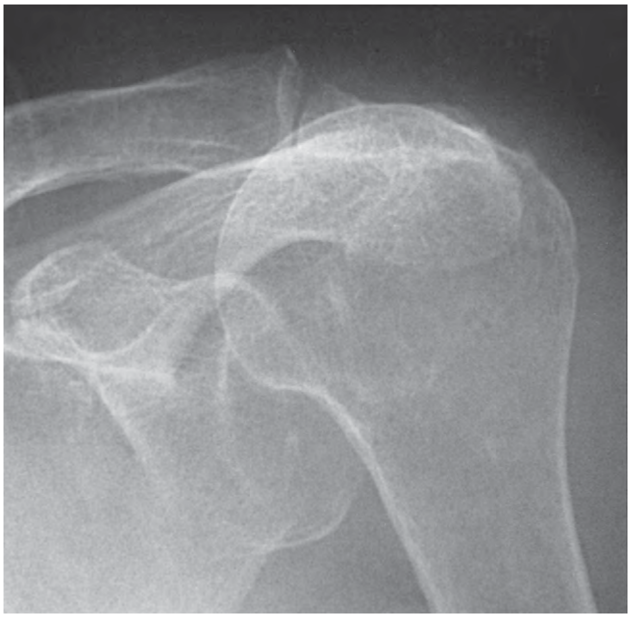

FIGURE 13–24 **Superior glenohumeral joint dislocation.**[37] Observe the elevation of the humeral head with respect to the glenoid cavity with acute superior dislocation of the humerus. Note that the inferior surface of the acromion is located inferiorly with respect to the superior aspect of the humeral head. This is a rare and unusual pattern of dislocation. Fractures of adjacent bones and injuries to the rotator cuff, joint capsule, biceps tendon, and surrounding muscles frequently complicate superior dislocations.

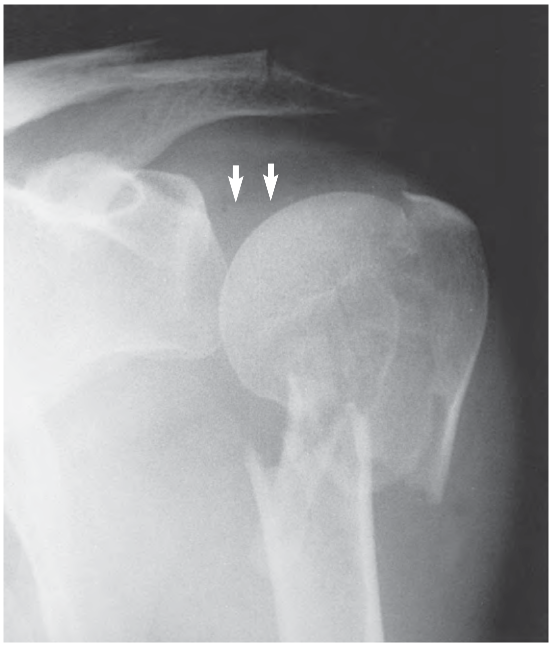

FIGURE 13–26 **Drooping shoulder: lipohemarthrosis associated with a fracture of the proximal portion of the humerus.**[39] This patient has sustained a comminuted, displaced fracture of the proximal portion of the humerus. On this frontal radiograph obtained with the patient standing, observe the fat-fluid level (lipohemarthrosis) *(arrows)* and inferior displacement of the humeral head (drooping shoulder). This finding strongly suggests the presence of an intraarticular fracture, the fat and blood being released from bone marrow after the fracture (see also Figure 12-17, *B*.)

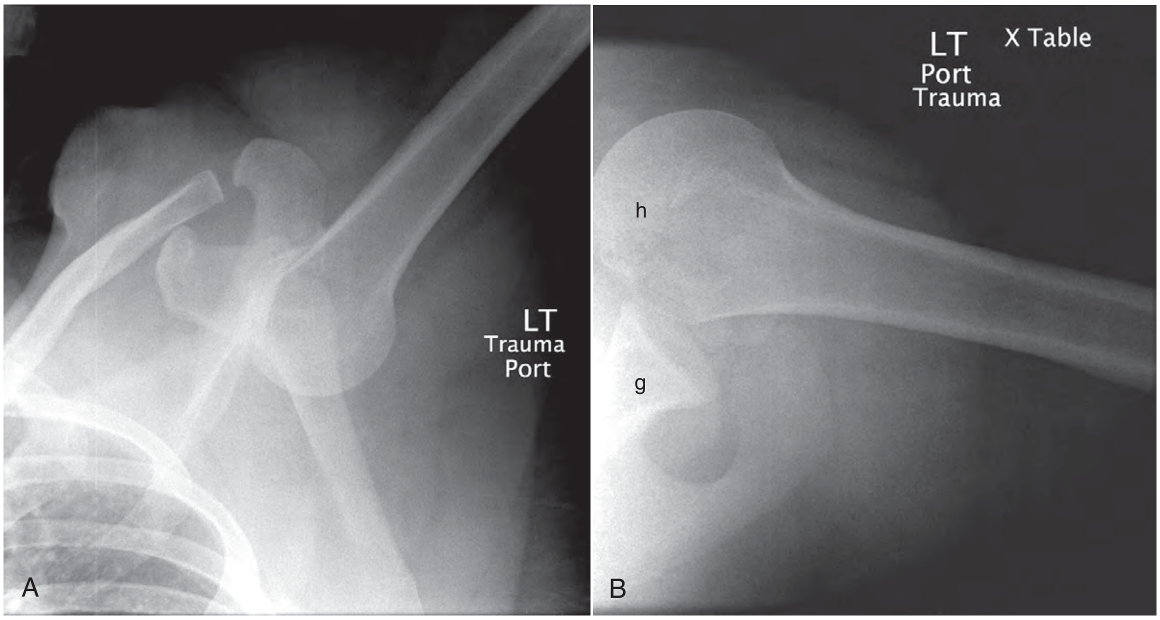

FIGURE 13–25 **Inferior glenohumeral joint dislocation: luxatio erecta.**[38] A frontal radiograph **(A)** of this 33-year-old man after a motorcycle crash reveals that the humerus is locked in a hyperabducted position with the humeral head driven downward in an inverted position below the glenoid. A cross-table axillary radiograph **(B)** documents that the humeral head is located anterior to the glenoid, that the articular surface of the humeral head is no longer in contact with the articular surface of the glenoid, and that the shaft of the humerus is positioned in a hyperextended position with respect to the scapula. The luxatio erecta is an extremely uncommon pattern of glenohumeral joint dislocation.

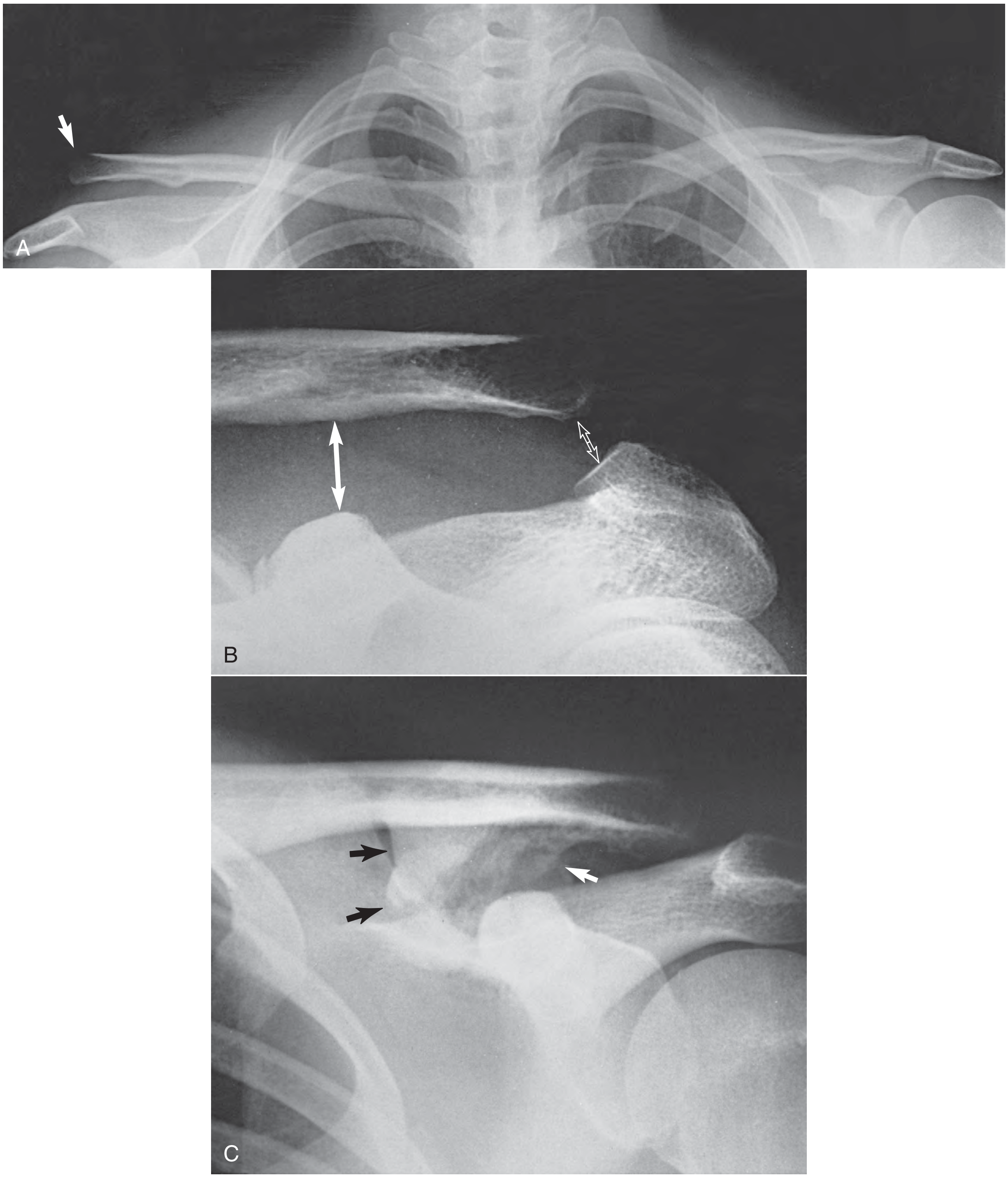

FIGURE 13–27 **Acromioclavicular joint dislocation.**[40,41,128,140,151] **A,** Acute grade V injury. Frontal stress radiograph obtained while the patient held a weight in both hands reveals marked widening of the coracoclavicular and acromioclavicular joint spaces, resulting in superior displacement of the clavicle *(arrow)*. The type V injury is a severe sprain characterized by disruption of both the acromioclavicular and coracoclavicular ligaments with acromioclavicular joint dislocation. The clavicle is elevated above the adjacent acromion. **B,** In another patient, a grade III or V acromioclavicular joint sprain (dislocation) is seen as widening of the coracoclavicular space *(double-headed white arrow)* and the acromioclavicular joint space *(double-headed open arrow)*. **C,** Chronic heterotopic ossification. Observe the extensive sheetlike ossification in the region of the coracoclavicular ligaments *(arrows)* in this man, who had sustained a severe acromioclavicular joint dislocation several years earlier. Posttraumatic heterotopic ossification is a well-known complication of such ligamentous injuries, but its presence does not appear to influence the eventual prognosis. In addition to radiographs taken with and without weights, anteroposterior shoulder radiographs obtained in internal rotation may also be used in diagnosing some grade III or V acromioclavicular joint dislocations. *(**B,** Courtesy T. Dobson, DC, Portland, Ore.)*

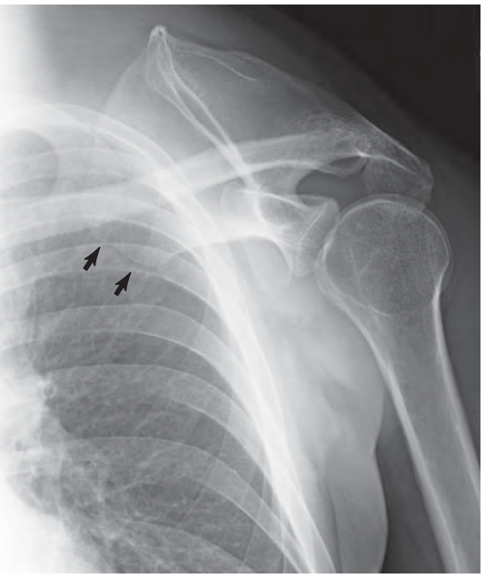

FIGURE 13–28 Scapulothoracic dissocation.[156] A frontal radiograph shows complete superior and lateral displacement of the scapula as a result of complete dissociation of the scapula from the thoracic cage. A subtle nondisplaced transverse fracture *(arrows)* of the inferior portion of the scapula is also present. *(Courtesy V. Khasgiwala, MD, Dallas.)*

TABLE 13-6 Internal Joint Derangements and Other Injuries Affecting the Shoulder*

Entity	Figure(s), Table(s)	Characteristics
Shoulder impingement syndrome[43,149]	Table 13-7	Repeated impingement and eventual tears of the rotator cuff tendons (RCT), the long head of the biceps brachii muscle, and other associated soft tissues of the shoulder
Rotator cuff tendon tear[44-46,145,150,160]	13-29 to 13-31	Full-thickness or partial-thickness tear of the supraspinatus (most common), infraspinatus, subscapularis, or teres minor tendons predominate in patients older than 40 years of age *Acute tears:* occur suddenly or as a result of a definite injury; fewer than 10% of all rotator cuff tears *Chronic tears:* present for months or years; most common type May complicate rheumatoid arthritis, ankylosing spondylitis, septic arthritis, and other articular disorders ***Depth of tear*** 1. *Full-thickness tear:* extends from bursal surface to articular surface 2. *Partial-thickness tear:* involves only the bursal or articular surface 3. *Intrasubstance tear:* confined within the substance of the tendon and does not extend to the surface Causes: trauma, attrition, ischemia, impingement ***Radiographic findings*** (chronic tears only) 1. Elevation of the humeral head related to narrowing of the acromiohumeral space 2. Inferior acromial concavity 3. Cyst formation and sclerosis within the apposing surfaces of the acromion and humeral head ***Advanced imaging*** Arthrography, ultrasonography, and MR imaging are useful techniques for evaluation of acute and chronic tears; more accurate in assessing full-thickness tears than partial-thickness tears MR imaging and ultrasound are also useful for long-term follow-up after surgery for rotator cuff tear; a normal appearance of the rotator cuff is correlated with good clinical outcome, whereas retear and tendinosis are associated with pain

---

* See also Table 1-5.

Continued

TABLE 13-6 Internal Joint Derangements and Other Injuries Affecting the Shoulder—cont'd

Entity	Figure(s), Table(s)	Characteristics
Rotator cuff tendinitis[47]		Ischemic or degenerative pathologic conditions of the tendon; the terms tendinosis and tendinopathy are more appropriate than tendinitis Common in manual laborers involved in occupations requiring frequent arm elevation and the use of hand tools and in athletes participating in sports involving frequent shoulder movement Routine radiographs not useful in evaluation ***MR imaging findings*** Increased signal intensity within tendon on T1-weighted and proton–density-weighted spin echo images and, to a lesser extent, on T2-weighted images
Calcific tendinitis and bursitis[64,65,131,142]	Table 13-8	See discussion on Calcium hydroxyapatite crystal deposition
Adhesive capsulitis[48]	13-32	Also termed *capsulitis, periarthritis*, and *frozen shoulder* Severe painful restriction of glenohumeral joint motion; usually self-limited, lasting about 12 to 18 months Most patients are between the ages of 40 and 70 years May be primary, with no apparent cause, or secondary, in patients with previous trauma *Predisposing factors:* trauma, hemiplegia, cerebral hemorrhage, diabetes mellitus, hyperthyroidism, cervical spondylosis, and immobilization Routine radiographs are usually not helpful; conventional or MR arthrography most useful
Biceps brachii tendinosis and tenosynovitis[49,50]	13-33	Inflammation of the tendon of the long head of the biceps may occur as a result of two mechanisms: 1. *Impingement:* tendon becomes trapped between the humeral head, the acromion, and the coracoacromial ligament during elevation and rotation of the arm 2. *Attrition:* stenosis of the bicipital groove related to periostitis leads to tendon attrition, peritendinous synovitis, and, in some cases, tendon rupture Most common in fifth or sixth decade of life Associated with activities such as golf, swimming, and throwing sports Symptoms include anterior shoulder pain, referred pain to the humeral insertion of the deltoid, and tenderness over the bicipital groove Radiographs not helpful; CT, arthrography, and MR imaging more useful
Rupture of long head of biceps brachii tendon[50]		*Complete rupture:* Usually occurs proximally within the extracapsular portion of the tendon of the long head of the biceps brachii muscle May result from impingement or tendon degeneration Clinical findings include audible pop, ecchymoses, and a change in contour of the soft tissues of the arm *Partial rupture:* Clinical findings more subtle MR imaging and ultrasonography are useful in evaluating both complete and partial ruptures of the tendon; arthrography less reliable
Capsular, ligamentous, and labral abnormalities[51]	13-34	Glenohumeral joint instability and dislocation are frequently associated with injuries of the capsule, ligaments, and labrum Computed arthrotomography and MR arthrography appear to be most useful in evaluation

TABLE 13-6 Internal Joint Derangements and Other Injuries Affecting the Shoulder—cont'd

Entity	Figure(s), Table(s)	Characteristics
Acromioclavicular joint synovial cysts[141,148]	13-35	Synovial cysts (or ganglia) are benign cystic tumors that communicate with the acromioclavicular joint space and appear in association with extensive rotator cuff tears, chronic degenerative arthropathy, and may also be associated with calcium pyrophosphate dihydrate (CPPD) crystal deposition disease May present as a palpable tumorlike mass Large synovial cysts may resemble a geyser with fluid arising from the acromioclavicular joint space
Erb-Duchenne paralysis[52]	13-36	Upper extremity palsy caused by brachial plexus injury at birth Hypoplasia of the glenoid neck, coracoid process, and humeral head, overhanging of the distal portion of the clavicle and acromion process
Parsonage-Turner syndrome[161,162]	13-37	*Synonym:* acute brachial neuritis Cause unknown Neuromuscular disorder associated with abrupt onset of shoulder pain followed by profound weakness involving shoulder girdle muscles supplied principally by the suprascapular nerve (97%), axillary nerve (50%) or rarely by the subscapular nerve (3%) ***MR imaging*** *Acute phase:* demonstrates myositis; T2-weighted hyperintensity in muscle *Chronic phase:* shows fatty atrophy of involved muscles
Posttraumatic osteolysis of the clavicle[53,54,146]	13-38	Progressive resorption of the distal end of the clavicle Usually begins after single or repeated episodes of local trauma Traumatic insult may be minor or related to chronic stress as in weight lifters Possible association also with spinal cord injury Symptoms include pain, local crepitation, and diminished strength and mobility Osteolysis begins as early as 2 weeks and as late as several years after injury and may be associated with a subtle distal clavicular subchondral fracture identified on MR imaging 0.5 to 3 cm of the distal part of the clavicle may undergo osteolysis over a 12- to 18-month period Other findings include soft tissue swelling and dystrophic calcification Findings are self-limited, resulting in eventual reconstitution over a period of 4 to 6 months; the acromioclavicular joint may remain permanently widened
Heterotopic ossification[55]	13-39	Periarticular heterotopic ossification occurs in patients after brain and spinal cord injury Osseous deposits begin as poorly defined opaque areas appearing 2 to 6 months after injury and progress to large radiodense lesions possessing trabeculae Complete osseous ankylosis of the shoulder may result

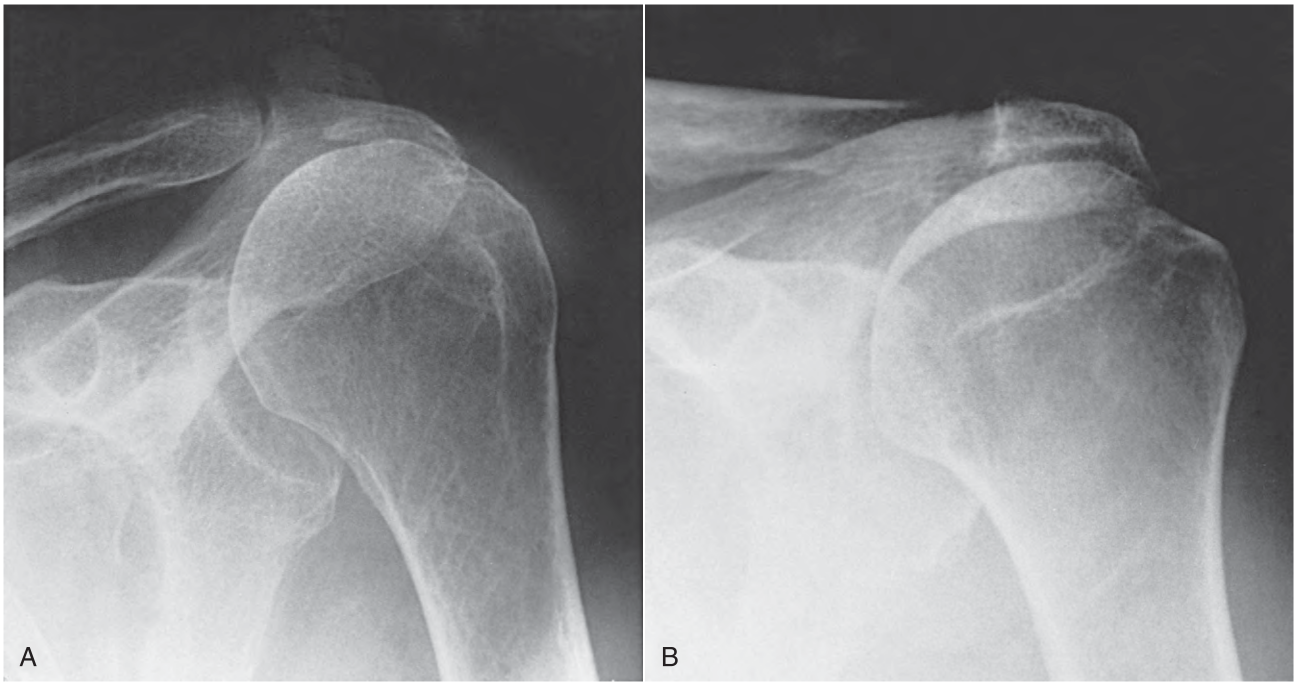

FIGURE 13–29 **Chronic degenerative rotator cuff tear: routine radiographic abnormalities.**[44,45,145] **A,** Radiograph of the shoulder in a patient with a chronic rotator cuff tear reveals elevation of the humeral head with respect to the glenoid, leading to obliteration of the acromiohumeral space, contact of the humeral head and the acromion, and scalloping of the inferior surface of the acromion. **B,** This 83-year-old man had chronic shoulder pain. Observe the narrowing of the acromiohumeral space and the concavity of the undersurface of the acromion and clavicle resulting from degenerative remodeling.

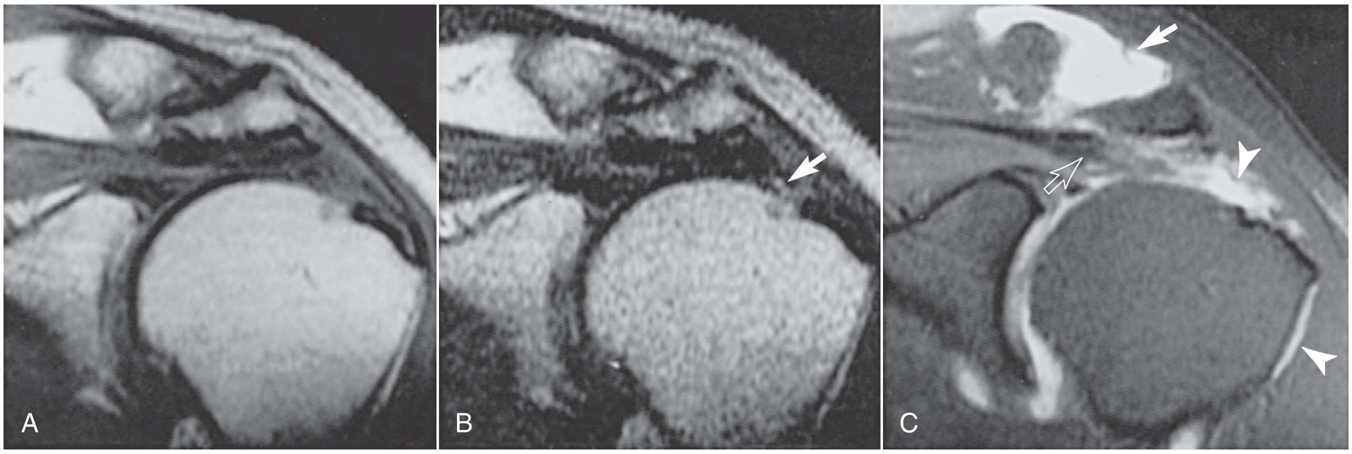

FIGURE 13–30 **Full-thickness rotator cuff tear: MR imaging and MR arthrography.**[45-47] **A-B,** Coronal oblique proton–density-weighted (TR/TE, 2000/20) **(A)** and T2-weighted (TR/TE, 2000/80) **(B)** spin echo MR images show osteoarthrosis of the acromioclavicular joint and an enlarged and irregular distal portion of the supraspinatus tendon. Only one region of the tendon, however, reveals increased signal intensity in **B** *(arrow)*. **C,** A coronal oblique T1-weighted (TR/TE, 650/20) spin echo MR image obtained with chemical presaturation of fat (ChemSat) after the intraarticular administration of a gadolinium compound revealed the high signal intensity of the contrast agent in the glenohumeral joint, subacromial-subdeltoid bursa *(arrowheads),* and acromioclavicular joint *(solid arrow)*. Note the completely torn and retracted supraspinatus tendon *(open arrow)*. *(From Resnick D, Kang HS, Pretterklieber ML: Internal derangements of joints. 2nd Ed. Philadelphia, Saunders, 2006, p 787.)*

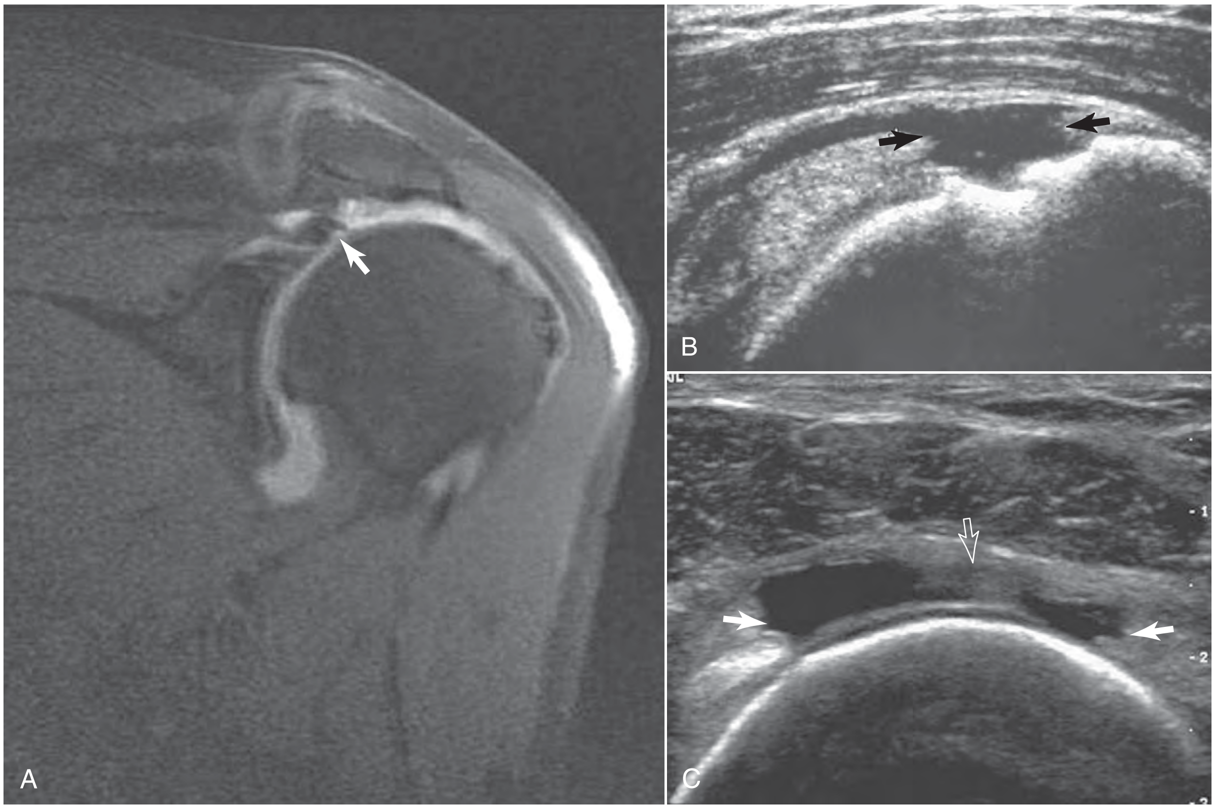

FIGURE 13–31 **Full-thickness rotator cuff tear: MR arthrography and ultrasonography.**[44-46,150,160] **A,** T1-weighted fat-suppressed MR image after an intraarticular injection of gadolinium in this 65-year-old man reveals a chronic full-thickness tear and retraction of the supraspinatus tendon *(arrow)*. **B,** In this coronal ultrasound image, observe the anechoic zone identified between the arrows that represents a complete tear of the supraspinatus tendon. **C,** This sagittal ultrasound view shows a large anechoic gap *(between white arrows)* with an intervening hyperechoic region *(open arrow)* indicating a fluid-filled full-thickness tear of the supraspinatus tendon, with inferior herniation of subdeltoid fat into the gap.

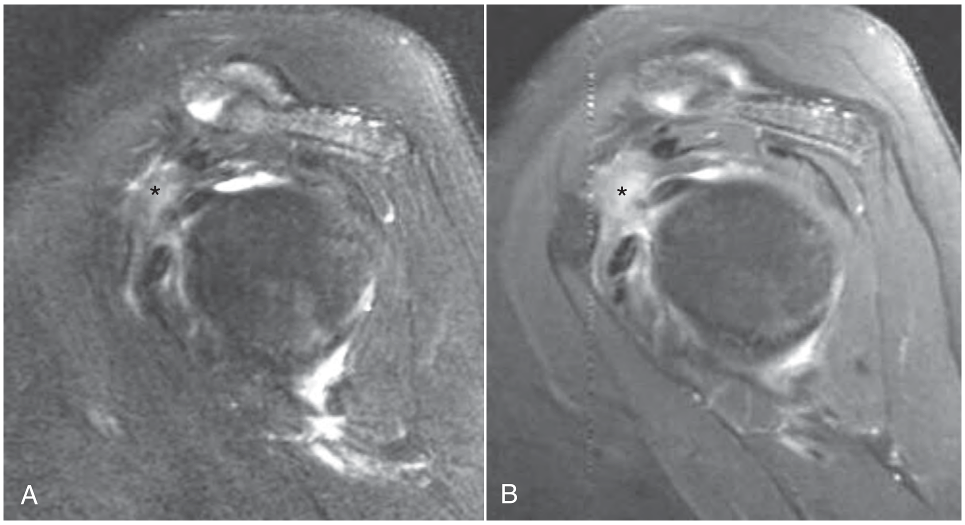

FIGURE 13–32 **Adhesive capsulitis: glenohumeral joint.**[48] This 50-year-old woman with a painful "frozen shoulder" and severe glenohumeral joint degenerative disease had an MR imaging examination including fat-suppressed sagittal T2-weighted **(A)** and T1-weighted images, the latter after intravenous gadolinium administration **(B)**. Inflammatory tissue of enhancing high signal intensity (*) within the rotator interval obscures the coracohumeral ligament. This finding, along with capsular and pericapsular edema, are useful MR imaging signs in some cases of adhesive capsulitis. On sagittal images (not shown), thickening of the joint capsule may also be observed.

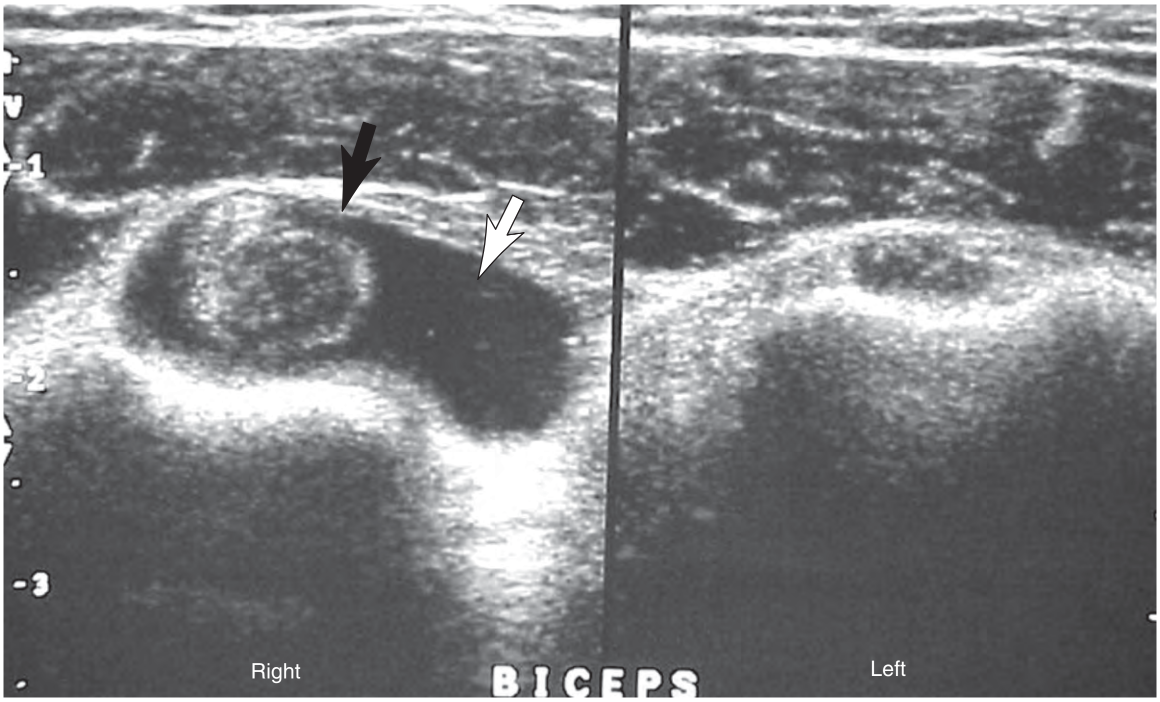

FIGURE 13–33 **Biceps brachii tendinosis and tenosynovitis: diagnostic ultrasound.**[49,50] Transverse ultrasonographic images of the right and left bíceps brachii tendon, long heads within the bicipital groove of the humerus, show tendon thickening *(black arrow)* and surrounding fluid within the tendon sheath *(white arrow),* findings that are clearly visible compared with the normal left side.

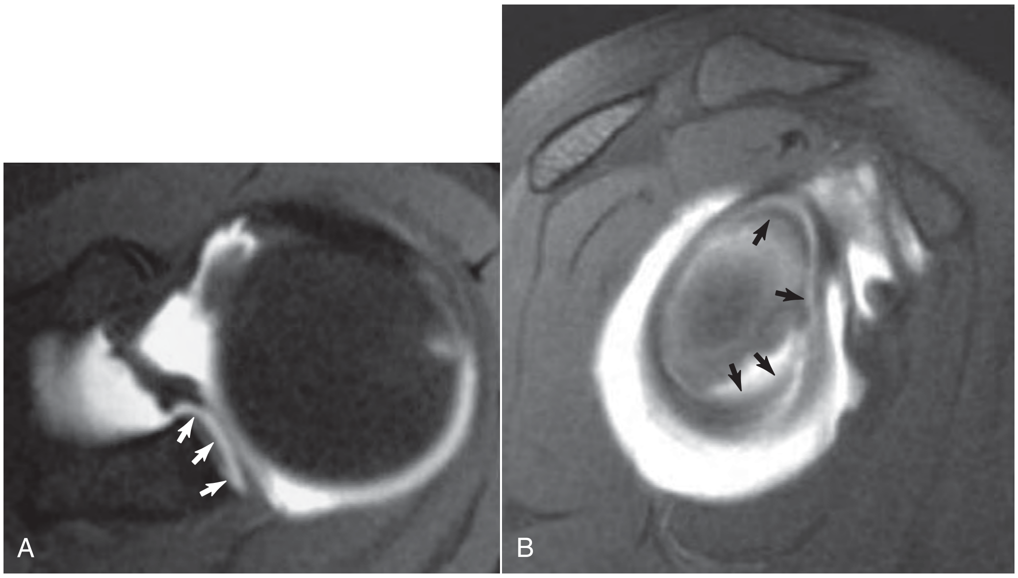

FIGURE 13–34 **Glenoid labrum injury: superior labral anterior and posterior (SLAP) tear.**[51] Transverse **(A)** and sagittal **(B)** fat-suppressed T1-weighted MR arthrographic images reveal high signal intensity fluid separating the labrum from the superior glenoid margin on both the axial and sagittal images *(arrows)*. On the sagittal image, the separation of the labrum extends from the top of posterosuperior margin and along the entire anterior margin *(arrows)*. Although the classification of glenohumeral instability and labral tear patterns seems infinite, this particular pattern of tear is designated SLAP Type V. *(For a more detailed description of labral abnormalities, see: Resnick D, Kang HS, Pretterklieber ML: Internal derangements of joints. 2nd Ed. Philadelphia, Saunders, 2006, pp 864-997.)*

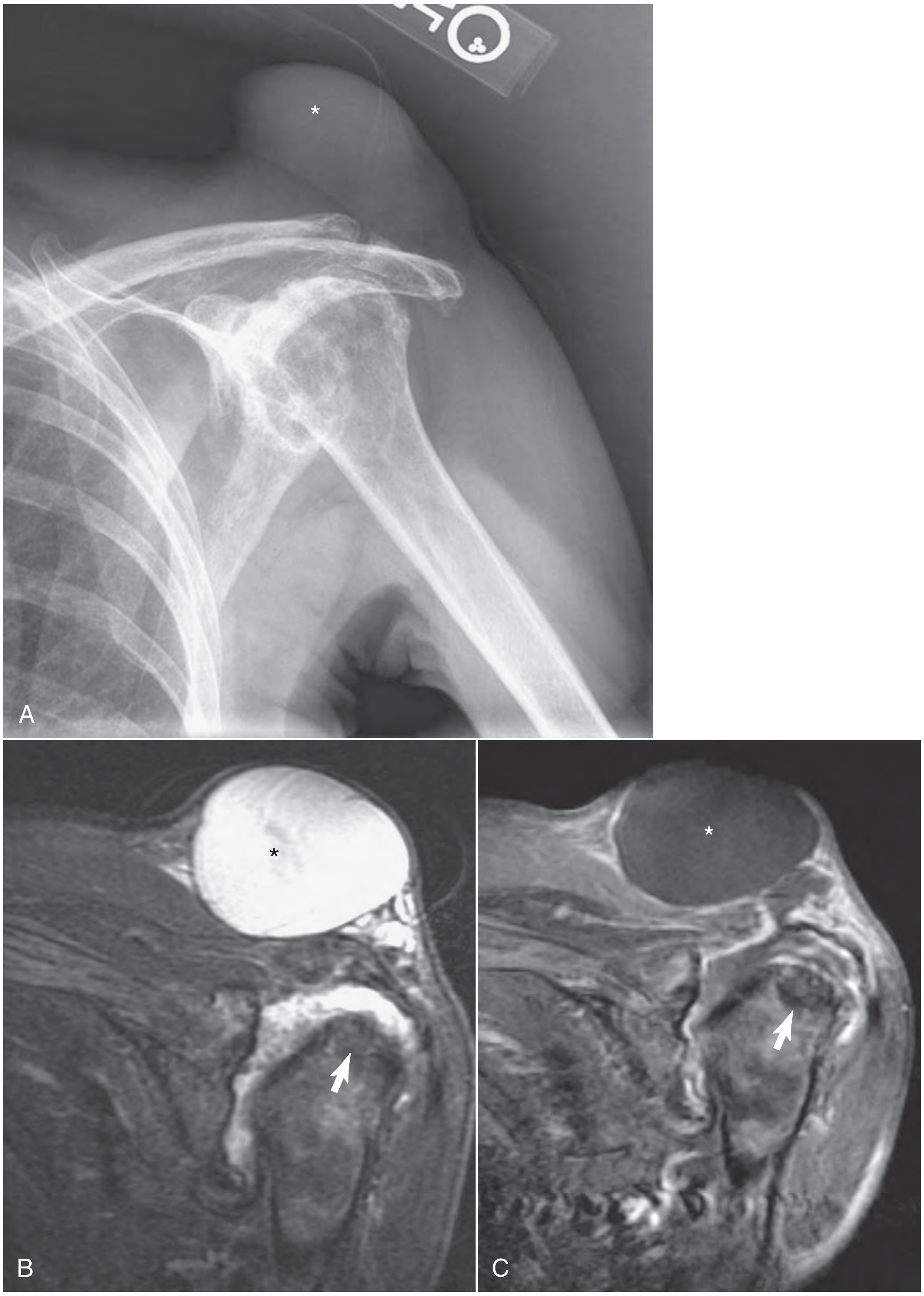

FIGURE 13–35 **Synovial cyst: acromioclavicular joint (geyser).**[141,148] This 84-year-old female has a large subcutaneous soft tissue mass overlying her shoulder. A frontal radiograph **(A)** shows a large ovoid water-density mass (*) immediately above the acromioclavicular joint and a severe glenohumeral joint degenerative disease and superior humeral head subluxation indicative of a chronic rotator cuff tear. Coronal MR images including fat-suppressed T2-weighted (STIR) **(B)** and T1-weighted sequences, the latter of which was obtained after intravenous gadolinium administration **(C),** show the well-defined cystic mass (*) above the acromioclavicular joint and extending into the subcutaneous tissues. The mass is a homogenous fluid-filled cavity that is hyperintense on the STIR image, and hypointense and nonenhancing on the postgadolinium T1-weighted image. Both images confirm the rotator cuff tear and severe degenerative erosion of the humeral head *(arrow)*. The resemblance of this type of synovial cyst to a geyser was first documented in reports of conventional glenohumeral joint arthrography. Most synovial cysts are quite small, never approaching this gigantic size.

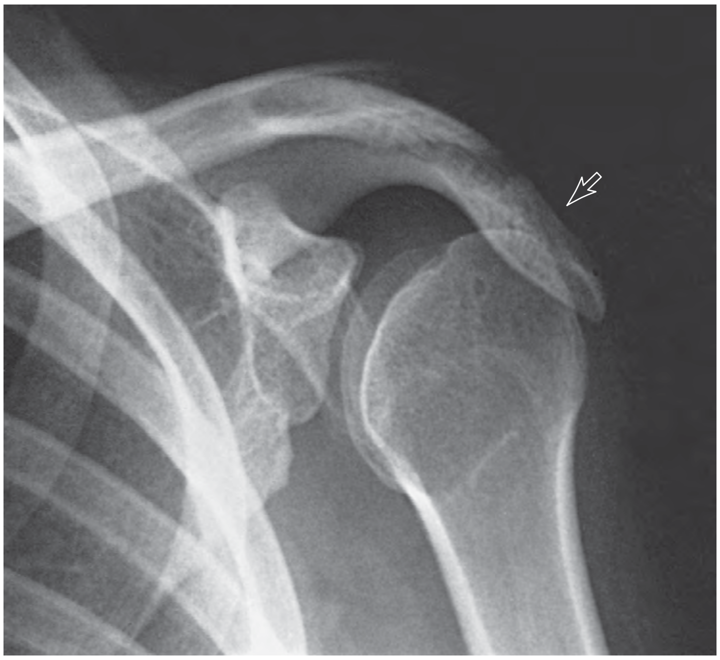

FIGURE 13–36 Erb-Duchenne paralysis.[52] Hypoplasia of the glenoid neck, coracoid process, and humeral head are associated with overhanging of the distal end of the clavicle and acromion process *(open arrow)*. These findings are characteristic in patients with Erb-Duchenne paralysis, an upper extremity palsy caused by a brachial plexus injury at birth.

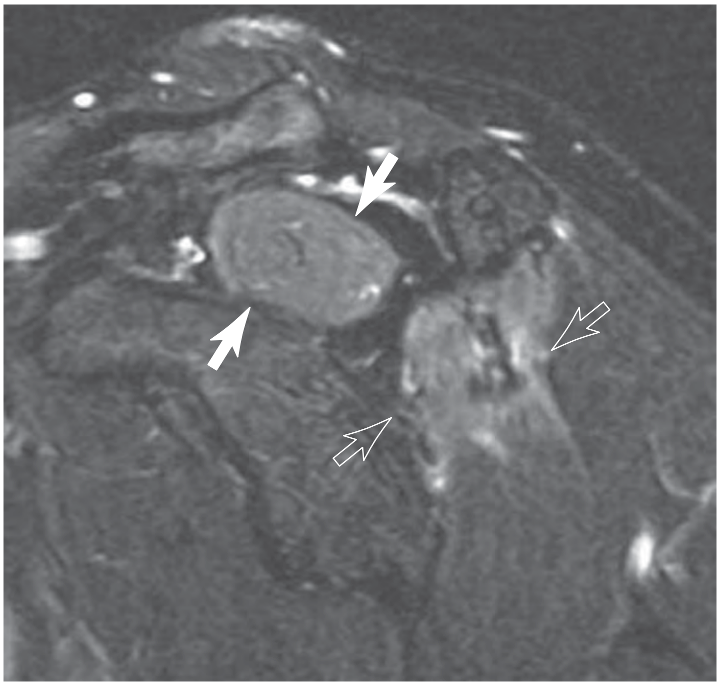

FIGURE 13–37 Parsonage-Turner syndrome.[161,162] A fat-suppressed proton–density-weighted sagittal MR image of the shoulder reveals diffuse high signal intensity within the supraspinatus *(arrows)* and infraspinatus *(open arrows)* muscles.

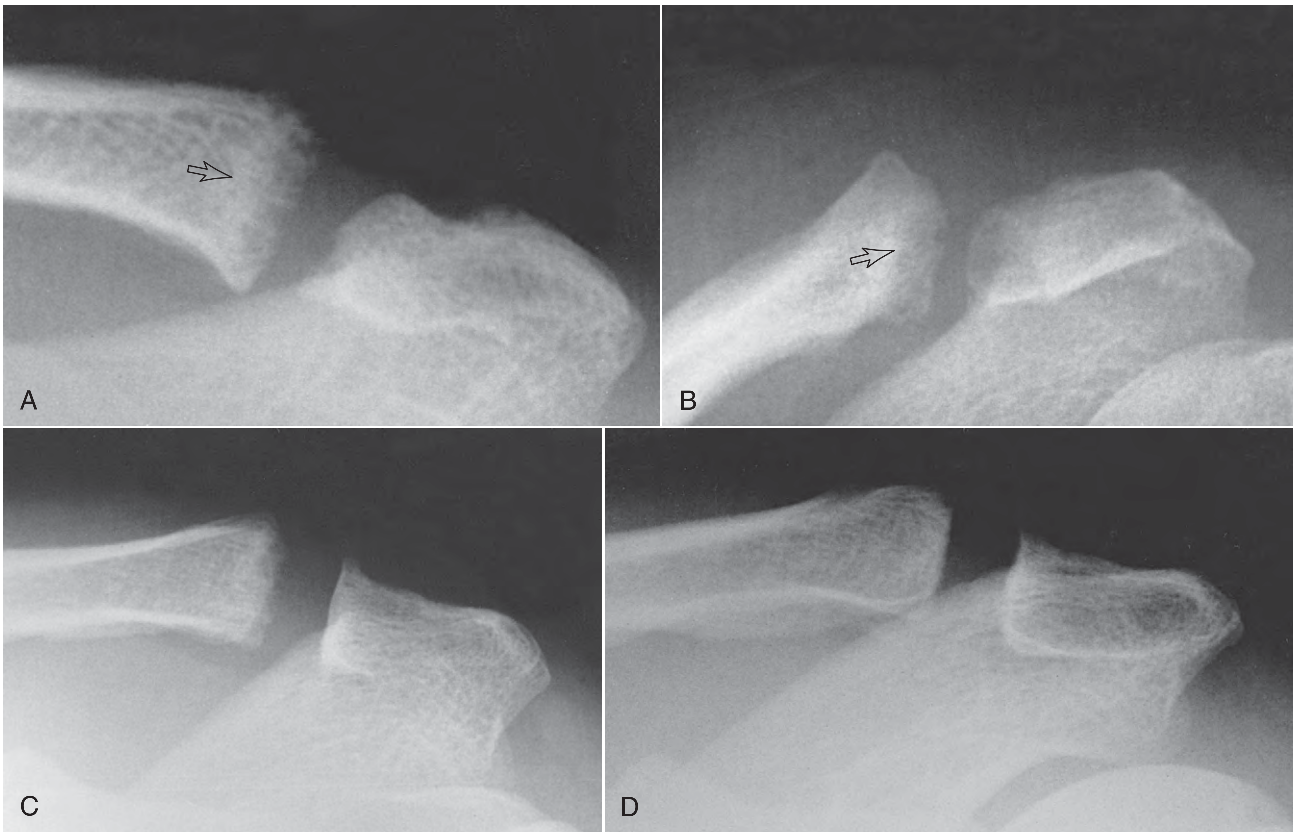

FIGURE 13–38 **Posttraumatic osteolysis of the clavicle.**[53,54,146] **A-B,** Two radiographs of the acromioclavicular joint in this competitive weight lifter show an indistinct articular surface of the distal end of the clavicle *(open arrow)* and minimal joint space widening. Stress radiographs failed to reveal acromioclavicular joint dislocation. **C-D,** A similar appearance is evident in another patient with shoulder pain that developed gradually after heavy lifting and participation in volleyball. In **C,** observe the widening of the acromioclavicular joint space and indistinct subchondral bone surface of the clavicle. In **D,** a radiograph obtained 6 months later when the patient was asymptomatic, reconstitution of the clavicular articular surface is evident, but the joint space remains widened. The appearance in these two patients is typical of posttraumatic osteolysis of the clavicle. *(**C-D,** Courtesy D. Lonquist, DC, Delta, Colo.)*

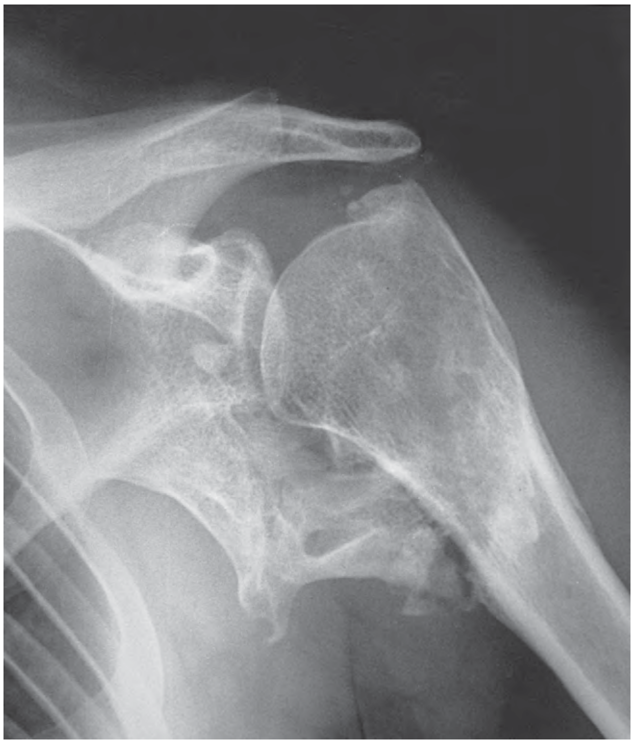

FIGURE 13–39 **Heterotopic ossification.**[55] This 43-year-old man sustained a head injury and was comatose for 3 days. Observe the extensive ossification surrounding the glenohumeral joint, resulting in almost complete osseous ankylosis. Brain and spinal cord injury may result in heterotopic ossification. This appearance may resemble the findings seen in fibrodysplasia ossificans progressiva.

TABLE 13-7 Shoulder Impingement Syndromes[43,149]

Syndrome	Causes and Clinical Features	MR Imaging and MR Arthrography Findings
Primary External (Extrinsic) Impingement		
A. Subacromial impingement	Pain caused by contact between the rotator cuff tendons (RCT) and abnormalities of the coracoacromial arch Pain is thought to be caused by irritation of the well-innervated subacromial-subdeltoid (SASD) bursa Occurs mainly in nonathletic persons over the age of 50 years Anterior or lateral shoulder pain produced by impingement of the SASD bursa and supraspinatus tendon between the greater tuberosity of the humerus and the coracoacromial arch during abduction and external rotation or during forward elevation and internal rotation	*MR imaging reveals:* a. acromioclavicular joint osteoarthrosis with subacromial enthesophyte b. developmental anomalies such as: os acromiale morphologic variations of acromion—types 2 and 3 downsloping acromion low-lying acromion c. posttraumatic abnormalities d. TRC tendinosis e. partial- or full-thickness tears of the anterior aspect of the supraspinatus tendon
B. Subcoracoid impingement	Pain caused by impingement of the subscapularis tendon, subcoracoid bursa, and joint capsule in the coracohumeral interval. Narrowing of the coracohumeral interval can be due to idiopathic, iatrogenic, or traumatic causes During internal rotation of the humerus, the coracoid process indents the superficial surface of the upper subscapularis tendon while stretching the deep surface of the tendon resulting in anteromedial shoulder pain and clicking during flexion, adduction, and internal rotation	*MR imaging reveals:* a. articular-sided subscapularis tendinosis and tear b. coracohumeral distance <6 mm on axial images c. subcoracoid bursal distention d. cortical irregularities of the lesser tuberosity e. Abnormalities of the long head of biceps
Secondary External (Extrinsic) Impingement	Pain caused by RCT impingement secondary to glenohumeral instability Occurs mainly in athletes involved in activities requiring repetitive overhead movements of the arm Stretched or lax joint capsule develops over time leading to increased workload on the rotator cuff resulting in cuff fatigue, superior migration of the humeral head, and narrowing of the supraspinatus outlet	*MR arthrography may help identify:* a. capsuloligamentous laxity b. causes of instability c. superior humeral head migration d. narrowing of supraspinatus outlet
Internal Impingement		
A. Posterosuperior impingement	Caused by friction between the glenoid and glenoid labrum, and the rotator cuff tendons Extreme abduction and external rotation (ABER) in athletes involved in overhead throwing activities results in excessive and repetitive impaction of the humeral head on the posterosuperior glenoid with entrapment of the posterior fibers of the supraspinatus tendon, anterior fibers of the infraspinatus tendon, and the posterosuperior labrum	MR arthrography performed in ABER position preferred a. cystic changes in posterolateral humeral head b. articular surface tears of the infraspinatus and posterior supraspinatus tendons c. tearing and fraying of the posterosuperior labrum including SLAP type 2 injuries
B. Anterosuperior impingement	Internal impingement of the biceps pulley system and the articular surface of the subscapularis tendon against the anterosuperior glenoid causing friction injury during anterior/horizontal elevation, adduction, and internal rotation of the shoulder	*MR imaging or MR arthrography demonstrate:* a. deep surface insertional subscapularis tear b. tear of the superior glenohumeral ligament—coracohumeral ligament complex c. subluxation of the long head of the biceps tendon d. superior labral tears

TABLE 13-8 Articular Disorders Affecting the Shoulder

Entity	Figure(s)	Characteristics
Degenerative and Related Disorders		
Osteoarthrosis: glenohumeral joint[56]	13-40	Primary osteoarthrosis occurs only infrequently Usually secondary to local trauma or disease processes, such as alkaptonuria, acromegaly, epiphyseal dysplasia, crystal deposition diseases, and hemophilia *Osteophytes:* glenoid, humeral head, and bicipital groove region Subchondral sclerosis Subchondral cysts *Elevation of humeral head:* secondary to rotator cuff degeneration and disruption
Osteoarthrosis: acromioclavicular joint[43,57]	13-41	Almost universal in elderly persons Diffuse pain or discomfort in the shoulder region; may radiate to upper arm; worse when arm is elevated between 120 and 180 degrees Joint space narrowing, osteophytes, and sclerosis Hypertrophy and superior subluxation of distal end of clavicle Osseous proliferation of superior surface of acromion Subacromial osteophytes may lead to impingement of the rotator cuff Osseous excrescences at site of coracoclavicular ligament may appear in elderly patients
Inflammatory Disorders		
Rheumatoid arthritis[58,59]	13-42	1. Glenohumeral joint Disability, pain, tenderness, restriction of motion, and soft tissue swelling Bilateral symmetric, concentric joint space narrowing Marginal subchondral erosions Cystic changes in superolateral region of humeral head adjacent to greater tuberosity Mild sclerosis of humeral head Elevation of humeral head secondary to rotatory cuff atrophy or tear Eventual deformity and flattening of humeral articular surface in severe disease Synovial cysts, rotator cuff tears, synovial abnormalities, and subacromial bursitis may be demonstrated by MR imaging or arthrography 2. Acromioclavicular joint Bilateral or unilateral involvement Pain, tenderness, and local soft tissue swelling Soft tissue swelling, subchondral osteopenia, erosions, subluxation Erosions predominate on the clavicle; may eventually result in extensive tapered or irregular osteolysis of the outer one third of the clavicle with apparent joint space widening 3. Coracoclavicular joint Elongated shallow erosions on the undersurface of the clavicle adjacent to the coracoid process (also seen in ankylosing spondylitis and hyperparathyroidism) Similar erosions within the upper ribs may also be observed
Juvenile idiopathic arthritis[60]		Diffuse concentric joint space narrowing, periarticular osteoporosis, bone enlargement, and erosions of the humeral head and subluxation
Ankylosing spondylitis[61]	13-43	1. Glenohumeral joint Thirty-two percent of patients with long-standing ankylosing spondylitis have glenohumeral joint involvement Bilateral > unilateral Osteoporosis and diffuse joint space narrowing Erosive changes of the superolateral portion of the humerus may be extensive, resulting in destruction of the entire outer aspect of the humerus (the hatchet sign) Elevation of humeral head secondary to rotator cuff atrophy and tear Joint ankylosis occurs infrequently 2. Acromioclavicular joint Bilateral erosive changes of distal end of clavicle may result in extensive resorption and widening of the joint space 3. Coracoclavicular joint Scalloped clavicular erosion similar to that of rheumatoid arthritis Ossification of coracoclavicular ligaments may infrequently occur

Continued

TABLE 13-8 Articular Disorders Affecting the Shoulder—cont'd

Entity	Figure(s)	Characteristics
Psoriatic arthropathy[62]	13-44	Shoulder involvement similar to, but less frequent than, ankylosing spondylitis Glenohumeral and acromioclavicular joints may be involved Findings range from minor erosions to severe osteolysis
Scleroderma (progressive systemic sclerosis)[63]	13-45	Globular accumulations of periarticular soft tissue calcinosis Bone resorption of the acromion and distal end of the clavicle Extensive osseous resorption may occur
Crystal Deposition and Metabolic Disorders		
Calcium hydroxyapatite crystal deposition[64,65,131,142]	13-46	Calcium hydroxyapatite crystal deposition in tendons, bursae, in capsules and ligaments about the shoulder, results in calcific tendinitis and bursitis May be asymptomatic or may be associated with painful episodes *Acute symptoms:* pain, tenderness on pressure, local edema or swelling, restricted active or passive motion and infrequently, mild fever *Chronic symptoms:* mild, nonincapacitating pain and tenderness Single or multiple cloudlike linear, triangular, or circular soft tissue calcifications within the rotator cuff tendons and subacromial and subdeltoid bursae Most frequently involved sites are the tendons of the supraspinatus, infraspinatus, teres minor, subscapularis, biceps, and pectoralis major muscles and the subacromial bursa Occasionally, large tumorlike accumulations of calcification will also be seen about the shoulder in patients with chronic renal disease or collagen vascular disorders Rare cause of inferior subluxation of humeral head (drooping shoulder) Chronic calcific tendinitis can infrequently lead to rotator cuff tear[152] and erosions of adjacent osseous structures[153]
Calcium pyrophosphate dihydrate (CPPD) crystal deposition[65,66]	13-47	Joint space narrowing, subchondral sclerosis, cysts, osteophytes, chondrocalcinosis; capsular, tendinous, and bursal deposits and rotator cuff tears Advanced destruction and fragmentation of the glenohumeral and acromioclavicular joints may occasionally resemble neuropathic osteoarthropathy in severe cases
Milwaukee shoulder syndrome[67,68]	13-48	Also termed *rapid destructive arthritis of the shoulder, hemorrhagic shoulder of the elderly,* or *apatite-associated destructive arthritis* Cause is unclear; believed to be related to a generalized process such as osteonecrosis or intraarticular deposition of mixed calcium phosphate crystals Predominates in elderly women with a history of trauma Symptoms mild in comparison with severe radiographic manifestations Severe rapid atrophic destruction of humerus and rotator cuff tear Bilateral in as many as 65% of patients *Differential diagnosis:* neuropathic joint disease, rheumatoid arthritis, secondary osteoarthrosis, CPPD crystal deposition disease, septic arthritis, or ochronotic arthropathy
Gouty arthropathy[69]	13-49	Involvement of glenohumeral and acromioclavicular joints is uncommon Soft tissue swelling, erosions, cysts, joint space narrowing, and proliferative changes of the glenohumeral joint; erosion of the distal end of the clavicle and irregular splaying of the acromioclavicular joint
Amyloid deposition[70,132]		Amyloid deposition within the soft tissues of the shoulder may occur as a primary process or in association with hemodialysis treatment, gout, inflammatory arthropathy, neoplasm, plasma cell myeloma, and collagen vascular disease Radiographic manifestations include osteoporosis, osteolytic lesions, pathologic fractures, osteonecrosis, soft tissue nodules and swelling, subchondral cysts and erosions, joint subluxations and contractures, and neuropathic osteoarthropathy Huge collections may result in hard rubbery masses about the shoulders, termed the *shoulder pad sign*
Hemochromatosis[71]	13-50	Rare disorder exhibiting findings identical to those of CPPD crystal deposition disease with chondrocalcinosis and secondary osteoarthrosis Prominent osteophytes, joint space narrowing, and irregularity of the humeral head may be seen

TABLE 13-8 Articular Disorders Affecting the Shoulder—cont'd

Entity	Figure(s)	Characteristics
Infectious Disorders		
Pyogenic septic arthritis[72,134-136]	13-51	Surgery, penetrating injury, immunosuppression, and debilitating illness, such as uncontrolled diabetes mellitus, all predispose to joint infection In intravenous drug abusers, the acromioclavicular joint frequently is involved, often with atypical organisms such as *Pseudomonas* ***Imaging findings*** Rapid concentric loss of joint space Poorly defined or "fuzzy" subchondral bone margins Periarticular osteoporosis Loss of definition and destruction of subchondral bone Capsular distention Erosions Slipped capital humeral epiphysis Metaphyseal osteomyelitis
Tuberculous arthritis[73,74]	13-52	Typically monoarticular disease in older patients Various degrees of soft tissue swelling Gradual joint space narrowing Juxtaarticular osteoporosis Peripherally located erosions Subchondral erosions Periarticular abscess Periostitis Subacromial (subdeltoid) bursitis may occur
Miscellaneous Disorders		
Pigmented villonodular synovitis[75,76,139]	13-53	Cystic erosions on both sides of the joint Hemorrhagic joint effusion Eventual osteoporosis Well-preserved joint space until late in the disease Extraarticular form is termed *giant cell tumor of the tendon sheath*
Idiopathic synovial (osteo)chondromatosis[77,78,163]	13-54	Multiple intraarticular or periarticular collections of calcification of variable size and density; monoarticular process Erosion of adjacent humerus and scapula may occur Secondary osteoarthrosis common Noncalcified bodies are best demonstrated with arthrography Secondary synovial osteochondromatosis may occur as a result of degenerative joint disease Extremely rare involvement of the acromioclavicular joint with large soft tissue mass and erosion of adjacent clavicle and acromion
Acromegalic arthropathy[79]	13-55	Abnormal cartilage proliferation results in secondary osteoarthrosis *Joint space:* widening in initial stages; narrowing in advanced stages Sclerosis, osseous fragmentation, and beaklike osteophytes on the inferior aspect of the humeral head
Hemophilic arthropathy[80,133]	13-56	Glenohumeral joint involvement includes secondary osteoarthrosis, osteoporosis, epiphyseal enlargement, joint space narrowing, and subchondral erosion, sclerosis, and cyst formation Rotator cuff disruption is a frequent finding
Neuropathic osteoarthropathy[81]	13-57	As many as 25% of patients with syringomyelia develop neuropathic osteoarthropathy, especially in the glenohumeral joint Fragmentation and sclerosis of the humeral head are common Cyst formation, dislocation, disorganization, and osseous debris Pathologic fractures of humerus, scapula, and clavicle

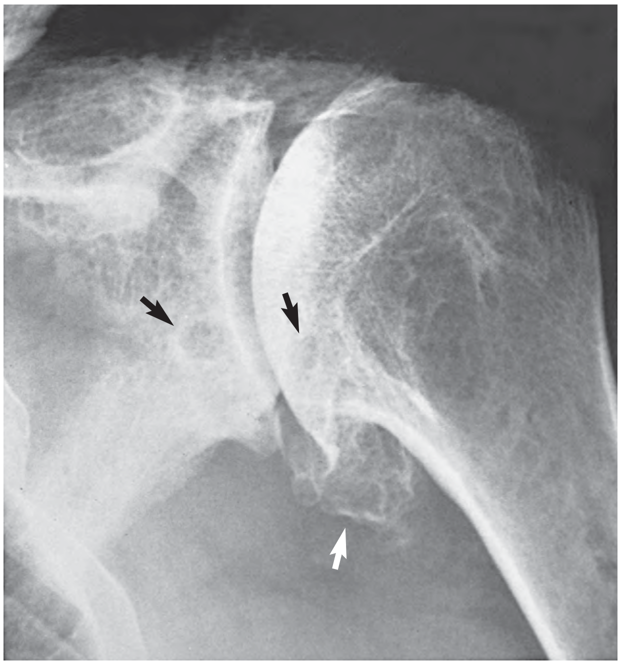

FIGURE 13–40 Osteoarthrosis (degenerative joint disease): glenohumeral joint.[56] In this patient with generalized osteoarthrosis of several joints, dramatic changes of the glenohumeral joint are seen. A large osteophyte *(white arrow),* nonuniform loss of joint space, subchondral sclerosis, and cyst formation *(black arrows)* are apparent. Poor visualization of the superolateral aspect of the humeral head is a photographic artifact and is not related to erosion or destruction. Degenerative disease of the glenohumeral joint is rare in the absence of trauma or other predisposing factors. *(Courtesy R. Shapiro, MD, Sacramento, Calif.)*

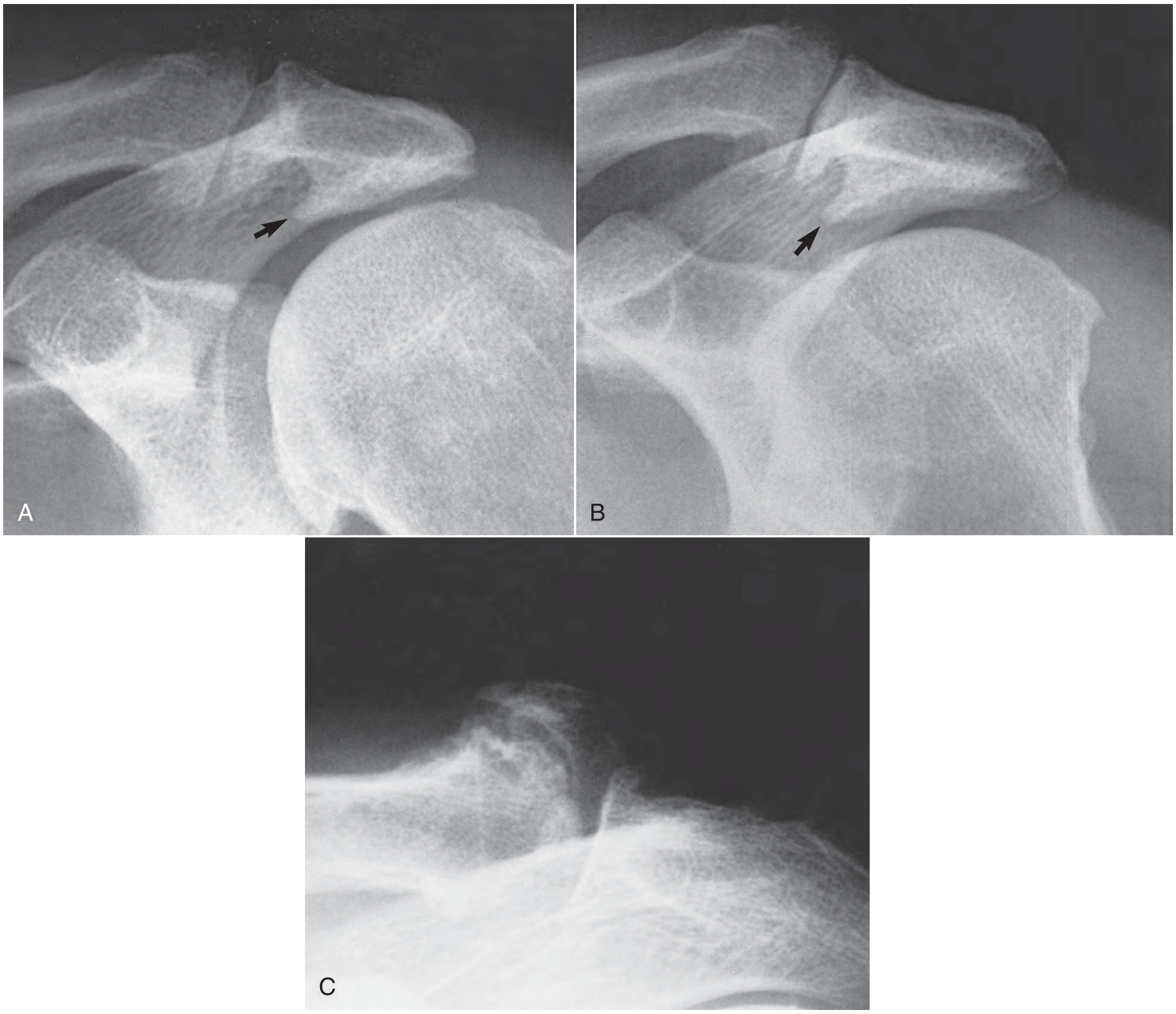

FIGURE 13–41 **Osteoarthrosis (degenerative joint disease): acromioclavicular joint.**[43,56,57] **A-B,** External rotation **(A)** and internal rotation **(B)** views of the shoulder reveal nonuniform joint space narrowing, osteophytes, subchondral sclerosis, and a large subacromial enthesophyte *(arrows)*. Enthesopathy at this site is implicated as an aggravating factor in the shoulder impingement syndrome and may contribute to rotator cuff tears.[149] **C,** In another patient with severe degenerative joint disease, extensive osteophyte formation and ossification of the intraarticular meniscus are present.

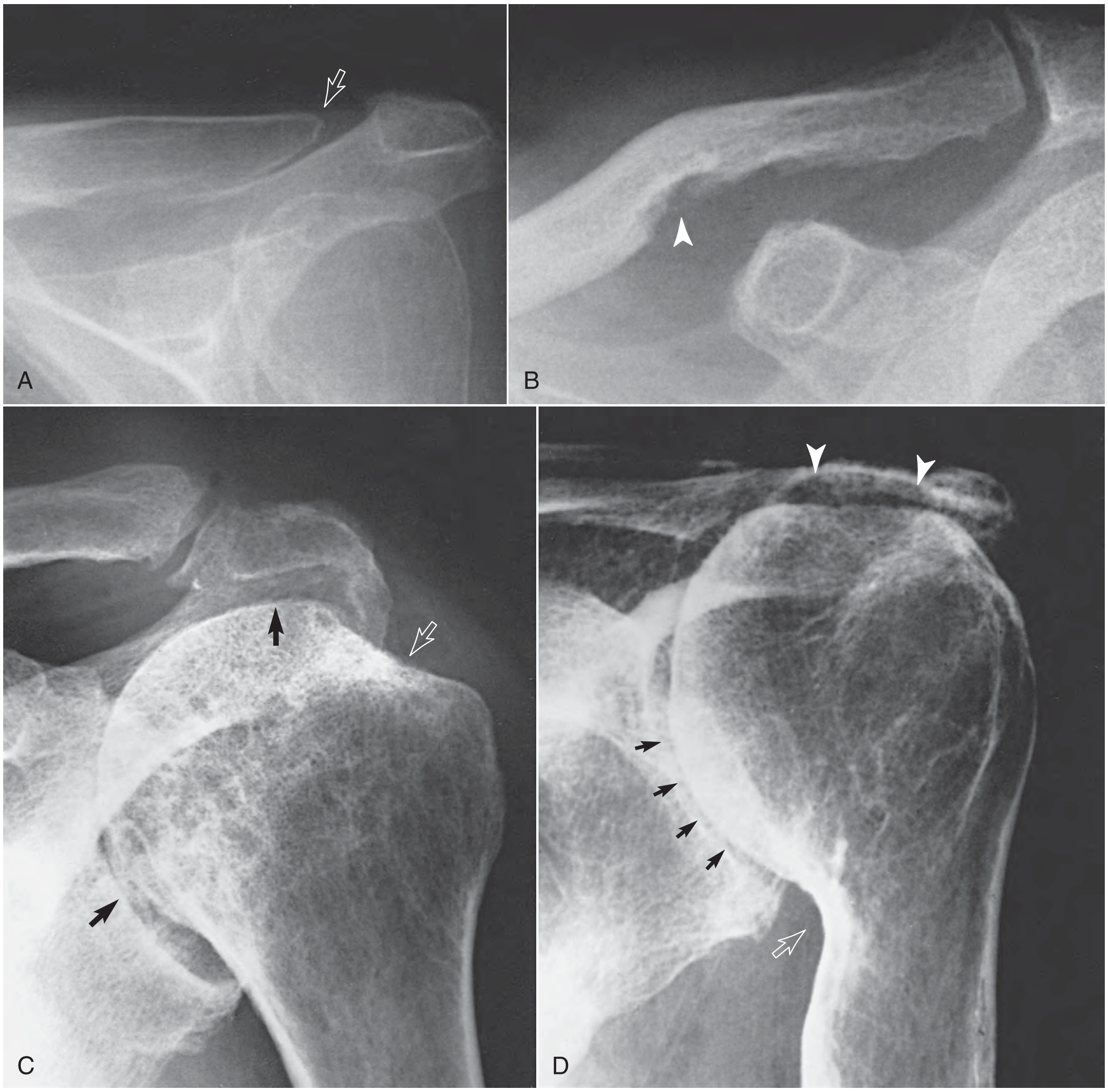

FIGURE 13–42 **Rheumatoid arthritis.**[58,59] **A-B,** Abnormalities of the acromioclavicular joint and clavicle. In **A,** resorption of the distal end of the clavicle results in tapering of the bone *(open arrow)* and widening of the acromioclavicular joint. In **B,** a prominent erosion is seen at the site of attachment of the coracoclavicular ligament *(arrowhead),* a frequent site of involvement in rheumatoid arthritis. A similar finding may be seen in hyperparathyroidism and ankylosing spondylitis. **C-D,** Abnormalities of the glenohumeral joint and acromiohumeral space. In **C,** the radiographic findings include superior subluxation of the humerus, acromiohumeral space and glenohumeral joint space narrowing *(arrows),* intraosseous cystic erosions within the humeral head and glenoid, and a large superolateral erosion of the humeral head resembling a Hill-Sachs fracture *(open arrow)*. In **D,** another patient with long-standing rheumatoid arthritis, observe the obliteration of the acromiohumeral space and glenohumeral joint space *(arrows),* diffuse osteopenia, erosion of the undersurface of the acromion *(arrowheads),* and a large erosion of the medial aspect of the humeral neck *(open arrow)*. Rotator cuff tear is common in rheumatoid arthritis and accounts for the narrowing of the acromiohumeral space and subsequent erosion of the inferior aspect of the acromion and distal end of the clavicle.

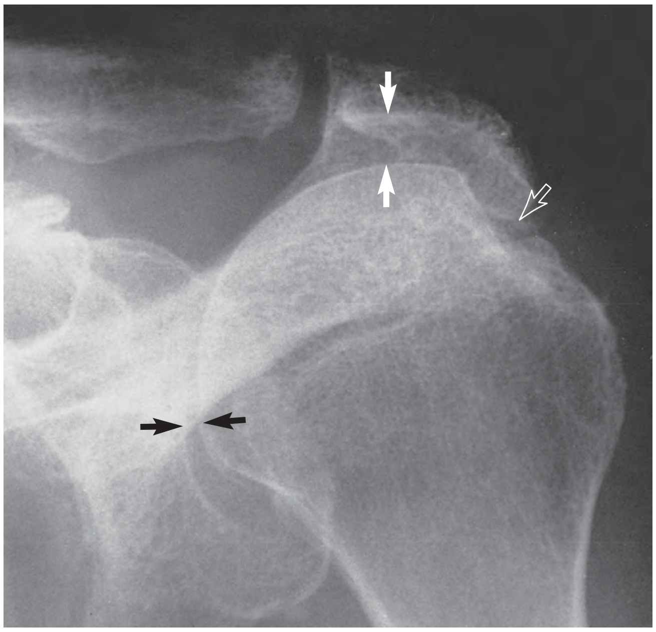

FIGURE 13–43 **Ankylosing spondylitis.**[61] Observe the elevation of the humerus and narrowing of the acromiohumeral space *(white arrows*) in this patient with ankylosing spondylitis and resultant rotator cuff tear. The glenohumeral joint space is narrowed *(black arrows)* and a large erosive defect is present along the lateral aspect of the humeral head *(open arrow)*. The glenohumeral joint is involved in approximately 32% of patients with long-standing ankylosing spondylitis.

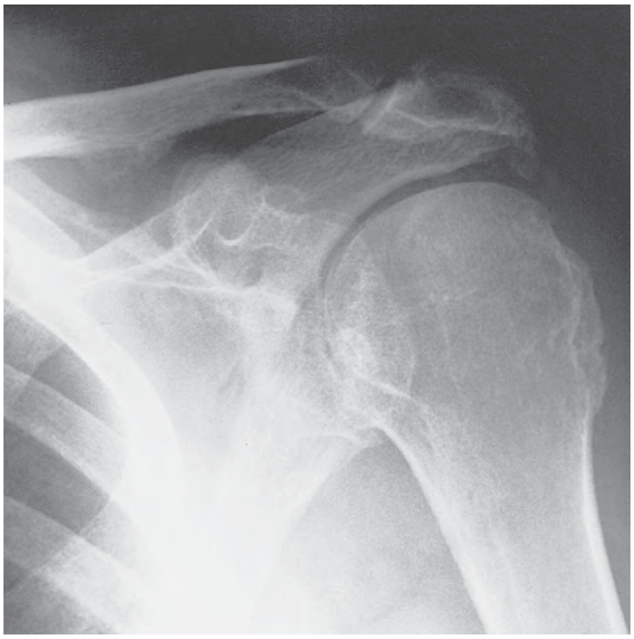

FIGURE 13–44 **Psoriatic arthropathy.**[62] This patient is a 49-year-old man with psoriasis and polyarticular joint disease. Frontal radiograph reveals fluffy bony excrescences arising from the humeral head, acromion, coracoid process, and site of attachment of the coracoclavicular ligament on the clavicle. The glenohumeral joint space is also narrowed. These findings are consistent with the appearance of a seronegative arthropathy.

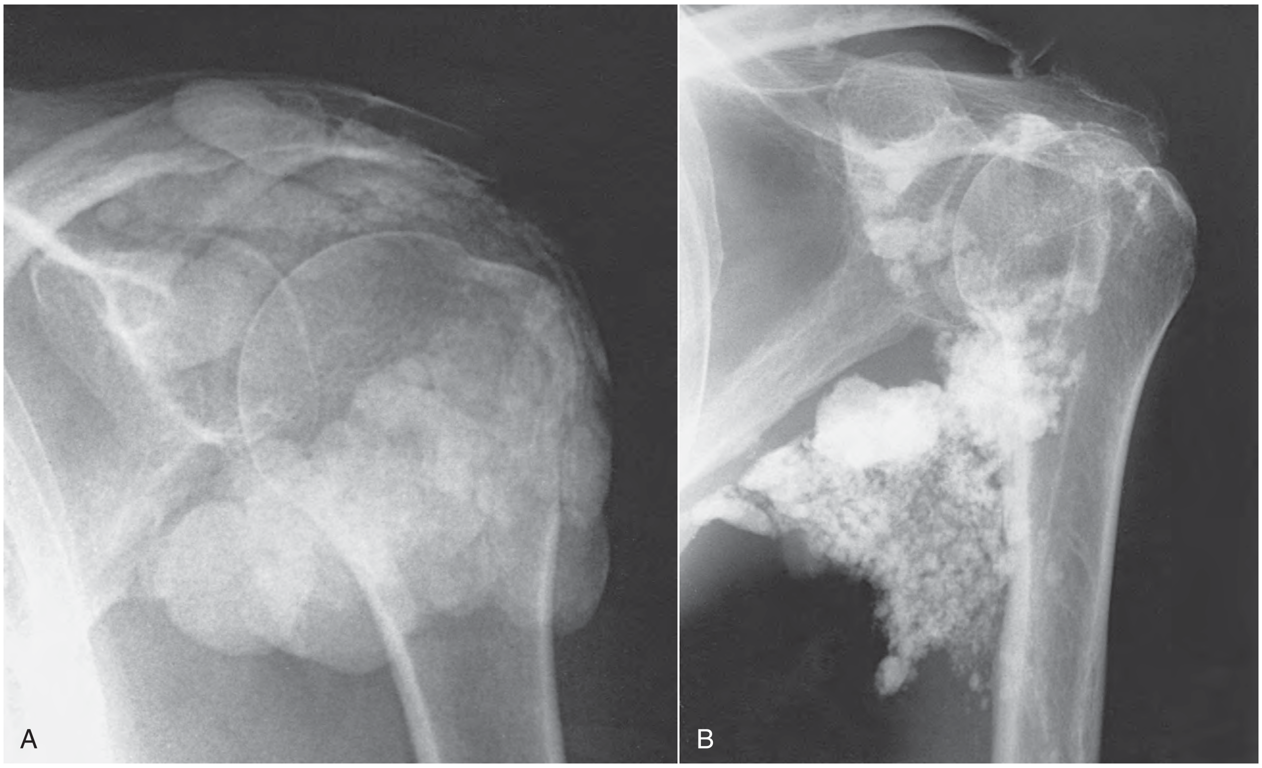

FIGURE 13–45 **Scleroderma (progressive systemic sclerosis).**[63] **A,** Cloudy accumulations of soft tissue calcification are seen adjacent to the glenohumeral joint and axilla in this 54-year-old man with polyarticular joint disease and esophageal abnormalities. **B,** In another patient, a sheetlike pattern of dense calcification predominates.

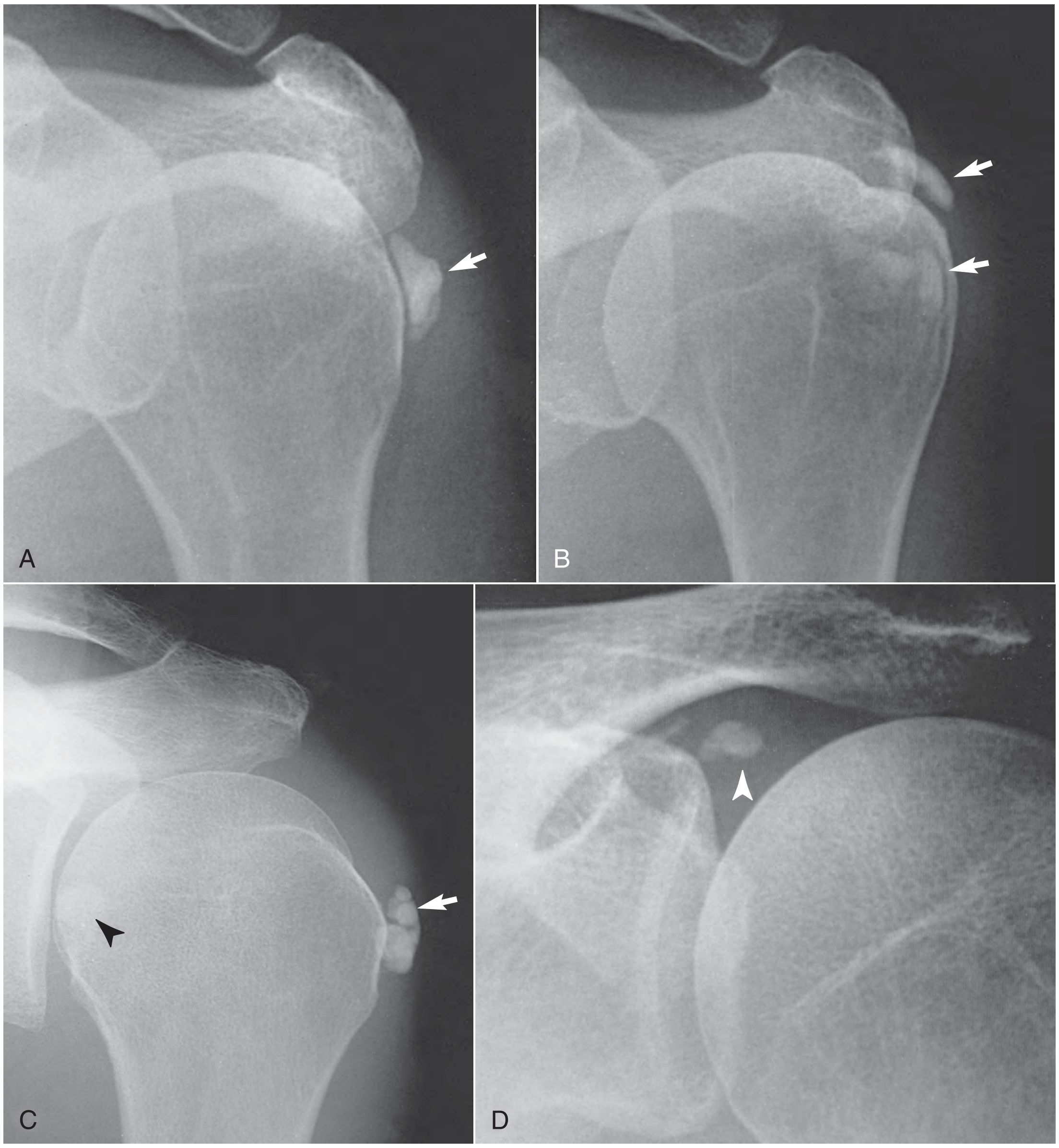

FIGURE 13–46 Calcium hydroxyapatite crystal deposition: calcific tendinitis.[64,65,131] **A-C,** Rotator cuff tendons. Internal rotation **(A)** and external rotation **(B)** radiographs reveal multiple accumulations of cloudlike calcification *(arrows)* within the tendons of the supraspinatus and infraspinatus muscles. In **C,** internal rotation radiograph shows globular calcification within the infraspinatus and teres minor tendons that appear lateral to the humeral head *(arrow)*. Another accumulation of calcification is present overlying the medial aspect of the humeral head *(arrowhead),* within the subscapularis tendon. **D,** Long head of the biceps brachii tendon. External rotation radiograph reveals calcification *(arrowhead)* in the vicinity of the biceps tendon near its attachment to the superior margin of the glenoid. (***A-B,*** *Courtesy D. Jones, MD, Southport, Australia.)*

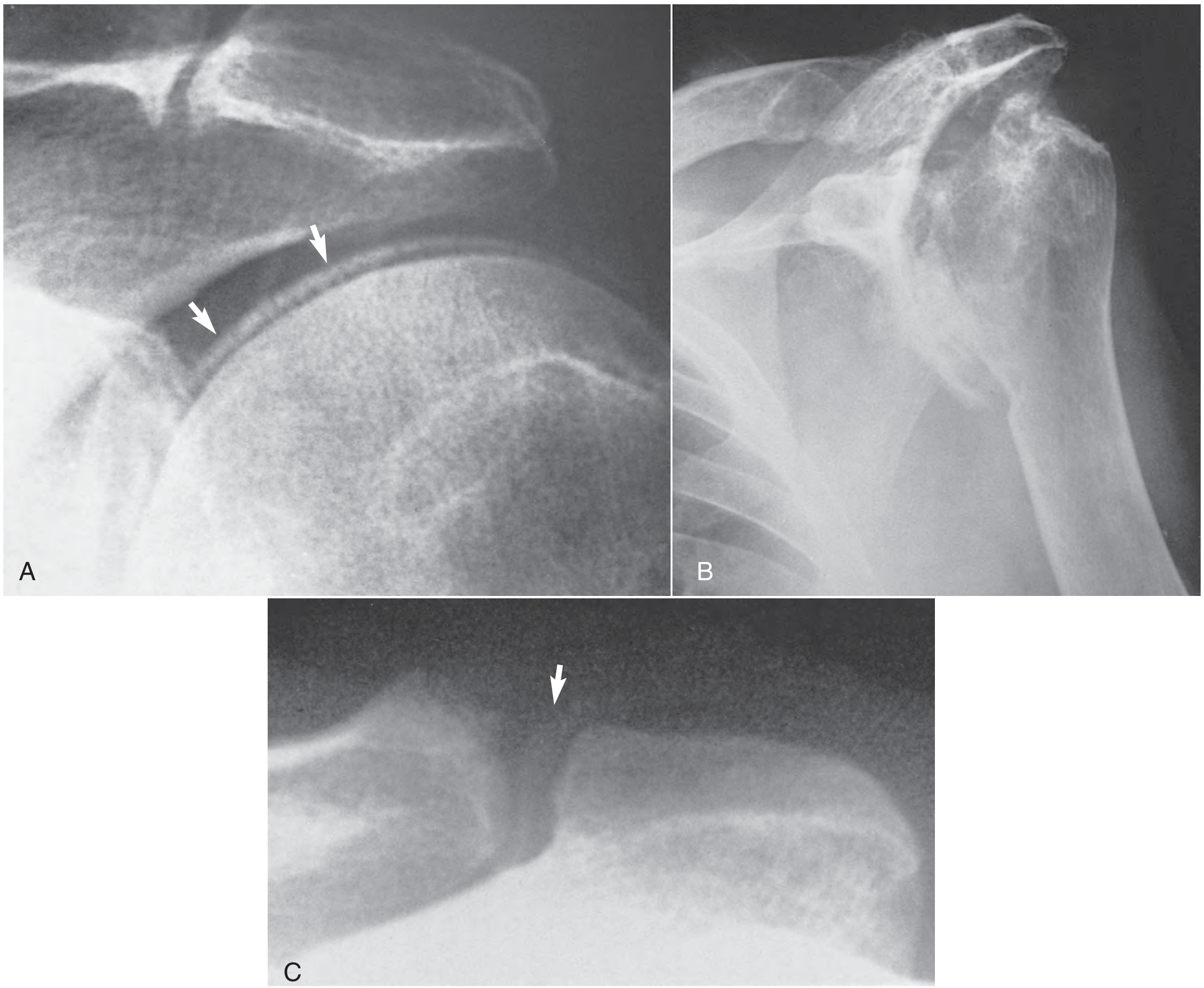

FIGURE 13–47 Calcium pyrophosphate dihydrate (CPPD) crystal deposition disease.[65,66,130] **A-B,** Glenohumeral joint. In **A,** chondrocalcinosis is present. Curvilinear calcification of the articular hyaline cartilage *(arrows)* within the glenohumeral joint parallels the humeral head. **B,** Pyrophosphate arthropathy. In another patient with CPPD crystal deposition disease, severe destructive osseous changes involving the proximal portion of the humerus, glenoid, and medial humeral metaphysis resemble the changes of neuropathic joint disease and Milwaukee shoulder syndrome. **C,** Acromioclavicular joint. Chondrocalcinosis is seen within the intraarticular cartilaginous disc of the acromioclavicular joint *(arrow)*. About 24% of patients with CPPD crystal deposition disease have acromioclavicular joint involvement. Other changes at this site may include soft tissue swelling, osseous sclerosis, joint space narrowing, and even tumorlike masses.

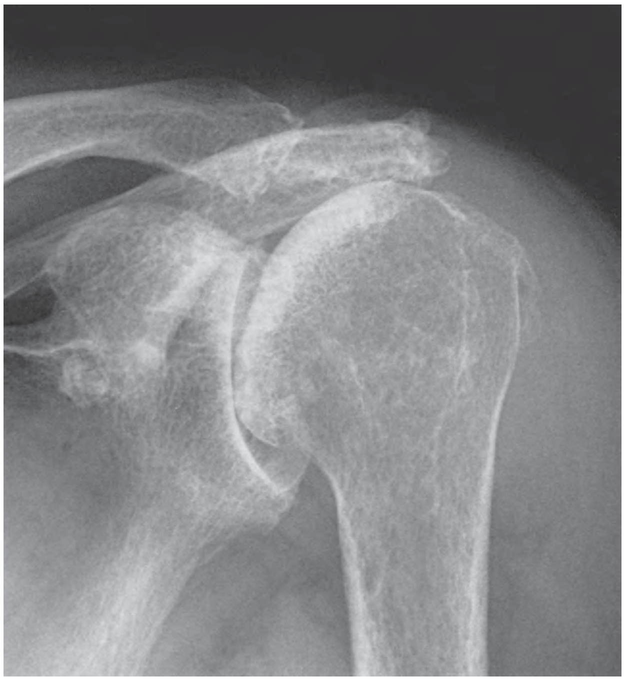

FIGURE 13–48 **Milwaukee shoulder syndrome: intraarticular crystal deposition.**[67,68] In a 75-year-old man, radiographic findings include joint space narrowing, elevation of the humerus from a rotator cuff tear, subchondral bone sclerosis, and flattening of the humeral head. Other findings include glenoid deformity, osteopenia, and erosions of the undersurface of the acromion. The Milwaukee shoulder syndrome refers to structural joint damage in patients with intraarticular accumulation of calcium hydroxyapatite and, to a lesser extent, calcium pyrophosphate crystals.

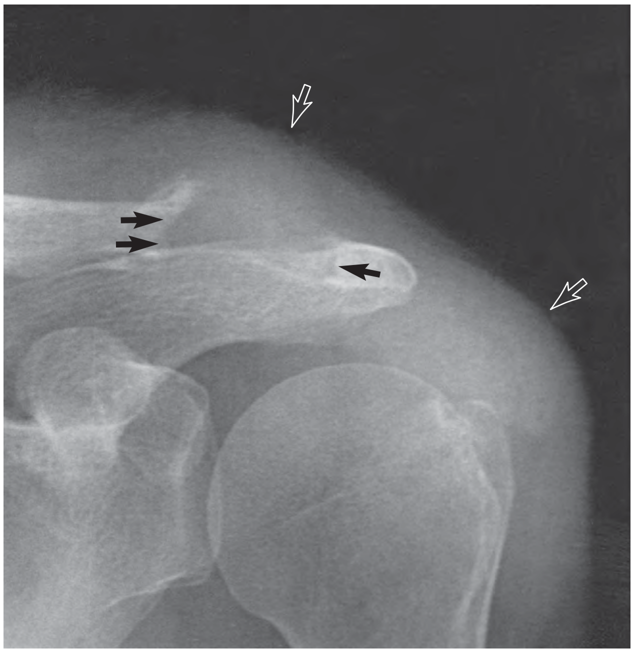

FIGURE 13–49 **Gouty arthropathy.**[69] This 53-year-old man has chronic tophaceous gout, gouty nephritis, and chronic renal insufficiency. Observe the extensive destruction of the subarticular bone about the acromioclavicular joint *(arrows)*. Large accumulations of radiodense soft tissue nodules in the subacromial-subdeltoid bursa and adjacent to the acromioclavicular joint *(open arrows)* may represent deposition of tophaceous material, calcium hydroxyapatite crystals, or amyloid secondary to chronic renal disease. *(Courtesy C. Chen, MD, Taipei, Taiwan.)*

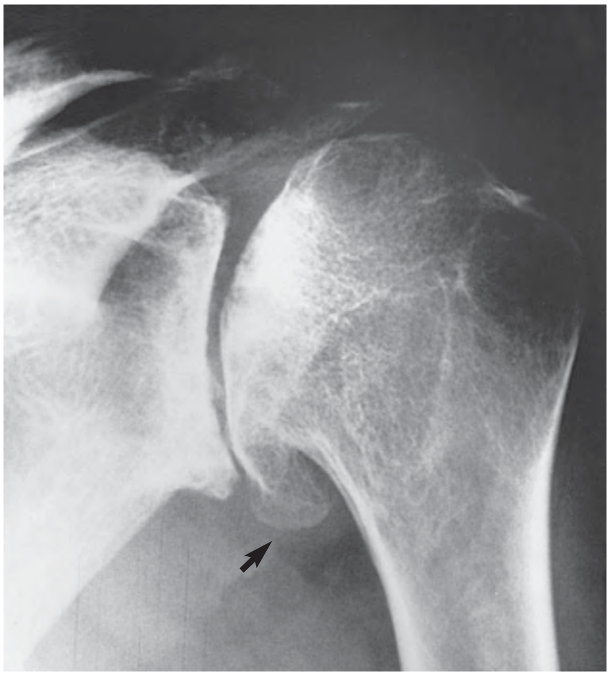

FIGURE 13–50 **Hemochromatosis.**[71] Radiographic findings in the shoulder include joint-space narrowing, subchondral sclerosis, deformity of the humeral head, and a large osteophyte arising from the inferior aspect of the humeral head *(arrow)*. *(Courtesy V. Vint, MD, San Diego.)*

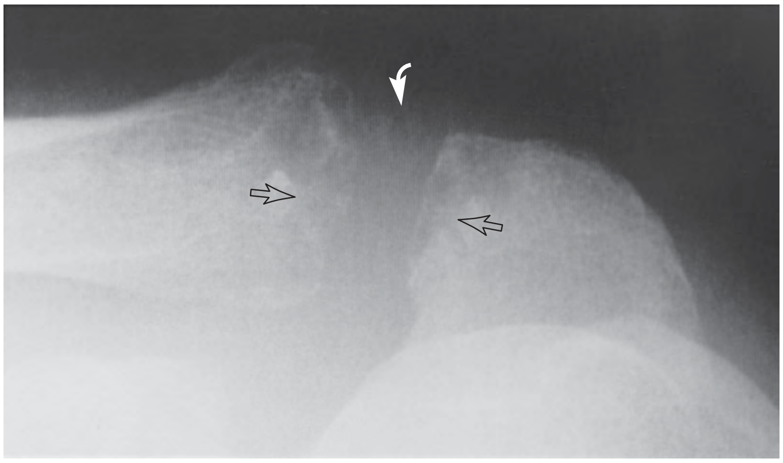

FIGURE 13–51 **Pyogenic septic arthritis: acromioclavicular joint.**[72,134-136] This intravenous heroin abuser developed gradual onset of shoulder pain. Frontal radiograph reveals widening of the joint space *(curved arrow)* and subchondral erosion of both the clavicle and the acromion *(open arrows)*. Joint aspirate contained *Pseudomonas* organisms. Intravenous drug abusers are predisposed to *Staphylococcus* and *Pseudomonas* infections of the acromioclavicular, sternoclavicular, spinal, and sacroiliac joints, as well as the symphysis pubis.

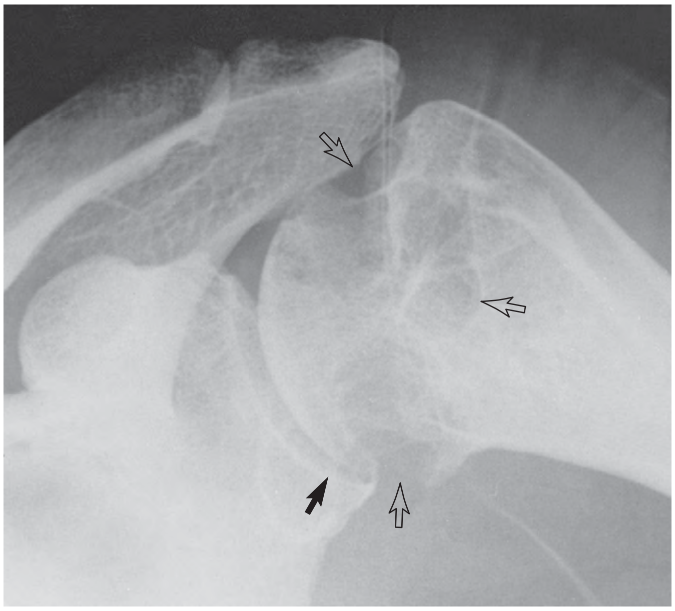

FIGURE 13–52 **Tuberculous arthritis: glenohumeral joint.**[73,74] Epiphyseal osteomyelitis is seen as widespread osteolytic cystlike erosions within the humeral head *(open arrows)*. The infection has disseminated to the glenohumeral joint and is characterized by marked joint-space narrowing *(small black arrow)*. The acromioclavicular joint does not appear to be affected.

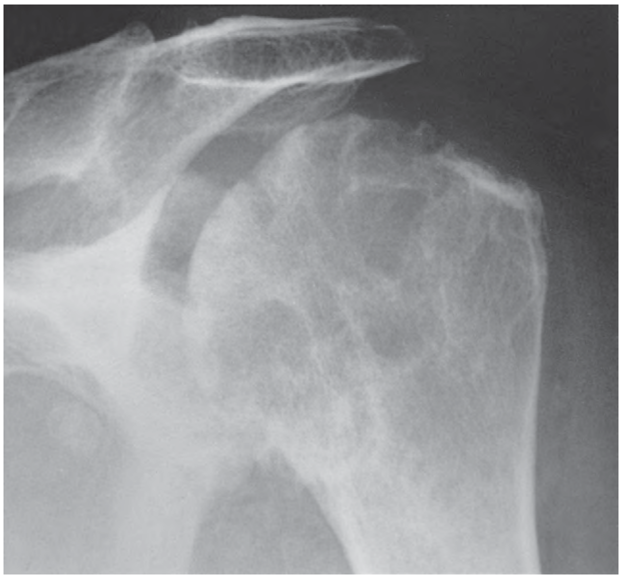

FIGURE 13–53 **Pigmented villonodular synovitis.**[75,76,139] The radiographic findings in this patient with chronic shoulder pain include large erosions involving the entire humeral head, widening of the glenohumeral joint space, and erosion of the subarticular bone of the glenoid. This synovial proliferative disorder of unknown cause is usually monoarticular, and 50% of patients report a history of previous trauma.

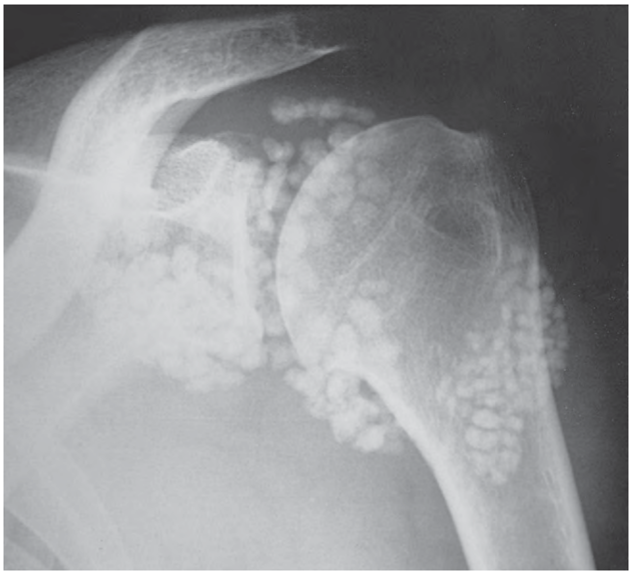

FIGURE 13–54 **Idiopathic synovial osteochondromatosis.**[77,78,163] Numerous juxtaarticular radiodense, osteocartilaginous bodies are present within the shoulder capsule. Idiopathic synovial osteochondromatosis represents metaplastic or neoplastic proliferation of cartilaginous bodies by the synovial membrane. It is typically discovered in patients between the ages of 20 and 40 years and is twice as common in men. Secondary synovial osteochondromatosis may also occur as a result of degenerative joint disease. *(Courtesy J. Slivka, MD, San Diego.)*

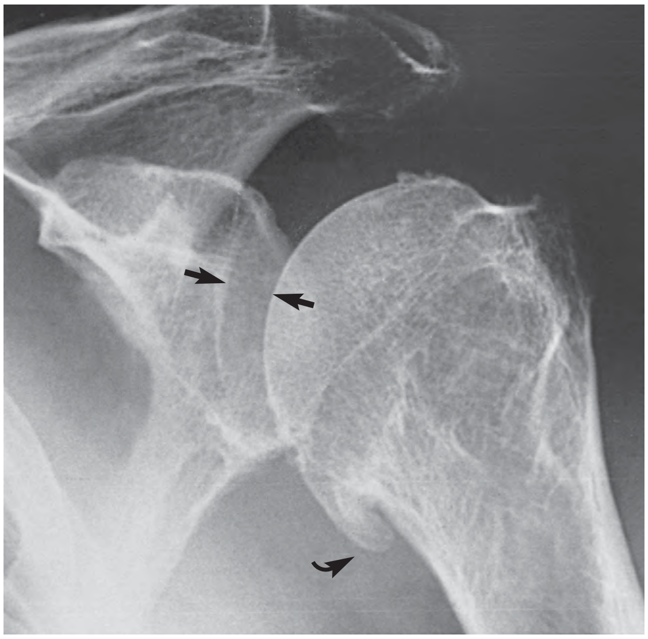

FIGURE 13–55 **Acromegalic arthropathy.**[79] Radiograph of the shoulder in this 53-year-old man reveals a large osteophyte *(curved arrow),* indicating accelerated degenerative joint disease of the glenohumeral joint. Cartilage proliferation has resulted in widening of the glenohumeral joint *(arrows)*. Most radiographic changes in acromegalic arthropathy relate to overgrowth of bone and soft tissues and resultant degenerative changes.

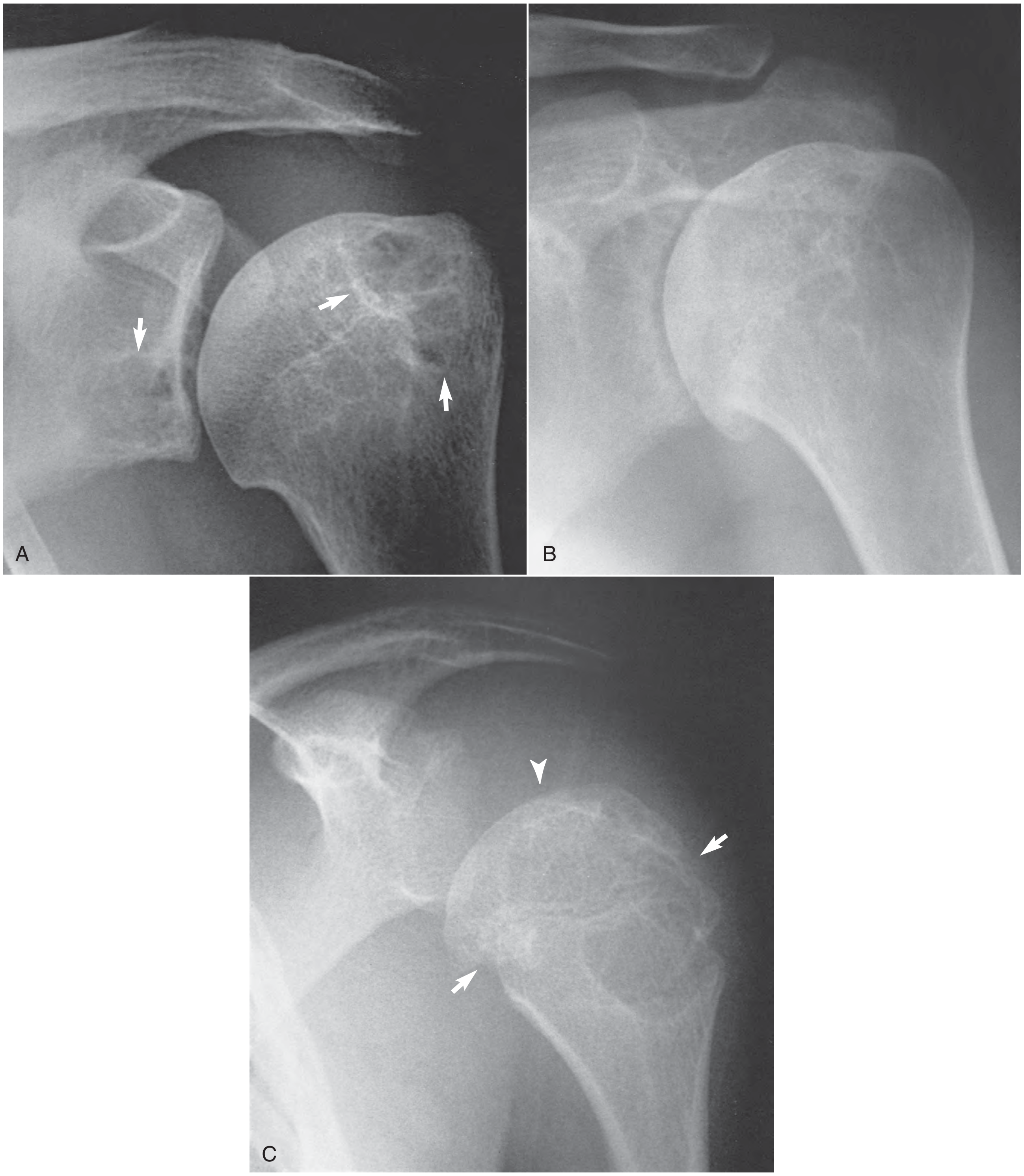

FIGURE 13–56 Hemophilic arthropathy.[80,133] **A,** This 29-year-old hemophilic man had a history of severe episodes of hemarthrosis of the glenohumeral joint. Observe the subchondral cysts within the glenoid and humeral head *(arrows)*. **B,** In another 29-year-old man, uniform joint space narrowing, sclerosis, osteophytosis, and cyst formation are seen. **C,** This 17-year-old boy has had long-standing hemophilia and has sustained several episodes of hemarthrosis. A frontal radiograph reveals a large joint effusion, probably a hemarthrosis, leading to inferior subluxation of the humeral head *(arrowhead)* with respect to the glenoid cavity. Significant articular surface erosions of the humeral head are apparent *(arrows)*. Both shoulders exhibited symmetric changes typical of hemophilic arthropathy. These changes closely resemble those of juvenile idiopathic arthritis.

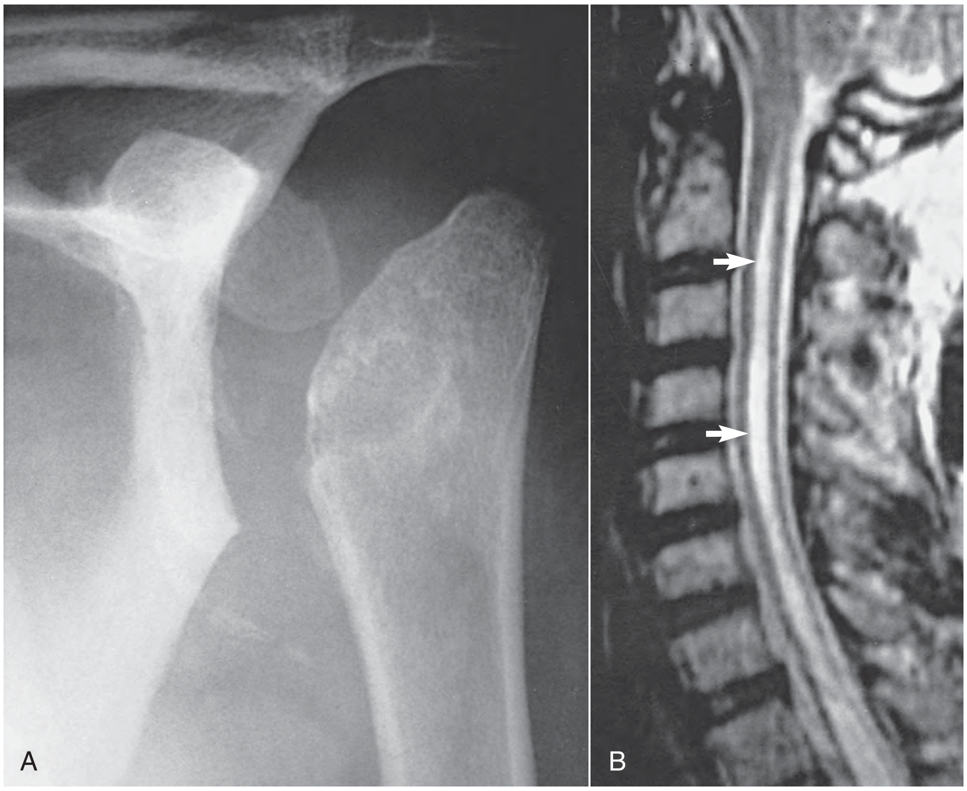

FIGURE 13–57 **Neuropathic osteoarthropathy: syringomyelia.**[81] **A,** Extensive atrophic destruction of the humeral head and glenoid is seen in this patient with a C3-C7 syrinx. Faint osseous debris is also present within the joint. **B,** In another patient, a sagittal T2-weighted (TR/TE, 3600/96) fast spin echo MR image reveals an expanded high signal intensity cerebrospinal fluid-filled cavity within the cervical and upper thoracic cord *(arrows)*. *(Courtesy D. Forrester, MD, and R. Kerr, MD, Los Angeles.)*

TABLE 13-9 Tumors and Tumorlike Lesions Affecting the Clavicle and Scapula

Entity	Figure(s)	Characteristics
Secondary Malignant Tumors of Bone		
Skeletal metastasis[82]	13-58	Osteolytic, osteoblastic, or mixed lesions occasionally occur within the scapula and clavicle Irradiation of primary breast or lung carcinoma may result in radiation-induced sarcoma, osteoporosis, and osteonecrosis
Primary Malignant Tumors of Bone		
Osteosarcoma[83,84]	13-59	One percent of osteosarcomas affect the scapula; fewer than 1% affect the clavicle Most osteosarcomas of the clavicle and scapula are secondary, arising from malignant transformation of Paget disease or irradiated bone
Osteoblastoma (aggressive)[85]		As many as 4% of aggressive osteoblastomas affect the scapula; fewer than 1% affect the clavicle Expansile osteolytic lesion that may be partially ossified or contain calcium
Chondrosarcoma[86]		Approximately 5% of chondrosarcomas affect the scapula; 1% affect the clavicle Tend to be osteolytic lesions sometimes containing a bulky cartilaginous cap and frequently containing calcifications Soft tissue masses common
Fibrosarcoma[87]		Approximately 2% of fibrosarcomas affect the scapula; 1% affect the clavicle
Ewing sarcoma[88]	13-60	As many as 5% of Ewing sarcomas affect the scapula; 2% affect the clavicle Aggressive permeative or moth-eaten pattern of bone destruction often associated with periostitis and soft tissue mass Most lesions central and metadiaphyseal in location

TABLE 13-9 Tumors and Tumorlike Lesions Affecting the Clavicle and Scapula—cont'd

Entity	Figure(s)	Characteristics
Myeloproliferative Disorders		
Plasma cell (multiple) myeloma[89]	13-61	Seventy-five percent of all plasma cell myeloma is the multiple form Approximately 5% of myeloma patients with skeletal lesions have scapular involvement; 10% have clavicular involvement Diffuse osteopenia or punctate osteolytic lesions
Solitary plasmacytoma[90]		Approximately 3% of plasmacytomas affect the scapula; 5% affect the clavicle
Hodgkin disease[91]		Approximately 3% of skeletal lesions in Hodgkin disease occur in the scapula; 1% occur in the clavicle
Primary lymphoma (non-Hodgkin)[92]		Approximately 4% of patients with primary non-Hodgkin lymphoma have scapular involvement; 2% have clavicular involvement May result in multiple moth-eaten or permeative osteolytic rib lesions Diffuse or localized sclerotic lesions are rare
Primary Benign Tumors of Bone		
Osteoid osteoma[93,94]		Rare occurrence within scapula and clavicle Central radiolucent nidus with surrounding reactive sclerosis
Osteoblastoma (conventional)[94]		Approximately 1% of conventional osteoblastomas affect the scapula; fewer than 1% affect the clavicle
Enchondroma (solitary)[95]		Approximately 1% of solitary enchondromas affect the scapula; fewer than 1% affect the clavicle
Maffucci syndrome[96]		More than 26% of patients with Maffucci syndrome have scapular lesions; fewer than 3% have clavicular lesions Soft tissue hemangiomas in addition to multiple enchondromas Higher risk of malignant transformation than solitary enchondroma
Chondroblastoma[97]		Approximately 2% of chondroblastomas involve the scapula; fewer than 1% involve the clavicle Radiolucent lesion, typically in a subchondral, epiphyseal, or apophyseal location Proximal humeral epiphysis is one of the most common sites (see Chapter 14)
Osteochondroma (solitary)[98,158]	13-62	Approximately 4% of solitary osteochondromas occur in the scapula; fewer than 1% occur in the clavicle Even though the scapula is a rare location for osteochondroma, the ventral surface of the scapula is the most common site of origin of bursa formation in association with osteochondroma
Hemangioma[99]	13-63	Approximately 2% of hemangiomas occur in the scapula; 1% occur in the clavicle Osseous expansion and trabecular striation within lesions
Aneurysmal bone cyst[100]	13-64	Approximately 2% of aneurysmal bone cysts involve the scapula and 3% involve the clavicle; one of the most common benign tumors of the clavicle Eccentric, thin-walled, expansile, multiloculated osteolytic lesion
Tumorlike Lesions		
Paget disease[101,102]	13-65	Paget disease involves the scapula and clavicle infrequently Usually polyostotic and may exhibit unilateral involvement
Neurofibromatosis 1 (von Recklinghausen disease)[103]		Involvement of scapula and clavicle is uncommon Clavicular pseudarthrosis may result from improper fracture healing
Monostotic fibrous dysplasia[104]		Approximately 2% of all monostotic lesions affect the scapula; fewer than 1% affect the clavicle Improper fracture healing may result in clavicular pseudarthrosis
Polyostotic fibrous dysplasia[104]	13-66	The scapula is involved in more than 33% of cases and the clavicle is involved in 10% of cases of polyostotic fibrous dysplasia Unilateral (or infrequently, bilateral asymmetric) involvement
Langerhans cell histiocytosis[105,106]	13-67	Five percent of lesions affect the clavicle and scapula Histiocytic infiltration of bone Eosinophilic granuloma is the most frequently encountered form

See also Tables 1-12 to 1-14.

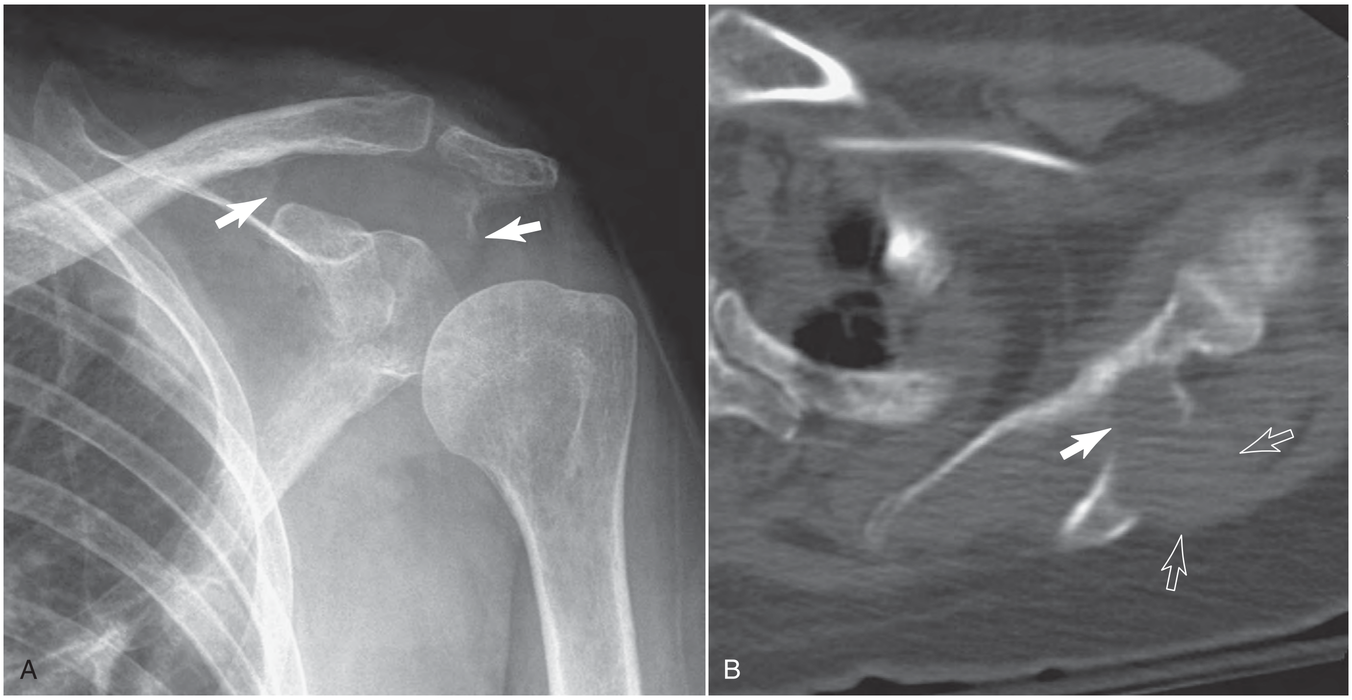

FIGURE 13–58 **Skeletal metastasis: scapula.**[82] This 49-year-old woman with a previous diagnosis of primary carcinoma of the thyroid gland had shoulder pain. **A,** A frontal radiograph reveals permeative osteolytic destruction of the superolateral aspect of the scapula including most of the spine of the scapula and proximal portion of the acromion *(arrows)*. **B,** A transverse CT bone window image reveals cortical destruction *(arrow)* and a large soft tissue mass *(open arrows)* projecting dorsally.

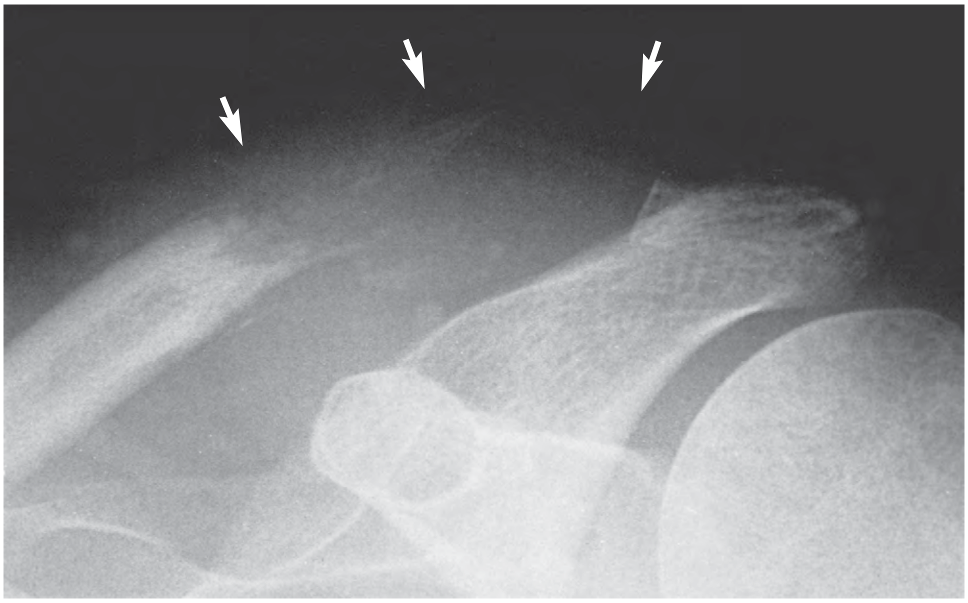

FIGURE 13–59 **Osteosarcoma.**[83,84] This 50-year-old man had severe shoulder pain. Radiographs reveal extensive osteolytic destruction of the distal end of the clavicle *(arrows)*. The histologic diagnosis was osteosarcoma.

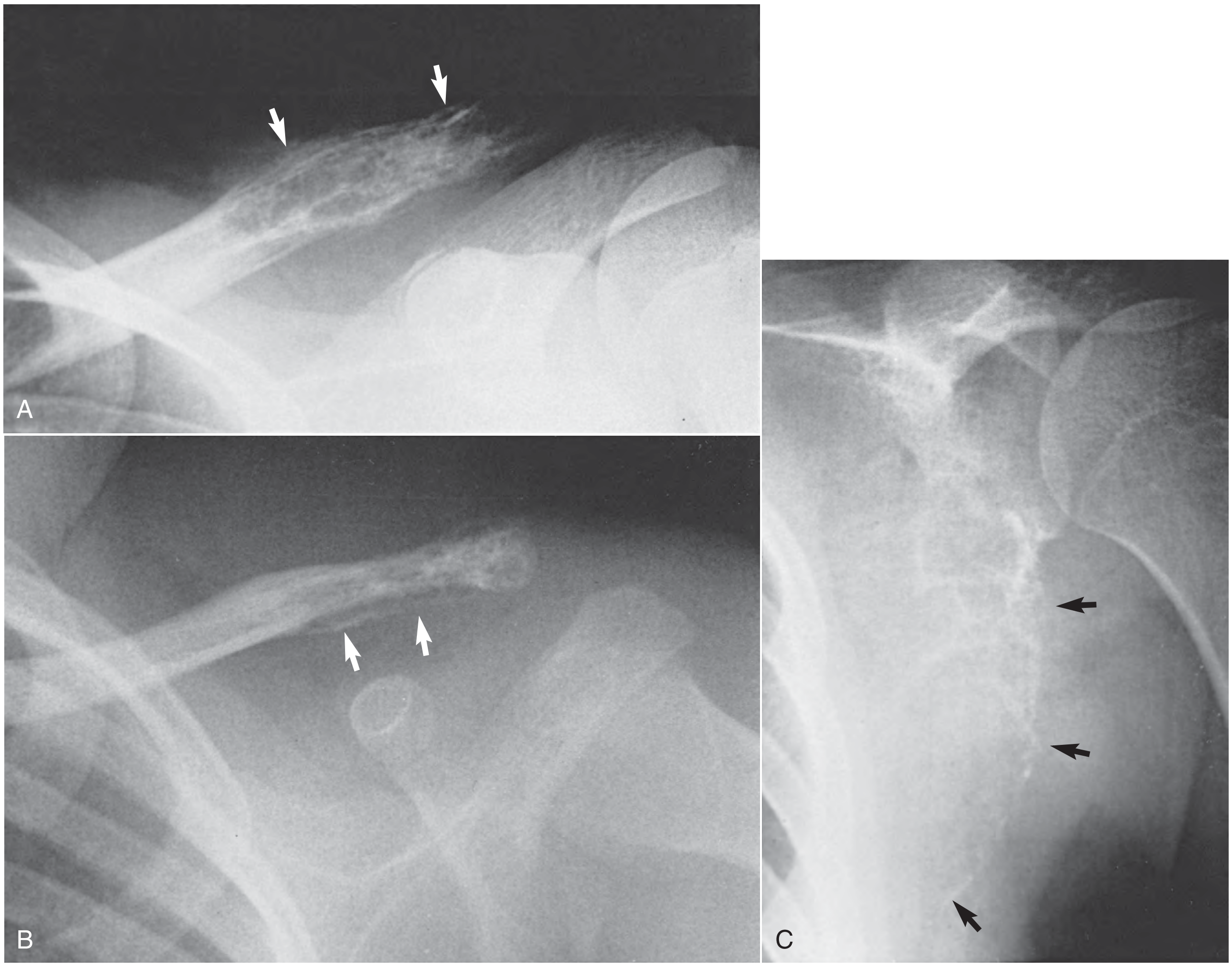

FIGURE 13–60 **Ewing sarcoma.**[88] **A,** Clavicle. In a 13-year-old girl, permeative osteolysis is seen within this expansile lesion of the clavicle *(arrows)*. **B,** Clavicle. A radiograph of the clavicle of this 3-year-old child with Ewing sarcoma shows a permeative pattern of osteolysis with a laminated periosteal response *(arrows)*. **C,** Scapula. A radiograph of the shoulder in this 15-year-old girl shows an expansile, multiloculated osteolytic lesion involving the majority of the body of the scapula *(arrows)*. (**C,** *Courtesy R. Kerr, MD, Los Angeles.)*

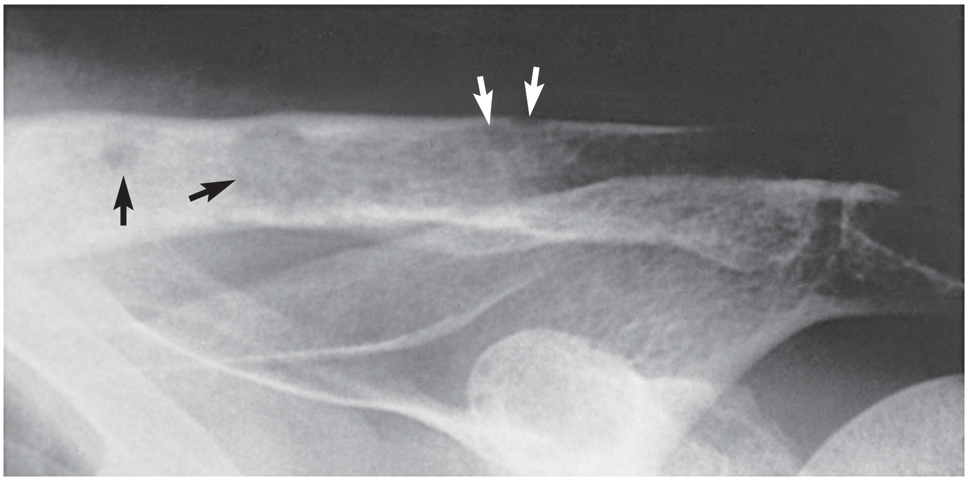

FIGURE 13–61 **Plasma cell myeloma.**[89] Several small and large punctate osteolytic lesions *(arrows)* are present throughout the clavicle.

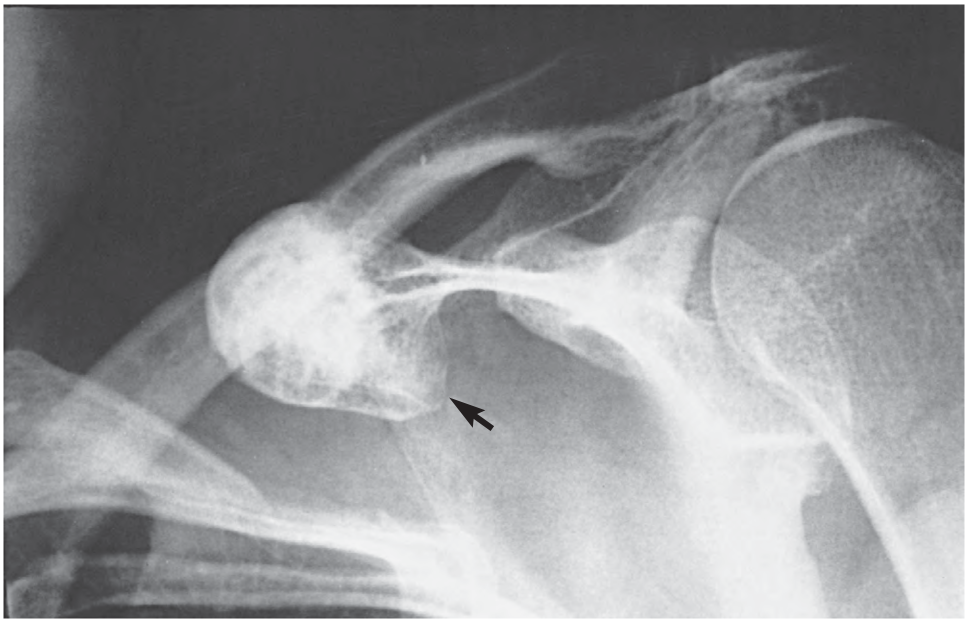

FIGURE 13–62 **Osteochondroma.**[98] Observe the bulbous osteochondroma arising from the medial border of the scapula *(arrow)* in this 34-year-old man with hereditary multiple exostoses.

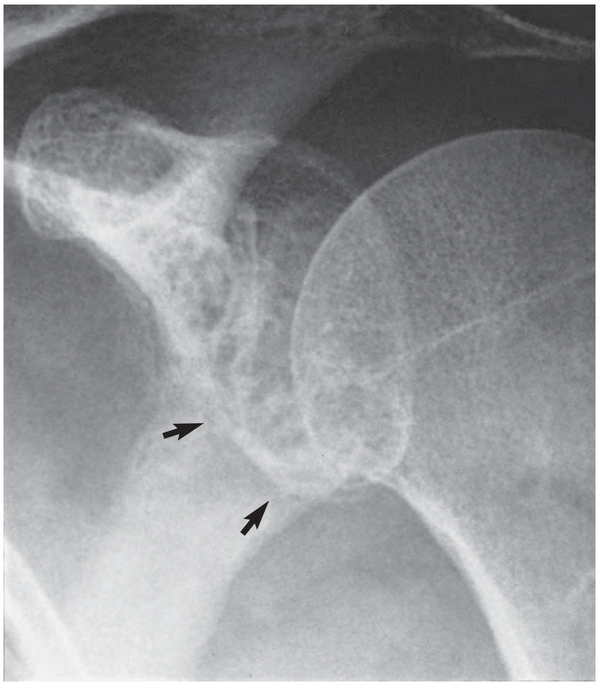

FIGURE 13–63 **Hemangioma.**[99] Note the trabeculated osteolytic lesion affecting the glenoid of the scapula *(arrows),* an incidental finding in this 55-year-old woman who was undergoing radiographic examination for evaluation of a shoulder injury.

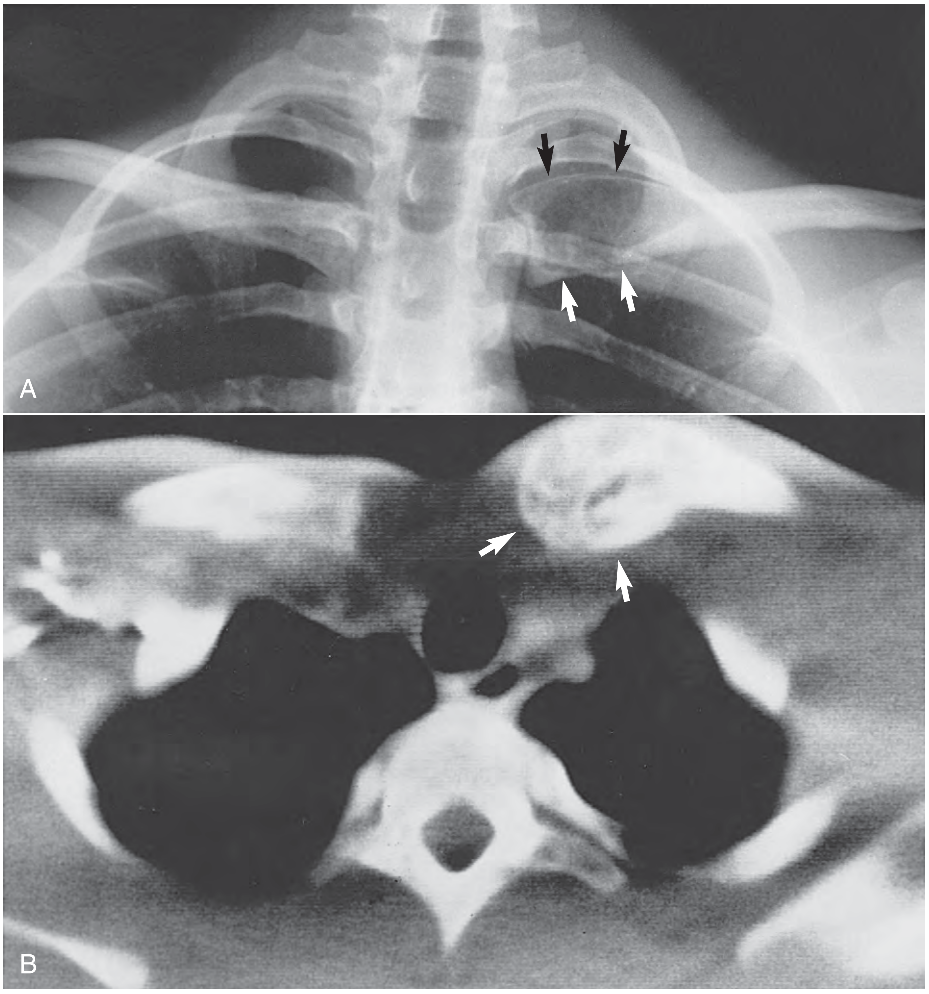

FIGURE 13–64 **Aneurysmal bone cyst.**[100] This 18-year-old man had sternoclavicular pain. **A,** Frontal radiograph. Comparison of the clavicles reveals an expansile osteolytic lesion involving the proximal portion of the left clavicle *(arrows)*. **B,** Transaxial CT image confirms the expansile osteolytic nature of the tumor *(arrows)* and demonstrates that the cortex is intact; no adjacent soft tissue mass is present. *(Courtesy M. Mitchell, MD, Halifax, Nova Scotia, Canada.)*

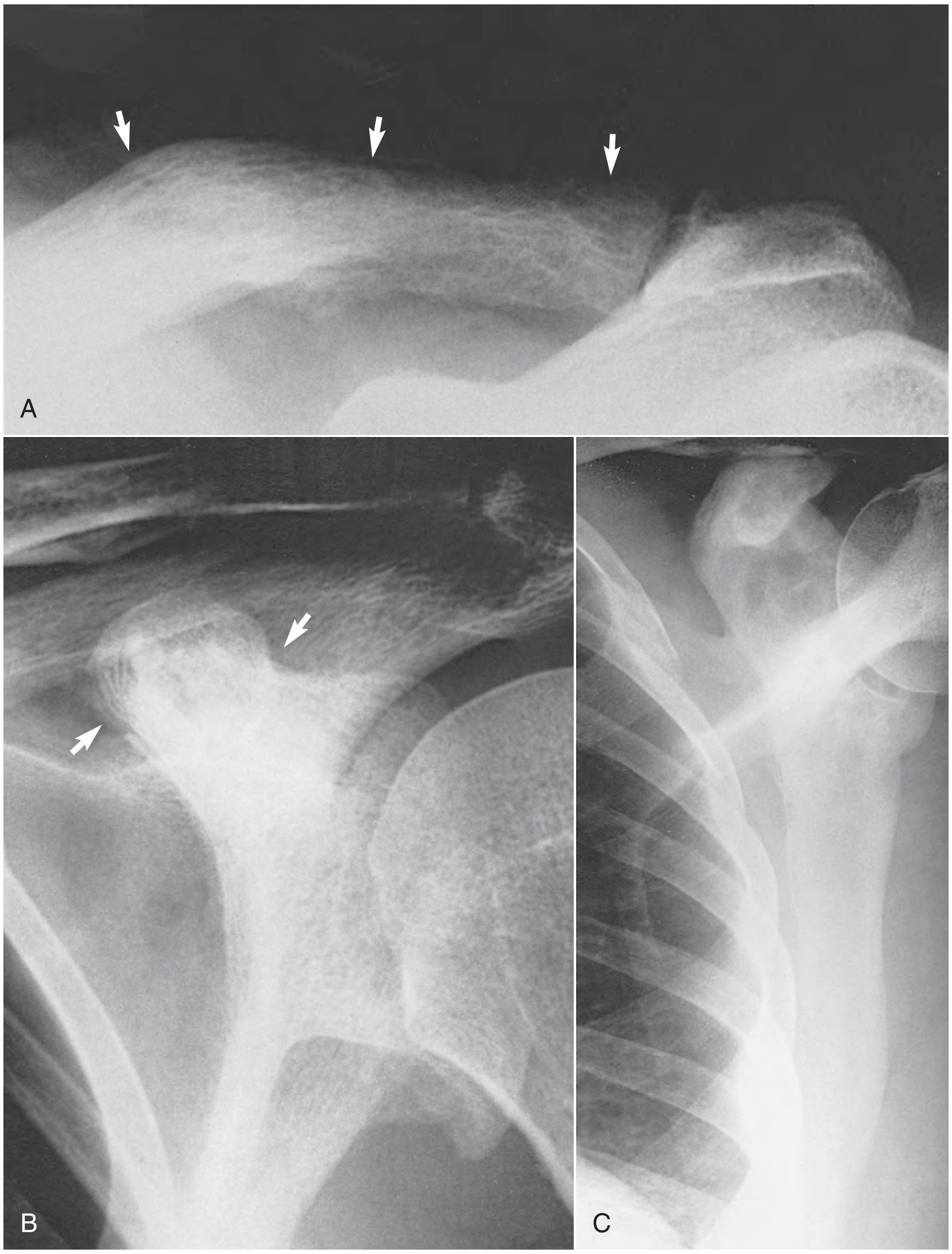

FIGURE 13–65 **Paget disease.**[101,102,137,138] **A,** Clavicle. Bone enlargement and trabecular coarsening *(arrows)* predominate in the clavicle of this patient with Paget disease. **B,** Scapula. Observe the osteosclerotic appearance and enlargement of the coracoid process *(arrows),* scapular neck, and glenoid. **C,** Body of the scapula. Note the osteosclerosis, cortical enlargement, and thickening and coalescence of the trabeculae throughout the scapula of this 65-year-old woman with Paget disease. The adjacent ribs and humerus were not affected. (**C,** *Courtesy E. Dal Mas, DC, Portland, Ore.)*

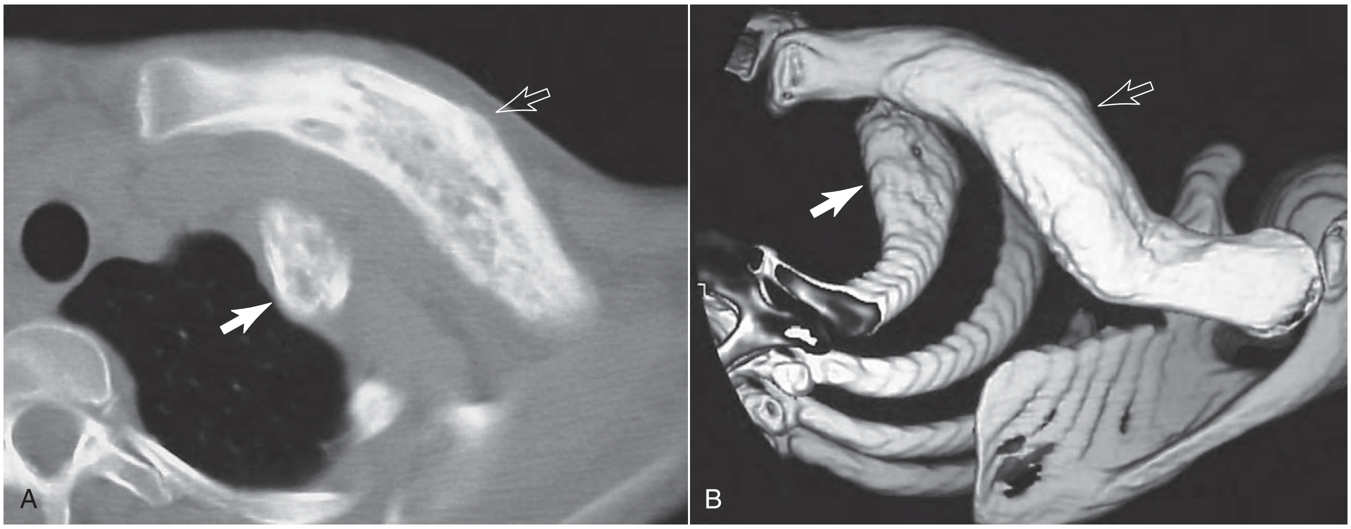

FIGURE 13–66 **Polyostotic fibrous dysplasia: clavicle.**[104] **A,** A transverse CT bone window scan shows enlargement of the clavicle *(open arrow)* and first rib *(arrow)* with cortical thickening and moth-eaten foci of osteolysis. **B,** A reconstructed 3-dimensional surface-rendered image viewed from above more clearly depicts the enlargement of the clavicle *(open arrow)* and first rib *(arrow)*.

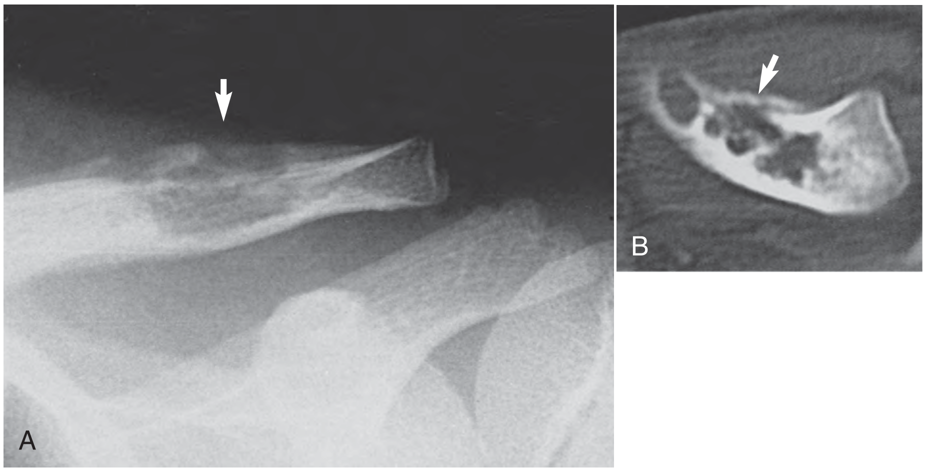

FIGURE 13–67 **Langerhans cell histiocytosis: eosinophilic granuloma.**[105,106] **A,** Frontal radiograph of a 9-year-old boy shows an expansile lesion with periostitis and a permeative pattern of osteolytic destruction involving the distal clavicular diaphysis *(arrow)*. **B,** Transaxial CT, image further documents the osteolytic, expansile, and septated appearance of the lesion *(arrow)*. Biopsy revealed eosinophilic granuloma of bone, the most frequent and mildest form of Langerhans cell histiocytosis. *(Courtesy G. Greenway, MD, Dallas.)*

TABLE 13-10 Metabolic, Hematologic, and Infectious Disorders Affecting the Shoulder

Disorder	Figure(s)	Characteristics
Generalized osteoporosis[107]	13-68	*Major complication:* fractures of the proximal portion of the humerus (see Chapter 14)
Osteomalacia[108]		Osteopenia Decreased trabeculae; remaining trabeculae appear prominent and coarsened Looser zones or pseudofractures
Rickets[108]		Findings most prominent in the proximal portion of the humerus *Metaphyseal demineralization:* frayed, widened, cupped metaphyses Bowing of bones Osteopenia
Hyperparathyroidism and renal osteodystrophy[109-111]	13-69	Bone resorption and erosion involving the distal end of the clavicle and the undersurface of the clavicle at the attachment site of the coracoclavicular ligaments Occasional bone sclerosis (more common with renal osteodystrophy) Chondrocalcinosis (CPPD crystal deposition) Brown tumors Soft tissue calcification Slipped capital humeral epiphysis Pathologic fracture
Milk-alkali syndrome[112]	13-70	Metastatic periarticular soft tissue calcification in persons who ingest large quantities of milk and alkaline substances Patients with chronic peptic ulcer disease and renal insufficiency Osseous tissues are normal Widespread calcification also occurs in blood vessels, kidneys, falx cerebri, and ligaments
Osteonecrosis[113,114]	13-71	Also termed *ischemic necrosis* or *avascular necrosis* of the humeral head Sclerosis, subchondral cysts, subchondral bone collapse, and eventual flattening of the humeral head; snowcap appearance may occur Predisposing factors include corticosteroid use, hemoglobinopathies, Gaucher disease, trauma, and alcoholism
Radiation changes of bone[115]	13-72	Radiation therapy for carcinoma of the breast and/or lung apex may result in radiation osteitis, osteonecrosis, and sarcoma formation Radiographic findings of osteitis and osteonecrosis include subchondral bone destruction, osseous debris, and joint disorganization resembling neuropathic osteoarthropathy
Pyogenic osteomyelitis[116,135]	13-73	Clavicle and scapula infrequently involved Initial latent period in which no radiographic signs are present—days to weeks *Early signs:* Soft tissue swelling with obliteration of soft tissue planes *Late signs:* Osteoporosis, osteolysis, cortical lucency, periostitis, involucrum formation, sequestration, and sinus tracts May be associated with septic arthritis of adjacent joints

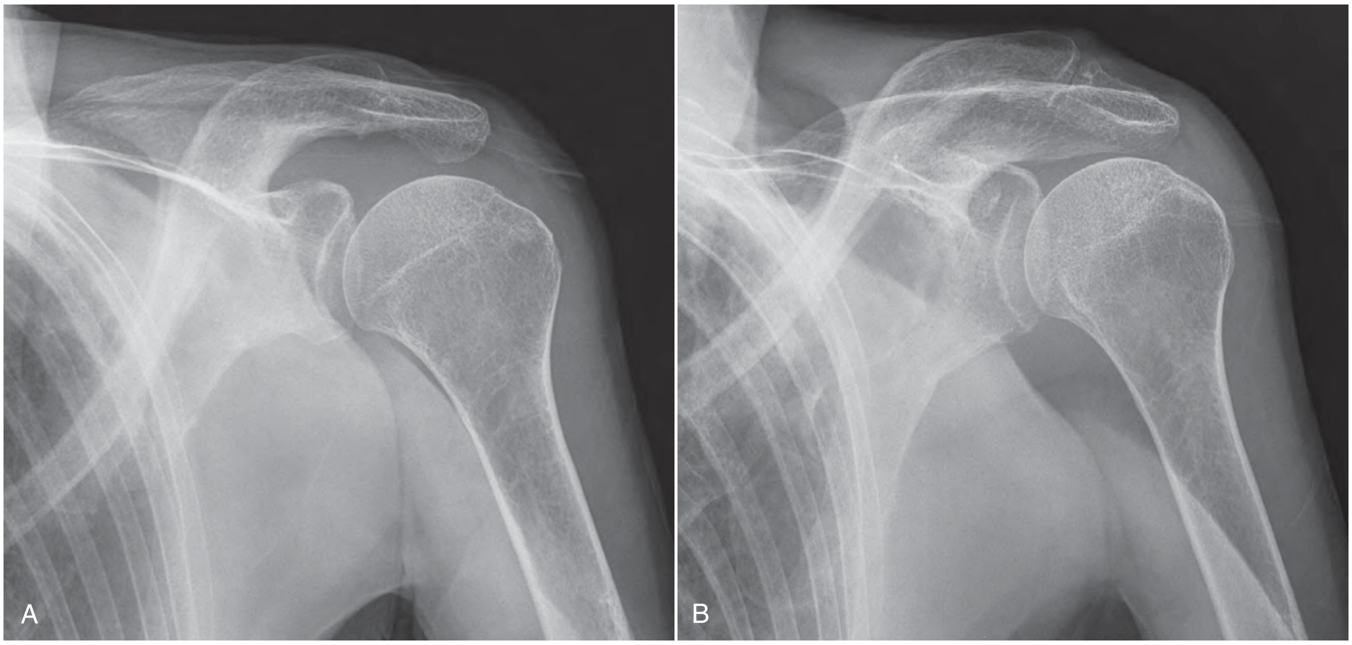

FIGURE 13–68 **Generalized osteoporosis.**[107] Anteroposterior neutral **(A)** and internal rotation **(B)** views of the shoulder in this 91-year-old woman depict prominent radiolucency and cortical thinning throughout the humerus, scapula, clavicle, and thoracic cage. No fractures are visible, but patients with severe osteoporosis are at considerably higher risk for fracture.

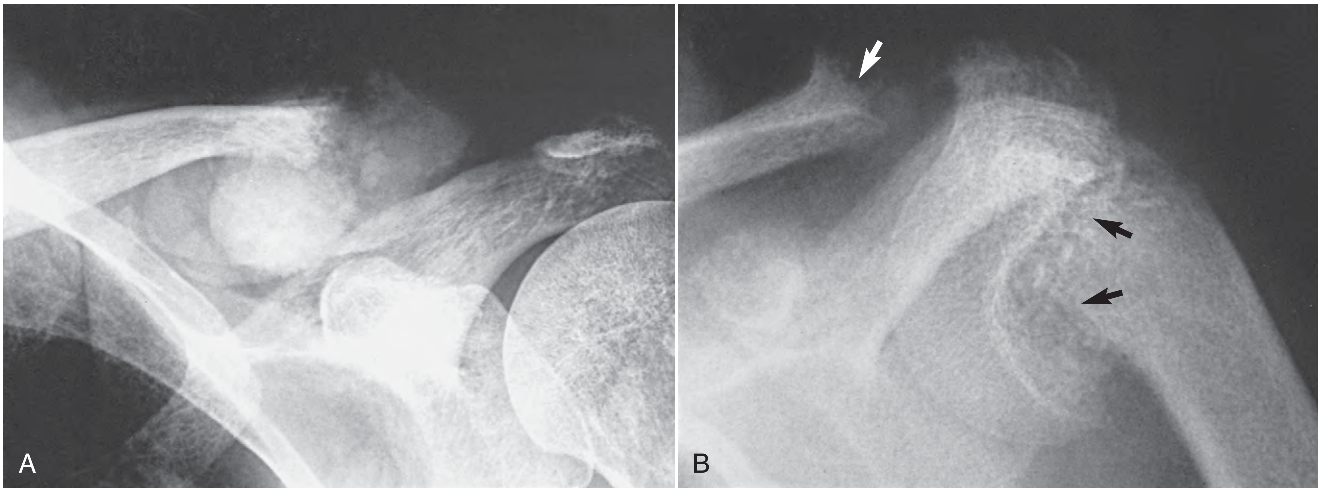

FIGURE 13–69 **Renal osteodystrophy.**[109–111] **A,** Observe the extensive erosion of the distal end of the clavicle and widening of the acromioclavicular joint in this 65-year-old renal transplant patient. Prominent soft tissue calcification also is present. **B,** Routine radiograph of this child's shoulder reveals osteopenia, widening of the physis, and a type I growth plate injury with displacement of the humeral epiphysis *(black arrows)*. These findings of subchondral resorption and resultant epiphyseal slippage are often seen in the proximal humeral epiphysis in children with chronic renal disease and resemble the physeal changes seen in rickets. Extensive resorption of the distal portion of the clavicle *(white arrow)* results in widening of the acromioclavicular joint. *(**B,** Courtesy M.N. Pathria, MD, San Diego.)*

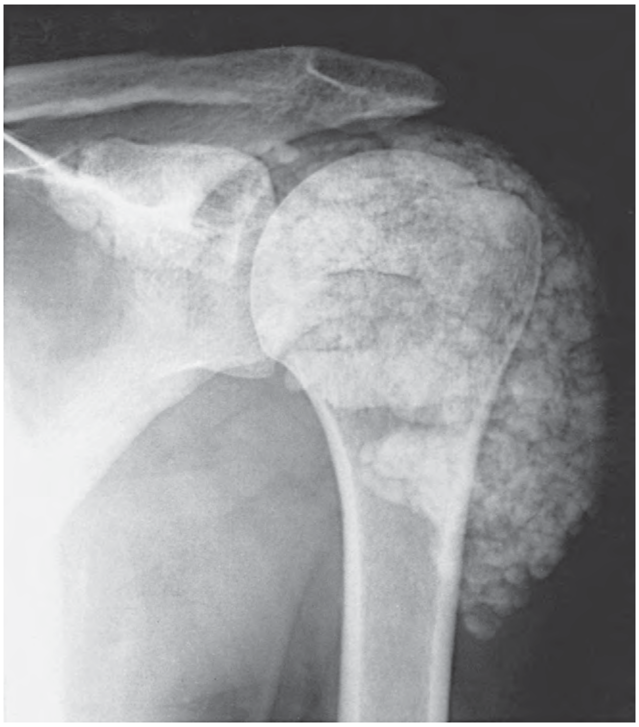

FIGURE 13–70 **Milk-alkali syndrome.**[112] Observe the extensive soft tissue calcinosis in this patient who was drinking excessive amounts of milk and calcium carbonate for his heartburn. Milk-alkali syndrome represents metastatic periarticular soft tissue calcification in persons who ingest large quantities of milk and alkaline substances.

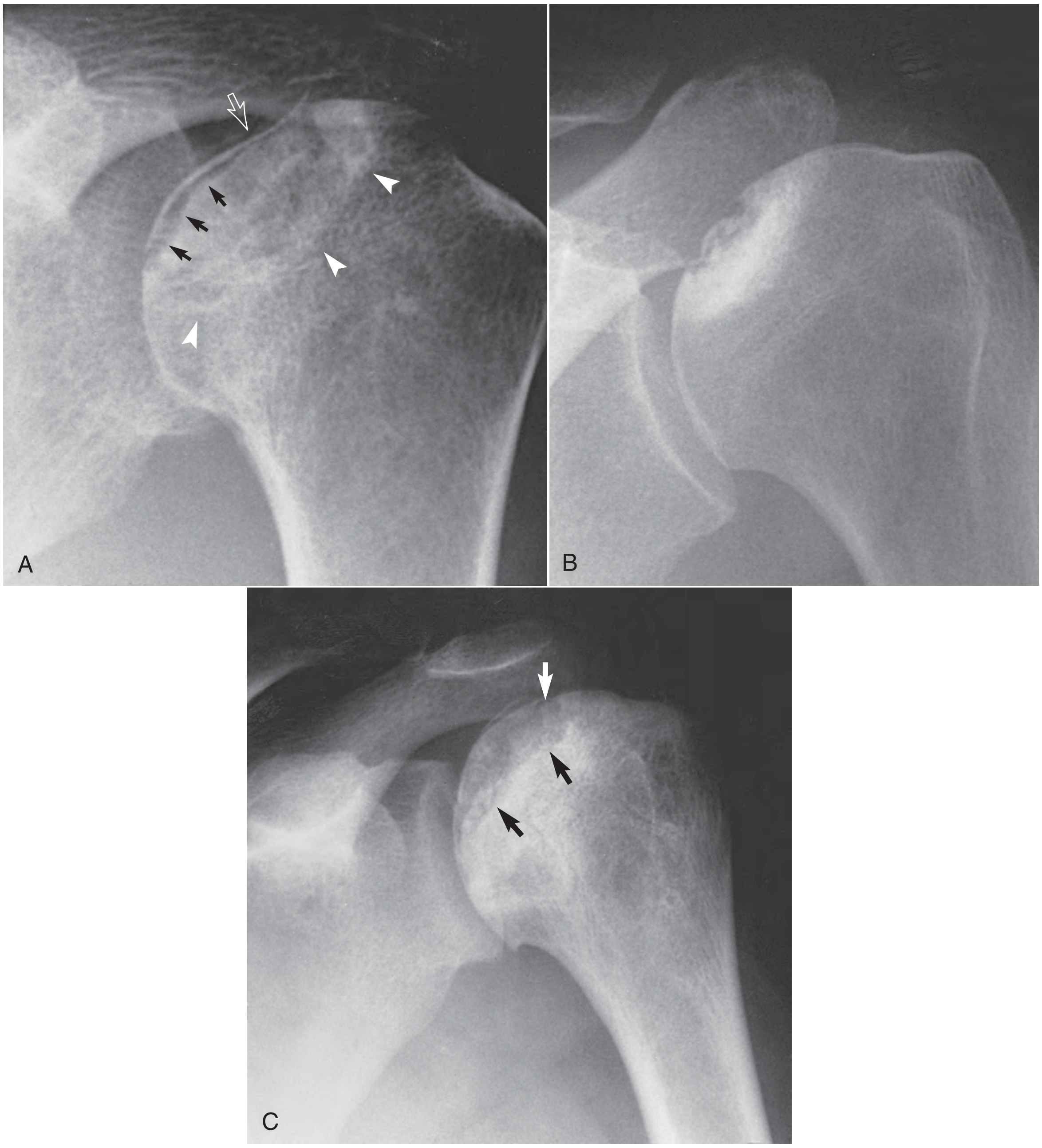

FIGURE 13–71 **Osteonecrosis.**[113,114] **A-B,** Corticosteroid-induced osteonecrosis. In **A,** a 47-year-old man with shoulder pain, the radiographic findings include collapse and fragmentation of the humeral head articular surface *(open arrow),* a curvilinear subarticular radiolucency (crescent sign) *(arrows),* and a combination of radiolucency and radiodensity in the humeral head *(arrowheads)*. In **B,** a radiograph of a 39-year-old woman on long-term corticosteroid therapy demonstrates a zone of sclerosis (snowcap appearance) with a small zone of radiolucent destruction of the proximal humeral articular surface. The glenohumeral joint space is preserved. **C,** Hemoglobinopathy. This 30-year-old woman with sickle cell anemia has an epiphyseal infarct, a common complication of vascular occlusion. Note the sclerotic zone adjacent to the subchondral radiolucent area *(black arrows)* and the articular collapse *(white arrow)*.

FIGURE 13–72 **Radiation changes.**[115] This patient underwent radiation therapy for carcinoma of the breast. Observe the destruction of subchondral bone in the humeral head, widening of the superior aspect of the glenohumeral joint space, and bursal distention with osseous debris *(arrows)*. Radiation osteitis and osteonecrosis are believed to be responsible for these changes. This appearance resembles that of neuropathic joint disease associated with syringomyelia.

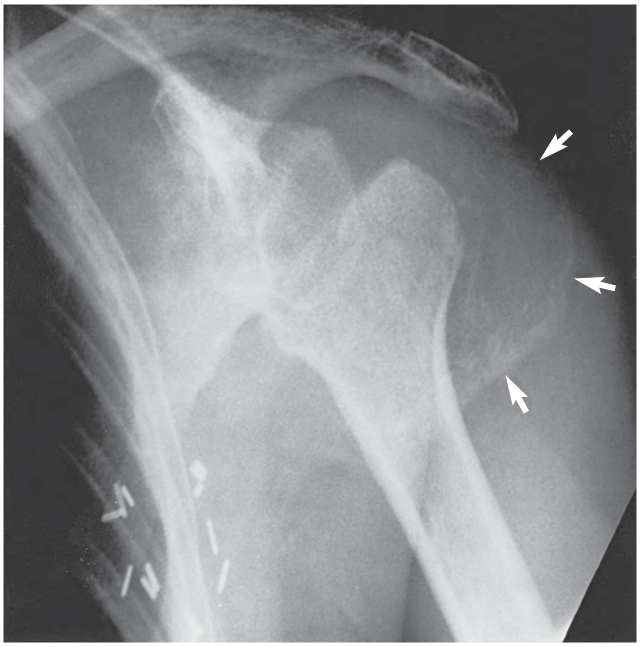

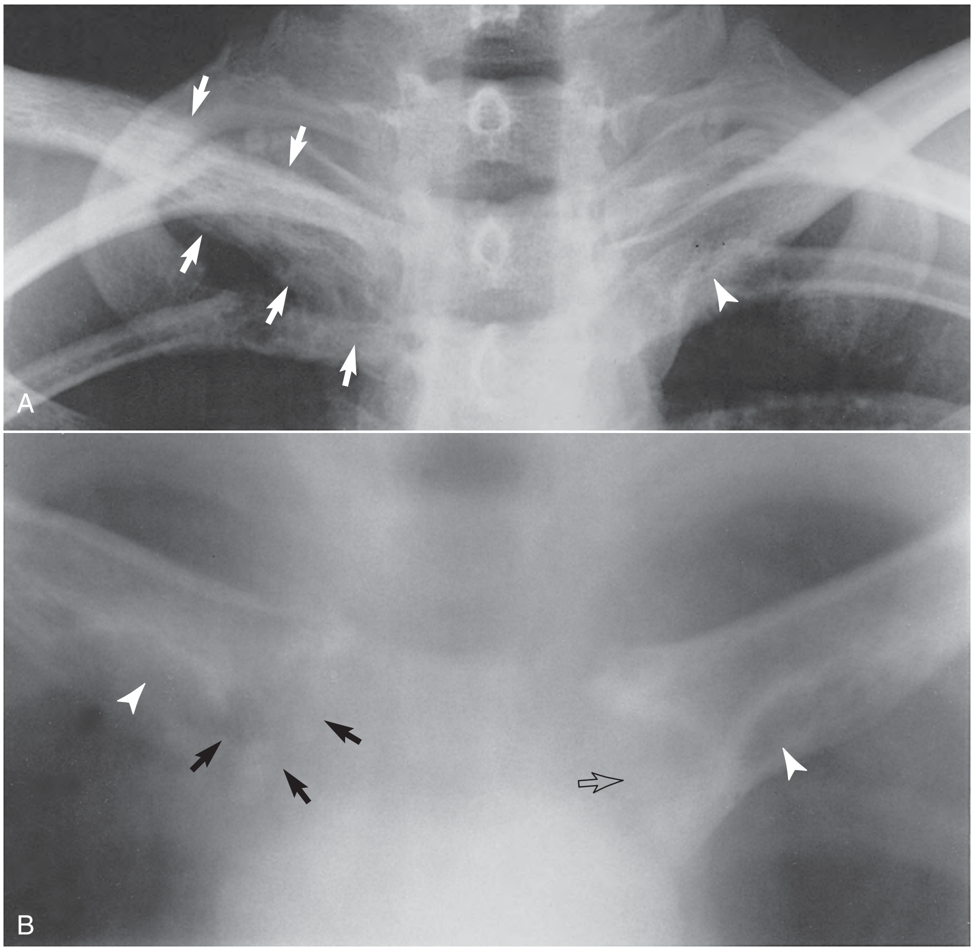

FIGURE 13–73 **Pyogenic osteomyelitis: clavicle.**[116] Frontal radiograph **(A)** and conventional tomogram **(B)** of the clavicles of this 18-year-old male patient show permeative destruction of the medial portion of the right clavicle with destruction of its articular end *(arrows)*. Of incidental note are bilateral rhomboid fossae *(arrowheads)* and a fork-shaped medial end of the left clavicle *(open arrow),* both of which are normal variants.

TABLE 13-11 **Miscellaneous Disorders Resulting in Clavicular Osteosclerosis, Periostitis, or Bone Enlargement**

Entity	Figure(s)	Typical Age of Onset (Years)	Characteristics
SAPHO syndrome[117]		Variable	SAPHO is an acronym for the findings of synovitis (S), acne (A), pustulosis (P), hyperostosis (H), and osteitis (O) Arthro-osteitis associated with acne or pustulosis palmaris et plantaris; closely related to sternocostoclavicular hyperostosis, psoriasis, and chronic recurrent multifocal osteomyelitis Prominent hyperostosis and painful osteitis of the clavicles and anterior chest wall along with synovitis of the nearby joints
Sternocostoclavicular hyperostosis[117,118]	13-74	40-60	Bilateral clavicle overgrowth and soft tissue ossification Associated with pustulosis palmaris et plantaris in 30% to 50% of patients (see SAPHO syndrome above) Men > women; cause unknown *Clinical findings:* pain, swelling, tenderness, and local heat overlying the anterior upper chest wall
Condensing osteitis of the clavicle[117,119,143]	13-75	20-50	Also termed *osteitis condensans clavicle* Painful swelling and sclerosis of the medial ends of the clavicles Encountered in young women involved in heavy lifting or sports Cause unknown
Chronic recurrent multifocal osteomyelitis[117,120,129]	13-76	5-10	Closely related to SAPHO syndrome Also termed *plasma cell osteomyelitis*, and *primary chronic osteomyelitis* Pain, tenderness, and swelling affecting the medial ends of the clavicles ***Radiographic findings*** Intense sclerosis, bone enlargement, osteolysis, and periostitis involving the clavicle
Friedrich disease[121,143]			Ischemic necrosis of the medial clavicular epiphysis Soft tissue swelling, tenderness to palpation over medial end of clavicle Osteosclerosis of entire clavicular head; often associated with notchlike defect of medial end of clavicle Benign, self-limited process
Infantile cortical hyperostosis (Caffey disease)[122]	Table 13-3	Younger than 5 months	Diffuse periostitis and cortical hyperostosis of the clavicles and, less commonly, the scapulae May become extreme
Acromegaly[123]		Older than 20	Osseous proliferation at ligament attachments on the undersurface of the distal end of the clavicle
Primary hypertrophic osteoarthropathy (pachydermoperiostosis)[124]		15-20	Diaphyseal, metaphyseal, and epiphyseal periostitis Shaggy, irregular excrescences Diaphyseal expansion
Secondary hypertrophic osteoarthropathy[125]	13-77	*Adults:* rare in children	Bilateral diaphyseal and metaphyseal periostitis of the clavicle Single layer or laminated, regular or irregular proliferation Periarticular osteoporosis, soft tissue swelling Underlying primary visceral disease such as bronchogenic carcinoma or mesothelioma
Hypervitaminosis A[126]		Older than 1 year	Megadoses of vitamin A in children may result in undulating diaphyseal periostitis of the tubular bones, including the clavicle Self-limited with cessation of vitamin A ingestion
Prostaglandin periostitis[127]		*Neonates:* within first 60 days of life	Prostaglandin E_1 and E_2 are medications used in the treatment of neonates with congenital heart disease Long-term infusion (40 days or more) or, rarely, short-term therapy (9 to 14 days) may result in bilateral periostitis and cortical thickening of tubular bones including the clavicle Self-limited; complete resolution usually occurs within 6 months to 1 year
Paget disease[101,102]	13-65; Table 13-9	Older than 55	Bilateral or unilateral trabecular coarsening, bone enlargement, osteosclerosis, osteolysis, or combined pattern of osteolysis and sclerosis

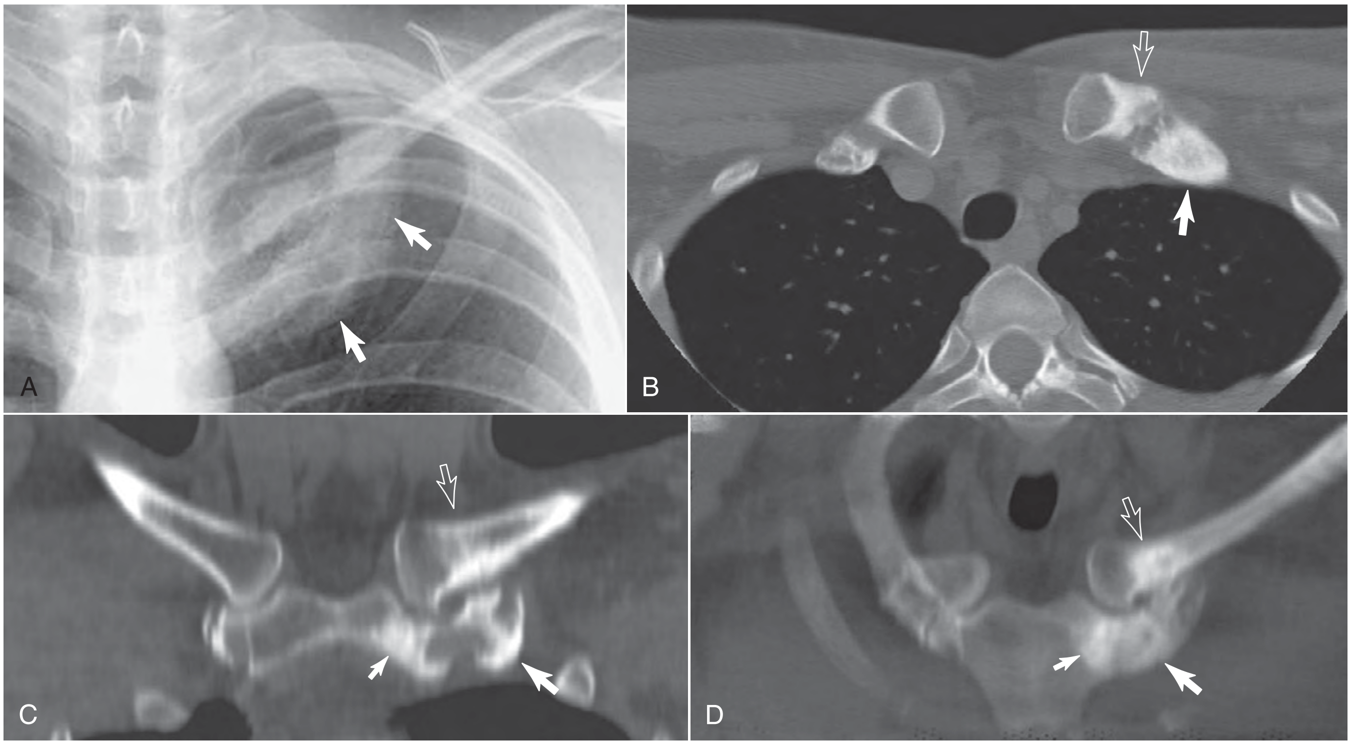

FIGURE 13–74 Sternocostoclavicular hyperostosis: conventional radiography and CT scanning.[117,118] A radiograph **(A)** of this 35-year-old woman complaining of anterior chest wall pain reveals enlargement and sclerosis of the left first rib *(arrows)*. A subsequent CT examination including axial bone window **(B)** and reconstructed coronal **(C-D)** scans reveal marked sclerosis and enlargement about the sternoclavicular and first costosternal joint on the left involving the sternum *(small arrows),* clavicle *(open arrows),* and first rib *(large arrows)*. The imaging findings of sternocostoclavicular hyperostosis closely resemble those of the SAPHO syndrome, and are often difficult to differentiate.

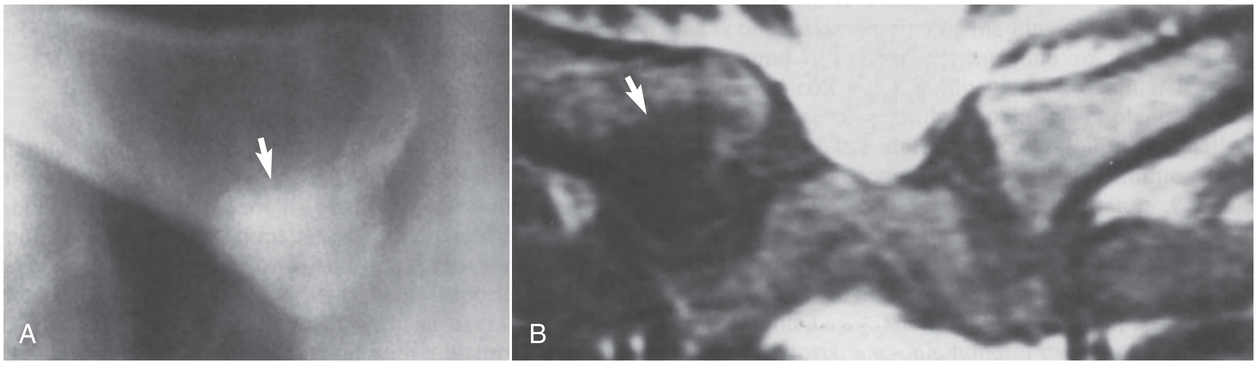

FIGURE 13–75 Condensing osteitis of the clavicle.[117,119,143] A 40-year-old woman developed pain and tenderness over the medial end of the right clavicle. **A,** Conventional tomography reveals bone sclerosis involving the inferomedial aspect of the bone *(arrow)*. **B,** Coronal T1-weighted (TR/TE, 300/11) spin echo MR image shows low signal intensity in this area *(arrow)*. The diminished signal intensity persisted on T2-weighted spin echo and gradient echo images (not shown). *(From Resnick D: Diagnosis of bone and joint disorders. 4th Ed. Philadelphia, Saunders, 2002.)*

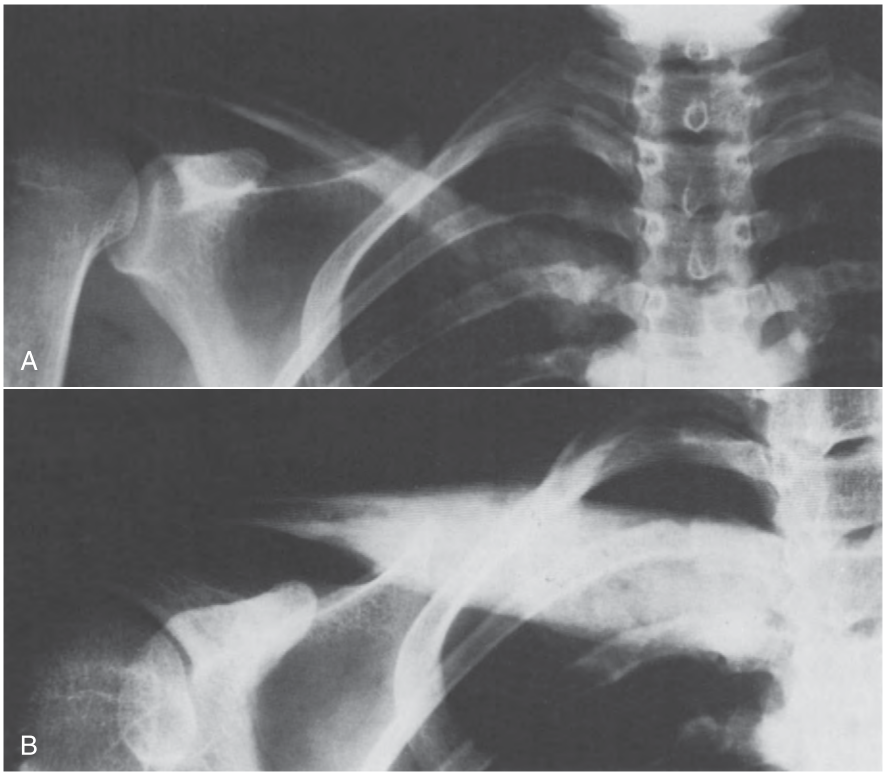

FIGURE 13–76 **Chronic recurrent multifocal osteomyelitis.**[117,120,129,143] A 16-year-old girl developed pain and progressive enlargement of the medial portion of the right clavicle over a 6-month period. She had no fever or erythema. Radiographs obtained 8 months apart reveal a process that is associated initially **(A)** with permeative bone destruction and subsequently **(B)** with massive enlargement of the clavicle. Biopsy and histologic evaluation indicated only chronic osteitis. Cultures were negative. *(From Resnick D: Diagnosis of bone and joint disorders. 4th E., Philadelphia, Saunders, 2002, p 2447.)*

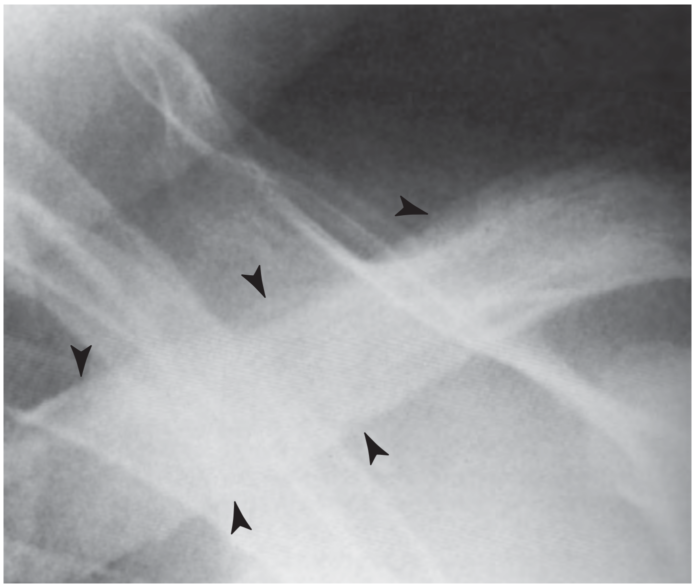

FIGURE 13–77 **Secondary hypertrophic osteoarthropathy: periostitis.**[125] Deposition of new bone *(arrowheads)* has resulted in diffuse enlargement of the clavicle. The process was bilateral and affected several tubular bones in this patient. *(From Resnick D: Diagnosis of bone and joint disorders. 4th Ed. Philadelphia, Saunders, 2002, p 4880.)*

CHAPTER 14

Humerus

DEVELOPMENTAL ANOMALIES, ANATOMIC VARIANTS, AND SOURCES OF DIAGNOSTIC ERROR

Very few developmental anomalies and anatomic variants affect the humerus. Table 14-1 and Figures 14-1 to 14-3 represent selected examples.

PHYSICAL INJURY

Acute fractures of the humeral diaphysis occur infrequently. The muscles of the upper arm are a frequent site for posttraumatic heterotopic ossification. These conditions are described in Table 14-2, and are illustrated in Figures 14-4 and 14-5. Injuries of the proximal and distal portions of the humerus are covered in Chapters 13 and 15, respectively.

BONE TUMORS

The humerus is a frequent site of malignant and benign tumors and tumorlike processes. Tables 14-3 to 14-5 list the major characteristics of these disorders. Their radiographic manifestations are illustrated in Figures 14-6 to 14-22.

METABOLIC, HEMATOLOGIC, AND INFECTIOUS DISORDERS

A number of metabolic, hematologic, and infectious disorders may involve the humerus. Table 14-6 lists some of the more common disorders and describes their characteristics. Their radiographic features are illustrated in Figures 14-23 to 14-28. Further manifestations of these disorders within the proximal and distal portions of the humerus are covered in Chapters 13 and 15, respectively.

TABLE 14-1 Developmental Anomalies, Anatomic Variants, and Sources of Diagnostic Error

Disorder	Figure(s)	Characteristics
Humeral pseudocyst[1]	13-2, *H*, 13-13	Zone of diminished trabeculae within the spongiosa bone of the greater tubercle of the humerus May simulate a destructive neoplasm, such as chondroblastoma
Supracondylar process[2-4]	14-1	Rare anomaly affecting less than 1% of population Anomalous elongated projection or flange of bone arising from the anteromedial cortical surface of the distal humeral metadiaphysis, projecting toward the elbow joint May be connected to the medial epicondyle of the humerus by a fibrous band termed the *ligament of Struthers* Median nerve and occasionally the brachial artery pass beneath this fibrous band Peripheral median nerve entrapment has been reported
Chevron sign[5]	14-2	Obliquely oriented trabeculae within the distal portion of the humerus may appear very prominent on frontal radiographs, simulating the appearance of osteoporosis or bone destruction This normal finding represents the typical herringbone or chevron pattern of trabecular bone and is of no clinical significance
Supracondylar foramen[6]	14-3	Failure of complete ossification of the thin membranous bone separating the olecranon fossa from the coronoid fossa of the distal portion of the humerus results in an unossified circular hole that is of no clinical significance Present in 4% to 13% of the population Left > right Women > men
Simulated periostitis[6]	See Figure 13-2, *G*	Periostitis of the proximal metaphysis of the humerus may be simulated by the intertubercular groove in neonates or by overlying projection of the cortices in adults Bilateral "physiologic periostitis of newborn infants" may be visible in the humeral diaphyses beginning about the age of 1 month and persisting throughout the first year of life Periostitis of the lateral epicondyle may be simulated by normal flanges of bone along the cortex of the distal humeral metaphyses Simulated periostitis may be mistaken for a pathologic condition but is of no clinical significance
Upper humeral notches[3,7]		Irregularity of the cortex of the medial aspect of the proximal humeral metaphysis in children between 10 and 16 years of age These notches may be bilateral and resemble cortical destruction Normal variant
Prominent deltoid tuberosity[3]		Insertion site of the deltoid muscle on the anterolateral aspect of the humeral diaphysis may appear as a prominent cortical outgrowth simulating a neoplasm

See also Table 1-1.

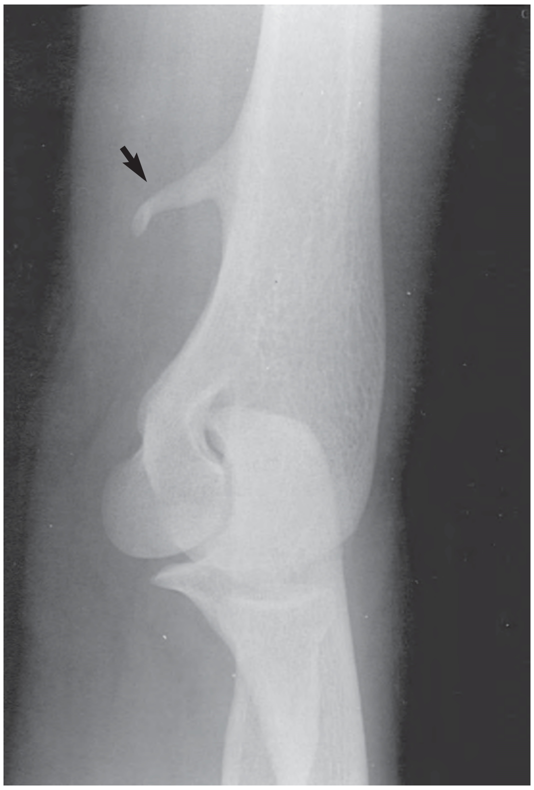

FIGURE 14–1 Supracondylar process.[2-4] An osseous outgrowth arises from the anteromedial surface of the distal portion of the humerus *(arrow)* approximately 5 to 7 cm above the medial condyle. This anomaly, present in 1% to 3% of the general population, is usually an incidental finding and does not cause signs or symptoms. The process may be joined to the medial epicondyle by the ligament of Struthers, a band of fibrous tissue that may occasionally lead to peripheral entrapment of the median nerve.

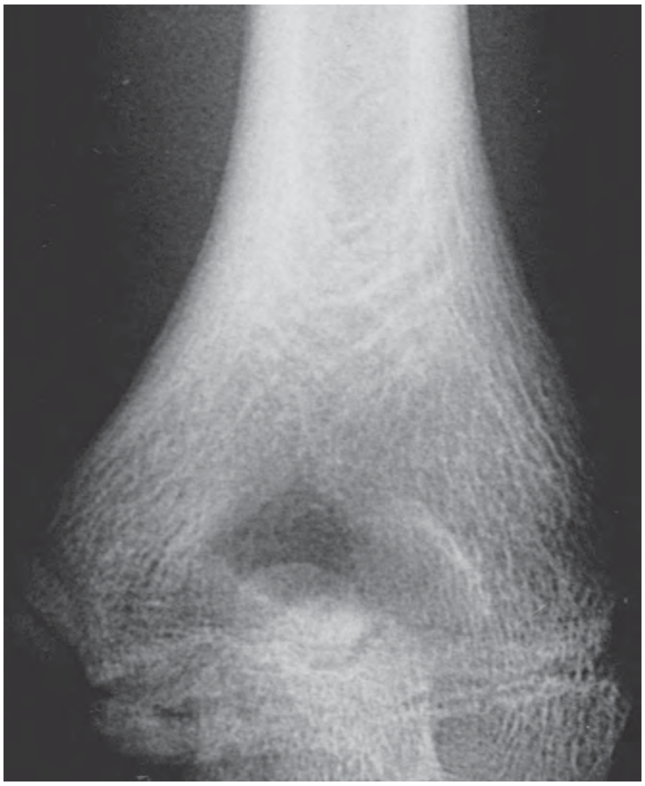

FIGURE 14–2 Chevron sign.[5] Observe the normal, obliquely oriented trabeculae within the cancellous bone of the distal portion of the humerus. This herringbone or chevron arrangement of trabeculae may simulate the appearance of osteoporosis or osteolytic destruction, but it is of no clinical significance.

FIGURE 14–3 Supracondylar foramen.[6] A well-defined circular radiolucency *(arrows)* in the supracondylar region of the humerus is typically visible on the anteroposterior **(A)** view but not on the lateral view **(B).** This normal variant is of no clinical significance, and should not be confused with a cyst, tumor, or other destructive lesion. The supracondylar foramen was an incidental finding in this 43-year-old man.

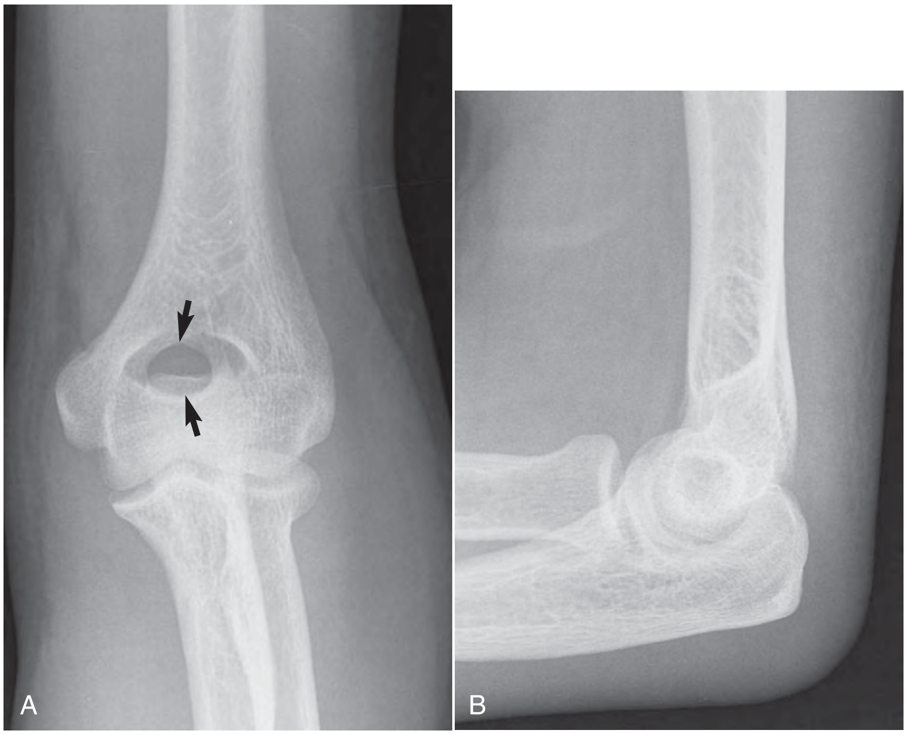

TABLE 14-2 Physical Injury: Humeral Diaphysis and Soft Tissues

Fractures	Figure(s)	Characteristics	Complications and Related Injuries
Fractures of the Humeral Diaphysis			
Acute fractures[8-10,68,70]	14-4	Fractures of the humeral diaphysis account for about 3% of all fractures Adults > children *Most common site:* junction of distal and middle thirds Transverse orientation—50 to 70% of all humeral diaphyseal fractures; oblique—20%; spiral—20% *Direct trauma:* automobile accidents, gunshot wounds, physical assault *Indirect trauma:* throwing a ball, shot putting, arm wrestling, childbirth injury in newborns *Ball-thrower fracture of the humerus:* minimally displaced spiral fracture in the mid to distal humerus resulting from severe muscular contraction during throwing of baseballs, hand grenades, javelins and even snowballs	Delayed union or nonunion when fracture is transverse or distracted Radial nerve injury in 5 to 15% of cases Brachial artery injury Characteristic displacements related to sites of muscular attachment Fractures above insertion of pectoralis major result in rotator cuff displacing proximal fragment into abduction and external rotation; fractures between insertion of pectoralis major proximally and the deltoid distally result in adduction of the proximal fragment; fractures distal to deltoid insertion result in abduction of the proximal fragment and proximal displacement of the distal fragment
Stress reaction[69]		*Rare condition:* marrow edema identified with MR imaging of the distal diaphysis of the humerus of the dominant arm in elite tennis players	
Child abuse[11]		Humerus is second only to the ribs as the most common site of fracture in child abuse Fractures may be single or multiple Spiral fractures of the humeral diaphysis are highly suggestive, but not invariably diagnostic, of abuse in children, especially the nonambulating infant; left-sided diaphyseal fractures most frequent; periosteal reaction suggests healing fracture Metaphyseal lesions of distal end of the humerus and epiphyseal displacement (Salter-Harris type I injury) of the distal humeral epiphysis suggestive of child abuse (see Chapter 13)	Fractures or injuries in other locations Fractures in different phases of healing
Soft Tissue Injury			
Posttraumatic heterotopic ossification[12]	14-5	Also termed *posttraumatic myositis ossificans* Faint calcific intermuscular or intramuscular shadow may appear within 2 to 6 weeks of injury Well-defined region of ossification aligned parallel to the long axis of the humerus may be evident within 6 to 8 weeks Associated periostitis may relate to subperiosteal hemorrhage	Limitation of motion May result in abnormal shoulder or elbow biomechanics and lead to premature degeneration May resemble aggressive neoplasms, such as osteosarcoma or Ewing sarcoma

See also Tables 1-4 and 1-5.

See Chapter 13 for injuries to the proximal portion of the humerus and Chapter 15 for injuries to the distal portion of the humerus.

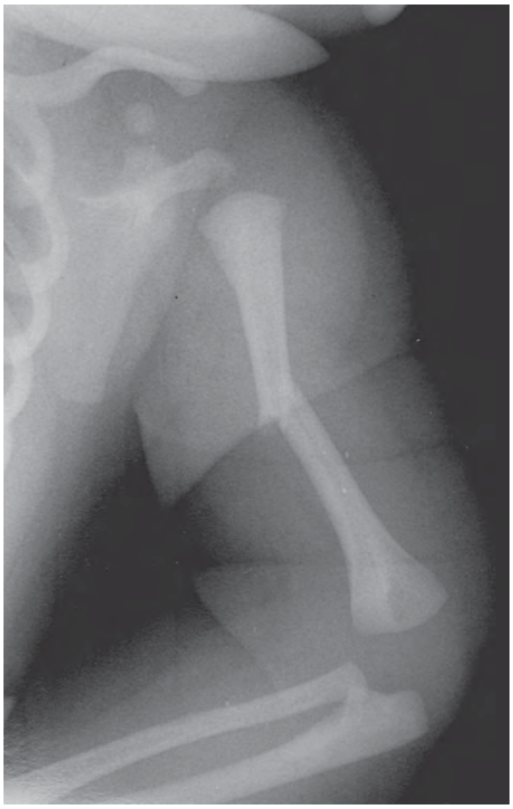

FIGURE 14–4 Humeral shaft fracture.[8-10] A difficult shoulder delivery resulted in a fracture of the humeral shaft in this newborn infant. Note the lateral displacement of the distal fragment. Radial nerve injury, and, less likely, vascular injury, malunion, and nonunion, may complicate humeral shaft fractures.

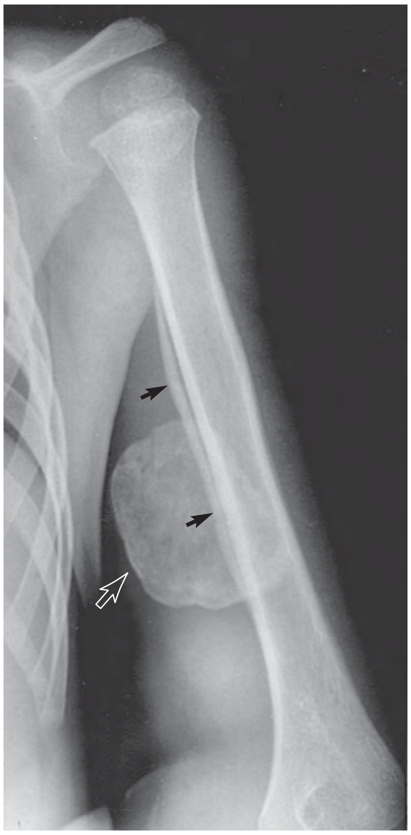

FIGURE 14–5 Heterotopic ossification: posttraumatic myositis ossificans.[12] This 4-year-old boy fell on his elbow. A radiograph taken 1 year later shows a well-organized hematoma *(open arrow)* with solid periosteal new bone formation *(arrows)* involving the medial humeral diaphysis. *(Courtesy D. Witte, M.D., Memphis.)*

TABLE 14-3 Malignant Tumors Affecting the Humerus*

Tumor	Figure(s)	Characteristics
Secondary Malignant Neoplasms of Bone		
Skeletal metastasis[13,14]	14-6	Fewer than 10% of skeletal metastatic lesions affect the humerus Seventy-five percent exhibit permeative or moth-eaten osteolysis Twenty-five percent exhibit diffuse or patchy osteosclerosis or a mixed pattern of lysis and sclerosis Usually multiple sites of involvement Pathologic fracture
		Cortical metastasis
		Prevalent in the long tubular bones of patients with metastasis, especially from bronchogenic carcinoma Small radiolucent, eccentric, saucer-shaped, scalloped erosions, which sometimes occur near the entrance of nutrient arteries into the bone, are referred to as "cookie bite" lesions
Malignant transformation of benign processes[15]	14-7	Several benign tumors and tumorlike lesions may undergo sarcomatous malignant transformation: Paget disease, fibrous dysplasia, neurofibromatosis, hereditary multiple exostoses, Ollier disease, Maffucci syndrome, and infrequently solitary primary benign tumors

* See also Table 1-12.

TABLE 14-3 Malignant Tumors Affecting the Humerus—cont'd

Tumor	Figure(s)	Characteristics
Primary Malignant Neoplasms of Bone		
Osteosarcoma (conventional)[16,62,63]	14-8	Ten to 15% of osteosarcomas occur in the humerus Osteolytic, osteosclerotic, or mixed patterns of medullary and cortical destruction Prominent periosteal reaction common Preference for the proximal metaphyseal region
Osteosarcoma (parosteal)[17,62,63]		Fifteen percent of parosteal osteosarcomas occur in the humerus Osteosclerotic surface lesion of bone Large radiodense, oval, sessile mass with smooth or irregular margins Peripheral portion of lesion may have cleavage plane separating it from the humerus Ossification begins centrally and progresses outward, opposite that of benign heterotopic bone formation (myositis ossification)
Chondrosarcoma (conventional)[18,19]		Ten percent of chondrosarcomas occur in the humerus Tend to be osteolytic lesions, sometimes containing a bulky cartilaginous cap and frequently containing calcifications May have soft tissue mass
Giant cell tumor (aggressive)[20]		More than 10% of aggressive giant cell tumors occur in the humerus Eccentrically located, metaphyseal lesion extending into the epiphysis and subarticular bone Cortical destruction and soft tissue mass are variable findings Radiographic appearance is an inaccurate guide to determining malignancy of lesion—bone biopsy is necessary
Fibrosarcoma[21]		Eleven percent of fibrosarcomas involve the humerus Purely osteolytic destruction with no associated sclerotic reaction or periostitis
Malignant fibrous histiocytoma[21]		Fewer than 10% of malignant fibrous histiocytomas involve the humerus Pathologic fracture common Metaphyseal location with frequent spread to epiphysis and diaphysis Moth-eaten or permeative osteolysis, frequently resembling fibrosarcoma
Ewing sarcoma[22]	14-9	Ten percent of Ewing sarcomas occur in the humerus Permeative or moth-eaten osteolysis, aggressive cortical erosion or violation, laminated or spiculated periostitis, and soft tissue masses Most lesions central and diametaphyseal in location
Myeloproliferative Disorders		
Plasma cell (multiple) myeloma[23]	14-10	Fifteen percent of multiple myeloma lesions occur in the humerus *Early:* Normal radiographs or diffuse osteopenia *Later:* Widespread, well-circumscribed osteolytic lesions with discrete margins, which appear uniform in size Ninety-seven percent osteolytic; 3% osteoblastic False-negative bone scans common
Solitary plasmacytoma[23]		Fourteen percent of solitary plasmacytomas occur in the humerus Solitary, geographic, expansile, osteolytic lesion that frequently results in pathologic fracture Seventy percent eventually develop into multiple myeloma
Primary lymphoma (non-Hodgkin)[24,25,59,61]	14-11	Approximately 11% of lesions in primary lymphoma occur in the humerus Multiple moth-eaten or permeative osteolytic lesions Diffuse or localized sclerotic lesions are rare Common cause of pathologic fracture
Leukemia[26]	14-12	Humerus frequently involved Diffuse osteopenia, radiolucent or radiodense transverse metaphyseal bands, osteolytic lesions, periostitis, and, infrequently, osteosclerosis Radiodense metaphyses more frequent in patients undergoing chemotherapy for leukemia; may resemble lead poisoning

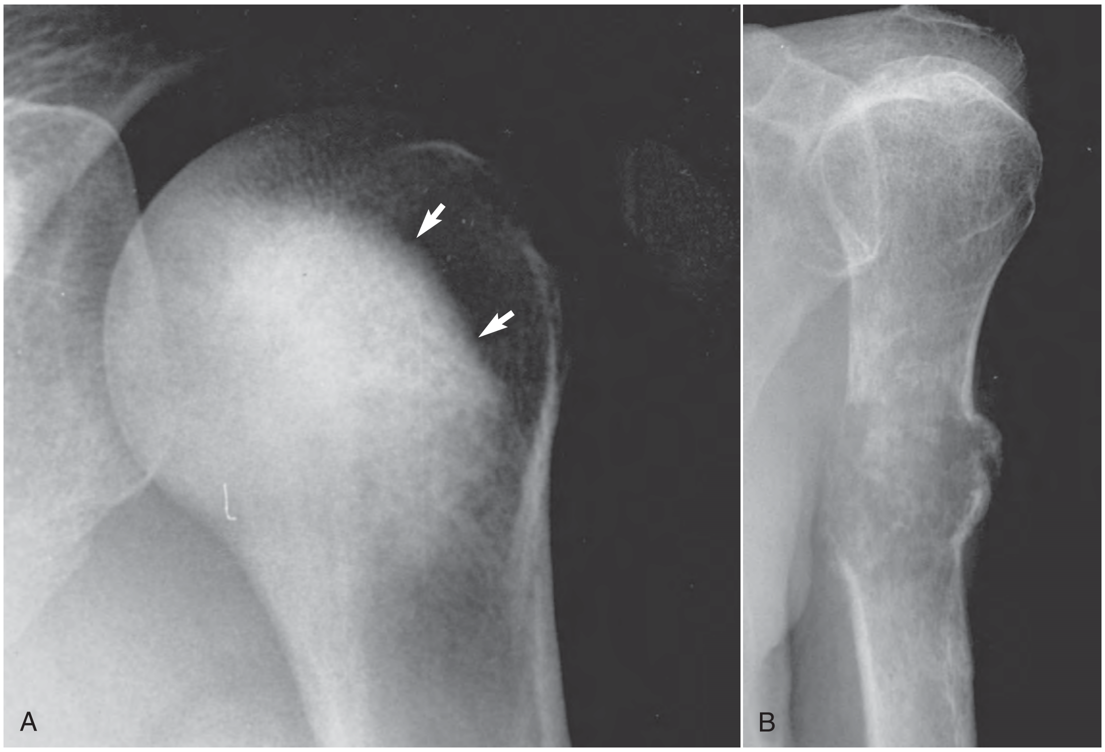

FIGURE 14–6 Skeletal metastasis: various patterns.[13,14] **A,** This 54-year-old man was diagnosed as having carcinoma of the prostate several years before this radiographic examination. The radiograph shows a zone of osteosclerosis within the head of the humerus *(arrows)*. **B,** In another patient, a 56-year-old man with carcinoma of the tonsils, a permeative pattern of osteolytic destruction involving the proximal portion of the humerus has resulted in a pathologic fracture.

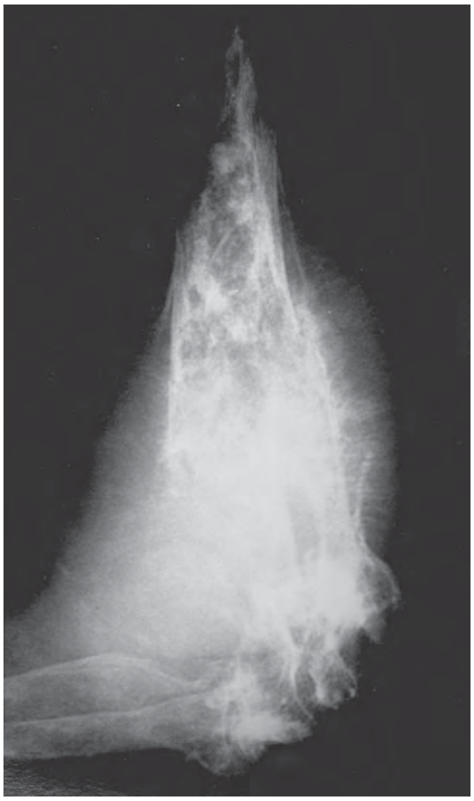

FIGURE 14–7 Secondary osteosarcoma: malignant transformation from fibrous dysplasia.[15,62,63] This patient with known fibrous dysplasia developed new onset of pain. Radiographs reveal a highly aggressive, destructive lesion involving the distal portion of the humerus. Bone expansion, cortical destruction, spiculated periostitis, and a soft tissue mass are evident. Biopsy revealed osteosarcoma developing in an area of fibrous dysplasia. Malignant transformation occurs in fewer than 1% of reported cases of fibrous dysplasia. Osteosarcoma and fibrosarcoma are the most frequently encountered tumor types, occurring in both monostotic and polyostotic fibrous dysplasia. *(Courtesy G. Greenway, M.D., Dallas.)*

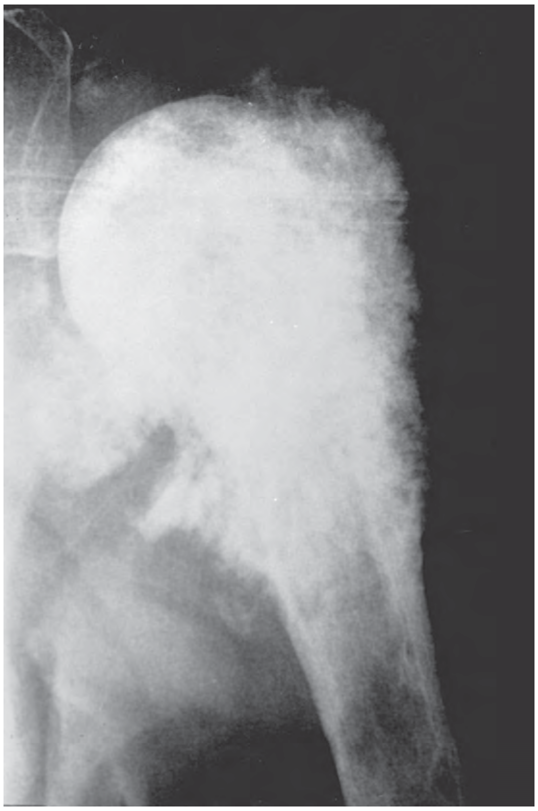

FIGURE 14–8 Conventional osteosarcoma.[16,62,63] An 80-year-old woman had shoulder pain. A frontal radiograph demonstrates extensive osteoblastic new bone deposition within the entire proximal portion of the humerus. The periosteal margins are spiculated, and the tumor appears very aggressive.

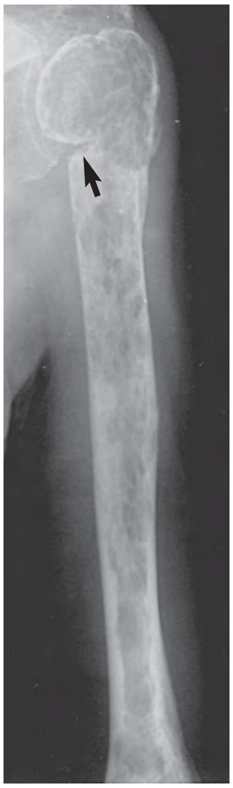

FIGURE 14–10 Plasma cell (multiple) myeloma.[23] Numerous osteolytic scalloped lesions are seen throughout the entire humerus. A pathologic fracture of the surgical neck has occurred *(arrow)*.

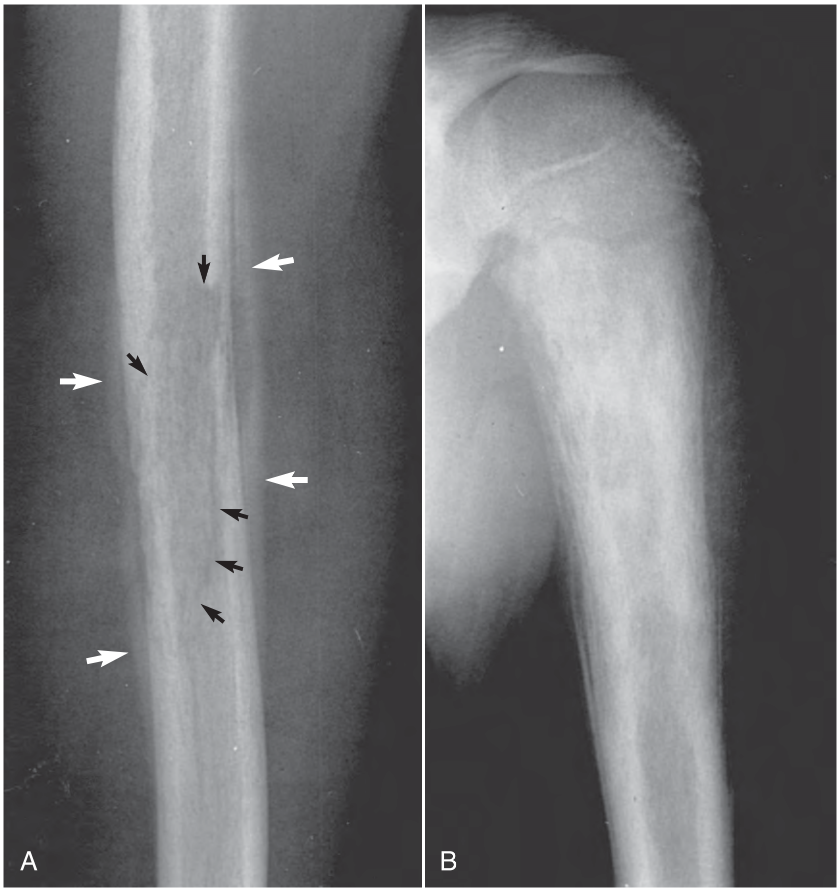

FIGURE 14–9 Ewing sarcoma.[22] **A,** Radiograph of the humerus shows a pathologic fracture *(black arrows)* through an area of extensive permeative destruction of the medullary and cortical bone. Observe also the thick periostitis throughout the diaphysis *(white arrows)*. **B,** Laminated periosteal response results in radiodensity of the humeral metadiaphysis in another patient with Ewing sarcoma. (***B,** Courtesy P.H. VanderStoep, M.D., St. Cloud, Minn.)*

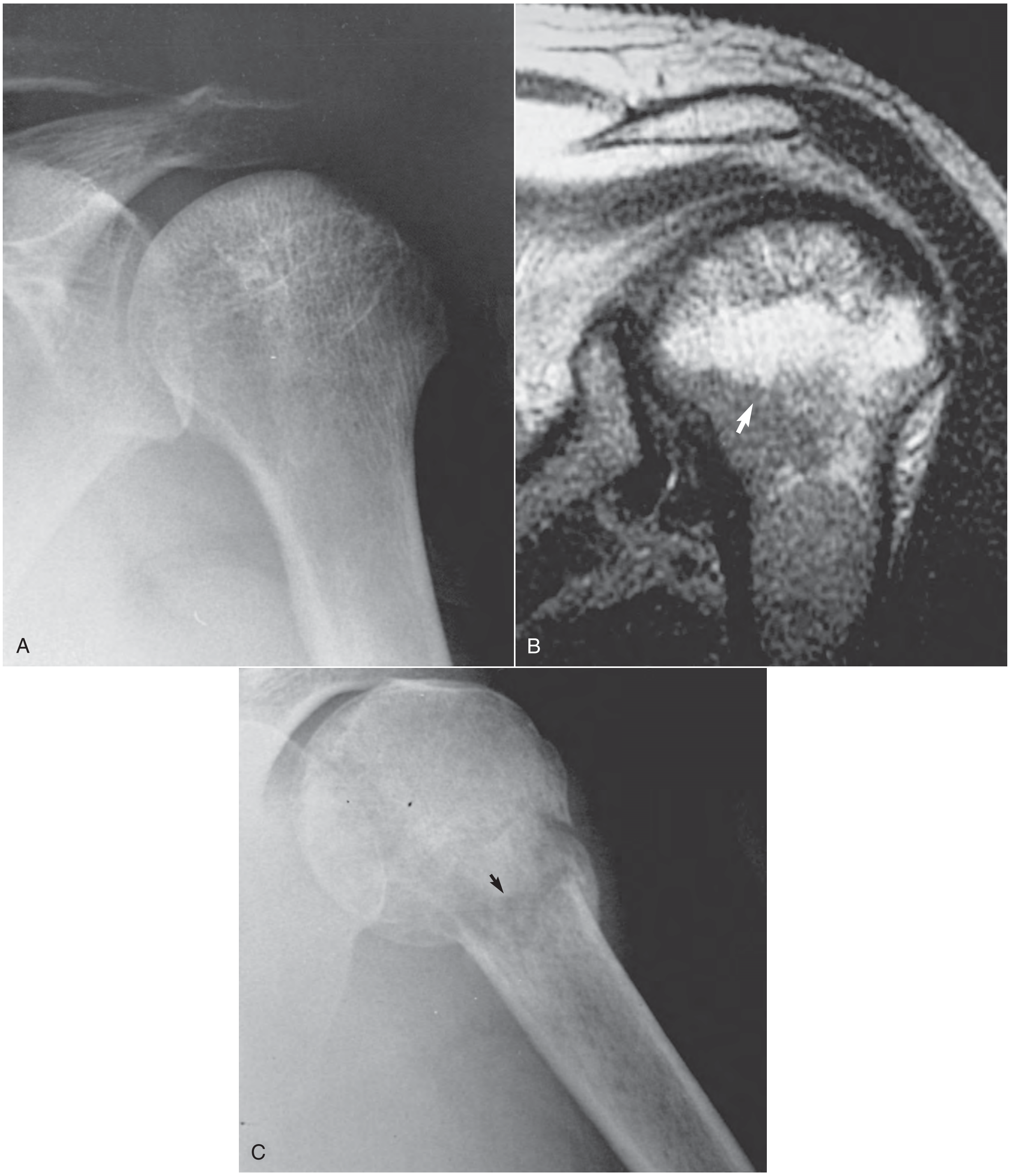

FIGURE 14–11 Non-Hodgkin lymphoma.[24,25,59,61] **A-B,** 53-year-old man with multiple organ system involvement. In **A,** a routine radiograph shows a subchondral zone of medullary bone sclerosis in the humeral head. In **B,** a coronal T2-weighted (TR/TE, 2000/70) spin echo MR image reveals high signal intensity of the bone marrow within the humerus *(arrow),* corresponding to the radiographic findings. **C,** In another patient with the histiocytic type of primary lymphoma, observe the permeative osteolysis and resultant transverse pathologic fracture *(arrow)* involving the proximal portion of the humerus.

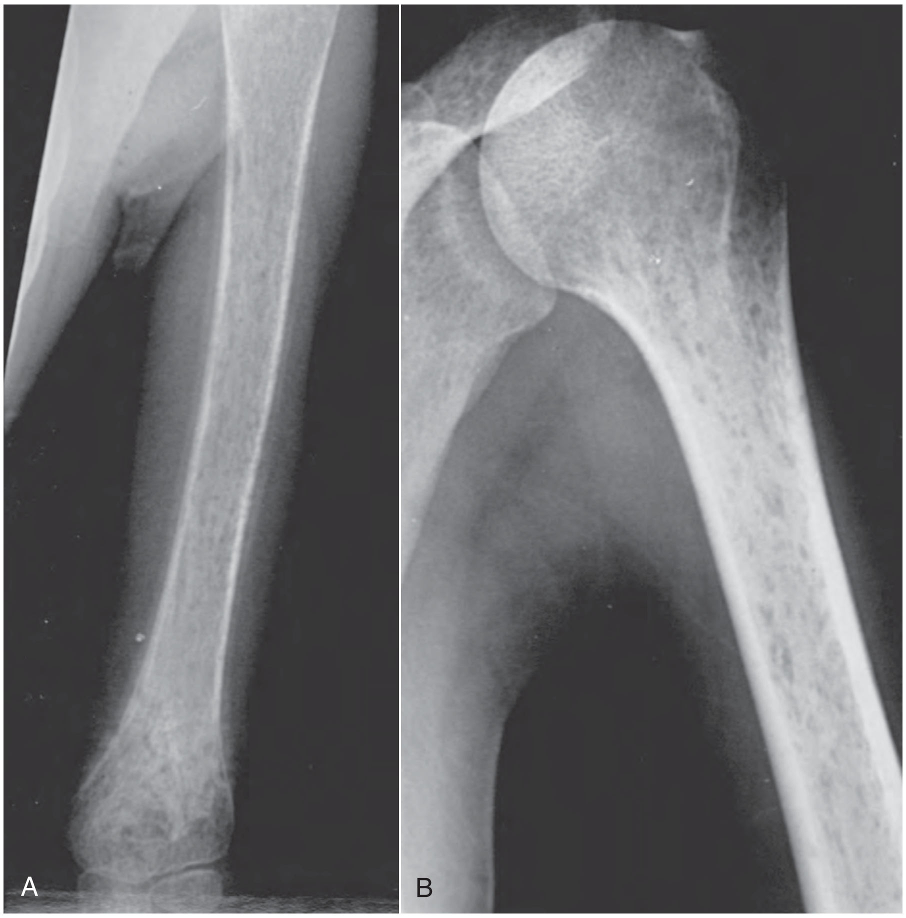

FIGURE 14–12 Acute childhood leukemia.[26] **A,** Permeative osteolysis with periostitis is seen throughout the humerus of this child with leukemia. **B,** In another patient with acute childhood leukemia, observe the moth-eaten osteolytic destructive lesions throughout the humeral diaphysis and metaphysis, resembling the punched-out lesions of plasma cell myeloma.

TABLE 14-4 Benign Tumors Affecting the Humerus*

Tumor	Figure(s)	Characteristics
Enostosis[27]		Fewer than 10% of enostoses (bone islands) occur in the humerus Solitary, rarely multiple, painless, discrete foci of osteosclerosis within the spongiosa of bone Round, ovoid, or oblong with brush border composed of radiating osseous spicules that intermingle with the surrounding trabeculae of the spongiosa
Osteoid osteoma[28,29]	14-13	Seven percent of osteoid osteomas occur in the humerus Cortical or subperiosteal lesion with reactive sclerosis surrounding central radiolucent nidus Nidus less than 1 cm in diameter and usually not visible on routine radiographs
Osteoblastoma (conventional)[30]		Fewer than 3% of conventional osteoblastomas involve the humerus Osteolytic, osteosclerotic, or both Expansile lesion that may be subperiosteal Partially calcified matrix in many cases Cortical thinning Often resembles large osteoid osteoma

* See also Table 1-13.

Continued

TABLE 14-4 Benign Tumors Affecting the Humerus—cont'd

Tumor	Figure(s)	Characteristics
Enchondroma (solitary)[31]	14-14	Approximately 7% of solitary enchondromas involve the humerus Central or eccentric, medullary osteolytic lesion Lobulated endosteal scalloping Approximately 50% have stippled calcification within the matrix
Enchondromatosis (Ollier disease)[31]		Multiple enchondromas; frequently involve the humerus
Maffucci syndrome[31]		Humerus is involved in more than 40% of cases of Maffucci syndrome Multiple enchondromas and soft tissue hemangiomas Unilateral distribution in 50% of cases
Chondroblastoma[32,33,57]	14-15	Approximately 22% of chondroblastomas affect the humerus Circular osteolytic lesion affecting predominantly the proximal humeral epiphyses May exhibit calcification in matrix Occasionally periosteal reaction and edema may be seen on MR imaging
Osteochondroma (solitary)[34,35]	14-16	As many as 20% of solitary osteochondromas arise from the humerus Pedunculated or sessile, cartilage-covered osseous excrescence arising from the surface of the metaphysis of the proximal or distal portion of the humerus Cortex and medulla are continuous with the host bone May occur spontaneously or after accidental or iatrogenic injury Typically grow away from the adjacent joint *Complications:* pathologic fracture, neurovascular compression, and malignant transformation (fewer than 1% of cases)
Hereditary multiple exostoses[36-38]	14-17	Multiple osteochondromas, sometimes numbering in the hundreds Proximal humeral metaphysis frequently involved May result in neurovascular compression or malignant transformation (fewer than 5% of cases)
Nonossifying fibroma and fibrous cortical defect[39]	14-18	Five percent of nonossifying fibromas and fibrous cortical defects involve the humerus Eccentric, multiloculated osteolytic lesion arising from the metaphyseal cortex Resembles a well-circumscribed, blisterlike shell of bone arising from the cortex Cortical thinning is often present Eventually disappears, filling in with normal bone Nonossifying fibromas are typically larger than fibrous cortical defects
Giant cell tumor (benign)[20]		Approximately 6% of benign giant cell tumors occur in the humerus Eccentric osteolytic neoplasm with a predilection for the subarticular region Often multiloculated and expansile Radiographs are inaccurate in distinguishing benign from aggressive giant cell tumors
Intraosseous lipoma[40,58]		Fewer than 10% of intraosseous lipomas occur in the humerus Osteolytic lesion surrounded by a thin, well-defined sclerotic border Central calcified or ossified nidus is common Occasional osseous expansion Cortical destruction and periostitis absent
Simple bone cyst[41,42]	14-19	Over half of all simple bone cysts occur in the humerus Mildly expansile, solitary osteolytic lesion within medullary cavity of proximal portion of humerus May be multiloculated Pathologic fracture with characteristic "fallen fragment" sign
Aneurysmal bone cyst[43]		Fewer than 10% of aneurysmal bone cysts occur in the humerus Eccentric, thin-walled, expansile osteolytic lesion of the humeral metaphysis Thin trabeculation with multiloculated appearance Buttressing at edge of lesion

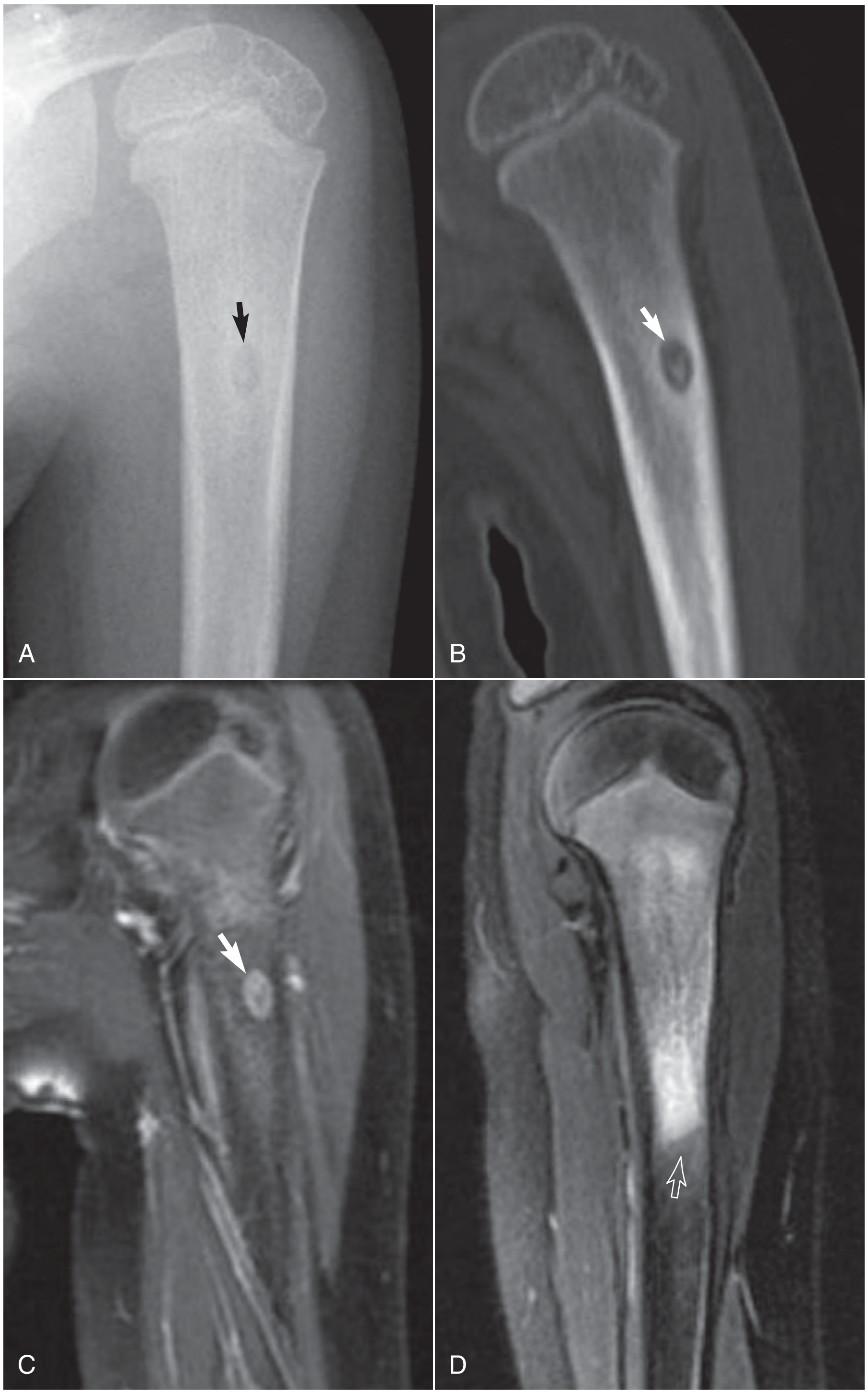

FIGURE 14–13 Osteoid osteoma.[28,29] This 9-year-old boy had a 2-year history of dull pain in his upper arm. A frontal radiograph **(A)** shows a well-defined ovoid radiolucency in the proximal metadiaphyseal region of the humerus *(arrow)*. A faint central radiodensity and minimal surrounding sclerosis are also evident. The radiolucent nidus *(arrow),* less than a centimeter in diameter, is much more conspicuous on a coronal reformatted CT scan bone window **(B),** which also reveals the central calcification and surrounding sclerosis. A fat-suppressed coronal T1-weighted MR image obtained after intravenous gadolinium administration **(C)** reveals high-signal enhancement of the nidus *(arrow)*. Marked bone marrow edema of the entire metaphysis is seen as high signal intensity *(open arrow)* on a fluid-sensitive, fat-suppressed coronal T2-weighted MR image **(D).** Higher intensity signal is evident in the region of the nidus.

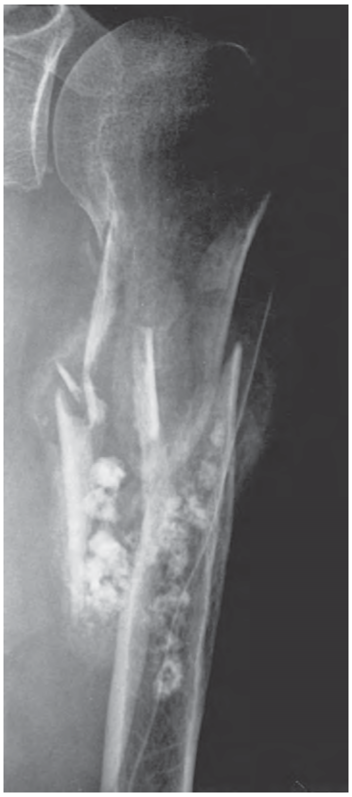

FIGURE 14–14 Enchondroma: pathologic fracture.[31] An 80-year-old male patient had fallen 1 month before these radiographs were obtained. He had decreased ranges of motion. An elongated, heavily calcified tumor with a healing, comminuted pathologic fracture is seen within the humeral diaphysis.

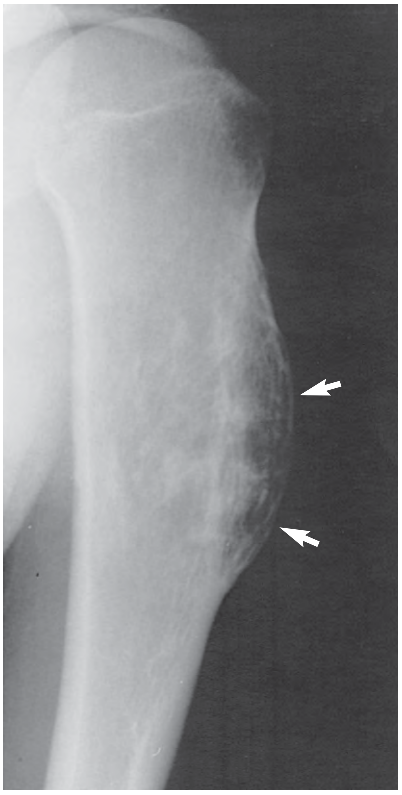

FIGURE 14–16 Solitary osteochondroma.[34,35] An expansile, sessile osteochondroma arising from the proximal metadiaphysis of the humerus is seen on a routine radiograph *(arrows).*

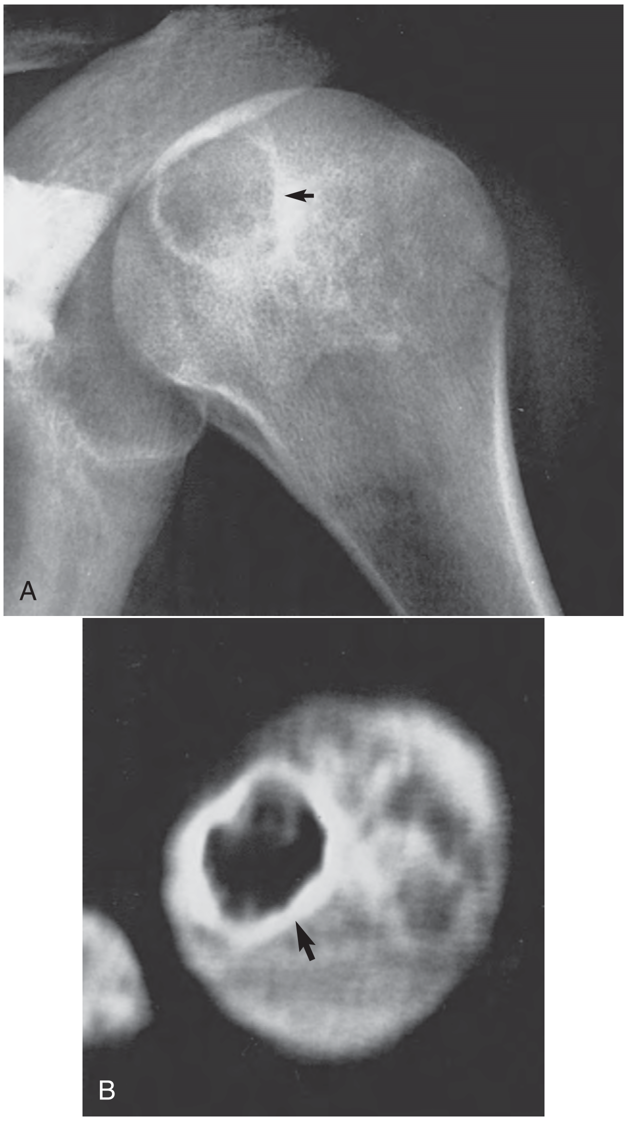

FIGURE 14–15 Chondroblastoma.[32,33,57] A 17-year-old boy with shoulder pain. **A,** Frontal radiograph of the humerus reveals a well-defined osteolytic epiphyseal lesion *(arrow),* that appears well defined. **B,** Transaxial CT scan clearly defines the lesion *(arrow)* and shows the sclerotic margin to good advantage. *(Courtesy R. Sweet, M.D., Pomona, Calif.)*

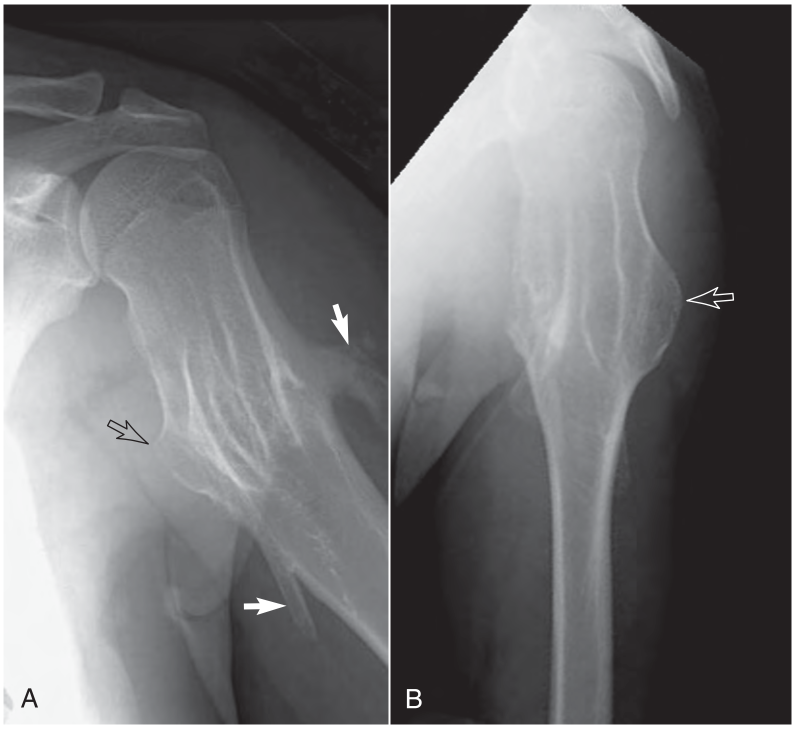

FIGURE 14–17 Hereditary multiple exostoses.[36-38] External **(A)** and internal **(B)** rotation radiographs of the humerus in this 13-year-old boy reveal multiple sessile *(open arrows)* and pedunculated *(arrows)* osteochondroma-like exostoses and significant metaphyseal widening. Similar findings were depicted bilaterally adjacent to several of the large joints.

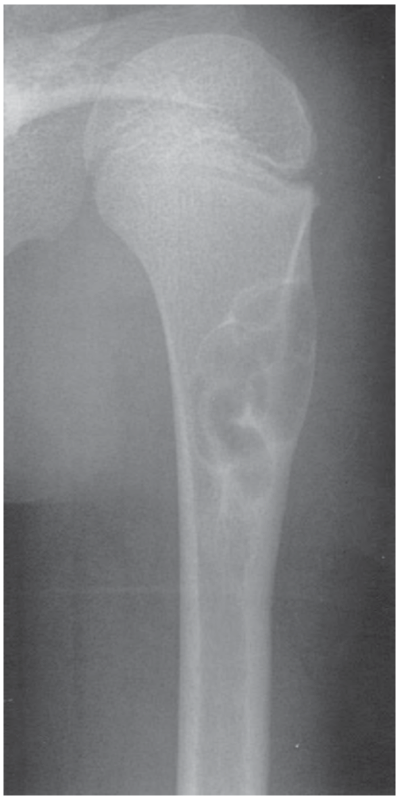

FIGURE 14–18 Nonossifying fibroma.[39] Routine radiograph of the proximal portion of the humerus in this 11-year-old girl reveals a large, eccentric, expansile, multiloculated, geographic osteolytic lesion. Cortical thinning and endosteal scalloping also are evident.

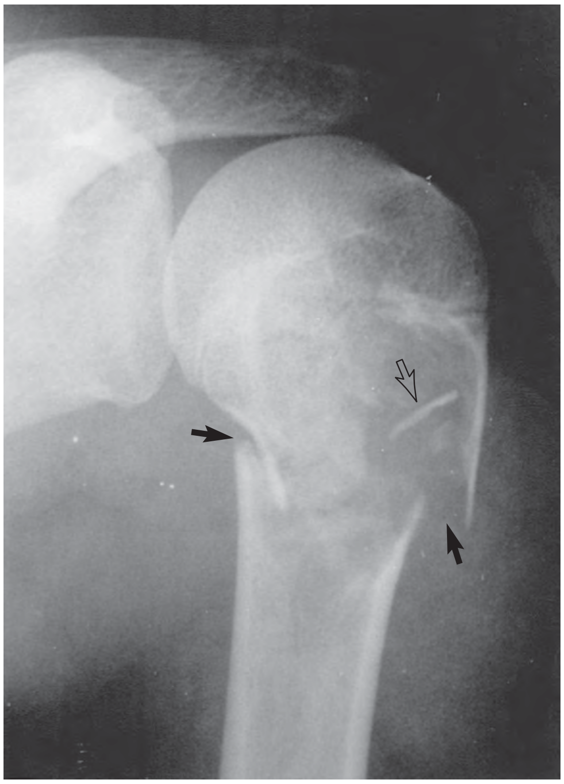

FIGURE 14–19 Simple bone cyst: pathologic fracture.[41,42] This young patient with a simple bone cyst in the proximal portion of the humerus sustained a transverse pathologic fracture through the weakened bone *(arrows)*. Routine radiograph exhibits the classic "fallen fragment sign," in which a sliver of fractured cortical bone migrates to a dependent position within the fluid matrix of the lesion *(open arrow)*. On serial radiographs of the humerus, simple bone cysts may appear to migrate away from the physis owing to normal longitudinal metaphyseal growth between the physis and the lesion. *(Courtesy D. Pate, D.C., San Diego and Terry R. Yochum, D.C., Denver, Colo.)*

TABLE 14-5 Tumorlike Lesions Affecting the Humerus*

Tumorlike Lesion	Figure(s)	Characteristics
Paget disease[44,45,64,65]	14-20	Humerus is a commonly affected site Usually polyostotic and may have unilateral involvement Coarsened trabeculae and bone enlargement Diaphyseal and metaphyseal involvement with extension into epiphysis *Stages of involvement:* osteolytic (50%), osteosclerotic (25%), and mixed (25%), malignant transformation (less than 2%) Pathologic fractures, deformities, pseudofractures
Monostotic fibrous dysplasia[46]	14-7, 14-21	Fewer than 4% of monostotic lesions affect the humerus Thick rim of sclerosis surrounding a radiolucent lesion Ground-glass appearance of fibrous matrix
Polyostotic fibrous dysplasia[46]		Fifty percent of patients have humeral lesions Unilateral or bilateral, asymmetric humeral involvement Lesions appear the same as monostotic form but are frequently larger, more expansile, and more multiloculated than monostotic lesions
Langerhans cell histiocytosis[47,48]	14-22	Humerus is involved in about 7% of cases Osteolytic lesions may be multiloculated and expansile Eosinophilic granuloma is the most frequent and mildest form of this disorder characterized by histiocytic infiltration of tissues

* See also Table 1-14.

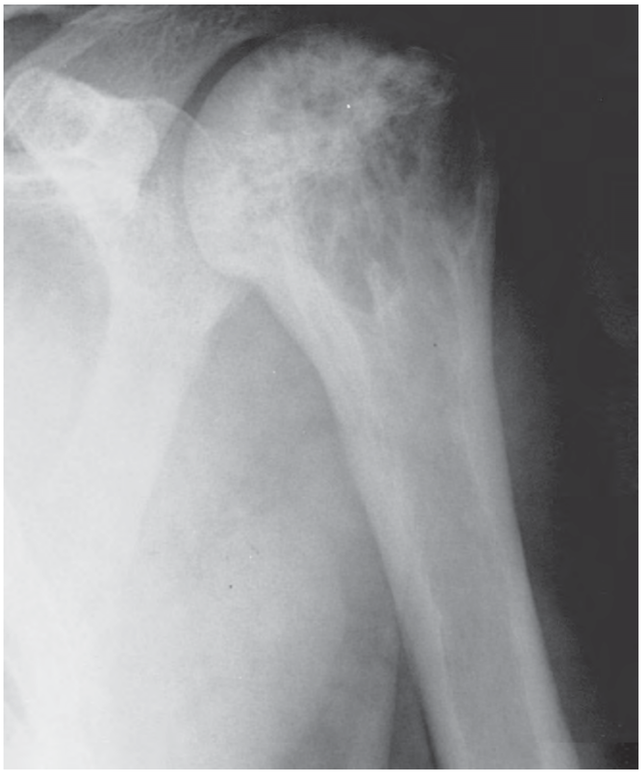

FIGURE 14–20 Paget disease: humerus.[44,45,64,65] Observe the areas of thickened, coarsely trabeculated bone with radiolucent regions of varying size extending into the subchondral region of the humerus. The combined stage of Paget disease, as seen in this patient, involves both osteolytic and osteosclerotic osseous changes.

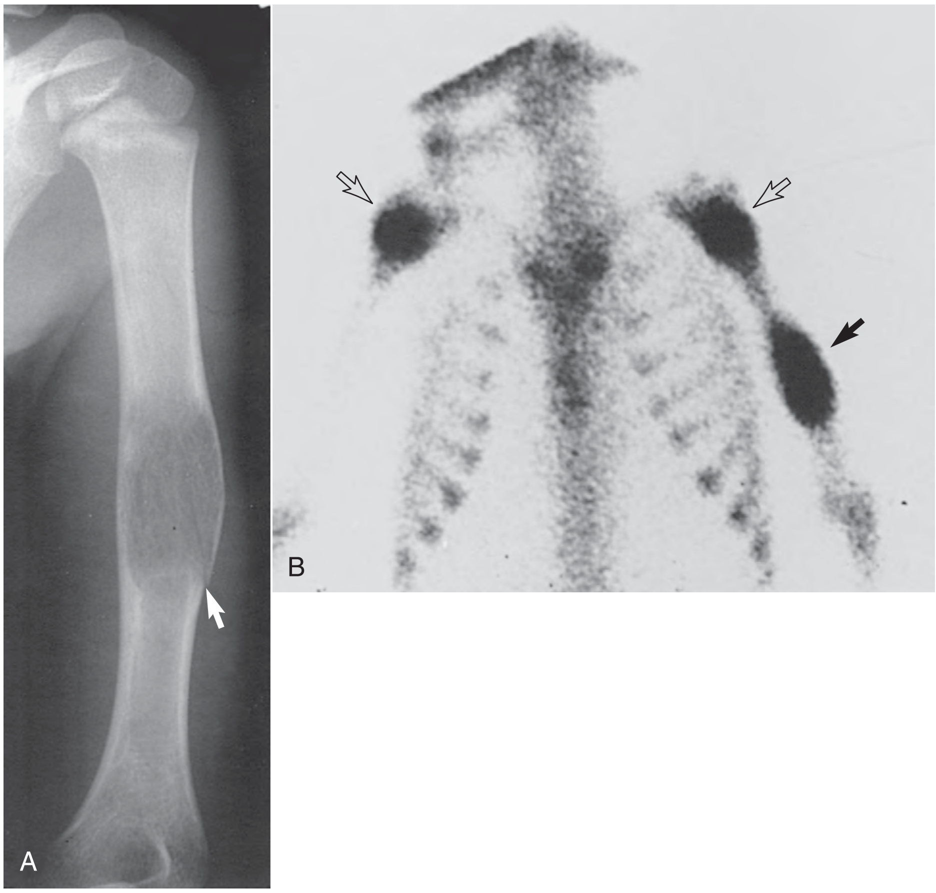

FIGURE 14–21 Monostotic fibrous dysplasia.[46] In a 4-year-old girl, a radiograph **(A)** shows an expansile diaphyseal lesion with endosteal scalloping, typical ground-glass hazy appearance of the matrix, and pathologic fracture *(arrow)*. A ^{99m}Tc-methylene diphosphonate bone scan **(B)** shows focal concentration of radionuclide in the vicinity of the lesion *(arrow)* and normal increased uptake at the growing epiphyses *(open arrows)*.

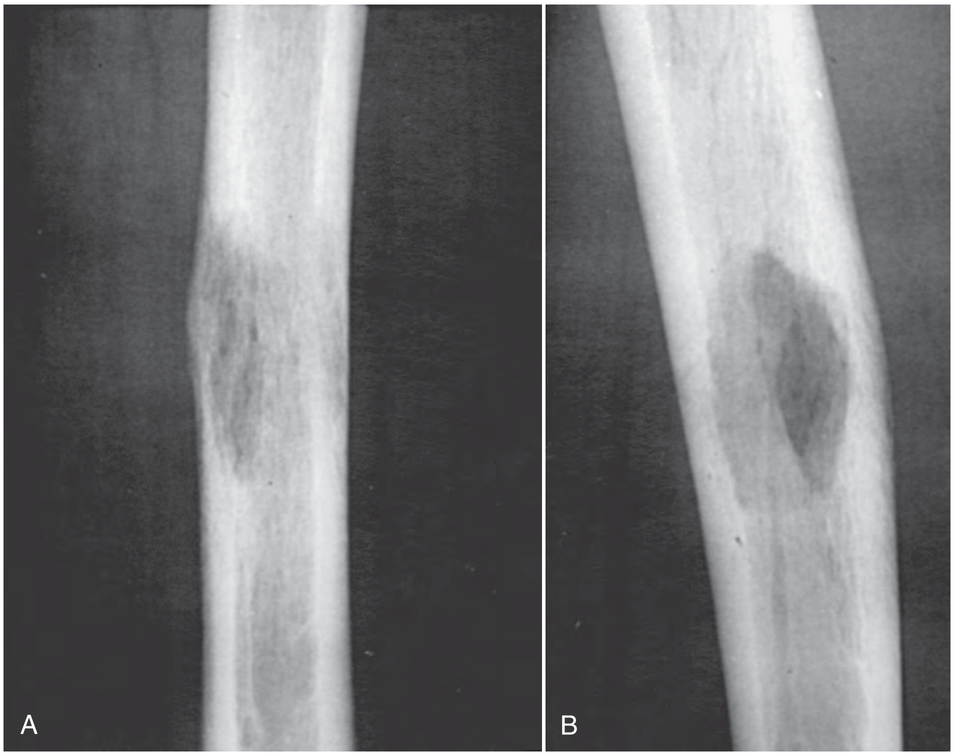

FIGURE 14–22 Langerhans cell histiocytosis: eosinophilic granuloma.[47,48] Anteroposterior **(A)** and lateral **(B)** radiographs of the humerus in this 23-year-old woman reveal a permeative pattern of osteolytic destruction. Biopsy analysis revealed eosinophilic granuloma. The lesion appears aggressive on the frontal radiograph **(A)** and shows geographic destruction on the lateral radiograph **(B).** Eosinophilic granuloma of bone is the most frequent and mildest form of Langerhans cell histiocytosis, a disease characterized by histiocytic infiltration of tissues. *(Courtesy R. Kerr, M.D., Los Angeles.)*

TABLE 14-6 Metabolic, Hematologic, and Infectious Disorders Affecting the Humerus*

Disorder	Figure(s)	Characteristics
Generalized osteoporosis[49]		Uniform decrease in radiodensity, thinning of cortices, accentuation of trabeculae May result in insufficiency fractures of the humerus
Osteogenesis imperfecta[50]	14-23	Osteoporosis and bone fragility Thin, gracile appearance of entire skeleton Severe deformities and fractures commonly affect the humerus
Osteomalacia[51,66]	14-24	Diffuse osteopenia Decreased trabeculae; remaining trabeculae appear prominent and coarsened Looser zones (pseudofractures)
Rickets[51,66]	14-24	Metaphyseal demineralization resulting in frayed metaphyses Bowing deformities Osteopenia Looser zones
Gaucher disease[52,67]	14-25	Marrow infiltration results in osteopenia, osteolytic lesions, cortical diminution, and medullary widening of tubular bones Osseous weakening results in pathologic fractures *Modeling deformities:* Erlenmeyer flask deformity (widening of the distal diametaphysis of the humerus) Osteonecrosis of humeral metadiaphysis and humeral head
Secondary hypertrophic osteoarthropathy[53]		Syndrome characterized by digital clubbing, arthritis, and bilateral symmetric periostitis of humerus and other tubular bones Complication of many diseases, including bronchogenic carcinoma, mesothelioma, and other intrathoracic and intraabdominal diseases
Acute osteomyelitis[54,60]	14-26	Acute pyogenic osteomyelitis frequently involves the metaphysis in children Poorly defined permeative bone destruction In infants and young children, streptococcal infection may be causative
Chronic osteomyelitis[55,60]	14-27	Humerus is a common site of this rare disease Osteosclerosis and cortical thickening Thick, single layer periosteal bone proliferation Poorly defined areas of osteolysis and osteosclerosis Sequestrum and involucrum Cloaca formation
Collagen vascular disease: soft tissue calcification[56]	14-28	Dermatomyositis, polymyositis, scleroderma, and other collagen vascular diseases may result in calcinosis in the soft tissues of the upper arm Differential diagnosis: hyperparathyroidism, neurologic injury, melorheostosis, posttraumatic heterotopic ossification, soft tissue neoplasms, fibrodysplasia ossificans progressiva

* See also Tables 1-15 to 1-19.

FIGURE 14–23 Osteogenesis imperfecta.[50] **A-B,** This 32-year-old female, who has suffered with osteogenesis imperfecta since early childhood, has new onset of upper arm pain in the absence of significant trauma. The humerus, radius, and ulna are all thin and bowed and the distal diaphysis of the humerus is fractured *(arrows)*. Observe the profound osteopenia involving all of the bones about the elbow.

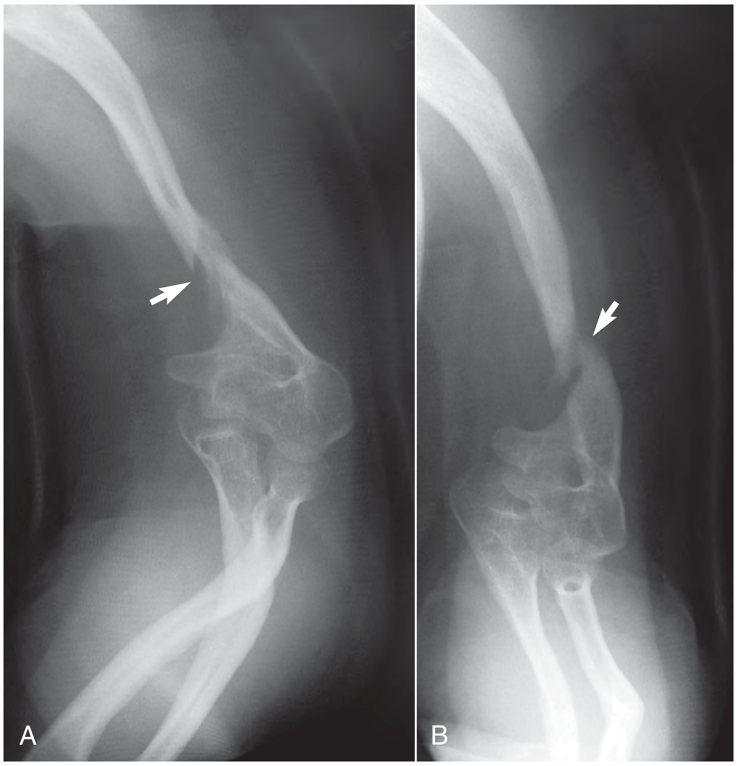

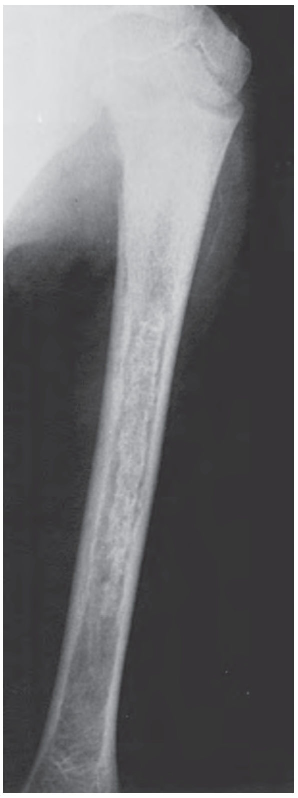

FIGURE 14–25 Gaucher disease: medullary infarct.[52,67] Radiograph of the humerus in this 10-year-old boy with Gaucher disease reveals diaphyseal medullary sclerosis characteristic of a medullary infarct. Gaucher disease may also be manifested as osteopenia, cortical thinning, or erosion, coarsened trabecular pattern, osteolytic lesions, modeling deformity (such as Erlenmeyer flask deformity), and epiphyseal osteonecrosis.

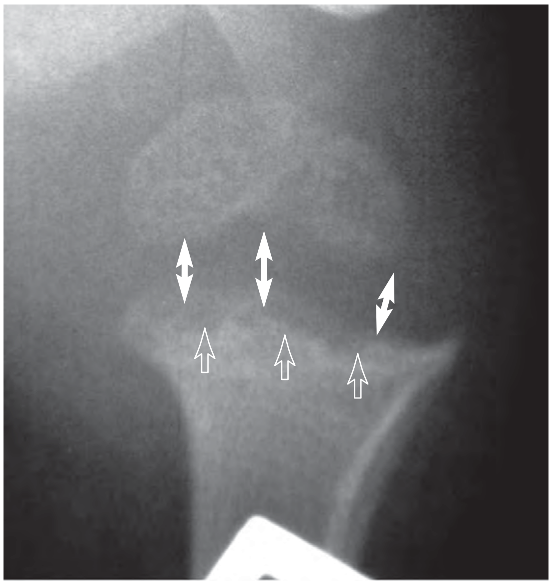

FIGURE 14–24 Rickets.[51,66] A single radiograph of the proximal end of the humerus in this child reveals widening of the physis *(double arrows)* with a frayed and widened metaphysis *(arrows)*. This appearance, seen in children with prolonged vitamin D deficiency, is designated the "paintbrush metaphysis."

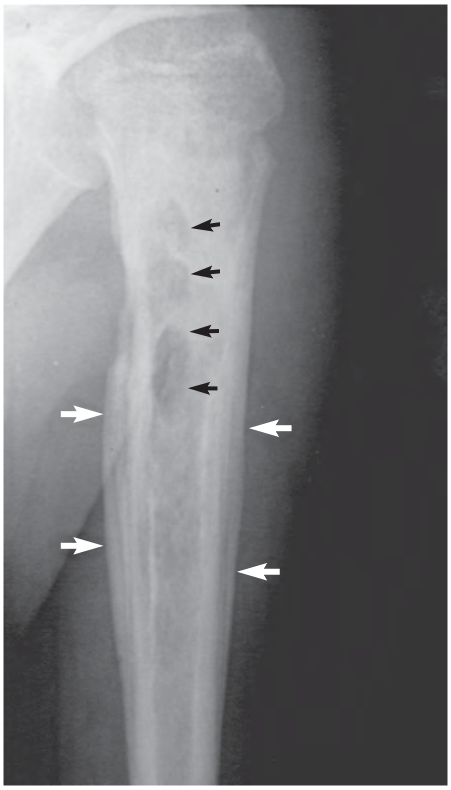

FIGURE 14–26 Acute pyogenic osteomyelitis.[54,60] In this 12-year-old patient, observe the diffuse solid layer of periosteal new bone formation *(white arrows),* the increased density, and the central, elongated osteolytic lesions *(black arrows)* within the proximal humeral metadiaphysis.

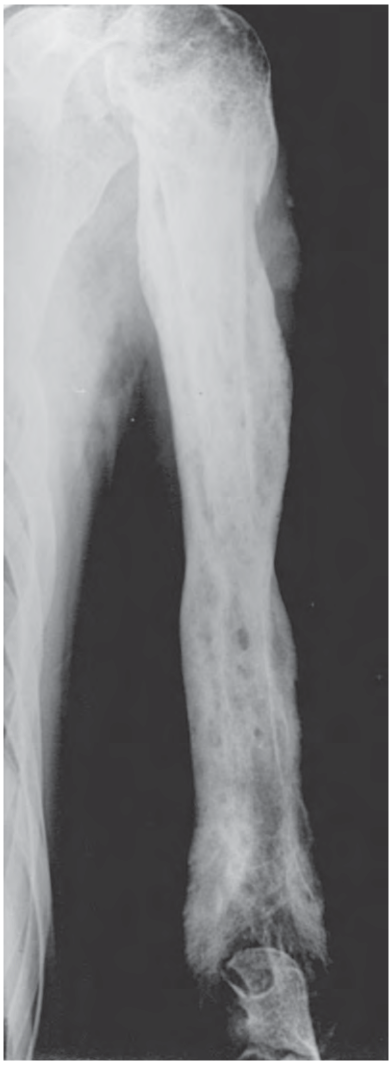

FIGURE 14–27 Chronic osteomyelitis: *Staphylococcus aureus.*[55,60] A bizarre cloak of ossification is seen surrounding the entire diaphysis and both metaphyses of the humerus. Circular osteolytic foci are present in the distal aspect of the shaft. This patient had longstanding chronic osteomyelitis that showed no change on serial radiographs. Radiographic signs of activity in chronic osteomyelitis include a change from previous radiographs, poorly defined areas of osteolysis, thin linear periostitis, and sequestration, none of which were present in this patient. *(Courtesy C. Pineda, M.D., Mexico City.)*

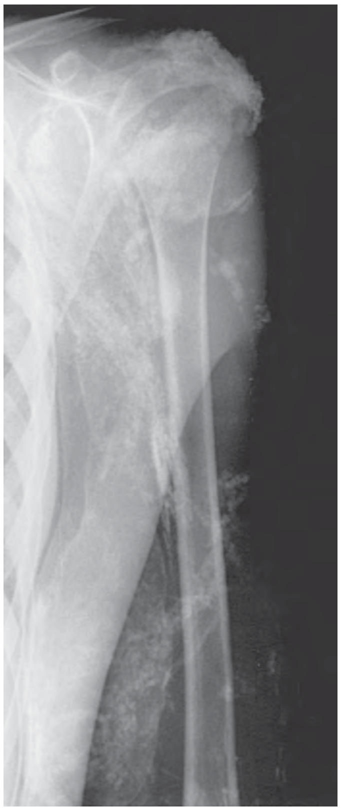

FIGURE 14–28 Collagen vascular disease: dermatomyositis and polymyositis.[56] Observe the sheetlike periarticular, muscular, and subcutaneous calcification adjacent to the humerus in this 16-year-old girl with dermatomyositis-polymyositis. A number of collagen vascular diseases may result in localized or diffuse soft tissue calcification. *(Courtesy C. Van Lom, M.D., San Diego.)*

CHAPTER 15

Elbow

NORMAL DEVELOPMENTAL ANATOMY

Accurate interpretation of radiographs of the pediatric elbow requires a complete understanding of normal developmental anatomy. Table 15-1 outlines the age of appearance and fusion of the primary and secondary ossification centers. Figures 15-1 and 15-2 demonstrate the radiographic appearance of many important ossification centers and other developmental landmarks at selected ages from birth to skeletal maturity. Figure 15-3 illustrates a special view for evaluating the radial head.

DEVELOPMENTAL ANOMALIES, ANATOMIC VARIANTS, SOURCES OF DIAGNOSTIC ERROR, AND SKELETAL DYSPLASIAS

Several anomalies, anatomic variants, skeletal dysplasias, and other sources of diagnostic error about the elbow may simulate disease and potentially result in misdiagnosis. Table 15-2 and Figures 15-4 to 15-7 represent selected examples of some of the more common processes affecting this region.

ELBOW JOINT EFFUSION: INTRACAPSULAR FAT PAD DISPLACEMENT

Displacement (elevation) of both the posterior and anterior intracapsular fat pads of the elbow indicates the presence of joint effusion. Table 15-3 lists a number of causes of joint effusion, and Figure 15-8 illustrates two examples.

DISLOCATIONS AND FRACTURES

Physical injury to the elbow region may result in a wide variety of dislocations and fractures. Table 15-4 lists the most common types of such injuries, and several examples of these are illustrated in Figures 15-9 to 15-21. Injuries to the humeral shaft are discussed in Chapter 14, and fractures of the diaphyses of the radius and ulna are discussed and illustrated in Chapter 16.

SOFT TISSUE INJURIES

The elbow is a frequent site of injuries to tendons, ligaments, and joint capsules. The more common injuries are listed in Table 15-5. Figures 15-22 to 15-26 illustrate several examples of these posttraumatic conditions.

ARTICULAR DISORDERS

The joints of the elbow are frequent target sites of involvement for many degenerative, inflammatory, crystal-induced, and infectious articular disorders. Table 15-6 outlines these diseases and their characteristics. Figures 15-27 to 15-35 illustrate the typical imaging manifestations of the most common articular disorders affecting the elbow.

METABOLIC, HEMATOLOGIC, AND INFECTIOUS DISORDERS

Several metabolic, hematologic, and infectious disorders affect the bones and soft tissue structures about the elbow region. Table 15-7 lists some of the more common disorders and describes their characteristics. Figures 15-38 to 15-39 illustrate the characteristic imaging findings of many of these disorders. Additionally, osteonecrosis of the juvenile capitulum (Panner's disease) is illustrated in Figure 15-39.

TABLE 15-1 **Elbow: Approximate Age of Appearance and Fusion of Ossification Centers**[1-5,69] **(Figures 15-1 to 15-3)**

Ossification Centers	Primary or Secondary	No. of Centers (Per Bone)	Age of Appearance* (Years)	Age of Fusion* (Years)	Comments
Capitulum epiphysis	S	1	1-2	13 12-13 16	Fuses to trochlea Fuses to lateral epicondyle Fuses to humerus
Medial humeral epicondyle	S	1	4-6	16	Fuses to humerus
Radial head epiphysis	S	1	4-5	16	Fuses to radius
Trochlear epiphysis	S	1	8-9	13 16	Fuses to capitulum Fuses to humerus
Olecranon epiphysis	S	1 or 2	8-9	12-15	Fuses to ulna
Lateral humeral epicondyle	S	1	10	12-13 15	Fuses to capitulum Fuses to humerus

P, Primary; *S,* secondary.

* Ages of appearance and fusion of ossification centers in girls typically precede those of boys. Ethnic differences also exist.

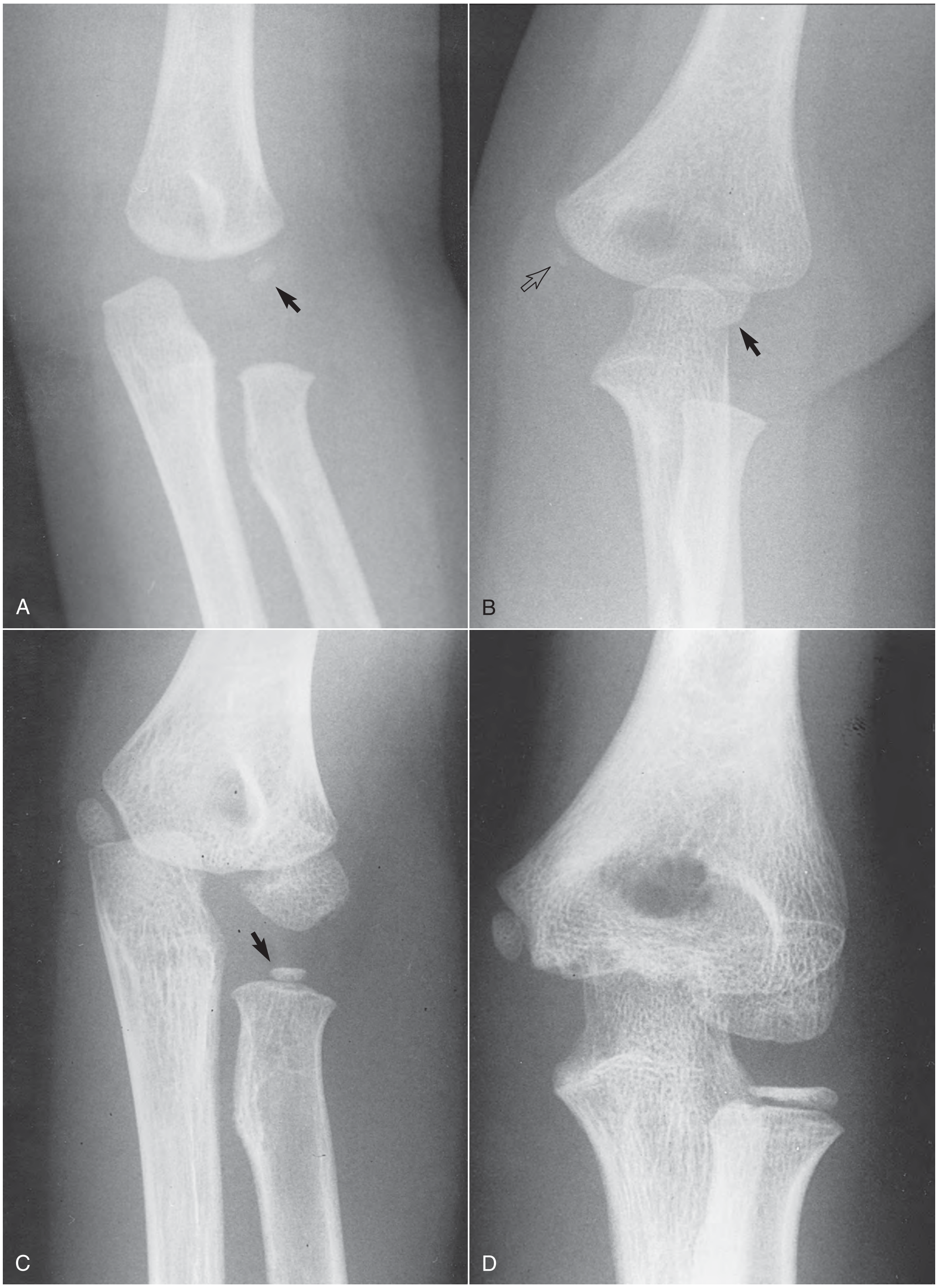

FIGURE 15–1 Skeletal maturation and normal development: anteroposterior elbow radiographs.[1-5] **A,** A 1-year-old girl. The secondary ossification center of the capitulum has begun to ossify *(arrow)*. **B,** A 2-year-old girl. The secondary ossification center of the medial epicondyle is beginning to ossify *(open arrow),* and the capitulum is larger *(arrow)*. **C,** A 5-year-old girl. The secondary ossification center of the radial head has begun to ossify *(arrow)*. **D,** An 8-year-old boy. The normal radial head ossification center is frequently radiodense, as in this case. The distal humeral metaphysis has widened significantly.

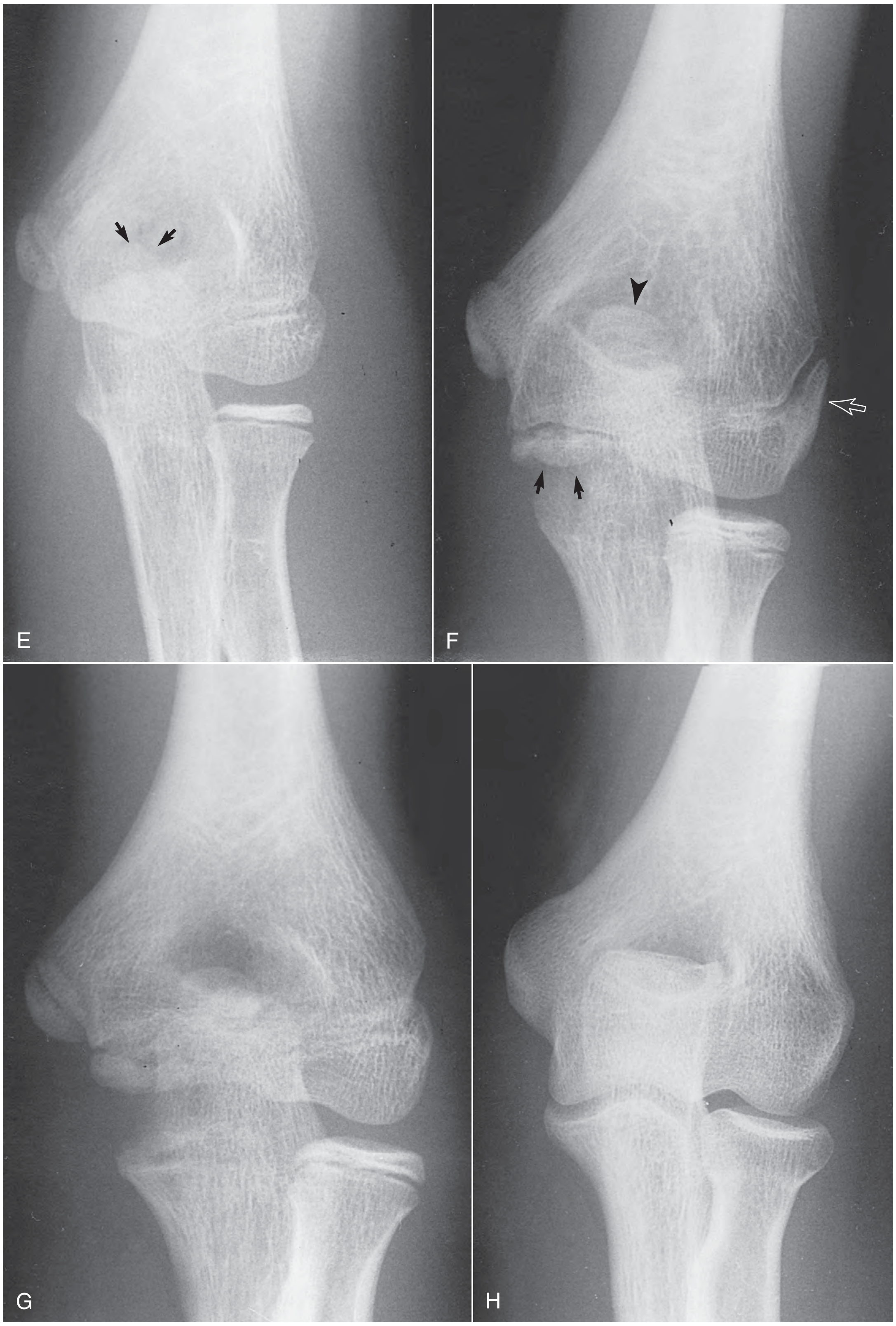

FIGURE 15–1, cont'd E, A 10-year-old girl. The existing ossification centers have enlarged and begun to conform to their adjacent metaphyses. The olecranon ossification center has begun to appear *(arrows),* a finding that is better seen on lateral radiographs. **F,** A 12-year-old girl. The secondary ossification center for the trochlea is beginning to ossify *(arrows),* and the center for the capitulum has a lateral projection that extends proximally along the humeral metaphysis *(open arrow)*. The olecranon ossification center is enlarging *(arrowhead)*. **G,** A 12-year-old boy. The ossification centers of the capitulum and trochlea have fused together, and the olecranon ossification center is large and prominent. **H,** A 16-year-old girl. Complete fusion of all ossification centers has occurred, and the elbow exhibits adult proportions.

Continued

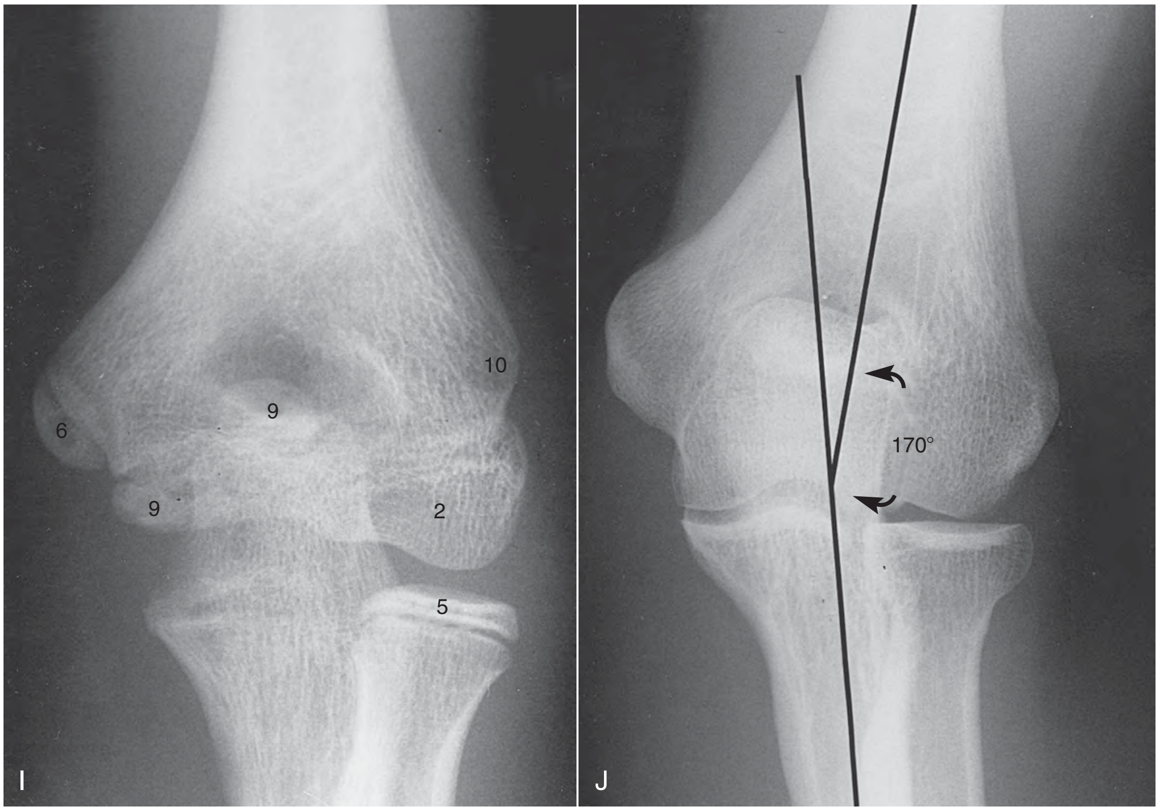

FIGURE 15–1, cont'd I, Normal pattern of ossification about the elbow. Numbers indicate approximate age in years at which the center begins to ossify (Table 15-1). **J,** Adult: 43-year-old man. The normal carrying angle of the elbow ranges from 154 to 178 degrees, averages 169 degrees, and may be altered as a result of fracture or other deformity.

Clinical Note: The normal appearances of the developing radial head and neck are often misinterpreted as evidence of trauma because (1) the radial neck of an infant is slightly angulated medially in the frontal projection, simulating a dislocation of the radial head; (2) the early physis of the proximal portion of the radius is wedge-shaped, mimicking an avulsion fracture of the head; and (3) notches and clefts in the metaphysis of the proximal portion of the radius may closely resemble posttraumatic abnormalities.[5]

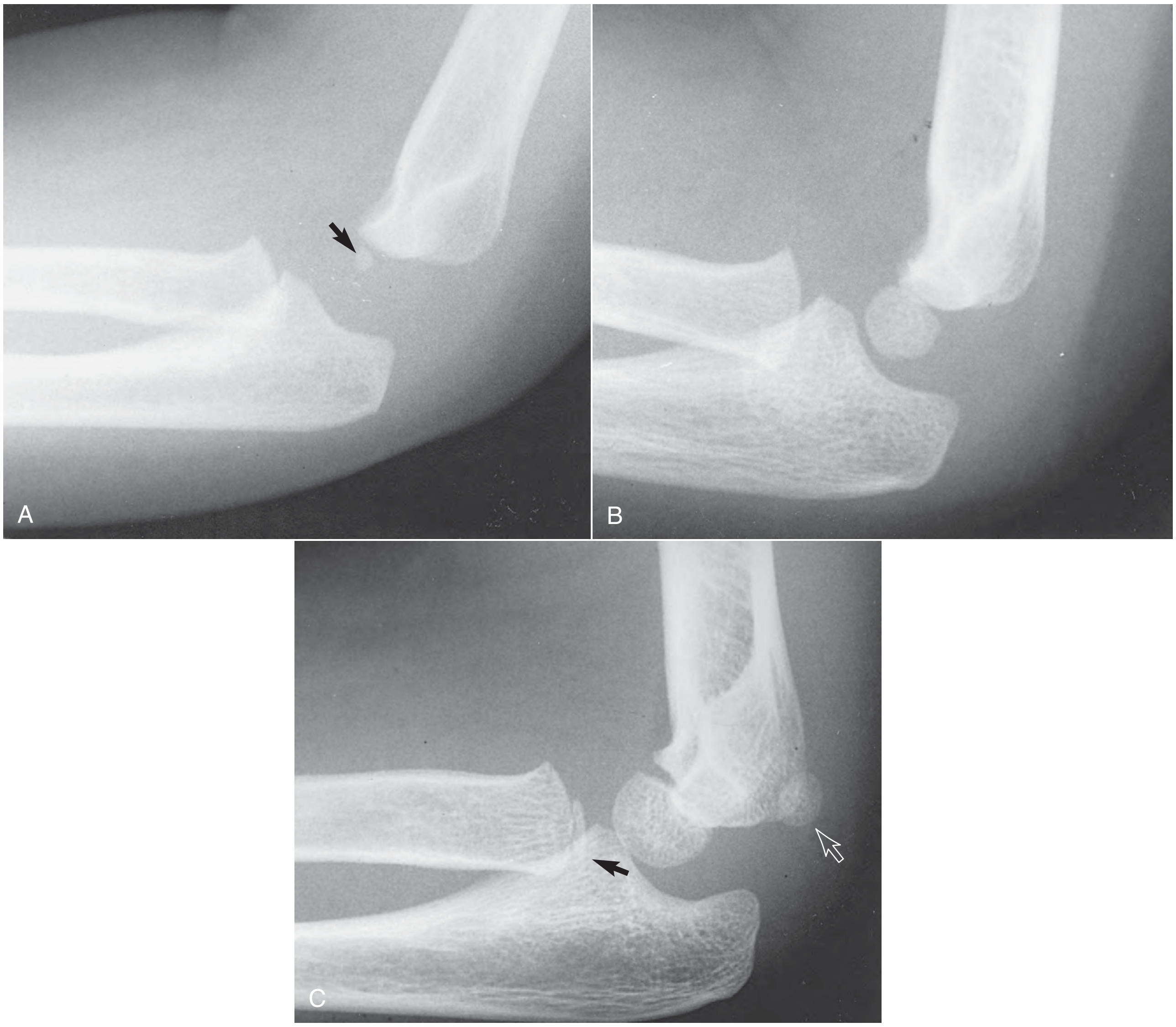

FIGURE 15–2 Skeletal maturation and normal development: lateral elbow radiographs.[1-5] **A,** A 1-year-old girl. Only the secondary ossification center for the capitulum is evident *(arrow)*. **B,** A 2-year-old girl. The ossification center for the capitulum is larger. **C,** A 5-year-old girl. The secondary ossification centers for the radial head *(arrow)* and medial epicondyle *(open arrow)* are present. These usually appear at the ages of 5 and 6 years, respectively.

Continued

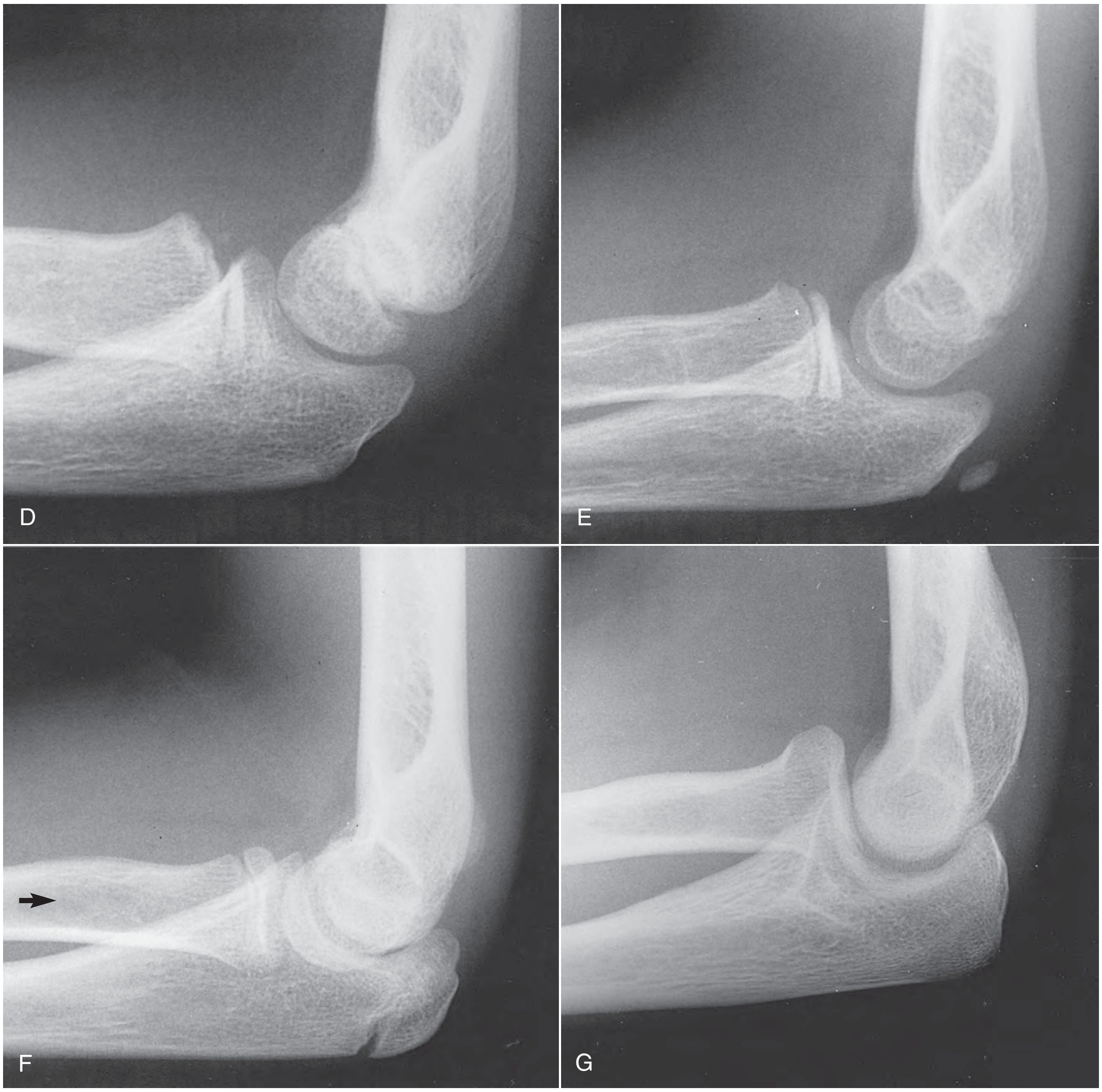

FIGURE 15–2, cont'd **D,** An 8-year-old boy. The radial head ossification center is normally radiodense, as in this case. The capitulum ossification center conforms to the shape of the humeral metaphysis. **E,** A 10-year-old girl. The secondary ossification center for the olecranon has begun to ossify. **F,** A 13-year-old boy. The secondary ossification center for the olecranon is beginning to fuse to the ulna. The radiolucent area in the radius represents the normal trabecular pattern in the cancellous bone of the radial tuberosity *(arrow)* and should not be mistaken for a destructive lesion. **G,** A 16-year-old girl. Complete fusion of all ossification centers has occurred, and the elbow exhibits adult proportions.

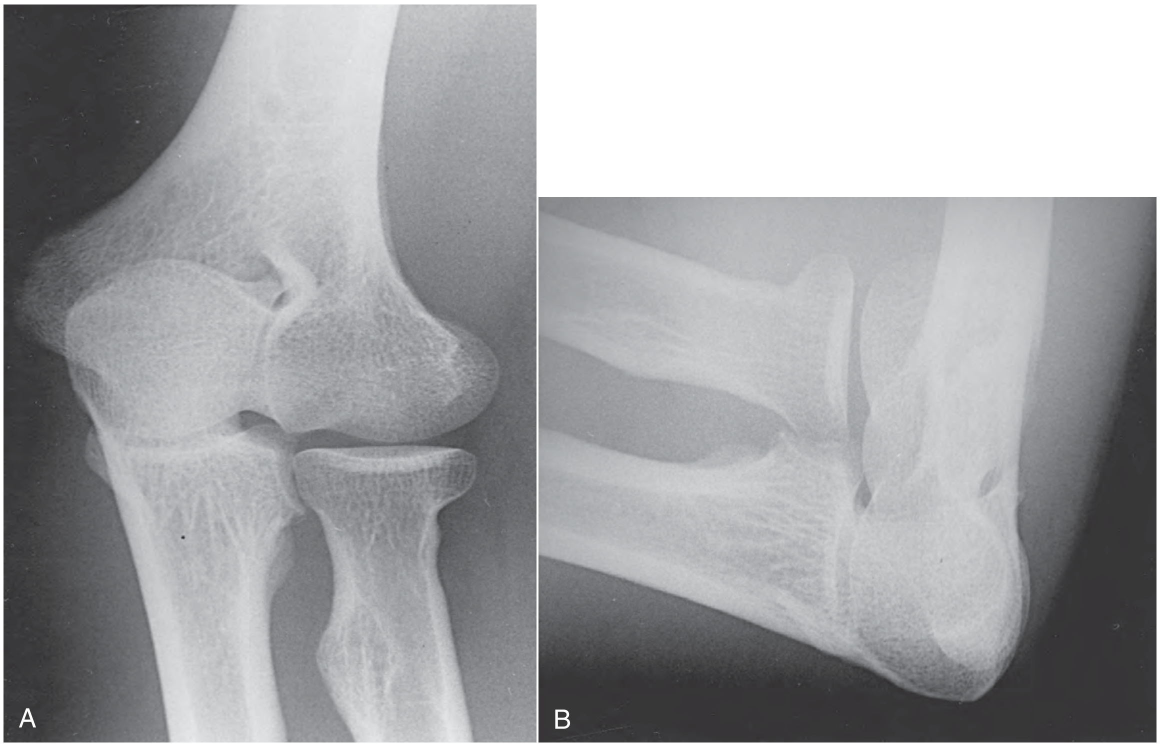

FIGURE 15–3 A-B, Normal radial head projections.[6] Special angulated views of the radial head clearly depict the anatomy of the proximal radioulnar region and are particularly useful in analyzing fractures of the radial head and neck.

TABLE 15-2 Developmental Anomalies, Anatomic Variants, Sources of Diagnostic Error, and Skeletal Dysplasias

Disorder	Figure(s)	Characteristics
Simulated periostitis[7,8]	13-2, *G*	See Table 14-1
Supracondylar process[7,8]	14-1	See Table 14-1
Chevron sign[9]	14-2	See Table 14-1
Supratrochlear foramen[7,8,10]	14-3	See Table 14-1
Radiolucent radial tuberosity[8]	15-2, *F*, 16-1	Normal radiolucency of the cancellous bone within the radial tuberosity may simulate a destructive lesion or a cyst No clinical significance
Incomplete union of ossification centers[8]	15-4	In children, incompletely fused ossification centers may simulate fractures *Common sites:* olecranon, epicondyles, trochlea, capitulum, radial head Irregularities of the growing epiphyses about the elbow are common Olecranon ossification center may arise from two or more nuclei, simulating a fracture Nonunion of ossification centers may persist into adulthood
Patella cubiti[11]		Sesamoid bone within the triceps tendon just above the olecranon Rare anomaly that may simulate heterotopic ossification or ununited olecranon avulsion fracture within the triceps tendon
Radioulnar synostosis[12]	15-5	Anomalous osseous fusion of the proximal portions of the radius and the ulna Bilateral in 60% of patients Restricts normal forearm supination and pronation Additional anomalies may accompany radioulnar synostosis
Hereditary osteo-onychodysostosis (HOOD syndrome)[13]	15-6	Dislocation of the radial head due to asymmetric development of the humeral condyles and hypoplasia of the radial head and capitulum Also termed *Fong syndrome* or *nail-patella syndrome* Associated abnormalities of the fingernails and toenails, absence or hypoplasia of the patella, and presence of iliac horns
Osteopoikilosis[14]	15-7	Multiple circular zones of osteosclerosis tend to accumulate in a periarticular distribution

See also Table 1-1.

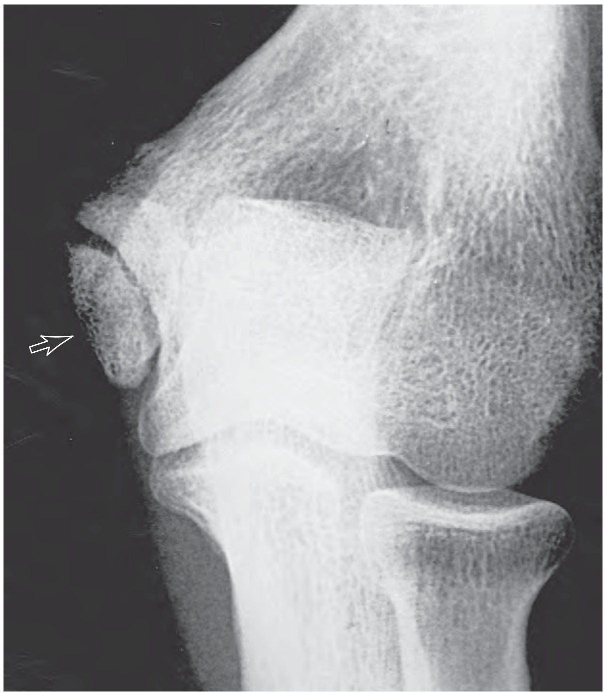

FIGURE 15–4 Unfused ossification center.[8] A well-corticated, ovoid osseous fragment is seen at the medial epicondyle of the humerus *(open arrow)* in this 35-year-old man. This ossicle represents failure of union of the ossification center. Ossification of the medial epicondyle usually begins to appear on radiographs between the ages of 4 and 6 years, and in most persons, fusion is complete by the age of 20 years.

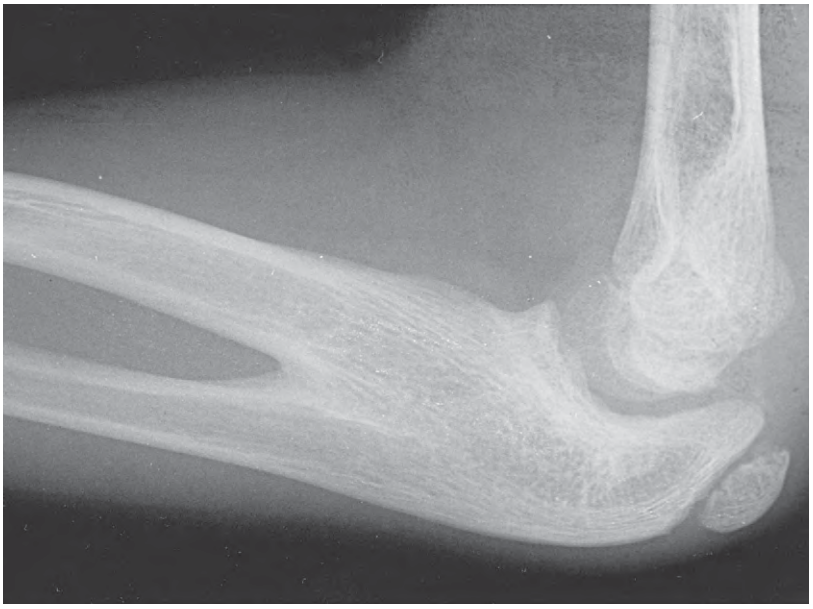

FIGURE 15–5 Radioulnar synostosis.[12] Complete osseous fusion of the proximal portions of the radius and ulna is seen. This anomaly, which is bilateral in 60% of patients, interferes with normal forearm supination. Additional anomalies may accompany radioulnar synostosis. (The olecranon ossification center has not yet fused in this child.)

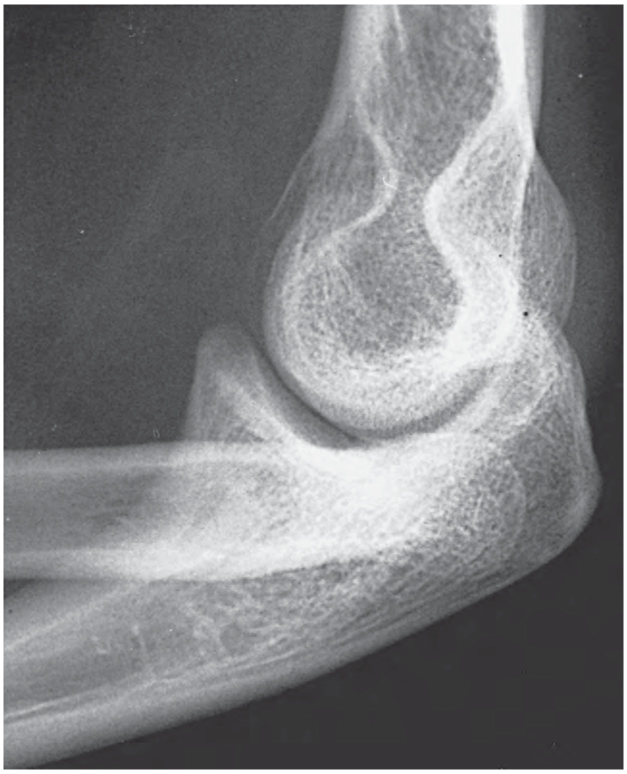

FIGURE 15–6 Hereditary osteo-onychodysostosis (HOOD syndrome).[13] Observe the dislocation of the radial head owing to asymmetric development of the humeral condyles and hypoplasia of the capitulum and radial head. This condition, also referred to as *Fong syndrome* or *nail-patella syndrome*, is characterized by associated abnormalities of the fingernails and toenails, absence or hypoplasia of the patella, and presence of iliac horns. *(Courtesy R. Sweet, MD, Pomona, Calif.)*

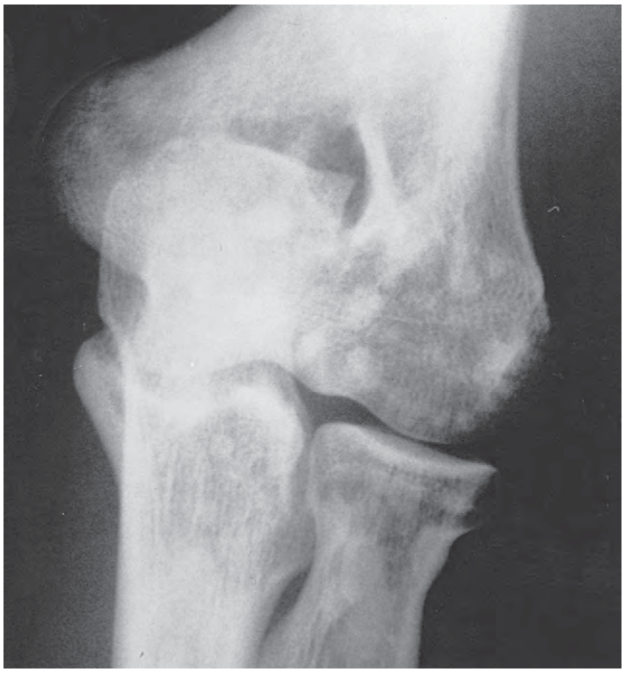

FIGURE 15–7 Osteopoikilosis.[14] Note the circular and ovoid osteosclerotic foci within the radius, ulna, and humerus. The symmetric, periarticular distribution is characteristic of this fairly common sclerosing dysplasia. Although the epiphysis may be affected, most lesions occur in the metaphysis. *(Courtesy L. Danzig, MD, Santa Ana, Calif.)*

TABLE 15-3 Some Causes of Intracapsular Fat Pad Displacement in the Elbow*[15-17] (Figure 15-8)

Blood	**Exudate**
Intraarticular fracture†	Infectious arthritis
Hemophilia	**Neoplasm**
Transudate	Leukemia
Rheumatoid arthritis	Metastasis
Other synovial arthropathies	Synovial sarcoma
Gout	Osteoid osteoma
Calcium pyrophosphate dihydrate (CPPD) crystal deposition	**Other**
Osteoarthrosis	Villonodular synovitis
Neuropathic osteoarthropathy	Synovial osteochondromatosis
	Osteochondritis dissecans

* Adapted from Murphy WA, Siegel MJ: Elbow fat pads with new signs and extended differential diagnosis. Radiology 124:659, 1977.

† Many pediatric fractures about the elbow are occult on conventional radiographs, revealing only a positive fat pad sign indicative of joint effusion. MR imaging is more sensitive and accurate than conventional radiography in diagnosing such subtle injuries.[71,78]

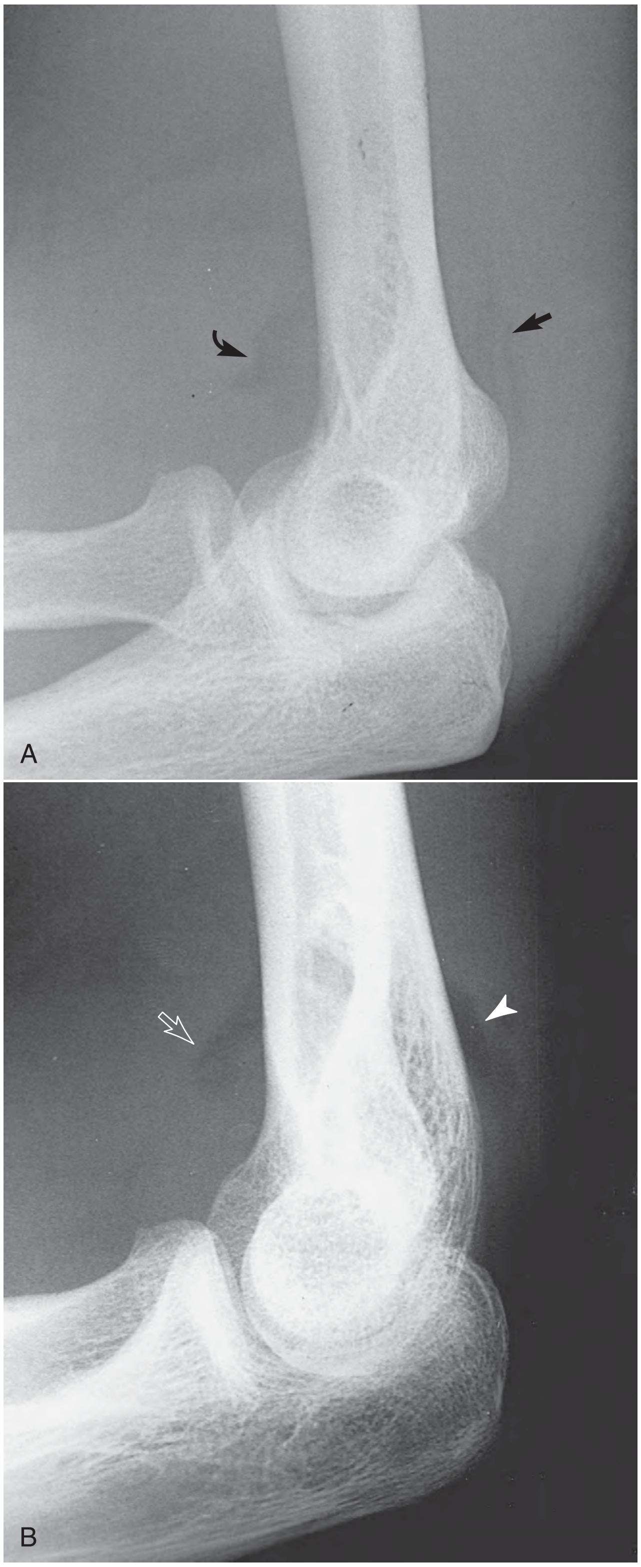

FIGURE 15–8 Elbow joint effusion: intracapsular fat pad displacement.[15-17] **A,** Elevation of both the anterior *(curved arrow)* and posterior *(arrow)* intracapsular fat pads of the elbow is evident in this patient with a radial head fracture (not seen). **B,** In another patient with an intraarticular fracture of the radial head (fracture not seen), elevation of both anterior *(open arrow)* and posterior *(arrowhead)* fat pads indicates a joint effusion. This sign usually reflects the existence of intracapsular fluid or blood and has traditionally been synonymous with an occult intraarticular fracture. Recent evidence has shown that visualization of joint effusion without evidence of fracture on initial radiographs after trauma does not correlate with the presence of occult fracture in 83% of pediatric cases. However, presence of persistent joint effusions on follow-up radiographs correlates with occult fractures.[17] Joint effusions may also be associated with a number of other pathologic processes (Table 15-4).

TABLE 15-4 Dislocations and Fractures About the Elbow[74]

Injury	Figure(s)	Characteristics	Complications and Related Disorders
Elbow Dislocation		Most frequent site of dislocation in children	
Posterior dislocation of elbow[18]	15-9	*Usual mechanism:* hyperextension Eighty percent to 90% are posterior dislocations of both ulna and radius in relation to the humerus	*Children:* Often associated with medial epicondyle avulsion *Adults:* Associated with fractures of the radial head and coronoid process of the ulna Median nerve entrapment
Radial head dislocation[19,69]	15-10	*Children:* "nursemaids' elbow" or "pulled elbow" is very common Sudden pull on child's arm while in pronated position Radial head dislocates anteriorly in relation to the capitulum The radiocapitular line drawn on a lateral radiograph of the elbow should always pass through the center of the capitulum regardless of the amount of elbow flexion; when the radial head is dislocated, the line will not pass through the center of the capitulum	Annular ligament entrapment (rare)
		Adults: Isolated radial head dislocation is rare May become chronic	Associated ulnar fracture
Monteggia fracture-dislocation[20,69]	See Figure 16-6	Common in adults; rare in children Radial head dislocation associated with ulnar fracture Four types have been described based on the location of the fracture and direction of dislocation See Table 16-2	All of the above plus heterotopic ossification Radial nerve injury (20% of cases)
Extraarticular Fractures of the Distal Portion of the Humerus			
Supracondylar fracture[21,69]	15-11, 15-12	Sixty percent of all elbow fractures in children Rare in adults Extension (95%) and flexion (5%) types Paradoxic posterior fat pad sign Supracondylar process, if present, may fracture Disruption of anterior humeral line on lateral radiograph	Brachial artery injury Median, ulnar, or radial nerve injury Alignment abnormalities Heterotopic ossification Volkmann ischemic contracture
Intraarticular Fractures of the Distal Portion of the Humerus			
Transcondylar fracture[21]		Intraarticular fracture resembling supracondylar fracture Horizontal through both condyles Extension and flexion varieties	Heterotopic ossification Coronoid process entrapment
Intercondylar fracture[21,22]	15-13	Most common in persons over the age of 50 years; rare fracture Vertical and horizontal or oblique component Comminuted with Y or T configuration	Nerve and vessel injury Instability Loss of elbow function Delayed union or nonunion Ischemic necrosis
Condylar fracture[21]		Relatively uncommon fracture seen most frequently in children Lateral condyle > medial condyle	Instability Restriction of motion

Continued

TABLE 15-4 Dislocations and Fractures About the Elbow[74]—cont'd

Injury	Figure(s)	Characteristics	Complications and Related Disorders
Capitulum fracture[23]	15-14	Rare injuries caused by direct forces applied through the radial head *Type I (Hahn-Steinthal type):* Displacement of large segment of bone *Type II (Kocher-Lorenz type):* Mainly displacement of cartilage	Tear of medial collateral ligament
Epicondylar fracture[21]		More frequent in children than adults Rare injury See growth plate injuries later	Ulnar nerve injury
Fractures of the Proximal Portion of the Ulna			
Olecranon process fracture[24]	15-15	Fracture through semilunar notch Proximal displacement of fragment from pull of triceps muscle Often comminuted	Disruption of triceps mechanism Decreased range of motion Degenerative joint disease Nonunion (5% of cases) Ulnar nerve damage (10% of cases)
Coronoid process fracture[25,76,77]	15-16	Rare isolated injury Often associated with posterior elbow dislocation Avulsion from brachialis tendon or impaction against the trochlea *Regan-Morrey classification:* *Type I:* simple avulsion *Type II:* fracture involving 50% of coronoid process *Type III:* fracture involving base of coronoid process (unstable) Alternative radiographic projections ensure correct imaging of the coronoid process[77]	Decreased range of motion Degenerative joint disease
Fractures of the Proximal Portion of the Radius		Radial head projections often helpful Joint effusion results in positive fat pad sign (Table 15-3)	
Radial head fractures[6,26,75]	15-17	Most common elbow fracture in adults From indirect trauma *Classification:* Four types after Mason I: undisplaced fractures II: marginal fractures with displacement III: comminuted fractures IV: fractures associated with dislocation Radiographic findings may be subtle Offset in cortical continuity of radial head and neck Vertical split of radial head termed chisel fracture	Limited ranges of motion Degenerative joint disease Heterotopic ossification May be associated with fractures of wrist and forearm (Monteggia fracture-dislocation) *May be a component of an Essex-Lopresti injury:* comminuted and displaced radial head fracture combined with diastasis of the distal radioulnar joint
Radial neck fractures[6]	15-18	Impaction fracture of radial neck without radial head fracture may be encountered frequently Findings of cortical offset may be subtle	Limited range of motion Degenerative joint disease Heterotopic ossification
Child Abuse[27]		Humerus is second most common site of fracture (ribs most common site) Subperiosteal hemorrhage with periostitis Metaphyseal corner fractures Physeal injuries Multiple fractures at different stages of healing	Continued morbidity and even death

TABLE 15-4 Dislocations and Fractures About the Elbow[74]—cont'd

Injury	Figure(s)	Characteristics	Complications and Related Disorders
Growth plate injuries			
Distal portion of the humerus[28]		*Common:* 16.7% of all physeal injuries	Growth arrest, joint deformity, and osteonecrosis
Medial epicondyle[29]	15-19	S-H Type I injuries most common: epiphysiolysis	Entrapment of epiphysis within joint
Lateral condyle[28,29]		S-H Type IV injuries in children younger than age 10 years	
Distal humeral epiphysis[28]		S-H Type I or II in children from birth to age 5 years	Cubitus varus deformity
Proximal portion of the radius[28]		Injury in children aged 8 to 13 years	
Stress injuries[30]		Stress (fatigue) fracture of the coronoid process of ulna from ball throwing	
Osteochondritis dissecans and osteochondral fractures[31,32]	15-20, 15-21	Usually involves capitulum or trochlea History of acute injury or chronic stress Frequently affects gymnasts	Joint locking Limited range of motion Degenerative joint disease Osteonecrosis

S-H, Salter-Harris.
See also Tables 1-4 and 1-5.

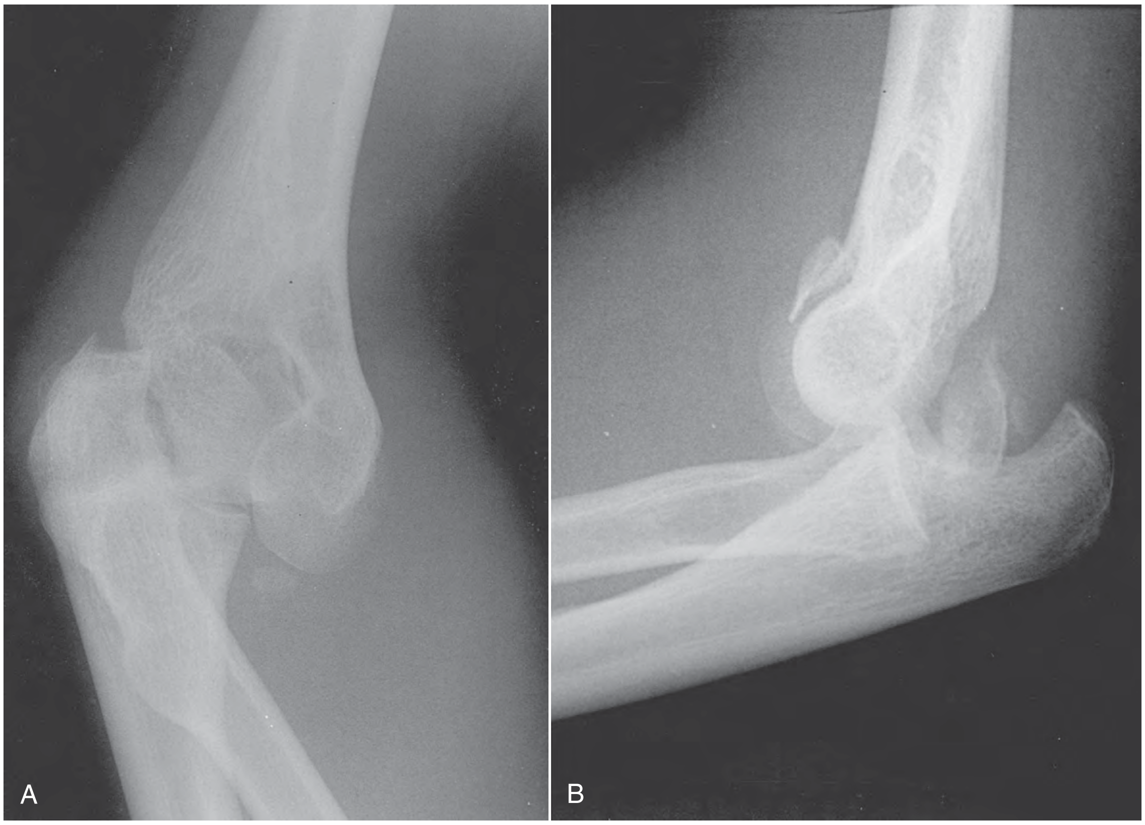

FIGURE 15–9 Posterior dislocation.[18] Frontal **(A)** and lateral **(B)** radiographs in this 28-year-old man reveal posterior dislocation of both the radius and the ulna with respect to the humerus. The lateral condyle of the humerus is fractured, and impingement of the radial head and capitulum is evident. This injury typically occurs from a fall on the outstretched hand while the elbow is hyperextended. The posterior type of dislocation represents about 80% to 90% of all elbow dislocations. Complications include coronoid process fractures in adults and fracture (and possible entrapment) of the medial condylar ossification center in children and adolescents. Median nerve entrapment also may occur after reduction.

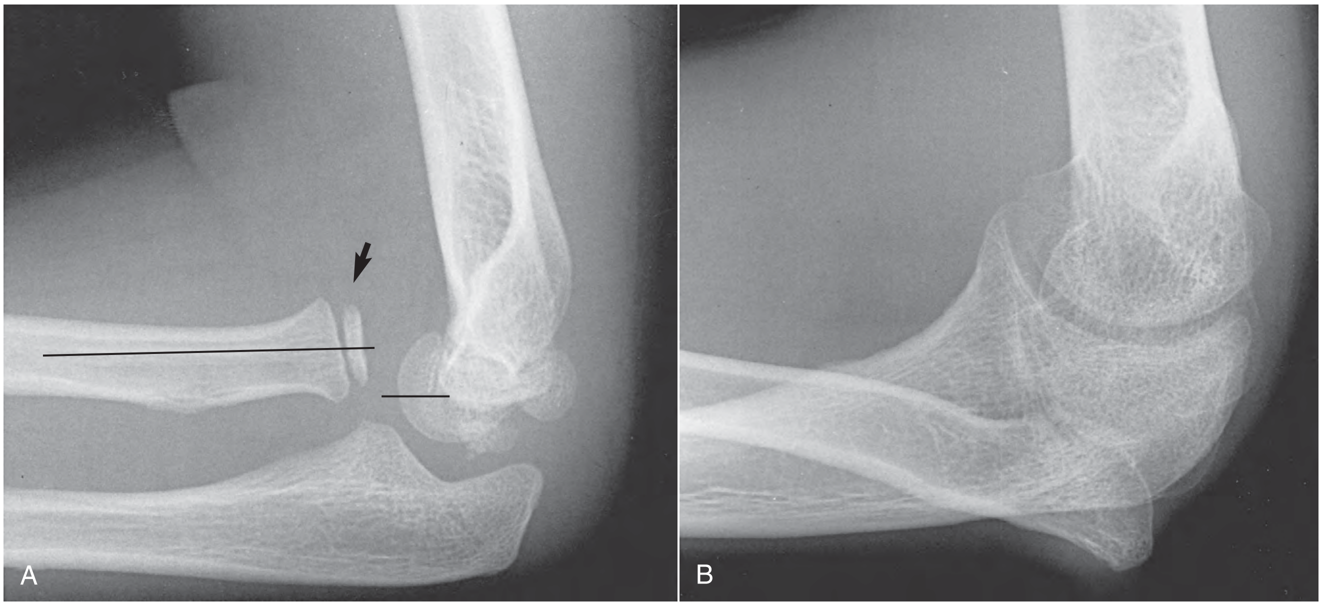

FIGURE 15–10 Traumatic radial head dislocation.[19] **A,** Nursemaids' elbow. In this infant, observe the abnormal separation of the radius and ulna and the isolated anterior dislocation of the radial head *(arrow)* with respect to the capitulum. A line constructed through the center of, and parallel to, the long axis of the radius (radiocapitular line) should intersect the center of the capitulum in all ranges of flexion and extension of the elbow. Note the offset in this line. Isolated radial head dislocation occurs most frequently in children; it is also termed *nursemaids' elbow* or *pulled elbow*. This injury is caused by a sudden pull of the child's arm, resulting in sudden elbow hyperextension and slipping of the radial head beneath the annular ligament, which is torn from its attachment to the radial neck. The dislocation usually reduces spontaneously or on supination of the forearm by a physician, but surgical reduction is occasionally required. **B,** Recurrent radial head dislocation. This 21-year-old man had recurrent traumatic radial head dislocations. Observe the posterior displacement of the radial head in relation to the ulna. The radial head appears small and dysplastic. Owing to the rarity of isolated radial head dislocations, all patients should undergo thorough investigation for associated ulnar fractures.

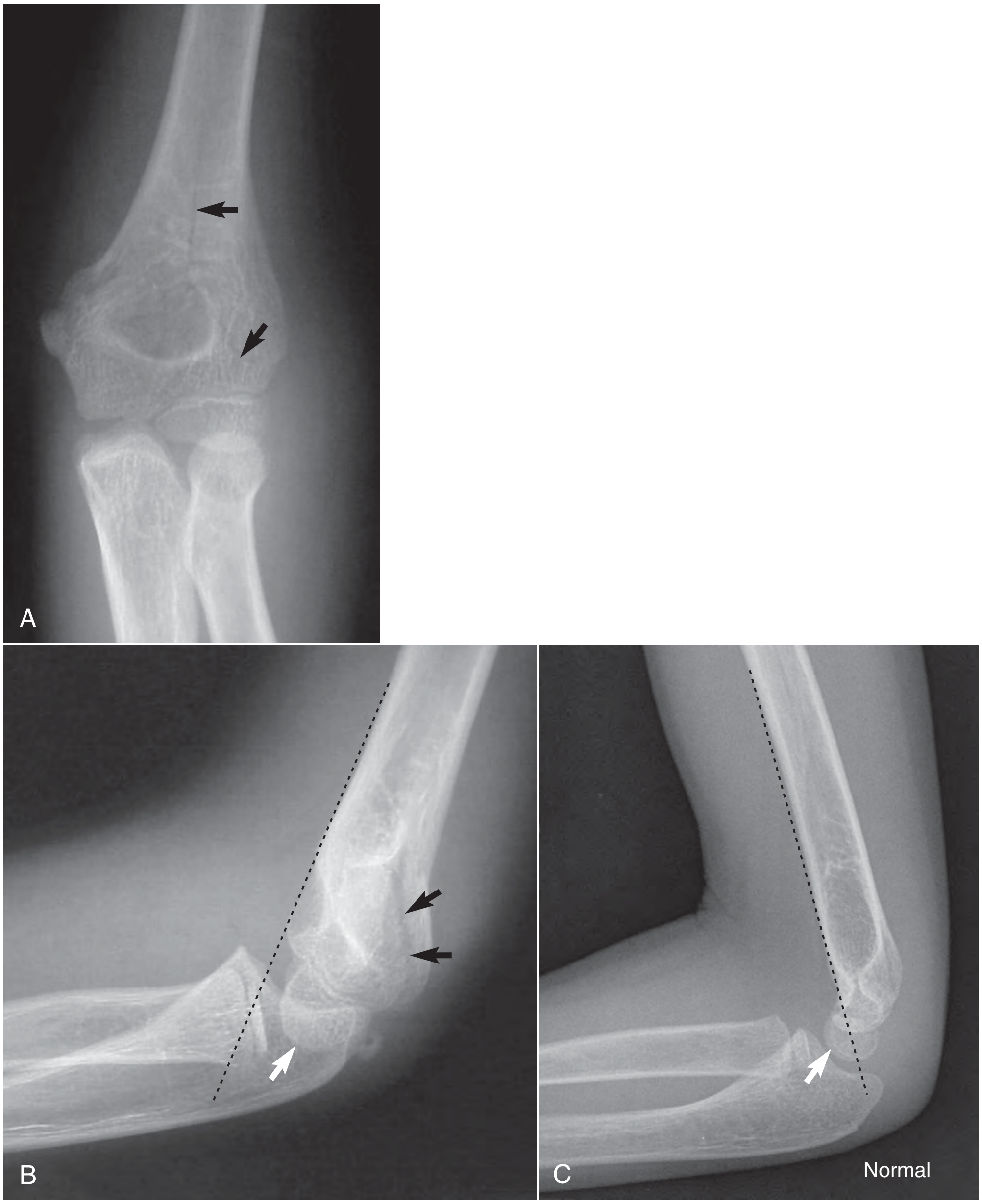

FIGURE 15–11 Supracondylar fracture: child.[21,69] This 5-year-old girl fell on an outstretched arm. The anteroposterior radiograph **(A)** shows a barely perceptible complex fracture line *(arrows)*. The lateral radiograph **(B)** reveals posterior displacement of the distal end of the humerus evidenced by a positive anterior humeral line. In the abnormal situation **(B)** the capitulum is displaced posterior to the line drawn along the anterior cortex of the humerus, whereas in the normal situation **(C),** the line intersects the mid third of the capitulum.

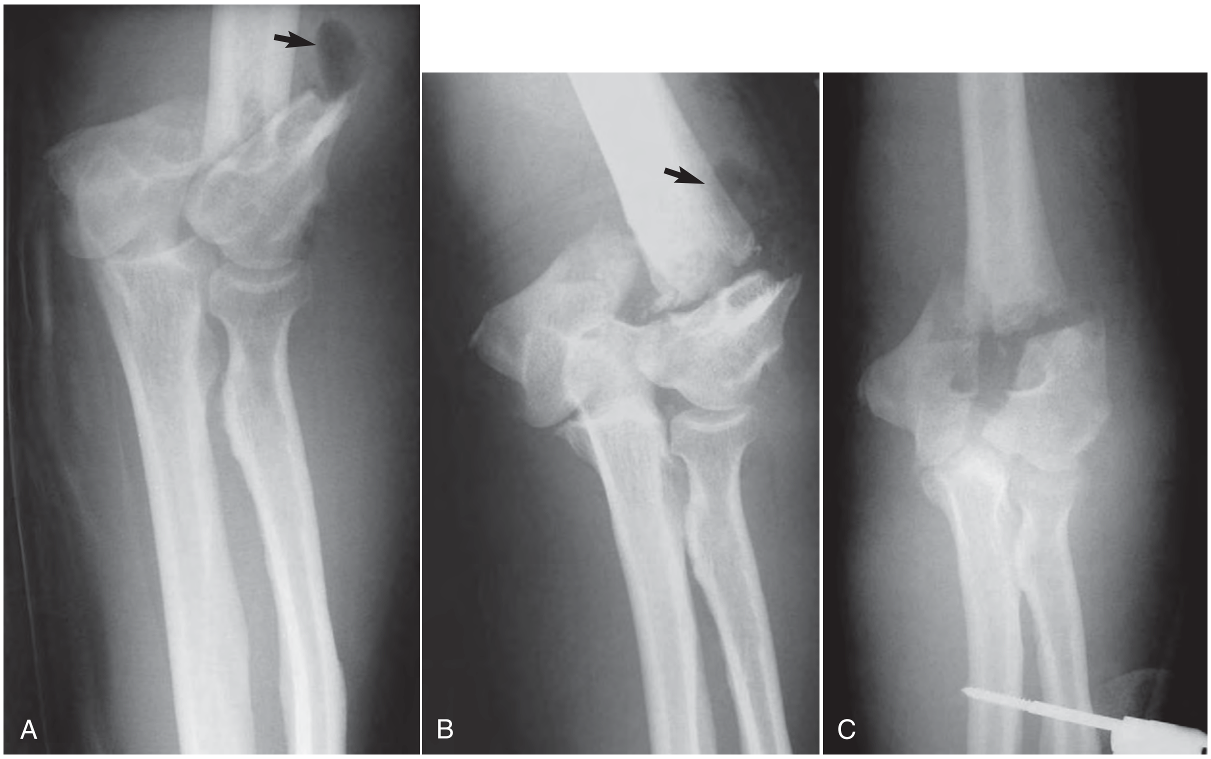

FIGURE 15–12 Supracondylar and intercondylar fracture: adult.[21,69] A displaced, comminuted, open supracondylar fracture in this 57-year-old man after trauma. The initial frontal **(A)** and oblique **(B)** radiographs shows a major transverse fracture and vertical splitting of the medial and lateral condyles. Air is seen in the soft tissues *(arrows)* as a result of the fracture fragments penetrating the skin. A postreduction radiograph **(C)** shows improvement in alignment, but the fracture fragments remain in less than ideal apposition requiring further surgical stabilization.

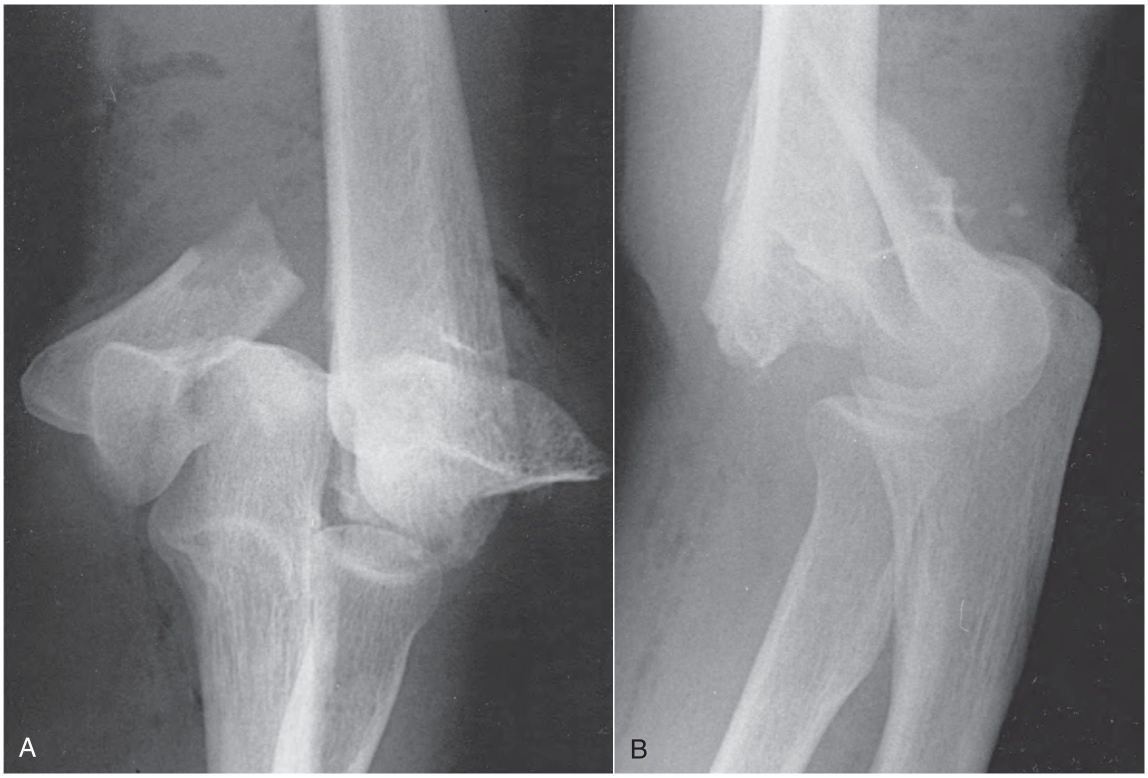

FIGURE 15–13 Intercondylar fracture.[21,22] Frontal **(A)** and lateral **(B)** radiographs show an open comminuted fracture, which has led to separation of the trochlear and capitular fragments. The shaft of the humerus is displaced anteriorly, and extensive soft tissue emphysema is evident. Intercondylar fractures are relatively rare, and occur primarily in patients older than 50 years of age. Rotation at the fracture site and incongruity of the articular surfaces are potential complications.

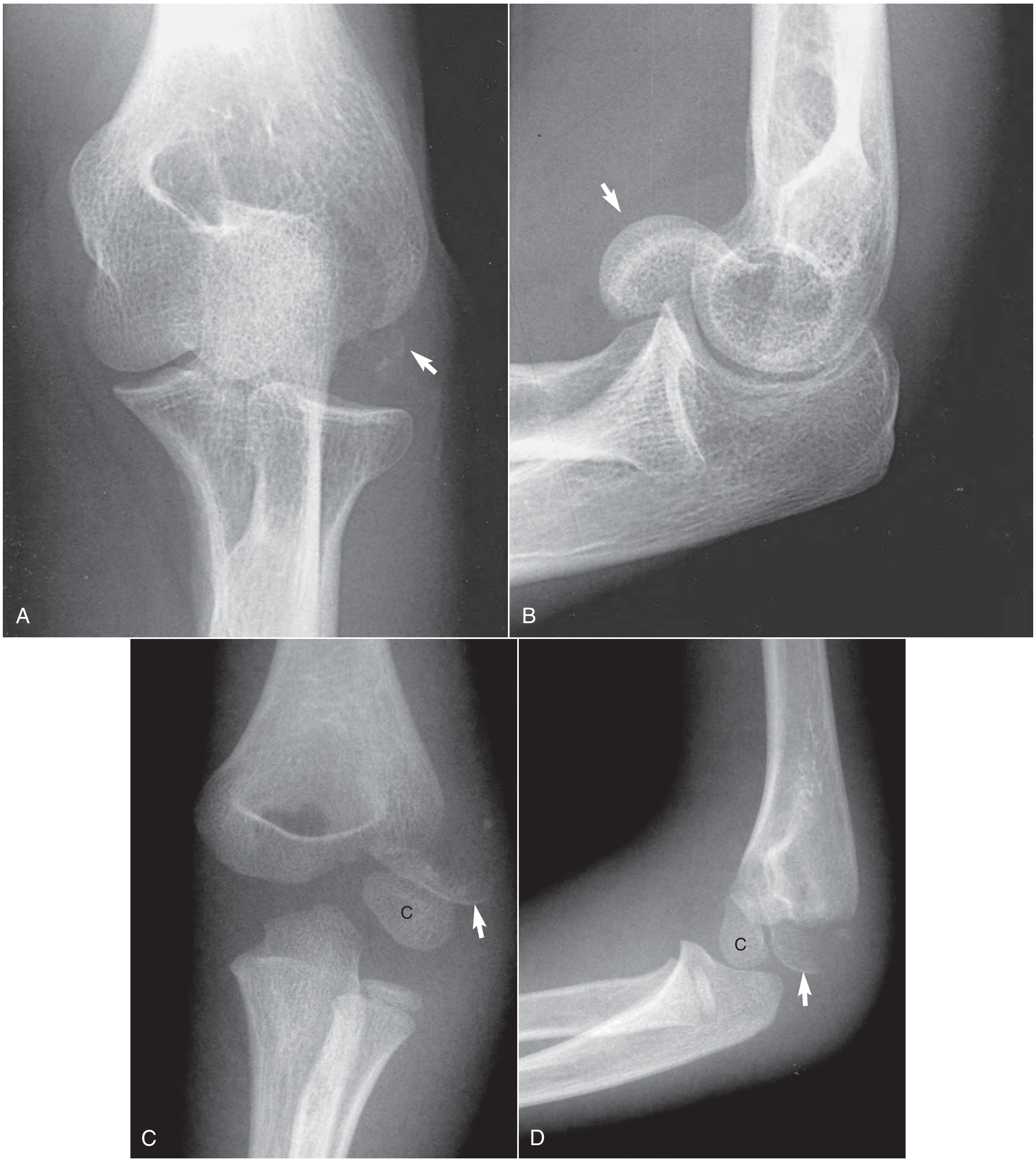

FIGURE 15–14 Fracture: capitulum.^{23} **A-B,** Adult. Frontal radiograph **(A)** shows absence of the capitulum adjacent to the lateral aspect of the distal end of the humerus. Small fragments of bone are evident *(arrow)*. **B,** Lateral radiograph shows displacement and rotation of the capitular fragment, which is lying within the radial fossa *(arrow)*. The injury in this patient is the type I (Hahn-Steinthal type) fracture involving a coronally oriented fracture of a large segment of the capitulum with characteristic anterior and superior displacement of the fracture fragment. The injury is difficult to visualize on anteroposterior radiographs. The half-moon appearance of the capitular fragment on lateral films, however, is characteristic of this injury. Type II fractures (not shown) involve fracture of only the articular cartilage and uncapping of the capitulum, a condition difficult to observe on routine radiographs. **C-D,** Child. This 5-year-old boy had a fall. The anteroposterior **(C)** and lateral **(D)** radiographs reveal the capitulum *(c)* and a corresponding attached fragment of the lateral humeral metaphysis *(arrows)* displaced from the humerus. The metaphyseal fracture fragment and the attached capitulum are distracted and rotated such that there is discontinuity of the radiocapitular line.

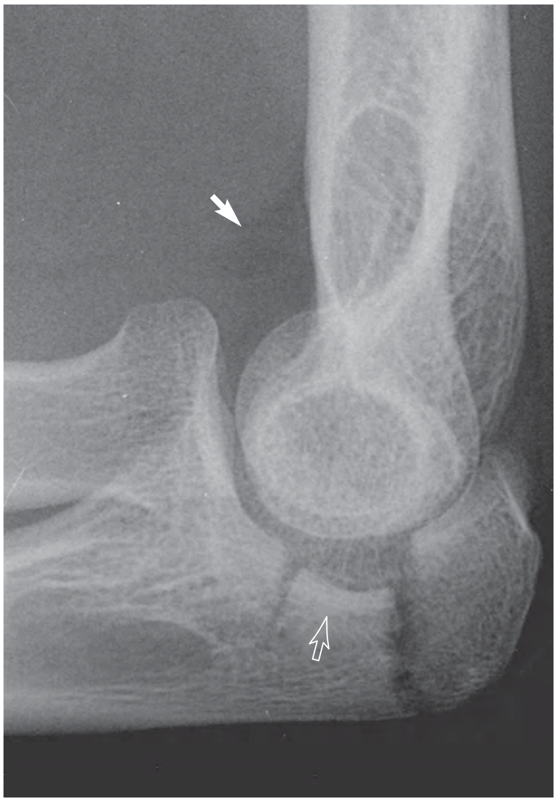

FIGURE 15–15 Olecranon process fracture.[24] Observe the comminuted intraarticular fracture with associated depression of the articular surface *(open arrow),* resulting in incongruity of the articular surface of the semilunar notch of the ulna. Also note elevation of the anterior intracapsular fat pad, indicating an associated joint effusion *(arrow)*. The combination of posterior displacement of the olecranon fragment with anterior movement of the remaining portion of the ulna and radial head is a serious injury termed *fracture-dislocation* of the elbow. Complications of olecranon fractures include decreased range of motion, osteoarthrosis, nonunion, and ulnar nerve damage.

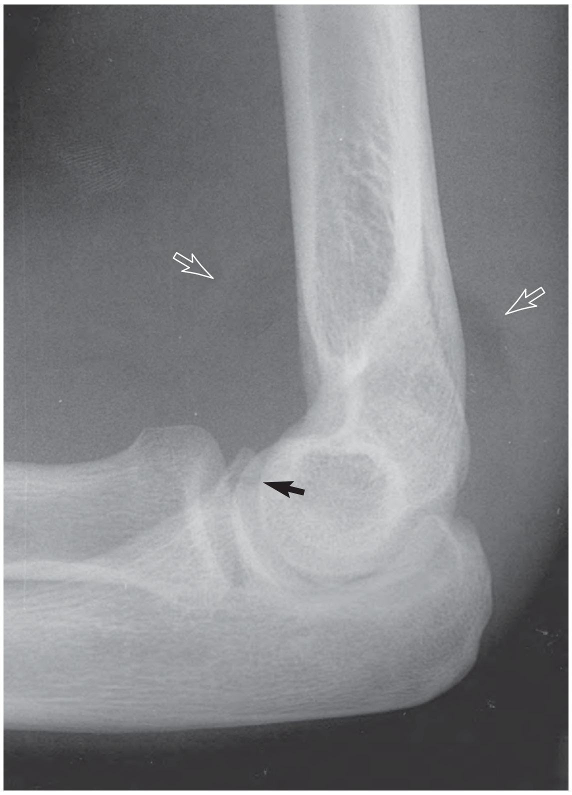

FIGURE 15–16 Coronoid process fracture.[25,76,77] A small, almost imperceptible fracture of the coronoid process is seen *(arrow)*. Elevation of both the anterior and posterior intracapsular fat pads *(open arrows)* is also present. Isolated fractures of the ulnar coronoid process are rare and occur as a result of avulsion from the brachialis tendon or direct impaction against the trochlea. Coronoid process fractures are more commonly associated with posterior elbow dislocations.

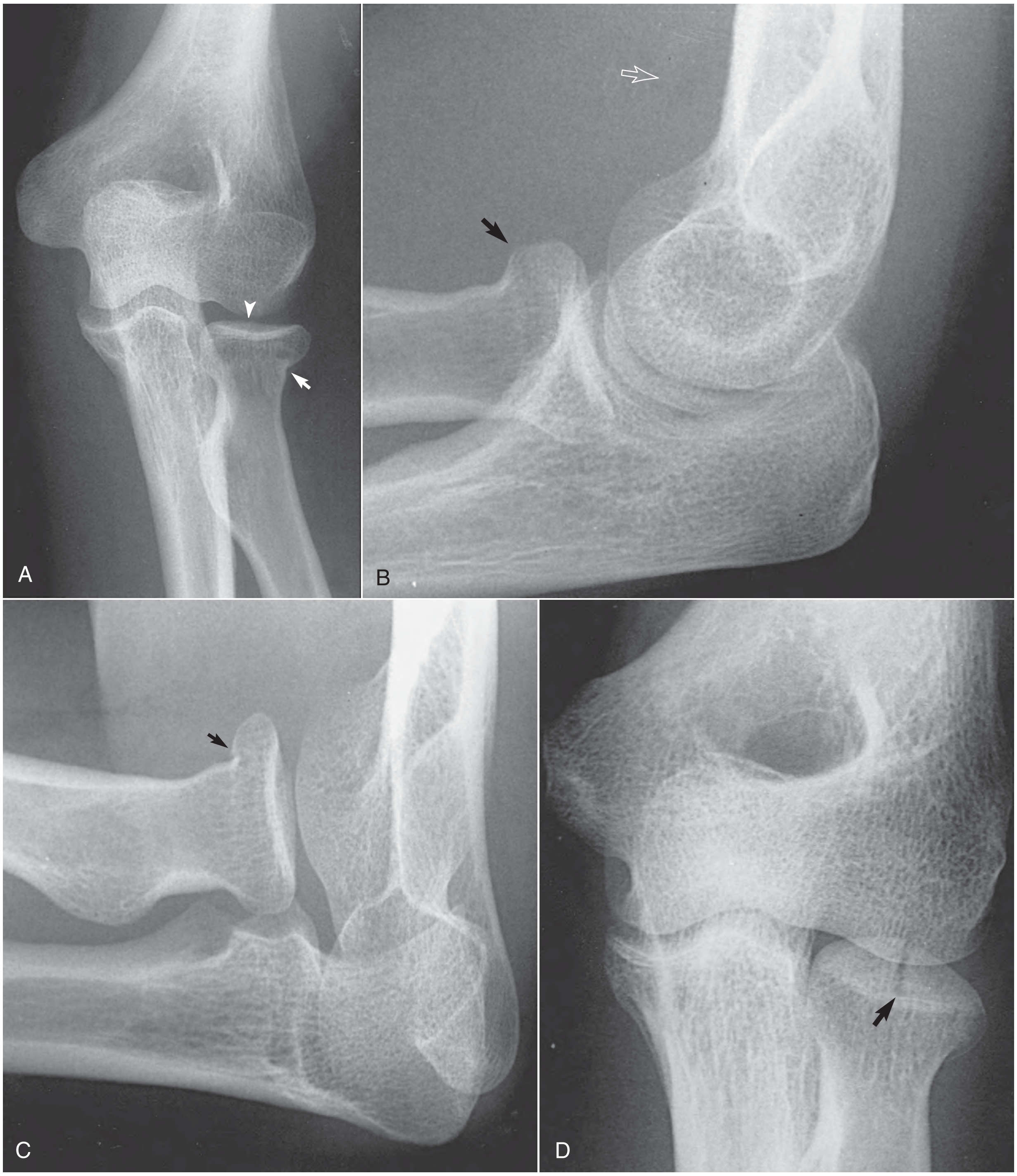

FIGURE 15–17 Radial head fracture.[6,26] **A-C,** This patient fell while skating. In **A,** a frontal radiograph shows a subtle longitudinal intraarticular fracture of the radial head *(arrowhead)* and an offset in the cortical margin of the head-neck junction *(arrow)*. In **B,** the routine lateral radiograph reveals a subtle anterior fat pad sign *(open arrow),* suggesting a fracture, but the head-neck junction appears essentially normal *(arrow)*. In **C,** a specialized radiographic projection, the radial head–capitulum view, projects the proximal portion of the radius away from the overlying ulna, allowing a clear depiction of the sharp, angular cortical defect characteristic of an impaction fracture *(arrow)*. **D,** In another patient, a longitudinal intraarticular fracture (chisel fracture) is seen *(arrow)*.

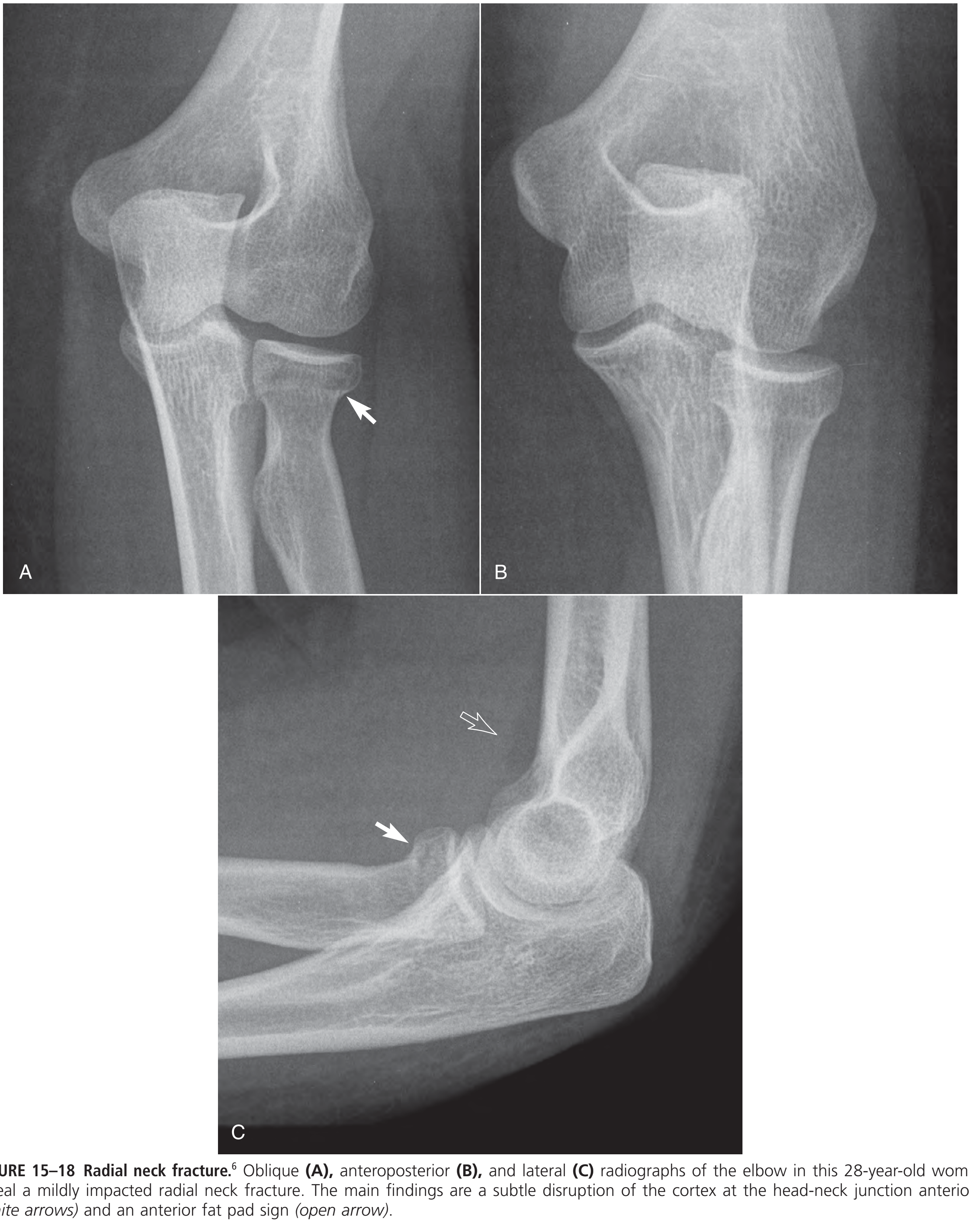

FIGURE 15–18 Radial neck fracture.[6] Oblique **(A),** anteroposterior **(B),** and lateral **(C)** radiographs of the elbow in this 28-year-old woman reveal a mildly impacted radial neck fracture. The main findings are a subtle disruption of the cortex at the head-neck junction anteriorly *(white arrows)* and an anterior fat pad sign *(open arrow)*.

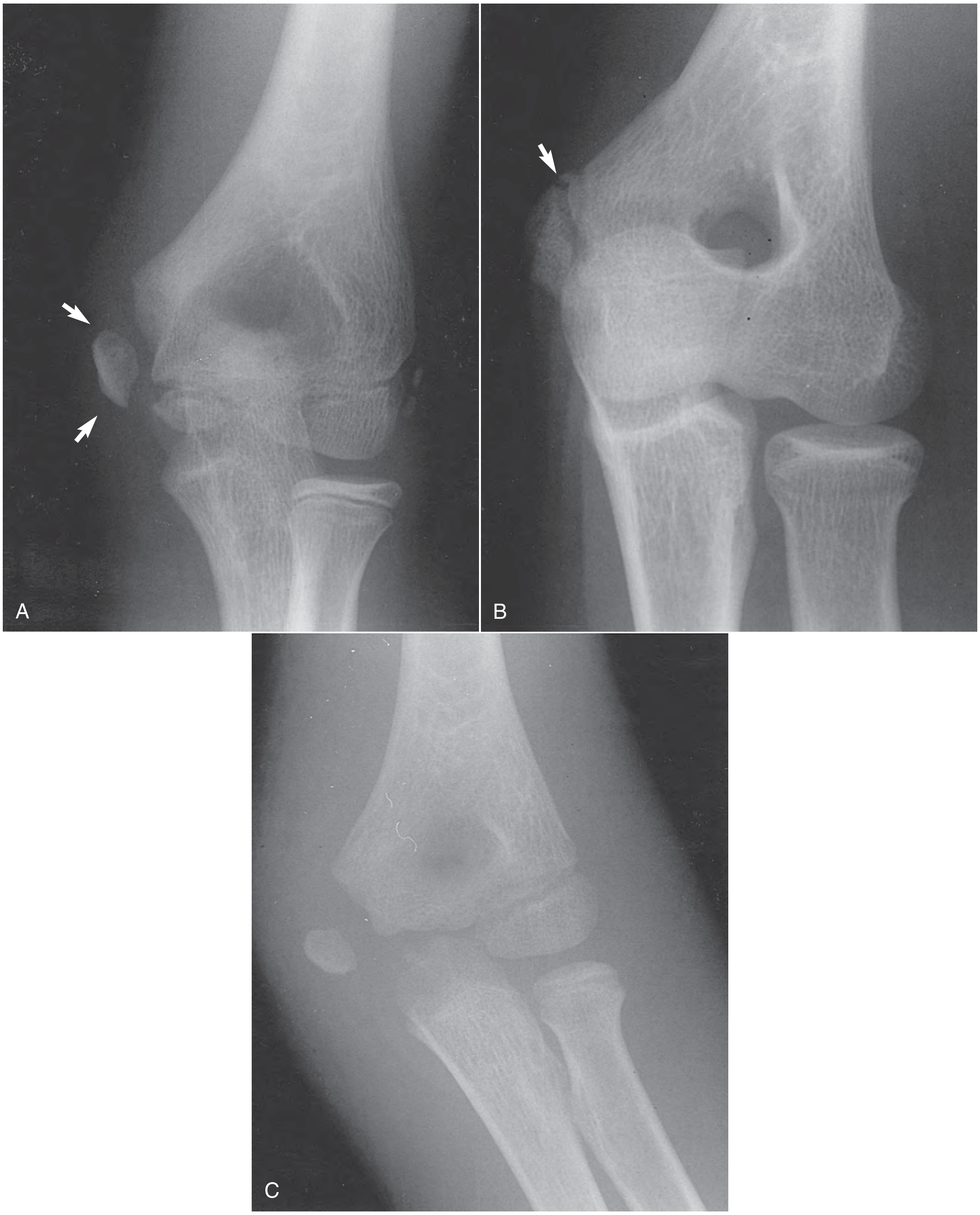

FIGURE 15–19 Medial epicondyle growth plate injury: Salter-Harris type I avulsion injury.[29] **A,** Observe the separation and displacement of the medial epicondyle *(arrows)* in this 14-year-old boy. **B,** In another boy, 15 years old, the medial epicondyle is fractured but not displaced *(arrow)*. **C,** This 11-year-old boy also has a separation of the medial epicondyle with extensive soft tissue swelling. This injury typically occurs as a result of valgus stress and consequent avulsion of the medial epicondyle ossification center by the attachment of the flexor pronator muscle group and the ulnar collateral ligament. The epicondyle may be drawn into the joint, becoming entrapped.

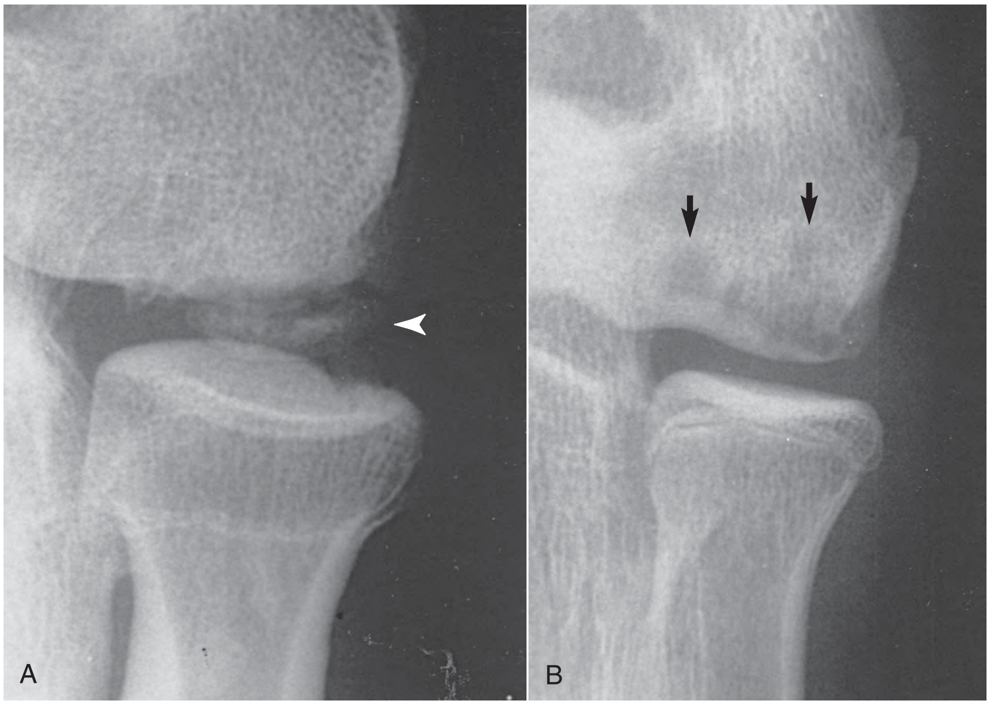

FIGURE 15–20 Osteochondritis dissecans: capitulum.[31,32] **A,** This 29-year-old man had progressive elbow pain. Frontal radiograph shows an intraarticular fragment adjacent to the articular surface of the capitulum *(arrowhead)*. **B,** In another patient, a 13-year-old high school football player, observe the radiolucent cystlike lesions involving the subchondral surface of the capitulum *(arrows)*. Although the radiographic appearance is similar, osteochondritis dissecans differs from Panner disease in that Panner disease occurs between the ages of 5 and 10 years, whereas osteochondritis dissecans occurs in adolescents and adults after ossification and fusion of the capitulum. *(**A,** Courtesy V. Vint, MD, San Diego. **B,** Courtesy T. Mick, DC, Bloomington, Minn.)*

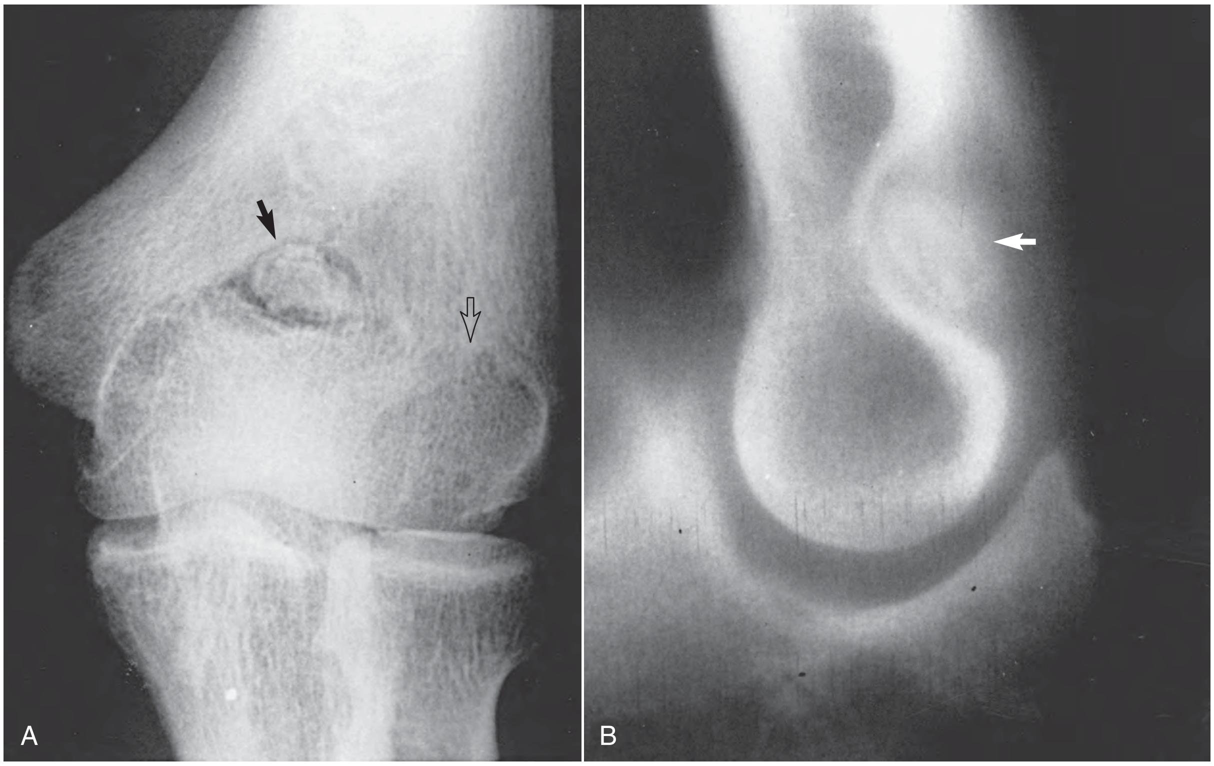

FIGURE 15–21 Osteochondral fracture: intraarticular osteochondral body.[31,32] This 20-year-old man with previous trauma noticed decreased ranges of motion in his elbow. **A,** Routine frontal radiograph demonstrates an ovoid osseous body overlying the olecranon and coronoid fossae *(arrow)*. The subchondral region of the capitulum appears somewhat radiolucent *(open arrow)*. **B,** Lateral conventional tomogram clearly reveals an osseous body deep within the olecranon fossa *(arrow)*. Subsequent surgery revealed loss of cartilage on the capitulum and radial head. Osteochondral bodies within the coronoid or olecranon fossa are often difficult to visualize on routine lateral radiographs owing to superimposed overlying structures. *(Courtesy G. Greenway, MD, Dallas.)*

TABLE 15-5 Soft Tissue Injuries About the Elbow*

Entity	Figure(s)	Characteristics
Ligamentous injuries[70,73]		
Medial elbow instability[33,67,68,73]	15-22	Injury of the medial (ulnar) collateral ligament Single acute injury or repetitive injuries such as those encountered in baseball pitchers May also result in muscle tears, avulsion fractures, and ulnar nerve damage Valgus stress radiography useful in revealing ligament injury; arthrography, dynamic sonography with valgus stress, and MR imaging are also useful methods for evaluating medial joint instability Degenerative changes develop in chronic elbow instability Heterotopic calcification may occur in the ulnar collateral ligament after trauma, the presence of which may be associated with partial or complete tears; conventional radiography is more sensitive than MR imaging in detecting heterotopic calcification
Lateral elbow instability[34,73]	15-23	Injury to the lateral collateral ligament complex Acute varus stress resulting in elbow dislocation is the most frequent cause of lateral elbow instability Repetitive injuries such as in throwing activities, not as frequent as acute injury *Other causes:* elbow subluxations, surgical injury MR imaging useful
Tendon injuries[70]		*Intratendinous tear:* partial or complete Avulsion injuries may occur at the site of tendon attachment to bone Chronic injuries (overuse syndromes) usually result from sporting activities Acute injuries Spontaneous tendon ruptures may occur in patients with hyperparathyroidism, systemic lupus erythematosus, rheumatoid arthritis, and osteogenesis imperfecta MR imaging most useful in evaluating such injuries
Lateral tendons (lateral epicondylitis)[35]	15-23	Common extensor tendon injuries Lateral epicondylitis more common than acute tears—most common injury of the elbow in athletes Backhand stroke in tennis; wrist maintained in extension and radial deviation (tennis elbow) *Radiographic changes:* calcification in as many as 30% of cases MR imaging may be helpful in diagnosis
Medial tendons (medial epicondylitis)[36,72]	15-24	Common flexor tendon injuries and tendinosis Medial epicondylitis more common than acute tears Medial epicondylitis also termed *medial tennis elbow, golfer's elbow*, or *pitchers' elbow* Also occurs in javelin throwers, racquetball and squash players, swimmers, and bowlers MR imaging demonstrates intermediate T1-weighted and intermediate to high T2-weighted signal intensity within the common flexor tendon and presence of peritendinous soft tissue edema
Anterolateral tendons[37]	15-25	Injuries of the distal end of the biceps brachii tendon Fewer than 5% of all biceps tendon injuries Single acute event may rupture biceps tendon or result in avulsion at the radial tuberosity *Weightlifters:* forceful hyperextension applied to a flexed and supinated forearm Partial tears more difficult to diagnose than complete tears
Posterior tendons[38]	15-26	Triceps brachii tendon injuries Uncommon injury Complete tears > partial tears Single acute event may rupture triceps tendon or result in avulsion of the olecranon process of the ulna Mechanism Deceleration force applied to extended arm with contraction of triceps (as in a fall) Direct blow to attachment at olecranon process (infrequent injury)

* See also Table 1-6.

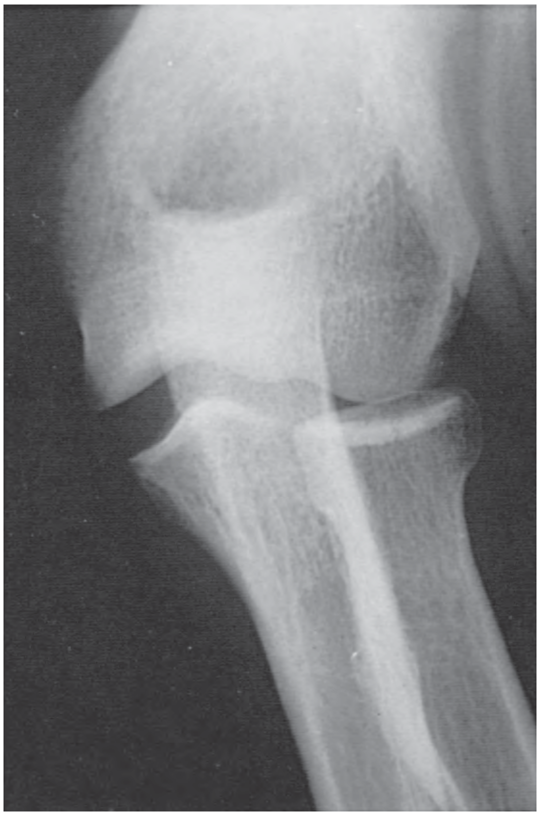

FIGURE 15–22 Medial elbow instability: stress radiograph.[33,73] Radiograph obtained during the application of valgus stress to a partially flexed elbow reveals widening of the medial aspect of the joint, indicative of injury to the medial collateral ligament. *(From Resnick D, Kang HS, Pretterklieber ML: Internal derangements of joints. 2nd Ed. Philadelphia, WB Saunders, 2006, p 1179.)*

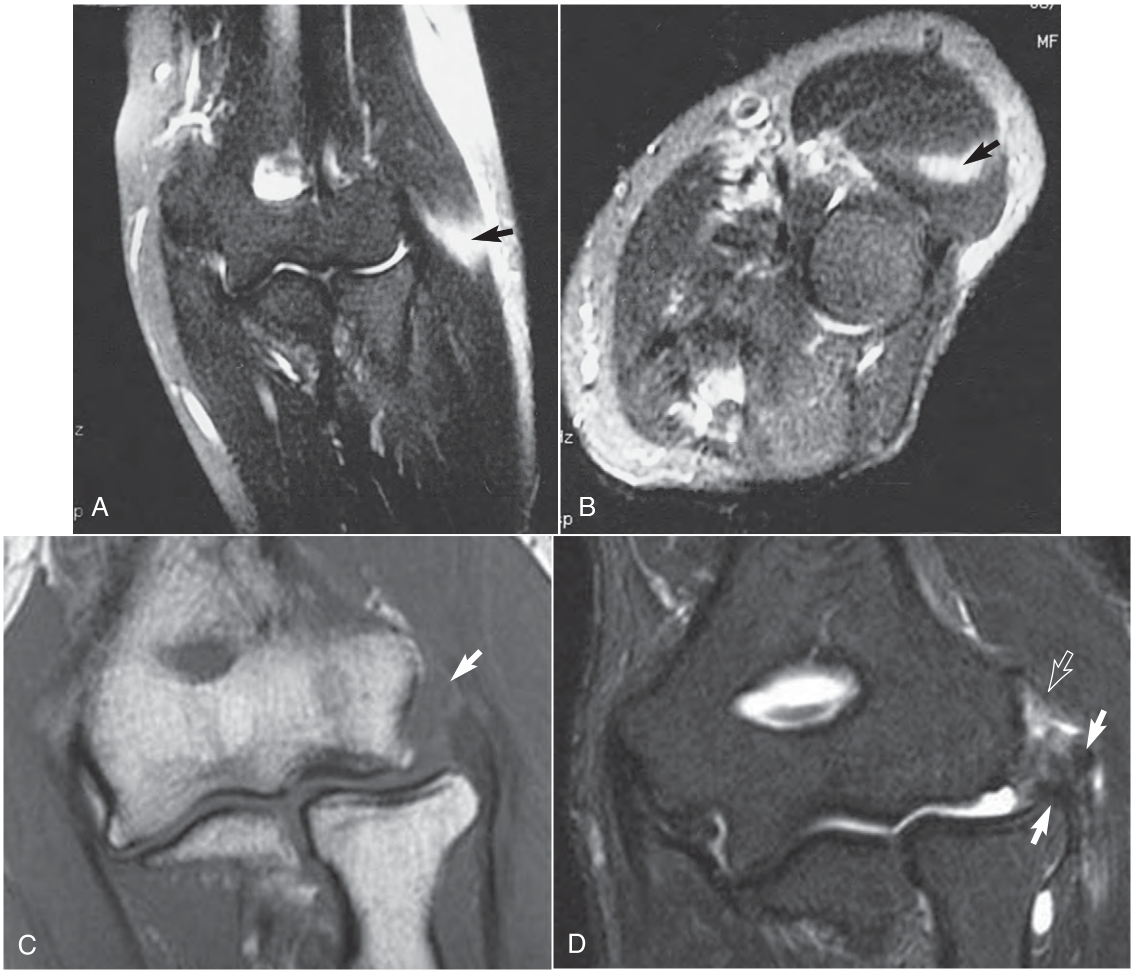

FIGURE 15–23 Lateral epicondylitis and tears of the common extensor tendon. A-B, Tears of the extensor carpi radialis brevis tendon and muscle.[35] These coronal (TR/TE, 3000/100) **(A)** and transaxial (TR/TE, 3000/90) **(B)** fat-suppressed fast spin echo MR images in a patient with tennis elbow show the site of injury *(arrows)* as a region of high signal intensity. **C-D,** Coronal T1-weighted MR image **(C)** reveals increased nonspecific intermediate signal intensity tissue adjacent to the lateral epicondyle and radiocapitular articulation *(arrow)*. The fat-suppressed coronal T2-weighted image **(D)** more clearly depicts disruption of the radial collateral ligament *(arrows)* and abnormally high signal intensity at the common extensor tendon attachment *(open arrow)*. (***A-B,*** *From Resnick D, Kang HS, Pretterklieber ML: Internal derangements of joints. 2nd Ed. Philadelphia, Saunders, 2006, p 1176.)*

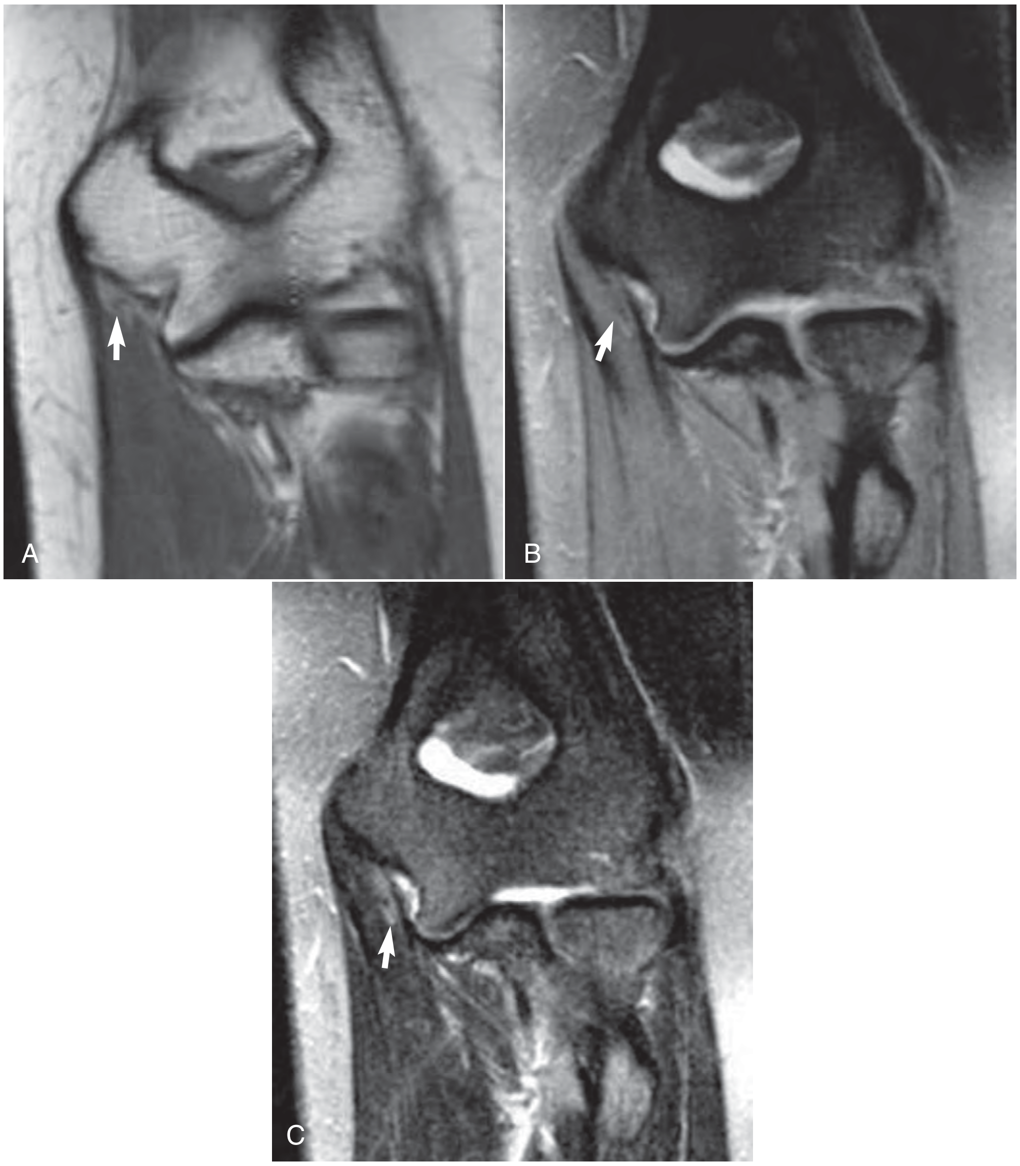

FIGURE 15–24 Medial epicondylitis: tendinosis of the common flexor tendon.[36,72] Coronal T1-weighted MR image **(A)** reveals a nonspecific indistinct appearance of the muscles attaching to the medial epicondyle *(arrow)*. The fat-suppressed coronal proton–density-weighted image **(B)** shows slightly increased signal intensity in the muscle just distal to its attachment *(arrow),* a finding that is more conspicuous *(arrow)* on a fat-suppressed coronal T2-weighted image **(C).**

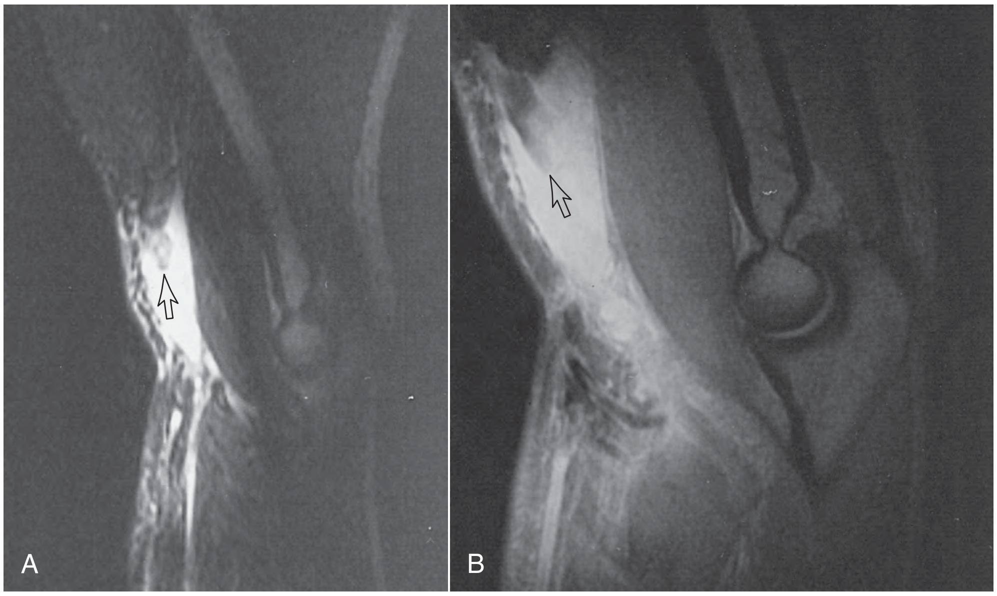

FIGURE 15–25 Biceps brachii tendon: tear of the distal end.[37] Complete rupture at distal insertion site in a 44-year-old man is evident. Sagittal STIR (GR/TE, 3000/38; inversion time, 150 ms) **(A)** and fat-suppressed fast spin echo (TR/TE, 3300/17) **(B)** MR images reveal the retracted tendon *(open arrows)* and high signal intensity characteristic of soft tissue edema and hemorrhage. *(From Resnick D, Kang HS, Pretterklieber ML: Internal derangements of joints. 2nd Ed. Philadelphia, Saunders, 2006, p 1171.)*

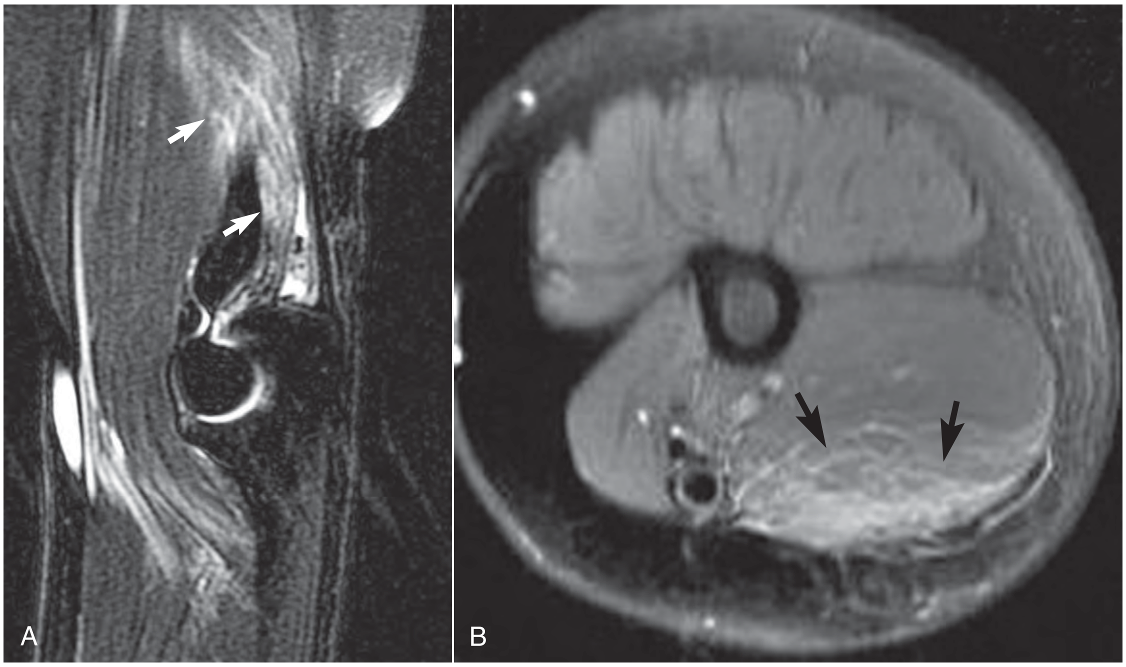

FIGURE 15–26 Injuries of the triceps brachii muscle and tendon. 48-year-old man.[38] **A,** A sagittal T2-weighted fat-suppressed (STIR) image reveals abnormal high signal intensity in the distal fibers of the triceps brachii muscle *(arrows)* proximal to its distal attachment on the olecranon. **B,** This 52-year-old weekend warrior sustained an injury playing recreational ice hockey. An axial fat-suppressed proton-density MR image reveals high signal intensity in the posterior portion of the triceps muscle (*arrows*) indicating a low-grade second degree strain of the muscle belly of the long head of the triceps brachii muscle.

TABLE 15-6 Articular Disorders Affecting the Elbow

Entity	Figure(s)	Characteristics
Degenerative and Related Disorders		
Osteoarthrosis[39]	15-27	Primary osteoarthrosis of the elbow occurs only infrequently Usually secondary to local trauma or disease processes, such as alkaptonuria, acromegaly, epiphyseal dysplasia, crystal deposition diseases, and hemophilia Osteophytes Subchondral sclerosis Subchondral cysts Occasional intraarticular osteochondral bodies
Diffuse idiopathic skeletal hyperostosis (DISH)[40]	15-28	Olecranon enthesophytes present in 48% of patients with DISH Hyperostosis along medial aspect of distal portion of the humerus
Inflammatory Disorders		
Rheumatoid arthritis[41]	15-29	Bilateral symmetric, concentric joint space narrowing Marginal subchondral erosions Cystic changes Mild sclerosis of apposing joint surfaces
Juvenile idiopathic arthritis[42]		Synonyms: Juvenile chronic arthritis or juvenile rheumatoid arthritis Diffuse concentric joint space narrowing Periarticular osteoporosis Erosions Subluxation
Ankylosing spondylitis[43,44]	15-30	Twelve percent of patients with long-standing ankylosing spondylitis have elbow joint involvement Bilateral or unilateral distribution Joint effusion Osteoporosis Diffuse joint space narrowing Osseous proliferation
Psoriatic arthropathy[44]		Elbow involvement rare Findings range from minor erosions to severe osteolysis
Scleroderma (progressive systemic sclerosis)[45]	15-31	Globular accumulations of periarticular soft tissue calcinosis Extensive osseous resorption may occur
Crystal Deposition and Metabolic Disorders		
Gouty arthropathy[46]	15-32	Bilateral soft tissue swelling over the extensor surface of elbow—bursal inflammation Marginal and eccentric erosions and cystlike lesions Osseous proliferation seen occasionally
Calcium pyrophosphate dihydrate (CPPD) crystal deposition[47,48]	15-33	*Chondrocalcinosis:* capsular, tendinous, and triceps tendon deposits Joint space narrowing, subchondral sclerosis, cysts, and osteophytes Osseous resorption of proximal portions of radius and ulna Advanced destruction and fragmentation may resemble neuropathic osteoarthropathy in severe cases
Infectious Disorders		
Pyogenic septic arthritis and bursitis[49,65]	15-34	Surgery, penetrating injury, immunosuppression, and debilitating illness, such as diabetes mellitus, all predispose to joint infection Rapid concentric loss of joint space Poorly defined or "fuzzy" subchondral bone margins Periarticular osteoporosis Loss of definition and destruction of subchondral bone Capsular distention Erosions Osteomyelitis of adjacent metaphyses

TABLE 15-6 Articular Disorders Affecting the Elbow—cont'd

Entity	Figure(s)	Characteristics
Tuberculous arthritis[50]		Typically monoarticular disease in older patients Various degrees of soft tissue swelling Gradual joint space narrowing Juxtaarticular osteoporosis Peripherally located erosions Subchondral erosions Periarticular abscess Periostitis Olecranon bursitis may occur
Miscellaneous Disorders		
Pigmented villonodular synovitis (PVNS)[51,52,66]		Cystic erosions on both sides of the joint Hemorrhagic joint effusion Eventual osteoporosis Well-preserved joint space until late in the disease Extraarticular form is termed *giant cell tumor of the tendon sheath*
Idiopathic synovial (osteo)chondromatosis[53,54]	15-35	Multiple intraarticular or periarticular collections of calcification of variable size and density Monoarticular process Erosion of adjacent bones may occur Secondary osteoarthrosis common Noncalcified bodies within the coronoid and olecranon fossae are best demonstrated with arthrography Secondary synovial osteochondromatosis may occur as a result of degenerative joint disease
Acromegalic arthropathy[55]		Abnormal cartilage proliferation results in secondary osteoarthrosis *Joint space:* widening in initial stages, narrowing in advanced stages Sclerosis, osseous fragmentation, and osteophytes
Hemophilic arthropathy[56]	15-36	Elbow joint involvement is frequent in hemophilia Secondary osteoarthrosis, osteoporosis, epiphyseal enlargement, joint space narrowing, and subchondral erosion, sclerosis, and cyst formation Trochlear and radial notches may be widened from erosion, and the radial head may be enlarged as a result of epiphyseal overgrowth
Neuropathic osteoarthropathy[57]	15-37	As many as 25% of patients with syringomyelia of the cervical cord develop neuropathic osteoarthropathy of the joints of the upper extremity Fragmentation, sclerosis, cyst formation, dislocation, disorganization, and osseous debris

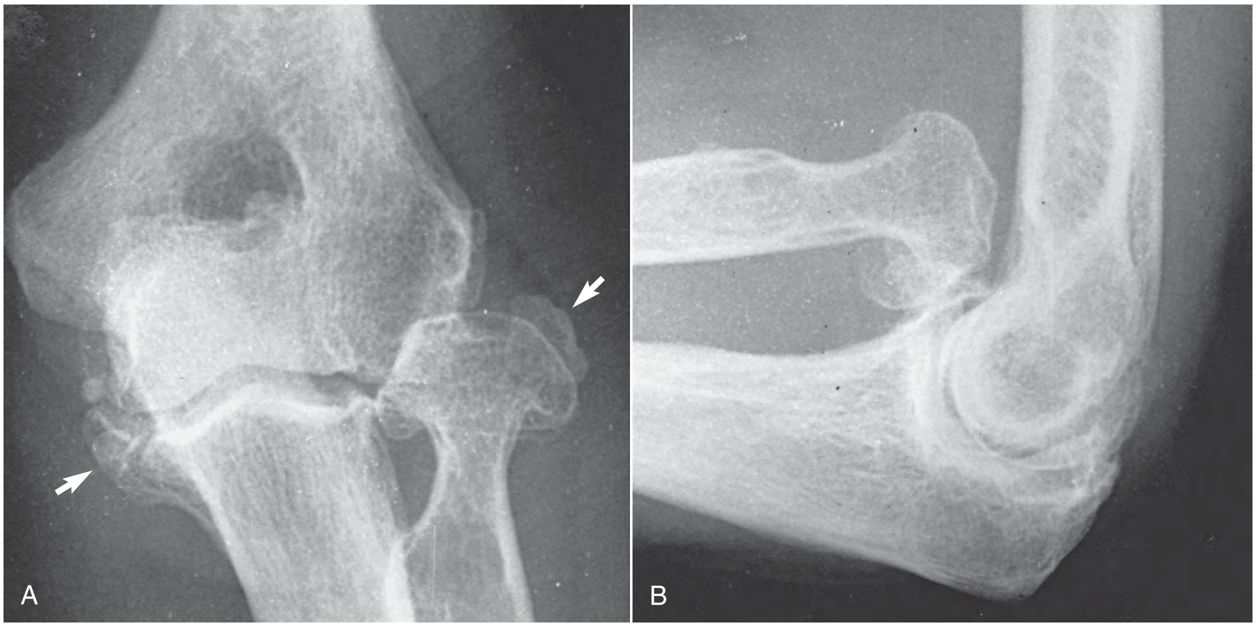

FIGURE 15–27 Osteoarthrosis.[39] This patient with a previous fracture and dislocation of the radial head had frontal **(A)** and lateral **(B)** radiographs of the elbow. They demonstrate nonuniform loss of joint space, radial head dislocation, and presence of osteophytes and intraarticular osseous bodies *(arrows)*. Degenerative joint disease of the elbow is uncommon, and is usually secondary to previous occupational or accidental trauma.

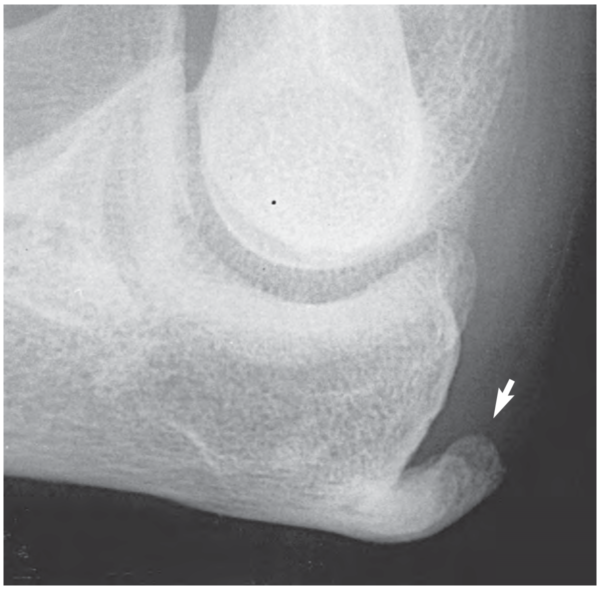

FIGURE 15–28 Diffuse idiopathic skeletal hyperostosis (DISH).[40] A prominent enthesophyte arises from the olecranon process *(arrow)* in this patient with DISH. The site of attachment of the triceps tendon is a characteristic location of enthesopathy in this disease, with involvement in about 48% of persons with DISH.

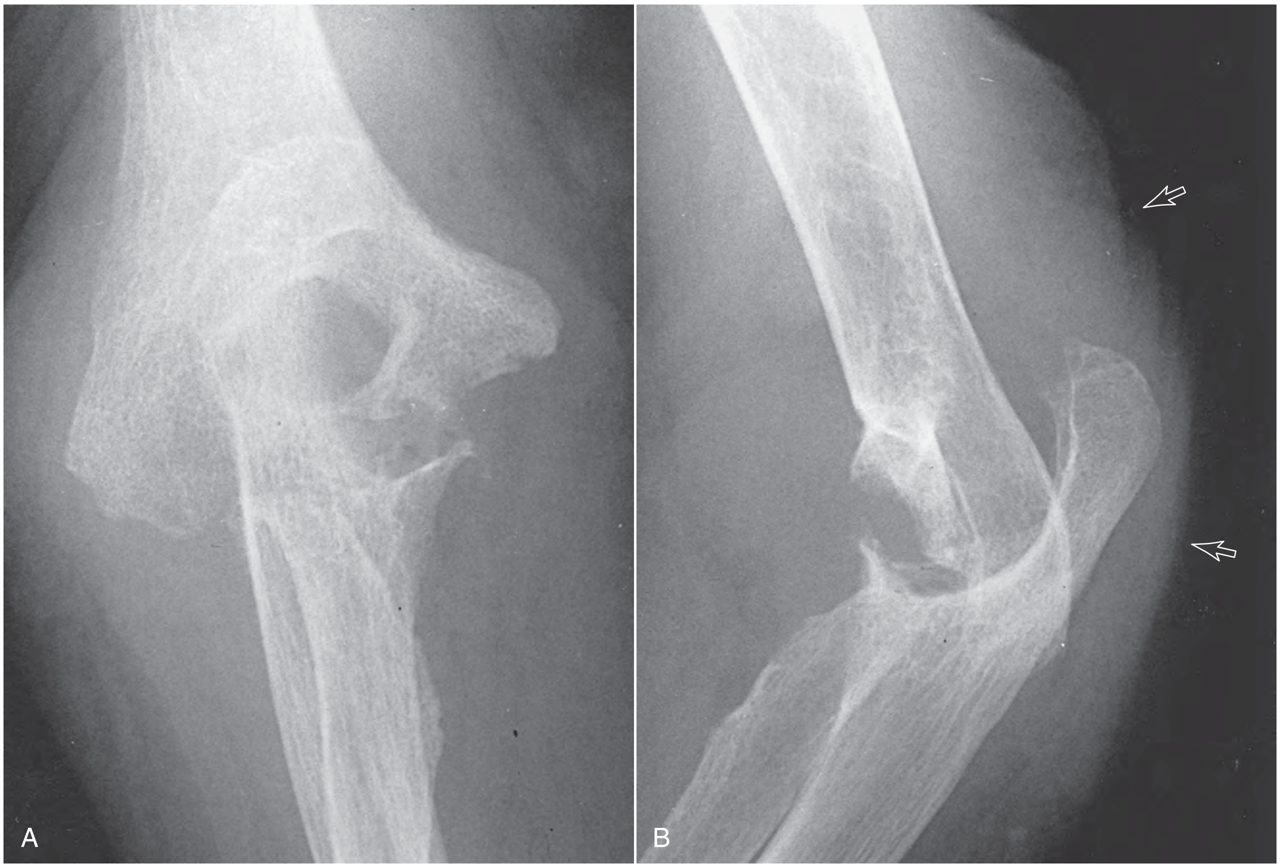

FIGURE 15–29 Rheumatoid arthritis.[41] A 55-year-old woman with a 20-year history of rheumatoid arthritis had severe elbow pain and swelling after twisting her arm. Frontal **(A)** and lateral **(B)** radiographs reveal marked erosive changes of the distal end of the humerus, olecranon, and radial head. Marked osteopenia is present, and there is no evidence of osteophyte formation. A large soft tissue prominence over the dorsal surface of the olecranon *(open arrows)* was proved by arthrography to be a synovial cyst. Culture of aspirated joint fluid yielded no evidence of infectious organisms. The elbow is involved in approximately 34% of patients with long-standing rheumatoid arthritis. Involvement is usually bilateral, but the process may be more advanced in the dominant extremity, or less involved in a paralyzed extremity.

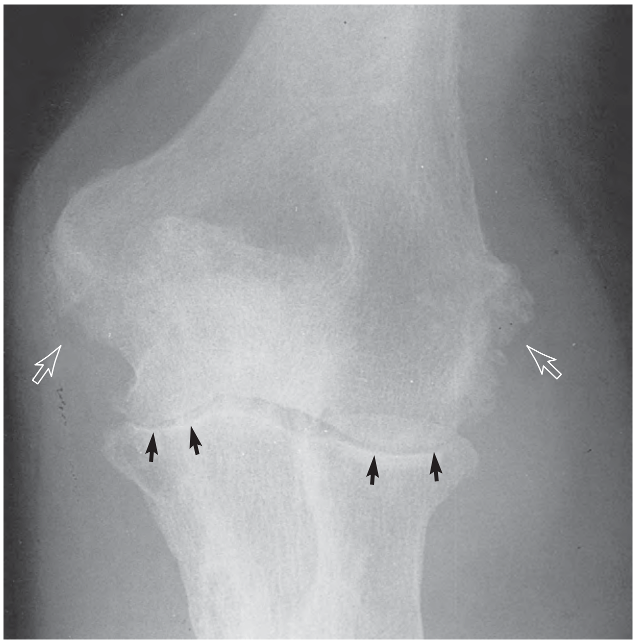

FIGURE 15–30 Ankylosing spondylitis.[43,44] Anteroposterior radiograph of the elbow of this 55-year-old man with severe ankylosing spondylitis reveals diffuse joint space narrowing *(arrows)* and fluffy periarticular periostitis *(open arrows)*. Elbow joint involvement occurs in only 12% of persons with long-standing ankylosing spondylitis.

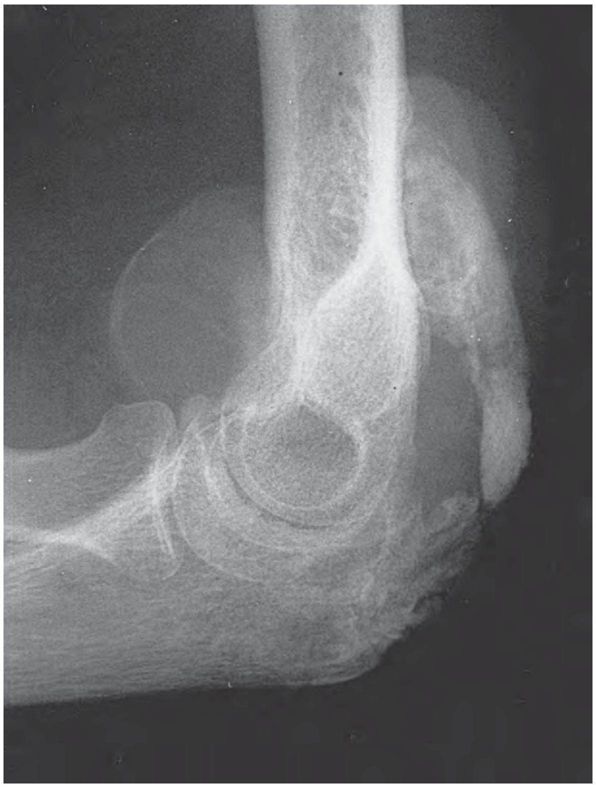

FIGURE 15–31 Scleroderma (progressive systemic sclerosis).[45] Prominent periarticular (and possibly intraarticular) calcinosis is seen in this patient with long-standing scleroderma. *(Courtesy V. Vint, MD, San Diego.)*

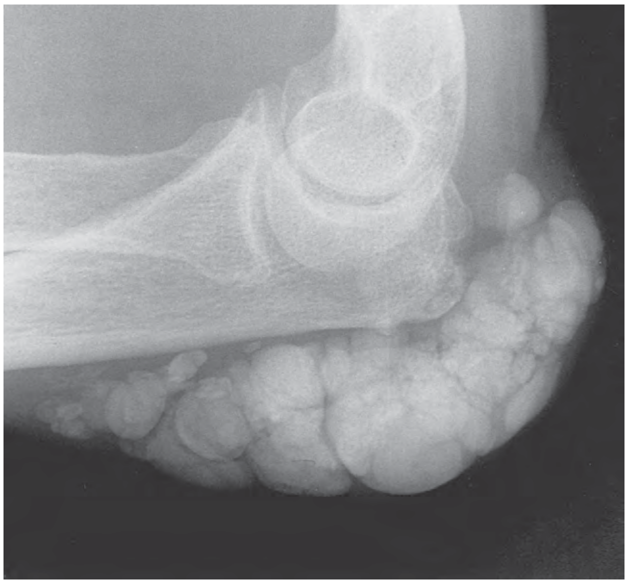

FIGURE 15–32 Gouty arthropathy.[46] Lateral radiograph of this 58-year-old man with long-standing gout and chronic renal disease reveals a large nodular collection of soft tissue calcification about the extensor surface of the olecranon. The calcification may represent tophi from gout, or, alternatively, it may represent calcium hydroxyapatite deposition secondary to chronic renal disease.

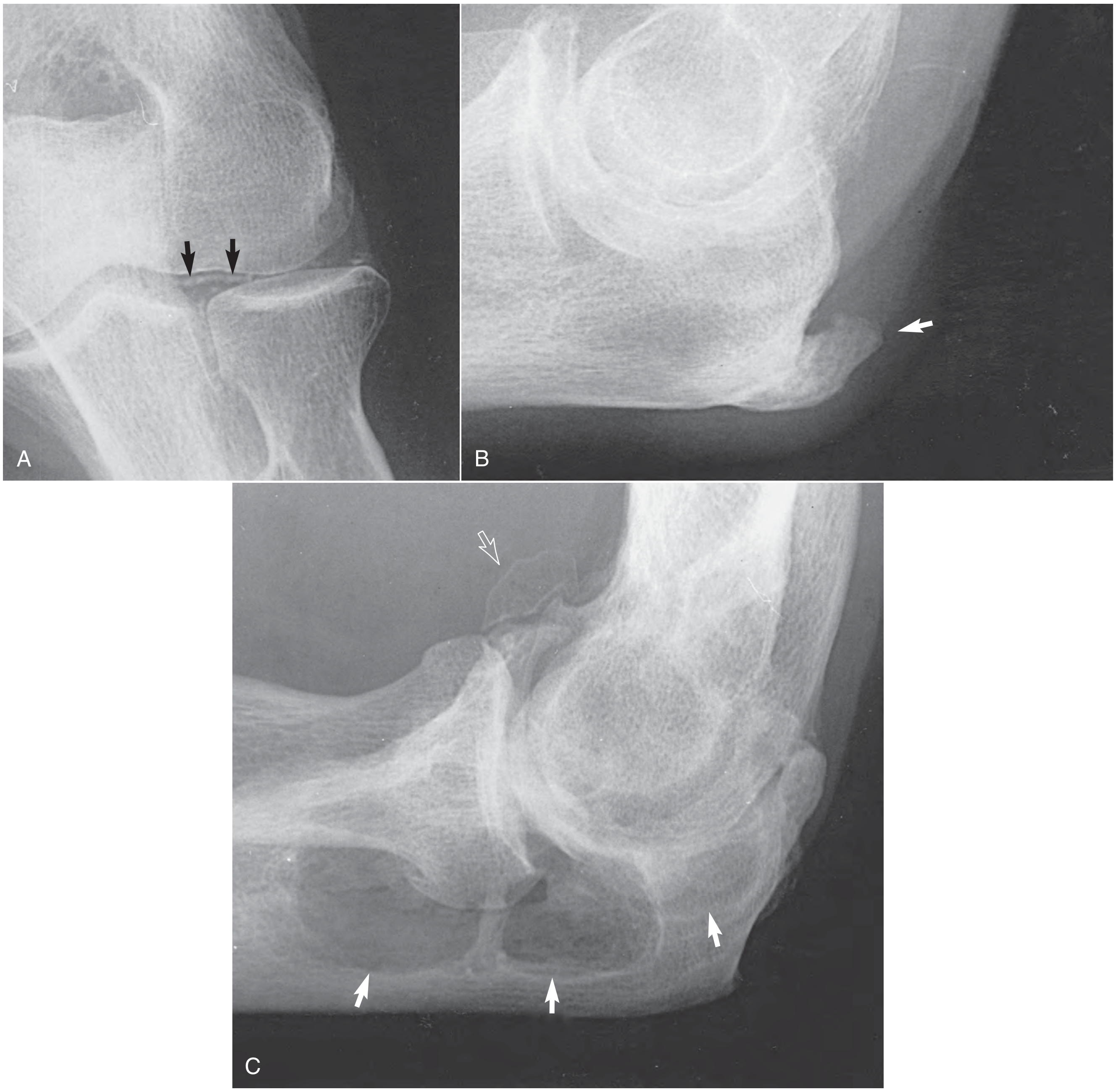

FIGURE 15–33 Calcium pyrophosphate dihydrate (CPPD) crystal deposition disease.[47,48] **A,** Chondrocalcinosis is seen in the distribution of the articular hyaline cartilage of the elbow *(arrows)* in this 82-year-old man. **B,** In another patient, a large olecranon enthesophyte *(arrow)* is seen arising from the attachment of the triceps tendon. **C,** In a third patient, large subchondral cysts *(arrows),* secondary degenerative changes, and intraarticular bodies *(open arrow)* are present.

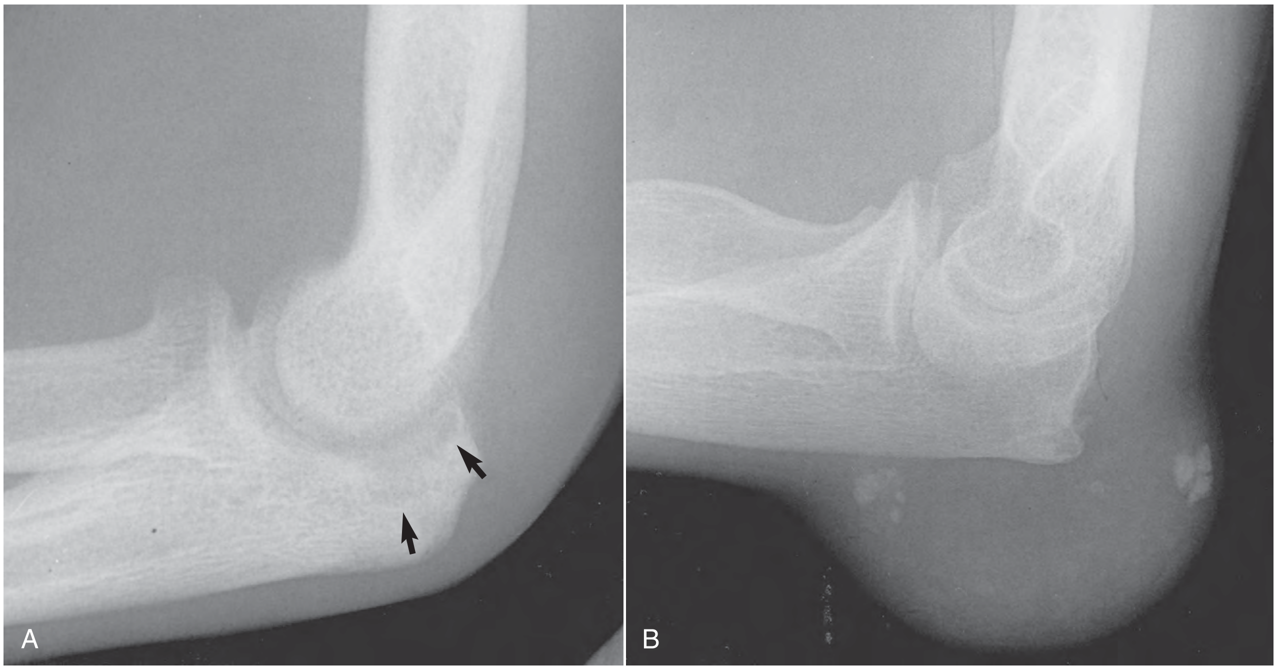

FIGURE 15–34 Pyogenic septic arthritis and bursitis.[49,65] **A,** Septic arthritis. This 21-year-old man had pain and swelling over the elbow for 3 months. Routine radiograph reveals indistinct subchondral bone margins, joint space narrowing, and erosions *(arrows)*. The joint was infected by *Pseudomonas,* presumably via hematogenous spread. **B,** Septic bursitis. Observe the massive soft tissue swelling and soft tissue edema caused by *Staphylococcus aureus* infection of the subcutaneous olecranon bursa (olecranon bursitis). Areas of calcification are present within the bursa.

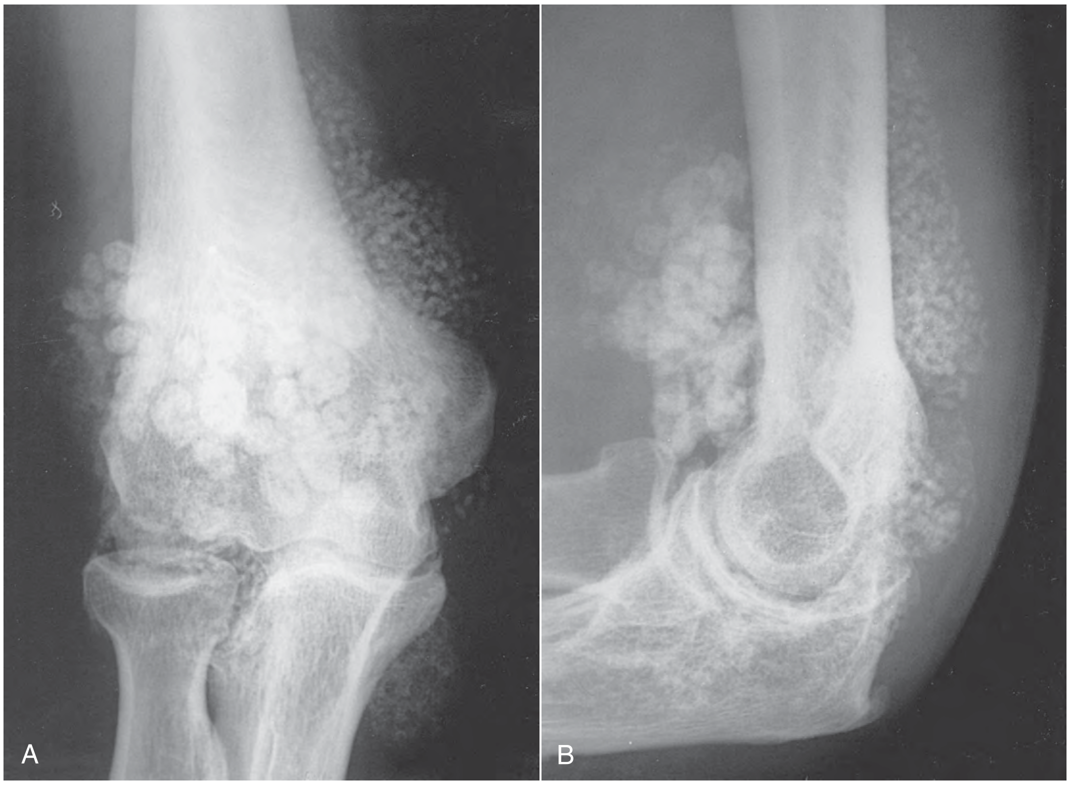

FIGURE 15–35 Idiopathic synovial osteochondromatosis.[53,54] Frontal **(A)** and lateral **(B)** radiographs reveal multiple juxtaarticular radiodense osteocartilaginous bodies within the synovial cavity of the elbow. Idiopathic synovial osteochondromatosis represents metaplastic or neoplastic proliferation of cartilaginous bodies by the synovial membrane. Secondary synovial osteochondromatosis may also occur as a result of degenerative joint disease. Noncalcified lesions are best evaluated with arthrography.

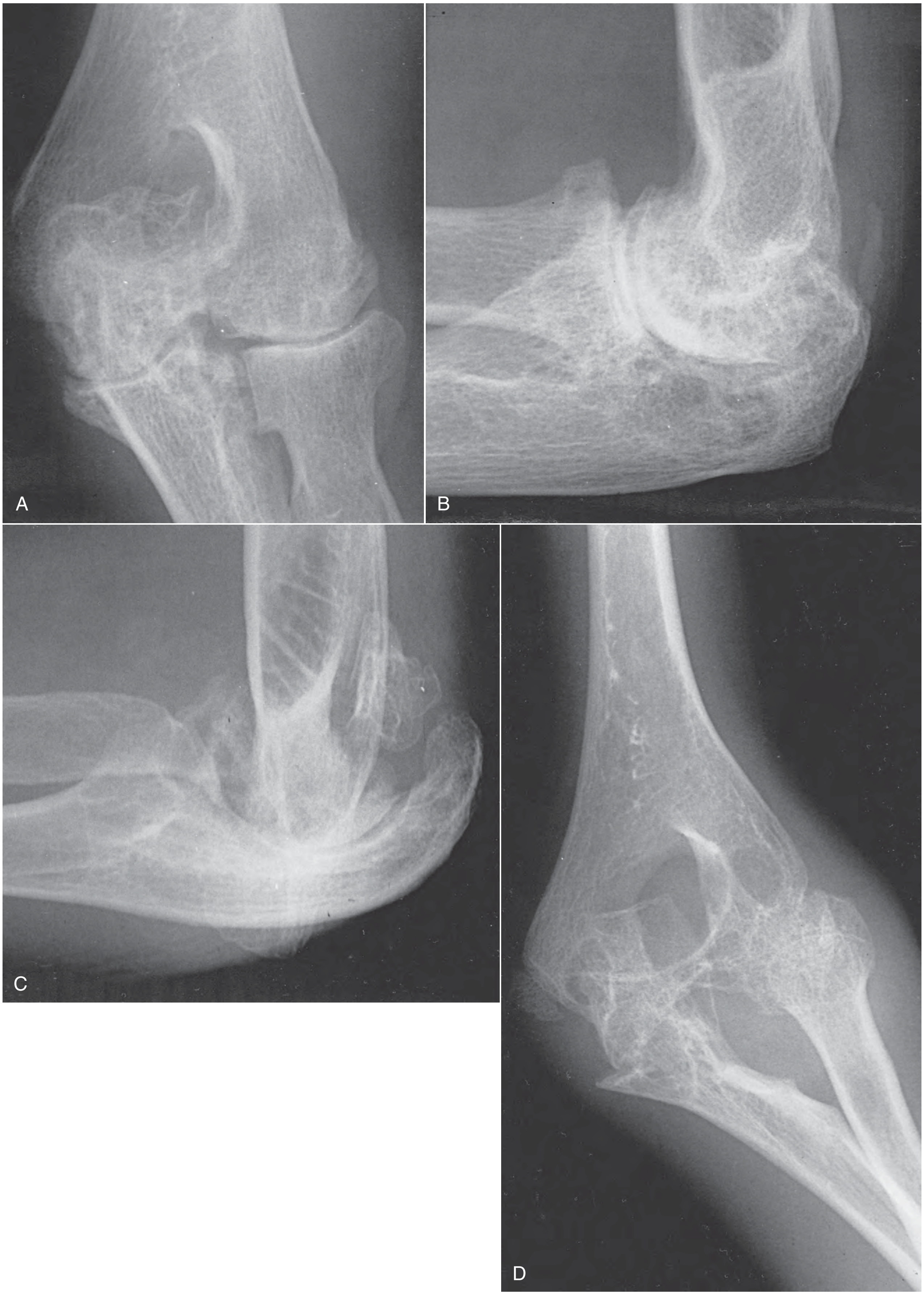

FIGURE 15–36 Hemophilic arthropathy.[56] **A-B,** Moderate changes. Radiographs of this 27-year-old man with hemophilia show osteopenia, joint space narrowing, and multiple subchondral cysts within the humerus, ulna, and radius. **C,** Severe changes. In a 40-year-old man, extensive articular destruction and subluxation have occurred. In this case, the pattern of joint involvement resembles that of neuropathic osteoarthropathy. **D,** Severe changes. This 17-year-old boy has had long-standing hemophilia and has sustained several episodes of hemarthrosis. The radiographs reveal severe articular destruction and subluxation. Both elbows exhibit symmetric changes that are characteristic of hemophilic arthropathy, but that also resemble the changes of juvenile idiopathic arthritis.

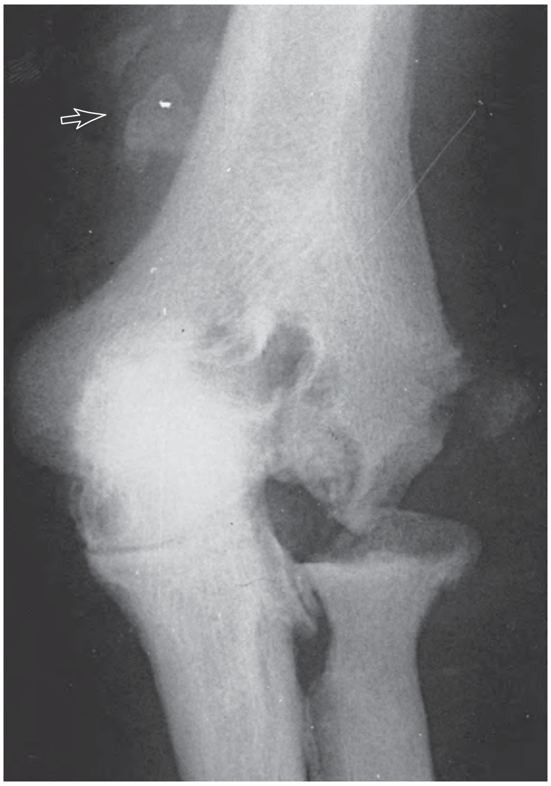

FIGURE 15–37 Neuropathic osteoarthropathy: syringomyelia.[57] Observe the extensive destruction of the capitulum, lateral epicondyle, and radial head in this patient with a cervical cord syrinx. Osseous debris is also evident *(open arrow)*.

TABLE 15-7 Metabolic, Hematologic, and Infectious Disorders Affecting the Elbow

Disorder	Figure(s)	Characteristics
Rickets[58]		Prominent findings in the metaphyses about the elbow in patients with long-standing rickets *Metaphyseal demineralization:* frayed, widened, cupped (paint brush metaphyses) Bowing of bones Osteopenia
Hyperparathyroidism and renal osteodystrophy[59-62]		Occasional bone sclerosis (more common with renal osteodystrophy) Chondrocalcinosis (calcium pyrophosphate dihydrate [CPPD] crystal deposition) Brown tumors Soft tissue calcification Pathologic fracture
Heterotopic ossification: Brain injury[63]	15-38	Brain and spinal cord injury (as in burns, mechanical trauma, and venous stasis) may result in heterotopic ossification about the elbow and other major joints Osseous deposits typically begin as poorly defined opaque areas appearing 2 to 6 months after the injury and progress to large radiodense lesions possessing trabeculae May eventually result in complete ankylosis of the joint
Osteonecrosis: Panner disease[64]	15-39	Osteonecrosis or altered sequence of ossification involving the capitulum of the humerus Occurs between the ages of 5 and 10 years, especially in gymnasts and baseball players Boys > girls Increased radiodensity, often with a peripheral zone of subchondral radiolucency Fragmentation and collapse of capitulum may result Complete regeneration and reconstitution of capitulum typically occur without residual deformity or disability Imaging appearance may resemble that of osteochondritis dissecans or osteochondral fracture

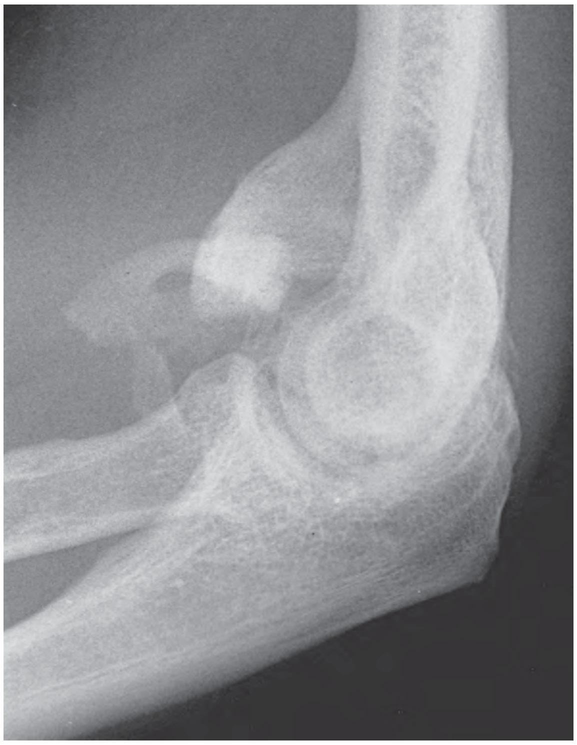

FIGURE 15–38 Heterotopic ossification.[63] This 43-year-old man sustained a head injury and was comatose for 3 days. In a radiograph taken several months after the injury, observe the extensive ossification surrounding the elbow joint. Such ossification may eventually result in complete osseous ankylosis. The ossification often involves several joints and may resemble the changes of fibrodysplasia ossificans progressiva.

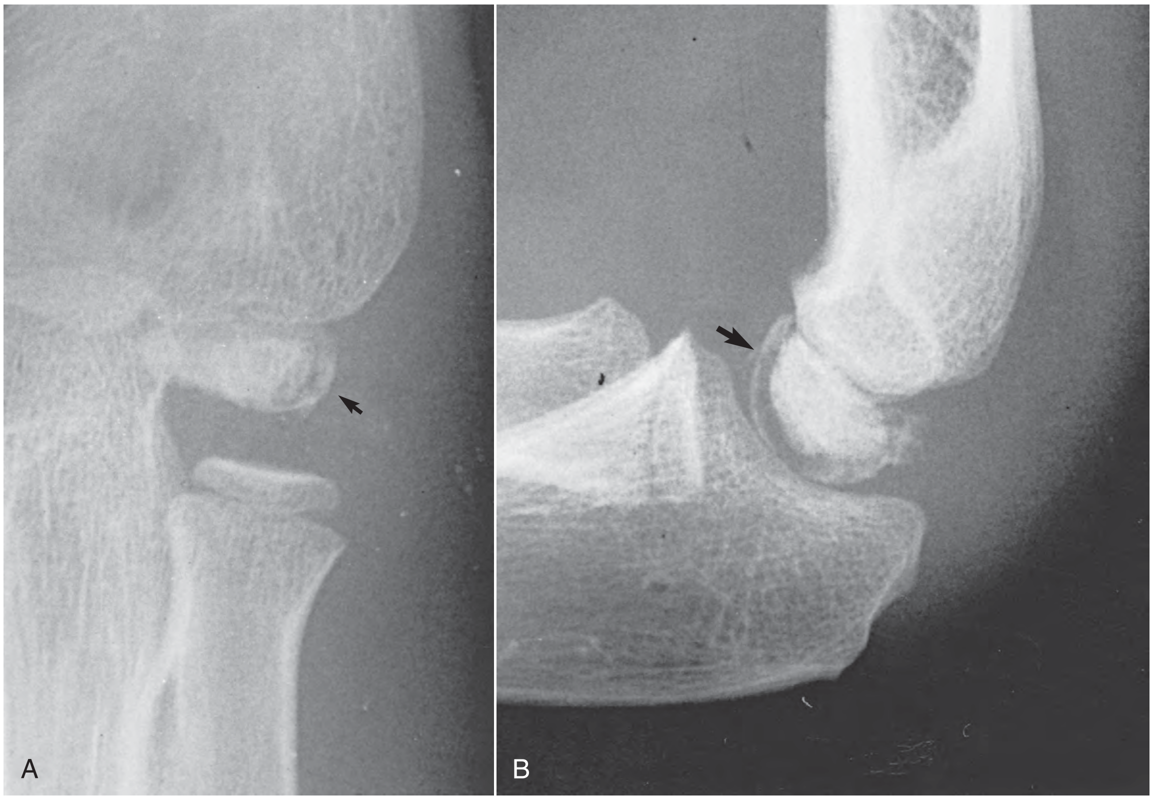

FIGURE 15–39 Panner disease.[64] Frontal **(A)** and lateral **(B)** radiographs of this 7-year-old boy with elbow pain and stiffness reveal a linear region of subchondral radiolucency and diffuse increased radiodensity involving the capitulum *(arrows)*. This osteonecrosis of the capitulum occurs in the juvenile epiphysis, typically between the ages of 5 and 10 years, and is more common in boys, especially baseball players and gymnasts. *(Courtesy E. Bosch, MD, Santiago, Chile;* ***B,*** *From Resnick D, Kang HS, Pretterklieber ML: Internal derangements of joints. 2nd Ed. Philadelphia, Saunders, 2006, p 1191.)*

CHAPTER 16

Radius and Ulna

DEVELOPMENTAL ANOMALIES, ANATOMIC VARIANTS, SOURCES OF DIAGNOSTIC ERROR, AND DYSPLASIAS

The most common developmental anomalies, anatomic variants, sources of diagnostic error, and skeletal dysplasias involving the radius and ulna are listed in Table 16-1. Figures 16-1 to 16-4 represent selected examples.

PHYSICAL INJURY

Fractures and other physical injuries to the radius and ulna are described in Tables 16-2 and 16-3. These injuries are illustrated in Figures 16-5 to 16-17. Injuries to the proximal portions of the radius and ulna are discussed in Chapter 15, and injuries of the wrist are discussed in Chapter 17.

BONE TUMORS

The radius and ulna are infrequent sites of malignant and benign neoplasms and tumorlike processes. Table 16-4 lists the major characteristics of these disorders. Their imaging manifestations are illustrated in Figures 16-18 to 16-32.

METABOLIC, HEMATOLOGIC, AND INFECTIOUS DISORDERS

A wide variety of metabolic, hematologic, and infectious disorders may involve the bones of the forearm. Table 16-5 lists some of the more common disorders and describes their characteristics. Their imaging features are illustrated in Figures 16-33 to 16-41. Further manifestations of these disorders within the proximal and distal portions of the radius and ulna are discussed in Chapters 15 and 17, respectively.

TABLE 16-1 Developmental Anomalies, Anatomic Variants, and Skeletal Dysplasias Affecting the Radius and Ulna

Disorder	Figure(s)	Characteristics
Radioulnar synostosis[1]	See Figure 15-5	Anomalous osseous fusion of the proximal portions of the radius and ulna Bilateral in 60% of patients Restricts normal forearm supination and pronation Additional anomalies may accompany radioulnar synostosis
Radiolucent radial tuberosity[2]	See Figure 15-2, *F* 16-1	Normal radiolucency of the cancellous bone within the radial tuberosity may simulate a destructive lesion or a cyst No clinical significance
Madelung deformity[3]	16-2	***Imaging findings*** *Radius:* Dorsal and ulnar curvature; decreased length; triangular distal epiphysis owing to premature fusion of medial half of epiphysis; ulnar and volar angulation of distal radial articular surface *Ulna:* Elongated ulna with dorsal subluxation; enlargement and distortion of ulnar head *Carpal bones:* Wedging of carpal bones between deformed radius and protruding ulna; triangular configuration of carpals with lunate at apex *Distal radioulnar joint:* Increased width of distal radioulnar joint *Radiocarpal joint:* V-shaped; decreased carpal angle Several forms of Madelung deformity have been identified: 1. *Isolated, idiopathic form:* females > males; bilateral > unilateral; asymmetric in severity 2. *Dysplastic form:* seen in association with multiple hereditary exostosis and dyschondrosteosis 3. *Genetic form:* seen with Turner syndrome 4. *Posttraumatic form:* from an extension injury to the radial epiphysis
Positive ulnar variance (ulnar abutment or impaction syndrome)[4-6,75]	16-3	Increased length of ulna in relation to the radius Results in limitation of rotation, subsequent ligamentous relaxation of the wrist, and a thinner triangular fibrocartilage complex (TFCC) Ulnar abutment (impaction) syndrome refers to the consequent degeneration, TFCC perforation, and lunotriquetral interosseous ligament disruption
Negative ulnar variance (ulna minus variant)[7-9,75]	16-4	Decreased length of ulna in relation to the radius measured at the distal end Present in about 20% of normal individuals Association between negative ulnar variance and Kienböck disease has been proposed, but the significance of the correlation remains controversial May also be associated with ulnar impingement syndrome May result in prominent fossa within the radial surface of the distal radioulnar articulation that may simulate focal destruction

See also Tables 1-1 and 1-2.

FIGURE 16–1 Normal radiolucent radial tuberosity.[2] **A-B,** Two views of the proximal portion of the radius show an expansile radiolucent region representing the normal radial tuberosity *(arrows)*. This appearance may mimic an osteolytic lesion, especially in the absence of a sclerotic margin.

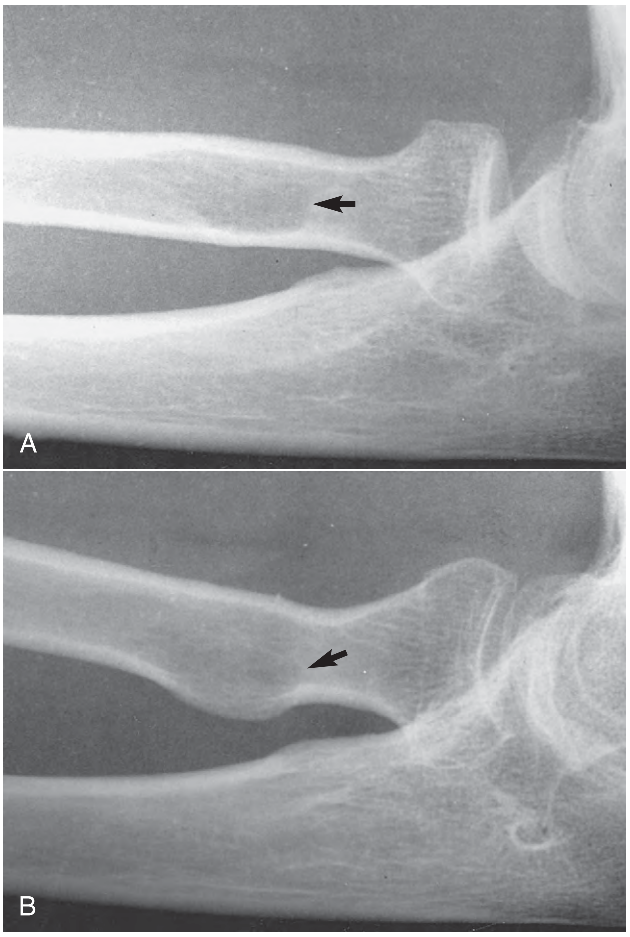

FIGURE 16–2 Madelung deformity.[3] Findings include an increased width between the distal portions of the radius and ulna, a relatively long ulna in comparison with the radius, a decreased carpal angle, triangularization of the distal radial epiphysis, an osseous excrescence at the metaphyses of the radius *(arrow),* and wedging of the carpal bones between the deformed radius and protruding ulna. The lunate bone is at the apex of the wedge. The isolated idiopathic form of Madelung deformity is more common in women and is more frequently bilateral than unilateral; the degree of severity is unequal on the two sides. *(Courtesy G. Greenway, M.D., Dallas.)*

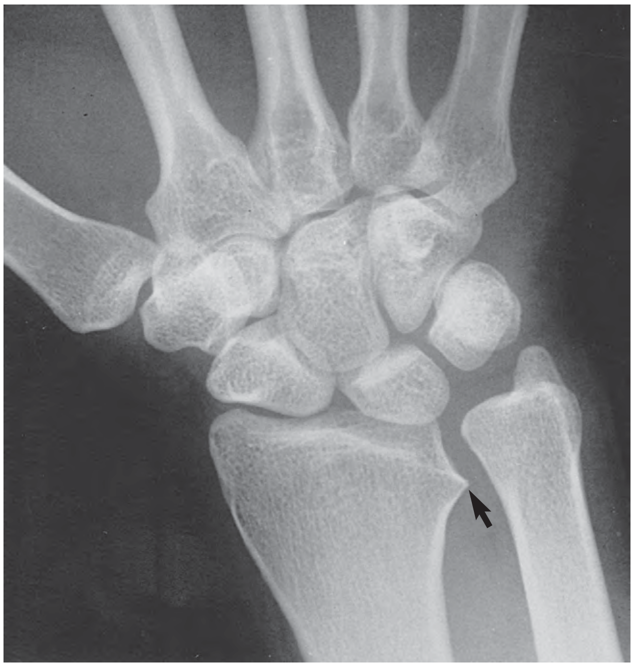

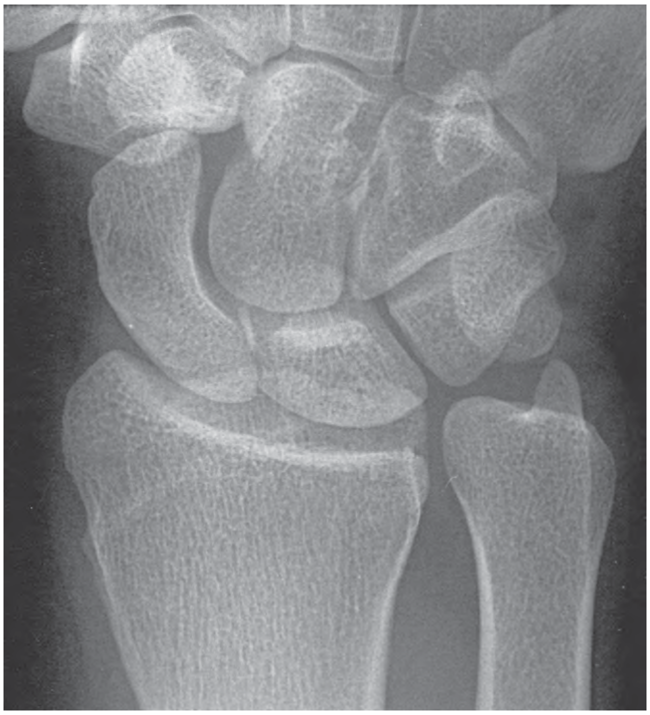

FIGURE 16–3 Positive ulnar variance: ulnar abutment (impaction) syndrome.[4-6,75] The ulna is relatively long in comparison with the radius, a finding termed *positive ulnar variance*. This form of variance results in limitation of rotation, subsequent ligamentous relaxation of the wrist, and a thinner triangular fibrocartilage complex (TFCC). The ulnar abutment (impaction) syndrome refers to the consequent degeneration, TFCC perforation, and lunotriquetral interosseous ligament disruption.

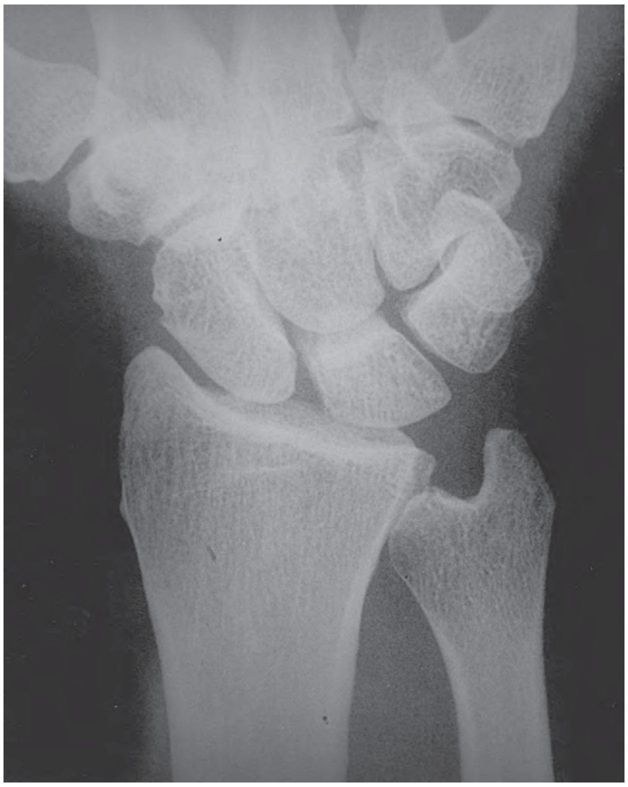

FIGURE 16–4 Negative ulnar variance (ulna minus).[7-9,75] On this posteroanterior radiograph of the wrist, the ulna is shorter than the radius, and mild osteoarthrosis of the distal radioulnar joint is evident. Note the discontinuity of the distal surfaces of the ulna and radius at the radiocarpal joint. Negative ulnar variance may lead to Kienböck disease (osteonecrosis of the lunate) or the ulnar impingement syndrome.

TABLE 16-2 Fractures and Dislocations of the Radial and Ulnar Diaphyses

Site	Figure(s)	Characteristics	Complications and Related Injuries
Ulna (Alone)			
"Nightstick" fracture[10]	16-5	Direct blow to forearm Distal third ulna > middle third ulna > proximal third	Displacement at fracture site (uncommon)
Monteggia fracture-dislocation[11,12]	16-6	*Type I:* fracture of middle or upper third of ulna with anterior dislocation of radial head (65% of cases) *Type II:* fracture of middle or upper third of ulna with posterior dislocation of radial head (18% of cases) *Type III:* fracture of ulna just distal to coronoid process with lateral dislocation of radial head (16% of cases) *Type IV:* fracture of upper or middle third of ulna with anterior dislocation of radial head and fracture of proximal portion of radius (1% of cases)	Injury to branches of radial nerve (20% of cases)
Radius (Alone)			
Proximal and middle segments[13]		*Uncommon:* usually associated with ulnar fracture	
Galeazzi injury[14]	16-7 See Figure 16-12	Fracture of the radial shaft with dislocation or subluxation of distal radioulnar joint Caused by direct blow or fall on the outstretched hand with pronation of forearm Variable degree of displacement at fracture site	Angulation Entrapment of extensor carpi ulnaris tendon Delayed union or nonunion Limitation of supination and pronation of forearm Fractures of ulnar head and styloid process
Radius and Ulna[15]		Closed or open Nondisplaced or displaced	Delayed union or nonunion (especially of ulna) Displacement more common in adults than in children Infection, especially in open fractures Nerve and vascular injuries, especially in open fractures and those with severe displacement Compartment syndromes Synostosis between radius and ulna (rare)
Stress Injuries[16,74]	16-8	Stress fractures or stress reactions in the ulna of rodeo riders, tennis players, baseball pitchers, volleyball players, weight lifters, baton twirlers, and patients using wheelchairs	

See also Tables 1-4 and 1-5, Chapter 15 for injuries to the proximal portion of the radius and ulna, and Chapter 17 for injuries to the wrist.

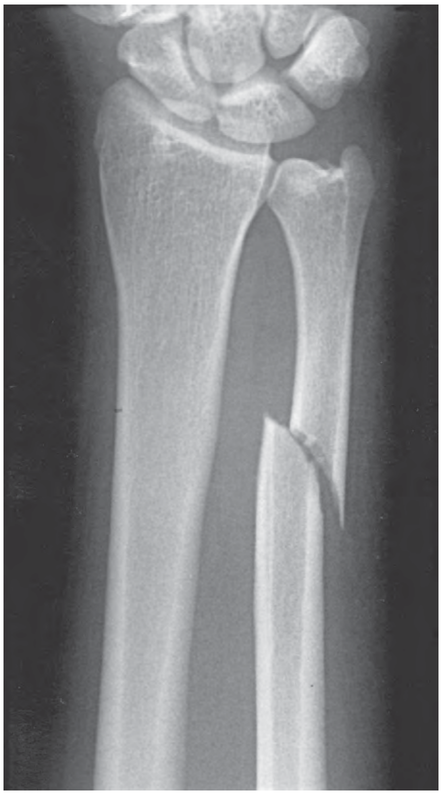

FIGURE 16–5 "Nightstick" fracture: Isolated fracture of the ulnar diaphysis.[10] Note the oblique, minimally displaced fracture of the distal portion of the ulna. The distal and proximal radioulnar joints and the radius were intact radiographically. These fractures occur as a result of a direct blow to the forearm during a violent assault by a hard object, such as a nightstick or club.

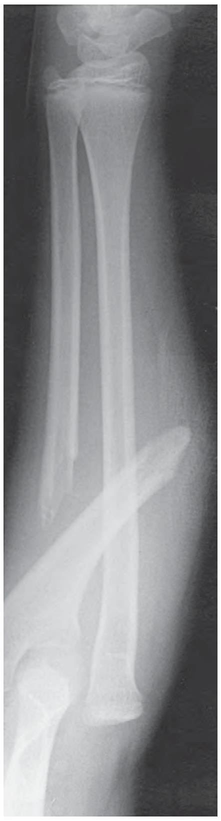

FIGURE 16–6 Monteggia fracture-dislocation (type I).[11,12] A displaced fracture of the proximal one third of the ulnar diaphysis and associated anterior dislocation of the radial head are evident in this 15-year-old boy. Monteggia injuries are common in adults but are rare and easily overlooked in children. Type I injuries represent 65% of cases, but variations including types II, III, and IV may also occur.

FIGURE 16–7 Galeazzi fracture-dislocation.[14] This 21-year-old woman has a comminuted distal radius fracture, diastasis of the distal radioulnar articulation *(arrow),* and a displaced fracture of the ulnar styloid process. The short oblique or transverse fracture usually occurs at the junction of the middle and distal thirds of the radial diaphysis, and the distal radial fragment is displaced in an ulnar direction. In addition to radioulnar diastasis, fractures of the ulnar head or styloid process often accompany the injury. Complications include nonunion, malunion, and limitation of supination and pronation ranges of motion. (See also FIGURE 16–12).

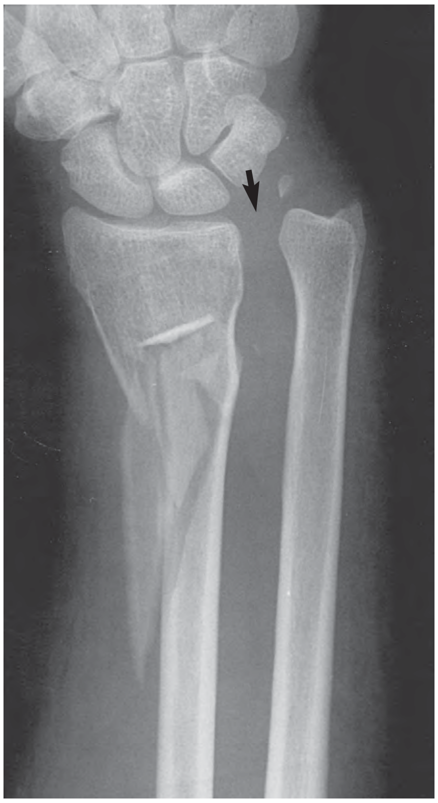

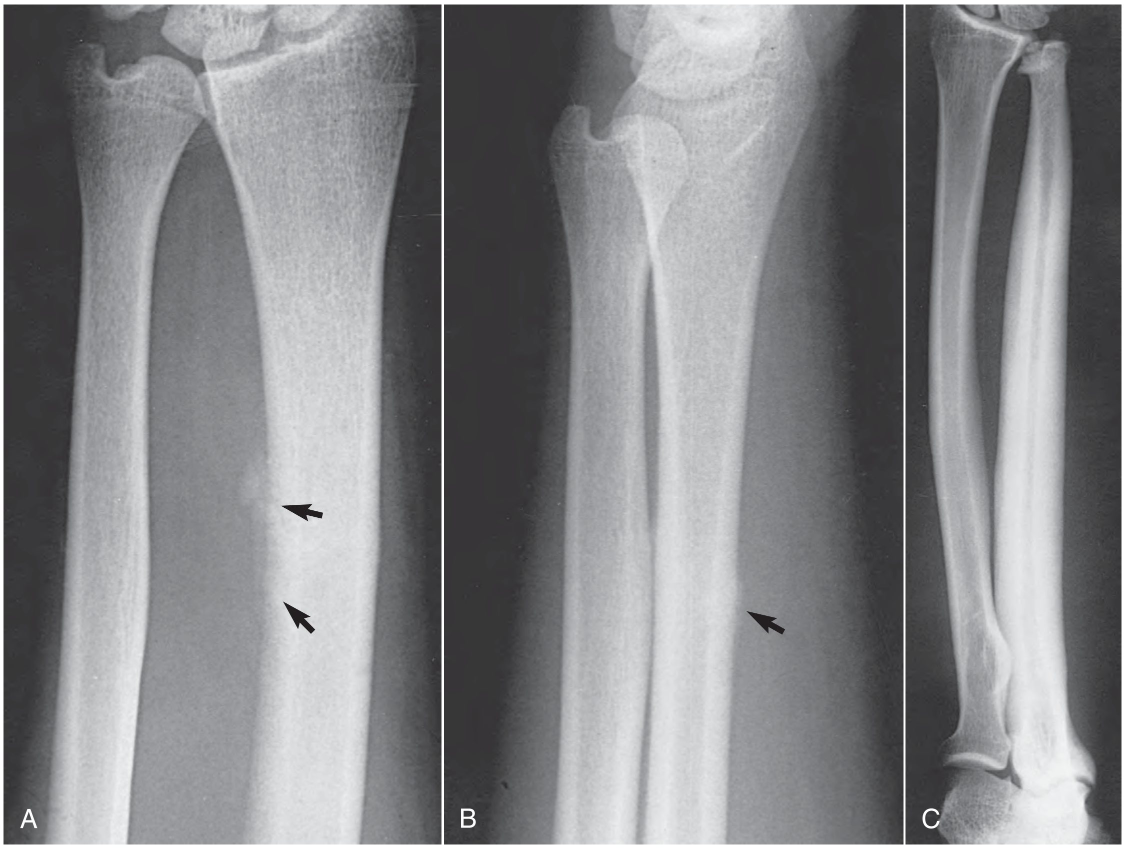

FIGURE 16–8 Reactions to stress.[16,74] **A** and **B,** Stress (fatigue) fracture. Frontal **(A)** and lateral **(B)** radiographs of this 22-year-old professional pool player illustrate periosteal new bone formation *(arrows)*. **C,** Stress reaction. In another patient, a 27-year-old rodeo cowboy, a radiograph of the ulna exhibits diffuse cortical hyperostosis, a complication seen in rodeo professionals. (*C, Courtesy G. Greenway, M.D., Dallas.)*

TABLE 16-3 Fractures and Dislocations About the Distal Portions of the Radius and Ulna

Fracture	Figure(s)	Characteristics	Complications and Related Injuries
Colles (Pouteau) fracture[17,73]	16-9	*Mechanism:* dorsiflexion Fracture of distal portion of radius with dorsal displacement Classification system based on extraarticular versus intraarticular location, presence or absence of ulnar fracture Varying amounts of radial displacement angulation, and shortening Ulnar styloid fracture in about 50% to 60% of cases Associated injuries to carpus, elbow, humerus, and femur (in osteoporotic patients), distal radioulnar joint	Deformity related to radial shortening and angulation Subluxation or dislocation of distal radioulnar joint Complex regional pain syndrome Injury to median or, less commonly, radial or ulnar nerve Osteoarthrosis Tendon rupture Secondary displacement of distal radius fractures increases with increasing patient age, primarily among fractures subject to closed reduction
Moore fracture[17]		Combination of Colles fracture, fracture of the ulnar styloid process, and disruption of the distal radioulnar joint	
Incomplete pediatric fractures[18]	16-10	*Mechanism:* longitudinal forces insufficient to cause complete discontinuity of the bone Incomplete fractures of the distal portion of the radius and ulna are common in children *Impaction fracture:* subtle increased zone of radiodensity at site of impaction *Torus fracture:* buckling of the metaphyseal cortex of the radius and/or ulna *Greenstick fracture:* buckling or bending of one side of the cortex, with fracture of the opposite side; diaphysis or metaphysis	May be initially overlooked, especially without evidence of buckling
Barton fracture[19]	16-11, 16-13	*Mechanism:* dorsiflexion and pronation Fracture of dorsal rim of radius with intraarticular extension	Similar to those of Colles fracture
Dislocation of the distal radioulnar joint[14]	16-12	*Isolated dislocation of the distal radioulnar joint:* rare injury *Galeazzi injury:* dislocation of the distal radioulnar joint combined with fracture of the radial shaft Fracture may be comminuted and severely displaced *Essex-Lopresti injury:* dislocation of the distal radioulnar joint combined with comminuted fracture of the radial head	Triangular fibrocartilage complex injury Fracture of ulnar head or styloid process Wrist and elbow instability
Radiocarpal fracture-dislocation[20]	16-11, 16-13	*Mechanism:* dorsiflexion Uncommon and severe injury Associated fractures of dorsal rim and styloid process of radius, and the ulnar styloid process May be irreducible	Entrapment of tendons and ulnar nerve and artery
Hutchinson (chauffeur's) fracture[21]	16-14	*Mechanism:* direct blow or avulsion by radial collateral ligament Fracture of styloid process of radius Usually nondisplaced	Scapholunate dissociation Degenerative joint disease Ligament damage
Smith (reverse Colles) fracture[22]	16-15	*Mechanism:* variable Fracture of distal portion of radius with palmar displacement Less common than Colles fracture Varying amounts of radial comminution, articular involvement	Complications similar to those of Colles fracture Extensor tendon injury Associated fracture of ulnar styloid process

Continued

TABLE 16-3 Fractures and Dislocations About the Distal Portions of the Radius and Ulna—cont'd

Fracture	Figure(s)	Characteristics	Complications and Related Injuries
Ulnar styloid process[23]	16-16	*Mechanism:* dorsiflexion or avulsion by ulnar collateral or triangular ligament Usually associated with radial fractures, infrequently isolated Usually nondisplaced	Nonunion Triangular fibrocartilage injury
Child abuse[24]	16-17	Incomplete or complete fracture of the radius or ulna may occur Epiphyseal injuries Other fractures at different stages of healing	Other injuries
Growth plate injuries: distal portion of radius[25]		*Mechanism:* chronic stress in gymnastic athletes or compression and rotation from upper limb weight-bearing *Fifty percent of all growth plate injuries:* distal portion of the radius is the most frequent site of physeal injuries *S-H Type I injury:* usually occurs between ages 9 and 14 years May resemble metaphyseal changes of rickets and dysplasias	Retardation of limb growth Positive ulnar variance Distal radioulnar joint abnormalities
Growth plate injuries: distal portion of ulna[25,26]		*Mechanism:* acute injury 5-7% of all growth plate injuries Ulna is not as common a site as radius S-H Type I injury most common Stress injuries of the distal ulnar epiphysis occurs in young gymnasts: radiodense reactive sclerosis	Retardation of limb growth

See also Tables 1-4 and 1-5.
S-H, Salter-Harris.

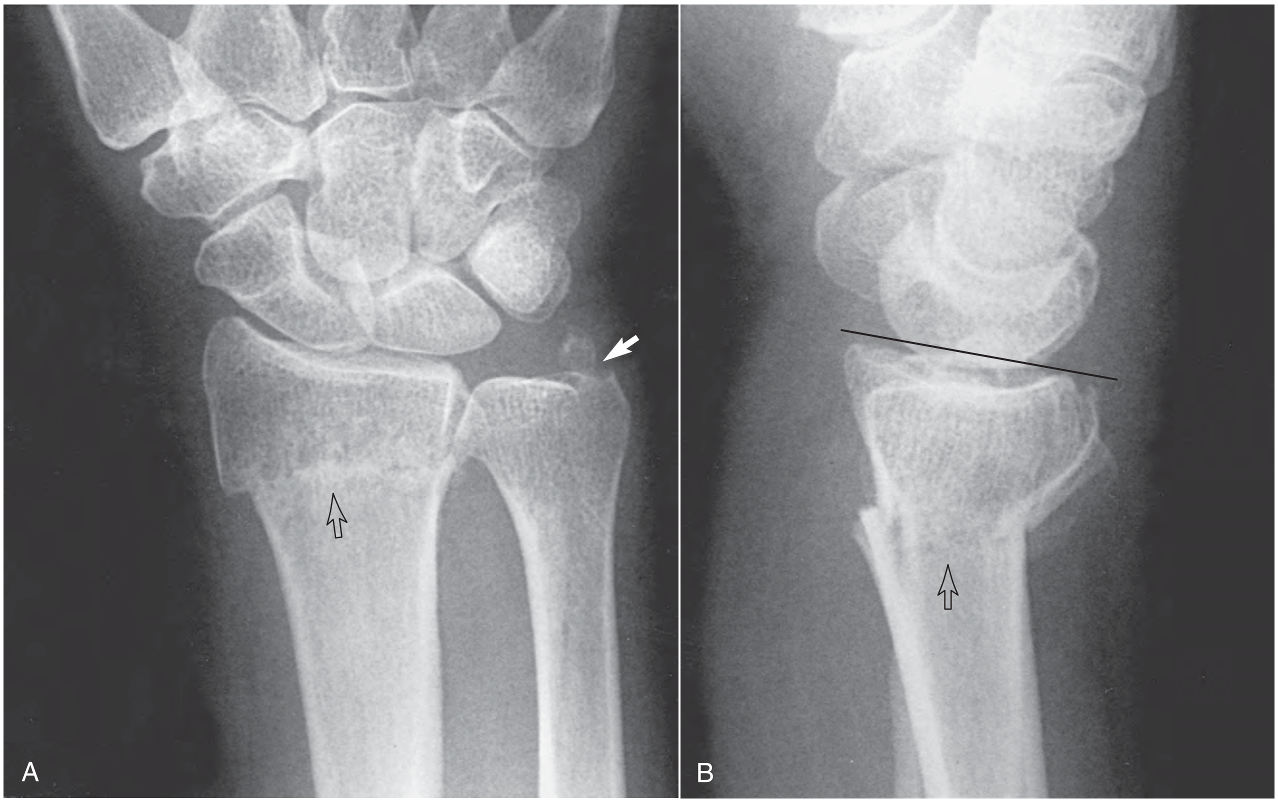

FIGURE 16–9 Colles fracture.[17,73] Frontal **(A)** and lateral **(B)** radiographs of this 61-year-old woman reveal a transverse fracture of the distal radial metaphysis *(open arrows)* with dorsal angulation of the distal radial articular surface *(line)*. The ulnar styloid also is fractured *(arrow)*, and prominent soft tissue swelling is observed. *(Courtesy A.L. Anderson, D.C., Portland, Ore.)*

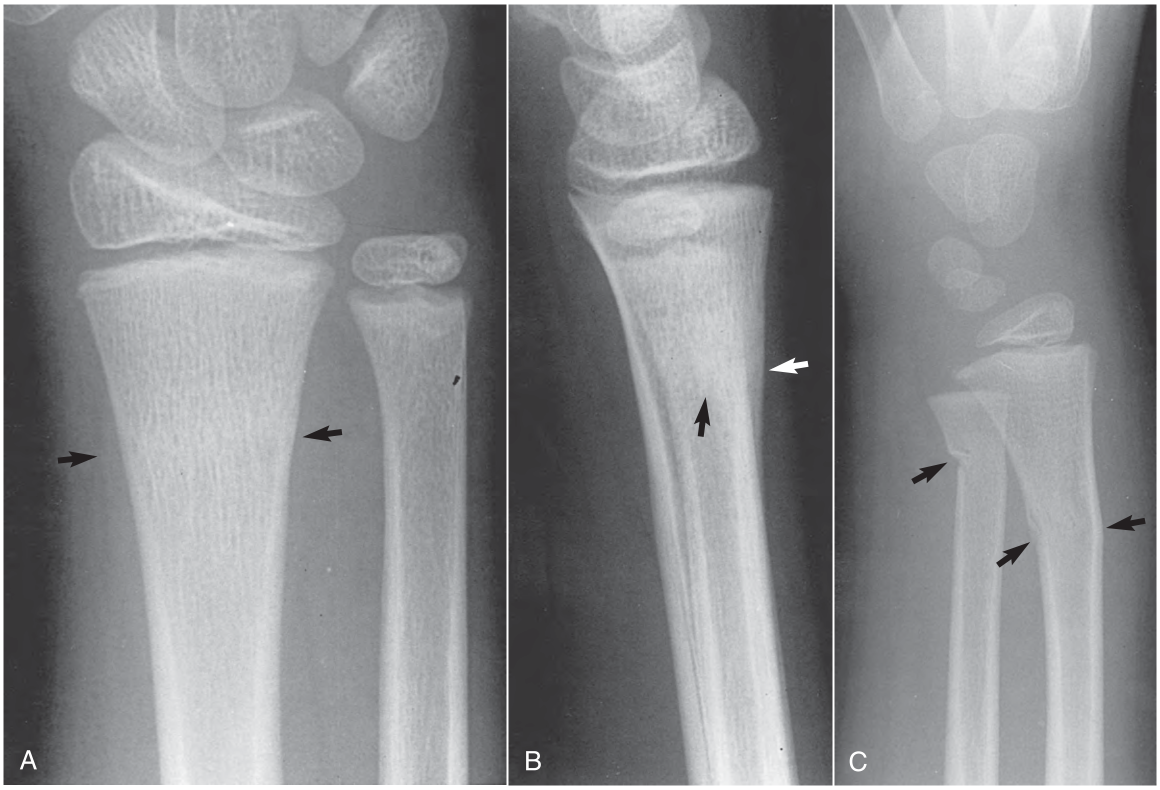

FIGURE 16–10 Pediatric fractures of the distal ends of the radius and ulna.[18] **A-B,** Impaction fracture. Frontal **(A)** and lateral **(B)** radiographs of this 13-year-old patient show an impaction fracture of the distal radial metaphysis manifested only as a subtle increased zone of density at the site of impaction *(arrows)*. **C,** Torus fracture. Note the buckling of the metaphyseal cortices of the radius and ulna *(arrows)* in this 8-year-old child who fell on an outstretched arm.

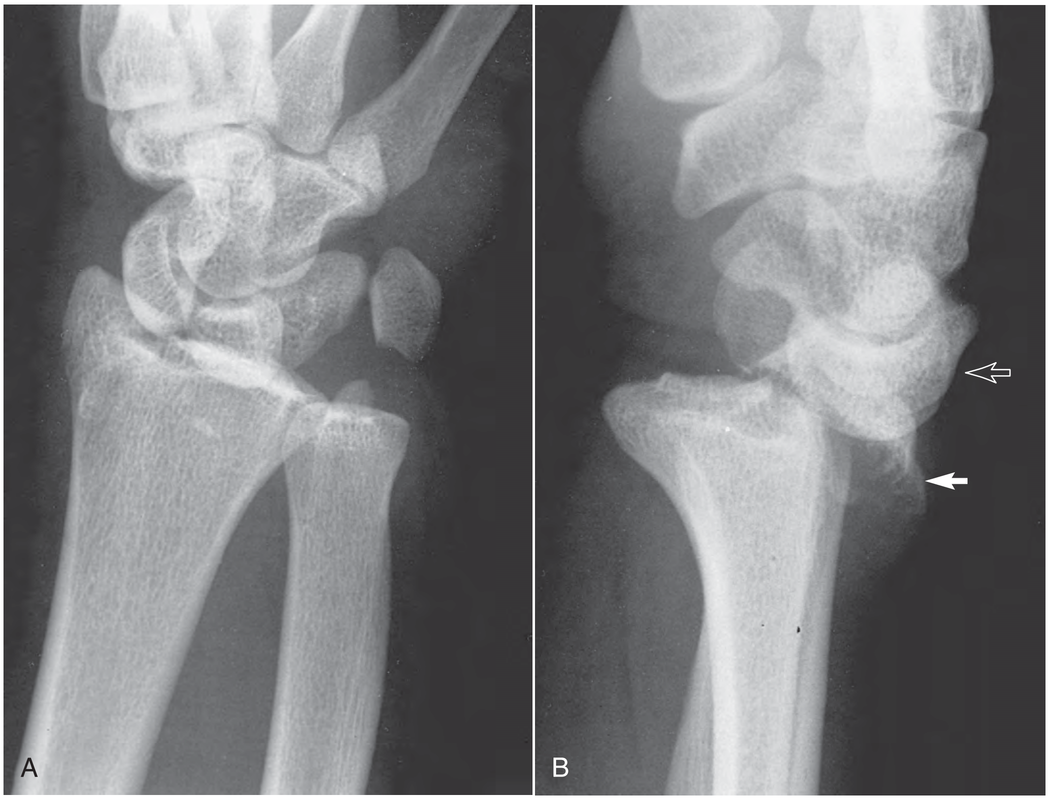

FIGURE 16–11 Barton fracture.[19] This 24-year-old man injured his wrist in a fall. Frontal **(A)** and lateral **(B)** radiographs reveal fracture of the dorsal rim of the radius *(arrow)* with intraarticular extension into the radiocarpal joint and dorsal dislocation of the radiocarpal articulations *(open arrow)*. These fractures are generally related to dorsiflexion and pronation of the forearm on the fixed wrist and occur frequently in young people involved in motorcycle accidents. (See Figure 16-13.)

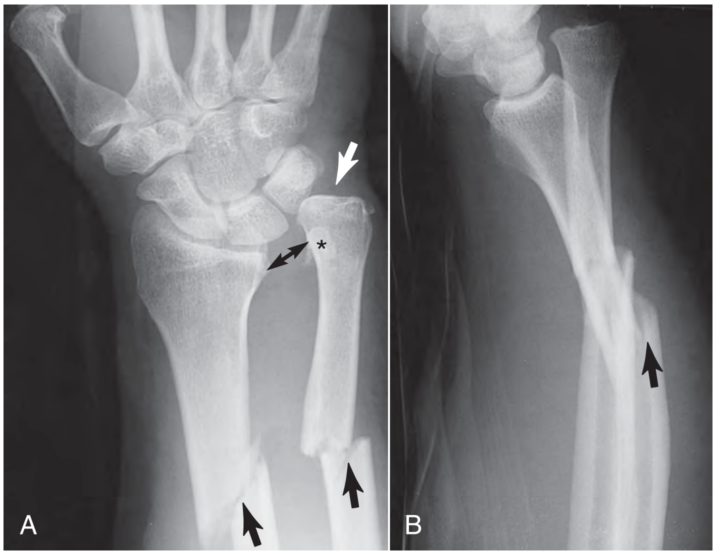

FIGURE 16–12 Dislocation of the distal radioulnar joint.[14] In this young adult patient with a variation of a Galeazzi fracture-dislocation, observe the widening of the distal radioulnar joint *(double-headed arrow)* and displacement of the distal ulnar fracture fragment *(white arrow)*. Both the radius and ulna are fractured in this patient *(black arrows)*. A classic Galeazzi fracture dislocation does not include an ulnar fracture. Note also the displacement of a fractured ulnar styloid process (*). (See Figure 16-7.)

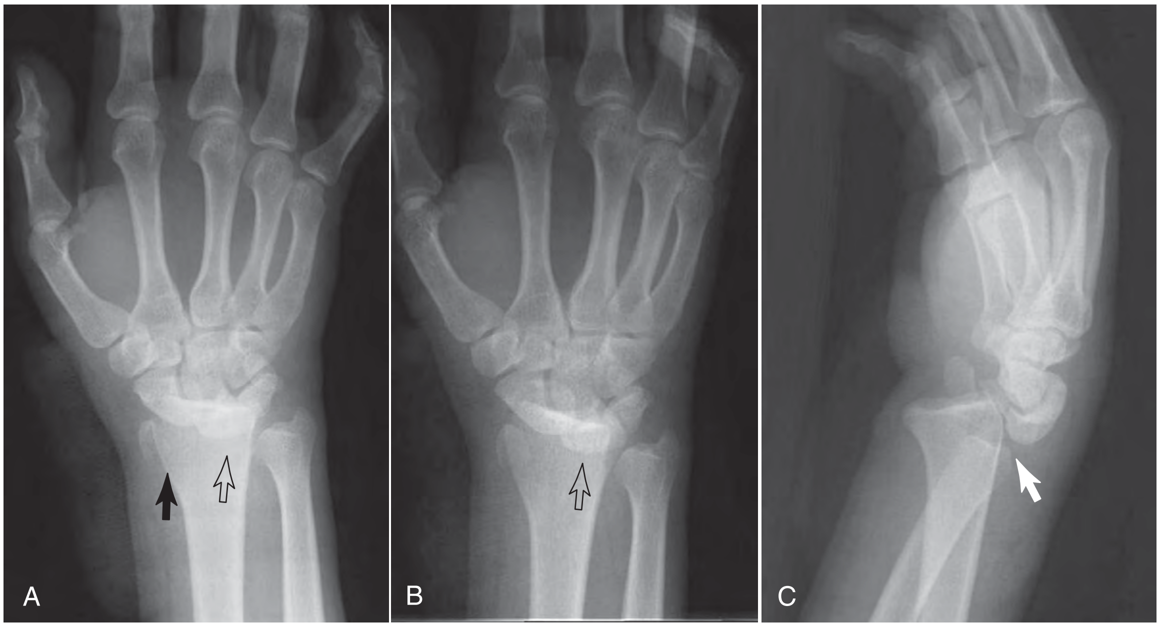

FIGURE 16–13 Radiocarpal fracture-dislocation.[20] A 33-year-old man. Anteroposterior **(A)** and oblique **(B)** radiographs reveal superimposition of the proximal carpal row and the distal radius *(open arrows),* along with a radial styloid fracture fragment *(black arrow)*. The lateral radiograph **(C)** clearly depicts dorsal dislocation of the radiocarpal joint *(white arrow)*. This is a variant of Barton fracture. (See Figure 16-11.)

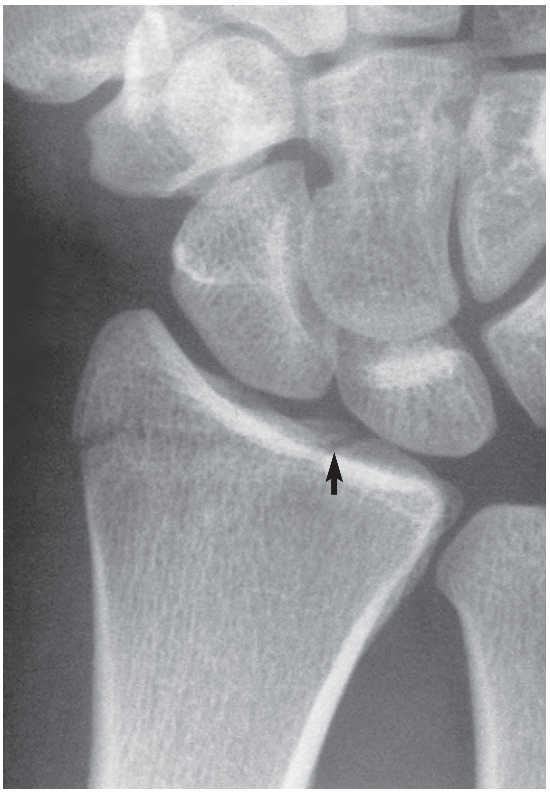

FIGURE 16–14 Hutchinson (chauffeur's) fracture: Radial styloid process.[21] Observe the large triangular fragment in this nondisplaced fracture. Intraarticular extension *(arrow)* is an important component of this fracture. Hutchinson fracture occurs as a result of a direct blow or as an avulsion of the radiocarpal or radial collateral ligament.

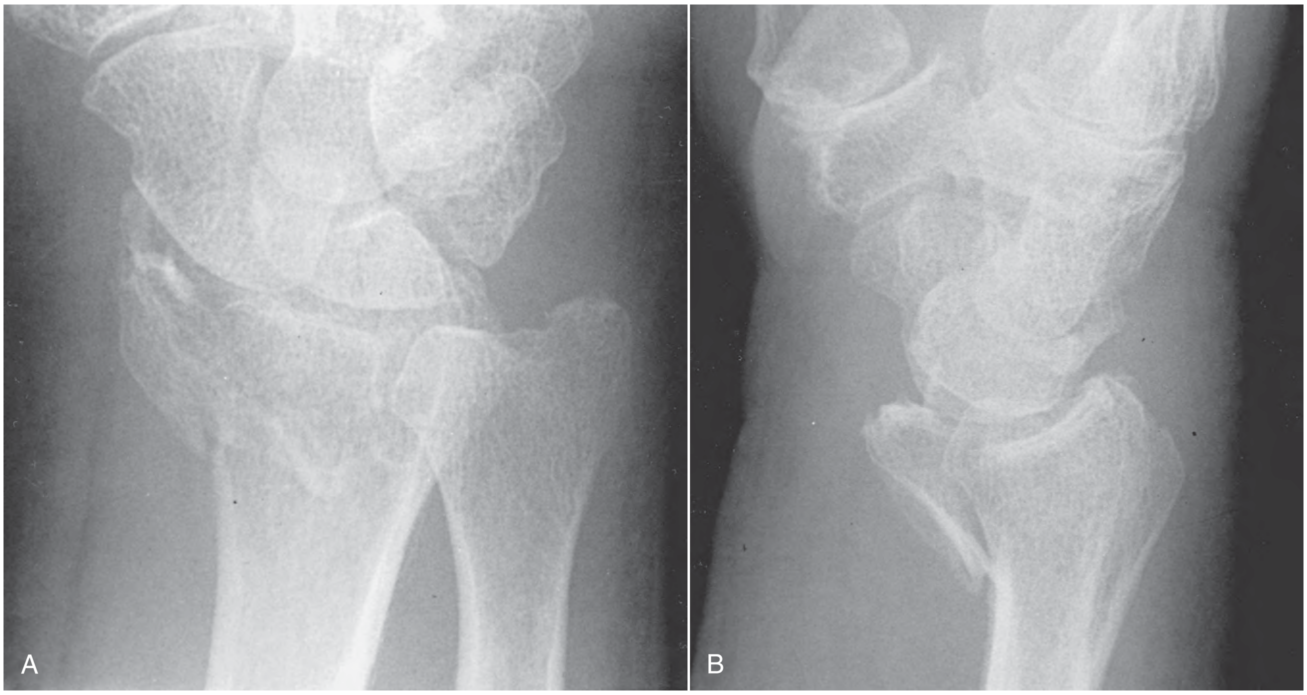

FIGURE 16–15 Smith fracture: reverse Colles fracture.[22] This 68-year-old woman had fallen, injuring her wrist. Frontal **(A)** and lateral **(B)** radiographs show a transverse fracture of the distal portion of the radius. The lateral radiograph **(B)** demonstrates mild volar and proximal displacement of the fracture fragment and the carpal bones, as well as soft tissue swelling. This injury is less common than Colles fracture and involves palmar angulation and anterior displacement of the distal radial surface. The fracture may be intraarticular or extraarticular, and it may be complicated by extensor tendon injury.

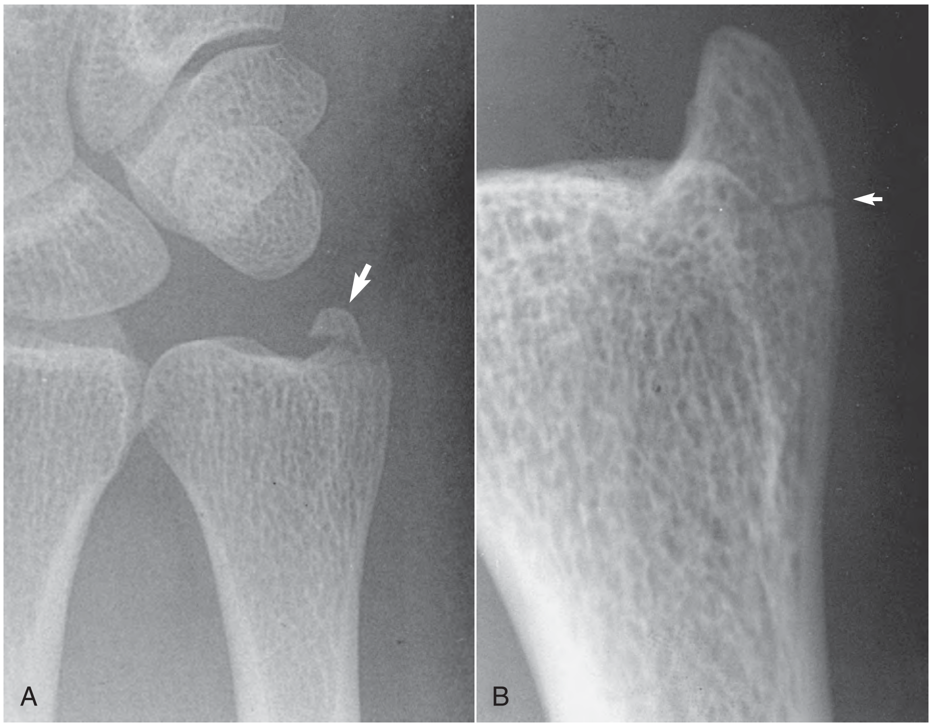

FIGURE 16–16 Isolated ulnar styloid process fracture.[23] **A,** This isolated fracture of the ulnar styloid process has minimal displacement *(arrow)*. **B,** In another patient, magnification radiography shows a nondisplaced transverse fracture *(arrow)*. Ulnar styloid process fractures are often a component of more complex wrist injuries, including Colles fracture, but may occur as an isolated phenomenon related to avulsion by the ulnar collateral or triangular ligaments. Nonunion of such fractures may be a source of chronic wrist pain, and may be difficult to differentiate from ununited ossification centers.

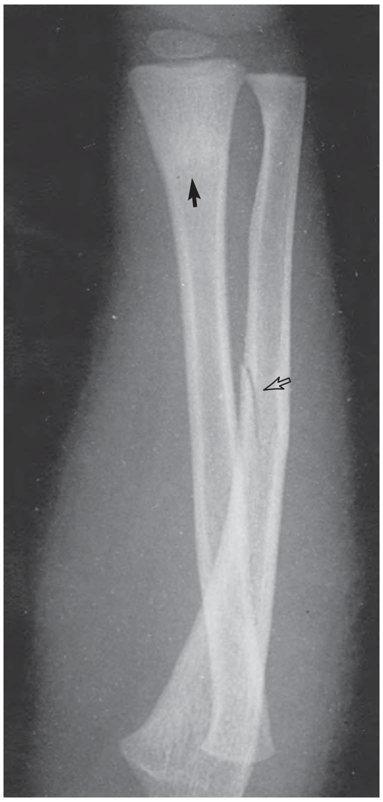

FIGURE 16–17 Child abuse.[24] An oblique ulnar fracture *(open arrow)* and an impacted radius fracture *(arrow)* are seen in this child who had been deliberately assaulted.

TABLE 16-4 Tumors Affecting the Radius and Ulna

Tumor	Figure(s)	Characteristics
Malignant Neoplasms of Bone		
Secondary malignant neoplasms of bone		
Skeletal metastasis[27,28]	16-18	*Acral metastasis rare:* fewer than 10% of skeletal metastatic lesions affect the radius and ulna Seventy-five percent permeative or moth-eaten osteolysis Twenty-five percent diffuse or patchy osteosclerosis or mixed pattern of lysis and sclerosis Usually multiple sites of involvement Pathologic fracture Cortical metastasis (“cookie-bite” lesions), especially from bronchogenic carcinoma
Primary malignant neoplasms of bone		
Osteosarcoma (conventional)[29,68,69]		Fewer than 1% of osteosarcomas occur in the radius and ulna Osteolytic, osteosclerotic, or mixed patterns of medullary and cortical destruction Prominent periosteal reaction common Preferential involvement of the metaphyseal region
Osteosarcoma (parosteal)[30,68,69]	16-19	Two percent of parosteal osteosarcomas occur in the radius and 1% occur in the ulna Osteosclerotic surface lesion of bone Large radiodense, oval, sessile mass with smooth or irregular margins Ossification begins centrally and progresses outward, opposite that of benign heterotopic bone formation (myositis ossification)
Giant cell tumor (aggressive)[31]	16-20	Approximately 4% of aggressive giant cell tumors occur in the distal portion of the radius Eccentrically located, subarticular osteolytic lesion extending into the metaphysis Cortical destruction and soft tissue mass are variable findings Radiographic appearance is an inaccurate guide to determining malignancy of lesion; biopsy is necessary
Ewing sarcoma[32]	16-21	Two percent of Ewing sarcomas occur in the radius and 1% occur in the ulna Permeative or moth-eaten osteolysis, aggressive cortical erosion or violation, laminated or spiculated periostitis, and soft tissue masses Most lesions central and diametaphyseal in location
Myeloproliferative disorders		
Plasma cell (multiple) myeloma[33]	16-22	Approximately 4% of multiple myeloma lesions occur in the radius and 1% occur in the ulna *Early:* normal radiographs or diffuse osteopenia *Later:* widespread, well-circumscribed osteolytic lesions with discrete margins, which appear uniform in size Ninety-seven percent osteolytic; 3% osteoblastic False-negative bone scans common
Primary lymphoma (non-Hodgkin)[34]	16-23	Approximately 2% of lesions in cases of primary lymphoma occur in the ulna Multiple moth-eaten or permeative osteolytic lesions Diffuse or localized sclerotic lesions are rare Common cause of pathologic fracture
Leukemia[35]	16-24	Radius and ulna occasionally involved Diffuse osteopenia, radiolucent or radiodense transverse metaphyseal bands, osteolytic lesions, periostitis, and, infrequently, osteosclerosis Radiodense metaphyses more frequent in patients undergoing chemotherapy for leukemia: may resemble lead poisoning

Continued

TABLE 16-4 Tumors Affecting the Radius and Ulna—cont'd

Tumor	Figure(s)	Characteristics
Benign Neoplasms of Bone		
Osteoid osteoma[36]		Three percent of osteoid osteomas occur in the ulna and 1% occur in the radius Cortical or subperiosteal lesion with reactive sclerosis surrounding central radiolucent nidus Nidus less than 1 cm in diameter and usually not visible on routine radiographs Intracapsular lesions provoke less reactive sclerosis and are more likely to cause joint pain
Osteoblastoma (conventional)[37]		Two percent of conventional osteoblastomas involve the ulna; 1% involve the radius Osteolytic, osteosclerotic, or both Expansile lesion that may be subperiosteal Partially calcified matrix in many cases Cortical thinning Often resembles large osteoid osteoma
Enchondroma (solitary)[38]		Approximately 2% of solitary enchondromas involve the radius; fewer than 1% involve the ulna Solitary, central or eccentric, medullary osteolytic lesion Lobulated endosteal scalloping Approximately 50% have stippled calcification within the matrix
Enchondromatosis (Ollier disease)[38]		Multiple enchondromas Occasionally involves the radius and ulna
Maffucci syndrome[38]		Radius and ulna are involved in more than 40% of cases of Maffucci syndrome Multiple enchondromas and soft tissue hemangiomas Unilateral distribution in 50% of cases
Osteochondroma (solitary)[39,40]	16-25	One percent of solitary osteochondromas arise from the radius and ulna Pedunculated or sessile cartilage-covered osseous excrescence arising from the surface of the metaphysis Cortex and medulla are continuous with the host bone May occur spontaneously or after accidental or iatrogenic injury Typically grow away from the adjacent joint *Complications:* pathologic fracture, and malignant transformation (fewer than 1% of cases)
Hereditary multiple exostosis[41,42]	16-26	Occasional involvement of bones of forearm Proximal or distal metaphyses may be involved Frequently results in Madelung deformity May result in malignant transformation (fewer than 5% of cases)
Nonossifying fibroma and fibrous cortical defect[43]	16-27	Nonossifying fibromas favor the lower extremity and infrequently occur in the radius or ulna Eccentric, multiloculated osteolytic lesion arising from the metaphyseal cortex Resemble a well-circumscribed, blisterlike shell of bone arising from the cortex Cortical thinning often is present Eventually disappear, filling in with normal bone Nonossifying fibromas are typically larger than fibrous cortical defects

TABLE 16-4 Tumors Affecting the Radius and Ulna—cont'd

Tumor	Figure(s)	Characteristics
Giant cell tumor (benign)[31]	16-28	Approximately 10% of benign giant cell tumors occur in the radius and 3% occur in the ulna Eccentric osteolytic neoplasm with a predilection for the subarticular region of the distal end of the radius Often multiloculated and expansile Radiographs are inaccurate in distinguishing benign from aggressive giant cell tumors
Intraosseous lipoma[44]		Fewer than 2% of intraosseous lipomas occur in the ulna; infrequently occur in the radius Osteolytic lesion surrounded by a thin, well-defined sclerotic border Central calcified or ossified nidus is common Occasional osseous expansion Cortical destruction and periostitis absent
Hemangioma (solitary)[45]	16-29	Rare in the radius and ulna Radiolucent, slightly expansile intraosseous lesion Radiating, latticelike or weblike trabecular pattern Occasional cortical thinning Rarely periostitis, soft tissue mass, or osteosclerosis Intracortical and periosteal forms of hemangioma are extremely rare
Aneurysmal bone cyst[46]	16-30	Four percent of aneurysmal bone cysts occur in the ulna and 3% occur in the radius Eccentric, thin-walled, expansile, osteolytic, metaphyseal lesion of the humeral metaphysis Thin trabeculation with multiloculated appearance Buttressing at edge of lesion
Tumorlike Lesions of Bone		
Paget disease[47,48,70,71]	16-31	Radius and ulna are rarely involved in Paget disease Usually polyostotic and may have unilateral involvement Coarsened trabeculae and bone enlargement Diaphyseal and metaphyseal involvement with extension into epiphysis Stages of involvement; osteolytic (50%), osteosclerotic (25%), and mixed (25%), malignant transformation (less than 2%) Bowing deformities occur frequently
Monostotic fibrous dysplasia[49]	16-32	Monostotic involvement of the radius or ulna is rare Thick rim of sclerosis surrounding a radiolucent lesion Ground-glass appearance of fibrous matrix
Polyostotic fibrous dysplasia[49]		Thirty percent to 40% of patients have lesions in the radius or ulna Unilateral or bilateral, asymmetric involvement Lesions appear the same as monostotic form but are frequently larger, more expansile, and more multiloculated than monostotic lesions
Langerhans cell histiocytosis[50,51]		Radius is involved in about 3% of cases; ulna rarely involved Osteolytic lesions may be multiloculated and expansile Eosinophilic granuloma is the most frequent and mildest form of this disorder

See also Tables 1-12 to 1-14.

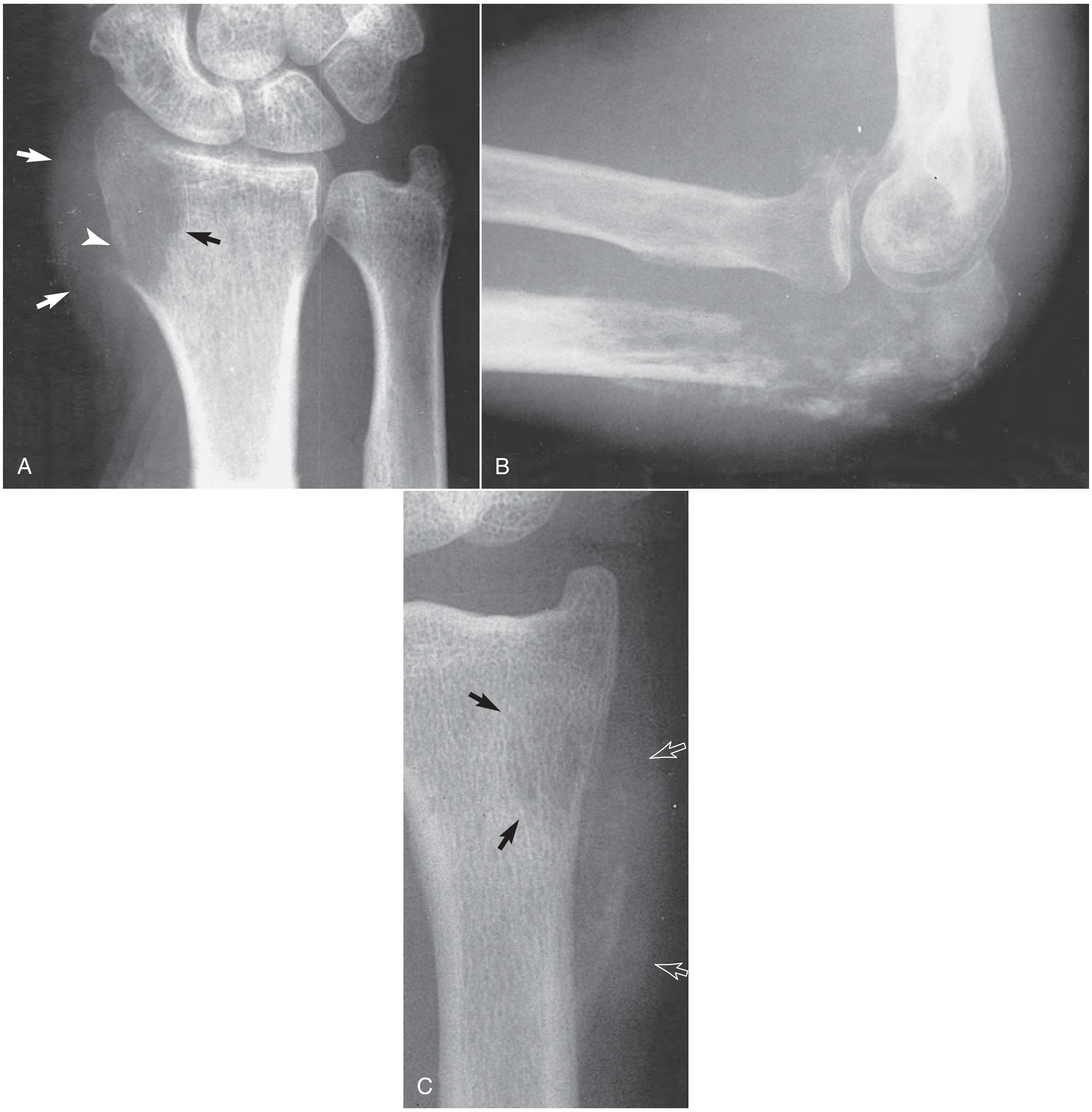

FIGURE 16–18 Skeletal metastasis.[27,28] **A,** This 63-year-old man with bronchogenic carcinoma developed wrist pain. A radiograph of the wrist reveals permeative osteolysis *(black arrow),* cortical perforation *(white arrowhead),* and a soft tissue mass *(white arrows)*. **B,** In another patient with bronchogenic carcinoma, severe, permeative osteolytic destruction of bone is accompanied by prominent soft tissue swelling overlying the proximal portion of the ulna. **C,** This 23-year-old man had pain and swelling over the distal ulna. He reported having had a "skin cyst" removed several years previously. A radiograph of the ulna shows a moth-eaten or permeative destructive lesion with osteolysis of the distal portion of the ulna *(arrows)* and associated periosteal proliferation and soft tissue swelling *(open arrows)*. At this time, no other osseous lesions were identified, and a preoperative diagnosis of a primary malignant tumor, probably Ewing sarcoma, was made. The patient underwent surgery that revealed a lesion containing melanin. The histologic evaluation showed malignant melanoma. The patient developed widespread skeletal metastasis within months. Periosteal reaction and involvement of bone beyond the elbow or knee are seen more commonly with primary malignant tumors and are infrequent findings in cases of skeletal metastasis.

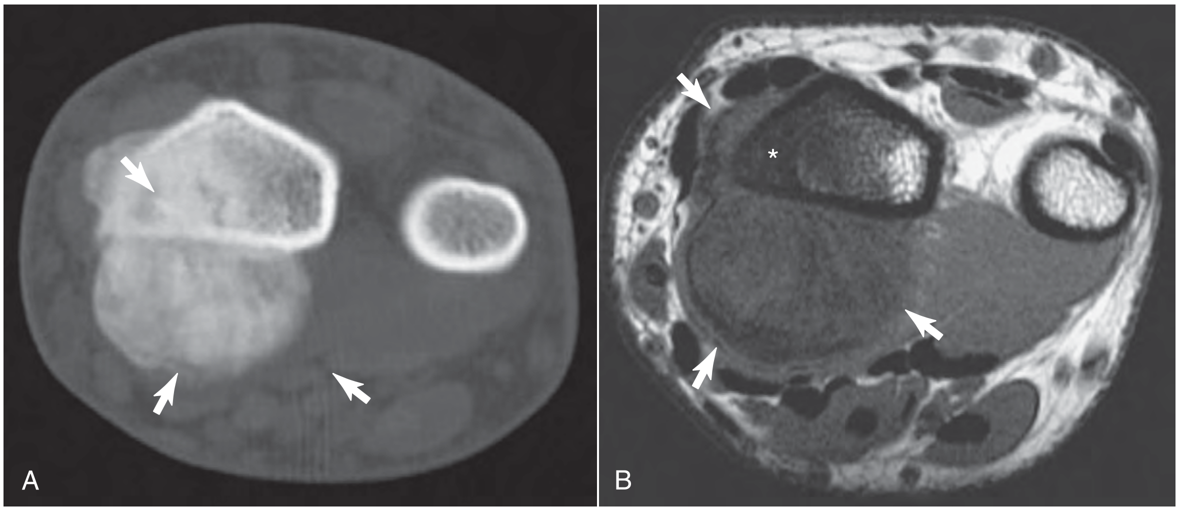

FIGURE 16–19 Parosteal osteosarcoma.[30,68,69] This 20-year-old man has a painful lump on his forearm. A transaxial CT scan, bone window **(A)** shows a large radiodense osseous mass arising from the volar and lateral cortical surfaces of the radius *(arrows)*. Increased radiodensity is also evident in the medullary cavity (*). The mass is seen as a low signal intensity bony protrusion *(arrows)* on a transverse T1-weighted MR image **(B).** The bone marrow of the radius also exhibits low signal intensity (*) corresponding with the increased density on the CT scan.

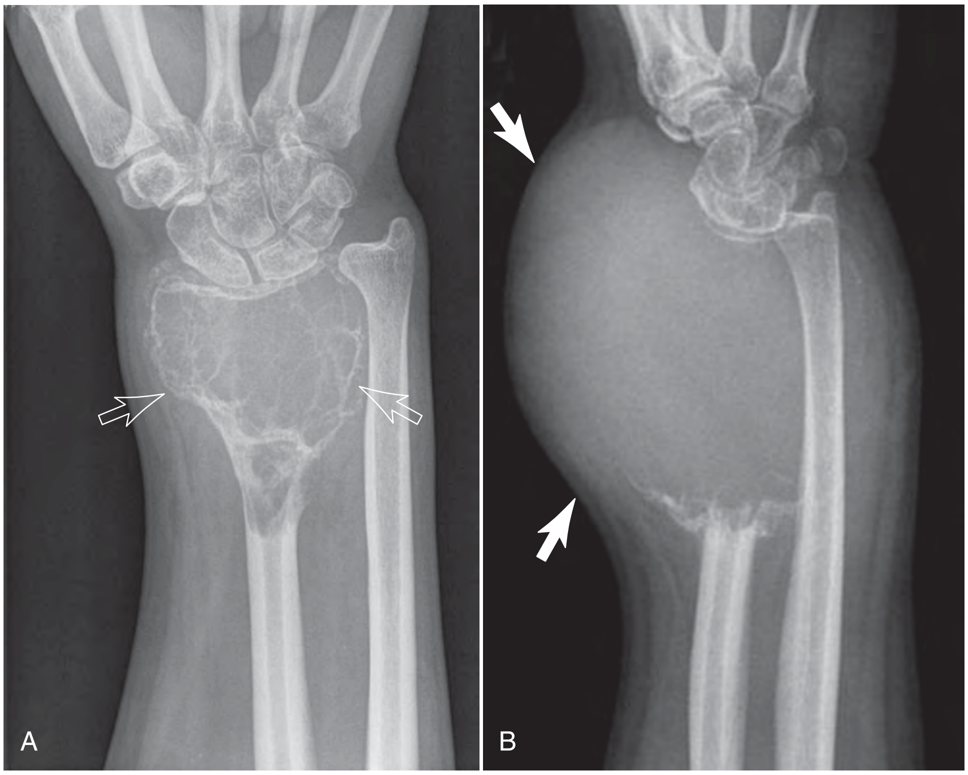

FIGURE 16–20 Aggressive giant cell tumor.[31] This 28-year-old woman presented with a painful enlarging mass on her forearm, just proximal to the wrist. The earlier radiograph **(A)** shows a multiloculated expansile lesion *(open arrows)* involving the distal metaphysis and subarticular region of the radius. The carpal bones exhibit disuse osteopenia and the radius appears shortened with respect to the ulna. A second radiograph obtained 5 months later **(B)** shows extensive permeative destruction of the entire end of the radius that has been replaced with a huge soft tissue mass *(arrows)*. The patient underwent a resection and fibular bone graft.

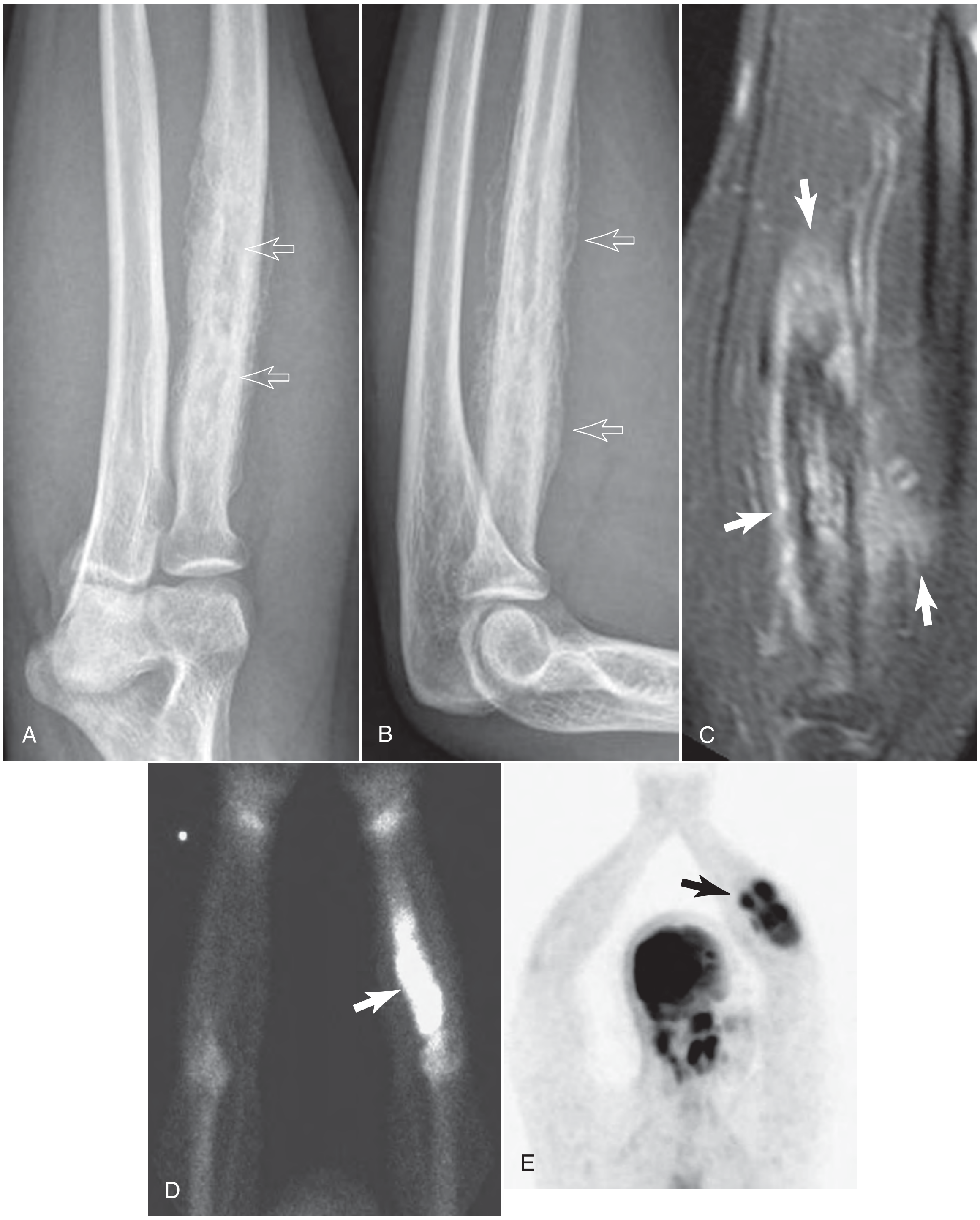

FIGURE 16–21 Ewing sarcoma: conventional radiography and radionuclide studies.[32] **A-B,** Radiographs of this 15-year-old boy with forearm pain show moth-eaten destruction with an irregular aggressive multilamellar periosteal reaction involving the proximal diaphysis of the radius *(open arrows)*. A coronal T1-weighted image **(C)** reveals high signal intensity enhancement of the marrow cavity and adjacent soft tissues *(arrows)* after intravenous gadolinium administration. A bone scan **(D)** shows an intense accumulation of radioisotope in the left forearm *(arrow)*. A positron emission tomography (PET) scan **(E)** using 18-fluorodeoxyglucose (FDG) shows increased uptake in the proximal portion of the radius *(arrow)* indicating increased metabolic turnover that uses glucose as the metabolite. (Increased uptake in the brain reflects normal metabolic activity.)

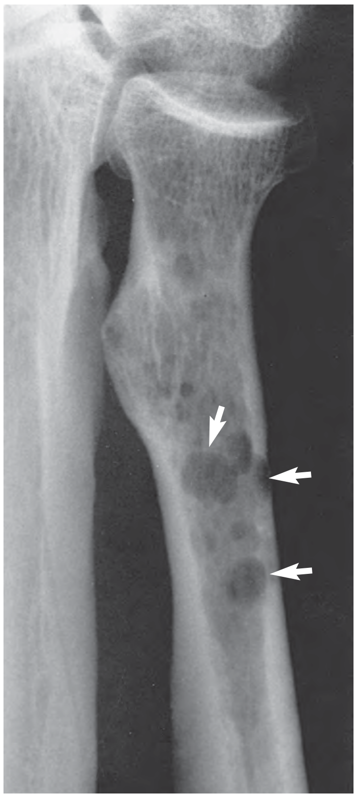

FIGURE 16–22 Plasma cell (multiple) myeloma.[33] This patient is a 60-year-old man. Multiple, well-circumscribed osteolytic lesions are evident in the proximal portion of the radius *(arrows)*. Diffuse involvement of several sites throughout the skeleton was observed.

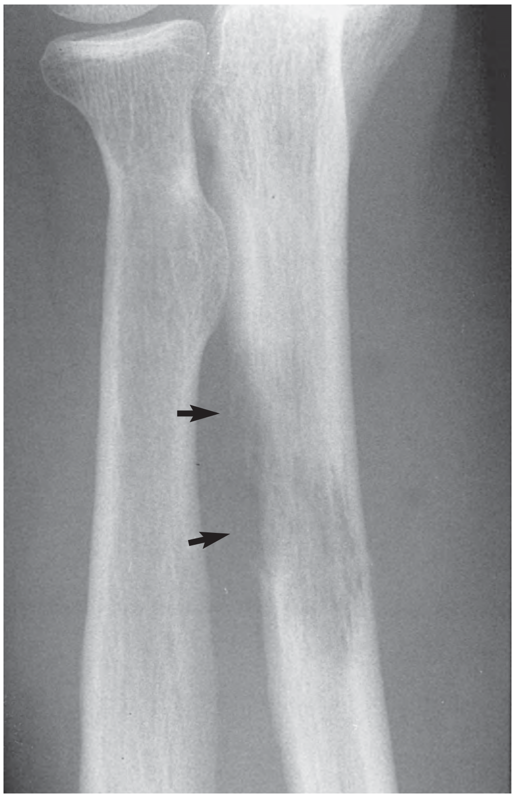

FIGURE 16–23 Lymphoma.[34] Observe the moth-eaten and permeative osteolysis with cortical perforation *(arrows)* involving the ulnar diaphysis of this 23-year-old man. Overall increased radiodensity of the ulna is also noted. The pathologic diagnosis was lymphoma, primary signet cell type. *(Courtesy T. Broderick, M.D., Orange, Calif.)*

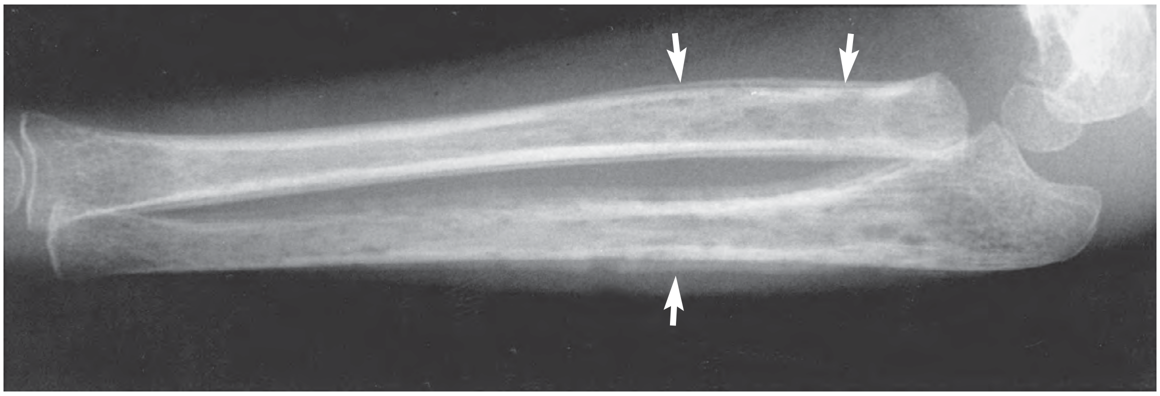

FIGURE 16–24 Acute childhood leukemia.[35] Permeative osteolysis with single layer periostitis *(arrows)* is seen throughout the radius and ulna of this child with leukemia. Radiographic changes in the skeleton occur in as many as 70% of persons with acute childhood leukemia.

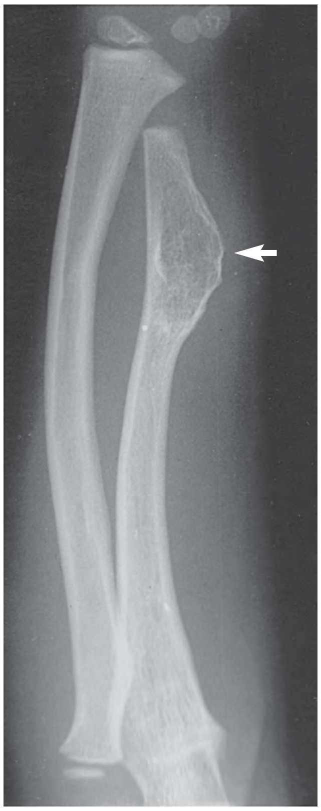

FIGURE 16–25 Solitary osteochondroma.[39,40] A sessile, expansile osseous outgrowth involving the distal ulnar metadiaphysis *(arrow)* is present in this 4-year-old boy with a short ulna (reverse Madelung deformity). The cortex overlying the lesion is intact, and no evidence of periosteal reaction or soft tissue mass is present. The ulna is an unusual location for a solitary osteochondroma. *(Courtesy G. Greenway, M.D., Dallas.)*

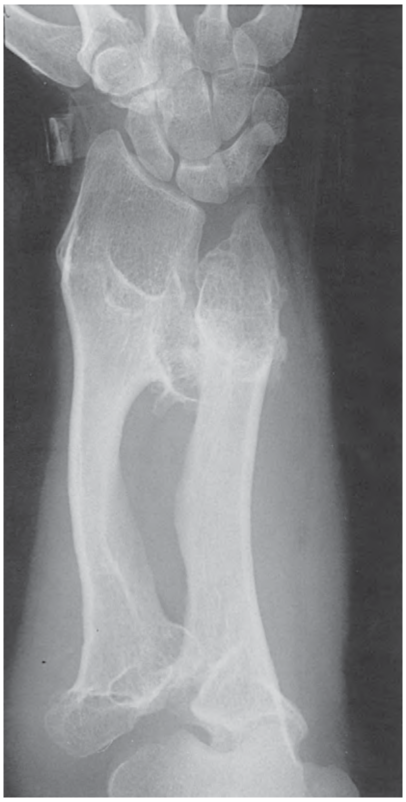

FIGURE 16–26 Hereditary multiple exostoses.[41,42] Marked deformity of the radius and ulna is seen with hereditary multiple exostoses. The abnormalities include bowing of the radius, metaphyseal osteochondromas, shortening of the ulna, and an angulated articular surface of the radius. *(Courtesy T. Broderick, M.D., Orange, Calif.)*

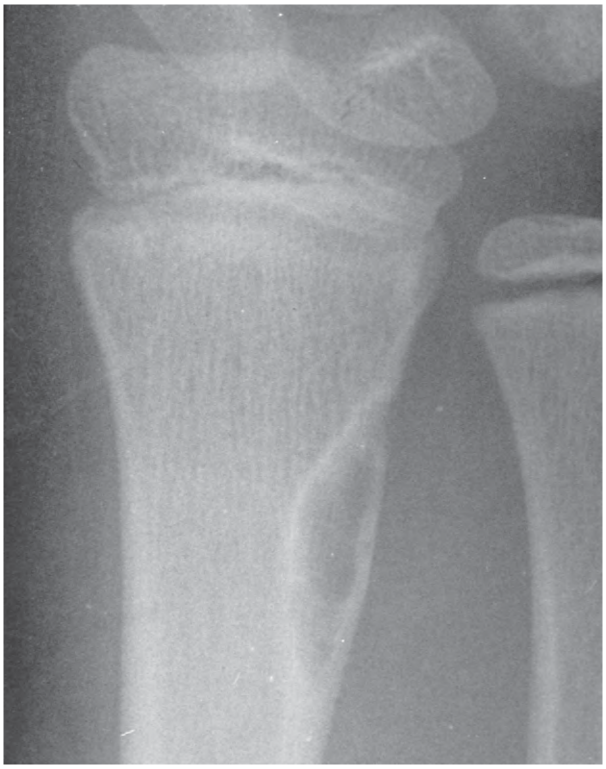

FIGURE 16–27 Nonossifying fibroma.[43] In this 11-year-old boy, an eccentric osteolytic lesion with a lobulated sclerotic margin is present in the metaphysis of the distal end of the radius.

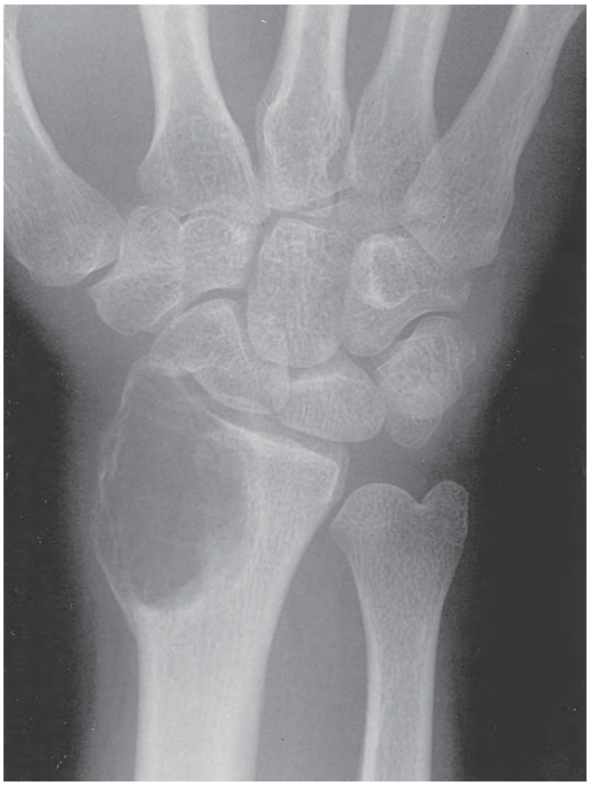

FIGURE 16–28 Giant cell tumor.[31] A radiograph of this 37-year-old man reveals an eccentric, osteolytic, geographic lesion extending into the subchondral region, producing cortical thinning and expansion and possessing a delicate trabecular pattern. Ten percent of giant cell tumors affect the radius. The radiographic appearance of the giant cell tumor is an inaccurate guide to the histologic composition and clinical behavior of the lesion. Benign lesions may appear aggressive and aggressive lesions may appear benign.

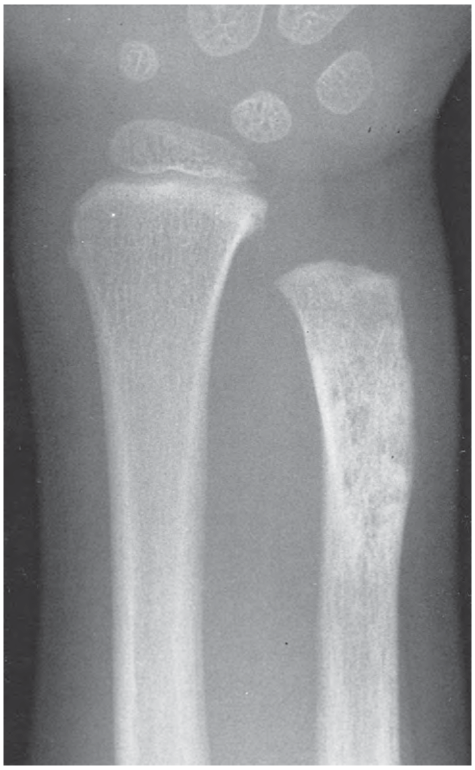

FIGURE 16–29 Hemangioma.[45] A radiograph of the forearm in this 5-year-old child shows a trabeculated lesion of the ulnar metadiaphysis. This benign hemangioma appears permeative and aggressive and should be considered possibly malignant until proved otherwise. The ulna is an extremely rare location for hemangioma.

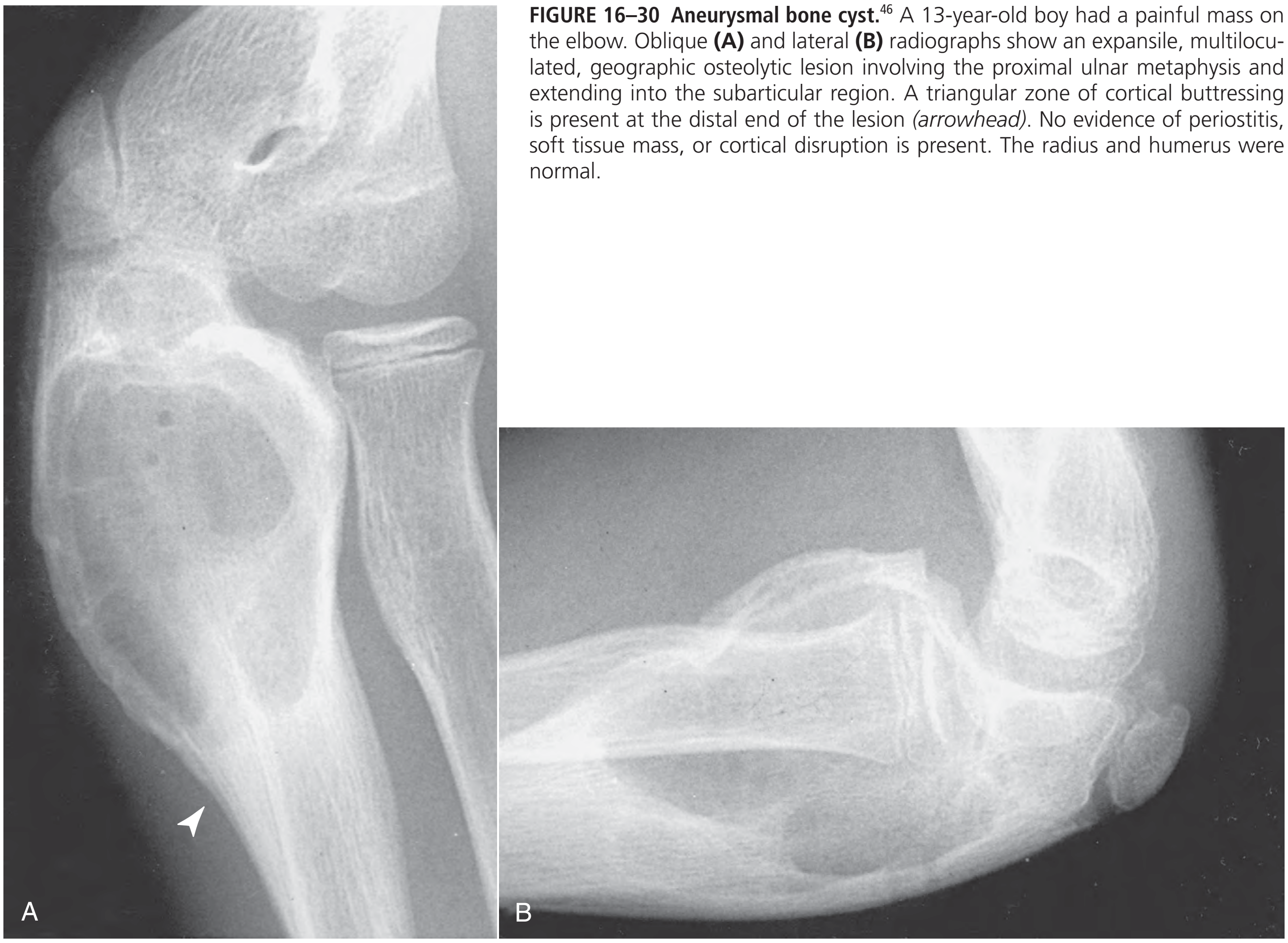

FIGURE 16–30 Aneurysmal bone cyst.[46] A 13-year-old boy had a painful mass on the elbow. Oblique **(A)** and lateral **(B)** radiographs show an expansile, multiloculated, geographic osteolytic lesion involving the proximal ulnar metaphysis and extending into the subarticular region. A triangular zone of cortical buttressing is present at the distal end of the lesion *(arrowhead)*. No evidence of periostitis, soft tissue mass, or cortical disruption is present. The radius and humerus were normal.

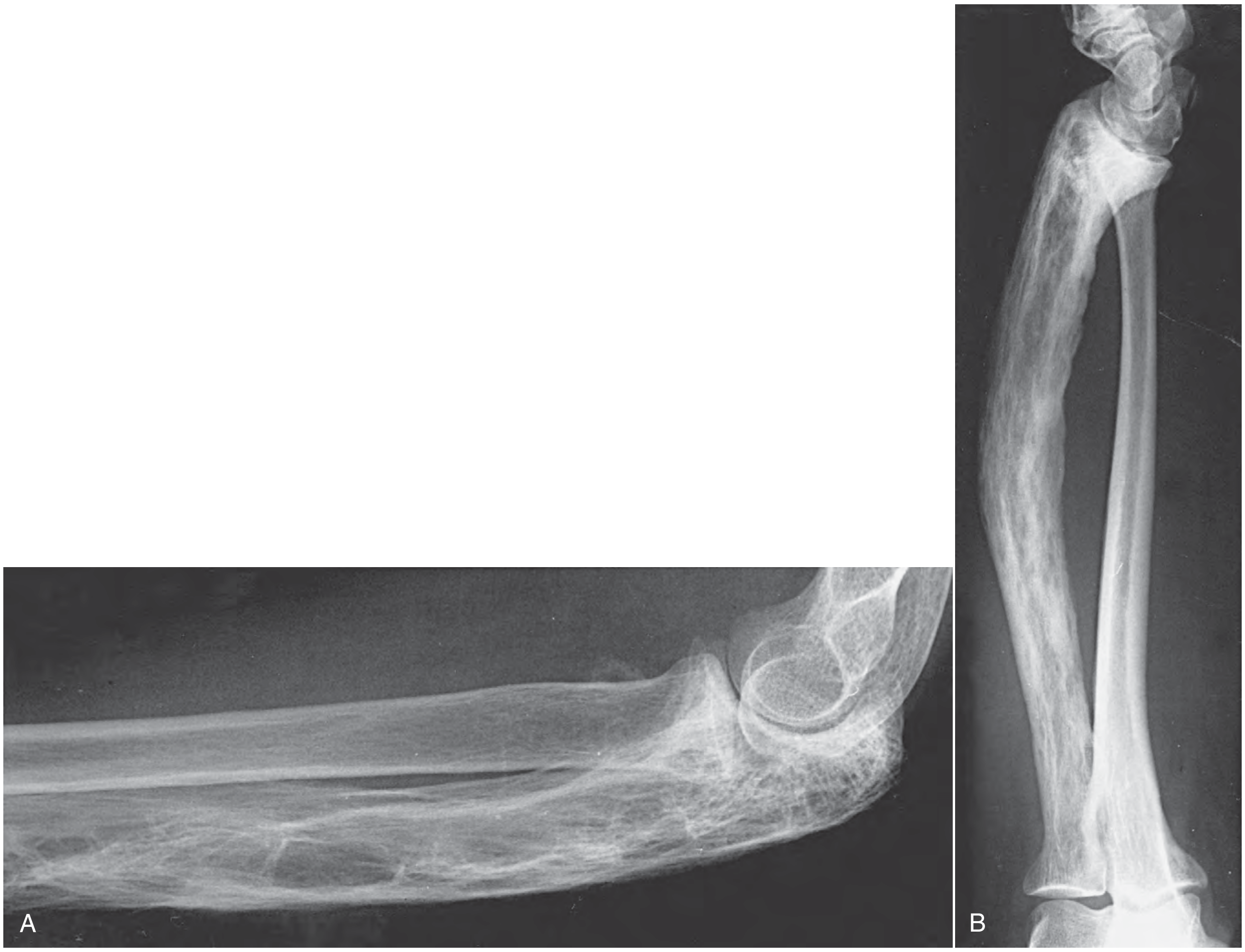

FIGURE 16–31 Paget disease.[47,48,70,71] **A,** Ulna. A combined pattern of osteolysis and osteosclerosis is evident. Note the characteristically coarsened trabeculae with combined areas of osteosclerotic bone and vacuous radiolucent regions. Also note the typical subchondral distribution of the bone changes. **B,** Radius. In another patient, observe the severe enlargement and bowing of the radius that often accompany this disease.

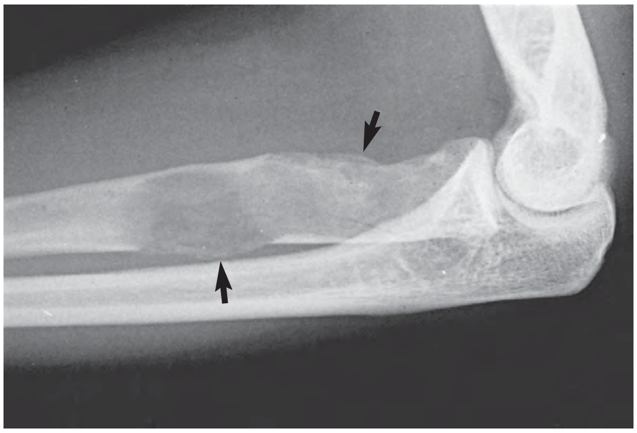

FIGURE 16–32 Monostotic fibrous dysplasia.[49] Endosteal thinning and a ground-glass appearance are noted in this slightly expansile metadiaphyseal lesion involving the proximal portion of the radius *(arrows). (Courtesy G. Bock, M.D., Winnipeg, Manitoba, Canada.)*

TABLE 16-5 Metabolic, Hematologic, and Infectious Disorders Affecting the Radius and the Ulna

Disorder	Figure(s)	Characteristics
Generalized osteoporosis[52,53]		Uniform decrease in radiodensity, thinning of cortices, accentuation of trabeculae *Osteoporosis predisposes to fractures of the distal end of the radius in elderly patients:* most common upper extremity fracture in patients with osteoporosis
Rickets[54,72]	16-33	Findings are most prominent in patients with chronic disease Metaphyseal demineralization resulting in frayed metaphyses Bowing deformities Osteopenia Looser zones
Osteomalacia[54,72]		Osteomalacia Diffuse osteopenia Decreased trabeculae; remaining trabeculae appear prominent and coarsened Looser zones (pseudofractures) rare in radius and ulna
Renal osteodystrophy and hyperparathyroidism[55-57]	16-34	*Brown tumor:* solitary or multiple expansile osteolytic lesions containing fibrous tissue and giant cells; may disappear after treatment for hyperparathyroidism Osteosclerosis more common in renal osteodystrophy Rickets-like physeal changes in patients with chronic renal disease
Primary hypertrophic osteoarthropathy (pachydermoperiostosis)[58]	16-35	Primary form of hypertrophic osteoarthropathy (3 to 5% of all cases of hypertrophic osteoarthropathy) Bilateral symmetric periostitis of the long tubular bones *Clinical syndrome:* enlargement of the hands and feet, digital clubbing, convexity of the nails, cutaneous abnormalities, and joint pains
Secondary hypertrophic osteoarthropathy[58]	16-36	Bilateral symmetric periostitis of radius and ulna as well as other tubular bones Syndrome characterized by digital clubbing, arthritis, and bilateral symmetric periostitis of radius, ulna, and other tubular bones Complication of many diseases including bronchogenic carcinoma, mesothelioma and other intrathoracic and intraabdominal diseases
Lead poisoning[59,60]	16-37	Prolonged ingestion, inhalation, or absorption of lead-containing materials Thick transverse radiodense metaphyseal lines in infants and children Similar radiodense lines may also be seen in the metaphyses, iliac crest, and vertebral bodies of adults Delayed skeletal development
Hemophilic pseudotumor[61,62]	16-38	Massive periosteal or intraosseous hemorrhage results in an expanded radiolucent pseudotumor Well-defined osteolytic lesion within radius, ulna, or other bones
Acute pyogenic osteomyelitis[63,66,67]	16-39	Acute pyogenic osteomyelitis frequently involves the metaphysis in children Poorly defined permeative bone destruction and soft tissue swelling
Chronic recurrent multifocal osteomyelitis (CRMO)[64]	16-40	Unknown cause This unusual entity is controversial—not certain whether it is truly infectious in nature Occurs mainly in children and adolescents Radiographic findings suggest acute or subacute osteomyelitis Initial osteolytic destruction of metaphysis adjacent to growth plate with no periosteal bone formation or sequestration May be associated with pustular skin lesions (synovitis-acne-pustulosis-hyperostosis-osteomyelitis [SAPHO] syndrome) Typically causes significant symptoms but regresses without residual change
Collagen vascular disease: soft tissue calcification[65]	16-41	Dermatomyositis, polymyositis, scleroderma, and other collagen vascular diseases may result in calcinosis in the soft tissues of the upper arm *Differential diagnosis:* hyperparathyroidism, neurologic injury, melorheostosis, posttraumatic heterotopic ossification, soft tissue neoplasms, fibrodysplasia ossificans progressiva

See also Tables 1-15 to 1-19.

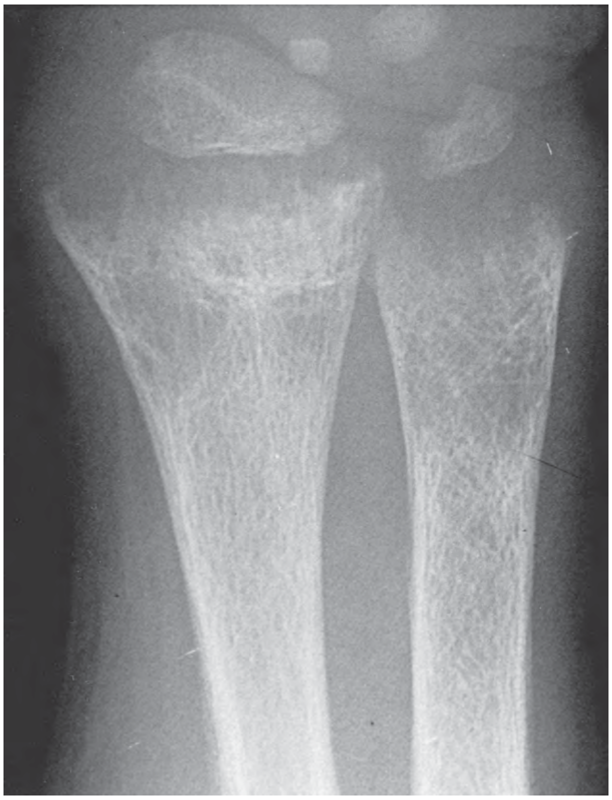

FIGURE 16–33 Rickets.[54] Physeal widening, metaphyseal disorganization, irregularity, and demineralization are characteristic findings in children with advanced rickets.

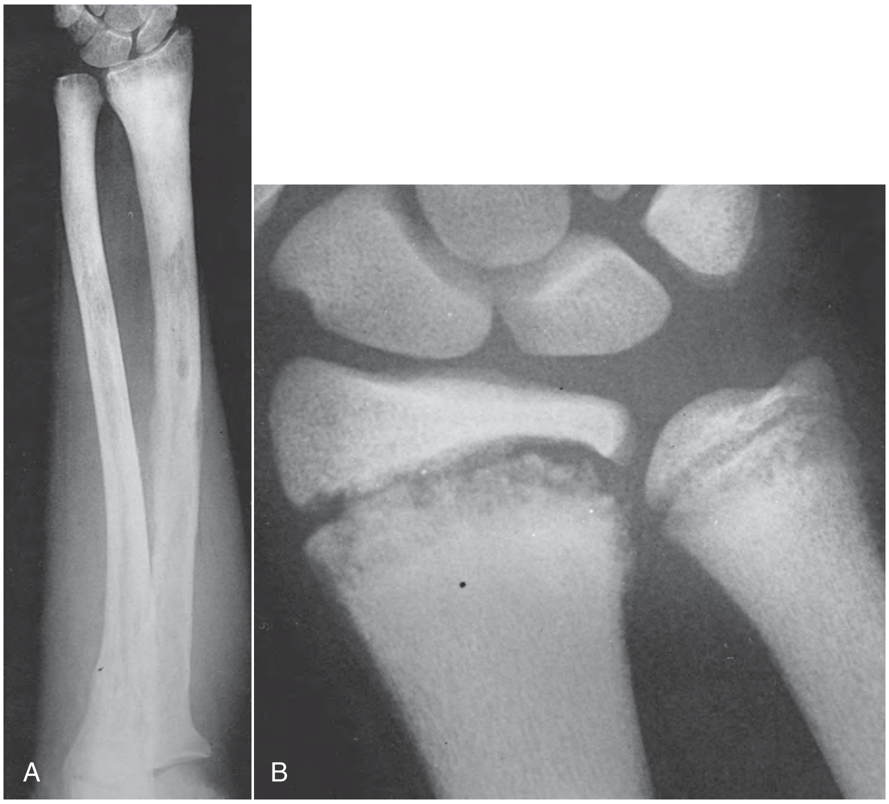

FIGURE 16–34 Renal osteodystrophy.[55-57] **A,** Osteosclerosis. Extensive osteosclerosis of the diaphysis and metaphysis of the radius and ulna are present in this patient with chronic renal disease. **B,** In a 15-year-old boy, observe the generalized osteosclerosis with widening and irregularity of the physes of the distal ends of the radius and ulna. These rickets-like physeal abnormalities, often seen in children with chronic renal disease, are associated with subphyseal bone resorption, and could relate to hyperparathyroidism alone or in combination with rickets. *(**A,** Courtesy L. Cooperstein, M.D., Pittsburgh, Penn.)*

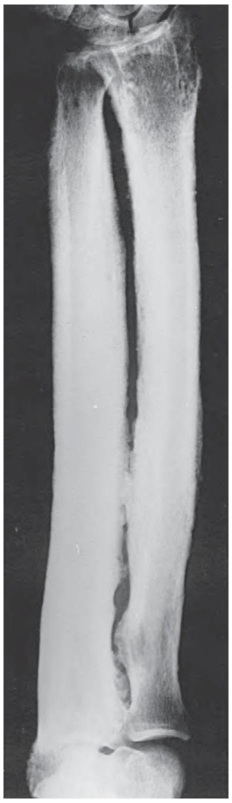

FIGURE 16–35 Primary hypertrophic osteoarthropathy: pachydermoperiostosis.[58] Widespread, prominent periostitis affects the radius and ulna. The findings in this patient were bilateral and symmetric and involved several tubular bones throughout the skeleton. *(Courtesy C. Chen, M.D., Kaohsiung, Taiwan, Republic of China.)*

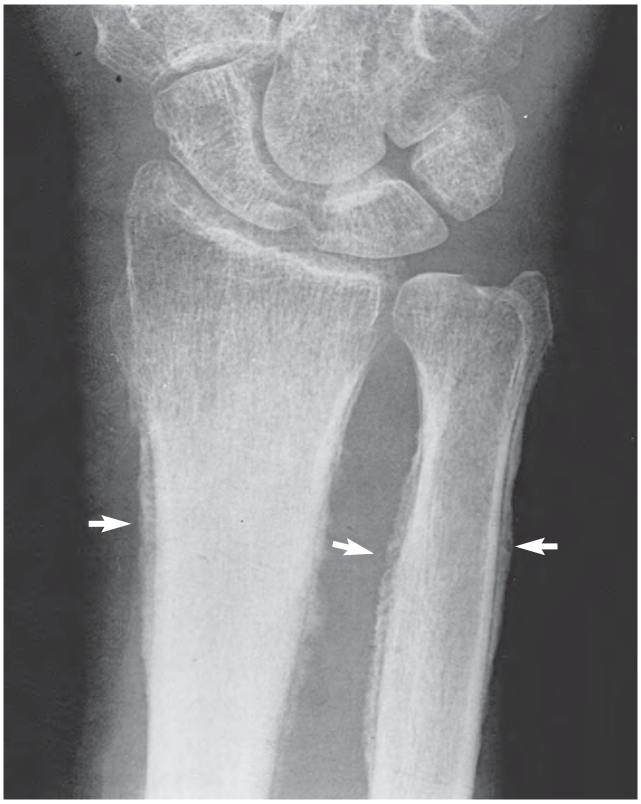

FIGURE 16–36 Secondary hypertrophic osteoarthropathy.[58] Radial and ulnar periostitis *(arrows)* is seen in this patient with bronchogenic carcinoma. The findings were bilateral and symmetric, and also involved the tubular bones of the lower extremities.

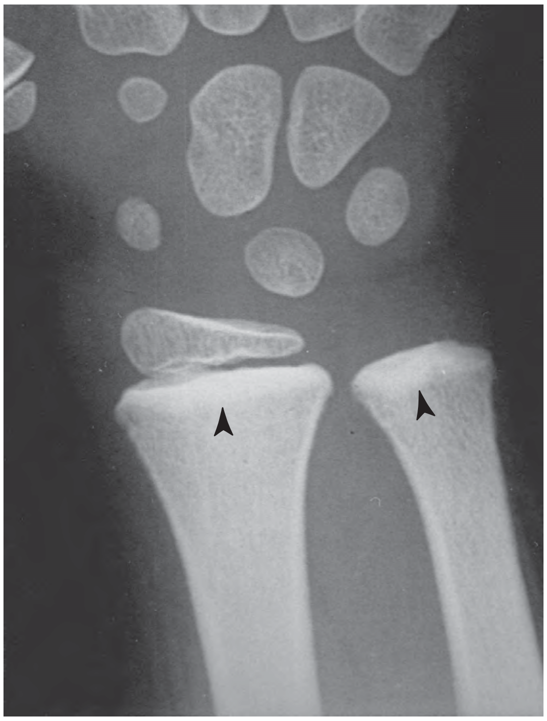

FIGURE 16–37 Lead poisoning.[59,60] This 6-year-old boy had been eating paint for 1 year when this radiograph was obtained. Observe the transverse sclerotic bands within the metaphyses of the radius and ulna *(arrowheads)*. These changes were present bilaterally. Other causes of metaphyseal density are treated rickets, scurvy, hypoparathyroidism, and hypervitaminosis A or D.

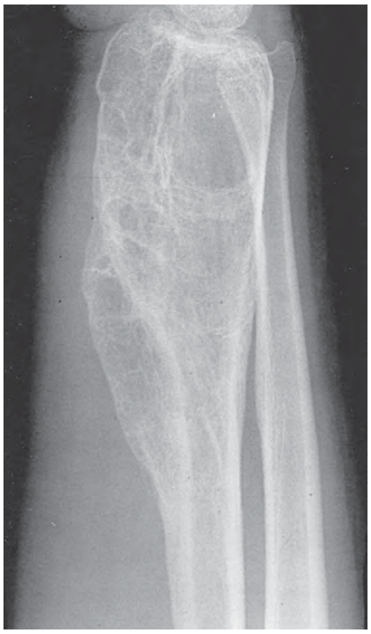

FIGURE 16–38 Hemophilia: pseudotumor.[61,62] A large multiloculated, expansile osteolytic lesion extending from the middiaphysis to the epiphysis of the radius in this 19-year-old man represents a pseudotumor that accompanies intraosseous or periosteal bleeding in hemophilia. This lesion also resembles an aneurysmal bone cyst or giant cell tumor. *(Courtesy A. Brower, M.D., Norfolk, Va.)*

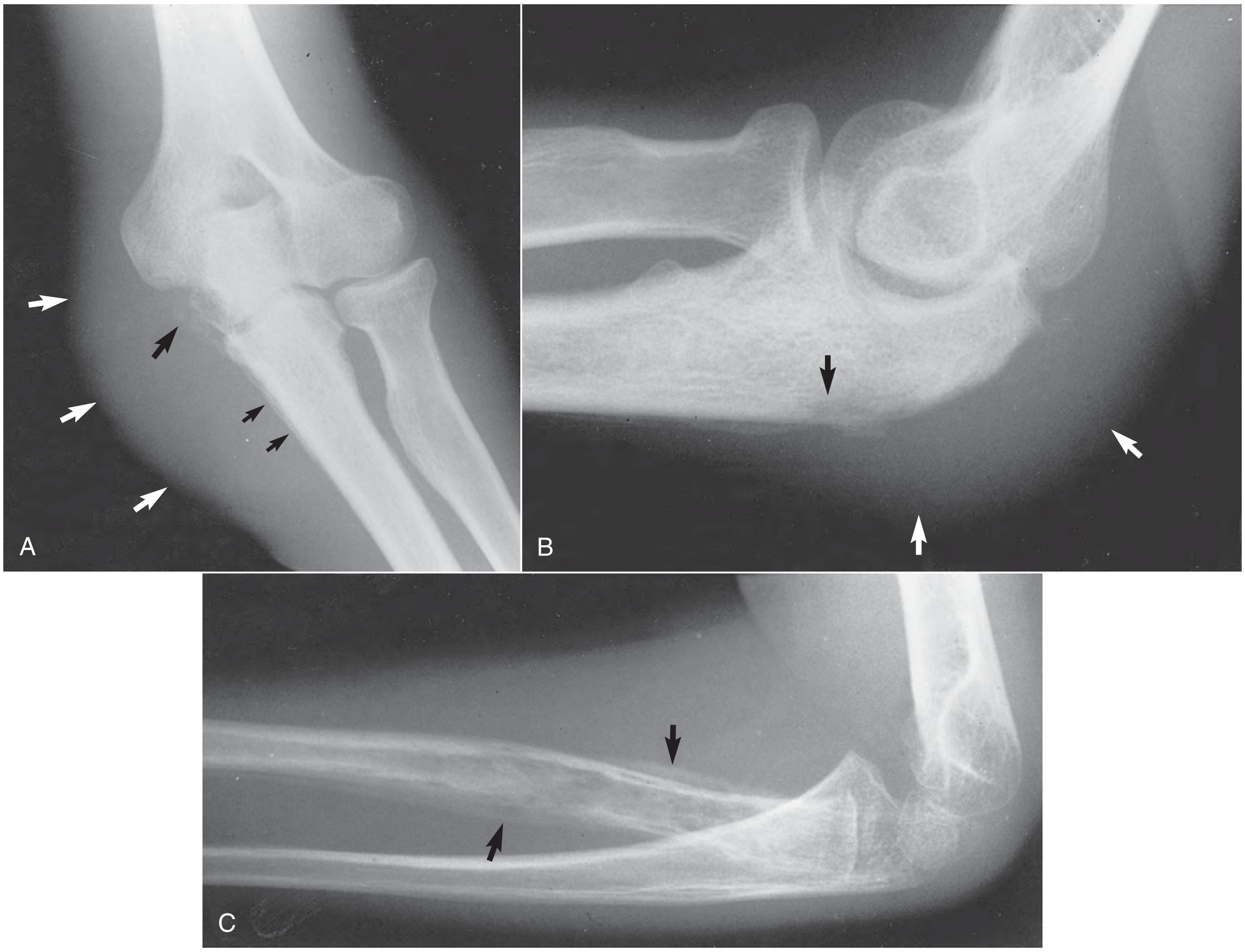

FIGURE 16–39 Acute pyogenic osteomyelitis.[63,66,67] **A-B,** This 23-year-old man complained of pain and swelling about the elbow and forearm. Frontal **(A)** and lateral **(B)** radiographs of the elbow show marked soft tissue swelling *(white arrows)* and diffuse sclerosis of the proximal portion of the ulna, prominent osseous erosions of the medial olecranon *(large black arrows),* and periostitis *(small black arrows)*. **C,** In another patient, a child, a permeative pattern of osteolytic destruction and single-layer periostitis *(arrows)* is evident in the radius.

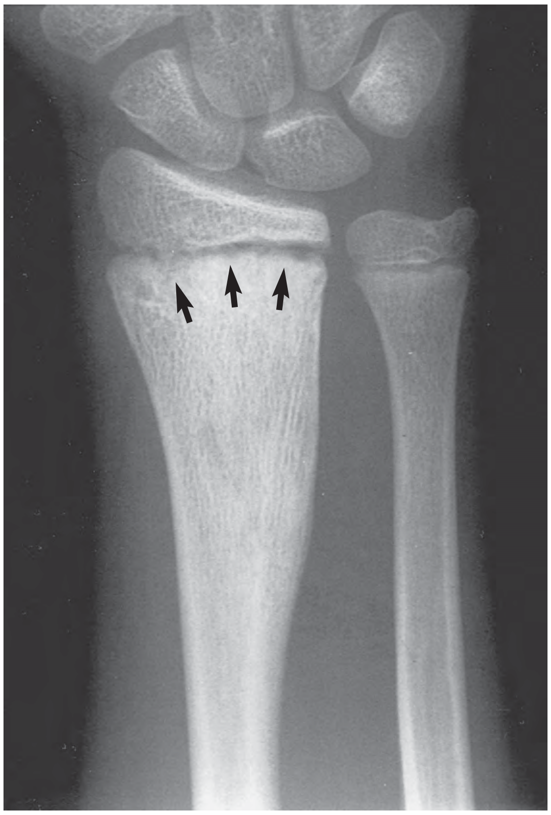

FIGURE 16–40 Chronic recurrent multifocal osteomyelitis.[64] This 12-year-old boy had unilateral wrist pain and swelling of 12 months' duration. Eight months after the wrist pain subsided, he developed unilateral ankle pain and swelling. The erythrocyte sedimentation rate was slightly elevated, but all other serologic test results were normal. Radiographs revealed similar changes in both locations. The findings include striking metaphyseal sclerosis, periosteal bone expansion, and subchondral osteolysis of the metaphysis adjacent to the growth plate *(arrows)*. *(Courtesy S. Cassell, M.D., Eugene, Ore.)*

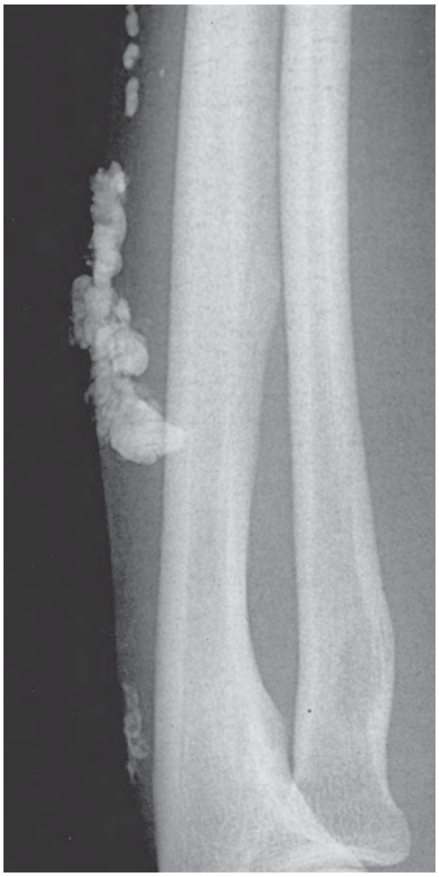

FIGURE 16–41 Scleroderma (progressive systemic sclerosis).[65] Globular masses of soft tissue calcification are seen adjacent to the dorsal surface of the ulna in this patient with long-standing scleroderma (progressive systemic sclerosis).

CHAPTER 17

Wrist and Hand

NORMAL DEVELOPMENTAL ANATOMY

A thorough understanding of normal developmental anatomy is essential for accurate interpretation of radiographs of the pediatric wrist and hand. Table 17-1 outlines the age of appearance and fusion of the primary and secondary ossification centers. Figure 17-1 illustrates examples of radiographs of children from 13 months to 15 years of age. Both the chronologic age and skeletal age are listed for each of these examples. These radiographs show the radiographic appearance of many important ossification centers and other developmental landmarks from infancy through adolescence. For precise assessment of skeletal age, the Greulich and Pyle atlas[1] or similar publications should be consulted.

Figure 17-2 shows the normal appearance of the phalangeal ungual tufts.

DEVELOPMENTAL ANOMALIES, ANATOMIC VARIANTS, AND SOURCES OF DIAGNOSTIC ERROR

The bones and soft tissues of the wrist and hand are frequent sites of anomalies, anatomic variations, and other sources of diagnostic error that may simulate disease and potentially result in misdiagnoses. Furthermore, many of these alterations may represent a component of a more complex developmental malformation syndrome or chromosomal abnormality. Table 17-2 and Figures 17-3 to 17-15 illustrate selected examples of some of the more common processes.

SKELETAL DYSPLASIAS AND OTHER CONGENITAL DISEASES

Table 17-3 outlines a number of the skeletal dysplasias and congenital disorders that may affect the wrist and hand. Figures 17-16 to 17-22 show the radiographic manifestations of some of these disorders.

PHYSICAL INJURY

Physical injury to the wrist and hand may result in a wide variety of fractures, dislocations, and soft tissue injuries. Table 17-4 and Figures 17-23 to 17-32 pertain to fractures and dislocations of the carpal bones. Table 17-5 and Figures 17-33 to 17-37 describe and illustrate the most common patterns of ligamentous instability of the wrist. Table 17-6 and Figures 17-38 to 17-45 refer to fractures and dislocations of the metacarpal bones and phalanges.

SOFT TISSUE DISORDERS

Several disorders of the soft tissues are encountered about the wrist and hand. Table 17-7 represents a list of some of the more frequently occurring conditions, some of which are illustrated in Figures 17-46 to 17-52.

ARTICULAR DISORDERS

The articulations of the wrist and hand are frequent target sites for degenerative, inflammatory, crystal induced, and infectious articular disorders. Table 17-8 outlines these diseases and their radiographic characteristics. Table 17-9 is a compartmental analysis emphasizing the target sites of joint involvement typical of some of the more common disorders. Figures 17-53 to 17-77 illustrate the typical radiographic manifestations of the most common articular disorders affecting this region.

TUMORS AND TUMORLIKE LESIONS

Malignant tumors of bone involve the bones of the hand and wrist much less frequently than benign tumors. Table 17-10 lists and characterizes these malignant neoplasms, many of which are illustrated in Figures 17-78 to 17-83. Table 17-11 describes benign tumors and tumorlike lesions that characteristically involve the bones of the wrist and hand. These are illustrated in Figures 17- 84 to 17-94.

METABOLIC, HEMATOLOGIC, VASCULAR, AND INFECTIOUS DISORDERS

Several metabolic, hematologic, vascular, and infectious disorders involve the bones of the wrist and hand and the surrounding soft tissue structures. Table 17-12 lists some of the more common disorders and describes their characteristics. Figures 17-95 to 17-107 illustrate the characteristic imaging findings of several of these disorders.

OSTEONECROSIS

Osteonecrosis of the bones about the wrist and hand may occur spontaneously or result from trauma or other predisposing factors. Table 17-13 discusses these disorders. Example of osteonecrosis of the lunate bone (Kienböck disease) and capitate bone are shown in Figures 17-108 and 17-109. Posttraumatic osteonecrosis of the scaphoid bone is illustrated earlier in the chapter (Figure 17-23, *D*).

ACQUIRED DEFORMITIES

Several well-recognized patterns of deformity occur about the wrist and hand. Most of these acquired deformities result from complications of inflammatory articular disorders or from physical injury. Table 17-14 describes a number of these deformities, many of which are illustrated throughout the chapter as they are manifested in several of the causative disorders.

PHALANGEAL RESORPTION

Table 17-15 lists the more common disorders that result in phalangeal resorption or acro-osteolysis and identifies the site of resorption characteristic of each disorder. Examples of phalangeal resorption are illustrated throughout the chapter as they characteristically appear in relation to many of the disorders. Figure 17-110 is a schematic diagram of the differential diagnosis of resorption.

SOFT TISSUE CALCIFICATION

Table 17-16 lists several disorders that result in soft tissue calcification about the terminal phalanges. Many examples of such calcification are illustrated throughout the chapter.

TABLE 17-1 **Wrist and Hand: Approximate Age of Appearance and Fusion of Ossification Centers[1-5] (Figures 17-1 and 17-2)**

Ossification Center	Primary or Secondary	No. of Centers	Age of Appearance*	Age of Fusion* (Years)
Wrist				
Capitate	P	1	Birth to 6 months	
Hamate	P	1	Birth to 6 months	
Triquetrum	P	1	1-3.5 years	
Lunate	P	1	1.5-4.5 years	
Navicular	P	1	3-9 years	
Trapezium	P	1	3-9 years	
Trapezoid	P	1	3-9 years	
Pisiform	P	1	7-13 years	
Distal radial epiphysis	S	1	6-24 months	20-25
Distal ulnar epiphysis	S	1	5.5-9.5 years	19-25
Hand				
Metacarpal heads (second through fifth)	S	4	10-24 months	14-21
Metacarpal base (first)	S	1	1-3.5 years	14-21
Phalangeal bases (second through fifth)	S	4	1-2.5 years	14-21
Phalangeal bases (first)	S	1	1-2.5 years	14-21

* Ages of appearance and fusion of ossification centers in girls typically precede those of boys. Ethnic differences also exist.
P, Primary; *S*, secondary.

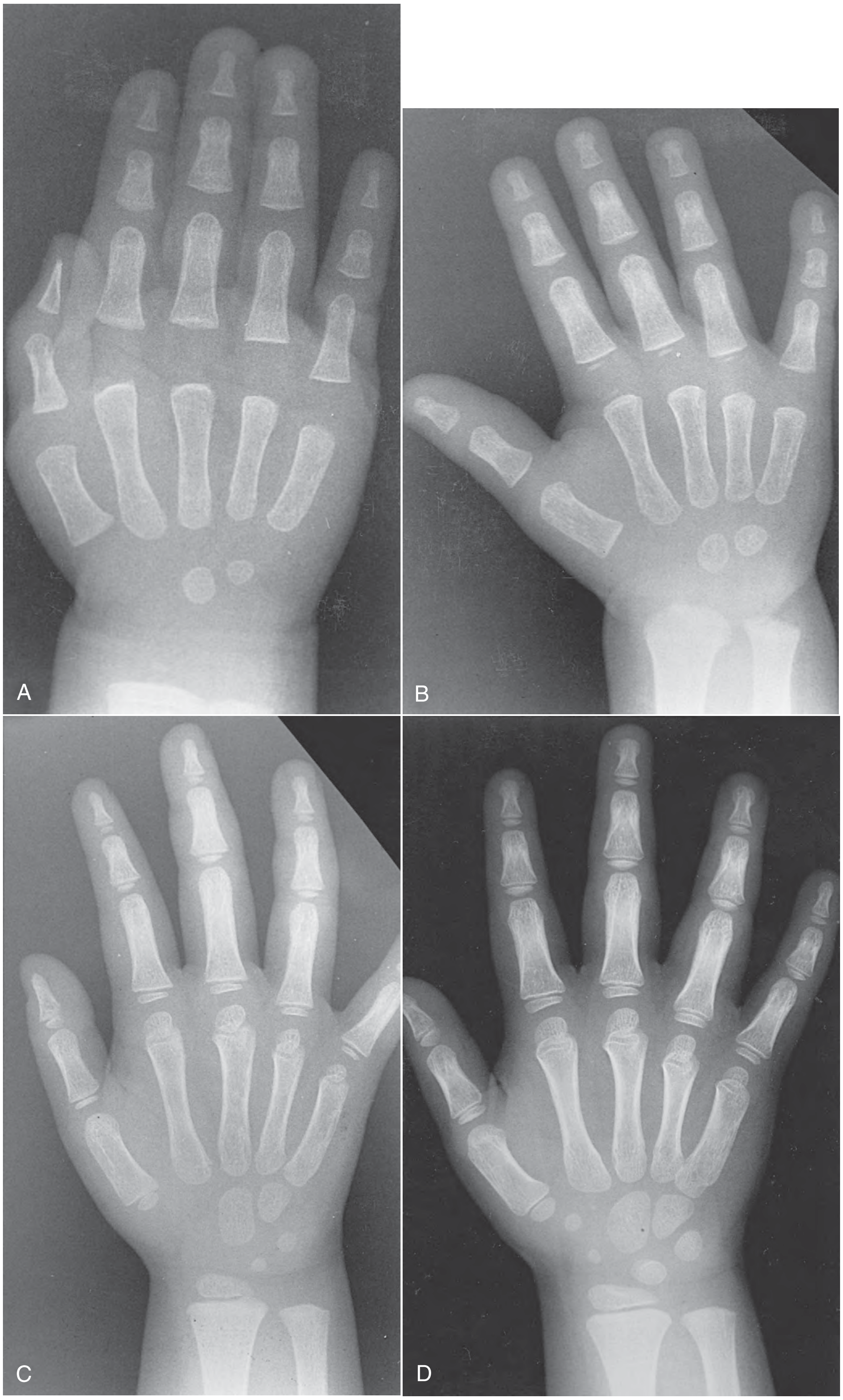

FIGURE 17–1 **Skeletal maturation and normal development: posteroanterior radiographs of the hand and wrist.**[1-5] **A,** Male; CA = 13 mo; SA = 15 mo; SD ± 2.1. **B,** Male; CA = 20 mo; SA = 18 mo; SD ± 2.7. **C,** Female; CA = 3 yr; SA = 3 yr; SD ± 6.0. **D,** Female; CA = 4 yr 5 mo; SA = 4 yr; SD ± 7.0.

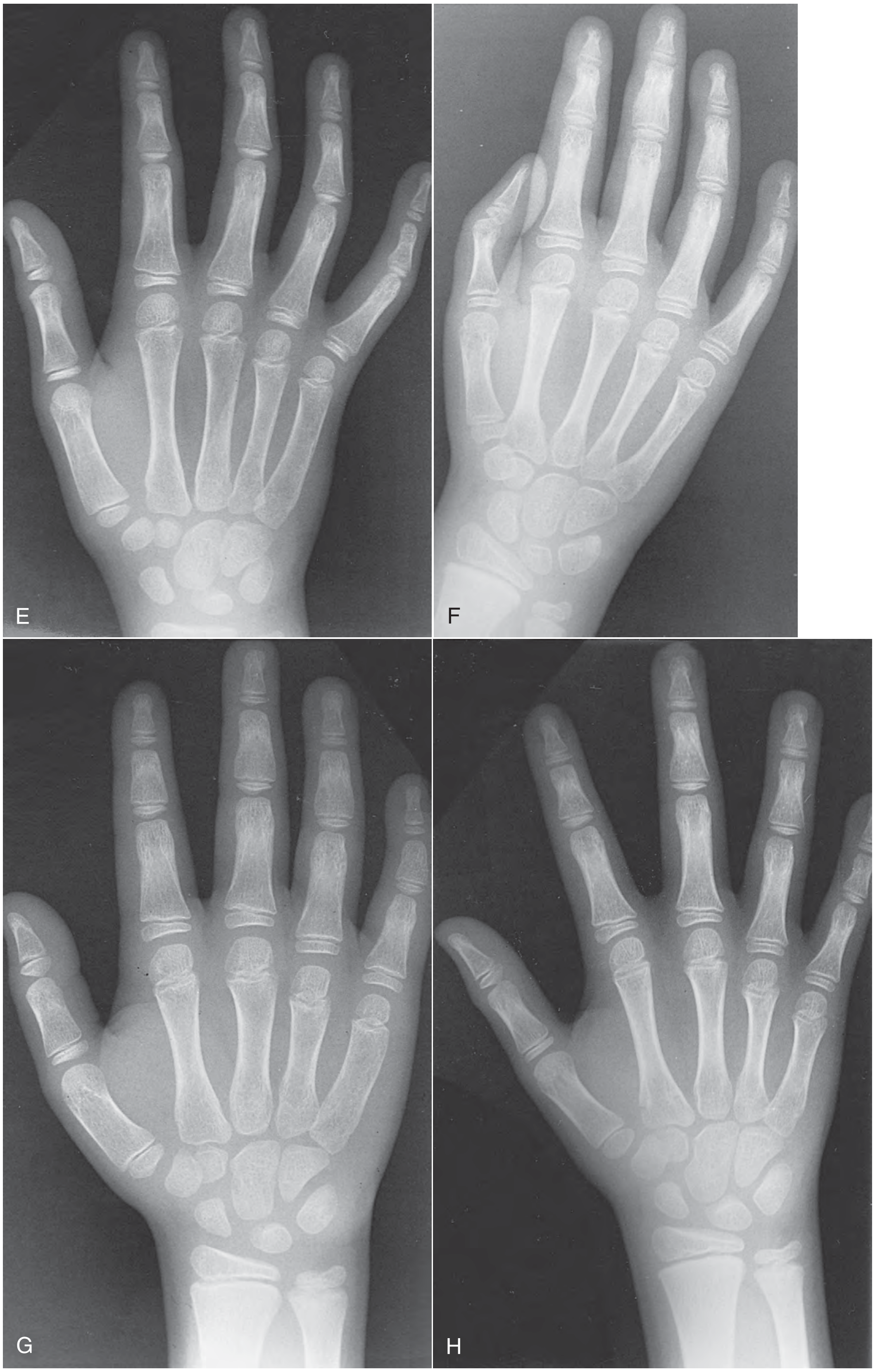

FIGURE 17–1, cont'd **E,** Male; CA = 7 yr; SA = 7 yr; SD ± 10.0. **F,** Female; CA = 8 yr; SA = 8 yr 6 mo; SD ± 10.9. **G,** Male; CA = 8 yr 4 mo; SA = 9 yr; SD ± 11.0. **H,** Male; CA = 10 yr; SA = 10 yr; SD ± 11.4.

Continued

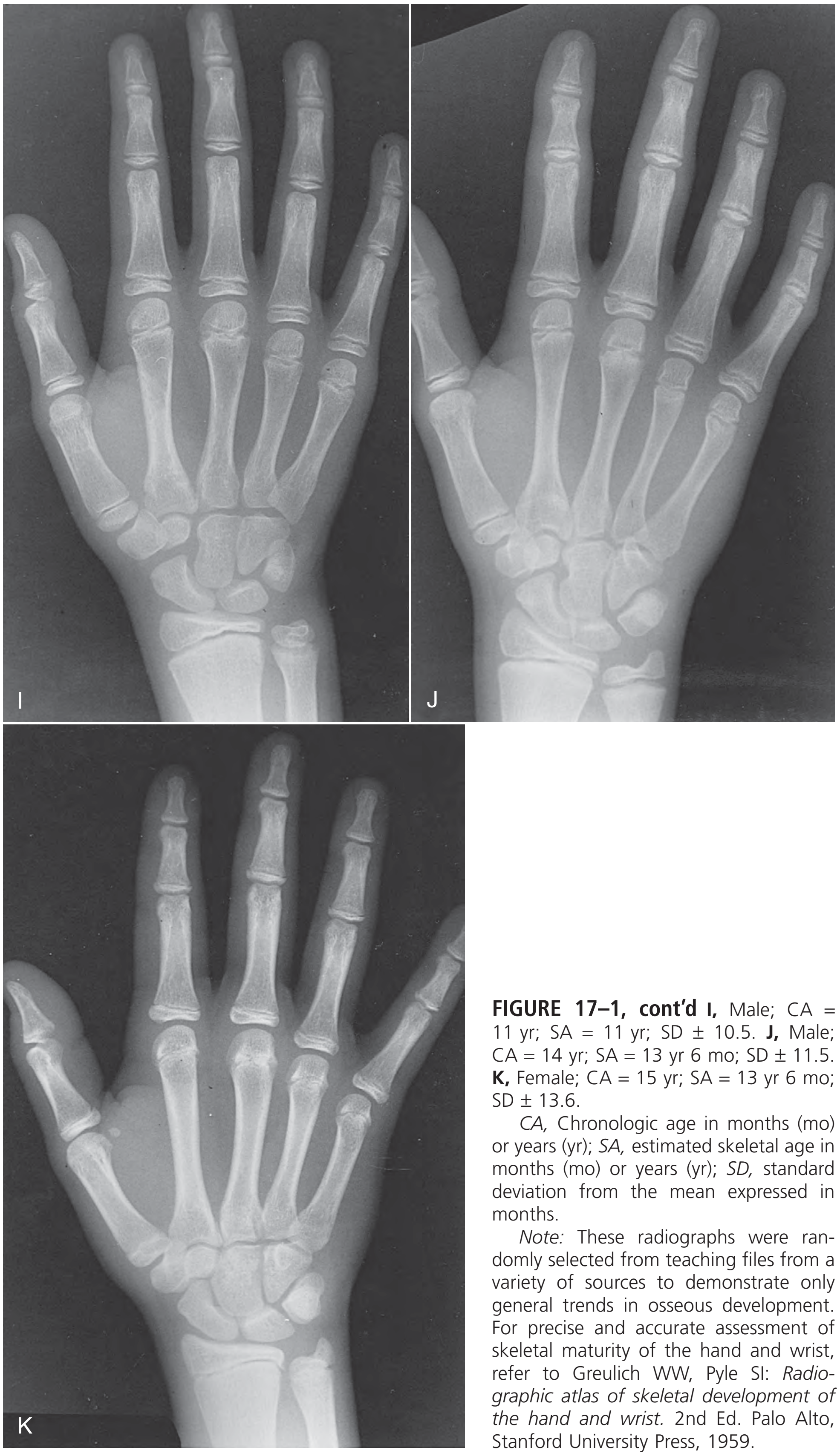

FIGURE 17–1, cont'd **I,** Male; CA = 11 yr; SA = 11 yr; SD ± 10.5. **J,** Male; CA = 14 yr; SA = 13 yr 6 mo; SD ± 11.5. **K,** Female; CA = 15 yr; SA = 13 yr 6 mo; SD ± 13.6.

CA, Chronologic age in months (mo) or years (yr); *SA,* estimated skeletal age in months (mo) or years (yr); *SD,* standard deviation from the mean expressed in months.

Note: These radiographs were randomly selected from teaching files from a variety of sources to demonstrate only general trends in osseous development. For precise and accurate assessment of skeletal maturity of the hand and wrist, refer to Greulich WW, Pyle SI: *Radiographic atlas of skeletal development of the hand and wrist.* 2nd Ed. Palo Alto, Stanford University Press, 1959.

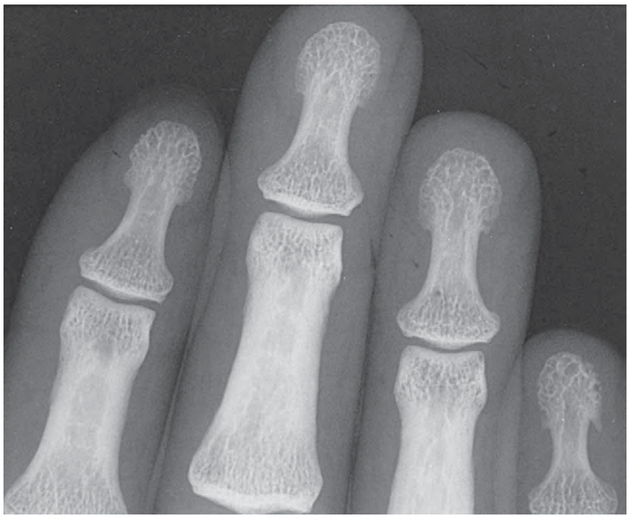

FIGURE 17–2 **Normal ungual tufts: terminal phalanges.**[2-5] Note the normally bulbous end of the terminal tuft. The trabeculae may appear somewhat lacelike and should not be confused with a pathologic condition.

TABLE 17-2 Developmental Anomalies, Anatomic Variants, and Sources of Diagnostic Error*

Entity	Figure(s)	Characteristics	Associated Syndromes or Disorders
Madelung deformity[6,7]	See Figure 16-2	***Radius*** Dorsal and ulnar curvature; decreased length; triangular distal epiphysis owing to premature fusion of medial half of epiphysis; ulnar and volar angulation of distal radial articular surface ***Ulna*** Elongated ulna with dorsal subluxation; enlargement and distortion of ulnar head Carpal bones Wedging of carpal bones between deformed radius and protruding ulna; triangular configuration of carpals with lunate at apex ***Inferior radioulnar joint*** Increased width of inferior radioulnar joint ***Radiocarpal joint*** V-shaped; decreased carpal angle See also Table 16-1	Isolated idiopathic form *Dysplastic form:* multiple hereditary exostosis and dyschondrosteosis *Genetic form:* Turner syndrome Posttraumatic form: extension injury to radial epiphysis
Carpal synostosis (coalition)[8,9,193]	17-3	*Lunate-triquetrum:* most frequent site; often bilateral *Capitate-hamate:* second most frequent site Synostoses of carpal bones in the same row are usually isolated anomalies of no clinical significance Occasional painful osteoarthrosis may develop at site of partial fusion Scapholunate space may be widened with intact scapholunate ligament in lunotriquetral coalition Synostosis of more than two carpal bones or of carpal bones across both rows may be related to congenital malformation syndromes Adjacent degenerative disease may result in the appearance of symptoms	Arthrogryposis Ellis-van Creveld syndrome Hand-foot-uterus syndrome Symphalangism Dyschondrosteosis Holt-Oram syndrome Cleft hand and foot Polydactyly Tarsal coalition *Acquired:* Inflammatory arthropathy may result in ankylosis

* For a more extensive discussion of these disorders, see Poznanski AK: The hand in radiologic diagnosis. 2nd Ed. Philadelphia, Saunders, 1984.

Continued

TABLE 17-2 Developmental Anomalies, Anatomic Variants, and Sources of Diagnostic Error—cont'd

Entity	Figure(s)	Characteristics	Associated Syndromes or Disorders
Scaphoid anomalies[10]		*Rare anomalies:* Bipartite scaphoid Hypoplastic scaphoid *Variants:* Irregular distal pole Normal scaphoid tubercle	Often mistaken for fractures or other pathologic condition
Accessory carpal bones[10]	17-4	Additional ossification centers result in extra carpal bones Unfused ossicles (accessory bones) represent normal anatomic variants that are usually of no clinical significance; infrequently result in symptoms; frequently simulate fractures Typical location and smooth, well-corticated margins help to distinguish ossicles from fractures	May be mistaken for fractures Occasionally syndrome-related
Bipartite carpal bones[10,176,177]		Any carpal bone may arise from more than one ossification center Bipartite scaphoid and hook of the hamate have been reported	May be mistaken for fractures
Os styloideum[11]	17-5	Also termed *carpal boss, carpe bossu,* or *dorsal boss* Accessory ossicle or dorsal bony prominence overlying the dorsal surface of the second and third carpometacarpal joints Often painful owing to bursitis, osteophyte, osseous proliferation, adjacent ganglion, or slippage of extensor tendon	May be mistaken for a ganglion
Brachydactyly (brachymesophalangy)[10]	17-6	Developmental shortening of middle phalanx Fifth digit most common *Normal variant:* 20% of Asian population; 1% of white population Occasionally related to syndrome	Trisomy 21 (60% of patients) Often accompanies clinodactyly
Short metacarpal bone[12]	17-7	Variant of brachydactyly Isolated or syndrome-related forms Usually affects fourth metacarpal bone Premature closure of metacarpal ossification centers Positive metacarpal sign	Isolated anomaly Turner syndrome Pseudohypoparathyroidism Pseudopseudohypoparathyroidism Sickle cell anemia
Epiphyseal variations[5,10]	17-8	Normal metacarpal and phalangeal epiphyses may be broad, irregular, asymmetric, divided by a cleft, or cone-shaped Additional metacarpal epiphyses occur infrequently Persistent unfused ossification center at the ulnar styloid is a common anomaly (os triangulare)	May mimic fracture or posttraumatic disorder *Trichorhinophalangeal syndrome of Giedion:* cone-shaped epiphyses Cleidocranial dysplasia
Syndactyly[10,188]	17-9	Developmental lack of differentiation between two or more digits Fusion of two digits may be partial or complete Osseous or soft tissue involvement Occurs as an isolated anomaly or in association with a generalized syndrome Syndactyly of the second and third digits is most likely an isolated anomaly	*May be associated with polydactyly:* synpolydactyly May be associated with Poland syndrome that also involves absent pectoral muscles Many associated chromosomal, craniofacial, and other syndromes may include syndactyly
Phalangeal synostosis (symphalangism)[10,198]	17-10	Nonsegmentation of one phalanx to another within the same digit usually related to absence of ossification centers Usually involves several digits of the same hand May be bilateral	Should not be mistaken for acquired fusion of inflammatory arthropathies

TABLE 17-2 Developmental Anomalies, Anatomic Variants, and Sources of Diagnostic Error—cont'd

Entity	Figure(s)	Characteristics	Associated Syndromes or Disorders
Polydactyly[10]	17-11	Developmental duplication of a digit *Postaxial:* duplicated digits on ulnar side of hand *Preaxial:* duplicated digits on radial side of hand	*Associated anomalies:* polydactyly, duplications, absent bones Most frequently an isolated anomaly but may be related to a generalized syndrome
Bifid thumb[10,14]	17-12	Form of polydactyly in which two terminal phalanges are present side by side or the terminal phalanx is bifurcated	Usually isolated anomaly Down syndrome Fanconi anemia Acrocephalosyndactyly syndromes
Triphalangeal thumb[10,14]	17-13	Rare normal variant Extra phalanx between proximal and distal phalanges of the thumb	*Associated anomalies:* polydactyly, duplications, absent bones *Associated syndromes:* Holt-Oram, trisomy 13-15, and Blackfan-Diamond anemia
Clinodactyly[10]	See 17-19	Medial or lateral curvature of a finger Most frequently an incidental finding associated with brachydactyly of the fifth digit	Infrequently associated with many different hand and foot syndromes, chromosomal disorders, and craniofacial syndromes Traumatic clinodactyly may also follow injury
Kirner deformity (dystelephalangy)[15]	17-14	*Normal variation:* palmar bending of the shafts of the fifth terminal phalanges Usually bilateral and painless	Usually isolated variant Epiphyseal separation may occur
Macrodactyly[16,17]	17-15	Also termed *localized* or *focal gigantism* Localized overgrowth of both soft tissues and osseous elements of a digit Isolated congenital form: present at birth	Neurofibromatosis Soft tissue hemangioma Macrodystrophia lipomatosa Lymphangioma Proteus syndrome

See also Table 1-1.

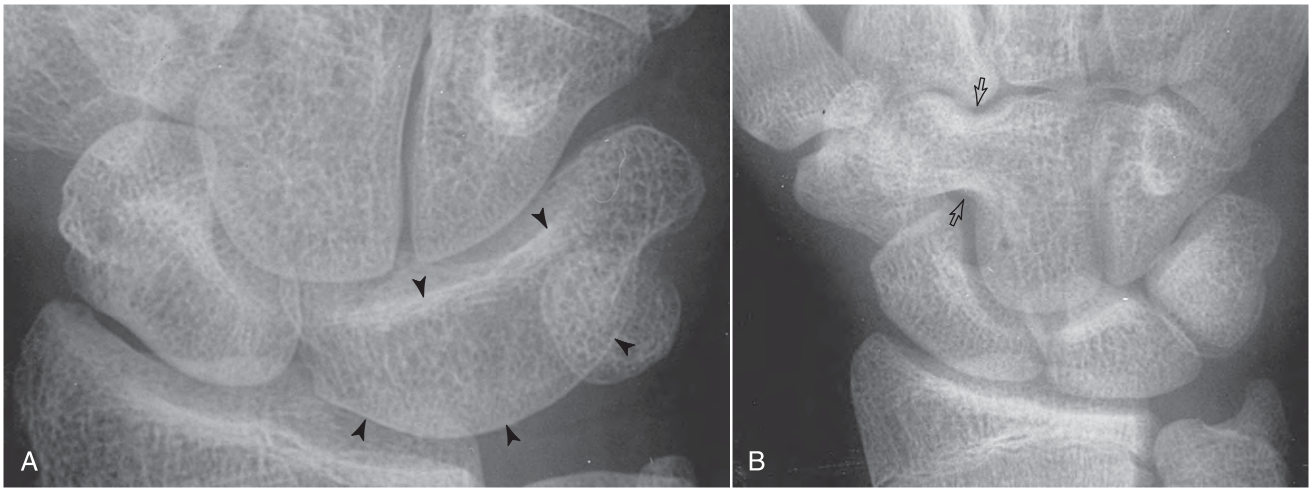

FIGURE 17–3 **Carpal synostosis (coalition).**[8,9] **A,** Lunotriquetral coalition. Osseous fusion of the lunate bone and the triquetrum is seen in this patient *(arrowheads)*. The lunotriquetral articulation is the most common site of carpal coalition. **B,** Capitate-trapezoidal coalition. Osseous ankylosis of the capitate and trapezoid bones, as seen in this patient *(open arrows),* is infrequent. Isolated fusions involving bones in the same carpal row (proximal or distal) are common and usually of no clinical significance. Fusion of carpal bones across different rows may be related to congenital malformation syndromes and deserves further investigation. Some carpal coalitions may become symptomatic secondary to degenerative changes.

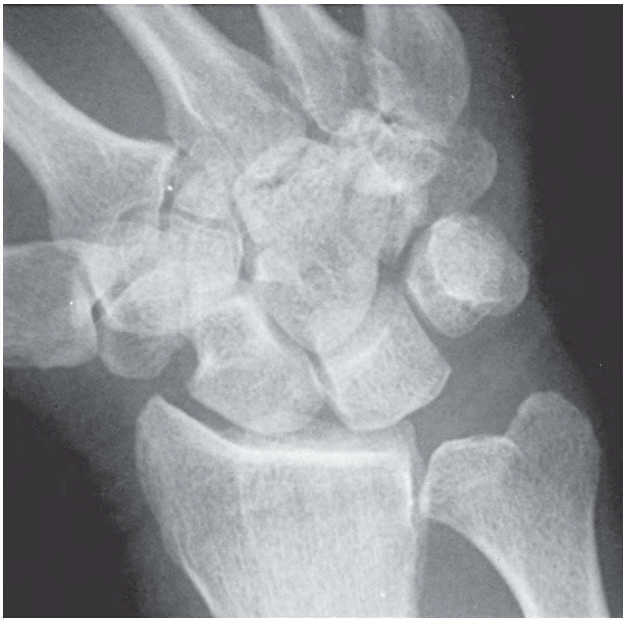

FIGURE 17–4 **Accessory carpal bones.**[10] Extra ossification centers may appear in the wrist, resulting in extra bones in addition to the eight normal carpal bones. These supernumerary carpal bones usually cause no symptoms or signs, but they must be differentiated from small fracture fragments. Accessory carpal bones occasionally may be found as a component of other heritable or congenital syndromes.

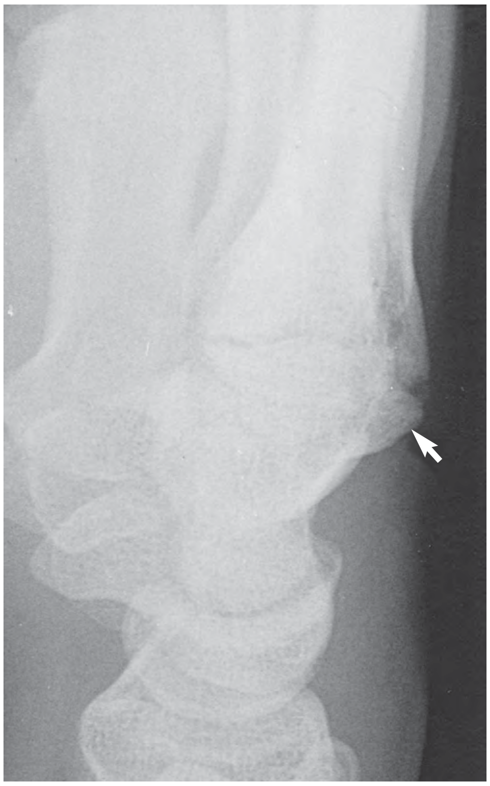

FIGURE 17–5 **Os styloideum (carpal boss).**[11] A typical os styloideum is seen as a triangular ossicle of bone on an angulated lateral radiograph *(arrow)*. The carpal boss, or carpe bossu, is located overlying the dorsum of the wrist at the bases of the second and third metacarpal bones. It may be asymptomatic or painful, resulting in limitation of hand motion.

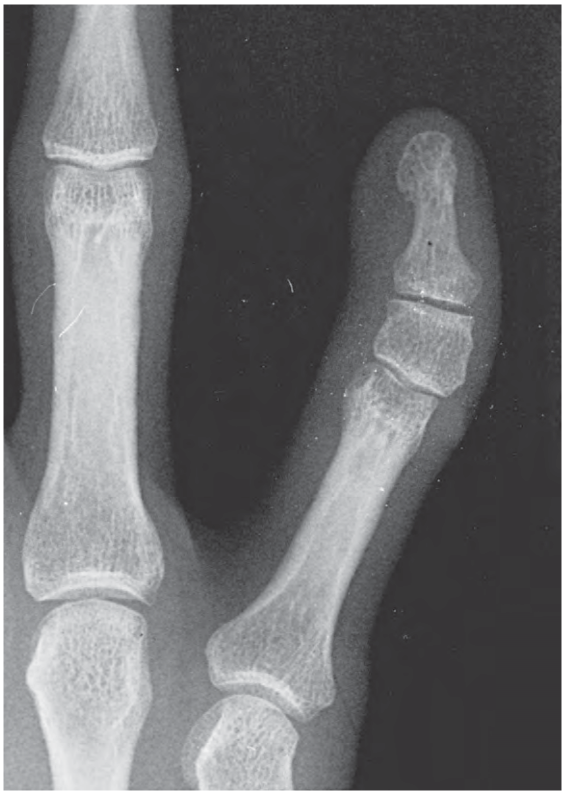

FIGURE 17–6 **Brachydactyly.**[10] The middle phalanx of the fifth digit is shorter on its radial side than on its ulnar side, resulting in slight radial clinodactyly. Shortening of the fifth middle phalanx is the most common form of phalangeal shortening and is also the most common hand anomaly. This anomaly is usually an isolated phenomenon, but it may be related to trisomy 21 and other syndromes. *(Courtesy G. Greenway, MD, Dallas.)*

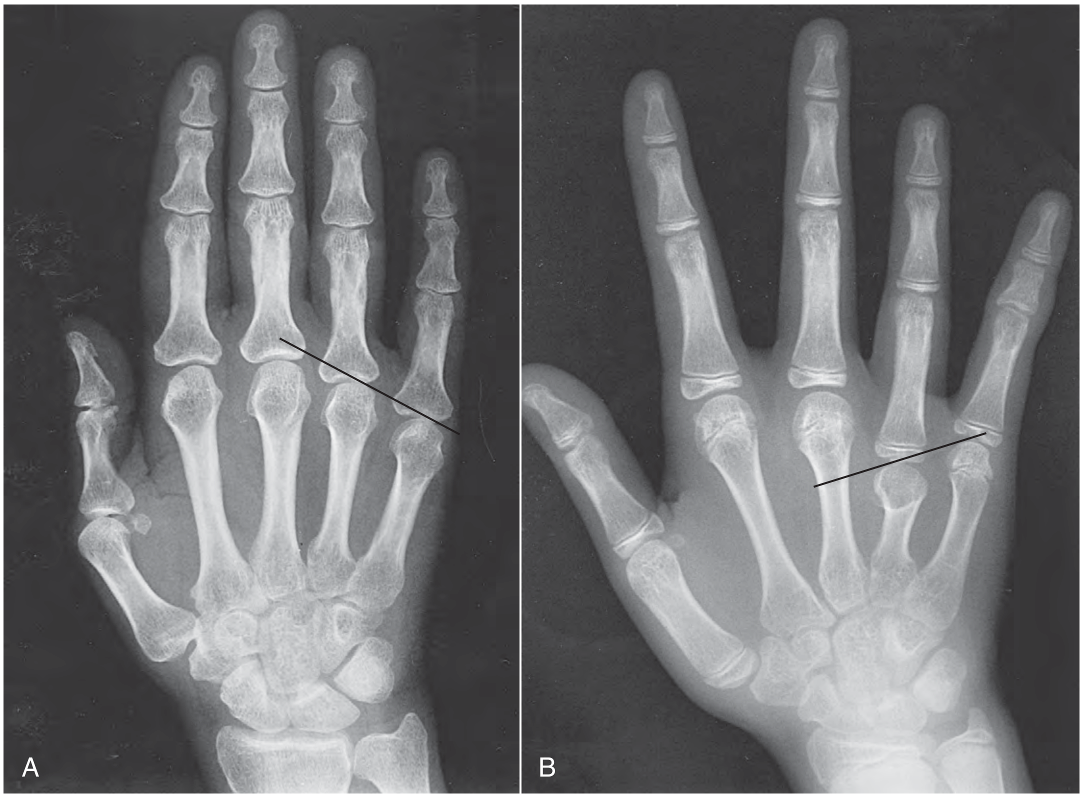

FIGURE 17–7 **Short fourth metacarpal bone.**[12,199] **A,** Metacarpal sign. In normal persons, a line drawn tangent to the distal ends of the fourth and fifth metacarpals should not intersect the end of the third metacarpal or should just contact its articular surface. In patients with a shortened fourth metacarpal bone, the line intersects the third metacarpal bone, a finding termed *positive metacarpal sign*. **B,** Isolated anomaly. Observe the shortened fourth metacarpal bone, resulting in a positive metacarpal sign (the line intersects the third metacarpal bone). This bilateral and symmetric anomaly was due to premature closure of the metacarpal ossification center in this 12-year-old girl. Metacarpal shortening, an anomalous variant is often seen as a familial trait in normal persons, but it may also be evident in persons with Turner syndrome (Figure 17-16).

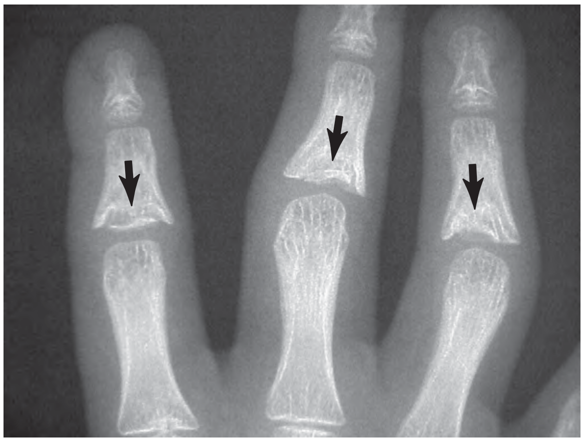

FIGURE 17–8 **Epiphyseal variations: cone-shaped epiphyses.**[5,10] In this 7-year-old girl born with trichorhinophalangeal syndrome of Giedion, observe the cone-shaped epiphyses of the middle *(arrows)* and distal phalanges.

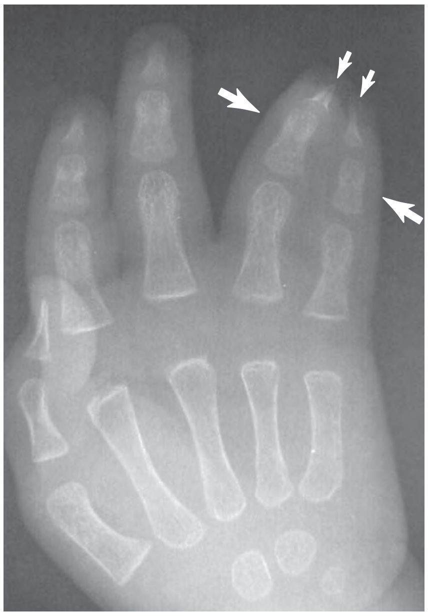

FIGURE 17–9 **Syndactyly.**[10,188] A radiograph of the hand in this 5-year-old girl; observe the complete lack of differentiation of the soft tissues of the fourth and fifth digits resulting in a fused or webbed appearance *(thick arrows)*. In this case, the underlying proximal and middle phalanges have developed normally, but the distal fourth and fifth phalanges appear hypoplastic *(small arrows),* and the fourth digit is deviated toward the fifth digit.

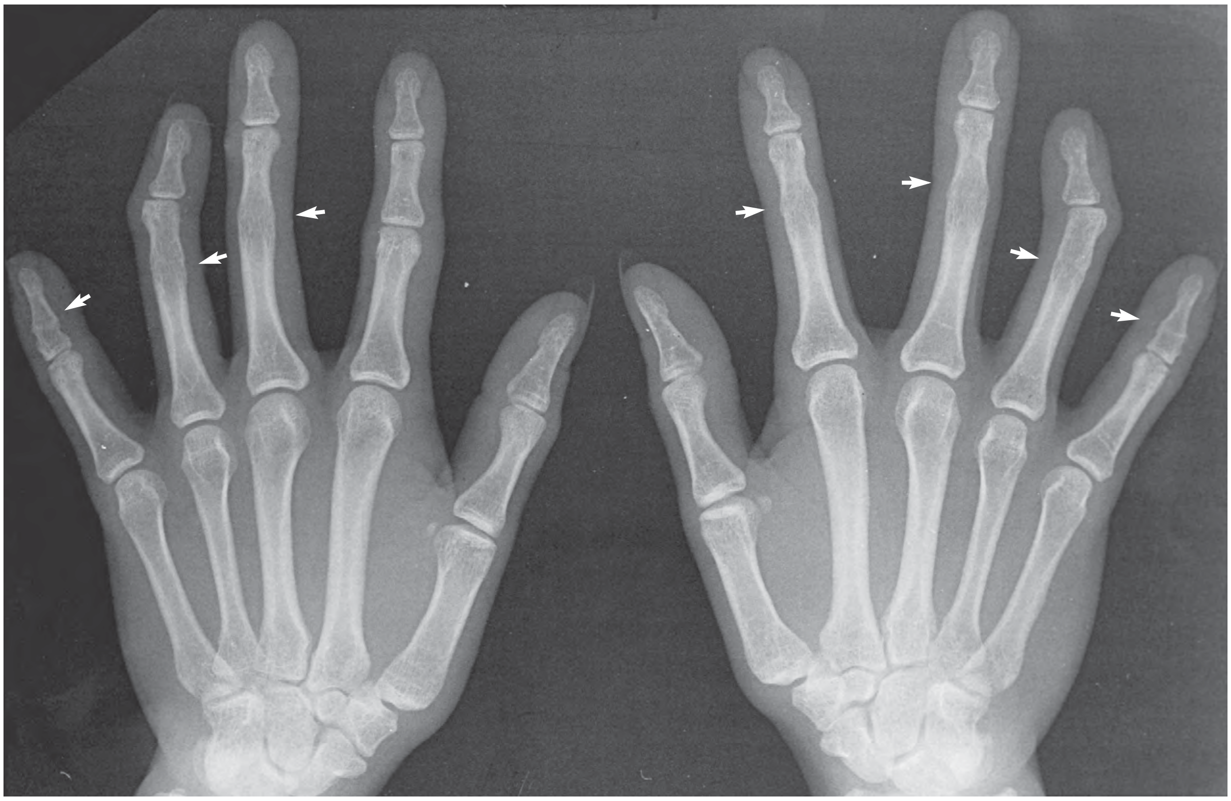

FIGURE 17–10 Phalangeal synostosis (symphalangism).[10,198] Observe the smooth bilateral osseous fusion of the proximal interphalangeal joints of the second to fourth fingers and the distal interphalangeal joints of the fifth fingers *(arrows)*. Occasionally, a small rudimentary lucent cleft is seen at the site of the articulation. This condition, which represents fusion of one phalanx to another within the same digit, usually is inherited as a dominant trait, but it may also be syndrome related. Symphalangism likewise must be differentiated from acquired intraarticular fusion, such as that seen in juvenile idiopathic rheumatoid arthritis and psoriatic arthritis.

FIGURE 17–11 Postaxial polydactyly.[10] A radiograph of this 3-day-old girl reveals an anomalous digit arising from the ulnar aspect of the fifth metacarpal. The supernumerary digit has three incompletely developed phalanges and is directed somewhat proximally with respect to the other digits *(arrow)*. (*Postaxial polydactyly* refers to an extra digit on the ulnar side of the extremity, whereas *preaxial polydactyly* involves the radial side.)

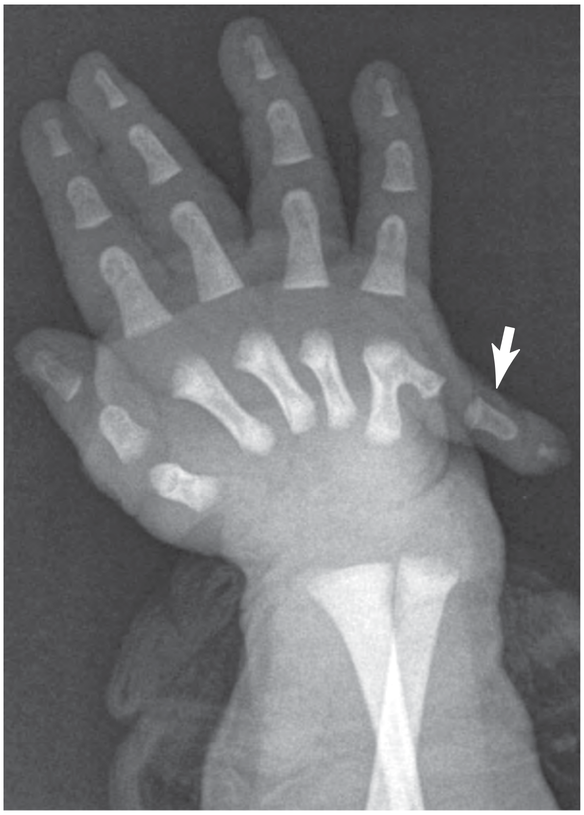

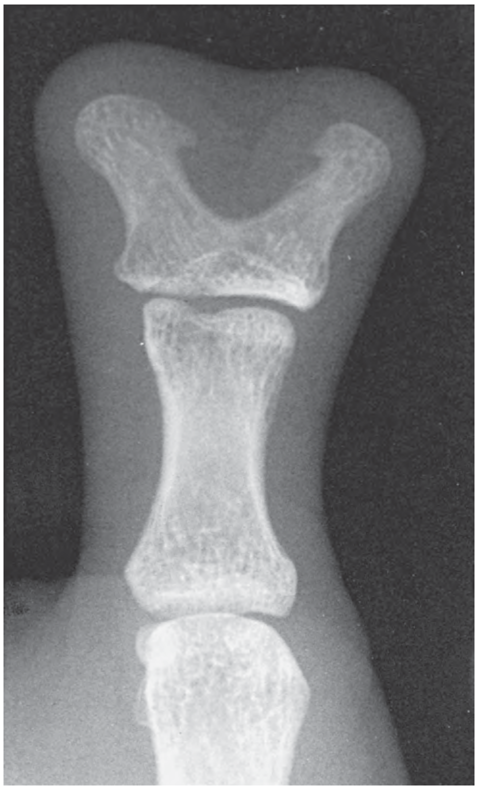

FIGURE 17–12 **Bifid thumb.**[10,14] Note the fork-shaped partial duplication of the terminal phalanx in this patient. This is a form of polydactyly, which may occur as an isolated anomaly or as an associated finding in Down syndrome, Fanconi anemia, and some other syndromes.

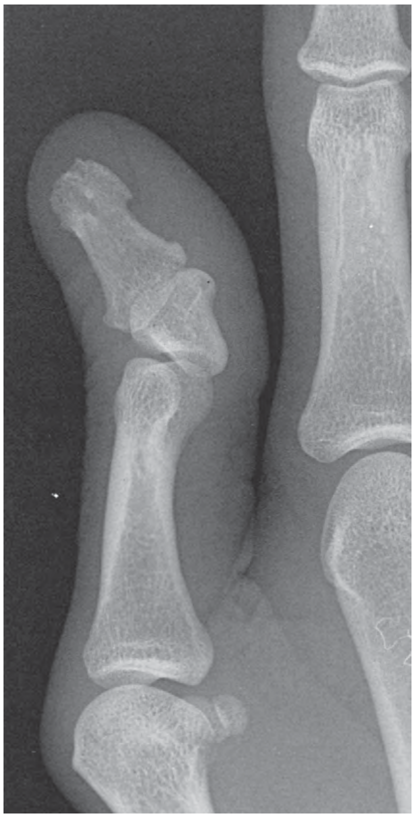

FIGURE 17–13 **Triphalangeal thumb.**[10,14] An extra phalanx is located between the proximal and distal phalanges of the thumb. This anomaly is a rare familial disorder that can occur as an isolated finding or in association with other anomalies, such as polydactyly, duplications, absent bones, and some syndromes (Holt-Oram syndrome, trisomy 13-15, and Blackfan-Diamond anemia).

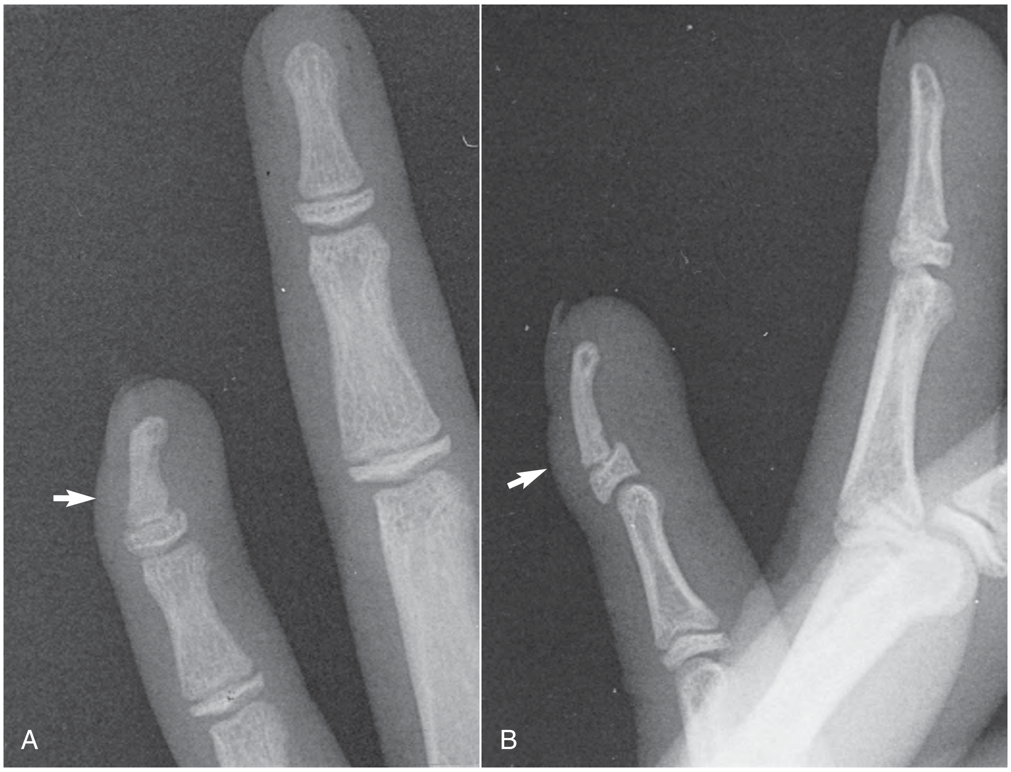

FIGURE 17–14 **Kirner deformity.**[15] **A,** Frontal radiograph. **B,** Lateral radiograph. Palmar bending of the shaft of the terminal fifth phalanx *(arrows)* was found incidentally in this 11-year-old girl. This deformity is usually bilateral and may occur in association with epiphyseal separation; however, it is usually painless and is considered a variation of normal.

FIGURE 17–15 **Macrodactyly (localized gigantism).**[16,17] In this 7-year-old girl, observe the characteristic overgrowth of both the bones and soft tissues of the third digit. Localized gigantism may be an isolated phenomenon or may be associated with vascular anomalies, neurofibromatosis, macrodystrophia lipomatosis, or the Proteus syndrome.

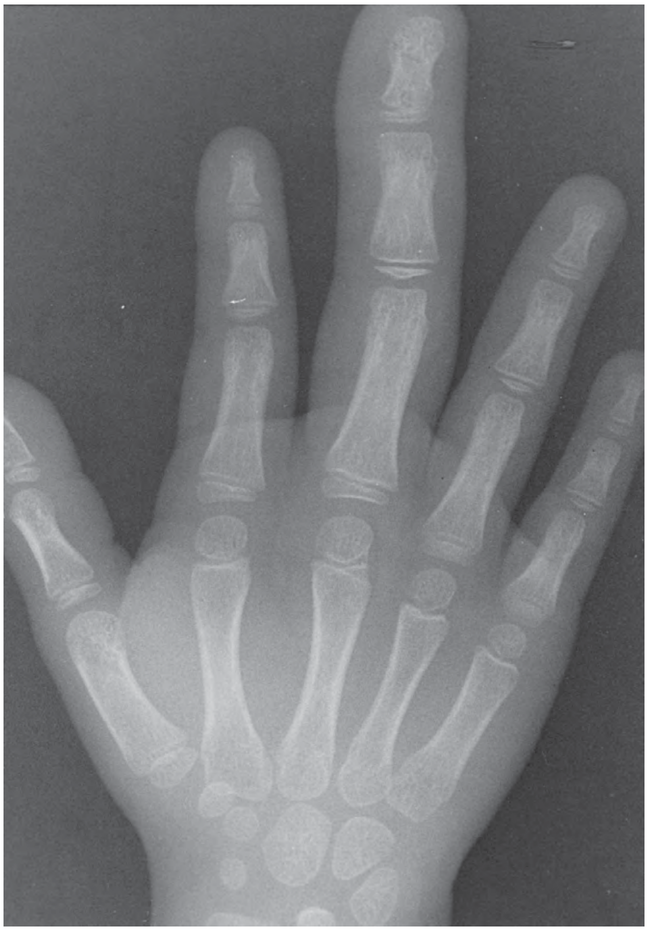

TABLE 17-3 Skeletal Dysplasias and Other Congenital Diseases Affecting the Wrist and Hand

Entity	Figure(s)	Characteristics
Turner syndrome[12,18]	17-16	Gonadal dysgenesis Short fourth metacarpal bone Delayed epiphyseal fusion Drumstick-shaped phalanges
Marfan sydrome[19-21]	17-17	*Arachnodactyly:* long slender fingers Hypermobility of wrist and finger joints *Elongated thumb:* when the hand is clenched, the thumb projects beyond the ulnar margin of the hand near the hypothenar eminence *Metacarpal index:* ratio of the length to midshaft width of the second to fifth metacarpal bones; ratio in normal men is less than 8.8; in normal women is less than 9.4; increased in patients with Marfan disease
Achondroplasia[22]	17-18	Short digits *Divergent fingers:* trident hand Metaphyseal cupping and irregularity Bones short but well formed in adults
Fibrodysplasia (myositis) ossificans progressiva[23]	17-19	*Multiple congenital anomalies:* hypoplasia of thumb, clinodactyly, polydactyly, and syndactyly
Osteogenesis imperfecta[24]		Bones of hand often are spared except in severe disease Osteoporosis with pencil-thin cortices Fractures seen occasionally *Rare cystic form:* ballooning of bone, metaphyseal flaring, and honeycombed appearance of thick trabeculae
Osteopoikilosis[25]	17-20	Multiple round or oval radiodense areas within spongiosa Periarticular location, especially in carpal bones
Melorheostosis[26,27]	17-21	Occasional involvement of hands Unilateral, hemimelic involvement is typical Cortical thickening and flowing hyperostosis resembling flowing candle wax extending from the forearm down the metacarpal bones and phalanges
Ehlers-Danlos syndrome[28]		Elongated ulnar styloid process *Acro-osteolysis:* rare Joint hypermobility
Hurler syndrome (MPS 1-H)[29]	17-22	Major changes appear about 1 year of age Tapering of the proximal portion of the metacarpal bones Widening of the proximal and middle phalangeal shafts Late appearance of carpal bones Flexion contractures of fingers V-shaped deformity of the distal portions of the radius and ulna Osteoporosis *Clinical findings:* clouding of the cornea, mental retardation, normal or slightly reduced stature, stiff joints, hirsutism, flexion of the hands, atlantoaxial subluxation, and aortic regurgitation
Macrodystrophia lipomatosa[16,17]	See Figure 17-52	Rare condition of unknown cause Bizarre digital overgrowth of fatty tissue within the soft tissues of the hand

See also Table 1-2.

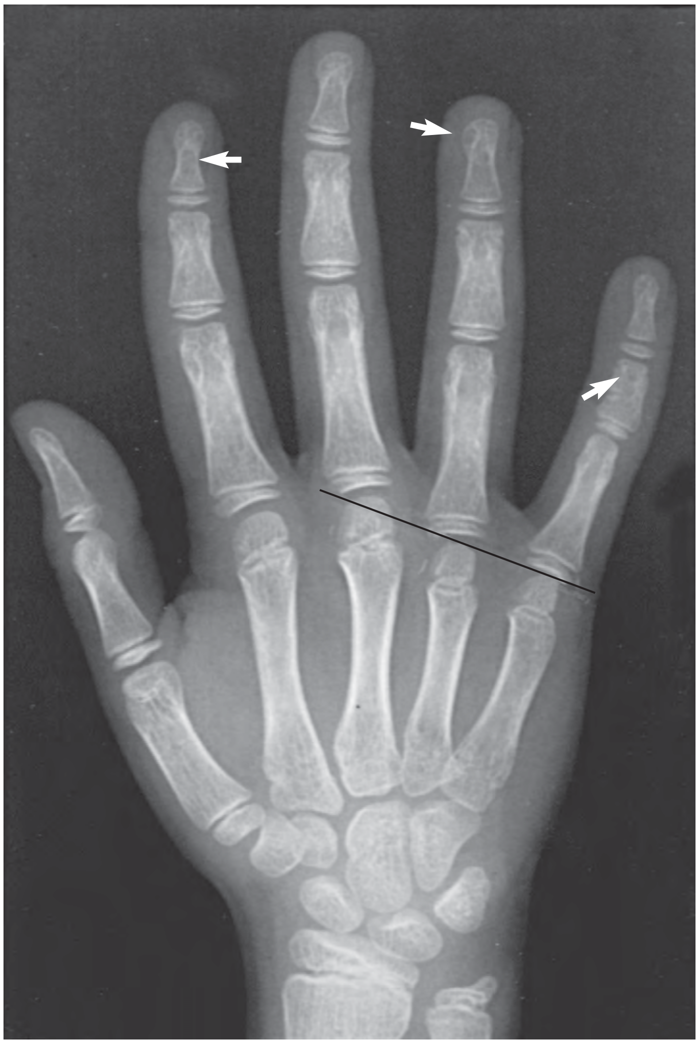

FIGURE 17–16 **Turner syndrome.**[12,18,199] The fourth metacarpal bone is short in relation to the adjacent metacarpal bones (positive metacarpal sign). Elongated phalanges, subtle cystlike changes in the phalanges *(arrows),* and osteopenia throughout the bones of the hand are evident in this 12½-year-old girl with gonadal dysgenesis. Other findings in Turner syndrome that may be observed are delayed epiphyseal fusion and drumstick-shaped phalanges.

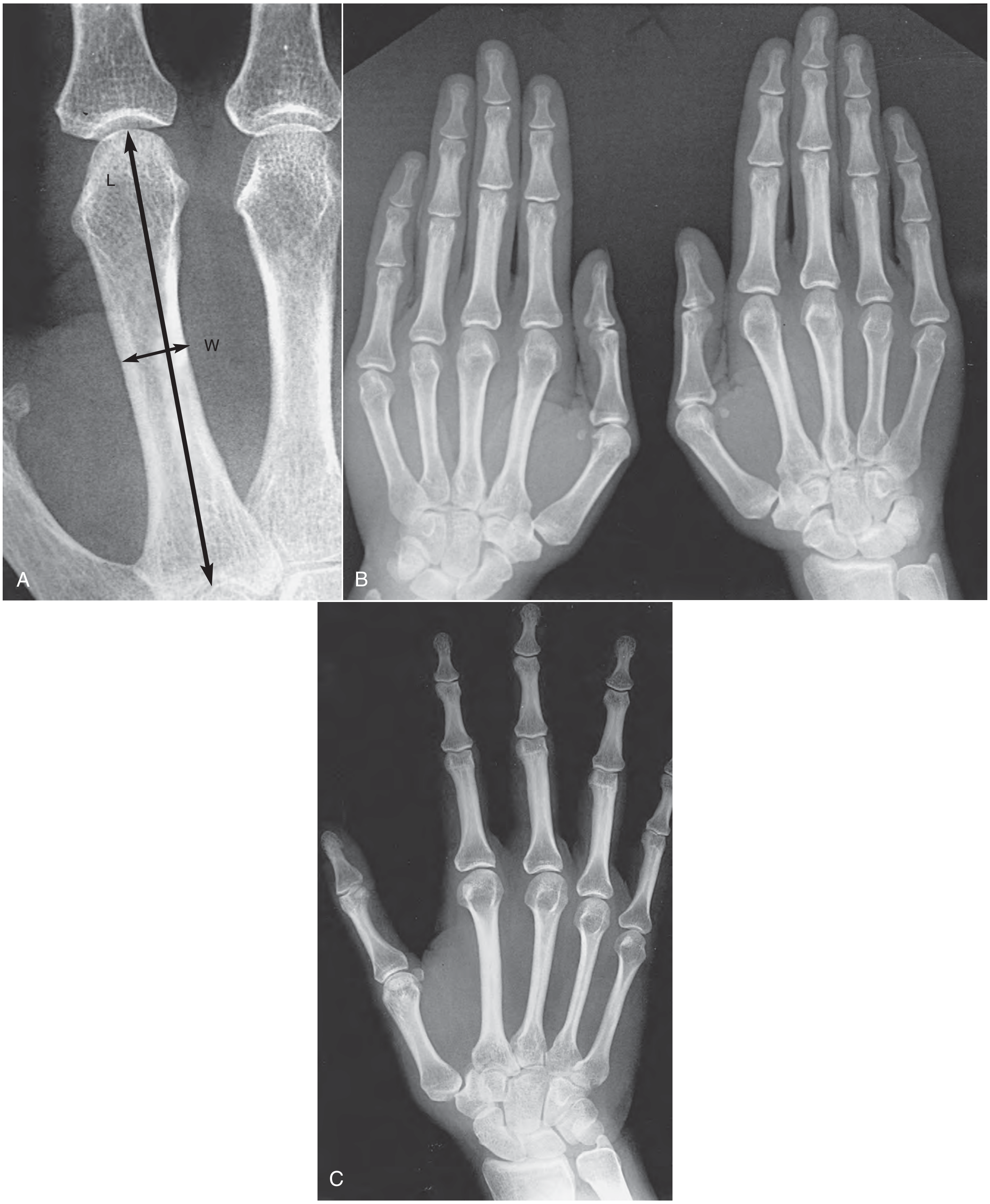

FIGURE 17–17 **Marfan syndrome: arachnodactyly.**[19-21] **A,** Metacarpal index: normal situation. The metacarpal index is used to determine the relative slenderness of the metacarpal bones. It is defined as the average of ratios of the length (L) divided by the midpoint widths (W) of the second to fifth metacarpal bones. In normal men, the ratio is less than 8.8; in normal women, it is less than 9.4. The ratio is typically increased in patients with Marfan syndrome. **B,** In this 27-year-old African-American woman, arachnodactyly is seen as elongation of the metacarpal bones and phalanges with normal bone density. **C,** In another patient with Marfan syndrome, observe the long slender metacarpal bones and phalanges and the relative absence of subcutaneous fat. *(**C,** Courtesy B.L. Harger, DC, Portland, Ore.)*

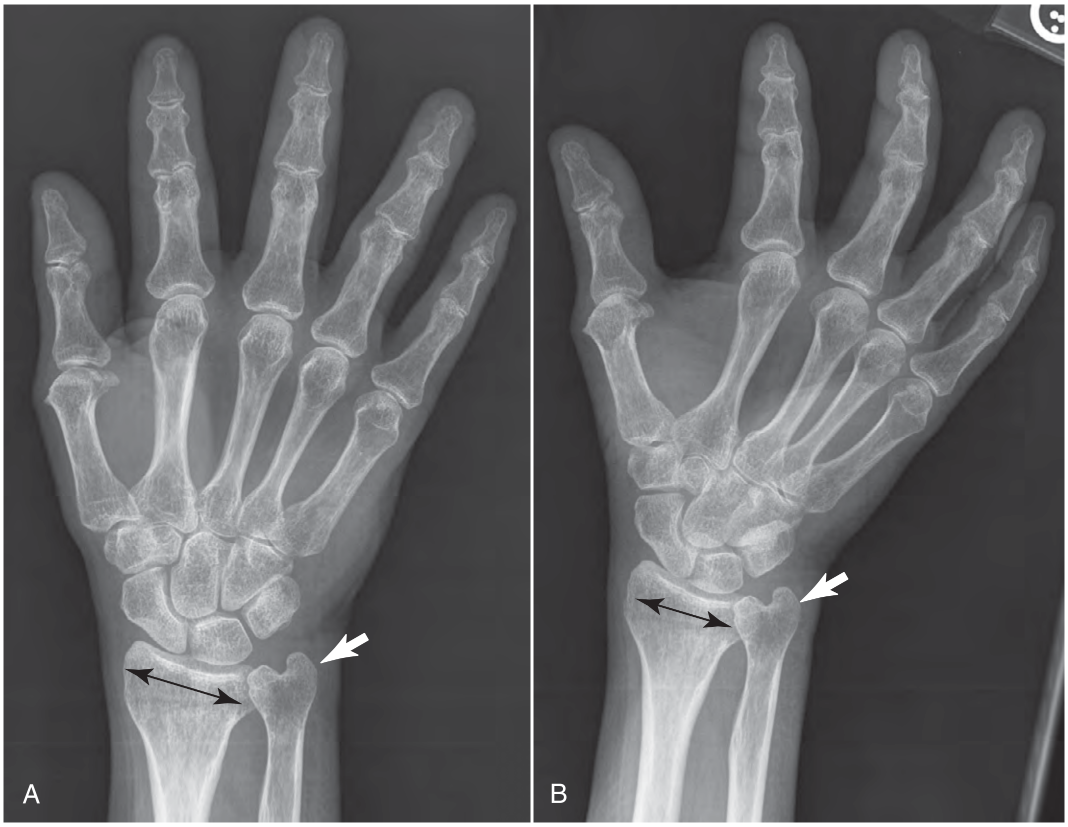

FIGURE 17–18 **Achondroplasia.**[22] Dorsopalmar **(A)** and oblique **(B)** radiographs of the hand in this 50-year-old woman born with heterozygous achondroplastic dwarfism reveal shortened tubular bones, elongated ulna with prominent styloid process *(arrows),* and minimal widening of the distal radial metaphysis *(double-headed arrows)*.

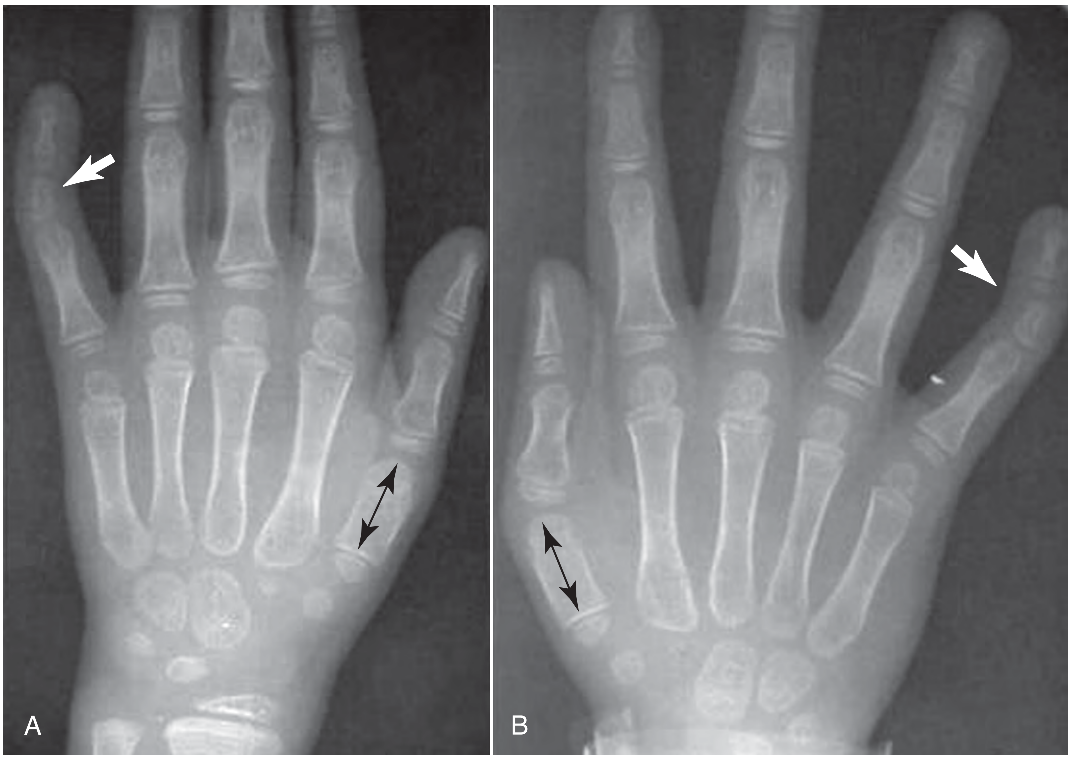

FIGURE 17–19 **Fibrodysplasia ossificans progressiva.**[23] **A-B,** Bilateral hand radiographs of this 3-year-old girl born with fibrodysplasia ossificans progressiva display the characteristic symmetric findings of hypoplastic first metacarpal *(double arrows)* and fifth middle phalanx, and radial deviation (clinodactyly) of the fifth middle and distal phalanges *(arrows)*.

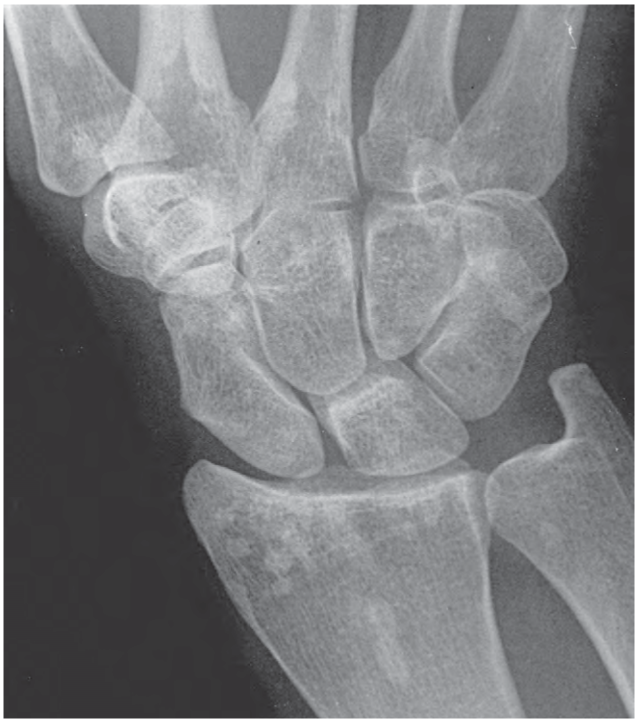

FIGURE 17–20 Osteopoikilosis.[25] Note the circular and ovoid osteosclerotic foci localized within the metacarpal and carpal bones, radius, and ulna. The symmetric periarticular distribution is characteristic of this fairly common sclerosing dysplasia. Although the epiphysis may be affected, most lesions usually predominate in the metaphysis.

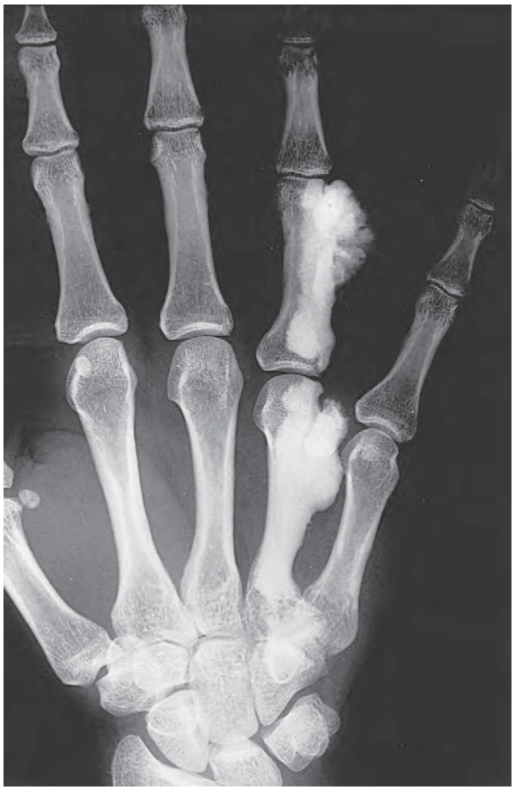

FIGURE 17–21 Melorheostosis.[26,27] Dramatic asymmetric periosteal and endosteal hyperostosis simulating flowing candle wax involves the ulnar side of the fourth metacarpal bone and proximal phalanx. The asymmetric hemimelic distribution of one digit is characteristic of this disease. Melorheostosis is a sclerosing dysplasia of bone that can result in joint swelling and contracture, pain, restriction of motion, growth disturbances, muscle weakness and atrophy, and skin changes. It may be positive on a bone scan. *(Courtesy A. Newberg, MD, Boston.)*

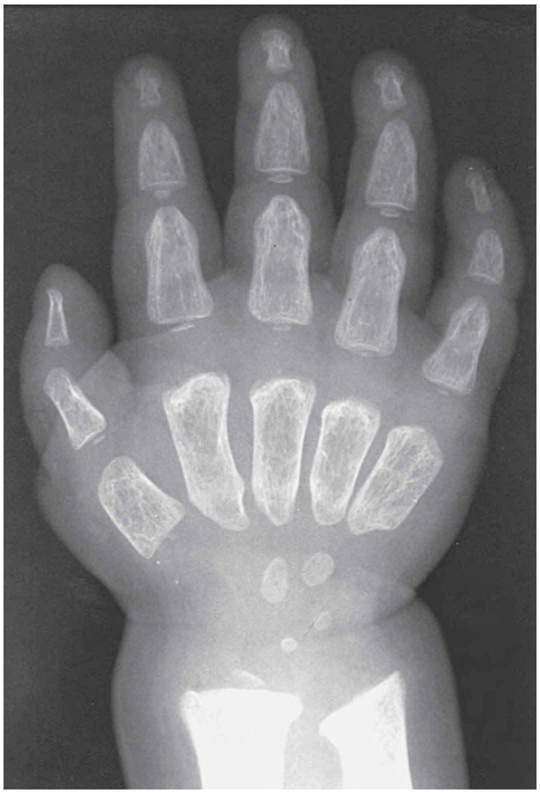

FIGURE 17–22 Hurler syndrome (MPS 1-H).[29] Radiograph of the hand in this 3-year-old girl with Hurler syndrome demonstrates osteopenia, pointing of the proximal portion of the metacarpal bones, widening of the proximal and middle phalangeal shafts, small carpal bones, flexion of the fingers, and a V-shaped deformity of the distal ends of the radius and ulna.

TABLE 17-4 Carpal Fractures and Dislocations[194]

Entity	Figure(s)	Characteristics	Complications and Related Injuries
Isolated Carpal Fractures			
Scaphoid fracture[30-33,183-186]	17-23	Sixty-five percent of wrist fractures involve the scaphoid Most common carpal fracture and most frequent site for occult fracture Usually occurs between ages 15 and 40 years *Mechanism* Fall on outstretched hand *Proximal pole:* (20%) *Waist:* (70%) *Distal (10%):* distal body, tuberosity, distal articular surface Waist fractures typically take 6 to 8 weeks or more to heal Tuberosity fractures typically take 4 to 6 weeks to heal Special radiographic projections to increase conspicuity of scaphoid fractures include: 1. PA* in ulnar deviation of wrist and fist position of hand 2. Oblique in 60 degrees pronation 3. Oblique in 60 degrees supination 4. Lateral view Multidetector CT is highly accurate in depicting occult scaphoid fractures and cortical involvement; MR imaging is superior to CT in depicting solely trabecular injury	*Nonunion in 5% to 15% of cases:* major factor for nonunion is delayed or inadequate immobilization Ischemic necrosis in 10% to 15% of cases; most common in proximal pole fractures; prevalence of ischemic necrosis increases by 30% to 40% in cases of nonunion Degenerative joint disease Tendon ruptures as a result of nonunion Occasionally associated with other wrist fractures and ligament disruptions Sixteen percent of scaphoid fractures are missed on initial radiographic evaluation; occult fractures are present in up to 40% of patients with suspected scaphoid fracture and normal initial radiographs
Triquetrum fracture[30,34]	17-24	Three percent to 4% of all carpal fractures Dorsal surface typically fractured *Mechanism* Contact with hamate or ulnar styloid process or avulsion by the dorsal radiotriquetral ligaments Best seen on lateral and steep oblique views	
Lunate fracture[30,34]		Two percent to 7% of all carpal fractures Dorsal or volar aspect or any portion of the body may fracture Usually avulsion fractures	Ischemic necrosis
Hamate fracture[30,34-36]	17-25	Two percent to 4% of all carpal fractures Hook is most common site of hamate fracture *Mechanism* Direct force from racquet, bat, or club; also from fall on a hyperextended wrist	Nonunion Ischemic necrosis Ulnar or median nerve injury Tendon rupture
Pisiform fracture[34,36]	17-26, *A*	*Mechanism* Direct crushing injury from fall on outstretched hand	Ulnar nerve injury
Capitate fracture[30,34]	17-26, *B*	Infrequent	May be combined with scaphoid fracture (scaphocapitate syndrome)

TABLE 17-4 Carpal Fractures and Dislocations[194]—cont'd

Entity	Figure(s)	Characteristics	Complications and Related Injuries
Trapezium fracture[30,34,203]	17-27	Infrequent The trapezial ridge may be fractured during a fall on an outstretched palm	Often overlooked on conventional radiographs May result in nonunion
Trapezoid fracture[30,34]		Infrequent	
Carpal Dislocations and Fracture-Dislocations			
Lesser arc injuries (lunate and perilunate dislocation)[37-39]	17-28, 17-29	*Lunate dislocation:* most common isolated carpal dislocation Hyperextension of the wrist Lateral view shows volar displacement and rotation of lunate; the capitate remains aligned with the radius Lunate appears triangular on the frontal view with the apex pointing distally ("pie sign") *Perilunate dislocation:* on the lateral view, the lunate remains aligned with the radius while the other carpal bones dislocate, usually dorsally On the frontal view, the capitate overlaps the lunate Often accompanies transscaphoid fracture (see greater arc injuries)	Wrist instability Osteonecrosis Predictable sequence of events after traumatic loading and impaction upon the thenar eminence, initially injuring the radial side of the wrist *Stage I:* scapholunate dissociation *Stage II:* perilunate instability owing to failure of radiocapitate ligament or radial styloid process fracture; leads to perilunate dislocation *Stage III:* further ligament disruption resulting in triquetral malrotation, triquetrolunate diastasis, or triquetral fracture *Stage IV:* Disruption of dorsal radiocarpal ligaments leading to lunate dislocation
Greater arc injuries[37,38,40]	17-28, 17-30	Predictable fracture-dislocation patterns passing through the greater arc consisting of scaphoid, capitate, hamate, and triquetrum *Examples:* Transscaphoid perilunate fracture-dislocation (relatively common) Transscaphoid, transcapitate, perilunate fracture-dislocation (scaphocapitate syndrome) Transscaphoid, transcapitate, transhamate, transtriquetral, perilunate fracture-dislocation (rare injury)	Complications similar to those of carpal dislocations and wrist instability
Scaphoid dislocation[41]		Infrequent injury *Two types:* 1. Isolated scaphoid dislocation—requires closed reduction 2. Dislocation in conjunction with axial carpal disruption—requires open reduction to stabilize carpals	Residual rotary subluxation of the scaphoid Median nerve compression
Common carpometacarpal joint dislocation[42]	17-31	Rare injury, typically involves ulnar aspect of wrist Dorsal dislocation, usually of 1 or 2 metacarpals in relation to the carpals CT useful in evaluation	Ulnar or median nerve injury Extensor tendon rupture Metacarpal fractures
First carpometacarpal joint dislocation[43]	17-32	Rare injury	Often associated with Bennett fracture-subluxation of the base of the first metacarpal bone

See also Tables 1-4 to 1-6.
* *PA,* Posterior to anterior

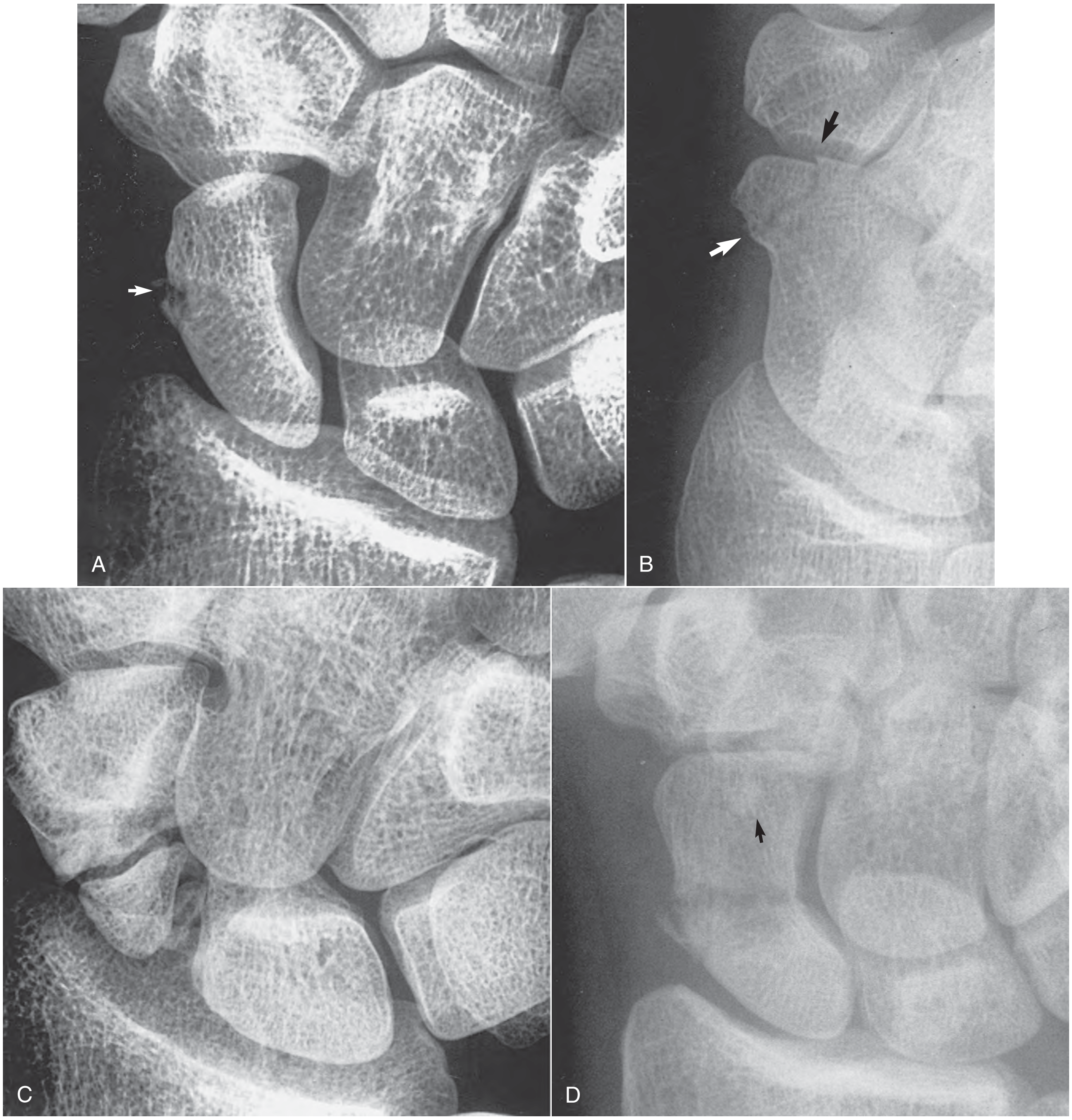

FIGURE 17–23 **Carpal fractures: scaphoid bone.**[30-33,183-186] **A,** Scaphoid waist fracture. A fracture line is seen traversing the midwaist of the scaphoid bone *(arrow)*. **B,** Distal scaphoid fracture. Oblique view shows a fracture of the scaphoid tuberosity *(arrows)*. **C,** Complication: nonunion. In another patient, observe the widened fracture cleft and the rounded sclerotic margins at the fracture site. Subchondral cyst formation and widening of the scapholunate articulation are also evident. **D,** Complication: osteonecrosis. A transverse radiolucent fracture line is evident through the waist of the scaphoid. The proximal fracture fragment is osteosclerotic, a sign of osteonecrosis. A small bone island (enostosis) is incidentally noted in the distal pole *(arrow)*. (***A, C,*** *Courtesy U. Mayer, MD, Klagenfurt, Austria.)*

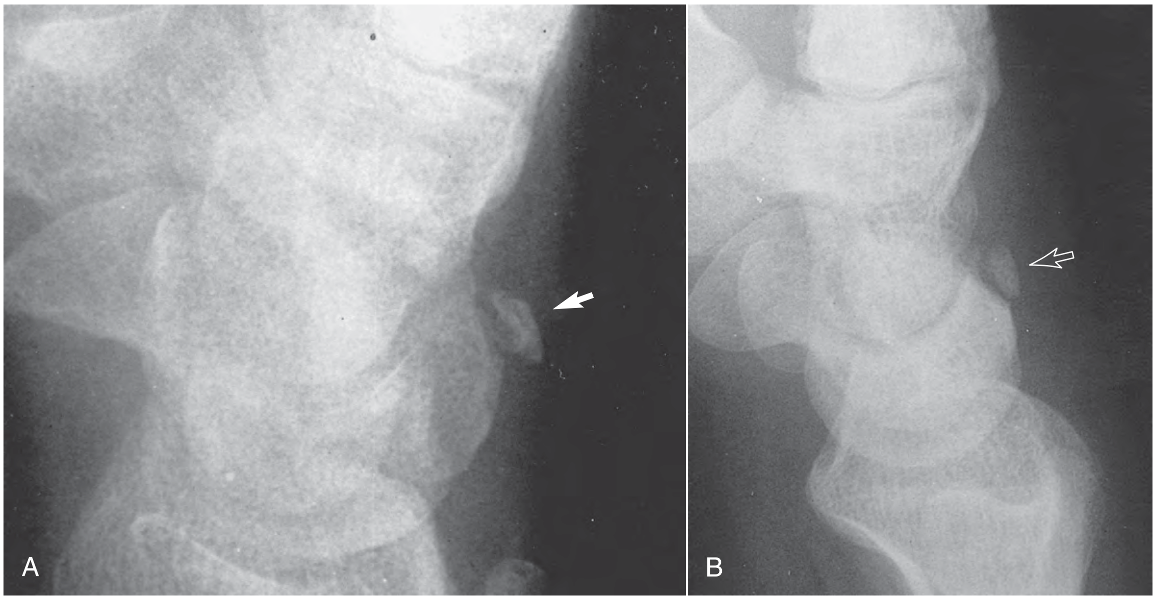

FIGURE 17–24 **Carpal fracture: dorsal surface of triquetrum.**[30,34] **A,** Lateral radiograph reveals the fracture fragment adjacent to the dorsal surface of the triquetrum *(arrow)*. **B,** A similar fracture of the triquetrum is evident in another patient *(open arrow)*.

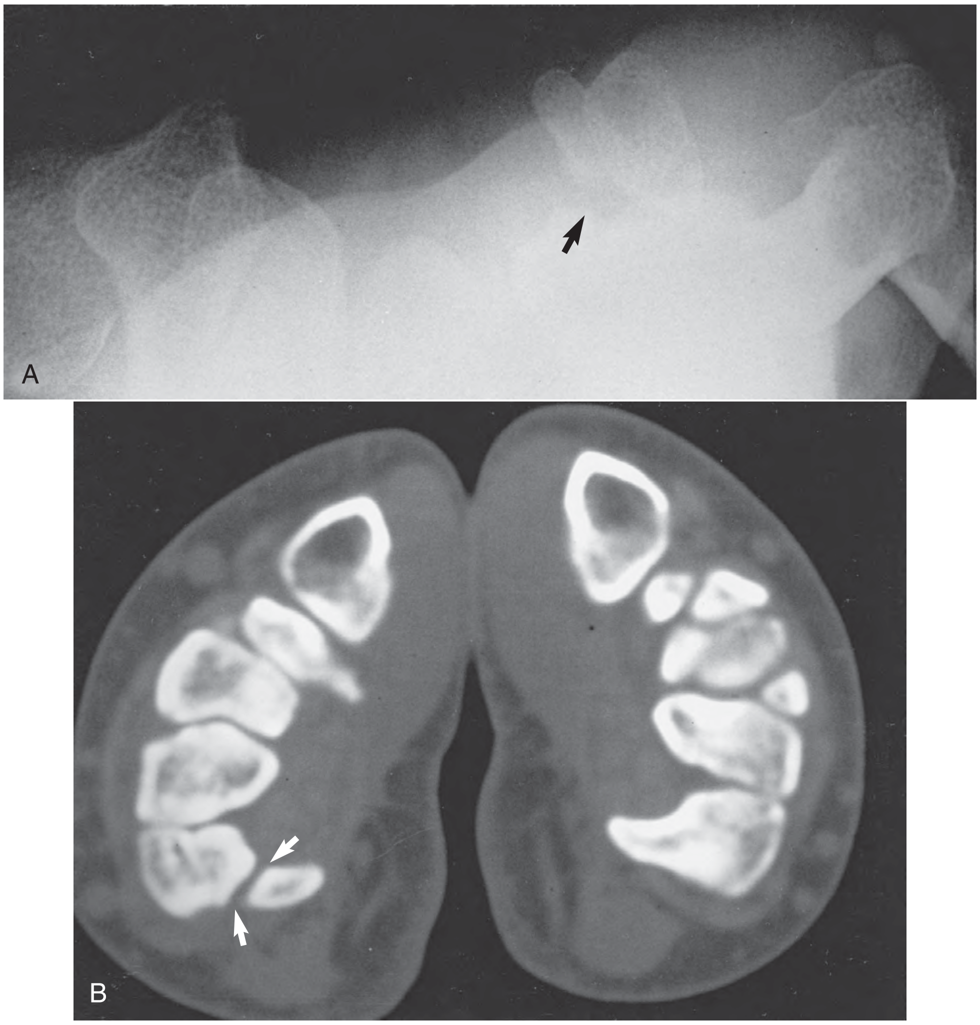

FIGURE 17–25 **Carpal fracture: hamate bone.**[30,34-36] This patient had several months of pain after an injury sustained while swinging a golf club. Carpal tunnel radiograph **(A)** and transaxial CT scan **(B)** reveal the fracture through the hook of the hamate bone *(arrows)*. Compare with the normal contralateral side in **B.** *(Courtesy G. Greenway, MD, Dallas.)*

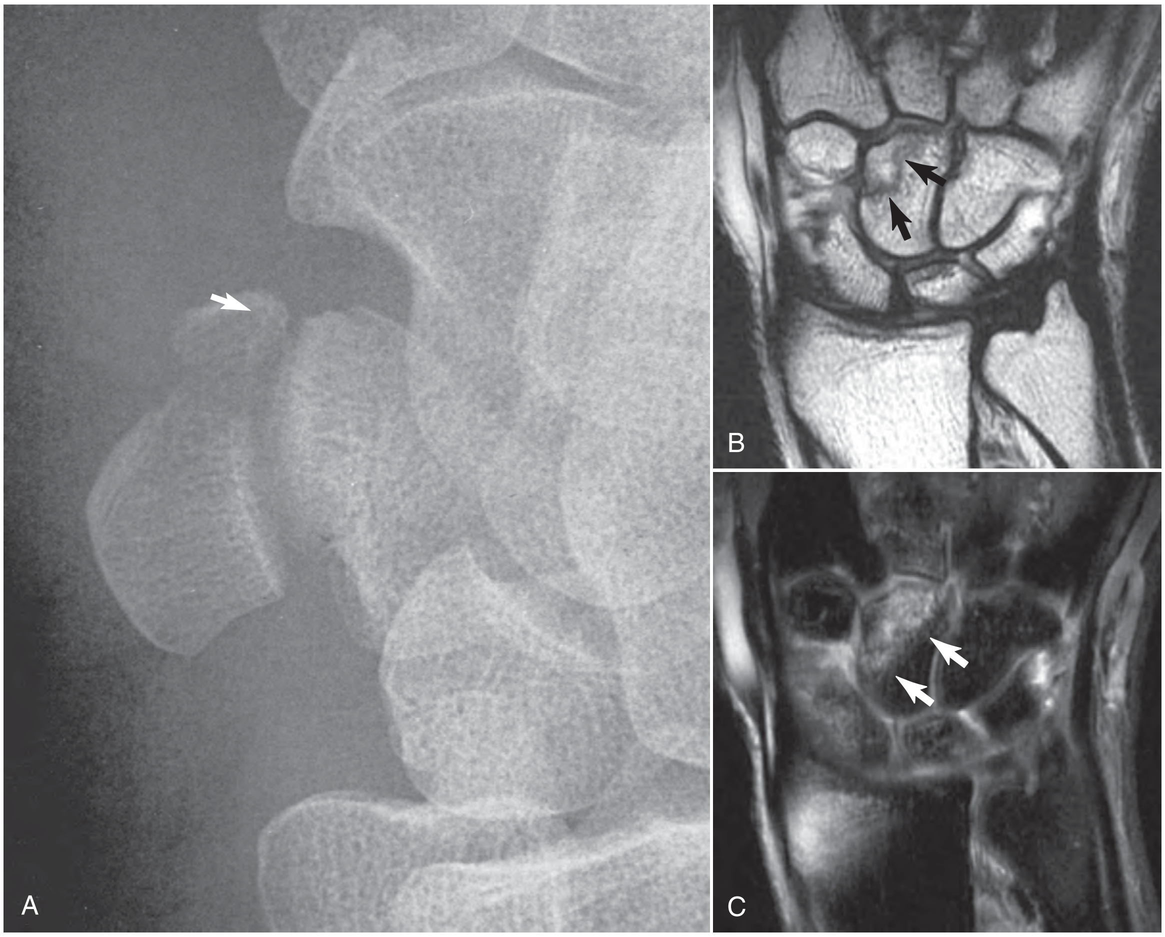

FIGURE 17–26 **Carpal fractures: pisiform and capitate bones.**[30,34,36] **A,** Pisiform. Semisupinated oblique radiograph reveals a minimally displaced fracture of the pisiform bone *(arrow)*. Pisiform fractures result from a crushing mechanism, usually sustained by breaking a fall with an outstretched hyperextended wrist, and may be complicated by ulnar nerve damage. **B-C,** Capitate. A 29-year-old man with wrist pain and swelling after a fall. A low signal intensity oblique fracture line *(arrows)* within the distal pole of the capitate is evident on a coronal proton–density-weighted MR image of the wrist **(B).** The fracture is seen as a zone of high signal intensity marrow edema *(arrows)* on a corresponding coronal fat-suppressed proton–density-weighted image **(C).** Many capitate fractures are occult on conventional radiographs.

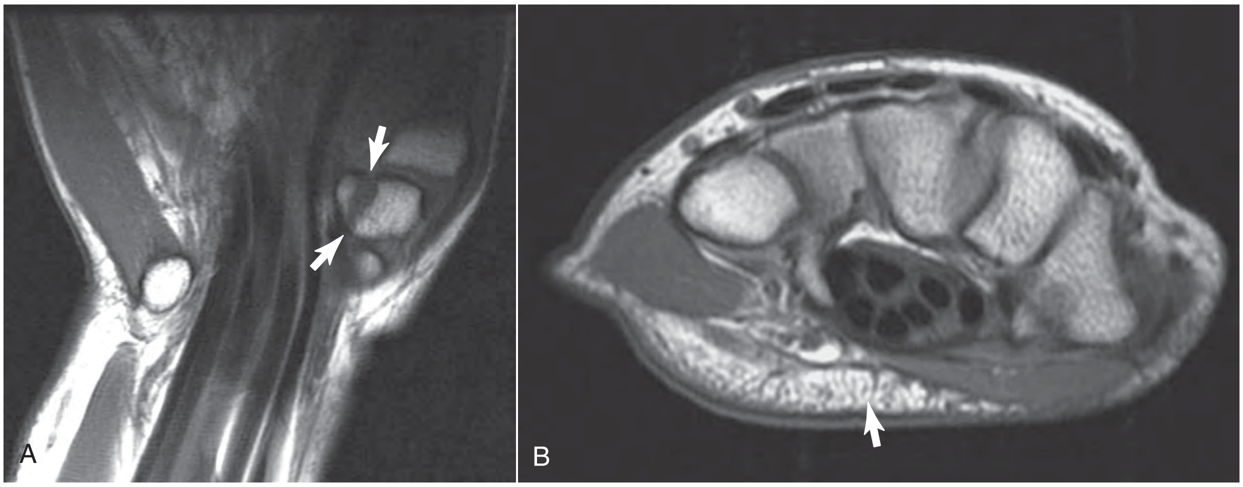

FIGURE 17–27 **Carpal fracture: trapezium bone.**[30,34,203] Coronal T1-weighted **(A)** and transaxial intermediate-weighted **(B)** MR images reveal a low-signal intensity vertical fracture line *(arrows)* between the trapezial ridge and the body of the trapezium. The trapezial ridge fracture is frequently missed on conventional radiographic studies, and often results in nonunion. It is seen to best advantage on carpal tunnel radiographs (not shown).

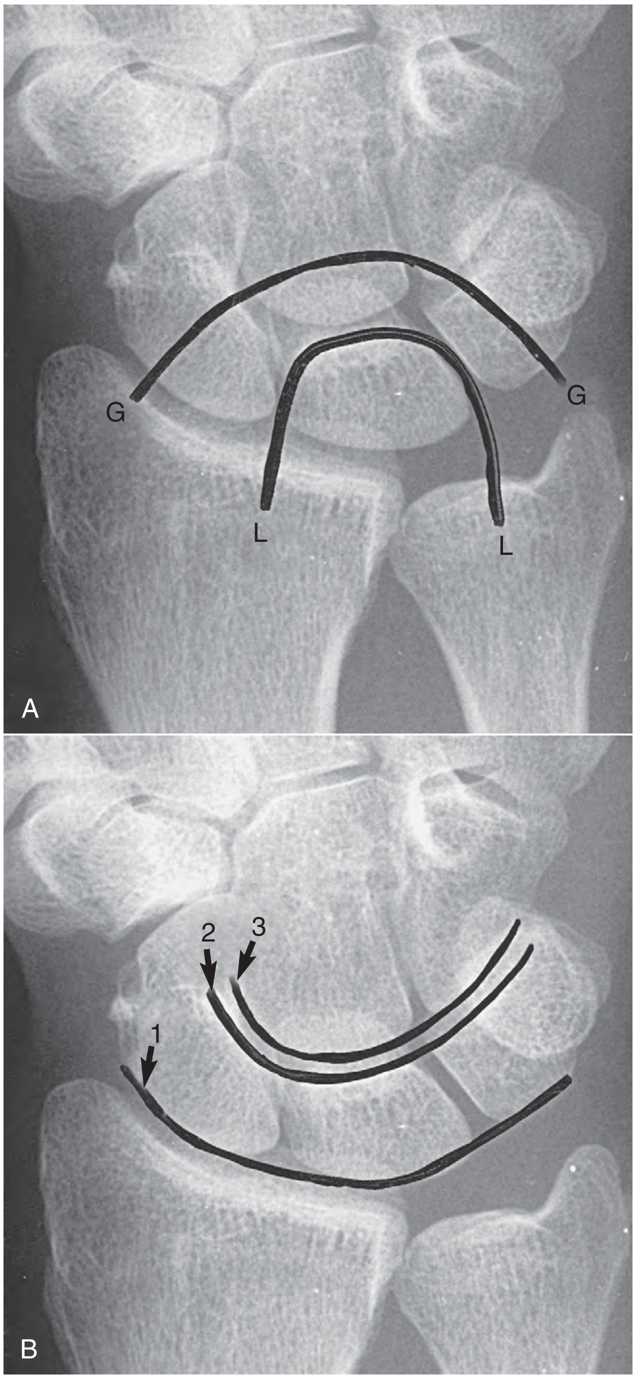

FIGURE 17–28 Wrist injuries: carpal relationships—the normal arcs.[37-40] **A,** Greater (G) and lesser (L) arc locations are shown. Fractures and dislocations along these arcs occur in predictable patterns. A pure greater arc injury consists of a transscaphoid, transcapitate, transhamate, transtriquetral fracture-dislocation. A pure lesser arc injury is a perilunate or lunate dislocation. Various combinations of these injury patterns are seen clinically. **B,** Normal arcs of proximal and distal carpal rows. On routine posteroanterior radiographs of the wrist, three arcs are demonstrated. Arc 1 (proximal carpal articular surfaces of the proximal carpal row) joins the outer curvatures of the proximal articular surfaces of the scaphoid, lunate, and triquetrum (1). Arc II (distal carpal articular surfaces of the proximal carpal row) connects the distal smooth curves of these same three bones (2). Arc III (proximal carpal articular surfaces of the distal carpal row) connects the distal smooth surfaces of the capitate and hamate bones (3).

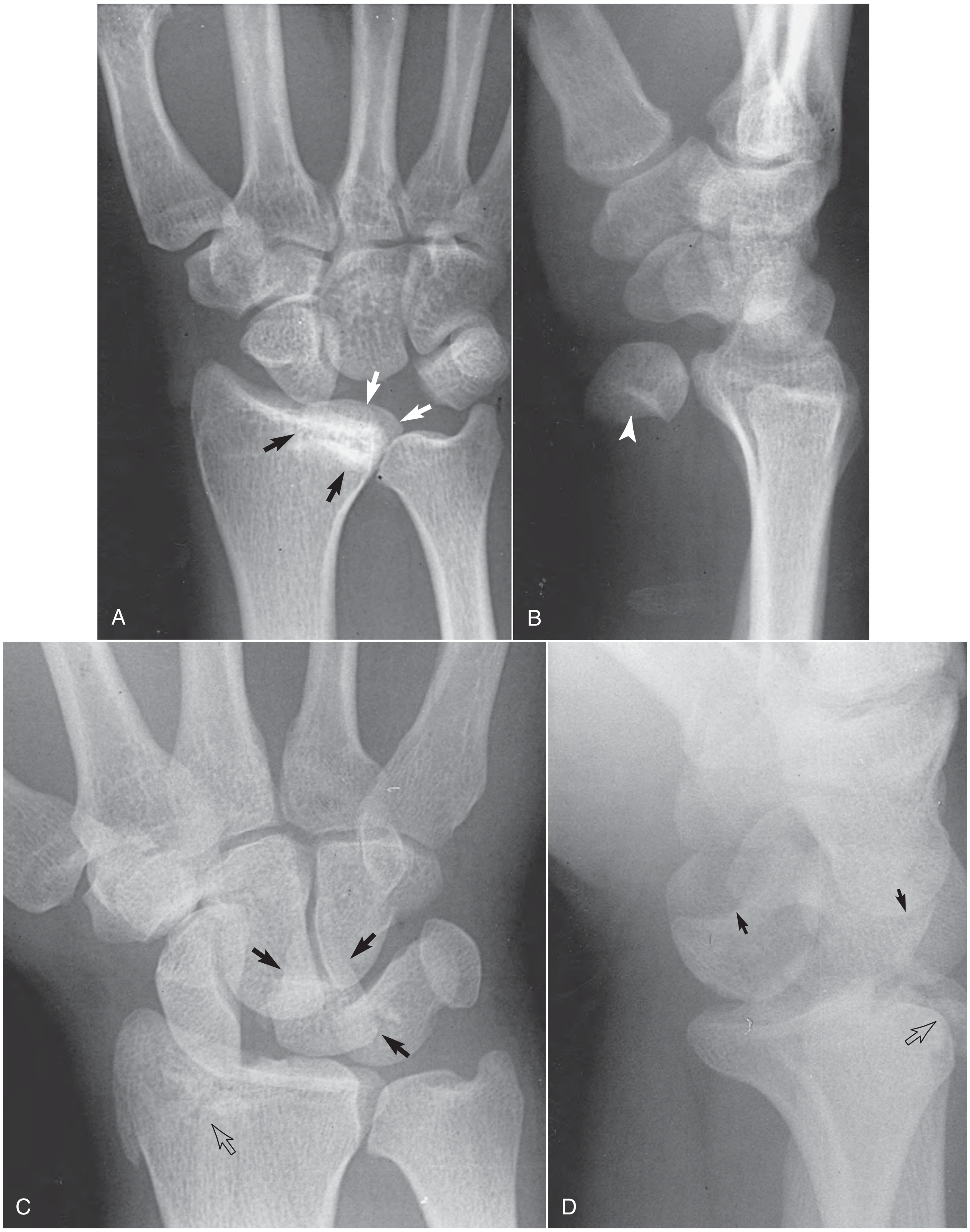

FIGURE 17–29 **Lesser arc wrist injuries.**[37-39] **A-B,** Lunate dislocation. In **A,** a frontal radiograph demonstrates volar dislocation of the lunate bone. The lunate bone is displaced proximally and overlies the volar surface of the distal end of the radius *(arrows)*. The space proximal to the capitate bone is vacant. In **B,** the lateral radiograph is most diagnostic, showing volar displacement. In addition, the lunate bone has rotated 180 degrees; therefore, the distal surface *(arrowhead)* is directed proximally. Neither the lunate nor the capitate bone is truly aligned with the distal surface of the radius, indicating the difficulty encountered in classifying such injuries as either lunate or perilunate dislocation. **C-D,** Perilunate dislocation. In **C,** a posteroanterior radiograph shows overlap of the lunate bone with respect to the capitate, hamate, and triquetrum *(arrows)*. A radial styloid fracture *(open arrows)* is also present. Observe the disruption of the lesser arc and the severe scapholunate dissociation. In **D,** the lateral radiograph clearly demonstrates the normal relationship between the lunate bone and the distal end of the radius, as well as the dorsal displacement of the capitate bone with respect to the lunate bone. (In the normal situation, the arrows within the capitate and lunate bones should be aligned.)

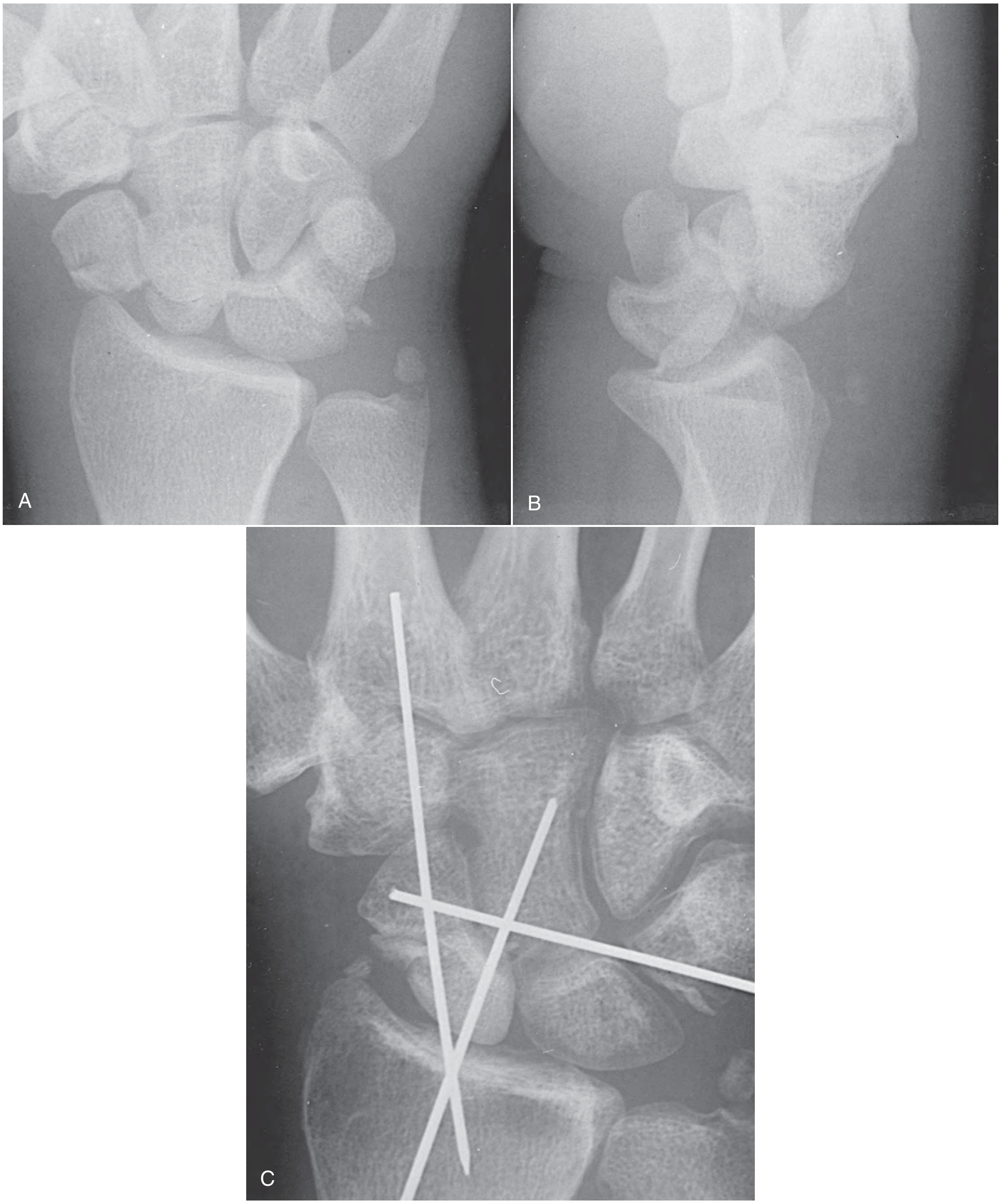

FIGURE 17–30 **Greater arc wrist injury.**[37,38,40] **A-B,** Frontal **(A)** and lateral **(B)** radiographs reveal a transscaphoid, transtriquetral, perilunate fracture-dislocation with ulnar styloid fracture. Also note the soft tissue swelling. **C,** Radiograph obtained after open reduction shows Kirschner wires used for stabilization. Marked disuse osteopenia is also present.

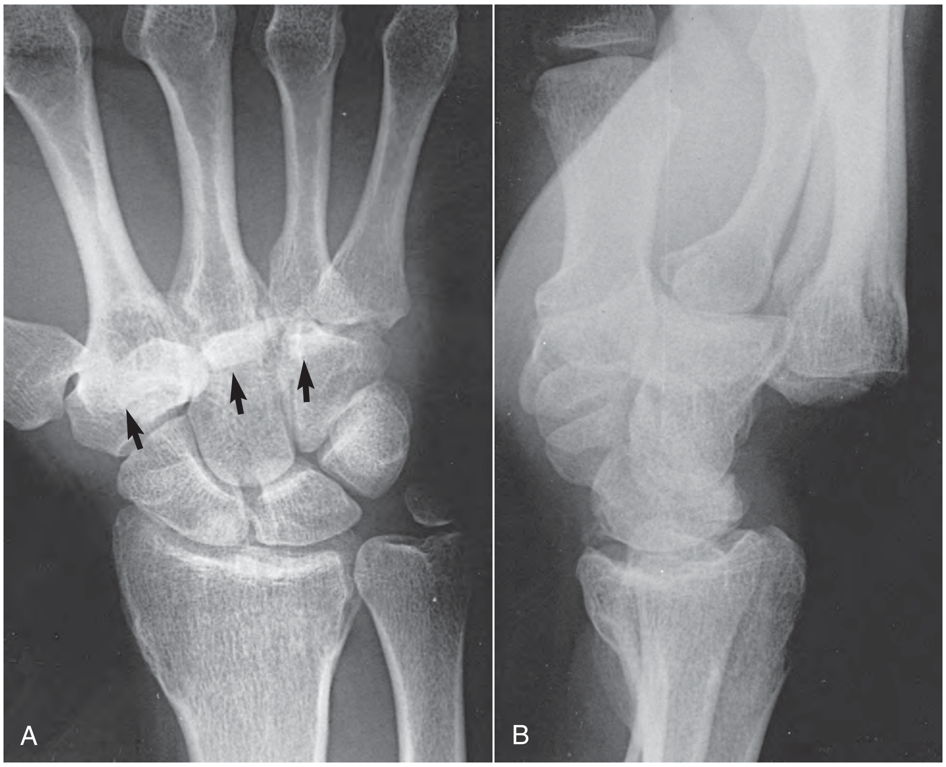

FIGURE 17–31 Dislocations of the common carpometacarpal joints.[42] Frontal **(A)** and lateral **(B)** radiographs show dorsal dislocation of the lateral four metacarpal bases with respect to the adjacent carpal bones. The metacarpal bases overlap the distal carpal row *(arrows)*. No associated fractures are evident.

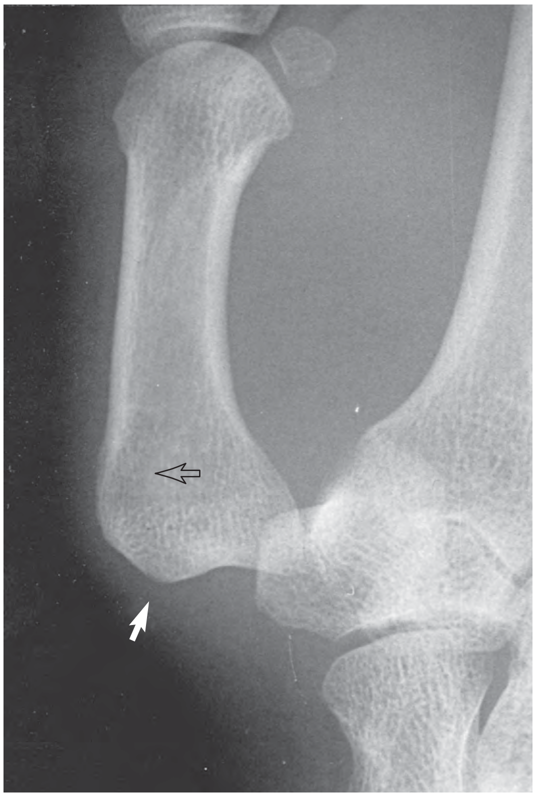

FIGURE 17–32 Dislocation of the first carpometacarpal joint.[43] Loss of continuity is seen between the trapezium and the base of the dorsally and medially dislocated first metacarpal bone *(arrow)*. The open arrow indicates the direction of displacement of the first metacarpal bone.

TABLE 17-5 Ligamentous Instability of the Wrist*

Entity	Figure(s)	Characteristics	Complications and Related Injuries and Disorders
Overview of wrist instability[44]		Several different patterns of instability have been identified *Criteria that suggest carpal instability:* abnormal carpal alignment on routine radiographs; scapholunate joint or ligament pain; reproducible painful clicking or popping; positive radiographic instability pattern in which abnormal motion is documented	*Complications of all types of instability:* Disabling wrist pain Osteoarthrosis Disability
Rotary subluxation of scaphoid and scapholunate dissociation[44-46]	17-33	*Rotary subluxation of the scaphoid:* most common type of wrist instability *"Ring" sign:* shortened scaphoid and ring produced by the cortex of the distal pole of the scaphoid on frontal radiograph Wide scapholunate joint Overlapping of scaphoid and capitate Increased scapholunate angle *Scapholunate dissociation:* frequent component of rotary subluxation of scaphoid and other patterns of instability Disruption of scapholunate interosseous ligament *Scapholunate separation on frontal radiograph:* 2 mm (suggested) or 4 mm (definite); "Terry Thomas" sign Occasionally, widened scapholunate joint may be a normal variant	*Predisposing disorders:* Acute and chronic trauma Rheumatoid arthritis Calcium pyrophosphate dihydrate (CPPD) crystal deposition disease Other patterns of wrist instability
Dorsal intercalated segmental instability (DISI)[44,47,48]	17-34	Common midcarpal instability Often associated with scapholunate dissociation Dorsally tilted lunate, flexed scaphoid, scapholunate angle greater than 80 degrees, and capitolunate angle greater than 30 degrees May occur with or without scapholunate dissociation	
Volar intercalated carpal instability (VISI)[44,47,48]	17-35	Less common than DISI Ventrally tilted lunate, scapholunate angle is less than 30 degrees, and capitolunate angle is greater than 30 degrees	
Scapholunate advanced collapse (SLAC wrist)[49]	17-36	Pattern of posttraumatic osteoarthrosis Narrowing of radioscaphoid and capitolunate spaces leading to scapholunate dissociation and eventual DISI	Associated with the following: Osteoarthrosis, calcium pyrophosphate dihydrate (CPPD) crystal deposition disease
Wrist subluxation: extrinsic ligament injury[204]	17-37	*Extrinsic ligaments of the wrist consist of:* • Radial and ulnar collateral ligaments • Volar radiocarpal ligaments • Meniscus homologue • Triangular fibrocartilage • Ulnolunate and ulnotriquetral ligaments • Dorsal ligaments Extrinsic ligaments of the wrist are stiffer and less capable of elongation than the intrinsic ligaments Disruption of extrinsic ligaments occurs with major trauma and typically results in ulnar translocation of the carpus	Severe wrist instability and degenerative disease

* Only the most frequent patterns are discussed here. For a more detailed discussion of wrist instability, see Yin Y, Mann FA, Hodge JC, et al: Roentgenographic interpretation of ligamentous instabilities of the wrist: Static and dynamic instabilities. In Gilula L, Yin Y (Eds): Imaging of the hand and wrist. Philadelphia, Saunders, 1996, p 203.

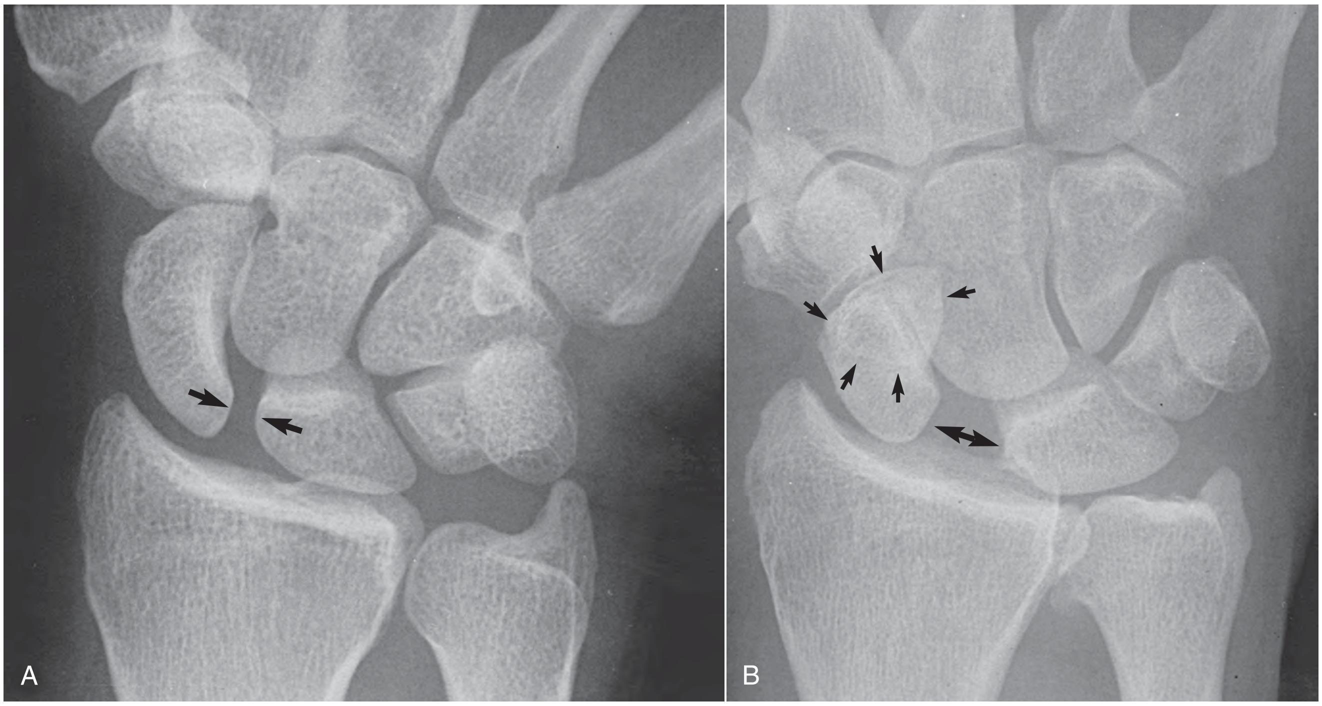

FIGURE 17–33 **Scapholunate dissociation (rotary subluxation of the scaphoid).**[44-46] **A,** The scapholunate distance is widened *(arrows)*. **B,** Radiograph of this 58-year-old man with wrist pain demonstrates widening of the scapholunate interosseous space *(double-headed arrow)* and a markedly shortened appearance of the scaphoid bone. Additionally, the distal pole of the scaphoid appears as a characteristic ringlike (Ring sign) structure owing to rotation of this bone *(small arrows)*. Scapholunate dissociation is suggested when the space between the scaphoid and lunate bones is 2 mm or wider, and it can be diagnosed with certainty if the distance is 4 mm or greater. Scapholunate separation results from perforation or disruption of the scapholunate interosseous ligament, and in cases in which the scaphoid has rotated in a palmar direction, a tear of the volar radiocarpal ligament is also present. In addition to routine radiographic projections, frontal radiographs should be obtained with ulnar deviation and radial deviation and with the patient's fist tightly clenched.

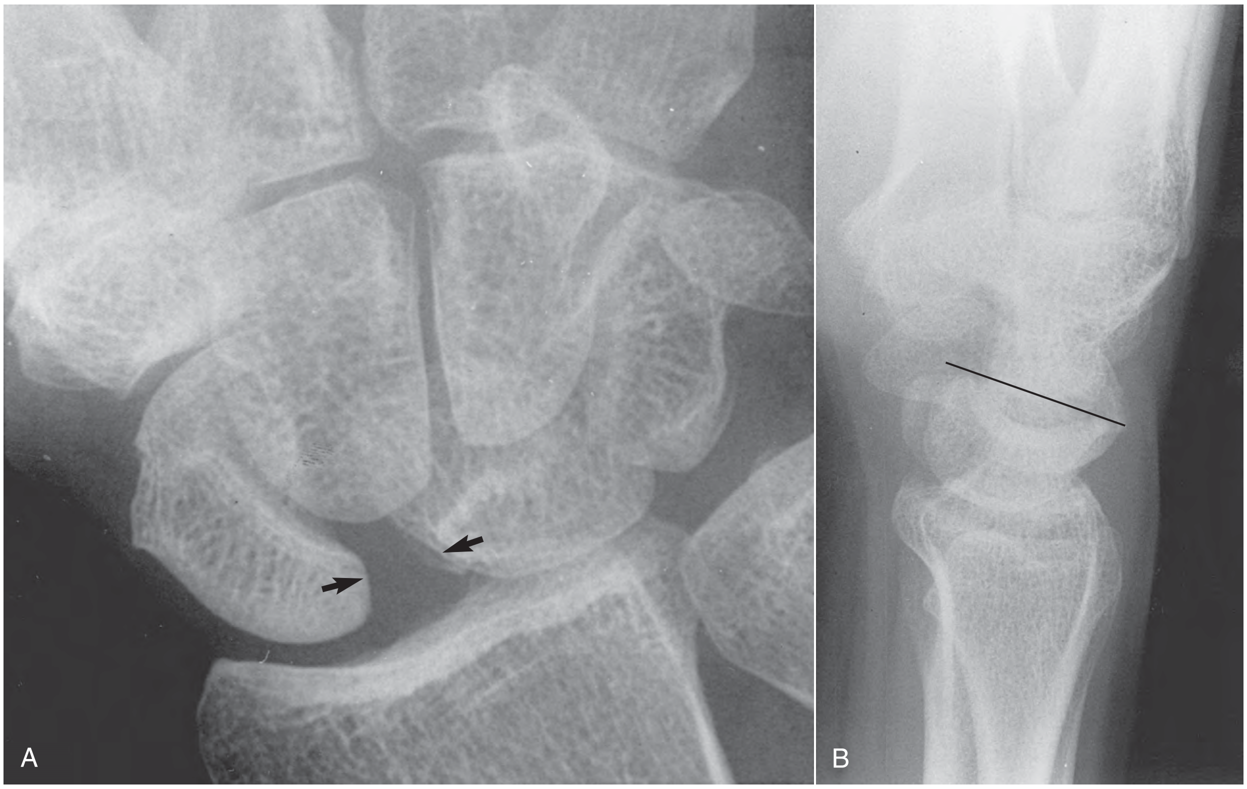

FIGURE 17–34 **Carpal instability: dorsal intercalated segmental instability (DISI).**[44,47,48] **A-B,** Findings include scapholunate joint space widening *(arrows)* and dorsiflexion of the lunate bone *(line)*. The radiocarpal and midcarpal joint spaces are narrowed.

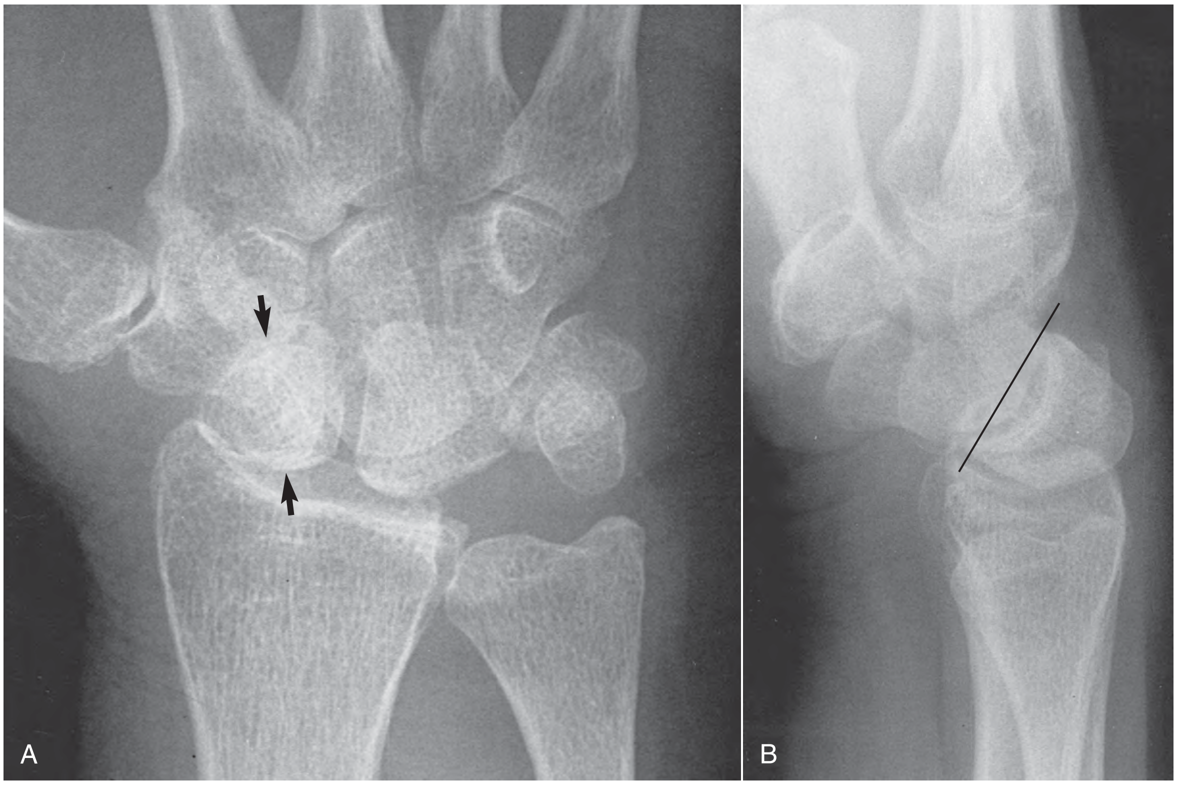

FIGURE 17–35 **Carpal instability: volar intercalated segmental instability (VISI).**[44,47,48] **A-B,** In this 72-year-old woman, the distal pole of the scaphoid bone shows palmar displacement, resulting in a ringlike shadow (Ring sign) *(arrows)* and volar tilting of the lunate bone *(line)*.

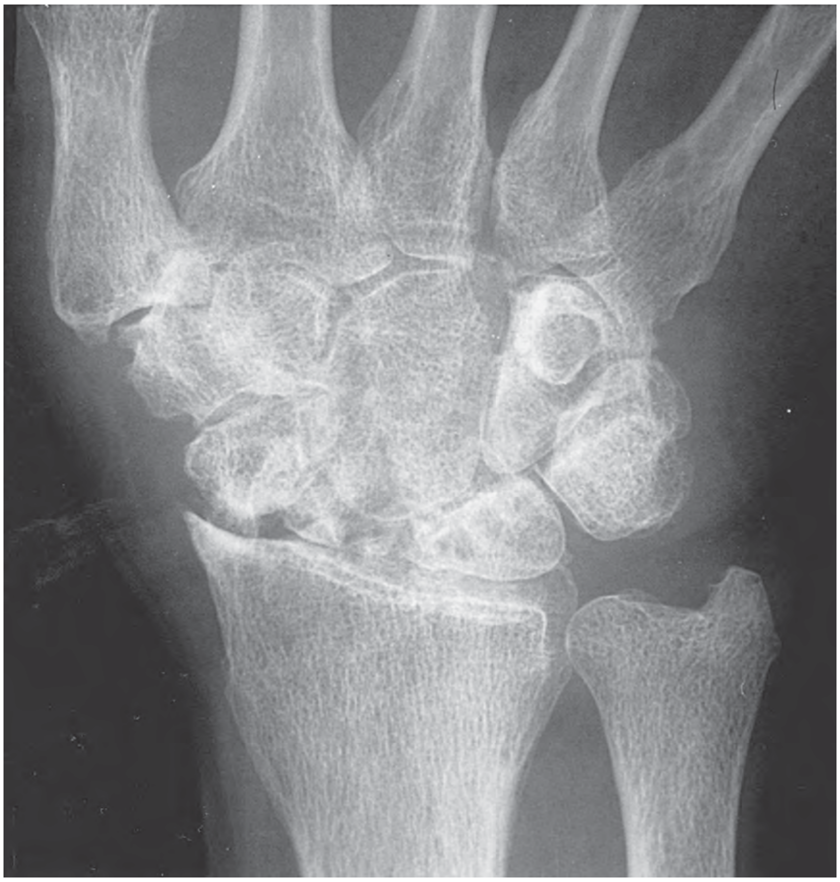

FIGURE 17–36 **Carpal instability: scapholunate advanced collapse (SLAC) wrist.**[49] In this patient with severe degenerative joint disease, observe the presence of scapholunate dissociation, narrowing of the radiocarpal and midcarpal articulations, and flattening of the scaphoid and lunate bones. These radiographic findings, seen in association with degenerative joint disease or calcium pyrophosphate dihydrate (CPPD) crystal deposition disease, are termed *SLAC wrist*.

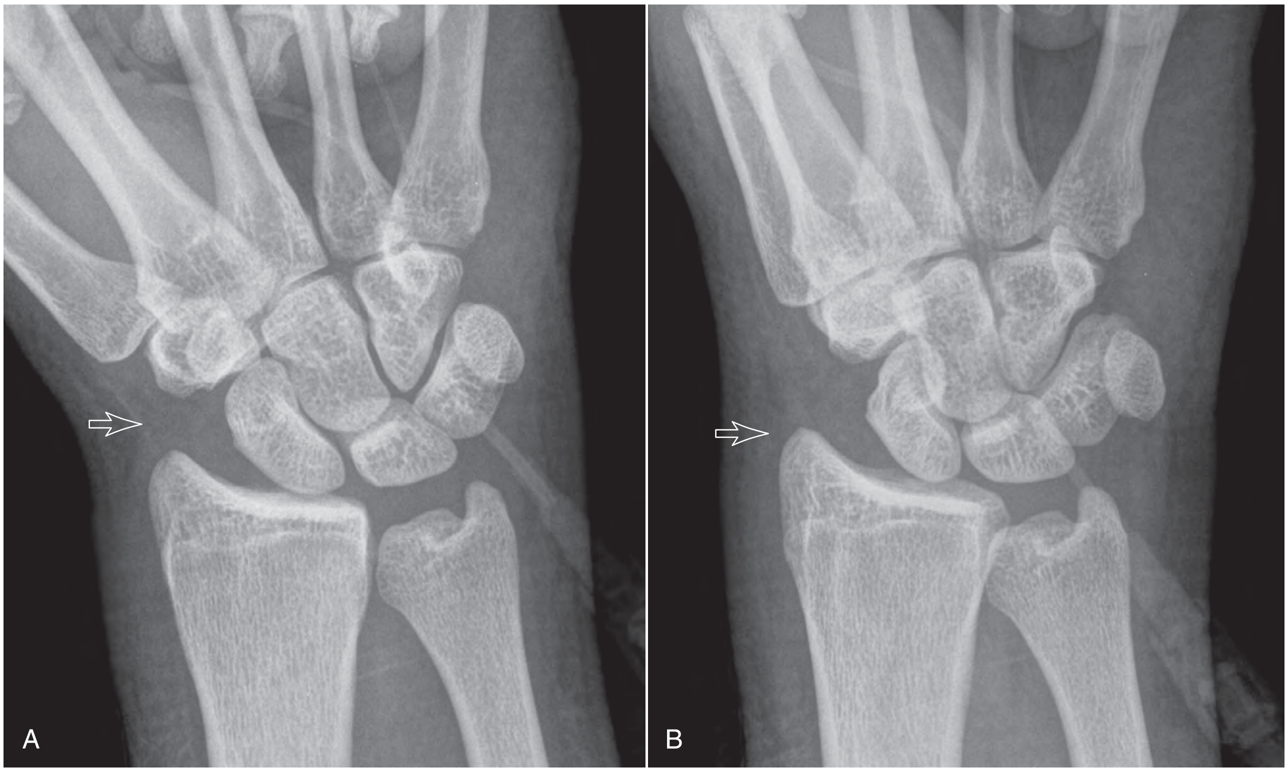

FIGURE 17–37 **Wrist subluxation: extrinsic ligament injury.**[204] This 24-year-old man was involved in a motor vehicle collision. Posteroanterior **(A)** and oblique **(B)** wrist radiographs reveal ulnar translocation (subluxation toward the ulnar side of the wrist in the direction of the *open arrows*) of all the carpals with respect to the radius and ulna. This injury results from severe trauma and involves disruption of the major extrinsic ligaments normally responsible for stabilizing the wrist.

TABLE 17-6 Fractures and Dislocations of the Hand*

Entity	Figure(s)	Characteristics	Complications and Related Injuries
Metacarpophalangeal (MCP) joint dislocations[30,50]		Second to fifth MCP joints ***Mechanism*** Forced hyperextension from fall on an outstretched hand Index finger most common site Classified as simple (reducible) or complex (potentially irreducible) Metacarpal head is usually displaced into the palm	Disruption of volar plate Interposition and entrapment of the volar plate or sesamoid bone
Interphalangeal joint dislocations[51]	17-38	Proximal interphalangeal joint dislocations very common Usually involve only one joint Posterior dislocation results from hyperextension injury Anterior dislocations less common	Associated phalangeal fracture Associated ligamentous and volar plate injuries common Intraarticular fracture-dislocation with joint instability Interposition of volar plate or flexor tendon Entrapment of sesamoid bone of thumb can prevent reduction
Bennett fracture-dislocation[52]	17-39	Intraarticular fracture of the base of the first metacarpal bone Axial blow to a partially flexed first metacarpal bone Fracture of a small fragment of the volar lip Base of metacarpal bone is displaced dorsally and radially	Osteoarthrosis
Rolando fracture[52,53]	17-40	Y- or T-shaped comminuted fracture of the base of the first metacarpal bone	Osteoarthrosis
Gamekeeper thumb[54-56,191]	17-41	Disruption of the ulnar collateral ligaments (UCL) of the first MCP joint A common mechanism is the ski pole injury—violent abduction-extension (valgus) force applied to the thumb; represents 6% of all ski injuries Unstable condition involving rupture of the ulnar collateral ligaments ***Clinical findings*** Pain, swelling, tenderness, edema, and pinch instability Routine radiographs cannot help differentiate between displaced and nondisplaced tears; however, MR imaging is effective in depicting such displacement Initial radiographs may appear normal, or they may show a small fragment of avulsed bone at the base of the proximal phalanx in some cases Multiple radiographic projections allow a more complete evaluation of alignment and apposition of phalangeal fractures	Pinch instability Avulsion of bone with rotation of fragments *Stener lesion:* abnormal folded position of the UCL in which the ligament becomes displaced and trapped superficially to the adductor pollicis aponeurosis; interferes with healing and necessitates surgery

* For a more detailed discussion of the distribution and type of hand fractures in children, see reference 195.

Continued

TABLE 17-6 Fractures and Dislocations of the Hand—cont'd

Entity	Figure(s)	Characteristics	Complications and Related Injuries
Dorsal dislocation of the first MCP joint[57]	17-42	Results from forcible hyperextension of the thumb	Ligament injury with instability Interposition and entrapment of a sesamoid bone
Metacarpal fractures[30,58,195]	17-43	Most commonly involve first and fifth metacarpal bones *Typical sites:* shaft and neck of fifth metacarpal (bar-room fracture) Shaft of third or fourth metacarpal bone (or both of these) (boxer's fracture)	Displacement, angulation, or rotation commonly encountered Rotation, if not corrected, may lead to serious disability
Phalangeal fractures[30,59,60,195]	17-44, *A*	More frequent than metacarpal fractures Distal phalanx most common, followed by proximal and middle phalanges	Associated tendon injuries and dislocations
	17-44 *B, C*	Fractures with intraarticular extension or rotational deformity Small intraarticular fractures may be subtle on routine radiographs and may require multiple projections	May result in marked disability or loss of functional capacity
	17-44, *D*	Mallet fracture: avulsion injury at the base of the dorsal surface of the terminal phalanx with disruption of the extensor mechanism	*Damage to the extensor tendon mechanism:* mallet finger with persistent flexion deformity and inability to extend the finger
	17-44, *E*	*Nailbed injury:* open skin surface may expose bone or joint	Secondary infection Growth plate injury in children
	17-44, *F*	*Growth plate fractures:* involve the distal phalangeal physes in children	Deformity and growth abnormalities
	17-44, *G*	*Volar plate fracture:* dorsal dislocation of a proximal interphalangeal joint is associated with an avulsion fracture in the middle phalanx at the site of attachment of the volar plate	Damage to the flexor tendon mechanism resulting in inability to flex the finger at proximal interphalangeal joint
Phalangeal stress injuries[61,62]	17-45	Extremely rare injuries *Phalanges:* bowlers *Phalangeal tufts:* guitar players	
Child abuse[63]		Torus fractures of the metacarpal bones and phalanges have been reported Most likely mechanism is forced hyperextension of fingers	Other fractures and injuries at different sites

See also Tables 1-4 and 1-6.

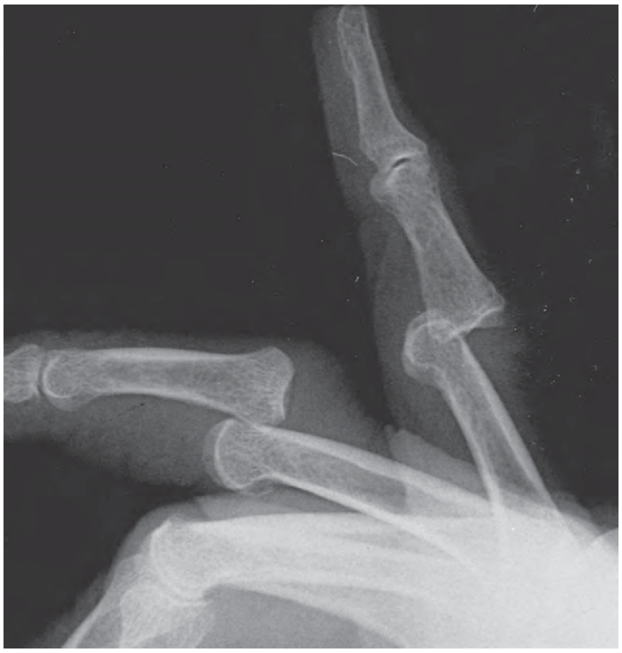

FIGURE 17–38 **Interphalangeal joint dislocation.**[51] Dorsal dislocations of the fourth and fifth proximal interphalangeal joints are evident. No associated fractures are observed. Such dislocations are common, occur as a result of hyperextension, and usually affect only one interphalangeal joint. Radiographs should be observed carefully for associated fractures.

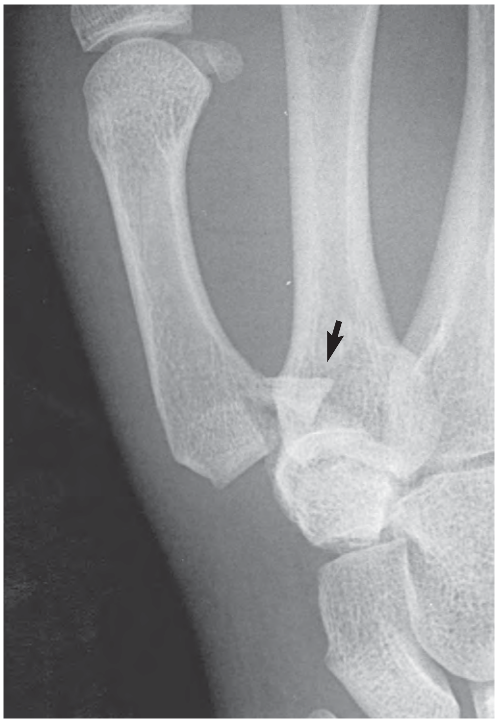

FIGURE 17–39 **Intraarticular injuries of the first metacarpal base: Bennett fracture-dislocation.**[52] A typical oblique fracture of the volar lip of the first metacarpal base with a single displaced fragment *(arrow)* is evident on this radiograph. Bennett fracture is a relatively common intraarticular injury that occurs at the base of the first metacarpal bone. It involves an axial force applied to a partially flexed metacarpal bone. The base of the metacarpal bone is pulled dorsally and radially and is separated by an oblique fracture line from a fragment of bone from the volar lip.

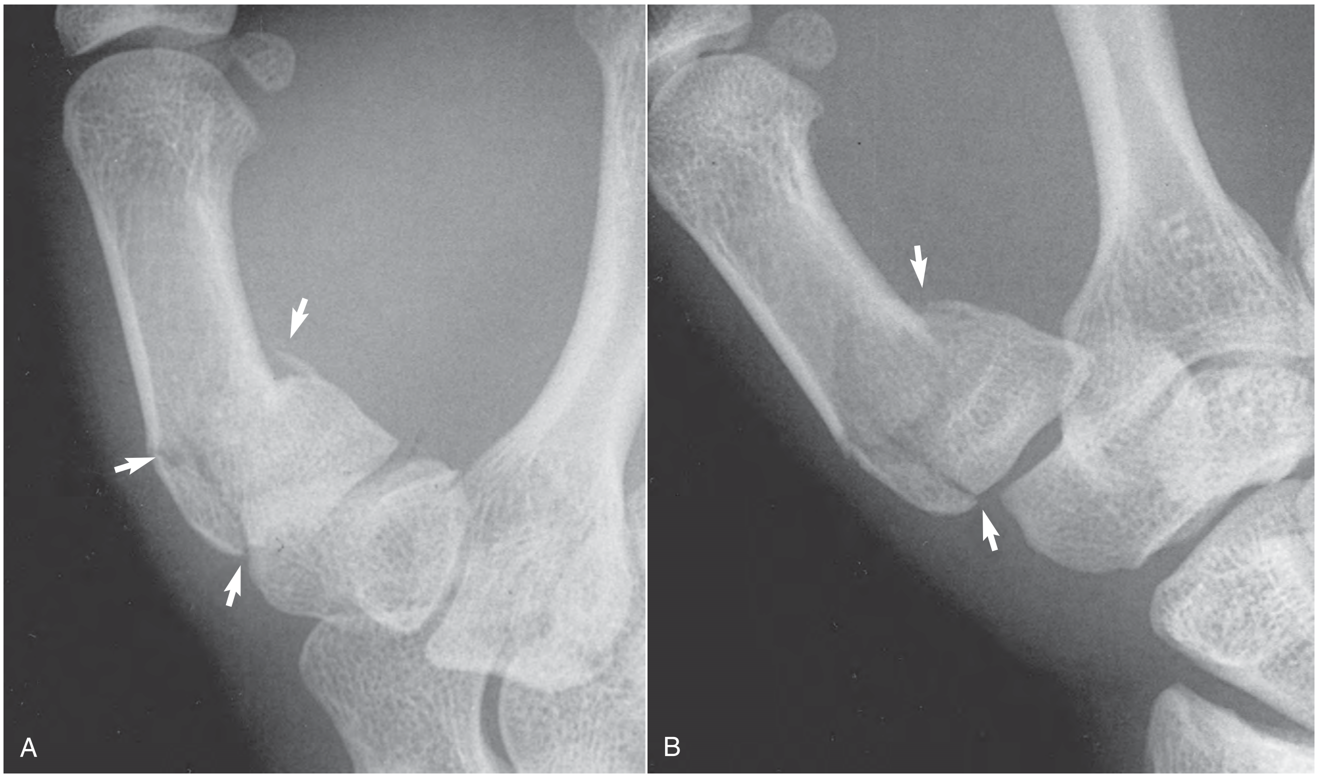

FIGURE 17–40 **Intraarticular injuries of the first metacarpal base: Rolando fracture.**[52,53] **A-B,** Two projections of the thumb reveal a comminuted intraarticular fracture at the base of the first metacarpal bone *(arrows)*.

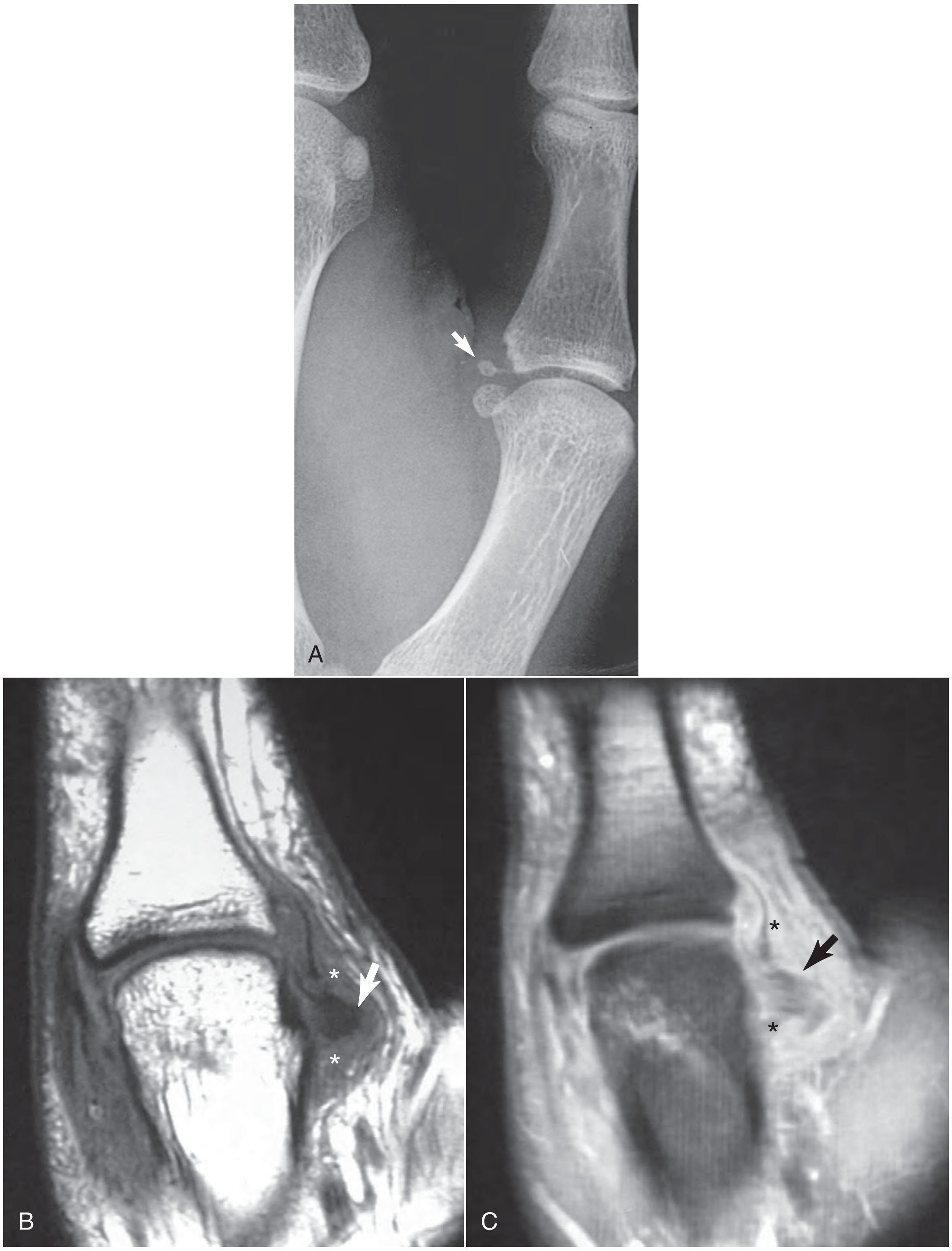

FIGURE 17–41 Gamekeeper's thumb.[54-56,191] **A,** Routine posteroanterior radiograph shows a small osseous fragment *(arrow)* avulsed from the base of the first proximal phalanx. **B-C,** Stener lesion**.** Coronal T1-weighted **(B)** and intermediate-weighted **(C)** MR images of the first metacarpophalangeal joint in another patient shows an abnormal folded position of the torn ulnar collateral ligament *(arrows)*. The ligament is displaced and trapped superficially to the adductor pollicis aponeurosis. The surrounding inflammatory edema (*) appears as low signal intensity on T1-weighting **(B)** and as high signal intensity on proton-density weighting **(C).** This abnormal ligament displacement, designated a Stener lesion, may interfere with healing and often requires surgical correction. The appearance of the retracted and balled up ulnar collateral ligament lying proximal and superficial to the adductor aponeurosis is referred to as the *yo-yo on a string* sign.

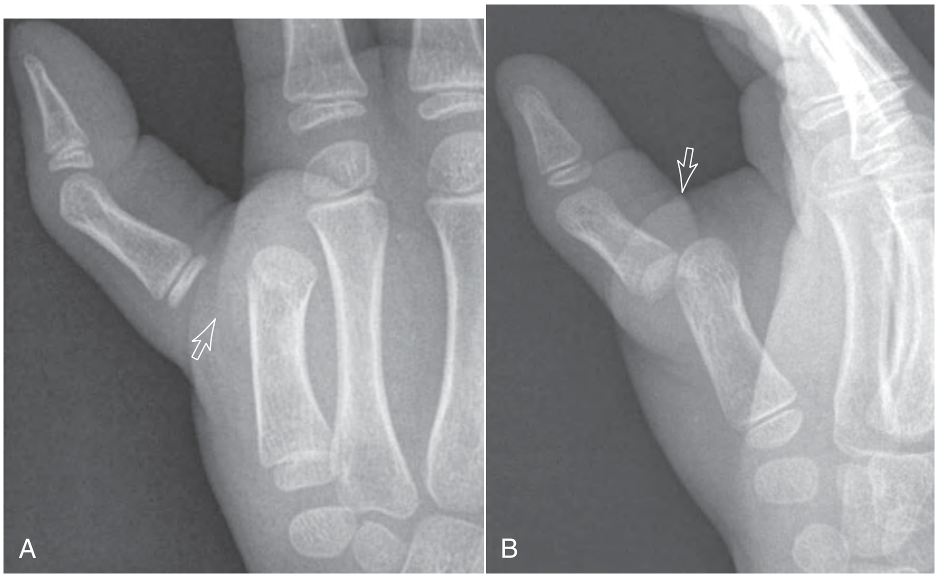

FIGURE 17–42 **Dislocation of first metacarpophalangeal joint.**[57] Radiographs of the hand obtained after a fall in this 7-year-old girl show dislocation of the first metacarpophalangeal joint *(open arrows)*. The proximal phalanx is displaced in a radial and slightly volar direction. There is no evidence of fracture or epiphyseal displacement.

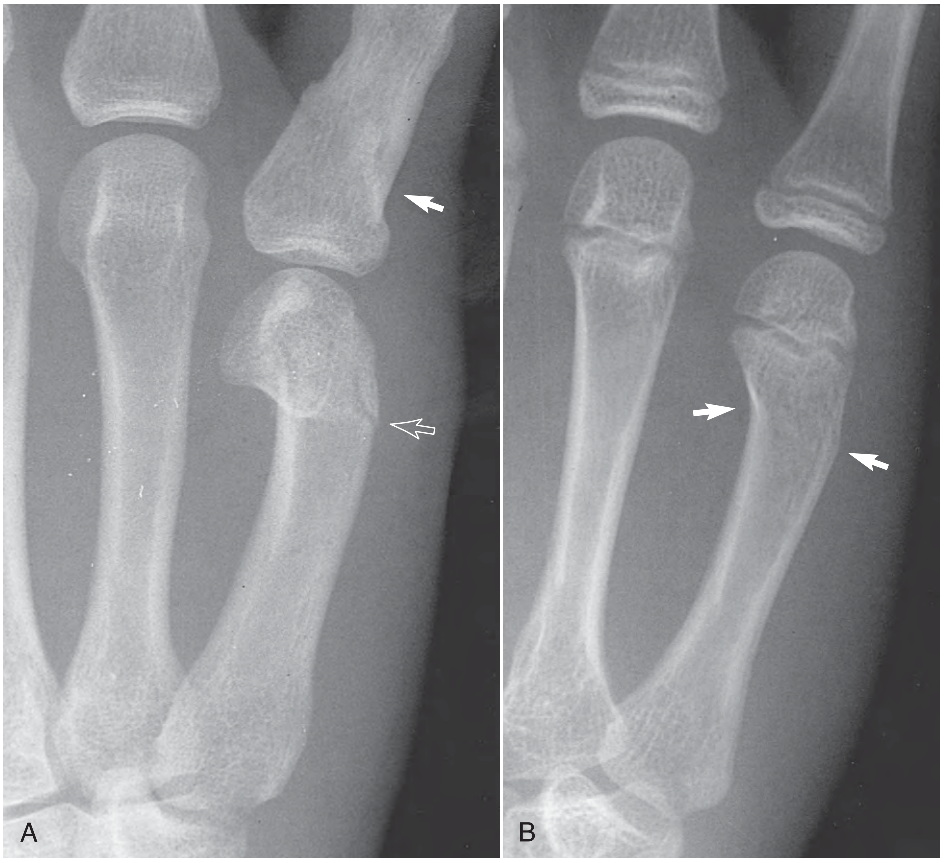

FIGURE 17–43 **Metacarpal fractures.**[30,58] **A,** This 21-year-old man fractured his distal fifth metacarpal bone *(open arrow)* in a fistfight. Volar angulation is associated with the fracture. Of incidental note is a previously healed oblique fracture of the fifth proximal phalanx *(arrow)*. **B,** In an 11-year-old girl, a fracture of the fifth metacarpal bone is seen as buckling of the cortex *(arrows)* and minimal radial displacement. Fractures of the metacarpal neck or shaft are sometimes referred to as *boxer's fractures* or *bar room fractures*. Rotation of the fracture fragment may lead to serious disability if not corrected.

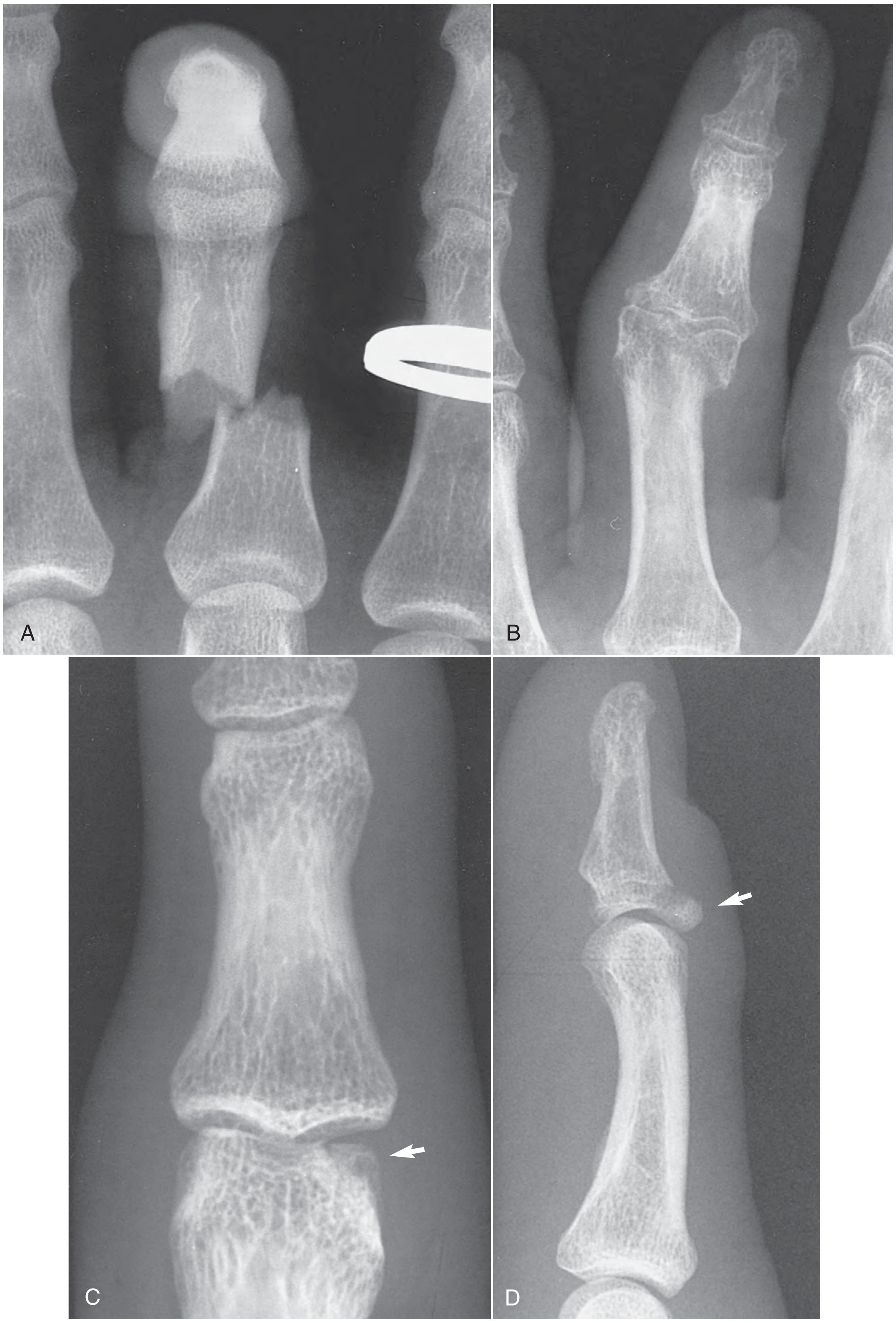

FIGURE 17–44 Phalangeal fractures.[30,59,60] **A,** Displaced fracture of the midshaft of the phalanx shows poor alignment and apposition. **B,** Radiograph of another patient shows a displaced intraarticular fracture of the distal end of the proximal phalanx with ulnar deviation of the distal fragment. **C,** In yet another patient, an intraarticular fracture of the head of the proximal phalanx is demonstrated *(arrow)*. **D,** Mallet finger. Observe the small fragment of bone at the proximal portion of the extensor surface of the distal phalanx *(arrow)*. This injury results from avulsion at the insertion of the extensor tendon mechanism. It is typically associated with a 40- to 45-degree flexion deformity, and the patient has loss of active extension at the distal interphalangeal joint.

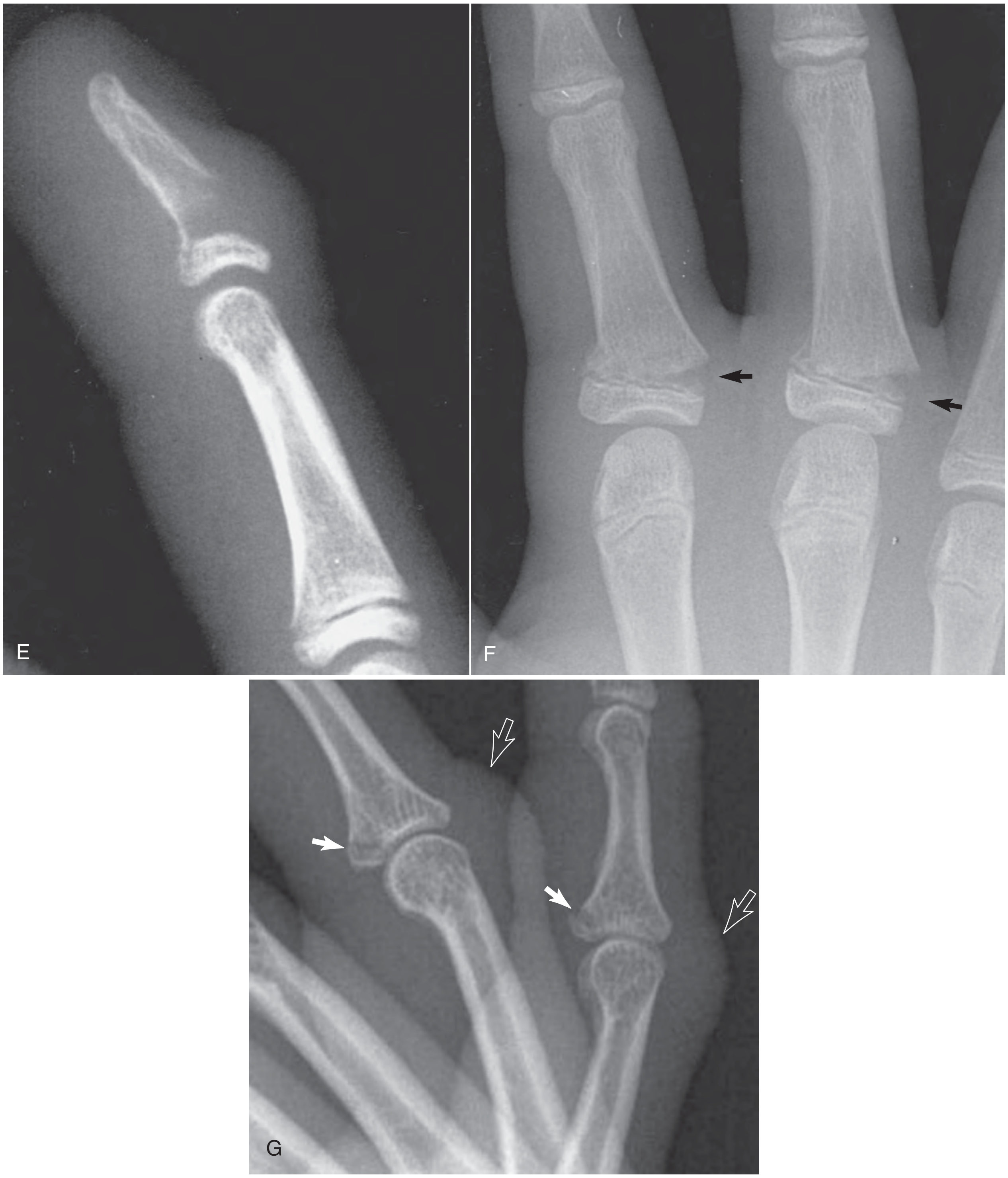

FIGURE 17–44, cont'd **E,** Nail-bed injury. This 14-year-old boy sustained a hyperflexion injury of his finger. A Salter-Harris type I fracture of the terminal phalanx is present, with epiphyseal displacement, bone resorption, and soft tissue swelling. This type of injury usually disrupts the nail bed, exposing the underlying tissues to the environment and rendering them susceptible to infection. **F,** Growth plate injuries. Salter-Harris type II fractures of the second and third proximal phalangeal bases are seen *(arrows)*. **G,** Volar plate fracture. This 39-year-old woman sustained a traumatic injury to the fingers. Oblique fractures of the volar corners of the middle phalanges of the fourth and fifth fingers *(arrows)* are accompanied by considerable soft tissue swelling *(open arrows)*.

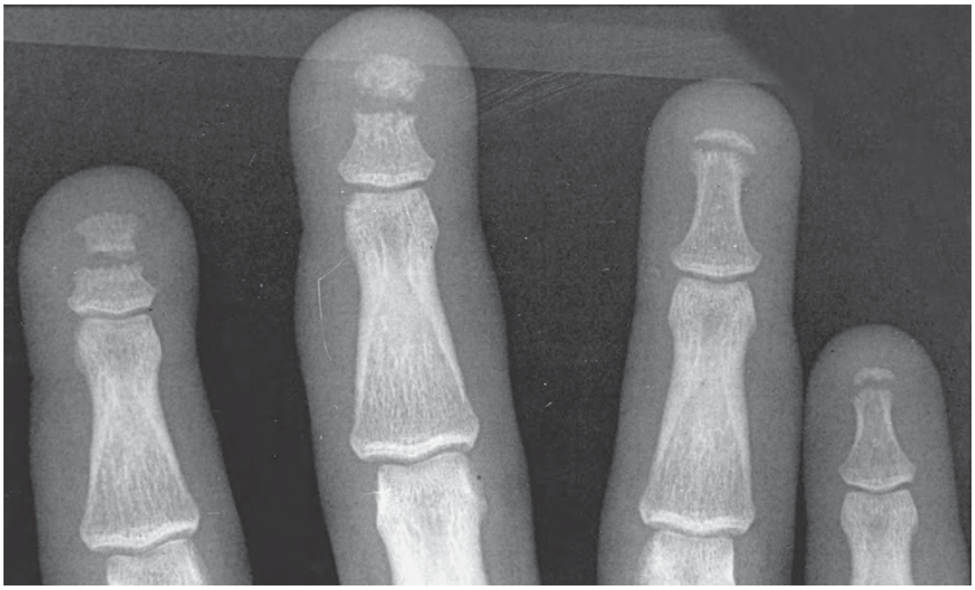

FIGURE 17–45 **Phalangeal stress fractures: guitar player acro-osteolysis.**[61,62] This enthusiastic guitar player sustained fatigue fractures of several terminal phalanges, a condition that has been termed *guitar player acro-osteolysis*. Observe the radiolucent bands traversing the terminal tufts.

TABLE 17-7 Soft Tissue Disorders Affecting the Wrist and Hand

Entity	Figure(s)	Characteristics
Ligament injuries[44]		See wrist instability (Table 17-5)
Lesions of the triangular fibrocartilage (TFC) complex[64,65]	17-46	Full-thickness and partial-thickness defects occur as a result of degeneration or trauma Traumatic avulsion from ulnar or radial attachments also may occur Arthrography and MR imaging have limited usefulness owing to the occurrence of communicating defects of the TFC complex in asymptomatic persons
Abnormalities of the extensor and flexor tendons and tendon sheaths[66]	17-47	*Spectrum of abnormalities:* Tendinitis and tenosynovitis: inflammation of tendons and tendon sheaths (i.e., De Quervain syndrome: tenosynovitis of the abductor pollicis longus and extensor brevis tendons) *Tendon rupture:* partial or complete disruption with retraction of tendon or avulsion of tendon sheath; may result in inability to extend or flex the fingers (i.e., mallet finger with disruption of extensor tendon resulting in persistent flexion deformity at distal interphalangeal joint [Figure 17-44, *D*]) MR imaging is the most useful imaging study for most of these disorders
Carpal tunnel syndrome (CTS)[67,195]	17-48, 17-52	Entrapment of median nerve within the carpal tunnel *Some causes:* tenosynovitis of the flexor tendon sheaths, rheumatologic disorders, infiltrative diseases, trauma, neoplasms, anatomic factors, diabetes mellitus, pregnancy, osteoarthrosis; idiopathic Clinical history, physical examination, and electromyography, usually diagnostic Ultrasonography is comparable to electrodiagnostic studies in diagnosis of CTS and should be considered as the initial test of choice for patients suspected of having CTS CT and MR imaging also play a role in evaluation: Swelling of median nerve (at level of pisiform bone) Flattening of median nerve (at level of hamate bone) Palmar bowing of flexor retinaculum (at level of hamate bone) Increased signal intensity of median nerve on T2-weighted images
Ganglion cyst[68,69]	17-49	Most commonly occurring soft tissue mass about the wrist Fibrous walled mass containing clear mucinous fluid Arises from joint capsules, tendons, or tendon sheaths, especially on extensor surface of wrist Ultrasonography and MR imaging often useful in evaluation
Glomus tumor[70,196]	17-50	Benign soft tissue lesion at base of nail that may involve the terminal phalanx Shallow well-marginated erosion of adjacent bone Approximately 27% of glomus tumors are recurrent after initial surgical removal MR imaging is useful in detecting recurrent glomus tumors and allows differentiation from scar tissue
Giant cell tumor of tendon sheath[71]	17-51	Benign giant cell tumors of soft tissues may arise from tendon sheaths about the wrist or, more frequently, in the fingers Closely resembles pigmented villonodular or nodular synovitis Soft tissue mass may result in erosion of adjacent bone
Fibrolipomatous hamartoma[201]	17-52	*Benign neoplasm of nerves:* anomalous growth of fibroadipose tissue of the nerve sheath Median nerve is the most commonly involved nerve *MR imaging features are pathognomonic:* A coaxial cablelike appearance on axial images Spaghetti-like appearance on coronal images

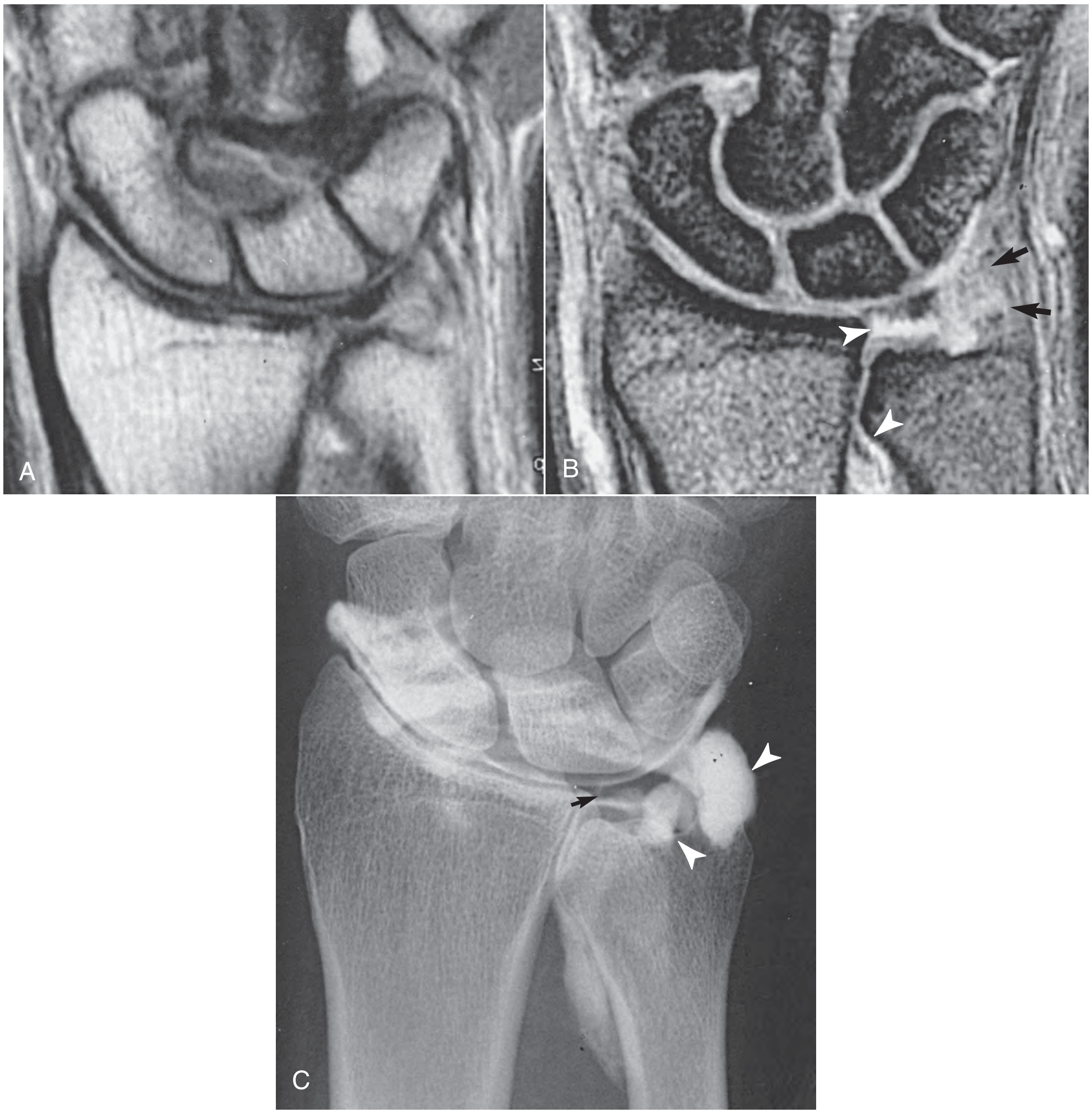

FIGURE 17–46 **Triangular fibrocartilage complex: ulnar detachment.**[64,65] **A-B,** Coronal proton-density–weighted (TR/TE, 2500/20) spin echo **(A)** and multiplanar gradient recalled (MPGR) (TR/TE, 549/15; flip angle, 35 degrees). **(B)** Magnetic resonance (MR) images show abnormal separation of the triangular fibrocartilage complex from the distal portion of the ulna and absence of visualization of the ulnar-sided attachments of the complex. In **B,** abnormal high signal intensity *(arrows)* is evident in this region, and fluid is present in the distal radioulnar joint *(arrowheads)*. **C,** Radiocarpal joint arthrogram shows a communicating defect in the triangular fibrocartilage complex *(arrow),* abnormal collections of contrast agent about the ulna *(arrowheads),* and proximal extravasation of contrast material from the distal radioulnar joint. *(From Resnick D, Kang HS, Pretterklieber ML: Internal derangements of joints. 2nd Ed. Philadelphia, Saunders, 2006, p 1258.)*

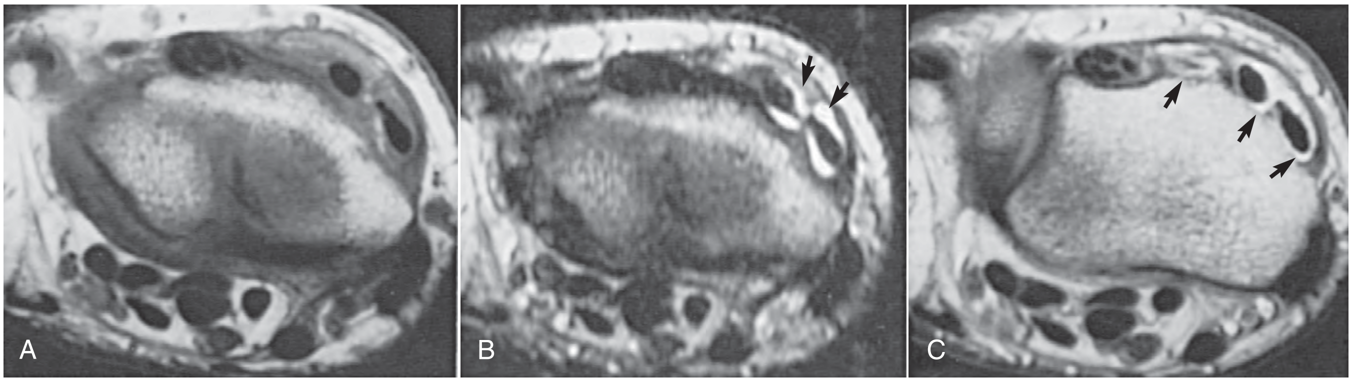

FIGURE 17–47 **Tenosynovitis of the tendon sheaths of the extensor pollicis longus and the extensor carpi radialis brevis and longus tendons: MR imaging.**[66] Transaxial T1-weighted (TR/TE, 700/17) **(A)** and T2-weighted (TR/TE, 2000/80) **(B)** spin echo MR images and a transaxial T1-weighted (TR/TE, 650/20) spin echo MR image after intravenous administration of gadolinium compound **(C)** show the enlarged tendon sheaths. The high signal intensity *(arrows)* in **B** and **C** is consistent with the presence of synovial inflammatory tissue. *(From Resnick D, Kang HS: Internal derangements of joints. Philadelphia, Saunders, 1997, p 448.)*

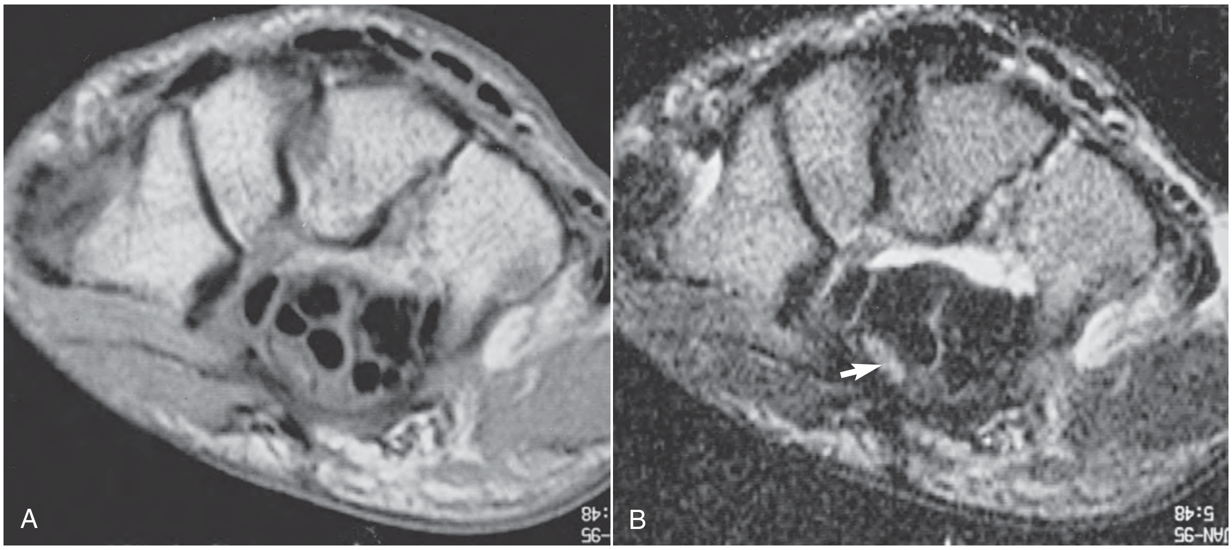

FIGURE 17–48 **Carpal tunnel syndrome: MR imaging.**[67,195] Transverse proton–density-weighted (TR/TE, 1800/20) **(A)** and T2-weighted (TR/TE, 1800/80) **(B)** spin echo MR images in a patient with clinical evidence of severe carpal tunnel syndrome, show bowing of the flexor retinaculum, fluid dorsal to the flexor tendons and sheaths, and increased signal intensity of the median nerve *(arrow)* in **B.** *(From Resnick D, Kang HS, Pretterklieber ML: Internal derangements of joints. 2nd Ed. Philadelphia, Saunders, 2006, p 1327.)*

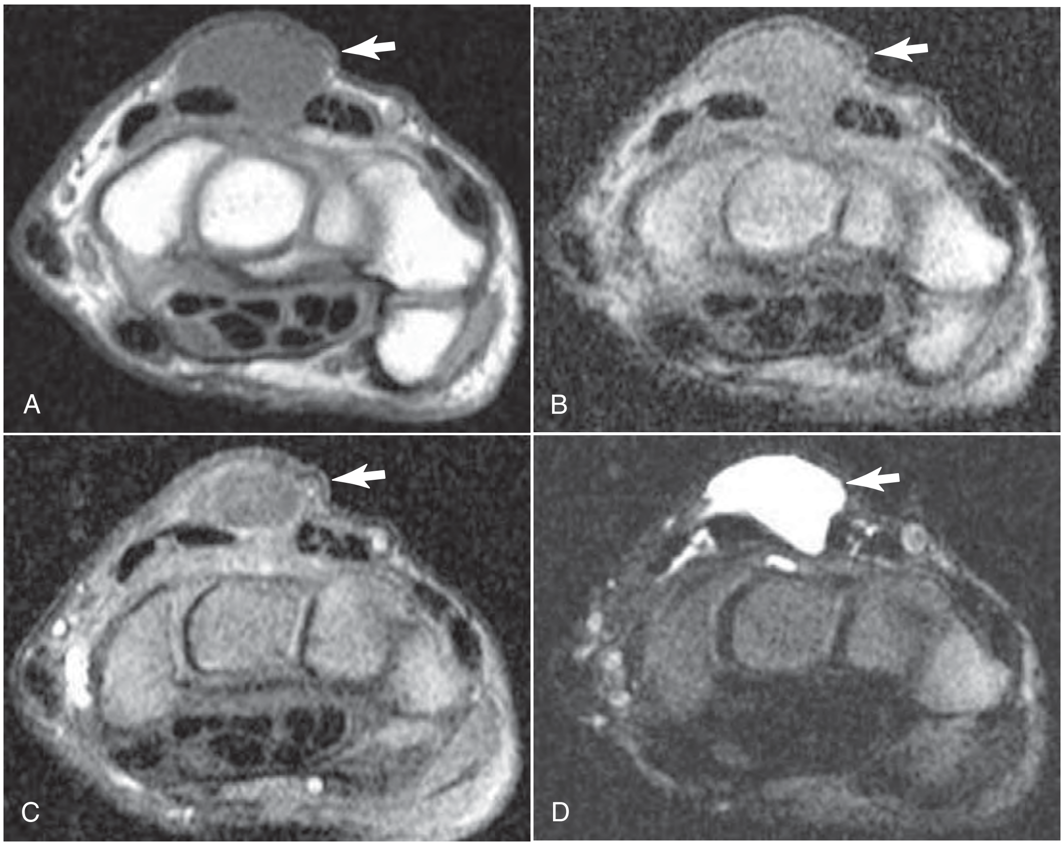

FIGURE 17–49 **Ganglion cyst.**[68,69] Multiple axial MR images of the wrist in this 45-year-old woman with a lump on the dorsum of her wrist reveal a homogenous subcutaneous soft tissue mass *(arrows)*. The mass is isointense to muscle on the T1-weighted image **(A);** it is of intermediate signal intensity (still isointense to muscle) on fat-suppressed T1-weighted images before intravenous gadolinium administration **(B)** and shows only minimal peripheral enhancement of the surrounding compressed tissues after gadolinium administration **(C).** The fluid-filled mass is most conspicuous as high signal intensity on the T2-weighted image with fat saturation **(D).**

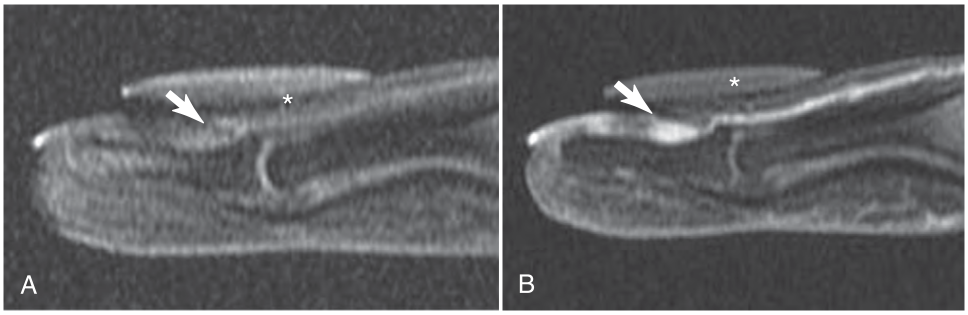

FIGURE 17–50 **Glomus tumor.**[70,196] A 43-year-old female with a painful distal ring finger. A sagittal fat-suppressed T1-weighted image **(A)** shows a mildly hyperintense ovoid soft tissue mass that erodes the dorsal cortical surface of the distal phalanx *(arrow)*. **B,** The enhancing lesion and the adjacent erosion are more conspicuous on an equivalent image after administration of intravenous gadolinium *(arrow)*. (The linear structure adjacent to the dorsal surface of the finger (*) is a marker to indicate the site of pain.)

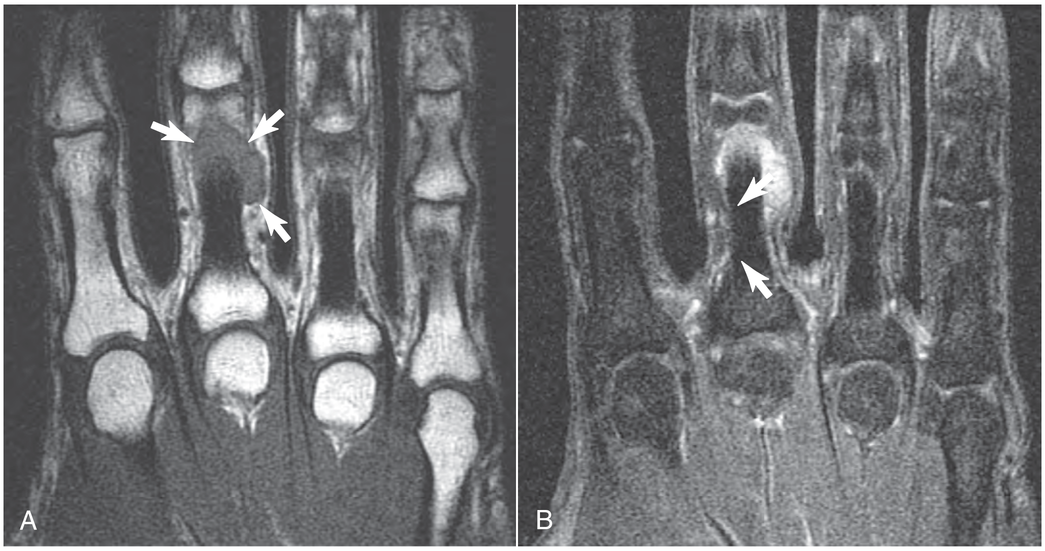

FIGURE 17–51 **Giant cell tumor of a tendon sheath.**[71] A 35-year-old man with painful mass in the third finger. Coronal T1-weighted images before **(A)** and after **(B)** fat suppression and intravenous gadolinium administration reveal a soft tissue mass *(arrows)* enveloping the metaphysis of the third proximal phalanx and creating a mass effect in the adjacent subcutaneous tissues. The mass appears isointense to muscle on the standard T1-weighted image, but exhibits significant enhancement after contrast administration.

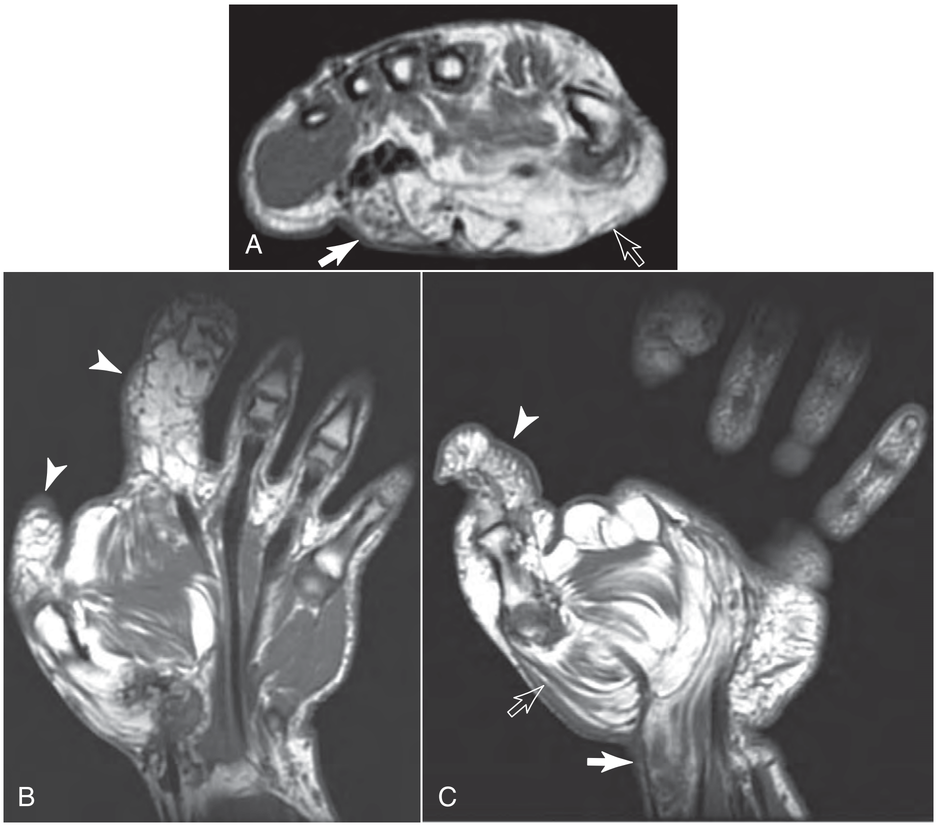

FIGURE 17–52 **Fibrolipomatous hamartoma**[201] **and macrodystrophia lipomatosa.**[16,17] This 39-year-old man presented with deformity and enlargement of the thumb and index finger and carpal tunnel syndrome. Axial **(A)** and coronal **(B-C)** T1-weighted MR images show grotesque enlargement of the first two digits with subcutaneous multiloculated collections of fat density *(arrowheads)* and swirls of fibrofatty infiltration within the thenar eminence *(open arrows),* all consistent with the appearance of macrodystrophia lipomatosa. In addition, linear low signal intensity strands intermixed with fatty tissue *(arrows)* envelop the median nerve within its distended sheath in the carpal tunnel. On the axial projection, these strands appear as a cluster of low signal intensity circular structures (arrow on Figure **A**). These strandlike findings represent the pathognomonic appearance of fibrolipomatous hamartoma (neural fibrolipoma), a rare benign condition characterized by fibroadipose tissue occupying the nerve sheath, most commonly involving the median nerve.

TABLE 17-8 Articular Disorders of the Wrist and Hand

Entity	Figure(s)	Characteristics
Degenerative and Related Disorders		
Primary osteoarthrosis[72-75,190]	17-53	Primary osteoarthrosis predominantly involves the interphalangeal joints and first carpometacarpal joints May also be age-related
Secondary osteoarthrosis[76,190]	17-54	Secondary osteoarthrosis may involve any previously injured joint Repeated trauma to the metacarpophalangeal joints in boxers and manual laborers is referred to as *boxer's arthropathy* or *Missouri metacarpal syndrome* Nonuniform joint space narrowing Subchondral sclerosis Osteophytes Subluxation Recent MR imaging analysis has revealed that marginal erosions typical of those seen in inflammatory arthritis are a more common feature of interphalangeal joint osteoarthrosis than conventional radiographs have previously indicated
Erosive (inflammatory) osteoarthritis[77-80,187]	17-55	Believed to be an inflammatory subset of osteoarthrosis characterized by acute painful inflammatory episodes in elderly patients Predilection for interphalangeal joints but may also involve the first carpometacarpal joint Central erosions Nonuniform joint space narrowing Subchondral sclerosis Osteophytes Subluxation
Inflammatory Disorders		
Rheumatoid arthritis[81,82]	17-56	Bilateral symmetric, concentric joint space narrowing, erosion, periarticular osteopenia, deformities and subluxation
Juvenile idiopathic arthritis[83,84]	17-57	Soft tissue swelling Diffuse, bilateral symmetric joint space loss and erosion, periarticular osteoporosis, ballooning of epiphyses, premature epiphyseal fusion, and joint ankylosis
Ankylosing spondylitis[85]	17-58	Erosions and periarticular enthesopathy (whiskering) predominates about the wrist Changes in fingers resemble those of psoriasis Infrequently, may result in partial or complete intraarticular osseous ankylosis
Psoriatic arthropathy[78,86-88,179]	17-59	Predilection for distal and proximal interphalangeal joints Central and peripheral erosions and fluffy, poorly defined periarticular periostitis *Ray pattern:* involvement of several joints within the same digit *Diffuse soft tissue swelling:* sausage digit Preservation of bone density
Reactive arthritis associated with Reiter syndrome[87-89,179]	17-60	Findings identical to those of psoriatic arthropathy but a greater predilection for lower extremity
Systemic lupus erythematosus[90]	17-61	Articular signs and symptoms present in as many as 90% of patients Deforming nonerosive arthropathy Myositis, polyarthritis, subchondral cysts, tendon weakening and rupture, soft tissue calcification, acrosclerosis, tuft resorption
Jaccoud arthropathy[91]	17-62	One form of nonerosive deforming arthropathy with reversible subluxations resulting from capsular inflammation and fibrosis; involves mainly the fourth and fifth metacarpophalangeal joints Seen in patients with rheumatic fever, systemic lupus erythematosus, scleroderma, and other collagen vascular disorders Nonerosive deforming arthropathy is seen less commonly in agammaglobulinemia, Ehlers-Danlos syndrome, sarcoidosis, and rheumatoid arthritis
Dermatomyositis and polymyositis[92]		Diffuse soft tissue calcification
Scleroderma (progressive systemic sclerosis)[93,200]	17-63	*Calcinosis:* Soft tissue, periarticular, tendinous, and intraarticular calcification Acro-osteolysis of the ungual tufts Periarticular erosions

TABLE 17-8 Articular Disorders of the Wrist and Hand—cont'd

Entity	Figure(s)	Characteristics
Crystal Deposition and Metabolic Diseases		
Gouty arthropathy[94-96]	17-64	May involve any joint in wrist or hand Periarticular erosions often with overhanging margins Soft tissue tophi
Calcium pyrophosphate dihydrate (CPPD) crystal deposition disease[97-99,178]	17-65	Periarticular and intraarticular calcification (chondrocalcinosis) Pyrophosphate arthropathy involving radiocarpal and metacarpophalangeal joints Scapholunate advanced collapse (SLAC wrist)
Hemochromatosis[100,101]	17-66	Rare involvement of wrist and hand Findings resemble those of CPPD crystal deposition disease Beaklike excrescences arising from radial aspect of metacarpal heads
Calcium hydroxyapatite crystal deposition disease[102,103]	17-67	Periarticular calcification of ligaments and tendons about the wrist may be encountered Masses may diminish in size or disappear Most common site of calcification in the wrist is within the flexor carpi ulnaris tendon and in the hands about the interphalangeal and metacarpophalangeal joints
Miscellaneous Disorders		
Multicentric reticulohistiocytosis[104]	17-68	Uncommon systemic disease of unknown cause that becomes apparent in adult life Characterized by proliferation of histiocytes in skin, mucosa, subcutaneous tissues, synovia, and, on occasion, bone and periosteum Bilateral symmetric central and marginal erosions of interphalangeal joints (75% of patients), resulting in apparent separation of joint surfaces Soft tissue swelling and eventual arthritis mutilans
Sarcoidosis[105-107]	17-69	Chronic, multisystem disease of unknown cause characterized by the development of noncaseating granulomas Honeycomb or latticework trabecular pattern predominating in the phalanges and metacarpal bones Cystic defects, pathologic fracture, subcutaneous nodules, and osteosclerosis Acro-osteolysis and phalangeal sclerosis
Idiopathic synovial osteochondromatosis[108,109]	17-70	Multiple intraarticular or periarticular collections of intracapsular osteochondral or chondral bodies of variable size and density May result in erosion of adjacent bone Idiopathic form more common than secondary form in hand
Neuropathic osteoarthropathy[110]	17-71	*Wrist and hand involvement:* leprosy, congenital insensitivity to pain, syringomyelia Prominent atrophic resorption of terminal tufts Joint space narrowing and obliteration, subluxation, disorganization, and destruction; bone fragmentation, destruction, and sclerosis
Frostbite[111,112]	17-72	Local tissue damage from cellular injury as a result of the freezing process itself or from vascular insufficiency Soft tissue swelling, osteoporosis, periostitis, secondary infection, arthritis secondary to cartilage injury, terminal tuft resorption, epiphyseal abnormalities, and premature physeal fusion in children Thumb frequently is spared
Thermal and electrical injuries[113]	17-73	Soft tissue swelling, loss, or contracture; osteoporosis, acro-osteolysis, periostitis, epiphyseal injury and growth disturbance, articular abnormalities, osteolysis, osteosclerosis, and periarticular calcification and ossification
Silicone synovitis[114,115]	17-74	Complication of silicone implant surgery for joint reconstruction Believed to be a reaction to shedded silicone particles embedded within the synovium, with resultant synovial hypertrophy and chronic inflammatory and giant cell infiltration of the synovial membrane Associated soft tissue swelling and preservation of cartilage spaces is often found Widespread joint destruction, cysts, and osseous fragmentation

Continued

TABLE 17-8 Articular Disorders of the Wrist and Hand—cont'd

Entity	Figure(s)	Characteristics
Fracture blisters[116]	17-75	Complication of fractures Irregular blisters and nodules about the wrist and hand
Epidermolysis bullosa[117]	17-76	Rare chronic skin disorder resulting from insufficient adherence of the epidermis to the dermis, leading to formation of vesicles, bullae, and ulcerations that occur spontaneously or after minor trauma
Osteolysis with detritic synovitis[118]	17-77	Rare disease characterized by pain, swelling, marked joint deformity, osseous resorption, osteolysis, erosion, and osseous debris

TABLE 17-9 Compartmental Analysis of Wrist and Hand Disease[*]

		Articulations[†]								
Entity	**Figure(s)**	**DIP**	**PIP**	**MCP**	**RC**	**DRU**	**MC**	**PT**	**CCMC**	**FIRST MCP**
Osteoarthrosis	17-53	+	+					+		+
Erosive (inflammatory) osteoarthritis	17-55	+	+				+			+
Rheumatoid arthritis	17-56		+	+	+	+	+	+	+	+
Scleroderma	17-63	+	+			+				+
Gouty arthropathy	17-64	+	+	+	+	+	+		‡	+
CPPD crystal deposition disease	17-65			+	+		+			+

[*] Only the typical locations for each disease are indicated.

[†] *DIP,* Distal interphalangeal; *PIP,* proximal interphalangeal; *MCP,* metacarpophalangeal; *RC,* radiocarpal; *DRU,* distal radioulnar; *MC,* midcarpal; *PT,* pisiform-triquetral; *CCMC,* common carpometacarpal; *MCP,* metacarpophalangeal; *CPPD,* calcium pyrophosphate dihydrate.

[‡] Very severe abnormalities may be present in this compartment.

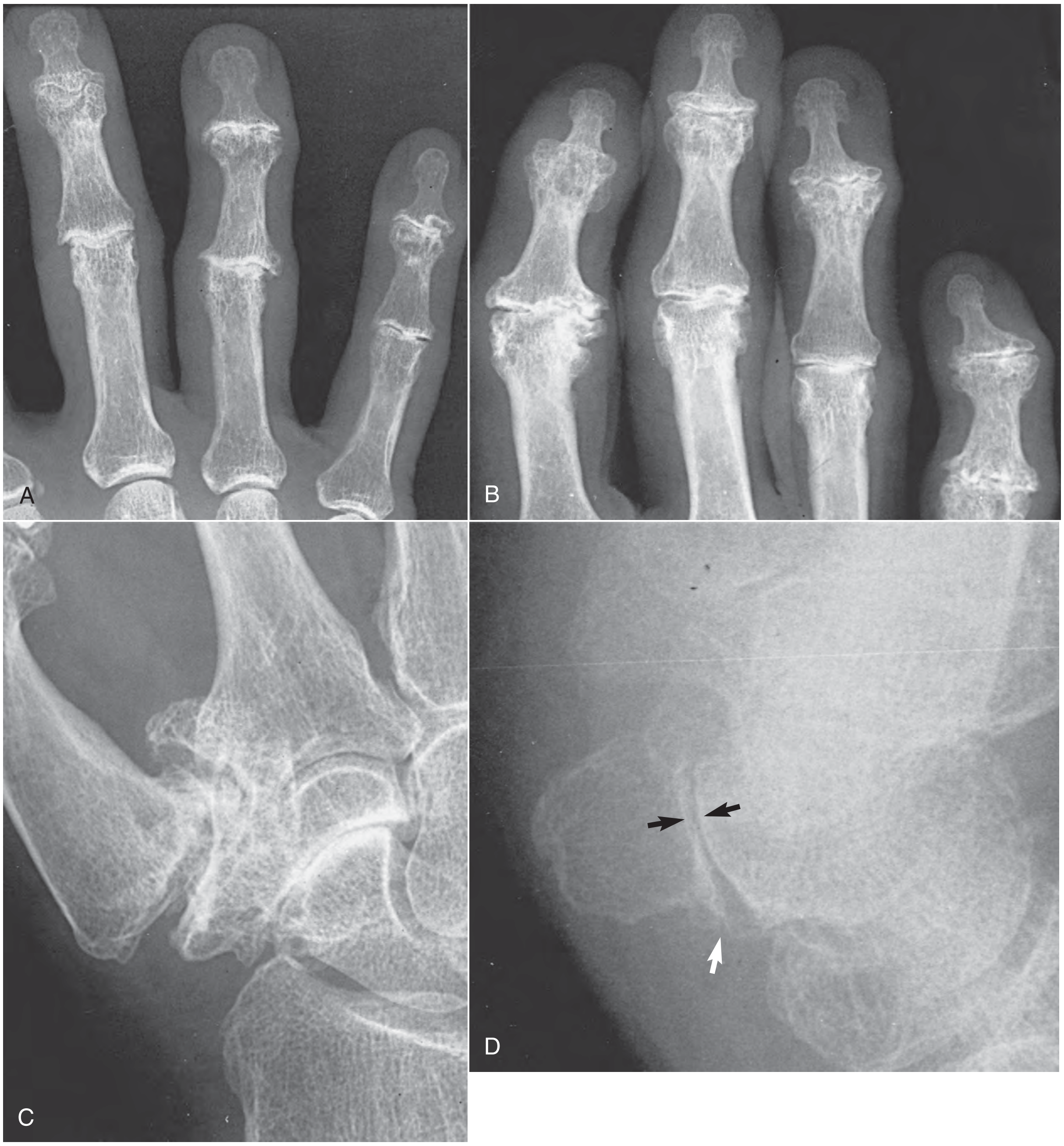

FIGURE 17–53 **Primary osteoarthrosis: typical sites.**[72-75,190] **A-B,** Interphalangeal joints. In **A,** degenerative joint disease of the interphalangeal joints is characterized by osteophytes, nonuniform loss of joint space, subchondral sclerosis, and soft tissue prominence overlying the terminal interphalangeal joints (Heberden nodes). The metacarpophalangeal joints are normal. In **B,** another patient, observe the prominent osteophytes, sclerosis, irregular joint space narrowing, and subluxations. **C,** First carpometacarpal region. Degenerative changes are seen in the trapeziometacarpal, trapezioscaphoid, and trapeziotrapezoid articulations, common sites of involvement for osteoarthrosis. The changes are characterized by radial subluxation of the base of the first metacarpal bone, subchondral sclerosis, joint space narrowing, osteophyte formation, subchondral cysts, and intraarticular osseous bodies. **D,** Pisiform-triquetral joint. Semisupinated oblique radiograph reveals joint space narrowing *(black arrows),* subchondral sclerosis, and osteophyte formation *(white arrow)* at the pisotriquetral articulation, a rare location for degenerative joint disease. The use of sonography has been described in the evaluation of pisotriquetral osteoarthrosis.[197] *(**D,** Courtesy R. Shapiro, MD, Sacramento, Calif.)*

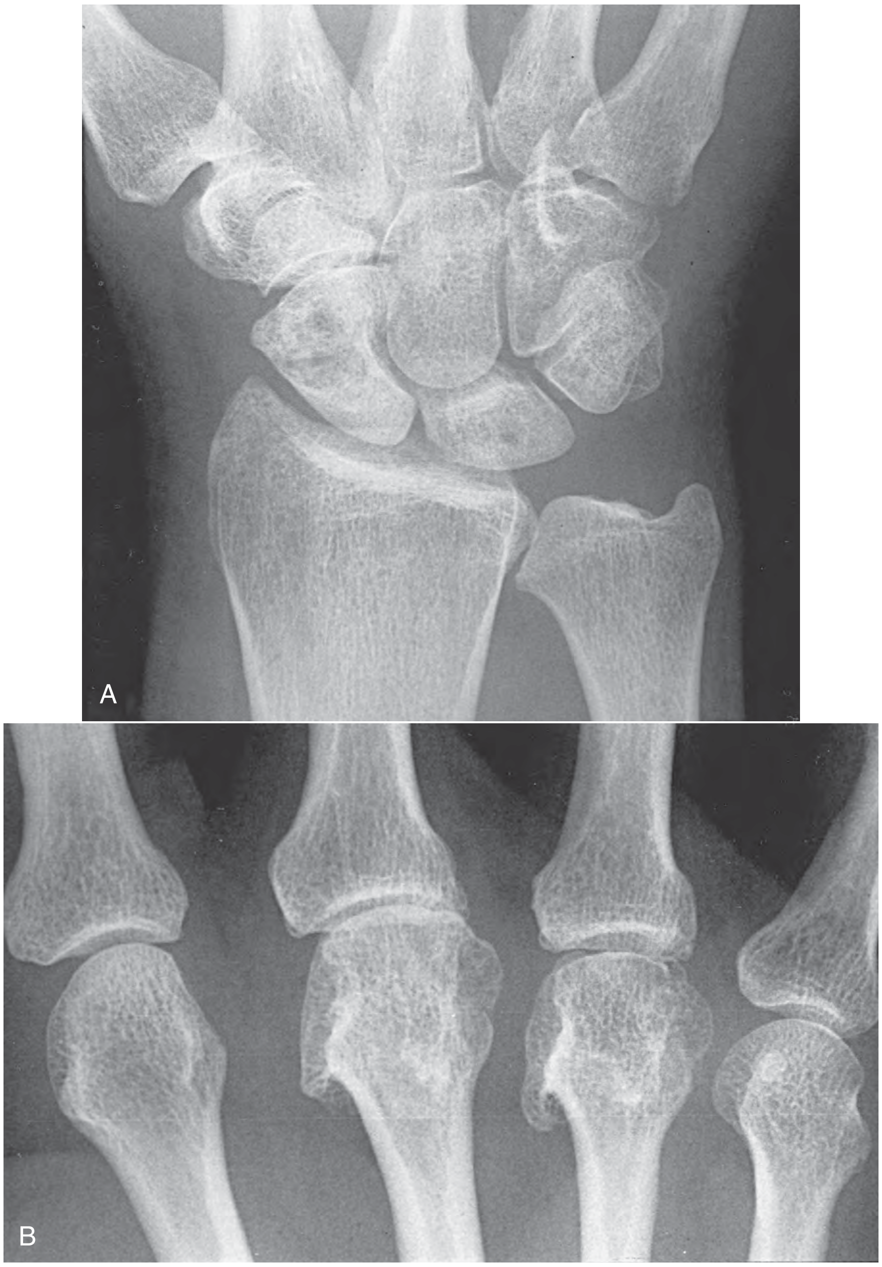

FIGURE 17–54 Secondary osteoarthrosis: posttraumatic.[76] **A,** This 50-year-old retired boxer had persistent wrist pain. Large subchondral cysts are seen in the scaphoid and lunate bones. Joint-space narrowing and osteophytes are not prominent in this patient. **B,** Metacarpophalangeal joints. Degenerative joint disease is evident, characterized by nonuniform loss of joint space and osteophyte formation, with no evidence of erosion. Degenerative disease at this site is seen after repeated trauma, such as that sustained in boxers or manual laborers, and has been referred to as *boxer's arthropathy* or *Missouri metacarpal syndrome*. It may resemble pyrophosphate arthropathy seen in calcium pyrophosphate dihydrate (CPPD) crystal deposition disease and hemochromatosis. *(**B,** Courtesy A. Brower, MD, Norfolk, Va.)*

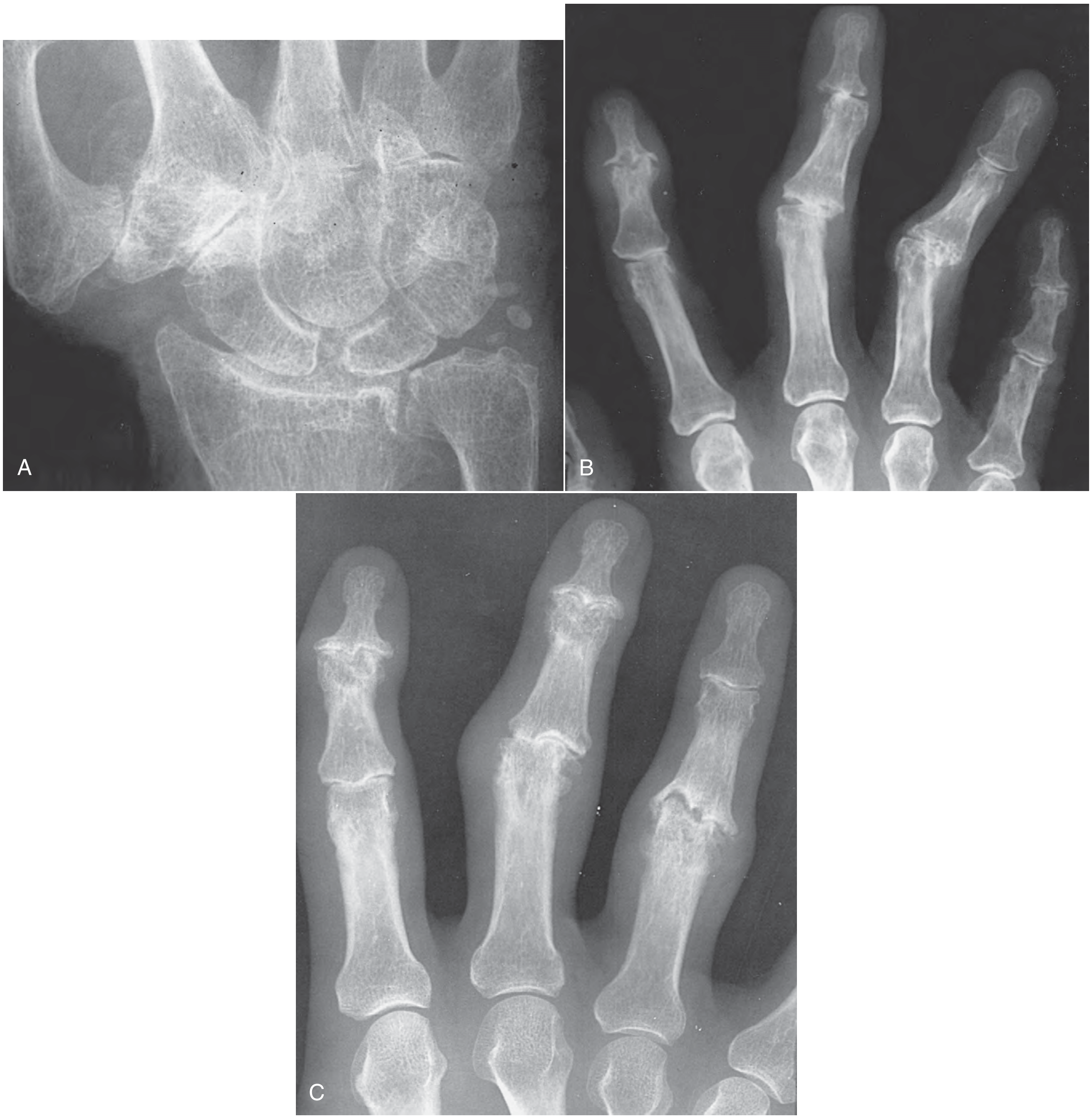

FIGURE 17–55 **Erosive (inflammatory) osteoarthritis.**[77-80,187] **A,** Wrist involvement. Observe the severe subluxation and degenerative changes at the first carpometacarpal, trapezioscaphoid, and distal radioulnar joints. Scapholunate dissociation is also present, indicating probable disruption of the interosseous scapholunate ligament. **B-C,** Interphalangeal joint involvement. In **B,** a 73-year-old woman, observe the central erosions of the subchondral bone, joint subluxations, soft tissue swelling, and preservation of the metacarpophalangeal joints. In **C,** another patient, similar changes are seen within the proximal and terminal interphalangeal joints. The metacarpophalangeal joints are not involved.

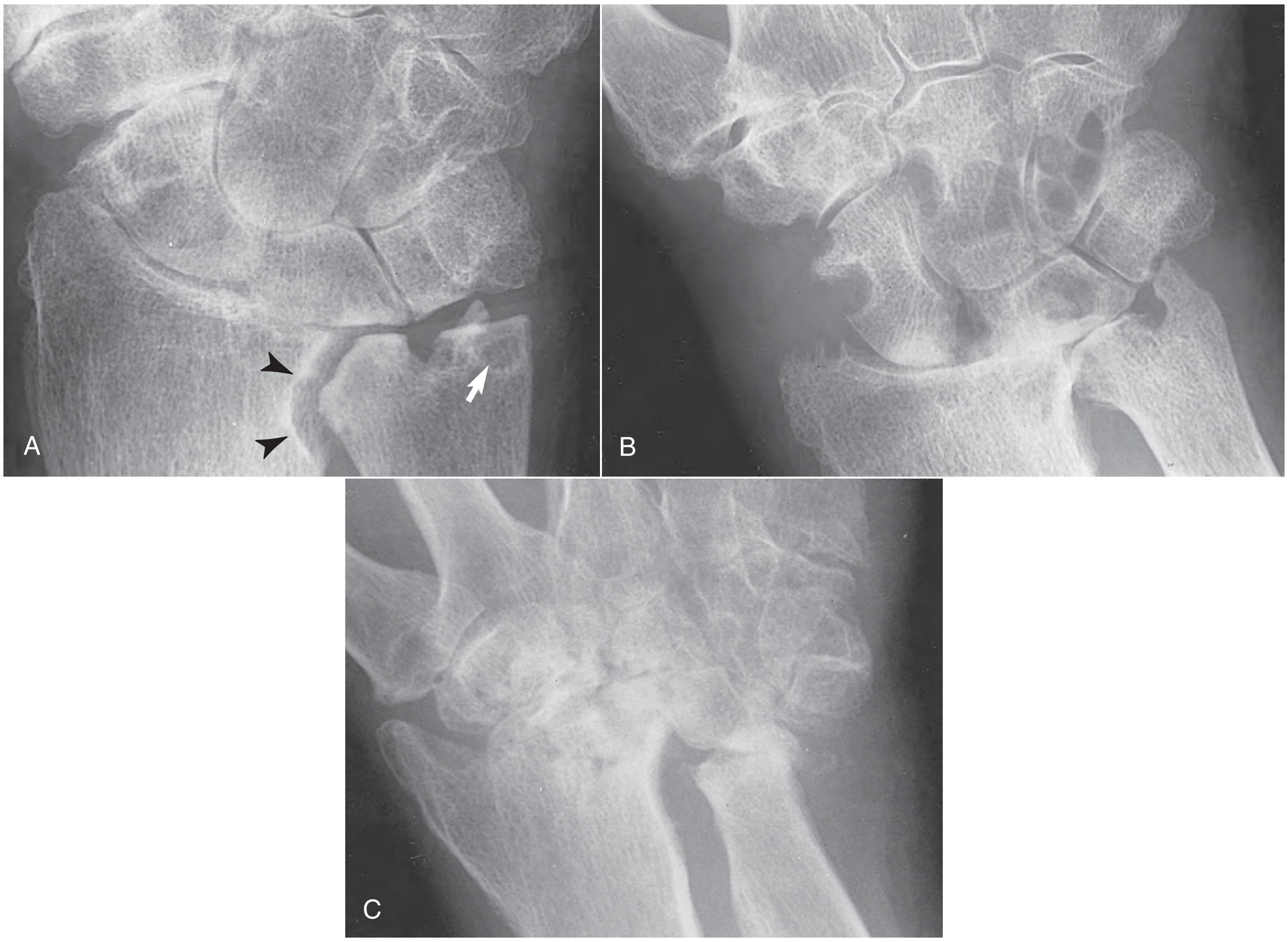

FIGURE 17–56 **Rheumatoid arthritis.**[81,82] **A-C** Carpal abnormalities. In **A,** moderate changes of rheumatoid arthritis are seen. Widespread radiocarpal, midcarpal, and pericapitate joint space narrowing predominates in this patient. Observe the characteristic erosions of the ulnar styloid process *(arrow)* and distal radioulnar joint *(arrowheads)*. In **B,** advanced changes (cystic form) are noted. The characteristic radiographic findings include soft tissue swelling, radiocarpal joint-space narrowing, scapholunate widening, and multiple marginal erosions and subchondral cysts involving the carpal bones and the distal ends of the radius and ulna. In **C,** severe changes (pan carpal destruction) are evident in another patient. Observe the widespread erosive destruction of the joint spaces and the fragmentation and collapse of the carpal bones, radius, and ulna.

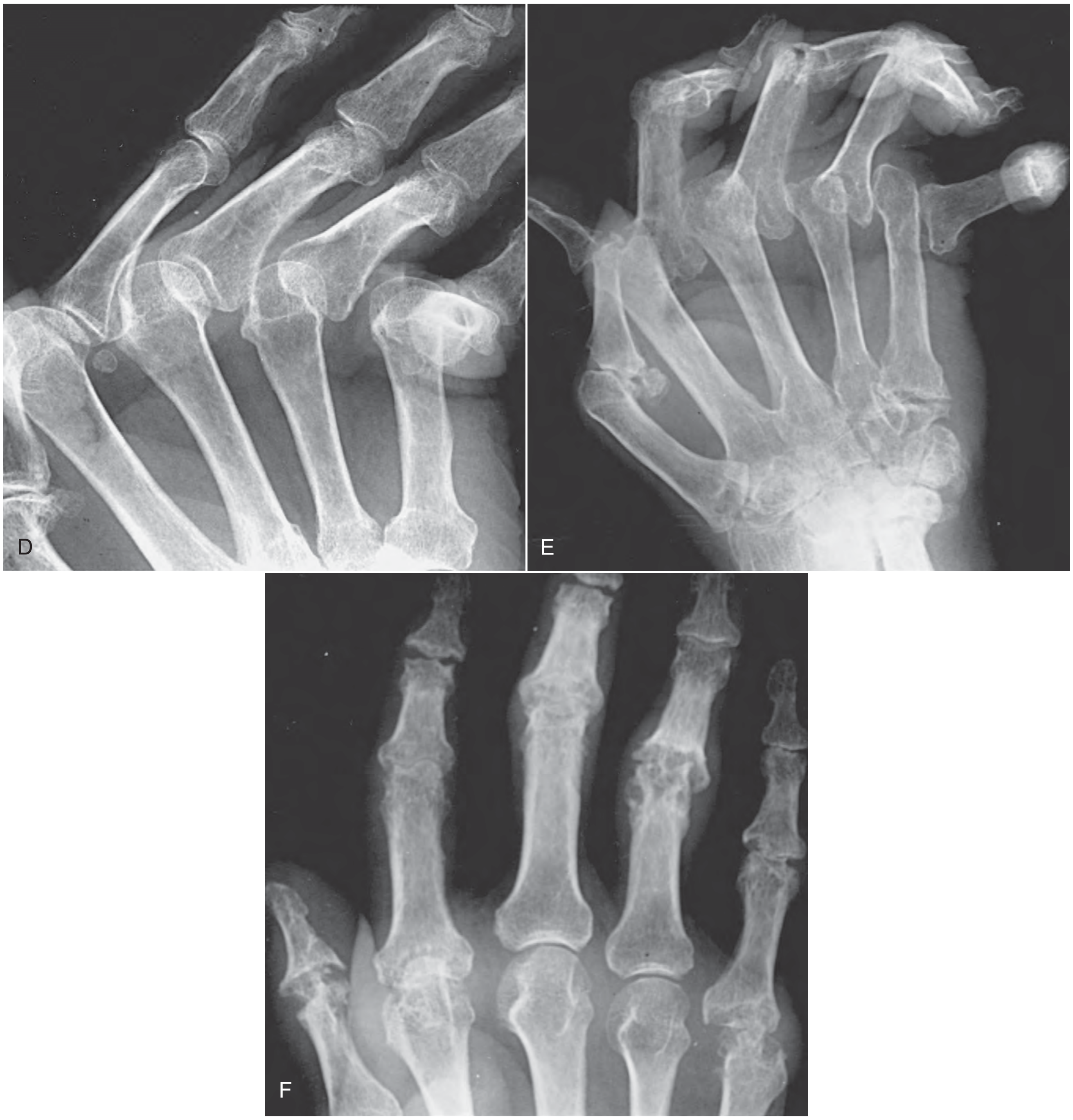

FIGURE 17–56, cont'd **D-F,** Hand abnormalities. In **D,** moderate deformities are evident. Ulnar deviation at the second to fifth metacarpophalangeal joints is a characteristic deformity found in rheumatoid arthritis. In **E,** advanced deformities in another patient include complete dislocation of the metacarpophalangeal joints and contractures of the interphalangeal joints. Widespread wrist destruction is also present. In **F,** advanced changes are characterized by erosions. In a third patient, observe the numerous marginal and central erosions involving the metacarpophalangeal and proximal interphalangeal joints. Note also the uniform loss of joint space and periarticular osteopenia. Such changes in rheumatoid arthritis tend to spare the distal interphalangeal joints until late in the disease.

Continued

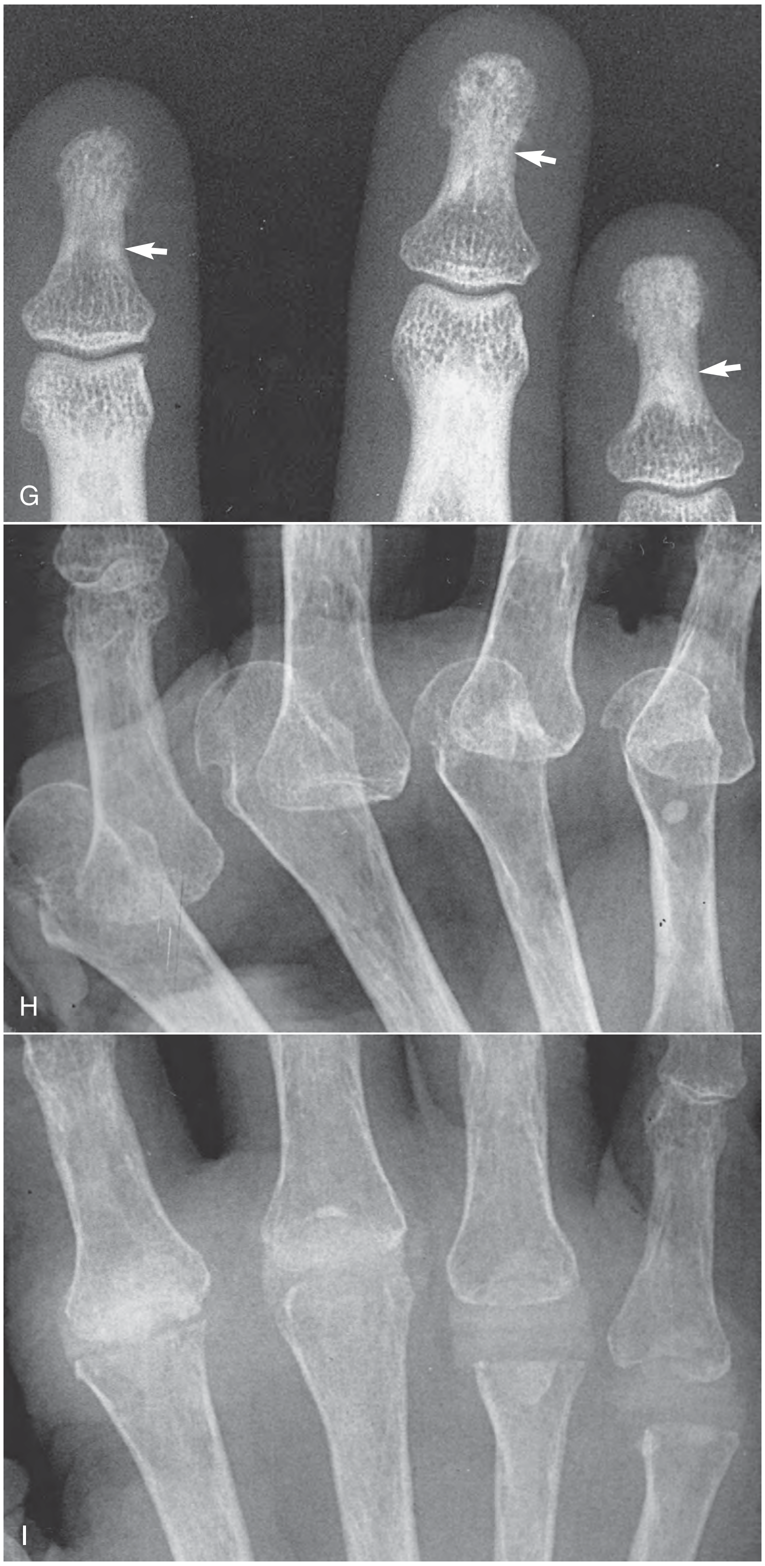

FIGURE 17–56, cont'd G, Phalangeal sclerosis. The terminal phalanges are sclerotic *(arrows),* an infrequent complication of rheumatoid arthritis and other inflammatory arthropathies. **H-I,** Surgical correction of deformities. In **H,** extensive volar dislocation of the second to fifth metacarpophalangeal joints is evident. In **I,** a postarthroplasty radiograph shows correction of the ulnar deviation and presence of joint prostheses.

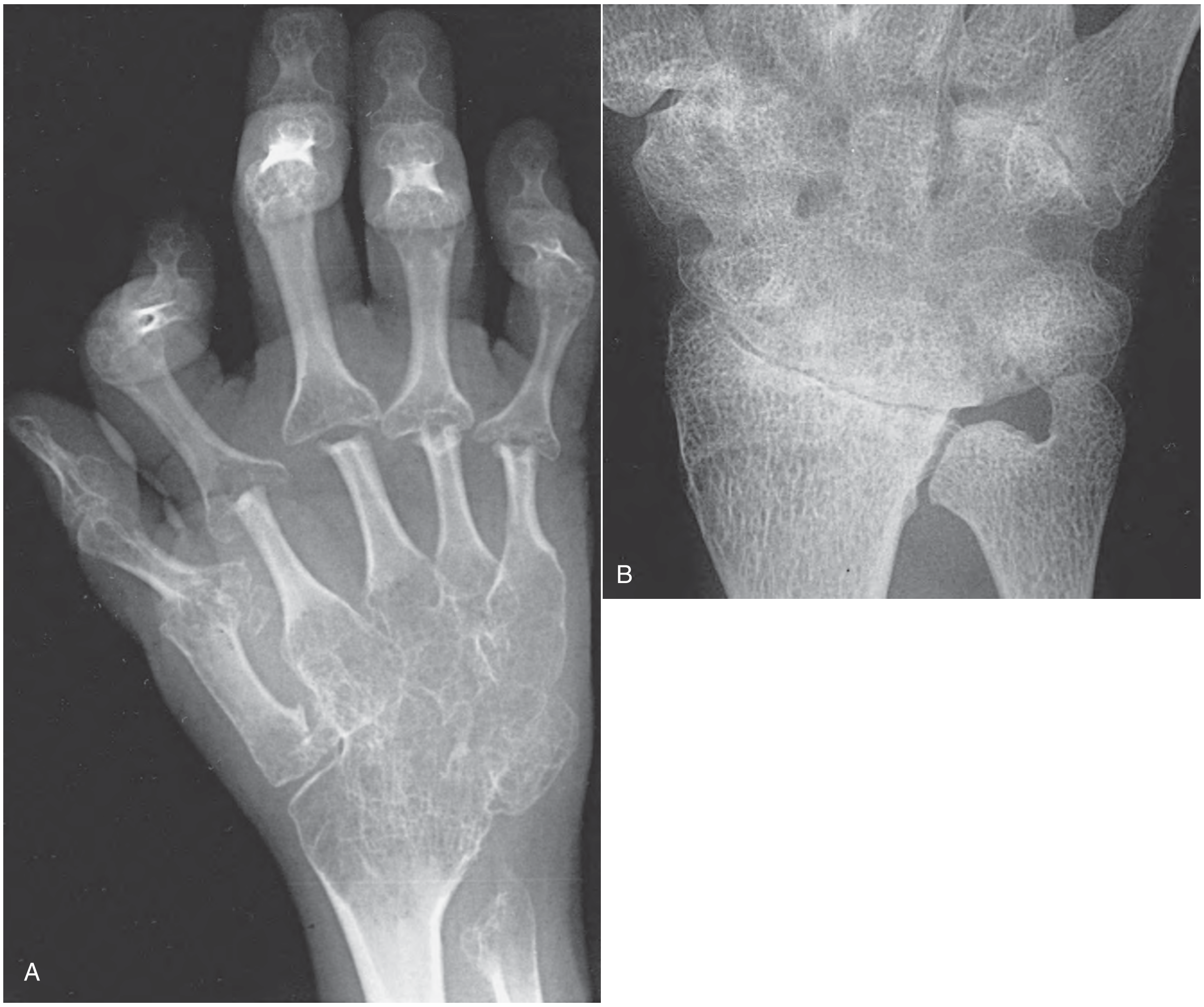

FIGURE 17–57 **Juvenile idiopathic arthritis: wrist and hand abnormalities.**[83,84] **A,** This 23-year-old woman with a 10-year history of Still disease has several characteristic radiographic findings, including periarticular osteopenia, wrist ankylosis, erosion and resorption of the distal end of the ulna, widespread joint-space narrowing, and soft tissue atrophy. Flexion deformities of the proximal interphalangeal joints are also prominent. All the findings were bilateral and symmetric (other hand not shown). Interpretation of the changes about the metacarpophalangeal joints is complicated by previous surgery. **B,** In this 27-year-old woman with juvenile rheumatoid arthritis, complete osseous ankylosis of the intercarpal and carpometacarpal articulations has occurred. The radiocarpal joint is severely narrowed. Some degree of carpal ankylosis has been reported in as many as 47% of persons with juvenile idiopathic arthritis.

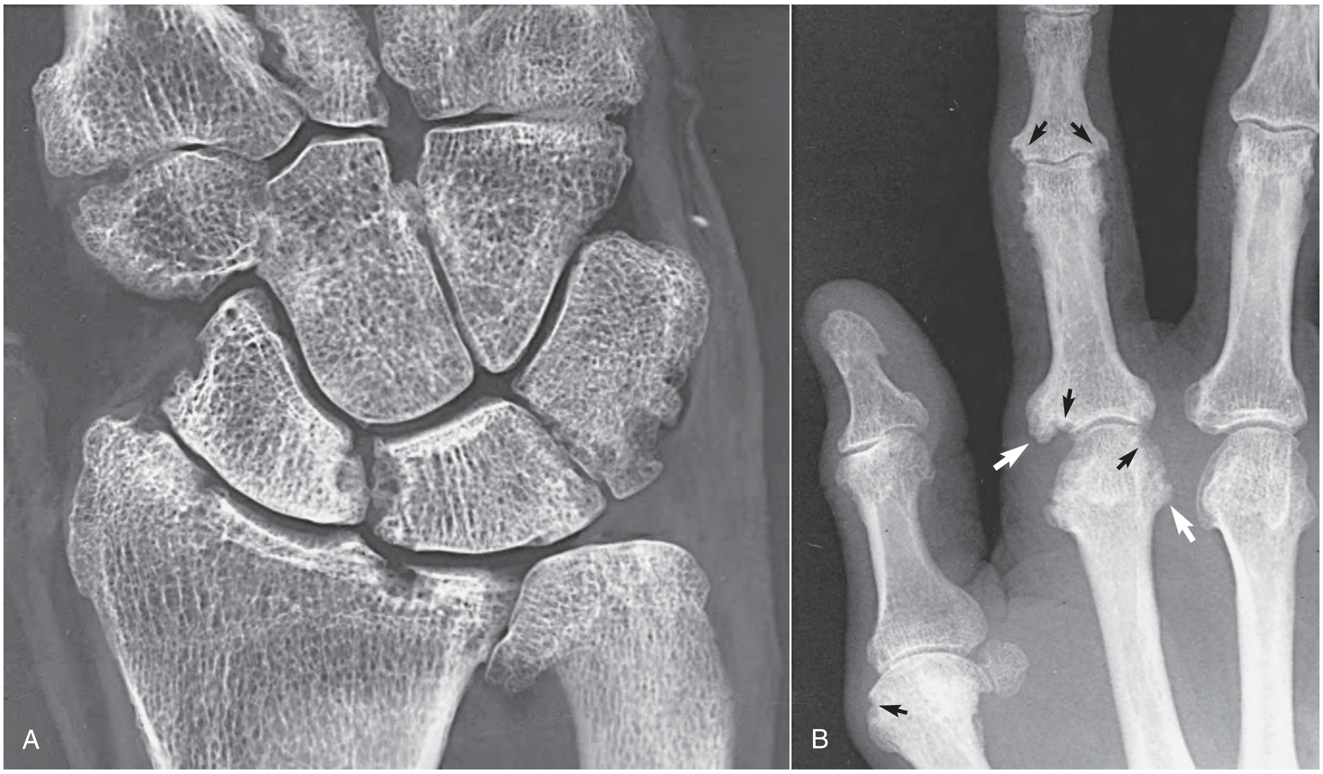

FIGURE 17–58 Ankylosing spondylitis.[85] **A,** Wrist abnormalities. Observe the widespread erosions of the scaphoid and lunate bones and the triquetrum, and the distal end of the radius in this radiograph of a coronal cadaveric section from a person with ankylosing spondylitis. **B,** Hand abnormalities. Prominent periarticular excrescences (enthesophytes) *(large white arrows)* are seen adjacent to the metacarpophalangeal and interphalangeal joints. Marginal erosions *(small black arrows)* and joint space narrowing also are evident. Note the absence of periarticular osteopenia. Asymmetric abnormalities of the hand and wrist occur in approximately 30% of patients with severe ankylosing spondylitis.

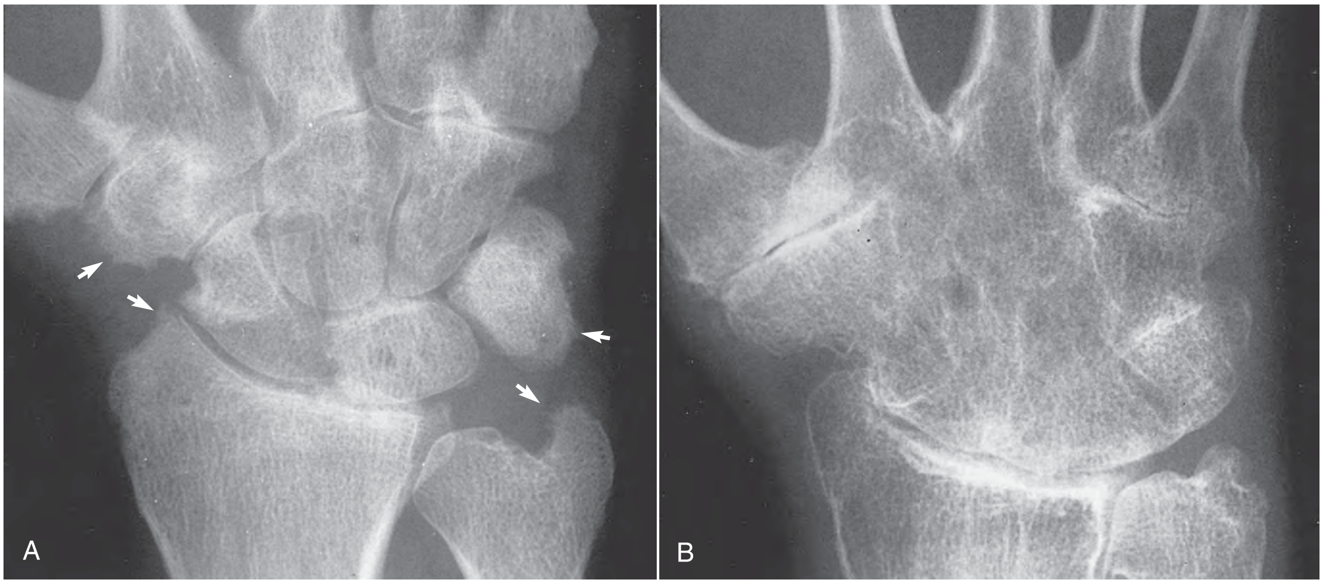

FIGURE 17–59 Psoriatic arthropathy.[78,86-88] **A-B,** Wrist abnormalities. In **A,** diffuse pancarpal joint space narrowing, cystic erosions, fluffy periostitis ("whiskering") *(arrows),* and absence of obvious osteopenia are typical features of the seronegative spondyloarthropathies. In **B,** diffuse osseous ankylosis of all intercarpal and carpometacarpal joints has occurred in a patient with advanced psoriatic arthritis.

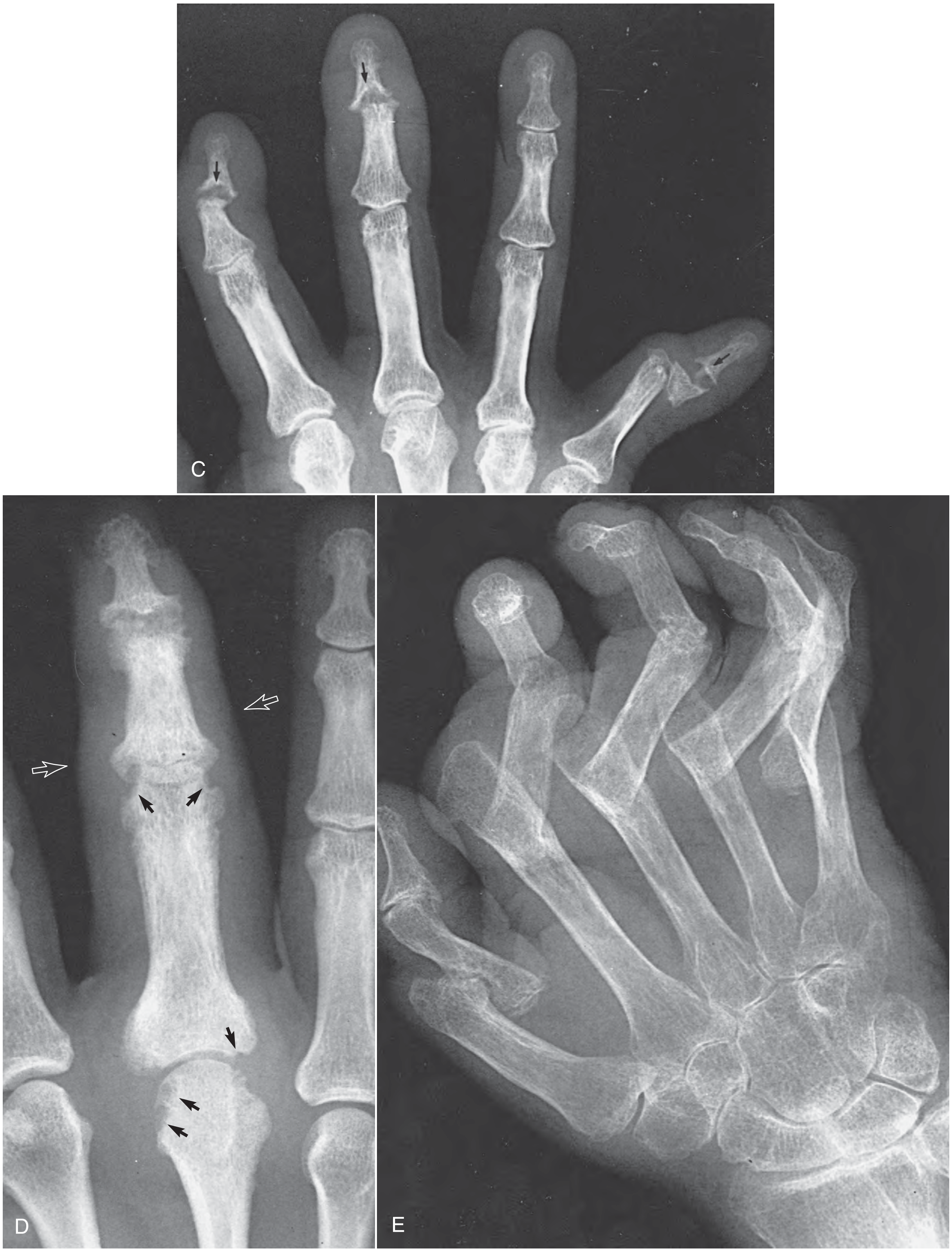

FIGURE 17–59, cont'd **C-E,** Hand abnormalities. In **C,** the interphalangeal joints show central joint erosions *(arrows)* and subluxation involving several distal interphalangeal joints and the fifth proximal interphalangeal joint. Prominent soft tissue swelling involving the second, third, and fifth digits is referred to as the "*sausage digit*" appearance. In **D,** the ray pattern is evident. Observe the prominent soft tissue swelling (sausage digit) *(open arrows)* and bone sclerosis rather than osteopenia. Marginal erosions *(arrows)* involving all the joints of the third digit with no evidence of involvement in the joints of the adjacent digits is referred to as the ray pattern and is typical of psoriasis and reactive arthritis. In **E,** a pattern of severely deforming resorptive arthropathy is evident in the hand of this 52-year-old woman with severe psoriasis. This pattern of deformity has been termed the *main en lorgnette* or *opera glass appearance* and involves a telescoping of the dislocated metacarpophalangeal joints and flexion contractures of the fingers. Diffuse osteopenia and tuft resorption are also present. Although this type of deformity may also occur in rheumatoid arthritis, absence of wrist involvement with such severe hand disease would be most unusual for rheumatoid arthritis. *(**B,** Courtesy P. Kindynis, MD, Geneva, Switzerland; **D,** Courtesy C. Pineda, MD, Mexico City.)*

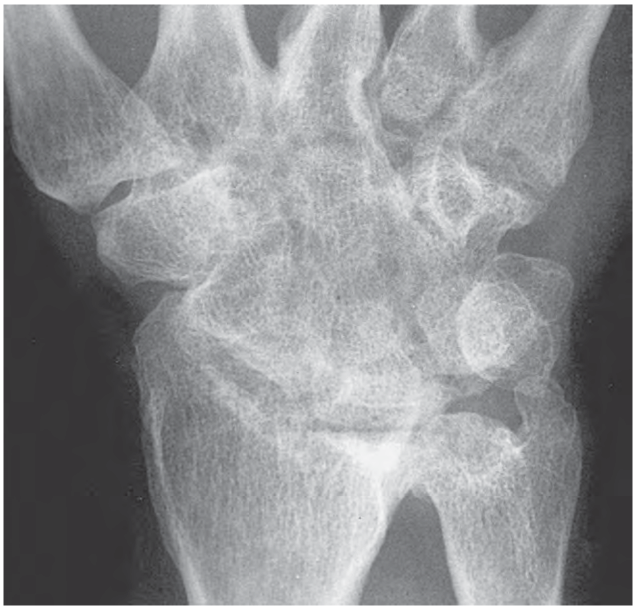

FIGURE 17–60 Reactive arthritis associated with Reiter syndrome: wrist abnormalities.[87-89] In this 42-year-old man with a long history of Reiter syndrome, pancarpal joint-space narrowing, erosions, and ankylosis are seen. Observe also the undulating and indistinct cortical margins of the carpal bones. *(Courtesy J. Schils, MD, Cleveland.)*

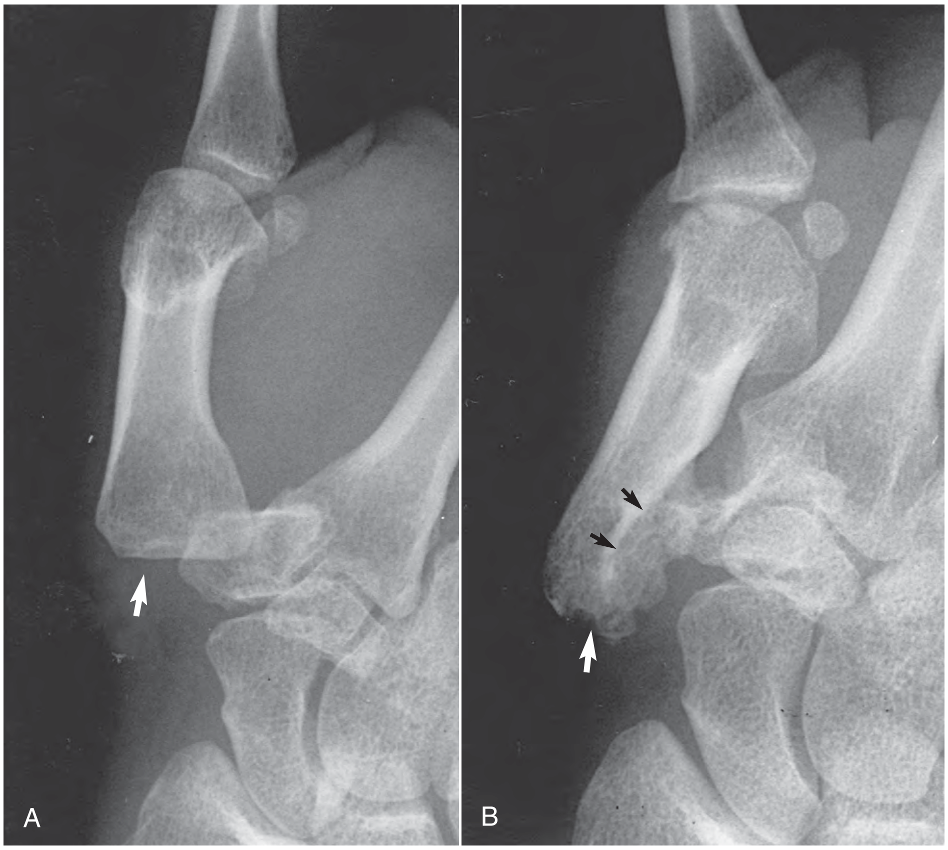

FIGURE 17–61 Systemic lupus erythematosus.[90] **A-B,** First carpometacarpal joint abnormalities. In **A,** persistent ligament laxity has resulted in subluxation of the first trapeziometacarpal articulation *(arrow)*. In **B,** a radiograph taken 5 years later reveals complete dislocation *(white arrow)* and mechanical erosion of the proximal portion of the first metacarpal bone *(black arrows)*. The trapezium appears to have been dissolved and resorbed.

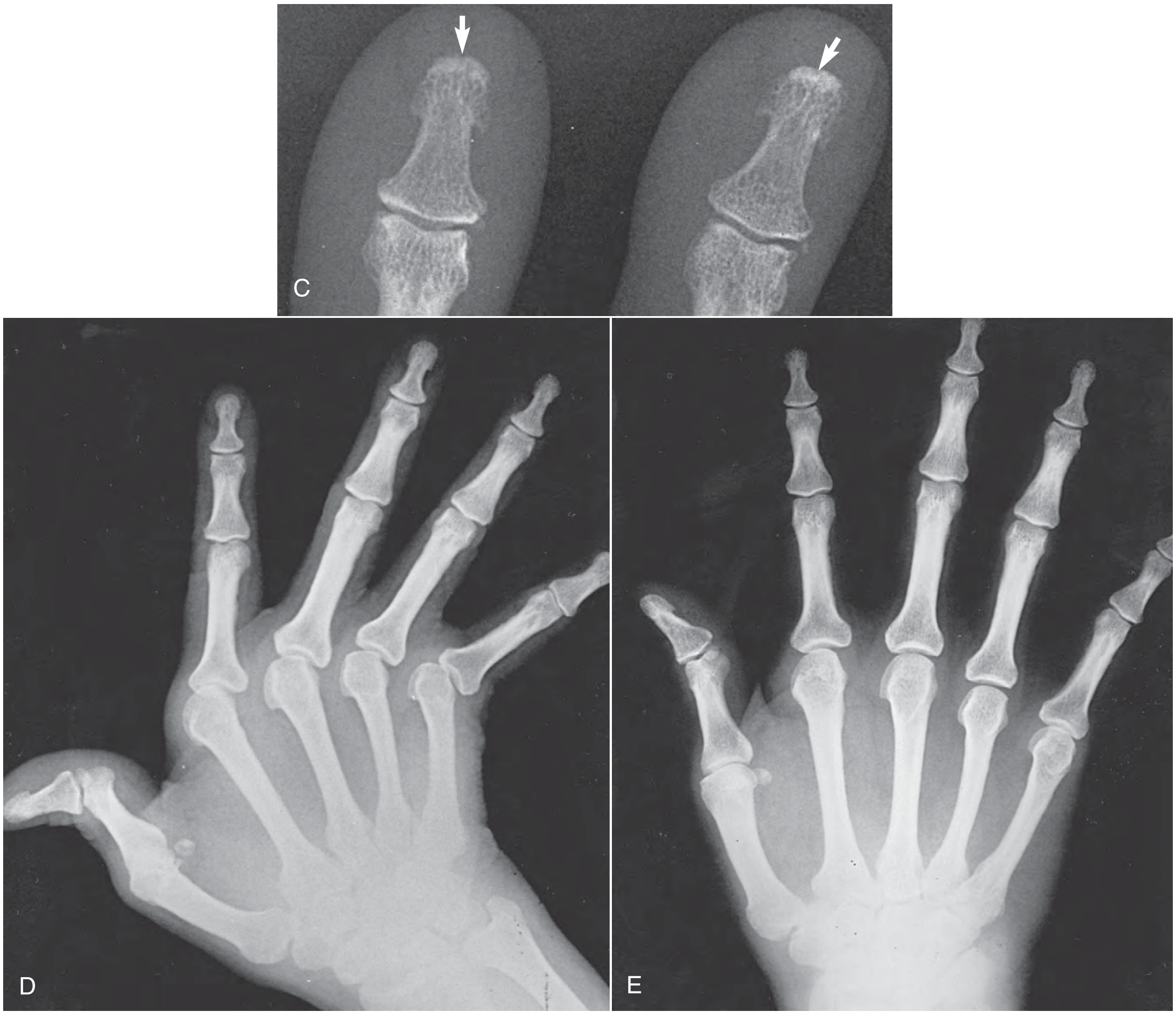

FIGURE 17–61, cont'd C, Phalangeal sclerosis. In another patient, observe the sclerosis of the tips of the phalangeal tufts *(arrows)*. **D-E,** Reversible subluxations. In another patient with long-standing lupus erythematosus, marked ulnar deviation at the metacarpophalangeal joints and boutonnière deformity of the thumb are evident on the initial radiograph **(D),** and the reversible nature of the subluxations can be appreciated when the hand is pressed against the cassette **(E).** *(**D-E,** Courtesy C. Pineda, MD, Mexico City.)*

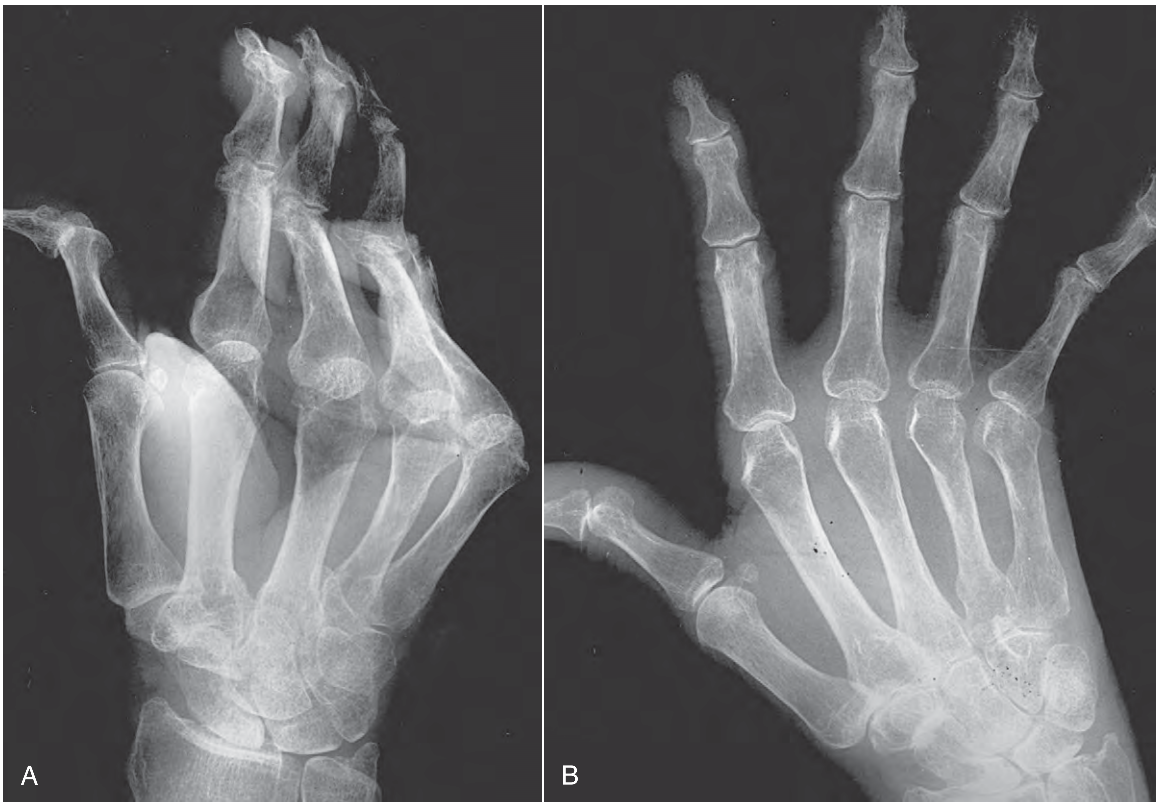

FIGURE 17–62 **Jaccoud arthropathy: nonerosive deforming arthropathy with reversible subluxations.**[91] This 64-year-old woman had injured her hand. Marked swan-neck deformities of the hands were seen clinically. The patient could not remember ever having been diagnosed as having rheumatic fever or systemic lupus erythematosus. **A,** Initial oblique radiograph shows osteoporosis and multiple swan-neck deformities with an absence of destructive or erosive lesions. **B,** Another radiograph obtained the next day, with the hand pressed on the cassette, shows a reversal of most of the deformities. Ulnar deviation of the metacarpophalangeal joints, especially the fifth, persists. *(Courtesy G. Greenway, MD, Dallas.)*

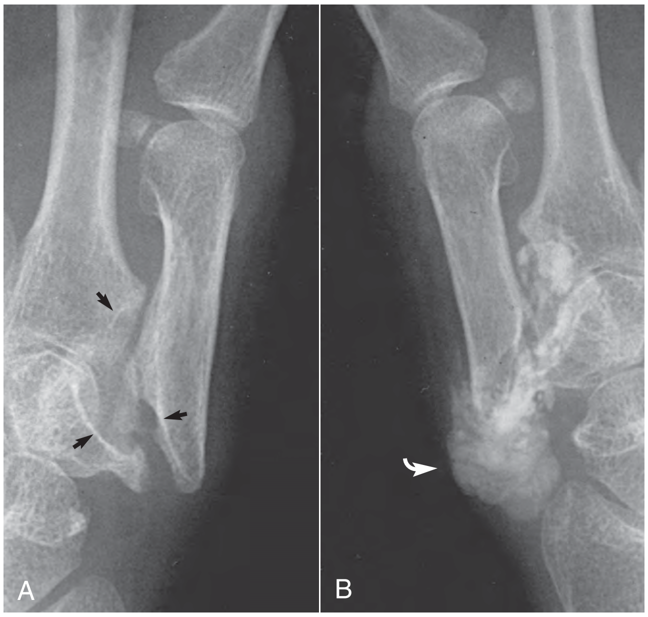

FIGURE 17–63 **Scleroderma (progressive systemic sclerosis).**[93,200] **A-B,** Carpometacarpal abnormalities. This 53-year-old woman has had long-standing scleroderma. Radiographs of both wrists show characteristic changes at the first carpometacarpal joint. On the left **(A),** scalloped erosions of the trapezium and the base of the metacarpal bones *(arrows)* are associated with dorsal and radial subluxation of the metacarpal base. Similar changes on the right **(B)** are accompanied by extensive intraarticular and periarticular globular calcification *(curved arrow)*.

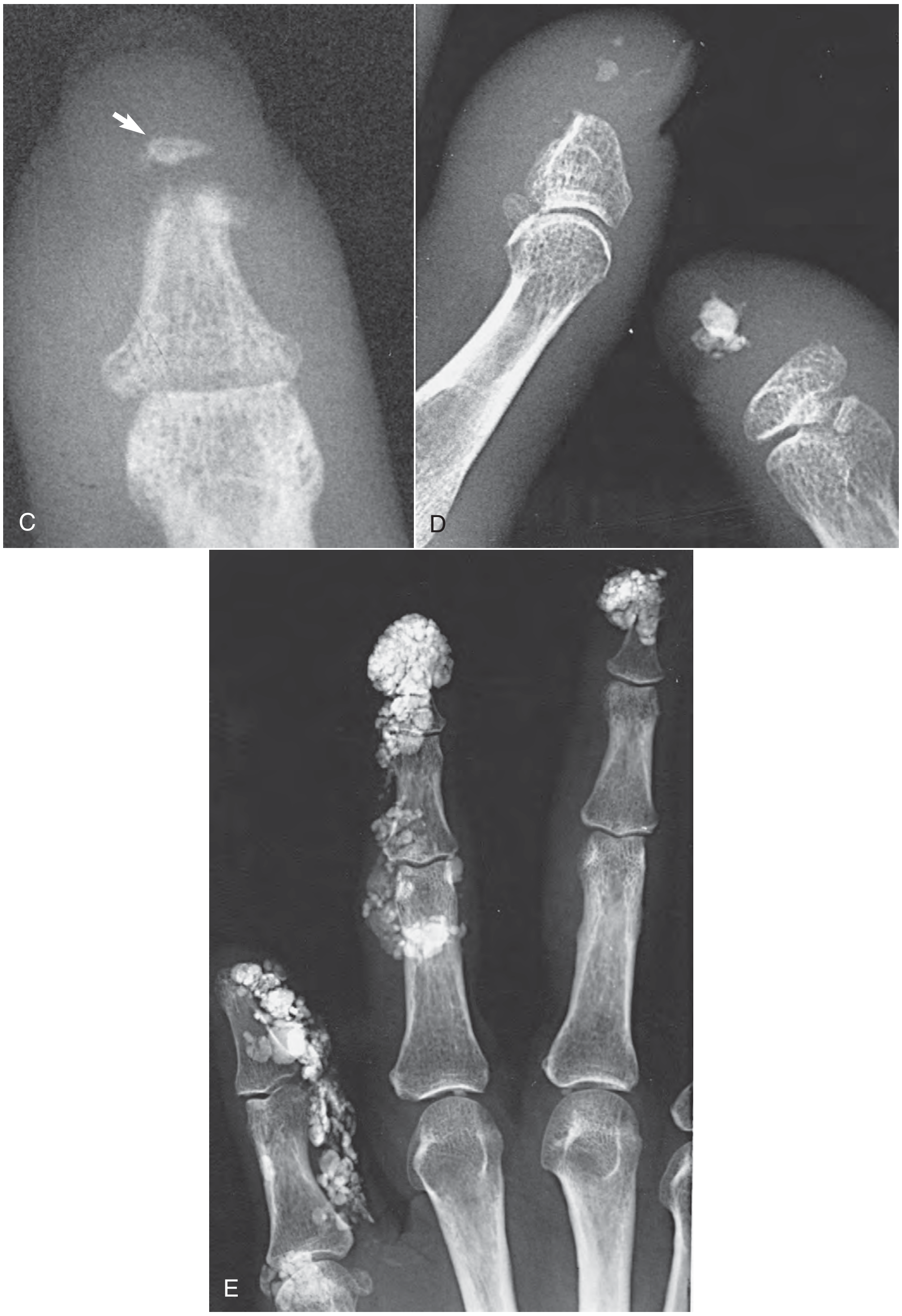

FIGURE 17–63, cont'd **C-E,** Hand abnormalities. In **C,** bandlike resorption of the terminal phalanx is seen *(arrow)*. In **D,** acro-osteolysis of the terminal tufts of both thumbs is present in this patient with long-standing scleroderma. In **E,** extensive subcutaneous calcification is present in another patient with scleroderma. (***A-B,*** *From Resnick D, Scavulli JF, Goergen TG, et al: Intraarticular calcification in scleroderma. Radiology 124:685, 1977;* ***D,*** *Courtesy V. Vint, MD, San Diego;* ***E,*** *Courtesy M. Alson, MD, Stanford, Calif.)*

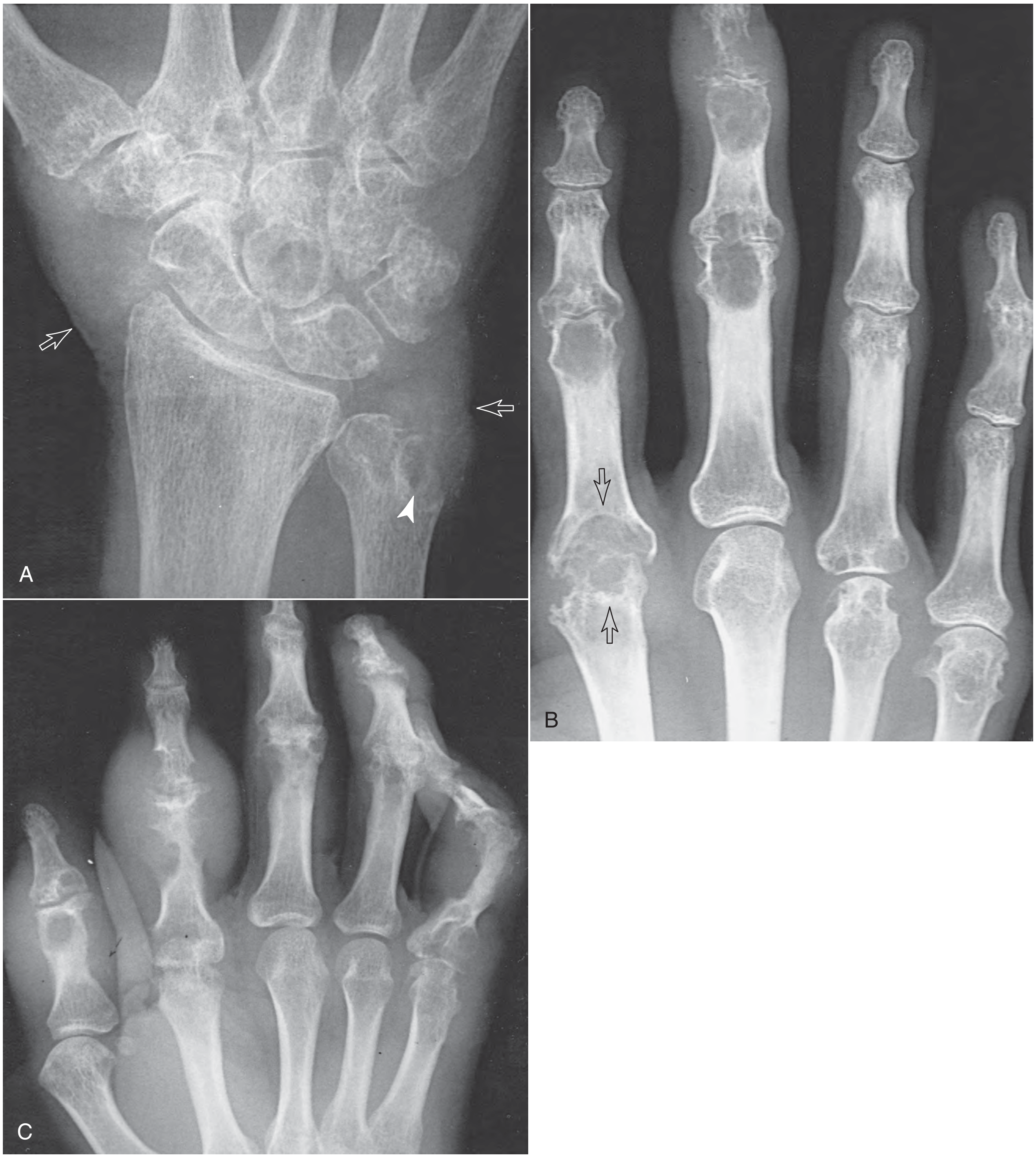

FIGURE 17–64 Gouty arthropathy.[94-96] **A,** Wrist abnormalities. Extensive periarticular soft tissue swelling *(open arrows)* and cystic erosions of the carpal bones are seen in this 84-year-old man with long-standing gout. Observe the extensive erosion of the ulnar styloid process *(arrowhead)*. **B-C,** Hand abnormalities. In **B,** multiple periarticular marginal erosions and cystic changes can be seen involving several joints. Severe intraarticular erosions and joint destruction are evident at the second metacarpophalangeal joint *(open arrows)*. Soft tissue swelling is also prominent, and the overall bone density is well preserved. In **C,** severe changes can be noted in another patient with chronic gout. Observe the extensive soft tissue swelling and marginal and nonmarginal erosions, some with overhanging margins. *(**A,** Courtesy T. Georgen, MD, San Diego.)*

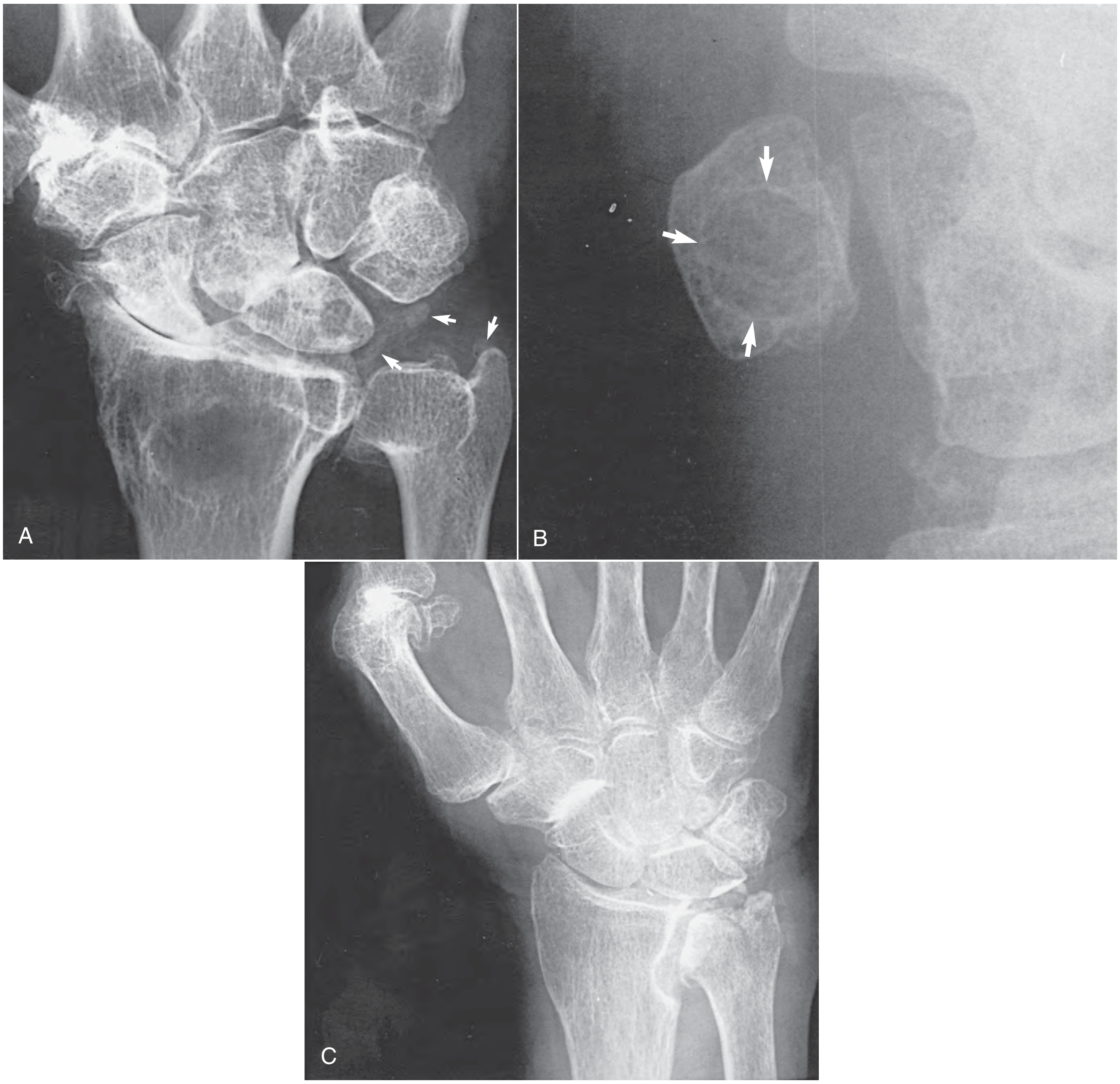

FIGURE 17–65 **Calcium pyrophosphate dihydrate (CPPD) crystal deposition disease.**[97-99,178] **A,** Diffuse chondrocalcinosis *(arrows),* huge subchondral cysts, joint-space narrowing, and scapholunate dissociation are evident in the wrist of this 67-year-old woman with CPPD crystal deposition disease. This pattern of carpal destruction and instability is termed *scapholunate advanced collapse (SLAC) wrist*. **B,** In another patient, a prominent subchondral cyst is seen in the pisiform bone *(arrows)*. **C,** Pyrophosphate arthropathy affecting the first metacarpophalangeal and trapezioscaphoid joints in this 64-year-old woman is characterized by marked subchondral sclerosis, joint space narrowing, and osteophyte formation. Observe also the radiocarpal joint-space narrowing and erosion of the radius at the distal radioulnar joint. Pyrophosphate arthropathy is found in more than 70% of wrists in patients with CPPD crystal deposition disease.

Continued

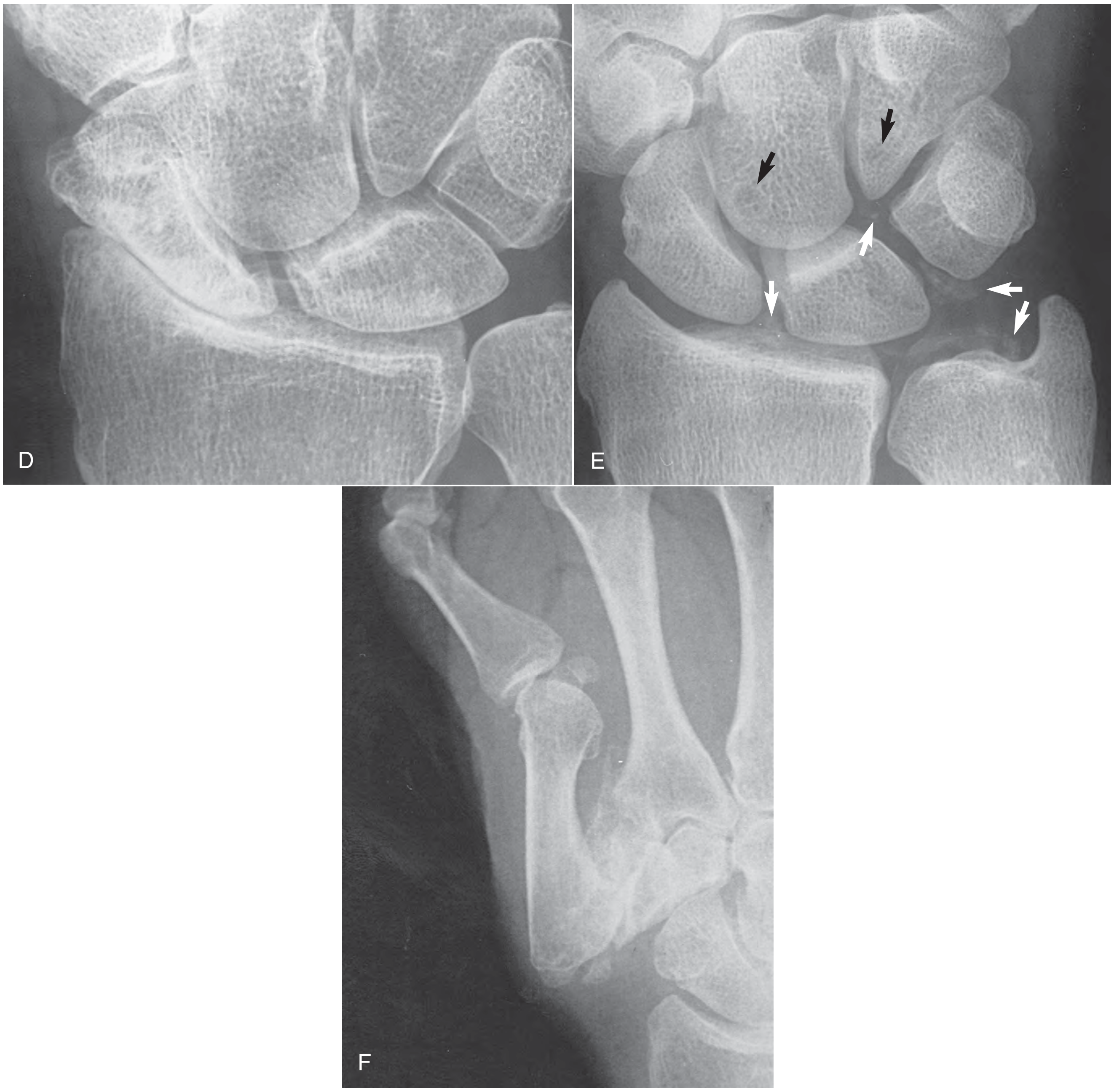

FIGURE 17–65, cont'd **D,** Pyrophosphate arthropathy is manifested in this patient as narrowing of the radioscaphoid articulation, a common site of involvement in patients with CPPD crystal deposition disease. Dense sclerosis of the scaphoid bone is also characteristic of pyrophosphate arthropathy. **E,** Chondrocalcinosis, seen as curvilinear articular cartilage calcification *(white arrows),* is found in more than 60% of wrists of patients with CPPD crystal deposition disease. Note also the subchondral cysts *(black arrows)*. **F,** First carpometacarpal joint involvement. Observe the typical pyrophosphate arthropathy with nonuniform joint space narrowing, subchondral sclerosis, large osteophytes, and subluxation.

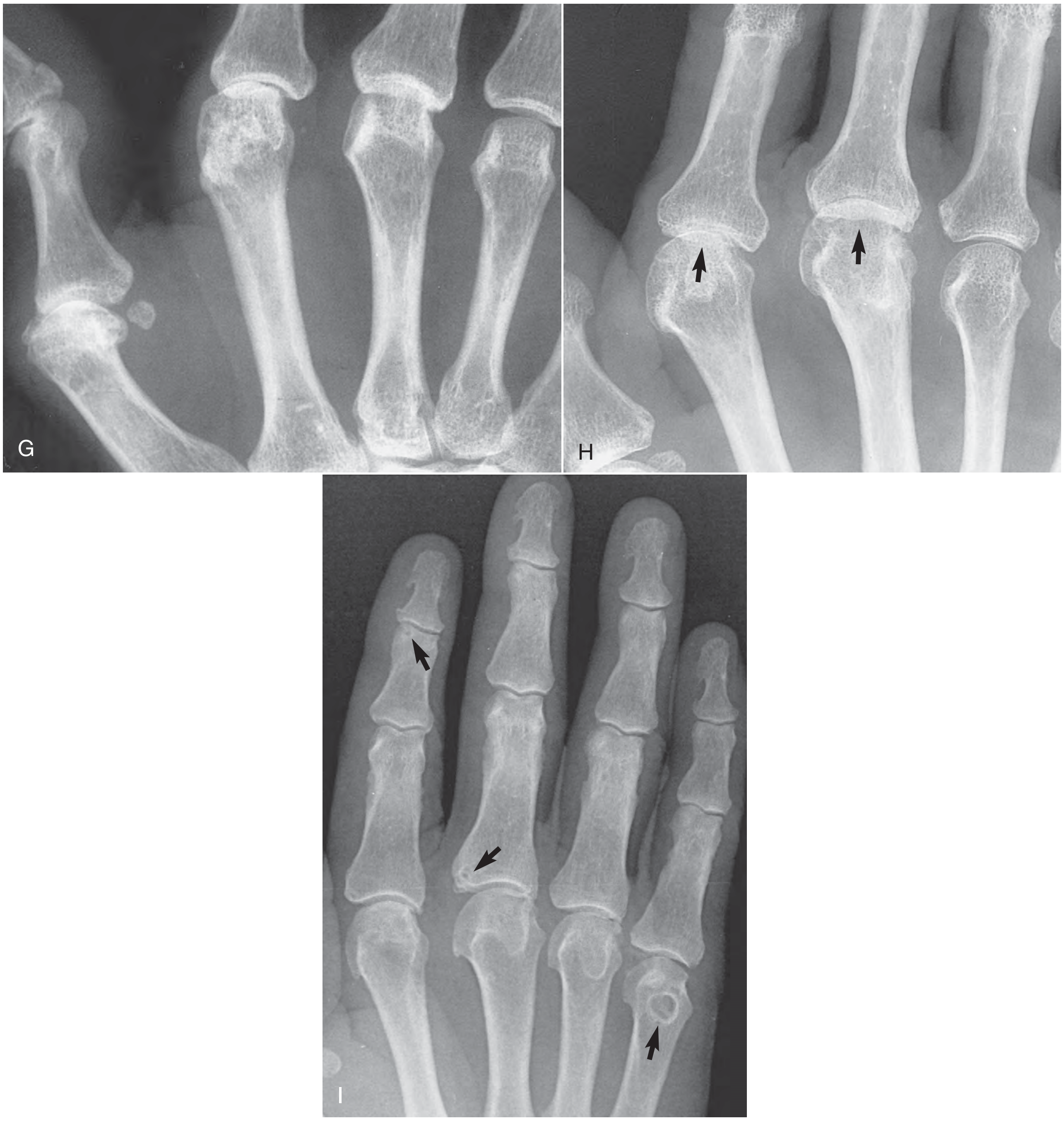

FIGURE 17–65, cont'd **G,** Pyrophosphate arthropathy involving the first, second, and third metacarpophalangeal joints is seen as nonuniform loss of joint space, subchondral sclerosis, and osteophyte formation. **H,** In another patient, an 80-year-old man, similar changes are identified in the second and third metacarpophalangeal joints *(arrows)*. **I,** In a 69-year-old man, cystic changes *(arrows)* predominate.

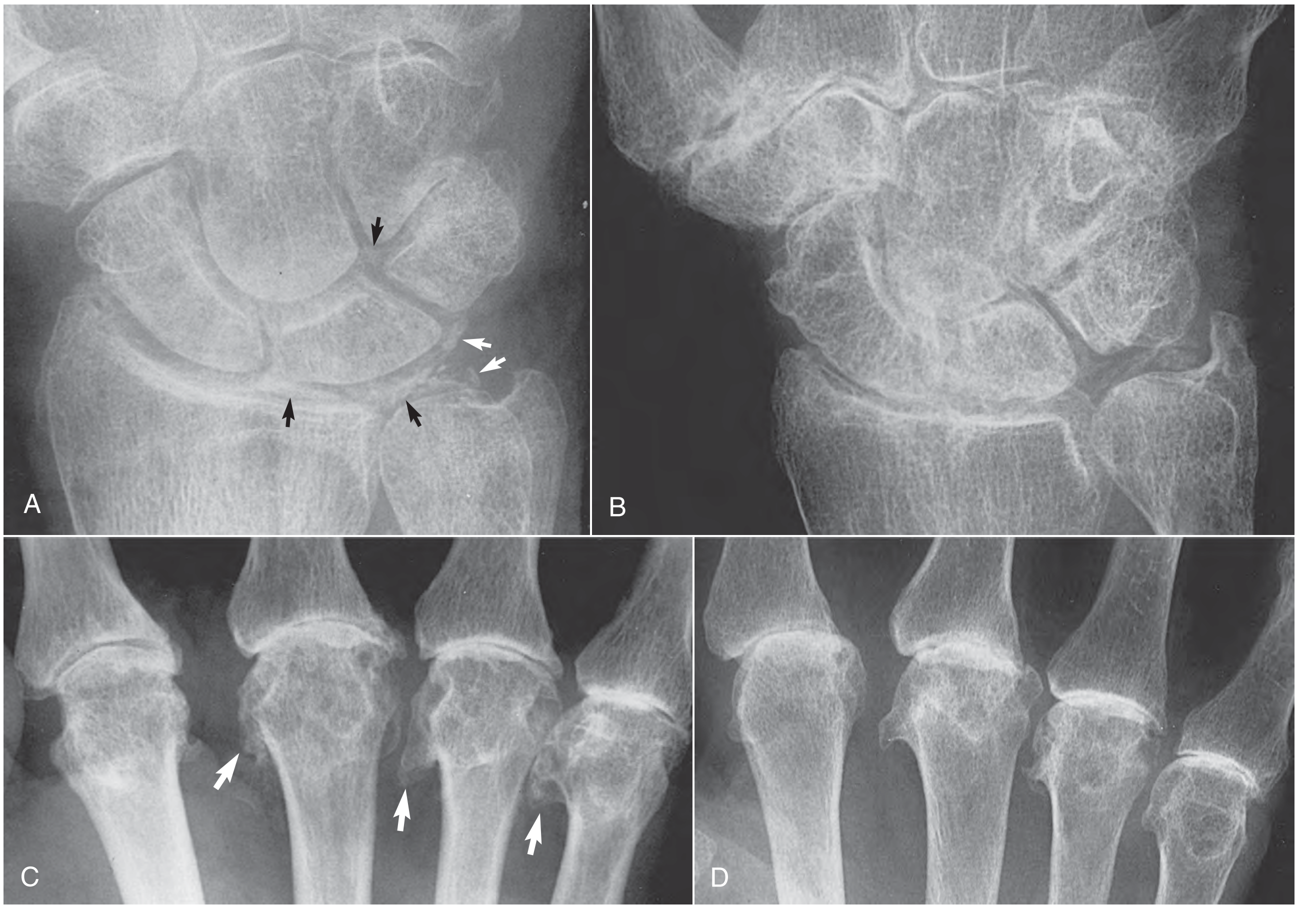

FIGURE 17–66 **Hemochromatosis.**[100,101] **A-B,** Wrist abnormalities. In **A,** chondrocalcinosis is manifested as linear calcification within the hyaline cartilage and fibrocartilage of the radiocarpal and midcarpal articulations and the triangular fibrocartilage complex *(arrows)*. In **B,** arthropathy and chondrocalcinosis are present in another patient with long-standing hemochromatosis. Observe the prominent pan-compartmental joint-space narrowing, osteopenia, and chondrocalcinosis. **C-D,** Metacarpophalangeal arthropathy. In **C,** nonuniform narrowing of the metacarpophalangeal joints is accompanied by subchondral sclerosis and prominent hook-shaped osteophytes *(arrows)*. This arthropathy is characteristic of hemochromatosis. In **D,** another patient, similar findings are evident. *(**C,** Courtesy V. Vint, MD, San Diego.)*

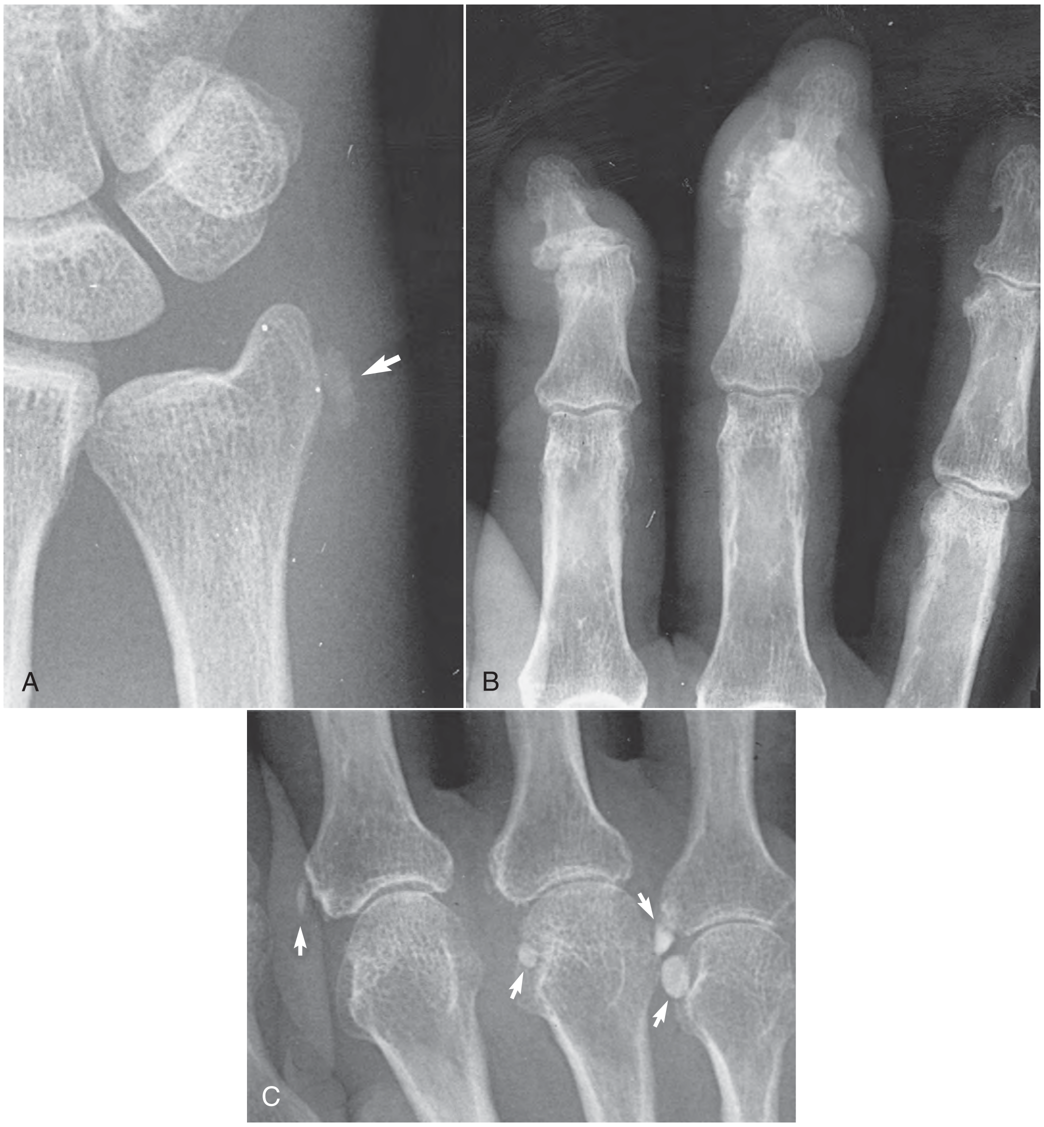

FIGURE 17–67 Calcium hydroxyapatite crystal deposition disease: calcific tendinitis.[102,103] **A,** Extensor carpi ulnaris tendon. Observe the globular accumulation of calcification adjacent to the ulnar aspect of the wrist *(arrow)* in this patient with persistent pain. **B,** Periarticular hydroxyapatite crystal deposition. Globular periarticular accumulations of calcification are seen surrounding the terminal interphalangeal joint and distal tuft in this patient. **C,** In another patient, observe periarticular, globular collections of calcification *(arrows)*. *(**B,** Courtesy V. Vint, MD, San Diego;* ***C,*** *Courtesy R. Shapiro, MD, Sacramento, Calif.)*

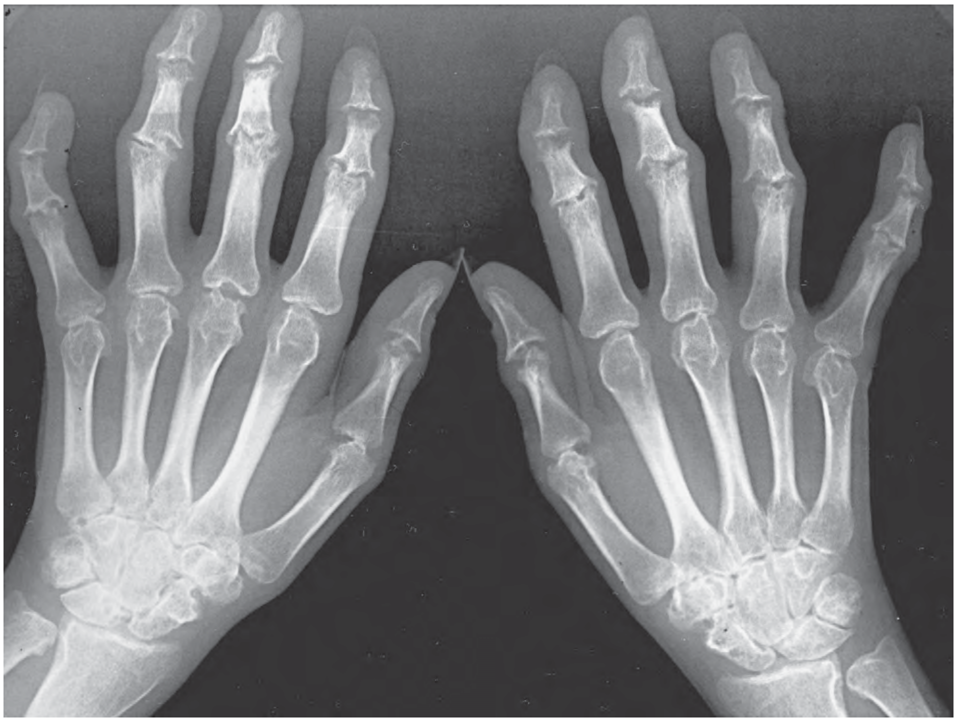

FIGURE 17–68 Multicentric reticulohistiocytosis.[104] Bilateral symmetric polyarticular joint disease is seen in this patient. Central articular erosions are present at all the interphalangeal joints and at many of the metacarpophalangeal joints. Similar erosions are seen in the carpal bones and the distal radioulnar joints. Periarticular osteopenia and minimal joint subluxations are also evident. *(Courtesy A. Brower, MD, Norfolk, Va.)*

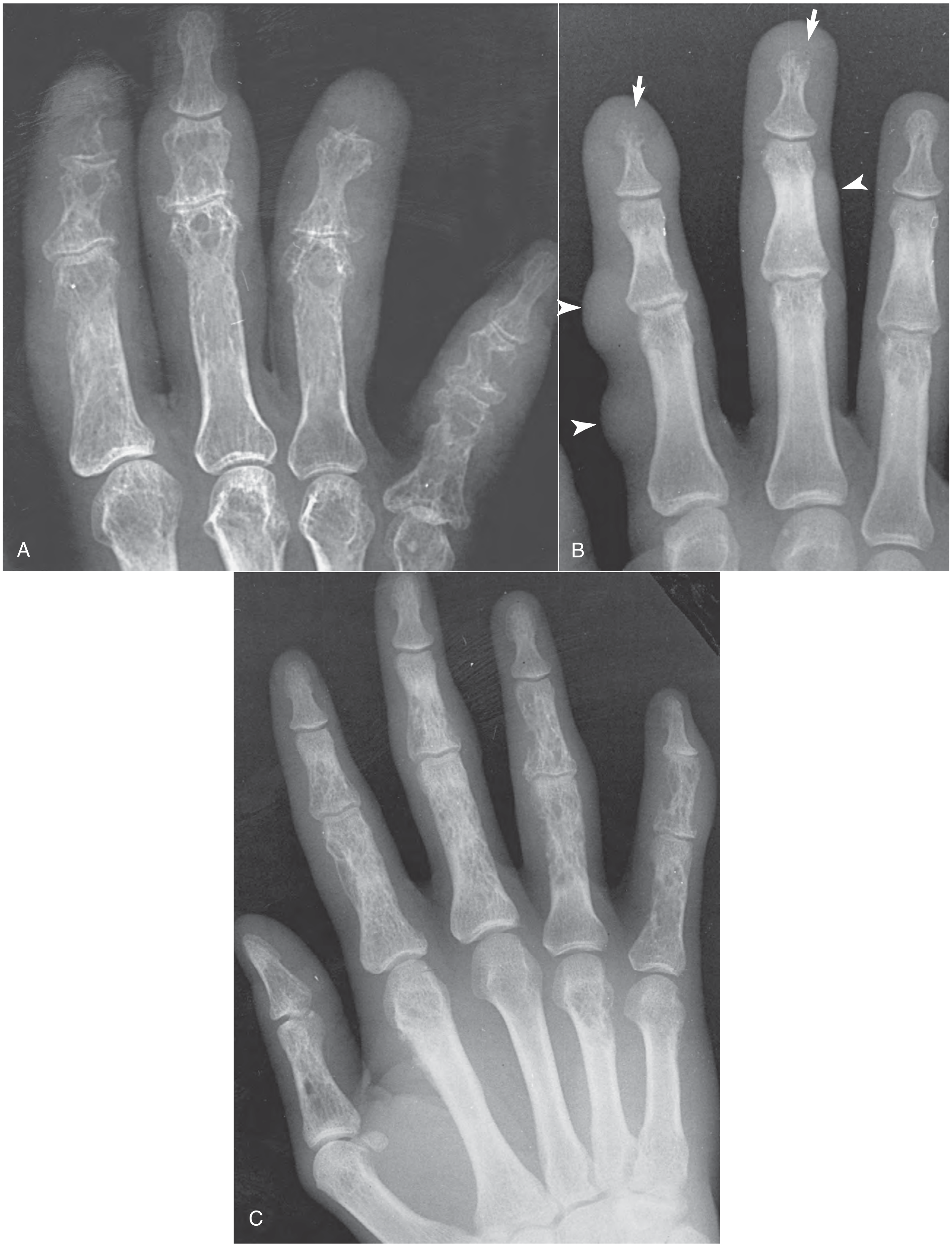

FIGURE 17–69 **Sarcoidosis.**[105-107] **A,** An abnormal, coarsened, reticulated, or lacelike trabecular pattern is evident in the phalanges. Acro-osteolysis of the distal phalanges and subcutaneous nodules also are seen. **B,** In another patient, observe the acro-osteolysis of the terminal tufts *(arrows)* and subcutaneous nodules *(arrowheads)*. **C,** In a third patient, lacelike trabeculae are present throughout the phalanges and metacarpal bones, frequent sites of involvement. (***A,*** *Courtesy M.N. Pathria, MD, San Diego;* ***C,*** *Courtesy B.N. Weissman, MD, Boston.)*

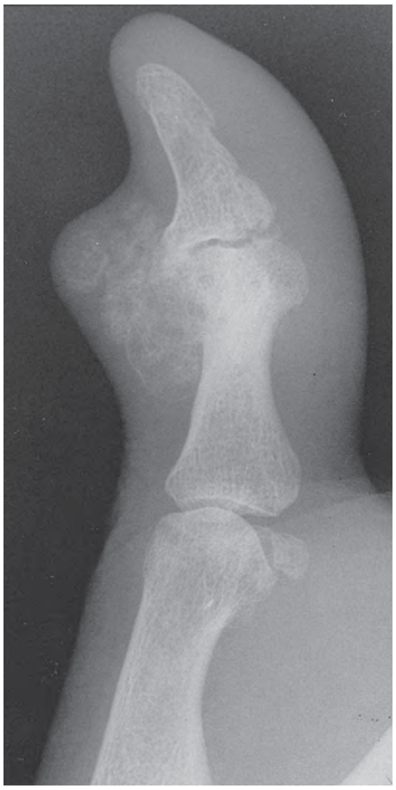

FIGURE 17–70 Extra-articular synovial osteochondromatosis.[108,109] Observe the large collection of ossified osteocartilaginous bodies adjacent to the interphalangeal joint of the thumb, creating a bizarre soft tissue deformity. This metaplastic disorder of the synovium usually produces intra-articular bodies.

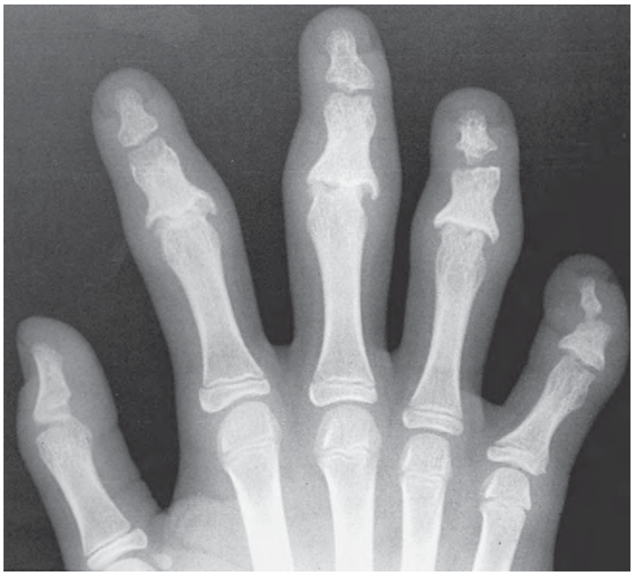

FIGURE 17–72 Frostbite.[111,112] Osseous and cartilaginous destruction of the interphalangeal joints is evident. Subchondral erosion, collapse, and joint-space narrowing simulate the findings of inflammatory (erosive) osteoarthritis. Soft tissue swelling is prominent, and deformity secondary to epiphyseal injury also is present. The thumb is spared because typically it is clenched in the fist and clasped within the palm during exposure to the cold. *(Courtesy R. Stiles, MD, Atlanta.)*

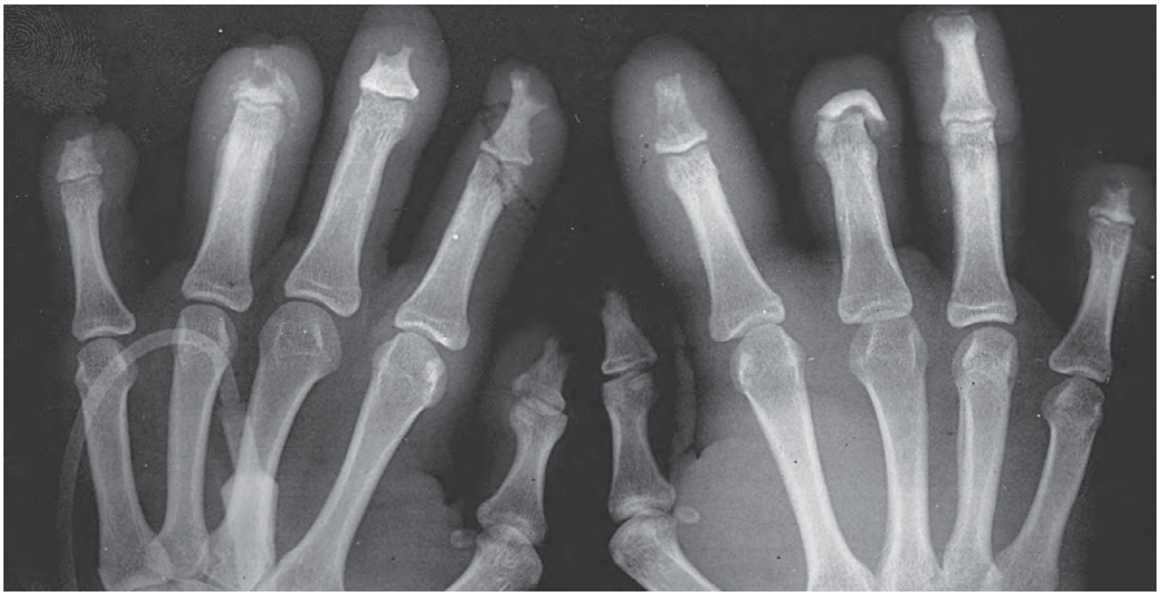

FIGURE 17–71 Neuropathic osteoarthropathy: congenital insensitivity to pain.[110] Radiographic findings include widespread bilateral acro-osteolysis involving the distal phalanges of every digit, and in some cases, the middle phalanges. Note that the soft tissues also are destroyed in this 17-year-old boy with type II congenital insensitivity to pain. *(Courtesy M. Mitchell, MD, Halifax, Nova Scotia, Canada.)*

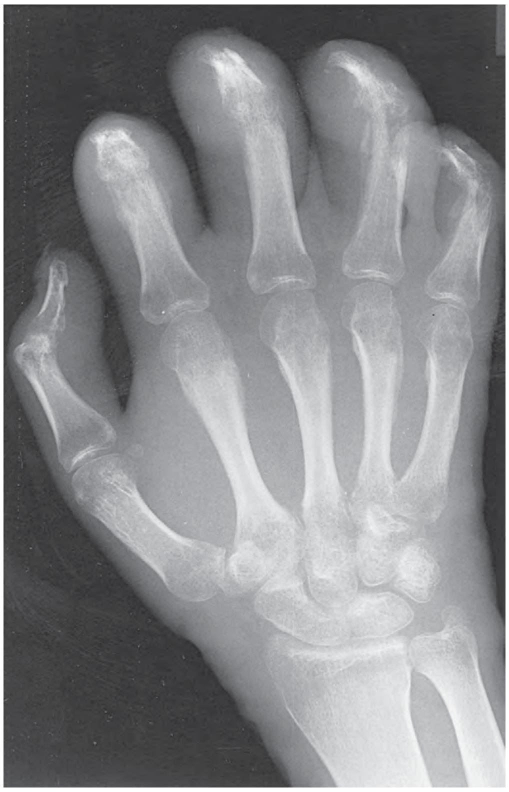

FIGURE 17–73 **Thermal injury: burns.**[113] In a patient who recently burned his hand, early changes are present, including diffuse soft tissue swelling, severe periarticular osteoporosis, and osseous fusion of the interphalangeal joints. Osteolysis of the terminal phalanges and phalangeal periostitis are also seen.

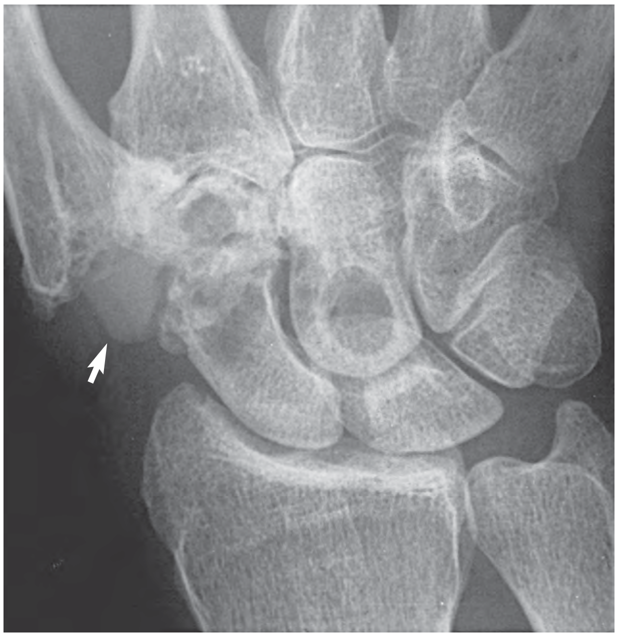

FIGURE 17–74 **Silicone synovitis.**[114,115] This patient with severe erosive osteoarthritis had a silastic prosthetic implant to replace the trapezium *(arrow)*. Observe the well-defined radiolucent defects and erosions in the adjacent carpal bones.

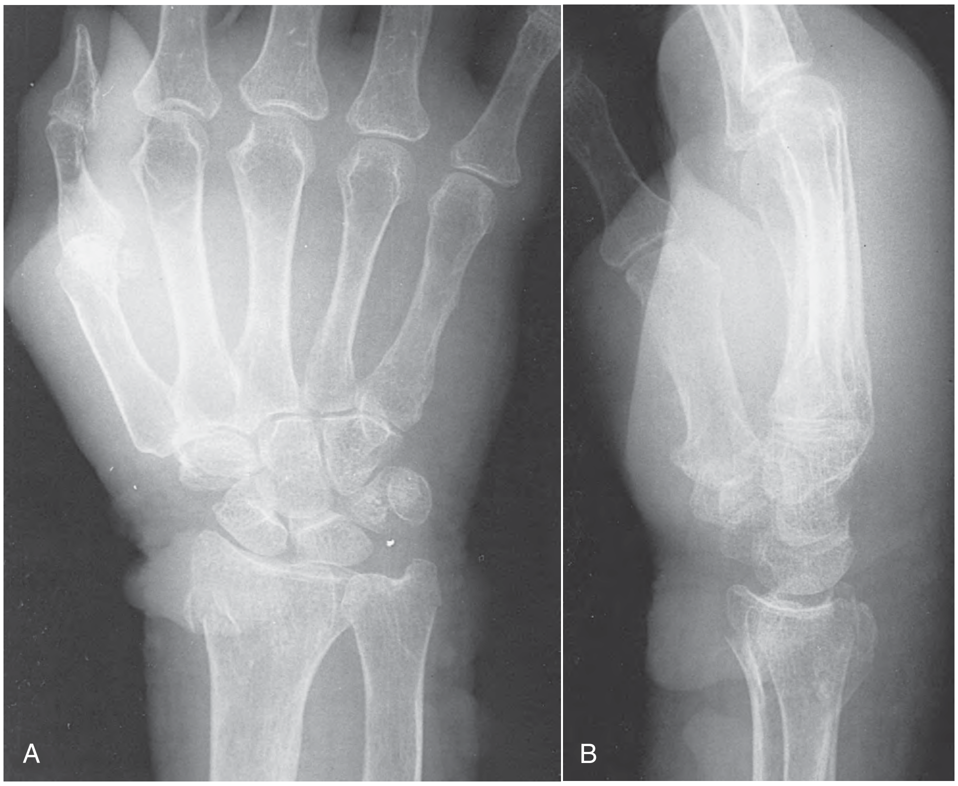

FIGURE 17–75 **Fracture blisters.**[116] **A-B,** This 79-year-old woman sustained a Colles fracture of the distal end of the radius and subsequently developed several irregular nodules about the wrist characteristic of fracture blisters. These blisters represent a complication of fractures and are more common in the ankle than the wrist.

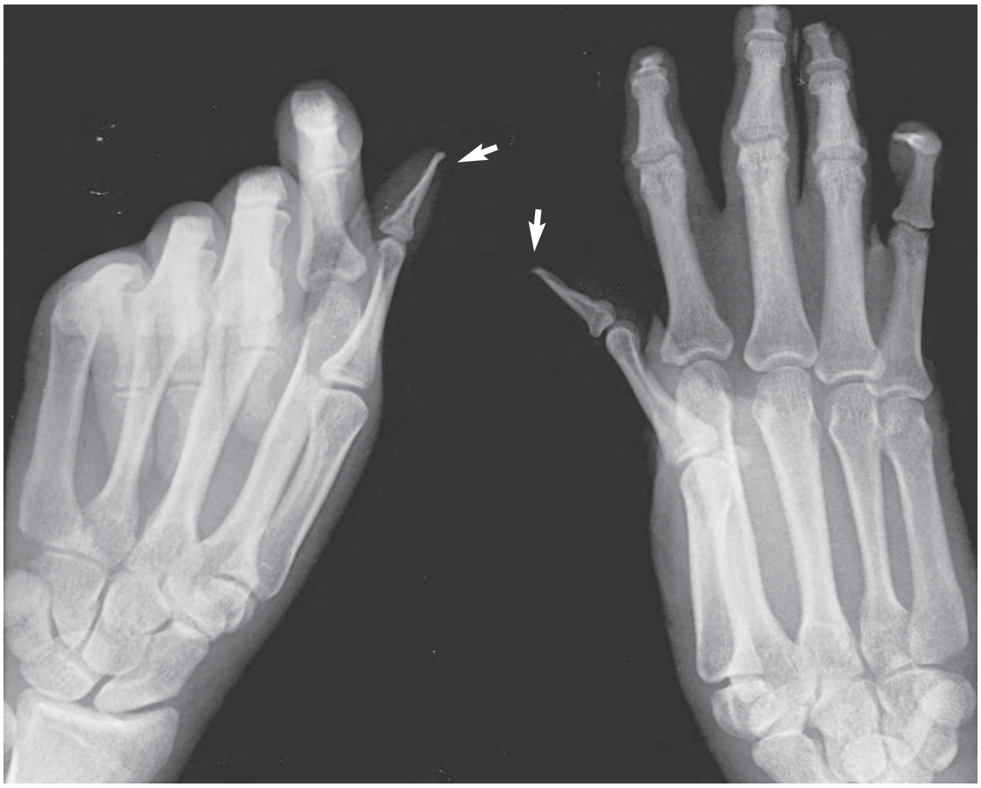

FIGURE 17–76 **Epidermolysis bullosum.**[117] Frontal view of both hands shows marked constriction around the metacarpal region with multiple flexion contractures. Close examination of the tufts reveals skin resorption, nonvisualization of the nails, and terminal phalangeal resorption, which is seen especially well on the thumbs *(arrows)*. This radiographic appearance is virtually pathognomonic of epidermolysis bullosum.

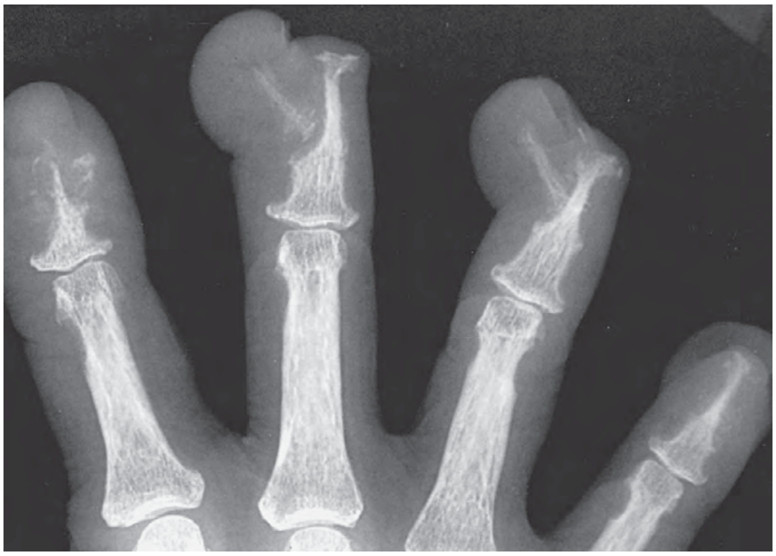

FIGURE 17–77 **Osteolysis with detritic synovitis.**[118] This 67-year-old woman developed pain and swelling of the interphalangeal joints of both hands. Radiographic findings were bilateral and symmetric and included severe resorption and osteolysis of the terminal tufts and, to a lesser extent, the middle and proximal phalanges of all fingers. Marked joint deformity is associated with osseous debris adjacent to the destructive lesions. Analysis of biopsy material revealed nonspecific inflammation. *(From Resnick D, Weisman M, Goergen TG, et al: Osteolysis with detritic synovitis. A new syndrome. Arch Intern Med 138:1003, 1978.)*

TABLE 17-10 Malignant Tumors Affecting the Bones of the Wrist and Hand

Entity	Figure(s)	Characteristics
Malignant Neoplasms		
Secondary malignant tumors		
Skeletal metastasis[119,120]	17-78	Fewer than 1% of metastatic lesions affect the bones of the wrist and hand; predilection for the distal phalanges Acral metastases occur most frequently in patients with carcinoma of the lung and bronchus Irregular osteolysis and cortical destruction
Primary malignant tumors		
Osteosarcoma (conventional)[121]	17-79	Fewer than 1% of osteosarcomas involve the bones of wrist and hand Osteolytic or osteosclerotic lesions or more frequently a mixed pattern Metaphyseal location preferred
Osteosarcoma (parosteal)[122]	17-80	Infrequently involves the bones of the wrist and hand Arises from surface of metaphyseal region Aggressive cortical destruction, periostitis, and soft tissue mass
Osteoblastoma (aggressive)[123]		Two percent of aggressive osteoblastomas affect the bones of the wrist and hand Expansile osteolytic lesion that may be partially ossified or contain calcium
Fibrosarcoma[124]		Fewer than 1% of fibrosarcomas affect the bones of the wrist and hand Purely osteolytic destruction with no associated sclerotic reaction or periostitis
Ewing sarcoma[125,192]	17-81	One percent of Ewing sarcomas affect the bones of wrist and hand Central diaphyseal lesions of the metacarpal and phalangeal bones predominate Aggressive permeative or moth-eaten pattern of bone destruction and cortical violation with laminated or spiculated periostitis and soft tissue mass; some degree of sclerotic activity may also be present
Synovial sarcoma[126]	17-82	Uncommon malignant neoplasm frequently found in the soft tissues in extraarticular locations More common in lower extremity than in upper extremity *Poor prognosis:* frequent recurrence and metastases, especially to the lung Large soft tissue mass and aggressive osteolytic destruction of adjacent bone Approximately 20% to 30% of synovial sarcomas contain calcification
Myeloproliferative Disorders of Bone		
Plasma cell (multiple) myeloma[127]	17-83	Only 1% of multiple myeloma lesions occur in the bones of the wrist and hand Diffuse osteopenia or discrete osteolytic lesions

See also Table 1-12.

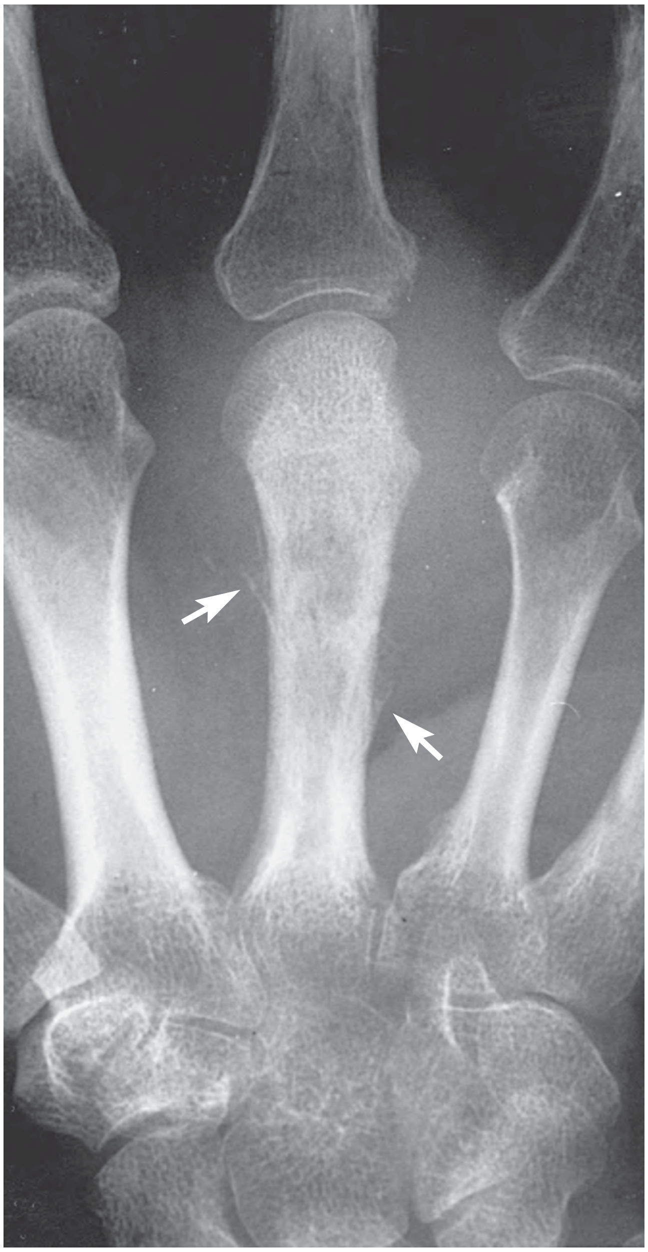

FIGURE 17–78 Skeletal metastasis: malignant melanoma.[119,120] This 23-year-old man had pain and swelling over the distal end of the ulna. He reported having a "skin cyst" removed several years previously. An initial lesion was found in the ulna. The patient underwent surgery, which revealed a lesion containing melanin. The histologic evaluation revealed malignant melanoma. The patient developed widespread skeletal metastasis within months. This radiograph from a subsequent skeletal survey revealed a destructive mixed lytic-sclerotic lesion of the metacarpal bone and the proximal phalanx of the third finger, with periostitis and soft tissue swelling *(arrows)*. Periosteal reaction and involvement of bone beyond the elbow or knee are seen more commonly in patients with primary malignant tumors and are infrequent findings in those with skeletal metastasis.

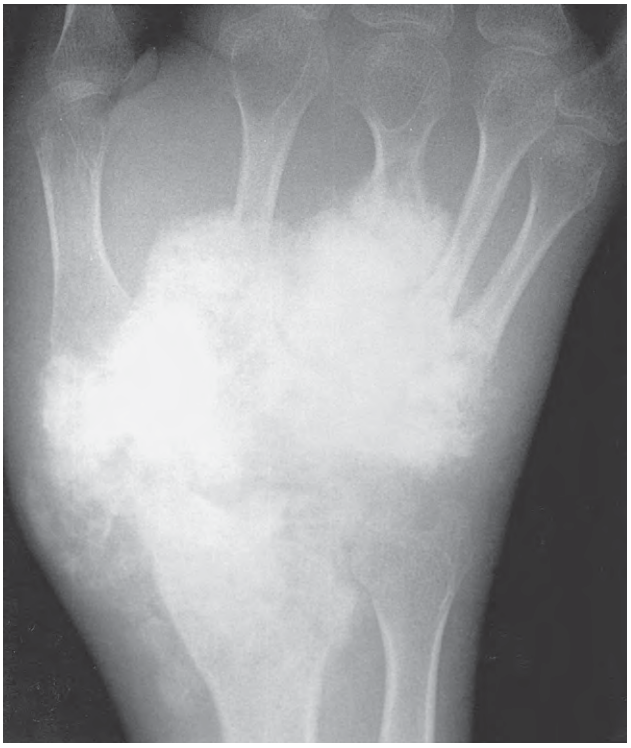

FIGURE 17–79 Conventional osteosarcoma.[121] Observe the widespread osteoblastic proliferation and destruction of the carpal bones with prominent soft tissue extension of osteosarcoma in this 19-year-old man. Osteosarcoma infrequently affects the carpal bones. *(Courtesy L. White, MD, Toronto, Ontario, Canada.)*

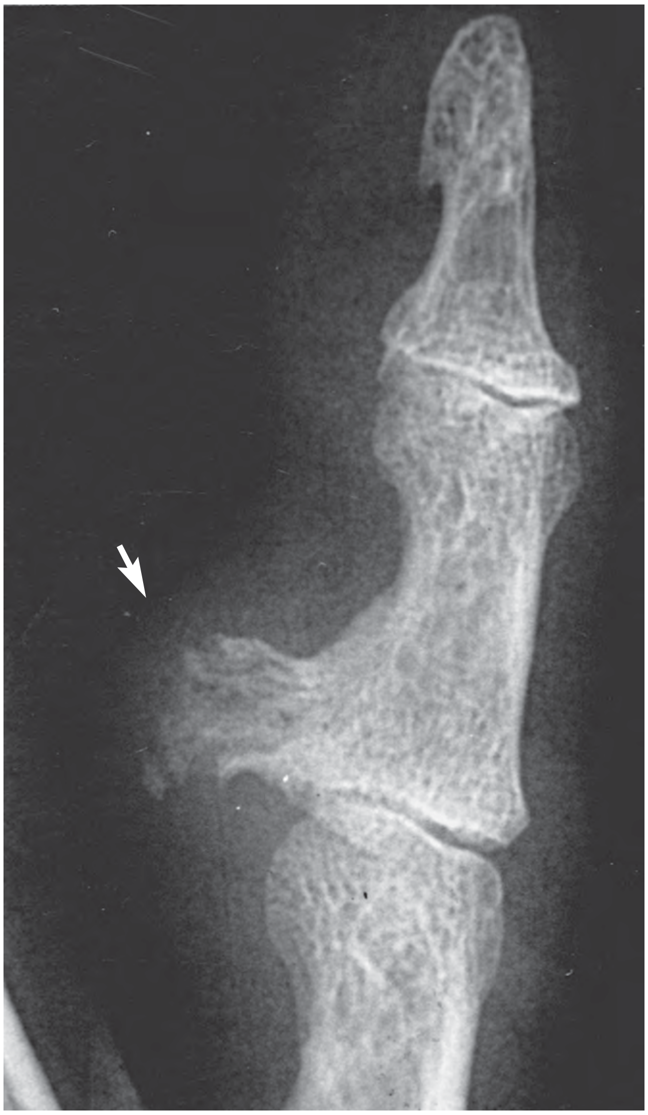

FIGURE 17–80 **Parosteal osteosarcoma.**[122] Routine radiograph of this 58-year-old man reveals a spiculated lesion growing horizontally from the cortex of the proximal portion of the middle phalanx *(arrow)*. Parosteal osteosarcomas generally affect patients between 20 and 40 years of age. *(Courtesy J. Slivka, MD, San Diego.)*

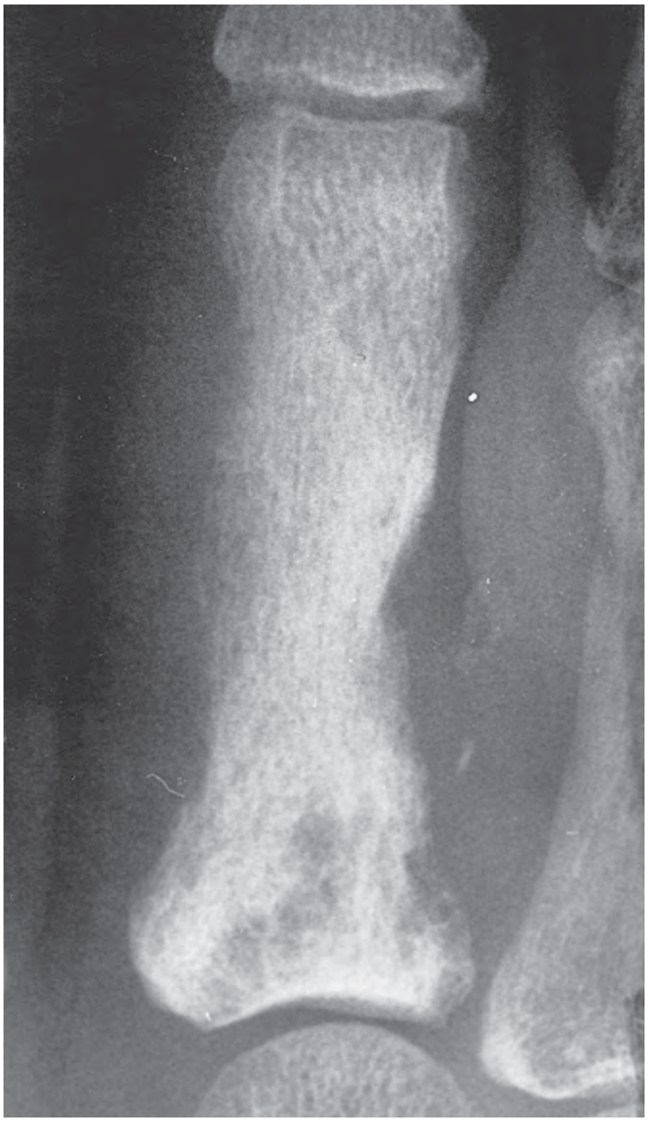

FIGURE 17–81 **Ewing sarcoma.**[125,192] Radiographic abnormalities in the third proximal phalanx include considerable sclerosis, permeative cortical destruction, and minimal periostitis. A previous biopsy is responsible for the large cortical defect and radiodensity within the soft tissues. *(Courtesy J. Rausch, MD, Fort Wayne, Ind.)*

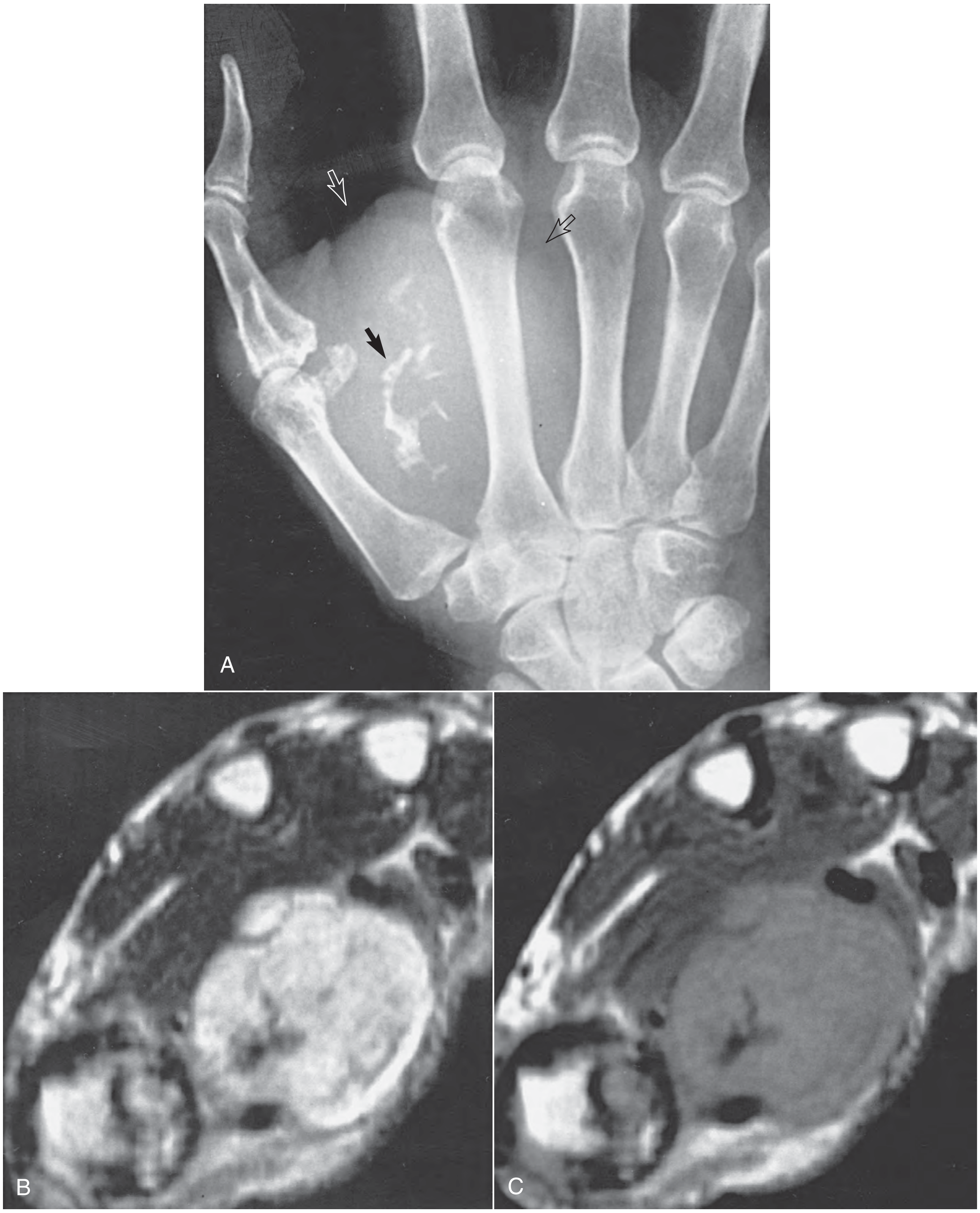

FIGURE 17–82 Synovial sarcoma.[126] A 75-year-old woman had an enlarging painful mass involving the thenar eminence. **A,** Frontal view of the hand shows a radiodense soft tissue mass *(open arrows)* with a central, irregular zone of soft tissue calcification *(arrow)*. **B-C,** A large soft tissue mass is of high signal intensity on the transaxial T2-weighted **(B)** (TR/TE, 1800/70) MR image and of intermediate signal intensity on the proton–density-weighted **(C)** (TR/TE, 1800/20) image. The magnetic resonance (MR) images help to delineate the nature and extent of this aggressive neoplasm.

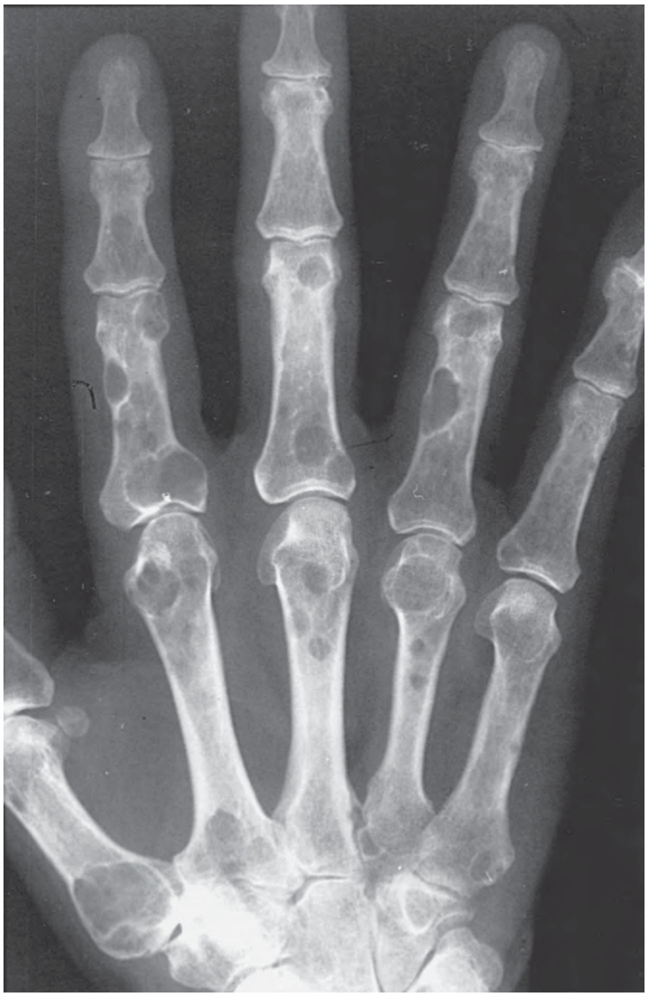

FIGURE 17–83 Plasma cell (multiple) myeloma.[127] Well-circumscribed osteolytic lesions are disseminated throughout the bones of the hand. Some of the radiolucent foci possess sclerotic margins.

TABLE 17-11 Benign Tumors and Tumorlike Lesions Affecting the Bones of the Wrist and Hand

Entity	Figure(s)	Characteristics
Primary Benign Tumors of Bone		
Enostosis[128]	17-23, *D*	Nine percent of enostoses affect the bones of the wrist and hand Circular or ovoid osteosclerotic focus
Osteoid osteoma[129-132,189]	17-84	Six to 13% of osteoid osteomas occur in the bones of the wrist and hand Extremely painful lesion classically relieved by salicylates Central radiolucent area (nidus) less than 1 cm in diameter surrounded by reactive sclerosis Diaphyseal location, but may affect metaphysis, epiphysis, or carpal bones
Subungual exostosis[133]	17-85, *A*	Approximately 20% of subungual exostoses involve the hand Solitary osteochondroma-like lesion arising from the dorsal surface of the distal phalanx Pressure on the undersurface of the nail may cause severe pain Lesion possesses smooth continuation of cortical and medullary bone Most frequently affects thumb and index finger
Bizarre parosteal osteochondromatous proliferation (BPOP)[202]	17-85, *B, C*	Also designated *Nora lesion* Well-marginated mass of heterotopic ossification arising from the periosteal surface of an intact cortex of a tubular bone, especially a phalanx or a metacarpal May result in a palpable mass, but there is no medullary bone involvement or cortical destruction *Differential diagnosis:* turret exostosis, florid reactive periostitis and malignant processes such as osteosarcoma and chondrosarcoma

Continued

TABLE 17-11 Benign Tumors and Tumorlike Lesions Affecting the Bones of the Wrist and Hand—cont'd

Entity	Figure(s)	Characteristics
Turret exostosis[134]		Infrequent osseous excrescence arising from the dorsal surface of a proximal or middle phalanx of a finger History of penetrating injury followed by pain and soft tissue swelling or lump Initial soft tissue swelling leading to immature periostitis and broad-based osseous protuberance on surface of bone
Enchondroma (solitary)[135,136]	17-86	Fifty-seven percent of solitary enchondromas affect the bones of the wrist and hand, especially the proximal phalanges, followed in decreasing frequency by the metacarpal bones, the middle phalanges, the terminal phalanges, and the carpal bones Solitary enchondroma is a benign neoplasm composed of hyaline cartilage that develops in the medullary cavity and is usually discovered in the third or fourth decade of life Most lesions are painless, and painful lesions should arouse the suspicion of malignant transformation, a complication that occurs only rarely in solitary lesions and as many as 20% to 30% of cases of multiple lesions (Ollier disease and Maffucci syndrome) Osteolytic metadiaphyseal lesions, endosteal scalloping, matrix calcification (50% of lesions)
Enchondromatosis (Ollier disease)[136,137]	17-87	More than 50% of patients with Ollier disease have lesions involving the wrist and hand Multiple enchondromas involving the metacarpal bones and phalanges Tubular radiolucent areas extending into the metaphysis from the physis Shortening and deformity of affected bones Frequent calcification of matrix
Maffucci syndrome[136,138]	17-88	Eighty-eight percent of patients with Maffucci syndrome have unilateral or bilateral lesions involving the wrist and hand Multiple enchondromas with soft tissue hemangiomas—multiple phleboliths in the soft tissues Multiple central or eccentric radiolucent lesions containing variable amounts of calcification Shortening and deformity of affected bones Frequently undergoes malignant transformation, principally to chondrosarcoma
Giant cell tumor (benign)[139]		Four percent of benign giant cell tumors are located in the bones of the wrist and hand, and an additional 4% of lesions are located in the distal portion of the radius Osteolytic subarticular lesion that extends to the metaphyseal region
Simple bone cyst[140]	17-89	Only 1% of simple bone cysts occur in the bones of the wrist and hand Multiloculated, eccentric lesion
Intraosseous lipoma[141]		Fewer than 1% of intraosseous lipomas occur in the bones of the wrist and hand Geographic osteolytic lesion with sclerotic margins, often containing a central calcified or ossified nidus
Aneurysmal bone cyst[142]	17-90	Five percent of aneurysmal bone cysts involve the bones of the wrist and hand Eccentric, thin-walled, expansile, multiloculated, osteolytic, metaphyseal lesion
Tumorlike Lesions of Bone		
Paget disease[143,144]	17-91	Infrequent involvement of the bones of the wrist and hand Usually polyostotic form
Fibrous dysplasia[145]	17-92	Involvement of the bones of the wrist and hand is rare in the monostotic form but present in about 55% of patients with polyostotic disease
Intraosseous ganglion cyst[146,147]	17-93	Intraosseous ganglia are often clinically silent; however, chronic pain, which sometimes increases with physical activity, may be evident Geographic cystlike lesions of various sizes within the carpal bones, especially the lunate bone
Epidermoid (inclusion) cyst[148]	17-94	Well-defined osteolytic lesion of terminal phalanx Sclerotic margin and mild expansion Usually 2 cm or less in diameter History of blunt or penetrating trauma

See also Tables 1-13 and 1-14.

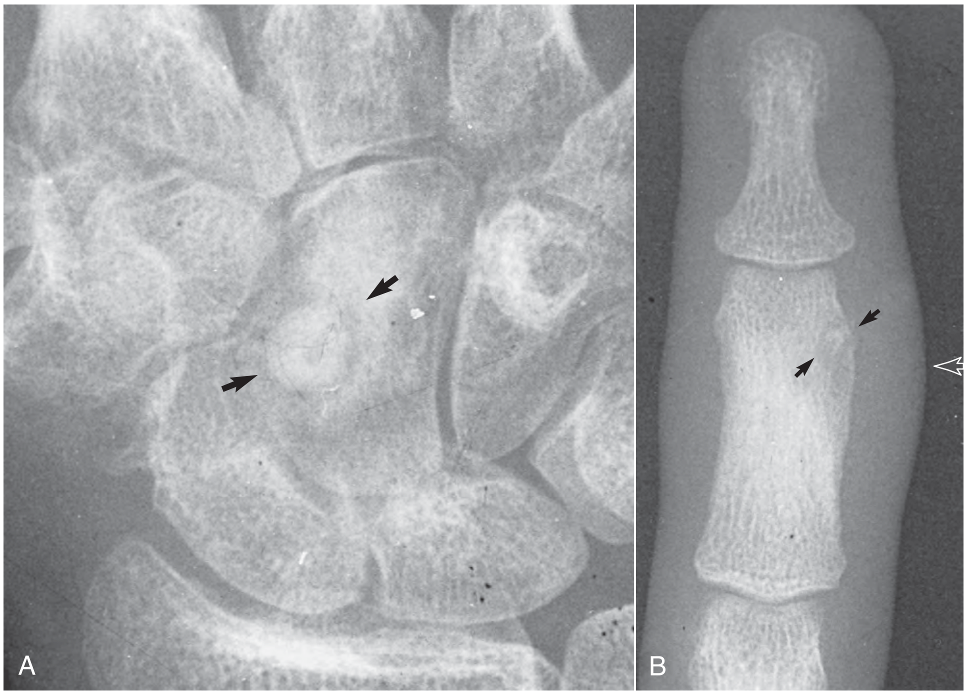

FIGURE 17–84 Osteoid osteoma.[129-132,188] **A,** Carpal involvement. An eccentric circular radiolucent area with a central zone of calcification *(arrows)* surrounded by reactive sclerosis is evident in the capitate bone. Diffuse periarticular osteopenia throughout the carpus is the result of disuse and hyperemia. **B,** Phalangeal involvement. A 23-year-old man had a painful swelling over the middle phalanx of the fourth finger. The radiograph reveals soft tissue swelling *(open arrow)* and an eccentric circular radiolucent area with a central zone of calcification *(arrows)* surrounded by reactive sclerosis. Approximately 9% of osteoid osteomas occur in the bones of the wrist and hand, but the capitate bone is not frequently involved.

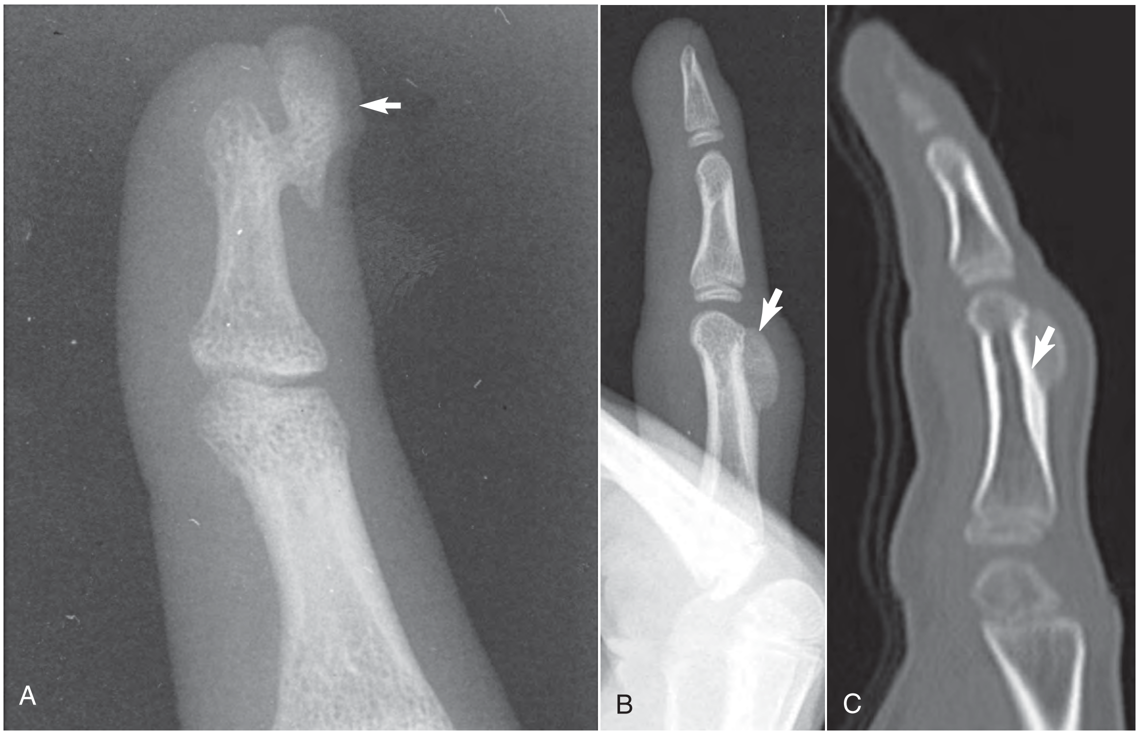

FIGURE 17–85 Osteochondroma-like processes. A, Subungual exostosis.[133] In this patient with a painful deformity of the fingernail, a pedunculated osseous excrescence arising from the dorsal surface of the terminal tuft is seen displacing the nail *(arrow)*. The subungual exostosis is an uncommon, solitary, benign bone neoplasm arising from a distal phalanx at or adjacent to the nail bed. Histologically, it is identical to an osteochondroma. **B-C,** Bizarre parosteal osteochondromatous proliferation (BPOP).[202] A lateral radiograph **(B)** and CT scan bone window **(C)** reveal a smooth, sessile, ovoid protuberance of bone *(arrows)* arising from the dorsal periosteal surface of the proximal phalanx of this 6-year-old girl. The cortex remains intact and there is no medullary bone involvement. The growth results in a mass effect of the overlying soft tissues, but no associated soft tissue swelling. BPOP is benign and is sequentially related to florid reactive periostitis.

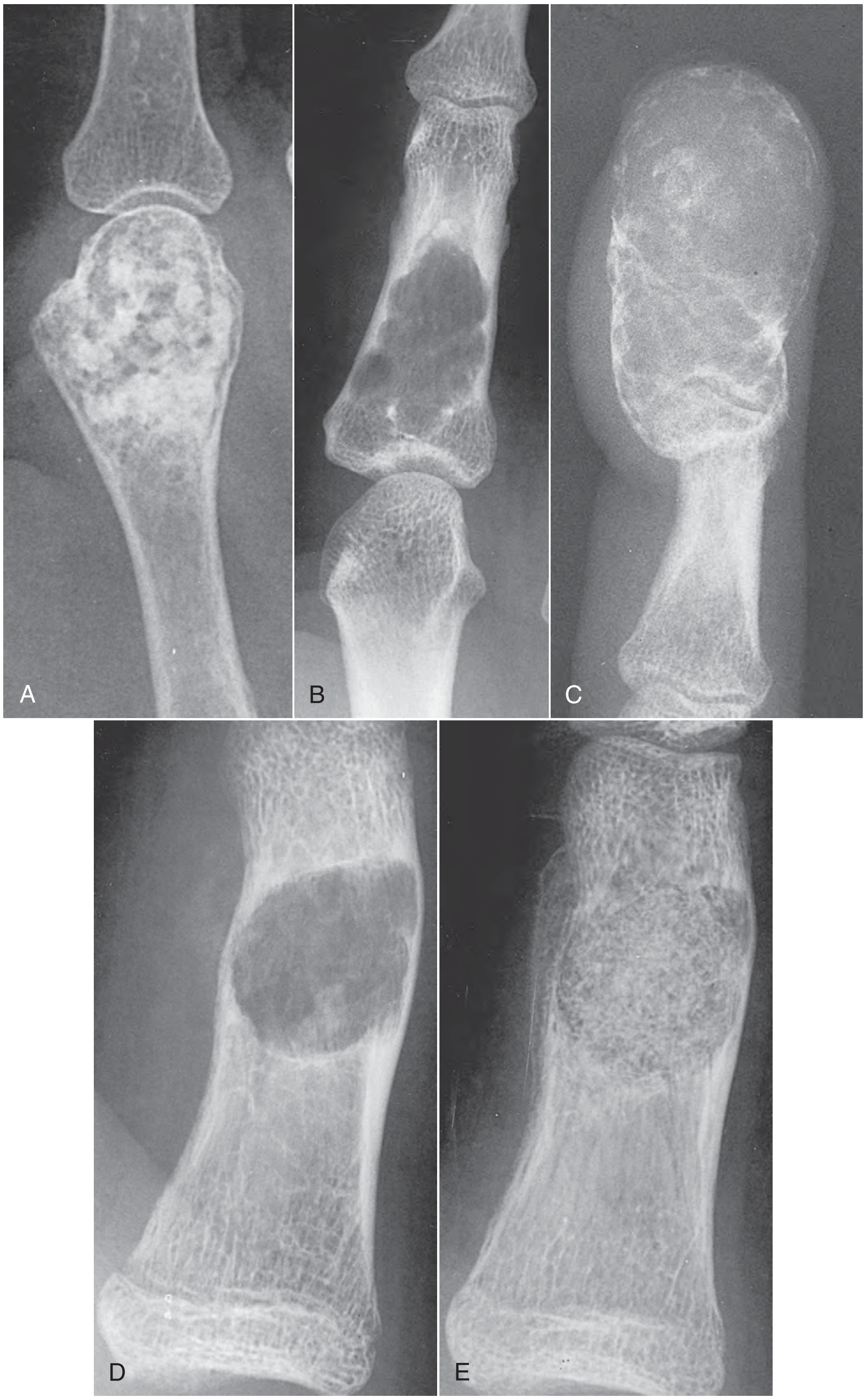

FIGURE 17–86 Solitary enchondroma: tubular bones of the hand.[135,136] **A,** Radiolucent lesion with endosteal scalloping involving the medullary cavity of the metaphysis and subchondral region of the metacarpal head is evident. Stippled calcification, present in about 50% of cartilaginous tumors, is seen within the matrix. **B,** Classic appearance of an enchondroma includes a radiolucent metadiaphyseal lesion with geographic margins, endosteal scalloping, and faint trabeculation. **C,** Enchondromas in the terminal phalanx are rare. Observe the marked expansion within this atypical lesion. **D-E,** In another patient, magnification radiographs of an enchondroma were taken before **(D)** and after **(E)** curettage and packing with bone chips. In **D,** this diaphyseal lesion is well circumscribed, with endosteal scalloping and faint trabeculation within the matrix. In **E,** the postsurgical radiograph reveals a mottled opacification of the matrix. This procedure is occasionally performed to strengthen the bone and to offset the likelihood of pathologic fracture. *(**A,** Courtesy S.K. Brahme, MD, San Diego; **D-E,** Courtesy U. Mayer, MD, Klagenfurt, Austria.)*

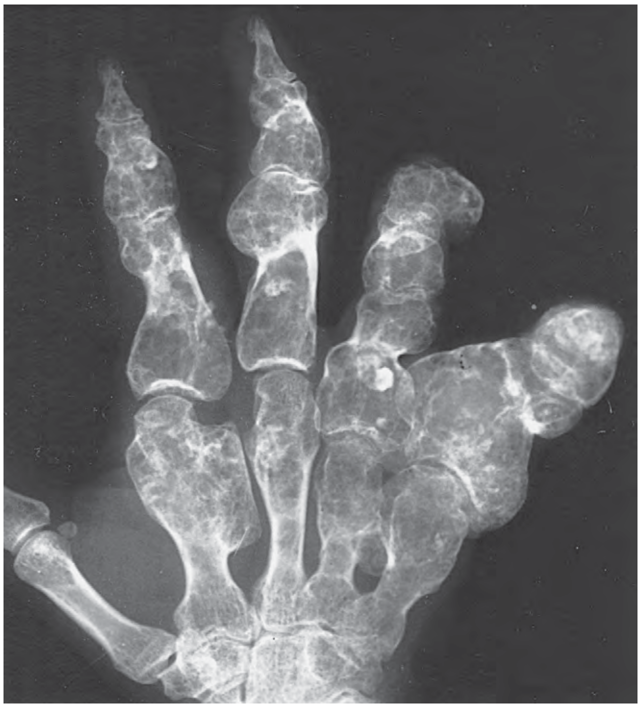

FIGURE 17–87 **Enchondromatosis (Ollier disease).**[136,137] Considerable deformity and multiple expansile, multiloculated radiolucent lesions are evident throughout most bones of the hand. Faint calcification is seen within the matrix. Malignant transformation to chondrosarcoma may occur in as many as 25% of patients by the age of 40 years.

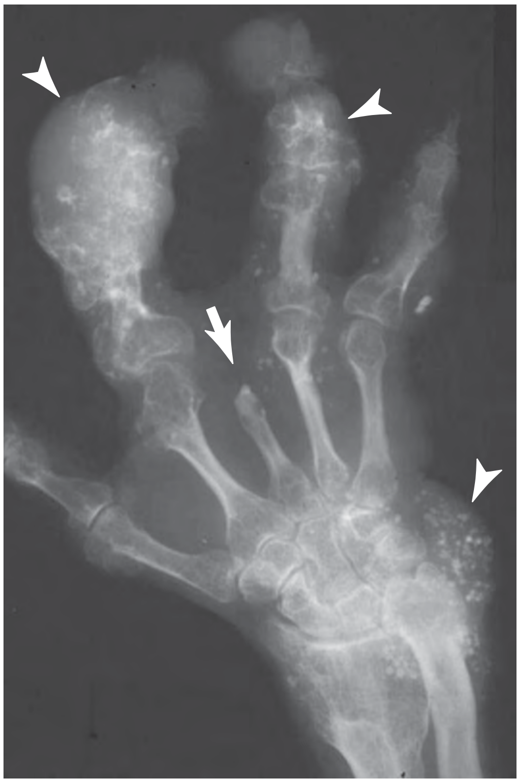

FIGURE 17–88 **Enchondromatosis (Maffucci syndrome).**[136,138] Bizarre osseous deformity and osteolytic destruction with accompanying soft tissue masses containing calcified phleboliths *(arrowheads)* are characteristic findings of Maffucci syndrome. The third digit has been surgically amputated *(arrow)*. This rare congenital, nonhereditary mesodermal dysplasia is characterized by multiple enchondromas, cavernous or capillary soft tissue hemangiomas, and other vascular soft tissue lesions. The disease is unilateral in 50% of patients, and frequently undergoes malignant transformation, usually to chondrosarcoma.

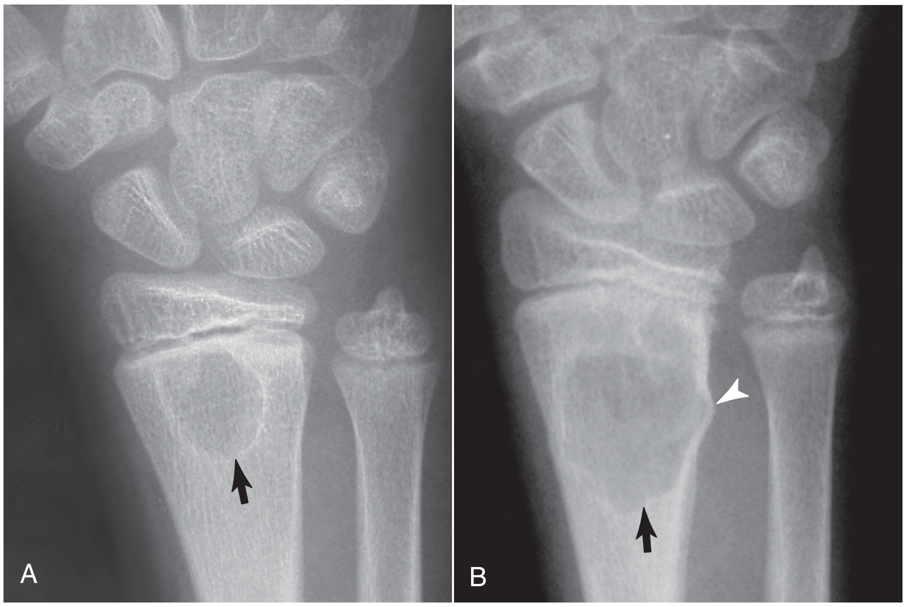

FIGURE 17–89 **Simple bone cyst.**[140] This 12-year-old boy had radiographs taken to evaluate an injury, and a circular geographic metaphyseal radiolucency *(arrow)* was discovered incidentally **(A)**. The painless lesion was diagnosed as a simple bone cyst and was left alone. Two years later, the boy injured his forearm and another set of radiographs was obtained **(B)** revealing a fracture seen best as cortical buckling on the ulnar side of the radius *(arrowhead)*. Furthermore, the lesion enlarged by about 50% in the intervening 2 years and the metaphysis of the radius grew in length distal to the lesion making it appear that the cyst has migrated proximally away from the physis.

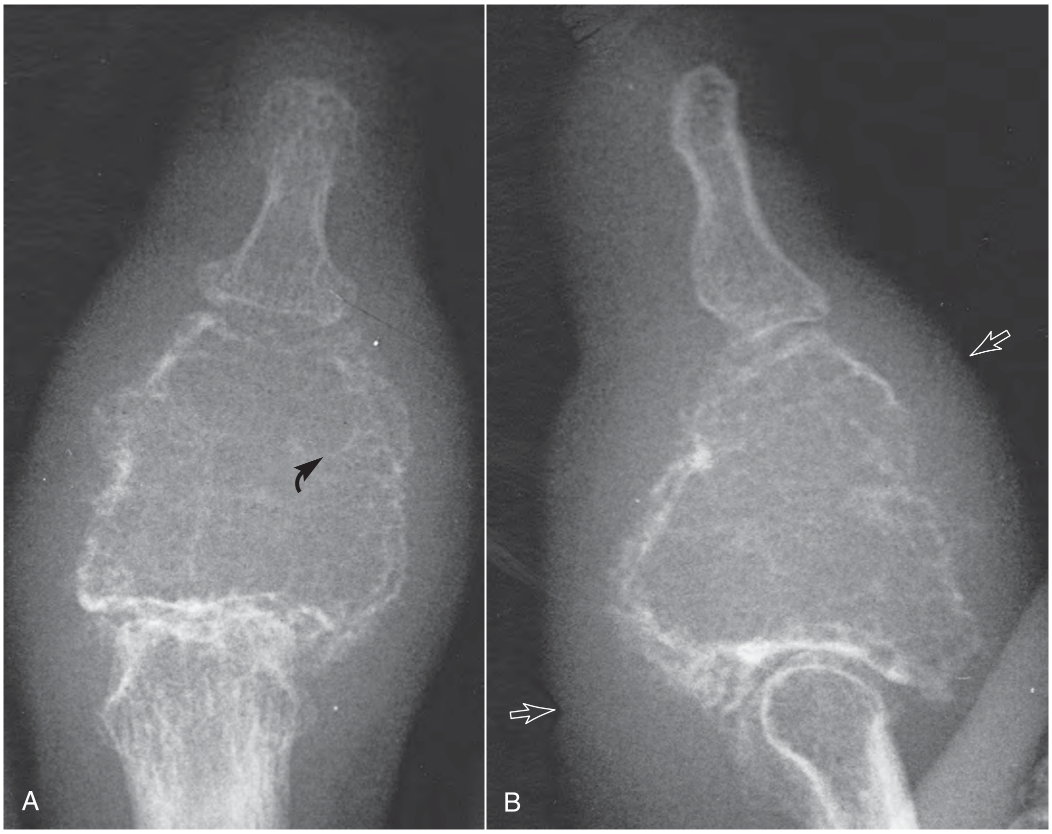

FIGURE 17–90 **Aneurysmal bone cyst.**[142] Frontal **(A)** and lateral **(B)** radiographs of the hand of this 57-year-old woman show an expansile, finely trabeculated *(curved arrow)* osteolytic lesion involving the entire middle phalanx of the third digit. Observe the prominent soft tissue displacement and swelling *(open arrows)*.

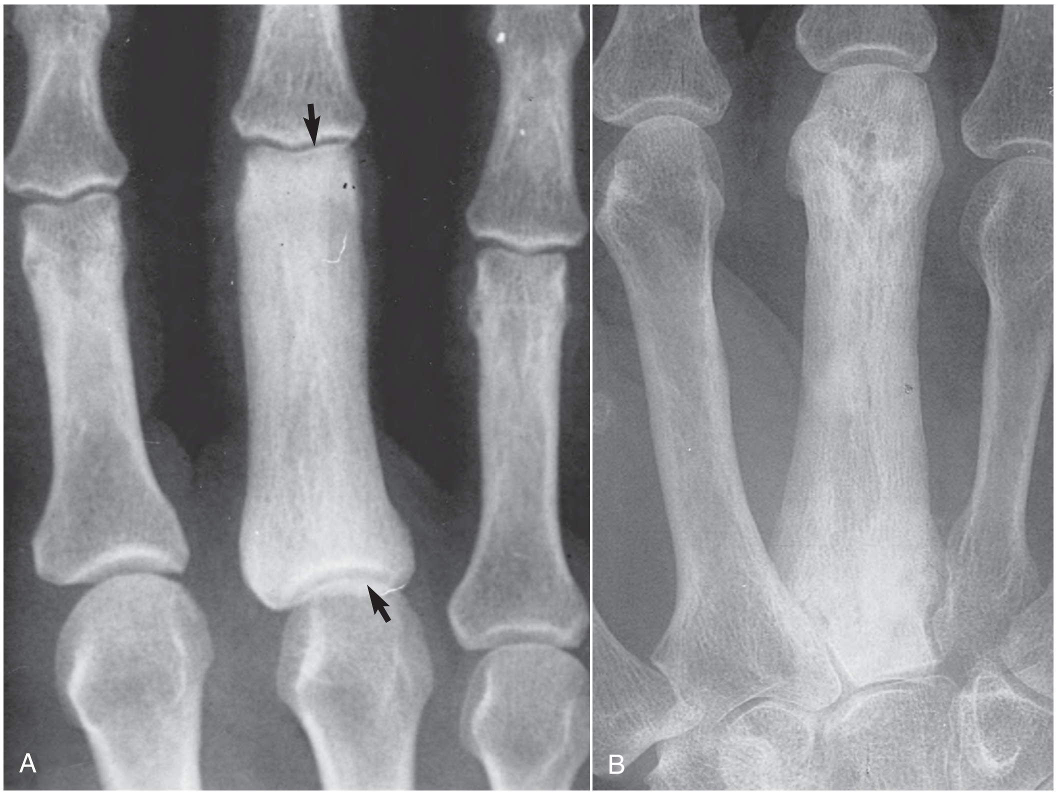

FIGURE 17–91 **Paget disease.**[143,144] **A,** Typical alterations of Paget disease in the proximal phalanx of this patient include diffuse increased sclerosis, bone enlargement, thickened and coarsened trabeculae, and subarticular distribution *(arrows)*. **B,** Posteroanterior radiograph of the metacarpal bone in this 86-year-old man reveals diffuse osseous enlargement, coarsened trabeculae, and increased radiodensity. When Paget disease affects the hand, involvement of a single hand or single bone is not uncommon.

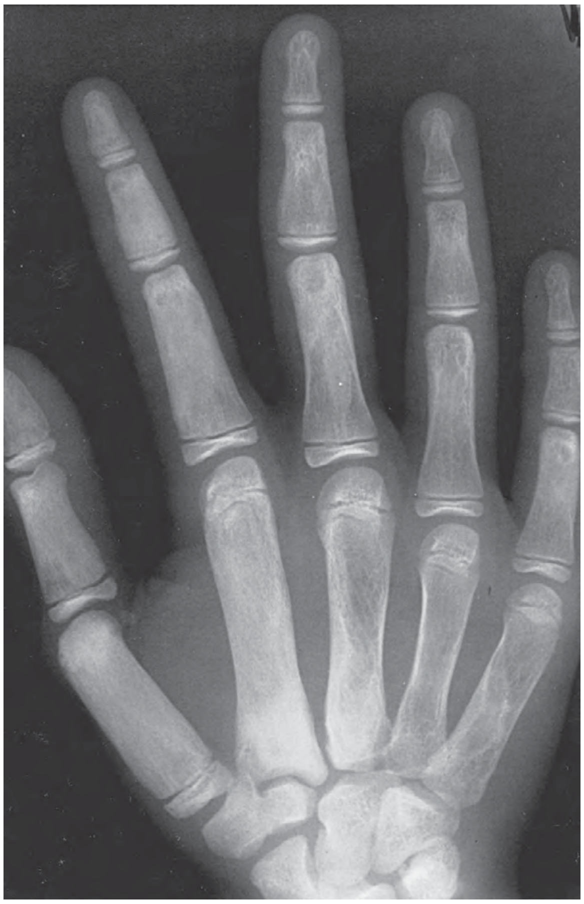

FIGURE 17–92 **Polyostotic fibrous dysplasia.**[145] Altered bone texture with osteosclerotic and osteolytic regions characterizes the bones of the hand in this child. The radiolucent lesions have the characteristic ground-glass appearance, and the more osteosclerotic lesions appear diffuse, with loss of definition between cortical and medullary bone.

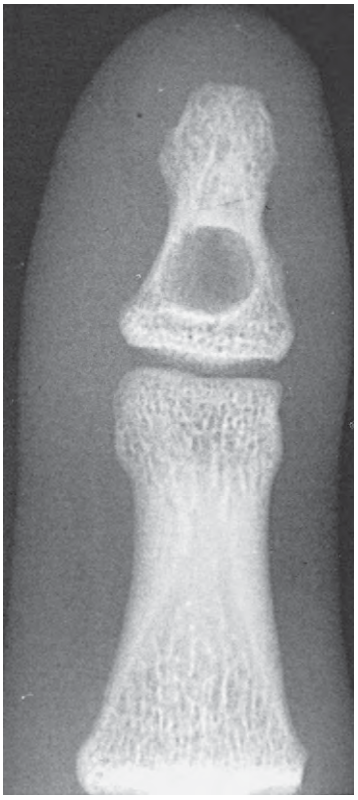

FIGURE 17–94 **Epidermoid (inclusion) cyst.**[148] A circular geographic osteolytic lesion with a sclerotic margin is seen in the terminal phalanx. It is believed that epidermoid cysts occur subsequent to implantation of ectodermal tissue after trauma to superficially located bone. They occur most frequently in the skull and the hand.

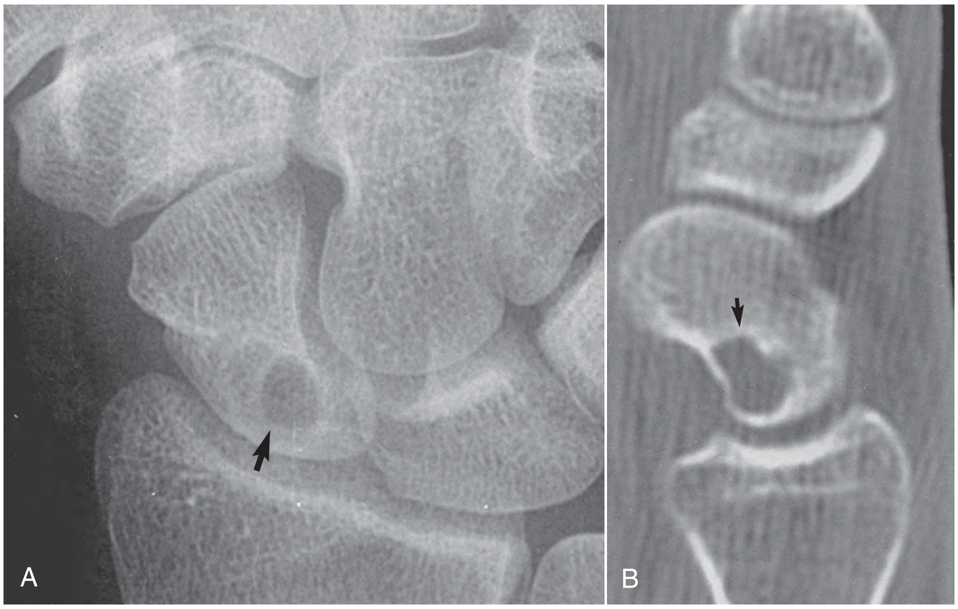

FIGURE 17–93 **Intraosseous ganglion cyst.**[146,147] This 29-year-old man had chronic wrist pain. **A,** Routine radiograph. A large, focal, well-marginated osteolytic lesion *(arrow)* is evident in the proximal pole of the scaphoid bone. **B,** Sagittal computed tomographic (CT) image. The scan clearly demonstrates the extent of the lesion and its fluidlike attenuation *(arrow)*.

TABLE 17-12 Metabolic, Hematologic, Vascular, and Infectious Disorders Affecting the Wrist and Hand

Entity	Figure(s)	Characteristics
Generalized osteoporosis[149-151]	17-95	Uniform decrease in radiodensity, thinning of cortices *Combined cortical thickness:* at the midshaft of the second metacarpal, the transverse thickness of both cortices should be equal to or greater than the transverse thickness of the medullary cavity; in osteoporosis, however, the transverse cortical thickness is diminished Routine radiographs may suggest the presence of osteoporosis, but bone densitometry is necessary to assess bone mineral content accurately
Regional osteoporosis[151-153]	17-96	Osteopenia confined to a specific anatomic region may occur as a result of disuse and immobilization after a fracture or other injury; also seen in complex regional pain syndrome, burns, frostbite, and paralysis Findings may be more widespread in paralyzed patients Bandlike, patchy, spotty, or periarticular osteopenia Subperiosteal and intracortical bone resorption Subchondral and juxtaarticular erosions
Hyperparathyroidism and renal osteodystrophy[154]	17-97	Brown tumors Subperiosteal resorption, especially radial side of second and third middle phalanges Metastatic soft tissue calcification and vascular calcification Tuft resorption—acro-osteolysis
Amyloid deposition[155]	17-98	Patients on long-term hemodialysis develop amyloid deposition Deposits in carpal tunnel may lead to carpal tunnel syndrome and extensive carpal bone erosion
Hypothyroidism[156]	17-99	Delayed skeletal maturation, epiphyseal dysgenesis, carpal tunnel syndrome, soft tissue edema, neuropathy, myopathy, osteoporosis, erosive arthritis, and calcium pyrophosphate dihydrate (CPPD) crystal deposition
Pseudohypoparathyroidism (PHP) and pseudopseudohypoparathyroidism (PPHP)[157]	17-100	Premature physeal fusion: metacarpal shortening Soft tissue calcification and ossification
Acromegaly[158,159]	17-101	*Soft tissue overgrowth:* prominent soft tissues of fingers, joint space widening, and clubbing of fingers *Osseous overgrowth:* enlargement of sesamoid bones and terminal tufts, periarticular excrescences Acromegalic arthropathy with eventual secondary osteoarthrosis
Primary hypertrophic osteoarthropathy[160]	17-102	Pachydermoperiostosis is the primary form of hypertrophic osteoarthropathy and represents only 3% to 5% of all cases *Clinical findings:* enlargement of the hands and feet, digital clubbing, convexity of the nails, cutaneous abnormalities, and joint pains *Radiographic findings:* bilateral symmetric periostitis of the long tubular bones and digital clubbing

TABLE 17-12 Metabolic, Hematologic, Vascular, and Infectious Disorders Affecting the Wrist and Hand—cont'd

Entity	Figure(s)	Characteristics
Secondary hypertrophic osteoarthropathy[161]	17-103	Most common form of hypertrophic osteoarthropathy Present in about 5% of patients with bronchogenic carcinoma *Predominant radiographic findings:* bilateral symmetric periostitis and digital clubbing
Acute pyogenic osteomyelitis[162,180,181]	17-104	Pyogenic infection of bones and joints usually spreads from contiguous sources of infection, such as a felon or paronychia Especially prevalent in patients with diabetes mellitus and immunocompromised patients Soft tissue swelling, osteolytic destruction, and periostitis
Acute pyogenic septic arthritis[162,163,180-182]	17-105	*Septic arthritis:* most joint infections begin as a monoarticular arthritis but frequently spread to adjacent bones and joints in the wrist or hand Rapid loss of joint space and destruction of subchondral bone Periarticular osteopenia, joint subluxation, and periostitis *Human bite injury:* direct implantation of organism into the metacarpophalangeal joint, usually resulting from a fistfight Most frequent organisms in this common type of infection are *Staphylococcus aureus*, *Streptococcus* species, and *Bacillus fusiformis*
Tuberculous osteomyelitis and arthritis[164,165]	17-106	Tuberculous infection is much less common than pyogenic infection in the wrist and hand; when it does occur, it has a predilection for the carpal region Mild symptoms and indolent course *Most common organism: Mycobacterium tuberculosis* *Osteomyelitis:* usually begins in epiphysis as an osteolytic lesion; may spread to metaphysis and diaphysis as moth-eaten or permeative pattern of destruction; may involve several bones of the hand *Spina ventosa:* tuberculous dactylitis; soft tissue swelling, bone destruction, periostitis, and bone expansion involving one or several digits; children > adults *Arthritis:* Juxtaarticular osteoporosis, joint space narrowing, joint effusion, and periarticular erosions
Unusual and atypical infections[166]	17-107	*Leprosy* (Mycobacterium leprae)*:* neuropathic osteoarthropathy—atrophic erosions of ungual tufts; osteomyelitis—periostitis and bone destruction; calcification of radial or ulnar nerves Leprosy is encountered infrequently in the United States but is more common in Africa, South America, and Asia *Coccidioidomycosis:* fungus found in Mexico and southwestern United States; results in osteolytic lesions; may be disseminated *Congenital syphilis* (Treponema pallidum)*:* diametaphyseal gummas result in periostitis and aggressive bone destruction

See also Tables 1-15, 1-16, and 1-19.

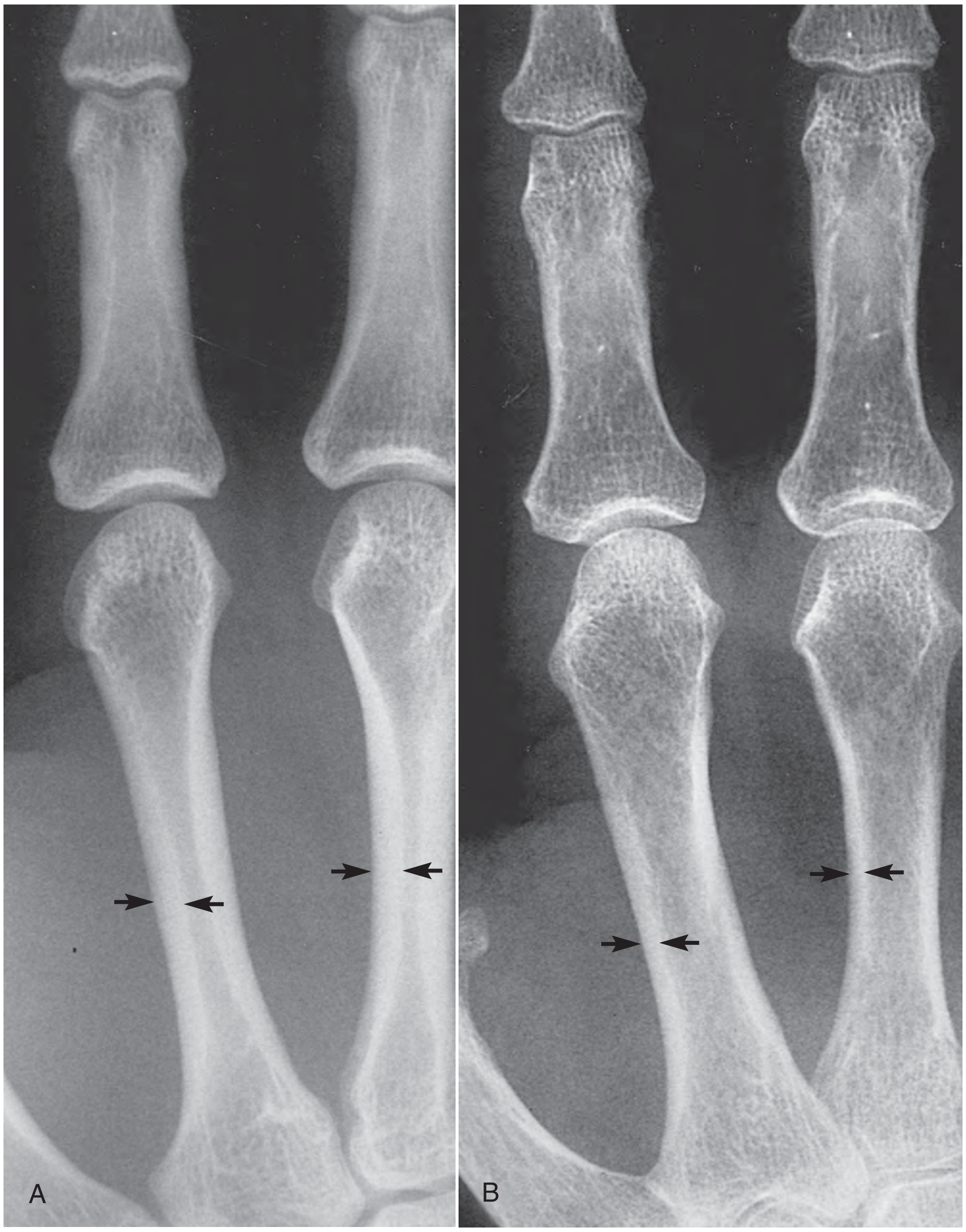

FIGURE 17–95 **Generalized osteoporosis: routine radiography.**[149-151] **A,** Normal bone density: 26-year-old man. Note the normal mineralization of the metacarpal bones and phalanges. The cortices are thick *(arrows),* and there is no evidence of bone resorption. **B,** Generalized osteoporosis: 71-year-old woman. Increased radiolucency and uniform thinning of all the cortices *(arrows)* are present.

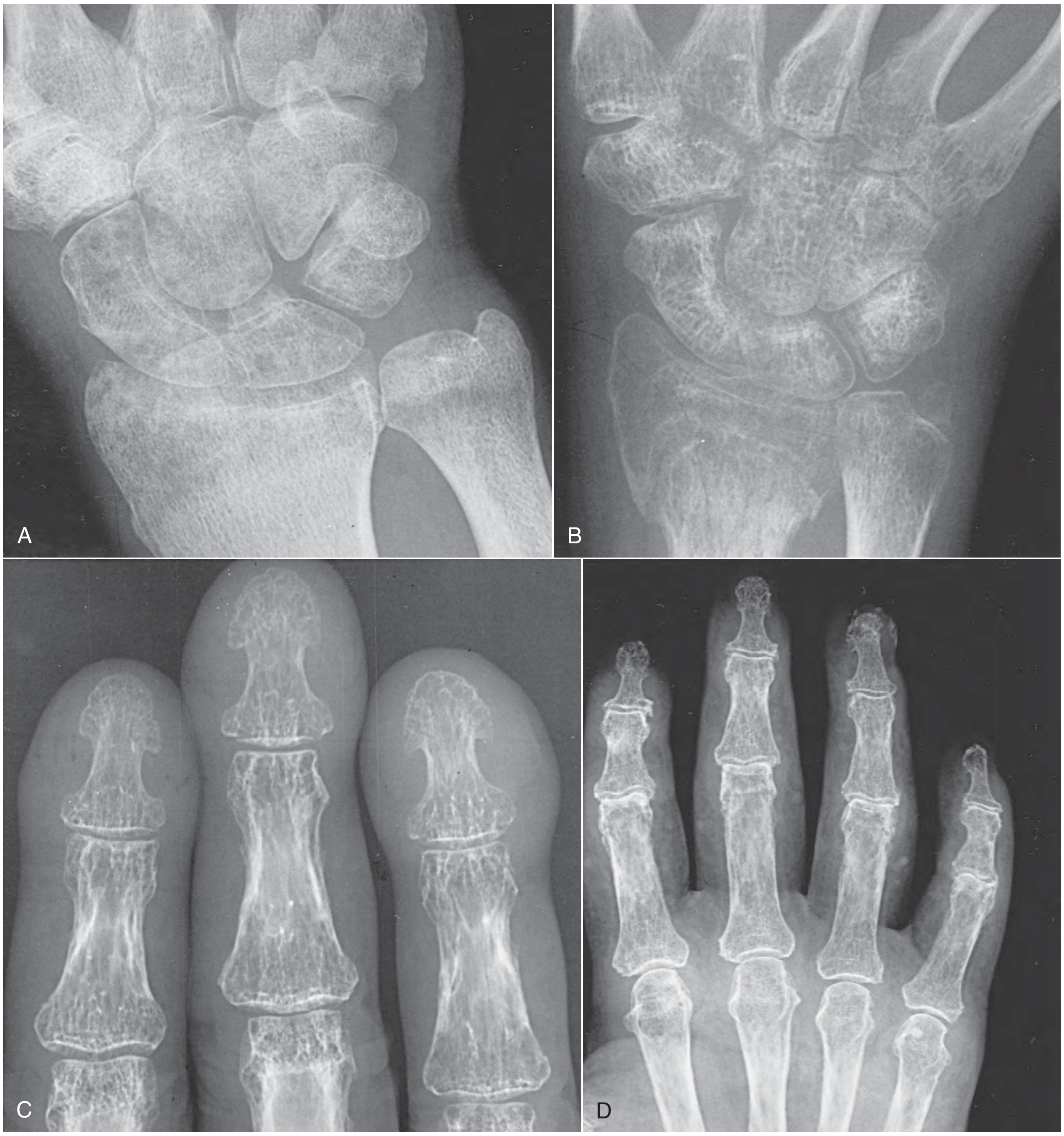

FIGURE 17–96 **Regional osteoporosis.**[151-153] **A-B,** Immobilization (disuse) osteoporosis. In **A,** this patient's forearm and wrist were in a cast for 6 weeks. The radiograph exhibits a patchy pattern of periarticular osteopenia throughout the bones of the distal forearm and wrist. A bandlike metaphyseal radiolucency is also recognized within the radius and ulna. In **B,** this 47-year-old woman with a Colles fracture was immobilized for 6 weeks. Observe the spotty, patchy, and bandlike osteopenia of the adjacent bones typical of disuse osteoporosis. This type of osteoporosis generally appears after 8 weeks of immobilization and may simulate the permeative appearance of malignancy. **C-D,** Complex regional pain syndrome (reflex sympathetic dystrophy). In **C,** findings include swelling of the soft tissues of the distal phalanges and osteoporosis characterized by subperiosteal, intracortical, and medullary resorption of bone. In **D,** a radiograph of another patient with complex regional pain syndrome reveals diffuse soft tissue swelling and a patchy, permeative pattern of osteopenia. Spotty, patchy, and bandlike bone resorption is typical of rapid-onset osteoporosis such as that also seen in disuse, burns, frostbite, or paralysis, an appearance that may simulate an aggressive neoplasm.

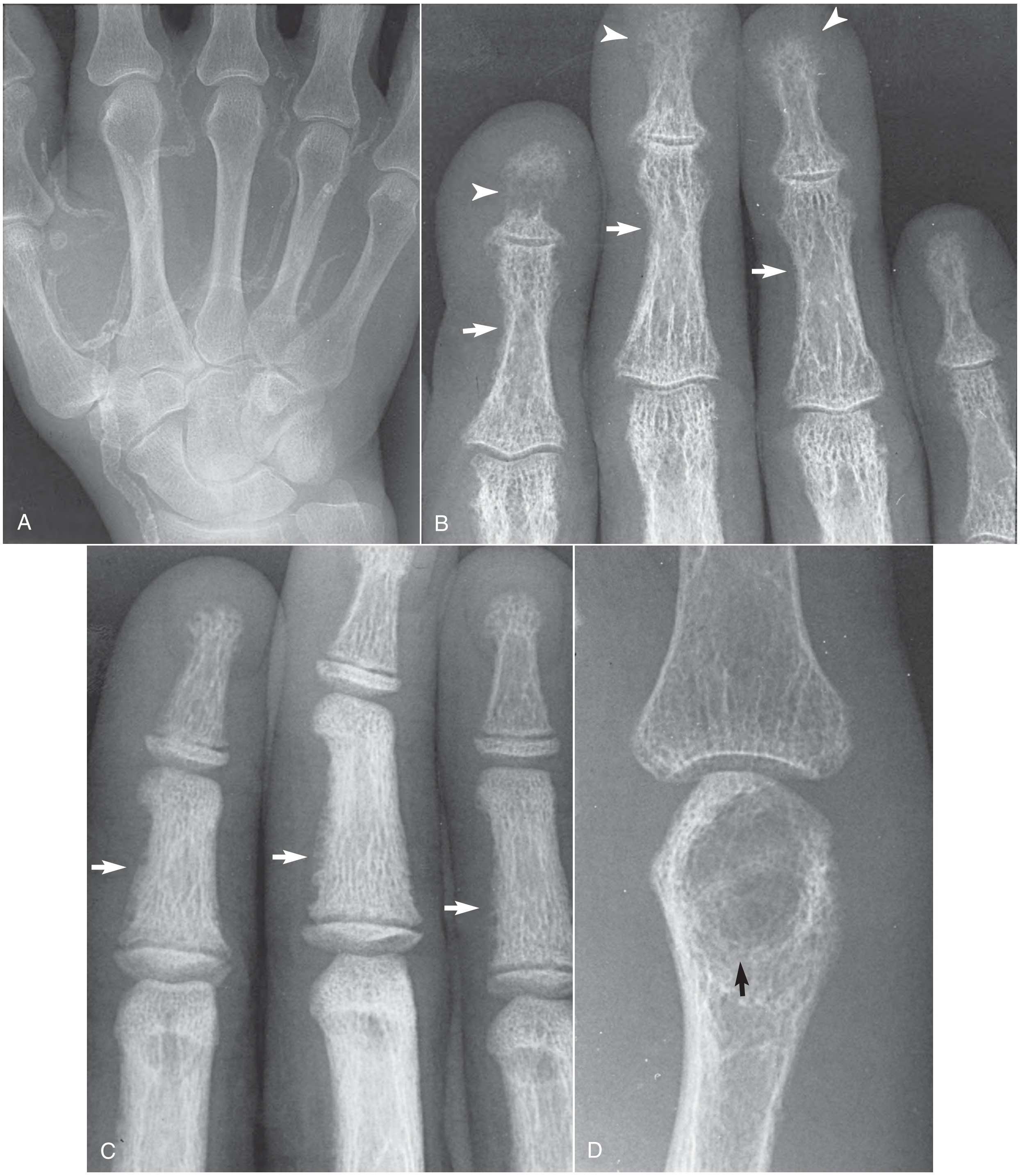

FIGURE 17–97 Hyperparathyroidism.[154] **A,** Vascular calcification. Observe the extensive vascular calcification, a finding occurring more frequently in patients undergoing hemodialysis. **B,** Subperiosteal resorption and acro-osteolysis. Subperiosteal resorption, predominantly on the radial aspect of the middle phalanges *(arrows),* and acro-osteolysis or tuft resorption *(arrowheads)* are frequent findings in hyperparathyroidism. **C,** Subperiosteal resorption. Subperiosteal resorption *(arrows)* and osteosclerosis are seen in this renal transplant patient with secondary hyperparathyroidism. **D,** Brown tumor. An osteolytic lesion with well-defined sclerotic margins is seen in the metacarpal bone *(arrow)*.

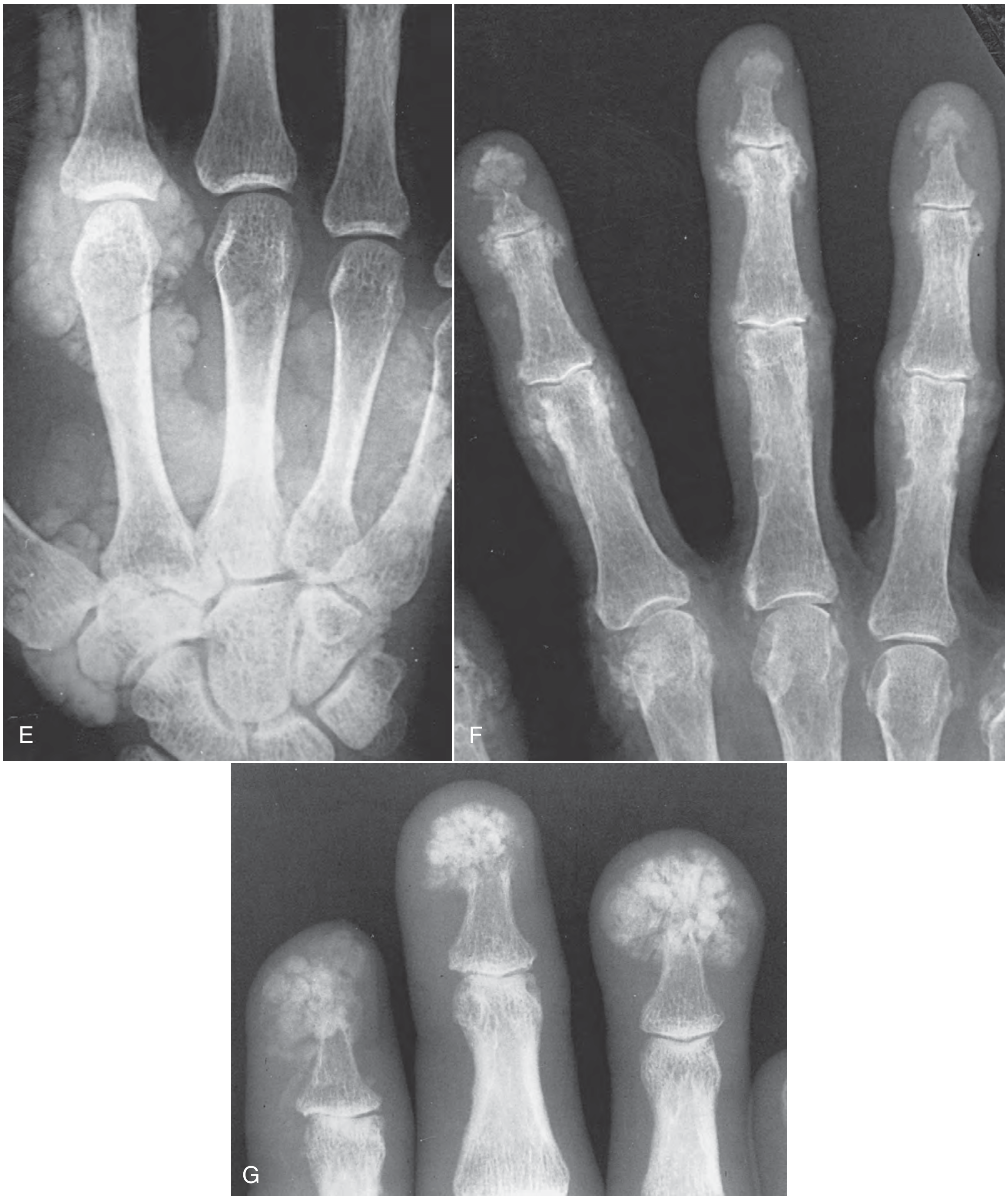

FIGURE 17–97, cont'd **E-G,** Soft tissue calcification. In **E,** observe the extensive lobulated calcinosis of the subcutaneous tissues in a patient with secondary hyperparathyroidism. In **F,** a 64-year-old woman has evidence of extensive periarticular calcification and acro-osteolysis. In **G,** a radiograph of a 49-year-old man shows tumoral calcification surrounding the distal tuft, another manifestation of chronic renal failure. These forms of metastatic soft tissue calcification are related to a disturbance in calcium or phosphorous metabolism and may accompany hyperparathyroidism and renal osteodystrophy. (*C, Courtesy U. Mayer, MD, Klagenfurt, Austria; F, Courtesy T. Broderick, MD, Orange, Calif.)*

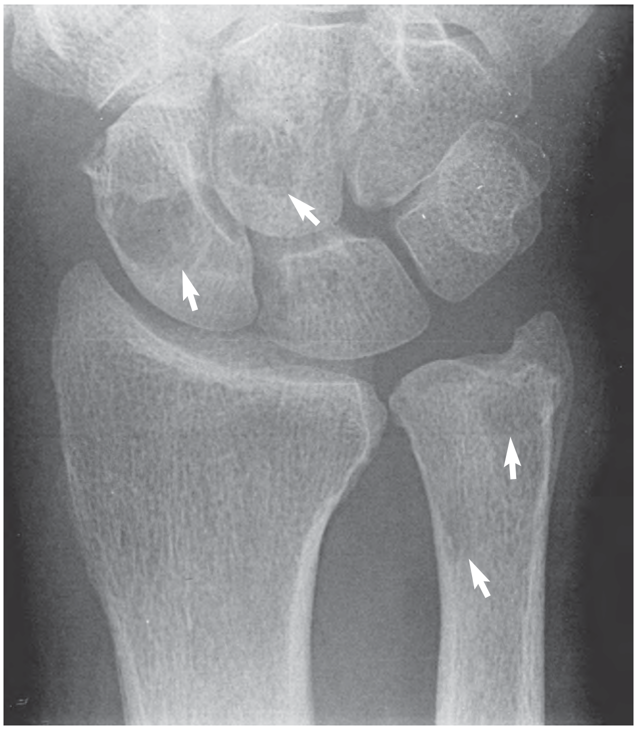

FIGURE 17–98 Amyloid deposition.[155] Long-term hemodialysis in a 55-year-old man with chronic renal failure. Multiple radiolucent cystlike lesions are present in several carpal bones *(arrows)*. Amyloid deposition is a well-established complication of hemodialysis. In the wrist, it may lead to multiple intraosseous osteolytic lesions, as in this patient, and carpal tunnel syndrome. *(Courtesy G. Greenway, MD, Dallas.)*

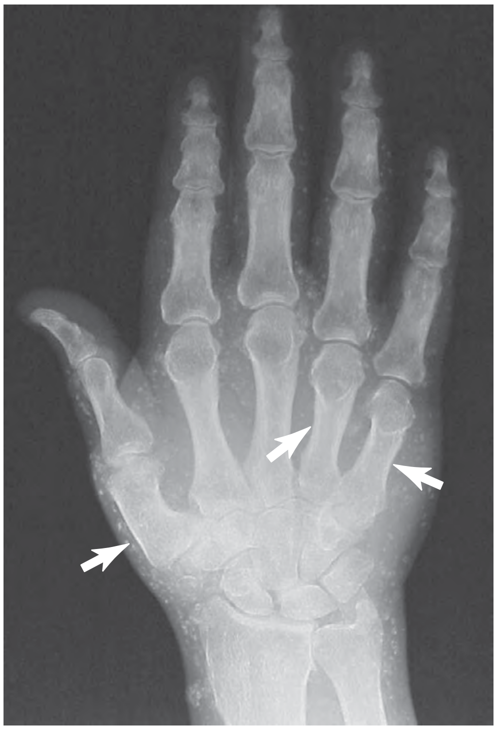

FIGURE 17–100 Pseudohypoparathyroidism.[157] An anteroposterior radiograph of a patient with pseudohypoparathyroidism reveals extensive subcutaneous soft tissue calcification and shortened metacarpals, particularly the first, fourth, and fifth *(arrows)*. Inflammatory connective tissue disorders should be considered in the differential diagnosis of such subcutaneous soft tissue calcification.

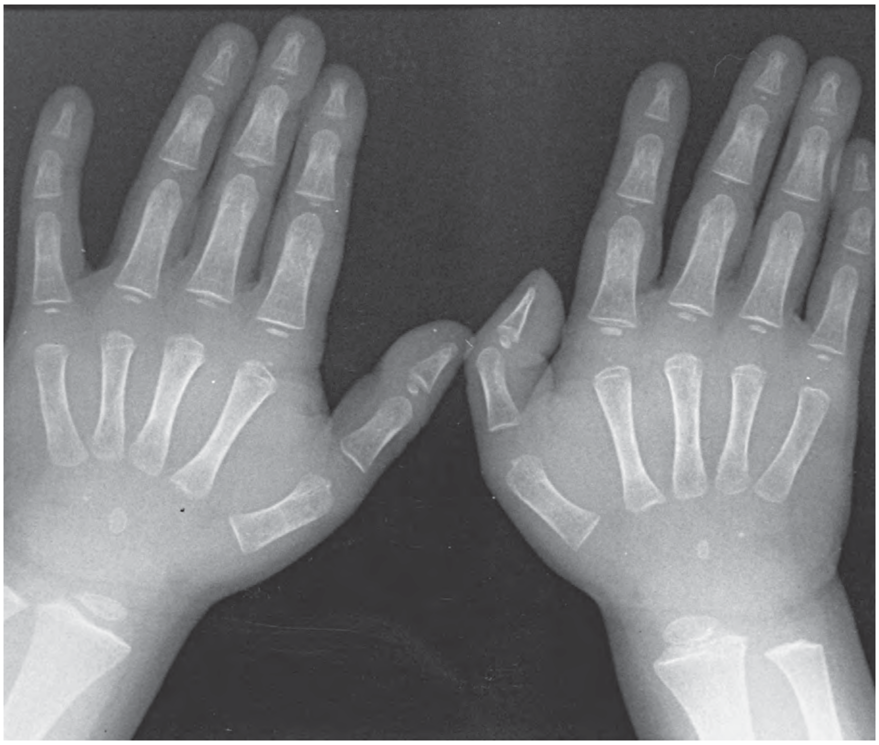

FIGURE 17–99 Hypothyroidism: delayed skeletal maturation.[156] This boy with cretinism had a chronologic age of 9 years, 9 months. Radiographs of both hands reveal a skeletal age of 2 years, 8 months.

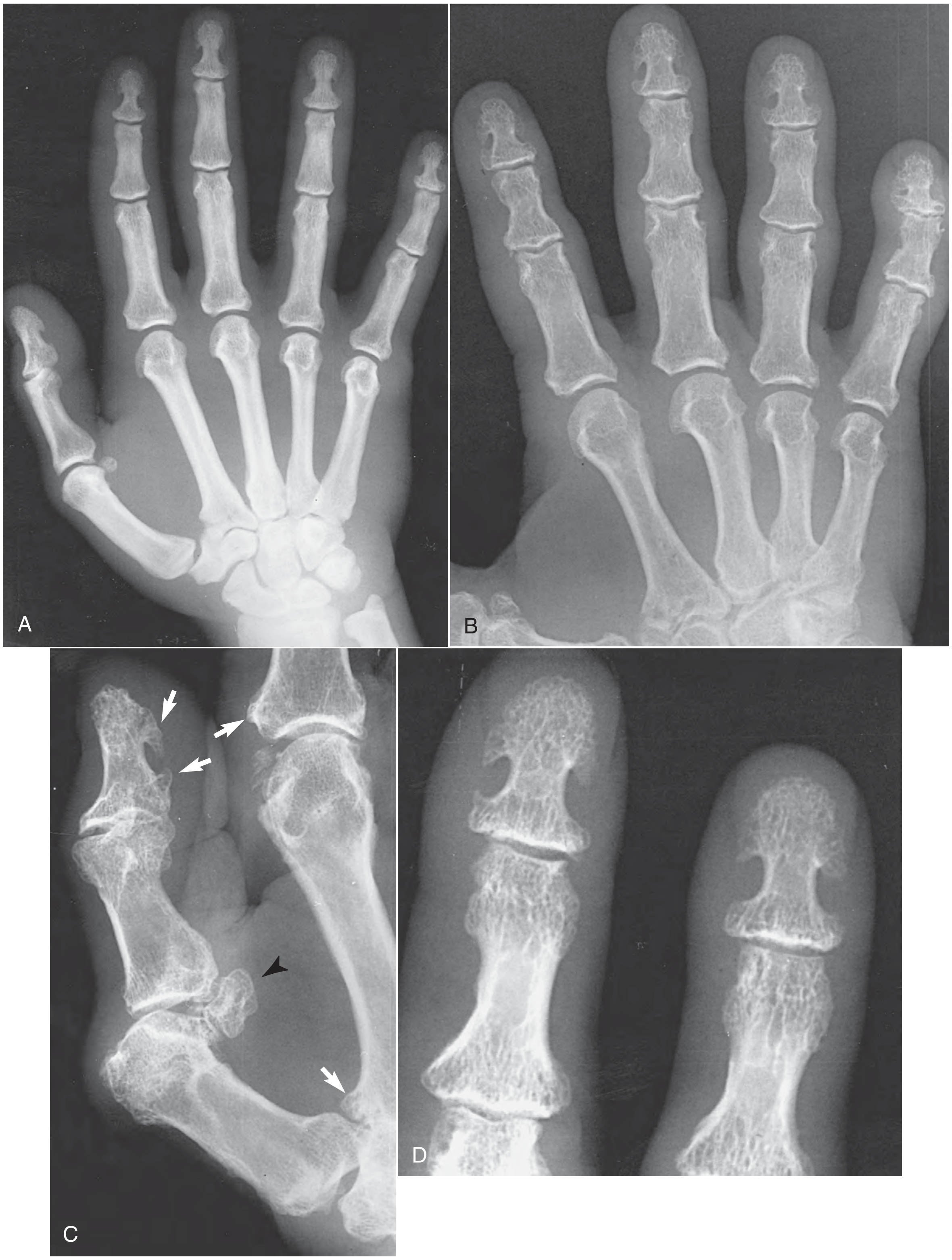

FIGURE 17–101 Acromegaly.[158,159] **A,** Diffuse soft tissue hypertrophy and widened metacarpophalangeal joint spaces are evident. **B,** In another patient, soft tissue hypertrophy, widened joint spaces, spade-shaped terminal tufts, and thickening of the proximal phalangeal diaphyses are seen. **C,** Hypertrophy of the sesamoid bones *(arrowhead),* as seen in this 62-year-old man, is a well-documented finding in acromegaly. Note also the periarticular and tuft bone proliferation *(arrows)*. **D,** Enlarged terminal tufts. The enlarged terminal phalanges are prominent and appear spade-shaped, a characteristic finding in acromegaly. Also note the prominent soft tissues.

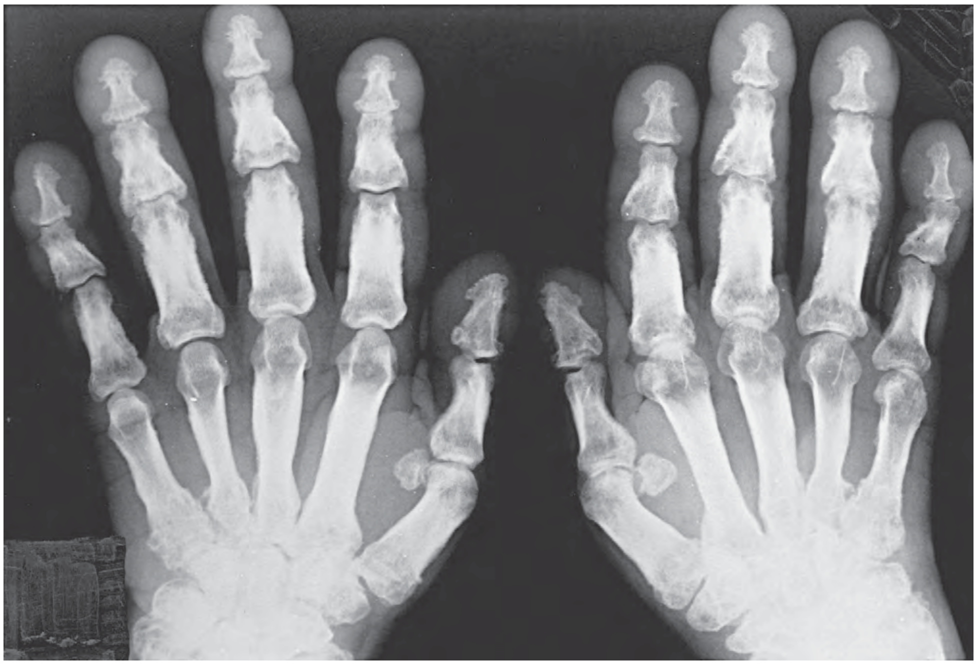

FIGURE 17–102 **Primary hypertrophic osteoarthropathy: pachydermoperiostosis.**[160] Observe the bilaterally symmetric and widespread soft tissue clubbing and prominent periostitis affecting the tubular bones of the hands. The findings in this patient were present in several tubular bones throughout the skeleton. *(Courtesy of C. Chen, MD, Kaohsi-ung, Taiwan.)*

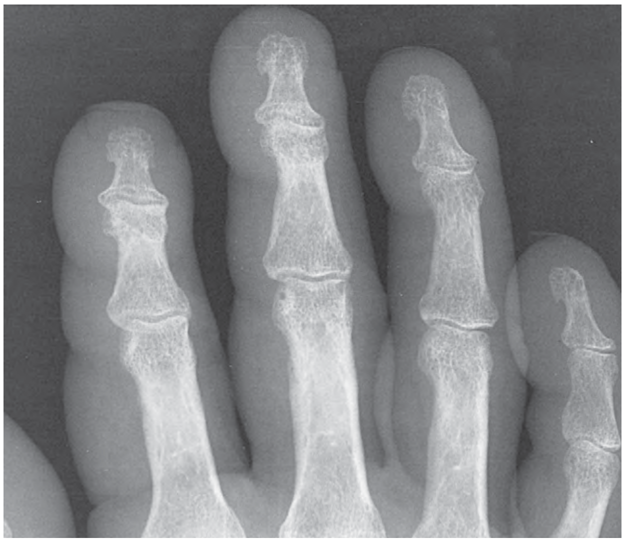

FIGURE 17–103 **Digital clubbing: secondary hypertrophic osteoarthropathy.**[161] This 60-year-old man was diagnosed as having bronchogenic carcinoma. Characteristic bulbous hypertrophy of the soft tissues overlying the terminal phalanges is seen. This finding relates to thickening of the fibroelastic tissue at the base of the nail bed and consequent increased curvature of the nail itself. It may result in tuft resorption or hypertrophy. It often accompanies hypertrophic osteoarthropathy, a condition that occurs in approximately 5% of patients with bronchogenic carcinoma and may also occur in many other diseases.

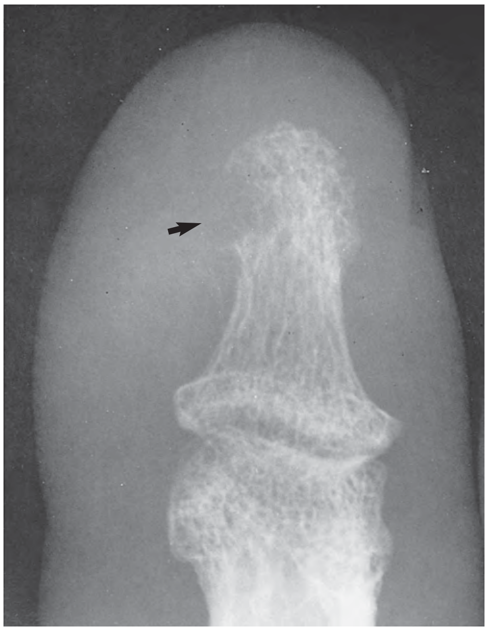

FIGURE 17–104 **Acute pyogenic osteomyelitis: spread from a contiguous source.**[162,180,181] Routine radiograph shows considerable soft tissue swelling. Infection from an adjacent felon has eroded into the tuft of the terminal phalanx *(arrow)*. A felon is an infection in the terminal pulp space, and a paronychia is a subcuticular abscess of the nail fold. When these soft tissue infections are neglected, organisms may spread to the contiguous bone, joint, or tendon sheath.

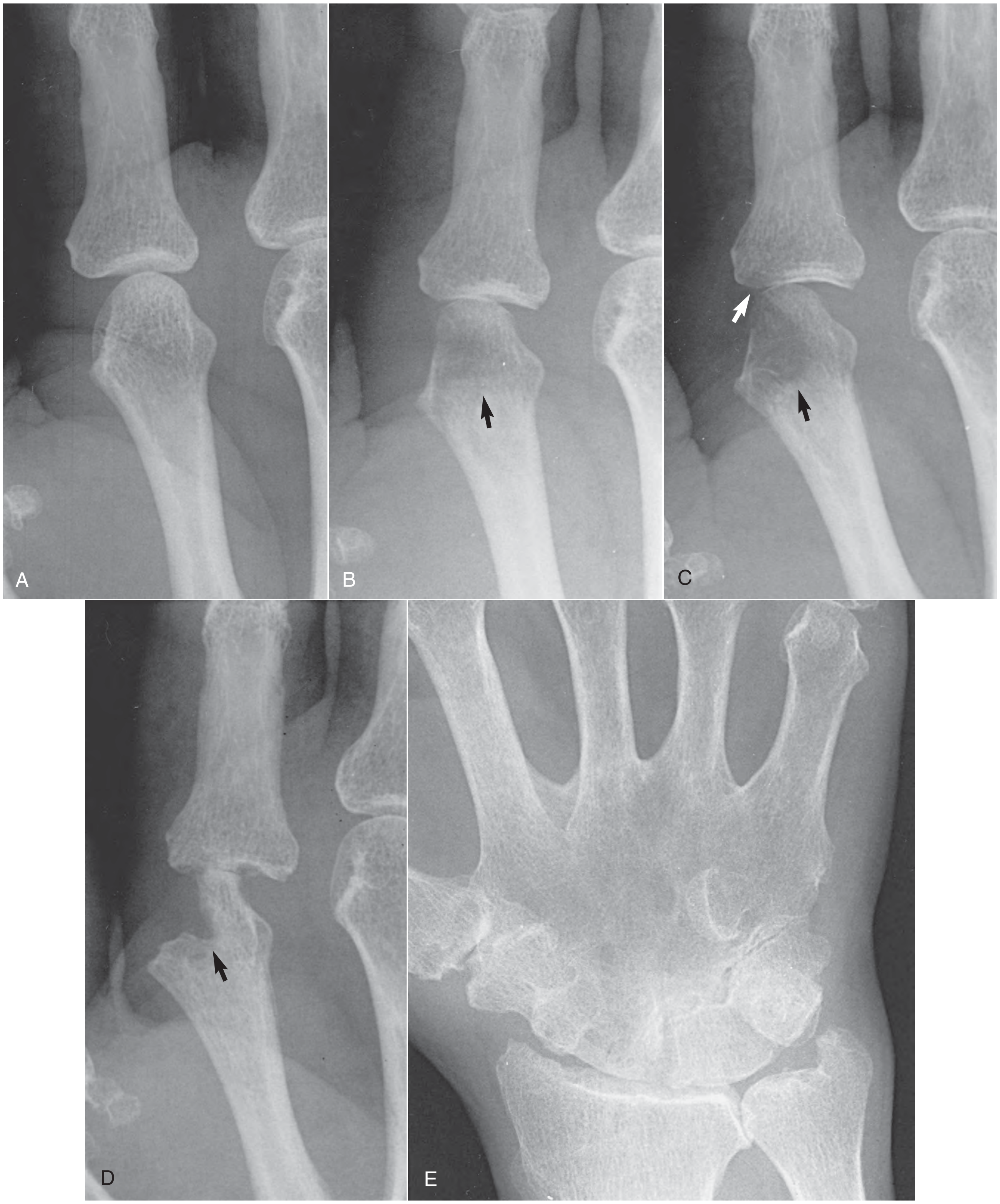

FIGURE 17–105 **Acute pyogenic septic arthritis.**[162,163,180-182] **A-D,** Direct implantation: human bite, progressive changes. This 47-year-old man was involved in a fistfight in which his hand was lacerated and he developed severe swelling and erythema over the dorsum of his second metacarpophalangeal joint. Serial radiographs were obtained. **A,** January 15: 1 week after the altercation, the radiograph appears essentially normal. **B,** February 5: the joint space is narrowed and the metacarpal head appears osteopenic *(black arrow)*. **C,** February 20: a large erosion is seen in the metacarpal head *(black arrow),* and an erosion of the subchondral bone of the proximal phalanx is becoming evident *(white arrow)*. **D,** May 14: 4 months after the initial injury, widespread destruction of the metacarpal head (*black arrow),* joint space narrowing, and subluxation are apparent despite antibiotic treatment. **E,** Wrist ankylosis. In another patient, complete osseous ankylosis of all the intercarpal and carpometacarpal articulations is consistent with the residual appearance of septic arthritis.

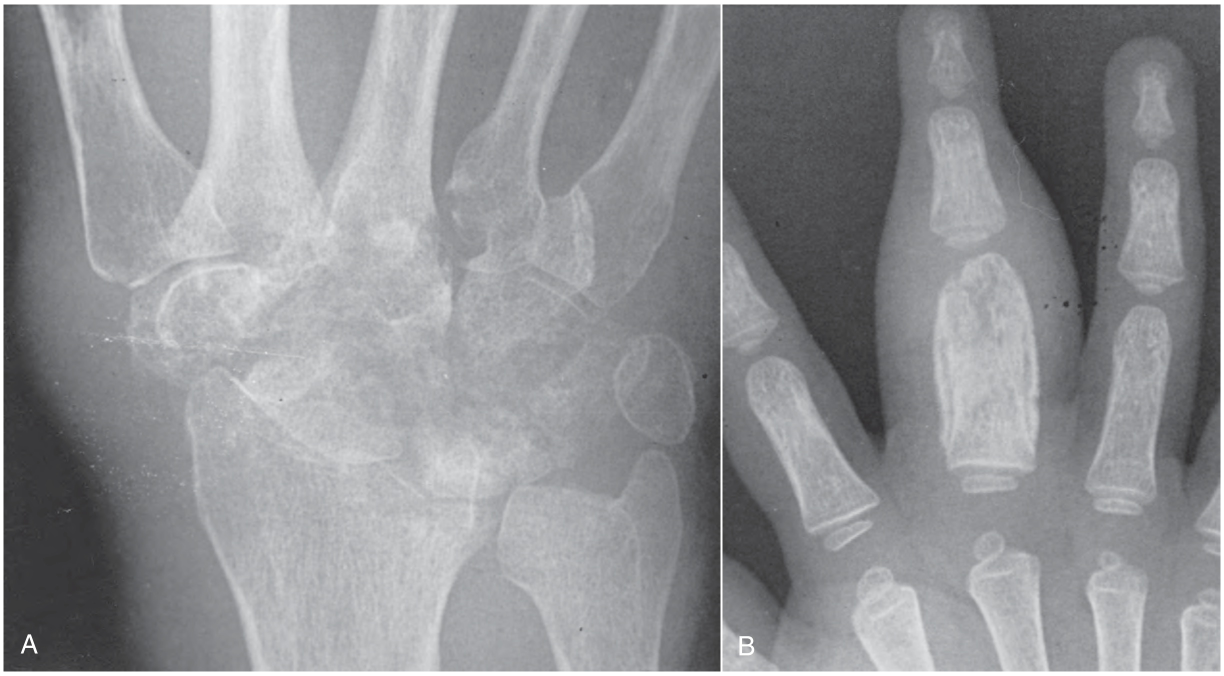

FIGURE 17–106 **Tuberculous infection.**[164,165] **A,** Tuberculous arthritis. In a 58-year-old man with long-standing pulmonary tuberculosis and wrist pain, abnormalities include soft tissue swelling, widespread joint space narrowing, periarticular osteopenia, osseous erosions, and collapse of the carpal bones and the distal articular surface of the radius. **B,** Tuberculous osteomyelitis: dactylitis. Prominent soft tissue swelling and exuberant periostitis and enlargement of the proximal phalanx are characteristic of tuberculous dactylitis (spina ventosa) in this child. Lytic lesions may also predominate in tuberculosis involving the digits. Radiographic changes are typically much more gradual in tuberculous infections than they are in pyogenic infections.

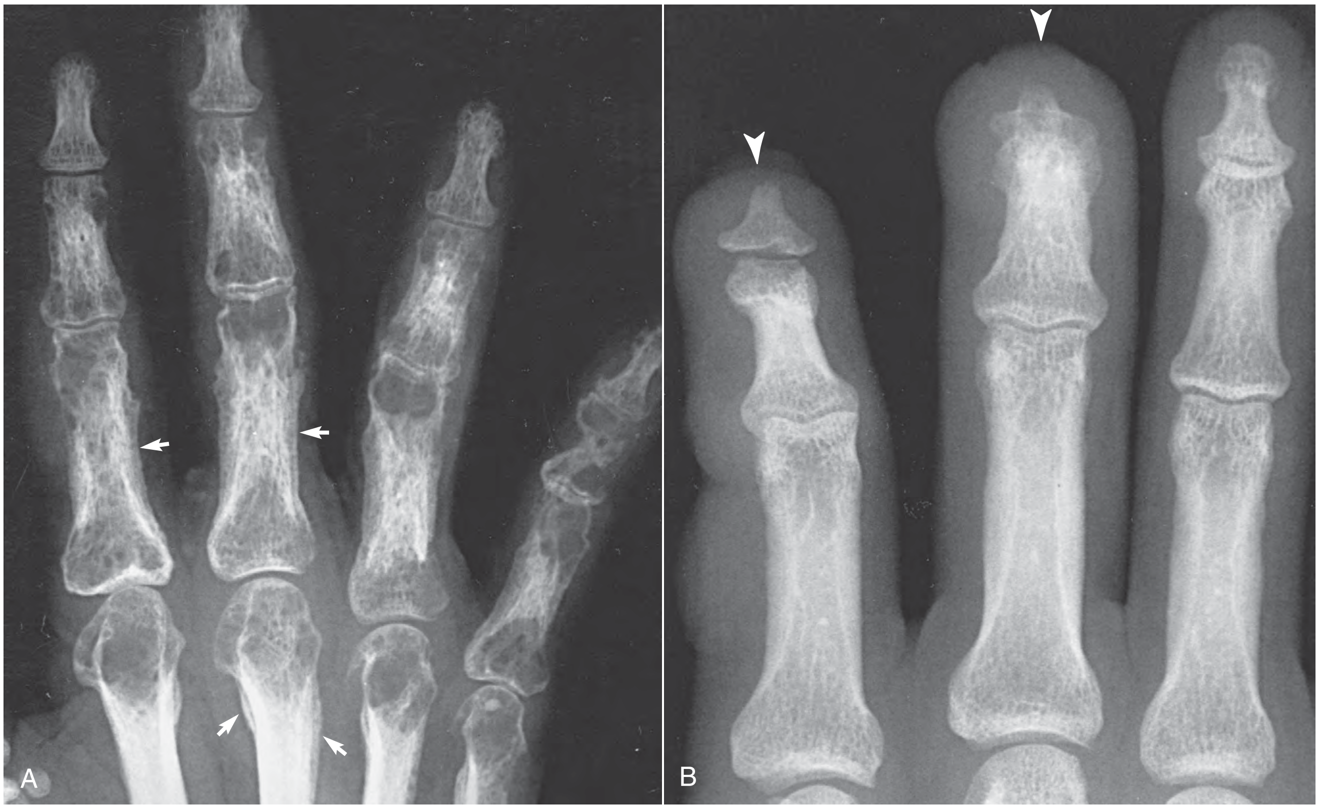

FIGURE 17–107 **Leprosy.**[166] **A,** Osteomyelitis. Periostitis *(arrows)* and moth-eaten and permeative destruction of several metacarpal bones and phalanges are present. **B,** Neuropathic lesions. In a second patient with long-standing leprosy, the tapered osseous surfaces of the second and third terminal phalanges represent phalangeal osteolysis (arrowheads). Note the soft tissue swelling of these two digits. Involvement in both cases was bilateral and symmetric.

TABLE 17-13 Osteonecrosis

Entity	Figure(s)	Characteristics
Lunate bone (Kienböck disease)[167]	17-108	Most frequent carpal bone to undergo osteonecrosis Magnetic resonance (MR) imaging most sensitive in comparison with radiography and scintigraphy More common in patients with negative ulnar variance Occurs between the ages of 20 and 40 years Pathologic fracture or collapse may occur
Scaphoid bone[168,169]	17-23, *D*	Idiopathic form (Preiser disease) or posttraumatic form (most common) Proximal portion affected most frequently after fracture of the waist of the scaphoid
Capitate bone[170]	17-109	Idiopathic or after an injury
Hamate bone[171,172]		Infrequent site of osteonecrosis Occurs after fractures of the body and hook of the hamate
Phalanges (Thiemann disease)[173]		Osteonecrosis of the phalangeal epiphyses secondary to trauma Occurs between the ages of 11 and 19 years May result in pain and swelling about the interphalangeal joints

See also Tables 1-17 and 1-18.

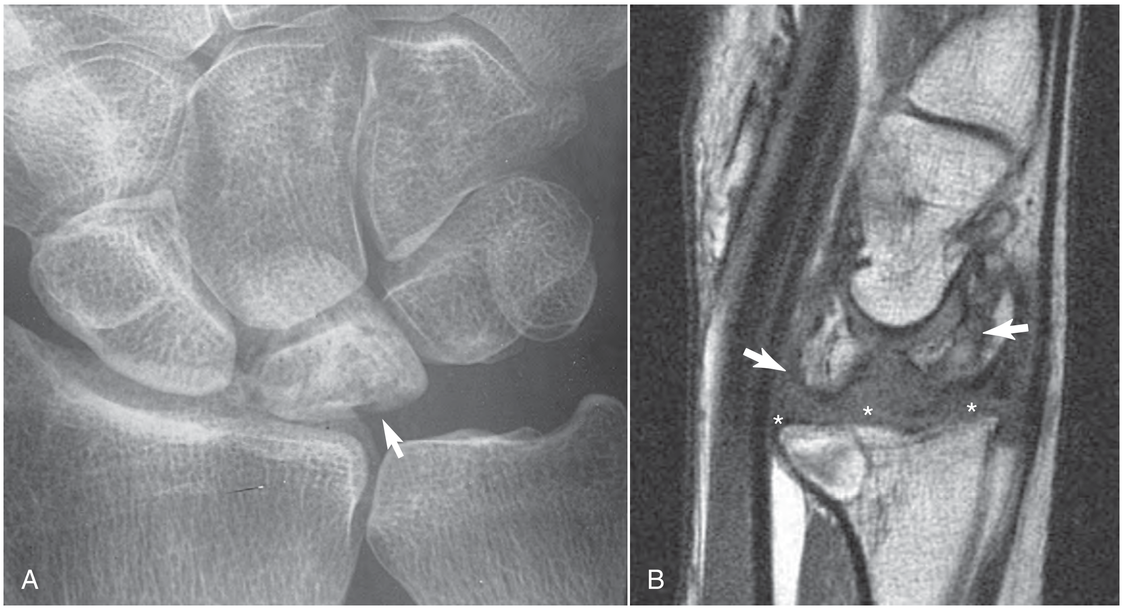

FIGURE 17–108 Kienböck disease.[167] **A,** Observe the sclerosis and fragmentation of the carpal lunate bone *(arrow)*. This form of osteonecrosis has a predilection for the right wrist and is especially prevalent in manual laborers. A history of trauma may be elicited, but this is not a constant feature. Progressive pain, swelling, and disability are the chief presenting clinical features. A short ulna (negative ulnar variance) is encountered in as many as 75% of cases. Radiographs may appear normal early in the course of the disease, in which case scintigraphy and MR imaging can be helpful. **B,** In another patient with Kienböck disease, a sagittal T1-weighted MR image reveals a pathologic fracture with fragmentation, low signal intensity of the two major fragments *(arrows),* and considerable intraarticular edema and effusion (*) that displaces the adjacent tendons. The dorsal and palmar displacement of the two fragments is designated "the broken canoe sign."

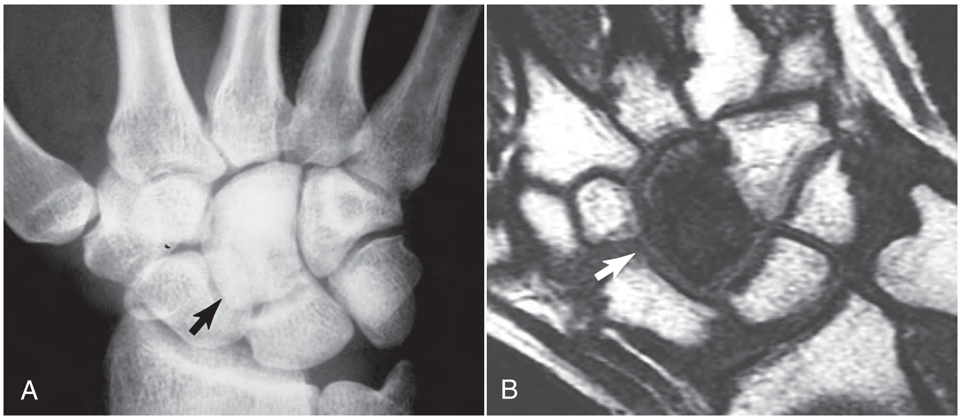

FIGURE 17–109 Osteonecrosis: capitate.[170] A frontal radiograph of the wrist **(A)** shows diffuse osteosclerosis of the capitate bone *(black arrow)*. Extremely low signal intensity of the capitate *(white arrow)* is evident on a corresponding T1-weighted coronal image **(B).** This replacement of normally high signal fatty marrow with dense low signal intensity is consistent with the appearance of osteonecrosis. *(Courtesy S. Ehara MD, DMSc, Morioka, Japan.)*

TABLE 17-14 Acquired Deformities of the Wrist and Hand[174]

Entity	Characteristics	Causes
Wrist Deformities		
Radial deviation of wrist	Carpal bones are displaced toward the radial side of the wrist in conjunction with ulnar deviation at the MCP joints See also zigzag deformity (below)	Rheumatoid arthritis
Ulnar deviation of wrist	Carpal bones are displaced toward the ulnar side of the wrist in conjunction with flexion deformity at the MCP joints	Juvenile idiopathic arthritis
Ulnar bayonet deformity	Ulnar migration of the carpal bones at the radiocarpal joint Ulna overrides the radius at the distal radioulnar joint	Juvenile idiopathic arthritis
Finger Deformities		
Boutonnière deformity	Hyperflexion at PIP joints and hyperextension at DIP joints	Rheumatoid arthritis Systemic lupus erythematosus
Flexion deformities	Hyperflexion at DIP and PIP joints	Rheumatoid arthritis Psoriatic arthritis Dupuytren contracture
Swan-neck deformity	Hyperextension at PIP joints and hyperflexion at DIP joints	Rheumatoid arthritis Systemic lupus erythematosus
Mallet finger	Persistent flexion at the DIP joints Loosening or disruption of the distal attachment of the extensor tendon to the terminal phalanx Uncommon deformity	Rheumatoid arthritis Traumatic extensor tendon rupture
Ulnar deviation of MCP joints	Deviation of proximal phalanges toward ulnar side in relation to metacarpal bones	Rheumatoid arthritis Psoriatic arthropathy
Zigzag deformity	Combination of ulnar deviation at MCP joints and radial deviation of wrist	Rheumatoid arthritis
Z-shaped deformity of thumb	Also termed *hitchhiker's thumb* *Boutonnière deformity of thumb:* hyperextension at the interphalangeal joint and hyperflexion at the MCP joint	Systemic lupus erythematosus Rheumatoid arthritis
Main-en-lorgnette deformity	Arthritis mutilans or opera glass hand In cases of severe phalangeal and metacarpal erosions, the soft tissues of the fingers telescope on each other as the underlying struts of bone are resorbed, resembling a collapsed opera glass	Psoriatic arthropathy Juvenile chronic arthritis Rheumatoid arthritis Neuropathic osteoarthropathy
Nonerosive deforming arthropathy	Jaccoud arthropathy Malalignment of joints in the absence of joint erosions *Reversible subluxations:* deformities may be present when the hand is gently placed on the image receptor and disappear when the hand is pressed firmly against the image receptor	Systemic lupus erythematosus Rheumatic fever Scleroderma Rare: Agammaglobulinemia Ehlers-Danlos syndrome Sarcoidosis Rheumatoid arthritis
Pencil-in-cup deformity	Resorption of distal end of metacarpal bone or phalanx with associated cuplike erosion of proximal articulating surface of adjacent phalanx, resembling a pencil in a cup	Psoriatic arthropathy Rheumatoid arthritis

DIP, Distal interphalangeal joint; *MCP,* metacarpophalangeal; *PIP,* proximal interphalangeal joint.

TABLE 17-15 Characteristic Sites of Terminal Phalangeal Resorption in Various Disorders[175] (Figure 17-110)

	Site*		
Entity	**Tuft**	**Midportion or Waist**	**Periarticular**
Scleroderma	+		+
Hyperparathyroidism	+	+	+
Thermal injury	+		+
Frostbite	+		+
Psoriasis	+		+
Epidermolysis bullosa	+		
Polyvinylchloride acro-osteolysis		+	
Neuropathic osteoarthropathy	+		
Multicentric reticulohistiocytosis	+		+
Inflammatory (erosive) osteoarthritis			+
Lesch-Nyhan syndrome	+		
Progeria	+		

* Only the characteristic sites of bone resorption are indicated, although in any single disease, considerable variability in these sites may exist.

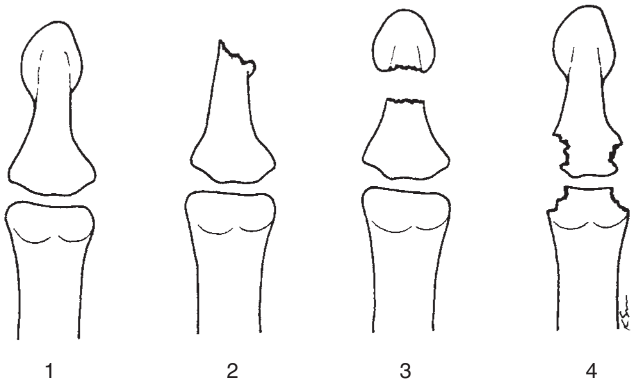

FIGURE 17–110 Phalangeal resorption: differential diagnosis.[175] The normal situation is depicted in diagram 1. Resorption of the tuft (2) can be seen in scleroderma, other collagen vascular disorders, thermal injuries, hyperparathyroidism, psoriasis, neuropathic osteoarthropathy, and epidermolysis bullosa. Bandlike resorption of the terminal phalanx (3) is seen in familial and occupational acro-osteolysis, collagen vascular disorders, and hyperparathyroidism. Erosions about the distal interphalangeal joint (4) can occur in psoriatic arthropathy, multicentric reticulohistiocytosis, gout, thermal injuries, scleroderma, and hyperparathyroidism. *(Resnick D: Scleroderma. From Resnick D [ed]: Diagnosis of bone and joint disorders. 4th Ed. Philadelphia, Saunders, 2002, p 1194.)*

TABLE 17-16 Some Causes of Soft Tissue Calcification About the Terminal Phalanges[174]

- Scleroderma
- Dermatomyositis
- Systemic lupus erythematosus
- Hyperparathyroidism
- Epidermolysis bullosa
- Raynaud disease
- Synovial osteochondromatosis
- Calcium hydroxyapatite crystal deposition
- Pseudohypoparathyroidism

REFERENCES

CHAPTER 1*

Introduction to Skeletal Disorders: General Concepts

Beaty JH, Kasser JR: Rockwood and Wilkins' fractures in children. 6th Ed. Philadelphia, Lippincott Williams & Wilkins, 2005.
Bucholz RW, Heckman JD, Court-Brown C: Rockwood and Green's fractures in adults. 6th Ed. Philadelphia, Lippincott Williams & Wilkins, 2006.
Chapman S, Nakielny R: Aids to radiological differential diagnosis: 4th Ed. Philadelphia, Saunders, 2003.
Chew FS, Roberts CC: Musculoskeletal imaging: a teaching file. 2nd Ed. Philadelphia, Lippincott Williams & Wilkins, 2005.
Dorfman HD, Czerniak B: Bone tumors. St Louis, Mosby, 1998.
Frymoyer JW, Wiesel SW, An HS, et al (editors): The adult and pediatric spine: an atlas of differential diagnosis. 3rd Ed. Philadelphia, Lippincott Williams & Wilkins, 2003.
Gehweiler JA Jr, Osborne RL Jr, Becker RF: The radiology of vertebral trauma. Philadelphia, Saunders, 1980.
Gilula LA, Yin Y: Imaging of the wrist and hand. Philadelphia, Saunders, 1996.
Greenspan A: Orthopedic imaging: a practical approach. 4th Ed. Philadelphia, Lippincott Williams & Wilkins, 2004.
Harris JH Jr, Mirvis SE: The radiology of acute cervical spine trauma. 3rd Ed. Baltimore, Williams & Wilkins, 1996.
Helms CA, Major NM, Anderson MW, et al: MRI. 2nd Ed. Philadelphia, Saunders, 2008.
Hilton SVW, Edwards DK: Practical pediatric radiology. 3rd Ed. Philadelphia, Saunders, 2006.
Huvos AG: Bone tumors: diagnosis, treatment and prognosis. 2nd Ed. Philadelphia, Saunders, 1991.
Jacobson JA: Fundamentals of musculoskeletal ultrasound. Philadelphia, Saunders, 2007.
Keats TE, Smith TH: An atlas of normal developmental roentgen anatomy. 2nd Ed. Chicago, Year Book Medical Publishers, 1988.
Keats TE: Atlas of normal roentgen variants that may simulate disease. 8th Ed. Chicago, Year Book Medical Publishers, 2006.
Kleinman PK: Diagnostic imaging of child abuse. 2nd Ed. Philadelphia, Mosby-Year Book, 1998.
Köhler A, Zimmer EA: Borderlands of normal and early pathologic findings in skeletal radiography. 4th Ed. New York, Thieme Medical Publishers, 1993.
Manaster BJ, May DA, Disler DG: Musculoskeletal imaging: the requisites. 3rd Ed. Philadelphia, Mosby-Year Book, 2006.
Manaster BJ, Roberts CC, Andrews CL, et al: Diagnostic and surgical anatomy: musculoskeletal. Philadelphia, Amirsys, 2006.
Manaster BJ, Crim J, Rosenberg ZS: Diagnostic and surgical anatomy: knee, ankle, foot. Philadelphia, Amirsys, 2007.
Marchiori D: Clinical Imaging: With skeletal, chest, and abdomen pattern differentials. 2nd Ed Philadelphia, Mosby-Year Book, 2004.
Miller TT, Schweitzer ME: Diagnostic musculoskeletal radiology. McGraw-Hill, 2005.
Morrissy RT, Weinstein S: Lovell and Winter's pediatric orthopedics. 6th Ed. Philadelphia, Lippincott Williams & Wilkins, 2005.
Pope T, Bloem HL, Beltran J, Morrison W: Imaging of the musculoskeletal system. 2008. Philadelphia, Saunders, 2008.
Resnick D, Kang HS, Pretterklieber ML: Internal derangements of joints. 2nd Ed. Philadelphia, Saunders, 2006.
Resnick D: Diagnosis of bone and joint disorders. 4th Ed. Philadelphia, Saunders, 2002.
Rogers LF: Radiology of skeletal trauma. 3rd Ed. New York, Churchill Livingstone, 2002.
Slovis TL, (ed): Caffey's pediatric diagnostic imaging. 11th Ed. Philadelphia, Mosby, 2008.
Stoller DW: Magnetic resonance imaging in orthopedic and sports medicine. 2006. 3rd Ed. Philadelphia, Lippincott Williams & Wilkins, 2006.
Taybi H, Lachman RS: Radiology of syndromes, metabolic disorders, and skeletal dysplasias. 5th Ed. St Louis, Mosby-Year Book, 2007.
Unni KK: Tumors of the bones and joints (atlas of tumor pathology series IV). Arp, 2005.
Wold LE, Unni KK, Sim FH, et al: Atlas of orthopedic pathology. 3rd Ed. Philadelphia, Saunders, 2008.
Yochum TR, Rowe LJ: Essentials of skeletal radiology. 3rd Ed. Baltimore, Williams & Wilkins, 2004.
Yu JS. Musculoskeletal imaging: case review series. 2nd Ed. Philadelphia, Mosby, 2008.

CHAPTER 2

Cervical Spine

1. Edeiken J, Dalinka M, Karasick D: Edeiken's roentgen diagnosis of diseases of bone. 4th ed. Baltimore, Williams & Wilkins, 1990.
2. Kahn SL, Gaskin CM, Sharp VL: Keats and Kahn's roentgen atlas of skeletal maturation. DVD-ROM Ed. Philadelphia, Lippincott Williams and Wilkins, 2007.
3. Greenfield GB: Radiology of bone diseases. 2nd ed. Philadelphia, JB Lippincott, 1975.
4. Smoker WRK: Craniovertebral junction: normal anatomy, craniometry, and congenital anomalies. RadioGraphics 14:255, 1994.
5. Keats TE: Atlas of normal roentgen variants that may simulate disease. 8th ed. Chicago, Year Book Medical Publishers, 2006.
6. Yochum TR, Rowe LJ: Essentials of skeletal radiology. 3rd ed. Baltimore, Williams & Wilkins, 2004.
7. Köhler A, Zimmer EA: Borderlands of normal and early pathologic findings in skeletal radiography. 4th ed. New York, Thieme Medical Publishers, 1993.
8. Gehweiler JA, Daffner RH, Roberts L: Malformations of the atlas simulating the Jefferson's fracture. AJR 140:1083, 1983.
9. Keats TE: Inferior accessory ossicle of the anterior arch of the atlas. AJR 101:834, 1967.
10. Daffner RH: Pseudofracture of the dens: mach bands. AJR 128:607, 1977.
11. Ramos LS, Taylor JAM, Lackey G, et al: Os odontoideum with sagittal and coronal plane instability: a report of three cases. Top Diagn Radiol Adv Imaging 3:5, 1996.
12. Swischuk LE, Hayden CK Jr, Sarwar M: The posteriorly tilted dens: a normal variation mimicking a fractured dens. Pediatr Radiol 8:27, 1979.
13. Bohrer P, Klein A, Martin W III: "V" shaped predens space. Skeletal Radiol 14:111, 1985.
14. Tredwell SJ, Newman DE, Lockitch G: Instability of the cervical spine in Down syndrome. J Pediatr Orthop 10:602, 1990.
15. Riebel GD, Bayley JC: A congenital defect resembling the hangman's fracture. Spine 16:1240, 1991.
16. Swischuk LE: Anterior dislocation of C2 in children: physiologic or pathologic? Radiology 122759, 1977.
17. Cattell ES, Filtzer DL: Pseudosubluxation and other normal variations in the cervical spine in children. J Bone Joint Surg [Am] 47:1295, 1965.
18. Massengill AD, Huynh SL, Harris JH Jr: C2-3 facet joint "pseudo-fusion": anatomic basis of a normal variant. Skeletal Radiol 26:27, 1997.
19. Chapman S, Nakielny R: Aids to radiological differential diagnosis. 3rd ed. Philadelphia, Saunders, 1995.
20. Applebaum Y, Gerald P, Bryk D: Elongation of the anterior tubercle of a cervical vertebral transverse process: an unusual variant. Skeletal Radiol 10:265, 1983.
21. Lapayowker MS: An unusual variant of the cervical spine. AJR 83:656, 1960.
22. Keats TE, Johnstone WH: Notching of the lamina of C7: a proposed mechanism. Skeletal Radiol 7:273, 1982.
23. Lovell WW, Winter RB: Pediatric orthopedics. Philadelphia, JB Lippincott, 1978.

---

* Only major reference sources, primarily textbooks, are listed here. More specific references pertaining to individual disorders are cited in subsequent chapters.

24. Karasick D, Schweitzer ME, Vaccaro AR: The traumatized cervical spine in Klippel-Feil syndrome: imaging features. AJR 170:85, 1998.
25. Black KS, Gorey MT, Seidman B, et al: Congenital spondylolisthesis of the 6th cervical vertebra: CT findings. J Comput Assist Tomogr 15:335, 1991.
26. Adson AW: Surgical treatment for symptoms produced by cervical ribs and the scalenus anticus syndrome. Clin Orthop 207:3, 1986.
27. Som PM, Bergeron RT: Head and neck imaging. St Louis, Mosby-Year Book, 1991, p 574.
28. Langlais R, Miles DA, Van Dis ML: Elongated and mineralized stylohyoid ligament complex: a proposed classification and report of a case of Eagle's syndrome. Oral Surg 61:527, 1986.
29. Kao SCS, Wazin MH, Smith WL, et al: MR imaging of the craniovertebral junction, cranium, and brain in children with achondroplasia. AJR 153:565, 1989.
30. Harding CO, Green CG, Perloff WH, et al: Respiratory complications in children with spondyloepiphyseal dysplasia congenita. Pediatr Pulmonol 9:49, 1990.
31. Thomas SL, Childress MH, Quinton B: Hypoplasia of the odontoid with atlantoaxial subluxation in Hurler's syndrome. Pediatr Radiol 15:353, 1985.
32. Holzgrave W, Grobe H, von Figura K, et al: Morquio syndrome: clinical findings of 11 patients with MPS IV-A and 2 patients with MPS IV-B. Hum Genet 57:360, 1981.
33. Bridges AL, Kou-Ching H, Singh A, et al: Fibrodysplasia (myositis) ossificans progressiva. Semin Arthritis Rheum 24:155, 1994.
34. Kovanlikaya A, Luiza Loro M, Gilsanz V: Pathogenesis of osteosclerosis in autosomal dominant osteopetrosis. AJR 168:929, 1997.
35. Kahler SG, Burns JA, Aylsworth AS: A mild autosomal recessive form of osteopetrosis. Am J Genet 17:451, 1984.
36. Benli IT, Akalin S, Boysan E, et al: Epidemiological, clinical, and radiological aspects of osteopoikilosis. J Bone Joint Surg [Br] 74:504, 1992.
37. Joseph KN, Kane HA, Milner RS, et al: Orthopedic aspects of the Marfan phenotype. Clin Orthop 277:251, 1992.
38. Harris JH, Carson GC, Wagner LK: Radiologic diagnosis of traumatic occipitovertebral dissociation: 1. Normal occipitovertebral relationships on lateral radiographs of supine subjects. AJR 162:881, 1994.
39. Harris JH, Carson GC, Wagner LK, et al: Radiologic diagnosis of traumatic occipitovertebral dissociation: 2. Comparison of three methods of detecting occipitovertebral relationships on lateral radiographs of supine subjects. AJR 162:887, 1994.
40. Shapiro R, Youngberg AS, Rothman SLG: The differential diagnosis of traumatic lesions of the occipito-atlanto-axial segment. Radiol Clin North Am 11:505, 1973.
41. Fielding JW, Stillwell WT, Chynn KY, et al: Use of computed tomography for the diagnosis of atlantoaxial rotatory fixation. J Bone Joint Surg [Am] 60:1102, 1978.
42. Kowalski HM, Cohen WA, Cooper P, et al: Pitfalls in the CT diagnosis of atlantoaxial rotary subluxation. AJNR 8:697, 1987.
43. Mirvis SE: Atlantoaxial relationships: questions and answers. AJR 170:1106, 1998.
44. Lee C, Woodring JH: Unstable Jefferson variant atlas fractures: an unrecognized cervical injury. AJR 158:113, 1992.
45. Suss RA, Bundy KJ: Unilateral posterior arch fracture of the atlas. AJNR 5:783, 1984.
46. Pathria M: Physical injury: Spine. In Resnick D: Diagnosis of bone and joint disorders. 4th ed. Philadelphia, Saunders, 2002, p 2934.
47. Hadley MN, Browner C, Sonntag VKH: Axis fractures: a comprehensive review of management and treatment in 107 cases. Neurosurgery 17:281, 1985.
48. Effendi B, Roy D, Cornish B, et al: Fractures of the ring of the axis: a classification based on the analysis of 131 cases. J Bone Joint Surg [Br] 63:319, 1981.
49. Pech P, Kilgore DP, Pojunas KW, et al: Cervical spine fractures: CT detection. Radiology 157:117, 1985.
50. Gehweiler JA Jr, Osborne RL Jr, Becker RF: The radiology of vertebral trauma. Philadelphia, Saunders, 1980.
51. Harris JH Jr, Mirvis SE: The radiology of acute cervical spine trauma. 2nd ed. Baltimore, Williams & Wilkins, 1995.
52. Fazl M, LaFebvre J, Willinsky RA, et al: Posttraumatic ligamentous disruption of the cervical spine, an easily overlooked diagnosis: presentation of three cases. Neurosurgery 26:674, 1990.
53. Salamone JA, Steele MT: An unusual presentation of bilateral facet dislocation of the cervical spine. Ann Emerg Med 16:1390, 1987.
54. Scher AT: Unilateral locked facet in cervical spine injuries. AJR 129:45, 1977.
55. Shanmuganathan K, Mirvis SE, Levine AM: Rotational injury of cervical facets: CT analysis of fracture patterns with implications for management and neurologic outcome. AJR 163:1165, 1994.
56. Andreshak JL, Dekutoski MB: Management of unilateral facet dislocations: a review of the literature. Orthopedics 20:917, 1997.
57. Cancelmo JJ Jr: Clay shoveler's fracture: a helpful diagnostic sign. AJR 115:540, 1972.
58. Kim KS, Chen HH, Russell HJ, et al: Flexion teardrop fracture of the cervical spine: Radiographic characteristics. AJR 152:319, 1989.
59. Edeiken-Monroe B, Wagner LK, Harris JH Jr: Hyperextension dislocation of the cervical spine. AJR 146:803, 1986.
60. Bohrer SP, Chen YM: Cervical spine anulus vacuum. Skeletal Radiol 17:324, 1988.
61. Davis SJ, Teresi LM, Bradley WG Jr, et al: Cervical spine hyperextension injuries: MR findings. Radiology 180:245, 1991.
62. Cintron E, Gilula LA, Murphy WA, et al: The widened disc space: a sign of cervical hyperextension injury. Radiology 141:639, 1981.
63. Lee C, Woodring JH: Sagittally oriented fractures of the lateral masses of the cervical vertebrae. J Trauma 31:1638, 1991.
64. Miller MD, Gehweiler JA, Martinez S, et al: Significant new observations on cervical spine trauma. AJR 130:659, 1978.
65. Harris JH Jr: Acute injuries of the spine. Semin Roentgenol 13:53, 1978.
66. Lee C, Kwang SK, Rogers LR: Sagittal fracture of the cervical vertebral body. AJR 139:55, 1982.
67. Schaaf RE, Gehweiler JA, Miller MD, et al: Lateral hyperflexion injuries of the cervical spine. Skeletal Radiol 3:73, 1978.
68. MacNab I: Cervical spondylosis. Clin Orthop 109:69, 1975.
69. Wilkinson HA, LeMay ML, Ferris EJ: Roentgenographic correlations in cervical spondylosis. AJR 105:370, 1969.
70. Lestini WF, Wiesel SW: The pathogenesis of cervical spondylosis. Clin Orthop 239:69, 1989.
71. Goldberg RP, Vine HS, Sacks BA, et al: The cervical split: a pseudofracture. Skeletal Radiol 7:267, 1982.
72. Halla JT, Hardin JG Jr: Atlantoaxial (C1-C2) facet joint osteoarthritis: A distinctive clinical syndrome. Arthritis Rheum 30:577, 1987.
73. Fletcher G, Haughton VM, Ho K-C, et al: Age-related changes in the cervical facet joints: Studies with cryomicrotomy, MR, and CT. AJNR 11:27, 1990.
74. Wong CC, Pereira B, Pho RWH: Cervical disc calcification in children: a long-term review. Spine 17:139, 1992.
75. Suzuki K, Ishida Y, Ohmori K: Long term follow-up of diffuse idiopathic skeletal hyperostosis in the cervical spine: analysis of progression of ossification. Neuroradiology 33:427, 1991.
76. Widder DJ: MR imaging of ossification of the posterior longitudinal ligament. AJR 153:194, 1989.
77. Kapila A, Lines M: Neuropathic spinal arthropathy: CT and MR findings. J Comput Assist Tomogr 11:736, 1987.
78. Boden SD, Dodge LD, Bohlman HH, et al: Rheumatoid arthritis of the cervical spine: a long-term analysis with predictors of paralysis and recovery. J Bone Joint Surg [Am] 75:1282, 1993.
79. Aisen AM, Martel W, Ellis JH, et al: Cervical spine involvement in rheumatoid arthritis: MR imaging. Radiology 165:159, 1987.
80. Espada G, Babini JC, Maldonado-Cocca JA, et al: Radiologic review: the cervical spine in juvenile rheumatoid

arthritis. Semin Arthritis Rheum 17:185, 1988.

81. Azouz EM, Duffy CM: Juvenile spondyloarthropathies: clinical manifestations and medical imaging. Skeletal Radiol 24:399, 1995.
82. Suarez-Almazor ME, Russell AS: Anterior atlantoaxial subluxation in patients with spondyloarthropathies: association with peripheral disease. J Rheumatol 15:973, 1988.
83. Amamilo SC: Fractures of the cervical spine in patients with ankylosing spondylitis. Orthop Rev 18:339, 1989.
84. Killebrew K, Gold RH, Sholkoff SD: Psoriatic spondylitis. Radiology 108:9, 1973.
85. Halla JT, Bliznak J, Hardin JG: Involvement of the craniocervical junction in Reiter's syndrome. J Rheumatol 15:1722, 1988.
86. Resnick D, Pineda C: Vertebral involvement in calcium pyrophosphate dihydrate crystal deposition disease: Radiographic-pathologic correlation. Radiology 153:55, 1984.
87. Steinbach LS, Resnick D: Calcium pyrophosphate dihydrate crystal deposition disease revisited. Radiology 200:1, 1996.
88. Hall FM, Docken WP, Curtis HW: Calcific tendinitis of the longus colli: diagnosis by CT. AJR 147:742, 1986.
89. Alarcon GS, Reveille JD: Gouty arthritis of the axial skeleton including the sacroiliac joints. Arch Intern Med 147:2018, 1987.
90. Justesen P, Andersen PE Jr: Radiologic manifestations in alkaptonuria. Skeletal Radiol 11:204:1984.
91. Osti OL, Fraser RD, Vernon-Roberts B: Discitis after discography: the role of prophylactic antibiotics. J Bone Joint Surg [Br] 72:271, 1990.
92. Dagirmanjian A, Schils J, McHenry M, et al: MR imaging of vertebral osteomyelitis revisited. AJR 167:1539, 1996.
93. Broom MJ, Beebe RD: Emphysematous septic arthritis due to *Klebsiella pneumoniae*. Clin Orthop 226:219, 1988.
94. Hsu LCS, Leong JCY: Tuberculosis of the lower cervical spine (C2 to C7): a report on 40 cases. J Bone Joint Surg [Br] 66:1, 1984.
95. Naito M, Ogata K, Nakamoto M, et al: Destructive spondyloarthropathy during long-term haemodialysis. J Bone Joint Surg [Br] 74:686, 1992.
96. Wong DA, Fornasier VL, MacNab I: Spinal metastases: The obvious, the occult, and the impostors. Spine 15:1, 1990.
97. Barwick KW, Huvos AG, Smith J: Primary osteogenic sarcoma of the vertebral column: a clinicopathologic correlation of ten patients. Cancer 46:595, 1980.
98. Mitchell M, Ackerman LV: Metastatic and pseudomalignant osteoblastoma: a report of two unusual cases. Skeletal Radiol 15:213, 1986.
99. Brien EW, Mirra JM, Kerr R: Benign and malignant cartilage tumors of bone and joint: their anatomic and theoretical basis with an emphasis on radiology, pathology and clinical biology. 1. The intramedullary cartilage tumors. Skeletal Radiol 26:325, 1997.
100. Dahlin DC: Giant cell tumor of bone: highlights of 407 cases. AJR 144:955, 1985.
101. Huvos AG, Higinbotham NL: Primary fibrosarcoma of bone: a clinicopathologic study of 130 patients. Cancer 35:837, 1975.
102. Dahlin DC, Coventry MB, Scanlon PW: Ewing's sarcoma: a critical analysis of 165 cases. J Bone Joint Surg [Am] 43:185, 1961.
103. Sudaresan N: Chordomas. Clin Orthop 204:135, 1986.
104. Kyle RA: Multiple myeloma: review of 869 cases. Mayo Clin Proc 50:29, 1975.
105. Franczyk J, Samuels T, Rubenstein J, et al: Skeletal lymphoma. J Can Assoc Radiol 40:75, 1989.
106. Hermann G, Klein MJ, Fikry Abdelwahab I, et al: MRI appearance of primary non-Hodgkin's lymphoma of bone. Skeletal Radiol 26:629, 1997.
107. Clayton F, Butler JJ, Ayala AG, et al: Non-Hodgkin's lymphoma in bone: pathologic and radiologic features with clinical correlates. Cancer 60:2494, 1987.
108. Epstein BS: Vertebral changes in childhood leukemia. Radiology 68:65, 1957.
109. Greenspan A: Bone island (enostosis): current concept—a review. Skeletal Radiol 24:111, 1995.
110. Zwimpfer TJ, Tucker WS, Faulkner JF: Osteoid osteoma of the cervical spine: case reports and literature review. Can J Surg 25:637, 1982.
111. Fielding JW, Ratzan S: Osteochondroma of the cervical spine. J Bone Joint Surg [Am] 55:640, 1973.
112. Karasick D, Schweitzer ME, Eschelman DJ: Symptomatic osteochondromas: imaging features. AJR 168:1507, 1997.
113. Schmale GA, Conrad EV, Raskind WH. The natural history of hereditary multiple exostosis. J Bone Joint Surg [Am] 76:986, 1994.
114. Dahlin DC: Giant cell tumor of bone: Highlights of 407 cases. AJR 144h55, 1985.
115. Laredo J-D, Reizine D, Bard M, et al: Vertebral hemangiomas: radiologic evaluation. Radiology 161:183, 1986.
116. De Dios AMV, Bond JR, Shives TC, et al: Aneurysmal bone cyst: a clinicopathologic study of 238 cases. Cancer 69:2921, 1992.
117. Papagelopoulos PJ, Currier BJ, Shaughnessy WJ, et al: Aneurysmal bone cyst of the spine management and outcome. Spine 23:621, 1998.
118. Hadjipavlou A, Lander P: Paget disease of the spine. J Bone Joint Surg [Am] 73:1376, 1991.
119. Mirra JM, Brien EW, Tehranzadeh J: Paget's disease of bone: review with emphasis on radiologic features. II. Skeletal Radiol 24:173, 1995.
120. Leeds NE, Jacobson HG: Spinal neurofibromatosis. AJR 126:617, 1976.
121. Mitchell GE, Lourie H, Berne AS: The various causes of scalloped vertebrae with notes on their pathogenesis. Radiology 89:67, 1967.
122. Resnik CS, Liniger JR: Monostotic fibrous dysplasia of the cervical spine: case report. Radiology 151:49, 1984.
123. Stull MA, Kransdorf MJ, Devaney KO: Langerhans' cell histiocytosis of bone. RadioGraphics 12:801, 1992.
124. Kilpatrick SE, Wenger DE, Gilchrist GS, et al: Langerhans' cell histiocytosis (histiocytosis X) of bone: a clinicopathologic analysis of 263 pediatric and adult cases. Cancer 76:2471, 1995.
125. Michel BA, Bjorkengren AG, Lambert E, et al: Estimating lumbar bone mineral density from routine radiographs of the lumbar spine. Clin Rheumatol 12:49, 1993.
126. Genant HK, Engelke K, Fuerst T, et al: Noninvasive assessment of bone mineral and structure: state of the art. J Bone Miner Res 11:707, 1996.
127. Resnick D, Niwayama G: Parathyroid disorders and renal osteodystrophy. In Resnick D: Diagnosis of bone and joint disorders. 4th ed. Philadelphia, Saunders, 2002, p 2043.
128. Mikawa Y, Watanabe R, Nishishita Y: Cervical myelopathy in acromegaly: report of a case. Spine 17:1542, 1992.
129. Wang Y, Yin Y, Gilula LA, et al: Endemic fluorosis of the skeleton: radiographic features in 127 cases. AJR 162:93, 1994.
130. Willing SJ: Atlas of neuroradiology. Philadelphia, Saunders, 1995.
131. Karasick D: Anterior cervical spine fusion: struts, plugs and plates. Skeletal Radiol 22:85, 1993.
132. Karasick D, Schweitzer ME, Vaccaro AR: Complications of cervical spine fusion: imaging features. AJR 169:869, 1997.
133. Sim FH, Svien HJ, Bickel WH, et al: Swan-neck deformity following extensive cervical laminectomy. J Bone Joint Surg [Am] 56:564, 1974.
134. Kricun R, Levitt LP, Winn HR: Tortuous vertebral artery shown by MR and CT. AJR 159:613, 1992.
135. Shaw M, Burnett H, Wilson A, et al: Pseudosubluxation of C_2 on C_3 in polytraumatized children—Prevalence and significance. Clin Radiol 54:377, 1999.
136. Garcia G, McCord GC, Kumar R: Hydroxyapatite crystal deposition disease. Semin Musculoskeletal Radiol 7:187, 2003.
137. Hwang S: Imaging of lymphoma of the musculoskeletal system. Radiol Clin N Am 46:379, 2008.
138. Tins BJ, Cassar-Pullicino VN: MR imaging of spinal infection. Semin Musculoskeletal Radiol 8:215, 2004.
139. Winterbottom AP, Shaw AS: Imaging patients with myeloma. Clin Radiol 64:1, 2009.
140. Moineuse C, Kany M, Fourcade D, et al: Magnetic resonance imaging findings in multiple myeloma: description and predictive value. Joint Bone Spine 68:334, 2001.

141. Stoker DJ: Osteopetrosis. Semin Musculoskeletal Radiol 6:299, 2002.
142. Whitehouse RW: Paget's disease of bone. Semin Musculoskeletal Radiol 6:313, 2002.
143. Whitten CR, Saifuddin A: MRI of Paget's disease of bone. Clin Radiol 58:763, 2003.
144. Gelineck J, Salomonsen M, Hviid C: Retropharyngeal tendinitis: radiographic and magnetic resonance imaging findings. Acta Radiol 47:806, 2006.
145. Johnson K, Gardner-Medwin J: Childhood arthritis: classification and radiology. Clin Radiol 57:47, 2002.
146. Azouz EM: Arthritis in children: conventional and advanced imaging. Semin Musculoskeletal Radiol 7:95, 2003.
147. Pratt H, Davies E, King L: Traumatic injuries of the C1/C2 complex: computed tomographic imaging appearances. Curr Probl Diagn Radiol 37:26, 2008.
148. Koivikko MP, Koskinen SK. MRI of cervical spine injuries complicating ankylosing spondylitis. Skeletal Radiol 37:813, 2008.
149. Nakstad PH, Server A, Josefsen R: Traumatic cervical injuries in ankylosing spondylitis. Acta Radiol 45:222, 2004.
150. Kovikko MP, Kiuru MJ, Koskinen SK. Multidetector computed tomography of the cervical spine fractures in ankylosing spondylitis. Acta Radiol 45:751, 2004.
151. Hirai T, Korogi Y, Takahashi M, et al: Ossification of the posterior longitudinal ligament and ligamentum flavum: imaging features. Semin Musculoskeletal Radiol 5:83, 2001.
152. Kim T-J, Bae K-W, Uhm W-S, et al: Prevalence of ossification of the posterior longitudinal ligament of the cervical spine. Joint Bone Spine 75:471, 2008.
153. Laiho K, Kauppi M, Savolainen A, et al: The cervical spine in mutilant juvenile chronic arthritis. Joint Bone Spine 68:425, 2001.
154. Roche CJ, O'Malley M, Dorgan JC, et al: A pictorial review of atlanto-axial rotatory fixation: key points for the radiologist. Clin Radiol 56:947, 2001.
155. Cheng SG, Blackmore CC, Mirza SK, et al: Rotatory subluxation and fracture at C1-C2. AJR 175:540, 2000.
156. Cabot J, Mosel L, Kong A, et al: Tophaceous gout in the cervical spine. Skeletal Radiol 34:803, 2005.
157. Abdulkarim JA, Dhigsa R, Finlay DBL: Magnetic resonance imaging of the cervical spine: frequency of degenerative changes in the intervertebral disc with relation to age. Clin Radiol 58:980, 2003.
158. Tins BJ, Cassar-Pullicino VN. Imaging of acute cervical spine injuries: review and outlook. Clin Radiol 59:865, 2004.
159. Stiell IG, Clement CM, McKnight D, et al: The Canadian C-spine rule versus the NEXUS low-risk criteria in patients with trauma. N Engl J Med 349:2510, 2003.
160. Benedetti PF, Fahr LM, Kuhns LR, et al: MR imaging findings in spinal ligamentous injury: pictorial essay. AJR 175:661, 2000.
161. Bouchard-Chabot A, Lioté F: Cervical spine involvement in rheumatoid arthritis: a review. Joint Bone Spine 69:141, 2002.
162. Roche CJ, Eyes BE, Whitehouse GH: The rheumatoid cervical spine: signs of instability on plain cervical radiographs. Clin Radiol 57:241, 2002.
163. Karhu JO, Parkkola RK, Koskinen SK. Evaluation of flexion/extension of the upper cervical spine in patients with rheumatoid arthritis: an MRI study with a dedicated positioning device compared to conventional radiographs. Acta Radiol 46:55, 2005.
164. Ergun T, Lakadamyali H, Lakadamyali H, et al: Acute spinal cord compression from an extraosseous vertebral hemangioma with hemorrhagic components: a case report. J Manipulative Physiol Ther 20:602, 2007.
165. Leone A, Sundaram M, Cerase A, et al: Destructive spondyloarthropathy of the cervical spine in long term hemodialyzed patients: a five-year clinical radiological prospective study. Skeletal Radiol 20:431, 2001.
166. Krakenes J, Kaale BR, Nordli H, et al: MR analysis of the transverse ligament in the late stage of whiplash injury. Acta Radiol 44:637, 2003.
167. Pathria M. Imaging of spine instability. Semin Musculoskeletal Radiol 9:88, 2005.
168. Dell'Atti C, Cassar-Pullicino VN, Lalam RK, et al: The spine in Paget's disease. Skeletal Radiol 36:609, 2007.
169. Mays S: Absent cervical spine pedicle: Report of a case in a mediaeval skeleton. Skeletal Radiol 36:773, 2007.
170. Varma R, Lander P, Assaf A: Imaging of pyogenic infectious spondylodiscitis. Rad Clin N Am 39:203, 2001.
171. Baudrez V, Galant C, Vande Berg BC: Benign vertebral hemangioma. Skeletal Radiol 30:442, 2001.
172. White AA, Panjabi MM. Clinical biomechanics of the spine, 2nd ed. Philadelphia, Lippincott, 1990.
173. Rumboldt Z: Degenerative disorders of the spine. Semin Roentgenol 41:327, 2006.
174. Lury K, Smith JK, Castillo M: Imaging of spinal infections. Semin Roentgenol 41:363, 2006.
175. Salgad R, Van Goethem JW, van den Hauwe L, et al: Imaging the postoperative spine. Semin Roentgenol 41:312, 2006.
176. Laredo J-D, Vuillemin-Bodaghi V, Boutry N, et al: SAPHO syndrome: MR appearance of vertebral involvement. Radiology 242:825, 2007.
177. Takigawa T, Tanaka M, Nakanishi K, et al: SAPHO syndrome associated spondylitis. Eur Spine J 17:1391, 2008.
178. Shah BK, Saifuddin A, Price GJ: Magnetic resonance imaging of spinal plasmacytoma. Clin Radiol 55:439, 2000.
179. Qaiyum M, Tyrrell PNM, McCall IW, et al: MRI detection of unsuspected vertebral injury in acute spinal trauma: incidence and significance. Skeletal Radiol 30:299, 2001.
180. Green RAR, Saifuddin A: Whole spine MRI in the assessment of acute vertebral body trauma. Skeletal Radiol 33:129, 2004.
181. Fournié B: Pathology and clinicopathologic correlations in spondyloarthropathies. Joint Bone Spine 71:525, 2003.
182. Lee Bennett D, Ohashis K, El-Khoury GY: Spondyloarthropathies: ankylosing spondylitis and psoriatic arthritis. Radiol Clin N Am 42:121, 2004.
183. Ilaslan H, Sundaram M, Unni KK, et al: Primary vertebral osteosarcoma: imaging findings. Radiology 230:697, 2004.
184. Denaro V, Denaro L, Papalia R, et al: Surgical management of cervical spine osteoblastomas. Clin Orthop Relat Res, 455:190, 2007.

CHAPTER 3

Thoracic Spine

1. Edeiken J, Dalinka M, Karasick D: Edeiken's Roentgen diagnosis of diseases of bone. 4th Ed. Baltimore, Williams & Wilkins, 1990.
2. Kahn SL, Gaskin CM, Sharp VL: Keats and Kahn's Roentgen atlas of skeletal maturation. DVD-ROM Ed. Philadelphia, Lippincott Williams and Wilkins, 2007.
3. Greenfield GB: Radiology of bone diseases. 2nd Ed. Philadelphia, JB Lippincott, 1975.
4. Köhler A, Zimmer EA: Borderlands of normal and early pathologic findings in skeletal radiography. 4th Ed. New York, Thieme Medical Publishers, 1993.
5. Keats TE: Atlas of normal roentgen variants that may simulate disease. 8th Ed. Chicago, Year Book Medical Publishers, 2006.
6. Magora A, Schwartz A: Relation between the low back pain syndrome and x-ray findings. 3. Spina bifida occulta. Scand J Rehabil Med 12:9, 1980.
7. Yochum TR, Rowe LJ: Essentials of skeletal radiology. 3rd Ed. Baltimore, Williams & Wilkins, 2004.
8. Ozonoff MB: Spinal anomalies and curvatures. In Resnick D: Diagnosis of bone and joint disorders. 4th Ed. Philadelphia, Saunders, 2002, p 4534.
9. Langer LO, Baumann PA, Gorlin RJ: Achondroplasia. AJR 100:12, 1967.
10. Langer LO: Spondyloepiphyseal dysplasia tarda, hereditary chondrodysplasia with characteristic vertebral configuration in the adult. Radiology 82:833, 1964.
11. Watts RWE, Spellacy E, Kendall BE, et al: Computed tomography studies on patients with mucopolysaccharidosis. Neuroradiology 21:9, 1981.

12. Holzgrave W, Grobe H, von Figura K, et al: Morquio syndrome: Clinical findings of 11 patients with MPS IV-A and 2 patients with MPS IV-B. Hum Genet 57:360, 1981.
13. Kovanlikaya A, Loro ML, Gilsanz V: Pathogenesis of osteosclerosis in autosomal dominant osteopetrosis. AJR 168:929, 1997.
14. Kahler SG, Burns JA, Aylsworth AS: A mild autosomal recessive form of osteopetrosis. Am J Genet 17:451, 1984.
15. Benli IT, Akalin S, Boysan E, et al: Epidemiological, clinical, and radiological aspects of osteopoikilosis. J Bone Joint Surg [Br] 74:504, 1992.
16. Magid D, Pyeritz RE, Fishman EK: Musculoskeletal manifestations of the Marfan syndrome: Radiologic features. AJR 155:99, 1990.
17. Root L: The treatment of osteogenesis imperfecta. Orthop Clin North Am 15:775, 1984.
18. Wardinski TD, Pagon RA, Powell BR, et al: Rhizomelic chondrodysplasia punctata and survival beyond one year: A review of the literature and five case reports. Clin Genet 38:84, 1990.
19. Fon GT, Pitt MJ, Thies AC Jr: Thoracic kyphosis: Range in normal subjects. AJR 134:979, 1980.
20. Rajasekaran S, Shanmugasundaram TK: Prediction of the angle of gibbus deformity in tuberculosis of the spine. J Bone Joint Surg [Am] 69:503, 1987.
21. Lund PJ, Ruth JT, Dzioba R, et al: Traumatic thoracolumbar facet instability: Characteristic imaging findings. Skeletal Radiol 26:360, 1997.
22. Kumar UK, Sahsasranam KV: Mitral valve prolapse syndrome and associated thoracic skeletal abnormalities. J Assoc Physicians India 39:536, 1991.
23. Lowe TG: Scheuermann's kyphosis. Neurosurg Clin North Am 18:305, 2007.
24. Perdriolle R, Vidal J: Thoracic idiopathic scoliosis curve: Evolution and prognosis. Spine 10:785, 1985.
25. McMaster MJ, Ohtsuka K: The natural history of congenital scoliosis: A study of two hundred and fifty-one patients. J Bone Joint Surg [Am] 64:1128, 1982.
26. Hsu LCS, Lee PC, Leong JCY: Dystrophic spinal deformities in neurofibromatosis. J Bone Joint Surg [Br] 66:495, 1984.
27. Robin GC, Brief LP: Scoliosis in childhood muscular dystrophy. J Bone Joint Surg [Am] 53:466, 1971.
28. Mayfield JK, Riseborough EJ, Jaffe N, et al: Spinal deformity in children treated for neuroblastoma. The effect of radiation and other forms of treatment. J Bone Joint Surg [Am] 63:183, 1981.
29. Cohen MD, Harrington TM, Ginsbury WW: Osteoid osteoma: 95 cases and a review of the literature. Semin Arthritis Rheum 12:265, 1983.
30. DeSousa AL, Kalsbeck JE, Mealey J Jr, et al: Intraspinal tumors in children: A review of 81 cases. J Neurosurg 51:437, 1979.
31. Ryan RW, Lally JF, Kozic Z: Asymptomatic calcified herniated thoracic discs: CT recognition. AJNR 9:363, 1988.
32. Giles LGF, Taylor JR: Lumbar spine structural changes associated with leg length inequality. Spine 7:159, 1982.
33. Thometz JG, An HS: Luque instrumentation with sublaminar wiring. In An HS, Cotler JM (eds): Spinal instrumentation. Baltimore, Williams & Wilkins, 1992, p 93.
34. El-Khoury G, Whitten CG: Trauma to the upper thoracic spine: Anatomy, biomechanics, and unique imaging features. AJR 160:95, 1993.
35. Kaplan PA, Orton DF, Asleson RJ: Osteoporosis with vertebral compression fractures, retropulsed fragments, and neurologic compromise. Radiology 165:533, 1987.
36. Stabler A, Bellan M, Weiss M, et al: MR imaging of enhancing intraosseous disc herniation (Schmorl's nodes). AJR 168:933, 1997.
37. Gehweiler JA, Osborne RL Jr, Becker RF: The radiology of vertebral trauma. Philadelphia, Saunders, 1980.
38. Baker LL, Goodman SB, Perkash I, et al: Benign versus pathologic compression fractures of vertebral bodies: Assessment with conventional spin-echo, chemical-shift, and STIR MR imaging. Radiology 174:495, 1990.
39. Dupuy DE, Palmer WE, Rosenthal DI: Vertebral fluid collection associated with vertebral collapse. AJR 167:1535, 1996.
40. Saifuddin A, Noordeen J, Taylor BA, et al: The role of imaging in the diagnosis of thoracolumbar burst fractures: Current concepts and a review of the literature. Skeletal Radiol 25:603, 1996.
41. Lund PJ, Ruth JT, Dzioba R, et al: Traumatic thoracolumbar facet instability: Characteristic imaging findings. Skeletal Radiol 26:360, 1997.
42. Smith KS, Kaufer H: Patterns and mechanisms of lumbar injuries associated with lap seat belts. J Bone Joint Surg [Am] 51:239, 1988.
43. Terk MR, Hume-Neal M, Fraipont M, et al: Injury of the posterior ligament complex in patients with acute spinal trauma: Evaluation by MR imaging. AJR 168:1481, 1997.
44. Emery SE, Pathria MN, Wilber RG, et al: Magnetic resonance imaging of posttraumatic spinal ligament injury. J Spinal Disord 2:229, 1989.
45. Kleinman PK, Marks SC: Vertebral body fractures in child abuse: Radiologic-histopathologic correlates. Invest Radiol 27:715, 1992.
46. Resnick D: Degenerative disease of the spine. In Resnick D: Diagnosis of bone and joint disorders. 4th Ed. Philadelphia, Saunders, 2002, p 1382.
47. Weinberger A, Myers AR: Intervertebral disc calcification in adults: A review. Semin Arthritis Rheum 8:69, 1978.
48. Resnick D, Shaul SR, Robins JM: Diffuse idiopathic skeletal hyperostosis (DISH): Forestier's disease with extraspinal manifestations. Radiology 115:513, 1975.
49. Weinfeld RM, Olson PN, Maki DD, et al: The prevalence of diffuse idiopathic skeletal hyperostosis (DISH) in two large American Midwest metropolitan hospital populations. Skeletal Radiol 26:222, 1997.
50. Hendrix RW, Melany M, Miller F, et al: Fracture of the spine in patients with ankylosis due to diffuse idiopathic skeletal hyperostosis: Clinical and imaging findings. AJR 162:899, 1994.
51. Quagliano PV, Hayes CW, Palmer WE: Vertebral pseudoarthrosis associated with diffuse idiopathic skeletal hyperostosis. Skeletal Radiol 23:353, 1994.
52. Widder DJ: MR imaging of ossification of the posterior longitudinal ligament. AJR 153:194, 1989.
53. Kapila A, Lines M: Neuropathic spinal arthropathy: CT and MR findings. J Comput Assist Tomogr 11:736, 1987.
54. Pascual E, Castellano JA, Lopez E: Costovertebral joint changes in ankylosing spondylitis with thoracic pain. Br J Rheumatol 31:413, 1992.
55. Peh WCG, Ho TK, Chan FL: Case report: Pseudoarthrosis complicating ankylosing spondylitis-appearances on magnetic resonance imaging. Clin Radiol 47:359, 1993.
56. Sundaram M, Patton JT: Paravertebral ossification in psoriasis and Reiter's disease. Br J Radiol 48:628, 1975.
57. Martel W, Braunstein EM, Borlaza G, et al: Radiologic features of Reiter's disease. Radiology 132:1, 1979.
58. Czirjak L, Nagy Z, Szegedi G: Systemic sclerosis in the elderly. Clin Rheumatol 11:483, 1992.
59. Resnick D: Dermatomyositis and polymyositis. In Resnick D: Diagnosis of bone and joint disorders. 4th Ed. Philadelphia, Saunders, 2002, p 1221.
60. Resnick D, Pineda C: Vertebral involvement in calcium pyrophosphate dihydrate crystal deposition disease: Radiographic-pathologic correlation. Radiology 153:55, 1984.
61. Steinbach LS, Resnick D: Calcium pyrophosphate dihydrate crystal deposition disease revisited. Radiology 200:1, 1996.
62. Justesen P, Andersen PE Jr: Radiologic manifestations in alkaptonuria. Skeletal Radiol 11:204, 1984.
63. Dagirmanjian A, Schils J, McHenry M, et al: MR imaging of vertebral osteomyelitis revisited. AJR 167:1539, 1996.
64. Hoffman EB, Crosier JH, Cremin B: Imaging in children with spinal tuberculosis: A comparison of radiography, computed tomography and magnetic resonance imaging. J Bone Joint Surg [Br] 75:233, 1993.
65. Travlos J, Du Toit G: Spinal tuberculosis: Beware the posterior elements. J Bone Joint Surg [Br] 72:722, 1990.
66. Wong DA, Fornasier VL, MacNab I: Spinal metastases: The obvious, the occult, and the impostors. Spine 15:1, 1990.
67. Algra PR, Heimans JJ, Valk J, et al: Do metastases in vertebrae begin in the body or the pedicles? Imaging study in 45 patients. AJR 158:1275, 1992.

68. Garrett IR: Bone destruction in cancer. Semin Oncol 20:4, 1993.
69. Barwick KW, Huvos AG, Smith J: Primary osteogenic sarcoma of the vertebral column: A clinicopathologic correlation of ten patients. Cancer 46:595, 1980.
70. Kyle RA: Multiple myeloma: Review of 869 cases. Mayo Clin Proc 50:29, 1975.
71. Lecouvet FE, Vande Berg BC, Maldague BE, et al: Vertebral compression fractures in multiple myeloma. Part I: Distribution and appearance at MR imaging. Radiology 204:195, 1997.
72. Bouroncle BA, Doan CA: Myelofibrosis: Clinical, hematologic and pathologic study of 110 patients. Am J Med Sci 243:697, 1962.
73. Franczyk J, Samuels T, Rubenstein J, et al: Skeletal lymphoma. J Can Assoc Radiol 40:75, 1989.
74. Epstein BS: Vertebral changes in childhood leukemia. Radiology 68:65, 1957.
75. Greenspan A: Bone island (enostosis): Current concept—a review. Skeletal Radiol 24:111, 1995.
76. Gamba JL, Martinez S, Apple J, et al: Computed tomography of axial skeletal osteoid osteomas. AJR 142:769, 1984.
77. Dahlin DC: Giant cell tumor of bone: Highlights of 407 cases. AJR 144:955, 1985.
78. Graham JJ, Yang WC: Vertebral hemangioma with compression fracture and paraparesis treated with preoperative embolization and vertebral resection. Spine 9:97, 1984.
79. Hadjipavlou A, Lander P: Paget disease of the spine. J Bone Joint Surg [Am] 73:1376, 1991.
80. Mirra JM, Brien EW, Tehranzadeh J: Paget's disease of bone: Review with emphasis on radiologic features, part II. Skeletal Radiol 24:173, 1995.
81. Leeds NE, Jacobson HG: Spinal neurofibromatosis. AJR 126:617, 1976.
82. Mitchell GE, Lourie H, Berne AS: The various causes of scalloped vertebrae with notes on their pathogenesis. Radiology 89:67, 1967.
83. Gibson MJ, Middlemiss JH: Fibrous dysplasia of bone. Br J Radiol 44:1, 1971.
84. Jee W-H, Choi K-Y, Choe B-Y, et al: Fibrous dysplasia: MR imaging characteristics with radiopathologic correlation. AJR 167:1523, 1996.
85. Stull MA, Kransdorf MJ, Devaney KO: Langerhans' cell histiocytosis of bone. Radiographics 12:801, 1992.
86. Kilpatrick SE, Wenger DE, Gilchrist GS, et al: Langerhans' cell histiocytosis (histiocytosis X) of bone: A clinicopathologic analysis of 263 pediatric and adult cases. Cancer 76:2471, 1995.
87. Ryan PJ, Fogelman I: Osteoporotic vertebral fractures: Diagnosis with radiography and bone scintigraphy. Radiology 190:669, 1994.
88. Mankin HJ: Rickets, osteomalacia, and renal osteodystrophy. Orthop Clin North Am 21:81, 1990.
89. Resnick D: Thyroid disorders. In Resnick D: Diagnosis of bone and joint disorders. 4th Ed. Philadelphia, Saunders, 2002, p 2026.
90. Resnick D, Niwayama G: Parathyroid disorders and renal osteodystrophy. In Resnick D (ed): Diagnosis of bone and joint disorders. 4th Ed. Philadelphia, Saunders, 2002, p 2043.
91. Tigges S, Nance EP, Carpenter WA, et al: Renal osteodystrophy: Imaging findings that mimic those of other diseases. AJR 165:143, 1995.
92. Lang EK, Bessler WT: The roentgenologic features of acromegaly. AJR 86:321, 1961.
93. Wang Y, Yin Y, Gilula LA, et al: Endemic fluorosis of the skeleton: Radiographic features in 127 cases. AJR 162:93, 1994.
94. Rohlfing BM: Vertebral end-plate depression: Report of two patients with hemoglobinopathy. AJR 128:599, 1977.
95. Malghem J, Maldague B, Labaisse M-A, et al: Intravertebral vacuum cleft: Changes in content after supine positioning. Radiology 187:483, 1993.
96. Wong CC, Pereira B, Pho RWH: Cervical disc calcification in children: A long-term review. Spine 17:139, 1992.
97. Moura B, Tubach F, Sulpice M, et al: Bone mineral density in Marfan syndrome. A large case-control study. Joint Bone Spine 73:733, 2006.
98. Tins BJ, Cassar-Pullicino VN: MR imaging of spinal infection. Semin Musculoskeletal Radiol 8:215, 2004.
99. Winterbottom AP, Shaw AS: Imaging patients with myeloma. Clin Radiol 64:1, 2009.
100. Moineuse C, Kany M, Fourcade D, et al: Magnetic resonance imaging findings in multiple myeloma: Description and predictive value. Joint Bone Spine 68:334, 2001.
101. Stoker DJ: Osteopetrosis. Semin Musculoskeletal Radiol 6:299, 2002.
102. Whitehouse RW: Paget's disease of bone. Semin Musculoskeletal Radiol 6:313, 2002.
103. Whitten CR, Saifuddin A: MRI of Paget's disease of bone. Clinical Radiology 58:763, 2003.
104. Quek S-T, Peh WCG: Radiology of osteoporosis. Semin Musculoskeletal Radiol 6:197, 2002.
105. Madani G, Papadopouluo AM, Holloway B, et al: The radiological manifestations of sickle cell disease. Clin Radiol 62:528, 2007.
106. Dell'Atti C, Cassar-Pullicino VN, Lalam RK, et al: The spine in Paget's disease. Skeletal Radiol 36:609, 2007.
107. Varma R, Lander P, Assaf A: Imaging of pyogenic infectious spondylodiscitis. Rad Clin N Am 39:203, 2001.
108. Baudrez V, Galant C, Vande Berg BC: Benign vertebral hemangioma. Skeletal Radiol 30:442, 2001.
109. Levine DS, Forbat SM, Sifuddin A: MRI of the axial skeletal manifestations of ankylosing spondylitis. Clin Radiol 59:400, 2004.
110. Girard CJ, Schweitzer ME, Morris WB, et al: Thoracic spine disc-related abnormalities: Longitudinal MR imaging assessment. Skeletal Radiol 33:216, 2004.
111. Guermazi A, Mohr A, Grigorian M, et al: Identification of vertebral fractures in osteoporosis. Semin Musculoskeletal Radiol 6:241, 2002.
112. Woo EK, Mansoubi H, Alyas F: Incidental vertebral fractures on multidetector CT images of the chest: Prevalence and recognition. Clin Radiol 63:160, 2008.
113. Armingeat T, Pham T, Legre V, et al: Coexistence of intravertebral vacuum and intradiscal vacuum. Joint Bone Spine 73:428, 2006.
114. Briggs AM, Wrigley EA, Tully PE, et al: Radiographic measures of thoracic kyphosis in osteoporosis: Cobb and vertebral centroid angles. Skeletal Radiol 36:761, 2007.
115. Prat C, Lemaire O, Bret J, et al: Morquio syndrome: Diagnosis in an adult. Joint Bone Spine 75:495, 2008.
116. Caro PA: Magnetic resonance imaging in children with scoliosis. Semin Musculoskeletal Radiol 3:257, 1999.
117. Javier R-M, Moser T, Dietemann J-L, et al: Multiple vertebral osteonecrosis. Joint Bone Spine 75:341, 2008.
118. Kim DH, Vaccaro AR: Osteoporotic compression fractures of the spine: Current options and considerations for treatment. Spine J 5:479, 2006.
119. Deramond H, Mathis JM: Vertebroplasty in osteoporosis. Semin Musculoskeletal Radiol 6:263, 2002.
120. Guglielmi G, Andreula C, Muto M, et al: Percutaneous vertebroplasty: Indications, contraindications, technique, and complications. Acta Radiol 46:256, 2005.
121. Peh WC, Munk PL, Rashid F, et al: Percutaneous vertebral augmentation: Vertebroplasty, kyphoplasty and skyphoplasty. Radiol Clin North Am 46:611, 2008.
122. Lavelle WF, Khaleel MA, Cheney R, et al: Effect of kyphoplasty on survival after vertebral compression fractures. Spine J 8:763, 2008.
123. Gilmore A, Thompson GH: Radiographic evaluation of children and adolescents with a spinal deformity. Semin Musculoskeletal Radiol 3:349, 2000.
124. Redla S, Sikdar T, Saifuddin A: Magnetic resonance imaging of scoliosis. Clin Radiol 56:360, 2001.
125. White AA, Panjabi MM: Clinical Biomechanics of the Spine, 2nd Ed. Philadelphia, Lippincott, 1990.
126. Kim CW, Perry A, Garfin SR: Spinal instability: The orthopedic approach. Semin Musculoskeletal Radiol 9:77, 2005.
127. Bernstein MP, Mirvis SE, Shanmuganathan K: Chance-type fractures of the thoracolumbar spine: Imaging analysis in 53 patients. AJR 187:859, 2006.
128. Daeubler BF, Carrel T, Kujawksi T, et al: Alterations for the thoracic spine in Marfan's syndrome. AJR 186:1246, 2006.
129. Bahloul K, Xhumari A, Feydy A, et al: Thoracic spine osteoid osteoma. Eur J Radiol 46:74, 2003.

130. Kim DH, Vaccaro AR: Osteoporotic compression fractures of the spine: Current options and considerations for treatment. Spine J 6:479, 2006.
131. Ilaslan H, Sundaram M, Unni KK, et al: Primary vertebral osteosarcoma: Imaging findings. Radiology 230:697, 2004.

CHAPTER 4

Lumbar Spine

1. Edeiken J, Dalinka M, Karasick D: Edeiken's Roentgen diagnosis of diseases of bone. 4th Ed. Baltimore, Williams & Wilkins, 1990.
2. Kahn SL, Gaskin CM, Sharp VL. Keats and Kahn's roentgen atlas of skeletal maturation. DVD-ROM Ed. Philadelphia, Lippincott Williams and Wilkins, 2007.
3. Greenfield GB: Radiology of bone diseases. 2nd Ed. Philadelphia, JB Lippincott, 1975.
4. Köhler A, Zimmer EA: Borderlands of normal and early pathologic findings in skeletal radiography. 4th Ed. New York, Thieme Medical Publishers, 1993.
5. Keats TE: Atlas of normal roentgen variants that may simulate disease. 5th Ed. Chicago, Year Book Medical Publishers, 1992.
6. Magora A, Schwartz A: Relation between the low back pain syndrome and x-ray findings. 3. Spina bifida occulta. Scand J Rehabil Med 12:9, 1980.
7. Yochum TR, Rowe LJ: Essentials of skeletal radiology. 3rd Ed. Baltimore, Williams & Wilkins, 2004.
8. Ozonoff MB: Spinal anomalies and curvatures. In Resnick D (ed): Diagnosis of bone and joint disorders. 4th Ed. Philadelphia, Saunders, 2002, p 4534.
9. Greenspan A: Orthopedic radiology: A practical approach. Philadelphia, JB Lippincott, 1988.
10. Chan KK, Sartoris DJ, Haghighi P, et al: Cupid's bow contour of the vertebral body: Evaluation of pathogenesis with bone densitometry and imaging-histopathologic correlation. Radiology 202:253, 1997.
11. Lovell WW, Winter RB: Pediatric orthopedics, Philadelphia, JB Lippincott, 1978.
12. Cowell MJ, Cowell HR: The incidence of spina bifida occulta in idiopathic scoliosis. Clin Orthop 118:116, 1976.
13. Goobar JE, Erickson F, Pate D, et al: Symptomatic clasp-knife deformity of spinous processes. Spine 13:953, 1988.
14. Mitchell R: Congenital absence of a lumbosacral facet. Topics Diagn Radiol Adv Imaging 1:3, 1993.
15. Tini PG, Wieser C, Zinn WM: The transitional vertebra of the lumbosacral spine: Its radiological classification, incidence, prevalence, and clinical significance. Rheumatol Rehabil 16:180, 1977.
16. Kim NH, Suk KS: The role of transitional vertebrae in spondylolysis and spondylolytic spondylolisthesis. Bull Hosp Joint Dis 56:161, 1997.
17. van Tulder MW: Spinal radiographic findings and nonspecific low back pain. Spine 22:427, 1997.
18. Castillo M: MRI of diastematomyelia. MRI Decisions, Sept/Oct, 1991, p 12.
19. Langer LO, Baumann PA, Gorlin RJ: Achondroplasia. AJR 100:12, 1967.
20. Langer LO: Spondyloepiphyseal dysplasia tarda, hereditary chondrodysplasia with characteristic vertebral configuration in the adult. Radiology 82:833, 1964.
21. Watts RWE, Spellacy E, Kendall BE, et al: Computed tomography studies on patients with mucopolysaccharidosis. Neuroradiology 21:9, 1981.
22. Holzgrave W, Grobe H, von Figura K, et al: Morquio syndrome: Clinical findings of 11 patients with MPS IV-A and 2 patients with MPS IV-B. Hum Genet 57:360, 1981.
23. Kahler SG, Burns JA, Aylsworth AS: A mild autosomal recessive form of osteopetrosis. Am J Genet 17:451, 1984.
24. Kovanlikaya A, Loro ML, Gilsanz V: Pathogenesis of osteosclerosis in autosomal dominant osteopetrosis. AJR 168:929, 1997.
25. Weisz GM: Lumbar spinal canal stenosis in osteopoikilosis. Clin Orthop 166:89, 1982.
26. Benli IT, Akalin S, Boysan E, et al: Epidemiological, clinical, and radiological aspects of osteopoikilosis. J Bone Joint Surg [Br] 74:504, 1992.
27. Tallroth K, Malmivaara A, Laitinen M-L, et al: Lumbar spine in Marfan syndrome. Skeletal Radiol 24:337, 1995.
28. Mitchell GE, Lourie H, Berne AS: The various causes of scalloped vertebrae with notes on their pathogenesis. Radiology 89:67, 1967.
29. Taylor JAM, Greene-DesLauriers K, Tanaka DI: Ehlers-Danlos syndrome. J Manip Phys Therap 13:273, 1990.
30. Root L: The treatment of osteogenesis imperfecta. Orthop Clin North Am 15:775, 1984.
31. Wardinski TD, Pagon RA, Powell BR, et al: Rhizomelic chondrodysplasia punctata and survival beyond one year: A review of the literature and five case reports. Clin Genet 38:84, 1990.
32. Poussa M, Merikanto J, Ryoppy S, et al: The spine in diastrophic dysplasia. Spine 16:881, 1991.
33. Wiltse LL, Newman PH, MacNab I: Classification of spondylolysis and spondylolisthesis. Clin Orthop 117:23, 1976.
34. Meyerding HW: Low backache and sciatic pain associated with spondylolisthesis and protruded intervertebral disc. J Bone Joint Surg [Am] 23:461, 1941.
35. Frederickson BE, Baker D, McHollick WJ, et al: The natural history of spondylolysis and spondylolisthesis. J Bone Joint Surg [Am] 66:699, 1984.
36. Langston JW, Gavant ML: Incomplete ring sign: A simple method for CT detection of spondylolysis. J Comput Assist Tomogr 9:728, 1985.
37. Bellah RD, Summerville DA, Treves ST, et al: Low-back pain in adolescent athletes: Detection of stress injury to the pars interarticularis with SPECT. Radiology 180:509, 1991.
38. Saifuddin A, Burnett SJD: The value of lumbar spine MRI in the assessment of the pars interarticularis. Clin Radiol 52:666, 1997.
39. Kauppila LI, Eustace S, Kiel DP, et al: Degenerative displacement of lumbar vertebrae: A 25-year follow-up study in Framingham. Spine 23:1868, 1998.
40. Khanchandani BA: Albers-Schonberg's disease with multiple-level lumbar spondylolysis: A case report. Eur J Chiropr 37:5, 1989.
41. Yochum TR, Sellers LT, Oppenheimer DA, et al: The sclerotic pedicle-how many causes are there? Skeletal Radiol 19:411, 1990.
42. Wood KB, Popp CA, Transfeldt EE, et al: Radiographic evaluation of instability in spondylolisthesis. Spine 19:1697, 1994.
43. Pitkänen M, Manninen HI, Lindgren K, et al: Limited usefulness of traction-compression films in the radiographic diagnosis of lumbar spinal instability: Comparison with flexion-extension films. Spine 22:193, 1997.
44. Friberg O: Lumbar instability: A dynamic approach by traction-compression radiography. Spine 12:119, 1987.
45. Ohmori K, Ishida Y, Tkatsu T, et al: Vertebral slip in lumbar spondylolysis and spondylolisthesis: Long-term follow-up of 22 adult patients. J Bone Joint Surg [Br] 77:771, 1995.
46. Weinstein SL, Ponseti IV: Curve progression in idiopathic scoliosis. J Bone Joint Surg [Am] 65:447, 1983.
47. Taylor JAM, Hoffman LE: The geriatric patient: Diagnostic imaging of common musculoskeletal disorders. Top Clin Chiropr 3:23, 1996.
48. Giles LGF, Taylor JR: Lumbar spine structural changes associated with leg length inequality. Spine 7:159, 1982.
49. Joseph KN, Kane HA, Milner RS, et al: Orthopedic aspects of the Marfan phenotype. Clin Orthop 277:251, 1992.
50. DeSmet AA, Robinson RG, Johnson BE, et al: Spinal compression fractures in osteoporotic women: Patterns and relationship to hyperkyphosis. Radiology 166:497, 1988.
51. Petersilge CA, Pathria MN, Emery SE, et al: Thoracolumbar burst fractures: Evaluation with MR imaging. Radiology 194:49, 1995.
52. Terk MR, Hume-Neal M, Fraipont M, et al: Injury of the posterior ligament complex in patients with acute spinal trauma: Evaluation by MR imaging. AJR 168:1481, 1997.
53. Sturm JT, Perry JF: Injuries associated with fractures of the transverse processes of lumbar vertebrae. Radiology 134:627, 1980.
54. Jackson DW: Unilateral osseous bridging of the lumbar transverse processes

following trauma. J Bone Joint Surg [Am] 57:125, 1975.
55. Denis F: The three column spine and its significance in the classification of acute thoracolumbar spinal injuries. Spine 8:817, 1983.
56. Graves VB, Keene JS, Strother CM, et al: CT of bilateral lumbosacral facet dislocation. AJNR 9:809, 1988.
57. Wagner A, Albeck MJ, Madsen FF: Diagnostic imaging in fracture of lumbar vertebral ring apophyses. Acta Radiol 33:72, 1992.
58. Bonic EE, Taylor JAM, Knudsen JT: Posterior limbus fractures: Five case reports and a review of selected published cases. J Manip Phys Therap 21:281, 1998.
59. Lafforgue PF, Chagnaud CJ, Daver LMH, et al: Intervertebral disc vacuum phenomenon secondary to vertebral collapse: Prevalence and significance. Radiology 193:853, 1994.
60. Ross JS, Modic MT: Current assessment of spinal degenerative disease with magnetic resonance imaging. Clin Orthop 279:68, 1992.
61. Cohn EL, Maurer EJ, Keats TE, et al: Plain film evaluation of degenerative disc disease at the lumbosacral junction. Skeletal Radiol 26:161, 1997.
62. Modic MT, Steinberg PM, Ross JS, et al: Degenerative disc disease: Assessment of changes in vertebral body marrow with MR imaging. Radiology 166:193, 1988.
63. Firooznia H, Benjamin V, Kricheff II, et al: CT of lumbar spine disc herniation: Correlation with surgical findings. AJR 142:587, 1984.
64. Mortensen WW, Thorne RP, Donaldson WF III: Symptomatic gas-containing disc herniation: Report of four cases. Spine 16:190, 1991.
65. Thornbury JR, Fryback DG, Turski PA, et al: Disc-caused nerve compression in patients with acute low back pain: Diagnosis with MR, CT myelography, and plain CT. Radiology 186:731, 1993.
66. Stäbler A, Bellan M, Weiss M, et al: MR imaging of enhancing intraosseous disc herniation (Schmorl's nodes). AJR 168:933, 1997.
67. Yagan R: CT diagnosis of limbus vertebra. J Comput Assist Tomogr 8:149, 1984.
68. Blumenthal SL, Roach J, Herring JA: Lumbar Scheuermann's disease: A clinical series and classification. Spine 12:929, 1987.
69. Kirkaldy-Willis WH, Farfan HF: Instability of the lumbar spine. Clin Orthop 165:110, 1982.
70. Fitzgerald JAW, Newman PH: Degenerative spondylolisthesis. J Bone Joint Surg [Br] 58:184, 1976.
71. Sanderson PL, Fraser RD: The influence of pregnancy on the development of degenerative spondylolisthesis. J Bone Joint Surg [Br] 78:951, 1996.
72. Wiltse LL, Guyer RD, Spencer CW, et al: Alar transverse process impingement of the L5 spinal nerve: The far-out syndrome. Spine 9:31, 1984.
73. Dihlmann W, Delling G: Spondylosclerosis hemisphaerica. ROFO 138:592, 1983.
74. Lee CK, Rauschning W, Glenn W: Lateral lumbar spinal canal stenosis: Classification, pathologic anatomy, and surgical decompression. Spine 13:313, 1988.
75. Carrera GF, Haughton VM, Syvertsen A, et al: Computed tomography of the lumbar facet joints. Radiology 134: 145, 1980.
76. Cone RO, Resnick D: Diffuse idiopathic skeletal hyperostosis (DISH). Contemp Diagn Radiol 6:1, 1983.
77. Broudeur P, Larroque CH, Passeron R, et al: The iliolumbar syndrome. Rev Rhum Mal Osteoartic 50:393, 1982.
78. Kapila A, Lines M: Neuropathic spinal arthropathy: CT and MR findings. J Comput Assist Tomogr 11:736, 1987.
79. Heywood AWB, Meyers OL: Rheumatoid arthritis of the thoracic and lumbar spine. J Bone Joint Surg [Br] 68:362, 1986.
80. Kahn MS: Pathogenesis of ankylosing spondylitis. J Rheumatol 20:1273, 1993.
81. Sparling MJ, Bartleson JD, McLeod RA, et al: Magnetic resonance imaging of arachnoid diverticula associated with cauda equina syndrome in ankylosing spondylitis. J Rheumatol 16: 1335, 1989.
82. Sundaram M, Patton JT: Paravertebral ossification in psoriasis and Reiter's syndrome. Br J Radiol 48:628, 1975.
83. Park Y-H, Huang G-S, Taylor JAM, et al: Patterns of vertebral ossification and pelvic abnormalities in paralysis: A study of 200 patients. Radiology 188:561, 1993.
84. Resnick D, Pineda C: Vertebral involvement in calcium pyrophosphate dihydrate crystal deposition disease: Radiographic-pathologic correlation. Radiology 153:55, 1984.
85. Steinbach LS, Resnick D: Calcium pyrophosphate dihydrate crystal deposition disease revisited. Radiology 200:1, 1996.
86. Justesen P, Andersen PE Jr: Radiologic manifestations in alkaptonuria. Skeletal Radiol 11:204, 1984.
87. Yagan R, Khan MA: The coexistence of ochronosis and ankylosing spondylitis. J Rheumatol 18:1639, 1991.
88. Alarcon GS, Reveille JD: Gouty arthritis of the axial skeleton including the sacroiliac joints. Arch Intern Med 147:2018, 1987.
89. Dagirmanjian A, Schils J, McHenry M, et al: MR imaging of vertebral osteomyelitis revisited. AJR 167:1539, 1996.
90. Rohde V, Meyer B, Schaller C, et al: Spondylodiscitis after lumbar discectomy: Incidence and a proposal for prophylaxis. Spine 23:615, 1998.
91. Travlos J, Du Toit G: Spinal tuberculosis: Beware the posterior elements. J Bone Joint Surg [Br] 72:722, 1990.
92. Graves VB, Schrieber MH: Tuberculous psoas muscle abscess. J Can Assoc Radiol 24:268, 1973.
93. Algra PR, Bloem JL, Tissing H, et al: Detection of vertebral metastases: Comparison between MR imaging and bone scintigraphy. RadioGraphics 11:219, 1991.
94. Wong DA, Fornasier VL, MacNab I: Spinal metastases: The obvious, the occult, and the impostors. Spine 15:1, 1990.
95. Mirra JM: Lymphoma and lymphoma-like disorders. In Mirra JM, Picci P, Gold RH (eds): Bone tumors: clinical, radiologic, and pathologic considerations. Lea & Febiger, London, 1989, p 1177.
96. Algra PR, Heimans JJ, Valk J, et al: Do metastases in vertebrae begin in the body or the pedicles? Imaging study in 45 patients. AJR 158:1275, 1992.
97. Sudaresan N: Chordomas. Clin Orthop 204:135, 1986.
98. Barwick KW, Huvos AG, Smith J: Primary osteogenic sarcoma of the vertebral column: A clinicopathologic correlation of ten patients. Cancer 46:595, 1980.
99. Kyle RA: Multiple myeloma: Review of 869 cases. Mayo Clin Proc 50:29, 1975.
100. Lecouvet FE, Vande Berg BC, Maldague BE, et al: Vertebral compression fractures in multiple myeloma. Part I: Distribution and appearance at MR imaging. Radiology 204:195, 1997.
101. Franczyk J, Samuels T, Rubenstein J, et al: Skeletal lymphoma. J Can Assoc Radiol 40:75, 1989.
102. Epstein BS: Vertebral changes in childhood leukemia. Radiology 68:65, 1957.
103. Greenspan A: Bone island (enostosis): Current concept—a review. Skeletal Radiol 24:111, 1995.
104. Esposito PW, Crawford AH, Vogler C: Solitary osteochondroma occurring on the transverse process of the lumbar spine: A case report. Spine 10:398, 1985.
105. Karasick D, Schweitzer ME, Eschelman DJ: Symptomatic osteochondromas: Imaging features. AJR 168:1507, 1997.
106. De Dios AMV, Bond JR, Shives TC, et al: Aneurysmal bone cyst: A clinicopathologic study of 238 cases. Cancer 69:2921, 1992.
107. Papagelopoulos PJ, Currier BJ, Shaughnessy WJ, et al: Aneurysmal bone cyst of the spine: Management and outcome. Spine 23:621, 1998.
108. Laredo J-D, Reizine D, Bard M, et al: Vertebral hemangiomas: Radiologic evaluation. Radiology 161:183, 1986.
109. Hadjipavlou A, Lander P: Paget disease of the spine. J Bone Joint Surg [Am] 73:1376, 1991.
110. Mirra JM, Brien EW, Tehranzadeh J: Paget's disease of bone: Review with emphasis on radiologic features, part II. Skeletal Radiol 24:173, 1995.
111. Angtuaco EJ, Binet EF, Flanigan S: Value of CT myelography in neurofibromatosis. Neurosurgery 13:668, 1983.

112. Stull MA, Kransdorf MJ, Devaney KO: Langerhans cell histiocytosis of bone. RadioGraphics 12:801, 1992.
113. Kilpatrick SE, Wenger DE, Gilchrist GS, et al: Langerhans' cell histiocytosis (histiocytosis X) of bone: A clinicopathologic analysis of 263 pediatric and adult cases. Cancer 76:2471, 1995.
114. Ryan PJ, Fogelman I: Osteoporotic vertebral fractures: Diagnosis with radiography and bone scintigraphy. Radiology 190:669, 1994.
115. Genant HK, Engelke K, Fuerst T, et al: Noninvasive assessment of bone mineral and structure: State of the art. J Bone Miner Res 11:707, 1996.
116. Resnick D: Disorders of other endocrine glands and of pregnancy. In Resnick D (ed): Diagnosis of bone and joint disorders. 4th Ed. Philadelphia, Saunders, 2002, p 2112.
117. Pacifici R, Rupich R, Griffin M, et al: Dual energy radiography versus quantitative computer tomography for the diagnosis of osteoporosis. J Clin Endocrinol Metab 70:705, 1990.
118. Mankin HJ: Rickets, osteomalacia, and renal osteodystrophy. Orthop Clin North Am 21:81, 1990.
119. Resnick D: Thyroid disorders. In Resnick D (ed): Diagnosis of bone and joint disorders. 3rd Ed. Philadelphia, Saunders, 1995, p 2005.
120. Resnick D, Niwayama G: Parathyroid disorders and renal osteodystrophy. In Resnick D (ed): Diagnosis of bone and joint disorders. 4th Ed. Philadelphia, Saunders, 2002, p 2043.
121. Parikh M, Iyer K, Elias AN, et al: Spinal stenosis in acromegaly. Spine 12:627, 1987.
122. Wang Y, Yin Y, Gilula LA, et al: Endemic fluorosis of the skeleton: Radiographic features in 127 cases. AJR 162:93, 1994.
123. De Gennes C, Kuntz D, De Vernejoul MC: Bone mastocytosis: A report of nine cases with a bone histomorphometric study. Clin Orthop 279:281, 1992.
124. Schwartz AM, Homer MJ, McCauley RGK: "Step-off" vertebral body: Gaucher's disease versus sickle cell hemoglobinopathy. AJR 132:81, 1979.
125. Moseley JE: Skeletal changes in the anemias. Semin Roentgenol 9:169, 1974.
126. Marlow TJ, Brunson CY, Jackson S, et al: "Tower vertebra": A new observation in sickle cell disease. Skeletal Radiol 27:195, 1998.
127. Barton CJ, Cockshott WP: Bone changes in hemoglobin SC disease. AJR 88:523, 1962.
128. Resnick D: Hemoglobinopathies and other anemias. In Resnick D (ed): Diagnosis of bone and joint disorders. 4th Ed. Philadelphia, Saunders, 2002, p 2147.
129. Malghem J, Maldague B, Labaisse M-A, et al: Intravertebral vacuum cleft: Changes in content after supine positioning. Radiology 187:483, 1993.
130. Steinmann JC, Herkowitz HN: Pseudoarthrosis of the spine. Clin Orthop 284:80, 1992.
131. Garfin SR, Glover M, Booth RE, et al: Laminectomy: A review of the Pennsylvania hospital experience. J Spinal Disord 1:116, 1988.
132. Katz JN, Lipson SJ, Larson MG, et al: The outcome of decompressive laminectomy for degenerative lumbar stenosis. J Bone Joint Surg [Am] 73:809, 1991.
133. Rothman SLG, Glenn WV, Kerber CW: Postoperative fractures of the lumbar articular facets: Occult cause of radiculopathy. AJR 145:779, 1985.
134. Kahanovitz N, Arnoczky SP: The efficacy of direct current electrical stimulation to enhance canine spinal fusions. Clin Orthop 251:295, 1990.
135. Pleumeekers HJCM, Hoes AW, van der Does E, et al: Epidemiology of abdominal aortic aneurysms. Eur J Vasc Surg 8:119, 1994.
136. Yochum TR, Guebert GM, Kettner NW: Abdominal aortic aneurysm—the total picture. Appl Diagn Imag 1:1, 1989.
137. Kleinman PK, Marks SC: Vertebral body fractures in child abuse: Radiologic-histopathologic correlates. Invest Radiol 27:715, 1992.
138. Crock HV: Internal disc disruption. In Frymoyer JW (ed): The adult spine: Principles and practice. New York, Raven Press, 1991, p 2015.
139. Tyler PA, Madani G, Chaudhuri R, et al: The radiological appearances of thalassaemia. Clin Radiol 61:40, 2006.
140. Hwang S: Imaging of lymphoma of the musculoskeletal system. Radiol Clin N Am 46:379, 2008.
141. Rossi A, Gandolfo C, Morana G, et al: Current classification and imaging of congenital spinal abnormalities. Semin Roentgenol 41:250, 2006.
142. Klecker RJ, Weissman BN: Imaging features of psoriatic and Reiter's syndrome. Semin Musculoskeletal Radiol 7:115, 2003.
143. Tins BJ, Cassar-Pullicino VN: MR imaging of spinal infection. Semin Musculoskeletal Radiol 8:215, 2004.
144. Winterbottom AP, Shaw AS: Imaging patients with myeloma. Clin Radiol 64:1, 2009.
145. Moineuse C, Kany M, Fourcade D, et al: Magnetic resonance imaging findings in multiple myeloma: Description and predictive value. Joint Bone Spine 68:334, 2001.
146. Ruzek KA, Wenger DE: The multiple faces of lymphoma of the musculoskeletal system. Skeletal Radiol 33:1, 2004.
147. Stoker DJ: Osteopetrosis. Semin Musculoskeletal Radiol 6:299, 2002.
148. Whitehouse RW: Paget's disease of bone. Semin Musculoskeletal Radiol 6:313, 2002.
149. Whitten CR, Saifuddin A: MRI of Paget's disease of bone. Clin Radiol 58:763, 2003.
150. Madani G, Papadopouluo AM, Holloway B, et al: The radiological manifestations of sickle cell disease. Clin Radiol 62:528, 2007.
151. Wenstrup RJ, Roca-Espiau M, Weinreb NJ, et al: Skeletal aspects of Gaucher disease: A review. Br J Radiol 75 (Suppl 1):A2, 2002.
152. Dell'Atti C, Cassar-Pullicino VN, Lalam RK, et al: The spine in Paget's disease. Skeletal Radiol 36:609, 2007.
153. Varma R, Lander P, Assaf A: Imaging of pyogenic infectious spondylodiscitis. Rad Clin N Am 39:203, 2001.
154. Baudrez V, Galant C, Vande Berg BC: Benign vertebral hemangioma. Skeletal Radiol 30:442, 2001.
155. Levine DS, Forbat SM, Saifuddin A: MRI of the axial skeletal manifestations of ankylosing spondylitis. Clin Radiol 59:400, 2004.
156. Kim CW, Perry A, Garfin SR: Spinal instability: The orthopedic approach. Semin Musculoskeletal Radiol 9:77, 2005.
157. Wang Y-C, Jeng C-M, Wu C-Y, et al: Dynamic effects of axial loading on the lumbar spine during magnetic resonance imaging in patients with suspected spinal stenosis. J Formos Med Assoc 107:334, 2008.
158. Francis RM: Mini-symposium: Osteoporosis (ii) Fracture risk assessment. Curr Orthop 22:322, 2008.
159. Dunn AJ, Campbell RSD, Mayor PE, et al: Radiological findings and healing patterns of incomplete stress fractures of the pars interarticularis. Skeletal Radiol 37:443, 2008.
160. Vialle R, Schmit P, Dauzac C, et al: Radiological assessment of lumbosacral dystrophic changes in high-grade spondylolisthesis. Skeletal Radiol 34:528, 2005.
161. Yue WM, Brodner W, Gaines RW: Abnormal spinal anatomy in 27 cases of surgically corrected spondyloptosis: Proximal sacral endplate damage as a possible cause of spondyloptosis. Spine 30 (6 Suppl):S22, 2005.
162. Athiveraham A, Yen D, Scott C, et al: Clinical correlation of radiological spinal stenosis after standardization for vertebral body size. Clin Radiol 62:776, 2007.
163. Arslan G, Çeken K, Çubuk M, et al: Vertebral pneumatocysts. Acta Radiol 42:20, 2001.
164. Nakayama T, Ehara S, Hama H: Spontaneous progression of vertebral intraosseous pneumatocysts to fluid-filled cysts. Skeletal Radiol 30:523, 2001.
165. Jinkins JR: Acquired degenerative changes of the intervertebral segments at and suprajacent to the lumbosacral junction: A radioanatomic analysis of the nondiskal structures of the spinal column and perispinal soft tissues. Radiol Clin N Am 39:73, 2001.
166. Ricq G, Laroche M: Acquired lumbar kyphosis caused in adults by primary paraspinal myopathy. Epidemiology, computed tomography findings, and outcomes in a cohort of 23 patients. Joint Bone Spine 67:528, 2000.
167. World Health Organization: Assessment of fracture risk and its application to screening for postmenopausal osteoporosis: Technical report series 843. Geneva WHO, 1994.

168. Kanis JA, Bluer CC, for the Committee of Scientific Advisors, International Osteoporosis Foundation: An update on the diagnosis and assessment of osteoporosis with densitometry. Osteoporos Int 11:192, 2000.
169. Blake GM, Fogelman I: The role of DXA bone density scans in the diagnosis and treatment of osteoporosis. Postgrad Med 83:509, 2007.
170. Wu H-TH, Morrison WB, Schweitzer ME: Edematous Schmorl's nodes on thoracolumbar imaging: Characteristic patterns and changes over time. Skeletal Radiol 35:212, 2006.
171. Coulier B: Giant fatty Schmorl's nodes: CT findings in four patients. Skeletal Radiol 34:29, 2005.
172. Pfirmann CWA, Resnick D: Schmorl's nodes of the thoracic and lumbar spine: Radiographic-pathologic study of prevalence, characterization, and correlation with degenerative changes of 1,650 spinal levels in 100 cadavers. Radiology 219:368, 2001.
173. Chung CB, Vande Berg BC, Tavernier T, et al: Endplate marrow changes in the asymptomatic lumbosacral spine: Frequency, distribution and correlation with age and degenerative changes. Skeletal Radiol 33:399, 2004.
174. Dorsay TA, Helms CA: MR imaging of epidural hematoma in the lumbar spine. Skeletal Radiol 31:677, 2002.
175. Sokolowski MJ, Garvey TA, Perl J, et al: Prospective study of postoperative lumbar epidural hematomas: Incidence and risk factors. Spine 33:108, 2008.
176. Butt S, Saifuddin A: The imaging of lumbar spondylolisthesis. Clin Radiol 60:533, 2005.
177. Wiltse LL, Rothman SG. Lumbar and lumbosacral spondylolisthesis, classification, diagnosis and natural history. In: Wisel SW, Weinstein JN, Herkowitz HN et al, editors. In: Lumbar spine, 2nd ed, vol. 2. Philadelphia PA: W.B. Saunders; 1996. p. 621-51.
178. Michel-Batôt C, Dintinger H, Blum A, et al: A particular form of septic arthritis: Septic arthritis of facet joint. Joint Bone Spine 75:78, 2008.
179. Campbell RSD, Grainger AJ, Hide IG, et al: Juvenile spondyloysis: A comparative analysis of CT, SPECT, and MRI. Skeletal Radiol 34:63, 2005.
180. Aydogan M, Karatoprak Om, Mirzanli C, et al: Severe erosion of lumbar vertebral body because of a chronic ruptured abdominal aortic aneurysm. Spine J 8:394, 2008.
181. Hui C, Cox I: Two unusual presentations of Baastrup's disease. Clin Radiol 62:495, 2007.
182. Groves CJ, Cassar-Pullicino VN, Tins BJ, et al: Chance-type flexion-distraction injuries in the thoracolumbar spine: MR imaging characteristics. Radiology 236:601, 2005.
183. Khalatbari K, Ansari H: MRI of degenerative cysts of the lumbar spine. Clin Radiol 63:322, 2008.
184. Kang CH, Shin MJ, Kim SM, et al: MRI of paraspinal muscles in lumbar degenerative kyphosis patients and control patients with chronic low back pain. Clin Radiol 62:479, 2007.
185. Chanchalrujira K, Chung C, Kim JY, et al: Intervertebral disc calcification of the spine in an elderly population: Radiographic prevalence, location, and distribution and correlation with spinal degeneration. Radiology 230:499, 2004.
186. Pitkänen MT, Manninen HI, Lindgren K-AJ, et al: Segmental lumbar spine instability at flexion-extension radiography can be predicted by conventional radiography. Clin Radiol 57:632, 2002.
187. Nizard RS, Wybier M, Laredo J-D: Radiologic assessment of lumbar intervertebral instability and degenerative spondylolisthesis. Radiol Clin N Am 39:55, 2001.
188. Santiago FR, Arnau IM, Cuevas CO, et al: Unilateral facet dislocation at the lumbosacral spine. Eur J Radiol Extra 57:23, 2006.
189. Wybier M: Imaging of lumbar degenerative changes involving structures other than disc space. Radiol Clin N Am 39:101, 2001.
190. Ilaslan H, Sundaram M, Unni KK, et al: Primary vertebral osteosarcoma: Imaging findings. Radiology 230:697, 2004.
191. Suk K-S, Kim K-T, Lee S-H, et al: Tophaceous gout of the lumbar spine mimicking pyogenic discitis. Spine J 7:94, 2007.
192. Dimar JR, Glassman SD, Carreon LY: Juvenile degenerative disc disease: A report of 76 cases identified by magnetic resonance imaging. Spine J 7:332, 2007.
193. Saifuddin A: The imaging of lumbar spinal stenosis. Clin Radiol 55:58, 2000.
194. Hughes RJ, Saifuddin A: Imaging of lumbosacral transitional vertebrae. Clin Radiol 59:984, 2004.
195. Hughes RJ, Saifuddin A: Numbering of lumbosacral transitional vertebrae on MRI: Role of iliolumbar ligaments. AJR 187:W59, 2005.
196. Pande RL, Beckman JA: Abdominal aortic aneurysm: Populations at risk and how to screen. J Vasc Interv Radiol 19 [6 Suppl]:S2, 2008.
197. Pathria MN, Garfin SR: Imaging after spine surgery. In Resnick D (ed): Diagnosis of bone and joint disorders. 4th Ed. Philadelphia, Saunders, 2002, p 521.
198. Peng B, Hou S, Wu W, et al: The pathogenesis and clinical significance of a high-intensity zone (HIZ) of lumbar intervertebral disc on MR imaging in the patient with discogenic low back pain. Eur Spine J 15:583, 2005.
199. Ross JS: Spinal imaging. In Resnick D (ed): Diagnosis of bone and joint disorders. 4th Ed. Philadelphia, Saunders, 2002, p 459.
200. McCall I: Degenerative disorders of the spine. In Pope TL, Bloem HL, Beltran J, et al (ed): Imaging of the musculoskeletal system. Philadelphia, Saunders Elsevier, 2008, p 1074.
201. Weishaupt D, Zanetti M, Hodler J, et al: MR imaging of the lumbar spine: Prevalence of intervertebral disc extrusion and sequestration, nerve root compression, endplate abnormalities and osteoarthritis of the facet joints in asymptomatic volunteers. Radiology 209:1913, 1998.
202. Stadnik TW, Lee RR, Coen HL, et al: Annular tears and disc herniation: Prevalence and contrast enhancement on MR images in the absence of low back pain or sciatica. Radiology 206:49, 1998.
203. Boos N, Rieder R, Schade V, et al: 1995 Volvo Award in clinical sciences. The diagnostic accuracy of magnetic resonance imaging, work perception, and psychosocial factors in identifying symptomatic disc herniations. Spine 20:2613, 1995.
204. Jensen MC, Brant-Zawadzki MN, Obuchowski N, et al: Magnetic resonance imaging of the lumbar spine in people without back pain. N Engl J Med 331:69, 1994.
205. Boden SD, Davis DO, Dina TS, et al: Abnormal magnetic-resonance scans of the lumbar spine in asymptomatic subjects: A prospective investigation. J Bone Joint Surg Am 72:403, 1990.
206. Weinreb JC, Wobarsht LB, Cohen JM, et al. Prevalence of lumbosacral intervertebral disc abnormalities on MR images in pregnant and asymptomatic nonpregnant women. Radiology 170:125, 1989.

CHAPTER 5

Sacrococcygeal Spine and Sacroiliac Joints

1. Edeiken J, Dalinka M, Karasick D: Edeiken's roentgen diagnosis of diseases of bone. 4th Ed. Baltimore, Williams & Wilkins, 1990.
2. Kahn SL, Gaskin CM, Sharp VL: Keats and Kahn's roentgen atlas of skeletal maturation. DVD-ROM Ed. Philadelphia, Lippincott Williams and Wilkins, 2007.
3. Dihlmann W: Diagnostic radiology of the sacroiliac joints. Chicago, Year Book Medical Publishers, 1980.
4. Broome DR, Hayman LA, Herrick RC, et al: Postnatal maturation of the sacrum and coccyx: MR imaging, helical CT, and conventional radiography. AJR 170:1061, 1998.
5. Schemmer D, White PG, Friedman L: Radiology of the paraglenoid sulcus. Skeletal Radiol 24:205, 1995.
6. Köhler A, Zimmer EA: Borderlands of normal and early pathologic findings in skeletal radiography. 4th Ed. New York, Thieme Medical Publishers, 1993.
7. Keats TE: Atlas of normal roentgen variants that may simulate disease. 8th Ed. Chicago, Year Book Medical Publishers, 2006.
8. Hadley LA: Accessory sacroiliac articulations with arthritic changes. Radiology 55:403, 1950.

9. Magora A, Schwartz A: Relation between the low back pain syndrome and x-ray findings. 3. Spina bifida occulta. Scand J Rehabil Med 12:9, 1980.
10. Yochum TR, Rowe LJ: Essentials of skeletal radiology. 3rd Ed. Baltimore, Williams & Wilkins, 2004.
11. Renshaw TS: Sacral agenesis: A classification and review of twenty-three cases. J Bone Joint Surg [Am] 60:373, 1978.
12. Tini PG, Wieser C, Zinn WM: The transitional vertebra of the lumbosacral spine: Its radiological classification, incidence, prevalence, and clinical significance. Rheumatol Rehabil 16: 180, 1977.
13. Montana MA, Richardson ML, Kilcoyne RF, et al: CT of sacral injury. Radiology 161:499, 1986.
14. Kane WJ: Fractures of the pelvis. In CA Rockwood Jr, DP Green (eds): Fractures in Adults. 2nd Ed. Philadelphia, JB Lippincott, 1984, p 1093.
15. Newhouse KE, El-Khoury GY, Buckwalter JA: Occult sacral fractures in osteopenic patients. J Bone Joint Surg [Am] 74:227, 1992.
16. Dasgupta B, Shah N, Brown H, et al: Sacral insufficiency fractures: An unsuspected cause of low back pain. Br J Rheumatol 37:789, 1998.
17. Mammone JF, Schweitzer ME: MRI of occult sacral insufficiency fractures following radiotherapy. Skeletal Radiol 24:101, 1995.
18. Sty JR, Starshak RJ: The role of bone scintigraphy in the evaluation of the suspected abused child. Radiology 146:369, 1983.
19. Taylor JAM, Hoffman LE: The geriatric patient: Diagnostic imaging of common musculoskeletal disorders. Top Clin Chiropr 3:23, 1996.
20. Resnick D, Niwayama G, Goergen TG: Comparison of radiographic abnormalities of the sacroiliac joint in degenerative disease and ankylosing spondylitis. AJR 128:189, 1977.
21. Olivieri I, Gemignani G, Camerini E, et al: Differential diagnosis between osteitis condensans ilii and sacroiliitis. J Rheumatol 17:1504, 1990.
22. Durback MA, Edelstein G, Schumacher HR Jr: Abnormalities of the sacroiliac joints in diffuse idiopathic skeletal hyperostosis: Demonstration by computed tomography. J Rheumatol 15:1506, 1988.
23. DeCarvalho A, Graudal H: Sacroiliac joint involvement in classical or definite rheumatoid arthritis. Acta Radiol Diagn 21:417, 1980.
24. Forrester DM: Imaging of the sacroiliac joints. Radiol Clin North Am 28:1055, 1990.
25. Murphey MD, Wetzel LH, Bramble JM, et al: Sacroiliitis: MR imaging findings. Radiology 180:239, 1991.
26. Jayson MIV, Bouchier IAD: Ulcerative colitis with ankylosing spondylitis. Ann Rheum Dis 27:219, 1968.
27. Russell AS, Suarez-Almazor ME: Sacroiliitis in psoriasis: Relationship to peripheral arthritis and HLA B27. J Rheumatol 17:804, 1990.
28. Russell AS, Davis P, Percy JS, et al: The sacroiliitis of acute Reiter's syndrome. J Rheumatol 4:293, 1977.
29. Hooge WA, Li D: CT of the sacroiliac joints in secondary hyperparathyroidism. J Can Assoc Radiol 31:42, 1981.
30. Murphy MD, Sartoris DJ, Quale JL, et al: Musculoskeletal manifestations of chronic renal insufficiency. RadioGraphics 13:357, 1993.
31. Sundaram M: Renal osteodystrophy. Skeletal Radiol 18:415, 1989.
32. Vyskocil JJ, McIlroy MA, Brennan TA, et al: Pyogenic infection of the sacroiliac joint: Case reports and review of the literature. Medicine 70:188, 1991.
33. Wong DA, Fornasier VL, MacNab I: Spinal metastases: The obvious, the occult, and the impostors. Spine 15:1, 1990.
34. Rafii M, Firooznia H, Golimbu C, et al: CT of skeletal metastasis. Semin Ultrasound CT MR 7:371, 1986.
35. Sudaresan N: Chordomas. Clin Orthop 204:135, 1986.
36. Kyle RA: Multiple myeloma: Review of 869 cases. Mayo Clin Proc 50:29, 1975.
37. Greenspan A: Bone island (enostosis): Current concept—a review. Skeletal Radiol 24:111, 1995.
38. Dahlin DC: Giant cell tumor of bone: Highlights of 407 cases. AJR 144:955, 1985.
39. Matfin G, McPherson F: Paget's disease of bone: Recent advances. J Orthop Rheumatol 6:127, 1993.
40. Mirra JM, Brien EW, Tehranzadeh J: Paget's disease of bone: Review with emphasis on radiologic features, part II. Skeletal Radiol 24:173, 1995.
41. Angtuaco EJ, Binet EF, Flanigan S: Value of CT myelography in neurofibromatosis. Neurosurgery 13:668, 1983.
42. Klecker RJ, Weissman BN: Imaging features of psoriatic arthritis and Reiter's syndrome. Semin Musculoskeletal Radiol 7:115, 2003.
43. Dell'Atti C, Cassar-Pullicino VN, Lalam RK, et al: The spine in Paget's disease. Skeletal Radiol 36:609, 2007.
44. Puhakka KB, Jurik AG, Egund N, et al: Imaging of sacroiliitis in early seronegative spondyloarthropathy: Assessment of abnormalities by MR in comparison with radiography and CT. Acta Radiol 44:218, 2003.
45. Puhakka KB, Melsen F, Jurik AG, et al: MR imaging of normal sacroiliac joint with correlation to histology. Skeletal Radiol 33:15, 2004.
46. White JH, Hague C, Nicolaou S, et al: Imaging of sacral fractures. Clin Radiol 58:914, 2003.
47. Blake SP, Connors AM: Sacral insufficiency fracture. Br J Radiol 77:891, 2004.
48. Major NM, Helms CA: Sacral stress fractures in long-distance runners. AJR 174:727, 2000.
49. Tuite MJ: Sacroiliac joint imaging. Semin Musculoskeletal Radiol 12:72, 2008.
50. Llauger J, Palmer J, Amores S, et al: Primary tumors of the sacrum: Diagnostic imaging. AJR 174:417, 2000.
51. Sung MS, Lee GK, Kang HS, et al: Sacrococcygeal chordoma: MR imaging in 30 patients. Skeletal Radiol 34: 87, 2005.
52. Gerber S, Ollivier L, Leclère J, et al: Imaging of sacral tumors. Skeletal Radiol 37:277, 2008.

CHAPTER 6

Pelvis and Symphysis Pubis

1. Edeiken J, Dalinka M, Karasick D: Edeiken's roentgen diagnosis of diseases of bone. 4th Ed. Baltimore, Williams & Wilkins, 1990.
2. Kahn SL, Gaskin CM, Sharp VL: Keats and Kahn's roentgen atlas of skeletal maturation. DVD-ROM Ed. Philadelphia, Lippincott Williams and Wilkins, 2007.
3. Greenfield GB: Radiology of bone diseases. 2nd Ed. Philadelphia, JB Lippincott, 1975.
4. Köhler A, Zimmer EA: Borderlands of normal and early pathologic findings in skeletal radiography. 4th Ed. New York, Thieme Medical Publishers, 1993.
5. Risser JC: The iliac apophysis: An invaluable sign in the management of scoliosis. Clin Orthop 175:111, 1958.
6. Keats TE: Atlas of normal roentgen variants that may simulate disease, 8th Ed. Chicago, Year Book Medical Publishers, 2006.
7. Greenspan A, Norman A: The "pelvic digit"—an unusual developmental anomaly. Skeletal Radiol 9:118, 1982.
8. Yochum TR, Rowe LJ: Essentials of skeletal radiology. 3rd Ed. Baltimore, Williams & Wilkins, 2004.
9. Langer LO, Baumann PA, Gorlin RJ: Achondroplasia. AJR 100:12, 1967.
10. Diamond LS, Lynne D, Sigman B: Orthopedic disorders in patients with Down's syndrome. Orthop Clin North Am 12:57, 1981.
11. Kovanlikaya A, Loro ML, Gilsanz V: Pathogenesis of osteosclerosis in autosomal dominant osteopetrosis. AJR 168:929, 1997.
12. Benli IT, Akalin S, Boysan E, et al: Epidemiological, clinical, and radiological aspects of osteopoikilosis. J Bone Joint Surg [Br] 74:504, 1992.
13. Watts RWE, Spellacy E, Kendall BE, et al: Computed tomography studies on patients with mucopolysaccharidosis. Neuroradiology 21:9, 1981.
14. Root L: The treatment of osteogenesis imperfecta. Orthop Clin North Am 15:775, 1984.
15. Jarvis JL, Keats TE: Cleidocranial dysostosis: A review of 40 cases. AJR 121:5, 1974.
16. Guidera KJ, Satterwhite Y, Ogden JA, et al: Nail-patella syndrome: A review

of 44 orthopaedic patients. J Pediatr Orthop 11:737, 1991.

17. Sundar M, Carty H: Avulsion fractures of the pelvis in children: A report of 32 fractures and their outcome. Skeletal Radiol 23:85, 1994.
18. Kane WJ: Fractures of the pelvis. In CA Rockwood Jr, DP Green (eds): Fractures in adults. 2nd Ed. Philadelphia, JB Lippincott, 1984.
19. Montana MA, Richardson ML, Kilcoyne RF, et al: CT of sacral injury. Radiology 161:499, 1986.
20. Mumber MP, Greven KM, Miner Haygood T: Pelvic insufficiency fractures associated with radiation atrophy: Clinical recognition and diagnostic evaluation. Skeletal Radiol 26:94, 1997.
21. Hosono M, et al: MR appearance of parasymphyseal insufficiency fractures of the os pubis. Skeletal Radiol 26:525, 1997.
22. Mammone JF, Schweitzer ME: MRI of occult sacral insufficiency fractures following radiotherapy. Skeletal Radiol 24:101, 1995.
23. Berg PM: Acute pelvic disruption, the bucking horse injury. Orthop Trans 3:271, 1979.
24. Failinger MS, McGanity PLJ: Unstable fractures of the pelvic ring. J Bone Joint Surg [Am] 74:781, 1992.
25. Dalal SA, Burgess AR, Siegel JH, et al: Pelvic fracture in multiple trauma: Classification by mechanism is key to pattern of organ injury, resuscitative requirements, and outcome. J Trauma 29:981, 1989.
26. Gill K, Bucholz RW: The role of computerized tomographic scanning in the evaluation of major pelvic fractures. J Bone Joint Surg [Am] 66:34, 1984.
27. Potok PS, Hopper KD, Umlauf MJ: Fractures of the acetabulum: Imaging, classification, and understanding. RadioGraphics 15:7, 1995.
28. Brandser E, Marsh JL: Acetabular fractures: Easier classification with a systematic approach. AJR 171:1217, 1998.
29. Pavlov H, Nelson TL, Warren RF, et al: Stress fractures of the pubic ramus: A report of twelve cases. J Bone Joint Surg [Am] 64:1020, 1982.
30. Otte MT, Helms CA, Fritz RC: MR imaging of supra-acetabular insufficiency fractures. Skeletal Radiol 26:279, 1997.
31. Haller J, Resnick D, Miller CW, et al: Diffuse idiopathic skeletal hyperostosis: Diagnostic significance of radiographic abnormalities of the pelvis. Radiology 172:835, 1989.
32. Prescher A, Bohndorf K: Anatomical and radiological observations concerning ossification of the sacrotuberous ligament: Is there a relation to spinal diffuse idiopathic skeletal hyperostosis (DISH)? Skeletal Radiol 22:581, 1993.
33. Resnick D, Shaul SR, Robins JM: Diffuse idiopathic skeletal hyperostosis (DISH): Forestier's disease with extraspinal manifestations. Radiology 115: 513, 1975.
34. Coventry MB, Mitchell WC: Osteitis pubis: Observations based on a study of 45 patients. JAMA 178:898, 1961.
35. Fricker PA, Taunton JE, Ammann W: Osteitis pubis in athletes: Infection, inflammation or injury? Sports Med 12:266, 1991.
36. Kormano M: Symphysial changes in rheumatoid arthritis. Scand J Rheumatol 4:17, 1975.
37. Scott DL, Eastmond CJ, Wright V: A comparative radiological study of the pubic symphysis in rheumatic disorders. Ann Rheum Dis 38:529, 1979.
38. Resnick D: Dermatomyositis and polymyositis. In Diagnosis of bone and joint disorders. 4th Ed. Philadelphia, Saunders, 2002, p 1221.
39. Resnick D, Niwayama G, Georgen TG, et al: Clinical, radiographic, and pathologic abnormalities in calcium pyrophosphate dihydrate deposition disease (CPPD): Pseudogout. Radiology 122:1, 1977.
40. Steinbach LS: Calcium pyrophosphate dihydrate and calcium hydroxyapatite crystal deposition diseases: Imaging perspectives. Radiol Clin N Am 42: 185, 2004.
41. Faraawi R, Harth M, Kertesz A, et al: Arthritis in hemochromatosis. J Rheumatol 20:448, 1993.
42. Justesen P, Andersen PE Jr: Radiologic manifestations in alkaptonuria. Skeletal Radiol 11:204, 1984.
43. Sundaram M: Renal osteodystrophy. Skeletal Radiol 18:415, 1989.
44. Murphy MD, Sartoris DJ, Quale JL, et al: Musculoskeletal manifestations of chronic renal insufficiency. RadioGraphics 13:357, 1993.
45. Bouza E, Winston DJ, Hewitt WL: Infectious osteitis pubis. Urology 12: 663, 1978.
46. Habermann ET, Lopez RA: Metastatic disease of bone and treatment of pathologic fractures. Orthop Clin North Am 20:469, 1989.
47. Wong DA, Fornasier VL, MacNab I: Spinal metastases: The obvious, the occult, and the impostors. Spine 15:1, 1990.
48. Dahlin DC, Unni KK: Osteosarcoma of bone and its important recognizable varieties. Am J Surg Pathol 1:61, 1977.
49. Mitchell M, Ackerman LV: Metastatic and pseudomalignant osteoblastoma: A report of two unusual cases. Skeletal Radiol 15:213, 1986.
50. Henderson ED, Dahlin DC: Chondrosarcoma of bone—a study of two hundred and eighty-eight cases. J Bone Joint Surg [Am] 45:1450, 1963.
51. Brien EW, Mirra JM, Kerr R: Benign and malignant cartilage tumors of bone and joint: Their anatomic and theoretical basis with an emphasis on radiology, pathology and clinical biology. 1. The intramedullary cartilage tumors. Skeletal Radiol 26:325, 1997.
52. Eckardt JJ, Grogan TJ: Giant cell tumor of bone. Clin Orthop 204:45, 1986.
53. Huvos AG, Higinbotham NL: Primary fibrosarcoma of bone: A clinicopathologic study of 130 patients. Cancer 35:837, 1975.
54. Dahlin DC, Coventry MB, Scanlon PW: Ewing's sarcoma: A critical analysis of 165 cases. J Bone Joint Surg [Am] 43:185, 1961.
55. Kyle RA: Multiple myeloma: Review of 869 cases. Mayo Clin Proc 50:29, 1975.
56. Franczyk J, Samuels T, Rubenstein J, et al: Skeletal lymphoma. J Can Assoc Radiol 40:75, 1989.
57. Hermann G, Klein MJ, Fikry Abedlewahab I, et al: MRI appearance of primary non-Hodgkin's lymphoma of bone. Skeletal Radiol 26:629, 1997.
58. Clayton F, Butler JJ, Ayala AG, et al: Non-Hodgkin's lymphoma in bone: Pathologic and radiologic features with clinical correlates. Cancer 60:2494, 1987.
59. Benz G, Brandeis WE, Willich E: Radiological aspects of leukemia in childhood: An analysis of 89 children. Pediatr Radiol 4:201, 1976.
60. Greenspan A: Bone island (enostosis): Current concept—a review. Skeletal Radiol 24:111, 1995.
61. Cohen MD, Harrington TM, Ginsbury WW: Osteoid osteoma: 95 cases and a review of the literature. Semin Arthritis Rheum 12:265, 1983.
62. Kroon HM, Schurmans J: Osteoblastoma: Clinical and radiologic findings in 98 new cases. Radiology 175:783, 1990.
63. Schiller AL: Diagnosis of borderline cartilage lesions of bone. Semin Diagn Pathol 2:42, 1985.
64. Karasick D, Schweitzer ME, Eschelman DJ: Symptomatic osteochondromas: Imaging features. AJR 168:1507, 1997.
65. Shapiro F, Simon S, Glimcher MJ: Hereditary multiple exostoses: Anthropometric, roentgenographic, and clinical aspects. J Bone Joint Surg [Am] 61:815, 1979.
66. Sanjay BKS, Frassica FJ, Frassica DA, et al: Treatment of giant-cell tumor of the pelvis. J Bone Joint Surg [Am] 75:1466, 1993.
67. Chigira M, Maehara S, Arita S, et al: The aetiology and treatment of simple bone cysts. J Bone Joint Surg [Br] 65:633, 1983.
68. De Dios AMV, Bond JR, Shives TC, et al: Aneurysmal bone cyst: A clinicopathologic study of 238 cases. Cancer 69:2921, 1992.
69. Matfin G. McPherson F: Paget's disease of bone: Recent advances. J Orthop Rheumatol 6:127, 1993.
70. Mirra JM, Brien EW, Tehranzadeh J: Paget's disease of bone: Review with emphasis on radiologic features, part II. Skeletal Radiol 24:173, 1995.
71. Moore TE, King AR, Kathol MH, et al: Sarcoma in Paget disease of bone: Clinical, radiologic, and pathologic features in 22 cases. AJR 156: 1199, 1991.
72. Crawford AH Jr, Bogamery N: Osseous manifestations of neurofibromatosis

in childhood. J Pediatr Orthop 6:72, 1986.

73. Gibson MJ, Middlemiss JH: Fibrous dysplasia of bone. Br J Radiol 44:1, 1971.
74. Kilpatrick SE, Wenger DE, Gilchrist GS, et al: Langerhans' cell histiocytosis (histiocytosis X) of bone: A clinicopathologic analysis of 263 pediatric and adult cases. Cancer 76:2471, 1995.
75. Stull MA, Kransdorf MJ, Devaney KO: Langerhans cell histiocytosis of bone. RadioGraphics 12:801, 1992.
76. Taylor JAM, Resnick D, Sartoris D. Osteoporosis: radiologic-pathologic correlation. In Sartoris D (ed): Osteoporosis: Current and future concepts. New York, Marcel Dekker, 1996.
77. Mankin HJ: Rickets, osteomalacia, and renal osteodystrophy. Orthop Clin North Am 21:81, 1990.
78. Chew FS, Huang-Hellinger F: Brown tumor. AJR 160:752, 1993.
79. Bronsky D, Kushner DS, Dubin A, et al: Idiopathic hypoparathyroidism and pseudohypoparathyroidism: Case reports and review of the literature. Medicine 37:317, 1958.
80. De Gennes C, Kuntz D, De Vernejoul MC: Bone mastocytosis: A report of nine cases with a bone histomorphometric study. Clin Orthop 279:281, 1992.
81. Barton CJ, Cockshott WP: Bone changes in hemoglobin SC disease. AJR 88:523, 1962.
82. Resnick D: Hemoglobinopathies and other anemias. In Resnick D: Diagnosis of bone and joint disorders. 4th Ed. Philadelphia, Saunders, 2002, p 2147.
83. Jaovisidha S, Nam Ryu K, Hodler J, et al: Hemophilic pseudotumor: Spectrum of MR findings. Skeletal Radiol 26:468, 1997.
84. Wilson DA, Prince JR: MR imaging of hemophilic pseudotumors. AJR 150: 349, 1988.
85. Marcus NA, Grace TG, Hodgin UG: Osteomyelitis of the sacrum and sepsis of the hip complicating pelvic actinomycosis. Orthopedics 4:645, 1981.
86. Hancock DA, Reed GW, Atkinson PJ: Bone and soft tissue changes in paraplegic patients. Paraplegia 17:267, 1979-1980.
87. Butler MS, Robertson WW Jr, Rate W, et al: Skeletal sequelae of radiation therapy for malignant childhood tumors. Clin Orthop 251:235, 1990.
88. Blomlie V, Rofstad EK, Talle K, et al: Incidence of radiation-induced insufficiency fractures of the female pelvis: Evaluation with MR imaging. AJR 167:1205, 1996.
89. Bencardion JT, Hassankhani A: Calcium pyrophosphate dihydrate crystal deposition disease. Semin Musculoskeletal Radiol 7:175, 2003.
90. Tyler PA, Madani G, Chaudhuri R, et al: The radiological appearances of thalassaemia. Clin Radiol 61:40, 2006.
91. Ruzek KA, Wenger DE: The multiple faces of lymphoma of the musculoskeletal system. Skeletal Radiol 33:1, 2004.
92. Stoker DJ: Osteopetrosis. Semin Musculoskeletal Radiol 6:299, 2002.
93. Andresen KJ, Sundaram M, Unni KK, et al: Imaging features of low-grade central osteosarcoma of the long bones and pelvis. Skeletal Radiol 33:373, 2004.
94. Whitehouse RW: Paget's disease of bone. Semin Musculoskeletal Radiol 6:313, 2002.
95. Whitten CR, Saifuddin A: MRI of Paget's disease of bone. Clin Radiol 58:763, 2003.
96. Williams TR, Puckett ML, Denison G, et al: Acetabular stress fractures in military endurance athletes and recruits: Incidence and MRI and scintigraphic findings.
97. Rossi F, Dragoni S: Acute avulsion fractures of the pelvis in adolescent competitive athletes: Prevalence, location and sports distribution in 203 cases collected. Skeletal Radiol 30:127, 2001.
98. Zajick DC, Zoga A, Omar IM, et al: Spectrum of MRI findings in clinical athletic pubalgia. Semin Musculoskeletal Radiol 12:3, 2008.
99. Besjakov J, von Scheele C, Ekberg O, et al: Grading scale of radiographic findings in the pubic bone and symphysis in athletes. Acta Radiol 44:79, 2003.
100. Kesek P, Ekberg O, Westlin N: Herniographic findings in athletes with unclear groin pain. Acta Radiol 43:79, 2002.
101. Albers SL, Spritzer CE, Garrett Jr WE, et al. MR findings in athletes with pubalgia. Skeletal Radiol 30:270, 2001.
102. Shortt CP, Zoga AC, Kavanagh EC, et al: Anatomy, pathology, and MRI findings in the sports hernia. Semin Musculoskeletal Radiol 12:54, 2008.
103. Cunningham PM, Brennan D, O'Connell M, et al: Patterns of bone and soft-tissue injury at the symphysis pubis in soccer players: Observations at MRI. AJR 188:W291, 2007.
104. O'Connell MJ, Powell T, McCaffrey NM, et al: Symphyseal cleft injection in the diagnosis and treatment of osteitis pubis in athletes. AJR 179:955, 2002.
105. Iqbal A, McKenna D, Hayes R, et al: Osteomyelitis of the ischiopubic synchondrosis; imaging findings. Skeletal Radiol 33:176, 2004.
106. O'Connor PJ, Barron D: MRI assessment of pelvic trauma. Semin Musculoskeletal Radiol 10:345, 2006.
107. Sanders TG, Zlatkin MB: Avulsion injuries of the pelvis. Semin Musculoskeletal Radiol 12:42, 2008.
108. Brittenden J, Robinson P: Imaging of pelvic injuries in athletes. Br J Radiol 78:457, 2005.
109. Theodorou SJ, Theodorou DJ, Schweitzer ME, et al: Magnetic resonance imaging of para-acetabular insufficiency fractures in patients with malignancy. Clin Radiol 61:181, 2006.
110. Campbell SE, Fajardo RS: Imaging of stress injuries of the pelvis. Semin Musculoskeletal Radiol 12:62, 2008.
111. Durkee NJ, Jacobsen J, Jamadar D, et al: Classification of common acetabular fractures: Radiographic and CT appearances. AJR 187:915, 2006.
112. Bui-Mansfield LT, Chew FS, Lenchik L, et al: Nontraumatic avulsions of the pelvis. AJR 178:423, 2002.
113. Topuz S, Citill I, Iyibozkurt AC, et al: Pubic symphysis diastasis: Imaging and clinical features. Eur J Radiol Extra 59:127, 2006.
114. Jajic Z, Jajic I, Grazio S: Radiological changes of the symphysis in ankylosing spondylitis. Acta Radiol 41:307, 2000.
115. Shingade VU, Song H-R, Lee S-H: The sagging rope sign in achondroplasia-different from Perthes' disease. Skeletal Radiol 35:923, 2006.

CHAPTER 7

Hip

1. Edeiken J, Dalinka M, Karasick D: Edeiken's roentgen diagnosis of diseases of bone. 4th Ed. Baltimore, Williams & Wilkins, 1990.
2. Kahn SL, Gaskin CM, Sharp VL: Keats and Kahn's Roentgen Atlas Of Skeletal Maturation. DVD-ROM Ed. Philadelphia, Lippincott Williams and Wilkins, 2007.
3. Greenfield GB: Radiology of bone diseases. 2nd Ed. Philadelphia, JB Lippincott, 1975.
4. Köhler A, Zimmer EA: Borderlands of normal and early pathologic findings in skeletal radiography. 4th Ed. New York, Thieme Medical Publishers, 1993.
5. Pitt MJ, Graham AR, Shipman JH, et al: Herniation pit of the femoral neck. AJR 138:1115, 1982.
6. Daenen B, Preidler KW, Padmanabhan S, et al: Symptomatic herniation pits of the femoral neck: Anatomic and clinical study. AJR 168:149, 1997.
7. Keats TE: Atlas of normal roentgen variants that may simulate disease. 8th Ed. Chicago, Year Book Medical Publishers, 2006.
8. Yochum TR, Rowe LJ: Essentials of skeletal radiology. 3rd Ed. Baltimore, Williams & Wilkins, 2004.
9. Swischuk LE: Differential diagnosis in pediatric radiology. Baltimore, Williams & Wilkins, 1984.
10. Chapman S, Nakielny R: Aids to radiological differential diagnosis. 4th Ed. Philadelphia, Saunders, 2003.
11. Weinstein JN, Kuo KN, Millar EA: Congenital coxa vara: A retrospective review. J Pediatr Orthop 4:70, 1984.
12. D'Arcy K, Ansell BM, Bywaters EGL: A family with primary protrusio acetabuli. Ann Rheum Dis 37:53, 1978.
13. Meals RA, Hungerford DS, Stevens MB: Malignant disease mimicking arthritis of the hip. JAMA 239:1070, 1978.
14. Armbruster TG, Guerra J Jr, Resnick D, et al: The adult hip: An anatomic study. Part I. The bony landmarks. Radiology 128:1, 1978.

15. Poul J, Bajerova J, Sommernitz M, et al: Early diagnosis of congenital dislocation of the hip. J Bone Joint Surg [Br] 74:695, 1992.
16. Gerscovich EO: A radiologist's guide to the imaging in the diagnosis and treatment of developmental dysplasia of the hip. I. General considerations, physical examination as applied to real-time sonography and radiography. Skeletal Radiol 26:386, 1997.
17. Gerscovich EO: A radiologist's guide to the imaging in the diagnosis and treatment of developmental dysplasia of the hip. II. Ultrasonography: Anatomy, technique, acetabular angle measurements, acetabular coverage of femoral head, acetabular cartilage thickness, three-dimensional technique, screening of newborns, study of older children. Skeletal Radiol 26:447, 1997.
18. Resnick D, Kang SK: Pelvis and hip. In Resnick D, Kang HS, Pretterklieber ML: Internal derangements of joints. 2nd Ed. Philadelphia, Saunders, 2006.
19. Erb RE, Steele JR, Nance EP Jr, et al: Traumatic anterior dislocation of the hip: Spectrum of plain film and CT findings. AJR 165:1215, 1995.
20. Potok PS, Hopper KD, Umlauf MJ: Fractures of the acetabulum: Imaging, classification, and understanding. RadioGraphics 15:7, 1995.
21. Brandser E, Marsh JL: Acetabular fractures: Easier classification with a systematic approach. AJR 171:1217, 1998.
22. Cooperman DR, Charles LM, Pathria MN, et al: Post-mortem description of slipped capital femoral epiphysis. J Bone Joint Surg [Br] 74:595, 1992.
23. Tountas AA, Waddell JP: Stress fractures of the femoral neck: A report of seven cases. Clin Orthop 210:160, 1986.
24. Anderson MW, Greenspan A: Stress fractures. Radiology 199:1, 1996.
25. Reading JM, Sheehan NJ: Spontaneous fractures of the lower limb in chronic rheumatoid arthritis. J Orthop Rheumatol 4:173, 1991.
26. Haramati N, Staron RB, Barax C, et al: Magnetic resonance imaging of occult fractures of the proximal femur. Skeletal Radiol 23:19, 1994.
27. Schwappach JR, Murphey MD, Kokmeyer SF, et al: Subcapital fractures of the femoral neck: Prevalence and cause of radiographic appearance simulating pathologic fracture. AJR 162:651, 1994.
28. Roback DL: Posttraumatic osteolysis of the femoral neck. AJR 134:1243, 1980.
29. DeLee JC: Fractures and dislocations of the hip. In CA Rockwood Jr, DP Green (eds): Fractures in adults. 2nd Ed. Philadelphia, JB Lippincott Co, 1984, p 1211.
30. Altman R, Alarcon G, Appelrouth D, et al: The American College of Rheumatology criteria for the classification and reporting of osteoarthritis of the hip. Arthritis Rheum 34:505, 1991.
31. Preidler KW, Resnick D: Imaging of osteoarthritis. Radiol Clin North Am 34:259, 1996.
32. Martel W, Braunstein EM: The diagnostic value of buttressing of the femoral neck. Arthritis Rheum 21:161, 1978.
33. Haller J, Resnick D, Miller CW, et al: Diffuse idiopathic skeletal hyperostosis: Diagnostic significance of radiographic abnormalities of the pelvis. Radiology 172:835, 1989.
34. Resnick D, Niwayama G: Rheumatoid arthritis. In Resnick D (ed): Diagnosis of bone and joint disorders. 4th Ed. Philadelphia, Saunders, 2002, p 891.
35. Pellman E, Kumari S, Greenwald R: Rheumatoid iliopsoas bursitis presenting as unilateral leg edema. J Rheumatol 13:197, 1986.
36. Dwosh IL, Resnick D, Becker MA: Hip involvement in ankylosing spondylitis. Arthritis Rheum 19:683, 1976.
37. Scarpa R, Oriente P, Pucino A, et al: Psoriatic arthritis in psoriatic patients. Br J Rheumatol 23:246, 1984.
38. Pachman LN: Juvenile dermatomyositis. Pediatr Clin North Am 33:1097, 1986.
39. Czirjak L, Nagy Z, Szegedi G: Systemic sclerosis in the elderly. Clin Rheumatol 11:483, 1992.
40. Olivieri I, Gemignani G, Balagi M, et al: Concomitant systemic lupus erythematosus and ankylosing spondylitis. Ann Rheum Dis 49:323, 1990.
41. Resnick D, Niwayama G, Goergen TG, et al: Clinical, radiographic and pathologic abnormalities in calcium pyrophosphate dihydrate deposition disease (CPPD): Pseudogout. Radiology 122:1, 1977.
42. Steinbach LS, Resnick D: Calcium pyrophosphate dihydrate crystal deposition disease revisited. Radiology 200:1, 1996.
43. Archer BD, Friedman L, Stilgenbauer S, et al: Symptomatic calcific tendinitis at unusual sites. J Can Assoc Radiol 43:203, 1992.
44. Bock GW, Garcia A, Weisman MH, et al: Rapidly destructive hip disease: Clinical and imaging abnormalities. Radiology 186:461, 1993.
45. Borg EJT, Rasker JJ: Gout in the elderly, a separate entity? Ann Rheum Dis 46:72, 1987.
46. Faraawi R, Harth M, Kertesz A, et al: Arthritis in hemochromatosis. J Rheumatol 20:448, 1993.
47. Justesen P, Andersen PE Jr: Radiologic manifestations in alkaptonuria. Skeletal Radiol 11:204, 1984.
48. Vincent GM, Amirault JD: Septic arthritis in the elderly. Clin Orthop 251:241, 1990.
49. Betz RR, Cooperman DR, Wopperer JM, et al: Late sequelae of septic arthritis of the hip in infancy and childhood. J Pediatr Orthop 10:365, 1990.
50. Torres GM, Cernigilaro JG, Abbitt PL, et al: Iliopsoas compartment: Normal anatomy and pathologic processes. RadioGraphics 15:1285, 1995.
51. Garland DE, Blum CE, Waters RL: Periarticular heterotopic ossification in head-injured adults: Incidence and location. J Bone Joint Surg [Am] 62:1143, 1980.
52. Garland DE: A clinical perspective on common forms of acquired heterotopic ossification. Clin Orthop 263:13, 1991.
53. van der Hoeven H, Keesen W, Kuis W: Idiopathic chondrolysis of the hip. A distinct clinical entity? Acta Orthop Scand 60:661, 1989.
54. Cotton A, Flipo R-M, Chastanet P, et al: Pigmented villonodular synovitis of the hip: Review of radiographic features in 58 patients. Skeletal Radiol 24:1, 1995.
55. Hughes TH, Sartoris DJ, Schweitzer ME, et al: Pigmented villonodular synovitis: MRI characteristics. Skeletal Radiol 24:7, 1995.
56. Thomas S: Synovial chondromatosis of the hip: Case with long-term follow up. SD J Med 30:7, 1977.
57. Prager RJ, Mall JC: Arthrographic diagnosis of synovial chondromatosis. AJR 127:344, 1976.
58. Kramer J, Recht M, Deely DM, et al: MR appearance of idiopathic synovial osteochondromatosis. J Comput Assist Tomogr 17:772, 1993.
59. Singh M, Nagrath AR, Maini PS: Changes in the trabecular pattern of the upper end of the femur as an index of osteoporosis. J Bone Joint Surg [Am] 52:457, 1970.
60. Schwappach JR, Murphey MD, Kokmeyer SF, et al: Subcapital fractures of the femoral neck: Prevalence and cause of radiographic appearance simulating pathologic fracture. AJR 162:651, 1994.
61. Kerr R, Resnick D, Sartoris DJ, et al: Computed tomography of proximal femoral trabecular patterns. J Orthop Res 4:45, 1986.
62. Grampp S, Jergas M, Lang P, et al: Quantitative assessment of osteoporosis: Current and future status. In Sartoris DJ (ed): Osteoporosis: diagnosis and treatment. New York, Marcel Dekker, 1996, p 233.
63. Potter H, Moran M, Schneider R, et al: Magnetic resonance imaging in diagnosis of transient osteoporosis of the hip. Clin Orthop 280:223, 1992.
64. Hayes CW, Conway WF, Daniel WW: MR imaging of bone marrow edema pattern: Transient osteoporosis, transient bone marrow edema syndrome, or osteonecrosis. RadioGraphics 13: 1001, 1993.
65. Mankin HJ: Rickets, osteomalacia, and renal osteodystrophy. Orthop Clin North Am 21:81, 1990.
66. Heyerman W, Weiner D: Slipped epiphysis associated with hypothyroidism. J Pediatr Orthop 4:569, 1984.
67. Resnick D, Niwayama G: Parathyroid disorders and renal osteodystrophy. In Resnick D (ed): Diagnosis of bone and joint disorders. 4th Ed. Philadelphia, Saunders, 2002, p 2043.

68. Tigges S, Nance EP, Carpenter WA, et al: Renal osteodystrophy: Imaging findings that mimic those of other diseases. AJR 165:143, 1995.
69. Johanson NA, Vigorita VH, Goldman AB, et al: Acromegalic arthropathy of the hip. Clin Orthop 173:130, 1983.
70. Hernigou P, Galacteros F, Bachir D, et al: Deformities of the hip in adults who have sickle-cell disease and had avascular necrosis in childhood: A natural history of fifty-two patients. J Bone Joint Surg [Am] 73:81, 1991.
71. Wenger DR, Ward WT, Herring JA: Legg-Calvé-Perthes disease. J Bone Joint Surg [Am] 73:778, 1991.
72. Takatori Y, Kokubo T, Ninomiya S, et al: Avascular necrosis of the femoral head: Natural history and magnetic resonance imaging. J Bone Joint Surg [Br] 75:217, 1993.
73. Van de Berg BE, Malghem JJ, Labaisse M-A, et al: MR imaging of avascular necrosis and transient marrow edema of the femoral head. RadioGraphics 13:501, 1993.
74. Dalinka MK, Edeiken J, Finkelstein JB: Complications of radiation therapy: Adult bone. Semin Roentgenol 9:29, 1974.
75. Weiner ES, Abeles M: Aseptic necrosis and glucocorticosteroids in systemic lupus erythematosus: A reevaluation. J Rheumatol 16:604, 1989.
76. Amstutz HC: The hip in Gaucher's disease. Clin Orthop 90:83, 1973.
77. Laorr A, Greenspan A, Anderson MW, et al: Traumatic hip dislocation: Early MRI findings. Skeletal Radiol 24:239, 1995.
78. Ryu KN, Kim EJ, Yoo MC, et al: Ischemic necrosis of the entire femoral head and rapidly destructive hip disease: Potential causative relationship. Skeletal Radiol 26:143, 1997.
79. Askin SR, Bryan RS: Femoral neck fractures in young adults. Clin Orthop 114:259, 1976.
80. Garden RS: Reduction and fixation of subcapital fractures of the femur. Orthop Clin North Am 5:683, 1974.
81. Evans EM: The treatment of trochanteric fractures of the femur. J Bone Joint Surg [Br] 31:190, 1949.
82. Seinsheimer F: Subtrochanteric fractures of the femur. J Bone Joint Surg [Am] 60:300, 1978.
83. Greenspan A, Tehranzadeh J: Imaging of infectious arthritis. Radiol Clin N Am 39:267, 2001.
84. Marin C, Sanchez-Alegre ML, Gallego C, et al: Magnetic resonance imaging of osteoarticular infections in children. Curr Probl Diagn Radiol 33:43, 2004.
85. Al-Nakshabandi NA, Ryan AG, Choudur H, et al: Pigmented villonodular synovitis. Clin Radiol 59:414, 2004.
86. Quek S-T, Peh WCG: Radiology of osteoporosis. Semin Musculoskeletal Radiol 6:197, 2002.
87. Toms AP, Marshall TJ, Becker E, et al: Regional migratory osteoporosis: A review illustrated by five cases. Clin Radiol 60:425, 2005.
88. Madani G, Papadopouluo AM, Holloway B, et al: The radiological manifestations of sickle cell disease. Clin Radiol 62:528, 2007.
89. Wenstrup RJ, Roca-Espiau M, Weinreb NJ, et al: Skeletal aspects of Gaucher disease: A review. Br J Radiol 75 (Suppl 1):A2, 2002.
90. Beall DP, Sweet CF, Martin HD, et al. Imaging findings of femoroacetabular impingement syndrome. Skeletal Radiol 34:691, 2005.
91. Pulido L, Parvizi J: Femoroacetabular impingement: Semin Musculoskeletal Radiol 11:66, 2007.
92. Pfirrmann CWA, Mengiardi B, Dora C, et al: Cam and pincer femoroacetabular impingement: Characteristic MR arthrographic findings in 50 patients. Radiology 240:778, 2006.
93. Kassarjian A, Yoon LS, Belzile E, et al: Triad of MR arthrographic findings in patients with cam-type femoroacetabular impingement. Radiology 236:588, 2005.
94. James LJ, Ali K, Malara F, et al: MRI findings of femoroacetabular impingement. AJR 187:1412, 2006.
95. Leunig M, Beck M, Kalhor M, et al: Fibrocystic changes at anterosuperior femoral neck: Prevalence in hips with femoracetabular impingement. Radiology 236:237, 2005.
96. James SLJ, Connell DA, O'Donnell P, et al: Femoroacetabular impingement: Bone marrow oedema associated with fibrocystic change of the femoral head and neck junction. Clin Radiol 62:472, 2007.
97. Tannast M, Siebenrock KA, Anderson SE: Femoroacetabular impingement: Radiographic diagnosis—what the radiologist should know. AJR 188: 1540, 2007.
98. Blankenbaker DG, Tuite MJ: The painful hip: New concepts. Skeletal Radiol 35:352, 2006.
99. James S, Miocevic M, Malara F, et al: MR imaging findings of acetabular dysplasia in adults. Skeletal Radiol 35:378, 2006.
100. Ömeroglu H, Biçimoglu A, Agus, et al: Measurement of center-edge angle in developmental dysplasia of the hip: A comparison of two methods in patients under 20 years of age. Skeletal Radiol 31:25, 2002.
101. Grissom LE, Harcke T: Developmental dysplasia of the pediatric hip with emphasis on sonographic evaluation. Semin Musculoskeletal Radiol 3:359, 1999.
102. Blake GM, Fogelman I: Dual energy x-ray absorptiometry and its clinical applications. Semin Musculoskeletal Radiol 6:207, 2002.
103. Francis RM: Mini-symposium: Osteoporosis (ii) fracture risk assessment. Curr Orthop 22:322, 2008.
104. Yu JS: Hip and femur trauma. Semin Musculoskeletal Radiol 4:205, 2000.
105. Blankenbaker DG, Ullrick SR, Davis KW, et al: Correlation of MRI findings with clinical findings of trochanteric pain syndrome. Skeletal Radiol 37:903, 2008.
106. Segal NA, Felson DT, Torner JC, et al: Greater trochanter pain syndrome: Epidemiology and associated factors. Arch Phys Med Rehabil 88:988, 2007.
107. Kong A, Van der Vliet A, Zadow S: MRI and US of gluteal tendinopathy in greater trochanteric pain syndrome. Eur Radiol 17:1772, 2007.
108. Garcia-Morales F, Seo GS, Chengazi V, et al: Collar osteophytes: A cause of false-positive findings in bone scans for hip fractures. AJR 181:191, 2003.
109. Boutry N, Paul C, Leroy X, et al: Rapidly destructive osteoarthritis of the hip: MR imaging findings. AJR 179:657, 2002.
110. Cannon J, Sivlestri S, Munro M: Imaging choices in occult hip fracture. J Emerg Med, 2008 Oct 27 [Epub ahead of print].
111. Petersilge CA: MR arthrography for evaluation of the acetabular labrum. Skeletal Radiol 30:423, 2001.
112. Hong RJ, Hughes TH, Gentilli A, et al: Magnetic resonance imaging of the hip. J Magn Reson Imaging 27:435, 2008.
113. Gross GW, Articolo GA, Bowen JR: Legg-Calvé-Perthes disease: Imaging evaluation and management. Semin Musculoskeletal Radiol 3:379, 1999.
114. Gupta KB, Duryea J, Weissman BN: Radiographic evaluation of osteoarthritis. Radiol Clin N Am 42:11, 2004.
115. Saini A, Saifuddin A: MRI of osteonecrosis. Clin Radiol 59:1079, 2004.
116. Sanders TG, Zlatkin MB: Avulsion injuries of the pelvis. Semin Musculoskeletal Radiol 12:42, 2008.
117. Yamamoto T, Schneider R, Bullough PG: Subchondral insufficiency fracture of the femoral head: Histopathologic correlation with MRI. Skeletal Radiol 30:247, 2001.
118. Billing L, Bogren HG, Henrikson B, et al: Slipped capital femoral epiphysis. The mechanical function of the periosteum: New aspects and theory including bilaterality. Acta Radiol 45 Suppl 431:1, 2004.
119. Resnick D et al: Pelvis and hip. In: Resnick D, Kang HS, Pretterklieber ML (eds): Internal derangements of joints. 2nd Ed. Philadelphia, Saunders, 2006, p 1498.
120. Hammani BK, Ghorbel H, Abid F, et al: Psoas abscess of the adult: Study of 38 cases. Tunis Med 85:631, 2007.

CHAPTER 8

Femur

1. Horsfield D, Jones SN: Assessment of inequality in length of the lower limb. Radiography 52:233, 1986.
2. Huurman WW, Jacobsen FS, Anderson JC, et al: Limb-length discrepancy measured with computerized axial tomographic equipment. J Bone Joint Surg [Am] 69:699, 1987.
3. Mannello DM: Leg length inequality. J Manip Physiol Ther 15:576, 1992.

4. Levinson ED, Ozonoff MB, Royers PM: Proximal femoral focal deficiency (PFFD). Radiology 125:197, 1977.
5. Kovanlikaya A, Loro ML, Gilsanz V: Pathogenesis of osteosclerosis in autosomal dominant osteopetrosis. AJR 168:929, 1997.
6. Benli IT, Akalin S, Boysan E, et al: Epidemiological, clinical, and radiological aspects of osteopoikilosis. J Bone Joint Surg [Br] 74:504, 1992.
7. Bass HN, Weiner JR, Goldman A, et al: Osteopathia striata syndrome: Clinical, genetic, and radiologic considerations. Clin Pediatr 19:369, 1980.
8. Campbell CJ, Papademetriou T, Bonfiglio M: Melorheostosis: A report of the clinical, roentgenographic, and pathological findings in fourteen cases. J Bone Joint Surg [Am] 50:1281, 1968.
9. Yu JS, Resnick D, Vaughan LM, et al: Melorheostosis with an ossified soft tissue mass. Skeletal Radiol 24:367, 1995.
10. Whyte MP, Murphy WA, Fallon MD, et al: Mixed-sclerosing-bone-dystrophy: Report of a case and review of the literature. Skeletal Radiol 6:95, 1981.
11. Rogers LF. Radiology of Skeletal Trauma. 3rd Ed. New York, Churchill Livingstone, 2002.
12. Johansson C, Ekenman I, Tönkvist H, et al: Stress fractures of the femoral neck in athletes: The consequence of a delay in diagnosis. Am J Sports Med 18:524, 1990.
13. Anderson MW, Greenspan A: Stress fractures. Radiology 199:1, 1996.
14. Nuovo MA, Norman A, Chumas A, et al: Myositis ossificans with atypical clinical, radiographic, or pathologic findings: A review of 23 cases. Skeletal Radiol 21:87, 1992.
15. Greenspan A, Norman A: Osteolytic cortical destruction: An unusual pattern of skeletal metastasis. Skeletal Radiol 17:402, 1988.
16. Taylor JAM, Harger BL, Resnick D: Diagnostic imaging of common hip disorders: A pictorial review. Top Clin Chiropr 1:8, 1994.
17. Resnik C, Garver P, Resnick D: Bony expansion in skeletal metastasis from carcinoma of the prostate as seen by bone scintigraphy. South Med J 77: 1331, 1984.
18. Dahlin DC, Unni KK: Osteosarcoma of bone and its important recognizable varieties. Am J Surg Pathol 1:61, 1977.
19. Ritschl P, Wurnig C, Lechner G, et al: Parosteal osteosarcoma. 2-23-year follow-up of 33 patients. Acta Orthop Scand 62:195, 1991.
20. Mitchell M, Ackerman LV: Metastatic and pseudomalignant osteoblastoma: A report of two unusual cases. Skeletal Radiol 15:213, 1986.
21. Henderson ED, Dahlin DC: Chondrosarcoma of bone—a study of two hundred and eighty-eight cases. J Bone Joint Surg [Am] 45:1450, 1963.
22. Brien EW, Mirra JM, Kerr R: Benign and malignant cartilage tumors of bone and joint: Their anatomic and theoretical basis with an emphasis on radiology, pathology and clinical biology. 1. The intramedullary cartilage tumors. Skeletal Radiol 26:325, 1997.
23. Dahlin DC: Giant cell tumor of bone: Highlights of 407 cases. AJR 144:955, 1985.
24. Taconis WK, Mulder JD: Fibrosarcoma and malignant fibrous histiocytoma of long bones: Radiographic features and grading. Skeletal Radiol 11:237, 1984.
25. Dahlin DC, Coventry MB, Scanlon PW: Ewing's sarcoma: A critical analysis of 165 cases. J Bone Joint Surg [Am] 43:185, 1961.
26. Kyle RA: Multiple myeloma: Review of 869 cases. Mayo Clin Proc 50:29, 1975.
27. Franczyk J, Samuels T, Rubenstein J, et al: Skeletal lymphoma. J Can Assoc Radiol 40:75, 1989.
28. Hermann G, Klein MJ, Fikry Abdelwahab I, et al: MRI appearance of primary non-Hodgkin's lymphoma of bone. Skeletal Radiol 26:629, 1997.
29. Clayton F, Butler JJ, Ayala AG, et al: Non-Hodgkin's lymphoma in bone: Pathologic and radiologic features with clinical correlates. Cancer 60: 2494, 1987.
30. Benz G, Brandeis WE, Willich E: Radiological aspects of leukemia in childhood: An analysis of 89 children. Pediatr Radiol 4:201, 1976.
31. Greenspan A: Bone island (enostosis): Current concept—a review. Skeletal Radiol 24:111, 1995.
32. Kattapuram SV, Kushner DC, Phillips WC, et al: Osteoid osteoma: An unusual cause of articular pain. Radiology 147:383, 1983.
33. Shankman S, Desai P, Beltran J: Subperiosteal osteoid osteoma: Radiographic and pathologic manifestations. Skeletal Radiol 26:457, 1997.
34. Kayser F, Resnick D, Haghighi P, et al: Evidence of the subperiosteal origin of osteoid osteomas in tubular bones: Analysis by CT and MR imaging. AJR 170:609, 1998.
35. Lichtenstein L, Sawyer WF: Benign osteoblastoma: Further observations and report of twenty additional cases. J Bone Joint Surg [Am] 46:755, 1964.
36. Schiller AL: Diagnosis of borderline cartilage lesions of bone. Semin Diagn Pathol 2:42, 1985.
37. Bloem JL, Mulder JD: Chondroblastoma: A clinical and radiological study of 104 cases. Skeletal Radiol 14:1, 1985.
38. Weatherall PT, Maale GE, Mendelsohn DB, et al: Chondroblastoma: Classic and confusing appearance at MR imaging. Radiology 190:467, 1994.
39. Wilson AJ, Kyriakos M, Ackerman LV: Chondromyxoid fibroma: Radiographic appearance in 38 cases and in a review of the literature. Radiology 179:513, 1991.
40. Milgram JW: The origins of osteochondromas and enchondromas: A histopathologic study. Clin Orthop 174:264, 1983.
41. Karasick D, Schweitzer ME, Eschelman DJ: Symptomatic osteochondromas: Imaging features. AJR 168:1507, 1997.
42. Shapiro F, Simon S, Glimcher MJ: Hereditary multiple exostoses: Anthropometric, roentgenologic and clinical aspects. J Bone Joint Surg [Am] 61:815, 1979.
43. Solomon L: Chondrosarcoma in hereditary multiple exostosis. S Afr Med J 48:671, 1974.
44. Schmale GA, Conrad EV, Raskind WH: The natural history of hereditary multiple exostosis. J Bone Joint Surg [Am] 76:986, 1994.
45. Ritschl P, Karnel F, Hajek P: Fibrous metaphyseal defects—determination of their origin and natural history using a radiomorphological study. Skeletal Radiol 17:8, 1988.
46. McInerney DP, Middlemiss JH: Giant-cell tumour of bone. Skeletal Radiol 2:195, 1978.
47. Milgram JW: Intraosseous lipoma: A clinicopathologic study of 66 cases. Clin Orthop 231:277, 1988.
48. Chigira M, Maehara S, Arita S, et al: The aetiology and treatment of simple bone cysts. J Bone Joint Surg [Br] 65:633, 1983.
49. De Dios AMV, Bond JR, Shives TC, et al: Aneurysmal bone cyst: A clinicopathologic study of 238 cases. Cancer 69:2921, 1992.
50. Matfin G, McPherson F: Paget's disease of bone: Recent advances. J Orthop Rheumatol 6:127, 1993.
51. Mirra JM, Brien EW, Tehranzadeh J: Paget's disease of bone: Review with emphasis on radiologic features. Part II. Skeletal Radiol 24:173, 1995.
52. Crawford AH Jr, Bogamery N: Osseous manifestations of neurofibromatosis in childhood. J Pediatr Orthop 6:72, 1986.
53. Gibson MJ, Middlemiss JH: Fibrous dysplasia of bone. Br J Radiol 44:1, 1971.
54. Stull MA, Kransdorf MJ, Devaney KO: Langerhans cell histiocytosis of bone. RadioGraphics 12:801, 1992.
55. Kilpatrick SE, Wenger DE, Gilchrist GS, et al: Langerhans' cell histiocytosis (histiocytosis X) of bone: A clinicopathologic analysis of 263 pediatric and adult cases. Cancer 76:2471, 1995.
56. Kerr R, Resnick D, Sartoris DJ, et al: Computed tomography of proximal femoral trabecular patterns. J Orthop Res 4:45, 1986.
57. Chew FS, Huang-Hellinger F: Brown tumor. AJR 160:752, 1993.
58. Greenfield GB: Bone changes in chronic adult Gaucher's disease. AJR 110:800, 1970.
59. Bouroncle BA, Doan CA: Myelofibrosis: clinical, hematologic and pathologic study of 110 patients. Am J Med Sci 243:697, 1962.
60. Yu JS, Greenway G, Resnick D: Myelofibrosis associated with prominent periosteal bone apposition: Report of two cases. Clin Imaging 18:89, 1994.

61. Pineda C: Diagnostic imaging in hypertrophic osteoarthropathy. Clin Exp Rheumatol 10:27, 1992.
62. Nerubay J, Pilderwasser D: Spontaneous bilateral distal femoral physiolysis due to scurvy. Acta Orthop Scand 55:18, 1984.
63. Westcott MA, Dynes MC, Remer EM, et al: Congenital and acquired orthopedic abnormalities in patients with myelomeningocele. RadioGraphics 12: 1155, 1992.
64. Ogden JA: Growth slowdown and arrest lines. J Pediatr Orthop 4:409, 1984.
65. Gold RH, Hawkins RA, Katz RD: Bacterial osteomyelitis: Findings on plain radiography, CT, MR, and scintigraphy. AJR 157:365, 1991.
66. Jurik AG, Egund N: MRI in chronic recurrent multifocal osteomyelitis. Skeletal Radiol 26:230, 1997.
67. Pachman LN: Juvenile dermatomyositis. Pediatr Clin North Am 33:1097, 1986.
68. Root L: The treatment of osteogenesis imperfecta. Orthop Clin North Am 15:775, 1984.
69. Mankin HJ: Rickets, osteomalacia, and renal osteodystrophy. Orthop Clin North Am 21:81, 1990.
70. Kaim AH, Hugli R, Bonél HM, et al: Chondroblastoma and clear cell chondrosarcoma: Radiological and MRI characteristics with histopathological correlation. Skeletal Radiol 31:88, 2002.
71. Propeck T, Bullard MA, Lin J, et al: Radiologic-pathologic correlation of intraosseous lipomas. AJR 175:673, 2000.
72. Hwang S: Imaging of lymphoma of the musculoskeletal system. Radiol Clin N Am 46:379, 2008.
73. Vanel D, Picci P, De Paolis M, et al: Radiological study of 12 high-grade osteosarcomas. Skeletal Radiol 30:667, 2001.
74. Marin C, Sanchez-Alegre ML, Gallego C, et al: Magnetic resonance imaging of osteoarticular infections in children. Curr Probl Diagn Radiol 33:43, 2004.
75. Christian S, Kraas J, Conway WF: Musculoskeletal infections. Semin Roentgenol 42:92, 2007.
76. Ruzek KA, Wenger DE: The multiple faces of lymphoma of the musculoskeletal system. Skeletal Radiol 33:1, 2004.
77. Stoker DJ: Osteopetrosis. Semin Musculoskeletal Radiol 6:299, 2002.
78. Andresen KJ, Sundaram M, Unni KK, et al: Imaging features of low-grade central osteosarcoma of the long bones and pelvis. Skeletal Radiol 33:373, 2004.
79. Suresh S, Saifuddin A: Radiological appearances of appendicular osteosarcoma: a comprehensive pictorial review. Clin Radiol 62:314, 2007.
80. Whitehouse RW: Paget's disease of bone. Semin Musculoskeletal Radiol 6:313, 2002.
81. Whitten CR, Saifuddin A: MRI of Paget's disease of bone. Clin Radiol 58:763, 2003.
82. Berry JL, Davies M, Mee AP: Vitamin D metabolism, rickets and osteomalacia. Semin Musculoskeletal Radiol 6:173, 2002.
83. Wenstrup RJ, Roca-Espiau M, Weinreb NJ, et al: Skeletal aspects of Gaucher disease: A review. Br J Radiol 75 (Suppl. 1):A2, 2002.
84. Kiuru MJ, Pihlajamäki HK, Ahuvuo JA. Bone stress injuries. Acta Radiol 45:317, 2004.
85. Theodorou SJ, Theodorou DJ, Resnick D: Imaging findings in symptomatic patients with femoral diaphyseal stress injuries. Acta Radiol 47:377, 2006.
86. Hwang B, Fredericson M, Chung CB, et al: MRI findings of femoral diaphyseal stress injuries in athletes. 185:166, 2005.
87. Maraval A, Grados F, Royant V, et al: Longitudinal femoral shaft fracture due to bone insufficiency. A review of three cases. Joint Bone Spine 70:526, 2003.
88. Flemming DJ, Murphey MD, Shekitka KM, et al: Osseous involvement in calcific tendinitis: A retrospective review of 50 cases. AJR 181:965, 2003.
89. Anderson MW, Kaplan PA, Dussault RG: Adductor insertion avulsion syndrome (thigh splints): Spectrum of MR imaging features. AJR 177:673, 2001.
90. Tshering-Vogel D, Waldherr C, Schindera ST, et al: Adductor insertion avulsion syndrome, "thigh splints": Relevance of radiological follow-up. Skeletal Radiol 34:355, 2005.
91. Allen SD, Saifuddin A: Imaging of intra-articular osteoid osteoma. Clin Radiol 58:845, 2003.
92. Fitzpatrick KA, Taljanovic MS, Speer DP, et al: Imaging findings of fibrous dysplasia with histopathologic and intraoperative correlation. AJR 182:1389, 2004.
93. Tanigawa N, Kariya S, Kojima H, et al: Lower limb ischemia caused by fractured osteochondroma of the femur. Br J Radiol 80;e78, 2007.
94. Winterbottom AP, Shaw AS: Imaging patients with myeloma. Clin Radiol 64:1, 2009.

CHAPTER 9

Knee

1. Edeiken J, Dalinka M, Karasick D: Edeiken's Roentgen diagnosis of diseases of bone. 4th Ed. Baltimore, Williams & Wilkins, 1990.
2. Ogden JA: Radiology of postnatal skeletal development. X. Patella and tibial tuberosity. Skeletal Radiol 11:246, 1984.
3. Kahn SL, Gaskin CM, Sharp VL. Keats and Kahn's roentgen atlas of skeletal maturation. DVD-ROM Ed. Philadelphia, Lippincott Williams and Wilkins, 2007.
4. Greenfield GB: Radiology of bone diseases. 2nd Ed. Philadelphia, JB Lippincott, 1975.
5. Köhler A, Zimmer EA: Borderlands of normal and early pathologic findings in skeletal radiography. 4th Ed. New York, Thieme Medical Publishers, 1993.
6. Keats TE: Atlas of normal roentgen variants that may simulate disease, 8th Ed. Chicago, Year Book Medical Publishers, 2006.
7. Yochum TR, Rowe LJ: Essentials of skeletal radiology. 3rd Ed. Baltimore, Williams & Wilkins, 2004.
8. Ogden JA, McCarthy SM, Jokl P: The painful bipartite patella. J Pediatr Orthop 2:263, 1982.
9. van Holsbeeck M, Vandamme B, Marchal G, et al: Dorsal defect of the patella: Concept of its origin and relationship with bipartite and multipartite patella. Skeletal Radiol 16:304, 1987.
10. Resnick D, Greenway G: Distal femoral cortical defects, irregularities, and excavations: A critical review of the literature with the addition of histologic and paleopathologic data. Radiology 143:345, 1982.
11. Yamazaki T, Maruoka S, Takahashi S, et al: MR findings of avulsive cortical irregularity of the distal femur. Skeletal Radiol 24:43, 1995.
12. Yochum TR, Sprowl CG, Barry MS: Double patella syndrome with a form of multiple epiphyseal dysplasia. J Manip Physiol Ther 18:407, 1995.
13. Guidera KJ, Satterwhite Y, Ogden JA, et al: Nail patella syndrome: A review of 44 orthopaedic patients. J Pediatr Orthop 11:737, 1991.
14. Keret D, Spatz DK, Caro PA, et al: Dysplasia epiphysealis hemimelica: Diagnosis and treatment. J Pediatr Orthop 12:365, 1992.
15. Lang IM, Azouz EM: MRI appearances of dysplasia epiphysealis hemimelica of the knee. Skeletal Radiol 26:226, 1997.
16. Taylor JAM, Greene-DesLauriers K, Tanaka DI: Ehlers-Danlos syndrome. J Manip Physiol Therap 13:273, 1990.
17. Wardinski TD, Pagon RA, Powell BR, et al: Rhizomelic chondrodysplasia punctata and survival beyond one year: A review of the literature and five case reports. Clin Genet 38:84, 1990.
18. Helfet DL: Fractures of the distal femur. In Browner BD, Jupiter JB, Levine AM, et al (eds): Skeletal trauma: Fractures, dislocations, ligamentous injuries. Philadelphia, Saunders, 1992, p 1643.
19. Hohl M, Larson RL, Jones DC: Fractures and dislocations of the knee. In Rockwood CA Jr, Green DP (eds): Fractures in adults. 2nd Ed. Philadelphia, JB Lippincott, 1984, p 1429.
20. Lewis SL, Pozo JL, Muirhead-Allwood WFG: Coronal fractures of the lateral femoral condyle. J Bone Joint Surg [Br] 71:118, 1989.
21. Lotke PA, Ecker ML: Transverse fractures of the patella. Clin Orthop 158:180, 1981.
22. Mason RW, Moore TE, Walker CW, et al: Patellar fatigue fractures. Skeletal Radiol 25:329, 1996.
23. Bates DG, Hresko MT, Jaramillo D: Patellar sleeve fracture: Demonstration

with MR imaging. Radiology 193:825, 1994.

24. Lloyd-Roberts GC, Jackson AM, Albert JS: Avulsion of the distal pole of the patella in cerebral palsy: A cause of deteriorating gait. J Bone Joint Surg [Br] 67:252, 1985.
25. Anglen JO, Healy WL: Tibial plateau fractures. Orthopedics 11:1527, 1988.
26. Tscherne H, Lobenhoffer P: Tibial plateau fractures: Management and expected results. Clin Orthop 292:87, 1993.
27. Barrow BA, Fajman WA, Parker LM, et al: Tibial plateau fractures: Evaluation with MR imaging. RadioGraphics 14:553, 1994.
28. Sonin AH, Fitzgerald SW, Hoff FL, et al: MR imaging of the posterior cruciate ligament: Normal, abnormal, and associated injury patterns. RadioGraphics 15:551, 1995.
29. Bock GW, Bosch E, Mishra DK, et al: The healed Segond fracture: A characteristic residual bone excrescence. Skeletal Radiol 23:555, 1994.
30. Kleinman PK, Marks SC Jr: A regional approach to the classic metaphyseal lesion in abused infants: The distal femur. AJR 170:43, 1998.
31. Kleinman PK, Marks SC Jr: A regional approach to the metaphyseal lesion in abused infants: Proximal tibia. AJR 166:421, 1996.
32. Harcke HT, Snyder M, Caro PA, et al: Growth plate of the normal knee: Evaluation with MR imaging. Radiology 183:119, 1992.
33. Frankl U, Waisilewski SA, Healy WL: Avulsion fracture of the tibial tubercle with avulsion of the patellar ligament: Report of two cases. J Bone Joint Surg [Am] 72:1411, 1990.
34. Ogden JA, Tross RB, Murphy MJ: Fractures of the tibial tuberosity in adolescents. J Bone Joint Surg [Am] 62:205, 1980.
35. Kujala UM, Kvist M, Heinonen O: Osgood-Schlatter’s disease in adolescent athletes: Retrospective study of incidence and duration. Am J Sports Med 13:236, 1985.
36. Milgram JW: Injury to articular cartilage joint surfaces: Displaced fractures of underlying bone. Clin Orthop 206:236, 1986.
37. Hodler J, Resnick D: Current status of imaging of articular cartilage. Skeletal Radiol 25:703, 1996.
38. Milgram JW: Radiological and pathological manifestations of osteochondritis dissecans of the distal femur: A study of 50 cases. Radiology 126:305, 1978.
39. Brossman J, Preidler K-W, Baenen B, et al: Imaging of osseous and cartilaginous intraarticular bodies in the knee: Comparison of MR imaging and MR arthrography with CT and CT arthrography in cadavers. Radiology 200:509, 1996.
40. DeSmet AA, Ilahi OA, Graf BK: Untreated osteochondritis dissecans of the femoral condyles: Prediction of patient outcome using radiographic and MR findings. Skeletal Radiol 26:463, 1997.
41. Pfeiffer WH, Gross ML, Seeger LL: Osteochondritis dissecans of the patella: MRI evaluation and a case report. Clin Orthop 271:207, 1991.
42. Kaufman SL, Martin LG: Arterial injuries associated with complete dislocation of the knee. Radiology 184:153, 1992.
43. Yu JS, Goodwin D, Salonen D, et al: Complete dislocation of the knee: Spectrum of associated soft-tissue injuries depicted by MR imaging. AJR 164:135, 1995.
44. Kirsch MD, Fitzgerald SW, Friedman H, et al: Transient lateral patellar dislocation: Diagnosis with MR imaging. AJR 161:109, 1993.
45. Kaneko K, De Mony EH, Robinson AE: Distribution of joint effusion in patients with knee joint disorders: MRI assessment. Clin Imaging 17:176, 1993.
46. Butt WP, Lederman H, Chuang S: Radiology of the suprapatellar region. Clin Radiol 34:511, 1983.
47. Maffulli N, Binfield PM, King JB, et al: Acute hemarthrosis of the knee in athletes: A prospective study of 106 cases. J Bone Joint Surg [Br] 75:945, 1993.
48. Kier R, McCarthy SM: Lipohemarthrosis of the knee: MR imaging. J Comput Assist Tomogr 14:395, 1990.
49. Lugo-Olivieri CH, Scott WW Jr, Zerhouni EA: Fluid-fluid levels in injured knees: Do they always represent lipohemarthrosis? Radiology 198:499, 1996.
50. Ryu KN, Jaovisidha S, De Maeseneer M, et al: Evolving stages of lipohemarthrosis of the knee: Sequential magnetic resonance imaging findings in cadavers with clinical correlation. Invest Radiol 32:7, 1997.
51. Janzen DL, Peterfy CG, Forbes JR, et al: Cystic lesions around the knee joint: MR imaging findings. AJR 163:155, 1994.
52. Butler MG, Fuchigami KD, Chako A: MRI of posterior knee masses. Skeletal Radiol 25:309, 1996.
53. Huang G-S, Chan WP, Taylor JAM, et al: Ganglion cysts of the cruciate ligaments: MR findings with clinical correlation. Acta Radiol 43:419, 2002.
54. Nokes SR, Koonce TW, Montanez J: Ganglion cysts of the cruciate ligaments of the knee: Recognition on MR images and CT-guided aspiration. AJR 162:1503, 1994.
55. Johnson DP, Eastwood DM, Witherow PJ: Symptomatic synovial plicae of the knee. J Bone Joint Surg [Am] 75:1485, 1993.
56. Myllymäki T, Tikkakoski T, Typpö T, et al: Carpet-layer’s knee: An ultrasonographic study. Acta Radiol Diagn 34:496, 1993.
57. Flandry F, McCann SB, Hughston JC, et al: Roentgenographic findings in pigmented villonodular synovitis of the knee. Clin Orthop 247:208, 1989.
58. Hughes TH, Sartoris DJ, Schweitzer ME, et al: Pigmented villonodular synovitis: MRI characteristics. Skeletal Radiol 24:7, 1995.
59. Kramer J, Recht M, Deely DM, et al: MR appearance of idiopathic synovial osteochondromatosis. J Comput Assist Tomogr 17:772, 1993.
60. Hodler J, Haghighi P, Pathria MN, et al: Meniscal changes in the elderly: Correlation of MR imaging and histologic findings. Radiology 184:221, 1992.
61. Stark JE, Siegel MJ, Weinberger E, et al: Discoid menisci in children: MR features. J Comp Assist Tomogr 19: 608, 1995.
62. Tyson LL, Daughters TC Jr, Ryu RKN, et al: MRI appearance of meniscal cysts. Skeletal Radiol 24:421, 1995.
63. Yu JS, Resnick D: Meniscal ossicle: MR imaging appearance in three patients. Skeletal Radiol 23:637, 1994.
64. Schnarkowski P, Tirman PFJ, Fuchigama KD, et al: Meniscal ossicle: Radiographic and MR imaging findings. Radiology 196:47, 1995.
65. Stoller DW, Martin C, Crues JV III, et al: Meniscal tears: Pathologic correlation with MR imaging. Radiology 163:731, 1987.
66. Mesgarzadeh M, Moyer R, Leder DS, et al: MR imaging of the knee: Expanded classification and pitfalls in the interpretation of meniscal tears. RadioGraphics 13:489, 1993.
67. Firooznia H, Golimbu C, Rafii M: MR imaging of the menisci: Fundamentals of anatomy and pathology. MRI Clin North Am 2:325, 1994.
68. Wright DH, De Smet AA, Norris M: Bucket-handle tears of the medial and lateral menisci of the knee: Value of MR imaging in detecting displaced fragments. AJR 165:621, 1995.
69. Schweitzer ME, Tran D, Deely DM, et al: Medial collateral ligament injuries: Evaluation of multiple signs, prevalence and location of associated bone bruises, and assessment with MR imaging. Radiology 194:825, 1995.
70. Garvin GJ, Munk PL, Vellet AD: Tears of the medial collateral ligament: Magnetic resonance imaging findings and associated injuries. J Can Assoc Radiol 44:199, 1993.
71. Ruiz ME, Erickson SJ: Medial and lateral supporting structures of the knee: Normal MR imaging anatomy and pathologic findings. MRI Clin North Am 2:381, 1994.
72. Speer KP, Warren RF, Wickiewicz TL, et al: Observations on the injury mechanism of anterior cruciate ligament tears in skiers. Am J Sports Med 23:77, 1995.
73. Liu SH, Osti L, Henry M, et al: The diagnosis of acute complete tears of the anterior cruciate ligament: Comparison of MRI, arthrometry, and clinical examination. J Bone Joint Surg [Br] 77:586, 1995.
74. Yu JS, Bosch E, Pathria MN, et al: Deep lateral femoral sulcus: Study of 124 patients with anterior cruciate ligament tear. Emerg Radiol 2:129, 1995.

75. Brandser EA, Riley MA, Berbaum KS, et al: MR imaging of anterior cruciate ligament injury: Independent value of primary and secondary signs. AJR 167:121, 1996.
76. Sonin AH, Fitzgerald SW, Friedman H, et al: Posterior cruciate ligament injury: MR imaging diagnosis and patterns of injury. Radiology 190:455, 1994.
77. Johnson DP, Wekely CJ, Watt I: Magnetic resonance imaging of patellar tendinitis. J Bone Joint Surg [Br] 78: 452, 1996.
78. Yu JS, Popp JE, Kaeding CC, et al: Correlation of MR imaging and pathologic findings in athletes undergoing surgery for patellar tendinitis. AJR 165:115, 1995.
79. Siwek CW, Rao JP: Ruptures of the extensor mechanism of the knee joint. J Bone Joint Surg [Am] 74:435, 1992.
80. Kuivila TE, Brems JJ: Diagnosis of acute rupture of the quadriceps tendon by magnetic resonance imaging: A case report. Clin Orthop 262:236, 1991.
81. Berg EE, Mason SL, Lucas MJ: Patellar height ratios: A comparison of four measurement methods. Am J Sports Med 24:218, 1996.
82. Shellock FG, Mink JH, Deutsch AL, et al: Patellofemoral joint: Identification of abnormalities with active-movement, “unloaded” versus “loaded” kinematic MR imaging techniques. Radiology 188:575, 1993.
83. Brossman J, Muhle C, Büll CC, et al: Evaluation of patellar tracking in patients with suspected patellar malalignment: Cine MR imaging vs. arthroscopy. AJR 162:361, 1994.
84. Ficat RP, Hungerford DS: Disorders of the patello-femoral joint. Baltimore, Williams & Wilkins, 1977.
85. Conway WF, Hayes CW, Loughran T, et al: Cross-sectional imaging of the patellofemoral joint and surrounding structures. RadioGraphics 11:195, 1991.
86. Barrett JP Jr, Rashkoff E, Sirna EC, et al: Correlation of roentgenographic patterns and clinical manifestations of symptomatic idiopathic osteoarthritis of the knee. Clin Orthop 253:179, 1990.
87. Preidler KW, Resnick D: Imaging of osteoarthritis. Radiol Clin North Am 34:259, 1996.
88. Resnick D, Shaul SR, Robins JM: Diffuse idiopathic skeletal hyperostosis (DISH): Forestier’s disease with extraspinal manifestations. Radiology 115:513, 1975.
89. Resnick D: Diagnosis of bone and joint disorders. 4th Ed. Philadelphia, Saunders, 2002.
90. Fiszman P, Ansell BM, Renton P: Radiological assessment of knees in juvenile chronic arthritis (juvenile rheumatoid arthritis). Scand J Rheumatol 10:145, 1981.
91. Azouz EM, Duffy CM: Juvenile spondyloarthropathies: Clinical manifestations and medical imaging. Skeletal Radiol 24:399, 1995.
92. Schurman JR II, Wilde AH: Total knee replacement after spontaneous osseous ankylosis: A report of three cases. J Bone Joint Surg [Am] 72:455, 1990.
93. Martel W, Braunstein EM, Borlaza G, et al: Radiologic features of Reiter’s syndrome. Radiology 132:1, 1979.
94. Pritchard CH, Berney S: Patellar tendon rupture in systemic lupus erythematosus. J Rheumatol 16:786, 1989.
95. Pachman LN: Juvenile dermatomyositis. Pediatr Clin North Am 33:1097, 1986.
96. Shiokawa S, Yasuda M, Kikuchi M, et al: Mixed connective tissue disease associated with lupus lymphadenitis. J Rheumatol 20:147, 1993.
97. Basanti M, Hardin JG: Undifferentiated, overlapping, and mixed connective tissue diseases. Am J Med Sci 305:114, 1993.
98. Resnick D, Niwayama G, Georgen TG, et al: Clinical, radiographic and pathologic abnormalities in calcium pyrophosphate dihydrate deposition disease (CPPD): Pseudogout. Radiology 122:1, 1977.
99. Mitrovic DR, Stankovic A, Iriarte-Borda O, et al: The prevalence of chondrocalcinosis in the human knee joint: An autopsy survey. J Rheumatol 15: 633, 1988.
100. Steinbach LS: Calcium pyrophosphate dihydrate and calcium hydroxyapatite crystal deposition diseases: Imaging perspectives. Radiol Clin N Am 42: 185, 2004.
101. Recht MP, Seragini F, Kramer J, et al: Isolated or dominant lesions of the patella in gout: A report of seven patients. Skeletal Radiol 23:113, 1994.
102. Faraawi R, Harth M, Kertesz A, et al: Arthritis in hemochromatosis. J Rheumatol 20:448, 1993.
103. Handelsman JE: The knee joint in hemophilia. Orthop Clin North Am 10:139, 1979.
104. Vincent GM, Amirault JD: Septic arthritis in the elderly. Clin Orthop 251:241, 1990.
105. Haygood TM, Williamson SL: Radiographic findings of extremity tuberculosis in childhood: Back to the future? RadioGraphics 14:561, 1994.
106. Rougraff BT, Kneisl JS, Simon MA: Skeletal metastases of unknown origin: A prospective study of a diagnostic strategy. J Bone Joint Surg [Am] 75:1276, 1993.
107. Kyle RA: Multiple myeloma: Review of 869 cases. Mayo Clin Proc 50:29, 1975.
108. Bloem JL, Mulder JD: Chondroblastoma: A clinical and radiological study of 104 cases. Skeletal Radiol 14:1, 1985.
109. Weatherall PT, Maale GE, Mendelsohn DB, et al: Chondroblastoma: Classic and confusing appearance at MR imaging. Radiology 190:467, 1994.
110. De Dios AMV, Bond JR, Shives TC, et al: Aneurysmal bone cyst: A clinicopathologic study of 238 cases. Cancer 69:2921, 1992.
111. Stuhl MA, Moser RP Jr, Vinh TN, et al: Paget’s disease of the patella. Skeletal Radiol 19:407, 1990.
112. Mirra JM, Brien EW, Tehranzadeh J: Paget’s disease of bone: Review with emphasis on radiologic features. Part II. Skeletal Radiol 24:173, 1995.
113. Mankin HJ: Rickets, osteomalacia, and renal osteodystrophy. Orthop Clin North Am 21:81, 1990.
114. Pineda C: Diagnostic imaging in hypertrophic osteoarthropathy. Clin Exp Rheumatol 10:27, 1992.
115. Sprague PL: Epiphyseo-metaphyseal cupping following infantile scurvy. Pediatr Radiol 4:122, 1976.
116. Kricun ME, Resnick D: Patellofemoral abnormalities in renal osteodystrophy. Radiology 143:667, 1982.
117. Tigges S, Nance EP, Carpenter WA, et al: Renal osteodystrophy: Imaging findings that mimic those of other diseases. AJR 165:143, 1995.
118. Chew FS, Huang-Hellinger F: Brown tumor. AJR 160:752, 1993.
119. Wolfson BH, Capitanio MA: The wide spectrum of renal osteodystrophy in children. CRC Crit Rev Diagn Imaging 27:297, 1987.
120. Bjorkengren AG, AlRowaih A, Lindstrand A, et al: Spontaneous osteonecrosis of the knee: Value of MR imaging in determining prognosis. AJR 154:331, 1990.
121. Phillips KA, Nance EP Jr, Rodriguez RM, et al: Avascular necrosis of bone: A manifestation of Cushing’s disease. South Med J 79:825, 1986.
122. Lee KR, Cox GG, Neff JR, et al: Cystic masses of the knee: Arthrographic and CT evaluation. AJR 148:329, 1987.
123. Applegate KE, Finkelstein MS, Gross GW: Child abuse: Imaging findings pertaining to the musculoskeletal system. Semin Musculoskeletal Radiol 3:351, 1999.
124. Bencardion JT, Hassankhani A: Calcium pyrophosphate dihydrate crystal deposition disease. Semin Musculoskeletal Radiol 7:175, 2003.
125. Kerr R: Imaging of musculoskeletal complications of hemophilia. Semin Musculoskeletal Radiol 7:127, 2003.
126. Greenspan A, Tehranzadeh J: Imaging of infectious arthritis. Radiol Clin N Am 39:267, 2001.
127. Al-Nakshabandi NA, Ryan AG, Choudur H, et al: Pigmented villonodular synovitis. Clin Radiol 59:414, 2004.
128. Abreu M, Johnson K, Chung C, et al: Calcification in calcium pyrophosphate dihydrate (CPPD) crystalline deposits in the knee: Anatomic, radiographic, MR imaging, and histologic study in cadavers. Skeletal Radiol 33:392, 2004.
129. Toye LR, Cummings PD, Armendariz G: Adult tibial intercondylar eminence fracture: Evaluation with MR imaging. Skeletal Radiol 31:46, 2002.
130. Davies NH, Niall D, King LJ, et al: Magnetic resonance imaging of bone bruising in the acutely injured knee—short term outcome. Clin Radiol 59: 439, 2004.

131. Mandalia V, Fogg AJB, Chari R, et al: Bone bruising of the knee. Clin Radiol 60:627, 2005.
132. Kijowski R, Blankenbaker DG, Stanton PT, et al: Radiographic findings of osteoarthritis versus arthroscopic findings of articular cartilage degeneration of the tibiofemoral joint. Radiology 239:818, 2006.
133. Yamanaka N, Takahashi T, Ichikawa N, et al: Posterior-anterior weight-bearing radiograph in 15° knee flexion in medial osteoarthritis. Skeletal Radiol 32:28, 2003.
134. Ditchfield A, Sampson MA, Taylor GR: Ultrasound diagnosis of sleeve fracture of the patella. Clin Radiol 55:721, 2000.
135. Peace KAL, Lee JC, Healy J: Imaging of the infrapatellar tendon in the elite athlete. Clin Radiol 61:570, 2006.
136. Elias DA, White LM: Imaging of patellofemoral disorders. Clin Radiol 59:543, 2004.
137. Forster BB, Lee JS, Kelly S, et al: Proximal tibiofibular joint: An often-forgotten cause of lateral knee pain. AJR 188:W359, 2007.
138. Kavanaugh EC, Zoga A, Omar I: MRI findings in bipartite patella. Skeletal Radiol 36:209, 2007.
139. Mansour R, Kausik M, McNally E: MRI of knee injury. Semin Musculoskeletal Radiol 10:328, 2006.
140. Hirano A, Fukubayashi T, Ishii T, et al: Magnetic resonance imaging of Osgood-Schlatter disease: The course of the disease. Skeletal Radiol 31:334, 2002.
141. Mendes LFA, Pretterklieber ML, Cho JH, et al: Pellegrini-Stieda disease: A heterogenous disorder not synonymous with ossification/calcification of the tibial collateral ligament-anatomic and imaging investigation. Skeletal Radiol 35:916, 2006.
142. Winterbottom AP, Shaw AS: Imaging patients with myeloma. Clin Radiol 64:1, 2009.

CHAPTER 10

Tibia and Fibula

1. Horsfield D, Jones SN: Assessment of inequality in length of the lower limb. Radiography 52:233, 1986.
2. Huurman WW, Jacobsen FS, Anderson JC, et al: Limb-length discrepancy measured with computerized axial tomographic equipment. J Bone Joint Surg [Am] 69:699, 1987.
3. Mannello DM: Leg length inequality. J Manipulative Physiol Ther 15:576, 1992.
4. Greene WB: Infantile tibia vara. J Bone Joint Surg [Am] 75:130, 1993.
5. Kovanlikaya A, Loro ML, Gilsanz V: Pathogenesis of osteosclerosis in autosomal dominant osteopetrosis. AJR 168:929, 1997.
6. Benli IT, Akalin S, Boysan E, et al: Epidemiological, clinical, and radiological aspects of osteopoikilosis. J Bone Joint Surg [Br] 74:504, 1992.
7. Bass HN, Weiner JR, Goldman A, et al: Osteopathia striata syndrome: Clinical, genetic, and radiologic considerations. Clin Pediatr 19:369, 1980.
8. Campbell CJ, Papademetriou T, Bonfiglio M: Melorheostosis: A report of the clinical, roentgenographic, and pathological findings in fourteen cases. J Bone Joint Surg [Am] 50:1281, 1968.
9. Yu JS, Resnick D, Vaughan LM, et al: Melorheostosis with an ossified soft tissue mass. Skeletal Radiol 24:367, 1995.
10. Whyte MP, Murphy WA, Fallon MD, et al: Mixed-sclerosing-bone-dystrophy: Report of a case and review of the literature. Skeletal Radiol 6:95, 1981.
11. Hanscom DA, Winter RB, Lutter L, et al: Osteogenesis imperfecta: Radiographic classification, natural history and treatment of spinal deformity. J Bone Joint Surg [Am] 74:598, 1992.
12. Kumar B, Murphy WA, Whyte MP: Progressive diaphyseal dysplasia (Englemann disease): Scintigraphic-radiographic-clinical correlations. Radiology 140:87, 1981.
13. Gershuni DH, Skyhar MJ, Thompson B, et al: A comparison of conventional radiography and computed tomography in the evaluation of spiral fractures of the tibia. J Bone Joint Surg [Am] 67:1388, 1985.
14. Sarmiento A, Gersten LM, Sobol PA, et al: Tibial shaft fractures treated with functional brace: Experience with 780 fractures. J Bone Joint Surg [Br] 71:602, 1989.
15. Conway JJ, Poznanski AP: Acute compression injuries of bone, or the toddler's fracture revisited. Pediatr Radiol 17:85, 1987.
16. Daffner RH, Martinez S, Gehweiler JA Jr, et al: Stress fractures of the proximal tibia in runners. Radiology 142:63, 1982.
17. Datir AP, Saini A, Connell A, et al: Stress-related bone injuries with emphasis on MRI. Clin Radiol 62:828, 2007.
18. Mulligan ME, Shanley DJ: Supramalleolar fatigue fractures of the tibia. Skeletal Radiol 25:325, 1996.
19. Davies AM, Evans N, Grimer RJ: Fatigue fractures of the proximal tibia simulating malignancy. Br J Radiol 61: 903, 1988.
20. Umans HR, Kaye JJ: Longitudinal stress fractures of the tibia: Diagnosis by magnetic resonance imaging. Skeletal Radiol 25:319, 1996.
21. Reading JM, Sheehan NJ: Spontaneous fractures of the lower limb in chronic rheumatoid arthritis. J Orthop Rheumatol 4:173, 1991.
22. Schneider R, Kaye JJ: Insufficiency fractures and stress fractures of the long bones occurring in patients with rheumatoid arthritis. Radiology 116: 595, 1975.
23. Lock TR, Schaffer JJ, Manoli A II: Maisonneuve fracture: Case report of a missed diagnosis. Ann Emerg Med 16:805, 1987.
24. Nuovo MA, Norman A, Chumas A, et al: Myositis ossificans with atypical clinical, radiographic, or pathologic findings: A review of 23 cases. Skeletal Radiol 21:87, 1992.
25. Neugut AI, Casper ES, Godwin A, et al: Osteoblastic metastases in renal cell carcinoma. Br J Radiol 54:1002, 1981.
26. Greenspan A, Norman A: Osteolytic cortical destruction: An unusual pattern of skeletal metastasis. Skeletal Radiol 17:402, 1988.
27. Eklof O, Mortensson W, Sandstedt B, et al: Bone metastases in Wilm's tumor: Occurrence and radiological appearance. Ann Radiol 27:97, 1984.
28. Dahlin DC, Unni KK: Osteosarcoma of bone and its important recognizable varieties. Am J Surg Pathol 1:61, 1977.
29. Ritschl P, Wurnig C, Lechner G, et al: Parosteal osteosarcoma: 2-23-year follow-up of 33 patients. Acta Orthop Scand 62:195, 1991.
30. Mitchell M, Ackerman LV: Metastatic and pseudomalignant osteoblastoma: A report of two unusual cases. Skeletal Radiol 15:213, 1986.
31. Henderson ED, Dahlin DC: Chondrosarcoma of bone—a study of two hundred and eighty-eight cases. J Bone Joint Surg [Am] 45:1450, 1963.
32. Dahlin DC: Giant cell tumor of bone: Highlights of 407 cases. AJR 144:955, 1985.
33. Huvos AG, Higinbotham NL: Primary fibrosarcoma of bone: A clinicopathologic study of 130 patients. Cancer 35:837, 1975.
34. Taconis WK, Mulder JD: Fibrosarcoma and malignant fibrous histiocytoma of long bones: Radiographic features and grading. Skeletal Radiol 11:237, 1984.
35. Kahn LB: Adamantinoma, osteofibrous dysplasia and differentiated adamantinoma. Skeletal Radiol 32:245, 2003.
36. Dahlin DC, Coventry MB, Scanlon PW: Ewing's sarcoma: A critical analysis of 165 cases. J Bone Joint Surg [Am] 43:185, 1961.
37. Kyle RA: Multiple myeloma: Review of 869 cases. Mayo Clin Proc 50:29, 1975.
38. Franczyk J, Samuels T, Rubenstein J, et al: Skeletal lymphoma. J Can Assoc Radiol 40:75, 1989.
39. Hermann G, Klein MJ, Abdelwahab IF, et al: MRI appearance of primary non-Hodgkin's lymphoma of bone. Skeletal Radiol 26:629, 1997.
40. Clayton F, Butler JJ, Ayala AG, et al: Non-Hodgkin's lymphoma in bone: Pathologic and radiologic features with clinical correlates. Cancer 60:2494, 1987.
41. Benz G, Brandeis WE, Willich E: Radiological aspects of leukemia in childhood: An analysis of 89 children. Pediatr Radiol 4:201, 1976.
42. Greenspan A: Bone island (enostosis): Current concept—a review. Skeletal Radiol 24:111, 1995.
43. Cohen MD, Harrington TM, Ginsbury WW: Osteoid osteoma: 95 cases and a

review of the literature. Semin Arthritis Rheum 12:265, 1983.

44. Shankman S, Desai P, Beltran J: Subperiosteal osteoid osteoma: Radiographic and pathologic manifestations. Skeletal Radiol 26:457, 1997.
45. Kayser F, Resnick D, Haghighi P, et al: Evidence of the subperiosteal origin of osteoid osteomas in tubular bones: Analysis by CT and MR imaging. AJR 170:609, 1998.
46. Lichtenstein L, Sawyer WF: Benign osteoblastoma: Further observations and report of twenty additional cases. J Bone Joint Surg [Am] 46:755, 1964.
47. Wang J-W, Shih C-H, Chen W-J: Osteofibrous dysplasia (ossifying fibroma of long bones): A report of four cases and review of the literature. Clin Orthop 278:235, 1992.
48. Schiller AL: Diagnosis of borderline cartilage lesions of bone. Semin Diagn Pathol 2:42, 1985.
49. Bloem JL, Mulder JD: Chondroblastoma: A clinical and radiological study of 104 cases. Skeletal Radiol 14:1, 1985.
50. Weatherall PT, Maale GE, Mendelsohn DB, et al: Chondroblastoma: Classic and confusing appearance at MR imaging. Radiology 190:467, 1994.
51. Wilson AJ, Kyriakos M, Ackerman LV: Chondromyxoid fibroma: Radiographic appearance in 38 cases and in a review of the literature. Radiology 179:513, 1991.
52. Milgram JW: The origins of osteochondromas and enchondromas: A histopathologic study. Clin Orthop 174:264, 1983.
53. Karasick D, Schweitzer ME, Eschelman DJ: Symptomatic osteochondromas: Imaging features. AJR 168:1507, 1997.
54. Schmale GA, Conrad EV, Raskind WH: The natural history of hereditary multiple exostosis. J Bone Joint Surg [Am] 76:986, 1994.
55. Ritschl P, Karnel F, Hajek P: Fibrous metaphyseal defects—determination of their origin and natural history using a radiomorphological study. Skeletal Radiol 17:8, 1988.
56. Ehara S, Tamakawa Y, Nishida J, et al: Cortical defect of the distal fibula: Variant of ossification. Radiology 197:447, 1995.
57. Tehranzadeh J, Murphy BJ, Mnaymneh W: Giant cell tumor of the proximal tibia: MR and CT appearance. J Comput Assist Tomogr 13:282, 1989.
58. Milgram JW: Intraosseous lipoma: A clinicopathologic study of 66 cases. Clin Orthop 231:277, 1988.
59. Kenan S, Abdelwahab IF, Klein MJ, et al: Hemangiomas of the long tubular bones. Clin Orthop 280:256, 1992.
60. Chigira M, Maehara S, Arita S, et al: The aetiology and treatment of simple bone cysts. J Bone Joint Surg [Br] 65:633, 1983.
61. De Dios AMV, Bond JR, Shives TC, et al: Aneurysmal bone cyst: A clinicopathologic study of 238 cases. Cancer 69:2921, 1992.
62. Bone HG, Kleerekoper M: Paget's disease of bone. J Clin Endocrinol Metab 7:1179, 1992.
63. Mirra JM, Brien EW, Tehranzadeh J: Paget's disease of bone: Review with emphasis on radiologic features, part II. Skeletal Radiol 24:173, 1995.
64. Yochum TR, Rowe LJ: Essentials of skeletal radiology. 3rd Ed. Baltimore, Williams & Wilkins, 2004.
65. Crawford AH Jr, Bogamery N: Osseous manifestations of neurofibromatosis in childhood. J Pediatr Orthop 6:72, 1986.
66. Morrissy RT: Congenital pseudoarthrosis of the tibia. Clin Orthop 166: 14, 1982.
67. Gibson MJ, Middlemiss JH: Fibrous dysplasia of bone. Br J Radiol 44:1, 1971.
68. Kilpatrick SE, Wenger DE, Gilchrist GS, et al: Langerhans' cell histiocytosis (histiocytosis X) of bone: A clinicopathologic analysis of 263 pediatric and adult cases. Cancer 76:2471, 1995.
69. Taylor JAM, Resnick D, Sartoris DJ: Radiographic-pathologic correlation. In Sartoris DJ (ed): Osteoporosis: diagnosis and treatment. New York, Marcel Dekker, 1996, p 147.
70. Schwarzman RJ, McLellan TL: Reflex sympathetic dystrophy: A review. Arch Neurol 44:555, 1987.
71. Mankin HJ: Rickets, osteomalacia, and renal osteodystrophy. Orthop Clin North Am 21:81, 1990.
72. Chew FS, Huang-Hellinger F: Brown tumor. AJR 160:752, 1993.
73. Resnick D, Niwayama G: Parathyroid disorders and renal osteodystrophy. In Resnick D (ed): Diagnosis of bone and joint disorders. 4th Ed. Philadelphia, Saunders, 2002, p 2043.
74. Tigges S, Nance EP, Carpenter WA, et al: Renal osteodystrophy: Imaging findings that mimic those of other diseases. AJR 165:143, 1995.
75. Bronsky D, Kushner DS, Dubin A, et al: Idiopathic hypoparathyroidism and pseudohypoparathyroidism: Case reports and review of the literature. Medicine 37:317, 1958.
76. Lambert RGW, Becker EJ: Diffuse skeletal hyperostosis in idiopathic hypoparathyroidism. Clin Radiol 40:212, 1989.
77. Nerubay J, Pilderwasser D: Spontaneous bilateral distal femoral physiology due to scurvy. Acta Orthop Scand 55: 18, 1984.
78. Sprague PL: Epiphyseo-metaphyseal cupping following infantile scurvy. Pediatr Radiol 4:122, 1976.
79. Bell RS, Mankin HJ, Doppelt SH: Osteomyelitis in Gaucher's disease. J Bone Joint Surg [Am] 68:1380, 1986.
80. Resnick D, Niwayama G: Enostosis, hyperostosis, and periostitis. In Resnick D (ed): Diagnosis of bone and joint disorders. 4th Ed. Philadelphia, Saunders, 2002, p 4844.
81. Pineda C: Diagnostic imaging in hypertrophic osteoarthropathy. Clin Exp Rheumatol 10:27, 1992.
82. Schumacher HR Jr: Hypertrophic osteoarthropathy: Rheumatologic manifestations. Clin Exp Rheumatol 10:35, 1992.
83. Ogden JA: Growth slowdown and arrest lines. J Pediatr Orthop 4:409, 1984.
84. Weinberger A, Kaplan JG, Myers AR: Extensive soft tissue calcification (calcinosis universalis) in systemic lupus erythematosus. Ann Rheum Dis 38: 384, 1979.
85. Davidson JK: Dysbaric disorders: Aseptic bone necrosis in tunnel workers and divers. Clin Rheumatol 3:1, 1989.
86. Gold RH, Hawkins RA, Katz RD: Bacterial osteomyelitis: Findings on plain radiography, CT, MR, and scintigraphy. AJR 157:365, 1991.
87. Tumeh SS, Aliabadi P, Weissman BN, et al: Disease activity in osteomyelitis: Role of radiography. Radiology 165: 781, 1987.
88. Stephens MM, MacAuley P: Brodie's abscess: A long-term review. Clin Orthop 234:211, 1988.
89. Rosenberg ZS, Shankman S, Klein M, et al: Chronic recurrent multifocal osteomyelitis. AJR 151:142, 1988.
90. Jurik AG, Egund N: MRI in chronic recurrent multifocal osteomyelitis. Skeletal Radiol 26:230, 1997.
91. Haygood T, Williamson SL: Radiographic findings of extremity tuberculosis in childhood: Back to the future? Radiographics 14:561, 1994.
92. Sachdev M, Bery K, Chawla S: Osseous manifestations in congenital syphilis: A study of 55 cases. Clin Radiol 33:319, 1982.
93. Dunn RA, Zenker PN: Why radiographs are useful in evaluation of neonates suspected of having congenital syphilis. Radiology 182:639, 1992.
94. Karat S, Karat ABA, Foster R: Radiological changes in the bones of the limbs in leprosy. Lepr Rev 39:147, 1968.
95. Cockshott WP, Martin R, Friedman L, et al: Focal fibrocartilaginous dysplasia and tibia vara: A case report. Skeletal Radiol 23:333, 1994.
96. Anderson MW, Ugalde V, Batt M, et al: Shin splints: MR appearance in a preliminary study. Radiology 204:177, 1997.
97. Kaim AH, Hugli R, Bonél HM, et al: Chondroblastoma and clear cell chondrosarcoma: Radiological and MRI characteristics with histopathological correlation. Skeletal Radiol 31:88, 2002.
98. Spitz DJ, Newberg AH: Imaging of stress fractures in the athlete. Radiol Clin N Am 40:313, 2002.
99. Propeck T, Bullard MA, Lin J, et al: Radiologic-pathologic correlation of intraosseous lipomas. AJR 175:673, 2000.
100. Hwang S: Imaging of lymphoma of the musculoskeletal system. Radiol Clin N Am 46:379, 2008.
101. Christian S, Kraas J, Conway WF: Musculoskeletal infections. Semin Roentgenol 42:92, 2007.

102. Marin C, Sanchez-Alegre ML, Gallego C, et al: Magnetic resonance imaging of osteoarticular infections in children. Curr Probl Diagn Radiol 33:43, 2004.
103. Ruzek KA, Wenger DE: The multiple faces of lymphoma of the musculoskeletal system. Skeletal Radiol 33:1, 2004.
104. Stoker DJ: Osteopetrosis. Semin Musculoskel Radiol 6:299, 2002.
105. Andresen KJ, Sundaram M, Unni KK, et al: Imaging features of low-grade central osteosarcoma of the long bones and pelvis. Skeletal Radiol 33:373, 2004.
106. Suresh S, Saifuddin A: Radiological appearances of appendicular osteosarcoma: A comprehensive pictorial review. Clin Radiol 62:314, 2007.
107. Whitehouse RW: Paget's disease of bone. Semin Musculoskeletal Radiol 6:313, 2002.
108. Whitten CR, Saifuddin A: MRI of Paget's disease of bone. Clin Radiol 58:763, 2003.
109. Berry JL, Davies M, Mee AP: Vitamin D metabolism, rickets and osteomalacia. Semin Musculoskeletal Radiol 6:173, 2002.
110. Wenstrup RJ, Roca-Espiau M, Weinreb NJ, et al: Skeletal aspects of Gaucher disease: A review. Br J Radiol 75 (Suppl. 1):A2, 2002.
111. Ameen S, Staub L, Ulrich, et al: Harris lines of the tibia across the centuries: A comparison of two populations, medieval and contemporary in Central Europe. Skeletal Radiol 34:279, 2005.
112. Kiuru MJ, Pihlajamäki HK, Ahuvuo JA. Bone stress injuries. Acta Radiol 45:317, 2004.
113. Craig JG, Widman D, van Holsbeeck M: Longitudinal stress fracture: Patterns of edema and the importance of the nutrient foramen. Skeletal Radiol 32:22, 2003.
114. Gaeta M, Minutoli F, Vinci S, et al: High-resolution CT grading of tibial stress reactions in distance runners. AJR 187:789, 2006.
115. Gaeta M, Minutoli F, Scribano E, et al: CT and MR imaging findings in athletes with early tibial stress injuries: Comparison with bone scintigraphy findings and emphasis on cortical abnormalities. Radiology 235:553, 2005.
116. Woods M, Kijowski R, Sanford M, et al: Magnetic resonance imaging findings in patients with fibular stress fractures. Skeletal Radiol 37:835, 2008.
117. Tigges S, Fajman WA: Injuries about the knee and tibial/fibular shafts. Semin Musculoskeletal Radiol 4:221, 2000.
118. Park HS, Kim JR, Lee SY: Symptomatic giant (10-cm) bone island of the tibia. Skeletal Radiol 34:347, 2005.
119. Winterbottom AP, Shaw AS: Imaging patients with myeloma. Clin Radiol 64:1, 2009.

CHAPTER 11

Ankle and Foot

1. Edeiken J, Dalinka M, Karasick D: Edeiken's roentgen diagnosis of diseases of bone. 4th Ed. Baltimore, Williams & Wilkins, 1990.
2. Kahn SL, Gaskin CM, Sharp VL. Keats and Kahn's roentgen atlas of skeletal maturation. DVD-ROM Ed. Philadelphia, Lippincott Williams and Wilkins, 2007.
3. Greenfield GB: Radiology of bone diseases. 2nd Ed. Philadelphia, JB Lippincott, 1975.
4. Köhler A, Zimmer EA: Borderlands of normal and early pathologic findings in skeletal radiography. 4th Ed. New York, Thieme Medical Publishers, 1993.
5. Keats TE: Atlas of normal roentgen variants that may simulate disease, 6th Ed. Chicago, Year Book Medical Publishers, 1996.
6. Griffiths H, Wandtke J: Tibiotalar tilt—a new slant. Skeletal Radiol 6:193, 1981.
7. Forrester DM, Kricun ME, Kerr R: Imaging of the foot and ankle. Rockville, Md, Aspen, 1988.
8. Takakura Y, Tamai S, Masuhara K: Genesis of the ball-and-socket ankle. J Bone Joint Surg [Br] 68:834, 1986.
9. Wesely MS, Barenfeld PA, Shea JM, et al: The congenital cavus foot: A follow-up report. Bull Hosp Joint Dis 47:217, 1982.
10. Scott G, Wilson DW, Bentley G: Roentgenographic assessment in hallux valgus. Clin Orthop 267:143, 1991.
11. Eustace S, Williamson D, Wilson M, et al: Tendon shift in hallux valgus: Observations at MR imaging. Skeletal Radiol 25:519, 1996.
12. Bridges AL, Kou-Ching H, Singh A, et al: Fibrodysplasia (myositis) ossificans progressiva. Semin Arthritis Rheum 24:155, 1994.
13. Stormont DM, Peterson HA: The relative incidence of tarsal coalition. Clin Orthop 181:28, 1983.
14. Wechsler RJ, Schweitzer ME, Deely DM, et al: Tarsal coalition: Depiction and characterization with CT and MR imaging. Radiology 193:447, 1994.
15. Kumar SJ, Guille JT, Lee MS, et al: Osseous and non-osseous coalition of the middle facet of the talocalcaneal joint. J Bone Joint Surg [Am] 74:529, 1992.
16. Lateur LM, Van Hoe LR, Van Ghillewe KV, et al: Subtalar coalition: Diagnosis with the C sign on lateral radiographs of the ankle. Radiology 193:847, 1994.
17. Wakeley CJ, Johnson DP, Watt I: The value of MR imaging in the diagnosis of the os trigonum syndrome. Skeletal Radiol 25:133, 1996.
18. Karasick D, Schweitzer ME: The os trigonum syndrome: Imaging features. AJR 166:125, 1996.
19. Reichmister JP: The painful os intermetatarseum: A brief overview and case reports. Clin Orthop 153:201, 1980.
20. Smith AD, Carter JR, Marcus RE: The os vesalianum: An unusual cause of lateral foot pain: A case report and review of the literature. Orthopedics 7:86, 1984.
21. Lawson JP, Ogden JA, Sella E, et al: The painful accessory navicular. Skeletal Radiol 12:250, 1984.
22. Miller TT, Staron RB, Feldman F, et al: The symptomatic accessory tarsal navicular bone: Assessment with MR imaging. Radiology 195:849, 1995.
23. Taylor JAM, Sartoris DJ, Huang GS, et al: Painful conditions affecting the first metatarsal sesamoid bones. RadioGraphics 13:817, 1993.
24. Resnick D: Talar ridges, osteophytes, and beaks: A radiologic commentary. Radiology 151:329, 1984.
25. Lyritis G: Developmental disorders of the proximal epiphysis of the hallux. Skeletal Radiol 10:250, 1983.
26. Turra S, Frizziero P, Cagnoni G, et al: Macrodactyly of the foot associated with plexiform neurofibroma of the medial plantar nerve. J Pediatr Orthop 6:489, 1986.
27. Nogami H: Polydactyly and polysyndactyly of the fifth toe. Clin Orthop 204:261, 1986.
28. Laurent Y, Brombart M: Variation trecs rare de l'ossification des phalanges des orteils. J Belge Radiol 36:102, 1953.
29. Keret D, Spatz DK, Caro PA, et al: Dysplasia epiphysealis hemimelica: Diagnosis and treatment. J Pediatr Orthop 12:365, 1992.
30. Root L: The treatment of osteogenesis imperfecta. Orthop Clin North Am 15:775, 1984.
31. Benli IT, Akalin S, Boysan E, et al: Epidemiological, clinical, and radiological aspects of osteopoikilosis. J Bone Joint Surg [Br] 74:504, 1992.
32. Campbell CJ, Papademetriou T, Bonfiglio M: Melorheostosis: A report of the clinical, roentgenographic, and pathological findings in fourteen cases. J Bone Joint Surg [Am] 50:1281, 1968.
33. Yu JS, Resnick D, Vaughan LM, et al: Melorheostosis with an ossified soft tissue mass. Skeletal Radiol 24:367, 1995.
34. Joseph KN, Kane HA, Milner RS, et al: Orthopedic aspects of the Marfan phenotype. Clin Orthop 277:251, 1992.
35. Ainsworth SR, Aulicino PL: A survey of patients with Ehlers-Danlos syndrome. Clin Orthop 286:250, 1993.
36. Goldman AB, Kaye JJ: Macrodystrophia lipomatosa: Radiographic diagnosis. AJR 128:101, 1977.
37. Nielsen J Ø, Dons-Jenson H, S ø rensen HT: Lauge-Hansen classification of malleolar fractures: An assessment of the reproducibility in 118 cases. Acta Orthop Scan 61:385, 1990.
38. Verma S, Hamilton K, Hawkins HH, et al: Clinical application of the Ottawa ankle rules for the use of radiography in acute ankle injuries: An independent site assessment. AJR 169:825, 1997.
39. Lock TR, Schaffer JJ, Manoli A II: Maisonneuve fracture: Case report of a missed diagnosis. Ann Emerg Med 16:805, 1987.
40. Rogers LF. Radiology of skeletal trauma. 3rd Ed. New York, Churchill Livingstone, 2002.

41. Resnick D: Diagnosis of bone and joint disorders. 4th Ed. Philadelphia, Saunders, 2002.
42. Kleinman PK, Marks SC Jr: A regional approach to classic metaphyseal lesions in abused infants: The distal tibia. AJR 166:1207, 1996.
43. MacNealy GA, Rogers LF, Hernandez R, et al: Injuries of the distal tibial epiphysis: Systematic radiographic evaluation. AJR 138:683, 1982.
44. Rogers LF, Poznanski AK: Imaging of epiphyseal injuries. Radiology 191:297, 1994.
45. Petite P, Panuel M, Faure F, et al: Acute fracture of the distal tibial physis: Role of gradient-echo MR imaging versus plain film examination. AJR 166:1203, 1996.
46. Reading JM, Sheehan NJ: Spontaneous fractures of the lower limb in chronic rheumatoid arthritis. J Orthop Rheumatol 4:173, 1991.
47. Molinari M, Bertoldi L, De March L: Fracture-dislocation of the ankle with the fibula trapped behind the tibia: A case report. Acta Orthop Scand 61:471, 1990.
48. Wechsler RJ, Schweitzer ME, Karasick D, et al: Helical CT of calcaneal fractures: Technique and imaging features. Skeletal Radiol 27:1, 1998.
49. Renfrew DL, El-Khoury GY: Anterior process fractures of the calcaneus. Skeletal Radiol 14:121, 1985.
50. Brijs S, Brijs A: Calcaneal avulsion: A frequent traumatic foot lesion. Fortschr Rontgenstr 156:495, 1992.
51. Sneppen O, Christensen SB, Krogsoe O, et al: Fracture of the body of the talus. Acta Orthop Scand 48:317, 1977.
52. Wechsler RJ, Schweitzer ME, Karasick D, et al: Helical CT of talar fractures. Skeletal Radiol 26:137, 1997.
53. Loomer R, Fisher C, Lloyd-Smith R, et al: Osteochondral lesions of the talus. Am J Sports Med 21:13, 1993.
54. Zimmer TJ, Johnson KA: Subtalar dislocations. Clin Orthop 238:190, 1989.
55. Rogers LF, Campbell RE: Fractures and dislocations of the foot. Semin Roentgenol 12:157, 1978.
56. Dines DM, Hershon SJ, Smith N, et al: Isolated dorsomedial dislocation of the first ray at the medial cuneonavicular joint of the foot: A rare injury to the tarsus. Clin Orthop 186:162, 1984.
57. Kiss ZS, Khan KM, Fuller PJ: Stress fractures of the tarsal navicular bone: CT findings in 55 cases. AJR 160:111, 1993.
58. Datir AP, Saini A, Connell A, et al: Stress-related bone injuries with emphasis on MRI. Clin Radiol 62:828, 2007.
59. Faciszewski T, Burks RT, Manaster BJ: Subtle injuries of the Lisfranc joint. J Bone Joint Surg [Am] 72:1519, 1990.
60. Preidler KW, Brossman J, Daenen B, et al: MR imaging of the tarsometatarsal joint: Analysis of injuries in 11 patients. AJR 167:1217, 1996.
61. Richli WR, Rosenthal DI: Avulsion fracture of the fifth metatarsal: Experimental study of pathomechanics. AJR 143:889, 1984.
62. Torg JS, Balduini FC, Zelko RR, et al: Fractures of the base of the fifth metatarsal distal to the tuberosity: Classification and guidelines for non-surgical and surgical management. J Bone Joint Surg [Am] 66:209, 1984.
63. Galant JM, Spinosa FA: Digital fractures: A comprehensive review. J Am Podiatr Assoc 81:593, 1991.
64. Eisele SA, Sammarco GJ: Fatigue fractures of the foot and ankle in the athlete. J Bone Joint Surg [Am] 75:290, 1993.
65. Chowchuen P, Resnick D: Stress fractures of the metatarsal heads. Skeletal Radiol 27:22, 1998.
66. Anderson MW, Greenspan A: Stress fractures. Radiology 199:1, 1996.
67. Galant JM, Spinosa FA: Digital fractures: A comprehensive review. J Am Podiatr Assoc 81:593, 1991.
68. Pinckney LE, Currarino G, Kennedy LA: The stubbed great toe: A cause of occult compound fracture and infection. Radiology 138:375, 1981.
69. Katayama M, Murakami Y, Takahashi H: Irreducible dorsal dislocation of the toe: Report of three cases. J Bone Joint Surg [Am] 70:769, 1988.
70. Towbin R, Dunbar JS, Towbin J, et al: Teardrop sign: Plain film recognition of ankle effusion. AJR 134:985, 1980.
71. Karlsson J, Lansinger O: Lateral instability of the ankle joint. Clin Orthop 276:253, 1992.
72. Weinstabl R, Stiskal M, Neuhold A, et al: Classifying calcaneal tendon injury according to MRI findings. J Bone Joint Surg [Br] 73:683, 1991.
73. Ouzounaian TJ, Anderson R: Anterior tibial tendon rupture. Foot Ankle 16:406, 1995.
74. Karasick D, Schweitzer ME: Tear of the posterior tibial tendon causing asymptomatic flatfoot: Radiologic findings. AJR 161:1237, 1993.
75. Sammarco GJ: Peroneus longus tendon tears: Acute and chronic. Foot Ankle 16:245, 1995.
76. Innis PC, Krackow KH: Weightbearing roentgenograms in arthritis of the ankle: A case report. Foot Ankle 9:54, 1988.
77. Resnick D, Feingold ML, Curd J, et al: Calcaneal abnormalities in articular disorders: Rheumatoid arthritis, ankylosing spondylitis, psoriatic arthritis and Reiter's syndrome. Radiology 125:355, 1977.
78. Karasick D, Wapner KL: Hallux rigidus deformity: Radiologic assessment. AJR 157:1029, 1991.
79. Malhotra CM, Lally EV, Buckley WM: Ossification of the plantar fascia and peroneus longus tendons in diffuse idiopathic skeletal hyperostosis (DISH). J Rheumatol 13:215, 1986.
80. Kirkup JR: Ankle and tarsal joints in rheumatoid arthritis. Scand J Rheumatol 3:50, 1974.
81. Kirkup JR, Vidigal E, Jacoby RK: The hallux and rheumatoid arthritis. Acta Orthop Scand 48:527, 1977.
82. Garcia-Morteo O, Gusis SE, Somma LF, et al: Tarsal ankylosis in juvenile and adult onset rheumatoid arthritis. J Rheumatol 15:298, 1988.
83. Azouz EM, Duffy CM: Juvenile spondyloarthropathies: Clinical manifestations and medical imaging. Skeletal Radiol 24:399, 1995.
84. Resnick D: Patterns of peripheral joint disease in ankylosing spondylitis. Radiology 110:523, 1974.
85. Martel W, Stuck KJ, Dworin AM, et al: Erosive osteoarthritis and psoriatic arthritis: A radiologic comparison in the hand, wrist, and foot. AJR 134:125, 1980.
86. Resnick D, Niwayama G: On the nature and significance of bony proliferation in "rheumatoid variant" disorders. AJR 129:275, 1977.
87. Forrester DM, Kirkpatrick J: Periostitis and pseudoperiostitis. Radiology 118:597, 1976.
88. Martel W, Braunstein EM, Borlaza G, et al: Radiologic features of Reiter's syndrome. Radiology 132:1, 1979.
89. Mizutani W, Quismorio FP: Lupus foot: Deforming arthropathy of the feet in systemic lupus erythematosus. J Rheumatol 11:80, 1984.
90. Pachman LN: Juvenile dermatomyositis. Pediatr Clin North Am 33:1097, 1986.
91. Czirjak L, Nagy Z, Szegedi G: Systemic sclerosis in the elderly. Clin Rheumatol 11:483, 1992.
92. Resnick D, Niwayama G, Georgen TG, et al: Clinical, radiographic and pathologic abnormalities in calcium pyrophosphate dihydrate deposition disease (CPPD): Pseudogout. Radiology 122:1, 1977.
93. Steinbach LS, Resnick D: Calcium pyrophosphate dihydrate crystal deposition disease revisited. Radiology 200:1, 1996.
94. Archer BD, Friedman L, Stigenbauer S, et al: Symptomatic calcific tendinitis at unusual sites. J Can Assoc Radiol 43:203, 1992.
95. Resnick D: Gouty arthritis. In Diagnosis of bone and joint disorders. 4th Ed. Philadelphia, Saunders, 2002, p 1519.
96. Jonge-Bok JMD, Macfarlane JD: The articular diversity of early haemochromatosis. J Bone Joint Surg [Br] 69:41, 1987.
97. Holm CL: Primary synovial chondromatosis of the ankle: A case report. J Bone Joint Surg [Am] 58:878, 1976.
98. Kramer J, Recht M, Deely DM, et al: MR appearance of idiopathic synovial osteochondromatosis. J Comput Assist Tomogr 17:772, 1993.
99. Gamble JG, Bellah J, Rinsky LA, et al: Arthropathy of the ankle in hemophilia. J Bone Joint Surg [Am] 73:1008, 1991.
100. Jensen BN, Christensen KS: Diabetic osteoarthropathy: Rapid osteoarthropathic progression in the tarsal and tarso-metatarsal joints. J Orthop Rheumatol 5:179, 1992.

101. Gold RH, Tong DJF, Crim JR, et al: Imaging of the diabetic foot. Skeletal Radiol 24:563, 1995.
102. Hasegawa Y, Ninomiya M, Yamada Y, et al: Osteoarthropathy in congenital sensory neuropathy with anhidrosis. Clin Orthop 258:232, 1990.
103. Horibe S, Tada K, Nagano J: Neuroarthropathy of the foot in leprosy. J Bone Joint Surg [Br] 70:481, 1988.
104. Bjorkengren AG, Weisman M, Pathria MN, et al: Neuroarthropathy associated with chronic alcoholism. AJR 151:743, 1988.
105. Brown FE, Spiegel PK, Boyle WE Jr: Digital deformity: An effect of frostbite in children. Pediatrics 71:955, 1983.
106. Atkinson RE, Smith RJ: Silicone synovitis following silicone implant arthroplasty. Hand Clin 2:291, 1986.
107. Bornstein DL, Weinberg AN, Swartz MN, et al: Anaerobic infections—review of current experience. Medicine 43:207, 1964.
108. Morrison WB, Schweitzer ME, Wapner KL, et al: Osteomyelitis in feet of diabetics: Clinical accuracy, surgical utility, and cost-effectiveness of MR imaging. Radiology 196:557, 1995.
109. Beltran J, Campanini DS, Knight C, et al: The diabetic foot: Magnetic resonance imaging evaluation. Skeletal Radiol 19:37, 1990.
110. Mendelson EB, Fisher MR, Deschler TW, et al: Osteomyelitis in the diabetic foot: A difficult diagnostic challenge. RadioGraphics 3:248, 1983.
111. Gold RH, Hawkins RA, Katz RD: Bacterial osteomyelitis: Findings on plain radiography, CT, MR, and scintigraphy. AJR 157:365, 1991.
112. Feldman F, Auerbach R, Johnston A: Tuberculous dactylitis in the adult. AJR 112:460, 1971.
113. Resnick D: Osteomyelitis, septic arthritis, and soft tissue infection: Organisms. In Resnick D: Diagnosis of bone and joint disorders. 4th Ed. Philadelphia, Saunders, 2002, p 2510.
114. Libson E, Bloom RA, Husband JE, et al: Metastatic tumours of bones of the hand and foot: A comparative review and report of 43 additional cases. Skeletal Radiol 16:387, 1987.
115. Miyayama H, Sakamoto K, Ide M, et al: Aggressive osteoblastoma of the calcaneus. Cancer 71:346, 1993.
116. Huvos AG, Higinbotham NL: Primary fibrosarcoma of bone: A clinicopathologic study of 130 patients. Cancer 35:837, 1975.
117. Dahlin DC, Coventry MB, Scanlon PW: Ewing's sarcoma: A critical analysis of 165 cases. J Bone Joint Surg [Am] 43:185, 1961.
118. Buck P, Mickelson MR, Bonfiglio M: Synovial sarcoma: A review of 33 cases. Clin Orthop 156:211, 1981.
119. Kyle RA: Multiple myeloma: Review of 869 cases. Mayo Clin Proc 50:29, 1975.
120. Greenspan A: Bone island (enostosis): Current concept—a review. Skeletal Radiol 24:111, 1995.
121. Loizaga JM, Calvo M, Barea FL, et al: Osteoblastoma and osteoid osteoma: Clinical and morphological features of 162 cases. Pathol Res Pract 189:33, 1993.
122. Muse G, Rayan G: Subungual exostosis. Orthopedics 9:997, 1986.
123. Brien EW, Mirra JM, Kerr R: Benign and malignant cartilage tumors of bone and joint: Their anatomic and theoretical basis with an emphasis on radiology, pathology and clinical biology. 1. The intramedullary cartilage tumors. Skeletal Radiol 26:325, 1997.
124. Moore TM, Roe JB, Harvey JP: Chondroblastoma of the talus: A case report. J Bone Joint Surg [Am] 59:830, 1977.
125. Weatherall PT, Maale GE, Mendelsohn DB, et al: Chondroblastoma: Classic and confusing appearance at MR imaging. Radiology 190:467, 1994.
126. Dahlin DC: Giant cell tumor of bone: Highlights of 407 cases. AJR 144:955, 1985.
127. Södegard J, Karaharju EO: Calcaneal cysts: Diagnosis and treatment. Fr J Orthop Surg 4:424, 1990.
128. Milgram JW: Intraosseous lipoma: A clinicopathologic study of 66 cases. Clin Orthop 231:277, 1988.
129. De Dios AMV, Bond JR, Shives TC, et al: Aneurysmal bone cyst: A clinicopathologic study of 238 cases. Cancer 69:2921, 1992.
130. Matfin G. McPherson F: Paget's disease of bone: Recent advances. J Orthop Rheumatol 6:127, 1993.
131. Mirra JM, Brien EW, Tehranzadeh J: Paget's disease of bone: Review with emphasis on radiologic features. Part II. Skeletal Radiol 24:173, 1995.
132. Gibson MJ, Middlemiss JH: Fibrous dysplasia of bone. Br J Radiol 44:1, 1971.
133. Taylor JAM, Resnick D, Sartoris DJ: Radiographic-pathologic correlation. In Sartoris DJ: Osteoporosis: diagnosis and treatment. New York, Marcel Dekker, 1996, p 147.
134. Clouston WM, Lloyd HM: Immobilization-induced hypercalcemia and regional osteoporosis. Clin Orthop 216:247, 1987.
135. Resnick D: Neuromuscular disorders. In Resnick D: Diagnosis of bone and joint disorders. 4th Ed. Philadelphia, Saunders, 2002, p 3479.
136. Mankin HJ: Metabolic bone disease. J Bone Joint Surg [Am] 76:760, 1994.
137. Tigges S, Nance EP, Carpenter WA, et al: Renal osteodystrophy: Imaging findings that mimic those of other diseases. AJR 165:143, 1995.
138. Edmondson ME, Morrison N, Laws JW, et al: Medial arterial calcification and diabetic neuropathy. Br Med J 284:928.
139. Lang EK, Bessler WT: The roentgenologic features of acromegaly. AJR 86:321, 1961.
140. Gonticas SK, Ikkos DG, Stergiou LH: Evaluation of the diagnostic value of heel-pad thickness in acromegaly. Radiology 92:304, 1969.
141. Greenfield GB: Bone changes in chronic adult Gaucher's disease. AJR 110:800, 1970.
142. Stevens MCG, Padwick GR, Serjeant GR: Observations on the natural history of dactylitis in homozygous sickle cell disease. Clin Pediatr 20:311, 1981.
143. Morris HD: Aseptic necrosis of the talus following injury. Orthop Clin North Am 5:177, 1974.
144. Donnelly EF: The Hawkins sign. Radiology 210:195, 1999.
145. Williams GA, Cowell HR: Köhler's disease of the tarsal navicular. Clin Orthop 158:53, 1981.
146. Haller J, Sartoris DJ, Resnick D, et al: Spontaneous osteonecrosis of the tarsal navicular in adults: Imaging findings. AJR 151:355, 1988.
147. Hoskinson J: Freiberg's disease: A review of long-term results. Proc R Soc Med 67:106, 1974.
148. Gentilli A: Advanced imaging of gout. Semin Musculoskeletal Radiol 7:165, 2003.
149. O'Sullivan PJ, Harris AC, Munk PL: Radiologic features of synovial cell sarcoma. Br J Radiol 81:346, 2008.
150. Spitz DJ, Newberg AH: Imaging of stress fractures in the athlete. Radiol Clin N Am 40:313, 2002.
151. Aliabadi P, Nikpoor N, Alparsian L: Imaging of neuropathic arthropathy. Semin Musculoskeletal Radiol 7:217, 2003.
152. Propeck T, Bullard MA, Lin J, et al: Radiologic-pathologic correlation of intraosseous lipomas. AJR 175:673, 2000.
153. Klecker RJ, Weissman BN: Imaging features of psoriatic and Reiter's syndrome. Semin Musculoskeletal Radiol 7:115, 2003.
154. Kerr R: Imaging of musculoskeletal complications of hemophilia. Semin Musculoskeletal Radiol 7:127, 2003.
155. Marin C, Sanchez-Alegre ML, Gallego C, et al: Magnetic resonance imaging of osteoarticular infections in children. Curr Probl Diagn Radiol 33:43, 2004.
156. Christian S, Kraas J, Conway WF: Musculoskeletal infections. Semin Roentgenol 42:92, 2007.
157. Greenspan A, Tehranzadeh J: Imaging of infectious arthritis. Radiol Clin N Am 39:267, 2001.
158. Gil H, Morrison WB: MR imaging of diabetic foot infection. Semin Musculoskeletal Radiol 8:189, 2004.
159. Mulligan ME: Ankle and foot trauma: Semin Musculoskeletal Radiol 4:241, 2000.
160. Robinson P, White LM, Salonen DC, et al: Anterolateral ankle impingement: MR arthrographic assessment of the anterolateral recess. Radiology 221:186, 2001.
161. Cerezal L, Abascal F, Canga A, et al: MR imaging of ankle impingement syndromes. AJR 181:551, 2003.
162. Peace KAL, Hillier JC, Hulme A, et al: MRI features of posterior ankle impingement syndrome in ballet dancers: A review of 25 cases. Clin Radiol 59:1025, 2004.
163. Taniguchi A, Tanaka Y, Kadono K, et al: C sign for diagnosis of talocalca-

neal coalition. Radiology 228:501, 2003.

164. Brown RR, Rosenberg ZS, Thornhill BA. The C sign: More specific for flatfoot deformity than subtalar coalition. Skeletal Radiol 30:84, 2001.
165. Crim JR, Kjeldsberg KM: Radiographic diagnosis of tarsal coalition. AJR 182:323, 2004.
166. Petrover D, Schweitzer ME, Laredo JD: Anterior process calcaneal fractures: A systematic evaluation of associated conditions. Skeletal Radiol 36:627, 2007.
167. Davila JA, Amrami KK, Sundaram M, et al: Chondroblastoma of the hands and feet. Skeletal Radiol 33:582, 2004.
168. Levinsohn EM, Shrimpton AE, Cady RB, et al: Congenital vertical talus in four generations of the same family. Skeletal Radiol 33:649, 2004.
169. Franco M, Albano L, Kacso I, et al: An uncommon cause of foot pain: The cuboid insufficiency stress fracture. Joint Bone Spine 72:76, 2005.
170. Schweitzer ME, Morrison WB: MR imaging of the diabetic foot. Radiol Clin N Am 42:61, 2004.
171. Karchevsky M, Schweitzer ME: Accuracy of plain films, and the effect of experience, in the assessment of ankle effusions. Skeletal Radiol 33:719, 2004.
172. Juan Mas A, Rotés-Querol J: Erosive osteoarthritis of the feet: Description of two patients. Joint Bone Spine 74:296, 2007.
173. Baraga JJ, Amrami KK, Swee RG, et al: Radiographic features of Ewing's sarcoma of the bones of the hands and feet. Skeletal Radiol 30:121, 2001.
174. Theodorou DJ, Theodorou SJ, Kakitsubata Y, et al: Fractures of the proximal portion of fifth metatarsal bone: Anatomic and imaging evidence of a pathogenesis of avulsion of the plantar aponeurosis and the short peroneal muscle tendon. Radiology 226:857, 2003.
175. Mellado JM, Ramos A, Salvadó E, et al: Accessory ossicles and sesamoid bones of the ankle and foot: Imaging findings, clinical significance and differential diagnosis. Eur Radiol Suppl 6:L164, 2003.
176. Mellado JM, Salvadó E, Camins A, et al: Painful os sustentaculi: Imaging findings of another symptomatic skeletal variant. Skeletal Radiol 31:53, 2002.
177. Foo LF, Raby N: Tumours and tumourlike lesions in the foot and ankle. Clin Radiol 60:308, 2005.
178. Pao DG, Keats TE, Dussault RG: Avulsion fracture of the base of the fifth metatarsal not seen on conventional radiography of the foot. AJR 175:549, 2000.
179. Sayed MN, Kondekar S, Jaiswal S, et al: Giant cell tumor of talus, a case report of a rare sit. Europ J Rad Extra 61:73, 2007.
180. Bezza A, Niamane R, Amine B, et al: Involvement of the foot in patients with psoriatic arthritis. A review of 26 cases. Joint Bone Spine 71:546, 2004.
181. Beeson P, Phillips C, Corr S, et al: Classification systems for hallux rigidus: A review of the literature. Foot Ankle, Int 29:407, 2008.
182. Chhaya SA, Brawner M, Hobbs P, et al: Understanding hallux valgus deformity: What the surgeon wants to know from the conventional radiograph. Curr Probl Diagn Radiol 37:127, 2008.
183. Sariali E, Lelièvre JF, Catonné Y: Fractures of the lateral process of talus. Retrospective study of 44 cases. Rev Chir Orthop Reparatrice Appar Mot. 94 :527 Epub 2008.
184. Gupta RT, Wadhwa RP, Learch TJ, et al: Lisfranc injury: Imaging findings for this important but often-missed diagnosis. Curr Probl Diagn Radiol 37:115, 2008.
185. Delfault EM, Rosenberg ZS, Demondion X: Malalignment at the Lisfranc joint: MR features in asymptomatic and cadaveric specimens. Skeletal Radiol 31:499, 2002.
186. Abreu MR, Chung CB, Mendes L, et al: Plantar calcaneal enthesophytes: New observations regarding sites of origin based on radiographic MR imaging, anatomic, and paleopathologic analysis. Skeletal Radiol 32:13, 2003.
187. Mazlout O, Saudan M, Fethi Ladeb M, et al: Osteoid osteoma of the talar neck: A diagnostic challenge. Eur J Radiol Extra 49:67, 2004.
188. Campbell RSD, Grainger AJ, Mangham DC, et al: Intraosseous lipoma: Report of 35 new cases and a review of the literature. Skeletal Radiol 32:209, 2003.
189. Miller TT: Painful accessory bones of the foot. Semin Musculoskeletal Radiol 6:153, 2002.
190. Muthukumar T, Butt SH, Cassar-Pullicino VN: Stress fractures and related disorders in foot and ankle: Plain films, scintigraphy, CT, and MR imaging. Semin Musculoskeletal Radiol 9:210, 2005.
191. Hopper MA, Robinson P: Ankle impingement syndromes. Radiol Clin N Am 46:957, 2008.
192. Naran KN, Zoga AC: Osteochondral lesions about the ankle. Radiol Clin N Am 46:995, 2008.
193. Donovan A, Schweitzer ME: Current concepts in imaging diabetic pedal osteomyelitis. Radiol Clin N Am 46:1105, 2008.
194. Bancroft LW, Peterson JJ, Kransdorf MJ: Imaging of soft tissue lesions about the foot. Radiol Clin N Am 46:1093, 2008.
195. Sanders TG, Kabir Rathur S: Imaging of painful conditions of the hallucal sesamoid complex and plantar capsular structures of the first metatarsophalangeal joint. Radiol Clin N Am 46:1079, 2008.
196. Crim J: Imaging of tarsal coalition. Radiol Clin N Am 46:1017, 2008.
197. Lee A, Taylor JAM, Sherwood W: Acute fracture and diastasis of a bipartite os peroneum. Topics in diagnostic radiology and advanced imaging. 11:4, 2007.
198. Berg EE: The symptomatic os subfibulare. Avulsion fracture of the fibula associated with recurrent instability of the ankle. J Bone Joint Surg Am. 73:1251, 1991.
199. Champagne IM, Cook DL, Kestner SC, et al: Os subfibulare. Investigation of an accessory bone. J Am Podiatr Med Assoc. 89:5320, 1999.
200. Mellado JM, Salvadó E, Camins A, et al: Painful os sustentaculi: Imaging findings of another symptomatic skeletal variant. Skeletal Radiol 31:53, 2002.
201. Resnick D: Osteomyelitis, septic arthritis, and soft tissue infection: Organisms. In Resnick D: Diagnosis of bone and joint disorders. 4th Ed. Philadelphia, Saunders, 2002, p 2581.
202. dePalma L, Gigante A, Specchia N: Subungual exostosis of the foot. Foot Ankle Int 17:758, 1996.

CHAPTER 12

Ribs, Sternum, and Sternoclavicular Joints

1. Edeiken J, Dalinka M, Karasick D: Edeiken's roentgen diagnosis of diseases of bone. 4th Ed. Baltimore, Williams & Wilkins, 1990.
2. Kahn SL, Gaskin CM, Sharp VL: Keats and Kahn's roentgen atlas of skeletal maturation. DVD-ROM Ed. Philadelphia, Lippincott Williams and Wilkins, 2007.
3. Köhler A, Zimmer EA: Borderlands of normal and early pathologic findings in skeletal radiography. 4th Ed. New York, Thieme Medical Publishers, 1993.
4. Keats TE: Atlas of normal roentgen variants that may simulate disease. 6th Ed. Chicago, Year Book Medical Publishers, 1996.
5. Yochum TR, Rowe LJ: Essentials of skeletal radiology. 2nd Ed. Baltimore, Williams & Wilkins, 1996.
6. Adson AW: Surgical treatment for symptoms produced by cervical ribs and the scalenus anticus syndrome. Clin Orthop 207:3, 1986.
7. Weinstein AS, Mueller CF: Intrathoracic rib. AJR 94:587, 1965.
8. Stark P, Lawrence DD: Intrathoracic rib—CT features of a rare chest wall anomaly. Comput Radiol 6:365, 1984.
9. Kelleher J, O'Connell DJ, MacMahon H: Intrathoracic rib: Radiographic features of two cases. Br J Radiol 52:181, 1979.
10. Senac MO, Lee FA, Gilsnaz V: Early costochondral calcification in adolescent hyperthyroidism. Radiology 156: 375, 1985.
11. Resnik CS, Brower AC: Midline circular defect of the sternum. Radiology 130:657, 1979.
12. Larsen LL, Ibach HF: Complete congenital fissure of the sternum. AJR 87:1062, 1962.
13. Morse RP, Rockenmacher S, Pyeritz RE, et al: Diagnosis and management

of infantile Marfan's syndrome. Pediatrics 86:888, 1990.

14. Eisenberg RL: Clinical imaging: An atlas of differential diagnosis. Rockville, Md, Aspen, 1988.
15. Mariacher-Gehler S, Michel BA: Sonography: A simple way to visualize rib fractures. AJR 163:1268, 1994.
16. Kattan KR: Trauma to the bony thorax. Semin Roentgenol 13:69, 1978.
17. Kinasewitz GT: Pneumothorax. Semin Respir Crit Care Med 16:293, 1995.
18. Kleinman PK, Marks SC, Nimkin K, et al: Rib fractures in 31 abused infants: Postmortem radiologic-histopathologic study. Radiology 200:807, 1996.
19. Leventhal JM, Thomas SA, Rosenfeld NS, et al: Fractures in young children: Distinguishing child abuse from unintentional injuries. Am J Dis Child 147: 87, 1993.
20. Strouse PJ, Owings CL: Fractures of the first rib in child abuse. Radiology 197:763, 1995.
21. Roberge RJ, Morgenstern MJ, Osborn H: Cough fracture of the ribs. Am J Emerg Med 2:513, 1984.
22. Gurtler R, Pavlov H, Torg JS: Stress fracture of the ipsilateral first rib in a pitcher. Am J Sports Med 13:277, 1985.
23. Sacchetti AD, Beswick DR, Morse SK: Rebound rib: Stress-induced first rib fracture. Ann Emerg Med 12:177, 1983.
24. Huang G-S, Park Y-H, Taylor JAM, et al: Hyperostosis of ribs: Association with vertebral hyperostosis. J Rheumatol 20:2073, 1993.
25. Spence EK, Rosato EF: The slipping rib syndrome. Arch Surg 118:1330, 1983.
26. Jurik AG, Justesen T, Graudal H: Radiographic findings in patients with clinical Tietze's syndrome. Skeletal Radiol 16:517, 1987.
27. Brookes JG, Dunn RJ, Rogers LR: Sternal fractures: A retrospective analysis of 272 cases. J Trauma 35:46, 1993.
28. Chen C, Chandnani V, Kang HS, et al: Insufficiency fracture of the sternum caused by osteopenia: Plain film findings in seven patients. AJR 154:1025, 1990.
29. Levinsohn EM, Bunnell WP, Yuan HA: Computed tomography in the diagnosis of dislocations of the sternoclavicular joint. Clin Orthop 140:13, 1979.
30. Gopalakrishnan KC, El Masri WS: Fractures of the sternum associated with spinal injury. J Bone Joint Surg [Br] 68:178, 1986.
31. Felson B: Chest roentgenology. Philadelphia, Saunders, 1973.
32. Greenfield GB: Radiology of bone diseases. 2nd Ed. Philadelphia, JB Lippincott, 1975.
33. Kier R, Wain SL, Apple J, et al: Osteoarthritis of the sternoclavicular joint. Invest Radiol 21:227, 1986.
34. Brossmann J, Stöbler A, Preidler KW, et al: Sternoclavicular joint: MR imaging-anatomic correlation. Radiology 198:193, 1996.
35. Kalliomaki JL, Viitanen S-M, Virtama P: Radiological findings of sternoclavicular joints in rheumatoid arthritis. Acta Rheumatol Scand 14:233, 1968.
36. Laitenen H, Saksanen S, Suoranta H: Involvement of the manubriosternal articulation in rheumatoid arthritis. Acta Rheumatol Scand 16:40, 1970.
37. Schils JP, Resnick D, Haghighi PN, et al: Pathogenesis of discovertebral and manubriosternal junction abnormalities in rheumatoid arthritis: A cadaveric study. J Rheumatol 16:291, 1989.
38. Jurik AG: Anterior chest wall involvement in seronegative arthritides: A study of the frequency of changes at radiography. Rheumatol Int 12:7, 1992.
39. Grosbois B, Paxlotsky Y, Chales G, et al: Clinical and radiological study of the manubrio-sternal joint. Rev Rhum Mal Osteoartic 49:232, 1982.
40. Reuler JB, Girard DE, Nardone DA: Sternoclavicular joint involvement in ankylosing spondylitis. South Med J 71:1480, 1978.
41. Boutin RD, Resnick D: The SAPHO syndrome: An evolving concept for unifying several idiopathic disorders of bone and skin. AJR 170:585, 1998.
42. Candardjis G, Saudan Y, DeBosset P: Etude radiologique de l'articulation manubrio-sternale dans la pelvispondylite rhumatismale et le syndrome de Reiter. J Radiol Electrol Med Nucl 59:93, 1978.
43. Hernandez RJ, Keim DR, Sullivan DB, et al: Magnetic resonance imaging appearance of the muscles in childhood dermatomyositis. J Pediatr 117:546, 1990.
44. Brancós MA, Peris P, Miroc JM, et al: Septic arthritis in heroin addicts. Semin Arthritis Rheum 21:81, 1991.
45. Kleinman GM, Hochberg FH, Richardson EP Jr: Systemic metastases from medulloblastoma: Report of two cases and review of the literature. Cancer 48:2296, 1981.
46. Wong DA, Fornasier VL, MacNab I: Spinal metastases: The obvious, the occult, and the impostors. Spine 15:1, 1990.
47. Garrett IR: Bone destruction in cancer. Semin Oncol 20:4, 1993.
48. Dahlin DC, Unni KK: Osteosarcoma of bone and its important recognizable varieties. Am J Surg Pathol 1:61, 1977.
49. Abdulrahman RE, White CS, Templeton PA, et al: Primary osteosarcoma of the ribs: CT findings. Skeletal Radiol 24:127, 1995.
50. St James AT: Resection of multiple metastatic pulmonary lesions of osteogenic sarcoma. JAMA 169:943, 1959.
51. Mitchell M, Ackerman LV: Metastatic and pseudomalignant osteoblastoma: A report of two unusual cases. Skeletal Radiol 15:213, 1986.
52. Nakashima Y, Unni KK, Shives TC, et al: Mesenchymal chondrosarcoma of bone and soft tissue: A review of 111 cases. Cancer 57:2444, 1986.
53. Brien EW, Mirra JM, Kerr R: Benign and malignant cartilage tumors of bone and joint: Their anatomic and theoretical basis with an emphasis on radiology, pathology and clinical biology. 1. The intramedullary cartilage tumors. Skeletal Radiol 26:325, 1997.
54. Levine E, Levine C: Ewing tumor of rib: Radiologic findings and computed tomography contribution. Skeletal Radiol 9:227, 1983.
55. Kyle RA: Multiple myeloma: Review of 869 cases. Mayo Clin Proc 50:29, 1975.
56. Franczyk J, Samuels T, Rubenstein J, et al: Skeletal lymphoma. J Can Assoc Radiol 40:75, 1989.
57. Hermann G, Klein MJ, Fikry Abdelwahab I, et al: MRI appearance of primary non-Hodgkin's lymphoma of bone. Skeletal Radiol 26:629, 1997.
58. Greenspan A: Bone island (enostosis): Current concept—a review. Skeletal Radiol 24:111, 1995.
59. McGuire MH, Mankin HJ: Osteoid osteoma: An unusual presentation as a rib lesion. Orthopedics 7:305, 1984.
60. Shankman S, Desai P, Beltran J: Subperiosteal osteoid osteoma: Radiographic and pathologic manifestations. Skeletal Radiol 26:457, 1997.
61. Kayser F, Resnick D, Haghighi P, et al: Evidence of the subperiosteal origin of osteoid osteomas in tubular bones: Analysis by CT and MR imaging. AJR 170:609, 1998.
62. Lichtenstein L, Sawyer WF: Benign osteoblastoma: Further observations and report of twenty additional cases. J Bone Joint Surg [Am] 46:755, 1964.
63. Keating RB, Wright PW, Staple TW: Enchondroma protuberans of the rib. Skeletal Radiol 13:55, 1985.
64. Geirnaerdt MJA, Bloem JL, Eulderink F, et al: Cartilaginous tumors: Correlation of gadolinium-enhanced MR imaging and histopathologic findings. Radiology 186:813, 1993.
65. Milgram JW: Intraosseous lipoma: A clinicopathologic study of 66 cases. Clin Orthop 231:277, 1988.
66. Sherman RS, Wilner D: The roentgen diagnosis of hemangioma of bone. AJR 86:1146, 1961.
67. De Dios AMV, Bond JR, Shives TC, et al: Aneurysmal bone cyst: A clinicopathologic study of 238 cases. Cancer 69:2921, 1992.
68. Mirra JM, Brien EW, Tehranzadeh J: Paget's disease of bone: Review with emphasis on radiologic features. Part II. Skeletal Radiol 24:173, 1995.
69. Crawford AH Jr, Bogamery N: Osseous manifestations of neurofibromatosis in childhood. J Pediatr Orthop 6:72, 1986.
70. Gibson MJ, Middlemiss JH: Fibrous dysplasia of bone. Br J Radiol 44:1, 1971.
71. Kilpatrick SE, Wenger DE, Gilchrist GS, et al: Langerhans' cell histiocytosis (histiocytosis X) of bone: A clinicopathologic analysis of 263 pediatric and adult cases. Cancer 76:2471, 1995.

72. Taylor JAM, Resnick D, Sartoris DJ: Radiographic-pathologic correlation. In Sartoris DJ (ed): Osteoporosis: diagnosis and treatment. New York, Marcel Dekker, 1996, p 147.
73. Hanscom DA, Winter RB, Lutter L, et al: Osteogenesis imperfecta: Radiographic classification, natural history and treatment of spinal deformity. J Bone Joint Surg [Am] 74:598, 1992.
74. Mankin HJ: Rickets, osteomalacia, and renal osteodystrophy. Orthop Clin North Am 21:81, 1990.
75. Chew FS, Huang-Hellinger F: Brown tumor. AJR 160:752, 1993.
76. Simpson W, Kerr DNS, Hill AVL, et al: Skeletal changes in patients on regular hemodialysis. Radiology 107:313, 1971.
77. Cameron EW, Resnik CS, Light PD, et al: Hemodialysis-related amyloidosis of the sternoclavicular joint. Skeletal Radiol 26:428, 1997.
78. Resnick D: Hemoglobinopathies and other anemias. In Resnick D (ed): Diagnosis of bone and joint disorders. 3rd Ed. Philadelphia, Saunders, 1995, p 2128.
79. Bouroncle BA, Doan CA: Myelofibrosis: clinical, hematologic and pathologic study of 110 patients. Am J Med Sci 243:697, 1962.
80. Gentry RR, Rust RS, Lohr JA, et al: Infantile cortical hyperostosis of the ribs (Caffey's disease) without mandibular involvement. Pediatr Radiol 13:236, 1983.
81. Tecce PM, Fishman EK: Spiral CT with multiplanar reconstruction in the diagnosis of sternoclavicular osteomyelitis. Skeletal Radiol 24:275, 1995.
82. Jurik AG, Egund N: MRI in chronic recurrent multifocal osteomyelitis. Skeletal Radiol 26:230, 1997.
83. Applegate KE, Finkelstein MS, Gross GW: Child abuse: Imaging findings pertaining to the musculoskeletal system. Semin Musculoskeletal Radiol 3:351, 1999.
84. Kemp AM, Butler A, Morris S, et al: Which radiological investigations should be performed to identify fractures in suspected child abuse? Clin Radiology 61:723, 2006.
85. Hyodoh K, Sugimoto H: Pustulotic arthro-osteitis: Defining the radiologic spectrum of the disease. Semin Musculoskeletal Radiol 5:89, 2001.
86. Berry JL, Davies M, Mee AP: Vitamin D metabolism, rickets and osteomalacia. Semin Musculoskeletal Radiol 6:173, 2002.
87. Heye S, Matthijs P, Wallon J, et al: Cat-scratch disease osteomyelitis. Skeletal Radiol 32:49, 2003.
88. Aslam M, Rajesh A, Entwisle J, et al: MRI of the sternum and sternoclavicular joints. Br J Radiol 75:627, 2002.
89. Hattingh L: Non-accidental injury. Curr Orthop 21:301, 2007.
90. Tateishi U, Gladish GW, Kusumoto M, et al: Chest wall tumors: Radiologic findings and pathologic correlation. Part 1. Benign tumors. RadioGraphics 23:1477, 2003.
91. Hughes EK, James SLJ, Butt S, et al: Benign primary tumours of the ribs. Clin Radiol 61:314, 2006.
92. Briccoli A, Malaguti C, Iannetti C, et al: Giant cell tumor of the rib. Skeletal Radiol 32:107, 2003.
93. Yamaguchi T, Shimizu K, Koguchi Y, et al: Skeletal Radiol 34:490, 2005.
94. Arslan G, Cevicol C, Karaali K, et al: Single rib sclerosis as a sequel of compression fracture of adjacent vertebra and costovertebral joint ankylosis. Eur J Radiol Extra 51:43, 2004.
95. Dragoni S, Giombini A, Di Cesare A, et al: Stress fractures of the ribs in elite competitive rowers: A report of 9 cases. Skeletal Radiol 36:951, 2007.
96. O'Sullivan P, O'Dwyer H, Flint J, et al: Soft tissue tumors and mass-like lesions of the chest wall: A pictorial review of CT and MR findings. Br J Radiol 80: 574, 2007.
97. McCulloch P, Henley BM, Linnau KF: Radiographic clues for high-energy trauma: Three cases of sternoclavicular dislocation. AJR 176:1534, 2001.
98. Yekeler E, Tunaci M, Tunaci A, et al: Frequency of sternal variations and anomalies evaluated by MDCT. AJR 186:956, 2006.

CHAPTER 13

Clavicle, Scapula, and Shoulder

1. Edeiken J, Dalinka M, Karasick D: Edeiken's Roentgen diagnosis of diseases of bone. 4th Ed. Baltimore, Williams & Wilkins, 1990.
2. Kahn SL, Gaskin CM, Sharp VL: Keats and Kahn's roentgen atlas of skeletal maturation. DVD-ROM Ed. Philadelphia, Lippincott Williams and Wilkins, 2007.
3. Greenfield GB: Radiology of bone diseases. 2nd Ed. Philadelphia, JB Lippincott, 1975.
4. Köler A, Zimmer EA: Borderlands of normal and early pathologic findings in skeletal radiography. 4th Ed. New York, Thieme Medical Publishers, 1993.
5. Keats TE: Atlas of normal roentgen variants that may simulate disease. 6th Ed. Chicago, Year Book Medical Publishers, 1996.
6. Yochum TR, Rowe LJ: Essentials of skeletal radiology. 3rd Ed. Baltimore, Williams & Wilkins, 2004.
7. Schnall SB, King JD, Marrero G: Congenital pseudoarthrosis of the clavicle: A review of the literature and surgical results of six cases. J Pediatr Orthop 8:316, 1988.
8. Juhl JH, Kuhlman JE: Methods of examination, techniques, and anatomy of the chest. In Juhl JH, Crummy AB, Kuhlman JE (eds): Paul and Juhl's essentials of radiologic imaging. 7th Ed. Philadelphia, Lippincott-Raven, 1998, p 800.
9. Haramati N, Cook RA, Raphael B, et al: Coraco-clavicular joint: Normal variant in humans. A radiographic demonstration in the human and non-human primate. Skeletal Radiol 23: 117, 1994.
10. Ogden JA, Conlogue GJ, Phillips SB, et al: Sprengel's deformity: Radiology of the pathologic deformation. Skeletal Radiol 4:204, 1979.
11. Trout TE, Resnick D: Glenoid hypoplasia and its relationship to instability. Skeletal Radiol 25:37, 1996.
12. Edelson JG, Zuckerman J, Hershkovitz I: Os acromiale: Anatomy and surgical implications. J Bone Joint Surg [Br] 74:551, 1993.
13. Park JG, Lee JK, Phelps CT: Os acromiale associated with rotator cuff impingement: MR imaging of the shoulder. Radiology 193:255, 1994.
14. Resnick D, Cone RO: The nature of humeral pseudocysts. Radiology 150: 27, 1984.
15. Langer LO, Baumann PA, Gorlin RJ: Achondroplasia. AJR 100:12, 1967.
16. Machlachlan AK, Gerrard JW, Houston CS, et al: Familial infantile cortical hyperostosis in a large Canadian family. Can Med Assoc J 130: 1172, 1984.
17. Cramer SF, Ruehl A, Mandel MA: Fibrodysplasia ossificans progressiva: A distinctive bone-forming lesion of the soft tissue. Cancer 48:1016, 1981.
18. Benli IT, Akalin S, Boysan E, et al: Epidemiological, clinical, and radiological aspects of osteopoikilosis. J Bone Joint Surg [Br] 74:504, 1992.
19. Kovanlikaya A, Loro ML, Gilsanz V: Pathogenesis of osteosclerosis in autosomal dominant osteopetrosis. AJR 168:929, 1997.
20. Yu JS, Resnick D, Vaughan LM, et al: Melorheostosis with an ossified soft tissue mass. Skeletal Radiol 24:367, 1995.
21. Chitayat D, Hodgkinson KA, Azouz EM: Intrafamilial variability in cleidocranial dysplasia: A three generation family. Am J Med Genet 42:298, 1992.
22. Kilcoyne RF, Shuman WP, Matsen FA III, et al: The Neer classification of displaced proximal humeral fractures: Spectrum of findings on plain radiographs and CT scans. AJR 154:1029, 1990.
23. Ovesen J, Nielsen S: Experimental distal subluxation in the glenohumeral joint. Arch Orthop Trauma Surg 104: 78, 1985.
24. Barnett LS: Little League shoulder syndrome: Proximal humeral epiphysiolysis in adolescent baseball pitchers. J Bone Joint Surg [Am] 67:495, 1985.
25. Rogers LF, Poznanski AK: Imaging of epiphyseal injuries. Radiology 191:297, 1994.
26. Weinberg B, Seife B, Alonso P: The apical oblique view of the clavicle: Its usefulness in neonatal and childhood trauma. Skeletal Radiol 20:201, 1991.
27. Robinson CM: Fractures of the clavicle in the adult: Epidemiology and classification. J Bone Joint Surg [Br] 80:476, 1998.
28. Ada JR, Miller ME: Scapular fractures: Analysis of 113 cases. Clin Orthop 269:174, 1991.

29. Froimson AI: Fracture of the coracoid process of the scapula. J Bone Joint Surg [Am] 60:710, 1978.
30. Herscovici D Jr, Fiennes AGTW, Allgöwer M, et al: The floating shoulder: Ipsilateral clavicle and scapular neck fractures. J Bone Joint Surg [Br] 74:362, 1992.
31. Strouse PJ, Owings CL: Fractures of the first rib in child abuse. Radiology 197:763, 1995.
32. Deutsch AL, Resnick D, Mink JH, et al: Computed tomography of the glenohumeral joint: Normal anatomy and clinical experience. Radiology 153: 603, 1984.
33. Richards RD, Sartoris DJ, Pathria MN, et al: Hill-Sachs lesion and normal humeral groove: MR imaging features allowing their differentiation. Radiology 190:665, 1994.
34. Workman TL, Burkhard TK, Resnick D, et al: Hill-Sachs lesion: Comparison of detection with MR imaging, radiography, and arthroscopy. Radiology 185:847, 1992.
35. Gonzalez D, Lopez RA: Concurrent rotator-cuff tear and brachial plexus palsy associated with anterior dislocation of the shoulder: A report of two cases. J Bone Joint Surg [Am] 73:620, 1991.
36. Hawkins RJ, Neer CS II, Pianta RM, et al: Locked posterior dislocation of the shoulder. J Bone Joint Surg [Am] 69:9, 1987.
37. Downey EF Jr, Curtis DJ, Brower AC: Unusual dislocations of the shoulder. AJR 140:1207, 1983.
38. Davids JR, Talbott RD: Luxatio erecta humeri: A case report. Clin Orthop 252:144, 1990.
39. Arger PH, Oberkircher PE, Miller WT: Lipohemarthrosis. AJR 121:97, 1974.
40. Väätäinen U, Pirinen A, Mäkelä A: Radiologic evaluation of the acromioclavicular joint. Skeletal Radiol 20:115, 1991.
41. Vanarthos WJ, Ekman EF, Bohrer SP: Radiographic diagnosis of acromioclavicular joint separation without weight bearing: Importance of internal rotation of the arm. AJR 162:120, 1994.
42. Levinsohn EM, Bunnell WP, Yuan HA: Computed tomography in the diagnosis of dislocations of the sternoclavicular joint. Clin Orthop 140:13, 1979.
43. Jim YF, Chang CY, Wu JJ, et al: Shoulder impingement syndrome: Impingement view and arthrography based on 100 cases. Skeletal Radiol 21:449, 1992.
44. DeSmet AA, Ting YM: Diagnosis of rotator cuff tear on routine radiographs. J Can Assoc Radiol 28:54, 1977.
45. Patte D: Classification of rotator cuff lesions. Clin Orthop 254:81, 1990.
46. Patten RM, Spear RP, Richardson ML: Diagnostic performance of magnetic resonance imaging for the diagnosis of rotator cuff tears using supplementary images in the oblique and sagittal plane. Invest Radiol 29:87, 1994.
47. Rafii M, Firooznia H, Sherman O, et al: Rotator cuff lesions: Signal patterns at MR imaging. Radiology 177: 817, 1990.
48. Resnick D: Frozen shoulder. Ann Rheum Dis 44:805, 1985.
49. Middleton WD, Remus WR, Totty WG, et al: Ultrasonographic evaluation of the rotator cuff and biceps tendon. J Bone Joint Surg [Am] 68:440, 1986.
50. van Leersum M, Schweitzer ME: Magnetic resonance imaging of the biceps complex. MRI Clin North Am 1:77, 1993.
51. Schweitzer ME: MR arthrography of the labral-ligamentous complex of the shoulder. Radiology 190:641, 1994.
52. Pollock AN, Reed MH: Shoulder deformities from obstetrical brachial plexus paralysis. Skeletal Radiol 18: 295, 1989.
53. Kaplan PA, Resnick D: Stress-induced osteolysis of the clavicle. Radiology 158:139, 1986.
54. Roach NA, Schweitzer ME: Does osteolysis of the distal clavicle occur following spinal cord injury? Skeletal Radiol 26:16, 1997.
55. Garland DE, Blum CE, Waters RL: Periarticular heterotopic ossification in head-injured adults: Incidence and location. J Bone Joint Surg [Am] 62: 1143, 1980.
56. Neer CS II: Replacement arthroplasty for glenohumeral osteoarthritis. J Bone Joint Surg [Am] 56:1, 1974.
57. Brossman J, Preidler KW, Pedowitz RA, et al: Shoulder impingement syndrome: Influence of shoulder position on rotator cuff impingement. AJR 167:1511, 1996.
58. Resnick D, Niwayama G: Resorption of the undersurface of the distal clavicle in rheumatoid arthritis. Radiology 120:75, 1976.
59. Babini JC, Gusis SE, Babini SM, et al: Superolateral erosions of the humeral head in chronic inflammatory arthropathies. Skeletal Radiol 21:515, 1992.
60. Reed MH, Wilmot DM: The radiology of juvenile rheumatoid arthritis: A review of the English language literature. J Rheumatol 18:2, 1991.
61. Resnick D: Patterns of peripheral joint disease in ankylosing spondylitis. Radiology 110:523, 1974.
62. Resnick D, Niwayama G: On the nature and significance of bony proliferation in “rheumatoid variant” disorders. AJR 129:275, 1977.
63. Czirjak L, Nagy Z, Szegedi G: Systemic sclerosis in the elderly. Clin Rheumatol 11:483, 1992.
64. Holt PD, Keats TE: Calcific tendinitis: A review of the usual and unusual. Skeletal Radiol 22:1, 1993.
65. Steinbach LS: Calcium pyrophosphate dihydrate and calcium hydroxyapatite crystal deposition diseases: Imaging perspectives. Radiol Clin N Am 42: 185, 2004.
66. Huang G-S, Bachmann D, Taylor JAM, et al: Calcium pyrophosphate dihydrate crystal deposition disease and pseudogout of the acromioclavicular joint: Radiographic and pathologic features. J Rheumatol 20:2077, 1993.
67. Halverson PB, Carrera GF, McCarthy DJ: Milwaukee shoulder syndrome: Fifteen additional cases and a description of contributing factors. Arch Intern Med 150:677, 1990.
68. Nguyen VD: Rapid destructive arthritis of the shoulder. Skeletal Radiol 25:107, 1996.
69. Miller-Blair D, White R, Greenspan A: Acute gout involving the acromioclavicular joint following treatment with gemfibrozil. J Rheumatol 19:166, 1992.
70. Katz GA, Peter JB, Pearson CM, et al: The shoulder pad sign—a diagnostic feature of amyloid arthropathy. N Engl J Med 288:354, 1973.
71. Faraawi R, Harth M, Kertesz A, et al: Arthritis in hemochromatosis. J Rheumatol 20:448, 1993.
72. Brancós MA, Peris P, Miró JM, et al: Septic arthritis in heroin addicts. Semin Arthritis Rheum 21:81, 1991.
73. Antti-Poika I, Vankka E, Santavirta S, et al: Two cases of shoulder joint tuberculosis. Acta Orthop Scand 62:81, 1991.
74. Haygood T, Williamson SL: Radiographic findings of extremity tuberculosis in childhood: Back to the future? RadioGraphics 14:561, 1994.
75. Schwartz HS, Unni KK, Pritchard DJ: Pigmented villonodular synovitis: A retrospective review of affected larger joints. Clin Orthop 247:243, 1989.
76. Hughes TH, Sartoris DJ, Schweitzer ME, et al: Pigmented villonodular synovitis: MRI characteristics. Skeletal Radiol 24:7, 1995.
77. Varma BP, Ramakrishna YJ: Synovial chondromatosis of the shoulder. Aust NZ J Surg 46:44, 1976.
78. Kramer J, Recht M, Deely DM, et al: MR appearance of idiopathic synovial osteochondromatosis. J Comput Assist Tomogr 17:772, 1993.
79. Melo-Gomes J, Viana-Queiroz M: Acromegalic arthropathy: A reversible rheumatic disease. J Rheumatol 14: 393, 1987.
80. MacDonald PB, Locht RC, Lindsay D, et al: Haemophilic arthropathy of the shoulder. J Bone Joint Surg [Br] 72:470, 1990.
81. Kolawole T, Banna M, Hawass N, et al: Neuropathic arthropathy as a complication of post-traumatic syringomyelia. Br J Radiol 60:702, 1987.
82. Garrett IR: Bone destruction in cancer. Semin Oncol 20:4, 1993.
83. Dahlin DC, Unni KK: Osteosarcoma of bone and its important recognizable varieties. Am J Surg Pathol 1:61, 1977.
84. Logan PM, Munk PL, O’Connell JX, et al: Post-radiation osteosarcoma of the scapula. Skeletal Radiol 25:596, 1996.
85. Mitchell ML, Ackerman LV: Metastatic and pseudomalignant osteoblastoma: A report of two unusual cases. Skeletal Radiol 15:213, 1986.
86. Smith J, McLachlan DL, Huvos AG, et al: Primary tumors of the clavicle and scapula. AJR 124:113, 1975.

87. Taconis WK, Mulder JD: Fibrosarcoma and malignant fibrous histiocytoma of long bones: Radiographic features and grading. Skeletal Radiol 11:237, 1984.
88. Dahlin DC, Coventry MB, Scanlon PW: Ewing's sarcoma: A critical analysis of 165 cases. J Bone Joint Surg [Am] 43:185, 1961.
89. Kyle RA: Multiple myeloma: Review of 869 cases. Mayo Clin Proc 50:29, 1975.
90. McLauchlan J: Solitary myeloma of the clavicle with long survival after total excision: Report of a case. J Bone Joint Surg [Br] 55:357, 1973.
91. Franczyk J, Samuels T, Rubenstein J, et al: Skeletal lymphoma. J Can Assoc Radiol 40:75, 1989.
92. Hermann G, Klein MJ, Fikry Abedlewahab I, et al: MRI appearance of primary non-Hodgkin's lymphoma of bone. Skeletal Radiol 26:629, 1997.
93. Mosheiff R, Liebergall M, Ziv I, et al: Osteoid osteoma of the scapula: A case report and review of the literature. Clin Orthop 262:129, 1991.
94. Loizaga JM, Calvo M, Barea FL, et al: Osteoblastoma and osteoid osteoma: Clinical and morphologic features of 162 cases. Pathol Res Pract 189:33, 1993.
95. Schiller AL: Diagnosis of borderline cartilage lesions of bone. Semin Diagn Pathol 2:42, 1985.
96. Ben-Itzhak I, Denolf FA, Versfeld GA, et al: The Maffucci syndrome. J Pediatr Orthop 8:345, 1988.
97. Kurt AM, Unni KK, Sim FH, et al: Chondroblastoma of bone. Hum Pathol 20:965, 1989.
98. Schmale GA, Conrad EV, Raskind WH: The natural history of hereditary multiple exostosis. J Bone Joint Surg [Am] 76:986, 1994.
99. Sherman RS, Wilner D: The roentgen diagnosis of hemangioma of bone. AJR 86:1146, 1961.
100. De Dios AMV, Bond JR, Shives TC, et al: Aneurysmal bone cyst: A clinicopathologic study of 238 cases. Cancer 69:2921, 1992.
101. Matfin G, McPherson F: Paget's disease of bone: Recent advances. J Orthop Rheumatol 6:127, 1993.
102. Mirra JM, Brien EW, Tehranzadeh J: Paget's disease of bone: Review with emphasis on radiologic features. II. Skeletal Radiol 24:173, 1995.
103. Crawford AH Jr, Bogamery N: Osseous manifestations of neurofibromatosis in childhood. J Pediatr Orthop 6:72, 1986.
104. Gibson MJ, Middlemiss JH: Fibrous dysplasia of bone. Br J Radiol 44:1, 1971.
105. Stull MA, Kransdorf MJ, Devaney KO: Langerhans cell histiocytosis of bone. RadioGraphics 12:801, 1992.
106. Kilpatrick SE, Wenger DE, Gilchrist GS, et al: Langerhans' cell histiocytosis (histiocytosis X) of bone: A clinicopathologic analysis of 263 pediatric and adult cases. Cancer 76:2471, 1995.
107. Taylor JAM, Resnick D, Sartoris DJ: Radiographic-pathologic correlation. In Sartoris DJ (ed): Osteoporosis: Diagnosis and treatment. New York, Marcel Dekker, 1996, p 147.
108. Mankin HJ: Rickets, osteomalacia, and renal osteodystrophy. Orthop Clin North Am 21:81, 1990.
109. Wolfson BJ, Capitanio MA: The wide spectrum of renal osteodystrophy in children. CRC Crit Rev Diagn Imaging 27:297, 1987.
110. Resnick D, Niwayama G: Subchondral resorption of bone in renal osteodystrophy. Radiology 118:315, 1976.
111. Tigges S, Nance EP, Carpenter WA, et al: Renal osteodystrophy: Imaging findings that mimic those of other diseases. AJR 165:143, 1995.
112. Schuman CA, Jones HW III: The "milk-alkali" syndrome: Two case reports with discussion of pathogenesis. Q J Med 55:119, 1985.
113. Kofoed H: Revascularization of the humeral head: A report of two cases of fracture-dislocation of the shoulder. Clin Orthop 179:175, 1983.
114. Lee DK, Hansen HR: Post-traumatic avascular necrosis of the humeral head in displaced proximal humerus fractures. J Trauma 21:788, 1984.
115. Langlands AO, Souter WA, Samuel E, et al: Radiation osteitis following irradiation for breast cancer. Clin Radiol 28:93, 1977.
116. Gersovich EO, Greenspan A: Osteomyelitis of the clavicle: Clinical, radiologic, and bacteriologic findings in ten patients. Skeletal Radiol 23:205, 1994.
117. Boutin RD, Resnick D: The SAPHO syndrome: An evolving concept for unifying several idiopathic disorders of bone and skin. AJR 170:585, 1998.
118. Köhler H, Uehlinger E, Kutzner K, et al: Sternocostoclavicular hyperostosis: Painful swelling of the sternum, clavicles, and upper ribs: Report of two new cases. Ann Intern Med 87:192, 1977.
119. Greenspan A, Gerscovich E, Szabo RM, et al: Condensing osteitis of the clavicle: A rare but frequently misdiagnosed condition. AJR 156:1011, 1991.
120. Rosenberg ZS, Shankman S, Klein M, et al: Chronic recurrent multifocal osteomyelitis. AJR 151:142, 1988.
121. Levy M, Goldberg I, Fischel RE, et al: Friedrich's disease: Aseptic necrosis of the sternal end of the clavicle. J Bone Joint Surg [Br] 63:539, 1981.
122. Holzman D: Infantile cortical hyperostosis of the scapula presenting as an ipsilateral Erb's palsy. J Pediatr 81:785, 1972.
123. Melo-Gomes J, Viana-Queiroz M: Acromegalic arthropathy: A reversible rheumatic disease. J Rheumatol 14: 393, 1987.
124. Herbert DA, Fessel WJ: Idiopathic hypertrophic osteoarthropathy (pachydermoperiostosis). West J Med 134: 354, 1981.
125. Kroon HMJA, Pauwels EKJ: Bone scintigraphy for the detection and follow-up of hypertrophic osteoarthropathy. Diagn Imaging 51:47, 1982.
126. Gamble JG, Ip SC: Hypervitaminosis A in a child from megadosing. J Pediatr Orthop 5:219, 1985.
127. Høst A, Halken S, Andersen PE Jr: Reversibility of cortical hyperostosis following long-term prostaglandin E_1 therapy in infants with ductus-dependent congenital heart disease. Pediatr Radiol 18:149, 1988.
128. Miller ME, Ada JR: Injuries to the shoulder girdle. In Browner BD, Jupiter JB, Levine AM, et al (eds): Skeletal trauma: fractures, dislocations, ligamentous injuries. Philadelphia, Saunders, 1992, p 1306.
129. Jurik AG: Chronic recurrent multifocal osteomyelitis. Semin Musculoskeletal Radiol 8:243, 2004.
130. Bencardion JT, Hassankhani A: Calcium pyrophosphate dihydrate crystal deposition disease. Semin Musculoskeletal Radiol 7:175, 2003.
131. Garcia G, McCord GC, Kumar R: Hydroxyapatite crystal deposition disease. Semin Musculoskeletal Radiol 7:187, 2003.
132. Sheldon PJ, Forrester DM: Imaging of amyloid arthropathy. Semin Musculoskeletal Radiol 7:195, 2003.
133. Kerr R: Imaging of musculoskeletal complications of hemophilia. Semin Musculoskeletal Radiol 7:127, 2003.
134. Marin C, Sanchez-Alegre ML, Gallego C, et al: Magnetic resonance imaging of osteoarticular infections in children. Curr Probl Diagn Radiol 33:43, 2004.
135. Christian S, Kraas J, Conway WF: Musculoskeletal infections. Semin Roentgenol 42:92, 2007.
136. Greenspan A, Tehranzadeh J: Imaging of infectious arthritis. Radiol Clin N Am 39:267, 2001.
137. Whitehouse RW: Paget's disease of bone. Semin Musculoskeletal Radiol 6:313, 2002.
138. Whitten CR, Saifuddin A: MRI of Paget's disease of bone. Clinical Radiology 58:763, 2003.
139. Al-Nakshabandi NA, Ryan AG, Choudur H, et al: Pigmented villonodular synovitis. Clin Radiol 59:414, 2004.
140. Antonio GE, Cho JH, Chung CB, et al: MR imaging appearance and classification of acromioclavicular joint injury. AJR 180:110, 2002.
141. Tshering Vogel DW, Steinbach LS, Hertel R, et al: Acromioclavicular joint cyst: Nine cases of a pseudotumor of the shoulder. Skeletal Radiol 34:260, 2005.
142. Prato N, Banderali A, Neumaier CE, et al: Calcific tendinitis of the rotator cuff as a cause of drooping shoulder. Skeletal Radiol 32:82, 2003.
143. Harden SP, Argent JD, Blaquiere RM: Painful sclerosis of the medial end of the clavicle. Clin Radiol 59:992, 2004.
144. Yamada K, Sugiura H, Suzuki Y: Stress fracture of the medial clavicle secondary to nervous tic. Skeletal Radiol 33:534, 2004.
145. Beaudreuil J, Bardin T, Orcel P: Natural history or outcome with conservative treatment of degenerative

rotator cuff tears [Editorial]. Joint Bone Spine 74:527, 2007.
146. Kassarjian A, Llopis E, Palmer WE: Distal clavicular osteolysis: MR evidence for subchondral fracture. Skeletal Radiol 36:17, 2007.
147. Sharma BG: Duplication of the clavicle with triplication of the coracoid process. Skeletal Radiol 32:661, 2003.
148. Moratalla MB, Gabarda RF: Acromioclavicular joint ganglion. Europ J Radiol Extra 63:21, 2007.
149. Mulyadi E, Harish S, O'Neill J, et al: MRI of impingement syndromes of the shoulder. Clinical Radiology 64:3, 2009
150. Kyrölä K, Niemitukia L, Jaroma H, et al: Long-term findings in operated rotator cuff tear. Acta Radiol 45:526, 2004.
151. Farid N, Bruce D, Chung CB: Miscellaneous conditions of the shoulder: Anatomical, clinical, and pictorial review emphasizing potential pitfalls in imaging diagnosis. Eur J Radiol 68:88, 2008.
152. Gotoh M, Higuchi F, Suzuki R, et al: Progression from calcifying tendinitis to rotator cuff tear. Skeletal Radiol 32:86, 2003.
153. Chan R, Kim DH, Millett PJ, et al: Calcifying tendinitis of the rotator cuff with cortical bone erosion. Skeletal Radiol 33:596, 2004.
154. MacDonald PB, Lapointe P: Acromioclavicular and sternoclavicular joint injuries. Orthop Clin N Am 39:535, 2008.
155. Alegre MLS, Marin C, Mardones GG: Duplication of the scapula. Skeletal Radiol 32:728, 2003.
156. Lapner PC, Uhthoff HK, Papp S: Scapula fractures. Orthop Clin N Am 39:459, 2008.
157. Tadros AMA, Lunsjo K, Czechowski J, et al: Usefulness of different imaging modalities in the assessment of scapular fractures caused by blunt trauma. Acta Radiol 48:71, 2007.
158. Gamanagatti S, Gufalani B, Singh N: Large bursa associated with osteochondroma of ventral surface of scapula. Eur J Radiol Extra 51:103, 2004.
159. Sanders TG, Jersey SL: Conventional radiography of the shoulder. Semin Roentgenol 40:207, 2005.
160. Opsha O, Malik A, Baltazar R, et al: MRI of the rotator cuff and internal derangement. Eur J Radiol 68:38, 2008.
161. Marshall GB, McKenna E, Mahallati H: Parsonage-Turner syndrome. Eur J Radiol 56:51, 2005.
162. Gaskin CM, Helms CA: Parsonage-Turner syndrome: MR imaging findings and clinical information of 27 patients. Radiology 240:501, 2006.
163. Kudawara I, Aono M, Ohzono K, et al: Synvovial chondromatosis of the acromioclavicular joint. Skeletal Radiol 33:600, 2004.
164. Lynch CJ, Taylor JAM, Buchberger DJ: Glenoid hypoplasia: a report of two patients. J Manip Phys Tharap 31:5, 2008.

CHAPTER 14

Humerus

1. Resnick D, Cone RO: The nature of humeral pseudocysts. Radiology 150: 27, 1984.
2. Wertsch JJ, Melvin J: Median nerve anatomy and entrapment syndromes: A review. Arch Phys Med Rehabil 63:623, 1982.
3. Keats TE: Atlas of normal roentgen variants that may simulate disease. 8th Ed. Chicago, Year Book Medical Publishers, 2006.
4. Yochum TR, Rowe LJ: Essentials of skeletal radiology. 3rd Ed. Baltimore, Williams & Wilkins, 2004.
5. Resnick D, Niwayama G: Osteoporosis. In Resnick D: Diagnosis of bone and joint disorders. 4th Ed. Philadelphia, Saunders, 2002, p 1783.
6. Köhler A, Zimmer EA: Borderlands of normal and early pathologic findings in skeletal radiography. 4th Ed. New York, Thieme Medical Publishers, 1993.
7. Ozonoff MB, Zeiter FM Jr: The upper humeral notch: A normal variant in children. Radiology 113:699, 1974.
8. Ward EF, Savoie FH, Hughes JL: Fractures of the diaphyseal humerus. In Browner BD, Jupiter JB, Levine AM, et al (eds): Skeletal trauma: fractures, dislocations, ligamentous injuries. Philadelphia, Saunders, 1992, p 1177.
9. Mast JW, Spiegel PG, Harvey JP Jr, et al: Fractures of the humeral shaft: A retrospective study of 240 adult fractures. Clin Orthop 112:254, 1975.
10. Rogers LF. Radiology of skeletal trauma. 3rd Ed. New York, Churchill Livingstone, 2002.
11. Thomas SA, Rosenfield NS, Leventhal JM, et al: Long-bone fractures in young children: Distinguishing accidental injuries from child abuse. Pediatrics 88:471, 1991.
12. Nuovo MA, Norman A, Chumas A, et al: Myositis ossificans with atypical clinical, radiographic, or pathologic findings: A review of 23 cases. Skeletal Radiol 21:87, 1992.
13. Greenspan A, Norman A: Osteolytic cortical destruction: An unusual pattern of skeletal metastasis. Skeletal Radiol 17:402, 1988.
14. Resnik C, Garver P, Resnick D: Bony expansion in skeletal metastasis from carcinoma of the prostate as seen by bone scintigraphy. South Med J 77: 1331, 1984.
15. Huvos AG, Higinbotham NL, Miller TR: Bone sarcomas arising in fibrous dysplasia. J Bone Joint Surg [Am] 54:1047, 1972.
16. Dahlin DC, Unni KK: Osteosarcoma of bone and its important recognizable varieties. Am J Surg Pathol 1:61, 1977.
17. Ritschl P, Wurnig C, Lechner G, et al: Parosteal osteosarcoma: 2-23 year follow-up of 33 patients. Acta Orthop Scand 62:195, 1991.
18. Henderson ED, Dahlin DC: Chondrosarcoma of bone—a study of two hundred and eighty-eight cases. J Bone Joint Surg [Am] 45:1450, 1963.
19. Brien EW, Mirra JM, Kerr R: Benign and malignant cartilage tumors of bone and joint: Their anatomic and theoretical basis with an emphasis on radiology, pathology and clinical biology. 1. The intramedullary cartilage tumors. Skeletal Radiol 26:325, 1997.
20. Dahlin DC: Giant cell tumor of bone: Highlights of 407 cases. AJR 144:955, 1985.
21. Taconis WK, Mulder JD: Fibrosarcoma and malignant fibrous histiocytoma of long bones: Radiographic features and grading. Skeletal Radiol 11:237, 1984.
22. Dahlin DC, Coventry MB, Scanlon PW: Ewing's sarcoma: A critical analysis of 165 cases. J Bone Joint Surg [Am] 43:185, 1961.
23. Kyle RA: Multiple myeloma: Review of 869 cases. Mayo Clin Proc 50:29, 1975.
24. Hermann G, Klein MJ, Fikry Abedlewahab I, et al: MRI appearance of primary non-Hodgkin's lymphoma of bone. Skeletal Radiol 26:629, 1997.
25. Clayton F, Butler JJ, Ayala AG, et al: Non-Hodgkin's lymphoma in bone: Pathologic and radiologic features with clinical correlates. Cancer 60: 2494, 1987.
26. Benz G, Brandeis WE, Willich E: Radiological aspects of leukemia in childhood: An analysis of 89 children. Pediatr Radiol 4:201, 1976.
27. Greenspan A: Bone island (enostosis): Current concept—a review. Skeletal Radiol 24:111, 1995.
28. Cronemeyer RL, Kirchmer NA, DeSmet AA, et al: Intraarticular osteoid osteoma of the humerus simulating synovitis of the elbow: A case report. J Bone Joint Surg [Am] 63:1172, 1981.
29. Kayser F, Resnick D, Haghighi P, et al: Evidence of the subperiosteal origin of osteoid osteomas in tubular bones: Analysis by CT and MR imaging. AJR 170:609, 1998.
30. Tonai M, Campbell CJ, Ahn GH, et al: Osteoblastoma: Classification and report of 16 cases. Clin Orthop 167:222, 1982.
31. Schiller AL: Diagnosis of borderline cartilage lesions of bone. Semin Diagn Pathol 2:42, 1985.
32. Bloem JL, Mulder JD: Chondroblastoma: A clinical and radiological study of 104 cases. Skeletal Radiol 14:1, 1985.
33. Weatherall PT, Maale GE, Mendelsohn DB, et al: Chondroblastoma: Classic and confusing appearance at MR imaging. Radiology 190:467, 1994.
34. Milgran JW: The origins of osteochondromas and enchondromas: A histopathologic study. Clin Orthop 174:264, 1983.
35. Karasick D, Schweitzer ME, Eschelman DJ: Symptomatic osteochondromas: Imaging features. AJR 168:1507, 1997.
36. Shapiro F, Simon S, Glimcher MJ: Hereditary multiple exostoses: Anthropometric, roentgenologic and clinical aspects. J Bone Joint Surg [Am] 61:815, 1979.

37. Solomon L: Chondrosarcoma in hereditary multiple exostosis. S Afr Med J 48:671, 1974.
38. Schmale GA, Conrad EV, Raskind WH: The natural history of hereditary multiple exostosis. J Bone Joint Surg [Am] 76:986, 1994.
39. Ritschl P, Karnel F, Hajek P: Fibrous metaphyseal defects—determination of their origin and natural history using a radiomorphological study. Skeletal Radiol 17:8, 1988.
40. Milgram JW: Intraosseous lipoma: A clinicopathologic study of 66 cases. Clin Orthop 231:277, 1988.
41. Chigira M, Maehara S, Arita S, et al: The aetiology and treatment of simple bone cysts. J Bone Joint Surg [Br] 65:633, 1983.
42. McGlynn FJ, Mickelson MR, El-Khoury GY: The fallen fragment sign in unicameral bone cysts. Clin Orthop 156:157, 1981.
43. De Dios AMV, Bond JR, Shives TC, et al: Aneurysmal bone cyst: A clinicopathologic study of 238 cases. Cancer 69:2921, 1992.
44. Matfin G, McPherson F: Paget's disease of bone: Recent advances. J Orthop Rheumatol 6:127, 1993.
45. Mirra JM, Brien EW, Tehranzadeh J: Paget's disease of bone: Review with emphasis on radiologic features. Part II. Skeletal Radiol 24:173, 1995.
46. Gibson MJ, Middlemiss JH: Fibrous dysplasia of bone. Br J Radiol 44:1, 1971.
47. Stull MA, Kransdorf MJ, Devaney KO: Langerhans cell histiocytosis of bone. RadioGraphics 12:801, 1992.
48. Kilpatrick SE, Wenger DE, Gilchrist GS, et al: Langerhans' cell histiocytosis (histiocytosis X) of bone: A clinicopathologic analysis of 263 pediatric and adult cases. Cancer 76:2471, 1995.
49. Taylor JAM, Resnick D, Sartoris DJ: Radiographic-pathologic correlation. In Sartoris DJ: Osteoporosis: diagnosis and treatment. New York, Marcel Dekker, 1996, p 147.
50. Root L: The treatment of osteogenesis imperfecta. Orthop Clin North Am 15:775, 1984.
51. Mankin HJ: Rickets, osteomalacia, and renal osteodystrophy. Orthop Clin North Am 21:81, 1990.
52. Greenfield GB: Bone changes in chronic adult Gaucher's disease. AJR 110:800, 1970.
53. Pineda C: Diagnostic imaging in hypertrophic osteoarthropathy. Clin Exp Rheumatol 10:27, 1992.
54. Gold RH, Hawkins RA, Katz RD: Bacterial osteomyelitis: Findings on plain radiography, CT, MR, and scintigraphy. AJR 157:365, 1991.
55. Tumeh SS, Aliabadi P, Weissman BN, et al: Disease activity in osteomyelitis: Role of radiography. Radiology 165:781, 1987.
56. Pachman LN: Juvenile dermatomyositis. Pediatr Clin North Am 33:1097, 1986.
57. Kaim AH, Hugli R, Bonél HM, et al: Chondroblastoma and clear cell chondrosarcoma: Radiological and MRI characteristics with histopathological correlation. Skeletal Radiol 31:88, 2002.
58. Propeck T, Bullard MA, Lin J, et al: Radiologic-pathologic correlation of intraosseous lipomas. AJR 175:673, 2000.
59. Hwang S: Imaging of lymphoma of the musculoskeletal system. Radiol Clin N Am 46:379, 2008.
60. Christian S, Kraas J, Conway WF: Musculoskeletal infections. Semin Roentgenol 42:92, 2007.
61. Ruzek KA, Wenger DE: The multiple faces of lymphoma of the musculoskeletal system. Skeletal Radiol 33:1, 2004.
62. Andresen KJ, Sundaram M, Unni KK, et al: Imaging features of low-grade central osteosarcoma of the long bones and pelvis. Skeletal Radiol 33:373, 2004.
63. Suresh S, Saifuddin A: Radiological appearances of appendicular osteosarcoma: A comprehensive pictorial review. Clin Radiol 62:314, 2007.
64. Whitehouse RW: Paget's disease of bone. Semin Musculoskeletal Radiol 6:313, 2002.
65. Whitten CR, Saifuddin A: MRI of Paget's disease of bone. Clin Radiol 58:763, 2003.
66. Berry JL, Davies M, Mee AP: Vitamin D metabolism, rickets and osteomalacia. Semin Musculoskeletal Radiol 6:173, 2002.
67. Wenstrup RJ, Roca-Espiau M, Weinreb NJ, et al: Skeletal aspects of Gaucher disease: A review. Br J Radiol 75 (Suppl 1):A2, 2002.
68. Callahan EB, Bennett DL, El-Khoury GY, et al: Ball-thrower's fracture of the humerus. Skeletal Radiol 33:355, 2004.
69. Lee JC, Malara FA, Wood T, et al: MRI of stress reaction of the distal humerus in elite tennis players. AJR 187:901, 2006.
70. Ridpath CA, Wilson AJ: Shoulder and humerus trauma. Semin Musculoskeletal Radiol 4:151, 2000.

CHAPTER 15

Elbow

1. Brodeur AE, Silberstein MJ, Graviss ER, et al: The basic tenets for appropriate evaluation of the elbow in pediatrics. Curr Probl Diagn Radiol 12:1, 1983.
2. Edeiken J, Dalinka M, Karasick D: Edeiken's roentgen diagnosis of diseases of bone. 4th Ed. Baltimore, Williams & Wilkins, 1990.
3. Kahn SL, Gaskin CM, Sharp VL: Keats and Kahn's roentgen atlas of skeletal maturation. DVD-ROM Ed. Philadelphia, Lippincott Williams and Wilkins, 2007.
4. Greenfield GB: Radiology of bone diseases. 2nd Ed. Philadelphia, JB Lippincott, 1975.
5. Silberstein MJ, Brodeur AE, Graviss ER: Some vagaries of the radial head and neck. J Bone Joint Surg [Am] 64:1153, 1982.
6. Greenspan A, Norman A: Radial head-capitellum view: An expanded imaging approach to elbow injury. Radiology 164:272, 1987.
7. Köhler A, Zimmer EA: Borderlands of normal and early pathologic findings in skeletal radiography. 4th Ed. New York, Thieme Medical Publishers, 1993.
8. Keats TE: Atlas of normal roentgen variants that may simulate disease, 6th Ed. Chicago, Year Book, 1996.
9. Resnick D, Niwayama G: Osteoporosis. In Resnick D: Diagnosis of bone and joint disorders. 4th Ed. Philadelphia, Saunders, 2002, p 1783.
10. Yochum TR, Rowe LJ: Essentials of skeletal radiology. 3rd Ed. Baltimore, Williams & Wilkins, 2006.
11. Kattan KR, Babcock DS: Bilateral patella cubiti. Skeletal Radiol 4:249, 1979.
12. Mital MA: Congenital radioulnar synostosis and congenital dislocation of the radial head. Orthop Clin North Am 7:375, 1976.
13. Guidera KJ, Satterwhite Y, Ogden JA, et al: Nail patella syndrome: A review of 44 orthopaedic patients. J Pediatr Orthop 11:737, 1991.
14. Benli IT, Akalin S, Boysan E, et al: Epidemiological, clinical, and radiological aspects of osteopoikilosis. J Bone Joint Surg [Br] 74:504, 1992.
15. Bohrer SP: The fat pad sign following elbow trauma. Its usefulness and reliability in suspecting invisible fractures. Clin Radiol 21:90, 1970.
16. Murphy WA, Siegel MJ: Elbow fat pads with new signs and extended differential diagnosis. Radiology 124:659, 1977.
17. Donnelly LF, Klostermeier TT, Klosterman LA: Traumatic elbow effusions in pediatric patients: Are occult fractures the rule? AJR 171:243, 1998.
18. Floyd WE III, Gebhardt MC, Emans JB: Intra-articular entrapment of the median nerve after elbow dislocation in children. J Hand Surg [Am] 12:704, 1987.
19. Triantafyllou SJ, Wilson SC, Rychak JS: Irreducible pulled elbow in a child. A case report. Clin Orthop 284:153, 1992.
20. Ring D, Jupiter JB, Simpson NS: Monteggia fractures in adults. J Bone Joint Surg [Am] 80:1733, 1998.
21. Beltran J, Rosenberg ZS, Kawelblum M, et al: Pediatric elbow fractures: MRI evaluation. Skeletal Radiol 23:277, 1994.
22. Gabel GT, Hanson G, Bennett JB, et al: Intraarticular fractures of the distal humerus in the adult. Clin Orthop 216:99, 1987.
23. Schild H, Muller HA, Klose K: The halfmoon sign. Australas Radiol 26:273, 1982.
24. Horne JG, Tanzer TL: Olecranon fractures: A review of 100 cases. J Trauma 21:469, 1981.

25. Regan W, Morrey B: Fractures of the coronoid process of the ulna. J Bone Joint Surg [Am] 71:1348, 1989.
26. Bock GW, Cohen MS, Resnick D: Fracture-dislocation of the elbow with inferior radioulnar dissociation: A variant of the Essex-Lopresti injury. Skeletal Radiol 21:315, 1992.
27. Leventhal JM, Thomas SA, Rosenfield NS, et al: Fractures in young children: Distinguishing child abuse from unintentional injuries. Am J Dis Child 147:87, 1993.
28. Rogers LF, Poznanski AK: Imaging of epiphyseal injuries. Radiology 191:297, 1994.
29. De Jager LT, Hoffman EB: Fracture-separation of the distal humeral epiphysis. J Bone Joint Surg [Br] 73:143, 1991.
30. Daffner RH, Pavlov H: Stress fractures: Current concepts. AJR 159:245, 1992.
31. Bauer M, Jonsson K, Josefsson PO, et al: Osteochondritis dissecans of the elbow: A long term follow-up study. Clin Orthop 284:156, 1992.
32. Patten RM: Overuse syndromes and injuries involving the elbow: MR imaging findings. AJR 164:1205, 1995.
33. Mirowitz SA, London SL: Ulnar collateral ligament injury in baseball pitchers: MR imaging evaluation. Radiology 185:573, 1992.
34. Morrey BF, O'Driscoll SW: Lateral collateral ligament injury. In BF Morrey (ed): The elbow and its disorders. 2nd Ed. Philadelphia, Saunders, 1993, p 573.
35. Caldwell GL Jr, Safran MR: Elbow problems in the athlete. Orthop Clin North Am 26:465, 1995.
36. Ho CP: Sports and occupational injuries of the elbow: MR imaging findings. AJR 164:1465, 1995.
37. Fitzgerald SW, Curry DR, Erickson SJ, et al: Distal biceps tendon injury: MR imaging diagnosis. Radiology 191:203, 1994.
38. Tiger E, Mayer DP, Glazer R: Complete avulsion of the triceps tendon: MRI diagnosis. Comput Med Imaging Graph 17:51, 1993.
39. Goodfellow JW, Bullough PG: The pattern of aging of the articular cartilage of the elbow joint. J Bone Joint Surg [Br] 49:175, 1967.
40. Beyeler CH, Schlapbach P, Gerber NJ, et al: Diffuse idiopathic skeletal hyperostosis (DISH) of the elbow: A cause of elbow pain? A controlled study. Br J Rheumatol 31:319, 1992.
41. Weston WJ: The synovial changes at the elbow in rheumatoid arthritis. Australas Radiol 15:170, 1971.
42. Reed MH, Wilmot DM: The radiology of juvenile rheumatoid arthritis: A review of the English language literature. J Rheumatol 18:2, 1991.
43. Resnick D: Patterns of peripheral joint disease in ankylosing spondylitis. Radiology 110:523, 1974.
44. Resnick D, Niwayama G: On the nature and significance of bony proliferation in "rheumatoid variant" disorders. AJR 129:275, 1977.
45. Czirjak L, Nagy Z, Szegedi G: Systemic sclerosis in the elderly. Clin Rheumatol 11:483, 1992.
46. Resnick D: Gouty arthritis. In Resnick D (ed): Diagnosis of bone and joint disorders. 4th Ed. Philadelphia, Saunders, 2002, p 1519.
47. Resnick D, Niwayama G, Georgen TG, et al: Clinical, radiographic and pathologic abnormalities in calcium pyrophosphate dihydrate deposition disease (CPPD): Pseudogout. Radiology 122:1, 1977.
48. Steinbach LS, Resnick D: Calcium pyrophosphate dihydrate crystal deposition disease revisited. Radiology 200: 1, 1996.
49. Ho G Jr, Mikolich DJ: Bacterial infection of superficial subcutaneous bursae. Clinics Rheum Dis 12:437, 1986.
50. Haygood TM, Williamson SL: Radiographic findings of extremity tuberculosis in childhood: Back to the future? RadioGraphics 14:561, 1994.
51. Schwartz HS, Unni KK, Pritchard DJ: Pigmented villonodular synovitis: A retrospective review of affected larger joints. Clin Orthop 247:243, 1989.
52. Hughes TH, Sartoris DJ, Schweitzer ME, et al: Pigmented villonodular synovitis: MRI characteristics. Skeletal Radiol 24:7, 1995.
53. Giustra PE, Furman RS, Roberts L, et al: Synovial chondromatosis involving the elbow. AJR 127:347, 1976.
54. Kramer J, Recht M, Deely DM, et al: MR appearance of idiopathic synovial osteochondromatosis. J Comput Assist Tomogr 17:772, 1993.
55. Melo-Gomes J, Viana-Queiroz M: Acromegalic arthropathy: A reversible rheumatic disease. J Rheumatol 14: 393, 1987.
56. Hôgh J, Ludlam CA, Macnicol MF: Hemophilic arthropathy of the upper limb. Clin Orthop 218:225, 1987.
57. Resnik CS, Reed WW: Hand, wrist, and elbow arthropathy in syringomyelia. J Can Assoc Radiol 36:325, 1985.
58. Mankin HJ: Rickets, osteomalacia, and renal osteodystrophy. Orthop Clin North Am 21:81, 1990.
59. Wolfson BJ, Capitanio MA: The wide spectrum of renal osteodystrophy in children. CRC Crit Rev Diagn Imaging 27:297, 1987.
60. Resnick D, Niwayama G: Subchondral resorption of bone in renal osteodystrophy. Radiology 118:315, 1976.
61. Tigges S, Nance EP, Carpenter WA, et al: Renal osteodystrophy: Imaging findings that mimic those of other diseases. AJR 165:143, 1995.
62. Murphy MD, Sartoris DJ, Quale JL, et al: Musculoskeletal manifestations of chronic renal insufficiency. RadioGraphics 13:357, 1993.
63. Garland DE, Blum CE, Waters RL: Periarticular heterotopic ossification in head-injured adults: Incidence and location. J Bone Joint Surg [Am] 62:1143, 1980.
64. Bauer M, Jonsson K, Josefsson PO, et al: Osteochondritis dissecans of the elbow: A long term follow-up study. Clin Orthop 284:156, 1992.
65. Greenspan A, Tehranzadeh J: Imaging of infectious arthritis. Radiol Clin N Am 39:267, 2001.
66. Al-Nakshabandi NA, Ryan AG, Choudur H, et al: Pigmented villonodular synovitis. Clin Radiol 59:414, 2004.
67. Mulligan SA, Schwartz ML, Broussard MF, et al: Heterotopic calcification and tears of the ulnar collateral ligament: Radiographic and MR imaging findings. AJR 175:1099, 2000.
68. De Smet AA, Winter TC, Best TM, et al: Dynamic sonography with valgus stress to assess elbow ulnar collateral ligament injury in baseball pitchers. Skeletal Radiol 31:671, 2002.
69. Jacoby SM, Herman MJ, Morrision WB, et al: Pediatric elbow trauma: An orthopaedic perspective on the importance of radiographic interpretation. Semin Musculoskeletal Radiol 11:48, 2007.
70. Cunningham PM: MR imaging of trauma: Elbow and wrist. Semin Musculoskeletal Radiol 10:28, 2006.
71. Pudas T, Hurme T, Mattila K, et al: Magnetic resonance imaging in pediatric elbow fractures. Acta Radiol 46: 636, 2005.
72. Kijowski R, De Smet AA: Magnetic resonance imaging findings in patients with medial epicondylitis. Skeletal Radiol 34:196, 2005.
73. Chung CB, Stanley AJ, Genitli A: Magnetic resonance imaging of elbow instability. Semin Musculoskeletal Radiol 9:67, 2005.
74. Sonin A: Fractures of the elbow and forearm. Semin Musculoskeletal Radiol 4:171, 2000.
75. Grayson DE: The elbow: Radiographic imaging pearls and pitfalls. Semin Roentgenol 40:223, 2005.
76. Pacelli LL, Guzman M, Botte MJ: Elbow instability: The orthopedic approach. Semin Musculoskeletal Radiol 9:56, 2005.
77. Tomás FJ: Alternative radiographic projections of the ulnar coronoid process. Br J Radiol 74:756, 2001.
78. Major NM, Crawford ST: Elbow effusions in trauma in adults and children: Is there an occult fracture? AJR 178: 413, 2002.

CHAPTER 16

Radius and Ulna

1. Mital MA: Congenital radioulnar synostosis and congenital dislocation of the radial head. Orthop Clin North Am 7:375, 1976.
2. Köhler A, Zimmer EA: Borderlands of normal and early pathologic findings in skeletal radiography. 4th Ed. New York, Thieme Medical Publishers, 1993, p 163.
3. Fagg PS: Wrist pain in the Madelung's deformity of dyschondrosteosis. J Hand Surg [Br] 13:11, 1988.

4. Friedman SL, Palmer AK: The ulnar impaction syndrome. Hand Clin 7:295, 1991.
5. Imaeda T, Nakamura R, Shionoya K, et al: Ulnar impaction syndrome: MR imaging findings. Radiology 201:495, 1996.
6. Escobedo EM, Bergman AG, Hunter JC: MR imaging of ulnar impaction. Skeletal Radiol 24:85, 1995.
7. Bonzar M, Firrell JC, Mah ET, et al: Kienböck disease and negative ulnar variance. J Bone Joint Surg [Am] 80:1154, 1998.
8. DeSmet L: Ulnar variance: Facts and fiction review article. Acta Orthop Belg 60:1, 1994.
9. Voorhees DR, Daffner RH, Nunley JA, et al: Carpal ligamentous disruptions and negative ulnar variance. Skeletal Radiol 13:257, 1985.
10. Goldberg HD, Young JWR, Reiner BI, et al: Double injuries of the forearm: A common occurrence. Radiology 185: 223, 1992.
11. Olney BW, Menelaus MB: Monteggia and equivalent lesions in childhood. J Pediatr Orthop 9:219, 1989.
12. Ring D, Jupiter JB, Simpson NS: Monteggia fractures in adults. J Bone Joint Surg [Am] 80:1733, 1998.
13. Alpar EK, Thompson K, Owen R, et al: Midshaft fractures of the forearm bones in children. Injury 13:153, 1981.
14. Walsh HPJ, McLaren CAN, Owen R: Galeazzi fractures in children. J Bone Joint Surg [Br] 69:730, 1987.
15. Watson FM, Eaton RG: Post-traumatic radio-ulnar synostosis. J Trauma 18:467, 1978.
16. Anderson MW, Greenspan A: Stress fractures. Radiology 199:1, 1996.
17. Cautilli RA, Joyce MF, Gordon E, et al: Classifications of fractures of the distal radius. Clin Orthop 103:163, 1974.
18. Light TR, Ogden DA, Ogden JA: The anatomy of metaphyseal torus fractures. Clin Orthop 188:103, 1984.
19. DeOliveira JC: Barton's fractures. J Bone Joint Surg [Am] 55:586, 1973.
20. Bilos ZJ, Pankovich AM, Yelda S: Fracture-dislocation of the radiocarpal joint. J Bone Joint Surg [Am] 59:198, 1977.
21. Helm RH, Tonkin MA: The chauffeur's fracture: Simple or complex? J Hand Surg [Br] 17:156, 1992.
22. Thomas WG, Kershaw CJ: Entrapment of the extensor tendons in a Smith's fracture: Brief report. J Bone Joint Surg [Br] 70:491, 1988.
23. Burgess RC, Watson HK: Hypertrophic ulnar styloid nonunions. Clin Orthop 228:215, 1988.
24. Kleinman PK, Marks SC Jr, Richmond JM, et al: Inflicted skeletal injury: Post mortem radiologic-histopathologic study in 31 infants. AJR 165:647, 1995.
25. Manoli A II: Irreducible fracture-separation of the distal radial epiphysis: Report of a case. J Bone Joint Surg [Am] 64:1095, 1982.
26. Chang CY, Shih C, Penn IW, et al: Wrist injuries in adolescent gymnasts of a Chinese opera school: Radiography survey. Radiology 195:861, 1995.
27. Greenspan A, Norman A: Osteolytic cortical destruction: An unusual pattern of skeletal metastasis. Skeletal Radiol 17:402, 1988.
28. Resnik C, Garver P, Resnick D: Bony expansion in skeletal metastasis from carcinoma of the prostate as seen by bone scintigraphy. South Med J 77: 1331, 1984.
29. Dahlin DC, Unni KK: Osteosarcoma of bone and its important recognizable varieties. Am J Surg Pathol 1:61, 1977.
30. Ritschl P, Wurnig C, Lechner G, et al: Parosteal osteosarcoma: 2-23-year follow-up of 33 patients. Acta Orthop Scand 62:195, 1991.
31. Dahlin DC: Giant cell tumor of bone: Highlights of 407 cases. AJR 144:955, 1985.
32. Dahlin DC, Coventry MB, Scanlon PW: Ewing's sarcoma: A critical analysis of 165 cases. J Bone Joint Surg [Am] 43:185, 1961.
33. Kyle RA: Multiple myeloma: Review of 869 cases. Mayo Clin Proc 50:29, 1975.
34. Clayton F, Butler JJ, Ayala AG, et al: Non-Hodgkin's lymphoma in bone: Pathologic and radiologic features with clinical correlates. Cancer 60:2494, 1987.
35. Benz G, Brandeis WE, Willich E: Radiological aspects of leukemia in childhood: An analysis of 89 children. Pediatr Radiol 4:201, 1976.
36. Kayser F, Resnick D, Haghighi P, et al: Evidence of the subperiosteal origin of osteoid osteomas in tubular bones: Analysis by CT and MR imaging. AJR 170:609, 1998.
37. Tonai M, Campbell CJ, Ahn GH, et al: Osteoblastoma: Classification and report of 16 cases. Clin Orthop 167:222, 1982.
38. Schiller AL: Diagnosis of borderline cartilage lesions of bone. Semin Diagn Pathol 2:42, 1985.
39. Milgran JW: The origins of osteochondromas and enchondromas: A histopathologic study. Clin Orthop 174:264, 1983.
40. Karasick D, Schweitzer ME, Eschelman DJ: Symptomatic osteochondromas: Imaging features. AJR 168:1507, 1997.
41. Burgess RC, Cates H: Deformities of the forearm in patients who have multiple cartilaginous exostosis. J Bone Joint Surg [Am] 75:13, 1993.
42. Schmale GA, Conrad EV, Raskind WH: The natural history of hereditary multiple exostosis. J Bone Joint Surg [Am] 76:986, 1994.
43. Ritschl P, Karnel F, Hajek P: Fibrous metaphyseal defects: Determination of their origin and natural history using a radiomorphological study. Skeletal Radiol 17:8, 1988.
44. Milgram JW: Intraosseous lipoma: A clinicopathologic study of 66 cases. Clin Orthop 231:277, 1988.
45. Sherman RS, Wilner D: The roentgen diagnosis of hemangioma of bone. AJR 86:1146, 1961.
46. De Dios AMV, Bond JR, Shives TC, et al: Aneurysmal bone cyst: A clinicopathologic study of 238 cases. Cancer 69:2921, 1992.
47. Matfin G, McPherson F: Paget's disease of bone: Recent advances. J Orthop Rheumatol 6:127, 1993.
48. Mirra JM, Brien EW, Tehranzadeh J: Paget's disease of bone: Review with emphasis on radiologic features, part II. Skeletal Radiol 24:173, 1995.
49. Gibson MJ, Middlemiss JH: Fibrous dysplasia of bone. Br J Radiol 44:1, 1971.
50. Stull MA, Kransdorf MJ, Devaney KO: Langerhans cell histiocytosis of bone. RadioGraphics 12:801, 1992.
51. Kilpatrick SE, Wenger DE, Gilchrist GS, et al: Langerhans' cell histiocytosis (histiocytosis X) of bone: A clinicopathologic analysis of 263 pediatric and adult cases. Cancer 76:2471, 1995.
52. Taylor JAM, Resnick D, Sartoris DJ: Radiographic-pathologic correlation. In Sartoris DJ: Osteoporosis: diagnosis and treatment. New York, Marcel Dekker, 1996, p 147.
53. Brien E, Healey JH: In Sartoris DJ: Osteoporosis: diagnosis and treatment. New York, Marcel Dekker, 1996, p 116.
54. Mankin HJ: Rickets, osteomalacia, and renal osteodystrophy. Orthop Clin North Am 21:81, 1990.
55. Wolfson BJ, Capitanio MA: The wide spectrum of renal osteodystrophy in children. CRC Crit Rev Diagn Imaging 27:297, 1987.
56. Tigges S, Nance EP, Carpenter WA, et al: Renal osteodystrophy: Imaging findings that mimic those of other diseases. AJR 165:143, 1995.
57. Sundaram M: Renal osteodystrophy. Skeletal Radiol 18:415, 1989.
58. Pineda C: Diagnostic imaging in hypertrophic osteoarthropathy. Clin Exp Rheumatol 10:27, 1992.
59. Sachs HK: The evolution of the radiologic lead line. Radiology 19:81, 1981.
60. Raber SA: The dense metaphyseal band sign. Radiology 211:773, 1999.
61. Jaovisidha S, Nam Ryu K, Hodler J, et al: Hemophilic pseudotumor: Spectrum of MR findings. Skeletal Radiol 26:468, 1997.
62. Wilson DA, Prince JR: MR imaging of hemophilic pseudotumors. AJR 150: 349, 1988.
63. Gold RH, Hawkins RA, Katz RD: Bacterial osteomyelitis: Findings on plain radiography, CT, MR, and scintigraphy. AJR 157:365, 1991.
64. Rosenberg ZS, Shankman S, Klein M, et al: Chronic recurrent multifocal osteomyelitis. AJR 151:142, 1988.
65. Czirjak L, Nagy Z, Szegedi G: Systemic sclerosis in the elderly. Clin Rheumatol 11:483, 1992.
66. Marin C, Sanchez-Alegre ML, Gallego C, et al: Magnetic resonance imaging of osteoarticular infections in children. Curr Probl Diagn Radiol 33:43, 2004.

67. Christian S, Kraas J, Conway WF: Musculoskeletal infections. Semin Roentgenol 42:92, 2007.
68. Andresen KJ, Sundaram M, Unni KK, et al: Imaging features of low-grade central osteosarcoma of the long bones and pelvis. Skeletal Radiol 33:373, 2004.
69. Suresh S, Saifuddin A: Radiological appearances of appendicular osteosarcoma: A comprehensive pictorial review. Clin Radiol 62:314, 2007.
70. Whitehouse RW: Paget's disease of bone. Semin Musculoskeletal Radiol 6:313, 2002.
71. Whitten CR, Saifuddin A: MRI of Paget's disease of bone. Clin Radiol 58:763, 2003.
72. Berry JL, Davies M, Mee AP: Vitamin D metabolism, rickets and osteomalacia. Semin Musculoskeletal Radiol 6:173, 2002.
73. Makhni EC, Ewald TJ, Kelly S, et al: Effect of patient age on the radiographic outcomes of distal radius fractures subject to nonoperative treatment. J Hand Surg 33A:1301, 2008.
74. Fines BP, Stacy GS: Stress fracture of the ulna in an adolescent baton twirler. Skeletal Radiol 31:116, 2002.
75. Schuurman AH, Maas M, Dijkstra PF, et al: Assessment of ulnar variance: A radiological investigation in a Dutch population. Skeletal Radiol 30:633, 2001.
76. Loredo RA, Sorge DG, Garcia G: Radiographic evaluation of the wrist: A vanishing art. Semin Roentgenol 40:248, 2005.

CHAPTER 17

Wrist and Hand

1. Greulich WW, Pyle SI: Radiographic atlas of skeletal development of the hand and wrist. 2nd Ed. Palo Alto, Stanford University Press, 1959.
2. Edeiken J, Dalinka M, Karasick D: Edeiken's roentgen diagnosis of diseases of bone. 4th Ed. Baltimore, Williams & Wilkins, 1990.
3. Kahn SL, Gaskin CM, Sharp VL. Keats and Kahn's roentgen atlas of skeletal maturation. DVD-ROM Ed. Philadelphia, Lippincott Williams and Wilkins, 2007.
4. Greenfield GB: Radiology of bone diseases. 2nd Ed. Philadelphia, JB Lippincott, 1975.
5. Köhler A, Zimmer EA: Borderlands of normal and early pathologic findings in skeletal radiography. 4th Ed. New York, Thieme Medical Publishers, 1993.
6. Keats TE: Atlas of normal roentgen variants that may simulate disease. 8th Ed. Chicago, Year Book Medical Publishers, 2006.
7. Fagg PS: Wrist pain in the Madelung's deformity of dyschondrosteosis. J Hand Surg [Br] 13:11, 1988.
8. Metz VM, Schimmerl SM, Gilula LA, et al: Wide scapholunate joint space in lunotriquetral coalition: A normal variant? Radiology 188:557, 1993.
9. Simmons BP, McKenzie WD: Symptomatic carpal coalition. J Hand Surg [Am] 10:190, 1985.
10. Poznanski AK: The hand in radiologic diagnosis: With gamuts and pattern profiles. 2nd Ed. Philadelphia, Saunders, 1984.
11. Conway, WF, Destouet JM, Gilula LA, et al: The carpal boss: An overview of radiographic evaluation. Radiology 156:29, 1985.
12. Bloom R: The metacarpal sign. Br J Radiol 43:133, 1970.
13. Elkington SG, Hunstman RG: The Talbot fingers: A study in symphalangism. Br Med J 1:407, 1967.
14. Wood VE: Congenital thumb deformities. Clin Orthop 195:7, 1985.
15. Blank E, Girdany BR: Symmetric bowing of the terminal phalanges of the fifth fingers in a family (Kirner's deformity). AJR 93:367, 1965.
16. Pear J, Viljoen D, Beighton P: Limb overgrowth—clinical observations and nosological considerations. S Afr J Med 64:905, 1983.
17. Wang YC, Jeng CM, Marcantonio DR, et al: Macrodystrophia lipomatosa: MR imaging in three patients. Clin Imaging 21:323, 1997.
18. Kosowicz J: The roentgen appearance of the hand and wrist in gonadal dysgenesis. AJR 93:354, 1965.
19. Rand TC, Edwards DK, Bay CA, et al: The metacarpal index in normal children. Pediatr Radiol 9:31, 1980.
20. Joseph KN, Kane HA, Milner RS, et al: Orthopedic aspects of the Marfan phenotype. Clin Orthop 277:251, 1992.
21. Morse RP, Rockenmacher S, Pyeritz RE, et al: Diagnosis and management of infantile Marfan's syndrome. Pediatrics 86:888, 1990.
22. Bailey JA: Orthopaedic aspects of achondroplasia. J Bone Joint Surg [Am] 52:1285, 1970.
23. Bridges AL, Kou-Ching H, Singh A, et al: Fibrodysplasia (myositis) ossificans progressiva. Semin Arthritis Rheum 24:155, 1994.
24. Root L: The treatment of osteogenesis imperfecta. Orthop Clin North Am 15: 775, 1984.
25. Benli IT, Akalin S, Boysan E, et al: Epidemiological, clinical, and radiological aspects of osteopoikilosis. J Bone Joint Surg [Br] 74:504, 1992.
26. Campbell CJ, Papademetriou T, Bonfiglio M: Melorheostosis: A report of the clinical, roentgenographic, and pathological findings in fourteen cases. J Bone Joint Surg [Am] 50:1281, 1968.
27. Caudle RJ, Stern PJ: Melorheostosis of the hand: A case report with long-term follow-up. J Bone Joint Surg [Am] 69:1229, 1987.
28. Ainsworth SR, Aulicino PL: A survey of patients with Ehlers-Danlos syndrome. Clin Orthop 286:250, 1993.
29. Watts RWE, Spellacy E, Kendall BE, et al: Computed tomography studies on patients with mucopolysaccharidosis. Neuroradiology 21:9, 1981.
30. Rogers LF. Radiology of skeletal trauma. 3rd Ed. New York, Churchill Livingstone, 2002.
31. Duppe H, Johnell O, Lundborg G, et al: Long-term results of fracture of the scaphoid: A follow-up study of more than thirty years. J Bone Joint Surg [Am] 76:249, 1994.
32. Calandra JJ, Goldner RD, Hardaker WT: Scaphoid fractures: Assessment and treatment. Orthopedics 15:931, 1992.
33. Hunter JC, Escobedo EM, Wilson AJ, et al: MR imaging of clinically suspected scaphoid fractures. AJR 168: 1287, 1997.
34. Cohen MS: Fractures of the carpal bones. Hand Clin 13:547, 1997.
35. Norman A, Nelson J, Green S: Fractures of the hook of the hamate: Radiographic signs. Radiology 154:49, 1985.
36. Lacey JD, Hodge JC: Pisiform and hamulus fractures: Easily missed fractures diagnosed on a reverse oblique radiograph. J Emerg Med 16:445, 1998.
37. Yin Y, Mann FA, Gilula LA, et al: Roentgenographic approach to complex bone abnormalities. In Gilula LA, Yin Y (eds): Imaging of the hand and wrist. Philadelphia, Saunders, 1996.
38. Johnson RP: The acutely injured wrist and its residuals. Clin Orthop 149:33, 1980.
39. Pai C-H, Wei D-C, Hu S-T: Carpal bone dislocation: An analysis of twenty cases with relative emphasis on the role of crushing mechanisms. J Trauma 35:28, 1993.
40. Yeager BA, Dalinka MK: Radiology of trauma to the wrist: Dislocations, fracture dislocations, and instability patterns. Skeletal Radiol 13:120, 1985.
41. Sides D, Laorr A, Greenspan A: Carpal scaphoid: Radiographic pattern of dislocation. Radiology 195:215, 1995.
42. Lawlis JF III, Gunther SF: Carpometacarpal dislocations: Long-term follow-up. J Bone Joint Surg [Am] 73:52, 1991.
43. Strauch RJ, Behrman MJ, Rosenwasser MP: Acute dislocation of the carpometacarpal joint of the thumb: An anatomic and cadaver study. J Hand Surg [Am] 19:93, 1994.
44. Yin Y, Mann FA, Hodge JC, et al: Roentgenographic interpretation of ligamentous instabilities of the wrist: Static and dynamic instabilities. In Gilula LA, Yin Y (eds): Imaging of the hand and wrist. Philadelphia, Saunders, 1996, p 203.
45. Cautilli GP, Wehbe MA: Scapholunate distance and cortical ring sign. J Hand Surg [Am] 16:501, 1991.
46. Watson H, Ottoni L, Pitts EC, et al: Rotary subluxation of the scaphoid: A spectrum of instability. J Hand Surg [Br] 18:62, 1993.
47. Zanetti M, Hodler J, Gilula LA: Assessment of dorsal or ventral intercalated segmental instability configurations of the wrist: Reliability of sagittal MR images. Radiology 206:339, 1998.

48. Truong NP, Mann FA, Gilula LA, et al: Wrist instability series: Increasing yield with clinical-radiologic screening criteria. Radiology 192:481, 1994.
49. Watson HK, Ballet FL: The SLAC wrist: Scapholunate advanced collapse pattern of degenerative arthritis. J Hand Surg [Am] 9:358, 1984.
50. Hubbard LF: Metacarpophalangeal dislocations. Hand Clin 4:39, 1988.
51. Lubahn JD: Dorsal fracture dislocations of the proximal interphalangeal joint. Hand Clin 4:15, 1988.
52. Pellegrini VD Jr: Fractures at the base of the thumb. Hand Clin 4:87, 1988.
53. Kontakis GM, Katonis PG, Steriopoulos KA: Rolando's fracture treated by closed reduction and external fixation. Arch Orthop Trauma Surg 117:84, 1998.
54. Spaeth HJ, Abrams RA, Bock GW, et al: Gamekeeper thumb: Differentiation of nondisplaced and displaced tears of the ulnar collateral ligament with MR imaging. Work in progress. Radiology 188:553, 1993.
55. Hinke DH, Erickson SJ, Chamoy L, et al: Ulnar collateral ligament of the thumb: MR findings in cadavers, volunteers, and patients with ligamentous injury (gamekeeper's thumb). AJR 163:1431, 1994.
56. Haramati N, Hiller N, Dowdle J, et al: MRI of the Stener lesion. Skeletal Radiol 24:515, 1995.
57. Miller RJ: Dislocations and fracture dislocations of the metacarpophalangeal joint of the thumb. Hand Clin 4:45, 1988.
58. McKerrell J, Bowen V, Johnston G, et al: Boxer's fractures-conservative or operative management. J Trauma 27: 486, 1987.
59. Street JM: Radiographs of phalangeal fractures: Importance of the internally rotated oblique projection for diagnosis. AJR 160:575, 1993.
60. Rogers LF, Poznanski AK: Imaging of epiphyseal injuries. Radiology 191:297, 1994.
61. Destouet JM, Murphy WA: Guitar player acroosteolysis. Skeletal Radiol 6:275, 1981.
62. Baran R, Tosti A: Occupational acroosteolysis in a guitar player. Acta Derm Venereol 73:64, 1993.
63. Nimkin K, Spevak MR, Kleinman PK: Fractures of the feet and hands in child abuse: Imaging and pathologic features. Radiology 203:233, 1997.
64. Skahen JR III, Palmer AK, Levinsohn EM, et al: Magnetic resonance imaging of the triangular fibrocartilage complex. J Hand Surg [Am] 15:552, 1990.
65. Miller RJ, Totterman SMS: Triangular fibrocartilage in asymptomatic subjects: Investigation of abnormal MR signal intensity. Radiology 196:22, 1995.
66. Glajchen N, Schweitzer M: MRI features in de Quervain's tenosynovitis of the wrist. Skeletal Radiol 25:63, 1996.
67. Mesgarzadeh M, Schneck CD, Boakdarpour A, et al: Carpal tunnel: MR imaging. II. Carpal tunnel syndrome. Radiology 171:749, 1989.
68. Miller TT, Potter HG, McCormack RR Jr: Benign soft tissue masses of the wrist and hand: MRI appearances. Skeletal Radiol 23:327, 1994.
69. Vo P, Wright T, Hayden F, et al: Evaluating dorsal wrist pain: MRI diagnosis of occult dorsal wrist ganglion. J Hand Surg [Am] 20:667, 1995.
70. Drapé JL, Idy-Peretti I, Goettmann S, et al: Subungual glomus tumors: Evaluation with MR imaging. Radiology 195:507, 1995.
71. Jelinek JS, Kransdorf MJ, Shmookler BM, et al: Giant cell tumor of the tendon sheath: MR findings in nine cases. AJR 162:919, 1994.
72. Buckland-Wright JC, MacFarlane DG, Lynch JA: Relationship between joint space width and subchondral sclerosis in the osteoarthritic hand: A quantitative microfocal radiographic study. J Rheumatol 19:788, 1992.
73. Menon J: The problem of trapeziometacarpal degenerative arthritis. Clin Orthop 175:155, 1983.
74. Cooke KS, Singson RD, Glickel SZ, et al: Degenerative changes of the trapeziometacarpal joint: Radiologic assessment. Skeletal Radiol 24:523, 1995.
75. Paley D, McMurtry RY, Cruickshank B: Pathologic conditions of the pisiform and pisotriquetral joint. J Hand Surg [Am] 12:110, 1987.
76. Williams WV, Cope R, Gaunt WD, et al: Metacarpophalangeal arthropathy associated with manual labor: Missouri metacarpal syndrome. Arthritis Rheum 30:1362, 1987.
77. Cobby M, Cushnaghan J, Creamer P, et al: Erosive osteoarthritis: Is it a separate disease entity? Clin Radiol 42:258, 1990.
78. Martel W, Stuck KJ, Dworin AM, et al: Erosive osteoarthritis and psoriatic arthritis: A radiologic comparison in the hand, wrist, and foot. AJR 134: 125, 1980.
79. Greenway G, Resnick D, Weisman M, et al: Carpal involvement in inflammatory (erosive) osteoarthritis. J Can Assoc Radiol 30:95, 1979.
80. Smith D, Braunstein EM, Brandt KD, et al: A radiographic comparison of erosive osteoarthritis and idiopathic nodal osteoarthritis. J Rheumatol 19: 896, 1992.
81. Buckland-Wright JC, Clarke GS, Walker SR: Erosion number and area progression in the wrists and hands of rheumatoid patients: A quantitative microfocal radiographic study. Ann Rheum Dis 48:25, 1989.
82. Sugimoto H, Takeda A, Masuyama J, et al: Early-stage rheumatoid arthritis: Diagnostic accuracy of MR imaging. Radiology 198:185, 1996.
83. Evans DM, Ansell BM, Hall MA: The wrist in juvenile arthritis. J Hand Surg [Br] 16:293, 1991.
84. Azouz EM, Duffy CM: Juvenile spondyloarthropathies: Clinical manifestations and medical imaging. Skeletal Radiol 24:399, 1995.
85. Resnick D: Patterns of peripheral joint disease in ankylosing spondylitis. Radiology 110:523, 1974.
86. Resnick D, Broderick RW: Bony proliferation of terminal phalanges in psoriasis: The "ivory" phalanx. J Can Assoc Radiol 28:187, 1977.
87. Resnick D, Niwayama G: On the nature and significance of bony proliferation in "rheumatoid variant" disorders. AJR 129:275, 1977.
88. Forrester DM, Kirkpatrick J: Periostitis and pseudoperiostitis. Radiology 118: 597, 1976.
89. Martel W, Braunstein EM, Borlaza G, et al: Radiologic features of Reiter's syndrome. Radiology 132:1, 1979.
90. Reilly PA, Evison G, McHugh NJ, et al: Arthropathy of the hands and feet in systemic lupus erythematosus. J Rheumatol 17:777, 1990.
91. Selby CL: Review and differential diagnosis of Jaccoud's arthropathy. IM 6:55, 1985.
92. Pachman LN: Juvenile dermatomyositis. Pediatr Clin North Am 33:1097, 1986.
93. Czirjak L, Nagy Z, Szegedi G: Systemic sclerosis in the elderly. Clin Rheumatol 11:483, 1992.
94. Garcia-Porrua C, Gonzalez-Gay MA, Vazquez-Caruncho M: Tophaceous gout mimicking tumoral growth. J Rheumatol 26:508, 1999.
95. Yu JS, Chung C, Recht M, et al: MR imaging of tophaceous gout. AJR 168: 523, 1997.
96. Holland NW, Jost D, Beutler A, et al: Finger pad tophi in gout. J Rheumatol 23:690, 1996.
97. Resnick D, Niwayama G, Georgen TG, et al: Clinical, radiographic and pathologic abnormalities in calcium pyrophosphate dihydrate deposition disease (CPPD): Pseudogout. Radiology 122:1, 1977.
98. Steinbach LS: Calcium pyrophosphate dihydrate and calcium hydroxyapatite crystal deposition diseases: Imaging perspectives. Radiol Clin N Am 42: 185, 2004.
99. Bourqui M, Vischer TL, Stasse P, et al: Pyrophosphate arthropathy in the carpal and metacarpophalangeal joints. Ann Rheum Dis 42:626, 1983.
100. Faraawi R, Harth M, Kertesz A, et al: Arthritis in hemochromatosis. J Rheumatol 20:448, 1993.
101. Jonge-Bok JMD, Macfarlane JD: The articular diversity of early haemochromatosis. J Bone Joint Surg [Br] 69:41, 1987.
102. Holt PD, Keats TE: Calcific tendinitis: A review of the usual and unusual. Skeletal Radiol 22:1, 1993.
103. McCarthy GM, Carrera GF, Ryan LM: Acute calcific periarthritis of the finger joints: A syndrome of women. J Rheumatol 20:1077, 1993.
104. Nakajima Y, Sato K, Morita H, et al: Severe progressive erosive arthritis in multicentric reticulohistiocytosis: Possible involvement of cytokines in synovial proliferation. Arthritis Rheum 19:1643, 1992.

105. Kalb RE, Epstein W, Grossman ME: Sarcoidosis with subcutaneous nodules. Am J Med 85:731, 1988.
106. Rivera-Sanfeliz G, Resnick D, Haghighi P: Sarcoidosis of hands. Skeletal Radiol 25:786, 1996.
107. Adelaar RS: Sarcoidosis of the upper extremity: Case presentation and literature review. J Hand Surg [Am] 8:492, 1983.
108. Ishizuki M, Isobe Y, Arai T, et al: Osteochondromatosis of the finger joints. Hand 9:198, 1977.
109. Kramer J, Recht M, Deely DM, et al: MR appearance of idiopathic synovial osteochondromatosis. J Comput Assist Tomogr 17:772, 1993.
110. Hasegawa Y, Ninomiya M, Yamada Y, et al: Osteoarthropathy in congenital sensory neuropathy with anhidrosis. Clin Orthop 258:232, 1990.
111. Brown FE, Spiegel PK, Boyle WE Jr: Digital deformity: An effect of frostbite in children. Pediatrics 71:955, 1983.
112. Reed MH: Growth disturbances in the hands following thermal injuries in children. 2. Frostbite. J Can Assoc Radiol 39:95, 1988.
113. Schiele HP, Hubbard RB, Bruck HM: Radiographic changes in burns of the upper extremity. Radiology 104:13, 1972.
114. Atkinson RE, Smith RJ: Silicone synovitis following silicone implant arthroplasty. Hand Clin 2:291, 1986.
115. Chan M, Chowchuen P, Workman T, et al: Silicone synovitis: MR imaging in five patients. Skeletal Radiol 27:13, 1998.
116. Resnick D: Soft tissue disorders. In Resnick D [ed]: Diagnosis of bone and joint disorders. 4th Ed. Philadelphia, Saunders, 2002, p 4635.
117. Wong WL, Pemberton J: The musculoskeletal manifestations of epidermolysis bullosa: An analysis of 19 cases with review of the literature. Br J Radiol 65:480, 1992.
118. Resnick D, Weisman M, Goergen TG, et al: Osteolysis with detritic synovitis, a new syndrome. Arch Intern Med 138:1003, 1978.
119. Galmarini CM, Kertesz A, Oliva R, et al: Metastasis of bronchogenic carcinoma to the thumb. Med Oncol 15: 282, 1998.
120. Gelberman RH, Stewart WR, Harrelson JM: Hand metastasis from melanoma: A case study. Clin Orthop 136:264, 1978.
121. Okada K, Wold LE, Beabout JW, et al: Osteosarcoma of the hand: A clinicopathologic study of 12 cases. Cancer 72:719, 1993.
122. Ritschl P, Wurnig C, Lechner G, et al: Parosteal osteosarcoma: 2-23-year follow-up of 33 patients. Acta Orthop Scand 62:195, 1991.
123. Lucas DR, Unni KK, McLeod RA, et al: Osteoblastoma: Clinicopathologic study of 306 cases. Hum Pathol 25:117, 1994.
124. Taconis WK, Mulder JD: Fibrosarcoma and malignant fibrous histiocytoma of long bones: Radiographic features and grading. Skeletal Radiol 11:237, 1984.
125. Reinus WR, Gilula LA, Shirley SK, et al: Radiographic appearance of Ewing sarcoma of the hands and feet: Report from the Intergroup Ewing Sarcoma Study. AJR 144:331, 1985.
126. Buck P, Mickelson MR, Bonfiglio M: Synovial sarcoma: A review of 33 cases. Clin Orthop 156:211, 1981.
127. Kyle RA: Multiple myeloma: Review of 869 cases. Mayo Clin Proc 50:29, 1975.
128. Greenspan A: Bone island (enostosis): Current concept—a review. Skeletal Radiol 24:111, 1995.
129. Riester J, Mosher JF: Osteoid osteoma of the capitate: A case report. J Hand Surg [Am] 9:278, 1984.
130. Shankman S, Desai P, Beltran J: Subperiosteal osteoid osteoma: Radiographic and pathologic manifestations. Skeletal Radiol 26:457, 1997.
131. Lamb DW, Del Castillo F: Phalangeal osteoid osteoma in the hand. Hand 13:291, 1981.
132. Kayser F, Resnick D, Haghighi P, et al: Evidence of the subperiosteal origin of osteoid osteomas in tubular bones: Analysis by CT and MR imaging. AJR 170:609, 1998.
133. Carroll RE, Chance JT, Inan Y: Subungual exostosis in the hand. J Hand Surg [Br] 17:569, 1992.
134. Rubin JA, Steinberg DR: Turret exostosis of the metacarpal: A case report. J Hand Surg [Am] 21:296, 1996.
135. Jewusiak EM, Spence KF, Sell KW: Solitary benign enchondroma of the long bones of the hand: Results of curettage and packing with freeze-dried cancellous-bone allograft. J Bone Joint Surg [Am] 53:1587, 1971.
136. Brien EW, Mirra JM, Kerr R: Benign and malignant cartilage tumors of bone and joint: Their anatomic and theoretical basis with an emphasis on radiology, pathology and clinical biology. 1. The intramedullary cartilage tumors. Skeletal Radiol 26:325, 1997.
137. Meinzer F, Minagi H, Steinbach HL: The variable manifestation of multiple enchondromatosis. Radiology 99:377, 1971.
138. Collins PS, Han W, Williams LR, et al: Maffucci's syndrome (hemangiomatosis osteolytica): A report of four cases. J Vasc Surg 16:364, 1992.
139. Dahlin DC: Giant cell tumor of bone: Highlights of 407 cases. AJR 144:955, 1985.
140. Lokiec F, Wientroub S: Simple bone cyst: Etiology, classification, pathology, and treatment. J Pediatr Orthop [Br] 7:262, 1998.
141. Blacksin MF, Ende N, Benevenia J: Magnetic resonance imaging of intraosseous lipomas: A radiologic-pathologic correlation. Skeletal Radiol 24:37, 1995.
142. De Dios AMV, Bond JR, Shives TC, et al: Aneurysmal bone cyst. A clinicopathologic study of 238 cases. Cancer 69:2921, 1992.
143. Friedman AC, Orcutt H, Madewell JE: Paget disease of the hand: Radiographic spectrum. AJR 138:691, 1982.
144. Mirra JM, Brien EW, Tehranzadeh J: Paget's disease of bone: Review with emphasis on radiologic features, part II. Skeletal Radiol 24:173, 1995.
145. Gibson MJ, Middlemiss JH: Fibrous dysplasia of bone. Br J Radiol 44:1, 1971.
146. Iwahara T, Hirayama T, Takemitu Y: Intraosseous ganglion of the lunate. J Hand Surg [Br] 15:297, 1983.
147. Magee TH, Rowedder AM, Degnan GG: Intraosseous ganglia of the wrist. Radiology 195:517, 1995.
148. Trias A, Beauregard G: Epidermoid cyst of bone. Can J Surg 17:1, 1974.
149. Bloom RA, Pogrund H, Libson E: Radiogrammetry of the metacarpal: A critical reappraisal. Skeletal Radiol 10:5, 1983.
150. Genant HK, Engelke K, Fuerst T, et al: Noninvasive assessment of bone mineral and structure: State of the art. J Bone Miner Res 11:707, 1996.
151. Taylor JAM, Resnick D, Sartoris DJ: Radiographic-pathologic correlation. In Sartoris DJ: Osteoporosis: diagnosis and treatment. New York, Marcel Dekker, 1996, p 147.
152. Clouston WM, Lloyd HM: Immobilization-induced hypercalcemia and regional osteoporosis. Clin Orthop 216:247, 1987.
153. Schwarzman RJ, McLellan TL: Reflex sympathetic dystrophy: A review. Arch Neurol 44:555, 1987.
154. Mankin HJ: Metabolic bone disease. J Bone Joint Surg [Am] 76:760, 1994.
155. Kurer MHJ, Baillod RA, Madgwick JCA: Musculoskeletal manifestations of amyloidosis: A review of 83 patients on haemodialysis for at least 10 years. J Bone Joint Surg [Br] 73:271, 1991.
156. Hernandez RJ, Poznanski AW, Hopwood NJ: Size and skeletal maturation of the hand in children with hypothyroidism and hypopituitarism. AJR 133:405, 1979.
157. Cherninkov Z, Cherninkova S: Two cases of pseudohypoparathyroidism in a family with type E brachydactylia. Radiol Diagn [Berlin] 30:57, 1989.
158. Lang EK, Bessler WT: The roentgenologic features of acromegaly. AJR 86: 321, 1961.
159. Bluestone R, Bywaters EGL, Hartog M, et al: Acromegalic arthropathy. Ann Rheum Dis 30:243, 1971.
160. Pineda C: Diagnostic imaging in hypertrophic osteoarthropathy. Clin Exp Rheumatol 10:27, 1992.
161. Vázquez-Abad D, Pineda C, Martinez-Lavin M: Digital clubbing: A numerical assessment of the deformity. J Rheumatol 16:518, 1989.
162. Resnick D: Osteomyelitis and septic arthritis complicating hand injuries and infections: Pathogenesis of roentgenographic abnormalities. J Can Assoc Radiol 27:21, 1976.
163. Gonzalez MH, Papierski P, Hall RF Jr: Osteomyelitis of the hand after a

human bite. J Hand Surg [Am] 18:520, 1993.

164. Robins RH: Tuberculosis of the wrist and hand. Br J Surg 54:211, 1967.
165. Feldman F, Auerbach R, Johnston A: Tuberculous dactylitis in the adult. AJR 112:460, 1971.
166. MacMoran JW, Brand PW: Bone loss in limbs with decreased or absent sensation: Ten year follow-up of the hands in leprosy. Skeletal Radiol 16:452, 1987.
167. Mirabello SC, Rosenthal DI, Smith RJ: Correlation of clinical and radiographic findings in Kienböck's disease. J Hand Surg [Am] 12:1049, 1987.
168. Gelberman RH, Menon J: The vascularity of the scaphoid bone. J Hand Surg [Am] 5:508, 1980.
169. Sherman SB, Greenspan A, Norman A: Osteonecrosis of the distal pole of the carpal scaphoid following fracture—a rare complication. Skeletal Radiol 9:189, 1983.
170. Arcalis AA, Pedemonte JJP, Massons AJM: Idiopathic necrosis of the capitate. Acta Orthop Belg 62:46, 1996.
171. Telfer JR, Evans DM, Bingham JB: Avascular necrosis of the hamate. J Hand Surg [Br] 19:389, 1994.
172. Failla JM: Osteonecrosis associated with nonunion of the hook of the hamate. Orthopedics 16:217, 1993.
173. Gewanter H, Baum J: Thiemann's disease. J Rheumatol 12:150, 1985.
174. Resnick D [ed]: Diagnosis of bone and joint disorders. 4th Ed. Philadelphia, Saunders, 2002.
175. Resnick D: Scleroderma (progressive systemic sclerosis). In Resnick D [ed]: Diagnosis of bone and joint disorders. 4th Ed. Philadelphia, Saunders, 2002, p 1194.
176. Doman AN, Marcus NW: Congenital bipartite scaphoid. J Hand Surg [Am] 15:869, 1990.
177. Pierre-Jerome C, Roug IK: MRI of bilateral bipartite hamulus. Surg Radiol Anat 20:299, 1998.
178. Bencardion JT, Hassankhani A: Calcium pyrophosphate dihydrate crystal deposition disease. Semin Musculoskeletal Radiol 7:175, 2003.
179. Klecker RJ, Weissman BN: Imaging features of psoriatic and Reiter's syndrome. Semin Musculoskeletal Radiol 7:115, 2003.
180. Marin C, Sanchez-Alegre ML, Gallego C, et al: Magnetic resonance imaging of osteoarticular infections in children. Curr Probl Diagn Radiol 33:43, 2004.
181. Christian S, Kraas J, Conway WF: Musculoskeletal infections. Semin Roentgenol 42:92, 2007.
182. Greenspan A, Tehranzadeh J: Imaging of infectious arthritis. Radiol Clin N Am 39:267, 2001.
183. Toth F, Sebestyen A, Balint L, et al: Positioning of the wrist for scaphoid radiography. Eur J Radiol 64:126, 2007.
184. Memarsadeghi M, Breitenseher MJ, Schaefer-Prokop C, et al: Occult scaphoid fractures: Comparison of multidetector CT and MR imaging—initial experience. Radiology 240:169, 2006.
185. Brydie A, Raby N: Early MRI in the management of clinical scaphoid fracture. Br J Radiol 76:196, 2003.
186. Loredo RA, Sorge DG, Garcia G: Radiographic evaluation of the wrist: A vanishing art. Semin Roentgenol 40:248, 2005.
187. Greenspan A: Erosive osteoarthritis. Semin Musculoskelet Radiol 7: 155, 2003.
188. Yucel A, Kuru I, Eray Bozan M, et al: Radiographic evaluation and unusual bone formations in different genetic patterns in synpolydactyly. Skeletal Radiol 34:468, 2005.
189. Laffosse J-M, Tricoire J-L, Cantagrel A, et al: Osteoid osteoma of the carpal bones. Two case reports. Joint Bone Spine 73:560, 2006.
190. Grainger AJ, Farrant JM, O'Connor PJ, et al: MR imaging of erosions in interphalangeal joint osteoarthritis: Is all osteoarthritis erosive? Skeletal Radiol 36:737, 2007.
191. Giele H, Martin J: The two-level ulnar collateral ligament injury of the metacarpophalangeal joint of the thumb. J Hand Surg [Br] 28:92, 2003.
192. Baraga JJ, Amrami KK, Swee RG, et al: Skeletal Radiol 30:121, 2001.
193. Haliloglu N, Sahin G: Symptomatic carpal coalition with degenerative changes: Report of two cases. Eur J Radiol Extra 63:11, 2007.
194. Lohan D, Cronin C, Meehan C, et al: Injuries to the carpal bones revisited. Current Probl Diagn Radiol 36:164, 2007.
195. Rajesh A, Basu AK, Vaidhyanath R, et al: Hand fractures: A study of their site and type in children. Clin Radiol 56:667, 2001.
196. Theumann NH, Goettmann S, Le Viet D, et al: Recurrent glomus tumors of fingertips: MR imaging evaluation. Radiology 223:143, 2002.
197. Santiago FR, Plazas PG, Sanchez FR, et al: Imaging study of pisotriquetral osteoarthritis. A role for ultrasound? Eur J Radiol Extra 52:33, 2004.
198. Joshi A, Nagaraj C, Singh S, et al: Symphalangism—role of physical therapy. Eur J Radiol Extra 65:101, 2008.
199. Laurencikas E, Söderman E, Davenport M, et al: Metacarpophalangeal pattern profile analysis as a tool for early diagnosis of Turner syndrome. Acta Radiol 46:424, 2005.
200. Erre GL, Marongiu A, Fenu P, et al: The "sclerodermic hand": A radiological and clinical study. Joint Bone Spine 75:426, 2008.
201. Jain TP, Srivastava DN, Mittal R, et al: Fibrolipomatous hamartoma of the median nerve. Australas Radiol 51: B98, 2007.
202. Dhondt E, Oudenhove L, Khan S, et al: Nora's lesion, a distinct radiological entity? Skeletal Radiol 35:497, 2006.
203. Botte MJ, von Schroeder HP, Gellman H, et al. Fracture of the trapezial ridge. Clin Orthop Relat Res 276:202, 1992.
204. Taleisnik J: Classification of carpal instability. Bull Hosp Jt Dis 44:51, 1984.

INDEX

A

Abscess
  Brodie, 41t, 614t, 665t, *667-668*
  of chest wall, 803t
  epidural
    cervical, *135*
    thoracic, *208*
  psoas, in tuberculosis, *310, 484*
  retropharyngeal, atlantoaxial instability and subluxation in, 59t
Abused child. *See* Child abuse
Acetabular index in developmental dysplasia of hip, 445, *446*
Acetabulum
  achondroplasia of, 388t, *389*
  in Down syndrome, 388t, *389*
  enostosis of, 414t, *421*
  in femoroacetabular impingement, 463t, *465-466*
  fractures of, 393t, *400-401,* 434, 440t, 453t
    hip dislocation in, 451t, *452*
  giant cell tumor of, *423*
  hyperostosis of, diffuse idiopathic skeletal, 468t, *472*
  labrum detachment and tears, 463t, *464*
  in Legg-Calvé-Perthes disease, *499*
  in mucopolysaccharidoses, 388t, *390*
  normal developmental anatomy of, 435t, *436*
  ossicles of, 384t, *385,* 438t
  ossification centers in, 435t, *436*
  osteonecrosis of, *433*
  perilabral ganglion cysts, 463t, *464*
  in pigmented villonodular synovitis, *487*
  protrusion of, 434, 440t, *442-443*
    in alkaptonuria, 469t, *481*
    in crystal deposition disease, 469t, *478*
    in fractures, 393t, *401*
    normal physiologic, *380*
    in osteogenesis imperfecta, 388t, *391*
    in Paget disease, 414t, *424*
    in plasma cell myeloma, *419*
    primary (Otto pelvis), 440t, *443*
    in psoriatic arthropathy, *476*
    in sickle cell anemia, 489t, *496*
  radiation-induced changes of, *433*
  simple bone cyst of, *423*
Achilles tendon disorders, 728t, *731,* 737t
  in ankylosing spondylitis, 737t, *742*
  in diffuse idiopathic skeletal hyperostosis, 737t, *739*
  in Reiter syndrome, *745*
  in scleroderma, 734t, *746*
Achondroplasia, 3t
  of cervical spine, 78t
  of humerus, 830t
  of knee, 557t, 558t
  of lumbar spine, 244t, *245,* 246t
  of pelvis, 388t, *389*
  of ribs, 781
  of thoracic spine, 170t
  of wrist and hand, 985t, *988*
Acne
  conglobata, 22t, *131*
  fulminans, 22t
Acne *(continued)*
  pustular, 15t, 22t
  and pustulosis palmaris et plantaris, *800*
  in synovitis-acne-pustulosis-hyperostosis-osteitis, 15t, 22t. *See also* SAPHO
Acromegaly, 37t
  ankle and foot disorders in, 737t, 768t, *771*
  cervical spine disorders in, *149,* 149t
  clavicle disorders in, 883t
  elbow disorders in, 935t
  hip disorders in, 489t, *496*
  knee disorders in, 600t, *610*
  lumbar spine disorders in, 246t, 327t, *333*
  rib disorders in, 814t
  shoulder disorders in, 859t, *868,* 883t
  skin and joint findings in, 23t
  thoracic spine disorders in, 221t, *224*
  wrist and hand disorders in, 1054t, *1061*
Acromioclavicular joint
  ankylosing spondylitis of, 857t
  crystal deposition disease of, 858t, *865*
  dislocation of, 842t, *846*
  gouty arthropathy of, 858t, *866*
  normal developmental anatomy of, *822-823*
  osteoarthrosis of, *850,* 857t, *861*
  in renal osteodystrophy, *879*
  rheumatoid arthritis of, 857t, *862*
  septic arthritis of, 859t, *867*
  synovial cysts of, 849t, *853*
Acromioclavicular ligament
  rupture of
    in acromioclavicular joint dislocation, 842t
    in clavicle fracture, *836*
  sprain of, 842t, *846*
Acromion process of scapula
  fractures of, 833t, *839*
  ossification centers in, 820t, *823*
Acro-osteolysis
  in guitar player, *1010*
  in hyperparathyroidism, 1054t, *1058, 1059*
  in sarcoidosis, 1017t, *1039*
  in scleroderma, *1031*
  in vinyl chloride exposure, 23t, 1067t
Acropachy, thyroid-associated, 37t
Actinomycosis, pelvic osteomyelitis in, *431*
Adamantinoma (angioblastoma), 26t
  of tibia and fibula, 636t, *640*
Adductor muscles of thigh
  athletic pubalgia syndromes of, 404t
  insertion avulsion syndrome of (thigh splints), 509t, *514*
Adhesive capsulitis of shoulder, 848t, *851*
Adolescents, scoliosis in
  lumbar, 259t, *260*
  thoracic, 177t, *180*
Adventitial bursa of ankle and foot, 759t
Agenesis, 2t
  of atlas
    anterior arch, 51t, *55*
    posterior arch, 51t, *54*
  caudal, 5t
  of lumbar articular process, 235t, *241*
  of odontoid process, 2t, 52t
    atlantoaxial instability in, 52t, 59t
    in mucopolysaccharidosis, 78t, *79*
  of sacrum, 349t, *351*
  of vertebral pedicle, 313t
Alcoholism, neuropathic osteoarthropathy of foot in, 735t, *752*
Alignment abnormalities of knee, 547, 557t-558t
Alkaptonuria, 19t
  cervical spine disorders in, 111t, *134*
  hip disorders in, 440t, 469t, *481*
    patterns of joint space narrowing in, 470t
  lumbar spine disorders in, 295t, *307*
  pelvic disorders in, 406t, *412*
  thoracic spine disorders in, 193t, *206*
Allergic reactions, 22t
Amyloid deposition
  in shoulder, 858t
  in wrist and hand, 1054t, *1060*
Anemia, sickle cell. *See* Sickle cell anemia
Aneurysm
  of aorta, abdominal, 229, 246t, 342t, *343*
  of iliac artery, 229, 342t, *344*
  of popliteal artery, 617t, *622*
  of vertebral artery, 159t, *160*
Aneurysmal bone cyst. *See* Cysts, aneurysmal bone
Angioblastoma (adamantinoma), 26t
  of tibia and fibula, 636t, *640*
Ankle, 672-775
  accessory ossicles of, 690t-691t, *694-699*
  anomalies and variants of, 672, 690t-692t, *692-695*
  articular disorders of, 672, 734t-737t, *738-753*
    in crystal deposition disease, 734t-735t, 737t, *747-749*
    degenerative, 734t, *738-739*
    differential diagnosis in, 737t
    distribution, symmetry, and preferential target sites of, 736t
    inflammatory, 734t, *740-746*
  ball-and-socket, 681t, *683*
  deformities of, 672, 681t, *683*
  dislocation of, 672, 710t, *713*
    talar, 715t, *720*
  dysplasias of, 672t, 703t
  fractures of, 672, 705, 709t-710t, *711-713*
    acute, *706-709,* 709t
    in child abuse, 710t, *711*
    Lauge-Hansen classification of, 705t, *706-709*
    natural history and complications in, *708*
    pronation-abduction, 705t
    pronation-dorsiflexion, 705t
    pronation-external rotation, 705t, *707-709*
    stress, 727t-728t
    supination-adduction, 705t, *706*
    supination-external rotation, 705t, *706*
  growth plate injuries of, 710t, *712*
  impingement syndromes of, 729t, *733*
    in os trigonum, 690t, *694-695,* 729t
  infections of, 672, 754t
  metabolic disorders of, 672, 768t, *768-771*
  normal developmental anatomy of, 672, 673t, *674-677*
  ossification centers in, 672, 673t
  osteochondral bodies in, intraarticular, 709t, *711*

Page numbers in *italics* refer to illustrations; page numbers followed by t refer to tables.

Ankle *(continued)*
  osteonecrosis and osteochondrosis of, 673, 772t, *773-775*
  soft tissue injuries of, 728t-729t, *730-733*
    instability in, 728t, *730*
    of ligaments, 728t, *730*
  tibiotalar slant of, 681t, *683, 741, 750*
  tumors and tumorlike lesions of, 672, 758t-760t, *761-767*
    benign, 759t, *762-765*
    malignant, 758t, *761, 767*
    metastatic, 758, *761*
    myeloproliferative, 758t, *762*
    tumorlike lesions, 759t-760t, *765-767*
  vascular calcification of, 768t, *770*
Ankylosing spondylitis, 14t
  of ankle and foot, 734t, 737t, *742*
    hallux valgus in, *687*
  of cervical spine, 109t, *127-130*
    atlantoaxial instability in, 109t, *127*
  of elbow, 934t, *937*
  of hip, 440t, 468t, *475*
    patterns of joint space narrowing in, 470t
  of knee, 599t, *605*
  of lumbar spine, 294t, *300-302*
    arachnoid diverticula in, 294t, *302*
  of manubriosternal junction, *799*
  of pelvis, 405t, *410*
  of sacroiliac joint, 356t, 357t, *365-366*
  of shoulder, 857t, *863*
  of sternoclavicular joint, 797t
  terminology related to, 201t
  of thoracic spine, 193t, 201t, *202-204*
    kyphosis in, 173t
    pseudarthrosis in, 193t, *204*
  of wrist and hand, 1016t, *1026*
Annular bulge in lumbar intervertebral disk disorders, 268t, *275*
Antiretroviral therapy, femoral head osteonecrosis in, *502*
Anulus fibrosus tears, lumbar, 268t, *278*
Aorta
  aneurysm of, lumbar spine disorders in, 229, 246t, 342t, *343*
  coarctation of, rib notching in, *787,* 787t
Aplasia, 2t
Apophyseal joints, vertebral
  cervical
    ankylosing spondylitis of, 109t, *128-130*
    dislocation of, 91t, *97, 98*
    fusion of C1-C2, *63*
    notching of, 67t, *71*
    osteoarthrosis of, 107t, *113, 117*
    pseudofusion of C2-C3, 52t, *66*
  lumbar
    asymmetry of, 234t, *241*
    gouty arthropathy of, 295t, *308*
    osteoarthrosis of, 294t, *296*
  lumbosacral, dislocation of, 262t, *266*
Apophysis. *See* Epiphysis
Apophysitis, differential diagnosis in, 404t
Arachnodactyly of hand, 985t, *987*
Arachnoid diverticula in lumbar ankylosing spondylitis, 294t, *302*
Arcuate foramen, 51t, *56*
Arthralgia, 22t
Arthritis
  erosive osteoarthritis, 11t
    of ankle and foot, 734t
    of wrist and hand, 1016t, 1018t, *1021,* 1067t
  gouty, 19t. *See also* Gout
  juvenile idiopathic, 13t, 22t

Arthritis *(continued)*
    of ankle and foot, 736t, *741*
    of cervical spine, 109t, *126*
    of elbow, 934t
    of hip, 468t, 470t
    of knee, 599t, *613-614*
    of shoulder, 857t
    of wrist and hand, 1016t, *1025,* 1066t
  psoriatic, 14t, 22t. *See also* Psoriatic arthropathy
  reactive, 15t. *See also* Reactive arthritis
  in Reiter syndrome, 15t, 23t. *See also* Reiter syndrome
  rheumatoid, 13t, 22t. *See also* Rheumatoid arthritis
  septic, 41t. *See also* Septic arthritis
  tuberculous. *See* Tuberculosis, arthritis in
Arthrodesis
  of cervical spine, 151t, *152-153*
    hydroxyapatite graft in, *152,* 155t
    occipito-cervical, *158*
    plates and screws in, 155t, *156*
  of lumbar spine, *337,* 337t
Arthro-osteitis, pustulotic, 15t, 22t
Arthropathy
  enteropathic, 15t
    of cervical spine, 109t
    of lumbar spine, 294t
    of sacroiliac joint, 356t, 357t, *367*
    of thoracic spine, 193t
  gouty, 19t. *See also* Gout
  in hemochromatosis, 19t, 23t. *See also* Hemochromatosis
  hemophilic, 20t. *See also* Hemophilia
  neuropathic osteoarthropathy, 20t. *See also* Osteoarthropathy, neuropathic
  ochronotic, 19t. *See also* Alkaptonuria
  psoriatic, 14t-15t. *See also* Psoriatic arthropathy
Arthrosis of cervical spine, 107t, *113-118*
Articular disorders, 10t-23t
  of ankle and foot, 672, 734t-737t, *738-753*
    differential diagnosis in, 737t
    distribution, symmetry, and preferential target sites of, 736t
  of cervical spine, 45, 107t-111t, *112-137*
  in crystal deposition. *See* Crystal deposition disorders
  of elbow, 906, 934t-935y, *936-942*
  of hip, 434, 468t-470t, *471-487*
  inflammatory, 13t-17t
  of knee, 547, 599t-600t, *601-613*
    compartmental analysis of, 603t
  of lumbar spine, 228, 294t-295t, *296-311*
  metabolic, 18t-21t
  of pelvis, 377, 405t-406t, *406-413*
  of sacrococcygeal spine and sacroiliac joints, 345, 356t-357t, *358-370*
  of shoulder, 819, 857t-859t, *860-870*
  with skin findings, 22t-23t
  of thoracic cage joints, 797t, *798-801*
  of thoracic spine, 161, 192t-194t, *194-209*
  traumatic, 10t
  of wrist and hand, 972, 1016t-1018t, *1019-1042*
    compartmental analysis of, 1018t
Articular process, vertebral
  cervical
    fracture of, 91t, *98*
    notching of, 67t, *71*
  lumbar
    agenesis of, 235t, *241*
    ossification centers in, 229t

Articular process, vertebral *(continued)*
    ununited ossification centers in, 234t, *241*
  thoracic, ossification centers in, 162t
Artifacts from hair in cervical spine imaging, 68t, *77*
Ascorbic acid deficiency, 36t
  femoral disorders in, 541t, *544*
  knee disorders in, 616t
  tibia and fibula disorders in, 657t, *661*
Assimilation
  atlanto-occipital, 51t, *53*
  lumbosacral, 235t
Atherosclerosis
  aortic aneurysm in, *343*
  of carotid artery, *159,* 159t
  of iliac artery, *344*
  Mönckeberg, of ankle and foot, 768t, *770*
Athletic activities
  clavicle osteolysis in, posttraumatic, 849t, *855*
  elbow injuries in, 929t, *933*
  femoral fractures in
    avulsion, 453t, *458*
    fatigue, 453t, *456*
  fibula fatigue fracture in, 629t, 710t
  humerus fracture in, 889t
  knee ligament injuries in, *595*
  Little League shoulder syndrome in, 832t, *835*
  metatarsal fatigue fracture in, 723t, *725*
  navicular fatigue fracture in, 715t, *721*
  osteitis pubis in, 405t
  patellar tendinosis in, 592t, *596*
  pelvic fatigue fractures in, 393t, *402,* 404t
  pubalgia syndromes in, 404t
  rib fatigue fractures in, 788t, *793*
  shin splints in, 629t
  shoulder impingement syndromes in, 856t
  sports hernia in, 404t
  tibia fatigue fracture in, *567,* 629t, *631-632,* 710t
  ulna stress injuries in, 948t, *950*
Atlantoaxial articulation
  anomalies and variants of, 52t, *63-64*
  instability and subluxation of, 44, 59t
    in ankylosing spondylitis, 109t, *127*
    in atlas assimilation, 51t, 59t
    causes of, 59t
    in crystal deposition disease, *132*
    in mucopolysaccharidosis, 78t, *79*
    in odontoid agenesis and hypoplasia, 52t, 59t
    in os odontoideum, 52t, 59t, *60*
    and pseudosubluxation of axis, 52t, *65*
    in psoriatic arthropathy, 109t, *131*
    in reactive arthritis, 109t, *132*
    in rheumatoid arthritis, 108t, 109t, *123-124, 125, 126*
    in spondyloepiphyseal dysplasia congenita, 78t, *79*
    surgical fusion in, 151t, *153*
    in trisomy 21, 52t, 59t
  osteoarthrosis of, *116*
  rotatory fixation of, 82t, *86*
Atlantodental interspace (predens space)
  in ankylosing spondylitis, *127*
  asymmetric, causes of, 85t
  in Jefferson fracture, 85t, *87*
  in osteoarthrosis, *116*
  in rheumatoid arthritis, *123-124*
  in rotatory atlantoaxial fixation, 85t, *86*
  in transverse ligament trauma, 82t, *85*
  in trisomy 21, *62*
  V-shaped, 52t, *61*

- Atlas (C1)
  - accessory ossicles of, 51t, *55*
  - anomalies and variants of, 51t, *53-57*
  - anterior arch of, 45t
    - agenesis of, 51t, *55*
    - fractures of, *55,* 83t
  - assimilation of, 51t, *53*
  - asymmetry of, 51t, *57*
  - in atlantoaxial articulation. *See* Atlantoaxial articulation
  - dislocation in juvenile rheumatoid arthritis, *126*
  - fractures of, 82t-83t, *87-88*
    - in anterior arch, *55,* 83t
    - burst or Jefferson, 82t, 85t, *87*
    - in lateral mass, 83t
    - in posterior arch, 82t, *88*
    - in transverse process, 83t
  - normal developmental anatomy of, 45t, *46*
  - and occipital condyle
    - dislocation of, 82t, *85*
    - fusion or assimilation of, 51t, *53*
  - ossification centers in, 45t
  - posterior arch of, 45t
    - agenesis of, 51t, *54*
    - fracture of, 82t, *88*
  - posterior ponticulus of, 51t, *56*
  - in rotatory atlantoaxial fixation, 82t, *86*
  - sclerotic anterior tubercle of, 51t, *56*
  - subluxation of, differential diagnosis in, *47*
  - traumatic injuries of, 82t-83t, *85-88*
- Avulsion injuries, 7t
  - of brachial plexus, 94t
  - cervical, 84t, 92t
  - of elbow, *927*
  - of femur, 453t, *458*
    - adductor insertion avulsion syndrome in, 509t, *514*
    - cortical irregularity in, 2t, 552t, *555*
  - of knee
    - patellar sleeve fracture in, 559t, *566*
    - tibial fractures in, 560t, 561t, *568, 571,* 591t
  - lumbar, 262t, *267,* 269t
  - pelvic, 392t, *394*
- Axis (C2)
  - anomalies and variants of, 51t-52t, *57-65*
  - in atlantoaxial articulation. *See* Atlantoaxial articulation
  - ball-and-socket articulation with C3, 52t, *65*
  - fractures of, 83t-84t, *88-90*
    - false appearance of, 2t, 51t, *57-59*
  - giant cell tumor of, benign, *144*
  - normal developmental anatomy of, 45t, *46-47*
  - odontoid process of. *See* Odontoid process
  - ossification centers in, 45t
  - osteochondroma of, solitary, *144*
  - pseudofusion with C3, 52t, *66*
  - pseudosubluxation of, 52t, *65*
  - in rotatory atlantoaxial fixation, 82t, *86*
  - spondylolysis of, congenital, 52t, *65*
  - transverse foramen of, 51t, *56*
  - traumatic injuries of, 83t-84t, *88-90*

B

- Baastrup disease, 281t, *288*
  - cysts associated with, 283t
- Back pain, thoracic scoliosis in, 178t
- Bacterial infections
  - Brodie abscess of tibia in, *668*
  - iliopsoas bursitis in, 469t, *483*
- Bacterial infections *(continued)*
  - osteomyelitis in, 43t
    - of femur, *546*
    - of humerus, *905*
    - of tibia, *666-667*
  - septic arthritis in
    - of hip, *481*
    - of sternoclavicular joint, *801*
  - septic bursitis of elbow in, *940*
  - skin and joint findings in, 23t
  - tuberculous. *See* Tuberculosis
- Baker cysts of knee, 578t, *582*
- Ball-and-socket articulation
  - in ankle, 681t, *683*
  - in cervical spine, 52t, *65*
- Ballooning of intervertebral disks in ankylosing spondylitis, 201t, *203*
- Balloon kyphoplasty in thoracic compression fractures, 226t, *227*
- Ball-thrower fracture of humerus, 889t
- Bamboo spine in ankylosing spondylitis, 201t, *300, 301*
- Bankart lesion, 833t, 841t, *844*
- Barlow maneuver in developmental dysplasia of hip, 444t, *448*
- Barton fracture, 951t, *953, 954*
- Bayonet apposition in clavicle fracture, *836, 837*
- Behçet syndrome, 22t
- Bennett fracture-dislocation, 1003t, *1005*
- Bent spine syndrome in degenerative lumbar kyphosis, 281t
- Biceps brachii tendon
  - calcific tendinitis of, 858t, *864*
  - rupture of
    - in distal end, 929t, *933*
    - in long head, 848t
  - tendinosis and tenosynovitis of, 848t, *852*
- Biceps femoris muscle and tendon injuries, 591t, *594*
- Bite wounds of hand, septic arthritis in, 1055t, *1063*
- Bizarre parosteal osteochondromatous proliferation in hand, 1047t, *1049*
- Blind vertebra sign in skeletal metastasis, *312*
- Blisters, as complication of wrist and hand fractures, 1017t, *1041*
- Block vertebrae, 2t
  - cervical
    - in lower segment, 67t, *72,* 73t, *74, 113*
    - in upper segment, 52t, *53, 66*
  - lumbar, 233t, *237*
  - thoracic, 167t
- Blount disease, 40t, 557t, 624t, *626*
- Bone cysts
  - aneurysmal. *See* Cysts, aneurysmal bone
  - simple. *See* Cysts, simple bone
- Bone islands. *See* Enostosis
- Bone marrow
  - edema of
    - of femur, transient migratory, 488t, *493*
    - of patella, in sleeve avulsion fracture, 559t, *566*
  - hyperplasia in ribs, in thalassemia, 814t, *818*
- Bone mineral density in osteoporosis, 327t, *330-331,* 331t, 488t, *491*
- Bone-within-bone appearance
  - in cervical osteopetrosis, 78t, *80*
  - in lumbar osteopetrosis, 244t, *246*
  - in pelvic osteopetrosis, 388t, *390*
  - in thoracic osteopetrosis, 170t, *171*
  - of tibia, *664*
- Bosworth fracture-dislocation of ankle, *713*
- Boutonnière deformity, 1066t
  - in lupus erythematosus, *1029*
- Bowlegs, 557t
  - in dysplasia epiphysealis hemimelica, *556,* 557t
- Boxer's arthropathy, 1016t, *1020*
- Boxer's fracture, 1004t, *1007*
- Brachial plexus injuries
  - in cervical spine injuries, 94t
  - Erb-Duchenne paralysis in, 849t, *854*
- Brachydactyly, 978t, *980*
- Brain injury, heterotopic ossification of elbow in, 942t, *943*
- Breast cancer
  - shoulder disorders from radiation therapy in, 878t, *882*
  - skeletal metastasis of
    - to ankle and foot, *761*
    - to femur, *518*
    - to pelvis, *416*
- Brodie abscess, 41t, 614t, 665t, *667-668*
- Bronchogenic carcinoma
  - secondary hypertrophic osteoarthropathy in
    - of femur, 541t, *544*
    - of radius and ulna, *969*
    - of tibia and fibula, 657t, *663*
    - of wrist and hand, 1055t, *1062*
  - skeletal metastasis of
    - to cervical spine, *140*
    - to femur, 515t, *517*
    - to pelvis, *416*
    - to radius and ulna, *960*
    - to tibia and fibula, 635t, *637*
- Brown tumors. *See* Osteoclastoma
- Bruises, bone, 7t
  - of cervical spine, 94t
  - of knee, *570, 577,* 579t, *584*
- Bullet vertebrae
  - in achondroplasia, 244t, *245*
  - in hypothyroidism, 221t, *223,* 327t, *332*
- Burns of hand, 1017t, *1041*
- Bursa, adventitial, of ankle and foot, 759t
- Bursitis, 18t
  - of ankle and foot, calcific, 734t, *747*
  - of elbow, septic, 934t, *940*
  - of hip
    - calcific, 469t, *479*
    - iliopsoas infectious, 469t, *483*
    - trochanteric pain syndrome in, *467*
  - of knee, 579t, *583*
    - prepatellar, 579t, *583*
  - retrocalcaneal
    - in ankylosing spondylitis, 737t, *742*
    - in Reiter syndrome, 737t, *745*
  - of shoulder, calcific, 848t, 858t
- Burst fractures
  - cervical
    - in atlas, 82t, 85t, *87*
    - in lower segment, 93t, *105*
  - lumbar, 228, 262t, *264,* 264t
    - instability in, 262t, 264t
    - surgery in, *340*
  - thoracic, 185t, *188*
  - thoracolumbar, 262t, *264*
- Butterfly vertebra
  - lumbar, 234t
  - thoracic, 167t, *169*

C

- Caffey disease
  - of clavicle and scapula, 830t, 883t
  - of ribs, 814t
- Calcaneocuboid joint, 736t
  - coalition of, 690t

Calcaneonavicular coalition, 690t, *692*
Calcaneus
  aneurysmal bone cyst of, *765*
  in ankylosing spondylitis, 734t, 737t, *742*
  in calcaneonavicular coalition, 690t, *692*
  deformity of, 681t
  enostosis of, *701, 762*
  enthesopathy of, 737t
    in diffuse idiopathic skeletal hyperostosis, 734t, 737t, *739*
  fibrosarcoma of, *761*
  fractures of, 714t, *716-717*
    extraarticular, 714t, *716*
    intraarticular, 714t, *717*
    stress, 714t, *716-717,* 728t
  giant cell tumor of, benign, *764*
  lipoma of, intraosseous, 759t, *765*
  in lupus erythematosus and corticosteroid therapy, *664*
  metastatic tumor of, *761*
  normal developmental anatomy of, 673t, *677,* 772t, *775*
  ossification centers in, 673t
  Paget disease of, 759t, *765*
  pseudocyst of, 2t, 691t, *701*
  in psoriatic arthropathy, *743*
  in Reiter syndrome, 734t, *745*
  secondarium, 690t, *695*
  simple bone cyst of, 759t, *764*
  in talocalcaneal coalition, 681t, *683,* 690t, *693, 739, 743*
Calcification
  of ankle and foot
    bursitis in, 734t, *747*
    in crystal deposition disease, 734t, 737t, *747*
    in dermatomyositis-polymyositis, 734t, *746*
    in hyperparathyroidism, 768t, *770*
    in intraosseous lipoma, 759t, *765*
    in scleroderma, 734t, *746*
    vascular, 768t, *770*
  of arm soft tissues in collagen vascular disorders, 903t, *905,* 967t, *971*
  bursitis in, 18t
    of ankle and foot, 734t, *747*
    of hip, 469t, *479*
    of shoulder, 848t, 858t
  of cervical intervertebral disk in childhood, 107t, *119*
  of cervical lymph nodes, 68t, *77*
  of chest wall in dermatomyositis-polymyositis, 797t, *801*
  of costochondral cartilage, 781t, *784-785*
  of elbow
    in crystal deposition disease, 934t, *939*
    in gout, *938*
    in scleroderma, 934t, *938*
  of hip
    bursitis in, 469t, *479*
    in crystal deposition disease, 469t, *478-479*
    in dermatomyositis-polymyositis, 468t, *477*
    in scleroderma, 468t, *477*
  of knee
    in crystal deposition disease, 600t, *607-608*
    in dermatomyositis-polymyositis, 599t, *606*
    in hemochromatosis, 600t, *610*
    in mixed connective tissue disease, 599t, *606*
  of leg soft tissues, 657t, *664*
Calcification *(continued)*
  lumbar, 282t, *290*
    in chondrodysplasia punctata, 244t, *247*
  of pectineal ligament, 384t, *387, 408*
  pelvic
    in dermatomyositis, 405t, *411*
    in hemochromatosis, *412*
    vascular, 384t, *386*
  of sacroiliac ligaments, 356t, *360*
  of shoulder
    bursitis in, 848t, 858t
    in crystal deposition disease, 858t, *864-865*
    in milk-alkali syndrome, 878t, *880*
  of stylohyoid ligament, 68t, *78*
  tendinitis in, 18t. *See also* Tendinitis, calcific
  of thoracic spine
    in alkaptonuria, *206*
    in childhood, 192t, *196-197*
    in crystal deposition disease, *206*
    in degenerative disorders, 192t, *196-197*
    in dermatomyositis-polymyositis, *205*
    in herniation, scoliosis in, 178t, *183*
    in soft tissues, *205*
  of tracheal cartilage, 68, *77,* 167t, *169*
  of wrist and hand, 973, 1067t
    causes of, 1067t
    in crystal deposition disease, 1017t, *1033-1035, 1037,* 1067t
    in dermatomyositis-polymyositis, 1016t, 1067t
    in hyperparathyroidism, 1054t, *1058, 1059,* 1067t
    in pseudohypoparathyroidism, 1054t, *1060,* 1067t
    in scleroderma, 1016t, *1030-1031,* 1067t
    vascular, 1054t, *1058*
Calcium hydroxyapatite crystal deposition disease, 18t
  of ankle and foot, 734t, 737t, *747*
  bursitis in, 18t
    of ankle and foot, 734t, *747*
    of hip, 469t, *479*
  of cervical spine, 110t, *133*
  of femur, 509t
  of hip, 469t, *479*
  of shoulder, 858t, *864, 866*
  tendinitis in, 18t
    of hip, 469t, *479*
    retropharyngeal, 110t, *133*
  of wrist and hand, 1017t, *1037,* 1067t
Calcium pyrophosphate dihydrate crystal deposition disease, 18t
  of ankle and foot, 734t, 737t, *747*
    hallux valgus in, *688*
  of cervical spine, 110t, *132*
  of elbow, 934t, *939*
  of hip, *439,* 440t, 469t, *478*
    patterns of joint space narrowing in, 470t
  of knee, 600t, 603t, *607-608*
  of lumbar spine, 295t, *306*
  of pelvis, 405t, *411, 428*
  of shoulder, 858t, *865, 866*
  of thoracic spine, 193t, *206*
  of wrist and hand, 1017t, 1018t, *1033-1035*
Callus of foot, 760t
Camurati-Engelmann disease, 4t, 624t, *628*
Canadian C-spine rule on diagnostic imaging, 80t-81t
Capitate
  fractures of, 990t, *994*
  in greater arc injuries, 991t
  ossification centers in, 973t
  osteonecrosis of, *1065,* 1065t
  synostosis with trapezoid, 977t, *979*
Capitulum of humerus
  fracture of, 918t, *923*
  ossification centers in, 907t, *908-909, 911-912*
  osteochondritis dissecans of, 919t, *928*
  Panner disease of, *928,* 942t, *943*
Capsulitis, adhesive, of shoulder, 848t, *851*
Carotid artery atherosclerosis, cervical spine in, *159,* 159t
Carpal bones
  accessory, 978t, *980*
  in ankylosing spondylitis, *1026*
  anomalies and variants of, 977t-978t, *979-980*
  bipartite, 978t
  in carpometacarpal dislocations, 991t, *998*
  fractures of, 990t-991t, *992-995*
  in gout, *1032*
  greater arc of, *995*
    injuries of, 991t, *997*
  in Hurler syndrome, 985t, *989*
  instability of, 999t, *1000-1002*
    dorsal intercalated segmental, 999t, *1000*
    scapholunate advanced collapse wrist in, 999t, *1001*
    ventral intercalated segmental, 999t, *1001*
  juvenile chronic arthritis of, *1025*
  lesser arc of, *995*
    injuries of, 991t, *996*
  in lupus erythematosus, *1028*
  Madelung deformity of, 945t, *946,* 977t
  ossification centers in, 973t
  osteoid osteoma of, *1049*
  osteonecrosis of, *1065,* 1065t
  osteopoikilosis of, 985t, *989*
  osteosarcoma of, *1044*
  in psoriatic arthropathy, *1026*
  reactive arthritis of, *1028*
  rheumatoid arthritis of, *1022*
  scleroderma of, *1030*
  synostosis of, 977t, *979*
Carpal boss, 978t, *980*
Carpal tunnel syndrome, 1011t, *1013*
  in amyloid deposition, 1054t, *1060*
Carpometacarpal joint, 1018t
  crystal deposition disease of, *1034*
  dislocation of, 991t, *998*
  erosive osteoarthritis of, 1016t, *1021*
  juvenile chronic arthritis of, *1025*
  in lupus erythematosus, *1028*
  osteoarthrosis of, in thumb, 1016t, *1019*
  psoriatic arthropathy of, *1026*
  scleroderma of, *1030*
  septic arthritis of, *1063*
Catterall classification of femoral involvement in Legg-Calvé-Perthes disease, 498t
Cavus deformity of foot, 682t, *686*
Celery stalk appearance of tibia and fibula, in congenital syphilis, 666t
Cellulitis of foot, *754,* 754t
Cerebral palsy, spastic paralysis and patellar injury in, 559t, *566*
Cervical carcinoma, pelvic insufficiency fracture after radiation therapy in, *433*

Cervical spine, 44-160
  anomalies and variants of, 2t, 44
    in lower segment, 67t-68t, *68-78*
    in upper segment, 51t-52t, *53-66*
  articular disorders of, 45, 107t-111t, *112-137*
    in crystal deposition disease, 110t-111t, *132-134*
    degenerative, 107t-108t, *112-122*
    infectious, 111t, *135-137*
    inflammatory, 108t-110t, *123-132*
  atlas in. *See* Atlas (C1)
  axis in. *See* Axis (C2)
  ball-and-socket articulation of C2 and C3 in, 52t, *65*
  congenital disorders of, 44, 78t, *79*
    spondylolisthesis in, 67t, *75*
    synostosis in, *66,* 73t, *74*
  dysplasias of, 44, 78t, *79*
  facet joint spaces in, *50*
  flattened vertebral body (vertebra plana) of, 67t, *69*
  fractures of
    in ankylosing spondylitis, *130*
    in atlas, *55,* 82t-83t, *87-88*
    burst
      in atlas, 82t, 85t, *87*
      in lower segment, 93t, *105*
    clay-shoveler's, 92t, *99*
    compression, 92t, 94t
    extension teardrop, 84t, 92t
    flexion teardrop, 92t, *100-101*
    hangman's, 84t, *90*
    in lower segment, 92t-94t, *98-101, 104-106*
    in metastatic bronchogenic carcinoma, *140*
    odontoid, 83t-84t, *88-90*
    pillar, 93t, *104-105*
    sagittal, of vertebral body, 94t, *106*
    screw fixation of, *89,* 155t
    simulation of, 2t, 51t, 52t, *57-59, 61,* 68t, *75*
  hair artifact in imaging of, 68t, *77*
  inflammatory disorders of, 108t-110t, *123-132*
    atlantoaxial instability and subluxation in, 59t
  instability of
    atlantoaxial. *See* Atlantoaxial articulation, instability and subluxation of
    in lower segment injuries, 91t, 94t, *95,* 96t, *103f*
  intervertebral disk disorders in. *See* Intervertebral disk disorders, cervical
  intervertebral foramen in, enlarged, 45, 146t
  in Klippel-Feil syndrome, 44, 73t, *74, 828*
  limbus vertebrae in, *75, 112*
  metabolic disorders affecting, 45, 149t, *149-150*
  normal developmental anatomy of, 44, 45t, *46-50*
  nuclear impressions of, 67t, *69*
  ossification centers in, 44, 45t, *46-50*
    age of appearance and fusion, 45t
    persistent unfused, 68t, *75*
  rheumatoid arthritis of. *See* Rheumatoid arthritis, of cervical spine
  sandwich vertebrae in, 78t, *80*
  spondylodiscitis of, 111t, *135-137*
    pyogenic, 111t, *135-136*
    tuberculous, 111t, *137*
Cervical spine *(continued)*
  sprain of
    hyperextension, 93t, *102*
    hyperflexion, 91t, 94t, *95*
    hyperflexion-hyperextension, *103*
  surgical procedures involving, 45, 151t, *152-154,* 155t, *156-158*
    fusion in, 151t, *152-153,* 155t, *156, 158*
    instrumentation and bone grafts in, *153,* 155t, *156-158*
    in intervertebral disk disorders, 45, 151t, *152,* 155t, *157*
    laminectomy and laminoplasty in, 151t, *154*
  synostosis (block vertebrae) of
    in lower segment, 67t, *72,* 73t, *74, 113*
    in upper segment, 52t, *53, 66*
  traumatic injuries of, 44
    Canadian rule on diagnostic imaging in, 80t-81t
    discovertebral, 92t, *101*
    instability in, 59t, 91t, 94t, *95,* 96t
    in lower segment, 91t-94t, *95-106*
    lucent annular cleft sign in, 92t, *101*
    nerve root or brachial plexus avulsion in, 94t
    risk criteria in, 80t-81t
    in upper segment, 82-85t, *85-90*
  tumors and tumorlike lesions of, 45, 138t-139t, *140-148*
    benign, 138t-139t, *143-145*
    enlarged intervertebral foramen in, 146t
    malignant, 138t, *140-141*
    myeloproliferative, 138t, *142*
    tumorlike lesions in, 139t, *146-148*
  vascular disorders affecting, 45, 159t, *159-160*
Champagne glass appearance in pelvic achondroplasia, 388t, *389*
Chance fracture, 185t, *189,* 262t
Charcot spine, *299, 304*
Chauffeur's fracture, 951t, *955*
Chest wall
  calcification in dermatomyositis-polymyositis, 797t, *801*
  tumors and tumorlike lesions of, 776, 803t, *813*
    in elastofibroma, 803t, *813*
Chevron sign of humerus, 887t, *888,* 913t
Child abuse, 9t
  ankle injuries in, 710t, *711*
  elbow injuries in, 918t
  humerus fracture in, 889t
  knee injuries in, 560t, *569*
  lumbar spine injuries in, 262t
  radius and ulna fractures in, 952t, *956*
  rib fractures in, 788t, *792*
  sacrococcygeal injuries in, 352t
  thoracic spine injuries in, 185t, *191*
  tibia and fibula fractures in, 710t, *711*
Children
  ankle and foot in
    in abused child, 710t, *711*
    in dermatomyositis-polymyositis, *746*
    growth plate injuries of, 710t, *712,* 723t, *725*
    in Köhler disease, 772t, *774*
    normal developmental anatomy of, 672, 673t, *674-680*
    in osteogenesis imperfecta, *703*
    in pes planus, *686*
    in talipes equinovarus, *684*
    in tarsal coalition, *692, 693*
Children *(continued)*
    in tibiotalar slant, *683*
    in tuberculous dactylitis, *757*
  arthritis in, juvenile idiopathic, 13t. *See also* Arthritis, juvenile idiopathic
  cervical spine in
    in calcification of intervertebral disks, 107t, *119*
    normal developmental anatomy of, 44, 45t, *46-50*
  elbow in
    in abused child, 918t
    dislocation of, 917t, *920*
    fractures of, 917t, 919t, *921, 923*
    growth plate injuries of, 919t, *927*
    normal developmental anatomy of, 906, 907t, *908-913*
    in osteochondritis dissecans, *928*
    in osteonecrosis, 942t, *943*
  epiphyseal disorders in, 40t
  femur in
    in aneurysmal bone cyst, *536*
    in avulsive cortical irregularity, 552t, *555*
    in chondroblastoma, *533*
    in collagen vascular disease, *546*
    in Ewing sarcoma, *525*
    in Gaucher disease, *543*
    growth resumption lines of, 541t, *545*
    in hereditary multiple exostoses, *534*
    in hyperparathyroidism, *542*
    in leukemia, *528-529*
    in limb length inequality, *505*
    in meningomyelocele, *545*
    in osteoblastoma, *532*
    in osteosarcoma, *519-520*
    in proximal focal deficiency, *507*
    in scurvy, 541t, *544*
  fractures in, 8t-9t
  growth recovery lines in, 37t
    of femur, 541t, *545*
    of tibia and fibula, 657t, *663, 683, 750*
  hip in
    in dermatomyositis-polymyositis, *477*
    in developmental dysplasia, 434, 444t-445t, *446-448*
    in hypothyroidism, *495*
    in infantile coxa vara, 440t, *442*
    in juvenile idiopathic arthritis, 468t
    in Legg-Calvé-Perthes disease, 497t, 498t, *499*
    normal developmental anatomy of, 434, 435t, *436-437*
    in renal osteodystrophy, *495*
    in septic arthritis and osteomyelitis, 469t, *482-483*
    in slipped capital femoral epiphysis, 453t, *454-455*
  humerus in
    in abused child, 889t
    in dermatomyositis-polymyositis, *905*
    in fibrous dysplasia, *901*
    fractures of, 889t, *890*
    in hereditary multiple exostoses, *899*
    in heterotopic ossification, *890*
    in leukemia, *895*
    in nonossifying fibroma, *899*
    in osteoid osteoma, *897*
    in osteomyelitis, 903t, *905*
    in rickets, *904*
  knee in
    in abused child, 560t, *569*
    in chondrodysplasia punctata, *556*
    growth plate injuries of, 560t-561t, *570-571*

- Children *(continued)*
    - in juvenile idiopathic arthritis, 599t, *613-614*
    - normal developmental anatomy of, 547, 548t, *549-551*
    - in Osgood-Schlatter disease, 561t, *572*
    - in patellar fractures, 559t, *565, 566*
  - lumbar spine in
    - in abused child syndrome, 262t
    - in chondrodysplasia punctata, *247*
    - in degenerative disk disease, 269t
    - in leukemia, *319*
    - normal developmental anatomy of, 228, 229t, *230-232*
    - in osteochondrosis, 269t, *279*
    - scoliosis of, 259t, *260*
    - in spondylolysis, 248t, *251*
    - in thalassemia, *335*
  - osteochondrosis in, 40t
  - pelvis in
    - in leukemia, *420*
    - normal developmental anatomy of, 377, 378t, *379-384*
    - in osteogenesis imperfecta, *391*
    - radiation-induced changes of, 427t, *433*
    - in β-thalassemia, *430*
  - radius and ulna in
    - in abused child, 952t, *956*
    - in aneurysmal bone cyst, *965*
    - fractures of, 951t, 952t, *953, 956*
    - in hemangioma, *965*
    - in leukemia, *963*
    - in nonossifying fibroma, *964*
    - in osteochondroma, *964*
    - in osteomyelitis, 967t, *970-971*
    - in renal osteodystrophy, *968*
    - in rickets, *968*
  - ribs and sternum in
    - in abused child, 788t, *792*
    - in infantile cortical hyperostosis, 814t
    - normal developmental anatomy of, 776, 777t, *778-780*
    - in osteogenesis imperfecta, *815*
    - in rickets, *816*
    - in synostosis of ribs, *783*
  - sacrococcygeal spine and sacroiliac joints in
    - in abused child, 352t
    - normal developmental anatomy of, 345, 346t, *346-348*
  - shoulder in
    - in chronic recurrent multifocal osteomyelitis, *885*
    - in clavicle fractures, *836, 837*
    - in congenital pseudarthrosis of clavicle, *827*
    - in eosinophilic granuloma, *877*
    - in Ewing sarcoma, *873*
    - in fibrodysplasia ossificans progressiva, *830*
    - in growth plate injuries of humerus, 832t, *835*
    - in infantile cortical hyperostosis, 830t, 883t
    - normal developmental anatomy of, 819, 820t, *821-823*
    - in prostaglandin periostitis of neonates, 883t
  - thoracic spine in
    - in abused child, 185t, *191*
    - in calcification of intervertebral disks, 192t, *196-197*
    - in chondrodysplasia punctata, *172*
    - in Hodgkin disease, *214*
    - in leukemia, *214*
- Children *(continued)*
    - in mucopolysaccharidoses, *171*
    - normal developmental anatomy of, 161, 162t, *162-166*
    - in osteogenesis imperfecta, *172*
    - in osteoid osteoma, *215*
    - in scoliosis, 177t, *180*
  - tibia and fibula in
    - in abused child, 710t, *711*
    - in Brodie abscess, 665t, *667-668*
    - in congenital syphilis, *670*
    - in fibrous dysplasia, *655*
    - in focal fibrocartilaginous dysplasia, *626*
    - fractures of, 628t, *630-631*
    - in Gaucher disease, *661*
    - growth recovery lines of, *663*
    - in hyperparathyroidism, *659-660*
    - in intraosseous lipoma, *651*
    - in leukemia, *643*
    - in osteoid osteoma, *645*
    - in osteomyelitis
      - acute, 665t, *666*
      - chronic recurrent multifocal, 666t, *669*
      - tuberculous, 666t, *669*
    - in osteosarcoma, *638-639*
    - in scurvy, *661*
    - varus deformity of, 624t, *626*
    - in Wilms tumor, *638*
  - wrist and hand in
    - in abused child, 1004t
    - in fibrodysplasia ossificans progressiva, *988*
    - in fibrous dysplasia, *1053*
    - in Hurler syndrome, *989*
    - in hypothyroidism, *1060*
    - in Kirner deformity, *984*
    - in macrodactyly, *984*
    - in metacarpal fractures, *1007*
    - normal developmental anatomy of, 972, 973t, *974-977*
    - in phalangeal fractures, 1004t, *1009*
    - in polydactyly, *982*
    - in simple bone cyst, *1051*
    - in syndactyly, *981*
    - in Turner syndrome, *986*
- Chisel fracture of radial head, 918t, *925*
- Chondroblastoma, 29t
  - of ankle and foot, 759t, *763*
  - of clavicle and scapula, 871t
  - of femur, 530t, *533*
  - of humerus, 896t, *898*
  - of knee, 614t, *615, 647*
  - of tibia and fibula, 644t, *647*
- Chondrocalcinosis, 19t, 23t
  - of elbow, 934t, *939*
  - of hip, 469t, *478, 480*
  - of knee, 600t, *607-608, 610*
  - of shoulder, 858t, *865*
  - of symphysis pubis, 405t, *411, 428*
  - of wrist and hand, 1017t, *1033-1035, 1036*
- Chondrodysplasia punctata, 4t
  - of knee, *555*t, *556*
  - of lumbar spine, 244t, *247*
  - of thoracic spine, 170t, *172*
- Chondrolysis of hip, idiopathic, 470t, *486*
- Chondromalacia patellae, 597t, *598*
- Chondroma of foot, 760t
- Chondromatosis, synovial, of foot, 760t
- Chondromyxoid fibroma, 29t
  - of femur, 530t
  - of tibia and fibula, 644t, *648*
- Chondrosarcoma, 25t
  - central, 413t
  - of cervical spine, 138t
  - of clavicle and scapula, 870t
  - of femur, 516t, *522*
  - of humerus, 891t
  - of knee, 614t
  - mesenchymal, 802t, *807*
  - of pelvis, 413t, *417*
  - peripheral, 413t
  - of ribs, 802t, *807*
    - extrapleural mass in, 791t, *807*
  - sacrococcygeal, 371t
  - of sternum, 802t
  - of tibia and fibula, 636t
- Chordoma, 26t
  - of cervical spine, 138t, *141*
  - ivory vertebra in, 313t, *315*
  - of lumbar spine, 312t, 313t, *315*
  - osteosclerosis in, 313t, *315*
  - of sacrococcygeal spine, 371t, *373*
- Christmas disease, 20t
- Clasp-knife deformity, 233t, *239,* 349t
- Clavicle, 819-885
  - in acromioclavicular joint. *See* Acromioclavicular joint
  - anomalies and variants of, 824t, *825-827*
  - cleidocranial dysplasia of, 830t, *831*
  - companion shadow of, 824t, *827*
  - dislocation of
    - in acromioclavicular joint, 842t, *846*
    - in sternoclavicular joint, 789t, *795*
  - duplication of, 824t
  - fork deformity of, 824t, *825*
  - fractures of, 832t, *836-837*
    - with scapular fracture, 833t, *839, 840*
  - hyperostosis of, infantile cortical, 830t, 883t
  - normal developmental anatomy of, 820t, *821*
  - oblique orientation in cervical spine radiographs, *49*
  - ossification centers in, 820t, *821*
    - ununited, 824t, *826*
  - osteitis of, condensing, 883t, *884*
  - osteolysis of, posttraumatic, 849t, *855*
  - osteomyelitis of
    - chronic recurrent multifocal, 814t, *818,* 883t, *885*
    - pyogenic, 878t, *882*
  - osteopetrosis of, 830t
  - Paget disease of, 871t, *876,* 883t
  - periostitis of, 883t, *885*
    - from prostaglandin therapy in neonates, 883t
  - pseudarthrosis of, congenital, 824t, *827*
  - in renal osteodystrophy, 878t, *879*
  - in rheumatoid arthritis, 857t, *862*
  - rhomboid fossa in, 2t, 824t, *826, 882*
  - in SAPHO syndrome, 797t, *800*
  - in sternoclavicular joint. *See* Sternoclavicular joint
  - in sternocostoclavicular hyperostosis, 797t, *800,* 883t, *884*
  - tumors and tumorlike lesions of, 819, 870t-871t, *872-877*
    - benign, 871t, *875*
    - malignant, 870t, *872-873*
    - metastatic, 870t
    - myeloproliferative, 871t, *873*
    - tumorlike lesions, 871t, *876-877*
- Claw toe, 682t
- Clay-shoveler's fracture, 92t, *99*

Cleidocranial dysplasia, 3t
  of hip, 440t
  of pelvis, 388t, *391*
  of shoulder, 830t, *831*
  of sternum, 781t, *786*
Clinodactyly, 979t, *988*
Clubbing of fingers, in secondary hypertrophic osteoarthropathy, 1055t, *1062*
Clubfoot, congenital, 681t, *684*
Cobb measurement method in lumbar scoliosis, *260*
Coccidioidomycosis, 23t
  of ankle and foot, 754t
  of lumbar facet joints, *311*
  of wrist and hand, 1055t
Coccyx, 345-376
  fractures of, 352t, 392t
  ossification centers in, 346t
  in sacrococcygeal spine. *See* Sacrococcygeal spine
Codman triangle, *519*
Cold injuries
  of foot, 735t, *753*
  of hand, 1017t, *1040*
    terminal phalangeal resorption in, 1067t
Colitis, ulcerative
  enteropathic arthropathy in, 15t
    of cervical spine, 109t
    of lumbar spine, 294t
    of sacroiliac joint, 356t, 357t, *367*
    of thoracic spine, 193t
  skin disorders in, 22t
Collagen vascular disorders, 22t
  of femur, 541t, *546*
  of hip, 440t, *477*
  of humerus, 903t, *905*
  of radius and ulna, 967t, *971*
  rib notching in, 787t
  of tibia and fibula, 657t, *664*
Collateral ligament injuries
  of elbow
    lateral, 929t, *931*
    medial, 929t, *930*
  of knee
    lateral, 591t, *594*
    medial, 557t, *584,* 590t, *593*
  of metacarpophalangeal joint, 1003t, *1006*
Colles fracture, 951t, *952*
  blisters as complication of, *1041*
  immobilization osteoporosis in, *1057*
  reverse, 951t, *955*
Complex regional pain syndrome, regional osteoporosis in
  of ankle and foot, 768t, *769*
  of tibia and fibula, 657t, *658*
  of wrist and hand, 1054t, *1057*
Compression fractures, 6t
  of cervical spine, 92t, 94t
  of lumbar spine, 262t, *263*
    in osteomalacia, 327t, *332*
    in osteoporosis, 327t, *328*
  of thoracic spine, 185t, *186-187,* 187t
    in hemangioma, *217*
    in osteogenesis imperfecta, 170t, *172*
    in osteoporosis, 221t, *222*
    surgical procedures in, 226t, *227*
Condylar fractures of humerus, 917t
  growth plate injuries in, 919t
Congenital disorders, 3t-4t
  of ankle and foot, 672t, 703t
    clubfoot in, 681t, *684*
    in congenital pain insensitivity, 735t, *752*
Congenital disorders *(continued)*
    in congenital syphilis, 754t
    talocalcaneal coalition in, *683*
    vertical talus and rocker-bottom foot in, 681t, *685*
  of cervical spine, 44, 78t, *79-80*
    enlarged intervertebral foramen in, 146t
    spondylolisthesis in, 67t, *75*
    synostosis in, *66,* 73t, *74*
  of clavicle, pseudarthrosis in, 824t, *827*
  of femur, *503,* 504t
  of knee, 547, *555*t
  of lumbar spine, 228, 244t, *245-247*
  pain insensitivity and neuropathic osteoarthropathy in
    of foot, 735t, *752*
    of wrist and hand, 1017t, *1040*
  of pelvis, 377, 388t, *389-391*
  rib pseudarthrosis in, 781t
  of shoulder, 819, 830t
  syphilis in, 42t
    ankle and foot disorders in, 754t
    tibia and fibula disorders in, 666t, *670*
    wrist and hand disorders in, 1055t
  of thoracic spine, 161, 170t, *170-172*
    scoliosis in, 177t, *181*
  of wrist and hand, 972, 985t
    in congenital pain insensitivity, 1017t, *1040*
    in congenital syphilis, 1055t
Connective tissue diseases, mixed, 17t
  of hip, 468t, *477*
  of knee, 599t, *606*
Conradi-Hünermann syndrome, 4t
Contusions, bone, 7t
  of cervical spine, 94t
  of knee, *570, 577,* 579t, *584*
Cookie-bite lesions in skeletal metastasis
  of radius and ulna, 957t
  of tibia and fibula, 635t
Coracoclavicular joint, 824t, *827*
  ankylosing spondylitis of, 857t
  rheumatoid arthritis of, 857t, *862*
Coracoclavicular ligament
  normal variants in region of, 824t, *827*
  rupture of
    in acromioclavicular joint dislocation, 842t
    in clavicle fracture, *836*
  sprain of, 842t, *846*
Coracoid process of scapula
  fractures of, 833t, *839*
  ossification centers in, 820t, *822-823*
Corduroy cloth appearance in hemangioma
  lumbar, *322*
  thoracic, *217*
Corner sign in metaphyseal fractures, 8t
Coronoid process fractures, 918t, *924*
Cortical defect, fibrous, 30t
  of femur, 530t, *535*
  of humerus, 896t
  of radius and ulna, 959t
  of tibia and fibula, 644t, *650*
Corticosteroid therapy
  femoral disorders in, *490, 502*
    in lupus erythematosus, 599t
  humeral head osteonecrosis in, 878t, *881*
  lumbar spine disorders in, 327t, *328, 330, 336*
  talus disorders in, 772t
  thoracic spine disorders in, *225*
  tibia disorders in, *622*
    in lupus erythematosus, *664*
Costal apophyses of sacrum, anterior and posterior, 346t
Costal processes of sacrum, 346t
Costochondral cartilage calcification or ossification, 781t, *784-785*
Costosternal joint
  articular disorders of, 776, 797t
  osteoarthrosis of, 797t, *798*
  in sternocostoclavicular hyperostosis, 797t, *884*
Costosternal syndrome (Tietze syndrome), 788t
Costovertebral joint
  articular disorders of, 776, 797t
  dislocation of, 788t
  osteoarthrosis of, 192t, *195-196,* 797t
Cough fracture of ribs, 788t, *792*
Coxa valga, 440t, *441*
  infantile (developmental), 440t, *442*
  in mucopolysaccharidoses, 388t, *390*
  in poliomyelitis, *432*
Coxa vara, 440t, *441-442*
  in achondroplasia, 388t, *389*
  in osteogenesis imperfecta, *542*
  in rickets, *494*
CPPD crystal deposition disease. *See* Calcium pyrophosphate dihydrate crystal deposition disease
Cranial settling in rheumatoid arthritis of cervical spine, *124*
Crescent sign in osteonecrosis
  of femoral head, 497t, 498t, *501*
  of humeral head, *881*
Crohn disease, enteropathic arthropathy in, 15t
Cruciate ligament tears
  anterior, *573,* 591t, *595*
  posterior, 557t, 591t, *595*
    with avulsion fracture of tibial eminence, *568,* 591t
Crystal deposition disorders, 18t
  of ankle and foot, 734t-735t, 737t, *747-749*
    hallux valgus in, 682t, *688*
  calcium hydroxyapatite. *See* Calcium hydroxyapatite crystal deposition disease
  calcium pyrophosphate dihydrate. *See* Calcium pyrophosphate dihydrate crystal deposition disease
  of cervical spine, 110t-111t, *132-134*
  of elbow, 934t, *939*
  of femur, 509t
  of hip, *439,* 440t, 469t, *478-479*
  of knee, 600t, 603t, *607-609*
  of lumbar spine, 295t, *306-308*
  of pelvis, 406t, *412, 428*
  of shoulder, 858t, *864-866*
    Milwaukee shoulder syndrome in, 858t, *865, 866*
  of thoracic spine, 193t, *206*
  of wrist and hand, 1017t, 1018t, *1033-1035, 1037*
Cuboid bone
  fractures of, 715t, *722*
    stress, 727t
  normal developmental anatomy of, 673t, *677-678*
  ossification centers in, 673t
  in talocuboid coalition, 690t, *694*
Cuneiform bones
  fractures of, 715t
    stress, 727t
  normal developmental anatomy of, 673t, *677-678*
  ossification centers in, 673t
Cuneonavicular joint, 736t

Cupid bow configuration of vertebrae, 2t, 233t, *237*
Curly toe, 682t
Cysts
  aneurysmal bone, 31t
    of ankle and foot, 759t, *765*
    of cervical spine, 139t, *145,* 146t
    of clavicle and scapula, 871t, *875*
    of femur, 530t, *536*
    of humerus, 896t
    of knee, 614t, *615, 652*
    of lumbar spine, *312t,* 321
    of pelvis, 414t, *423*
    of radius and ulna, 959t, *965*
    of ribs, 803t
    of sacrococcygeal spine, 371t
    of tibia and fibula, 644t, *652*
    of wrist and hand, 1048t, *1052*
  degenerative
    of knee, 614t
    of lumbar spine, 283t, *293*
  epidermoid (inclusion), of hand, 1048t, *1053*
  ganglion. *See* Ganglion cysts
  meniscal, 585t, *586*
  simple bone, 31t
    of ankle and foot, 759t, *764*
    of femur, 530t, *536*
    of humerus, 896t, *900*
    of pelvis, 414t, *423*
    of tibia and fibula, 644t, *652*
    of wrist and hand, 1048t, *1051*
  synovial. *See* Synovial cysts

D

Dactylitis
  sickle cell, 772t, *773*
  tuberculous
    of foot, 754t, *757*
    of hand, 1055t, *1064*
Dagger sign in ankylosing spondylitis, 201t
De Quervain syndrome, 1011t
Decompressive surgery
  of cervical spine, 151t, *154*
  of lumbar spine, 337t, *338-339*
Degenerative disorders, 11t-12t
  of ankle and foot, 734t, *738-739*
  of cervical spine, 107t-108t, *112-122,* 150t, *158*
  of elbow, 934t, *936*
  of hip, 468t, *471-472*
  of knee, 585t, 599t, *601-602*
  of lumbar spine. *See* Lumbar spine, degenerative disorders of
  of pelvis, 405t, *406-409*
  of sacroiliac joint, 356t, 357t, *358-363*
  of shoulder, *850,* 857t, *860-861*
  of thoracic cage joints, 797t, *798*
  of thoracic spine, 192t, *194-201*
  of wrist and hand, 1016t, *1019-1021*
Deltoid ligament rupture, 705t, *706, 707*
Deltoid tuberosity of humerus, 887t
Densitometry in osteoporosis, 327t, *330-331,* 331t, 488t, *491*
Dermal sinus, 5t
Dermatomyositis, 16t
  ankle and foot disorders in, 734t, *746*
  chest wall disorders in, 797t, *801*
  femoral disorders in, 541t, *546*
  hip disorders in, 468t, *477*
  humerus disorders in, 903t, *905*
  knee disorders in, 599t, *606*
  pelvic disorders in, 405t, *411*
  thoracic spine disorders in, 193t, *205*
  wrist and hand disorders in, 1016t, 1067t
Dermis disorders, 22t
Desmoid, juxtacortical, 552t, *555*
Diabetes mellitus
  ankle and foot disorders in
    cellulitis, *754,* 754t
    neuropathic osteoarthropathy, 735t, *751*
    pyogenic osteomyelitis and septic arthritis, 754t, *754-756*
    vascular calcification, 768t, *770*
  in hemochromatosis, 19t, 23t
Dialysis, 35t
  amyloid deposition in, 1054t, *1060*
  rib fractures in, 814t, *818*
  spondyloarthropathy in, 35t, 111t, *137*
  vascular calcification of hand in, *1058*
Diaphyseal dysplasia, progressive, 4t, 624t, *628*
Diaphyseal fractures
  of femur, 503, 509t, *510-515*
  of tibia, 628t-629t, *630-632*
Diastematomyelia, 5t
  lumbar, 235t, *243*
  thoracic, 177t, *182*
Diffuse idiopathic skeletal hyperostosis. *See* Hyperostosis, diffuse idiopathic skeletal
Direct current electrical stimulation in lumbar spine surgery, 339t, *340*
Discectomy, cervical, *152, 153*
Discitis in ankylosing spondylitis, 201t
Discoid meniscus, 585t, *586*
Discovertebral joints, 10t
  cervical, lucent annular cleft sign in trauma of, 92t, *101*
  lumbar
    ankylosing spondylitis of, 294t, *300*
    gouty arthropathy of, 295t, *308*
DISH. *See* Hyperostosis, diffuse idiopathic skeletal
Disk disorders, intervertebral. *See* Intervertebral disk disorders
Dislocations, 10t
  in ankle and foot, 672, 710t, *713*
    interphalangeal, 723t, *725, 727*
    metatarsophalangeal, 723t
    talar, 715t, *720*
  in cervical spine
    atlanto-occipital, 82t, *85*
    in lower segment, 91t, 93t, *97-98*
    in rheumatoid arthritis, *126*
  of costovertebral joint, 788t
  of elbow, 906, 917t, *919-920*
  in hand, 991t, *998,* 1003t-1004t, *1005, 1007*
  of hip. *See* Hip, dislocation of
  of knee, *547,* 557t, 575t, *576-577*
  of lumbosacral apophyseal joint, 262t, *266*
  of radioulnar joint, distal, 951t, *954*
  in sacrococcygeal spine, 352t
  of shoulder, 819, 841t-842t, *843-847*
  in wrist, 991t, *995-998*
Diverticula, arachnoid, in lumbar ankylosing spondylitis, 294t, *302*
Down syndrome
  atlantoaxial instability in, 52t, 59t
  atlantodental interspace in, *62*
  brachydactyly in, 978t, *980*
  pelvic disorders in, 388t, *389*
Drawer test in anterior ankle instability, *730*
Drooping shoulder, 841t, *845*
Dual energy x-ray absorptiometry in osteoporosis, 327t, *331,* 488t, *491*
Duchenne muscular dystrophy, thoracic scoliosis in, 178t, *182*
Duverney fracture of iliac wing, 392t, *395*
Dysgenesis, spinal segmental, 5t
Dysplasia, 3t-4t
  of ankle and foot, 672, *703,* 703t
    fibrous, 759t, *766*
  of cervical spine, 44, 78t, *79*
  cleidocranial, 3t
    of hip, 440t
    of pelvis, 388t, *391*
    of shoulder, 830t, *831*
    of sternum, 781t, *786*
  diaphyseal, progressive, 4t, 624t, *628*
  diastrophic, 3t
    of hip, 440t
    of lumbar spine, 244t, *247*
  epiphysealis hemimelica, 3t
    of ankle and foot, *703,* 703t
    of knee, 555t, *556,* 557t
  of femur, 503, 504t
    fibrous, *426,* 537t, *539, 656*
  fibrous. *See* Fibrous dysplasia
  of hip. *See* Hip, dysplasia of
  of knee, *547,* 555t, *556,* 557t
  of lumbar spine, 228, 244t, *247*
    and spondylolisthesis, 248t, *250*
  osteofibrous, 28t
    of tibia and fibula, 643t, *645*
  of pelvis, 377, 388t
    cleidocranial, 388t, *391*
    fibrous, 414t, *426*
    sclerosing, *390*
  of sacrococcygeal spine and sacroiliac joints, 345
  of scapula, 824t, *828*
  of shoulder, 819, 830t, *831*
  spondyloepiphyseal, 3t
    congenita, 3t, 78t, *79*
  of thoracic spine, 161, *170,* 170t
  of tibia, focal fibrocartilaginous, 624t, *626*
  of wrist and hand, 972, 985t
    fibrous, 1048t, *1053*
Dysraphisms, spinal, 5t
Dystelephalangy, 979t
Dystrophy
  Duchenne muscular, thoracic scoliosis in, 178t, *182*
  mixed sclerosing bone, 4t
    of femur, 504t, *627*

E

Eagle syndrome, 68t, *78*
Edema of bone marrow
  of femur, transient migratory, 488t, *493*
  of patella, in sleeve avulsion fracture, 559t, *566*
Effusions, joint, 10t
  in ankle and foot, 728t, *730*
    in gouty arthropathy, *748*
  in elbow, *916*
  in knee. *See* Knee, joint effusions in
  in shoulder, in hemophilic arthropathy, *869*
Ehlers-Danlos syndrome, 4t
  ankle and foot disorders in, 703t
  knee disorders in, 555t, 557t
  lumbar spine disorders in, 244t, 246t, *247*
  pectus excavatum in, 781t, *786*
  skin disorders in, 22t
  wrist and hand disorders in, 985t
Eisenstein measurement method in spinal stenosis, 234t, *240,* 293t
Elastofibroma of chest wall, 803t, *813*

Elbow, 906-943
  anomalies and variants of, 906, 913t, *914-915*
  articular disorders of, 906, 934t-935y, *936-942*
    in crystal deposition disease, 934t, *939*
    degenerative, 934t, *936*
    infectious, 934t-935t, *940*
    inflammatory, 934t, *937-938*
  dislocations of, 906, 917t, *919-920*
    in Monteggia fracture-dislocation, 917t
    posterior, 917t, *919*
    of radial head, 917t, *920*
  epicondylitis of
    lateral, 929t, *931*
    medial, 929t, *932*
  fat pad displacement in, 906, 915t, *916*
  fractures of, 906, 917t-919, *921-928*
    in child abuse, 918t
    of humerus, 917t-918t, *921-923*
    osteochondral, 919t, *928*
    of radius, 918t, *925-926*
    of ulna, 918t, *924*
  growth plate injuries of, 919t, *927*
  humerus at. *See* Humerus, distal
  instability of, 929t, *930-931*
    lateral, 929t, *931*
    medial, 929t, *930*
  metabolic disorders of, 906, 942t
  normal developmental anatomy of, 906, 907t, *908-913*
  nursemaids', 917t, *920*
  ossification centers in, 906, 907t, *908-912*
    age of appearance and fusion, 907t
    incomplete union of, 913t, *914*
  soft tissue injuries of, 906, 929t, *930-933*
    ligament, 929t, *930-931*
    tendon, 929t, *931-933*
  tennis elbow, 929t, *931*
Electrical injuries of hand, 1017t, *1041*
Electrical stimulation, direct current, in lumbar spine surgery, 339t, *340*
Enchondroma, 28t
  of clavicle and scapula, 871t
  of femur, 529t, *532*
  of foot, 759t, *763*
  of humerus, 896t, *898*
  of knee, 614t
  of pelvis, 414t
  of radius and ulna, 958t
  of ribs, 802t, *810*
  of tibia and fibula, 644t, *646*
  of wrist and hand, 1048t, *1050*
Enchondromatosis, 29t
  of femur, 440t, 529t
  of foot, 759t
  of humerus, 896t
  of pelvis, 414t
  of radius and ulna, 958t
  of tibia and fibula, 644t, *646*
  of wrist and hand, 1048t, *1051*
Endocrine disorders, 34t-37t
  hyperparathyroidism. *See* Hyperparathyroidism
  hypoparathyroidism
    pelvic disorders in, 427t, *429*
    tibia and fibula disorders in, 657t, *660*
  hypothyroidism. *See* Hypothyroidism
Endometrial carcinoma
  pelvic disorders in, *433*
  radiation-induced osteonecrosis in, *502*
End plate ring apophysis
  cervical, 45t, *48*
  thoracic, 162t
Enostosis, 28t
  of ankle and foot, 759t, *762*
    in calcaneus, *701, 762*
  of cervical spine, 138t
  of femur, 529t, *531*
  of humerus, 895t
  of lumbar spine, 312t, 313t, *319*
  of pelvis, 414t, *421*
  of ribs, 802t
  of sacrococcygeal spine, 371t, *374*
  of thoracic spine, 209t, *215*
  of tibia and fibula, 643t
  of wrist and hand, 1047t
    in scaphoid, *992*
Enteric fistula, dorsal, 5t
Enteropathic arthropathy, 15t
  of cervical spine, 109t
  of lumbar spine, 294t
  of sacroiliac joint, 356t, 357t, *367*
  of thoracic spine, 193t
Enthesopathy
  of acromioclavicular joint, *861*
  of ankle and foot, 737t, *739*
    calcaneal, 737t, *739*
    in diffuse idiopathic skeletal hyperostosis, 734t, 737t, *739*
    in Reiter syndrome, 734t, 737t, *745*
  of elbow
    in crystal deposition disease, *939*
    in diffuse idiopathic skeletal hyperostosis, 934t, *936*
  of hip, in diffuse idiopathic skeletal hyperostosis, 468t, *472*
  of knee, 599t, *601-602*
    in acromegaly, *610*
    in reactive arthritis, *605*
  of pelvis
    degenerative, 405t, *406, 407*
    in hypoparathyroidism, 427t, *429*
  sacroiliac, in diffuse idiopathic skeletal hyperostosis, 356t, 357t
  of wrist and hand, in ankylosing spondylitis, 1016t, *1026*
Eosinophilic granuloma. *See* Granuloma, eosinophilic
Epicondyles of humerus
  lateral
    growth plate injury of, 919t
    inflammation of, 929t, *931*
    ossification centers in, 907t
  medial
    growth plate injury of, 919t, *927*
    inflammation of, 929t, *932*
    ossification centers in, 907t, *908, 911*
      unfused, *914*
Epicondylitis
  lateral, 929t, *931*
  medial, 929t, *932*
Epidermis disorders, 22t
Epidermoid cyst of hand, 1048t, *1053*
Epidermolysis bullosa, hand disorders in, 1017t, *1042,* 1067t
  terminal phalangeal resorption in, *1067,* 1067t
Epiphysis, 8t, 40t
  of calcaneus, normal developmental anatomy of, 673t, *677*
  of clavicle, normal developmental anatomy of, 820t, *821*
  differential diagnosis in disorders of, 404t
  dysplasia epiphysealis hemimelica of, 3t
    in ankle and foot, *703,* 703t
    in knee, 555t, *556,* 557t
  of femur
    distal
Epiphysis *(continued)*
      in chondrodysplasia punctata, 555t, *556*
      dysplasia epiphysealis hemimelica of, 555t, *556*
      injuries of, 560t, *570*
      normal developmental anatomy of, 548t, *549-551*
    proximal, *379-380*
      in Legg-Calvé-Perthes disease, 498t, *499*
      normal developmental anatomy of, 435t, *436-437*
      slipped, 440t, 453t, *454-455,* 469t, *483,* 488t, *495*
  of fibula
    distal
      injuries of, 710t
      normal developmental anatomy of, 673t, *674-677*
    proximal, normal developmental anatomy of, 548t, *549-551*
  of humerus
    distal
      injuries of, 919t, *927*
      normal developmental anatomy of, 907t, *908-912*
    proximal
      injuries of, 832t, *835*
      normal developmental anatomy of, 820t, *822-823*
  of metatarsal bones, *679-680*
    anomalies and variants of, 691t
  in osteonecrosis, 40t
  of phalangeal bones in foot, *679-680*
    anomalies and variants of, 691t
    injuries of, 723t, *725*
  of phalangeal bones in hand
    anomalies and variants of, 978t, *981*
    cone-shaped, 978t, *981*
    injuries of, 1004t, *1009*
    in Kirner deformity, 979t, *984*
    in Turner syndrome, 985t, *986*
  of radius
    distal
      injuries of, 952t
      normal developmental anatomy of, 973t
    proximal
      injuries of, 919t
      normal developmental anatomy of, 907t, *908, 911-913*
  of scapula, normal developmental anatomy of, 820t, *822-823*
  of tibia
    distal
      dysplasia epiphysealis hemimelica of, *703,* 703t
      injuries of, 710t, *712*
      normal developmental anatomy of, 673t, *674-677*
    proximal
      dysplasia epiphysealis hemimelica of, 555t, *556*
      injuries of, 561t, *571*
      normal developmental anatomy of, 548t, *549-551*
      in Osgood-Schlatter disease, 561t
  of ulna
    distal
      injuries of, 952t
      normal developmental anatomy of, 973t
    proximal, normal developmental anatomy of, 907t, *912*

Equinus deformity of foot, 681t
Erb-Duchenne paralysis, shoulder in, 849t, *854*
Erlenmeyer flask deformity
  in Gaucher disease
    of ankle and foot, 768t
    of femur, 541t, *543*
    of humerus, 903t, *904*
    of tibia and fibula, 657t, *661*
  in osteopetrosis
    of femur, 504t, *507*
    of tibia and fibula, *626*
Essex-Lopresti injury, 951t
Evans classification of femoral fractures, 460t
Ewing sarcoma, 26t
  of ankle and foot, 758t, *761*
  of cervical spine, 138t
  of clavicle and scapula, 870t, *873*
  of femur, 516t, *525*
  of humerus, 891t, *893*
  of pelvis, 413t, *418*
  of radius and ulna, 957t, *962*
  of ribs, 802t, *808*
    extrapleural mass in, 791t, *808*
  of sacrococcygeal spine, 371t
  of tibia and fibula, 636t, *641*
  of wrist and hand, 1043t, *1045*
Exostoses
  hereditary multiple, 30t
    of cervical spine, 139t
    of femur, 440t, 530t, *534, 649*
    of humerus, 896t, *899*
    of pelvis, 414t
    of radius and ulna, 958t, *964*
    of tibia and fibula, 644t, *649*
  subungual
    of foot, 759t, *763*
    of hand, 1047t, *1049*
  Turret, of hand, 1048t
Expandable cages
  in cervical spine surgery, 155t
  in lumbar spine surgery, 339t
Extensor carpi radialis muscle and tendon
  tear of, *931*
  tenosynovitis of, *1013*
Extensor carpi ulnaris tendon, calcific tendinitis of, *1037*
Extensor pollicis longus tenosynovitis, *1013*
Extrapleural mass, etiologies of, 791t
Extrusion of lumbar intervertebral disk, 268t, *276*

F

Facetectomy of lumbar spine, 337t, *338*
Facet joints
  in cervical spine, *50*
    dislocation of, 91t, *97, 98*
    osteoarthrosis of, 107t
  in lumbar spine
    asymmetry of, 234t, *241*
    degenerative synovial cysts of, 283t, *293*
    septic arthritis of, 295t, *311*
    surgery of, 337t, *338*
  lumbosacral, asymmetry of, 349t
Factor VIII deficiency, 20t
Factor IX deficiency, 20t
Fallen fragment sign in simple bone cyst and pathologic fracture
  of humerus, 896t, *900*
  of tibia and fibula, 644t, *652*
Far-out syndrome in lumbar degenerative scoliosis, 281t, *287*
Fat pad displacement in elbow, 906, 915t, *916*
Fat pad sign in radial fractures, *925, 926*
Felon, acute pyogenic osteomyelitis of hand in, 1055t, *1062*
Femoroacetabular impingement, 463t, *465-466*
Femorotibial disorders, 603t
  in ankylosing spondylitis, *605*
  dislocation, 575t, *576*
Femur, 503-546
  anomalies and variants of, 503, 504t, *505-508*
  avulsive cortical irregularity of, 2t, 552t, *555*
  distal
    avulsive cortical irregularity of, 552t, *555*
    in dysplasia epiphysealis hemimelica, 555t, *556*
    in femorotibial dislocation, 575t, *576*
    fractures of, 558t, 560t, 562t, *562-563, 570, 573*
    growth plate injuries of, 560t, *570*
    normal developmental anatomy of, 548t, *549-551*
    osteochondritis dissecans of, 562t, *574*
    osteonecrosis of, *620-621*
    in patellofemoral disorders, 547, 597t, *597-598*
  distal epiphysis of
    in chondrodysplasia punctata, 555t, *556*
    in dysplasia epiphysealis hemimelica, 555t, *556*
    injuries of, 560t, *570*
    normal developmental anatomy of, 548t, *549-551*
  dysplasia of, 503, 504t
    fibrous, *426,* 537t, *539, 656*
  exostosis of, hereditary multiple, 530t, *534, 649*
  fractures of
    butterfly fragment in, *510*
    diaphyseal, 503, 509t, *510-515*
      in distal end, 509t, *512*
      fatigue, 509t, *513*
      in midshaft, 509t, *510-511*
      in proximal end, 509t, *510*
      in supracondylar region, 509t, *512*
    distal, 558t, *562-563*
      in child abuse, 560t, *569*
      condylar, 558t, 562t, *563, 573*
      intercondylar, 558t
      metaphyseal, 560t, *569*
      osteochondral, 562t, *573*
      supracondylar, 558t, *562*
    in leukemia, *528*
    in malignant fibrous histiocytoma, 516t, *524*
    in Paget disease, 537t, *538*
    in plasma cell myeloma, *526*
    proximal, 434, 453t, *454-459,* 460t-461t
      avulsion, 453t, *458*
      classification of, 460t
      fatigue, 453t, *456,* 460t
      insufficiency, 453t, *457,* 460t
      intertrochanteric, 460t, 461t, *462*
      intracapsular, *459,* 460t, *461,* 461t
      in neck, 440t
      nonunion and osteolysis in, *461*
      in osteoporosis, 453t, *457, 459,* 488t, *491*
      subcapital, *491*
      subtrochanteric, 460t, 461t, *462*
      sources of diagnostic errors in, 2t
Femur *(continued)*
  heterotopic ossification of, posttraumatic, 509t, *515*
  in leukemia, *420,* 516t, *528-529, 643*
  in limb length inequality, 504, *505-506,* 624t, *625*
  melorheostosis of, 504t, *508, 627*
  metabolic disorders of, 503, 541t
  osteogenesis imperfecta of, 541t, *542*
  osteomyelitis of, 541t, *546*
    acute pyogenic, 541t, *546*
    chronic recurrent multifocal, 541t
    proximal, 469t, *481-483*
  osteonecrosis of
    distal, *620-621*
      of lateral condyle, *621*
      of medial condyle, *620*
    proximal, 435, 497t-498t, *499-502*
      in adults, 497t, 498t, *500-502*
      computed tomography in, 497t, *501*
      disorders associated with, *502*
      in HIV infection and antiretroviral therapy, *502*
      in Legg-Calvé-Perthes disease, 497t, 498t, *499*
      magnetic resonance imaging in, 497t, *501*
      postoperative, *502*
      in radiation therapy, *433, 502*
      segmental pattern, *501*
      stages and grades of, 498t, *500*
  osteopathia striata of, 504t, *508*
  osteopetrosis of, 504t, *507*
  osteopoikilosis of, 504t, *508*
  osteoporosis of, 488t, 489t, *490-493*
    bone mineral density in, 488t, *491*
    fractures in, 488t, *491*
      insufficiency, 453t, *457*
      intracapsular, *459*
    generalized, 541t
    Singh index in, 488t, 489t
    transient, 488t, *492-493*
  in pigmented villonodular synovitis, *487, 583*
  proximal
    achondroplasia of, 388t, *389*
    in alkaptonuria, 469t, *481*
    bone marrow edema of, transient migratory, 488t, *493*
    in coxa vara and coxa valga, 440t, *441-442*
    in developmental dysplasia of hip, 434, 444t-445t, *446-451*
    in femoroacetabular impingement, 463t, *465-466*
    focal deficiency of, 504t, *507*
    fovea capitis of, 438t, *439*
    fractures of, 434, 453t, *454-459,* 460t-461t
    herniation pits of, *385, 438,* 438t
    in hyperparathyroidism, *495*
    in Langerhans cell histiocytosis, *427*
    in mucopolysaccharidoses, 388t, *390*
    in osteochondromatosis, idiopathic synovial, *487*
    osteoporosis of, 488t, 489t, *490-493*
    in pigmented villonodular synovitis, *487*
    in poliomyelitis, 427t, *432*
    positional variations of neck, 438t, *439*
    in psoriatic arthropathy, *476*
    in rheumatoid arthritis, 468t, *473-474*
    in septic arthritis and osteomyelitis, 469t, *481-483*

Femur *(continued)*
- proximal (capital) epiphyses, *379-380*
  - in Legg-Calvé-Perthes disease, 498t, *499*
  - normal developmental anatomy of, 435t, *436-437*
  - slipped, 440t, 453t, *454-455,* 469t, *483,* 488t, *495*
- radiation-induced changes of, *433, 502*
- in renal osteodystrophy, *495,* 541t
- in rheumatoid arthritis, 468t, *473-474*
  - insufficiency fracture of, 453t, *457*
  - synovial cyst of, *474*
- in rickets, *494,* 541t, *542*
- sclerosing dystrophy of, mixed, 504t, *627*
- in sickle cell disease, *430*
- trochanters of
  - greater
    - normal developmental anatomy of, *380,* 435t, *436-437*
    - pain syndrome of, 463t, *467*
  - lesser, normal developmental anatomy of, *380,* 435t, *436-437*
- tumors and tumorlike lesions of
  - benign, 503, 529t-530t, *531-536*
  - in leukemia, *420,* 516t, *528-529, 643*
  - malignant, 503, 515t-516t, *517-535*
  - metastatic, 515t, *517-518*
  - myeloproliferative, *419,* 516t, *526-529*
  - radiation-induced, *433*
  - tumorlike lesions, *427,* 537t, *538-540*
- Ward triangle of, 2t, *490*

Fibrocartilaginous dysplasia of tibia, 624t, *626*

Fibrodysplasia. *See* Fibrous dysplasia

Fibroma
- chondromyxoid, 29t
  - of femur, 530t
  - of tibia and fibula, 644t, *648*
- nonossifying, 30t
  - of femur, 530t, *535*
  - of humerus, 896t, *899*
  - of radius and ulna, 959t, *964*
  - of tibia and fibula, 644t, *650*
- ossifying, 28t
  - of tibia and fibula, 643t, *645*
- plantar, 760t, *767*

Fibromatosis
- of chest wall, 803t
- plantar, 760t, *767*

Fibrosarcoma, 25t
- of ankle and foot, 758t, *761*
- of cervical spine, 138t
- of clavicle and scapula, 870t
- of femur, 516t
- of humerus, 891t
- of pelvis, 413t, *418*
- of tibia and fibula, 636t, *640*
- of wrist and hand, 1043t

Fibrous cortical defect, 30t
- of femur, 530t, *535*
- of humerus, 896t
- of radius and ulna, 959t
- of tibia and fibula, 644t, *650*

Fibrous dysplasia, 33t
- of cervical spine, 139t, *148*
  - progressive ossifying, 78t
- of clavicle and scapula, 871t, *877*
- of femur, *426,* 537t, *539, 656*
- of foot, 759t, *766*
  - progressive ossifying, 682t, *688,* 703t
- of humerus, 900t, *901*
  - malignant transformation of, 890t, *892*
- monostotic, 33t, 139t
  - of clavicle and scapula, 871t
  - of femur, 537t, *539*

Fibrous dysplasia *(continued)*
  - of humerus, 900t, *901*
  - of pelvis, 414t, *426*
  - of radius and ulna, 959t, *966*
  - of ribs, 803t, *812*
  - of tibia and fibula, 653t, *655*
- of pelvis, 414t, *426*
- polyostotic, 33t, 139t
  - of clavicle and scapula, 871t, *877*
  - of femur, 537t, *539, 656*
  - of hand, *1053*
  - of humerus, 900t
  - of pelvis, 414t, *426*
  - of radius and ulna, 959t
  - of ribs, 803t, *812*
  - of tibia and fibula, 653t, *656*
- progressive ossifying, 3t
  - of cervical spine, 78t
  - of foot, 682t, *688,* 703t
  - of hand, 985t, *988*
  - of shoulder, *830,* 830t
- of radius and ulna, 959t, *966*
- of ribs, 803t, *812*
  - extrapleural mass in, 791t, *812*
- of thoracic spine, 209t, *219*
- of tibia and fibula, 653t, *655-656*
- of wrist and hand, 1048t, *1053*

Fibula, 623-671
- diaphyseal dysplasia of, progressive, 624t, *628*
- distal
  - dislocation of, *713*
  - fractures of, 705t, *706-709,* 710t, *711, 713*
    - stress, 728t
  - growth plate injuries of, 710t
  - metaphyseal injuries of, *711*
  - normal developmental anatomy of, 673t, *674-677*
  - ossicle of, 691t, *698*
  - in psoriatic arthropathy, *743*
- distal epiphysis
  - injuries of, 710t
  - normal developmental anatomy of, 673t, *674-677*
  - ossification centers in, 673t
- exostoses of, hereditary multiple, *534*
- fractures of, 623, 629t, *634*
  - in child abuse, 710t, *711*
  - distal, 705t, *706-709,* 710t, *711, 713*
    - stress, 728t
  - Maisonneuve, 629t, *634*
  - proximal, 560t, 629t, *634*
  - in simple bone cyst, *652*
  - stress, 728t
    - fatigue, 629t, *634,* 710t
    - insufficiency, 710t, *713*
- hematologic disorders of, 623, 657t
- heterotopic ossification of, posttraumatic, 629t, *635*
- infections of, 623, 665t-666t, *666-671*
- melorheostosis of, 624t, *627*
- metabolic disorders of, 623, 657t
- osteogenesis imperfecta of, 624t, *627*
- osteopetrosis of, 624t, *626*
- osteopoikilosis of, 624t, *627*
- periosteal reaction in, 657t, *662*
- proximal
  - in femorotibial dislocation, *576*
  - fractures of, 560t, 629t, *634*
  - normal developmental anatomy of, 548t, *549-551*
  - in tibiofibular dislocation, 575t
- proximal epiphysis, normal developmental anatomy of, 548t, *549-551*

Fibula *(continued)*
- tumors and tumorlike lesions of, 623
  - benign, 643t-644, *645-652*
  - malignant, 635t-636t, *637-641*
  - metastatic, 635t, *637-638*
  - myeloproliferative, 636t, *641-643*
  - tumorlike lesions, 653t, *653-656*

Filum terminale, tight, 5t

Fingers. *See* Hand

Fish vertebrae, lumbar
- in childhood leukemia, *319*
- in osteoporosis, *330*

Flail chest, 788t

Flatfoot deformity, 557t, 681t, *686*
- acquired, 681t, *686*
- hereditary, 681t, *686*

Floating shoulder, 833t, *839, 840*

Flowing candle wax appearance in melorheostosis
- of ankle and foot, 703t, *704*
- of femur, 504t, *508*
- of tibia and fibula, 624t, *627*
- of wrist and hand, 985t, *989*

Fluorosis, 36t, 313t
- of cervical spine, 149t, *150*
- of lumbar spine, 327t, *334*
- of thoracic spine, 221t, *224*

Fong syndrome, 4t
- of elbow, 913t, *915*
- of knee, 552t, 555t, *556*
- of pelvis, 388t, *391*

Foot, 672-775
- accessory ossicles of, 690t-691t, *694-699*
- anomalies and variants of, 672, 690t-692t, *692-702*
- articular disorders of, 672, 734t-737t, *738-753*
  - in crystal deposition disease, 734t-735t, 737t, *747-749*
  - degenerative, 734t, *738-739*
  - differential diagnosis in, 737t
  - distribution, symmetry, and preferential target sites of, 736t
  - inflammatory, 734t, *740-746*
- claw toes in, 682t
- curly toes in, 682t
- deformities of, 672, 681t-682t, *683-689*
- dysplasia of, 672t, 703t
  - fibrous, 759t, *766*
- fractures of, 672
  - metatarsal, *722,* 723t, *724-725, 726*
    - stress, 723t, *725,* 727t
  - phalangeal, 723t, *725*
  - stress, 723t, *725,* 727t-728t
  - tarsal, 714t-715t, *716-722*
- frostbite of, 735t, *753*
- hammer toe deformity of, 682t, *689*
- infections of, 672, 754t, *754-758*
- Madura, 754t, *758*
- mallet toes in, 682t
- metabolic disorders of, 672, 768t
- normal developmental anatomy of, 672, 673t, *677-680*
- ossification centers in, 672, 673t
- osteonecrosis and osteochondrosis of, 673, 772t, *773-775*
- rocker-bottom, 681t, *685*
- soft tissue injuries of, 728t-729t, *730-733*
- tumors and tumorlike lesions of, 672, 758t-760t, *761-767*
  - benign, 759t, *762-765*
  - malignant, 758t, *761, 767*
  - metastatic, 758, *761*
  - myeloproliferative, 758t, *762*
  - tumorlike lesions, 759t-760t, *765-767*

- Foramen
  - cervical intervertebral, 45, 146t
  - in humerus, 887t, *888,* 913t
  - in ribs, 780t
  - in sternum, 781t
- Fork deformity of clavicle, 824t, *825*
- Fovea capitis, 438t, *439*
- Fractures, 6t-9t
  - of acetabulum, 393t, *400-401,* 434, 440t, 453t
    - hip dislocation in, 451t, *452*
  - acute, 6t, 7t
  - of ankle. *See* Ankle, fractures of
  - avulsion, 7t
  - bowing, 8t
  - butterfly fragment, 6t
    - of femur, *510*
  - of carpal bones, 990t-991t, *992-995*
  - of cervical spine. *See* Cervical spine, fractures of
  - in children, 8t-9t
  - chondral, 7t
  - closed, 6t
  - comminuted, 6t
  - compression. *See* Compression fractures
  - delayed union of, 7t
  - depression, 6t
  - of elbow, 906, 917t-919, *921-928*
  - of femur. *See* Femur, fractures of
  - of fibula. *See* Fibula, fractures of
  - of foot. *See* Foot, fractures of
  - greenstick, 8t
  - of hand, 1003t-1004t, *1005-1010*
    - blisters as complication of, 1017t, *1041*
  - of humerus
    - diaphyseal, 886, 889t, *890*
    - distal, 917t-918t, *921-923*
    - proximal, 832t, *834-835*
  - impaction, 6t
  - insufficiency. *See* Insufficiency fractures
  - of knee, 547, 558t-562t, *562-574*
  - lead pipe, 8t
  - of lumbar spine. *See* Lumbar spine, fractures of
  - malunion of, 7t
  - nonunion of, 7t
    - in femoral intracapsular fracture, *461*
  - open, 6t
  - osteochondral, 7t
    - in knee injuries, 562t, *573*
  - of pelvis, 377, 392t-393t, *394-401*
    - fatigue, 393t, *402,* 404t
    - in metastasis, 413t, *416*
  - of radius. *See* Radius, fractures of
  - of ribs, 776, 788t, *790-793,* 833t
    - in hemodialysis, 814t, *818*
  - of sacrum, 352t, *353-355,* 392t, *397*
    - with pubic diastasis, *353, 395, 397*
  - segmental, 6t
  - of shoulder, 819, 832t-833t, *834-840*
  - in stress-related bone injuries, 6t, 8t. *See also* Stress-related bone injuries
  - of thoracic spine. *See* Thoracic spine, fractures of
  - of tibia. *See* Tibia, fractures of
  - torus, 8t
  - of ulna. *See* Ulna, fractures of
  - of wrist, 972, 990t-991t, *992-995*
    - blisters as complication of, 1017t, *1041*
- Freiberg infraction, 40t, 772t, *775*
- Friedreich disease, clavicle in, 883t
- Frostbite
  - of foot, 735t, *753*
  - of hand, 1017t, *1040*
    - terminal phalangeal resorption in, 1067t
- Frozen shoulder, 848t, *851*
- Fungal infections
  - of foot, 754t, *758*
  - of lumbar facet joints, *311*
  - osteomyelitis in, 43t
    - of pelvis, *431*
  - skin and joint findings in, 23t
  - of wrist and hand, 1055t
- Funnel chest, 781t, *786*
- Fusion surgery. *See* Arthrodesis

G

- Galeazzi fracture-dislocation, 948t, *950, 954*
- Gallie fusion wires in cervical spine surgery, *153,* 155t
- Gamekeeper's thumb, 1003t, *1006*
- Ganglion cysts
  - of ankle and foot, 759t
  - of knee, 585t
    - intraarticular, 578t, *582*
    - periarticular, 578t
  - perilabral, 463t, *464*
  - of posterior longitudinal ligament, lumbar, 283t
  - of wrist, 1011t, *1014,* 1048t, *1053*
- Ganglioneuroma, 803t
- Gangrene, gas, of foot, *754,* 754t
- Garden classification of femoral fractures, 460t
- Gas gangrene of foot, *754,* 754t
- Gaucher disease, 38t
  - of ankle and foot, 768t, *771*
  - of femur, 541t, *543*
  - of hip, 489t, *502*
  - of humerus, 903t, *904*
  - of lumbar spine, 327t, *334*
  - of tibia and fibula, 657t, *661*
- Genu recurvatum, 557t
  - in neuropathic osteoarthropathy, 557t, *613*
- Genu valgum, 557t
- Genu varum, 557t
  - in dysplasia epiphysealis hemimelica, *556,* 557t
- Geyser appearance in acromioclavicular joint synovial cyst, 849t, *853*
- Giant cell tumors
  - aggressive, 25t
    - of cervical spine, 138t
    - of femur, 516t, *523*
    - of humerus, 891t
    - of knee, 614t
    - of pelvis, 413t
    - of radius and ulna, 957t, *961*
    - of tibia and fibula, 636t
  - benign, 30t
    - of ankle and foot, 759t, *764*
    - of cervical spine, 139t, *144*
    - of femur, 530t, *535*
    - of humerus, 896t
    - of knee, 614t, *651*
    - of pelvis, 414t, *423*
    - of radius and ulna, 959t, *964*
    - of ribs, 803t
    - of sacrococcygeal spine, 371t, *375*
    - of thoracic spine, 209t, *216*
    - of wrist and hand, 1048t
  - of tendon sheaths
    - in foot, 760t
    - in hand, 1011t, *1015*
- Gibbus deformity, thoracolumbar, 170t, *171,* 173t
  - in hypothyroidism, 327t, *332*
- Gigantism, 2t, 37t
  - macrodactyly in, 979t, *984*
- Glenohumeral joint
  - acromegalic arthropathy of, *868*
  - in adhesive capsulitis, 848t, *851*
  - ankylosing spondylitis of, 857t, *863*
  - crystal deposition disease of, 858t, *865*
  - dislocation of, 841t, *843-845*
    - anterior, 841t, *843-844*
    - drooping shoulder in, 841t, *845*
    - inferior, 841t, *845*
    - posterior, 841t, *844*
    - superior, 841t, *845*
  - hemophilic arthropathy of, 859t, *869*
  - impingement syndrome in instability of, 856t
  - neuropathic osteoarthropathy of, 859t, *870*
  - osteoarthrosis of, 857t, *860*
  - psoriatic arthropathy of, 858t, *863*
  - rheumatoid arthritis of, 857t, *862*
  - in scleroderma, 858t, *863*
  - tuberculous arthritis of, 859t, *867*
- Glenoid cavity of scapula
  - fractures of, 833t, *838*
    - Bankart, 833t, 841t, *844*
  - hypoplasia of, 2t, 824t, *828*
  - labrum injury, 848t
    - SLAP tear in, *852*
  - ossification centers in, 820t
- Glomus tumor of hand, 1011t, *1014*
- Golfer's elbow, 929t
- Gout, 19t, 23t
  - of ankle and foot, 735t, 737t, *748-749,* 760t, *766*
    - distribution, symmetry, and preferential target sites of, 736t
    - hallux valgus in, *688*
  - of cervical spine, 110t, *133*
  - of elbow, 934t, *938*
  - of hip, 469t, *480*
  - intercritical, 19t
  - of knee, 600t, *609*
  - of lumbar spine, 295t, *308*
  - of shoulder, 858t, *866*
  - of wrist and hand, 1017t, 1018t, *1032*
- Granuloma, eosinophilic
  - of cervical spine, *148*
  - of clavicle and scapula, 871t, *877*
  - of femur, *540*
  - of humerus, 900t, *902*
  - of lumbar spine, *326*
  - of pelvis, 414t, *427*
  - of thoracic spine, *220*
- Greater trochanteric pain syndrome, 463t, *467*
- Greenstick fracture, 8t
- Grisel syndrome, atlantoaxial instability and subluxation in, 59t
- Ground-glass appearance in fibrous dysplasia
  - of femur, 537t, *539*
  - of hand, *1053*
  - of radius and ulna, 959t, *966*
  - of tibia and fibula, 653t, *655*
- Growth hormone hypersecretion, acromegaly in, *333. See also* Acromegaly
- Growth plate injuries, 8t
  - of ankle, 710t, *712*
  - of elbow, 919t, *927*
  - of foot, 723t, *725*
  - of hand, 1004t, *1009*
  - of humerus, 832t, *835*
  - of knee, 560t-561t, *570-571*
  - of radius, distal, 952t
  - of ulna, distal, 952t

Growth recovery lines (Harris lines), 37t
  of femur, 541t, *545*
  of tibia and fibula, 657t, *663, 683, 750*
Guitar player acro-osteolysis, *1010*

H

Hahn-Steinthal type of capitulum fracture, 918t, *923*
Hahn venous channels, 2t
  in lumbar spine, 233t, *236*
  in thoracic spine, *165,* 167t, *168*
Hair artifact in cervical spine imaging, 68t, *77*
Hallux rigidus, 734t, *739*
Hallux valgus, 682t, *687-688*
  in generalized osteoporosis, *768*
  in osteoarthrosis, 682t, *687,* 734t
Hallux varus in rheumatoid arthritis, *740*
Hamartoma, fibrolipomatous, of hand, 1011t, *1015*
Hamate
  fractures of, 990t, *993*
  in greater arc injuries, 991t
  ossification centers in, 973t
  osteonecrosis of, 1065t
Hammer toe deformity, 682t, *689*
Hand, 972-1067
  acquired deformities of, 973, 1066t
  anomalies and variants of, 978t-979t, *980-985*
  in arachnodactyly, 985t, *987*
  articular disorders of, 972, 1016t-1018t, *1019-1042*
    compartmental analysis of, 1018t
    in crystal deposition disease, 1017t, *1033-1035, 1037*
    degenerative, 1016t, *1019-1021*
    inflammatory, 1016t, *1022-1031*
  bizarre parosteal osteochondromatous proliferation in, 1047t, *1049*
  in brachydactyly, 978t, *980*
  in clinodactyly, 979t, *988*
  clubbing of fingers, 1055t, *1062*
  congenital disorders of, 972, 985t
  dislocations in, 991t, *998,* 1003t-1004t, *1005, 1007*
  dysplasias of, 972, 985t
    fibrous, 1048t, *1053*
  flexion deformities of, 1066t
  fractures of, 1003t-1004t, *1005-1010*
    in abused child, 1004t
    blisters as complication of, 1017t, *1041*
  gouty arthropathy of, 1017t, *1032*
  infections of, 972, 1055t, *1062-1064*
  Jaccoud arthropathy of, 1016t, *1030*
  in macrodactyly, 979t, *984*
  mallet finger in, 1004t, *1008,* 1066t
  metabolic disorders of, 972, 1054t-1055t, *1056-1062*
  normal developmental anatomy of, 972, 973t, *974-977*
  ossification centers in, 972, 973t
    age of appearance and fusion, 973t
  osteolysis with detritic synovitis, 1017t, *1042*
  osteonecrosis of, 973, 1065t
  phalangeal resorption in, 973, *1067,* 1067t
    in epidermolysis bullosa, *1042*
    in osteolysis with detritic synovitis, *1042*
    in scleroderma, *1031*
  in polydactyly, 979t, *982*
  sausage digit in psoriatic arthropathy, 1016t, *1027*
Hand *(continued)*
  soft tissue disorders of, 972, 1011t, *1012-1015*
    in calcification, 973, 1067t
    in frostbite, 1017t, *1040*
    in thermal and electrical injuries, 1017t, *1041*
  subungual exostosis of, 1047t, *1049*
  swan-neck deformity of, *1030,* 1066t
  in syndactyly, 978t, *981*
  terminal phalangeal tufts in, *977, 1010, 1031*
    in acromegaly, 1054t, *1061*
  tumors and tumorlike lesions of, 972
    benign, 1047t-1048t, *1049-1052*
    fibrolipomatous hamartoma, 1011t, *1015*
    giant cell tumor of tendon sheath, 1011t, *1015*
    glomus tumor, 1011t, *1014*
    malignant, 1043t, *1044-1046*
    metastatic, 1043t, *1044*
    myeloproliferative, 1043t, *1047*
    tumorlike lesions, 1048t, *1052-1053*
  zigzag deformity of, 1066t
Hand-foot syndrome in sickle cell anemia, 772t, *773*
Hangman's fracture, 84t, *90*
Harrington rod
  in lumbar spine surgery, *340*
  in thoracic scoliosis, *184*
Harris lines (growth recovery lines), 37t
  of femur, 541t, *545*
  of tibia and fibula, 657t, *663, 683, 750*
Head injury, heterotopic ossification of elbow in, 942t, *943*
Heberden nodes, *1019*
Heel spurs, 737t, *739*
Hemangioma, 31t
  of cervical spine, 139t, *145*
  of chest wall, 803t
  of clavicle and scapula, 871t, *874*
  of knee, 614t
  of lumbar spine, 312t, 313t, *322*
  of radius and ulna, 959t, *965*
  of rib, 802t, *811*
  of sacrococcygeal spine, 371t
  of thoracic spine, 209t, *217*
  of tibia and fibula, 644t
Hemarthrosis, 10t
  of ankle and foot, 728t, *730*
  in hemophilia, 20t, *612, 869*
  of knee, 578t, *612, 619*
  of shoulder, *869*
Hematologic disorders, 38t-39t
  in Gaucher disease, 38t. *See also* Gaucher disease
  in mastocytosis, 38t
    lumbar spine disorders in, 327t, *334*
    pelvic disorders in, 427t, *429*
  in myelofibrosis, 38t
    of femur, 541t, *543*
    of thoracic cage, 814t
    of thoracic spine, 209t, *214*
  in sickle cell anemia, 39t. *See also* Sickle cell anemia
  in thalassemia, 39t
    lumbar spine disorders in, 327t, *335*
    pelvic disorders in, 427t, *430*
Hematoma, lumbar epidural, 269t, *280*
Hemimyelocele, 5t
Hemimyelomeningocele, 5t
Hemivertebrae
  cervical, in Klippel-Feil syndrome, 73t
  lumbar, 234t, *241*
Hemivertebrae *(continued)*
    dorsal and ventral, 234t
    lateral, 234t, *241*
  thoracic, 167t, *168, 181*
    dorsal and ventral, 167t
    lateral, 167t, *168, 181*
Hemochromatosis, 19t, 23t
  ankle and foot disorders in, 735t
  hip disorders in, 469t, *480*
  knee disorders in, 600t, *610*
  pelvic disorders in, 405t, *412*
  shoulder disorders in, 858t, *866*
  wrist and hand disorders in, 1017t, *1036*
Hemodialysis
  amyloid deposition in, 1054t, *1060*
  rib fractures in, 814t, *818*
  spondyloarthropathy in, 35t, 111t, *137*
  vascular calcification of hand in, *1058*
Hemoglobin C disease
  lumbar spine disorders in, *335*
  pelvic disorders in, *430*
Hemophilia, 20t
  ankle and foot disorders in, 735t, *750*
    tibiotalar slant in, *683,* 735t, *750*
  elbow disorders in, 935t, *941*
  hip disorders in, 470t
  knee disorders in, 600t, *611-612*
  pseudotumors in
    of pelvis, 427t, *431*
    of radius and ulna, 967t, *969*
  shoulder disorders in, 859t, *869*
Herniation of intervertebral disks
  cervical, 45, 150t, *151*
  lumbar, 268t, *275-277*
    extrusion in, 268t, *276*
    protrusion in, 268t, *275, 277*
    sequestration in, 268t, *276-277*
  thoracic, ossification in, 192t, *197-198*
    and scoliosis, 178t, *183*
Herniation pits of femur, *385, 438,* 438t
Herringbone appearance of humerus, 887t, *888*
Heterotopic ossification. *See* Ossification, heterotopic
Hidradenitis suppurativa, 22t
Hilgenreiner line, *446*
Hill-Sachs fracture, 841t, *843-844*
Hip, 434-502
  acetabulum in. *See* Acetabulum
  anomalies and variants of, 434, 438t, *438-439*
  articular disorders of, 434, 468t-470t, *471-487*
    in crystal deposition disease, 469t, *478-479*
    degenerative, 468t, *471-472*
    infectious, 469t, *481-484*
    inflammatory, 468t, *473-477*
    metabolic, 469t, *480-481*
  deformities of, 434, 440t, *441-443*
  differential diagnosis in disorders of, 404t
  dislocation of, 434
    in acetabular fracture, *400,* 451t, *452*
    anterior, 451t, *452*
    in developmental dysplasia, 444t, *449, 450*
    in pelvic fracture, *452*
    posterior, 451t, *452*
    traumatic, 451t, *452*
  dysplasia of
    cleidocranial, 440t
    developmental, 434, 440t, 444t-445t, *446-451*
      acetabular index in, 445, *446*
      center-edge angle in, 445, *447*

- Hip *(continued)*
      - computed tomography in, 445t, *450*
      - in Down syndrome, 388t, *389*
      - magnetic resonance imaging in, 445t, *451*
      - medial joint space width in, 445, *447*
      - radiographic measurements in, 445, *446-447*
      - ultrasonography in, 445t, *450*
    - diastrophic, 440t
  - femoroacetabular impingement in, 463t, *465-466*
    - CAM type, 463t, *466*
    - pincer type, 463t, *465*
  - femur at. *See* Femur, proximal
  - fractures of, 453t, *454-459,* 460t-461t
    - in osteoporosis, 488t, *491*
  - in greater trochanteric pain syndrome, 463t, *467*
  - instability in developmental dysplasia, 444t
  - internal derangements of, 434, 463t, *464-467*
  - metabolic disorders of, 434-435, 488t-489t, *490-496*
    - articular, 469t, *480-481*
  - normal developmental anatomy of, 434, 435t, *436-437*
  - ossification centers in, 434, 435t, *436-437*
    - age of appearance and fusion, 435t
  - osteomalacia of, 488t, *494*
  - in osteonecrosis of femoral head, 435, 497t-498t, *499-502*
  - osteopoikilosis of, 388t, *390*
  - osteoporosis of, 488t, 489t, *490-493*
    - bone mineral density in, 488t, *491*
    - in chondrolysis, 470t, *486*
    - femoral fractures in, 488t, *491*
      - insufficiency, 453t, *457*
      - intracapsular, *459*
    - generalized, 488t, *490-491*
    - transient, 488t, *492-493*
  - patterns of joint space narrowing, 470t
  - perilabral ganglion cysts of, 463t, *464*
  - rapidly destructive disease of, 469t, *480*
  - rheumatoid arthritis of. *See* Rheumatoid arthritis, of hip
  - subluxation in developmental dysplasia, 444t, *450, 451*
  - traumatic injuries of, 434, 451t, *452,* 453t, *454-459,* 460t-461t
- Histiocytoma, malignant fibrous
  - of ankle and foot, 760t
  - of chest wall, 803t
  - of femur, 516t, *524*
  - of humerus, 891t
  - of tibia and fibula, 636t
- Histiocytosis, Langerhans cell. *See* Langerhans cell histiocytosis
- HIV infection and AIDS
  - antiretroviral therapy and femoral head osteonecrosis in, *502*
  - Hodgkin disease of femur in, *527*
- Hodgkin disease, 27t
  - of cervical spine, 138t
  - of clavicle and scapula, 871t
  - of femur, 516t, *527*
  - of lumbar spine, 312, 313t, *318*
  - of pelvis, 414t
  - of ribs, 802t
  - of sternum, 802t
  - of thoracic spine, 209t, *214*
  - of tibia and fibula, 636t
- Homocystinuria, alignment disorders of knee in, *557t*, 558t
- Homogentisic acid oxidase, 19t
- HOOD (hereditary osteo-onychodysostosis) syndrome, 4t
  - of elbow, 913t, *915*
  - of knee, *552t, 555t, 556*
  - of pelvis, 388t, *391*
- Housemaid's knee, 579t, *583*
- Humerus, 886-905
  - anomalies and variants of, 886, 887t, *888*
    - proximal, 825t, *829*
  - chevron sign of, 887t, *888,* 913t
  - deltoid tuberosity of, 887t
  - distal
    - fractures of, 917t-918t, *919, 921-923*
    - in hereditary osteo-onychodysostosis syndrome, 913t, *915*
    - ossification centers in, 907t, *908-909*
      - unfused, *914*
    - osteochondritis dissecans of, 919t, *928*
    - osteonecrosis of, 942t, *943*
    - Panner disease of, *928,* 942t, *943*
  - foramen of, 887t, *888,* 913t
  - fractures of
    - acute, 889t, *890*
    - ball-thrower, 889t
    - diaphyseal, 886, 889t, *890*
    - distal, 917t-918t, *919, 921-923*
      - of capitulum, 918t, *923*
      - condylar, 917t
      - epicondylar, 918t
      - intercondylar, 917t, *922*
      - with posterior elbow dislocation, *919*
      - supracondylar, 917t, *921-922*
    - in enchondroma, *898*
    - in Ewing sarcoma, *893*
    - fallen fragment sign in, 896t, *900*
    - in lymphoma, 891t, *894*
    - in metastasis, 890t, *892*
    - in plasma cell myeloma, *893*
    - proximal, 832t, *834-835*
      - acute, 832t, *834*
      - drooping shoulder in, 841t, *845*
      - in glenohumeral joint dislocation, 841t, *843-844, 845*
      - growth plate injuries in, 832t, *835*
      - Hill-Sachs, 841t, *843-844*
      - in osteopetrosis, *786*
      - in osteoporosis, 832t, *834*
      - with scapular fracture, *838*
      - trough line, 841t, *844*
    - in simple bone cyst, 896t, *900*
  - lateral epicondyle of
    - growth plate injury of, 919t
    - inflammation of, 929t, *931*
    - ossification centers in, 907t
  - medial epicondyle of
    - growth plate injury of, 919t, *927*
    - inflammation of, 929t, *932*
    - ossification centers in, 907t, *908, 911*
      - unfused, *914*
  - metabolic disorders of, 886, 903t, *904-905*
  - notches of, 887t
  - ossification centers in
    - distal, 907t, *908-909*
      - unfused, *914*
    - proximal, 820t
  - osteonecrosis of
    - distal, 942t, *943*
    - proximal, 878t, *881*
  - proximal
    - anomalies and variants of, 825t, *829*
    - fractures of, 832t, *834-835*
    - in glenohumeral dislocation, 841t, *843-845*
- Humerus *(continued)*
    - melorheostosis of, 830t
    - normal developmental anatomy of, 820t, *822-823*
    - ossification centers in, 820t
    - osteonecrosis of, 878t, *881*
    - osteopetrosis of, *786,* 830t
    - osteopoikilosis of, 830t, *831*
    - radiation-induced changes of, *882*
    - in renal osteodystrophy, *879*
    - in rheumatoid arthritis, 857t, *862*
  - pseudocyst of, 2t, *823,* 825t, *829,* 887t
  - simulated periostitis of, *823,* 887t
  - supracondylar process of, 887t, *888,* 913t
  - trochlea of, 907t, *909*
  - tumors and tumorlike lesions of, 886
    - benign, 895t-896t, *897-900*
    - malignant, 890t-891t, *892-893*
    - myeloproliferative, 891t, *893-895*
    - tumorlike lesions, 900t, *901-902*
- Hunter syndrome, 440t
- Hurler syndrome, 3t
  - cervical spine disorders in, 78t
  - lumbar spine disorders in, 244t, 246t
  - pelvic disorders in, 388t, *390*
  - thoracic spine disorders in, 170t, *171*
  - wrist and hand disorders in, 985t, *989*
- Hutchinson fracture, 951t, *955*
- Hydroxyapatite graft in cervical spine arthrodesis, *152,* 155t
- Hyperextended knees, 557t
  - in neuropathic osteoarthropathy, 557t, *613*
- Hyperostosis
  - diffuse idiopathic skeletal (DISH), 12t
    - of ankle and foot, 734t, 737t, *739*
    - of cervical spine, 107t-108t, *120-122*
    - of elbow, 934t, *936*
    - of hip, 468t, *472*
    - iliolumbar ligament ossification in, 294t, *298*
    - of knee, 599t, *602*
    - of lumbar spine, 294t, *297*
    - of pelvis, 405t, *406-408*
    - posterior longitudinal ligament ossification in, 107t, 108t, *120, 122,* 294t, *298*
    - of sacroiliac joint, 356, 357t, *363*
    - stylohyoid ligament ossification in, 68t, *78*
    - of thoracic spine, 192t, *199-200*
  - flowing
    - in diffuse idiopathic skeletal hyperostosis
      - of lumbar spine, 294t, *297*
      - of thoracic spine, 194t, *199*
    - in melorheostosis
      - of ankle and foot, 703t, *704*
      - of femur, 504t, *508*
      - of tibia and fibula, 624t, *627*
      - of wrist and hand, 985t, *989*
  - infantile cortical
    - of clavicle and scapula, 830t, 883t
    - of ribs, 814t
  - sternocostoclavicular, 797t, *800,* 883t, *884*
  - in synovitis-acne-pustulosis-hyperostosis-osteitis, 15t, 22t. *See also* SAPHO
- Hyperparathyroidism, 35t
  - ankle and foot disorders in, 737t, 768t, *770*
  - cervical spine disorders in, 149t
  - elbow disorders in, 942t
  - femoral disorders in, 541t, *542*
  - hip disorders in, 489t, *494, 495*

Hyperparathyroidism *(continued)*
  knee disorders in, 603t, 616t, *618, 619*
  lumbar spine disorders in, 327t, *333*
  pelvic disorders in, 427t, *428*
  radius and ulna disorders in, 967t
  rib disorders in, 814t, *817*
    notching in, 787t, 814t
  sacroiliac joint disorders in, 357t, *369*
  shoulder disorders in, 878t
  thoracic spine disorders in, 221t, *223*
  tibia and fibula disorders in, 657t, *659-660*
  wrist and hand disorders in, 1054t, *1058-1059,* 1067t
    terminal phalangeal resorption in, *1067,* 1067t
Hyperplasia, 2t
Hyperthyroidism, 37t
Hypertrophic osteoarthropathy
  primary. *See* Osteoarthropathy, primary hypertrophic
  secondary. *See* Osteoarthropathy, secondary hypertrophic
Hyperuricemia, gout in, 19t
Hypervitaminosis A, 36t
  clavicle disorders in, 883t
Hypervitaminosis D, 36t
Hypochondrogenesis, 3t, *79*
Hypoparathyroidism
  pelvic disorders in, 427t, *429*
  tibia and fibula disorders in, 657t, *660*
Hypophosphatemic rickets
  of femur, *542*
  of tibia and fibula, *659*
Hypoplasia, 2t
  of cervical intervertebral disk, *72*
  of odontoid process, 52t
    atlantoaxial instability in, 52t, 59t
    in spondyloepiphyseal dysplasia congenita, 78t, *79*
  of patella, 552t, 555t, *556*
  of vertebral pedicle, 313t
Hypothyroidism, 37t
  hip disorders in, 488t, *495*
  lumbar spine disorders in, 327t, *332*
  thoracic spine disorders in, 221t, *223*
  wrist and hand disorders in, 1054t, *1060*
Hypovitaminosis C, 36t
  femoral disorders in, 541t, *544*
  knee disorders in, 616t
  tibia and fibula disorders in, 657t, *661*

I

Iliac artery aneurysm, 229
  lumbar spine disorders in, 342t, *344*
Iliolumbar ligament ossification, 294t, *298*
Iliopsoas bursitis, infectious, 469t, *483*
Iliotibial tract injuries, *594*
Ilium
  achondroplasia of, 388t, *389*
  chondrosarcoma of, *417*
  crest of
    normal developmental anatomy of, 378t, *381-382*
    ossification centers in, 378t, *381-382*
  in Down syndrome, 388t, *389*
  fibrosarcoma of, *418*
  fractures of
    avulsion, 392t, *394*
    Duverney, 392t, *395*
    in wing, 392t, *395*
  hemophilic pseudotumor of, *431*
  metastasis of, *372, 416*
  normal developmental anatomy of, 378t, *379-380, 381-382*
Ilium *(continued)*
  nutrient artery groove in, 384t, *385*
  ossification centers in, 378t
    in crest apophysis, 378t, *381-382*
  osteitis condensans of, 356t, *361-362*
  osteochondroma of, *422*
  osteoid osteoma of, *422*
  osteo-onychodysostosis syndrome of, hereditary, 388t, *391*
  osteopetrosis of, 388t, *390*
  osteosarcoma of, *417*
  plasma cell myeloma of, *419*
  plasmacytoma of, solitary, *419*
  in renal osteodystrophy, *428*
  in sacroiliac joint. *See* Sacroiliac joint
  spine of
    avulsion fracture of, 392t, *394*
    ossification centers in, 378t
Immunologic disorders, 22t
Impingement syndromes
  in ankle, 729t, *733*
    anterior, 729t
    anterolateral, 729t, *733*
    anteromedial, 729t
    posterior, 729t
      in os trigonum, 690t, *694-695,* 729t
    posteromedial, 729t, *733*
  femoroacetabular, 463t, *465-466*
  in shoulder, 819, 847t, 856t
    biceps brachii tendinosis in, 848t
    external, 856t
    internal, 856t
Implant, penile, in impotence, 384t, *387*
Impotence, penile implant in, 384t, *387*
Incisors overlying odontoid, differentiated from fracture, 51t, *58*
Inclusion cyst of hand, 1048t, *1053*
Infarction
  epiphyseal, of shoulder, *881*
  intramedullary, of tibia, 657t, *665*
Infections, 41t-43t
  of ankle and foot, 672, 754t, *754-758*
  of cervical spine, 111t, *135-137*
  of elbow, 906, 934t-935t, *940,* 942t
  of femur, 503, 541t
  of fibula, 623, 665t-666t, *666-671*
  of hip, 469t, *481-484*
  of humerus, 886, 903t
  of knee, 600t, 603t, *613*
  of lumbar spine, 295t, *309-311,* 313t
  of pelvis, 378, 406t, *413,* 427t
  of radius, 944, 967t
  of ribs and sternum, 776, 814t
  of sacroiliac joint, 357t, *370*
  of shoulder, 820, 859t, *867,* 878t
  skin and joint findings in, 23t
  of thoracic cage joints, 797t, *801*
  of thoracic spine, 193t, *207-209*
  of tibia, 623, 665t-666t, *666-671*
  of ulna, 944, 967t
  of wrist and hand, 972, 1055t, *1062-1064*
Inflammatory bowel disease
  enteropathic arthropathy in, 15t
    of cervical spine, 109t
    of lumbar spine, 294t
    of sacroiliac joint, 356t, 357t, *367*
    of thoracic spine, 193t
  skin disorders in, 22t
Inflammatory disorders, 13t-17t
  of ankle and foot, 734t, *740-746*
  of cervical spine, 59t, 108t-110t, *123-132*
  of elbow, 934t, *937-938*
  of hip, 468t, *473-477*
  of knee, 599t, *603-606*
Inflammatory disorders *(continued)*
  of lumbar spine, 294t-295t, *299-305*
  of pelvis, 405t, *410-411*
  of sacroiliac joint, 356t, 357t, *364-368*
  of shoulder, 857t-858t, *862-863*
  of thoracic cage joints, 797t, *799-801*
  of thoracic spine, 193t, 201t, *202-205*
  of wrist and hand, 1016t, *1022-1031*
Infraspinatus tendon
  calcific tendinitis of, 858t, *864*
  impingement of, 856t
Inguinal hernia, 404t
Innominate bones
  Langerhans cell histiocytosis of, *427*
  radiation-induced changes of, *433*
Insall-Salvati measurement method in patellar displacement, *597,* 597t
Insufficiency fractures, 6t
  of calcaneus, 714t, *717*
  of femur
    diaphyseal, 509t
    proximal, 453t, *457,* 460t
  of fibula, 710t, *713*
  of pelvis, 393t, *403, 428*
    in radiation therapy, 393t, *403,* 427t, *433*
  of sacrum, 352t, *354*
  of sternum, 789t, *794*
  of tibia, 629t, *633,* 710t
    in osteomalacia, *658*
Interbody cage
  in cervical disk disorders, 155t, *157*
  in lumbar disk disorders, 339t
Interphalangeal joints of foot, 736t
  dislocation of, 723t, *725, 727*
  in hammer toe deformity, 682t, *689*
  osteolysis with detritic synovitis, *1042*
  psoriatic arthropathy of, *744*
  rheumatoid arthritis of, *740*
Interphalangeal joints of hand, 1018t
  ankylosing spondylitis of, *1026*
  dislocation of, 1003t, *1005*
  erosive osteoarthritis of, 1016t, *1021*
  juvenile chronic arthritis of, *1025*
  osteoarthrosis of, 1016t, *1019*
  psoriatic arthropathy of, 1016t, *1027*
  reticulohistiocytosis of, multicentric, 1017t, *1038*
  rheumatoid arthritis of, *1023-1024*
Intervertebral disk disorders
  cervical, 45, 150t, *151*
    calcification in childhood, 107t, *119*
    degenerative, 107t, *112-113,* 150t, *158*
    herniation, 45, 150t, *151*
    hypoplastic, *72*
    surgical procedures in, 45, 151t, *152,* 155t, *157*
      interbody cage in, 155t, *157*
      prosthesis in, 155t, *157*
  lumbar, 228, 268t-270t, *271-280*
    annular bulge in, 268t, *275*
    anulus fibrosus tears, 268t, *278*
    calcification in, 282t, *290*
    cysts, 283t
    degenerative, 268t, *271-275,* 282t, *290*
      juvenile, 269t
      MRI of vertebral body bone marrow in, 268t, 273t, *274*
    displacement in, 282t
    extrusion in, 268t, *276*
    herniation, 268t, *275-277*
    ossification in, 282t
    and prevalence of disk abnormalities in asymptomatic subjects, 274t
    protrusion in, 268t, *275, 277*

- Intervertebral disk disorders *(continued)*
    - sequestration in, 268t, *276-277*
    - surgery in, 339t, *341-342*
      - disk prosthesis in, 339t, *342*
  - thoracic
    - ballooning in ankylosing spondylitis, 201t, *203*
    - calcification in childhood, 192t, *196-197*
    - in crystal deposition disease, 193t, *206*
    - degenerative, 192t, *194, 196-197*
    - herniation and ossification in, 178t, *183,* 192t, *197-198*
- Intervertebral foramen, enlarged cervical, 45, 146t
- Inverted Napoleon hat sign in lumbar spondylolisthesis, *253, 258*
- Iron deposition in hemochromatosis, 19t
- Ischiopubic ramus
  - aneurysmal bone cyst of, *423*
  - fracture of, 392t, *396*
    - fatigue, *402*
    - Malgaigne, *398*
- Ischiopubic synchondroses
  - normal developmental anatomy of, *379-380, 384, 436*
  - unfused, *384,* 384t
- Ischium
  - fractures of, 392t, *396*
    - with acetabular fracture, *400, 452*
    - avulsion, 392t, *394*
    - with hip dislocation, *452*
  - normal developmental anatomy of, 378t, *383*
    - ischiopubic synchondrosis in, *379-380, 384, 436*
  - ossification centers in, 378t, *383*
  - osteochondroma of, *422*
  - osteomyelitis of, *431*
  - Paget disease of, *425*
  - tuberosity of
    - avulsion fracture of, 392t, *394*
    - ossification centers in, 378t
- Ivory vertebrae, 313t
  - in chordoma, 313t, *315*
  - in Hodgkin disease, 313t, *318*
  - in osteosarcoma, *213*
  - in Paget disease, 313t, *324*

J

- Jaccoud arthropathy of hand, 1016t, *1030,* 1066t
- Jefferson fracture of atlas, 82t, 85t, *87*
- Joint disorders, 10t-23t. *See also* Articular disorders
- Jones fracture, 723t, *724*
- Jumper's knee, 592t, *596*
- Juvenile arthritis, idiopathic. *See* Arthritis, juvenile idiopathic

K

- Kidney disorders
  - dialysis in, 35t
    - and amyloid deposition, 1054t, *1060*
    - and rib fractures, 814t, *818*
    - and spondyloarthropathy, 35t, 111t, *137*
    - and vascular calcification in hand, *1058*
  - osteodystrophy in. *See* Osteodystrophy, renal
  - osteonecrosis of knee in, *620*
  - renal cell carcinoma. *See* Renal cell carcinoma, metastatic
  - rickets and knee disorders in, *618*
- Kienböck disease, 40t, *1065,* 1065t
- Kirner deformity, 979t, *984*
- Kirschner wire stabilization in wrist injuries, *997*
- *Klebsiella pneumoniae* infections, cervical spondylodiscitis in, *136*
- Klippel-Feil syndrome
  - cervical rib in, 68t, 73t, 780t
  - cervical spine in, 44, 73t, *74, 828*
    - spina bifida occulta of, 67t, 73t
  - Sprengel deformity in, 73t, 824t, *828*
- Knee, 547-622
  - alignment abnormalities of, 547, 557t-558t
  - anomalies and variants of, 547, 552t, *553-556*
  - articular disorders of, 547, 599t-600t, *601-613*
    - compartmental analysis of, 603t
    - crystal deposition disease, 600t, 603t, *607-609*
    - degenerative, 599t, *601-602*
    - infectious, 600t, 603t, *613*
    - inflammatory, 599t, *603-606*
    - metabolic, 600t, *610-612*
  - bursitis of, 579t, *583*
    - prepatellar, 579t, *583*
  - chondroblastoma of, 614t, *615, 647*
  - congenital disorders of, 547, 555t
  - contusions of, *570, 577,* 579t, *584*
  - dislocation of, 547, 557t, 575t, *576-577*
    - femorotibial, 575t, *576*
    - patellar, 575t, *577*
    - tibiofibular, 575t
  - dysplasia of, 547, 555t
    - epiphysealis hemimelica, 555t, *556*
    - multiple epiphyseal, 557t
  - femur at. *See* Femur, distal
  - fibula at. *See* Fibula, proximal
  - fractures of, 547, 558t-562t, *562-574*
    - in child abuse, 560t, *569*
    - in distal femur, 558t, 560t, *562-563, 570*
    - osteochondral, 562t, *573*
    - in patella, 558t-559t, *564-566*
    - in proximal fibula, 560t, *634*
    - in proximal tibia, 559t-560t, 561t, *567-568, 571*
  - ganglion cysts of, 585t
    - intraarticular, 578t, *582*
    - periarticular, 578t
  - growth plate injuries of, 560t-561t, *570-571*
  - hemarthrosis of, 578t, *580, 612, 619*
  - hematologic disorders of, 547, 616t-617t
  - housemaid's, 579t, *583*
  - joint effusions in, *571, 573, 580, 584*
    - in aneurysmal bone cyst, *615*
    - in gout, 600t, *609*
    - in juvenile idiopathic arthritis, 599t, *604*
    - in osteoarthrosis, *601*
    - in renal osteodystrophy, *619*
    - in skeletal metastasis, *615*
    - in tuberculous arthritis, *613*
  - jumper's, 592t, *596*
  - ligament disorders of, 547, 590t-591, *593-595*
  - lipohemarthrosis of, 578t, *581*
  - melorheostosis of, *627*
  - meniscal disorders of, 547, 585t, *586-587,* 588t, *589-590*
  - metabolic disorders of, 547, 616t-617t
    - articular, 600t, *610-612*
  - neuropathic osteoarthropathy of, 557t, 600t, *613*
- Knee *(continued)*
  - normal developmental anatomy of, 547, 548t, *549-551*
  - ossification centers in, 547, 548t, *549-551*
    - accessory, 552t
    - age of appearance and fusion, 548t
    - in bipartite patella, 552t, *553*
  - osteoarthrosis of, 599t, *601-602*
  - osteochondritis dissecans of, 562t, *574*
  - osteonecrosis of, 617t, *620-622*
    - in chronic renal disease, *620*
    - corticosteroid-induced, *622*
    - spontaneous, *621*
  - osteopoikilosis of, 624t, *627*
  - patella in. *See* Patella
  - patellofemoral disorders of, 547, 597t, *597-598*
  - sclerosing bone dystrophy of, mixed, *627*
  - synovial disorders of, 547, 578t-579t, *580-584*
    - cysts, 578t, *582*
    - in idiopathic synovial osteochondromatosis, 579t, *584*
    - in juvenile idiopathic arthritis, *604*
    - in pigmented villonodular synovitis, 579t, *583*
    - plica, 579t, *583*
  - tendon disorders of, 547, 592t, *596*
  - tibia at. *See* Tibia, proximal
  - tumors and tumorlike lesions of, 547, 614t, *615-616*
    - benign, *535,* 614t, *615, 651*
    - metastatic, 614t, *615*
    - myeloproliferative, 614t, *615*
    - tumorlike lesions, 614t, *616*
  - vascular disorders of, 547, 616t-617t
- Knock-knees, 557t
- Kocher-Lorenz type of capitulum fracture, 918t
- Köhler disease of navicular bone, 40t, 772t, *773*
- Kohler teardrop in giant cell tumor of acetabulum, *423*
- Kyphoplasty, balloon, in thoracic compression fractures, 226t, *227*
- Kyphosis
  - cervical
    - in hyperflexion sprain, 91t, 94t, *95*
    - in neurofibromatosis type I, 139t, *147*
    - postlaminectomy, 151t, *154*
  - lumbar, degenerative, 281t
  - thoracic, 161, 173t, *174-176*
    - congenital, 173t
    - normal appearance of, 173t, *174*
    - in osteoporosis, 173t, *175,* 222
    - senile, 173t, *175*

L

- Laminectomy
  - of cervical spine, 151t, *154*
  - of lumbar spine, 337t, *338-339*
    - instability in, *338*
    - osteosclerosis in, 313t
    - stress fracture in, *339*
- Laminoplasty of cervical spine, 151t, *154*
- Langerhans cell histiocytosis, 33t
  - of cervical spine, 139t, *148*
  - of clavicle and scapula, 871t, *877*
  - of femur, 537t, *540*
  - of humerus, 900t, *902*
  - of lumbar spine, 312t, *326*
  - of pelvis, 414t, *427*
  - of radius and ulna, 959t
  - of ribs, 803t
  - of thoracic spine, 209t, *220*

- Lauge-Hansen classification of ankle fractures, 705t, *706-709*
- Lead poisoning, appearance of radius and ulna in, 967t, *969*
- Ledderhose disease, *767*
- Legg-Calvé-Perthes disease, 40t, 435, 440t, *441,* 497t, 498t, *499*
  - Catterall classification of femoral involvement in, 498t
- Leg length inequality. *See* Limb length inequality
- Leiomyosarcoma of ankle and foot, 760t
- Leprosy
  - neuropathic osteoarthropathy in
    - of foot, 735t, *752*
    - of hand, 1055t, *1064*
  - osteomyelitis in, 42t
    - of hand, *1064*
    - of tibia and fibula, 666t, *671*
  - skin and joint findings in, 23t
- Lesch-Nyhan syndrome, terminal phalangeal resorption in, 1067t
- Leukemia, 27t
  - of cervical spine, 138t
  - of femur, *420,* 516t, *528-529, 643*
  - of humerus, 891t, *895*
  - of lumbar spine, 312t, *319*
  - of pelvis, 414t, *420*
  - of radius and ulna, 957t, *963*
  - of thoracic spine, 209t, *214*
  - of tibia and fibula, 636t, *643*
- Liberty Bell chest, 814t, *815*
- Ligament disorders
  - of ankle, 728t, *730*
  - of cervical spine, 107t, 108t, *120, 122*
    - in stylohyoid ligament ossification, 68t, *78*
  - of elbow, 929t, *930-931*
  - of knee, 547, *590t-591, 593-595*
  - of lumbar spine, 283t, 294t, *298*
  - of posterior longitudinal ligament. *See* Longitudinal ligament, posterior
  - of thoracic spine, 192t, *201*
  - of wrist, 999t, *1000-1002*
    - external, subluxation in, 999t, *1002*
- Ligamentum flavum
  - cysts of, 283t
  - ossification of, 294t
- Limb length inequality, 504, *505-506*
  - etiologies of, 504t
  - femur in, 504, *505-506,* 624t, *625*
  - measurement techniques in, 504, *505-506,* 624t, *625*
  - scoliosis in
    - lumbar, 259t, *261*
    - thoracic, 178t
  - tibia in, 504, *505-506,* 624t, *625*
- Limbus vertebrae
  - cervical, *75, 112*
  - lumbar, 269t, *279*
- Lipohemarthrosis, 10t
  - of knee, 578t, *581*
  - of shoulder, *845*
- Lipoma
  - filar, 5t
  - intradural, 5t
  - intraosseous, 31t
    - of ankle and foot, 759t, *765*
    - of femur, 530t, *536*
    - of humerus, 896t
    - of knee, 614t
    - of radius and ulna, 959t
    - of ribs, 802t
    - of tibia and fibula, 644t, *651*
    - of wrist and hand, 1048t
- Lipoma *(continued)*
  - soft tissue
    - of ankle and foot, 760t
    - of chest wall, 803t
  - and spinal dysraphisms, 5t
- Lipomyelocele, 5t
- Lipomyelomeningocele, 5t
- Liposarcoma of chest wall, 803t
- Lisfranc fracture-dislocation of tarsometatarsal joints, 715t, *722, 751*
  - divergent pattern, *722*
  - homolateral pattern, *722*
- Little League shoulder syndrome, 832t, *835*
- Longitudinal ligament, posterior
  - ganglion cysts of, lumbar, 283t
  - ossification of
    - cervical, 107t, 108t, *120, 122*
    - lumbar, 294t, *298*
    - thoracic, 192t, *201*
- Lordosis, cervical, *48*
- Lucent annular cleft sign in cervical discovertebral injury, 92t, *101*
- Lumbarization of transitional lumbosacral segment, 235t
- Lumbar spine, 228-344
  - anomalies and variants of, 228, 233t-235t, *236-243*
  - articular disorders of, 228, 294t-295t, *296-311*
    - degenerative, *271-275,* 294t, *296-299*
    - infectious, 295t, *309-311*
    - inflammatory, 294t-295t, *299-305*
  - congenital disorders of, 228, 244t, *245-247*
  - degenerative disorders of, 281t-283t, *284-293*
    - articular, *271-275,* 294t, *296-299*
    - cysts in, 283t, *293*
    - disk disease in, 268t, *271-275,* 282t, *290*
      - juvenile, 269t
    - instability in, 281t, *284*
    - retrolisthesis in, 281t, *285-286*
    - scoliosis in, 259t, *260,* 281t, *287*
    - spinal canal stenosis in, 282t-283t, *291-293*
    - spondylolisthesis in, 248t-249t, *255,* 281t, *285*
  - dysplasias of, 228, 244t, *247*
  - fractures of, 228, 262t, *263-267*
    - burst, 228, 262t, *264,* 264t
      - surgery in, *340*
    - compression, 262t, *263*
      - in osteomalacia, 327t, *332*
      - in osteoporosis, 327t, *328*
    - with dislocation, 262t, *266*
    - stress, postoperative, *339*
  - instability of, 228, 281t, *284*
    - in burst fracture, 262t, *264*
    - checklist for diagnosis of, 267t
    - postoperative, in laminectomy, *338*
    - in spondylolisthesis, 249t, *257*
  - intervertebral disk disorders in. *See* Intervertebral disk disorders, lumbar
  - limbus vertebra in, 269t, *279*
  - metabolic disorders of, 229, 327t, *328-336*
  - normal developmental anatomy of, 228, 229t, *230-232*
  - nuclear impressions in, 233t, *236*
  - ossification centers in, 228, 229t, *230-232*
    - ununited, 234t, *241*
  - scalloping of vertebrae in. *See* Scalloping of lumbar vertebrae
  - scoliosis of, 228, 259t, *260-261*
- Lumbar spine *(continued)*
  - segmental sclerosis of vertebral bodies in, 282t, *289*
  - spondylolysis and spondylolisthesis of, 228, 248t-249t, *250-258*
    - degenerative, 248t-249t, *255,* 281t, *285*
    - high grade, 249t, *258*
    - Myerding measurement method in, *252,* 252t
    - pathologic, 249t, *255*
    - progressive, 249t, *257*
    - and spina bifida occulta, 233t, *238*
    - unilateral, 249t, *256*
  - surgical procedures involving, 329, 337t, *337-342*
    - in diastrophic dysplasia, *247*
    - in disk disorders, 339t, *341-342*
    - fusion in, *337,* 337t
    - instrumentation and bone grafts in, 339t, *340-342*
    - laminectomy and facetectomy in, 337t, *338-339*
    - spondylolisthesis after, 249t
  - and transitional lumbosacral segment, 235t, *242-243*
  - traumatic injuries of, 228, 262t, *263-267*
    - spondylolysis in, 249t
  - tumors and tumorlike lesions of, 228, 312t, *312-326*
    - benign, 312t, *319-322*
    - malignant, 312t, *312-319*
    - myeloproliferative, 312, *317-319*
    - in osteoblastic metastasis, *373*
    - tumorlike lesions, 312t, *323-326*
  - vascular disorders affecting, 329, 342t, *343-344*
- Lumbosacral spine
  - agenesis of articular process in, *241*
  - dislocation of apophyseal joint in, 262t, *266*
  - facet tropism in, 349t
  - transitional segment anomalies, 235t, *242-243,* 349t
- Lunate
  - dislocation of, 991t, *996*
  - fractures of, 990t
  - ossification centers in, 973t
  - osteonecrosis of, *1065,* 1065t
  - in scapholunate advanced collapse wrist, 999t, *1001*
    - in crystal deposition disease, 1017t, *1033*
  - in scapholunate dissociation, 999t, *1000, 1001*
  - synostosis with triquetrum, 977t, *979*
- Lungs
  - osteosarcoma metastatic to, 802t, *806*
  - secondary hypertrophic osteoarthropathy in cancer of
    - of femur, 541t, *544*
    - of radius and ulna, *969*
    - of tibia and fibula, 657t, *663*
    - of wrist and hand, 1055t, *1062*
  - skeletal metastasis in cancer of
    - to cervical spine, *140*
    - to femur, 515t, *517*
    - to pelvis, *416*
    - to radius and ulna, *960*
    - to ribs, 802t, *805*
    - to thoracic spine, *211*
    - to tibia and fibula, 635t, *637*
- Lupus erythematosus, 17t, 22t
  - ankle and foot disorders in, 734t
  - hip disorders in, 468t, *477, 502*
  - knee disorders in, 599t, *605, 606*

- Lupus erythematosus *(continued)*
  - rib notching in, 787t
  - skin disorders in, 17t, 22t
  - tibia and fibula disorders in, *664*
  - wrist and hand disorders in, 1016t, *1028-1029,* 1066t, 1067t
- Luque rods in scoliosis, *184*
- Luxatio erecta, 841t, *845*
- Lyme disease, 23t
- Lymph node calcification, cervical, 68t, *77*
- Lymphoma, 27t
  - of cervical spine, 138t, *142*
  - of chest wall, 803t
  - of clavicle and scapula, 871t
  - of femur, 516t, *527*
  - Hodgkin. *See* Hodgkin disease
  - of humerus, 891t, *894*
  - of knee, 614t
  - of lumbar spine, 246t
  - of pelvis, 414t
  - of radius and ulna, 957t, *963*
  - of ribs, 802t, *810*
  - of tibia and fibula, 636t, *642*

M

- Mach band effect simulating odontoid fractures, 2t, 51t, *58*
- Macrodactyly
  - of foot, 692t
  - of hand, 979t, *984*
- Macrodystrophia lipomatosa
  - of ankle and foot, 703t
  - of wrist and hand, 985tf, *1015*
- Madelung deformity, 945t, *946,* 977t
  - reverse, *964*
- Madura foot, 754t, *758*
- Maduromycosis, 754t, *758*
- Maffucci syndrome, 29t
  - of femur, 529t
  - of foot, 759t
  - of humerus, 896t
  - of pelvis, 414t
  - of radius and ulna, 958t
  - of ribs, 802t
  - of shoulder, 871t
  - of tibia and fibula, 644t
  - of wrist and hand, 1048t, *1051*
- Main-en-lorgnette deformity of hand, 1066t
  - in psoriatic arthropathy, *1027*
- Maisonneuve fracture, 560t, *634, 707*
- Malgaigne fractures, 393t, *398*
- Malleolus of tibia
  - medial, fracture of, 705t, *707-709*
    - stress, 728t
  - posterior, fracture of, *706*
- Mallet finger, 1004t, *1008,* 1066t
- Mallet toe, 682t
- Malunion of fractures, 7t
- Mamillary processes, vertebral
  - lumbar, 229t
  - sacral, 346t
- Manubriosternal junction, 776, 797t
  - ankylosing spondylitis of, *799*
  - dislocation of, 789t, *796*
  - normal developmental anatomy of, *779, 780*
  - psoriatic arthropathy of, 797t, *799*
  - rheumatoid arthritis of, 797t, *799*
  - trauma of, 10t
- Manubrium
  - normal developmental anatomy of, 777t, *779, 780*
  - ossification centers in, 777t
- March fracture of metatarsals, 723t, *725*
- Marfan syndrome, 4t
  - ankle and foot disorders in, 703t
  - arachnodactyly in, 985t, *987*
  - cervical spine disorders in, 78t
  - hip disorders in, 440t
  - lumbar spine disorders in, 244t, 246t, *247, 261*
    - scoliosis in, 259t, *261*
  - pectus excavatum in, 781t, *786*
  - rib notching in, 787t
  - thoracic spine disorders in, 170t, 177t
- Marjolin ulcer, 41t
- Mastocytosis, 38t
  - lumbar spine disorders in, 327t, *334*
  - pelvic disorders in, 427t, *429*
- Mastoid air cells in atlanto-occipital region, *48*
- Median nerve
  - in carpal tunnel syndrome, 1011t, *1013*
  - in fibrolipomatous hamartoma, 1011t, *1015*
- Medulloblastoma metastasis to ribs, *804*
- Melanoma, malignant, skeletal metastasis of
  - to ulna, *960, 1044*
  - to wrist and hand, *1044*
- Melorheostosis, 4t
  - of ankle and foot, 703t, *704*
  - of femur, 504t, *508, 627*
  - of shoulder, 830t
  - of tibia and fibula, 624t, *627*
  - of wrist and hand, 985t, *989*
- Meningocele, lumbosacral, 5t
- Meningomyelocele, 440t
  - femoral disorders in, 541t, *545*
- Meniscal disorders of knee, 547, 585t, *586-587,* 588t, *589-590*
  - cysts, 585t, *586*
  - degenerative, 585t
  - discoid meniscus in, 585t, *586*
    - classification of, 585t
  - ossicles, 585t, *587*
  - tears, 585t, 588t, *589-590*
    - classification of, 588t, *589*
    - grades of, 588t, *589-590*
    - longitudinal, 588t, *589*
    - magnetic resonance imaging in, 588t, *589-590*
    - radial, 588t, *589*
- Metabolic disorders, 18t-19t, 34t-37t
  - of cervical spine, 45, 149t, *149-150*
  - of elbow, 906, 942t
  - of femur, 503, 541t
  - of fibula, 623, 657t
  - of hip, 434-435, 488t-489t, *490-496*
    - articular, 469t, *480-481*
  - of humerus, 886, 903t
  - of knee, 547, 616t-617t
    - articular, 600t, *610-612*
  - of lumbar spine, 229, 327t, *328-336*
  - of pelvis, 378, 427t
    - articular, 406t, *412*
  - of radius, 944, 967t
  - of ribs and sternum, 776, 814t
  - of sacroiliac joint, 357t, *369*
  - of shoulder, 820, 858t, *866,* 878t
  - skin findings in, 23t
  - of thoracic spine, 161, 221t, *222-225*
  - of tibia, 623, 657t
  - of ulna, 944, 967t
  - of wrist and hand, 972, 1054t-1055t, *1056-1062*
- Metacarpal bones
  - in arachnodactyly, 985t, *987*
  - Bennett fracture-dislocation of, 1003t, *1005*
  - in carpometacarpal dislocations, 991t, *998*
  - enchondroma of, 1048t, *1050*
  - fractures of, 1004t, *1007*
    - in abused child, 1004t
  - in Hurler syndrome, 985t, *989*
  - in leprosy, *1064*
  - in lupus erythematosus, *1028*
  - in melorheostosis, 985t, *989*
  - metastatic tumor of, *1044*
  - ossification centers in, 973t
  - osteopoikilosis of, *989*
  - osteoporosis of, 1054t, *1056*
  - Paget disease of, *1052*
  - Rolando fracture of, 1003t, *1005*
  - in sarcoidosis, 1017t, *1039*
  - scleroderma of, *1030*
  - septic arthritis of, *1063*
  - short, 978t, *981*
- Metacarpal index, *987*
- Metacarpal sign
  - in short metacarpal bone, 978t, *981*
  - in Turner syndrome, *986*
- Metacarpophalangeal joint, 1018t
  - ankylosing spondylitis of, *1026*
  - crystal deposition disease of, 1017t, *1033, 1035*
  - dislocations of, 1003t
    - in thumb, 1004t, *1007*
  - gouty arthropathy of, *1032*
  - in hemochromatosis, *1036*
  - Jaccoud arthropathy of, 1016t, *1030*
  - in lupus erythematosus, *1029*
  - osteoarthrosis of, posttraumatic, 1016t, *1020*
  - psoriatic arthropathy of, *1027*
  - reticulohistiocytosis of, multicentric, *1038*
  - rheumatoid arthritis of, *1023-1024*
  - septic arthritis of, *1063*
  - of thumb, 1018t
    - dislocation of, 1004t, *1007*
  - ulnar deviation of, 1066t
- Metastasis, 24t
  - to ankle and foot, 758t, *761*
  - to cervical spine, 138t, *140*
    - enlarged intervertebral foramen in, 146t
  - to chest wall, 803t
  - to clavicle and scapula, 870t, *872*
  - to femur, 515t, *517-518*
    - osteoblastic, *518*
    - osteolytic, *517*
  - to fibula, 635t, *637-638*
  - to hip, acetabular protrusion in, 440t, *443*
  - to humerus, 890t, *892*
  - to knee, 614t, *615*
    - osteolytic, 614t, *615*
  - to lumbar spine, 312t, *312-315,* 313t
    - osteoblastic, 313t
    - osteolytic, *315*
  - to lungs, in osteosarcoma, 802t, *806*
  - to pelvis, 413t, *415-416*
    - osteolytic, *416*
  - to radius and ulna, 957t, *960*
  - to ribs, 802t, *804-805*
    - extrapleural mass in, 791t, *805*
  - to sacrococcygeal spine, 371t, *372-373*
    - osteoblastic, 371t, *373*
    - osteolytic, 371t, *372*
  - to thoracic spine, 209t, *210-212*
  - to tibia, 635t, *637-638*
  - to wrist and hand, 1043t, *1044*
- Metatarsals
  - accessory ossicles of, 690t-691t, *696-697*
  - adduction and varus position of, 682t, *687*

Metatarsals *(continued)*
  dislocation of, 715t, *722*
  Ewing sarcoma of, 758t, *761*
  fibrous dysplasia of, *766*
  fractures of, *722,* 723t, *724-725, 726*
    stress, 723t, *725,* 727t
  Freiberg infraction of, 772t, *775*
  normal developmental anatomy of, 673t, *678-680*
  ossification centers in, 673t
  osteomyelitis of, *755-757*
  osteoporosis of, *769*
  plasma cell myeloma of, *762*
  in sickle cell anemia, *773*
Metatarsophalangeal joints, 736t
  ankylosing spondylitis of, *742*
  crystal deposition disease of, *747*
  dislocation of, 723t
  gouty arthropathy of, 735t, *749*
  in hammer toe deformity, 682t, *689*
  osteoarthrosis of, 734t, *739*
  rheumatoid arthritis of, *740*
  silicone synovitis of, *753*
Milk-alkali syndrome, shoulder disorders in, 878t, *880*
Milwaukee shoulder syndrome, 858t, *865, 866*
Missing pedicle sign in metastasis to thoracic spine, *211*
Missouri metacarpal syndrome, 1016t, *1020*
Mönckeberg atherosclerosis of ankle and foot, 768t, *770*
Monteggia fracture-dislocation, 917t, 948t, *949*
Moore fracture, 951t
Morquio syndrome, 3t
  cervical spine disorders in, 78t, *79*
  lumbar spine disorders in, 244t, *245,* 246t
  pelvic disorders in, 388t
  thoracic spine disorders in, 170t, *171*
Morton interdigital neuroma, 760t, *766*
Mucopolysaccharidosis, 3t
  cervical spine disorders in, 78t, *79*
    in stylohyoid ligament ossification, 68t, *78*
  Hurler syndrome in, 3t. *See also* Hurler syndrome
  lumbar spine disorders in, 244t, *245*
  Morquio syndrome in, 3t. *See also* Morquio syndrome
  pelvic disorders in, 388t, *390*
  thoracic spine disorders in, 170t, *171*
  wrist and hand disorders in, 985t, *989*
Mueller-Weiss syndrome, 772t, *774*
Mycotic aneurysm of vertebral artery, cervical spine in, 159t, *160*
Myelocele, 5t
Myelocystocele, lumbosacral, 5t
Myelofibrosis, 38t
  of femur, 541t, *543*
  of thoracic cage, 814t
  of thoracic spine, 209t, *214*
Myeloma, plasma cell. *See* Plasma cell myeloma
Myelomeningocele, 5t
Myeloproliferative disorders, 26t-27t
  of ankle and foot, 758t, *762*
  of cervical spine, 138t, *142*
  of femur, 516t, *526-529*
  of humerus, 891t, *893-895*
  of knee, 614t, *615*
  of lumbar spine, 312, *317-319*
  of pelvis, 414t, *419-420*
  of radius and ulna, 957t, *963*
  of ribs and sternum, 802t, *809-810*
Myeloproliferative disorders *(continued)*
  of sacrococcygeal spine, 371t, *374*
  of thoracic spine, 209t, *213-214*
  of tibia and fibula, 636t, *641-643*
  of wrist and hand, 1043t, *1047*
Myerding measurement method in spondylolisthesis, *252,* 252t
Myopathy, thoracic scoliosis in, 178t, *182*
Myositis ossificans
  of femur, 509t, *515*
  of fibula, 629t, *635*
  of foot, 703t
    hallux valgus in, *688*
  of humerus, 889t, *890*

N

Nails
  in hereditary osteo-onychodysostosis (nail-patella) syndrome, 4t
    elbow disorders in, 913t, *915*
    knee disorders in, 552t, 555t, *556*
    pelvic disorders in, 388t, *391*
  and nail-bed injuries of hand in phalangeal fractures, 1004t, *1009*
  in subungual exostosis
    of foot, 759t, *763*
    of hand, 1047t, *1049*
Napoleon hat sign, inverted, in lumbar spondylolisthesis, *253, 258*
Navicular bone of foot
  accessory, 691t, *698*
  in calcaneonavicular coalition, 690t, *692*
  dislocation in congenital vertical talus, 681t, *685*
  fractures of, 715t, *720-721*
    stress, 715t, *721,* 727t
  Köhler disease of, 772t, *773*
  in Mueller-Weiss syndrome, 772t, *774*
  normal developmental anatomy of, 673t, *677-678*
  ossification centers in, 673t
  osteonecrosis of, *774*
Navicular bone of hand, 973t. *See also* Scaphoid bone
Neoplasia. *See* Tumors and tumorlike lesions
Nephroblastoma, *638. See also* Wilms tumor
Nerve root injuries in cervical spine trauma, 94t
Neural arch ossification centers
  cervical, 45t, *49*
  lumbar, 229t
  sacrococcygeal, *346,* 346t
  thoracic, *162,* 162t, *164, 165-166*
    in spina bifida occulta, *168*
Neurenteric cysts, 5t
Neuritis, acute brachial, 849t
Neuroblastoma, rib notching in, 787t
Neuroectodermal tumor of sacrococcygeal spine, primitive, 371t
Neurofibroma, 803t
Neurofibromatosis type I, 32t
  of cervical spine, 139t, *147*
  of clavicle and scapula, 871t
  of femur, 537t, *538*
  of lumbar spine, 312t, *325, 376*
  of pelvis, 414t
  of ribs, 787t, 803t, *811*
  of sacrococcygeal spine, 371t, *376*
  of thoracic spine, 209t, *218*
    scoliosis in, 177t, *181, 218*
  of tibia and fibula, 653t, *654*
Neurologic disorders
  of brachial plexus, 94t, 849t, *854*
  carpal tunnel syndrome in, 1011t, *1013*
  in cervical spine trauma, 94t
Neurologic disorders *(continued)*
  in fibrolipomatous hamartoma of hand, 1011t, *1015*
  heterotopic ossification in, 21t
    of elbow, 942t, *943*
    of hip, 470t, *485*
  lumbar spine disorders in, 295t, *299, 304-305*
  of median nerve, 1011t, *1013, 1015*
  osteoarthropathy in. *See* Osteoarthropathy, neuropathic
  in syphilis, *299,* 600t, *613*
  thoracic scoliosis in, 178t
Neuroma, Morton interdigital, 760t, *766*
Neuromuscular disorders
  knee alignment disorders in, *557t,* 558t
  thoracic scoliosis in, 178t, *182*
Neuropathy
  osteoarthropathy in. *See* Osteoarthropathy, neuropathic
  thoracic scoliosis in, 178t
Neurosyphilis, neuropathic osteoarthropathy in
  of knee, 600t, *613*
  of lumbar spine, *299*
Nightstick fracture of ulna, 948t, *949*
Nodules in ankle and foot, rheumatoid, 760t
Nonossifying fibroma. *See* Fibroma, nonossifying
Nonunion of fractures, 7t
  femoral intracapsular, *461*
Notching
  of humerus, 887t
  of ribs, 776, *787,* 787t
    in coarctation of aorta, *787,* 787t
Notochordal disorders, 5t
Nuclear impressions
  of cervical spine, 67t, *69*
  of lumbar spine, 233t, *236*
Nursemaids' elbow, 917t, *920*
Nutrient artery grooves in ilium, 384t, *385*
Nutritional disorders, 34t-37t
  rickets in, 35t. *See also* Rickets
  scurvy in, 36t. *See also* Scurvy
  skin and joint findings in, 23t

O

Occipital condyle
  assimilation of atlas with, 51t, *53*
  dislocation of atlas and, 82t, *85*
Occipitalization of atlas, 51t, *53*
Ochronosis, 19t, 23t
  cervical spine disorders in, *134*
  hip disorders in, *481*
  lumbar spine disorders in, *307*
  pigmentation changes in, 19t, 23t
O'Donoghue triad in anterior cruciate ligament injuries, 591t
Odontoid process
  agenesis of, 2t, 52t
    atlantoaxial instability in, 52t, 59t
    in mucopolysaccharidosis, 78t, *79*
  in assimilation of axis, *53*
  fractures of, 83t-84t, *88-90*
    atlantoaxial instability and subluxation in, 59t
    with distraction dislocation, 84t, *90*
    false appearance of, 2t, 51t, *58, 59*
    screw fixation of, *89,* 155t
    types of, 83t, *88*
  hypoplasia of, 52t
    atlantoaxial instability in, 52t, 59t
    in spondyloepiphyseal dysplasia congenita, 78t, *79*
  incisors overlying, 51t, *58*

Odontoid process *(continued)*
  incomplete fusion to axis, 52t, *60*
  Mach band effect of, 2t, 51t, *58*
  normal developmental anatomy of, 45t, *46-48*
  ossification centers in, 45t, *46-47*
    unfused, 51t, *59*
  paraodontoid notch of, 51t, *58*
  posterior inclination of, 52t, *61*
Olecranon of ulna
  in diffuse idiopathic skeletal hyperostosis, 934t, *936*
  fractures of, 918t, *924*
  ossification centers in, 907t, *912,* 913t
Ollier disease, 29t
  of femur, 440t, 529t
  of foot, 759t
  of humerus, 896t
  of pelvis, 414t
  of radius and ulna, 958t
  of tibia and fibula, 644t, *646*
  of wrist and hand, 1048t, *1051*
Omovertebral bone, 824t, *828*
Opera glass appearance of hand, 1066t
  in psoriatic arthropathy, *1027*
OPLL (ossification of posterior longitudinal ligament)
  cervical, 107t, 108t, *120, 122*
  lumbar, 294t, *298*
  thoracic, 192t, *201*
Oppenheimer ossicle, lumbar, 234t, *241*
Ortolani maneuver in developmental dysplasia of hip, 444t, *448*
Os acetabuli, 384t, *385,* 438t
Os acromiale, 825t, *828*
Os cervicalis, *164*
Os intermetatarseum, 690t, *696*
Os odontoideum, 52t, 59t, *60*
Os peroneum, 691t, *697, 768*
  stress fracture of, 727t
Os styloideum, 978t, *980*
Os subfibulare, 691t, *698*
Os supranaviculare, 691t
Os sustentaculi, 691t, *699*
Os terminale of Bergmann, *46,* 51t, *59*
Os tibialis externa, 691t, *698*
Os trigonum, 690t, *694-695*
  posterior ankle impingement in, 690t, *694-695,* 729t
  stress fracture of, 728t
Os vesalianum, 691t, *696*
Osgood-Schlatter disease, 40t, 561t, *572*
  alignment disorders of knee in, 557t, 558t
Ossicles
  of acetabulum, 384t, *385,* 438t
  acromial, 825t, *828*
  of ankle and foot, 690t-691t, *694-699*
  of atlas, 51t, *55*
  of meniscus, 585t, *587*
  odontoid, 52t, 59t, *60*
  Oppenheimer, 234t, *241*
  of patella, *554*
  of sternum, 781t
  of wrist, 978t, *980*
Ossification
  cervical, in diffuse idiopathic skeletal hyperostosis, 107t-108, *120-122*
  of costochondral cartilage, 781t, *784-785*
  heterotopic, 10t, 21t
    of elbow, 942t, *943*
    of femur, 509t, *515*
    of fibula, 629t, *635*
    of hip, 470t, *485*
    of humerus, 889t, *890*
    of shoulder, *846,* 849t, *855*
Ossification *(continued)*
  lumbar
    in diffuse idiopathic skeletal hyperostosis, 294t, *298*
    of iliolumbar ligament, 294t, *298*
    of intervertebral disks, 282t
    paravertebral, 295t, *302-303*
    of posterior longitudinal ligament, 294t, *298*
    in psoriatic spondyloarthropathy, 295t, *302-303*
    in reactive arthritis, 295t, *303*
    of transverse process, 262t, *265*
  paravertebral, 194t
    lumbar, 295t, *302-303*
  of pelvis, in diffuse idiopathic skeletal hyperostosis, 405t, *406-408*
  of posterior longitudinal ligament
    cervical, 107t, 108t, *120, 122*
    lumbar, 294t, *298*
    thoracic, 192t, *201*
  of quadriceps and patellar tendons, in acromegaly, 600t, *610*
  of sacroiliac joint, in diffuse idiopathic skeletal hyperostosis, 356, *363*
  of sacrotuberous ligament, 356t, *360*
  of shoulder, in fibrodysplasia ossificans progressiva, *830,* 830t
  of stylohyoid ligament, 68t, *78*
  thoracic
    in alkaptonuria, *206*
    in diffuse idiopathic skeletal hyperostosis, 192t, *199-200*
    in disk herniation, 178t, *183,* 192t, *197-198*
    in psoriatic spondyloarthropathy, *204*
    in reactive arthritis, *205*
Ossification centers
  in ankle and foot, 672, 673t, *674-680*
    age of appearance and fusion, 673t
  in cervical spine, 44, 45t, *46-50*
    age of appearance and fusion, 45t
    persistent unfused, 68t, *75*
  in clavicle, 820t, *821*
    ununited, 824t, *826*
  in elbow, 906, 907t, *908-912*
    age of appearance and fusion, 907t
    incomplete union of, 913t, *914*
  in hip, 434, 435t, *436-437*
    age of appearance and fusion, 435t
  in knee, *547,* 548t, *549-551*
    accessory, 552t
    age of appearance and fusion, 548t
    in bipartite patella, 552t, *553*
  in lumbar spine, 228, 229t, *230-232*
    age of appearance and fusion, 229t
    ununited, 234t, *241*
  in pelvis, 377, 378t, *379-384*
    age of appearance and fusion, 378t
  in ribs and sternum, 776, 777t, *778-780*
    age of appearance and fusion, 777t
  sacrococcygeal, 345, 346t, *346-348*
    age of appearance and fusion, 346t
  in scapula, 820t, *822-823*
    ununited, 824t
  in shoulder, 819, 820t, *821-823*
    age of appearance and fusion, 820t
    ununited, 824t
  in thoracic spine, 161, *162-166, 168*
    age of appearance and fusion, 162t
  in wrist and hand, 972, 973t
    age of appearance and fusion, 973t
    extra or additional, 978t, *980*
Osteitis
  in ankylosing spondylitis, 201t, *203*
  condensing
    of clavicle, 883t, *884*
    of sacroiliac joint, 356t, 357t, *361-362*
  pubis, 404t, 405t, *409*
    infective, 406t, *413*
    symphyseal cleft injection in, 404t
  in synovitis-acne-pustulosis-hyperostosis-osteitis, 15t, 22t. *See also* SAPHO
Osteoarthritis, erosive, 11t
  of ankle and foot, 734t
  of wrist and hand, 1016t, 1018t, *1021*
    terminal phalangeal resorption in, 1067t
Osteoarthropathy
  neuropathic, 20t
    of ankle and foot, 735t, *751-752*
      distribution, symmetry, and preferential target sites of, 736t
    of cervical spine, 111t
    of elbow, 935t, *942*
    of hand, in leprosy, *1064*
    of hip, patterns of joint space narrowing in, 470t
    of knee, 557t, 600t, *613*
      genu recurvatum in, 557t, *613*
    of lumbar spine, 294t, *299, 304*
      surgery in, *340*
    of shoulder, 859t, *870*
    of thoracic spine, 192t
    of wrist and hand, 1017t, *1040,* 1066t
      terminal phalangeal resorption in, *1067,* 1067t
  primary hypertrophic
    of clavicle, 883t
    of knee, 616t, *618*
    of radius and ulna, 967t, *969*
    of tibia and fibula, 657t, *662*
    of wrist and hand, 1054t, *1062*
  secondary hypertrophic
    of clavicle, 883t, *885*
    of femur, 541t, *544*
    of humerus, 903t
    of radius and ulna, 967t, *969*
    of tibia and fibula, 657t, *663*
    of wrist and hand, 1055t, *1062*
Osteoarthrosis, 11t
  of acromioclavicular joint, *850,* 857t, *861*
  of ankle and foot, 734t, *738-739*
    distribution, symmetry, and preferential target sites of, 736t
    hallux rigidus in, 734t, *739*
    hallux valgus in, 682t, *687,* 734t
  of cervical spine, 107t, *113-118*
  costovertebral, 192t, *195-196,* 797t
  of elbow, 934t, *936*
  of glenohumeral joint, 857t, *860*
  of hip, 440t, 468t, *471-472*
    in developmental dysplasia, *449*
    patterns of joint space narrowing in, 470t
  of knee, 557t, 599t, *601-602,* 603t
  of lumbar apophyseal joint, 294t, *296*
  of sternoclavicular joint, 797t, *798*
  of sternocostal joint, 797t, *798*
  of thoracic spine, 192t, *195-196*
  of wrist and hand, 1016t, 1018t, *1019-1020*
    primary, 1016t, *1019*
    secondary posttraumatic, 1016t, *1020*
Osteoblastoma
  aggressive, 24t
    of ankle and foot, 758t
    of cervical spine, 138t, *141*

- Osteoblastoma *(continued)*
    - of clavicle and scapula, 870t
    - of femur, 516t
    - of pelvis, 413t
    - of ribs, 802t
    - of tibia and fibula, 636t, *639*
    - of wrist and hand, 1043t
  - conventional, 28t
    - of cervical spine, 139t, *143*
    - of clavicle and scapula, 871t
    - of femur, 529t, *532*
    - of humerus, 895t
    - of pelvis, 414t
    - of radius and ulna, 958t
    - of ribs, 802t
    - of sacrococcygeal spine, 371t
    - of tibia and fibula, 643t
  - osteosclerosis in, 313t
- Osteochondral bodies, intraarticular
  - in ankle, 709t, *711*
  - in elbow, 919t, *928*
- Osteochondritis dissecans, 7t
  - of elbow, 919t, *928*
  - of knee, 562t, *574*
  - of talus, 715t, *719*
- Osteochondroma, 29t
  - of cervical spine, 139t, *144*
  - of clavicle and scapula, 871t, *874*
  - of femur, 530t, *533*
    - radiation-induced, *433*
  - of humerus, 896t, *898*
  - of lumbar spine, 312t, *320*
  - of pelvis, 414t, *422*
  - of radius and ulna, 958t, *964*
  - of ribs, 802t, *810*
  - of tibia and fibula, 644t, *648*
- Osteochondromatosis, idiopathic synovial, 21t
  - of ankle and foot, 735t, *750*
  - of elbow, 935t, *940*
  - of hip, 470t, *487*
  - of knee, 579t, *584*
  - of shoulder, 859t, *868*
  - of wrist and hand, 1017t, *1040,* 1067t
- Osteochondromatous proliferation in hand, bizarre parosteal, 1047t, *1049*
- Osteochondrosis, 2t, 40t
  - of ankle and foot, 673, 772t, *773-775*
  - of cervical spine, 107t
  - of knee, posttraumatic, 561t, *572*
  - of lumbar spine, 268t
    - intervertebral, 294t
    - juvenile, 269t, *279*
  - of thoracic spine, 192t
- Osteoclastoma (brown tumor)
  - of ankle and foot, 768t
  - of femur, 541t, *542, 619*
  - of hip, 489t
  - of knee, 616t
  - of pelvis, 427t, *428*
  - of radius and ulna, 967t
  - of ribs, 814t, *817*
    - extrapleural mass in, 791t, *817*
  - of tibia and fibula, 657t, *659*
  - of wrist and hand, 1054t, *1058*
- Osteodystrophy, renal, 35t
  - of ankle and foot, 768t, *770*
  - of cervical spine, 149t
  - of elbow, 942t
  - of femur, *495,* 541t
  - of hip, 440t, 489t, *495*
  - of knee, 616t, *619-620*
  - of lumbar spine, 327t, *333*
  - of pelvis, 406t, *412,* 427t, *428*
  - of radius and ulna, 967t, *968*
- Osteodystrophy, renal *(continued)*
  - of ribs, 814t
    - notching in, 787t
  - of sacroiliac joint, 357t, *369*
  - of shoulder, 878t, *879*
  - of thoracic spine, 221t, *222, 223*
  - of tibia and fibula, 657t, *660*
  - of wrist and hand, 1054t, *1058-1059*
- Osteofibrous dysplasia, 28t
  - of tibia and fibula, 643t, *645*
- Osteogenesis imperfecta, 4t
  - of ankle and foot, *703,* 703t
  - of femur, 541t, *542*
  - of hand, 985t
  - of hip, 440t
  - of humerus, 903t, *904*
  - of knee, *557t*
  - of lumbar spine, 244t
  - of pelvis, 388t, *391*
  - of ribs, 814t, *815*
  - of thoracic spine, 170t, *172*
  - of tibia and fibula, 624t, *627,* 657t
- Osteoid osteoma. *See* Osteoma, osteoid
- Osteolysis
  - with detritic synovitis of hand, 1017t, *1042*
  - posttraumatic, of clavicle, 849t, *855*
  - in skeletal metastasis
    - of femur, *517*
    - of knee, 614t, *615*
    - of lumbar spine, *315*
    - of pelvis, *416*
    - of sacrococcygeal spine, 371t, *372*
- Osteoma, osteoid, 28t
  - of ankle and foot, 759t, *762*
  - of cervical spine, 138t, *143*
  - of clavicle and scapula, 871t
  - of femur, 529t, *531*
  - of humerus, 895t, *897*
  - osteosclerosis in, 313t
  - of pelvis, 414t, *422*
  - of radius and ulna, 958t
  - of ribs, 802t, *810*
  - of thoracic spine, 209t, *215*
    - scoliosis in, 178t, *183*
  - of tibia and fibula, 643t, *645*
  - of wrist and hand, 1047t, *1049*
- Osteomalacia, 34t
  - of cervical spine, 149t
  - of femur, 541t
  - of hip, 440t, 488t, *494*
    - patterns of joint space narrowing in, 470t
  - of humerus, 903t
  - of lumbar spine, 327t, *332*
  - of pelvis, 427t, *428*
  - of radius and ulna, 967t
  - of ribs, 814t, *815*
  - of shoulder, 878t
  - of thoracic spine, 221t, *222*
  - of tibia and fibula, 657t, *658*
- Osteomyelitis, 41t, 42t, 43t
  - of ankle and foot, 754t, *754-757*
    - acute pyogenic, 754t, *754-756*
    - tuberculous, 754t, *757*
  - of clavicle
    - acute pyogenic, 878t, *882*
    - chronic recurrent multifocal, 814t, *818,* 883t, *885*
  - of femur, 541t, *546*
    - acute pyogenic, 541t, *546*
    - chronic recurrent multifocal, 541t
  - of hip, 469t, *482*
  - of humerus, 903t, *905*
    - acute pyogenic, 903t, *905*
    - chronic, 903t, *905*
- Osteomyelitis *(continued)*
  - magnetic resonance imaging findings in, 134t
  - of pelvis, 427t, *431*
  - of radius and ulna, 967t, *970-971*
    - acute pyogenic, 967t, *970*
    - chronic recurrent multifocal, 967t, *971*
  - of rib, 814t
  - of scapula, acute pyogenic, 878t
  - of sternoclavicular joint, 814t, *818*
    - acute pyogenic, 814t
    - chronic recurrent multifocal, *818*
  - of sternum, 814t
  - of tibia and fibula
    - acute pyogenic, 665t, *666*
    - chronic, 665t, *667*
      - recurrent multifocal, 666t, *669*
    - leprous, 666t, *671*
    - tuberculous, 666t, *669*
  - of wrist and hand, 1055t, *1062, 1064*
    - acute pyogenic, 1055t, *1062*
    - leprous, *1064*
    - tuberculous, 1055t, *1064*
- Osteonecrosis, 40t
  - of acetabulum, in radiation therapy, *433*
  - of ankle and foot, 673, 772t, *773-775*
    - in navicular bone, *774*
    - in talus, 772t, *773*
  - of femur. *See* Femur, osteonecrosis of
  - of humerus
    - distal, 942t, *943*
    - proximal, 878t, *881*
  - of knee, 617t, *620-622*
    - in chronic renal disease, *620*
    - corticosteroid-induced, *622*
    - spontaneous, *621*
  - medullary, 40t
    - of tibia and fibula, 657t, *665*
  - of scaphoid, *992*
  - of small or irregular bones, 40t
  - of tibia and fibula
    - corticosteroid-induced, *622*
    - medullary, 657t, *665*
  - vertebral body, 40t
    - lumbar, 327t, *336*
    - steroid-induced, *225,* 327t, *336*
    - thoracic, 221t, *225*
  - of wrist and hand, 973, *1065,* 1065t
- Osteo-onychodysostosis syndrome, hereditary, 4t
  - of elbow, 913t, *915*
  - of knee, 552t, *555t, 556*
  - of pelvis, 388t, *391*
- Osteopathia striata, 4t
  - of femur, 504t, *508*
  - of tibia, 624t
- Osteopenia
  - in poliomyelitis, 427t, *432*
  - World Health Organization definition of, 229, 331t
- Osteopetrosis, 3t, 313t
  - of cervical spine, 78t, *80*
  - of femur, 504t, *507*
  - of fibula, 624t, *626*
  - of lumbar spine, 244t, *246, 255*
  - of pelvis, 388t, *390*
  - of ribs, 781t, *786*
  - of shoulder, 830t
  - of thoracic spine, 170t, *171*
  - of tibia, 624t, *626*
- Osteophytes, 194t
  - in hip, 468t, *471-472*
    - in ankylosing spondylitis, 468t, *475*
  - lumbar, 268t, *271-272*
    - spinal canal stenosis in, 282t, *291-292*

Osteophytes *(continued)*
  in sacroiliac joint, 356t, *358-359*
  in shoulder
    in acromioclavicular joint, 857t, *861*
    in glenohumeral joint, 857t, *860*
    in hemochromatosis, 858t, *866*
Osteopoikilosis, 4t, 313t
  of ankle and foot, 703t, *704*
  of cervical spine, 78t
  of femur, 504t, *508*
  of knee, 624t, *627*
  of lumbar spine, 244t, *246*
  of pelvis, 388t, *390*
  of shoulder, 830t, *831*
  of thoracic spine, 170t
  of wrist and hand, 985t, *989*
Osteoporosis, 34t
  of ankle and foot, 768t, *768-769*
    generalized, *768,* 768t
    regional, 768t, *769*
  bone mineral density measurements in, 327t, *330-331,* 331t, 488t, *491*
  of cervical spine, *149,* 149t
  of femur. *See* Femur, osteoporosis of
  of hip. *See* Hip, osteoporosis of
  of humerus, 903t
  of knee, 616t, *617*
  of lumbar spine, 327t, *328-331*
    corticosteroid-induced, *328, 330*
    senile, *328*
  of pelvis, 427t
  of radius and ulna, 967t
  of ribs and sternum, 814t
    generalized, 814t
    insufficiency fracture of sternum in, 789t, *794*
    notching of ribs in, 787t
  of sacrum, fracture in, 352t, *354*
  of shoulder, 878t, *879*
  of thoracic spine, 221t, *222*
    kyphosis in, 173t, *175,* 222
  of tibia and fibula
    generalized, 657t
    insufficiency fracture in, 629t, *633*
    regional, 657t, *658*
  World Health Organization definition of, 229, 331t
  of wrist and hand, 1054t, *1056-1057*
    generalized, 1054t, *1056*
    regional, 1054t, *1057*
Osteosarcoma, 24t
  of cervical spine, 138t
  of clavicle and scapula, 870t, *872*
  of femur
    conventional, 515t, *519-521*
    parosteal, 515t, *522*
    pulmonary metastasis of, *806*
  of humerus, 891t, *892-893*
    conventional, 891t, *893*
    parosteal, 891t
    secondary, *892*
  of knee, 614t
  of lumbar spine, 312t, *316*
  of pelvis, 413t, *417*
    in Paget disease, *425*
  pulmonary metastasis of, 802t, *806*
  of radius and ulna, 957t, *961*
    conventional, 957t
    parosteal, 957t, *961*
  of ribs, 802t, *806*
    extrapleural mass in, 791t, *806*
  of sacrococcygeal spine, 371t
  of thoracic spine, 209t, *213*
  of tibia and fibula
    conventional, 635t, *638*
    parosteal, 635t, *639*
Osteosarcoma *(continued)*
  of wrist and hand, 1043t, *1044-1045*
    conventional, 1043t, *1044*
    parosteal, 1043t, *1045*
Osteosclerosis, 313t
  of cervical spine, 78t, *80*
  in chordoma, 313t, *315*
  in enostosis, 313t, *319*
  of femur in myelofibrosis, 541t, *543*
  in Hodgkin disease, 313t, *318*
  of lumbar spine, 228, 282t, *289,* 313t, *315, 316, 318*
  of pelvis, 388t, *390*
  of thoracic spine, *214, 215*
Otto pelvis, 440t, *443*
Ovarian carcinoma, 22t
  metastatic to tibia and fibula, *637*

P

Pachydermoperiostosis
  of clavicle, 883t
  of knee, 616t, *618*
  of radius and ulna, 967t, *969*
  of tibia and fibula, 657t, *662*
  of wrist and hand, 1054t, *1062*
Paget disease, 32t
  of ankle and foot, 759t, *765*
  of cervical spine, 139t, *146*
  of clavicle, 871t, *876,* 883t
  of femur, 537t, *538*
  of hip, 440t, *443*
    acetabular protrusion in, 440t, *443*
    patterns of joint space narrowing in, 470t
  of humerus, 900t, *901*
  ivory vertebra in, 313t, *324*
  of knee, 614t, *616*
  of lumbar spine, 312t, *323-324*
  of pelvis, 414t, *424*
    sarcomatous transformation of, *425*
  of radius and ulna, 959t, *966*
  of ribs, 803t, *811*
  of sacrococcygeal spine, 371t, *376*
  of scapula, 871t, *876*
  of thoracic spine, 209t, *218*
  of tibia and fibula, *653,* 653t
  of wrist and hand, 1048t, *1052*
Pain
  in complex regional pain syndrome, regional osteoporosis in
    of ankle and foot, 768t, *769*
    of tibia and fibula in, 657t, *658*
    of wrist and hand, 1054t, *1057*
  congenital insensitivity to, neuropathic osteoarthropathy in
    of foot, 735t, *752*
    of wrist and hand, 1017t, *1040*
  in hip, in greater trochanteric pain syndrome, 463t, *467*
  in knee, in patellofemoral pain syndrome, 597t
Pancoast tumor, skeletal metastasis of
  to ribs, 802t, *805*
  to thoracic spine, *212*
Panner disease, 40t, *928,* 942t, *943*
Paraglenoid sulcus, 349t
Paralysis
  Erb-Duchenne, shoulder in, 849t, *854*
  lumbar spine disorders in, 295t, *304-305*
  spastic, patellar injury in, 559t, *566*
Paraodontoid notch, 51t, *58*
Parathyroid disorders
  hyperparathyroidism. *See* Hyperparathyroidism
Parathyroid disorders *(continued)*
  hypoparathyroidism
    pelvic disorders in, 427t, *429*
    tibia and fibula disorders in, 657t, *660*
Parosteal osteochondromatous proliferation in hand, bizarre, 1047t, *1049*
Pars interarticularis
  elongated, spondylolisthesis in, 248t
  fractures of
    acute, 248t, *254,* 262t
    pathologic, *255*
    stress, 228, 259t
  unilateral defect in, 249t, *256*
Parsonage-Turner syndrome, 849t, *854*
Patella
  bipartite, 552t, *553*
  chondroblastoma of, 614t, *615*
  chondrodysplasia punctata of, 555t, *556*
  chondromalacia of, 597t, *598*
  dislocation of, 558t, 575t, *577*
  displacement of
    inferior (patella baja), 558t, *597,* 597t
    Insall-Salvati measurement method in, *597,* 597t
    lateral, 552t, 558t
    superior (patella alta), 558t, *597,* 597t
      in lupus erythematosus, *605*
      in tear of patellar tendon, *596*
  dorsal defect of, 552t, *554*
  duplication of, 552t
  fractures of, 558t-559t, *564-566*
    fatigue, 559t, *565*
    longitudinal, 558t, *564*
    sleeve, 558t, 559t, *566*
    stellate comminuted, 559t, *564*
    transverse, 558t, *564*
  in gout, *609*
  hypoplastic or aplastic, 552t, 555t, *556*
  lateral dystopia of, 552t
  normal developmental anatomy of, 548t, *550-551*
  ossicle of, *554*
  ossification centers in, 548t, *550-551*
    in bipartite patella, 552t, *553*
  osteochondritis dissecans of, 562t, *574*
  slipping, 552t
  squaring of
    in hemophilia, 600t, *612*
    in juvenile idiopathic arthritis, *604*
  subluxation of, 558t, *575t*
Patella cubiti of elbow, 913t
Patellar tendon
  in Osgood-Schlatter disease, 561t, *572*
  ossification in acromegaly, 600t, *610*
  rupture in lupus erythematosus, 599t, *605*
  tear of, 558t, 592t, *596*
  tendinosis of, 592t, *596*
Patellar tooth sign, *602*
Patellofemoral disorders, 547, 597t, *597-598,* 603t
  in ankylosing spondylitis, *605*
  in crystal deposition disease, *608*
  in gout, *609*
  instability, 558t, 597t, *598*
Pectineal ligament calcification of, 384t, *387, 408*
Pectus carinatum, 781t
Pectus excavatum, 781t, *786*
Pedicle, vertebral
  agenesis or hypoplasia of, 313t
  missing pedicle sign in metastasis to thoracic spine, *211*
  sclerotic, 313t
Pedicle screw fixation systems in lumbar spine surgery, 339t, *341*

Pelken spurs in scurvy, 541t, *544, 661*
Pellegrini-Stieda syndrome, 590t, *593*
Pelvic vein calcification, 384t, *386*
Pelvis, 377-433
  anomalies and variants of, 377, 384t, *384-387*
  articular disorders of, 377, 405t-406t, *406-413*
    in crystal deposition disease, 406t, *412*
    degenerative, 405t, *406-409*
    infectious, 406t, *413*
    inflammatory, 405t, *410-411*
    metabolic, 406t, *412*
  champagne glass appearance of, 388t, *389*
  congenital disorders of, 377, 388t, *389-391*
  digit anomaly, 384t, *385*
  dysplasia of, 377, 388t
    cleidocranial, 388t, *391*
    fibrous, 414t, *426*
    sclerosing, *390*
  fractures of, 377, 392t-393t, *394-401*
    avulsion, 392t, *394*
    with hip dislocation, *452*
    insufficiency, 393t, *403, 428*
      in radiation therapy, 393t, *403,* 427t, *433*
    Malgaigne, 393t, *398*
    in metastasis, 413t, *416*
    stress (fatigue), 393t, *402,* 404t
  hematologic disorders of, 378, 427t
  hyperostosis of, diffuse idiopathic skeletal, 405t, *406-408*
  ilium in. *See* Ilium
  infections of, 378, 427t
    articular, 406t, *413*
  ischium in. *See* Ischium
  metabolic disorders of, 378, 427t
    articular, 406t, *412*
  metastasis of, osteoblastic, *373*
  normal developmental anatomy of, 377, 378t, *379-384*
  ossification centers in, 377, 378t, *379-384*
    age of appearance and fusion, 378t
  pubis in. *See* Pubis
  traumatic injuries of, 377, 392t-393t, *394-401,* 404t-405t
    sprung pelvis in, *399*
    type I, 392t, *394*
    type II, 392t, *395*
    type III, 392t-393t, *395-398*
  tumors and tumorlike lesions of, 378, 413t-414t, *415-427*
    benign, 414t, *421-423*
    malignant, 413t, *415-418*
    myeloproliferative, 414t, *419-420*
    tumorlike lesions, 414t, *424-427*
Pencil-in-cup deformity
  of foot in psoriatic arthropathy, *744*
  of hand, 1066t
Penile implant in impotence, 384t, *387*
Periarteritis nodosa, systemic, 22t
Perilunate dislocation, 991t, *996*
Periosteal reaction in tibia and fibula, 657t, *662*
Periostitis
  of clavicle, 883t, *885*
    from prostaglandin therapy in neonates, 883t
  of radius, *970*
  simulated, 913t
    of humerus, *823,* 887t
  of wrist and hand
    in leprosy, *1064*
    in psoriatic arthropathy, *1026*
Peripheral nerve tumors of chest wall, 803t
Perkin line, *446*
Peroneal tendons
  injuries of, 728t, *732*
  in os peroneum, 691t, *697*
Pes planovalgus, 681t, *686*
Pes planus, 557t, 681t, *686*
  acquired, 681t, *686*
  hereditary, 681t, *686*
PFFD (proximal femoral focal deficiency), 504t, *507*
Phalangeal bones of foot
  fractures of, 723t, *725*
  growth plate injuries of, 723t, *725*
  normal developmental anatomy of, 673y, *678-680*
  ossification centers in, 673t
  osteoporosis of, *769*
Phalangeal bones of hand
  anomalies and variants of, 978t-979, *980-984*
  enchondroma of, 1048t, *1050*
  Ewing sarcoma of, 1043t, *1045*
  fractures of, 1004t, *1008-1010*
    in abused child, 1004t
  growth plate injuries of, 1004t, *1009*
  in Hurler syndrome, 985t, *989*
  in leprosy, *1064*
  in lupus erythematosus, *1029*
  in melorheostosis, 985t, *989*
  metastatic tumor of, *1044*
  normal developmental anatomy of, 973t, *977*
  ossification centers in, 973t
  osteoid osteoma of, *1049*
  osteonecrosis of, 1065t
  osteoporosis of, *1056*
  osteosarcoma of, *1045*
  resorption of, 973, *1067,* 1067t
    characteristic sites of, 1067t
    differential diagnosis in, *1067*
    in epidermolysis bullosa, *1042*
    in osteolysis with detritic synovitis, *1042*
    in scleroderma, *1031*
  rheumatoid arthritis of, *1024*
  in sarcoidosis, 1017t, *1039*
  in scleroderma, *1031*
  stress injuries of, 1004t, *1010*
  synostosis of, 978t, *982*
  terminal tufts of, *977, 1010, 1031*
    in acromegaly, 1054t, *1061*
  in Turner syndrome, 985t, *986*
Phenytoin therapy, osteomalacia in, *332*
Phleboliths, pelvic vein, 384t, *386*
Picture-frame vertebrae in Paget disease, *323*
Pie sign in lunate dislocation, 991t
Pigeon breast, 781t
Pigmented villonodular synovitis, 21t
  of elbow, 935t
  of foot, 760t
  of hip, 470t, *487*
  of knee, 579t, *583*
  of shoulder, 859t, *867*
Pillar fractures of cervical spine, 93t, *104-105*
Pisiform, 1018t
  in crystal deposition disease, *1033*
  fractures of, 990t, *994*
  ossification centers in, 973t
  osteoarthrosis of joint with triquetrum, *1019*
Pisiform-triquetral joint, 1018t
  osteoarthrosis of, *1019*
Pitchers' elbow, 929t
Pitt pits, *438,* 438t
Plasma cell myeloma, 26t
  of ankle and foot, 758t, *762*
  of cervical spine, 138t, *142*
  of clavicle and scapula, 871t, *873*
  of femur, 516, *526*
  of humerus, 891t, *893*
  of knee, 614t, *615*
  of lumbar spine, 312, *317*
  of pelvis, 414t, *419*
  of radius and ulna, 957t, *963*
  of ribs, 802t, *809*
    extrapleural mass in, 791t, *809*
  of sacrococcygeal spine, 371t
  of sternum, 802t
  of thoracic spine, 209t, *213*
  of tibia and fibula, 636t, *641*
  of wrist and hand, 1043t, *1047*
Plasmacytoma, 27t
  of cervical spine, 138t
  of femur, 516t, *526*
  of humerus, 891t
  of knee, 614t
  of lumbar spine, 312, *317*
  of pelvis, 414t, *419*
  of sacrococcygeal spine, 371t, *374*
  of thoracic spine, *213*
Plates in cervical spine surgery, 155, *156*
Platyspondyly
  in mucopolysaccharidosis, 78t, *79*
  in spondyloepiphyseal dysplasia congenita, 78t, *79*
Plica, synovial, of knee, 579t, *583*
Pneumolipohemarthrosis, 10t
Pneumothorax in rib fractures, *792*
Poliomyelitis, 42t
  coxa valga deformity in, 440t, *441*
  foot disorders in, 768t, *770*
  pelvic disorders in, 427t, *432*
  rib notching in, 787t
Polychondritis, relapsing, 22t
Polydactyly, 2t
  of foot, 692t, *702*
  of hand, 979t, *982*
    postaxial, 979t, *982*
    preaxial, 979t, *982*
Polymyositis, 16t
  ankle and foot disorders in, 734t, *746*
  chest wall disorders in, 797t, *801*
  femoral disorders in, 541t, *546*
  hip disorders in, 468t, *477*
  humerus disorders in, 903t, *905*
  knee disorders in, 599t, *606*
  pelvic disorders in, 405t
  thoracic spine disorders in, 193t, *205*
  wrist and hand disorders in, 1016t
Polyvinylchloride acro-osteolysis, terminal phalangeal resorption in, 1067t
Ponticulus of atlas, posterior, 51t, *56*
Popliteal artery aneurysm, posttraumatic, 617t, *622*
Popliteus muscle injuries, *594*
Predens space. *See* Atlantodental interspace
Pregnancy
  osteitis pubis after, 405t, *409*
  symphysis pubis diastasis after, 392t, *395*
Preiser disease, 1065t
Primitive neuroectodermal tumor, sacrococcygeal, 371t
Progeria, terminal phalangeal resorption in, 1067t
Prostaglandin therapy in neonates, periostitis of clavicle in, 883t

- Prostate carcinoma, metastatic
  - to femur, *518*
    - avulsion fracture in, *458*
  - to humerus, *892*
  - to lumbar spine, *313-314*
  - to pelvis, *415*
    - insufficiency fracture in, *403*
  - to ribs, *804*
  - to sacrococcygeal spine, *373*
  - to thoracic spine, *210*
- Prostate surgery, osteitis pubis after, 405t, *409*
- Prosthesis for intervertebral disk
  - cervical, 155t, *157*
  - lumbar, 339t, *342*
- Protrusion
  - of acetabulum. *See* Acetabulum, protrusion of
  - of lumbar intervertebral disk, 268t, *275, 277*
- Pseudarthrosis
  - of clavicle, congenital, 824t, *827*
  - of ribs, congenital, 781t
  - of thoracic spine in ankylosing spondylitis, 193t, *204*
  - of tibia and fibula in neurofibromatosis type I, 653t, *654*
- Pseudoacetabulum, in developmental dysplasia of hip, *449*
- Pseudocyst
  - of calcaneus, 2t, 691t, *701*
  - of humerus, 2t, *823,* 825t, *829,* 887t
- Pseudofracture of cervical spine, in degenerative disorders, *113, 114*
- Pseudohypoparathyroidism, wrist and hand disorders in, 1054t, *1060,* 1067t
- *Pseudomonas aeruginosa* infections, septic arthritis in
  - of elbow, *940*
  - of sacroiliac joint, *370*
- Pseudopseudohypoparathyroidism, wrist and hand disorders in, 1054t
- Pseudosubluxation of axis, 52t, *65*
- Pseudotumors, hemophilic
  - of pelvis, 427t, *431*
  - of radius and ulna, 967t, *969*
- Psoas abscess in tuberculosis, *310, 484*
- Psoriatic arthropathy, 14t-15t
  - of ankle and foot, 734t, 737t, *743-744*
  - of cervical spine, 109t, *131*
  - of elbow, 934t
  - of hip, 440t, 468t, *476*
    - patterns of joint space narrowing in, 470t
  - of knee, 599t
  - of lumbar spine, 295t, *302-303*
  - of manubriosternal junction, 797t, *799*
  - of pelvis, 405t, *411*
  - of sacroiliac joint, 356t, 357t, *367*
  - of shoulder, 858t, *863*
  - skin disorders in, 14, 22t
  - of sternoclavicular joint, 797t
  - of thoracic spine, 193t, *204*
  - of wrist and hand, 1016t, *1026-1027,* 1066t
    - terminal phalangeal resorption in, *1067,* 1067t
- Pubalgia syndromes, athletic, differential diagnosis of, 404t
- Pubis
  - classification and grading of changes in, 405t
  - cleidocranial dysplasia of, 388t, *391*
  - fibrosarcoma of, *418*
  - fibrous dysplasia of, *426*
- Pubis *(continued)*
  - fractures of, 392t
    - Malgaigne, 393t, *398*
    - in osteomalacia, *428*
    - straddle, 392t, *396*
    - stress (fatigue), *402*
  - and ischium synchondrosis
    - normal developmental anatomy of, *379-380, 384, 436*
    - unfused, *384,* 384t
  - metastasis to, *416*
  - ossification centers in, 378t
  - osteitis of, 404t, 405t, *409*
    - infective, 406t, *413*
    - symphyseal cleft injection in, 404t
  - osteomalacia of, *428*
  - simple bone cyst of, *423*
  - symphysis of. *See* Symphysis pubis
- Pustulosis
  - palmaris et plantaris, 797t, *800,* 883t
  - in synovitis-acne-pustulosis-hyperostosis-osteitis, 15t, 22t. *See also* SAPHO

Q

- Quadriceps tendon
  - ossification in acromegaly, 600t, *610*
  - tear of, 558t, *592, 596*

R

- Rachitic rosary in rickets of ribs, 814t, *816*
- Radiation therapy
  - hip disorders in, 440t, *502*
  - pelvic disorders in, 427t, *433*
    - insufficiency fracture in, 393t, *403,* 427t, *433*
  - sacral insufficiency fracture in, 352t, *354*
  - shoulder disorders in, 878t, *882*
  - thoracic scoliosis in, 178t, *182*
- Radiocarpal joint, 1018t
  - crystal deposition disease of, 1017t, *1033-1034*
  - fracture-dislocation of, 951t, *953, 954*
  - Madelung deformity of, 945t, *946,* 977t
- Radioulnar joint
  - distal, 1018t
    - crystal deposition disease of, *1033*
    - dislocation of, 951t, *954*
    - erosive osteoarthritis of, *1021*
    - in Galeazzi fracture-dislocation, 948t, *950*
    - Madelung deformity of, 945t, *946,* 977t
    - in negative ulnar variance, 945t, *947*
    - in positive ulnar variance, 945t, *947*
    - rheumatoid arthritis of, *1022*
  - proximal
    - normal developmental anatomy of, *913*
    - synostosis of, 913t, *914,* 945t
- Radius, 944-971
  - anomalies and variants of, 944, 945t, *946*
  - aplasia of, 2t
  - distal
    - fractures of, 951t-952t, *952-956*
      - in children, 951t, *953*
    - ossification centers in, 973t
    - rheumatoid arthritis of, *1022*
  - fractures of, 944
    - in child abuse, 952t, *956*
    - diaphyseal, 948t, *950*
    - distal, 951t-952t, *952-956*
      - in children, 951t, *953*
    - Galeazzi, 948t, *950*
    - proximal, 918t, *925-926*
    - in styloid process, 951t, *955*
  - in lead poisoning, 967t, *969*
  - Madelung deformity of, 945t, *946,* 977t
- Radius *(continued)*
  - metabolic, hematologic, and infectious disorders of, 944, 967t, *968-971*
  - ossification centers in
    - distal, 973t
    - proximal, 907t, *908, 911-912,* 913t
  - proximal
    - dislocation of, 917t, *919-920*
      - in Monteggia fracture-dislocation, 917t, 948t, *949*
      - osteoarthrosis in, *936*
    - fractures of, 918t, *925-926*
    - growth plate injury of, 919t
    - in hereditary osteo-onychodysostosis syndrome, 913t, *915*
    - normal developmental anatomy of, 907t, *908, 910-913*
    - ossification centers in, 907t, *908, 911-912,* 913t
    - synostosis with ulna, 913t, *914,* 945t
  - radiolucent tuberosity of, *912,* 913t, 945t, *946*
  - in radioulnar joint. *See* Radioulnar joint
  - tumors and tumorlike lesions of, 944, 957t-959t, *960-966*
    - benign, 958t-959t, *964-965*
    - malignant, 957t, *960-962*
    - myeloproliferative, 957t, *963*
    - tumorlike lesions, 959t, *966*
- Raynaud disease, 1067t
- Ray pattern in psoriatic arthropathy of hand, 1016t, *1027*
- Reactive arthritis, 15t
  - of ankle and foot, 734t, *745*
  - of cervical spine, 109t, *132*
  - of hip, 468t
  - of knee, 599t, *605*
  - of lumbar spine, 295t, *303*
  - of manubriosternal junction, 797t
  - of pelvis, 405t
  - of sacroiliac joint, 356t, 357t, *368*
  - of thoracic spine, 193t, *205*
  - of wrist and hand, 1016t, *1027, 1028*
- Rectus abdominis insertional tendinopathy, 404t
- Reflex sympathetic dystrophy, regional osteoporosis in
  - of ankle and foot, 768t, *769*
  - of tibia and fibula, 657t, *658*
  - of wrist and hand, 1054t, *1057*
- Reiter syndrome, 15t, 23t
  - ankle and foot disorders in, 734t, 737t, *745*
  - cervical spine disorders in, 109t, *132*
  - hip disorders in, 470t
  - knee disorders in, 599t, *605*
  - lumbar spine disorders in, 295t, *303*
  - manubriosternal junction disorders in, 797t
  - pelvic disorders in, 405t
  - sacroiliac joint disorders in, 356t, 357t, *368*
  - thoracic spine disorders in, 193t, *205*
  - wrist and hand disorders in, 1016t, *1028*
- Renal cell carcinoma, metastatic
  - to lumbar spine, *312*
  - to sacrococcygeal spine, *372*
  - to tibia, *637*
- Resorption
  - of phalangeal bones in hand, 973, *1067,* 1067t
    - characteristic sites of, 1067t
    - differential diagnosis in, *1067*
    - in epidermolysis bullosa, *1042*

Resorption *(continued)*
    in osteolysis with detritic synovitis, *1042*
    in scleroderma, *1031*
  subchondral, of sacroiliac joint
    in hyperparathyroidism, 357t, *369*
    in renal osteodystrophy, *369*
Reticulohistiocytosis, multicentric
  skin and joint findings in, 22t
  of wrist and hand, 22t, 1017t, *1038*
    terminal phalangeal resorption in, *1067,* 1067t
Retinoid exposure, 23t
Retrolisthesis of lumbar spine, degenerative, 281t, *285-286*
Rheumatoid arthritis, 13t, 22t
  of ankle and foot, 734t, 737t, *740*
    distribution, symmetry, and preferential target sites of, 736t
    hallux valgus in, *687*
    insufficiency fracture in, 710t, *713*
    nodules in, 760t
  of cervical spine, 108t-109t, *123-126*
    atlantoaxial instability in, 108t, 109t, *123-124, 125, 126*
    cranial settling in, *124*
    juvenile, 109t, *126*
    lower segment, 108t, *125*
  of elbow, 934t, *937*
  fibula insufficiency fracture in, 710t, *713*
  of hip, 440t, 468t, *473-474*
    acetabular protrusion in, 440t, *442*
    femoral insufficiency fracture in, 453t, *457*
    patterns of joint space narrowing in, 470t
    synovial cyst in, 468t, *474*
  juvenile, 22t. *See also* Arthritis, juvenile idiopathic
  of knee, 557t, 599t, *603,* 603t
  of lumbar spine, 294t, *299*
  of manubriosternal junction, 797t, *799*
  of pelvis, 405t
  rib notching in, 787t
  of sacroiliac joint, 356t, 357t, *364*
  of shoulder, 857t, *862*
  skin disorders in, 22t
  of sternoclavicular joint, 797t
  tibia insufficiency fracture in, 629t, *633,* 710t
  of wrist and hand, 1016t, 1018t, *1022-1024,* 1066t
Rhomboid fossa in clavicle, 2t, 824t, *826, 882*
Ribs, 776-818
  anomalies and variants of, 776, 780t-781t, *782-786*
    associated with spinal anomalies, 780t, *782*
  asymmetric, 780t, *782*
  bifurcation of, 780t
  cervical, 68t, *76,* 780t
    in Klippel-Feil syndrome, 68t, 73t, 780t
  foramen of, 780t
  fractures of, 776, 788t, *790-793,* 833t
    acute, 788t, *790-792*
    in child abuse, 788t, *792*
    extrapleural mass in, *791,* 791t
    fatigue, 788t, *792-793*
    in hemodialysis, 814t, *818*
    pneumothorax in, *792*
  horizontal, 780t, *782*
  intrathoracic, 780t, *782*
  lumbar, 233t, *238,* 780t, *782*
    ectopic, 384t, *385*
Ribs *(continued)*
  metabolic, hematologic, and infectious disorders of, 776, 814t
  normal developmental anatomy of, 776, 777t, *778-780*
  notching of, 776, *787,* 787t
    in coarctation of aorta, *787,* 787t
  ossification centers in, 776, 777t, *778, 778-780*
    age of appearance and fusion, 777t
  pelvic, 384t, *385*
  pseudarthrosis of, congenital, 781t
  in slipping rib syndrome, 788t
  in sternocostoclavicular hyperostosis, 797t, *800*
  synostosis of, 781t, *783*
  tumors and tumorlike lesions of, 776, 802t-803t
    metastatic, 802t, *804-805*
      extrapleural mass in, 791t, *805*
    in neurofibromatosis type I, 787t, 803t, *811*
Rickets, 35t
  of elbow, 942t
  of femur, *494,* 541t, *542*
  of hip, 440t, 488t, *494*
  of humerus, 903t, *904*
  of knee, 557t, 616t, *618*
  of radius and ulna, 967t, *968*
  of ribs, 814t, *816*
  of shoulder, 878t
  of tibia and fibula, 657t, *659*
Rider's bone in pelvic avulsion injuries, 392t, *394*
Ring apophysis, vertebral
  cervical
    in lower segment, 67t, *68,* 92t
    in upper segment, 45t, *48*
  lumbar, 229t, *230-232,* 233t
    posterior avulsion fracture of, 262t, *267,* 269t
  sacral, 346t
  thoracic, 162t, *163, 166,* 167t, *168*
Ring sign in wrist instability
  in scapholunate dissociation, 999t, *1000*
  in volar intercalated segmental instability, *1001*
Risser sign, *382*
Rocker-bottom foot, 681t, *685*
Rod fixation systems in lumbar spine surgery, 339t, *340*
Rolando fracture, 1003t, *1005*
Rösler sign in coarctation of aorta, *787,* 787t
Rotator cuff, 847t-848t, *850-851*
  impingement syndromes of, 856t
  tears of, 847t, *850-851*
    acute, 847t
    in ankylosing spondylitis, *863*
    chronic, 847t, *850*
    full-thickness, 847t, *850-851*
    partial-thickness, 847t
    in rheumatoid arthritis, 857t, *862*
  tendinitis of, 848t
    calcific, 858t, *864*
Rugger-jersey spine appearance, *817*
  of lumbar spine, 327t, *333*
  of thoracic spine, 221t, *223*

S

Saber-shin deformity in Paget disease of tibia, *653,* 653t
Sacralization of transitional lumbosacral segment, 235t, *242*
Sacrococcygeal spine, 345-376
  anomalies and variants of, 345, 349t, *350-351*
  articular disorders of, 345, 356t-357t, *358-370*
  dislocation in, 352t
  normal developmental anatomy of, 345, 346t, *346-348*
  traumatic injuries of, 345, 352t, *353-355*
  tumors and tumorlike lesions of, 345, 371t, *372-376*
    benign, 371t, *374-375*
    malignant, 371t, *372-373*
    myeloproliferative, 371t, *374*
    tumorlike lesions in, 371t, *376*
Sacroiliac joint, 345-376
  accessory, 349t, *351*
  degenerative disorders of, 356t, 357t, *358-363*
  diastasis of, 352t, *355,* 392t
    in ischiopubic fracture, *396*
    in Malgaigne fracture, 393t, *398*
    in sacral fracture, *397*
    in sprung pelvis, *399*
  infections of, 357t, *370*
  inflammatory disorders of, 356t, 357t, *364-368*
  metabolic disorders of, 357t, *369*
  normal developmental anatomy of, 345, *346-347*
  pseudonarrowing of, 349t, *350*
Sacroiliac ligament
  calcification and ossification of, 356t, *360*
  pubic diastasis in injuries of, 392t
Sacroiliitis
  in ankylosing spondylitis, 356t, 357t, *365*
  differential diagnosis in, 404t
  in enteropathic arthropathy, *367*
  in psoriatic spondyloarthropathy, 356t, *367*
  in reactive arthritis and Reiter syndrome, 356t, 357t, *368*
Sacrospinous ligament
  calcification and ossification of, 356t
  pubic diastasis in injuries of, 392t
Sacrotuberous ligament calcification and ossification, 356t, *360, 408*
Sacrum, 345-376
  agenesis of, 349t, *351*
  chordoma of, *373*
  enostosis of, *374*
  fibrosarcoma of, *418*
  fractures of, 352t, *353-355,* 392t, *397*
    insufficiency, 352t, *354*
    with pubic diastasis, *353, 395, 397*
    sacroiliac joint diastasis in, *397*
    stress, 352t, *355*
  giant cell tumor of, *375*
  in lumbosacral spine. *See* Lumbosacral spine
  metastatic tumors of
    osteoblastic, *373*
    osteolytic, *372*
  neurofibromatosis type I of, *376*
  ossification centers in, 346t, *347*
  Paget disease of, *376*
  plasmacytoma of, *374*
  in poliomyelitis, *432*
  in sacrococcygeal spine. *See* Sacrococcygeal spine
  in sacroiliac joint. *See* Sacroiliac joint
  wing or ala of
    fossa of, 349t, *350*
    ossification centers in, *347*
Sagging rope sign in pelvic achondroplasia, 388t, *389*

Sail sign, *162*
Salter-Harris fractures, 8t
  of ankle, 710t, *712*
  of elbow, 919t, *927*
  of knee, *570-571*
  of phalangeal bones in foot, *725*
  of phalangeal bones in hand, *1009*
  of radius, distal, 952t
  of ulna, distal, 952t
Sandwich vertebrae in osteopetrosis
  cervical, 78t, *80*
  lumbar, 244t, *246, 255*
  thoracic, 170t, *171*
SAPHO (synovitis-acne-pustulosis-hyperostosis-osteitis), 15t, 22t
  cervical spine disorders in, 110t
  clavicle disorders in, 883t
  thoracic cage joint disorders in, 797t, *800*
Sarcoidosis
  skin and joint findings in, 23t
  of wrist and hand, 1017t, *1039*
Sarcoma
  Ewing. *See* Ewing sarcoma
  fibrosarcoma. *See* Fibrosarcoma
  osteosarcoma. *See* Osteosarcoma
  synovial cell
    of ankle and foot, 758t, 760t, *761, 767*
    of wrist and hand, 1043t, *1046*
  undifferentiated pleomorphic, of ankle and foot, 760t
Sausage digit in psoriatic arthropathy of hand, 1016t, *1027*
Scalloping of lumbar vertebrae, 228, *325*
  in achondroplasia, 244t, *245*
  causes of, 246t
  in Ehlers-Danlos syndrome, 244t, 246t, *247*
  in Marfan syndrome, 244t, 246t, *247*
  in neurofibromatosis type I, 246t, *325*
  physiologic, *231,* 246t
Scaphoid bone
  anomalies and variants of, 978t
  in crystal deposition disease, *1034*
  dislocation of, 991t
  fracture of, 990t, *992*
    osteonecrosis in, *992,* 1065t
  in greater arc injuries, 991t, *997*
  ossification centers in, 973t
  osteonecrosis of, *992,* 1065t
  rotary subluxation of, 999t, *1000*
  in scapholunate advanced collapse wrist, 999t, *1001,* 1017t, *1033*
  in scapholunate dissociation, 999t, *1000, 1001*
Scapholunate advanced collapse wrist, 999t, *1001*
  in crystal deposition disease, 1017t, *1033*
Scapholunate dissociation, 999t, *1000, 1001*
Scapula, 819-885
  accessory ossicle of, 825t, *828*
  acromion process of
    fractures of, 833t, *839*
    ossification centers in, 820t, *823*
  anomalies and variants of, 824t-825t, *828-829*
  coracoid process of
    fractures of, 833t, *839*
    ossification centers in, 820t, *822-823*
  duplication of, 825t
  dysplasia of, 824t, *828*
    cleidocranial, 830t, *831*
  fractures of, 833t, *838-840*
    in acromion process, 833t, *839*
    in body, 833t, *838*
    with clavicle fracture, 833t, *839, 840*
Scapula *(continued)*
    in coracoid process, 833t, *839*
    floating shoulder in, 833t, *839, 840*
    in glenoid fossa, 833t, *838*
    in spine and neck, 833t, *840*
  glenoid cavity of. *See* Glenoid cavity of scapula
  hyperostosis of, infantile cortical, 830t, 883t
  melorheostosis of, 830t
  normal developmental anatomy of, 820t, *822-823*
  omovertebral bone of, 824t, *828*
  ossification centers in, 820t, *822-823*
    ununited, 824t
  osteomyelitis of, pyogenic, 878t
  osteopetrosis of, 830t
  osteopoikilosis of, 830t, *831*
  in scapulothoracic dissociation, 842t, *847*
  Sprengel deformity of, 73t, 824t, *828*
  tumors and tumorlike lesions of, 819, 870t-871t, *872-876*
    benign, 871t, *874*
    malignant, 870t, *873*
    metastatic, *872*
    myeloproliferative, 871t
    tumorlike lesions, 871t, *876*
  vascular channel in, prominent, 825t, *829*
Scapulothoracic dissociation, 842t, *847*
Scheuermann disease, 40t
  of lumbar spine, *279*
  Schmorl nodes in, 173t, *176,* 185t, 269t, *278, 279*
  thoracic kyphosis in, 173t, *174, 176*
Schmorl nodes
  of lumbar spine, *236,* 269t, *278, 279*
  in Scheuermann disease, 173t, *176,* 185t, 269t, *278, 279*
  of thoracic spine, 185t, *186*
Schwannoma, 803t
Scleroderma, 16t, 22t
  of ankle and foot, 734t, *746*
  of elbow, 934t, *938*
  of hip, 468t, *477*
  of radius and ulna region, 967t, *971*
  rib notching in, 787t
  of shoulder, 858t, *863*
  skin disorders in, 16t, 22t
  of thoracic spine, 193t, *205*
  of wrist and hand, 1016t, *1030-1031,* 1066t
    calcification in, 1016t, *1030-1031,* 1067t
    terminal phalangeal resorption in, *1067,* 1067t
Sclerosis
  osteosclerosis. *See* Osteosclerosis
  progressive systemic. *See* Scleroderma
  segmental, of lumbar vertebral bodies, 282t, *289*
Scoliosis
  in leg length inequality, 178t, 259t, *261*
  lumbar, 228, 259t, *260-261*
    congenital, in hemivertebrae, 234t, *241*
    degenerative, 259t, *260,* 281t, *287*
    in diastematomyelia, 235t
    idiopathic adolescent, 259t, *260*
    in leg length inequality, 259t, *261*
    in Marfan syndrome, 259t, *261*
  thoracic, 161, 177t-179t, *180-184*
    adolescent-onset, 177t, *180*
    congenital, *168,* 177t, *181*
    indications for additional imaging in, 179t
Scoliosis *(continued)*
    infantile-onset, 177t
    juvenile-onset, 177t
    in neurofibromatosis type I, 177t, *181, 218*
    in neuromuscular disorders, 178t, *182*
    surgical procedures in, 178t, *184*
    in trauma, 178t, *182*
    in tumors, 178t, *183, 215*
Screws
  in cervical spine surgery, *89,* 155t, *156*
  in femoral fracture repair, *462*
  in fibula fracture repair, *708*
  in lumbar spine surgery, 339t, *341*
Scurvy, 36t
  femoral disorders in, 541t, *544*
  knee disorders in, 616t
  tibia and fibula disorders in, 657t, *661*
Seat belt fracture of thoracolumbar spine, 185t, *189,* 262t
Sebaceous gland disorders, 22t
Segond injury of tibia, 560t, *568,* 591t
Seinsheimer classification of femoral fractures, 460t
Septic arthritis, 41t
  of acromioclavicular joint, 859t, *867*
  of ankle and foot, 754t, *755-757*
  of costosternal joint, 797t
  of elbow, 934t, *940*
  of hip, 469t, *481-483*
    with epiphysiolysis, *483*
    patterns of joint space narrowing in, 470t
  of knee, 600t
  of lumbar facet joints, 295t, *311*
  of manubriosternal junction, 797t
  of sacroiliac joint, 357t, *370*
  of sternoclavicular joint, 797t, *801*
  of wrist and hand, 1055t, *1063*
Septic bursitis of elbow, 934t, *940*
Sequestration of lumbar intervertebral disk, 268t, *276-277*
Serum sickness, 22t
Sesamoid bones
  of elbow, 913t
  of foot, 691t, *700*
    fractures of, 723t, *726,* 727t
    hallux, 691t, *700,* 723t, *726*
    in interphalangeal joint dislocation, *727*
  of hand, in acromegaly, 1054t, *1061*
Sever disease, 40t, 772t, *775*
Shenton line, *446*
Shin splints, 629t
Shiny corner sign in ankylosing spondylitis
  lumbar, *300*
  thoracic, 201t, *203*
Shoulder, 819-885
  adhesive capsulitis of, 848t, *851*
  anomalies and variants of, 819, 824t-825t, *825-829*
  articular disorders of, 819, 857t-859t, *860-870*
    in crystal deposition disease, 858t, *864-866*
    degenerative, 857t, *860-861*
    infectious, 859t, *867*
    inflammatory, 857t-858t, *862-863*
    metabolic, 858t, *866*
  clavicle in. *See* Clavicle
  congenital disorders of, 819, 830t
  dislocations of, 819, 841t-842t, *843-847*
    acromioclavicular, 842t, *846*
    glenohumeral, 841t, *843-845*
    sternoclavicular, 842t

- Shoulder *(continued)*
  - drooping, 841t, *845*
  - dysplasia of, 819, 830t, *831*
  - floating, 833t, *839, 840*
  - fractures of, 819, 832t-833t, *834-840*
  - frozen, 848t, *851*
  - humerus in. *See* Humerus, proximal
  - impingement syndromes of, 819, 847t, 856t
    - biceps brachii tendinosis in, 848t
    - external, 856t
    - internal, 856t
  - infections of, 820, 859t, *867,* 878t
  - internal derangements of, 819, 847t-849t, *850-855*
  - metabolic disorders of, 820, 858t, *866,* 878t
  - Milwaukee shoulder syndrome, 858t, *865, 866*
  - normal developmental anatomy of, 819, 820t, *821-823*
  - ossification centers in, 819, 820t, *821-823*
    - age of appearance and fusion, 820t
    - ununited, 824t
  - rotator cuff in. *See* Rotator cuff
  - scapula in. *See* Scapula
  - in scapulothoracic dissociation, 842t, *847*
  - tumors and tumorlike lesions of, 819, 870t-871t, *872-877*
- Shoulder pad sign in amyloid deposition, 858t
- Sickle cell anemia, 39t
  - ankle and foot disorders in, 772t, *773*
  - hip disorders in, 440t, 489t, *496*
  - humeral head osteonecrosis in, *881*
  - lumbar spine disorders in, 327t, *335*
  - pelvic disorders in, 427t, *430*
  - thoracic spine disorders in, 221t, *224*
- Silicone synovitis
  - of foot, 735t, *753*
  - of wrist and hand, 1017t, *1041*
- Sinding-Larsen-Johansson disease, 40t, 558t, 561t
- Singh index in femoral osteoporosis, 488t, 489t
- Sjögren syndrome, rib notching in, 787t
- Skin disorders, 22t-23t
  - in epidermolysis bullosa and hand disorders, 1017t, *1042*
  - in lupus erythematosus, 17t, 22t
  - in psoriasis, 14, 22t
  - in Reiter syndrome, 15t, 23t
  - in scleroderma, 16t, 22t
- Slipped capital femoral epiphysis, 440t, 453t, *454-455*
  - in hypothyroidism, 488t, *495*
  - in septic arthritis, 469t, *483*
- Slipping rib syndrome, 788t
- Smith fracture, 951t, *955*
- Snowcap appearance in humeral head osteonecrosis, 878t, *881*
- Soft tissue disorders
  - of ankle and foot
    - infectious, *754,* 754t, *758*
    - traumatic, 728t-729t, *730-733*
    - in tumors and tumorlike lesions, 759t-760t
      - in synovial cell sarcoma, 758t, *761, 767*
  - of chest wall, in dermatomyositis-polymyositis, 797t, *801*
  - of elbow, 906, 929t, *930-933*
    - in scleroderma, 934t, *938*
  - of humerus region
    - in collagen vascular disease, 903t, *905*
    - in trauma, 889t, *890*
- Soft tissue disorders *(continued)*
  - of ligaments. *See* Ligament disorders
  - of radius and ulna region, in scleroderma, 967t, *971*
  - of shoulder
    - in amyloid deposition, 858t
    - of biceps brachii, 848t, *852. See also* Biceps brachii tendon
    - in calcific tendinitis, 858t, *864*
    - in milk-alkali syndrome, 878t, *880*
    - of rotator cuff, 847t-848t, *850-851. See also* Rotator cuff
  - of tendons. *See* Tendon disorders
  - of thoracic spine, in calcification, *205*
  - of tibia and fibula region, in calcification, 657t, *664*
  - of wrist and hand, 972, 1011t, *1012-1015*
    - in calcification, 973, 1016t, *1030-1031,* 1067t
    - in crystal deposition disease, 1017t, *1037*
    - in dermatomyositis-polymyositis, 1016t
    - in epidermolysis bullosa, 1017t, *1042*
    - in frostbite, 1017t, *1040*
    - instability of wrist in, 999t, *1000-1002*
    - in pseudohypoparathyroidism, 1054t, *1060*
    - in pyogenic osteomyelitis, 1055t, *1062*
    - in scleroderma, 1016t, *1030-1031*
    - in thermal and electrical injuries, 1017t, *1041*
- Spastic paralysis, patellar injury in, 559t, *566*
- Spina bifida occulta
  - cervical, 67t, *75*
  - in Klippel-Feil syndrome, 67t, 73t
  - lumbar, *230,* 233t, *238*
    - and clasp-knife deformity, 233t, *239*
  - osteosclerosis in, 313t
  - sacrococcygeal, *347,* 349t, *351*
  - thoracic, 167t, *168*
- Spina ventosa, 754t, *757*
- Spinal canal stenosis
  - cervical, 67t, *73*
    - decompressive surgery in, 151t, *154*
    - in Klippel-Feil syndrome, *74*
  - lumbar, 234t, *240,* 282t-283t, *291-293*
    - central, 282t-283t, *291*
    - foraminal, 282t, 283t, *291-292*
    - lateral recess, 282t, 283t, *292-293*
    - measurement methods, 234t, *240,* 282t
- Spinal cord
  - in diastematomyelia, 5t
    - lumbar, 235t, *243*
    - thoracic, 177t, *182*
  - in syringomyelia, *870*
  - tumors of, thoracic scoliosis in, 178t
- Spine, 2t, 12t, 44-376
  - block vertebrae in. *See* Block vertebrae
  - cervical, 44-160. *See also* Cervical spine
  - cupid bow configuration of vertebral bodies in, 2t, 233t, *237*
  - dysraphisms of, 5t
  - Hahn venous channels in, 2t
    - lumbar, 233t, *236*
    - thoracic, *165,* 167t, *168*
  - lumbar, 228-344. *See also* Lumbar spine
  - osseous outgrowths of, 194t
  - osteomyelitis of, 134t
  - osteonecrosis of, 40t
    - lumbar, 327t, *336*
    - steroid-induced, *225,* 327t, *336*
    - thoracic, 221t, *225*
- Spine *(continued)*
  - sacrococcygeal, 345-376. *See also* Sacrococcygeal spine
  - thoracic, 161-227. *See also* Thoracic spine
  - thoracolumbar. *See* Thoracolumbar spine
- Spinous process, vertebral
  - cervical
    - fracture of, 84t, 92t, *99*
    - osteochondroma of, *144*
  - lumbar, 229t
  - sacral, 346t
  - thoracic, 162t
- Spondylitis
  - ankylosing, 14t. *See also* Ankylosing spondylitis
  - tuberculous, 42t, *208*
- Spondyloarthropathy
  - cervical, 45
    - in dialysis, 111t, *137*
    - psoriatic, 109t
  - in dialysis, 35t, 111t, *137*
  - lumbar, psoriatic, 295t, *302-303*
  - sacrococcygeal, 345
    - psoriatic, 356t, 357t, *367*
  - thoracic, psoriatic, 193t, *204*
- Spondylodiscitis
  - cervical, 111t, *135-137*
    - pyogenic, 111t, *135-136*
    - tuberculous, 111t, *137*
  - lumbar
    - pyogenic, 295t, *309*
    - tuberculous, 295t, *310*
  - thoracic
    - pyogenic, 193t, *207*
    - tuberculous, 173t, 193t, *208-209*
- Spondyloepiphyseal dysplasia congenita
  - cervical, 78t, *79*
  - lumbar, 244t
  - thoracic, *170,* 170t
- Spondylolisthesis
  - cervical
    - congenital, 67t, *75*
    - degenerative, 107t, *118, 152*
    - traumatic, 84t
  - lumbar, 228, 248t-249t, *250-258*
    - degenerative, 248t-249t, *255,* 281t, *285*
    - dysplastic, 248t, *250*
    - high grade, 249t, *258*
    - iatrogenic, 249t
    - instability in, 249t, *257*
    - Myerding measurement method, *252,* 252t
    - progressive, 249t, *257*
    - and spina bifida occulta, 233t, *238*
    - spondylolytic, 248t, *251-253, 257*
- Spondylolysis
  - cervical congenital, 52t, *65*
  - lumbar, 228, 248t-249t, *250-258*
    - acute, 248t, *254*
    - pathologic, 249t, *255*
    - and spina bifida occulta, 233t, *238*
    - traumatic, 249t
    - unilateral, 249t, *256*
  - osteosclerosis in, 313t
- Spondyloptosis, lumbar, 249t, *252*
- Spondyloschisis, cervical, *46, 65*
  - anterior, 51t, *55*
  - posterior, *54*
- Spondylosclerosis, hemispheric, of lumbar vertebral bodies, 282t, *289*
- Spondylosis
  - cervical, 45, 107t
    - chronic, 150t, *158*
    - fusion surgery in, *158*

- Spondylosis *(continued)*
  - lumbar, 268t, 294t
  - thoracic, 192t
- Sporotrichosis, 23t
- Sports activities. *See* Athletic activities
- Sprains, 10t
  - of cervical spine
    - hyperextension, 93t, *102*
    - hyperflexion, 91t, 94t, *95*
    - hyperflexion-hyperextension, *103*
  - of collateral ligament of knee, medial, 590t
  - of tibiofibular joint, proximal, 575t, *577*
- Sprengel deformity, 824t, *828*
  - in Klippel-Feil syndrome, 73t, 824t, *828*
- Sprung pelvis, *399*
- Squaring of vertebral body, in ankylosing spondylitis
  - lumbar, 294t, *300*
  - thoracic, 201t, *203*
- Srb's anomaly, 781t, *783*
- Staphylococcal infections
  - Brodie abscess of tibia in, *668*
  - iliopsoas bursitis in, 469t, *483*
  - osteomyelitis in
    - of femur, *546*
    - of humerus, *905*
    - of tibia, *666-667*
  - septic arthritis of sternoclavicular joint in, *801*
  - septic bursitis of elbow in, *940*
- Stener lesion in gamekeeper's thumb, 1003t, *1006*
- Sternoclavicular joint, 776-818
  - ankylosing spondylitis of, 797t
  - anomalies and variants of, 776
  - articular disorders of, 776, 797t
  - cleidocranial dysplasia of, 781t, *786*
  - dislocation of, 789t, *795,* 842t
    - anterior, 789t, *795,* 842t
    - posterior, 789t, 842t
  - normal developmental anatomy of, 776, *780*
  - osteoarthrosis of, 797t, *798*
  - osteomyelitis of, 814t
    - chronic recurrent multifocal, *818*
  - rheumatoid arthritis of, 797t
  - septic arthritis of, 797t, *801*
  - in sternocostoclavicular hyperostosis, 797t, *800,* 883t, *884*
  - trauma of, 776
- Sternocostal joint
  - articular disorders of, 776, 797t
  - osteoarthrosis of, 797t, *798*
  - in sternocostoclavicular hyperostosis, 797t, *884*
- Sternocostoclavicular hyperostosis, 797t, *800,* 883t, *884*
- Sternum, 776-818
  - accessory ossicles of, 781t
  - anomalies and variants of, 776, 781t, *786*
  - bifid, 781t
  - cleidocranial dysplasia of, 781t, *786*
  - fissure in, 781t
  - foramen and cleft in, 781t
  - fractures of, 776, 789t, *793-794*
    - acute, 789t, *793*
    - insufficiency, 789t, *794*
  - in manubriosternal junction dislocation, 789t, *796*
  - metabolic, hematologic, and infectious disorders of, 776, 814t
  - normal developmental anatomy of, 776, 777t, *778-780*
- Sternum *(continued)*
  - ossification centers in, 776, 777t, *778-780*
    - age of appearance and fusion, 777t
    - asymmetry of, 781t
  - in pectus carinatum, 781t
  - in pectus excavatum, 781t, *786*
  - in sternoclavicular joint. *See* Sternoclavicular joint
  - in sternocostoclavicular hyperostosis, 797t, *800*
  - tumors and tumorlike lesions of, 776, 802t-803t
- Still disease, *1025*
- Straddle fracture of pubic rami, 392t, *396*
- Straight back syndrome, 173t, *174*
- Streptococcal infections, septic arthritis of hip in, *481*
- Stress-related bone injuries, 6t
  - of ankle and foot, 710t, *713,* 715t, 727t-728t
    - in calcaneus, 714t, *716-717*
    - metatarsal, 723t, *725*
    - in navicular bone, 715t, *721*
  - of cervical spine, in anterior arch of atlas, *55*
  - in children, 8t
  - of clavicle, 832t, *837*
  - of elbow, 919t
  - of femur
    - diaphyseal, 509t, *513*
    - proximal, 453t, *456,* 460t
  - of fibula, 629t, *634,* 710t, *713*
  - of humerus, 889t
  - of lumbar spine, postoperative, in laminectomy, *339*
  - of pars interarticularis, 228
    - grading system for, 259t
  - of patella, 559t, *565*
  - of pelvis, 393t, *402,* 404t
  - of phalangeal bones in hand, 1004t, *1010*
  - of ribs, 788t, *792-793*
  - of sacrum, 352t, *355*
  - of sternum, 789t, *794*
  - of tibia, *567,* 629t, *631-632,* 710t
  - of ulna, 948t, *950*
- Stylohyoid ligament ossification, 68t, *78*
- Styloid process
  - of radius, fracture of, 951t, *955*
  - of ulna
    - fracture of, 952t, *956*
    - in gout, *1032*
    - rheumatoid arthritis of, *1022*
- Subluxation, 10t
  - atlantoaxial. *See* Atlantoaxial articulation, instability and subluxation of
  - of hip, in developmental dysplasia, 444t, *450, 451*
  - of scaphoid, rotary, 999t, *1000*
- Subscapularis tendon impingement, 856t
- Subtalar dislocation, 715t, *720*
- Subungual exostosis
  - of foot, 759t, *763*
  - of hand, 1047t, *1049*
- Supernumerary bones, 2t
- Supracondylar foramen of humerus, 887t, *888*
- Supracondylar process of humerus, 887t, *888,* 913t
  - fracture of, 917t, *921-922*
- Supraspinatus tendon
  - calcific tendinitis of, 858t, *864*
  - impingement of, 856t
  - tear of, 847t, *850, 851*
- Supraspinous ligament ossification, 294t
- Surgery
  - cervical spine, 45, 151t, *152-154,* 155t, *156-158*
    - fusion in, 151t, *152-153,* 155t, *156, 158*
    - instrumentation and bone grafts in, *153,* 155t, *156-158*
    - in intervertebral disk disorders, 45, 151t, *152,* 155t, *157*
    - laminectomy and laminoplasty in, 151t, *154*
  - in femoral fracture, intertrochanteric, *462*
  - lumbar spine, 329, 337t, *337-342*
    - in diastrophic dysplasia, *247*
    - in disk disorders, 339t, *341-342*
    - fusion in, *337,* 337t
    - instrumentation and bone grafts in, 339t, *340-342*
    - laminectomy and facetectomy in, 337t, *338-339*
    - spondylolisthesis after, 249t
  - thoracic spine, 161, 226t, *227*
    - in compression fractures, 226t, *227*
    - in scoliosis, 178t, *184*
- Sustentaculum tali, ossicle of, 691t, *699*
- Swan-neck deformity
  - cervical, postlaminectomy, *154*
  - of hand, *1030,* 1066t
- Sweat gland disorders, 22t
- Symphalangism
  - of foot, 692t
  - of hand, 978t, *982*
- Symphyseal cleft injection in osteitis pubis, 404t
- Symphysis pubis, 377
  - in alkaptonuria, 406t, *412*
  - ankylosing spondylitis of, 405t, *410*
  - calcium pyrophosphate dihydrate crystal deposition disease of, 405t, *411, 428*
  - chondrocalcinosis of, 405t, *411, 428*
  - classification and grading of changes in, 405t
  - diastasis of, 392t, *395*
    - postpartum, 392t, *395*
    - in sacral fracture, *353, 395, 397*
    - in sprung pelvis, *399*
  - hemochromatosis of, 406t, *412*
  - hyperostosis of, diffuse idiopathic skeletal, 405t, *408*
  - inflammatory disorders of, 405t, *410-411*
  - normal developmental anatomy of, 378t, *383*
  - ossification centers in, 378t, *383*
  - psoriatic arthropathy of, 405t, *411*
  - in renal osteodystrophy, 406t, *412*
  - rheumatoid arthritis of, 405t
  - trauma of, 10t, 377
- Symphysography in osteitis pubis, 404t
- Synchondroses, 8t
  - of cervical spine, *63*
  - ischiopubic
    - normal developmental anatomy of, *379-380, 384, 436*
    - unfused, *384,* 384t
- Syndactyly
  - of foot, 692t
  - of hand, 978t, *981*
- Syndesmophytes
  - of lumbar spine, 294t, *300-301*
  - of thoracic spine, 194t, 201t, *202, 203, 204*

Synostosis
  of carpal bones, 977t, *979*
  of cervical spine
    in lower segment, 67t, *72,* 73t, *74, 113*
    in upper segment, 52t, *53, 63, 66*
  of lumbar spine, developmental, 233t, *237*
  phalangeal, of hand, 978t, *982*
  of radioulnar joint, 913t, *914,* 945t
  of ribs, 781t, *783*
  sacrococcygeal, 349t
  of thoracic spine, 167t
Synovial cell sarcoma
  of ankle and foot, 758t, 760t, *761, 767*
  of wrist and hand, 1043t, *1046*
Synovial cysts
  of acromioclavicular joint, 849t, *853*
  of ankle and foot, 759t
  of elbow, *937*
  of hip, 468t, *474*
  of knee, 578t, *582*
  of lumbar juxtafacet joint, 283t, *293*
Synovial disorders
  of ankle and foot, 760t
    cysts, 759t
    in idiopathic synovial osteochondromatosis, 735t, *750*
    in pigmented villonodular synovitis, 760t
    in silicone synovitis, 735t, *753*
  of elbow
    cysts, *937*
    in idiopathic synovial osteochondromatosis, 935t, *940*
    in pigmented villonodular synovitis, 935t
  of hip
    cysts, 468t, *474*
    in idiopathic synovial osteochondromatosis, 470t, *487*
    in pigmented villonodular synovitis, 470t, *487*
  of knee, *547,* 578t-579t, *580-584*
    cysts, 578t, *582*
    in idiopathic synovial osteochondromatosis, 579t, *584*
    in juvenile idiopathic arthritis, *604*
    in pigmented villonodular synovitis, 579t, *583*
    plica, 579t, *583*
  of shoulder
    in idiopathic synovial osteochondromatosis, 859t, *868*
    in pigmented villonodular synovitis, 859t, *867*
  of wrist and hand
    in detritic synovitis and osteolysis, 1017t, *1042*
    in idiopathic synovial osteochondromatosis, 1017t, *1040*
    in silicone synovitis, 1017t, *1041*
Synovial osteochondromatosis, idiopathic, 21t
  of ankle and foot, 735t, *750*
  of elbow, 935t, *940*
  of hip, 470t, *487*
  of knee, 579t, *584*
  of shoulder, 859t, *868*
  of wrist and hand, 1017t, *1040,* 1067t
Synovitis
  detritic, and osteolysis of hand, 1017t, *1042*
  pigmented villonodular, 21t
    of elbow, 935t
    of foot, 760t
    of hip, 470t, *487*
Synovitis *(continued)*
    of knee, 579t, *583*
    of shoulder, 859t, *867*
  in rheumatoid arthritis, 13t, 22t
  silicone
    of foot, 735t, *753*
    of wrist and hand, 1017t, *1041*
  in synovitis-acne-pustulosis-hyperostosis-osteitis, 15t, 22t. *See also* SAPHO
Syphilis
  congenital, 42t
    ankle and foot disorders in, 754t
    tibia and fibula disorders in, 666t, *670*
    wrist and hand disorders in, 1055t
  neuropathic osteoarthropathy in
    of knee, 600t, *613*
    of lumbar spine, *299*
  skin and joint findings in, 23t
Syringomyelia, neuropathic osteoarthropathy in
  of elbow, 935t, *942*
  of shoulder, 859t, *870*

T

T score in osteoporosis, *331,* 331t
Talipes calcaneovalgus, 681t
Talipes equinovarus, 681t, *684*
Talocalcaneal joint
  coalition of, 681t, *683,* 690t, *693, 739, 743*
  in os sustentaculi, 691t, *699*
Talocalcaneonavicular joint, 736t
  dislocation of, *720*
Talocuboid coalition, 690t, *694*
Talonavicular joint
  coalition of, 690t
  in congenital vertical talus, *685*
  crystal deposition disease of, 734t, *747*
  osteoarthrosis of, *738*
  psoriatic arthropathy of, *743*
Talus
  accessory, 690t
  beak prominence of, 691t
  chondroblastoma of, 759t, *763*
  dislocation of, 715t, *720*
  fractures of, 714t, *718-720*
    osteochondral, 715t, *719*
    stress, 728t
  normal developmental anatomy of, 673t, *674, 677*
  ossification centers in, 673t
  osteochondritis dissecans of, 715t, *719*
  osteoid osteoma of, *762*
  osteonecrosis of, 772t, *773*
  in talocalcaneal coalition, 681t, *683,* 690t, *693, 739, 743*
  in talocuboid coalition, 690t, *694*
  in tibiotalar joint. *See* Tibiotalar joint
  vertical, rocker-bottom foot in, 681t, *685*
Target sequestrum in intraosseous lipoma, *536*
Tarsal bones
  coalition of, 2t, 690t, *692-694*
    calcaneonavicular, 690t, *692*
    talocalcaneal, 681t, *683,* 690t, *693, 739, 743*
    talocuboid, 690t, *694*
  dislocations of, 715t, *722, 751*
  fractures of, 714t-715t, *716-722*
  in Mueller-Weiss syndrome, 772t, *774*
  normal developmental anatomy of, *677-680*
  osteomyelitis of, *755-757*
  osteonecrosis of, *774*
  osteoporosis of, *769*
Tarsometatarsal joint, 736t
  ankylosing spondylitis of, *742*
  gouty arthropathy of, *748, 749*
  Lisfranc fracture-dislocation of, 715t, *722, 751*
  neuropathic osteoarthropathy of, *751*
  osteoarthrosis of, *738*
Tendinitis, 728t
  Achilles, *731*
  calcific, 18t
    of femur, 509t
    of hip, 469t, *479*
    retropharyngeal, 110t, *133*
    of shoulder, 848t, 858t, *864*
    of wrist and hand, 1017t, *1037*
  of rotator cuff, 848t, 858t, *864*
  of wrist and hand, 1011t, 1017t, *1037*
Tendon disorders
  of Achilles tendon. *See* Achilles tendon disorders
  of ankle and foot, 728t, *731-733*
    in giant cell tumor of tendon sheath, 760t
  of biceps brachii. *See* Biceps brachii tendon
  of elbow, 929t, *931-933*
    lateral epicondylitis in, 929t, *931*
    medial epicondylitis in, 929t, *932*
  of knee, *547,* 592t, *596*
  of rectus abdominis, 404t
  of shoulder, 848t, *852*
    in calcific tendinitis, 848t, 858t, *864*
    in rotator cuff, 847t-848t, *850-851. See also* Rotator cuff
  of triceps brachii, 929t, *933*
  of wrist and hand, 1011t, *1013*
    in calcific tendinitis, 1017t, *1037*
    in giant cell tumor of tendon sheath, 1011t, *1015*
Tendon sheath giant cell tumor
  in foot, 760t
  in hand, 1011t, *1015*
Tennis elbow, 929t, *931*
Tenosynovitis, 728t
  biceps brachii, 848t, *852*
  peroneal, *732*
  of wrist and hand, 1011t, *1013*
Teres minor tendinitis, calcific, 858t, *864*
Terminal ventricle, persistent, 5t
Tetralogy of Fallot, rib notching in, 787t
Thalassemia, 39t
  lumbar spine disorders in, 327t, *335*
  pelvic disorders in, 427t, *430*
  rib marrow hyperplasia in, 814t, *818*
Thermal injuries of hand, 1017t, *1041*
  terminal phalangeal resorption in, *1067,* 1067t
Thiemann disease, 40t, 1065t
Thigh splints, 509t, *514*
Thoracic cage, 776-818
  articular disorders of, 797t, *798-801*
  normal developmental anatomy of, 776, *778-780*
  ribs in. *See* Ribs
  sternum in. *See* Sternum
Thoracic spine, 161-227
  anomalies and variants of, 161, 167t, *168-169*
  articular disorders of, 161, 192t-194t, *194-209*
    in crystal deposition disorders, 193t, *206*
    degenerative, 192t, *194-201*
    infectious, 193t, *207-209*
    inflammatory, 193t, 201t, *202-205*

- Thoracic spine *(continued)*
  - butterfly vertebra in, 167t, *169*
  - congenital disorders of, 161, 170t, *170-172*
  - dysplasia of, 161, *170,* 170t
  - fractures of
    - in ankylosing spondylitis, 193t, *204*
    - burst, 185t, *188*
    - compression, 185t, *186-187,* 187t
      - in hemangioma, *217*
      - in osteogenesis imperfecta, 170t, *172*
      - in osteoporosis, 221t, *222*
      - surgical procedures in, 226t, *227*
    - in diffuse idiopathic skeletal hyperostosis, *200*
    - with dislocation, 185t, *190*
    - instability in, *189-190*
    - in middle segment, 185t, *186*
    - scoliosis in, 178t
    - in seat belt injuries, 185t, *189*
    - in upper segment, 185t
  - heaped-up appearance of vertebral bodies in, *170*
  - instability in
    - checklist for diagnosis of, 191t
    - in fractures, *189-190*
  - intervertebral disk disorders of. *See* Intervertebral disk disorders, thoracic
  - ivory vertebrae in, *213*
  - kyphosis of, 161, 173t, *174-176*
    - in osteoporosis, 173t, *175,* 222
  - metabolic disorders of, 161, 221t, *222-225*
  - normal developmental anatomy of, 161, 162t, *162-166*
  - osseous outgrowths of, 194t
  - scoliosis of, 161, 177t-179t, *180-184*
    - in tumors, 178t, *183, 215*
  - surgical procedures involving, 161, 226t, *227*
    - in compression fractures, 226t, *227*
    - in scoliosis, 178t, *184*
  - traumatic injuries of, 161, 185t, *186-191*
    - kyphosis in, 173t
    - scoliosis in, 178t, *182*
  - tumors and tumorlike lesions of, 161, 209t, *210-220*
    - benign, 209t, *215-217*
    - malignant, 209t, *210-214*
    - myeloproliferative, 209t, *213-214*
    - scoliosis in, 178t, *183, 215*
    - tumorlike lesions, 209t, *218-220*
- Thoracolumbar spine
  - fractures in, 185t, *187-190*
    - burst, 262t, 264t
    - with dislocation, 185t, *190*
  - in hypothyroidism, 221t, *223*
  - instability in, *189-190*
    - in burst fracture, 264t
    - checklist for diagnosis of, 191t
  - kyphosis in injuries of, 173t
  - seat belt injuries of, 185t, *189,* 262t
- Thumb
  - Bennett fracture-dislocation of, 1003t, *1005*
  - bifid, 979t, *983*
  - carpometacarpal osteoarthrosis of, 1016t, *1019*
  - gamekeeper's, 1003t, *1006*
  - metacarpophalangeal joint of, 1018t
    - dislocation of, 1004t, *1007*
  - triphalangeal, 979t, *983*
  - Z-shaped deformity of, 1066t
- Thurston-Holland fragment in metaphyseal fractures, 8t
- Thymus, sail sign of, *162*
- Thyroid disorders
  - acropachy, 37t
  - carcinoma metastatic to scapula, *872*
  - hyperthyroidism, 37t
  - hypothyroidism. *See* Hypothyroidism
- Tibia, 623-671
  - diaphyseal dysplasia of, progressive, 624t, *628*
  - diaphyseal fractures of, 628t-629t, *630-632*
  - distal
    - fractures of, 705t, *706, 708-709,* 709t-710t, *711*
      - stress, 710t
    - growth plate injuries of, 710t, *712*
    - metaphyseal injuries of, 710t, *711*
    - normal developmental anatomy of, 673t, *674-677*
    - ossification centers in, 673t
    - in psoriatic arthropathy, *743*
  - focal fibrocartilaginous dysplasia of, 624t, *626*
  - fractures of, 623, 628t-629t, *630-632*
    - in children, 628t, *630-631*
      - in abuse, 710t, *711*
    - diaphyseal, 628t-629t, *630-632*
    - distal, 705t, *706, 708-709,* 709t-710t, *711,* 728t
    - fatigue, *567,* 629t, *631-632,* 710t
    - insufficiency, 629t, *633,* 710t
      - in osteomalacia, *658*
    - in intercondylar eminence, 560t, *568*
    - lateral capsular avulsion, *568,* 591t
    - in plateau, 557t, 559t-560t, *567*
    - proximal, 559t-560t, 561t, *567-568, 571*
      - avulsion, 560t, 561t, *568, 571,* 591t
      - in child abuse, 560t, *569*
      - metaphyseal, 557t, 560t, *569*
    - Segond, 560t, *568,* 591t
  - hematologic disorders of, 623, 657t
  - in hereditary multiple exostoses, *534*
  - infections of, 623, 665t-666t, *666-671*
  - in limb length inequality, 504, *505-506,* 624t, *625*
  - melorheostosis of, 624t, *627*
  - metabolic disorders of, 623, 657t
  - osteogenesis imperfecta of, 624t, *627*
  - osteopathia striata of, 624t
  - osteopetrosis of, 624t, *626*
  - osteopoikilosis of, 624t, *627*
  - periosteal reaction in, 657t, *662*
  - proximal
    - in chondrodysplasia punctata, 555t, *556*
    - in dysplasia epiphysealis hemimelica, 555t, *556*
    - in femorotibial dislocation, 575t, *576*
    - fractures of, 559t-560t, 561t, *567-568, 571*
    - growth plate injuries of, 561t, *571*
    - normal developmental anatomy of, 548t, *549-551*
    - in Osgood-Schlatter disease, 561t, *572*
    - osteonecrosis of, corticosteroid-induced, *622*
    - in pigmented villonodular synovitis, *583*
    - in renal rickets, *618*
    - in tibiofibular dislocation, 575t
  - sclerosing bone dystrophy of, mixed, 624t, *627*
  - in shin splints, 629t
  - in tibiotalar joint. *See* Tibiotalar joint
  - tubercle apophysis, 548t, *550-551*
    - avulsion fracture of, 561t, *571*
- Tibia *(continued)*
  - tumors and tumorlike lesions of, 623
    - benign, 643t-644, *645-652*
    - malignant, 635t-636t, *637-641*
    - metastatic, 635t, *637-638*
    - myeloproliferative, 636t, *641-643*
    - tumorlike lesions, 653t, *653-656*
  - varus deformity of, 624t, *626*
- Tibialis tendon disorders
  - anterior, 728t, *732*
  - posterior, 728t, *732*
    - in diabetic neuropathic joint disease, *751*
- Tibiofibular joint
  - proximal, sprain and dislocation of, 575t, *577*
- Tibiotalar joint, 736t
  - fracture-dislocation of, 710t, *713*
  - hemophilic arthropathy of, *683,* 735t, *750*
  - osteoarthrosis of, *738*
  - osteochondromatosis of, idiopathic synovial, 735t, *750*
  - psoriatic arthropathy of, *743*
  - slant of, 681t, *683, 741, 750*
    - in hemophilic arthropathy, *683,* 735t, *750*
    - in juvenile idiopathic arthritis, *741*
- Tietze syndrome, 788t
- Tillaux fracture, 705t
- Toddler fractures, 8t, 628t, *631*
- Toes. *See* Foot
- Tonsillar carcinoma metastatic to humerus, *892*
- Tophaceous gout, 19t, 23t
  - of ankle and foot, 735t, 737t, *749,* 760t, *766*
  - of cervical spine, 110t, *133*
  - of hip, 469t, *480*
  - of lumbar spine, 295t, *308*
  - of shoulder, *866*
  - of wrist and hand, 1017t
- Tracheal cartilage calcification, 68, *77,* 167t, *169*
- Transverse foramen of axis, 51t, *56*
- Transverse ligament of cervical spine
  - absence of, 52t
  - traumatic disruption of, 82t, *85*
- Transverse process, vertebral
  - cervical, *56*
    - elongation of anterior tubercles, 67t, *70*
    - elongation of C7, 68t, *76, 164*
    - fracture of, 83t, 94t, *106*
    - ossification centers in, 45t, *46, 49-50*
  - coccygeal, 346t
  - hyperplasia of, 2t
  - lumbar
    - fracture of, 262t, *265*
    - osseous bridging of, 262t, *265*
    - ossification centers in, 229t
  - sacral, 346t
  - thoracic, ossification centers in, 162t, *164*
- Trapezium
  - fractures of, 991t, *994*
  - in lupus erythematosus, *1028*
  - ossification centers in, 973t
  - in scleroderma, *1030*
- Trapezoid bone
  - fractures of, 991t
  - ossification centers in, 973t
  - synostosis with capitate, 977t, *979*
- Trauma, 10t
  - of ankle and foot, 672, 705t, *706-709,* 709t-710t, *711-713*
    - metatarsal and phalangeal fractures and dislocations in, 723t, *724-727*

- Trauma *(continued)*
    - soft tissue injuries in, 728t-729t, *730-733*
    - tarsal fractures and dislocations in, 714t-715t, *716-722*
  - of cervical spine. *See* Cervical spine, traumatic injuries of
  - of elbow
    - fractures and dislocations in, 906, 917t-919t, *919-928*
    - soft tissue injuries in, 906, 929t, *930-933*
  - of femur, 503, 509t. *See also* Femur, fractures of
  - of hip, 434, 451t, *452,* 453t, *454-459,* 460t-461t
  - of humerus, 886, 889t, *890*
  - of knee
    - dislocations in, *547,* 575t, *576-577*
    - fractures in, *547,* 558t-562t, *562-574*
    - popliteal artery aneurysm in, 617t, *622*
  - of lumbar spine, 228, 262t, *263-267*
    - spondylolysis in, 249t
  - of pelvis, 377, 392t-393t, *394-401,* 404t-405t
  - of radius and ulna, 944
    - diaphyseal fractures and dislocations in, 948t, *949-950*
    - distal fractures and dislocations in, 951t-952t, *952-956*
  - of ribs and sternum, 776, 788t-789t, *790-796*
  - of sacrococcygeal spine and sacroiliac joints, 345, 352t, *353-355*
  - of shoulder, 819, 832t-833t, *834-840*
  - of thoracic spine, 161, 185t, *186-191*
  - of tibia and fibula, 623, 628t-629t, *630-635*
  - of wrist and hand, 972
    - carpal fractures and dislocations in, 990t-991t, *992-998*
    - ligament instability in, 999t, *1000-1002*
    - metacarpal and phalangeal fractures and dislocations in, 1003t-1004t, *1005-1010*
- Trevor disease
  - of ankle and foot, *703,* 703t
  - of knee, 555t, *556*
- Triangular fibrocartilage complex lesions, 1011t, *1012*
- Triceps brachii muscle and tendon injuries, 929t, *933*
- Trichorhinophalangeal syndrome of Giedion, 978t, *981*
- Triquetrum
  - fractures of, 990t, *993*
  - in greater arc injuries, 991t, *997*
  - ossification centers in, 973t
  - in pisiform-triquetral joint, 1018t
    - osteoarthrosis of, *1019*
  - synostosis with lunate, 977t, *979*
- Triradiate cartilage, normal developmental anatomy of, *379-380, 436*
- Trisomy 21
  - atlantoaxial instability in, 52t, 59t
  - atlantodental interspace in, *62*
  - brachydactyly in, 978t, *980*
  - pelvic disorders in, 388t, *389*
- Trochanters of femur
  - avulsion fracture of, 453t, *458*
  - normal developmental anatomy of, *380,* 435t, *436-437*
- Trochlea of humerus, ossification centers in, 907t, *909*
- Trolley track sign in ankylosing spondylitis
  - lumbar, *300*
  - thoracic, 201t
- Trough fracture in posterior glenohumeral dislocation, 841t, *844*
- Tuberculosis
  - arthritis in, 42t
    - of ankle and foot, 754t
    - of elbow, 935t
    - of hip, 469t, *484*
    - of knee, 600t, *613*
    - of shoulder, 859t, *867*
    - of wrist and hand, 1055t, *1064*
  - dactylitis in
    - of foot, 754t, *757*
    - of hand, 1055t, *1064*
  - osteomyelitis in, 42t
    - of ankle and foot, 754t, *757*
    - of tibia and fibula, 666t, *669*
    - of wrist and hand, 1055t, *1064*
  - spondylitis in, 42t
    - of thoracic spine, *208*
  - spondylodiscitis in
    - cervical, 111t, *137*
    - lumbar, 295t, *310*
    - thoracic, 173t, 193t, *208-209*
- Tuberosity of radius, radiolucent, *912,* 913t, 945t, *946*
- Tumors and tumorlike lesions, 24t-33t
  - of ankle and foot, 672, 758t-760t, *761-767*
  - of cervical spine, 45, 138t-139t, *140-148*
    - enlarged intervertebral foramen in, 146t
  - of clavicle, 819, 870t-871t, *872-877*
  - of femur. *See* Femur, tumors and tumorlike lesions of
  - of fibula. *See* Fibula, tumors and tumorlike lesions of
  - general characteristics and imaging findings in, 24t-33t
    - in benign bone tumors, 28t-31t
    - in malignant bone tumors, 24t-27t
    - in tumorlike lesions, 32t-33t
  - of hand. *See* Hand, tumors and tumorlike lesions of
  - of humerus. *See* Humerus, tumors and tumorlike lesions of
  - of knee, *535,* 547, 614t, *615-616*
  - of lumbar spine, 228, 312t, *312-326*
  - of pelvis, 378, 413t-414t, *415-427*
  - of radius and ulna, 944, 957t-959t, *960-966*
  - of ribs and sternum, 802t-803t, *804-813*
  - of sacrococcygeal spine, 345, 371t, *372-376*
  - of scapula, 819, 870t-871t, *872-877*
  - of shoulder, 819, 870t-871t, *872-877*
  - skin and joint findings in, 22t
  - of thoracic spine, 161, 209t, *210-220*
    - scoliosis in, 178t, *183, 215*
  - of tibia. *See* Tibia, tumors and tumorlike lesions of
  - of wrist. *See* Wrist, tumors and tumorlike lesions of
- Turner syndrome, wrist and hand disorders in, 985t, *986*
- Turret exostosis of hand, 1048t

U

- Ulcer, Marjolin, 41t
- Ulcerative colitis. *See* Colitis, ulcerative
- Ulna, 944-971
  - abutment or impaction syndrome of, 945t, *947*
- Ulna *(continued)*
  - anomalies and variants of, 944, 945t, *946-947*
  - distal
    - fractures of, 951t-952t, *952-956*
      - in children, 951t, *953*
    - in gout, *1032*
    - ossification centers in, 973t
    - rheumatoid arthritis of, *1022*
  - fractures of, 944
    - in child abuse, 952t, *956*
    - in coronoid process, 918t, *924*
    - diaphyseal, 948t, *949*
    - distal, 951t-952t, *952-956*
      - in children, 951t, *953*
    - in Monteggia fracture-dislocation, 917t, 948t, *949*
    - nightstick, 948t, *949*
    - proximal, 918t, *924*
    - stress, 948t, *950*
    - in styloid process, 952t, *956*
  - in lead poisoning, 967t, *969*
  - Madelung deformity of, 945t, *946,* 977t
  - metabolic, hematologic, and infectious disorders of, 944, 967t, *968-971*
  - olecranon process of. *See* Olecranon of ulna
  - ossification centers in
    - distal, 973t
    - proximal, 907t, *909, 912,* 913t
  - proximal
    - in diffuse idiopathic skeletal hyperostosis, 934t, *936*
    - dislocation of, 917t, *919-920*
    - fractures of, 918t, *924*
    - ossification centers in, 907t, *909, 912,* 913t
    - synostosis with radius, 913t, *914,* 945t
  - in radioulnar joint. *See* Radioulnar joint
  - tumors and tumorlike lesions of, 944, 957t-959t, *960-966*
    - benign, 958t-959t, *964-965*
    - malignant, 957t, *960-962*
    - myeloproliferative, 957t, *963*
    - tumorlike lesions, 959t, *966*
  - variance of
    - negative, 945t, *947*
    - positive, 945t, *947*
- Uncinate process
  - fracture of, 94t
  - hypertrophy and osteophyte formation, *113-115*
- Uncovertebral joint disorders, 107t, *113-115*
- Uric acid serum levels in gout, 19t
- Uterine carcinoma, metastatic, acetabular protrusion in, *443*

V

- Vacuum phenomenon, 40t
  - cervical, 107t, *113, 118, 152*
  - lumbar, 268t, 327t, *336*
  - sacroiliac, 356t, *359, 360*
  - thoracic, 192t, *206,* 221t, *225*
- Valgus deformity
  - of foot, 681t
    - in hallux valgus, 682t, *687-688*
  - of hip. *See* Coxa valga
  - of knee, 557t
- Valley fever, 23t. *See also* Coccidioidomycosis
- Van Neck disease, 40t
- Varus deformity
  - of foot, 681t
  - of hip. *See* Coxa vara

Varus deformity *(continued)*
  of knee, *556,* 557t
  of tibia, 624t, *626*
Vascular disorders
  of ankle and foot, 768t, *770*
  of cervical spine, 45, 159t, *159-160*
  of knee, 547, 616t-617t
  of lumbar spine, 329, 342t, *343-344*
  of tibia and fibula, 657t, *662*
  of wrist and hand, 1054t, *1058*
Venous insufficiency, periosteal reaction of tibia and fibula in, 657t, *662*
Vertebrae
  cervical
    block (synostosis)
      in lower segment, 67t, *72,* 73t, *74, 113*
      in upper segment, 52t, *53, 66*
    compression fracture of, 92t, 94t
    flattened (vertebra plana), 67t, *69*
    limbus, *75, 112*
    nuclear impressions of, 67t, *69*
    sagittal fracture of, 94t, *106*
    sandwich, in osteopetrosis, 78t, *80*
  lumbar
    block (synostosis), 233t, *237*
    bullet, 327t, *332*
    butterfly, 234t
    compression fracture of, 262t, *263*
    cupid bow contour of, 233t, *237*
    fish, *319, 330*
    ivory, *315, 318, 324*
    limbus, 269t, *279*
    nuclear impressions of, 233t, *236*
    osteonecrosis of, 327t, *336*
    picture-frame, *323*
    sandwich, 244t, *246, 255*
    scalloping of. *See* Scalloping of lumbar vertebrae
    segmental sclerosis of, 282t, *289*
    squaring of, 294t, *300*
    wasp-waist constriction of, *237*
  thoracic
    block (synostosis), 167t
    bullet, 221t, *223*
    butterfly, 167t, *169*
    compression fracture of, 185t, *186*
    heaped-up appearance of, *170*
    ivory, *213*
    osteonecrosis of, 221t, *225*
    sandwich, 170t, *171*
Vertebral artery abnormalities, 159t
  aneurysm, 159t, *160*
  enlarged cervical intervertebral foramen in, 146t
Vertebroplasty in thoracic compression fractures, 226t
Vinyl chloride exposure, acro-osteolysis in, 23t, 1067t
Viral infections, skin and joint findings in, 23t
Vitamin A excess, 36t
  clavicle disorders in, 883t
Vitamin C deficiency, 36t
  femoral disorders in, 541t, *544*
  knee disorders in, 616t
  tibia and fibula disorders in, 657t, *661*
Vitamin D
  deficiency of
    humerus in, *904*
    osteomalacia in, 34t
  excess of, 36t
Von Recklinghausen disease. *See* Neurofibromatosis type I

W

Ward triangle of femur, 2t, *490*
Wasp-waist constriction of lumbar vertebrae, *237*
Wilms tumor
  radiation therapy in
    pelvic disorders after, *433*
    thoracic scoliosis after, 178t, *182*
  skeletal metastasis to tibia and fibula, *638*
Wimberger sign
  in scurvy, 541t, *544, 661*
  in syphilis, congenital, *670*
Winking owl sign in skeletal metastasis, *312*
World Health Organization definition of osteoporosis and osteopenia, 229, 331t
Wrist, 972-1067
  acquired deformities of, 973, 1066t
  anomalies and variants of, 972, 977t-978t, *979-980*
  articular disorders of, 972, 1016t-1018t, *1019-1042*
    compartmental analysis of, 1018t
    in crystal deposition disease, 1017t, *1033-1035, 1037*
    degenerative, 1016t, *1019-1021*
    inflammatory, 1016t, *1022, 1025-1026, 1028*
  carpal tunnel syndrome of, 1011t, *1013*
  congenital disorders of, 972, 985t
  dislocations in, 991t, *995-998*
    lunate and perilunate, 991t, *996*
Wrist *(continued)*
  dysplasias of, 972, 985t
    fibrous, 1048t
  fractures of, 972, 990t-991t, *992-995*
    blisters as complication of, 1017t, *1041*
  ganglion cyst of, 1011t, *1014,* 1048t, *1053*
  gouty arthropathy of, 1017t, *1032*
  greater arc of carpal bones in, *995*
    injuries of, 991t, *997*
  infections of, 972, 1055t, *1063-1064*
  instability of, 999t, *1000-1002*
    in crystal deposition disease, 1017t, *1033*
    dorsal intercalated segmental, 999t, *1000*
    in external ligament injury, 999t, *1002*
    scapholunate advanced collapse wrist in, 999t, *1001,* 1017t, *1033*
    ventral intercalated segmental, 999t, *1001*
  lesser arc of carpal bones in, *995*
    injuries of, 991t, *996*
  metabolic disorders of, 972, 1054t-1055t
  normal developmental anatomy of, 972, 973t, *974-976*
  ossification centers in, 972, 973t
    age of appearance and fusion, 973t
    extra or additional, 978t, *980*
  osteonecrosis of, 973, *1065,* 1065t
  radial deviation of, 1066t
  soft tissue disorders of, 972, 1011t, *1012-1015*
    ligamentous, 999t, *1000-1002*
  tumors and tumorlike lesions of, 972
    benign, 1047t-1048t, *1049-1052*
    malignant, 1043t, *1044*
    metastatic, 1043t, *1044*
    tumorlike lesions, 1048t, *1052-1053*
  ulnar bayonet deformity of, 1066t
  ulnar deviation of, 1066t

X

Xiphoid process
  absent, 781t
  ossification centers in, 777t, *780*

Y

Yo-yo on a string sign in gamekeeper's thumb, *1006*

Z

Z score in osteoporosis, *331*
Z-shaped deformity of thumb, 1066t
Zigzag deformity of hand, 1066t